Bulletin of the Geological Society of Greece
Special Publication No. 7, 2019

Proceedings

of the

15th International Congress

of the

Geological Society of Greece



ERE 2019

15th International Congress of the Geological Society of Greece

Athens, 22-24 May 2019

EXPLORING AND PROTECTING OUR LIVING PLANET EARTH

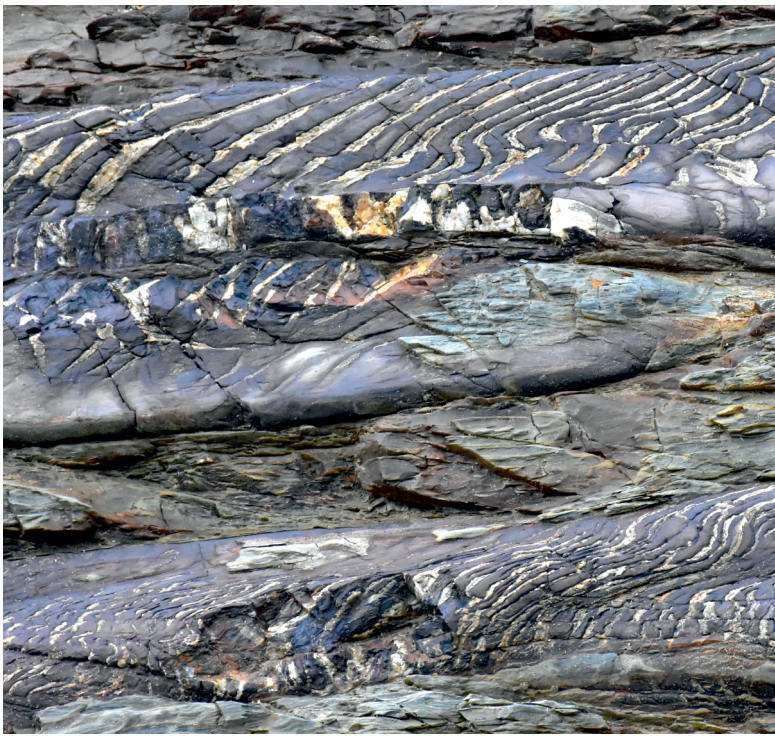

Athens, Greece | 22-24 May 2019

ΕΓΕ 2019
15th International Congress of the Geological Society of Greece
Athens, 22-24 May 2019
EXPLORING AND PROTECTING OUR LIVING PLANET EARTH
www.gsg2019.gr



Bulletin of the Geological Society of Greece
Special Publication No. 7, 2019
Volume Editor: Haralambos Kranis

Proceedings

of the 15th International Congress of the Gelogocial Society of Greece

Athens, Greece | 22-24 May 2019

GOLD SPONSOR

HHRM
HELLENIC HYDROCARBON RESOURCES MANAGEMENT

SILVER SPONSORS

Epiroc

HELLENIC PETROLEUM
GROUP OF COMPANIES

HellasGOLD

SPONSORS / EXHIBITORS

Marathon Data Systems

GEOSYSTEMS HELLAS

ΔΕΗ Ανανεώσιμες
Καινοτομία • Ανάπτυξη • Περιβάλλον

ΓΕΩΤΕΧΝΙΚΟ ΕΠΙΜΕΛΗΤΗΡΙΟ ΕΛΛΑΔΑΣ

hcmr
Ε Λ Κ Ε Θ Ε

Ο.Α.Σ.Π.
Οργανισμός Αντισεισμικού Σχεδιασμού & Προστασίας

ΙΓΜΕ

GEOLOGICAL SOCIETY OF GREECE

BOARD MEMBERS

(Elected at the GSG General Assembly, May 2018)

President:	
Spyros Pavlides, Professor	Aristotle University of Thessaloniki
Vice-President:	
Assimina Antonarakou, Professor	National and Kapodistrian University of Athens
Secretary General:	
Haralambos Kranis, Ass. Professor	National and Kapodistrian University of Athens
Executive Secretary:	
Hara Drinia, Professor	National and Kapodistrian University of Athens
Treasurer:	
Evgenia Moraiti, Dr. Geologist	Institute of Geology and Mineral Exploration
Trustee:	
Apostolos Arvanitis, Dr. Geologist	Institute for Geology and Mineral Exploration
Members:	
Athanassios Ganas, Research Director	National Observatory of Athens
Petros Koutsovitis, Dr. Geologist	CERTH
Kiki Makri, Dr Geologist	National Observatory of Athens

ΕΓΕ 2019

15th International Congress of the Geological Society of Greece

Athens, 22-24 May 2019

EXPLORING AND PROTECTING OUR LIVING PLANET EARTH

ORGANIZING COMMITTEE

Congress Chair:	
Efthymis Lekkas, Professor	National and Kapodistrian University of Athens
Vice-Chair:	
Issaak Parcharidis, Professor	Harokopio University of Athens
Secretariat:	
Assimina Antonarakou, Professor	National and Kapodistrian University of Athens
Hara Drinia, Professor	National and Kapodistrian University of Athens
Evangelia Kotsi, Ph.D.c.	Geotechnical Chamber of Greece
Treasurer:	
Haralambos Kranis, Ass. Professor	National and Kapodistrian University of Athens
Members:	
Theodora Rondoyianni, Professor	National Technical University of Athens
Athanassios Ganas, Research Director	National Observatory of Athens
Dimitris Sakellariou, Research Director	Hellenic Centre for Marine Research
Ioannis Papanikolaou, Assoc. Professor	Agricultural University of Athens
Loukas Georgalas, Dr. Geologist	Ministry of Environment and Energy
Spyros Lalechos, Dr. Geologist	Earthquake Planning and Protection Organization
Evgenia Moraiti, Dr. Geologist	Institute of Geology and Mineral Exploration
Nikolaos Nikolaou, Dr. Geologist	Institute of Geology and Mineral Exploration
Xenophon Stavropoulos, Dr. Geologist	Association of Greek Geologists

KEYNOTE TALKS

ΕΓΕ 2019 | 15th International Congress of the Geological Society of Greece
Athens, 22-24 May, 2019 | Harokopio University of Athens, Greece
Bulletin of the Geological Society of Greece, Sp. Publ. 7 **KEYNOTE TALK**



From Pangaea to the Active Hellenic Subduction Zone

Dimitrios Papanikolaou
National and Kapodistrian University of Athens, Greece

The Hellenides have been developed within a segment of the Tethys Ocean between Eurasia and Gondwana of the Pangaea configuration, since the Early Triassic. Their paleogeographic evolution was characterised by an opening phase throughout Early Triassic – Late Jurassic and a closing phase from Late Jurassic to present. The Tethyan realm was rather complicated as there were several microcontinents / terranes, drifting from the Gondwana / African passive margin to the European active margin. Thus, a number of distinct oceanic basins was opened and closed in between the northwards drifting continental fragments, which were gradually accreted to the European margin. Major subduction zones and orogenic arcs were associated to the Axios / Vardar oceanic basin in Late Jurassic-Early Cretaceous, sutured between the Rhodope and Pelagonian terranes, the Pindos / Cyclades basin in Late Cretaceous-Eocene, sutured between the Pelagonian / Internal and the Apulia / External Carbonate Platforms and the East Mediterranean basin, subducting since Late Miocene, between the External Carbonate Platform and Africa. The overall development of the orogenic wedges and the resulting new Hellenic continental crust is maintained through compressional and extensional detachments at subcrustal scale, involving tectonic wedges of shallow sedimentary and deeper metamorphic units.

Dimitrios Papanikolaou *was born in Athens and studied Natural Sciences and Geology at the University of Athens. He started his carrer as assistant at the Laboratory of Geology (1974), he obtained his PhD in Geology (1978) and became full professor of Dynamic, Tectonic Geology and Marine Geodynamics (1993) at the University of Athens. He served as President of the Geological Society of Greece (1988-1992, 1994-1996), Project Leader of IGCP 276 «Paleozoic Geodynamic Domains and their Alpidic Evolution in the Tethys» (1988-1995), President of the Karpatho-Balkan Geological Association (1993-1995), President of the Earthquake Planning and Protection Organization (1993-1998), President and General Director of the National Centre for Marine Research (1994-2000), Member of the board of CIESM in Monaco (1994-2000), Member of the Scientific Committee for International Continental Deep Drilling, in Potzdam (1998-2000), Secretary General for Civil Protection, at the Ministry of Interior (2000-2002). During 1979-1980 he was post-doc researcher in Lausanne, Switzerland and in 1982-1983 he was professeur associe in Reims, France. He was nominated Grosby professor at the Dept. of Earth, Atmospheric & Planetary Sciences in MIT, USA (2003) and Barnes Distinguished Lecturer in the Jackson School of Geosciences, at Texas University in Austin, USA (2008). He has published more than 70 papers in peer reviewed scientific journals, more than 120 papers in Proceedings of Congresses and more than 25 papers in books, fieldguides etc. with more than 2400 citations. He was the Director of Studies of the Master's program in Oceanography (2007-2016) and in Natural Hazards (2009-2016). Since 2016 he is Emeritus Professor of Geology at the University of Athens.*

ΕΓΕ 2019
15th International Congress of the Geological Society of Greece
Athens, 22-24 May, 2019 | Harokopio University of Athens, Greece
Bulletin of the Geological Society of Greece, Sp. Publ. 7 **KEYNOTE TALK**



From Earth to "Gaia". An earth system science

Spyros Pavlides

Aristotle University of Thessaloniki, Dept. of Geology 541 24 Thessaloniki. Greece

System is a set of things working together as parts of a mechanism or an interconnecting network forming a unified whole. A **complex system** is a system composed of many components which is organized for a common purpose, an infrastructure such as power grid of transportation or communication systems, they interact with each other in a complex whole. Examples of complex systems are Earth's atmosphere and the global climate, organisms, the animal's brains, ecosystems, a living cell and ultimately the entire universe. Can we consider the Earth as a complex System? Does it meet the criteria to be named system? Presents a great diversity? Consists of many parts? What are the properties links of its parts? What interdependence? Can one's sub-system work alone? Has an organization? These are some question concerning the Earth as a unity to be answered today.

Gaia, the ancient Greek goddess personifying the Earth in its role as the beginning of life, is self-existent and unborn, the Big Mother, the Almighty Goddess. Gaia actually personifies the general cosmic frame within life is being evolved, or better to say, Gaia itself constitutes an integral system with life. Furthermore, Gaia represents a significant, scientific hypothesis (theory) of the last forty years which views the Earth in its entirety as a hyper- organism. Which are though the facts that geoscientists have nowadays at their disposal in order to adopt a stance towards this conjunction and why do we turn to myths again? From cognitive and psychological view, every myth is catalytic for the human way of thinking, as it simplifies the inexplicit scientific approaches through narration. No matter how many doubts might have been raised concerning the myth, it is still considered to be a primary form of historicity. Carried by the word, it is a quite philosophical and mainly pedagogic way of conveying knowledge; an allegoric attestation.

Earth is regarded as a planet with life on its surface. However, a new view has already begun to emerge: Earth is a living planet itself where "inorganic" and "organic" forms and processes are integrated in a single, integral unity. It is a new approach regarding Earth's operation and the life which rises from it and develops billions of years now on its sheer and lissom crust and on the so called biosphere with indistinct and limited boundaries. The matter of the constantly renewable biosphere has been recycled many times, both on the surface and inside the Earth, so as to maintain a constant bidirectional relation between the "inorganic" and "organic" matter (see bio-geochemistry or bio-geosciences).

Geology explores an enormous and significant part of our natural world. As per its definition, Geology studies in fact the solid crust of the earth on which we live, move and create. A first contribution of Geology was the study and understanding of the so called "inorganic" world, namely the study and classification of the rocks of Earth's crust, the rocks' components, the minerals and the understanding of the structure of matter from the amorphous to the crystal level. However, beyond the description of the composition of Earth's crust and the structure of its components, the most important contribution of Geology towards this direction was the large extent of understanding of the formation, destruction, transformation and recycling of our planet's materials, where life itself is the main geological factor. The "geological cycle", that is the rocks and minerals transformation cycle, and the dynamics of this ceaseless procedure take place in the geological time dimension. There is a permanent and impressive mobility in geological time which is difficult to be anticipated by man, as he has formed the perception that Earth is static, inorganic, steady, a "terra firma", due to his restricted empirical perception of geological time.

Geological knowledge plays a significant role in understanding and partially explaining time. Geological time starts in present time and goes through the recorded history of humanity. It runs the paleontological history of human beings that goes up to 5 million years back, of mammals (60-100 million years), of life on land (500 million years), of the beginning of life on our planet (3,5 billion years), of Earth's generation (4,6 billion years). Within this period, the mountains, the valleys, the extension and the position of the seas, which seem ageless compared to the man's life scale, change rapidly and systematically so as if they are in a permanent motion under the influence of very strong powers. A geological evolution interdependent biological evolution.

The Earth has been divided in Geospheres from the deepest Nucleus, to Mantle, Lithosphere, Hydrosphere, Atmosphere, Biosphere etc. The knowledge of the inner structure of our planet - an achievement of the early 20th century, Alfred Wegener's "Theory of Continental Drift", the "Theory of Seafloor Spreading" and mainly the "Theory of Plate Tectonics", also known as the "Theory of New Global Tectonics", which integrates the big geological and geophysical phenomena into a coherent unity, only in the last quarter of the 20th century, offered a satisfying explanation for orogenesis, (mountain building), volcanism, seismic activity, petrogenesis (creation and development of rocks), mineralization and primarily the Earth's crust kinematics, an a holistic view of Earth's processes.

The above mentioned theories concede the continent's movement, i.e. the movement of land, a concept that is firmly established in man's consciousness as a reference point for stability. In this sense, these theories can be related to Galileo's theory supporting that "the earth moves", which had such a radical impact on the evolution of human thought. The recent "Theory of Plate Tectonics" that dominates today the world of geosciences and can be epistemological characterized as a "model", "assumption" or "paradigm (example)" after the statement of the historian of geosciences and philosopher Thomas Kuhn, has the characteristics

of a big and important scientific conception: Simplicity, Universality, Globality and Completeness, as it generalizes and unifies on a planet scale every single local geological effect. Before the formulation of the Theory of Plate Tectonics, there was a fragmentary approach to the single geological phenomenon while the relevant theories-assumptions were incomplete and non-generalized. The Theory provides now a single and clear mechanism to explain all geological phenomena. So, time is ripe to think globally, that is holistic view.

The Theory of Plate Tectonics constitutes a significant contribution of geosciences to human thought. The fact that it is tough on all educational levels and that it is widely spread on a scientific as well as a popular science level– mainly due to its simplicity- have made it very popular and show how significant it is. This Theory of Plate Tectonics, or better to say, "The generalized hypothesis", has provided the expert scientist with new tools of thinking and the average educated man with new possibilities of understanding his "home", planet Earth.

Earth's lithosphere, in particular the continental crust, constitutes a unique feature of our planet as it is not met in other planets of our solar system. It owes its uniqueness primarily to two basic facts: the existence of water, a basic element of life, and its tectonic mobility. The "richness" of the surface water, the atmospheric water as well as the groundwater is impressive. The hydrosphere constitutes also a space of joined organic and inorganic processes. "We can consider the global ocean surrounding the earth exactly as the petals on a flower".

Earth's magnetosphere, namely its substantial shield, extends up to 100 km over its surface. This is another outcome of the processes that take place in the inner part of earth, in particular in its core. The rest of the earth planets have inconsiderable magnetospheres. This exactly is another particularity of our planet Earth. However, the most significant uniqueness of our planet is life itself.

The "lithospheric plates" mobility generates the earthquakes and the volcanoes. A physiological process which influenced from the Earth's interior and affects the Earth's crust and surface. The volcanoes then generate, renew and partially recycle the lithosphere and the gasses of the atmosphere. If we consider our planet's age as equivalent to the average age of a man, the renewal of big parts of the crust takes place approximately every three years. This renewability of earth's crust influences the biosphere and generates geo-ecological system diversity, which is responsible for the amazing diversity in various forms of life. The crust's mobility is directly connected with life, or is even part of life.

The atmosphere's composition, as it was formed in the first phases of its geological history and as it is preserved for over 500 million years now within some limits, which are considered to be optimal for life, played a decisive role in earth's development into a living planet. The atmosphere constitutes in fact the main factor of life maintenance in cooperation with life itself. Its oxygen, a product of photosynthesis, bacterial fermentation and volcanic explosions is interdependent with life. The "Gaia" hypothesis points out that life is the climate regulator and the climate changes vary then within some limits, which are adequate for life maintenance.

The strong bacteria, which constitute a primeval form of life, play even today the most important role in the animal-inorganic recycling. Bacteria are ubiquitous in every habitat on earth, under the most extreme life maintenance conditions; in volcanic craters, up to 4 km deep in the Earth's crust, in the deepest points of oceans, in the deep thermal springs of the mid-ocean ridges. The bacteria participate even in the geological processes. Still, there are a lot of things concerning Earth's dynamic which we do not understand.

New scientific researches on the "geo-physiology" of the living planet provide a new way of viewing earth's function as well as life's function which is generated in earth and develops on its sheer crust, the so called biosphere. In fact, there is no biosphere in the sense we use the term for other geospheres –crust, mantel and core-. Life constitutes an integral part of the upper crust, mainly of its surface, and of the atmosphere. Life participates in the geological processes as a substantial factor. The development of this new scientific knowledge and view will offer us the possibility in the near future to obtain a better understanding of ourselves, as living objects within a broader object, our planet.

In a holistic view Earth as a whole is considered as a System of Systems, in the theory of Chaos and Complexity that is a Complex System, a new "Gaia", an Active Planet or a "Living Planet".

References

Αναγνώστου, Χ., and Χρόνης, Γ., 2002, Το γήινο σύστημα - εισαγωγή στις γεωεπιστήμες: Αθήνα, Εκδόσεις Χαμηλοθώρης, 172 p.

Back, P. 1996. «How Nature Works: The science of self-organized criticality». Springer-Verlag, New York.

Condie, C, K. 2005. «EARTH as an Evolving Planetary System». Elsevier.

Holmes, A., 1978, Principles of Physical Geology: Sunbury on Thames, Nelson, 730 p.

Lenton Tim, 2018. Earth System Science: A Very Short Introduction. Oxford University Press.

Lovelook, J.E. (2000). Gaia: A New Look at Life on Earth Oxford University Press.

Lovelock, J. E., «GAIA, Medicine for an ailing planet». Gaia books. 192pp. 3rd Ed. (2005).

Lovelock, J. E. and Margulis, L. 1984 «Gaia and Geognosy», In Global Ecology: Towards a Science of Biosphere. Rambler M.B. (Ed.), 72-79.

M'Pherson, P.K., 1974, A perspective on systems science and systems philosophy: Futures, v. 6, p. 219–239, Margulis, L., 1998, Symbiotic Planet: A New Look at Evolution. Kindle Edition. Basic books.

Παυλίδης, Σ., 1999, Η Συμβολή της Γεωλογικής Γνώστης στην Εξέλιξη της Ανθρώπινης Σκέψης: Scientific American - Ελληνική έκδοση, v. Α΄.

Παυλίδης, Σ., 2007, ΠΑΝ-ΓΑΙΑ, : μία διαφορετική βιο-γεωλογική διαδρομή στον πλανήτη Γη: Αθήνα, Leader Books, 290 p.

Παυλίδης, Σ. , Χατζηπέτρος, Α., 2018. ΓΕΩΣΥΣΤΗΜΑ «ΓΑΙΑ», Κατανοώντας τη δομή και λειτουργία του πλανήτη μας. Liberal Books. Press, F., Siever, R., Grotzinger, J., and Jordan, T.H., 2004, Understanding earth: W.H. Freeman.

Σαχτούρη, Ε., 1990, Γαία - Το ανθρώπινο ταξίδι από το χάος στη σκέψη: Αθήνα, Λιβάνης -Νέα Σύνορα, 379 p.

Στουρνάρας, Γ.Κ., 2017, Παμμήτειρα Γαία - Διαχρονική φυσιογνωστική και φιλοσοφική προσέγγιση: University Studio Press, 376 p.

ERE 2019
15th International Congress of the Geological Society of Greece
Athens, 22-24 May, 2019 | Harokopio University of Athens, Greece
Bulletin of the Geological Society of Greece, Sp. Publ. 7 **KEYNOTE TALK**



Exploring for energy resources and the role of the geosciences in Greece

Yannis Bassias
Hellenic Hydrocarbon Resource Management, Greece

At a time when sustainable development is by-and-large a fundamental requirement for economic growth and development, hydrocarbon exploration – and in particular natural gas exploration– is going to be a primary element of the Greek economy's energy mix. What is more, in tandem with the pipeline projects (Trans-Adriatic Pipeline, East-Med) they form the main concerns of the country's energy plans.

In that sense, geosciences play an important role in every stage of those projects. As they progressively develop even from the first exploration phases of the concession areas from basic desktop geological, geophysical and economical studies, activities will require a well-trained and highly-skilled competent workforce that will match the needs of the operating companies.

Needless to say, given the long-term investments in the E&P industry (25 to 30 years), there will have to be efficient and well-organized training plans in place coupled with the necessary conditions that will allow Greece to build a competitive workforce. This should and will open up a new chapter in geoscience education from today.

Yannis Bassias *was appointed in November 2016 Chairman and CEO of the Hellenic Hydrocarbon Resources Management SA (HHRM) for a five-year term. He has 30 years of international business experience in geology and geophysics, in technical projects and corporate management for reservoir evaluation, creating portfolio of oil and gas resources and the contribution of human resources and of international relations. Between 2012-2016 he consulted in the evaluations of research permits, with country authorities' partners and local stakeholders in frontier offshore hydrocarbon bearing sedimentary basins in West Africa, Mauritania, in the Mozambique Channel, the Central-Southern Atlantic, and the French overseas departments which are under European legislation. Between 1997 and 2012 he conducted an evaluation team prospecting in Texas, Colombia, Yemen, Senegal, Venezuela, Tunisia, Congo and created an exploration portfolio in the Paris Basin and in Tunisia. In the service business, he was President and CEO of the Georex group for 20 years, he demerered the exploration assets from the service activities in geology and geophysics and created subsidiaries for the provision of services in France, Tunisia, United Kingdom and Republic of Congo. He managed multiannual programs such as the creation of a database of hydrocarbon reservoirs for the CIS republics in cooperation with the Institutes IFP and VNIGNI, the merger of databases of companies Total, PetroFina and Elf, the digital storage of seismic data of the National Petroleum Company of the Republic of the Congo (SNPC). Before joining the petroleum industry, he had an academic career in the Free University of Berlin with main research focus the Pre-Cambrian of Anti-Atlas (Morocco) and then as Associate Professor in Geology at the National Museum of Natural History in Paris working on the sedimentary basins and ridges of the Indian Ocean. He holds a PhD in Geology (Paris 1984), degree in Geology from the University of Athens (1979), diploma in Economics from French Institute of Management, IFG (1994) and Management-Marketing Certificate from the Business School of Paris, Chamber of Commerce and Industry, CCIP (1989). He is author or co-author of more than 30 publications in international scientific or industry journals on the Indian Ocean, Central-South Atlatinc, France, Greece, Morocco, and co-editor of 3 reports of the TAAF (Terres Australes et Antarctiques Françaises) sea campaigns in the Indian Ocean.*

ERE 2019
15th International Congress of the Geological Society of Greece
Athens, 22-24 May, 2019 | Harokopio University of Athens, Greece
Bulletin of the Geological Society of Greece, Sp. Publ. 7 **KEYNOTE TALK**



The Opening of the Western Mediterranean during the Alpine Orogeny: a Perspective from Orogenic Peridotites and UHP Eclogites

Carlos J. Garrido
University of Granada, Spain

Talk outline

Any geodynamic model for the opening of the western Mediterranean should account for the exhumation and emplacement of the largest outcrops worldwide of subcontinental lithospheric mantle (SCLM) peridotites —and associated UHP eclogites— occurring in the western peri-Mediterranean Alpine chain. It must also explain the origin of the characteristic internal tectono-magmatic zoning of Betic-Rif-Tell orogenic peridotites, recording a polyphase P-T-t evolution from UHP cratonic-like SLCM to hyper-extended, oceanic-like mantle. Here, I present a model for the opening of the western Mediterranean largely segmented by inherited structures from the Mesozoic Paleo-Tethys Ocean. Late Cretaceous to Eocene N-directed subduction of the Tethys and subsequent continental collision occurred in a highly segmented subduction zone where the westernmost segments developed high-T UHP eclogites that did not occur in colder subduction eastern segments. The opening of the Ligurian-Provencal basin and the counter-clockwise rotation of the easternmost Sardinia-Corsica segment followed this contractional event. The easternmost Kabylian-Rif-Betic segment, however, underwent a SSE-directed pervasive back-arc extension during slab rollback leading to the final collision with the African margin. This model provides a common origin and accounts for the internal tectono-metamorphic evolution of orogenic peridotites in the Tell and Betics-Rif belts, and explains the high-T and UHP nature of associated eclogites.

Dr. Carlos J. Garrido *is a Senior Research Scientist at the Andalusian Institute of Earth Sciences (CSIC–Univ. Granada) and head of the Petrology and Geochemistry department. Carlos holds a M.Sc. and Ph.D. in Earth Sciences at the University of Granada. Before moving to Granada in 2002 as a Ramon y Cajal Fellow, he was a post-doctoral researcher at the Woods Hole Oceanographic Institution (USA) and a Marie-Curie Fellow at the University of Montpellier (France). During many years, he has served as a panelist of the European Research Council and a member of the editorial board of Lithos.*

ΕΓΕ 2019
15th International Congress of the Geological Society of Greece
Athens, 22-24 May, 2019 | Harokopio University of Athens, Greece
Bulletin of the Geological Society of Greece, Sp. Publ. 7 **KEYNOTE TALK**



Recent advances in landslides monitoring techniques

Daniele Giordan

Italian National Research Council – Research Institute for Hydrogeological Protection

The recent technological development has sharply increased the number of instruments that can be adopted for slope instabilities monitoring. Nowadays, a multiscale approach that considers satellites, aerial or UAVs systems and in place monitoring solutions can be considered state of the art for landslides monitoring. Satellites and aerial systems are good solutions for the first identification and characterization of active slides, and in situ monitoring networks are the best solution for a near real-time acquisition of a series of parameters that could support an early warning procedure. The use of early warning systems is essential in particular where the activation of large landslides can have a critical impact on infrastructure or population. In these cases, monitoring systems are usually a part of a more complex civil protection procedure that should also consider possible scenarios and risk reduction solutions. Even if the technological evolution offers complex and advanced monitoring instruments, the validation of monitoring results can always be done considering the geological model of the slope instability. When a validated result has been obtained, the last step for the effective use of these systems is a correct and dedicated communication strategy.

Daniele Giordan *holds a MSc and Ph.D. in Earth Science studying deep-seated gravitational slope deformations and landslides monitoring systems. He started to work at the Research Institute for Geo-Hydrological Protection of the Italian National Research Council in 2004, and he became a scientific researcher in 2009. Scientific coordinator of Geohazard Monitoring Group since 2015, he works in particular on the development of new methodologies and systems for geo-hydrological processes monitoring. In particular, he focused his attention on the use of monitoring systems for the improvement of the geological model of large slopes instabilities and correct management of early warning systems. He worked on the improvement of the effectiveness of monitoring systems defining a communication strategy for correct management and dissemination of monitoring results. Chairman of the Commission C35 "monitoring methods and approaches in engineering geology applications" of the International Association for Engineering Geology and the Environment, he has been editor of several books and special issues focused on natural hazards and engineering geology topics, and he is a co-author of more than 50 international papers and book chapters.*

ERE 2019
15th International Congress of the Geological Society of Greece
Athens, 22-24 May, 2019 | Harokopio University of Athens, Greece
Bulletin of the Geological Society of Greece, Sp. Publ. 7 **KEYNOTE TALK**



Soil Contaminant Baselines in the management of urban ecosystems

Andrew S. Hursthouse
University of the West of Scotland, UK

Talk outline

With increasing growth of the urban environment as population migration dominates land use, the resilience of urban ecosystem services is under critical pressure. Urban soils provide many significant functions for wider urban management and identifying their role as a source or sink of urban pollution is critical if we are to resolve their contribution to remediating and sustaining healthy urban ecosystems. A series of projects linked to defining the state and function of urban soils in a number of European cities provides opportunities to study source terms and baseline conditions for typical metallic (potentially toxic elements – PTEs) and organic pollutants (e.g. PAHs, PCBs). These studies highlight high levels of variability due to the wide range of inputs and the sources of contamination from air pollution through to direct introduction of wastes and the effects of urban management practice. Work includes the derivation of sources from the multivariate analysis of data on soil pollution from metallic elements, soil properties and basic indicators. The tools developed to assess impacts on desired soil function e.g. in supporting urban green infrastructure such as forestry, agriculture and recreational space and must form part of the management strategy to ensure reliable clean up and maintenance of urban ecosystems.

Professor Hursthouse *is an environmental geochemist, applying an "earth-systems" approach to his research which covers the transport/behaviour of pollutants in the environment, evaluating their impact on ecosystems and for human health. He undertook PhD and postdoc research on actinide geochemistry associated with nuclear waste processing facilities, developing analytical tools and applying them to study environmental transport processes. Subsequently his research has applied these principles in studies of the impact of wastes and development of management systems, resource recovery strategies and exposure assessment. He holds a high-end expert fellowship at the Regional Key Laboratory for Shale Gas Exploitation, Hunan University of Science & Technology, Xiangtan, China. He is a Trustee of Environmental Protection Scotland (http://www.ep-scotland.org.uk/) and Past President of the Society for Environmental Geochemistry & Health (www.segh.net).*

ΕΓΕ 2019
15th International Congress of the Geological Society of Greece
Athens, 22-24 May, 2019 | Harokopio University of Athens, Greece
Bulletin of the Geological Society of Greece, Sp. Publ. 7 **KEYNOTE TALK**

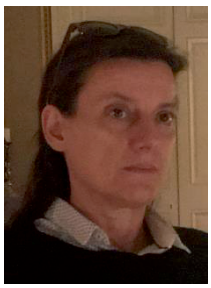

Meteorology in formal education: Necessity and teaching suggestions

Vassiliki Kotroni
National Observatory of Athens, Greece

Meteorology is a branch of Physical Sciences. It is mainly applied physics and every branch of physics finds an application in it. What gives rise to our weather is an *extremely* complex set of interactions involving fluid mechanics and thermodynamics. Physics also comes in to play when we use the principles from optics to explain how the atmosphere reflects and refracts light giving rise to phenomena as rainbows, coronas, glories, etc. and we use electrodynamics to try to understand lightning and phenomena associated with it, like red sprites and blue jets.

Weather phenomena influence everyday live and economy while severe weather phenomena may cause serious property and infrastructure damages, disruptions in economic and social activities, and human fatalities. The education of the citizens and namely of the pupils on the risks from natural hazards related to weather events and the increase of awareness on preparatory measures and precautions to protect themselves is actually needed.

The NOA's (National Observatory of Athens/ meteo.gr) scientific team of educational meteorology, named "*Peri Anemon & Ydaton*", has started in 2016 its effort to popularize the science of Meteorology for Junior and Senior High School pupils. The developed program aims to help the pupils understand how weather phenomena occur, based on the Physics' curriculum of each school grade. The "*Peri Anemon & Ydaton*" is currently under assessment through the completion of questionnaires by both teachers and pupils. In the frame of this presentation we will also discuss the results of the program assessment scores, by the teachers of the participating schools.

Dr. Vassiliki KOTRONI, *Research Director at the National Observatory of Athens, born in 1965, has a PhD in Dynamic Meteorology (University Clermont-Ferrand, 1993). She has acted as Research Associate at the University Athens (Meteorology Laboratory, Physics Dept.) during the period 1993-1998, while since 1999 she joined the National Observatory of Athens. She has more than 25 years of experience on numerical weather prediction. She has authored or co-authored 125 papers published in refereed international journals, and 4 book chapters in the fields of dynamic meteorology, numerical weather prediction (including dust forecasting), weather monitoring, atmospheric electricity, climatology, dynamics and societal impacts of weather related natural hazards. Her citation report includes 2019 citations and an h-index 25 (12/2018). She has worked extensively with a number of meteorological models (RAMS, MM5, BOLAM, WRF, WRF-CHEM). She coordinates: (a) the operational weather prediction and related activities at NOA based on MM5, WRF and WRF-CHEM models, (b) the operation of ZEUS lightning detection network; (c) in collaboration with Dr. K. Lagouvardos, the concept, development and operation of www.meteo.gr. This activity integrates specialized forecasts and observations over Greece, it was founded in 2002 and during the last years is constantly among the top-5 (in terms of average daily visitors) sites in the Greek internet (ref: www.ened.gr). This activity has been self-financed since 2006 and has attracted funding from the private sector that exceeds in total 4.000.000 €. Since 2016 she coordinates the educational program «Περί Ανέμων και Υδάτων - About Winds and Waters".*

ERE 2019
15th International Congress of the Geological Society of Greece
Athens, 22-24 May, 2019 | Harokopio University of Athens, Greece
Bulletin of the Geological Society of Greece, Sp. Publ. 7 **KEYNOTE TALK**



GEMAS: Geochemistry of European Soil for Producing Good Quality Food

Anna Ladenberger
Geological Survey of Sweden, Uppsala, Sweden

Assessment of risks to human health and the environment, related to exposure of metals in agricultural soil (arable land) and grazing land soil (grassland), is one of the requirements under the European Commission's REACH (Registration, Evaluation, Authorisation and Restriction of Chemicals) regulation. The regulation required the development of pan-European harmonised soil geochemical data sets for agricultural and grazing land and, thus, the emergence of the GEMAS project (GEocheMistry of Agricultural and grazing land Soil) of the EuroGeoSurveys Geochemistry Expert Group. The project addressed the data gap and data quality requirements imposed by REACH, *i.e.*, monitoring data were collected for metals in agricultural soil (arable land 0-20 cm) and grazing land soil (grassland 0-10 cm) from 33 European countries, using a harmonised sampling protocol, and all samples were prepared and analysed at the same laboratory for the same suite of determinands. Geochemical maps display a distinct element concentration break between northern and southern Europe delineating the limit of the last glaciation. This concentration break can be recognised for many elements, both nutrients (*e.g.*, P, Mg, Zn, Cu) and toxic ones (*e.g.*, Pb, As, Hg, Cd), and it is strongly controlled by underlying geology and climatic conditions. The signature from fertilisers and other land-use play subordinate role at the continental scale.

***Anna Ladenberger** is a senior research geochemist at the Geological Survey of Sweden (SGU). She received her PhD from the Jagiellonian University, Krakow, Poland, in the field of isotope geochemistry. Anna's research has focused on isotope geochemistry of volcanic rocks and Pb-U geochronology, and then moved into low temperature geochemistry with emphasis on geochemical mapping using various sample types (soil, till, plants, water) and analytical methods (acid leach, total concentrations and isotopic systems).*

Anna is Deputy chair of the EuroGeoSurveys Geochemistry Expert Group and a member of the Swedish Chemicals Agency's Toxicological Council, which identifies and evaluates signals of the New Emerging Risk Chemicals (NERC). She is author or co-author of more than 70 publications appearing as both SGU reports and papers in international peer-reviewed scientific journals.

ΕΓΕ 2019
15th International Congress of the Geological Society of Greece
Athens, 22-24 May, 2019 | Harokopio University of Athens, Greece
Bulletin of the Geological Society of Greece, Sp. Publ. 7 **KEYNOTE TALK**



Modern Issues of Geoethics

Gerassimos A. Papadopoulos
National Observatory of Athens, Greece

Geoethics is an emerging multidisciplinary field dealing with problems of Ethics applied to the Geosciences. Geoethics consists of research and reflection on the values which underpin appropriate behaviours and practices, wherever human activities interact with the Earth system. Geoethics deals with the ethical, social and cultural implications of geoscience knowledge, education, research, practice and communication, providing a point of intersection for geosciences, sociology, philosophy and economy. In addition, geoethics represents an opportunity for geoscientists to become more conscious of their social role and responsibilities in conducting their activity in education, in research as well as in the daily professional life. On the other hand, geoethics is a tool to influence the awareness of society regarding problems related to geo-resources and geo-environment. In this presentation two important examples of geoethical issues will be examined: geonservation and public communication of georisks. The examination will be made from several perspectives including research, education, professionalism, applications and operations. The first is an excellent example referring to geoconservation with the Phalasarna geoarchaeological area in NW Crete taken as a case study. The other example is about the early warning systems for earthquakes and tsunamis and the geoethical issues they open for consideration.

Gerassimos Papadopoulos *is an earthquake and tsunami scientist. Studies at the University of Thessaloniki, post-doc at MIT, USA. Visiting Researcher at NIED, Visiting Professor at Tohoku University (both in Japan), Research Director at the National Observatory of Athens. More than 150 published papers, 7 books, 3800 citations. He serviced in a long number of Committees, Societies and Working Groups of EU, UNESCO, Council of Europe, American Geophysical Union etc. He is Chairman of the NE Atlantic and Mediterranean Tsunami Warning System (UNESCO), Member of the Seismic Hazard Assessment Committee (EPPO), and Greek national representative of the International Association for the Promotion of Geoethics.*

ΕΓΕ 2019
15th International Congress of the Geological Society of Greece
Athens, 22-24 May, 2019 | Harokopio University of Athens, Greece
Bulletin of the Geological Society of Greece, Sp. Publ. 7 **KEYNOTE TALK**



Analysis of GPS Network Data for Detecting Anomalies and Geohazards

Panos Psimoulis
Nottingham Geospatial Institute, University of Nottingham, UK

The advances of GPS technology, such as the expansion of dense GPS networks with high sampling rate (even up to 10Hz), and the broader development of other satellite systems (GLONASS, BeiDou, etc.) have made GNSS an important tool in deformation monitoring applications in geohazards and potentially in early warning systems. Recent studies have shown the potential contribution of GPS in estimating earthquakes characteristics (magnitude, PGV, etc.). However, most of them are based on the analysis of the GPS coordinate time series aiming to determine the characteristics of the deformation and relate them to the current phenomenon. A recent approach has been developed, which is based on the analysis of GPS network data using temporal and spatial analysis algorithm for the detection anomalies potentially related to geohazards. The application of artificial neural networks and the spatial regression model are adopted to detect changes through the analysis of the time-history of the GPS records and their spatial correlation. Through their application in different case studies, it is shown that the temporal analysis is more effective for rapid, short-period changes, while the spatial analysis is more suitable for slowly developed anomalies.

Panos Psimoulis *began his academic life as civil engineer, with a degree from University of Patras in 2004, where he continued for an MSc and PhD degree focusing on geodetic applications in deformation monitoring of stiff civil engineering structures. After a year in Athens University of Applied Sciences, as Teaching and Research Associate, he left to continue his research as Research Fellow at the Geodesy and Geodynamics Lab in ETH Zurich, focusing on the application of high-rate GPS on seismology. Since 2013, he holds the position of Assistant Professor at the Nottingham Geospatial Institute of University of Nottingham. His research explores applications of deformation monitoring related to civil engineering structures and geohazards.*

ΕΓΕ 2019
15th International Congress of the Geological Society of Greece
Athens, 22-24 May, 2019 | Harokopio University of Athens, Greece
Bulletin of the Geological Society of Greece, Sp. Publ. 7 **KEYNOTE TALK**



The GEO - Geohazard Supersites and Natural Laboratories Initiative

Stefano Salvi
Istituto Nazionale di Geofisica e Vulcanologia, Italy

The Geohazard Supersites and Natural Laboratory initiative (GEO-GSNL) is a voluntary international partnership aiming to improve, through an Open Science approach, geophysical scientific research and geohazard assessment in support of Disaster Risk Reduction. This goal is pursued promoting broad international scientific collaboration and open access to a variety of space- and ground-based data, focusing on areas with high geohazard and risk levels. GEO-GSNL coordinates a global network of eleven geohazard Supersites, over which an international effort is carried out: space agencies provide satellite imagery at no cost for scientific use, monitoring agencies provide ground-based data, the international scientific community employs these data to generate new scientific results which are eventually delivered to national decision makers by the Supersite coordinators.

Stefano Salvi *is Technological Director at INGV-ONT Rome, Italy. He is expert in the application of optical and radar remote sensing to different Solid Earth applications, and in particular for crustal deformation studies and active tectonics. He coordinated several research projects in those fields. He founded the INGV Remote Sensing Laboratory and directed it for several years. He coordinates INGV operational services based on satellite EO data during seismic crises. He is Chair of the Geohazard Supersites and Natural Laboratory initiative of GEO and co-lead of the Seismic Demonstrator of the CEOS Working Group on Disasters.*

ΕΓΕ 2019
15th International Congress of the Geological Society of Greece
Athens, 22-24 May, 2019 | Harokopio University of Athens, Greece
Bulletin of the Geological Society of Greece, Sp. Publ. 7 **KEYNOTE TALK**



Stochastic Models in Seismology

George Tsaklidis
Aristotle University of Thessaloniki, Greece

Stochastic models accept that some aspects of a physical process cannot be explained or incorporated into the model and must be represented by some random process, in order to cope with the uncertainties. The stochastic model is used as a basis for planning, data analysis and prediction (or decision making -depending on the process). In that sense, stochastic models can be useful in seismology.

A seismic sequence can be interpreted as a realization of a point process through the consideration of the conditional intensity function, which characterizes the process completely. The corresponding models, known as Stress Release Models (SRMs), are the probabilistic translation of Reid's theory of the elastic rebound. According to these models an earthquake produces a sudden decrease of the amount of stress present along the fault; then the tectonic strain rebuilds gradually over time. The next event occurs when the stress exceeds the strength of the medium. Many versions of these stress release models have been established, based on different conjecture on the physical process evolving on regional scale. Using the SRMs the investigation of various statistical features of seismic activity can be carried out.

Markov processes constitute a wide category of models for studying the evolution of physical phenomena. These models do not take into account the dependencies on the time elapsed since the last event, due to the memoryless property of the geometric distribution (in the discrete-time case) or the exponential distribution (in the continuous-time case), which characterize these models. The semi-Markov models constitute a generalization of the Markov models; they can combine both the aforementioned dependencies and can be applied to characterize location-specific patterns of earthquake recurrence, based on strain accumulation and intermittent times. The Markov and semi-Markov properties allow for modeling of both the magnitude and time between successive earthquakes by taking into account the amount of strain energy released by the events, by means of the magnitude of the previous event. The main advantage of semi-Markov modeling is that it allows for different types of sojourn (interevent) time distributions; the parameters of the distributions as long as the transition probabilities can be estimated by means of the maximum likelihood estimation (MLE) method.

Hidden Markov models- abbreviated as "HMMs"-are considered to be generalizations of the abovementioned models. Especially, HMMs can be used in order to reveal hidden (unobservable) states through a timeseries of observations that depend on the hidden states through a given function (law). The dependence structure is still considered Markovian, thus allowing for using efficient computational methods. The HMMs have a wide range of applications, e.g., speech recognition, computational biology, signal processing etc. In seismology, the hidden states can represent any non-observable or not directly observed status of the physical process, e.g. the stress level, while the observations timeseries can represent the earthquakes magnitudes, or space coordinates related with the earthquakes, or any quantities associated with the physical process. The main problems arising in dealing with the HMMs, are the estimation, the evaluation and the decoding problem. There are available methodologies to face these problems, to estimate the parameters of the model and derive the underlying stochastic process, e.g., the underlying timeseries of stress levels associated with an earthquake sequence.

A drawback of HMMs is the inflexibility in dealing with the time spent in a given state, which is considered to be geometrically or exponentially distributed (for the discrete and continuous time, respectively). In order to face this problem, an extension of the HMMs, the hidden semi-Markov models (HSMMs) can be used; the HSMMs allow for considering any type of sojourn (interevent) time distribution of the underlying semi-Markov process. HSMMs have been applied in several scientific areas, e.g., speech recognition, human activity recognition, handwriting recognition, network anomaly detection, meteorology etc. In seismology the HMMSs can be used in the same way as the HMMs and despite their computational cost compared to the HMMs (due to the additive estimation burden), they can derive more reliable results, if enough data is available.

The Markovian Arrival Process (MAP) models can be applied to describe time-varying earthquake activity. The hidden states of MAPs can correspond to different levels of seismicity. The MAPs with phase type distributed interevent times are very flexible and often outperform the models with other distributions. Important indicators of the underlying Markov process can be estimated, e.g., change points concerning the underlying process.

References

Extended list of references can be found in:

Pertsinidou, C.-E., 2017. Stochastic models for the estimation of the seismic hazard. Ph.D. Thesis, University of Thessaloniki and Universite de Technologie de Compiegne, Thessaloniki, 199pgs.

Votsi, E,, 2013. Seismic Hazard Assessment through Hidden Markov and Semi-Markov Modeling and Statistical Estimation. Ph.D. Thesis, University of Thessaloniki and Universite de Technologie de Compiegne, Thessaloniki, 198pgs.

***Prof. George Tsaklidis** - Short CV: Education: B.Sc (4 years studies) in Mathematics, PhD in Mathematics (Probabilistic Modelling-Operat.Research) in the Aristotle University of Thessaloniki (AUTH), Greec; Personal skills : University Professor in Mathematics (AUTH): Statistical-Probabilistic Modeling (Markov and semi-Markov modeling, Hidden Markov and Hidden semi Markov modeling, Linear and Non-linear filtering and Applications (in Seismology, Finance, video-Tracking, Continuum Mechanics), Dynamics, Matrix Theory; PhD thesis supervision: 5 completed, 3 in progress; Publications: 43 in international scientific journals. 3 scientific books (one of them in english) Conference talks: More than 70.*

GENERAL SESSION

T1 Stratigraphy, Palaeontology and Sedimentology

15th International Congress of the Geological Society of Greece
Athens, 22-24 May, 2019 | Harokopio University of Athens, Greece
Bulletin of the Society Society of Greece, Sp. Pub. **7** Ext. Abs. GSG2019-063

The Tectono-stratigraphic Units of the Sofrana Insular Complex, Dodecanese Islands, Greece

A. Photiades[1], N. Carras[2]

(1) IGME, Olympic Village, Acharnae, Greece, fotiadis@igme.gr, (2) IGME, Olympic Village, Acharnae, Greece, nicarras@igme.gr

The geological mapping on the Sofrana insular complex, in the SE Aegean Sea, sheds some light on the geological history gap on that part of the Carpathian Sea, which extends among Astypalea, Karpathos and Cretan basin. We recognize two tectono-stratigraphic units that correlated with the geotectonic units of the external Hellenides on the adjacent islands, such as a parautochthonous unit at the base, tectonically overlain by an upper unit as follow:

A) The parautochthonous unit of the insular complex consists, from base to top, of a) basal recrystallized or dolomitic limestones and dolomites, overlain by a succession of fine-grained to mixed with big clasts, locally dolomitized, of grainstones, packstones and wackestones, as well as of Thaumatoporella bindstone, similar to the Ionian "Pantokrator" facies, of Late Triassic-Middle Lias age, occurring on the islets of Mikro Sofrano, Divounia and Astakida, and having a thickness up to 600m; b) Upwards, Upper Lias to Middle Jurassic platy to thin-platy, white, pelagic to sublithographic limestones occur, of mudstone texture, like the Ionian Sinies facies, 100m approximately thick, in the islets of Mikro Sofrano and Astakida, and c) at the top of the islets of Mikro Sofrano, Karavonisia, Avgo, Sial, Astakida and Astakidopoulo, an Upper Jurassic – Cenomanian sequence occurs, significantly recrystallized, with thin-to-mid-bedded, multifolded, green, pelagic limestones bearing silex intercalations and nodules, similar to the Ionian Vigla limestone facies, over than 500m in thickness.

B) The tectonically overlying upper unit consists, from base to top, of the following distinguished members: a) Medium- to thick-bedded, fine- to coarse-grained and brecciated limestones, slightly recrystallized, with rudist and coral fragments and, towards the base, micritic with bioclasts, of Cenomanian age. They occur on the islands Megalo Sofrano, Astakida (klippe) and Chamili, having a 500m apparent thickness; b) On Megalo Sofrano and Chamili islets develop upwards micritic to fine-clastic limestones (mudstones and wackestones), of early Senonian age, tending to emerge. The thickness is 100m approximately; c) At the top on Megalo Sofrano and Chamili islets develop Upper Campanian bioclastic limestones, with fine- to coarse-grained packstones, characterized by mild recrystallization, of 200m approximate thickness; d) Paleocene-Middle Eocene nummulitic bioclastic limestones, 150m approximately thick, occurring on the last two islets and, finally, e) a Middle (?) - Upper Eocene flysch sequence, with thin- to medium-bedded, fine- to medium-grained turbiditic sandstones with foliated argillite intercalations occurs solely on the Megalo Sofrano islet, exceeding 50m in thickness.

The above stratigraphy and stacking order of the Sofrana insular complex consists of a parautochthonous unit, which outcrops in Mikro Sofrano, Karavonisia, Avgo, Sial, Divounia, Astakida and Astakidopoulo islets, and is correlated to the Ionian geotectonic zone. Besides, the upper tectonic unit, occurring in Megalo Sofrano, Chamili and Astakida (as klippe) is correlated to the Gavrovo-Tripolis geotectonic zone and more precisely to the Gavrovo sub-zone.

This stacking setting, characterized by a thin-skinned thrusting, would occur in the late Miocene times, during the southward detachment of the Plattenkalk unit (Crete - Kassos - eastern Rhodes) that is implicated, in turn, in an inter-thrusting under the Ionian zone (Sofrana insular complex) and over the pre-Apulian zone (Ro - Strongyli – Kastellorizo complex).

Acknowledgements

This work is dedicated to the Hellenic Navy and especially to the Officers and crew of the Oceanographic Vessel Nautilus during 2008-2009.

Bulletin of the Geological Society of Greece, Sp. Pub. 7 Ext. Abs. GSG2019-162

Dachstein-type loferitic facies in the Upper Triassic-Lower Jurassic carbonate platform of the Eastern Greece Zone.

V. Kostopoulou[1], F. Pomoni-Papaioannou[1], A. Zambetakis-Lekkas[1]

(1) Department of Geology & Geoenvironment, University of Athens, Panepistimiopolis, 157 84 Athens, Greece, vakofil@gmail.com

This study aimed at the careful sedimentological analysis of the shallow-water carbonate sediments (Dachstein-type loferitic facies of "Pantokrator" Formation) developed during the Upper Triassic-Lower Jurassic times at the carbonate platform (referred to in this work as Pelagonian palaeoplatform) that geotectonically belongs to the zone of the internal Hellenides known as Eastern Greece. The neritic carbonates (limestones, dolomitic limestones) have been studied in order to determine their depositional environment and investigate their cyclic pattern.

The sedimentary facies of the chosen platform sections – which are located in the SW part of the Argolis peninsula (Didymi Mountains, Karnezeika area) as well as, in the SE part of the Corinthia (Korfos and Sofiko areas) and in the area of central Greece opposite Chalkis (Euboea) – have been studied in detail (Kostopoulou 2018). Loferitic facies have been described in the Didymi (Pomoni-Papaioannou, 2008) and Karnezeika (Varti-Mataranga and Matarangas, 1991) areas.

Eleven vertical profiles were systematically sampled for sedimentological analysis, using stained thin sections (Kostopoulou, 2018). The carbonate classification follows the schemes of Dunham (1962) and Folk (1959, 1962). Microfacies analysis is based on Wilson (1975) and Flügel (1982, 2004).

Macroscopic observations and microscopic characteristics lead to the definition of thirty eight carbonate microfacies and four facies zones (depositional environments). The described in detail microfacies (microfacies types/MF) can be classified into the following three facies associations that correspond, respectively, to the members C, B and A of the Fischer's (1964) typical Lofer cyclothem.

The lagoonal-shallow subtidal facies association generally consists of wackestones, packstones, packstones/grainstones and boundstones with diverse marine fauna and flora (e.g. megalodonts, dacycladacean algae, involutinids) (Fig. 1c). Peloids, microcoprolites, oncoids, aggregate grains, cortoids, small ooids and intraclasts are included in the observed non-skeletal particles.

The intertidal facies association mainly comprises of microbial (algal) laminated bindstones and fenestral algal bindstones/algal mat loferites (Fig. 1b). They are characterized by planar or crinkled well-developed laminations, abundant fenestrae with geopetal filling and a variety of desiccation structures. Pellet loferites also commonly occur and stromatolite intrabreccia are subordinately observed.

The supratidal-pedogenic facies association is represented by microfacies containing abundant subaerial diagenesis-related features, which reflect emersion events of different duration and subsequent weak or stronger early meteoric modification. Pisoids, circumgranular cracks, meniscus and microstalactitic cements, alveolar-septal structure, black pebbles, and rhizolite-like structures are included among the recognized diagenetic micromorphological characters (Fig. 1a).

The facies zones (FZ) correspond to lagoonal, intertidal, supratidal and emerged tidal/coastal areas of the platform internal sector. Very shallow areas with little circulation that periodically were flooded by marine waters constituted the intertidal and supratidal areas. They were covered by microbial mats and their deposits commonly were subaerially exposed and modified. Adjacent to them, shallow lagoons were developed up to the backreef/marginal sector of the paleoplatform.

Micropalaeontological analysis of the loferitic facies discussed in this study has revealed the presence of dasycladacean green algae and benthic foraminifers (e.g. involutinids, duostominids). Mollusc shell-fragments (gastropods and bivalves), ostracods, porostromate algae and thaumatoporellids are also present. In many cases, Megalodon-bearing subtidal beds (floatstones) can be observed along exposed sections. A Late Triassic (Norian-Rhaetian) age for the studied sediments can be accepted. Particularly, as regards the organism Thaumatoporella, its presence is dominant and exclusive in subtidal layers lacking benthic foraminifers, dasycladaceans and megalodontids. A Late Triassic-?Lower Jurassic age is presumable for these distinct loferitic successions, on the basis of the fossil assemblages distribution across the T/J boundary (e.g. Barattolo & Romano 2005).

In the investigated carbonate successions the detected basic facies pattern and meter-scale (lofer) cyclicity closely resemble that described in the type locality of the Dachstein Limestone Formation (Northern Calcareous Alps). The observed cycles usually deviate from the ideal symmetrical lofer cycle (sensu Haas 1991). Although various stacking patterns are recognized, including symmetric and asymmetric incomplete cycles, the deepening-upward facies arrangement is prevalent. In the Didymi area, cyclothems showing shallowing-upward trend have been also distinguished (Pomoni-Papaioannou 2008).

The cycles are generally bounded by subaerial exposure-related discontinuity surfaces that point to changes and interruptions in sedimentation. In several cases, the vadose meteoric diagenetic features (e.g. microkarstic features) overprint the subtidal strata below the subaerial disconformities, implying periodic sea-level drop and supporting allocyclic control of the cyclicity (i.e. eustatic control) in the study area. Nevertheless, the contribution of autocyclic

processes and/or tectonic motions cannot be excluded.

In the examinated sections the cycles display common basic characteristics. However, significant differences concerning the (micro)facies of their subtidal members are noted. Oncoidal microfacies – corresponding to the oncoidal facies of Dachstein limestones (oncoidal Dachstein Limestone) – were developed in the more external lagoonal area, near the backreef/marginal zone of the platform. In contrast, rich in bioclasts and peloids subtidal microfacies were formed in the internal lagoonal area, far from the platform margin.

Furthermore, syndepositional tensional features (e.g. fractures, small faults, sedimentary dykes, internal/synsedimentary breccias) overprint the topmost Upper Triassic loferitic successions of the "Pantokrator" Formation (Karnezeika area). They are regarded as the result of the synsedimentary extensional tectonic activity that took place at the Triassic/Jurassic boundary.

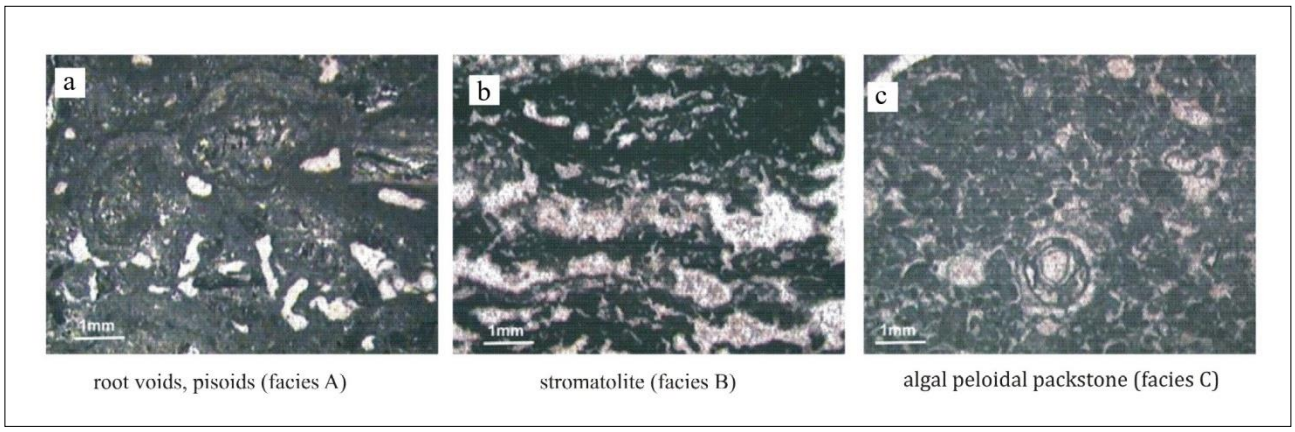

Fig. 1: Characteristic microfacies recognized in the studied sections.

Finally, the comparison between the investigated lofer cyclothems and those reported from distant and different palaeogeographic segments of the western Neotethys realm (e.g. Northern Calcareous Alps, Transdanubian Range, Southern Alps, Dinarides) reveals conspicuous similarities in rhythmic sedimentation, cycle thickness, litho- and biofacies. The considerable analogies support eustasy, as the prevailing lofer cycle-forming mechanism, although the influence of other factors (e.g. autocyclic processes) cannot be ruled out (Haas *et al.* 2009).

References

Barattolo, F., Romano, R. 2005. Shallow carbonate platform bioevents during the Upper Triassic-Lower Jurassic: an evolutive interpretation. Bolletino Societa Geologica Italiana, 124, 123-142.

Dunham, R.J. 1962. Classification of carbonate rocks according to depositional texture. American Association Petroleum Geologists, Memoir, 1, 108-121.

Fischer, A.G. 1964. The Lofer cyclothems of the Alpine Triassic, in: Merriam, D.F. (Ed.) Symposium on cyclic sedimentation. Kansas Geological Survey Bulletin 169, 107-149.

Flügel, E. 1982. Microfacies Analysis of Limestones. Springer.

Flügel, E. 2004. Microfacies of carbonate rocks: Analysis, interpretation and application. Springer.

Folk, R.L. 1959. Practical petrographic classification of limestones. American Association Petroleum Geologists Bulletin, 43, 1-38.

Folk, R.L.1962. Spectral subdivision of limestone types. American Association Petroleum Geologists, Memoir, 1, 62–84

Haas, J., 1991. A basic model for lofer cycles, in: Einsele, G., Ricken, W., Seilacher, A. (Eds.), Cycles and Events in Stratigraphy, 722–732.

Haas, J., Pomoni-Papaioannou, F., Kostopoulou, V. 2009. Comparison of the Late Triassic carbonate platform evolution and Lofer cyclicity in the Transdanubian Range, Hungary and Pelagonian Zone, Greece. Central European Geology, 52, 153–184.

Kostopoulou, V. 2018. Lofer cycles in the Upper Triassic-Lower Jurassic carbonate platform of the Eastern Greece zone. Ph.D. Thesis, National & Kapodistrian University of Athens, Athens, 362 p.

Pomoni-Papaioannou, F. 2008. Facies analysis of Lofer cycles (Upper Triassic), in the Argolis Peninsula (Greece). Sedimentary Geology, 208, 79-87.

Varti-Mataranga, M., Matarangas, D. 1991. Depositional facies and diagenetic phenomena in "Pantokrator Limestones" of Argolis Peninsula (Tasoulaika-Karnazaiika area). Bulletin Geological Society Greece, XXXV/I, 339–354.

Wilson, J.L. 1975. Carbonate facies in geologic history. Springer.

Late Oligocene and Early Miocene Paleoenvironmental Analysis of the Mesohellenic Basin (Grevena area, NW Greece)

D. Thivaiou[1]*, E. Koskeridou[1], M. Harzhauser[1], H. Drinia[1], Th. Tsourou[1], D. Mantzouka[1]

(1) National and Kapodistrian University of Athens, University Campus, 157 84, Zografou, Greece, dthivaiou@geol.uoa.gr

(2) Naturhistorisches Museum Wien, Burgring 7, 1010 Wien, Austria

The Mesohellenic Basin (MHB) is a synorogenic molasse-type basin of NW Greece active from the late-Eocene (late Lutetian) through the mid-Miocene (Langhian). The MHB has been studied since the late 19th century with few mentions of its fossil content (Wielandt-Schuster et al., 2004); in the 1950's Brunn (1956) presented a synthetic work that analyzed all the characteristics of the basin.

In the present study, a multidisciplinary paleoenvironmental approach, based on sedimentological and paleontological analyses, is attempted in newly studied sections. Particularly, the material comes from two new sections and one new locality of the greater Grevena area in NW Greece. One section and locality are of late Oligocene age (Chattian), and one section is of the early Miocene age (Aquitanian). The sections belong to Eptachori and Pentalofo formations (Zelilidis et al. 2002), and are mainly composed of fine marls, marly sands to conglomerating sands. Most of the fossiliferous beds are fine-grained, with only one coquina bed found during our investigation in the known Dotsiko section (Wielandt-Schuster et al., 2004).

Fossil content in the region include mollusks, benthic foraminifers, ostracods and wood fragments. The detailed sedimentary facies analysis together with the taxonomic analysis of mollusks, benthic foraminifers and ostracods has yielded two different environments, one of brackish-mudflat character, and one where shallow marine conditions prevailed.

For mollusks, new occurrences of 17 species are noted in the Aquitanian, as well as 5 new species (Thivaiou et al. in press). For the Oligocene, three species of bivalves are reported for the first time from Dotsiko section of Wielandt-Schuster et al. (2004), as well as two species of micromorphic gastropods. The gastropod species Bellatara lozoueti Harzhauser, 2004 is found in shallow marine assemblages of three Oligocene locations of the studied area, in addition to the original location of Dotsiko village (Harzhauser, 2004). Species of Terebralia Swainson, 1840 infer proximity to mangrove environments and (Houbrick, 1991; Raw et al., 2017; Reid et al., 2008). In the study area, two occurrences are noted, one in the Chattian and one in the Aquitanian.

Benthic foraminifers and ostracods provide stronger support of differences between the brackish-mudflat assemblage and the shallow marine assemblage, as their taxonomic diversity and relative numbers vary. They also are reflecting well the fluctuating environments especially for the Aquitanian section. Interestingly, the ostracod assemblages also point towards the presence of mangrove environments in the same section. The combined results, help retrace the sea level fluctuations and add information to the evolution of the MHB, for example the details of the subsidence curve of (Ferrière et al., 2004).

Lastly, the analysis of fossil wood fragments has shown transportation and strong boring from Teredo Linnaeus, 1758 for specimens collected in the Oligocene. Samples from the early Miocene found within the brackish-mudflat assemblage correspond to an "evergreen Quercus type" wood (Fagaceae), inferring such nearby forests.

In summary, the present study has brought new information relative to sea-level changes that occurred in the MHB, with changing environments between shallow marine and bracksish–coastal mudflats.

References

Brunn, J., 1956. Contribution à l'étude du Pinde septentrional et d'une partie de la Macédoine occidentale. Ann. Géologiques du Pays Helléniques, 7: 1-358.

Ferrière, J., Reynaud, J.-Y., Pavlopoulos, A., Bonneau, M., Migiros, G., Chanier, F., Proust, J.-N., Gardin, S., 2004. Geologic evolution and geodynamic controls of the Tertiary intramontane piggyback Meso-Hellenic basin, Greece. Bull. la Soc. Géologique Fr. 175, 361–381. https://doi.org/10.2113/175.4.361

Harzhauser, M., 2004. Oligocene gastropod faunas of the eastern Mediterranean (Mesohellenic Trough/Greece and Esfahan-Sirjan Basin/Central Iran). CFS Cour. Forschungsinstitut Senckenb.

Houbrick, R.S., 1991. Systematic review and functional morphology of the mangrove snails Terebralia and Telescopium (Potamididae; Prosobranchia). Malacologia 33, 289–338.

Raw, J.L., Perissinotto, R., Miranda, N.A.F., Peer, N., Raw, J.L., Perissinotto, R., Miranda, N.A.F., Peer, N., 2017. Feeding dynamics of Terebralia palustris (Gastropoda : Potamididae) from a subtropical mangrove ecosystem Feeding dynamics of Terebralia palustris (Gastropoda : Potamididae) from a subtropical mangrove ecosystem. Molluscan Res. 37, 258–267. https://doi.org/10.1080/13235818.2017.1323370

Reid, D.G., Dyal, P., Lozouet, P., Glaubrecht, M., Williams, S.T., 2008. Mudwhelks and mangroves: The evolutionary history of an ecological association (Gastropoda: Potamididae). Mol. Phylogenet. Evol. 47, 680–699. https://doi.org/10.1016/j.ympev.2008.01.003

Thivaiou D., Harzhauser, M. and Koskeridou, E. (in press). Early Miocene gastropods from the Felli section (Proto-Mediterranean Sea, NW Greece). Geodiversitas.

Wielandt-Schuster, U., Schuster, F., Harzhauser, M., Mandic, O., Kroh, A., Rögl, F., Reisinger, J., Liebtrau, V., Steininger, F.F., Piller, W.E., 2004. Stratigraphy and palaeoecology of Oligocene and Early Miocene sedimentary sequences of the Mesohellenic Basin (NW Greece). CFS Cour. Forschungsinstitut Senckenb.

Zelilidis, A., Piper, D.J.W., Kontopoulos, N., 2002. Sedimentation and basin evolution of the Oligocene-Miocene Mesohellenic basin, Greece. Am. Assoc. Pet. Geol. Bull. 86, 161–182. https://doi.org/10.1306/61eeda6c-173e-11d7-8645000102c1865d

15th International Congress of the Geological Society of Greece
Athens, 22-24 May, 2019 | Harokopio University of Athens, Greece
Bulletin of the Geological Society of Greece, Sp. Pub. 7 Ext. Abs. GSG2019-386

A GIS-based Evaluation of Grain Roundness

I. Vakalas[1] & I. Zananiri[2]

(1) Hellenic Survey of Geology & Mineral Exploration, Spirou Loui 1, 13677 Acharnae, Greece; vakalasjohn@gmail.com
(2) Hellenic Survey of Geology & Mineral Exploration, Spirou Loui 1, 13677 Acharnae, Greece; izanan@igme.gr

Background and Objectives

In sedimentary studies one of the physical properties of the examined samples is grain roundness; a critical parameter providing information about the depositional environment and the physical processes that the material has undergone since its deposition. This paper describes an attempt to provide an automatic and accurate method to measure roundness of clastic particles from sediments. The technique, developed at the Marine Geology laboratory of HSGME, is based on the Waddel (1935) methodology, traditionally applied through laborious microscopic examination. To provide an automatic and out of the box routine Model Building tools and script development using Python Libraries in an ArcMap environment were involved. GIS was chosen as a practical solution for data elaboration and mapping both in marine and terrestrial sedimentary studies.

Methodology

According to Wadell (1935) the average roundness of a grain is calculated using the formula: Roundness = $(\Sigma r_i/n)/R_{max}$, where r_i is the radius of curvature of every angle of the grain, n is the number of angles and R_{max} is the maximum inscribed to grain circle (Fig. 1a). Taking that into account, the toolbox design in ArcGIS involved the following concepts:

- Use of simple equations of differential geometry for the calculation of radius of curvature (r_i).
- A set of three vertices is used at each calculation step to define a triangle and a circumscribed circle (Fig 1b).
- The radius of the circumscribed circle corresponds to the radius of curvature at the part of the grain boundary curve defined by the three active vertices.
- Successive sets of three (3) vertices are used for every calculation step.

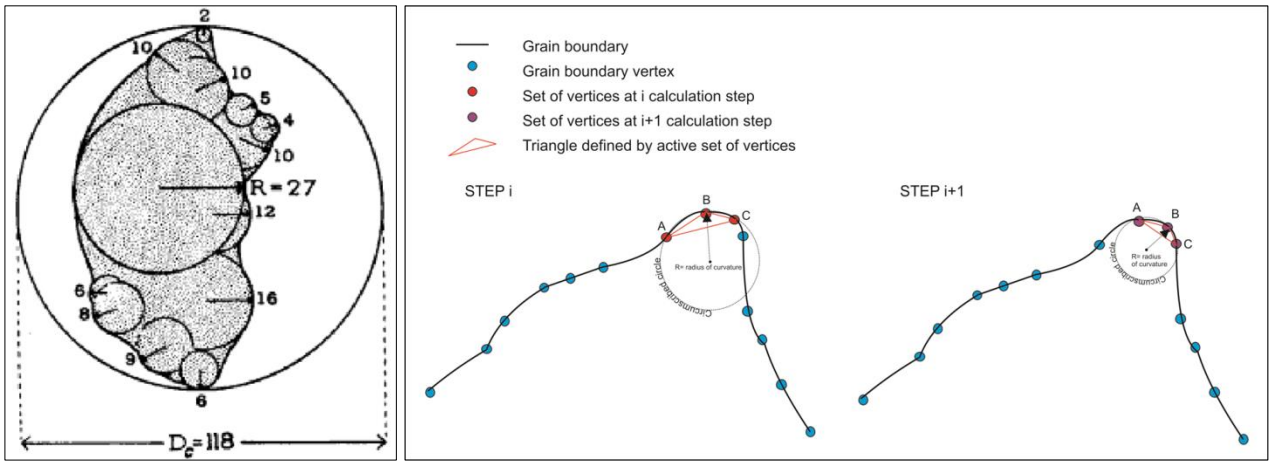

Figure 1. The basic concept of the Wadell (1935) methodology (left) and its application through the ArcGIS tooldbox (right).

For the practical application of the above methodology a high resolution image – captured during optical microscopy examination – of the studied sample is required. To ease the processing, before import in ArcGIS the raster undergoes image analysis, using Python scripting, by application of Gaussian filtering and the Otsu (1979) thresholding method, to "extract" the grain boundaries in the form of a black and white binary image. Possible restriction may, however, arise in cases of polymictic grains, exhibiting a variety of colours which may complicate image processing.

The calculation of specimen roundness in ArcGIS, from its microscopic image, is accomplished using an in-house custom-made Toolbox (*"Roundness.tbx"*), using the following tools: spatial analyst, conversion, editing, geoprocessing by model builder and Python calculations.

To test the applicability, validity and accuracy of the aforementioned methodology the roundness of the published prototype grains by Wadell (1935) was calculated (Fig. 2) and compared to that, measured manually, quoted in the publication. Additionally, a set of 20 individual grains was used, with nominal roundness ranging from 0.1 to 0.9 and the mean deviation from Wadell values was 0.02 (Fig. 2).

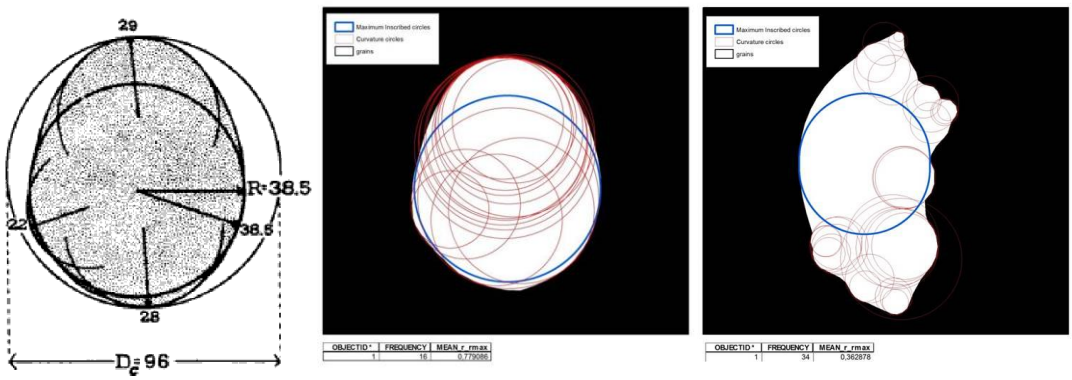

Figure 2. Validation using Waddell (1935) "grains" for a round (Waddell R=0.81, Model R=0.78) and an angular (Waddell R=0.30, Model R=0.36) grain.

Conclusions

The proposed methodology can accurately calculate the roundness of sediment samples, irrespective of their nature and environment. It is fast, cost-effective, totally automatic and thus free from user bias and random errors. The created toolbox is user-friendly and its application in a GIS environment – broadly adopted in data processing in earth science worldwide - does not involve any other special software.

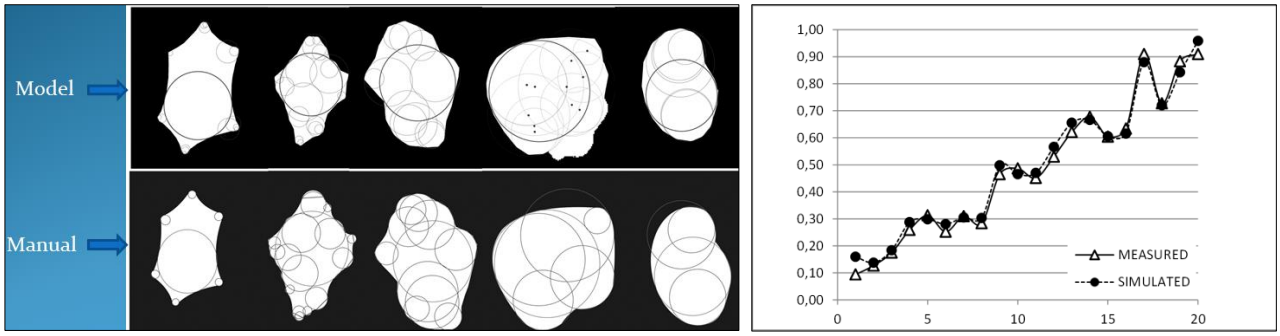

Figure 3. Model validation using a set of 20 grains of optimum roundness; manual data from Waddell (1935).

This novel approach, using GIS not only for geospatial data management and representation, but also for the generation of original data can be taken one step further. Future work will focus on using the tool for batch image processing images and embedding the *Roundness* Toolbox into an integrated tool for storing and mapping the results. Thus, for a set of samples from a region, after roundness calculation, the resulting data will be correlated with the required geospatial information (sample coordinates) and the corresponding map will be drawn allowing a combined interpreatation.

Acknowledgments

Part of this work has been carried out through the support of European Commission contract No.SI2.658129 ("European Marine Observation and Data Network – Lot 2 Geology").

References

Otsu, N., 1979. "A threshold selection method from gray-level histograms". IEEE Trans. Sys., Man., Cyber 9 (1), 62-66. doi:10.1109/TSMC.1979.4310076

Wadell, H., 1935. "Volume, Shape and Roundness of Rock Particles". Journal of Geology 43, 250-280.

SPECIAL SESSION

T1.S1 Updating Paleontology and Stratigraphy in Greece and the Eastern Mediterranean

Conveners: **Maria Triantafyllou (NKUA)**
Dimitris Kostopoulos (AUTH)
George Iliopoulos (UPAT)

Co-organized by the Palaeontology-Stratigraphy Committee of the G.S.G.

15th International Congress of the Geological Society of Greece
Athens, 22-24 May, 2019 | Harokopio University of Athens, Greece
Bulletin of the Geological Society of Greece, Sp. Pub. 7 Ext. Abs. GSG2019-022

Mammuthus meridionalis from Apollonia-1 (Mygdonia Basin, Northern Greece) and its Importance within the Early Pleistocene Mammoth Evolution in Europe

G.E. Konidaris[1], D.S. Kostopoulos[2], G.D. Koufos[2]

(1) Palaeoanthopology, Senckenberg Centre for Human Evolution and Palaeoenvironment, Eberhard Karls University of Tübingen, Rümelinstr. 23, 72070 Tübingen Germany, geo.konidaris@gmail.com
(2) Laboratory of Geology and Palaeontology, Department of Geology, Aristotle University of Thessaloniki, 54124 Thessaloniki, Greece

Introduction-Fossiliferous locality

Mammoths originated in Africa at the end of the Miocene and during the late Pliocene migrated through the Levant to Eurasia, where they thrived until the Late Pleistocene. Eurasian mammoths show significant morphological adaptations through time, related to the general dietary trend from browse-dominated mixed feeding towards grazing, as a response to the changing environments of the Pleistocene (Lister & Sher, 2001). These adaptations are related to biomechanical advantages for grazing and increased resistance to abrasion, and are evident in skull and dental morphology: shortening and heightening of the cranium and mandible, enamel thinning, and increase in the height of the molar crown (hypsodonty) and the number of enamel plates in the molars (Lister, 1996). Mammoths (*Mammuthus*) are distinguished in Europe into four species: 1) a primitive morph, commonly, but tentatively, attributed to *M. rumanus* (early Villafranchian, late Pliocene); 2) the southern mammoth *M. meridionalis* (middle Villafranchian–Epivillafranchian, Early Pleistocene); 3) the steppe mammoth *M. trogontherii* (Middle Pleistocene); and 4) the wooly mammoth *M. primigenius* (late Middle–Late Pleistocene). Although most of the mammoth species are properly defined, the time and mode of the transitions/replacements are still open issues, and several intermediate/mosaic morphotypes or subspecies have been proposed by various researchers. Here, we conduct a preliminary study on the mammoth from Apollonia-1, and we discuss its evolutionary and biostratigraphic importance within the evolution of the Early Pleistocene European mammoths.

The fossiliferous locality Apollonia-1 (APL) is located in Mygdonia Basin (Northern Greece), about 45 km east of Thessaloniki. The locality was discovered in 1991 (Koufos *et al.*, 1992) and subsequently excavated in 1992–1996 and 2012–2014, and provided a wealth of mammal fossils. APL is situated within the Platanachori Formation (Pre-Mygdonian Group), which consists of sands, sandstones, conglomerates, silty sands, silts, clays, marls and marly limestones, indicating the local development of small lakes and swamps (Koufos *et al.*, 1995). The APL fauna is younger than Dmanisi (~1.8 Ma; Georgia) and older than Untermaßfeld (~1.0 Ma, Epivillafranchian; Germany), showing similarities with Pirro Nord (1.5–1.2 Ma; Italy); therefore, a correlation to the second half of the late Villafranchian is possible for the locality.

Description-Comparison

The APL sample includes a hemi-mandible with the third lower molar (m3) (Figure 1), an isolated m3, two isolated upper third molar (M3) fragments (Fig. 2) and a maxilla fragment with deciduous dentition (DP2–DP3), the latter briefly discussed in Athanassiou & Kostopoulos (2001). The m3 of the hemi-mandible (Fig. 1) is characterized by PN (plate number): >11, LF (lamellar frequency): 4.6 and ET (enamel thickness): 3.1; the M3 (Fig. 2) by PN: >13, LF: 5.5, ET: 2.8 and HI (hypsodonty index): 1.48; the DP2 and DP3 bear 4 and 8 plates, respectively. The APL molars are different from those of *M. rumanus*, the latter having lower PN, LF and HI, and higher ET values. On the other side, the APL molars are also clearly outside the range of the *M. trogontherii* sample from its type locality Süßenborn (Germany) and the sample of *M. primigenius* from Předmostí (Czech Republic), which have higher PN, LF and HI values, and thinner enamel. The values of all these parameters of the APL molars are comfortably within the range of *M. meridionalis*, showing the diagnostic features of this species (Lister, 1996), and unambiguously indicate an attribution to the southern mammoth, in accordance with the morphology of the mandible, e.g., caudal border of the ramus posteriorly inclined (Fig. 1).

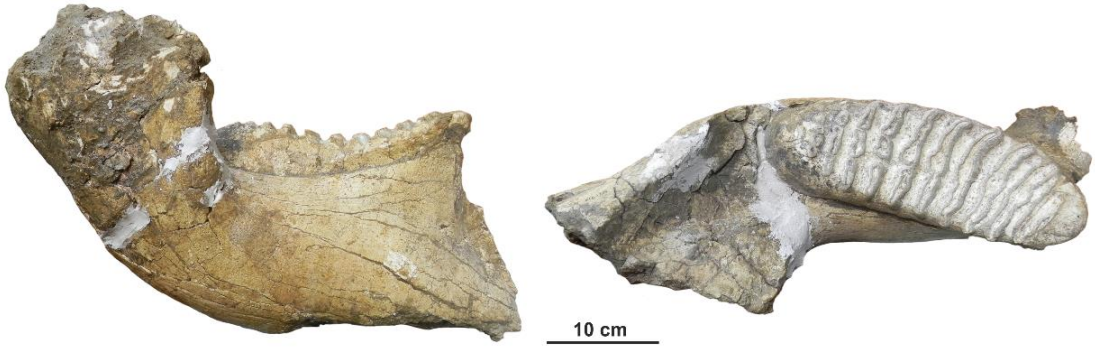

Figure 1. Right hemi-mandible with m3 of *Mammuthus meridionalis* from Apollonia-1 in lateral and dorsal view. Anterior to the right.

Within *M. meridionalis*, the APL molar sample is more derived than *M. m. gromovi* from Liventsovka (middle

Villafranchian, Russia). On the other side, it is more primitive from the post-Jaramillo–pre-Brunhes specimens from Imola (Italy) and Dorst (The Netherlands) [both "*M. meridionalis* advanced" according to Lister et al. (2005) and Palombo & Ferretti (2005)], which show a higher HI in their M3s, within the range of *M. trogontherii*, and they could alternatively belong to the steppe mammoth as in the case of the Voigtstedt and Edersleben specimens (Germany; Van Essen, 2011). The APL mammoth fits well within the late Villafranchian *M. m. meridionalis* (typical) sample from Upper Valdarno (Italy), however, occupying its upper range in terms of PN and LF, and slightly surpassing its HI values (data from Van Essen, 2003). On the other side, the APL molars are plotted at the lower values of *M. m. tamanensis* from Sinyaya Balka (Russia; Baygusheva & Titov, 2012). The best match of the APL molars is perhaps with the sample from the post-Upper Valdarno late Villafranchian localities from Italy, correlated to the Farneta Faunal Unit and attributed to *M. m. vestinus* by Azzaroli (1977) [although the validity of this subspecies is questioned (Palombo & Ferretti, 2005)], as well as with the Epivillafranchian (Jaramillo) *M. m. depereti* from St. Prest (France) sample. Finally, the eight plates of the APL DP3, combined with its large length, is unique so far within *M. meridionalis*.



Figure 2. Left M3 fragment of *Mammuthus meridionalis* from Apollonia-1 in occlusal and labial view. Anterior to the left.

Taxonomic and biostratigraphic conclusions

The dentognathic remains of the APL mammoth permit its attribution to *M. meridionalis*. The relatively deep mandibular corpus is a derived condition. The dental features also indicate an evolutionary stage somewhat more derived than the Upper Valdarno mammoth (beginning of late Villafranchian) in terms of the higher NP in the DP3 and the marginally higher HI in the M3. In this aspects, the APL mammoth fits better with corresponding specimens from localities correlated to the second half of the late Villafranchian and the Epivillafranchian. Whether this sample should be distinguished at subspecific level is open to discussion. These results are in agreement with the existing biochronological correlation of the APL fauna and further support the potential biostratigraphic significance of *M. meridionalis* within the Early Pleistocene, although conclusions based on limited/fragmentary sample should always be taken with caution.

Acknowledgements

Research in Apollonia-1 was supported by the Research Committee of the Aristotle University of Thessaloniki (Projects 1396 and 87845) awarded to G. Koufos and D. Kostopoulos, and by the European Research Council StG 283503 (PaGE) awarded to K. Harvati. GK is supported by the European Research Council CoG 724703 (CROSSROADS) awarded to K. Harvati.

References

Azzaroli, A., 1977. Evolutionary patterns of Villafranchian elephants in Central Italy. Atti della Accademia Nazionale dei Lincei 14, 149-168.

Athanassiou, A., Kostopoulos, D.S., 2001. Proboscidea of the Greek Pliocene-Early Pleistocene faunas: biochronological and palaeoecological implications. The world of elephants-1st International Congress, Rome, Italy, pp. 85-90.

Baygusheva, V.S., Titov, V., 2012. The evolution of Eastern European meridionaloid elephants' dental characteristics. Quaternary International 255, 206-216.

Koufos, G.D., Syrides, G.E., Kostopoulos, D.S., Koliadimou, K.K., 1992. Apollonia, a new vertebrate site in the Pleistocene of the Mygdonia basin, Macedonia (Greece); the first fossil fresh-water mollusks in the area. Comptes Rendus Académie des Sciences Paris 315, 1041-1046.

Koufos, G.D., Syrides, G.E., Kostopoulos, D.S., Koliadimou, K.K., 1995. Preliminary results about the stratigraphy and the palaeoenvironment of Mygdonia Basin, Macedonia, Greece. Geobios M.S. 18, 243-249.

Lister, A.M., 1996. Evolution and taxonomy of Eurasian mammoths, in: Shoshani, J., Tassy, P. (Eds.), The Proboscidea: Evolution and palaeoecology of elephants and their relatives, 203-213.

Lister, A.M., Sher, A.V., 2001. The origin and evolution of the woolly mammoth. Science 294, 1094-1097.

Lister, A.M., Sher, A.V., van Essen, H., Wei, G., 2005. The pattern and process of mammoth evolution in Eurasia. Quaternary International 126-128, 49-64.

Palombo, M.R., Ferretti, M.P., 2005. Elephant fossil record from Italy: knowledge, problems, and perspectives. Quaternary International 126-128, 107-136.

Van Essen, H., 2003. Tooth morphology of *Mammuthus meridionalis* from the southern bight of the North Sea and from several localities in the Netherlands. Deinsea 9, 453-511.

Van Essen, H., 2011. Tracing transitions. An overview of the evolution and migrations of the genus *Mammuthus* Brookes, 1828 (Mammalia, Proboscidea). Ph.D. Thesis, Leiden University, Leiden, 270 p.

15th International Congress of the Geological Society of Greece
Athens, 22-24 May, 2019 | Harokopio University of Athens, Greece
Bulletin of the Geological Society of Greece, Sp. Pub. 7 Ext. Abs. GSG2019-024

The Lower Pleistocene Primate-Bearing Fossil Site of Dafnero (W. Macedonia, Greece): New Data from classic and Innovative Approaches

D. S. Kostopoulos[1], E. Aidona[1], M., Benammi[2], A.Gkeme[1], L. Grasset[2], F. Guy[2], G. Koufos[1], Z. Kynigopoulou[1,3], A. Le Maitre[2,4], A. Novello[5], Ch.-A. Plastiras[1,2], G. Merceron[2]

(1)School of Geology, Aristotle University of Thessaloniki, 54124 Thessaloniki, Greece, dkostop@geo.auth.gr
(2) PALEVOPRIM, University of Poitiers, France
(3) School of GeoSciences, Grant Institute, University of Edinburgh, UK
(4) Department of Theoretical Biology, University of Vienna, Austria,
(5) CEREGE,Europole Mediterraneen de l'Arbois BP80 - 13545 Aix-en-Provence Cedex 4, France

Introduction

Well hidden in an intricate system of deep ravines crossing the Aliakmon River Valley -one of the most beautiful and wildest landscapes in NW Greece- is the fossil locality of Dafnero (Dafnero-1), nearby the homonymous village (Fig. 1A). Discovered in 1990 and originally explored between 1990 and 1994 (Koufos *et al.*, 1991), the locality has yielded a limited but significant Early Pleistocene fossil mammal assemblage.

A Greek-French partnership between the Aristotle University of Thessaloniki (Lab of Palaeontology) and the University of Poitiers (PALEVOPRIM), came back to this area in 2010 and started a new field campaign that soon allowed locating two additional fossil sites. Dafnero-3 has proven to be extremely promising in terms of quality and density of fossils (Fig. 1C) and four years later (summer 2014) a fairly complete skull of a large baboon-like monkey was unearthed (Fig; 1C), upgrading the locality to a primate-bearing one. After seven years of intense field and lab work new data on the Dafnero fauna, flora, stratigraphy, and age picture altogether an astonishing mammal palaeocommunity at the gates of Europe.



Figure 1. Overall view of Dafnero fossil locality (A); discovery of primate cranium (B) and fossil preparation on field (C).

The Dafnero Fauna and Age

Earlier works allowed identifying within the Dafnero fauna the carnivores Chasmaporthetes lunensis, Baranogale cf. helbingi, Nyctereutes megamastoides, Vulpes alopecoides, and Ursus cf. etruscus, the equid Equus stenonis cf. vireti, the giraffid Palaeotragus inexspectatus, the cervids Metacervoceros ex gr. rhenanus, and Eucladoceros tegulensis, and the bovids Gallogoral meneghinii, Gazella bouvrainae, and Gazellospira torticornis. The 2011-2018 mission in Dafnero-3 allows us to add at the moment the hysticid Hystrix sp., the rhino Stephanorhinus sp., the machairodontine felid Homotherium latidens (Koufos et al., in press), and the cercopothecid Paradolichopithecus aff. arvernensis (Kostopoulos et al. 2018; Fig. 2A). This mammal assemblage as a whole match perfectly those recovered previously from Volakas (Drama), Vatera (Lesvos Island), and Sesklo (Thessaly), keeping strong affinities with contemporaneous mammal communities from SW Europe and W Asia, and suggesting the establishment across this latitudinal belt of a rather homogeneous and characteristic South Alpine mammal palaeocoenosis.

Preliminary data based on mammal biochronology allow suggesting for Dafnero mammal assemblage a middle-late Villafranchian age, European Land Mammal zone MN 17b. An extensive magnetostratigraphic sampling conducted in 2016 and 2017 from 31 horizons in two partially overlapping lithostratigraphic sections allowed reconstructing the local

magnetostratigraphy, which includes two long reverse units interrupted by a short normal one. Correlation with GPTS is still in progress but preliminary data suggest a better match within C2r (i.e., within post-Olduvai Matuyama Chron) (Benami et al. in progress).

Innovative Palaeoecological Approaches

In order to further address phylogenetic and ecological questions related to the cercopithecid Paradolichopithecus aff. arvernensis based mainly on the characteristics of the internal structure of the cranium LGPUT DFN3-150 from Dafnero-3 we applied micro-CT scan imaging analysis i) the inner ear anatomy (Fig. 2B), ii) the development of maxillary sinuses and iii) the enamel thickness (Fig. 2C). These approaches are combined by dental microwear texture analysis (DMTA; Fig. 2D) which provides a glance on its dietary preferences. The results allow us to propose Paradolichopithecus as a terrestrial omnivore "opportunist", a European Early Pleistocene analogue of extant baboons, and to call into question the traditional hypothesis of a Macaca-Paradolichopithecus relationship (Le Maitre et al., submitted).

Investigation for palynomorphs/phytoliths within the sedimentary sequence of Dafnero has provided poor results. Instead, we applied botanical palaeochemotaxonomy as a complementary proxy for palaeoflora and palaeoclimate reconstruction. According to our preliminary results, the overall extractable lipid distribution from Dafnero fossil horizon is characterized by n-alkan-1-ols, phytosterols, fatty acids, series of aromatics typical of charred wood residues and an important amount waxy nalkanes in the C15-C37 range (Grasset et al., in progress).

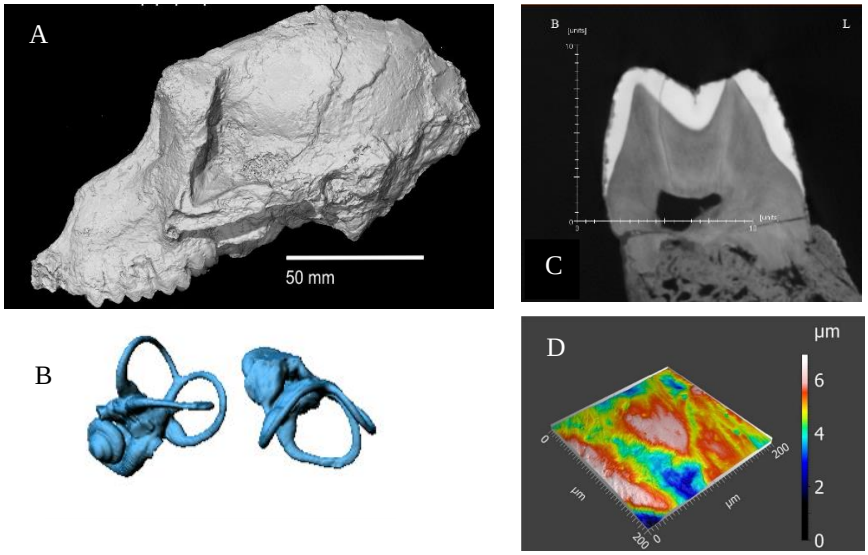

Figure 2. Digital reconstruction of outer (A) and inner (B, C, D) features of *Paradolichopithecus* from Dafnero 3.

Discussion

Planned field work over the next few years at Dafnero focuses on the improvement of the local fossil record in order to identify with the utmost precision and safety the taxinomic content and the composition of the fauna and its paleozoogeographic relations with adjacent areas. At the same time the forthcoming magnetochronology and updated biochronology will provide accurate dating of the fauna allowing an important review of the local-scale biostratigraphy and a refinement of regional to continental-scale correlations. The per species analysis of the dietary preferences of the mammals recorded in the Dafnero fauna along with independent paleoecological approaches will finally lead to the reconstitution of the local palaeoenvironment, triggering further discussions about temporal and spatial oscillations of environmental factors controlling primate distribution.

Acknowledgements

Excavations at Dafnero were supported by the Lab of Paleontology, AUTh, the CNRS, France [grant number PICS5185; 2010-2013]; and the National Geographic Society [grant 9903-16; 2016-2017]. ALM studies were partly supported by the Austrian Science Fund [FWF grant number P29397] and ChAP studies by Eiffel scholarship program of excellence.

References

Kostopoulos D.S., Guy, F., Kynigopoulou, Z., Koufos, G., Valentin, X., Merveron, G. 2018. A 2Ma old baboon-like monkey from Northern Greece and new evidence to support the *Paradolichopithecus – Procynocephalus* synonymy (Primates: Cercopithecidae). Journal of Human Evolution 121, 178-192.

Koufos, G.D., Kostopoulos, D.S., Merceron, G., The saber-toothed cat *Homotherium latidens* (Owen, 1864) from the Lower Pleistocene locality Dafnero, Western Macedonia, Greece. Geodiversitas (in press).

Koufos, G.D., Kostopoulos, D.S., Koliadimou, K., 1991. Un nouveau gisement de mammiferes dans le Villafranchien de Macedoine occidentale (Grèce). Comptes Rendus de l'Académie des Sciences de Paris 313, 831-836.

Le Maitre, A., Kynigopoulou, Z., Plastiras Ch.-A., Guy, F., Merceron, G. Kostopoulos, D.S. (submitted). Inner cranial anatomy of *Paradolichopithecus* aff. *arvernensis* from Dafnero 3 (Lower Pleistocene, Greece) as inferred from microCT-scan imaging analyses. Journal of Anatomy (submitted).

15th International Congress of the Geological Society of Greece
Athens, 22-24 May, 2019 | Harokopio University of Athens, Greece
Bulletin of the Geological Society of Greece, Sp. Pub. 7 Ext. Abs. GSG2019-028

Detrital Zircon Record on the Stratigraphy of Meta-Carbonate Rocks in the Circum-Rhodope Belt: U-Pb LA-ICP-MS Geochronology Data from the Mandritsa Unit, Bulgaria

N. Bonev[1], P. Filipov[2], R. Raicheva[2]

(1) Sofia University "St. Kliment Ohridski", 15Tzar Osvoboditel Bd., Sofia, Bulgaria, niki@gea.uni-sofia.bg
(2) Geological Institute, Acad. G. Bonchev Str., Bl. 24. Sofia, Bulgaria

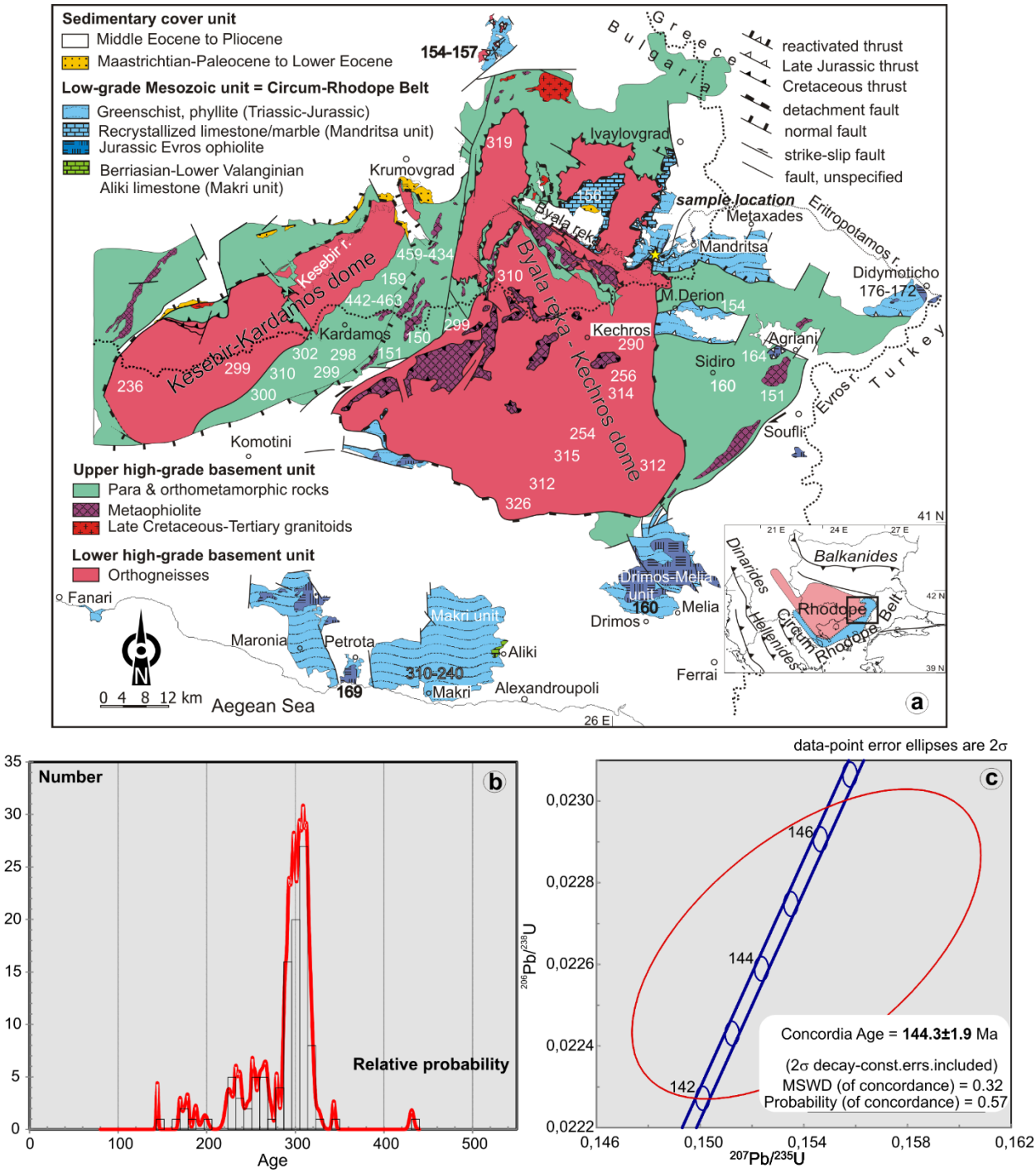

Figure 1. a) Geological map of the Eastern Rhodope-Thrace region of Bulgaria-Greece (adapted from Bonev et al., 2015a) and the U-Pb, 40Ar/39Ar and Rb-Sr geochronology there labeled by numbers in Myr., b) Density probability diagram, c) concordia diagram of the youngest detrital zircon in greywacke sample.

Background, Objectives and Methods

Latest Jurassic-Early Cretaceous sedimentary rocks and Jurassic arc/back-arc related ophiolitic rocks constitute various units of the Cicrum-Rhodope Belt (CRB) in Bulgaria and Greece (e.g. Meinhold and Kostopoulos, 2013, Ivanova et al.,

2015; Bonev et al., 2015a,b, and references therein). In Bulgaria, the basal strata of the Mandritsa unit of the CRB are built of recrystallized limestone to marble, which preserved their primary depositional layering (Fig. 1a). The marble hosts greywacke ranging in size from pebbles to blocks (Bonev, 2005). Both lithologies are metamorphosed to medium greenschist-facies and experienced ductile shear deformation (Bonev and Stampfli, 2011). These marble strata of the Mandritsa unit are considered to be Triassic in age by lithological similarity to fossil-bearing marble strata of the Makri unit exposed in the CRB of Thrace region in Greece (Boyanov et al., 1990). The depositional age of the basal marble strata in the Mandritsa unit is unknown. Here, we present U-Pb geochronology results from the greywacke hosted by marble, which provide necessary insights into the timing of the deposition of the marble strata at the base of the CRB Mandritsa unit, in Bulgaria. We applied U-Pb LA-ICP-MS technique on detrital zircons from the greywacke, following standard density and heavy liquids separation methods and cathodoluminescence (CL) imaging to obtain internal structure of the dated zircons. LA-ICP-MS analyses were performed in geochronology laboratory of the Geological Institute of the Bulgarian Academy of Sciences. Details on analytical procedures can be found in Bonev et al., (2019).

Results and Conclusions

Zircon grains range in size between 80 μm and 300μm showing irregular fragments or crystals with a slightly rounded shape in CL images, which altogether suggest a short transport from the source area. In the CL images, the zircon grains display well-defined oscillatory zoning, as well as slightly obliterated homogeneous zoning patterns. The range of Th/U ratio in dated zircons varies between 0.11 and 0.75 except for two analyses in recrystallized zircon grains with Th/U ratios of 0.07 and 0.09. The obtained ages of detrital zircons range from 431.3 Ma to 144.3 Ma (Fig. 1b). Dominant age cluster comprises Carboniferous-Permian zircons whose analyses yielded concordant ages at 317.1±1.4 Ma to 257.1±2.9 Ma. Minor age clusters yielded Triassic ages (242.9±7.6 Ma, 233.7±3.6 Ma), a single Silurian age of 431.3 Ma and a concordant Jurassic age of 171.4±2.6 Ma defined by two analyses (Th/U=0.07 and 0.15). The only youngest zircon out of 105 zircon grains analyzed in the greywacke sample yielded an age of 144.3±1.9 Ma (Th/U=0.09), and hence, defines the maximum depositional age of the greywacke and the marble (Fig. 1c). The Paleozoic and Triassic detrital zircons age clusters are time-correspondent to the protolith ages of the meta-granitoids that build the Rhodope high-grade metamorphic basement underlying the CRB (Fig.1a). Jurassic arc-related magmatic rocks are also known from the CRB in Thrace region (Bonev et al., 2015a). Therefore, both Rhodope high-grade metamorphic basement and CRB magmatic rocks must have been the source for clastic sedimentary deposition of the greywacke in the basal marble of the Mandritsa unit. Berriasian ammonite of first appearance in Tithonian was reported in schist of the Makri unit of the CRB in Greece (Dimadis and Nikolov, 1997). Thus, biostratigraphic constraint and the maximum deposition radiometric age in this study reveal latest Late Jurassic sedimentation in the CRB of the Thrace region. Thus, we have reached the following conclusions:

- In the CRB of Thrace region, the basal marble of the Mandritsa unit deposited in latest Late Jurassic (Tithonian).
- Both Rhodope basement and CRB Jurassic rocks must have been the sedimentary source of continental provenance.

Acknowledgements

The study was supported by the National Science Foundation of Bulgaria through grant DN04/6.

References

Bonev, N., 2005. Siliciclastic knockers in marbles of the Eastern Rhodope, Bulgaria: significance for depositional environment and tectonic setting. Annuaire de l'Universite de Sofia « St. Kliment Ohridski », Faculte de Geologie et Geographie, livre 1 Geologie 98, 29-42.

Bonev, N., Stampfli, G., 2011. Alpine tectonic evolution of a Jurassic subduction-accretionary complex: deformation, kinematics and 40Ar/39Ar age constraints on the Mesozoic low-grade schists of the Circum-Rhodope Belt in the eastern Rhodope-Thrace region, Bulgaria-Greece. Journal of Geodynamics 52, 143-167.

Bonev, N., Marchev, P., Moritz, R., Collings, D., 2015a. Jurassic subduction zone tectonics of the Rhodope Massif in the Thrace region (Northern Greece) as revealed by new U-Pb and 40Ar/39Ar geochronology of the Evros ophiolite and high-grade basement rocks. Gondwana Research 27, 760-775.

Bonev, N., Marchev, P., Moritz, R., Filipov, P., 2015b. Timing of igneous accretion, composition, and temporal relation of the Kassandra-Sithonia rift-spreading center within the eastern Vardar suture zone, Northern Greece: insights into Jurassic arc/back-arc systems evolution at the Eurasian plate margin. International Journal of Earth Sciences 104, 1837-1864.

Bonev, N., Filipov, P., Raicheva, R., Moritz, R., 2019. Timing and tectonic significance of Paleozoic magmatism in the Sakar unit of the Sakar-Strandzha Zone, SE Bulgaria. International Geology Review. https://doi.org/10.1080/00206814.2019.1575090.

Boyanov, I., Ruseva, M., Toprakchieva, V., Dimitrova, E., 1990. Lithostratigraphy of the Mesozoic rocks from the Eastern Rhodope. Geologica Balcanica 20, 3-28.

Dimadis, E., Nikolov, T., 1997. An ammonite find in the Makri unit (Berriasian, southeast Rhodopes, northeast Grece). Comptes Rendus de l'Academie bulgare des Sciences 50, 71-74.

Ivanova, D., Bonev, N., Chatalov, A., 2015. Biostratigraphy and tectonic significance of lowermost Cretaceous carbonate rocks of the Circum-Rhodope Belt (Chalkidiki Peninsula and Thrace region, NE Greece). Cretaceous Research 52, 25-63.

Meinhold, G., Kostopoulos, D.K., 2013. The Circum-Rhodope Belt, northern Greece: Age, provenance, and tectonic setting. Tectonophysics 595-596, 55-68.

15th International Congress of the Geological Society of Greece
Athens, 22-24 May, 2019 | Harokopio University of Athens, Greece
Bulletin of the Geological Society of Greece, Sp. Pub. 7 Ext. Abs. GSG2019-037

Discovery of Capitanian-Wuchiapingian (Middle-Late Permian) Calcareous Algae and Foraminiferan assemblages from Chios Island (Greece). Paleogeographic implications

G. Grigoryan[1,2], D. Vachard[2], T. Tsourou[3] D, A. Zambetakis-Lekkas[3], T. Danelian[2]

(1) Institute of Geological Sciences, National Academy of Sciences of Armenia, Bagramyan ave., 24, Yerevan, Armenia, gevgrigg@gmail.com
(2) UMR 8198 Evo-Eco-Paléo CNRS – University of Lille, Cité Scientifique, Bât. SN5, Villeneuve d'Ascq, France, danielvachard@gmail.com, taniel.danelian@univ-lille.fr.
(3) Department of Historical Geology - Paleontology, National and Kapodistrian University of Athens, Zografou, 15784, Athens, Greece, ttsourou@geol.uoa.gr, zambetaki@geol.uoa.gr

The sedimentary and fossil record of Chios Island (eastern Aegean Sea) holds key evidence to understand the geodynamic and paleogeographic evolution of the Eastern Mediterranean area, as well as all the complex geological events that led to the closure of the Palaeotethys Ocean and subsequent opening of Neotethys in the south.

Two tectonostratigraphic units are distinguished since the synthesis of Besenecker et al. (1968) on the geology of the island. The Lower (relative autochthonous) Unit is made of siliciclastic turbidites, which contain olistolithes of various lithologies, ranging in age between the Silurian and the Carboniferous; they are overlain by a Mesozoic carbonate sequence. The Upper, allochthonous Unit is thrust over the Lower Unit and is only preserved in a number of isolated klippes. It is composed of Upper Carboniferous turbidites, Lower Permian sandy/marly limestones and Middle Permian shallow-water carbonates, which are overlain by red siltstones and Jurassic platform carbonates. According to Zanchi et al. (2003), the Upper Palaeozoic sequence of the Lower Unit is of Laurasian affinity, while Angiolini et al. (2005) suggested a Gondwanan affinity for the Upper Unit, based on the Brachiopods found in the Middle Permian limestones. We here provide for the first time evidence of the presence of Upper Permian shallow water carbonates within the Upper Unit, in which the identified foraminiferan record is also suggestive of North-Gondwanan affinity.

Studied material

Three nearly 3m-thick sections of Permian limestones and marls of the Upper Unit were observed and sampled along the east coast of the Marmaro Bay, situated in the north-eastern part of the Chios island (Kardamyla, N 38°32'29.76", E 26° 7'5.67"). The access to the area is easy by car as a settlement has been developed. The total length of the outcrop is 283 m and it is interrupted by several small faults and landslides.

Results

The three studied sections may be assigned to the latest Capitanian/earliest Wuchiapingian, latest substage of the Middle Permian (= Guadalupian) and/or oldest stage of the Late Permian (= Lopingian). Two of them are characterized by abundant gymnocodiacean algae, which are associated with some rare smaller foraminifers, miliolates, nankinellins and nodosariates. The well-characterized Capitanian/Wuchiapingian strata display interesting bioaccumulated perireefal microfacies with richthofeniid brachiopods and inozoan calcisponges. They are biostratigraphically characterized by an assemblage of *Reichelina* cf. *media*, *Dunbarula*? sp., *Altineria alpinotaurica*, *Labioglobivalvulina*, *Frondina* and *Robuloides*. Other perireefal microfacies show abundant elements of a new tubiphytid genus and species.

Discussion and conclusions

The palaeogeographical distribution of *Altineria alpinotaurica* includes now Chios, the Taurus mountains in Turkey, the NW and central Iran, whereas primitive forms of the genus are also known from Tunisia and Armenia. All these areas were part of the Perigondwanan border during the Wuchiapingian, which would suggest that the opening of the Neo-Tethys did not begin prior to the Changshingian (= latest Permian).

Acknowledgements

The micropaleontological and microfacies observations were conducted during the Master 2 studies of G. Grigoryan in Lille, with the financial support of the French Embassy in Yerevan and of the University of Lille.

References

Angiolini, L., Carabelli, L., Gaetani, M., 2005. Middle Permian brachiopods from Greece and their palaeobiogeographical significance: a new evidence for a Gondwanan affinity of the Chios island Upper Unit. Journal of Systematic Palaeontology, 3, 169-185.

Besenecker, H., Durr, S., Herget, G., Jacobshagen, V., Kauffman, G., Ludtke, G., Roth, W, Tietze, K.V., 1968. Geologie von Chios (Agais). Geol. Palaeontolog. 2, 121-150.

Zanchi, A., Garzanti, E., Larghi, C., Angiolini, L., Gaetani, M., 2003. The Variscan orogeny in Chios (Greece): Carboniferous accretion along a Palaeotethyan active margin. Terra Nova, 15, 213-223.

15th International Congress of the Geological Society of Greece
Athens, 22-24 May, 2019 | Harokopio University of Athens, Greece
Bulletin of the Geological Society of Greece, Sp. Pub. 7 Ext. Abs. GSG2019-038

Paleoecologic and neotectonic evolution of SE Rhodes (Greece) during the early Pleistocene

Yvonne Milker[1], Frans J. Jorissen[2], Ulrich Riller[1], Klaus Reicherter[3], Jürgen Titschack[4,5], Manuel F. G. Weinkauf[6], Marc Theodor[1], Gerhard Schmiedl[1]

(1) Center for Earth System Research and Sustainability, Institute for Geology, University of Hamburg, Bundesstrasse 55, 20146 Hamburg, Germany, yvonne.milker@uni-hamburg.de
(2) UMR CNRS 6112 LPG-BIAF Bio-Indicateurs Actuels et Fossiles, Université d'Angers, Angers Cedex 1, France
(3) Institute of Neotectonics and Natural Hazards, RWTH Aachen University, Lochnerstrasse 4-20, 52064 Aachen, Germany
(4) MARUM - Center for Marine Environmental Sciences, Leobener Strasse 8, 28359 Bremen, Germany
(5) Senckenberg am Meer, Marine Research Department, Südstrand 44, 26382 Wilhelmshaven, Germany, (6) Department of Earth Sciences, University of Geneva, Rue des Maraîchers 13,1205 Genève, Switzerland

Introduction

The recent Eastern Mediterranean Sea is characterized by oligotrophic conditions but little is known whether trophic conditions were comparable in the northeastern Mediterranean Sea region during older time periods such as the early Pleistocene. The Neogene climatic and hydrologic evolution of the Eastern Mediterranean Sea is influenced by orbital changes, leading to the periodic deposition of sapropels. The sapropels formed at times of Northern Hemisphere summer insolation maxima and are linked to phases of enhanced African monsoon activity (e.g., Hilgen, 1991; Rossignol-Strick et al., 1982) resulting in changes in the oxygenation of bottom and pore waters. Changes in trophic conditions and oxygenation of bottom and pore waters, in turn, influence the distribution and microhabitats of benthic foraminifera, particularly in deep-sea environments (Jorissen et al., 1995).

The Eastern Mediterranean Sea is tectonically active since the late Cretaceous closure of the Tethys where the African plate is subducted beneath the Anatolian plate along the Hellenic trench and its eastern extensions, the Pliny and Strabo trenches (Fig. 1A). In this geotectonic context, the island of Rhodes has been affected by two long-term subsidence and uplift phases, one in the early and one prevailing middle Pleistocene, and counterclockwise/anticlockwise rotations in the Plio- and middle Pleistocene (e.g., Van Hinsbergen et al., 2007; Cornée et al., 2019). The early Pleistocene neotectonic evolution of the eastern part of the island of Rhodes is recorded in various onshore sedimentary units consisting of marine sediments. These sediments reflect large-scale subsidence and uplift phases in individual and mostly fault-bound paleo-valleys, although remains unclear to what extent the different paleo-valleys underwent diachronous tectonic motions (e.g., Cornée et al., 2019).

Aims & Methods

Major aim of the study was to provide new insights into the paleoecologic and neotectonic evolution of the southeastern part of the island of Rhodes. In this context, we studied fossil benthic foraminiferal assemblages in 164 sediment samples from a marine sediment section from the Lindos Bay Formation (Pefka E section) deposited at the SE coast of the Island of Rhodes (Fig. 1A) during the early Pleistocene. We further developed a benthic foraminiferal-based transfer function to reconstruct tectonically-driven changes in paleo-water depths.

Results & Discussion

We found a high and constant concentration of eutrophic/low oxygen tolerant species in conjunction with a generally high diversity in the Pefka E sediment section (Fig. 1B). This observation suggests that mesotrophic conditions, with well oxygenated bottom waters, prevailed in the NE Mediterranean Sea region during the early Pleistocene which is in contrast to the recent oligotrophic conditions. The higher food availability might be the consequence of enhanced riverine nutrient influx into the Rhodes basin which led to increased surface productivity and related organic matter fluxes during the early Pleistocene. We further orbital-driven fluctuations in the individual abundances of the most important benthic foraminiferal species. Obliquity-driven changes were found in the relative abundance of *Cassidulina carinata* s.l. in the upper part of the section and are related to a higher food availability during glacial compared to interglacial periods in the Eastern Mediterranean region. Precession-driven changes were observed in the relative abundances of *C. carinata* s.l., *Cibicidoides pseudoungerianus* and *Cibicidoides mundulus*. These changes likely reflect enhanced rain fall and associated prolonged near-coastal phytoplankton blooms at times of Northern-Hemisphere insolation maxima. Most the early Pleistocene deep-sea sapropel intervals are characterized by an increase in eutrophic/low oxygen tolerant taxa and a decrease in oligotrophic taxa in the studied section (Fig. 1B). This suggest a higher and seasonally prolonged riverine runoff and associated phytodetritus fluxes rather than dysoxic conditions at the sea floor at estimated water depths between ~200 and ~600 m during times of sapropel formation in the Eastern Mediterranean deep-sea basins.

Precession-corrected paleo-water depth estimates (Milker et al., 2017) in the Pefka E section indicate a series of substantial vertical tectonic motions during the early Pleistocene with averaged vertical rates between 4 and ~8-10 mm/yr for the respective subsidence-uplift cycles (Fig. 1B). These rates of tectonic movements are rather fast compared to other estimates from Rhodes with 0.32 to 2.4 mm/yr (Cornée et al., 2019) and likely portray local vertical motions of an individual paleovalley rather than long-term vertical tectonic motion of the entire island of Rhodes.

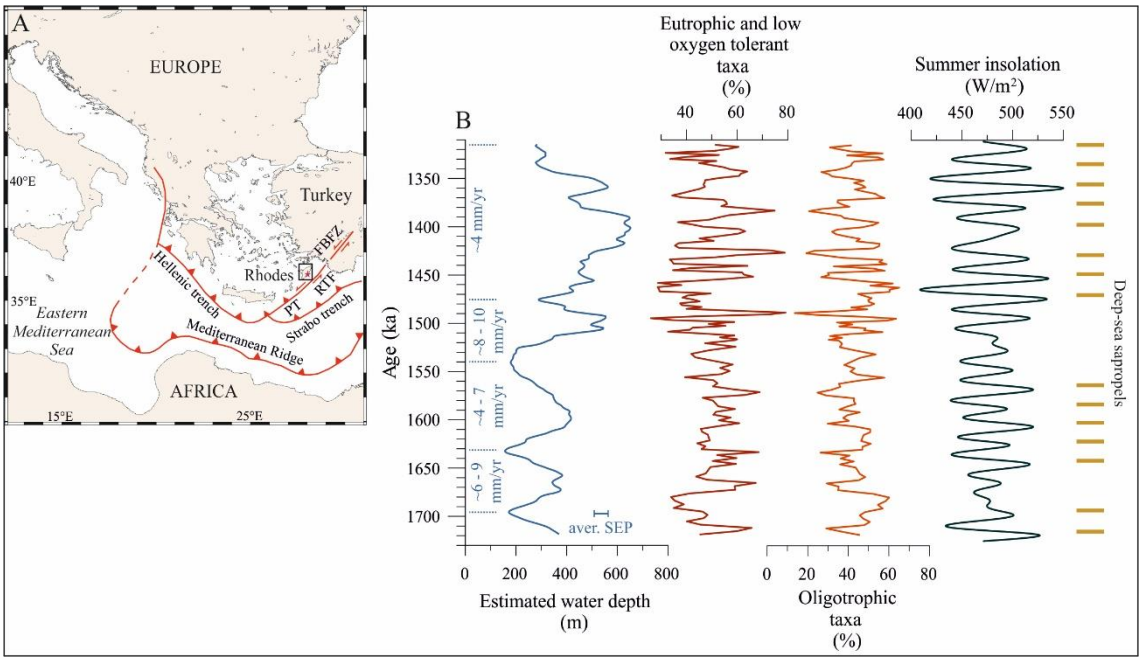

Figure 1. A. Main tectonic features in the Eastern Mediterranean region after Dilek and Sandvol (2009), and Görgün et al. (2014) and references therein (PT = Pliny trench, RTF = Rhodes transform fault; FBFZ = Fethiye-Burdur fault zone). Base map has been created with Ocean Data View (ODV), v. 4.7.10 (Schlitzer, 2017; https://odv.awi.de). B. Precession-corrected paleo-water depths with averaged squared error of prediction (SEP) of the original estimates (Milker et al., 2017) and quantified vertical motions, and relative abundance of eutrophic/low oxygen tolerant and oligotrophic taxa in the Pefka E section versus age. Northern Hemisphere summer (21 June) daily insolation after Laskar et al. (2004). Deep-sea sapropels after Kroon et al. (1998).

Acknowledgements

We thank the former students Franziska Schmidtke, Maurice Ballein and Benedikt Walker for sample preparation and for some counting of the samples. The sampling campaigns and sample preparation benefitted from funds of the German Research Foundation (DFG) project Fr 1134/7. The DFG is also acknowledged for financial support in the frame of the Cluster of Excellence CliSAP (Integrated Climate System Analysis and Prediction) at the University of Hamburg.

References

Cornée, J.-J., Quillévéré, F., Moissette, P., Fietzke, J., Lopez Otalvaro, G.E., Melinte-Dobrinescu, M., Philippon, M., van Hinsbergen, D., Agiadi, K., Koskeridou, E., Münch, P., 2019. Tectonic motions in oblique subduction forearcs: insights from the revisited middle and upper Pleistocene deposits of Rhodes (Greece). Journal of the Geological Society 176, 78-96.

Dilek, Y., Sandvol, E., 2009. Seismic structure, crustal architecture and tectonic evolution of the Anatolian-African Plate Boundary and the Cenozoic Orogenic Belts in the Eastern Mediterranean Region. Geological Society of London, Special Publication 327, 127-160.

Görgün, E., Zang, A., Kalafat, D., Kekovalı, K., 2014. The 10 June 2012 Fethiye Mw 6.0 aftershock sequence and its relation to the 24–25 April 1957 Ms 6.9–7.1 earthquakes in SW Anatolia, Turkey. Journal of Asian Earth Sciences 93, 102–112.

Hilgen, F.J., 1991. Astronomical calibration of Gauss to Matuyama sapropels in the Mediterranean and implication for the Geomagnetic Polarity Time Scale. Earth and Planetary Science Letters 104, 226-244.

Jorissen, F.J., de Stigter, H.C., Widmark, J.G.V., 1995. A conceptual model explaining benthic foraminiferal microhabitats. Marine Micropaleontology 26, 3-15.

Kroon, D., Alexander, I., Little, M., Lourens, L.J., Matthewson, A., Robertson, A.H.F., Sakamoto, T., 1998. Oxygen isotope and sapropel stratigraphy in the eastern Mediterranean during the last 3.2 million years, in: Robertson, A.H.F., Emeis, K.-C., Richter, C., Camerlenghi, A. (Eds.), Proceedings of the Ocean Drilling Program, Scientific Results, 181-189.

Laskar, J., Robutel, P., Joutel, F., Gastineau, M., Correia, A.C.M., Levrard, B., 2004. A long term numerical solution for the insolation quantities of the Earth. Astronomy and Astrophysics 428, 261-285.

Milker, Y., Weinkauf, M.F.G., Titschack, J., Freiwald, A., Krüger, S., Jorissen, F.J., Schmiedl, G., 2017. Testing the applicability of a benthic foraminiferal-based transfer function for the reconstruction of paleowater depth changes in Rhodes (Greece) during the early Pleistocene. PLoS ONE 12, e0188447.

Rossignol-Strick, M., Nesteroff, W., Olive, P., Vergnaud-Grazzini, C., 1982. After the deluge: Mediterranean stagnation and sapropel formation. Nature 295, 105-110.

Van Hinsbergen, D.J.J., Krijgsman, W., Langereis, C.G., Cornée, J.-J., Duermeijer, C.E., van Vugt, N., 2007. Discrete Plio-Pleistocene phases of tilting and counterclockwise rotation in the southeastern Aegean arc (Rhodes, Greece): early Pliocene formation of the south Aegean left-lateral strike-slip system. Journal of the Geological Society 164, 1133-1144.

15th International Congress of the Geological Society of Greece
Athens, 22-24 May, 2019 | Harokopio University of Athens, Greece
Bulletin of the Geological Society of Greece, Sp. Pub. 7 Ext. Abs. GSG2019-068

First evidence of *Mesopithecus monspessulanus* (Mammalia: Cercopithecidae) in the Late Miocene of Macedonia, Greece

G.D. Koufos
Aristotle University of Thessaloniki, Department of Geology, Laboratory of Geology and Palaeontology, 54124 Thessaloniki, Greece

Introduction - Fossiliferous site

The cercopithecid Mesopithecus is common in the late Miocene of Greece, recognized in several localities of the country. It was found in all Turolian localities of Axios Valley (Macedonia, Greece); two certain taxa M. delsoni and M. pentelicus, as well as a third one M. cf. monspessulanus have been described (Koufos, 2009a and references therein). The latter taxon was recognized in the material from the locality Dytiko 2 (DIT) by the mandibular fragment DIT-22 (Fig. 1c), which has smaller mandibular and dental dimensions than the typical M. pentelicus. The single known specimen and the badly preserved rest material from Dytiko 2 prevented a definite attribution and thus it was described as M. cf. monspessulanus (see Bonis et al., 1990; Koufos, 2009a, b). A re-examination of the Dytiko Mesopithecus sample allowed the recognition of another small-sized specimen from the locality Dytiko 1 (DTK). The specimen DTK-276 (it is wrongly mentioned as DTK-240 in Bonis et al., 1990: fig. 7, appendix 1) is a maxillary fragment in functional connection with the corresponding mandibular fragment and was not described. Recently, the maxillary and mandibular fragments of DTK-276 were separated (Fig. 1a, b), making possible to see their morphology, measure the teeth and make detailed comparisons.

Three different fossiliferous sites are known from the area of Dytiko village, about 65 km northeast of Thessaloniki city, and all are situated into the Dytiko Formation, which consists of alternating yellowish-gray marls, sandy marls, gravels, and fresh-water massive marly limestones at the top (Koufos, 1990). They were biochronologically correlated to the late Turolian, MN 13; more exactly the faunal comparison with the well dated Late Miocene-Early Pliocene localities of Ptolemais Basin suggested an age between 7.0-6.0 Ma (Koufos & Vassileiadou, 2015 and references therein).

The cercopithecids originated from Victoriapithecidae (Frost et al., 2017) and migrated to Eurasia from Africa during late Miocene; there are some discussed indications for their Vallesian presence, but they are certainly present at the beginning of the Turolian. The main Eurasian Late Miocene cercopithecid is Mesopithecus, expanded from the Iberian Peninsula to China. The earliest presence of Mesopithecus in Greece is mentioned from the locality Nikiti 2, NIK (Macedonia, Greece), dated at the beginning of early Turolian, MN 11 (8.7-8.2 Ma) (Koufos et al., 2016). The open, warm and dry environment of the Mediterranean region during Turolian was suitable for Mesopithecus, a semiterrestrial and opportunistic feeder, that often-consumed hard seeds (Merceron et al., 2009; Youlatos et al., 2012). The small and more arboreal form M. monspessulanus appeared later in the Pliocene (Szalay & Delson, 1979).

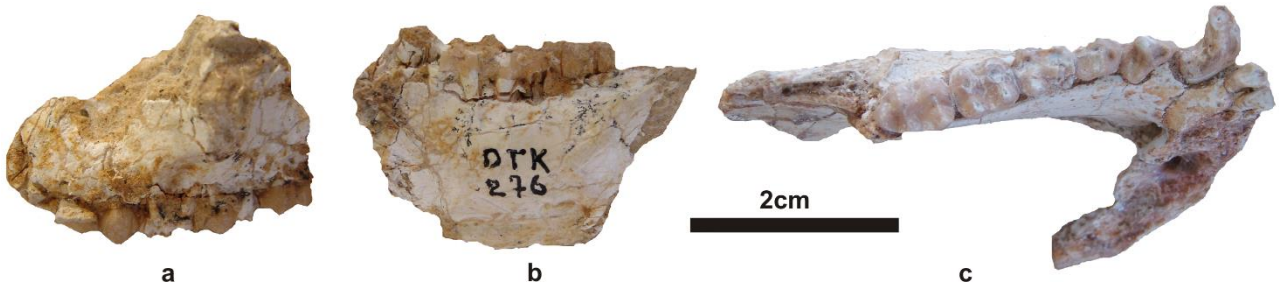

Figure 1. Mesopithecus monspessulanus, Dytiko, Axios Valley, Macedonia, Greece; Late Turolian, MN 13; a-b. Left maxillary (a) and mandibular (b) fragment, DTK-276 and c. mandibular fragment, DIT-22.

Description

The maxillary fragment of DTK-276 preserves part of the left maxilla with the tooth row P3-M3 (Fig. 1a); the dentition is moderately worn, indicating an adult individual; the base of the zygomatic arc is well distinguished, and its anterior margin is situated above the M1 and M2 contact; the premolars are asymmetric (the P3 more than the P4) and bears two main cusps; the molars have the typical morphology of Mesopithecus with four main cusps. The mandibular fragment of DTK-276 preserves a small part of the mandibular corpus with the tooth row M1-M3 and that of DIT-22 the left mandibular corpus with i1-m3 and the beginning of the right mandibular corpus without teeth (Fig. 1b, c). The height of the mandibular corpus is small (~10.0 mm below the middle of the m2); the transverse torus is weak; the incisors are smaller than those of M. pentelicus; the premolars are asymmetric; the p3 has a single main cuspid; the p4 has two cuspids; large honing facet in the p3; the molars are not well preserved but they bear the Mesopithecus morphology and are smaller than those of M. pentelicus.

Comparisons

The dental morphology of the Dytiko specimens is like that of Mesopithecus pentelicus and the differences are mainly restricted in the size between the two species. A principal component analysis of the lower dental dimensions of the Dytiko specimens in comparison with M. pentelicus from Pikerni and M. monspessulanus from Europe helps the attribution of the studied material. PC2 separates M. pentelicus from M. monspessulanus, while PC1 separates males from

females in both taxa (Fig. 2a). The specimens DTK-276 and DIT 22 match with the males of M. monspessulanus. Therefore, the small-sized Mesopithecus from Dytiko can be definitely attributed to M. monspessulanus and the available material belongs to male individuals. Although the available sample of the upper dentition of M. monspessulanus is small, a similar analysis indicates that DTK-276 is out of the convex hulls of males and females of M. pentelicus from Pikermi. Moreover, the dimensions of the preserved lower canine of DIT-22 are close to the males of M. monspessulanus and smaller than the corresponding ones of male M. pentelicus (Fig. 2b), confirming the above attribution.

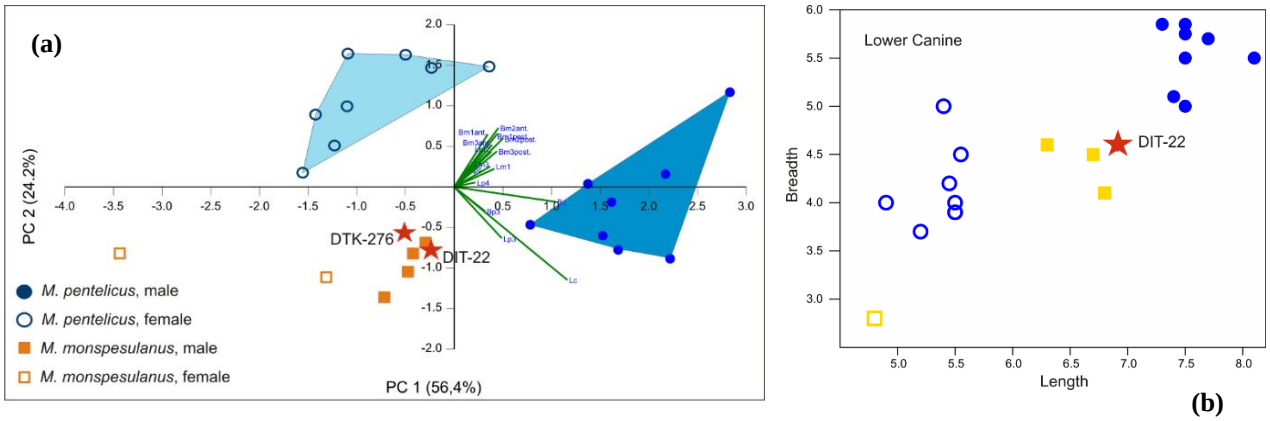

Figure 2. a. Principal component analysis comparing the lower dental dimensions of DTK-276 and DIT-22 with M. pentelicus and M. monspessulanus; b. Scatter plot comparing the lower canine of DTK-22 with M. pentelicus and M. monspessulanus, symbols as in Fig. 2a. Data sources: PRIMO (https://primo.nycep.org/) for M. monspessulanus; personal dataset for M. pentelicus.

Remarks

The re-consideration of the Dytiko small-sized Mesopithecus indicated that this material belongs to the small-sized M. monspessulanus a species which was unknown in Greece. Considering that: a) M. monspessulanus is known from the Pliocene of Europe, and b) the age of the Dytiko localities is late Turolian, MN 13, the studied material represents the earliest evidence of this species in Greecee. Based on the Turolian material of Mesopithecus in the Balkan Peninsula, there is a decrease in the size of the genus during that time span. The large-sized early Turolian M. delsoni continues with the middle Turolian M. pentelicus and then with the small-sized M. monspessulanus from late Turolian to Pliocene (Bonis et al., 1990; Koufos, 2009a, b). This early occurrence of the more arboreal form M. monspessulanus (see Szalay & Delson, 1979) agrees with the estimated environmental conditions (wetter with more closed microhabitats) in Macedonia, Greece during late Turolian and became more wet at the Miocene/Pliocene transition (Bonis et al., 1992; Koufos & Vasileiadou, 2015 and references therein).

Acknowledgements

Financial support for comparative studies was provided to me by the European Commission's Research Infrastructure Action (EU-SYNTHESYS: AT-TAF-702, FR-TAF-3102, GBTAF-1842) and the NSF-RHOI. Thanks to Mrs S. Veldemiri who separated the maxilla and mandible of the specimen DTK-276. I am indebted to A. Currant, G. Daxner-Höck, M. Harzhauzer, K. Heissig, S. Roussiakis, S. Sen, C. Soligo, P. Tassy and G. Theodorou, for giving me access to the collections at their disposal and for their great hospitality and help during my visit to their institutions.

References

Bonis de L., Bouvrain, G., Geraads, D., Koufos, G.D., 1990. New remains of Mesopithecus (Primates, Cercopithecidae) from the late Miocene of Macedonia with the description of a new species. Journal of Vertebrate Paleontology 10, 473-483.

Bonis, L.de, Bouvrain, G., Geraads, D., Koufos, G.D., 1992. Diversity and palaeoecology of Greek Late Miocene mammalian faunas. Palaeogeography, Palaeoclimatology, Palaeoecology 91, 99-121.

Frost, S.R., 2017. Evolution of the Cercopithecidae, in Fuentes A. (ed), The International Encyclopedia of Primatology, 1-3. DOI: 10.1002/9781119179313.wbprim0064

Koufos, G.D. 1990. The hipparions of the lowerAxios valley (Macedonia, Greece). Implications for the Neogene stratigraphy and the evolution of hipparions, in Lindsay E., Fahlbusch V., Mein P. (Eds), European Neogene Mammal Chronology, 321-338.

Koufos, G.D. (2009a). The Neogene cercopithecids (Mammalia, Primates) of Greece. Geodiversitas 31(4), 817-850.

Koufos, G.D., 2009b. The genus Mesopithecus (Primates, Cercopithecidae) in the late Miocene of Greece. Bollettino della Società Paleontologica Italiana 48(2), 157-166.

Koufos, G.D., 2016. Primates, in Koufos, G.D., Kostopoulos, D.S. (Eds), Palaeontology of the upper Miocene vertebrate localities of Nikiti (Chalkidiki Peninsula, Macedonia, Greece). Geobios 49(1-2), 45-51.

Koufos, G. D., Vasileiadou, K., 2015. Miocene/Pliocene mammal faunas of southern Balkans: implications for biostratigraphy and palaeoecology. Palaeobiodiversity and Palaeoenvironments 95, 285–303.

Merceron, G., Koufos, G.D., Valentin, X., 2009. Feeding habits of the first European colobine, Mesopithecus (Mammalia, Primates): evidence from a comparative dental microwear analysis with modern cercopithecids. Geodiversitas, 31(4):865-878.

Szalay F. & Delson E., 1979. Evolutionaty history of the Primates, 1-580.

Youlatos, D., Couette, S., Koufos, G.D., 2012. A functional multivariate analysis of Mesopithecus (Primates: Colobinae) humeri from the Turolian of Greece. Journal of Human Evolution 63, 219-230.

15th International Congress of the Geological Society of Greece
Athens, 22-24 May, 2019 | Harokopio University of Athens, Greece
Bulletin of the Geological Society of Greece, Sp. Pub. 7 Ext. Abs. GSG2019-104

Karnezeika (Argolis, Peloponnese): preliminary data concerning a new Villafranchian locality of Southern Greece

M. Kokotini[1], N. Kargopoulos[2], G. Iliopoulos[3], S. Roussiakis[2], P. Skandalos[2], D. Michailidis[4], G. Svorligkou[2], P. Kampouridis[5] and G. Theodorou[2]

(1) Aristotle University of Thessaloniki, School of Geology, 54124, Thessaloniki, Greece, kmariann@geo.auth.gr
(2) National and Kapodistrian University of Athens, Faculty of Geology and Geoenvironment, Panepistimiopolis, 15784, Athens, Greece
(3) University of Patras, Department of Geology, 26504 Rio Achaia, Greece
(4) American School of Classical Studies at Athens, The Malcolm H. Wiener Laboratory for Archaeological Science, Souidias 54, 10676, Athens, Greece
(5) Eberhard Karls University of Tübingen, Department of Geosciences, Sigwartstr. 10, 72074 Tübingen, Germany

Introduction

Karnezeika is a Villafranchian locality, situated in the northern part of southern Argolis. No proper excavations have been conducted in the locality. Geologically, the fossils are enclosed in fine-grained red sediments, which filled a small doline in a late Triassic – early Jurassic limestone. The locality of Karnezeika has been discovered in 2005 and the collected material has been stored in both Athens Museum of Palaeontology and Geology (AMPG) and the Laboratory of Palaeontology and Stratigraphy, Department of Geology, University of Patras. The material housed at the University of Patras was studied in the contexts of an Undergraduate dissertation (Kokotini, 2018). The present study is a combined effort from both Institutes to resume the up to now results on the prepared material.

Results

Despite the fragmentary nature and the scarcity of the material, the biodiversity of the site seems to be significantly high, including at least 22 genera, belonging to 17 families. The preliminary faunal list is provided on Table 1.

Table 1. Preliminary faunal list of Karnezeika

Class **Reptilia**	Order **Carnivora**
Order **Testudines** indet.	Family **Canidae**
Order **Squamata**	***Vulpes*** sp.
Clade **Lacertoidea** indet.	***Canis*** sp.
Clade **Ophidia** indet.	Family **Felidae**
Class **Aves**	***Panthera gombaszoegensis***
Order Accipitriformes	Family **Hyaenidae**
Family Accipitridae	***Pachycrocuta brevirostris***
Order **Passeriformes**	Order **Perissodactyla**
Family **Corvidae**	Family **Rhinocerotidae**
Pyrrhocorax sp.	***Stephanorhinus*** sp.
Class **Mammalia**	Family **Equidae**
Order **Artiodactyla**	***Equus*** sp.
Family **Bovidae**	Order **Rodentia**
Gazella borbonica	Family **Arvicolidae**
Gazellospira torticornis	***Kislangia*** sp.
Gallogoral meneghinii	***Kalymnomys*** sp.
Pliotragus sp.	Family **Muridae**
Family **Cervidae**	***Apodemus*** cf. ***dominans***
Eucladoceros sp.	Family **Gliridae** indet.
Order **Primates**	Order **Lagomorpha**
Family **Cercopithecidae**	Family **Leporidae**
Papionini indet.	***Hypolagus*** sp.

The majority of the identified taxa indicate an age approximately at the border between middle to late Villafranchian (Kostopoulos, 1996; Rook & Martínez-Navarro, 2010; Koufos, 2014; Doukas & Papayianni, 2016; Koufos & Kostopoulos, 2016). The coexistence of mammalian carnivores and herbivores of varying size, micromammals, birds and reptiles offers a great opportunity to study the Villafranchian faunas of Greece in more detail. Another interesting finding is the presence of a proximal radius, belonging to one of the macaque-like species occurring in this period.

Conclusions

The studied locality preserves high interest because of the following:

- It is the most comprehensively studied Villafranchian locality in southern Greece, offering new insights on biochronology and biogeography
- It comprises a rich fauna including macro-mammals, micro-mammals, birds and reptiles
- It is the first locality in Greece with remains of *Hypolagus*
- It includes some rare taxa such as *Eucladoceros*, *Gallogoral*, *Pliotragus* and the papionin primate
- In contrast to other Villafranchian localities it includes very few equid remains

The study of the bulk of the material which is still unprepared will certainly provide further and more complete data on the Villafranchian of Karnezeika. Thus, more precise conclusions will be made concerning the palaeoecology of the locality and its relationship with other Villafranchian sites in Greece.

Acknowledgements

We would like to thank Christos Rigas who first discovered the fossiliferous site and was responsible for the first collection of the material housed at AMPG and the owner of the quarry, Thanasis Iliopoulos, for extracting a large portion of the bone assemblage and maintaining it in the quarry, as well as Dimitrios Kostopoulos and Nikolai Spassov for their useful comments, concerning taxonomic identifications.

References

Athanassiou, A., 1998. Contribution to the Study of the Fossil Mammals of Thessaly, Faculty of Geology. Ph.D. Thesis, National and Kapodistrian University of Athens, Athens, 354 p.

Doukas, C., Papayianni, K., 2016. Small mammals in the Plio/Pleistocene sediments of Greece, in: Harvati, K., Roksandic, M. (Eds.), Palaeoanthropology of the Balkans and Anatolia: Human evolution and its context, 291-302.

Kokotini, M., 2018. Osteological study of Pleistocene Mammals from the locality Karnezeika, S. Argolis, Department of Geology, Bachelor Thesis, University of Patras, Patras, 60 p.

Kostopoulos, D., 1996. The Plio-Pleistocene Artiodactyls of Macedonia (Greece): Systematic-Palaeoecology-Biochronology-Biostratigraphy. School of Geology, Ph.D. Thesis, Aristotle University of Thessaloniki, Thessaloniki, 612 p.

Koufos, G., 2014. The Villafranchian carnivoran guild of Greece: implications for the fauna, biochronology and paleoecology. Integrative Zoology 9, 444-460.

Koufos, G., Kostopoulos, D., 2016. The Plio-Pleistocene large mammal record of Greece: Implications for early human dispersals into Europe, in: Harvati, K., Roksandic, M. (Eds.), Palaeoanthropology of the Balkans and Anatolia: Human evolution and its context, 269-280.

Rook, L., Martínez-Navarro, B., 2010. Villafranchian: The long story of a Plio-Pleistocene European large mammal biochronologic unit. Quaternary International 219(1-2), 134-144.

Late Glacial and Holocene Vegetation History and Climate Variability in Southwestern Balkans

K. Panagiotopoulos[1], K. Kouli[2], O. Peyron[3], S. Kyrikou[1,2], A. Francke[4], N. Leicher [1], B. Wagner[1]

(1) Institute of Geology and Mineralogy, University of Cologne, Germany, panagiotopoulos.k@uni-koeln.de
(2) Department of Geology and Geoenvironment, National and Kapodistrian University of Athens, Greece
(3) Institut des Sciences de l'Evolution de Montpellier, Université de Montpellier, Montpellier, France
(4) School of Earth and Environmental Sciences, University of Wollongong, Australia

New insights into the floristic composition, vegetation changes and climate variability over the last 17000 years are provided by the two new high-resolution pollen records from lakes Ohrid and Prespa. The Lake Ohrid (DEEP core) pollen record is the first continuous Late Glacial-Holocene sequence from Lake Ohrid, as existing Late Glacial and Holocene records from Lake Ohrid suffer from discontinuities in sedimentation (Sadori *et al.*, 2016). This centennial resolution pollen record along with an increased resolution in the pollen archive of the adjacent Lake Prespa allow to examine the evolution of local and regional vegetation patterns at an unprecedented scale. Subsequently, we employ the modern analogue technique (MAT) on the new pollen data to reconstruct climate variability in the area over the study interval. Moreover, thirty modern surface (moss) samples collected across an altitudinal transect within the catchments of Ohrid and Prespa were analyzed and integrated in the calibration dataset to improve the local vegetation-climate relationship.

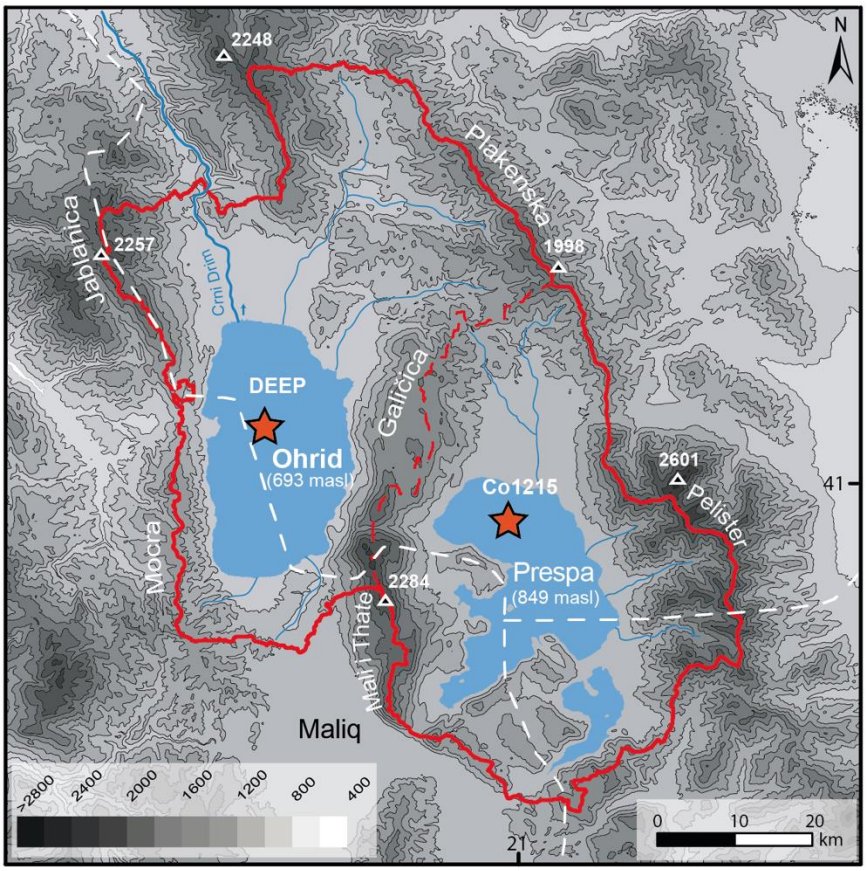

Figure 1: Topographic map of the study region showing the catchment of Lake Ohrid and Lake Prespa and the coring locations of the DEEP (Ohrid) and Co1215 (Prespa) sites (after Panagiotopoulos 2013.

In the Last Glacial period (from 17000 cal BP onwards), pollen spectra from both lakes suggest a rather open landscape dominated by steppe elements (mainly *Artemisia* and Chenopodiaceae) along with grasslands. Pines appear to be the dominant trees in the region during this interval, while relatively high oak percentages suggest their local presence in both catchments. During the Bølling/Allerød deciduous oaks dominate arboreal tree percentages at Ohrid, while at Prespa pines remain dominant throughout this period. During the Bølling/Allerød, deciduous oaks dominate tree percentages at Ohrid, while at Prespa pines remain dominant over this period (Panagiotopoulos *et al.*, 2013). Throughout the Younger Dryas (12900 – 11600 cal BP), the resurgence of steppe elements accompanied by *Betula*, *Ephedra* and *Hippophae* in both pollen records suggest that cold and arid conditions prevailed. Mean annual precipitation values reconstructed applying the MAT method yield values above 400 mm/year during the last 17000 years. These findings imply that moisture availability was most likely not a limiting factor for tree growth and support the refugial character of the region

(Panagiotopoulos *et al.*, 2014).

The Holocene is characterized by an estimated twofold increase of mean annual precipitation compared to the Younger Dryas. The onset of the Holocene is characterized by the gradual expansion of mixed deciduous woodland dominated by oaks indicating the presence of dense deciduous oak forests in the surroundings of Lakes Ohrid and Prespa. A markedly short-term shift highlighted by an abrupt rise of *Artemisia* percentages, corresponding to the centennial 8.2 cooling event is registered in the pollen records of both lakes. During the Middle and Late Holocene, the closed forests diversify and percentages of other deciduous taxa such as *Acer*, *Alnus*, *Carpinus*, *Fagus*, *Ostrya* increase in both records, especially at Prespa. Although Lake Ohrid is situated a 150 m lower than Lake Prespa at 693 m asl, the presence of Mediterranean elements such as *Pistacia* and *Phillyrea* in Ohrid pollen spectra is rather limited compared to Prespa. Intensifying anthropogenic activities during the last two millennia can be inferred in both records from the decline of tree percentages and the coeval increase in pollen of cultivated plants such as walnuts and cereals.

These two pollen records from mid-altitudes in southwestern Balkan suggest that the vegetation response in the region is highly sensitive to sub-millennial climate shifts and improve our understanding on plant diversity dynamics, evolution and resilience over the last 17000 years.

Acknowledgements

This study was funded by a DFG Grant No. PA2664/2-2 (Konstantinos Panagiotopoulos) and by a Grant No. GSGS-2018A-SUH03 of the Graduate School of Geosciences, University of Cologne (Styliani Kyrikou).

References

Panagiotopoulos, K., Aufgebauer, A., Schäbitz, F., Wagner, B., 2013. Vegetation and climate history of the Lake Prespa region since the Lateglacial. Quaternary International 293, 157-169.

Panpagiotopoulos, K., 2013. Late Quaternary ecosystem and climate interactions in SW Balkans inferred from Lake Prespa sediments. PhD thesis, Universität zu Köln, Cologne, Germany,

Panagiotopoulos, K., Böhm, A., Leng, M.J., Wagner, B., Schäbitz, F., 2014. Climate variability over the last 92 ka in SW Balkans from analysis of sediments from Lake Prespa. Climate of the Past 10, 643-660.

Sadori, L., Koutsodendris, A., Masi, A., Bertini, A., Combourieu-Nebout, N., Francke, A., Kouli, K., Joannin, S., Mercuri, A.M., Panagiotopoulos, K., Peyron, O., Torri, P., Wagner, B., Zanchetta, G., Donders, T.H., 2016. Pollen-based paleoenvironmental and paleoclimatic change at Lake Ohrid (SE Europe) during the past 500 ka. Biogeosciences 13, 1423–1437.

15th International Congress of the Geological Society of Greece
Athens, 22-24 May, 2019 | Harokopio University of Athens, Greece
Bulletin of the Geological Society of Greece, Sp. Pub. 7 Ext. Abs. GSG2019-109

Benthic foraminifera as a tool for Environmental Evaluation in Thermaikos Gulf, NW Aegean Sea

O. Koukousioura[1], S. Georgiou[1], M.D. Dimiza[2], I. Michailidis[1], E. Aidona[1], M. Seferlis[3], C. Christoforidis[4], M. Evgenakis[4], M.V. Triantaphyllou[2]

(1) Aristotle University of Thessaloniki, School of Geology, 54124, Thessaloniki, Greece, okoukous@geo.auth.gr
(2) National and Kapodistrian University of Athens, Faculty of Geology and Geoenvironment, 15784, Athens, Greece
(3) The Goulandris National History Museum, Greek Biotope/Wetland Centre, 57001 Thermi, Thessaloníki, Greece
(4) Aristotle University of Thessaloniki, School of Chemistry, 54124, Thessaloniki, Greece

Thermaikos Gulf is a semi-enclosed, shallow basin in the northwestern part of the Aegean Sea (Fig. 1A). The environmental setting of the area is defined by the three major rivers, two minor ones and several ephemeral streams (Lykousis *et al*., 2005) that flow into the basin, while the gulf is characterized by eutrophication being one of the most anthropogenically impacted coastal regions of Greece. During the high precipitation period (January-May), the freshwater intrusion can extend southwards enough to seal a major part of the gulf's surface waters (salinities <25 psu). On the other hand, more saline waters from the northern Aegean Sea flow towards the northeast, entering the inner Thermaikos Gulf (Kontoyannis *et al.*, 2003; Fig. 1B).

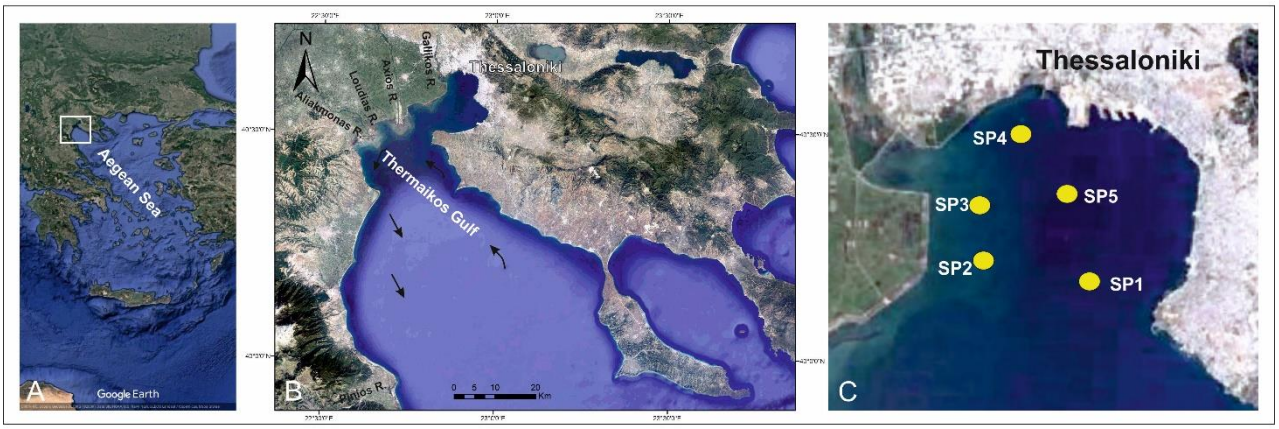

Figure 1. A) Location map of Thermaikos Gulf, B) water circulation and main rivers discharging in the gulf, C) sampling stations at the inner part of the gulf.

The aim of this study is to explore changes in the foraminiferal abundance and composition, as compared to a multi-parameter environmental dataset (temperature, salinity, pH and nutrients), magnetic susceptibility and metal content, during a twelve-month monitoring. Sampling of the top 2 cm of the surface sediment was carried out on a monthly basis (December 2015-December 2016) at one station (SP1), and at 5 stations (SP1-SP5) during winter (February 2016) and spring (April 2016), located in Thessaloniki Bay (inner part of the Thermaikos Gulf). Sampling followed the standardized FOBIMO method (Schönfeld *et al*., 2012), while field measurements at the maximum depth of each station were also conducted. Furthermore, the Foram Stress Index (FSI; Dimiza *et al*., 2016) was calculated, in order to evaluate the environmental status.

Foraminiferal assemblages were dominated mostly by *Bulimina* spp., *Bolivina* spp., *Uvigerina* spp. and various species of agglutinated foraminifera, such as *Textularia bocki*, *Eggereloides scaber*, and *Leptohalysis scotti*. The foraminiferal assemblage also included *Ammonia tepida*, *Haynesina depressula*, *Nonionella turgida*, *Lobatula lobatula* and miliolids.

During late spring-summer (April to August), foraminiferal densities and relative percentages of the living specimens displayed the highest values, while high diversities (Shannon-Wiener index) were observed during winter. The investigated samples for February and April sampling periods were variable with respect to both abiotic parameters and the foraminiferal assemblage, characterized by a mix of stress-tolerant and more sensitive taxa. Samples from the western part of the gulf were characterized by a diverse assemblage that included *Bulimina* spp., *Bolivina* spp., agglutinants, miliolids and a variety of small, epiphytic rotaliid taxa. The rest of the gulf presented a monotonous fauna, dominated mostly by stress-tolerant species. FSI values suggested poor/bad to moderate conditions prevailing, while good environmental status has been defined during April at only one station from the western part of the gulf.

The variability in foraminiferal composition reflects the exceptional environmental conditions that prevailed in inner Thermaikos Gulf, thus providing further evidence for the species' seasonality in comparison with the anthropogenic impact.

Acknowledgments

Financial support for this study was provided by Municipality of Thessaloniki.

References

Dimiza, M.D., Triantaphyllou, M.V., Koukousioura, O., Hallock, P., Simboura, N., Karageorgis, A.P., Papathanasiou, E., 2016. The Foram Stress Index: A new tool for environmental assessment of soft-bottom environments using benthic foraminifera. A case study from the Saronikos Gulf, Greece, Eastern Mediterranean. Ecological Indicators 60, 611-621.

Kontoyiannis, H., Kourafalou, V.H., Papadopoulos, V., 2003. Seasonal characteristics of the hydrology and circulation in the northwest Aegean Sea (eastern Mediterranean): Observations and modelling. Journal of Geophysical Research 108, No. C9, 3302.

Lykousis, V., Karageorgis, A.P., Chronis, G.Th., 2005. Delta progradation and sediment fluxes since the last glacial in the Thermaikos Gulf and the Sporades Basin, NW Aegean Sea, Greece. Marine Geology 222-223, 381-397.

Schönfeld, J., Alve, E., Geslin, E., Jorissen, F., Korsun, S., Spezzaferri, S. and Members of the FOBIMO group, 2012. The FOBIMO (FOraminiferal BIo-MOnitoring) initiative-Towards a standardised protocol for soft-bottom benthic foraminiferal monitoring studies. Marine Micropaleontology 94-95, 1-13.

15th International Congress of the Geological Society of Greece
Athens, 22-24 May, 2019 | Harokopio University of Athens, Greece
Bulletin of the Geological Society of Greece, Sp. Pub. 7 Ext. Abs. GSG2019-110

Benthic foraminifera contribution to the stratigraphic and paleoenvironmental evolution of the coastal area of Farasan Al-Kabir Island (Saudi Arabia)

O. Koukousioura[1], K. Pavlopoulos[2], M. Triantaphyllou[3], D. Vandarakis[4], S. Marion de Procé[5], V. Chondraki[3], V. Kapsimalis[4], E. Fouache[2]

(1) Aristotle University of Thessaloniki, School of Geology, 54124, Thessaloniki, Greece, okoukous@geo.auth.gr
(2) Paris Sorbonne University Abu Dhabi, Geography and Planning Department, P.O. 38044, Abu Dhabi, United Arab Emirates
(3) National and Kapodistrian University of Athens, Faculty of Geology and Geoenvironment, 15784, Athens, Greece
(4) Hellenic Centre for Marine Research, Institute of Oceanography, 46.7 km Athens-Sounio Ave, 19013, Anavyssos, Greece
(5) Université Paris 1-Panthéon Sorbonne, Archéologies et Sciences de l'Antiquité, (équipe APOHR, UMR 7041), Nanterre, France.

Holocene environmental changes of coastal areas with a high temporal resolution, can be derived by the multi-proxy analysis of sediment cores (e.g., Morhange *et al.*, 2000; Triantaphyllou *et al.*, 2010; Di Rita *et al.*, 2011), while the study of benthic foraminifera assemblages together with radiocarbon dating is evidently the best tool to reveal the succession of past environmental conditions and, therefore, the alteration of physiographical settings (e.g., Cann *et al.*, 2000; Horton *et al.*, 2007; Koukousioura *et al.*, 2012; Xiang *et al.*, 2008).

The Farasan Al Kabir island is one of the two main islands of the Farasan Bank, which lies in the southeastern part of the Red Sea, offshore the southwest Saudi Arabian coast (Fig. 1A), and consists of more than 128 islands covering a total land area of approximately 600 km^2 (Khalil, 2012).

In order to reconstruct the coastal paleoenvironments since the mid Holocene, a 3.3-m long sediment core sampling, was conducted and Matar-1 core was analyzed. A multidisciplinary approach was selected to reveal short-term changes, combining micropalaeontological (benthic foraminifera), stratigraphical, lithological, element geochemical, bulk mineralogical, and isotopic dating (^{14}C) analyses. Thirty nine (39) samples were used for micropaleontological analysis and over than forty foraminiferal species were identified. Benthic foraminiferal assemblages of the studied core samples were generally rich, but a lot of broken specimens were observed. Thus, the broken-reworked ratio was calculated.

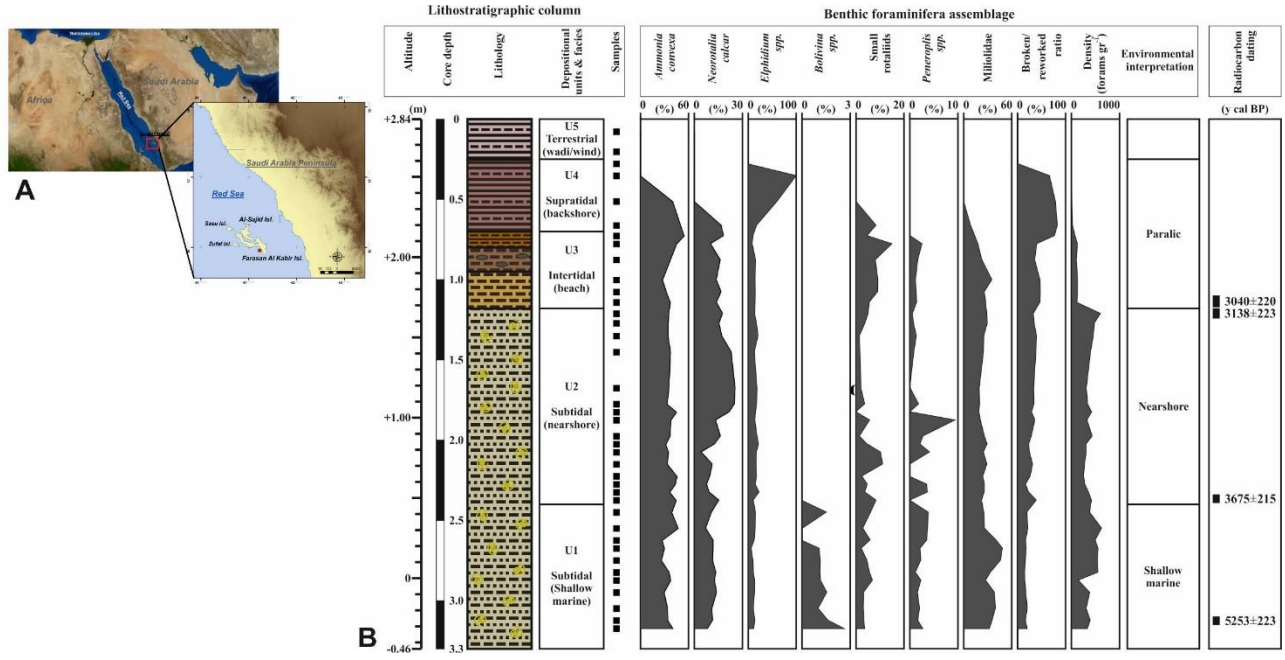

Figure 1. A) Location map of Farasan Al-Kabir Island, B) stratigraphy and benthic foraminiferal assemblages of Matar-1 core (modified from Pavlopoulos *et al.*, 2018).

The southeast coast of the Farasan Al Kabir Island is formed from uplifted reefal limestone. The arid low-lying topography includes hard rock formations, such as coral limestone plateau, cliffs and pediments, as well as soft-sediment formations, such as playa-like depressions located on plateau surfaces, alluvial fans and bajada, and sandy beaches.

The mid Holocene evolution of the borehole area is resulted from the detailed analysis of five sedimentary units detected along the core Matar-1, and includes three distinct stages:

(a) from 5253 ± 223 y cal BP to 3138 ± 223 y cal BP, carbonate coarse-grained material consisting of coral fragments, molluscs, calcareous algae and benthic foraminifera are deposited on a shallow marine fringing reefal platform.

Foraminiferal density presents high values, while the fauna is characterized by the dominant *Ammonia convexa* and miliolids, along with the small rotaliids, elphidiids and *Bolivina* spp. (Fig. 1B). Faunal composition varies at around 3675 ± 215 y cal BP, consisting mainly by *Neorotalia calcar* and *A. convexa* and by fluctuating percentages of small rotaliids, *Peneroplis* spp. and miliolids. Density reaches high values and broken-reworked tests increase significantly suggesting a high energy environment, in accordance with the Farasan modern analogue (Abu-Zied et al., 2011), pointing to a nearshore backreef, and later (around 3138 ± 223 y cal BP) a reef ramp.

(b) since 3040 ± 220 y cal BP foraminiferal density decreases abruptly, with broken-reworked tests presenting their highest values, suggesting that the borehole area obtains the characteristics of a high-energy beach that receives increasing inputs of terrigenous material;

(c) subsequently, a supratidal backshore setting is established influenced mostly by terrestrial processes and occasionally by marine processes, as it is indicated by the decreasing and sometimes sporadic presence of benthic foraminifera, and recently, a sedimentary veneer consisting of terrigenous, carbonate and evaporite material is formed by terrestrial, mainly wadi and aeolian, processes.

Acknowledgements

The authors would like to thank Prof. F. Villeneuve and Dr. M. Mouton for their full support and collaboration during the research survey. We are indebted to HRH Prince Sultan Bin Salman Bin Abdulaziz Al Saud (President and Chairman of the Directors Board of the Saudi Commission for Tourism and Antiquities, SCTA), as well as to Dr Al-Saud, Professor Ali Al-Ghabbān (Vice-President of SCTA) and Dr Jamal Al Omar (Director General of SCTA), for granting permission to carry out the fieldwork. We also gratefully acknowledge the cooperation and help of Dr Al-Modare, Dr Mofareh and M. Aqīlī, members of SCTA in Jizān and Farasān.

References

Cann, J.H., Bourman, R.P., Barnett, E.J., 2000. Holocene foraminifera as indicators of relative estuarine-lagoonal and oceanic influences in estuarine sediments of the River Murray, South Australia. Quaternary Research 53(3), 378-391.

Di Rita, F., Simone, O., Caldara, M., Gehrels, W.R., Magri, D., 2011. Holocene environmental changes in the coastal Tavoliere Plain (Apulia, southern Italy): a multiproxy approach. Palaeogeography, Palaeoclimatology, Palaeoecology 310(3), 139-151.

Horton, B.P., Culver, S.J., Hardbattle, M.I., Larcombe, P., Milne, G.A., Morigi, C., Whittaker, J.E., Woodroffe, S.A., 2007. Reconstructing Holocene sea-level change for the central Great Barrier Reef (Australia) using subtidal foraminifera. Journal of Foraminiferal Research 37(4), 327-343.

Khalil, H.M., 2012. Pliocene-Pleistocene stratigraphy and macrofauna of the Farasan islands, south East Red Sea, Saudi Arabia. Arabian Journal of Geosciences 5(6), 1223-1245.

Koukousioura, O., Triantaphyllou, M.V., Dimiza, M.D., Pavlopoulos, K., Syrides, G., Vouvalidis, K., 2012. Benthic foraminiferal evidence and paleoenvironmental evolution of Holocene coastal plains in the Aegean Sea (Greece). Quaternary International 261, 105-117.

Morhange, C., Goiran, J.P., Bourcier, M., Carbonel, P., Le Campion, J., Rouchy, J.M., Yon, M., 2000. Recent holocene paleo-environmental evolution and coastline changes of Kition, Larnaca, Cyprus, Mediterranean sea. Marine Geology 170(1), 205-230.

Pavlopoulos, K., Koukousioura, O., Triantaphyllou, M., Vandarakis, D., Marion de Procé, S., Chondraki, V., Fouache, E., Kapsimalis, V., 2018. Geomorphological changes in the coastal area of Farasan Al-Kabir Island (Saudi Arabia) since mid Holocene based on a multi-proxy approach. Quaternary International 493, 198-211.

Triantaphyllou, M.V., Kouli, K., Tsourou, T., Koukousioura, O., Pavlopoulos, K., Dermitzakis, M.D., 2010. Paleoenvironmental changes since 3000 BC in the coastal marsh of Vravron (Attica, SE Greece). Quaternary International 216(1), 14-22.

Xiang, R., Yang, Z., Saito, Y., Fan, D., Chen, M., Guo, Z., Chen, Z., 2008. Paleoenvironmental changes during the last 8400 years in the southern Yellow Sea: benthic foraminiferal and stable isotopic evidence. Marine Micropaleontology 67(1), 104-119.

Taxonomy and stratigraphy of the Eocene nummulitic deposits of Greece: a biometric analysis approach

V.-G. Dimou[1], O. Koukousioura[1], M.D. Dimiza[2], M.V. Triantaphyllou[2], G. Less[3], F. Pomoni-Papaioannou[2], G. Syrides[1]

(1) Aristotle University of Thessaloniki, School of Geology, 54124, Thessaloniki, Greece, dimouvaso@geo.auth.gr
(2) National and Kapodistrian University of Athens, Faculty of Geology and Geoenvironment, 15784, Athens, Greece
(3) University of Miskolc, Department of Geology and Mineral Resources, H-3515, Miskolc-Egyetemváros, Hungary

Nummulitid banks and depositional models have been the subject of many studies in Greece already since 19$_{th}$ century (eg., Philippson, 1890). Although numerous studies deal with nummulitid presence mainly in the Greek Thrace basin, the Mesohellenic basin and the external Hellenides, systematic morphometrical analysis has never performed.

This study was undertaken to define biometric and morphological features of Greek nummulitids and to test the relative taxonomic importance of internal and external features for distinguishing biostratigraphically significant species.

Nummulitid assemblages from six different localities in Greece were morphometrically investigated for the first time (Fig. 1). The aforementioned localities belong to alpine (Perivoli Grevena, Manoliasa Ioannina, Dervenakia and Tripoli) and molassic (Kirki Thrace from Thrace basin and Vasiliki Trikala from Mesohellenic basin) formations.

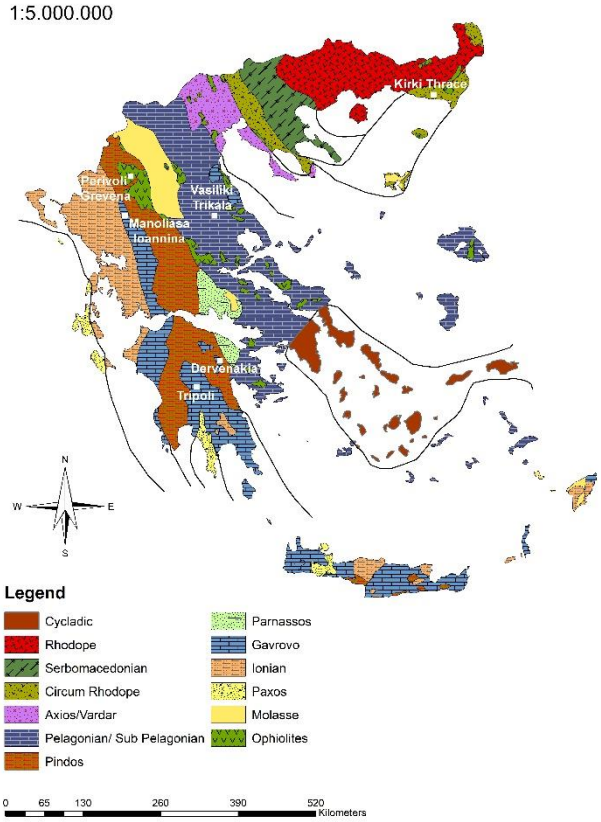

Figure 1. Generalized geological map of Greece and location of the studied sites (modified by IGME, 1983).

The micropaleontological material was examined in thin sections, except for isolated specimens collected within the molassic deposits in the area of Kirki Thrace, which were studied in polished sections and split specimens.

The scheme of identification includes the study of the external morphology of the isolated specimens (the shape of the test, the shape of septa filaments, the presence or the absence of the granules, their type of arrangement and the measurements on diameter and test thickness). Furthermore, the study of the internal morphology in equatorial sections, is including the observations on the shape of septa and the architecture of the chambers.

Biometrical analysis has been performed on the morphological characteristics of both megalospheric and microspheric forms. The conducted measurements refer to thickness, diameter and radius of the whole test and all internal whorls. Specific measurements refer to the dimensions of the protoconch (only for A-form). The scheme for the identification of *Nummulites* is based mainly in Blondeau (1972), Less (1998), Less *et al*. (2011), Less and Özcan (2012), Özcan *et al.* (2009) and Schaub (1981).

Statistical analysis of the biometric data, combined with the established systematic taxonomy, enabled us to identify eight different morphotypes potentially associated with different nummulitid species.

Among them the most commonly identified was *Nummulites perforatus* group, with *N. perforatus* de Montfort (SBZ 17; Serra-Kiel *et al*., 1998) being its main representative together with *Assilina exponens*, dominating in the molassic sediments of Vasiliki Trikala and Kirki Thrace. Additionally, faunas from Dervenakia and Tripoli present identical species associations pointing to a Bartonian age. Furthermore, three different assemblages have been observed from Perivoli Grevena area, suggesting three distinguished deposits forming a continuous succession spanning Early to Late Eocene time interval. Although Manoliasa Ioannina nummulitic bank corresponds to a redeposited formation, it shows significant similarities to the Early Eocene Perivoli Grevena fauna. Our results contribute to a refined stratigraphic assessment and high resolution local and interregional correlations of studied alpine and post- alpine Eocene carbonate deposits from the Hellenic peninsula.

References

Blondeau, A., 1972. Les Nummulites. Librairie Vuibert.

IGME, 1983. Geological Map of Greece, scale 1:5.000.000. Institute of Geology and Mineral Exploration, Athens.

Less, G., 1998. Statistical data of the inner cross protoconch diameter of Nummulites and Assilina from the Schaub collection. Opera Dela Slovenska Akademija Znanosti in Umetnosti (4)34, 183-202.

Less, G., Özcan, E., 2012. Bartonian-Priabonian larger benthic foraminiferal events in the Western Tethys. Austrian Journal of Earth Sciences Volume 105/1, 129-240.

Less, G., Özcan, E., Okay, I.-A., 2011. Stratigraphy and Larger Foraminifera of the Middle Eocene to Lower Oligocene Shallow-Marine Units in the Northern and Eastern Parts of the Thrace Basin, NW Turkey. Turkish Journal of Earth Sciences 20, 793-845.

Özcan, E., Less, G., Baldi-Beke, M., Kollanyi, K., Acar, F., 2009. Oligo-Miocene foraminiferal record (Miogypsinidae, Lepidocyclinidae and Nummulitidae) from the Western Taurides (SW Turkey): biometry and implications for the regional geology. Journal of Asian Earth Sciences 34, 740-760.

Philippson, A., 1890. Über die Altersfolge der Sedimentformationen in Griechenland. Zeit. Deutsch. Geol. Gessel. 42, 150-159.

Schaub, H., 1981. Nummulites et Assilines de la Téthys Paléogène; taxinomie, phylogenèse et biostratigraphie. Mémoires suisses de Paléontologie, Birkhäuser Bâle.

Serra-Kiel, J., Hottinger, L., Caus, E., Drobne, K., Ferràndez, C., Jauhri, A.K., Less, G., Pavlovec, R., Pignatti, J., Samsó, J.M., Schaub, H., Sirel, E., Strougo, A., Tambareau, Y., Tosquella, J., Zakrevskaya, E., 1998. Larger foraminiferal biostratigraphy of the Tethyan Paleocene and Eocene. Bulletin de la Société Géologique de France 169, 281-299.

Faunal Diversity at the Turolian locality of Kerassia (Northern Euboea, Greece)

P. Kampouridis[1], S. Roussiakis[2], N. Kargopoulos[2], I. Giaourtsakis[3], G. Dimakopoulos[2], G. Iliopoulos[4], G. Svorligkou[2] and G. Theodorou[2]

(1) Eberhard-Karls University of Tübingen, Department of Geosciences, Sigwartstr. 10, 72074, Tübingen, Germany, panagiotis.kampouridis@student.uni-tuebingen.de
(2) National and Kapodistrian University of Athens, Department of Geology and Geoenvironment, Panepistimiopolis, 15784, Athens, Greece
(3) Ludwig-Maximilians-Universität München, Department of Earth and Environmental Sciences, Paleontology & Geobiology, Richard-Wagner-Str. 10, 80333 München, Germany
(4) University of Patras, Department of Geology 26504, Rio Patras, Greece

The fossiliferous sites of Kerassia are located in northern Euboea, Greece. The first excavation was conducted in 1982 by H. de Bruijn, A. van der Meulen (University of Utrecht) and C. Doukas (National and Kapodistrian University of Athens; NKUA). They were not continued until 1992, when G. Theodorou (NKUA) began a series of recurring systematic excavations in the area, revealing seven fossiliferous sites, which can be allocated into two distinct stratigraphical horizons (Iliopoulos, 2003; Theodorou *et al.*, 2003). The lower horizon contains the sites K2, K3, K4 and K5. The upper horizon comprises the sites K1, K6, as well as the site Ke of the initial excavation of 1982. In the present study, the majority of the material from Kerassia, which is housed in the collections of the Museum of Palaeontology and Geology of the NKUA, has been evaluated, shedding light on the faunal composition of the two fossiliferous horizons (Fig. 1), and updating the taxonomic identifications based on a greater sample of specimens (Kampouridis & Dimakopoulos, 2018).

The bovid material consists mostly of fragmentary mandibles, whereas crania and horns are rare, making their identification quite difficult. Currently, two main groups can be distinguished: one of a large-sized bovid, resembling the species *Tragoportax amalthea*, and one of a smaller-sized, resembling *Gazella capricornis*. It seems that in the lower horizon the bigger bovid is the dominant taxon, while in the upper horizon the smaller one is more frequent. In the upper horizon, a partially preserved skull differs from the rest of the *G.* cf. *capricornis* material and resembles *Gazella deperdita*. In the lower horizon two more bovid taxa can be preliminary referred, ?*Palaeoreas lindermayeri* and ?*Protragelaphus skouzesi*.

The hipparionine horses are well-represented in Kerassia. However, similar to the bovids, the cranial material is scarce. The postcranial material can be separated into two main groups, a robust and a slender one. The robust postcranials can be assigned to *Hippotherium brachypus*, which is the most common robust hipparionine species in Greece during the Turolian. The identification of the slender hipparionine material is more delicate, due to the existence of several potential taxa, which are usually identified based on cranial and dental material. Only two fragmentary crania have been found so far. Neither of them can be assigned to *H. brachypus*, whereas both of them differ significantly from each other to be assigned to the same species. A juvenile cranium, from the site K4, has a single, well-developed, and deep preorbital fossa, which is situated near the orbit. These features are typical for the *Cremohipparion* lineage, in particular *Cremohipparion mediterraneum*. An adult cranium, originating from the initial excavation site (Ke), features a weakly developed preorbital fossa without posterior pocketing, placed far from the orbit, whereas its upper dentition is moderately plicated. These features resemble closer the *Hipparion dietrichi* - *Hipparion prostylum* lineage. Thus, it may be assumed that Kerassia was inhabited by two slender hipparionine species. In the lower horizon the slender hipparionines are more frequent, while in the upper horizon the robust *H. brachypus* is more common.

The Rhinocerotidae from Kerassia have been studied in detail (Giaourtsakis *et al*., 2006; Athanassiou *et al*., 2014), and are represented by three species: the tandem-horned rhinocerotids "*Diceros*" *neumayri* and *Dihoplus pikermiensis*, along with the hornless species *Acerorhinus neleus*. "*Diceros*" *neumayri* is the dominant rhinocerotid taxon, and the only one that occurs in both fossiliferous horizons, so far. The family Chalicotheriidae is represented in both horizons by a few specimens, which are attributed to the schizotheriine *Ancylotherium pentelicum* (Kampouridis & Dimakopoulos, 2018).

The family Giraffidae is well-represented in Kerassia. Five different species have been identified: *Palaeotragus rouenii*, *Palaeotragus* sp., *Helladotherium duvernoyi*, *Bohlinia attica* and *Samotherium major* (Iliopoulos, 2003). Notably, four species coexist in each fossiliferous horizon (Fig. 1).

The carnivorans include seven species, the hyaenids *Plioviverrop*s sp., cf. *Ictitherium pannonicum*, *Hyaenotherium wongii*, *Adcrocuta eximia*, the felids *Amphimachairodus giganteus*, *Metailurus parvulus* and the mustelid ?*Promeles palaeatticus* (Iliopoulos, 2003; Roussiakis & Theodorou, 2003; Roussiakis *et al*., 2006).

The proboscideans are scarce but diverse, comprising three species: *Deinotherium* cf. *proavum*, *Konobelodon atticus* and *Choerolophodon* sp. (Theodorou *et al.*, 2001; Kampouridis & Dimakopoulos, 2018; Konidaris *et al.*, 2014). Some additional rare taxa have been recovered so far from the upper horizon, including the suid *Hippopotamodon erymanthius*, the tragulid *Dorcatherium* sp., and the tubulidentate *Amphiorycteropus gaudryi*. Interestingly, remnants of a large-sized bird, attributed to *Struthio* sp., have been reported from both horizons, while another bird *Pavo archiaci*, has been only found in the site K4 (Kampouridis & Dimakopoulos, 2018).

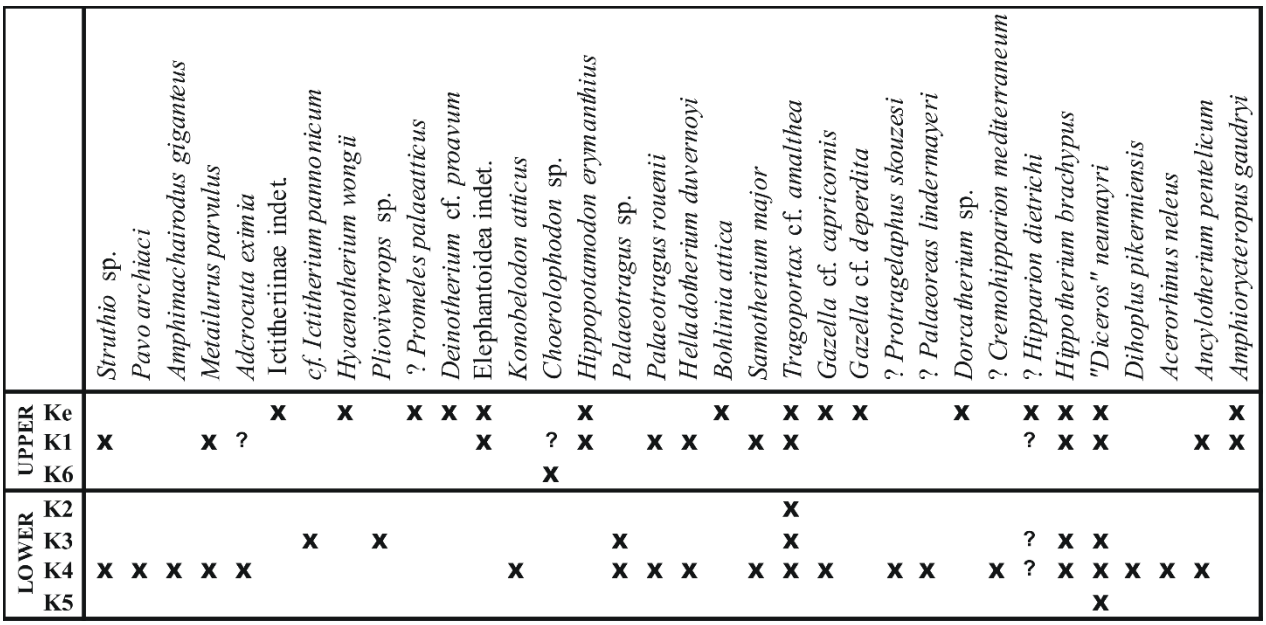

Figure 1. Updated faunal list of the Kerassia fossiliferous sites.

Based on the faunal composition, a middle Turolian (MN12) age has been suggested for the fossiliferous sites of Kerassia, although an early Turolian (MN11) age cannot be decisively excluded (Athanassiou *et al*., 2014; Iliopoulos, 2003; Theodorou *et al.*, 2003). Thus far, the available data are not sufficient for a more precise biochronological differentiation between the two fossiliferous horizons. The biogeographical and palaeoecological implications are of particular interest, since Kerassia seems to feature some transitional elements in its faunal composition with respect to the classical localities of Pikermi and Samos (Koufos *et al.*, 2009). The fauna of Kerassia includes taxa like the giraffid *Samotherium* and the tubulidentate *Amphiorycteropus*, which are typically known from Samos but are notably absent in Pikermi. Conversely, Kerassia lacks the hornless rhinocerotid *Chilotherium*, which is characteristic for Samos, and includes *Acerorhinus neleus*, which occurs in Pikermi. The coexistence of numerous and dietary diverse ungulates within the faunal association of Kerassia (Iliopoulos, 2003; Solounias *et al*., 2010; Athanassiou *et al*., 2014), indicates a heterogeneous vegetational regime providing suitable dietary niches for each one of these species, and suggests a mosaic habitat of widespread open woodlands with intermittent bushlands and grassy herbaceous landscapes.

Acknowledgements

We would like to thank all students that participated in the excavations and in the preparation of the material. The excavations between 1992 and 2015 were funded by local authorities, the General Secretariat for Research and Technologies of Greece and the NKUA Research Account projects 70/4/1394, 70/3/2842, 70/3/3922, 70/3/8567 and 70/3/12301. Participation in the conference has been supported by the Palaeontological Association.

References

Athanassiou, A., Roussiakis, S., Giaourtsakis, I., Theodorou, G., Iliopoulos, G., 2014. A new hornless rhinoceros of the genus *Acerorhinus* (Perissodactyla: Rhinocerotidae) from the Upper Miocene of Kerassiá (Euboea, Greece), with a revision of related forms. Palaeontographica, Abt. A: Palaeozoology – Stratigraphy 303 (1-3), 23-59.

Giaourtsakis, I., Theodorou, G., Roussiakis, S., Athanassiou, A., Iliopoulos, G., 2006. Late Miocene horned rhinoceroses (Rhinocerotinae, Mammalia) from Kerassia (Euboea, Greece). N. Jb. Geol. Palaont. Abh. 239, 367-398.

Iliopoulos, G., 2003. The Giraffidae (Mammalia, Artiodactyla) and the study of histology and chemistry of fossil mammal bone from the Late Miocene of Kerassia (Euboea Island, Greece). Ph.D. Thesis, University of Leicester, Leicester, 147 p.

Kampouridis, P., Dimakopoulos, G., 2018. Taxonomic identification of the Turolian fauna of Kerassia, Euboea (Greece). Undergraduate Thesis, National and Kapodistrian University of Athens, Athens, 131 p.

Konidaris, G., Roussiakis, S., Theodorou, G., Koufos, G., 2014. The Eurasian occurrence of the shovel-tusker *Konobelodon* (Mammalia, Proboscidea) as illuminated by its presence in the Late Miocene of Pikermi (Greece). Journal of Vertebrate Paleontology 34 (6), 1437-1453.

Koufos, G., Kostopoulos, D., Merceron, G., 2009. The Late Miocene Mammal Faunas of the Mytilinii Basin, Samos Island, Greece: New Collection 17. Palaeoecology – Palaeobiogeography. Beiträge zur Paläontologie 31, 409-430.

Roussiakis, S., Theodorou, G., 2003. Carnivora from the Late Miocene of Kerassia (Northern Euboea, Greece). Deinsea 10, 469-497.

Roussiakis, S., Theodorou, G., Iliopoulos, G., 2006. An almost complete skeleton of *Metailurus parvulus* (Carnivora, Felidae) from the Late Miocene of Kerassia (Northern Euboea, Greece). Geobios 39, 563-584.

Solounias, N., Rivals, F., Semprebon, G. M., 2010. Dietary interpretation and paleoecology of herbivores from Pikermi and Samos (late Miocene of Greece). Paleobiology 36 (1), 113-136.

Theodorou, G., Athanassiou, A., Iliopoulos, G., 2001. Proboscidea from the Late Miocene of Kerassiá (Euboea, Greece). 45th Annual Meeting of the Palaeontological Association, Copenhagen. The Palaeontology Newsletter 48 (suppl.), p. 50.

Theodorou, G., Athanassiou, A., Roussiakis, S., Iliopoulos, G., 2003. Preliminary remarks on the Late Miocene herbivores of Kerassia (Northern Euboea, Greece). Deinsea 10, 519-530.

15th International Congress of the Geological Society of Greece
Athens, 22-24 May, 2019 | Harokopio University of Athens, Greece
Bulletin of the Geological Society of Greece, Sp. Pub. 7 Ext. Abs. GSG2019-127

The use of X-ray Computed Tomography (CT) on varved lake sediments for the identification of different sedimentological facies

Alexandros Emmanouilidis[1], Gerasimos Messaris[3], Epameinondas Ntzanis[2], Petros Zampakis[2], Pavlos Avramidis[1]

(1) Department of Geology, University of Patras, 26504 Rio Patras, Greece, alexandros.emmanouilidis@upnet.gr
(2) Department of Medical Physics, University of Patras, 26504 Rio Patras, Greece.
(3) Department of Radiology / Medical School, University of Patras, 26504 Rio Patras, Greece

Background

The use of non-destructive high-resolution analysis in sediment cores has been continuously increasing through out the years, due to the introduction of new techniques that can attribute to the visualization of different sediment structures, composition etc. Specifically, in paleoclimatic and paleoenvironmental studies, the use of Computed tomography (CT), can provide useful information concerning depositional changes, climatic driven events and short scale depositional changes that would not be recognized macroscopically. In order to distinguish density changes, complex sedimentary structures as well as grain size in lacustrine and marine sediment cores, the evaluation of the CT imaging has been widely used (Dewanckele et al., 2012; Gualda et al., 2010; Ketcham et al., 2010).

Apart from the 3D visualization of a sediment core, one of the most important parameters produced by the CT scanning is the Radiodensity. It is related to the bulk density and chemical composition of the core and has been widely used to describe bulk density (Kenter, 1989), periodic bedding patterns (Boespflug et al., 1995) as well as porosity and permeability (Mena et al., 2015).

Objectives

Sediment cores characterized by the presence of complex micro structures like varves, are most of the times difficult to be examined by conventional means, so the use of a more high-resolution techniques like CT scanning, seems necessary. The main aim of the present study is to distinguish different sedimentary structures (varve sequences, bioturbation, organic layers) and sedimentological phases, in a 6 m sediment core.

Methods

For the present study, a 6 m sediment core, retrieved from Vouliagmeni Lake in central Greece, was used. The acquiring of the CT images was conducted on General University Hospital of Patras in Greece, using a General Electric lightspeed 16x CT scanner. The acquisition parameters were set as follows: 0.8 gantry rotation time, 16*0.625 mm detector configuration, 8 Images per rotation, Axial thickness 1.25 mm, 120 kV and 175 mA. To enhance the density contrast of the CT acquisitions, the soft tissue and bone kernel were used. For every 1m sediment sequence that was scanned, around 1800 DICOM files were extracted. The raw DICOM files were then processed through the MATLAB based software SedCT v.1.01 (Reilly et al., 2017) and high-resolution Hounsfield Unit (HU) profiles were calculated. Hu values produced are determined by the attenuation of the X-rays, the density of the core and the atomic number.

In order to have a better understanding of the additional information provided from the CT scanner, the sediment core was also scanned with a jAi 3CCD RGB line scan camera, with resolution 4096*1px. Profile plots of the RGB colors were created, with the maximum possible resolution, using ImageJ software.

Results

From the analysis performed at the DICOM files that were extracted from the CT scanning, 4 different lithological facies and two different varve types were recognized (Fig. 1). The laminated sediments that were recognized (Phase A and D), present Hu values ~200 and~ 700 respectively, whereas the silty clay material (Phase C) presents Hu values above 1000 (Fig. 1). Organic rich layers (Phase B) in the core are attributed to HU values 200-400, indicating lower bulk density compared to the other units (Fig. 1).

The 3D intensity model that was compiled through the medical software Inobitec DICOM Viewer, provide robust information concerning bioturbation, organic matter and lamination boundaries. Darker areas which correspond to higher density values, attribute to silty clay barren material, whereas the green areas correspond to the $CaCO_3$ rich layers (white layers). Representative images as shown in Figure 1, shows 3 clear laminations with calcite rich material, whereas only one of them can be clearly visible through the line scan camera. Thus, formations that may be disturbed or overlapped in the surface of the core, can now be thoroughly examined.

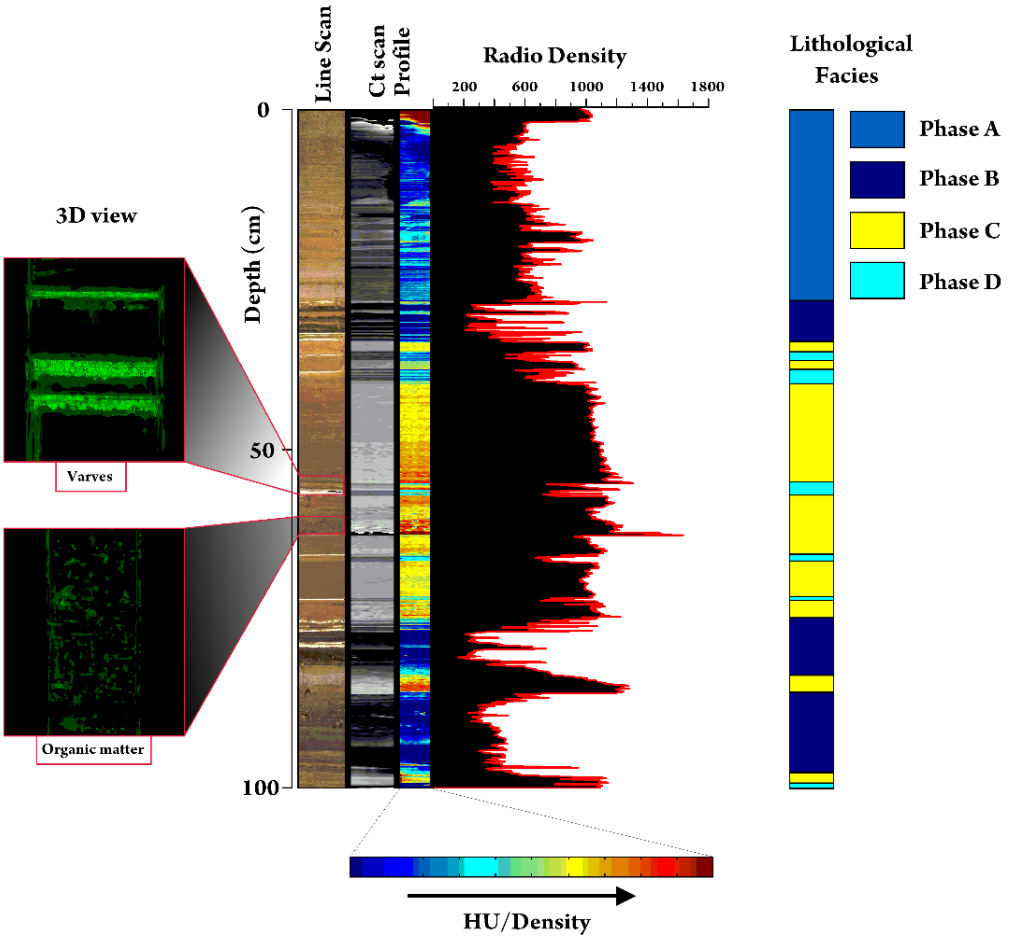

Figure 1. Representative Lithological Phases identified for the first 1 m of Vouliagmeni core.

Conclusion

Three-dimensional quantitative analysis using X-ray computed tomography combined with line scan digital core images was used for effective core characterization. Internal structure and different sedimentological facies such as (a) organic rich layers, (b) varves and (c) clay rich material were recognized. The applied methodology provide efficient information concerning high resolution sampling strategy avoiding core degradation. The development of new software for the processing of DICOM files and the development of new, more high-resolution CT scanners opens new possibilities in the reconstruction of past environmental changes from lacustrine or marine environments.

Acknowledgements

This research is financed by Greece and the European Union (European Social Fund- ESF) through the Operational Programme «Human Resources Development, Education and Lifelong Learning» in the context of the project "Strengthening Human Resources Research Potential via Doctorate Research" (MIS-5000432), implemented by the State Scholarships Foundation (IKY).

References

Boespflug,X., Long,B.F.N., Occheitti, S., 1995. CAT-scan in marine stratigraphy: A quantitive approach. Marine Geology 122, 281-301.

Dewanckele, J., De Kock, T., Boone, M.A., Cnudde, V., Brabant, L., Boone, M.N., Fronteau, G., Van Hoorebeke, L., Jacobs, P., 2012. 4D imaging and quantification of pore structure modifications inside natural building stones by means of high resolution X-ray CT. Science of the Total Environment, 416,436–48.

Gualda, G.A.R., Pamukcu, A.S., Claiborne, L.L., Rivers, M.L., 2010. Quantitative 3D petrography using X-ray tomography 3:documenting accessory phases with differential absorption tomography. Geosphere 6,782-792.

Kenter, J.A.M., 1989. Applications of computerized tomography in sedimentology. Marine Geotechnology 8, 201-211.

Ketcham, R.A., Slottke, D.T., Sharp, J.M., 2010. Three-dimensional measurement of fractures in heterogeneous materials using high resolution X-ray computed tomography. Geosphere 6, 499-514.

Mena, A., Frences, G., Perez-Arlucea, M., Aguiar, P., Barreiro-Vazquez, J.D., Iglesias, A., Barreiro-Lois, A., 2015. A novel sedimentological method based on CT scanning:Use for tomographic characterization of the Galicia Interior Basin. Sedimentary Geology 321, 123-138.

Reilly, B.T., Stoner, J.S., Wiest, J., 2017. SedCT: Matlab tools for standardized and quantitative processing of sediment core computed tomography (CT) data collected using a medical CT scanner. Geochemistry, Geophysics, Geosystems 18, 3231-3240.

15th International Congress of the Geological Society of Greece
Athens, 22-24 May, 2019 | Harokopio University of Athens, Greece
Bulletin of the Geological Society of Greece, Sp. Pub. 7 Ext. Abs. GSG2019-134

Palaeoenvironmental Interpretation Based on Taphonomic Indices of Pleistocene Ostracods

K. Karanika[1], M. Tsoni[1], P. Papadopoulou[1], G. Iliopoulos[1]

(1) Department of Geology, University of Patras, University Campus 26504, Rio Achaia, Greece, kostantinapat@gmail.com

Introduction

This work involves the paleoecological study of Pleistocene deposits from Magoula (northwestern Peloponnesus, Greece, Fig. 1), based on the analysis of microfaunal elements (basically ostracods). The study area has been chosen not only as a site of significant palaeontological interest where plant fossils, mammal bones and a wide range of different kinds of invertebrate and microfossils occur, but mainly because it belongs to the tectonically interesting Rio –Antirio basin, which is part of the Corinth rift. Rio basin is an asymmetric graben with a NW-SE trending, located between the mainland of Greece and NW Peloponnesus (Kontopoulos & Zelilidis 1997). The basin formed during the Upper Pliocene to Lower Pleistocene, due to WNW normal faults and NNE transfer faults (Doutsos et al. 1988, Parcharidis et al. 2009).

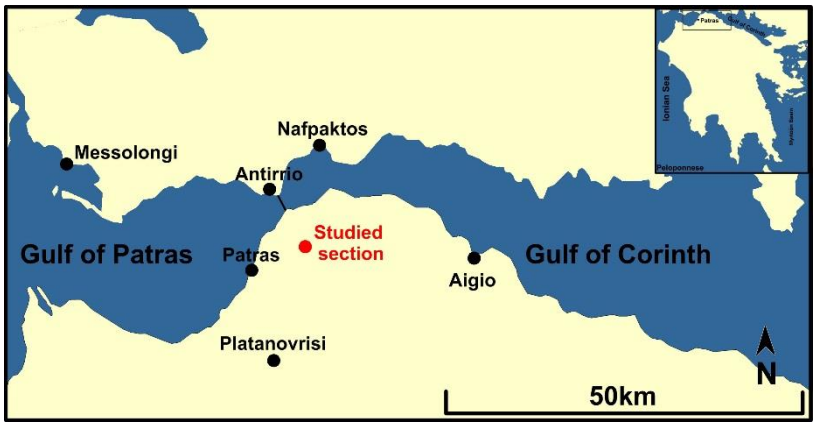

Figure 1. Map illustrating the position of the studied section.

Material & Methodology

Microfaunal analyses were carried out on 133 samples collected every 20-40cm from a natural section in the area of Magoula (2.5 kilometers SE of University of Patras) with a total thickness of 31.30 meters. Sediment samples were washed through 500 and 63 μm mesh sieves. Microfossils were collected and studied under the stereoscope. Species determined based on previous studies of Mediterranean benthic taxa. The collected data were analyzed, relative abundance diagrams were prepared for each species. Furthermore, taphonomic indices (Right/Left valve ratio, Sex ratio, Adult/Juvenile ratio and Carapace/Disarticulated Valves ratio) were calculated for the most abundant species.

Results and Discussion

Out of the 133 sediment samples, 75 contained sufficient numbers of tests and valves (>10%) for quantitative analyses, 53 were barren and 6 contained scarce specimens. According to the microfaunal analysis, 6 ostracod taxa (*Cyprideis torosa* (both un-noded and noded morphotypes), *Candona neglecta*, *Ilyocypris spp.*, *Tyrrhenocythere amnicola*, *Aurila convexa and Cypridopsis vidua*) were recorded in the studied samples. The most abundant were *Cyprideis torosa* and *Candona neglecta*. Two benthic foraminifera taxa (*Ammonia tepida* and *Haynesina depressula*), as well as some charophyte gyrogonites, freshwater gastropods, gastropod opercula and fragments were identified as well. Generally, a lagoonal environment with several variations in the salinity and the mean depth occurred. Based on the relative abundance diagrams and the taphonomic indices three main units can be distinguished (Fig. 2). Unit 1 (0-14.60 m) is mainly characterised by the presence of *C. torosa* and the minor contribution of *C. neglecta* and *Ilyocypris spp*. Based on the taphonomic indices of *C. neglecta*, Unit 1 is characterized by the locally focused deposition of more easily transported juvenile valves (A/J ratio < 1:25 & R/L ratio > 1), thus representing hydrodynamic transport, whereas the taphonomic indices of *C. torosa* (Fig. 2) may represent an in situ death assemblage, with reduced taphonomic removal of juveniles which therefore can be characterized as a life assemblage (A/J ratio 1:12-1:4 & R/L ratio ≈1). At 5.30 m the presence of *Ilyocypris spp*. and the A/J ratio (0.5) of *C. torosa* indicate a freshwater influx. Unit 2 (14.61-23.50 m) consists of barren coarse grained sediments (Fig. 2), while Unit 3 (23.51-31.30 m) is represented mainly by *C. torosa*, *C. neglecta* and small numbers of *Ilyocypris spp*. valves (Fig. 2). Based on the taphonomic indices of *C. neglecta* (A/J ratio < 1:25, R/L ratio ≈1 & C/D ratio >0), Unit 3 may reflect not only low-energy conditions, but also potential mass kill events associated with increased sedimentation rates (smothering via settling of fine-grained sediment from river flood discharge). On the other hand, based on the taphonomic indices of *C. torosa* (A/J ratio 1:10-1:2, R/L ratio ≈1 & C/D ratio >0 at 24.30 m) an in situ death assemblage can be considered, where possibly the taphonomic removal of most juveniles occurred (Fig. 2). Also in this unit at 25.7 m, the presence of *Ilyocypris spp*. and the C/V ratio (0.1) of *C. neglecta* and at 29.90 m, the presence of

Ilyocypris spp. and the A/J ratio (0.56) of *C. torosa* indicate a freshwater influx. Unit 1 can be characterized as a lagoon environment with freshwater influxes. Unit 2 represents river mouth deposits from a river outflowing in the lagoon. Unit 3 can be characterized as a lagoon environment with strong freshwater influxes and the appearance of a possible flood event (24.10-24.30 m).

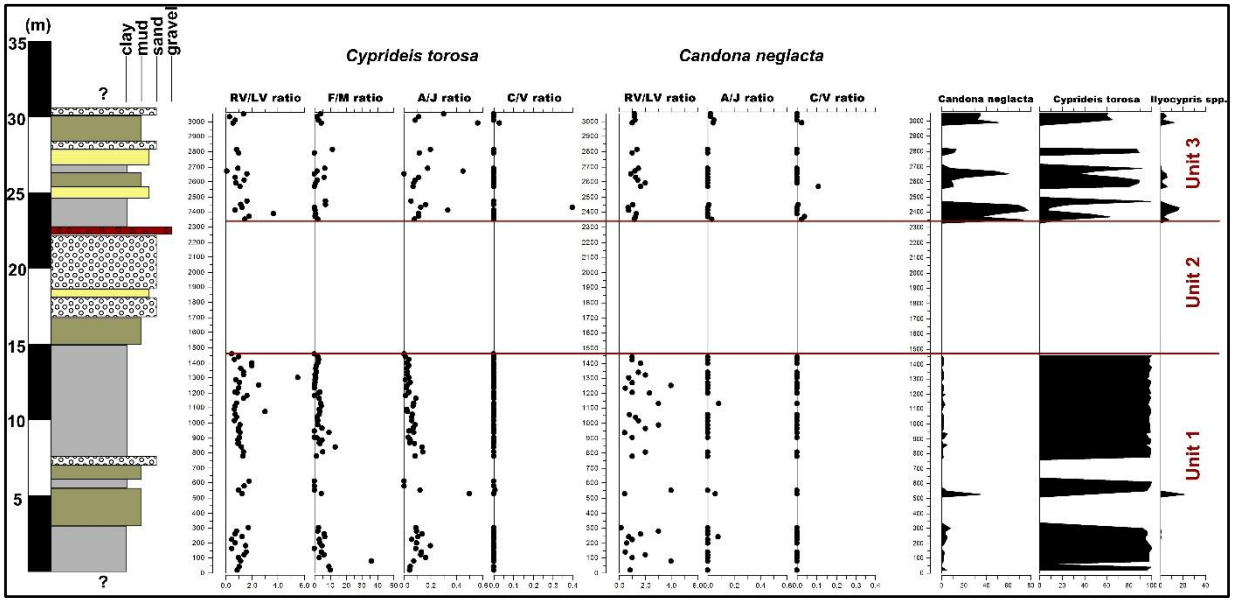

Figure 2. Stratigraphic column of the study section, taphonomic indices and relative abundance diagrams of selected species.

Conclusions

According to micropalaeontological and taphonomic analysis palaeonvironmental changes occurred due to eustatism. Initially a lagoon system, turned gradually into a lagoonal river mouth environment (barren layers) due to sea level drop and finally when sea level rose became again a lagoonal environment influenced by a river system with strong freshwater influxes. Moreover, the relative abundance diagrams and the taphonomic indices in combination with the stratigraphic column characterize a possible flood event at 24.10-24.30 meters.

Acknowledgements

I would like to thank the members of the laboratory of Palaeontology and Stratigraphy (Department of Geology, University of Patras).

References

Kontopoulos N., Zelilidis A., 1997. Depositional environments of the coarse-grained lower Pleistocene deposits in the Rio-Antirio basin, Greece. Proceedings International Symposium on Engineering Geology and the Environment, IAEG, Athens.

Doutsos T., Kontopoulos N., Poulimenos G., 1988. The Corinth-Patras rift as the initial stage of continental fragmentation behind an active island arc (Greece). Basin Research, v. 1(3), p. 177–190.

Parcharidis I., Kokkalas S., Fountoulis I., Foumelis M., 2009. Detection and Monitoring of active faults in Urban environments: Time series interferometry on the cities of Patras and Pyrgos (Peloponnese, Greece). Remote Sensing Journal, v. 1, p. 676-696.

15th International Congress of the Geological Society of Greece
Athens, 22-24 May, 2019 | Harokopio University of Athens, Greece
Bulletin of the Geological Society of Greece, Sp. Pub. 7 Ext. Abs. GSG2019-137

Palaeoenvironmental evolution of Rio basin during the Middle Pleistocene

M. Tsoni[1], G. Iliopoulos[1], I. Koukouvelas[1], S. Kostopoulou[1], N. Kontopoulos[1]

(1) Department of Geology, University of Patras, University Campus 26504, Rio Achaia, Greece, mariatsoni@upatras.gr

Study area

The structural grain of Greece is traversed by a 140-km-long system of grabens that includes three members namely the Corinth graben in the east, the Patras graben in the west and the bridging with the Rion graben in the middle (Doutsos et al. 1988). Rio graben is an asymmetric graben with a NE trending Peloponnesian border fault hosting significant offset between the mainland of Greece and NW Peloponnesus (Kontopoulos & Zelilidis 1997). The basin is severely tectonised by a dense fault array comprising WNW normal faults and NE-trending transfer faults (Doutsos et al. 1988).

Rio basin is also a region of significant stratigraphical and palaeontological interest. For this reason, several authors have studied sediments from NW Peloponnesus trying to address the geological evolution of the recent past and proposed different ages and palaeoenvironmental interpretations. The study area is located between the villages of Sychena and Velvitsi on the west side of Charadros River and the name of the studied section is Vigla. The purpose of this work is to determine the sedimentary environments and the palaeo-ecological conditions of the studied section and to unravel the Middle - Upper Pleistocene environmental changes.

Material and methods

Microfaunal analyses were carried out on 121 samples collected every 20-40cm from a natural section in the area of Vigla (east of Sichena village) with a total thickness of about 34 meters. Sediment samples were washed through 500 and 63 μm mesh sieves. When abundant microfaunal elements were present, a combined total of 300 specimens of benthic foraminifera and ostracod tests were collected. Out of the 121 sediment samples, 88 contained sufficient numbers of specimens for quantitative analyses and 33 were barren or contained scarce specimens (<10%). Species and their ecological characteristics were mainly determined based on previous studies of Mediterranean benthic taxa (Cimerman & Langer 1991, Relative volumes of Stereo-atlas of ostracod shells). Species were grouped based on their ecological characteristics and relative abundance diagrams were prepared for each group. Furthermore, 2 smear slides were produced for sediments of marine orgin in order to investigate the presence of calcareous nannofossils.

For statistical purposes, the data matrix was standardized to percentages of the entire sample. Four measures of species diversity were calculated: (1) species richness (S), (2) Simpson's index (1-D), (3) the Shannon–Wiener index [H(s)] and (4) the evenness index, using the PAST3 software (Hammer et al., 2001; version 3.19, 2018). Cluster analysis was run for samples (Q mode) and different outputs of the dendrogram have been compared in order to find the most homogeneous clusters or groups. In addition, correspondence analysis (CA) was also used to correlate taxa and samples. Furthermore, stratigraphic columns were produced. The colors of the depicted layers in the columns were selected based on the Munsell colour system. Sediments were analysed in situ and Munsell colour notations were collected with the use of a Minolta CM-2002 reflectance spectrophotometer.

Results

In order to check the continuity of the layers we collected samples from three closely spaced well exposed sequences from the same area (Fig. 1). Through the micropalaeontological analysis, four different facies were identified. This allowed us to establish the presence of two normal faults and a disconformity that intercept the sequences. For this reason, in this study, the results are expounded separately for Sequence 1, 2, 3 and 4 (Fig.1). As a general picture, microfossils were abundant in the samples from Sequence 2 and 3, whereas they were scarce or absent in the samples from Sequence 1 and Sequence 4 was barren.

- Sequence 1 has a total thickness of 1110 cm and is mainly composed of olive green silts. According to the microfaunal analysis, 4 ostracod taxa have been identified in the studied samples and the total absence of benthic foraminifera is remarkable. Based on the percentage abundance diagrams, statistical analysis and the microfaunal composition of the layers of Sequence 1, six main units (1-6) can be distinguished, 3 of which are barren (Units 2-4-6). The microfauna of this section reflects a primarily brackish environment.
- Sequence 2 is mainly composed of gray clays and silts and has a total thickness of 1200 cm. This sequence is rich in micro- and macrofauna as well. According to the microfaunal analysis this section is composed of 28 different taxa of benthic foraminifera and 20 different ostracod taxa. According to the relative abundance diagrams and statistical analysis as well, for this Sequence there is a clear division into two main units, a brackish and a marine unit After calcareous nannofossil analysis from the marine unit's sediments, *Emiliana huxleyi* was identified.
- Sequence 3 is mainly composed of grey silts nevertheless at the upper part the grain size increases to sand. This sequence has a total thickness of 1855 cm and is rich in micro and macro fauna as well. Based on the microfaunal analysis, 11 different ostracod species and 7 different foraminifera species were identified. Based on the percentage abundance diagrams and the micro-faunal composition of the layers of Sequence 3, three main units that reflect a primarily brackish environment can be distinguished.
- Sequence 4 constitutes the last 8 meters of the section. This sequence consists of a massive, mainly matrix supported

barren red conglomerate that overlies uncomformably the sediments of Unit 3.

Discussion

Detailed analyses of benthic foraminifera and ostracoda of a 33.60 meters section have been performed. The employed micropalaeontological analysis and the respective statistical methods that were used, indicate that the microfaunal assemblages of the lower sequence 1 reflect a low salinity lagoon environment. The remaining part of the sequence 1 corresponds to a lagoon with low salinity and freshwater influxes. The microfaunal assemblages of this part of this sequence, reflect the continental-end member of a lagoonal environment. In Sequence 2, the fauna of the lower unit is characteristic of a lagoon with periodic freshwater influxes. The upper part of this section has been characterised as marine. The marine unit can be separated further into two subunits, an open lagoon with good connection to the open sea and a shallow marine environment. In conclusion, the first 4 m of Sequence 2 are indicative of a lagoon ecosystem, but the remaining part of the section is indicative of a closed gulf. At Sequence 3, the main part is indicative of a restricted lagoon with high salinity water influxes that changed gradually to an open lagoon and later again to a closed lagoon. It has been observed that there are repetitive environmental changes from brackish to more or less marine environments, especially between Sequences 2 and 3. The last sequence overlies uncomformably the other three sequences. Sequence 4 is barren of micro or macrofauna and indicates an alluvial fan environment.

The palaeonvironmental changes that have been recorded in our study area are the result of eustatism and tectonism as well. Hence, the uplift or subsidence events that took place during the middle and late Pleistocene control the evolution of the palaeoenvironments and the depositional history across the Rio basin.

Based on the stratigraphic analysis of the studied section, Vigla presents roughly the same stratigraphic features with Aravonitsa-Location 11 that Palyvos et al. (2010) described. According to them at the base of MNN21a Corinth Gulf was expectedly a lake, isolated from the sea by a sill. The lowest occurrence of *E. huxleyi* in the Corinth Gulf is expected at the MIS7e highstand, as only then sea water with *E. huxleyi* had the chance to enter the gulf. The presence of *E. huxleyi* in Vigla section and its stratigraphic resemblance with Aravonitsa 11, lead us to conclude that this highstand affected both the western part of Corinth Gulf and Rio Basin as well.

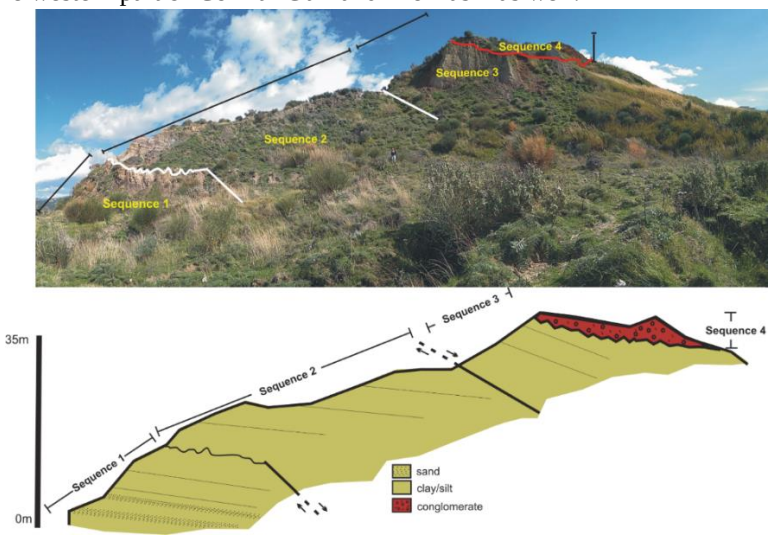

Figure 1. Figure and schematic section of the studied section with depiction of sedimentary sequences. With white line are symbolized the faults and with red disconformity.

Acknowledgement

This project is funded by the Operational Program "Human Resources Development, Education and Lifelong Learning" and is co-financed by the European Union (European Social Fund) and Greek national funds.



References

Cimerman, F., Langer, M., 1991. Mediterranean foraminifera. Ljubljana: Slovenska akademija znanosti in umetnosti, 593.1/2/091638

Doutsos, T., Kontopoulos, N., Poulimenos, G., 1988 The Corinth-Patras rift as the initial stage of continental fragmentation behind an active island arc (Greece), Department of Geology, University of Patras, Greece. https://doi.org/10.1111/j.1365-2117.1988.tb00014.x

Hammer, O., Harper, D.A.T., Ryan P.D., 2001. PAST: paleontological statistics software package for education and data analysis. Paleontologia Electronica 4, 1-9.

Kontopoulos, N., Zelilidis, A., 1997. Depositional environments of the coarse- grained lower Pleistocene deposits in the Rio-Antirio basin, Greece. Proceedings International Symposium on Engineering Geology and the Environment, IAEG, Athens.

Palyvos, N., Mancini, M., Sorel, D., Lemeille, F., Pantosti, D., Julia. R., Triantaphyllou, M., De Martini, P.M., 2010. Geomorphological, stratigraphic and geochronological evidence of fast Pleistocene coastal uplift in the westernmost part of the Corinth Rift (Greece). Geological Journal 45 78-104.

15th International Congress of the Geological Society of Greece
Athens, 22-24 May, 2019 | Harokopio University of Athens, Greece
Bulletin of the Geological Society of Greece, Sp. Pub. 7 Ext. Abs. GSG2019-138

The palaeoenvironment of *Homo neanderthalensis* during the Late Pleistocene: preliminary results of the *KalPal project,* the palaeoecological and taphonomical study of the Upper Pleistocene fauna from the Kalamakia cave (Mani Peninsula, Greece)

M. Kolendrianou[1], S. Ligkovanlis[1], M. Tzortzi[1], I. Maniakas[1,2], G. Iliopoulos[1]

(1) Department of Geology, University of Patras, GR- 26504, Rio, Patras, Greece, kolendrianou@upatras.gr
(2) Department of Geology, Aristotle University of Thessaloniki, GR-54124, Thessaloniki, Greece

Presenting the *KalPal Project*

The *KalPal Project* includes the study of microfaunal and macrofaunal skeletal elements from the Upper Pleistocene deposits of the Kalamakia cave in the Mani Peninsula, in order to extract conclusions on the palaeoenvironment and taphonomical history of the site. The cave was inhabited during the Middle Palaeolithic period by humans and, specifically, by individuals of the species *Homo neanderthalensis*, whose remains were also found during past excavations.

The aim of the project is to identify the palaeo-ecological relationships between the different vertebrate species, including the Neanderthals, living in the area during the time of deposition and, at the same time, the taphonomic processes that affected the samples over time and how they defined the characteristics of the studied fossils. In addition, an attempt will also be made to identify the possible interaction between the people living in the cave with the animals from which the material originated.

Study area

Kalamakia cave is located 2km northwest of Areopolis, in the southern part of Itilo Bay, Mani Peninsula, southern Peloponnese. In this location, the vertical cliff that stands above the coast subsides leaving a small cove and, thus, creating a small plateau by the shore. The cave itself is located above that plateau (that is interpreted as a Tyrrhenean terrace) along with several smaller caves that surround it, either communicating with one another or not. The entrance, which is 7m wide and 8m long, lies at the foothill of a limestone cliffside 2m above sea level, 10m away from the shore, whereas the cave cavity is 20m deep. Excavations in Kalamakia were conducted from 1993 to 2006 by the Ephorate of Paleoanthropology and Speleology (Greek Ministry of Culture) in collaboration with the University of Athens and the Muséum National d'Histoire Naturelle (Paris) (Darlas et al., 1998).

Former research

The excavation in Kalamakia is one of the most important palaeontological / paleoanthropological excavations that have been conducted so far in Greece because of the skeletal remains of *Homo neanderthalensis* found in the cave (Darlas et al., 1998, 2004; Harvati et al., 2013). During the excavation, plenty of samples showed that the cave was used during the Middle Palaeolithic period, and more specifically 100-40 kya BP, as a periodic habitat of hunters and gatherers (Harvati et al. 2013).

The identified large mammal fauna of Kalamakia comprises of 17 taxa. Fallow deer dominates the assemblage while ibexes and wild boars follow. Carnivores were also present, although low in numbers, throughout the stratigraphic sequence, with red fox being the most common species. The site also yielded the remains of several smaller vertebrate taxa, including abundant land tortoise remains (mostly *Testudo marginata*) (Darlas et al., 2008; 2016). A previous study of the microvertebrates of Kalamakia, especially rodents, indicated a generally open landscape surrounding the cave with dry and relatively warm climatic conditions (Roger et al., 2008). On the basis of both pollen and faunal data, during at least the first half of the last glacial, the climate in Kalamakia is considered to have been mild. The surrounding landscape was covered with maquis vegetation and some Mediterranean presteppic forest taxa (Lebreton et al. 2008).

Material and Methodology

Different approaches have been selected to decipher the scientific questions of this project and more specifically to provide palaeoecological interpretations, hence each subject of the project (lithic artifacts, microfaunal remains, macrofaunal remains examined taphonomicaly and animal teeth) follows its own protocol:

- Lithic artifacts: a digital application for the listing of archaeological material was created, in which the parameters were set according to the project's priorities: stratigraphic origin, characteristics of the raw material, data on morphology, technology and typology.
- Microfauna: remains are observed stereoscopically and are identified taxonomically based on literature and the LPS's comparative skeleton collection. Detailed lists for the identified fossils are kept for each specimen reporting the following: stratigraphic origin, type of skeletal element, relative position on the skeleton, taxon identified, preservation state.
- Taphonomic and geochemical analyses of macrofaunal remains: for the evaluation of the site's taphonomical history, the samples are examined macroscopically and microscopically using a stereoscope and scanning electron microscope, while taphonomical indices will also be calculated and analyzed statistically. For the geochemical study, samples are collected and examined under a scanning electron microscope, using nondestructive analytical techniques such as

Raman spectroscopy, Fourier Transform Infrared Spectroscopy (FTIR) and of X-ray fluorescence (XRF) spectroscopy.

- Microwear and mesowear study of ruminant teeth: The procedure for microwear analyses involves upper and lower second molar cleaning with acetone for the removal of dust, and also of any other chemical residues used in the field or during fossil preparation. Dental facets are molded and consequently photomicrographic scans are taken directly on the molds under a stereomicroscope in order to render the surface of the dental wear facets. For mesowear, the procedure has already been done by evaluating the occlusal relief and the cusp shape of the upper and lower molars (M1-M3, m1-m3) through digital photography with the aid of the software tpsDig2 2.17 (Fortelius et al., 2000).

Results and Discussion

So far, 20.500 lithic artifacts have been studied, 14.951 microfaunal specimens have been identified, 54 microfaunal and macrofaunal remains have been examined using X-ray fluorescence (XRF) spectroscopy and 134 samples of maxillar and mandibular specimens (from adult animals) were taken into account for mesowear analyses.

- As far as the type of the cultural material is concerned, stone-knapping from Kalamakia cave seems to have all the components that characterize the lithics in the area of Southeastern Europe during the Middle Paleolithic Age, but it also presents some particularities. What can be said with relative certainty, in relation to human occupation and activity in the cave, is that these were only periodical and that the exploitation of lithic resources was not the attractive factor for human groups (the vast majority of the raw materials are of poor quality and there is occasional use of "circumstantial" lithic backgrounds as tool materials, such as limestone raw material or core leftovers).
- The results concerning the identifications of microvertebrates have revealed the presence of 3 different species of amphibians, 18 different reptile taxa, 3 insectivore species, 2 bat taxa and 6 rodent taxa through the whole sequence. From the taxa identified so far in the assemblage, the majority reflects an open environment. No species, considered typical of colder climates, have been identified yet leading to an estimate that the climate must have been relatively temperate during the depositional periods of the studied material.
- The XRF results obtained so far from the examination of the bones from both small vertebrate and large mammal taxa, suggest that the main elements of the samples are calcium and phosphorus, obviously derive from the biomineral of bone (apatite). Nevertheless the enrichment in Fe, Al, Zn, Sr, Ba, Y and Sn at varying levels, is ascribable to the taphonomic processes that affected the bones post-burially.
- Summary statistics for mesowear data for each taxon and among different strata have revealed a dietary range from browsing to mixed feeding strategy. The vast majority of the samples analyzed, belonged to *Capra* sp. and *Dama* sp. The predominant mesowear pattern over all strata among fossil samples of the two aforementioned taxa is high cusp relief associated with rounded cusp apices. Overall mesowear scores (Fortelius et al., 2000) in *Dama* sp. reflect a slight tendency to browsing but, in terms of average wear signal comparisons of *Capra* sp. and *Dama* sp. among different strata populations, it is rather reasonable to conclude that there were no siginificant variations through time.

Acknowledgements

The authors would like to thank Dr. Andreas Darlas, Director of the Ephorate of Palaeoanthropology and Speleology of Greece, for his consent to study the material and all his support during the ongoing studies and Dr. Eleni Psathi for her help with the study of the larger animals.



This project is funded by the Operational Program "Human Resources Development, Education and Lifelong Learning" and is co-financed by the European Union (European Social Fund) and Greek national funds.

References

Darlas, A., de Lumley, H., 1998. Fouilles franco-helléniques de la grotte de Kalamakia (Aréopolis; Péloponnèse). Bull. Corresp. Hellénique 122, 655-661.

Darlas, A., de Lumley, H., 2004. La grotte de Kalamakia (Aréopolis, Grèce). Sa contribution à la connaissance du Paléolithique moyen de Grèce, vol. 1239. BAR, pp. 225-233.

Darlas, A., Psathi, E., 2008. Le Paléolithique supérieur dans la péninsule du Mani (Péloponnèse, Grèce). In: Darlas, A., Mihailovic, D. (Eds.), The Palaeolithic of the Balkans, vol. 1819. BAR, pp. 51-59.

Fortelius, M.., Solounias, N., 2000. Characterization of ungulate molars using the abrasion-attrition wear gradient: a new method for reconstructing paleodiets. American Museum Novitates 3301, 1-36.

Harvati, K., Darlas, A., Bailey, S.E., Rein, T.R., El Zaatari, S., Fiorenza, L., Kullmer, O., Psathi, E., 2013. New Neanderthal remains from Mani peninsula, Southern Greece: The Kalamakia Middle Paleolithic cave site. Journal of Human Evolution 64, 486-499.

Lebreton, V., Psathi, E., Darlas, A., 2008. Environnement végétal des néandetaliens de la grotte de Kalamakia (Arépolis, Grèce). In: Darlas, A., Mihailovic, D. (Eds.), The Palaeolithic of the Balkans, vol. 1819. BAR, pp. 61-68.

Roger, T., Darlas, A., 2008. Microvertébrés, paléo environnement et paléoclimat de la grotte de Kalamakia (Péloponnèse, Grèce). In: Darlas, A., Mihailovic, D. (Eds.), The Palaeolithic of the Balkans, vol. 1819. BAR, pp. 77-84.

15th International Congress of the Geological Society of Greece
Athens, 22-24 May, 2019 | Harokopio University of Athens, Greece
Bulletin of the Geological Society of Greece, Sp. Pub. 7 Ext. Abs. GSG2019-146

Study of Pleistocene ostracods from central and southern Greece- Digital imaging of a palaeoenvironmental tool (PLOSTRAC): Preliminary results

P. Papadopoulou[1], M. Tsoni[1], G.Iliopoulos[1]

(1) University of Patras, Department of Geology, Laboratory of Palaeontology and Stratigraphy, Panepistimioupoli, Rio, Greece, 26504, penelpapadop@upatras.gr

Introduction

The Pleistocene has been a period of continuous universal climatic turmoil due to the establishment of glacial and interglacial periods and their periodic alteration (Millankovic cycles) which stigmatized Quaternary climates and ecosystems. Ostracods can be found in a wide variety of environments from alpine lakes to abyssal basins (Schellenberg, 2007) being excellent palaeoenvironmental indicators (Rodriguez-Lazaro and Ruiz-Munoz, 2012). Their highly calcified bivalve carapace can be easily fossilized. Actually, they are among the small number of organisms that can be found not only in great numbers especially in transitional environments, but also they are environmentally sensitive to several factors such as salinity, water chemistry, substrate characteristics, temperature, oxygen and nutrient availability (Frenzel and Boomer, 2005). All these factors cause severe changes in the composition of the ostracod assemblages, even in the intraspecific level, and high endemism.

The project's main objective is to study the Pleistocene ostracods deriving from sedimentary successions from central and southern Greece. The different species that dominate each ecological niche, their morphology, distribution, systematics, history and ecological preferences are examined. Moreover, high quality SEM images of the respective ostracod species have been produced and can serve as reference point for future studies. The results of this project will cover a significant gap in the Greek ostracod record which is rather incomplete compared to that of central Europe.

Material and Methods

A bibliographic review of Pleistocene sediments that can be found in central and southern Greece took place in order to detect possible sampling sites. The location of the selected sedimentary sequences was mapped and at least 10 samples from each study site were collected. The samples were transported and stored at the Laboratory of Palaeontology and stratigraphy of the University of Patras. Sediment samples were appropriately processed (using tap water and/or suitable chemicals such as perydrol and dried), using standard methods. The fossils were handpicked and sorted under a stereoscope. After the determination of the tests, down to the species level, using appropriate atlases and keys (e.g. Stereo Atlas), representative valves of each ostracod species were cleaned and SEM photographed. Additionally, published literature that concerns the identified species and their distribution and palaeoecology is being studied as a comparative tool for the results of the project.

Results & Discussion

Pleistocene sediments have been recorded in several places throughout central and southern Greece (Fig.1). Lower Pleistocene sedimentary sequences have been found in Atalanti (Central Greece), in Messinia and Lakonia (Southern Peloponnese) and also in Kefalonia (Ionian Sea) and Kos islands (Aegean Sea). Lower to Middle Pleistocene sequences have been recorded in Megalopolis (Southern Peloponnese) and in Zakynthos Island (Ionian Sea) while Middle Pleistocene sediments can be found in Lesvos Island (Aegean Sea). In Ioannina and Kopais (central Greece) sediments of Middle to Early Pleistocene age can be found. Finally Upper Pleistocene sediments have been recorded all over Crete Island and in Argos (NE Peloponnese). In Elis (West Peloponnese) and across the Southern margin of the Corinth Gulf (Northern Peloponnese) sediments that cover all Pleistocene can be found as it is also the case for Rhodes Island and for Cyprus. For this reason these areas are considered particularrly important for the study of the Pleistocene evolution in central and Southern Greece.

Most of the recorded Pleistocene sedimentary sequences were deposited in marine environments. Lacustrine sequences have been recorded in Megalopolis Basin and on Lesvos and Kos islands. Across the Southern margin of Corinth Basin and also in Cyprus the sedimentary sequences show marine, transitional and lacustrine characteristics.

Currently, micropalaeontological analysis has been conducted in samples from the southern margin of the Corinth Gulf (Rion and Corinth Basin), and from Kefalonia and Lesvos islands. Ostracods belonging to 17 different families have been identified (Candonidae, Cushmanideidae, Cyprididae, Cytherellidae, Cytherideidae, Cytheruridae, Darwinulidae, Eucytheridae, Hemicytheridae, Leptocytheridae, Limnocytheridae, Loxoconchinidae, Neocytherideidae, Paradoxostomatidae, Pontocyprididae, Trachyleberididae,, Xestoleberididae) and characteristic SEM photos are presented herein.

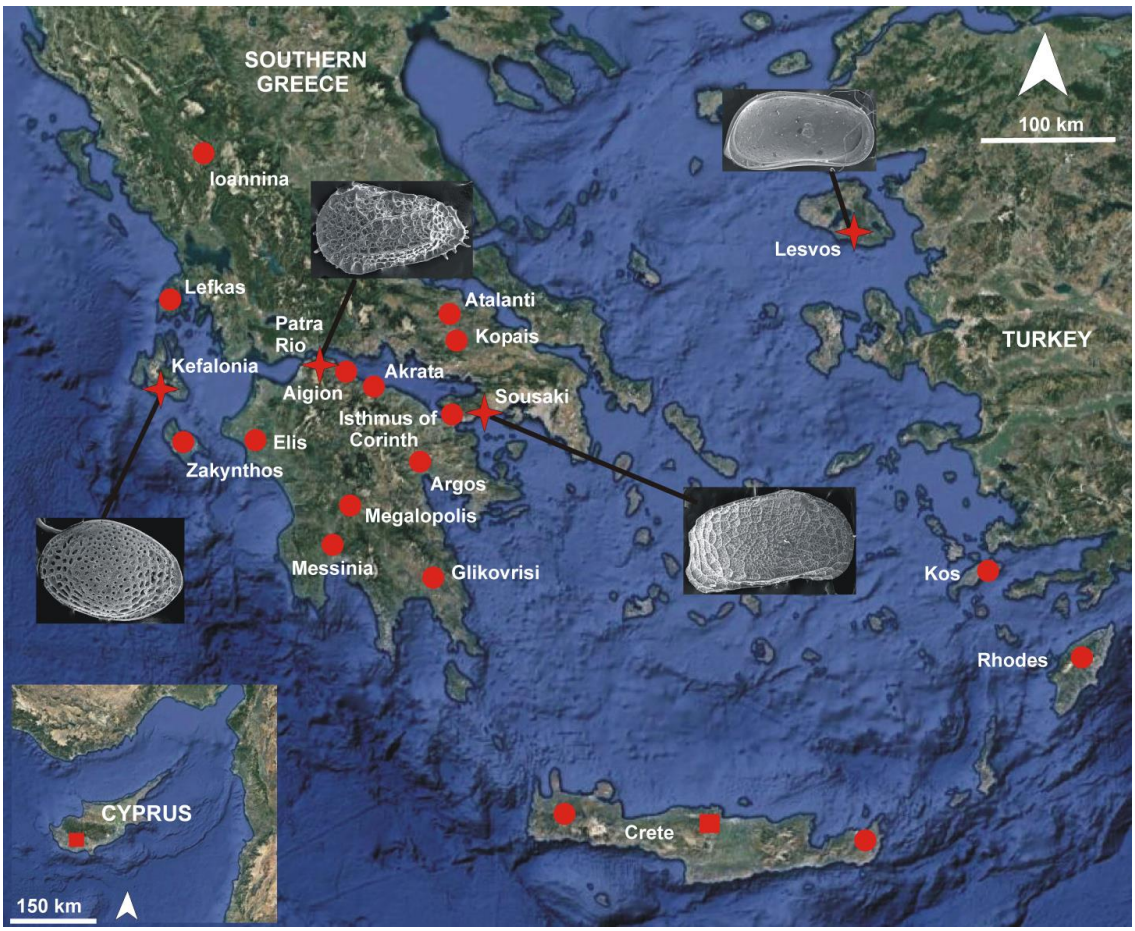

Figure 1. Satellite image (Google Earth) of central and southern Greece and Cyprus, depicting the geographic distribution of the Pleistocene sediments that have been recorded until now. Stars: studied sections, squares: under study sections, circles: other Pleistocene sections. Characteristic SEM images of Pleistocene ostracods from the studied sections are shown (Patra-Rio: Trachyleberididae, Kefalonia: Loxoconchinidae, Sousaki: Hemicytheridae, Lesvos: Candonidae).

Future perspectives

Represenative Pleistocene sedimentary successions from marine, transitional and lacustrine palaeoenvironments will be selected and sampled in order to acquire robust information about the Pleistocene ostracods of central and Southern Greece. Samples from Crete and Cyprus are already under study while two other Pleistocene sites (Elis and Megalopolis) have already been planned for sampling. This project will produce a digital collection with characteristic SEM photos of the identified ostracod species and respective information about their systematics, their ecology and distribution. A catalog with the bibliography on Greek Pleistocene ostracods will also be included. This collection intends to promote the communication between specialists and will greatly facilitate future research in the study of Pleistocene palaeoenvironments. At the same time, the gathering of published literature and the new data that will emerge will allow a future comparison of the Pleistocene ostracod species of central and southern Greece with the European Pleistocene ostracod record in order to ascertain possible relationships.

Acknowledgements

The authors would like to sincerely thank Ac. Prof. Koskeridou E. and Dr. Agiadi K. for providing us the samples from Kefalonia. We would also like to thank Dr. Tsiolakis E. for providing us the samples from Cyprus. This project is implemented through the Operational Program "Human Resources Development, Education and Lifelong Learning" and is co-financed by the European Union (European Social Fund) and Greek national funds.



References

Frenzel, P., Boomer, I., 2005. The use of ostracodes from marginal marine, brackish waters as bioindicators of modern and Quaternary environmental change. Palaeogeography, Palaeoclimatology, Palaeoecology 225, 68– 92. https://doi.org/10.1016/j.palaeo.2004.02.051

Rodriguez-Lazaro, J. and Ruiz-Muñoz, F.: A General Introduction to ostracods: morphology, distribution, fossil record and applications, in: Ostracoda as proxies for Quaternary climate change, edited by: Horne, D. J., Holmes, J. A., Rodriguez-Lazaro, J., and Viehberg, F., Developments in Quaternary Science, 17, Elsevier, 1–14, 2012.

Schellenberg, S., 2007. Marine Ostracods S A, Palaeolimnology, 2046-2062.

15th International Congress of the Geological Society of Greece
Athens, 22-24 May, 2019 | Harokopio University of Athens, Greece
Bulletin of the Geological Society of Greece, Sp. Pub. 7 Ext. Abs. GSG2019-149

New Material of the Hornless Rhinocerotid *Chilotherium* (Mammalia, Perissodactyla) from the Turolian Fauna of Samos Island, Greece

Georgia Svorligkou[1], Ioannis Giaourtsakis[2], Socrates Roussiakis[1]

(1) National and Kapodistrian University of Athens, Department of Geology and Geoenvironment, Section of Historical Geology and Palaeontology, Panepistimiopolis, GR-15784 Athens, Greece, geosvorligk@geol.uoa.gr

(2) Ludwig-Maximilians-Universität München, Department of Earth and Environmental Sciences, Paleontology & Geobiology, Richard-Wagner-Str. 10, 80333 München, Germany

The paleontological wealth of the island of Samos, Greece had sparked the interest of researchers since the middle of the 19th century (Solounias, 1981; Koufos, 2009). The diverse fauna of this renowned Late Miocene locality is characterized by the notable presence of the hornless rhinocerotid *Chilotherium* (Ringström, 1924), along with the two-horned species *Dihoplus pikermiensis* (Toula, 1906) and "*Diceros*" neumayri (Osborn, 1900). In this preliminary report, we examine and evaluate for the first time previously undescribed specimens of the hornless rhinocerotid *Chilotherium* excavated during the first decade of the 1900s by Prof. Theodore Skoufos in Samos, which are stored at the collections of the Museum of Palaeontology and Geology in Athens (AMPG).

The presence of two different two-horned rhinocerotids on Samos has been known since their first dedicated study by Weber (1904). *"Diceros" neumayri*, is a common element of the Late Miocene mammal faunas of the Eastern Mediterranean, and it is the dominant tandem-horned rhinocerotid on Samos Island. The frequently sympatric *Dihoplus pikermiensis* is also present in Samos fauna, but in a significant lower percentage (Giaourtsakis, 2009).

Weber (1905) was also the first author to recognize the presence of hornless rhinocerotids (subfamily Aceratheriinae) in the fauna of Samos, which he assigned to two different new species, *Aceratherium schlosseri* and *Aceratherium samium*. Andree (1920) named two additional hornless species based on material from Samos, *Aceratherium wegneri* and *Aceratherium angustifrons*. Ringström (1924) included all aforementioned hornless species into his newly erected genus *Chilotherium*. Later, Heissig (1975) merged *C. wegneri* with *C. schlosseri*, and attributed *C. angustifrons* to *C. kowalevskii* (Pavlow, 1913). Recently, Giaourtsakis (2009) suggested that both *C. wegneri* and *C. angustifrons* might be junior synonyms of *C. schlosseri*, thus recognizing the presence of only two hornless species in Samos, *C. schlosseri* and *C. samium*. Since the current nomenclatural status of the Eastern Mediterranean chilotheres and their systematic affinities remain unsettled, we have preliminary limited our specimens' assignment at generic level.

Among the most impressive specimens of the AMPG collection is a well-preserved *Chilotherium* cranium with associated mandible, currently under preparation (Fig. 1.1). The cranium, which is missing the nasals and the occipital region, is characterized by the following salient features: the flattened and hornless frontals, the retracted nasal notch that terminates above the mesial half of the P4, the highly placed orbital fossa with a rostral margin located above the M1, and the very short distance between the orbit and the nasal notch. On the contrary, the crania of the sympatric horned species *Dihoplus pikermiensis* and "*Diceros*" *neumayri* are characterized by the presence of a frontal horn boss, the markedly less retracted nasal notch, the relatively lower placed orbits, and the longer distance between the orbit and the nasal notch (Geraads, 1988; Giaourtsakis, 2009).

Another interesting specimen of the AMPG collection is a partial mandible missing the ascending rami and the caudal half of the mandibular body, but preserving the symphysis (Fig. 1.2). It belongs to a female individual, as deduced by the relatively small size of the second lower incisors, which are partially preserved. The mandibular symphysis is notably widened, demonstrating one of the most prominent apomorphic features of the genus *Chilotherium*. It is also characterized by a rather long diastema with a marked crest along the interalveolar margin, and a concave ventral profile. The mandible of *Dihoplus pikermiensis* is characterized by a narrower symphyseal region, featuring significantly smaller second lower incisors (Giaourtsakis *et al*., 2006). The symphyseal region of "*Diceros*" *neumayri* is abbreviated, and permanent second lower incisors are missing (Giaourtsakis, 2009). The postcranial material of the AMPG collection is of particular interest, as it includes several partially associated specimens that are presently under preparation. The postcranial elements of *Chilotherium* can be readily distinguished from the ones of the sympatric horned species, since they have significantly smaller size and relatively more robust proportions (Fig. 1.3, 1.4).

The biogeographical and paleoecological implications of the rhinocerotid dispersal during the Late Miocene in Greece are of particular interest. The hornless genera *Chilotherium* and *Acerorhinus* migrated into Greece from Central Asia through Anatolia, at the beginning of the Vallesian (Heissig, 1975; Giaourtsakis, 2003). The Vallesian locality of Pentalophos-1 is the only Greek site where both *Acerorhinus* and *Chilotherium* are found sympatric, along with the horned rhinocerotid "*Diceros*" *neumayri* (Geraads & Koufos, 1990; Athanassiou *et al*., 2014). The Greek Turolian localities have yielded only one of the two hornless genera, thus far. Furthermore, in Turolian localities where both of the horned taxa *Dihoplus pikermiensis* and "*Diceros*" *neumayri* co-occur, one of them is usually more abundant, signifying a clear interspecific dominance (Giaourtsakis *et al*., 2006; Giaourtsakis, 2009). In Samos, "*Diceros*" *neumayri* is the dominant horned species, *Dihoplus pikermiensis* is rare, and hornless *Chilotherium* is present. On the contrary, in the locality of Pikermi, *Dihoplus pikermiensis* emerges as the dominant horned species, "*Diceros*" *neumayri* is less frequent, whereas *Acerorhinus* is the sole hornless rhinocerotid taxon present.



Fig. 1: (1) Chilotherium sp. cranium and mandible in left lateral view. (2) Chilotherium sp. mandible in dorsal view; note the widened symphysis, arrows indicate the position of the partially preserved second lower incisors. (3) Chilotherium sp. calcaneus in lateral view. (4) "Diceros" neumayri calcaneus in lateral view. (All specimens from AMPG collections).

These marked differences observed in the relative distribution and abundance of rhinocerotid taxa among the Turolian localities of Greece and adjacent regions appear to have been primarily influenced by environmentally controlled provincial differences. The relatively slender and brachydont *Acerorhinus* and *Dihoplus pikermiensis* seem to have preferred more closed and temperate niches, whereas the more robust and specialized "*Diceros*" *neumayri* and *Chilotherium* favoured more open and dry habitats. In cases of sympatry, a potential resource partitioning with limited dietary competition has been suggested (Giaourtsakis *et al*., 2006; Giaourtsakis, 2009; Athanassiou *et al*., 2014).

Acknowledgements

For fascilitating access to comparative material, we kindly acknowledge G. Theodorou, V. Karakitsios (Athens Museum of Palaeontology and Geology, AMPG); G. Koufos, D. Kostopoulos (Laboratory of Geology and Palaeontology, Aristotle University, Thessaloniki); P. Tassy (Muséum National d'Histoire Naturelle, Paris); K. Heissig, G. Rössner (Bayerische Staatssammlung für Paläontologie und Geologie, München); J. Hooker, (Natural History Museum, London); G. Höck, U. Göhlich,(Naturhistorisches Museum, Wien). Financial support for comparative studies was provided to I.G. by the European Commission's Research Infrastructure Action (under EU-SYNTHESYS grants GB-TAF 574, FR-TAF 1226, FR-TAF 2545, AU-TAF 5710).

References

Andree, J., 1921. Rhinocerotiden aus dem Unterpliozän von Samos. Paläontologische Zeitschrift, 20, 189-212.

Athanassiou, A., Roussiakis, S. J., Giaourtsakis, I. X., Theodorou, G. E., Iliopoulos, G., 2014. A new hornless rhinoceros of the genus Acerorhinus (Perissodactyla, Rhinocerotidae) from the Upper Miocene of Kerassia (Euboea, Greece), with a revision of related forms. Palaeontographica, Abt. A: Palaeozoology - Stratigraphy 303 (1-3), 23-59.

Geraads, D., 1988. Révision des Rhinocerotinae (Mammalia) du Turolien de Pikermi. Comparaison avec les formes voisines. Annales de Paléontologie 74, 13-41.

Geraads, D., Koufos, G., 1990. Upper Miocene Rhinocerotidae (Mammalia) from Pentalophos-1, Macedonia, Greece. Palaeontographica, Abt. A: Palaeozoology – Stratigraphy 210, 151– 168.

Giaourtsakis, I.X., 2003. Late Neogene Rhinocerotidae of Greece: distribution, diversity and stratigraphical range. Deinsea 10, 235-253.

Giaourtsakis, I.X., 2009. The Late Miocene Mammal Faunas of the Mytilinii Basin, Samos Island, Greece: New Collection. 9. Rhinocerotidae. Beiträge zur Paläontologie 31, 157-187.

Giaourtsakis, I., Theodorou, G. Roussiakis, S., Athanassiou, A. & Iliopoulos, G., 2006: Late Miocene horned rhinoceroses (Rhinocerotinae, Mammalia) from Kerassia (Euboea, Greece). - N. Jb. Geol. Palaont. Abh., 239: 367-398.

Heissig, K., 1975. Rhinocerotidae aus dem Jungtertiär Anatoliens. Geologisches Jahrbuch (B) 15, 145-151.

Koufos, G.D., 2009. The Late Miocene Mammal Faunas of the Mytilinii Basin, Samos Island, Greece: New Collection. 1. History of the Samos Fossil Mammals. Beiträge zur Paläontologie 31, 1-12.

Osborn, H.F., 1900. Phylogeny of the rhinoceroses of Europe. Bulletin of the American Museum of Natural History, 12: 229–267.

Pavlow, M.W., 1913. Mammifères tertiaires de la Nouvelle Russie, 1. Partie: Artiodactyla, Perissodactyla (Aceratherium kowalevskii n.s.). Nouveaux Mémoires de la Société Impériale des Naturalistes de Moscou 17, 1-68.

Ringström, T., 1924. Nashörner der Hipparion-Fauna Nord-Chinas. Palaeontologia Sinica, C, 1(4), 1-156.

Solounias, N. 1981. The Turolian fauna from the Island of Samos, Greece - with special emphasis on the hyaenids and the bovids. Contributions to Vertebrate Evolution 6, 1-232.

Toula, F., 1906. Das Gebiss und Reste der Nasenbeine von Rhinoceros (Ceratorhinus Osborn) hundsheimensis. Abhandlungen der k.k. Geologischen Reichsanstalt, Wien 20 (2), 1-38.

Weber, M., 1904. Über tertiäre Rhinocerotiden von der Insel Samos I. Bulletin de la Société Impériale des Naturalistes de Moscou 17, 477-501.

Weber, M., 1905. Über tertiäre Rhinocerotiden von der Insel Samos II. Bulletin de la Société Impériale des Naturalistes de Moscou 18, 345-363.

15th International Congress of the Geological Society of Greece
Athens, 22-24 May, 2019 | Harokopio University of Athens, Greece
Bulletin of the Geological Society of Greece, Sp. Pub. 7 Ext. Abs. GSG2019-179

A fieldwork update on the new palaeontological excavations at the classical Turolian locality of Pikermi (Attica, Greece)

P. Filis[1], S. Roussiakis[1], I. Giaourtsakis[2], P. Kampouridis[3], N. Kargopoulos[1], P. Skandalos[1], S. Sklavounou[1], I. Koumoutsea[1], G. Svorligkou[1], N. Tsoukalas[1], S. Kirdis[1] and G. Theodorou[1]

(1) National and Kapodistrian University of Athens, Department of Geology and Geoenvironment, Panepistimiopolis, 15784, Athens, Greece, panagfilis@gmail.com
(2) Ludwig-Maximilians-Universität München, Department of Earth and Environmental Sciences, Paleontology & Geobiology, Richard-Wagner-Str. 10, 80333 München, Germany
(3) Eberhard Karls University of Tübingen, Department of Geosciences, Sigwartstr. 10, 72074, Tübingen, Germany

The classical locality of Pikermi (Attica, Greece) is considered to be one of the most important fossiliferous localities in Europe. The fossils occur along the Megalo Rema ravine, locally known as Valanaris. The first fossils were discovered by the Scottish historian G. Finlay in 1836. Subsequently, excavations were carried out by many naturalists and palaeontologists, namely A. Lindermayer in 1843, J. Roth in 1852, H. Mitzopoulos in 1853 and 1860-1861, A. Gaudry during the winter of 1855-56 and summer of 1860, W. Dames in 1882, M. Neumayr and L. v. Tausch in 1885, A. S. Woodward and Th. Skouphos in 1901, O. Abel in 1912 and others, whereas N. Symeonidis, F. Bachmayer and H. Zapfe excavated in a nearby locality known as Kisdari or Chomateri from 1972 to 1980 (Roth & Wagner, 1854; Gaudry, 1862-67; Dames, 1883; Weithofer, 1888; Woodward, 1901; Abel, 1922; Symeonidis *et al.*, 1973; Bachmayer *et al.*, 1982). These excavations led to the acquisition of very important palaeontological collections of specimens from Pikermi by almost all major natural history museums of Europe (Paris, London, Athens, Munich, Berlin, Vienna etc.). The collected material has been used extensively as a reference for comparative studies in numerous publications up till now and resulted in numerous publications, including some very important ones for the early development of mammalian palaeontology (e.g. Wagner, 1839, 1840; Roth & Wagner, 1854; Gaudry, 1862-1867).

Since 2008, almost two centuries after the first excavations, the National and Kapodistrian University of Athens (NKUA) resumed fieldwork in Pikermi, with a series of new systematic excavations under the direction of Prof. George Theodorou (Theodorou *et al.*, 2010, 2013). Several new and prolific fossiliferous sites like PV1 (Fig. 1) and PV3 have been revealed. In particular, the site PV1, located about 0.5 km east of the classical site, has been thoroughly explored during the last decade. Systematic excavations have been carried out almost annually, each one lasting up to a period of three months. Until 2018, over fifty students from the Department of Geology and Geoenvironment of the NKUA, as well as other institutions, have received training or participated in the fieldwork campaigns, and more than 2000 fossil specimens have been collected.

The preliminary study of the collected material from PV1 shows a rich and diverse mammalian fauna with representatives of most macromammalian groups that inhabited Greece during the Turolian. The age of the locality has been recently refined to about 7.27 Mya (Böhme *et al.*, 2017). The most frequent mammalian representatives are hipparionine horses and bovids, but rhinocerotids and giraffids are also well represented. The faunal list includes two species of hipparionine horses, the slender *Cremohipparion mediterraneum* and the robust *Hippotherium brachypus*, the bovids *Tragoportax amalthea*, *Gazella capricornis*, *Protragelaphus skouzesi*, *Palaeoryx pallasi* and *Palaeoreas lindermayeri*, the cercopithecid *Mesopithecus pentelicus*, the felids *Amphimachairodus giganteus* and an unidentified felid in the size of *Metailurus major*, the hyaenid *Adcrocuta eximia*, the mustelid *Promeles palaeatticus*, the zygodont proboscidean *"Mammut"* sp., the two-horned rhinocerotids *"Diceros" neumayri* and *Dihoplus pikermiensis*, the giraffids *Bohlinia attica*, *Palaeotragus rouenii* and *Helladotherium duvernoyi*, the suid *Hippopotamodon erymanthius* and the rodent *Hystrix primigenia*. Complementing the list of mammalian taxa is a relatively smaller number of representatives of the class Aves, including *Pavo archiaci* (Phasianidae), as well as of the class Reptilia with *Testudo* cf. *marmorum* (Testudinae) and *Varanus* sp. (Squamata) (Theodorou *et al.*, 2010, 2013; Roussiakis *et al.*, 2014). Recent palaeoecological reconstructions place the aforementioned fauna in a wooded grassland-to woodland habitat of a savannah biome (Böhme *et al.*, 2017), supporting the initial environmental interpretations put forward by A. Gaudry (1862-1867).

Pikermi is one of most significant Late Miocene localities in Europe. The detailed study of the newly excavated material is essential for improving the understanding of the taphonomical, biogeographical and palaeoecological context of the locality, as well as for the evaluation of the systematic affinities and phylogenetic position of the Pikermian taxa. In particular, one of the key objectives based on this stratigraphically well-calibrated material is the assessment of the potential existence of multiple stratigraphic levels, as opposed to the commonly regarded biochronological and taxonomic homogeneity of the Pikermian fauna (Theodorou & Nicolaides, 1988).



Figure 1. A fossiliferous bone assemblage at the PV1 site (left), and the palaeontological exhibition in Pikermi (right).

Currently, a preliminary exhibition featuring specimens from the new excavations and selected reconstructions is housed in the Rafina-Pikermi Municipality's Urban Planning Building (Fig. 1). This exhibition has achieved to generate public interest and awareness on the scientific significance of the locality, through numerous visits by schools and non-profit organizations. Imminent plans of the project include the annual continuation of the excavations, with an expansion to other sites including PV3 and Chomateri, as well as the thorough preparation of the material and its scientific evaluation. The primary objectives encompass the establishment of a multidisciplinary and educational protected Geopark at Pikermi, as well as the founding of a local Palaeontological Museum, where the material of the excavations and a new permanent exhibition shall be housed.

Acknowledgements

We would like to thank all participants of the new excavations at Pikermi, in particular the students. The fieldwork campaings at PV1 from 2009 to 2018 were supported by the Municipality of Rafina-Pikermi, several private sponsors, and the NKUA-Special Account Research Grant project no. 70/3/12977.

References

Abel, O., 1922. Lebensbilder aus der Tierwelt der Vorzeit. Jena, 644 p.

Bachmayer, F., Symeonidis, N., Zapfe, H., 1982. Die Ausgrabungen in Pikermi-Chomateri bei Athen. Eine Dokumentation. Annalen des Naturhistorischen Museums in Wien 84, 7-12.

Böhme, M., Spassov, N., Ebner, M., Geraads, D., Hristova, L., Kirscher, U., *et al.*, 2017. Messinian age and savannah environment of the possible hominin *Graecopithecus* from Europe. PLoS ONE 12 (5), e0177347.

Gaudry, A., 1862-1867. Animaux fossiles et géologie de l'Attique. F. Savy, Paris, 475 p.

Dames, W., 1883. Hirsche und Mäuse von Pikermi in Attica. Zeitschrift der Deutschen Geologischen Gesellschaft 35 (1), 92-100.

Roth, J., Wagner, A., 1854. Die fossilen Knochenüberreste von Pikermi in Griechenland. Abhandlungen der Bayerischen Akademie der Wissenschaften 7 (2), 371-464.

Roussiakis, S., Athanassiou, A., Michailidis, D., Mitsopoulou, V., Solomos, Ch., Theodorou, G., 2014. Remarks on new proboscidean remains from the classical Late Miocene locality of Pikermi and their associated fauna. Scientific Annals, School of Geology, Aristotle University of Thessaloniki, Greece, VIth International Conference on Mammoths and their Relatives, Grevena - Siatista 102, 171-172.

Symeonidis, N., Bachmayer, F., Zapfe, H., 1973. Ausgrabungen in Pikermi bei Athen, Griechenland. Annalen des Naturhistorischen Museums in Wien 77, 125-132.

Theodorou, G., Nicolaides, S., 1988. Stratigraphic horizons at the classic mammal locality of Pikermi, Attica, Greece. Modern Geology 13, 177-181.

Theodorou, G., Roussiakis S., Athanassiou, A., Filippidi A., 2010. Mammalian remains from a new site near the classical locality of Pikermi (Attica, Greece). Scientific Annals, School of Geology, Aristotle University of Thessaloniki 99, 109-119.

Theodorou, G., Roussiakis, S., Athanassiou, A., Mitsopoulou, V., Solomos, Ch., Lychounas, A., 2013. Pikermi; new excavations at a classical locality. 14th R.C.M.N.S. Congress "Neogene to Quaternary Geological Evolution of Mediterranean, Paratethys and Black Sea", Istanbul, Turkey, Abstracts, p. 128.

Wagner, A., 1839. Fossile Ueberreste von einem Affenschädel und andern Saügthieren aus Griechenland. Gelehrte Anzeigen 8, 305-311.

Wagner, A., 1840. Fossile Ueberreste von einem Affen und einigen andern Säugthieren aus Griechenland. Abhandlungen der Bayerischen Akademie der Wissenschaften 2Kl. 3 (1), 155-170.

Weithofer, A., 1888. Beiträge zur Kenntniss der Fauna von Pikermi bei Athen. Beiträge zur Paläontologie Österreich-Ungarns und des Orients 6, 225-292.

Woodward, A. S., 1901. On the bone beds of Pikermi, Attica and on similar deposits in Northern Euboea. Geological Magazine 8, 481-486.

15th International Congress of the Geological Society of Greece
Athens, 22-24 May, 2019 | Harokopio University of Athens, Greece
Bulletin of the Geological Society of Greece, Sp. Pub. 7 Ext. Abs. GSG2019-180

A high resolution multidisciplinary study of palaeoenvironmental changes in the Gulf of Elefsis, Attica, Greece during the last 300 years

A. Papaioannou[1,2], K. Kouli[1,*], C.S. Parinos[2], M. Dimiza[1], M.V. Triantaphyllou[1], K. Miaritis[1], M. Dasenakis[3], A. Gogou[2]

(1) Department of Geology and Geoenvironment, National and Kapodistrian University of Athens, Panepistimiopolis, 157 84 Athens, Greece, akouli@geol.uoa.gr
(2) Institute of Oceanography, Hellenic Center for Marine Research, 190 13 Anavyssos, Attiki, Greece
(3) Department of Chemistry, National and Kapodistrian University of Athens, Panepistimioupolis, 157 84 Athens, Greece

Introduction

We hereby present the first high resolution palaeoenvironmental record of the last 300 years from the area of Attica, South Greece. The very recent environmental changes and the imprint of human activity in marine palaeoenvironmental records are still poorly understood, despite the increasing number of archives from Greece during the last decades (e.g. Kouli *et al.*, 2012; Gogou *et al.*, 2016; and references therein).

Objectives

Through the study of alkenone paleothermometry and a plethora of geochemical, micropaleontological and pollen proxy-indices obtained from the marine multi-core WFS2, we aim to provide insights into the prevailing environmental and climatic dynamics in this region i.e. variabilities in temperature, salinity, humidity vs. aridity, redox conditions, changes in marine productivity and land vegetation patterns throughout the last 300 years, as also as the development of the anthropogenic signal (i.e. inputs of fossil fuel hydrocarbons and their combustion-derived compounds) after the Industrial Revolution Era.

Methodology

The multi-core was sampled at 0.5 cm resolution and the sediment samples have been stored at -20ºC. 52 dried samples were extracted with mixture of organic solvents and analyzed by column chromatography and gas chromatography coupled to mass spectrometry for the determination of lipid biomarkers, namely *n*-alkanes, *n*-alkanols, sterols, alkenones, diols and keto-ols, fatty acids. For the reconstruction of past Sea Surface Temperatures (SSTs) the alkenone unsaturation index ($U^{k'}_{37}$) was calculated according to Gogou *et al.* (2016). Land plant wax *n*-alkanes (Ter *n*-alkanes) as well as steroidal alcohols (sterols) were used as proxies (Gogou *et al.*, 2007) to track ecosystemic and environmental changes in the terrestrial and marine realm. The productivity from Prymnesiophyte and other nannoplankton algal species is reflected by the abundance of long-chain alkenones and diols/ keto-ols, respectively (Marlowe *et al.*,1984).

The Unresolved Complex Mixture (UCM) of aliphatic hydrocarbons, a commonly observed persistent contaminant mixture in marine sediments consisting of branched alicyclic hydrocarbons (Gough and Rowland, 1990), is used as an indicator of the contribution from anthropogenic activities i.e. chronic oil pollution (Wang *et al.*, 1999).

The Carbon Preference Index of long chain *n*-alkanes (CPI_{NA}) has been used as indicator of terrestrial organic matter supply with CPI values in fresh leaves being typically >4 (Collister *et al.*, 1994), while fossil fuel *n*-alkanes present CPI_{NA} values ~1 (Wang *et al.*, 1999).

Fifty samples were prepared and analyzed for stable isotopic composition of C and N ($\delta^{13}C$ and $\delta^{15}N$).

Pollen analysis was performed on 46 samples. Pretreatment followed classical palynological protocol including spiking and sieving through a 10 μm mesh. Pollen concentrations were calculated based on the known amount of "exotic" spores added and is expressed as grains or cysts per gram of dry sediment. Percentage and concentration pollen diagrams were constructed using TILIA Graph software. The PDI (Pollen Disturbance Index: Kouli, 2015) sum includes selected anthropogenic indicators (e.g. *Centaurea*, Cichorieae, *Plantago, Pteridium, Sarcopoterium*) and is used to explore pastoral activities in the borderlands of Elefsis Bay.

Results & Discussion

The alkenone-derived SSTs at Elefsis Bay drop by almost 1ºC from the end of the 17th to the beginning of the 18th century. This cooling is probably synchronous to one of the coldest intervals (ad 1645–1715) of the 'Little Ice Age' (LIA), characterized by a prolonged episode of volcanic and low solar activity known as 'Maunder minimum' (MM) (Xoplaki *et al.*, 2005). After that and throughout the 18th century, SSTs stabilize at a mean temperature of 23ºC. During the 19th century a gradual increase of SSTs is observed. After the last decades of the 19th century (marking the beginning of the Industrial Era in Greece) the SST turns back to an increasing mode. The trend of the SST values shows a decrease during the 20th century, possibly reflecting the result of a combination of events that have thereafter affected the temperature and other physicochemical characteristics of the study area.

The significant population rise and the related urban activities in the Athens metropolitan area during the second half of the 19th century resulted to a noticeable decrease of CPI, and a radical increase of UCM, attributed to enhanced terrestrial inputs (Ter *n*-alkanes) thus marking the entrance to the Industrial Era.

During the same interval, an increase in the abundance of alkenones and of specific sterols, reflects the higher productivity

from algal species linked to enhanced continental inputs and consequently increased nutrient supply to the coastal environment.

Pollen assemblages indicate the existence of a diverse Mediterranean plant landscape, while prominent is the imprint of the human activities on the vegetation. Evergreen *Quercus*, accompanied by *Pistacia* and *Phillyrea*, are the most conspicuous taxa featuring the occurrence of Mediterranean macchia. Thermophilous deciduous oaks woodlands compose a significant part of the vegetation, especially at the lower part of our record. Mountainous forest is underlined by the presence of *Abies*, while a big variety of herb taxa fill in the landscape. *Olea* is a major component of the vegetation throughout the entire record. Olive cultivation is intensified after the first quarter of the 18th century and seems to be one of the major human activities in the area. Anthropogenic indicator pollen implies the decrease of pastoral activities during the 19th century and since the end of the 20th century. During the 19th and most of the 20th century the impact of grazing activities on vegetation is more pronounced. A very distinct transitory drop in human indicators is recorded in mid- 18th century. This temporal retreat in olive cultivation and grazing activities can be connected with the societal instability during the Greek War of Independence. Finally since the last quarter of the 19th century and until the mid-20th century a gradual retreat of *Pinus* is recorded, probably associated with the start of the Industrial Period in Greece and the increased requirement for fuel like firewood.

Conclusions

Our study revealed marine and terrestrial environmental and ecosystem responses to climatic variability along with land-ocean interactions in the Elefsis Bay, South Greece, during the last 300 years. Distributions of the lipid markers indicated the impact of both marine and terrestrially derived organic matter inputs in the study area, which were highly intensified after the onset of the Industrial Era in Greece. Vegetation patterns denote the significant role of human activities in shaping the landscape of the Elefsis region.

Acknowledgements

We sincerely thank Dr. Nikos Lampadariou and the Officers and Crew of R/V Aegaeo (HCMR, Greece) for retrieving the WF-S2 multicore in the frame of the EU 'Water Framework Directive' Program.

References

Collister, J., Rieley, G., Stern, B., Eglington, G., Fry, B., 1994. Compound-specific d13C of leaf lipids from plants with differing carbon dioxide metabolisms. Organic Geochemistry 21, 619-627

Gogou, A., Bouloubassi, I., Lykousis, V., Arnaboldi, M., Gaitani, P., Meyers, P.A., 2007. Organic geochemical evidence of Late Glacial–Holocene climate instability in the North Aegean Sea. Palaeogeography Palaeoclimatology Palaeoecology, 256, 1–20.

Gogou, A., Triantaphyllou, M., Xoplaki, E., Izdebski, A., Parinos, C., Dimiza, M., Bouloubassi, I., Luterbacher, J., Kouli, K., Martrat, B., Toreti, A., Fleitmann, D., Rousakis, G., Kaberi, H., Athanasiou, M., Lykousis, V., 2016. Climate variability and socio-environmental changes in the northern Aegean (NE Mediterranean) during the last 1500 years. Quaternary Science Reviews 136, 209–228.

Gough, M.A., Rowland, S.J., 1990. Characterization of unresolved complex mixture of hydrocarbons in petroleum. Nature 344, 648-650.

Kouli, K., 2015. Plant landscape and land use at the Neolithic lake settlement of Dispilió (Macedonia, northern Greece). Plant Biosystems 149, 195–204.

Kouli, K., Gogou, A., Bouloubassi, I., Triantaphyllou, M.V., Ioakim, C., Katsouras, G., Roussakis, G., Lykousis, V., 2012. Late postglacial paleoenvironmental change in the northeastern Mediterranean region: Combined palynological and molecular biomarker evidence. Quaternary International 261, 118–127.

Marlowe, I.T., Green, J.C., Neal, A.C., Brassell, S.C., Eglington, G., Course P.A., 1984. Long chain alkenones in the Prymnesiophyceae. Distribution of alkenones and other lipids and their taxonomic significance. British Phycological Journal 19, 203-16.

Wang, Z., Fingas, M., Shu, Y. Y., Sigouin, L., Landriault, M., Lambert, P., Turpin, R., Campagna, P., Mullin, J., 1999. Quantitative Characterization of PAHs in Burn Residue and Soot Samples and Differentiation of Pyrogenic PAHs from Petrogenic PAHs-The 1994 Mobile Burn Study. Environmental Science and Technology 33, 3100-3109

Xoplaki, E., Luterbacher, J., Paeth, H., Dietrich, D., Steiner, N., Grosjean, M., Wanner, H., 2005. European spring and autumn temperature variability and change of extremes over the last half millennium. Geophysical Research Letters 32, L15713

15th International Congress of the Geological Society of Greece
Athens, 22-24 May, 2019 | Harokopio University of Athens, Greece
Bulletin of the Geological Society of Greece, Sp. Pub. 7 Ext. Abs. GSG2019-182

The upper Cretaceous palaeo-slope transition: an integrated calcareous nannofossil and microfacies approach (Ionian Islands, Preapulian Zone, Western Greece)

Ioulietta Mikellidou[1], Stefano Patruno[2], Maria V. Triantaphyllou[1], Fotini Pomoni-Papaioannou[1]

(1) Department of Geology and Geoenvironment, University of Athens, Panepistimiopolis 15784, Athens, Greece, julietmikellides@gmail.com
(2) Oranje-Nassau Energie, London, UK

The Ionian islands are situated on the west portion of the Hellenic Arc, part of the most active plate margins in the Mediterranean. The westerly-verging Hellenides fold-and-thrust belt in this area comprises the deformed Meso-Cenozoic basinal succession of the Ionian Zone, which thrusts over the time equivalent slope unit of the Preapulian Zone.The basal front of this tectonic contact outcrops along the eastern edges of Kefalonia and Zakynthos (Zante) islands.

The palaeoenvironmental transition between the Late Cretaceous persistent carbonate platform 'Apulian' facies and the time-equivalent 'Pre-Apulian' facies is very close to the westernmost edge of the islands of Zakynthos (Zante) and Cephalonia (c.f., Bosellini, 2002; Karakitsios, 2013); however these islands are thought to be composed almost entirely of Pre-Apulian facies (with Ionian facies confined to the easternmost fringes of the island, in the hangingwall of the main overthrust.

We carried out a geological _fieldwork in the islands of Zakynthos in 2012 and Cephalonia in 2015, with the aim to describe a rarely described near-continuous distal-to-proximal transition from a pelagic slope (eastwards) to a neritic platform (west). Our work focuses predominantly (albeit not exclusively) on the Cretaceous sections, with nannoflora analyses conducted for the first time. Also, Cretaceous microfacies are investigated to interpret the changes of palaeoenvironments from platform margin to distal slope. Stratigraphic sections were logged on the field, and a total of 267 samples were collected along 6 east-to-west transects for successive biostratigraphic analyses: 95 samples in Zakynthos and 172 samples in Cephalonia.

This study shows thin-bedded, 'platform slope' formations to the east of Zakynthos (Campanian-Maastrichtian), and thicker bedded, carbonate platform-like calcareous formations westwards (usually ?Cenomanian-Turonian). A paleoenvironmental transition between the two facies was recognized, with a gradual general increase of proximality and 'platform influence' in slope facies towards the west (Fig. 1). The presence of gradually older rocks towards the east is explained by the consistent westerly monoclinal dip of the outcropping strata; a potential hiatus is present between the Campanian-Maastrichtian and the ?Cenomanian-Turonian packages. Presence of gradually shallower-marine and more proximal palaeo-facies towards the west are explained by the close vicinity of the edge of the Apulia platform. Accordi et al. (2014) argue that southern Zakynthos in the Late Cretaceous was characterized by a toe-of-slope sequence. Our analyses of the Agalas sectionn (southern Zakynthos), however, point out to a more proximal depositional setting, becoming increasingly shallower to the west, where we recognized potential occurrences of in-situ neritic carbonates.

In Cephalonia similar palaeoenvironmental trends were also identified, with even clearer outcrops of inner carbonate platform facies identified to the west of the island, around Argostoli (hereby named "Argostoli Platform"). This is characterized by evidence of inner carbonate platform facies, including peritidal cycles and development of redded palaeosol layers encased between thick-bedded or massive fine-grained carbonate units. Arguably, the Argostoli Platform represents the easternmost edge of the Apulian platform, and these facies belong to the Apulian facies domain rather than to the transitional Preapulian ones. Elsewhere in Cephalonia, similar to Zakynthos, from west to east there is a transition between very proximal slope facies dominated by massive megabreccias with neritic clasts and distal slope to basinal facies on the eastern coast of the island (e.g., Agia Efimia location)

The biostratigraphic and microfacies analyses are still ongoing for the Cephalonia samples. The final aim of this study is to reconstruct the position of the Apulian platform edge in western Greece, which may have significant implications in oil exploration.

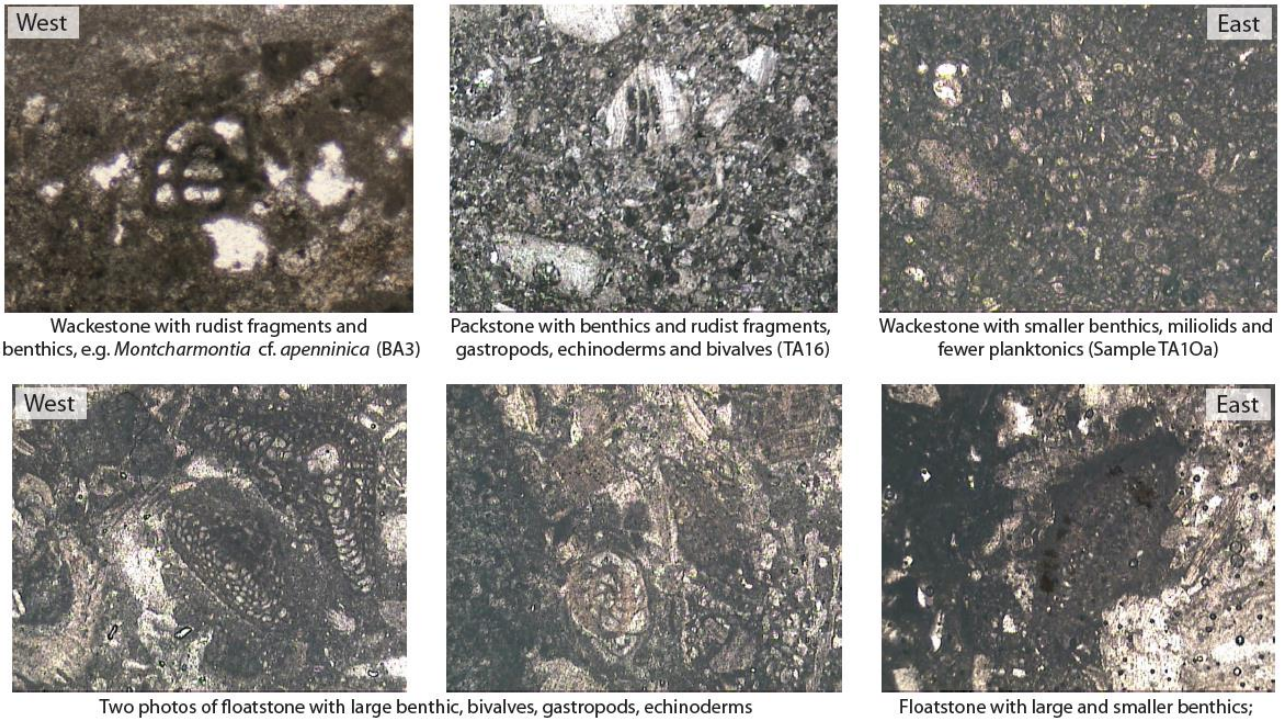

Figure 1. Examples of typical Preapulian upper Cretaceous microfacies transitions from the east (distal slope) to the west (proximal slope) in the Island of Zakynthos. Agalas section (southern Zakynthos)

References

Accordi et al, 2014. Microfacies analysis of deep-water breccia clasts:a tool for interpreting shallow v.s. deep-ramp Palaeogene sedimentation in Cephalonia and Zakynthos (Ionian Islands, Greece). Facies, Vol.60, Issue 2, 445 – 466

Bosellini, A., 2002. Dinosaurs ''re-write'' the geodynamics of the eastern Mediterranean and the paleogeography of the Apulia Platform. Earth-Science Reviews, 59, 211– 234

Danelian, T., Tsikos, H., et al., 2004. Global and regional palaeoceanographic changes as recorded in the mid-Cretaceous (Aptian–Albian) sequence of the Ionian zone (NW Greece). Journal of the Geological Society, London, 161, 703–709

Etiope, G., Papatheodorou, G., et al., 2006. Methane and hydrogen sulfide seepage in the northwest Peloponnesus petroliferous basin (Greece): Origin and geohazard. AAPG Bulletin, 90, no. 5, 701–713

Karakitsios, V., 2003. Evolution and Petroleum Potential of the Ionian Basin (Northwest Greece). AAPG Search and Discovery Article #90017©2003 AAPG International Conference, Barcelona, Spain, September 21-24, 2003

Karakitsios, V., and Rigakis, N., 2007. Evolution and Petroleum potential of Western Greece. Journal of Petroleum Geology, 30 (3), 197 – 218

Karakitsios, V., Triantaphyllou, M. et al., 2010. Preliminary study of the slump structures of the Early Oligocene sediments of the Pre – Apullian zone (Antipaxos Island, North Western Greece). Bulletin of the Geological society of Greece, Proceedings of the 12th International Conference Patras, 2010

Karakitsios, V., 2013. Western Greece and Ionian Sea – conventional and unconventional hydrocarbon potential. Presentation

15th International Congress of the Geological Society of Greece
Athens, 22-24 May, 2019 | Harokopio University of Athens, Greece
Bulletin of the Geological Society of Greece, Sp. Pub. 7 Ext. Abs. GSG2019-186

The Höwenegg fossil turtle assemblage (Late Miocene, South Germany): preliminary results on taxonomic composition and diversity

Irena Pappa[1], Eberhard Frey[2], Evangelos Vlachos[3], George Iliopoulos[1]

(1) Department of Geology, University of Patras, University Campus, Rio, Greece; geo08108@upnet.gr , iliopoulosg@upatras.gr
(2) Department of Biology, Karlsruhe Institute of Technology, University of Karlsruhe,
Kaiserstraße 1276131, Karlshrouhe, Germany, State Museum of Natural History Karlsruhe, Erbprinzenstraße 13
76133 Karlsruhe, Germany, dinofrey@aol.com
(3) CONICET and Museo Paleontológico Egidio Feruglio, Trelew, Chubut, Argentina, evlacho@mef.com.ar

Introduction

During the Late Cenozoic (Tertiary, Quaternary) the Western Palearctic region experienced a number of climatic changes (e.g., Ice Ages), geotectonic changes (e.g., final rise of the Alpes; extension and formation of sedimentary basins) as well as more complex events (e.g., Messinian salinity crisis; changes in sea level; Middle Miocene climatic Optimum). These events had a significant impact on the evolution of flora and fauna in this region during those periods. Ectothermic reptiles, such as turtles, are more susceptible to these changes and can be used as palaeoecological indicators. Also, and mainly due to the presence of their carapace, turtles have an excellent fossil record which provides the ability of exporting considerable inferences. Nevertheless, compared to other vertebrate groups (e.g., mammals), the turtle fossils have been rarely studied elaborately.

Particularly in Europe, the fossil record of the turtles is mostly complete, from the Tertiary to the Present (e.g., Lapparent de Broin 2001; Danilov, 2005). Therefore, the study of fossilized turtles can provide insights regarding the effect of climate and environmental changes on the evolution, diversity, and anatomy of the turtles.

Objective and study area

Herein, we present some preliminary results of the doctoral study of the first author. The purpose of this study is to contribute and strengthen the knowledge of classification, evolution, taphonomy and palaeoecology of the Neogene of the western Palearctic, focused on the study of the rich and diverse fossilized turtle's record of the Höwenegg region, Germany.

Höwenegg is a locality found 2.5 Km from Immendingen, which is part of the Hegau, a volcanic area in Southern Germany. Höwenegg locality is noteworthy for its Late Miocene fauna (MN9) with well-preserved and almost complete skeletons of vertebrates, invertebrates and plant fossils. Höwenegg fossils belong to the Vallesian stage, and more specifically to the MN9 biozone (Munk *et al.*, 2007; Giersch *et al.*, 2010; Wolf *et al*., 2012).

The most important vertebrate findings are the mammals (*Miotragocerus pannoniae, Hippotherium primigenium, Aceratherium incisivum*), a big amount of fishes, as well as a remarkable number of turtle samples (Bernor *et al*., 1997; Giersch *et al*., 2010; Schleich 1985). The taxonomy and diversity of the chelonian assemblage is one of the primary objectives of this study.

Methodology

- Preparation, conservation and cataloguing of the fossilized skeletal material will be carried out primarily at the Department of Geology of the University of Patras, Greece, as well as in several Natural History Museums and Collections of Germany (Karlsruhe, Mainz, Freiburg and Darmstadt) where the skeletal material is stored.
- Taxonomic analysis. For the taxonomic determination of Höwenegg's turtle fauna standard anatomical and paleontological techniques will be used.
- Phylogenetic analysis. Cladistic analyses will be carried out and the most comprehensive taxa will be analyzed in a phylogenetic context.
- Taphonomic study. The taphonomic study concerns the collection and analysis of various quantitative and qualitative data, as well as their final connection to the taphonomic history of the skeletal material.
- Diversity. Study the diversity of fossilized turtles both locally (α-) and regionally (β- and γ-diversity).
  Palaeocological analysis. Palaecological inferences will be made through the study of skeletal anatomy, sedimentology, and palaeohistology.

Results

The preliminary study of the Höwenegg's turtle fauna reveals the presence of several cryptodiran clades of turtles. Most of them appear to be represented by a single taxon (Pan-Trionychidae, Pan-Chelydridae, Emydidae, Geoemydidae), whereas tortoises (Testudinidae) are apparently represented by a small and a medium-to-large taxon. Our preliminary assessment, therefore, identifies up to six different turtle species surviving in Höwenegg during the Late Miocene. These clades were quite diverse in Central Europe during the Neogene, and Höwenegg appears to be one of the most diverse localities of that period. The preservation of the fossils in many cases is fairly good. The majority of the specimens correspond to partial shell and isolated shell fragments, whereas limb elements are few. Of particular highlight of the Höwenegg assemblage is a partial skeleton of a chelydrid taxon, preserving skull, shell and associated limb bones.

Starting with Höwenegg, the results of this thesis will be compared and correlated with those of other coeval localities in detail, as well as with other adjacent regions from Central (e.g., Switzerland, Austria) and South Europe (e.g., Italy, Greece) with available data. The study of fossilized turtles from Höwenegg, combined with other local and European localities where fossilized turtles have been found, will make a significant contribution to the knowledge of the diversity and evolution of turtles in Central and Northern Europe during the Neogene. Finally, particular emphasis will be given on the comparison of the occurrence and diversity of the various turtle clades between Central and Southern Europe. Information from rich and diverse places with detailed geological / stratigraphic and faunal backgrounds, such as Höwenegg, could contribute significantly to the assessment of the origin and evolution of the Neogene European turtles. The results of this study will contribute also to the interpretation of the evolutionary and palaeoecological model at a regional and continental level.

Acknowledgements

I would like to thank Natural History Museums of Karlsruhe, Mainz, Freiburg and Darmstadt for giving me permission to study Höwenegg's skeletal material. Furthermore, I would like to thank the stuff of Natural History Museum of Karlsruhe for all their help and particularly Wolfgang Munk who was responsible for the Howenneg's collection. Finally, I must thank Erasmus + Placement Program under which I was able to visit the collections in the Natural History Museum of Karlshruhe and study part of material.

References

Bernor, R.L., Tobien, H., Hayek, L.-A.C., Mittmann, H.-W. 1997. *Hippotherium primigenium* (Equidae, Mammalia) from the Late Miocene of Höwenegg (Hegau, Germany). Adrias 10, 1–230.

Danilov, I.G. 2005. Die fossilen Schildkröten Europas. In: U.Fritz, ed. Handbuch der Reptilien und Amphibien Europas, Part 3/IIIB: Schildkröten (Testudines) II. Wiebelsheim, Germany: Aula-Verlag. pp. 329–448.

Giersch, S., Munk, W. and Ziegler, R. 2010. The first record of a beaver – *Trogontherium (Euroxenomys) minutum* – in the Höwenegg fauna (Miocene, southern Germany). Palaeodiversity 3, 235–239.

Lapparent de Broin, F., 2001. The European turtle fauna from the Triassic to the Present. Dumerilia 4(3), 155–217.

Munk, W., Bernor, R.L., Heizmann, E.P.J.,Mittmann, H., 2007. Excavations at the Late Miocene NM9 (10.3 Ma) Locality of Höwenegg (Hegau) Southwest-Germany 2004-2006. Carolinea 65, 5–14.

Schleich, H., 1985. Neogene testudines of Germany. Studia Geologica Salmanticensia, Volume especial 1. Studia Palaeochelonologica I, 249–267.

Wolf, D., Semprebon, G.M., Bernor, R.L., 2012. New observations on the paleodiet of the late Miocene Howenegg (Hegau, Germany) *Hippotherium primigenium* (Mammalia, Equidae). Bolletino del la Società Paleontologica Italiana 51(3), 185–191.

ΕΓΕ 2019
15th International Congress of the Geological Society of Greece
Athens, 22-24 May, 2019 | Harokopio University of Athens, Greece
Bulletin of the Geological Society of Greece, Sp. Pub. 7 Ext. Abs. GSG2019-240

New stratigraphic data of the Limnos volcano-sedimentary sequence and correlations with the Thrace Basin

D. Papanikolaou[1], M. Triantaphyllou[1]

(1) Department of Geology and Geoenvironment, National and Kapodistrian University of Athens, Panepistimioupolis, 15784 Athens, Greece, mtriant@geol.uoa.gr

Introduction

The geological structure of Limnos Island comprises a clastic sedimentary sequence of Oligocene age with extensive volcanic rocks of Lower Miocene age (Innocenti et al., 1994, 2009). The available geological maps (Roussos, 1994; Innocenti et al., 2009) do not comprise a stratigraphic subdivision with distinct stratigraphic formations but a description of the dominant lithology. The available stratigraphic and sedimentological studies (e.g., Caracciolo et al., 2011; Maravelis and Zelilidis, 2012; Kostopoulou et al., 2018) do not present a coherent tectono-stratigraphic structure of the island and their conclusions are referring to an Upper Eocene - Oligocene stratigraphic range with a total thickness of less than 800 m.

Our research comprised geological mapping, combined with several stratigraphic sections from the lower to the upper horizons and tectonic analysis combined with calcareous nannofossil biostratigraphy (Martini, 1971; Agnini et al., 2014).

Results

Our results have shown that: 1) Limnos volcano-sedimentary sequence exceeds 2200 m of thickness and 2) the stratigraphic range extends from the Late Eocene (nannofossil biozone NP17, around 38–40 Ma) to the Oligocene/Miocene boundary (nannofossil biozone NP25 around 24–25 Ma and up to 23 Ma within biozone NN1).

Characteristic stratigraphic assemblages are:

- The lower horizons, cropping out in Southeast Limnos at Bay Agias, are more than 300 m thick and their age is of Late Eocene (NP17), comprising a nannofossil assemblage of Helicosphaera compacta, Sphenolithus predistentus, S. spiniger and S. obtusus.

- An overlying distinct horizon, cropping out along the crest of the NW-SE trending hill of Southeast Limnos east of Fissini, consists of a blocky formation with olistolites of Nummulitic neritic limestones. This horizon occurs about 100–120 m above the lowermost rhythmic alternations of turbiditic sandstones and pelites belonging to the Late Eocene (nannofossil biozone NP17) with H. compacta, S. obtusus, Dictyococcites bisectus and Reticulofenestra umbilicus.

- Another distinct horizon about 150–200 m higher than the blocky formation consists of several interlayering volcanic tuffs within a cyclical sedimentary sequence exposed at Cape Ag. Eirini. It has been dated as Late Eocene-Early Oligocene up to biozone NP23 determined from the presence of Sphenolithus predistentus and S. distentus (27.14–30.0 Ma). Radiochronological data from the lower volcanic intercalations have revealed an age of ~36 Ma (Maravelis et al., 2016).

- Several hundred meters upward in the sequence there is a change to thick sandstones-conglomerates of variable thickness, depending on the position of the area within the lobes of submarine fans. An average thickness of the conglomerates at the central part of Eastern Limnos is 150–200 m. Its age has been determined as Late Oligocene (27.14–26.81 Ma, biozone NP24), based on the contemporaneous presence of Sphenolithus ciperoensis and S. distentus.

The stratigraphic sequence continues into the Late Oligocene until the Oligocene/Miocene boundary, with a characteristic N-S section along the western part of Limnos, without important tectonic breaks, from Kaspakas to the northwestern cape of Mourtzouflos at the area of Vigla. The younger ages have been determined at this northwestern part of Limnos with characteristic assemblages of NP25 in between 26.81–24.36 Ma, such as S. ciperoensis and D. bisectus and even up to 23 Ma (biozone NN1) based on the presence of Sphenolithus delphix.

Impressive volcanic dikes and lava flows become frequent towards the upper horizons. However, the most extensive volcanic extrusions occur at the central-southern part of Limnos and they are dated as Early Miocene (18–22 Ma; Pe-Piper and Piper, 2002). Thick pyroclastic deposits cover unconformably the previous sedimentary sequence in central Limnos, producing characteristic morphological cliffs due to their erosional style.

The overall stratigraphic sequence of Limnos together with its equivalent sequence of Thrace shows a molassic type deep marine environment within a back-arc basin (Papanikolaou, 1993, 2013) as this is shown: 1) by the unconformable deposition of the Paleogene clastic sediments on a varietated Alpine basement, belonging either to the Circum Rhodope belt along its northern margin, deformed during the Late Jurassic with deposition of unconformable neritic limestones in Early Cretaceous (Aliki Limestones, west of Alexandroupolis), or to the Eastern Greece unit of the Internal Hellenides along the southern margin, deformed in Early Eocene, 2) by the co-existence of the volcanic arc within this North Aegean - Thrace Basin. In fact, flysch type deposits during this period of Late Eocene - Oligocene occur at the fore-arc basins of the External Hellenides fold and thrust belt (e.g. Tripolis, Ionian etc.).

Correlations with the Thrace Basin

The above stratigraphic sequence of Limnos can be correlated with the stratigraphy of the similar sequences around Alexandroupolis in the Western Thrace basin (Papanikolaou and Triantaphyllou, 2010). The Limnos sequence can be correlated with the upper Group of the Pylaea formation, whereas the Lower group of the Kirki formation is not cropping out on Limnos, but it could occur deeper. The characteristic formation of the Upper Eocene Avantas neritic limestones, separating the two clastic sequences in Alexandroupolis can be correlated with the olistolite horizon of Southeast Limnos, where the same neritic limestones occur as blocks, slided within a deep basin. Generally, the sedimentary facies of the Limnos clastic sequence corresponds to a much deeper setting than that of the Alexandroupolis area.

Volcanism is also present in Alexandroupolis in the Upper Eocene-Oligocene Kirki sequence (related also to the metalliferous deposits of Kirki) but also in the higher horizons of the Oligocene Pylaea sequence with volcanic extrusions also in the Early Miocene.

The Lower Miocene volcanic breccia of Limnos, unconformably overlying the Limnos clastic sequence, can be correlated to the Aghios Efstratios pyroclastic sequence as well as to the pyroclastic sequences of Northern Lesbos Island.

References

Agnini, C., Fornaciari, E., Raffi, I., Catanzariti, R., Pälike, H., Backman, J., Rio, D., 2014. Biozonation and biochronology of Paleogene calcareous nannofossils from low and middle latitudes. Newsletters on Stratigraphy 47/2, 131–181.

Caracciolo, L., Critelli, S., Innocenti, F., Kolios, N., Manetti, P., 2011. Unraveling provenance from Eocene–Miocene sandstones of the Thrace Basin, NE Greece. Sedimentology 58, 1988–2011.

Innocenti, F., Manetti, P., Mazzuoli, R., Pertusati, P., Fytikas, M., Kolios, N., 1994. The geology and geodynamic significance of the Island of Limnos, North Aegean Sea, Greece. N. Jb. Geol. Palaont. Mh. 11, 661–691.

Innocenti, F., Manetti, P., Mazzuoli, R., Pertusati, P., Fytikas, M., Kolios, N., Vougioukalakis, G.E., Androulakakis, N., Critelli, S., Caracciolo, L., 2009. Geological map (scale 1:50,000) of Limnos island (Greece): explanatory notes. Acta Vulcanol. 20, 87–97.

Kostopoulou, S., Maravelis, A.G., Zelilidis, A., 2018. Biostratigraphic analysis across the Eocene–Oligocene boundary in the southern Hellenic Thrace basin (Lemnos Island, north Aegean Sea). Turkish J. Earth Sci. 27, 232–248.

Maravelis, A.G., Boutelier, D., Catuneanu, O., Seymour, KSt., Zelilidis, A., 2016. A review of tectonics and sedimentation in a forearc setting: Hellenic Thrace Basin, north Aegean Sea and northern Greece. Tectonophysics 674, 1–19.

Maravelis, A., Zelilidis, A., 2012. Paleoclimatology and Paleoecology across the Eocene/Oligocene boundary, Thrace Basin, Northeast Aegean Sea, Greece. Palaeogeogr. Palaeoclimatol. Palaeoecol. 365–366, 81–98.

Martini, E., 1971. Standard Tertiary and Quaternary calcareous nannoplankton zonation. In: Farinacci, A. (Ed.),

Proceedings 2nd International Conference Planktonic Microfossils Roma: Rome (Ed. Tecnosci.) 2, 739–785.

Papanikolaou, D. 1993. Geotectonic evolution of the Aegean. Bull. Geol. Soc. Greece 28, 33-48.

Papanikolaou, D. 2013. Tectono-stratigraphic models of the Alpine terranes and subduction history of the Hellenides. Tectonophysics 595-596, 1-24.

Papanikolaou D., Triantaphyllou M., 2010. Tectonostratigraphic observations in the western Thrace Basin in Greece and correlations with the eastern part in Turkey. XIX Congress of the Carpathian Balkan Geological Association. Thessaloniki, Greece, 23-26 September 2010, Geologica Balcanica 39 1-2, 293–294.

Pe-Piper, G., Piper, D.J.W., 2002. The Igneous Rocks of Greece. The Anatomy of an Orogen. Gebrüder Borntraeger, Berlin.

Roussos, N., 1993. Geological Map of Limnos Island, Scale 1.50,000, Athens, IGME.

15th International Congress of the Geological Society of Greece
Athens, 22-24 May, 2019 | Harokopio University of Athens, Greece
Bulletin of the Geological Society of Greece, Sp. Pub. 7 Ext. Abs. GSG2019-241

IODP Expedition 381: The potential of the new high-resolution palaeoenvironmental and palaeoclimatic record from the Corinth Gulf

K. Kouli[1], K. Panagiotopoulos[2], M. Geraga[3], M. Phillips[4], A. Cvetkoska[5], P. Diz[6], S.A. Oflaz[7], J. Everest[8], G. Carter[8], D. Shillington [9], L. McNeill[10] and Expedition 381 Scientists

(1) Department of Geology and Geoenvironment, National and Kapodistrian University of Athens, Greece, akouli@geol.uoa.gr
(2) University of Cologne, Germany
(3) Department of Geology, University of Patras, Greece
(4) University of Texas at Austin, USA
(5) Justus Liebig University, Germany
(6) Universidad de Vigo, Spain
(7) Christian-Albrechts-Universität zu Kiel, Germany
(8) ECORD Science Operator, British Geological Survey, Lyell Centre, Edinburgh, United Kingdom
(9) Lamont-Doherty Earth Observatory, Columbia University, Palisades NY, USA
(10) University of Southampton, Ocean and Earth Science, Southampton, United Kingdom

The International Ocean Discovery Program Expedition 381: Corinth Active Rift Development was conducted in late 2017 (offshore phase-drilling campaign) and early 2018 (onshore phase-Bremen Core Repository). The primary objectives of the Expedition 381 were to target the active continental Corinth Rift (Greece) in order to: a) obtain high spatial and temporal resolution records of the rifting process dynamics, b) to study the interaction of climate and tectonics on sedimentary and surface processes in a rift zone, c) to improve regional hazard assessments in one of the most seismically active regions of Europe and d) to generate a new high resolution record of Quaternary paleoclimate and paleoenvironment evolution from a semi-isolated basin dominated at present by typical Mediterranean ecosystems.

During IODP Exp. 381, three sites (Figure 1) located along the Gulf of Corinth, were drilled and logged, sampling in high resolution the syn-rift sedimentary sequence back to ~1.5 Ma or more (Shillington *et al.*, 2019; McNeill et al., 2019a). Preliminary results produced during the onshore phase of the expedition confirmed that the retrieved deposits contain a rich and complex record of the tectonics, climate and palaeoenvironment interplay in the syn-rift basin. The connection of the Gulf of Corinth to the Mediterranean is controlled by basin sills resulting in alternating aquatic conditions. These vary between open ocean/marine and isolated phases as sea level fluctuates in response to climate forcing (glacial-interglacial cycles). As a result, a unique range of paleoenvironmental gradients is encountered across the central (M0078 and M0079) and eastern (M0080) rift impacting depositional processes, sediment and water chemistry and composition of microfossil assemblages such as calcareous nannofossils, foraminifera, diatoms and dinoflagellate cysts (Shillington et al., 2019; McNeill et al., 2019a), while pollen assemblages from the same intervals record alternating periods of forest or herb vegetation in the borderlands of the Gulf of Corinth.

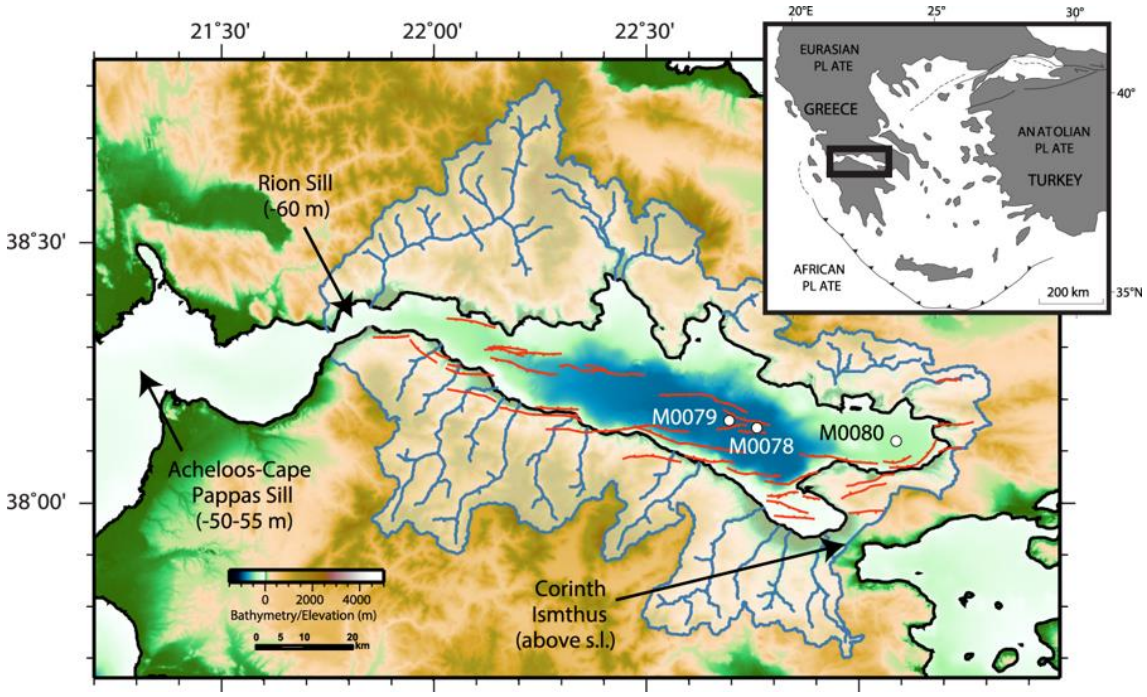

Figure 1: Map of the Gulf of Corinth and Corinth Rift system showing the locations of the three sites drilled during the IODP Expedition 381. The position of bounding sills of the Gulf, primary active faults (Nixon *et al.*, 2016) and primary catchment areas and main rivers discharging into the Gulf (Watkins *et al.*, 2018) are included. Inset: tectonic setting of Corinth rift in Aegean region, Eastern Mediterranean Sea (from Mc Neill *et al.*, 2019b).

During interglacial periods, when the sea level was high, the Gulf was connected to the global ocean and marine microfossil assemblages including foraminifera, diatoms, calcareous nannoplankton, and dinoflagellate cysts were observed. High abundances of foraminifera were recorded, while benthic foraminifer abundance was generally higher than that of planktonic foraminifers. The dominant planktonic foraminifera species (neogloboquadrinids and *T. quinqueloba*) suggest high fertility in surface waters. High abundances of buliminids and bolivinids in the benthic assemblages suggest increased organic fluxes to the seafloor. During isolated/semi-isolated periods, when the Gulf appears to have been fully or partially cut off from the global ocean complex aquatic microfossil assemblages, mainly constituted by non-marine diatoms and organic dinoflagellate cysts, suggest brackish paleoenvironmental conditions. Foraminifers tend to be absent or in low abundances, although brief intervals with higher foraminifer abundance were also observed. The transitions between the marine and isolated/semi-isolated intervals expressed in the micropaleontological and sedimentary record are particularly complex and varied in their length and character.

Preliminary pollen and terrestrial non-pollen palynomorph (NPP) assemblages analyzed during the onshore phase of the expedition allow to establish a direct link between the response of terrestrial and aquatic environments (Mc Neill et al., 2019b; Shillington et al., 2019). The Arboreal/Non Arboreal Pollen ratio (AP/NAP) fluctuates at orbital scale suggesting the alternation of forested and open landscapes in the borderlands of the Gulf of Corinth. The first palynological results point to increased AP percentages during marine intervals (interglacials), however, further analyses and a higher temporal resolution are required to understand the vegetation response at orbital and sub-orbital time scales. Quercus dominates the deciduous trees percentages, but other mesophilous trees such as Corylus, Ulmus, Carpinus, Tilia, and Acer are also encountered. Cedrus appears to be the dominant conifer tree in the older part of the sequence, while Abies in the upper. Relict pollen taxa (e.g. Carya, Pterocarya, and Liquidambar) were also encountered in the sequence. Steppic elements (e.g., Artemisia and Ephedra) are more abundant during isolated/semi-isolated intervals (glacials) and suggest the occurrence of a rather open landscape. Mediterranean sclerophyllous vegetation increases towards the top of the sequence, depicting the significant role of Mediterranean maquis in the modern vegetation surrounding the Gulf of Corinth.

Combined multiproxy results produced during the onshore phase showed the existence of significant variations in sedimentation rates in the Corinth Gulf basin between glacial and interglacial periods. These findings confirm the dominant role of Quaternary climate forcing and eustatic sea level fluctuations in shaping the paleoenvironment in the Corinth Gulf basin. Analyses of M0079 sediments revealed that during glacial periods sedimentation rates were 2 to 7 times higher than during interglacial periods (McNeill *et al.,* 2019b). Higher sedimentation rates during glacials are most likely associated with increased erosion and runoff driven by the decrease and change of vegetation cover during the glacial, also observed in other existing long Mediterranean palaeovegetation records (Sadori *et al., 2016*; Tzedakis *et al.*, 2006).

This new high-resolution palaeoenvironmental and palaeoclimatic sedimentary record can provide new insights to the the long-term vegetation dynamics in response to glacial/interglacial cycles during the last ~1Ma. Situated at a key location at the southernmost tip of the Balkan Peninsula, the Corinth Rift deposits have the potential to be an invaluable palaeo-archive that will improve our understanding concerning the the evolution of marine and terrestrial ecosystems in the Mediterranean and allow to infer lead and lag relationships between the land and sea ecosystem response.

References

McNeill, L.C., Shillington, D.J., Carter, G.D.O., and the Expedition 381 Participants, 2019a. Corinth Active Rift Development. Proceedings of the International Ocean Discovery Program, 381: College Station, TX (International Ocean Discovery Program). https://doi.org/10.14379/iodp.proc.381.101.2019

McNeill, L.C., Shillington, D.J., Carter, G.D.O., Everest, J., Gawthorpe, R., Miller, C., Phillips, M., Collier, R., Cvetkoska, A., De Gelder, G., Diz Ferreiro, P., Doan, M.-L., Ford, M., Geraga, M., Gillespie, J., Hemelsdael, R., Herrero-Bervera, E., Ismaiel, M., Janikian. L., Kouli, K., Le Ber, E., Li, S., Maffione, M., Mahoney, C., Machlusm M.L., Michas, G., Nixon, C., Oflaz, S.A., Omale, A.P., Panagiotopoulos, K., Pechlivanidou, S., Sauer, S., Seguin, J., Sergiou, S., Zhakarova, N., Green, S., 2019b. High-resolution record reveals climate-driven environmental and sedimentary changes in an active rift. Scientific Reports 9, 3116.

Nixon, C.W., McNeill, L.C., Bull, J.M., Bell, R.E., Gawthorpe, R.L., Henstock, T.J., Christodoulou, D., Ford, M., Taylor, B., Sakellariou, D., Ferentinos, G., Papatheodorou, G., Leeder, M.R., Collier, R.E.L., Goodliffe, A.M., Sachpazi, M., Kranis, H., 2016. Rapid spatiotemporal variations in rift structure during development of the Corinth Rift, central Greece. Tectonics 35, 1225-1248.

Sadori, L., Koutsodendris, A., Masi, A., Bertini, A., Combourieu-Nebout, N., Francke, A., Kouli, K., Joannin, S., Mercuri, A.M., Panagiotopoulos, K., Peyron, O., Torri, P., Wagner, B., Zanchetta, G., Donders, T.H., 2016. Pollen-based paleoenvironmental and paleoclimatic change at Lake Ohrid (SE Europe) during the past 500 ka. Biogeosciences 13, 1423–1437.

Shillington, D.J., McNeill, L.C., Carter, G.D.O., and the Expedition 381 Participants, 2019. Expedition 381 Preliminary Report: Corinth Active Rift Development. International Ocean Discovery Program. https://doi.org/10.14379/iodp.pr.381.2019

Tzedakis, P.C., Hooghiemstra, H., Pälike, H., 2006. The last 1.35 million years at Tenaghi Philippon: revised chronostratigraphy and long-term vegetation trends. Quaternary Science Reviews 25, 3416–3430.

Watkins, S.E., Whittaker, A.C., Bell, R.E., McNeill, L.C., Gawthorpe, R.L., Brooke, S.A.S., Nixon, C.W., 2018. Are landscapes buffered to high-frequency climate change? A comparison of sediment fluxes and depositional volumes in the Corinth Rift, central Greece, over the past 130 k.y.. GSA Bulletin 131 (3-4), 372–388.

IODP Expedition 381: Development of the active Corinth Rift

K. Kouli[1], M. Geraga[2], G. Michas[3], K. Panagiotopoulos[4], S. Pechlivanidou[5], S. Sergiou[2], J. Everest[6], G. Carter[6], D. Shillington [7], L. McNeill[8] and Expedition 381 Scientists

(1) Department of Geology and Geoenvironment, National and Kapodistrian University of Athens, Greece, akouli@geol.uoa.gr
(2) Department of Geology, University of Patras, Greece
(3) Institute of Geology and Mineralogy, University of Cologne, Germany
(4) Department of Earth Science, University of Bergen, Norway
(5) Laboratory of Geophysics and Seismology, TEI Crete, Greece
(6) ECORD Science Operator, British Geological Survey, Lyell Centre, United Kingdom
(7) Lamont-Doherty Earth Observatory, Columbia University, Palisades NY, USA
(8) Ocean and Earth Science, University of Southampton, United Kingdom

International Ocean Discovery Program (IODP) Expedition 381 was operated as a Mission Specific Platform onboard the industry drilling vessel Fugro Synergy between October and December 2017 in the Gulf of Corinth, Greece. The objective of the expedition was to retrieve a record of early continental rifting and basin evolution from the Corinth rift in order to:

- obtain high spatial and temporal resolution records of the dynamics of the rifting process and its evolution,
- study the interaction of climate and tectonics on sedimentary and surface processes in a rift zone,
- generate a new high-resolution Quaternary paleoenvironment and palaeoclimate record from an active basin, and
- to improve regional hazard assessments in one of the most seismically active regions of Europe.

The Corinth Rift, one of Europe's most seismically active areas, is a region of rapid, localised extension, exhibiting today some of the highest extension rates in the world. The young rift (~5 Ma) has evolved in 3 main phases identified by integration of onshore depositional records and offshore seismic stratigraphy (e.g. Leeder *et al.*, 2002; Lykousis *et al.*, 2007; Ford *et al.*, 2013; Nixon *et al.*, 2016; Gawthorpe *et al.*, 2017). Corinth's high rates of tectonic activity, high sediment fluxes, closed drainage system and preservation of the syn-rift record make it a unique laboratory for the study of extension, sedimentation and paleoenvironment in a young rift.

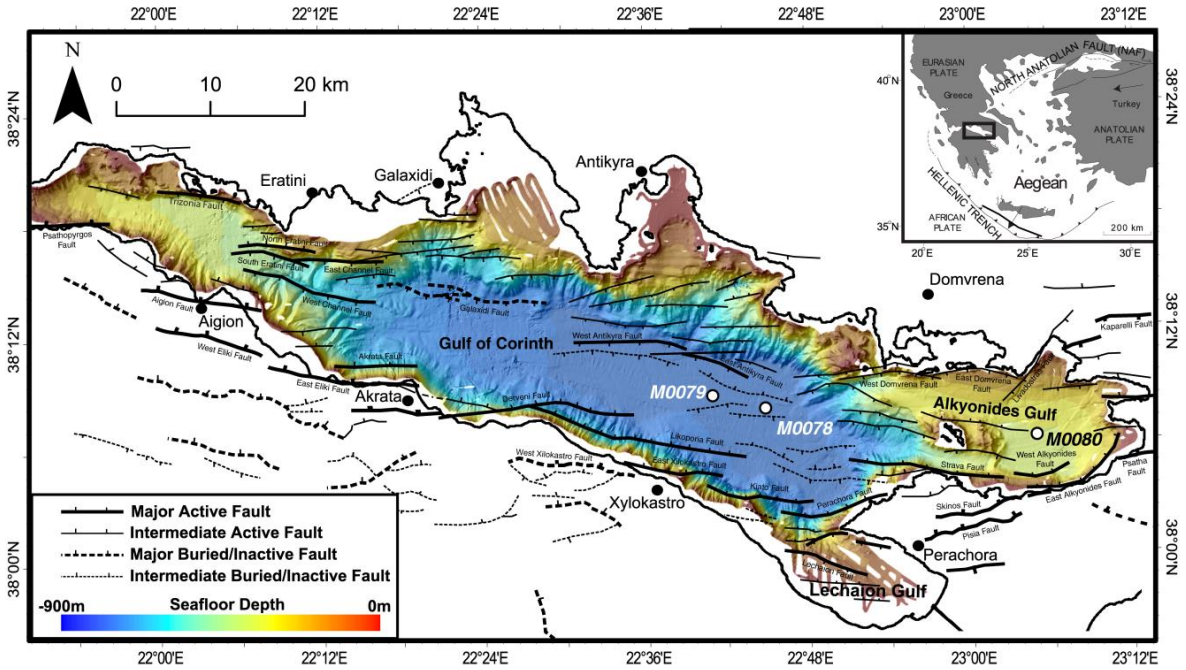

Figure 1: Bathymetric map showing the locations of the three sites drilled during the IODP Expedition 381. Sites M0078 and M0079 are located in the central basin, while site M0080 is in the east in the Alkyonides Gulf. (Shillington *et al.*, 2019). Offshore fault traces taken from Nixon *et al.* (2016). Onshore fault traces are derived from Ford et al. (2007, 2013) and Skourtsos and Kranis (2009). Inset: tectonic setting of Corinth rift in Aegean region, Eastern Mediterranean Sea. Bathymetry data provided by the Hellenic Centre for Marine Research and collected for R/V *Aegaeo* cruises (Sakellariou *et al.*, 2007).

During IODP Exp. 381, three sites (Figure 1) located along the Gulf of Corinth, were drilled, sampled and logged. A total of 1645 m of sediments were retrieved from 1900 m of cored section (an average recovery of 86%), sampling in high resolution the syn-rift sedimentary sequence back to ~1.5 Ma or more. During the onshore phase that took place in Bremen, Germany in February 2018, 35 scientists from 10 countries described, sampled and analyzed the recovered deposits and data (McNeill et al., 2019a). Cores recovered together provide (1) a longer rift history (Sites M0078 and

M0080), (2) a high resolution record of the most recent phase of rifting (Site M0079), and (3) the spatial variation of rift evolution (all sites; Shillington *et al.*, 2019; McNeill et al., 2019a). The deposits contain a rich and complex record of changing sedimentation, sediment and pore water geochemistry, and environmental conditions from combined micropaleontological and palynological assemblages. This is the longest and highest resolution sedimentary record from a young extensional basin at the point of connection to the global oceans, and it provides the first constraints on the age of the full rift sequence, syn-rift stratigraphy, rates and timings of rift tectonic processes, sediment fluxes and basin environmental conditions.

First results produced during the onshore phase confirmed the basin environment fluctuations between marine conditions during eustatic highstands and isolated conditions during eustatic lowstands - when the basin was cut off by basin-bounding sills. During interglacials, when the basin was connected with the Mediterranean Sea, sedimentation rates were lower, and bioturbation and organic carbon concentration higher. During glacials, the basin was isolated from the ocean, and sedimentation rates were 2 to 7 times higher than during interglacials (McNeill *et al.*, 2019b). The higher sedimentation rates during glacials may signify increased erosion and basin sediment influx driven by the decrease and change of vegetation cover during the glacial, as also recorded in other existing long Mediterranean palaeovegetation records (Sadori *et al., 2016*; Tzedakis *et al.*, 2006).

Post-cruise analysis of the IODP Exp. 381 data will allow the investigation of the relative roles of and feedbacks between tectonics, climate, and eustasy in sediment flux and basin evolution. Furthermore, the Corinth rift boreholes will provide the first long Quaternary record of Mediterranean-type climate in the region. The potential range of scientific applications for this unique data set is very large, encompassing tectonics, sedimentary processes, paleoenvironment, paleoclimate, paleoecology, geochemistry, and geohazards.

References

Ford, M., Rohais, S,, Williams, E.A., Bourlange, S., Jousselin, D., Backert, N., Malartre, F., 2013. Tectono-sedimentary evolution of the western Corinth rift (Central Greece). Basin Research 25, 3-2.

Ford, M., Williams, E.A., Malartre, F., Popescu, S.M., 2007. Stratigraphic architecture, sedimentology and structure of the Vouraikos Gilbert-type delta, Gulf of Corinth, Greece. in: Paola, C., Nichols, G.J., Williams, E.A. (Eds.), Spec. Publ. Int. Assoc. Sedimentologists, Blackwell, 44-90.

Gawthorpe, R.L., Leeder, M.R., Kranis H., Skourtsos, E., Andrews, J.E., Henstra, G.A., Mack, G.H., Muravchik, M., Turner, J.A., Stamatakis, M., 2017. Tectono-sedimentary evolution of the Plio-Pleistocene Corinth rift, Greece. Basin Research 30, 448-479.

Leeder, M., Collier, R., Abdul Aziz, L.H., Trout, M., Ferentinos, G., Papatheodorou, G., Lyberis, E., 2002. Tectono-sedimentary processes along an active marine/lacustrine half-graben margin: Alkyonides Gulf, E. Gulf of Corinth, Greece. Basin Research 14, 25-41

Lykousis, V., Sakellariou, D., Moretti, I., Kaberi, H., 2007. Late Quaternary basin evolution of the Gulf of Corinth: Sequence stratigraphy, sedimentation, fault slip and subsidence rates: Tectonophysics 440, 29-51.

McNeill, L.C., Shillington, D.J., Carter, G.D.O., and the Expedition 381 Participants, 2019a. Corinth Active Rift Development. Proceedings of the International Ocean Discovery Program, 381: College Station, TX (International Ocean Discovery Program). https://doi.org/10.14379/iodp.proc.381.101.2019

McNeill, L.C., Shillington, D.J., Carter, G.D.O., Everest, J., Gawthorpe, R., Miller, C., Phillips, M., Collier, R., Cvetkoska, A., De Gelder, G., Diz Ferreiro, P., Doan, M.-L., Ford, M., Geraga, M., Gillespie, J., Hemelsdael, R., Herrero-Bervera, E., Ismaiel, M., Janikian. L., Kouli, K., Le Ber, E., Li, S., Maffione, M., Mahoney, C., Machlusm M.L., Michas, G., Nixon, C., Oflaz, S.A., Omale, A.P., Panagiotopoulos, K., Pechlivanidou, S., Sauer, S., Seguin, J., Sergiou, S., Zhakarova, N., Green, S., 2019b. High-resolution record reveals climate-driven environmental and sedimentary changes in an active rift. Scientific Reports 9, 3116.

Nixon, C.W., McNeill, L.C., Bull, J.M., Bell, R.E., Gawthorpe, R.L., Henstock, T.J., Christodoulou, D., Ford, M., Taylor, B., Sakellariou, D., Ferentinos, G., Papatheodorou, G., Leeder, M.R., Collier, R.E.L., Goodliffe, A.M., Sachpazi, M., Kranis, H., 2016. Rapid spatiotemporal variations in rift structure during development of the Corinth Rift, central Greece. Tectonics 35, 1225-1248.

Sadori, L., Koutsodendris, A., Masi, A., Bertini, A., Combourieu-Nebout, N., Francke, A., Kouli, K., Joannin, S., Mercuri, A.M., Panagiotopoulos, K., Peyron, O., Torri, P., Wagner, B., Zanchetta, G., Donders, T.H., 2016. Pollen-based paleoenvironmental and paleoclimatic change at Lake Ohrid (SE Europe) during the past 500 ka. Biogeosciences 13, 1423–1437.

Sakellariou, D., Lykousis, V., Alexandri, S., Kaberi, H., Rousakis, G., Nomikou, P., Georgiou, P., Ballas, D., 2007, Faulting, seismic-stratigraphic architecture and late Quaternary evolution of the Gulf of Alkyonides basin – East Gulf of Corinth, Central Greece. Basin Research 19, 273-295.

Shillington, D.J., McNeill, L.C., Carter, G.D.O., and the Expedition 381 Participants, 2019. Expedition 381 Preliminary Report: Corinth Active Rift Development. International Ocean Discovery Program. https://doi.org/10.14379/iodp.pr.381.2019

Skourtsos, E., Kranis, H., 2009. Structure and evolution of the western Corinth Rift, through new field data from the Northern Peloponnesus. in: Ring U. and Wernicke B. (Eds.), Extending a Continent: Architecture, Rheology and Heat Budget. Geological Society London, Special Publication 321, 119-138.

Tzedakis, P.C., Hooghiemstra, H., Pälike, H., 2006. The last 1.35 million years at Tenaghi Philippon: revised chronostratigraphy and long-term vegetation trends. Quaternary Science Reviews 25, 3416–3430.

15th International Congress of the Geological Society of Greece
Athens, 22-24 May, 2019 | Harokopio University of Athens, Greece
Bulletin of the Geological Society of Greece, Sp. Pub. 7 Ext. Abs. GSG2019-245

Geochemical Distribution and Foraminiferal Analysis from a Basin in SE Aegean Sea

C. Kozanoglou[1], G. Rousakis[1], M. Geraga[2], G. Papatheodorou[2], A. Arabas[3], A. Gogou[1], C. Parinos[1], M. Triantaphyllou[4]

(1) Hellenic Centre for Marine Research, Institute of Oceanography, 19013 Anavyssos, Attiki, Greece, ckozanoglou@yahoo.gr
(2) Laboratory of Marine Geology and Physical Oceanography, Department of Geology, University of Patras, 26100, Rion-Patra, Greece
(3) Institute of Geological Sciences, Polish Academy of Sciences, Research Centre in Kraków, ul. Senacka 1, Kraków 31-002, Poland
(4) Faculty of Geology and Geoenvironment, National and Kapodistrian University of Athens, Panepistimioupolis 15784, Athens, Greece

Introduction

This study concerns an area located in the basin between Tilos and Symi, near Kos and Rhodes, southeast Aegean Sea, in the SE Mediterranean (Figure 1). The Aegean Sea is distant and almost isolated from the North Atlantic oceanic circulation and is considered a key region as it reflects high and low latitude climate changes, through an intense atmospheric connection. Reconstructions of climate during the Holocene have revealed the occurrence of determining episodes of severe cooling also on multi-centennial to millennial timescales (Rohling et al., 2002; Casford et al., 2003). The study area is also near the Rhodes gyre where formation of Levantine intermediate waters occurs. Here we present high resolution measurements of organic carbon Corg, nitrogen Ntot concentrations and micropaleaontological results focusing on planktonic foraminifera during the S1 deposition. Sapropel S1, deposited during the Holocene Climate Optimum is characterized by strongly dysoxic conditions punctuated by reventilation events in the Aegean sea (e.g., Abu-Zied et al., 2008; Filippidi et al., 2016).

Material and methods

The chronostratigraphy of the studied core is based on accelerator mass spectroscopy (AMS) ^{14}C dating performed on planktonic foraminiferal assemblages. Core ST5 (3.81 m long) retrieved from 688 m depth, has been photographed and visually described. Samples for organic carbon and nitrogen analysis were collected with 0.5–4 cm resolution. Samples for planktonic foraminiferal analysis were separated at a high resolution sampling interval of 0.5 cm, were disaggregated using hydrogen peroxide and then wet sieved through a 125 μm mesh. The dried material was split into aliquots using an Otto microsplitter. At least 200 specimens were picked and identified for each sample. In all, 35 samples were collected for stable isotope analyses ($\delta^{18}O$) using the tests of the handpicked planktonic foraminifera *Globigerinoides ruber*.

Results and Discussion

The core ST5 contains a dark color mud that corresponds to sapropel S1 consisting of two discrete layers, the lower layer S1a and the upper layer S1b which are separated by the lighter-colored S1 interruption.

The organic carbon values downcore fluctuate and suggest that subtle changes actually occur during the deposition period. The lower part (S1a) and the upper part of the sapropel (S1b) have similar Corg average concentrations (1.2%) while the interruption interval has an average Corg=0.7%. High organic carbon content in sapropels shows an increase in primary productivity due to enhanced nutrient availability.

The ratio Corg/Ntot in S1a, S1b and Si is respectively 11.6, 10.3 and 9.7. Above S1 we calculated a Corg/Ntot=9.3 and below S1 the ratio increased to 9.9. The difference in Corg/Ntot ratios between sapropels and background sediments could indicate changes in the source of organic matter: algal or land-plant derived organic matter (Arnaboldi et al., 2006; Gogou et al., 2007). The study includes qualitative and quantitative analysis of planktonic foraminifera as the composition of their assemblages reflects water mass conditions (e.g., Casford et al., 2003). The benthic foraminifera are very good indicators of conditions prevailing in the sea bottom (dysoxic /anoxic) and the water masses circulation. In each sample we determined the abundances and some key benthic foraminifera groups.

The determined planktonic foraminiferal assemblages are composed mostly of *Globigerinoides ruber* (*alba* and *rosea*), *Globigerina bulloides, G. falconensis, Globigerinella calida, G. siphonifera, Globigerinita glutinata, G. uvula, Globigerinoides conglobatus, G. sacculifer, G. trilobus, Globorotalia inflata, Gl. truncatulinoides,Globoturborotalita rubescens, Hastigerina, Neogloboquadrina incompta, N. dutertrei, N. pachyderma, Orbulina universa, Turborotalita quinqueloba.* The species belonging to the SPRUDTS group (Rohling et al., 1997) and *G. ruber* (*alba* and *rosea*) dominate warm and oligotrophic summer mixed layers in subtropical regions and the eastern Mediterranean and consequently the downcore variation of their percentages is considered an indicator of SST variability (Pujol et al., 1995; Triantaphyllou et al., 2016). The warm planktonic foraminifera group ranges from 41 to 65% during the S1a deposition, while it varies in-between 54 and 89% within the S1b deposition interval.

Above the sapropel, the planktonic foraminifera abundance pattern reveals at least two distinct episodes of successive increased and decreased warm water species abundances. This observation due to a high resolution analysis may capture and reveal more detailed information for climatic changes in the area and consequently needs further investigation compiled with the δO^{18} measurements on *Globigerinoides ruber* tests.

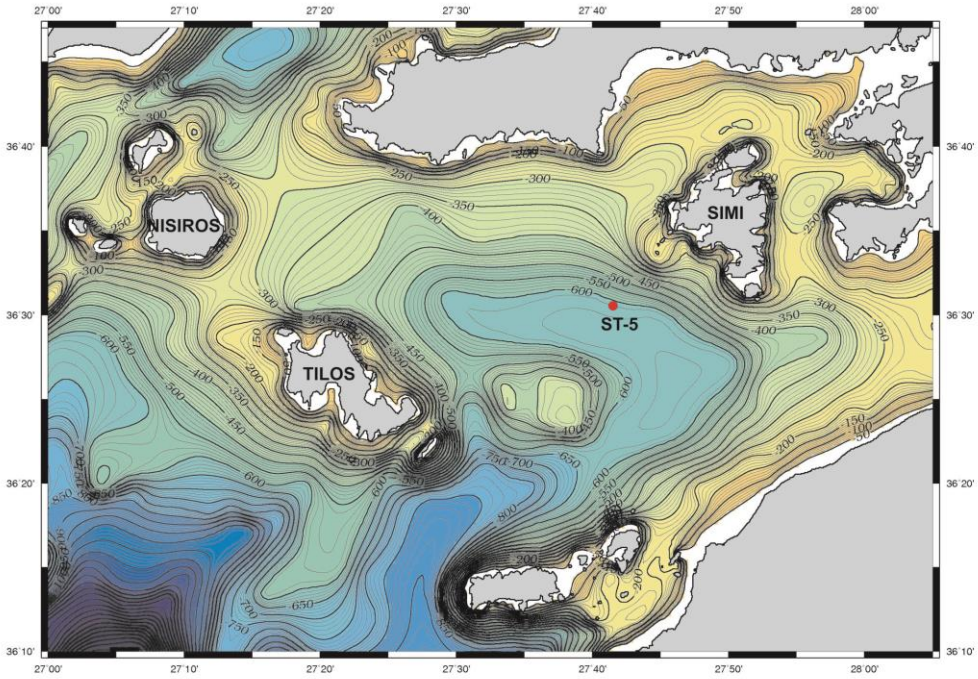

Figure 1. Conventional bathymetry of the Nisyros – Tilos – Symi – Chalki region and location of the studied core.

Acknowledgements

The authors sincerely acknowledge Dr. V. Lycousis for his precious and constructive scientific support.

References

Rohling, E.J., Jorissen, F.J., De Stigter, H.C., 1997. 200 Year interruption of Holocene sapropel formation in the Adriatic Sea. J. Micropalaeontol. 16, 97–108.

Rohling, E.J., Mayewski, P.A., Hayes, A., Abu-Zied, R.H., Casford, J.S.L., 2002. Holocene atmosphere-ocean interactions: records from Greenland and the Aegean Sea. Clim. Dyn. 18, 587–593.

Casford, J.S.L., Rohling, E.J., Abu-Zied, R.H., Jorissen, F.J., Leng, M., Thomson, J., 2003. A dynamic concept for eastern Mediterranean circulation and oxygenation during sapropel formation. Palaeogeogr. Palaeoclimatol. Palaeoecol. 190, 103–119.

Abu-Zied, R.H., Rohling, E., Jorissen, F.J., Fontanier, C., Casford, J.S.L., Cooke, S., 2008. Benthic foraminiferal response to changes in bottom-water oxygenation and organic carbon flux in the eastern Mediterranean during LGM to Recent times. Mar. Micropaleontol. 67, 46–68

Arnaboldi, M., Meyers, P.A., 2006. Patterns of carbon and nitrogen stable isotopic compositions of latest Pliocene sapropels from six locations across the Mediterranean. Palaeogeog. Palaeoclimatol. Palaeoecol. 235, 149–167.

Filippidi, A., De Lange, G, Triantaphyllou, M.V., 2016…

Gogou, A., Bouloubassi, I., Lykousis, V., Arnaboldi, M., Gaitani, P., Meyers, P.A., 2007. Organic geochemical evidence of abrupt late glacial-Holocene climate changes in the North Aegean Sea. Palaeogeogr. Palaeoclimatol. Palaeoecol. 256, 1–20

Pujol, C., Vergnaud-Grazzini, C., 1995. Distribution of live planktic foraminifers as related to regional hydrography and productive systems of the Mediterranean Sea. Mar. Micropaleontol. 25, 187–217

Triantaphyllou, M.V., Gogou, A., Dimiza, M.D., Kostopoulou, S., Parinos, C., Roussakis, G., Geraga, M., Bouloubassi, I., Fleitmann, D., Zervakis, V., Velaoras, D., Diamantopoulou, A., Sampatakaki, A., Lykousis, V., 2016. Holocene climatic optimum centennial-scale paleoceanography in the NE Aegean (Mediterranean Sea). Geo-Mar. Lett. 36, 51-66.

15th International Congress of the Geological Society of Greece
Athens, 22-24 May, 2019 | Harokopio University of Athens, Greece
Bulletin of the Geological Society of Greece, Sp. Pub. 7 Ext. Abs. GSG2019-257

Pleistocene Palaeogeography and Palaeolithic Archaeology: The Tectonically Active North Aegean Sea Case Study

D. Papanikolaou[1], P. Nomikou[1], I. Papanikolaou [2], M. Triantaphyllou[1], N. Galanidou[3], M. Dimiza[1], C. Tzedakis[4]

(1) Department of Geology and Geoenvironment, National and Kapodistrian University of Athens, Panepistimioupolis, 15784 Athens, Greece, mtriant@geol.uoa.gr
(2) Laboratory Mineralogy-Geology, Agricultural University of Athens, Iera Odos 75,11855 Athens, Greece
(3) Department of History & Archaeology, University of Crete, University Campus Gallou, Rethymno, 74100, Greece
(4) Environmental Change Research Centre, Department of Geography, University College London, London WC1E 6BT, UK

Introduction

The Aegean area was part of the Hellenic orogenic system throughout the early Tertiary with continuous landmasses between mainland Greece and Western Anatolia. This continental status, known by Philippson as "Agaeis" (Philippson, 1901), lasted until the late Miocene, when mammal migrations of the 'Pikermi' fauna (*Hipparion* as characteristic fossil) occurred. At this period, the last Tethyan oceanic remnant of the Ionian Basin entered the Hellenic subduction zone and resulted in the acceleration of the African plate subduction (from 1 to 5 cm/year) and created the individualization of the Aegean microplate, south of the North Aegean Basin (e.g., Royden and Papanikolaou, 2011). The above geodynamic change gradually produced a thinning of the Aegean continental crust causing subsidence, which became more extensive during the Quaternary. Data based on lithoseismic profiles in the North Aegean (Skyros Basin) indicate that towards the Skyros and Limnos Platform there is no sedimentary cover or a very thin cover (e.g of several tens of meters) resting on top of the Alpine basement. According to published sedimentation rates obtained from coring, the older sediments might extend back to 400-500 Ka in extended areas of the Central - North Aegean Sea (Papanikolaou *et al*., 2019). The availability of high resolution bathymetric and seismic reflection data revealed that several of North Aegean islands would be connected by stretches of land allowing terrestrial animals to travel between them. The existence of such land passages would have affected connectivity and thus biodiversity and colonization rhythms. The overall aim of this study is to provide a synthesis of the North Aegean palaeogeography during the Pleistocene and examine its role as a southeastern entrance to hominin movements out of Asia and into Europe and subsequent occupations and migrations.

State-of-the art

New high resolution bathymetric and seismic reflection data, bolstered with tectonic data on active faults have enriched our understanding of the palaeogeography of the North Aegean. Regional subsidence rates at the Aegean margins during the last 400 Ka have been investigated using high-resolution seismic reflection profiles, indicating a gradual process, based on successive glacial sea-level lowstand systems of Marine Isotope Stages (MIS) 2, 6, 8, 10 and probably 12 (Lykousis, 2009). Higher subsidence rates were calculated for MIS 12–8 at the North Aegean margins (1.46–1.88 m/Ka) whereas sedimentological and mineralogical analyses in commercial boreholes in the northern Aegean revealed sediment deposition under riverine-lake conditions throughout the Pliocene and the Early Pleistocene.

In world prehistory, the questions of geography and process of the first penetrations to Europe by late Early Pleistocene hominins and later colonization by Middle Pleistocene hominins remain wide open. In Iberia, several pre-1 Ma and post-1 Ma archaeological sites indicate a very early presence of hominin groups. By comparison, the very sparse and contested Balkan archaeological record from the same periods meant that, until recently, the role of the Balkan Peninsula as a gateway to Europe has been unclear. The question became all the more pressing by the discovery a *Homo erectus* skull near Kocabaş in the province of Denizli, Aegean Turkey, dating to around 1.1 Ma.

Results and Discussion

More recently, archaeological work at Rodafnidia, Lisvori, near the Gulf of Kalloni on the island of Lesbos, ~300 km to the west of Kocabaş, returned absolute dates and evidence of Middle Pleistocene hominin activity from ~500 ka (Galanidou *et al*., 2013). The archaeological variability has indicated repeated hominin occupations on Lesbos over long periods of time from at least the early stages of the Middle Pleistocene. The stone tools from the site belong to the Acheulean and have close industrial affinities with material excavated at Gesher Benet Y'aaqov on the bank of the Jordan River in northern Israel, which dates to 800 Ka and the lower strata at Kaletepe Deresi 3 on a seasonal drainage in the Göllüdağ area near Cappadocia. The verterbrate palaeontology of Lesbos (Villanfrancian fauna) suggests that animal crossings from Anatolia to the Aegean began much earlier. Two possible, though not mutually exclusive, routes for early hominin dispersals from Anatolia to Europe therefore emerge: through the, inadequately explored, northern Balkan territories, or through a southern route in the North Aegean. Thus, the extensive submerged landscapes of the Aegean hold clues to understanding the early Pleistocene hominin expansions 'Out of Asia' into Europe.

A second issue concerns the situation after the submergence of the N. Aegean, when migrations depended on land connections exposed during glacial sea-level lowstands. These coastal landscapes may have provided relatively fertile and productive refugia for plants, land mammals and hominins. The Palaeolithic sites discovered in the last 20 years on the islands of Crete, Thasos, Limnos, the Inner Ionian Archipelago and Lesbos suggest that land-bridge crossings become more frequent in the late Middle and Late Pleistocene, as glacial lowstands reached ~120 m below present.

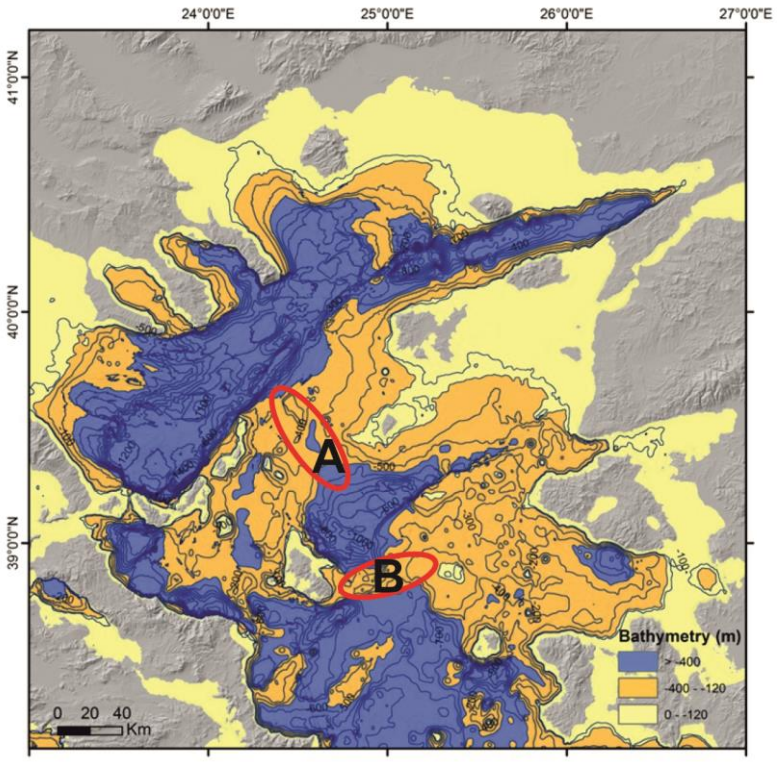

Fig.1 Bathymetric map of the North Aegean area showing the areas: 0-120 m depth, where the paleocoastline was located 20 Ka ago during MIS 2, 120-400 m depth, where palinspastic tectonics show the existence of land bridges during MIS 4, 6 and 8, and depths more than 400 m, where palinspastic tectonics show the existence of marine basins.

Some answers related to the questions on the evidence for land bridges during glacial sea-level lowstands of the late Middle and Late Pleistocene and their importance for human migrations may be obtained from the study of the North Aegean Sea and especially of the Northern Sporades - Limnos platform, which might serve as a major land bridge from Northwestern Anatolia to southeast Thessaly (Fig. 1, area A). Here the maximum depth is about 350 m, between the islands of Aghios Efstratios and Kyra Panagia - Youra. Another probable land bridge might have been south of the Skyros Basin, between Lesbos and Skyros – Evia, where the maximum depth is around 250m (Fig. 1, area B). The study of the active faults surrounding this area of the two North Aegean platforms has shown that the fault throws are several hundred m or even more than 1.0 –1.5 km. Especially in the case of area B the NW-SE faults forming a graben structure with fault lengths more than 8–11 km east of Skyros Island have probably caused the tectonic subsidence of the platform to 250 m depth. Taking into account the available chronological data in combination with the available sedimentation rates we may conclude that several active faults have been activated during the last 200–400 Ka, with slip rates ranging around 3mm/yr. Thus, the presently maximum depths within the North Aegean platforms did not exist during the previous lowstands in MIS 4, 6 and 8.

In conclusion, land bridges between the western coastlines of Minor Asia and the eastern coastlines of continental Greece probably existed during the lowstands of MIS 4, 6 and 8, due to the regional subsidence combined with the tectonic subsidence caused by the normal/oblique faulting especially of the NW-SE trending faults within the platform areas (Papanikolaou *et al*., 2019). Thus, hominin migrations were possible through the North Aegean until the late most Middle Pleistocene around 140 Ka.

References

Philippson, A., 1901. Beitrage zur Morphologie Griechenlands. Geogr. Abh. 3, 1-96.

Galanidou, N., Cole, J., Iliopoulos, G., McNabb, J. 2013. East meets west: the Middle Pleistocene site of Rodafnidia on Lesvos, Greece. Antiquity 87(336).

Lykousis, V., 2009. Sea-level changes and shelf break prograding sequences during the last 400ka in the Aegean margins: subsidence rates and palaeogeographic implications. Continental Shelf Research 29(16), 2037-2044.

Royden, L.H., Papanikolaou, D.J., 2011. Slab segmentation and late Cenozoic disruption of the Hellenic arc. Geochem. Geophys. Geosyst. 12, Q03010, doi: 10.1029/2010GC003280.

Papanikolaou, D., Nomikou, P., Papanikolaou, I., Lampridou D., Rousakis, G., Alexandri, M., 2019. Active Tectonics and Seismic Hazard in Skyros Basin, North Aegean Sea, Greece. Marine Geology 407, 94–110.

15th International Congress of the Geological Society of Greece
Athens, 22-24 May, 2019 | Harokopio University of Athens, Greece
Bulletin of the Geological Society of Greece, Sp. Pub. 7 Ext. Abs. GSG2019-273

Multi-proxy Analysis of the Corinth Isthmus Pleistocene Sediments: a case study of paleoenvironmental reconstruction in a tectonically active domain

A. Pallikarakis[1], M. Triantaphyllou[2], I. Papanikolaou[1], M. Dimiza[2], K. Reicherter[3], G. Migiros[1]

(1) Laboratory Mineralogy - Geology, Department of Natural Resources Management & Agricultural Engineering, Agricultural University of Athens, Athens, Greece, agpall@aua.gr
(2) Hist. Geology-Paleontology Department, Faculty of Geology and Geoenvironment, National and Kapodistrian University of Athens, Athens, Greece
(3) Institute of Neotectonics and Natural Hazards, RWTH Aachen University, Aachen, Germany

Introduction

Fossil associations are an essential tool for studying past sea-level changes in coastal areas (e.g. Pallikarakis *et al*., 2018). The Corinth Isthmus located at the eastern part of Corinth Gulf is influenced both by glacioeustatic sea level changes and tectonic movements, resulting into a complex lithostratigraphic pattern (e.g. Freyberg, 1973; Collier, 1990; Pallikarakis *et al*., 2018). The study area is controlled by major fault structures such as the South Alkyonides fault zone, the Loutraki, the Agios Vassileios and the Kenchreai faults and by shorter local faults, like the Kalamaki–Isthmia fault (e.g. Roberts *et al*., 2009; Papanikolaou *et al*., 2015). As a result the Corinth Isthmus is constantly uplifted 0.3 mm/yr during at least the last 200 ka (Collier *et al*., 1992; Dia *et al*., 1997). The sedimentary facies in Corinth Isthmus consists of marls, sandstones and conglomerates representing offshore, shoreface and coastal paleoenvironments, organized in six transgressive-regressive cycles ranging from marine isotope stages 11 to 5 (e.g. Freyberg, 1973; Collier, 1990; Pallikarakis *et al*., 2018).

Materials and Methods

An approximately 70 m deep borehole core (Bh-3) extracted at 19.20 m above the present sea level, is characterized by lithological alternations of clay, marl clayey sand, sand, sandstone, conglomerate and soil horizons reflecting low-energy to high-energy depositional environments. Fifty five samples extracted from the sedimentary sequence have been analyzed for their micropaleontological content, following standard procedures (e.g. Triantaphyllou *et al.*, 2010). Foraminiferal species have been subjected into two-way cluster analysis to highlight biofacies. Thirteen samples of fine-grained sediments were examined by Scanning Electron Microscopy (SEM) for their calcareous nannoplankton content. Furthermore magnetic susceptibility (MS) within the core was measured with the Bartington MS2 system with the MS2K sensor, where sixty one MS measurements have been carried out from various lithological alternations within the core.

Results and Discussion

Fourteen benthic foraminiferal taxa comprised more than 90% of the total assemblage (e.g. *Ammonia* spp., *Elphidium* spp., *Discorbis* spp., *Asterigerinata* spp., miliolids). Based on the microfossils analysis three distinctive clusters have been described as separate biofacies. Cluster I indicated shallow marine assemblage (regional estimated sea paleodepth ~40 m), Cluster II indicated lagoon assemblage (regional estimated sea paleodepth ~0-20 m) and Cluster III was associated with a shallow marine assemblage with fresh water influence (regional estimated sea paleodepth ~20-40 m). The identified calcareous nannoplankton specimens were dominated by the presence of small *Reticulofenestra* spp. (~40%) and small *Gephyrocapsa* spp. (~30%) coccoliths, while *Emiliania huxleyi* species was relatively scarce (5-8% of the total assemblage), but consistently present. Furthermore the magnetic susceptibility in Bh-3 sediments ranged from 1 to 207 ×10-5 (SI units), where clayey and fine coarse sediments displayed lower MS signal than gravely and coarse sediments.

Based on the lithological, microfaunal and MS analysis, the paleoenvironment and the palaeobathymetry within the borehole were interpreted, describing successions of lagoonal to shallow marine deposits (highstand) with terrestrial deposits (lowstand). Within the borehole core five successive sedimentary sequences have been defined, indicating the onset of transgressive-regressive (T-R) conditions. Correlating the glacioeustatic sea level change curve of Siddall *et al.* (2003) with the uplift rate 0.3 mm/yr for the Corinth Isthmus area (e.g. Collier *et al*., 1992; Dia *et al*., 1997), it appears that marine deposits would have been expected to be preserved during the high stands within MIS 5.5, 6.5, MIS 7 and MIS 9 with maximum depths ranging between ~20 and 80 m (e.g. Siddall *et al*., 2003), while the study area is expected to be emerged above sea level during MIS 2.21, MIS 6.0 and MIS 7.0. Transgressive stacking patterns therefore, would have been expected to be deposited during the high stands MIS 5.5, 6.5, 7, 9.

The continuous existence of *E. huxleyi* throughout the borehole core indicates that depositional ages are younger than 265 ka (e.g., Raffi *et al*., 2006), limiting the marine sedimentation to MIS 5.5, MIS 6.5 and MIS 7 high stands. Three possible scenarios can describe the sedimentation processes. In the first scenario, the entire sequence can be associated with the MIS 7 highstand, where marine sedimentation processes are interrupted by terrestrial sediments due to relative sea level fluctuations associated with the sub-stages MIS 7.1, 7.3, 7.4 and 7.5. In the second scenario the described sediments are correlated with MIS 5.5 and MIS 7, while the third scenario involves sedimentation in all three possible MIS periods (MIS5.5, MIS 6.5 and MIS 7). Scenarios 2 and 3 are relatively similar and can be distinguished only by absolute dating data. The third scenario is considered as the most favorable to describe the sedimentation processes based on the described sea water paleodepths within the core (Pallikarakis *et al*., 2018) and the modeled shoreline elevations described in Papanikolaou *et al*. (2015).

Conclusions

Through multi-proxy analysis of the borehole core the paleoenvironment has been described, where based on two way cluster analysis of the foraminiferal assemblages three distinct biofacies were described, Cluster I (shallow marine), Cluster II (lagoonal) and Cluster III (transition from lagoon to shallow marine conditions). The presence of *E. huxleyi* (NN21a biozone), indicates that Bh-3 sediments are younger than MIS 8. Based on the glacioeustatic sea level changes, along with the measured uplift rate of the area, MIS 7, MIS 5.5 and possible MIS 6.5 highstands are described in the eastern part of the Corinth Isthmus.

Acknowledgements

The Academy of Athens scholarship (Mitsopoulos Fund) is thanked for financial support.

References

Collier, R.E.L., 1990. Eustatic and tectonic controls upon Quaternary coastal sedimentation in the Corinth Basin, Greece. Journal of the Geological Society, 147, 301-314.

Collier, R.E.L.; Leeder, R.M.; Rowe, P., Atkinson, T., 1992. Rates of tectonic uplift in the Corinth and Megara basins, Central Greece. Tectonics, 11(6), 1159-1167.

Dia, A.N.; Cohen, A.S.; O'Nions, R.K., Jackson, J.A., 1997. Rates of uplift investigated through 230Th dating in the Gulf of Corinth (Greece). Chemical Geology, 138(3-4), 171-184.

Freyberg, V., 1973. Geologie des Isthmus von Korinth, Erlangen Geologische Ablhandlungen, Heft 95. Junge und Sohn, Universitats Buchdruckerei Erlangen,183p.

Pallikarakis, A., Triantaphyllou, M., Papanikolaou, I., Dimiza, M., Reicherter, K., Migiros, G., 2018. Age Constraints and Paleoenvironmental Interpretation of a Borehole Sedimentary Sequence at the Eastern Part of Corinth Isthmus, Greece. Journal of Coastal research, 34,3

Papanikolaou I.D.; Triantaphyllou, M.; Pallikarakis A., Migiros, G., 2015. Active faulting at the Corinth Canal based on surface observations, borehole data and paleoenvironmental interpretations. Passive rupture during the 1981 earthquake sequence?. Geomorphology, 237, 65-78

Raffi, I.; Backman, J.; Fornaciari, E.; Palike, H.; Rio, D.; Lourens, L., Hilgen, F., 2006. A review of calcareous nannofossil astrobiochronology encompassing the past 25 million years. Quaternary Science Reviews, 25(23), 3113–3137.

Roberts, G.P.; Houghton, S.L.; Underwood, C.; Papanikolaou, I.; Cowie, P.A.; van Calsteren, P.; Wigley, T.; Cooper, F.J., McArthur, J.M., 2009. Localization of Quaternary slip rates in an active rift in 105 years: an example from central Greece constrained by 234U-230Th coral dates from uplifted paleoshorelines. Journal of Geophysical Research, 114(B104). Doi:org/10.1029/2008JB0058.

Siddall, M.; Rohling, E.J.; Almogi-Labin, A.; Hemleben, Ch.; Meischner, D.; Schmelzer, I., Smeed, D.A., 2003. Sea-level fluctuations during the last glacial cycle. Nature, 423, 853-858.

Triantaphyllou, M.V.; Kouli, K.; Tsourou, T.; Koukousioura, O.; Pavlopoulos, K., Dermitzakis, M.D., 2010. Paleoenvironmental changes since 3000 BC in the coastal marsh of Vravron (Attica, SE Greece). Quaternary International, 216(1-2), 14-22.

15th International Congress of the Geological Society of Greece
Athens, 22-24 May, 2019 | Harokopio University of Athens, Greece
Bulletin of the Geological Society of Greece, Sp. Pub. 7 Ext. Abs. GSG2019-280

Living coccolithophores at an anthropogenically impacted neritic site of Thermaikos Gulf, NW Aegean Sea

M.D. Dimiza[1], M.V. Triantaphyllou[1], O. Koukousioura[2], I. Michailidis[2], V.-G. Dimou[2], V. Navrozidou[2], K. Aligizaki[3], M. Seferlis[4]

(1) Department of Geology and Geoenvironment, National and Kapodistrian University of Athens, Panepistimiopolis, 15784 Athens, Greece, mdimiza@geol.uoa.gr
(2) Aristotle University of Thessaloniki, School of Geology, Thessaloníki 541 24, Greece
(3) Aristotle University of Thessaloniki, School of Biology, Thessaloníki 541 24, Greece
(4) The Goulandris Natural History Museum, Greek Biotope/Wetland Centre, 57001 Thermi, Thessaloníki, Greece

Background

Coccolithophores constitute a significant component of the phytoplankton communities in the oligotrophic environments of the Aegean Sea, especially in the south Aegean (Ignatiades *et al.*, 2002; Triantaphyllou *et al.*, 2004). In particular, *Emiliania huxleyi* is a key taxon for the coccolithophore productivity in the marine environment of Aegean Sea, but also numerous species of *Syracosphaera* spp., Rhabdosphaeraceae and holococcolithophores show significant contributions mainly in relatively diverse summer assemblages (e.g., Triantaphyllou *et al.*, 2004; Malinverno *et al.*, 2009; Dimiza *et al.*, 2015; Karatsolis *et al.*, 2017; Skampa *et al.*, 2019). These studies showed that coccolithophore dynamics display a highly seasonal variability primarily driven by the local water circulation pattern, changes in temperature and nutrient availability. Despite the well-studied coccolithophore assemblages in various marine ecosystems of the Aegean Sea, little is known about the coccolithophore species composition and variability in anthropogenically impacted neritic regions. In a recent study on the late-winter coccolithophore assemblages from the industrial zone of Elefsis-Saronikos Gulf, Dimiza *et al.* (2014) reported significantly lower abundance and species diversity compared with off-shore assemblages of the Aegean Sea, with nearly monospecific assemblages of *Helicosphaera carteri*, which behaved like an opportunistic taxon.

Objectives

In the present study, we investigated the living coccolithophore abundance, community structure and key species of coccolithophores from a 12 monthly time series in the Thessaloniki Bay, a polluted bay located in the inner part of Thermaikos Gulf (Northwestern Aegean Sea). The aims of this research were to examine the seasonal variation of coccolithophorres and determine the effects of environmental factors on their abundance, species composition and distribution in a restricted environment with intense anthropogenic activity.

Materials and methods

The monitoring site is located near the outer edge of the Thessaloniki Bay (Inner Thermaikos Gulf), about 7 km south of the Thessaloniki city (station SP1: 40°35'11.72" N and 22°55'1.20" E) and is approximately 22 m in depth. Water samples have been collected by pumping, on a monthly basis between January and December 2016. During each sampling campaign, water temperature and salinity measurements were obtained with a CTD device. Monthly-averaged data for satellite chlorophyll a (Chl-*a*) concentration from MODIS-Aqua (MODerate resolution imaging spectroradiometer) were obtained from the National Aeronautic and Space Administration (NASA) Giovanni website (http://disc.sci.gsfc.nasa.gov/techlab/giovanni/).

Phytoplankton counts (cells, colonies, and filaments) were performed on subsample volume of 25 ml of seawater per sample using a Zeiss inverted light microscope (LM) following the sedimentation method described by Utermohöl (1958).

The coccolithophore composition and community structure was evaluated through Scanning Electron Microscopy. The samples were examined in a Jeol JSM 6360 Scanning Electron Microscope (SEM) (University of Athens, Faculty of Geology and Geoenvironment) and the coccospheres per liter was calculated following the methodology of Jordan and Winter (2000).

Results and Discussion

The sea surface temperatures exhibited a seasonal cycle with low values ~11°C in wintertime and maxima of approximately 26°C during the summer months. Sea surface salinity values (< 22.5) were low from January through to May indicating significant freshwater supply and increased gradually to 34.7 in the following months. Satellite measurements of Chl-*a* concentrations in this area were quite high (> 2.5 mg m^{-3}) throughout the year with a spring peak reaching 33 mg m^{-3}.

The phytoplankton community was composed mainly of diatoms, dinoflagellates, coccolithophores, cryptophytes, silicoflagellates and euglenophytes. The total phytoplankton abundance ranged from 2×10^4 cells l^{-1} to 1.5×10^6 cells l^{-1} and averaging 3.5×10^5 cells l^{-1}. The seasonal pattern showed a main peak in April-May and a secondary increase in October. Diatoms were the most abundant component of the phytoplankton community, whereas coccolithophores were the second significant element of the community. Dinoflagellates were abundant mostly in July.

Coccolithophore assemblages were dominated mostly by *Emiliania huxleyi*, a typical opportunistic species; well known for its quick response to nutrient enrichment, even in oligotrophic areas (e.g., Dimiza *et al.*, 2015). This species displayed

concentrations of up to 24 × 10^3 coccospheres l^{-1} during winter-early spring, similar to the typical *E. huxleyi* Aegean values. However, extremely high cell densities of *E. huxleyi* (420 × 10^3 coccospheres l^{-1}) were observed in April, following Chl-*a* maxima. *Gephyrocapsa oceanica*, a well-known species for its preference for warm, high-nutrient, less saline waters (e.g., Andruleit and Rogalla, 2002), represented a major component (210 × 10^3 coccospheres l^{-1}) to coccolithophore abundance in July. Its abundance is unusually high for the coccolithophore assemblages of the Aegean Sea, where this species has been rarely reported. *Helicosphaera carteri*, and various species of *Syracosphaera*, such as *S. protrudens*, *S. molischii* represented minor components of the coccolithophore assemblages.

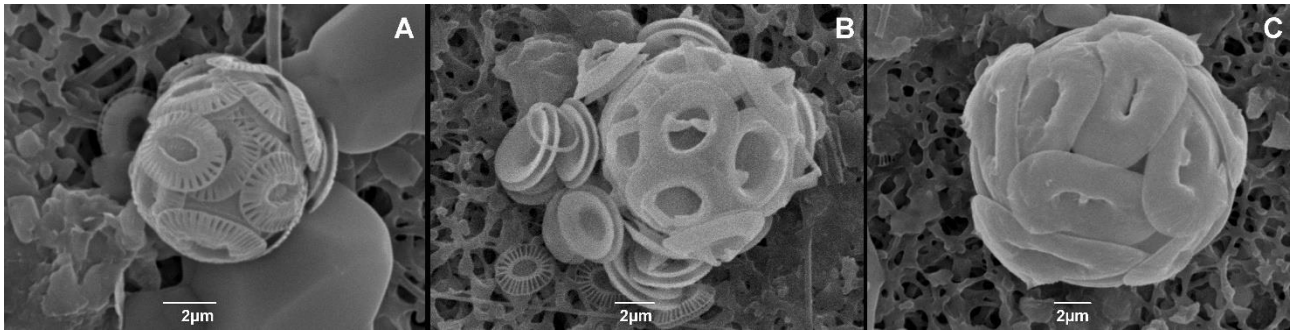

Fig.1 Coccolithophore species A *Emiliania huxleyi* (Lohmann) Hay and Mohler var. *huxleyi*, SP1, February 2016; B *Gephyrocapsa oceanica* Kamptner, SP1, April 2016; C *Helicosphaera carteri* (Wallich) Kamptner, SP1, February 2016.

The seasonal variation of living coccolithophores reflects the exceptional environmental conditions that prevailed in the semi-closed inner Thermaikos Gulf with respect to the open Aegean Sea, thus providing further evidence of the species' biogeography.

Acknowledgments

Financial support for this study was provided by Municipality of Thessaloniki.

References

Andruleit, H., Rogalla, U., 2002. Coccolithophores in surface sediment of Arabian Sea in relation to environmental gradients in surface waters. Marine Geology, 186, 505–526.

Dimiza M.D., Triantaphyllou M.V., Malinverno E., 2014. New evidence for the ecology of *Helicosphaera carteri* in polluted coastal environments (Elefsis Bay, Saronikos, Greece). Journal of Nannoplankton Research, 34: 37–43.

Dimiza, M., Triantaphyllou, M.V., Malinverno, E., Psarra, S., Karatsolis, BT., Mara, P., Lagaria, A., Gogou, A., 2015. The composition and distribution of living coccolithophores in the Aegean Sea (NE Mediterranean). Micropaleontology 61, 521–540.

Ignatiades, L., Psarra, S., Zervakis, V., Pagou, K., Souvermezoglou, E., Assimakopoulou, G., Gotsis-Skretas, O., 2002. Phytoplank ton size-based dynamics in the Aegean Sea (Eastern Mediterranean). J. Mar. Sys., 36, 11–28.

Jordan, R.W., Winter, A., 2000. Assemblages of coccolithophorids and other living microplankton off the coast of Puerto Rico during January-May 1995. Mar. Micropaleontol. 39, 113–130.

Karatsolis, B.-Th., Triantaphyllou, M.V., Dimiza, M. D., Malinverno, E., Lagaria, A., Mara, P., Archontikis, O., Psarra, S., 2017. Coccolithophore assemblage response to Black Sea Water inflow into the North Aegean Sea (NE Mediterranean). Continental Shelf Research 149, 138–150.

Malinverno, E, Triantaphyllou, M.V., Stavrakakis, S., Ziveri, P., Lykousis, V., 2009. Seasonal and spatial variability of coccolithophore export production at the South-Western margin of Crete (Eastern Mediterranean). Marine Micropaleontology 7, 131–147.

Skampa, E., Triantaphyllou, M.V., Dimiza, M.D., Gogou, A., Malinverno, E., Parinos, C., Panagiotopoulos, I.P., Baumann, K.-H., 2019. Coupling plankton-sediment trap-surface sediment coccolithophore regime in the North Aegean Sea (NE Mediterranean). Marine Micropaleontology, https://doi.org/10.1016/j.marmicro.2019.03.001.

Triantaphyllou, M.V., Ziveri, P., Tselepides, A., 2004. Coccolithophore export production and response to seasonal surface water variability in the oligotrophic Cretan Sea (NE Mediterranean). Micropaleontology 50, 127–144.

Utermöhl, H., 1958. Zur Vervollkommnung der quantitativen Phytoplankton. Methodik. Mit. lnt. Verein. Theor.Angew. Limnology, 9, 1-38.

15th International Congress of the Geological Society of Greece
Athens, 22-24 May, 2019 | Harokopio University of Athens, Greece
Bulletin of the Geological Society of Greece, Sp. Pub. 7 Ext. Abs. GSG2019-287

A multi-proxy approach for reconstructing environmental dynamics since the mid Holocene, in Ismarida Lake (N. Greece)

O. Koukousioura[1], K. Kouli[2], K. Vouvalidis[1], E. Aidona[1], G. Karadimou[1], G. Syrides[1]

(1) Aristotle University of Thessaloniki, Department of Geology, 54124, Thessaloniki, Greece, okoukous@geo.auth.gr
(2) National and Kapodistrian University of Athens, Department of Geology and Geoenvironment, 15784, Athens, Greece

During the last decades, a great number of studies have been conducted in the Holocene coastal plains of the Aegean Sea, using multi-proxy approaches. In particular, the combination of benthic foraminiferal, palynological and molluscan analysis, along with stratigraphical, sedimentological, magnetic susceptibility and radiocarbon dating techniques, have been proven to be an invaluable tool box for such researches (e.g., Pavlopoulos *et al*. 2010; Theodorakopoulou *et al*., 2009; Triantaphyllou *et al*. 2010, 2016; Vouvalidis *et al*., 2010). However, limited information is available for the north coastal zone of Greece (Karadimou *et al*., 2016; Koukousioura *et al*., 2012; Pavlopoulos, 2010).

Lake Ismarida, known also by Herodotus description, is located in the lowlands of Thrace near the north Aegean coast. Therefore, it is a valuable archive for reconstructing palaeoenvironmental changes in the area. The lake is placed 20 Km south of Komotini city (Thrace, N. Greece), in the western side of Filiouris River valley, bordered on the west by Neogene sediments and on the east by the alluvial sediments of the Filiouris plain. The ISMR-2 5.8-m long sediment core was retrieved from Lake Ismarida area, in order to reconstruct the paleoenvironments and paleovegetation since mid-Holocene. Systematic stratigraphic, sedimentological, and paleontological analyses were performed, while the magnetic susceptibility of the recovered deposits was measured. More than 50 samples were used for combined micropaleontological and palynological analysis and 190 for mollusc analysis (Karadimou *et al*., 2016). Furthermore, four horizons were radiometrically dated with AMS ^{14}C.

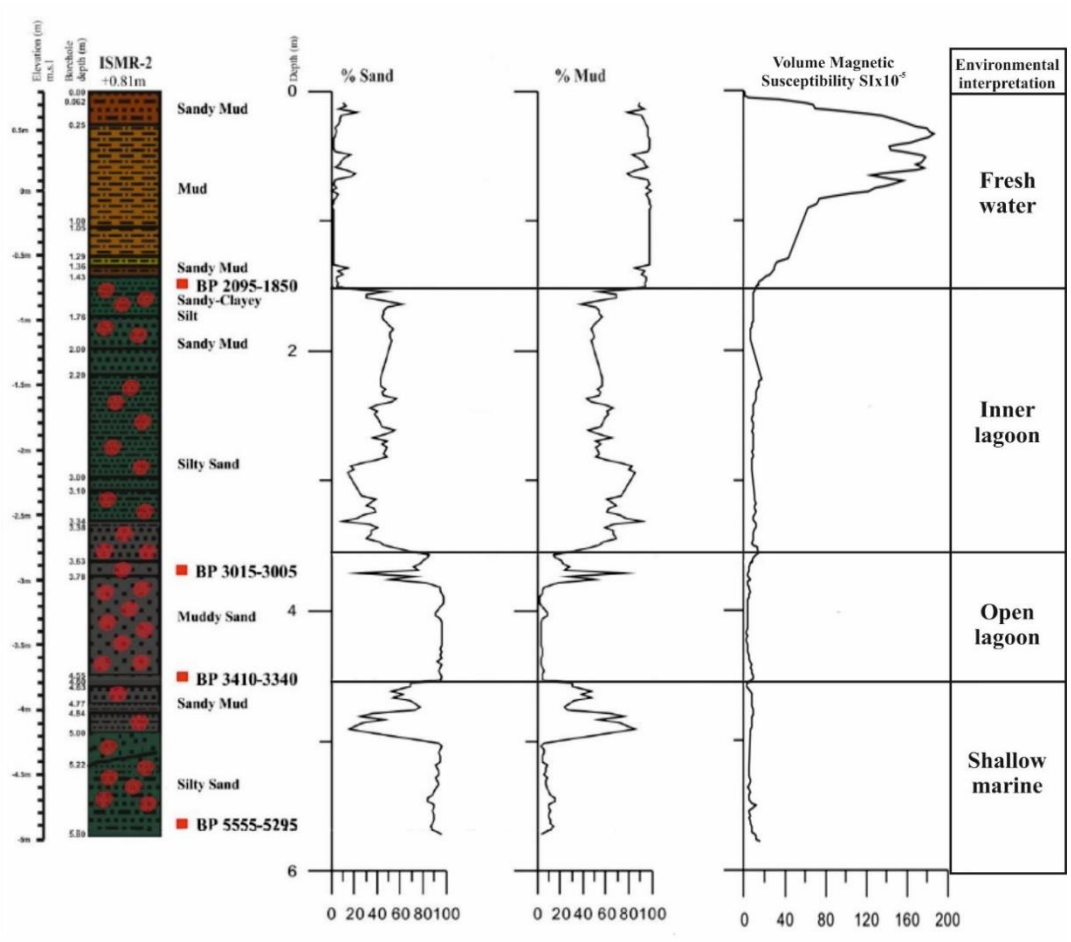

Figure 1. Lithostratigraphy, relative frequencies of sand and mud and magnetic susceptibility measurements of ISMR-2 core (modified from Karadimou *et al*., 2016).

The analysis of paleontological, stratigraphical, sedimentological and magnetic susceptibility data as well as the evaluation of ^{14}C datings, revealed four well-distinguished evolutionary phases in the mid-Holocene Ismarida Lake succession:

(i) from ~5500 to ~3500 cal BP silty sand with coarse sand horizons was deposited bearing mainly marine foraminiferal and mollusc species and high abundances of marine dinoflagellate cysts. Magnetic susceptibility values were low (Fig. 1), confirming a shallow marine environment in accordance with fauna and flora findings

(ii) between ~3500 and 3000 cal BP the distinct lagoon features recorded are indicating the isolation of the area. Nevertheless, the communication with the sea is still evident in both fauna and flora. Benthic foraminiferal assemblage is characterized by a mixture of mainly marine but also some euryhaline species, while macrofauna and flora present a similar composition. The low magnetic susceptibility values agree with an open lagoonal environment, in good communication to the sea

(iii) subsequently the isolation of the core area took place with the establishment of an inner lagoon with limited communication to the sea, until ~2000 cal BP. The overall aquatic palynomorph and mollusk assemblages reflect a complex depositional environment with both marine and fresh water inputs. Furthermore, benthic foraminiferal species composition represents mesohaline to oligohaline biofacies, showing clear similarities to modern Aegean closed lagoons (e.g., Koukousioura *et al.*, 2012; Dimiza *et al.*, 2016)

(iv) after ~2000 cal BP, the silty clay was deposited, exhibits high magnetic susceptibility and the highest mud values of the sedimentary sequence (Fig. 1), in a fresh-water environment with possible river discharges. No fauna was detected in this phase, while fresh-water indicators and aquatic pollen were encountered in an environment analogue to today's Ismarida Lake.

Acknowledgements

The authors would like to thank the "Molyvoti Project" headed by Professor Nathan Arrington, Department of Art and Archeology, Princeton University, for the financial support of the fieldwork and AMS datings.

References

Dimiza, M.D., Koukousioura, O., Triantaphyllou, M.V., Dermitzakis, M.D., 2016. Live and dead benthic foraminiferal assemblages from coastal environments of the Aegean Sea (Greece): Distribution and diversity. Revue de Micropaléontologie 59(1), 19-32.

Karadimou, G., Vouvalidis, K., Syrides, K., Koukousioura, O., Aidona, E., 2016. Geomorphological and paleoenvironmental changes of Ismarida Lake during Holocene (N. Greece). Bulletin of the Geological Society of Greece 50(1), 424-433.

Koukousioura, O., Triantaphyllou, M.V., Dimiza, M.D., Pavlopoulos, K., Syrides, G., Vouvalidis, K., 2012. Benthic foraminiferal evidence and paleoenvironmental evolution of Holocene coastal plains in the Aegean Sea (Greece). Quaternary International 261, 105-117.

Pavlopoulos, K., Triantaphyllou, M., Karkanas, P., Kouli, K., Syrides, G., Vouvalidis, K., Palyvos, N., Tsourou, T., 2010. Paleoenvironmental evolution and prehistoric human environment, in the embayment of Palamari (Skyros Island, Greece) during Middle-Late Holocene. Quaternary International 216, 41-53.

Theodorakopoulou, K., Pavlopoulos, K., Triantaphyllou, M., Kouli, K., Tsourou, T., Bassiakos, Y., Zacharias, N., Hayden, B., 2009. Geoarchaeological studies in coastal area in Istron-Kalochorio (gulf of Mirabello-Eastern Crete): landscape evolution and palaeoenvironmental reconstruction. Zeitschrift für Geomorphologie 53(1), 55-70.

Triantaphyllou, M.V., Kouli, K., Tsourou, T., Koukousioura, O., Pavlopoulos, K., Dermitzakis, M.D., 2010. Paleoenvironmental changes since 3000 BC in the coastal marsh of Vravron (Attica, SE Greece). Quaternary International 216, 14-22.

Triantaphyllou, M.V., Pavlopoulos, K.P., Kouli, K., Koukousioura, O., Dimiza, M.D., Aidona, E., Syrides, G., Pallikarakis, A., Goiran, J.-P., Fouache, E., 2016. Multiproxy paleoenvironmental reconstruction: the Piraeus coastal plain case study. Bulletin of the Geological Society of Greece 50(1), 478-487.

Vouvalidis, K., Syrides, G., Pavlopoulos, K., Papakonstantinou, M., Tsourlos, P., 2010. Holocene palaeoenvironmental changes in Agia Paraskevi prehistoric settlement, Lamia, Central Greece. Quaternary International 216, 64-74.

15th International Congress of the Geological Society of Greece
Athens, 22-24 May, 2019 | Harokopio University of Athens, Greece
Bulletin of the Geological Society of Greece, Sp. Pub. 7 Ext. Abs. GSG2019-289

Summer coccolithophore community in the Western Black Sea

A. Ravani[1] M.D. Dimiza[1], M.V. Triantaphyllou[1], E. Malinverno[2], B.-T. Karatsolis[3], A. Lagaria[4], S. Psarra[4]

(1) Department of Geology and Geoenvironment, National and Kapodistrian University of Athens, Panepistimiopolis, 15784 Athens, Greece, mdimiza@geol.uoa.gr
(2) University of Milan – Bicocca, Department of Earth and Environmental Sciences, Piazza della Scienca 4, Milano, Italy
(3) Uppsala University, Geocentrum, Villav 16, Sweden
(4) Hellenic Centre for Marine Research, Institute of Oceanography, 190 13 Anavyssos, Attiki, Greece

Background

Coccolithophores have a widespread distribution in the photic zone, ranging from polar to tropical waters, but overall show preference to warm, low productivity regions (e.g., Winter et al., 1994; Karatsolis et al., 2017). Most coccolithophore taxa are more diverse and abundant in low and middle latitude warm, and stratified oligotrophic waters. However, certain species, such as *Emiliania huxleyi*, reveal an opportunistic and r-selected behavior (e.g., Tyrrell and Merico, 2004) thriving in high productivity areas and often form intense blooms over large areas of the ocean (e.g., Westbroek et al., 1993).

The Black Sea is the largest semi-enclosed marginal sea and receives drainage from almost one-third of continental Europe. Intensive coccolithophore blooms (*Emiliania huxleyi*, primarily) are typical events for the Black Sea. According to satellite observations, on a temporal scale the most extended bloom occurs in May-June, although differences in intensity and area of coverage have been recorded (e.g., Cokacar et al., 2004; Kopelevitch et al., 2014; Triantaphyllou et al., 2014; Mikaelyan et al., 2015). These blooms can be detected by ocean color sensors as a result of light being scattering by the coccolith plates that are detached from cells. The optical signature of coccolithophore blooms on satellite true color images is a very bright patch of water with a milky turquoise color. The Black Sea is an ideal site in which to study the effect of biogeochemical properties on coccolithophore blooms.

Objectives

The main aim of this study was to determine the spatial and vertical distribution patterns of living coccolithophores from the oxic surface zone in the western part of the Black Sea in June 2016.

Materials and methods

The present study focuses on the analysis of 95 seawater samples from 33 stations from the inner (<50 m depth), outer (50–200 m depth) self and the open sea (>200 m depth), in the western part of the Black Sea, that was undertaken in June 2016 (2–24/06). For each sampling station, a surface sample was taken from 1 m depth and 1-4 more depths within the surface layer (5 m – 50 m), adjusted to bottom topography and bathymetry. Water samples were taken with a 5 L Niskin bottles positioned in a rosette over the CTD system of the ship.

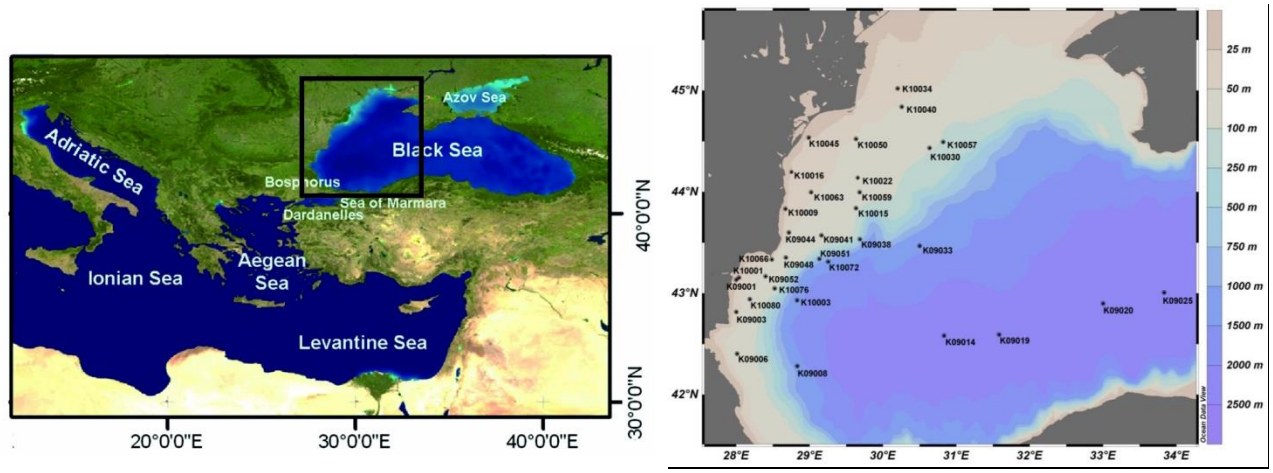

Figur3 1. Map of the study area and location of the stations sampled for coccolithophore analysis at the western part of the Black Sea.

Several physico-chemical parameters including temperature, salinity profiles were measured at most of the stations using a SBE-19 CTD-Rosette System. The amount of chlorophyll-a (Chl *a*) that corresponded to the 0.2-2.0 μm and >2.0 μm size classes was measured fluorometrically (Holm-Hansen et al., 1965).

The coccolithophore composition and community structure was evaluated through Optical Microscopy. The samples were examined in a Leica DMLSP polarizing light microscope and the coccospheres per liter were calculated following the methodology of Jordan and Winter (2000).

Results and Discussion

At the northern areas of the inner shelf the sea surface temperature ranged from 16 to 22 °C. In the outer shelf region the temperature increased reaching the values of ~21°–24 °C, whereas in the open sea the values fluctuate from 21 to 22 °C. The sea surface salinity was relatively low, both in the shelf and open sea areas. Generally, the salinity values ranged from the minima of < 17.5, near the northern shelf area reflecting the influx of fresh water from the Danube River to the maxima of 17.5–18.9 in the open sea.

The spatial distribution (1 m depth) of Chl *a* was revealed from the seventeen samples collected mainly from the south-western part of the studied areas. Total Chlorophyll-*a* concentrations in surface waters ranged from 0.147 μg l^{-1} to 5.764 μg l^{-1}. The values of Chl *a* were increased near the self-region with maxima in the northern stations, with decreasing trend towards the open sea stations.

Living coccolithophores showed excessively high densities ranging from $2.44x10^4$ to $7.63x10^6$ coccospheres l^{-1}. *Emiliania huxleyi* lightly calcified morphotypes ($1.24x10^4$–$7.38x10^6$ coccospheres l^{-1}) dominated in the surface assemblage and constituted the 98% of the coccolithophore community. Differences in spatial distribution between inner self and open-sea environments were observed that are primarily associated with freshwater inputs and nutrients influx from the Danube River. A significant positive correlation between *E. huxleyi* density and Chl *a* concentrations (Pearson $r=0.255$, $p<0.05$) indicate a direct relationship between coccolithophores and chlorophyll-*a*.

In general, *Emiliania huxleyi* was usually higher in the surface layer (up to around 35 m), and tended to decrease in density below ~35 m water depth, while *Algirosphaera robusta* occurred in high densities in the deeper parts (up to $7.94x10^6$ coccospheres l^{-1}), indicating low light availability below the thermocline.

The present study suggests that some Syracosphaeraceae and Rabdosphaeraceae taxa such as *Syracosphaera dilatata*, *Syracosphaera molischii*, *Acanthoica acanthifera*, *Acanthoica quattrospina* and few holococcolithophores (*Syracosphaera arethusae* HOL and *Helladosphaera cornifera*) that have also been identified in the studied Black Sea water samples prove to thrive well in low salinities and relative eutrophic conditions.

Acknowledgments

The material studied for coccolithophore analysis was provided during the BIO-OPT-2016 EUROFLEETS cruise, onboard the R/V Akademik.

References

Cokacar, T., Oguz, T., Kubilay, N. 2004. Satellite-detected early summer coccolithophore blooms and their interannual variability in the Black Sea. Deep-Sea Research Part I, 54: 1017–1031.

Holm-Hansen, O., Lorenzen, C.J., Holmes, R.W., Strickland, J.D.H., 1965. Fluorometric Determination of Chlorophyll. ICES J Mar Sci. 30(1), 3–15.

Jordan, R.W., Winter, A., 2000. Assemblages of coccolithophorids and other living microplankton off the coast of Puerto Rico during January-May 1995. Mar. Micropaleontol. 39, 113–130.

Karatsolis, B.-Th., Triantaphyllou, M.V., Dimiza, M. D., Malinverno, E., Lagaria, A., Mara, P., Archontikis, O., Psarra, S., 2017. Coccolithophore assemblage response to Black Sea Water inflow into the North Aegean Sea (NE Mediterranean). Continental Shelf Research 149, 138–150.

Kopelevich, O.V., Burenkov, V.I., Sheberstov, S.V., Vazyulya, S.V., Kravchishina, M., Pautova, L.A., Silkin, V.A., Artemiev, V., Grigoriev, A. 2014. Satellite monitoring of coccolithophore blooms in the Black Sea from ocean color data. Remote Sensing of the Environment, 146: 113–123.

Mikaelyan, A.S, Pautova, L.A., Chasovnikov, V.K., Mosharov, S.A., Silkin, V.A. 2015. Alternation of diatoms and coccolithophores in the northeastern Black Sea: a response to nutrient changes. Hydrobiologia, 755: 89–105.

Triantaphyllou, M.V., Malinverno, E., Dimiza, M.D., Gogou, A., Athanasiou, A., Skampa, E., Tselenti, D., Thanassoura, E., Birli, A., Stavrakaki, I., Stavrakakis, S., Corselli, C., Lykousis, V. 2014. Coccolithophore biogeographic trends and export production in the Eastern Mediterranean and Black Seas. Journal of Nannoplankton Research, 34: 97–98.

Tyrrell, T., Merico, A., 2004. Coccolithophores—From Molecular Processes to Global Impact, Ed. by H. R. Thierstein & J. R. Youngs (Springer, 2004), pp. 75–97.

Westbroek, P., Brown, C. W., Bleijswijkbrownlee, J. Van C., Brummer, G. J., Conte, M., Egge, J., Fernandez, E., Jordan R., Knappertsbusch, M., Stefels, J., Verdhuis, M., Van Der Wal, P., Young, J., 1993. A model system approach to biological climate forcing: the example of Emiliania huxleyi. Global and Planetary Change, 8, 27-46.

Winter, A., Jordan, R. W. & Roth P., 1994. Biogeography of living Coccolithophores in oceanic waters. In: A. Winter & W.G. Siesser (eds), Coccolithophores, p. 13-27, Cambridge University Press.

15th International Congress of the Geological Society of Greece
Athens, 22-24 May, 2019 |Harokopio University of Athens, Greece
Bulletin of the Geological Society of Greece, Sp. Pub. 7 Ext. Abs. GSG2019-294

The flora of NW Peloponnese during the Middle Pleistocene (Vigla Sychainon, Rio-Antirio Basin) - Preliminary results

E.Liapi[1], D.Karanikolas[1], E. Tokmaktsi[1], M. Tsoni[1], G. Zidianakis[1], G. Iliopoulos[1]

(1) Palaeontology and Stratigraphy Lab., Department of Geology, University of Patras, 26504, Rio, Greece, eleni.lia.2093@gmail.com

Introduction

The Pleistocene sediments of the Rio-Antirio Basin (Achaia, Greece) have yielded several terrigenous plant assemblages. In this study, numerous plant fossils as disarticulated parts, mainly leaves and defoliate shoots, have been collected from two fossiliferous sites in the Vigla Sychainon area (Vigla I and III). Based on recent data from the micropalaeontological analysis of marine sediments found stratigraphically bellow the plant bearing sediments and especially the presence of the coccolithophore *Emiliana huxley* (Tsoni et al., this volume), a late Middle Pleistocene age can be inferred for the examined plant material. Our main objectives include the description and taxonomic identification of the plant remains, the determination of the palaeoflora and the reconstruction of the regional palaeovegetation.

Methods

More than 1.500 plant macro-remains, mainly foliage and shoot impressions, were collected by the Paleontology and Stratigraphy laboratory team of the University of Patras. The remains were quite fragmentary and lack organic material preventing cuticular analysis. Initially, the collected material was prepared carefully with thin needles and soft brushes. Afterwards, acrylic resin (Paraloid B72) was used for the conservation of morphological details. The taxonomic determinations and systematic affinities were based mainly on leaf morphology by recording the basic macro-morphological features of the fossils in protocols (e.g. laminar shape, margin type, venation). For the reconstruction of the vegetation, the published data on European plant palaeoassemblages, the autoecology of modern allies and the taphonomical processes that affected the examined material were taken under consideration.

Results

About 1/3 of the collected plant remains were identified to family or genus level. The great majority of them represents Angiosperm taxa of trees or shrubs [tab. 1, fig. 2]. Fagaceae predominates the assemblage with a deciduous oak which is characterized by lobed leaves (*Quercus*) [fig. 3]. At least two additional oak species, one of them evergreen, also occur. Ulmaceae is represented by *Zelkova* and possibly an elm (*Ulmus*) species [fig. 1]. Moreover, broad-leaved elements such as *Platanus*, *Acer* and *Populus* are identified. Rarely needles of Gymnosperm origin (possibly Pinaceae) are present.

Conclusions-Discussion

According to the preliminary results from the study of Vigla palaeoflora it can be concluded that:

- The plant assemblage is profoundly dominated by a deciduous oak with lobed leaves.
- The genus *Zelkova* it seems to survive through most of the middle Pleistocene in NW Peloponnese while in central Europe it had disappeared much earlier. Today *Zelkova* is found as a relict species in the Mediterranean area with two endemic species in Crete and Sicily respectively.
- The severe fragmentation of the plant remains probably indicates allochthonous fossil deposition (leaf transportation by winds or likely water currents).
- The assemblage represents a gallery forest with *Platanus*, *Populus*, *Ulmus* and possibly *Zelkova* and *Quercus* that might thrived across an active river channel or a lake. In the lowland surrounding area, a mixed mesophytic forest mostly with deciduous elements such as oaks, maples and *Zelkova* likely occurs.

Further research is required in order to conclude a final definition of the palaeoflora and the palaeovegetional reconstruction. For a more purposeful systematic affinity of the identified taxa, the future study will focus on their comparison to the modern Mediterranean allies and determination to species level.

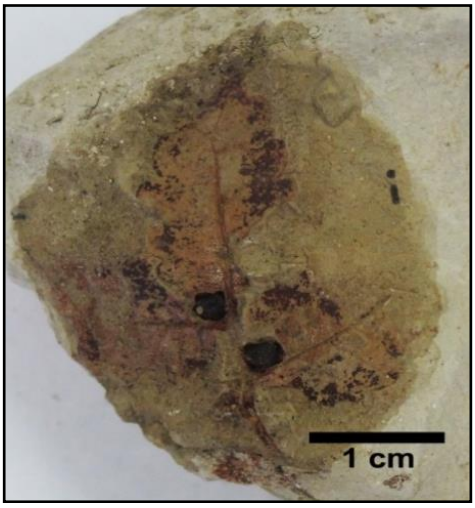

Figure 1: *Zelkova* sp., twig with attached leaves and fruits.

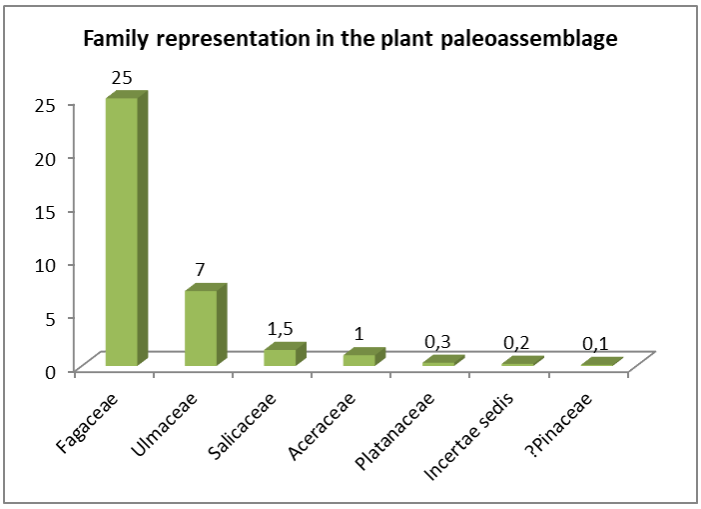

Figure 2: The Vigla Sychainon palaeoassemblage, plant family representation (%).

Table 1. The Vigla Sychainon palaeoassemblage, flora list and frequencies.

Family	Genus	Family Frequency
Gymnospermae		
? Pinaceae	indet.	rare
Angiospermae		
Platanaceae	*Platanus*	rare
Ulmaceae	?*Ulmus* *Zelkova*	common
Fagaceae	*Quercus*	abundant
Aceraceae	*Acer*	rare
Salicaceae	*Populus*	rare
indet.	*Dicotylophyllum*	rare



Figure 3: *Quercus sp.*, lobed leaf.

References

Kleinhölter, K., 1994. Die neogenen Floren der Peloponnes. Ph.D. Thesis, Münster University, Münster.

Kleinhölter, K., 1995. Oberpliozäne Makroflorenaus dem Bereich des Patras-, Rion- und Korinth-Grabens (Peloponnes und SW-Kontinentalgriechenland). Münster. Forsch. Geol. Paläont., 77: 467-478.

Knobloch, E., Velitzelos, E., 1986. Die pliozäne Flora Von Skoura bei Sparta auf dem Peloponnes (Griechenland). Documenta Naturae, 29: 21-28.

Kontopoulos, N., Zelilidis, A., 1992. Upper Pliocene lacustrine environments in the intramontane Rio graben basin, NW Peloponnesus, Greece. N. Jb. Geol. Paläont. Mh., H.2: 102-114.

Tsoni, M., Iliopoulos, G., Koukouvelas, I., Kostopoulou, S., Kontopoulos, N., 2019. Palaeonvironmental evolution of Rio basin during the Middle Pleistocene. In this volume.

Velitzelos, D., Bouchal, M.J., Denk, T., 2014. Review of the Cenozoic floras and vegetation of Greece. Rev. Palaeobot. Palynol., 204: 56-117.

Velitzelos, E., Gregor, H.J., 1990. Some aspects of the Neogene floral History in Greece. Rev. Palaeobot. Palynol., 62: 291-307.

15th International Congress of the Geological Society of Greece
Athens, 22-24 May, 2019 | Harokopio University of Athens, Greece
Bulletin of the Geological Society of Greece, Sp. Pub. 7 Ext. Abs. GSG2019-302

High Resolution Stratigraphy and Evolution of Sperchios Delta Plain-Greece Based on Optical Dating of Quartz and Feldspar

E. Tsakalos[1,2], M. Kazantzaki[2], Y. Bassiakos[2] , E. Filippaki[2]

(1) Department of Geophysics, Division of Earth and Planetary Sciences, Graduate School of Science, Kyoto University, Kyoto 606-8502, Japan
(2) Laboratory of Luminescence dating, Institute of Nanoscience and Nanotechnology, National Centre for Scientific Research, N.C.S.R. "Demokritos", Aghia Paraskevi, Athens 153 10, Greece, e.tsakalos@inn.demokritos.gr

The establishment of the Holocene stratigraphic configuration of deltaic successions around the Mediterranean has been the study of several researchers over the last few decades (e.g., Bruno et al., 2015), with much of the associated research being focused on sedimentological and geochemical analyses (e.g., Pechlivanidou et al., 2014), tectonics and geodynamics (e.g., Lafuerza et al., 2005) as well as seismic profile analyses (e.g., Styllas, 2014).

Sperchios delta plain is located in central Greece and covers an area of 121.5 km^2. The hydrological regime in the area and the tectonic activity in the basin have forced the river's main channel to shift its course several times in the past, leading to the development of many deltaic prolongations and the creation of an extensive deltaic plain (Poulos et al., 1997). Earlier studies in Sperchios delta plain have primarily been focused on the reconstruction of the shoreline at the time of the ancient battle terrain of Thermopylae (Kraft et al., 1987; Vouvalidis et al., 2010a), while more recently the palaeogeography of the Late stages Holocene Sperchios delta plain has been described by Pechlivanidou et al. (2014) and Tsakalos et al. (2016), based on palaeontological, geochemical and sedimentological analyses on deltaic deposits.

However, numerical ages of the different deltaic sedimentary faces have been very limited, bringing uncertainties on the sequential history of the upper part of Sperchios delta plain. Previous chronological research in the delta (Pechlivanidou et al., 2014; Vouvalidis et al., 2010b) was based on archaeological and radiocarbon dates, with 14C ages bearing a number of limitations (e.g., sample contamination and uncertainties associated with the estimation of the C-14 to C-12 ratio). Furthermore, even though the luminescence dating techniques are now extensively applied to variety of sedimentary environments (e.g., aeolian, fluvial and marine), their application on fluvial and deltaic deposits still limited, since incomplete bleaching of sediment grains may be apparent. In such environments, sunlight exposure of sediments transported by fluvial processes may be very short-time and/or water turbulence may not allow direct sunlight exposure and thus full resetting of their luminescence signal (Dietlefsen, 1992; Rendell et al., 1994).

In this regard, an absolute dating study by Tsakalos et al., (2018) examined the applicability of the Optically Stimulated Luminescence (OSL) technique on sand sized (coarse) quartz from Sperchios delta deposits and provided a reliable chronological framework for the upper (~20 m) sedimentary deposits of Sperchios delta plain. This study also revealed that the distributions of the "equivalent dose" (D_E) values of the dated coarse grained quartz are over-dispersed, which may be considered as typical for fluvial sediments (e.g., Arnold et al., 2009). However, this problem of obtaining the best estimate of D_E and thus calculating a reliable age was overcome by the use of a number of statistical approaches.

Here we present a new-detailed Holocene chronological framework for the Sperchios delta along with sedimentation rates of its depositional sequences. Our approach is based on an enhanced chronological model which builds on the earlier set of luminescence ages on coarse quartz produced in the area by Tsakalos et al. (2018). The current study adopts the systematic employment of the luminescence dating techniques on fine (4-11 μm) quartz and coarse (80-125 μm) feldspar grains. The use of fine quartz will allow checking the hypothesis of a more effective resetting mechanism of the fine grained fraction (as opposed to coarser) during transportation and deposition. For age consistency check, samples dated here are exactly the same as the ones dated using the conventional Single Aliquot Regenerative (SAR)-OSL protocol in the study by Tsakalos et al., (2018). Samples were collected from five boreholes and are associated with different sedimentary facies (transgressive and regressive deposits that overlay late Pleistocene deposits) Fig. 1. To this end, the produced ages put additional strain on the applicability and reliability of the different luminescence techniques for dating deltaic deposits.

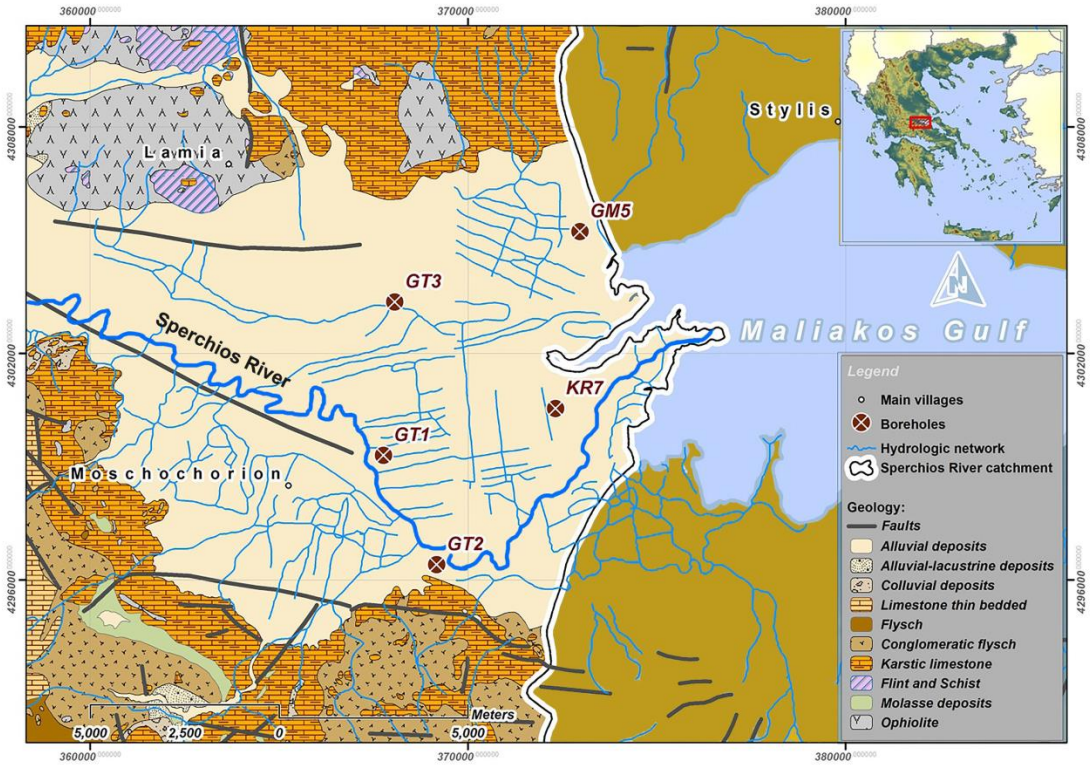

Fig. 1 Study area and sampling sites of the five cores (after Tsakalos et al., 2018).

Our luminescence dating results provided evidence of an Early to Late Holocene deposition for the upper 20 m of the delta and shorted in chronostratigraphic order. Further, the absolute ages derived by both fine quartz and coarse feldspar grains the are in agreement with independent previous choronological studies (radiocarbon dating) conducted in the area (Pechlivanidou et al., 2014) and in great consistency with the coarse quartz OSL ages by Tsakalos et al. (2018). The produced information adds to the widely accepted consensus regarding a consistent late Pleistocene to Holocene stratigraphic configuration of Mediterranean deltas while at the same time further contribute to the development of an evolutionary model of Mediterranean low-lying coastal areas subject to rising sea level rates.

References

Arnold, L.J., Roberts, R.F., Galbraith, S.B., DeLong, S.B., 2009. A revised burial dose estimation procedure for optical dating of young and modern-age sediments. Quaternary Geochronology 4 (4), 306-325.

Bruno, L., Amorosi, A., Severi, P., and Bartolomei, P., 2015. High-frequency depositional cycles within the late Quaternary alluvial succession of Reno River (northern Italy). Italian Journal of Geosciences 134, 339-354.

Ditlefsen, C., 1992. Bleaching of K-feldspars in turbid water suspensions: a comparison of photo- and thermoluminescence signals. Quaternary Science Reviews 11, 33-38.

Kraft, J., Rapp, G., Szemler, G., Tziavos, Ch., and Kase, E., 1987. The pass of Thermopylae, Greece. Journal of Field Archaeology 14, 181-198.

Lafuerza, S., Canals, M., Casamor, J.L., Devincenzi, J.M., 2005. Characterization of deltaic sediment bodies based on in situ CPT/CPTU profiles: A case study on the Llobregat delta plain, Barcelona, Spain. Marine Geology 222-223, 497-510.

Pechlivanidou, S., Vouvalidis, K., Løvlie, R., Nesje, A., Albanakis, K., Pennos, C., Syrides, G., Cowie, P., Gawthorpe, R., 2014. A multi-proxy approach to reconstructing sedimentary environments from the Sperchios delta, Greece. The Holocene 24 (12), 1825-1839.

Poulos, S., Leontaris, S., Collins, M.B., 1997. Sedimentological and clay mineralogical investigations in Maliakos Gulf, eastern Greece. Bollettino di Geofisica Teorica ed Applicata 38 (3-4), 267-279.

Rendell, H.M., Webster, S.E., Sheffer, N.L., 1994. Underwater bleaching of signals from sediment grains: New experimental data. Quaternary Science Reviews 13, 433-435.

Styllas, M., 2014. A simple approach for defining Holocene sequence stratigraphy using borehole and cone penetration test data. Sedimentology 61, 444-460.

Tsakalos E., Dimitriou E., Triantaphyllou M., Kouli K., Dimiza M., Anagnostou C., Kazantzaki M., 2016. Late Pleistocene-Holocene environmental changes on Sperchios delta plain-central Greece. The MedCLIVAR 2016 conference, 26-30 Sept 2016, book of Abstracts, Athens, Greece.

Tsakalos, E., Dimitriou, E., Kazantzaki, M., Anagnostou Ch., Christodoulakis J., Filippaki E., 2018. Testing optically stimulated luminescence dating on sand-sized quartz of deltaic deposits from Sperchios delta plain, Greece. Journal of Palaeogeography 7, 130-145.

Vouvalidis, K., Syrides, G., Pavlopoulos, K., Papakonstantinou, M., Tsourlos, P., 2010b. Holocene palaeoenvironmental changes in Agia Paraskevi prehistoric settlement, Lamia, Greece. Quaternary International 216, 64-74.

Vouvalidis, K., Syrides, G., Pavlopoulos, K., Pechlivanidou, S., Tsourlos, P., Papakonstantinou, M., 2010a. Palaeogeographical reconstruction of the battle terrain in Ancient Thermopylae, Greece. Geodinamica Acta 23 (5-6), 241-253.

15th International Congress of the Geological Society of Greece
Athens, 22-24 May, 2019 | Harokopio University of Athens, Greece
Bulletin of the Geological Society of Greece, Sp. Pub. 7 Ext. Abs. GSG2019-304

Middle Pleistocene Luminescence Ages on Coastal Sediments from North Evoikos Gulf: Overcoming Quartz Saturation by Elevated-temperature Infrared Stimulated Luminescence (IRSL) from Feldspars

M. Kazantzaki[1], E. Tsakalos[1], Th. Rondoyanni[2], Y. Bassiakos[1], E. Filippaki[1]

(1) National Centre for Scientific Research, NCSR "Demokritos", Athens, Greece, m.kazantzaki@inn.demokritos.gr
(2) National Technical University of Athens, Athens, Greece

The employment of luminescence dating techniques on coastal sediments from North Evoikos Gulf (Central Greece) revealed that Optically Stimulated Luminescence (OSL) and Isothermal Thermoluminescence (ITL) natural signals of quartz grains are close to saturation (Figure 1a,1b) and also yielding broadly scattered equivalent dose (De) values, thus perplexing the calculation of reliable luminescence ages. To overcome this problem, Infrared Stimulated Luminescence (IRSL) dating of feldspar was attempted, which was proven more suitable for such sediments, as it showed higher saturation levels. Natural luminescence signal from feldspar grains (Figure 2) produced accurate De values, the reliability of which was confirmed by the properly corrected sensitivity changes that take place during measurements, as well as a number of validation tests (namely, dose recovery and preheat plateau tests). The post-IRSL SAR protocol after Thiel et al. (2011) was employed which use an elevated temperature both during preheating and stimulating of the feldspar samples. Our luminescence dating results on the coastal samples provided ages that go back to the Middle Pleistocene (Figure 3). The reliability of the post-IRSL ages are further confirmed by a number of previous palaeontological studies in the area (Kumadakis, 1969; Keraudren, 1975; Phillip, 1974; Lemeille, 1977; Rondoyanni-Tsiambaou, 1984; Genre 1999; Mauridis et al., 2006), as they provided ages which are in fair agreement with the dating results of this study. Based on the derived absolute ages, the mean sedimentation rate in the study area was also determined, which could be considered as being relatively low, ranging from 0.15 to 0.7 cm/yr, similar to the sedimentation rate estimated by previous studies in the area (Kamperi and Sakellariou, 2006). In addition, a mean uplift rate of 0.11 to 0.15 mm/y was calculated for the southern part of North Evoikos Gulf since the Middle Pleistocene.

During the Middle Pleistocene, North Evoikos Gulf was periodically becoming a lake, when the sea level was low enough, not exceeding the maximum depth of Lichades Strait, while a change to a lagoon environment was taking place when seawater from the Aegean Sea entered the Gulf. Probably, the first entry of seawater into the North Evoikos Gulf took place at the beginning of the Middle Pleistocene, as indicated by the presence of brackish deposits, sitting on layers of successive lacustrine and terrestrial deposits of an older age. This is also confirmed by the presence of mollusk fauna, which is also present on the Caspian and Black Sea, thus signifying a connection between Evoikos Gulf and the Black Sea and the Caspian Sea, through the Marmara Sea and the Dardanelles Strait respectively.

This study revealed that post-IRSL dating was a reliable technique for establishing the chronological framework of North Evoikos Gulf and an alternative trustworthy dating technique when OSL on quartz suffers from saturation. Furthermore, the produced post-IRSL ages are the first Middle Pleistocene ages reported for Greek clastic sediments using the luminescence dating techniques.

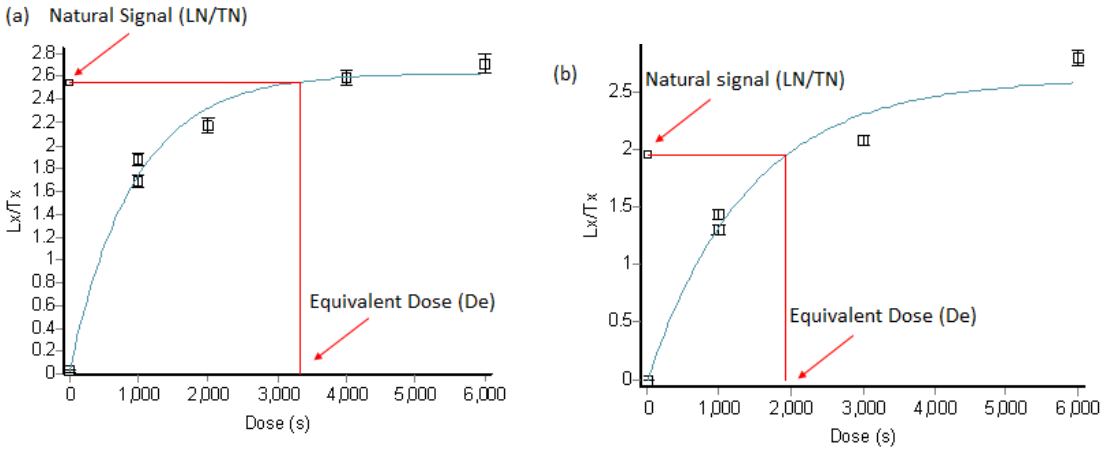

Figure 1. Growth curves of a quartz aliquot close to saturation using (a) the OSL and (b) the ITL dating techniques.

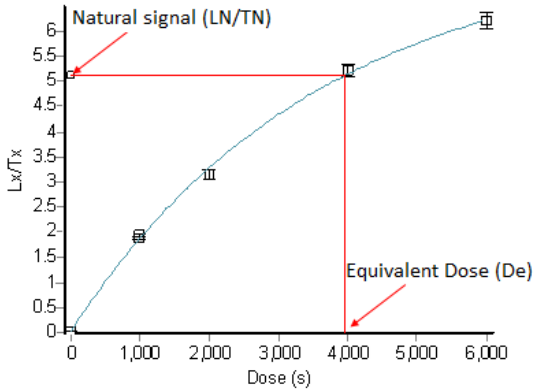

Figure 2. Growth curve of an aliquot containing feldspar grains using the post-IRSL protocol.

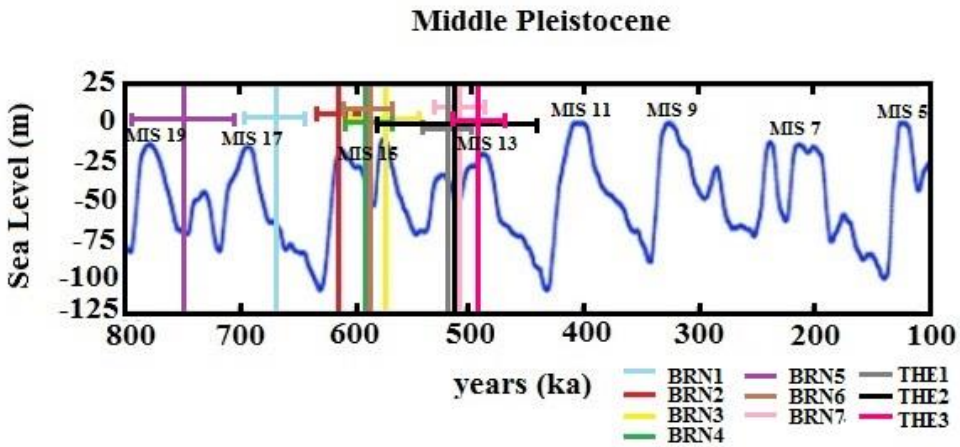

Figure 3. post-IRSL Middle Pleistocene ages of North Evoikos Gulf, plotted on an eustatic curve (modified after Bintanja et al., 2005).

Acknowledgements

This study was supported by the National Technical University of Athens, faculty of Geological Sciences, School of Mining and Metallurgical engineering.

References

Genre, C., 1999. Neotectonics and Late Holocene terraces. The example of Euboea (Central Eastern Greece). Geomofphologie: relief, processus, environement 2, 143-158.

Kamperi, E., Sakellariou, D., 2006. Active sedimentation rates in N. Evoikos Gulf and Gulf of Alkyonides. Comparison with Pb-210 method, 8th Panhellenic Symposium of Oceanography and Fishing, Hellenic Centre for Marine Research, Thessaloniki. (In Greek)

Keraudren, B., 1975. Essai de stratigraphie et de paleogeographie du Plio-Pleistocene egeen. Bulletin de la Société géologique de France VII (17), 1110-1120.

Kumandakis I., 1969. The geology of Grammousa Island (N. Evoikos Gulf). Annales Géologique des Pays Helléniques 22, 295-299. (In Greek)

Lemeille, F., 1977. Etudes neotectoniques en Grece centrale nord-orientale (Eubee centrale, Attique, Beotie, Locride). Thèse Doctorat - de 3eme cycle, Université de Paris, Paris, XI, 173 p.

Mavrides, A., 2006. Geological map of Greece scale 1:50.000, Chalkida sheet, IGME, Athens.

Philip, H., 1974. Etude néotectonique des rivages égéens en Locride et en Eubée nord orientale, Thèse de 3eme cycle, Académie de Montpellier, Paris.

Rondoyanni-Tsiambaou, Th., 1984. Etude néotectonique des rivages occidentaux du canal d' Atalandi (Grèce Centrale). Thèse Doctorat, Université de Paris sud Centre d' Orsay, Paris.

Thiel, C., Buylaert, J.P., Murray, A.S., Terhorst, B., Hofer, I., Tsukamoto, S., Frechen, M. 2011. Luminescence dating of the Stratzing loess profile (Austria) - Testing the potential of an elevated temperature post-IR IRSL protocol, Quaternary International 234(1-2), 23-31.

15th International Congress of the Geological Society of Greece
Athens, 22-24 May, 2019 | Harokopio University of Athens, Greece
Bulletin of the Geological Society of Greece, Sp. Pub. 7 Ext. Abs. GSG2019-307

Late Quaternary Evolution of a Tabular Relief in the Sicily Channel through the Study of Foraminifera and Ostracods

F. Giovenzana[1], V. A. Bracchi[1], M.V. Triantaphyllou[2], M. Dimiza[2], Th. Tsourou[2], A. Savini[1], C. Corselli[1], E. Malinverno[1]

(1) University of Milano-Bicocca, Department of Earth and Environmental Sciences, Piazza della Scienza, 4, Milano, Italy, f.giovenzana3@campus.unimib.it
(2) National and Kapodistrian University of Athens, Faculty of Geology and Geoenvironment, Panepistimioupolis 15784, Athens, Greece

Background

The Malta Plateau is an area of particular interest since it is affected by active gas venting phenomena, which lead to the formation of mud volcanoes. Furthermore, tabular reliefs occur in this area (Fig. 1) and are the objective of this work. Previous studies focused on the morphological description of this feature (Savini *et al.*, 2009) and on its evolution basing upon paleontological, sedimentological and mineralogical analyses (Bracchi *et al.*, 2019).

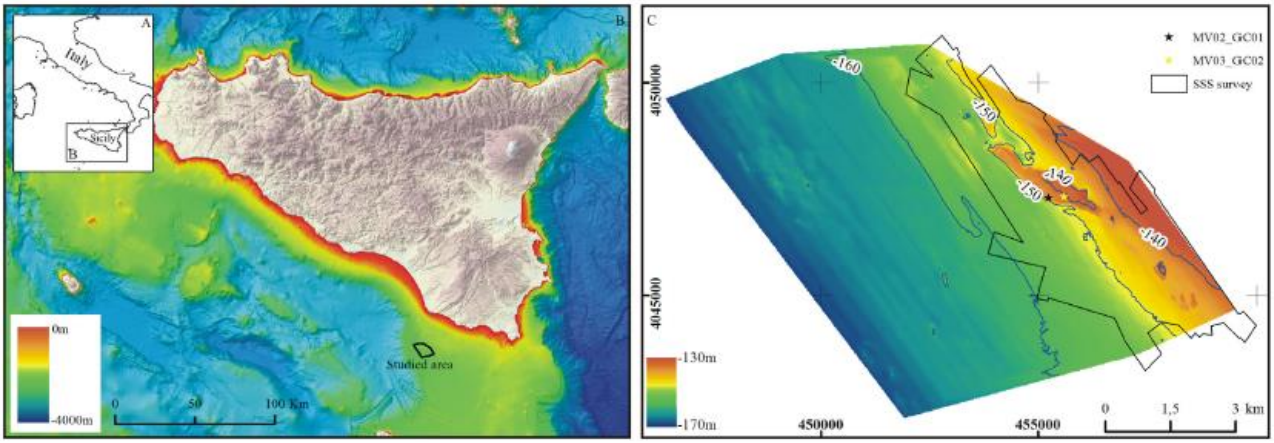

Fig. 1. Location of the investigated tabular relief. Black star indicates the core site (modified from Bracchi et al., 2019).

Objectives

This work proposes a quantitative description of the variation of foraminifera and ostracod assemblages throughout a sedimentary core, in order to detail the paleoenvironmental evolution of this tabular relief.

Methods

Core MV02_GC01 (36°34.2147′N; 14°30.2232′E), 176 cm long, was sampled on the flank of the tabular relief at 141 m depth and divided into two sections: section 1 from cm 0 to cm 76 cm, and section 2 from cm 76 to cm 176. Samples for micropaleontology were collected at 10 cm resolution, with a total of 17 samples from the top to the bottom. For each sample, 3 g of sediment were wet-sieved and splitted. Benthic foraminifera were hand-picked, identified and counted, whereas planktonic foraminifera and ostracods are still under study. Six samples (10-20-40-50-100-160 cm) have been collected and analyzed for nannofossil biostratigraphy.

Results

A total of 7218 benthic foraminifera were identified, belonging to 70 species. According to their habitat requirements, benthic foraminifera were grouped in four ecological categories, whose relative abundance was assessed: transported, lagoonal, marine and epiphytes. The downcore variations of these categories are described below and shown in Fig. 2:

- Transported: group composed by reworked Miliolids, *Ammonia beccarii* and *Elphidium crispum*. These specimens are characterized by an altered coloration and an intense abrasion on their tests. Two or even three cycles of upward-decreasing abundance can be identified. The relative abundance of this category is remarkably large in the lower section of the core, with a maximum value of 37,89% at -160 cm, then it decreases until -80 cm, where there is another peak of 33,04%; finally, it decreases again towards the top, reaching the 0% at -10 cm.

- Lagoonal: group composed by *Haynesina depressula*, *H. germanica*, *Pararotalia* spp., *Ammonia tepida*, *Elphidium granosum* and *E. translucens*; this category has a stable relative abundance of about 10-15% throughout the whole core, with a maximum value of 22,92% at -30 cm.

- Marine: group composed by in situ Miliolids (small and with a white and well-preserved test), *Bolivina* spp., *Cassidulina carinata*, *Globocassidulina subglobosa*, *Bulimina* spp., *Uvigerina* spp., *Valvulineria* spp., *Discorbis* spp., *Cibicides*

refulgens and *Nonion* spp.; the relative abundance of this category has an upward increasing trend, with a maximum value of 70,00% at -20 cm.

- Epiphytes: group composed by *Textularia* spp., *Reussella spinulosa*, *Neoconorbina terquemi*, *Rosalina* spp. and *Asterigerinata mamilla*; this category is directly connected to the marine one regarding the ecological meaning, since most of these identified epiphytes is related, in the Mediterranean, to a fully marine environment with *Posidonia oceanica*; the relative abundance of this category has an upward increasing trend, with a large peak corresponding to 33,02% at -60 cm.

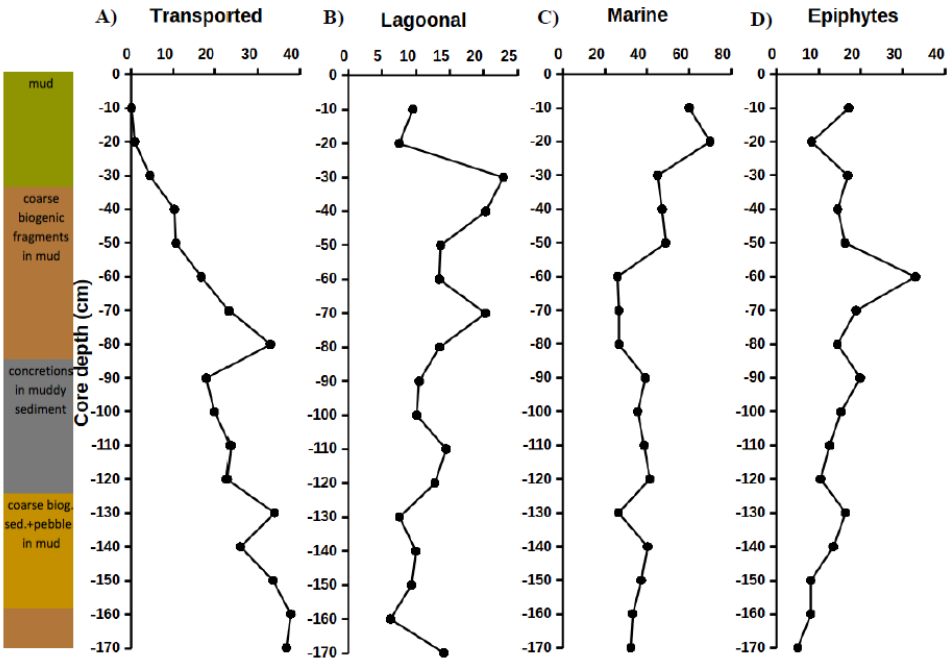

Fig. 2 Plots showing the relative abundance of the four ecological categories (A: transported; B: lagoonal; C: marine; D: epiphytes) along the sedimentary core expressed as percentage (%).

The ratio of planktonic foraminifera vs total foraminifera (%P) corrected for infaunal species, expressed as percentage (van der Zwaan et al., 1990) is notably large in the lower section of the core, with values around 80% from -150 to -90 cm and a maximum of 84,35% at -140 cm, while, starting from -90 cm, this ratio decreases towards the top, with a relevant increase in the last two samples.

Conclusions

The variation in the relative abundance of ecological groups is interpreted as a transgressive cycle from the Last Glacial Maximum or previous glacial phases. The upward decrease in the transported tests is coupled with an increase in the percentage of marine and epiphytes: this suggests an upward deepening trend. Such results well agree with the data of Bracchi et al. (2019), although the analysis of planktonic foraminifera and ^{14}C dating will allow a better constrain of the evolution of the tabular relief. High values of %P in the lower section of the core are still debated. They could result from: an intense erosional activity during glacial phases, vertical migration of older material in correspondence of mud volcanoes or peculiar paleoecological conditions.

Acknowledgements

We acknowledge the shiptime through the 2006-2007 Italian PRIN 'MESC' program, funded by the Italian Ministry of Research and Technology (MIUR). FG benefitted from a grant through the Erasmus Traineeship Program to work at the University of Athens. This is a scientific contribution of Italian Project MIUR - Dipartimenti di Eccellenza 2018-2022

References

Bracchi V.A. Basso D., Savini A., Corselli C., 2019. Algal reefs (Coralligenous) from glacial stages: Origin and nature of a submerged tabular relief (Hyblean Plateau, Italy). Marine Geology, 411:119-132.

Savini, A., Malinverno, E., Etiope, G., Tessarolo, C., Corselli, C., 2009. Shallow seep related seafloor features along the Malta plateau (Sicily channel – Mediterranean Sea): Morphologies and geo-environmental control of their distribution. Mar. Pet. Geol. 26, 1831–1848.

Van der Zwaan, G.J., Jorissen, F.J., De Stigter, H.C., 1990. The depth dependency of planktonic/ benthic foraminiferal ratios: constraints and applications. Marine Geology 95, 1–16.

Cranial Sinuses of Bovidae from Late Miocene of Greece

D. Liakopoulou[1], S. Roussiakis[1]

(1) National and Kapodistrian University of Athens, Department of Geology and Geoenvironment, Panepistimioupoli Zografou, 15784 Athens, Greece, dliakopoulou@geol.uoa.gr

Cranial morphology of Late Miocene bovid species is presented, as part of a greater project, with the use of computed tomographic methods. The non-destructive nature of this method allows (3D) digital representation of cranial internal features of fossilized material in high resolution, thus giving the unique opportunity to examine otherwise inaccessible parts of the skull.

The cranial internal structures of fossilized mammals are to this day one of the most poorly described features. Most studies of internal morphology concern extant species and the majority of them have focused on primates (Rae and Koppe, 2003; Farke, 2007, Rae, 2008; Kostopoulos *et al*., 2018; Miguel *et al.*, 2018). Indeed, cranial sinuses – air-filled chambers resulting from the removal of bone by a pneumatic diverticulum – have yet to be studied for fossil taxa in order to assess their functional role (Edinger, 1950; Farke, 2010). Frontal sinuses, as part of the paranasal sinuses, are believed to form as pneumatic spaces that develop opportunistically where bone is not mechanically necessary, leading to reduction of the skull mass and so improvement of its performance (Curtis *et al*., 2014). Their function is not well understood, it has been suggested that frontal sinuses might aid the absorption of shock and/or dissipation of stress during feeding and combat (Badlangana *et al.*, 2011; Farke, 2008; Snively and Theodor, 2011; Alsafy *et al.*, 2013; Curtis, 2014).

Fossil bovids from the Late Cenozoic are studied in order to extract data that will clarify the mysterious functions and evolutionary development of internal cranial features. Bovidae are used because of the exceptional diversity in cranial characters in terms of size and shape, which consists an excellent opportunity for identifying the most important morphological aspects. Furthermore, the Late Cenozoic consists a period with major climatic changes and variations, which put these animals under big selective pressure. Therefore, the most successful animals were those that were adapted to specific conditions, which possibly led to their diversification.

This project is extensively using X-ray computed tomography. The skulls of several bovid species were chosen to be subjected to CT imaging. This method was chosen because it is the only high-resolution and non-invasive/non-destructive one available that provides information to inaccessible areas and structures of the skull. Additionally, it gives the opportunity to work on available Museum/University specimens, thus providing more information to the final results. Therefore, a Philips CT 64-slice tomographer from the Konstantopouleio General Hospital ‘Agia Olga’ and an Optima LG CT 64-slice tomographer from the University General Hospital of Thessaloniki ‘AHEPA’ were used. The CT data obtained are imported to advance imaging software (Avizo 8.1 and Mimics) to provide the digital reconstructions of the skulls internally and externally, that allow all digital measurements, volumetric and linear ones.

The results will consist a base for further studies on other groups of mammals, both for the identification of the most useful morphological characters, and for the establishment of a novel methodological framework for this type of work. Lastly, the phylogenetic relationships of bovids will be analysed and provide an explanation of the morphological diversity of the recent species of the group.

Herein we present an example of certain specimens that reveals these sinuses in their entity, and we comment on the expectations of this project in terms of interpreting the function of these features and whether these features add on phylogenetic interpretations.

Acknowledgements

For access to material from Aristotle University of Thessaloniki and permission to CT scan them we thank Prof. D. Kostopoulos. Special thanks deserve to Dr. Maniatis P. and his team (especially to Dr. Moschouris P. and Dr. Tsipra E.) at the Konstantopouleio General Hospital ‘Agia Olga’ and Dr. Kalogera A. and her team at the University General Hospital of Thessaloniki ‘AHEPA’, both for giving us access to CT medical equipment.

References

Alsafy, M.A.M., El-Gendy, S.A.A., El Sharaby, A.A., 2013. Anatomic reference for computed tomography of paranasal sinuses and their communication in the Egyptian buffalo (*Bubalus bubalis*). Journal of Veterinary Medicine Series C: Anatomia Histologia Embryologia,Anat. Histologia Embryol., 42(3), 220-231.

Badlangana, N. L., Adams, J.W., Manger, J.R., 2011. A Comparative Assessment of the Size of the Frontal Air Sinus in the Giraffe (*Giraffa Camelopardalis*). The Anatomical Record 294, 931–940.

Curtis, A.A., Lai, G., Wei, F., Van Valkenburgh, B., 2014. Repeated loss of frontal sinuses in arctoid carnivorans. Journal of Morphology 276, 22-32

Curtis, A.A., 2014. A three-dimensional quantitative investigation of frontal sinus morphology and function in mammalian carnivores. Ph.D. Thesis in Biology, University of California, 128 p.

Edinger, T., 1950. Frontal sinus evolution particularly in the Equidae. Bulletin of the Museum of Comparative Zoology at Harvard 103, 409-496.

Farke, A.A., 2007. Morphology, constraints, and scaling of frontal sinuses in the hartebeest, *Alcelaphus buselaphus* (Mammalia:

Artiodactlya, Bovidae). Journal of Morphology 268, 243–253
Farke, A.A., 2008. Frontal sinuses and head-butting in goats: a finite element analysis. Journal of Experimental Biology 211, 3085–3094.
Farke, A.A., 2008. Function and evolution of the cranial sinuses in bovid mammals and ceratopsian Dinosaurs. Ph.D. Thesis in Anatomical Sciences, Stony Brook University.
Farke, A.A., 2010. Evolution and functional morphology of the frontal sinuses in Bovidae (Mammalia: Artiodactyla), and implications for the evolution of cranial pneumaticity. Zoological Journal of the Linnean Society, 159, 988-1014.
Kostopoulos, D.S., Guy, F., Kynigopoulou, Z., Koufos, G.D., Valentin, X., Merceron, G., 2018. A 2Ma old baboon-like monkey from Northern Greece and new evidence to support the *Paradolichopithecus - Procynocephalus* synonymy (Primates : Cercopithecidae). Journal of Human Evolution 121, 178–192.
Miguel, R., Higgins, P. O., 2018. The biomechanical significance of the frontal sinus in Kabwe 1 (*Homo heidelbergensis*). Journal of Human Evolution, 114, 141–153. doi: 10.1016/j.jhevol.2017.10.007.
Rae, T.C., Koppe, T., 2003. The term 'lateral recess' and craniofacial pneumatization in Old World monkeys (Mammalia, Primates, Cercopithecoidea). Journal of Morphology 258, 193–199.
Rae, T. C., 2008. Paranasal pneumatization in extant and fossil Cercopithecoidea. Journal of Human Evolution, 54(3): 279–286.
Snively, E., Theodor, J.M., 2011. Common Functional Correlates of Head-Strike Behavior in the Pachycephalosaur *Stegoceras validum* (Ornithischia, Dinosauria) and Combative Artiodactyls. PloS ONE 6:e21422

15th International Congress of the Geological Society of Greece
Athens, 22-24 May, 2019 | Harokopio University of Athens, Greece
Bulletin of the Geological Society of Greece, Sp. Pub. 7 Ext. Abs. GSG2019-317

Towards a Biostratigraphic-Controlled Chronostratigraphic Framework for the Aegean Sea (Eastern Mediterranean)

G. Gkaniatsa[1], A. Antonarakou[1], G. Kontakiotis[1], V. Lianou[1], G. Anastasakis[1]

(1) Department of Geology & Geoenvironment, Section of Historical Geology-Paleontology, National & Kapodistrian University of Athens, Panepistimiopolis, Zografou, 15784, Greece

The last half-century considerable interest has developed on the role of the (sub) tropical oceans in climate change, and in particular, oceanic sub-basins and marginal seas that are often more responsive to paleoceanographic and paleoclimatic changes than broader global ocean basins, because of their smaller size and partial isolation (Kontakiotis, 2016; Kontakiotis *et al*., 2013; Marino *et al*., 2009; Antonarakou *et al.,* 2015, 2019). As an example, the small volume of the Mediterranean Sea, compared with ocean basins, causes changes in its climatic forcing to be recorded virtually instantaneously in palaeoceanographic proxy data, such as stable isotope and other geochemical ratios, and microfossil abundances. The basin's limited communication with the open ocean implies that any climatic signals will be recorded in an amplified fashion in Mediterranean properties, such as temperature, salinity and specific elemental concentrations (Kontakiotis, 2012). Especially the eastern Mediterranean is ideal for addressing proposed forcing mechanisms of tropical climate variability (Kontakiotis, 2016; Casford *et al*., 2007) due to its intermediate position between the higher-latitude (i.e. North Atlantic-influenced) and lower-latitude (i.e. monsoonally influenced) climate systems. This heightened sensitivity to the effects of climate variations seems to be especially true for the Aegean Sea, because of the combination of its semi-isolation from the rest of the Mediterranean Sea, its small size, large topographic contrasts acting as specific boundary conditions, the abundance of local freshwater inputs and the regional climate.

To better understand the impact of these parameters on the regional climate, a number of studies has focused on the paleoceanographic evolution of the basin during the late Quaternary (e.g., Drinia *et al*., 2016; Kontakiotis, 2016; Koutrouli *et al*., 2018). However, the reconstruction of the variability of late Quaternary climate needs a detailed chronostratigraphic control. In this respect, a notable contribution is particularly required by micropaleontological, biogeochemical, and sedimentological studies. In particular, morphological and compositional changes in the planktonic foraminiferal assemblages recorded in marine sediments and/or the water column provide detailed information on the physical and chemical properties of the surrounding water masses and their relationships with climatic variability (Antonarakou *et al*., 2015; Kontakiotis, 2016; Zarkogiannis *et al*., 2019). They also allow the definition of a detailed sequence of regional eco-bioevents for the late Quaternary, reflecting the climatic oscillations that represent an important tool for an accurate subdivision of the late Quaternary stratigraphic record and facilitate correlations between sites in the different sub-basins (Casford *et al*., 2007; Budillon *et al*., 2009; Triantaphyllou *et al*., 2009; Siani *et al*., 2010; Lirer *et al*., 2013; Antonarakou *et al*., 2019).

This study aimed at achieving high resolution sediment cores at sub-centennial to centennial scale, and therefore highlights the planktonic foraminiferal abundance variations during the last glacial cycle from two gravity cores (M-22-67and NS-18) along the Aegean Sea. In particular, the relative abundance of selected climate-sensitive planktonic foraminiferal species have led us to identify several eco-bioevents in *G. ruber alba, G. ruber rosea, G. bulloides, G. inflata, T.quinqueloba, N. pachyderma, N durtertrei, O. universa, G. sihonifera, G. trilobus, G. scitula, G. rubescens, G. glutinata,* and *G. trucatulinoides*. All faunal events have been defined by morphospecies evolution, first local occurrences and disappearances of a given species, prominent changes in coiling direction, frequency shifts and strong inflections in the faunal record, with reference to the pioneer work of Casford *et al*. (2007). The similarity between the two north and south Aegean records underlines the utility to support conventional dating methodologies with different constraints, and further reveals a powerful tool for reliably correlating marine records between comparable deep-sea marginal settings and/or an original dating tool for coeval sequences of this region. Overall, the bioevents chronology combined with ^{14}C-AMS data could be used to define an updated and comprehensive age model that can be considered as a useful paleoclimatic and stratigraphic reference record for the entire eastern Mediterranean Sea.

References

Antonarakou, A., Kontakiotis, G., Mortyn, P.G., Drinia, H., Sprovieri, M., Besiou, E., Tripsanas, E., 2015. Biotic and geochemical (δ^{18}O, δ^{13}C, Mg/Ca, Ba/Ca) responses of *Globigerinoides ruber* morphotypes to upper water column variations during the last deglaciation, Gulf of Mexico. Geochim. Cosmochim. Acta 170, 69–93, doi: 10.1016/j.gca.2015.08.003.

Antonarakou, A., Kontakiotis, G., Karageorgis, A.P., Besiou, E., Zarkogiannis, S., Drinia, H., Mortyn, P.G., Tripsanas, E., 2019. Eco-biostratigraphic advances on late Quaternary geochronology and paleoclimate: The marginal Gulf of Mexico analogue. Geol. Quart. 63 (1).

Budillon, F., Lirer, F., Iorio, M., Macri, P., Sagnotti, L., Vallefuoco, M., Ferraro, L., Garziglia, S., Innangi, S., Sahabi, M., Tonielli, R., 2009. Integrated stratigraphic reconstruction for the last 80 kyr in a deep sector of the Sardinia Channel (Western Mediterranean). Deep-Sea Res. II 56, 725–737.

Casford, J.S.L., Abu-Zied, R.H., Rohling, E.J., Cooke, S., Fontanier, C., Leng, M., Millard, A., Thomson, J., 2007. A stratigraphically controlled multiproxy chronostratigraphy for the eastern Mediterranean. Paleoceanography, 22, PA4215,

doi:10.1029/2007PA001422.
Drinia, H., Antonarakou, A., Tsourou, T., Kontakiotis, G., Psychogiou, M., Anastasakis, G., 2016. Foraminifera eco-biostratigraphy of the southern Evoikos outer shelf, central Aegean Sea, during MIS 5 to present. Cont. Shelf. Res. 126, 36–49.
Kontakiotis, G., 2012. Palaeoceanographic and palaeoclimatic study of Eastern Mediterranean during Late Quaternary, based on planktonic foraminiferal assemblages, PhD Thesis, National & Kapodistrian University of Athens, Greece, pp. 1–247.
Kontakiotis, G., 2016. Late Quaternary paleoenvironmental reconstruction and paleoclimatic implications of the Aegean Sea (eastern Mediterranean) based on paleoceanographic indexes and stable isotopes. Quater. Internat. 401, 28–42, doi:10.1016/j.quaint.2015.07.039.
Koutrouli, A., Anastasakis, G., Kontakiotis, G., Ballengee, S., Kuehn, S., Pe-Piper, G., Piper, D.J.W., 2018. The early to mid-Holocene marine tephrostratigraphic record in the Nisyros-Yali-Kos volcanic center, SE Aegean Sea. J. Volc. Geoth. Res., 366, 96–111.
Lirer, F., Sprovieri, M., Ferraro, L., Vallefuoco, M., Capotondi, L., Cascella, A., Petrosino, P., Insinga, D.D., Pelosi, N., Tamburrino, S., Lubritto, C., 2013. Integrated stratigraphy for the Late Quaternary in the eastern Tyrrhenian Sea. Quat. Int. 292, 71–85.
Marino, G., Rohling, E.J., Sangiorgi, F., Hayes, A., Casford, J.L., Lotter, A.F., Kucera, M., Brinkhuis, H., 2009. Early and middle Holocene in the Aegean Sea: interplay between high and low latitude climate variability. Quat. Sci. Rev. 28, 3246–3262.
Siani, G., Paterne, M., Colin, C., 2010. Late Glacial to Holocene planktic foraminifera bioevents and climatic record in the South Adriatic Sea. J. Quat. Sci. 25(5), 808–821.
Triantaphyllou, M.V., Antonarakou, A., Kouli, K., Dimiza, M., Kontakiotis, G., Papanikolaou, M.D., Ziveri, P., Mortyn, P.G., Lianou, V., Lykousis, V., Dermitzakis, M.D., 2009. Late Glacial-Holocene ecostratigraphy of the south-eastern Aegean Sea, based on plankton and pollen assemblages. Geo. Mar. Lett. 29(4), 249–267.
Zarkogiannis, S.D., Antonarakou, A., Tripati, A., Kontakiotis, G., Mortyn, P.G., Drinia, H., Greaves, M., 2019. Influence of surface ocean density on planktonic foraminifera calcification. Scientific Reports, 9, 533, DOI:10.1038/s41598-018-36935-7.

15th International Congress of the Geological Society of Greece
Athens, 22-24 May, 2019 | Harokopio University of Athens, Greece
Bulletin of the Geological Society of Greece, Sp. Pub. 7 Ext. Abs. GSG2019-318

Biogenic sedimentation in the North Aegean Sea and climatic implications

E. Skampa[1], M.V. Triataphyllou[1], M.D. Dimiza[1], A. Gogou[2], E. Malinverno[3], S. Stavrakakis[2], I.P. Panagiotopoulos[1, 2], C. Parinos[2], K.-H. Baumann[4]

(1) National and Kapodistrian University of Athens, Department of Geology and Geoenvironment, Panepistimiopolis 15784 Athens, Greece, elskampa@geol.uoa.gr
(2) Hellenic Centre for Marine Research, Institute of Oceanography, PO Box 712, 19013 Anavyssos, Greece
(3) University of Milano-Bicocca, Department of Earth and Environmental Sciences, Italy
(4) University of Bremen, Department of Geosciences, PO Box 33 04 40, 28334 Bremen, Germany

Background-Objectives

Coccolithophore assemblages that are recorded in marine sediments generally comprise a successful palaeontological tool for the reconstruction of the paleoclimatic and paleoceanographic conditions in the geological past (e.g., Triantaphyllou et al., 2009; Gogou et al., 2016), as they represent reliable indicators of environmental conditions (e.g., Baumann et al., 2000). However, little is known about the transformation of living coccolithophore communities into coccolith assemblages within the underlying sediments.

In the oligotrophic waters of the Eastern Mediterranean Sea, the high seasonality of the oceanographic parameters affects the coccolithophore abundance and productivity (e.g., Dimiza et al., 2015). The North Aegean Sea (NE Mediterranean) displays less oligotrophic characteristics during the highest productivity spring period (Ignatiades et al., 2002). In the North Aegean Sea, surface Black Sea water outflows from the Dardanelles and meets the salty Levantine waters coming from the southern part of The Aegean. Due to the hydrographic regime, North Aegean supported a deep-water formation, under the influence of anomalously cold winters, known as the Eastern Mediterranean transient (EMT), which has been proven to ventilate the water column of the basin from the surface down to 650 m (Velaoras et al., 2017).

The present study uses new data from the North Aegean sampling site M2, provided by sediment trap time series (Skampa et al., 2019), surface sediments combined with plankton samples (Dimiza et al., 2015) and a sediment core record (Gogou et al., 2016), in order to make a synthesis of the coccolithophores' regime in the photic zone and assess their contribution to the sinking matter towards the seafloor, their preservation as surface sediment particles and, finally, their impact to the sedimentary record (Skampa et al., 2019). The understanding of the modifications between the plankton vs. the exported assemblages and the sediment taphocoenoses can further establish coccolithophores as valuable proxies for the investigation of water column response to paleoceanographic changes (e.g., dense water formation events) in the North Aegean and analogous oceanic sites of deep water formation.

Methods

Quantitative coccolithophore analyses were performed on plankton samples datasets from the Athos basin in the North Aegean Sea (Athos basin-M2 site), which have been collected during January and May 2011 (Dimiza et al., 2015). In addition, the sinking particulate matter derived from a sediment trap deployed at 500 m depth in the Athos basin (M2 site) was examined in order to estimate export fluxes for the time interval January- December 2011 (Triantaphyllou et al., 2014) and October 2014-November 2015 (Skampa et al., 2019). Coccolithophore analyses of surface and core sediments from a 48-cm long multicore (M2), retrieved in 2011 from the same site in the North Aegean Sea (Athos basin, water depth 1018 m), have been conducted in a decadal to multi-decadal high resolution record (Gogou et al., 2016).

Results and Discussion

Emiliania huxleyi was the dominant species in all sampling types, occurring in high relative abundances in the current plankton (~90%) and sediment trap samples (~70%), especially during the low-temperature, high precipitation and max Chl-a winter-spring period. *Emiliania huxleyi* prevailed in the plankton samples with the subordinate presence of Syracosphaeraceae. The species *Florisphaera profunda* was not included in the upper water column plankton assemblage, most probably due to sampling depth limitations, but was present in the sediment traps and surface sediments, presuming to flourish in nutrient-enriched layers below the sampled 100 m water column depth. Plankton samples revealed a well-developed upper euphotic zone community but several fragile *Syracosphaeraceae* and holococcolithophore species were not present in the sinking assemblage or on the seafloor; apparently, currents and circulation patterns of the North Aegean have an impact on the distribution of coccolithophore assemblages and convert them while sinking from the euphotic zone to the seafloor. However, the main features of the living assemblages were generally preserved (Skampa et al., 2019).

Sediment trap calcareous nannoplankton multiannual mean fluxes documented similar values to the accumulation rates recorded in the surface sediment (Skampa et al., 2019). Apart from the loss of the more fragile holococcolithophore species and the delicate *Algirosphaera robusta*, the main features of the living assemblages were generally preserved on the seafloor, pointing out calcareous nannoplanktons' importance as reliable proxy for paleoenvironmental reconstructions.

The coccolithophore assemblage of the past 500 years revealed a periodic occurrence of "*E. huxleyi* dominance" intervals (~60%), indicating strong water column convection EMT-like events, which have been described in the recent fossil

record (last 500 years; Gogou et al., 2016; Incarbona et al., 2016), coupled with positive shifts of the North Atlantic Oscillation (NOA) and volcanic activity within the Dalton solar minimum (Skampa et al., 2019). In contrast, the analogous occurrence of "*F. profunda* dominance" intervals may be linked to increased sea surface temperatures, and stratified conditions in the water column potentially associated with Black Sea Water intrusions (Skampa et al., 2019).

Acknowledgements

The funding for the fulfilment of this study was provided by the Greek National Project KRIPIS (Integrated Observatories in the Greek Seas - IO, HCMR-MIS 451724; NSRF), the European Research Project MedEcos (MarinERA, EU/FP6) and the IKYDA program of the DAAD (project 57260124 AegeanCocco). The first author E. Skampa has been granted with a scholarship from the State Scholarships Foundation. This research is co-financed by Greece and the European Union (European Social Fund- ESF) through the Operational Programme «Human Resources Development, Education and Lifelong Learning» in the context of the project "Strengthening Human Resources Research Potential via Doctorate Research" (MIS-5000432), implemented by the State Scholarships Foundation (IKY). Also, we would like to thank the two anonymous reviewers and the journal chief editor Dr Richard Jordan for their constructive comments that significantly helped us to improve the quality of this manuscript during the revision process.







References

Baumann, K.-H., Andruleit, H.A., Samtleben, C., 2000. Coccolithophores in the Nordic Seas: comparison of living communities with surface sediment assemblages. Deep-Sea Research II 47, 1743–1772.

Dimiza, M., Triantaphyllou, M.V., Malinverno, E., Psarra, S., Karatsolis, BT., Mara, P., Lagaria, A., Gogou, A., 2015: The composition and distribution of living coccolithophores in the Aegean Sea (NE Mediterranean). Micropaleontology 61, 521–540.

Gogou, A., Triantaphyllou, M., Xoplaki, E., Izdebski, A., Parinos, C., Dimiza, M., Bouloubassi, I., Luterbacher, J., Kouli, K., Martrat, B., Toreti, A., Fleitmann, D., Rousakis, G., Kaberi, H., Athanasiou, M., Lykousis, V., 2016: Climate variability and socio-environmental changes in the northern Aegean (NE Mediterranean) during the last 1500 years. Quaternary Science Reviews 136, 209–228

Ignatiades, L., Psarra, S., Zervakis, V., Pagou, K., Souvermezoglou, E., Assimakopoulou, G., Gotsis-Skretas, O., 2002. Phytoplankton size-based dynamics in the Aegean Sea (Eastern Mediterranean). Journal of Marine Systems 36, 11–28.

Incarbona, A., Matrat, B., Mortyn, G.P., Sprovieri, M., Ziver,i P., Gogou, A., Jorda, G., Xoplaki, E., Luterbacher, J., Langone, L., Marino, G., Rodriguez-Sanz, L., Triantaphyllou, M., Di Stefano, E., Grimalt, J.O., Tranchida, G., Spriovieri, R., Mazzola, S., 2016. Mediterranean circulation perturbations over the last five centuries: Relevance to past Eastern Mediterranean Transient-type events, Scientific Reports 6, 29623.

Skampa, E., Triantaphyllou, M.V., Dimiza, M.D., Gogou, A., Malinverno, E., Stavrakakis, S., Panagiotopoulos, I.P., Parinos, C., Baumann, K.-H., 2019. Coupling plankton - sediment trap - surface sediment coccolithophore regime in the North Aegean Sea (NE Mediterranean). Marine Micropaleontology, in press, DOI: https://doi.org/10.1016/j.marmicro.2019.03.001

Triantaphyllou, M.V., Gogou, A., Bouloubassi, I., Dimiza, M., Kouli, K., Rousakis, G., Kotthoff, U., Emeis, K.C., Papanikolaou, M., Athanasiou, M., Parinos, C., Ioakim, C., Lykousis, V., 2014. Evidence for a warm and humid Mid-Holocene episode in the Aegean and northern Levantine Seas (Greece, NE Mediterranean). Regional Environonmental Change 14, 1697–1712.

Triantaphyllou, M.V., Ziveri, P., Gogou, A., Marino, G., Lykousis, V., Bouloubassi, I., Emei,s K.C., Kouli, K., Dimiza, M., Rosell-Mele, A., Papanikolaou, M., Katsouras, G., Nunez, N., 2009. Late Glacial-Holocene climate variability at the south-eastern margin of the Aegean Sea. Marine Geology 266, 182–197.

Velaoras, D., Papadopoulos, V.P., Kontoyiannis, H., Papageorgiou, D., Pavlidou, A., 2017. The response of the Aegean Sea (Eastern Mediterranean) to the Extreme 2016–2017 Winter. Geophysical Research Letters, 44, doi.org/10.1002/2017GL074761.

15th International Congress of the Geological Society of Greece
Athens, 22-24 May, 2019 | Harokopio University of Athens, Greece
Bulletin of the Geological Society of Greece, Sp. Pub. 7 Ext. Abs. GSG2019-321

Marine Geomorphology and environmental status of Elefsis Bay and inner Saronikos Gulf, Greece. A multidisciplinary analysis.

A. Katsigera[1], M. Dimiza[1], O. Koukousioura[1], A.-I. Anastasiadis[3], K. Pavlopoulos[4], M. Triantaphyllou[1]

(1) Department of Geology and Geoenvironment, National and Kapodistrian University of Athens, Panepistimiopolis 15784 Athens, Greece, annakat@geol.uoa.gr
(2) Aristotle University of Thessaloniki, School of Geology, 54124, Thessaloniki, Greece
(3) Laboratory Mineralogy-Geology, Agricultural University of Athens, Iera Odos 75, 11855 Athens, Greece
(4) Paris Sorbonne University Abu Dhabi, Geography and Planning Department, P.O. 38044, Abu Dhabi, United Arab Emirates

Introduction

Saronikos Gulf is located in the Aegean Sea between Attica and eastern Peloponnese Peninsula and is considered as a hot spot site for the particular environmental conditions and sea floor morphology. Through the ages, the coastal areas surrounding the gulf where used for economic and strategic purposes, with the most important of these being the Pireaus port and Elefsis Bay. Both are located on the north eastern part of the gulf and are strongly linked to human activities since the beginning of the ancient greek civilization. The area holds a great geomorphological and environmental interest, due to the human intervention since the ancient times but also due to the various landforms and processes that form its amazing underwater and coastal landscapes. In addition, the industrial activities along the coast of Elefsis Bay in the north east of Saronikos Gulf, affect the ecosystems, leaving traces of human activity that impacts the environmental status of the inner Saronikos Gulf.

Foraminifera are one of the most spread and diverse group of meiofauna. Especially benthic foraminifera are commonly used as bio-indicators of both natural and human-stressed environments and are increasingly used in environmental monitoring in coastal and marginal marine ecosystems (e.g., Dimiza *et al.*, 2016a, b).

Objectives

The main aim of this study is to create bathymetry maps in order to record the coastal and marine geomorphology of the gulf and to show the dynamic evolution of the coastline for the past 11.500 years. In addition, the study of foraminiferal thanatocoenoses in relation with their bathymetric distribution aims to relate the marine landforms with the recent processes and environmental conditions and efficiently describe the environmental profile of the area.

Materials and methods

For the creation of the bathymetry map we used a combination of data collected from field studies and available archive data from the Hellenic Center for Marine Research (HCMR) and the Institute of Geology and Mineral Exploration (IGME). Gis techniques (ArcGis from ESRI) were used to record the bathymetry of the gulf. Concerning the foraminiferal analysis, sediments were collected as small push-cores (mean depth about 10 cm) from box corers onboard the R/V Aegaeo from 12 sampling stations, four in Elefsis Bay and eight in Saronikos Gulf in February 2016, at water depths ranging from 15 to 95 m. Surface sediments (0-1 cm) from each station were collected and were immediately stained with rose Bengal dissolved in 70% ethanol (2g l^{-1}) to facilitate the distinction between live and dead foraminifera. Approximately 2g of each sample was washed in the laboratory and sieved over 125μm and 63μm mesh and oven dried. A total of up to 300 not stained (dead) handpicked benthic foraminifera for each sample were obtained using an Otto microsplitter. All subsamples were examined under a Leica APO S8 stereoscope, following Cimerman and Langer (1991), Dimiza *et al.* (2016a), Milker *et al.* (2009) and Sgarrella and Moncharmont Zei (1993) for species classification and species relative abundances have been calculated. Proportional Similarity (PS) between the species composition of dead and living foraminiferal associations was calculated using the Renkonen index (Renkonen, 1938).

Results – Discussion

The benthic foraminiferal assemblage structure (*H'* index) and the ecological quality classification tool, Foram Stress Index (FSI) as plotted in the georeferenced maps indicated an environmental amelioration for Inner Saronikos Gulf; e.g., upgrade of Ecological Quality Status (EcoQS) from moderate to good quality during the investigated time interval 2012-2016. In contrast, the central part of the Elefsis Bay evidenced an on-going poor environment status throughout the monitoring period. As this part of Saronikos Gulf is experiencing severe oxygen depletion due to limited water circulation during summer, further sampling during the summer period is needed to explore any seasonal difference that can be recorded in the foraminiferal assemblages.

A low-diversity assemblage, dominated by stress-tolerant *Ammonia tepida* and *Bulimina* spp., was characteristic of samples from Elefsis Bay. Samples from the western and central part of Saronikos Gulf were the most variable, characterized by a mix of stress-tolerant and more sensitive taxa, especially *Bulimina* spp. and *Nonion fabum*. In contrast, samples from the coast of Salamis and at the eastern sector of the gulf were characterized by a diverse assemblage that mostly included miliolids and small, epiphytic rotaliid taxa, and the dominant species *Haynesina germanica* and *Bulimina aculeata*.

According to the foraminiferal distribution, it appears that north east Elefsis Bay the high levels of *Bulimina* spp. indicate

periods of anoxic events along with eutrophic conditions while western and central Saronikos is more variable with areas affected by stress and low oxygen periods in the south east of Salamis island and less stress environments in the north east of the island. In the shallow shelf environments of the Mediterranean Sea, the main environmental parameters affecting the distribution pattern of the benthic foraminifera are temperature, salinity and substrate type (Basso and Spezzaferri, 2000; Hyams-Kaphzan et al., 2008; Milker *et al.*, 2009; Samir *et al.*, 2003). Several ecological studies have demonstrated that the environmental variables controlling the distribution pattern of benthic foraminiferal assemblages vary with water depth (e.g., De Rijk *et al.*, 2000; Rossi and Horton, 2009), while Milker *et al.* (2009) showed distinct benthic foraminifera bathymetric zonation linked to substrate, water turbulence and food availability. According to Dimiza *et al.* (2016a) several environmental conditions impact on the taphonomic processes. The studied assemblages provided us concerning the relation of dead fauna and bathymetry when considering Renkonen index. The calculated PS exhibited high degree of similarity with an average value of PS= 67 ±6.8 in Elefsis Bay and intermediate similarity values with an average of PS= 31 ±5.9 in the inner Saronikos, suggesting negligible transport processes in the shallower parts of the gulf.

References

Basso, D., Spezzaferri, S., 2000. The distribution of living (stained) benthic foraminifera in Iskenderun Bay (eastern Turkey): a statistical approach. Soc. Paleontol. Ital. 39, 359–379.

Cimerman, F., and Langer, M.R. (1991). Mediterranean foraminifera. Acad. Sci. Artium Slov. Dela Opera 30 Cl. IV Hist. Nat. 118, pls. 93.

De Rijk, S., Jorissen, F.J., Rohling, E.J., Troelstra, S.R., 2000. Organic flux control on bathymetric zonation of Mediterranean benthic foraminifera. Mar. Micropaleontol. 40, 151–166.

Dimiza, M. D., Koukousioura, O., Triantaphyllou, M. V., Dermitzakis, M. D., 2016a. Live and dead benthic foraminiferal assemblages from coastal environments of the Aegean Sea (Greece): Distribution and diversity. Revue de Micropaléontologie, 59(1), 19–32.

Dimiza, M.D., Triantaphyllou, M.V., Koukousioura, O., Hallock, P., Simboura, N., Karageorgis, A.P., Papathanasiou, E., 2016b. The Foram Stress Index: A new tool for environmental assessment of soft-bottom environments using benthic Foraminifera. A case study from the Saronikos Gulf, Greece, Eastern Mediterranean. Ecological Indicators 60, 611–621.

Hyams-Kaphzan, O., Almogi-Labin, A., Sivan, D., Benjamini, C., 2008. Benthic foraminifera assemblage change along the southeastern Mediterranean inner shelf due to fall-off of Nile-derived siliciclastics. Neues Jb. Geol. Paläontol. Abh. 248, 315–344.

Milker, Y., Schmiedl, G., Betzler, C., Römer, M., Jaramillo-Vogel, D., and Siccha, M. (2009). Distribution of recent benthic foraminifera in shelf carbonate 52 environments of the Western Mediterranean Sea. Mar. Micropaleontol. 73, 207–225.

Renkonen, O., 1938. Statisch-okologische Untersuchungen uber die terrestiche kaferwelt der finnischen bruchmoore. Annales Botanici Societatis Zoologicæ-Botanicæ Fennicæ “Vanamo” 6, 1–231.

Rossi, V., Horton, B.P., 2009. The application of subtidal foraminifera-based transfer function to reconstruct Holocene paleobathymetry of the Po Delta, northern Adriatic Sea. J. Foraminifer. Res. 39, 180–190.

Samir, A.M., Abdou, H.F., Zazou, S.M., El-Menhawey,W.H., 2003. Cluster analysis of recent benthic foraminifera from the northwestern Mediterranean coast of Egypt. Rev. Micropalaeontol. 46, 111–130.

Sgarrella, F., and Moncharmont Zei, M. (1993). Benthic Foraminifera of the Gulf of Naples (Italy): systematics and autoecology. Boll. Della Soc. Paleontol. Ital. 32, 145–264.

Abiotic Forcing On Planktonic Foraminifera Shell Mass Variations

S. D. Zarkogiannis[1], A. Antonarakou[1], G. Kontakiotis[1], H. Drinia[1], P.G. Mortyn[2,3]

(1) National and Kapodistrian University of Athens, University Campus- Zografou, Athens, Greece, stergiosz@geol.uoa.gr
(2) Institute of Environmental Science and Technology (ICTA), Universitat Autònoma de Barcelona (UAB), Edifici Z - Carrer de les Columnes, Barcelona, Spain
(3) Department of Geography, Universitat Autònoma de Barcelona, Campus de la UAB, Barcelona, Spain

Planktonic foraminifera are known to alter their shell mass at glacial/interglacials cycles as a function of changing CO_2 concentrations in the ocean/atmosphere system. Nevertheless, preliminary results have shown that under similar atmospheric CO_2 concentrations planktonic foraminifera alter their mass as a function of latitude (Zarkogiannis et al., 2019b). Our analysis shows that it is ambient seawater density changes that influence calcification and causes observed planktonic foraminifera shell mass increases during glacial times relative to interglacials. The reconstruction of planktonic foraminifera shell volumes from X-ray tomography scans and ambient seawater densities from Mg/Ca and $\delta^{18}O$ data showed that a heavier shell would need to be precipitated in glacial climates in order for the increased buoyant force of a denser glacial ocean to be counteracted (Zarkogiannis et al., 2019a). The relationship between shell mass and density allows reconstructions of past ocean stratification and may have implications on the uptake of atmospheric CO_2 by the oceans.

References

Zarkogiannis, S. D., Antonarakou, A., Tripati, A., Kontakiotis, G., Mortyn, P. G., Drinia, H. and Greaves, M., 2019a. Influence of surface ocean density on planktonic foraminifera calcification. Scientific Reports 9(1): 533.

Zarkogiannis, S. D., Kontakiotis, G., Antonarakou, A., Mortyn, P. G. and Drinia, H., 2019b. Latitudinal Variation of Planktonic Foraminifera Shell Masses During Termination I. IOP Conference Series: Earth and Environmental Science 221: 012052.

15th International Congress of the Geological Society of Greece
Athens, 22-24 May, 2019 | Harokopio University of Athens, Greece
Bulletin of the Geological Society of Greece, Sp. Pub. 7 Ext. Abs. GSG2019-338

Spatial distribution of epibenthic molluscs on a Tortonian reef in central Crete, Greece

C. Psarras[1], E. Koskeridou[1], D. Merle[2], A. Antonarakou[1], G., Kontakiotis[1], I. Kyriakoulis[1]

(1) National and Kapodistrian University of Athens, Department of Geology and Geoenvironment, Section of Hist. Geology-Paleontology, Athens (Greece) cpsarras@geol.uoa.gr
(2) Muséum national d'Histoire naturelle, Département Histoire de la Terre, Unité de Paléontologie, UMR 5143 du CNRS, case postale 38, 57 rue Cuvier, F-75231 Paris cedex (France)

Coral reefs are hosts of a remarkable variety of animals and plants, ranging from a few hundred species living in the Amazon Reef, to thousands of species living in the Great Barrier Reef. The structures are made mainly from corals and shelter many species that are endangered, while some are endemic to specific niches. The health, abundance and diversity of the organisms that make up a coral reef are directly linked to the surrounding terrestrial and marine environments. For this reason, molluscs are used as bioindicators in reef ecosystems, because they are situated in a variety of ecological niches in hard substrate environments (Zuschin, 2001, Koskeridou *et al*. 2017). In this study, the community structure of Tortonian coral reef associated molluscs from Central Crete (Greece) is investigated.

In Messara basin, near Filippi village (Crete), in proximity to the reef, mollusc fossils were extracted from pebbly sandstone deposits. When evaluating the abundance of mollusc species, we detected a dominance of carnivore gastropods (53% of the species), hosting 34 species belonging to 25 genera. Some examples of carnivore species are included in families like Cassidae which feed on echinoids (Tewfik, 2013), Conidae that feed mainly on polychaete worms (Jiménez-Tenorio *et al*. 2019) and Muricidae with Naticidae that drill to feed on mollusc shells (Sawyer & Zuschin, 2011). Also, we observed a striking presence of bivalve suspension feeders, for example *Megacardita sp*., which require relatively high hydrodynamics. Furthermore, herbivore species like *Persististrombus sp*. and *Alvania sp*., as well as the spongivore *Cerithiopsis sp*. were present. Finally, considering the small coral parts and red algae in the deposits, the samples indicate a well oxygenated shallow marine paleoenvironment on a sandy bottom, with sponges, coral patches and seagrasses.

Additionally, skeletal parts of fish, as well as echinoid spines were found in sieved material. According to previous published studies, a sirenian fossil has been found in Filippi (Svana *et al*. 2010), an herbivore sea mammal, similar to those existing today on tropical coral reefs. We also gathered information about other animals living in the ecosystem, without obtaining any fossils, either because their bodies were not found or they did not have hard parts to be fossilized. The shells form habitats for a series of organisms (Alberti & Reich, 2018). Trace fossils of *Entobia* and *Caulostrepsis* are formed from sponges and boring polychaetes, respectively (Alberti & Reich, 2018). Broken and healed shells are indications of crustaceans preying on gastropod shells (Lindström & Peel, 2005, Alberti & Reich, 2018).

We are aware that our sampling material is not enough for estimating species richness (Kusworo *et al*. 2015). Despite of that fact, by taking into account the information on spatial variability and distribution patterns of organisms in modern coral reef environments (Taylor, 1968), we can address our material to a specific ecological niche in this Tortonian coral ecosystem. Using statistical analysis on our quantitative and qualitative results of the fossil fauna, we identified the ecosystem of the coral reef, for the first time in Greece. Our findings point towards a sandy environment between the beach and the reef, with a proximity towards the reef. Trophic relationships, of the organisms living in ecosystems such as the present one, have been recently discussed (Alberti & Reich, 2018). Using a similar model, we can show the trophic food chain of the niche and the complexity of the life in a Tortonian coral reef in the Mediterranean Sea. Further research will compare this material with other Miocene sampling areas, for example the Gatun locality in Panama (Alberti & Reich, 2018), and their paleoenvironmental implications, improving our knowledge about how such ecosystems functioned in the past.



Figure 1. A: Mark of a Naticid drilling mark. B: Balanid and ichnofossils *Entobia*. C: *Caulostrepsis* ichnofossils.

Acknowledgments

We thank the Special Account for Research Grants and the National and Kapodistrian University of Athens for funding our attendance to this Conference.

References

Alberti, M. & Reich, S., 2018. A palaeoecological review of the lower Gatun Formation (Miocene) of Panama with special emphasis on trophic relationships. Palaeobio Palaeoenv 98: 571.

Jiménez-Tenorio, M, Abalde, S, Uribe, J, Zardoya, R., 2019. Conidae phylogenomics and evolution. Zoologica Scripta. 48. 194-214.

Koskeridou, E., Giamali, C., Antonarakou, A., Kontakiotis, G., Karakitsios, V., 2017. Early Pliocene gastropod assemblages from the eastern Mediterranean (SW Peloponnese, Greece) and their palaeobiogeographic implications, Geobios, 50: 267–277.

Kusworo, A., Reich, S., Wesselingh, F., Santodomingo, N.,Johnson, K.,Todd, J.,Renema, W., 2015. Diversity and paleoecology of Miocene coral-associated mollusks from East Kalimantan (Indonesia). Palaios. 30. 116-12.

Lindström, A. and Peel, J.S. 2005. Repaired injuries and shell form in some Palaeozoic pleurotomarioid gastropods. Acta Palaeontologica Polonica 50 (4): 697–704.

Sawyer J., Zuschin M., 2011. Drilling predation in mollusks from the lower and middle Miocene of the central Paratethys. Palaios, 26, p. 284–297.

Svana K., Iliopoulos G., Fassoulas C., 2010. New Sirenian findings from Crete Island. Bulletin of the Geological Society of Greece, 43, 746-753.

Taylor, J., 1968. Coral Reef and Associated Invertebrate Communities (Mainly Molluscan) Around Mahe, Seychelles. Philosophical Transactions of the Royal Society B: Biological Sciences. 254. 129-206.

Tewfik, A., 2013. Ecology of the King Helmet, Cassis tuberosa (L.), in South Caicos. Caribbean Naturalist. 2. 1-10.

Zuschin, M., Hohenegger, J., Steininger, F., 2001. Molluscan assemblages on coral reefs and associated hard substrata in the Northern Red Sea. Coral Reefs. 20. 107-116.

15th International Congress of the Geological Society of Greece
Athens, 22-24 May, 2019 | Harokopio University of Athens, Greece
Bulletin of the Geological Society of Greece, Sp. Pub. 7 Ext. Abs. GSG2019-358

Micropalaeontological analysis and Palaeoenvironmental interpretation of the sedimentary sequence in the central Corinth Isthmus (central Greece)

Th. Tsourou[1], S. Cheilaris[2], E.G. Fatourou[2], I. Michailidis[2], A.P. Nikitas[2], M.A. Tzortzopoulou[2], M. Dimiza[1], M.V. Triantaphyllou[1]

(1) Section of Historical Geology – Palaeontology, Department of Geology and Geoenvironment, National and Kapodistrian University of Athens, Panepistimiopolis 15784, Athens, Greece, ttsourou@geol.uoa.gr
(2) Department of Geology - Aristotle University of Thessaloniki, 54124 Thessaloniki, Greece

Background

Corinth Isthmus is one of the fastest extending regions worldwide as it is a highly active extensional tectonic environment (Briole et al., 2000). More than 40 faults can be recognized along the Corinth Canal most of them being normal and oblique normal with fault planes dipping westwards and eastwards from the central horst, towards the Corinth and Saronic Gulfs respectively (Freyberg, 1973, Papanikolaou et al., 2015). Although the depositional patterns of the sedimentological sequences in Corinth Canal are of great interest as six transgressive-regressive cycles were recognized by Collier (1990), there are few detailed palaeoenvironmental studies based on micropalaeontological evidence (e.g. Krstic and Dermitzakis 1981; Papanikolaou et al., 2015; Pallikarakis et al., 2018).

Objectives

Purpose of this study is to contribute with detailed micropalaeontological evidence to the reconstruction of the depositional environments of the sedimentary sequence exposed in the central part of Corinth Isthmus.

Methods

The study area is located at the central part of Corinth Isthmus and includes the sedimentary sequence exposed at about 70 m elevation along the north side of the Corinth Canal (Fig. 1). The sequence is consisted of two different formations from the bottom to the top: about 10 m of beige marls and yellow sandy marls and about 5 m of sandstones and conglomerates. The two formations are bounded by an unconformity surface. Just before the unconformity, the marly sequence ends up with a sandy bed rich in *Cladocora caespitosa* stems and bivalves and it was dated at MIS11 by Pierini et al. (2016).

A total of 22 samples were collected from the marls and the *C. caespitosa* bed for micropalaeontological analysis. The samples were disaggregated with a 5% H_2O_2 solution, washed over 0.125 mm mesh sieves, and the residues were oven-dried at approximately 40 °C. Dried material was splitted and microfossils (ostracods and benthic foraminifera) were hand-picked, identified and counted and a detailed quantitative and qualitative micropalaeontological analysis was performed. Additionally, two samples have been prepared for nannofossil biostratigraphy.

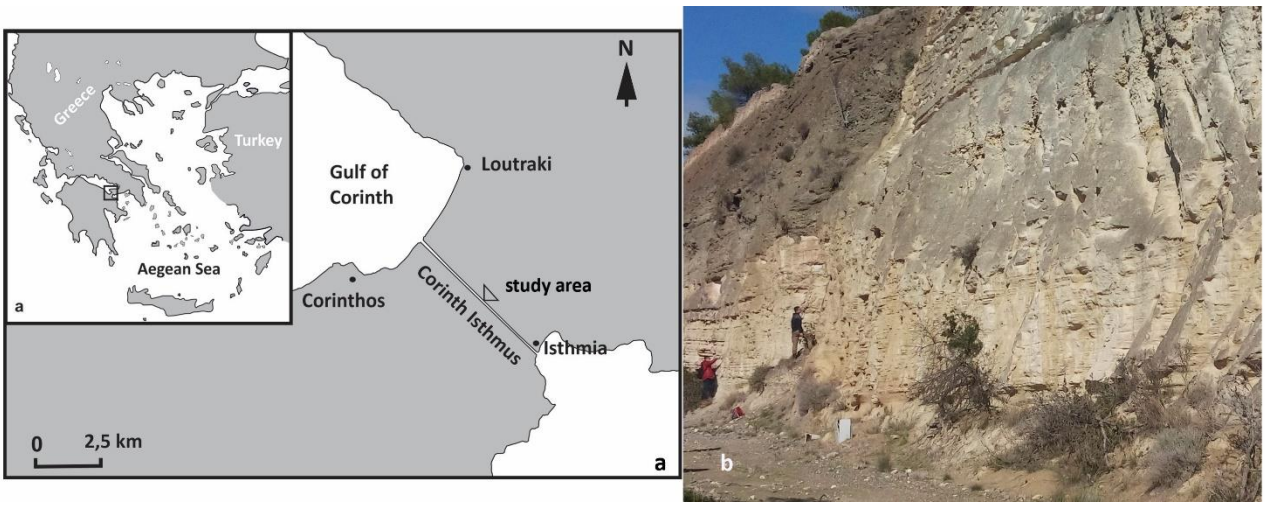

Figure 1. a. Location map and position of the study area. b. The under study sedimentary sequence.

Results and Discussion

Ostracods are the most abundant group in most of the samples, while benthic foraminifera are dominant in the samples from the bed with *C. caespitosa*. A total of 17 ostracod species were identified. The most common and abundant taxa in all the marly and sandy marly layers are the mesohaline *Cyprideis torosa*, *Cyprideis* sp., *Tyrrhenocythere amnicola*, *Loxoconcha* aff. *L. elliptica*, *Euxinocythere schuldtae* and the fresh water-oligohaline species *Candona neglecta*, *C. angulata*. A total of 28 benthic foraminiferal species were identified; specimens are considered transported when showing scarce presence and bad state of preservation. The euryhaline taxa *Ammonia beccarii*, *A. tepida* and *Elphidium* spp. are

considered in situ and are present in low numbers in most of the marly layers.

The combined study of ostracods and benthic foraminifera demonstrated four main micropalaeontological assemblages:

Oligohaline assemblage: Includes high abundances of *C. torosa* and *Candona* spp. There are not benthic foraminifera present. This assemblage indicates a closed lagoonal environment with very limited communication with the sea and significant fresh water input.

Mesohaline assemblage: Characterized by the presence of mesohaline ostracod taxa and very low frequencies of euryhaline benthic foraminifera. This assemblage indicates a closed lagoonal environment with limited communication with the sea and fresh water input. This is the most frequent assemblage in the studied samples.

Polyhaline assemblage: Identified by the presence of both mesohaline and shallow marine ostracod taxa (*Aurila convexa*, *Loxoconcha* spp., *Xestoleberis* spp., *Leptocythere multipunctata*). Accordingly, benthic foraminifera present their higher diversity and abundance in this open lagoonal environment represented by euryhaline and marine taxa: *Ammonia* spp., *Elphidium* spp., *Asterigerinata mamilla*, *Cibicides lobatulus*, *C. refulgens*, *Cancris auriculus* and *Neoconorbina* sp.

Coastal open marine assemblage: Characterized by high frequencies of coastal marine ostracod and benthic foraminifera taxa. It is present only in the samples from the sandy bed with *C. caespitosa* and bivalves. Represents a normal salinity-high energy, shallow-coastal open marine environment.

Conclusions

The distribution patterns of the identified ostracod and foraminiferal assemblages combined with the sedimentary facies reflect the various depositional environments which alternate along the studied section. Consequently, the lower formation (beige marls and yellow sandy intercalations) of the sedimentary sequence exposed at the central part of Corinth Isthmus corresponds to a brackish lagoonal environment with salinity alternations due to the communication with the sea (closed-, semi-closed-, open-lagoon) and the fresh water input. At the top of this formation a sandy bed rich in macro- and micro-fossils indicates a radical environmental change: the opening of the lagoon and the establishment of a shallow marine coastal environment, expressing the beginning of a regressive circle.

References

Briole, P., Rigo, A., Lyon-Caen, H., Ruegg, J.C., Papazissi, K., Mitsakaki, C., Balodimou, A., Veis, A., Hatzfeld, D., Deschamps, A., 2000. Active deformation of the Corinth rift, Greece: results from repeated Global Positioning System surveys between 1990 and 1995. J. Geophys. Res. Solid Earth, 21, 25,605–25,625.

Collier, R.E.L., 1990. Eustatic and tectonic controls upon Quaternary coastal sedimentation in the Corinth Basin, Greece. Journal of the Geological Society, 147(2), 301–314.

Freyberg, V., 1973. Geologie des Isthmus von Korinth. Erlangen Geologische Ablhandlungen, Heft 95. Junge und Sohn, Universitats Buchdruckerei Erlangen (183 pp., in German).

Krstic, N., Dermitzakis, M.D., 1981. Pleistocene fauna from a section in the channel of Corinth (Greece). Annales Geologiques des Pays Helleniques, 1e Serie, 30(2), 473–499.

Pallikarakis, A., Triantaphyllou, M., Papanikolaou, I.D., Dimiza, M.D., Reicherter, K., Migiros, G., 2018. Age Constraints and Paleoenvironmental Interpretation of a Borehole Sedimentary Sequence at the Eastern Part of Corinth Isthmus, Greece, Journal of Coastal Research, 34(3), 602-617.

Papanikolaou, I.D., Triantaphyllou, M., Pallikarakis, A., Migiros, G., 2014. Active faulting at the Corinth Canal based on surface observations, borehole data and paleoenvironmental interpretations. Passive rupture during the 1981 earthquake sequence? Geomorphology, 237, 65–78.

Pierini, F., Demarchi, B., Turner, J., Penkman, K., 2016. *Pecten* as a new substrate for IcPD dating: The quaternary raised beaches in the Gulf of Corinth, Greece, Quaternary Geochronology, 31, 40-52.

15th International Congress of the Geological Society of Greece
Athens, 22-24 May, 2019 | Harokopio University of Athens, Greece
Bulletin of the Geological Society of Greece, Sp. Pub. 7 Ext. Abs. GSG2019-387

Mineral Staining In Excavated Bone: The Case of Dispilio, Greece

E. Stathopoulou[1,2], M. Mallouchou1, E. Margariti[1]

(1) Department of Historical Geology & Palaeontology, Faculty of Geology & Geoenvironment, University of Athens, Panepistimiopolis, 15784 Zographou, Greece, estathop@geol.uoa.gr
(2)Wiener Laboratory, American School of Classical Studies at Athens ASCSA, 54, Souidias str., 106 76 Athens, Greece.

Background

Mineral staining of buried bone is a diagenetic procedure, which involves mainly Fe and Mn oxides (Stermer et al., 1995; Stathopoulou et al., 2013; Bradfield, 2018). Manganese is usually the most present in soil and can occur in several oxidation states, each resulting in different colouration of the bone surface with which it has come into close proximity. Specifically, reduced manganese will tend to produce darker brown to black stains (Dupras and Schultz, 2014). Iron oxides in the sediment typically result in bone turning a deep chocolate brown colour, while well-drained soils conducive to oxidizing conditions can result in bright red to brown discolourations. The mineral composition of soils, soil solution, unique chemistry and pH play an important role on bone staining (Shahack-Gross et al., 1997). Moist, acidic conditions are conducive to corrosion (Janaway, 2008) and it is in these environments that a variety of bone discolourations are expected.

Possible causes of oxide staining may include: 1) microbial activity and more specifically activity of Mn, Fe-oxiding bacteria. The optimal conditions preferred by these bacteria are moist environments that are aerobic with near neutral pH. Manganese origin is often associated with soil humification following a human occupation. The presence of clay minerals is also important, since the bacteria can adsorb on them and use nutrients that also absorb on clay. The bacteria concentrate metals from their environment, most probably from water. The bones themselves may serve as a source of nutrients for the Mn- oxidizing bacteria (Marin Arroyo et al., 2008; Shahack-Gross et al., 1997), and 2) alterations of pH and Eh that may cause precipitation of Fe –Mn oxides. For instance, iron oxides can be produced due to the oxidation of pyrite. Bacterial solubilization and oxidation of iron from pyrite has also been determined. An increase in pH and intensification of oxidizing conditions (associated with dry, well-aerated soils) may favour a change in manganese towards insoluble forms. On the contrary, with a decrease in pH, the manganese may be reduced, increasing its solubility. An increase in the pH can, in turn, be due to burial causes, lack of humidity, the evolution of the soil itself, or other types of causes that may have an anthropogenic origin, such as combustion produced in hearths (Caldeira et al., 2010; Marin Arroyo et al., 2008).

The identification of mineral staining at a site is important, as bone discolouration may also be connected to burning. The use of fire within a prehistoric settlement or site is one of the major issues of geoarchaeological research (Asmussen, 2009), as it proves the presence of man. The identification of archaeological burnt bones has commonly been based on changes such as their colour, crystallinity, shape, histology, as well as the presence of cracks and a black char with characteristic chemical properties. The most easily identified colour, indicative of burning, is also black (Shipman et al., 1984).

Objectives

This paper presents the interdisciplinary study on the origin of “black bones” at the Neolithic lakeside settlement of Dispilio, Greece (5500–3500 BC), where discoloured animal bones have been recovered from a waterlogged and organic soil-matrix containing charcoal, ash and burnt cultural remains. In the past, this has been interpreted as the result of the destruction of the village by fire and abandonment. This study aims to examine whether the colouration of the material at the site can be explained by this theory, through the distinction of burnt vs. oxide stained bones.

Material-Methods

Forty four (44) groups of fish bones and nineteen (19) mammal bone samples were selected for this study. The fish bones included fragments from the neurocranium, the branchiocranium and the spine (vertebrae, costae, etc) as well as bone parts from the pectoral, pelvic and fin skeleton. The species most represented were Cyprinus carpio and Silurus glanis. The mammal bone samples were shafts of long bones (tibia, humerus, etc), and of metapodials, as well as fragments of short bones. They were pieces not identified to species, and pertained predominantly to smaller animals. Material was mainly chosen based on colour, in an attempt to cover all types of bone discolouration present at Dispilio (light-coloured/yellow to dark-coloured/black), but also the different cultural contexts found at the site (lacustrine phase C, early-pre-destruction and late-destruction) and amphibian phase B (post-destruction layer; terrestrial phase). By means of comparison, two modern bone reference samples were used (NIST bone meal sample Reference material 1486 and an exhumed relatively fresh bovine bone).

All bone samples were examined through Optical Microscopy, Scanning Electron Microscopy (SEM), X-ray Microanalysis (EDS), X-ray Diffraction (XRD) - Rietveld Analysis, Infrared Spectroscopy (ATR, NIR) and chemical analyses (ICP-MS). Alterations of histology, mineralogy, chemistry, crystallinity and structural parameters due to diagenesis and/or possible burning are presented and correlated to the intriguing regional geochemical context.

Results-Conclusions

The various analytical techniques employed on mammal and fish bones did not offer any proof that any of the chosen material is burnt, based on specific features described in relevant bibliography. Rather, all the observed alterations concerning cracking, histology, colour, crystallinity etc. in the samples, could be attributed to diagenesis.

Our study showed that bones have certainly been affected by Mn and Fe oxide staining and owe their colour to this procedure. The soil-matrix at the site, which is very rich in charcoal and ash but at the same time waterlogged and organic, may have played a role in bone colouration, in combination with the aforementioned phenomena. Oxide staining is a very common phenomenon in sites that appear rich in organic matter abandoned as a result of consumption activities. With respect to the origin of Mn and Fe in the area and based on the mineral phases traced within the surrounding sediment in the polished sections, it can be suggested that these elements come from the rocks and sediments of the surrounding area. It is also possible that part of the Mn does not have a geological origin, and an anthropogenic source should be considered, namely the accumulation of vegetable and animal organic matter. Ions of the metal could be released during decomposition of the organic matter, and then enter the sediments in which the bones are buried (Marin-Arroyo et al., 2008; Shahack-Gross et al., 1997).

Regarding the colour based grouping (dark vs. light-coloured bones), it also corresponded to a number of different diagenetic features. In general, light-coloured bones seem to be less affected by diagenesis and exhibit features concerning chemistry, crystallinity etc, that resemble those of fresh bone, which proves that these bones were buried in a totally different geochemical environment to the dark-coloured ones.

On the other hand, fish samples exhibited some different characteristics to those of mammal bones. This can be explained by the different histological structure of fish bones, in terms of increased porosity and thus higher susceptibility to dissolution, degradation and interaction with the surrounding sediment.

Concerning the stratigraphy of the studied samples, there does not seem to be a specific diagenetic trend, other than those described based on the colour of the bones. Light-coloured bones, come mainly from phase B which represent the terrestrial part of the site, while dark-coloured material derived from all phases, but mostly C early and C late which represent the waterlogged part.

Acknowledgements

The authors are indebted to late Prof. G. H. Hourmouziadis for providing access to the material, to Panayiotis Karkanas for geting the project off the ground. Funding was provided by the Wiener Laboratory (American School of Classical Studies at Athens). Thanks are owed to Dr. G. D. Chryssikos and Dr. V. Gionis from the Applied Spectroscopy Laboratory, of the Theoretical and Physical Chemistry Institute at the National Hellenic Research Foundation, for their ideas and specialized knowledge, as well as for the application of vibrational techniques on our material.

References

Asmussen, B., 2009. Intentional or incidental thermal modification? Analysing site occupation via burned bone. Journal of Archaeological Science 36, 528–536.

Bradfield, J., 2018. Some thoughts on bone artefact discolouration at archaeological sites. Journal of Archaeological Science: Reports 17, 500–509.

Caldeira, C.L., Ciminelli, V.S.T., Osseo-Asare, K., 2010. The role of carbonate ions in pyrite oxidation in aqueous systems. Geochimica et Cosmochimica Acta 74, 1777–1789.

Dupras, T., Schultz, J., 2014. Taphonomic bone staining and color changes in forensic contexts. In: Pokines, J., Symes, S. (Eds.), Manual of Forensic Taphonomy. CRC Press, Florida, 315–340.

Janaway, J., 2008. The Decomposition of Materials Associated with Buried Cadavers. In: Tibbett, M., Carter, D. (Eds.), Soil Analysis in Forensic Taphonomy: Chemical and Biological Effects of Buried Human Remains. CRC Press, Florida, 153–201.

Marin Arroyo, A.B., Landete Ruiz, M.D., Vidal Bernabeu, G., Seva Román, R., González Morales, M. R., Straus, L.G., 2008. Archaeological implications of human-derived manganese coatings: a study of blackened bones in El Mirón cave, Cantabrian Spain. Journal of Archaeological Science 35, 801–813.

Shahack-Gross, R., Bar-Yosef, O., Weiner, S., 1997. Black-coloured bones in Hayonim Cave, Israel: differentiating between burning and oxide staining. Journal of Archaeological Science 24, 439–446.

Shipman, P., Foster, G., Schoeninger, M., 1984. Burned bones and teeth: An experimental study of color, morphology, crystal structure and shrinkage. Journal of Archaeological Science 11, 307–325.

Stathopoulou, E. T., Theodoropoulou, T. and Phoca-Cosmetatou, N., 2013. Black fish bones in waterlogged deposits: the case of the Neolithic lake settlement of Dispilio, Greece. Archaeofauna 22, 51-74.

Stermer, E., Risnes, S., Fischer, P., 1995. Trace element analysis of blackish staining on the crowns of human archaeological teeth. Eur. J. Oral Sci. 104, 253–261.

SPECIAL SESSION

T1.S2 Sedimentary Processes, Depositional Settings and Basin analysis

Conveners: **G. Anastasakis (NKUA)**
P. Avramidis (UPAT)
A. Zelilidis (UPAT)

Co-organized by the Hellenic Sedimentological Association

15th International Congress of the Geological Society of Greece
Athens, 22-24 May, 2019 | Harokopio University of Athens, Greece
Bulletin of the Geological Society of Greece, Sp. Pub. 7 Ext. Abs. GSG2019-008

Lithological and Mineralogical study of Quaternary Clastic Materials of the Internal Thermaikos Gulf

A. Livas[1,2], N. Kantiranis[2], M. Kati[3], and L. Papadopoulou[2]

(1) Imperial College London, Royal School of Mines, Department of Earth Science and Engineering, SW7 2BP, London, United Kingdom, agis.livas17@imperial.ac.uk
(2) Aristotle University of Thessaloniki, Faculty of Sciences, School of Geology, Department of Mineralogy - Petrology - Economic Geology, GR-54124, Thessaloniki, Greece
(3) University of Athens, Faculty of Geology and Geoenvironment, Department of Mineralogy and Petrology, University Campus - Zografou GR-15784, Athens, Greece

Location & Geological Background

The basin of Thermaikos Gulf is located at the Northwestern part of the Aegean Sea, North Greece (Fig. 1). It is a tectonic draft with a varying depositional environment, formed as a result of the NNW-SSE trending tectonic rifting movements, which developed in this area during Tertiary. During the Pliocene to Pleistocene, the basement was effected by relatively rapid submergence. Consequently, the appropriate conditions were formed for the transportation and the deposition of sediments within the basin.



Figure 1. Location of the study area on the maps of Greece (upper right corner) and of the broader area of Thessaloniki (lower right corner). On the left, the positions of the wells of the drilling program "Widening of Coastal Avenue of Thessaloniki", which was executed in the Internal Thermaikos Gulf, close to the city of Thessaloniki. The yellow well names indicate the drillings from which borehole core samples were tested in laboratory (source: Google Earth).

Methodology & Results

In the present work, ten (10) samples of borehole cores from 7 different wells were studied to examine their mineralogical, textural and lithological features. These drillings were perforated in the spring of 1979 in order to study the subsoil of the Thermaikos Gulf, as part of the "Widening of Coastal Avenue of Thessaloniki" project. In this way, a drilling program was carried out involving seventeen (17) wells, which were numbered from Γ13 to Γ29 (Fig. 1). In-situ engineering geological tests, such as S.P.T. (Standard Penetration Test) were performed, and samples of borehole cores were collected.

Table 1. Grain size distribution (% w/w) of the studied samples. The double line frame includes the samples of the drilling Γ14, which was chosen for the vertical study of the sediment succession.

Sample *(depth)*	**Gravel** (>2mm)	**Sand** (2mm-63μm)	**Silt** (63μm-2μm)	**Clay** (<2μm)	**C.O.I.***	**Total**
Γ13 *(22.30-22.60m)*	4.1	49.4	22.4	16.0	8.1	100.0
Γ14 (1) *(14.85-15.15m)*	10.6	39.1	28.0	15.8	6.5	100.0
Γ14 (2) *(19.50-19.80m)*	7.1	45.8	21.5	14.3	11.3	100.0
Γ14 (3) *(25.20-25.50m)*	4.3	41.5	18.5	30.0	5.7	100.0
Γ14 (4) (31.20-31.50m)	3.6	26.7	27.5	31.3	10.9	100.0
Γ15 *(19.10-19.40m)*	8.7	42.1	22.1	15.9	11.2	100.0
Γ16 *(20.80-21.10m)*	19.4	33.0	23.5	17.4	6.7	100.0
Γ23 *(18.20-18.50m)*	22.4	24.8	30.3	13.9	8.6	100.0
Γ24 *(20.45-20.75m)*	9.9	32.5	28.9	23.0	5.7	100.0
Γ26 *(26.40-27.40m)*	15.4	41.5	15.1	22.7	5.3	100.0

* C.O.I.: Carbonates + Organic matter & MnO_2 + Iron (Fe) oxides and hydroxides

The ten samples were examined macroscopically and were sieved in ≥2 and <2 mm subsamples (Table 1). The ≥2 mm pebbles were inspected and characterized by using stereoscope and their textural and morphological characteristics were recorded. The <2 mm subsamples were treated according to Jackson techniques (1974), and sand, silt and clay fractions were measured (Table 1). The mineralogical composition of these fractions was studied by using X-ray diffraction (XRD) (Fig. 2).

According to Folk *et al.*, 1970 textural classification, the clastic materials of the studied area can be characterized as gravelly mud, sandy mud, gravelly muddy sand or muddy sand (Fig. 3). Their pebbles comprise of schist-gneiss (1.1-16.7% wt), quartz (0.5-6.2% wt) and limestone (0.1-4.6% wt). The Quaternary clastic materials display almost the same horizontal and vertical mineralogical composition regarding the whole samples. On the contrary, significant variations between sand, silt and clay fractions were observed (Table 1). Quartz (39-56% wt), feldspars (plagioclase 8-16% wt and K-rich 1-4% wt), chlorite (±kaolinite) (14-31% wt), illite (in the clay fraction) + muscovite (6-13% wt), illite/chlorite (2-13% wt), amphiboles (1% wt), pyroxenes (1% wt), calcite (1% wt) and dolomite (1-2% wt) were identified in three fractions (Fig. 2).

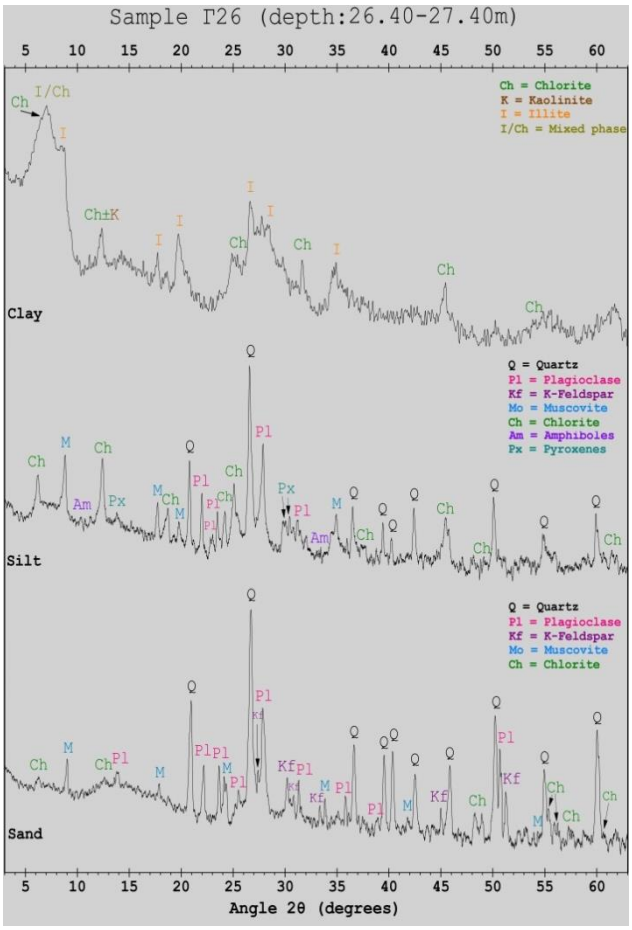

Figure 2. Representative X-Ray Diffraction patterns of sand, silt and clay of the sample Γ26.

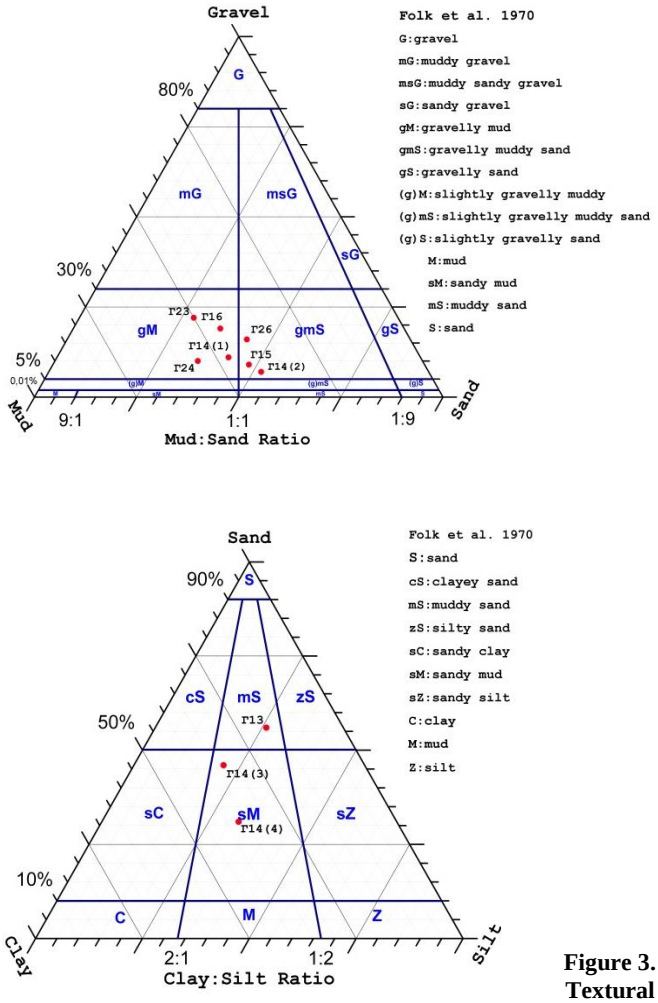

Figure 3. Textural classification (Folk *et al.* 1970): Gravel-bearing (upper) and gravel-free samples (lower).

Conclusions

All the above methods show that the deposition within the study area took place in a coastal marine depositional environment, in conjunction with the rapid transportation of sediments by the rivers and large streams, which leaked mainly through the hydrological basin of Thessaloniki and of Dendropotamos to some extent. The composition of Quaternary clastic materials of the Internal Thermaikos Gulf can be mainly considered as a result of the weathering which took place in the neighboring hydrological basins, where igneous and metamorphic rocks prevail. In addition, boulders of the Tertiary series (mainly from the Red beds) were also found.

References

Folk, R.L., Andrews, P.B., Lewis, D.W, 1970. Detrital sedimentary rock classification and nomenclature for use in New Zealand, New Zealand Journal Geology and Geophysics, v.13, p. 937-968.

Jackson, M.L., 1974. Soil chemical analysis: Advanced Course, 1st ed. Parallel Press, University of Wisconsin – Madison Libraries, Wisconsin, 690 p.

15th International Congress of the Geological Society of Greece
Athens, 22-24 May, 2019 | Harokopio University of Athens, Greece
Bulletin of the Geological Society of Greece, Sp. Pub. 7 Ext. Abs. GSG2019-040

Paleoenvironmental conditions and hydrocarbon potential assessment on the Late Miocene evaporitic sediments of Zakynthos Island (Greece)

V. Karakitsios[1], N. Kafousia[1], G. Kontakiotis[1], K. Agiadi[1], A. Antonarakou[1]

(1) Department of Historical Geology and Paleontology, Faculty of Geology and Geoenvironment, National and Kapodistrian University of Athens, Panepistimiopolis, 15784, Athens, Greece, vkarak@geol.uoa.gr

In the present study, we investigate the stable oxygen ($\delta^{18}O$) and carbon ($\delta^{13}C$) isotope ratios, the total organic carbon (TOC) content, and the petroleum potential of the pre-evaporitic and evaporitic Messinian deposits (6.46–5.33 Ma) from continuous sections on Zakynthos Island, Greece. The pre-evaporitic sequence mainly consists of alternating massive and laminated marls with rare calcareous marl and calcarenite intercalations. It is conformably followed by the gypsum unit. Particularly, the study is focused on Kalamaki and Agios Sostis sections (Kontakiotis et al., 2016; Karakitsios et al., 2017; Vasiliev et al., 2019; Fig. 1).

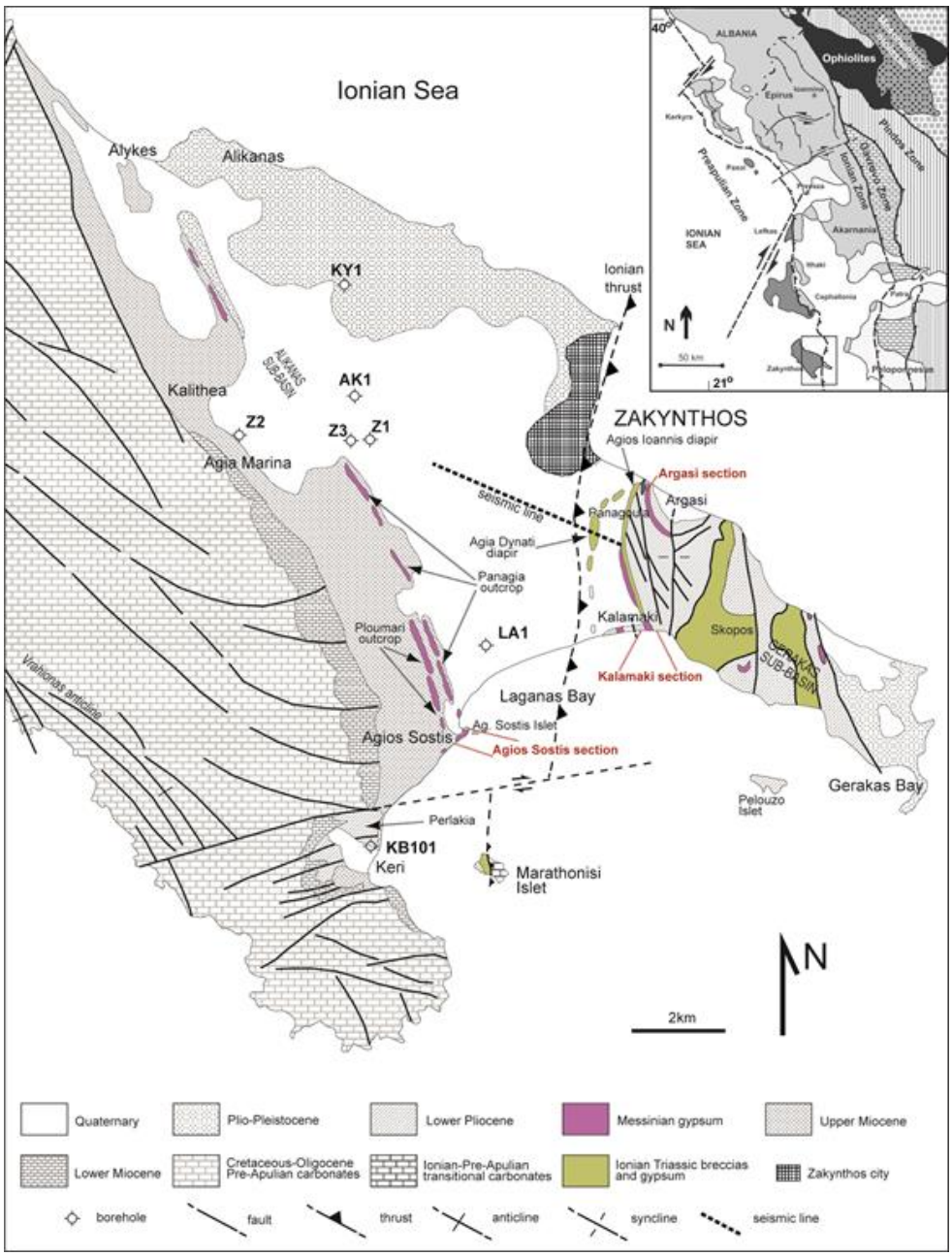

Figure 1 Geological map of Zakynthos Island (Karakitsios et al., 2017). The regional location is indicated in the inset map. Z1, Z2, Z3, LA1, KB101, AK1, KY1 correspond to boreholes.

In Kalamaki section, the gypsum unit corresponds to Primary Lower Gypsum (PLG) deposits, consisting of a 108-m thick succession with eight gypsum-marl cycles and different gypsum facies (Karakitsios et al., 2017). In Agios Sostis section the gypsum unit is more than16 m thick, consisting of several alternations of primary and clastic gypsum which derived from the resedimentation of older PLG deposits (Karakitsios et al., 2017). The isotopic bulk values are greatly variable: in Kalamaki section, -3.75 to +8.8‰ for $\delta^{18}O$, and -9.42 to -0. 93‰ for $\delta^{13}C$, whereas in Agios Sostis section, -3.54 to -0.31‰ for $\delta^{18}O$ and -7.74 to +0.08‰ for $\delta^{13}C$ respectively. Isotope values of the Agios Sostis section clearly show a marine environment, whereas in Kalamaki, the relevant values imply influence of continental fresh water in an environment of highly evaporated solutions. The origin of continental water is also confirmed by the organic matter type (type III kerogen) and the presence of plant remains (leaves) in the samples. Total organic carbon (TOC) values in Kalamaki section range from 0.15 to 1.31 wt% in the pre-evaporitic sequence, and from 0.07 to 0.95 wt% in the shale layers of the Primary Lower Gypsum, whereas in in the post-evaporitic from 0.03 to 0.3 wt%. In terms of petroleum potential, many of the samples are immature, whereas some of them correspond to the mature oil stage. Nevertheless, the pre-evaporitic and evaporitic sequence present a fair to good hydrocarbon-generating potential. Although the onshore source rocks are partially immature due to insufficient thickness of the overburden sediments that does not preclude the possibility that the same source rocks are mature for oil generation in the offshore area (between Zakynthos-and Peloponnesus) where they are covered by more than 3 km of Pliocene-Pleistocene sediments.

Acknowledgements

This research has been co-financed by the European Union (European Social Fund – ESF) and Greek National Funds through the Operational Program 'Education and Life-long Learning' of the National Strategic Reference Framework (NSRF) – Research Funding Program: THALIS-UOA-'Messinian Salinity Crisis: the greatest Mediterranean environmental perturbation and its repercussions to the biota'.

References

Karakitsios, V., Roveri, M., Lugli, S., Manzi, V., Gennari, R., Antonarakou, A., Triantaphyllou, M., Agiadi, K., Kontakiotis, G., Kafousia, N., De Rafelis, M., 2017. A record of the Messinian Salinity Crisis in the eastern Ionian tectonically active domain (Greece, eastern Mediterranean). Basin Research 29(2): 203–233. DOI: 10.1111/bre.12173.

Kontakiotis, G., Karakitsios, V., Mortyn, P.G., Antonarakou, A., Drinia, H., Anastasakis, G., Agiadi, K., Kafousia, N., De Rafelis, M., 2016. New insights into the early Pliocene hydrographic dynamics and their relationship to the climatic evolution of the Mediterranean Sea. Palaeogeography, Palaeoclimatology, Palaeoecology 459: 348–364.

Vasiliev, I., Karakitsios, V., Bouloubassi, I., Agiadi, K., Kontakiotis, G., Antonarakou, A., Triantaphyllou, M., Gogou, A., Kafousia, N., de Rafélis, M., Zarkogiannis, S., Kaczmar, F., Parinos, C., Pasadakis, N., 2019. Large sea surface temperature, salinity, and productivity-preservation changes preceding the onset of the Messinian Salinity Crisis in the eastern Mediterranean Sea. Paleoceanography and Paleoclimatology. https://doi.org/10.1029/2018PA003438.

15th International Congress of the Geological Society of Greece
Athens, 22-24 May, 2019 | Harokopio University of Athens, Greece
Bulletin of the Geological Society of Greece, Sp. Pub. 7 Ext. Abs. GSG2019-132

Preliminary results for the possibility of Lower Cretaceous Vigla shales to be a major source formation for the production of hydrocarbons in the Ionian basin

N. Bourli[1], Ch. Stauropoulou[1], A. Maravelis[1], N. Pasadakis[2], E. Chamilaki[2], A. Zelilidis[1]

(1) Department of Geology, University of Patras, 2650 Patras, Greece, n_bourli@upnet.gr
(2) Department of Mineral Resources Engineering, Technical University of Crete, Chania, Greece, pasadaki@mred.tuc.gr

Introduction – Geological setting

The field observations of the Lower Cretaceous "Vigla formation" in NW Peloponnesus (Gianniskari beach) and according to Bourli et al., (2019), indicate a fault-controlled formation that was accumulated into restricted basins. These basins were formed from normal faults with NNW-SSE direction and were influenced from ENE-WSW directed transfer faults. According to Bourli et al., 2019 the subdivision of the Ionian basin into asymmetric grabens resulted in variations in geometry and water depth and thus, sedimentary successions with different thicknesses were accumulated. The deeper deposits occur in the central part of each asymmetric graben, where the "Vigla shales" were deposited. The Lower Cretaceous "Vigla formation", along the Gianiskari beach consists of two different members, the lower one made of "Vigla limestones" and the upper one made of strongly deformed "Vigla shales". Vigla shales consist of thinly interbedded chert and shales, up to 60 m thick. The chert is mostly reddish but is also black or green, that characterizes in general cherts. Synsedimentary faults produced slumping within Vigla shales, during sedimentation. This slumping is up to 30m long and up to 40cm relief high. Synsedimentary faults have a general southward direction and strong deformation internally to the deposits. Finally, some of the faults produced also flower structures producing accommodation space that was filled up by successive deposits.

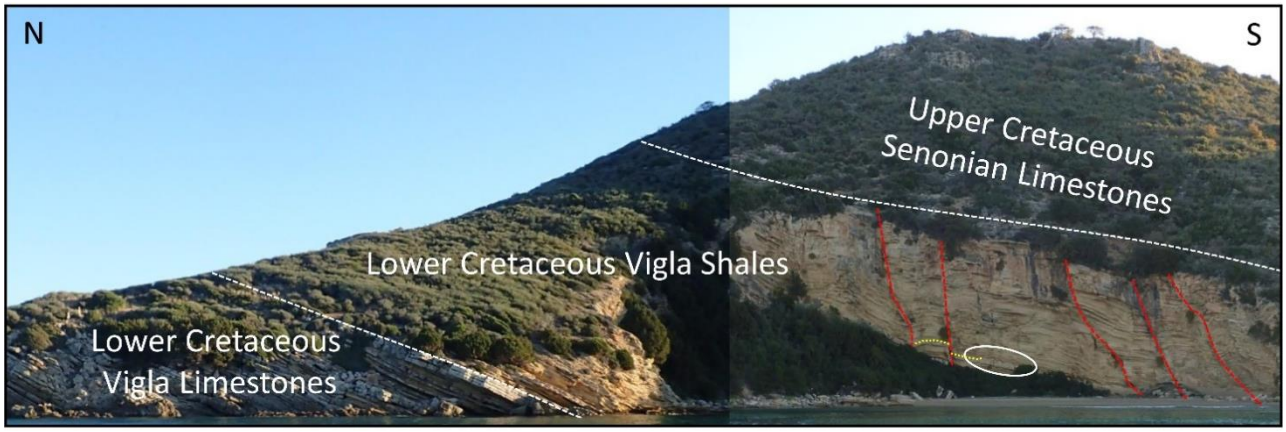

Figure 1. The studied outcrop along the Gianiskari coast with the lower Cretaceous "Vigla Shales" overlying lower Cretaceous "Vigla limestones" and underlying the upper Cretaceous "Senonian limestones" (white dashed lines mark the two boundaries). Many normal faults cross-cut the sedimentary association of Vigla shales (red dashed lines) during sedimentation producing synsedimentary slumps (white circle).

Data analysis - Results

Geochemical analysis in 31 samples with Rock-Eval VI, from the up to 60m thick succession, showed that there are at least eight (8) samples with more or close to 0.50% TOC (Table 1). From these results and according to the analytical restriction (when S2 is <0.2 then Tmax is not considered accurate), we concentrate on the Tmax values of three samples (G1R, G4 and G5).They indicate that the contained organic matter is immature.

Although there are samples with high enough TOC content, the respective S1 and S2 values are very low. The visual inspection of the FID pyrolysis signals of the samples revealed a wide pattern of the S2 peak in most samples, without a clear maximum point. In several samples two different distributions may be identified within the S2 peak, corresponding to immature and over-mature organic matter. These distributions are shown for the samples G10 and G30 in Fig. 2. The presence of the over-mature kerogen may be attributed to transported reworked material before deposition in the current location. The low concentration of kerogen in the studied samples does not allow for the reliable determination of its origin and therefore a more detailed study is advisable to reveal the sedimentation history of the studied Vigla shales samples.

Considering the above results and taking into account that Vigla shales are proposed as one of the possible sources for hydrocarbon production in the Ionian basin, further studies are needed to document their real hydrocarbon generation potential.

Table 1: The Rock Evall VI geochemical results from 31 samples along the Gianiskari coast in NW Peloponnesus

Sample	Qty - (mg)	S1 - (mg/g)	S2 - (mg/g)	Tmax(°C)	S3 - (mg/g)	TOC(%)	MINC(%)
G1	63.4	0.01	0.04	370	0.55	0.04	5.94
G2	67.9	0.00	0.00		0.00	0.20	7.68
G3	63.8	0.02	0.03		0.33	0.07	1.95
G4	64.9	0.01	0.12	370	0.62	0.38	2.43
G5	62.3	0.01	0.07	372	0.28	0.16	0.65
G6	69.7	0.00	0.03		0.31	0.45	6.96
G7	68.4	0.00	0.01		0.34	0.59	7.47
G8	64.4	0.00	0.02		0.53	0.22	5.87
G9	62.4	0.02	0.04		0.24	0.03	5.73
G10	65.1	0.00	0.04		0.41	0.07	5.38
G11	58.8	0.02	0.06		1.90	0.13	3.06
G12	63.5	0.04	0.07		1.48	0.14	5.56
G13	69.6	0.01	0.03		0.43	0.56	7.96
G14	61.1	0.01	0.00		0.21	0.28	7.25
G15	67.5	0.02	0.06		0.59	0.53	7.36
G16	69.4	0.00	0.03		0.39	0.29	7.57
G17	60.7	0.05	0.07		0.55	0.52	7.42
G18	66.9	0.04	0.12		0.38	0.16	7.34
G19	67.3	0.02	0.05		0.43	0.33	7.00
G20	63.8	0.02	0.08		0.78	0.03	3.94
G21	63.3	0.01	0.03		0.34	0.09	6.64
G22	59.6	0.00	0.01		0.66	0.12	5.66
G23	60.4	0.01	0.02		0.86	0.13	5.86
G24	64	0.00	0.01		0.64	0.12	5.20
G25	69.6	0.00	0.00		1.08	0.24	6.42
G26	65.4	0.00	0.00		0.51	0.01	5.39
G27	62.4	0.00	0.01		0.23	0.08	5.67
G28	64.1	0.00	0.00		0.23	0.01	5.32
G29	64.5	0.00	0.00		0.71	0.19	6.04
G30	64.9	0.01	0.09		0.65	0.13	4.93
G31	63.2	0.01	0.02		0.60	0.72	6.83

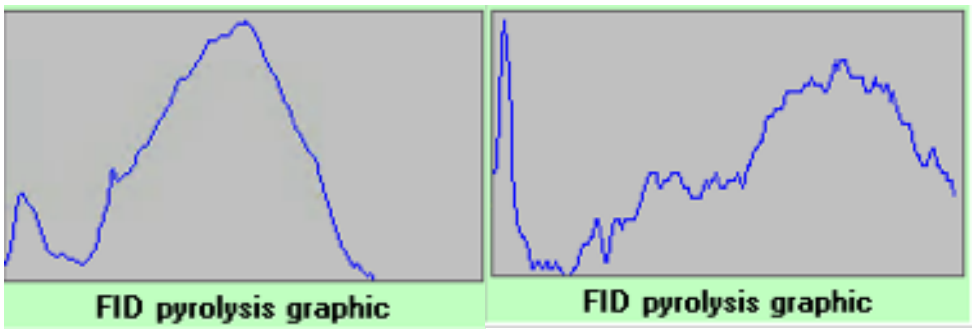

Figure 2: S.1 and S2 images for G30 and G10 samples showing immature and overmature-reworked kerogen respectively

Acknowledgements

Nicolina Bourli is a PhD student and she was financially supported by the "Andreas Mentzelopoulos Scholarships for the University of Patras".

References

Bourli, N., Pantopoulos, G., Maravelis, A.G., Zoumpoulis, E., Iliopoulos, G., Pomoni-Papaioannou, F., Kostopoulou, S., Zelilidis, A., 2019. Late Cretaceous to Early Eocene geological history of the eastern Ionian Basin, southwestern Greece: An integrated sedimentological and bed thickness statistics analysis. Cretaceous Research 98, 47-71.

15th International Congress of the Geological Society of Greece
Athens, 22-24 May, 2019 | Harokopio University of Athens, Greece
Bulletin of the Geological Society of Greece, Sp. Pub. 7 Ext. Abs. GSG2019-155

Evolution of the Coastal Environment of the Marathon Bay Based on the Shoreline Displacement Rate for the Last 80 Years

G. Kourliaftis[1], E.Vassilakis[1], V.Kapsimalis[2], S.Poulos[1], D. Vandarakis[2]

(1) Section of Geography & Climatology, National & Kapodistrian University, Panepistimiopolis Zografou, Athens 15784, Greece; kourliaf@gmail.com
(2) Hellenic Centre for Marine Research, Institute of Oceanography, 46.7th km Athens-Sounion Ave., 19013 Anavyssos, Attica, Greece

Introduction

The purpose of the study is the determination of the shoreline changes and the sediment processes along the beach of Marathon Bay, which is located at northeast Attica. In the wider on shore area the Schinias National Park, at the northeast of the bay, the Olympic Rowing Centre, military bases, archeological sites, museums etc. are encountered. The area is also characterized by high touristic activity during summer. In the area there are specific locations and constructions endangered due to coastal retreat. A lagoon was established in the study area 3.500 years BP (Pavlopoulos *et al.*, 2006) as it is characterized by low elevations, gentle slopes and fine sediments.

Methods

A survey of the coastal and marine geomorphology was carried out by acoustic scanning of the seafloor with an echo sounder and sonar side scan topographical sections perpendicular to the shoreline along with collection and analysis of surface sediments. The quantification of long-term shoreline displacements was carried out by comparing historical and contemporary aerial photographs (1945, 1960, 1969, 1988, 1996, 2001, 2010) along with very high resolution satellite imagery (2012, 2014, 2015, 2016, 2017, 2018), not to mention the tracing of the coastline (2013) with Real Time Kinematics equipment (RTK-GNSS). The quantification of long-term shoreline displacements was made with the use of the add-on application of Digital Shoreline Analysis System (DSAS) within the GIS platform ArcMap 10.6 (Thieler *et al.*, 2009). This was accomplished by drawing 261 transects (every 50 meters), except those neighboring anthropogenic structures, perpendicularly to the historical shorelines from a stable baseline (Tsokos *et al.*, 2018). At each transect the rate of displacement was measured.

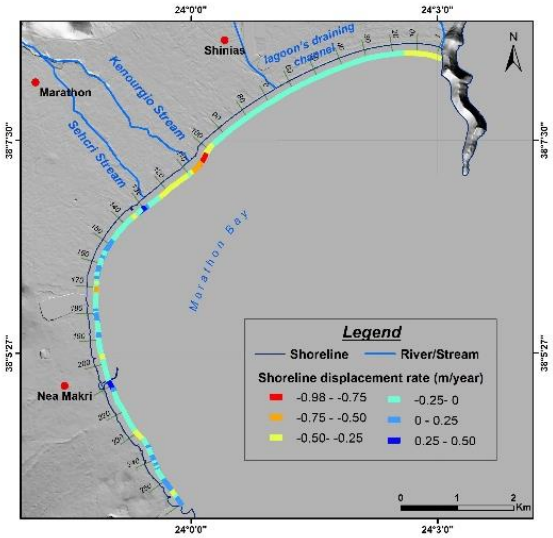

Figure 1. Shoreline displacement rates at Marathon Bay

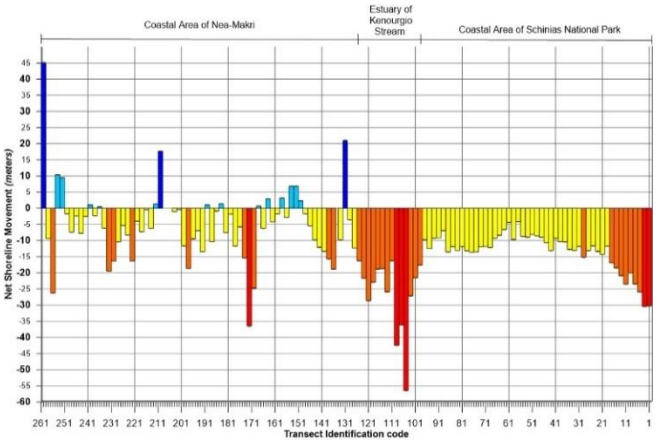

Figure 2. Distance between oldest and youngest shorelines

Results

Throughout the Marathon Bay relatively gentle slopes are formed onshore, combined with shallow depths not exceeding the maximum measured depth of-40 m. An extended submerged alluvial fan seems to have been created mainly by Oinoi River (which is divided into Kenourgio and Sechri streams). The types of substrate and habitats were mainly constructed by non-cohesive materials (mainly sand). An extended meadow of Posidonia Oceanica is observed (from 5 to 27 m depth) and Penicillus capitatus from 2 to 15 m depth as patches and as beds from 27 to 35 m depth. From 35 to 40 m, mud is mostly prevailed. Specific locations with course sand, gravel and rock are noticed at the westernmost section of the Bay (north and south of Nea Makri marina), mostly by the human structures along the shoreline and by destroyed beachrocks. The estuary of Kenourgio stream consists mainly of sand and pebbles. At the coastal area of Nea Makri, several zones of beach rocks were found from 1 to -3 m depth (Koutsomichou *et al.*, 2009). Also an intense underwater berm is observed, about 50 meters from the shore, along the part of the coastline which is mostly exposed to south waves. The biggest part

of Marathon Bay seems to be subjected to coastal erosion (Figure 1). At the center of the Bay, at the estuary of Kenourgio stream, the maximum rates of coastal retreat is noticed (-0,35m/yr) from the mid-40's to 70's. At Nea Makri, a variation of displacements occurs due to anthropogenic structures which affect the nearshore sedimentation (Dimou *et al.*, 2014).

Conclusions

The exposition of the coast to the southern waves, the reduced sediment supply from local rivers, due to the Marathon's Dam and finally the morphology of their riverbeds, they have been filled because of the sea level rise, the sediment's composition and the sediment transport from the beach to the submerged berm due to Marathon coastal hydrodynamic regime are mainly responsible for the coastal retreat. A lower and steady rate of retracement seems to have prevailed since the 1970s and beyond.

Acknowledgements

The authors are grateful to the HCMR for the provision of the aerial photographs and to BSc I. Stavrakaki for the contribution in the sedimentological analysis of the samples collected, held in the laboratory of the sedimentological analysis of HCMR.

References

Dimou, A., Vassilakis, E., Antoniou, B., Evelpidou, N., 2014. An assessment of the coastal erosion at Marathon, east Attica (Greece). I10th Congress of the Hellenic Geographical Society, Thessaloniki, Greece, p. 1579-1587.

Koutsomichou, I., Poulos, S., Evelpidou, N., Anagnostou, C., Ghionis, G., Vassilopoulos, A., 2009. The role of beach rock formations in the evolution of embayed coastal zones of Attica (Greece) in relation to sea level rise. The case of Kalyvia beach zone. Geografica Fisica Dinamica Quaternaria, 32, 49–56.

Pavlopoulos, K., Karkanas, P., Triantaphyllou, M., Karymbalis, E., Tsourou, T., Palyvos, N., 2006. Paleoenvironmental Evolution of the Coastal Plain of Marathon, Greece, during the Late Holocene: Depositional Environment, Climate, and Sea Level Changes. Journal of Coastal Research, 424-438.

Thieler, E.R., Himmelstoss, E.A., Zichichi, J.L., and Ergul, Ayhan, 2009. Digital Shoreline Analysis System (DSAS) version 4.0 — An ArcGIS extension for calculating shoreline change: U.S. Geological Survey Open-File Report 2008-1278.

Tsokos A., Kotsi E., Petrakis S. Vassilakis E., 2018. Combining series of multi-source high spatial resolution remote sensing datasets for the detection of shoreline displacement rates and the effectiveness of coastal zone protection measures. Journal of Coastal Conservation, 22(2):431-441

15th International Congress of the Geological Society of Greece
Athens, 22-24 May, 2019 | Harokopio University of Athens, Greece
Bulletin of the Geological Society of Greece, Sp. Pub. 7 Ext. Abs. GSG2019-164

Revealing the Eocene-Oligocene transition in Pindos Foreland Basin, western Greece

S. Kostopoulou[1], A.G. Maravelis[1], C. Mpotziolis[1], A. Zelilidis[1]

(1) Laboratory of Sedimentology, Department of Geology, University of Patras, 26504 Rion, Greece, kost.sofia@hotmail.com

Introduction-Geological setting

The middle Eocene to early Oligocene transition (EOT) is of particular interested because it corresponds to significant climatic changes in the Cenozoic (Maravelis and Zelilidis, 2012). The EOT marks the shift from greenhouse to icehouse conditions and the last major extinction of marine fauna (Miller et al., 1992). Calcareous nannofossils are abundant in submarine fan deposits and are regarded as very good biostratigraphic indicators (Winter and Siesser, 1994). Thus, calcareous nannofossil analysis has been employed for determining the age of such sediments. The submarine fan deposits in the Pindos Foreland Basin, western Greece offer a case study to precisely define the EOT and investigate potential fingerprints of this climatic change at low latitude settings. The basin is bounded to the east by the Pindos Thrust and to the west by the Ionian thrust and is further dissected by smaller thrusts (Gavrovo, internal and middle Ionian thrusts). Although the studied deposits are Eocene to Oligocene in age, detailed biostratigraphic analysis to define their time span has not been yet conducted and the EOT has not been documented. In view of the absence of such data, calcareous nannofossil analysis has been carried out, adding constraints on the depositional age of the submarine fan deposits in Pindos Foreland Basin and documenting the EOT in western Greece.

Material and methods

For calcareous nannofossil analysis, 70 samples were collected from the submarine fan deposits in Pindos Foreland Basin. These deposits correspond to the infill of the basin, as a result of the growing Pindos Thrust (Konstantopoulos and Zelilidis, 2012). The submarine fan system documents progradation and therefore, outer fan deposits are stratigraphically below inner fan sediments (Konstantopoulos and Zelilidis, 2012). Prior to sample selection and collection, systematic field work was performed to assure that the samples are placed to the right stratigraphic position and cover the entire sedimentary succession. The sample preparation was made using standard smear slide techniques, as described in Bown and Young (1998) and Giunta *et al*. (2003). Smear slides were analyzed with an optical Optica Italy B-1000POL microscope at 1250× magnification. Calcareous nannofossils were generally abundant and well preserved. The biostratigraphy was based on the biozonal definitions of Martini (1971) and Agnini *et al*. (2014).

Results and conclusions

The biostratigraphic analyses of more than 70 samples in outer fan deposits, until now, calcareous nannofossils (Fig.1; Fig.2) confirm the late Eocene to early Oligocene time interval. The studied samples referred to a 221 m total sequence that rest uncomfortably over the Eocene limestones. The transition zone from carbonates to clastic deposits showed a late Eocene age.

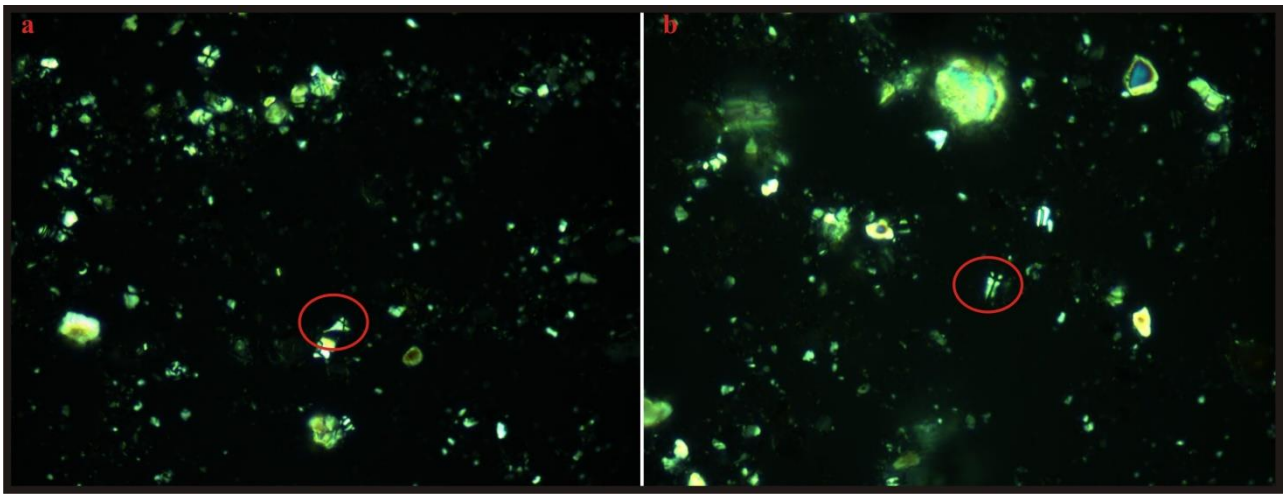

Figure 1. Sphenolithus species. a) Sphenolithus ciperoensis, sample AGX 31; b) Sphenolithus predistentus, sample AGX 20.

The Eocene-Oligocene boundary is observed in the lower part of the turbiditic system. In particular, the presence of *Discoaster barbadiensis*, *Discoaster saipanensis*, *Ericsonia formosa*, *Cyclicargolithus floridanus*, *Reticulofenestra floridana*, and *Sphenolithus predistentus* confirms late Eocene. The presence of *C. floridanus*, *Reticulophenestra bisecta*,

R. floridana, *S. predistentus*, *Sphenolithus distentus* and *Sphenolithus ciperoensis* in combination with the absence of *D. barbadiensis*, *D. saipanensis* indicates the early Oligocene time interval in the middle/upper part of outer fan deposits. In conclusion, the sedimentation in western Greece started on late Eocene and continues on early Oligocene. Subsequently, further investigation is to be conducted for:

- The biostratigraphic analysis of outer and inner fan deposits using calcareous nannofossils and planktonic foraminifera.
- The foraminiferal analysis (both planktonic and benthic foraminifera) because of the palaeoclimatological, palaeoenvironmental and palaeoecological interest of Eocene-Oligocene epoch.

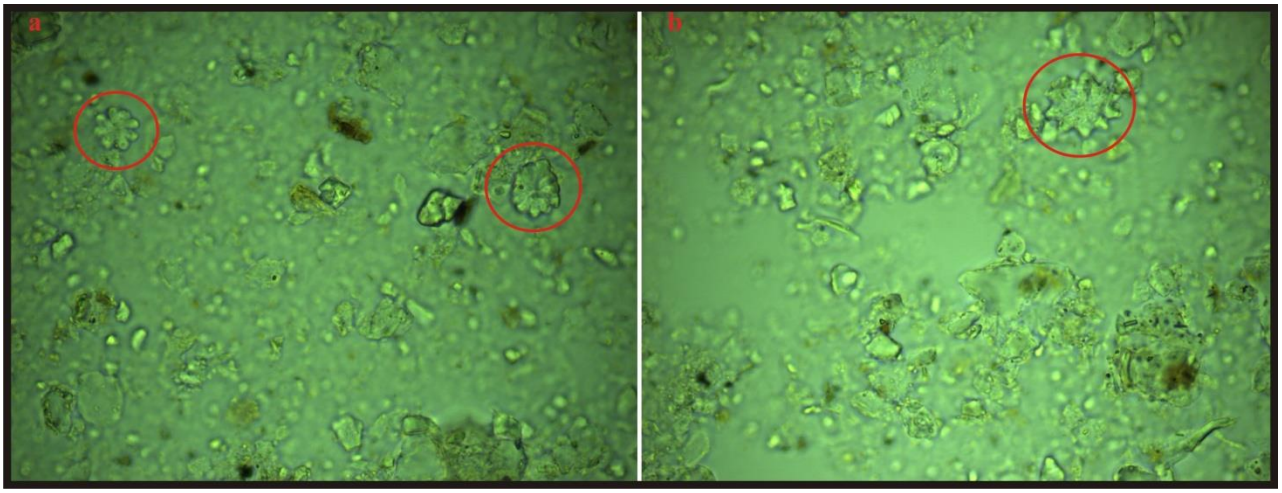

Figure 2. Discoaster species. a) Discoaster barbadiensis, sample AM 1; b) Discoaster barbadiensis, sample AM 35.

Acknowledgements

This work was funded by the H.F.R.I. (Hellenic Foundation for Research & Innovation) and GSRT (General Secretarial for Research and Technology) through the research project "Global climate and sea-level changes across the Latest Eocene-Early Oligocene, as reflected in the sedimentary record of Pindos foreland and Thrace basin, Greece, 80591".

References

Agnini, C., Fornaciari, E., Raffi, I., Catanzariti, R., Pälike, H., Backman, J. Rio, D. 2014. Biozonation and biochronology of Paleogene calcareous nannofossils from low and middle latitudes. Newsletters on Stratigraphy 47, 131–181.

Bown, P.R., Young, J.R., 1998. Techniques, in: Bown, P.R. (Ed.), Calcareous Nannofossil Biostratigraphy. British Micropalaeontology Society Series. London, UK: Chapman & Hall, p. 16-28.

Giunta, S., Negri, A., Morigi, C., Capotondi, L., Combourieu-Nebout, N., Emeis, K.C., Sangiorgi, F., Vigliotti, L., 2003. Coccolithiphorid ecostratigraphy and multi-proxy paleoceanographic reconstruction in the Southern Adriatic Sea during the last deglacial time (Core AD91-17). Palaeogeography, Palaeoclimatology, Palaeoecology 190, 39-59.

Konstantopoulos, P., Zelilidis, A., 2012. Sedimentation of submarine fan deposits in Pindos foreland basin, from late Eocene to early Oligocene, West Peloponnesus peninsula, Greece. Geol. J., doi:10.1002/gj.2450**.**

Maravelis, A., Zelilidis, A., 2012. Paleoclimatology and paleoecology across the Eocene–Oligocene boundary, Thrace Basin, northeast Aegean Sea, Greece. Palaeogeography, Palaeoclimatology, Palaeoecology 365-366, 81-98.

Martini, E., 1971. Standard Tertiary and Quaternary calcareous nannoplankton zonation, in: Farinacci, A. (Ed.), Second Planktonic Conference Proceedings, Roma 1970. Second Planktonic Conference Proceedings, Roma 1970. Rome: Edizioni Tecnoscienza, p. 739-785.

Miller, KG. 1992. Middle Eocene to Oligocene stable isotopes, climate and deepwater history: The Terminal Eocene Event? See Prothero and Berggren 1992, pp. 60-77.

Pälike, H., Norris, R.D., Herrle, J.O., Wilson, P.A., Coxall, H.K., Lear, C.H., Shackleton, N.J., Tripati, A.K., Wade, B.S. 2006. The heartbeat of the Oligocene climate system. Science 314(5807), 1894-1898.

Winter, A., Siesser, W.G., 1994. Coccolithophores. Cambridge University Press, 242.

Zachos, J., Pagani, M., Sloan, L., Thomas, E., Billups, K., 2001. Trends, rhythms, and aberrations in global climate 65 Ma to Present. Science 292, 686-693.

15th International Congress of the Geological Society of Greece
Athens, 22-24 May, 2019 | Harokopio University of Athens, Greece
Bulletin of the Geological Society of Greece, Sp. Pub. 7 Ext. Abs. GSG2019-202

Climate reconstruction and environmental changes during the Holocene period based on a varved sediment record from Vouliagmeni lake, Corinth Gulf, Greece

Alexandros Emmanouilidis[1], Ingmar Unkel[2], Pavlos Avramidis[1]

(1) Department of Geology, University of Patras, 26504 Rio Patras, Greece, alexandros.emmanouilidis@upnet.gr
(2) Institute for Ecosystem Research, Christian-Albrechts-University, 24118 Kiel, Germany

Background

The eastern Mediterranean region has long been a region of interest concerning palaeoclimatic (Kaniewski et al., 2013; Triantaphyllou et al., 2014) and palaeoenvironmental (Pavlopoulos et al., 2012; Kouli et al., 2012; Avramidis et al., 2017) studies, due to climate heterogeneity and complex atmospheric circulation patterns that produce regional precipitation and temperature fluctuations. Studies of coastal sedimentological environments allow the recognition of coastline changes and give information about the rate of sedimentation, eustatic sea level changes and tectonic movements.

Annually laminated lake sediments (varves), have proven to be excellent geoarchivies in order to interpret changes that occurred during the Holocene period, regarding elemental fluxes, palaeoclimate reconstruction, sea level fluctuation, tectonic activity etc. The distinct color, composition, texture structure and thickness, contained in all varve types, corresponds to different climatic driven mechanisms. Thus, the study of varved sedimentary records, can provide annually to seasonal climatic variations and mirrors sedimentological and environmental conditions taking place in the catchment.

Objectives

The study area is located at the east part of the Gulf of Corinth, an active rift and one of the most seismically active regions in the world. Until the 19th century, when an artificial channel was opened, lake Vouliagmeni lake completely separated from the sea. Anoxic conditions seem to prevail throughout the year, at least below 38 m water depth. Human occupancy in the area, as indicated from archaeological findings in the area, is recorded during the Bronze Age (3100-1700 BC) and Early Iron Age (1075-750 BC).

The aim of the present study is the high-resolution analysis of a 6m varved core retrieved from Vouliagmeni Lake, covering the last ~ 12000 years, in order to extract regional and long scale palaeoclimatic data.

Methods

Standard sedimentological analysis was conducted on 90 samples, including grain size analysis, Total Organic Carbon (TOC) and Calcium Carbonate content. For the X-ray Diffraction (XRD) analysis, a Brucker D8 device was used. XRF core log analysis was performed with a step of 0.5 cm, at the Institute of Geosciences at Kiel University (Germany), using an Avaatech system. Core scanning was performed with a Molybdenium tube set at 10 kV and 30 kV with an integration time of 60 second per measurement. The chronological framework of the core was determined by 8 AMS ^{14}C radiocarbon dating, combined with laminae counting. For the exact determination of each lamination boundaries as well as an estimation of the bulk density throughout the core, CT scanning was performed, at General University Hospital of Patras in Greece.

Results

Through varve counting in the sediment core, combined with the AMS radiocarbon dating, the accumulation rates in the study area seem to change at around 3 ka BP (Fig. 1). Varved sediments interrupted by non laminated silty clay sequences were recognized in all core Units. Calcite rich layers alternating with organic rich layers, correspond to summer and winter depositions. Varve thickness was determined through the CT scan models that were produced for the core and was used as a seasonal intensity interval.

Representative elemental ratios were constructed in order to recognize the different sedimentary processes taking place in the study area (Fig. 1). Some long-scale climatic events (8.2 ka BP, 6-5 ka BP, 3.2-3.8 ka BP) seem to be well reflected into the elemental composition of the core. Rb/Sr ratio which is a suitable indicator for precipitation/physical erosion in the catchment area, shows distinct climatic driven fluctuations. The aragonite rich laminations that occur in the core, are documented in the Ca/Sr ratio, with increased values distinguishing a terrigenous supply of $CaCO_3$. The S and Pb content were used for marine inundations.

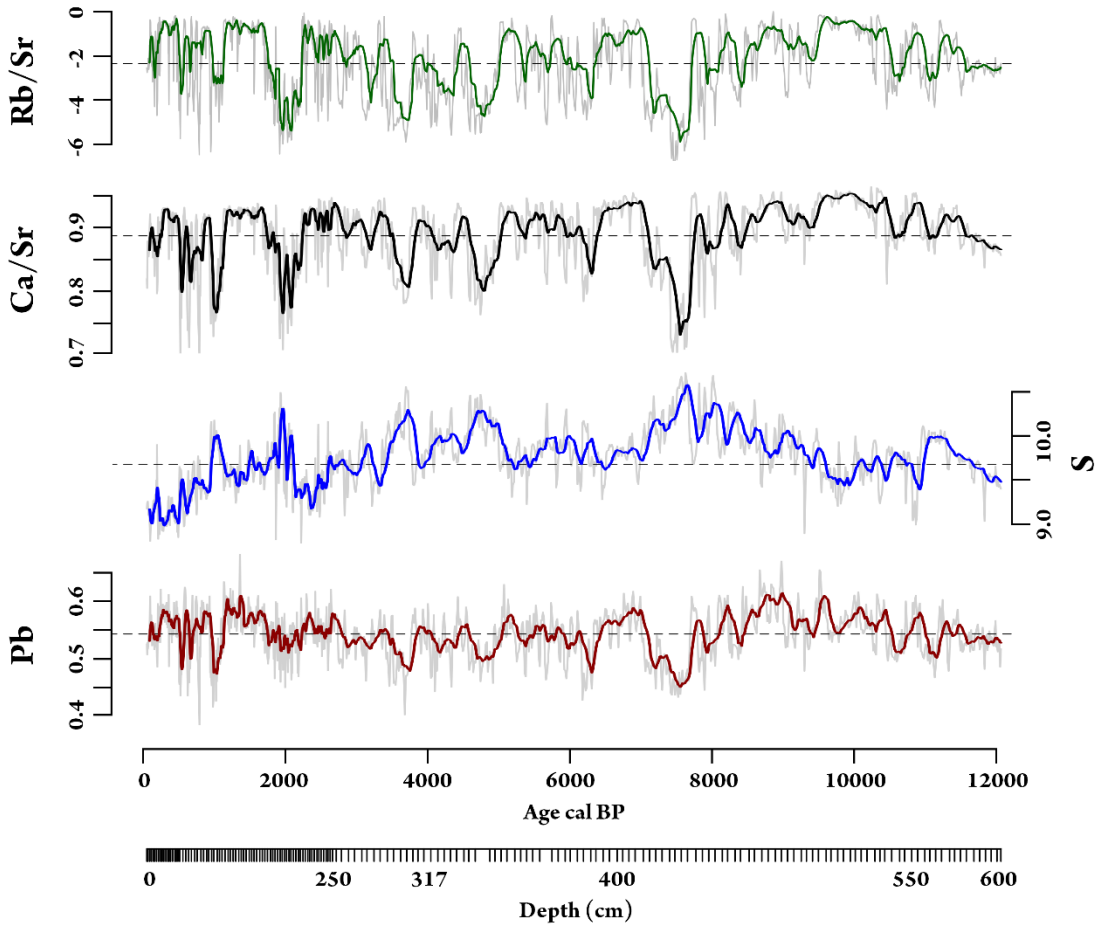

Figure 1. Representative geochemical proxies from Vouliagmeni core.

Conclusion

Vouliagmeni core, presents the oldest geoachive in Greece concerning varved sediments. Sedimentation rate of the study area seems to completely change at around 3000 cal BP and can be strongly associated with the relative sea level change at around that time. Paleoclimatic signals detected through the geochemical analysis conducted in the core, pronounce clear interaction between elemental composition and temperature/precipitation fluctuations. Future analysis and microscale examination especially in the varved sequences, will provide even more details regarding regional climatic fluctuations and will increase the spatial coverage on the already existing palaeoclimatic datasets.

Acknowledgements

This research is financed by Greece and the European Union (European Social Fund- ESF) through the Operational Programme «Human Resources Development, Education and Lifelong Learning» in the context of the project "Strengthening Human Resources Research Potential via Doctorate Research" (MIS-5000432), implemented by the State Scholarships Foundation (IKY).

References

Avramidis, P., Iliopoulos, G., Nikolaou, K., Kontopoulos, N., Koutsodentris, A., Wijngaarden, G. J., 2017. Holocene sedimentology and coastal geomorphology of Zakynthos Island, Ionian sea: A history of a divided Mediterranean island. Palaeogeography Palaeoclimatology Palaeoecology 487, 340-354.

Kaniewski, D., Campo, E. V., Morhange, C., Guiot, J., Zviely, D., Shaked, I., Otto, T., Artzy, M., 2013. Early urban impact on Mediterranean coastal environments. Scientific Reports 3, 3540.

Kouli, K., Gogou, A., Bouloubassi, I., Triantaphyllou, M. V., Ioakim, C., Katsouras, G., Roussakis, G., and Lykousis, V., 2012. Late postglacial paleoenvironmental change in the northeastern Mediterranean region: Combined palynological and molecular biomarker evidence. Quaternary International 261, 118–127.

Pavlopoulos, K., Kapsimalis, V., Theodorakopoulou, K., Panagiotopoulos, I.P., 2012. Vertical displacement trends in the Aegean coastal zone (NE Mediterranean) during the Holocene assessed by geo-archaeological data. Holocene 22, 717-728.

Triantaphyllou, M.V., Gogou, A., Bouloubassi, I., Dimiza, M., Kouli, K., Papanikolaou, M., Kotthoff, U., Emeis, K. C., Roussakis, G., Athanasiou, M., Parinos, K., Ioakim, C., Lykousis, V., 2014. Evidence for a warm and humid Mid-Holocene episode in the Aegean and northern Levantine Seas (Greece, NE Mediterranean). Regional Environmental Change 14 (5), 1697-1712.

15th International Congress of the Geological Society of Greece
Athens, 22-24 May, 2019 | Harokopio University of Athens, Greece
Bulletin of the Geological Society of Greece, Sp. Pub. 7 Ext. Abs. GSG2019-207

New sedimentological finding studying the Cretaceous deposits along the new Ionian road around the Amphilochia and Arta sections

N. Dimopoulos[1], E. Georgoulas[1], S. Peridis[1], G. Iliopoulos[1], N. Bourli[1], A. Zelilidis[1]
(1) University of Patras, Department of Geology, Laboratory of Sedimentology, 26504, Patras, Greece,
nikos.dhmopoulos@gmail.com

Introduction – Geological setting

Upper Cretaceous–Lower Eocene deposits of the Ionian basin are the major target in hydrocarbon exploration as they represent the reservoir rocks. These deposits mostly are composed of calciturbidites interbedded with breccia-microbreccia deposits. According to Bourli et al., 2019 the studied outcrops from Araxos area (internal Ionian sub-basin) showed that the breccia - microbreccia deposits are structureless, with a channelized geometry and calciturbiditic blocks internally to the channels; whereas most of the clasts were sourced from the underlying Lower Cretaceous "Vigla limestones". Moreover, microfacies analysis indicate deep-water deposits and reworked shelf deposits. The intense extensional tectonic activity in the Ionian basin during the early Cretaceous, with synthetic and antithetic faults, produced active platform margins and asymmetrical grabens. During the late Cretaceous, the uplifted margins of the grabens caused erosion of the pre-existing deposits of the early Cretaceous "Vigla formation".

Analysis of the studied sections – Field work

In order to have a better understanding of Upper Cretaceous-Lower Eocene evolution of the Ionian basin, two new-outcropped sections were selected around Amphilochia – Arta area (middle Ionian sub-basin). Amphilochia section is directed parallel to the thrust faults (NNW-SSE), whereas Arta section is directed parallel to the transfer or strike slip faults (NE-SW).

In the new Ionian road, Amphilochia section, and although geological map showed the presence only of the Upper Cretaceous deposits, in the new sections the lower stratigraphic deposits correspond to the Lower Cretaceous Vigla shales or Vigla limestones, whereas Upper Cretaceous limestones rest unconformably over the Lower Cretaceous sediments. Lower Cretaceous deposits are characterized by strong discontinuity along the NNW direction, that mostly influenced by syn-sedimentary transfer faults. In addition, slumps were observed throughout the sections with E-W direction with a sliding from the east. These slumps are result of an instability probably produced from the N-S directed normal faults (Figure 1a). The dip direction of the beds is NNE-SSW.

In the new Ionian road the Arta section, with a NNE-SSW direction, is strongly deformed due to many reverse faults, probably branches of the major thrust fault, situated west of the studied section. The above deformation is owed to the compressional regime (Eocene to Miocene) that influenced the whole area after the sedimentation. These deformations are recorded in many outcrops along the Ionian road and their general dip is 230º/50º (Figure 1b).

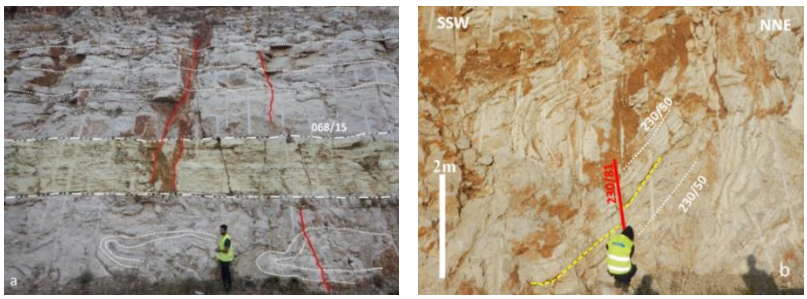

Figure 1: This figure shows: (a) the slumps on the lower stratigraphic layers and the non-deformed sediments above them (Amphilochia section), (b) the intense deformation of the sediments due to reverse faults. The sediments as a result of the deformation have dip and dip direction, respectively, 230º/50º (Arta section).

Microfacies analysis of thin sections

Microfacies analysis carried out in thin sections from selected samples from Amphilochia, Arta and Kerasonas showed that most of the sediments deposits belong to deep marine environment (FZ 1 **&** 2), some of them showed a slope to shelf environment (FZ 3 **&** 4) and only a few showed shallow water environment. The main textural and compositional characteristics, as well as the sedimentary features of the distinguished microfacies are summarized in Table 1, corresponding to different depositional environments or facies zones (FZ: Flügel, 2010). More specifically, the "Vigla limestones" were classified as packstones/wackestones with scattered planktonic foraminifera and radiolarian limestones (standard microfacies SMF 3), indicating a deep-sea basin environment (FZ 1). Upper Cretaceous incudes pelagic wackestones with planktonic foraminifera (SMF3); microbreccia biolithoclastic packstones to grainstones (bioclasts, planktonic and benthic foraminifera (SMF4) indicating slope environment (FZ4) – toe of slope (FZ3), and, allochthonous

bioclastic packstone to rudstone/floatstone breccia containing rudist and gastropod fragments, planktonic and benthic foraminifera, geopetal fractures (SMF5) indicating a slope environment (FZ4). Fenestral cavities and geopetal fractures in allochthonous material may indicate a source from a restricted or shallow shelf environment (FZ4) with the influence of meteoric water. The Paleocene pelagic grainstone containing planktonic and benthic foraminifera (SMF2), corresponding to a deep shelf environment (FZ 2) and finally, Eocene pelagic wackestones with planktonic foraminifera (SMF3), indicating a toe of slope environment (FZ3).

Table 1. Detailed description of studied smear slides where depositional facies, lithology, fossils and the age of the studied deposits are presented (SMF= Standard Microfacies Type, FZ= Facies Zone, Pl.z.= Planktonic zone, foraminifera=forams).

No. of Samples	Facies Description	Fossils	Lithology	Stage
Amphil. sec.: 1	Pelagic wackestone with planktonic forams (SMF3). alaeoenvironment: Toe of slope (FZ3)	Planktonic forams (*Subbotina inaequispira, Globorotalia centralis, Morozovella aragonensis*)	Thin-bedded limestones with chert intervals	Eocene - [Lutetian (P1.z. 11a) - Lutetian (P1.z. 11b)]
Arta sec.: 1	Pelagic grainstone with benthic and planktonic forams (SMF2). Palaeoenvironment: Deep shelf (FZ2)	Benthic & planktonic forams (*Acarinina subsphaerica, Morozovella angulata)*	Micro brecciated limestones	Paleocene - [Selandian (Pl.z. 3b)- Thanetian (Pl.z. 5a)]
Amphil. sec.: 2 Arta sec.: 2	Allochthonous bioclastic packstone to rudstone/floatstone breccia. Rudist and gastropod fragments, planktonic and benthic forams, geopetal fractures (SMF5). Palaeoenvironment: Slope (FZ4)	Planktonic forams *(Globotruncana falsostuari, Siderolites calcitrapoides)* & benthic forams *(*Miliolidae, *Orbitoides midea, Cuneolina sp.),* rudist & gastropod fragments, algae	Micro brecciated limestones	Upper Cretaceous – Maastrichtian
Arta sec.: 8, Amphil. sec.: 3, Keras. sec.: 1	Two facies: 1. Pelagic wackestones with planktonic forams (SMF3). 2. Microbreccia biolithoclastic packstones to grainstones. Bioclasts, planktonic and benthic forams (SMF4). Palaeoenvironment: Slope (FZ4) – Toe of slope (FZ3)	1. Benthic and planktonic forams (*Sigalitruncana sigali, Marginotruncana pseudolinneana*) 2. Benthic and planktonic forams (*Globotruncanita stuartiformis,Marginotruncana renzi)*	1. Thin-bedded limestones with chert fragments 2. Micro brecciated limestones	Upper Cretaceous – [Turonian (Pl.z. 1) – Campanian (Pl.z. 2)]
Arta sec.: 10, Amphil. sec.: 5, Keras. sec.: 15	Bioclastic pelagic packstones and wackestones that contain scattered pelagic microfossils. Palaeoenvironment: Deep-sea basin (FZ1)	Radiolarians and planktonic forams (Calpionella sp.)	Vigla limestones and shales	Lower Cretaceous
Amphil. sec.: 4 Keras. sec.: 2	Palaeenvironment: (FZ9) Evaporitic/brackish platform interior – Restricted platform interior (FZ8)	Benthic forams (Miliolidae, Rotalidae) Algae	Pantokrator limestones	Lower Jurassic

Discussion and conclusions

In the Amphilochia new cross-section, with a N-S direction, the lower Cretaceous Vigla limestones and Vigla shales were outcropped for first time. This section is directed parallel to the paleo Ionian basin axis and the fact of the lateral discontinuity of Vigla limestones and Vigla shales indicate that during the sedimentation of these two formations there was a restriction along the paleo basin axis, probably due to synsedimentary transfer fault activity.

In the Arta new cross-section, with a NE-SW direction, the upper Cretaceous Senonian deposits showed strong deformation that took place during the compressional regime that affected the Ionian basin after sedimentation. This deformation is stronger in the western part, close to a major thrust, and seems that this deformation could produce a high secondary porosity increase of upper Cretaceous deposits.

The unconformably overlying Upper Cretaceous Senonian limestones are characterized by micro-breccia, calciturbidites and slumps, as recognized and in other areas (Bourli et al., 2019).

Microfacies analysis showed in general a deep-sea environment with few exceptions with shallow environment character, introducing the existence of platforms, close to the studied sections.

References

Bourli, N., Pantopoulos, G., Maravelis, A.G., Zoumpoulis, E., Iliopoulos, G., Pomoni-Papaioannou, F., Kostopoulou, S., Zelilidis, A., 2019. Late Cretaceous to Early Eocene geological history of the eastern Ionian Basin, southwestern Greece: An integrated sedimentological and bed thickness statistics analysis. Cretaceous Research 98, 47-71.

Flügel, E., 2010. Microfacies Analysis of Carbonate Rocks. Springer Verlag, Berlin, 745p

15th International Congress of the Geological Society of Greece
Athens, 22-24 May, 2019 | Harokopio University of Athens, Greece
Bulletin of the Geological Society of Greece, Sp. Pub. 7 Ext. Abs. GSG2019-210

Sedimentary facies recognition using XRF core scanner, on two former lagoonal systems of western Peloponnese, Greece

Ioannis Prevedouros [1], Alexandros Emmanouilidis[1], Pavlos Avramidis[1]
(1) Department of Geology, University of Patras, 26504 Rio Patras, Greece, giannhspre@hotmail.com

Background

The understanding of palaeoenvironmental changes through sedimentological, palaeontological, geochemical and mineralogical studies provide information regarding depositional environments, elemental fluxes, palaeoclimate reconstruction, sea level fluctuation, tsunamigenic phenomena and tectonic activity (Kontopoulos and Avramidis 2003; Vött, et.al., 2009, 2011; Avramidis et al., 2013; Emmanouilidis et al., 2018). Coastal aquatic systems are considered environmentally sensitive areas formed behind sand or gravel barrier shorelines, at the terminal area of the coastal alluvial plains or at river mouths. They are shallow and highly dynamic ecosystems at the interface between coastal and marine environments, which can be permanently open or intermittently closed off.

The study of sedimentary facies in lagoonal systems reveal transition patterns concerning sediment runoff, physical erosion in the catchment area, human activity etc. High resolution geochemical profiles, relative changes and altering trends of elemental concentration imprint these palaeoenvironmental changes as well as micro facies that would not be detected otherwise. Many researchers use geochemical proxies such as Rb/Sr, Fe/Mn, Ca/Ti, Sr/Ti, Zr/Rb, Zr/Ti to delineate existing physical, sedimentological and geochemical processes such as evaporation, precipitation, dissolution of solid phases, Eh and pH changes, chemical and physical weathering.

Objectives

Mouria and Agoulinitsa lagoons are located in western Peloponnese, Greece. Palaeoenvironmental studies conducted in western Greece, reveal continuous transitions in the geomorphological evolution of coastal aquatic systems. Marine inundations, human activity and fluvial influx comprise major aspects into the lifespan of those systems. In this framework, the present study reveals such sedimentary transitions in both studied sites based on sedimentological and geochemical proxies.

Methods

Two sediment cores were retrieved using an Eijelkamp vibrating corer with closed barrel tubes. After the extraction, the cores were sealed with cling film and transported for analysis in the laboratory of sedimentology, University of Patras, Greece.

Standard sedimentological analyses were carried out, on a total of 80 sediment samples including: (1) grain size analysis and calculation of moment measures such as mean, sorting, kurtosis and skewness, (2) color determination and RGB profile plot, (3) Total Organic Carbon (T.O.C.), (4) Total Carbon (T.C.), (5) Total Nitrogen (T.N.), (6) Calcium Carbonate Content (CaCO3), (7) Total Phosphorus (T.P.) content and (8) Magnetic susceptibility measurements.

U-channels were extracted from the sediment cores for XRF core-log analysis using the Avaatech system at the Institute of Geosciences of Kiel University. Core scanning was performed with a Molybdenum tube set at 10 kV and 30 kV with a step of 0.5 cm and an integration time of 60 second per measurement.

Results

Compiling all the sedimentological and geochemical data, 3 main lithological units were distinguished for Mouria core (Fig. 1) and 2 for Agoulinitsa core.

For Mouria core, Units 1 and 2 consist of coarser material and present the highest values in geochemical ratios Si/Ti, Ca/Fe, Sr, Cl, S, Zr/Rb (Fig. 1). The increase of Cl and S indicate the marine influence in the study area whereas Mn/Fe ratio reflects the oxic conditions (Fig. 1). Magnetic susceptibility is mostly associated with terrestrial input in the study area, thus presenting the lowest values at these units (Fig. 1). Unit 3 consist of fine organic rich sediment. Elemental ratios such as Ti and Rb/Sr are strongly associated with clay minerals and provide a clear signal concerning the physical erosion and fine sediment deposition in the study area.

Concerning Agoulinitsa core, the two sediment units that were recognized, present similar trends with Mouria core. The first two meters of the core, are characterized by organic rich sediment, presenting high values for the terrigenous elements. Mn/Fe ratio, indicates anoxic conditions, validating the high organic content and thus presents a more lacustrine environment. Sandy units at the lower parts of the core (>2 m) present an open lagoonal environment. Higher values of S, Cl and Br indicate constant marine inundations into the system.

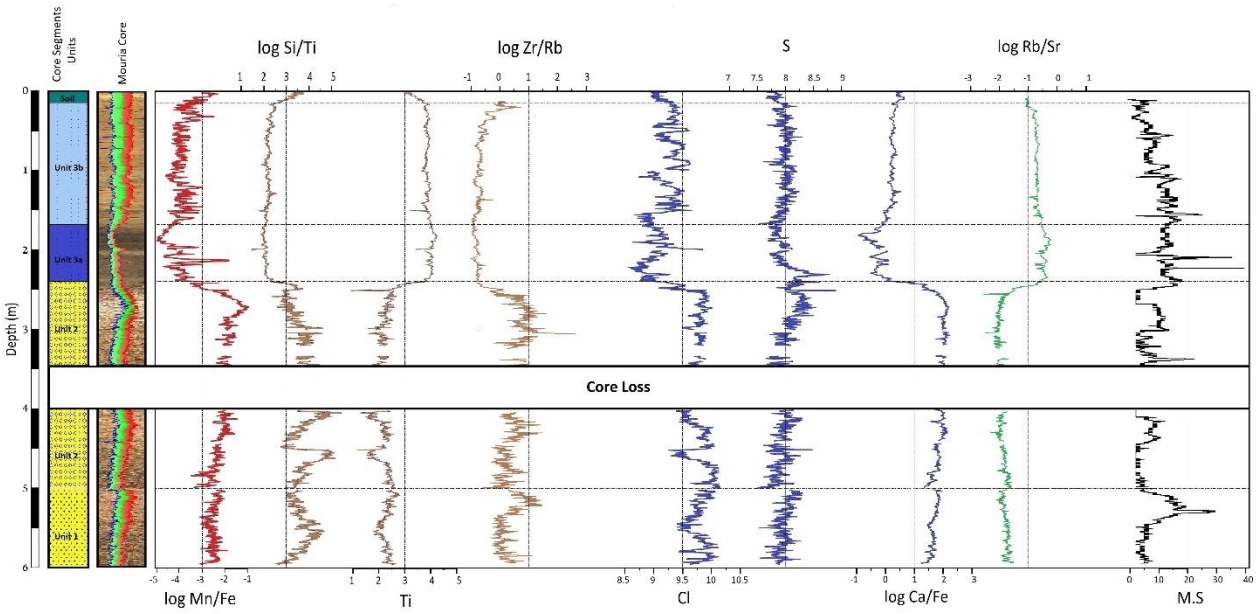

Figure 1. Representative geochemical proxies from Mouria lagoon

Conclusion

The sedimentological, geochemical and magnetic susceptibility measurements from both sediment cores (ML-1 and AG-1), indicate different sediment transport and depositional processes. Non-destructive analysis conducted on both cores, imprints all the palaeoenvironmental and palaeogeomorphological changes that occurred in the study area as well as the interplay between those coastal aquatic systems and marine environment.

References

Avramidis, P., Iliopoulos, G., Kontopoulos, N., Panagiotaras, D., Barouchas, P., Nikolaou, K. Papadopoulou, P., 2015. Deposotional environments, sediment characteristics, palaeoecological analysis and environmental assessment of an internationally protected shallow Mediterranean lagoon, Gialova lagoon Navarino Bay, Greece. Earth and Environ. Sci. Trans. Royal Soci. Endinburgh 105, 189-206.

Avramidis, P., Iliopoulos, G., Nikolaou, K., Kontopoulos, N., Koutsodendris, A., van Wijngaarden, G.J., 2017. Holocene sedimentology and coastal geomorphology of Zakynthos Island, Ionian Sea: a history of a divided Mediterranean island. Palaeogeogr. Palaeoclimatol. Palaeoecol. 487, 340-354.

Balascio, N., Zhang, Z., Bradley, R., Perren, B., Dahl, S., Bakke, J., 2011. A multi-proxy approach to assessing isolation basin stratigraphy from the Lofoten Islands, Norway. Quat. Res. 75, 288-300.

Chatziapostolou, A.; Siavalas, G.; Kalaitzidis, S.; Cristanis, K.;2013. Geological study for a wetland restoration: the case of the drained Mouria Lake (W. Peloponnese). Bulletin of the Geological Society of Greece, [S.l.], v. 47, n. 1, p. 72-81.

Emmanouilidis, A.; Katrantsiotis, C.; Norstrom, E.; Risbeng, J.; Kylander, M.; Sheik, T.A.; Iliopoulos, G.; Avramidis, P.;2018 Middle to late Holocene palaeoenvironmental study of Gialova Lagoon, SW Peloponnese, Greece. Quaternary International Volume 476, 46-62

Folk, R.I., 1974. Petrology of Sedimentary Rocks. Hamphill, Austin, Texas.

Haenssler, E., Unkel, I., Dorfler, W., Nadeau, M.-J., 2014. Driving mechanisms of Holocene lagoon development and barrier accretion in Northern Elis, Peloponnese, inferred from the sedimentary record of the Kotychi Lagoon. Quat. Sci. J. 63, 60-77.

Kraft, J.C, Rapp, G, Gifford, J.A., Aschenbrenner, S.E.; 2005, Coastal Change and Archaeological Settings in Elis, Hesperia: The Journal of the American School of Classical Studies at Athens; Vol. 74, No. 1 (Jan. – Mar., 2005), pp. 1-39

Vott, A., Kelletat, D., 2015. Holocene palaeotsunami landfalls and neotectonic dynamics in the western and southern Peloponnese (Greece). Zeitschrift fur Geomorphologie 59, 1-5.

Vott, A., 2007. Relative sea level changes and regional tectonic evolution of seven coastal areas in NW Greece since the mid-Holocene. Quat. Sci. Rev. 26, 894-919.

15th International Congress of the Geological Society of Greece
Athens, 22-24 May, 2019 | Harokopio University of Athens, Greece
Bulletin of the Geological Society of Greece, Sp. Pub. 7 Ext. Abs. GSG2019-211

Spatial Sedimentological, Geochemical and Mineralogical Characterization of Vouliagmeni Coastal Lake, Greece

D.Bassukas[1], A.Emmanouilidis[1], D.Panagiotaras[2], P.Avramidis[1]

(1) Department of Geology, University of Patras, 26504 Rio Patras, Greece, d.basoukas@upnet.gr
(2) Department of Mechanical Engineering, Technological Educational Institute of Western Greece, 26334, Patras, Greece

Background

Coastal lakes and lagoons are highly dynamic and prone to changes like human impact, climatic influences or changes in depositional environments and many more all of which are imprinted in the sediment characteristics and chemistry. Grain size distribution and moment measurements provide an insight into transport-deposition processes while pointing out driving forces (Gao and Collins, 1992; le Roux, 1994,). Sedimentological analyses are generally coupled with geochemical focusing on major oxides, trace elements as well as mineralogy which provide information concerning the provenance and geochemical processes of the sedimentological basement (Panagiotaras et al., 2012). Preserved organic matter in sediments comprises carbon assessed mainly as Total Organic Carbon (TOC) and nutrients as Total Phosphorus (TP) and Total Nitrogen (TN) with organic as well as inorganic sources.

Objectives

Vouliagmeni is a coastal lake located in the SW Perachora peninsula extending into the eastern Gulf of Corinth (Greece) while with a maximum depth of around 49m (Katsanevakis, 2005). At the northern and southern part of the lake, due to normal dipping faults, the lake is characterized by steep bathymetry unlike the eastern and western part where the transition is smoother. Until the late 19th century the lake was separated from the Gulf of Corinth by an isthmus when a narrow (18m) canal was constructed leading to the present lagoonal state. In the current study we present a spatial characterization of the lake bottom sediments based on sedimentological, geochemical and mineralogical analyses providing an insight into depositional environments and processes presently active in the lagoon.

Methods

A total of nineteen (19) samples consisting of upper 1-2cm lake bottom sediments were collected. For the grain size analysis, coarser material (>4 Φ) was dry sieved whereas finer (<4 Φ) was measured with the use of a Malvern Mastersizer 2000 followed by the moment measures' calculation using GRADISTAT V.4. (Blott and Pye, 2001). The $CaCO_3$ content was measured with a FOG II/Digital hand-held soil calcimeter (BD Inventions), the TOC using the (Walkley and Black 1934, Avramidis *et al*., 2015) tritation method, TN content was measured using a Carlo Erba CHNS-O EA 1108 Elemental Analyzer while the TP content was measured using a HACH photometer, based on APHA 2005-4500-P.

In a geochemical framework, concentrations of 10 major elements (Si, Al, Ca, Mg, Mn, P, Fe, Na, K and Ti) and 19 trace elements (Sc, V, Cr, Co, Ni, Cu, Zn, Rb, Sr, Y, Zr, Nb, Ba, Hf, W, Pb, La, Ce and Th) were measured by comparison of X-ray intensities for each element with calibration lines constructed from the analysis of known concentrations in 32 international standards. Powdered samples where pressed into pellets and analyzed with a RIGAKU ZSX PRIMUS II wavelength dispersive spectrometer equipped with a 4KW Rh X-ray tube which is located at the Laboratory of Electron Microscopy and Microanalysis of the University of Patras, Greece. A predominant mineralogical composition was determined for each of the nineteen samples by powder X-Ray diffraction (XRD) using a Bruckner D8 advance diffractometer with Ni-filtered CuKα radiation and analyzing the results with the DIFFRACplus EVA 12 software.

Results

The central part of the lagoon is characterized by fine sediment, whereas the shallower parts of the lagoon are mostly associated with coarser material. In samples located near the artificial channel and at the north east part of the lagoon, the coarser material is attributed to bivalve assemblages. These bivalve assemblages, which represent around the 70 % of these samples, are highly linked to the hydrological regime of the lagoon, since they show clear evidence of transport before their burial (broken bivalves, cracks). Samples from depth less than 20 m present higher $CaCO_3$ being attributed to the high presence of micro-macrofaunal assemblages (Fig. 1d). Low $CaCO_3$ content is apparent in the deep horizons of the lake. Higher TOC, TN and TP concentrations are observed in the depths beyond 20m sediments (Fig. 1a, b, c).

Statistical analysis on the geochemical data shows that all elements are associated with the organic content and the clay fraction of the sediments except that for Na, Sr and Co. High correlation ($r>0.83$) for Ni, Cu, Pb, Zn and Rb with the Al_2O_3 shows the same origin of these metals and their association with the detrital materials from the catchment. The elements Fe, Mn, Mg, K, Ti, P and TP are well correlated with the aluminosilicate fraction of the sediments. However, Ca and $CaCO_3$ show complex geochemical association with high negative loadings ($r>-0.95$) been observed with Al_2O_3. Negative loadings ($r=-0.56$ and $r=-0.66$) have been found between TOC and $CaCO_3$ and TOC and CaO respectively. This finding implies both a non biogenic and a biogenic origin of these components. The same geochemical feature is observed with the TN. High positive correlation ($r=0.83$) is found between TOC and TN and also a positive correlation is apparent ($r=0.66$) between TN and Al_2O_3.

The mineralogical composition showed little spatial diversity throughout the samples and was mostly represented by Quartz (mean: 33.7%), Aragonite (mean: 30.5%), Calcite (mean: 18.2%), Biotite (mean: 13.7%), Halite (mean: 6.5%) and Pyrite (mean: 11.4%, in samples 5, 6, 7) indicating anoxic/hypoxic conditions.

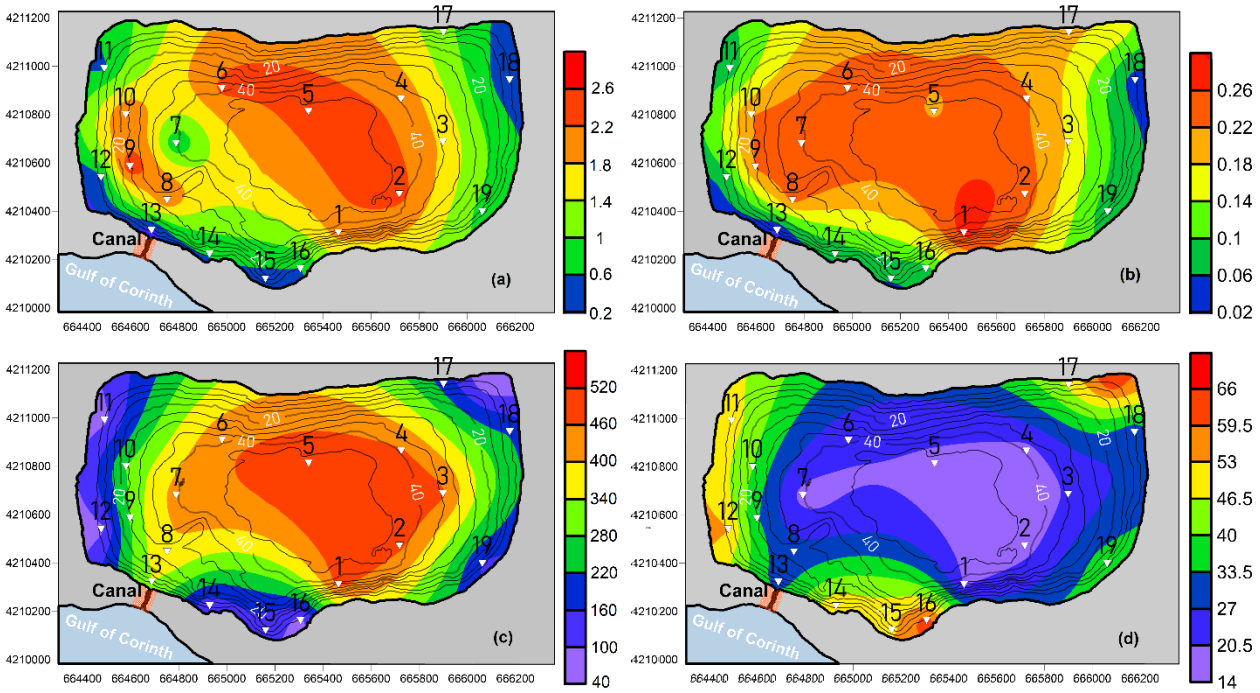

Figure 1. Bathymetry modified after Katsanevakis, 2005 a) TOC(%) b) TN(%) c) TP(mg/kg) d) $CaCO_3$(%)

Conclusions

Based on grain size analysis, sedimentological, geochemical and mineralogical analyses a division of the lake in two distinct environments by depth is recognized, shallow (0-20m) and deep (>20m). The grain size distribution, from coarse to fine progressing from the coast (until 20m) to the deeper part is controlled by the hydrodynamic regime. The oxidation conditions in the deep part due to the preservation of organic matter as well as the existence of Pyrite below 35m indicate anoxia.

References

Avramidis, P., Nikolaou, K., Bekiari, V., 2015. Total Organic Carbon and Total Nitrogen in Sediments and Soils: A Comparison of the Wet Oxidation – Titration Method with the Combustion-Infrared Method. Agriculture and Agricultural Science Procedia 4, 425–430.

Blott, S.J., Pye, K., 2001. GRADISTAT: a grain size distribution and statistics package for the analysis of unconsolidated sediments. Earth Surface Processes and Landforms 26, 1237–1248.

Gao, S., Collins, M., 1992. Net sediment transport patterns inferred from grain-size trends, based upon definition of "transport vectors." Sedimentary Geology 81, 47–60.

Katsanevakis, S., 2005. Population ecology of the endangered fan mussel Pinna nobilis in a marine lake. Endangered Species Research 1, 1–9.

Panagiotaras, D., Papoulis, D., Kontopoulos, N., Avramidis, P., 2012. Geochemical processes and sedimentological characteristics of Holocene lagoon deposits, Alikes Lagoon, Zakynthos Island, western Greece. Geological Journal 47, 372–387

Roux, J.P. le, 1994. An alternative approach to the identification of net sediment transport paths based on grain-size trends. Sedimentary Geology 94, 97–107.

Walkley, A., Black, I.A., 1934. An examination of the Degtjareff method for determining soil organic matter, and a proposed modification of the chromic acid titration method. Soil Science 37, 29-38.

15th International Congress of the Geological Society of Greece
Athens, 22-24 May, 2019 | Harokopio University of Athens, Greece
Bulletin of the Geological Society of Greece, Sp. Pub. 7 Ext. Abs. GSG2019-217

Facies Associations Review Of Depositional Environments In The External Hellenides Isopic Zones, Ionian Sea And Western Greece Margin

G. Makrodimitras[1], V. Kosmidou[1]

(1) Hellenic Hydrocarbon Resources Management S.A., Dimitriou Margari 18, 11525, Athens, Greece,
g.makrodimitras@greekhydrocarbons.gr

Background & Methods

The studied area of the Ionian Sea and the Western Greece margin, running from the Diapondia Islands-north of Corfu Island, to Filiatra in Southern Peloponnese, is characterized by the most external Hellenides zones and the Apulian Platform. It is well known that during the Tethyan rifting, taphrogenetic processes divided the uniform carbonate platform into shallower parts (the Apulian Platform, its margin the Pre-Apulian zone, and the Gavrovo-Tripolitza Platform) and deeper parts (the Ionian basin). From that time, different sedimentary evolution processes took place in each part, thus the zones exhibit distinct lithostratigraphic columns with different petroleum systems (Karakitsios, 2013).

The external Hellenides units are separated by NW-SE trending thrusts. In the offshore areas of the Ionian Sea, a system of NE-SW strike-slip faults cross-cuts the Apulian, Pre-Apulian and Ionian units. The most important of these strike-slip faults is the Kefalonia Transform Fault Zone (KTFZ), dividing the offshore area in two (2) segments; the north and the south segments. For the purpose of this study, eight (8) wells have been selected in order to cover both geographically the three segments and stratigraphically the external Hellenides zones which are present in the area. In the north segment: East Ericoussa-1, Yanadhes-1, Paxos Gaios-1X, and Parga-1; and in the south segment: South Kefallinia-1, Agios Kirikos-1, Sosti-1 and Peristeri-1.

A hierarchical approach to sedimentological description and interpretation has been applied to generate the present lithotypes/lithofacies (LTs/LFs) through cuttings and core data. The LTs/LFs have been grouped in bed-set scale units-depositional packages (DPs) with similar characteristics and internal organization. The vertical and lateral organization of the depositional packages can define the bed-set stack scale facies associations (FAs) with specific geometries and dimensions. These facies can be assigned to specific depositional environments.

Results & Conclusions

The wells which have been drilled on the Ionian zone, exhibit a wide range of both clastic and carbonate depositional environments, ranging from shallow marine, coastal, deltaic, to deep-water (Table 1). On the other hand, the wells which have been drilled on the Pre-Apulian unit, exhibit shallow marine carbonate deposits overlaid by deep-water to shallow-marine clastic sediments. Consequently, the aforementioned depositional environments have their distinct FAs and DPs in different proportions through geological time.

The differences between north Segment and south Segment might be due to:

- Different isopic domains (Jurassic, Ionian → deep Vs Pre-Apulian → shallow)
- Rifting and paleogeography (Cretaceous to Eocene, development of new platforms in the area)
- Shallowing (Oligocene-Miocene, relatively shallowing of northern Ionian domain, compared to the southern)
- Coverage and well position issues (Oligocene-Miocene, higher coverage from well data in north segment)
- KTZ juxtapose of FAs (Pliocene – Pleistocene, juxtaposition of deeper FAs of south segment westwards compared to northern segment)

The depositional environments interpretation of this study, confirms the onshore data studies (Karakitsios et al, 2010b; Makrodimitras, 2011; Maravelis et al, 2014).

The available log data can give a first impression of the FAs with the best reservoir properties, such as the upper shoreface, proximal lower shoreface, channel, lobe and shallow shelf deposits. However, the hydrocarbon shows during the drilling program, might range and be present in a wide range of FAs (asterisk * in Table 1).

This model confirms previous studies in western Greece areas (Getsos et al., 2007), where Pre-Apulian Zone deposits were assigned to inner carbonate ramp, and external to middle Ionian Zone assigned to middle to outer carbonate ramp conditions. The well data which correspond to inner ramp conditions are the evaporitic, sabkha, lagoonal and tidal flat deposits of Paxos Gaios-1X and South Kefalinia-1. The middle to outer ramp conditions represented by the slope and base of slope deposits, were observed mostly in South Kefalinia-1.

The tectonism of the External Hellenides, which is moving to the SW, along with the presence of the major strike slip faults, leads to a juxtaposition of depositions from different geological environments, making them present quite far from the place initially deposited and even further from the source of sedimentation regarding the clastic sediments. Due to the structural setting of the area and the distance between the wells, any attempt to correlate specific FAs among wells is very speculative, leading us to correlate only coeval deposits in terms of age.

Table 1. Facies Association log signature in selected wells from Western Greece. Asterisk (*) on hydrocarbon shows.

Depositional system	Facies Associations	GR log characteristic	GR Log curve
Coastal Plain	Floodplain channel	Moderate to low amplitude due to sandstone presence. Abrupt high spikes due to mudstone.	
	Floodplain valley*	High to very high amplitude (60-150 GAPI). Profile range from funnel to irregular blocky shape	
	Swamp*	High amplitudes due to mudstone. Sandstone and lignite contribute to typical irregular shape.	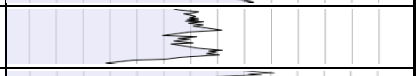
	Bay/Lagoon*	Very high amplitude (80-100 GAPI) with serrated shape due to mudstone.	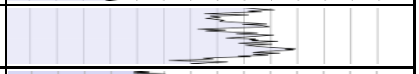
Delta Plain	Prodelta	High amplitude (50-60 GAPI) with serrated shape due to mudstone. Rare higher/lower peaks	
Shallow marine	Upper Shoreface*	Low amplitude (30-40 GAPI) due to sandstone domination, rarely serrated shape	
	Lower Shoreface proximal*	Typically, low amplitude (40 GAPI) for sandstones and higher for mudstone layers	
	Lower Shoreface distal*	High amplitude (40-60 GAPI) due to mudstone domination, and "U" shaped profile for sandstone	
	Offshore Transition Zone*	Typically, high values (50-55 GAPI) with homogenous profile	
	Debritic Sheets	Moderate to low amplitude with "U" shape. When siltstone is present, higher amplitudes	
Deepwater	Basin/Offshore*	Low to very low (5-20 GAPI), homogenous to serrated amplitude.	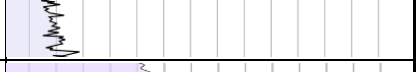
	Channel-fill*	Moderate (20-50 GAPI) Blocky "U" shaped to locally upward-dirtying responses.	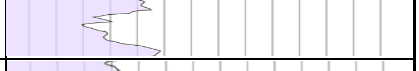
	Lobe sandsheet	Clear sandstone responses with blocky to serrated profile (~40GAPI).	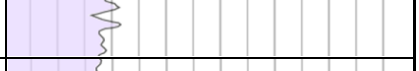
	Lobe sandsheet fringe	Moderate (30-40 GAPI) upward-dirtying responses, or "U" shape among higher amplitude.	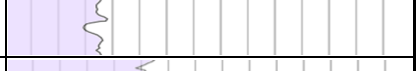
	Inter-lobe mudrock sheets*	High (50-60 GAPI) homogenous to serrated trendless amplitude.	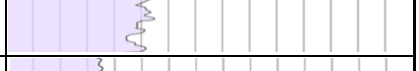
	Calcareous gravity mass deposit	Low (5-10 GAPI), "U" shape amplitude, easily distinguished among higher amplitude.	
Carbonate Platform / ramp	Evaporites	Moderate to low amplitude with box shape. Profile might be homogenously low when evaporites becomes thick.	
	Sabkha	Irregular shape ranging from "U" shape (due to evaporite precipitation?) to serrated.	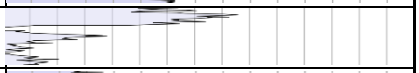
	Lagoon*	Irregular to serrated shape with moderate to low amplitude. Rare spikes due to clay material.	
	Tidal Flat*	Very low amplitude (5-15 GAPI) with minor spikes above 20 GAPI	
	Slope*	Moderate to low amplitude (20-30 GAPI) with spikes up to 40 GAPI. Serrated shape.	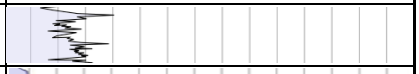
	Base of Slope*	Very low amplitude (5-15 GAPI) with minor spikes above 15 GAPI	

References

Getsos, K., Pomoni-Papaioannou, F. & Zelilidis, A., 2007. A carbonate ramp evolution in the transition from the Apulia platform to the Ionian basin during Early to Late Cretaceous (NW Greece). Proceedings of the 11th Intern. Congress of the Geological society of Greece, Bull of the Geol. Soc. Greece, v. XXVII, 53-63.

Karakitsios, V., Triantafyllou, M. & Panoussi, P 2010b. Preliminary study on the slump structures of the early Oligocene sediments of the pre-Apulian zone (Antipaxos Island, northwestern Greece): Bulletin of Geological society of Greece, v. 43, No 2, 634-642.

Karakitsios, V., 2013. Western Greece and Ionian Sea petroleum systems. AAPG Bulletin, v. 97, No. 9, 1567-1595.

Makrodimitras, G., 2011. The detailed sedimentological and petrographical research of the flysch deposits on Diapondia Islands, NW Greece. Paleogeographic evolution of the NW part of the Ionian Sea with respect to hydrocarbon field formation. PhD Thesis, University of Patras, Greece.

Maravelis, A., Makrodimitras, G. & Zelilidis, A. 2014. Stratigraphic evolution and source rock potential of a Lower Oligocene-Lower/Middle Miocene continental slope system, Hellenic Fold and Thrust Belt, Ionian Sea, northwest Greece. Geological magazine, 151(3): 394-413.

15th International Congress of the Geological Society of Greece
Athens, 22-24 May, 2019 | Harokopio University of Athens, Greece
Bulletin of the Geological Society of Greece, Sp. Pub. 7 Ext. Abs. GSG2019-222

A Regional Study of the Ionian Sea and its Hydrocarbon Prospectivity, Offshore W Greece

V. Kosmidou[1], G. Makrodimitras[1], S. Bellas[1]

(1) Hellenic Hydrocarbon Resources Management S.A., Dim. Margari 18, Athens, Greece, v.kosmidou@greekhydrocarbons.gr

Background & Approach

The Ionian Sea can be distinguished in the northern and the southern part. The north part, above the Kefalonia Transform Fault (KTF), is characterized by the obduction of the Hellenides Thrust and Fold Belt (HTFB) to the Apulian margin (continental crust). The southern segment, south of the KTF, is characterized by the activity of two dextral strike-slip faults, the subduction of a thinned continental-oceanic crust below the HTFB (continental crust) and the development of the Mediterranean Ridge (MR), the Backstop and the Hellenic Trench. The methodology followed was the study of the available literature, the interpretation of the well data and the 2D seismic survey acquired by PGS in 2012, the 2D modelling and the integration in order to establish a framework for the assessment of the hydrocarbon prospectivity.

Results & Conclusions: Geological Evolution, Petroleum System and Plays

North Ionian Sea covers the southern margin of the greater Apulian platform. Seismic interpretation led to the development of a 2D model that simulates the evolution of the area. The reconstruction enables us to visualize and validate our seismic interpretation. North Ionian Sea has mainly carbonate plays equivalent to the ones in the Adriatic Sea and Italy the source rocks are expected to be Upper Triassic (Burano Fm.), Jurassic (Complesso Anidritico Fm. and Calcare di Aptici Fm.), Toarcian to Aalenian (Rosso Ammonitico Fm.), Late Valanginian to Hauterivian (Maiolica Fm.), Early Aptian (Selli OAE, Marne a Fucoidi Fm.) and Late Santonian to Early Campanian pelagic sediments (shales) (Beicip, 2014; Nikolaou, 2001; Kosmidou, 2018). Geochemical analysis from well samples suggest type I-II oil-prone source rocks with higher TOC values in the Cretaceous and Jurassic series (up to 11.7% and 19.1%); and Triassic shale fragments (up to 16.1%). Play A: Oligocene-Late Miocene shallow-water carbonate build-ups (eq. Castro Fm. and Novaglie Fm.) sealed by fine-grained pelagic marls. The trap is stratigraphic pinch-outs. Analogues are the Giove and Medusa discoveries in Italy. Outcrop data in Italy suggest efficient vertical communication between the Cretaceous karstified reservoir and the overlying Oligocene – Miocene carbonates. Play B: Reservoirs of microbreccious limestone and/or calcareous gravity-mass deposits (slope-fan) with locally bioclastic base-of-slope aprons (eq. Scaglia). The trap is stratigraphic pinch-outs sealed by muddy-cherty deep-sea sediments. The main challenges associated with this play are the lateral extent and the distribution of the reservoir quality properties. Analogue discoveries are the Aquila, Rovesti and Griffone in the Adriatic Sea. Secondarily; Play C: Intra-platform plays rimmed platform deposits/reefs with stratigraphic traps (pinch outs) with lagoonal silty sediments in the Cretaceous series. Play D: Karstified sections sealed by pelagic sediments.

The South Ionian Sea is the area offshore western Peloponnese which is subdivided into the MR to the west and the HTFB and its offshore extension. important unconformities (Burdigalian and Messinian) and mass transport deposits overlie the Mesozoic carbonates. The depositional environment is shallow marine/platform (eq. Gavrovo Fm. and Paxi Fm.) changing westwards to distal slope and deformed ramp anticlines have been interpreted. The presence of the Apulia platform south of the KTF is estimated only in offshore Kefalonia. The Burano evaporites play a key role as a decollement but they are found in three main geometric configurations: in place, as diapirs, and reworked. They are believed to have facilitated the migration of the hydrocarbons in the carbonate reservoirs. The Messinian evaporites are deformed, due to the westward movement of the MR. Both Triassic and Messinian evaporites act as cap rock in specific leads. The Backstop is the extension of the lower Hellenic continental margin and its geometry is a pop–up structure with a flat summit. Geophysical data suggest a unit of high seismic velocity. To the west, there is the MR, an accretionary wedge with fluidized mud from the decollement zone(s). The upper part is characterized by highly deformed Plio- Pleistocene sediments and Messinian Evaporites. There are signs of two decollement levels and structural elements in the Mesozoic carbonate units. The area is highly tectonized with intensive shortening and imbrication. The plays are mainly carbonate with clastic plays in channels originated from the Hellenides. The carbonate plays can be summarized in the following: Type A: Carbonate slope deposits/ reefs; the reservoirs are expected to be of Middle Jurassic - Eocene age charged by thermogenic mature type I-II source rocks Lower Cretaceous Vigla shales and Triassic Breccias. Type B: Carbonate faulted blocks with karstified tops sealed by evaporitic and shale deposits. It is believed to have the same source rocks as Play type A. Type C: Middle-Upper Pliocene intercalations of (calcareous) sandstone and shales/siltstone with gas shows with expected source rock in the Paleogene-Neogene clastic basins.

References

Beicip Franlab, 2014. New Exploration Opportunities in Offshore Western Greece and South of Crete.

Kosmidou, V., Bellas, S., Bassias, Y., 2018. Offshore Western Peloponnese: Structural Elements and differences from Northern Ionian, Greece. First EAGE Workshop on Geophysical and Geological Challenges in the Hydrocarbon Provinces of the Eastern Mediterranean, St. Julian's, Malta.

Kosmidou, V., Makrodimitras, G., Papatheodorou, N., 2018. Depositional Environments and Hydrocarbon Potential of Northern Ionian Sea. AAPG GTW Alpine Folded Belts and Extensional Basins, Granada, Spain.

Nikolaou, K.A., 2001. Προέλευση και Μηχανισμός Μετανάστευσης των Κυριότερων Ενδείξεων Υδρογονανθράκων της Δυτικής Ελλάδας. Bulletin of the Geological Society of Greece, Vol. XXXIV/3, Proceedings of the 9th International Congress, Athens, Greece, p. 1213-1219

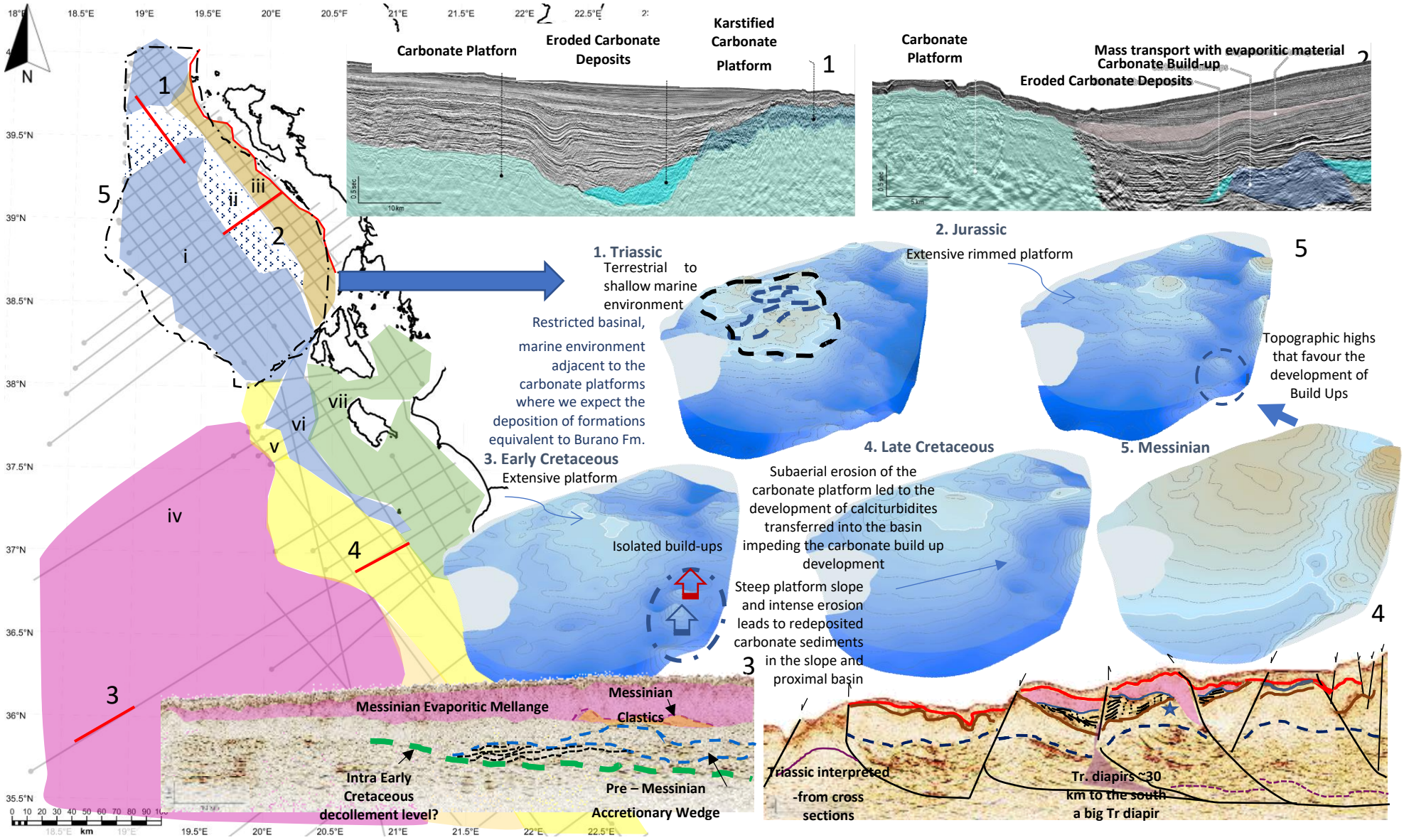

Figure 1. Geological interpretation from the 2D seismic data. i. Apulian Platform, ii. Rimmed margin, slope and redeposited carbonates, iii. deep pelagic basin, foreland basin after Oligocene, iv. Mediterranean Ridge, v. Backstop – Hellenic Trench, vi. Carbonate Platform, vii. Carbonate Platform, foreland(?) basin after the Oligocene

15th International Congress of the Geological Society of Greece
Athens, 22-24 May, 2019 | Harokopio University of Athens, Greece
Bulletin of the Geological Society of Greece, Sp. Pub. 7 Ext. Abs. GSG2019-228

Preliminary Results from Soft-sediment Deformation of Lower Cretaceous Vigla Limestones of Kastos Island and Their Support to Basin Evolution.

N.Bourli[1], A. Zelilidis[1]

(1) Department of Geology, University of Patras, 2650 Patras, Greece, n_bourli@upnet.gr

Introduction

Soft-sediment deformation structures formed during, or immediately after deposition, during the first stages of the sediment's solidification. These structures are formed mainly in shallow marine areas and in deep basins with the presence of turbiditic currents. This is because these environments have high deposition rates, which allows the sediments to pack loosely. The deformation is related mostly to the drastic decrease in shear resistance in water saturated and unconsolidated sediments.

Geological setting

The Cretaceous succession differs between the three sub-basins of the Ionian zone. The lower Cretaceous Vigla limestone in the external Ionian sub-basin, where the studied Kastos Island is situated, consist of white, light grey to yellowish micrites and radiolarian biomicrites (wackestones to packstones and rarely mudstones). Usually they are thin-bedded to platy with chert intercalations and chert nodules. (Skourtsis-Coroneou et al., 1995).

In Kastos Island, the lower Cretaceous Vigla formation outcrops on the east side of the island, and consists of, in the lower part, carbonates in restricted outcrops with estimated thickness up to 350 m, whereas the upper part with interbedded cherts and shales (Vigla shales) is up to 100 m thick. The Vigla limestones, consist of thin to medium bedded limestones, with up to three strongly deformed horizons, internally to undisturbed limestones, representing slumps. This deformation appears stronger than in the NW Peloponnesus (Bourli et al., 2019) and is interpreted as syn-sedimentary slumping.

Data analysis

According to Bourli et al., (2019) Vigla limestones in NW Peloponnesus are characterized by synsedimentary deformation. On the upper part of this deformation paleo relief filled up by breccia showing that, sedimentation was active during and after the deformation. Measurements of this deformations showed that there is a “fold” axis with E-W direction. Moreover, the steep side of this deformation dips northwards. The above introduce that slumps directed northwards and produced from transfer faults with E-W direction (Fig. 1).

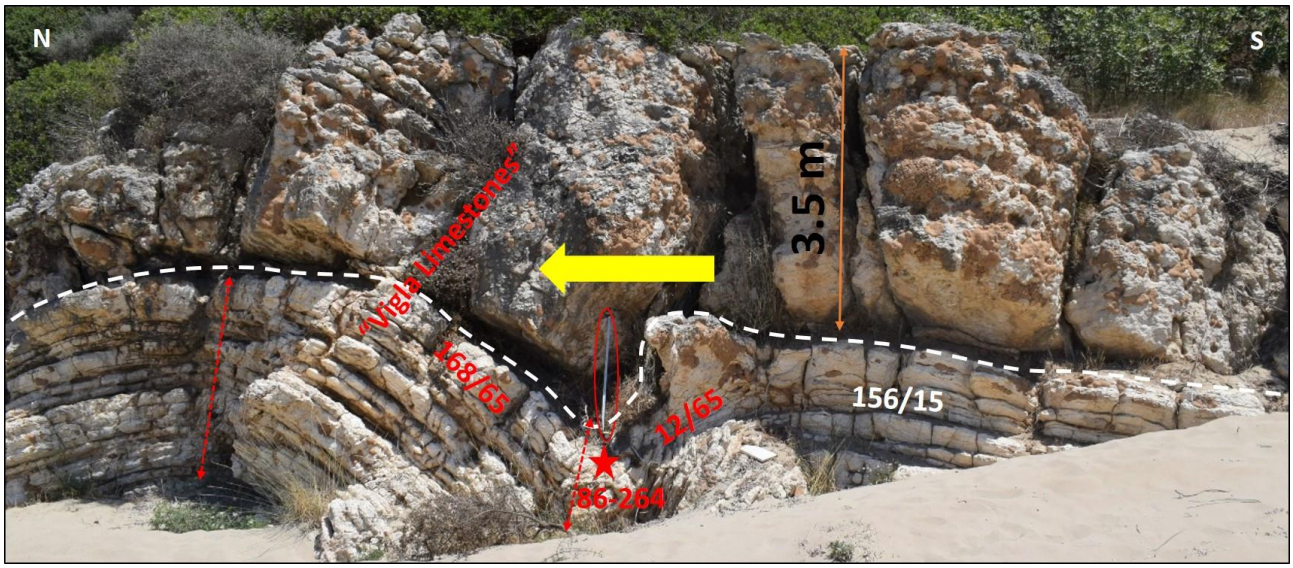

Figure 1. Vigla limestones with intense synsedimentary deformation. The red lines show the axes, the yellow arrow marks the kinematic direction of deformation, the white line shows the different lithologies, and the star indicates the fold axis.

In Kastos island and although the estimated thickness for Vigla limestones is about 350m only 30m are outcropped along the eastern cost of the island. Vigla limestones are unconformably underlines Vigla shales and this contact is characterized by strong deformation. This deformation has different laterally thickness ranging from 1 to 3m thick. Such horizons also were recognized internally to Vigla limestones.

In two studied sections with NW-SE and SW-SE directions (Figs 2, 3), two different directed slump horizons were recognized. In the NW-SE section, an E-W deformation axis was recognized, probably related with a transfer fault activity; whereas in the SW-NE section deformation is stronger with two or three different directed axes (either N-S or E-W) introducing slump development from both normal and transfer faults activity. It seems that the slumps produced

from the normal fault activity are thicker and strongly deformed in contrast to these that produced from transfer faults.



Figure 2. A slump horizon 1m thickness on the top of Vigla limestones and in contact with the undeformed Vigla shales. The star shows the fold axis and the white line marks the above contact.

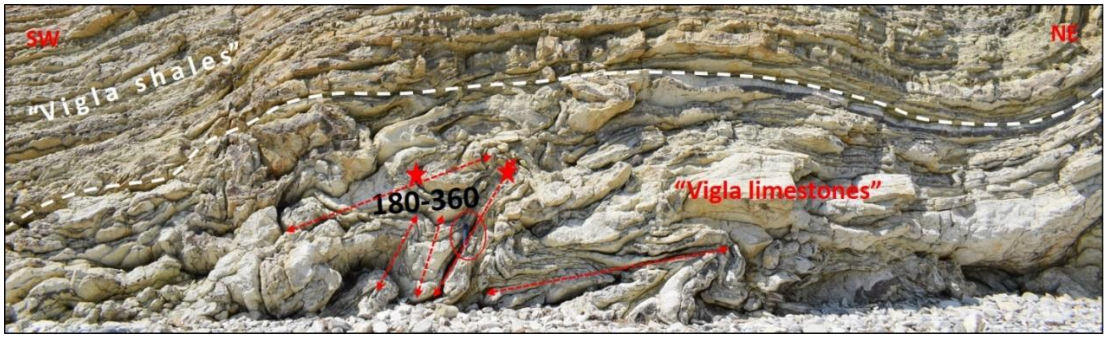

Figure 3. A slump horizon 3m thickness on the top of Vigla limestones and in contact with the undeformed Vigla shales. The stars show the fold axes and the white line marks the above contact. See the intensive deformation within slump horizon with different axes directions.

Except of Vigla limestones also within Vigla shales slump horizons were recognized. In these horizons paleo relief produced from slumping is up to 40cm (Gianniskari Vigla shales in Bourli et al., 2019); whereas in Kastos Island this paleo relief is up to 1m? or more (Fig. 4).



Figure 4. Vigla shales with lower deformation in Kastos Island.

Results

From the above we conclude that in both areas (NW Peloponnesus and Kastos island) Vigla limestones are characterized by intensive deformation during sedimentation due to both normal and transfer faults activity. Further study is needed in order to show how and when this deformation took place.

It is obvious that deformations of Vigla shales is lower and the reasons for the above is under investigation.

Acknowledgements

Nicolina Bourli is a PhD student and she was financially supported by the "Andreas Mentzelopoulos Scholarships for the University of Patras".

References

Bourli, N., Pantopoulos, G., Maravelis, A.G., Zoumpoulis, E., Iliopoulos, G., Pomoni-Papaioannou, F., Kostopoulou, S., Zelilidis, A., 2018. Late Cretaceous to Early Eocene geological history of the eastern Ionian Basin, southwestern Greece: An integrated sedimentological and bed thickness statistics analysis. Cretaceous Research 98, 47-71.

Skourtsis-Coroneou, V., Solacious, N., Constantinidis, I., 1995. Cretaceous stratigraphy of the Ionian Zone, Hellenides, western Greece. Cretaceous Research 16, 539-558.

15th International Congress of the Geological Society of Greece
Athens, 22-24 May, 2019 | Harokopio University of Athens, Greece
Bulletin of the Geological Society of Greece, Sp. Pub. 7 Ext. Abs. GSG2019-230

Approaching the porosity values of Cretaceous carbonate deposits in Araxos peninsula and Kastos Island (North-Western Peloponnese, Greece) for the characterization of reservoir quality.

N. Bourli[1], M. Kokkaliari[1], I. Iliopoulos[1], A. Zelilidis[1]
(1) Department of Geology, University of Patras, 26504 Patras, Greece, n_bourli@upnet.gr

Introduction

According to Bourli et al., (2019) upper Cretaceous–Lower Eocene deposits of the Ionian basin is the major target in hydrocarbon exploration as they represent the expected reservoir rocks. These deposits are mostly composed of calciturbidites interbedded with breccia-microbreccia deposits. Calciturbidites can be of great economic importance and they can serve as viable reservoir rocks because of their high porosity and permeability values, which can be additionally enhanced by the development of nodules that in turn increase secondary porosity. Studied Cretaceous limestones in Araxos peninsula (NW Peloponnesus, internal Ionian sub-basin) and Kastos Island (external Ionian sub-basin) showed that both lower Cretaceous "Vigla limestones" and upper Cretaceous "Senonian limestones" are characterized by the presence of siliceous nodules. Siliceous nodules within the Vigla limestones are of smaller in relation to the Senonian limestones. The above difference in nodules size could be related with the different porosity of hosted deposits. Pelagic limestones of lower Cretaceous Vigla limestones must have reduced pores or lower porosity than the porosity of calciturbidites.

Material and methods

Nitrogen absorption-desorption was performed with the Quantachrome Nova 2200e at the Research Laboratory of Minerals and Rocks, Department of Geology, University of Patras. The relative pressure against the nitrogen adsorption was used and a full isotherm diagram was produced based on the adsorption and the desorption isotherms. For determination of the specific surface area, the BET equation (Brunauer, Emmett, & Teller, 1938) was used in the form of a linear plot. The BJH method (Barrett, Joyner, & Halenda, 1951) was applied within the range from 2 to 50 nm and average cumulative surface of pores (S_{BJH}), average volume of mesopores (V_{BJH}) and average diameter of mesopores (D_{BJH}) were calculated. According to IUPAC (Sing et al., 1985), pores are classified into three groups according to their diameter: micropores (diameter < 2 nm, mesopores (diameter 2 - 50 nm), and macropores (diameter > 50 nm). Moreover, results processing with software NovaWin helped us classify isotherms according to Sing et al. (1985), where five (5) groups (I to V) were determined and isotherm hysteresis loops into four types (H1-H4).

Data analysis

Lower Cretaceous limestone samples (V1, V3, I5, GN1 and GN2) and Upper Cretaceous limestone samples (S1, Ark7 and Ar40d), from both studied areas were analyzed for their specific surface area (S_{BET}) and the average diameter of mesopores (D_{BJH}) by Nitrogen porosimetry. Porosity measurements for both areas showed that the isotherms of the samples, according to IUPAC classification (Sing et al., 1985), are type IV, indicating mesoporous (2 – 50 nm) studied rocks. The characteristic feature of type IV isotherm is the presence of the hysteresis loop, typical for the mesoporous material, which is associated with pore condensation (Fig. 1). The hysteresis loop of the studied type IV isotherms classified in the H3 type, indicating pores with slit shape overall of the sample, from non-rigid aggregated of platy particles. Also, if the network consists of macropores, then these are not completely filled with the condensate (Thommes et al., 2015). Furthermore, the H3 loop hysteresis suggests the presence of mainly accessible pore network, because otherwise it would not create hysteresis (Liu et al., 2014). The adsorption and desorption branches of some

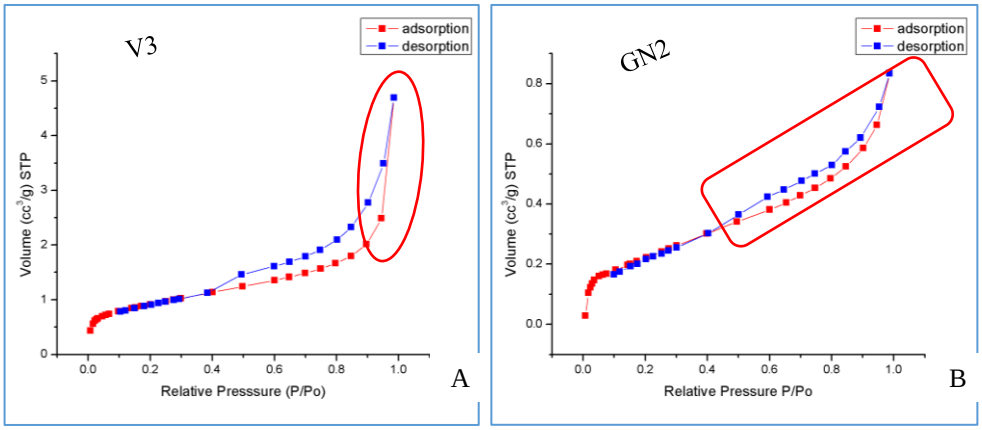

Figure 1. Representative diagrams of N2 adsorption of samples V3 (Lower Cretaceous shales from Kastos Island) and GN2 (Upper Cretaceous calciturbidites from NW Peloponnesus).

samples approach a nearly vertical direction above the 0.8 relative pressure indicating the presence of outer surface, which is characteristic of isotherm II (red circle in figure 1A). The above could support the idea that although the studied samples were classified into the type IV due to the presence of the hysteresis loop, the pores present broad size distribution and could also suggest the presence of some larger porous, perhaps of type II. In cases where an incomplete equilibrium during the measurements occur, an open loop hysteresis is observed (Bertier et al., 2016) at very low relative pressure (red circle in Fig. 2) that refers to the slow diffusion of adsorptive in micropores, structural deformation of the sample or even chemisorption (Rouquerol et al. 2014). On the other hand, the hysteresis loop for the rest of the samples has a narrower shape indicating the presence of slit-shaped mesopores with a non-uniform size (red box in Fig. 1B).

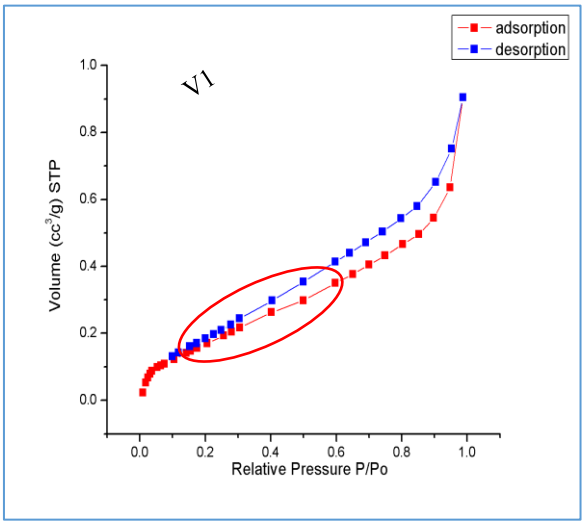

Figure 2: Representative diagrams of N2 adsorption of sample V1 (Lower Cretaceous shales from Kastos Island)

Nitrogen sorption isotherms of the studied samples have similar shape, classified as an H3 of the type IV isotherm. According to the BJH method the pore volume (V_{BJH}) ranges from 0.001 to 0.002 cc/g, the pore diameter (D_{BJH}) ranges from 3.550 to 3.663 nm and the cumulative surface area (S_{BJH}) ranges from 0.376 to 0.826 m^2/g while the total specific area (S_{BET}) through the BET calculations ranges from 0.577 to 0.933 m^2/g. Only one sample had different values as far as the BJH pore volume (0.007 cc/g) and the BJH cumulative surface area (2.321 m^2/g), even though the BJH pore diameter is 3.550 nm, while the BET specific surface area with the BET calculation is 3.193 m^2/g.

Results

According to the above and taking into account that both, Early Cretaceous Vigla limestones and Late Cretaceous Senonian calciturbidites, showed that now they are mesoporous, a secondary higher increase of pores within Early Cretaceous Vigla limestones than in Late Cretaceous calciturbidites, could be caused due to fracturing owed to the nodules development, as suggested by Spence and Finch (2015).

Acknowledgements

Nicolina Bourli is a PhD student and she was financially supported by the "Andreas Mentzelopoulos Scholarships for the University of Patras".

References

Barrett, E.P., Joyner, L.G., Halenda, P.P., 1951. The Determination of Pore Volume and Area Distributions in Porous Substances. I. Computations from Nitrogen Isotherms. Journal of the American Chemical Society 73, 373-380.

Bertier, P., Schweinar, K., Stanjek, H., Ghanizadeh, A., Clarkson, C.R., Busch, A., Kampman, N., Prinz, D., Amann-Hildenbrand, A., Krooss, B., Pipich, V., 2016. On the use and abuse of N2 physisorption of the pore structure of shales. The Clay Minerals Society Workshop Lectures Series 21, 151–161.

Bourli, N., Pantopoulos, G., Maravelis, A.G., Zoumpoulis, E., Iliopoulos, G., Pomoni-Papaioannou, F., Kostopoulou, S., Zelilidis, A., 2019. Late Cretaceous to Early Eocene geological history of the eastern Ionian Basin, southwestern Greece: An integrated sedimentological and bed thickness statistics analysis. Cretaceous Research 98, 47-71.

Brunauer, S., Emmet, P.H., Teller, E., 1938. Adsorption in gases in multimolecular lyers. Journal of the American Chemical Society 60, 309-319.

Liu, J.Y., Qiu, Z.S., Huang, W.A., Luo, Y., Song, D.D., 2014. Nano-pore structure characterization of shales using gas adsorption and mercury intrusion techniques. Journal of Chemical and Pharmaceutical Research 6, 850–857.

Rouquerol, F., Rouquerol, J., Sing, K.S.W., Llewellyn, P., Maurin, G., 2014. Adsorption by Powders and Porous Solids: Principles, Methodology and Applications, 2nd ed. Academic Press, Oxford, UK.

Sing, K., Everett, D., Moscou, L., Pierotti, R., Rouquerol, J., Siemieniewska, T., 1985. Reporting physisorption data for gas/solid systems with special reference to the determination of surface area and porosity International union of pure and applied chemistry. Pure and Applied Chemistry 57, 603-619.

Thommes, M., Kaneko, K., Neimark, A.V., Olivier, J.P., Rodriguez-Reinoso, F., Rouquerol, J., Sing, K.S.W., 2015. Physisorption of gases, with special reference to the evaluation of surface area and pore size distribution (IUPAC Technical Report). Pure and Applied Chemistr, 87, 9–10.

15th International Congress of the Geological Society of Greece
Athens, 22-24 May, 2019 | Harokopio University of Athens, Greece
Bulletin of the Geological Society of Greece, Sp. Pub. 7 Ext. Abs. GSG2019-315

Evidence of Strong Sea Surface Temperature and Salinity Decline after the Tortonian-Messinian Boundary based on Paired Foraminiferal Sr/Ca and $\delta^{18}O$ Analyses

E. Besiou[1], G. Kontakiotis[1], A. Antonarakou[1], P. G. Mortyn[2,3], H. Drinia[1], E. Koskeridou[1], V. Karakitsios[1]

(1) Faculty of Geology & Geoenvironment, School of Earth Sciences, Department of Historical Geology-Paleontology, National & Kapodistrian University of Athens, Panepistimiopolis-Zografou, 15784, Greece, wwweua@hotmail.com
(2) Institute of Environmental Science and Technology (ICTA), Universitat Autònoma de Barcelona (UAB), Edifici Z - Carrer de les Columnes, Bellaterra 08193, Spain.
(3) Department of Geography, Universitat Autònoma de Barcelona (UAB), Spain

Objectives

The late Miocene has been considered as one of the most climatically stable periods of the Cenozoic, characterized by minor long-term cooling and ice growth (Zachos *et al*., 2001). Especially, the Tortonian-Messinian Transition (TMT) is recognized as a priority for paleoenvironmental reconstruction and climate modelling due to the significant paleoenvironmental changes preceding the Messinian Salinity Crisis (MSC) (Blanc-Valleron *et al*., 2002; Drinia *et al*., 2007) and the development of the modern Mediterranean-type climate (Mertz-Kraus *et al*., 2009) respectively. This time window is of particular importance for the paleoceanographic evolution of the entire Mediterranean Sea, because it covers the successive closure of the marine Mediterranean-Atlantic gateways, which culminated in the onset of the MSC. The basin experienced a dramatic hydrological and biological crisis induced by a powerful combination of geodynamic and climatic drivers (Roveri *et al*., 2014; Karakitsios *et al*., 2017a; Krijgsman *et al*., 2018). The change of the Mediterranean's connections with both the Atlantic Ocean and the freshwater Paratethyan basins, caused high-amplitude fluctuations in the hydrology of its basins (Karakitsios *et al*., 2017b; Vasiliev *et al*., 2019), which had a great impact on the subsequent geological history of the Mediterranean area, and on the salinity of the global oceans. The geological expression of this evolution was the omnipresent cyclic marl/sapropel succession because freshwater input was not constant, but strongly pulsed at precessional time-scales (Hilgen *et al*., 1995). In the present study, we present an integrated study based on sedimentological, micropaleontological, and geochemical data from the pre-evaporitic sedimentary sequence of the Faneromeni section (Crete Island, eastern Mediterranean), which provides an excellent illustration of the progressive restriction of the Mediterranean basin in response to paleoclimate. The observed sedimentary cyclicity corresponds to lithological alternations from laminated to indurated homogeneous marls and clayey limestones, and covers the late Tortonian and earliest Messinian stages (7.6-6.7 Ma; Moissette *et al*., 2018). Outcropping marine sediments in Crete, which preserve the foraminiferal signal intact, provide windows into the Mediterranean that have not been recovered by deep sea drilling, because the late Miocene sedimentary record from this area is buried under thick layers of salt deposited when the Mediterranean desiccated.

Methods

The tools used by the Miocene palaeoclimate community have changed over time, and researchers continue to use the most sophisticated and independent techniques available for reconstruction. Proxies have been developed to estimate different aspects of the environment, but surface ocean temperatures and salinities are by far the primary data generated, since together they control ocean water density and thereby thermohaline circulation. Initially, the foraminiferal record was qualitatively evaluated for dissolution by X-ray micro-computed tomography. Stable oxygen ($\delta^{18}O$) and carbon ($\delta^{13}C$) isotopes were also used to estimate salinities, and indirectly ice volume. Moreover, primary temperature proxies, including foraminiferal Mg/Ca and Sr/Ca ratios, were utilized for the paleotemperature reconstruction. Those proxy techniques have strengths and limitations (Kontakiotis *et al*., 2011, 2016; Antonarakou *et al*., 2019), but each plays an important role in our conceptual understanding of the late Miocene Earth. The use of multiple proxies is of great benefit to gaining more robust and detailed estimates of the palaeoenvironment as long as the relative limitations of various techniques are recognized.

Results

We present the first evidence for changes in the upper water column reflected by sea surface temperature (SST) and salinity (SSS) variations that correlate with pronounced paleoclimatic fluctuations. Our planktonic isotope record, in combination with paired mixed layer Sr/Ca-derived SST data, reveal that the very warm late Tortonian interval was followed by a strong long-term cooling and desalination trend (up to 10^0C and 10‰ respectively) during the earliest Messinian. This change in the upper water column just after the T/M boundary attributed to the paroxysmal phase of the so-called “siphon” event. Especially, the climate shift that occurred at the end of a global carbon isotope decrease suggests that changes in the carbon cycle were instrumental in driving late Miocene climate dynamics (cooling and aridity) in the progressively isolated eastern Mediterranean Sea. The observed salinity variability during that time interval also provides further insights about seasonal freshwater inputs, and gives new support to the much-debated hydrological regime preceding the deposition of evaporites.

Conclusions

This study focuses on and further extends the application of the foraminiferal Sr/Ca paleothermometer to late Miocene Mediterranean sections, and inserts the climate history of this setting into the framework of global climate through this time period. Our findings reveal a non-gradual increase in sea surface salinity prior to the onset of the MSC, but substantial variability in response to climatic oscillations, supporting the concept of a stepwise restriction of the Mediterranean Sea.

References

Antonarakou, A., Kontakiotis, G., Vasilatos, C., Besiou, E., Zarkogiannis, S., Drinia, H., Mortyn, P.G., Tsaparas, N., Makri, P., Karakitsios, V., 2019. Evaluating the effect of marine diagenesis on Late Miocene pre-evaporitic sedimentary successions of eastern Mediterranean Sea. IOP Conference Series: Earth and Environmental Sciences, 221: 012051.

Blanc-Valleron, M.M., PierreI, C., Caulet, J.P., Caruso, A., Rouchy, J.M., Cespuglio, G., Sprovieri, S., Pestrea, S, Di Stefano, E., 2002. Sedimentary, stable isotope and micropaleontological records of paleoceanographic change in the Messinian Tripoli Formation (Sicily, Italy). Palaeogeogr. Palaeoclimatol. Palaeoecol., 185, 255–286.

Drinia, H., Antonarakou, A., Tsaparas, N., Kontakiotis, G., 2007. Palaeoenvironmental conditions preceding the Messinian Salinity Crisis: A case study from Gavdos Island. Geobios, 40, 251–265.

Hilgen, F.J., Krijgsman, W., Langereis, C.G., Lourens, L.J., Santarelli, A., Zachariasse, W.J., 1995. Extending the astronomical (polarity) time scale into the Miocene. Earth Planet. Sci. Lett., 136, 495–510.

Karakitsios, V., Cornée, J.-J., Tsourou, T., Moissette, P., Kontakiotis, G., Agiadi, K., Manoutsoglou, E., Triantaphyllou, M., Koskeridou, E., Drinia, H., Roussos, D., 2017b. Messinian salinity crisis record under strong freshwater input in marginal, intermediate, and deep environments: The case of the North Aegean. Palaeogeogr., Palaeoclimatol., Palaeoecol., 485, 316–335.

Karakitsios, V., Roveri, M., Lugli, S., Manzi, V., Gennari, G., Antonarakou, A., Triantaphyllou, M., Agiadi, K., Kontakiotis, G., Kafousia, N., de Rafelis, M., 2017a. A record of the Messinian salinity crisis in the eastern Ionian tectonically active domain (Greece, eastern Mediterranean). Bas. Res., 29, 203–233.

Kontakiotis, G., Mortyn, P.G., Antonarakou, A., Drinia, H., 2016. Assessing the reliability of foraminiferal Mg/Ca thermometry by comparing field-samples and culture experiments: A review. Geol. Quart., 60 (3), 547–560.

Kontakiotis, G., Mortyn, P.G., Antonarakou, A., Martínez-Botí, M.À., Triantaphyllou, M.V., 2011. Field-based validation of a diagenetic effect on G. ruber Mg/Ca paleothermometry: core top results from the Aegean Sea (eastern Mediterranean). Geochem. Geophys. Geosyst., 12 (9), Q09004.

Krijgsman, W., Capella, W., Simon, D., Hilgen, F.J., Kouwenhoven, T.J., Meijer, P.Th., Sierro, F.J., Tulbure, M.A., van den Berg, B.C.J., van der Schee, M., Flecker, R., 2018. The Gibraltar Corridor: Watergate of the Messinian Salinity Crisis. Mar. Geol., 403, 238–246.

Mertz-Kraus, R., Brachert, T.C., Reuter, M., Galer, S.J.G., Fassoulas, C., Iliopoulos, G., 2009. Late Miocene sea surface salinity variability and paleoclimate conditions in the Eastern Mediterranean inferred from coral aragonite δ18O. Chem. Geol., 262 (3-4), 202–216.

Moissette, P., Cornée, J.-J., Antonarakou, A., Kontakiotis, G., Drinia, H., Koskeridou, E., Tsourou, T., Agiadi, K., Karakitsios, V., 2018. Palaeoenvironmental changes at the Tortonian/Messinian boundary: A deep-sea sedimentary record of the eastern Mediterranean Sea. Palaeogeogr. Palaeoclimatol. Palaeoecol., 505, 217–233.

Roveri, M., Flecker, R., Krijgsman, W., Lofi, J., Lugli, S., Manzi, V., Sierro, F.J., Bertini, A., Carnerlenghi, A., De Lange, G., Govers, R., Hilgen, F.J., Hubscher, C., Meijer, P.T., Stoica, M., 2014. The Messinian Salinity Crisis: Past and future of a great challenge for marine sciences. Mar. Geol., 352, 25–58.

Vasiliev, I., Karakitsios, V., Bouloubassi, I., Agiadi, K., Kontakiotis, G., Antonarakou, A., Triantaphyllou, M., Gogou, A., Kafousia, N., de Rafélis, M., Zarkogiannis, S., Kaczmar, F., Parinos, C., Pasadakis, N., 2019. Large sea surface temperature, salinity, and productivity-preservation changes preceding the onset of the Messinian Salinity Crisis in the eastern Mediterranean Sea. Paleoceanography and Paleoclimatology. 34.

Zachos, J., Pagani, M., Sloan, L., Thomas, E., Billups, K., 2001. Trends, rhythms, and aberrations in global climate 65 Ma to present. Science, 292(5517), 686–693.

15th International Congress of the Geological Society of Greece
Athens, 22-24 May, 2019 | Harokopio University of Athens, Greece
Bulletin of the Geological Society of Greece, Sp. Pub. 7 Ext. Abs. GSG2019-316

Integrated Stratigraphy and Paleoceanographic Reconstruction for the Messinian Sedimentary Sequence in a Marginal Sector of the Eastern Mediterranean: Agios Myron Section (Crete Island)

A. Kostis[1], A. Antonarakou[1], G. Kontakiotis[1], E. Koskeridou[1], H. Drinia[1]

(1) National & Kapodistrian University of Athens, School of Earth Sciences, Department of Geology & Geoenvironment, Section of Historical Geology-Paleontology, Panepistimiopolis-Zografou, 15784, Greece, andkos@geol.uoa.gr

The Messinian was a period of drastic paleoenvironmental and paleoceanographic changes in the Mediterranean. During this time interval, tectonic processes together with glacio-eustatic sea level oscillations led to the Mediterranean isolation from the Atlantic Ocean triggering the formation of thick evaporite successions during the so-called "Messinian Salinity Crisis" (MSC, 5.97-5.33 Ma; Krijgsman *et al.*, 1999; Roveri *et al.*, 2014). Studies of Messinian sediments preserved in marginal and/or peripheral Mediterranean sub-basins have provided much information on the sedimentology, cyclostratigraphy, palaeontology, and geochemistry of that period (Karakitsios *et al.*, 2017a,b; Moissette *et al.*, 2018; Antonarakou *et al.*, 2019; Vasiliev *et al.*, 2019). Especially the cyclic bedded biosiliceous deposits of the Tripoli Formation that preceded the MSC (6.96-5.98 Ma) records an important depositional change that occurred after the monotonous deposition of Tortonian to lowermost Messinian marls in deep open marine conditions, and consists of lithological alterations of marls, limestones, diatomites and organic-rich sapropelitic layers. Overall, this typical Late Miocene cyclic succession likely resulted from orbitally-driven variations in freshwater input due to the African Summer Monsoon modifications, reflects precessionally-controlled dry-wet climate fluctuations influencing the hydrological budget of the entire Mediterranean Sea (Rohling *et al.*, 2015).

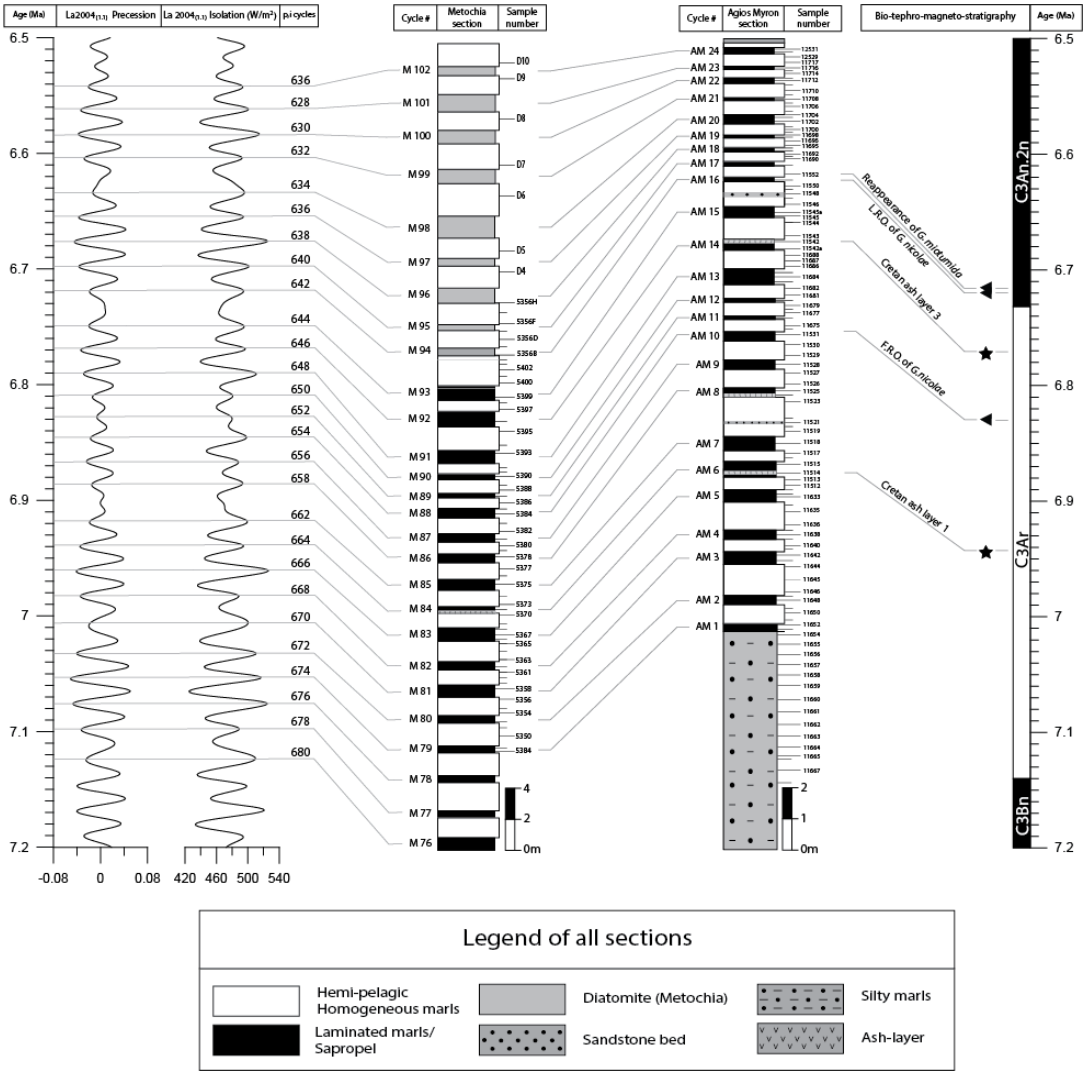

Figure 1. Cyclostratigraphic correlation between Metochia and Agios Myron sections

We present the first continuous non-diatomaceous Messinian record in eastern Mediterranean based on the combined sedimentological, micropaleontological, and geochemical approach, recovered from sampling the Agios Myron section.

The study section, is located in the north-central Crete, and consists of a continuous, pelagic sedimentation (alternations of hemipelagic homogenous marls and sapropels) covering the ~7.2-6.5 Ma time interval. To ascertain the potential correlation between the increase in calcareous sediments on Crete and the beginning of the diatomite sequences on Gavdos, we further compare our results from the time-equivalent interval with one of the most suitable, well-astronomically dated, and complete Miocene sections in the Mediterranean Sea, the Metochia section (Schenau *et al.*, 1999; Drinia *et al.*, 2007). An integrated correlation between Agios Myron and Metochia sections is shown in Figure 1. The sections were correlated using their characteristic sedimentary cyclic pattern, planktonic foraminiferal biostratigraphy and the ash layers. Both sections were characterized by the same sedimentary cluster pattern, with the only difference of the presence/absence of the diatomite sequence at the top. The characteristic sedimentary cycles have been also correlated to the astronomical target curve, in particular the precession interference pattern in isolation curve. Astronomically calibrated biostratigraphic events were used as reference points in order to check the correct sequence of sedimentary cycles. We have identified 3 planktonic foraminiferal bioevents: the First and the Last Common Occurrence (FCO and LCO) of *Globorotalia nicolae* and the re-appearance of *Globorotalia miotumida* group (Fig. 1). We also detected two different tephra layers in the Agios Myron section: the Cretan ash-layers 1 and 3 which have an astronomical age of 6.941 Ma and 6.771 Ma respectively (Hilgen *et al.*, 1997; Kuiper *et al.*, 2004).

The resulting integrated stratigraphy for the lower Messinian at Agios Myron, including biostratigraphy, cyclostratigraphy, and tephrostratigraphy, is consistent with both bio- and magneto-stratigraphic dated pre-MSC sections in eastern Mediterranean Sea. Finally, we further complement this study with stable isotope ($\delta^{18}O$, $\delta^{13}C$) and distributional planktonic foraminiferal data with the aim to monitor the mutual interplay between paleoclimatic/paleoceanographic evolution and the sedimentary environment across the pre-MSC time interval in this marginal setting.

References

Antonarakou, A., Kontakiotis, G., Vasilatos, C., Besiou, E., Zarkogiannis, S., Drinia, H., Mortyn, P.G., Tsaparas, N., Makri, P., Karakitsios, V., 2019. Evaluating the effect of marine diagenesis on Late Miocene pre-evaporitic sedimentary successions of eastern Mediterranean Sea. IOP Conference Series: Earth and Environmental Sciences, 221: 012051 doi:10.1088/1755-1315/221/1/012051.

Drinia, H., Antonarakou, A., Tsaparas, N., Kontakiotis, G., 2007. Palaeoenvironmental conditions preceding the Messinian Salinity Crisis: A case study from Gavdos Island. Geobios, 40, 251–265.

Hilgen, F.J., Krijgsman, W., Wijbrans, J.R., 1997. Direct comparison of astronomical and $^{40}Ar/^{39}Ar$ ages of ash beds: potential implications for the age of mineral dating standards, Geophys. Res. Lett., 24, 2043–2046.

Karakitsios, V., Roveri, M., Lugli, S., Manzi, V., Gennari, G., Antonarakou, A., Triantaphyllou, M., Agiadi, K., Kontakiotis, G., Kafousia, N., de Rafelis, M., 2017a. A record of the Messinian salinity crisis in the eastern Ionian tectonically active domain (Greece, eastern Mediterranean). Bas. Res., 29, 203–233.

Karakitsios, V., Cornée, J.-J., Tsourou, T., Moissette, P., Kontakiotis, G., Agiadi, K., Manoutsoglou, E., Triantaphyllou, M., Koskeridou, E., Drinia, H., Roussos, D., 2017b. Messinian salinity crisis record under strong freshwater input in marginal, intermediate, and deep environments: The case of the North Aegean. Palaeogeogr., Palaeoclimatol., Palaeoecol., 485, 316–335.

Krijgsman, W., Hilgen, F.J., Marabini, S., Vai, G.B., 1999. New paleomagnetic and cyclostratigraphic age constraints on the Messinian of the Nothern Apenines (Vera del Gesso Basin, Italy). Mem. Soc. Geol. It., 54, 25–33.

Kuiper, K.F., Hilgen, F.J., Steenbrink, J., Wijbrans, J.R., 2004. $^{40}Ar/^{39}Ar$ ages of tephras intercalated in astronomically tuned Neogene sedimentary sequences in the eastern Mediterranean. Earth Planet. Sci. Lett., 222, 583–597.

Moissette, P., Cornée, J.-J., Antonarakou, A., Kontakiotis, G., Drinia, H., Koskeridou, E., Tsourou, T., Agiadi, K., Karakitsios, V., 2018. Palaeoenvironmental changes at the Tortonian/Messinian boundary: A deep-sea sedimentary record of the eastern Mediterranean Sea. Palaeogeogr. Palaeoclimatol. Palaeoecol., 505, 217–233.

Rohling, E.J., Marino, G., Grant, K.M., 2015. Mediterranean climate and oceanography, and the periodic development of anoxic events (sapropels). Earth-Sci. Rev. 143, 62–97.

Roveri, M., Flecker, R., Krijgsman, W., Lofi, J., Lugli, S., Manzi, V., Sierro, F.J., Bertini, A., Carnerlenghi, A., De Lange, G., Govers, R., Hilgen, F.J., Hubscher, C., Meijer, P.T., Stoica, M., 2014. The Messinian Salinity Crisis: Past and future of a great challenge for marine sciences. Mar. Geol., 352, 25–58.

Schenau, S.J., Antonarakou, A., Hilgen, F.J., Lourens, L.J., Nijenhuis, I.A., Van Der Wejden, C.H., Zachariasse, J.W., 1999. Organic rich layers in the Metochia section (Gavdos, Greece): Evidence for a single sapropel formation mechanism in the eastern Mediterranean during the last 10 Myr. Paleoceanography, 153, 117–135.

Vasiliev, I., Karakitsios, V., Bouloubassi, I., Agiadi, K., Kontakiotis, G., Antonarakou, A., Triantaphyllou, M., Gogou, A., Kafousia, N., de Rafélis, M., Zarkogiannis, S., Kaczmar, F., Parinos, C., Pasadakis, N., 2019. Large sea surface temperature, salinity, and productivity-preservation changes preceding the onset of the Messinian Salinity Crisis in the eastern Mediterranean Sea. Paleoceanography and Paleoclimatology. 34.

15th International Congress of the Geological Society of Greece
Athens, 22-24 May, 2019 | Harokopio University of Athens, Greece
Bulletin of the Geological Society of Greece, Sp. Pub. 7 Ext. Abs. GSG2019-331

Hydrocarbon Potential, Sediment Characteristics and Facies Analysis of a Lower Jurassic-Eocene Carbonate Succession in Western Greece

L. Moforis[1], V. Karakitsios[1], G. Kontakiotis[1], D. Galanakis[2] and A. Antonarakou[1]

(1) National & Kapodistrian University of Athens, Department of Geology & Geoenvironment, Section of Historical Geology-Paleontology, Panepistimioupolis-Zografou, Athens, Greece, leomof@geol.uoa.gr
(2) Institute of Geology & Mineral Exploration, Spirou Loui, Acharnai, Athens, Greece

Introduction

The thrust belt in the Balkan Peninsula along the margin of the Apulian foreland is known as the External Hellenides in Greece,which has been divided into three tectonostratigraphic zones which are from east to west: the Gavrovo Zone, the Ionian Zone and the Pre-Apulian (or Paxoi) Zone.

The rock successions in these zones consist of Mesozoic and Cenozoic strata, which have been thrust westwards onto the Apulian foreland. Form Eocene to Miocene, the migrating internal Hellenide orogeny to the west caused the simultaneous migration and the compressional deformation of the foreland in front of the orogen. (Underhill, 1985; Karakitsios, 1995; Karakitsios and Rigakis, 2007; Karakitsios, 2013)

The major structural trends are recognized in Western Greece. In the first place, major thrust fault trend NNW-SSE. These are locally offset by east-west oriented faults, some of which, such as those in the Gulf of Corinth, may have been inherited from Early Mesozoic rifting (Robertson et al., 1991). In the Cenozoic, they acted either as wrench faults during thrusting (e.g. the Petoussi Fault) or as basin bounding normal faults (e.g. in the Gulf of Patras). Thirdly, a series of dextral NE-SW trending strike-slip faults are presented in Cephalonia fault in the South. These strike-slip faults appear to have taken up relative motion in the Neogene between the Anatolian-Aegean Plate and the African-Apulian Plate north of the Hellenides subduction zone (Walcott and White, 1998).

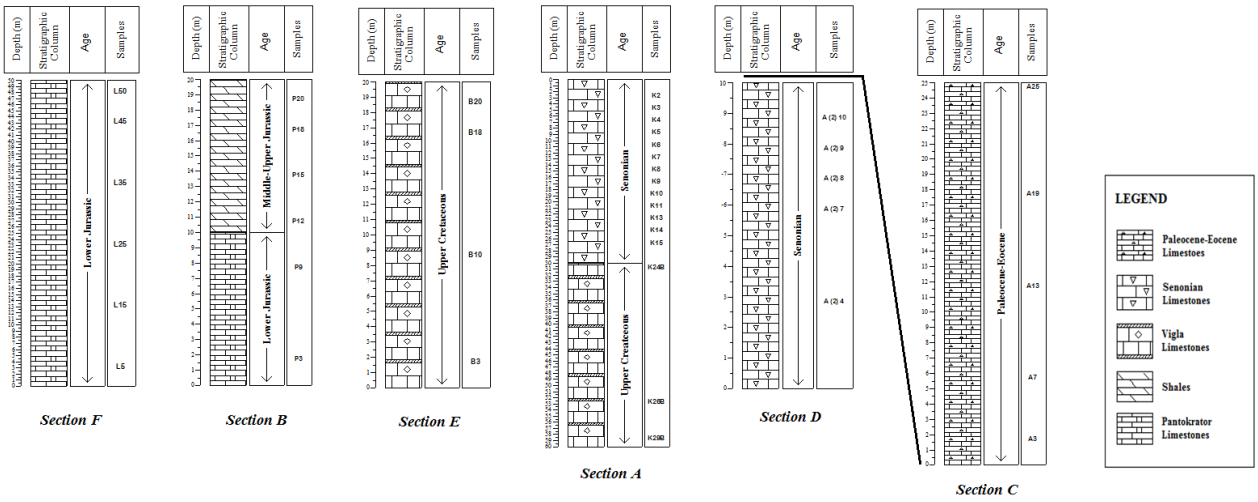

Figure 1. Stratigraphic columns of study sections (A to F). The stratigraphic columns are presented by aging order, from the older (Lower Jurassic) to the younger (Paleocene-Eocene) formation.

Materials & Methods

For the purpose of this study, a detailed investigation has been made in the Ionian zone. Six sections have been studied, and 150 samples collected in order to make extended laboratory analyses. The reservoir parameters that examined are porosity and permeability through an Accupyc 1330 pycnometer and a Geopyc 1360, from Micrometrics respectively. Furthermore, thin sections have been constructed in order to verify the sedimentological characteristics of the involved carbonate rocks.

Results

The principal lithofacies of Section F (Louros Section) is *biolithitic (boundstone)*. Section B (Perivleptos Section) is characterized by the lithofacies *biosparite (grainstone)*. The Pantokrator limestones give evidence of a depositional environment characterized by a carbonate platform with characteristics of both intertidal and subtidal settings. Vadose diagenesis of some redeposited carbonate clasts points a partly subaerial exposure. Section E (Vigla Section) consists of *radiolarian biomicrite (wackestone)* characterizing a low energy deep environment. In Section A (Koloniati Section), *pisoid lithoface*, is the only distinguished from all the other lithofacies. Pisoids have been described in the classical paper of Dunham (1962) and interpreted as caliche soil pisoids formed by subaerial vadose diagenesis during episodic lowstands of sea level. The range of depositional interpretations of these pisoids includes caliche formation in continental or coastal-

spray-zone, supratidal settings, vadose-marine inorganic precipitation in inter and subtidal environments of formation in marine seepage or groundwater springs (Flugel, 2010). Within this section, the following lithofacies have been observed as well: *biomicrite (mudstone-wackestone)* which refers to deep depositional environment. In Section D (Aspрageli-2 Section), the following three lithofacies have been observed: *bioclastic (packstone)*, which represents a medium energy environment. Possibly, sediments have been transported within the basin from the platform, *biomicrite (wakestone-packstone-floatstone)* with plaktonic foraminifera, deposited in a medium energy pelagic depositional environment and *biolithitic (bounstone)* corresponding to the margin of the platform. In Section C (Aspрageli-1 Section) the lithofacies that have been identified is *biomicritic (packstone).* Within this lithofacies pelagic foraminifera have been observed, that represent a medium energy environment, possibly corresponding to a deep depositional environment.

Although it is natural to assume that permeability values depend on porosity, it is not simple to determine which the appropriate relationship is since this would require a detailed knowledge of size distribution and spatial arrangement of the pore channels in the porous medium. Generally, it is known that the higher the porosity, the higher permaebility we should have. However, because of the complexity and the large number of related parameters no simple single functions can exist. In our samples, it has been observed that as the porosity increases the permeability values seem to decrease. For instance, in Section E (Vigla Section), sample B3 with porosity 6,85% has higher permeability value (2,7017) than sample B10 which presented a higher porosity value (23,1%) but a lower permeability measurement (2,6811). This principle can be observed in several samples within our study area.
For section F, the average porosity is 3,92%, while permeability values range between 2,6496 (sample Λ45) and 2,7319 (sample Λ25). For Section B the average porosity is 8,46%. According to the permeability measurements, for Section B, range between 2,6496 (sample Π18) and 2,7319 (sample Π12). For Section E the average porosity is 8,67%. For the permeability measurements, sample B1 showed the highest value (2,7277), while sample B10 showed the lowest value (2,6811). The average porosity from section's A samples is 7,57%. On the other hand, permeability measurements range between 2,6707 (sample K28) and 2,718 (sample K8). For Section D the average porosity is 11,59%. Permeability values, for Section D, range between 2,6204 (sample $A_2$9) and 2,7411 (sample $A_2$4). For Section C the average porosity is 6,29%. The highest porosity value has been reported in sample A1 (16,88%) and the lowest value within the sample A13 (2,50%). For the permeability measurements, the highest value presented in sample A23 (2,7193), while the lowest appeared within sample A3 (2,5799).

References

Dunham, R.J., 1962. Classification of Carbonate Rocks According to Depositional Texture. In W.E. Hamm (ed.), Classification of Carbonate Rocks, A Symposium, American Association of Petroleum Geologists, p. 108-121.

Flugel, E., 2010. Macrofacies of Carbonate Rocks. Springer-Verlag Berlin Heilderberg.

Karakitsios, V., 1995. The influence of preexisting structure and halokinesis on organic matter preservation and thrust system evolution in the Ionian basin, northwestern Greece: AAPG Bulletin, vol. 79, p. 960–980.

Karakitsios, V., and Rigakis, N., 2007. Evolution and petroleum potential of western Greece: Journal of Petroleum Geology, vol. 30, no. 3, p. 197–218.

Karakitsios, V., 2013. Western Greece and Ionian Sea petroleum systems. AAPG Bulletin, vol. 97, no. 9, p. 1567-1595.

Robertson et al., 1991. Paleogeographic and paleotectonic evolution of the Eastern Mediterranean Neotethys. Paleogeography, Paleoclimatology, Paleoecology. 87, p. 289-343.

Underhill, J.R., 1985. Neogene and Quaternary tectonics and sedimentation in Western Greece. Ph.D Thesis. University of Wales, Cardiff.

Walcott, C.R. and White, S.H., 1998. Constraints on the kinematics of post-orogenic extension imposed by stretching lineations in the Aegean region. Tectonophysics, 298, p. 155-175.

15th International Congress of the Geological Society of Greece
Athens, 22-24 May, 2019 | Harokopio University of Athens, Greece
Bulletin of the Geological Society of Greece, Sp. Pub. 7 Ext. Abs. GSG2019-332

Seismic Stratigraphy of North Aegean Trough: Indicative Evidence of Messinian Evaporites, Preliminary Results

A. Varesis[1], G. Anastasakis[1]

(1) Section of Historic Geology-Paleontology, Department of Geology and Geoenvironment, National and Kapodistrian University of Athens, Panepistimiopolis, Zografou 15784, avaresis@geol.uoa.gr

Introduction

The North Aegean Trough (NAT), is a ENE – WSW trending structural deep, that forms along the westward propagation of the North Anatolian Fault (NAF) (Le Pichon et al., 1984). Structural and basin analysis of NAT addressed mainly the tectonic fragmentation that led to the development of sub – basins forming in the Uppermost Miocene (Lalechos and Savoyat, 1979; Mascle and Martin, 1990). Moreover, the discovery of the Prinos and Espilon hydrocarbon fields to the NE of NAT in the 70s, led to an increased interest of the Upper Cenozoic evolution of the broader region. (Laigle *et al.*, 2000; Beniest *et al.*, 2016; Ferentinos *et al.*, 2018).

Objectives

This study, focused on the western and central NAT, is derived exclusively from deep penetrating seismic reflection data. By processing and interpreting the digitally available data – set we proceed to the qualitative identification of the stratigraphic top, of the Upper Miocene (Messinian) and describe the seismic stratigraphy of the identified depositional units. A refined understanding of the sedimentary column, for the various depocenters in the area under investigation, will enhance the geological perception of the region and will update the knowledge on the structural mechanisms that formed the basins.

Methods

The available data set consists, by several two-dimensional (2D) seismic profiles (multichannel, PSDM). They were acquired as part of the SEISGRECE campaign (Vigner, 2002). The acquisition parameters consist of a 16-fold coverage with a source of 16 generator – injector air guns with a total volume of 31L, operated in single bubble mode along a multi-channel streamer (96 channels, 2.4 km long streamer). We focus on an area of 600 km^2 defined as Central NAT (Fig.1). Characteristics such as: (a) the reflection continuity, (b) the geometry and architecture, (c) the frequency and (d) the amplitude of the reflectors are used in order to enhance the seismic stratigraphy of the region.

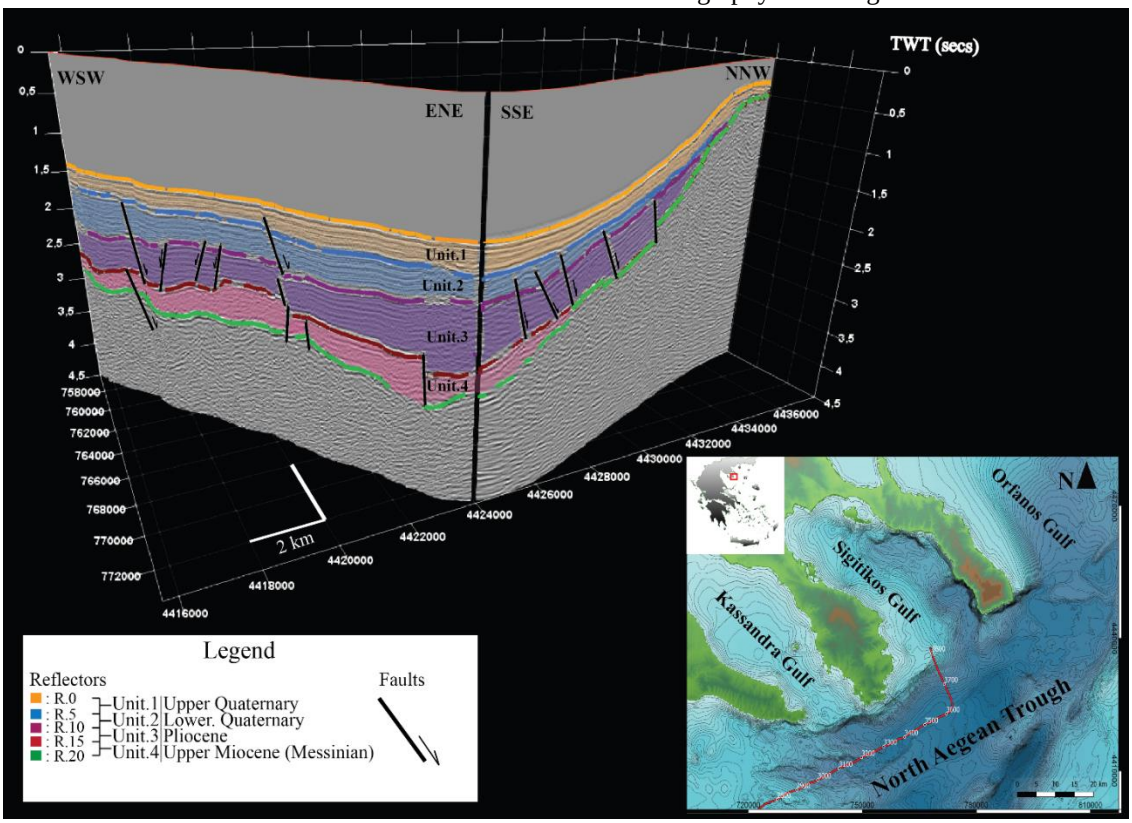

Figure. 1 Visual representation of the interpreted area (3D perspective).

Results

The utilised seismic reflection system, achieved an acquisition penetration down to approximately 17 secs (Vigner, 2002). Due to the fact that the resolution diminishes below the upper 6 seconds and because we were interested in Upper

Cenozoic seismic stratigraphy, the seismic profiles were processed vertically so that the upper 4 secs (TWT) were distinguished, allowing a more detailed insight in the upper sedimentary column. In the under-evaluation area (Central NAT), four major seismic stratigraphic units have been recognized (Fig.1) and characterized by different seismic signatures, separated by three major unconformities, as distinguished in other parts of the Aegean. The uppermost unit (Unit. 1) is characterized, by densely spaced, parallel reflectors, with relative high amplitude and continuity. The thickness of the unit, ranges from 150 ms along slope, increasing to 250 ms at the center of the basin. The underlying, second unit (Unit.2), demonstrates a similar seismic response with a set of rather well stratified reflector packages up to 500 ms, that rest unconformably over the underlying units. The third unit (Unit.3) interpreted below is bounded by a pronounced unconformity better expressed along slopes. A chaotic seismic response and intense faulting characterize this unit. It is predominantly differentiated by lower frequencies and its thickness varies from 150 to more than 650 ms basin-ward. Finally, the lower fourth unit (Unit. 4), is clearly distinguished due to, (a) an increase in seismic amplitude, (b) a characteristic internal signal blanking and (c) the presence of distinctive up – doming structures. The average thickness of this unit is around 300ms.

Conclusions

The mapped uppermost three seismic units in Central NAT are attributed to the Plio-Quaternary sediment fill of the basin. They are separated by two major unconformities that overlap the slopes of the basin. On the basis of the regional stratigraphy we attribute the three units to Upper Quaternary, Lower Quaternary and Pliocene respectively (Fig.01). The fourth unit represents the Upper Miocene (Messinian). In our proposed interpretation we highlight this distinct Unit 4 seismic reflector package, that overlaps unconformably over the basement and displays the acoustic characteristics of an evaporitic sequence (prominent acoustically turbulent-transparent unit). Available literature for the broad area of North Aegean Trough reports sceptical about the presence of Messinian evaporites in the western and central regions. Here we recognize a unit that displays clear reflection characteristics of an evaporitic sequence. Even though our study relies solely on the interpretation of seismic profiles, the proposed scenario is further supported by the identification through refraction tomography of an interval, of high velocity (4.1 km/s) between the unconsolidated sediment cover and the Alpine basement at the vicinity of the area (Le Pichon *et al.*, 1984). This, correlates also, with the calculated PSDM velocities of 4.43 km/s by Vigner (2002) that are compatible with an evaporitic sequence. Moreover doming-like structures, visible in low penetration medium resolution records (Ferentinos, 1990; Rodriguez *et al.*, 2018), clearly emanate from our clearly distinguished Unit 4. In the broader area of NAT there are some references hinting the presence of Messinian evaporates (Ferentinos, 1990; Mascle and Martin, 1990; Lalechos, 2000; Koukouvelas and Aydin, 2002; Sakellariou and Tsampouraki-Kraounaki, 2019).

Acknowledgements

We thank Professor Hirn from the Institut de Physique du Globe de Paris, for making available the multichannel seismic profiles.

References

Beniest, A. *et al.* (2016) 'Interaction between trench retreat and Anatolian escape as recorded by neogene basins in the northern Aegean Sea', *Marine and Petroleum Geology*. Elsevier Ltd, 77, pp. 30–42. doi: 10.1016/j.marpetgeo.2016.05.011.

Ferentinos, G. (1990) 'Offshore geological hazards in the Hellenic arc', *Marine Geotechnology*, 9(4), pp. 261–277. doi: 10.1080/10641199009388244.

Ferentinos, G. *et al.* (2018) 'Propagation and termination of a strike slip fault in an extensional domain: The westward growth of the North Anatolian Fault into the Aegean Sea', *Tectonophysics*. Elsevier, 745(April), pp. 183–195. doi: 10.1016/j.tecto.2018.08.003.

Koukouvelas, I. K. and Aydin, A. (2002) 'Fault structure and related basins of the North Aegean Sea and its surroundings', *Tectonics*, 21(5), pp. 10-1-10–17. doi: 10.1029/2001TC901037.

Laigle, M. *et al.* (2000) 'North Aegean crustal deformation: An active fault imaged to 10 km depth by reflection seismic data', *Geology*, 28(1), pp. 71–74. doi: 10.1130/0091-7613(2000)28.

Lalechos, N. (2000) 'Aegean Sea,Possible Oil Bearing Areas - Petroleum Geology', *Mineral Wealth*, 115, pp. 43–70.

Lalechos, N. and Savoyat, E. (1979) 'La sedimentation Neogene dans le Fosse Nord Egeen', *VI Colloquiim on the Geology of the Aegean Region*, 2, pp. 591–603.

Mascle, J. and Martin, L. (1990) 'Shallow structure and recent evolution of the Aegean Sea: A synthesis based on continuous reflection profiles', *Marine Geology*, 94(4), pp. 271–299. doi: 10.1016/0025-3227(90)90060-W.

Le Pichon, X., Lybéris, N. and Alvarez, F. (1984) 'Subsidence history of the North Aegean Trough', *Geological Society, London, Special Publications*, 17(1), pp. 727–741. doi: 10.1144/GSL.SP.1984.017.01.58.

Rodriguez Mathieu, Dimitris Sakellariou, Christian Gorini, Nicolas Chamot-Rooke, Elia d'Acremont, Alexandre Nercessian, Konstantina Tsampouraki Kraounaki, Davide Oregioni, Matthias Delescluse, and A. J. (2018) 'Seismic profiles across the North Anatolian Fault in the Aegean Sea', *EGU General Assembly Conference Abstracts*, 20, p. 7426. doi: 10.13140/RG.2.2.17993.24164.

Sakellariou, D. and Tsampouraki-Kraounaki, K. (2019) 'Plio-Quaternary Extension and Strike-Slip Tectonics in the Aegean', in *Transform Plate Boundaries and Fracture Zones*. Elsevier, pp. 339–374. doi: 10.1016/B978-0-12-812064-4.00014-1.

Vigner, A. (2002) *Images sismiques par réflexions verticale et grand-angle de la croûte en contexte extensif : les Cyclades et le Fossé Nord-Egéen*. Paris, Institut de physique du globe. p.269.

15th International Congress of the Geological Society of Greece
Athens, 22-24 May, 2019 | Harokopio University of Athens, Greece
Bulletin of the Geological Society of Greece, Sp. Pub. 7 Ext. Abs. GSG2019-337

Lithostratigraphic response of the last sea level cycle in the Saronikos shelf

A. Bougiouris[1], P. Foutrakis[1], G. Kontakiotis[1], G. Anastasakis[1]

(1) Section of Historic Geology-Paleontology, Department of Geology and Geoenvironment, National and Kapodistrian University of Athens, Panepistimiopolis, Zografou 15784, Greece, abougiouris@geol.uoa.gr

Introduction

Quaternary sea level cycles are well imprinted in the marine sediments of continental margins worldwide. The Aegean hosts several locations where excellent preservation of these cycles is manifested on seismic reflection records (Lykousis, 2009; Anastasakis and Piper, 2013). Seismic records of medium and high resolution are not capable to fully resolve and describe the complete association of sedimentary lithofacies that normally develop around 4th and 5th order sea level fluctuations. This is only possible by direct sampling and studying of the sedimentary sequences formed in response to sea level fluctuations. Reworking of the sediments can locally distort the lithostratigraphic continuity, but such processes can readily be identified on the basis of textural and compositional parameters.

Objectives

The objective of this study is to establish a core transect across the outer shelf and shelf break of the Saronikos Gulf in order to establish and evaluate the sedimentary sequences developed during the last sea level cycles. Compositional and textural parameters are established in relation to the sea level curve.

Methodology

Four gravity cores (SAR3, 4, 5 and 6) presented in this study were retrieved by the Department of Historic Geology-Paleontology, during the 2011 Saronic research expedition utilizing a trawler boat. The cores were scanned for their magnetic susceptibility, split and photographed. Cores were sampled at a few cm resolution based on macroscopic and susceptibility differentiations. Samples were oven dried at 45ºC. Carbonate content (%) was measured on all samples following the Muller and Gastner (1971) method. Organic carbon content was measured on selected samples using a combustion technique. Selected samples were also picked for grain size analysis. Core SAR5, recovered at 160m water depth, which displays the well-established Eastern Mediterranean lithostratigraphy, was chosen for detailed X-ray bulk mineralogy. Carbonate minerals were estimated by measuring peak areas of main peaks on diffractograms and utilizing published calibration curves. Other well crystallized minerals were measured using peak heights and mineral correction factors (Muller and Mann, 1979).

Results

SAR-3 was recovered at 110 m depth and is entirely composed of bioclastic sands dominated by coarse calcareous algae fragments, bivalves and gastropods. Carbonate contents range in-between 60-80%. At the base of the core an unconformity is observed. The basal section of this core displays a significant percentage of well rounded, sub-spherical terrigenous grains, plus many iron-coated mostly foraminifera tests. Coarse biogenic grains are broken and rounded. All the above suggest exposure to a sub-aerial wave dominated coastal environment.

SAR-4, retrieved at 138 m depth, consists of medium to fine carbonate sands with frequent large sized shells. Generally carbonate contents are decreasing upwards ranging from 50-70%.

SAR-5 obtained at 160 m depth, on the slope, displays well developed cyclothematic lithoface associations starting from the bottom with coarse grained carbonate sands, enriched on biogenic fragments and their carbonate content to range from 90% at the base to 55% on the top of the core. A well-developed sapropelic layer is developed on the upper section of the core. Grain size mean diameters are around-1φat the lower half of the core, due to coarse biogenic tests and rapidly decrease upwards from below the sapropelic sequence to the top of the core. There is also a concomitant to the grain size decrease in carbonate contents.

Detailed bulk mineralogy of this core also displays well expressed trends. Terrigenous minerals score highest percentages at the upper section of this core. Illite is the most dominant mineral varying from 3 to 17 %, quartz is the second in abundance scoring 2-16% respectively. There are two levels with enhanced feldspar contents, around 7%, most likely associated with cryptotephras. Carbonate minerals consist mostly from Mg-rich calcite, calcite and aragonite while dolomite is present in trace amounts. From top of the core until below the sapropelic layer Mg-calcite varies from 20-38%, calcite scores 16-21% and aragonite varies from 6-15%. At a well expressed stratigraphic interval below the sapropelic lithoface, there is a coarse calcareous algae sand lithoface that presents aragonite contents up to 32%. Below this layer, there is a step-wise increase of Mg-rich calcite paralleled by a concomitant decrease of calcite and aragonite. Mg-rich calcite scores up to 74%.

SAR-6 is located at 212 m depth within the basin of South Saronikos. It is generally composed of a fine sandy marl with carbonate contents generally decreasing upwards from 65-45%. A thin 6 cm sapropelic horizon is developed on the uppermost section, from 26-32 cm. Carbonate contents score the highest percentages of 68% around 10-20 cm below the sapropelic layer and then steadily decrease to the bottom of the core varying in-between 40-50%. Grain size shows little variability along this core with the finest sediments attaining median diameters of around 3,7φ at the top 10 cm.

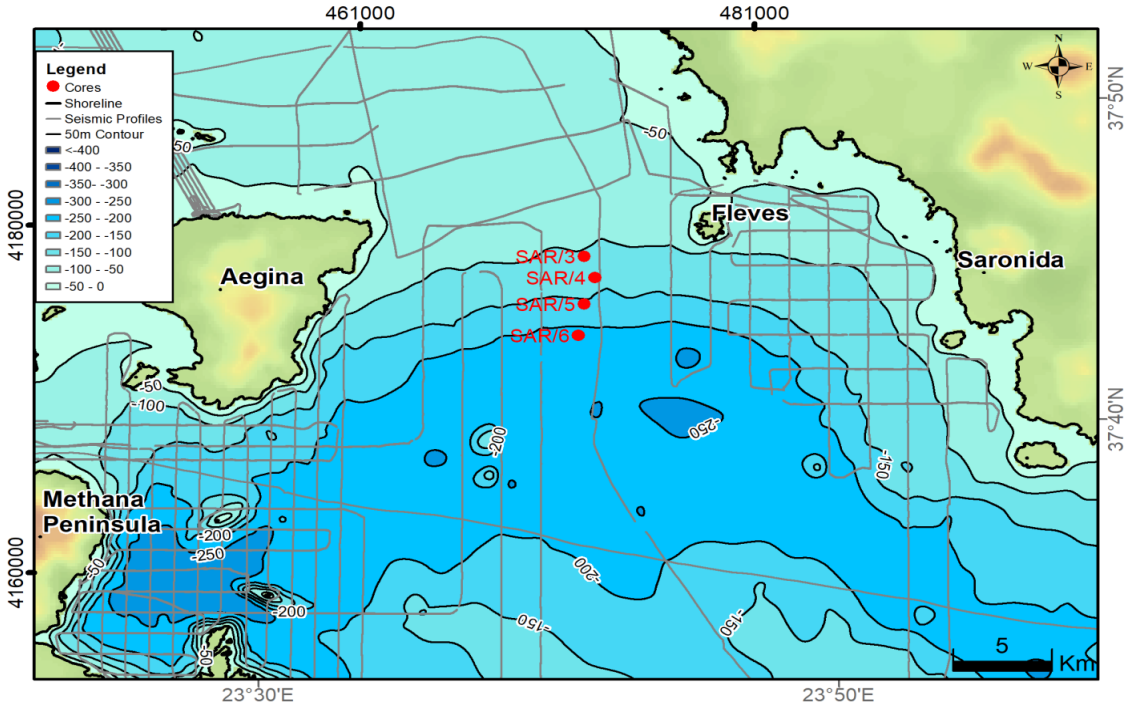

Fig.1 - Bathymetric map of the study area with core locations presented in this study.

An indicative high resolution chirp profile along the bathymetric transect established along the coring stations presented in this study shows:

a. A 8-20 m thick horizon developed in water depths greater than 190m.
b. A less than 1m thick surface horizon developed in-between 190-120m.
c. A clinoform package developed at 115-120 m attributed to the last glacial sea level strandline. This clinoform package is bounded to the north by a ca 5-m high sandy barrier.

Conclusions

A bathymetric transect in-between water depths of 110-212 m, obtained by coring stations along the South Saronikos shelf revealed the following:

1. There is direct evidence of subaerial exposure in core SAR-3 recovered in water depth of 110 m. Terrigenous grains at the time of this exposure suggest littoral transport along this paleo-coast presumably developed during the last glacial sea level drop as mapped on seismics by the identification of a clinoform wedge at 115-120 m.
2. Cores recovered down to water depths of around 140m display a coarse sandy carbonate facies.
3. Deeper cores display cyclothematic lithofacies associations with a thin sapropelic layer developed in the upper 30 cm. Texture of sediments becomes coarser below the uppermost sapropelic horizon, as a result mostly of coarser biogenic grains precipitated in shallower water depths during reduced sea levels of MIS 2 and 3. There appears to be terrigenous sediment trapping landwards to the north, behind a sediment barrier developed in Saronikos shelf during the lowest and lower sea levels.
4. Mg-calcite contents at a core recovered at 160 m water depth display slightly reduced percentages at the colder stratigraphic interval of MIS 2 and further show a drastic increase throughout MIS 3 as compared to MIS 1. This paradox can be attributed to the enhanced contribution to the biogenic carbonate factory of Mg-calcite secreting organisms, such as coralline red algae, bryozoans and echinoids. This is due to the fact thatMIS 3 sea level consisted of an initial rise to a level of approximately 60 m for the first half of MIS 3 and subsequent drop to 80 m for the remainder.

References

Anastasakis, G., Piper, D.J.W., 2013. The changing architecture of sea-level lowstand deposits across the Mid-Pleistocene Transition: South Evoikos Gulf, Greece. QuaternaryScience Reviews 73, 103–114. doi:10.1016/j.quascirev.2013.04.018

Lykousis, V., 2009. Sea-level changes and shelf break prograding sequences during the last 400ka in the Aegean margins: Subsidence rates and palaeogeographic implications. Continental Shelf Research 29, 2037–2044. doi:10.1016/j.csr.2008.11.005

Mann, U., Müller, G., 1979. X-ray mineralogy of Deep Sea Drilling Project Legs 51 through 53, western North Atlantic. Initial Rep. Deep Sea Drill. Proj. 51–53, 721–729.

Müller, G., Gastner, M., 1971. The “Carbonate Bomb, a simple device for the determination of the carbonate content in sediments, soils, and other materials. N. Jb. Mineral., vol. 10, pp. 466–469.

15th International Congress of the Geological Society of Greece
Athens, 22-24 May, 2019 | Harokopio University of Athens, Greece
Bulletin of the Geological Society of Greece, Sp. Pub. 7 Ext. Abs. GSG2019-352

Provenance of deep sea turbidites in two South Aegean basins

O. Koumoutsakou[1], G. Anastasakis[1], A. Antonarakou

(1) Section of Historic Geology-Paleontology, Department of Geology and Geoenvironment, National and Kapodistrian University of Athens, Panepistimiopolis, Zografou 15784, Greece, okoumout@geol.uoa.gr

Introduction

Gravitative sedimentation dominates deep basins in the Mediterranean and so far has received little attention in the Aegean Sea. An increase in sedimentation rates by a few orders of magnitude has been reported along the Hellenic Trench (Blanpied and Stanley, 1981; Anastasakis and Piper, 1991) and also in the South Aegean Sea (Koumoutsakou and Anastasakis, 1997). Especially in the South Aegean Sea volcaniclastic sedimentation within certain stratigraphy intervals can locally overprint any other sediment source (Anastasakis, 2006). However it is evident that there must be significant sediment source contributions from the recycled orogen.

Objectives

The purpose of this study is to present and discuss unequivocal evidence for the different provenance of turbiditic sequences that were deposited in the deepest two basins of the South Aegean Sea, the Karpathos Basin and the east Karpathos Basin, during the Late Quaternary. A tight stratigraphic control, based on sapropel stratigraphy and tephrostratigraphy (Koumoutsakou and Anastasakis, 1997; 2017), provides a chronological framework in order to evaluate sediment parameters such as texture and provenance.

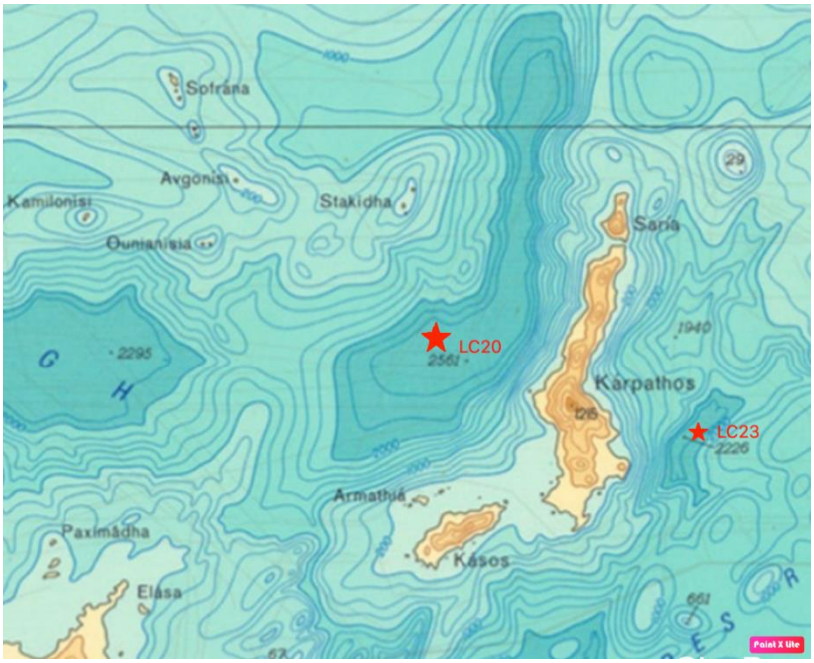

Figure 1. Bathymetric map of the study area with core locations presented in this study.

Two long Kullenberg piston cores, LC20 and LC23, were retrieved during Marion Dufresne Cruise 81 (MAST II PALAEOFLUX PROGRAMME EU-funded, 1995). The cores were scanned for magnetic susceptibility and then were sampled directly on board immediately after retrieval and splitting. Sediment color was determined using the 'Revised Standard Color Chart' (1991). Samples were oven dried at 40□C at the Department of Historic Geology-Paleontology. Calcium carbonate content (%) was measured using the carbonate bomb method (Muller and Gastner, 1971). Grain size analyses were performed by wet sieving, for any sand fraction present and then using a Sedigraph 5100 with a MasterTech 051 auto sampler. Bulk mineralogy was determined by powder X-ray diffraction (XRD) (Siemens D8000, CuKα radiation, graphite monochromator, 35 kV and 35 mA, using a 0.02□ step size and 1s per step counting time), on randomly oriented samples ground with a pestle and mortar. Minerals were estimated by measuring peak areas of main peaks on diffractograms and peak heights using the Muller and Mann (1979) method.

Core No	Location	Latitude	Longitude	Water Depth	Core Length
LC-20	Karpathos Basin	35 40.05'N	26 52.10'E	2490m	23.70m
LC-23	East Karpathos Basin	35 31.48'N	27 22.08'E	2154	19.33m

Results

Four main sediment types were recognized in the two cores and were distinguished on the basis of magnetic susceptibility, colour, grain size and composition. They are: 1) Hemipelagic sediments, 2) dark-coloured organic rich sapropel layers, 3) tephra and volcaniclastic layers and 4) turbidites that interrupt and distort all other lithologies.

Hemipelagic muds consist mostly of yellowish (10YR6/3) to brownish grey (10YR3/2) biogenic clayey marls and marly clays, with 25-65% CaCO3 and fine silt median diameter grain size. They are characterized by bioturbation and frequent foram tests.

Turbidites are recognized on the basis of sedimentary structures such as erosional bases, lamination and further verified by textural analysis. The basal coarser fraction is mainly composed of quartz, dolomite, and mostly biogenic grains. Many mm to cm turbidite layers have been identified and many of them have been analyzed for grain size (Koumoutsakou & Anastasakis 1997).

Distinctive organic rich sapropel layers occur in both cores. They were classified based on the definitions by Kidd et al. (1978) and found to be severely affected by reworking processes as described by Anastasakis and Stanley (1984). They are mostly well laminated with variable thicknesses of turbidite units developed over erosional bases.

Tephra and volcanic debris layers are characterized mostly by high susceptibility, contain elevated to overwhelming amounts of volcanic grains often reworked forming turbiditic sequences.

In between and within the above lithologies are deposited mostly base cut out turbiditic units of Tde and rarely of Tbe and Tce Bouma sequence development. Median and modal diameters of turbidites range from 500 μm to 1,1 mm.

Bulk mineralogy of all lithologies has revealed that the most important provenance indicator is dolomite. All turbidites with a medium sized sand to coarse silt base display dolomite contents higher than 7% reaching as high as 30%. Core LC-20 retrieved in the deepest Karpathos Basin contains a higher proportion of coarse based, dolomite rich turbidites apparently originating from the west Karpathos and north Kasos shelf and flowing along the steep slopes.

Conclusions

We clearly distinguish that both basins are dominated by gravitative sedimentation and we identify a high proportion of base cut out turbiditic sequences that display excellent textural sorting and fining upward grain size trends. With the exception of a few volcaniclastic coarser turbidites starting with a base of all other coarser than medium silt turbidites contain significantly enhanced dolomite contents, clearly denoting provenance of the sediments from the surrounding island shelves. Sedimentation rates in the studied cores are at least one order of magnitude higher than the surrounding margins. Turbidites are more frequent during rapid initial stages of transgressions, but seismicity appears to be triggering gravitative sedimentation time synchronous events.

References

Anastasakis, G. C., & Stanley, D. J. (1984). Sapropels and organic-rich variants in the Mediterranean: sequence development and classification. Geological Society, London, Special Publications, 15(1), 497–510.

Anastasakis, G., Piper, D.J.W., 2005. Late Neogene evolution of the western South Aegean volcanic arc: sedimentary imprint of volcanicity around Milos. Marine Geology 215, 135–158.

Blanpied, Christian and Stanley, Daniel J. 1981. "Uniform Mud (Unifite) Deposition in the Hellenic Trench, Eastern Mediterranean." Smithsonian Contributions to the Marine Sciences. 13:1–40

Koumoutsakou O. and Anastasakis G., 1997. Lithostratigraphic framework of dynamic sedimentation in the SE Aegean Sea. 5th Symposium of Oceanography and Fishery, Athens, 1997.

Koumoutsakou O., Anastasakis G., Smith V.C., Vougioukalakis G., Economou G. 2017 Tephrostratigraphic framework of sedimentation in the Karpathos basin, SE Aegean Sea. 5th RCMNS Conference "Exploring a "physical laboratory": the Mediterranean Basin" 2017. Athens.

Mann, U., Müller, G., 1979. X-ray mineralogy of Deep Sea Drilling Project Legs 51 through 53, western North Atlantic. Initial Rep. Deep Sea Drill. Proj. 51–53, 721–729.

Müller, G., Gastner, M., 1971. The "Carbonate Bomb, a simple device for the determination of the carbonate content in sediments, soils, and other materials. N. Jb. Mineral., vol. 10, pp. 466–469.

GENERAL SESSION

T2 Geodynamics, Tectonics and Structural Geology

Conveners: **Alexandros Chatzipetros (AUTH)**
Haralambos Kranis (NKUA)

Co-organized by the Structural Geology and Tectonics Committee, G.S.G.

15th International Congress of the Geological Society of Greece
Athens, 22-24 May, 2019 | Harokopio University of Athens, Greece
Bulletin of the Geological Society of Greece, Sp. Pub. 7 Ext. Abs. GSG2019-027

Intra oceanic subduction initiation

M. Delagas[1]
(1) Utrecht University, Princetonplein 6, 3508 TA, Utrech, The Nederlands, m.delagas@students.uu.nl

Subduction is key for driving for plate tectonics. Yet it is still unclear where and how subduction initiates in the oceanic domain. It is widely accepted that it critically depends on the rheology of the oceanic lithosphere (Nikolaeve et al., 2010) and can occur upon failure of the load-bearing crustal and mantle layers. When oceanic lithosphere is too strong, high shear strength of the oceanic lithosphere does not permit failure, and subduction may occur by deforming a passive margin at ocean-continent transition. However, weakening processes such as zones of serpentinized mantle may affect the strain localization (Maffione et al., 2015; Stern, 2004). Therefore, a series of experiments conducted to determine the favourable rheological and kinematic conditions that lead to the development of subduction zones in the intra-oceanic domain. These experiments involving both oceanic and continental domains which incorporate weak zones of realistic dimensions in the oceanic crust. Model results show that the key factor for the strain localisation is the difference in strength between the continental and oceanic upper crust. Analysis of deformation is used to define a boundary of rheological conditions enabling subduction in oceanic or in continental domain. Additionally, addition of a weak zones in a thick and strong oceanic lithosphere doesn't affect the deformation pattern. However, presence of a weak zone in a relatively younger oceanic lithosphere (60 ± 10 My) may induce strain localization in the oceanic crust rather than at passive margin. This shows the importance of geological inheritance and thermo-mechanical feed-backs for the locus and evolution of subduction zone.

Acknowledgments

This study has been supported by the Tectonic Laboratory of Utrecht University providing the materials and the equipment for the experiments. Antoine Auzemery supervised the progress of this study and helped with his fruitful discussions and his expertise on the subduction as well as with his contribution on the experimental procedure.

References

Maffione, M., Thieulot, C., Van Hinsbergen, D.J., Morris, A., Plümper, O. and Spakman, W., 2015. Dynamics of intraoceanic subduction initiation: 1. Oceanic detachment fault inversion and the formation of supra-subduction zone ophiolites. *Geochemistry, Geophysics, Geosystems*, *16*(6), pp.1753-1770.

Nikolaeva, K., Gerya, T.V. and Marques, F.O., 2010. Subduction initiation at passive margins: Numerical modeling. *Journal of Geophysical Research: Solid Earth*, *115*(B3).

Stern, R.J., 2004. Subduction initiation: spontaneous and induced. *Earth and Planetary Science Letters*, *226*(3-4), pp.275-292.

15th International Congress of the Geological Society of Greece
Athens, 22-24 May, 2019 | Harokopio University of Athens, Greece
Bulletin of the Geological Society of Greece, Sp. Pub. 7 Ext. Abs. GSG2019-116

Architecture of the Alpine Deformation and Geotectonic Setting of the Hellenides. A synthesis

A. Kilias
Aristotle University of Thessaloniki, Department of Geology, Kilias@geo.auth.gr

Introduction

The Hellenic orogen, as a branch of the broader Alpine orogenic belt in Laurasia, were resulted from the convergence and final continental collision of Europe and Apulia plates in a complicated, multiphase deformational regime, with the questions around, the existence of one or more Tethys ocean basins between Europe and Apulia continents and the origin of the old Paleozoic Crystalline fragments incorporated in the Hellenides to remain under debate until today (**Fig. 1;** Gawlick et al. 2008, Robertson 2012, Papanikolaou 2013). The goal of this work was to present the main geological structure and architecture of the Hellenic orogenic belt, as well as the new aspects for its geotectonic evolution during the Alpine orogeny. We based on our recent studies about the deformational history of the Hellenides but also on the more modern views, published from others colleagues, concerning the Alpine geotectonic reconstruction of the Hellenides.

Architecture of Deformation

The Alpine structural evolution in Hellenides starts with the continental rifting of the Pangaea Super-continent during the Permo-Triassic and the opening of the Neotethyan Ocean. Subsequently, deformation history and metamorphism are recorded in six main tectonic events from the Middle Jurassic to present day (D1-D6; Kilias et al. 2010, 2013). The structural evolution from the Permo-Triassic to the recent is briefly described below (Kilias et al. 2010, 2013). Older Paleozoic deformational events have been strongly overprinted by the Alpine deformation. They are recognized only as rests in some places in the Paleozoic basement rocks of the Internal Hellenides.

1. **Permo-Triassic**: continental rifting, bimodal magmatism and A-type granite intrusion.
2. **Triassic-Jurassic**: passive margins extension and sedimentation.
3. **Middle Jurassic**: intraoceanic subduction, amphibolite sole, ophiolite mélanges, island arc magmatism.
4. **Mid-Late Jurassic**: ophiolite obduction, ophiolite mélanges formation at the front of the advanced ophiolites, high-pressure metamorphism, retrogression from greenschist to amphibolite facies metamorphic conditions, W-ward and E-ward sense of movement and crustal imbrication at the western (Pelagonian) and eastern (Serbo-Macedonian) marginal parts respectively of the Neotethyan realm, **D1.**

- Deposition during extension? of the **Upper Jurassic-Lower Cretaceous** sediments above or at the front of the obducted ophiolites.

5. **Albian-Aptian (upper Early Cretaceous)**: W-ward and E-ward crustal imbrication, syn-tectonic low grade metamorphism, **D2.**
6. **Upper Cretaceous:** extension, shallow water carbonate sedimentation terminated in the Paleocene with the internal Hellenides flysch, **D3.** Starting of subduction of the Axios/Vardar ocean remnants under the European margin.
7. **Tertiary (Paleocene-Eocene)**: compression, W-ward sense of movement, HP/LT metamorphism and building of the Internal Hellenides high pressure belt of Paleocene-Eocene age (Olympos-Ossa, Cyclades), progressively emplacement during the **Eocene-Oligocene** of the Pelagonian nappe together with the *HP/LT internal metamorphic belt* on the External Hellenides, **D4**. Syn-orogenic extension associated with high-temperature metamorphism, migmatization and magmatism in the Serbo-Macedonian/Rhodope metamorphic province, **D4.**
8. **Oligocene-Miocene:** HP/LT metamorphism and building of the *External Hellenides high pressure belt* associated with compression and nappe stacking in the External Hellenides, **D5**. Syn-orogenic extension, high-temperature metamorphism and magmatism in the Internal Hellenides (**D5;** Olympos-Ossa, Kyklades and Serbo-Macedonian/Rhodope metamorphic province).
9. **Neogene-Quaternary**: active Hellenic subduction, extension and intramontagne basin formation, **D6**. Recent neo-tectonic activity.

As it is concluded by the above structural description, compression, nappe stacking and high-pressure metamorphism alternated progressively through time with extension, orogenic collapse and medium- to high-temperature metamorphism. Extension was leading to uplift and exhumation of deep crustal levels as tectonic windows and metamorphic core complexes. The deformation during the extensional stages were progressively evolving from ductile to brittle conditions. An S- to SW-ward migration of the dynamic peer compression vs extension is clearly recognized during the Tertiary in the Hellenides. In any case extension and crustal uplift follow burial, compression and nappe stacking (Kilias et al. 2010, 2013, Burg 2012). The kinematic pattern of the extension and compression tectonics appears to be complicated, but nevertheless for both stages, compressional and extensional, the recognized stretching lineation and associated movement direction are roughly perpendicular to the Hellenic arc; these are NE-SW trending in the west and N-S trending in the center, with a main movement direction, at least for the compressional tectonics, SW- and S-ward respectively (Kilias et al. 2002, 2010, Papanikolaou 2013). The sense of shear during the extensional stages of deformation and the nappes' collapse appears in many places bivergent (SW- to S-ward and NE- to N-ward), indicating an important component of bulk coaxial deformation during extension (Fig. 1; Kilias et al. 2002, 2010, 2013).

Geotectonic reconstruction- Conclusions

According to our more recent structural works (Kilias et al. 2010, 2013, Michail et al. 2016), as well as a lot of studies from others researchers, concerning the geodynamic evolution of the Hellenides (e.g. Gawlick et al. 2008, Froitzheim et al. 2014), all ophiolite belts in the Hellenides, as well as the Middle-Late Jurassic island arc magmatic products during the Neotethyan intra-oceanic subduction (Michail et al. 2016), subsequently incorporated inbetween the Axios/Vardar zone units and the Circum-Rhodope belt, were originated from a single source and this was the Neotethyan Axios /Vardar ocean basin. The latter closed finally during the Late Cretaceous-Paleocene subducted totally E-ward under the European

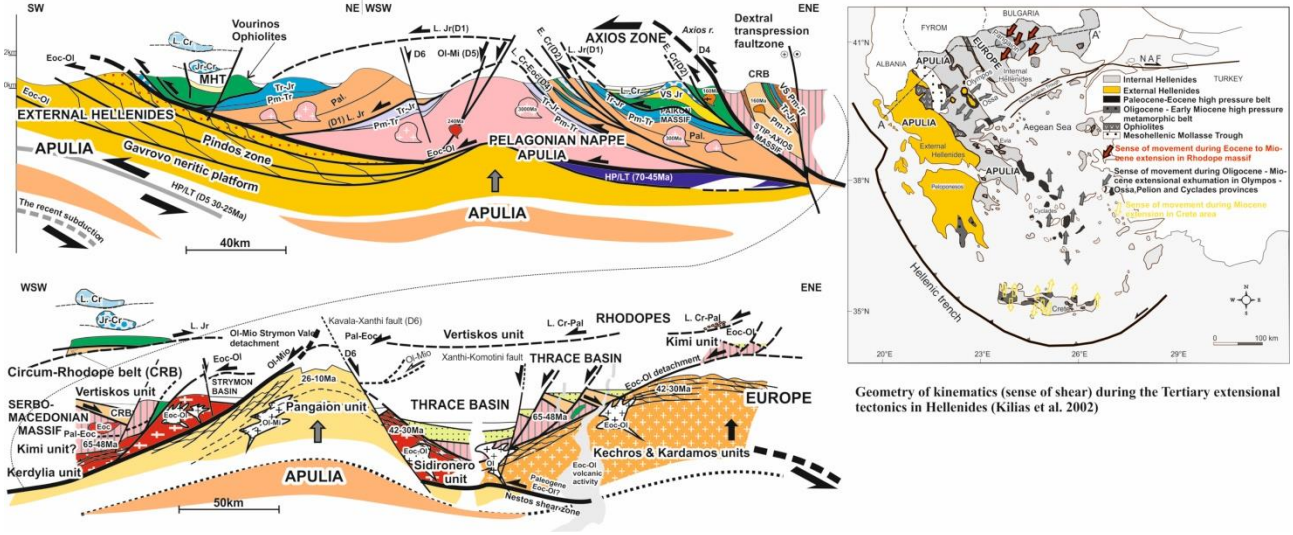

Figure 1. Geological cross-section (A-A`) through the Hellenides (A-A` is indicated on the geological map of Greece, right). The geometry and kinematics of deformation is also shown (D1 to D6 events). 26-10Ma cooling ages (after Kilias et al. 2013)

continental margin, including the Serbo-Macedonian and Strandja/Sredna Gora massifs (Fig. 1). In this content, the ophiolite nappes (e.g. the Vourinos ophiolite complex etc.) and the island arc magmatic products (e.g. Fanos granite, Chortiatis magmatic series etc.) should be considered as far-travelled nappes on the Hellenides continental parts (Pelagonian nappe and Serbo-Macedonian massif, Fig. 1; Gawlick et al. 2008, Kilias et al. 2010). Furthermore, the deposition of the Upper Jurassic sedimentary carbonate series (Gawlick et al. 2008, Robertson 2012) on the top of the obducted ophiolite nappe clearly determine the upper limit of the ophiolite emplacement in the ?Kimmeridgian/Tithonian (Fig. 1). In this scenario we assume that the Vardar/Axios ophiolites are also allochthones and the Axios/Vardar suture zone should be traced in-between the Rhodopes nappes, more eastern (Fig. 1; Froitzheim et al. 2014). Additionally, regarding this structural architecture and evolution the lower-most Pangaion Rhodope unit, today exhumed as an Oligocene-Miocene metamorphic core complex, should be the marginal part of the Apulia plate (Pelagonia?), which was unterthrusted below the Serbo-Macedonian massif and the Rhodope nappes stack during the Cretaceous-Tertiary, subsequently following the Upper Cretaceous subduction of the Neotethyan Axios/Vardar ocean (Fig. 1; Froitzheim et al. 2014). The Apulia carbonate platform is also exhumed in the Olympos-Ossa window and the Attico-Cycladic massif below the Paleocene-Eocene high pressure belt and the Pelagonian nappe (Jolivet et al. 2004, Kilias et al. 2010). Additionally, in the Cyclades area is also exhumed the Paleozoic basement of the Apulia plate as a metamorphic core complex under the carbonate platform and the overlain Internal Hellenides nappe stack. Cretaceous-Tertiary nappe stacking and crustal thickening in the Internal Hellenides were followed by syn-to late-orogenic extension, crustal thinning and exhumation of the deeper structural units as tectonic windows or metamorphic core complexes (Fig. 1; Burg 2012, Kilias et al. 2013, Froitzheim et al. 2014). High-temperature metamorphism, partly migmatization and intense magmatism associated the Tertiary extensional tectonic regime (Burg 2012, Kilias et al. 2013). Extension occurred simultaneously with compression and W-ward verging nappes' stacking in the External Hellenides (Jolivet et al. 2004, Kilias et al. 2010, Froitzheim et al. 2014). A retreating subduction zone and roll back of the subducted lithospheric slab under the Hellenides nappes stack and collapse of an overthickened crust or mantel delamination (Burg 2012, Froitzheim et al. 2014) could well explain the Tertiary extensional tectonics in the Internal Hellenides taken place simultaneously with compression in the External Hellenides and the Hellenic foreland.

References

Burg, J.P., 2012. Rhodope: From Mesozoic convergence to Cenozoic extension. Review of petro-structural data in the geochronological frame. J. Virtual Explorer. 42.

Froitzheim, N., Jahn-Awe, S., Frei, D., Wainwright, A.N., Maas, R., Georgiev, N., Nagel, T.J., Pleuger, J., 2014. Age and composition of meta-ophiolite from the Rhodope Middle Allochthon (Satovcha, Bulgaria): A test for the maximum-allochthony hypothesis of the Hellenides. Tectonics 33, 1477–1500.

Gawlick, H.J., Frisch, W., Hoxha, L., Dumitrica, P., Krystyn, L., Lein, R., Missoni, S., Schlagintweit, F., 2008. Mirdita Zone ophiolites and associated sediments in Albania reveal Neotethys Ocean origin. Int. J. Earth Sci. 97, 865–881.

Jolivet, L., Rimmele, G., Oberhansli, R., Goffe, B., Candan, O., 2004. Correlation of syn-orogenic tectonic and metamorphic events in the Cyclades, the Lycian nappes and the Menderes massif. Geodynamic implications. Bull. Soc. Geol. Fr. 175, 217–238.

Kilias, A., Tranos, M.D., Orozco, M., Alonso-Chaves, F.M., Soto, J.I., 2002. Extensional collapse of the Hellenides: A review. Rev. la Soc. Geol. Espana 15, 129–139.

Kilias, A., Frisch, W., Avgerinas, A., Dunkl, I., Falalakis, G., Gawlick, H.-J., 2010. Alpine architecture and kinematics of deformation of the northern Pelagonian nappe pile in the Hellenides. Austrian J. Earth Sci. 103, 4–28.

Kilias, A., Falalakis, G., Sfeikos, A., Papadimitriou, E., Vamvaka, A., Gkarlaouni, C., 2013. The Thrace basin in the Rhodope province of NE Greece - A tertiary supradetachment basin and its geodynamic implications. Tectonophysics 595–596, 90–105.

Michail, M., Pipera, K., Koroneos, A., Kilias, A., Ntaflos, T., 2016. New perspectives on the origin and emplacement of the Late Jurassic Fanos granite, associated with an intra-oceanic subduction within the Neotethyan Axios-Vardar Ocean. Int. J. Earth Sci. 105, 1965–1983.

Papanikolaou, D., 2013. Tectonostratigraphic models of the Alpine terranes and subduction history of the Hellenides. Tectonophysics 595–596,

Robertson, A.H.F., 2012. Late Palaeozoic–Cenozoic tectonic development of Greece and Albania in the context of alternative reconstructions of Tethys in the Eastern Mediterranean region. Int. Geol. Rev. 54, 373–454.

15th International Congress of the Geological Society of Greece
Athens, 22-24 May, 2019 | Harokopio University of Athens, Greece
Bulletin of the Geological Society of Greece, Sp. Pub. 7 Ext. Abs. GSG2019-170

Dating the varnishes of active Petousi-Souli fault zone (Northwestern Greece) using Portable XRF

D. Ntokos[1,2], P. Ntokou[3]

(1) Department of Civil Engineering, School of Engineering, University of Thessaly, Pedion Areos, GR-38334, Volos, Greece, ntokos@uth.gr; dimitriosntokos@yahoo.gr
(2) Department of Geosciences, School of Mining and Metallurgical Engineering, National Technical University of Athens, Zografou Campus, GR-15780, Athens, Greece
(3) Department of Mathematics, School of Science, University of Ioannina, University Campus, GR-45110, Ioannina, Greece

In this paper, the dating of Petousi-Souli fault zone (PSFZ) is being studied through a chemical analysis of the rock varnishes which identified in the outer fault surface. Several attempts have been made to identify the ages of geological and tectonic phenomena that develop on the surface of the earth. Other times using absolute dating methods, such as Radiocarbon dating (^{14}C) and Luminescence dating, and others through the use of more qualitative analyzes which, although they lag behind in accuracy, outweigh the speed at which the result is obtained. Such a method is the dating from the observations and the chemical analysis of rock varnishes.

Methods

The methodology applied to determine the ages of Petousi-Souli fault zone is based on the chemical analysis of rock varnishes with the methods from Dorn (1983; Eq. 1) and the calibration of Nobbs and Dorn (1988; Eq. 2):

$$R_C = {(Ca^{2+} + K^{+})}/{Ti^{4+}} \quad (1)$$

where, Ca^{2+}: is the percentage concentration of Calcium (%), K^{+}: is the percentage concentration of Potassium (%), and Ti^{4+}: is the percentage concentration of Titanium (%).

$$T = e^{\frac{16.218 - R_C}{1.137}} \quad (2)$$

where, T: is time and R_C: is the cation-ratio, resulting from above equation (2).

It is a method that has been applied in many areas of the world and especially in petroglyphs, using either a Scanning Electron Microscope or Portable X-Ray Fluorescence. More specifically, in this study the chemical analysis was applied using the EDX POCKET III P730 - QUALITEST XRF mobile spectrometer.

Study Area

As the study area determined the PSFZ, which located on the central part of northwestern Greece (Fig. 1A). The PSFZ features one of its largest tectonic structures, of a total length of approximately 36.5 km, generally trending E-W, with a southern inclination. The Petousi-Souli fault zone constitutes the largest fault zone of northwestern Greece, while forming at the same time a natural boundary between its northern and southern part.

It is classified as active because of its intense morphology and the impressive surface trace consisting of well-preserved fault surfaces which has deep and well-marked striations and canellures (Fig. 1B and C).

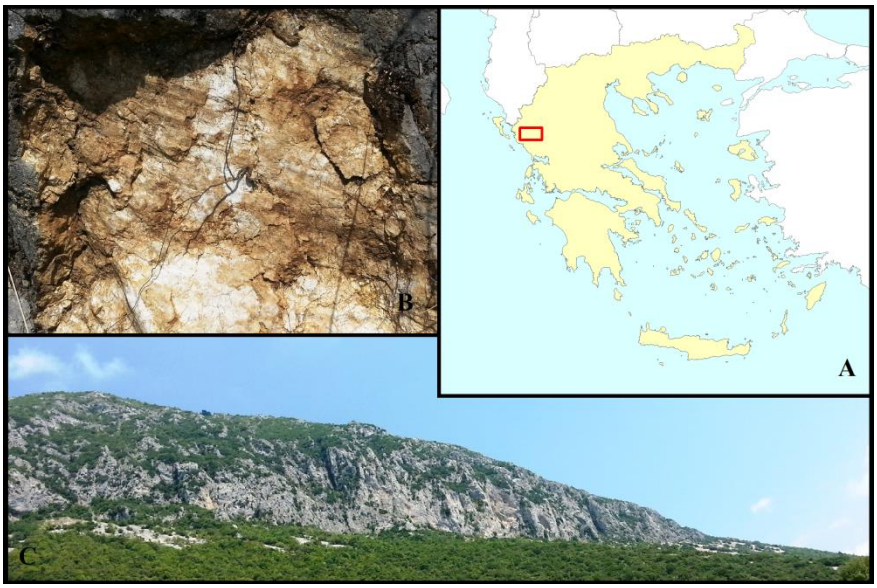

Figure 1. (A) Study area and (B and C) field photographs of the PSFZ surfaces in the area of Souli.

This tectonic structure has caused the displacement of pre-existing structures, such as the synclines and anticlines formed during the Alpine fold, as well as recent Quaternary deposits (Ntokos, 2017a, 2018a). It has affected the morphology and relief of a large area, while a typical example of the displacements it has caused can be found in the syncline structure of Voutsaras, which is transversely intersected in the middle, by the Petousi-Souli fault. The Voutsaras syncline seems to present a displacement in the order of 2 km to the east, while the displacements of the geological boundaries, along the length of the fault's trace, often exceed 4 km.

The western and eastern ends of the Petousi-Souli strike-slip active fault feature a series of minor normal and strike-slip active faults, running in a parallel direction to the orientation of the fault, whose high concentration is similar to an enechelon layout, which is typically observed in strike-slip zones. Observations show that this tectonic structure fans out into numerous smaller branches, typical in cases on strike-slip faults (imbricate fans). Since these faults are consistently oriented from E-W to NE-SW (right stepping faults) they may well constitute Riedel faults, which have impacted the sedimentary nappe and which are associated with a large-scale sinistral movement of the bedrock.

The impact and the tectonic regime, which created the Petousi-Souli strike-slip fault, has left its imprint throughout the area, where many minor faults, trending E-W were observed, as well as other faults, which are affected by the same regime that caused the rupture of the main fault, albeit developing in a different direction. A number of surfaces were detected; the nature however of the geological materials at their contact did not enable the identification of kinematic evidence, since their surfaces and tectonic striations have largely disintegrated due to erosion.

Results

Due to its well-preserved fault surfaces and the limited erosion effect, this tectonic structure is indicated to apply the R_C method. Specifically, by fieldwork, rock varnishes were found both in the Petousi-Souli segment, Agia Maura segment and in Saloniki ones. According to the methodology, calcium, titanium, and potassium cations were analyzed, and their concentration was determined in percentages at 21 sites. From these measurements using the Dorn's equation (1; 1983), the R_C ratio takes values between 2.1 and 110.1 corresponding to ages from 10.000 to 3.8 Ma years ago (Table 1).

Table 1. Distribution of the R_C ratio by fault and the varnish age based on the Nobbs and Dorn (1988).

Fault	R_C	Dating
Petousi-Souli	2.4 - 110.1	10,000 - 2.2 Ma
Agia Mavra	2.2 - 62.6	220,000 - 3 Ma
Saloniki	2.1 - 13.3	10,000 - 3.8 Ma

Discussion - Conclusions

Tectonic and geological observations made in the field, geomorphological features (Ntokos, 2018a), paleomagnetic data (Kissel *et al.*, 1985), paleoseismological data (Boccaletti *et al.*, 1997), and recent microseismicity records (Pavlides, Caputo, Zouros, Mountrakis and Boccaletti (1992), Tselentis *et al.*, 2006) all indicate recent fault activity. According to Boccaletti *et al.* (1997), over the last 30,000 years, at least three tectonic paleo-events are particularly associated with the Petousi-Souli Fault. Initial fault activation, based on recent tectonic geomorphological data on the evolution of northwestern Greece (Ntokos (2018a), dates to between the Miocene and Pliocene, which is similar to the rock varnish ages.

In addition, it is worth mentioning that in the Petousi-Souli Fault the dating of the rock varnishes gave better results compared to other areas, e.g. Arkitsa (Ntokos, 2019) and Epirus, Greece (Ntokos, 2018), where the same method was applied to faults due to the well-preserved fault surface, verifying the application of the method to tectonic structures.

References

Boccaletti, M., Caputo, R., Mountrakis, D., Pavlides, S., Zouros, N., 1997. Paleoseismicity of the Souli Fault, Epirus, Western Greece. Journal of Geodynamics, 24(1–4), 117–127.

Dorn, R.I., 1983. Cation-ratio dating: A new rock varnish age determination technique. Quaternary Research, 20, 49-73.

Kissel, C., Laj, C., Muller, C., 1985. Tertiary geodynamical evolution of northwestern Greece, Paleomagnetic results. Earth Planet. Sa. Lett, 72, 190-204.

Nobbs, M.F., Dorn, R.I., 1988. Age determinations for rock varnish formation within petroglyphs: cation-ratio dating of 24 motifs from the Olary region, South Australia. Rock Art Res., 5, 108-146.

Ntokos, D., 2018a. Formulation of the conceptual model for the tectonic geomorphological evolution of an area: five main rivers of Greece as a case study. CATENA, 167, 60-77.

Tselentis, G., Sokos, E., Martakis, N., Serpetsidaki, A., 2006. Seismicity and seismotectonics in Epirus, western Greece: results from a microearthquake survey. Bull. Seismol. Soc. Am., 96, 1706-1717.

Ntokos. D., 2019. Dating the varnishes of active Kamena Vourla - Arkitsa fault zone (Northwestern Evoikos Gulf, Central Greece) using Portable XRF. 7th International Conference on Coupled Thermo-Hydro-Mechanical-Chemical (THMC) Processes, University of Utrecht, Utrecht, Netherlands, 03-05 July 2019 (In press).

Ntokos, D., 2018b. Can cation-ratio dating of rock varnishes be applied in faults? 9th International Symposium on Eastern Mediterranean Geology, Akdeniz University, Antalya, Turkey, 07-11 May 2018, p. 221.

Ntokos, D., 2017a. Neotectonic - Geomorphological study of Epirus, Northwestern Greece and compiling of neotectonic map, by use of Geographic Information Systems. Ph.D. Thesis, National Technical University of Athens, Athens, 404 p. (In Greek).

15th International Congress of the Geological Society of Greece
Athens, 22-24 May, 2019 | Harokopio University of Athens, Greece
Bulletin of the Geological Society of Greece, Sp. Pub. 7 Ext. Abs. GSG2019-172

Mid-Miocene Strike Slip in Continental Greece

A. Faucher[1], F. Gueydan[1], M. Jolivet[2], M. Alsaif[1]

(1) Géosciences Montpellier, UMR5243CNRS, Université de Montpellier, rue Eugène Bataillon, 34095 Montpellier, France, agathe.faucher@umontpellier.fr
(2) Laboratoire Géosciences Rennes, CNRS-UMR6118, Université Rennes 1, avenue Général Leclerc, 35042, Rennes, France.

The Aegean system and Continental Greece are marked by back-arc extension that is commonly viewed as occurring in two stages: 1/ classical back-arc extension with N150 normal faults (e.g parallel to the trench) during miocene 2/ followed by mainly N50 dextral strike-slip (North Anatolian fault-NAF) with E-W normal faults (Gulf of Evvia and Corinth) since 5 Ma marking the impact of the NAF in the tectonic system (Armijo et *al*., 1999; Hubert-Ferrari et *al*., 2002). However, some published structural data in the Cyclades show that N50 dextral strike-slip were already active during mid-Miocene time (e.g. during granite intrusion between 15 and 10 Ma; Kokkalas and Aydin, 2013), questioning this classical view of the Aegean extension. In this study, we wish to constrain the potential activity of dextral strike slip faulting during Mid-Miocene in Continental Greece.

Geological Setting

Central Greece is characterized by the stacking of two units, from bottom to top: 1/ the Cycladic Unit made of HP rocks so-called the Cycladic Blueschist Unit (C.B.U) and 2/ the Pelagonian unit made of metasediment covered by Trias-Jurassic marble and limestone (Fig. 1). The boundary between these two terranes is characterized by the N50 Pelagonian fault (Xypolias et *al*., 2003). In order to constrain the potential mid-Miocene activity of N50 dextral faults and achieve our objective, we focus on Evvia, Attic and, Continental Greece, to understand the tectonic context of the deposition of two mid-Miocene basins 1/ in the south of Evvia and Attic which border the N50 Pelagonian fault and 2/ in the north of Evvia far from N50 structures. We complete field data with Apatite Fission track currently non-existent in the area.

Geological Data

The Northern Miocene basin shows N150 normal faults and late E-W normal faults. The major N150 faults are systematically associated with larger amount of sedimentation indicating syn-kinematical filling of the basin. This suggests N150 faulting during mid Miocene. Field arguments do not allow us to know the chronology of the appearance and activities of the E-W faults. However, they have the same orientations and characteristics as the normal faults bordering the Gulf of Corinth as well as the faults mapped by (Royden and Papanikolaou, 2011). These faults are therefore supposed to have been active since the Pliocene and are younger than the N150 faults.

The Southern Miocene basin is located near the roughly N50 Pelagonia fault between the Cycladic Blueschist Unit and the Pelagonian unit. The entire Mid-Miocene basin is located on Pelagonian rocks. It is bounded to the south by the Pelagonian fault and does not extend beyond it. This particular geometry shows an overlap of this basin by the fault that delimits it and indicates that it predates the functioning of the fault. However, the bedding in the basin are sub-horizontal, even close the fault, suggesting a deposition after the fault activity. Faults and folds analysis demonstrates the existence of a major dextral slip kinematic associated with this N50 fault. All these data allow us to argue for a dextral strike slip activity of the Pelagonian fault during mid Miocene time.

Apatite Fission Track Data

Times Samples for the apatite fission track (AFT) method were collected along a cross line perpendicular to the Pelagonian fault and along the N150 and N-E faults. This sampling logic aims to better constrain the large-scale deformation associated with the formation of the Miocene basin and to indirectly date the activity of the Pelagonian fault by comparing the Cycladic and Pelagonian AFT ages (AFT data in the Cyclades from Hejl et *al*., 2008, 2003; Ring et *al*., 2007). The study of AFT averages reveals a first tectonic event during the Oligocene to early Miocene (Fig. 1). This one stands out on the majority of the rocks imposing an event impacting the whole of Continental Greece important. Two sample (G11-G16) show younger mean age with a last stage of exhumation in the middle Miocene. These two samples are located on the hanging-wall of the N150 fault, allowing a dating of the activity of these faults at mid-Miocene time, an interpretation that is consistent with the findings from the basin analysis. These new data in Continental Greece highlight a major change in age distribution between the C.B.U. rocks exhumed during the Mio-Pliocene and the Oligo-Miocene Pelagonian rocks. This difference is attributed to a recent exhumation event affecting only the Cyclades at the end of the Miocene. From these results, we can hypothetise that the N50 Pelagonian fault was active since the mid-Miocene, as a major strike slip fault that potentially accommodate strain partitioning during back arc extension.

Discussion

This study provides new field and dating data allowing a better understanding of the evolution of Continental Greece since the Oligocene. It could be describe in three steps:

- A generalized extension over the entire Aegean domain in the Eo-Oligocene period, creating a first episode of slow exhumation of deep rocks followed by the formation of metamorphic Core Complex.
- A change in back-arc extension at mid Miocene time, implying the coeval activity of N50 dextral strike slip and N150

normal faults.

- A second change in back arc dynamics at 5Ma with the interplay between NAF and back arc extension and the formation of the Corinth and Evvia rifts system with E-W normal faults.

The origin of such strain partitioning during mid-Miocene time between N150 extensional fault and N50 dextral strike slip is most probably the interplay between the extension related to the retreat of the slab and the onset at around 15 Ma of westward extrusion of Anatolia.

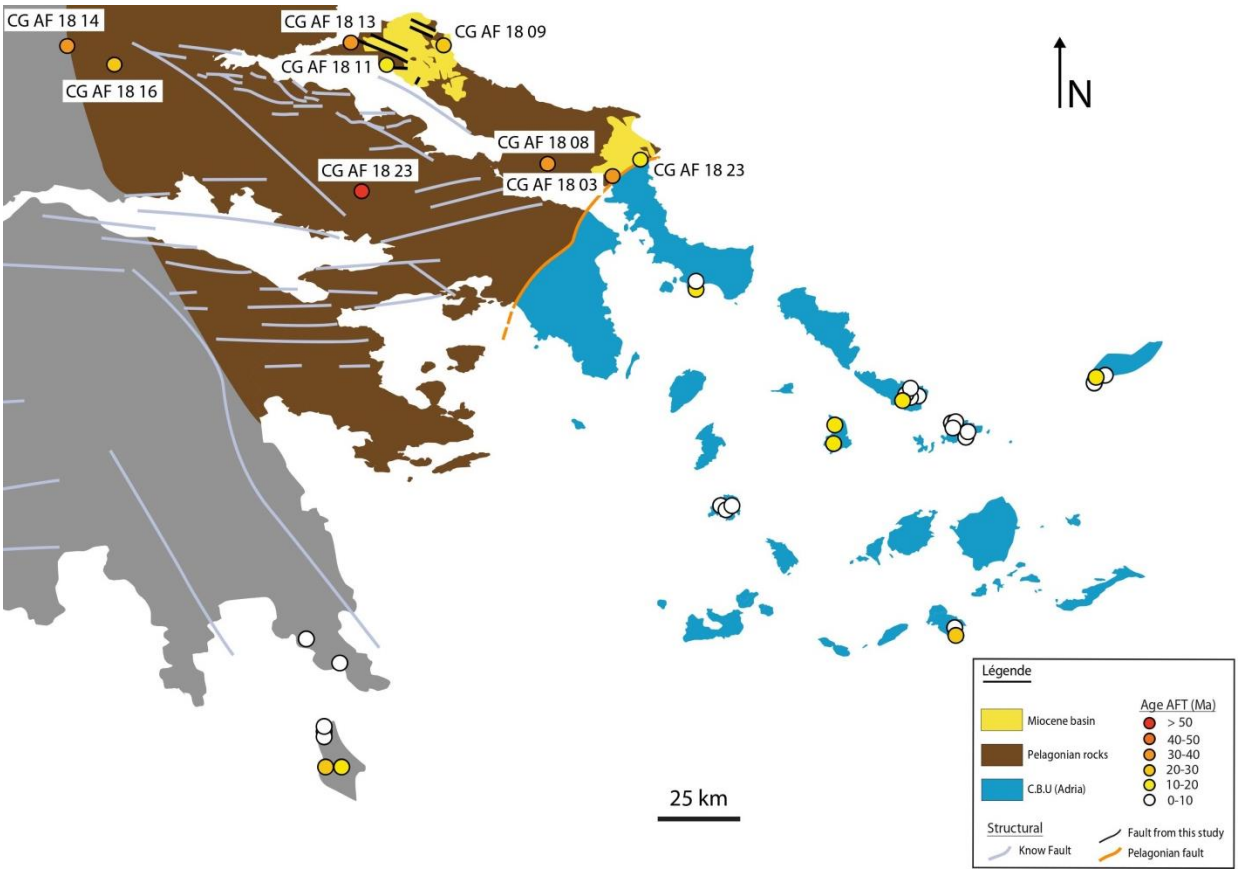

Figure 1. Geological Map of Greece with new structural (black line) and AFT data (circle in Continental Greece)

References

Armijo, R., Meyer, B., Hubert, A., Barka, A., 1999. Westward propagation of the North Anatolian fault into the northern Aegean: Timing and kinematics. Geology 27, 267. https://doi.org/10.1130/0091-7613(1999)027<0267:WPOTNA>2.3.CO;2

Hejl, E., de Grave, J., Riedl, H., Weingartner, H., Van den haute, P., 2008. Fission-track thermochronology of the Middle Aegean Island Bridge – implications for Neogene geomorphology and palaeogeography [Spaltspuren-Thermochronologie der Mittelägäischen Inselbrücke – ein Beitrag zur Kenntnis der geomorphologischen und paläogeografi schen Entwicklung während des Neogens.]. Zeitschrift der Deutschen Gesellschaft für Geowissenschaften 159, 495–512. https://doi.org/10.1127/1860-1804/2008/0159-0495

Hejl, E., Sekyra, G., Friedl, G., 2003. Fission-track dating of the south-eastern Bohemian massif (Waldviertel, Austria): thermochronology and long-term erosion. International Journal of Earth Sciences 92, 677–690. https://doi.org/10.1007/s00531-003-0342-y

Hubert-Ferrari, A., Armijo, R., King, G., Meyer, B., Barka, A., 2002. Morphology, displacement, and slip rates along the North Anatolian Fault, Turkey: THE NORTH ANATOLIAN FAULT. Journal of Geophysical Research: Solid Earth 107, ETG 9-1-ETG 9-33. https://doi.org/10.1029/2001JB000393

Kokkalas, S., Aydin, A., 2013. Is there a link between faulting and magmatism in the south-central Aegean Sea? Geological Magazine 150, 193–224. https://doi.org/10.1017/S0016756812000453

Ring, U., Glodny, J., Will, T., Thomson, S., 2007. An Oligocene extrusion wedge of blueschist-facies nappes on Evia, Aegean Sea, Greece: implications for the early exhumation of high-pressure rocks. Journal of the Geological Society 164, 637–652. https://doi.org/10.1144/0016-76492006-041

Royden, L.H., Papanikolaou, D.J., 2011. Slab segmentation and late Cenozoic disruption of the Hellenic arc: DISRUPTION OF THE HELLENIC ARC. Geochemistry, Geophysics, Geosystems 12, n/a-n/a. https://doi.org/10.1029/2010GC003280

Xypolias, P., Kokkalas, S., Skourlis, K., 2003. Upward extrusion and subsequent transpression as a possible mechanism for the exhumation of HP/LT rocks in Evia Island (Aegean Sea, Greece). Journal of Geodynamics 35, 303–332. https://doi.org/10.1016/S0264-3707(02)00131-X

15th International Congress of the Geological Society of Greece
Athens, 22-24 May, 2019 | Harokopio University of Athens, Greece
Bulletin of the Geological Society of Greece, Sp. Pub. 7 Ext. Abs. GSG2019-208

Active Faults and Seismic Hazard Assessment at the Mygdonia, Strymon and Drama Basins, Northern Greece, based on Paleoseismic Trenching and Radiometric Dating

I. Papanikolaou[1], G. Deligiannakis[1], P. Dafnis[2], J. Hengesh[3], A. Panagopoulos[2], E. Lymperis[4]

(1) Mineralogy-Geology Laboratory, Department of Natural Resources Development and Agricultural Engineering, Agricultural University of Athens, 75 Iera Odos Str., 118-55 Athens, Greece. Email: i.pap@aua.gr
(2) Geoskopio SA – EDAFOMICHANIKI GROUP, 19 Emmanouil Papadaki Str., 141 21 N. Iraklio, Greece
(3) Interface Geohazard Consulting LLC, 20 Plumeria Pl., Lahaina, HI 96761 USA
(4) Edafos Engineering Consultants SA, 9 Iperidou Str, 10558 Athens, Greece

Introduction

The NW–SE trending fault-bounded Axios, Mygdonia, Strymon and Drama basins dominate the Central and Eastern Macedonia landscape and geological structure (Mercier et al. 1989, Mountrakis *et al.*, 2006, Tranos 2011). They were formed during the Late Miocene to Pliocene NE–SW directed extensional stresses, which primarily activated NW–SE striking normal faults. Since the Quaternary the stress field has changed and is now dominated by N-S extension, resulting to the formation of E-W trending normal faults, reshaping the pre-existing basins (e.g. Lyberis 1984, Pavlides & Kilias 1987). Isoseismal data from past earthquakes indicate that both the NW-SE faults (e.g. 1902 M=6.6 Assiros and 1932 M=7.0 Ierrisos earthquakes) and the E-W trending faults (e.g. 1932 M=6.2 Sochos and 1978 M=6.5 Volvi earthquakes) are active (Papazachos *et al.*, 1979, Voidomatis *et al.*, 1990). Limited paleoseismic investigations have been carried out along some of the E-W oriented fault zones in northern Greece (e.g. Chatzipetros *et al.*, 2005), yet none have previously applied on the NW-SE oriented fault zones in this region.

4 paleoseismic studies were carried out to assess the location, geometry, kinematics, and past surface displacements of the NW-SE trending Symvoli-Fotolivos (SFFZ – Drama Basin), Tholos-Nea Zichni fault zone (TNFZ – Strymon Basin), Assiros Krithia fault (ASFZ – Mygdonia Basin) and Drymos fault zone (DRFZ – Mygdonia Basin) (Figure 1).

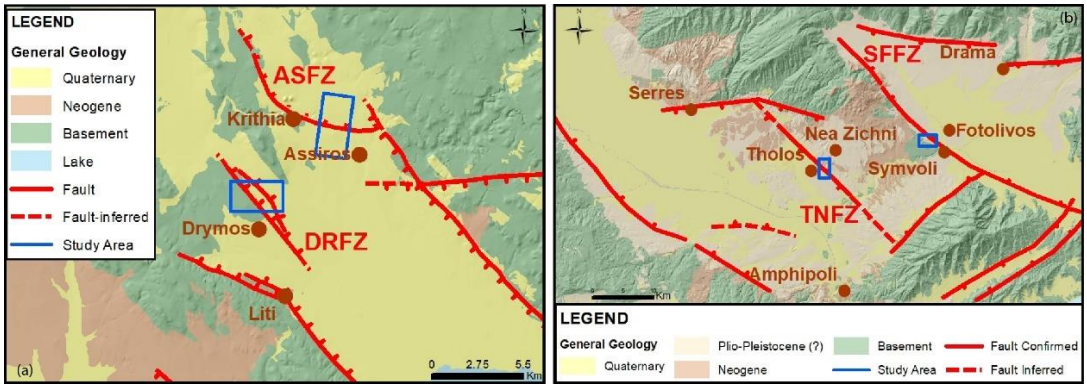

Figure 1. Simplified geological map showing the main faults of the Mygdonia basin (a) and Drama and Strymon Basins (b).

Methodology

The largest paleoseismic study has been performed in Northern Greece in order to assess whether NW-SE trending basin bounding faults are Holocene active with important implications in seismic hazard assessment. Kinematics and past surface displacements associated with these fault traces were assessed by detailed geomorphological, geological and paleoseismic trench investigations. For the SFFZ a 221 m long and 3 m deep trench was excavated, while for the TNFZ the trench was 153 m long and 1.5 - 3 m deep. Paleoseismic observations for ASFZ and DRFZ were performed along targeted sections of an existing 3 m deep, two-side sloped construction trench. All trenches were cleaned, gridded, photographed, georeferenced and logged. Samples also were collected for radiocarbon dating where evidence for active faulting was found.

Results & Discussion

The SFFZ has a segment length of 32 km and yields an average magnitude value of Mw=6.61. 2 events are inferred with vertical displacements of 66 cm (penultimate event ~11350±40 BP) and 75 cm (most recent event ~5620 ± 30 BP) implying an approximate 0.12 mm/yr throw-rate and 0.14 mm/yr slip-rate, respectively (Figure 2). Geological and geomorphological data for TNFZ strongly support a 15 km long fault segment, which represents the preferred rupture scenario. Radiometric dating provides limiting ages of surface displacements along a synthetic fault plane about 4950 ± 30 years ago, and along an antithetic fault plane about 2840 ± 30 to 6300 ± 30 years ago. As a result, 1 or 2 events appear to have occurred along this fault in the past 6300 years, implying slip-rate of 0.20 ± 0.1 mm/yr, with recurrence intervals of ~3000 yrs (Figure 3).

Holocene deformation occurred along both the ASFZ and DRFZ. 2 events have occurred in ASFZ, around 4540 and 7900 years BP. The total displacement over the last 7900 years is 121 cm, implying a 0.15 mm/yr slip-rate, with a recurrence interval of 3360 yrs. The DRFZ is an 8 to 10 km long structure with a slip-rate on the order of 0.1-0.3 mm/yr. The fault could produce average displacements of 13 to 28 cm and maximum displacements of 24 cm to 40 cm. We interpreted 3 possible paleo-events with vertical displacements exceeding 40 cm, implying a possible multi-segment rupture scenario involvinh the Gerakarou-Liti fault zone, which is parallel to DRFZ with a step over of only 2 km. The DRFZ is characterized by distributed deformation with 8 major and secondary fault planes observed at four different sites (T1-T4) across the trench. Dating results confirm that 4 of these fault planes have produced displacements between approximately 4000 and 9000 ybp (Figure 4).

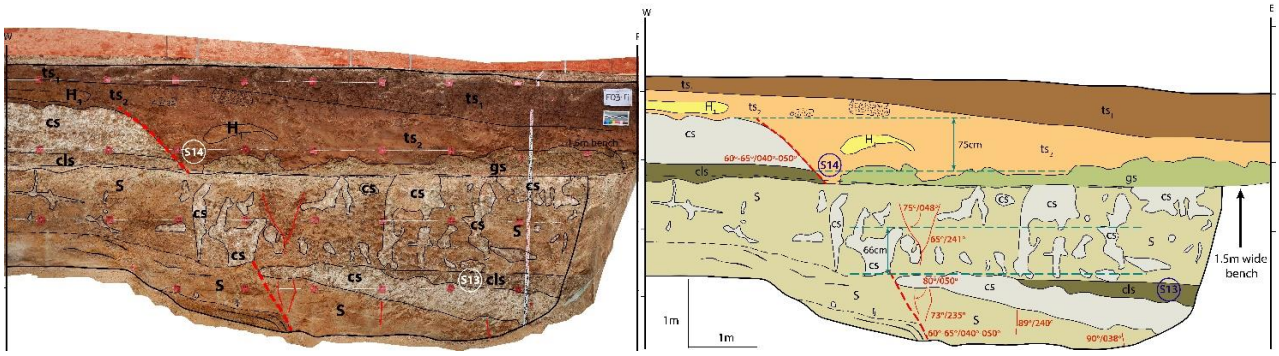

Figure 2. Left: Orthomosaic of the 9m long active fault area (from 212 up to 221m) of the SFFZ trench. Right: Two events are inferred with 75 cm (most recent) and 66 cm (penultimate) of vertical displacement. Sampling locations shown inside circles.

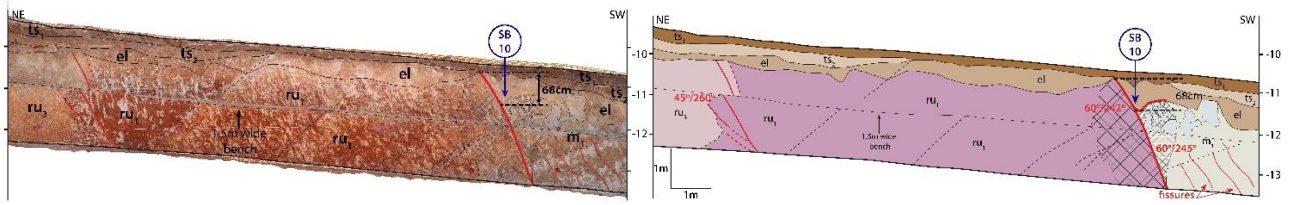

Figure 3. Left: Orthomosaic of the TNFZ trench from 109 to 123 m, showing the main fault plane. Right: Final logging, depicting all major boundaries, trench stratigraphy, displacement scenario and sampling locations for radiocarbon dating.

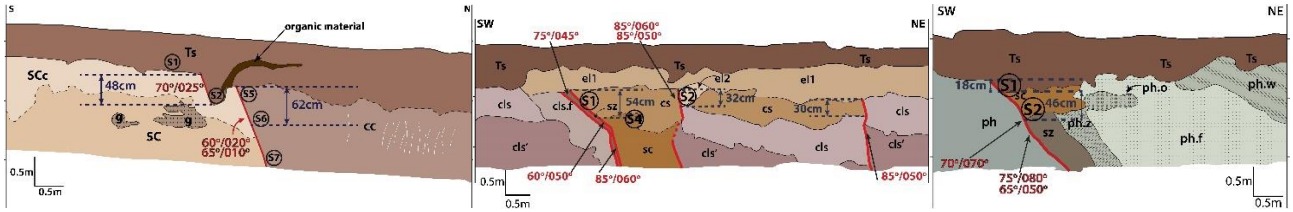

Figure 4. Left: Interpretation of the ASFZ trench with 2 inferred events. Middle: Interpretation of section T1 of DRFZ with 3 inferred events. Right: Interpretation of section T4 of DRFZ with 2 inferred events.

Acknowledgements

We would like to thank all personnel involved to excavating and cleaning these trenches.

References

Chatzipetros, A., Kokkalas, S., Pavlides, S., Koukouvelas, I., 2005. Palaeoseismic data and their implication for active deformation in Greece. Journal of Geodynamics 40, 170-188.

Lyberis, N., 1984. Tectonic evolution of the North Aegean trough. Geological Society of London, Special Publications 17, 709-725.

Mercier, J.-L., Simeakis, K., Sorel, D., Vergély, P., 1989. Extensional tectonic regimes in the Aegean basins during the Cenozoic. Basin Research 2, 49–71.

Mountrakis, D., Tranos, M., Papazachos, C., Thomaidou, E., Karagianni, E., Vamvakaris, D., 2006. New neotectonic and seismological data about the main active faults and stress regime of Northern Greece. Geological Society of London, Sp. Publications 260, 649–670.

Papazachos, B., Mountrakis, D., Psilovikos, A., Leventakis, G. 1979. Surface fault traces and fault plane solutions of the May-June 1978 major shocks in the Thessaloniki area, Greece. Tectonophysics 53, 171-183.

Pavlidis, S.B., Kilias, A.A.,1987. Neotectonic and active faults along the Servomacedonian zone (SE Chalkidiki, northern Greece). Ann. Tecton. I 2, 9–104.

Tranos, M.D., 2011. Strymon and Strymonikos Gulf basins (Northern Greece): Implications on their formation and evolution from faulting. Journal of Geodynamics 51, 285–305.

Voidomatis Ph.S, Pavlides S.B., G.A. Papadopoulos 1990. Active deformation and seismic potential in the Serbomacedonian zone, northern Greece. Tectonophysics 179, 1-9.

15th International Congress of the Geological Society of Greece
Athens, 22-24 May, 2019 | Harokopio University of Athens, Greece
Bulletin of the Geological Society of Greece, Sp. Pub. 7 Ext. Abs. GSG2019-218

Carbonate -platform Basin systems evolved through compression tectonics: Examples from the Mediterranean region

N.Papadimitriou[1,2], C. Gorini[2], V. Kosmidou[1], Y. Bassias[1]

(1) Hellenic Hydrocarbon Resources Management S.A.
(2) iSTEP, UMR 7193, UPMC, F-75005 Paris (France)

Carbonate platforms have been a subject of research for more than twenty years. Much research work has focused on the effects that sea-level change, oceanographic factors and climate have on carbonate platform stratigraphic characteristics. In this contribution we aim to better understand the tectonostratigraphy of Carbonate platforms by showing examples from the eastern (Levant Basin) and the western Mediterranean (Offshore Greece; Papadimitriou et al., 2018). In particular, we propose that by comparing the evolution and the geometries of carbonate platform we can have a better of Carbonate platform basin systems.

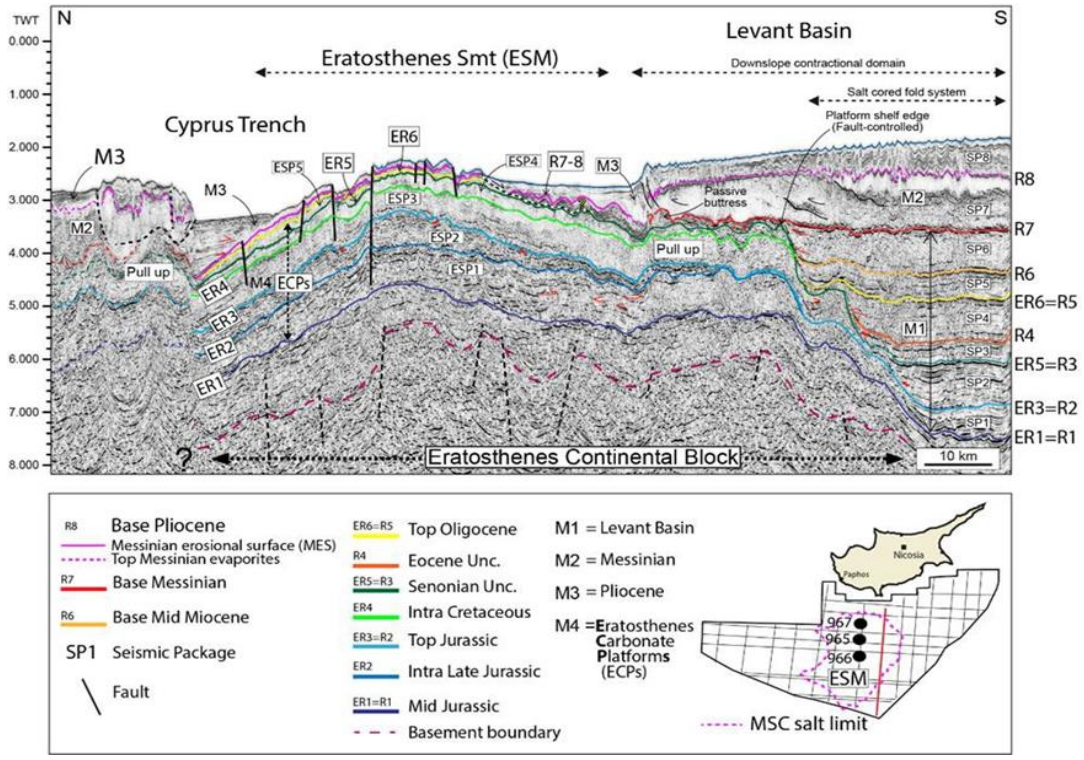

Figure 1: Interpreted seismic profile that intersects the Eratosthenes Seamount and illustrates the four mega-sequences (M1-M4) and the main seismic boundaries identified in the western part of the Levant Basin.

Four carbonate platforms (three Mesozoic and one Cenozoic) separated by main seismic surfaces have been identified on top of a basement high at the western margin of the Levant and western Greece (Figs. 1 and 2). The main seismic boundaries identified on top of carbonate platforms refer to erosional truncations, major flooding surfaces, downlap surfaces and slope onlap surfaces, whereas the seismic sequences in the deep basin are marked only by flooding and geometric unconformities (marine onlaps).

The Tethyan Carbonate platform shows a lot of differences. For instance, to the east the Egyptian and the Levant platforms were invaded by terrigenous siliciclastics during the Jurassic- Cretaceous interval (Fig 3; Hawie et al., 2013; Tassy et al., 2015a). In contrast, the Eratosthenes and Apulia platforms located in a long distance from the continent were free from the continental influence (Fig. 3; Borgomano, 2000). Finally, the Mesozoic carbonate pile within the Cretan margin, is more likely associated to the Gavrovo-Tripolitza carbonate platform, which is well- known from studies in western Greece showing reservoirs in Early Jurassic and Cretaceous limestones. The seismic interpretation offshore Crete shows isolated carbonate buildups which appeared beneath the Messinian salt.

The Tethyan carbonate platforms seem have been developed on basements highs. The position of basement-high is controlled by structures inherited from the Tethyan rifting (i.e., transform faults and a different crustal thickness between the Eratosthenes Seamount and the Levant Basin; Sagy et al., 2015; Granot 2016). Furthermore, the distance of the paleo-relief from the continent has a fundamental role in the evolution of a carbonate platform. For instance, these platforms have either been isolated (e.g., Apulia platform) or attached to the continent (Levant and Egyptian platforms).

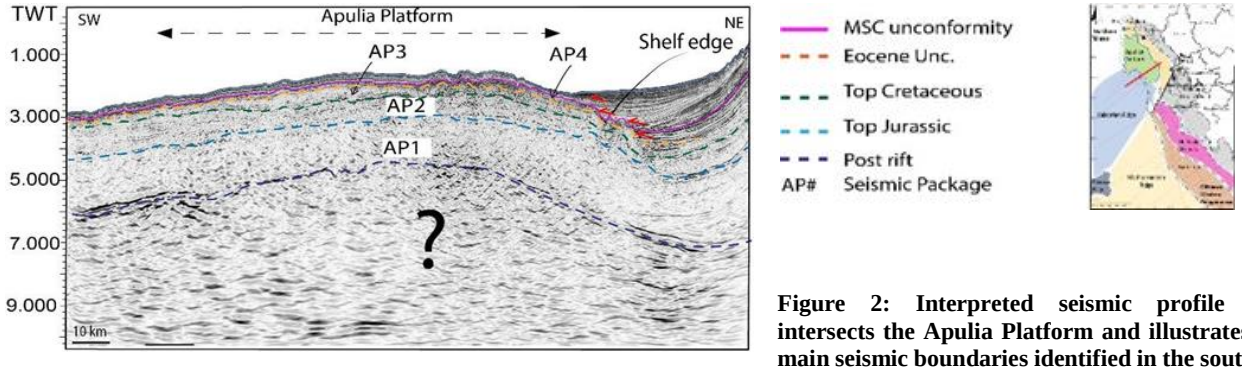

Figure 2: Interpreted seismic profile that intersects the Apulia Platform and illustrates the main seismic boundaries identified in the southern Part of Hellenides thrust belt.

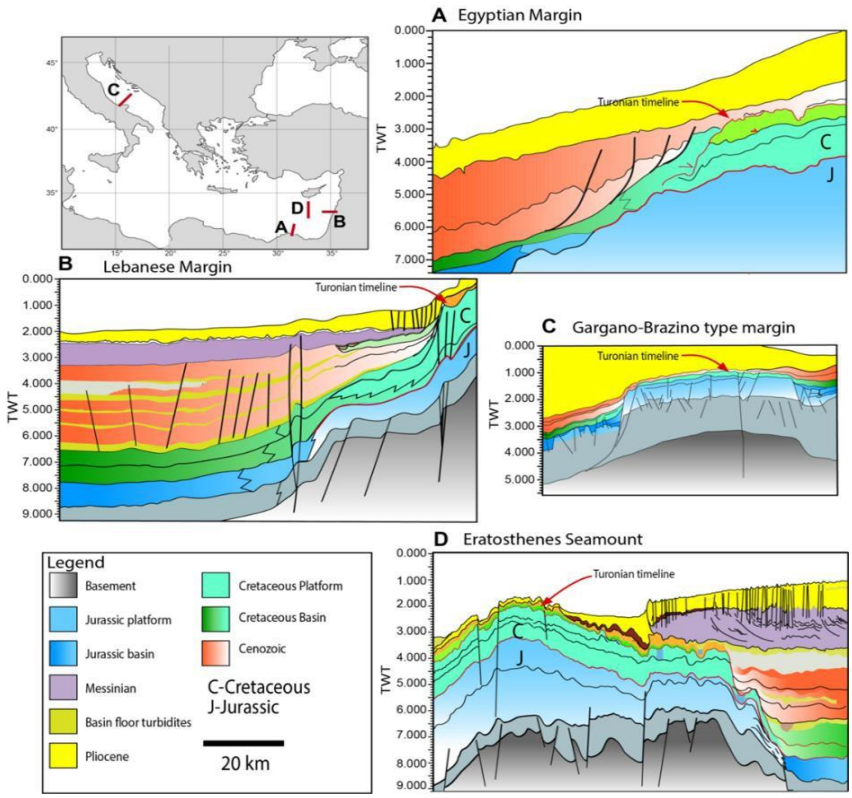

Figure 3: Seismic profiles of four Tethyan carbonate platforms: (A) Egyptian margin (Tassy et al., 2015a); (B) Lebanese margin (Hawie et al., 2013); (C) Apulia platform (Santantonio et al., 2013); (D) Eratosthenes carbonate platform.

Despite their differences, the Tethyan carbonate platforms show some similarities. They were all drowned during the Late Cretaceous. The drowning of the carbonate platforms coincided with the global reorganization of the oceans depicting that the demise and the onset of the carbonate factory are depended on the global sea level changes in response to long-term, deep processes such as rifting collision and not only by the eustatism (Robertson, 1998).

Hence, this study can be used as a paradigm for further understanding of the predominant factors that control carbonate factories for other Carbonate platforms that can be found in the region.

References

Borgomano, J., 2000. The Upper Cretaceous carbonates of the Gargano-Murge region, southern Italy: A model of platform-to-basin transition. AAPG Bulletin, 84, pp. 1561-1588

Hawie, N., Gorini, C., Deschamps, R., Nader, F. H., Montadert, L., Granjeon, D. and Baudin, F., 2013. Tectono-stratigraphic evolution of the northern Levant Basin (offshore Lebanon), Marine and Petroleum Geology. Elsevier Ltd, 48, pp. 392–410. doi: 10.1016/j.marpetgeo.2013.08.004.

Papadimitriou, N, C. Gorini, F.H. Nader, R. Deschamps, V. Symeou, J.C. Lecomte, 2018. Tectono- stratigraphic evolution of the western margin of the Levant Basin (offshore Cyprus), Marine and Petroleum Geology, 91, 683-705, ISSN 0264-8172, https://doi.org/10.1016/j.marpetgeo.2018.02.006.

Robertson, A. H. F., 1998. Tectonic significance of the Eratosthenes Seamount: A continental fragment in the process of collision with a subduction zone in the eastern Mediterranean (Ocean Drilling Program Leg 160), Tectonophysics, 298(1–3), 63–82. doi: 10.1016/S0040-1951(98)00178-4.

Sagy, Y., Gvirtzman, Z., Reshef, M. and Makovsky, Y., 2015. The enigma of the Jonah high in the middle of the Levant basin and its significance to the history of rifting', Tectonophysics. Elsevier B.V., 665, 186–198.

Santantonio, M., Scrocca, D. and Lipparini, L., 2013. The Ombrina-Rospo Plateau (Apulian Platform): Evolution of a Carbonate Platform and its Margins during the Jurassic and Cretaceous. Marine and Petroleum Geology, 42, pp.4–29.

Tassy, A., Crouzy, E., Gorini, C., Rubino, J. L., Bouroullec, J. L. and Sapin, F., 2015. Egyptian Tethyan margin in the Mesozoic: Evolution of a mixed carbonate-siliciclastic shelf edge (from Western Desert to Sinai), MPG, pp, .565–581.

15th International Congress of the Geological Society of Greece
Athens, 22-24 May, 2019 | Harokopio University of Athens, Greece
Bulletin of the Geological Society of Greece, Sp. Pub. 7 Ext. Abs. GSG2019-226

Seismic Character as a Tool to Identify Different Geotectonic Zones in the Frontier Area Offshore South of Crete, Greece

K. Oikonomopoulos[1], G. Makrodimitras[1], N. Papadimitriou[1], Y. Bassias[1]

(1) Hellenic Hydrocarbon Resources Management SA (HHRM SA), Dim. Margari 18, Athens, Greece, k.oikonomopoulos@greekhydrocarbons.gr

Abstract

Although the geotectonic zones in western Greece are clearly thrusted on top of each other from east to west, in Crete these nappes are piled up cropping out thanks to tectonic windows. In western Greece, the Ionian islands provide a lot of information with regards to the most external parts of the Hellenides Thrust-and-Fold Belt (TFB). In addition, several wells and a dense seismic grid confirm the geological knowledge of the area and mitigate the uncertainty about the petroleum system there. In contrast, the area south of Crete includes only four (4) very small islands providing scattered information of the geological setting in the Cretan margin, along with a sparse seismic grid and the lack of wells.

Despite more than forty (40) years of geological and geophysical work in the region, the geodynamic and tectonic processes have been debatable and controversial. An initial attempt to distinguish and outline the geotectonic zones present in the area south of the island of Crete has been done based on the integration of seismic data and onshore geology. However, because of the above-mentioned limitations the attempt remains speculative.

The use of the seismic data allowed for a more accurate mapping of the three (3) distinct geological areas south of Crete; Cretan margin, Backstop and Mediterranean Ridge. The Cretan margin includes stacked nappes similar to those onshore Crete, the Backstop includes probably the most external Hellenides, while the Mediterranean Ridge cannot be assigned to any of the known Hellenides.

Introduction

Following the convergence between the African and Eurasian plate, which initiated in the Late Jurassic, successive orogenic belts were produced. The orogenic systems of the Hellenides which are a segment of the Alpine Orogenic Belt developed along the European active margin. In particular, on the island of Crete a stack of five (5) tectonic units are related to the Hellenides. There are two (2) sets of nappes according to their position and metamorphism which are separated by a low-angle detachment fault. These two (2) sets are: the lower metamorphic set of nappes, consisting of clastic Phyllites-Quartzites together with the carbonate para-autochthonous Plattenkalk unit and the upper non-metamorphic set consisting of Tripolitza, Pindos and the uppermost nappes.

Previous studies have shown that the Cretan margin is bound to the north by the Cretan coastline and by Ptolemy trough to the southwest and the Pliny trough to the southeast, while the Backstop extends from the Pliny trough to the overthrusted Mediterranean Ridge (Huguen et al., 2001).

Results

This study used seismic data, acquired by Petroleum Geo-Services (PGS) in 2012 and the reprocessed legacy data integrated with the onshore geology of Crete (Fig. 1). Comparison of the seismic characters from Crete and western Greece led to the following results as is shown in Fig. 2 and Table 1:

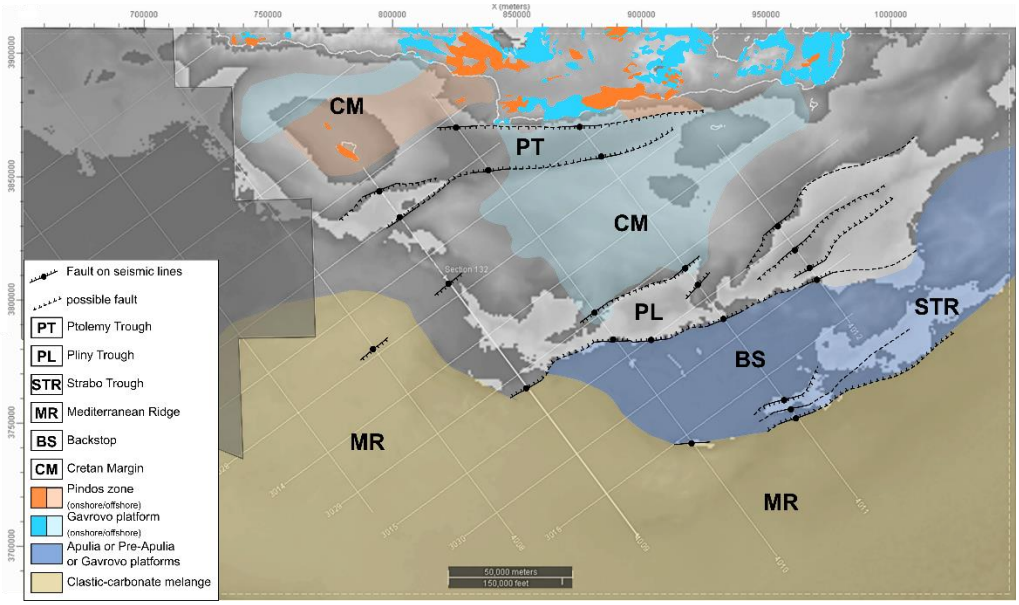

Figure 1: Geotectonic zones and geomorphological elements south of Crete.

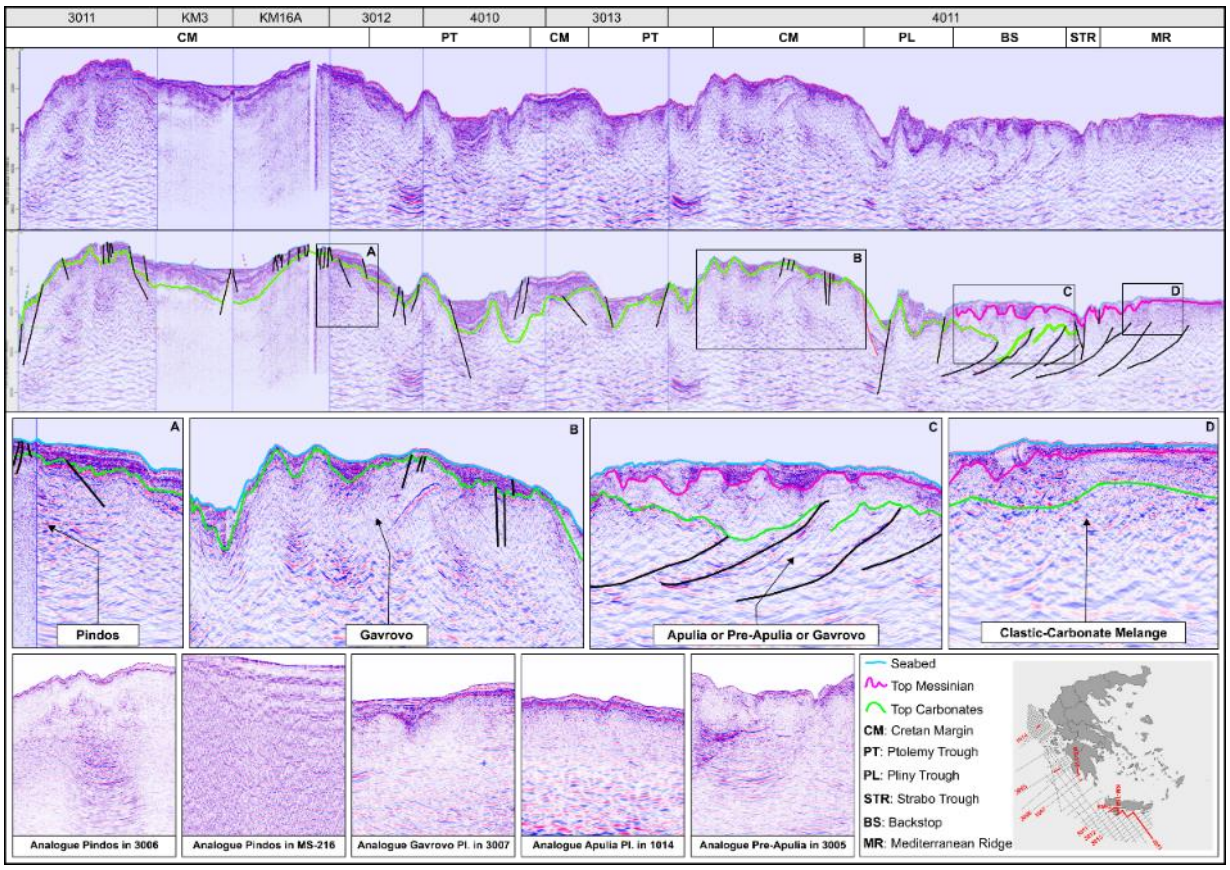

Figure 2: Seismic character of the geotectonic zones south of Crete compared to data from offshore western Greece.

Table 1. Seismic character identified in the distinct geological areas south of Crete.

South of Crete geological units		Cretan Margin		Backstop	Mediterranean Ridge
		West	East		
Pleistocene	Amplitude	High	High	High	High
	Frequency	High	High	High	High
	Continuity	Continuous	Continuous	Continuous	Continuous to discontinuous
Messinian-Pliocene	Amplitude	High	High	Low	Low to High
	Frequency	High	High	Low	Low to High
	Continuity	Continuous	Continuous	Transparent	Chaotic
Pre-Messinian	Amplitude	High	High	N/A	**
	Frequency	High	High	N/A	**
	Continuity	Continuous to discontinuous	Continuous to discontinuous	N/A	**
Carbonate*	Amplitude	Low	High	Locally High	Low
	Frequency	Low	Continuous to discontinuous	Low	Low
	Continuity	Transparent discontinuous	Transparent continuous to discontinuous	Chaotic to transparent	Chaotic

**The Mediterranean Ridge cannot be assigned to any known Hellenides zone. Mud volcanoes studies indicate a clastic/carbonate melange (Akhmanov et al., 2003) and perhaps Cretaceous to Pleistocene sediments according to Chaumillon et al. (1996).*

***Pre-Messinian series cannot be found in available seismic data, however it has been described by Akhmanov et al. (2003).*

References

Akhmanov, G. G., I. Premoli Silva, E. Ebra and M. B. Cita, 2003, Sedimentary succession and evolution of the Mediterranean Ridge western sector as derived from lithology of mud breccia clasts: Marine Geology, v. 195, no. 1-4, p. 277-299.

Chaumillon, E., J. Mascle and H., J., Hofmann, 1996, Deformation of the western Mediterranean Ridge: Importance of Messinian evaporitic formations: Tectonophysics, v. 263, p. 162-190.

Huguen, C., J. Mascle, E. Chaumillon, J. Woodside, J Benkhelil, A. Kopf, and A. Volkonskaya, 2001, Deformational styles of the Eastern Mediterranean Ridge and surrounding from combined swath mapping and seismic reflection profiling: Tectonophysics, v 343, p. 21-47.

15th International Congress of the Geological Society of Greece
Athens, 22-24 May, 2019 | Harokopio University of Athens, Greece
Bulletin of the Geological Society of Greece, Sp. Pub. 7 Ext. Abs. GSG2019-238

Interaction of Strike-Slip Faulting and Salt Wall Formation in the Katakolo area, NW Peloponnese, Greece

L. Gouliotis[1], G. Panagopoulos[1], K. Nikolaou[1], D. Anestoudis[1]
(1) Energean Oil and Gas S.A., Athens Greece, lgouliotis@energean.com

In this paper we integrate offshore and onshore data from the Katakolo area, NW Peloponnese, Greece, in order to examine the interaction of strike slip faulting and salt diapirism. Reprocessing of the legacy 3D seismic data in the offshore area show that the previously identified salt diapir (Monopolis & Armoutidis, 1983) is a narrow, elongated NNE-SSW to N-S trending salt wall that penetrates the Plio-Quaternary sedimentary rocks (Figure 1). The overburden adjacent to the salt structure is deformed by a series of NE-SW striking conjugate extensional faults. The later, close to the salt wall display a progressive ~20°-30° counter-clockwise rotation resulting in NNE-SSW strike which is consistent with a dextral shearing. Some faults show growth strata and listric geometry, while other are planar domino-style normal faults that root into deeper faults and the alpine rocks of the Ionian unit (Figure 1). In order to trace the northward continuation of the offshore faults we performed geological mapping in 1:5.000 scale at the Katakolo peninsula. We mapped two formations: i) The lower "Vounargos" formation and ii) the upper "Katakolo" formation (Streif, 1980). The contact between them is marked by an angular unconformity that can be nicely observed in the western part of the peninsula. The unconformity dips to the west-southwest and is submerged at the southern and southwestern part. The overall geometry of the Plio-Quaternary rocks shows that the whole peninsula is a fault block, tilted to the west-southwest and is bounded by a NNE-SSW trending fault at the southern part and an N-S trending fault at the eastern. Along these faults thermogenic gas seepages indicate connection with a deeper salt structure. Systematic fracture analysis on omnipresent extensional fracture sets from the Katakolo formation resulted in the calculation of the minimum horizontal stress that has a NW-SE strike, consistent with extension within a NNE-SSW trending dextral shear zone. From the geometry and the faulting pattern of the Plio-Quaternary sedimentary rocks in the offshore and onshore Katakolo, we conclude that the salt wall is supported by a deeper feeder and is formed along an active strike slip zone.

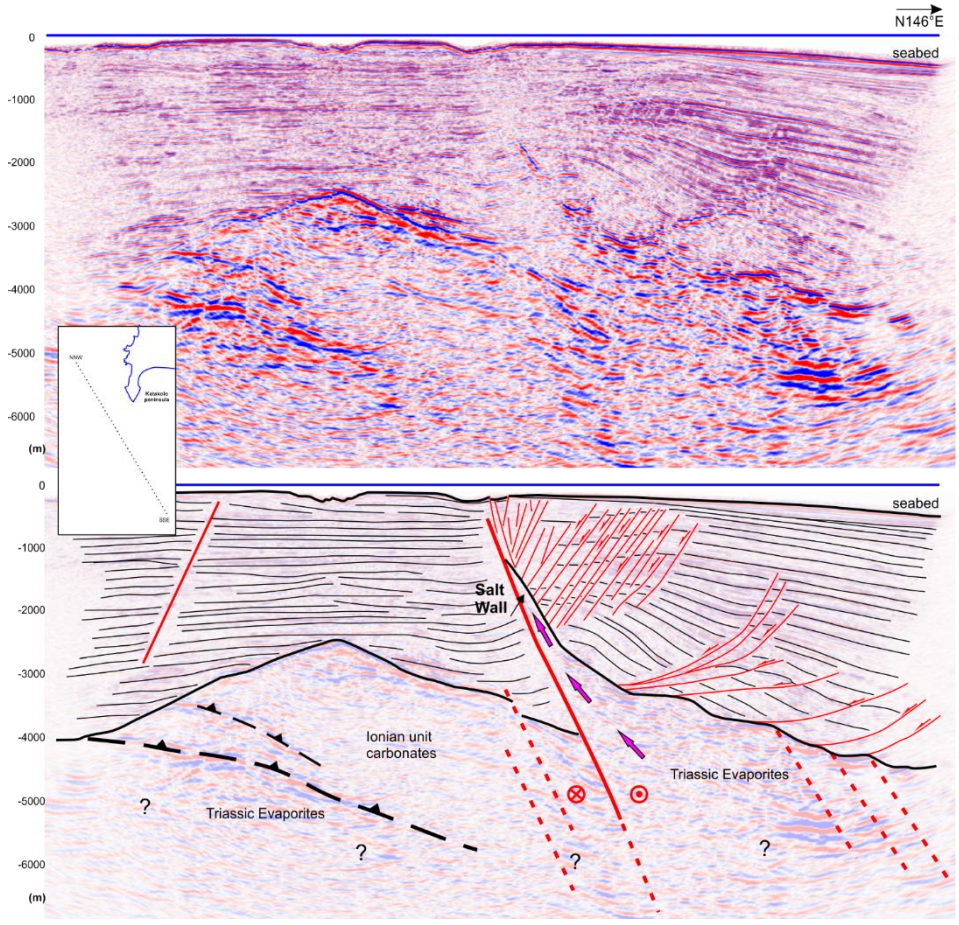

Figure 1. Seismic section (top) and Seismic interpretation (bottom) of the reprocessed pre-stack depth migrated (PSDM) legacy 3D seismic data from the offshore Katakolo area. 1) Dashed black lines - Early/Middle Miocene thrusts, 2) Solid thick black lines - Top of the alpine rocks of the Ionian unit, 3) Solid and dashed red lines – Plio-Quaternary faults and inferred continuation.

References

Monopolis, D., & Armoutidis, Ch., 1983. Evaluation of the Gas-Oil Field "West Katakolo", Provisional Geological Report, Public Petroleum Corporation of Greece S.A., Athens, Greece.

Streif, H., 1980. Geological map of Greece, scale 1:50 000, Pyrgos sheet, Institute of Geology and Mineral Exploration, Athens, Greece.

15th International Congress of the Geological Society of Greece
Athens, 22-24 May, 2019 | Harokopio University of Athens, Greece
Bulletin of the Geological Society of Greece, Sp. Pub. 7 Ext. Abs. GSG2019-303

Absolute Dating of Neotectonic Events: A Feasibility Study on Gouge Material from the Nojima and Asano Faults, NW Awaji Island, Japan

E. Tsakalos[1], A. Lin[2], M. Kazantzaki[1] Y. Bassiakos[1], E. Filippaki[1] T. Nishiwaki[2]

(1) Laboratory of Luminescence dating, Institute of Nanoscience and Nanotechnology, National Centre for Scientific Research, N.C.S.R. "Demokritos", Aghia Paraskevi, Athens 153 10, Greece, e.tsakalos@inn.demokritos.gr
(2) Department of Geophysics, Division of Earth and Planetary Sciences, Graduate School of Science, Kyoto University, Kyoto 606-8502, Japan

Determining the absolute age of the past faulting activity is crucial for assessing seismic hazards in a particular area. Historical records can be used for such purposes, however they only provide a relatively recent picture of fault activity, which is generally inadequate for drawing concrete conclusions on the seismicity of an area. As such, geochronology approaches try to address this problem using appropriate dating techniques on earthquake-disturbed materials prior to the time of recorded information.

The employment of the luminescence dating techniques is now widely applied to variety of materials and sedimentary environments (e.g., quartz and feldspar from heated archaeological material, sand-dunes and fluvial sediments), their application however on fault-deformed materials still limited, since full resetting (due to mechanical crushing/sliding or frictional heat) of their luminescence signal, during a rupture event, cannot be easily established (e.g., Toyoda et al., 2000), but also due to the limited access to appropriate material (e.g., fault gouges; crushed and ground-up rock produced by friction between the two sides when a fault moves). No systematic effort has been made up to now on the use of luminescence in directly dating material from the brittle zone of a fault which is related to faulting or the earthquake event.

To this end, the current study explore the use of both Isothermal Thermoluminescence (ITL) and Optically Stimulated Luminescence (OSL) to date past seismic deformed features which are directly linked to past seismic events and develop detailed protocols and methodological approaches on the use of the two techniques, so that the long-term temporal behavior of seismically active faults could be realistically evaluated and modeled. This work is part of a feasibility study using fault gouge and breccia material acquired from a drilled core of the Nojima Fault Zone, as well from an exposed outcrop of the Asano Fault, which belong in one of the most active fault systems in southwest Japan (Research Group For Active Faults of Japan, 1991). Our approach is based on an enhanced chronological model which builds on the earlier set of luminescence ages on quartz and feldspar produced by Tsakalos et al. (2018).

Microstructural observations on the Nojima Fault core revealed that the fault gouge zone is made of thin layers (mm to cm) of different colour, with each layers most probably corresponding at least to one seismic slip event (Lin and Nishiwaki, 2019). Thus, to assess the age of the gouge layers, we tried to sample each one individually. As for the Asano Fault, sampling was achieved by hammering steel cylinders in an exposed gouge formation. In the case of Asano, gouge layering was not very clear and thus collected sub-samples most probably contained several gouge layers. Intercalated breccia samples were also collected from both faults.

The Single-Aliquot-Regenerative-dose (SAR) approach (Table 1 and 2) was employed for both ITL (Choi et al., 2006) and OSL (Murray and Wintle 2003) measurements on quartz and feldspar.

Table 1. The SAR-OSL protocol applied to quartz grains.

Step	Treatment
1	Give dose
2	Preheat, 10 s at 240 ˚C
3	Blue-LED stimulation, 40 s at 125 ˚C
4	Give test dose
5	Cut-heat, 0 s at 200 ˚C
6	Blue-LED stimulation, 40 s at 125 ˚C
7	IR diodes stimulation, 100 s at 125 °C
8	Return to Step 1

Table 2. The SAR-ITL measurement protocol applied to quartz and feldspar grains.

Step	Treatment
1	Give dose, D_i [(a)]
2	Heat to 310°C, (hold for 300 s)
3	Give test dose, D_t [(b)]
4	Heat to 310°C, (hold for 300 s)
5	Return to step 1

[(a)] D_0 = natural dose; [(b)] D_t= Fixed test dose

Typical examples of decay and growth curves of the ITL and OSL signals appear in Fig. 1. Their natural dose and their dose response curves are well described by fitting of a saturating exponential function.

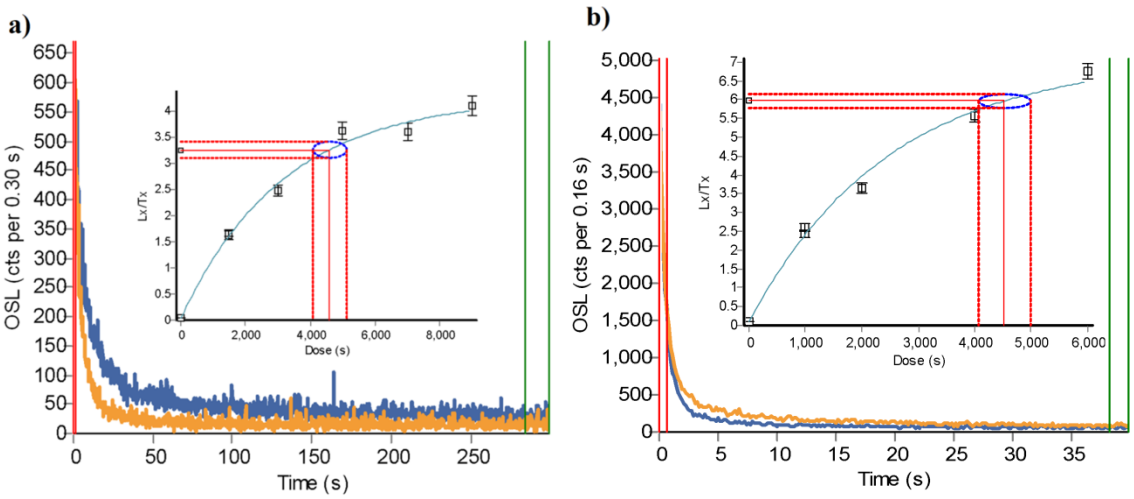

Figure 1. Representative dose response curves and luminescence decay curves for the ITL and OSL signal measured in a) feldspar and b) quarts grain aliquots. Lx/Tx is the corrected luminescence signal for the equivalent radiation dose (D_E).

Luminescence dating results on fault gouge revealed that both techniques could produce reliable results giving very similar ages on the same samples and indicating a continuing activity of the two faults during the Middle-Upper Pleistocene. However, ITL ages were slightly older than the OSL ages, most probably suggesting partial resetting of the ITL signal. It should also be stressed here that, some mixing of the different gouge layers during sub-sampling might be apparent and thus gouge ages may represent a mixture of fault raptures. On the other hand, observations of the OSL and ITL signals of breccia samples appear unusual, not following the expected signal decay behaviour and thus they were excluded from further analysis.

This study is a fundamental advancement in the field of palaeoseismology, as it provides evidence of the potential of the luminescence dating techniques to be used for assessing the neotectonic activity of an area while its methodological approach could become a principal part for geo-hazards evaluations.

Acknowledgments

This research project was supported by the Secretariat of the Nuclear Regulation Authority of Japan and partially by JSPS KAKENHI Grant Number JP18H01309. Part of this study has also received funding from the State Scholarships Foundation (IKY) co-financed by the European Union (European Social Fund-ESF) and Greek national funds through the action entitled “Reinforcement of Postdoctoral Researchers”.

References

Choi, J.H., Murray, A.S., Cheong C.S., Hong D.G., Chang, H.W., 2006. Estimation of equivalent dose using quartz isothermal TL and the SAR procedure. Quaternary Geochronology, 1, 101-108.

Lin, A., Nishiwaki, T., 2019. Repeated seismic slipping events recorded in a fault gouge zone: evidence from the Nojima Fault drill holes, SW Japan. Geophysical Research Letters, 46, https://doi.org/10.1029/2019GL081927.

Murray, A.S., Wintle, A.G., 2000. Luminescence dating of quartz using an improved single-aliquot regenerative-dose protocol. Radiation Measurements, 32, 57-73.

Research Group for Active Faults of Japan, 1991. Active Faults in Japan-Sheet Maps and Inventories (revised edition). University Tokyo Press, Tokyo, Japan 437. (in Japanese with English summary).

Toyoda, S., Rink J., Schwarcz P., Rees-Jones J., 2000. Crushing effects on TL and OSL on quartz: Relevance to fault dating, Radiation Measurements 32, 667-672.

Tsakalos E., Kazantzaki M., Lin A., Nishiwaki T., 2018. Luminescence and ESR dating of fault gouge materials from the Nojima fault - Japan. American Geophysical Union (AGU Fall Meeting 2018), December 10-14, Washington, Maryland, USA.

15th International Congress of the Geological Society of Greece
Athens, 22-24 May, 2019 | Harokopio University of Athens, Greece
Bulletin of the Geological Society of Greece, Sp. Pub. 7 Ext. Abs. GSG2019-326

Late Quaternary extension in eastern Mirabello bay, Ierapetra Fault Zone, Crete, Greece

S. Valkaniotis[1], L. Gouliotis[2], S. Pavlides[3], S. Skovolas[4]

(1) Trikala, Greece, valkaniotis@yahoo.com
(2) Depaertment of Geology and Geoenvironment - National & Kapodistrian University of Athens, Athens, Greece
(3) Department of Geology - Aristotle University, Thessaloniki, Greece (4) Athens, Greece

Extended Abstract

The island of Crete is located at the southern part of the Hellenic Arc, where active extension occurs at the overriding plate of the Africa – Eurasia retreating subduction. Onshore and offshore faults in Crete display significant morphological features formed by the Pleistocene to present extensional activity, while their strike is both arc-parallel and arc-normal (Angelier, 1979; Armijo et al., 1992).

The study area is located in the eastern Mirabello bay, Lasithi District, where Late Quaternary normal faults NNE-SSW to NE-SW trending are exposed around Mirabello bay. The most significant fault structure is the Ierapetra Fault Zone (IFZ), a NNE-SSW normal fault zone that extends from the northern to the southern coast of Crete (Fortuin, 1978; Fytrolakis & Dermitzakis 1996, Caputo et al., 2010). IFZ consists of multiple normal fault segments, parallel and overlapping. The main IFZ is divided (from north to south) into Kavousi segment, Ha Gorge and Vainia segments, while Lastros and Sfaka faults are encountered to the east, along IFZ footwall (Caputo et al., 2006, Gaki-Papanastassiou et al., 2009, Mason et al., 2016, Veliz et al., 2018). A second, less well defined, fault zone is developed along the coast of eastern Mirabello bay; Pachia Ammos coastal fault and Psira offshore fault to the north. These faults are parallel to the IFZ and follow the eastern coast and bathymetric relief.

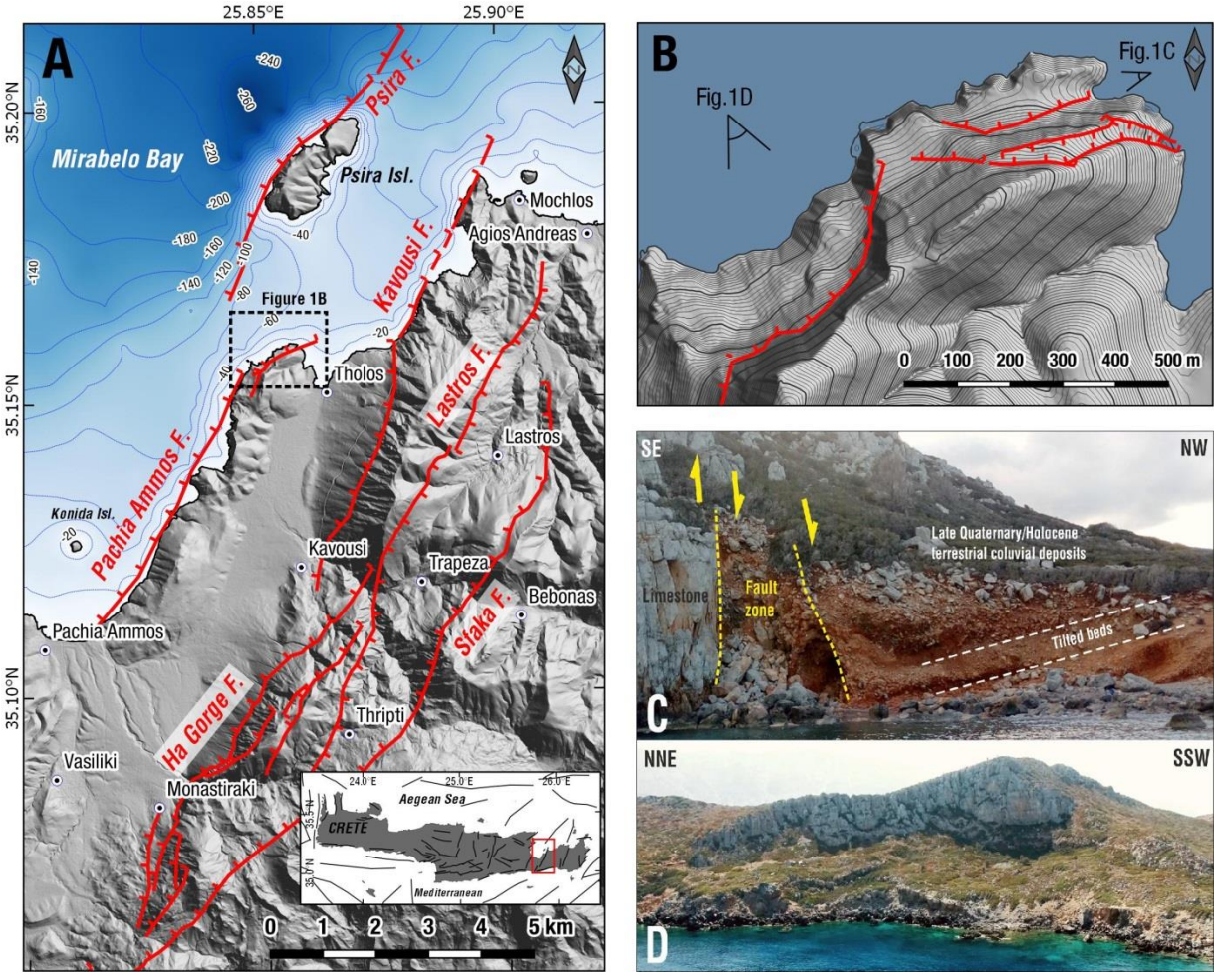

Figure 1. A) Late Quaternary faults in the area of study (eastern Mirabello bay, Ierapetra, Crete). B) Detailed fault traces mapped in the Tholos site. C) Profile of the main normal fault in Tholos site, with Late Quaternary colluvial sediments deformed and rotated on the hangingwall. D) View of the fault scarp in the southern Tholos site, with part of the footwall removed from a paleo-landslide.

In this study, we examine in detail a section of the Pachia Ammos fault zone. The site is located at the northernmost tip of the steep coast of east Mirabello bay, near Tholos site (Figure 1). Footwall lithology is comprised by carbonate Alpine rocks, mainly dolomites and dolomitic limestones of Triassic age (Papastamatiou et al. 1959). Different generations of Quaternary debris and colluvial terrestrial sediment scree can be found along the fault scarps and on the western slopes of the site. The morphology is dominated by the steep bedrock scarps formed by normal faulting or landslide erosion. Coastal erosion and a large paleo-landslide at the southern part of the site have removed part of the colluvial sediments and the fault scarp (Figure 1C-D).

Fault traces were mapped in a 1:2000 scale (Figure 1B) and reveal a composite fault structure with parallel fault scarps, and fault setbacks showing a variation in fault strike from west to east. The change in the fault strike from NNE-SSW to NE-SW occurs at the northern edge of the Pachia Ammos footwall and we examine two different scenarios to interpret this change of geometry:

- related to the development of a brecciated relay ramp between the Pachia Ammos fault and the Kavousi fault.
- different geometry and probable left-stepping overlap between Pachia Ammos and Psira faults.

Adjacent to the faults, deformed outcrops of the fault zones reveal deformed and tilted late Quaternary terrestrial deposits, a clear indication of recent fault activity. Although there is a lack of detailed offshore surveys in the area, we interpret the Pachia Ammos and Psira footwalls as part of a series of backtilted fault blocks towards the IFZ.

Although the coastal/offshore faults of Pachia Ammos and Psira preserve a lower morphological imprint due to coastal erosion and submergence of the hanging-wall than the IFZ, their structural features, geometry and segmentation contributes to the better understanding of the active extension in the eastern Mirabello bay. We conclude that paleoseismological and displacement features and observations is crucial for the further improvement our current understanding on the seismic hazard assessment of a rapidly developing area and a popular tourist destination.

References

Angelier, J., 1979. Neotectonique de l'Arc Egeen, Soc. Geol. Du Nord, 3, 418.

Armijo, R., Lyon-Caen, H., Papanastassiou, D., 1992. East-west extension and Holocene normal-faults scarps in the Hellenic arc, Geology, 20, 491–494.

Caputo, R., Monaco, C., Tortorici, L., 2006. Multiseismic cycle deformation rates from Holocene normal fault scarps on Crete (Greece). Terra. Nova 18, 181–190.

Caputo, R., Catalano, S., Monaco, C., Romagnoli, R., Tortorici, G., Tortorici, L., 2010. Active faulting on the island of Crete (Greece). Geophys. J. Int. 183, 111–126.

Fortuin, A.R., 1978. Late Cenozoic History of Eastern Crete and implications for the geology and geodynamics of the southern Aegean Area. Geologie en Mijnbouw 57(3), 451-464.

Fytrolakis, N., Dermitzakis, M., 1996. Map of Active Faults of the area of Crete Island. Earthquake Protection and Planning Organization, Athens.

Gaki-Papanastassiou, K., Karymbalis, E., Papanastassiou, D., Maroukian, H., 2009. Quaternary marine terraces as indicators of neotectonic activity of the Ierapetra normal fault SE Crete (Greece). Geomorphology 104, 38–46.

Mason, J., Schneiderwind, S., Pallikarakis, A., Wiatr, T., Mechernich, S., Papanikolaou, I., Reicherter, K., 2016. Fault structure and deformation rates at the Lastros-Sfaka Graben, Crete. Tectonophysics 683, 216–232.

Papastamatiou, I., Vetoulis, D., Tataris, A., Bornovas, I., Christodoulou, G., Katsikatsos, G., 1959. Geological Map of Greece in 1:50000 scale. Map Sheet Ierapetra – Kato Chorion. IGME, Athens.

Veliz, V., Mouslopoulou, V., Nicol, A., Fassoulas, Ch., Begg, J., Oncken, O., 2018. Millennial to million year normal-fault interactions in the forearc of a subduction margin, Crete, Greece. Journal of Structural Geology 113, 225-241.

15th International Congress of the Geological Society of Greece
Athens, 22-24 May, 2019 | Harokopio University of Athens, Greece
Bulletin of the Geological Society of Greece, Sp. Pub. 7 Ext. Abs. GSG2019-328

Contemporary Kinematics of the South Aegean Area Detected with Differential GNSS Measurements

C. Doxa[1], V. Sakkas[1], A. Tzanis[1], H. Kranis[1]

(1) Department of Geology and the Geoenvironment, National and Kapodistrian University of Athens, Panepistimiopoli, Zografou 15784, Greece, chrysadoxa@geol.uoa.gr

The south Aegean Sea and its adjacent areas is a highly segmented tectonically active domain, characterized by high-rate extension and severe crustal thinning. The different segments (blocks) that make up the south Aegean crust are bounded by significant fault zones and/or dislocation surfaces whose their relative motion varies in size and direction. The present study studies the kinematic characteristics of the southern Aegean crustal segments using geodetic data of 47 permanent GNNS stations distributed over the eastern Peloponnesus, Attica, Cyclades, Dodecanese, Crete and the coast of western Anatolia.

The data used herein comprise:

- Primary (unprocessed/raw) data from 24 permanent stations operated by METRICA S.A. (https://www.metrica.gr), spanning the period 2011-2018 and generously provided by said organization.
- Primary data, from 8 stations of the HEPOS (Hellenic Positioning System) facility, Hellenic National Cadaster (http://www.hepos.gr), spanning the period 2013-2017 and generously provided by said organization.
- Primary data from one station, operated by the RING network of Italy (Rete Integrata Nationale GPS - http://ring.gm.ingv.it), spanning the period 2017-2018.
- Primary data from one station operated by UNAVCO (https://www.unavco.org/), spanning the period 2011-2017.

All primary data were processed with the Bernese v5.2 software (Dach et al., 2007**)**.

- Processed data (displacement time series) from 4 stations operated by the Geodetic Laboratory of Nevada, spanning the periods 2009-2018 (http://geodesy.unr.edu/NGLStationPages/gpsnetmap/GPSNetMap_MAG.html).
- Velocity vectors from 7 stations located in Attica and Peloponnesus, extracted from Chousianitis et al., (2013) and spanning a period of approx. five years.
- Velocity vectors from 2 stations operated by the National Technical University of Athens (NTUA), spanning the period 2012-2015 and kindly provided by Dr. J. Galanis (personal communication, 2018).

Hitherto studies of the kinematics of the Aegean Plate have mainly focused on the analysis of the regional strain field and large-scale relative motion between the Aegean, Anatolian and Eurasian plates, either using the ITRF coordinate frame or remote poles of rotation located in Western Europe or Africa. This approach does not facilitate discrimination of local-scale relative motion between tectonic blocks. Inasmuch as we are mainly interested in studying *local-scale* effects in the south and eastern Aegean region, we have based our analysis on a *local* reference point situated at Anavyssos, Attica and indicated with a red square in Fig.1.

Given the reference point, it is apparent that to the west of longitude 24°E, relative block motion is somewhat uncertain because the majority of estimated relative velocities are associated with large errors. Nevertheless, at least four well estimated vectors clearly indicate that the eastern Peloponnese slides in a roughly N210°–N220° direction, expectedly and approximately normal to the strike of the western half of the Hellenic Trench.

Eastward of longitude 24°E things appear to be quite different; the errors associated with the relative velocity vectors are rather small and the distribution of velocities allows the identification of four and tentatively five major blocks with different kinematics, whose boundaries are illustrated in Fig. 1 with blue dashed lines. Thus:

- Block 1 (Cyclades) experiences approximately N220° dislocation at an average velocity of 1.48 mm/yr.
- Block 2 (soth-western Cyclades) experiences approximately N210° dislocation at average velocity of 3.25 mm/yr.
- Block 3 (northern Dodecanese) experiences approximately N150° dislocation at an average velocity of 3.02 mm/yr.
- Block 4 (Cretan Sea/Crete) experiences approximately N160° dislocation at an average velocity of 2.00 mm/yr.
- Block 5 (southern Dodecanese) experiences approximately N120° dislocation at an average velocity of 7.35 mm/yr.

According to this kinematic setting, the relative horizontal motion between individual blocks is as follows:

- *Left-lateral* between Blocks 1/ 2 and the area extending beyond their northern boundaries (marked as “Block 6” in Fig. 1).
- *Left-lateral* between Blocks 1 and 3.
- *Right-lateral* between Blocks 1 and 2.
- *Extension* (divergence) in an approx. N-S direction between Blocks 2/ 3 on one hand, and 4/ 5 on the other. The onset of the divergence coincides with the onset of severe crustal thinning in the Cretan Sea
- *Unknown* between tentative Blocks 4 and 5 which appear to be distinguished by the *very* significant difference in the velocities observed between Crete on one hand and the Dodecanese islands on the other.

In conclusion, the area of the south Aegean appears to exhibit a rather complex kinematic pattern, the origin of which remains to be confirmed and validated with future research.

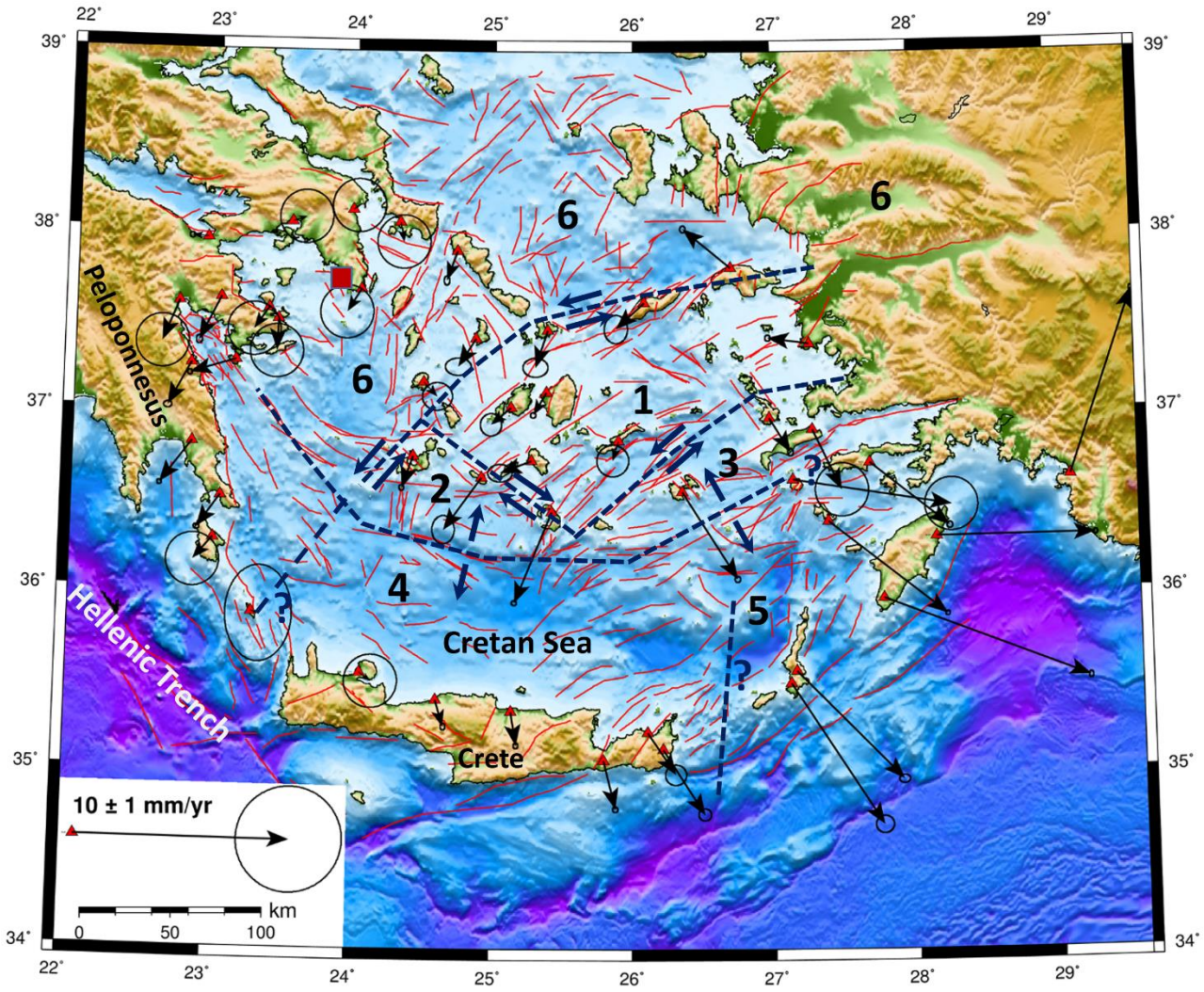

Figure 1. Velocity vectors relative to Anavyssos station (red square); ellipses at the tips of the vectors indicate the 95% confidence region. Blue dashed lines indicate the boundaries of the kinematic discontinuities identified herein. Known or inferred faults are shown with red lines; information was extracted from Sakellariou and Tsampouraki (2019), Kokkalas and Aydin (2013) and IGME (1989). The bathymetry was extracted from the EMODNet (2016) data base.

References

Chousianitis K., Ganas A. And Gianniou,M, 2013. Kinematic interpretation of present-day crustal deformation in central Greece from continuous GPS measurements. J. Geodyn., 71, 1-13. https://doi.org/10.1016/j.jog.2013.06.004.

Dach, R., Hugentobler, U., Fridez, P., Meindl, M., 2007. Bernese GPS Software Version 5.0. Astronomical Institute, University of Bern, Bern.

EMODnet Bathymetry Consortium (2016): EMODnet Digital Bathymetry (DTM). https://doi.org/10.12770/c7b53704-999d-4721-b1a3-04ec60c87238.

IGME (Institute of Geology and Mining Exploration), 1989. Seismotectonic map of Greece, 1:500,000 scale.

Kokkalas S. and Aydin, A., 2013. Is there a link between faulting and magmatism in the south-central Aegean Sea? Geological Magazine, 150 (2), 193-224. https://doi.org/10.1017/S0016756812000453.

Sakellariou D. and Tsampouraki-Kraounaki K., 2019. Plio-Quaternary Extension and Strike-Slip Tectonics in the Aegean, in: Duarte J.C. (Ed), Transform Plate Boundaries and Fracture Zones, 339-374. https://doi.org/10.1016/B978-0-12-812064-4.00014-1.

15th International Congress of the Geological Society of Greece
Athens, 22-24 May, 2019b | bHarokopio University of Athens, Greece
Bulletin of the Geological Society of Greece, Sp. Pub. 7 Ext. Abs. GSG2019-344

Active deformation pattern of the Peloponnese region, based on geostatistical analysis of primary geodetic data

I. Lazos[1], A. Chatzipetros[1], S. Pavlides[1], S. Bitharis[2], C. Pikridas[2]

(1) Department of Geology, School of Geology, Aristotle University of Thessaloniki, 54124, Thessaloniki, Greece, ilialazo@geo.auth.gr
(2) Department of Geodesy and Surveying, School of Rural and Surveying Engineering, Aristotle University of Thessaloniki, Greece

Peloponnese area is in the broader South Aegean region, one of the most tectonically active regions in eastern Mediterranean. Peloponnese exhibits a profound extensional regime, which caused crustal thinning and the evolution of multiple tectonic windows. This extension has been ongoing in the neotectonic period as well (Papanikolaou et al., 1988), forming three major NNW – SSE trending normal fault zones at its southern part (largely controlling Messiniakos, Lakonikos and Argolikos Gulfs), while its northern part is deformed by primarily NW-SE and E – W trending normal fault zones, associated mainly to the tectonic activity of the Corinth Gulf. The area undergoes active deformation, as documented by several seismic events, such as Alkyonides (1981, M_w 6.7), Kalamata (1986, M_w 5.9), Aigion (1995 M_w 6.4) in 1995 and Andravida (2008, M_w 6.4) earthquakes (Jackson et al., 1982; Papanikolaou et al., 1988; Roumelioti 2004; Koukouvelas et al., 2010; GreDaSS Pavlides et al., 2010).

One of the most reliable ways of estimating the level of active deformation of an area is Satellite Geodesy, based on permanently installed GPS/GNSS stations and collecting geodetic data (specifically East and North velocity components of the station). Data processing is then implemented by dedicated software packages (UNAVCO), leading to the quantitative and qualitative determination of the uppermost crustal deformation of the study area. Primary data from 59 GPS/GNSS stations were used for extrapolating the deformation pattern of the broader Peloponnese area. They consist of timeseries for seven consecutive years (2008 – 2014), while the data analysis was carried out using 30-sec daily GPS observations. The reference frame of the geodetic data is the European Terrestrial Reference Frame 2000 (ETRF2000), which is coincident with the stable part of the Eurasian plate.

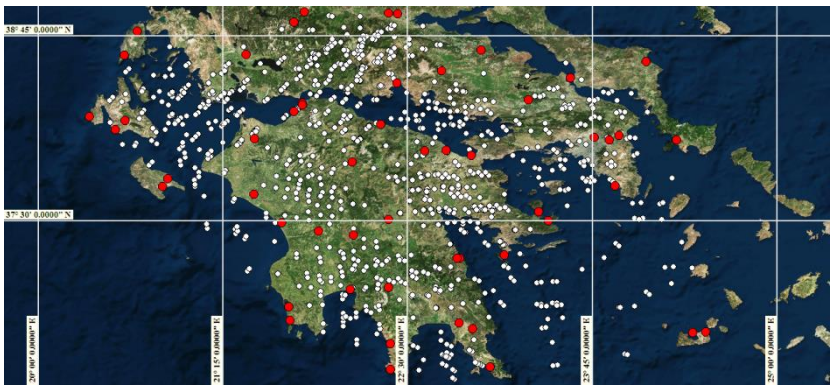

Figure 1. Location of the 59 permanently installed GPS/GNSS stations (red dots) and the 932 triangular centroids (white dots) within the study area.

Two main sets of methodologies were applied on the collected datasets. The first method is based on a triangulation process, taking into account the data of three different stations, which form a different each time triangle. Each station is located on a triangle vertex and is characterized by a specific velocity value, recorded for the aforementioned time. The intersection of the triangle medians defines the triangle centroid, which is then used as the centre of an inner, inscribed circle, expressing the initial and undeformed triangle. Taking into consideration the motion of the GPS/GNSS stations, which is imprinted on the corresponding velocity vectors of each station, the inner circle is morphed into an ellipse. By using equations, combining the major and minor axes of the inner circle and the ellipse, respectively, a series of parameters related to strain assessment can be calculated. The estimated parameters are: a) maximum and minimum horizontal extension, b) total velocity, c) maximum shear strain, d) area strain and e) rotation. In the frame of this study, 932 different triangles were taken into account, using the 59 permanently installed GPS/GNSS stations (Fig. 1).

Using the parameters from the first stage a second set of methodologies is implemented, leading to interpolation of missing or incomplete data. Interpolation is a reliable way of geostatistical process, as the distribution of each parameter throughout the study area is calculated with an acceptable confidence range. The geostatistically extracted parameters provide information leading to the interpretation of the neotectonic and the geodynamic setting of the study area.

The maximum and minimum horizontal extension parameters are identifying indicators of the extensional and compressional regime in a study area, respectively. The interpolated results show maximum horizontal extension values concentrated at the broader area of Corinth Gulf, as well as the northwestern part of Peloponnese, effectively the meisoseismal area of the 2008 Andravida earthquake sequence, which is contained in the recoding period. Furthermore,

high maximum horizontal extension values are observed at the southwestern part of Peloponnese, probably related to offshore faults, located further to the West. Nevertheless, the maximum extension values of the study area, with the exception of the aforementioned areas, are generally low, indicating a rather tectonically quiescent area (Figure 2). Similarly, the main concentration of minimum extension values (i.e. associated with compression) is again located near the epicentral area of the Andravida earthquake. The concurrent maximum extension and maximum compression values are in good agreement with the focal mechanisms of the main event, which attribute it to the reactivation of a deep strike-slip fault.

The total velocity is associated to the motion and therefore the geodynamic evolution of the study area. The statistically processed results show an increase of total velocity values from the north-northeastern part to the south-southwestern part of Peloponnese area. These results are comparable and compatible with the general geodynamic setting of the area, as the south-southwestern part of Peloponnese is closer to the subduction zone, extended southwestwards into the offshore area, where African plate is subducted beneath the Eurasian one; it is therefore expected that it is deformed at a higher rate.

The maximum shear strain is associated to the deformation of the upper crust, caused by seismic, landslide or creeping phenomena. The areas where the highest values of maximum shear strain are observed are the same with the ones where maximum horizontal extension is observed.

The area strain expresses the dilatation and the compaction of the area, associated to extension and compression, respectively. Based on this parameter, a general extensional regime can be identified, while compressional effects are limited and located at the western part of the study area, where the transition from an extensional to a compressional regime is evident from other indicators (geological, structural, seismic, etc.). In general, the low to medium area strain values are compatible with a low activity character of the mainland Peloponnese area.

Finally, estimation of the areal rotation can indirectly contribute to the knowledge of the recent geodynamic evolution of area. To this end, the rotation pattern was modelled for three periods (1, 5 and 10 Myr BP), showing a dominant clockwise rotation of the study area. The results of the rotation analysis are preliminary in adequately good agreement with palaeomagnetic data for the broader area (Lazos et al., 2018).

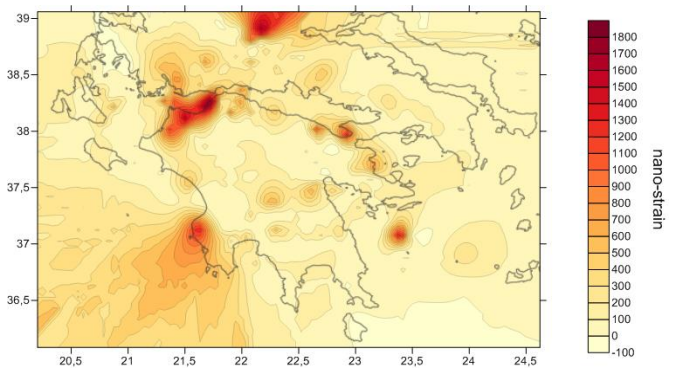

Figure 2. Interpolation of the maximum horizontal extension values of the study area. The highest values are concentrated at the northwestern part, where the epicentral area of the Andravida, 2008 earthquake is. Although this event did not produce significant ground deformation, its predominantly strike-slip regime was marked by performing parametric analyses on the primary data of the permanently installed GPS/GNSS network.

Acknowledgements

Metrica S.A., National Cadastre and Mapping Agency S.A., National Observatory of Athens (Ganas et al., 2011) and National Technical University of Athens are acknowledged for providing the primary GPS/GNSS data.

References

Ganas, A., Chousianitis, K., Drakatos, G. Papanikolaou, M., Argyrakis, P., Kolligri, M., Petrou, Panagiota., Batsi, E., Tsimi, C., 2011. NOANET. High-rate GPS Network for Seismology and Geodynamics in Greece. Geophysical research abstracts, 13.

Jackson, J.A., Gagnepain, J., Houseman, G., King, G.C.P., Papadimitriou, P., Soufleris, C., Virieux, J., 1982. Sesimicity, normal faulting, and the geomorphological development of the Gulf of Corinth (Greece): the Corinth earthquakes of February and March 1981. Earth Planet. Sci. Lett. 57, 377–397.

Koukouvelas, I., Kokkalas, S., Xypolias, P., 2010. Surface deformation during the Mw 6.4 (8 June 2008) Movri Mountain earthquake in the Peloponnese, and its implications for the seismotectonics of western Greece. Inter. Geol. Review 52, 249 – 268.

Lazos, I., Kondopoulou, D., Chatzipetros, A., Pavlides, S., Bitharis, S., Pikridas, C., 2018. Rotation rates of the South Aegean region, Greece, based on primary geodetic data - Comparison between geodetic and palaeomagnetic results. 9th International INQUA Meeting on Paleoseismology, Active Tectonics and Archeoseismology (PATA), Possidi, Greece, 141-144.

Papanikolaou, D., Lykousis, V., Chronis, G., Pavlakis, P., 1988. A comparative study of neotectonic basins across the Hellenic arc: the Messiniakos, Argolikos, Saronikos and Southern Evoikos Gulfs. Basin Res. 1, 167–176.

Pavlides, S., Caputo, R., Sboras, S., Chatzipetros, A., Papathanasiou, G., Valkaniotis, S., 2010. The Greek Catalogue of Active Faults and Database of Seismogenic Sources. Bull. Geol. Soc. Greece 43, 486–494.

Roumelioti, Z., Benetatos, C., Kiratzi, A., Stavrakakis, G., Melis, N., 2004. A study of the 2 December 2002 (M5.5) Vartholomio (western Peloponnese, Greece) earthquake and of its largest aftershocks. Tectonophysics 387, 65–79.

15th International Congress of the Geological Society of Greece
Athens, 22-24 May, 2019 | Harokopio University of Athens, Greece
Bulletin of the Geological Society of Greece, Sp. Pub. 7 Ext. Abs. GSG2019-349

Pattern of Active Deformation in the Area of Thermaikos Gulf and Pieria (Northern Greece), Based on Morphotectonics and Satellite Geodesy

A. Zervopoulou[1], A. Chatzipetros[1], S. Pavlides[1] and I. Lazos[1]
(1) Department of Geology, Aristotle University of Thessaloniki, 54124, Greece, annezervo@gmail.com

The present-day tectonic stress pattern in Northern Greece has been active since Pleistocene, showing a slightly radial crustal extension with variable trend (N-S to NNW-SSW) in central Macedonia. The fault pattern is almost perpendicular to the stress field, crosscutting the older NW-SE alpine deformation structures (Sboras *et al.*, 2017). The current active stress field in the broader area of Thessaloniki has its extensional axis directed N-S, while the corresponding active faults are generally E-W trending. In the past couple of decades, GNSS measurements are widely used as a well-established tool in earth crustal deformation studies. The synergy between geodesy and geophysics can provide some very promising discussions about the Earth's upper crustal processes (Lazos et al., 2018). In this paper the extension of Anthemous fault zone at the broader Thessaloniki area is examined, using an integrated geodetic and geomorphologic approach.

The largest part of the study area is covered by Quaternary deposits, which were developed at the northern side of Anthemous river basin and the basins of Gallikos, Axios, Loudias and Aliakmon rivers (Thessaloniki plain). The deposits are mainly fluvial - torrential sediments containing marsh – marine or fluvial – deltaic layers. The Neogene Sandstone – Marl formation Series underlies the Quaternary sediments. This series consists of layers of very dense sand and sandstone, alternating with clay and silt of light brown to light green color. This formation covers a large part of the broader area. In the study area, this series is extended along the main fault zone from Galarinos to the East, up to the west shoreline of Thermaikos Gulf at the area of Aiginio and Melini. This series is in tectonic contact with the Quaternary deposits of Anthemous basin and the Thessaloniki plain sediments. The oldest Neogene Red Clay Series outcrops at the eastern part of the fault zone. This series consists of alternations of red color very stiff clays, sand and gravel layers and lenses.

The largest active fault zone in the immediate vicinity of Thessaloniki metropolitan area, is the Anthemous normal fault zone, which is located *ca.* 15 km to the south (F-An). The general strike of the zone is E-W, dipping to the north, while its total mapped length is *ca.* 32 km. It can be divided into three discrete segments, namely the Galarinos - Neo Risio, the Aggelochori area (Zervopoulou, 2010) and a possible third one, which is considered to be an extension to Thermaikos Gulf, detected from geophysical (seismic) investigations (Chronis, 1986). In this paper, the existence of a probable fourth segment in Aiginio area is also discussed. The activity of this fault zone is inferred by several indications. It defines the contact between the Neogene series at the south and the Holocene sediments at the central and north part of the basin. The application of quantitative geomorphic indices shows that the relief is responding to a relatively recent activity, as documented by various factors. The dissimilar development of the tributary network between the north and the south banks of Anthemous River, shows a tilting to the south along the surface fault trace. In addition, the asymmetry index of the basin, as well as the poor water channel development at the south part of the basin, indicate that the area has been subjected to rather recent deformation. Mountain front sinuosity is low, also suggesting a relatively high uplift rate of the footwall. The Aggelochori area segment shows indications of higher activity, as is suggested by steep slopes (cliffs). Some other indirect signs of neotectonic activity are the existence of hot springs in the Souroti area, with travertine deposits aligned along the fault line (Zervopoulou & Pavlides, 2005). This fault is also probably associated to the M 6.2 earthquake of Vasilika, as well as with aseismic creep along the fault line at Peraia area. The aseismic cracks follow the fault trace, however they have been attributed to overpumping.

The western extension of Anthemous fault zone towards Aiginio area is a research objective that has not yet been confidently resolved. To this end, a geodetic approach has been applied by extrapolating the active geodynamic state of the area by using primary geodetic data. They have been recorded for seven years (2008-2014) by 18 permanent GPS/GNSS stations in the broader area. Data were recorded daily in 30-second increments. The reference frame of these data is ETRF2000, which assumes that Eurasia is stable. The data processing involved GPS triangulation of three different GPS/GNSS stations, based on the vector analysis of East and North velocity components and their uncertainties. Any given three stations form a triangle, while each of them is located on a triangle vertex., The triangle centroid is determined by taking into consideration the intersection of the triangle medians and the inner circle of the triangle is inscribed. Then, the triangle vertices (GPS/GNSS stations) are relocated, based on their recorded velocity vectors, leading to the deformation of the inner circle into an ellipse. The combination of the major and minor axes of the inner circle and the ellipse, respectively, using specific equations, results in the calculation of certain parameters related to the active deformation of the area (e.g. Lazos et al., 2018). The combination of these 18 GPS/GNSS stations of the broader area led to the construction of 348 different triangles (http://www.unavco.org/).

The maximum horizontal extension is one of the parameters that is directly associated with the determination of the tectonic regime of a study area (extensional or compressional). The calculated maximum horizontal extension values, as well as their geostatistical process (interpolation), confirm that the probable western Anthemous fault zone prolongation is characterized by the highest values of the study area (approximately 200-230 nano-strain), Figure 1. In addition, high values are observed at the eastern part of Thessaloniki city, where numerous faults have been mapped. These high maximum horizontal extension values however, cannot be attributed to a specific fault, as they are concentrated within a limited area.

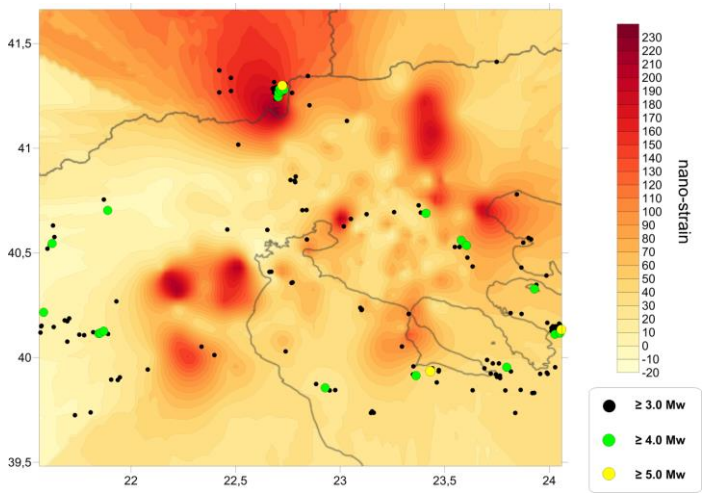

Figure 1. Maximum horizontal extension and recent seismic events of the study area.

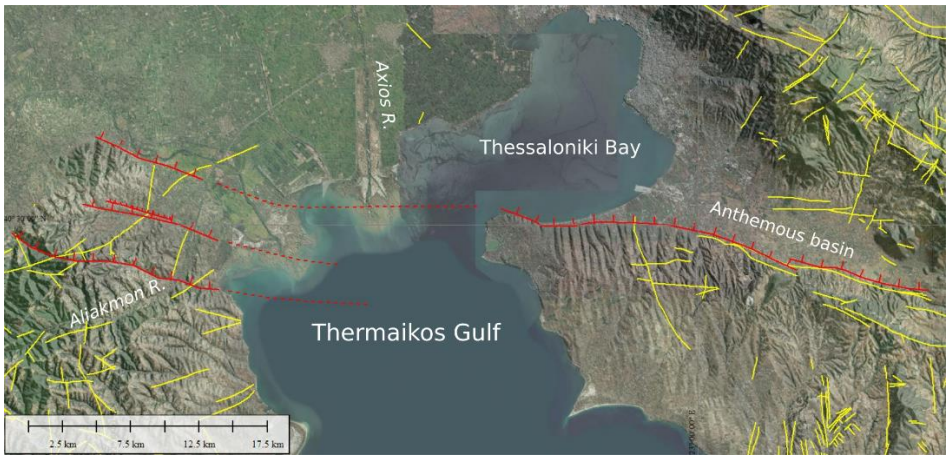

Figure 2. Summary map of faulting in the area of Thermaikos Gulf. Yellow lines show the mapped faults from published IGME geological maps, while red solid and dashed lines show the faults, lineaments and probable faults discussed in this paper.

While geodetic analysis shows that there is a considerable active deformation at the westward probable extension of Anthemous fault zone towards Aiginio area, the continuation cannot be verified due to the lack of precise offshore information. Nevertheless, a geomorphological assessment of Aiginio area shows that there are ESE-WNW to E-W trending linear features that are in good agreement with the expected fault pattern (Fig. 2). They form a low relief with no significant linear scarps, indicating thus that this probable segment is of lower activity level. Further research is needed in the area in order to establish a reliable correlation between the different fault strands.

Acknowledgements

Metrica S.A, National Cadastre and Mapping Agency S.A, National Observatory of Athens (Ganas et al. 2011) and National Technical University of Athens are acknowledged for providing GPS data.

References

Chronis G.Th. 1986. Modern dynamics and the recent Holocene sedimentation at the inner side of Thermaikos bay. School of Geology, faculty of Geography, Ph.D. Thesis (in Greek), Athens.

Ganas, A., Chousianitis, K., Drakatos, G. Papanikolaou, M., Argyrakis, P., Kolligri, M., Petrou, Panagiota, Batsi, E., Tsimi, C., 2011. NOANET. High-rate GPS Network for Seismology and Geodynamics in Greece. Geophysical research abstracts, 13.

Lazos I., Stergiou C., Chatzipetros A., Pikridas C., Bitharis S., Melfos, V. 2018. Active tectonics (extensional regime and rotations) and Tertiary mineralization occurrences within Central Macedonia, Greece. 9th International INQUA Meeting on Paleoseismology, Active Tectonics and Archeoseismology (PATA).

Sboras S., Chatzipetros A., Pavlides S. 2017. North Aegean Active Fault Pattern and the 24 May 2014, Mw6.9 Earthquake. Active Global Seismology: Neotectonics and Earthquake Potential of the Eastern Mediterranean Region, Geophysical Monograph 225, First Edition. İbrahim Çemen and Yücel Yılmaz. American Geophysical Union. Published by John Wiley & Sons, Inc.

Zervopoulou A., Pavlides S. 2005. Morphotectonic study of the broader area of Thessaloniki for the cartography of neotectonic faults. Bulletin of the Geological Society of Greece vol. XXXVIII, 2005.

Zervopoulou A. 2010. Neotectonic faults of the broader area of Thessaloniki and foundation on them. School and faculty of Geology, Ph.D. Thesis (in Greek), A.U.Th.

http://www.unavco.org/

15th International Congress of the Geological Society of Greece
Athens, 22-24 May, 2019 | Harokopio University of Athens, Greece
Bulletin of the Geological Society of Greece, Sp. Pub. 7 Ext. Abs. GSG2019-350

Active Tectonics and Pliocene-Pleistocene volcanic rocks of Almopia and Charopo (Sitsi-Kamen) areas in Northern Greece

I. Lazos[1], C. Stergiou[2], A. Chatzipetros[1], V. Melfos[2], P. Voudouris[3], C. Pikridas[4]

(1) Department of Geology, School of Geology, Aristotle University of Thessaloniki, 54124, Thessaloniki, Greece, ilialazo@geo.auth.gr
(2) Department of Mineralogy-Petrology-Economic Geology, Aristotle University of Thessaloniki, 54124, Thessaloniki, Greece
(3) Department of Mineralogy-Petrology, National and Kapodistrian University of Athens, 15784, Athens, Greece
(4) Department of Geodesy and Surveying, School of Rural and Surveying Engineering, Aristotle University of Thessaloniki, Greece

Several episodes of magmatic activity characterize the Paleogene-Quaternary geological history of Greece. Set in a back-arc geotectonic environment, this activity is the result of the south-southwestward migration of the post-collisional geodynamic settings of the Alpine orogeny (Agostini et al., 2010). The undergoing widespread regional extension of the geodynamical Northern Aegean region has been active since Eocene-Early Miocene and has resulted in the formation of distinct magmatic rock groups of plutonic to volcanic origin (Melfos and Voudouris, 2017; Sakellariou and Tsampouraki-Kraounaki, 2019). Specifically, the Cenozoic rocks of volcanic origin comprise: a) the Lower to Middle Miocene shoshonites and adakites of the northeastern Aegean region, b) the Middle Miocene to Pliocene volcanic rocks of the southeastern Aegean region, c) the Pliocene-Quaternary volcanic rocks of the northwestern Aegean region, d) the lamproites and alkaline basalts of the Aegean Islands and western Anatolia, and e) the subduction-related volcanic rocks of the southern Aegean volcanic arc (Pe-Piper and Piper, 2007).

The Pliocene to Quaternary volcanic rocks at Almopia, Charopo (Sitsi-Kamen), Doirani, Strymonikon, Euboecos, Psathoura, Vlichades, and Mikrothive belong to the group of the northwestern Aegean region (Vougioukalakis et al., 2004; Pe-Piper and Piper, 2007). This refer area corresponds with the geodynamical Northern Aegean region where the North Anatolian trough fault zone has a major role in structural control dynamics. According to Pe-Piper and Piper (2007) these rocks are the result of a slab tear at the depth of 300 km spanning from Albania to the Gulf of Corinth.

The present study focuses on the Almopia and Charopo trachytic to rhyolitic rocks which are the northernmost volcanic rocks of Pliocene to Pleistocene age found in northern Greece (Fig. 1) (Pe-Piper and Piper, 2007). They are located at Voras mountains and Aridaia plain and at the northern part of the Strymon basin respectively and their occurrences are strongly structurally controlled (Maratos, 1966; Vougioukalakis et al., 2004). At the area of Voras, the volcanic activity initiated at 6.5 Myr and terminated at 1.8 Myr shifting from east to west in an area of approximately 70 km^2. Dacites, trachytes, latites, and andesites and a rhyolitic dome describe the Voras volcanic rocks (Vougioukalakis et al., 2004). In addition, volcanic tuffs and lapilli deposits cover large areas both around these rocks and Aridaia plain (Vougioukalakis et al., 2004). The Quaternary Charopo (Sitsi-Kamen) volcanic outcrops are located near Charopo village covering an area of approximately 12 km^2 (Maratos, 1966). Rhyolitic tuffs constitute the main volcanic rocks at Sitsi-Kamen, while lavas are scarce at the surface (Maratos, 1966). The Pliocene-Quaternary hydrothermal activity is documented by the present day low-enthalpy geothermal fields occurring in both areas (Karydakis et al., 2005; Lambrakis et al., 2014).

Geological mapping at both areas has revealed the significant relation between the volcanic activity and the regional structural control mechanisms (Maratos, 1966; Vougioukalakis et al., 2004). Both regions are characterized by limited fault zones exhibiting NW-SE, NNW-SSE, and NE-SW orientations. Nevertheless, NE-SW and E-W trending remarkable fault zones highlight the predominant structural settings at the Voras and the Sitsi-Kamen areas, respectively. At Almopia region, the Voras and Aridaia volcanic activity were structurally controlled by several fault zones fragmenting the metamorphic rocks of the Almopia Subzone (Axios Zone) at the footwalls of the North Almopia-Promachi and South Almopia fault zones. The volcanic material at Charopo was extruded through the fault zone defining the border between the metamorphic rocks of the Rhodope Massif and the Quaternary sediments of the Strymon basin (Kastanoussa-Petritsi fault) (Caputo and Pavlides, 2013).

One of the most reliable and accurate ways of determining the neotectonic activity is satellite geodesy, based on permanently installed GPS/GNSS stations. Regarding the study area of Voras, 12 different stations record the primary geodetic data, including the east and north velocity components, while the corresponding stations, collecting geodetic data for the wider Sitsi-Kamen region, are totally 15. It is mentioned that the aforementioned data was collected for the seven-year time period 2008 – 2014, while the recording was implemented every 30 seconds in a daily basis. The reference frame of geodetic data is European Terrestrial Reference Frame 2000 (ETRF2000) that is coincident with the stable part of the Eurasian Plate. Concerning the data processing, the triangulation method was applied in order to extract a series of parameters (results), revealing information about the neotectonic and geodynamic setting. The principal of the triangulation method is based on the combination of the primary geodetic data of three different GPS/GNSS stations, forming a triangle (each station is located on a triangle vertex), while the use of the triangle medians leads to the estimation of the triangle centroid (Lazos et al., 2018). The implementation of the primary geodetic data into equations, expressing the surficial deformation, results in an extraction of parameters for the triangle centroid. The calculated parameters are the following: 1) maximum horizontal extension, b) minimum horizontal extension, c) area strain and d) rotation (http://www.unavco.org/). Based on the combinations of the GPS/GNSS stations of the study area, 190 different triangles were constructed (Figure 1), while the aforementioned parameters were calculated for each triangle centroid. The

extracted parameter values were geostatistically processed in a grid pattern in order to be distributed throughout the study area.

The analysis of the parameters shows that the volcanic rocks within the two study areas are directly associated with the active tectonics of the broader area. In particular, the combination of the maximum and minimum horizontal extension values confirms the regional extensional regime which favored the extrusion of the volcanic rocks. Furthermore, the area strain parameter reveals the dilatation, related to the dominant extension of the study areas. Regarding the rotational regime, the counter-clockwise rotation dominates in both areas (approximately 67% of the triangle centroids show counter-clockwise rotation) in contrast with the general clockwise rotational regime of Northern Greece. The transition from the clockwise to the counter-clockwise rotational regime documents the neotectonic activity of the study area, related to the volcanic rocks presence. In conclusion, the Pliocene-Quaternary volcanic activity of northern Greece is directly associated with the extensional regional neotectonic setting.

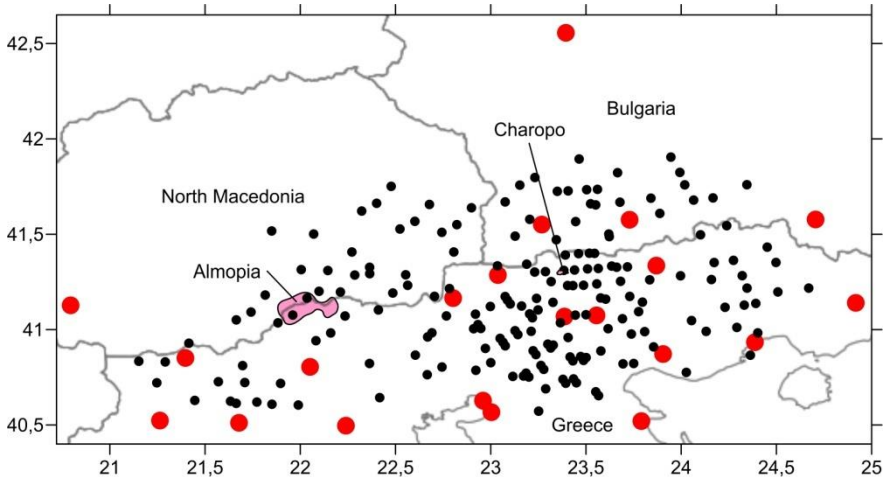

Figure 1. Permanently installed GPS/GNNS stations (red dots) and the 190 different triangle centroids (black dots) of the study area. The occurrence areas of the Almopia and Charopo (Sitsi-Kamen) volcanic rocks are highlighted.

Acknowledgements

The Metrica S.A, National Cadastre and Mapping Agency S.A, National Observatory of Athens (Ganas et al. 2011) and National Technical University of Athens are acknowledged for providing GPS data.

References

Agostini, S., Doglioni, C., Innocenti, F., Manetti, P., Tonarini, S., 2010. On the geodynamics of the Aegean rift. Tectonophysics 488, 7-21.

Caputo, R., Pavlides, S., 2013. The Greek Database of Seismogenic Sources (GreDaSS), version 2.0.0: A compilation of potential seismogenic sources (Mw > 5.5) in the Aegean Region. http://gredass.unife.it/, doi:10.15160/unife/gredass/0200.

Ganas, A., Chousianitis, K., Drakatos, G. Papanikolaou, M., Argyrakis, P., Kolligri, M., Petrou, Panagiota., Batsi, E., Tsimi, C., 2011. NOANET. High-rate GPS Network for Seismology and Geodynamics in Greece. Geophysical research abstracts, 13.

Kamvisis, I.N.G., 2010. Occurrences of lamprophyric rocks in Greece. Neues Jahrbuch für Mineralogie-Abhandlungen: Journal of Mineralogy and Geochemistry 187, 225-234.

Karydakis, G., Arvanitis, A., Andritsos, N., Fytikas, M., 2005. Low enthalpy geothermal fields in the Strymon basin (Northern Greece). World Geothermal Congress, Antalya, Turkey, 24-29.

Lazos, I., Stergiou, L.C., Chatzipetros, A., Pikridas, C., Bithris, S., Melfos, V., 2018. Active tectonics (extensional regime and rotations) and Tertiary mineralization occurrences within Central Macedonia, Greece. 9th International INQUA Meeting on Paleoseismology, Active Tectonics and Archeoseismology (PATA), Possidi, Greece, 145-148.

Lambrakis, N., Katsanou, K., Siavalas, G., 2014. Geothermal fields and thermal waters of Greece: An overview. in: Baba, A., Bundschuh, J., Chandrasekharam, D. (Eds.), Geothermal Systems and Energy Resources: Turkey and Greece, 25-46.

Maratos, G., 1966. The Sitsi-Kamen Volcano on the Angistron mountain. Age and relation with the metallogenesis and the hot springs. Bulletin of the Geological Society of Greece VII(1), 93-106.

Melfos, V., Voudouris, P., 2017. Cenozoic metallogeny of Greece and potential for precious, critical and rare metals exploration. Ore Geology Reviews 89, 1030-1057.

Pe-Piper, G., Piper, D.J.W., 2007. Neogene backarc volcanism of the Aegean: New insights into the relationship between magmatism and tectonics, in: Beccaluva, L., Bianchini, G., Wilson, M. (Eds.), Cenozoic Volcanism in the Mediterranean Area: Geological Society of America Special Paper 418, 17–31.

Sakellariou, D., Tsampouraki-Kraounaki, K., 2019. Plio-Quaternary Extension and Strike-Slip Tectonics in the Aegean, in: Duarte, J.C. (Eds.), Transform Plate Boundaries and Fracture Zones. Elsevier, 339-374.

Vougioukalakis, G., Eleftheriadis, G., Christofides, G., Pavlides, S., Fytikas, M., Villa, I., 2004. Volcanological study of the Almopias Pliocene volcanic formations (N Greece). 5th International Symposium on Eastern Mediterranean Geology, Thessaloniki, Greece, 3, 1318–1321.

http://www.unavco.org/

15th International Congress of the Geological Society of Greece
Athens, 22-24 May, 2019 | Harokopio University of Athens, Greece
Bulletin of the Geological Society of Greece, Sp. Pub. 7 Ext. Abs. GSG2019-353

Intra-Mountainous Late Orogenic High-Angle Normal Faulting in Parnon Mt Tectonic Window, Peloponnesus, Greece

E. Skourtsos[1], A. Alexopoulos[1], S. Lekkas[1]

(1) National and Kapodistrian University of Athens, Department of Geology and Geoenvironment, Panepistimiopolis Zografou 15784, Athens, Greece, eskourt@geol.uoa.gr

The outer part of the Hellenic arc undergoes a late-orogenic extension since the Miocene, which was installed in an area that had initially undergone the stacking of a number of thrust nappes. This build-up was the direct result of the orogenic process caused by the subduction of the African plate to the south beneath the Eurasian plate in the north, which culminated in the Upper Tertiary, simultaneously eliminating a large number of paleogeographical domains that were part of the Tethys' ocean.

This late-orogenic extension was expressed: a) by the exhumation of the deepest tectonic units metamorphosed in low-grade conditions in the Upper Oligocene - Lower Miocene, constituting the footwall of low-angle normal faults (detachment faults) and building up the core of the large tectonic windows in the high mountain ranges of Crete and the Peloponnese; b) the creation of tectonic post-alpine basins defined by high-angle normal faults and filled by syn-rift sediments of Upper Miocene-Quaternary age.

This paper describes an intra-mountainous high-to moderate-angle normal fault system that constitutes the eastern margin of the tectonic window of Mt Parnon in the eastern Peloponnese. It is a significant tectonic structure which is at the same time a) the main eastern marginal fault of the metamorphic rocks of the deepest Plattenkalk Unit and b) the morphological boundary between the high topographic area of the mountain range and the lower hills of the Kynouria sector. With a length of 35 km striking NW-SE and having NE dips, it consists of four segments separated by lateral NE-SW high-angle normal faults that have cut the northern part of the metamorphic core. Its central segment, the Platanaki fault, controls an impressive slope of about 500m height (Fig. 1).

This fault system is the last expression of the late-orogenic extension that affected the area, overprinting the earlier detachment faults formed in the Middle Miocene-Lower Pliocene. Although an intra-mountainous one it must be regarded as contemporary with those faults that control the western margin of Mt Parnon that led to the final exhumation of the marbles of Plattenkalk Unit on the earth surface and its elevation at altitudes >1800m, feeding material to the Upper Pliocene-Quaternary basins of the southern Peloponnese.



Figure 1. The Platanaki fault segment. View from the north (Google Earth image).

15th International Congress of the Geological Society of Greece
Athens, 22-24 May, 2019 | Harokopio University of Athens, Greece
Bulletin of the Geological Society of Greece, Sp. Pub. 7 Ext. Abs. GSG2019-371

Gravity Driven Slope-Failures along Late Cenozoic Basin Margins in the Outer Hellenic Arc

Apostolos Alexopoulos[1], Emmanuel Skourtsos[1], Haralambos Kranis[1]

(1) National and Kapodistrian University of Athens, Department of Geology and Geoenvironment, Panepistimiopolis Zografou, 15784, Athens, Greece, aalexopoulos@geol.uoa.gr

Introduction

Tectonic activity is a factor that affects the stability of fault-controlled escarpments in three ways (Brideau et al., 2005, 2009): (i) weakness zones develop along faults; (ii) it is associated with high relief and steep gradients and (iii) it can transfer can transfer inherited structures into the rocks to sites that are more susceptible to failures, e.g. they cause tilting of the fault-blocks by increasing the dips of the bedding. The relationship between active tectonics and landslide occurrence along marginal normal fault has been well established and described. However, the finding of such phenomena in older sedimentary sequences is more problematic.

The occurrence of compressional structures within the Neogene and Quaternary deposits in the post-orogenic basins on the frontal part of the Hellenic arc has been observed and described in the last 4 decades (e.g. Meulenkamp et al., 1988; Alexopoulos 1990). Notwithstanding, their interpretation and the involvement of alpine rocks in these remains to be clarified. They have been described as structures of local importance, associated with faults that have significant horizontal displacement component (e..g. Fassoulas, 1999; ten Veen and Postma, 1999), or that they form part of syn-sedimentary landslide complexes (Meulenkamp et al., 1988). Recently, an older view, expressed by Mercier (1976) and re-emerged, in the sense that these structures are associated with large-scale compressional events that took place in the Upper Miocene- Pliocene, affecting the post-orogenic basins, in the form of out-of-sequence thrust faults (Tortorici et al., 2010). This paper focuses on a number of cases where compressional structures are observed within syn-tectonic deposits or, where alpine rocks are found to overlie Late Miocene – Pliocene sediment in basins of central Crete and the Northern Peloponnese.

Tectonic setting

The Peloponnese and Crete are the topographically higher frontal parts of the mountain chain that has been formed during the subuction of the African plate beneath the Eurasian one in Greece. Their evolution since the Upper Oligocene includes a series of tectonic episodes, through the formation of large compressional nappes, the exhumation of metamoprhics through extensional detachment faults and the formation of hanging-wall syn-tectonic basins; and ultimately the development of a complex network of high-angle brittle faults that bound the active tectonic basins (e.g. van Hinsbergen et al., 2006).

Description and interpretation of the compressional structures

A series of E-W trending, fault-controlled basins (terrestrial or marine ones) were formed in central Crete in the Upper Miocene. Sedimentation in these basins lasted until the Pliocene. One such example is the Spili basin, where Tortonian conglomerates are steeply tilted against the Spili boundary fault, at the foot of Mt Kedros. These conglomerates are overlain by Mesozoic carbonates of the Tripolis unit and the whole structure is covered by lateral scree and colluvial wedges. Such positioning of the Tripolis carbonates is attributed to landsliding that occurred at the late stages of rifting. The Apostolon-Amari basin (close to the Fourfouras village), located along the south-western flanks of Mt Psiloreitis, the geometry of the Tefelia and Vrysses formations is fault-controlled, and display N-NNE dips which become S-SSW close to the basin margin. The deposition in this basin took place on a highly faulted basement with intense palaeorelief and was controlled by a normal NW-SE fault that caused local dragging folds in the syn-rift sediemnts. Nowadays, along this fault zone, Late Pleistocene lateral scree has covered most of these structures. To the north, in the Rethymno basin and to the south of Perama, there are sediments of the Vrysses Group with slight northern slopes. Locally, small south-dipping reverse faults are also observed: these are related slumping events that occurred on the weakness planes defined by the bedding of the post-alpine deposits.

Two more cases are examined, at Northern Peloponnese, along the southern margin of the Corinth rift. At the southern flanks of Mt Ziria (Kyllini) and north of Lake Stymfalia, a strip of Tripolis carbonates in sandwiched between steeply tilted (>30o) synrift conglomerates. North of Mt Khelmos, east of Kalavrita, fluvial conglomerates are capped by Tripolis and Pindos carbonates, which in turn are covered by thick cohesive multimictic breccia, related to glacier erosion. Such positioning of the Mesozoic carbonates is attributed to landsliding that occurred at the early stages of rifting, during the deposition of the conglomerates. The ensuing flank uplift associated with the Corinth rift evolution cause the southward tilting of the early synrift deposits, while from the geomorphological viewpoint it led to the formation of the closed hydrological basin of Stymfalia.

Conclusions

The tectonic activity on the outer part of the Hellenic Arc since the Middle Miocene has led to the formation of basins bounded by normal faults. The continuing activity on these faults led to the formation of weakness zones, high relief, and the necessary depositional space. Locally –and where conditions were favorable- slides along the then marginal faults transported blocks of alpine rocks downhill, where they were finally emplaced atop the syn-tectonic sediments. The

stratigraphic context of these slides (i.e. the age of the syn-tectonic sediments they are associated with), suggests that such activity took place during the late stages of basin evolution. The parallelism of the landslides with the margins of the basins highlights their close relationship, eventually rejecting the scenario for occurrence of a broad compressional event in the Upper Messinian- Lower Pliocene.

References

Alexopoulos, A., 1990. Peculiar Neogene deposits in Central-eastern Crete and their significance for the tectonic and paleogeographic evolution of Crere. Bull. Geol.Soc.Greece, 26, 67-76 (in Greek with English abstract).

Brideau, M., Stead, D., Kinakin, D. and Fecova, K., 2005. Influence of tectonic structures on the Hope Slide, British Columbia, Canada. Engineering Geology, 80, 242–259.

Brideau, M., Yan, M. and Stead, D., 2009. The role of tectonic damage and brittle rock fracture in the development of large rock slope failures, Geomorphology, 103, 30–49.

Fassoulas, C., 1999. The structural evolution of central Crete: insight into the tectonic evolution of the south Aegean (Greece). J. Geodyn. 27, 23–43.

van Hinsbergen, D.J.J., Meulenkamp, J.E., 2006. Neogene supradetachment basindevelopment on Crete (Greece) during exhumation of the South Aegean corecomplex. Basin Res. 18, 103–124. doi:10.1111/j.1365-2117.2005.00282.x.

Mercier, J.L., 1976. La Neotectonique, ses methods et ses buts. Un exemple: L' Arc Egeen (Mediterranee orientale). Rev. Geogr. Phys. Geol. Dyn. V. XVIII, 323-346.

Meulenkamp, J.E., Wortel, M.J.R., van Wamel, W.A., Spakman, W., Hoogerduyn Strating, E., 1988. On the Hellenic subduction zone and the geodynamic evolution of Cretesince the late Middle Miocene. Tectonophysics 146, 203–215.

ten Veen, J.H., Postma, G.,1999. Neogene tectonics and basinfill patterns in the Hellenic outer-arc (Crete, Greece). Basin Res. 11, 223–241.

Tortorici, L., et al., 2010. Late Neogene to Quaternary contractional structures in Crete (Greece)." Tectonophysics 483, 203-213.

15th International Congress of the Geological Society of Greece
Athens, 22-24 May, 2019 | Harokopio University of Athens, Greece
Bulletin of the Geological Society of Greece, Sp. Pub. 7 Ext. Abs. GSG2019-378

The Upper Miocene sediments of Anoghia: their Significance for the Tectonic Evolution of Crete, Greece.

E. Moraiti[1] & A. Alexopoulos[2]

(1) Hellenic Survey of Geology and Mineral Exploration (H.S.G.M.E.). Spirou Loui 1, 13677 Acharnae, Greece, moraiti@igme.gr
(2) National and Kapodistrian University of Athens; aalexopoulos@geol.uoa.gr

Crete lies close to the convergence boundary of African and Euro-Asiatic continents (Fig.1.C) and consists of a series imbricate tectonic units (nappes), which consist of Alpine formations (Creuzburg and Seidel 1975, Bonneau 1976, Fig. 1A, B). These formations were formed in different palaeo environments but each unit has its own deformational and metamorphic history. Except these sediments there occur post-alpine sediments where the Neogene sediments dominate. The nowadays configuration of Crete is the result of several tectonic processes. The main processes are:

a) A compressional tectonic phase which accumulated the tectonic nappes and caused the metamorphism of some units under HP/LT conditions in Oligocene (Seidel et al., 1982),

b) The consequent fragmentation of the emergent areas due to the extension, which caused the formation of trenches and horsts and the deposition of Neogene sediments. (Meulenkamp et al., 1994).

c) The post-Miocene warping of the crust, which led to the exhumation of metamorphic complex of Crete and the formation of detachment faults. (Fassoulas et al., 1994).

The Neogene sediments south of Anoghia

The Neogene sediments south of Anoghia are limited along the way from Anoghia to Nida plateau (fig.1D) and their outcrop is relatively small as well of small thickness. In Vathia area 1.5 Km south of Anogia the thickness of Neogene ranges from 10 to 50 cm and they comprise well-cemented micro conglomerates masse and brown yellow marls with numerous small size limestone pieces. In fact they are unconformably overlying the carbonates of Crete-Mani unit or the tectonic contact of Tripolis and Crete-Mani carbonates. The ages of Upper Miocene –L.Pliocene are indicated. Southwards the thickness and width of the outcrop increases. The conglomerate-breccia with clay-sandstone matrix dominates. They are well cemented and overlying unconformably both Crete-Mani and Tripolis carbonates as well as phyllite-quartzite horizons.

Biostratigraphically, the most important Neogene sediments outcrop is the one next to the chapel St. Marina close to the spring of the Zomythos. Their thickness is about six meters and from depth to the upper surface the following members can be distinguished (fig. 2): (i) An alternation of thin-layered sandstones, marls saprophytes and fine grained conglomerates of total thickness 1.5 meters (sample D2 is part of thin-layered marls), (ii)Microbreccia of total thickness 20 cm. At its base yellow marls of 5cm thickness occur (sample D3), (iii) Carbonate breccia of 2 m thick in a sandstone-marl matrix, (iv) Alternation of thin layered microbreccia yellow marls and well cemented sandstones (sample D4), (v) 2m polymixed breccia with lateral transition to coarse-thin grained alternation of sandstones (sample D5) phyllitic marls and microbreccia. In the proximity of St. Marina the Neogene sediments overlie unconformably phyllite-quartzite series and near the spring “Zomythos”, partly cover the tectonic contact of Tripolis carbonates and phyllite - quartzite series. Southwesterly of the spring, the Neogene sediments overlie unconformably the contact of the meta-flysch of the plattenkalk and the phyllite -quartzite series (sample D1).

Biostratigraphical data

The results of the study of samples D1-D5 of the previous section can be seen in tables P1 and P5 (see also fig. 3). Combining the results of tables P2 to P5 leads to the Neogene sediments age determination that is Messinian. (biozones NN11a-b, NN11b). From table P1 it is concluded that sample D1 determines the biozone NN11b. Our biostratigraphical analysis was partly based on the previously published data of Schmidt (1979) and partly on present observations. Unfortunately, the later author has not differentiated between the various Helicosphaera and furthermore he did not identify any circular Reticulofenestrids or Reticulofenestra rotaria. Moreover, he reported the FAO (First Absolute Occurrence) of Amaurolithus delicatus long before that of Discoaster quinqueramus, the latter species shown very scarce distribution in the published charts. It is known for defining the homonymous calcareous nannoplankton zone (NN 11) sensu Martini (1971) or alternatively in the scheme of Okada & Bukry (1980) the base of the equivalent CN9 Zone is defined by the FO of both D. berggrenii and D. Surculus and the top by the LO of D. quinqueramus. Therefore and due to the scarcity of the nominate species, although present to the top of the section, the nannofossill assemblage of Anogia was originally placed in the NN11, or CN9 zones and it was impossible further refinement with the presently available data set (cf. Schmidt, 1979 as well). New events like the re-occurrence of R. pseudoublilica are important, because the large variety (>7μm) has been used as an additional event for subdivision of the NN11 a, b (CN9a, b) subzones. A re-entrance of this large variety is placed within the R.rotaria zone of Theodorides (1984), below the FO of A. amplificus (CN9Bb subzzone) and immediately after the absent interval of R. pseudoumbilica (sensu Raffi & Flores, 1995).

For the lower stratigraphic interval of Anogia section, truncation of bimodality between the two varieties is present at 6 μm, while for the upper part it was estimated at ca. 7μm. Considering a constant and relatively uniform occurrence of the large variety (R.pseudoumblilica >7μm), one can use this subordinate event in distinguishing firstly the CN9b (NN11b)

subzone. Occurrence of R. rotalia points to the Tortonian/Messinian boundary of the Late Miocene and to the homonymous zone sensu Theodoridis (1984) and Young et al. (1994) various biostratigraphic data compilation for the Neogene. Key species: Discoaster quinqueramus (FAD, marks the base of CN9 or NN11), Amaurolithus delicatus (FAD) marks the base of the NN11b subzone.

Discussion-conclusions

The aforementioned observations show that this is the first time that marine Neogene deposits are found at high altitudes, south of Anoghia.

The age of these sediments, based on their microfauna and nannoplankton content is Late Tortonian to Middle-Late Messinian (NN11a-b or CN9a-b biozones). It is also highly likely that their age is even younger, reaching up to the Lower Pliocene.

The fact that these outcrops have limited extent and thickness, in respect to other isochronous deposits in other, lower-lying areas of Crete, suggest either a pause in sedimentation (owing to emergence of the broader area), or high, post-emergence erosion rate.

The occurrence of these deposits at such altitude is indicative of the magnitude of the uplift that took place in post-Messinian times.

Such uplift cannot be attributed to normal faulting (in which case the cumulative fault throw should exceed 1,400 m), but must be related to a regional doming at the area of Crete, and close to the accretionary prism, possibly related to an abrupt change in the geometry and/or the volume of the subducting African plate.

Such doming, which is also held responsible for the formation or the reactivation of large detachment faults and is connected to the exhumation of the metamorphic complex in Crete, is believed to have lasted well after the deposition of the Messinian sediments at Anoghia.

Thus, we suggest that the tectonic and structural post-alpine history of Crete should be reconsidered, by incorporating these new data.

References

Alexopoulos, A., Markopoulou – Diakadoni, A.. 1996. La presence du Calabrien au plateau Impros (Crete occidentale, Greece) et sa signification pour l'evolution tectonique de Crete. Revue de Paleobiologie, 15, 349-355.

Bonneau, M. 1976. Esquisse structurale de la Crète alpine. Bulletin de la Société géologique de France, 18, 351-353.

Creutzburg, N., Seidel, E. 1975. Zum Stand der Geologie des Präneogens auf Kreta. Neues Jahrbuch für Geologie und Paläontologie, Abhandlungen, 141, 259-285.

Fassoulas, C., Kilias, A., Mountrakis, D. 1994. Postnappe staking extension and exhumation of high-pressure/low-temperature rocks in the island of Crete, Greece. Tectonics, 13, 127-138.

Gartner, S., J. (1973). Absolute chronology of the Late Neogene calcareous nannofossil succession in the Equatorial Pacific: Geol. Soc. Am. Bull., 84, p. 2021-2034.

Meulenkamp, J. E., Van Der Zwaan, G. J., Van Wamel, W. A. 1994. On Late Miocene to resent vertical motions in the Cretan segment of the Hellenic arc. Tectonophysics, 234, 53-72.

Martini, E., 1971. Standar Tertiary and Quaternary calcareous nannoplankton zonation: Second Plank. Conf. Proc., Roma 1970, v.2, p.739-785.

Müller, C., 1972. Kalkiges Nannoplankton aus Tiefseekernen des Ionischen Meers: "Meteor" Forsch-Ergebnisse, Reihe C, v.10, p. 75-95.

Okada, H., Bukry, D., 1980. Supplementary modification and introduction of code numbers to the low-latitude coccolith biostratigraphic zonation (Bukry, 1973, 1975). Mar. Miicropaleontol., 5 (3): 321-325; Amsterdam.

Raffi, I., Flores, J.-A. (1995). Pleistocene through Miocene calcareous nannofossils from eastern Equatorial Pacific Ocean. In: Pisias, N. G. Mayer, L. A., Janecek, T.R., Palmer-Julson, A & van Andel, T. H. (eds), Proceedings of the O.D.P., Sci. Results, 138: 233-286: College Station, Tx (Ocean Drilling Program).

Raffi, I., Rio, D., 1981. Coccolithus pelagicus (Wallich): a paleotemperature indicator in the late Pliocene Mediterranean deep sea record. In: Wezel, F.C. (ed.), "Sedimentary Basins of Mediterranean Margins": 187-190; C.N.R. Italian Project of Oceanography, Tectoprint, Bologna.

Raffi, I., Backman, J., Rio, D., Shackleton, N.J., 1983. Plio-Pleistocene nannofossil biostratigraphy and calibration to oxyden isotope stratigraphiew from Deep Sea Drilling Project Site 607 and Ocean Drilling Program Site 677. Paleoceanography, 8 (3): 387-408; American Geophysical Union.

Schmidt, R., R., 1973. A calcareous nannoplankton zonation for Upper Miocene-Pliocene deposits from the southern Aegean area, with a comparison to Mediterranean stratotype localities: Kon. Ned. Akad. Wettensch. Proc. Ser. B, v. 76, p. 288-309.

Seidel, E., Kreuzer, H., Harre, W. 1982. A late Oligocene/Early Miocene high pressure belt in the External Hellinides. Geologisches Jahrbuch,, E23, 165-206.

Stradner, H., 1973. Catalogue of calcareous nannoplankton from sediments of Neogene age in the eastern North Atlantic and Mediterranean Sea. In Ryan, W. B. F., Hsu K. J., et al., Initial reports of the Deep Sea Drilling Project, Volume 13; Wasington (U.S. Government Printing Office), p. 1137-1199.

15th International Congress of the Geological Society of Greece
Athens, 22-24 May, 2019 | Harokopio University of Athens, Greece
Bulletin of the Geological Society of Greece, Sp. Pub. 7 Ext. Abs. GSG2019-388

Rheological Transects Across the Aegean Region: a Contribution to the Seismotectonics of the Area

M. Maggini[1,2], R. Caputo[1,2]

(1) University of Ferrara, Dept. of Physics and Earth Sciences, Ferrara, Italy, massimiliano.maggini@unife.it

(2) Centro inteRUniversitario per la Sismotettonica Tridimensionale, CRUST-UR Ferrara, Italy

Introduction

The Aegean Region is characterized by a dense pattern of seismogenic faults, whose terminations at depths are not always well defined. Rheological modelling, by means of strength profiles calibration and realization, is used to determine the depth of the brittle-ductile transition (hereinafter BDT) within the broader area. In the present paper we focus on the Hellenides fold and thrust belt and Hellenic subduction zone comparing our results (in terms of BDT depth) with the depth of the recorded seismicity. The primary aim is to constrain some of the principal seismotectonic parameters for better defining the seismogenic potential of the active faults.

Data and Methods

We realized eight transects in the Aegean Region (see Fig. 1a). The first three start offshore Corfu (western Greece) and terminate around Thessaloniki (northeastern Greece) thus entirely crossing a continental collision setting. A second group of three transects is almost parallel but it has been traced across the active western Hellenic subduction zone of oceanic Nubian/Ionian lithosphere below the Aegean microplate; it initiates offshore of southwestern Peloponnesus and ends in the Attica region. Two more transects have been designed parallel to the axis of the Hellenides fold and thrust belt in order to cross and link the other two groups; one runs in a distal offshore position and the other mainly onland. The crosscutting geometry of the transects array allows to use the two intersections both as control points and as 3D-view insights on the thermo-rheological characteristics of the western Hellenides region. Each transect (except for the NNW-SSE trending ones, which are longer) has a total length of ~430 km and results from the projection of well-calibrated 1D strength profiles onto the transect direction (mean inter-space between the 1D profiles along a transect is ~10 km). By interpolating the closely-spaced strength profiles we obtained BDT depth, strength and temperature distributions at depth (here we limit the analysis to the first 100 km) for the eight transects. In order to realize the rheological transects we collected literature data for the values of the input parameters of the constitutive rheological equations from different studies, methods and sources. The literature data were then integrated with our geological and tectonic considerations in order to select the proper values and obtain reliable profiles. For the purposes of thermo-rheological modelling we used the simplified approach first proposed by Brace and Kohlstedt (1980) and then widely used in the literature (e.g. Ranalli and Murphy, 1987; Ranalli, 1995). Such a method consists in taking into account only the frictional sliding (brittle) deformation mechanism and the dislocation creep one, for respectively, the brittle and the ductile behavior.

Results

As regards the BDT depth, in the western 180-200 km the southern group of profiles (profile EE', see Fig. 1c) displays a deeper transition than the northern one, with values comprised between 35 and 40 km. This is probably due to the (cold and old) oceanic nature of the crust in those sectors. After the 200 km mark, the sudden shallowing of the BDT to depths comprised between 15 and 10 km in the Oichalia and Kalamata regions is related to the upward shift of the rheological transition from the downgoing Ionian plate to the overriding Aegean plate. In the northern group of profiles (profile BB', Fig. 1b) a similar trend of rapid shallowing of the BDT after *ca* 170-180 km is also observed. In this case however, the BDT is no ever deeper than 33 km even in the low surface heat-flow region at the western end (Corfu area). Such a behaviour is related to the continental nature of the crust within the undergoing plate and the associated intermediate/felsic typical lithologies (we selected quartzite and granulite for the upper and the lower crust, respectively) which tend to yield at lower shear stresses (and therefore minor pressures and depths) with respect to mafic lithotypes. After the 200 km mark the BDT shallows to depths comprised between 15 and 20 km, being therefore deeper than the corresponding sectors of the southern profiles. This could be explained by the lower surface heat-flow characterizing Epirus and northern Hellenides area with respect to Attica and northeastern Peloponnesus regions. From a rheological point of view the comparison between continental collision (BB') and oceanic subduction (EE') settings emphasizes the following differences and peculiarities: i) the occurrence of a deeper brittle layer just below the uppermost one in the continental settings, which is instead absent in the oceanic crust; ii) a thinner brittle layer in the back-arc region for the oceanic subduction setting; iii) the presence in the continental settings of brittlely deforming layers occurring in the intermediate and lower crust even below considerably thick ductile layers, especially when geothermal gradient and surface heat-flow are particularly low.

Application to seismotectonics

We used the depth of the BDT as a tool for constraining the geometrical (width and hence expected maximum magnitude) characteristics of some selected seismogenic sources taken from the GreDaSS database (Caputo *et al*., 2012). The selected sources crosscut either the transect BB' or the EE' and correspond to the South Kourveleshi Thrust (composite source, BB'), Paleochori Fault (individual source, BB'), Pamisos Fault (composite source, EE') and the Fili Fault (individual

source, EE'). The South Kourveleshi Thrust lies in the central-western sector of the BB' transect, where on average the BDT is ~21-22 km deep; assuming a dip angle of 45° for this reverse fault and using empirical relationships a maximum expected magnitude of 7.1-7.2 is obtained which is consistent with the estimate of the GreDaSS database. The Paleochori Fault lies instead in the central-eastern portion of the BB' transect. Here aftershocks of the 1995 Kozani-Grevena earthquake are distributed down to depths of ca 15-16 km (Rigo *et al*., 2004; Resor *et al*., 2005), being consistent with the BDT depth from our rheological modelling equal to ca 16 km. The maximum expected magnitude is in the order of 6.8, which is slightly higher than the value of Mw=6.5 of the 1995 earthquake. However, the estimate is considered to be acceptable, also considering that the 1995 earthquake did not produce surface ruptures and aftershocks did not occur any shallower than 4 km (Resor *et al*., 2005), indicating that probably the seismogenic rupture did not propagate for the entire thickness of the seismogenic layer (while our estimate are always conservative meaning that all the seismogenic thickness is ruptured coseismically). As regards the Pamisos Fault, this lies on the central sector of the EE' transect; also in this case the seismological data are in agreement with the BDT depth obtained from the rheological modelling, which is around 16 km. The calculated maximum expected magnitude corresponds to values around 6.8, which is consistent with the estimate given in the GreDaSS database equal to 6.7. The last selected source, corresponding to the Fili Fault is located close to the eastern termination of the EE' transect. The BDT in this region is quite shallow, with depth of *ca* 9-10 km, consistent with the focal depth of the 1999 Athens earthquake being on average ~10-11 km and most of the aftershocks occurring above 11-12 km (e.g. Louvari and Kiratzi, 2001; Papadimitriou *et al*., 2002; Papadopoulos *et al*, 2004). We obtained a maximum expected magnitude of 6.3-6.4, which is slightly greater than the value of the 1999 mainshock. Also in this case however, it must be taken into account that the rupture only propagated upwards to depths as shallow as 3-5 km, and therefore the maximum magnitude associated to the Fili Fault could be greater and comparable to our estimate in the case of a rupture fully propagating throughout the entire seismogenic layer.

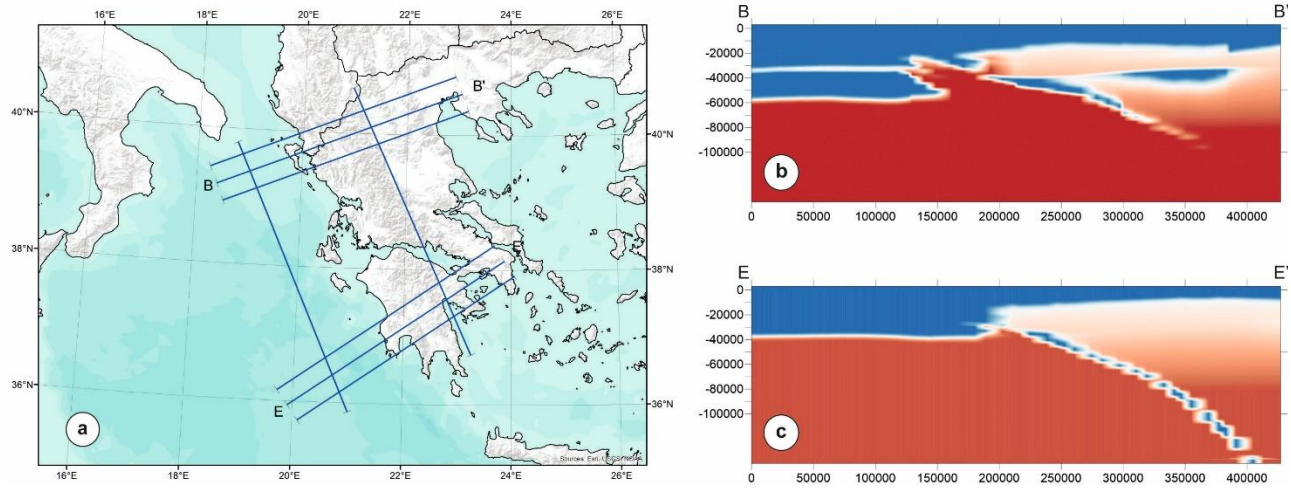

Figure 1. a) Terrain map of the Central-Eastern. Mediterranean Region showing the position of the investigated profiles; b) section of the difference between brittle (blue) and ductile (red) strength for the BB' profile. The whitish colors indicate the brittle-ductile transition zones; c) same as b) but for the EE' profile.

References

Brace W.E., Kohlstedt D., 1980. Limits on lithospheric stress imposed by laboratory experiments. J. Geophys. Res. 85, 6248-6252.

Caputo R., Chatzipetros A., Pavlides S., Sboras S., 2012. The Greek Database of Seismogenic Sources (GreDaSS): state-of-the-art for northern Greece. Ann. Geophys. 55(5), 859-894.

Louvari, E., Kiratzi, A., 2001. Source parameters of the 7 September 1999 Athens (Greece) earthquake based on teleseismic data. Journal of the Balkan Geophysical Society 4(3), 51-60.

Papadimitriou, P., Voulgaris, N., Kassaras, I., Kaviris, G., Delibasis, N., Makropoulos, K., 2002. The Mw= 6.0, 7 September 1999 Athens earthquake. Natural Hazards 27(1-2), 15-33.

Papadopoulos, G. A., Matsumoto, H., Ganas, A., Karastathis, V., Pavlides, S., 2004. Deformation patterns associated with the M5.9 Athens (Greece) earthquake of 7 September 1999. Journal of Seismology 8(3), 381-394.

Ranalli G., 1995. Rheology of the earth. 2nd ed. Chapman & Hall.

Ranalli G., Murphy D.C., 1987. Rheological stratification of the lithosphere. Tectonophys. 132, 281-295.

Resor P.G., Pollard D.D., Wright T.J., Beroza G.C., 2005. Integrating high-precision aftershock locations and geodetic observations to model coseismic deformation associated with the 1995 Kozani-Grevena earthquake, Greece. J. Geophys. Res. 110, B09402.

Rigo A., de Chabalier J.-B., Meyer B., Armijo R., 2004. The 1995 Kozani-Grevena (northern Greece) earthquake revisited: An improved faulting model from synthetic aperture radar interferometry. Geophys. J. Int. 157, 727-736.

SPECIAL SESSION

T2.S1 The Hellenic Subduction, the North Anatolian Fault and the Aegean back-arc deformation: how do they interact in space and time?

Conveners: **Dimitris Sakellariou (HCMR)**
Nicholas Chamot-Rook (Ec. Sup. Paris)
Laurent Jolivet (Univ. P.M Curie)

15th International Congress of the Geological Society of Greece
Athens, 22-24 May, 2019 | Harokopio University of Athens, Greece
Bulletin of the Geological Society of Greece, Sp. Pub. 7 Ext. Abs. GSG2019-023

Geodetic evidence for shear instability in the west part of the North Aegean Trough, in a 100+ years scale

SC Stiros
Departmentt of Civil Engineering, Patras University, Patras 26500, stiros@upatras.gr

Overview

GPS data describe well deformation of the crust in tectonically active regions, but they cover a period of up to few decades only, and this interval is very short compared to geological processes and the repeat intervals of earthquakes. A possibility to expand this geodetic record is to exploit historical geodetic data.
In this article we analyze triangulation data covering the west edge of the North Aegean Trough (NAT), an area of complicated tectonics, and document an instability in the kinematics of the study area in time scale of a few tens of years. This result is consistent with the distribution of earthquakes and may provide some clues on the termination of major strike slip faults.

The North Aegean Trough (NAT)

The North Aegean Trough (NAT) is a prominent, about 1000m deep, tectonically active marine basin in North Aegean, at the continuation of the North Anatolian Fault (Taymaz et al, 1991; Kreemer et al, 2004; Saltogianni et al, 2015). At its eastern part, at the continuation of the North Anatolian Fault, NAT is identified with a narrow basin which hosted, among others, the 2014, strike slip M_w6.9 Samothraki-Imvros (Gokceada) earthquake (Saltogianni et al, 2015). At its middle part, the NAT is overprinted by a transtensional basin, while farther west its width increases and becomes a rather diffuse, double half-graben structure (Papanikolaou et al. 2002; Georgiou et al. 2016), also marked by essentially strike slip earthquakes but with more diffuse pattern (Taymaz et al, 1991; Roumelioti et al, 2004; Ganas et al, 2005). The overall pattern is confirmed by displacement vectors of the HEPOS GPS network, the first homogeneous and well-tested permanent GPS network analyzed in this area (Mouslopoulou et al 2014).
In the past, it was thought that NAT and the North Anatolian Fault continue through the Greek mainland, but this seems not likely. First, the active tectonic and morphotectonic pattern of continental Greece do not support this hypothesis. Second, the streamlines of slip vectors from the permanent HEPOS GPS are characterized by bending near the coast of the Greek mainland, indicating a kind of barrier in the kinematics and deformation of the area (Mouslopoulou et al, 2014).

Historical geodetic (triangulation) data and tectonic information

High quality triangulation data cover southern and central Greece and part of the Sporades Isles. These data were collected during three major surveys, in the 1890's, 1920's and 1960's, are homogeneous and of exceptionally high quality, and many of the pillars of the first survey were also used in the two later surveys so that a comparison of data of successive surveys can be made. Available historical triangulation data are reliable, especially because they cover all three angles of triangles, so that the error control in excellent (Stiros, 1991).
The problem with triangulation data is that they do not provide information on the scale (distances between triangulation stations), and for this reason it is not possible to derive displacement vectors (unless certain a priori assumptions are made), and among the three elements describing the deformation tensor, only shear can be computed (Stiros et al 2013). This is, however, an ideal information for strike-slip environments (Fig. 1).

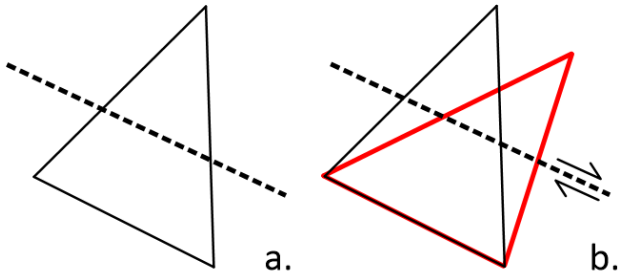

Figure 1. Conceptual model for derivation of shear from triangulation data. Fault activity tends to deform angles of a triangle crossed by a strike slip fault. Inversely, from the analysis of measured angles in historical triangulation data (i.e. of angles in triangles), shear deformation can be identified and quantified.

Analysis of data from the western part of the NAT

The available triangulation data were analyzed using the algorithm summarized in Stiros et al (2013) and there have been computed estimates of shear for the two different intervals, 1890's-1920's and 1930's-1960's.
During the second interval, between the 1920's-1960's, shear deformation was found compatible with that derived from modern GPS data and morphotectonic and seismological observations. On the contrary, during the first interval, 1890's-1920's, no evidence of significant estimate of shear deformation exists.
These results are statistically significant and reliable, and likely to indicate true contrasts in the kinematics of the study area.

Seismotectonic and structural constraints and implications

The inferred instability in the deformation pattern derived from historical geodetic data is intriguing because short-term (of the order of tens of years) fluctuations in the deformation pattern are not expected in a major strike slip fault.
Still, the inferred change in shear is consistent with changes in seismicity (e.g. Papazachos and Papazachou, 1997). The interval 1890's-1920's of no shear is marked by seismic quiescence at least for the western part of the NAT, while the interval 1930's-1960's is characterized by moderate and strong earthquakes, and such a correlation may have a structural significance.
On these grounds and based on the morphotectonics of the west edge of the NAT, and on the pattern of streamlines of the GPS-derived tectonic displacements (Mouslopoulou et al, 2014), we can propose the following scenario.
The west part of the NAT represents a structurally composite area (cf. Papanikolaou et al., 2002; Georgiou et al, 2016) and not a simple strike slip-controlled environment, and its overall deformation reflects the cumulation of different tectonic processes at different stages, as well as the influence of adjacent tectonic provinces (boundary effects). Superimposition of the deformation rates from these effects and sources may temporarily obscure certain regional effects (e.g. shear from the east), emphasize transient effects and lead to alternation of clusters of strong earthquakes with relatively short aseismic intervals.

Structural and tectonophysical implications: how strike-slip faults terminate?

Deformation of this area may also provide some clues for the problem of how major strike slip faults terminate. In fact, this is a question of both theoretical and practical (seismic hazard) importance, but for lack of data, no convincing answers have been given so far. The kinematics of the western part of the NAT may shed some light to this important problem.

Acknowledgements

Historical triangulation data were mined from the archives of GYS. ontributions in calculations by A. Gavrilaki, D. Chiotis and F. Moschas are acknowledged.

References

Ganas, A., G. Drakatos, S. Pavlides, G. Stavrakakis, M. Ziazia, E. Sokos, V.Karastathis. 2005. The 2001 Mw = 6.4 Skyros earthquake, conjugate strike-slip faulting and spatial variation in stress within the central Aegean Sea Journal of Geodynamics 39, 61–77

Georgiou, N., Dimas, X., Sergiou, S., Christodoulou, D., Papatheodorou, G., Ferentinos, G., 2016. Fault geometry and kinematics at the termination of the North Anatolian Fault: Sporades Basin and surrounding area, North Aegean Sea, Eastern Mediterranean. Poster presentation, Geol Soc Gr Conference.

Kreemer, C, Chamot-Rooke, N, Le Pichon, X., 2004. Constraints on the evolution and vertical coherency of deformation in the Northern Aegean from a comparison of geodetic, geologic and seismologic data. Earth Planet Sci Lett, 225, 329-346

Mouslopoulou, V, Saltogianni, V., Gianniou, M., Stiros, S., 2014. Geodetic evidence for tectonic activity on the Strymon Fault System, northeast Greece, Tectonophysics, 633, 246-255.

Papanikolaou, D., Alexandri, M., Nomikou, P., Ballas, D., 2002. Morphotectonic structure of the western part of the North Aegean Basin based on swath bathymetry. Marine Geology, 190, 465-492

Papazachos, B., and C. Papazachou 1997, The Earthquakes of Greece., Ziti and Co., Thessaloniki, Greece.

Roumelioti, Z., A. Kiratzi, and D. Dreger. 2004. The source process of the 2001 July 26 Skyros Island (Greece) earthquake, *Geophys. J. Int.*, *156*(3), 541–548

Saltogianni, V., Gianniou, M., Taymaz, T., Yolsal-Çevikbilen, S., Stiros, S., 2015. Fault-Slip Source Models for the 2014 *Mw* 6.9 Samothraki-Gökçeada Earthquake (North Aegean Trough) Combining Geodetic and Seismological Observations, J Geophys. Res. (Solid Earth), 120(12).

Stiros, S., 1991. Kinematics and deformation of central and southwestern Greece from historical triangulation data and implications for the active tectonics of the Aegean, Tectonophysics, 220, 283-300.

Stiros, S., Moschas, F., Feng, L. Newman, A., 2013. Long-term versus short-term deformation of the meizoseismal area of the 2008 Achaia-Elia (M_W 6.4) earthquake in NW Peloponnese, Greece: Evidence from historical triangulation and morphotectonic data., Tectonophysics, 592, 150–158.

Taymaz, T., J. Jackson, D. McKenzie, 1991, Active tectonics of the north and central Aegean Sea, Geophys. J. Int., 106(2), 433–490.

15th International Congress of the Geological Society of Greece
Athens, 22-24 May, 2019 | Harokopio University of Athens, Greece
Bulletin of the Geological Society of Greece, Sp. Pub. 7 Ext. Abs. GSG2019-080

Constraints on the onset of the Aegean back-arc extension using Oligocene NE-directed ductile shearing in the Cyclades

P. Xypolias[1], V. Chatzaras[2], N. Gerogiannis[1], E. Aravadinou[1]

(1) Department of Geology, University of Patras, 26500 Patras, Greece; p.xypolias@upatras.gr
(2) School of Geosciences, The University of Sydney, Sydney, NSW, Australia

Objectives

Several studies (e.g., Jolivet *et al.*, 2010) suggest that the Cyclades in central Aegean region have been affected by back-arc extension triggered by the retreat of the Hellenic subduction slab. However, the initiation time of the Aegean back-arc extension remains controversial. Specifically, post-orogenic back-arc extension in Cyclades is considered to have begun either in late Eocene/early Oligocene (Jolivet *et al.*, 2010; Laurent *et al.*, 2017) or late Oligocene/early Miocene (Avigad *et al.*, 1997) or late Miocene (Chatzaras *et al.*, 2011) or potentially in lower Pliocene (Boronkay and Doutsos, 1994). In order to shed light on this controversy, we focus on the Oligocene deformation history of the Cycladic Blueschist Unit.

Tectonic framework

The Cycladic Blueschist Unit suffered blueschist to eclogite facies metamorphism at early Eocene (Bröcker *et al.*, 2013 and references therein). Subsequent ductile-stage exhumation of the unit initiated at blueschist facies conditions and progressively continued and completed at greenschist facies conditions until early Miocene (Bröcker *et al.*, 2013). The Oligocene exhumation-related ductile deformation is mainly expressed by a penetrative foliation and an associated NE-trending stretching lineation. It is broadly accepted that top-to-the-NE shearing was dominant in west Cyclades during this deformation phase (Fig. 1: inset map) (e.g., Jolivet *et al.*, 2010).

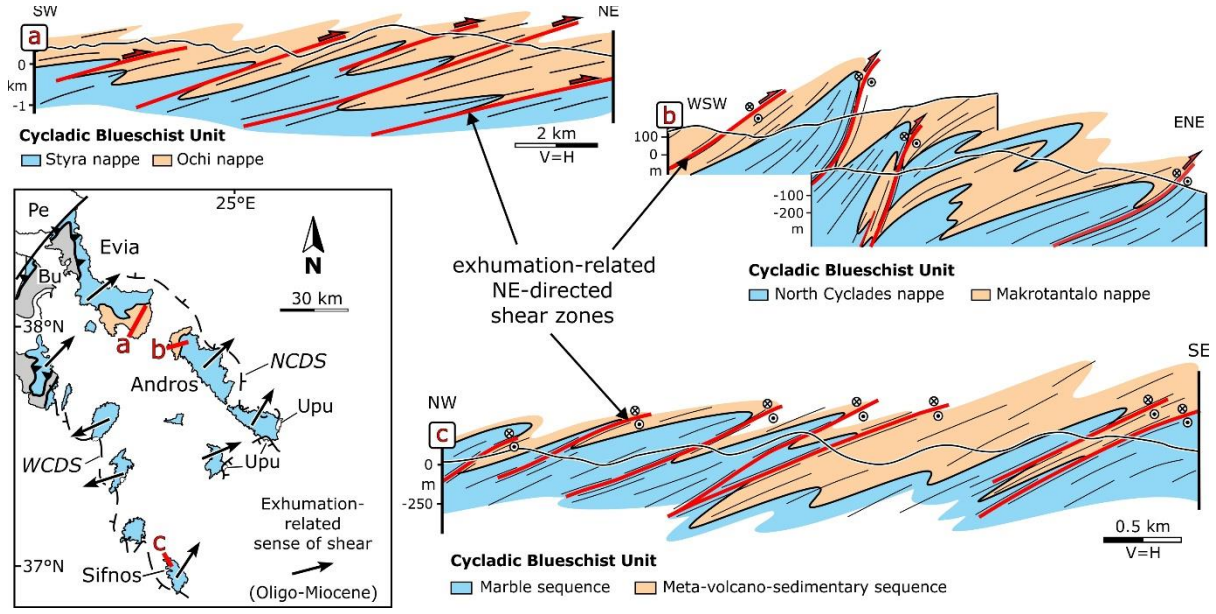

Figure 1. Cross-sections from (a) south Evia (after Xypolias *et al.*, 2012), (b) north Andros (after Gerogiannis *et al.*, 2019) and (c) north Sifnos (after Aravadinou *et al.*, 2016) illustrating the internal structural architecture of the Cycladic Blueschist Unit. Inset shows a simplified geological map of Cyclades indicating the sense of shear in the Cycladic Blueschist Unit during Oligocene-Miocene as well as the position of the cross sections (a-c). Bu, Basal unit; Pe, Pelagonian; Upu, Uppermost unit; NCDS and WCDS, North and West Cycladic Detachment System, respectively.

However, the tectonic context in which this shearing occurred remains controversial. Specifically, it has been suggested that the Oligocene NE-directed shearing has: (a) a normal-sense and reflects the motion of the upper NE-dipping detachment formed during SW-wards Oligocene extrusion/exhumation of the Cycladic Blueschist Unit under overall orogenic compression (Ring *et al.*, 2007); (b) a normal-sense and genetically linked with the formation of the North Cycladic Detachment System due to overall, back-arc related extension (Laurent *et al.*, 2017); and (c) a thrust-sense and reflects the direction of extrusion/exhumation of the Cycladic Blueschist Unit under overall orogenic compression (Xypolias *et al.*, 2012).

Key structural observations

Outcrop-scale kinematic indicators indicating top-down-to-NE and top-up-to-NE sense of shear cannot be used to discriminate between large-scale normal- and thrust-sense of shearing during exhumation. Post-orogenic doming in

Cyclades has probably masked the original orientation of the foliation formed during exhumation. Therefore, other criteria should be used to discriminate between the above assumptions.

The absence of Oligocene extensional sedimentary basins and magmatism, as well as the absence of downward increase in the metamorphic pressure, do not support the interpretation that NE-directed shearing was linked with normal-sense movements under an overall extension. Moreover, in many Cycladic islands, the NE-directed shearing is associated with the restacking of the early nappe pile of the Cycladic Blueschist Unit, which formed during the burial stage. In south Evia and north Andros, for example, we have mapped a series of NE-directed shear zones that cut up-section in their transport direction and have brought the lower North Cyclades nappe (also known as Styra nappe in Evia) over the upper Ochi-Makrotantalo nappe (Fig. 1a, b). Such a deformation pattern is to be expected in contractional belts, and therefore, it seems that the NE-directed shear zones have operated as ductile thrusts. Chemical analysis of amphiboles defining the mylonitic foliation in these shear zones has shown that thrust-sense movements started at blueschist facies conditions and progressively continued until the completion of the greenschist facies metamorphism at early Miocene. A similar situation has also been observed in northern Sifnos. There, a lower marble sequence was thrust over an upper meta-volcano-sedimentary sequence via a series of NE-directed shear zones that operated under blueschist facies to greenschist facies conditions (Fig. 1c).

Conclusions

Our structural observations show that NE-directed shearing in the Cycladic Blueschist Unit had a thrust-sense until the early Miocene when the greenschist facies metamorphism was completed. Therefore, the Oligocene NE-directed shearing within the Cycladic Blueschist Unit was associated with thrust-sense movements that occurred under overall orogenic contraction. This finding implies that the Cyclades area was affected by back-arc extension not earlier than early Miocene times.

References

Aravadinou, E., Xypolias, P., Chatzaras, V., Iliopoulos, I., Gerogiannis, N., 2016. Ductile nappe stacking and refolding in the Cycladic Blueschist Unit: insights from Sifnos Island (south Aegean Sea). Int J Earth Sci 105, 2075-2096.

Avigad, D., Garfunkel, Z., Jolivet, L., Azañon, J.M., 1997. Back arc extension and denudation of Mediterranean eclogites. Tectonics 16, 924-941.

Boronkay, K., Doutsos, T., 1994. Transpression and transtension within different structural levels in the central Aegean region. J Struct Geol 16, 1555-1573.

Bröcker, M., Baldwin, S., Arkudas, R., 2013. The geological significance of $^{40}Ar/^{39}Ar$ and Rb-Sr white mica ages from Syros and Sifnos, Greece: a record of continuous (re)crystallization during exhumation? J Metamorph Geol 31, 629-646.

Chatzaras, V., Xypolias, P., Kokkalas, S., Koukouvelas, I., 2011. Oligocene-Miocene thrusting in central Aegean: insights from the Cycladic island of Amorgos. Geol J 46, 619-636.

Gerogiannis, N., Xypolias, P., Chatzaras, V., Aravadinou, E., Papapavlou, K., 2019. Deformation within the Cycladic subduction–exhumation channel: new insights from the enigmatic Makrotantalo nappe (Andros, Aegean). Int J Earth Sci, doi.org/10.1007/s00531-019-01680-3

Jolivet, L., Lecomte, E., Huet, B., Denèle, Y., Lacombe, O., Labrousse, L., Le Pourhiet, L., Mehl, C., 2010. The North Cycladic Detachment System. Earth Planet Sci Lett 289, 87-104.

Laurent, V., Huet, B., Labrousse, L., Jolivet, L., Monié, P., Augier, R., 2017. Extraneous argon in high-pressure metamorphic rocks: Distribution, origin and transport in the Cycladic Blueschist Unit (Greece). Lithos 272-273, 315-335.

Ring, U., Glodny, J., Will, T., Thomson, S.N., 2007. An Oligocene extrusion wedge of blueschist-facies nappes on Evia, Aegean Sea, Greece: implications for the early exhumation of high-pressure rocks. J Geol Soc Lond 164, 637-652.

Xypolias, P., Iliopoulos, I., Chatzaras, V., Kokkalas, S., 2012. Subduction- and exhumation-related structures in the Cycladic Blueschists: insights from south Evia Island (Aegean region, Greece). Tectonics 31, TC2001. doi.org/10.1029/2011TC002946.

15th International Congress of the Geological Society of Greece
Athens, 22-24 May, 2019 | Harokopio University of Athens, Greece
Bulletin of the Geological Society of Greece, Sp. Pub. 7 Ext. Abs. GSG2019-103

From slow to fast deformation in the Marmara Sea: the SMARTNET network

V.Durand[1], P.Martinez-Garzon[1], M.Bohnhoff[1], T.Turkmen[2]

(1) GFZ, Telegrafenberg, Potsdam, Germany, vdurand@gfz-potsdam.de
(2) AFAD, Yalova, Turkey

The strain energy accumulated in the Earth's crust is released by a continuum of slip processes ranging from completely aseismic (i.e., slow and continuous) to fully seismic (i.e. instant rupture with km/s propagation resulting in corresponding ground motions) through several types of intermediate signals such as episodic tremor or slow earthquakes (e.g. Shelly et al., 2006, 2007; Ide et al., 2007; Rubinstein et al., 2007; 2009; Peng and Gomberg, 2010). While it is generally accepted that the occurrence of aseismic vs. seismic deformation is controlled by the fault structure (i.e. frictional properties, existence and size of asperities) (Scholz, 2002; Rubin and Ampuero, 2005; Rubin, 2008), our current process understanding on which of these deformation types dominates under which conditions is still incomplete (Harris, 2017). Furthermore, the aseismic energy release or fault creep has been usually considered in seismic hazard models as a factor reducing the amount of energy available to produce large earthquakes (Field et al., 2014). Whether aseismic slip really leads to a decreased seismic hazard also depends on many factors, such as the fraction of the fault on which creep occurs and the effect of aseismic deformation on potentially loading nearby faults. Furthermore, recent studies have shown that large earthquakes may be preceded by an acceleration of the slow slip on the interface (Bouchon et al. 2011, 2013, Kato et al. 2012, Ruiz et al. 2014), and that moderate to large earthquakes can be triggered by the propagation of a slow deformation (Durand et al. 2014). In consequent, it is important to understand how slow and fast slip interact, and what is controlling the type of slip on a fault.

The ICDP-GONAF geophysical observatory started operating in 2015 with the main goal of characterizing the deformation in the eastern Sea of Marmara region in direct vicinity of Istanbul metropolitan region and its > 15 Million inhabitants. GONAF includes seven borehole seismic arrays at different locations of the eastern Sea of Marmara as well as four boreholes equipped with strainmeters operated by UNAVCO. Recently, a large strain signal lasting for 50 days has been found in the strainmeter data recorded at the GONAF-Esenkoy station in 2016 (Martinez-Garzon et al., 2019), suggesting that the slow slip source could be located within the nearby Cinarcik segment, an intermediate branch of the North Anatolian Fault. The offset observed in the strain signal is concomitant with the occurrence of a MW4.4 earthquake located 30km away in the Cinarcik basin. This signal also corresponds to an increase of the seismic moment released in the region, including eight earthquakes of magnitude greater than 3.5. On another hand, the strain signal does not correlate with known environmental parameters such as changes of sea level, rainfall or temperature. By consequence, we infer that this signal could indicate local slow slip on the Cinarcik fault. Before the same M_W4.4 earthquake, a sequence of foreshocks has been observed (Malin et al. 2018). These foreshocks exhibit waveforms strikingly similar to the one of the mainshock. This similarity may mean that the source area of the mainshock is failing in a repetitive way before the occurrence of the main earthquake, maybe under the action of a transient forcing, like slow slip. Furthermore, identifying clusters of seismicity based on the rescaled nearest neighbor distance between events, we show that the Cinarcik region is particularly prone to the presence of foreshocks. All these observations are in favor of the existence of interplay between slow and fast deformation in the Cinarcik fault region. It is of particular interest to understand the processes controlling the deformation in this region because the Cinarcik fault could have hosted the M6.3 earthquake which occurred in 1963, and so is contributing to increase the seismic hazard to which Istanbul is exposed.

In January 2019, in order to intensify the seismic coverage of the Armutlu Peninsula in the eastern Sea of Marmara, we deployed a temporal seismic network directly on top of the Cinarcik fault, located roughly -50 km away from the Istanbul metropolitan region. We installed at total of 20 short-period stations (1Hz and 4.5Hz) and 5 broadband stations to capture a broader frequency range and reach a good azimuthal coverage for locating microseismicity and creep processes along the onshore portion of the Cinarcik fault. The main objective of this experiment is to characterize the seismic and aseismic deformation of this eventually creeping fault which is in direct vicinity to the recent 2016 M_W 4.4 earthquake (Malin et al., 2018) and the slow-slip episode recorded in the strainmeter in relation to the MW 4.4 event (Martinez-Garzon et al., 2019)

Acknowledgements

VD and PMG acknowledge funding from the Helmholtz Association in the frame of the Young Investigators Group VH-NG-1232 (SAIDAN). We also want to thank S.Bentz and C.Marx for their help during the installation of the stations, the collecting and the management of the data.

References

Bouchon, M., Karabulut, H., Aktar, M., Özalaybey, S., Schmittbuhl, J., & Bouin, M.-P. 2011. Extended Nucleation of the 1999 Mw 7.6 Izmit Earthquake. Science 331, 877–880.

Bouchon, M., Durand, V., Marsan, D., Karabulut, H., & Schmittbuhl, J. 2013. The long precursory phase of most large interplate earthquakes. Nature Geoscience 6, 299–302.

Durand, V., Bouchon, M., Floyd, M.A., Thodulidis, N., Marsan, D., Karabulut, H., & Schmittbuhl, J. 2014. Observation of the spread of slow deformation in Greece following the breakup of the slab. Geophysical Research Letters 41, 7129-7134.

Field, E. H., Arrowsmith, R. J., Biasi, G. P., Bird, P., Dawson, T. E., Felzer, K. R., et al. 2014. Uniform California Earthquake Rupture Forecast, Version 3 (UCERF3)—The Time-Independent Model. Bulletin of the Seismological Society of America 104, 1122–1180.

Harris, R. A. 2017. Large earthquakes and creeping faults. Reviews of Geophysics 2016RG000539.

Ide, S., Beroza, G. C., Shelly, D. R., & Uchide, T. 2007. A scaling law for slow earthquakes. Nature 447, 76–79.

Kato, A., Obara, K., Igarashi, T., Tsuruoka, H., Nakagawa, S., & Hirata, N. 2012. Propagation of Slow Slip Leading Up to the 2011 Mw 9.0 Tohoku-Oki Earthquake. Science 335, 705-708.
Malin, P. E., Bohnhoff, M., Blümle, F., Dresen, G., Martínez-Garzón, P., Nurlu, M., et al. 2018. Microearthquakes preceding a M4.2 Earthquake Offshore Istanbul. Scientific Reports 8, 16176.
Martínez-Garzón, P., Bohnhoff, M., Mencin, D., Kwiatek, G., Dresen, G., Hodgkinson, K., et al. 2019. Slow strain release along the eastern Marmara region offshore Istanbul in conjunction with enhanced local seismic moment release. Earth and Planetary Science Letters 510, 209–218.
Peng, Z., & Gomberg, J. 2010. An integrated perspective of the continuum between earthquakes and slow-slip phenomena. Nature Geoscience, 3, 599–607.
Rubin, A. M., & Ampuero, J.-P. 2005. Earthquake nucleation on (aging) rate and state faults. Journal of Geophysical Research: Solid Earth 110, B11312.
Rubin, A. M. 2008. Episodic slow slip events and rate-and-state friction. Journal of Geophysical Research: Solid Earth 113, B11414.
Rubinstein, J. L., Vidale, J. E., Gomberg, J., Bodin, P., Creager, K. C., & Malone, S. D. 2007. Non-volcanic tremor driven by large transient shear stresses. Nature 448, 579–582.
Rubinstein, J. L., Shelly, D. R., & Ellsworth, W. L. 2009. Non-volcanic Tremor: A Window into the Roots of Fault Zones. In S. Cloetingh & J. Negendank (Eds.), New Frontiers in Integrated Solid Earth Sciences, 287–314. Springer Netherlands.
Ruiz, S., Metois, M., Fuenzalida, A., Ruiz, J., Leyton, F., Grandin, R., Vigny, C., Madariaga, R., & Campos, J. 2014. Intense foreshocks and a slow slip event preceded the 2014 Iquique Mw 8.1 earthquake. Science 345, 1165-1169.
Scholz, C. H. 2002. The mechanics of earthquakes and faulting, 2nd ed. Cambridge University Press.
Shelly, D. R., Beroza, G. C., Ide, S., & Nakamula, S. 2006. Low-frequency earthquakes in Shikoku, Japan, and their relationship to episodic tremor and slip. Nature 442, 188–191.
Shelly, D. R., Beroza, G. C., & Ide, S. 2007. Non-volcanic tremor and low-frequency earthquake swarms. Nature 446, 305–307.

15th International Congress of the Geological Society of Greece
Athens, 22-24 May, 2019 | Harokopio University of Athens, Greece
Bulletin of the Geological Society of Greece, Sp. Pub. 7 Ext. Abs. GSG2019-119

Post-Miocene Deformation in the South Aegean: Insights from Seafloor Morphology and Seismic Profiling Data

K. Tsampouraki-Kraounaki[1,2], D. Sakellariou[1]

(1) Inst. Oceanography, Hellenic Centre for Marine Research, 19013 Anavyssos, Greece, tsampourakik@hcmr.gr
(2) Department of Geology, University of Patras, 26504 Rio Patra, Greece

Introduction

Geodetic surveys and kinematic models indicate that the western, larger part of South Aegean, along with Peloponnese behaves as a rigid body which translates SSW-wards at 33-34 mm yr-1 while SE Aegean moves at 10 mm yr-1 toward SE, away from the latter (Kreemer & Chamot-Rooke, 2004; Reilinger *et al*., 2010). Seismological data show a rather week or at least not frequent seismic activity with normal and oblique faulting earthquake focal mechanisms and more or less stable, WNW-ESE trending T-axis (Kiratzi & Louvari, 2003). Old and recent marine geological-geophysical campaigns revealed a complicate seafloor morphology and geological structure indicating that deformation in the South Aegean is active and the long-term kinematics and tectonic movements follow a more complex patter than anticipated by the short-term geodetic and seismological observations (Sakellariou & Tsampouraki-Kraounaki, 2019 and references therein). This paper aims to contribute to the understanding of the post-Miocene evolution and active tectonics in the South Aegean in the framework of the ongoing Hellenic subduction and the effect of the westward propagating North Anatolian Fault.

Methods

The bathymetric relief published recently by EMODNET Bathymetry (https://emodnet.eu/bathymetry) includes literally all available swath bathymetry data and reprocessed GEBCO bathymetry and provides a reliable base for geomorphological analysis (Fig. 1). Old and recent seismic reflection profiles available at HCMR (Fig. 1A) have been used to extract information on the shallow geological structure and seismic stratigraphy.

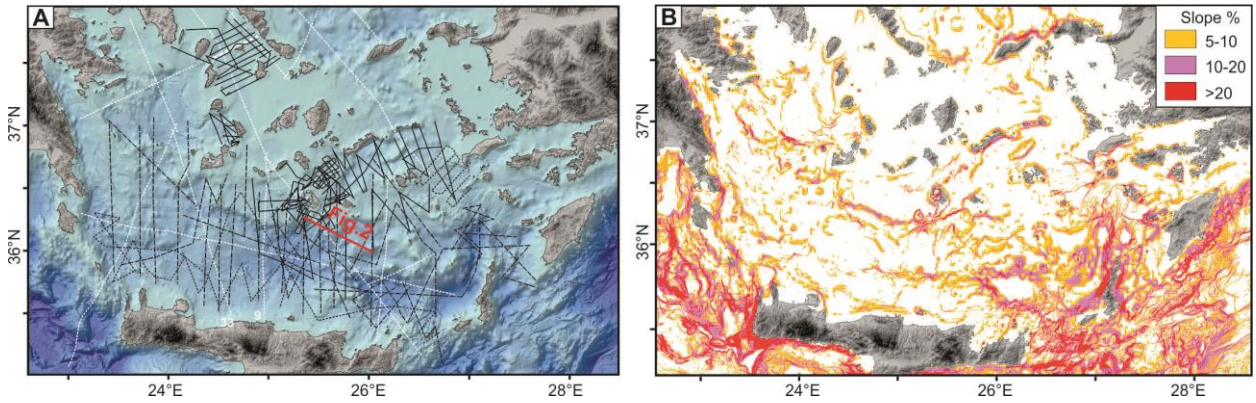

Figure 1. (A) Bathymetry and location of seismic profiles in the South Aegean. (B) Slope map highlighting the complicate morphological structure of the South Aegean.

Results

The seafloor morphology of the South Aegean is characterized by isolated basins with rhomboid, elliptical, trapezoid or spindle shape and dimension of a few tens of kilometers. They are aligned predominantly in NE-SW to ENE-WSW and secondarily in NW-SE to WNW-ESE directions, which coincide with the orientation of the steep slopes and are separated from each other by shallow ridges (Fig. 1B). The southern margin of the Cyclades Plateau is characterized by less than 1000 m deep basins. Maximum depths, between 2000 m and 2500 m, occur at the southeastern part of the South Aegean, while in the western part the depth of the major basins ranges between 1000 m and 2000 m.

Numerous, major and secondary faults cross cut the seafloor of the South Aegean, they group in two main directions, NE-SW to ENE-WSW and NW-SE to WNW-ESE and coincide with the prevailing steep slopes (Fig. 3A). They are largely responsible for the relief of the seafloor and control the margins of the topographic basins and the ones of the active sedimentary basins. A major unconformity M occurs throughout the South Aegean (Fig. 2). Below the margins, it marks the erosional surface of the basement exposed during the Messinian. Below the basins, it represents the top of the Messinian evaporites. A second, widespread unconformity U has been observed in DSDP 378 drill hole in the Cretan Basin (Hsű *et al*., 1978) and in the sedimentary infill of most of the basins in the South Aegean (Bartole *et al*., 1983; Mascle & Martin, 1990; Piper & Perissoratis, 2003; Anastasakis & Piper, 2005, Tsampouraki-Kraounaki & Sakellariou, 2017). It marks a major change in the tectonic regime, which led to rearrangement and faulting of the Pliocene basins, basin inversion, local subsidence and/or uplift and the development of the present morphological structure.

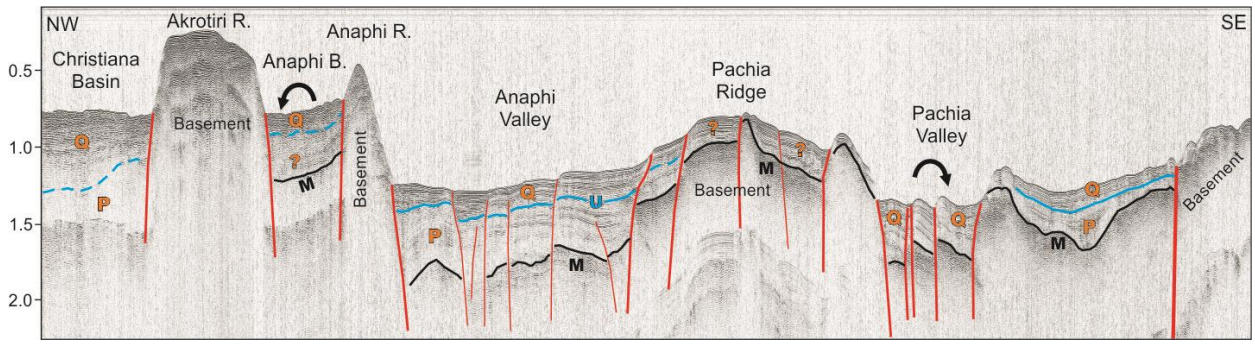

Figure 2. Seismic reflection profile (see Fig. 1A for location). The major unconformity U between the Pliocene (P) and Quaternary (Q) deposits is shown in blue. Note the dense faulting and the opposite sense of basins asymmetry between the northern and southern parts. M: Messinian unconformity

Conclusions

The configuration of the fault network, the spatial distribution of the morphological and sedimentary basins (local subsidence) and ridges and islands (local uplift), along with the seismological data point to a dual kinematic pattern in the South Aegean (Fig. 3B). The southeastern part undergoes transtensional deformation along NE-SW to ENE-WSW sinistral strike slip to oblique faulting, in accordance to the kinematics of the Pliny and Strabo Trenches. The rest of the South Aegean experiences transtenional deformation along NE-SW dextral strike slip to oblique faulting and conjugate NW-SE predominantly normal faulting. The unconformity U in Late Pliocene / Early Quaternary marks the onset of this kinematic pattern which remains active presently. We suggest that the establishment of the present kinematic regime has been triggered by the gradual propagation of the North Anatolian Fault into the Aegean and accommodates the SSW-ward movement and general NNE-SSW extension in the South Aegean.

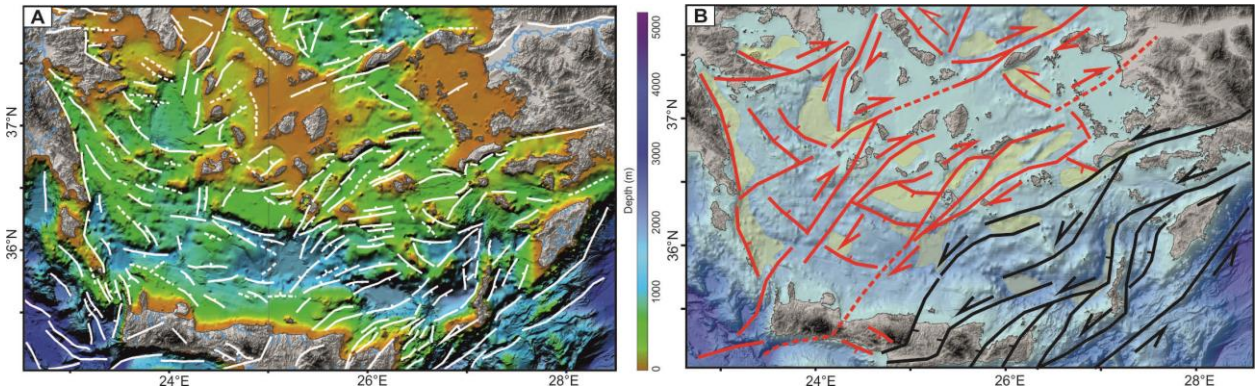

Figure 1. (A) Processed bathymetry and tetwork of main active faults in the South Aegean. (B) Main Plio-Quaternary depocenters (in yellow) and interpreted active, composite, dextral (black) and sinistral (red) fault/shear zones.

Acknowledgements

We are grateful to our colleagues in HCMR and the captain and crew of R/V AEGAEON for their continuous support during the research cruises in the South Aegean and during data processing.

References

Anastasakis, G., Piper, D. J. W., 2005. Late Neogene evolution of the western South Aegean volcanic arc: sedimentary imprint of volcanicity around Milos. Marine Geology 215, 135-158.

Bartole, Catani, R., Lenardon, G., Vinci, A., 1983. Tectonics and sedimentation of the Southern Aegean Sea. Bolletino di Oceanologia Teorica et Applicata, 4, 319-340.

Hsu, K.J., Montadert, L., Bernouilli, D., Bizon, G., Cita, M., Erickson, A., Fabricius, F., Garrison, R.E., Kido, R.B., Mellieres, F., Muller, C., Wright, R.C., 1978. Site 378: Cretan basin. Init. Rep. Deep Sea Drill. Proj. 42 (1), 321–357.

Kiratzi, A., Louvari, E., 2003. Focal mechanisms of shallow earthquakes in the Aegean Sea and the surrounding lands determined by waveform modelling: a new database. J. Geodyn. 36 (1–2), 251–274.

Kreemer, C. & Chamot-Rooke, N. 2004, Contemporary kinematics of the southern Aegean and the Mediterranean Ridge. Geophysical Journal International 157, 1377-1392.

Mascle, J. & Martin, L. 1990. Shallow structure and recent evolution of the Aegean Sea: a synthesis based on continuous seismic reflection profiles. Marine Geology 94, 271–299.

Piper, D.J.W., Perissoratis, C., 2003. Quaternary neotectonics of the South Aegean arc. Marine Geology 198, 259-288.

Reilinger, R., McClusky, S., Paradissis, D., Ergintav, S., Vernant, P., 2010. Geodetic constraints on the tectonic evolution of the Aegean region and strain accumulation along the Hellenic subduction zone. Tectonophysics 488, 22–30.

Sakellariou, D., Tsampouraki-Kraounaki, K., 2019. Plio-Quaternary extension and strike-slip tectonics in the Aegean. In: J. Duarte (Ed.): Transform Plate Boundaries and Fracture Zones, Chapter 14, p. 339-374, ELSEVIER, 2019, ISBN: 978-0-12-812064-4

Tsampouraki-Kraounaki, K., Sakellariou, D., 2017. Strike-slip deformation behind the Hellenic subduction: The Amorgos Shear Zone, South Aegean Sea. Proc. 8th Intern. INQUA Meeting Paleoseismology, Active Tectonics and Archeoseismology, 392-395.

15th International Congress of the Geological Society of Greece
Athens, 22-24 May, 2019 | Harokopio University of Athens, Greece
Bulletin of the Geological Society of Greece, Sp. Pub. 7 Ext. Abs. GSG2019-169

Late, brittle faulting in the Cyclades: a combination of strike slip and high angle normal faulting since the Mid-Miocene

Manar Alsaif [1], Frederic Gueydan[1], Dimitris Sakellariou [2] and Agathe Faucher[1]

(1) Géosciences Montpellier, Université de Montpellier, UMR 5243, Montpellier, France, Frederic.gueydan@umontpellier.fr
(2) Institute of Oceanography, Hellenic Centre for Marine Research, 19013 Anavyssos, Greece

Introduction

Back-arc extension in the Greek Cyclades has been widely studied and its extensional style seems to have evolved through time. The earliest stages started with high-pressure, low-temperature rock exhumation, and metamorphic core complex exhumation in the Late Oligocene – Early Miocene (Jolivet et al., 2013, Brun et al., 2016). It has since progressed to low angle normal faulting, and through to high angle normal faulting estimated since the Late Miocene (Jolivet et al, 2013, Philippon et al., 2012). Recent studies suggest that the latest brittle stage is more complex, as strike slip faulting may have been active in the Cyclades since the Mid-Late Miocene (Kokkalas and Aydin, 2013). This study aims to constrain the relationship between strike slip and normal faulting in the Cyclades.

Methods

We combine offshore data in the Cyclades with field data from the island of Syros to better understand the tectonic pattern and how it has evolved since the Miocene. Our data from Syros consists of structural measurements of high angle faults. These are used in combination with other published data, such as lithological and geochronological data (compilation in Philippon et al., 2012), to understand fault kinematics.

Results

In Syros, we find two dominant directions of high angle (apparently normal) faults at the scale of the island: NNW-SSE (with some oblique component) and NW-SE (mostly pure normal component).

Offshore in the Cyclades, we interpret legacy shallow seismic reflection data provided by the Hellenic Centre for Marine Research. We use this in combination with bathymetry to constrain the present day tectonics in the Cyclades. Similar to Syros, we find two directions of normal faults: NNW-SSE and NW-SE (Fig. 1). However, syn-kinematic sediments within the faulted grabens show broad folding and local inversion. We suggest that this indicates oblique slip along these high angle normal faults. From the offshore data, we also interpret two strike slip faults trending NE-SW, and locally trending NNE-SSW. The northern strike slip is a negative flower structure creating a major strike slip trough across the northern Cyclades. The southern strike slip fault is smaller and only locally affects the surrounding geology.

Discussion

We suggest that the two directions of normal faulting are a result of progressive rotation within the strike slip zones. The first set opens in the direction of maximum stretching (NW-SE) due to slab rollback. As the block is bound by dextral strike slip faults, it rotates clockwise, rotating the faults to their current NNW-SSE position, while a new set of NW-SE faults starts to open. Since the rotated faults are no longer aligned with the direction of maximum stretching, they experience oblique slip and hence create local inversion in former graben systems.

This scenario is compatible with palaeomagnetic data that show that north of the Mid-Cycladic lineament, the Cyclades have rotated 22-23 degrees clockwise since the Miocene (Avigad et al., 1998; Morris and Andersen, 1996). The data from Syros also shows activity around the mid-Miocene (Philippon et al., 2012) which can be explained by our tectonic interpretation.

Conclusion

Our results support the idea that strike slip faulting has been active in the Cyclades since the Miocene (Kokkalas and Aydin, 2013), making it much younger than the NAF, which has only been active since the Pliocene (Armijo et al., 1999). We also conclude that coeval with this strike slip faulting, the Cyclades are affected by distributed, high angle faults, which create tilted blocks and sedimentary basins. Our interpretation suggests that these faults are still presently active in the Cyclades and experience dominantly oblique slip, accommodating strike slip components from Anatolian extrusion and normal components from the retreating Hellenic subduction zone.

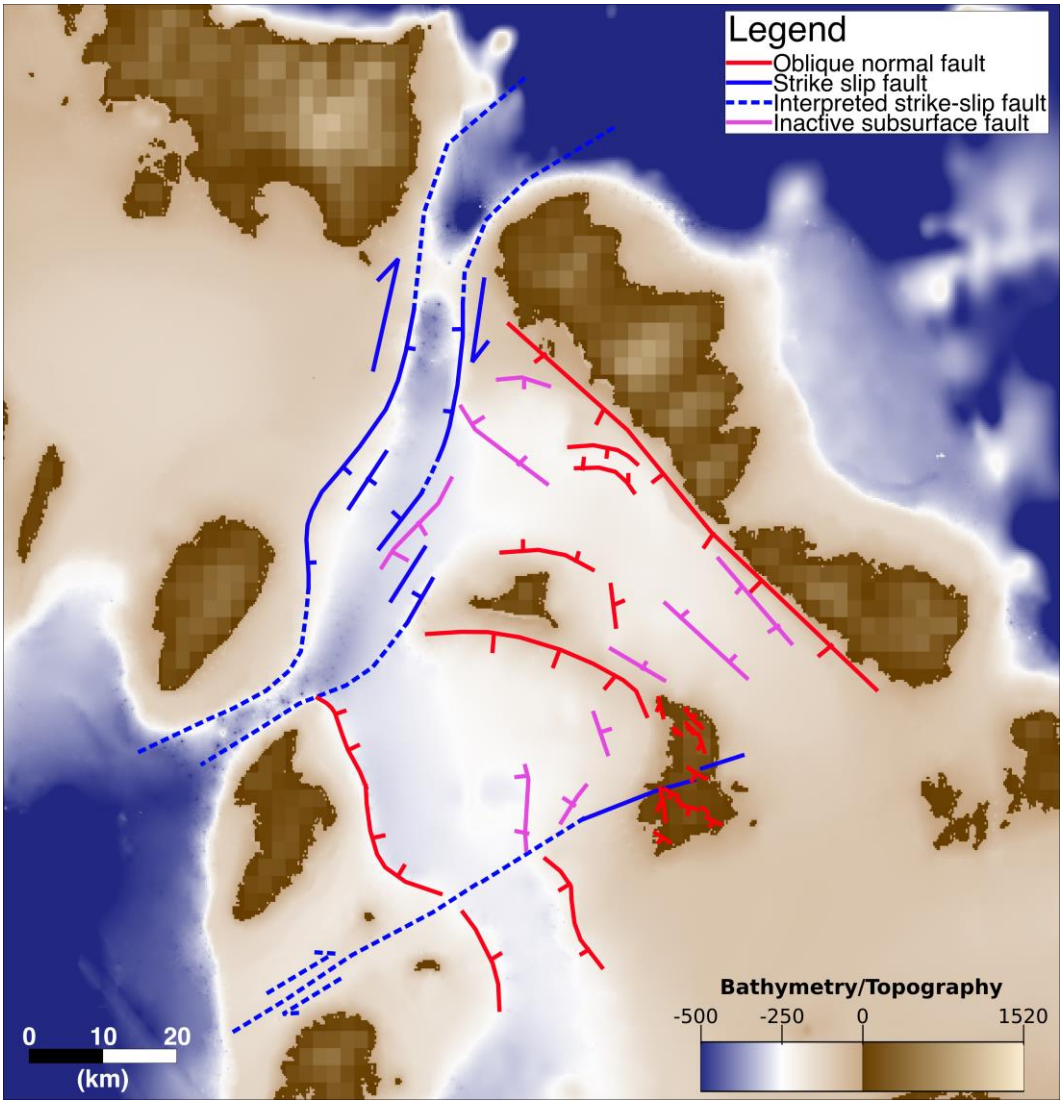

Figure 1-Tectonic map inferred from seismic lines analysis and field work in Syros.

References

Avigad, D., Baer, G. & Heimann, A., 1998. Block rotations and continental extension in the central Aegean Sea: palaeomagnetic and structural evidence from Tinos and Mykonos (Cyclades, Greece). Earth and Planetary Science Letters, 157(1), pp.23–40.

Morris, A. & Anderson, M., 1996. First palaeomagnetic results from the Cycladic Massif, Greece, and their implications for Miocene extension directions and tectonic models in the Aegean. Earth and Planetary Science Letters, 142(3–4), pp.397–408.

Armijo, R., Meyer, B., Hubert, A., & Barka, A. (1999). Westward propagation of the North Anatolian fault inoto the northern Aegean: Timing and kinematics. Geology, 27(3), 267–270.

Brun, J.-P., Faccenna, C., Gueydan, F., Sokoutis, D., Philippon, M., Kydonakis, K., & Gorini, C. (2016). The two-stage Aegean extension, from localized to distributed, a result of slab rollback acceleration. Canadian Journal of Earth Sciences, 53(11). https://doi.org/10.1139/cjes-2015-0203

Jolivet, L., Faccenna, C., Huet, B., Labrousse, L., Le Pourhiet, L., Lacombe, O., Driussi, O. (2013). Aegean tectonics: Strain localisation, slab tearing and trench retreat. Tectonophysics, 597–598. https://doi.org/10.1016/j.tecto.2012.06.011

Kokkalas, S., & Aydin, A. (2013). Is there a link between faulting and magmatism in the south-central Aegean Sea ? Geological Magazine, 150, 193–224. https://doi.org/10.1017/S0016756812000453

Philippon, M., Brun, J. P., & Gueydan, F. (2012). Deciphering subduction from exhumation in the segmented Cycladic Blueschist Unit (Central Aegean, Greece). Tectonophysics, 524–525, 116–134. https://doi.org/10.1016/j.tecto.2011.12.025

Philippon, M., Brun, J.-P., Gueydan, F., & Sokoutis, D. (2014). The interaction between Aegean back-arc extension and Anatolia escape since Middle Miocene. Tectonophysics, 631(C). https://doi.org/10.1016/j.tecto.2014.04.039.

15th International Congress of the Geological Society of Greece
Athens, 22-24 May, 2019 | Harokopio University of Athens, Greece
Bulletin of the Geological Society of Greece, Sp. Pub. 7 Ext. Abs. GSG2019-177

Deformation pattern and structural analysis along the western termination of the North Anatolian Fault

G. Trikalinou[1], H. Kranis[1], D. Sakellariou[2]

(1) National and Kapodistrian University of Athens, 15784 Panepistimiopolis Athens, Greece, gtrikalinou@geol.uoa.gr
(2) Hellenic Centre for Marine Research, Institute of Oceanography, 47th km Athens-Sounio Ave. 19013 Anavyssos

The North Aegean Trough (NAT) is considered to be an expression of the prolongation of the North Anatolian Fault (NAF) into the Aegean Sea (McKenzie, 1970; Lyberis, 1984; Armijo et al., 1999; Papanikolaou et al., 2002, 2006; Brun et al., 2016). The NAF is divided into eastern and western branch, with mean strike N70°E and N40°E respectively, and the turning point is been located NW of Lemnos Island (Sakellariou and Tsampouraki-Kraounaki, 2018). These two branches of the fault are responsible for the formation of the eastern and the western North Aegean basins, respectively. The present study is specialized in the western termination of the NAT, in order to analyze the tectonic structures that consist the North Anatolian Fault.

The database utilized in this analysis, i.e. swath bathymetry data and seismic profiles, was acquired in the framework of the nationally funded "YPOTHER/Aegean Explorations" project, implemented by the Institute of Geology & Mining Exploration (IGME) and the Hellenic Centre for Marine Research (HCMR). Swath bathymetry data were acquired with a 20 kHz SeaBeam 2120 (L3 ELAC Nautic), hull-mounted, multibeam system and were complemented with data obtained by HCMR in 2000, reprocessed at 25m grid. The fault network across the western branch of NAF was analyzed using 53 seismic profiles, of which 38 are airgun 10 in^3 seismic profiles and 15 are airgun 40 in^3 seismic profiles.

The analysis of the submarine morphology and the structural analysis along the western termination of the NAF, revealed that it consists a fault – controlled area. The western NAF is not a major, linear brittle structure, but rather a zone of numerous, parallel to sub – parallel, undulating fault segments, overlapping with others with soft – linkage, forming the western NAF zone. The fault segments are arranged in a mean strike N40°E, they are very steep or nearly vertical, their direction of dip is towards NW or SE and they accommodate a combination of shear and dip slip component, with the latter being greater towards the southwestern segments. The results of the seismic profiles analysis of the area, implied that the fault segments consist the upper parts of negative and positive flower structures that are created due to the oblique slip accommodating by the main strike – slip faults. Furthermore, the pure dextral strike – slip motion with a dip – slip component is verified by the determined focal mechanisms for all the earthquakes with magnitude Mw > 3.5 that occurred in the vicinity of the study area from 2006 until present (Figure 1B).

The submarine morphology of the NE – SW oriented marginal zone is rather complex and disparate. In particular, subsided areas with relatively greater water depth and uplifted areas with relatively smaller water depth can be observed. In other words, the southern marginal zone of NAT consists of a series of spatially alternating structural highs and lows. Specifically, three morphological depressions and two ridges can be distinguished from SW to NE: Alonissos Deep, Psathoura Ridge, Psathoura Deep and Myrina Ridge and Lemnos Deep. Alonissos Deep is the last structure before the SW end of the NAF zone and corresponds to a tectonic half – graben. The master marginal fault is located along the southern margin of the deep. This marginal fault accommodates significant normal component, with dip direction towards NW. The uplifted footwall is composed of the alpine basement and the basin is formed on the subsided hanging wall block. The direction of the extension of the basin is almost N44°W. The depression is characterized by enhanced subsidence, due to the contemporary activity of the NE – SW trending strike – slip fault segments of the NAF zone with the normal component, dipping towards NW and the normal Pelion – Skiathos Fault with direction NW – SE, dipping NE (Papanikolaou et al., 2006; Sakellariou et al., 2016). The area between Alonissos Deep and Psathoura Ridge is a submarine hill with the SE area being uplifted. The hill is formed by parallel, NE – SW trending faults segments with normal component, dipping NW. Psathoura Ridge is located east of the islet Psathoura, and represents a structural high that is formed by two parallel fault segments that accommodate normal dip – slip component and have opposite direction of dip, i.e. the major northern marginal fault has dip direction towards NW and the southern one has dip direction towards SE. Between the two aforementioned faults, a tectonic horst is pushed upwards. Psathoura Deep consists a tectonic graben by arranged strike – slip NAF segments with normal component that dip towards the center of the depression. The northern NE – SW margin is composed of two overlapping marginal fault segments that have a dip direction towards SE. The direction of the extension of the basin is almost N42°W. The area between Psathoura Deep and Myrina Ridge is quite complex and only few insufficient data were available, thus detailed structural analysis and therefore, submarine mapping, could not be possible. However, on Myrina Ridge, two major, parallel fault segments were mapped. These faults dip NW and accommodate normal component that uplifts the footwall block of both of them (SE block) and subsides the hanging wall block (NW block). There were not data available further NE, to investigate the possibility of the existence of an antithetic NE – SW trending fault that dips SE and might be the marginal fault of a horst structure, like the one on Psathoura Ridge. A major landslide affected Lesvos Deep, creating a characteristic submarine morphology and thus, the original structure of the deep cannot be determined.

Further analysis of the submarine morphology was made by constructing a slope map of the study area. The abrupt change of slope usually reflects the location of active tectonic structures, thus corresponds to their location and the negligible change of slope corresponds to the location of flat-lying areas that are tectonically inactive (Papanikolaou et al., 2002;

Sakellariou et al., 2018) Consequently, the slope map of Figure 2 confirms the results of the structural analysis through the seismic reflection profiles, that is the area along the western NAT consist of many active tectonic elements.

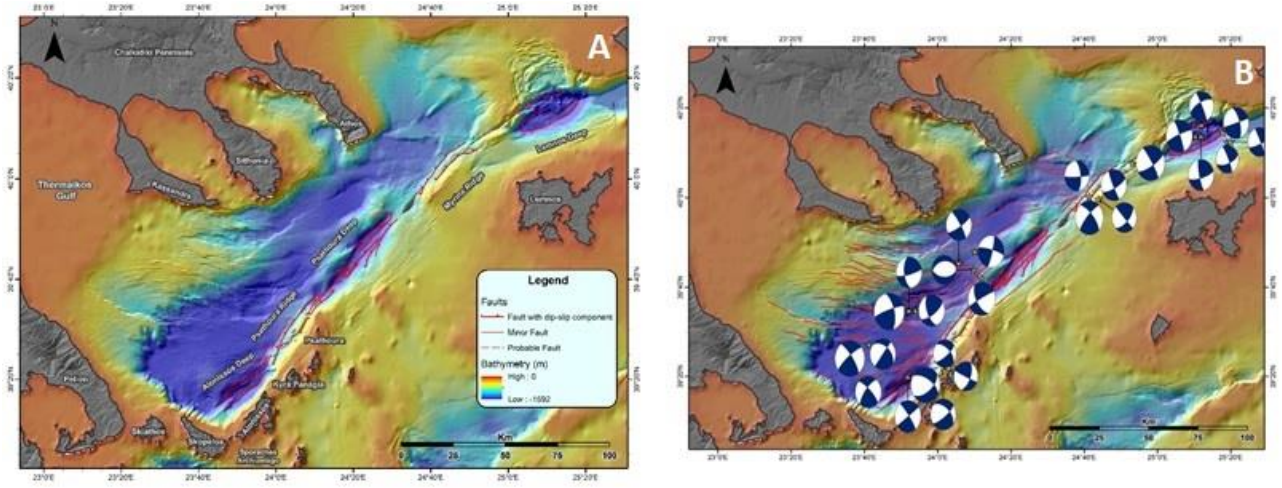

Figure 1. A) Morphotectonic map of the western North Aegean Trough. The North Anatolian Fault Zone is mapped in detail. B) Morphotectonic map of the western North Aegean Trough (NAT). The detailed fault network of the NAF zone, as long as the faults that occur in the wider NAT, from Sakellariou et al. (2018), are illustrated by red lines. The epicenters of the earthquakes (yellow stars) and the corresponding fault plane solutions that occurred in the area, are also indicated. The seismic data were acquired from the Seismological Laboratory of NKUA (http://dggsl.geol.uoa.gr/en_index.html).

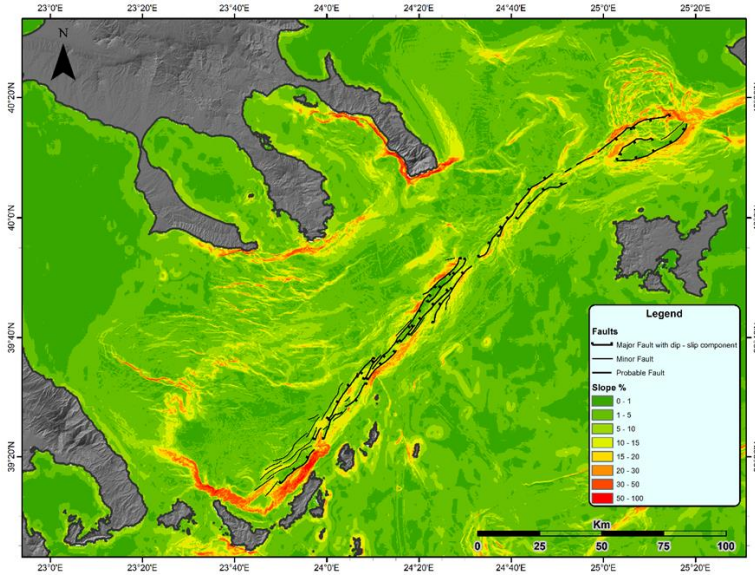

Figure 2. Slope map of western North Aegean Trough. Slope values distinguished in eight categories. The black lines correspond to the mapped North Anatolian Fault segments.

References

Armijo, R., Meyer, B., Hubert, A., & Barka, A. (1999). Westward propagation of the North Anatolian Fault into the northern Aegean: Timing and kinematics. Geology, 27(3), 267-270. doi:10.1130/0091-7613(1999)027<0267:WPOTNA>2.3.CO;2.

Brun, J.-P., Faccenna, C., Gueydan, F., Sokoutis, D., Philippon, M., Kydonakis, K., & Gorini, C. (2016). The two-stage Aegean extension, from localized to distributed, a result of slab rollback acceleration. Canadian Journal of Earth Sciences, 53(11), 1142-1157. doi:10.1139/cjes-2015-0203.

Lyberis, N. (1984). Tectonic evolution of the North Aegean Trough. In: Dixon, J.E., Robertson A.H.F. (eds.), The Geological Evolution of the Eastern Mediterranean. Geological Society, London, Special Publications, 17, 709–725. doi:10.1144/GSL.SP.1984.017.01.57

McKenzie, D. P. (1970). Plate tectonics of the Mediterranean region. Nature, 226(5242), 239-243. doi:10.1038/226239a0.

Papanikolaou, D., Alexandri, M., Nomikou, P., & Ballas, D. (2002). Morphotectonic structure of the western part of the North Aegean basin based on swath bathymetry. Marine Geology, 190(1-2), 465-492. doi:10.1016/S0025-3227(02)00359-6.

Papanikolaou, D., Alexandri, M., & Nomikou, P. (2006). Active faulting in the North Aegean Basin. Geological Society of America Bulletin, 409, 189-209. doi:10.1130/2006.2409(11).

Sakellariou, D., & Tsampouraki-Kraounaki, K. (2016). Offshore Faulting in the Aegean Sea: a Synthesis Based on Bathymetric and Seismic Profiling Data. Bulletin of the Geological Society of Greece, 50(1), 134-143. doi:10.12681/bgsg.11712.

Sakellariou, D., Rousakis, G., Morfis, I., Panagiotopoulos, I., Ioakim, C., Trikalinou, G., Tsampouraki-Kraounaki, K., Kranis, H., & Karageorgis, A.P. (2018). Deformation and kinematics at the termination of the North Anatolian Fault: The North Aegean Trough. INQUA Focus Group Earthquake Geology and Seismic Hazards. Possidi, Greece, 237–240.

15th International Congress of the Geological Society of Greece
Athens, 22-24 May, 2019 | Harokopio University of Athens, Greece
Bulletin of the Geological Society of Greece, Sp. Pub. 7 Ext. Abs. GSG2019-341

Determination of the rotational regime in the North Aegean region based on palaeomagnetic and geodetic data

I. Lazos[1], D. Kondopoulou[2], S. Pavlides[1], A. Chatzipetros[1], C. Pikridas[3], S. Bitharis[3]

(1) Department of Geology, Aristotle University of Thessaloniki, 54124, Thessaloniki, Greece, ilialazo@geo.auth.gr
(2) Department of Geophysics, Aristotle University of Thessaloniki, 54124, Thessaloniki, Greece
(3) Department of Geodesy and Surveying, School of Rural and Surveying Engineering, Aristotle University of Thessaloniki, Greece

North Aegean is in the broader Eastern Mediterranean region. The general geodynamic evolution of the area is related to the westward tectonic escape of the Anatolia plate, which is interacting with the Arabian plate, as well as with the ongoing subduction of the African plate beneath the Eurasian one. This coupled interaction is causing the southwestern movement of the Aegean region (McKenzie, 1978; Le Pichon and Angelier, 1979). The recorded, by permanently installed GPS/GNSS stations, geodetic data confirm this movement (McClusky et al., 2000; Hollenstein et al., 2008). The surficial deformation of the area can also be estimated by using the recorded GPS/GNSS velocities.

Regarding the tectonic setting of the study area, numerous onshore and offshore active tectonic structures have been documented (Sboras, 2011 and references therein). The dominant one is the ENE – WSW trending North Aegean Trough (NAT) fault zone, while fault zones of different strikes (Thrace, Drama, Belles, Mygdonia, Aliakmonas, Tyrnavos, etc.) associated to the Oligocene – Miocene extensional regime are deforming parts of the northern Greek mainland (e.g. Mountrakis et al., 2006; Sboras et al., 2017). Several of these fault zones are associated with modern or historical seismic events.

Palaeomagnetic research in the broader Aegean area (including continental Greece and western Anatolia) has provided a considerable amount of data, a part of which covers the presently studied area (Kondopoulou, 2000 and references therein; van Hinsbergen et al., 2005; Kaymakci et al., 2007; Zananiri et al., 2013). The pattern arising from these studies for the last 5 to 20Myr clearly defines a fast, clockwise rotating block at the north-western part of the studied area. The pattern is less precise at its eastern and northern parts with a mixture of counter-clockwise and no rotations. The northern Greece deformation appearing from palaeomagnetic data has also been documented by independent models (Brun and Sokoutis, 2018).

The use of Satellite Geodesy is a reliable way for estimating the current activity pattern, as well as the crustal deformation of a study area. To this end, a dense network of permanently installed GPS/GNSS is necessary to collect the geodetic data. The study area is covered by 77 different GPS/GNSS stations collecting primary geodetic data. A subset covering a seven-year period (2008 – 2014) was used in this study, using data recorded during 30-sec daily GPS observations. The European Terrestrial Reference Frame 2000 (ETRF2000), which considers Eurasia plate as stable, is the geodetic data reference frame.

Based on the primary geodetic data, including the East and North velocity components and their uncertainties, derived from the permanently installed GPS/GNSS stations, both the rotation rate and the orientation were calculated, implementing the triangulation method. The combination of 77 stations resulted in the construction of 1,610 different triangles and therefore the extraction of 1,610 different rotation rate vectors.

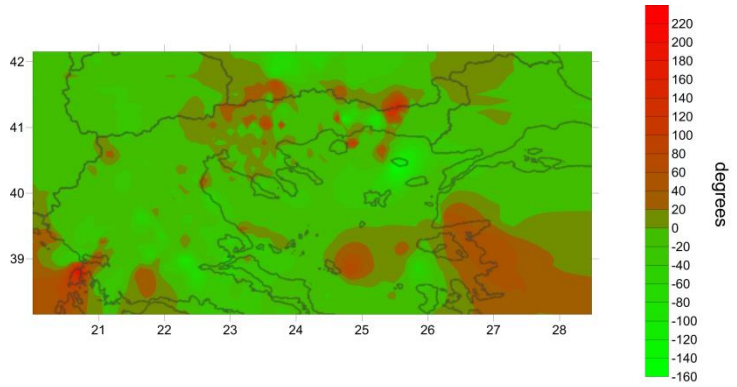

Figure 1. Interpolation of the rotation rate values of the study area, extracted from the primary geodetic data, for a -5 Myr time period.

Based on this process, the annual rotation rate and type (clockwise rotation, counter-clockwise rotation, zero rotation) were calculated for the triangular centroids. The rate of annual rotation is minimal, therefore it cannot be visualized properly, nor can it lead to the construction of rotation models. By assuming that the rotation rate of the study area is constant, the annual rotation rate values were extrapolated, resulting in the extraction of the rotation models of -5, -10, -15 and -20 Myr (Lazos et al., 2018). The results were then geostatistically processed, using interpolation methods, in order for the entirety of the study area to be covered (Figure 1). The extrapolated rotation model has then been compared

to the one suggested from palaeomagnetic data, so that it can be validated and checked for each of the time periods under consideration, to provide information about the geodynamic evolution of the study area.

Based on the combination of palaeomagnetic and geodetic rotational models, the North Aegean region can been divided into five distinct blocks (Figure 2). Blocks 1 and 3 are characterized by clockwise rotation, while Blocks 2 and 4 show counter-clockwise rotation. Although Blocks 1 and 3 both show clockwise rotational behavior, they are considered separate based on their different rotation rate. Block 5 delimits an area, where the rotational regime is not clear; this block however is subjected to the general clockwise rotation of the broader area.

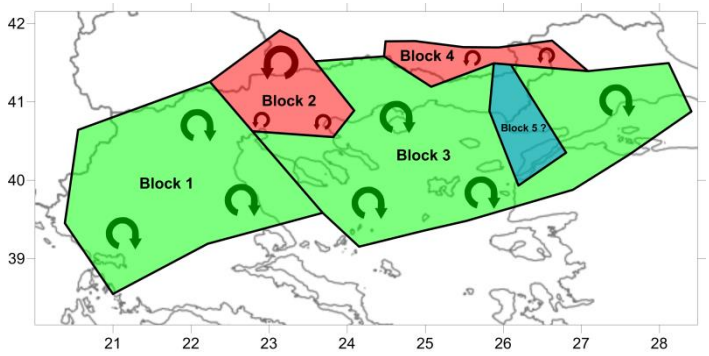

Figure 2. Classification of the study area into distinct rotational blocks, based on palaeomagnetic and geodetic data. Green blocks (1 and 3) are characterized by clockwise rotation, while red blocks (2 and 4) show counter-clockwise rotation. The rotational regime of the blue block (5) is not clear.

Acknowledgements

The authors would like to thank Metrica S.A, National Cadastre and Mapping Agency S.A, National Observatory of Athens (Ganas et al. 2011) and National Technical University of Athens for providing GPS data. In addition, Despina Kondopoulou, Christos Pikridas, Stylianos Bitharis acknowledge partial support by the project HELPOS (MIS 5002697) co-financed by Greece and the European Union.

References

Brun, J.-P., Sokoutis, D., 2018. Core Complex Segmentation in North Aegean, A Dynamic View. Tectonics 37, 1797–1830.

Ganas, A., Chousianitis, K., Drakatos, G. Papanikolaou, M., Argyrakis, P., Kolligri, M., Petrou, Panagiota., Batsi, E., Tsimi, C., 2011. NOANET. High-rate GPS Network for Seismology and Geodynamics in Greece. Geophysical research abstracts, 13.

Hollenstein, C., Müller, M.D., Geiger, A., Kahle, H.G., 2008. Crustal motion and deformation in Greece from a decade of GPS measurements, 1993-2003. Tectonophysics 449, 17–40.

Kaymakcı, N., Langereis, C., Özkaptan, M., Özacar, A., Gülyüz, E., Uzel, B., Sözbilir, H., 2018. Paleomagnetic evidence for upper plate response to a STEP fault, SW Anatolia. Earth Planet. Sci. Lett. 498, 101–115.

Kondopoulou, D., 2000. Palaeomagnetism in Greece: Cenozoic and Mesozoic components and their geodynamic implications. Tectonophysics 326, 131–151.

Lazos, I., Kondopoulou, D., Chatzipetros, A., Pavlides, S., Bitharis, S., Pikridas, C., 2018. Rotation rates of the South Aegean region, Greece, based on primary geodetic data - Comparison between geodetic and palaeomagnetic results. 9th International INQUA Meeting on Paleoseismology, Active Tectonics and Archeoseismology (PATA), Possidi, Greece, 141-144.

Le Pichon, X., Angelier, J., 1979. The hellenic arc and trench system: A key to the neotectonic evolution of the eastern mediterranean area. Tectonophysics 60, 1–42.

McClusky, S., Balassanian, S., Barka, A., Demir, C., Ergintav, S., Georgiev, I., Gurkan, O., Hamburger, M., Hurst, K., Kahle, H., Kastens, K., Kekelidze, G., King, R., Kotzev, V., Lenk, O., Mahmoud, S., Mishin, A., Nadariya, M., Ouzounis, A., Paradissis, D., Peter, Y., Prilepin, M., Reilinger, R., Sanli, I., Seeger, H., Tealeb, A., Toksöz, M.N., Veis, G., 2000. Global Positioning System constraints on plate kinematics and dynamics in the eastern Mediterranean and Caucasus. J. Geophys. Res. 105, 5695.

McKenzie, D., 1978. Active tectonics of the Alpine—Himalayan belt: the Aegean Sea and surrounding regions. Geophys. J. R. Astron. Soc. 55, 217–254.

Mountrakis, D., Tranos, M., Papazachos, C., Thomaidou, E., Karagianni, E., Vamvakaris, D., 2006. New neotectonic and seismological data about the main active faults and stress regime of Northern Greece. Geol. Soc. London, Spec. Publ. 260, 649–670.

Sboras, S., Chatzipetros, A., Pavlides, S., 2017. North Aegean Active Fault Pattern and the 24 May 2014, Mw 6.9 Earthquake, in: Active Global Seismology: Neotectonics and Earthquake Potential of the Eastern Mediterranean Region. John Wiley & Sons, Inc., pp. 239–272.

Sboras, S., 2011. The Greek Database of Seismogenic Sources: seismotectonic implications for North Greece. Ph.D. Thesis, University of Ferrara, Ferrara, 274 p.

Taymaz, T., Jackson, J., McKenzie, D., 1991. Active tectonics of the north and central Aegean Sea. Geophys. J. Int. 106, 433–490.

van Hinsbergen, D.J.J., Langereis, C.G., Meulenkamp, J.E., 2005. Revision of the timing, magnitude and distribution of Neogene rotations in the western Aegean region. Tectonophysics 396, 1–34.

Zananiri, I., Kondopoulou, D., Dimitriadis, S., Kilias, A., 2013. Insights into the geotectonic evolution of the southern Rhodope as inferred from a combined AMS, microtextural and paleomagnetic study of the Tertiary Symvolon and Vrondou plutons. Tectonophysics 595–596, 106–124.

GENERAL SESSION

T3 Geophysics and Seismology

15th International Congress of the Geological Society of Greece
Athens, 22-24 May, 2019 | Harokopio University of Athens, Greece
Bulletin of the Geological Society of Greece, Sp. Pub. 7 Ext. Abs. GSG2019-090

Rating Seismicity In Terms of Radiated Energy of Earthquakes

Olatunde Isaiah POPOOLA[1] and Olumide Akinwale ADEDEJI[1]
(1) Department of Physics, University of Ibadan, Nigeria. itundepopoola@yahoo.com

Abstract
In the world of seismology, a major tool for seismicity study is the Gutenberg – Richter (G-R) relation whereby the G-R constants a and b are determined from earthquake catalogue to assess the seismicity of the region of interest. However the G-R relation does not accommodate information about the spatial coverage of the region concerned hence it will not suitably compare seismic activities of two or more regions that have unequal spatial coverage. Moreover, the method breaks down for any region where earthquake events are virtually of the same magnitude since constants a and b are indeterminate in this case. In addition the relation gives the rate of seismicity in terms of the total number N of earthquakes which makes a region having unusually few but large earthquakes to be underestimated. In this work, two mathematical models for rating seismicity in terms of radiated energy per unit area per unit time of earthquakes in a given region over a period of time were developed. One of the models takes care of situations where the G-R constants may not be defined. The two models were applied to ten regions in the world seismic zones. Both models rated the seismicity of the regions in the same order that is different from rating obtained from the a value of the G-R relation.

Keywords: Earthquakes, seismicity, Gutenberg – Richter's relation, radiated energy

Introduction

Seismicity is the world -wide or local distribution of earthquake epicentres in space and time. It is a general term for the number of earthquakes in unit time, or for a relative earthquake activity. It is very obvious that the rate of earthquake occurrence varies from one region to another. Some regions are known to be very active; some are moderately active while some are inactive. However, in the absence of a suitable method of describing the manner of occurrence of earthquakes with respect to time and space, comparison of seismicity of any two regions could be difficult. The empirical formula: LogN(M) = a - bM known as the Gutenberg-Richter (G-R) magnitude-frequency relationship after Gutenberg and Richter (1954) is a common tool in seismicity study The constants a and b,usually referred to as the G-R constants are positive and real. For a certain region and time interval, the G-R relation provides the number of earthquakes, N, with magnitudes greater than or equal to M, **a** describes the seismic activity; b which is typically close to unity for the whole earth, describes the relative abundance of large to smaller shocks. The implications of several properties of the Earth interior as well as pattern of occurrence of earthquake clusters on the b- value has been extensively studied (Nakaya, 2004; Mogi, 1962; Suyehiro et al., 1964). In its original form, G-R relationship was based on the seismicity of the whole Earth but over the years, it has been found to fit into regional seismicity and other studies. E.g. Molchan et. al (1999) used the frequency-magnitude relation to construct a multi-scale seismicity model for the main shock in seismic risk assessment. The use of G-R relationship for studying regional seismicity has the following limitations:
1. It does not include information about the geographical area covered by the epicenters of earthquakes so it is possible to have the same values of a and b for two regions of different geographical areas; this implies that information about the clustering or sparseness of epicentres is lost.
2. It assumes that both constants a and b can be determined. However, occurrence of earthquakes with close magnitude range within a region of interest will yield a situation where the constants are indeterminate since G-R curve will be almost parallel to the vertical axis. In this work, we develop two mathematical models for rating the seismicity of any region over a period of time. The models take care of the limitations of G-R relation. It has an additional advantage of rating seismicity from energy of the earthquakes and yield a numerical value for the seismicity as is the case for earthquake magnitudes. This approach provides a better platform for comparing seismic activities of two or more regions.

Methodology

Model 1. This takes care of situations where the G-R constants are indeterminate. Considering an arbitrary region of coverage area A, where N earthquakes have occurred over a period T, total radiated energy per unit area per unit time is defined as:

$$\Im_1 = \sum_i^N E_i \big/ TA$$

where E_i is the energy radiated by the *i*th earthquake.

The E_i was expressed in terms of earthquake moment magnitude m_i as $E_i = 10^{(1.5m_i+11.8)}$. (Gutenberg, 1956; Lowrie, 1997) A second model, $\Im_2$, which incorporates the G-R constants was developed by dividing T into k equal sub-periods, and substituting for m in the G-R relation to yield:

$$\Im_2 = \frac{1}{TA}\sum_{j=1}^{k}\frac{10^{1.5a_j/b_j}}{N_j^{1/b_j}} \times 10^{11.8}$$

where aj and bj are the G-R constants for each sub - period k

The two models were applied to fifty-year (1956 - 2005) earthquake data for 10 selected regions in the world seismic zones and were rated accordingly.

Results

The two models ratted the seismicity of the regions in the same order which is different from the rating obtained by using the a - value of the G –R relation.

Conclusion

The models could suitably categorise seismic activities of two or more selected areas in terms of energy rather than number of earthquakes which the G-R a-value represents. Counting earthquakes of different magnitudes together is equivalent to combining unlike terms since a single large earthquake is equivalent to thousands of small earthquakes

References

Bath, M. 1966. Earthquake energy and magnitude. In Fundamentals of Geophysics of Geophsics, Lowrie, W. Cambridge University Press, Cambridge. pp. 127.

Gutenberg, B. 1956. The energy of earthquakes. Quarterly Journal of Geological Society, London, 112, 1-14.

Gutenberg, B. and Richter, C.F. 1956. Seismicity of the Earth an associated phenomena, Princeton University Press, Princeton.

Nakaya, S. 2004. A zone of anomalously low b-value within the subduction slap prior to the September 26, 2003 Tochachi – Oki, Japan earthquake (M = 8), EOS Trans. AGU, 85:47, Fall meeting suppl Abstract S13Am 1028.

Lowrie, W. 1997. Fundamentals of Geophysics, Cambridge University Press, Cambridge.

Mogi, K. 1962. Magnitude – frequency relationship for elastic shocks accompanying fractures of various materials and some related problems in earthquakes. Bulletin of Earthquake Research Institute, University of Tokyo, 40: 831-883.

Molchan, G.M., Kronrod, T.L. and Nekrasova, A.K. 1999. Immediate foreshocks: Time variation of the b – value. Phys. Inter. 111, 229-240.

Suyehiro, S., Asada, T. and Ohtake, M. 1964. Foreshocks and aftershocks accompanying a perceptible earthquake in central Japan: On the peculiar nature of foreshocks. Pap. Metrol. Geophys. 19: 427- 435.

15th International Congress of the Geological Society of Greece
Athens, 22-24 May, 2019 | Harokopio University of Athens, Greece
Bulletin of the Geological Society of Greece, Sp. Pub. 7 Ext. Abs. GSG2019-093

Urban Gravity Measurements for the Subsurface Investigation of Athens Basin (Greece)

Spyridon Dilalos, John D. Alexopoulos
NKUA, Department of Geology and Geoenvironment, Panepistimiopolis, Zografou, Greece, sdilalos@geol.uoa.gr

Introduction

Taking into consideration the major damage caused by the disastrous earthquake of 7th September 1999 (5.9R), the need for further and deeper investigation of the geological structure of the subsurface came up. The damage distribution of an earthquake is usually related to the tectonic structures of the area (Dilalos and Alexopoulos, 2017). Unfortunately, since the areas are covered with artificial surfaces, such as buildings, industrial infrastructures, roads, bridges and generally artificial surfaces, the geological research is quite complicated. The missing geological information for the deep subsurface can only be retrieved using geophysical methods. Given the fact that the 54.5% of Athens basin is covered with artificial surfaces (Dilalos, 2018), not all the geophysical methods can be applied. The land gravity measurements seem like the most applicable method for such a deep geotectonic investigation.

Geological regime

In Figure 1, a simplified geology map of the area (Dilalos, 2018) is provided, mostly based on the geotectonic study by Papanikolaou D. *et al.,* (2002). The autochthonous Metamorphic Unit is compiled mainly of dolomites, marbles and shales. On the other hand, the "*Ypopelagoniki"* unit consists of Triassic-Jurassic limestones and some base clastic formations from Paleozoic. The *Athens Unit* (upper allochthonous unit) is comprised of two main parts, the upper one which is basically limestones and the lower one, called "*Athens Schists*" which is basically a geological mélange that consists of sandstones, shales, phyllites, limestones and marls. The "*Alepovouni"*, located tectonically between the autochthonous metamorphic unit and the "*Athens"* unit, consists of limestones (upper part) and additionally schists and phyllites in the base, because of its low metamorphism. The post-alpine geological formations cover the biggest part of the basin. More than ten different post-alpine, Quaternary and Neogene geological formations had been proposed by Papanikolaou D. *et al.,* (2002), but here they are observed simplified in groups that will help the gravity survey, based on Dilalos (2018).

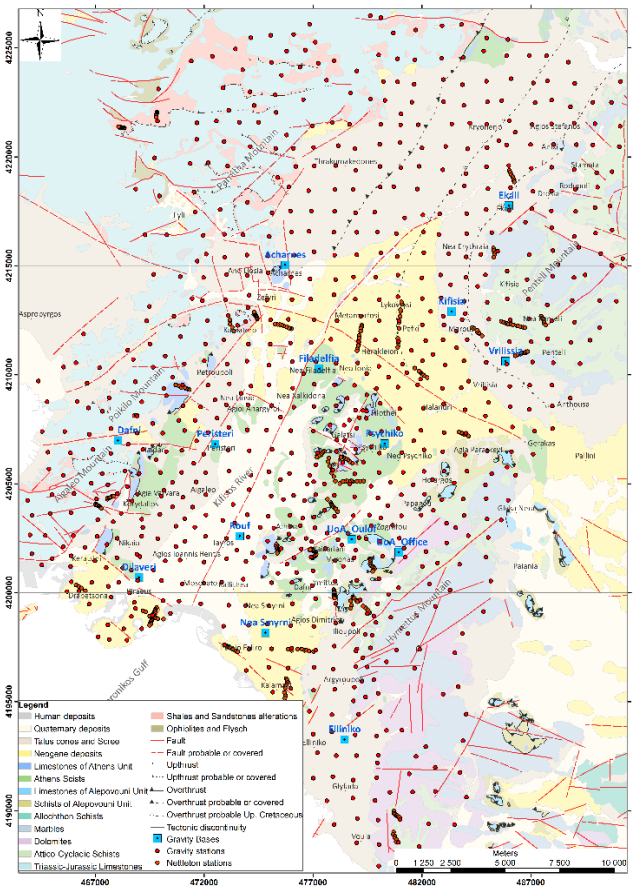

Figure 1. Geological and tectonic map along with the locations of the gravity stations and gravity bases.

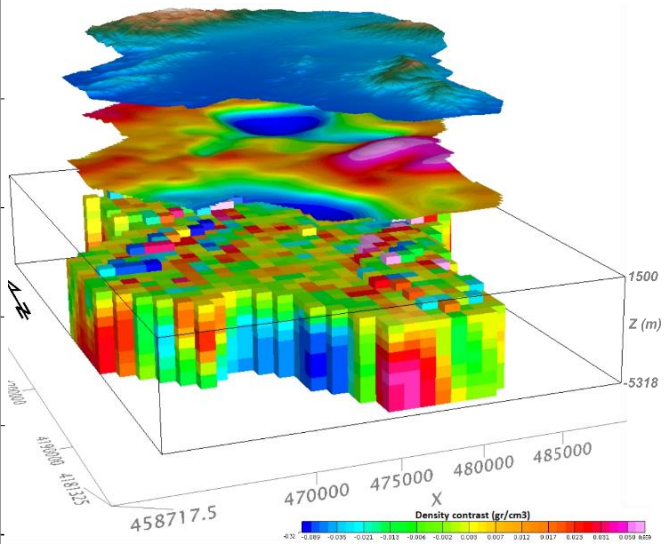

Figure 2. 3D gravity inversion of Athens basin, with cell size of 1000m. The upper plane is the area DEM and the lower is the grid of the Residual Anomaly.

Establishment of gravity bases and data acquisition

Taking into account the traffic jam of this over-populated metropolis and the increasing time that we would spend moving among the stations and the base re-measurements, we planned and established very cautiously the gravity base network, distributing spatially **fourteen (14) gravity bases** (Fig. 1-blue squares). The entire gravity base network is referred to the IGSN'71 datum (Morelli *et al*., 1974) as it was tied with repeated measurements (ABABA type) to an already established gravity base in the University of Athens (Hipkin *et al*., 1988).

Due to the complicated geology of the area and the urban environment, the gravity measurements were planned on a grid, with a station grid spacing set to 1km. Afterwards, some stations were added among the first ones, in order to clarify the status of some ambiguous areas. The gravity database is comprised of 1122 gravity stations (Fig. 1), acquired with the LaCoste & Romberg G-496 gravity meter. The essential coordinates of the gravity stations and bases were determined with high precision, using a Differential Global Positioning System (dGPS) and the *static* technique.

Table 1: Established gravity bases in Athens along with their determined absolute values.

Gravity base name	Absolute gravity (mGal)	Standard Deviation (mGal)	Easting (Egsa '87,m)	Northing (Egsa '87, m)	Elevation (m)
UoA_Office	980010.745	±0.00	480948.310	4201848.100	252.000
UoA_Oulof	980029.856	±0.03	478772.001	4202445.816	134.792
Rouf	980049.351	±0.04	473639.680	4202590.600	20.239
Psychiko	980017.268	±0.03	480288.710	4206831.900	179.091
Nea Smyrni	980043.877	±0.04	474819.600	4198156.400	42.662
Peristeri	980044.151	±0.07	472514.450	4206815.757	51.888
Dilaveri	980052.977	±0.08	469013.766	4200694.898	7.536
Kifisia	979991.509	±0.04	483373.599	4212901.998	287.379
Filadelfia	980029.065	±0.04	477276.990	4210270.695	116.118
Elliniko	980039.123	±0.07	478453.689	4193259.660	80.884
Acharnes	980017.082	±0.07	475726.609	4215036.626	168.425
Ekali	979981.326	±0.07	485997.896	4217756.564	344.891
Vrilissia	979997.111	±0.07	485846.098	4210619.196	269.935
Dafni	980031.436	±0.05	468050.208	4206980.671	109.281

Results and Conclusion

A geologically constrained 3D gravity modelling was produced (Fig. 2) using the "*VOXI*" Earth modelling module, based on the Complete Bouguer Anomaly calculated after the standard data reduction and the application of the innovative Building Correction (Dilalos *et al.*, 2018). The subsurface was discretized in a 3D block mesh, where all blocks have a cell size equal to 1000m for X-Y and 500m for Z direction. The produced block mesh (Fig. 2) is constituted by a total of 12760 blocks of individual density contrast. The density contrast ranges from -0.32 gr/cm^3 (bluish colors) to 0.669 gr/cm^3 (reddish colors), with a maximum depth of almost 6800m. The evaluation of this density model, given the fact of the geological formations' densities (Dilalos, 2018) provide valuable information for the subsurface geological structure of Athens basin. It verifies the existence of faults mapped as possible but also indicates the location of possible new ones.

Acknowledgements

The fieldwork was partially supported by the NKUA-SARG (contract no. 70/4/9254). The authors would like to thank Ms. Achtypi S., Ms. Kaplanidi H., Mr. Mavroulis S., Mr. Michelioudakis D.and Ms. Drosopoulou E. for their contribution during the field measurements. We would also like to gratitude Mr. Stylianos Chailas for the kind supply of the established gravity base data.

References

Dilalos, S., 2018. Application of geophysical technique to the investigation of tectonic structures in urban and suburban environments. A case study in Athens basin. *Ph.D. Thesis*, National and Kapodistrian University of Athens, 321p. Athens, Greece.

Dilalos, S. and Alexopoulos, J.D., 2017. Indications of correlation between gravity measurements and isoseismal maps. A case study of Athens basin (Greece). *Journal of Applied Geophysics*, 140, 62-74. https://doi.org/10.1016/j.jappgeo.2017.03.012

Dilalos, S., Alexopoulos, J.D., Tsatsaris, A., 2018. Calculation of Building Correction for urban gravity surveys. A case study of Athens metropolis (Greece). *Journal of Applied Geophysics*. 159(C), 540-552. https://doi.org/10.1016/j.jappgeo.2018.09.036

Hipkin, R.G., Lagios, E., Lyness, D., Jones P., 1988. Reference gravity stations on the IGSN71 standard in Britain and Greece. *Geophysical Journal International*, 92(1), 143-148. https://doi.org/10.1111/j.1365-246X.1988.tb01128.x

Morelli, C., Gantar, C., Honkasalon, T., McConnel, K., Tanner, J.G., Szabo, B., Uotila, U., Whalen, C.T., 1974. *The International Standardization Net 1971 (IGSN71)*. IUGG-IAG Publ. Spec. 4. Int. Union of Geod. and Geophysics

Papanikolaou, D., Lozios, S., Sideris, C., Kranis, H., Danamos, G., Soukis, K., Skourtsos, E., Bassi, E., Marinos, P., Tsiampaos, G., Boukovalas, G., Sabatakakis, N., Antoniou, A., Provia, K., 2002. Geological – Geotechnical study of Athens basin. OASP Applied research program, 152p., Athens (In Greek).

15th International Congress of the Geological Society of Greece
Athens, 22-24 May, 2019 | Harokopio University of Athens, Greece
Bulletin of the Geological Society of Greece, Sp. Pub. 7 Ext. Abs. GSG2019-144

Geophysical Measurements for Upraising the Geological Model at the Katakolo Peninsula

P. Tsourlos[1], P. Karmis[2], G. Vargemezis[2], G. Panagopoulos[3], L. Gouliotis[3], K. Nikolaou[3]

(1) Department of Geophysics, School of Geology, Aristotle University of Thessaloniki, Thessaloniki Greece, tsourlos@geo.auth.gr
(2) Institute of Geology and Mineral Exploration (I.G.M.E.), Athens Greece
(3) Energean Oil and Gas S.A., Athens Greece

Introduction

In this work we present the results of the geophysical survey that took place in 2018 at the Katakolo peninsula aiming into obtaining supplementary information regarding the subsurface geological configuration of the wider Katakolo peninsula.

The post-alpine rocks of the Katakolo area are part of the wider Pyrgos basin. The Pyrgos basin is a first order tectonic graben that is bounded to the north and to the east by the Erymanthos and Tropaia horsts, and to the south by the Lapithas horst. In the Katakolo peninsula, two basic formations crop out: 1) The lower fine grain Vounargos formation and 2) The Katakolo calcarenitic formation. The contact between these two is designated by an angular unconformity that is visible at the western part of the peninsula. The Katakolo formation crops out in the whole peninsula covering large areas on top of the Vounargos fine grain formation. It is in general a strong calcarenitic to calciruditic member that dips towards the west in the northern and western part of the peninsula and towards the south in the southern part reaching its highest onshore width near the western coastline. The Katakolo formation was subjected to weathering processes that generated a weathering brown/red clayey mantle <2m thick. In some areas the Katakolo formation is locally absent and the Vounargos formation is topped by a thick (>3m) younger fluvial deposits.

The main aim of the geophysical survey was to determine the thickness of the top Katakolo formation and to investigate the possible existence of salt diapir below the wider Katakolo peninsula area up to a depth of 500m. The technique of electrical resistivity tomography was applied over the entire Katakolo Peninsula to map the subsurface at depths up to 250m in order to locate geoelectrical units and discontinuities and then correlate them with the geological/geotectonic setting of the area. Additionally, a large number of Transient Electromagnetic (TEM) method soundings were collected and interpreted in an attempt to map the deeper geoelectrical structure (i.e. up to 500m depth) of the peninsula and locate possible diapir intrusions.



Figure 1. The location of the ERT lines and the TEM centers.

Geophysical Measurements

A total of 9 long ERT lines (total length of 9450m) were measured: lines K51-K512 are distributed all over at the Katakolo peninsula. The exact location of the lines is depicted in Fig. 1. All ERT lines had a 50m electrode separation and a typical length of 1000m (21 electrodes) while some lines were longer and they are the result of the merging of two 1000m roll-along lines. Data were obtained using the multiple gradient and the dipole-dipole electrode arrays and were inverted using standard 2D inversion software (Kim, 2017). The inversion results were extracted from all 2D lines and every inversion

point was georeferenced to its actual coordinates. Georeferenced inversion data were combined into a single interpolated 3D grid from which slices for specific elevations were extracted. A typical geoelectrical colored map slice for the elevation of z=-10m is shown in Fig.2a using a rainbow color scale (blue-low, red-high). Areas of high resistivity (red) correspond to the Katakolo formation which is thicker at the NW part of the peninsula. Further clear lateral geoelectrical variations can be seen which can be correlated to WSW-ENE and SSE-NNW tectonic lines which are also depicted in Fig.2a.

A total of 34 TEM soundings were conducted at the area of investigation. The location of the soundings is shown in Fig.1. Typical loop sizes used were 100x100 m and sometimes 50x50 in certain "noisy" areas. The delay time reached 500 msec in noise free areas, such as the southern tip of the peninsula. The data were inverted with a 1D scheme assuming models of 3 to 5 layers, with the Terra software developed by Karmis (2004). A typical TEM sounding and its interpretation is shown in Fig2b. The sounding TA2 was conducted at the southern part of the peninsula. Loop size is 120x120 m and the induced current was 4.7 Amps. The interpreted geoelectrical layer model is also shown at the bottom of in Fig.2b. The top layer with resistivity of 14 Ohm-m is underlain by conductive layers of low resistivity values, reaching sea-water resistivity. There is no indication of large resistivity formation (i.e. possible diaper intrusion) up to a depth exceeding 432 m.

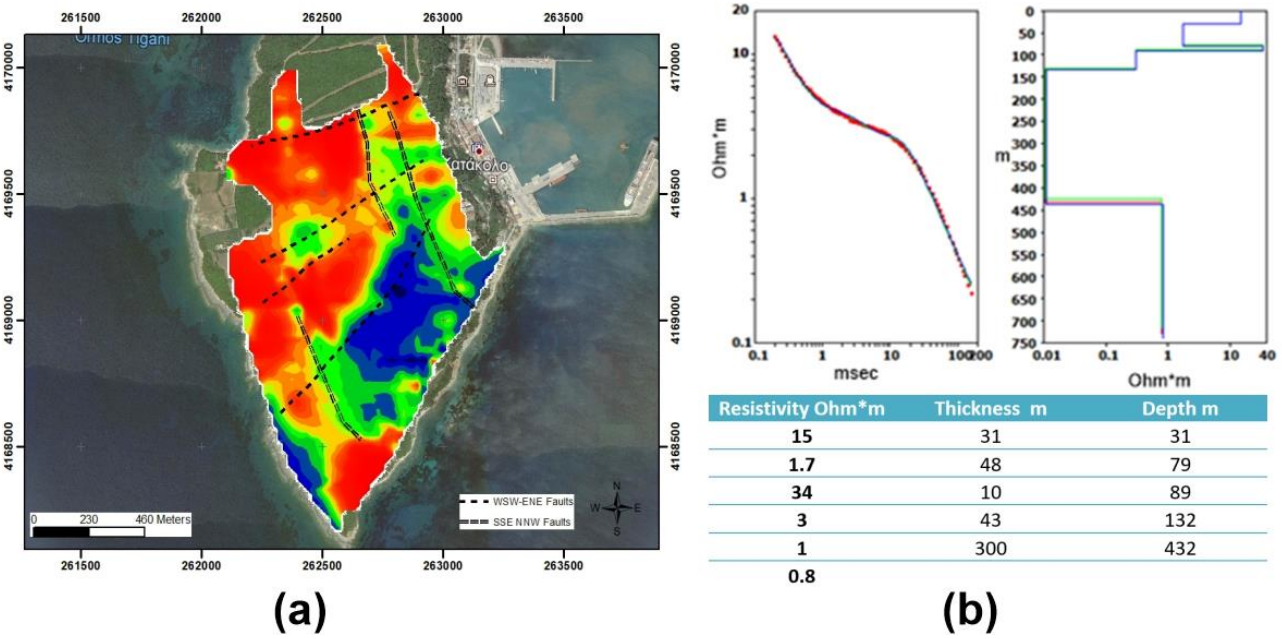

Resistivity Ohm*m	Thickness m	Depth m
15	31	31
1.7	48	79
34	10	89
3	43	132
1	300	432
0.8		

Figure 2. (a) Geoelctrical depth slice at the elevation of Z=-10m. (b) Typical TEM sounding curve (TA2) and its interpretation.

Concluding Remarks

By inspecting the individual and combined inversion results of the long ERT lines it is evident that there is clear distinction in view of resistivities of the top geological Katakolo formation. The formation appears to be generally more resistive and it is geoelectrically heterogeneous and at parts appears to be quite resistive (resistivities > 100 Ohm-m). The thickness of this formation ranges from few meters to 2-3-decades of meters but is on average 10m. The Katakolon formation is followed by deeper formations which are generally more conductive to moderately resistive and are probably related to clays, sandy clays and maybe sandstones. The combined depth slices and 3D views of all lines illustrate clearly that the thickness of the Katakolo formation is limited at the south-eastern and south parts of the peninsula but it increases significantly towards north-west. The particular change in thickness seems to be also related to the existence of tectonic lines.

The general pattern of all TEM soundings is the succession of a resistive layer as overburden with thickness of 20 to 30 m, followed by a conductive formation with resistivity values 2 to 10 Ohm*m. This is probably attributed to silty clayey deposits with sand intercalations in places. At larger depths, the formations are becoming very conductive with resistivity values below 1 Ohm*m indicating sea water intrusion. There is no evidence of a salt diapir intrusion in the whole area of investigation. This result applies for the first approximately 500 m of depth, within which the results are considered as reliable.

References

Karmis P., 2003. Automatic interpretation of Transient EM surveys, PhD Thesis, Athens University, Greece.
Kim J.H., 2017. DC2DPro: 2D Inversion of ERT data. User's Manual. Korea Institute of Geoscience and Mineral Resources, S. Korea.

15th International Congress of the Geological Society of Greece
Athens, 22-24 May, 2019 | Harokopio University of Athens, Greece
Bulletin of the Geological Society of Greece, Sp. Pub. 7 Ext. Abs. GSG2019-190

Stochastic simulation of the intermediate earthquakes using the 3D attenuation model for the southern Aegean subduction zone

C. Kkallas[1], C. Ventouzi[1], C. Papazachos[1]

(1) Geophysical Laboratory, Aristotle University of Thessaloniki, Thessaloniki, Greece, chkkalla@geo.auth.gr

It is well-known that low body-wave velocities (Papazachos and Nolet, 1997) and quality factor (high attenuation) (Ventouzi et al., 2014) have been observed beneath the Southern Aegean volcanic arc, at the depth of ~60–90 km. This is usually attributed to the subduction process of the Eastern Mediterranean lithosphere under the Aegean microplate, resulting in the partial melting above the subducting slab. As a result, P and S waves from intermediate-depth earthquakes are strongly attenuated along the South Aegean Sea volcanic arc. On the other hand, P and S waves from in-slab events, propagating toward the outer Hellenic arc, exhibit relatively high-frequency amplifications (Fig. 1). More recently, Ventouzi et al. (2018) confirmed the existence of the high attenuation mantle wedge beneath the volcanic arc by calculating a new 3D attenuation (Q_P and Q_S) model. This 3D-model has been determined by the tomographic inversion of the linear decay of acceleration spectra at high frequencies, t_S*, calculated for body waves and assuming an ω^2 earthquake source model

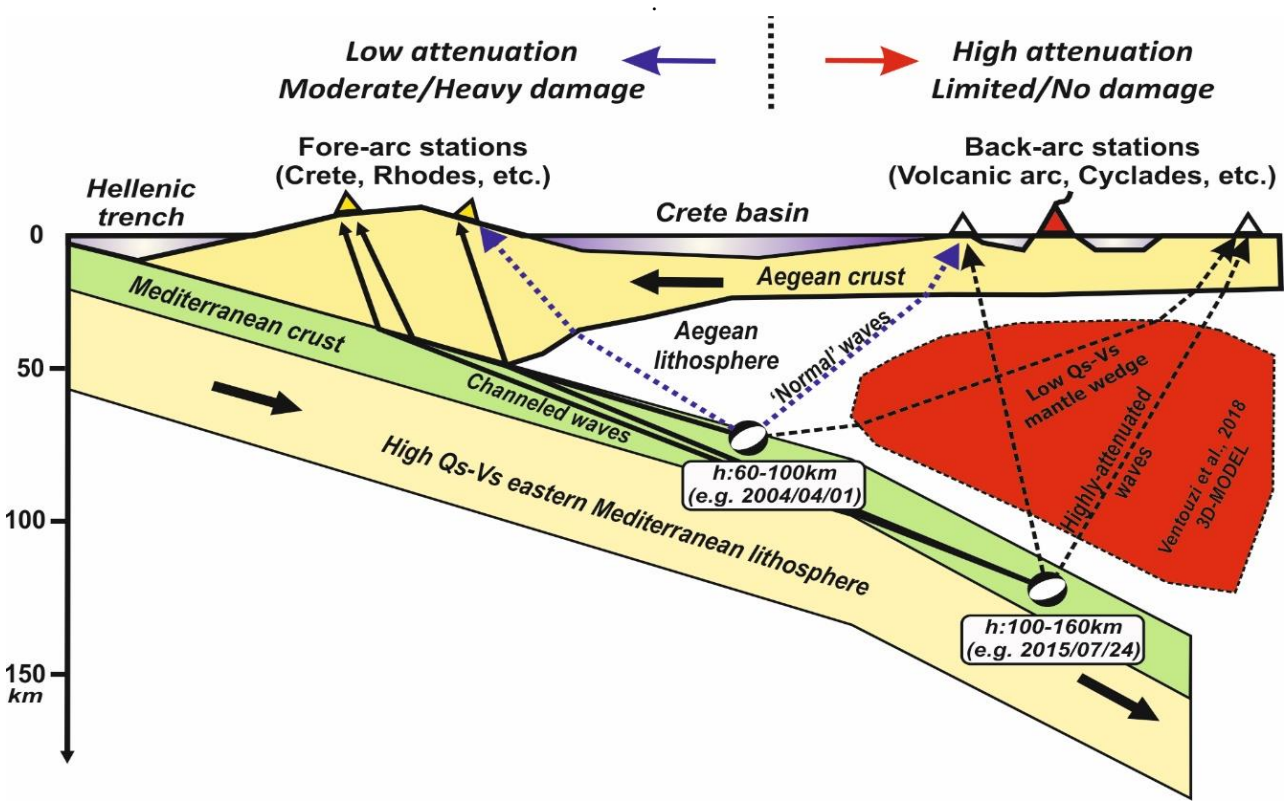

Figure 1. Schematic representation of the seismic wave propagation pattern of intermediate-depth events occurring at the Hellenic arc along a cross section parallel to the subduction direction for earthquakes occurring at the subducted slab of the Eastern Mediterranean lithosphere at different depths. Seismic rays from in-slab events travelling through the low Q_S–V_S back-arc mantle wedge or the high Q_S–V_S subducting eastern Mediterranean slab are depicted by dashed and solid lines, respectively. Seismic energy from deep events (h ≥100 km) is strongly attenuated in the back-arc area and channeled through the slab, resulting in larger damage in the fore-arc region than in the epicentral area (back-arc area) above the slab. For shallower events (h~ 60–100 km) this pattern is prominent only at larger distances, since short-distance propagation is not affected by the mantle wedge presence (blue dotted rays). The vertical projections of typical fault-plane solutions are also shown (modified from Skarlatoudis et al., 2013).

The main target of this study is to compare the new 3D anelastic attenuation model for the upper mantle of the southern Aegean Sea subduction area (Ventouzi et al., 2018) with the Ground Motion Prediction Equations, GMPEs (Skarlatoudis et al., 2013) and to employ this model into the stochastic simulation approach developed by Kkallas et al. (2018a, b), in order to generate realistic seismic waveforms for intermediate depth events occurring in the southern Aegean subduction area. For this purpose, we initially used a synthetic dataset of intermediate-depth events recorded by the same seismological stations later used in the stochastic simulation and calculated the theoretically expected Q_S values based on the 3D anelastic attenuation model of Ventouzi et al. (2018). The results were compared with the corresponding anelastic attenuation coefficient values of the GMPE from Skarlatoudis et al. (2013), showing a good agreement.

In order to predict several expected ground motion measures, for example peak ground acceleration (PGA) and peak

ground velocity (PGV) as a function of distance and magnitude, we used the results obtained from the stochastic simulation approach. These simulations were performed with the EXSIM code (Motazedian and Atkinson, 2005), as adapted by Boore (2009), taking into account finite-fault effects for ground-motion modelling. The main concept is based on the summation of the contributions to ground motion over all of the sub-sources comprising the fault at the observation site, considering proper delays of sub-sources due to rupture propagation. Several researchers have investigated the seismotectonic setting, strong ground motion attenuation and source properties that control seismic motions for the intermediate-depth earthquakes of the south Aegean Sea (e.g. Boore et al., 2009; Skarlatoudis et al., 2009, 2013; Kkallas et al., 2013, 2018a, b). These studies provide constraints on several source and propagation path parameters for this class of events, namely the stress parameter, expected fault dimensions, quality factor of the Aegean mantle, geometrical spreading etc. In the present study, these results have been incorporated in order to perform a realistic stochastic finite-fault modelling of intermediate depth earthquakes in the South Aegean Sea.

To confirm the stability and effectiveness of the employed 3D attenuation model, we model the PGA and PGV distribution of three intermediate depth earthquakes of the southern Aegean Sea subduction zone, namely the 2011 intermediate-depth earthquake (M 6.1, h~75 km), the 2004 M = 5.5 event (southeast of Astypalaia), and the more recent 2015 M = 5.0 Nisyros intermediate earthquake (h~130km), which all exhibit spatially anomalous seismic motion and macroseismic (damage) patterns. In general, there is a good agreement between peak ground-motion measures (PGA/PGV) and synthetic values for the entire dataset. Finally, the approach allowed us to explore simulation for future, larger magnitude events in the study area. A typical application example of the proposed methodology was considered for the scenario of a Mw=7.5 intermediate-depth event which will occurr near the islands of Kos and Nisyros (eastern Hellenic arc). The obtained results are promising, confirming the significant differences of fore-arc and back-arc damage distributions, suggesting that the role of intermediate-depth earthquakes should be further explored using the updated 3D attenuation model.

References

Boore, D. M. (2009), Comparing Stochastic Point-Source and Finite-Source Ground-Motion Simulations: SMSIM and EXSIM, Bull. Seism. Soc. Am., 99(6), 3202-3216, doi: 10.1785/0120090056.

Kkallas, H., C. Papazachos, E. Skordilis, V. Margaris (2013), Re-examining the stress field of the broader Southern Aegean subduction area using an updated focal mechanism database, Bull. Geol Soc. Greece., 47(2), 563-573.

Kkallas Ch., Papazachos C.B., Margaris B.N., Boore D., Ventouzi Ch. and Skarlatoudis A. (2018a) Stochastic strong ground motion simulation of the Southern Aegean Sea Benioff zone intermediate-depth earthquakes, Bull Seismol Soc Am, 108(2), 946-965.

Kkallas Ch., Papazachos C.B., Boore D., Ventouzi Ch., and Margaris B.N. (2018b) Historical intermediate-depth earthquakes in the southern Aegean Sea Benioff zone: Modeling their anomalous macroseismic patterns with stochastic ground-motion simulations, Bull. Earth. Eng., doi: 10.1007/2Fs10518-018-0342-8

Motazedian, D., and G. M. Atkinson (2005), Stochastic Finite-Fault Modeling Based on a Dynamic Corner Frequency, Bulletin of the Seismological Society of America, 95(3), 995-1010, doi:10.1785/0120030207.

Papazachos, C., and G. Nolet (1997). P and S deep velocity structure of the Hellenic area obtained by robust nonlinear inversion of travel times, J. Geophys. Res. 102, no. B4, 8349–8367.

Skarlatoudis, A.A., Papazachos, C.B., Margaris, B.N., Papaioannou, C., Ventouzi, C., Vamvakaris, D., Bruestle, A., Meier, T., Friederich, W., Stavrakakis, G. and Taymaz, T., (2009), Combination of acceleration-sensor and broadband velocity-sensor recordings for attenuation studies: The case of the 8 January 2006 Kythera intermediate-depth earthquake, Bulletin of the Seismological Society of America, 99(2A), 694-704.

Skarlatoudis, A. A., C. B. Papazachos, B. N. Margaris, C. Ventouzi, and I. Kalogeras (2013), Ground-Motion Prediction Equations of Intermediate-Depth Earthquakes in the Hellenic Arc, Southern Aegean Subduction Area, Bulletin of the Seismological Society of America, 103(3), 1952-1968, doi:10.1785/0120120265.

Ventouzi, C., C. B. Papazachos, C. Papaioannou, P. Hatzidimitriou, and the EGELADOS working group (2014). QP and QS attenuation models of the southern Aegean subduction area, 15th European Conf. on Earthquake Engineering & 34th General Assembly of the European Seismological Commission, Istanbul, Turkey, 25–29 August 2014.

Ventouzi, C., Papazachos, C., Hatzidimitriou, P., Papaioannou, C., & EGELADOS Working Group. (2018). Anelastic P-and S-upper mantle attenuation tomography of the southern Aegean Sea subduction area (Hellenic Arc) using intermediate-depth earthquake data. Geophysical Journal International, 215(1), 635-658.

15th International Congress of the Geological Society of Greece
Athens, 22-24 May, 2019 | Harokopio University of Athens, Greece
Bulletin of the Geological Society of Greece, Sp. Pub. 7 Ext. Abs. GSG2019-244

Contemporary Tectonic Deformation in the Santorini Volcanic Complex, Greece.

A. Tzanis[1], V. Sakkas[1], S. Chailas[1], E. Lagios[1]

(1) Section of Geophysics and Geothermy, National and Kapodistrian University of Athens, Panepistimiopoli, Zografou 15784, Greece, atzanis@geol.uoa.gr

Tectonic deformation is difficult to study in the Santorini Volcanic Complex which comprises a cluster of small and awkwardly shaped islands covered by pyroclastic deposits: seismicity is generally absent and tell-tale markers of tectonic activity are swiftly erased by surface processes. We address the problem by combining geophysical exploration methods to assess the long-term effects of tectonic deformation and time-lapse Differential GPS (DGPS) and kinematic modelling to directly evaluate present-day deformation. 3-D modeling of gravity data is used to strip the gravity effect of pyroclastic and extrusive volcanic formations, reconstruct the morphology of the Alpine basement and delineate markers of tectonic activity such as fault steps, grabens and horsts. Spatial analysis of magnetotelluric data is used to map *epiphenomenal* conductivity anomalies generated by thermal fluid circulation along active faults. Finally, the DGPS observations span the period 1994–2005 during which the SVC was in repose and no volcanic activity whatsoever was reported before, during and immediately after the measurements. These measurements are used to resolve relative displacements (deformation) of the surface with nearly sub-millimetric precision, while their numerical modeling determines the nature and kinematics of the active fault zones generating this deformation. The following active fault configuration was determined:

The **Trans-Santorin Divide** (TSD) develops lengthwise of the line joining the areas of Vlychada/Cape Exomytis, the Kammeni islets and the Oia – Therassia strait. In the topography of the Alpine basement it appears as a series of dents and depressions aligned in an approximately N330° direction (Fig.1a, 1b). At depths greater than 500m, it is collocated with a major sub-vertical conductivity apparently associated with fluid circulation interface and defined by the current concentration pointed to by the real induction vectors and the mutual configuration of the maximum electric field polarization state (Fig. 1a). Contemporary deformation identifies the TSD as an aseismic segmented right-lateral dislocation surface that splits the SVC into NE and SW halves (Fig. 1c). Faulting with analogous geometrical characteristics may also exist in eastern Thera as well as along the caldera wall between Mts. Mikros Prof. Elias and Megalo Vouno where they and may be associated with the extrusion of Peristeria Volcano lavas: the deep dent in the Alpine basement at that location is thought to represent the volcanic vent.

The **Columbo Fault Zone** (CFZ) develops in a NE-SW direction between Mts. Mikros Prof. Elias and Megalo Vouno at north Thera and terminates on the TSD. It comprises a pair of parallel sub-vertical south-westerly dipping normal-sinistral faults (Fig. 1c): the Cape Columbo Fault (CCF) to the north and the Mikros Prof. Elias fault (MPEF) to the south. CFZ may be associated with thermal fluid injection into the shallow crust, possibly occurring at depths of 2-3 km via a TSD-like fissure beneath the coastline (caldera wall) and the pipe of the Peristeria Volcano. Onshore, it does not have a clear signature in the gravity field; offshore, it appears to have formed a significant NE-SW depression beneath the North Basin that terminates against the TSD (Fig. 1a-1c). The CFZ also appears to have limited effect on the electrical conductivity of the SVC crust (Fig. 1a).

The **Anhydros Fault Zone** (AFZ) is a very significant NE-SW system forming the NW flank of the Santorini–Amorgos Ridge; it has been detected off the northeast coast of Thera Island and is thought to traverse the SVC. On Thera, its presence is confirmed by its footprint on the Alpine basement, where it is seen to comprise a set of parallel, north-westerly dipping faults located between the Athinios–Monolithos line and Fira (Fig. 1a-1c). The morphological characteristics of the Alpine basement in the area of the Akrotiri Volcano indicate that AFZ may have had a role in the extrusion of the Akrotiri lavas (Fig. 1a-1c). The AFZ does not appear to affect electrical conductivity structure, meaning that it is *not* associated with active circulation (Fig. 1a). It also appears to insignificantly contribute to the observed horizontal displacement field, which can be entirely explained by the TSD and CFZ faults. These observations indicate that the AFZ may not have been particularly active in the recent geological past.

The CFZ and AFZ have antithetic throws and generate a graben-like structure that contains the Kammeni Line and the volcanic centre of the Kammeni islets. Given the observed kinematics of the TSD and CFZ, it can be safely concluded that the AFZ, as well as *any* NE-SW fault in the vicinity of the SVC, can only have *left-lateral* heave.

The arrangement of NNW-SSE right-lateral (TSD) and NE-SW normal left-lateral faults (CFZ) can be explained *only* if the NNW-SSE faulting direction comprises the synthetic (dextral) Riedel-R shear and the NE-SW direction the antithetic (sinistral) Riedel-R′ shear. This configuration can only be generated by N-S σ_1 and E-W σ_3 principal stress axes (Fig. 1c), therefore *secondary* E-W compressional and N-S extensional failure is also expected.

The strain field computed from GPS observations indicates E-W extension lengthwise of a zone stretching from Cape Exomytis to Athinios port and along the east flank of the caldera, up to Imerovigli. The same computations indicate NNE-SSW compression at south Thera and along the Akrotiri peninsula. The footprint of the caldera on the Alpine basement is a parallelogram with N-S long side and WNW-ESE short side. All this evidence indicate that the east flank of the caldera may have formed by collapse along secondary westerly dipping N-S normal faults and the WNW-ESE short side of the parallelogram by collapse along WNW-ESE “inverse faults”.

The observed configuration of active faulting and associated principal strain/stress axes can only be driven by NW-SE right-lateral shearing of the broader SVC area, the exact geographical extent of which as well as its role and contribution to the regional tectonic and kinematic setting of the south Aegean Sea cannot be determined with the present data.

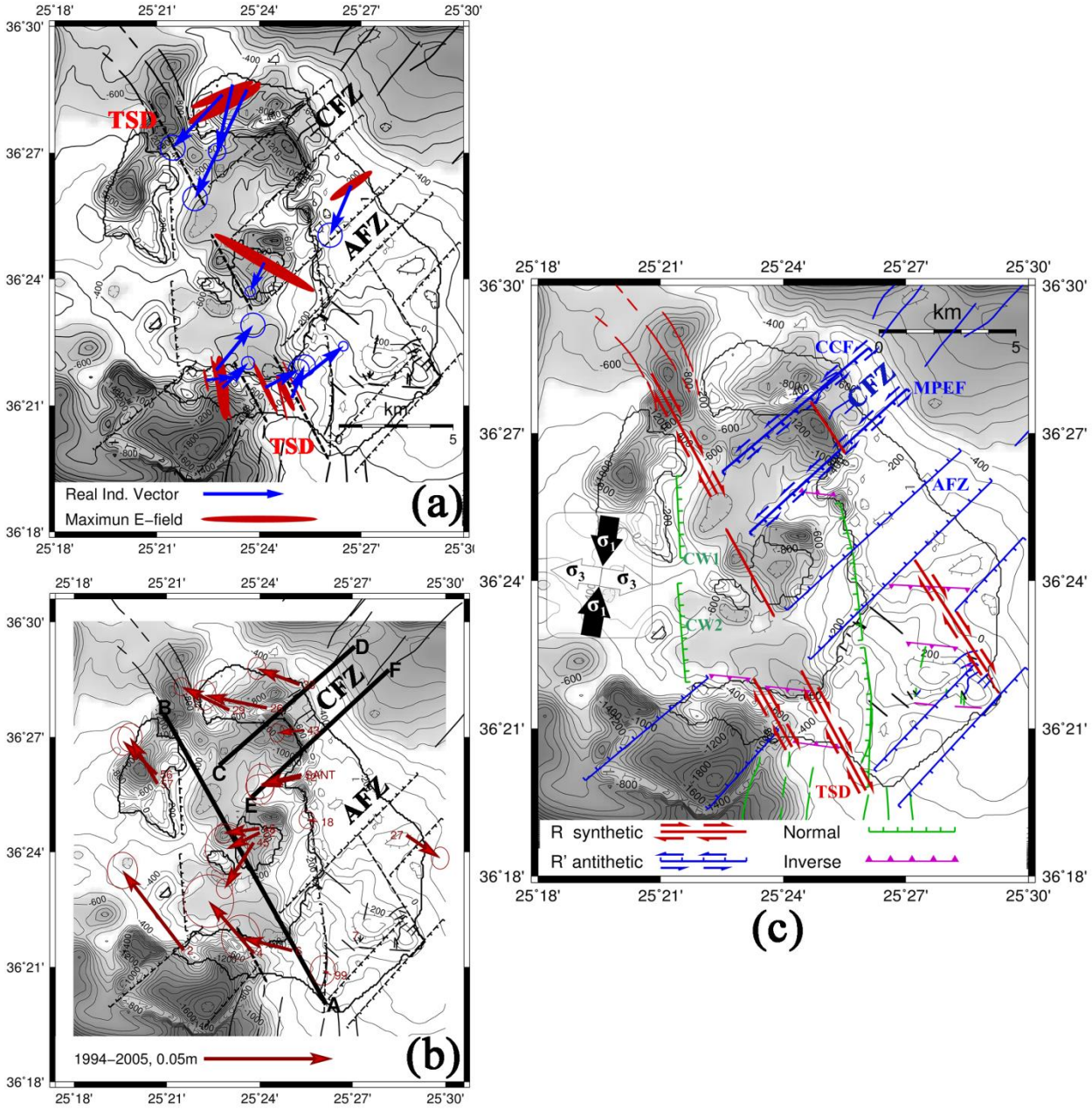

Figure 1. (A) Polarization of the maximum electric field (red ellipses) and the Real Induction Vectors (blue arrows); both are shown as averages over the bandwidth 1–100s and are superimposed on the model of the Alpine basement. (B) Aggregate horizontal displacement vectors relative to Station 7, measured over the periods 1994-2005 and superimposed on the model of the Alpine basement. AB, CD and EF are the surface traces of the model faults used in modelling the surface deformation sensed by the GPS data; they represent the TSD, the CCF and the MPEF respectively. Solid black lines indicate the traces of known faults and dashed lines the traces of inferred faults; throw/dip direction is shown whenever possible. (C) The horizontal stress axes σ_1, σ_3 and the principal (R/R′) and secondary (normal/inverse) tectonic and kinematic elements in the SVC. They are all superimposed on the model of the surface of the Alpine basement.

Acknowledgements

We sincerely appreciate insightful discussions with Dr Haralambos Kranis (National and Kapodistrian University of Athens). We are grateful to Prof. Dr Tim Druitt (University Clermont Auvergne) for valuable comments and recommendations.

15th International Congress of the Geological Society of Greece
Athens, 22-24 May, 2019 | Harokopio University of Athens, Greece
Bulletin of the Geological Society of Greece, Sp. Pub. 7 Ext. Abs. GSG2019-250

Stochastic Simulation of Seismic Motion and Site-Effects Studies of Ambient Noise and Seismic Data: The Case of the Vrisa Settlement and the 2017 M=6.3 Lesvos Earthquake

N. Chatzis[1], Ch. Kkallas[1], C. Papazachos[1], M. Anthymidis[1], Em. Rovithis[2], Ch. Karakostas[2], Ch. Papaioannou[2]

(1) Department of Geophysics, School of Geology, Aristoteles University of Thessaloniki, Thessaloniki, Greece, chatniko@geo.auth.gr
(2) Institute Of Engineering Seismology & Earthquake Engineering, Elaionon 28, Pylaia, Thessaloniki, Greece

A strong earthquake with magnitude M6.3 struck on June 12, 2017 the island of Lesvos and the surrounding area, situated at the north-east part of the Aegean Sea. While the mainshock epicenter was estimated to be ~15 km off the southern coast of Lesvos island with a focal depth to 12 Km, relatively limited damage was reported along the coastal Lesvos area. An exception was the historical settlement of Vrisa, where extensive damage (including a large number of collapsed masonry houses) was observed, mainly in the northwestern part of the village, which was located on recent (Holocene) sediments. On the contrary, for the remaining part of the village, founded on stiffer Neogene deposits, limited damage was reported. Moreover, the earthquake affected mainly the historical, masonry buildings of the village, with a negligible impact on the (fewer) reinforced concrete modern constructions.

To explain the presence of such localized damage phenomena, we employ the stochastic finite-fault modelling approach of Motazedian and Atkinson (2005), as adapted by Boore (2009), for the simulation of Fourier Amplitude Spectra (FAS) of the 2017 Lesvos earthquake. To calibrate the necessary model parameters of the stochastic finite-fault method, we used waveform data from both acceleration and broadband-velocity sensor instruments within ~100km from the earthquake fault. To constrain the mainshock focal parameters, we have computed an updated 1-D velocity model for the study area following Kissling et al. (1994), and relocated the Lesvos 2017 aftershock sequence in order to determine the main geometrical features of the earthquake's fault. Preliminary relocations were performed with the HYPOINVERSE (Klein, 2002) program, and hypoDD (Waldhauser, 2001) relocations allowed to obtain an improved aftershock sequence distribution. From the relocation procedure we constrained the main fault dimensions, strike and dip, in good agreement with fault plane solutions published for this event, and used them in the stochastic simulation approach. Using the previous source information, as well as appropriate path and generic site-effect information for the Aegean area, we solved for the mainshock stress-parameter value, in an attempt to fit the FAS of the mainshock recorded waveforms. To estimate the stress parameter ($\Delta\sigma$), we adopted a trial-and-error approach and tested different stress-drop values, through comparison of simulated and observed acceleration Fourier spectra.

Since the previously described damage pattern for the Vrisa settlement is indicative for the presence of strong site-effect phenomena, we have employed a large number of surface geophysical measurements, recording mainly of surface waves from both active and passive sources, in order to study the shallow geophysical structure and examine the spatial distribution of the expected site effects on seismic motions for the Vrisa area.

To determine the 1-D shear-wave velocity structure, a circular Noise-Array was realized in the northern (Holocene) Vrisa area (with a radius of 10, 40 and 100 m for the inner, the middle and the outer circle radius, respectively). Moreover, 23 lines of MASW were realized with the use of 4.5 Hz vertical geophones. This dataset was complemented by the performance of nearly 70 single station ambient noise measurements, which were conducted with the use of broad-band seismometers (CMG-6TD or CMG-40T-60 sec with Reftek 130 digitizers). Horizontal-to-Vertical Spectral Ratio (HVSR, Nakamura, 1989) curves were calculated for all noise recording sites, while dispersion curves were determined with the use of the f-k method, both for the MASW and the Noise-Array data.

For the final 1-D shear-wave velocity model determination we employed a joint inversion of Rayleigh wave dispersion curve and Rayleigh ellipticity information. For this reason, Rayleigh wave ellipticity was extracted from the noise recordings using the approach of Hobiger et al. (2009). Ellipticity was jointly inverted with the reconstructed Rayleigh dispersion curves, in order to increase the Vs-model penetration depth, as well as to reduce the non-uniqueness of the model inversion. The joint inversion was performed with the use of a Monte-Carlo approach, namely the neighborhood algorithm, as adapted by Wathelet et al. (2008) and realized through the *Geopsy* software tools (http://www/geopsy.org).

The final Vs models (figure 1) show the presence of a very soft layer (Vs<300 m/sec, in most cases <200m/s for the uppermost 10-15m), with a typical thickness of ~20-25 m for the northwestern part of Vrisa, clearly corresponding to the Holocene formations of the study area. This layer is underlain by a stiffer layer (Vs>500 m/sec, locally >700-800m/sec), which outcrops in the Vrisa southeastern section, corresponding to the Neogene formations. The transition from Neogene to Holocene formations is rather abrupt, suggesting the presence of a NE-SW normal fault that creates the local basin, which is filled with Holocene formations. Preliminary 1D site response analysis in the frequency domain for the final geophysical model of the Vrisa area confirms the presence of strong amplification of seismic motions in the northwestern Vrisa area, in good agreement with the damage pattern of the June 12, 2017 M6.3 earthquake.

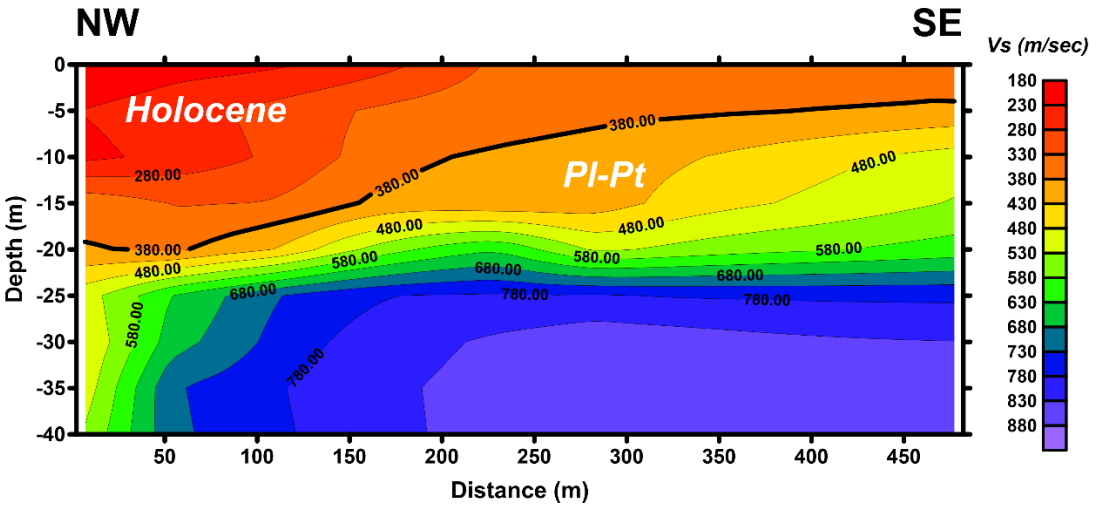

Figure 1. Final 2D model of shear-waves velocity along a NW-SE profile in the Vrisa area. The Holocene sediments with low S-wave velocities are located on the NW part of the study area, where the main damages and amplification of seismic motions from the strong earthquake at 12 June 2017 (M6.3) mainly occurred.

The HVSR results revel a strong spatial variation of the soil fundamental frequency, f_0, and maximum HVSR amplitudes, A_0^{HVSR}, with almost flat HVSR curves in the southeast Vrisa (Neogene sediments) and large A_0^{HVSR} values (locally larger than 5) in the Holocene sediments at frequencies f_0~2.5-3 Hz. Considering that A_0^{HVSR} values generally provide a low threshold of local amplifications, we expect seismic motions to be significantly amplified in the Holocene sediments section of the village. This was confirmed by computing Standard Spectral Ratios (SSR, Borcherdt, 1970) from aftershock records in both Neogene and Holocene deposits, which showed that peak amplifications, A_0, are almost double than the values provided by A_0^{HVSR}, though the resonant frequency, f_0, and spectral shapes of the SSR and HVSR curves were nearly identical. The spectral slopes (Anderson and Hough, 1984) were computed for all the sites with aftershock records, in order to compute kappa factors and the SSR curve correlations. By quantitative comparison of the HVSR and SSR results for several sites it was possible to determine an appropriate scaling factor and reduce all HVSR curves to equivalent SSR curves. Using these equivalent SSR amplifications, we employed the stochastic simulation method for the determination of complete ground motion simulations throughout a dense virtual receiver grid in the Vrisa area, and reconstructed the detailed spatial variation of several ground motion measures (PGA, PGV, etc.), as well as expected damages (IMM) in the broader Vrisa area. The results show that the while the southeastern part of the Settlement (Neogene deposits) exhibited values around IMM=6+ to 7, the northwestern Holocene section experienced damage levels of the order of IMM=8+ to 9, in excellent agreement with the observed damage distribution.

References

Anderson, J.G., Hough, S.E., 1984. A model for the shape of the Fourier amplitude spectrum of acceleration at high frequencies. Bulletin of the Seismological Society of America, 74(5), 1969-1993.

Boore, D.M., 2009. Comparing stochastic point-sou rce and finite-source ground-motion simulations: SMSIM and EXSIM. Bulletin of the Seismological Society of America, 99(6), 3202-3216.

Borcherdt, R.D., 1970. Effects of local geology on ground motion near San Francisco Bay. Bulletin of the Seismological Society of America, 60(1), 29-61.

Kissling, E., Ellsworth, W.L., Eberhart-Phillips, D., Kradolfer, U., 1994. Initial reference models in local earthquake tomography. Journal of Geophysical Research: Solid Earth, 99(B10), 19635-19646.

Klein, F.W., 2002. User's guide to HYPOINVERSE-2000, a Fortran program to solve for earthquake locations and magnitudes, USGS Open-File Report 2002-171, https://doi.org/10.3133/ofr02171

Hobiger M., Bard P-Y, Cornou C., Le Bihan N., 2009. Single station determination of Rayleigh wave ellipticity by using the random decrement technique (RayDec). Geophys. Res. Lett., 36, doi:10.1029/2009GL038863.

Motazedian, D., Atkinson, G.M., 2005. Stochastic finite-fault modeling based on a dynamic corner frequency. Bulletin of the Seismological Society of America, 95(3), 995-1010.

Nakamura, Y., 1989. A method for dynamic characteristics estimation of subsurface using microtremor on the ground surface. QR Railway Tech. Res. Inst., 30(1), 25-33.

Waldhauser, F., 2001. hypoDD--A program to compute double-difference hypocenter locations.

Wathelet, M., 2008. An improved neighborhood algorithm: Parameter conditions and dynamic scaling. Geophys. Res. Lett., 35, doi:10.1029/ 2008GL033256.

15th International Congress of the Geological Society of Greece
Athens, 22-24 May, 2019 | Harokopio University of Athens, Greece
Bulletin of the Geological Society of Greece, Sp. Pub. 7 Ext. Abs. GSG2019-252

Improving Station Characterisation for the Accelerometric Network of the National Observatory of Athens

O.-J. Ktenidou[1], I. Kalogeras[1]

(1) Institute of Geodynamics, National Observatory of Athens, Greece, olga.ktenidou@noa.gr

Abstract

The accelerometric network of the National Observatory of Athens (NOA) covers most Greek territory with 164 strong-motion stations. For few of those, site conditions are known in detail through measurements. However, most of them are still characterised merely through 1:50,000 geological maps. Considering: 1. the progress made in recent years with sophisticated ground motion models, 2. the move towards large open-access strong-motion databases, and 3. that Greek-provenance data represent a significant percentage of European seismic data, better site characterisation of this network's stations has become imperative. In-situ-characterisation campaigns impose unattainable time/budget constraints, so we implement alternative approaches using the recordings themselves. We consider triggering-mode stations with an adequate number of recordings and use the empirical horizontal-to-vertical spectral ratio technique to estimate amplification. The computed transfer functions show that the response within site categories as defined by seismic design codes (e.g. Eurocode 8) is often not homogeneous. The results shed light onto the seismic behaviour of particular stations and hope to aid in the quest for a more harmonised site characterisation throughout Greece.

Background and Objectives

The accelerometric network of the Institute of Geodynamics of the NOA had its first strong-motion stations installed in the 1970s, and today covers most of the country's territory with 164 strong-motion stations (https://accelnet.gein.noa.gr,). In March 2019, the network consists of 91 stations operating in continuous mode with live data transmission and 73 stations operating with low-resolution instruments in triggering mode. For a few of these stations, site conditions are known in great detail thanks to nearby boreholes, geophysical in situ and/or geotechnical laboratory investigations. For some others, Vs_{30} values have been inferred from proxies, such as topography. Margaris et al. (2014) provide a brief history of the characterisation of Greek stations with boreholes, geophysical campaigns and microtremors, while Stewart et al. (2014) compile values of Vs_{30} and other geological data for some of the stations. However, to date, most of these stations are still characterized merely through 1:50,000 scale geological maps. Today, characterising the network's stations has become a necessity, not only due to the upgrade of the instrumentation leading to more and better-quality data, but also given the state of the art in ground motion prediction and simulation, where the prevalent type of classification used up to now (geological maps) has become obsolete.

Methods

Despite the strong need for site characterisation, performing in-situ measurements (boreholes, geophysical campaigns, geotechnical testing) at all stations imposes unattainable time/budget constraints. Hence, we turn to alternative approaches and estimate amplification functions (aka transfer functions), with the horizontal-to-vertical spectral ratio (HVSR) introduced by Lermo and Chavez-Garcia (1993), the empirical technique available in the absence of a reference station. Here we focus on the triggering-mode accelerometric stations. At the end of 2018, over 1000 strong-motion recordings had been processed and individually inspected for quality assurance. Recordings up to 1999 are included in the unified Hellenic Accelerogram Database HEAD (Theodulidis et al., 2004), while recordings from 2000 to 2018 are not in public databases so far. We begin with the best-populated stations choosing a minimum number of 10 events per station, resulting in 19 stations and about 700 usable recordings. Few of these stations appear in the Vs compilation of Stewart et al. (2014). After standard corrections and processing, ratios of the Fourier amplitude spectra (FAS) of acceleration were computed between the horizontal components and to the vertical. For each station these were logarithmically averaged per component, yielding amplification functions for the longitudinal and transverse component. An additional set of analyses was performed in order to assess the sensitivity of the amplification to orientation. We followed the procedure of Ktenidou et al. (2015), incrementally rotating the pairs of components, and recomputing the transfer functions.

Results

Fig. 1 shows the mean transfer functions computed for each station and their directional dependence per rotational increment. The shaded areas represent values of HVSR between 0.5 and 2.0, which considering typical uncertainties are practically equivalent to unity. An example of considerable directional dependence/sensitivity of the HVSR is ARGA, while an example of stability with orientation is VLSA. Around 3 Hz, ARGA exhibits statistically the same amplification in both components, if the as-installed recordings are rotated by 10°, but shows a difference of a factor of 2 if rotated by 40°. This is particularly interesting, as ARGA is one of the few stations on rock (class-A site as per EC8, CEN, 2003). Considering the high number of recordings at the site, and the significant separation of the standard error bands, this is not likely to be an artefact and so further investigation is recommended. On the other hand, VLSA exhibits considerable stability with orientation, and also remains flat and close to unity over the entire range of frequencies below 6 Hz. Of the rock stations studied, VLSA is the only one that may be considered a reference station, at least out to 6 Hz. Of the 2 stiff

soil sites, AIGA exhibits the typical behaviour of a B-class site, while the fact that no strong directionality is observed there seems to confirm previous conclusions that topographic effects are not prominent at Aegion (Ktenidou, 2010); MALA, on the other hand, does not exhibit significant amplification. Finally, of the soft-soil (class C) sites, site AMAA shows a clear peak around 1 Hz, much as expected, while PATA is interesting due to its stability with orientation and its lack of significant amplification.

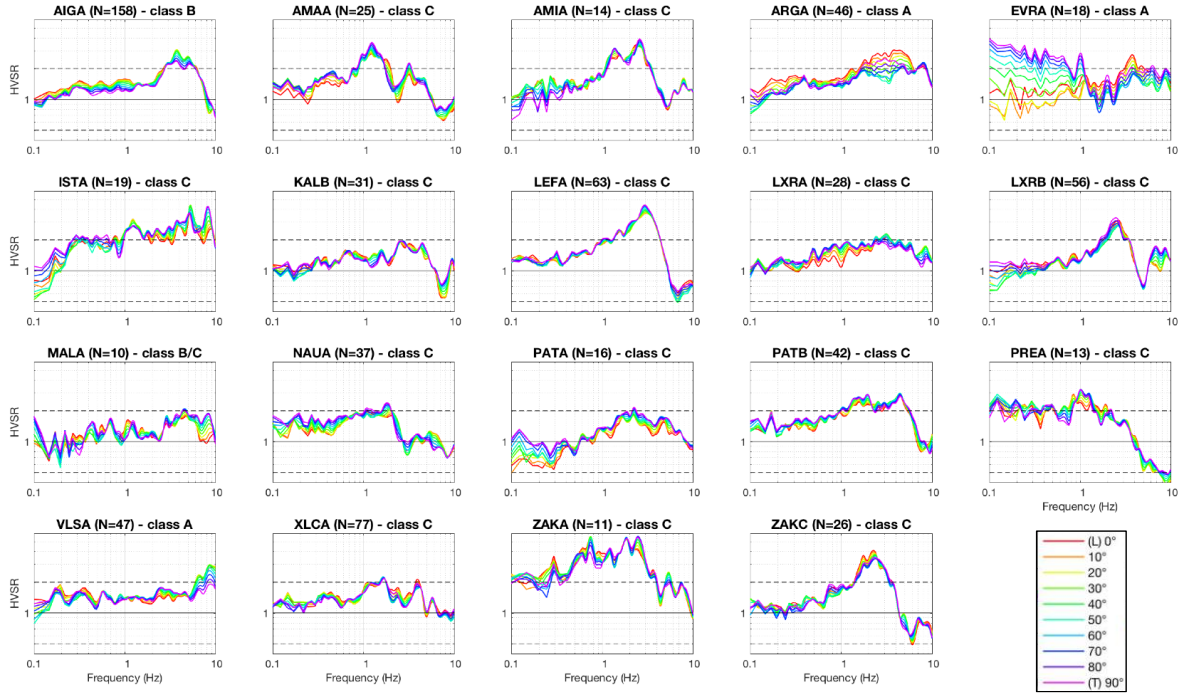

Figure 1. Mean HVSR and directional sensitivity at stations that recorded more than 10 earthquakes.

Conclusions

The hard sites in this subset do not behave in the same way, nor is their response independent of orientation. This calls for further investigation into the local site conditions and an effort to understand the provenance of any directional dependence. The majority of sites studied are soft-soil sites, and again their response exhibits variability: some stations have an identifiable resonance, others have more complex or broadband amplification patterns, while others show no significant amplification. We do not focus on absolute amplitude, as HVSR has often been shown to yield unreliable amplitudes (Field & Jacob, 1996). Finally, low-frequency uncertainties are likely due to the fact that some of the recordings came from analog instruments (Kinemetrics SMA-1) or from low-resolution digital Kinemetrics QDR or Teledyne A800 sensors, whose low-frequency content is known to be limited.

Acknowledgements

All recordings and catalogue information come from the Institute of Geodynamics. Some plots were made using Generic Mapping Tools v.3.4 (Wessel and Smith 1998).

References

CEN 2003 Eurocode 8: design of structures for earthquake resistance. Part 1: general rules, seismic actions and rules for buildings. EN 1998-1: 2004. Brussels.

Field, E, and K. Jacob 1995. A comparison and test of various site-response estimation techniques, including three that are not reference-site dependent. Bull. Seism. Soc. Am. 85, 1127-1143.

Ktenidou O-J 2010 Experimental and theoretical study of seismic ground motion in the city of Aegion, Greece, focusing on local site and topographic effects. PhD thesis, Aristotle University Thes/ki. http://ikee.lib.auth.gr/record/124050/files/GRI-2010-5489.pdf.

Ktenidou O.-J., F.J. Chávez-García, D. Raptakis and K.D. Pitilakis 2015. Directional dependence of site effects observed near a basin edge at Aegion, Greece. Bull. Earthq. Eng. 14, 623-645.

Lermo, J., F.-J. Chávez-García 1993. Site effect evaluation using spectral ratios with only one station, BSSA 83, 1574-1594.

Margaris, B., I. Kalogeras, Ch. Papaioannou, A. Savvaidis, N. Theodoulidis 2014. Evaluation of the national strong motion network in Greece: deployment, data-processing and site characterization. Bull. Earthq. Eng., 12, 237-254.

Stewart, JP, Klimis, N, Savvaidis, A, Theodoulidis, N, Zargli, E, Athanasopoulos, G, Pelekis, P, Mylonakis, G & Margaris, B 2014. Compilation of a local Vs profile database and its application for inference of Vs30 from geologic- and terrain-based proxies Bull. Seismol. Soc. Am. 104, 2827-2841.

Theodoulidis N., Kalogeras I., Papazachos C., Karastathis V., Margaris B., Papaioannou Ch., Skarlatoudis A. 2004 HEAD 1.0: a unified Hellenic accelerogram database. Seismol. Res. Lett. 75, 36–45.

Wessel P, Smith WHF 1998. New, improved version of the generic mapping tools released. EOS Trans AGU 79:579.

15th International Congress of the Geological Society of Greece
Athens, 22-24 May, 2019 | Harokopio University of Athens, Greece
Bulletin of the Geological Society of Greece, Sp. Pub. 7 Ext. Abs. GSG2019-279

Improved Generalized Inversion Technique (GIT) and its implementation to a synthetic dataset, to retrieve seismic source, propagation path and site factors

I. Grendas[1,2], N. Theodoulidis[2], F. Hollender[3] and P. Hatzidimitriou[1]

(1) Laboratory of Geophysics, Aristotle University of Thessaloniki, Greece, igrendas@geo.auth.gr
(2) Institute of Engineering. Seismology and Earthquake Engineering, Elaionon, 28 ,Pylaia, Greece,
(3) CEA Cadarache, French Alternative Energies and Atomic Energy Commission, St. Paul Les Durance

Introduction

Generalized Inversion Technique (GIT) first introduced and applied by Andrews (1986), consists a seismological "tool" where seismic source, site effect and propagation path spectral terms, is feasible to be separated from the Fourier Spectra of an S-wave earthquake record. The application of this technique requires a dataset of Fourier spectra based on a satisfactory number of seismic records from several common earthquakes and stations at a non-extended area. The last is theoretically considered so that the assumption of an average representative attenuation for the investigated area to be tested. Several studies have been achieved under this assumption by the application of the GIT, concluding in encouraging results about the three controlling terms (source, path, site), in comparison with other methods. Drouet et al. 2008a first applied the non-linear Gauss-Newton inversion method, at a parametric Generalized Inversion Technique in order to investigate for a set of earthquakes in France-Alps, the site spectral amplification where the recording stations were located and an average wave attenuation for the study area. In Greece the GIT method was applied by *Drouet et al. 2008b*, aiming at the estimation of the station site effect in Lefkas island and by Grendas et al. 2018 investigating seismic sources, average attenuation and site effect of the ITSAK (Institute of Engineering Seismology and Earthquake Engineering) accelerometric stations. The intention of this study is to introduce a reasonable way of spatially separating and studying the attenuation model. The goal of this effort is to improve the parameterization of the attenuation and consequently the GIT computing precision of the study parameters (seismic source, attenuation, site effect). At the end, a synthetic dataset was created and inverted by the new inversion algorithm that was developed following the one by Drouet et al. 2008a.

Method

GIT inversion developed here is based on the fundamental Eq. [1], where the first term of the product refers to the seismic sources (*Brune, 1970*), the second and the third refer to the attenuation and the last term consists the site effect. The product of these terms is equal to the Fourier spectrum A_{ijk} of the S-wave record. The investigated parameters are the seismic moment M_o and corner frequency f_c for each i earthquake, the $\gamma(r_{ij})$, Q_{sn} and a_n parameters for the attenuation as mentioned below and the non-parametric site spectral amplification for the specific k frequencies at each station j. Gauss-Newton inversion algorithm (Tarantolla, 2004) uses the partial derivatives of Eq. [1] in relation to the above investigated parameters, as well as the initial values for these parameters and their corresponding a priori covariance values. Wave attenuation is controlled by the geometrical spreading and anelastic attenuation. The first one is analyzed and studied here as a distance dependent factor, controlled by a distance dependent gamma factor ($\gamma(r_{ij})$) that is investigated (Eq. [1]). The second one is separately studied for the different n sub-divided areas (Figure 1b), controlled by the frequency dependent quality factor $Q_n(f) = Q_{sn}\, f^{\,an}$, as well as by the specific epicentral distance r_{ijn} that passes through each specific "rectangular".

$$A_{ijk}(f_k) = \left(\frac{\boldsymbol{M_{o_i}} \times \left({}^{2R_{\theta\varphi}}\!/_{4\pi\rho\beta^3} \right)}{\left[1 + (f_k/\boldsymbol{f_{c_i}})^2\right]} \right) \times \left(\frac{1}{r_{ij}^{\,\gamma(r_{ij})}} \right) \times \prod_1^n \left(exp\left(- \frac{\pi\, r_{ijn} f_k}{\boldsymbol{Q_{s_n}} f_k^{\boldsymbol{a_n}} v_{s_n}} \right) \right) \times \left(\boldsymbol{S_{jk}}(f_k) \right) \qquad (1)$$

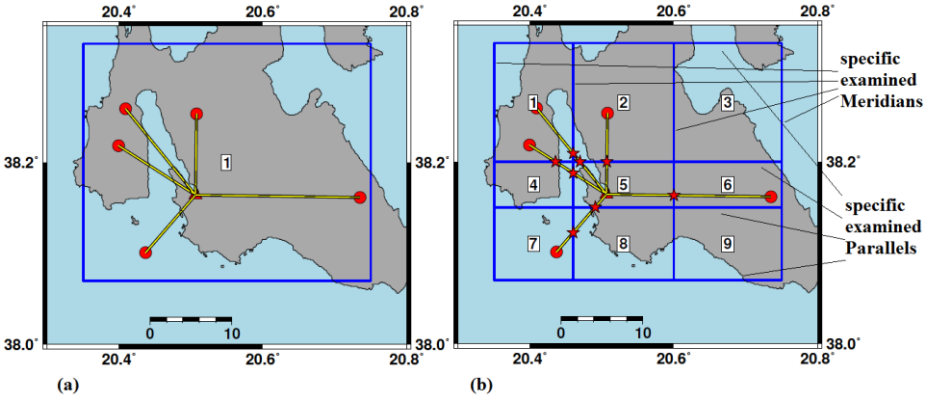

Figure 1. An example (Cephalonia island) of the separation of a (a) unique attenuation model-area to (b) more than one (nine here) attenuation model-areas. With red circles and triange are some random earthquakes and station, respectively, while with red asterisks are the intersection points of the ray paths (yellow lines) with specific Paralles and/or Meridians, in order to contribute at the part distance ray path r_{ijn}.

Results & Conclusions

The developed inversion algorithm in this work was applied to a synthetic dataset of 4313 spectra created by eq. [1] for 126 synthetic seismic sources (M_o and f_c) "recorded" at 60 random stations with specific site amplifications, for 20 frequencies (0.5 -15 Hz). The initial values needed for the inversion method were considered to be unknown, taking reasonable initial values and quite large *a priori* covariance values. The only exception was the moment magnitudes that were considered to be the synthetic values affected by a random factor up to 0.2 as can be understandable in Fig. 2a. The use of *a priori known* moment magnitudes, with their standard deviations (~±0.2) from different methods, for a real dataset is a common practice in GIT. Thus, affecting the synthetic values by a common computed factor up to 0.2, an actual practice was implemented.

The results are encouraging enough for the correct process of the algorithm and also for the attenuation separation concept. This can be confirmed in Fig. 2 where the source parameters results are presented. Inverted moment magnitudes $\boldsymbol{M_w}$ (corresponds to inverted seismic moments $\boldsymbol{M_o}$), are equal to the synthetic $\boldsymbol{M_w}$ values (Fig. 2a), as well as the computed corner frequencies, at least for M_w >2 corresponds to stress drop 100 bar, which is the synthetic stress drop value. For M_w < 2 the corner frequencies and stress drop are not well estimated in comparison to synthetic values, but this is more or less a reasonable result since the data are limited at frequencies up to 15 Hz and the inversion process can not easy compute corner frequencies greater than this limit. Attenuation parameters were computed close enough, with a short deviation, to the synthetic values, while site amplifications were computed satisfing enough, having the same "shape" but with a low underestimation as it is presented in Fig. 3 for 5 of the 60 stations. It is worth noting that in case where some of the initial values were considered to be known, the final results were exactly the same as the synthetic values.

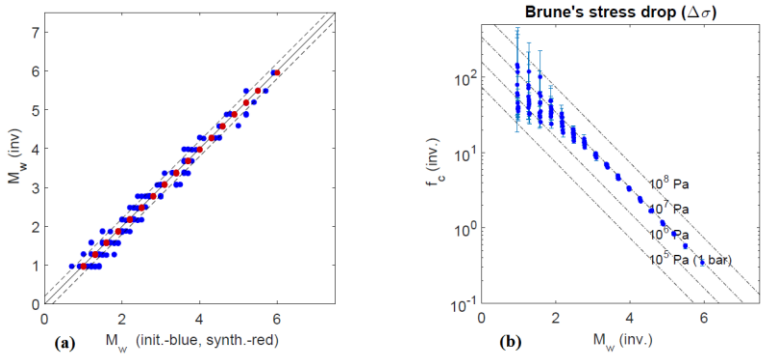

Figure 2. (a) The comparison of the inversion computed moment magnitude M_w (inv.) to the initial values of M_w (blue points) and to the synthetic M_w (red points). (b) The comparison between the corner frequencies f_c and moment magnitude M_w, both computed from the inversion.

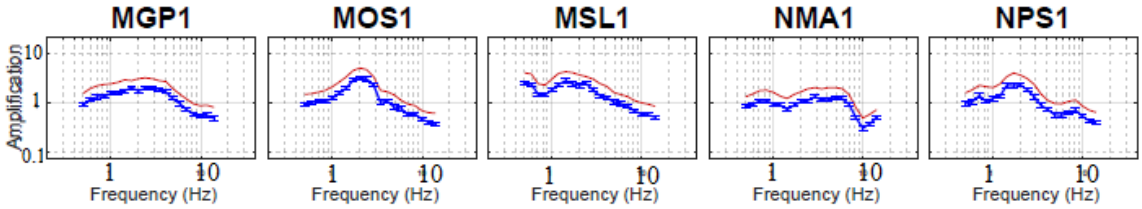

Figure 3. Site spectral amplification of 5 stations that used for the synthetic data. With red line is depicted the synthetic values, while with blue line is depicted the computed from the inversion values.

Acknowledgements

This study consists a part of a doctoral dissertation, the implementation of which was co-funded through the action: "Human research potential support through doctoral research implementation", from financial resources of the operational Program "Human resources development, Education and Lifelong learning", 2014-2020.

References

Andrews, D., J., (1986). Objective determination of source parameters and similarity of earthquakes of different size. Earthquakes Source Mechanics. American Geophysical Monograph 37, 259-267.

Brune, J., N., (1970). Tectonic stress and the spectra of seismic shear waves from earthquakes, J. Geophys. Res. 75, 26, 4997–5009.

Drouet, S., Chevrot, S., Cotton, F. and Souriau, A., (2008a). Simultaneous inversion of source spectra, attenuation parameters and site responses: Application to the data of the French accelerometric network. Bull. Seism. Soc. Am. 98, 1, 198-219.

Drouet, S., Triantafyllidis, P., Savvaidis, A. and Theodulidis, N., (2008b). Comparison of Site -Effects estimation methods using the Lefkas, Greece 2003 earthquake aftershocks, Bull. Seism. Soc. Am. 98, 1198 - 219.

Grendas, I., Theodoulidis, N., Hatzidimitriou, P., Margaris, B., & Drouet, S. (2018). Determination of source, path and site parameters based on non-linear inversion of accelerometric data in Greece. *Bulletin of Earthquake Engineering*, *16*(11), 5061-5094.

Tarantola, A., (2004). Inversion Problem Theory and Methods for Model Parameters Estimation, SIAM, Philadelphia, 342 p.

15th International Congress of the Geological Society of Greece
Athens, 22-24 May, 2019 | Harokopio University of Athens, Greece
Bulletin of the Geological Society of Greece, Sp. Pub. 7 Ext. Abs. GSG2019-314

Geophysical Investigation of Zerelia Twin-Lakes (Central Greece): Two Possible Meteorite Craters

V. Sakkas[1], S. Chailas[1], VJ. Dietrich[2], E. Lagios[1], E. Gartzos[3], K. Kyriakopoulos[1]

(1) Section of Geophysics-Geothermics, National & Kapodistrian University of Athens, Panepistimiopolis, Athens, Greece, vsakkas@geol.uoa.gr
(2) Institute of Geochemistry and Petrology, Swiss Federal Institute of Technology, Zurich, Switzerland
(3) Laboratory of Mineralogy-Geology, Agricultural University of Athens, Athens, Greece

Two circular permanent lakes of 150 and 250m diameter and 6-8m depth to an unconsolidated muddy bottom occur 250 m apart from each other, isolated in the agricultural fields SW of the town of Almyros (Thessaly, central Greece) (Fig. 1) (Dietrich et al., 2017). Geological outcrops that exhibit possible underground structures are missing in the area. The age of the lakes is assumed to be Late Pliocene to Early Holocene with a minimum age of approx. 7000 years BP.



Figure 1. The Magoula Zerelia twin-lakes in the agricultural fields SW of the town of Almiros (Thessaly) with the hillsite of the prehistoric Magoula Zerelia settlement, which was occupied from the Middle Neolithic period until Late Bronze Age. Red stippled line mark the distribution of the "fallback breccia" as deposits due to the impact of the projects. SP 1 and 2 mark sampling points at small trenches within the walls of the fallback breccias.

The halo-type embankments of the lakes, excavated in two trenches down to 8 m depth, are made up of yellow to brownish, clay-rich and whitish marly soil with pedogenic characteristics and weak stratification. The southern parts of the halos contain angular and spherical clasts of various, up to decimeter size, which are made up of polymict, quartz-rich hard carbonate breccia with marly and calcite feathery, pseudospherulitic fibrous calcite to micro-sparitic textures, besides abundant quartz and chert fragments, as well as spheroidal shaped solidified, calcite veined "septariantype" carbonate clasts. The carbonatic matrix includes small xenomorphic phases, such as chromspinel, zircon with blurred granular and skeletal textures, skeletal rutile and ilmenite, which are interpreted as relicts of partial melting and quenching under high temperatures of 1240-1800°C. Only a few quartz fragments exhibit indistinct planar fractures. In several cases they include exotic Al-Si- and sulfur bearing Fephases, <1-10 mm as globules. The carbonaceous textures, small calcareous porcelain fragments and calcite globules in quartz are interpreted as possible carbonate melting, quenching, devitrification and recrystallization.

Geophysical Survey

A gravity survey was carried out in the area around the two lakes to form the Gravity Anomaly Field. About 80 gravity measurements were taken by the use of the LaCoste & Romberg G-496 gravity meter. The Gravity Anomaly Map of the area is presented in Figure 2. It was found that a surface density of about 2 gr/cm3 was appropriate to reduce the gravity anomaly values after fitting a 2nd and 3rd polynomial fit to the observed gravity anomaly field. It can be seen that two gravity lows are associated with the localities of the two lakes, reaching values of about 120 gravity units (gu). The modelled "Residual Gravity" profiles through the lakes indicate negative gravity anomalies of bowl-type structures down to 150 m for the eastern lake and down to 250 m for the larger western lake.

Total field magnetic measurements were also conducted to determine the Total Magnetic Field at an effort to detect magnetic anomalies relating to the probable presence of a magnetic body supporting the meteorite impact hypothesis. Total field magnetic readings were performed using total field magnetometers of the GEOMETRICS G-856 type along 12 profiles at a spacing of 10 m. Magnetic measurements were also taken peripherally around the two lakes. Corrections for the normal field and the diurnal variation were made to form the magnetic anomaly value for each station. As can be seen from the magnetic anomaly map (Fig. 2), the eastern part of the area, as well as the half northern and southern part

is characterized by positive anomalies, which should be attributed to the basement geological formations. The same positive feature extending N-S is the ridge separating the two lakes, forming actually a part of the basement. The two lakes are also associated with two magnetic anomalies. The eastern lake is dominated by a large negative magnetic anomaly encompassing even a region outside the lake. There is also another positive anomaly at its eastern flank, but this should rather be attributed to as part of basement characteristics. Magnetic readings have not been taken on the surface of the two lakes, so the values over them have been produced by the interpolation routine.

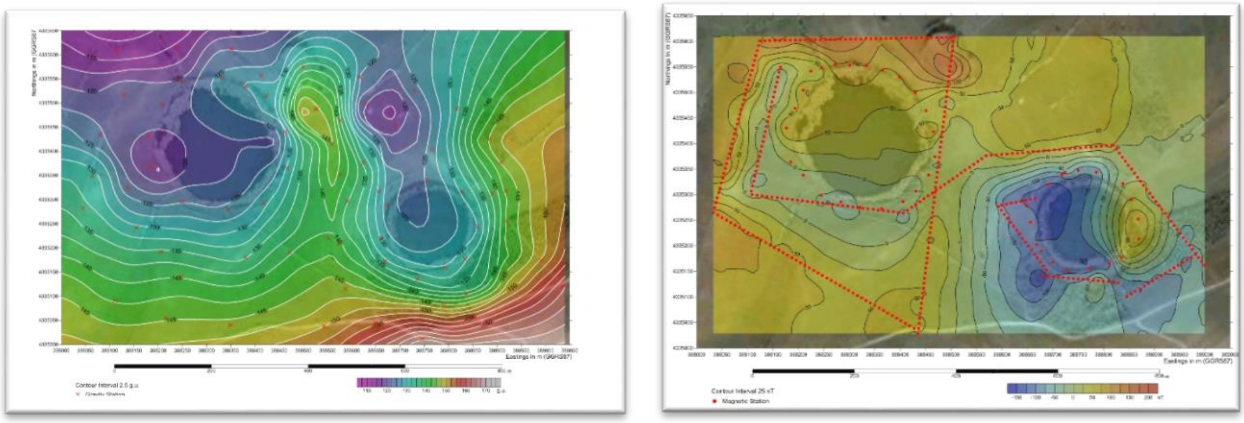

Figure 2. Gravity Anomaly Map referred to IGSN'71 and GRF'67 (Left) and Total Field Magnetic Anomaly Map (Right) superimposed on the Google Image.

The situation on the western lake is almost the same. A negative anomaly dominates its southern flank which swings to the west along its western part. However, most the lake is covered by positive anomaly values that have to be treated with caution since they are deduced by interpolation. Therefore, the magnetic anomaly map should only qualitatively be considered.

Discussion

Several hypotheses can be drawn upon to explain the origin of these enigmatic twin-lakes: a) Maar-type volcanic craters; b) Hydrothermal or CO_2/hydrocarbon and methane gas explosion craters, producing mud-volcanoes; d) Doline holes due to karstification; or e) Small meteorite impact craters, the latter being a plausible explanation due to geologic, petrologic, and geophysical evidence. However, an underground gas explosion cannot be excluded. The morphology and dimensions of the lakes, as well as the density contrast tomography of the bedrock favour a meteorite impact hypothesis of a projectile, which may has split into two fragments before reaching the surface.

Acknowledgements

Project of the John S. Latsis Benefit Foundation, Athens May 2011.

References

Dietrich, VJ., Lagios, E., Reusser, E., Sakkas, V., Gartzos, E., Kyriakopoulos, K., 2017. The Zerelia twin-lakes (Central Greece): Two Possible Meteorite Craters." LAP LAMBERT Academic Publishing. ISBN-13: 978-3-659-64693-5, 116p.

SPECIAL SESSION

T3.S1 Statistical Seismology

Conveners: **Eleftheria Papadimitriou (AUTH)**
G. Tsaklidis (AUTH)
R. Console (INGV)

15th International Congress of the Geological Society of Greece
Athens, 22-24 May, 2019 | Harokopio University of Athens, Greece
Bulletin of the Geological Society of Greece, Sp. Pub. 7 Ext. Abs. GSG2019-031

Physics-based simulation of spatiotemporal patterns of earthquakes in the Corinth Gulf fault system

R. Console[1,2], R. Carluccio[2], M. Murru[2], E. Papadimitriou[3], V. Karakostas[3]

(1) Centro di Geomorfologia Integrata per l'Area del Mediterraneo, Potenza, Italy, rodolfo.console@ingv.it
(2) Istituto Nazionale di Geofisica e Vulcanologia, Rome, Italy
(3) Aristotle University of Thessaloniki, Geophysics Department, Thessaloniki, Greece.

Introduction

In the last decade new and more complex physics-based simulators were developed and have acquired a growing interest as a tool for comprehension and testing of seismic process models. The earthquake simulators differ in the type of methodology developed within them and for the geometry type of the grid used in the fault model. A recent paper by Field (2019) supports the usefulness of physics-based earthquake simulators for improving overall testing procedures for earthquake forecasting.

Here we apply an earthquake simulation algorithm of new generation and study its potential for modelling the long-term spatiotemporal process of strong earthquakes preparation. The algorithm of our simulator was initially introduced by Console et al. (2014), and successively modified by Console et al. (2017, 2018). In this improved version a specific seismogenic structure is modelled by quadrilateral faults constituted by thousands of cells with sides of 1 km or less. Note that modelling the seismic sources by numerous segments of rectangular or trapezoidal shape is just a convenient tool for the simplicity of the algorithm used in the physics-based simulator code, but definitely does not limit a rupture to expand beyond the edges of such segments.

The physical model on which the latest version of our simulation algorithm is based also includes, besides tectonic stress loading and static stress transfer as in the previous versions, the Rate & State constitutive law. The simulator code needs relatively modest computer resources and is capable for simulating tens of thousands of years of seismic activity producing catalogues of tens of thousands of events in a wide magnitude range. The resulting synthetic catalogues exhibit typical magnitude, space and time features, which are comparable with those of real observations.

In this study we applied the simulator code to a physical model for the Corinth Gulf (Greece) fault system, a well-known seismic structure about 100 km long, where several earthquakes of magnitude larger than 6.0 occurred in the last few centuries. This structure is typically modelled after being subdivided into eight major fault segments characterized by different slip-rates, which can rupture either separately or simultaneously (Console et al., 2015). The results of this simulation provide interesting inferences on the spatiotemporal properties of seismic activity in the study area. In particular, the recurrence time of the larger events and their spatial relation are investigated.

Application to the seismicity of the Corinth Gulf fault system

By means of a set of preliminary trials, the values of the free parameters characterizing the simulation algorithm were set up in order to obtain a synthetic catalogue reproducing realistic features of the real observations, including the *b*-value of the frequency-magnitude distribution. The simulation was run over a period of 100 kyr, preceded by a warm up period of 10 kyr not used in the output catalogue. Some results of the synthetic catalog are reported in Table 1.

Table 1. Features of the 100,000 yr synthetic catalogue in the Corinth Gulf fault system

Number of earthquakes of $M \geq 4.0$	158,923
Number of earthquakes of $M \geq 5.0$	68,321
Number of earthquakes of $M \geq 6.0$	3,931
Number of earthquakes of $M \geq 6.5$	632
Maximum likelihood *b*-value ($M \geq 4.5$)	0.80
Largest magnitude M_{max}	6.81
Annual seismic moment M_0 ($M \geq 4.0$)	2.66E+17 Nm/yr
Number of earthquakes of $M \geq 6.0$ rupturing only one segment	2,365
Number of earthquakes of $M \geq 6.0$ rupturing at least two segment	1,566
Largest number of segments ruptured in one earthquake of $M \geq 6.0$	5

Recurrence of large magnitude earthquakes in the synthetic catalogue

We examined the statistical features of the synthetic catalogue referring to the long term series of large magnitude earthquakes for some specific seismogenic faults of the study area. In order to carry out a statistical analysis of the earthquake recurrence intervals, we need a quantitative, even if somehow arbitrary, definition to identify in a seismic catalogue the events to which we want to apply such analysis. For a more in-depth discussion of this issue, we refer to Field (2015) addressing the "recurrence of what?" question.

There could be two ways for associating earthquakes to specific segments. These ways can be termed either "nucleation" or "participation" (Parsons et al., 2018). Once we have selected a segment to be studied, by the nucleation criterion we take only earthquakes encompassed in the considered segment. In this case, each earthquake can be associated to one segment only, even if it has substantially ruptured more than one segment. This criterion may lead to underestimation of the hazard assessment of a specific site, because a very large earthquake rupturing a segment close to that site might be ignored in the analysis, if its hypocenter was located into a different source. Moreover, we should consider the fact that frequently seismic catalogues provide the hypocentral coordinates of a large earthquake outside any segment reported in the adopted geological model.

By the participation criterion we associate to a specific segment all the large earthquakes that have ruptured a substantial part of this seismic source. In this way, any single earthquake can be counted more than once in the recurrence analysis of different sources. The participation criterion can be applied to the synthetic catalogue generated by our simulation algorithm because the output file contains the number of cells ruptured by each earthquake for any segment.

In this analysis, we have adopted the participation criterion by applying the following empirical rules: 1) a magnitude threshold of 6.0 for the considered earthquake is assigned; 2) the earthquake is initially assigned to the segment containing the nucleation cell of the earthquake; 3) if the equivalent magnitude estimated by the number of cells ruptured by the earthquake in one of any other segments is larger than the minimum magnitude assigned by rule 1, then this segment can be associated to the same earthquake; 4) if the earthquake ruptured at least 70% of the cells of a segment, then this segment can also be associated to this particular earthquake. In this way, we counted through the whole 100 kyr synthetic catalogue the number of times that a given fault segment has participated in any $M \geq 6.0$ earthquake alone (2,365 times) or jointly with other segments (1,566 times). In six cases, five segments ruptured all together in one single very large earthquake (Table 1).

In order to assess whether the earthquake occurrence time on single segments in the synthetic catalogue behaves either as a Poisson process or it rather exhibits some pseudo-periodical feature, we carried out a statistical analysis of the inter-event times for the entire 100 kyr simulation. The analysis focused on the sources listed in Table 2, which displays the mean inter-event time, the standard deviation, and the coefficient of variation of each analysed segment, for the earthquakes fulfilling the four above-mentioned empirical rules. This Table also reports the results of the difference between the log likelihood computed by the Brownian Passage Time (BPT) renewal model and the Poisson time-independent model ($d\log L$). For the likelihood estimation we adopted the values of Tr and Cv reported in Table 2 for each segment.

Table 2. Statistical parameters obtained for some sources of the 100,000 yr synthetic catalogue associated to earthquakes of $M \geq 6.0$

Segment Number	T_r (yr)	σ (yr)	C_v	$d\log L$
S01 (Psathopyrgos)	169.2	108.4	0.64	208.5
S02 (Aigion)	172.9	124.1	0.72	173.6
S05 (Xylokastro)	106.6	49.9	0.47	262.0
S07 (Skinos)	226.4	99.3	0.44	172.9

The results reported in Table 2 show a moderate pseudo-periodical behaviour of strong earthquakes in all the selected sources, with a significant over-performance of the renewal BPT model with respect to the time-independent Poisson model. Other tests carried out in a similar way with different magnitude thresholds show that smaller magnitudes exhibit a less periodical and more clustered behaviour.

References

Console, R., Carluccio, R., Papadimitriou, E. & Karakostas, V., 2014. Synthetic earthquake catalogs simulating seismic activity in the Corinth Gulf, Greece, fault system, *J. Geophys. Res.*, 120(1), 326-343, doi: 10.1002/2014JB011765.

Console, R., Nardi, A., Carluccio, R., Murru, M., Falcone, G. & Parsons, T., 2017. A physics-based earthquake simulator and its application to seismic hazard assessment in Calabria (Southern Italy) region, *Acta Geophys*., 65, 243-257, doi: 10.1007/s11600-017-0020-2.

Console, R., Vannoli, P. & Carluccio, R., 2018. The seismicity of the Central Apennines (Italy) studied by means of a physics-based earthquake simulator, *Geophys. J. Int*., 212, 916-929, doi: 10.1093/gji/ggx451.

Field, E.H., 2015. Computing Elastic-Rebound-Motivated Earthquake Probabilities in Unsegmented Fault Models: A New Methodology Supported by Physics-Based Simulators, *Bull. Seism. Soc. Am.*, 105(2A), 544-559, doi:10.1785/0120140094.

Field, E.H., 2019. How Physics-Based Earthquake Simulators Might Help Improve Earthquake Forecasts, *Seism. Res. Lett.*, Published online 9 January 2019, doi: 10.1785/0220180299.

Parsons, T., Geist, E. L., Console, R. and Carluccio, R., 2018. Characteristic earthquake magnitude frequency distributions on faults calculated from consensus data in California, *J. Geoph. Res.*123, 12, 10,761-10,784, doi: 10.1029/2018JB016539.

15th International Congress of the Geological Society of Greece
Athens, 22-24 May, 2019 | Harokopio University of Athens, Greece
Bulletin of the Geological Society of Greece, Sp. Pub. 7 Ext. Abs. GSG2019-059

Earthquake Recurrence Intervals in Complex Seismogenetic Systems: A Proemial Analysis

A. Tzanis, A. Efstathiou

Section of Geophysics and Geothermy, National and Kapodistrian University of Athens, Panepistimiopolis, Zografou 15784, Greece, atzanis@geol.uoa.gr

Principles and Objectives

A recurrence interval (RI) is a statistical estimate of the likelihood of an earthquake to occur, typically based on historical data; its standard definition is the number of years on record plus one divided by the number of events, and assumes that the events are generated by Poissonian processes so that events of similar size are mutually independent and have a stationary probability of occurrence. The number of events is typically taken from, or estimated on the basis of the Frequency–Magnitude distribution or its modifications/ extensions. Although indisputable, the F-M distribution is static and says *nothing* about the dynamic state of fault networks. Accordingly, standard and "improved" RI estimators are mere *approximations* of the *long-term average*. This might lead to misestimation if the dynamics of a seismogenetic system is *not* Poissonian.

A parameter *obviously* associated with the RI *and* the dynamic state is the *interevent time* (IT), i.e. the lapse between consecutive earthquakes over a given area and above a magnitude threshold. The IT has generally *not* been used in the estimation of earthquake recurrence intervals. This may be due to a majority endorsement of the idea that seismogenesis is Poissonian in time. If so, the statistics of IT should observe the exponential distribution whereas they generally *do not*: contrary to "expectation", Frequency–Interevent Time distributions are power laws that cannot possibly fit into the Poissonian context. Several Authors attempted to resolve the contradiction by working out *ad hoc* theories that are generally well formulated and elegant, albeit unavoidably multi-parametric, unnecessarily complicated and possibly defying the principle of maximum parsimony.

An alternative approach is Complexity. In this view seismicity expresses a fault network (system) that evolves in a fractal-like spacetime and may be sustainably *non-equilibrating* (Complex), sustainably equilibrating (Poissonian), or transitioning between equilibrating and non-equilibrating states. Complex States require a significant proportion of successive earthquakes to be *dependent* through short and long range interaction that introduces delayed feedback: this is known as *correlation* and confers memory manifested by power-law distributions of dynamic parameters such as interevent times. The statistical and entropic properties of Complex States can be studied with Non-Extensive Statistical Physics (NESP), which is a direct generalization of Boltzmann-Gibbs thermodynamics to non-equilibrating systems (e.g. Tsallis, 2009).

Previous studies (Efstathiou *et al*., 2017, 2015; Efstathiou and Tzanis, 2018; Tzanis *et al.*, 2018; Tzanis and Tripoliti, 2019) have appraised the dynamics of seismogenesis on the basis of correlation, as this is specified by the *temporal entropic index* associated with the distribution of IT: it was found that it can be very different, from SOC to Poissonian, that the level of correlation may be influenced by the geodynamic setting and that it can change with time. Herein we revisit the temporal entropic index, but this time in direct association with another important dynamic parameter, the *q-relaxation interval* (*q*RI) which is the NESP generalization of the relaxation time and comprises an *alternative definition* of the RI: it is the *characteristic time* required to produce an earthquake above a given magnitude and is expected to relay information about the dynamic state of the system. For instance, a critical system should generate earthquakes of *any* magnitude *shortly* after *any* event. Conversely, a Poissonian system should generate earthquakes within intervals exponentially increasing with event size.

We examine many different seismogenetic systems of the northern Circum-Pacific Belt: the transformational plate boundaries and inland seismic regions of California, Alaska and Southwest Japan, the convergent plate boundaries and Wadati-Benioff zones of the Aleutian, Ryukyu, Izu-Bonin and Honshū arcs, and the divergent plate boundary of the Okinawa Trough. Objectives are: a) to confirm and clarify results of previous work; b) to explore how and why the geodynamic setting may affect the entropic state of seismogenetic systems; c) to assess the statistical effects of blending the seismicity of different systems in a single catalogue.

Method of analysis

NESP predicts that the Cumulative Probability Function associated with a real variable $\Delta t \in [0,\infty)$ is

$$P(>\Delta t) = \exp_q\left(-\Delta t \cdot \Delta t_0^{-1}\right) = \left[1-(1-q_T)\left(-\Delta t \cdot \Delta t_0^{-1}\right)\right]^{(1-q_T)^{-1}}$$

where Δt represents the IT, Δt_0 the *q-relaxation interval* and q_T the *temporal entropic index*; $\exp_q(.)$ is the *q-exponential function* which for $q_T \neq 1$ is a Zipf-Mandelbrot power law, while for $q_T=1$ $\exp_q(-\Delta t/\Delta t_0) = \exp(-\Delta t/\Delta t_0)$ reducing to the exponential distribution (Poissonian process). Our analysis comprises modelling of empirical functions $P(>\Delta t : M \geq M_{th})$ from many different seismogenetic systems, so as to enable a comparative study of the resulting $\Delta t_0(M_{th})$ and $q_T(M_{th})$; M_{th} is a magnitude threshold. Because $\Delta t_0>0$ and $q_t \in [1, 2]$, modelling is performed with the trust-region reflective algorithm together with least absolute residual minimization to suppress possible outliers.

Results and Conclusions

The joint examination of Δt_0 and q_T assumes that they are indivisibly associated with the dynamic state of a system which, in turn, can be evaluated by the level of correlation (q_T) and classified as: *insignificant* when $q_T<1.15$, in which case the system is Poissonian; *weak* when $1.15\leq q_T<1.3$, *moderate* when $1.3\leq q_T<1.4$ and *significant* when $1.4\leq q_T<1.5$, in which cases the system is Complex and possibly non-critical; *strong* when $1.5\leq q_T<1.6$ and *very strong* when $1.6\leq q_T$, in which cases the system is Complex and possibly critical.

Our results indicate that the *q*-exponential distribution is a *universal descriptor* of IT statistics. It is also clear that the duration of *q*-relaxation intervals is *reciprocal* to the level of correlation (q_T). Both parameters may change with time and across boundaries so that neighbouring systems may co-exist in *drastically* different dynamic states.

Crustal systems in transformational plate boundaries are generally correlated: 56.3% of q_T estimators indicate correlation above moderate, 46.6% above significant and 37.9% above strong. However, the cases of very strong correlation are quasi-stationary and the corresponding *q*-relaxation intervals very short, very slowly increasing with magnitude and vastly incomparable to the exponentially increasing standard RI: on occurrence of any event, such systems appear to respond swiftly by generating any magnitude anywhere within their boundaries – these are hallmarks of Self-Organized Criticality.

Crustal systems in convergent and divergent plate margins are generally weakly–moderately correlated: approximately 56.9% of q_T estimators indicate weak, 17.6% moderate 19.6% significant to strong correlation. In *significantly to strongly correlated crustal* systems, the *q*-relaxation and standard recurrence intervals both increase exponentially with magnitude but diverge, with the standard RI escalating much faster than the *q*-RI. In *insignificantly to significantly correlated crustal* systems, the *q*-RI and standard RI both increase exponentially with magnitude and generally congruent within the range of observations and possibly beyond.

- Given that the standard RI assumes Poissonian statistics while Complexity accommodates a broad range of dynamic states, the above observations imply that fault networks with moderate to strong correlation and *q*-relaxation intervals exponentially increasing but *shorter* than the standard, are Complex and but possibly sub-critical or non-critical.

Sub-crustal and Wadati-Benioff zone systems are definitely uncorrelated (quasi-Poissonian); in these cases the *q*-relaxation and standard recurrence intervals increase exponentially with magnitude and are *congruent*. Finally, the blending of earthquake populations from adjacent but dynamically different fault networks *randomizes* the statistics of the mixed catalogue and over large seismogenetic provinces, *reduces the apparent level of Complexity*.

A partial explanation of our results is based on simulations of small-world fault networks and posits that free boundary conditions at the surface allow for self-organization and possibly criticality to develop, while fixed boundary conditions at depth do not. The development of criticality in transformational crustal fault networks may be associated with the degree of connectivity and synchronization of the contiguous segments of large transform faults that continuously "push" against each other and facilitate longitudinal, long-range transfer of stress. In the crust of convergent plate boundaries the large faults are essentially low-angle mega-thrusts whose contiguous segments do *not* push against each other and are thus *not* as highly connected as large transform faults. Finally, the physical conditions of sub-crustal fault networks inhibit connectivity, only allowing earthquakes to occur as a series of quasi-independent events. Future research will show if all this holds water!

The standard RI may overestimate the seismicity rate of non-Poissonian systems and for what it is worth, underestimate earthquake hazard. There is no doubt that the information introduced by *q*-relaxation intervals, regarding the effect of the dynamic state on the RI, might be useful in improving earthquake hazard analysis. Exactly how it can be applied, however, requires significant additional research: it is certain that nothing new has to be done if a system turns out to be quasi-Poissonian but in the general case of Complexity things are far more complicated.

References

Efstathiou A. and Tzanis A., 2018. An examination of the nature and dynamics of seismogenesis in South California, USA, based on Non-Extensive Statistical Physics, Phys. Earth Planet. In., 284, 51–71. Doi: 10.1016/j.pepi.2018.08.013.

Efstathiou A., Tzanis A. and Vallianatos F., 2017. On the nature and dynamics of the seismogenetic systems of North California, USA: An analysis based on Non-Extensive Statistical Physics, Phys. Earth Planet. In., 270, 46–72. Doi: 10.1016/j.pepi.2017.06.010.

Efstathiou A., Tzanis A. and Vallianatos, F, 2015. Evidence of Non-Extensivity in the evolution of seismicity along the San Andreas Fault, California, USA: An approach based on Tsallis Statistical Physics, Phys. Chem. Earth, Parts A/B/C, 85–86, 56–68. Doi: 10.1016/j.pce.2015.02.013.

Tsallis, C., 2009. Introduction to Nonextensive Statistical Mechanics: Approaching a Complex World. Springer, Berlin

Tzanis A. and Tripoliti E., 2019. On the Statistical Nature and Dynamics of Seismogenesis in the NW Circum-Pacific Belt: A Study Based on Non-Extensive Statistical Physics, arXiv:1901.09628v1.

Tzanis A., Efstathiou A. and Vallianatos, F., 2018. Are seismogenetic systems random or organized? A treatise of their statistical nature based on the seismicity of the north-northeast Pacific Rim, in: Chelidze, T., Vallianatos, F., Telesca, L. (Eds.), Complexity of Seismic Time Series, 365–418. Doi: 10.1016/B978-0-12-813138-1.00011-0.

15th International Congress of the Geological Society of Greece
Athens, 22-24 May, 2019 | Harokopio University of Athens, Greece
Bulletin of the Geological Society of Greece, Sp. Pub. 7 Ext. Abs. GSG2019-128

Monitoring Earthquake Network Measures in Aftershock Sequences in Greece

D. Chorozoglou[1], E. Papadimitriou[1]
(1) Aristotle university of Thessaloniki, Campus 54124, Thessaloniki, Greece, chorozod@geo.auth.gr

Abstract

Strong earthquakes ($M \geq 6.0$) may be followed by numerous aftershocks, which steadily decrease in frequency according to Omori law. The stronger aftershock usually causes catastrophic consequences as the strong earthquake that preceded has reduced the durability of buildings. The identification of certain occurrence patterns of strong aftershocks is then of both scientific and societal significance and effective tools are seeking for this scope. The monitoring of complex earthquake networks that are formed from Greek seismicity, based on the evolution of their measures, such as global efficiency, betweenness centrality and clustering coefficient is performed, aiming to identify when these networks exhibit distinct evolution between the main shock and strongest aftershocks occurrence. As network nodes the 2D seismic cells in which the study area was appropriately divided are considered and their connections among the nodes are given by the succession of earthquakes. The data are taken from a seismic catalog comprising crustal earthquakes (focal depth less than 50 km) of magnitude $M \geq 3.0$ that occurred in the territory of Greece in between 1999-2017. During this period twenty two (22) main shocks of $M \geq 6.0$ occurred, and is examined the evolution of network measures on earthquake networks before the strongest aftershocks. The earthquake networks are formed on sliding windows of a few days for monitoring the network measures variation. To assess whether the values of network measures are statistically significant the construction of randomized networks is required, and the same network measures are calculated for comparison purposes. The monitoring of network measures revealed that their values were found statistically significantly different from the corresponding values of the randomized networks shortly before the strongest aftershocks.

Objectives

- The investigation of the complex seismicity behaviour constitutes a major scientific challenge and an indispensable component in improving our knowledge concerning seismogenesis and earthquake forecasting.
- One approach for investigating the spatial and temporal complexity of seismicity is effected through the construction of earthquake networks, given that graph theory provides a framework to investigate the structure and dynamics of a complex system.
- The examination of basic network measures, such as global efficiency and clustering coefficient, will unveil properties of spatio-temporal seismicity structure and give a new perspective for the seismic hazard assessment.
- The scope of this work is the monitoring of evolution of eight (8) basic network measures for six (6) of 22 aftershock sequences that occurred during 1999-2017 in Greek territory by strong earthquakes with $M \geq 6.0$, and the identification of potential patterns in the distinct evolution of the earthquake networks structure before the strongest aftershock. We study six (6) of them for which the interevent period was sufficiently long for the network measures to be robustly computed.

Method

- The construction of earthquake networks is based on the Abe and Suzuki (2004a). The study area is divided into $2D$ cells that are considered as nodes of the earthquake networks inside which the earthquakes occurred, and the connections are given by the succession of earthquakes.
- For the monitoring of earthquake network structure for aftershock sequences that examined, the eight (8) different network measures that are considered and computed, are: clustering coefficient, characteristic path length, global efficiency, betweenness centrality, eigenvector centrality, assortativity, eccentricity and diameter.
- The investigation of evolution of these network measures values for aftershock sequences, requires checking of statistical significance of these values in each time interval (sliding window per day) after comparing them with the corresponding values of randomized networks.
- A randomization setting requires the preservation of the degree of each node in the original network based on the shuffling of the connections of the original network and is called RNnoddeg (Maslov and Sneppen 2002). In a different approach, the random network is not formed by randomizing the connections of the original network, but it is built according to the Erdős and Rényi (1959) model with preset probability of connections as in the original network, which essentially corresponds to the preservation of the average degree and is called RNpoisson.

Randomization significance test

- Since the asymptotic null distribution of each statistics is not known, meaning each one of the (eight) 8 network measures, a randomization significance test is applied and the empirical null distributions for each statistics is formed from the values of the statistics computed on the B randomized networks (for any of the 2 approaches for network randomization which are used).

- The null hypothesis H_0 that the network measure values of both the original and randomized networks are similar (i.e. $p-value > 0.05$, see eq. (1)) is considered. To establish the statistical significance of the network measures values the test should reject the null hypothesis H_0 (i.e. $p-value < 0.05$, see eq. (1)).
- The p-value is calculated, and the test decision is reached at the significance level $\alpha = 0.05$. Denoting q_0 the test statistics computed for the original network, and $q_1, \dots, q_B$ for the B randomized ones (in the computations we set $B = 100$), the p-value is

$$p=\begin{cases} \frac{2r_0}{B+1}, \text{ if } r_0 \leq \frac{B+1}{2} \\ \frac{2(1-r_0)}{B+1}, \text{ if } r_0 > \frac{B+1}{2} \end{cases} \quad (1)$$

where r_0 is the rank of q_0 in the ordered list of $q_0, q_1, \dots, q_B$.

Results

- The percentages of rejection of H_0 are computed from the average of the corresponding rejections of H_0 that are derived for each one of the 6 examined cases in each non-overlapping time window (Figure 1).
- It was found that the values of most of the network measures are different than the corresponding values of the randomized networks in the last time window, with higher percentages of rejection of H_0 than in the other time intervals, before the upcoming strongest aftershocks.

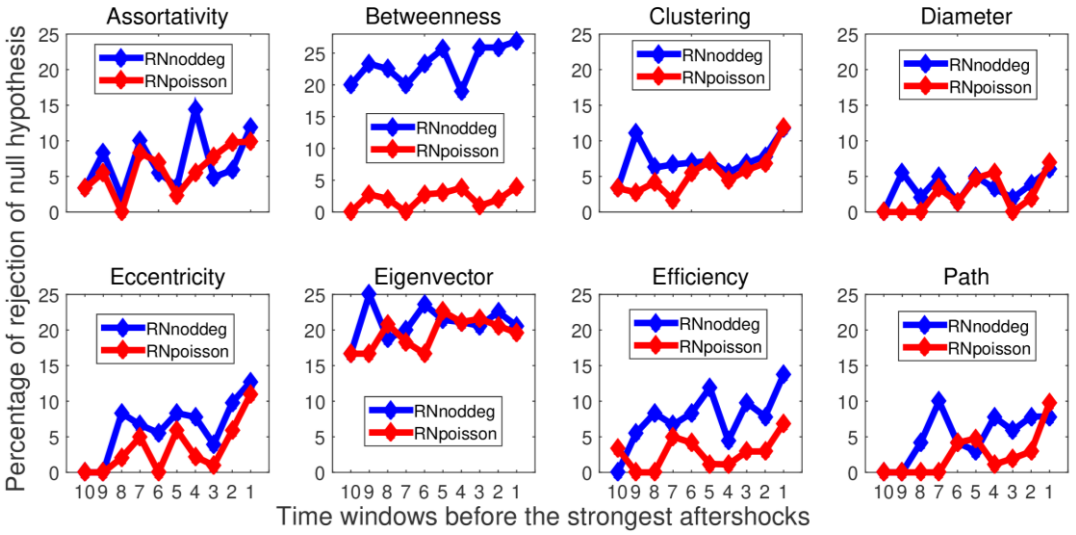

Figure 1. The percentage of rejection of H_0, that the values for each of the 8 network measures and the 2 randomization approaches of original and randomized networks are similar, based on all the 6 strongest aftershocks which are considered.

Conclusions

- The evolution of network measures revealed that the values for the original earthquake networks are different, i.e. there is statistical significance, from the corresponding values for randomized networks in the last time interval before the aftershocks.
- The application of the network theory is found to be a powerful tool for the investigation of complex phenomena, such as seismic activity as the changes in the network structure can reveal certain seismicity behavior a few days before an aftershock occurrence.

Acknowledgements

The critical reading of the abstract by Prof. Kugiumtzis is greatly appreciated. The financial support by the European Union and Greece (Partnership Agreement for the Development Framework 2014-2020) for the project "Development and application of time-dependent stochastic models in selected regions of Greece for assessing the seismic hazard" is gratefully acknowledged, MIS5004504.

References

Abe, S., Suzuki, N., 2004a. Small-world structure of earthquake network. Physica A 337, 357-362.
Erdős, P., Rényi, A., 1959. On random graphs. Publicationes Mathematicae Debrecen 6, 290-297.
Maslov, S., Sneppen, K., 2002. Specificity and stability in topology of protein networks. Science 296, 910-913.

15th International Congress of the Geological Society of Greece
Athens, 22-24 May, 2019 | Harokopio University of Athens, Greece
Bulletin of the Geological Society of Greece, Sp. Pub. 7 Ext. Abs. GSG2019-133

Earthquake clusters in Corinth Gulf, Greece: Identification through a Markovian arrival process (MAP)

P. Bountzis[1], E. Papadimitriou[1], G. Tsaklidis[2]

(1) Department of Geophysics, Aristotle University of Thessaloniki, 54124 Thessaloniki, Greece, pmpountzp@geo.auth.gr
(2) Department of Mathematics, Aristotle University of Thessaloniki, 54124 Thessaloniki, Greece

Clustering of earthquakes both in time and space is a vital aspect of seismicity, which provide information on the earthquake dynamics. For the study of the seismicity patterns and clustering characteristics in Corinth Gulf, Greece, we applied a Markovian Arrival Process (MAP) (Neuts, 1979), which is a temporal bivariate point process $(N_t, J_t)_{t\in R^+}$, with an intensity rate driven by a Markov one with unobservable states. The counting process, N_t, counts the number of events in a time interval $[0, t)$, which are associated with the evolution of the underlying Markov process J_t, at time $t \geq 0$; that is, the hidden states indicate the seismicity rate. The parameters of the MAP are estimated through an EM algorithm (Dempster *et al.*, 1977), which is iterative in that at each step it computes the log-likelihood function and reaches a local maximum after a predefined number of iterations or a convergence criterion. We followed a special structure of the rate matrices (Horvath and Okamura, 2013) where transitions among the hidden states are allowed only when arrivals are taken place. The information criterion of Akaike (Akaike, 1974) is used to determine the number of distinct seismicity rates that characterize each earthquake catalog. Residual analysis is applied to assess the goodness-of-fit of the model (Ogata, 1988), and the most likely sequence of the hidden states under which the observations occurred is computed via a local decoding algorithm. For the implementation of the algorithm the forward-backward equations are used (Mac Donald and Zucchini, 1997) and the robustness of the method is verified on synthetic catalogs where the hidden path is known. MAP is applied in the Corinth Gulf, Greece, which is a region with high seismic activity. In the study, we used the data from the catalog compiled by the Geophysics Department of the Aristotle University of Thessaloniki (Permanent Regional Seismological Network (1981)). The study area is divided in the eastern and western parts, based on seismotectonic criteria and the model is tested for different periods and magnitude thresholds in both subareas. A complete cluster analysis of the revealed path of the hidden states (Figures 1 and 2) is given for the 135 and 139 earthquakes with $M \geq 4.5$ that occurred from 1964 to 2017 in the eastern and western parts, respectively, and the correspondence of the hidden states to the major earthquake sequences is addressed. Three states seem sufficient to describe the temporal fluctuations of earthquake occurrences for both subareas, with the lowest seismicity rate corresponding to the first one (state 1). The third state corresponds in most cases to main shocks and their immediate aftershocks. In the western part, 10 to 13 events with $M \geq 5.5$ occurred in state three, which suggests that an aftershock with $M \geq 4.5$ is expected during next hours. Our results show that the model can capture the behavior of active seismic periods revealing seismic sequences and swarms, as well periods of seismic quiescence and might be introduced as a model for change point detection able to reveal seismic clusters.

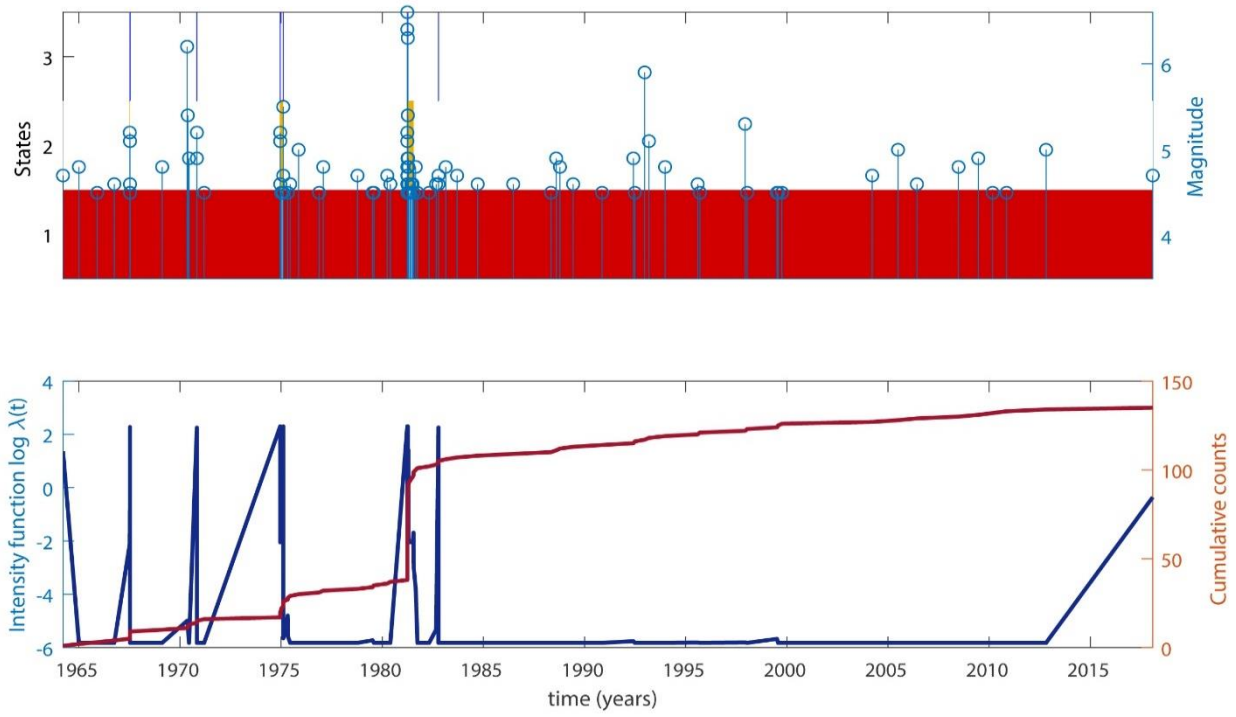

Figure 1. *Top:* Most probable state of the underlying process, J_t, of the eastern subarea, for magnitudes, $M \geq 4.5$. *Bellow:* Logarithm of the intensity function of the counting process, N_t, and cumulative number of the events.

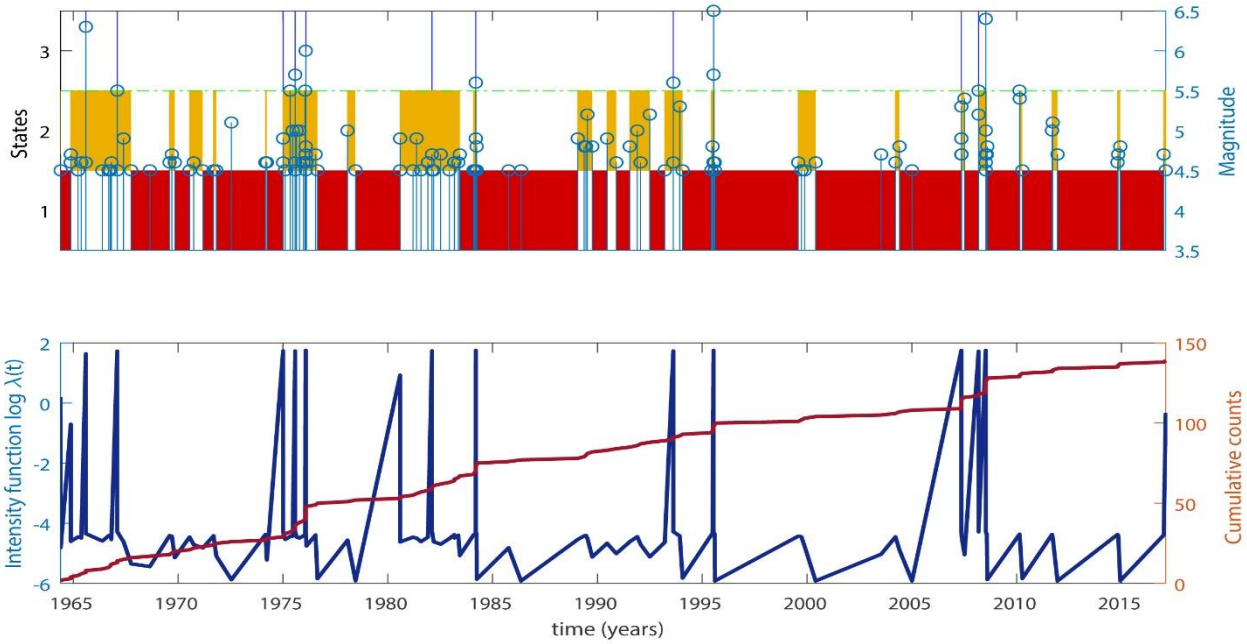

Figure 2. *Top:* Most probable state of the underlying process, J_t, of the western subarea, for magnitudes, $M \geq 4.5$. *Bellow:* Logarithm of the intensity function of the counting process, N_t, and cumulative number of the events.

Acknowledgements

This research is co-financed by Greece and the European Union (European Social Fund- ESF) through the Operational Programme «Human Resources Development, Education and Lifelong Learning» in the context of the project "Strengthening Human Resources Research Potential via Doctorate Research" (MIS-5000432), implemented by the State Scholarships Foundation (IKY).

Ευρωπαϊκή Ένωση
European Social Fund

Operational Programme
Human Resources Development,
Education and Lifelong Learning
Co-financed by Greece and the European Union

ΕΣΠΑ 2014-2020
ανάπτυξη - εργασία - αλληλεγγύη

References

Akaike, H., 1974. A new look at the statistical model identification. IEEE Transactions on Automatic Control 19, 716-723.

Dempster, A.P., Laird, N.M., Rubin, D.M., 1977. Maximum likelihood from incomplete data via the EM algorithm. Journal of the Royal Statistical Society: Series B (Statistical Methodology). 39, 1-38.

Horvath, G., Okamura, H., 2013. A fast EM algorithm for fitting marked markovian arrival processes with a new special structure, in: Computer Performance Engineering, EPEW, Springer, Berlin, Heidelberg. pp. 119-133.

MacDonald, I.L., Zucchini, W., 1997. Hidden Markov and other models for discrete-valued time series. Chapman & Hall, London, U.K.

Neuts, M.F., 1979. A Versatile Markovian Point Process. Journal of Applied Probability. 16, 764-779.

Ogata, Y., 1988. Statistical models for earthquake occurrences and residual analysis for point processes. Journal of the American Statistical Association. 83, 9-27.

Permanent Regional Seismological Network, 19811 (operated by the Aristotle University of Thessaloniki). International Federation of Digital Seismograph Networks. dataset available at https://doi.org/10.7914/SN/HT.

15th International Congress of the Geological Society of Greece
Athens, 22-24 May, 2019 | Harokopio University of Athens, Greece
Bulletin of the Geological Society of Greece, Sp. Pub. 7 Ext. Abs. GSG2019-135

A physics-based simulator application in Southern Thessaly Fault System, Greece

C. Kourouklas[1], R. Console[2,3], E. Papadimitriou[1], M. Murru[2], V. Karakostas[1]

(1) Geophysics Department, School of Geology, Aristotle University of Thessaloniki, Thessaloniki, Greece, ckouroukl@geo.auth.gr
(2) Istituto Nazionale di Geofisica e Vulcanologia (INGV), Rome, Italy
(3) Center of Integrated Geomorphology for the Mediterranean Area (CGIAM), Potenza, Italy

The development of fault-based long-term earthquake models is one of the key components of probabilistic hazard assessment. The main input parameter of such models is the recurrence time of strong earthquakes above a predefined magnitude threshold (e.g. $M \geq 6.0$) on specific faults or fault segments. These earthquakes, so called characteristic (Schwartz and Coppersmith, 1984), are considered to be identical for a given fault segment, that is to rupture the majority of the fault area, resulting in events with similar physical mechanism. Using the determined recurrence time of each segment on a given region, then one can develop an Earthquake Rupture Forecast (ERF), which returns the likelihood of the occurrence of a characteristic event in a specific time span. This forecast model can be considered either a memoryless Poisson or a renewal one, constraining the occurrence time of a future event with the date of the last one. That latter kind of models represent an elastic rebound motivated forecast (Field, 2015), in accordance with Reid's theory (Reid, 1911). The real situation in fault zones is much more different leading the recurrence time to a complex behavior due to the interactions among fault segments due to the permanent and temporal stress perturbations (Dieterich, 1994; Stein *et al.*, 1997), which is a potential factor that can move a fault towards or away from a future rupture.

According to this conclusion, the study of recurrence time should be treated with the application of statistical approaches, rather than deterministic ones, which require the compilation of as many as possible strong earthquakes occurred in individual fault segments from all possible records, including historical, paleoseismological and instrumental catalogs. In fact, these observational data are limited because of the large interevent times between successive strong earthquakes in a given segment and consequently the related catalogs are short and incomplete. The development of earthquake simulators, introduced and applied in California (Tullis, 2012) is one powerful tool to overcome these difficulties and limitations, and can provide information on earthquake occurrence combining approximations of the known physics concerning the stress transfer, frictional properties, fault parameters and kinematics. This concept became very popular over the years due to its ability to model and reproduce long earthquake occurrence records (starting from thousands to millions of years). Following this concept, Console *et al.* (2015) have developed a physics-based simulator algorithm based on the modeling of the rupture growth, taking into account the long-term slip rate constrains on fault segments and without using any rheological parameter. Over the years, the simulation algorithm had an evolutionary improvement. These improved versions of the algorithm were successfully applied to simulate the Italian seismicity (Console *et al.*, 2017, 2018a, b). In this study, a new version of the above mentioned simulation algorithms is applied, embodying in the physical processes the effect of the Rate and State Constitutive law proposed by Dieterich (1994), that contributes in the resembling of stress transfer and fault interaction in short time scales. The current version is applied in Southern Thessaly Fault Zone (Figure 1), which consists in the southern margin of Thessaly basin and belongs to the extensional back-arc Aegean region, that formed due to the subduction of Eastern Mediterranean oceanic lithosphere under Aegean Sea. The regional stress field is characterized by a N-S extension with relatively moderate slip rates (about 4.1 – 4.6 ± 0.5 mm/yr) as derived from GPS measurements (Muller *et al.*, 2013; among others). The stress is mainly accumulated on and released by six normal faults with an E-W to WNW-ESE strike as obtained from geodetic studies, fault plane solutions and field observations (Papadimitriou and Karakostas, 2003 and the references therein).

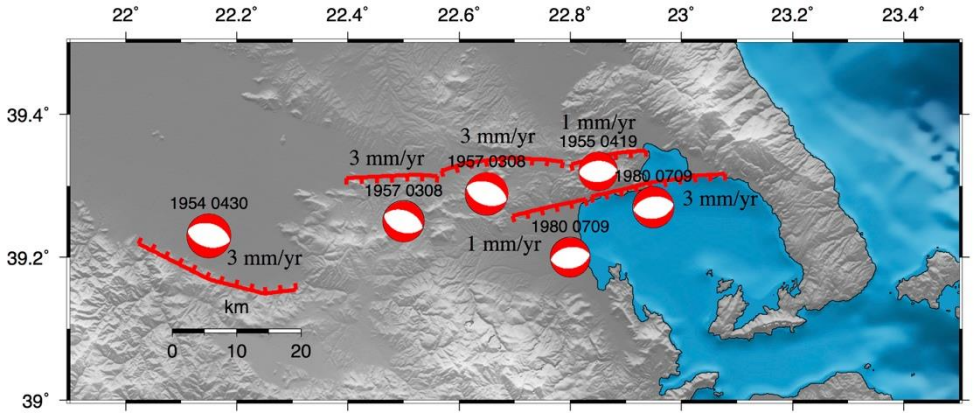

Figure 1. The six major segments of Southern Thessaly Fault System. Focal mechanisms are taken from Papadimitriou and Karakostas (2003) and plotted as lower-hemisphere equal-area projections. The occurrence date of each event is annotated on the top of focal spheres. Slip rates are taken from Muller *et al.* (2013).

Several strong earthquakes $M_w \geq 6.0$ have occurred in the past as inferred from both historical and instrumental earthquake catalogs. Historical information related with strong earthquake occurrence are available since the 16th century (Papazachos and Papazachou, 2002). As revealed from this information, a sequential pattern of active and inactive clustering periods is observed over the years. Focusing on the latest one during the 20th century, Papadimitriou and Karakostas (2003) showed that the stress transfer dominates the occurrence of strong earthquakes. This fact provokes the detailed study of both short and long term behavior of strong earthquakes by the application of the simulation algorithm.

The simulation is implemented by modeling each one of the six fault segments as rectangular source, considered as a grid of 0.75x0.75 km squared cells. The thickness of the seismogenic layer, which is equal to 3-15 km (Hatzfeld *et al.*, 1999), is constrained by the long-term slip rate. Taking into account that only the 60% of the total slip is released coseismically (Davies et al., 1997) the corresponding slip rate of each segment is calculated and given in Figure 1. Additionally, three free parameters must be specified before the simulation processes. These are the product $A\sigma$ of Rate and State law, the Strength Reduction (S-R) coefficient, which refers to the fault weakening and the Aspect Ratio (A-R), which discourages the rupture propagation over long distances. The selection of the three parameters is made by the application of the algorithm multiple times with different combinations among them and the comparison of each resulting catalog with a real one using the two sample Kolmogorov-Smirnov goodness of fit test. The duration of each simulation is 10kyr with a warm up period of 2kyr. The minimum magnitude generated by a two cell rupture is selected to be equal to 4.0. Based on these results, the best fitted synthetic catalog is built and used for the investigation of the strong earthquakes recurrence behavior and the renewal model was tested whether it performs better than the Poisson one. The interactions and possible triggering behavior between adjacent fault segments is studied and compared with the observed episodic occurrence of strong events. For modeling the recurrence times of each segment as a renewal process the Brownian Passage Time (BPT) distribution (Matthews *et al.*, 2002) is adopted against the memoryless exponential one. The comparison between the models is made in terms of their log-likelihood values.

Acknowledgements

The GMT software (Wessel *et al.*, 2013) was used to plot the map. We acknowledge support of this work by the project "HELPOS – Hellenic System for Lithosphere Monitoring" (MIS 5002697) which is implemented under the Action "Reinforcement of the Research and Innovation Infrastructure", funded by the Operational Programme "Competitiveness, Entrepreneurship and Innovation" (NSRF 2014-2020) and co-financed by Greece and the European Union (European Regional Development Fund).

References

Console, R., Carluccio, R., Papadimitriou, E., Karakostas, V., 2015. Synthetic earthquake catalogs simulating seismic activity in the Corinth Gulf, Greece, fault system, Journal of Geophysical Research., 120, 326-343. doi:10.1002/2014JB011765.

Console, R., Nardi, A., Carluccio, R., Murru, M, Falcone, G., Parsons, T., 2017. A physics-based earthquake simulator and its application to seismic hazard assessment in Calabria (Southern Italy) region, Acta Geophysica., 65, 243-257. doi:10.1007/s11600-017-0020-2.

Console, R., Vannoli, P., Carluccio R., 2018a. The seismicity of Central Apennines (Italy) studied by means of a physics-based earthquake simulator, Geophysical Journal International, 212, 916-929. doi: 10.1093/gji/ggx451.

Console, R., Chiappini, M., Minelli, L., Speranza, F., Carluccio, R., Greco M., 2018b, Seismic hazard in southern Calabria (Italy) based on the analysis of a synthetic earthquake catalog, Acta Geophysica., 66, 931-943. doi:10.1007/s11600-018-0181-7.

Davis, R., England, P., Parsons, B., Billiris, H., Paradisis, D., Veis, G., 1997. Geodetic strain in Greece in the interval 1892-1992, Journal of Geophysical Research., 102, 24571-24588.

Dieterich, J.H., 1994. A constitutive law for rate of earthquake production and its application to earthquake clustering, Journal of Geophysical Research, 99, 2601-2618.

Field, E.H., 2015. Computing Elastic-Rebound-Motivated Earthquake Probabilities in Unsegments Fault Models: A New Methodology Supported by Physics-Based Simulators, Bulletin of the Seismological Society of America, 105, 544-559. doi:10.1785/01201140094.

Hatzfeld, D., Ziazia, M., Kementzetzidou, D., Hatzidimitriou, P., Panagiotopoulos, D., Makropoulos, K., Papadimitriou, P., Deschamps, A., 1999. Microseismicity and focal mechanisms at the western termination of the North Anatolian Fault and their implications for continental tectonics, Geophysical Journal International, 137, 891-908.

Matthews, M. V., Ellsworth, W. L., Reasenberg, P. A., 2002. A Brownian model for recurrent earthquakes, Bulletin of the Seismological Society of America, 92(6), 2233-2250. doi:10.1785/0120010267.

Muller, M.D., Geiger, A., Kahle, H.-G., Veis, G., Billiris, H., Paradissis, D, Felekis, S., 2013. Velocity and deformation fields in the North Aegean domain, Greece, and implications for fault kinematics, derived from GPS data 1993-2009, Tectonophysics, 597-598, 34-49. doi:10.1016/j.tecto.2012.08.003.

Papadimitriou, E. Karakostas, V., 2003. Episodic occurrence of strong (Mw≥6.2) earthquakes in Thessalia area (central Greece), Earth and Planetary Science Letters, 215, 395-409. doi:10.1016/S0012-812X(03)00456-4.

Papazachos, B, Papazachou, C., 2002. The earthquakes of Greece, Ziti Publications

Reid, H.F., 1911. The elastic-rebound theory of earthquakes, University of California Publications. Bulletin of Department of Geological Science., 6, 413-444.

Schwartz, D.P., Coppersmith, K.J., 1984. Fault behavior and characteristic earthquakes: examples from Wasatch and San Andreas fault zones, Journal of Geophysical Research, 89, 5681-5698.

Stein, R.S., Barka, A.A., Dieterich, J.H., 1997. Progressive failure on the North Anatolian fault since 1939 by earthquake stress triggering, Geophysical Journal International, 128, 594-604.

Tullis, T.E., 2012. Preface to the focused issue on earthquake simulators, Seismological Research Letters, 83, 957-958.

Wessel, P., Smith, W. H. F., Scharroo, R., Luis, J., Wobbe, F., 2013. Generic Mapping Tools: Improved Version Released, EOS, Transactions American Geophysical Union, 94, 409-410.

15th International Congress of the Geological Society of Greece
Athens, 22-24 May, 2019 | Harokopio University of Athens, Greece
Bulletin of the Geological Society of Greece, Sp. Pub. 7 Ext. Abs. GSG2019-136

A ten-year study (2008-2017) of short-term clustering features of Greek Seismicity

C. Kourouklas[1], O. Mangira[1], A. Iliopoulos[1], D. Chorozoglou[1], E. Papadimitriou[1]

(1) Department of Geophysics, School of Geology, Aristotle University of Thessaloniki, Thessaloniki, Greece, ckouroukl@geo.auth.gr

Studying the clustering features of seismicity both in space and time is one of the most important factors of earthquake forecasting. Earthquake occurrence exhibits short and long term clustering (Kagan and Jackson, 1991; Dieterich, 1994) due to the physical processes related with seismogenesis (e.g. fault interactions and heterogeneity). Focusing on short-term clustering, the seismicity can be considered as the summation of background seismicity of spontaneous earthquakes and triggered one, which dominated by foreshocks, mainshocks and aftershocks or swarm like excitations. The time span of such clustering typically ranges from several months to few years and is spatially distributed mostly around a strong event (e.g. a mainshock) of the order of a few km.

Earthquake occurrence can be represented as a stochastic point process in which the occurrence rate, λ, gives the instantaneous probability of event occurrence (Daley and Vere-Jones, 2003). Despite the fact that many purely temporal models are developed, only few spatiotemporal ones have been proposed, namely the ETAS (Ogata, 1998; Console and Murru, 2001), the EEPAS (Rhoades and Evison, 2004), the double branching model (Marzocchi and Lombardi, 2008). The Epidemic Type Aftershock Sequences (ETAS) model is the most popular one for such studies and is suggested as the best for describing the short-term seismicity (Console *et al.*, 2007).

The spatiotemporal ETAS model, which is an extension of the temporal ETAS model (Ogata, 1988), is formulated as follows:

$$\lambda(t,m,x,y|H_t) = \lambda(t,x,y|H_t) f_m =$$

$$= \left[\mu \cdot u(x,y) + \sum_{T_i<t} \frac{k \cdot e^{\alpha(M_i - M_c)}}{(t-T_i+c)^p} \frac{c^i_{d,q,\gamma}}{[r_i^2 + d^2 e^{2\gamma(M_i - M_c)}]^q}\right] f_m \quad (1)$$

where $u(x,y)$ is the spatial probability density function (pdf) of background events, $\{\mu, k, p, c, \alpha, d, q, \gamma\}$ are the 8 parameters to be estimated, r_i is the distance between location (x,y) and the epicenter of the ith event (in kms), $c^i_{d,q,\gamma}$ is a normalization constant, depending on parameters $\{d, q, \gamma\}$, M_c is the completeness magnitude of the given dataset and f_m is the magnitude pdf representing the Gutenberg-Richter law, given by:

$$f_m = \beta e^{-\beta(M - M_c)} \quad (2)$$

with $\beta = bln(10)$ linked to the b-value of the dataset.

Using this model, a thorough study of the clustering features of crustal seismicity (h≤50 km) in Greece is conducted in both space and time during the period from 2008 up to 2017, when 17 strong events with Mw≥6.0 occurred. The earthquake catalog is compiled based on the recordings of the Geophysics Department of Aristotle University of Thessaloniki (GD-AUTh). With a completeness threshold of M_c=3.5 and b-value equal to 1.17 (b=1.17), 7455 events are comprised in the data set (Figure 1) provoking the detailed analysis of the spatiotemporal characteristics of short – term clustering behavior.

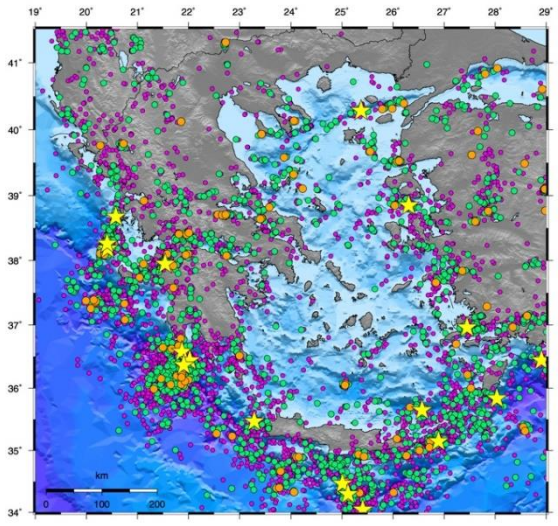

Figure 1. Epicentral distribution of crustal (h≤50km) seismicity with M_c≥3.5 of the broader Greek territory during the period 2008 to 2017. Small magenta, moderate green and large orange circles depict earthquakes in the magnitude ranges 3.5≤M<4.0, 4.0≤M<5.0 and 5.0≤M<6.0, respectively. Yellow stars depict the M≥6.0 events.

The estimation of the model parameters is made via the MLE technique using a simulated annealing approach proposed by Lombardi (2015) implemented in the software package SEDA (Lombardi, 2017), dividing the study area by a regular grid of 0.2ºx0.2º, resulted in 2080 cells in total. The meaning of estimated parameters is discussed and interpreted in connection with the physical processes related with strong earthquakes occurrence. The model is then tested by applying a residual analysis procedure. The initial estimated model including the entire dataset, underestimates the observed seismicity, while it seems to be unstable, leading to an explosive one (in other words a model with infinite decay rate). Specifically, the underestimation is observed during 2008, when five $Mw \geq 6.0$ occurred. Excluding the events in 2008, the estimated model exhibits good agreement with the observed seismicity. In order to develop a stable model including the 2008 seismicity, a different set of constrains concerning the 8 parameters estimation is adopted.

Regarding the final suggested model, the classification between background and triggered events is made by measuring the contribution of each class to the total seismicity using the stochastic declustering method (Zhuang *et al.*, 2002). Individual earthquake sequences occurred in different tectonic regimes are identified and compared using the stochastic reconstruction method (Zhuang *et al.*, 2002). The stationarity of the background seismicity rate is investigated for these different areas along with the recognition of seismicity bursts or quiescence before and after major earthquakes. The present model can be considered as a reference one for the Greek territory with many potential applications including declustering the Greek earthquake catalog for time independent studies, identification of possible triggering patterns and forecasting of future strong earthquakes.

Acknowledgements

The authors would like to express their sincere appreciation to Dr. A.M. Lombardi for her help concerning some technical issues of SEDA package. The GMT software (Wessel et al., 2013) was used to plot the map. The financial support by the European Union and Greece (Partnership Agreement for the Development Framework 2014-2020) for the project "Development and application of time-dependent stochastic models in selected regions of Greece for assessing the seismic hazard" is gratefully acknowledged, MIS5004504.







References

Console, R., Murru, M., 2001. A simple and testable model for earthquake clustering, Journal of Geophysical Research, 106, 8699-8711.

Console, R., Murru, M., Catalli, F., Falcone, G., 2007. Real time forecasts through an earthquake clustering model constrained by the rate-and-state constitutive law: comparison with the purely stochastic ETAS model, Seismological Research Letters, 78(1), 49-56.

Daley, D.J., Vere-Jones, 2003. An introduction to the Theory of Point Processes, vol.1, 2nd ed., Springer-Verlag.

Dieterich, J.H., 1994. A constitutive law for rate of earthquake production and its application to earthquake clustering, Journal of Geophysical Research, 99, 2601-2618.

Kagan, Y.Y., Jackson, D.D., 1991. Long-term earthquake clustering, Geophysical Journal International., 104, 117-133.

Lombardi, A.M., Estimation of the parameters of ETAS models by Simulated Annealing, Scientific Reports, 5, 8414, doi: 10.1038/srep084147.

Lombardi, A.M., 2017. SEDA: A software package for the Statistical Earthquake Data Analysis, Scientific Reports, 7, 44171, doi:10.1038/srep44171.

Marzocchi, W., Lombardi, A.M., 2008. A double branching model for earthquake occurrence, Journal of Geophysical Research, 113, B08, 317, doi:10.1029/2007JB005472.

Ogata, Y., 1988. Statistical models for the earthquake occurrences and residual analysis for point processes, Journal of the American Statistical Association, 83, 9-27.

Ogata, Y., 1998. Space-time point-process models for earthquake occurrences, Annals of the Institute of Statistical Mathematics, 50, 379-402.

Permanent Seismological Network operated by the Aristotle University of Thessaloniki, doi:10.7914/SN/HT.

Rhoades, D.A., Evison, F.F., 2004. Long-range earthquake forecasting with every earthquake a precursor according to scale, Pure and Applied Geophysics, 161, 47-72, doi:10.1007/s00024-003-2434-9.

Wessel, P., Smith, W. H. F., Scharroo, R., Luis, J., Wobbe, F., 2013. Generic Mapping Tools: Improved Version Released, EOS, Transactions American Geophysical Union, 94, 409-410.

Zhuang, J., Ogata, Y., Vere-Jones, D., 2002. Stochastic declustering of space-time earthquake occurrences, Journal of the American Statistical Association, 97(3), 369-380.

Zhuang, J., Ogata, Y., Vere-Jones, D., 2004. Analyzing earthquake clustering features by using stochastic reconstruction, Journal of Geophysical Research, 109(3), B05301.

15th International Congress of the Geological Society of Greece
Athens, 22-24 May, 2019 | Harokopio University of Athens, Greece
Bulletin of the Geological Society of Greece, Sp. Pub. 7 Ext. Abs. GSG2019-142

Studying aftershock sequences generated through a physics-based simulator

O. Mangira[1], R. Console[2,3], E. Papadimitriou[1], M. Murru[2], V. Karakostas

(1) Department of Geophysics, School of Geology, Aristotle University of Thessaloniki, GR54124 Thessaloniki, Greece, omangira@geo.auth.gr
(2) Istituto Nazionale di Geofisica e Vulcanologia, Via Vigna Murata 605, I-00143 Rome, Italy
(3) Center of Integrated Geomorphology for the Mediterranean Area, Via F. Baracca 175, I-85100 Potenza, Italy

The area of Central Ionian Islands, comprising Kefalonia and Lefkada Islands, consists the most active zone in the Aegean and the surrounding area, characterized by high seismic moment rate release and frequent occurrence of strong ($M \geq 6.0$) earthquakes. The last strong event (M_w6.5) occurred on 17 November 2015 at the south western part of Lefkada Island, in less than 2 years after the occurrence in 2014 of a doublet along the western part of Kefalonia Island (with M_w6.1 and M_w6.0), with the two main events being separated temporally by seven days and associated with adjacent fault segments (Karakostas *et al.*, 2015; Papadimitriou *et al.*, 2017).

The above agrees with the observation that one of the most important features of seismic activity is its tendency to clustering. It is widely recognized that the seismicity rate increases after a large earthquake for several years and at distances distinctly larger than the fault length. Since the area under study is characterized by remarkable temporal closeness of strong events, their tight clustering implies significant interaction on adjacent fault segments (Papadimitriou *et al.*, 2017) and can be explained through stress transfer (Papadimitriou, 2002). Since strong events in the region have caused severe damage and numerous casualties, it is important to set up a real time evaluation of the evolution of aftershock activity.

Aiming to investigate short-term interactions and find seismicity patterns, even if the information contained in a good historical catalog cannot be substituted, physics-based simulators created with characteristics based on the Central Ionian Islands faulting properties can overcome the lack of long historical data and provide us reliable information. In order to investigate clustering features in a larger time window in comparison to the short duration of historical and instrumental records thus, the use of a newly developed earthquake simulator is proposed providing the opportunity of dealing with a catalog lasting 10kyr, i.e., of much larger duration (Console *et al.*, 2015, 2017, 2018a, b). The free parameters of the simulator are the strength reduction coefficient (S-R), which is a weakening mechanisms, the aspect ratio coefficient (A-R), which controls the rupture propagation, and $A\sigma$ related to the Rate and State Constitutive law. A synthetic catalog with time, space and magnitude behavior comparable to the observed seismicity is compiled, where substantial similarity is observed between the observed (magenta line) and the calculated annual rate (red line in Figure 1).

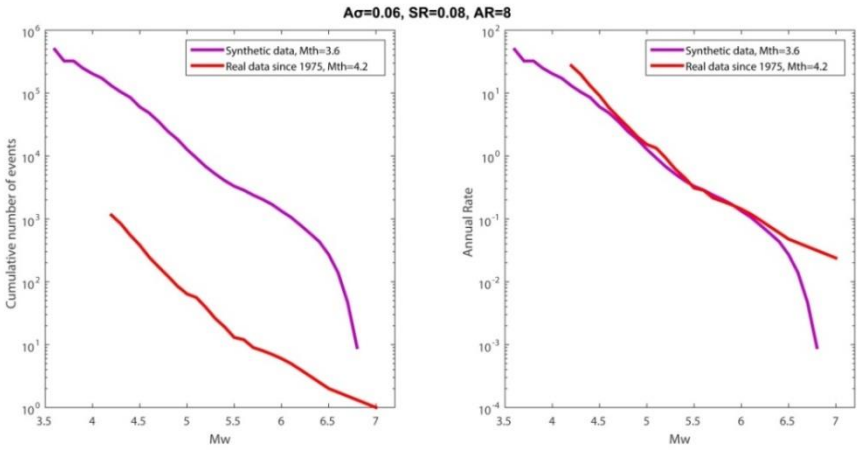

Figure 1. (left) The frequency magnitude distribution and (right) the annual rate of events using the synthetic data (magenta line) with Aσ=0.06, S-R=0.08 and A-R=8 and the real data since 1975 (red line).

A temporal feature obtained from the simulator algorithm can be explored by analyzing the statistical distribution of the time by which an event can precede or follow a strong earthquake. For that purpose a stacking technique is applied and all events with $M \geq 6.0$ included in the 10kyr catalog, are scanned for a time period of 0.5 years before and 0.5 years after the occurrence of the main shock. The total number of events with $M \geq 3.6$ preceding and following the mainshock in each bin for the whole time period considered is shown in Figure 2. A sudden raise is clearly observed soon after the occurrence of a large event, indicating the presence of a feature resembling the aftershock activity.

The clustering features and patterns of the synthetic seismicity are also investigated by means of the spatio-temporal Epidemic Type Aftershock Sequence (ETAS) branching model that has been widely and successfully applied to quantify earthquake interrelations (Console and Murru, 2001; Console *et al.*, 2003). The synthetic data are subdivided in smaller

periods in order to test the performance of the model within periods of equivalent duration to the real case. Comparison is performed with the results provided by the application of the ETAS model in the Central Ionian Islands fault system, using as a learning period the period from 2008 until 2014, i.e. approximately 7 years. Although the synthetic data adequately match the real data as shown by statistical tests (Kolomogorov Smirnov test, Wilcoxon rank sum test), some discrepancy is observed between the estimated parameters when the ETAS model is applied. This could be explained by the fact that the study period in the real case is characterized by intense seismic activity with 3 strong events ($M_w \geq 6.0$) in a period of 2 years, which is not the case in the subdivided periods of 7 years in the simulated data.

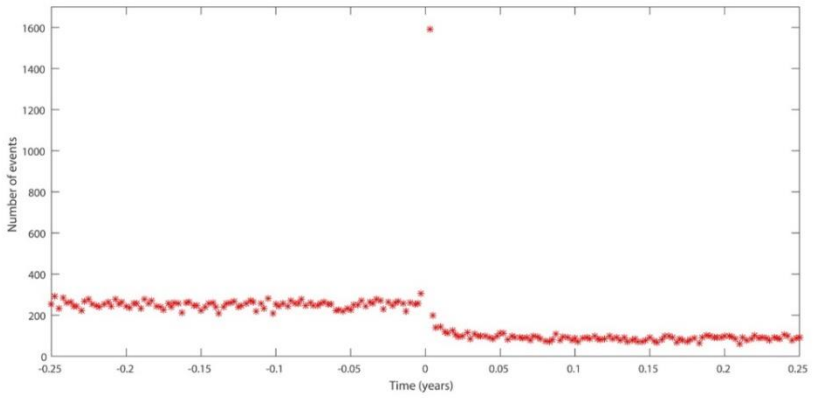

Figure 2. Stacked number of earthquakes with $M \geq 3.6$ preceding and following an M6.0 earthquake, obtained from the 10kyr simulation in a short-time scale, 0.5 years before and after the occurrence of the strong 2015 M_w6.5 Lefkada event.

Conclusions

Our preliminary results show that the spatial rather than the temporal features of the model are more stable. It is intriguing exploiting more deeply the performance of the clustering model using the synthetic catalog generated through the physics-based simulator in order to find features and patterns – both temporal and spatial – of short-term seismicity.

Acknowledgements

This research is co-financed by Greece and the European Union (European Social Fund- ESF) through the Operational Programme «Human Resources Development, Education and Lifelong Learning» in the context of the project "Strengthening Human Resources Research Potential via Doctorate Research" (MIS-5000432), implemented by the State Scholarships Foundation (IKY).

Ευρωπαϊκή Ένωση
European Social Fund

Operational Programme
Human Resources Development,
Education and Lifelong Learning
Co-financed by Greece and the European Union

ΕΣΠΑ 2014-2020
ανάπτυξη - εργασία - αλληλεγγύη

References

Console, R., Murru, M., 2001. A simple and testable model for earthquake clustering. Journal of Geophysical Research, 106, 8699–8711.

Console, R., Murru, M., Lombardi, A. M., 2003. Refining earthquake clustering models. Journal of Geophysical Research, 108, 2468, doi: 10.1029/2002JB002130.

Console, R., Carluccio, R., Papadimitriou, E. & Karakostas, V., 2015. Synthetic earthquake catalogs simulating seismic activity in the Corinth Gulf, Greece, fault system, Journal of Geophysical Research, 120(1), 326–343.

Console, R., Nardi, A., Carluccio, R., Murru, M., Falcone, G., Parsons, T., 2017. A physics-based earthquake simulator and its application to seismic hazard assessment in Calabria (Southern Italy) region. Acta Geophysica, 65, 243–257.

Console, R., Chiappini, M., Minelli, L., Speranza, F., Carluccio, R. & Greco, M., 2018a. Seismic hazard in Southern Calabria (Italy) based on the analysis of a synthetic earthquake catalog. Acta Geophysica, doi: 10.1007/s11600-018-0181-7.

Console, R., Chiappini, M., Minelli, L., Speranza,F., Carluccio, R., Greco, M., 2018b. Seismic hazard in Southern Calabria (Italy) based on the analysis of a synthetic earthquake catalog. Acta Geophysica, doi: 10.1007/s11600-0181-7.

Karakostas, V., Papadimitriou, E., Mesimeri, M., Gkarlaouni, Ch., Paradisopoulou, P. 2015. The 2014 Kefalonia doublet (Mw6.1 and Mw6.0) central Ionian Islands, Greece: seismotectonic implications along the Kefalonia transform fault zone. Acta Geophysica, 63, 1–16, doi:10.2478/s11600-014-0227-4.

Papadimitriou, E. E., 2002. Mode of strong earthquake occurrence in central Ionian Islands (Greece). Possible triggering due to Coulomb stress changes generated by the occurrence of previous strong shocks. Bulletin of Seismological Society of America, 92, 3293–3308.

Papadimitriou, E., Karakostas, V., Mesimeri, M., Chouliaras, G., Kourouklas, Ch., 2017. The Mw6.5 17 November 2015 Lefkada (Greece) Earthquake: Structural Interpretation by Means of the Aftershock Analysis. Pure & Applied Geophysics, 174, 3869–3888.

15th International Congress of the Geological Society of Greece
Athens, 22-24 May, 2019 | Harokopio University of Athens, Greece
Bulletin of the Geological Society of Greece, Sp. Pub. 7 Ext. Abs. GSG2019-219

Scaling Properties and Stochastic Modelling of Earthquake Time Series

G. Michas[1], F. Vallianatos[1,2]

(1) UNESCO Chair on Solid Earth Physics and Geohazards Risk Reduction, Technological Educational Institute of Crete, Chania, Greece, gmichas@hotmail.com
(2) Department of Geophysics–Geothermics, Faculty of Geology and Geoenvironment, National and Kapodistrian University of Athens, Athens, Greece

Earthquake time series are widely used to characterize the main features of regional seismicity and to provide useful insights into the earthquake dynamics. Furthermore, the temporal properties of seismicity have important implications regarding earthquake physics and probabilistic earthquake hazard assessment studies. As such, the temporal properties of seismicity have been the subject of intensive study during the past years. Research focused on whether waiting times, i.e. the time intervals between successive earthquakes, for various threshold magnitudes and spatial scales present particular scaling properties described by "universal" distributions (e.g., Bak *et al*., 2002; Corral, 2004), the form and the physical mechanism of which are of great importance in earthquake modeling and hazard assessments. Another main research question related to this topic is whether earthquakes occur randomly in time, following a Poisson process, or they possess some kind of "memory", where the time of the next earthquake is related to the time of the previous ones.

The present work seeks to contribute in this field. We study earthquake time series from the Corinth Rift (Greece), as well as from the Southern California and Japan. In such tectonically active regions, properties such as intermittency, fractality/multifractality and non-stationary clustering are common in earthquake time series, highlighting the complex nature of the earthquake generation process (e.g., Michas *et al*., 2013; Michas *et al.*, 2015; Vallianatos *et al*., 2016). The probability density function of waiting times, for various time periods, spatial scales and threshold magnitudes in all three regions, exhibits bimodality and a gradual crossover between two power-law regimes at short and long waiting times, respectively (Fig.1), suggesting that the distribution is a mixture of correlated events at short timescales, induced by aftershock sequences and earthquake swarms, and correlated background activity at long timescales. Such properties indicate clustering effects at all timescales and memory in the seismogenic process.

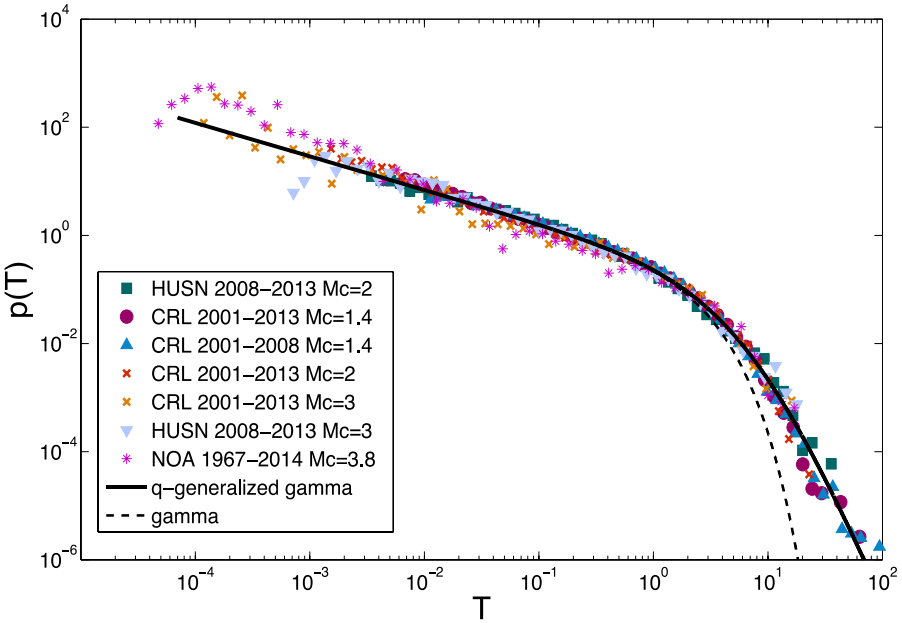

Figure 1. Probability density p(T) of the rescaled waiting times T in the Corinth Rift for various earthquake catalogues (HUSN, CRL, NOA) and for various time periods and threshold magnitudes. The solid line represents the corresponding fit according to the q-generalized gamma function, while the dashed line represents the corresponding fit according to the gamma function (from Michas, 2016).

To model this behavior, we introduce a stochastic model with memory effects that reproduces the temporal scaling behavior observed in regional seismicity (Michas & Vallianatos, 2018). For nonstationary earthquake activity, where the average seismic rate fluctuates, the solution of the stochastic model is the q-generalized gamma function that presents two power-law regimes for short and long waiting times, respectively, while for stationary activity it reduces to the standard gamma function, frequently observed in stationary earthquake timeseries (Corral, 2004). The application of the derived model to the aforementioned earthquake timeseries shows that for various threshold magnitudes and spatial areas and after rescaling with the mean waiting time, the normalized probability density functions fall onto a unique curve, which is characterized by two power-law regimes for short and long waiting times, respectively, a scaling behavior that

can exactly be recovered by the derived q-generalized gamma function (Fig.1). The results seem robust for nonstationary earthquake time series, despite the possible incompleteness of the earthquake catalogs, the selected threshold magnitude, or the spatial size of the chosen area, further signifying self-similarity in the temporal structure of seismicity. The results show the validity of the stochastic model and the derived scaling function, further signifying both short- and long-term clustering effects and memory in the evolution of seismicity.

Acknowledgements

This work is supported by the project HELPOS (MIS 5002697) which is implemented under the Action “Reinforcement of the Research and Innovation Infrastructure”, funded by the Operational Programme "Competitiveness, Entrepreneurship and Innovation" (NSRF 2014-2020) and co-financed by Greece and the EU.

References

Bak, P., Christensen, K., Danon, L., Scanlon, T., 2002. Unified scaling law for earthquakes. Physical Review Letters 88, 178501.

Corral, A., 2004. Long-term clustering, scaling, and universality in the temporal occurrence of earthquakes. Physical Review Letters 92, 108501.

Michas, G., 2016. Generalized statistical mechanics description of fault and earthquake populations in Corinth Rift (Greece). PhD Thesis, University College London.

Michas, G., Vallianatos, F., Sammonds, P., 2013. Non-extensivity and long-range correlations in the earthquake activity at the West Corinth rift (Greece). Nonlinear Processes in Geophysics 20, 713–724.

Michas, G., Sammonds, P., Vallianatos, F., 2015. Dynamic multifractality in earthquake time series: Insights from the Corinth rift, Greece. Pure and Applied Geophysics 172, 1909-1921.

Michas G., Vallianatos F., 2018. Stochastic modelling of non-stationary earthquake time series with long-term clustering effects. Physical Review E 98, 042107.

Vallianatos F., Papadakis G., Michas G., 2016. Generalized statistical mechanics approaches to earthquakes and tectonics. Proc. R. Soc. A 472, 20160497.

SPECIAL SESSION

T3.S2 Seismicity & Geodynamics in the Ionian Islands and the Corinth Gulf

Conveners: **Vasileios Karakostas (AUTH)**
George Kaviris (NKUA)
Efthymios Sokos (UPAT)
Pierre Briole (Ec. Norm. Sup./CNRS)

15th International Congress of the Geological Society of Greece
Athens, 22-24 May, 2019 | Harokopio University of Athens, Greece
Bulletin of the Geological Society of Greece, Sp. Pub. 7 Ext. Abs. GSG2019-029

Spatial Variations of Seismic Anisotropy in the Western Gulf of Corinth

I. Spingos[1], G. Kaviris[1], C. Millas[1], V. Kapetanidis[1], P. Papadimitriou[1], N. Voulgaris[1], K. Makropoulos[1]

(1) Section of Geophysics–Geothermics, Department of Geology and Geoenvironment, National and Kapodistrian University of Athens, 15784 Panepistimiopolis, Zografou, Athens, Greece, ispingos@geol.uoa.gr

The Western Gulf of Corinth (WGoC) is the most active rift in Europe, having hosted a large number of destructive earthquakes (Makropoulos *et al.*, 2012), as well as multiple swarms (Kapetanidis *et al.*, 2015). It comprises of fault systems striking approximately WNW-ESE, while the focal mechanisms in the area are almost exclusively normal in nature. This complicated structure characterizes the rift as a semi-graben, with the southern coasts of Northern Peloponnesus being uplifted (Armijo *et al.*, 1996). The intense seismic activity in the area has led to significant interest from researchers worldwide.

Seismic anisotropy refers to the wave velocity dependence from changes in the polarization direction. A widely studied branch of the above phenomenon is Shear-wave Splitting (SwS), which refers to velocity variations in shear-waves. Upon entering an anisotropic medium, shear-waves undergo splitting and two components of polarization can be distinguished; (a) the one propagating faster (S_{fast}) and (b) the one lagging behind (S_{slow}). SwS is quantified by determining two parameters, i.e. the polarization direction of the S_{fast} (φ) and the time-delay between the arrivals of the two split shear-waves (t_d). SwS is a featured phenomenon in areas where the crust is permeated by vertical fluid-filled microcracks. According to the Anisotropic Poro-Elasticity (APE) model (Crampin and Zatsepin, 1997; Zatsepin and Crampin, 1997), stress variations in a given rock volume and changes in the characteristics of the fluids affect the geometry of the microcracks. This affects SwS by altering both φ and t_d. Microcracks are usually controlled by the maximum horizontal compressive stress component (σ_{Hmax}). However, local structures can also have an effect on microcracks, leading to spatial differences in the distribution of φ (Li and Peng, 2017). In the WGoC, splitting has been previously studied, exhibiting polarization directions mostly aligned to σ_{Hmax}, i.e. WNW-ESE (e.g. Giannopoulos *et al.*, 2015; Kaviris *et al.*, 2017, 2018). However, deviations from this orientation have yet to be fully explored. The current study aims to clarify whether these outliers can be attributed to anisotropy controlled by structural factors.

The development and operation of dense seismological networks in the WGoC have a significant impact in the above, permitting the continuous recording of events by broadband seismological stations all around the rift. The Hellenic Unified Seismological Network (HUSN) is a joint venture of the operators of seismological networks in Greece and has been active since 2008, covering a significant portion of the gulf. The Corinth Rift Laboratory Network (CRLN) is the result of the partnership between Greek and French institutes with its main focus being the study of seismicity within the gulf. Data by both networks are used in the presented work.

The large dataset of event-station pairs was analyzed automatically. Initial locations of foci (acquired from the Seismological Laboratory of the National and Kapodistrian University of Athens) were used to determine candidate rays for analysis, i.e. ones with a maximum angle of incidence equal to 45°, in order to avoid converted and scattered phases. Then, two techniques were employed for the SwS analysis, through the Pytheas software (Spingos, 2019). The Eigenvalue (EV) method (Silver and Chan, 1991) utilizes a grid search approach, searching for the pair of φ and t_d that best minimizes the smallest eigenvalue λ_2 of the covariance matrix between the (corrected for anisotropy) horizontal components. To implement this, a signal window for analysis must be provided. Commonly, this is specified by the analyst. However, to fully automate the selection and accommodate a large number of recordings, the Pytheas software has followed a Cluster Analysis (CA) approach (Teanby *et al.*, 2004). Measurements with the EV method are repeatedly conducted for a range of candidate signal windows around the S-wave arrival. The outer bounds of the windows' range are defined by the S-P times and the period of the shear-waves. Thus, a population of measurements with coordinates (φ, t_d) is acquired, where clusters are formed, indicating stable solutions. A hierarchical agglomerative clustering is initially performed to determine the clusters. The optimal one is selected, based on the degree of constraint. The selected signal window is the one corresponding to the measurement with the smallest uncertainties, included in the most constrained cluster. Results from this analysis were then used to obtain the spatial variation of φ, with the use of the TESSA program (Johnson *et al.*, 2011). For a selected grid, the average of the polarization direction is calculated for each cell, by taking into account the φ value attributed to each passing ray and weighting their contribution according to t_d.

Results of the above analysis indicate that shear-wave splitting in the WGoC is mostly influenced by stress. While this was evident for the coastal areas (due to the stations being located on land), the spatial distribution of φ confirms this for the offshore region within the rift. However, the area surrounding the Mornos delta, to the NW, offers a different perspective, with polarization directions oriented NE-SW, perpendicular to σ_{Hmax}. While this could be interpreted as the microcracks reaching a critical state, where their aspect-ratio is inverted due to increased fluid pressure causing φ to flip by 90°, the time-independent nature of this change offers refuting evidence to the hypothesis. We attribute this difference in direction to local structures in the broader Mornos delta area, where both topographical and tectonic data indicate NE-SW trending structures. Distinguishing between the factors influencing SwS is a decisive step in seeking relations between fluid-related processes, such as diffusion/migration and splitting, enabling the latter to function as a monitoring tool.

Acknowledgements

The authors would like to thank the personnel of all cooperating institutes of both HUSN and CRLN (doi: 0.15778/RESIF.CL) for the operation of the respective networks. We acknowledge support of this study by the project "HELPOS – Hellenic Plate Observing System" (MIS 5002697) which is implemented under the Action "Reinforcement of the Research and Innovation Infrastructure", funded by the Operational Programme "Competitiveness, Entrepreneurship and Innovation" (NSRF 2014-2020) and co-financed by Greece and the European Union (European Regional Development Fund).

References

Armijo, R., Meyer, B., King, G., Rigo, A., Papanastassiou, D., 1996. Quaternary evolution of the Corinth Rift and its implications for the Late Cenozoic evolution of the Aegean. Geophys. J. Int. 126, 11–53. doi: 10.1111/j.1365-246X.1996.tb05264.x

Crampin, S., Zatsepin, S., 1997. Modelling the compliance of crustal rock—II. Response to temporal changes before earthquakes. Geophys. J. Int. 129, 495–506. doi: 10.1111/j.1365-246X.1997.tb04489.x

Giannopoulos, D., Sokos, E., Konstantinou, K.I., Tselentis, G.-A., 2015. Shear wave splitting and VP/VS variations before and after the Efpalio earthquake sequence, western Gulf of Corinth, Greece. Geophys. J. Int. 200, 1436–1448. doi: 10.1093/gji/ggu467

Johnson, J.H., Savage, M.K., Townend, J., 2011. Distinguishing between stress-induced and structural anisotropy at Mount Ruapehu volcano, New Zealand. J. Geophys. Res. Solid Earth 116, 1–18. doi: 10.1029/2011JB008308

Kapetanidis, V., Deschamps, A., Papadimitriou, P., Matrullo, E., Karakonstantis, A., Bozionelos, G., Kaviris, G., Serpetsidaki, A., Lyon-caen, H., Voulgaris, N., Bernard, P., Sokos, E., Makropoulos, K., 2015. The 2013 earthquake swarm in Helike, Greece: Seismic activity at the root of old normal faults. Geophys. J. Int. 202, 2044–2073. doi: 10.1093/gji/ggv249

Kaviris, G., Millas, C., Spingos, I., Kapetanidis, V., Fountoulakis, I., Papadimitriou, P., Voulgaris, N., Makropoulos, K., 2018. Observations of shear-wave splitting parameters in the Western Gulf of Corinth focusing on the 2014 Mw = 5.0 earthquake. Phys. Earth Planet. Inter. 282, 60–76. doi: 10.1016/j.pepi.2018.07.005

Kaviris, G., Spingos, I., Kapetanidis, V., Papadimitriou, P., Voulgaris, N., Makropoulos, K., 2017. Upper crust seismic anisotropy study and temporal variations of shear-wave splitting parameters in the Western Gulf of Corinth (Greece) during 2013. Phys. Earth Planet. Inter. 269, 148–164. doi: 10.1016/j.pepi.2017.06.006

Li, Z., Peng, Z., 2017. Stress- and Structure-Induced Anisotropy in Southern California From Two Decades of Shear Wave Splitting Measurements. Geophys. Res. Lett. 44, 9607–9614. doi: 10.1002/2017GL075163

Makropoulos, K., Kaviris, G., Kouskouna, V., 2012. An updated and extended earthquake catalogue for Greece and adjacent areas since 1900. Nat. Hazards Earth Syst. Sci. 12, 1425–1430. doi: 10.5194/nhess-12-1425-2012

Silver, P.G., Chan, W.W., 1991. Shear Wave Splitting and Subcontinental Mantle Deformation. J. Geophys. Res. 96, 16429–16454. doi: 10.1029/91JB00899

Spingos, I., 2019. Development of a shear-wave splitting parameters determination software suite for upper crust seismic anisotropy studies: Application in tectonic and volcanic regimes, Department of Geology and Geoenvironment. MSc Thesis, National and Kapodistrian University of Athens, Athens, 95 p.

Teanby, N., Kendall, J.-M., van der Baan, M., 2004. Automation of shear-wave splitting measurements using cluster analysis. Bulliten Seismol. Soc. Am. 94, 453–463. doi: 10.1785/0120030123

Zatsepin, S., Crampin, S., 1997. Modelling the compliance of crustal rock—I. Response of shear-wave splitting to differential stress. Geophys. J. Int. 129, 477–494. doi: 10.1111/j.1365-246X.1997.tb04488.x

15th International Congress of the Geological Society of Greece
Athens, 22-24 May, 2019 | Harokopio University of Athens, Greece
Bulletin of the Geological Society of Greece, Sp. Pub. 7 Ext. Abs. GSG2019-108

Spatiotemporal analysis of the early 2019 seismic excitation offshore north Lefkada Island

V. Karakostas[1], E. Papadimitriou[1], T. Kostoglou[1], O. Mangira[1], P. Bountzis[1]

(1) Geophysics Department, School of Geology, Aristotle University of Thessaloniki, GR54124 Thessaloniki, Greece, vkarak@geo.auth.gr

A moderate magnitude M_w5.4, earthquake occurred on the 5th of February 2019 in the offshore area north of Lefkada Island, strongly felt in the Lefkada city and the onshore continental area to the east, with no major damage or injuries reported. The main shock was followed by a very productive aftershock sequence with more than 400 recorded, and about 370 of them being relocated, by the 15 March 2019. An M_w4.2 earthquake has occurred on the 15th of January 2019, to the northeast of the 05/02/2019 event, also followed by several aftershocks. The affected area has been frequently visited by moderate earthquakes in the last decades with no one of them exceeding in magnitude M6.0.

The activated area is located at the boundary between the Kefalonia Transform Fault Zone (KTFZ) to the south and the Adriatic – Eurasian Collision to the north. The continental collision is expressed by a belt of thrust faulting with a NE – SW direction of the axis of maximum compression, runs along the eastern coastline of Adriatic Sea and terminates just north of Lefkada Island. The KTFZ is a major dextral strike slip fault zone that accommodates frequent strong earthquakes, clustered in space and time probably due to the stress transfer between the fault segments comprised in the fault system (Papadimitriou, 2002). The northernmost fault segment of KTFZ was activated in 2003 with an M_w6.2 main shock and a rich aftershock sequence, the accurate location of which provided for the first time the indication that the major fault segments bound the western coastlines and the contemporaneously activated secondary ones lie onshore (Karakostas *et al*., 2004).

The investigation of this activity is challenging to shed light in the seismogenic setting and the complex geodynamics of the area, prerequisite for any seismic hazard assessment study. Its location is critical to decipher how these secondary structures play a role in accommodating strain at the borderline of the KTFZ, an area where also reverse focal mechanisms were determined for moderate earthquakes that occurred in the last few decades.

Seismicity relocation and spatial characteristics

Seismicity was relocated after manually picking the P and S arrivals and using the 1–D velocity model along with a recalculated v_p/v_s ratio suggested by Papadimitriou *et al*. (2017) for the relocation of the 2015 Lefkada aftershock sequence. Station delays were calculated for further refining the locations, following a procedure described in Karakostas *et al*. (2014) and the HYPOINVERSE (Klein, 2002) computer program. The relocated seismicity allowed refined and more reliable picture than the disperse epicentral distribution derived from the regional catalogue, revealing seismicity concentrations mainly close to the stronger earthquakes' epicentres (Figure 1). The total earthquake set includes ~370 events that could be detected by an adequate number of seismological stations and relocated.

The first strong M_w4.2 earthquake triggered the activity in the northern cluster, with a comparatively noticeable aftershock frequency and magnitudes, with 15 aftershocks in the first 24 hours and additional 20 in the next five days. It is noteworthy that the activity continued and even intensified at this location after the M_w5.4 main shock. The close distance of the two concentrations could be investigated through interaction of small – magnitude earthquakes within the sequence.

The February aftershocks delineate an ~10 km long zone, which seems larger than expected from known scaling laws connecting rupture length with earthquake magnitude. Given that the locations are highly accurate, it implies that several secondary fault segments were activated in a cascade mode through stress transfer firstly due to the main shock coseismic slip and in the following among the activated fault patches. Independently of the moderate main shock magnitude this seismic sequence appeared remarkably productive with an M_w4.2 aftershock, a handful of $M \geq 3.0$ aftershocks and numerous smaller magnitude events (shown with different symbol size and colour, according to their magnitude). The sequence behaves as a foreshock – mainshock – aftershock – like sequence, with a 3 located foreshocks in the five days preceding the main shock occurrence and about 163 events occurred in the first five days, an interval taken the same in length for comparison reasons, the 72 of them being occurred in the first 24 hours.

The fault plane solutions of all the three stronger earthquakes, which are depicted in Figure 1 as lower hemisphere equal area projections, exhibit strike slip motion either dextral on an almost N–S striking fault plane, or sinistral on an E–W conjugate one. Although the N–S fault strike and the dextral motion is compatible with KTFZ geodynamic properties, motion on the conjugate faults cannot be ruled out and further investigation is stimulating.

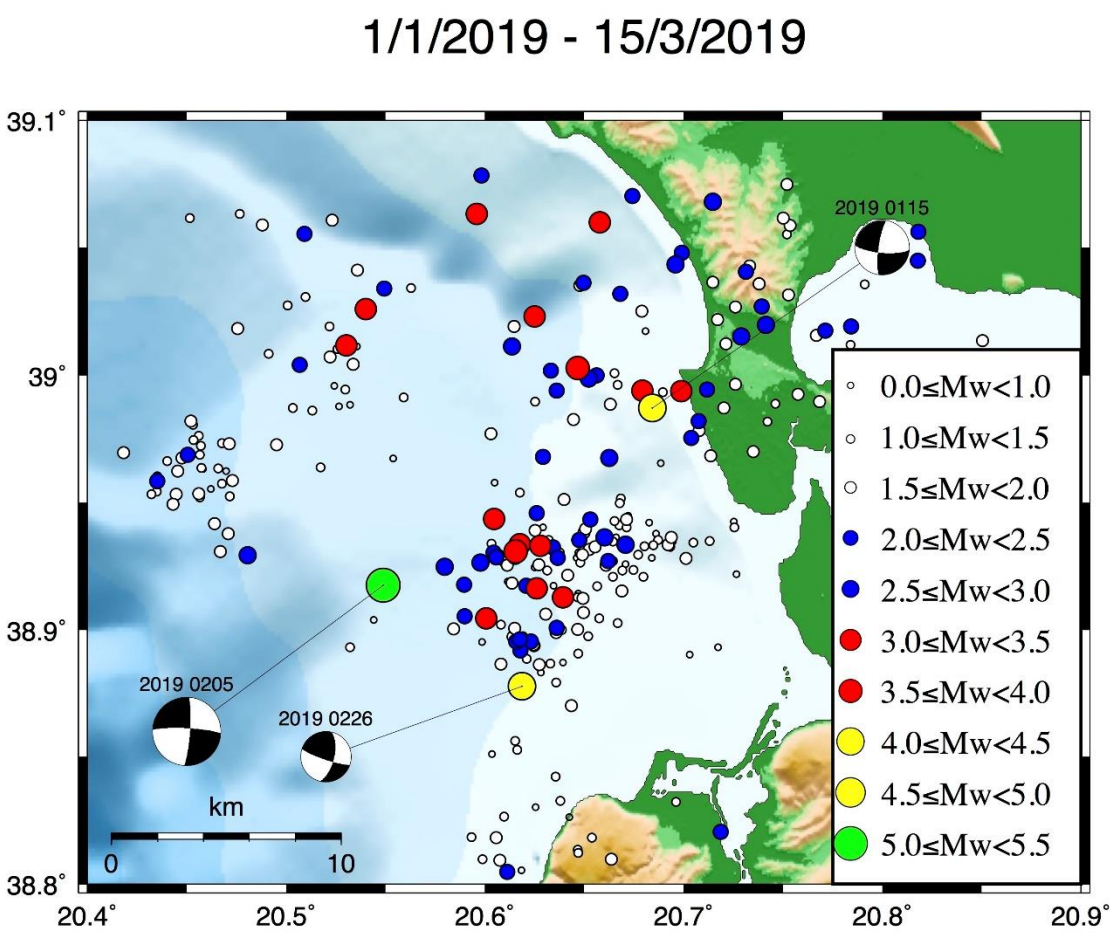

Figure 1. Relocated seismicity in the study area along with the fault plane solutions of the 3 stronger earthquakes shown as equal area lower hemisphere projections.

Summary

The as much as possible accurately relocated intense activity that observed in the first few weeks of the year (2019) beyond the northern termination of the KTFZ, forms distinctive clusters, the most prominent of which is associated with the 05/05/2019 M_w5.4 earthquake. The spatial distribution and the fault plane solutions of the three (3) stronger events evidence the prevalence of strike slip motion in this area, as a continuation of the KTFZ to the north of Lefkada Island. The complexity of the active structures, which in addition to the primary segments of the KTFZ are capable of producing disastrous earthquakes, highlights the need for intensive maintenance and careful analysis of the seismicity.

Acknowledgements

The financial support by the European Union and Greece (Partnership Agreement for the Development Framework 2014 -2020) under the Regional Operational Programme Ionian Islands 2014-2020, for the project "Telemachus – Innovative Operational Seismic Risk Management System in the Region of Ionian Islands" is gratefully acknowledged.

References

Karakostas, V.G., Papadimitriou, E.E., Papazachos, C.B., 2004. Properties of the 2003 Lefkada, Ionian Islands, Greece, earthquake seismic sequence and seismicity triggering. Bulletin Seismological Society America 94, 1976–1981.

Karakostas, V.G., Papadimitriou, E.E., Gospodinov, D., 2014. Modeling the 2013 North Aegean (Greece) seismic sequence: geometrical and frictional constraints, and aftershock probabilities, Geophysical Journal International 197, 525–541, doi: 10.1093/gji/ggt523.

Klein, F.W., 2000. User's Guide to HYPOINVERSE–2000, a Fortran program to solve earthquake locations and magnitudes, U. S. Geological Survey Open File Report 02–171 Version 1.0.

Papadimitriou, E.E., 2002. Mode of strong earthquake occurrence in central Ionian Islands (Greece). Possible triggering due to Coulomb stress changes generated by the occurrence of previous strong shocks. Bulletin Seismological Society America 94, 3293–3308.

Papadimitriou, E., Karakostas, V., Mesimeri, M., Chouliaras, G., Kourouklas, Ch., 2017. The M_w6.7 17 November 2015 Lefkada (Greece) earthquake: structural interpretation by means of aftershock analysis. Pure & Applied Geophysics, DOI 10.1007/s00024–07–1601–3.

15th International Congress of the Geological Society of Greece
Athens, 22-24 May, 2019 | Harokopio University of Athens, Greece
Bulletin of the Geological Society of Greece, Sp. Pub. 7 Ext. Abs. GSG2019-112

The 2018 Zakynthos Island, Greece, Earthquake Sequence: Implications in a Region of Distributed Deformation

V. Karakostas[1], E. Papadimitriou[1], A. Kostoglou[1], D. Chorozoglou[1]
(1) Geophysics Department, Aristotle University of Thessaloniki, GR54124 Thessaloniki, Greece, vkarak@geo.auth.gr

An M_w6.8 earthquake occurred on 25 October 2018, 30 km offshore of the west-southwest coastlines of Zakynthos Island. The aftershock sequence being still in progress, appeared very productive with 6 aftershocks of $M \geq 5.0$ in the first month and tens of $M \geq 4.0$ ones. Centroid moment tensor solutions (https://www.globalcmt.org/CMTsearch.html) for the main shock are predominantly indicative of thrust faulting in response to northeast – southwest compression, with a very low angle plane (dip=24º) for a significant dextral strike slip component (rake=165º), alike for the the largest aftershock (M_w5.9, dip=7º, rake=169º) that occurred five days afterwards.

The affected area occupies the northwesternmost part of the Hellenic Arc – Trench System is characterized by remarkably high seismic activity, with frequent strong (M>6.0) earthquakes that have caused severe casualties and damage during the last six centuries since historical information is available. The recurrence of these shocks is rather in the order of few decades, given that in the vicinity of the main rupture, an M_w=6.6. occurred in 1997. The 2018 Zakynthos earthquake and accompanying activated secondary faults suggest strong distributed crustal deformation in the area, highlighting the need for better understanding of active faulting and seismic hazard in this region.

Aftershock Location and Evolution of the Sequence

The Hellenic Arc–Trench System was recognized as a subduction zone with the oceanic plate of eastern Mediterranean being subducted under the Aegean microplate and constitutes the most prominent seismotectonic feature of the broader Aegean region. The seismicity is well delineated along the subduction front with the stronger events exhibiting thrust faulting along NW–SE striking faults and NE–SW striking axis of the maximum compression, placed perpendicular to this front in the study area. West – Northwest of the Zakynthos Island the Kefalonia Transform Fault Zone (KTFZ), with dextral strike slip motion, connects the oceanic subduction with the continental collision between the Outer Hellenides and the Adriatic microplate. This dextral strike–slip faulting was recognized as a major discontinuity between the Apulian platform and the western Hellenic Arc and was firstly suggested by Scordilis *et al*. (1985).

The properties of the activated structure were investigated with accurate relocated data and the available fault plane solutions of some of the stronger events. Station delays were calculated for further refining the locations of the aftershocks provided by the catalogs of Geophysics Department of the Aristotle University of Thessaloniki (GD–AUTh), following a procedure described in Karakostas *et al*. (2014) and the HYPOINVERSE (Klein, 2002) computer program. The double–difference location technique along with a cross – correlation algorithm was employed for further refining the locations, revealing a seismogenic layer extending from 3 to 15 km depth, whereas all the aftershock locations do not obviously align with the strike or dip of the mainshock focal mechanism; however, location uncertainties are expected in this region, with the depth control of the smaller events to be difficult constrained.

Figure 1 shows the relocated aftershock spatial distribution where different magnitude ranges are depicted with different symbols and the main shock epicenter by the star. The activity is spreading offshore the southwestern Zakynthos coastline, and persistently in an area activated since the first hours of the emergence of this seismic excitation, which is remarkably continuing with frequent M3.0 and M4.0 aftershocks for almost six months. The general trend of the relocated seismicity shows a strike agreeing well with the northwest–striking plane from the moment tensor solutions. The location refinement contributes in documenting kinematic details of the seismicity in relation to the active structures, whereas the inclusion of smaller magnitude earthquakes in the relocated data set provide the means for a more detailed analysis of the spatiotemporal evolution of the sequence.

Both the distribution of seismicity and fault plane solutions show that thrusting with strike slip motion are both present in low angle fault segments. The segmentation of the activated structure could be attributed to the faulting complexity combining the regional compressive tectonics with the dextral strike slip motion, mainly manifested along the KTFZ. Investigation of the spatial and temporal behavior of seismicity revealed possible triggering of adjacent fault segments that may fail individually thus preventing coalescence in a large main rupture. Multiple activation of secondary faults is observed, since the activity is extended over 60 km, an area well above from what is expected from known scaling laws expressing the fault length and rupture area as a function of the main shock magnitude. This implies that strain energy was not solely released on a main fault only, but on secondary and adjacent fault segments as well. The as much as possible reliable definition of their geometry forms the basis for the structural interpretation of the local fault network.

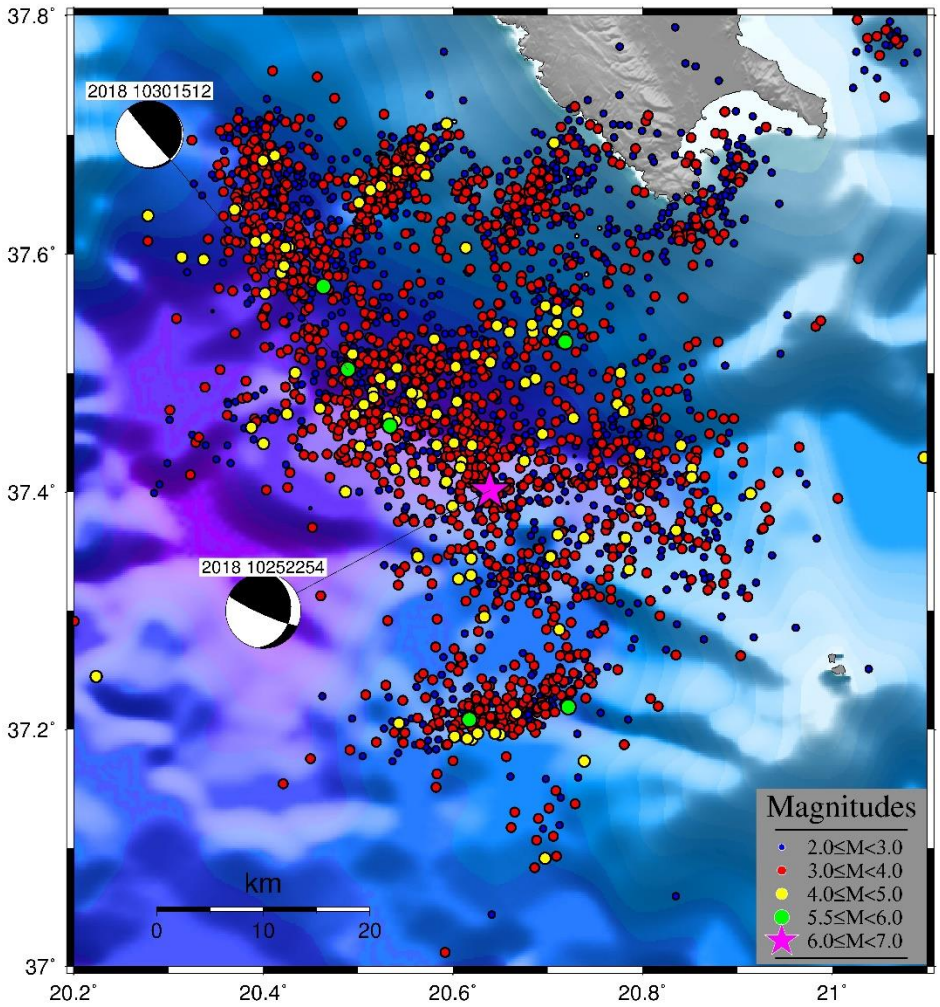

Figure 1. The 2018 Zakynthos relocated aftershock sequence in the first three months after the main shock occurrence, along with the focal mechanisms of the main shock and its largest aftershock shown as equal area lower hemisphere projections.

Summary

The 2018 M_w6.8 Zakynthos earthquake and its largest aftershock were crustal thrust – faulting events. The stress axes orientations are consistent with the regional stress field and with the focal mechanisms of past regional events (Papadimitriou, 1993). Complex earthquake sequences are common in the study area, where multiple adjacent and conjugate faults are contemporaneously activated. The abundance of aftershock activity appears to be correlated with structural complexity, in the sense that aftershock populations reflect fault populations surrounding major faults.

Acknowledgements

The plots were made using the Generic Mapping Tools version 5.4.4 (Wessel et al., 2013). Support is acknowledged by "HELPOS – Hellenic System for Lithosphere Monitoring" (MIS 5002697) project, implemented under the Action "Reinforcement of the Research and Innovation Infrastructure", funded by the Operational Programme "Competitiveness, Entrepreneurship and Innovation" (NSRF 2014-2020) and co-financed by Greece and the European Union (European Regional Development Fund).

References

Karakostas, V.G., Papadimitriou, E.E., Gospodinov, D., 2014. Modeling the 2013 North Aegean (Greece) seismic sequence: geometrical and frictional constraints, and aftershock probabilities, Geophysical Journal International 197, 525–541, doi: 10.1093/gji/ggt523.

Klein, F.W., 2000. User's Guide to HYPOINVERSE–2000, a Fortran program to solve earthquake locations and magnitudes, U. S. Geological Survey Open File Report 02–171 Version 1.0.

Papadimitriou, E.E., 1993. Focal mechanism along the convex side of the Hellenic Arc and its tectonic significance. Bolletino di Geofisica Teorica ed. Applicata 35, 401–426.

Permanent Regional Seismological Network operated by the Aristotle University of Thessaloniki, doi:10.7914/SN/HT.

Scordilis, E.M., Karakaisis, G.F., Karakostas, B.G., Panagiotopoulos, D.G., Comninakis, P.E., Papazachos, B.C., 1985. Evidence for transform faulting in the Ionian Sea: The Cephalonia Island earthquake sequence. Pure Applied Geophysics 123, 388–397.

Wessel P., Smith W.H.F., Scharroo R., Luis J.F., Wobbe F., 2013. Generic Mapping Tools: Improved version released. EOS Trans AGU, 94, 409–410.

15th International Congress of the Geological Society of Greece
Athens, 22-24 May, 2019 | Harokopio University of Athens, Greece
Bulletin of the Geological Society of Greece, Sp. Pub. 7 Ext. Abs. GSG2019-143

Temporal variations of b-values in Central Ionian Islands

O. Mangira[1], E. Papadimitriou[1], V. Karakostas[1], G. Vasiliadis[2]

(1) Department of Geophysics, School of Geology, Aristotle University of Thessaloniki, GR54124 Thessaloniki, Greece, omangira@geo.auth.gr
(2) Department of Informatics Engineering, TEI of West Macedonia, 52100, Kastoria, Greece

Our study investigates the temporal patterns of b-values in Central Ionian Islands during the last decade. This data-rich case study includes the January-February 2014 earthquake doublet of Kefalonia Island and the associated earthquakes and the 2015 sequence of Lefkada Island (Karakostas *et al*., 2015; Papadimitriou *et al.*, 2017). For the interpretation of the temporal variations of b-values it is crucial to use high quality data and consistent earthquake catalogs compiled based on a homogeneous monitoring network. For that purpose we use a dataset with events occurred in Central Ionian Islands for the period between 2008 and 2017. The magnitude of completeness is computed through the application of the goodness-of-fit method (Wiemer and Wyss, 2000, Figure 1). For safety we add 0.1 and consequently, the magnitude threshold is set $M_{th} = 2.8$.

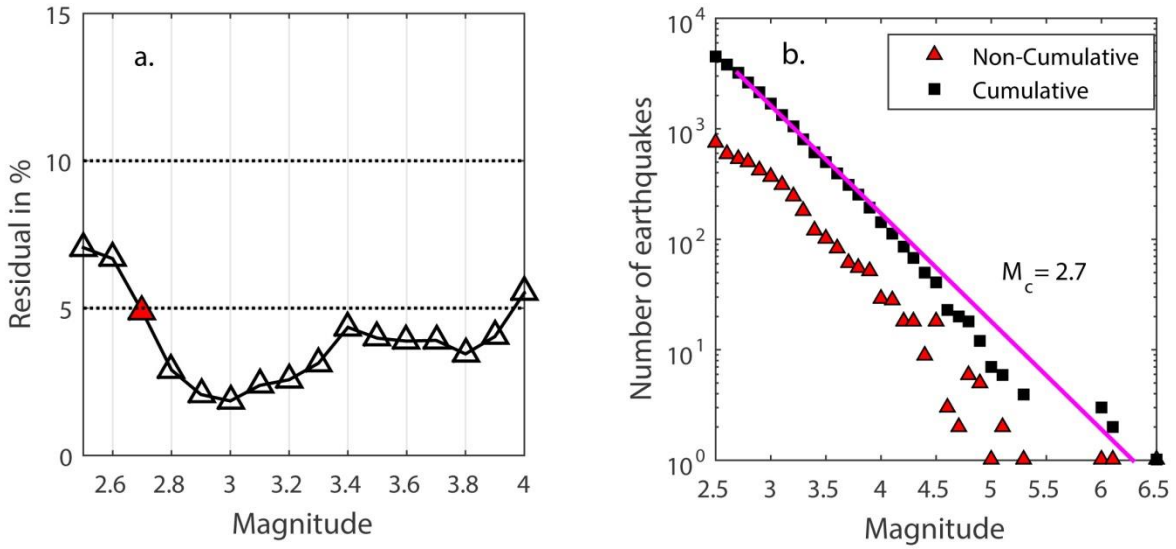

Figure 1a. Residual plot between the observed frequency magnitude distribution (FMD) and the perfect fit of the power law for each magnitude bin. Red triangle shows the completeness magnitude *Mc*. b. Incremental (triangles) and cumulative (squares) FMD, respectively, of the Central Ionian Islands earthquake catalog. The line represents the best fitting model after the application of GFT method.

The temporal evolution of b-values is analyzed by means of two different techniques (Tormann *et al*., 2013). The former is the constant – time – windows technique, where fixed length time windows are used to estimate b-values through time, and the latter is the fixed – number – of events approach. When applying the fixed – number – of – events approach we are based on the average annual number of events occurred in the selected period with $M \geq M_{th}$. In our case, it is found that $\overline{N}_{ann} = 265$ earthquakes. We show that changing the value of the number of events within reasonable limits (-50, 50) does not change the shape of the time-series. For the constant – time – windows technique, a wider variety of time windows is examined since both seismic excitation and relative quiescence are present in the dataset and an average period cannot be applied. The time windows range from a few months to 2 years.

We argue that when significantly varying seismicity rates are observed in a region, like in the case examined, the approach of constant – time – windows is biased. On the one hand, small time windows are able to capture abrupt changes but then, when seismicity is relatively low, many empty bins are created, and on the other, large time windows fill all the bins but are not able to track immediate changes and provide detailed information. The red line in Figure 2, for example, which corresponds to a time window of 2 years, does not seem able to capture b-value variations due to the 2014 Kefalonia doublet and the 2015 Lefkada main shock, which are apparent to the black line.

The overlap between successive b-value estimates is also investigated within different ranges from no overlap to continuously moving the window by one event at a time. The larger is the overlap the smaller is the sensitivity of choosing the starting point of the analysis and the larger are the details depicted in the time-series. Figure 2 shows an example of 80% overlap between successive windows.

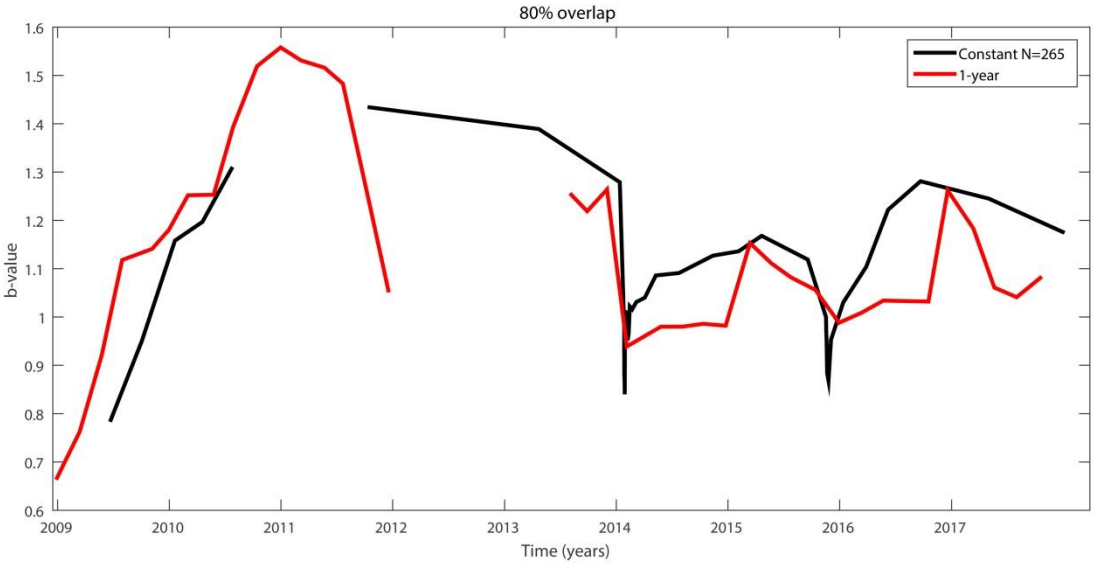

Figure 2. Comparison of b-value time-series for different sampling techniques: constant number, N, of events (black) versus constant time T, windows (red). N is set 265 events, i.e. the annual average number of events and T=1 years. 80 %overlapping is set for both cases.

Summary

In this study different techniques are investigated for a detailed analysis of the temporal evolution of b-values in the Central Ionian Islands area. This is particularly intriguing, since monitoring the evolution of b-values through time rather than a mere comparison of absolute b-values could be translated into changes in stress levels.

Acknowledgements

The financial support by the European Union and Greece (Partnership Agreement for the Development Framework 2014 -2020) under the Regional Operational Programme Ionian Islands 2014-2020, for the project "Telemachus – Innovative Operational Seismic Risk Management System in the Region of Ionian Islands" is gratefully acknowledged.

References

Cao, A M., Gao, S.S., 2002. Temporal variations of seismic b-values beneath northeastern Japan island arc. Geophysical Research Letters, 29(9), doi:10.1029/2001GL013775.

Karakostas, V., Papadimitriou, E., Mesimeri, M., Gkarlaouni, Ch., Paradisopoulou, P. 2015. The 2014 Kefalonia doublet (Mw6.1 and Mw6.0) central Ionian Islands, Greece: seismotectonic implications along the Kefalonia transform fault zone. Acta Geophysica, 63, 1–16., doi:10.2478/s11600-014-0227-4.

Papadimitriou, E., Karakostas, V., Mesimeri, M., Chouliaras, G., Kourouklas, Ch., 2017. The Mw6.5 17 November 2015 Lefkada (Greece) Earthquake: Structural Interpretation by Means of the Aftershock Analysis. Pure & Applied Geophysics, 174, 3869–3888.

Tormann, T., Wiemer, S., Hardebeck, J., 2012. Earthquake recurrence models fail when earthquakes fail to reset the stress field. Geophysical Research Letters, 39, doi:10.1029/2012GL052913.

Tormann,T., Wiemer, S., Metzger, S., Michael, A. J., Hardebeck, J. L., 2013. Size distribution of Parkfield's microearthquakes reflects changes in surface creep rate. Geophysical Journal International, 193, 1474–1478.

Wiemer, S., Wyss, M., 1997. Mapping the frequency-magnitude distribution in asperities: an improved technique to calculate recurrence times? Journal of Geophysical Research, 102, 15115–15128

Wiemer, S., Wyss, M., 2000. Minimum magnitude of complete reporting in earthquake catalogs: examples from Alaska, the western United States, and Japan. Bulletin of Seismological Society of America, 90, 859–869.

15th International Congress of the Geological Society of Greece
Athens, 22-24 May, 2019 | Harokopio University of Athens, Greece
Bulletin of the Geological Society of Greece, Sp. Pub. 7 Ext. Abs. GSG2019-201

Detailed Microseismicity Analysis of the Central Ionian Islands

A. Kostoglou[1], V. Karakostas[1], E. Papadimitriou[1]

(1) Department of Geophysics, School of Geology, Aristotle University of Thessaloniki, 54124 Thessaloniki, Greece, akostogl@geo.auth.gr

The Central Ionian Islands, namely Kefalonia and Lefkada, consists the most seismically active area in the Mediterranean. The main tectonic characteristic is the dextral strike slip motion caused by the Kefalonia Transform Fault Zone (KTFZ) (Scordilis et al., 1985) along which strong earthquakes occur regularly for the past 600 years at least. Since 2003 four strong earthquakes (M_W > 6.0) occurred in the area, both in Kefalonia (26/1/2014 and 3/2/2014) and Lefkada (14/8/2003 and 17/11/2015) and their aftershock sequences were adequately recorded and located since a local seismological network has been installed the day after the 2003 main shock (Karakostas *et al*., 2004), whereas the last one of them was recorded by an adequate number of permanent seismic stations, since the network was substantially improved since 2003. A permanent dense seismic network is in operation since mid-2014 (Hellenic Unified Seismological Network), resulted to microseismicity monitoring sufficient to reveal the complex faulting properties of the area. From September 2016 to December 2018 all recorded earthquakes in the area are manually picked and then located resulting in a adequately accurate earthquake catalog comprising about 13000 events (Fig. 1), most of them along the Kefalonia Transform Fault.

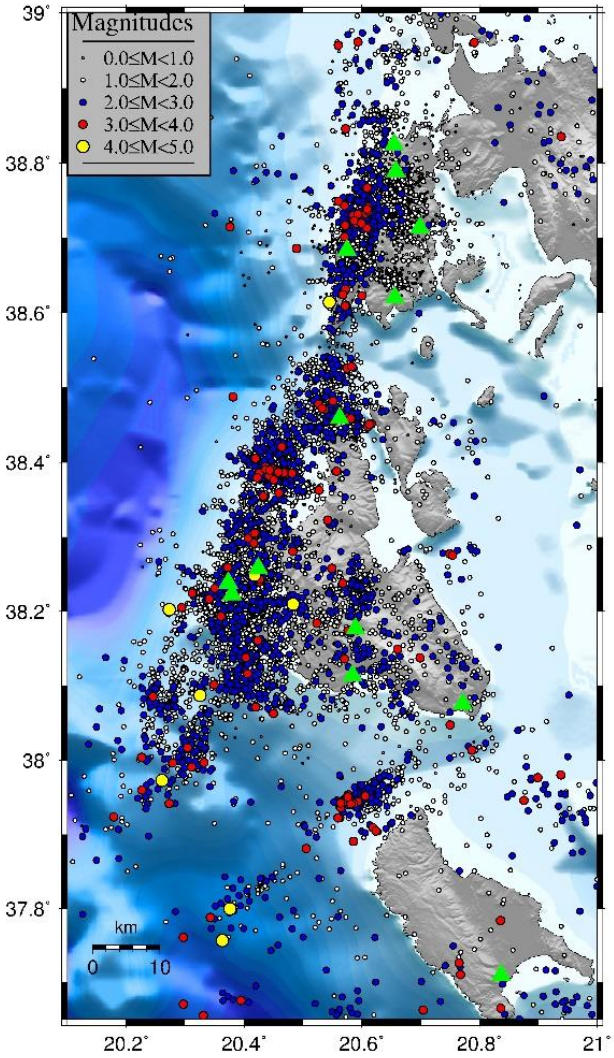

Figure 1. Located seismicity in the Ionian Islands from September 2016 to December 2018. Green triangles indicate the stations of HUSN in the area used in the manual picking and relocation.

The earthquakes are relocated using a recent 1D velocity model (Papadimitriou *et al*., 2017) considering station time delays by an iterative procedure (Karakostas and Papadimitriou, 2010) in order to account for the lateral crustal variations. The Double – Difference method is then applied and a cross – correlation algorithm (Waldhauser and Ellsworth, 2000, Schaff and Waldhauser, 2005) is implemented. The resulting spatial distribution is examined using strike parallel and strike normal cross sections detailing the major seismically active structures as well as the adjacent minor faults along the

KTFZ. Benefiting from the azimuthal coverage of the seismic network focal mechanisms are calculated using moment tensor inversion (Sokos and Zahradnik, 2008) or first motion polarities (Reasenberg and Oppenheimer, 1985) in order to determine the rupture properties of the active structures in the area and, along with the relocated seismicity, reveal the kinematic properties of the faults.

Seismicity on Lefkada Island is observed along the main fault zone as well as on several conjugate structures where mostly microseismicity is manifested with focal depths ranging from 5 to 15 km. In Kefalonia Island the seismicity follows more complex patterns. In its northern part and in the gulf of Myrtos seismicity reveals the existence of step overs between the two islands, in accordance with Karakostas *et al*., (2015), whereas along the Paliki Peninsula seismicity patterns appear more scattered, revealing small structures following the trend of the KTFZ with focal depths ranging from 5 to 18 km. In the offshore area South of Kefalonia several M_L >4.0 were recorded and the resulting seismic activity is manifested by small clusters that follow the main fault zone at focal depths reaching about 20 km. In the area between Zakynhtos and Kefalonia a seismic excitation over a two month period led to the mapping of a well – defined cluster striking NE – SW with focal depths ranging between 15 and 20 km. The results contribute to the precise mapping of smaller active seismic sources, that are capable of producing light to moderate earthquakes and should be taken into account in seismic hazard assessment.

Acknowledgements

This work gas been supported by the project "Helpos – Hellenic System for Lithosphere Monitoring" (MIS 5002697) which is implemented under the Action "Reinforcement of the Research and Innovation Infrastructure" funded by the Operational Programme "Competitiveness, Entrepreneurship and Innovation" (NSRF 2014 – 2020) and co-financed by Greece and the European Union (European Regional Development Fund)

References

Karakostas, V., Papadimitriou, E., Mesimeri, M., Gkarlaouni, C., Paradisopoulou, P., 2015. The 2014 Kefalonia Doublet (Mw6.1 and Mw6.0), central Ionian Islands, Greece: Seismotectonic implications along the Kefalonia transform fault zone. Acta Geophysica 63, 1–16. https://doi.org/10.2478/s11600-014-0227-4

Karakostas, V.G., Papadimitriou, E.E., 2010. Fault complexity associated with the 14 August 2003 Mw6.2 Lefkada, Greece, aftershock sequence. Acta Geophysica 58, 838–854. https://doi.org/10.2478/s11600-010-0009-6

Karakostas, V.G., Papadimitriou, E.E., Papazachos, C.B., 2004. Properties of the 2003 Lefkada, Ionian Islands, Greece, earthquake seismic sequence and seismicity triggering. Bull. Seismol. Soc. Am. 94, 1976–1981. https://doi.org/10.1785/012003254

Papadimitriou, E., Karakostas, V., Mesimeri, M., Chouliaras, G., Kourouklas, C., 2017. The Mw6.5 17 November 2015 Lefkada (Greece) Earthquake: Structural Interpretation by Means of the Aftershock Analysis. Pure Applied Geophysics 174, 3869–3888. https://doi.org/10.1007/s00024-017-1601-3

Reasenberg, P., Oppenheimer, D.H., 1985. FPFIT, FPPLOT and FPPAGE; Fortran computer programs for calculating and displaying earthquake fault-plane solutions. U.S. Geological Survey Open-File Rep. 85-739. https://doi.org/10.3133/OFR85739

Schaff, D.P., Waldhauser, F., 2005. Waveform cross-correlation-based differential travel-time measurements at the northern California seismic network. Bulletin of the Seismological Society of America 95, 2446–2461. https://doi.org/10.1785/0120040221

Scordilis, E.M., Karakaisis, G.F., Karacostas, B.G., Panagiotopoulos, D.G., Comninakis, P.E., Papazachos, B.C., 1985. Evidence for transform faulting in the Ionian sea: The Cephalonia island earthquake sequence of 1983. Pure Applied Geophysics 123, 388–397. https://doi.org/10.1007/BF00880738

Sokos, E.N., Zahradnik, J., 2008. ISOLA a Fortran code and a Matlab GUI to perform multiple-point source inversion of seismic data. Computers & Geosciences 34, 967–977. https://doi.org/10.1016/j.cageo.2007.07.005

Waldhauser, F., Ellsworth, W.L., 2000. A Double-difference Earthquake location algorithm: Method and application to the Northern Hayward Fault, California. Bulletin of the Seismological Society of America 90, 1353–1368. https://doi.org/10.1785/0120000006

15th International Congress of the Geological Society of Greece
Athens, 22-24 May, 2019 | Harokopio University of Athens, Greece
Bulletin of the Geological Society of Greece, Sp. Pub. 7 Ext. Abs. GSG2019-216

Stochastic Modelling of Anomalous Earthquake Diffusion in the 2001 Agios Ioannis Earthquake Swarm (Corinth Rift)

G. Michas[1], F. Vallianatos[1,2]

(1) UNESCO Chair on Solid Earth Physics and Geohazards Risk Reduction, Technological Educational Institute of Crete, Chania, Greece, gmichas@hotmail.com
(2) Department of Geophysics–Geothermics, Faculty of Geology and Geoenvironment, National and Kapodistrian University of Athens, Athens, Greece

The Corinth Rift (central Greece) is one of the most seismically active areas in Europe due to rapid continental extension that reaches the rate of ~15mm/year in its western part. In contrast to the eastern part, the western part of the rift presents intense microseismic activity and frequent earthquake swarms that have been associated with pore-fluid pressure diffusion at depth (Bourouis & Cornet, 2009). Such an earthquake swarm occurred on 2001 in the SW margin of the rift, in the area of Agios Ioannis, near the city of Aigion. The swarm initiated on 2001 March 28 with a sudden increase in the regional seismicity rate and involved more than 2900 events over a period of 100 days. The largest event of the swarm occurred on 2001 April 8, 10 days after the initiation of the swarm, with the moderate size of M_w4.3. The spatial distribution of the swarm and the focal mechanism of the largest event indicated the activation of a SW–NE fault plane dipping at ∼40◦ to the north-west, which coincides with the unexposed Kerinitis fault (Pacchiani & Lyon-Caen, 2010). The spatiotemporal evolution of the swarm indicated the spatial migration of activity towards the surface with time. This migration pattern is consistent with a pore-fluid pressure diffusion mechanism, where the initial pore-fluid pressure perturbation occurred at some point near the early events of the swarm and progressively migrated at negative pressure gradients towards the surface along the active fault structures.

According to the Mohr-Coulomb failure criterion, increased pore-fluid pressure can reduce the effective normal stress along a fault zone triggering earthquakes. Here we investigate the diffusion properties of the Agios Ioannis earthquake swarm and the applicability of such mechanism in triggering the earthquake activity. We consider a probabilistic approach and a stochastic framework that generates the key properties of earthquake diffusion. Within this context, a well-established stochastic framework for modelling anomalous diffusion phenomena in complex heterogeneous media, where linear diffusion equations and Fick's second law might no longer be applicable, is the continuous-time random walk (CTRW) model (Berkowitz *et al*., 2006). Within the CTRW context, we consider earthquake occurrence as a point-process in time and space and we map earthquake diffusion with a joint probability density function of spatial jumps and waiting times between successive earthquakes. The analysis of the swarm within this context indicates a broad probability density of waiting times with asymptotic power-law behavior, as well as the power-law growth of the mean square displacement of seismicity with time, with a diffusion exponent well below unity that marks normal diffusion (Fig.1). Such properties are intrinsic characteristics of anomalous diffusion and indicate the slow propagation of seismicity according to a sub-diffusive process.

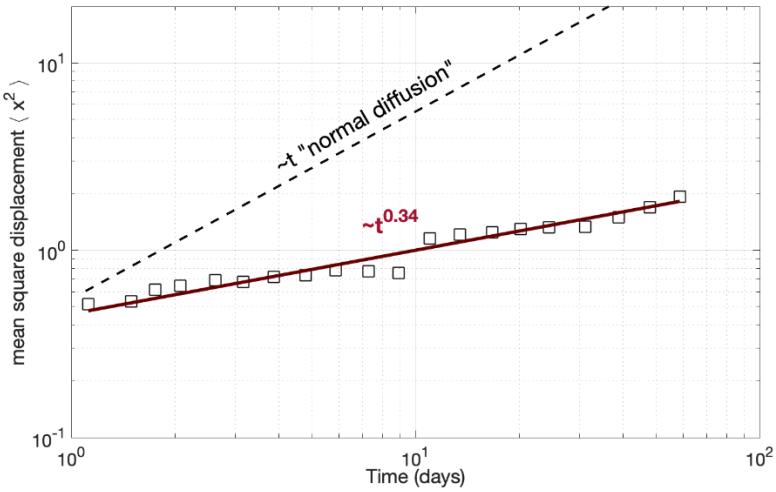

Figure 1. Mean square displacement of the earthquake swarm with time (squares) in logarithmically spaced bins and in double logarithmic axes. The solid line indicates the best-fitting solution of ~t^a for the value of a = 0.34 ± 0.04, while the dashed line indicates ~t that marks normal diffusion (modified after Michas & Vallianatos, 2018).

In addition, we combine the CTRW model with fractional kinetics and the time-fractional diffusion equation to provide an analytic description of the spatial migration of seismicity with time. According to the results for various time periods, the derived stochastic model can successfully predict the main features of anomalous earthquake diffusion, indicating a

peak of earthquake concentration close to the origin and a stretched exponential decay for the concentration of distant events. Our results are consistent with pore-fluid pressure diffusion as the triggering mechanism of the earthquake swarm. In this case, our results can be understood as a 'non- Fickian' relaxation of an initial pore-fluid pressure perturbation that reduces the effective normal stress along the active fault structure triggering the seismicity. The results further indicate that the CTRW model and the fractional diffusion equation can efficiently be used to model anomalous earthquake diffusion in the highly heterogeneous crust.

Acknowledgements

This work is supported by the project HELPOS (MIS 5002697) which is implemented under the Action "Reinforcement of the Research and Innovation Infrastructure", funded by the Operational Programme "Competitiveness, Entrepreneurship and Innovation" (NSRF 2014-2020) and co-financed by Greece and the EU.

References

Berkowitz, B., Cortis, A., Dentz, M., Scher, H., 2006. Modeling non-Fickian transport in geological formations as a continuous time random walk,.Rev. Geophys. 44, RG2003.

Bourouis, S., Cornet, F.H., 2009. Microseismic activity and fluid fault interactions: some results from the Corinth Rift Laboratory (CRL), Greece. Geophys. J. Int. 178, 561–580.

Michas G., Vallianatos F., 2018. Modelling earthquake diffusion as a continuous-time random walk with fractional kinetics: the case of the 2001 Agios Ioannis earthquake swarm (Corinth Rift). Geophys. J. Int. 215, 333–345.

Pacchiani, F., Lyon-Caen, H., 2010. Geometry and spatiotemporal evolution of the 2001 Agios Ioanis earthquake swarm (Corinth rift, Greece). Geophys. J. Int. 180, 59–72.

15th International Congress of the Geological Society of Greece
Athens, 22-24 May, 2019 | Harokopio University of Athens, Greece
Bulletin of the Geological Society of Greece, Sp. Pub. 7 Ext. Abs. GSG2019-224

The 25th October, 2018 Zakynthos Earthquake

P. Papadimitriou[1], V. Kapetanidis[1], A. Karakonstantis[1], I. Spingos[1], K. Pavlou[1], G. Kaviris[1], I. Kassaras[1] and N. Voulgaris[1]

(1) Section of Geophysics–Geothermics, Department of Geology and Geoenvironment, National and Kapodistrian University of Athens, 15784 Panepistimiopolis, Zografou, Athens, Greece, ppapadim@geol.uoa.gr

The geodynamic regime in western Greece manifested by intense seismic activity results from the convergence between the African and Eurasian lithospheric plates (e.g. Armijo *et al.*, 1992), while the westward motion of the Turkish plate imposes an important contribution (e.g., Armijo et al., 1996). The region hosts both continental collision to the north and oceanic slab subduction to the south; these features are connected by the right-lateral Cephalonia Transform Fault (CTF). Active tectonics involves all types of faulting. Reverse and strike-slip faulting characterize the interplate type of deformation (Papadimitriou et al., 2006; 2012; Kassaras et al., 2016), while normal and strike-slip faulting prevails in intraplate regions (Kassaras et al., 2014a, 2014b), forming pull-apart basins (King et al., 1993) and the rapidly spreading Corinth Rift (Kapetanidis & Papadimitriou, 2011; Kapetanidis et al., 2015). GPS measurements demonstrate rapid deformation to the south (~35 mm·yr^{-1}) and a slower one of the order 5–8 mm·yr^{-1} in NW Greece (Chousianitis *et al.*, 2015). Deformation across the area of Western Greece is mainly accommodated within the accretionary sediments comprising the external Paxi, Gavrovo and Ionian geotectonic units, escarped from the African margin and colliding against the un-deformed Eurasian hinterland (e.g. Royden and Papanikolaou, 2011).

Zakynthos Island is located at the front of the present-day Hellenic Trench, which is formed along the convergent zone of the plate boundaries between the subducting oceanic lithosphere of Tethys and the overriding Eurasian plate. The high level of seismic activity in the area is the result of the intense crustal deformation in the Central Ionian Sea, which leads to the occurrence of moderate to strong events. The most recent events include the November 18th, 1997 (Mw=6.5) earthquake, SW of Zakynthos Island, the December 2nd, 2002 (Mw= 5.5) earthquake, a sequence of earthquakes on October 2005 (Mw=5.6) and April 2006 (Mw=5.5–5.7) south of Zakynthos, the June 8th, 2008 (Mw= 6.4) Andravida earthquake, the January 26th, 2014 (Mw= 6.1) Paliki earthquake and the November 17th, 2016 (Mw= 6.4) Lefkas earthquake.

A strong earthquake of moment magnitude Mw=6.8 occurred on 25 October 2018, ~50 km to the SW of Zakynthos Island, causing some damage in the municipality of Zakynthos and on the islands of Strofades. This event was one of the largest that have occurred in the vicinity of Zakynthos Island since 1983. It was strongly felt in Western Greece but also in other parts of the Greek mainland. More than 4,000 aftershocks were located in the framework of this study. The aftershock zone covers a region about 60-70 km long in a N110°E direction and ~80 km towards N20°E.

In this work we attempt to highlight the nature and dynamics of the earthquake sequence, the driving forces that acted during its evolution and potential consequences of its occurrence on the regional hazard. To this aim, a comprehensive dataset of recordings from the Hellenic Unified Seismological Network (HUSN) and the Hellenic Strong Motion Network (HSMN; Theodulidis et al. 2004) was compiled and the following tasks were carried out: (a) determination of precise hypocentral locations employing a custom velocity model, followed by double-difference relocation, (b) spatiotemporal analysis of the sequence, (c) regional moment tensor inversion for the determination of the source parameters of the mainshock and the larger events, (d) inversion of focal mechanisms to investigate the local stress-field distribution and (e) computation of Coulomb stress transfer to identify regions and receiver faults that were loaded with additional stress.

After the manual determination of P- and S-wave phase arrivals, a dataset of 900 best located earthquakes, between 26 October and 30 November 2018, was compiled and a local velocity model was obtained using a travel-time residual and location errors minimization method (e.g. Kissling et al., 1994). Locations were recalculated with the new model and relocated with the use of a double-difference algorithm. The spatial distribution of epicenters revealed several distinct clusters, some of which are in general agreement with the geometry of known mapped faults and compatible with the strike of Quaternary faults.

Regional moment tensor inversion revealed a focal mechanism with a strike of N16°E, a dip of 25° and a rake of 166°. Most of the determined focal mechanisms of the sequence followed this trend. Nevertheless, the largest aftershock displayed strike-slip characteristics. In addition, focal mechanisms, including events of past activity (Kassaras et al., 2016), were inverted to determine the regional stress field (Hardebeck and Michael, 2006). A complex stress field in the broader area of Central Ionian Sea, related to both thrust and strike-slip faulting was revealed.

Acknowledgements

We acknowledge support of this study by the project "HELPOS – Hellenic Plate Observing System" (MIS 5002697) which is implemented under the Action "Reinforcement of the Research and Innovation Infrastructure", funded by the Operational Programme "Competitiveness, Entrepreneurship and Innovation" (NSRF 2014-2020) and co-financed by Greece and the European Union (European Regional Development Fund).

References

Armijo, R., Lyon-Caen, H., Papanastassiou, D., 1992. East-west extension and Holocene normal-fault scarps in the Hellenic arc. Geology 20, 491–494.

Armijo, R., Meyer, B., King, G.C.P., Rigo, A., Papanastassiou, D., 1996. Quaternary evolution of the Corinth Rift and its implications for the Late Cenozoic evolution of the Aegean. Geophys. J. Int. 126, 11–53.

Chousianitis, K., Ganas, A., Evangelidis, C.P., 2015. Strain and rotation rate patterns of mainland Greece from continuous GPS data and comparison between seismic and geodetic moment release. J. Geophys. Res. Solid Earth 120, 3909–3931.

Hardebeck, J.L. and Michael, A.J., 2006. Damped regional-scale stress inversions: Methodology and examples for southern California and the Coalinga aftershock sequence. J. Geophys. Res. Solid Earth, 111, B11310.

Kapetanidis, V., Papadimitriou, P., 2011. Estimation of arrival-times in intense seismic sequences using a Master-Events methodology based on waveform similarity. Geophys. J. Int. 187, 889–917.

Kapetanidis, V., Deschamps, A., Papadimitriou, P., Matrullo, E., Karakonstantis, A., Bozionelos, G., Kaviris, G., Serpetsidaki, A., Lyon-Caen, H., Voulgaris, N., Bernard, P., Sokos, E., Makropoulos, K., 2015. The 2013 earthquake swarm in Helike, Greece: seismic activity at the root of old normal faults. Geophys. J. Int. 202, 2044–2073.

Kassaras, I., Kapetanidis, V., Karakonstantis, A., Kaviris, G., Papadimitriou, P., Voulgaris, N., Makropoulos, K., Popandopoulos, G., Moshou, A., 2014a. The April-June 2007 Trichonis Lake earthquake swarm (W. Greece): New implications toward the causative fault zone. J. Geodyn. 73, 60–80.

Kassaras, I., Kapetanidis, V., Karakonstantis, A., Kouskouna, V., Ganas, A., Chouliaras, G., Drakatos, G., Moshou, A., Mitropoulou, V., Argyrakis, P., Lekkas, E., Makropoulos, K., 2014b. Constraints on the dynamics and spatio-temporal evolution of the 2011 Oichalia seismic swarm (SW Peloponnesus, Greece). Tectonophysics 614, 100–127.

Kassaras, I., Kapetanidis, V. and Karakonstantis, A., 2016. On the spatial distribution of seismicity and the 3D tectonic stress field in western Greece. Phys. Chem. Earth, Parts A/B/C, 95, 50–72.

King, G., Sturdy, D., Whitney, J., 1993. The landscape geometry and active tectonics of northwest Greece. Geol. Soc. Am. Bull. 105, 137–161.

Kissling, E. et al., 1994. Initial reference models in local earthquake tomography. J. Geophys. Res. 99: 19635-19646.

Papadimitriou, P., G. Kaviris and K. Makropoulos, 2006. The Mw=6.3 2003 Lefkada Earthquake (Greece) and induced transfer changes. Tectonophysics, 423, 73-82.

Papadimitriou, P., Chousianitis, K., Agalos, A., Moshou, A., Lagios, E. and Makropoulos, K., 2012. The spatially extended 2006 April Zakynthos (Ionian Islands, Greece) seismic sequence and evidence for stress transfer. Geophysical Journal International, 190 (2), 1025-1040.

Royden, L.H., Papanikolaou, D.J., 2011. Slab segmentation and late Cenozoic disruption of the Hellenic arc. Geochemistry, Geophys. Geosystems 12(3).

Theodulidis N. et al., 2004. HEAD1.0 : A unified accelerogram database", Seism. Research. Lett, 75, 41-50.

15th International Congress of the Geological Society of Greece
Athens, 22-24 May, 2019 | Harokopio University of Athens, Greece
Bulletin of the Geological Society of Greece, Sp. Pub. 7 Ext. Abs. GSG2019-290

Seismotectonic study in Vilia, Eastern Gulf of Corinth, Greece

A. Billia[1],I. Spingos[1], H. Kranis[1], G. Kaviris[1]

(1) Department of Geology and Geoenvironment, National and Kapodistrian University of Athens, 15784 Panepistimiopolis, Zografou, Athens, Greece, alexandrabillia@gmail.com

The Gulf of Corinth (GoC) is a unique site for seismotectonic studies in Europe.The eastern side of the GoC (Fig. 1) is subject to extensional directions similar to the western, i.e. NNE-SSW (Armijo *et al.*, 1996). The highest extensional rate is located in the western side (15 mm/yr), while in the eastern part it is constrained at 10 mm/yr. The main part of the deformation is found offshore, within the gulf (Briole *et al.*, 2003). The gulf is dominated by normal faulting trending WNW-ESE. The geologic substratum in the eastern side is comprised of Permian and Upper Carboniferous formations. Lithology is generally dominated by limestones (Triassic-Cretaceous). Overlying, Pleistocene and Pliocene deposits are found. Recent scree and alluvial deposits cover locally the aforementioned formations (IGME, 1971, 1984).

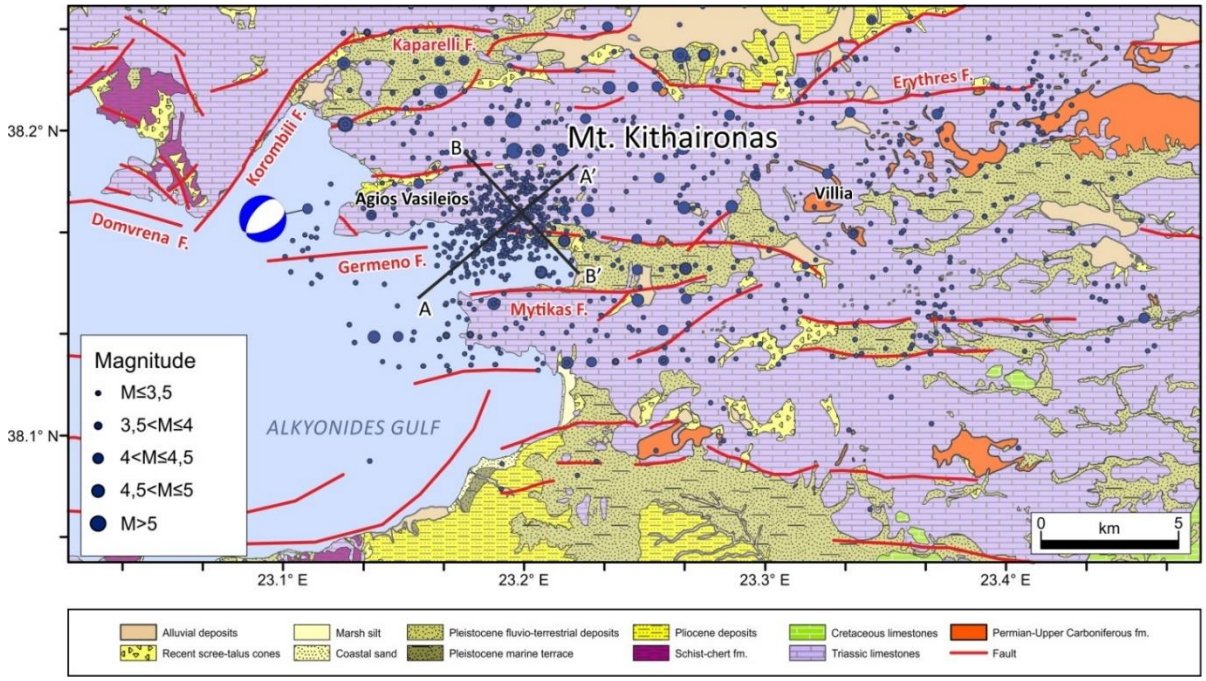

Figure 1.Seismotectonic map of the broader study area. Blue dots indicate epicenters between 1900 and 2017. Focal mechanism of the 20 September 2013 (M_L=4.4) is also shown. Lines AA' and BB' denote the foci cross-sections in Fig. 2.

The extension in the Eastern Gulf of Corinth (EGoC) is related to a highly segmented fault system. The main strike of these faults is E-W, although secondary directions (NW-SE and NE-SW) are also observed. The major structures in the study area are the Kaparelli, Erithres, Germeno and Mytikas faults (Ganas *et al.*, 2013). The Kaparelli fault is an approximately E-W striking, south dipping normal fault which consists of three segments (Kokkalas *et al.*, 2005).

Active tectonics in the EGoC have led to several major earthquakes since 1900, with moment magnitudes (M_w) ranging between 4.1 and 6.2 (Makropoulos *et al.*, 2012). The largest events are the main shocks of the Alkyonides sequence of February-March 1981, with three M_w>6.0 earthquakes causing extensive damage to buildings and infrastructure in the EGoC, as well as to Athens (Papazachos and Papazachou, 2003). Since then, seismicity has been scarce (e.g. Papadimitriou *et al.*, 1999). However, small episodes of seismic outburst have been recorded. A prime example is the sequence that occurred close to the town of Vilia. A total of 560 events were located in 2013, with local magnitudes (M_L) between 0.5 and 4.4 (Kaviris *et al.*, 2014).

The current study incorporates a comprehensive seismic catalogue from 1900 up to 2017 for the broader area of Vilia. Event information was acquired from four sources: (a) the updated and extended catalogue of Makropoulos *et al.* (2012) between 1900 and 2009, (b) the catalogue of the Seismological Laboratory of the National and Kapodistrian University of Athens between 2009 and 2016, (c) the detailed catalogue of the 2013 Vilia sequence (Kaviris *et al.*, 2014) and (d) newly located events of a local sequence near Vilia during 2017. For the latter, the arrivals of the P- and S-waves were manually determined from local and regional recordings of stations belonging to the Hellenic Unified Seismological Network (HUSN). The location of the foci was later acquired using a local velocity model (Kaviris *et al.*, 2014) and the Hypoinverse software (Klein, 2002). The 2017 catalogue contains 53 events.

The spatial features of the 2013 sequence do not present a definite correlation with the faults mapped in the area. The plane defined by the spatial distribution of hypocenters is striking N58°E and dipping SE (Fig. 2), whereas the focal mechanism of the main shock indicated a similar fault with a 46° dip, a N64°E strike and a -71° rake. Both, however,

indicate the existence of NE-SW, SE-dipping structures. This is in agreement with the depths of the foci (concentrated between 7 and 15 km). However, it is important to note that the accuracy of the hypocentral locations is compromised by the sparse network. Only one station (VILL) was located in a small distance from the seismogenic area (approximately 12 km). Thus, the causative fault(s) for the 2013 sequence could be a blind normal fault, or the NE-SW, SE-dipping Korombili fault. The latter suggestion can be valid if we accept a much steeper fault than the one indicated by the focal mechanism of the main shock; indeed, field mapping shows that this is a very steep fault (dip>65°), which could have a bi-planar or curved geometry, flattening downdip. In addition, a smaller, SSE dipping fault is also observed near Agios Vasileios village: this could also be connected to the 2013 sequence.

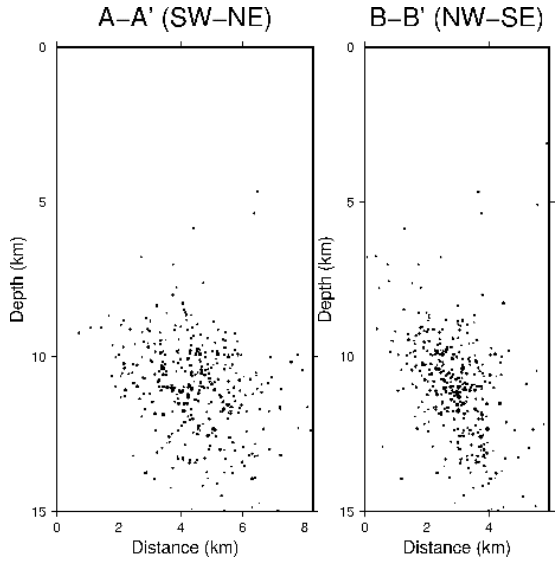

Figure 2. Cross-sections of the foci that belong to the 2013 sequence, as indicated in Fig. 1.

Placed in a broader tectonic context, the fault(s) responsible for the 2013 events is located between major E-W normal and oblique-normal faults, such as the Erythres fault to the east, the Kaparelli fault to the north, the Mytikas and Germeno faults tothe south and the Domvrena fault to the west, the latter being the northern marginal fault in the eastern part of the active GoC. The 2013 seismic activity, attributed to NE-SW faults, such as the Korombili fault and/or possible blind structures indicates a possible linkage between major E-W faults, such as the Kaparelli-Erythres and Domvrena faults. If this assumption is valid, then Mt Kithaironas can be considered as a transfer zone between major E-W faults; Korombili fault can be acting as a link between the Kaparelli and Domvrena faults, defining the western border of the transfer zone; its eastern border is much less well defined, however, with only a few NE-SW minor faults mapped.

The study of faulting in the EGoC is of great importance. As evidenced by the events of 1981, the knowledge of seismotectonics in an active area close to Athens, the largest metropolitan area in Greece, is crucial for improving the estimates of seismic hazard and for taking steps towards risk mitigation and refining the building code. A more detailed mapping of the faults in the area and the densification of the network can aid in identifying potential sources of intense tectonic activity.

References

Armijo, R., Meyer, B., King, G., Rigo, A., Papanastassiou, D., 1996. Quaternary evolution of the Corinth Rift and its implications for the Late Cenozoic evolution of the Aegean. Geophys. J. Int. 11–53.

Briole, P., Avallone, A., Billiris, H., Charade, O., 2003. A ten years analysis of deformation in the Corinthian Gulf via GPS and SAR Interferometry. 11th International Symposium Deformation Measurements.

Ganas, A., Oikonomou, A.I., Tsimi, C., 2013. NOAFAULTS : a Digital Database for Active Faults in Greece. Bull. Geol. Soc. Greece XLVII, 518–530.

IGME 1971. Erithres 1:50.000 Geological Sheet, Athens, Greece.

IGME 1984. Kaparellion 1:50.000 Geological Sheet, Athens, Greece.

Kaviris, G., Kapetanidis, V., Kravvariti, P., Karakonstantis, A., Bozionelos, G., Papadimitriou, P., Voulgaris, N., Makropoulos, K., 2014. Anisotropy Study in Villia (E. Corinth Gulf, Greece). 2nd European Conference on Earthquake Engineering and Seismology, Istanbul.

Klein, F.W., 2002. User's Guide to HYPOINVERSE-2000, a Fortran Program to Solve for Earthquake Locations and Magnitudes. U.S. Geol. Surv. Open File Rep. 02-171 123 pp.

Kokkalas, S., Pavlides, S.,Koukouvelas, I., Ganas, A., Stamatopoulos, L., 2007.Paleoseismicity of the Kaparelli fault (eastern Corinth Gulf): evidence for earthquake recurrence and fault behavior. Boll.Soc.Geol.It. (Ital.J.Geosci.), Vol. 126, No. 2 (2007), pp. 387-395, 6 figs., 1 tab.

Makropoulos, K., Kaviris, G., Kouskouna, V., 2012. An updated and extended earthquake catalogue for Greece and adjacent areas since 1900. Nat. Hazards Earth Syst. Sci. 12, 1425–1430. doi: 10.5194/nhess-12-1425-2012

Papadimitriou, P.,Kaviris, G., Makropoulos, K., 1999. Evidence of shear wave splitting in the eastern Corinthian Gulf (Greece). Physics of the Earth and Planetary Interiors, 114, 3-13.

Papazachos, V., Papazachou, K., 2003. The earthquakes of Greece, Ziti Publications Co.(in Greek).

15th International Congress of the Geological Society of Greece
Athens, 22-24 May, 2019 | Harokopio University of Athens, Greece
Bulletin of the Geological Society of Greece, Sp. Pub. 7 Ext. Abs. GSG2019-319

Ground Deformation from GNSS Data Following Strong Ionian Sea Earthquakes in 2014 and 2015: Co-seismic Offsets and Station Baseline Changes

Eleni I. Partheniou[1,2], Athanassios Ganas[1], and Vassilis Sakkas[2]

(1) Institute of Geodynamics, National Observatory of Athens, hparth83@gmail.com; aganas@noa.gr
(2) Department of Geophysics and Geothermics, National and Kapodistrian University of Athens, vsakkas@geol.uoa.gr

Extended abstract

In this study we used geodetic data from two Greek GNSS networks, operating during the 2014-2015 period when three (3) strong and shallow seismic events occurred in the central Ionian islands, Greece. The earthquakes occurred on 26 January 2014 13:55 UTC (moment magnitude M_w=6.1; Fig. 1), 3 February 2014 03:08 UTC (M_w=5.9) and 17 November 2015 07:10 UTC (M_w=6.4). The 2014 events occurred onshore Cephalonia (Fig. 1; e.g. Karastathis et al. 2015), while the 2015 event occurred onshore south Lefkada (Ganas et al. 2016). To study the ground deformation due to the three events we used daily observations from the GPS satellite constellation sampled at 30-s intervals. The daily data are provided by the network operators in the form of rinex version 2.11 files. The stations are equipped with dual-frequency geodetic receivers and belong to NOANET (Ganas et al., 2008; 2013), HxGN SmartNet Greece, EUREF and NKUA networks (Sakkas and Lagios, 2015, 2017). The GNSS data are processed using the Bernese 5.1 software following the double-difference approach. Details of the processing can be found in Sakkas and Lagios (2017). For each station we obtained daily estimates of IGb08 positions (X, Y, Z). We then converted the positions in EGSA 1987 (Greek national projection) coordinates using the Leica Geo-office software. We normalized the position data dividing each component by the mean position of all the years (for example, for station VLSM the data coverage is 2009-2018; see station location in Fig. 1). Then, we took the mean value (and its standard deviation) of the normalized position one week before and one week after the event (in all components), and we calculated the offset and the quadratic error of the offset. We found that cm-size co-seismic horizontal offsets were recorded by the continuous GPS stations operating at both Cephalonia and Lefkada islands, in agreement with previous studies. Mm-size offsets were detected in stations located in western Peloponnese and Akarnania regions. In Table 1 we present the offsets due to the 26 January 2014 M_w=6.1 event (see Fig. 1 for vector plots).

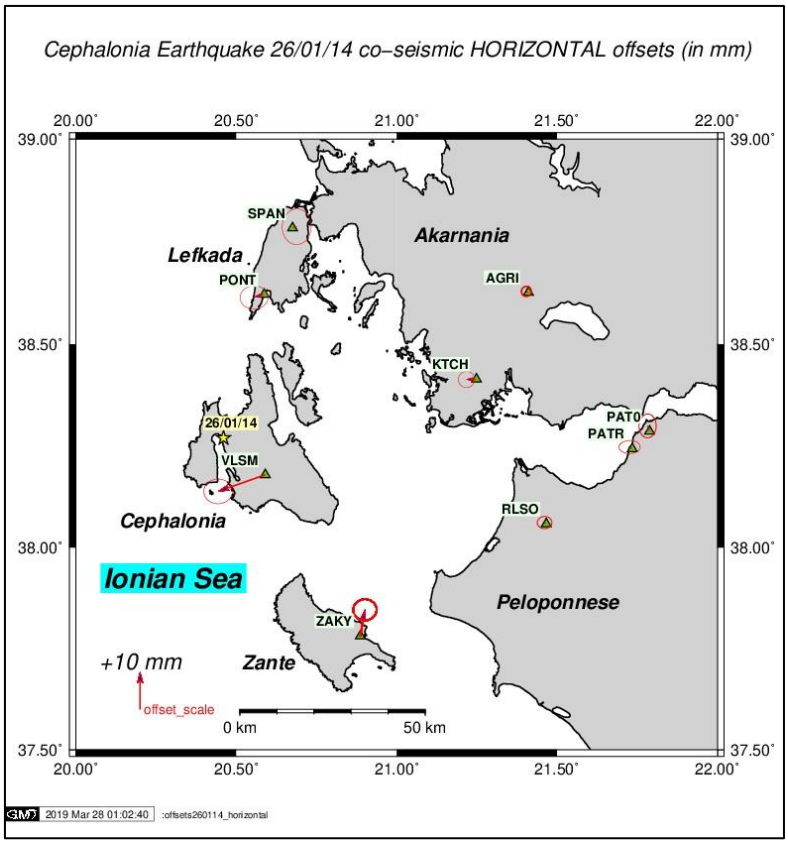

Figure 1. Map of central Ionian Islands and western Greece showing the location of GNSS stations (green triangles) that recorded the January 26, 2014 earthquake (yellow star). The co-seismic offsets are shown as vectors with error ellipses. The map was done with GMT software v5.0 (Wessel et al. 2013).

We also studied the change of station baselines with time, i.e. we calculated a) the baseline (horizontal distance) between all stations within our network and b) how this distance varies over the study period (2006-2018). It is expected that station baselines will change after the occurrence of a strong earthquake as station positions change. In addition, after the earthquake the baseline may show a delay before obtaining a stable trend because of post-seismic motions that may affect the GNSS station. It is of interest to study if baseline changes can be detected before strong earthquakes, so that the GNSS data may be used for earthquake forecasting. The Ionian Sea is a region with high seismic activity due to the occurrence of the Cephalonia strike-slip fault, a transform fault between the Eurasia and African tectonic plates so the GNSS data are crucial for monitoring ground motions before, during and after earthquakes.

Table 1. List of GNSS stations that recorded the 26 January 2014 earthquake (M=6.1) and their co-seismic offsets. Lon, LAT indicates station location in decimal degrees longitude, latitude, respectively. A_E, A_N & A_{UP} indicate East-West, North-South and Up-Down offsets, respectively. Stations are depicted in Fig. 1.

Station	Network	LON	LAT	26/01/2014 Mw=6.1		
				A_E mm	A_N mm	A_{UP} mm
AGRI	HxGN	21.410664	38.626618	-0.56 ± 0.97	0.26 ± 0.99	2.92 ± 4.52
KTCH	PPGNET	21.248555	38.414210	-2.66 ± 1.60	-0.09 ± 1.60	0.82 ± 3.57
PAT0	EUREF	21.788366	38.286275	-0.52 ± 1.70	1.44 ± 2.35	0.98 ± 4.55
PATR	HxGN	21.734591	38.243478	-0.73 ± 2.09	0.45 ± 1.29	2.84 ± 5.67
PONT	NOANET	21.781232	38.370106	-2.69 ± 2.76	-0.81 ± 2.28	4.75 ± 6.84
RLSO	NOANET	20.586785	38.621631	-0.46 ± 1.44	0.37 ± 1.21	6.1 ± 6.24
SPAN	NOANET	21.466366	38.058459	1.11 ± 2.86	0.33 ± 3.52	3.44 ± 8.33
VLSM	NOANET	20.590243	38.179464	-12.58 ± 2.82	-4.44 ± 2.44	-3.77 ± 2.68
ZAKY	HxGN	20.886645	37.781794	3.59 ± 2.31	1.2 ± 2.10	6.98 ± 7.16

Acknowledgements

We thank Nikolaos Voulgaris, Chrysa Doxa and Varvara Tsironi for comments. We thank the Greek networks for GNSS data.

We acknowledge support of this research by the project “HELPOS - Hellenic Plate Observing System” (MIS 5002697) which is implemented under the Action “Reinforcement of the Research and Innovation Infrastructure”, funded by the Operational Programme "Competitiveness, Entrepreneurship and Innovation" (NSRF 2014-2020) and co-financed by Greece and the European Union (European Regional Development Fund).

References

Ganas, A. et al. 2016. Coseismic deformation, field observations and seismic fault of the 17 November 2015 M = 6.5, Lefkada Island, Greece earthquake, Tectonophysics, 687, 210-222, http://dx.doi.org/10.1016/j.tecto.2016.08.012.

Ganas, A., G. Drakatos, S. Rontogianni, C. Tsimi, P. Petrou, M. Papanikolaou, P. Argyrakis, K. Boukouras, N. Melis and G. Stavrakakis, 2008. NOANET: the new permanent GPS network for Geodynamics in Greece. Geophysical Research Abstracts, Vol. 10, EGU2008-A-04380

Ganas, A., Marinou A, Anastasiou D., Paradissis D., Papazissi K., Tzavaras P., Drakatos G. 2013. GPS-derived estimates of crustal deformation in the central and north Ionian Sea, Greece: 3-yr results from NOANET continuous network data. Journal of Geodynamics, 67, 62– 71. http://dx.doi.org/10.1016/j.jog.2012.05.010

Karastathis, V. K., Mouzakiotis, E., Ganas, A., and Papadopoulos, G. A. 2015. High-precision relocation of seismic sequences above a dipping Moho: the case of the January–February 2014 seismic sequence on Cephalonia island (Greece), Solid Earth, 6, 173-184, doi:10.5194/se-6-173-2015

Sakkas V, Lagios E. 2017. Ground Deformation Effects from the ~M6 Earthquakes (2014-2015) on Cephalonia-Ithaca Islands (W. Greece) deduced by GPS Observations, Acta Geophysica (doi.: 10.1007/s11600-017-0017-x)

Sakkas, V., and Lagios, E. 2015. Fault Modelling of the Early-2014 ~M6 Earthquakes in Cephalonia Island (W. Greece) Based on GPS Measurements, Tectonophysics, DOI 10.1016/j.tecto.2015.01.010.

Wessel, P., W. H. F. Smith, R. Scharroo, J. F. Luis, and F. Wobbe, 2013. Generic Mapping Tools: Improved version released, EOS Trans. AGU, 94, 409-410.

15th International Congress of the Geological Society of Greece
Athens, 22-24 May, 2019 | Harokopio University of Athens, Greece
Bulletin of the Geological Society of Greece, Sp. Pub. 7 Ext. Abs. GSG2019-320

SAR multi-temporal interferometry for precise ground deformation mapping of the Corinth rift, Greece. Deriving parameters of Rio-Patra oblique slow slipping fault

P. Elias[1], P. Briole[2]

(1) National Observatory of Athens, Greece, pelias@noa.gr
(2). École normale supérieure, Paris, France

The Corinth Rift (Greece) is one of the narrowest and fastest extending continental regions worldwide, and has one of the highest seismicity rates in the Euro-Mediterranean region. At its western termination, several active faults are located beneath the city of Patras and the surrounding area, a region of major socio-economic importance for Greece.

The Corinth Rift (Greece) is one of the narrowest and fastest extending continental regions worldwide. It is bounded on both sides by active normal faults, on- and off-shore (Moretti et al., 2003; Palyvos et al., 2007) with cumulated offset ~3 km and a series of tilted blocks along the south coast (Doutsos and Poulimenos, 1992; Koukouvelas et al., 1999). It has one of the highest seismicity rates in the Euro-Mediterranean region with, on average, one Mw > 6 earthquake per decade. Recent large earthquakes include Alkyonides 1981 (M = 6.7), Galaxidi 1992 (Mw = 5.8), Aigion 1995 (Mw = 6.1) and Movri 2008 (Mw = 6.4). This last event is located outside of the rift, but is connected to it and is crucial for deciphering the deformation processes at the western termination of the rift and its junction with the Gulf of Patras, where, several active faults are located beneath the city of Patras and the surrounding area, a region of major socio-economic importance for Greece. Previous geodetic studies conducted, which were based on GPS observations observations, revealed North – South extension rates across the gulf of up to about 1.5 cm/yr [Clarke et al., 1997; Briole et al., 2000; Avallone et al., 2004] during the last 20 years.

The Corinth Rift Laboratory (CRL) institution (http://crlab.eu) is based on the joint efforts of various European institutions to study fault mechanics and related hazards in the study area. It is included in Geohazards Natural Laboratories of the GEO Supersites and will be one of the Near Fault Observatories (NFO) of European Plate Observing System (EPOS).

Displacement rates for the period 2002-2010 obtained from ascending and descending ASAR/ENVISAT multi-temporal interferometry are combined with Global Positioning System measurements from permanent and campaign stations to produce a map of vertical and east-west ground velocities. More specifically initial datasets derived from Persistent Scatterers and Small baselines Subsets techniques. These datasets has been doubled by performing a second running with different initial parameters. Combination of ascending and descending tracks has been used to calculate the east-west and vertical deformation components rates. The wealth of information provided by the availability of eight measurements per original pixel and the combination of several original pixels, allows tracking efficiently the unwrapping errors. Finally improved vertical and east-west velocities were calculated by using an averaging filter and a cutoff threshold based on r.m.s. scattering.

In the city of Patras and through the gulf of Patras, the northern continuation of the 2008 Movri earthquake fault (Serpetsid;aki et al., 2014) is connected to the oblique transform zone of Rio. The Rio-Patras fault is off-shore, in front of downtown Patras and penetrates inland between Patras and Rio. Then it rotates progressively and connects with the Psathopyrgos normal fault at the entrance to the Corinth rift. To model the GPS and InSAR velocities, we assume a fault system locked in part of the crust and slowly slipping elsewhere. The deformation shape of the Rio-Patras fault indicates a shallow locking depth and suggests slow slipping below that depth. The large gradient of strike-slip velocities between the south and the north coast at both ends of the Rio-Antirio bridge support a model of deformation accumulation in a very narrow locked layer in the crust, with the rest being unlocked, and therefore not associated with strong seismicity (at least in the last decades until present).

References

Avallone, A., Briole, P., Agatza-Balodimou, A. M., Billiris, H., Charade, O., Mitsakaki, C. A., et al. (2004). Analysis of eleven years of deformation measured by GPS in the Corinth Rift Laboratory area. Comptes Rendus Geoscience. https://doi.org/10.1016/j.crte.2003.12.007.

Briole, P., Rigo, A., Lyon-Caen, H., Ruegg, J.C., Papazissi, K., Mitsataki, C., et al. (2000). Active deformation of the Corinth rift, Greece: Results from repeated Global Positioning System surveys between 1990 and 1995. Journal of Geophysical Research, 105(B11), 25,605-25,625. https://doi.org/10.1029/2000JB900148.

Clarke, P., Davies, R., England, P., Parsons, B., Billiris, H., Paradissis, D., et al. (1997). Geodetic estimate of seismic hazard in the Gulf of Korinthos. Geophysical Research Letters, 24(11). https://doi.org/10.1029/97GL01042.

Doutsos T., & Poulimenos G. (1992). Geometry and kinematics of active faults and their seismotectonic significance in the western Corinth - Patras Rift (Greece). Journal of Structural Geology, 14(6), 689-699. https://doi.org/10.1016/0191-8141(92)90126-H

Koukouvelas, I., Asimakopoulos, M., & Doutsos T. (1999). Fractal characteristics of active normal faults: an example of the eastern Gulf of Corinth, Greece. Tectonophysics, 308(1-2), 263-274. https://doi.org/10.1016/S0040-1951(99)00087-6.

Moretti, I., Sakellariou, D., Lykousis, V., & Micarelli L. (2003). The Gulf of Corinth: an active half graben? Journal of Geodynamics, 36(1-2), 323-340. https://doi.org/10.1016/S0264-3707(03)00053-X.

Palyvos, N., Pantosti, D., Stamatopoulos, L., & De Martini, P. M. (2007). Geomorphological reconnaissance of the Psathopyrgos and Rion-Patras fault zones (Achaia, NW Peloponnesus). Bulletin of the Geological Society of Greece, 40, 1586-1598.

Serpetsidaki, A., Elias, P., Ilieva, M., Bernard, P., Briole, P., Deschamps, A., et al. (2014). New Constraints from Seismology and Geodesy on the Mw=6.4 2008 Movri (Greece) Earthquake. Evidence for a Growing Strike Slip Fault System. Geophysical Journal International, 198(3), 1373-1386. https://doi.org/10.1093/gji/ggu212.

15th International Congress of the Geological Society of Greece
Athens, 22-24 May, 2019 | Harokopio University of Athens, Greece
Bulletin of the Geological Society of Greece, Sp. Pub. 7 Ext. Abs. GSG2019-342

Environmental effects and ESI-07 seismic intensities of the October 26, 2018, Mw 6.8 offshore southwestern Zakynthos earthquake and comparison with all known destructive historical and recent earthquakes in the southern Ionian Islands (Greece)

S. Mavroulis[1], E. Stanota[1], E. Lekkas[1]

(1) Faculty of Dynamic Tectonic Applied Geology, Department of Geology and Geoenvironment, School of Sciences, National and Kapodistrian University of Athens, Panepistimiopolis, 15784, Athens, Greece, smavroulis@geol.uoa.gr

Zakynthos Island is located in the external part of the Hellenic Arc and in the east of the Hellenic Trench, which represents the convergence boundary between the African and Eurasian plates, and is one of the most tectonically and seismically active parts of the Mediterranean region (Papazachos and Papazachou, 1989, 1997, 2003; Lekkas et al., 1996-1997).

Based on the seismicity catalogues of the permanent regional seismological network operated by the Aristotle University of Thessaloniki (AUTH, 2019) covering the period from 550 BC to 2018, it is concluded that many earthquakes with magnitudes larger than 5.0 have been concentrated in four zones around Zakynthos Island. These zones include significant seismic sources with high productivity and frequent occurrence of destructive earthquakes during historical and recent times (Lekkas et al., 1996-1997; Papazachos and Papazachou, 1989, 1997, 2003) and they are the following:

(a) The western offshore Cephalonia and Lefkada area, where the prevailing active tectonic structure is the Cephalonia Transform Fault Zone (Scordilis et al., 1985).

(b) Within the Zakynthos channel and the respective structural basin between Zakynthos Island and Peloponnese, which are affected by the westward offshore extensions of onshore faults to onshore western Peloponnese. More specifically for the area offshore eastern Zakynthos, major normal faults bound continental fault blocks and are characterized as active tectonic structures as revealed from the integration results of onshore neotectonic mapping (Lekkas et al., 2000; Papanikolaou et al., 2007) and local seismological observations (Papoulia et al., 2014).

(c) The area south and southeast of Zakynthos Island, where Vp-velocity models and their tectonic interpretation showed that the southwestward extension of the NE-SW striking dextral strike-slip Western Achaia Fault Zone (WAFZ) from Northwestern Peloponnese to offshore southern Zakynthos prevails (Makris and Papoulia, 2014).

(d) The area southwest of Zakynthos Island. This zone constitutes a downthrown block of the external Hellenides at the northern end of the Hellenic Trench and comprises tectonic structures like flat thrusts, strike-slip faults and normal faults, whose reactivations have resulted moderate seismicity (SEAHELLARC Working Group, 2014). More specifically, thrusting prevails over strike – slip or normal faulting (Kokinou et al., 2005, 2006), with the most important feature of this area being a 46-km-long NW-SE trending thrust system (SEAHELLARC Working Group, 2014). This system is responsible for the generation of the 1997 Mw 6.6 earthquake (SEAHELLARC Working Group, 2014) as well as for the October 26, 2018 Mw 6.8 offshore Zakynthos earthquake. Thrust events are also observed along the Hellenic subduction zone located west and southwest of Zakynthos Island (Kiratzi and Louvari, 2003).

The last major episode of the geodynamic evolution of the Central Ionian Islands is the October 26, 2018, Mw 6.8 Zakynthos earthquake. It was generated offshore southwestern Zakynthos and it was predominantly felt on Zakynthos and throughout the Ionian Islands, Peloponnese and the mainland Greece fortunately with no casualties or injuries reported.

As regards the environmental effects induced by the 2018 Zakynthos earthquake, secondary earthquake environmental effects were observed including slope failures, a small tsunami and asphalt-pitch seepages. Landslides and rockfalls were mainly generated in various parts of the island and more specifically along the steep coastal slopes and scarps in its northwestern part (e.g. Navagio beach, $VII_{ESI\ 2007}$), in its southwestern part (e.g. along Mizithres beach, $VII_{ESI\ 2007}$), in its central-eastern part (e.g. Panagoula and Kryoneri areas, VI-$VII_{ESI\ 2007}$ and $VI_{ESI\ 2007}$ respectively). A small tsunami wave was generated offshore southwestern Zakynthos and was detected based on sea level changes (offset: 0.549 m) ($VI_{ESI\ 2007}$) that occurred after the earthquake and were recorded by the Katakolo (offshore central western Peloponnese) station of the Sea Level Station Monitoring Facility (https://goo.gl/wURcNs). Based on several witnesses, an increase in sea level of about half a meter were observed along the coast between Santa Maria di Leuca Cape and Otranto located in the eastern coast of the Salento peninsula (Italy).

Data on historical and recent earthquakes generated in the Central Ionian Sea and the western Peloponnese and on their EEEs induced on Zakynthos Island were obtained from the following sources: (a) all major academic databases, search engines and sources for scientific research including GeoRef, Sciencedirect, Scopus, Springer, JSTOR etc, (b) official earthquake catalogues from universities, seismological institutes and observatories, (c) books and scientific articles containing catalogues or information of earthquakes and their EEEs in Zakynthos (e.g. Papazachos and Papazachou, 2003) or in the broader Zakynthos area (e.g. Lekkas et al., 1996-1997), (d) official field survey and reconnaissance reports (e.g. Lekkas and Mavroulis, 2018) and (e) official reports of scientific research projects (e.g. Lekkas, 1993).

The complete seismic history of destructive historical and recent earthquakes comprises 20 significant earthquakes generated not only onshore Zakynthos Island but also offshore with great impact on population, natural environment, buildings and infrastructures. The impact on the natural environment comprises mainly secondary effects including

hydrological anomalies, anomalous waves/tsunamis, ground cracks, slope movements, tree shaking and liquefaction phenomena. Primary effects have also been reported after strong earthquakes in Zakynthos Island including reactivation of faults and coseismic surface ruptures.

In Zakynthos Island: (a) primary effects comprised fault reactivation during the 1513 earthquake and formation of coseismic surface ruptures during the January 1893 earthquake, (b) the observed hydrological anomalies included rising of the ground water level, increased discharge in wells, increased river flow, overflow of streams and subsequent flooding of the adjacent area and sulphureous gas emissions along with flames and burning of the adjacent vegetation, (c) the anomalous waves/tsunamis included sea withdrawal, roughness and violent agitation of the sea surface and small scale tsunamis resulting in cape sweeping by sea waves, coastal submergence and coastal inundation, (d) the detected ground cracks were observed in areas with loose recent sediments and instability conditions along river banks, close to geotechnically unstable areas and along with liquefaction phenomena and sulphureous gas emissions, (e) the triggered slope movements are classified as rockfalls, rockslides and landslides along high and steep inland and coastal slopes and scarps, (f) severe tree shaking and damage to vegetation due to the earthquake shaking was limited, (g) liquefaction phenomena were also limited to ejection of sand/water mixture along ground cracks and coastal subsidence, (h) phenomena related to the presence of asphalt-pitch in the coastal mire/swamp zone of Keri were also triggered by the generated earthquakes. These phenomena included boiling of asphalt and asphalt-pitch seepages in various sites of the earthquake-affected area and more specifically in the eastern onshore and offshore part of the Keri bay fault block.

The following summarizing and concluding remarks are made. Anomalous waves/tsunamis are the most frequently reported EEE in the 20 historical and recent earthquakes of this study (11 out of 20 events), followed by the slope movements (10 out of 20), ground cracks (7 out of 20), hydrological anomalies (6 out of 20), liquefaction phenomena (4 out of 20) and hydrocarbon-related phenomena (4 out of 20). Primary effects are limited to fault reactivation (1 out of 20 events) and coseismic surface ruptures (1 out of 20).

The maximum assigned local environmental seismic intensities are VIII-IX$_{ESI\ 2007}$ for the Northern Zakynthos fault block, VII$_{ESI-07}$ for the western part of the Central Zakynthos fault block, VIII-IX$_{ESI\ 2007}$ for the eastern part of the Central Zakynthos fault block, IX$_{ESI\ 2007}$ for the Keri Bay fault block, VII$_{ESI\ 2007}$ for the Southern Zakynthos fault block and VIII$_{ESI\ 2007}$ for the Skopos Mt fault block.

The most susceptible areas to the generation of EEE are the Skopos Mt fault block, which has been affected by EEE during 11 earthquakes, followed by the eastern part of the Central Zakynthos fault block with EEE during 9 earthquakes, the Keri Bay fault block affected by EEE during 5 earthquakes, the western part of the Central Zakynthos fault block affected 4 times, the Southern Zakynthos fault block affected 3 times and the Northern Zakynthos fault block only once.

References

Aristotle University of Thessaloniki (AUTH) (2019). Permanent regional seismological network operated by the Aristotle University of Thessaloniki. https://doi.org/10.7914/sn/ht

Kiratzi, A., Louvari, E., 2003. Focal mechanisms of shallow earthquakes in the Aegean Sea and the surrounding lands determined by waveform modeling: a new database. Journal of Geodynamics, 36, 251-274, https://doi.org/10.1016/S0264-3707(03)00050-4

Kokinou, E., Papadimitriou, E., Karakostas, V., Kamberis, E., Vallianatos, F., 2006. The Kefalonia Transform Zone (offshore Western Greece) with special emphasis to its prolongation towards the Ionian Abyssal Plain. Marine Geophysical Research, 27 241-252, https://doi.org/10.1007/s11001-006-9005-2

Kokinou, E., Kamberis, E., Vafidis, A., Monopolis, D., Ananiadis, G., Zelilidis, A., 2005. Deep Seismic Reflection Data from Offshore Western Greece: A New Crustal Model for the Ionian Sea. Journal of Petroleum Geology, 28 (2), 185-202, https://doi.org/10.1111/j.1747-5457.2005.tb00079.x

Lekkas, E., Fountoulis, I., Papanikolaou, D., 2000. Intensity Distribution and Neotectonic Macrostructure Pyrgos earthquake data (26 March 1993, Greece). Natural Hazards, 21, 19-33, https://doi.org/10.1023/A:1008153620842

Lekkas, E., Kolyva, M., Antonopoulos, G., Kopanas, I., 1996-1997. The earthquakes of Zakynthos. An interpretation of the descriptions of earthquakes and correlation with the existing geological structure. Annales Géologiques des Pays Hélléniques, 1 (37), 1033-1073.

Makris, J., Papoulia, J., 2014. The backstop between the Mediterranean Ridge and western Peloponnese, Greece: its crust and tectonization. An active seismic experiment with ocean bottom seismographs. Bollettino di Geofisica Teorica ed Applicata, 55 (2) 249-279, DOI 10.4430/bgta0125

Papanikolaou, D., Fountoulis, I., Metaxas, C., 2007. Active faults, deformation rates and Quaternary paleogeography at Kyparissiakos Gulf (SW Greece) deduced from onshore and offshore data. Quaternary International, 171-172, 14-30, https://doi.org/10.1016/j.quaint.2007.04.005

Papazachos, B., Papazachou, C., 1989, 2003. The Earthquakes of Greece, Ziti Publications, Thessaloniki, Greece (in Greek).

Papazachos, B., Papazachou, C., 1997. The Earthquakes of Greece, Ziti Publications, Thessaloniki, Greece

Papoulia, J., Makris, J., Tsambas, A. (2014). Microseismicity and crustal deformation of the Kyparissiakos Gulf, south-western Hellenic Arc, using an “amphibious” seismic array and a 3D velocity model obtained from active seismic observations. Bollettino di Geofisica Teorica ed Applicata, 55 (2), 281-302, DOI: 10.4430/bgta0086

Scordilis, E.M., Karakaisis, G.F., Karacostas, B.G., Panagiotopoulos, D.G., Comninakis, P.E., Papazachos, B.C., 1985. Evidence for transform faulting in the Ionian Sea: the Cephalonia island earthquake sequence of 1983. Pure and Applied Geophysics, 123, 388-397, https://doi.org/10.1007/BF00880738

SEAHELLARC Working Group, 2014. A new seismogenic model for the Kyparissiakos Gulf and western Peloponnese (SW Hellenic Arc). Bollettino di Geofisica Teorica ed Applicata, 55 (2), 405-432, DOI 10.4430/bgta0127

GENERAL SESSION

T3.S3/T11.S3 HELPOS: Hellenic Plate Observation System

Conveners: **Panagiotis Papadimitriou (NKUA)**
Vassileios Sakkas (NKUA)
Christos Evangelidis (NOA)

15th International Congress of the Geological Society of Greece
Athens, 22-24 May, 2019 | Harokopio University of Athens, Greece
Bulletin of the Geological Society of Greece, Sp. Pub. 7 Ext. Abs. GSG2019-033

The Significance of Local Networks in Shear-wave Splitting: The Case of the Gulf of Corinth

G. Kaviris[1], I. Spingos[1], V. Kapetanidis[1], C. Millas[1], P. Papadimitriou[1], N. Voulgaris[1], K. Makropoulos[1]

(1) Section of Geophysics–Geothermics, Department of Geology and Geoenvironment, National and Kapodistrian University of Athens, 15784 Panepistimiopolis, Zografou, Athens, Greece, gkaviris@geol.uoa.gr

Abstract

The Gulf of Corinth (GoC) is an active tectonic rift located in central Greece. Its unique seismotectonic properties have rendered it a prime candidate for tectonic (e.g. Bell *et al*., 2008), seismic (e.g. Stefatos *et al*., 2002) and seismological (e.g. Rigo *et al*., 1996) studies. Its long history of both moderate-to-strong events (Makropoulos *et al*., 2012) and seismic swarms (Kapetanidis *et al*., 2015; Mesimeri *et al*., 2016) has been the main instigator for installing and operating dense local networks. The intense observation period of the GoC started in 1995, with the installation of the permanent Cornet seismological network (Papadimitriou et al., 2010) by the Seismological Laboratory of the National and Kapodistrian University of Athens (SL-NKUA). This network was located at the eastern tip of the rift, monitoring an area that featured the destructive Alkyonides sequence of 1981 (Jackson *et al*., 1982). The four digital stations that comprised Cornet recorded over 6,300 events until 2008. Near the western part of the GoC, the Corinth Rift Laboratory Network (CRLN) was installed in 2000 (Lyon-Caen *et al*., 2004) to monitor the area surrounding the focus of the 1995 Aigion earthquake (Bernard *et al*., 1997). The CRLN has since facilitated numerous studies of seismicity in the area, providing local recordings of thousands of events every year. Today, the network is comprised of six borehole and eight surficial stations. The above networks have been complemented by broadband stations operated by the SL-NKUA, the Geodynamic Institute of the National Observatory of Athens (GI-NOA) and the Seismological Laboratory of the University of Patras (SL-UP). In 2008, the Hellenic Unified Seismological Network (HUSN) launched, providing prompt and uninterrupted access to the continuous data recorded by stations of the three institutes.

The extensive record of monitoring in the GoC has permitted the detailed study of seismic properties. Shear-wave Splitting (SwS) is the phenomenon of velocity dependence from the propagation direction of shear-waves. The latter undergo splitting and are distinguished into two components; the S_{fast} travelling with a higher velocity and the S_{slow}. It is a prominent characteristic of media with strong anisotropic features, such as finely-layered rocks (Valcke *et al*., 2006). However, it has long been debated that the cause of SwS in the upper crust can be attributed to the existence of vertical microcracks, saturated with fluids. These microcracks are sensitive to both pore-fluid and local stress variations, as described by the Anisotropic Poro-Elasticity (APE) model (Crampin and Zatsepin, 1997; Zatsepin and Crampin, 1997). Thus, the polarization direction of the S_{fast} (φ) can be used as an indicator of the regional maximum horizontal stress component (σ_{Hmax}) and the time-delay between the arrivals of the split waves (t_d) can be viewed as a representation of the pore stress state.

SwS has been studied in the GoC since the 1990s (Bouin *et al*., 1996). In the current study, we combine results obtained from recordings of Cornet, CLRN and HUSN, to delineate the anisotropic features of the whole GoC. The database constructed in the presented work is composed of 281 events measurements between 1996-1997 from the eastern GoC (Kaviris, 2003; Papadimitriou *et al*., 1999), 201 measurements from the Villia sequence of 2013 (Kaviris *et al*., 2014), 663 pairs from events of 2013 (Kaviris *et al*., 2017) and 1,642 measurements from events of 2014 (Kaviris *et al*., 2018) in the western GoC. The dataset was further improved by including new measurements from recent events.

The mean φ (in most stations) seems to agree with the general WNW-ESE direction of σ_{Hmax}, as determined by seismotectonic data in the area (Armijo *et al*., 1996; Rigo *et al*., 1996; Bernard *et al*., 1997; Elias and Briole, 2018). However, there are significant deviations from this direction. A group of stations in the NW edge of the GoC exhibits directions perpendicular to the above, i.e. NE-SW. Time-delays do not exhibit a specific trend, which is an expected feature, given that they are affected by factors with a periodicity far smaller than the length of the database. Clarifying the characteristics of seismic anisotropy in the GoC is pivotal for monitoring stress variations through SwS (Crampin *et al*., 1999) and constraining focal mechanisms with shear-wave polarizations, after the effect of anisotropy is corrected. The presented detailed report of SwS properties in the whole of the GoC would be impossible without the operation of dense local networks. Splitting studies involve a rigid and strict event selection procedure and an even stricter analysis regime, leading to a significant percentage of rejected candidates. Without the provision of thousands of events, the number of results would be poor, leading to an inconclusive interpretation of the phenomenon. The need of constantly improving and densifying the networks is paramount for such studies. Initiatives, such as the HELlenic Plate Observing System (HELPOS), have enhanced the ability of conducting SwS surveys by expanding data availability and contributing to the operation of the participating networks.

Acknowledgements

The authors would like to thank the personnel of all cooperating institutes of both HUSN and CRLN (doi: 0.15778/RESIF.CL) for the operation of the respective networks. We acknowledge support of this study by the project "HELPOS – Hellenic Plate Observing System" (MIS 5002697) which is implemented under the Action "Reinforcement of the Research and Innovation Infrastructure", funded by the Operational Programme "Competitiveness, Entrepreneurship and Innovation" (NSRF 2014-2020) and co-financed by Greece and the European Union (European Regional Development Fund).

References

Armijo, R., Meyer, B., King, G., Rigo, A., Papanastassiou, D., 1996. Quaternary evolution of the Corinth Rift and its implications for the Late Cenozoic evolution of the Aegean. Geophys. J. Int. 126, 11–53. doi: 10.1111/j.1365-246X.1996.tb05264.x

Bell, R.E., McNeill, L.C., Bull, J.M., Henstock, T.J., 2008. Evolution of the offshore western Gulf of Corinth. Bull. Geol. Soc. Am. 120, 156–178. doi: 10.1130/B26212.1

Bernard, P., Briole, P., Meyer, B., Gomez, J., Tiberi, C., Berge, C., Cattin, R., Hatzfeld, D., Lachet, C., Lebrun, B., Deschamps, a., Courboulex, F., Larroque, C., Rigo, a., Massonnet, D., Papadimitriou, P., Kassaras, J., Diagourtas, D., Makropoulos, K., Veis, G., Papazisi, E., Mitsakaki, C., Karakostas, V., Papadimitriou, E., 1997. The Ms=6.2, June 15, 1995 Aigion earthquake (Greece): evidence for low-angle normal faulting in the Corinth rift. J. Seismol. 1, 131–150. doi: 10.1023/A:1009795618839

Bouin, M., Téllez, J., Bernard, P., 1996. Seismic anisotropy around the Gulf of Corinth, Greece, deduced from three-component seismograms of local earthquakes and its relationship with crustal strain. J. Geophys. Res. 101, 5797. doi: 10.1029/95JB03464

Crampin, S., Volti, T., Stefánsson, R., 1999. A successfully stress-forecast earthquake. Geophys. J. Int. 1–5.

Crampin, S., Zatsepin, S., 1997. Modelling the compliance of crustal rock—II. Response to temporal changes before earthquakes. Geophys. J. Int. 129, 495–506. doi: 10.1111/j.1365-246X.1997.tb04489.x

Elias, P., Briole, P., 2018. Ground Deformations in the Corinth Rift, Greece, Investigated Through the Means of SAR Multitemporal Interferometry. Geochemistry, Geophysics, Geosystems, 19 (12), pp. 4836-4857. doi: 10.1029/2018GC007574

Jackson, J. A., Gagnepain, J., Houseman, G., King, G.C.P., Papadimitriou, P., Soufleris, C., Virieux, J., 1982. Seismicity, normal faulting, and the geomorphological development of the Gulf of Corinth (Greece): the Corinth earthquakes of February and March 1981. Earth Planet. Sci. Lett. 57, 377–397. doi: 10.1016/0012-821X(82)90158-3

Kapetanidis, V., Deschamps, A., Papadimitriou, P., Matrullo, E., Karakonstantis, A., Bozionelos, G., Kaviris, G., Serpetsidaki, A., Lyon-Caen, H., Voulgaris, N., Bernard, P., Sokos, E., Makropoulos, K., 2015. The 2013 earthquake swarm in Helike, Greece: seismic activity at the root of old normal faults. Geophys. J. Int. 202, 2044–2073. doi: 10.1093/gji/ggv249

Kaviris, G., 2003. Study of seismic source properties of the eastern Gulf of Corinth, Faculty of Geology. Doctoral Dissertation, National and Kapodistrian University of Athens, Athens, 402 p.

Kaviris, G., Kapetanidis, V., Kravvariti, P., Karakonstantis, A., Bozionelos, G., Papadimitriou, P., Voulgaris, N., Makropoulos, K., 2014. Anisotropy Study in Villia (E. Corinth Gulf, Greece). 2nd European Conference on Earthquake Engineering and Seismology, Istanbul, Turkey.

Kaviris, G., Millas, C., Spingos, I., Kapetanidis, V., Fountoulakis, I., Papadimitriou, P., Voulgaris, N., Makropoulos, K., 2018. Observations of shear-wave splitting parameters in the Western Gulf of Corinth focusing on the 2014 Mw = 5.0 earthquake. Phys. Earth Planet. Inter. 282, 60–76. doi: 10.1016/j.pepi.2018.07.005

Kaviris, G., Spingos, I., Kapetanidis, V., Papadimitriou, P., Voulgaris, N., Makropoulos, K., 2017. Upper crust seismic anisotropy study and temporal variations of shear-wave splitting parameters in the Western Gulf of Corinth (Greece) during 2013. Phys. Earth Planet. Inter. 269, 148–164. doi: doi: 10.1016/j.pepi.2017.06.006

Lyon-Caen, H., Papadimitriou, P., Deschamps, A., Bernard, P., Makropoulos, K., Pacchiani, F., Patau, G., 2004. First results of the CRLN seismic network in the western Corinth Rift: evidence for old-fault reactivation. Comptes Rendus - Geosci. 336, 343–351. doi: 10.1016/j.crte.2003.12.004

Makropoulos, K., Kaviris, G., Kouskouna, V., 2012. An updated and extended earthquake catalogue for Greece and adjacent areas since 1900. Nat. Hazards Earth Syst. Sci. 12, 1425–1430. doi: 10.5194/nhess-12-1425-2012

Mesimeri, M., Karakostas, V., Papadimitriou, E., Schaff, D., Tsaklidis, G., 2016. Spatiotemporal properties and evolution of the 2013 Aigion earthquake swarm (Corinth Gulf, Greece). J. Seismol. 20 (2), 595–614. http://dx.doi.org/10.1007/s10950-015-9546-4

Papadimitriou, P., Kaviris, G., Karakonstantis, A., Makropoulos, K., 2010. The Cornet seismological network : 10 years of operation, recorded seismicity and significant applications. Ann. Geol des Pays Hell. 45, 193–208.

Papadimitriou, P., Kaviris, G., Makropoulos, K., 1999. Evidence of shear-wave splitting in the eastern Corinthian Gulf (Greece). Phys. Earth Planet. Inter. 114, 3–13.

Rigo, A., Lyon-Caen, H., Armijo, R., Deschamps, A., Hatzfeld, D., Makropoulos, K., Papadimitriou, E., Kassaras, I., 1996. A microseismic study in the western part of the gulf of Corinth (Greece) implication for large-scale normal faulting mecanisms. Geophys. J. Int. 126, 663–688.

Stefatos, A., Papatheodorou, G., Ferentinos, G., Leeder, M., Collier, R., 2002. Seismic reflection imaging of active offshore faults in the Gulf of Corinth: their seismotectonic significance. Basin Res. 14, 487–502. doi: 10.1046/j.1365-2117.2002.00176.x

Valcke, S.L.A., Casey, M., Lloyd, G.E., Kendall, J.-M., Fisher, Q.J., 2006. Lattice preferred orientation and seismic anisotropy in sedimentary rocks. Geophys. J. Int. 166, 652–666. doi: 10.1111/j.1365-246X.2006.02987.x

Zatsepin, S., Crampin, S., 1997. Modelling the compliance of crustal rock—I. Response of shear-wave splitting to differential stress. Geophys. J. Int. 129, 477–494. doi: 10.1111/j.1365-246X.1997.tb04488.x

15th International Congress of the Geological Society of Greece
Athens, 22-24 May, 2019 | Harokopio University of Athens, Greece
Bulletin of the Geological Society of Greece, Sp. Pub. 7 Ext. Abs. GSG2019-079

Real-Time Shaking Maps of PGA and PGR in Greece

G. Sakkas[1], V. Kouskouna[1], G. Kaviris[1], N. Sakellariou[1], I. Misailidis[1]

(1) Section of Geophysics-Geothermics, Department of Geology and Geoenvironment, National and Kapodistrian University of Athens, Panepistimiopolis, 15784, Zografou, Athens, Greece, sakkasg@geol.uoa.gr

The use of real-time in natural disasters is on the rise. Earthquake real-time applications have proved to be a useful tool for acquiring a rapid estimation of ground shaking immediately after an earthquake occurrence. USGS ShakeMaps (Wald *et al.*, 2005) and PAGER (Wald *et al.*, 2010) applications are two of the most known. In Greece, the Earthquake Planning and Protection Organization – Institute of Engineering Seismology and Earthquake Engineering (EPPO-ITSAK) provides PGA maps for moderate and large earthquakes using the ShakeMaps application within 30 minutes (Wald *et al.*, 2005). In 2015, the National and Kapodistrian University of Athens (NKUA) was the first institution in Greece that developed its own application, in Matlab environment, for creating rapid PGA maps in the case of earthquake occurrence (Kouskouna *et al.*, 2014). This application was further upgraded by Sakkas (2016) and Sakkas *et al.* (2018), taking into account modern GMPEs for calculating PGA and Peak Ground Rotations – torsion and rocking (PGR) – incorporating, in addition to moment magnitude (M_w), epicentral distance (R_{epi}) and focal depth (h), also the soil type (rock, stiff or soft soil) and focal mechanism type (normal and strike-slip or thrust). The real-time application is hosted by NKUA and publicly available online at http://macroseismology.geol.uoa.gr/realtime/ (the home page is presented in Figure 1). The application presents PGA and PGR maps in a user-friendly environment with google maps as base maps, zoom-in and zoom-out options, as well as activation and deactivation of the PGA and PGR thematic layers. Maps are created in a few seconds in a run-of-the-mill personal computer. The algorithm utilizes the internet, RSS feeds, XML DOM elements, HTML and Matlab mathematical, scripting and plotting capabilities.

Within the framework of HELPOS project, NKUA, as official partner, will host both its own application and ShakeMaps (Wald *et al.*, 2005). In this context, we present the Sakkas (2016) and Sakkas *et al.* (2018) upgrade. The latter incorporates the most recent regional GMPEs for Greece. Specifically, PGA and PGR maps are produced in real-time for both shallow and intermediate depth earthquakes with M≥4.0. More specifically, for shallow earthquakes, five (5) GMPEs (Skarlatoudis *et al.*, 2003; Danciu and Tselentis, 2007; Segou and Voulgaris, 2013; Sakkas, 2016; Chousianitis *et al.*, 2017) are used for the calculation of PGA in different thematic layers. For intermediate depth earthquakes, GMPEs proposed by Skarlatoudis et al. (2013) are applied. For the calculation of PGR, the GMPEs for shallow and intermediate depth earthquakes of Sakkas (2016) and Sakkas et al. (2018) are used. Soil types are based on the 1:500.000 Geotechnical map of Greece and focal mechanism type on Papazachos *et al.* (1998), Benetatos *et al.* (2004) and Giardini *et al.* (2013), taking also in account the interface and in-slab zones proposed in Kkallas *et al.* (2018). PGA values for all GMPEs adopted in this study are presented in Figure 2.

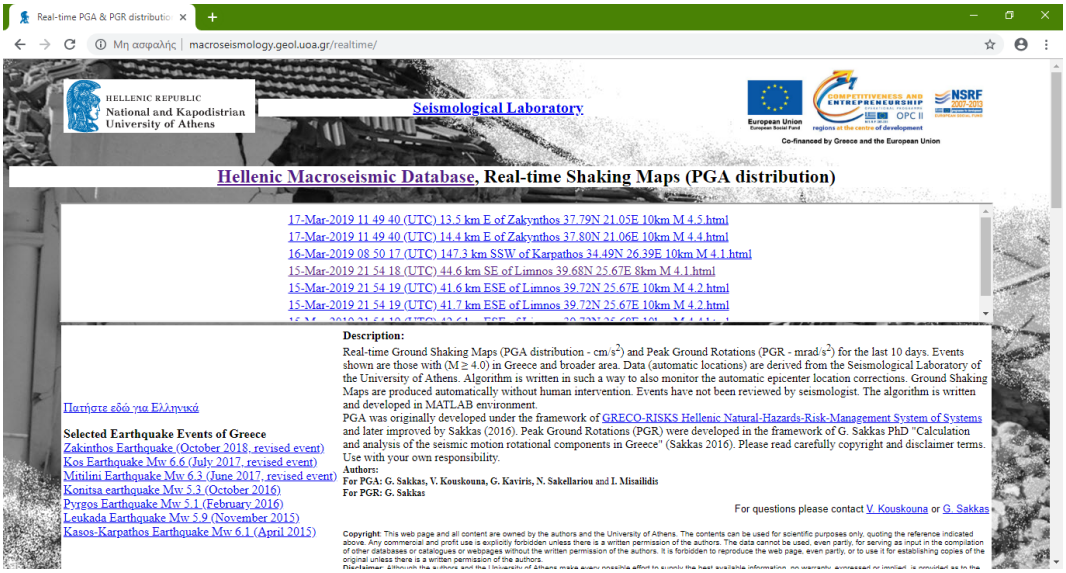

Figure 1. The home page of the real-time application hosted in NKUA.

Future development of the algorithm will incorporate real-time PGA measurements from accelerographs and seismographs, belonging to the national infrastructure of the HELPOS project. In addition, residuals of GMPEs compared to observed measurements will be embedded and open-source software and improved mapping capabilities of GIS software will be examined for better representation of PGA and PGR maps.

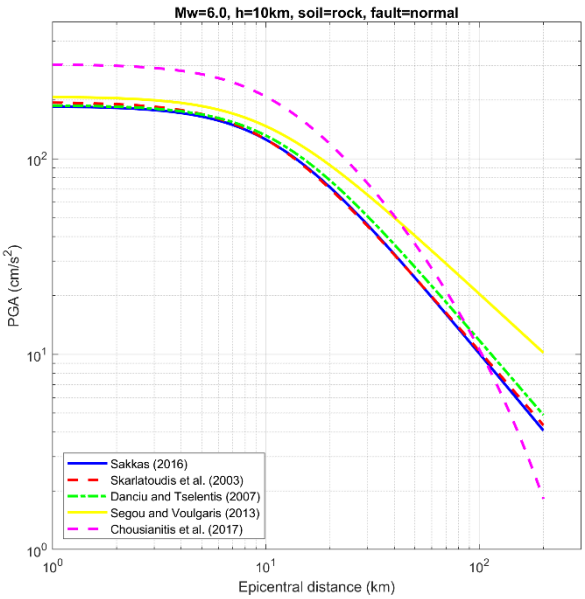

Figure 2. GMPEs for shallow earthquakes used in this study (M_w6.0, focal depth 10km, normal fault, rock soil type).

Acknowledgements

We acknowledge support of this study by the project "HELPOS – Hellenic Plate Observing System" (MIS 5002697) which is implemented under the Action "Reinforcement of the Research and Innovation Infrastructure", funded by the Operational Programme "Competitiveness, Entrepreneurship and Innovation" (NSRF 2014-2020) and co-financed by Greece and the European Union (European Regional Development Fund). Funding of the original version of the application was provided through the "Greco-Risks - Hellenic Natural-Hazards Risk-Management System of Systems" project which was jointly funded by Greece and the European Union, European Regional Development Fund (ERDF), National Action "Cooperation 2011 – Partnerships of Production and Research Institutions in Focused Research and Technology Sectors", (former) Ministry of Education, Lifelong Learning and Religious Affairs, Operational Programmes "Competitiveness and Enterpreneurship" (EPAN II) and Regions in Transition, National Strategic Reference Framework NSRF 2007–2013.

References

Benetatos, C., Kiratzi, A., Papazachos, C., Karakaisis, G., 2004. Focal mechanisms of shallow and intermediate depth earthquakes along the Hellenic Arc. Journal of Geodynamics 37, 253–296.

Chousianitis, K., Del Gaudio, V., Pierri, P., Tselentis, G.A., 2017. Regional ground-motion prediction equations for amplitude-, frequency response-, and duration-based parameters for Greece. Earthquake Engng Struct Dyn. 47, 2252–2274.

Danciu, L., Tselentis, GA., 2007. Engineering Ground-Motion Parameters Attenuation Relationships for Greece. Bulletin of the Seismological Society of America 97,1B, 162–183.

Giardini, D., et al. 2013. Seismic Hazard Harmonization in Europe (SHARE): Online Data Resource, doi:10.12686/SED-00000001-SHARE.

Kkallas, Ch., Papazachos, C.B., Margaris, B.N., Boore, D., Ventouzi, Ch., Skarlatoudis, A.A., 2018. Stochastic Strong Ground Motion Simulation of the Southern Aegean Sea Benioff Zone Intermediate-Depth Earthquakes. Bulletin of the Seismological Society of America, 108(2), 946–965, doi: 10.1785/0120170047.

Kouskouna, V., Kaviris, G., Pomonis, A., Kallidromitou, D., Kassela, A., Bonazountas, M., Makropoulos, K., Holevas, K., Lagios, E., Kyriakopoulos, K., Drakatos, G., Sakkas, V., Dellino, P., Sakkas, G., Sakellariou, N., Misailidis, I., 2014. "GRECO-RISKS" Hellenic Natural-Hazards Risk Mitigation System (A Real Time Operational Platform)". Abstract, 2nd ECEES, Istanbul, Turkey.

Papadimitriou, P., Kaviris, G., Makropoulos, K., 2006. The Mw=6.3 2003 Lefkada earthquake (Greece) and induced stress transfer changes., Tectonophysics 423, 73-82.

Papazachos, B.C., Papadimitriou, E.E., Kiratzi, A.A., Papazachos, C.B., Louvari, E. K., 1998. Fault plane solutions in the Aegean Sea and the surrounding area and their tectonic implication. Bolletino di Geofisica Teorica ed Applicata 39(3), 199-218.

Sakkas, G., Kouskouna, V., Kaviris, G., Sakellariou, N., Misailidis, I., 2018. A Real-Time PGA and PGR Distribution Application for Greece. European Seismological Commission, 36th General Assembly, Valetta, Malta.

Sakkas, G., 2016. Calculation and analysis of the seismic motion rotational components in Greece. Ph.D. Thesis, National and Kapodistrian University of Athens, Athens, 278 p.

Skarlatoudis, A.A., Papazachos, C.B., Margaris, B.N., Ventouzi, C., Kalogeras, I., the EGELADOS Group, 2013. Ground-Motion Prediction Equations of Intermediate-Depth Earthquakes in the Hellenic Arc, Southern Aegean Subduction Area. Bulletin of the Seismological Society of America, 103(3), 1952–1968, doi: 10.1785/0120120265.

Skarlatoudis, A.A., Papazachos, C.B., Margaris, B.N., Theodulidis, N., Papaioannou, Ch., Kalogeras, I., Scordilis, E.M., Karakostas, V., 2003. Empirical Peak Ground-Motion Predictive Relations for Shallow Earthquakes in Greece. Bulletin of the Seismological Society of America, 93(6), 2591-2603.

Segou, M., Voulgaris, N. 2013. The Use of Stochastic Optimization in Ground Motion Prediction. Earthquake Spectra, 29(1), 283-308.

Wald, D.J., Jaiswal, K., Marano, K.D., Bausch, D., Hearne, M., 2010. PAGER—Rapid Assessment of an Earthquake's Impact. United States Geological Survey, Fact Sheet 2010-3036.

Wald, D.J., Worden, B.C., Quitoriano, V.C., Pankow, K.L., 2005. ShakeMap manual: technical manual, user's guide, and software guide: U.S. Geological Survey Techniques and Methods, United States Geological Survey, book 12, section A, chap. 1, 132 p.

15th International Congress of the Geological Society of Greece
Athens, 22-24 May, 2019 | Harokopio University of Athens, Greece
Bulletin of the Geological Society of Greece, Sp. Pub. 7 Ext. Abs. GSG2019-087

Seismic Vulnerability Categorization of the Greek Building Stock

N. Sakellariou[1], A. Pomonis[2], V. Kouskouna[1], G. Kaviris[1], G. Sakkas[1], I. Misailidis[1], M. Tzouxanioti[1]

(1) Section of Geophysics-Geothermics, Department of Geology and Geoenvironment, National and Kapodistrian University of Athens, Panepistimiopolis, 15784, Zografou, Athens, Greece
(2) Cambridge Architectural Research Limited, Gwydir St, Cambridge CB1 2LG, United Kingdom, nsakel@geol.uoa.gr

The essential goal of vulnerability assessment of buildings and other assets to ground shaking is to estimate their expected performance to ground motion. This will in turn affect the life quality and safety of people living or working inside them, being in their vicinity or depending upon their functionality. Seismic vulnerability of assets, i.e. buildings, critical facilities, lifelines etc., is thus defined as the likelihood of damage from future earthquakes. Vulnerability is an integral component of seismic risk assessment (i.e. the probabilistic estimation of economic loss, life loss or injury, downtime and business interruption). Relationships that define vulnerability are typically classified into empirical, analytical or hybrid, according to the type of data and method used for their determination.

In most cases researchers emphasize on fragility and vulnerability assessment of standard buildings, given that they are the most common among the elements at risk. For the existing Greek building stock, fragility curves have been proposed from hybrid methodologies (Kappos et al., 2006; Kappos and Panagopoulos, 2010), based on a combination of real observed damage data and analytical models. Karababa and Pomonis (2011) have proposed a set of empirical fragility curves resulting from the 2003 Lefkada earthquake observed damage data. Following, Pomonis et al. (2013) presented a database of observed damage to 29,000 Greek reinforced concrete (RC), unreinforced masonry (URM) and mixed structure buildings compiled from post-earthquake damage surveys carried-out by government authorities and University researchers after four damaging crustal earthquakes (Kalamata 1986, Pyrgos 1993, Aegion 1995 and Lefkada 2003).

A successful attempt to categorize the entire country's building stock in vulnerability classes and for each municipality was performed during the implementation of the research project "Greco-Risks" (Kouskouna et al., 2014). In detail, the structural characteristics of the Greek building stock, derived from the December 2000 Building Census was analyzed, using parameters, such as the construction material, the period of construction and the number of floors. This led to building classification according to the vulnerability classes proposed by the European Macroseismic Scale (EMS-98).. The level of analysis was set to the Kallicratis municipality administrative system. The full combinations resulted in 368 building sub-classes, many of which (79 sub-classes) contain zero or less than 10 buildings (77 sub-classes). To further simplify the analysis, from the seismic risk point of view, the existing buildings can be grouped into:

- 3 periods of construction (before 1961, 1961-1995, after 1995 incl. under construction), according to the evolution of the Greek earthquake code (the first compulsory seismic design code of Greece was introduced in March 1959 and the second in January 1995 – although interim guidelines were also developed in 1986 following experiences of the 1981 Corinth Gulf earthquakes of February-March 1981);
- 3 classes of height (low-rise i.e. buildings with 1 to 3 floors incl. the ground floor; medium-rise i.e. buildings with 4 to 6 floors incl. the ground floor; and high-rise (i.e. buildings with 7+ floors incl. the ground floor) and
- 6 construction material classes (wood, metal, reinforced concrete, stone, brick or concrete block, other materials).

This grouping results in 54 seismic vulnerability classes. It is worth noting though that only 12 classes contain 97.8% of the Greek building stock. More than a third of the country's building stock (34.3%) is in one class, i.e. low-rise reinforced concrete buildings built in 1961-1995.

In the framework of the HELPOS project, the National and Kapodistrian University of Athens (NKUA) is carrying out research, based on the above procedure. The results of the vulnerability assessment will be updated by using, after homogenization, the most recent data of the Greek building stock, derived from the February 2011 Building Census which contains 4.053.451 buildings. The data are categorized in 11 periods of construction, 5 height classes (number of floors) and 5 construction material classes. It should be noted that 52.186 buildings "under construction" and 77.263 of "Other" construction material were also enumerated (the class "under construction" will be excluded from the analysis, the class "Other material" warrants further investigation as to its definition, given that it may include highly vulnerable buildings, such as aging adobe or rammed earth buildings). Regarding seismic risk assessment, the buildings will be grouped into 4 periods of construction (before 1961, 1961-1995, 1995-2005 and after 2005, as a new seismic code came into force in 2004), 3 classes of height (low-, medium- and high-rise) and 5 classes of construction material (wood, metal, reinforced concrete, stone, brick or concrete block). The analytical final results of the aforementioned methodology will present the categorization of the Greek building stock and the percentage of vulnerability classes at municipality and prefecture level.

An example of this implementation is shown in Figure 1a,b for the Prefecture of Eastern Attica, which includes 13 municipalities. During the period 2001-2008, the area experienced a building boom, which led to an increase of modern buildings, according to the revised Greek seismic design code (2004). A decrease of buildings belonging to the EMS-98 vulnerability classes A, B is observed, which is due to their replacement by new constructions and the increase in the size of the stock. Also, a decrease by about a quarter of the incidence of vulnerability classes C and D, respectively, was more than compensated by the increase of class E, which reached 23%. Further investigation of such results may also reveal

possible societal changes.

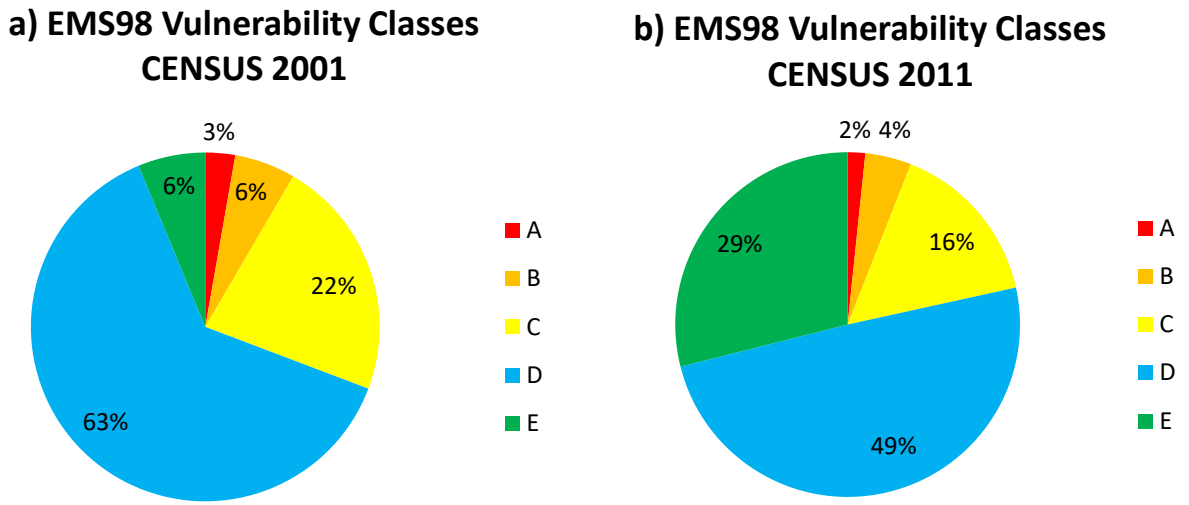

Figure 1. Vulnerability categorization for the Eastern Attica building stock, based on the a) 2001 Census and b) 2011 Census

The procedure will be applied to the entire Greek building stock and all the municipalities, with a detailed table of how the census data are mapped to the EMS-98 classes. We expect that the results will show that the country's present stock consists in large part of better designed and more resistant buildings, while municipalities with aging and vulnerable stock will also be identified.

Acknowledgements

We acknowledge support of this study by the project "HELPOS – Hellenic Plate Observing System" (MIS 5002697) which is implemented under the Action "Reinforcement of the Research and Innovation Infrastructure", funded by the Operational Programme "Competitiveness, Entrepreneurship and Innovation" (NSRF 2014-2020) and co-financed by Greece and the European Union (European Regional Development Fund). Funding of the research for the 2001 Census data was provided through the project "Greco-Risks - Hellenic Natural-Hazards Risk-Management System of Systems", jointly funded by Greece and the EU, European Regional Development Fund (ERDF), National Action "Cooperation 2011 – Partnerships of Production and Research Institutions in Focused Research and Technology Sectors", Ministry of Culture, Education and Religious Affairs, Operational Programmes "Competitiveness and Entrepreneurship" (OPCE II) and Regions in Transition (ROP Attica), National Strategic Reference Framework NSRF 2007-2013. Census data were provided by the Hellenic Statistical Authority (EL.STAT).

References

Grünthal, G. (Editor), 1998. European Macroseismic Scale 1998 (EMS-98), 101 pp., Luxembourg, 1998.

Kappos A. and Panagopoulos G., 2010. Fragility curves for reinforced concrete buildings in Greece. Struct. Infrastruct. Eng., 6, 39-53.

Kappos, A., Panagopoulos, G., Panagiotopoulos, Ch., Penelis G., 2006. A hybrid method for the vulnerability assessment of R/C and URM buildings, Bull Earthquake Engineering, vol. 4, p. 391–413.

Karababa F. and Pomonis A. 2011. Damage data analysis and vulnerability estimation following the August 14, 2003 Lefkada Island, Greece, Earthquake. Bull. Earthquake Eng., 9, 1015-1046.

Kouskouna, V., Kaviris, G., Pomonis, A., Kallidromitou, D., Kassela, A., Bonazountas, M., Makropoulos, K., Holevas, K., Lagios, E., Kyriakopoulos, K., Drakatos, G., Sakkas, V., Dellino, P., Sakkas, G., Sakellariou, N., Misailidis, I., 2014. "GRECO-RISKS" Hellenic Natural-Hazards Risk Mitigation System (A Real Time Operational Platform)". Abstract, 2nd ECEES, Istanbul, Turkey.

Pomonis, A., Gaspari, M. and Karababa, F., 2013. Seismic vulnerability assessment for buildings in Greece based on observed damage data sets, Bolletino di Geofisica Teorica de Applicata, Vol. 54, no. X, DOI 10.4430/bgta0069.

15th International Congress of the Geological Society of Greece
Athens, 22-24 May, 2019 | Harokopio University of Athens, Greece
Bulletin of the Geological Society of Greece, Sp. Pub. 7 Ext. Abs. GSG2019-095

Earthquake Early Warning application in Central Greece

V. Kapetanidis[1], P. Papadimitriou[1], G. Kaviris[1]

(1) Section of Geophysics–Geothermics, Department of Geology and Geoenvironment, National and Kapodistrian University of Athens, 15784 Panepistimiopolis, Zografou, Athens, Greece, vkapetan@geol.uoa.gr

Greece is the most seismically active country in Europe, with an estimated 50% of Europe's and 2% of the world's annual seismic energy being released on major active faults that cross the Greek territory (Bath, 1983). Several strong earthquakes during the last decades have caused serious damage and loss of human lives. With operational short-term earthquake forecasting still being an elusive prospect, Earthquake Early Warning (EEW) is currently one of the most important developing technologies in applied seismology. These systems are focused on acquiring information from the faster seismic phases, including arrival time, peak-to-peak displacement amplitude and, optionally, pulse duration to estimate location and magnitude based on probabilistic and other approaches before the slower but destructive seismic waves arrive. Depending on the density of the seismological network and the latency of waveform data transmission, an operational EEW system can generate and transmit alerts for impending seismic strong motion at target sites of significant importance and inform the authorities, companies or even the public to take specific risk/damage mitigation measures within the short time window between the warning signal and the arrival of the strong shear or surface waves.

In the framework of the Hellenic Plate Observing System (HELPOS) research project, the National and Kapodistrian University of Athens has been working on the application of EEW focused in Central Greece. The monitored region includes major active fault systems, such as the Cephalonia-Lefkada Transform Fault Zone (CLTFZ; Stiros *et al.*, 1994; Papadimitriou *et al.*, 2006; Karakostas *et al.*, 2015) and the thrust faults near Zakynthos island (Papadimitriou *et al.*, 2012) in the west, the Andravida fault (Ganas *et al.*, 2009; Papadopoulos *et al.*, 2010) in NW Peloponnese, the Corinth Rift (Bernard *et al.*, 1997; Kapetanidis *et al.*, 2015; Kaviris *et al.*, 2017, 2018), the pull-apart fault system in Lake Trichonis (Kassaras *et al.*, 2014) and, towards the east, the fault systems surrounding the capital, Athens (Papadimitriou *et al.*, 2002), and the fault systems in Atalanti (Pantosti *et al.*, 2001) and Evia rift (Ganas *et al.*, 2016).

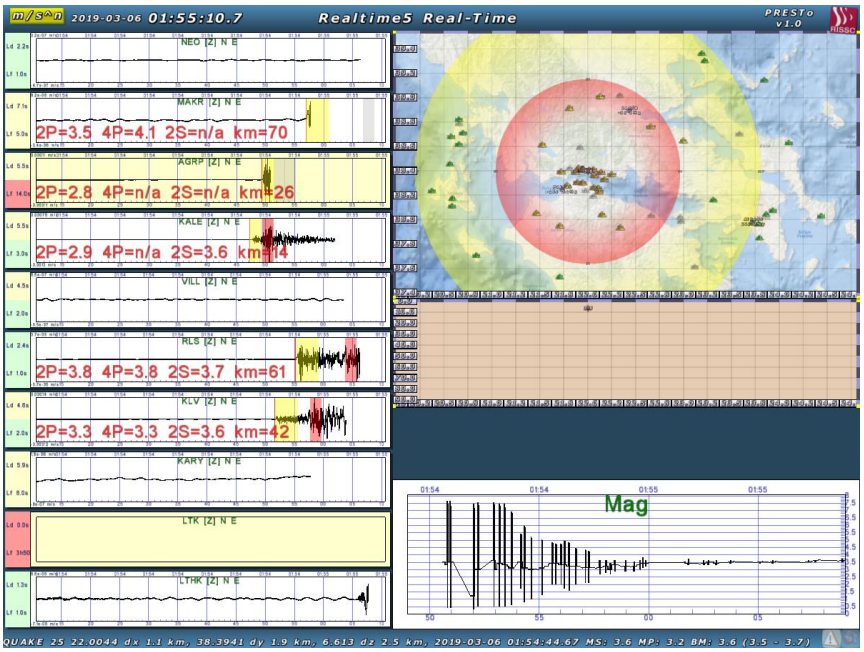

Figure 1. Example of a real-time alert from PRESTo EEW for an event that occurred in the WGoC. The first solution was available only 6 sec after the origin time, allowing for a 4 sec window before the S-waves arrival at the city of Patras, at an epicentral distance of 30 km.

In this work we present preliminary results of a pilot application using the PRESTo EEW software (Satriano *et al.*, 2011). We incorporate data from seismological stations of the Hellenic Unified Seismological Network (HUSN), along with stations of the local Corinth Rift Laboratory Network (CRLN; Lyon-Caen *et al.*, 2004) installed in the Western Gulf of Corinth (WGoC). The target sites are major cities of central Greece, including Athens, Patras, Aigion, Corinth and Agrinion. However, we chose to use a much broader area, to avoid strong earthquakes that occur outside the true region of interest being mislocated inside the latter and producing false alerts.

The playback feature of the EEW software was used to fine-tune the automatic location algorithm of PRESTo and to calibrate the equations used to calculate the magnitude, by employing a large dataset of significant earthquakes recorded during the past years in the study area. We estimated the absolute capacity of the currently available network to detect

and locate earthquakes promptly. To this purpose, we also take into account the latency of data transmission, given that waveforms have to be transferred to the central server running the EEW software before being processed. The EEW system works best in areas where the seismological network is dense enough for first arrivals to be picked in at least 4 stations within a reasonable travel-time. During the real-time application we recorded examples of earthquakes in which the EEW system produced its first alert promptly and with adequate precision allowing for a 4 sec time-window before the shear waves arrive at a major target city at a minimum 30 km epicentral distance (e.g. Fig. 1).

Acknowledgements

The authors would like to thank the personnel of all cooperating institutes of both HUSN and CRLN (doi: 0.15778/RESIF.CL) for the operation of the respective networks. We acknowledge support of this study by the project "HELPOS – Hellenic Plate Observing System" (MIS 5002697) which is implemented under the Action "Reinforcement of the Research and Innovation Infrastructure", funded by the Operational Programme "Competitiveness, Entrepreneurship and Innovation" (NSRF 2014-2020) and co-financed by Greece and the European Union (European Regional Development Fund).

References

Båth, M., 1983. The seismology of Greece. Tectonophysics 98, 165–208.

Bernard, P., Briole, P., Meyer, B., Gomez, J., Tiberi, C., Berge, C., Cattin, R., Hatzfeld, D., Lachet, C., Lebrun, B., Deschamps, a., Courboulex, F., Larroque, C., Rigo, a., Massonnet, D., Papadimitriou, P., Kassaras, J., Diagourtas, D., Makropoulos, K., Veis, G., Papazisi, E., Mitsakaki, C., Karakostas, V., Papadimitriou, E., 1997. The Ms=6.2, June 15, 1995 Aigion earthquake (Greece): evidence for low-angle normal faulting in the Corinth rift. J. Seismol. 1, 131–150.

Ganas, A., Serpelloni, E., Drakatos, G., Kolligri, M., Adamis, I., Tsimi, C., Batsi, E., 2009. The Mw 6.4 SW-Achaia (Western Greece) Earthquake of 8 June 2008: Seismological, Field, GPS Observations, and Stress Modeling. J. Earthq. Eng. 13, 1101–1124.

Ganas, A., Mouzakiotis, E., Moshou, A., Karastathis, V., 2016. Left-lateral shear inside the North Gulf of Evia Rift, Central Greece, evidenced by relocated earthquake sequences and moment tensor inversion. Tectonophysics 682, 237–248.

Kapetanidis, V., Deschamps, A., Papadimitriou, P., Matrullo, E., Karakonstantis, A., Bozionelos, G., Kaviris, G., Serpetsidaki, A., Lyon-Caen, H., Voulgaris, N., Bernard, P., Sokos, E., Makropoulos, K., 2015. The 2013 earthquake swarm in Helike, Greece: seismic activity at the root of old normal faults. Geophys. J. Int. 202 (3), 2044–2073.

Karakostas, V., Papadimitriou, E., Mesimeri, M., Gkarlaouni, C., Paradisopoulou, P., 2015. The 2014 Kefalonia Doublet (Mw6.1 and Mw6.0), Central Ionian Islands, Greece: Seismotectonic Implications along the Kefalonia Transform Fault Zone. Acta Geophys. 63, 1–16.

Kassaras, I., Kapetanidis, V., Karakonstantis, A., Kaviris, G., Papadimitriou, P., Voulgaris, N., Makropoulos, K., Popandopoulos, G., Moshou, A., 2014. The April-June 2007 Trichonis Lake earthquake swarm (W. Greece): New implications toward the causative fault zone. J. Geodyn. 73, 60–80.

Kaviris, G., Spingos, I., Kapetanidis, V., Papadimitriou, P., Voulgaris, N., Makropoulos, K., 2017. Upper crust seismic anisotropy study and temporal variations of shear-wave splitting parameters in the Western Gulf of Corinth (Greece) during 2013. Phys. Earth Planet. Inter. 269, 148–164.

Kaviris, G., Millas, C., Spingos, I., Kapetanidis, V., Fountoulakis, I., Papadimitriou, P., Voulgaris, N., Makropoulos, K., 2018. Observations of shear-wave splitting parameters in the Western Gulf of Corinth focusing on the 2014 Mw = 5.0 earthquake. Phys. Earth Planet. Inter. 282, 60–76.

Lyon-Caen, H., Papadimitriou, P., Deschamps, A., Bernard, P., Makropoulos, K., Pacchiani, F., Patau, G., 2004. First results of the CRLN seismic network in the western Corinth Rift: evidence for old-fault reactivation. Comptes Rendus Geosci. 336, 343–351.

Pantosti, D., De Martini, P.M., Papanastassiou, D., Palyvos, N., Lemeille, F., Stavrakakis, G., 2001. A reappraisal of the 1894 atalanti earthquake surface ruptures, Central Greece. Bull. Seismol. Soc. Am. 91, 760–780.

Papadimitriou, P., Voulgaris, N., Kassaras, I., Kaviris, G., Delibasis, N., Makropoulos, K., 2002. The Mw= 6.0, 7 September 1999 Athens earthquake. Nat. Hazards 27, 15–33.

Papadimitriou, P., Kaviris, G., Makropoulos, K., 2006. The Mw = 6.3 2003 Lefkada earthquake (Greece) and induced stress transfer changes. Tectonophysics 423, 73–82.

Papadimitriou, P., Chousianitis, K., Agalos, A., Moshou, A., Lagios, E., Makropoulos, K., 2012. The spatially extended 2006 April Zakynthos (Ionian Islands, Greece) seismic sequence and evidence for stress transfer. Geophys. J. Int. 190, 1025–1040.

Papadopoulos, G.A., Karastathis, V., Kontoes, C., Charalampakis, M., Fokaefs, A., Papoutsis, I., 2010. Crustal deformation associated with east Mediterranean strike-slip earthquakes: The 8 June 2008 Movri (NW Peloponnese), Greece, earthquake (Mw6.4). Tectonophysics, 492, 201–212.

Satriano, C., Elia, L., Martino, C., Lancieri, M., Zollo, A., Iannaccone, G., 2011. PRESTo, the earthquake early warning system for Southern Italy: Concepts, capabilities and future perspectives. Soil Dyn. Earthq. Eng. 31, 137–153.

Serpetsidaki, A., Elias, P., Ilieva, M., Bernard, P., Briole, P., Deschamps, A., Lambotte, S., Lyon-Caen, H., Sokos, E., Tselentis, G.A., 2014. New constraints from seismology and geodesy on the Mw = 6.4 2008 Movri (Greece) earthquake: Evidence for a growing strike-slip fault system. Geophys. J. Int. 198, 1373–1386.

Sokos, E., Kiratzi, A., Gallovič, F., Zahradník, J., Serpetsidaki, A., Plicka, V., Janský, J., Kostelecký, J., Tselentis, G.-A., 2015. Rupture process of the 2014 Cephalonia, Greece, earthquake doublet (Mw6) as inferred from regional and local seismic data. Tectonophysics 656, 131–141.

Stiros, S.C., Pirazzoli, P.A., Laborel, J., Laborel-Deguen, F., 1994. The 1953 earthquake in Cephalonia (Western Hellenic Arc): coastal uplift and halotectonic faulting. Geophys. J. Int. 117, 834–849.

15th International Congress of the Geological Society of Greece
Athens, 22-24 May, 2019 | Harokopio University of Athens, Greece
Bulletin of the Geological Society of Greece, Sp. Pub. 7 Ext. Abs. GSG2019-100

Shear velocity structure of the Hellenic upper mantle from Rayleigh-wave dispersion

I. Kassaras, V. Kapetanidis, I. Spingos, A. Karakonstantis, G. Kaviris, P. Papadimitriou
Department of Geophysics & Geothermics, NKUA, Panepistimiopolis, 15784 Athens, Greece, kassaras@geol.uoa.gr

The dynamics of the Hellenic lithosphere has been extensively studied over the last decades. However, tomographic investigations on the seismic structure of its upper mantle have yielded controversial interpretations, mostly related to restraints due to poor resolution, especially for the intermediate depth range down to 150 km. This study provides new constraints on the intermediate depth, upper-mantle shear velocity structure of Greece using broadband Rayleigh-wave recordings. The analysis is a three-step procedure: acquisition of waveform recordings, dispersion curve estimation, and inversion. The data are constituted of broadband waveforms of over 670 events recorded by ~200 broadband stations of the Hellenic Unified Seismological Network (HUSN; http://www.gein.noa.gr/en/networks/husn) and Kandilli Observatory and Earthquake Research Institute network (KOERI, 2001) between 2010 and 2018. Additional recordings were acquired from stations of the Corinth Rift Laboratory (CRL), operating in Central Greece, as well as of GEOFON and MEDNET.

Phase-velocity dispersion curves were derived using a multichannel cross-correlation technique, applying the Automated Surface-Wave Measuring System algorithm (ASWMS; Jin and Gaherty, 2015), based on the Generalized Seismological Data Functionals (GSDF) proposed by Gee & Jordan (1992). In this method, phase delays are measured between all combinations of neighboring stations of the network to avoid systematic biases due to propagation effects, rather than only for pairs that are aligned with the epicenter, within a few degrees of tolerance along a common great circle path; an assumption that greatly reduces the number of quasi-valid measurements. Phase-velocities were determined in terms of apparent and structural velocities, approximated by the application of the Eikonal and Helmholtz equation, respectively. Phase-velocity maps were generated in a grid cell of cell-dimensions 0.2º×0.2º over the period range 30 to 90 s (Fig. 1a). Checkerboard tests yielded adequate horizontal resolution to distinguish anomalies of about 130×130 km² for the obtained tomograms.

The phase-velocity maps were then inverted in order to acquire the vertically polarized shear-velocity (V_{SV}) distribution with depth, using the *surf96* code (Herrmann, 1994), derived by a Monte-Carlo scheme on perturbations over initial 1-D models, as implemented in the ASWSM suite (Jin, 2015), modified to take into account the region's crustal structure (CRUST1.0; Laske *et al.*, 2013). The most prevalent features in the phase velocity maps (Fig. 1) are the Hellenic Subduction Zone (HSZ) and the North Anatolia Trench system (NAT), manifested by high and low velocities, respectively. Low velocities along the outer Hellenic Arc at low periods are pertinent to the thick crust and sedimentation along the HSZ (Laske *et al.*, 2013). Fast velocities beneath the Cephalonia-Lefkas-Akarnania Block (CLAB, Fig. 1), considered a microplate (Perouse *et al.*, 2017) are indicative for deep lithospheric roots. A high velocity anomaly extends below the Greek mainland and the South Aegean Active Volcanic Arc (SAAVA), consistently with other tomographic studies (e.g. Papazachos & Nolet, 1997).

Cross-sections across the 3-D absolute V_{SV} model (Fig. 2) highlight a low velocity zone hosting intermediate depth seismicity, above a high velocity surrounding upper mantle material deeper than 90 km. This finding is compatible with Spakman and Nolet (1988) and Granet and Trampert (1989), who interpreted a low velocity anomaly at similar depth as representing a possible detachment zone along the slab, and with Suckale *et al.* (2009) who found a low-velocity layer at the western part of the HSZ at depths 40-90 km, explained as the hydrated crust of the Hellenic slab. The upper mantle of North Aegean is dominated by slow velocities, compatible with mantle wedge, asthenospheric flow and surface magmatism observed throughout the region. The latter observation, also complies with high crustal stress ratio values (Kapetanidis and Kassaras, 2019), indicative of a stable $\mathbf{S}_3$ axis, exhibiting extension in a SSW-NNE direction.

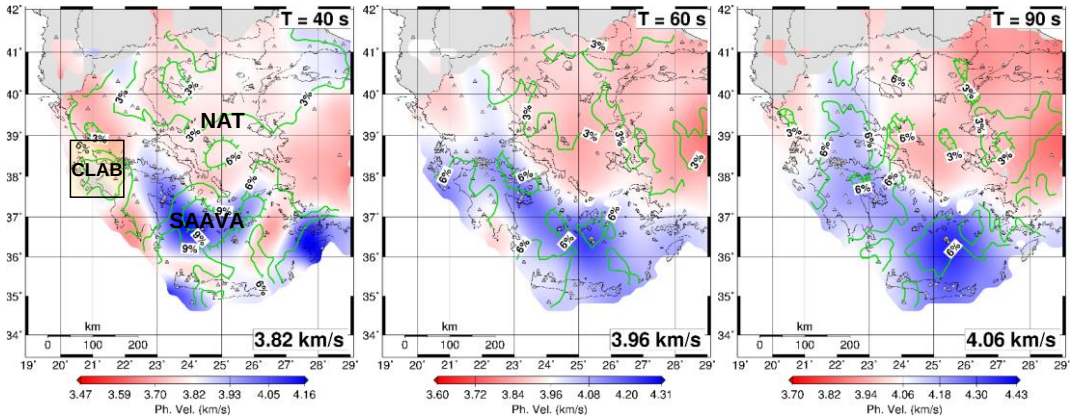

Figure 1. Rayleigh-wave structural (Helmholtz) phase velocity maps at various periods of interest. The color scale varies with period T, with white color corresponding to the average phase velocity as given in the lower right corner of each map. Green contours indicate relative error (%) with respect to the average phase velocity per period. Tick lines on the contours indicate the direction of relative error reduction.

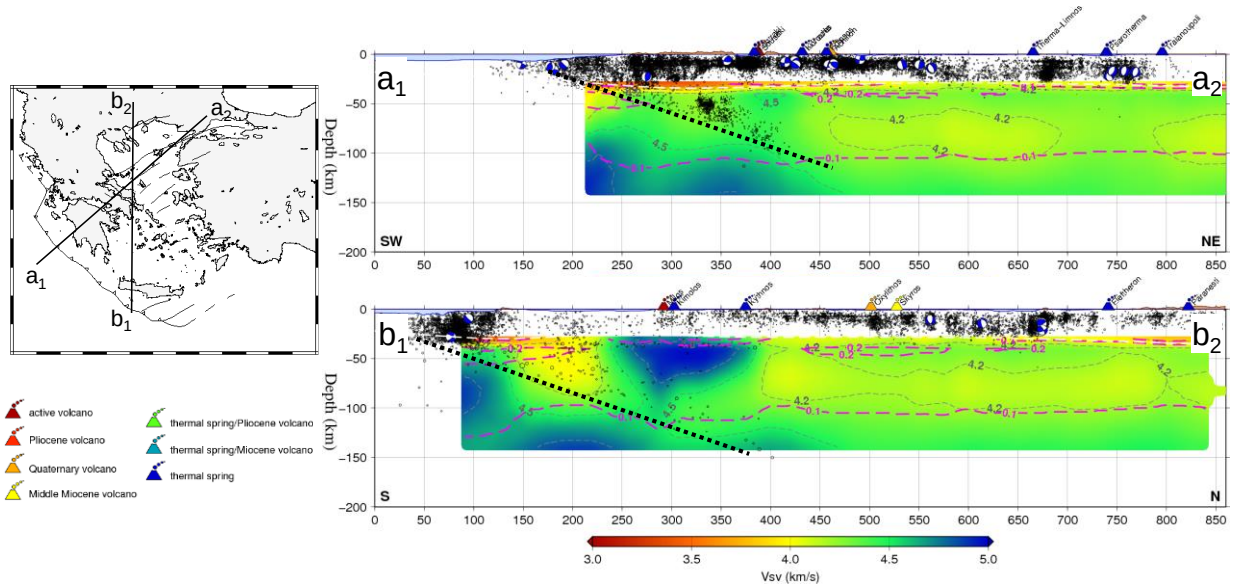

Figure 2. Cross sections of preliminary results on the 3-D absolute V_{SV} model along profiles shown on the left map. Purple dashed lines are contours of the Resolution matrix Diagonal Element (RDE), with results in regions within RDE>0.1 generally considered as reliable. Seismicity (Karakonstantis, 2017; Bocchini, 2018), focal mechanisms (Kapetanidis & Kassaras, 2019) and volcanics (Siebert & Simkin, 2002) are superimposed.

Acknowledgements

We acknowledge support of this study by the project "HELPOS - Hellenic Plate Observing System" (MIS 5002697) which is implemented under the Action "Reinforcement of the Research and Innovation Infrastructure", funded by the Operational Programme "Competitiveness, Entrepreneurship and Innovation" (NSRF 2014-2020) and co-financed by Greece and the European Union (European Regional Development Fund). We thank EIDA for providing data from regional networks HL (doi: 10.7914/SN/HL), HT (doi: 10.7914/SN/HT), HA (doi: 10.7914/SN/HA), HP (doi: 10.7914/SN/HP), HC (doi: 10.7914/SN/HC), CQ (doi:10.7914/SN/CQ), Z3 (doi:10.14470/M87550267382), and CL (doi:10.15778/RESIF.CL). We are greatly indebted to Ge Jin, Natalie Accardo for clarifications on the ASWSM suite and A. Ganas for discussions.

References

Bocchini, G.M., 2018. Big or Small Earthquakes along the Subduction Interface: Impact on Natural Hazards, PhD Thesis, National and Kapodistrian University of Athens, p.249.

Gee, L.S. & Jordan, T.H., 1992. Generalized seismological data functionals, Geophys. J. Int., 111(2), 363–390.

Granet, M. And Trampert, J., 1989. Large scale P-velocity structures in the EuroMediterranean area, Geophysical Journal International, 99, 583–594.

Herrmann, R.B., 1994. Computer programs in Seismology, User's manual. St. Louis University, Missouri.

Jin, G. & Gaherty, J.B., 2015. Surface wave phase-velocity tomography based on multichannel cross-correlation, Geophys. J. Int. (2015) 201, 1383–1398, doi: 10.1093/gji/ggv079.

Jin, G., 2015. Surface-wave analysis and its application to determining crustal and mantle structure beneath regional arrays, PhD Thesis, Columbia University, USA, pp. 126.

Kapetanidis, V., Kassaras, I., 2019. Contemporary crustal stress of the Greek region deduced from earthquake focal mechanisms, J. of Geodynamics, DOI: 10.1016/j.jog.2018.11.004.

Karakonstantis, A., 2017. 3-D simulation of crust and upper mantle structure in the broader Hellenic area through Seismic Tomography, PhD Thesis, National and Kapodistrian University of Athens, (in Greek).

KOERI, 2001. Bogazici University Kandilli Observatory and Earthquake Research Institute. International Federation of Digital Seismograph Networks. Other/Seismic Network. 10.7914/SN/KO, https://doi.org/10.7914/SN/KO

Laske, G., Masters, G., Ma, Z. and Pasyanos, M., 2013. Update on CRUST1.0 - A 1-degree Global Model of Earth's Crust, Geophys. Res. Abstracts, 15, Abstract EGU2013-2658.

Papazachos, C.B., Nolet, G. 1997. P and S deep structure of the Hellenic area obtained by robust nonlinear inversion of travel times. Journal of Geophysical Research, 102, 8349–8367.

Pérouse E., et al., 2017. Transition from collision to subduction in Western Greece: The Katouna-Stamna active fault system, Int. J. Earth Sci., 106, 967-989.

Siebert, L., Simkin, T., 2002–present. Volcanoes of the World: an Illustrated Catalog of Holocene Volcanoes and their Eruptions. Smithsonian Institution, Global Volcanism Program Digital Information Series, GVP-3 (http://www.volcano.si.edu).

Spakman, W., Nolet, G. (1988). Imaging algorithms, accuracy and resolution in delay time tomography. In N.J. Vlaar, G. Nolet, M.J.R. Wortel, & S.A.P. Cloetingh (Eds.), Mathematical geophysics: A survey of recent developments in seismology and geodynamics (pp. 155–187). Netherlands: Springer.

Suckale, J., et al., 2009. High-resolution seismic imaging of the western Hellenic subduction zone using teleseismic scattered waves, Geophys. J. Int., 178, 775–791, doi: 10.1111/j.1365-246X.2009.04170.x.

15th International Congress of the Geological Society of Greece
Athens, 22-24 May, 2019 | Harokopio University of Athens, Greece
Bulletin of the Geological Society of Greece, Sp. Pub. 7 Ext. Abs. GSG2019-165

Crustal stress-field in Greece and implications on faulting mechanisms

V. Kapetanidis[1], I. Kassaras[1]

(1) Section of Geophysics–Geothermics, Department of Geology and Geoenvironment, National and Kapodistrian University of Athens, 15784 Panepistimiopolis, Zografou, Athens, Greece, vkapetan@geol.uoa.gr

Greece is widely recognized as one of the most rapidly deforming regions in the world. Significantly large strain-rates are observed along the Hellenic Arc, owing to the active subduction of the eastern Mediterranean lithosphere beneath the Aegean, but also in the North Aegean Trough, caused by the westwards propagation of the North Anatolian Fault. In the framework of the HELPOS project, we collected a massive dataset of over 1900 focal mechanisms (Kapetanidis & Kassaras, 2019a) of $M_w \geq 3.5$ earthquakes that have occurred at focal depths of $Z \leq 30$ km to resolve the stress-field in a grid with node-spacing 0.25°, covering the entire region of Greece, using a damped least-squares inversion (Hardebeck & Michael, 2006). We then investigated the properties of the stress-field in terms of its principal stress axes orientations and stress-ratio to determine the main tectonic features across the Greek territory.

The resulting stress-field is presented in Fig. 1a, interpolated in regions with insufficient data, such as the southern Aegean and the respective part of the volcanic arc, which are generally characterized by very low seismicity. NW Greece and Corfu Island are mainly affected by NE-SW contraction, favoring NW-SE reverse faulting and, in addition, strike-slip faulting, mainly in Epirus. Northern/central Greece and the Corinth Rift are primarily characterized by E-W normal faulting (Fig. 1b). Central Aegean, including Lesvos (e.g. Papadimitriou et al., 2018), Chios and Samos islands, is mainly governed by SW-NE dextral strike-slip faulting but also N-S extension (transtensional tectonics), with a very stable minimum principal stress axis ($\mathbf{S}_3$) in northern Aegean, also producing E-W normal faulting which becomes dominant near Dodecanese. The southern part of the Hellenic Arc around Crete is dominated by SW-NE sinistral strike-slip faulting with the presence of E-W reverse faulting, in the vicinity of the subduction zone. In W. Greece (e.g. Kassaras et al., 2016), SW-NE dextral strike-slip dominates along the Cephalonia-Lefkada Transform Fault Zone.

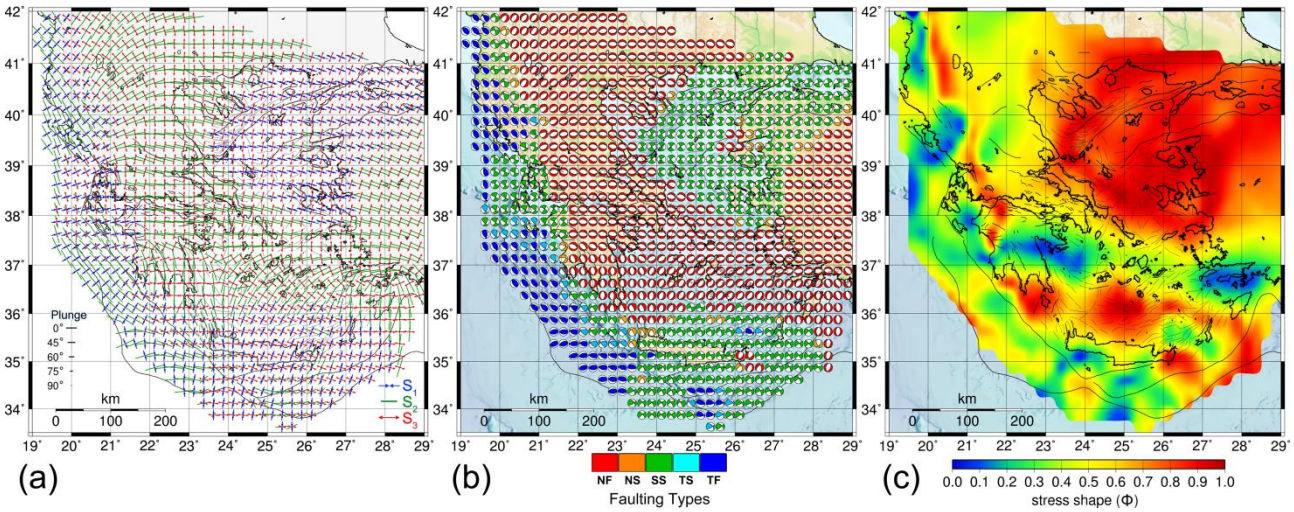

Figure 1. a) Principal stress axes S_1, S_2, and S_3 of the resolved stress-field, b) Expected faulting types for faults optimally oriented to the stress-field (NF/SS/TF: Normal/Strike-Slip/Thrust faulting, NS/TS: Oblique-Normal/Thrust faulting, U: undefined), c) Distribution of the stress-shape, $\Phi=(\sigma_2-\sigma_3)/(\sigma_1-\sigma_3)$. Fault lines from Karakonstantis and Papadimitriou (2010) and Sakellariou and Tsampouraki-Kraounaki (2016).

The stress-field, and in particular the component of maximum horizontal compression, $\mathbf{S}_{Hmax}$, was found in good agreement with the respective principal strain-rate axes determined by GPS/GNSS data, such as the Global Strain Rate Model (GSRM; Kreemer *et al.*, 2003). Some differences are observed in areas of low strain-rate magnitude, as, for example in NW Greece, near Corfu, where the stress-field suggests compression more transverse to the Apulian collision front than the strain-rate field implies, and SW Aegean, where the strain-rate tensor is overwhelmed by the contraction along the Hellenic Arc, whereas the stress-field is related to strike-slip faulting near Crete and N-S normal faulting in southern Peloponnese and near Rhodes Island.

To investigate the effects of the stress-field on the kinematics of known faults, the stress-tensor was applied on the fault-sources (FS) of the European Seismic Hazard Model 2013 (ESHM13; Woessner *et al.*, 2015). In most regions, our results were found to be compatible with the ESHM13 FS, in terms of orientation and expected faulting type (Fig. 2), which was examined by imposing the direction of maximum shear on the fault plane as the direction of slip. Some differences were observed in regions of low strain-rate, such as the southern Aegean, where left-lateral strike-slip E-W faulting is expected, in contrast to the registered E-W normal FS. Discrepancies were also found in areas with complex tectonics, such as pull-

apart basins in Western Greece, where the resolution of the regional stress-field is insufficient to explain local stress heterogeneities, or near the boundaries between regions with different tectonic regimes. Nevertheless, such areas were highlighted by anomalies in the stress-shape, Φ (Fig. 1c), which is strongly dependent on the variation of one principal stress axis while another remains relatively stable. A high Φ-value anomaly runs along the Andravida fault zone, which hosted the 8 June 2008 M_w=6.4 earthquake (e.g. Ganas *et al.*, 2009) and further north along the normal and strike-slip zones of Lake Trichonis (e.g. Kassaras *et al.*, 2014) and Amvrakikos gulfs. On the other hand, a low Φ-value, E-W oriented anomaly marks a significant rotation of the stress-field by 90° that occurs along the latitude=37°N, turning from E-W (in the north) to N-S (in the south) normal faulting in southern Peloponnese and Dodecanese Islands, as well as from dextral to sinistral SW-NE strike-slip faulting in northern and southern Aegean, respectively. The regional stress-tensor, which is available online at http://dx.doi.org/10.17632/sm8bj39nfy.1 (Kapetanidis & Kassaras, 2019b), can provide first-order knowledge that is useful for further studies involving focal mechanisms / fault kinematics, Coulomb stress transfer and seismic hazard assessment.

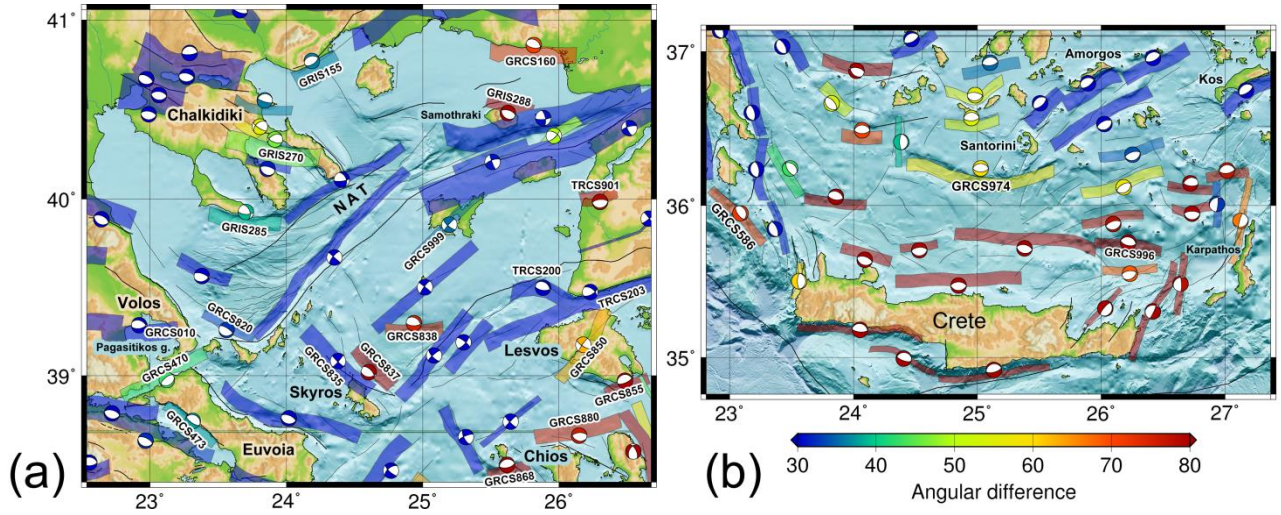

Figure 2. ESHM13 Fault Sources (polygons) with their kinematics represented by beachballs. Colors indicate the minimum angular difference between the orientation of the FS's "equivalent moment tensor" principal axes (P, N, T) and the respective axes (S_1, S_2, S_3) of the stress-tensor, a) in northern Aegean, b) in southern Aegean.

Acknowledgements

We acknowledge support of this study by the project "HELPOS – Hellenic Plate Observing System" (MIS 5002697) which is implemented under the Action "Reinforcement of the Research and Innovation Infrastructure", funded by the Operational Programme "Competitiveness, Entrepreneurship and Innovation" (NSRF 2014-2020) and co-financed by Greece and the European Union (European Regional Development Fund).

References

Ganas, A., Serpelloni, E., Drakatos, G., Kolligri, M., Adamis, I., Tsimi, C., Batsi, E., 2009. The Mw 6.4 SW-Achaia (Western Greece) Earthquake of 8 June 2008: Seismological, Field, GPS Observations, and Stress Modeling. J. Earthq. Eng. 13, 1101–1124.

Hardebeck, J.L. and Michael, A.J., 2006. Damped regional-scale stress inversions: Methodology and examples for southern California and the Coalinga aftershock sequence. J. Geophys. Res. Solid Earth, 111, B11310.

Kapetanidis, V., Kassaras, I., 2019a. Contemporary crustal stress of the Greek region deduced from earthquake focal mechanisms. J. Geodyn. 123, 55–82. doi:10.1016/j.jog.2018.11.004

Kapetanidis, V., Kassaras, I., 2019b. Data for: Contemporary crustal stress of the Greek region deduced from earthquake focal mechanisms, Mendeley Data, v1 http://dx.doi.org/10.17632/sm8bj39nfy.1

Karakonstantis, A. & Papadimitriou, P., 2010. Earthquake relocation in Greece using a unified and homogenized seismological catalogue. Bull. Geol. Soc. Greece, 43, 2043-2052, doi: 10.12681/bgsg.11394.

Kassaras, I., Kapetanidis, V., Karakonstantis, A., Kaviris, G., Papadimitriou, P., Voulgaris, N., Makropoulos, K., Popandopoulos, G., Moshou, A., 2014. The April-June 2007 Trichonis Lake earthquake swarm (W. Greece): New implications toward the causative fault zone. J. Geodyn. 73, 60–80.

Kassaras, I., Kapetanidis, V., Karakonstantis, A., 2016. On the spatial distribution of seismicity and the 3D tectonic stress field in western Greece. Phys. Chem. Earth, Parts A/B/C 95, 50–72. doi:10.1016/j.pce.2016.03.012

Kreemer, C., Holt, W.E. & Haines, A.J., 2003. An integrated global model of present-day plate motions and plate boundary deformation. Geophys. J. Int., 154, 8–34.

Papadimitriou, P., et al., 2018. The 12 th June 2017 M w = 6.3 Lesvos earthquake from detailed seismological observations. J. Geodyn. 115, 23–42. doi:10.1016/j.jog.2018.01.009

Sakellariou, D. & Tsampouraki-Kraounaki, K., 2016. Offshore faulting in the Aegean sea: a synthesis based on bathymetric and seismic profiling data. Bull. Geol. Soc. Greece, 50, 134, doi: 10.12681/bgsg.11712.

Woessner, J., et al., 2015. The 2013 European Seismic Hazard Model: key components and results. Bull. Earthq. Eng., 13, 3553–3596.

15th International Congress of the Geological Society of Greece
Athens, 22-24 May, 2019 | Harokopio University of Athens, Greece
Bulletin of the Geological Society of Greece, Sp. Pub. 7 Ext. Abs. GSG2019-204

A GIS platform for Rapid Seismic Risk Assessment in Greece – Case study Cephalonia Isl.

I. Kassaras1, D. Kazantzidou-Firtinidou[1], V. Kapetanidis[1], G. Sakkas[1], S. Vassilopoulou[1], D. Theodorakatou[1], S. Hadjiefthymiades[2], P. Papadimitriou[1]

(1) Department of Geophysics & Geothermics, NKUA, Panepistimiopolis, 15784 Athens, Greece, kassaras@geol.uoa.gr
(2) Department of Informatics & Telecommunications, NKUA, Panepistimiopolis, 15784 Athens, Greece

The term Seismic Risk Assessment (SRA) is defined as the combination of a specified level of ground motion at a site (seismic hazard), the degree of damage expected to occur in its structures after an earthquake (seismic fragility) and the assets exposed (economic exposure). Given that the issue of the accurate prediction of earthquakes is strongly argued at present and physical limitations of Earthquake Early Warning Systems (EEWS) often impose restraints on their feasibility (Thelen et al., 2016), implementation of Rapid Seismic Risk Assessment (RSRA), highlighting urban regions prone to damage within the affected area, may crucially facilitate targeted emergency actions to be taken immediately after a disaster. To this aim, a GIS computer platform for semi-automatic deterministic RSRA is under development in the frame of HELPOS project, with the prospect to be linked to the near-realtime ShakeMap application of the Seismological Laboratory of NKUA towards acquiring an efficient, site-tailored, structural RSRA system. Herein we present its basic structure and an offline application on Cephalonia (Ionian Islands) that will be used as a baseline scenario of the platform's validation at a later stage. Computational tasks within the system consist of Deterministic Seismic Hazard Assessment (DSHA) for a given earthquake taking into account site-effects and a combination of the derived Intensity Measures (IMs) with a predefined macroseismic EMS-98 vulnerability model (Grünthal, 1998). The output product includes spatial models (maps) of EMS-98 Damage Grades (DGs) and their probability to occur at the building block level. Key-point the platform is stressed to, is short delay in producing output, reduction of error-prone conversions and adaptations between modules/systems and a fully automated workflow (Fig. 1).

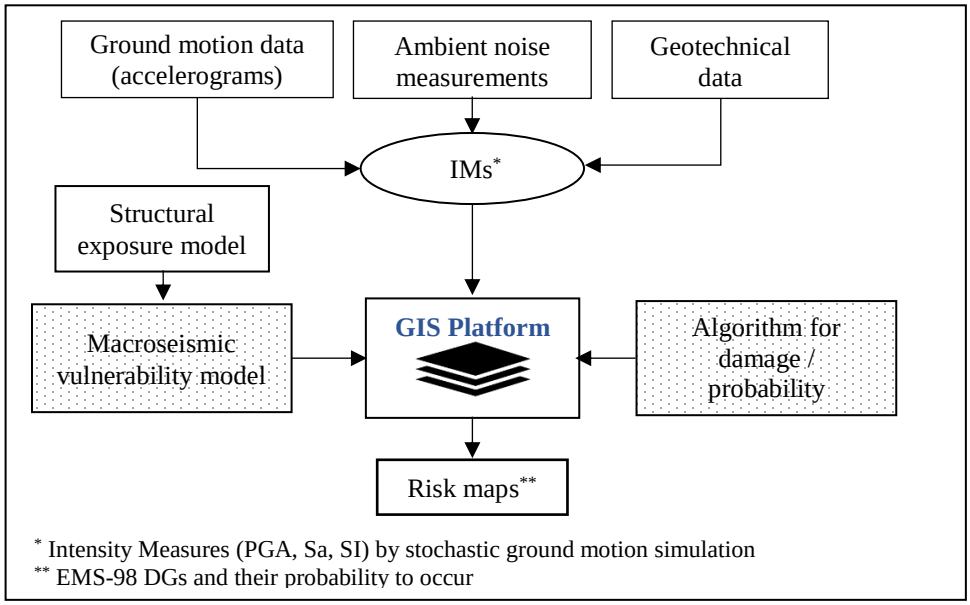

Figure 1. Basic design of the GIS platform.

As mentioned above, platform output is fully localized, which requires site-specific parameterization regarding seismic sources, Ground Motion Prediction Equations (GMPEs), soil conditions and buildings taxonomy. Seismic source, i.e. its location, geometry, kinematics and its magnitude is the only variable in the workflow, input to a DSHA based on stochastic ground motion simulation implemented through the EXSIM module (Motazedian & Atkinson, 2005). Prior to automatic simulations, the appropriate GMPEs and soil conditions have been pre-determined by applying synthetic IMs generated by considering historical, instrumental and nearest Maximum Credible Earthquakes (MCEs), after validation with real damage observations. Path-effects are assumed after empirical GMPEs; site effects are approximated by experimental Horizontal to Vertical Spectral Ratios - HVSRs (Nakamura, 1989) and geotechnical borehole data. Hence, the platform's EXSIM parameterization is considered to accurately resolve DSHA's IMs, i.e. Peak Ground Acceleration (PGA), Velocity (PGV) or

Displacement (PGD), Spectral Acceleration (Sa), Seismic Intensity (SI), defined as equivalent Modified Mercalli Intensity - MMI), however only by neglecting near-source effects and non-linear soil response.

Vulnerability is input as indices, integrated into the platform in tabular form, linked to specific building classes and characteristics, and consists of a static component of the risk assessment application. This architecture allows flexibility for the input of different exposure files, renders the platform extendable to other areas and provides guidelines for structural data collection and exposure modelling in a standardized way. The structural vulnerability method selected to be implemented in the platform is the macroseismic semi-empirical method proposed by Giovinazzi & Lagomarsino (2004) that takes into account the EMS-98 classification (Grünthal, 1998) and additional typological-specific and seismic behavior modifiers, i.e. height, irregularities, building position, etc. The final outcome includes risk maps, in terms of collapse maps, distribution of number of buildings per EMS-98 DGs with maximum probability of occurrence. Consistently with international scientific practices for risk assessment studies at territorial level, the lowest tract at which the end product is provided, is seismic risk at building-block scale, because of the numerous uncertainties risk assessment is related to and also social privacy issues.

The components that we put together have demonstrated good performance in the past when operated individually into several target sites in the Greek territory, i.e. Lefkada (Kassaras et al., 2015), Kalamata (Kassaras et al., 2018), Aigion (Giannaraki et al., 2018), Fira-Santorini (Kazantzidou-Firtinidou et al., 2018), yielding good agreement with real damage observations. Herein, we showcase seismic risk assessment of W. Cephalonia, pivotal for the platform's validation, by exploiting damage observations due to the 26.1.2014 (Mw=6.1) and 3.2.2014 (Mw=5.9) earthquakes, ambient noise measurements during a post-seismic campaign and geotechnical data. Regarding the buildings' inventory it was available by EPANTYK (2009) at building scale for the towns of Argostoli and Lixouri and aggregates per municipal district for the rest of the island. The derived IMs by the EXSIM scheme were found consistent with observed MMIs. Scenario DGs derived from the macroseismic approach were compared to the accumulated damage of the 2014 events, manifesting a satisfactory behavior of the constructions throughout the island, and a successful stress testing of the intended approach.

Acknowledgements

This work is being developed within the project HELPOS - Hellenic Plate Observing System (MIS 5002697) which is implemented under the Action Reinforcement of the Research and Innovation Infrastructure, funded by the Operational Programme "Competitiveness, Entrepreneurship and Innovation" (NSRF 2014-2020), co-financed by Greece and the EU.

References

EPANTYK (2009) Development of GIS software for the representation of the structural wealth of the municipalities of the country and of its structural vulnerability in buildings block level. YP.ES.A, H.D, KEDKE, TEE, pp 39 (in Greek)

Giannaraki, G., et al., 2018. Deterministic seismic risk assessment in the city of Aigion (W. Corinth Gulf, Greece) and juxtaposition with real damage due to the 1995 Mw6.4 earthquake, Bull. Earthq. Engin., doi: 10.1007/s10518-018-0464-z

Giovinazzi, S, Lagomarsino, S., 2004. A macroseismic method for the vulnerability assessment of buildings, 3th WCEE, Vancouver, BC, Canada, August 1–6, paper No 896.

Grünthal, G. (Ed.), 1998. European Macroseismic Scale 1998 (EMS-98). Cahiers du Centre Europeen de Geodynamique et de Seismologie 15, Centre Europeen de Geodynamique et de Seismologie, Luxembourg, 99 pp.

Kassaras, I., et al., 2015. Seismic damage scenarios in Lefkas old town (W. Greece), Bull. Earthq. Engin., DOI:10.1007/s10518-015-9789-z.

Kassaras, I., et al., 2018. Seismic risk and loss assessment for Kalamata (SW Peloponnese, Greece) from neighboring shallow sources, Bollettino di Geofisica Teorica e Applicata, 59, 1:1-26, doi: 10.4430/bgta0222.

Kazantzidou-Firtinidou, D., et al., 2018. Empirical seismic vulnerability, deterministic risk and monetary loss assessment in Fira (Santorini, Greece), Nat. Hazards, doi: 10.1007/s11069-018-3350-8.

Motazedian,D., Atkinson, G.M., 2005. Stochastic finite-fault modeling based on a dynamic corner frequency, BSSA, 95(3):995–1010

Nakamura, Y., 1989. A method for dynamic characteristics estimation of subsurface using microtremor on the ground surface. QR Railway Tech. Res. Inst., 30, 25-33.

Thelen, W.A., et al., 2016. Feasibility study of EEW in Hawaii: U.S. Geological Survey, USGS O-F Report 2016–1172, 30 p.

15th International Congress of the Geological Society of Greece
Athens, 22-24 May, 2019 | Harokopio University of Athens, Greece
Bulletin of the Geological Society of Greece, Sp. Pub. 7 Ext. Abs. GSG2019-215

Directivity effect on strike slip faults at North Aegean area, Greece

D. Kementzetzidou[1], A.A. Panou[1], P. Papadisopoulou[1]

(1) Aristotle University of Thessaloniki, Department of Geology, 54124, Thessaloniki, Greece, dkementz@geo.auth.gr, arpanou@geo.auth.gr, ppara@geo.auth.gr

This study examines the ground motion pulses during events which occurred in strike slip faults in order to show rupture directivity. Earthquake directivity is the focusing of wave energy along the fault in the direction of rupture. Observations from previous studies have displayed the effects of near-fault ground motions and suggested the forward and backward rupture directivity (Cocco, 1997; Somerville et al., 1997; Koketsu and Miyake, 2008; Poiata et al., 2012; Kane et al., 2013). Forward rupture directivity effects occur when the rupture front propagates toward the site, and the direction of slip on the fault is aligned with the site. Conversely backward directivity effects occur when the rupture propagates away from the site. Rupture directivity effects cause spatial variations in ground motion amplitudes and duration around faults. If a site is located in the forward direction of the rupture most of the seismic energy will arrive in a large brief pulse. Backward directivity effects are recorded as long duration motions with low amplitudes at long periods.

Considering the aforementioned works, an attempt is made here to explain the effects of rupture directivity using waveforms from earthquakes which occurred in the study area (North Aegean, Figure 1). Digital recordings were taken from the broadband seismological stations belonging to the Hellenic Unified Seismological Network (HUSN, network codes: HL, HT, HP, HA). Waveform data have been processed to form individual events corresponding to the initial earthquakes, and have been associated with the appropriate response information for the time period of the event. The deconvoluted data is shown in ground velocity units.

A demonstration of the effect of the ground motion directivity pulses is given in Figure 1 for the Lemnos earthquake (M 5.9). The earthquake occurred on January 8th 2013 in North Aegean Sea on a right lateral strike slip fault. The fault plane solution estimated by NOA (National Observatory of Athens) and it indicates a right lateral strike slip faulting mechanism in a NE-SW direction (strike: 60^0), moment magnitude of 5.7 and a shallow hypocenter (8 km), at only 42 km epicentral distance from the Lemnos island. The locations of the stations used for this study and the recorded ground motions (north south component) as well as the focal mechanism of the earthquake are presented in Figure 1. The main aspects of the rupture configuration contributing to the generation of fault ground motions pulses during a strike-slip faulting event are studied here.

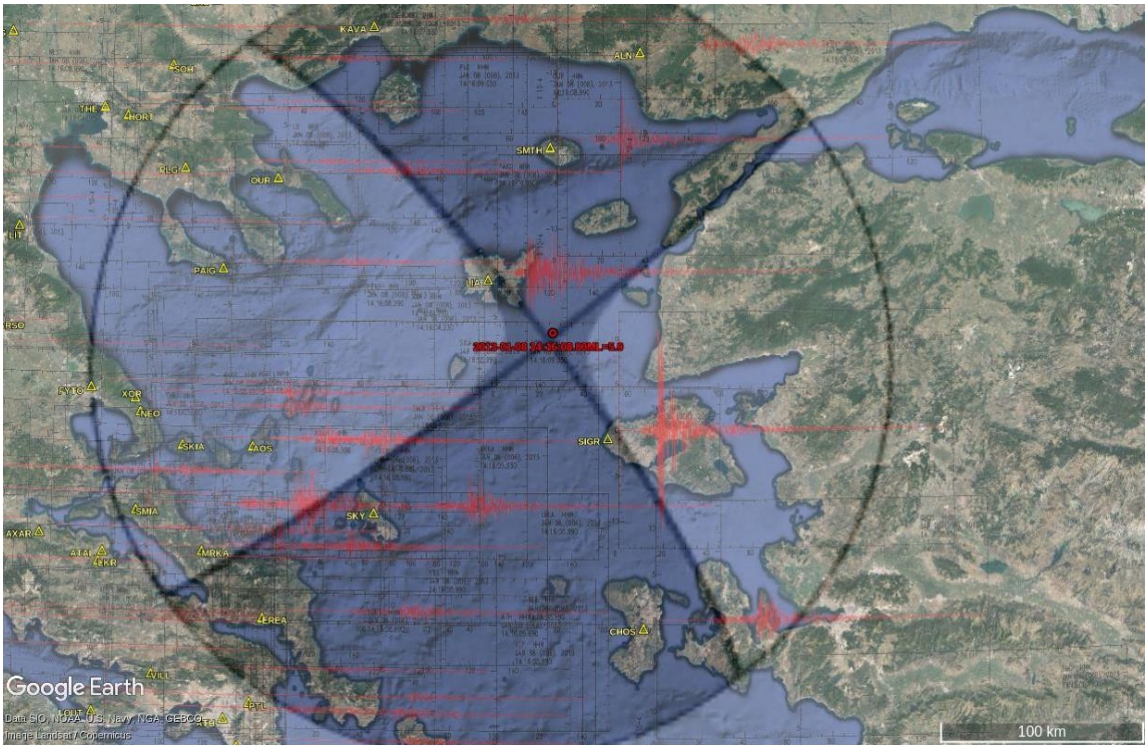

Figure 1. Map showing the epicenter and the focal mechanism of the 20130108_141608. Distribution of the stations (yellow triangles) and observed displacement time series (red lines) are also marked in the figure.

According to the focal mechanism we expect that forward rupture directivity effects propagate along strike. Therefore, stations recordings located in compression (grey) areas will present the forward rupture directivity effect whereas the recordings placed in dilatation (light) areas will show the backward directivity effect. Figure 1 points out the influence of rupture directivity effects at the recording sites. Despite similar epicentral distances, stations located at N and NNW as well as S and SE from the epicenter have amplitudes much larger than those located at E and W. Some representative stations along with the corresponding recordings and their rupture directivity classification are shown in Table 1. For example, the SIGR record is displayed where ground motions have a large amplitude and a short duration (forward directivity effect). On the other hand, the ground motion in station AOS is characterized by a longer duration and a lower amplitude ground motions (backward directivity effect).

Table 1. Ground velocity time histories of selective stations and their rupture directivity characterization.

a/a	Station	R (km)	Recordings	Directivity
1	LIA	44		Forward
2	SIGR	55	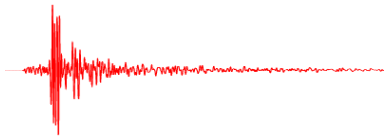	Forward
3	SMTH	89		Forward
4	AOS	159		Backward
5	OUR	157		Backward
6	PAIG	167		Backward

Acknowledgements

We acknowledge support of this work by the project “HELPOS – Hellenic System for Lithosphere Monitoring” (MIS 5002697) which is implemented under the Action “Reinforcement of the Research and Innovation Infrastructure”, funded by the Operational Programme "Competitiveness, Entrepreneurship and Innovation" (NSRF 2014-2020) and co-financed by Greece and the European Union (European Regional Development Fund).

References

Cocco, M., 1997. Seismic Hazard assessment: Rupture propagation modeling for ground motion prediction. Seismic Risk SERINA, 21-27 September, Thessaloniki, Greece.

Kane, D.L., Shearer, P.M., Goertz-Allmann, B.P., Vernon, F.L., 2013. Rupture directivity of small earthquakes at Parkfield. J. Geophysical Research. 118, 212-221.

Koketsu, K., Miyake H., 2008. A seismological overview of long-period ground motion. J. Seismol. 12, 133-143.

Somerville, P.G., Smith, N.F., Graves, R.W., Abrahamson, N.A., 1997. Modification of empirical strong ground motion attenuation relations to include the amplitude and duration effects of rupture directivity. Seismol. Res. Lett. 68, 199–222.

Poiata, N., Miyake, H., Koketsu, K., 2012. Generation Mechanism of Near-Fault Ground Motion for Dip-Slip Faulting. 15th World Conference on Earthquake Engineering, Lisbon, Portugal, p. 5071.

15th International Congress of the Geological Society of Greece
Athens, 22-24 May, 2019 | Harokopio University of Athens, Greece
Bulletin of the Geological Society of Greece, Sp. Pub. 7 Ext. Abs. GSG2019-237

Methana volcanic observatory: Towards a seismic and geodetic network deployment to monitor seismicity, seismic velocity changes and deformation

C.P. Evangelidis[1], E. Sokos[2], A. Ganas[1], K. Chousianitis[1], K. Kontakos[1], S. Liakopoulos[1], M. Samios[1], K. Boukouras[1], I. Karamitros[1] and G.-A. Tselentis[1]

(1) Institute of Geodynamics, National Observatory of Athens, Athens, Greece, cevan@noa.gr
(2) Department of Geology, University of Patras, Rio, Greece.

An effort to monitor seismicity and deformation across the Methana volcanic complex is under implementation. Our target is to monitor continuously any potential volcanic activity and deformation across the volcano using pilot applications of innovative seismic and geodetic methods. Aim of the project "GEORISK – Developing Infrastructure and Provision of Services through Actions of Excellence to Reduce the Impact of Geodynamic Hazards" is to assess the volcanic risk in the broader area that may affect maritime and air transport, in order to determine preventive measures. Even in the case of volcanic quiescence, seismological and geodetic data, derived from a permanent and temporary infrastructure, will define the level of volcanic status, hence the continuous (background) seismic-volcanic activity. We are deploying a network of permanent broadband seismic stations at the volcano and the neighboring islands. These stations will be incorporated in the Hellenic Unified Seismic Network (HUSN). A complementary deployment of temporary seismic stations will cover the entire volcanic complex aiming at the microseismicity monitoring and its association with tectonic or volcanic processes. In recent years, ambient noise interferometry (ANI) methods have been successfully used to detect temporal seismic velocity changes in volcanoes. Travel times between neighboring seismic stations are constantly obtained from their cross-correlation function (CCF) of ambient seismic noise. Thus, relative velocity changes in the Earth crust are likely to be caused by the change of stress and/or volume within the volcano and are accounted as precursors to volcanic events. The ground motions in the Methana volcanic complex will be also investigated geodetically by means of a non-permanent GNSS network along with one continuously recording GNSS station. An extensive experience on similar studies and network deployments in Santorini, Milos and Nisyros volcanic complexes assists on the optimal design of the seismic and geodetic network able to monitor, in a cost effective way, temporal changes across Methana volcano.

Methana volcano

Methana peninsula, located in the Saronicos Gulf at the westernmost part of the South Aegean active volcanic arc and 50km south of Athens, shows a long recorded volcanic history from Upper Pliocene to recent times. It is composed by andesitic and dacitic volcanic rocks with the more recent dated at 0.2 ± 0.3 Ma (Pe-Piper and Piper, 2013). The latest eruption giving andesitic lava is described by the ancient geographer Strabo at about 230 BCE. Moreover, Pausanias volcanic field is the offshore continuation of northern Methana and is comprised of six cones or domes (Foutrakis and Anastasakis, 2018). The long lived volcanic field is characterized by relatively low rates of magma supply and absence of Plinian phreatomagmatic eruptions. Recent tomographic results of the Hellenic arc show a thinned lithosphere associated with an horizontal slab tear that coincides with the volcanic centers in this area (Hansen et. al., 2018).

Volcanic observatory network

Current permanent seismic networks are not covering adequately the Saronikos Gulf area. Thus, the magnitude completeness of the recorded microseismicity is considered high. Our aim is to develop a local network surrounding the Methana peninsula able to detect microseismicity (Fig. 1). Additionally, our target is to monitor continuously any potential volcanic activity and deformation across the volcano using innovative ANI methods. The inter-station paths of such a local network will be able to sample with adequate resolution this part of the Saronic Gulf (Fig. 1). Within the project "GEORISK", the first phase of seismic station deployment was succeeded. Three temporary short -period stations were installed at Agious Theodorous (MET4), Makriloggos (MET5) and Megalochori (MET6) at Methana peninsula on February 2019 (Fig. 1). The vaults of two permanent broadband seismic stations are under construction at Methana village (MET1) and Kameni Chora (MET2) and the stations will be installed on May 2019 Fig. 1). The vault design of the broadband seismic stations is developed by NOA engineers and forms a totally independent free-field installation site (Fig. 1). The seismometer will be placed in bedrock totally independent from the cemented vault cell. Within the vault a higher level in a "step-wise" design will ensure that the rest of the equipment would be placed safely avoiding potential flooding but also having the adequate distance from the thermally insulated seismic sensor itself. In site MET1 a permanent GNSS station will be also stably installed (Fig. 2), following strict criteria on selecting an unobstructed horizon site (Fig. 2)..

Apart from monitoring the ongoing microseismicity in the area, we are interested in monitoring volcanic edifices for temporal changes of the velocity of the seismic waves. When magma pressure increases inside a volcano, the added pressure results into the inflation of the volcano, and small cracks around the magma chamber will decrease the velocity of seismic waves. That small decrease in velocity can be detected successfully using ambient noise interferometry (ANI) techniques. Based on previous ANI studies in Milos and Santorini (Daskalakis et. Al, 2016) we can resolve any potential velocity change of ±0.1%.

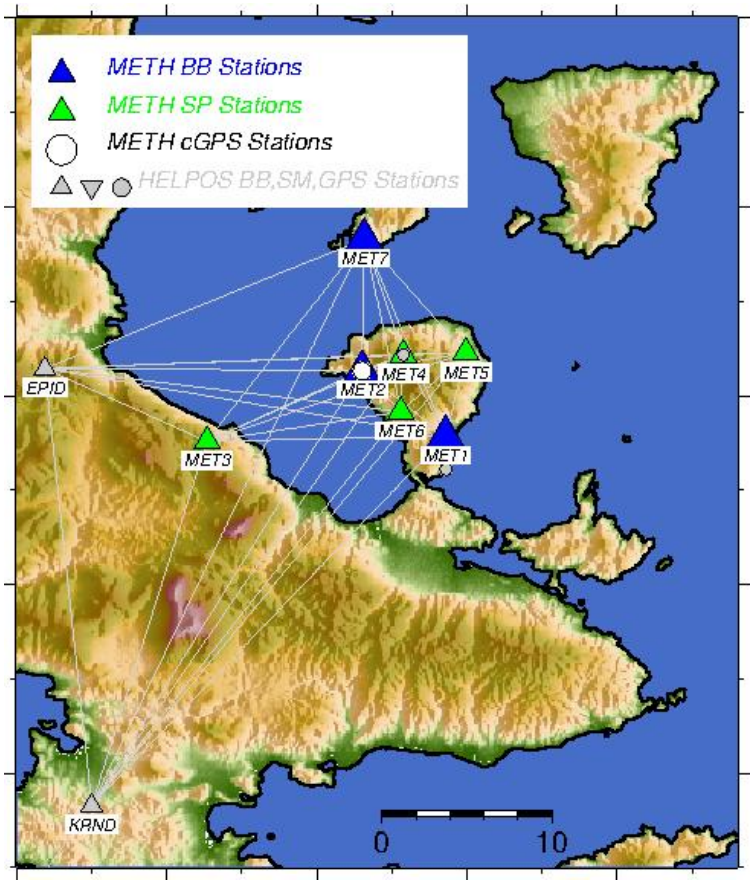

Figure 1. Network of permanent (blue) and temporary (green) seismic stations in Methana and their inter-station paths.



Figure 2. MET2 seismic vault under construction. The GNSS antenna will be installed on the concrete pillar.

Acknowledgements

The local municipality of Troizinia-Methana is supporting the network deployment in terms of granting land permissions, seismic vault construction, power supply and telecommunication links. We acknowledge support of this abstract by the project "GEORISK – Developing Infrastructure and Provision of Services through Actions of Excellence to Reduce the Impact of Geodynamic Hazards" (MIS 5002541).

References

Daskalakis, E., C.P. Evangelidis, J. Garnier, N.S. Melis, G. Papanicolaou and C. Tsogka, 2016. Robust seismic velocity change estimation using ambient noise recordings, Geophys.J.Int, doi: 10.1093/gji/ggw142.

Foutrakis, P., Anastasakis, G., 2018.The active submarine NW termination of the South Aegean Active Volcanic Arc: The Submarine Pausanias Volcanic Field, Journal of Volcanology and Geothermal Research.

Hansen S., C.P. Evangelidis, G.A. Papadopoulos, Imaging Slab Detachment within the Western Hellenic Subduction Zone, Geochemistry, Geophysics, Geosystems, under review.

Pe-Piper, G., Piper, D.J.W., 2013. The effect of changing regional tectonics on an arc volcano: Methana, Greece, Journal of Volcanology and Geothermal Research 260, 146-163.

15th International Congress of the Geological Society of Greece
Athens, 22-24 May, 2019 | Harokopio University of Athens, Greece
Bulletin of the Geological Society of Greece, Sp. Pub. 7 Ext. Abs. GSG2019-305

A new improved version of the Aeromagnetic Map of Greece

S. Chailas[1], A. Tzanis[1]

(1) Section of Geophysics, Department of Geology and Geoenvironment, National and Kapodistrian University of Athens, Panepistimiopolis, Zografou 157 84, Greece, schailas@geol.uoa.gr

Introduction

Chailas et al. (2010) presented a unified and homogenized aeromagnetic map of the Greek mainland. In the frame of HELPOS a new enriched, re-interpreted and homogenized, aeromagnetic map of Greece is being compiled. In the new version new areas were added to the previous map, and the data were re-assessed prior to the final compilation in order to both use incorporate the definite IGRF model and, diminish the effect of topography. As it will be shown here the improvement of the resulted map is of the order of some tens of nT.

Data Sources

The compilation of the unified and homogeneous aeromagnetic map of Greece is based on the 1:50,000 map series of IGME, produced by ABEM AB and Hunting Geology and Geophysics Ltd.

The ABEM maps (ABEM, 1967), were produced with measurements at a nominal constant ground clearance (GC) of 275±75m above ground level (AGL) i.e. in constant ground clearance mode. The direction of the flight lines (tracks) was NE-SW and the mean distance between them was about 1km. Connection (tie) lines for crossover adjustment of the data were also flown at NE-SW direction, with a mean distance of 10km.

Hunting Geology and Geophysics Ltd. has generally used a magnetic field measurement spacing of 200–250m and has flown on a NE-SW direction, but at different GC's and track densities depending on the topography. The data collection schemes are as follows (also see Fig. 1):

- Areas A1 and A2: Nominal GC 150m AGL at a nominal distance of 400m between tracks.
- Area B: Nominal GC l 150m above mean sea level (AMSL) at a nominal distance of 400m.
- Areas C1, C2a and C3: Nominal GC 300m AGL at a nominal distance of 800m.
- Exception is the area of Mt. Olympus, (area C2b) where the flight level was 3000m AMSL with the same nominal distance between lines.
- Areas D1 and D2: Nominal flight level was 2300m AMSL and 2100m AMSL respectively at a distance of 1000m between tracks.

In all cases, connection lines were flown at a NE-SW direction and a spacing of 10km. The IGRF correction was based on the IGRF model for the epoch 1977.3. A constant value of 150nT was added to the magnetic anomaly values prior to plotting the contour maps.

Additional Data Non Aeromagnetic Data

In order to complete the area coverage for large scale maps, an additional dataset is going to be incorporated (Pavlakis et al., 1993). It consists of digitized marine magnetic anomalies, covering the Aegean Sea area.

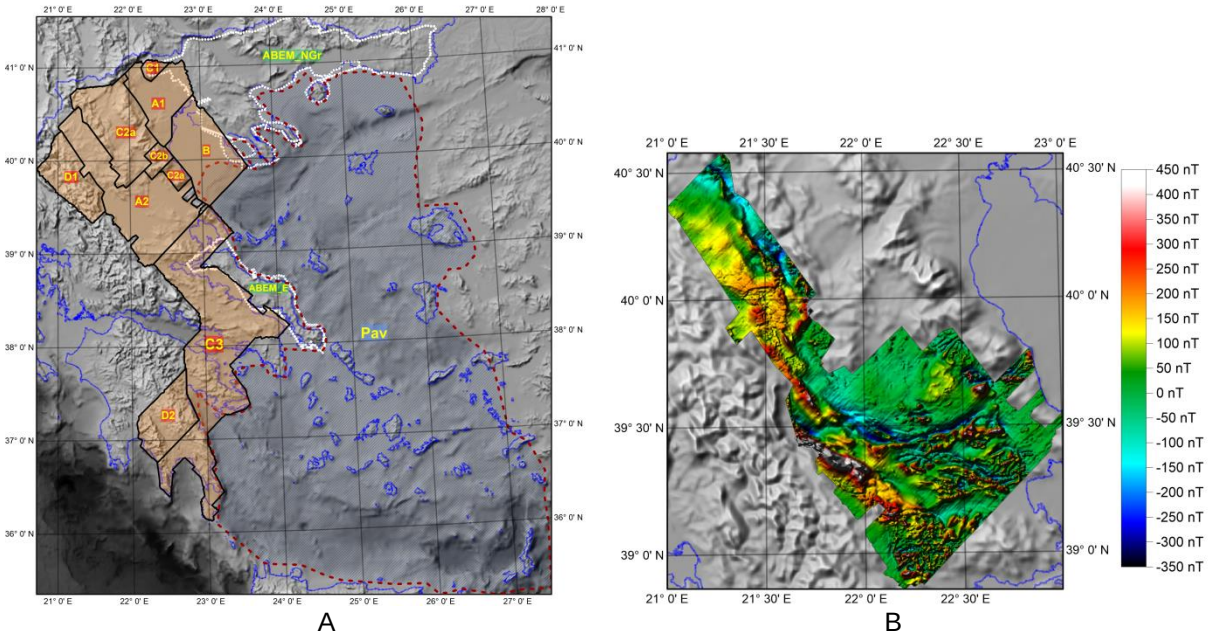

Figure 1: A. Map showing the area coverage of the aeromagnetic data. B. Map showing the reproduced map based on the digitized values of the original aeromagnetic maps for area A2.

Aeromagnetic Anomalies Data re-processing

In the present attempt and, prior to the homogenization, the digitized aeromagnetic anomalies subjected to an additional correction procedure:

- For the Hunting maps (as an example, the map of the area A2 is given in Fig. 1B), the 150 nT value which had originally been added was now subtracted from the grids.
- The IGRF model for the epoch 1977.3 for the Hunting Maps and for the epoch 1966.5 for the ABEM maps was recalculated for the entire area and for 0 m elevation and then was added to the grids. Thus we attempted to reproduce, as close as possible, the original Total Magnetic Intensity maps.

The next step was to recalculate the Magnetic Anomaly maps using this time the definite IGRF for the corresponding epochs and for the flying elevations in each area. As a DEM we used the SRTM model of 3 seconds after re-gridding it from its original ~90m interval to the 250m of our own grids. So we,

- computed the definite IGRF model at the flying elevation, for each area (the resulted map for the area A2 is given in Figure 2A) and for its nominal epoch of surveying.
- the definite IGRF was then subtracted from the reproduced Total Magnetic Intensity maps (the resulted map for the area A2 is given in Fig. 2B).

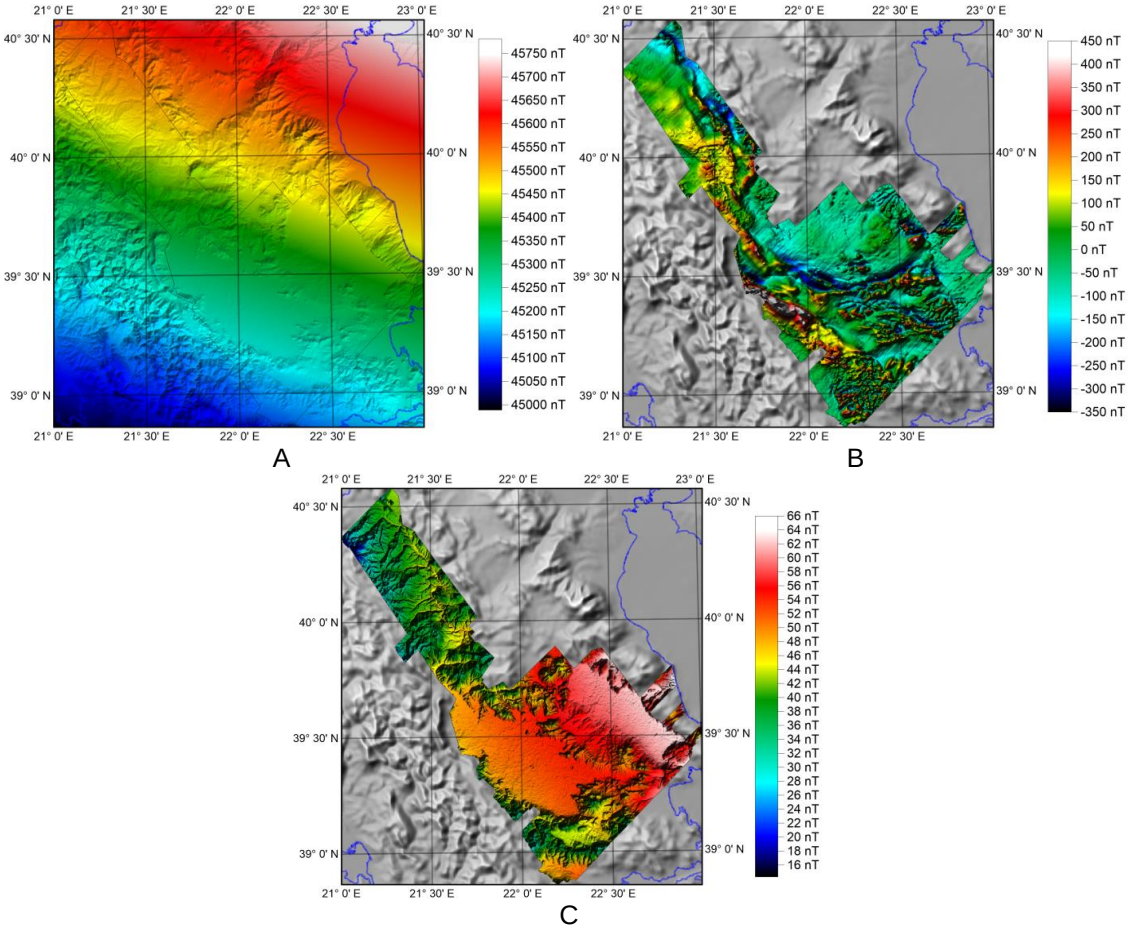

Figure 2: A. Map showing the calculated dGRF values on the flying height for the area A2. B. The final dIGRF corrected map for area A2. C. Map resulted by the subtraction of the final dIGRF corrected map from the original for area A2.

The improvement of our new data, compared to the original ones (Chailas et al., 2010) becomes obvious in Fig. 2C. The original maps, at least for the lower elevations, seem to give magnetic anomaly values overestimated by some tens of nT.

Acknowledgements

This work is partly supported by the project "HELPOS – Hellenic Plate Observing System" (MIS 5002697) which is implemented under the Action "Reinforcement of the Research and Innovation Infrastructure", funded by the Operational Programme "Competitiveness, Entrepreneurship and Innovation" (NSRF 2014-2020) and co-financed by Greece and the European Union (European Regional Development Fund)

References

Chailas, S., Tzanis, A., Kranis, H., Karmis, P., 2010. Compilation of a Unified and Homogeneous Aeromagnetic Map of the Greek Mainland. 12th Int. Conference of the Geol. Soc. Greece, Bull. Geol. Soc. Greece, XLIII, No4, pp. 1919- 1929.

Pavlakis, P. Makris, J., Alexandrie, M., 1993. Proceeding of Marine Geophysical Mapping of Aegean Sea. 2nd International Congress, Hellenic Geophysical Union. Florina, Greece, May 5-7, pp. 400-411.

15th International Congress of the Geological Society of Greece
Athens, 22-24 May, 2019 | Harokopio University of Athens, Greece
Bulletin of the Geological Society of Greece, Sp. Pub. 7 Ext. Abs. GSG2019-310

Probabilistic Seismic Hazard Assessment for Lesvos Island Using Multiple Seismic Source Models Combined in a Logic Tree to Account for Epistemic Uncertainty

N. Vavlas[1], A. Kiratzi[1], B. Margaris[2], G. Karakaisis[1]

(1) Aristotle University of Thessaloniki, Dept of Geophysics, Thessaloniki, Greece navavlas@geo.auth.gr
(2) Institute of Earthquake Engineering and Engineering Seismology, (EPPO), Thessaloniki, Greece

We carry out a new probabilistic seismic hazard analysis (PSHA) for Lesvos Island, in the northern Aegean Sea. Being the most densely populated island and hosting the capital of the prefecture, its seismic potential has significant social-economic meaning. The new version of R-CRISIS module is used for the hazard estimation (Ordaz *et al.*, 2017) which has high efficiency and flexibility in model selection. We incorporate into the calculations several different source models, as well as Ground Motion Prediction Equations (GMPEs) using a Logic Tree approach. This approach allows capturing the epistemic uncertainties in different input models by employing-considering alternative models in the hazard estimation (Bommer *et al*., 2005).

The earthquake source models (Fig. 1) include both line sources, representing seismogenic faults of the broader region, as well as area sources representing seismic zones. The hazard from these sources is computed based on the standard Cornell approach (Cornell, 1968). The assumption of the module is that within a source zone, seismicity is evenly distributed by unit area and thus all points might be potential earthquake focus. The sources corresponding to seismogenic faults are those included in the SHARE Database (Giardini *et al*., 2013), alongside those proposed by Papazachos *et al*., (2001). These are modeled both as area and line sources, with the latter resulting from the intersection of the fault with the ground surface.

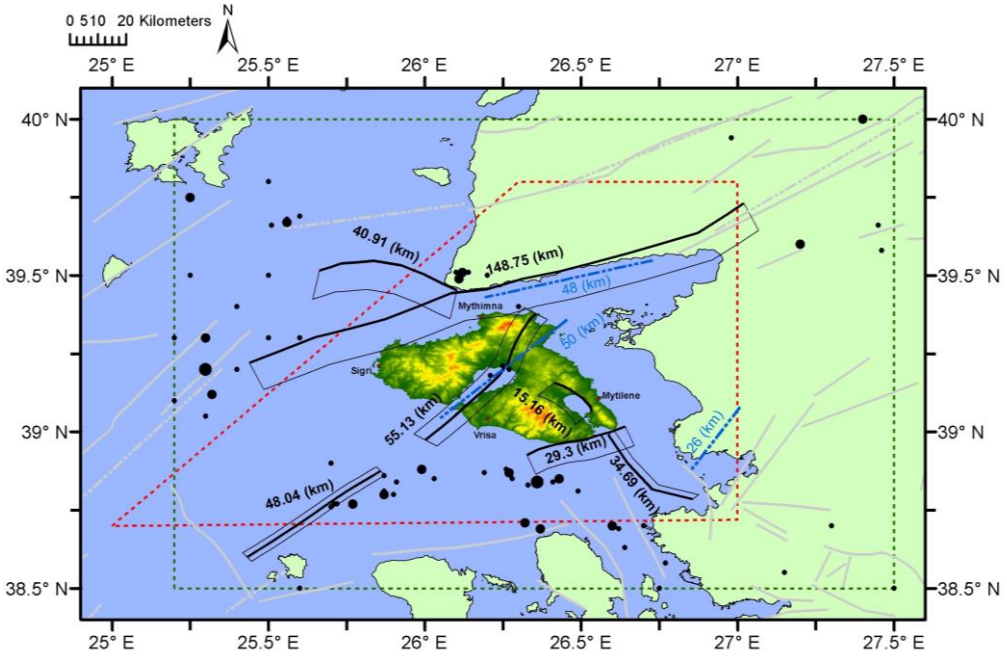

Figure 1. Seismic sources used in the hazard assessment. Black circles denote the seismicity (M≥4.5) for the period 1964-2019. The red dashed lines delineate the Lesvos Zone (Papaioannou and Papazachos, 2000). The black lines denote the SHARE seismic sources, while the blue dashed lines denote the line sources from Papazachos *et al.*, (2001).

The seismicity parameters, from a complete earthquake catalog spanning 106 years, were calculated within the area delimited by the green dashed line in Figure 1. The Lesvos Zone no (61), as proposed by Papaioannou and Papazachos, (2000) was also considered as an alternative zone model to the aforementioned. Using the Logic Tree approach, the six (6) in total different source models are combined into a single one, to account for the epistemic uncertainty in the hazard estimation.

The intensity measures used are Peak Ground Acceleration, (PGA), Peak Ground Velocity, (PGV), and Spectral Acceleration, (SA at T=0.2 sec). We calculated hazard curves for selected sites on the island: the capital Mytilene (Fig. 2), the village of Vrisa, in southeastern coast, which was partially ruined by the 12 June 2017 Mw 6.3 earthquake (Kiratzi, 2018 among others), Mythimna and Sigri, in the northwestern and southwestern part of the island, respectively. Hazard Maps are also presented in terms of all three intensity measures, for mean return period of 475 years (or 10% probability of exceedance in 50 years, assuming a Poisson process).

The spatial distribution of PGA in the hazard maps, using equal weights to all models, is between 0.27 g and 0.48 g, for

PGV between 19 cm/s and 30 cm/s while the spectral values SA (0.2 sec) between 0.62 g and 1.0 g. According to the New Greek Seismic Code (EAK, 2003), Lesvos belongs to Zone II of 0.24 g.

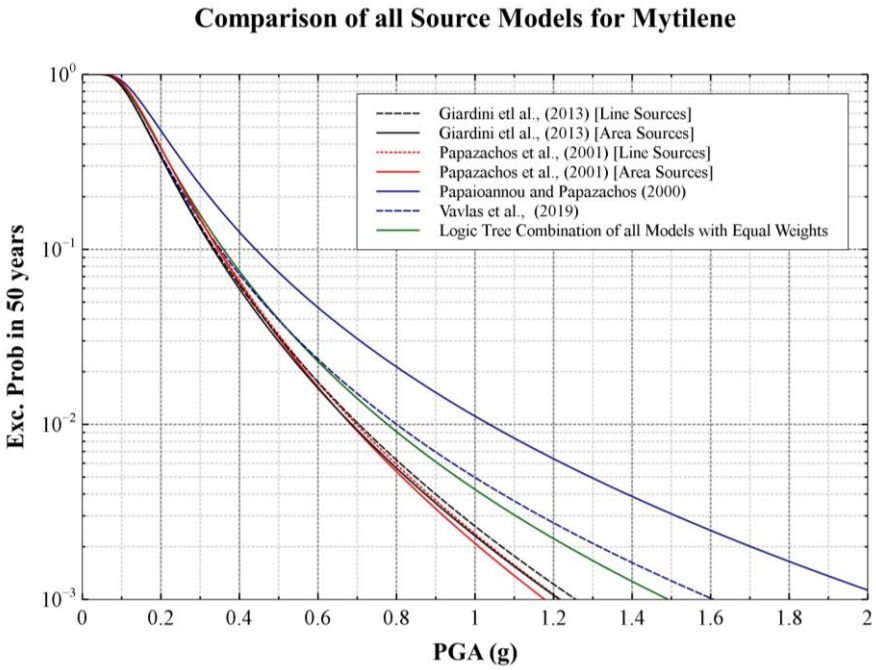

Figure 2. Seismic hazard (PGA) curves for the capital city of Mytilene for individual models and combined logic tree model.

Finally, the results regarding the two (2) area source models, which represent seismogenic faults, were disaggregated to depict the relative contribution of different earthquake sources and magnitudes to the results. The Edremit fault, right opposite of the northern shore of Lesvos, seems to contribute the most in the northern part of the island, which is something to be expected, being one of the most hazardous seismic sources in the broader region. The Agia Paraskevi right lateral fault (Chatzipetros *et al*., 2013), that cuts off the central part of Lesvos from N to S, has a significant contribution around the central part of the island, and especially in the village of Vrisa where small distance and big magnitude bins show elevated values.

The sources proposed by Giardini *et al*., (2013), except the two ones already mentioned, do not seem to contribute much to the final result. The most important factor leading to this are the activity rates, which, calculated from the average slip rate, are relatively low (<0.01 eq/yr). For a mean return period of 475 years, activity rates that low appeared insignificant in the calculations.

Acknowledgements

We acknowledge support of this work by the project "HELPOS – Hellenic System for Lithosphere Monitoring" (MIS 5002697) which is implemented under the Action "Reinforcement of the Research and Innovation Infrastructure", funded by the Operational Programme "Competitiveness, Entrepreneurship and Innovation" (NSRF 2014-2020) and co-financed by Greece and the European Union (European Regional Development Fund).

References

Bommer, J., Scherbaum, F., Bungum, H., Cotton, F., Sabetta, F. and Abrahamson, N., 2005. On the Use of Logic Trees for Ground-Motion Prediction Equations in Seismic-Hazard Analysis. Bulletin of the Seismological Society of America, 95(2), pp.377-389.

Chatzipetros, A., Kiratzi, A., Sboras, S., Zouros, N., Pavlides, S., 2013. Active faulting in the north-eastern Aegean Sea Islands. Tectonophysics, 597-598, pp.106-122

Cornell, C.A., 1968. Engineering seismic risk analysis. Bull. Seism. Soc. Am., 58, 1503-1606.

EAK, 2003. Greek Seismic Code. Earthquake Planning & Protection Organization. Athens-Greece, ed., 72 pp and 7 appendixes (in Greek).

Giardini D. *et al*., 2013, Seismic Hazard Harmonization in Europe (SHARE): Online Data Resource, doi: 10.12686/SED-00000001-SHARE, 2013.

Kiratzi, A., 2018. The 12 June 2017 Mw 6.3 Lesvos Island (Aegean Sea) earthquake: Slip model and directivity estimated with finite-fault inversion. Tectonophysics, 724-725, pp.1-10.

Ordaz, M., Salgado-Gálvez, M.A., 2017. R-CRISIS Validation and Verification Document. Technical Report. Mexico City, Mexico.

Papaioannou, Ch. A. and Papazachos, B.C., 2000. Time-independent and time-dependent seismic hazard in Greece based on seismogenic sources, Bull. Seism. Soc. Am., 90, 22-33.

Papazachos, B.C., Mountrakis, D.M., Papazachos, C.B., Tranos, M.D., Karakaisis, G.F. and Savvaidis, A.S., 2001. The faults that caused the known strong earthquakes in Greece and surrounding areas during 5th century B.C. up to present, Proc. 2nd Conf. Earthquake Eng. and Eng. Seism., 2-30 September 2001, Thessaloniki, Greece, 1, 17-26 (in Greek).

15th International Congress of the Geological Society of Greece
Athens, 22-24 May, 2019 | Harokopio University of Athens, Greece
Bulletin of the Geological Society of Greece, Sp. Pub. 7 Ext. Abs. GSG2019-311

GPS Networks in Seismically Active Areas of Western Greece: The Case of Zakynthos Earthquake (Mw=6.8) of October 25, 2018

V. Sakkas[1], K. Pavlou[1], S. Vassilopoulou[1], E. Lagios[1]

(1) Section of Geophysics-Geothermics, National & Kapodistrian University of Athens, Panepistimiopolis, Zografou, Athens, Greece, vsakkas@geol.uoa.gr

Ground deformation studies based on satellite geodetic measurements (GPS/GNSS) have been proved a unique tool to measure ground deformation in seismically active areas aiming to study the tectonic motions associated with earthquake procedures. The Central Ionian Islands is an area of high seismicity accompanied with large ground deformation due to the intense tectonic activity occurring in the area. In order to measure pre- co- and post-seismic activity in this area several local GPS networks have been established since 2001 covering the islands of Cephalonia, Ithaca and Zakynthos. Periodic GPS campaigns provided vital information of the motions that occurred prior and after strong earthquakes, such as are the Cephalonia events in 2014, and the Lefkadian event in 2015 (Sakkas and Lagios 2015; 2017).

Late October 2018, a strong seismic event (Mw=6.8) occurred offshore ~40km SW of Zakynthos Island (Fig. 1). The post seismic activity that started that day continued for many months, comprised by several events of lower magnitude ~M5 and hundreds other smaller events. The post seismic activity that took place during the first few days after the main event was in the epicentral area, but also extended to the NE along three zones with a SW-NE extension that cross-cut the central and southern part of the island.

The October 25, 2018 Zakynthos Earthquake is a typical example of a strong event that caused intense deformation in the broader epicentral area, revealing significant tectonic structures in the island.

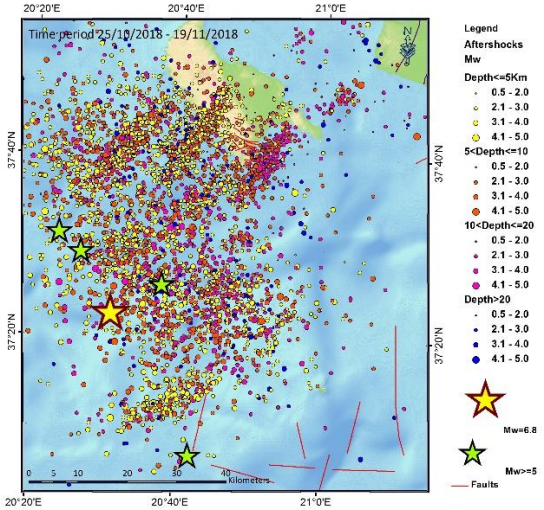

Figure 1. The October 25th, 2018 Zakynthos Earthquake and the post seismic activity during the following days.

Brief Geotectonic Setting

The Central Ionian islands in western Greece play an important role in the kinematic processes of the Eastern Mediterranean. They are situated within a very active seismotectonically complex area which is undergoing rapid and intense ground deformation. The highest seismic activity in Europe currently takes place in that region, constituting part of the Eastern Mediterranean Lithosphere that is subducting beneath the Aegean Lithosphere along the Hellenic Arc. The subduction zone terminates against the Cephallonia Transform Fault, a major strike-slip fault that links the subduction boundary to the continental collision between the Apulian microplate and the Hellenic foreland, and plays a key role in the region's geodynamic complexity (Brooks and Ferentinos, 1984).

Zakynthos Island consists of rocks of two zones, the Pre-Apulian or Paxos Zone and the Ionian Zone. Both zones lie to the west of the Pindos thrust and the boundary between them is the Ionian thrust which is generally considered to represent the most external Hellenides structure (Underhill, 1989). This thrust is not well exposed in Zakynthos, because the absence of Mesozoic carbonates and the occurrence of a thick Pliocene cover make the boundary between these zones difficult to define. The Pre-Apulian Zone is characterized by Upper Cretaceous to Miocene sediments (limestones, marly limestones etc.), whereas the Ionian zone, which appears in the southeastern part of the island, consists of limestones and evaporitic rocks of Triassic age. The post Alpine deposits are marls of Pliocene age and Quaternary marine and continental formations.

The GPS Measurements

The GPS network (14 stations) in Zakynthos was first installed in 2005 and re-measured in 2006, 2012, 2015, May 2018 and after the earthquake November 2018. Overall rms errors of about 1.0-7.0 mm and 2.0-8.1 mm for the horizontal and vertical components of displacement, respectively, were achieved for the majority of the stations (at a 90% confidence level) using the Bernese v5.2 software. Station No. 73 was chosen as a local reference station for the periods prior to 2010. Late 2013 a continuous GNSS site has been established by METRICA SA in the city of Zakynthos, and since then this site has been used as local reference station, showing a velocity vector with respect to ITRF2008 (V_{East}=12.7±1.1 mm/yr and V_{North}=-3.1±0.7 mm/yr) that is consistent with the anticipated regional motion (Hollenstein et al. 2008).

For the first re-measurement periods 2005-2015, the horizontal deformation is consistent with the anticipated southwestern motion of the area with respect to the ITRF. However, at the northern half of the island, the vectors show a westward motion (about 80 mm), while to the south a southwestern motion of the same amplitude prevails. The vertical deformation shows significant subsidence for the whole of the island. The strong differentiation in the motion between the northern and the southern parts of the island, observed mainly in the first re-measurement period (2005-2006), but also in the second period (2006-2015), highlights the different kinematic status of the two areas, as has been described also in previous works (Lagios et al. 2007).

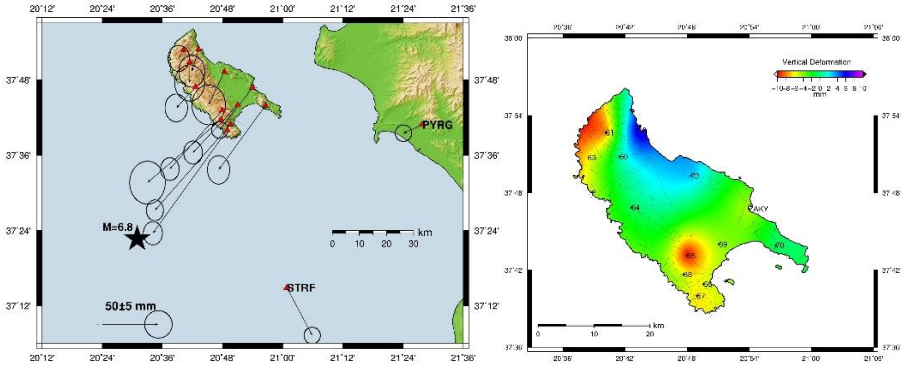

Figure 2. Horizontal (left) and Vertical (vertical) displacements (mm) of the Zakynthos GPS network observed for the period May to November 2018

The last remeasurements of the network took place during May and November 2018, before and after the strong earthquake. The deformation results of these two re-measurement periods may be considered as representing the co-seismic deformation occurred in the island (Fig. 2). The horizontal vector shows SW motion of about 110mm is the southern stations and less (~30mm) in the northern stations. Results from two other permanent stations that operate in the broader area, the PYRG station (METRICA SA) in western Peloponnese and the STRF station in Strofades islet (RING network http://ring.gm.ingv.it) show SW and SE horizontal motion, respectively. The most distinctive characteristic of the horizontal vectors is the differentiation of the motion vectors, in both amplitude and direction, between the northern and southern part of the island that has also been observed during the pre-seismic observational periods. The zone that marks the change of type of motion is across the northern line that forms the post seismic events (see Fig. 1) showing that there is a clear tectonic lineament that cross-cuts Zakynthos in its central area, and causes this different type of motion between the northern and southern part of the island.

Acknowledgements

The last GPS network remeasurement was performed on the framework of "HELPOS – Hellenic Plate Observing System" (MIS 5002697) which is implemented under the Action "Reinforcement of the Research and Innovation Infrastructure", funded by the Operational Programme "Competitiveness, Entrepreneurship and Innovation" (NSRF 2014-2020) and co-financed by Greece and the European Union (European Regional Development Fund). METRICA SA provided the raw GNSS data for the ZAKY and PYRG stations.

References

Brooks, M., Ferentinos, G. 1984. Tectonics and sedimentation in the Gulf of Corinth and the Zakynthos and Kefallinia channels, Western Greece. Tectonophysics, 101(1-2), 25-54.

Hollenstein, CH., Müller, M.D., Geiger, A., Kahle H.-G. 2008. Crustal motion and deformation in Greece from a decade of GPS measurements, 1993–2003. Tectonophysics, 449, 17-40.

Lagios, E., Sakkas, V., Papadimitriou, P., Parcharidis, I., Damiata, B.N., Chousianitis, K., Vassilopoulou, S. 2007. Crustal deformation in the Central Ionian Islands (Greece): Results from DGPS and DInSAR analyses (1995-2006). Tectonophysics, 444 (1-4), 119-145.

Sakkas, V., Lagios, E. 2017. Ground deformation effects from the~ M6 earthquakes (2014–2015) on Cephalonia–Ithaca Islands (Western Greece) deduced by GPS observations. Acta Geophysica, 65,1, 207-222, Springer.

Sakkas, V., Lagios, E. 2015. Fault modelling of the early-2014~ M6 Earthquakes in Cephalonia Island (W. Greece) based on GPS measurements. Tectonophysics, 644, 184-196, Elsevier.

Underhill, J.R. 1989. Late Cenozoic deformation of the Hellenide foreland, western Greece. Bull. Soc. Geol. Am. 101, 613-634.

15th International Congress of the Geological Society of Greece
Athens, 22-24 May, 2019 | Harokopio University of Athens, Greece
Bulletin of the Geological Society of Greece, Sp. Pub. 7 Ext. Abs. GSG2019-355

Shakemaps from the urban Strong Ground Motion of Chania

G. Chatzopoulos[1], F. Vallianatos[1,2], I. Papadopoulos[1,3]

(1) UNESCO Chair on Solid Earth Physics & Geohazards Risk Reduction, Laboratory of Geophysics & Seismology, Technological Educational Institute of Crete, Greece, ggh1983@hotmail.com
(2) Department of Geophysics–Geothermics, Faculty of Geology and Geoenvironment, National and Kapodistrian University of Athens, Athens, Greece, fvallian@geol.uoa.gr
(3) Seismic Research Centre, The University of the West Indies, St. Augustine, Trinidad & Tobago.

Introduction

The project HELPOS – Hellenic System for Lithosphere Monitoring, Greece aims to create/upgrade a unified network to record the ground motion with the use of a variety of sensors. Among the HELPOS goals is to build urban accelerometer networks such as the dense Strong Ground Motion (SGM) network that have been installed in the Chania basin. The dense SGM networks aiming to continuously monitor the ground motion in urban environments and present the results in enhanced detail shakemaps, especially in areas where high variations in the Peak Ground Acceleration (PGA) values due to the local site effects are observed.

The geology of the investigation area

The Crete island has a complex geology of Crete which is characterised by continuous nappe units, a product of the different stress fields that acted since upper Oligocene-Miocene, due to the tectonic plates collision, which have placed the extensive tectonic nappes on Plattenkalk limestone of the Talea Ori unit (Mountrakis, 1986; Kilias et al. 1999). In the Chania area, at the southern part there are thick recrystallized limestones and marbles which are considered as the lowest units of Crete and above them there are Neogene sediments mainly consisted of marles, sandstones and limestones. Most of the Chania southern basin is covered with Quaternary alluvial deposits and in the northern part where the urban area is located, there are Neogene sediments such as marles with sandstones and limestones (Mountrakis, 2012).

The utilized sensors

Aiming to monitor the Peak Ground Acceleration distribution in the different geological formations, a dense strong ground motion network started operating in the Chania broader basin area as well as the crucial parts of the urban area and the old Venetian town. The first two types of sensors that have been installed have similar recording capabilities, the REF TEK 130 ANSS/02 and the 130 SM. To provide a detailed information regarding the ground motion during earthquakes six accelerometers were utilized in the area of interest with sampling rate at 250Hz. The initial results of the SGM network suggested that the sensor grid should be denser to provide better spatial resolution. Aiming to enhance the resolution of the results more REF TEK accelerometers were installed and afterwards we start using the cost-effective choice, the Satways' GSense. Examples of the monitoring installation of each sensor type are provided in figure 1.



Figure 1. The three types of accelerometer installed for the SGM network, the Ref Tek 130 ANSS/02(left) the 130 SM (middle) and the GSense (right).

Interpolation Method for shakemaps

The ArcGIS environment has been adopted to present the PGA values recorded from the SGM network in shakemaps. Among the available interpolators in the software, the geostatistical Kriging which uses a linear combination of weighted measured values to estimate the value at a point was preferred. Microtremors H/V spectral ratio studies that were performed in the location of each SGM station. The obtained predominant frequency f0 and amplitude A0 values (the largest peak) are used as variables to give a trend to the Ordinary Co-Kriging interpolation method. The PGA along with f0 and A0 variables which reflect the thickness and material properties of the geological formations are fitted in empirical semivariograms aiming to find the optimal fitting between observed and empirical values. An example of the interpolation results is illustrated in figure 2.

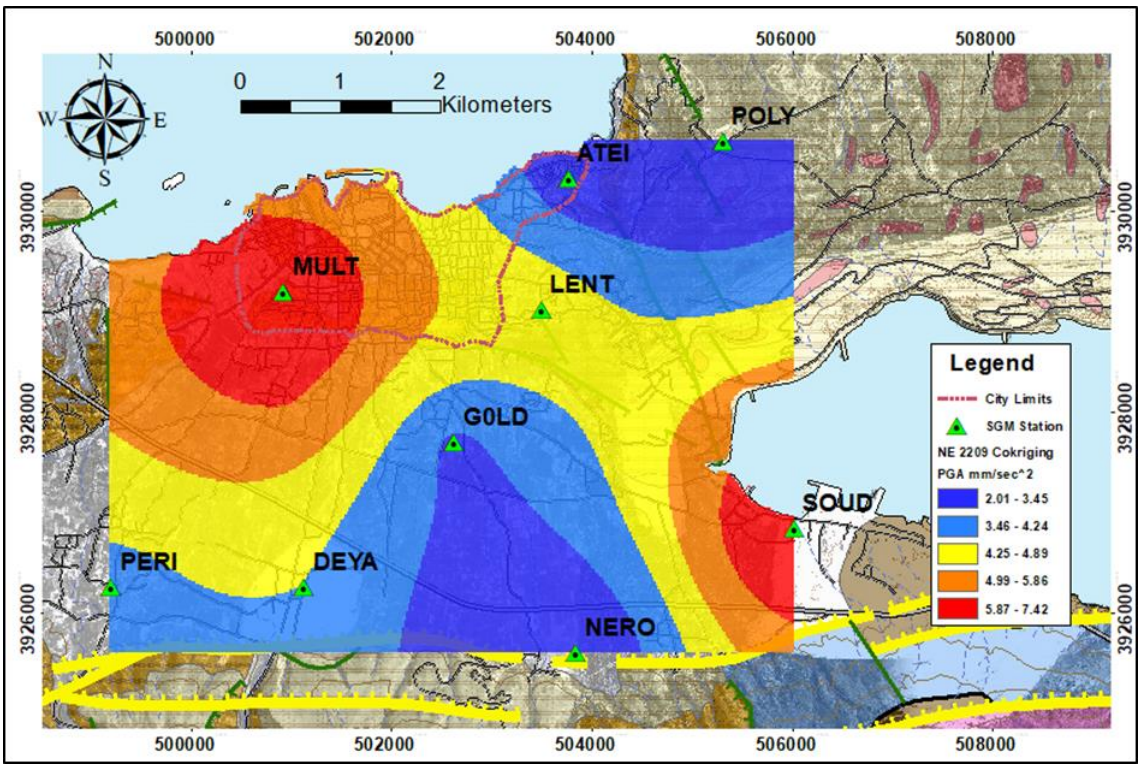

Figure 2. The PGA distribution obtained with the Ordinary Cokriging interpolation method for a local magnitude 4.1 earthquake (26/01/2018 22:09 UTC), located 64 km away northeast of Chania.

Results

The dense network of fourteen SGM station in the broader area Chania permits to monitor the PGA distribution the different parts of the urban. The SGM instruments are constantly recording the ground motions which enables the construction of detailed shakemaps. The use of ground parameters related with the geology and local site effects, f0 and A0 obtained by microtremors studies can improve the interpolation results.

Acknowledgements

We acknowledge support of this work by the project ''HELPOS – Hellenic System for Lithosphere Monitoring, Greece'' (MIS 5002697) which is implemented under the Action ''Reinforcement of the Research and Innovation Infrastructure'', funded by the Operational Programme ''Competitiveness, Entrepreneurship and Innovation, Greece'' (NSRF 2014–2020) and co-financed by Greece and the European Union (European Regional Development Fund).

References

Kilias A, Falalakis G and Mountrakis D, 1999. Cretaceous-Tertiary structures and kinematics of the Serbomacedonian metamorphic rocks and their relation to the exhumation of the Hellenic Hinterland (Macedonia, Greece). International Journal of Earth Sciences 88, 513-531

Mountrakis D, 1986. The Pelagonian zone in Greece: A polyphase deformed fragment of the Cimmerian continent and its role in the geotectonic evolution of the Eastern Mediterranean. Journal of Geology 94, 335-347.

Mountrakis D, Killias A, Pavlaki A, Fassoulas C, Thomaidou E, Papazachos C, Papaioannou C, Roumeliozi Z, Benetatos C, Vamvakaris D, 2012. Neotectonic study of Western Crete and implications for seismic hazard assessment. Journal of the Virtual Explorer 42, 19–20.

15th International Congress of the Geological Society of Greece
Athens, 22-24 May, 2019 | Harokopio University of Athens, Greece
Bulletin of the Geological Society of Greece, Sp. Pub. 7 Ext. Abs. GSG2019-366

Seismicity: A tool in forecasting Volcanic eruptions

P. Papadimitriou[1], A. Karakonstantis[1], V. Kapetanidis[1], K. Pavlou[1], I. Sotiriadis[1] and I. Spingos[1]

(1) Section of Geophysics–Geothermics, Department of Geology and Geoenvironment, National and Kapodistrian University of Athens, 15784 Panepistimiopolis, Zografou, Athens, Greece, ppapadim@geol.uoa.gr

The recent activity in the broader area of Hellenic Volcanic Arc (HVA) highlights the importance of continuous monitoring of selected volcanic centers (Papadimitriou et al., 2015). Volcanic activity is often accompanied by precursors which are related to the movement of magma, causing localized increase of stress, developing cracks and fissures in the crust and triggering seismicity. These effects can be investigated by local seismological networks that permit earthquakes and ambient seismic motions to be recorded and analyzed. The construction of high precision catalogues of earthquake hypocenters can enhance the spatiotemporal distribution, highlighting activated structures and revealing pertinent seismicity migration patterns that may be related to the diffusion of magmatic process. Due to lack of data in the HVA, the case of 2018 Kilauea eruption will be examined, where high-quality seismological data were used in order to recognize certain seismic precursory patterns.

Kīlauea is an active shield volcano and the most active of the five volcanoes that form the island of Hawaii. Located along the southern shore of the island, the volcano is between 210,000 and 280,000 years old and emerged above sea level about 100,000 years ago. It is the second youngest product of the Hawaiian hotspot and the current eruptive center of the Hawaiian-Emperor seamount chain. Kilauea Volcano nestles on the southeast slope of Mauna Loa and merges so imperceptibly with its giant neighbor that significant dimensions cannot be assigned. Hawaiian volcanoes can erupt either at their summits or on their flanks. Summit eruptions of Kilauea occur within or near its caldera. Flank eruptions usually take place along rift zones, which are highly fractured zones of weakness within the volcano (e.g. Bevins *et al.*, 1988; Carey *et al.*, 2015). The most recent major eruption at Kīlauea had the longest duration of any other observed eruption. The current Kīlauea eruption began on January 3rd, 1983, along the eastern rift zone and resulted in the construction of the Pu'u'O'o cone. In 1986, activity shifted down the rift to a new vent, named Kūpa'ianahā, where it took on a more effusive character (Bevins *et al.*, 1988).

The Island of Hawaii experiences intense microseismic activity each year. Most of Hawaii's earthquakes are directly related to volcanic activity. These events may occur before or during an eruption, or they may result from the underground movement of magma that comes close to the surface but does not erupt. During the last decades (1983-today) the area of Kilauea has been characterized by intense seismic activity (Kirby and Klein, 2006). In this study, we collected and processed earthquake waveforms recorded by the Hawaiian Volcano Observatory (HVO) seismological network, providing P- and S-wave phase arrival-time data for events that occurred in the period April 2018-May 2018. The obtained catalogue contains phase data for more than 500 microearthquakes. A preliminary hypocenter location has been performed for the seismicity of the broader area, using the HYPOINVERSE code (Klein, 1989) and a custom 1-D velocity model. The waveform data of HVO were acquired from the Incorporated Research Institutions for Seismology (IRIS) (http://service.iris.edu/) via the International Federation of Digital Seismograph Networks web-services (FDSN-WS) data request protocol, facilitating prompt data availability. A subset of the phase data was employed in order to investigate the average Vp/Vs ratio and local 1-D velocity structure, using the mean travel-time residuals and location uncertainties (RMS, ERH, ERZ) minimization method (e.g. Kissling *et al.*, 1994).

The broader area of Kilauea and the Lower East Rift Zone (LERZ) showed several signs of volcano unrest leading up to the events of May-August 2018. Clustered activity of VT-earthquakes along a ENE-WSW fault zone, in Lower East Rift Zone (LERZ), has been identified during April 30th-May 3rd, 2018. The density of the HVO seismic network made feasible the categorization of the event type according to the source properties and, hence, the origin of the excitation (either volcanic or tectonic). During LERZ eruption, three main classes of seismic signals were discriminated: Volcano-Tectonic (VT), Long-Period (LP) and Hybrid (HB) earthquakes (Zobin, 2003). The classification of volcanic earthquakes was performed by visual inspection. The signals were selected from nearby seismic stations of the HVO at distances of 0.5 km to 20 km from the active fissures respectively. High amplitude volcanic tremor began on May 2nd following a swarm of VTs, as the real-time seismic amplitude measurement (RSAM) plot clearly showed. May 4th, 2018 M6.9 earthquake resulted to the collapse of the Pu'u'O'o cone, opening twenty (20) new fissures and to the interaction of magma with the water table in Halema'uma'u crater. Since May 17th, this interaction has led to a series of volcanic explosions of energy equivalent to M5.0 earthquakes that were connected to the inflation-deflation cycles of Kilauea volcano (USGS, 2018; Neal *et al.*, 2019).

References

Bevins, D., Takahashi, T. J. & Wright, T. L., 1988. The early serial publications of the Hawaiian Volcano Observatory: Volume 3, Monthly Bulletin of the Hawaiian Volcano Observatory (1821-1929), 1224 pp.

Carey, R. J., Cayol, V., Poland, M., Weis, D., 2015. Hawaiian Volcanoes: From Source to Surface. Geophysical Monograph Series doi:10.1002/9781118872079

Klein, F.W., 1989. HYPOINVERSE, a program for VAX computers to solve for earthquake locations and magnitudes. U.S. Geological Survey Open-File Report: 89-314.

Kirby, S. H., and Klein, F. W., 2006. The 15 October 2006-to-present earthquakes beneath the island of Hawaii: implications for Pacific plate flexure and geomechanical effects of ascendingCO2 that embrittles the Pacific plate mantle, Eos Transactions AGU,87(52), Fall MeetingSupplement, Abstract 253E-07.

Kissling, E., Ellsworth, W.L., Eberhart-Phillips, D. and Kradolfer, U., 1994. Initial reference models in local earthquake tomography. J. Geophys. Res. 99, 19635-19646.

Neal, C. A. et al., 2019. The 2018 rift eruption and summit collapse of Kīlauea Volcano, Science, Vol. 363, Issue 6425, pp. 367-374 DOI: 10.1126/science.aav7046

Papadimitriou, P., Kapetanidis, V., Karakonstantis, A., Kaviris, G., Voulgaris, N. and Makropoulos, K., 2015. The Santorini Volcanic Complex: A detailed multi-parameter seismological approach with emphasis on the 2011-2012 unrest period. J. Geodynamics, 85, 32-57.

USGS, 2018. Preliminary Analysis of the ongoing Lower East Rift Zone (LERZ) eruption of Kīlauea Volcano: Fissure 8 Prognosis and Ongoing Hazards, COOPERATOR REPORT TO HAWAII COUNTYCIVIL DEFENSE, 15 pp.

Zobin, V.M., 2003. Introduction to Volcanic Seismology, Elsevier Science, 308pp.

15th International Congress of the Geological Society of Greece
Athens, 22-24 May, 2019 | Harokopio University of Athens, Greece
Bulletin of the Geological Society of Greece, Sp. Pub. 7 Ext. Abs. GSG2019-367

Recent Significant Seismic Activity in Greece

P. Papadimitriou[1], K. Pavlou[1], A. Karakonstantis[1], V. Kapetanidis[1], I. Spingos[1], G. Kaviris[1], I. Kassaras[1] and N. Voulgaris[1]

(1) Section of Geophysics–Geothermics, Department of Geology and Geoenvironment, National and Kapodistrian University of Athens, 15784 Panepistimiopolis, Zografou, Athens, Greece, ppapadim@geol.uoa.gr

Greece is located in the eastern end of Europe where a variety of geological procedures take place such as the Alpine orogenesis. The creation of the Alpine mountain chain, which is one of the most important geological features, is caused by the collision between Europe and Africa. Furthermore, the intense deformation observed in Greece and surrounding areas produces significant seismicity concentrated along active seismic zones such as the Hellenic Arc and the North Anatolian fault (Papazachos et al., 2000). In addition, the gulfs of Corinth, Evoikos and Saronikos also present important seismic activity. Since 2018, more than 10,000 events have been recorded by stations of the Hellenic Unified Seismological Network (HUSN; Papanastassiou, 2011) and were analyzed by the Seismological Laboratory of the National and Kapodistrian University of Athens. Recently, data from the Hellenic Strong Motion Network (HSMN; Theodulidis et al. 2004) were included in the framework of HELPOS project. The "scolv" tool of the SeisComP3 software was used in order to manually revise the automatically located events. The initial catalogue was further enriched with events that weren't automatically detected, by extracting waveform data according to an initial origin time after visual inspection of the 24-hour recordings on reference stations.

In the present study we mainly focus on significant seismic activity that occurred during 2018-2019. In North Aegean, shallow aftershock activity associated with the earthquakes that occurred on the 6th February and 12th of June 2017, in the broader area of Lesvos Island, is still present in 2018. More than 200 events since June, manually analyzed, were used to obtain an optimized local velocity model. The newly developed seismic catalogue revealed distinct spatial ~E-W oriented seismic clusters, compatible with the strike of Quaternary faults in the area south-west of Canakkale and along the southern coasts of Lesvos Island, related to Lesvos-Psara pull-apart basins (e.g. Kiratzi, 2014).

In Central Greece, the greatest part of the seismicity is located in the southern termination of Saronikos gulf and in Attica area. The seismic activity in Saronikos gulf is concentrated around Leuces islands, north of Aegina and Methana in E-W striking neotectonic fault zones. In addition, a swarm located along the Poros Fault System (PFS) took place in 2016-2017. In Attica area a microseismic activity occurred in January 2018, north of Mt Penteli (Kaviris et al., 2018), Marathon Bay, Thriassion fault and its continuation in Athens basin. 450 events were located in the vicinity of Attica during 2018-2019 with magnitudes mainly between 1.8 and 2.6. Sporadic seismicity was also detected along the southern shores of Attica. The most notable events of this region occurred on 18 January 2018 (ML=4.2) and 1 May 2018, in the areas NNE of Mt Penteli and Oropos, respectively.

The earthquake activity in the broader area of Santorini volcanic center is strongly connected with the tectonic regime, as well as with the volcanic process (Bohnhoff et al., 2006; Dimitriadis et al., 2010; Papadimitriou et al., 2015). The highest rate of seismic activity in this area has been observed along the NE-SW striking Santorini-Columbo volcano-tectonic line, a deep-seated, strike-slip feature (Bohnhoff et al., 2006; Sakellariou et al., 2013; Nomikou et al., 2018). Within this zone, the submarine Columbo volcano exhibits strong seismic and hydrothermal activity which could be linked to the magma reservoir and therefore to the migration of magma and fluids towards the surface (Bohnhoff et al., 2006; Sigurdsson et al., 2006). A similar pattern of seismic activity is observed NE of Columbo, with small-scaled activity spots that might represent local pathways of upward migrating fluids or even developing volcanic activity within this zone of crustal weakness (Bohnhoff et al. 2006). The majority of the recorded seismic activity was located 38.2 km NE of Thira, SSW of Amorgos (Mw=4.5). This cluster lies on the southern boundary of the activated fault during the 1956 tsunamigenic M7.2 earthquake of Amorgos. Another significant portion of the seismic activity (13-14/01/2019) was located south of Akrotirion, 17.1 km SSW of Thira, aligned in a general WSW-ENE direction. The most notable event of this group occurred on 13 January 2019 (ML=3.6).

On October 25th, 2018 (22:54 GMT), an M6.8 earthquake occurred 57.0 km SW of Zakynthos Island, at a focal depth of ~11km. The mainshock was widely felt to the island and in many areas of Central Greece. More than 4,000 aftershocks were manually located. A local 1-D velocity model was developed upon a selected dataset (1,000 earthquakes). The aftershock locations reveal a complex hypocentral distribution, which indicates the activation of more than one structure in the area, with five main spatial groups being identified: one situated in the area around the mainshock; another likely associated with the southern prolongation of Cephalonia Transform Fault (CTF) WNW of Zakynthos (Papadimitriou et al., 2006; 2012); a third ~20km to the NNE of the mainshock; a forth in Laganas bay (Southern Zakynthos) and a fifth close to Strofades islands, where the 1997 M6.6 earthquake took place. The obtained results highlight a complex fault pattern in Southern Ionian Sea, as a result of the intense deformation of the overriding crust.

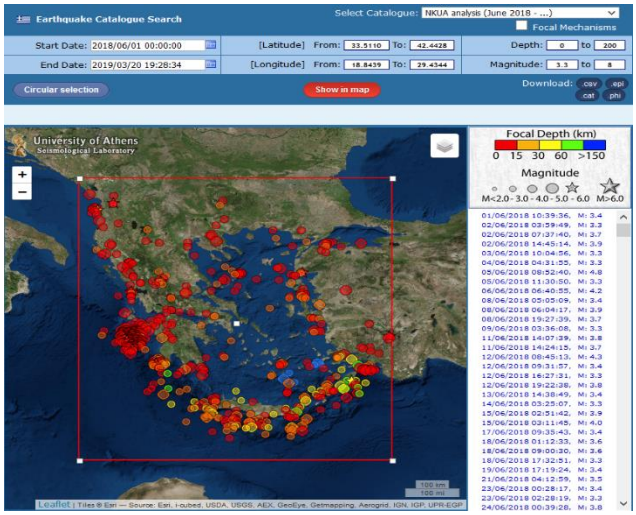

Figure 1. Seismic activity of earthquakes with M≥3.3 for the period Jun 2018 – March 2019 resolved by SL-NKUA, as presented in the catalogue search platform available online at: http://www.geophysics.geol.uoa.gr/stations/gmapv3_db/index.php

Acknowledgements

We acknowledge support of this study by the project "HELPOS – Hellenic Plate Observing System" (MIS 5002697) which is implemented under the Action "Reinforcement of the Research and Innovation Infrastructure", funded by the Operational Programme "Competitiveness, Entrepreneurship and Innovation" (NSRF 2014-2020) and co-financed by Greece and the European Union (European Regional Development Fund).

References

Dimitriadis, I. et al., 2010. P and S velocity structures of the Santorini-Colombo volcanic system (Aegean Sea, Greece) obtained by non-linear inversion of travel times and its tectonic implications. J. Volcanol. Geotherm. Res. 195 (1), 13–30

Kaviris, G., Spingos, I., Millas, C., Kapetanidis, V., Fountoulakis, I., Papadimitriou, P., Voulgaris, N., Drakatos, G., 2018. Effects of the January 2018 seismic sequence on shear-wave splitting in the upper crust of Marathon (NE Attica, Greece). Phys. Earth Planet. Inter. 285, 45–58.

Kiratzi, A., 2014. Mechanisms of Earthquakes in Aegean, Encyclopedia of Earthquake Engineering, 1-22, Springer Berlin Heidelberg, DOI: 10.1007/978-3-642-36197-5_299-1

Nomikou, P. et al., 2018. Expanding extension, subsidence and lateral segmentation within the Santorini - Amorgos basins during Quaternary: Implications for the 1956 Amorgos events, central - south Aegean Sea, Greece. Tectonophysics 722:138-153, DOI: 10.1016/j.tecto.2017.10.016.

Papadimitriou, P. et al., 2015. The Santorini Volcanic Complex: A detailed multi-parameter seismological approach with emphasis on the 2011–2012 unrest period. J. Geodyn., 85, 32–57, doi: 10.1016/j.jog.2014.12.004.

Papadimitriou, P. et al., 2018. The 12th June 2017 Mw=6.3 Lesvos earthquake from detailed seismological observations, Journal of Geodynamics, Volume 115, April 2018, Pages 23-42, ISSN 0264-3707, https://doi.org/10.1016/j.jog.2018.01.009.

Papanastassiou D. 2011. Earthquake detection-location capability of the Hellenic Unified Seismological Network (HUSN) operating by the Institute of Geodynamics, National Observatory of Athens. Hellenic J Geosc 45: 209–216.

Papazachos, B.C., Karakostas, V.G., Papazachos, C.B., Scordilis, E.M., 2000. The geometry of the Wadati-Benioff zone and the lithospheric kinematics in the Hellenic arc. Tectonophysics 319, 275–300.

Sakellariou, D. et al., 2013. Strike slip tectonics and transtensional deformation in the Aegean region and the Hellenic arc: preliminary results. Bulletin of the Geological Society of Greece, XLVII, Proceedings of the 13th International Congress, Chania, Sept. 2013.

Sigurdsson H.et al., 2006. Marine Investigations of Greece's Santorini Volcanic Field, EOS, Vol 87 N. 34, 22 August 2006.

Theodulidis N. et al., 2004. HEAD1.0: A unified accelerogram database", Seism. Research. Lett, 75, 41-50.

15th International Congress of the Geological Society of Greece
Athens, 22-24 May, 2019 | Harokopio University of Athens, Greece
Bulletin of the Geological Society of Greece, Sp. Pub. 7 Ext. Abs. GSG2019-369

Focal mechanisms database of moderate and strong events in the broader area of Greece

P. Papadimitriou[1], V. Kapetanidis[1], A. Karakonstantis[1], I. Spingos[1], K. Pavlou[1] and I. Kassaras[1]

(1) Section of Geophysics–Geothermics, Department of Geology and Geoenvironment, National and Kapodistrian University of Athens, 15784 Panepistimiopolis, Zografou, Athens, Greece, ppapadim@geol.uoa.gr

The Aegean is the most rapidly deforming region in the Mediterranean, as evidenced from seismological and geodetic observations (McKenzie,1972; 1978; Jackson, 1994; Jackson and McKenzie, 1988). The Aegean is located between two lithospheric plates, the Eurasian and the African, that are converging in an approximately N-S direction with a rate ranging 2-4 cm/yr (Floyd et al., 2010). The deformation becomes more complicated, due to the collision of the Arabian plate with Eurasia, resulting to the westward motion of Turkey towards the Aegean. All the above-mentioned movements lead to a complex deformation pattern: (a) the northern Aegean is dominated by the right lateral strike-slip motion of the westernmost part of the North Anatolian fault (McNeill et al., 2004), (b) the central part of the Aegean is characterized by normal faulting and extension in an approximately N-S direction and (c) the southern part is characterized by a subduction zone along the Hellenic Arc, where intermediate depth earthquakes occur, leading to the formation of the Volcanic Arc. The average distance between the two arcs is 120 km. The subduction zone is characterized by a general NE dip direction. However, the located events along the Benioff zone indicate that the slip and the shape vary along an amphitheatric, asymmetrical scheme, presenting significant differences between its eastern and western parts. The above-mentioned complex deformation results in high seismic activity consisting of small-intermediate as well as large earthquakes (Papazachos et al., 1998).

In a such complex environment, it is crucial to determine earthquake focal mechanisms of intermediate, as well as of large magnitude events for understanding physical processes on faults during earthquakes. It is worth noting that since 2007 all Greek seismological networks have been integrated into the Hellenic Unified Seismological Network (HUSN; Papanastassiou, 2011). This important effort has contributed to the increase of detectability as well as to the improvement of the location parameters of earthquakes. The Seismological Laboratory of the National and Kapodistrian University of Athens (SL-NKUA), by taking into account phases from Greek Seismological institutions, has compiled a data set of more than 180.000 events and 1000 focal mechanisms located in Greece and the surrounded areas for the time period 1996-2018. Since 2018, more than 20,000 events have been recorded by HUSN stations and ~150 fault plane solutions have been analyzed by SL-NKUA.

The determination of the seismic source parameters is based on a software developed at SL-NKUA (Papadimitriou et al., 2012). Two different techniques were applied to determine the source parameters of the selected earthquakes:

a) Teleseismic body-wave modelling using waveforms at epicentral distances between 30□ and 90□ was employed for the large events (Mw > 5.8). Synthetic seismograms of P, SV and SH were calculated, taking into account the geometric spreading, the Earth's radius, the radiation pattern of the considered component, the density, the angle of incidence at the source and the receiver as well as the free surface effect.

b) For local to regional distances, the method of the P-wave first-motion polarities has been, for several years, the only one to constrain focal mechanisms. The installation of regional seismological networks worldwide, gave the opportunity to develop new methods based on the generation of synthetic waves using inversion techniques (Dreger and Helmberger, 1990; Fukuyama and Dreger, 2000; Ichinose et al., 2003; Kiratzi and Louvari, 2003). The main advantage of this approach is that moderate events can be analyzed in order to obtain reliable solutions. Thus, the knowledge on the type of the earthquake rupture is increased and contributes to the seismotectonic analysis of the study area. These techniques are based on the calculation of synthetics representing the complete wavefield, using the frequency–wavenumber method at local-regional distances (Bouchon, 2003). This method, applied in the present study, calculates synthetic waveforms directly comparable with the observed ones for a given velocity structure. Synthetics were generated by computing 9 fundamental Green's functions, which are then combined with the elements of a moment tensor to produce the tangential, radial and vertical component of motion.

The number of fault plane solutions based on moment tensor inversion for moderate magnitude events (M>3.5) is increasing the last years due to the quality and the density of broad band seismological stations. In this study, well-constrained focal mechanisms using the above-mentioned moment tensor inversion technique are presented and analyzed. The determined focal mechanisms can be viewed, selected and exported through an online platform at the web-site of the Department of Geophysics-Geothermics of NKUA (Fig. 1). The local-regional stress deducing from the focal mechanisms improves the knowledge of the physical state of the local seismogenic structures. This is important, considering that, in the same area, the type of the fault plane solutions of the moderate events has no significant differences in comparison with the type of the large ones. The recent calculated focal mechanisms in the broader area of Zakynthos (not only the aftershocks) indicate small differences from the main event of the 25 November 2018. Complexity of the focal mechanisms type is observed mainly southern of Greece along the Hellenic Arc.

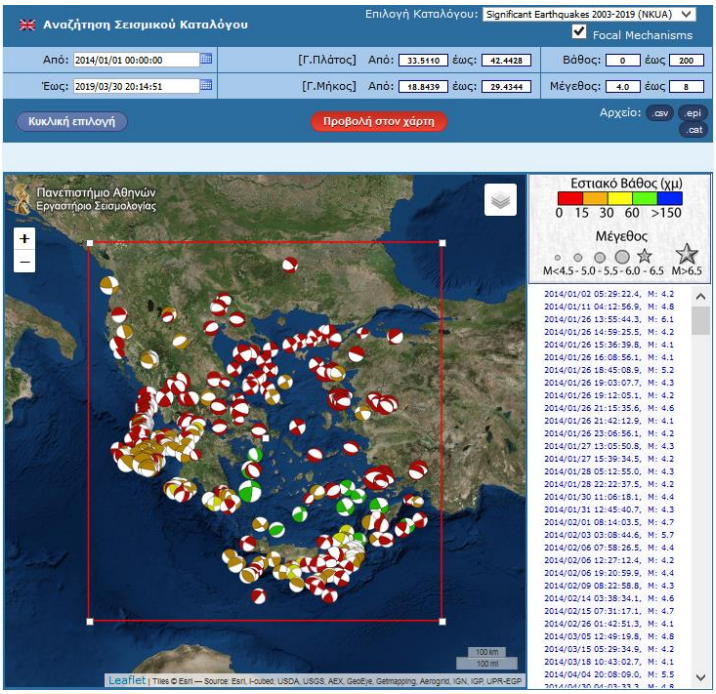

Figure 1. Focal mechanisms of earthquakes with $M_w \geq 4.0$ for the period 2014 – March 2019 resolved by SL-NKUA, as presented in the catalogue search platform available online at: http://www.geophysics.geol.uoa.gr/stations/gmapv3_db/index.php.

Acknowledgements

We acknowledge support of this study by the project "HELPOS – Hellenic Plate Observing System" (MIS 5002697) which is implemented under the Action "Reinforcement of the Research and Innovation Infrastructure", funded by the Operational Programme "Competitiveness, Entrepreneurship and Innovation" (NSRF 2014-2020) and co-financed by Greece and the European Union (European Regional Development Fund).

References

Bouchon, M., 2003. A Review of the Discrete Wavenumber Method. Pure Appl. Geophys. 160, 445–465.

Dreger, D., and Helmberger, D., 1990. Broadband modelling of local earthquakes. Bull. Seismol. Soc. Am.,. 80, 1162–1179.

Fan, G., Ni, J.F., Wallace, T.C., 1994. Active tectonics of the Pamirs and Karakorum. J. Geophys. Res. 99, 7131–7160.

Floyd, M.A., Billiris, H., Paradissis, D., Veis, G., Avallone, A., Briole, P., McClusky, S., Nocquet, J.-M., Palamartchouk, K., Parsons, B., England, P.C., 2010. A new velocity field for Greece: Implications for the kinematics and dynamics of the Aegean. J. Geophys. Res. 115, B10403. doi:10.1029/2009JB007040

Fukuyama, E. & Dreger, D.S., 2000. Performance test of an automated moment tensor determination system for the future "Tokai" earthquake, Earth Planets Space, 52, 383–392.

Ichinose, G., Anderson, J., Smith, K. & Zeng, Y., 2003. Source parameters of Eastern California and Western Nevada earthquakes from regional moment tensor inversion, Bull. Seism. Soc. Am., 93, 61–84.

Jackson, J., 1994. Active Tectonics of the Aegean Region. Annu. Rev. Earth Planet. Sci. 22, 239–271.

Jackson, J. and McKenzie, D., 1988. Rates of active deformation in the Aegean Sea and surrounding regions. Basin Res., 1, 121-128.

Kiratzi, A., and Louvari, E., 2003. Focal mechanisms of shallow earthquakes in the Aegean Sea and the surrounding lands determined by waveform modelling: a new database. J. Geodyn., 36, 251–274.

McKenzie, D., 1972. Active tectonics of the Mediterranean region. Geophys. J. R. astr. Soc., 30, 109-185.

McKenzie, D., 1978. Some remarks on the development of sedimentary basins. Earth Planet. Sci. Lett. 40, 25–32.

McNeill, L.C., Mille, A., Minshull, T.A., Bull, J.M., Kenyon, N.H., Ivanov, M., 2004. Extension of the North Anatolian Fault into the North Aegean Trough: Evidence for transtension, strain partitioning, and analogues for Sea of Marmara basin models. Tectonics 23, TC2016. doi:10.1029/2002TC001490

Papadimitriou, P., Chousianitis, K., Agalos, A., Moshou, A., Lagios, E., Makropoulos, K., 2012. The spatially extended 2006 April Zakynthos (Ionian Islands, Greece) seismic sequence and evidence for stress transfer. Geophys. J. Int. 190, 1025–1040.

Papadimitriou, P., et al., 2018. The 12 th June 2017 M w = 6.3 Lesvos earthquake from detailed seismological observations. J. Geodyn. 115, 23–42. doi:10.1016/j.jog.2018.01.009

Papanastassiou D. 2011. Earthquake detection-location capability of the Hellenic Unified Seismological Network (HUSN) operating by the Institute of Geodynamics, National Observatory of Athens. Hellenic J Geosc 45: 209–216.

Papazachos, B.C., Papadimitriou, E.E., Kiratzi, A.A., Papazachos, C.B. and Louvari, E., 1998. Fault plane solutions in the Aegean Sea and the surrounding area and their tectonic implication. Boll. Geof. Teor. App., 39, 199-218.

GENERAL SESSION

T4 Geochemistry, Mineralogy, Petrology, Economic Geology, Volcanology

15th International Congress of the Geological Society of Greece
Athens, 22-24 May, 2019 | Harokopio University of Athens, Greece
Bulletin of the Geological Society of Greece, Sp. Pub. 7 Ext. Abs. GSG2019-003

Silica polymorphs in the mineral assemblage of fossil plant samples from Lesvos Petrified Forest

A. Iordanidis[1], J. Garcia-Guinea[2], N. Zouros[3], A. Asvesta[1]
(1) Department of Geotechnology and Environmental Engineering, Western Macedonia University of Applied Sciences, Kila, 50100 Kozani, Greece andior@teiwm.gr & aiordanidis@yahoo.co.uk
(2) Museo Nacional Ciencias Naturales, CSIC, Abascal 2, 28006 Madrid, Spain
(3) Department of Geography, University of the Aegean, 81100 Mytilene, Greece

The Lesvos Petrified Forest was formed by silicification process of plants during the Lower Miocene era, when intense volcanic activity occurred in that region. It is situated in the western part of Lesvos Island (NE Greece) and consists of hundreds of standing and lying fossilized tree trunks, covering an area of 150 km^2. It is one of the most important natural heritage monuments in the world and in 2004 the area was included in the Global Geoparks Network. The Natural History Museum of the Lesvos Petrified Forest is the management body of Lesvos Geopark (Zouros, 2010). During the last three decades, a great number of excavations are taking place in the area, revealing important fossil plants and providing crucial palaeobotanical and volcano-sedimentological information. Despite its significance, the conduction of extensive geochemical and mineralogical analyses on fossil plant samples from this area has merely commenced (Pe-Piper et al., 2019), providing information on the permineralization process.

The present study aims to shed light on the silicification of the Lesvos fossil woods, by analyzing the silica polymorphs comprising the latter samples. Seventeen fossil plant samples were collected from the Sigri pyroclastic formation within the Lesvos Petrified Forest. Several analytical techniques were employed. A Philips QUANTA 200 Environmental Scanning Electron Microscope (ESEM), coupled with an Oxford INCA Energy 200 Energy Dispersive System (EDS) was used for imaging and chemical analyses. For the Raman spectroscopy, a Thermo Scientific DXR Raman Microscope with a 780 nm laser beam was employed. The power value of the sample irradiation was ranging from 6 mW to 12 mW. The average spectral resolution in the Raman shift range of 100-3000 cm^{-1} was 5cm^{-1} (grating 400 lines/mm, spot size 2μm). Cathodoluminescence (CL) spectra were collected on polished slabs, at low vacuum mode without coating, using a Gatan MonoCL3 detector with a PA-3 photomultiplier attached to the SEM. For the X-ray diffraction (XRD), a Phillips PW1710/00 diffractometer was used with a CuKα radiation source, equipped with a graphite monochromator. The XRD patterns were obtained by step scanning from 2º to 64º (2θ in steps of 0.020º; 4 s per step). Block sections (Figure 1) of each sample were used for the ESEM-EDS, SEM-CL and Raman spectroscopy analyses, while a ground to powder portion of the same samples was used for the XRD analysis.

SEM imaging and EDS spectra provided a first appraisal of the chemical composition of the samples, focusing on silica-rich zones, which were abundant not only in geode-like structures (Figure 1), but also in white, black and green-coloured parts of the fossil plants. While some textural features were evident by ESEM-EDS, the determination of the exact types of silica polymorphs was managed by employing XRD, Raman spectroscopy and CL-SEM methods.

Quartz, opal, cristobalite and tridymite were determined by XRD technique (Figure 2). Opal is a micro to non-crystalline form of hydrated silica with high degree of structural disorder. Cristobalite and tridymite are both more common as components of opal than as individual minerals and may form metastable phases in silica-rich volcanic and sedimentary environments (Pe-Piper et al., 2019).

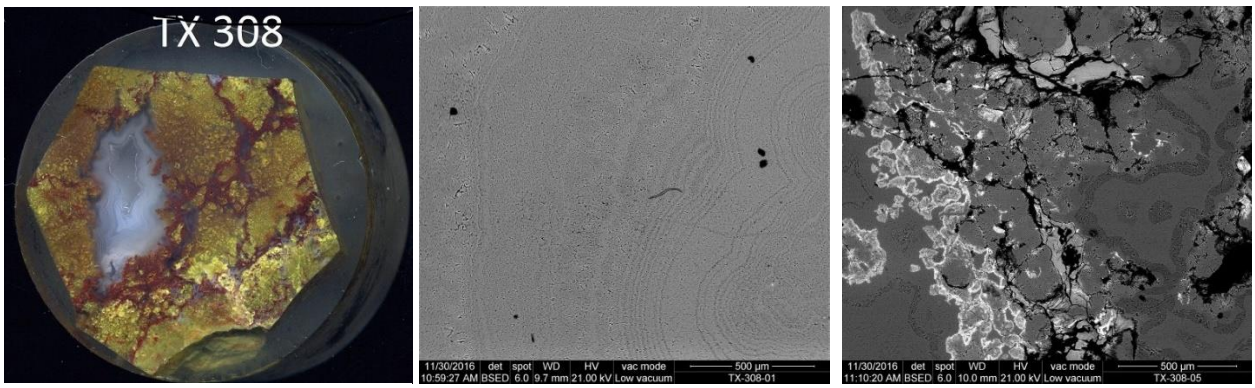

Figure 1. Polished block section of the TX308 fossil plant sample [left] and characteristic SEM images of the same sample showing different silica-rich zones [middle] and geode-like, Si-rich microstructure (various hues of grey colour) and Fe-rich parts (white colour hues) [right].

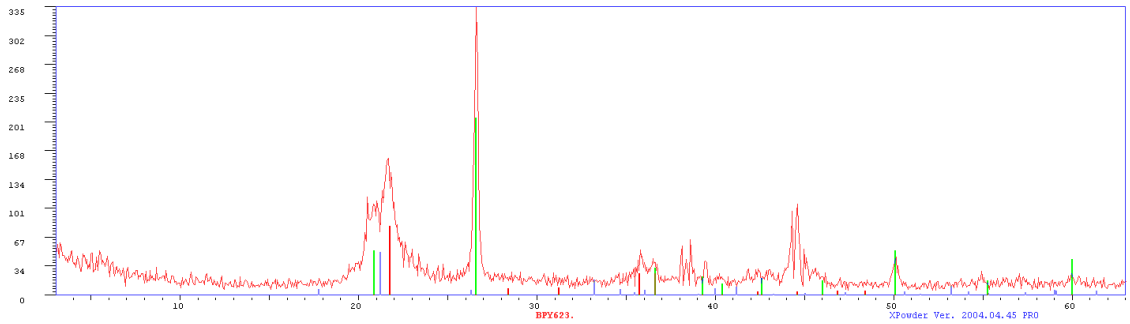

Figure 2. XRD pattern of a fossil plant sample, showing the mineral phases of quartz (green bars) and opal (red bars).

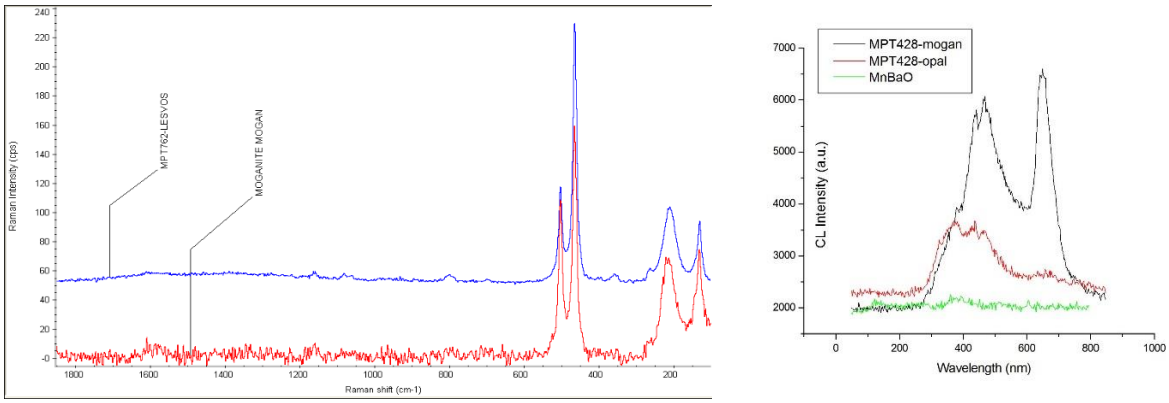

Figure 3. Raman spectra of a standard moganite mineral (red) and the moganite mineral phase found in a fossil plant sample (blue) [left] and CL spectra of moganite, opal and a Mn and Ba-rich phase found in another fossil plant sample [right].

Raman spectroscopy confirmed the presence of opal and quartz. Thus, quartz was revealed with its intensive band at 465 cm^{-1} and the secondary bands at 123, 203 and 497 cm^{-1}, while opal showed a characteristic hump between 200 and 500 cm^{-1}, with distinct, strong peaks at 350, 784 and 1590 cm^{-1} (Iordanidis et al., 2014). Furthermore, moganite, which is a meta-stable silica polymorph typically intergrown with cryptocrystalline quartz, was also determined by Raman spectroscopy, revealing its characteristic peak at 502 cm^{-1} and the three other shifts at 464, 206 and 123 cm^{-1}. Figure 3 shows the assignment of moganite mineral phase compared to the Raman spectrum of an original, standard moganite sample, collected from Mogan, Gran Canaria, Spain.

The cathodoluminescence (CL) technique was employed as a complementary method to all the aforementioned techniques (ESEM-EDS, XRD, Raman) to investigate the fossil wood samples. Quartz, opal and moganite showed distinctive CL spectra. An intensive peak at 650 nm (aprx. 12000 a.u.) and two lower, broader peaks at 430 and 460 nm are determined for quartz (Aparicio and Bustillo, 2012). Opal revealed a CL spectrum with a broad hump between 300 and 500 nm, showing a rather low intensity (aprx. 3500 a.u.), while moganite presented a characteristic double peak at 440 and 470 nm and another at 650 nm with equal intensity (aprx. 6500 a.u.). Additionally, the CL spectrum of a manganese and barium rich phase with very low luminescence is also shown in Figure 3.

In conclusion, the utilization of complementary techniques (ESEM-EDS, Raman, CL-SEM and XRD) provided substantial information for the identification of the silica polymorphs comprising the Lesvos petrified wood samples.

Acknowledgements

This research received support from the SYNTHESYS Project (ES-TAF-5318), which http://www.synthesys.info/ is financed by European Community Research Infrastructure Action under the FP7 "Capacities" Programme at the Museo Museo Nacional de Ciencias Naturales (CSIC), Madrid, Spain.

References

Aparicio, A., Bustillo, M.A., 2012. Cathodoluminescence Spectral Characteristics of Quartz and Feldspars in Unaltered and Hydrothermally Altered Volcanic Rocks (Almeria, Spain). Spectroscopy Letters 45(2), 104-108.

Iordanidis, A., Garcia-Guinea, J., Strati, A., Gkimourtzina, A., 2014. A comparative study of pigments from the wall paintings of two Greek Byzantine churches. Analytical Letters 4(16), 2708-2721.

Pe-Piper, G., Imperial, A., Piper, D.J.W., Zouros, N.C., Anastasakis, G., 2019. Nature of the hydrothermal alteration of the Miocene Sigri Petrified Forest and host pyroclastic rocks, western Lesbos, Greece. Journal of Volcanology and Geothermal Research 369, 172-187.

Zouros, N., 2010. Lesvos Petrified Forest geopark, Greece: Geoconservation, Geotourism and Local development. Journal of Parks, Protected Areas and Cultural sites 27, 19-28.

15th International Congress of the Geological Society of Greece
Athens, 22-24 May, 2019 | Harokopio University of Athens, Greece
Bulletin of the Geological Society of Greece, Sp. Pub. 7 Ext. Abs. GSG2019-005

Geochemical characteristics and Tectonic significance of Permo-Triassic Silicic Volcanic rocks from Circum-Rhodope Belt, Vardar (Axios) Zone, northern Greece

A. Asvesta[1], S. Dimitriadis[2]

(1) Department of Geotechnology and Environmental Engineering, Western Macedonia University of Applied Sciences, Kila, 50100 Kozani, Greece, asvesta@teiwm.gr & argyasve@gmail.com
(2) Department of Geology, Aristotle University of Thessaloniki, 54006 Thessaloniki, Greece

Introduction and Geological setting

The Circum-Rhodope Belt (CRB) in Greece comprises the eastern part of Peonias subzone of the Vardar (Axios) Zone. It is a complex imbricated belt that borders the Palaeozoic high-grade crystalline basement of Serbo-Macedonian massif. It mainly consists of Upper Palaeozoic to Mesozoic greenschist-facies metamorphosed sedimentary successions, igneous rocks and ophiolites (Asvesta and Dimitriadis, 2010; Meinhold and Kostopoulos, 2013; and references therein), among them, a Permo-Triassic Silicic Volcano-Sedimentary (SVS) succession that crops out discontinuously in NNW-SSE direction. The SVS succession is an important part of the CRB, as it probably represents the early stages of the opening of a post-Variscan, neo-Tethyan oceanic strand (Vardar -Axios- oceanic basin) which was finely eliminated during some stage of the Tertiary Alpine orogeny (Asvesta, 1992; Dimitriadis and Asvesta, 1993; Asvesta and Dimitriadis, 2010, 2013). The SVS succession is laid stratigraphically between the Permian Examili Formation (terrigenous sediments) and the Triassic Svoula Formation (neritic carbonate sediments). From base to top it comprises mainly rhyolitic to rhyodacitic pyroclastic rocks, aphyric and porphyritic lavas, as well as domes intruded and sills embedded into formerly wet unconsolidated neritic carbonate sedimentary facies forming peperites, hyaloclastites and polymictic epiclastic sedimentary rocks. This facies architecture suggests an acid volcanic activity in a transitional subaerial-coastal to shallow submarine environment, which was still active when the neritic carbonate sedimentation began (Asvesta and Dimitriadis, 2010, 2013). Moreover, minor occurrence of tholeiitic basalts and dolerites (Triassic Rift Basic Volcanics: Asvesta, 1992; Dimitriadis and Asvesta, 1993; Asvesta and Dimitriadis, 2013) are temporally and spatially related with the SVS succession, as they are found interstratified with the Upper Triassic pelagic chert and carbonate sediments of Metallikon and Megali Sterna units as well as in the Akritas rhyodacitic lavas of the SVS succession.

Results and Discussion

Silicic Volcanic rocks (63 samples) from the SVS succession, outcropping near the villages Akritas, Metallikon, Kolchida, Nea Santa and Sana, were studied geochemically for major and trace elements in order to investigate their origin and geotectonic environment. The rocks (SiO_2 range from 62.30 to 85.42 wt.%) are classified predominantly as rhyolites, rhyodacites and much less as dacites (Figure 1a). They are corundum-normative, peraluminous (molar A/CNK ratios range from 0.99 to 1.37), enriched in total alkalis, depleted in MgO and CaO and have high FeO_t/MgO ratios. They are enriched in HFS elements, like Zr, Nb and Y.

On primordial mantle normalised multi-element spider diagrams (Figure 1b), samples of all areas show similar patterns revealing origin from the same magma. It is indicated that feldspar (negative Ba and Sr anomalies), apatite (negative P anomaly) and Fe-Ti oxides (negative Ti anomaly) were fractionated from the magma. The presence of significant positive Th and Pb anomalies indicates evidence of a significant crustal component in their magma source. In granite discriminate diagram of Whalen *et al.* (1987), all samples of the volcanic rocks fall almost exclusively in the field of A-type granite (Figure 1c). On the tectonic discrimination diagram (Y+Nb) *vs.* Rb for granites, the majority of samples lie in the within-plate granite field but all the samples straddle at the triple junction boundary of the within-plate, volcanic arc and syn-collision granites (Figure 1d) that is the post-collision granite field (Pearce, 1996). This also provides support for an A-type character magma, as A-type is considered emplaced in post-collisional or within plate settings; i.e., an extensional environment (Whalen *et al.*, 1987; Eby, 1992).

Eby (1992) divided the A-type granitoids into two groups (A1 and A2). Granitoids that are associated with true anorogenic (within plate) settings and interpreted as differentiates of basaltic magma derived from an OIB-like source (A1 group: Y/Nb<1.2), and granitoids that are often emplaced in post-collisional, post-orogenic settings and were derived from the subcontinental lithosphere or lower crust (A2 group: Y/Nb>1.2). All samples of the studied silicic volcanic rocks surpass the 1.2 value of Y/Nb ratios (1.87-4.75, average 3.36) and plot in the A2 granite field (Figure 1e) on the (Nb-Y-Ce) discrimination diagram of Eby (1992), implying dominant crustal magma sources derivation and emplacement in a post-collisional environment. Furthermore, Ce/Nb *vs.* Y/Nb discrimination diagram is used to estimate possible genetic links of the A-type granitoids with crustal sources or mantle-derived magmas (Eby, 1992). In this diagram, the rhyolite samples plot well into the field for rocks derived by crustal anatexis, characteristic for A2 group (Figure 1f). The sources, from which these granitoids were extracted, were originally formed by subduction or continent-continent collision (Eby, 1992).

The role of mantle-derived mafic magmas, to provide heat and/or material, seems essential in the generations of the A-type granitoid melts (Eby, 1992). The investigated silicic volcanic rocks have relatively high magma temperatures (average Zr saturated temperature: T_{zr}=886°C) indicating that the crustal source rocks should have been underplated and heated by mantle-derived mafic magmas. The presence of the nearby minor outcrops of tholeiitic basalt and dolerite with a transitional MORB to within-plate character (Triassic Rift Basic Volcanics: Asvesta, 1992; Dimitriadis and Asvesta,

1993; Asvesta and Dimitriadis, 2013) provides supportive evidence for the existence of underplating magmatism. Furthermore, limited magma mixing microtextures in dacites and mafic microgranular enclaves in rhyolites of Metallikon area support the coexisting mafic and felsic volcanism. The Triassic volcanism in CRB was in fact bimodal (A2-subtype rhyolites-dacites and minor tholeiites).

Moreover, A2-subtype post-collisional granites (Arnea and Kerkini suits) of Late Permian to Early Triassic age have intruded the nearby western Vertiskos unit of Serbo-Macedonian massif (Poli *et al*., 2009) and are likely the deep level equivalents of the Permo-Triassic volcanic rocks studied here (Poli *et al*., 2009; Asvesta and Dimitriadis, 2010).

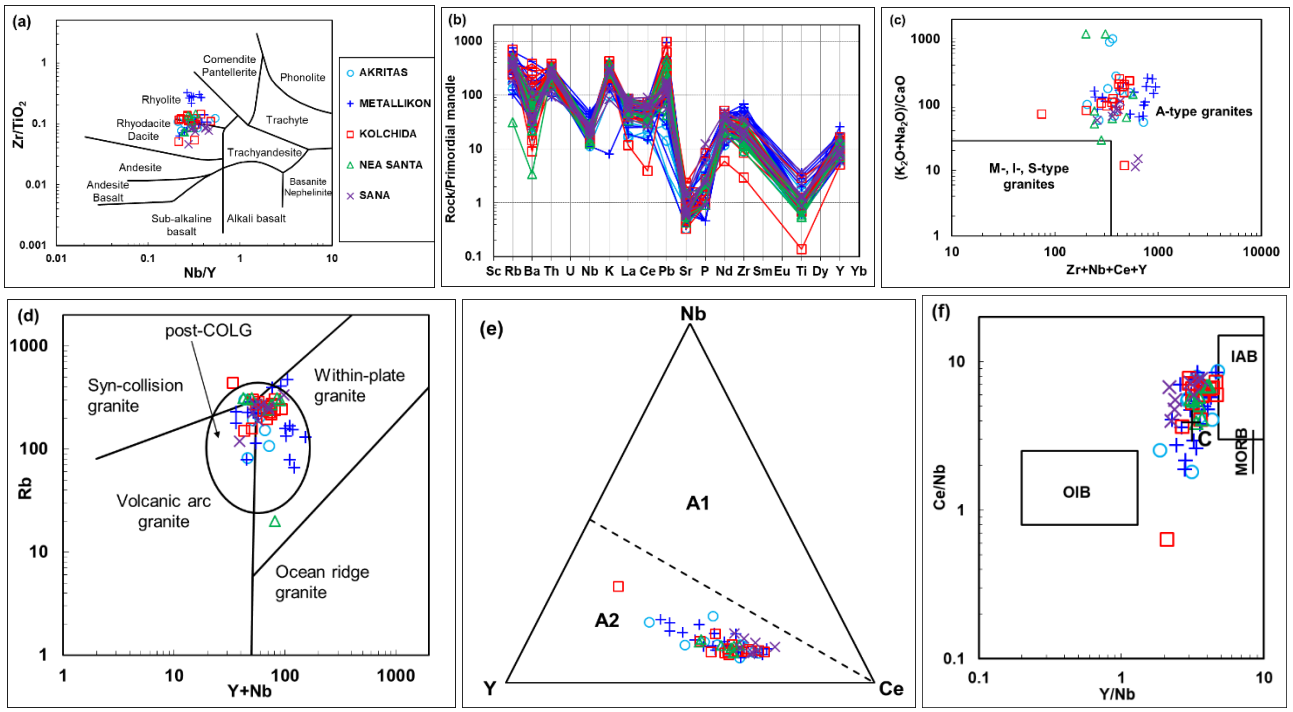

Figure 1. (a) Zr/TiO_2 *vs.* Nb/Y classification diagram (Winchester and Floyd, 1977), (b) primitive mantle normalised trace element patterns (normalisation values after Sun and McDonough, 1989), (c) $(K_2O+Na_2O)/CaO$ *vs.* (Zr+Nb+Ce+Y) discrimination diagram (Whalen *et al*., 1987), (d) tectonic discrimination diagram (Y+Nb) *vs.* Rb for granites, post-COLG=post-Collision Granites (Pearce, 1996), (e) Nb-Y-Ce ternary diagram (dashed line corresponds to Y/Nb ratio of 1.2) (Eby, 1992), (f) Ce/Nb *vs.* Y/Nb discrimination diagram, OIB: oceanic island basalts, black cross labelled C: average crustal composition, IAB: island arc basalts, MORB: mid-ocean ridge basalts (Eby, 1992).

Conclusions

The Permo-Triassic Silicic Volcanic rocks from Circum-Rhodope Belt are A2-subtype rhyolites-dacites and are probably the extrusive facies of the coeval and similar geochemically Arnea and Kerkini granites. It is suggested that silicic volcanism in CRB was evolved during a post-collision extensional stage of a Variscan progeny, leading to attenuated continental lithosphere and continental rifting during the Permo-Triassic which created the Vardar (Axios) oceanic strand. Silicic magma was produced by crustal anatexis of Serbo-Macedonian basement (Vertiskos unit) that was underplated and heated by mantle-derived mafic magma, represented by the minor dolerites and basaltic extrusions in the CRB.

References

Asvesta, A., 1992. Magmatism and associated sedimentation during the first stage of the opening of the Vardar oceanic basin in Triassic times. Ph.D. Thesis, Department of Geology, Aristotle University of Thessaloniki, Greece, 439 p. (in Greek with English summary).

Asvesta, A., Dimitriadis, S., 2010. Facies architecture of a Triassic rift-related Silicic Volcano-Sedimentary succession in the Tethyan realm, Peonias subzone, Vardar (Axios) Zone, northern Greece. J. Volcanol. Geotherm. Res. 193, 245-269.

Asvesta, A., Dimitriadis, S., 2013. Magma-sediment interaction during the emplacement of syn-sedimentary silicic and mafic intrusions and lavas into and onto Triassic strata (Circum-Rhodope Belt, northern Greece). Geologica Carpathica 64(3), 181-194.

Dimitriadis, S., Asvesta, A., 1993. Sedimentation and magmatism related to the Triassic rifting and later events in the Vardar-Axios zone. Bull. Geol. Soc. Greece XXVIII(2), 149-168.

Eby, G.N., 1992. Chemical subdivision of the A-type granitoids: petrogenetic and tectonic implications. Geology 20, 641-644.

Meinhold, G., Kostopoulos, D.K., 2013. The Circum-Rhodope Belt, northern Greece: Age, provenance, and tectonic setting, Tectonophysics 595-596, 55-68.

Pearce, J.A., 1996. Sources and settings of granitic rocks. Episodes 19, 120-125.

Poli, G., Christofides, G., Koroneos, A., Soldatos, T., Perugini, D., Langone, A., 2009. Early Triassic granitic magmatism – Arnea and Kerkini granitic complexes – in the Vertiskos unit (Serbo-Macedonian massif, north-eastern Greece) and its significance in the geodynamic evolution of the area. Acta Vulcanologica 21(1-2), 47-70.

Sun, S.-S., McDonough, W.F., 1989. Chemical and isotopic systematics of oceanic basalts: Implications for mantle composition and processes. Geol. Soc. London, Spec. Publ. 42, 313-345.

Whalen, J.B., Currie, K.I., Chappell, B.W., 1987. A-type granites: geochemical characteristic, discrimination and petrogenesis. Contrib. Mineral. Petrol. 95, 407-419.

Winchester, J.A., Floyd, P.A., 1977. Geochemical discrimination of different magma series and their differentiation products using immobile elements. Chem. Geol. 20, 325-343.

15th International Congress of the Geological Society of Greece
Athens, 22-24 May, 2019 | Harokopio University of Athens, Greece
Bulletin of the Geological Society of Greece, Sp. Pub. 7 Ext. Abs. GSG2019-009

Study of Neogene and Quaternary Terrestrial and Marine Sediments from Macedonia and Thrace, Greece

A. Tsirambides

Aristotle University of Thessaloniki, School of Geology, Department of Mineralogy-Petrology-Economic Geology, 54124 Thessaloniki, Greece, ananias@geo.auth.gr

Introduction

The Neogene and Quaternary sediments of Macedonia and Thrace lie unconformably over the folded alpine basement and are of fluvial, lacustrine or marine origin. These sediments are deposited into grabens or other neotectonic basins and are not connected to orogenetic procedures. The Post Alpine formations are widespread and are characterized by a wide lithological and facies variation. The Holocene sedimentation in the eastern Mediterranean is strongly affected by changes in the sea surface level associated with global paleoclimatic changes at the end of the Quaternary (Mountrakis, 2010).

The area of Macedonia and Thrace is a complex of grabens and horsts arranged in a NW-SE trend. Intermountain high level basins with elevation 400-500 m or low level basins with elevation 150-250 m, large coastal basins and plains were filled with Neogene and Quaternary sediments. Red beds are the most characteristic of them. They can be traced in the subsurface of the central parts of the basins. The widespread red beds and the associated rich mammalian fauna offer a good basis for stratigraphic and paleogeographic correlation with other sedimentary deposits in the Mediterranean (Psilovikos et al., 1987).

The coastline of Macedonia and Thrace incorporates the mouths of many small and large rivers. Most of them drain the mainland, except Evros, Nestos, Strymon and Axios that expand their network to neighboring countries. Evros River is the largest supplier of continental clastic material (8.5 × 106 tons/year) in the coastal region of NE Aegean. Similarly, in the Thermaikos Gulf, the rivers Gallikos, Axios, Aliakmon and Pinios discharge (25-30) × 106 tons/year of clastic terrestrial material (Poulos et al., 2000). The total suspended material in the NW Aegean is (484-830) × 103 tons/year (Karageorgis & Anagnostou, 2003).

Results and discussion

The fluvial sediments are climatically uniform in their setting and prograding into the north Aegean Sea. Tidal activity is negligible and the waves play a secondary role compared to the high sediment discharge of the rivers. Sand is the predominant (>60%) constituent of the river mouths (top sets), while the prodelta area consists mainly of silt- and clay-sized (>70%) particles (Poulos & Chronis, 1997).

The extended presence of quartz, feldspars and micas in the discharged material of the Evros is expected because it constitutes the weathering products of the large drainage basin of the river (extended in NE Greece and south Bulgaria), where igneous and metamorphic rocks predominate. The presence, in significant amounts, of zeolites is justified by the extended presence of volcaniclastic sediments in this drainage basin (Tsirambides & Kantiranis, 1998).

Evros is the largest supplier of fine grained Fe-Al-rich continental detritus to the offshore area. The modern sediments of the Alexandroupolis Gulf have adopted their characteristic zonal distribution in response to the coastal topography, the water motion and the quality of the supplied material. Acid and mafic igneous (especially volcanic), as well as metamorphic rocks cover the western and central parts of the Evros river drainage basin; Neogene sediments cover the eastern part and the coastal zone (Perissoratis et al., 1987).

The abundance of illite and smectite in the offshore sediments is mainly due to the weathering of primary Fe-Mg minerals of the drainage basin rocks and their transport and deposition in the Gulf. Especially, the abundance of smectite is enhanced by the high Fe and organic content, which results in a rapid flocculation and settling out of smectite grains. Kaolinite content expresses the strong climatic dependence controlled by the intensity of hydrolysis of continental rocks which occur in the drainage basin. However, the low content of kaolinite may be due to unfavorable climatic and physicochemical conditions, as well as to the detrital origin, rapid transport and deposition of the weathered material in the Gulf. Furthermore, the low percentage of the interstratified illite/smectite, as well as some presence of amphiboles in the clay fraction of the discharged material, confirm the limited reworking and weathering of the primary ferromagnesian minerals because of the high river discharge over short time periods and rapid deposition in the Gulf (Pehlivanoglou et al., 2000).

The most likely source materials for the formation of red beds at the Cedar Hills of Thessaloniki are feldspars, micas, and various Fe-Mg silicates, which are primary constituents of the metamorphic and ultramafic rocks predominating in these hills such as the greenschists (Tsirambides, 2004).

During Holocene, the rivers Gallikos, Axios, Aliakmon and Pinios discharged into the Thermaikos Gulf terrestrial clastic sediments with a mean accumulation rate 2.2 × 106 tons/yr. The maximum thickness of the sediments in the Gulf reaches 25-30 m. The estimated mean sedimentation rate ranges from 5 cm/ka to 15 cm/ka. The main minerals present in decreasing abundance are: quartz, feldspars (plagioclases > K-feldspars), Fe-Mg minerals, micas, and clay minerals. On average, the clay fraction (<2 μm) consists of: 48% illite, 26% smectite, 18% (chlorite + kaolinite), 3% quartz, 3%

feldspars and 2% Fe-Mg minerals. The origin of dolomite and calcite is mostly biogenic. Ordered and randomly interstratified phases of I/S are present. The abundance of smectite is enhanced by the high Fe and organic content of the terrigenous input, as well as by the physicochemical conditions of the seawater, which result in rapid flocculation and settling of smectite flocks. The low content of kaolinite may be due to unfavorable climatic and physicochemical conditions, as well as to the detrital origin, rapid transport and deposition of the weathered material in the Gulf. Furthermore, the presence of amphiboles observed even in the coarse clay fraction (2-0.25 μm) confirms the limited reworking and weathering of the primary ferromagnesian minerals because of the high river discharge over short time periods and rapid deposition in the Gulf. Finally, the significant presence of interstratified illite/smectite confirms the limited reworking and weathering of the primary minerals during their transport and deposition from the drainage basins of the rivers to the Gulf (Lykousis et al., 1981; Lykousis & Chronis, 1989; Karageorgis & Anagnostou, 2001; Pehlivanoglou et al., 2004).

The recent sediments of the Thermaikos Gulf have adopted their characteristic zone distribution in response to the coastal topography, the water circulation, and the prevailing climate in the region. The composition and dispersal of the suspended load of the rivers into the Gulf is controlled by the prevailing seasonal meteorological conditions at their catchment areas and the coastal area. The aggregation and distribution of clay particles in the Gulf is least controlled by the organic content of the terrigenous input because its presence is limited (Poulos et al., 2000).

Conclusions

All terrestrial sediments from Macedonia and Thrace are coarse grained and poorly sorted, with angular to sub-angular grains. These are mainly composed of quartz and feldspars, followed by micas, calcite and Fe-Mg minerals. Among the clay minerals illite predominates over smectite and smectite over vermiculite (+chlorite+kaolinite). In addition, the interstratifications I/S, Ch/V and S/V are present in significant amounts in the clay fraction (<2 μm), signifying the incomplete character of the weathering of the primary minerals. Mixing during transportation, flocculation, differential settling processes and organic matter are the main mechanisms for the distribution of the discharged terrigenous load into the North Aegean Gulfs.

All gulf bottom samples are coarse to fine grained and medium sorted, and their grains are angular to sub-angular. Quartz and feldspars predominate. In addition, biogenic carbonates (calcite+dolomite), micas and various Fe-Mg minerals exist as primary and/or accessory minerals. Among clay minerals, illite predominates over smectite and smectite over kaolinite. Almost in all sediments of the gulf bottoms the interstratified phase I/S is apparent.

The presence of feldspars and Fe-Mg minerals, as well as the high content of clay minerals and the polymodal grain-size distribution with angular to sub-angular grains, signify mineralogical and textural immaturity of all the examined terrestrial and marine sediments, as well as predominance of mild climatic conditions and thus mild weathering processes. The quartz content in these sediments is usually <65%. Therefore, a sedimentation cycle of these materials has not been completed.

References

Karageorgis, A., Anagnostou, Ch., 2001. Particulate matter spatial-temporal distribution and associated surface sediment properties: Thermaikos Gulf and Sporades Basin, NW Aegean Sea. Continental Shelf Research 21, 2141-2153.

Karageorgis, A., Anagnostou, Ch., 2003. Seasonal variation in the distribution of suspended particulate matter in the northwest Aegean Sea. J. Geophysical Research 108, No C8, 3274, doi: 10.1029/2002JC001672.

Lykousis, B., Chronis, G., 1989. Mechanisms of sediment transport and deposition: sediment sequences and accumulation during the Holocene on the Thermaikos Plateau, the continental slope, and basin (Sporades Basin), NW Aegean Sea, Greece. Marine Geology 87, 15-26.

Lykousis, B., Collins, M.B., Ferentinos, G., 1981. Modern sedimentation in the NW Aegean Sea. Marine Geology 43, 111-130.

Mountrakis, D., 2010. Geological and geotectonic evolution of Greece. University Studio Press, Thessaloniki (in Greek).

Pehlivanoglou, K., Tsirambides, A., Trontsios, G., 2000. Origin and Distribution of Clay Minerals in the Alexandroupolis Gulf, Aegean Sea, Greece. Estuarine Coastal & Shelf Science 51, 61-73.

Pehlivanoglou, K., Trontsios, G., Tsirambides, A., 2004. Grain size distribution, clay mineralogy and chemistry of bottom sediments from the outer Thermaikos Gulf, Aegean Sea, Greece. Mediterranean Marine Science 5(1), 43-53.

Perissoratis, C., Moorby, S.A., Papavassiliou, C., Cronan, D.S., Angelopoulos, I., Sakellariadou, F., Mitropoulos, D., 1987. The geology and geochemistry of the surficial sediments off Thraki, Northern Greece. Marine Geology 74, 209-224.

Poulos, S.E., Chronis, G.T., 1997. The importance of the river systems in the evolution of the Greek coastline. Bulletin of Institute of Oceanography Monaco 18, 75-96.

Poulos, S.E., Chronis G.T., Collins, M.B., Lykousis, V., 2000. Thermaikos Gulf Coastal System, NW Aegean Sea: an overview of water/sediment fluxes in relation to air–land–ocean interactions and human activities. J. Marine Systems 25, 47-76.

Psilovikos, A., Koufos, G., Syrides, G., 1987. The problem of red-beds in Northern Greece. Ann. Inst. Geol. Publ. Hung. LXX, 509-516.

Tsirambides, A., 2004. Genesis and physical characteristics of the Neogene red beds from the cedar hills of Thessaloniki, Macedonia, Greece. Bull. Geol. Soc. Greece 36, 708-716.

Tsirambides, A., Kantiranis, N., 1998. Composition and origin of the recent fluvial deposits of Evros (Thrace, Greece). Bull. Geol. Soc. Greece 32(2), 329-337.

15th International Congress of the Geological Society of Greece
Athens, 22-24 May, 2019 | Harokopio University of Athens, Greece
Bulletin of the Geological Society of Greece, Sp. Pub. 7 Ext. Abs. GSG2019-010

Sb- Bi-Bearing Metallogeny of the Serbomacedonian-Rhodope Metallogenic Belt (SRMB)

A. Tsirambides, A. Filippidis

Aristotle University of Thessaloniki, School of Geology, Department of Mineralogy-Petrology-Economic Geology, 54124 Thessaloniki, Greece, ananias@geo.auth.gr, anestis@geo.auth.gr

Introduction

The Alpine-Balkan-Carpathian-Dinaride (ABCD) metallogenic and geodynamic belt is considered Europe's premier Pb-Zn-Cu (-Mo-Sb-Ag-Au) province. It is divided in three spatially and temporally distinct tectonic and metallogenic belts. One of them, the Serbomacedonian-Rhodope Metallogenic Belt (SRMB), intersects with a NNW-SSE trend south-western Serbia, Kosovo, F.Y.R.O.M., north-eastern Greece and south Bulgaria. This arcuate belt is about 500 km long and 130-180 km wide. Deposits of carbonate-replacement Pb-Zn-Ag-Au, of porphyry Cu-Mo-Au, of stratiform volcano-sedimentary, of isolated magmatic-hydrothermal and skarns, as well as intrusion-related, epithermal and Carlin-type, compose this belt. All are genetically related to Oligocene-Miocene post-subduction magmatism (Kalogeropoulos et al., 1989; Marchev et al., 2005; Serafimovski et al., 2010; Tsirambides & Filippidis, 2016; Voudouris et al., 2018).

Native Bi is a relatively common mineral, native Sb is less abundant, and Sb-Bi alloys are relatively rare phases in nature. Sb-Bi alloys and Ag-Cu-Pb-Sb-Bi sulfosalts have been discovered in some metal assemblages in the SRMB. Stibnite (Sb_2S_3) is the predominant ore mineral of Sb. The most important ores of Bi are bismuthinite (Bi_2S_3) and bismite (Bi_2O_3). Trace metallic minerals like Bi-sulfosalts and Bi- sulfotellurides, precious- and base metal tellurides are usually associated with Au-bearing ores and can be considered as pathfinder minerals for Au (Melfos & Voudouris, 2012).

The European Union (EU) is highly dependent on critical and rare metals which are very important for a sustainable development. However, European industry is not able to cover its demands from native sources and it imports commodities from third countries. The various types of deposits of the SRMB are promising targets for future exploration and exploitation in Sb, Te, Mo, Re, Ga, In, REE and PGE. Therefore, the mineral wealth of this belt can contribute significantly to a sustainable and a competitive economy of Europe (Tsirambides & Filippidis, 2012, 2016).

Results and discussion

The Au-As-Sb-Tl Alshar deposit of Carlin type in F.Y.R.O.M. is located at the intersection of the Axios (Vardar) and Aridea-Kozuf metallogenic zones at the western side of the Vardar Graben and the Pelagonian crystalline massif, approximately 3 km from the Greek-F.Y.R.O.M. border. The deposit is composed of several ore deposits and occurrences, which are characterized by specific assemblages of elements and minerals. More than 40 minerals have been identified in this ore deposit. Stibnite occurs in the form of crystals up to 2 × 5 mm in size and frequently cements quartz and marcasite grains, indicating its younger age in comparison to pyrite–marcasite assemblage. A probable temperature of about 200°C is accepted for the formation of the main Au-ore. The Alshar deposit is undoubtedly related to the action of post-volcanic hydrothermal fluids. The ore field covers an area of 21 km2. It is considered a very significant deposit containing economic grades of Sb (up to 2.5 wt%), As (up to 1.5 wt%), Tl (up to 0.5 wt%) and Au (about 1 g/t). The indicated stibnite reserves exceed 20,000 t (av. Sb=0.5 wt%) (Volkov et al., 2006).

In the regions of Macedonia and Thrace in Greece there is a large number of occurrences and ores of Pb, Zn, and Cu, which are often accompanied by Mo, Sb, Bi, W, Ag, Au and other metals. Some of these ores are economically very significant. Except stibnite, antimony is also contained in many sulfosalts which are common in porphyry-, epithermal- and intrusion-related systems at the Rhodope Massif. In some cases samples contain up to 0.2 wt% Sb (Voudouris et al., 2011; Melfos & Voudouris, 2012; Tsirambides & Filippidis, 2016).

The Vertiskos Unit of the Serbomacedonian massif (SMM) hosts several Oligocene-Miocene ore deposits and mineralization occurrences. Some of these contain significant amounts of metals such as Sb, Bi, Te, Co, REEs and PGMs. At the northern part of the SMM there are porphyry-epithermal (Vathi, Palatiano, Gerakario, Pontokerasia, Doirani), skarn/carbonate replacement (Myriofyto, Petrades, Monolithi) and epithernal vein (Rodonas) ore type occurrences (Stergiou et al., 2018).

The most important porphyry-epithermal ore occurrences in the Regional Unit of Kilkis are (Stergiou, 2016):

- The Vathi Cu- Au- U±Mo-deposit is associated with a high-K calc-alkaline monzonite intrusion. Its probable and indicated reserves are 0.15 Mt ore with up to 0.3 wt% Cu and up to 0.8 ppm Au. Other constituents of this deposit are: 20-977 ppm Pb, 9-156 ppm Zn, up to 341 ppm Mo, up to 239 ppm Bi, up to 11 ppm Sb and up to 4.6 ppm Ag.
- The Gerakario Cu- Au-deposit is hosted in a calc-alkaline syenite and granodiorite intrusion. Its probable and indicated reserves are 0.13 Mt ore with up to 0.3 wt% Cu and up to 1.4 ppm Au.
- The Pontokerasia Cu- Mo- Au-deposit is associated with a calc-alkaline syenite intrusion. It contains up to 0.3 wt% Cu and up to 0.2 ppm Au.
- The Rizana/Lachanas porphyry-epithermal deposit is considered the most important stibnite ore in Greece. It is related to sheeted quartz veins, usually of small dimensions, that crosscut Paleozoic metamorphic rocks such as gneisses and amphibolites. Many occurrences of minerals of antimony and some of tungsten exist at the broader area.

These sheeted veins are the most spread type of ore mineralization. The paragenesis minerals of the ore are quartz, pyrite, calcite, dolomite, sericite, chlorite, stibnite and wolframite. This mineral assemblage reinforces the aspect that this ore has an epithermal hydrothermal origin. The difficulty in the dissolution of the hosted rocks by the thermal solutions prevented the creation of extended stibnite and wolframite ore (Paraskevopoulos, 1958). However he suggested that additional research is needed at the broader area for the evolution of Sb- W-metallogeny in deeper horizons. In the period of 1930-50 about 9,000 tons of stibnite ore and some tons of wolframite ore have been extracted from rough tunnels of 350 m total length. The Sb concentration reached 40% for half of the total production. The mineralization is spread over an area of 50 km long and 30 km wide, and today presents high potential for future exploitation (Paraskevopoulos, 1958). The proven reserves of stibnite are 5000 t (av. Sb=0.3 wt%) and its indicated reserves are 50,000-100,000 t of the same Sb concentration. The proven reserves of wolframite are 1000 t (Liatsikas *et al.*, 1947).

- The Kimmeria Xanthi intrusion-related Mo-Cu-W-Bi-Au deposit is associated with an Oligocene (25-30 My) pluton, which consists of granodiorite and minor outcrops of tonalite, quartz-diorite, monzonite and gabbroic rocks. The pluton intruded gneiss, mica schist, amphibolite and marble of the Rhodope Massif. Two different ore types are genetically connected with the magmatic intrusion: 1. Massive Au-bearing skarn-type mineralization and 2. Mo-Cu-Bi-W quartz vein mineralization. An extensive skarn formation outcrops 2-3 km NNE of Kimmeria consisting mainly of garnet, epidote, hematite, wollastonite, vesuvianite and secondary amphibole, quartz and calcite. The intrusion-related polymetallic system includes sheeted quartz veins and stockworks crosscutting the granitic pluton. Bulk chemical analyses of vein-type mineralization resulted in the following composition: ~1 wt% Cu, ~0.2 wt% Mo, up to 2.7 g/t Au, up to 80 g/t W, up to 457 g/t Bi, and up to 4 g/t Te (Theodoridou *et al.*, 2016).

Conclusions

Antimony-bismuth alloys and Ag-Cu-Pb-Sb-Bi sulfosalts have been discovered in some metal assemblages in the SRMB. The European Union (EU) is highly dependent on critical and rare metals, such as Sb and Bi, which are very important for a sustainable development. Greece is one of the EU countries with the most potential for supplying the strategic metal Sb in the future, since it hosts a significant ore deposit at Rizana/Lachanas (central Macedonia, Greece). Here, the stibnite reserves (proven+indicated) are 50,000-100,000 t with average Sb=0.3 wt% and the wolframite reserves (proven) are 1000 t. Another promising Sb-bearing mineral assemblage exists at Alshar (F.Y.R.O.M.). Here, the stibnite indicated reserves are >20,000 t with average Sb=0.5 wt%. At both mineralization districts further investigations are needed to determine the grade and the proven reserves of the critical metal Sb. Until today none encouraging site has been located in the SRMB for remarkable Bi-bearing ore sites.

References

Kalogeropoulos, S., Kilias, S., Bitzios, D., Nicolaou, M., Both, R., 1989. Genesis of the Olympias carbonate-hosted Pb-Zn (Au, Ag) sulphide ore deposit, eastern Chalkidiki Peninsula, northern Greece. Economic Geology 84(5), 1210-1234.

Liatsikas, N., Solomos, I., Kogevinas, S., Andreakos, G., 1947. The mineral wealth of Greece. U.N.R.R.A., Athens (in Greek).

Marchev, P., Kaiser-Rohrmeier, M., Heinrich, C., Ovtcharova, M., Von Quadt, A., Raicheva, R., 2005. Hydrothermal ore deposits related to post-orogenic extentional magmatism and core complex formation: The Rhodope Massif of Bulgaria and Greece. Ore Geology Reviews 27, 53–89.

Melfos, V., Voudouris, P., 2012. Geological, Mineralogical and Geochemical Aspects for Critical and Rare Metals in Greece. Minerals 2, 300-317, doi:10.3390/min2040300.

Paraskevopoulos, G., 1958. Genesis of the W- and Sb-bearing ores of Lachanas area in the central Macedonia. Ann. Geol. Pays Helleniques 9, 227-241 (in Greek).

Serafimovski, T., Stefanova, V., Volkov, A.V., 2010. Dwarf Copper-Gold Porphyry Deposits of the Buchim-Damian-Borov Dol Ore District, Republic of Macedonia (FYROM). Geology of Ore Deposits 52(3), 179-195.

Stergiou, C.L., 2016. Mineralogical, geochemical and structural – control study of the hydrothermal alterations and the ore mineralization at Vathi porphyry Cu - Au ± U ± Mo system, N. Greece. Master Thesis, School of Geology, Aristotle University of Thessaloniki, 118 p.

Stergiou, C.L., Melfos, V., Voudouris, P., 2018. A Review on the Critical and Rare Metals Distribution throughout the Vertiskos Unit, N. Greece. Conf. Proc. IECMS, 9 p.

Theodoridou, S., Melfos, V., Voudouris, P., Miscovic, A., 2016. Mineralogical and Geochemical Characterization of the Kimmeria Intrusion-Related Deposit, Xanthi, NE Greece. Geophysical Research Abstracts, 18, EGU2016-8933.

Tsirambides, A., Filippidis, A., 2012. Metallic mineral resources of Greece. Central European J. Geosciences 4(4), 641-650.

Tsirambides, A., Filippidis, A., 2016. Gold metallogeny of the Serbomacedonian-Rhodope Metallogenic Belt (SRMB). Bull. Geol. Soc. Greece 40, 2037-2046.

Volkov, A.V., Serafimovski, T., Kochneva, N.T., Tomson, I.N., Tasev, G., 2006. The Alshar Epithermal Au–As–Sb–Tl Deposit, Southern Macedonia. Geology of Ore Deposits 48(3), 175-192.

Voudouris, P., Melfos, V., Spry, P.G., Moritz, R., Papavassiliou, C., Falalakis, G., 2011. Mineralogy and geochemical environment of formation of the Perama Hill high-sulfidation epithermal Au-Ag-Te-Se deposit, Petrota Graben, NE Greece. Mineralogy & Petrology 103, 79-100.

Voudouris, P., Spry, P.G., Melfos, V., Haase, K., Klemd, R., Mavrogonatos, C., Repstock, A., Alfieris, D., 2018. Gold deposits in Greece: Hypogene ore mineralogy as a guide for precious and critical metal exploration. Conf. Proc. IECMS, 13 p.

15th International Congress of the Geological Society of Greece
Athens, 22-24 May, 2019 | Harokopio University of Athens, Greece
Bulletin of the Geological Society of Greece, Sp. Pub. 7 Ext. Abs. GSG2019-013

Plagioclase hosted melt inclusion in hypabyssal rocks in Torud-Amad Abad magmatic belt.

FazilatYousefi[1*], Papadopoulou Lambrini[2], Mahmoud Sadeghian[1], Christina Wanhainen[3], Glenn Bark [3]
(1)Faculty of Earth Sciences, Shahrood University of Technology, Shahrood, Iran. Email: f.yousefi87@gmail.com
(2) Department of Mineralogy-Petrology-Economic Geology, Aristotle University of Thessaloniki, Thessaloniki, Greece
(3) Department of Civil, Environmental and Natural Resource Engineering, Lulea University of Technology, Lulea, Sweden

In this study, we investigated the melt inclusions (MI) that are hosted in constituent minerals of the hypabyssal rocks in in Torud-Ahmad Abad magmatic rocks in south-southeast of Shahrood (Northern part of central Iran structural zone) for the first time (Figure 1). Based on previous studies, the composition of hypabyssal rocks in Torud-ahmad Abad are andesite, dacite and basaltic andesite (Yousefi et al., 2016a). The mineral assemblages and the composition of minerals in magmatic rocks are related to the composition and evolving conditions of the melt during crystallization (Yousefi et al., 2016b).Melt inclusions represent liquids that were trapped along growth zone (primary) or healed fractures of mineral phases, which crystallized from the silicate liquid as it cooled. Based on SEM analysis of these melt inclusions, their compositions are dacite, andesite and basaltic andesite. The chemical composition of these melt inclusions is determined by the Scanning Electron Microscope Laboratory, using a SEM (JEOL JSM-840A) equipped with an energy dispersive spectrometer (EDS, Oxford INCA 250) at Aristotle University of Thessaloniki. Thus, with the use of melt inclusions in the volcanic rocks of Torud-Ahmad Abad magmatic belt, we show the compositional evolution and origin of magma. The effective factors on evolution of these magma, are magma mixing, fractional crystallization and crustal contamination. Melt inclusions are hosted in many, virtually all, igneous-related minerals, but are mostly studied in those minerals where they are more abundant and/or better preserved and or/more visible. It follows that common host minerals are quartz and plagioclase in felsic igneous rocks, and olivine, pyroxene and plagioclase in mafic/ultramafic igneous rocks (Cesare et al., 2015). Our results best fit a model in which similar basaltic andesites and andesite rocks are repeatedly generated from mantle magma batches during their ascent as they mix with resident magmas, fractionate, and recycle older crystals and the dacite rocks, which have more silica than the others, originate from melting of Neo-TethyanOceanic crust (Figure 2).In figure 3, backscattered electron image of melt inclusions is shown.

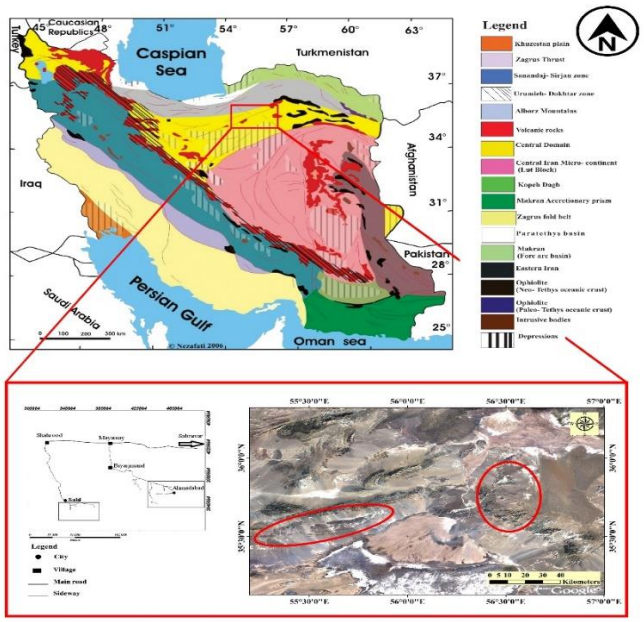

Figure 1. Distribution of Middle and late Eocene hypabyssal rocks of TAMB (Torud-Ahmad Abad Magmatic Belt).

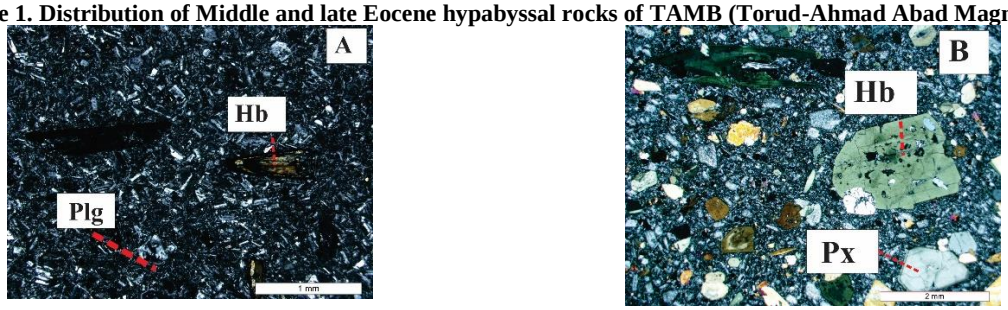

Fig 2: Photomicrographs of the studied rocks. A: Trachydacite rock; B: Porphyritic texture within basaltic andesite.

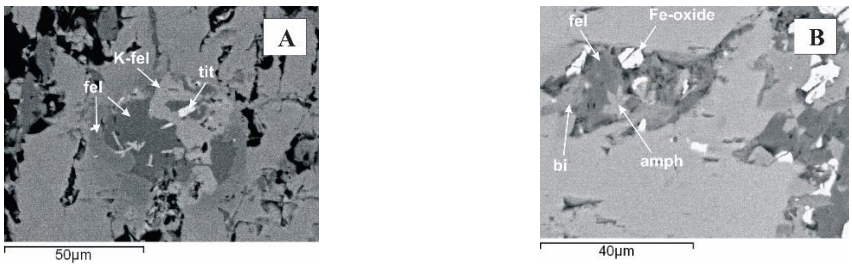

Fig 3: Backscattered electron image of melt inclusion in host mineral of plagioclase and amphibole.

Based on analysis of melt inclusions in these dacite, andesite and basaltic andesite rocks, their composition are andesite, basaltic andesite and dacite (Figure 4). The melt inclusions in these rocks were trapped during the simultaneous growth of the host minerals. We came to this result based on the chemical composition of these melt inclusions after analysis by SEM and drawing the classification diagram. The Harker diagrams of melt inclusions illustrate negative correlation of Al_2O_3 and CaO vs. SiO_2 that can be due to crystal differentiation during crystallization of magma (Figure 4). In figure 4 the classification diagrams of rocks and melt inclusions are shown (Le Bas et al., 1986).

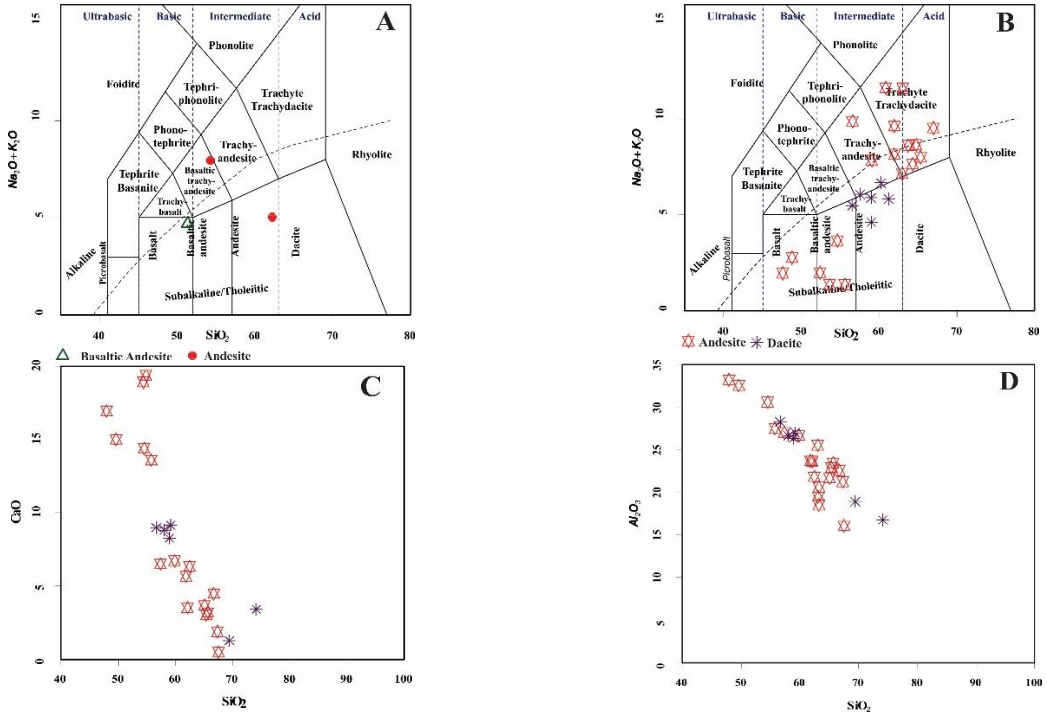

Fig 4: A: Composition of whole rocks. B: Composition of MI in plagioclase in andesite, dacite, basaltic andesite.

In general, the results are: 1) based on the obtained results of geochemical analysis, the studied rocks have chemical compositions varying from andesite, trachyandesite, basaltic andesite and dacite. 2) The composition of melt inclusions is andesite, basaltic andesite and dacite. 3) The melt inclusions in these rocks are small droplets of melt that are trapped in minerals.

Acknowledgements

Dr Papadopoulou Lambrini is acknowledged for doing SEM analysis at Aristotle University of Thessaloniki and presenting the article. Authors wish to thank Professor Christina Wanhainen and Dr Glenn Bark for providing favorable residence conditions for Fazilat Yousefi in Sweden and conducting the whole rocks and microprobe analysis at Lulea University of Technology.

References

Cesare, B., Acosta-Vigil, A., Bartoli, O., Ferrero, F., 2015. What can we learn from melt inclusions in Migmatites and granulites? Lithos, 186-216.

Harker, A., 1909. The Natural History of Igneous Rocks. 255 p. Methuen, London.

Le Bas, M.J., Le Maitre, R.W., Streckeisen, A., Zanettin, B., 1986. A chemical classification of volcanic rocks based on the total alkali-silica diagram. Journal of Petrology, 27, 745-750.

Yousefi, F., Sadeghian, M., Wanhainen, Ch., Ghasemi, H., Frei, D., 2016 a. Geochemistry, Petrogenesis and tectonic setting of middle Eocene hypabyssal rocks of the Torud-Ahmad Abad magmatic belt: An implication for evolution of the northern branch of Neo-Tethys Oceanic in Iran. 1-15. Journal of Geochemical Exploration, 178, 1-15.

Yousefi, F., Sadeghian, M., Wanhainen, Ch., Ghasemi, H., Lambrini, P., Bark, G., RezaiKakhhaei, M., Koroneos, A., 2016b. Mineral chemistry and P-T conditions of the adakitic rocks from Torud-AhmadAbad magmatic belt, S-SE Shahrood, Iran. 110-120. J.G.E., 182, DOI: 10.1016/j.gexplo.2017.09.006.

15th International Congress of the Geological Society of Greece
Athens, 22-24 May, 2019 | Harokopio University of Athens, Greece
Bulletin of the Geological Society of Greece, Sp. Pub. 7 Ext. Abs. GSG2019-017

Precious and critical metal phases in the Agios Filippos high-sulfidation epithermal system, Kirki, Thrace, NE Greece

Stavros Triantafyllidis

National Technical University of Athens, School of Mining and Metallurgical Engineering, Iroon Polytechneiou 9, 157 80 Zografou, Athens, Greece, striantafyllidis@metal.ntua.gr

Geologic setting

The Agios Filippos (Kirki) high-sulfidation epithermal deposit is located in Thrace, NE Greece, approximately 19 km to the NNW of Alexandroupolis city. The mineralization is hosted in the Eocene-Oligocene rock sequences of SE Evros county, and is associated to orogenic calc-alkaline to shosonitic magmatism as a result of subduction of the African plate below the Eurasian plate. The deposit is developed between two sub-parallel faults forming the western and the eastern part of the open pit (Skarpelis, 1999), and the low-grade ore body is hosted within a rhyolite dyke and the nearby hydrothermally altered volcano-sedimentary and sedimentary formations.

Sampling – Analytical methods

Drill core samples down to depths of approximately 180m from the surface were selected and used for the mineralogical investigation of primary epithermal mineralization, hydrothermal alteration assemblages and supergene mineral phases. Scanning electron microscopy was performed using a Jeol JSM 5600 scanning electron microscope combined with energy dispersive X-ray spectrometry (OXFORD ISIS Link electron microprobe) and equipped with a Jeol Analytical back-scattered electron detector at the Laboratory of Economic Geology and Geochemistry, Department of Geology and Geoenvironment, University of Athens. Operating conditions for the SEM were 20 kV accelerating voltage and 0.5 nA beam current. Counting time for each analysis was 50 sec, with 15-sec dead time.

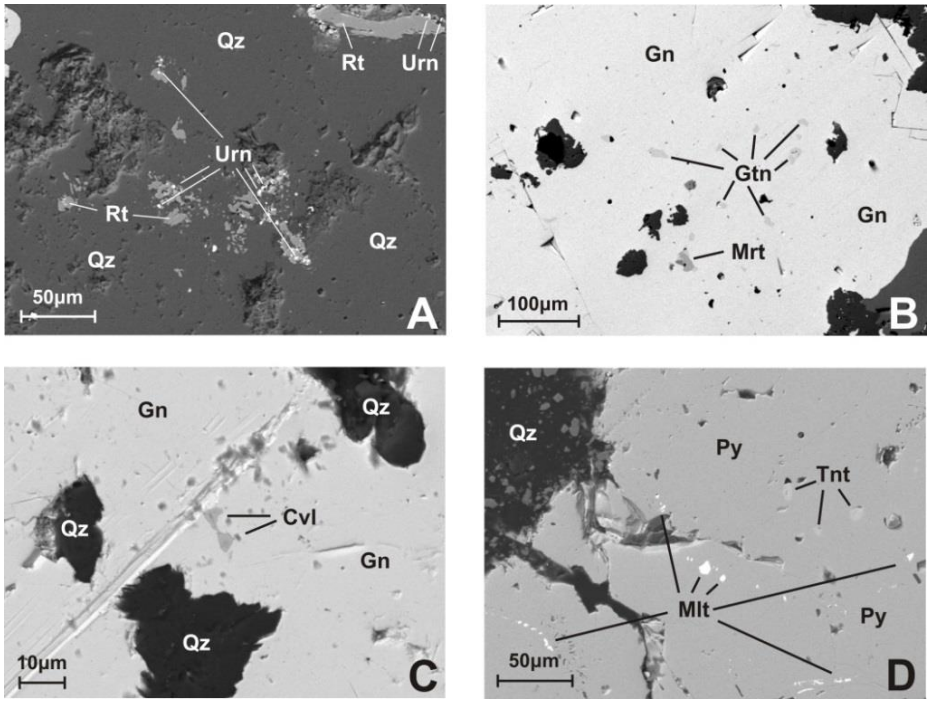

Figure 1. Back-scattered electron SEM images from the Agios Filippos high sulfidation epithermal system. A. Disseminated fine-grained uraninite (Urn) in association with anhedral rutile (Rt) in silicified host-rock. B. Anhedral gratonite (Gtn) and marrite (Mrt) inclusions in galena (Gn). C. Anhedral cervelleite (Cvl) inclusions in galena (Gn). D. Anhedral tennantite (Tnt) and matildite (Mlt) inclusions in pyrite (Py). Abbreviations for quartz, uraninite, rutile, galena, tennantite and pyrite after Whitney and Evans (2010).

Results and discussion

Uraninite (UO_2) is reported for the first time in the Agios Filippos epithermal system and is identified at the upper part of the deposit, forming disseminated subhedral to euhedral crystals with size ranging between 2 and 10 μm. Uraninite is associated to TiO_2, pyrite and barite in silicified to advanced argillic altered sectors of the deposit (Figure 1A). Marrite ($PbAgAsS_3$) is identified in samples from the upper part of the Agios Filippos deposit, and in particular within the rhyolite intrusion at the eastern part of the mineralized zone**,** forming anhedral inclusions within galena crystals (Figure 1B, Table 1). Cervelleite (Ag_4TeS) is also identified for the first time in the Agios Filippos epithermal system, and in particular in

samples from the upper - eastern part of the deposit where bedded acidic tuffs have suffered silicic to advanced argillic alteration. Cervelleite is mainly found forming inclusions in galena (Figure 1C, Table 1), and based on semi-quantitative SEM-EDS analyses shows enrichment in Sn (up to 5.4 wt%). In Greece, cervelleite type phases are also reported in the vein-hosted Panormos Bay system in Tinos (Spry et al., 2006). Matildite ($AgBiS_2$) is identified in samples from the lower sector of the Agios Filippos deposit, and within bedded acidic tuffs. Matildite forms anhedral inclusions with size ranging between 1 and 10μm within pyrite (Figure 1D, Table 1). The presence of cervelleite, marrite and matildite in the Agios Filippos epithermal system may indicate evolution from early high-sulfidation state to late intermediate sulfidation state (Baksheev et al., 2018; Mehrabi et al., 2016). Cuprobismutite ($Cu_{10}Bi_{12}S_{23}$) is identified at the lower sector of the Agios Filippos deposit, and within bedded acidic tuffs. Cuprobismutite forms anhedral inclusions within pyrite and is closely associated to matildite. Based on SEM-EDS analyses, cuprobismutite shows enrichment in Ag up to 4.6 wt% (Table 1). Besides primary critical and precious metal bearing phases, Ga-bearing beudantite [endmember chemical formula $PbFe_3(AsO_4)(SO_4)(OH)_6$] is identified at the upper part of the oxidation zone. In the Agios Filippos system, beudantite is fine grained and its composition varies showing enrichment in Ga, In and Sb. The Ga content of beudantite crystals analyzed from the Agios Filippos epithermal system ranges from 1.2 to 5.6 wt% (as Ga_2O_3), and in several occasions In is also detected, ranging from 0.7 to 1.2 wt% (as In_2O_3), whereas the Sb content of beudantite (as Sb_2O_5) ranges from 3 to 5.9 wt% (Triantafyllidis, 2006).

Table 1: Representative semi-quantitative SEM-EDS analyses (in wt%) of critical and precious metal ore phases from the Agios Filippos high-sulfidation epithermal system.

Phase	**S**	**Fe**	**Pb**	**Te**	**Cu**	**Ag**	**Sn**	**Bi**	**As**	**Total**
Matildite	16.09	1.65	n.d.	n.d.	n.d.	27.61	n.d.	55.06	n.d.	100.41
Cuprobismuthite	18.01	3.15	n.d.	n.d.	10.10	4.58	n.d.	63.98	n.d.	99.82
Marrite	19.01	n.d.	44.37	n.d.	n.d.	21.43	n.d.	n.d.	15.38	100.19
Cervelleite	5.85	n.d.	n.d.	21.51	n.d.	66.96	5.44	n.d.	n.d.	99.76
	Molecular proportions									**No of ions**
Matildite	1.91	0.11	-	-	-	0.97	-	1.00	-	4.00
Cuprobismuthite	22.45	2.25	-	-	6.35	1.70	-	12.24	-	45.00
Marrite	2.94	-	1.06	-	-	0.98	-	-	1.02	6.00
Cervelleite	1.08	-	-	0.99	-	3.66	0.27	-	-	6.00
n.d.: not detected										

The Agios Filippos deposit has been a target of exploitation for base metals (Pb, Zn and Cu), and only in recent years the presence of elevated concentrations of Critical and Precious Metals was revealed (Skarpelis, 1995; Voudouris et al., 2005). In this study, mineralogical investigation of drill core samples from the Agios Filippos epithermal system revealed the presence of rare and uncommon Critical and Precious metal bearing phases including uraninite, cervelleite, marrite, matildite and cuprobismutite (Figure 1, Table 1), that could provide further insights on the mode of formation of the Agios Filippos deposit and its correlation with the Northern Greece metallogeny, as well as further information on the Critical and Precious Metal potential of Greek mineral deposits and mineralizations.

Acknowledgements

Part of the research work was funded through the program ‘‘IRAKLEITOS—Fellowships for Research of National and Kapodistrian University of Athens—ENVIRONMENT.’’ The author would also like to thank emeritus professor Nikolaos Skarpelis for providing the drill-core samples for mineralogical investigation during the progress of the author’s PhD Thesis.

References

Baksheev, I.A., Vlasov, E.A., Nikolaev, Y.N., Krivitskaya, N.N., Koshlyakova, N.N., Nagornaya, E.V., Kara, T.V., Dzhedzheya, G.T., 2018. Mineralogy of the Tumanny Au-Ag-Te-Hg epithermal veins, Western Chukchi Peninsula, Russia. Ore Geology Reviews, 101, 293-311.

Mehrabi, B., Siani, M.G., Goldfarb, R., Azizi, H., Ganerod, M., Marsh, E.E., 2016. Mineral assemblages, fluid evolution, and genesis of polymetallic epithermal veins, Glojeh district, NW Iran. Ore Geology Reviews, 78, 41-57.

Skarpelis, N., 1999. The Agios Filippos ore deposit, Kirki (Western Thrace). A base metal part of a high sulfidation epithermal system, Bull. Geol. Soc. Greece, XXXIII, 51-60.

Skarpelis, N., 1995. Minor elements in the base metals part of an epithermal system: the Kirki (St. Philippe) mine, Thrace, Northern Greece. EUG 8, Strasbourg, Abstract Supplement No 1 to TERRA Nova, 7, 293.

Spry, P.G., Tombros, S.F., Seymour, K.St., Zouzias, D.P., 2006. Geology, mineralogy and geochemistry of granite-hosted gold telluride mineralization at Panormos Bay, Tinos Island, Greece. Geol. Soc. Amer. Abstr. Prog. 38, 55.

Triantafyllidis, S., 2006. Environmental risk assessment of mining and processing activities and rehabilitation proposals in Evros and Rhodope prefectures (Thrace, NE Greece). PhD Thesis, Faculty of Geology & Geoenvironment, University of Athens, 361p.

Voudouris, P., Papavasiliou, C., Melfos, V., 2005. Silver mineralogy of St. Philippos deposit (NE Greece) and its relationship to a Te-bearing porphyry-Cu-Mo mineralization. Bulgarian Academy of Sciences, Geochemistry, Mineralogy and Petrology, 43, IGCP Project 486, 2005 Field Workshop, Kiten, Bulgaria, 14-19 September 2005.

Whitney, D.L., Evans, B.W., 2010. Abbreviations for names of rock-forming minerals. American Mineralogist, 95, 185-187.

15th International Congress of the Geological Society of Greece
Athens, 22-24 May, 2019 | Harokopio University of Athens, Greece
Bulletin of the Geological Society of Greece, Sp. Pub. 7 Ext. Abs. GSG2019-018

Electrum (Au-Ag±Cu) in association with Ag-Au and Ag tellurides and Bi-Te-Se phases in the intermediate conglomerate, Perama Hill epithermal Au deposit, Thrace, NE Greece

Stavros Triantafyllidis

National Technical University of Athens, School of Mining and Metallurgical Engineering, Iroon Polytechneiou 9, 157 80 Zografou, Athens, Greece, striantafyllidis@metal.ntua.gr

Geologic setting

The Perama Hill epithermal Au deposit is located approximately 30 km west-northwest of the city of Alexandroupolis (Thrace, NE Greece), at the eastern margin of the N-S trending Petrota Graben. According to Lescuyer et al. (2003) and Juras et al. (2010), the deposit is mushroom shaped, and two major sectors may be recognized, the upper, oxide sector (Perama sandstone) with free Au (Triantafyllidis & Skarpelis, 2015) which is the target of exploitation (Juras et al., 2010), and the lower, refractory ore in the underlain andesites, whereas a volcanoclastic conglomerate unit with ranging thickness lies between the upper oxidized and the lower refractory ore. According to Juras et al. (2010), the calculated reserves (proven and probable) in the oxidized ore (Perama sandstone) are 9.4 Mt with average Au and Ag grades 3.20 gr/t and 3.75 gr/t respectively.

Sampling – Analytical methods

Drill core samples from the intermediate volcanoclastic conglomerate of the Perama Hill epithermal Au deposit were selected and used for the mineralogical investigation of ore and hydrothermal alteration phases. Scanning Electron Microscopy was carried out at the Laboratory of Mineralogy, Petrology and Economic Geology, Section of Geological Sciences, School of Mining and Metallurgical Engineering, National Technical University of Athens. It involved the use of a JEOL JSM 6380LV scanning electron microscope combined with energy dispersive X-ray spectrometry (OXFORD ISIS Link electron microprobe) and equipped with a Jeol Analytical back-scattered electron detector. Operating conditions for the SEM were 20 kV accelerating voltage, 20mm working distance and 1.0 nA beam current. Counting time for each analysis was 50 sec, with 15 sec dead time.

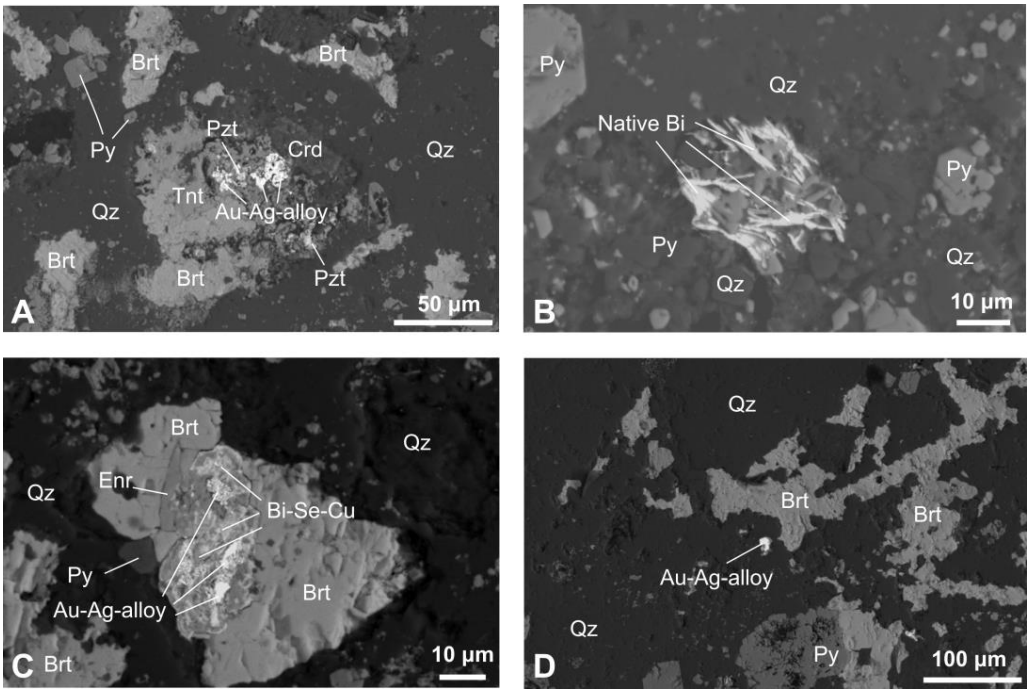

Figure 1. A. Electrum (Au-Ag±Cu alloy) in association with petzite (Pzt), anhedral tennantite (Tnt) and disseminated euhedral pyrite (Py) in silicified sectors of the intermediate conglomerate. Barite (Brt) and crandallite (Crd) are also identified. B. Needle shaped native Bi in association with euhedral to subhedral pyrite (Py). C. Electrum (Au-Ag±Cu alloy) in association with barite (Brt), enargite (Enr) and un-identified Bi-Se-Cu phases in silicified rock. D. Electrum (Au-Ag±Cu alloy) in association with abundant euhedral coarse-grained barite (Brt) and pyrite (Py) aggregates in silicified intermediate conglomerate. Abbreviations for barite, pyrite, tennantite, enargite and quartz after Whitney and Evans (2010).

Results and discussion

Previous studies on the mineralogy of the lower refractory ore from Voudouris et al. (2011) and Skarpelis et al., (2006) revealed the presence of Bi-Te-Se±(Au,Ag) mineralization in the southern and central part of the Perama Hill epithermal

system hosted in the lower andesitic breccia. Mineralogical investigation of drill core samples from the intermediate volcanoclastic conglomerate indicates the presence of Au-Ag-Bi-Te-Se mineralization in several parts of the Perama Hill epithermal system, and in particular the southern and central part, where the main hypogene feeder zones are located. Relative to studies performed on the lower refractory ore, the intermediate volcanoclastic conglomerate is characterized by higher concentrations of precious metals, as evident by the presence of electrum (Au-Ag±Cu alloy, Figure 1A,1C,1D) and precious metal tellurides, including petzite and hessite (Figure 1A, Figure 2). This observation supports the statement of Juras et al. (2010) that the Au content in the Perama epithermal system is not uniformly distributed, and the highest Au grades are identified in drill core samples from the upper and the lower part of the epithermal system scheduled for exploitation.

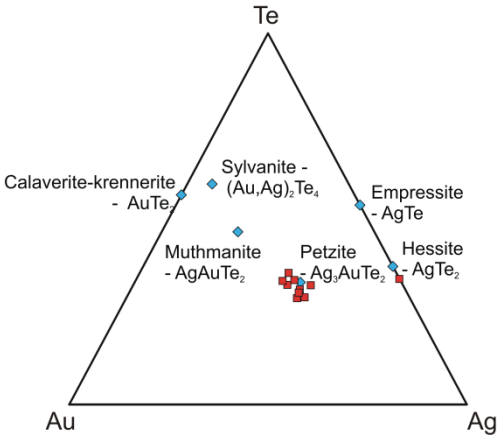

Figure 2. Ternary Au-Ag-Te diagram of typical Au, Ag and Au-Ag tellurides (blue rhombs), and Au-Ag and Ag tellurides (red squares) from the intermediate volcanoclastic conglomerate of the Perama Hill epithermal Au deposit.

The relatively increased precious and critical metal load of the intermediate volcanoclastic conglomerate may be attributed to sudden changes in hydraulic conductivity between the lower and cohesive andesitic breccia (refractory ore) and the upper, unconsolidated and highly porous felsic sandstone. According to Lescuyer et al. (2003), the Perama mineralization is considered contemporaneous to the host rocks, hence the ascending, rich in precious and critical metals hydrothermal fluids may have unloaded a significant part of their precious and critical metal load in such locations where the hydraulic conductivity changes rapidly, resulting in a late stage Au-Ag-Bi-Te-Se mineralization, including electrum, precious metal tellurides, Bi-Te-Se phases as well as native Bi (Figure 1B). This hypothesis is also supported by the high content of barite in all samples examined where disseminations and swarms of coarse-grained euhedral barite are identified (Fig. 1C, 1D).

The absence of any evidence of supergene alteration further supports the hypothesis of hypogene origin of precious metals and in particular Au-Ag alloys. No alteration of primary sulfides is observed (Figure 1), whereas the presence of APS-type phases in the intermediate conglomerate is not related to supergene phenomena but to hypogene hydrothermal alteration procedures that led to the formation of such phases probably after dissolution of primary phosphates in the host rock, as suggested by Voudouris et al. (2011). The presence of APS-type phases combined with the presence of enargite and unaltered pyrite in the intermediate conglomerate may be related to circulation of oxidative hydrothermal fluids and the development of an advanced argillic gangue assemblage (Dill, 2001).

Acknowledgements

The author would like to thank emeritus professor Nikolaos Skarpelis for providing a number of drill core samples for this research.

References

Dill, H.G., 2001. The geology of aluminium phosphates and sulphates of the alunite group minerals: a review. Earth-Science Reviews, 53, 35-93.

Lescuyer, J.L., Baily, L., Cassard, D., Lips, A.L.W., Piantone, P., McAlister, M., 2003. Sediment-hosted gold in south-eastern Europe: the epithermal deposit of Perama, Thrace, Greece. 7th Biennial SGA Meeting, Mineral Exploration and Sustainable Development, Athens, 499-502.

Juras, S., Miller, R., Perkins, P., 2010. Technical Report, of the Perama Hill Project, Thrace, Greece. Unpublished Report, Eldorado Gold Corporation, 144p.

Skarpelis, N., Triantafyllidis, S., Falalakis, G., 2006. The Perama intermediate sulfidation epithermal Au system (Thrace, Greece): Hypogene mineralogy and supergene alteration. Neogene Magmatism of the Central Aegean and Adjacent Areas: Petrology, Tectonics, Geodynamics, Mineral Resources and Environment, Milos, Cyclades, Greece, p37.

Triantafyllidis, S., Skarpelis, N., 2015. Supergene alteration of a refractory gold mineralization: The Perama hill deposit, NE Greece. Bull. Geol. Soc. Greece, 49, 59-75.

Voudouris, P.C., Melfos, V, Spry, P.G., Moritz, R., Papavassiliou, C., Falalakis, G., 2011. Mineralogy and geochemical environment of formation of the Perama Hill high-sulfidation epithermal Au-Ag-Te-Se deposit, Petrota Graben, NE Greece. Miner. Petrol., 103, 79-100.

Whitney, D.L., Evans, B.W., 2010. Abbreviations for names of rock-forming minerals. American Mineralogist, 95, 185-187.

15th International Congress of the Geological Society of Greece
Athens, 22-24 May, 2019 | Harokopio University of Athens, Greece
Bulletin of the Geological Society of Greece, Sp. Pub. 7 Ext. Abs. GSG2019-019

Mineralogical and geochemical investigation of the Ermioni VMS supergene alteration zone, Argolis, Greece

Stavros Triantafyllidis

National Technical University of Athens, School of Mining and Metallurgical Engineering, Iroon Polytechneiou 9, 157 80 Zografou, Athens, Greece, striantafyllidis@metal.ntua.gr

Ore deposit geology, exploitation history and production

The Ermioni volcanogenic massive sulfide ore, with pyrite and minor chalcopyrite and sphalerite, was a target of exploitation from the early 20th century for the production of sulfuric acid for fertilizers. Outcrops of the massive, stockwork and disseminated ore have suffered extensive supergene alteration resulting in the formation of iron caps that were used in the past as indicators of the sub-surface primary ore (Aronis, 1951). Small-scale exploitation took place namely prior World War II (Aronis, 1951; Mousoulos, 1958), whereas after the war, production dropped significantly until the cease of the Ermioni mines in the late 70s (Sideris and Skounakis, 1987).

Sampling – Analytical methods

The present study was focused on the most important mine sites, Karakasi and Roro. Samples were collected from locations where outcrops of the supergene alteration zones are still preserved, and from abandoned mine wastes. Sampling included massive to semi-massive oxidized ore samples, and oxidized samples from both the stringer and leached ore zones from Karakasi and Roro. Mineralogy was determined by combination of transmitted and reflected light optical microscopy, Raman Spectroscopy, X-ray Diffractometry and Scanning Electron Microscopy. Primary and secondary ore samples were commercially analyzed by ICP-AES for determination of Au grades.

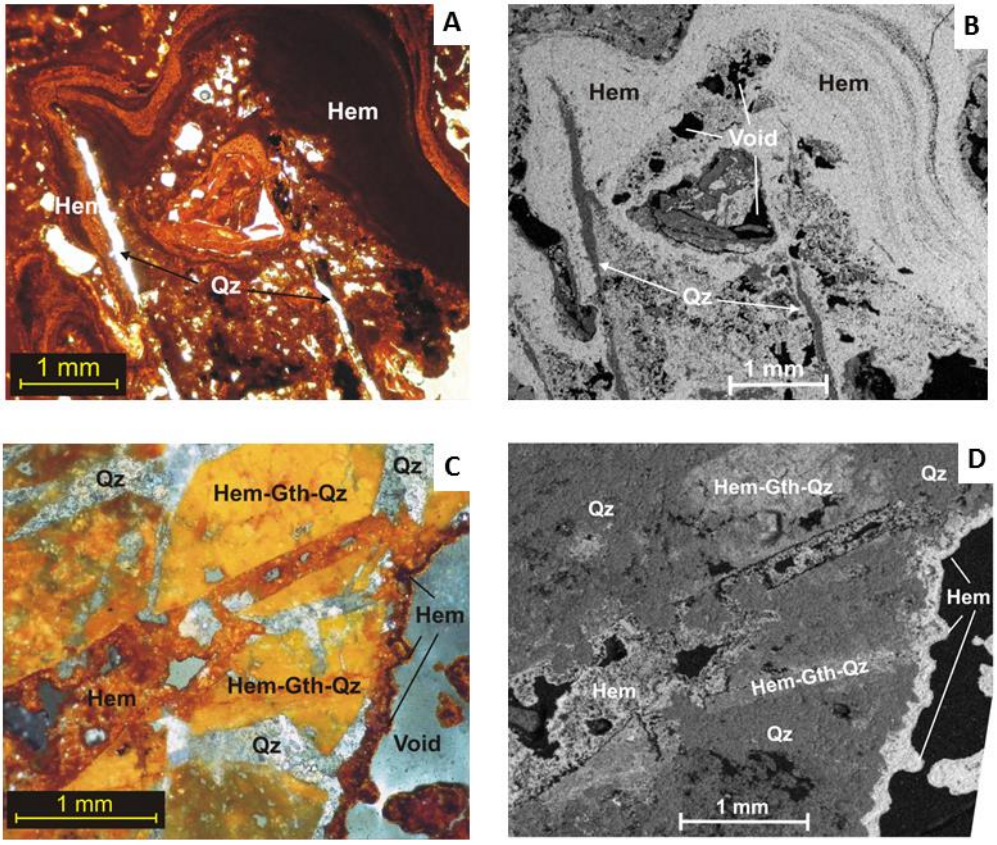

Figure 1. Optical and Backscattered Electron Microscopy images of the Ermioni supergene alteration zone. A-B. Roro oxidation zone. Extensive hematite colloform banding (Hem) is observed with minor quartz (qz) fragments and quartz veinlets. The highly porous texture of the rock is observed. C-D. Karakasi oxidation zone. Primary quartz stockwork is preserved, providing the highly cohesive character to the rock. Primary ore phases are pervasively altered and replaced by hematite (Hem) with minor goethite (Gth). Occasionally, colloform bands and porous veinlets of predominant hematite are developed between hematite-goethite-quartz masses. Abbreviations after Whitney and Evans (2010).

Results and discussion

Mineralogical investigation of Ermioni oxidized massive ore samples revealed the high degree of supergene alteration with hematite and minor goethite being the major secondary phases identified, whereas only traces of pyrite and chalcopyrite relicts are still present. SEM studies revealed that both hematite and goethite from Karakasi and Roro show no enrichment in other metals. Minor jarosite is also observed by XRD and SEM studies in the partially altered stockwork ore at Karakasi and Roro. At Roro, rock samples from the oxidation zone are both porous and brittle, and extensive hematite colloform banding is observed (Figure 1A, 1B). The supergene alteration zone at Roro is occasionally rich in secondary Cu phases (azurite and malachite) as a result of weathering of primary ore rich in chalcopyrite. At Karakasi, the samples from the supergene alteration zone show higher silica content relative to Roro. Hematite forms fine-grained aggregates between quartz stockwork, whereas occasional colloform bands are observed around voids (Figure 1C, 1D). In contrast to Roro, the Karakasi iron cap samples are very cohesive although highly porous, an observation that is related to the siliceous nature of the Karakasi primary ore (Mousoulos, 1958). The supergene alteration zones at Karakasi and Roro are characterized by very limited Au enrichment that is related to both the small size of the primary ore bodies, and the very low Au content in the primary ore (Table 1). The higher Au grades are identified in samples collected from Roro, whereas at Karakasi, the Au content of the supergene alteration zone is even lower (Table 1).

Table 1: Au grades (in gr/t) from the Ermioni massive ore and supergene alteration zones at Karakasi and Roro locations.

Sample type	Au grade
Roro massive sulfide ore	0.431
Roro massive sulfide ore	0.504
Roro massive sulfide ore	0.548
Roro oxidized ore	0.727
Roro oxidized ore	0.744
Roro oxidized ore	0.722
Karakasi oxidized ore	0.002
Karakasi oxidized ore	0.110
Karakasi oxidized ore	0.113
Karakasi oxidized ore	0.104
*Karakasi primary ore	0.2
*Roro primary ore	0.4
*Data from Mousoulos (1958)	

Concluding, hematite predominates in the Ermioni oxidation zone followed by lower amounts of goethite. Their formation is directly related to the presence of pyrite in the primary ore, but also to the predominant physicochemical conditions of the near-surface environment. Typical secondary phases Fe in oxidation zones include ferrihydrite, schwertmannite, jarosite, goethite and hematite, and the stability of those minerals depends on the gradually evolving physicochemical conditions of the surface environment. Newbrough and Gammons (2002) and Fukushi et al. (2003) state that with increasing pH and decreasing sulfate load the series of replacement are as follows:

Jarosite → schwertmannite → ferrihydrite → goethite → hematite

Hematite and goethite are the most stable secondary Fe(III) phases in mildly acidic to alkaline and oxidative conditions (Nordstrom & Alpers, 1999). It is therefore reasonable to assume that as supergene alteration phenomena progressed, the geochemical environment of the Ermioni oxidation zone gradually changed from highly oxidative with increased sulfate load, to mildly acidic and oxidative with very low sulfate content.

References

Aronis, G., 1951. Research on the iron-pyrite deposits in the Hemioni mining district, Geological and geophysical surveys, Subsurface Research Department, Ministry of Coordination, Athens, 153-188.

Mousoulos, L., 1958. Les gisements pyriteux du district minier d'Hermione. Étude sur leur gèologie et minéralogie. Le problème de leur genèse, Ann. Géol. Pays Hellén., 9, 119-164.

Fukushi, K., Sasaki, M., Sato, T., Yanase, N., Amano, H., Ikeda, H., 2003. A natural attenuation of arsenic in drainage from an abandoned arsenic mine dump. Applied Geochemistry, 18, 9, 1267-1278.

Newbrough, P., Gammons, C.H., 2002. An experimental study of water-rock interaction on acid rock drainage in the Butte mining district, Montana. Environmental Geology, 41, 705-719.

Nordstrom, D.K., Alpers, C.N., 1999. Geochemistry of acid mine waters, in: Plumlee, G.S., Logsdon, M.J., (Eds.), Reviews in Economic Geology, 6A. The Environmental Geochemistry of Mineral Deposits. Part A: Processes, Techniques, and Health Issues, Society of Economic Geologists, 133-160.

Sideris, C., Skounakis, S., 1987. Metallogeny in the Basic Rocks of a Paleosubduction Area – The Case of Ermioni Cu-bearing Pyrite Mines (East Peloponnesos, Greece). Chem. Erde, 47, 93-96.

Whitney, D.L., Evans, B.W., 2010. Abbreviations for names of rock-forming minerals. American Mineralogist, 95, 185-187.

15th International Congress of the Geological Society of Greece
Athens, 22-24 May, 2019 | Harokopio University of Athens, Greece
Bulletin of the Geological Society of Greece, Sp. Pub. 7 Ext. Abs. GSG2019-020

Trace element geochemistry, mineralogy and texture of the Ermioni VMS mineralization host volcanics, and new insights on the geotectonic setting of volcanism, Argolis, Greece

Stavros Triantafyllidis

National Technical University of Athens, School of Mining and Metallurgical Engineering, Iroon Polytechneiou 9, 157 80 Zografou, Athens, Greece, striantafyllidis@metal.ntua.gr

Introduction

Several studies have been performed on the trace element geochemistry of the mafic volcanics of the "Ermioni Complex" (Bortolotti et al., 2002; Robertson et al, 1987) in order to clarify the geotectonic setting of the Southeast Argolis Peninsula. Yet, the complex lithology and tectonism of the "Ermioni Complex" combined with the diversity in the geochemical character identified, including both Island Arc Tholeiites (IAT) and Mid-Ocean Ridge Basalts (MORB), create significant issues in providing solid results on the distinction of the geotectonic setting of the Southeast Argolis area. This study is focused on the volcanic rocks that host the Ermioni VMS mineralization in an attempt to specify the geotectonic setting of volcanism and the corresponding type of mineralization.

Sampling – Analytical methods

Samples were collected from the most important mine sites, Karakasi and Roro, and were primarily screened for the exclusion of the highly altered ones. The remaining were crushed, pulverized and homogenized, and were commercially analyzed by ICP-AES and ICP-MS for major, minor and trace elements (84 in total). The host rock mineralogy and texture was determined by combination of transmitted and reflected light optical microscopy, Raman Spectroscopy, X-ray Diffractometry and Scanning Electron Microscopy carried out at the Laboratory of Mineralogy, Petrology and Ore Deposit Geology, Section of Geological Sciences, School of Mining and Metallurgical Engineering, National Technical University of Athens.

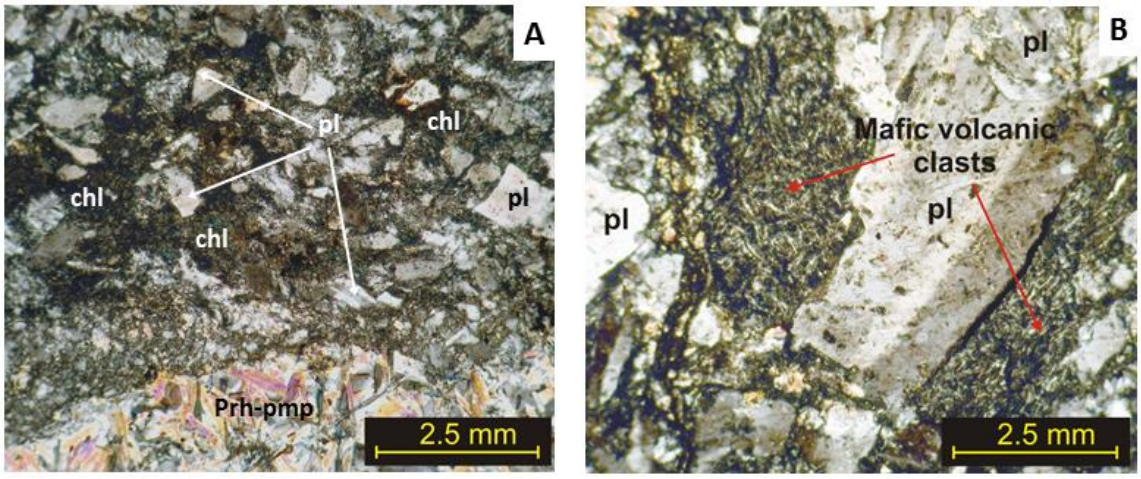

Figure 1. Transmitted light optical microscopy images of the Ermioni VMS mineralization host volcanics. A. Propylitized mafic volcanic tuffs with angular to sub-angular Ca-plagioclase (pl) fragments altered to albite, in a ground mass dominated by chlorite (chl) ± quartz (qz). Late stage prehnite (prh)-pumpellyite (pmp) ± quartz (qz), and quartz veins and veinlets cut the propylitized rock. B. Mafic volcanic clasts with plagioclase microlaths between coarse-grained plagioclase crystals within the host volcanic tuffs. Abbreviations after Whitney and Evans (2010).

Results and discussion

The Ermioni VMS mineralization is hosted in mafic volcanic tuffs and terrigenous turbidites of the "Ermioni Complex. The host mafic volcanics are gray-green in color, cohesive, indurated and massive, and geochemically range between basalts and andesites. The mineralogy of the Ermioni host volcanics is rather monotonous, with predominant angular to subangular coarse-grained albite crystals after hydrothermal alteration of primary Ca-plagioclase (Figure 1). The size of the albite crystals ranges from several μm to a few mm, and their angular shape indicates small-scale transportation of detritus. Primary mafic phases are highly altered and the matrix is dominated by fine-grained chlorite, epidote, prehnite – pumpellyite and minor quartz (Figure 1). Scarce Ti phases include rutile/anatase, sphene and ilmenite. Angular to subangular clasts of mafic volcanics with plagioclase microlaths are also observed within the Ermioni host volcanics, indicating limited transportation of volcanic material (Figure 1B). Hydrothermal propylitic alteration is evident by the presence of prehnite – pumpellyite ± quartz (Figure 1A), and quartz – epidote veins and veinlets that cut the host volcanics, which in turn are cross-cut by late stage coarse-grained quartz and quartz – calcite veins.

Examination of the trace element geochemistry of the Ermioni VMS host mafic volcanics indicates a calc-alkaline to tholeiitic, and subduction related character (Figure 2). The geochemistry of the host mafic volcanics at Karakasi and Roro is characteristic of a supra-subduction zone setting in close proximity to the continental margin, as identified by the high

silica content of the Ermioni host turbidites (Triantafyllidis and Diamantakis, 2018). The Ermioni host volcanics show similar trend to island arc volcanic rocks, with moderate LREE and relatively constant HREE values. Moreover, the Ermioni volcanics show enrichment in LILs and depletion in HFS (e.g. Ti, Y and Zr), although depletion in K and Rb is also observed, most probably related to hydrothermal alteration phenomena that have affected the footwall host volcanics (Misra, 2012). A negative Nb-Ta anomaly is observed and considered as subduction-related magma signature, and the trend is typical for subduction zone related volcanics, and in particular calc-alkaline volcanic arc basalts (Pearce et al., 1984).

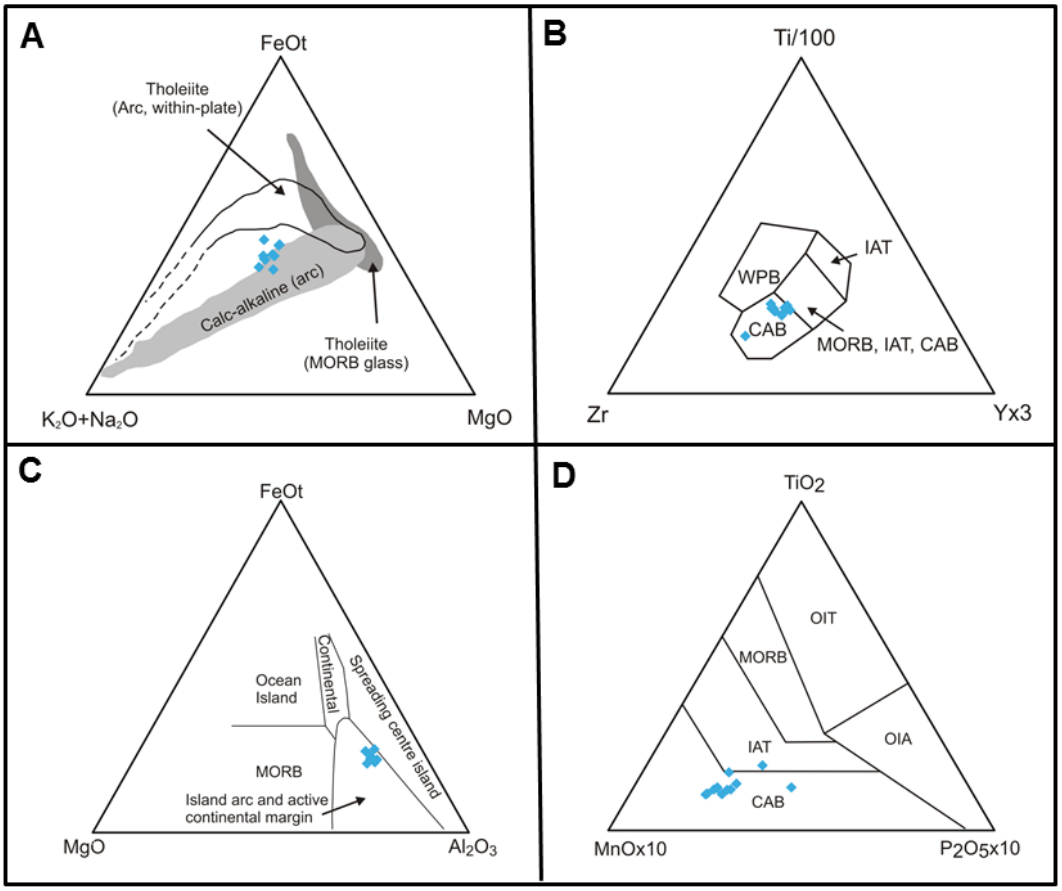

Figure 2. Major and trace elements ternary diagrams from the Ermioni VMS host mafic volcanics. A. AFM diagram. B. Ti-Zr-Y diagram. C. FeOt-Al_2O_3-MgO diagram. D. TiO_2-P_2O_5x10-MnOx10 diagram.

Concluding, the trace element geochemistry, texture and alteration of the Ermioni VMS host volcanics indicates a different geotectonic setting of volcanism relative to the typical geotectonic setting of ophiolites that host Cyprus-type mineralizations, as formerly proposed for the Ermioni VMS ore (Robertson et al., 1987). Based on the results of this study related to host rock lithology, mineralogy, texture and geochemistry, there are strong arguments for classification of the Ermioni VMS mineralization as "Besshi-type" (Höy, 1991). Yet, due to the complex tectonism and deformation of the Southeast Argolis Peninsula only geochronological data may provide solid arguments on the geotectonic setting and age of the "Ermioni Complex" volcanism, as well as the type of the Ermioni mineralization.

References

Bortolotti, V. Carras, N., Chiari, M., Fazzuoli, M., Marcucci, M. Photiades, A., Principi, G., 2002. New Geological Observations and Biostratigraphic Data on the Argolis Peninsula: Paleographic and Geodynamic Implications, Ofioliti, 27, 43-46.

Höy, T., 1991. Volcanogenic Massive Sulphide Deposits in British Columbia, in: Ore Deposits, Tectonics and Metallogeny in the Canadian Cordillera, B.C., McMillan, W.J. (Ed.). Ministry of Energy, Mines and Petroleum Resources, 1991-4, 89-123.

Misra, K.C., 2012. Introduction to Geochemistry: Principles and Applications. Wiley-Blackwell, West Sussex.

Pearce, J.A., Lippard, S.J., Roberts, S., 1984. Characteristics and tectonic significance of supra-subduction zone (SSZ) ophiolites, in: Kokelaar, B.P., Howells, M.F.(Eds). Marginal basin geology; volcanic and associated sedimentary tectonic processes in modern and ancient marginal basins, Geological Society of London, Special publication 16, 77-94.

Robertson, A.H.F., Varnavas, S.P., Panagos, A.G., 1987. Ocean Ridge Origin and Tectonic Setting of Mesozoic Sulphide and Oxide Deposits of the Argolis Peninsula of the Peloponnesus, Greece. Sedimentary Geology, 53, 1-32.

Triantafyllidis, S. Diamantakis, N., 2018. New insights on the Ermioni VMS ore based on ore texture and host rock lithology and geochemistry (SE Argolis Peninsula, Peloponnese, Greece). 1st Conference of the Arabian Journal of Geosciences, Hammamet, Tunisia, 7, 141-143.

Whitney, D.L., Evans, B.W., 2010. Abbreviations for names of rock-forming minerals, American Mineralogist, 95, 185-187.

15th International Congress of the Geological Society of Greece
Athens, 22-24 May, 2019 | Harokopio University of Athens, Greece
Bulletin of the Geological Society of Greece, Sp. Pub. 7 Ext. Abs. GSG2019-021

Multidisciplinary investigation of seabed sediments in revealing the exploitation history and ore-types exploited, Lavrion, Greece

Filothei Pappa[1], Stavros Triantafyllidis[2]

(1) Institute of Oceanography, Hellenic Center of Marine Research, 46.7 km Athens-Sounio Ave., 19013, Anavyssos, Attiki, Greece, fkpappa@hcmr.gr
(2) National Technical University of Athens, School of Mining and Metallurgical Engineering, Iroon Polytechneiou 9, 157 80 Zografou, Athens, Greece, striantafyllidis@metal.ntua.gr

Introduction – geology

Lavreotiki Peninsula is known for its mining activities from ancient times until late 20th century. First traces of exploitation go back to 3.000 B.C., whereas the first mines operated during the Classical period (6th to 4th century B.C.) for exploitation of Ag-bearing galena for the production of Ag, which contributed to the power of ancient Athens (Conophagos, 1980). During that period, the metallurgical process of "cupellation" was first established. The Lavrion mines re-opened during the mid-19th century and exploitation continued until the 1980s. The distinctive geotectonic evolution and hydrothermal activity in the Lavrion area resulted in the formation of several major and minor hydrothermal type sulfide ores including carbonate-replacement Pb-Zn-Ag, Skarn type, porphyry-style and vein-type mineralizations (Bonsall et al., 2011).

The aim of the present study is to correlate the radionuclide and geochemical data with the mineralogical investigation of core sediments in an attempt to provide new insights on the history of exploitation as well as the ore type exploited.

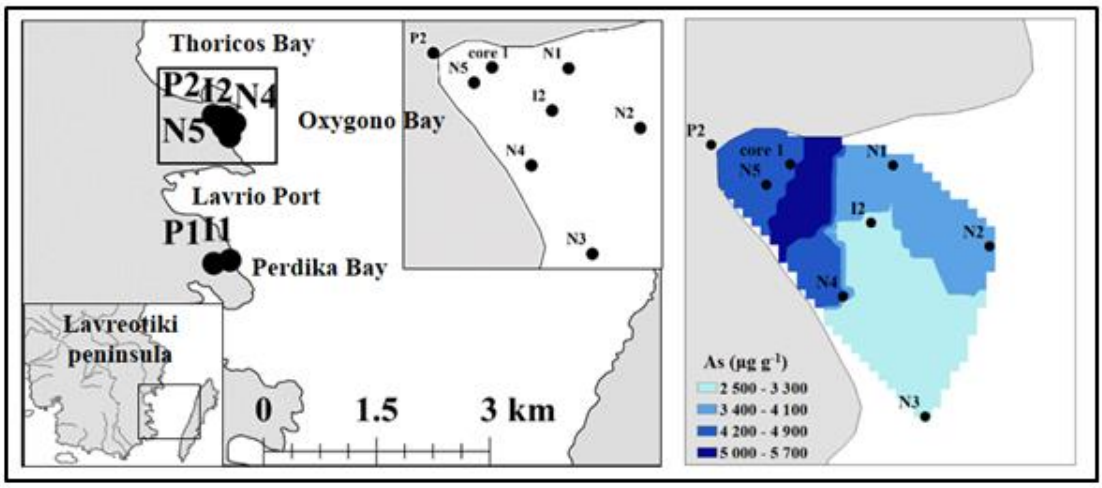

Figure 1. Sampling map of surface beach sands and seabed sediments (left), and spatial distribution of As (right) at Oxygono Bay, Lavrion (Pappa et al., 2018).

Sampling-Analytical methods

One seabed sediment core (core 1) of approximately 50 cm length was collected in 2014 at 50 m distance from the shore of Oxygono Bay. Sampling also included surficial beach sands and marine sediments (Fig. 1). The samples were primarily cleaned, sieved, and the fraction below 2mm was pulverized for radionuclide, geochemical and mineralogical analyses. The fine-grained fraction was selected for the mineralogical analysis in order to better correlate the geochemistry with the mineralogical assemblage of the samples. The radionuclide concentrations were determined via gamma ray spectroscopy at the Nuclear Laboratory of Physics, National Technical University of Athens utilizing a High-Purity Ge Detector (HPGe). The major elements and trace metals concentrations were calculated by means of X-ray Fluorescence at the Geochemistry Laboratory of the Hellenic Centre for Marine Research, whereas optical and Scanning Electron Microscopy was employed for the mineralogical investigation, and was carried out at the Laboratory of Mineralogy, Petrology and Economic Geology, Section of Geological Sciences, School of Mining and Metallurgical Engineering, National Technical University of Athens.

Results – Discussion

The spatial distribution of metals indicated a more contaminated area near the coast, as it is evident by the indicative spatial distribution map of As (Figure 1). Therefore a temporal study was performed in the coastal core (core 1) utilizing the metal profiles in combination with radio-chronological models. These models and in particular the sedimentation rate (SR) estimation based on natural radionuclides were employed for dating analysis (details in Pappa et al., 2018) resulting in the identification of three periods of mining activities in the Lavrion area (1860-1900, 1900-1930, 1930-1980), as well as a post-mining period (1980-2014). The corresponding depths for each period are 38-52 cm, 28-38 cm, 12-28 cm and 0-12 cm respectively (Fig. 2).

During the first period (1860-1900) the ancient slags were primarily utilized for the production of Ag and Pb, as evident by the very low Pb, As, Zn, Cu and Mn content of the sediments (Figure 2). Mineralogical investigation revealed that the sediments are dominated by silicate clasts, carbonates and biofragments, whereas only traces of authigenic framboidal pyrite are identified. In later years (1875-1900) exploitation was expanded to the primary sulfide ores also for the production of Ag and Pb, resulting in a slight increase in the sediment metal load. During the second and third period (1900-1930 and 1930-1980), a new flotation method was adopted mainly for the exploitation of Ag-bearing galena, whereas the other ore phases and metals (e.g. As, Zn, Mn) were not retrieved and were disposed. This observation is directly related to the geochemistry and mineralogy of the sediment core between 35 and 10 cm depth. In particular, the As, Zn and Mn content increases rapidly and remains constant until the surface (Figure 2). The mineralogy identified includes in ranging content primary ore phases (mainly pyrite and arsenopyrite with minor galena and sphalerite), waste rock clasts, slag fragments, gangue phases (quartz, micas, chlorite, ankerite-siderite, dolomite, barite), secondary phases [smithsonite, mimetite - $Pb_5(AsO_4)_3Cl$], and W-bearing phases (scheelite - $CaWO_4$, ferberite - $FeWO_4$, and hubnerite - $MnWO_4$). At the same time, the concentration of natural radionuclide (^{226}Ra) shows similar trend to As, Zn and Mn, indicating possible correlation. The presence of ^{226}Ra in the sediment may be related to the granitoids surrounding the primary ores, and in particular the Skarn-type mineralization (Leleu et al., 1973; Economou et al., 1981; Voudouris et al., 2008). The granitoids were extracted during exploitation along with the ore and were disposed as wastes.

Based on the mineralogy and geochemistry of the sediment core, as well as its radionuclide content, it is reasonable to assume that at some points during the second (1900-1930) and the third period (1930-1980), exploitation of the Plaka intrusion related system, and in particular the skarn type mineralization took place. The primary sulfide ore was mainly exploited by floatation for the extraction of Ag-bearing galena whereas the rest of the material including primary ore phases (arsenopyrite, sphalerite and pyrite), gangue (including carbonates and W-bearing phases), and waste granodiorite (as evident by the presence of natural radionuclide ^{226}Ra) were disposed and are now enriched in the sediment core at depths between 10 and 35 cm.

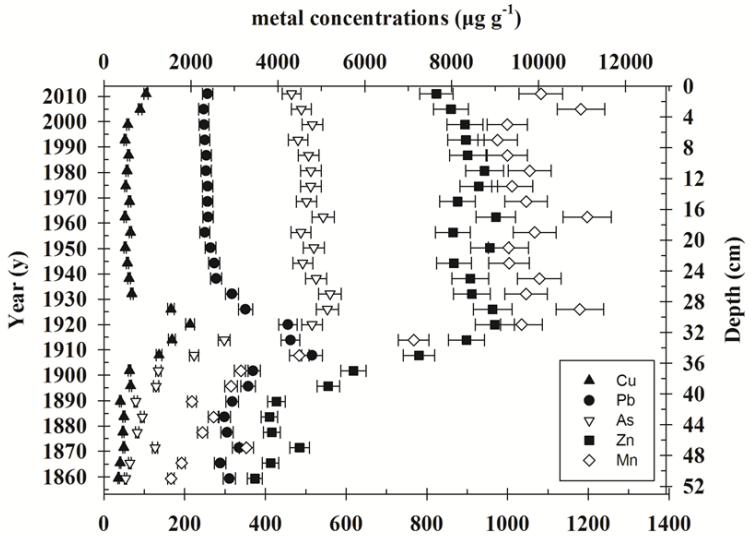

Figure 2. Vertical distribution of As, Pb, Cu, Zn and Mn in the sediment core from Oxygono Bay, Lavrio.

Acknowledgements

The authors would like to acknowledge A.G. Leventis foundation for the financial support of Mrs Pappa's PhD Thesis.

References

Bonsall, T.A., Spry, P.G., Voudouris, P., Tombros, S., Seymour, K., Melfos, V., 2011. Footwall mineralization during Late Miocene extension along the West Cycladic Detachment System, Lavrion, Greece. Terra Nova, 25, 181-191.

Conophagos, C., 1980. The Lavrion and the ancient Greek techniques for silver production. Athens, Ekdotiki Athinon, 458p.

Economou, M., Skounakis, S., Papathanasiou, C., 1981. Magnetite deposits of skarn type from the Plaka area of Laurium mines, Greece. Chemie der Erde, 40, 241-252.

Leleu, M., Morikis, A., Picot, P., 1973. Sur les mineralisations de type skarn au Laurium (Grèce). Mineralium Deposita, 36, 477-489.

Pappa, F.K., Tsabaris, C., Patiris, D.L., Androulakaki E.G., Eleftheriou, G., Betsou, C., Michalopoulou, V., Kokkoris, M., Vlastou, R., 2018. Historical trends and assessment of radionuclides and heavy metals in sediments near an abadonded mine, Lavrio, Greece. Environ Sci Pollut Res., 25, 30084-30100.

Voudouris, P., Melfos, V., Spry, P.G., Bonsall, T., Tarkian, M., Economou-Eliopoulos, M., 2008. Mineralogical and fluid inclusion constraints on the evolution of the Plaka intrusion-related ore system, Lavrion, Greece. Mineral. Petrol. 93, 79–110.

15th International Congress of the Geological Society of Greece
Athens, 22-24 May, 2019 | Harokopio University of Athens, Greece
Bulletin of the Geological Society of Greece, Sp. Pub. 7 Ext. Abs. GSG2019-041

Mineralogical and Fluid Inclusions Study of Epithermal Type Veins Intruding the Volcanic Rocks of the Kornofolia Area, Evros, NE Greece (Preliminary results).

F. Aravani[1], L. Papadopoulou[1], V. Melfos[1], T. Soldatos[1], T. Zorba[2], P. Voudouris[3]

(1) Department of Mineralogy-Petrology-Economic Geology, School of Geology, Aristotle University of Thessaloniki, 54124 Thessaloniki, Greece, faravani@geo.auth.gr
(2) Solid State Physics Section, Department of Physics, Aristotle University of Thessaloniki, Greece
(3) Department of Mineralogy-Petrology, Faculty of Geology and Geoenvironment, National and Kapodistrian University of Athens, 15784, Greece

The aim of the present research is the mineralogical and microthermometric study of epithermal type veins that intrude the volcanic rocks of the Kornofolia area, Evros. The volcanic host rocks are high-K calc-alkaline andesites that penetrate the boundary between the Rhodope Massif and the Circum-Rhodope Belt in eastern Thrace, NE Greece. The host rocks of the Kornofolia area have been dated with the K/Ar method at 30.7 Ma (Christofides *et al*. 2004). They show indications of hydrothermal alteration (Voudouris *et al.* 2018). Optical (polarized and reflected) and scanning microscopy were employed to determine the mineralogical and textural characteristics of the host rocks and the veins. Additionally, the samples were analyzed with Fourier-transform infrared spectrometer (FT-IR) in order to determine any structural differences among the various vein minerals

Mineralogical and fluid inclusion studies have been conducted on the amethyst occurrences in the same veins by Voudouris *et al*. 2018.

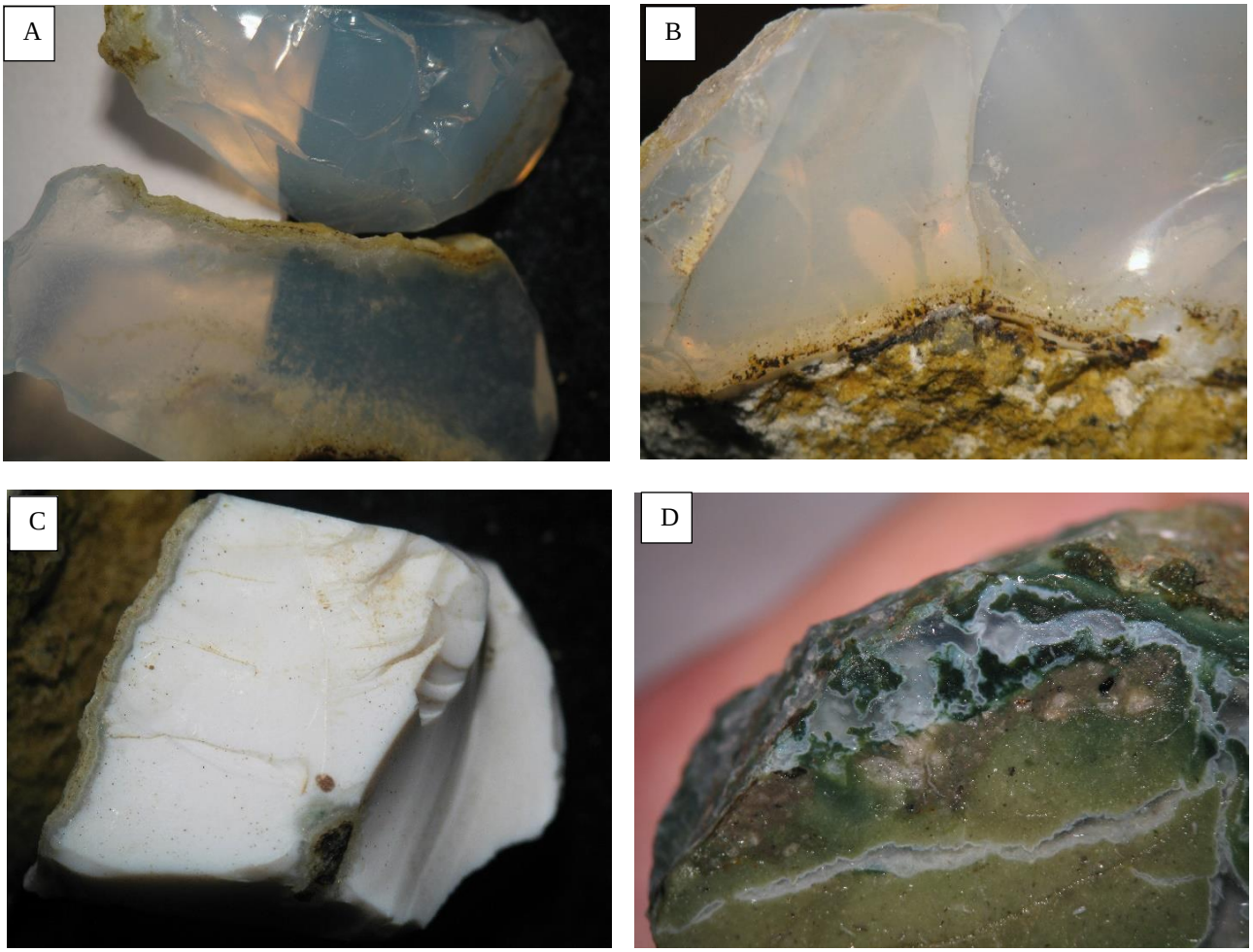

Figure 1. Photos of the three opal samples (X6.5). A, B: transparent opal, C: white opal, D: green opal

The andesite host rock comprises a hydrothermal breccia (Sillitoe 1985). The rock is generally silicified and the rock's matrix is zeolitized. The main mineral assemblage of the host rock, emerging from macroscopic and microscopic observations as well as microanalysis, is zoned plagioclase, magnesiohornblende, biotite and celadonite. The veins consist of quartz, chalcedony, three different types of opal (white, green and transparent), calcite and zeolites (clinoptilolite and mordenite). The veins show lateral zonation. The succession of the mineral phases in the veins, outwards to inwards, is

unaltered andesite – celadonite - clinoptilolite and/or quartz - chalcedony - mordenite and (sometimes) euhedral clinoptilolite. The relation between the calcite and the other minerals has not been determined yet.

As mentioned above, three different opal types have been recognized in the veins of Kornofolia: transparent opal, green opal with a dull lustre and white milky opal (Figure 1).

FT-IR analysis was performed on the three opal types from the veins in order to determine variations in the crystallinity of the samples. The FT-IR spectra displayed significant variations among the three opal types (Figure 2), which are attributed to differences in their crystal structure (Adamo *et al.* 2010). The crystal structure of the white and the transparent opal is identical with that of christobalite (Farmer 1974) suggesting a well-ordered structure (opal-C) (Jones *et al.* 1971). On the contrary, the spectrum acquired from the green opal approaches the spectrum of quartz and is more amorphous (not well-ordered) (opal-CT, opal-A) (Jones *et al.* 1971) compared to the other opal samples. Moreover, the spectrum of the green opal displays indications of impurities, possibly clay minerals that may be responsible for its color. However, further investigation on the opals is required in order to extrapolate definite conclusions on the composition of the impurities.

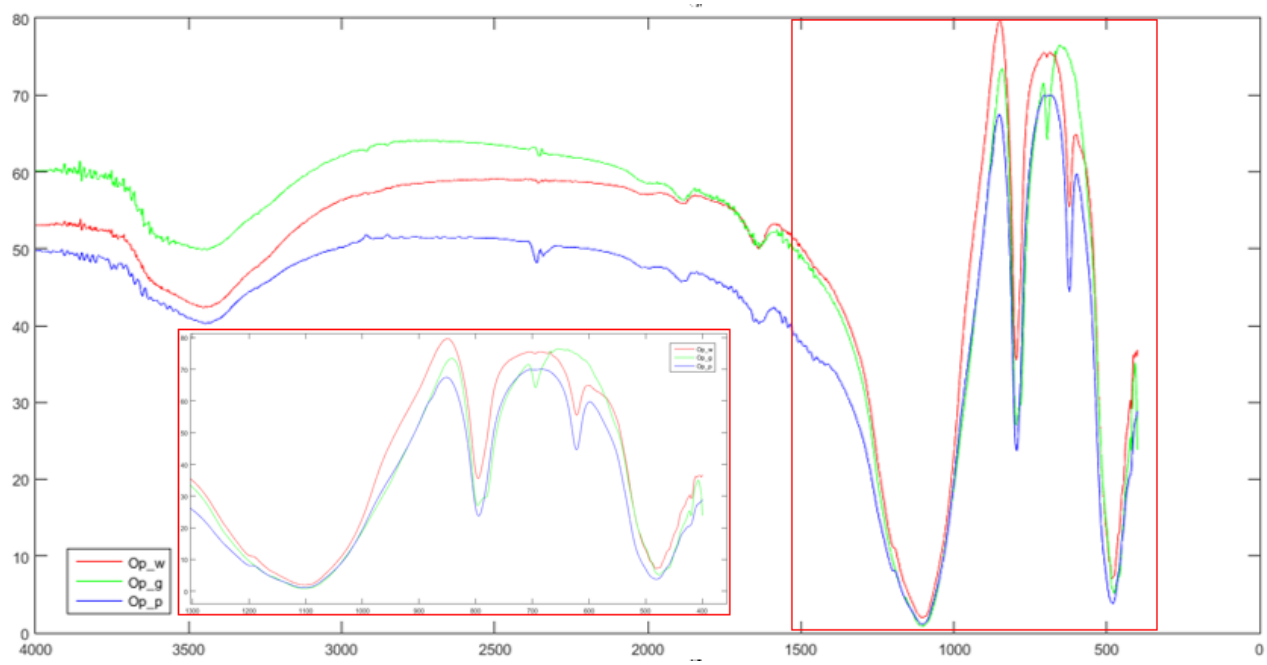

Figure 2. FT-IR spectra from the opal samples. Op_w: white opal, Op_g: green opal and Op_p: transparent opal

References

Adamo, I., Ghisoli, C., Caucia, F., 2010. A contribution to the study of FTIR spectra of opals. N. Jb. Miner. Abh. 187/1, 63-68.

Christofides, G., Pecskay, Z., Eleftheriadis, G., Soldatos, T., Koroneos, A., 2004. The Tertiary Evros volcanic rocks (Thrace, northeastern Greece): Petrology and K/Ar geochronology. Geologica Carpathica 55(5), 397-410.

Farmer V.C., 1974. The infrared spectra of minerals, in: Moenke H.H.W. (Ed.), Mineralogical Society Monograph 4. Silica, the three-dimentional silicates, borosilicates and beryllium silicates, 16, 365-370.Jones, J.B., Segnit, E.R., 1971. The nature of opal I. Nomenclature and constituent phases. Journal of the Geological Society of Australia 18, 57-68.

Sillitoe, R.H., 1985. Ore-Related Breccias in Volcanoplutonic Arcs. Economic Geology 80(6), 1467-1514

Voudouris, P., Melfos, V., Mavrogonatos, C., Tarantola, A., Götze, J., Alfieris, D., Psimis, I., 2018. Amethyst occurrences in Tertiary volcanic rocks of Greece: Mineralogical, fluid inclusion and oxygen isotope constraints on their genesis. Minerals 8, 324, p. 26.

15th International Congress of the Geological Society of Greece
Athens, 22-24 May, 2019 | Harokopio University of Athens, Greece
Bulletin of the Geological Society of Greece, Sp. Pub. 7 Ext. Abs. GSG2019-042

Studying the Local Distribution of Thorium in Eudialyte Deposits Associated with Peralkaline Igneous Rocks (Greenland) by Electron Microscopy & Spectroscopic Techniques

P.N. Gamaletsos[1,2], A.M. Borst[3], T. Kasama[2], A.A. Finch[3], A. Godelitsas[4], I.T. Tzifas[5], Y. Pontikes[1], A. Filippidis[6]

(1) Department of Materials Engineering, KU Leuven, Kasteelpark Arenberg 44, 3001 Leuven, Belgium, platon.gkamaletsos@kuleuven.be
(2) National Centre for Nano Fabrication and Characterization, Technical University of Denmark, 2800 Kongens Lyngby, Denmark
(3) School of Earth & Environmental Sciences, University of St Andrews, Irvine Building, North Street, KY16 9AL, St Andrews, UK
(4) Department of Geology & Geoenvironment, National & Kapodistrian University of Athens, Zografou Campus, 15784 Athens, Greece
(5) Institute of Earth Sciences, Heidelberg University, Im Neunheimer Feld 234, 69120 Heidelberg, Germany
(6) Department of Geology, Aristotle University of Thessaloniki, 54124 Thessaloniki, Greece

Rare Earth Elements (REEs) are considered to be strategic metals, having a wide range of technological applications (e.g., Hatch, 2012). Due to high demand in industry and technology, the European Union (EU) has identified the study of REE resources as a top priority (e.g., Binnemans *et al.*, 2018). As we are exploring for alternative REE deposits (e.g. Gamaletsos *et al.*, 2019 and references therein), it is important to consider the environmental challenges associated with their exploitation, such as studying the spatial distribution of elements like thorium / Th (e.g. Gamaletsos *et al.*, 2011). Eudialyte deposits, associated with peralkaline igneous rocks, are the dominant EU alternatives to currently exploited Chinese REE deposits from ion adsorption clays and carbonatites (e.g., Smith *et al.*, 2016). Due to relatively low Th contents in peralkaline igneous rocks, typically sub-continental crust (<100 ppm Th), eudialyte exploitation could avoid potential issues of radioactive contamination in tailings that bedevil, e.g. monazite and xenotime extraction. However, the partitioning of Th and REEs at the micro-/nano-scale in eudialyte deposits is poorly studied. Here we utilize the technical advance of combining synchrotron radiation (SR) μ-XRF/-XAFS and electron microscopic (SEM-EDS/-WDS, EPMA, SEM-FIB, TEM/HRTEM) techniques (Fig. 1), along with LA-ICP-MS to study the local distribution of Th in one of the largest European eudialyte deposits, i.e. the Ilímaussaq Complex in South Greenland (Larsen and Sørensen, 1987).

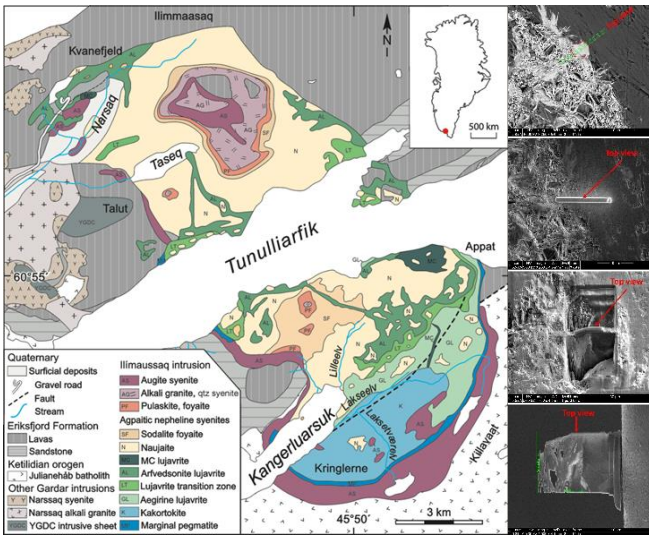

Figure 1. Geological map of the Ilímaussaq complex (modified after Borst et al., 2019 and references therein) and SEM-FIB preparation of a representative sample undergone TEM/HRTEM study.

The Ilímaussaq complex is an oval-shaped peralkaline composite intrusion, part of the Mesoproterozoic Gardar province in South Greenland (**Fig. 1**). During at least four intrusive pulses, augite syenites, alkali-to-peralkaline granites, quartz syenites and volumetrically layered eudialyte-bearing nepheline syenites ("kakortokite") crystallized (e.g., Larsen & Sørensen, 1987; Borst *et al.*, 2019). The kakortokites comprise alkali feldspar, nepheline, sodalite, aegirine, arfvedsonite and eudialyte, with aenigmatite, rinkite-group minerals, fluorite, apatite and analcime as common accessory phases (e.g., Borst *et al.*, 2018). Of particular economic interest are the eudialyte-group minerals (EGM), i.e. a group of complex Na-Ca-zirconosilicates which occur as major phases and contain wt.% significant concentrations of rare earth elements (ca. 2.5 wt.% REE_2O_3). A proportion of the primary EGM have been partially-to-fully replaced by fine intergrowths of variety of EGM alteration products (i.e. catapleiite, aegirine, nacareniobsite-(Ce) and other REE-rich secondary phases), resulting from late-magmatic hydrothermal alteration (e.g. Karup-Møller & Rose-Hansen., 2013; Borst *et al.*, 2016).

Preliminary SR (Fig. 2) and e-microscopic observations at altered EGM domains reveal the presence of Th-bearing phases at the micro-/submicro-/nano-scale. Similar micro-scale heterogeneity is observed for the REEs in eudialyte replacement

products. We also collected Th L_{III}-edge μ-XAFS spectral data of Th-enriched micro-areas, previously identified by SR μ-XRF mapping that confirmed the heterogeneous distribution of the actinide, which provide information on the local structural environment of Th within altered EGM domains. Several Th-bearing phases were detected along altered margins of eudialyte, in secondary phases, and interstitial to primary phases such as feldspar, amphibole and eudialyte. In fresh magmatic EGM, Th is undetectable by SR μ-XRF; however, actinides are detected in fresh EGM crystals by means of LA-ICP-MS indicating very low concentrations typically below 40 ppm. Furthermore, LAICPMS detected all the REE, including Y and Sc in fresh EGM crystals. Significant variation of Ta and Nb and less of LREE in fresh EGM is recorded by LA-ICP-MS. HREE variations are within analytical uncertainty. Similar variation in Ce concentration was additionally recorded by SR μ-XRF mapping. The above variations might be associated with the sector zoning in fresh EGM as it is demonstrated by Borst *et al.* (2018).

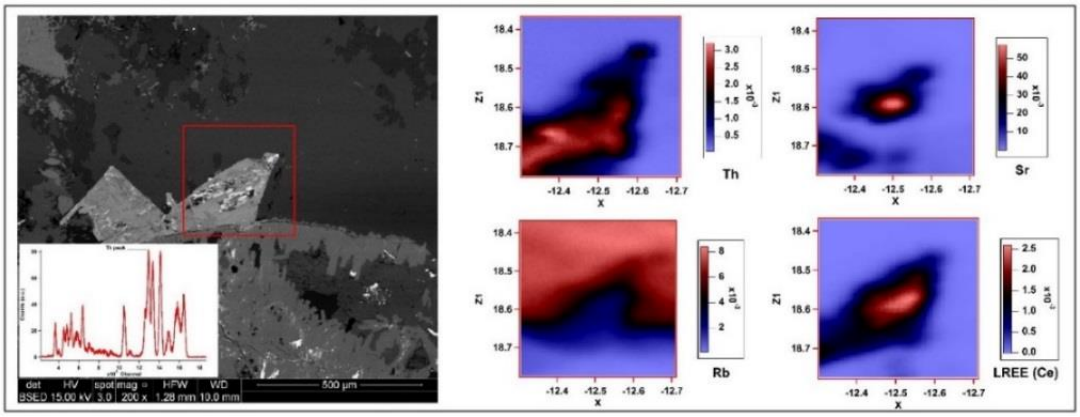

Figure 2. SR μ-XRF data of a representative sample from the eudialyte deposit of the Ilímaussaq Complex, demonstrating relative heterogeneity of Th, Sr, Rb and Ce concentrations in altered rinkite and eudialyte.

Regardless of low bulk contents of Th in peralkaline igneous rocks, we find localized relative enrichments of Th at the micro-/nano-scale associated with hydrothermal alteration products after rinkite and EGM, probably. Either thorium, which is enriched in the melt until the final stages of magmatic crystallization, partitions into the late-magmatic fluids at the hydrothermal stage as part of further cooling or it is redistributed from the eudialyte during alteration. Further research of how elements like Th, which are at low concentrations in bulk and are localized at the micro-/nano-scale, are transported and distributed within the ore and gangue minerals of peralkaline deposits will be important to inform and enhance the development of sustainable metallurgical processing routines for these ore types. Since traces of Th may be transferred into the metallurgical residues, the monitoring of its paths from the ore feed towards to the residues is needed.

Acknowledgements

This research has been received funding from the People Programme (Marie Curie Actions) of the European Union's Seventh Framework Programme (FP7/2007-2013) under REA grant agreement no. 609405 (COFUNDPostdocDTU). We thank Dr. J. Göttlicher and Dr. R. Steininger for provision of beamtime at the SUL-X beamline (ANKA Synchrotron Facility/KIT, Germany). We acknowledge Dr. Hiroki Mukai and Dr. Yoshiaki Kon (AIST, Japan) for assistance with EPMA and LA-ICP-MS measurements.

References

Binnemans, K., Jones P.T., Müller, T., Yurramendi, L., 2018. Rare earths and the balance problem: How to deal with changing markets? *Journal of Sustainable Metallurgy 4*, 126-146.

Borst, A.M., Friis, H., Andersen, T., Nielsen, T.F.D., Waight, T.E., Smit, M.A., 2016. Zirconosilicates in the kakortokites of the Ilímaussaq complex, South Greenland: Implications for fluid evolution and high-field-strength and rare-earth element mineralization in agpaitic systems. Mineralogical Magazine 80, 5-30.

Borst, A.M., Friis, H., Nielsen, T., Waight, T.E., 2018. Bulk and mush melt evolution in agpaitic systems: Insights from compositional variations in eudialyte-group minerals of the Ilímaussaq complex, South Greenland. Journal of Petrology 59 (4), 589-612.

Borst, A.M., Waight, T.E., Finch, A.A., Storey, M., Roux, P.J.L., 2019. Dating agpaitic rocks: A multi-system (U/Pb, Sm/Nd, Rb/Sr and $^{40}Ar/^{39}Ar$) isotopic study of layered nepheline syenites from the Ilímaussaq complex, Greenland. Lithos 324-325, 74-88.

Gamaletsos, P., Godelitsas, A, Mertzimekis, T.J., Göttlicher, J., Steininger, R., Xanthos, S., Berndt, J., Klemme S., Bárdossy, G., 2011. Thorium partitioning in Greek industrial bauxite investigated by synchrotron radiation and laser-ablation techniques, *Nuclear Instruments and Methods in Physics Research B 269*, 3067-3073.

Gamaletsos, P.N., Godelitsas, A., Filippidis, A., Pontikes, Y., 2019. The Rare Earth Elements Potential of Greek Bauxite Active Mines in the Light of a Sustainable REE Demand. *Journal of Sustainable Metallurgy 5*, 20-47.

Hatch, G.P., 2012. Dynamics in the global market for rare earths. *Elements 8*, 341-346.

Karup-Møller, S., Rose-Hansen, J., 2013. New data on eudialyte decomposition minerals from kakortokites and associated pegmatites of the Ilímaussaq complex, South Greenland. *Bulletin of Geological Society of Denmark 61*, 47-70.

Larsen, L.M., Sørensen, H., 1987. The Ilímaussaq intrusion-progressive crystallization and formation of layering in an agpaitic magma. *Geological Society*, London, Special Publications 30, 473-488.

Smith, M.P., Moore, K., Kavecsánszki, D., Finch, A.A., Kynicky, J., Wall, F., 2016. From mantle to critical zone: A review of large and giant sized deposits of the rare earth elements. *Geochemical Frontiers 7*, 315-334.

15th International Congress of the Geological Society of Greece
Athens, 22-24 May, 2019 | Harokopio University of Athens, Greece
Bulletin of the Geological Society of Greece, Sp. Pub. 7 Ext. Abs. GSG2019-048

Tourmaline from the Fakos porphyry-epithermal Cu-Mo-Au-Te prospect, Limnos island, Greece: Mineral-chemistry and genetic implications

P. Voudouris[1], I.A. Baksheev[2], C. Mavrogonatos[1], P.G. Spry[3], A. Djiba[4], U. Bismayer[4], K. Papagkikas[1], A. Katsara[1]

(1) National and Kapodistrian University of Athens, 15780 Athens, Greece, voudouris@geol.uoa.gr, kmavrogon@geol.uoa.gr, k.papagkikas@gmail.com, anthikatsara@yahoo.com
(2) Geology Department, Moscow State University, Leninskie Gory, Moscow 119991, Russia, ivan.baksheev@gmail.com
(3) Department of Geological and Atmospheric Sciences, Iowa State University, Ames IA 50011-1027, USA; pgspry@iastate.edu
(4) Institute of Mineralogy and Petrology, University of Hamburg, 20146 Hamburg, Germany, alioudjiba209@hotmail.com, mi4a001@uni-hamburg.de

The Fakos Cu-Mo-Au prospect, in Limnos island, NE Aegean Sea, comprises the first occurrence of porphyry-related tourmaline in Greece (Voudouris & Alfieris, 2005; Fornadel et al., 2012). The prospect is a telescoped porphyry-epithermal system hosted in lower Miocene alkaline to sub-alkaline igneous rocks and middle Eocene to lower Miocene sandstones. Tourmaline occurs within E-trending hydrothermal breccias (Fig. 1a) and quartz-tourmaline veins related to quartz+sericite+tourmaline alteration of the Fakos monzonite (Fig. 1b), as well as disseminations within sericite-altered sandstones. This study presents EPMA data on the Fakos tourmaline and attempts to record any chemical differentiations, which may reflect variations of the ore-forming fluids. Tourmaline occurs as isolated crystals (with size up to 0.5cm) or as radial aggregates. The crystals are optically zoned, usually with a darker core and nearly colorless rim (Fig. 1c). The lighter coloration is caused by a lower concentration of Fe. Due to the minor amount of Ca in all analyzed tourmalines (Fig. 2a; no higher than 0.02 apfu), the optimal plot to distinguish any different species is the binary $Fe_{tot}/(Fe_{tot} + Mg)$ *versus* X-site vacancy/(Na + X-site vacancy) (Fig. 2b). This diagram does not distinguish among OH-, F-, and O-bearing species, however, F contents are either below detection, or very low in all analyzed grains, and therefore the *W* site is dominated by O^{2-} or OH^-. Consequently, the magnesio-foitite, dravite, schorl, and foitite fields could be considered as "oxy-magnesiofoitite", oxy-dravite, oxy-foitite, and oxy-schorl fields, respectively. This diagram shows that tourmaline from the sandstones falls into the dravite/oxy-dravite and schorl/oxy-schorl fields, whereas those from the breccia and the quartz veins are restricted to the dravite--oxy-dravite field only. However, the vein-related tourmaline is characterized by higher X-site vacancy/(Na + X-site vacancy) and lower $Fe_{tot}/(Fe_{tot} + Mg)$ values than those in the other tourmalines studied here.

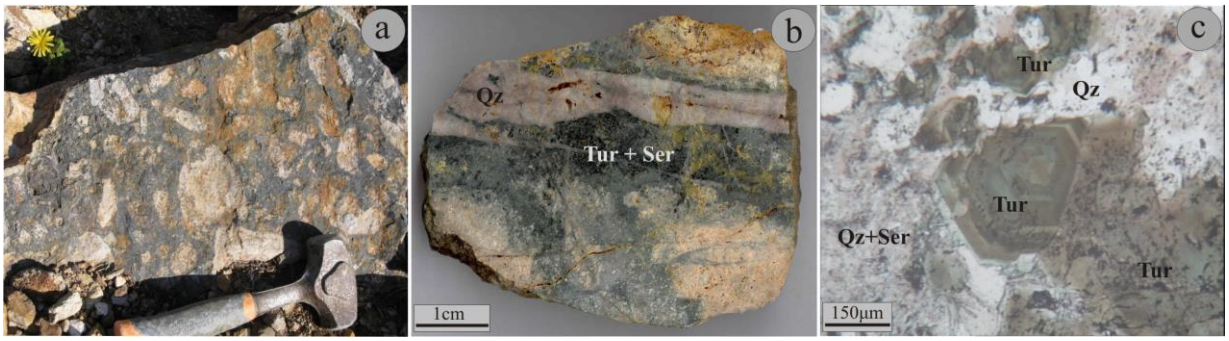

Figure 1. (a) Tourmaline breccia with fragments of phyllic-altered monzonite; (b) Hand specimen of quartz vein associated with tourmaline (Tur) and sericite (Ser) alteration halo, crosscutting phyllic-altered monzonite; (c) Microphotograph of zoned tourmaline (Tur) in association with (Qz) and sericite (Ser) (plane-polarized light; Tourmaline breccia).

In a plot of X-site vacancy versus Al diagram (Fig. 2c), the compositions of tourmaline from the sandstones and the breccia plot parallel to $FeAl_{-1}$, and $AlO(FeOH)_{-1}$ vectors, whereas those from the quartz veins scatter between the two vectors $AlO(R(OH))_{-1}$ and $Al(NaR)_{-1}$. In the (charge excess) *versus* (Fe + Mg + *X* vacancy) plot (Fig. 2d) it is obvious that the $FeAl_{-1}$ vector is predominant for the tourmaline in the sandstones. In addition, this diagram shows two compositional groups in excess charge: below -1 and ~ -0.3 to ~0.1. In the second group, most compositions have charge deficiency. Similarly most compositions of tourmaline from the breccia plot parallel to the $FeAl_{-1}$ vector and have charge deficiency and plot close to the second compositional group of the tourmaline from the sandstones. However, tourmaline compositions from the quartz veins are parallel to the $AlO(R(OH))_{-1}$ vector and have no charge deficiency. This testifies to negligible Fe^{3+} content in the tourmaline, although a Mössbauer study is required to test this hypothesis. The Fe_{tot} *versus* Mg diagram (Fig. 2e) and the ternary plot in terms of Fe-Al-Mg (Fig. 2f) show that tourmaline compositions from the sandstones and the breccia parallel the $FeAl_{-1}$ vector and the oxy-dravite / povondraite (OP) trend, respectively. In contrast to the first- and second-types of tourmaline, the compositions of the quartz vein-related tourmaline parallel the $FeMg_{-1}$ vector. Thus, they plot over the schorl-dravite join and are not parallel to the OP trend (Fig. 2f). The tourmaline compositions from the quartz veins are characterized by the $AlO(R(OH))_{-1}$, $Al(NaR)_{-1}$, and $FeMg_{-1}$ exchange vectors, probable negligible Fe^{3+} concentration, and are not parallel to the OP trend.

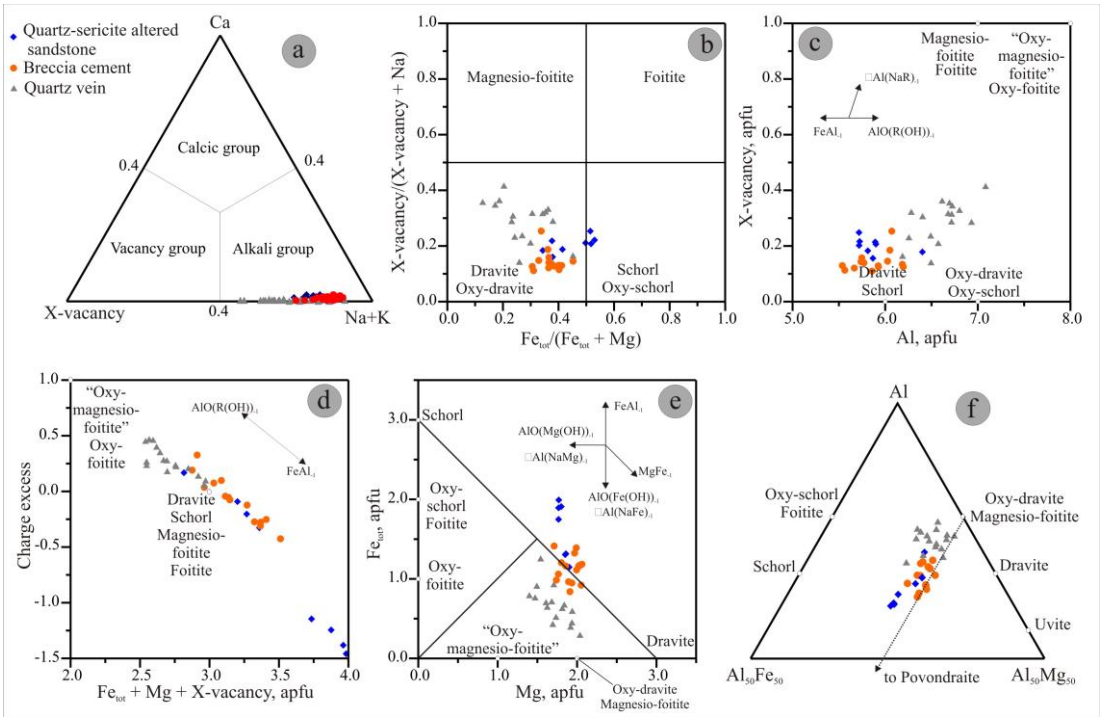

Figure 2. Chemical compositions of analyzed tourmalines from the Fakos prospect in terms of: (a) Ca – (X-vacancy) – (Na+K); (b) X-vacancy/(X-vacancy +Na) vs Fetot/(Fetot+Mg); (c) X-vacancy vs Al; (d) Charge excess vs Fetot+Mg+X-vacancy; (e) Fetot vs Mg; (f) Al-Fe-Mg.

Tourmaline from the Fakos area is Ca-poor that is attributed to Ca deficiency in the host rocks. Tourmaline from altered sandstone and breccia cement have similar major exchange vector substitution FeAl-1 corresponding to isomorphic substitution Fe3+ ↔ Al and parallel to the OP trend. Similarly, tourmaline with the same features have been described from other porphyry deposits (Baksheev et al., 2012; Lynch and Ortega, 1997; Yavuz et al., 1999). Difference in excess charge value between tourmalines from sandstone and breccia cement may be explained by more reducing conditions of tourmaline crystallization in the breccia cement. This more reducing environment may be caused by an increase in the H2S fugacity, which resulted in sulfide deposition. In turn, the latter caused a decrease in the Fe content of the cement tourmaline, because Fe fractionated into sulfide minerals.

Tourmaline from alteration adjacent to quartz-tourmaline veins is different in terms of composition and isomorphic substitutions compared to the previous two types. For these tourmalines, the compositions follow the FeMg-1 vector, which is quite unusual in tourmaline from porphyry systems, but rather represents a major exchange observed in tourmalines from mesothermal gold deposits, greisen, mesothermal tin deposits, and base metal deposits. This is in accordance with field observations at Fakos where quartz-tourmaline veins are transitional from the porphyry to the epithermal environment. Future work will focus on the tourmaline chemistry from Limnos and will be used as a possible vector towards new mineralized (Au-rich) centers in the broader area, as has been suggested for other tourmaline-bearing, porphyry-style alteration assemblages elsewhere.

References

Baksheev I., Prokof'ev V.Y., Zaraisky G., Chitalin A., Yapaskurt V., Nikolaev Y., Tikhomirov P., Nagornaya E., Rogacheva L., Gorelikova N., Kononov O. 2012. Tourmaline as a prospecting guide for the porphyry-style deposits. European Journal of Mineralogy, 24, 957-979.

Fornadel A.P., Voudouris P., Spry P.G., Melfos V. 2012. Mineralogical, stable isotope and fluid inclusion studies of spatially related porphyryCu-Mo and epithermal Au-Te mineralization, Fakos Peninsula, Limnos Island, Greece. Mineralogy Petrology, 105, 85-111.

Lynch G., Ortega J. Hydrothermal alteration and tourmaline-albite equilibria at the Coxheath porphyry Cu-Mo-Au deposit, Nova Scotia. 1997. Canadian Mineralogist 35:79-94.

Voudouris, P. and Alfieris, D. 2005. New porphyry-Cu-Mo occurrences in northeastern Aegean/Greece: Ore mineralogy and transition to epithermal environment. In: Mao J, Bierlein FP (eds) Mineral deposit research: Meeting the global challenge. Springer Verlag, pp. 473-476.

Yavuz, F., Iskenderglu, A., Jiang, S.Y. 1999. Tourmaline compositions from the Salikvan porphyry Cu-Mo deposit and vicinity. Canadian Mineralogist, 37, 1007–1024.

15th International Congress of the Geological Society of Greece
Athens, 22-24 May, 2019 | Harokopio University of Athens, Greece
Bulletin of the Geological Society of Greece, Sp. Pub. 7 Ext. Abs. GSG2019-050

Cave pearls from Almopia Speleopark (Greece): preliminary results

G. Lazaridis[1], L. Papadopoulou[1], M.-O. Voudouri[1]
(1) Aristotle University of Thessaloniki, School of Geology, Thessaloniki, 54124, Greece, geolaz@geo.auth.gr

Cave pearls are speleothems concentrically developed around a nucleus in shallow cave pools (Hill and Forti, 1997). Their name derives from their structure and appearance that commonly resembles pearls produced by mollusks. However, their shape varies greatly from spherical to cylindrical, cubic, hexagonal and disc-shaped. Their size can range from smaller than sand to about 20 cm in diameter and they can grow in few decades. They are commonly composed by calcite. However, the nucleus may be fragments of speleothems, rocks, organic material such as bones, wood etc. In contrast to most speleothems, cave pearls are not cemented on the substrate they are formed due to small occasional vibrations. Their shape, structure and texture is indicative of formation conditions.

In Greece, cave pearls have been studied only in few caves (Dermitzakis et al., 1993). In this study a number of cave pearls have been sampled from the Almopia Speleopark caves (Lazaridis, 2005, 2006) in order to investigate their structure and composition.

Methods

The cave pearls have been divided into categories and the conditions of formation are interpreted according to Table 1.

Electron microprobe analyses were carried out in the Scanning Microscope Laboratory, A.U.Th., using a JEOL JSM-840A Scanning Electron Microscope (SEM) equipped with an Energy Dispersive Spectrometer (EDS) with 20kV accelerating voltage and 0.4mA probe current. Pure Co was used as an optimization element. For SEM observations, the samples were coated with carbon - to an average thickness of 200 A° - using a vacuum evaporator JEOL-4X.

Table 1. Variation in the shape, texture and structure of cave pearls in respect to the corresponding conditions of formation (according to Hill and Forti, 1999 and references therein).

Shape	cubic, hexagonal	round	cementation to the floor	formation of cave cup	random
conditions	restricted precipitate supply, regular packing, calm mode of deposition or precipitation due to water freezing	small size	water pool level below the base	water pool level below the top	nucleus shape
Texture	smooth, polished surface		rough surface		
conditions	rapid water circulation		slow water circulation		
Structure	porosity variation				
conditions	strong water agitation, composition, abnormal rates of precipitation, high temperature				

Results

In total, more than 70 specimens were measured and examined macroscopically. More than 10 specimens were cut in order to examine their internal structure and two were studied in SEM. Their large diameter ranges from about 6.6 to 47.3 mm. According to their shape and texture, they are divided in the following categories.

- Round to irregular shape with smooth to polished surface; cave caps absent, their base may be less polished but smooth with facets due to contact with adjacent cave pearls. Small to intermediate size. Condition: Fast to rapid water circulation, possibly dense packing of cave pearls.
- Oval-shaped with coarse surface covered by coralloids. Intermediate size. Condition: slow water circulation.
- Oval-shaped with smooth to polished surface. Large size. Condition: Rapid water circulation, high water pool level.
- Disc-shaped with smooth to polished surface. Intermediate to large size. Condition: fast water circulation, high water level.
- Disc-shaped with coarse surface and cave cups. Their edge may be irregular. Intermediate to large size. Condition: relatively fast water circulation at early stages of development succeeded by a stage of pool level fluctuations.

Regarding the nucleus of the examined cave pearls it has been found to consist of speleothem fragments, aggregate of fine-grained sediment, tooth fragment or coal. The latter has been found in cave pearls from the Bear Cave, where two samples of coal have been dated with radiocarbon in 4920-4720 B.C. and another in 5220-5050 B.C. (Kambouroglou et

al., 2006).

As far as their structure is concerned, a variation in their porosity related to conditions seen in Table 1 has been noticed. In four out of six rounded to irregular shaped with polished surface pearls, layers of fine-grained clastic sediment are noticed. These layers are separating a more porous cave pearl from a less porous external layer. In three of those the nucleus consists of similar sediment. The other two cave pearls with polished surfaces are more porous close to the nucleus and the clastic sediment is absent. Another two cave pearls with irregular shape and coralloids on their surface have a porous part in their core and more dense external layers. Five disc-shaped specimens are more porous in comparison to the external layers of polished cave pearls. Their porosity varies among layers. The structure of a cave cup in some of them is clearly seen. Apart from the clastic material, only calcium carbonate was found in the layers of the analyzed specimens.

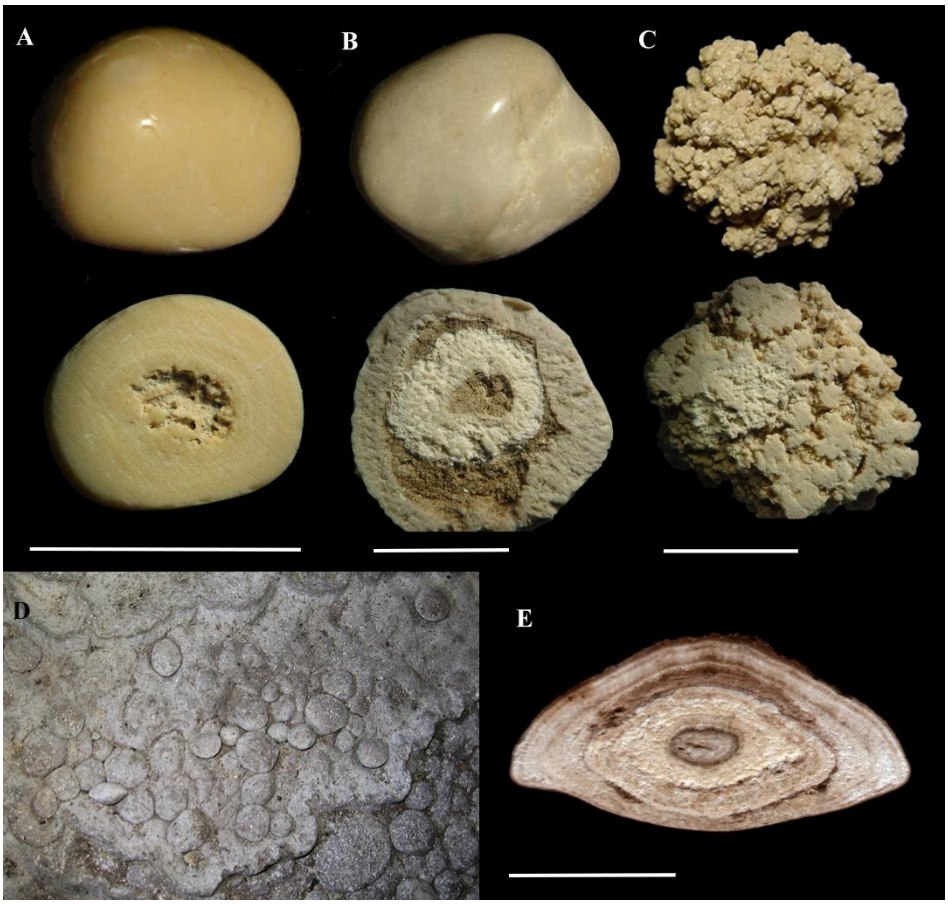

Figure 1. Cave pearls and their cross-sections: A. Almost rounded and polished cave pearl with porous core and probably dissolved nucleus; B. Almost rounded and polished cave pearl with clastic nucleus and one layer that separates internal relatively porous layers and external dense layers; C. Oval-shaped with coarse surface covered by coralloids and a more porous core; D. Disc-shaped cave pearls in situ; E. Longitudinal section of a disc-shaped cave pearl; dark layers on the upper half represent cave caps. Scale bar is 1 cm.

Conclusions

Cave pearls in the Almopia Speleopark caves display a significant variation that depends on the sampling site and the conditions during their development. Despite their differences, specimens from the same chambers are clustered together according to their characteristics, such as shape, texture and structure or by similar nucleus. Based on the cave pearls with coal nucleus, it is estimated that their radius is increased with at least a mean rate of 1.2 mm/1000 years.

References

Hill, C.A. & Forti, P., 1997. Cave minerals of the world (2nd ed.). 1-463, National Speleological Society, Huntsville, Alabama.

Dermitzakis, M., Tsipoura-Vlachou, M. & Basiakos, I. 1993. Cave-pearls: mineralogy and geochemistry. Bulletin of the Hellenic Speleological Society, 21, 140-158.

Kambouroglou E., Bassiakos, Y., Bouzas, D., 2006. Paleontological-sedimentological excavational research in 2004 and dating results of Cave A' Loutraki, Aridea, in: "The Archaeological Survey in Macedonia and Thrace", 18 (2004): 573-589, Thessaloniki (in Greek with English abstract).

Lazaridis, G., 2005. Speleological research in the loutra arideas area (Macedonia, Greece). –Neue Forschungen zum Höhlenbären in Europa, Naturhistorische Gesellschaft Nürnberg e. V., 45: 57-64, Nürnberg.

Lazaridis, G., 2006. Almopia Speleopark (Pella, Macedonia, Greece): Morphology-Speleogenesis of the caves. –Scientific annals, School of geology, Aristotle University of Thessaloniki, Special Volume 98: 33-40, Thessaloniki.

15th International Congress of the Geological Society of Greece
Athens, 22-24 May, 2019 | Harokopio University of Athens, Greece
Bulletin of the Geological Society of Greece, Sp. Pub. 7 Ext. Abs. GSG2019-062

Petrology and Geochemistry of Volcanic Rocks from Hisarlıkaya region (SW of Ankara) Central Anatolia, Turkey

E.Varol[1], A.Korkmaz[1], G.D. Doğan Külahcı[1], S. Tatar Erkül[2]

(1) Hacettepe University, Department of Geological Engineering, 06800, Beytepe Campus, Ankara, Turkey, aslihan.korkmaz12@hacettepe.edu.tr (2) Akdeniz University, Department of Geological Engineering, 07058, Antalya, Turkey

Abstract

The study area is located in Hisarlıkaya region, Southwest (SW) of Ankara, Central Anatolia. Units cropping out throughout large areas consist of different sized and shaped xenoliths having a polygenetic origin in certain areas. Macroscopically blackish-greenish-greyish-greenish colored and porphyritic textured rocks contained mainly plagioclase, amphibole, opaque microlites and rarely pyroxene crystals. Plagioclases are generally euhedral in shape and are predominantly zoned. They show sieved texture at the rims and/or cores. The amphiboles have been completely or partly replaced by Fe-Ti oxides. According to the microprobe analysis, it was determined that the plagioclases in the host rocks are andesine and the amphiboles are calcic-chermakite in characters. As a result of geochemical analyses, volcanic rocks have been identified as trachytic rocks with calc-alkaline character. Major, trace element Harker variation diagrams indicate an effective fractional crystallization process in the formation of these rocks. SiO_2 (62.6-63.7%), Al_2O_3 (16.5-17.2 %), Na_2O (4.9-5.6 %), Sr (1249-1397 ppm), Y (13.1-14.2 ppm) contents of these trachytic rocks indicate typical adakitic rocks features. Previous works in the study and vicinity areas revealed the presence of volcanic products carrying the evidences of post collisional Early Miocene magmatism. It is thought that the Hisarlıkaya volcanic rocks, having trachytic character, were formed in this period.

Introduction

Hisarlıkaya region is located in SW of Ankara, Central Anatolia is about 45 km from the city center, and situated at the northern part of İzmir - Ankara - Erzincan suture zone which formed by the closure of the northern branch of Neotethys. The volcanism that develops with the closure of the northern branch of the Neo-Tethys, convergence, subduction and collision, has been spreading in large areas in many parts of Central Anatolia (Şengör and Yılmaz, 1981; Okay and Tüysüz, 1999). The aim of this study is to investigate the mineralogical-petrographic and geochemical characteristics of the Hisarlıkaya volcanic rocks which are thought to be formed during the Neogene period.

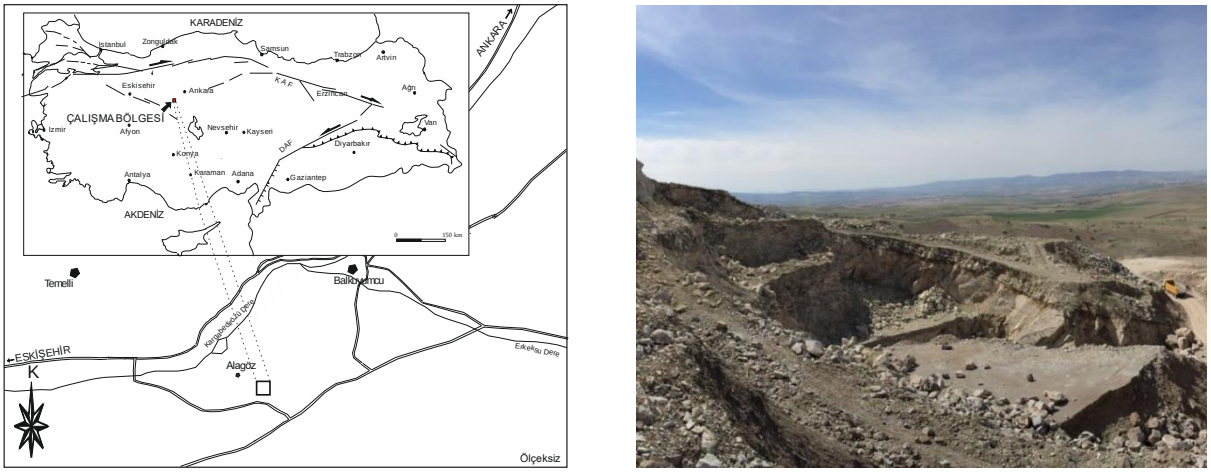

Figure 1. Simplified map and a general view of the study area (Hisarlıkaya, Ankara, Central Anatolia)

Mineralogy

The Hisarlıkaya volcanic rocks are macroscopically blackish-grayish-greenish colored and show porphyritic texture. These rocks mostly contain plagioclase, amphibole, opaque microlites and rarely pyroxene. Plagioclases are generally euhedral and are zoned. They show sieved texture at the rims and/or cores. Amphiboles are opaque completely or as from the edges. According to microprobe analyzes, it was determined that the plagioclase crystals are andesine and the amphiboles are calcic-chermakite. These volcanic rocks, which are cropped out in Hisarlıkaya region, contain polygenetic xenoliths in different sizes and compositions. They consist of pyroxene, garnet and plagioclase phenocrysts. The garnets observed in xenoliths are macroscopically red-brown colored and their size varies between 0.2 mm to 1 cm. According to the microprobe analysis of xenoliths, pyroxenes are diopside and hedenbergite; plagioclases are labrador and andesine and garnets are andradite-grossular in compositions.



Figure 2. The host rock and the xenoliths.

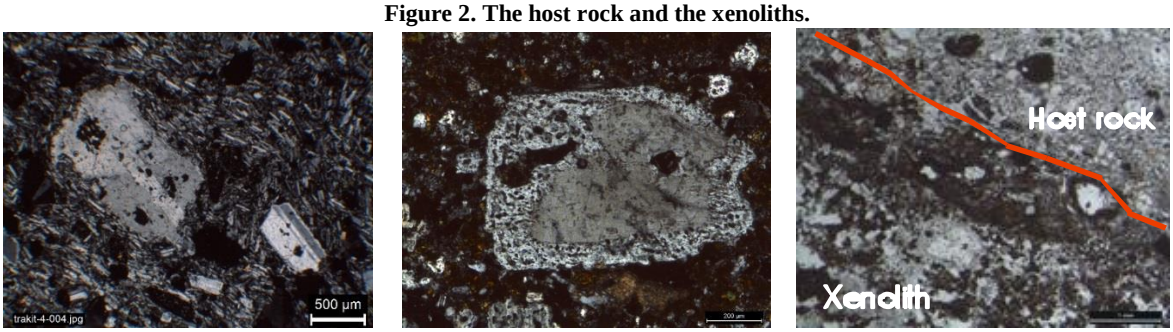

Figure 3. Photomicrographs from the host rocks and the xenolith

Geochemistry

As a result of the geochemical analyses on the Hisarlıkaya volcanic rocks, the SiO_2 contents ranges from 62.6 to 63.7% and the LOI values were between 0.23-0.96 %. According to the total alkali-silica diagram (Le Bas et al., 1986), it was determined that the samples have sub-alkaline trachytic character due to the normative quartz value being <20%. FeO_t-Na_2O + K_2O-MgO diagram shows that all of them have a calc-alkaline in character. It has been observed that fractional crystallization is an effective process during the formation of these Hisarlıkaya volcanic rocks according to the major and trace element Harker variation diagrams. SiO_2 (62.6-63.7 %), Al_2O_3 (16.5-17.2 %), Na_2O (4.9-5.6 %), Sr (1249-1397 ppm), Y (13.1-14.2 ppm) values reveal that samples have features similar to adakitic rocks.

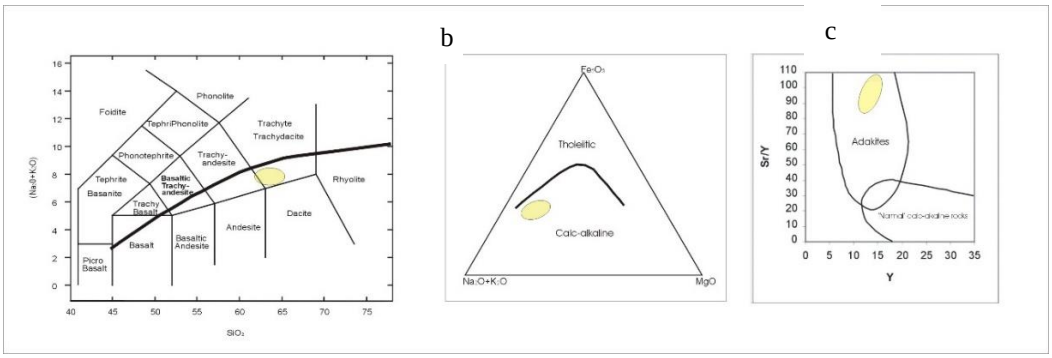

Figure 4. a)Total alkali-silis (Le Bas and others 1986), b)AFM (Irvine and Baragar, 1975), c) Sr/Y vs Sr (Defant and Drummond, 1990) diagrams

Conclusion

Hisarlıkaya calc-alkaline trachytic rocks consist of polygenetic xenoliths. They have adakitic features and fractional crystallization process is significant process during their formation.

Acknowledgements

We thank Dr. Yusuf Kaan KADIOĞLU, Dr. Kıymet DENİZ for their help with the geochemical analysis at YEBİM laboratories and E. YAVUZ and M. AKAGÜNDÜZ with the preparation of samples to the analysis.

References

Defant, M.J., Drummond, M.S., 1990. Derivation of some modern arc magmas by melting of young subducted lithosphere. Nature, 347, 662–665.

Irvine, T.N., Baragar,W.R.A., 1971. A guide of to the chemical classification of the common volcanic rocks. Canadian Journal of Earth Sciences, 8, 523–548.

Şengör, A. M. C., Yılmaz Y. 1981. Tethyan Evolution of Turkey: A Plate Tectonic Approach, Tectonophysics, 75, 181-241.

Okay, A., Tüysüz, O. 1999. Tethyan Sutures of Northern Turkey, Geological Society London Special Publications, 156(1):475-515.

Le Bas, M.J., Le Maitre, R.W., Streckeisen, A., Zanettin, B., 1986. A chemical classification ofvolcanic rocks based on the total alkali–silica diagram. Journal of Petrology. 27, 745–750.

15th International Congress of the Geological Society of Greece
Athens, 22-24 May, 2019 | Harokopio University of Athens, Greece
Bulletin of the Geological Society of Greece, Sp. Pub. 7 Ext. Abs. GSG2019-082

Mineralogical Study of the vein style Cu-Pb-Zn-Bi-As-Au mineralization hosted in the carbonates of Myriofyto, Vertiskos Unit, N. Greece

E. Petika[1], V. Melfos[1], L. Papadopoulou[1], P. Voudouris[2]

(1) Department of Mineralogy, Petrology, Economic Geology, Aristotle University of Thessaloniki, 54124, Thessaloniki, Greece, eppetika@geo.auth.gr
(2) Department of Mineralogy-Petrology, National and Kapodistrian University of Athens, Athens 15784, Greece

Introduction

The long-debated Serbo-Macedonian Massif belongs to the complex tectonomagmatic terrain which forms the northern part of the Hellenides or the North Aegean Domain and is represented by the Vertiskos Unit (Kydonakis *et al.*, 2015). It is dominated by a Paleozoic sequence of gneiss and mica gneiss and rarely some marble exposures. A Mesozoic two-mica and generally deformed granite with fine grained aplitic offsets to the north, outcrops at Myriofyto. According to Christofides *et al.* (2007), the Myriofyto granite belongs to the Kerkini Granitic Complex, and is enriched in Zr, Nb, Y, Ga and REE but not in metallic elements. These plutonic rocks are chemically associated with the Arnaia granite which displays low metallic content. Vertiskos Unit was intruded by Oligocene-Miocene magmatic rocks which were strictly related to an extensional regime set in back-arc environment conditions (Stergiou *et al.* 2018). Extended complex shear and fault structures as well as incorporating fragmented sequences of metamorphosed mafic and ultramafic rocks are found in the Vertiskos Unit (Sidiropoulos, 1991; De Groot *et al.*, 1996).

The strongly sheared marble-gneiss contact zones and the post-shear subvertical faults and related breccia zones in gneisses of the northern part of Vertiskos, host several gold-bearing sulfide mineralizations in Drakontio, Koronouda, Stefania, Laodikino, and Myriofyto (Melfos and Voudouris, 2017). These deposits are part of the Kilkis ore district which includes porphyry, carbonate-replacement and vein style mineralizations enriched in gold. Herodotus and other ancient writers mention the importance of this area, around Dysoron mountain, for the gold rich deposits since the times of Alexander I (6th century B.C.)

According to Melfos and Voudouris (2017) the gold-bearing sulfide deposits of the Vertiskos Unit are associated with the Cenozoic magmatism. The present paper focuses on the study of the gold-bearing sulfide mineralization in the Myriofyto area.

Materials and Methods

For the purposes of optical microscopy, a total of 17 thin, 8 polished and 4 thin-polished sections were prepared and studied under a Leitz LABLORLUX 12 POL dual reflected-transmitted light polarizing microscope at the Department of Mineralogy, Petrology, Economic Geology of the Faculty of Geology, Aristotle University of Thessaloniki. The chemical composition of the non-metallic and the metallic minerals was determined by Scanning Electron Microscopy (SEM), using a JEOL 840 equipped with an ISIS 300 OXFORD energy dispersive spectrometer (EDS) at the Scanning Electron Microscopy Laboratory of Aristotle University of Thessaloniki. The study of the fluid inclusions was carried out at the Aristotle University of Thessaloniki, using the freezing-heating stage of LINKAM THM 600, attached at a LEITZ SM-LUX-POL microscope and a temperature control system TMS 90. Finally, to identify the major elements content of the mineralization and the host rock, six samples were analyzed by X-ray fluorescence (XRF) at the School of Sciences, Aristotle University of Thessaloniki.

Results

The rocks of the Myriofyto area consist mainly of marbles intruded by hydrothermal quartz veins with a thickness of 30-40 cm. The marbles appear white, coarse-grained, massive and folded at some places due to shear. On the basis of the petrographic study, three types of marbles are recognized: i) slightly impure calcitic marble, ii) dark grey laminated calcitic marble, and iii) very coarsely-crystalline, white calcitic marble. The mineralogical composition of the marbles consists mainly of calcite, with minor dolomite and ankerite. The carbonate minerals are accompanied by traces of quartz, white mica, chlorite, amphibole, epidote, clinozoisite, zircon and apatite.

The mineralization is hosted by the marbles and the quartz veins which intrude the marbles. The ore minerals form disseminations mostly in the quartz veins and include pyrite, chalcopyrite, sphalerite and galena with minor magnetite, tennantite, pyrrhotite (Fig. 1a, b). Arsenopyrite, galenobismutite and native gold are found in traces. Pyrite is the most dominant sulfide and demonstrates euhedral crystals including various inclusions of the other sulfides (Fig. 1a,b). Chalcopyrite appears in crystals and often as inclusions in pyrite. Sphalerite and galena form overgrowths over pyrite crystals and galena appears either with the other sulfides or as the dominant ore mineral in the host rocks. Other ore minerals are magnetite which occurs in characteristic euhedral crystals and accompanies the other sulfides (Fig.1b), tennantite and pyrrhotite which are relevant to chalcopyrite, arsenopyrite which is associated mostly with galena, chalcopyrite and galenobismutite. Galenobismutite is relevant to arsenopyrite and often carries Ag. Finally native gold appears at the margins of chalcopyrite grains included in pyrite. The primary mineralization has been replaced by chalcocite, covellite, malachite and goethite in the oxidized zone.

Chemical analysis of the host marble shows that the MgO content varies among the three different types of the marbles

and is higher in the samples of the second type (dark grey laminated calcitic marble). The first type displays high concentrations of FeO and Al_2O_3 because of the amphiboles and the phyllosilicate minerals which are possibly attributed to the hydrothermal alteration. The third type of the marble appears pure and mostly consists of CaO. The enrichment of MgO in the second type of marble is possibly attributed to the grey layers alternating with the white calcitic ones. The high concentration of SiO_2 reflects the presence of the quartz veins associated with the ore mineralization. The study of the fluid inclusions showed homogenization temperatures between 200 and 240 ºC, with a peak at 220 ºC, and salinities from 7.11 to 14.36 wt% NaCl eq. These conditions are attributed to post mineralization processes, e.g. tectonics with the development of extended shear zones, which affected the primary fluid inclusions.

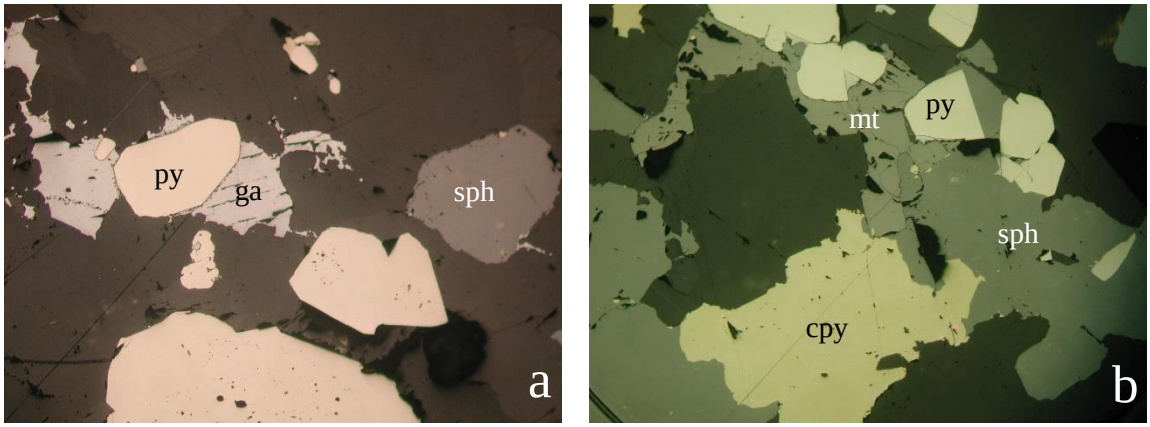

Figure 1. Photomicrographs of the primary ore mineralization. a. Pyrite (py), galena (ga) and sphalerite (sph). b. Chalcopyrite (Cpy), pyrite (py), sphalerite (sph) and magnetite (mt).

Discussion

The ore mineralogical composition and the fluid inclusions in the mineralization of the Myriofyto area are very similar to the Stanos Cu-Au-Bi-Te deposit at the southern part of Vertiskos. According to Bristol et al. (2015) this mineralization in Stanos is dated in early Miocene (19 Ma) and is probably related to a magmatic event which was developed along a shear zone. It was affected by the subsequent metamorphic processes of greenschist to lower amphibolite grade, due to shear, and is characterized by the lack of any magmatic rocks exposure. Magmatic related deposits with elevated Te-Bi-Au are found also at the northern part of Vertiskos, in the Kilkis ore district, and are possibly related to shear zones and normal and strike-slip faults which enhanced the hydrothermal fluids circulation derived from the Oligocene-Miocene magmas (Gilg, 1993; Bristol et al., 2015; Melfos and Voudouris, 2017; Stergiou *et al.*, 2018). It is very probable the shear-related Cu-Pb-Zn-Bi-As-Au mineralization in Myriofyto, hosted in quartz veins and the marbles of the Vertiskos Unit, to have a genetic affiliation to a magmatic rock of a possible Oligocene-Miocene age, not exposed in the area. The ore bodies are mainly associated with quartz veins that were emplaced along shear and strike-slip zones, operated under ductile-to-brittle conditions. This is the reason that the measured fluid inclusions in Myriofyto are not representatives of the primary mineralized fluids but of the subsequent fluids circulated along the tectonic structures.

Acknowledgements

The authors would like to thank Former Professor K. Michailidis, for pointing out the study area, his assistance in sampling and his suggestions.

References

Bristol, S.K., Spry, P.G., Voudouris, P.Ch., Melfos, V., Fornadel, A.P., Sakellaris, G.A., 2015. Geochemical and geochronological constraints on the formation of shear-zone hosted CuAu-Bi-Te mineralization in the Stanos area, Chalkidiki, northern Greece. Ore Geology Reviews 66, 266-282.

Christofides G., Koroneos A., Liati A., and Kral J., 2007. The A-type Kerkini granitic complex in north Greece: Geochronology and geodynamic implications. Bulletin of the Geological Society of Greece XXXX, 700-711.

De Groot, P.A., Arvanitidis, N.D., Baker, J.H., 1996. Regional carbon, oxygen and Sulphur isotopic values in the Serbo-Macedonian and Rhodope massifs. Mineral Wealth 98, 17-23.

Gilg, H.A., 1993, Geochronology (K–Ar), fluid inclusion, and stable isotope (C, O, H) studies of skarn, porphyry copper, and carbonate hosted Pb–Zn (Ag–Au) replacement deposits in the Kassandra mining district (eastern Chalkidiki, Greece), Swiss Federal Institute of Technology (ETH) Zurich, Switzerland, Unpublished Ph.D. thesis, 153 p.

Kydonakis, K., Brun, J. P., Sokoutis, D., and Gueydan, F., 2015. Kinematics of Cretaceous subduction and exhumation in the western Rhodope (Chalkidiki block), Tectonophysics, v. 665, p. 218-235.

Melfos V. and Voudouris P., 2017. Cenozoic metallogeny of Greece and potential for precious, critical and rare metals exploration. Ore Geology Reviews 89, 1030-1057.

Sidiropoulos 1991. Lithology, geochemistry, structural geology and metamorphism of the NW part of Vertiskos Formation, Disoro Mt (Krousia), N.Kilkis. Ph.D, Thesis, Aristotle University of Thessaloniki, 592 p.

Stergiou C., Lazos I., Melfos V., Chatzipetros A., Voudouris P., Pikridas C., Bitharis S., 2018. Links between the neotectonics regime and the Tertiary mineralization of the Vertiskos and Kerdylion Units, N. Greece. XXI International Congress of the CBGA, Salzburg, Austria.

15th International Congress of the Geological Society of Greece
Athens, 22-24 May, 2019 | Harokopio University of Athens, Greece
Bulletin of the Geological Society of Greece, Sp. Pub. 7 Ext. Abs. GSG2019-089

Geochemical characterization of groundwater quality in Hellenic karst systems

L. Li Vigni[1], K. Daskalopoulou[2,3], W. D'Alessandro[1], C. Cardellini[4], S. Calabrese[1,2]

(1) Istituto Nazionale di Geofisica e Vulcanologia, via Ugo La Malfa 153, Palermo, Italy, livignilorenza@gmail.com
(2) University of Palermo, via Archirafi 36, Palermo
(3) National and Kapodistrian University of Athens, Panepistimioupolis, Ano Ilissia, 15784, Athens, Greece
(4) University of Perugia, Piazza dell'Università, Perugia, Italy

Karst aquifers are considered to be one of the most important aquifer types, as they constitute the main drinking water resource for the majority of the global population (Ford et al., 2007). They are generated from the dissolution of carbonate rocks (e.g. limestone, dolomite, marble etc.), a phenomenon commonly known as "karstification". This process is mainly caused by the acidity of water enriched in dissolved CO_2, with the concentration of the latter being dependent on both the temperature and the CO_2 partial pressure of the atmosphere in contact with the water (Bakalowicz, 2005).

Carbonate rocks cover about 35% of the land surface of Greece and are mainly located in the western, central and southern parts of the country (Daskalaki et al., 2008). The Hellenic karst aquifer resources are more abundant in the western part of Greece, which receives the highest amount of precipitation (1800 mm/a) (Mimikou, 2005). The karst system constitutes a strategic resource of water in the region and preserving its quantity and quality is of the utmost importance for the sustainability of the area.

Seventy samples of natural water were collected from karst springs in the northern (Macedonia-Thrace) and in the central parts of Greece, during 3 campaigns from 2016 to 2018. Sampling sites were selected on the basis of the springs flow rates (> 50 L/s). Water temperature, pH, Eh and electric conductivity were measured in situ with portable instruments; major ions were determined by Ionic Chromatography (IC) on filtered (anions) or filtered and acidified (cations) samples, whereas trace elements were determined by Inductively Coupled Plasma Mass Spectrometry (ICP-MS) on filtered and acidified samples. All analyses were performed at the laboratories of INGV of Palermo.

Chemical compositions were compared with the limits fixed by the Directive 98/83/EC, which is the most recent EU legislation that sets quality standards for drinking water. Regulations concerning the quality of drinking water as established by the Directive allow Member States to adapt the monitoring of water quality to local conditions (Karavoltsos et al., 2008).

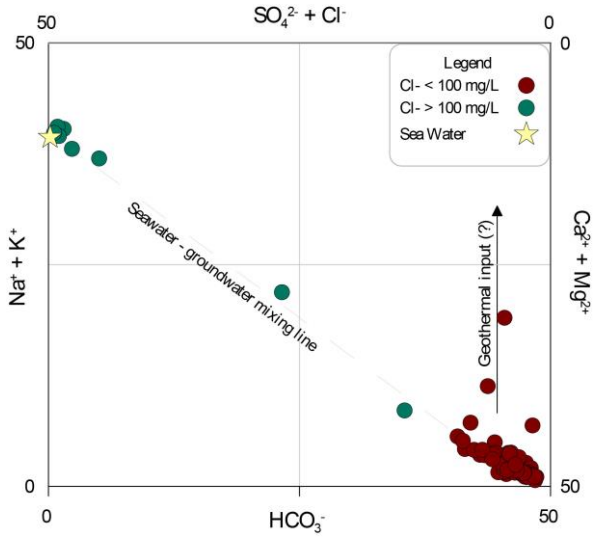

Figure 1. Langelier Ludwig diagram showing the chemical composition of the sampled karstic groundwater of northern and central Greece.

Temperatures of the sampled waters ranged from 8 to 25 °C, pH from 6.5 to 8.4, whilst Total Dissolved Solids (TDS) from 206 to 15,418 mg/L. The highest concentrations of sodium, potassium, chloride and sulfate were found in the karst springs of Central Greece (26.6-5610 mg/L; 1.56-204 mg/L; 81.06-9467 mg/L; 15-2420 mg/L, respectively), where values had sometimes exceeded the limits set by the Directive 98/83/EC, indicating a contamination due to sea water intrusion. Based on the chloride concentrations, samples were subdivided into low (Cl^- < 100 mg/L) and high (Cl^- > 100 mg/L) chloride karst waters. All water samples were plotted in a Langelier Ludwig diagram (Fig. 1) with the low chloride waters presenting a typical alkaline-earth bicarbonate composition. Exception is the samples of Kaliakuda, Sidirokastro and Koromilia that display enrichment in alkalis possibly due to hydrothermal activity. On the other hand, the most chloride-rich waters plot close to the sea water composition point while two samples (Rema, Mylos Kokkosi) are aligned

along the seawater-groundwater mixing line (Fig. 1).

Concentration ranges of major and trace elements for all waters are presented in Fig. 2, with low and high chloride samples being plotted with different symbols. High chloride group displays much higher values for Mg, SO_4, Cl, Na, K, Sr, B, Li, Rb and Cs with respect to low chloride, with differences in the median values between two and three orders of magnitude. Species deriving from carbonate dissolution (Ca and HCO_3) show the lowest range of concentrations both for low and high chloride waters (Fig. 2). Low chloride waters show a wide range of concentrations (three to four orders of magnitude) for trace elements such as Li, Fe, Rb, As, Mn, Cu and Cs.

Trace elements were above the legislation limits (Directive 98/83/EC) mostly in the case of high chloride karst springs, showing elevated concentrations of Boron (up to 1861 μg/L), Strontium (up to 5026 μg/L) and Arsenic (up to 12.1 μg/L). In terms of Boron and Strontium, the exceeding values seem to be generally related to the intrusion of sea water. On the other hand, Arsenic, whose maximum admissible level is 10 μg/L, was above limit also in the low chloride water (17 μg/L) of Tempi, Thessalia. Few low chloride waters show a metal enrichment, such as Tempi (Sr = 242 μg/L, Mo = 2.27 μg/L, and Cs = 1.57 μg/L) and Kaliakuda (V = 3.89 μg/L, Mn = 3.65 μg/L, Fe = 71.26 μg/L, Cu = 11.55 μg/L, Zn = 22.61 μg/L, Rb = 54.7 μg/L), whilst nitrate concentrations that could indicate contamination from fertilizers or from septic tanks, are always below the maximum admissible value (50 mg/L).

Most of the analyzed waters can be considered suitable for human consumption. Water quality deterioration of Hellenic karst springs is mainly due to sea water intrusion, whilst only few low chloride waters show significant enrichments in trace metals that rarely exceeds the drinking water standards. These higher contents are probably of natural origin due to local geological setting.

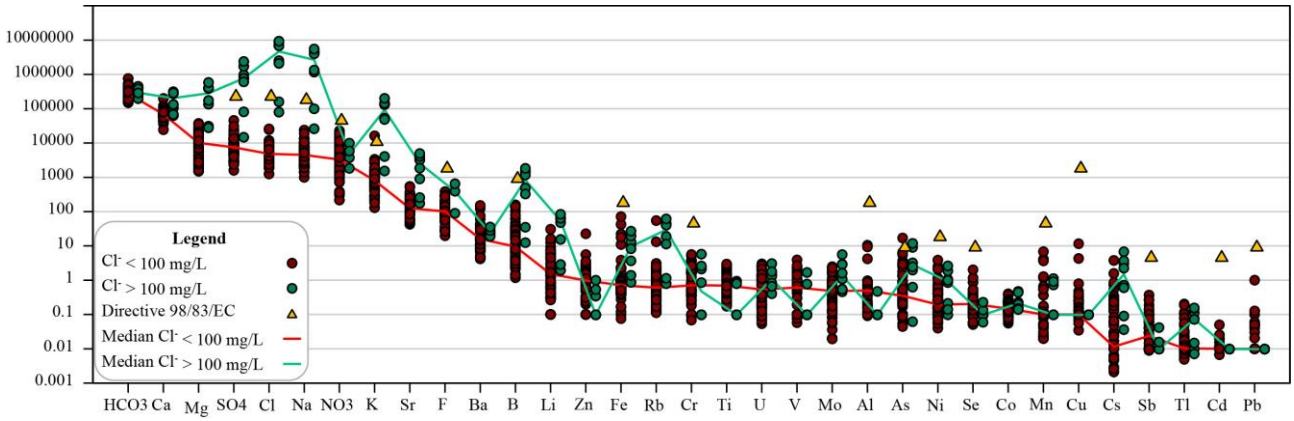

Figure 2. Distribution of major and trace elements in μg/L. Limits set by the Directive 98/83/EC are plotted with yellow triangles.

References

Bakalowicz, M., 2015. Karst groundwater: A challenge for new resources. Hydrogeology Journal, 13, 148-160.

Ford, D.C., Williams, P.W. 2007. Karst Geomorphology and Geomorphology, John Wiley and Sons Inc.

Daskalaki, P., Voudouris, K. 2008. Groundwater quality of porous aquifer in Greece: a synoptic review. Environmental Geology, 54, 505-513.

Mimikou, M.A., 2005. Water resources in Greece: present and future. Global NEST Journal, 7, 313-322.

Karavoltsos, S., Sakellari, A., Mihopoulos, N., Dassenakis, M., Scoullos, M.J., 2008. Evaluation of the quality of drinking water in regions of Greece. Desalination, 224, 317-329.

EU, Council Directive 98/83/EC, 1998.

15th International Congress of the Geological Society of Greece
Athens, 22-24 May, 2019 | Harokopio University of Athens, Greece
Bulletin of the Geological Society of Greece, Sp. Pub. 7 Ext. Abs. GSG2019-091

Synthetic zeolites from lignite fly ash and biomass ash for agricultural applications

M. Andreadi[1], C. Vasilatos[1]

(1)Department of Economic Geology and Geochemistry, Faculty of Geology and Geoenvironment, National and Kapodistrian University of Athens, Athens, Greece, vasilatos@geol.uoa.gr

The production of zeolites is one of the potential applications of fly ash production to obtain high value industrial products with environmental technology utilization (Querol et al, 2001). The synthesis of zeolite products from fly ash is analogous to the formation of natural zeolites from volcanic deposits or other high-Si-Al rocks, rich in amorphous phases, by the interaction of hot alkaline water on the glass fraction of the rocks. That zeolite development process may take thousands of years in order to form natural zeolites. In the laboratory, the process can be speeded up (to days or hours) for both volcanic and fly ash.

Previous studies have demonstrated the utilization of lignite fly ash Na bearing synthetic zeolitic materials for the removal of heavy metals from wastewater (e.g. Koukouzas*et al.*, 2010), for mine-water treatment (Itskos *et al.*, 2015) and as soil amendments in acid mining soils (Giannatou *et al.*, 2017, 2018). Since K is considered as a nutritient in agriculture (e.g. Stamatakis *et al.*, 2016), in the present study KOH was selected as an activation solution, in order to develop a K-rich synthetic zeolite suitable for utilization in agriculture.

In the current study we are evaluating the results of the hydrothermal activation of lignite fly ash and biomass asses from Greece, by KOH in order to produce synthetic zeolites, for agricultural applications.

As KOH solutions present lower conversion efficiency than the respective NaOH under the same temperature (Itskos *et al.*, 2015) the experimental conditions were modified from those proposed by Koukouzas *et al*. (2010) Itskos *et al.* (2015) and Giannatou *et al.* (2017, 2018), by using a 6N KOH as activation solution and extending the treatment period to 72h. Lignite fly ash samples from Meliti (MEL-FA) and Megalopoli (MEG-FA) Electric Power Stations and biomass ash from sawdust (SAWD-ASH), reed (REED-ASH) and olive kernel (OL-ASH) were used as raw materials that underwent the alkaline hydrothermal treatment at 100ºC. The applied techniques mainly aimed at the dissolution of Al-Si bearing phases of the ashes and the subsequent precipitation of the zeolitic minerals.

Both the initial materials and the final solid products, were subjected to X-ray diffraction (XRD) analysis and scanning electron microscopy (SEM) study along with electron microbe microanalysis [Energy Dispersive System (EDS)] for the identification of their mineral phases at the Laboratory of Economic Geology and Geochemistry, National and Kapodistrian University of Athens. The cation exchange capacity (CEC) of the original and the hydrothermally treated materials had been determined in the same Laboratory. Furthermore, X-ray fluorescence analysis for the determination of the materials' chemical changes after the thermalalkali digestion, has been carried out at the R&D Department of the Titan Cement Company.

Table 1: Effect of hydrothermal treatment (HT-) in the mineralogical composition of the biomass and lignite fly- ashes

Mineral phase	REED-ASH	HT-REED-ASH	SAWD-ASH	HT-SAWD-ASH	OL-ASH	HT-OL-ASH	MEG-FA	HT-MEG-FA	MEL-FA	HT-MEL-FA
Zeolite-F($KAlSiO_4 1,5H_2O$)								✓		✓
Anhydrite	✓	✓					✓	✓	✓	✓
Arcanite (K_2SO_4)	✓	✓			✓	✓				
Calcite	✓	✓	✓	✓	✓	✓	✓	✓	✓	✓
Gehlenite	✓	✓								
Hematite	✓	✓	✓	✓			✓	✓	✓	✓
Periclase	✓		✓							
Portlandite	✓						✓	✓	✓	✓
Feldspars	✓	✓	✓	✓	✓	✓	✓	✓	✓	✓
Sylvite (KCl)	✓		✓		✓					
Bassanite			✓		✓	✓				
Fairchildite ($K_2Ca(CO_3)_2$)					✓					
Cristobalite			✓				✓			
Diopside			✓							
Gismondine			✓				✓	✓	✓	✓
Muscovite			✓							
Ankerite					✓	✓				
Quartz	✓	✓		✓	✓	✓	✓	✓	✓	✓
Maghemite									✓	✓
Magnetite							✓	✓		
Gypsum		✓					✓	✓	✓	✓
Amorphous phase	✓	✓	✓	✓	✓	✓	✓	✓	✓	✓

Amorphous phases were present in all initial biomass and lignite fly ash samples. The synthetic zeolite produced from both lignite fly ashes was the K-bearing Zeolite-F [$KAlSiO_4 1,5H_2O$] (Table 1). The formation of the synthetic zeolite from lignite fly ashes was also confirmed by the SEM investigation. The effect of hydrothermal treatment in the mineralogical composition of the biomass and lignite fly- ashes is abstracted in Table 1.

Table 2 presents the impact of the alkaline activation in the chemical composition of the initial fly ashes. Biomass ashes failed to develop any zeolitic material after the low temperature hydrothermal alkaline treatment due to their primary shortage of Al_2O_3

The cation exchange capacity of the initial and the hydrothermally treated (HT-) ashes is presented in Table 3. The hydrothermally treated lignite fly ashes exhibit more than ten times higher CEC values than the initial materials due to the Zeolite-F presence.

No major phase conversion has been identified in the treated biomass ash samples probably due to their initial low Al_2O_3 content (Table 2) as a result of the minorpresence of aluminum bearing mineral phases in the initial ashes.

Table 2: Effect of hydrothermal treatment (HT-) in the major chemical compounds of the treated fly- and biomass ashes

Sample	MEG-FA	HT-MEG-FA	MEL-FA	HT-MEL-FA	REED-ASH	HT-REED-
SiO_2	41.15	32.10	51.82	37.58	49.42	37.71
Al_2O_3	15.67	13.07	17.98	16.09	1.62	2.76
Fe_2O_3	11.09	10.11	7.12	7.27	1.24	2.77
MgO	2.52	2.28	2.36	3.10	4.11	7.60
CaO	16.12	14.53	9.94	9.66	10.14	7.73
Na_2O	0.60	0.23	1.54	0.66	0.54	0.23
K_2O	1.66	10.72	1.98	11.95	14.14	18.75
TiO_2	0.72	0.66	0.79	0.85	0.10	0.19
P_2O_5	0.32	0.13	0.11	0.12	1.66	1.70
MnO	0.09	0.08	0.10	0.09	0.06	0.12
Cr_2O_3	-	-	0.02	-	-	-
TOT/C	-	-	0.95	-	-	-
TOT/S	7.28	0.30	0.44	0.25	3.72	0.36
LOI	4.21	14.65	2.10	11.52	12.63	19.76
Sum	101.43	98.86	99.96	99.14	99.38	99.68

Table 3: Cation exchange capacity of raw and hydrothermally treated (HT-) materials

Sample	CEC meq/100g
MEG-FA	11.02
MEL-FA	15.61
OL-ASH	24.79
REED-ASH	17.45
SAWD-ASH	11.02
HT-MEG-FA	145.10
HT-MEL-FA	152.45
HT-OL-ASH	32.14
HT-REED-ASH	17.45
HT-SAWD-ASH	92.75

Concluding, the synthetic zeolite produced by both lignite fly ashes was Zeolite-F. The cation exchange capacity of those synthetic materials is improved with respect to the initial ashes.Chemical and mineralogical properties of those lignite fly ashes treated, make them a suitable raw material for the synthesis of hybrid zeolitic products with upgraded potential for agricultural applications.On the contrary, biomass ashes failed to develop zeolitic material after the low temperature hydrothermal alkaline treatment due to their primary shortage of Al_2O_3.

The synthesized Zeolite-F rich materials will be tested in the near future for their performance as soil amendments and slow release fertilizers.

Acknowledgements

The Centre for Research & Technology, Hellas (Chemical Process & Energy Resources Institute), BiogypsKarvelis S.A. and Polyeco S.A are thanked for providing the fly ash, olive kernel and sawdust samples respectively. Mr D. Cheimarios is thanked for providing the reed samples.Titan Cement Company is kindly thanked for the XRF analysis. National and Kapodistrian University of Athens is acknowledged for supporting this work.

References

Giannatou, S., Vasilatos, C., Mitsis, I., Koukouzas, N., Itskos, G., Stamatakis, M., 2017. Reduction of toxic element mobility in acid mine soils by zeolitic amendments. Bulletin of the Geological Society of Greece 50(4), 2127-2136.

Giannatou, S., Vasilatos C., Mitsis, I., Koukouzas, N., 2018. Utilization of natural and synthetic zeolitic materials as soil amendments in abandoned mine sites. Bulletin Geological Society of Greece 53(1), 78-98.

Itskos, G., Koutsianos, A., Koukouzas, N., Vasilatos, C., 2015. Zeolite development from fly ash and utilization in lignite mine-water treatment. International Journal of Mineral Processing 139, 43-50.

Koukouzas, N., Vasilatos, C., Itskos, G., Mitsis, I., Moutsatsou, A., 2010. Removal of heavy metals from wastewater using CFB-coal fly ash zeolitic materials", in the Journal of Hazardous Materials 173(1-3), 581-588.

Querol, X., Umana, J.C, Plana, F., Alastuey, A., Lopez-Soler, A., Medinaceli, A., Valero, A., Domingo, M., Garcia-Rojo, E., 2001.Synthesis of Na zeolites from fly ash in a pilot plant scale.Examples of potential environmental applications. Fuel 80(6), 857-865.

Stamatakis, M., Stamataki, I., Giannatou, S., Vasilatos, C., Drakou, F., Mitsis, I., Xinou, K., 2016. Characterization and evaluation of chabazite- and mordenite-rich tuffs, and their mixtures as soil amendments and slow release fertilizers. Archives of Agronomy and Soil Science, 63(6), 735-747.

15th International Congress of the Geological Society of Greece
Athens, 22-24 May, 2019 | Harokopio University of Athens, Greece
Bulletin of the Geological Society of Greece, Sp. Pub. 7 Ext. Abs. GSG2019-092

Actinides and Rare Earth Elements (REE) in Sedimentary Formations of Greece: A Review

I.T. Tzifas[1], P.N. Gamaletsos[2], A. Papadopoulos[3], A. Godelitsas[4], N. Kantiranis[3], P. Misaelides.[5], A. Filippidis[3]

(1) Institute of Earth Sciences, Heidelberg University, Im Neunheimer Feld 234, 69120 Heidelberg, Germany
ioannis.tzifas@geow.uni-heidelberg.de
(2) Department of Materials Engineering, KU Leuven, Kasteelpark Arenberg 44, 3001 Leuven, Belgium
(3) Department of Geology, Aristotle University of Thessaloniki, 54124 Thessaloniki, Greece
(4) Department of Geology & Geoenvironment, National & Kapodistrian University of Athens, Zografou 15784 Athens, Greece
(5) Department of Chemistry, Aristotle University of Thessaloniki, 54124 Thessaloniki, Greece

The rare earth elements (REEs) have been characterized by European Union (EU) as critical raw materials with a significant risk of supply due to their wide utilization in many new technological applications. The growing demand for REE has spiked the research initiatives on new potential REE resources in Europe and is also linked to the increasing exploitation efforts from various geological settings. Regarding on that fact, Greece could play an important role in REE market by targeting the potential evaluation of sedimentary formations such as bauxites, phosphorites, placers and laterites. The present study is providing a review based on the distribution and quantification of the REEs in various sedimentary formations of Greece and, specifically, in the black costal sands near Kavala granitoids, the bauxite deposit of Parnassos-Ghiona, the phosphate rocks of Epirus and, finally, the lateritic ores of Evia and Larymna. The uranium (U) and thorium (Th) content of these formations was also extensively investigated because of its close geochemical association with the REEs. In order to contribute to better understanding of the nature of REE and the above-mentioned actinides from micro- to nano-meter scale a number of analytical techniques were applied. In particular, electron microscopic techniques (SEM-EDS, EPMA, TEM/HRTEM) were combined with synchrotron radiation (SR)- methods (μ-XRF and μ-XANES) as well as with single-crystal XRD and ICP-MS/ LA-ICP-MS.

The allanite-bearing black coastal sands close to Kavala granitoids (N. Greece) have gained the attention displaying a total REE (ΣREE+Y) content ranging from 4010 to 10810 ppm, while Th was also enhanced (236-1205 ppm). The chemistry of the sand mineral components showed that the main Th- and REE- hosting phases were allanite and titanite and, to a lesser extent, monazite, zircon and apatite (Tzifas 2017 doctoral dissertation, Papadopoulos *et al*., 2016). In addition, chemical analyses of the magnetic and non-magnetic fractions of the sands exhibited higher Light REE (LREE: La-Gd) concentration in the latter (1908 ppm and 12470 ppm respectively) due to the relatively higher presence of the afore-mentioned REE-bearing minerals. Tzifas *et al*. (2017) also studied coastal sands of the volcanic island of Nisyros and found relative enrichment in High Field Strength Elements / HFSE (Nb, Ta) compared to actinides (namely U and Th) and REEs. The same authors interpreted this as combination of background geology (provenance) and mineralogical composition of the sands controlling the particular endowment in critical metals. Papadopoulos (2018) extensively studied the REE and actinide content in various coastal areas near granitoids revealing that in Mykonos and Naxos Islands the REE content was also enhanced (ΣREE: 64-9620 ppm and 74-4700 ppm respectively) and comparable with those of the ones of Kavala.

Greek bauxites from the Parnassos-Ghiona active mines studied by Gamaletsos *et al*. (2019) demonstrated an increased content in LREE (varying from 106 to 913 ppm) compared to the relatively lower content of the HREE (ΣHREE- from Tb to Lu including Y- varying between 45 and 179 ppm; ΣHREE = 95 ppm). The overall REE concentration (ΣREE + Y+Sc) varied from 192 to 1109 ppm. However, it should be pointed out that significant variations were observed between the Fe-depleted (avg. 268 ppm) and the Fe-rich bauxites (avg. 569 ppm). This differentiation of the REE concentration in Fe-rich bauxites can be attributed to the higher participation of (diagenetic and/or epigenetic) REE minerals, mainly LREE-fluorocarbonates as indicated by the SEM-EDS investigation. It is worthy to be mentioned that the REE-content of the Greek bauxite metallurgical residues / BR (also known as "red mud") seems to be remarkably increased by almost two times compared to that of the Parnassos-Ghiona bauxite parent material. The data presented by Gamaletsos *et al*. (2019) showed similar REE values compared to karst-type bauxites of the globe. The actinide content, and particularly of Th, is also relatively increased in the bauxites. The Fe-depleted samples contained up to 63 ppm Th whereas the corresponding content of the Fe-rich samples is lower (Gamaletsos *et al*., 2011; Gamaletsos *et al.*, 2016).

Organic-rich phosphatized limestones from Epirus region were found to present enhanced phosphorous content (27 wt.%) and natural uranium enrichment (647 ppm). Their relatively high ΣREE + Y content (56-280 ppm) can be linked, on the basis of the mineralogical and geochemical investigations, with the presence of carbonate-apatites and/or organic matter (Tzifas *et al.*, 2014). The REEs average concentration values were compared to those of phosphate deposits of other countries (i.e., Israel, Egypt, Tunisia) demonstrating that, regardless of the observed similar trends, the Epirus samples were not especially enriched.

Nickeliferous laterite ores from two typical central Greece deposits of Larymna and Evia (Samouhos *et al*., 2019), exhibited ΣREE = 774 ppm and 76 ppm respectively, while their clay fraction demonstrated significant enrichment in contrast to the initial ore (ΣREE = 1014 and 40 ppm, respectively). The scandium (Sc) concentrations found to present similar values in both mining areas (64 and 42 ppm, respectively). The mineralogical investigation of laterites indicated

that both materials contain crystalline hematite- and chlorite group phyllosilicates, whereas the Evia sample additionally illite. Transmission electron microscopy investigations revealed that laterite ores consisted of complex nanoscale aggregates of the above-mentioned phases.

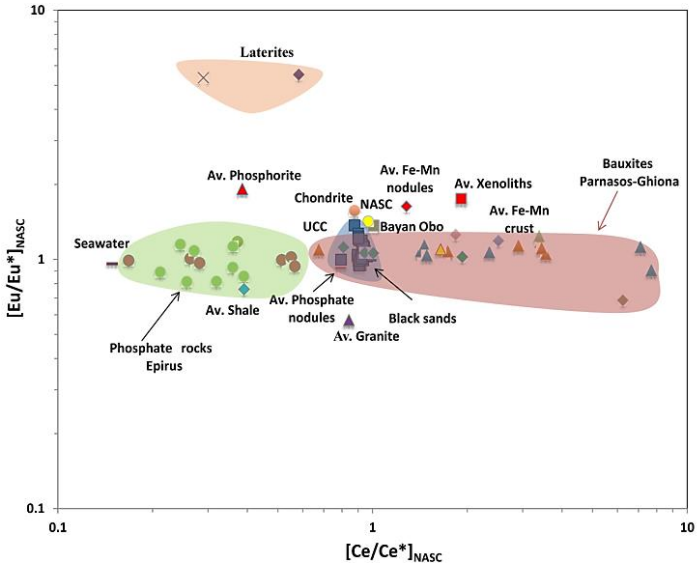

Figure 1. REE discrimination diagrams for bauxites, laterites, phosphates, black sands compared to various geological materials of the globe.

To the extent that Eu/Eu* - Ce/Ce* bivariate diagrams for sedimentary geomaterials provide information about their origin as Leybourne & Johannesson (2008) suggested, similar diagrams were constructed for the same reason in the case of bauxites, laterites, phosphorites and Kavala black sands. The average values of various geomaterials of the globe were also used for comparison (Fig. 1). The black sands showed that the samples are not located close to the field of the average granite as they were influenced from various geological processes. In the case of the bauxites, it is revealed that the Ce/Ce* ratios significantly varies. This fact might be attributed to the $Ce^{3+} \leftrightarrow Ce^{4+}$ and the LREE re-mobilization during the supergene/epigenetic processes. The lateritic samples exhibited high Eu/Eu* ratios as a matter of the fact that they do not exclusively originate in ultrabasic -ophiolitic- rocks as previously considered, while the organic-rich phosphatized limestones are not typical phosphorites, covering a rather large range as a result of the impact of surface waters.

References

Gamaletsos, P. N., Godelitsas, A., Filippidis, A., Pontikes, Y., 2019. The Rare Earth Elements Potential of Greek Bauxite Active Mines in the Light of a Sustainable REE Demand. Journal of Sustainable Metallurgy, 5, 20-47.

Gamaletsos, P., Godelitsas, A., Mertzimekis, T.J., Göttlicher, J., Steininger, R., Xanthos, S., Berndt, J., Klemme, S., Kuzmin, A. and Bárdossy, G., 2011. Thorium partitioning in Greek industrial bauxite investigated by synchrotron radiation and laser-ablation techniques. Nuclear Instruments and Methods in Physics Research Section B: Beam Interactions with Materials and Atoms 269(24), 3067-3073.

Gamaletsos, P.N., Godelitsas, A., Kasama, T., Kuzmin, A., Lagos, M., Mertzimekis, T.J., Göttlicher, J., Steininger, R., Xanthos, S., Pontikes, Y. and Angelopoulos, G.N., 2016. The role of nano- perovskite in the negligible thorium release in seawater from Greek bauxite residue (red mud). Scientific Reports, 6, p.21737.

Leybourne, M.I., & Johannesson, K.H., 2008. Rare earth elements (REE) and yttrium in stream waters, stream sediments, and Fe–Mn oxyhydroxides: fractionation, speciation, and controls over REE+ Y patterns in the surface environment. Geochimica et Cosmochimica Acta, 72(24), 5962-5983.

Papadopoulos, A., 2018. Geochemistry and REE content of beach sands along the Atticocycladic coastal zone, Greece. Geosciences Journal, 1-19.

Papadopoulos, A., Koroneos, A., Christofides, G., Papadopoulou, L., 2016. Geochemistry of beach sands from Kavala, Northern Greece. Italian Journal of Geosciences, 135(3), 526-539.

Samouhos, M., Godelitsas, A., Nomikou, Chr., Taxiarchou, M., Tsakiridis, P., Zavašnik, J., Gamaletsos, P.N., Apostolikas, Th., 2018. New insights into nanomineralogy and geochemistry of Ni-laterite ores from Central Greece (Larymna and Evia deposits). Chemie der Erde – Geochemistry, 2019 – In press.

Tzifas I.T, 2017. Study and distribution of actinides in REE-bearing geological materials from Greece, Ph.D. Thesis, Aristotle University of Thessaloniki, Department of Chemistry, Thessaloniki 347 p.

Tzifas, I.T., Godelitsas, A., Magganas, A., Androulakaki, E., Eleftheriou, G., Mertzimekis, T.J., Perraki, M., 2014. Uranium-bearing phosphatized limestones of NW Greece. Journal of Geochemical Exploration, 143, 62-73.

Tzifas, I.T, Misaelides, P., Godelitsas, A., Gamaletsos, P.N., Nomikou, Chr., Karydas, A.G., Kantarelou, V., Papadopoulos, A., 2017. Geochemistry of coastal sands of Eastern Mediterranean: The case of Nisyros volcanic materials. Chemie der Erde-Geochemistry 77(3), 487-501.

15th International Congress of the Geological Society of Greece
Athens, 22-24 May, 2019 | Harokopio University of Athens, Greece
Bulletin of the Geological Society of Greece, Sp. Pub. 7 Ext. Abs. GSG2019-115

Origin of the geogenic gases and preliminary estimation of the carbon release of Greece

K. Daskalopoulou[1,2], S. Calabrese[1,3], A.L. Gagliano[3], L. Li Vigni[3], W. D'Alessandro[3]

(1) University of Palermo, via Archirafi 36, Palermo, Italy, kikdaskalopoulou@gmail.com
(2) National and Kapodistrian University of Athens, University Campus, Zografou, Athens, Greece
(3) Istituto Nazionale di Geofisica e Vulcanologia, via Ugo La Malfa 153, Palermo, Italy

Volatiles are transported from the deep crust or mantle to the surface in geodynamically active areas where seismic, volcanic and geothermal activity is present; the circulation of hydrothermal fluids in the crust is enhanced. In such areas, faults may act as preferential pathways for advective gas-carrying fluid transport. Towards the surface, pressure decrease allows the gases to escape from the fluids into soil gas and eventually into the atmosphere (King, 1986). The migration of carbon-bearing crustal and mantle fluids contributes to Earth's carbon cycle (Berner & Kothavala 2001). However, till now, the mechanisms, magnitudes and time variations of carbon transfer from depth to the surface remain the least understood parts of the global carbon budget. Carbon dioxide and methane are the main contributors of the total amount of C-degassing from geological (volcanic and non-volcanic) sources. From the beginning of the last century, high attention has been paid to the reservoirs of CO_2 and CH_4 in the atmosphere because they represent the most dangerous species in terms of global warning. The increased amount of carbon dioxide and methane in the atmosphere has important implications for the energy balance and the chemical composition of the atmosphere. Mörner and Etiope (2002) calculated that 10^2-10^3 Mt of CO_2 are presumably involved in the carbon cycle every year. This estimation though, is affected by high uncertainty as a number of sources and C-degassing environments that account for this high leakage were not taken into consideration.

Greece belongs to the most geodynamically active regions of the world and as such, it has to be considered an area of intense geogenic degassing. Regarding carbon, the territory is characterized by the high hydrothermal and volcanic activity of the South Aegean Active Volcanic Arc (SAAVA), and by widespread geological seeps of buried carbon dioxide and methane. In the present work, we present more than 700 literature data of free gases spread along the whole Hellenic territory to get insight on geographic distribution and composition of the released fluids. Moreover, we review all the published studies on CO_2 and/or CH_4 output of high degassing areas of Greece that are mainly concentrated along the SAAVA in a first attempt to estimate the total geologic output of the nation.

Helium isotope data propose that the highest mantle contribution (50 to 90%) is found along the SAAVA, whereas the lowest in continental Greece (0-20%), with the atmospheric contribution being mostly negligible. Based on the geographical distribution of the gases, it is evident that the R/R_A ratios and CO_2 concentrations increase in areas characterized by: i) thin crust; ii) elevated heat flow values; iii) recent (Pleistocene-Quaternary) volcanic activity; and iv) deep routed extensional or transtensional regional faults. The highest values are therefore found along the SAAVA and the lowest in the western part of Greece where CH_4 emission is prevailing. Furthermore, it was noticed that the majority of the samples present a prevailing limestone C component, whilst only few samples have a prevailing mantle C component (Sano and Marty, 1995). It seems barely possible though to distinguish CO_2 deriving from crustal and slab-related limestones. Additionally, due to the complex geodynamic history, the mantle C isotope composition could be affected by subduction-related metasomatism and, similarly to the nearby Italian area (Martelli et al., 2008), the C isotope composition could be more positive. In this case, the mantle contribution is probably underestimated.

In terms of geogenic carbon degassing, the best studied and most exhaling area is the SAAVA, which releases 104,090 t/a of CO_2 and 20.26 t/a of CH_4. Continental Greece on the contrary, is much less studied but may release CO_2 in the same order of magnitude in its eastern-central and northern part. The western and south-western parts of Greece are conversely the main area of methane and higher hydrocarbon degassing. Methane output of Greece is much less constrained but the presence on its territory of one of the biggest thermogenic gas seepages of Europe releasing about 200 t/a of CH_4 to the atmosphere underscores its potentially high contribution.

Approximately 114,310 t/a of CO_2 and 221 t/a of CH_4 are released from the whole Hellenic territory (Daskalopoulou et al., submitted). This estimation though, should be considered minimum as there are processes and sources that have not been taken into consideration yet. More specifically, in the submarine manifestations found at greater depths, gases cannot reach the sea surface due to the dissolution process that takes place along the water column; this is especially true for CO_2 that is more soluble in water respect to other gases (eg. Milos - Dando et al., 1995; Kolumbo - Rizzo et al., 2016 etc). Moreover, the geological and geodynamic regime can contribute in the formation of CO_2 reservoirs. This is the case of Florina Basin (Pearce et al., 2004) where more than one CO_2 reservoirs were created, with one of them being exploited by the company Air Liquide Greece. It is worth noting that this reservoir, found at a depth of approximately 300 m, produces 30,000 t/a of CO_2 (Pearce et al., 2004). Moreover, in the same area, water is also used for water supply and irrigation purposes. This water though contains a great amount of dissolved CO_2 great part of which is released to the atmosphere when the water is pumped to the surface. Another source that should be underscored is the quantification of geogenic CO_2 dissolved in big karstic aquifers. Chiodini et al. (1999, 2000) demonstrated that the relatively high solubility of CO_2 in water plays an important role in the quantification of carbon. This approach was proved for central Italy and it might be the case for continental Greece due to the similar geodynamic history. Finally, in ophiolitic sequences where serpentinization takes place, if and when the conditions are adequate (i.e. presence of effective catalysts – Etiope and

Ionescu, 2015) an abiogenic origin for CH_4 seems to be favored even at low temperatures. Ophiolitic sequences crop out widely in Greece along two N-S trending belts, whilst more hyperalkaline springs or dry seeps may be present. However, their flux in generally is very low and therefore their contribution to the total natural CH_4 output has probably to be considered negligible.

References

Berner, R.A., Kothavala, Z., 2001. GEOCARB III: a revised model of atmospheric CO2 over Phanerozoic time. American Journal of Science, 301, 182-204.

Chiodini, G., Fondini, F., Kerrick, D.M. Rogie, J., Parello, F., Peruzzi, L. & Zanzari, A.R., 1999. Quantification of deep CO2 fluxes from central Italy: Examples of carbon balance for regional aquifers and soil degassing, Chemical Geology, 159, 205-222.

Chiodini, G., Frontini, F., Cardellini, C., Parello, F. & Peruzzi, L., 2000. Rate of diffuse carbon dioxide Earth degassing estimated from carbon balance of regional aquifers: The case of central Apennine, Italy. Journal of Geophysical Research, 105(B4), 8423-8434.

Dando, P.R., Hughes, J.A., Leahy, Y., Niven, S.J., Taylor, L.J. & Smith, C., 1995. Gas venting rates from submarine hydrothermal areas around the island of Milos, Hellenic Volcanic Arc. Continental Shelf Research, 15, 913–929.

Daskalopoulou, K., Calabrese, S., Gagliano, A.L., D'Alessandro, W., Submitted. Estimation of the geogenic carbon degassing of Greece. Applied Geochemistry.

Etiope, G., Ionescu, A., 2015. Low-temperature catalytic CO2 hydrogenation with geological quantities of ruthenium: a possible abiotic CH4 source in chromite-rich serpentinized rocks. Geofluids 15, 438-452.

King, C.Y. (1986). Gas Geochemistry Applied to Earthquake Prediction: An Overview. Journal of Geophysical Research, 91, 12,269-12,281.

Martelli, M., Nuccio, P.M., Stuart, F.M., Di Liberto, V., Ellam, R.M., 2008. Constraints on mantle source and interactions from He-Sr isotope variation in Italian Plio-Quaternary volcanism. G3, Volume 9, 2.

Mörner, N.A., Etiope, G., 2002. Carbon degassing from the lithosphere, Global. Planet. Change, 33, 185–203.

Pearce, J.M., Czernichowski-Lauriol, I., Lombardi, S., Brune, S., Nador, A., Baker, J. et al., 2004. A review of natural CO2 accumulations in Europe as analogues for geological sequestration. Geology Society of London Special Pubblication, 233, 29–41

Rizzo, A.L., Caracausi, A., Chavagnac, V., Nomikou, P., Polymenakou, P.N., Mandralakis, M., Kotoulas, G., Magoulas, A., Castillo, A., Lampridou, D., 2016. Kolumbo submarine volcano (Greece): An active window into the Aegean subduction system. Scientific Reports 6:28013. doi: 10.1038/srep28013

15th International Congress of the Geological Society of Greece
Athens, 22-24 May, 2019 | Harokopio University of Athens, Greece
Bulletin of the Geological Society of Greece, Sp. Pub. 7 Ext. Abs. GSG2019-117

Gas hazard related to CO_2 degassing at Loutra Ypatis, Greece

W. D'Alessandro[1], K. Daskalopoulou[2,3], S. Calabrese[1,2], L. Li Vigni[1], H. Pfanz[4]

(1) Istituto Nazionale di Geofisica e Vulcanologia, via Ugo La Malfa 153, Palermo, Italy, walter.dalessandro@ingv.it
(2) University of Palermo, via Archirafi 36, Palermo, Italy
(3) National and Kapodistrian University of Athens, Panepistimioupolis, Ano Ilissia, 15784, Athens, Greece
(4) University of Duisburg-Essen, Campus Essen, 45117 Essen, Germany

Introduction

Earthquakes and volcanic eruptions represent a hazard. However, the impact of gases released in geodynamically active areas should not be underestimated. It is commonly known that geogenic sources release great amounts of gases, which, apart from having an important influence on the global climate, can also have a strong impact on human health causing both acute and chronic effects. In particular, CO_2 and sulphur gases (mainly H_2S and SO_2) are the main compounds responsible for acute mortality due to their asphyxiating and/or toxic properties. One of the most known and also worst episodes occurred, took place on the 21th of August 1986 at Lake Nyos, Cameroon, when about 1700 people were killed and 850 injured by a massive CO_2 release (D'Alessandro, 2006).

Like other geodynamically active areas, Greece is also affected by a large number of geogenic gas manifestations (Daskalopoulou *et al*., 2018a). These occur either in the form of point sources (fumaroles, mofettes, bubbling gases) or of diffuse soil gas emanations (Daskalopoulou *et al*., 2018b). D'Alessandro and Kyriakopoulos (2013) made a preliminary estimation of the risk related to geogenic gases in Greece for the time period of 1992-2011; the whole population of the country was considered. In that period, at least two fatal episodes with a total of three victims took place, likely caused to the exposure to geogenic gases (specifically CO_2). This would give a risk of 1.3×10^{-8} fatality from geogenic gas manifestations per annum. This value, although probably underestimated, is much lower than many other natural or anthropogenic risks. Since deaths due to natural gases are often wrongly attributed, it cannot be excluded that some fatal episode has not been recognized and thus that the risk is somewhat higher than assessed. Although very low, this risk should not be neglected, not only because it is possibly underestimated, but also because simple countermeasures could be adopted for risk reduction. Dangerous areas could be easily identified and delimited by geochemical prospecting and their hazards properly highlighted.

Apart from the sites where fatal episodes occurred, many other hazardous sites have been recognized in Greece. Here we present data collected at Loutra Ypatis (central Greece).

Study area

Sperchios Basin – Evoikos Gulf Graben is a 130 km long actively spreading graben in Central Greece (1 cm/a). The high geothermal gradient of the area is evident by the presence of many thermal springs with temperatures that vary from 24 to 82 °C. In the waters of these springs, discharging along the normal faults bordering the graben, an abundant gas phase is bubbling. Loutra Ypatis is one of the emerging springs and its waters (31 °C) are exploited by a spa. The water is currently drained by a gallery and therefore the water level is about 5 m below ground at the bottom of a funnel-like hole (Fig. 1 left). For safety reasons the hole was covered by a closed building (Fig. 1 left and center). The gas, which is vigorously bubbling in the spring, is mostly (> 96%) composed of CO_2 (D'Alessandro *et al*., 2014). The walls of the hole are covered of sulfur that derives from the partial oxidation of the H_2S (2500 ppm) contained in the released gas (D'Alessandro *et al*., 2014).



Figure 1. The thermal spring inside the building (left); Measurements of the atmospheric concentrations of CO_2 outside the building in October 2015 (center); A dead bird close to a small opening of the building (right).

Methods

In October 2015 atmospheric concentrations of CO_2 were measured with a Licor LI820 NDIR spectrometer (range 0 to 20,000 ppm, accuracy of 2%), whilst in April 2016, the atmospheric concentrations of CO_2 and H_2S were measured with a Multi-GAS analyser manufactured by INGV-Palermo equipped with Licor LI-840 NDIR spectrometer (CO_2 0-20,000 ppm) and an EZ3H electrochemical sensor by City Technology Ltd. (H_2S 0–100 ppm). Simultaneous CO_2, CH_4 (both 0-100%), CO, H_2S (both 0-500 ppm) and O_2 (0 – 25%) concentrations within the building were measured with a portable gas analyser GA2000 (Geotechnical Instruments).

Results and discussion

Due to the fact that a building covers the thermal spring, the intense bubbling activity of its waters creates a strong gas accumulation inside. The main component of the released gases is CO_2, which has a higher density with respect to atmospheric air, thus creating the conditions for gas accumulation. About 2 m above the water level, CO_2 concentrations of >95% and non-detectable O_2 concentrations were measured. At higher levels above the water, CO_2 concentrations were decreased but never below 50%. Such concentrations within the building are lethal for both animals and human beings. Of course, access is forbidden, but as the building is not perfectly sealed, the gases permeate to the outside through fissures and cracks. Figure 2 shows the CO_2 concentrations measured in the air on October 2015 at 1.5 m height while walking around the walls of the edifice at about 2 m distance. Leaking of CO_2 from the edifice is made evident by concentrations reaching values of more than 6000 ppm. The highest values were measured close to the entrance of the edifice were fissures and cracks are concentrated. Due to the tendency of CO_2 to accumulate at lower levels, in this place, close to the ground, CO_2 levels lethal to small animal can be reached. This was made evident by a dead bird found in that occasion (Fig. 1).

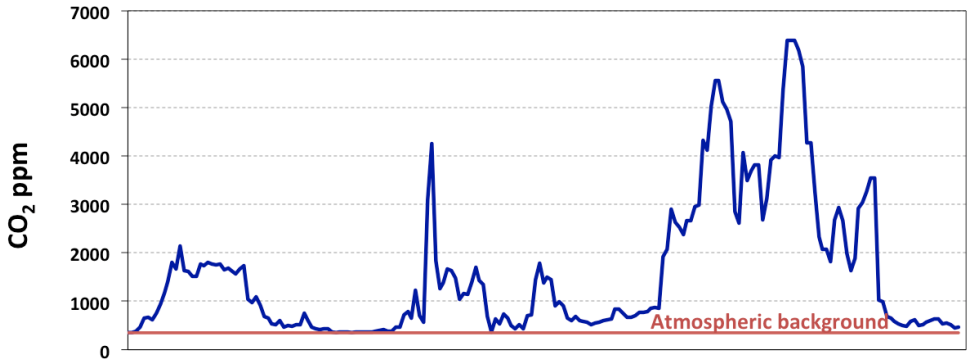

Figure 2. Atmospheric CO_2 concentrations at 1.5m height around the building of Fig. 1 in October 2015

In April 2016, due to the much windier conditions, CO_2 concentrations at the same places reached values never exceeding 1000 ppm while H_2S was always below 1 ppm. These values sharply increased getting closer to the fissures around the main entrance of the building and reached saturation of the sensors (CO_2 > 20,000 ppm and H_2S > 100 ppm) at a distance of few centimeters.

The intense CO_2 degassing observed at Loutra Ypatis may be responsible for elevated levels that can have an impact on human beings. It is worth noting that values measured in the atmosphere close to the building exceed the Occupational Recommended Exposure Limit of 5000 ppm (NIOSH, 2005). In closed spaces lethal levels can be easily reached. An older inhabitant of the close by village told us that in his childhood a playmate died by going inside the gallery that drains the thermal water out of the spa due to the high CO_2 levels. Such episode underscores the need not to disregard the gas hazard created by intense natural gas manifestations like the thermal spring of Loutra Ypatis.

References

D'Alessandro, W., 2006. Gas hazard: an often neglected natural risk in volcanic areas, in: Martin-Duque, J.F., Brebbia, C.A., Emmanouloudis, D.E., Mander, U. (Eds.), Geo-Environment & Landscape Evolution II. WIT Press Southampton, Ashurst Lodge, Ashurst, Southampton, pp. 369-378.

D'Alessandro, W., Kyriakopoulos, K., 2013. Preliminary gas hazard evaluation in Greece. Natural Hazard 69, 1987-2004.

D'Alessandro, W., Brusca, L., Kyriakopoulos, K., Bellomo, S., Calabrese, S., 2014. A geochemical traverse along the "Sperchios Basin — Evoikos Gulf" Graben (Central Greece): origin and evolution of the emitted fluids. Marine and Petroleum Geology 55, 295-308

Daskalopoulou, K., Calabrese, S., Grassa, F., Kyriakopoulos, K., Parello, F., Tassi, F., D'Alessandro, W., 2018a. Origin of methane and light hydrocarbons in natural fluid emissions: a key study from Greece. Chemical Geology 479, 286-301.

Daskalopoulou, K., Gagliano, A.L., Calabrese, S., Longo, M., Hantzis, K., Kyriakopoulos, K., D'Alessandro, W., 2018b. Gas geochemistry and CO_2 output estimation of the Island of Milos, Greece. Journal of Volcanology and Geothermal Research 365, 13-22

NIOSH (2005) National Institute for Occupational Safety and Health pocket guide to chemical hazards. DHHS (NIOSH) publication No. 2005-149

15th International Congress of the Geological Society of Greece
Athens, 22-24 May, 2019 | Harokopio University of Athens, Greece
Bulletin of the Geological Society of Greece, Sp. Pub. 7 Ext. Abs. GSG2019-120

Mineralogical, Petrological and Geochemical Study of the Agios Ioannis Lavas, at Kamena Vourla Area, Greece

Ch. Kanellopoulos[1,2], G. Vougioukalakis[3], C. Mavrogonatos[4], I. Megremi[4], I. Iliopoulos[1]

(1) Department of Geology, University of Patras, 26500, Rio-Patra, Greece, e-mail: ckanellopoulos@gmail.com morel@upatras.gr
(2) Ministry of Environment and Energy, 119 Mesogeion Avenue, 11526, Athens, Greece.
(3) Hellenic Survey of Geology and Mineral Exploration (H.S.G.M.E.), 1st Spirou Louis St., Olympic Village, 13677, Acharnae, Greece, e-mail: gvoug@igme.gr
(4) Department of Geology and Geoenvironment, National and Kapodistrian University of Athens, Panepistimiopolis, Ano Ilissia, 15784 Athens, Greece, e-mails: kmavrogon@geol.uoa.gr megremi@geol.uoa.gr

The volcanic center of Lichades is located in the Northern Euboean Gulf and consists of a complex of volcanic islands and lava outcrops named Agios Ioannis and Vromolimni at the Kamena Vourla area, in mainland (Georgalas, 1938). Different theories have been proposed about Lichades volcanic center geological setting. Innocenti et al. (2010) based on Sr–Nd–Pb isotopic data, related this volcanic center with the large volcanic belt that developed north of the Pelagonian–Attic–Cycladic–Menderes massifs, encompassing a 35 Ma timespan which is widespread over a large area from NW Greece–Macedonia to the Aegean–western Anatolia. According to the above authors, the Euboea-Kamena Vourla volcanic products are orogenic in character and partially contemporaneous with the south Aegean active volcanic arc, but with different geochemical features, related to distinct magma sources. The volcanic center of Lichades are located along the major tectonic structures in the area (Kranis, 1999). Karastathis et al. (2011) showed that there is a magma chamber under the North Euboean Gulf area using low seismic P-wave velocity values and high Poisson ratios at depths below 8 km, also coincident with a Curie surface estimated at 7-8 km depth. Kanellopoulos et al. (2017a, 2017b) suggested that the volcanic center of Lichades and the associated magmatic chamber is the heating source and contributes with a portion of deep magmatic fluid to the geothermal fluid of Euboea-Sperchios system, alongside with seawater and only limited meteoric water contribution.



Figure 1. Agios Ioannis lava outcrop at Kamena Vourla area.

Detailed petrographic analysis of volcanic rock samples collected from Agios Ioannis was conducted in thin sections, using polarized optical microscope (OM). Mineral composition has been determined by Scanning Electron Microscopy-Energy Dispersive Spectroscopy (SEM-EDS) and powder X-ray powder diffraction (XRPD). The volcanic rocks are characterized by vitrophyric texture. Their matrix is dominated by glass, numerous, randomly oriented microlites of plagioclase and minor sanidine, clinopyroxene and amphibole (Fig, 2a, b). Phenocrysts are commonly plagioclase, olivine, quartz, clinopyroxene and amphibole. Plagioclase occur as large euhedral to subhedral grains, displaying patchy or concentric zonation. At places, plagioclase phenocrysts are rimmed by a thin rind of K-rich feldspar (sanidine, Fig. 2c), which can rarely be found as phenocryst as well. Olivine is usually found as large, euhedral to subhedral grains or they can form glomerophyric aggregates along with clinopyroxene crystals. Sometimes, zoning and the existence of embayments in the crystals may indicate reactions with the host melt, as the crystallization was evolving through time. Amphiboles, mostly hornblende, is usually forming euhedral grains with characteristic zoning. Locally, replacement by opaque phases suggest minor opacitization processes. Resorbed quartz phenocrysts are uncommon, but they are always rimmed by clinopyroxene crystals. Vesicles are abundant and, in some cases, amygdules filled with euhedral clinopyroxene may occur. Clinopyroxene is also present as euhedral phenocrysts or even as glomerophyric aggregates. Sphene may occur as a rare accessory mineral. Finally, opaque phases, commonly spinel, magnetite and rutile are quite abundant, scattered in the vitreous matrix.

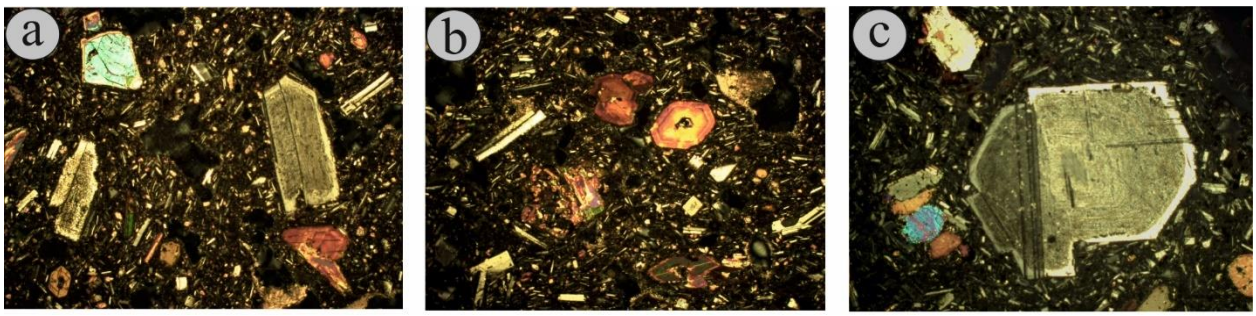

Figure 2. Photomicrographs of the studied volcanic rocks, taken under crossed nicols (a and b) Their matrix is dominated by glass, numerous, randomly oriented microlites of plagioclase and minor sanidine , clinopyroxene, amphibole grains and (c) Plagioclase appears as phenocrysts and commonly are rimmed by a thin rind of K-rich feldspar (sanidine).

A study of the bulk geochemical composition of selected samples was conducted by X-ray Fluorescence (XRF) and Inductively Coupled Plasma-Mass Spectroscopy (ICP-MS). Major elements in the studied samples show a limited range of variation such as SiO_2 (57.3-58.8 wt%), TiO_2 (0.7 wt%) and Al_2O_3 (17– 17.5 wt%), MgO (3.1–3.4 wt%) and CaO (5.8–6.1 wt%). The volcanic rocks from Agios Ioannis plot in the fields of trachyandesites on the total alkali-silica (TAS) diagram. In the K_2O vs SiO_2 classification diagram, the studied samples plot in the field of high-K calc-alkaline series. Their trace-element patterns show relatively high Th and Ta contents, pronounced negative P anomaly and significant negative Rb, K, Ti and Y anomalies.

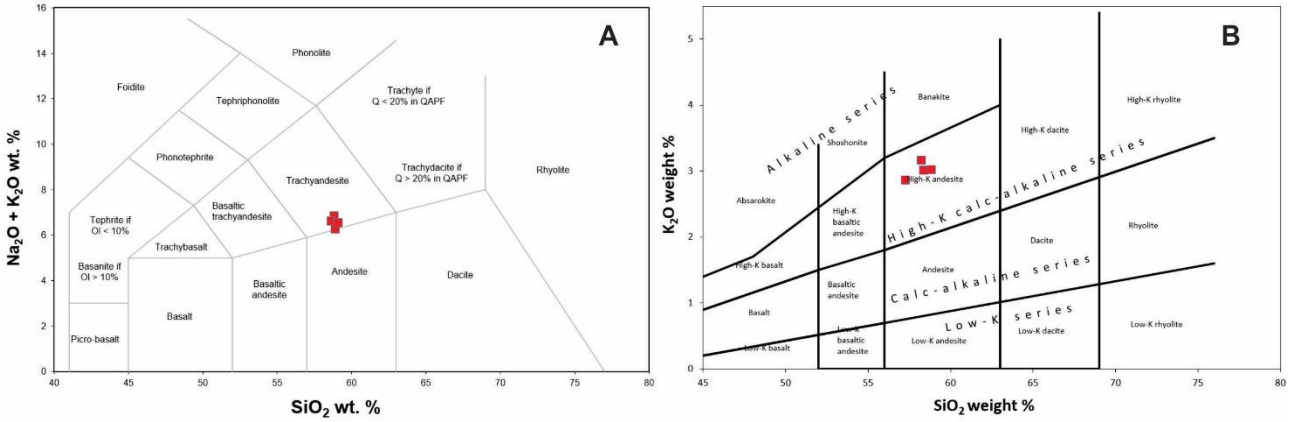

Figure 3. Classification diagrams (A) Total alkalis–silica (TAS) and (B) K_2O vs SiO_2.

The petrographic characterization and the geochemical signature of the Aghios Ioannis volcanics let us draw some preliminary conclusions of their petrological affinities, helping us to make some first inferences about their geotectonic evolution and their emplacement regime. The studied features are similar to geochemical characteristics of subduction-related rocks, with high normalized abundances of LIL elements and troughs in the normalized trace element plots at Nb, Sr, P and Ti. The small size of the volcanic centre of the studied area and the strong enrichment in incompatible elements suggest that the magmas resulted from small degrees of partial melting of an enriched subcontinental lithospheric mantle.

References

Georgalas, G.C., 1938. Le volcan des îles Likhades et de Hagios Ioannis (Kammena Vourla). Praktika Academia Athinion, 13, 86–98.

Innocenti, F., Agostini, S., Doglioni, C., Manetti, P., Tonarini, S., 2010. Geodynamic evolution of the Aegean: constraints from the Plio-Pleistocene volcanism of the Volos–Evia area. J. Geol. Soc., London, 167, 475–489.

Kanellopoulos C., Stouraiti C., Xenakis M., Vakalopoulos P., Vougioukalakis G., 2017b. The geothermal system of northwestern Euboea Island and eastern Sperchios areas, Greece: Geological characteristics and suggested direct use applications. 11th International Hydrogeological Congress of Greece, vol. 2, 263-273.

Kanellopoulos, C., Mitropoulos, P., Valsami-Jones, E., Voudouris, P., 2017a. A new terrestrial active mineralizing hydrothermal system associated with ore-bearing travertines in Greece (northern Euboea Island and Sperchios area). Journal of Geochemical Exploration 179, 9-24, DOI: 10.1016/j.gexplo.2017.05.003.

Karastathis, V.K., Papoulia, J., Di Fiore, B., Makris, J., Tsambas, A., Stampolidis, A., Papadopoulos, G.A., 2011. Deep structure investigations of the geothermal field of the North Euboean Gulf, Greece, using 3-D local earthquake tomography and Curie Point Depth analysis. Journal of Volcanology and Geothermal Research, 206, 106–120.

Kranis, H., 2002. Kinematics of active faults in Lokris, central Greece – block rotation within a crustal-scale shear zone? Geologica Carpathica, 53, 157-159.

15th International Congress of the Geological Society of Greece
Athens, 22-24 May, 2019 | Harokopio University of Athens, Greece
Bulletin of the Geological Society of Greece, Sp. Pub. 7 Ext. Abs. GSG2019-124

Determination of amorphous matter in industrial minerals with X-ray diffraction using Rietveld refinement

G. E. Christidis[1], K. Paipoutlidi[1], I. Marantos[2], V. Perdikatsis[1]

(1)Technical University of Crete, School of Mineral Resources Engineering, 73100 Chania, Greece
(2) Institute of Geology and Mineral Exploration (IGME), Spyrou Loui 1, 13677 Acharnes, Greece. christid@mred.tuc.gr

The presence of amorphous matter in industrial minerals and rocks during the quantitative analysis with X-Ray diffraction (XRD) is not always visible and its exact quantification may be difficult. This results to an overestimation of the remaining crystalline phases, because the quantitative analysis is normalized to 100 % for the crystalline phases, thus rendering the analysed sample not representative. Therefore, determination of the amorphous matter is an important task for complete assessment of industrial minerals. In this work we applied Rietveld refinement to determine and quantify the amorphous matter in a series of synthetic samples. The samples were examined on a Bruker D8 Advance Diffractometer equipped with a Lynx Eye strip silicon detector, using Ni-filtered CuKα radiation (35 kV, 35 mA). Data were collected in the range 3–70° 2θ with a step size of 0.02° and counting time 1 s per strip step (total time 63.6 s per step). The XRD traces were analyzed and interpreted with the Diffract Plus software package from Bruker and the Powder Diffraction File (PDF). The quantitative analysis was performed on random powder samples (side loading mounting) emplaced in Al-holders, by the Rietveld method using the BGMN computer code. The code performs quantitative analysis by varying the particle size and preferred orientation parameters.

Two series of experiments were performed. The first series included mixtures of synthetic quartz and calcite at 1:1 ratio containing 5, 10, 20, 25, 30, 40, 50 and 80% amorphous material. The second series included natural calcite and quartz at the same ratio and the same proportion of glass. In both experimental series corundum (α-Al_2O_3) internal standard with particle size <1 μm was added. The main difference between the two series of the experiments was particle size. The synthetic quartz and calcite had comparable particle size as the internal standard, whereas their natural counterparts were considerably coarser, being derived from a quartzite and a coarse grained marble respectively. Consequently they were ground with an agate pestle and mortar. The natural samples were free of impurities, within the accuracy of the XRD method. The aims of the work were to determine the accuracy in the determination of the amorphous matter, to evaluate the influence of particle size in the accuracy of the measurements and to identify the amount of glass at which the presence of the hump at 18-30 °2θ, the criterion to identify amorphous matter, becomes visible.

The accuracy of the quantitative determinations depends on the particle size of the minerals present in the mixtures (quartz and calcite) due to the microabsorption effect, and the difference between the particle size of the internal standard and the minerals. In the experiments with synthetic quartz and calcite without glass, the amounts of the minerals determined by quantitative analysis were comparable to the calculated values of the mixtures assuming particle size <1 μm (error ± 1-2%). In the mixtures with natural quartz and calcite similar error values between the experimental and the calculated abundances were observed for particle size <10 μm. In the synthetic samples good agreement between the calculated and the actual content was observed for assuming preferred orientation for calcite. By in contrast, in the natural samples good agreement between the calculated and the actual contents (error ± -2%) was observed for assuming preferred orientation for both minerals. In all cases increasing particle size led to increase of the calcite content and decrease of the quartz and the corundum (internal standard) contents.

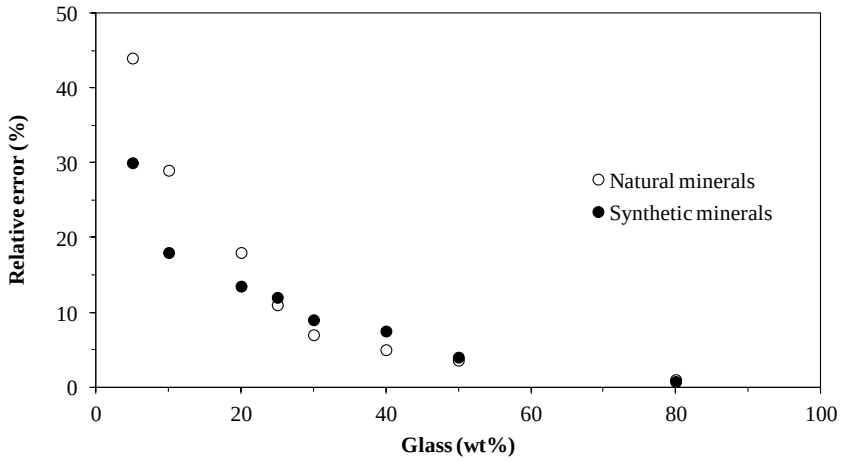

Figure 1. Relative error of determination of amorphous matter in mixtures natural and synthetic minerals.

The mixtures containing glass also showed similar trends in the mixtures of both the synthetic and natural minerals. In the experiments with synthetic quartz and calcite minimum errors were observed in experiments assuming particle size <1 μm, whereas in the experiments with natural quartz and calcite minimum errors were obtained assuming particle size <10 μm. In addition, particle size affects the absolute error of determination of amorphous matter. The relative error in natural samples was higher for amorphous matter contents lower than 20% (Figure 1). As expected, for higher amorphous matter contents the relative error decreased due to decreased uncertainty and it was comparable in the two sets of experiments (Fig. 1).

The XRD traces of the mixtures of both the synthetic and natural minerals showed the existence of a hump in the range 18-30 °2θ characteristic of the amorphous matter in mixtures containing more than 25% glass. For lower glass contents the hump was hot visible. The only indication for the presence of an additional phase undetected by X-rays was the gradual decrease of the intensities of the diffraction maxima of both calcite and quartz, with increasing amorphous matter content. This indicates that the lack of the hump is not a safe criterion for the recognition amorphous matter at low amorphous matter contents and that the presence of amorphous matter should be verified and quantified by the use of an internal standard. Rietveld refinement is a very promising technique in this aspect. Nevertheless, particle size should be carefully controlled for optimum results. It is suggested that particle size for more accurate determinations of amorphous matter should be lower than 10μm, preferably less than 5μm and that sample preparation should be carefully made to avoid preferred orientation of mineral phases.

15th International Congress of the Geological Society of Greece
Athens, 22-24 May, 2019 | Harokopio University of Athens, Greece
Bulletin of the Geological Society of Greece, Sp. Pub. 7 Ext. Abs. GSG2019-126

Knowledge-driven Predictive Mapping of Copper Prospectivity in the part of the Khorasan Razavi Province, NE of Iran

Hooman Dadashzadeh Ahari[1], Omid Ardabili[2]

(1) Geological Survey of Iran, Tehran Province, Tehran, District 9, Meraj Blvd, Tehran, Iran, hooman_ir2001@yahoo.com
(2) Geological Survey of Iran, Tehran Province, Tehran, District 9, Meraj Blvd, Tehran, Iran

Abstract

Integrate various evidential maps that obtained from spatial data set of great scientific significance and has considerable value for mineral prospectivity mapping (MPM). Mineral prospectivity mapping by considering the various aspect of data set layers and information can be used to make mineral exploration less expensive, more efficient, and more accurate, it is important to move beyond traditional concepts and establish a rapid, efficient, and intelligent method of predicting the existence and location of minerals. Over the past years, two contrasting analytical approaches have been used to produced mineral prospectivity mapping. one is a conceptual knowledge-driven approach, and the other is an empirical data-driven approach. The knowledge-driven approach in exploration is carried out by extracting the spatial factors from exploration dataset on the basis of the exploration model, quantification of spatial factors and finally integration of these factors through map combination processes. In this study the integration process includes the weighting and scoring of different layers affecting the copper mineralization at studied area (Khorasan Razavi province SE of central Iran structural-metamorphic zone.) carried out by Index Overlay method as one of the knowledge- driven approaches within GIS environment. According to obtained results, we could achieve an initial guideline for effectively prospecting copper mineralization in the studied area

Introduction

Mineral exploration is a sophisticated process that seeks to discover new mineral deposits in a region of interest. Utilization of geographic information (GIS) provides the capacity to integrate and combine multiple layers such as geological, geochemical, remote sensing and air-borne geophysical surveys and will be consequence to the mineral prospectivity mapping (MPM) that will be make the mineral exploration process more accurate and easier than exploration by conventional methods. The MPM is a multistage procedure for generation of evidential maps consisting of extracted and weighted features representing the existence of the ore deposit-type sought within combining the evidential maps and classification of prospects for further exploration. Numerous modelling methods for producing mineral prospectivity maps using a GIS or other software have been developed over the past 20 years. These methods can be divided into two basic categories: knowledge-driven as a conceptual technique and data driven as an empirical technique respectively. Data-driven mineral prospectivity mapping is appropriate for moderately- to well-sampled mineralized areas. Known deposit-type locations are a dataset of situations with great chance for mineral deposit existence in a mineralized landscape. The conventional data-driven methods are weights of evidence, neural networks, evidential belief functions and logistic regression which used for brown fields with high values of exploratory data. The other technique is called knowledge-driven which is applicable for areas with low value exploration and geological data entitled green fields In ‘green fields’ cases where no known occurrences of the deposit type being modeled or the number of the deposits is too low to make valid statistical calculations, a conceptual (or knowledge-driven) approach can be used. In techniques for conceptual spatial modeling, expert opinions are used to define the thresholds. The knowledge-driven techniques include applications of fuzzy logic, evidential belief function, the Dempster-Shafer model and the decision tree approach. In this study the integration process includes the weighting and scoring of various exploratory layers such as geochemical, geophysical, remote sensing and geological data carried out by Index Overlay method as one of the knowledge- driven approaches within GIS environment. to prepare a MPM affecting the copper mineralization at studied area (Khorasan Razavi province SE of central Iran structural-metamorphic zone) (Fig.1). According to obtained results, we could achieve an initial guideline for effectively prospecting copper mineralization in the studied area.

Index Overlay Method

In this method, the evidence (factors) consists of a set of exploration dataset (maps) and weights are estimated from the measured association between known mineral occurrences and the exploration model for a particular terrain. The hypothesis then repeatedly evaluates all possible location of the maps using the weight and in turn produce a mineral potential map in which the evidences of several map layers are combined by this map combination rule in the index overlay method, each input map (layer of evidence) to be used as evidence is assigned a different score (weight), as well as the maps are receiving different weight depending on the exploration model. An area that is geologically well explored with a relatively well-understood exploration model in hand (the present study area), assignment of weight on different themes or maps ought to be through knowledge driven approach. This not only help in developing a clear understanding of relationship between datasets (both geological, geophysical or geochemical) but this also give flexibility to an exploration geologist to manipulate weight on different elements or evidence maps through geological knowledge about the terrain in different stages of analysis. This is advantageous for developing perhaps a variety of scenarios for different

weight schemes, reflecting differences in opinion amongst experts, and allows the evaluation of sensitivity of the mineral potential maps to such differences. After defining the score by knowledge driven approach for elements or maps, the average score (index weight) is then defined by

$$\bar{S} = \frac{\sum_{i}^{n} Sjjwi}{\sum_{i}^{n} wi}$$

Where S is the weighted score for an area object, Wi is the weight for the i-th input map, and Sij is the score for the j -th class of the i-th map, the value of j depending on the class actually occurring at the current location.

Discussion and Conclusion

The results obtained by the Index Overlay (Multi-Class Maps) indicate a lot of exploration targets related to the copper mineralization hosted by volcanic rocks such as andesite, dacite, and tuff that affected by the heat source and geodynamic occurrences as the controlling factors. Regarding the mineral prospectively map created by the integration of various evidence maps, we could identify and delineated 10 promising areas in the study area. These targets could be as copper mineralization anomalies as soon as possible by complementary activities such as drilling.

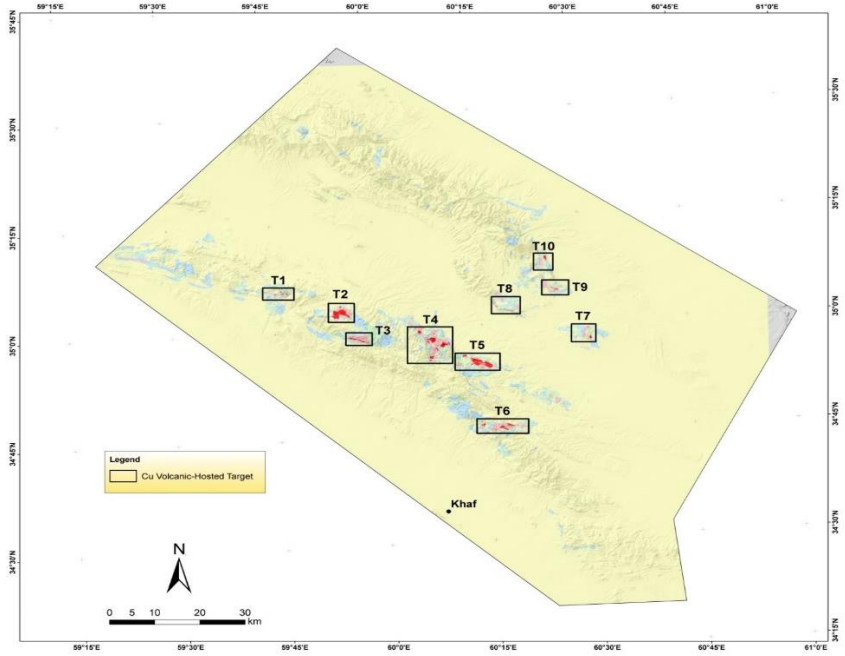

Figure 1. Mineral Prospectivety Map of coper mineralizations.

References

Afzal, P., Mirzaei, M., Yousefi, M., Adib, A., Khalajmasoumi, M., Zia Zarifi, A., Foster, P., Yasrebi, A.B., 2016. Delineation of geochemical anomalies based on stream sediment data utilizing fractal modeling and staged factor analysis. Journal of African Earth Sciences 119, 139-149.

Carranza, E.J.M., 2008, Geochemical anomaly and mineral prospectivity mapping in GIS. Handb. Explor. Environ. Geochem., Elsevier, Amsterdam, Netherland, 368 p

Bonham-Carter, G.F., 1994, Geographic information systems for geoscientists: modeling with GIS. Pergamon Press, Oxford, UK, 398 p.

Chung, C.F., and Moon, W.M., 1990, Combination rules of spatial geoscience data for mineral exploration. Geoinformat., v. 2, p. 159-169.

Bonham-Carter, G.F., Agterberg, F.P., and Wright, D.F., 1989. Weights-of-evidence modelling: a new approach to mapping mineral potential. In: Agterberg F.P. and Bonham-Carter G.F. (eds), Stat. Appl. Earth Sci., Geol. Surv. Canada, Paper 89-90, p. 171-183.

15th International Congress of the Geological Society of Greece
Athens, 22-24 May, 2019 | Harokopio University of Athens, Greece
Bulletin of the Geological Society of Greece, Sp. Pub. 7 Ext. Abs. GSG2019-130

Comparative Study of the Cesium Uptake Ability between HEU-type (Clinoptilolite-Heulandite) Zeolitic Tuff and Pure Heulandite

C. Mytiglaki[1], N. Kantiranis[1], P. Misaelides[2], F. Noli[2] and A. Filippidis[1]

(1) Aristotle University, Faculty of Sciences, School of Geology, Dept. of Mineralogy-Petrology-Economic Geology
(2) School of Chemistry, 54124 Thessaloniki, Greece, michristi@geo.auth.gr, kantira@geo.auth.gr, misailid@chem.auth.gr, noli@chem.auth.gr, anestis@geo.auth.gr

Introduction and Objectives

The zeolitic volcaniclastic rock deposit corresponds to a rock which contains high amounts of one or more from the different (more then 65) phases of zeolites. The zeolitic rock with numerous applications is the high quality HEU-type (clinoptilolite-heulandite) zeolitic tuff. Among other quality characteristics, only HEU-type zeolitic tuff with ≥80 wt% clinoptilolite-heulandite, ≤20 wt% clay minerals, free of fibres (e.g., fibrous zeolites such as erionite, mordenite, roggianite, mazzite, etc) and free of SiO_2 minerals (quartz, cristobalite, tridymite) can be used as feed additive for all animal species and consequently as nutrition supplement for humans. For all other environmental, industrial and agricultural applications, the zeolitic tuff, among others, should contain ≤20 wt% clay minerals (except for the uses in construction and cement industry) and ≥80 wt% clinoptilolite-heulandite (EU Regulation No 651/2013; Filippidis *et al.*, 2016a; Filippidis, 2016 and references therein). The HEU-type (clinoptilolite-heulandite) shows tabular crystals and contains micro/nano-pores in a framework of channels with 10- and 8-memers rings, in dimensions of 7.5x3.1 Å, 4.6x3.6 Å, 4.7x2.8 Å (Baerlocher *et al.*, 2007; Mitchell *et al.*, 2012). Natural zeolites are characterized by enhanced high cation exchange capacity and selectivity, higher for monovalent cations and lower for bivalent cations. Therefore, zeolitic rocks have already been proposed and successfully applied to the removal of fission products (e.g., Cs, Sr) and actinides (e.g., Th, U, Np, Pu) from effluents of the nuclear industry (e.g., Misaelides *et al.*, 1995a,b, 2018; Godelitsas *et al.*, 1996; Rajec *et al.*, 1999; Misaelides, 2011). Zeolitic rocks, ontaining e.g. clinoptilolite, chabazite, were used for the remediation of the consequences of the Three Miles Island, Chernobyl and Fukushima nuclear accidents and, along with clay minerals, were proposed as potential hosts for nuclear waste and as permeable reactive barriers for the cleaning of contaminated ground waters (e.g., Misaelides 2019). HEU-type (clinoptilolite-heulandite) zeolitic tuffs have effectively been used, to remove trace elements from wastewaters, and other different environmental, industrial and agricultural applications (e.g., Filippidis & Kantiranis, 2007; Vogiatzis *et al.*, 2012; Filippidis *et al.*, 2015a,b; 2016a,b; Filippidis 2016; Floros *et al.*, 2018; Kalaitzis *et al.*, 2019). The aim of this study was the comparison of the cesium sorption ability between pulverized high quality HEU-type (clinoptilolite-heulandite) zeolitic tuff and pulverized heulandite crystals.

Materials and methods

The high quality HEU-type (clinoptilolite-heulandite) zeolitic tuff (sample NA11) was obtained from specific continuous layers of zeolitic tuff in Ntrista stream location of Petrota area of Evros region (sample NA11) whereas pure heulandite crystals (sample HEU1) from the collection of the Dept. of Mineralogy-Petrology-Economic Geology (Aristotle Univ.). The mineralogical composition of the samples was determined by X-Ray Diffraction (XRD). The sample NA11 consists of 86 wt% HEU-type zeolite, 4 wt% micas + clay minerals, 4 wt% christobalite and 4 wt% feldspars, while the sample HEU1 is pure (100 wt%) heulandite. The combined methods of SEM-EDS, thermal treatment and XRD (Kantiranis *et al.*, 2006, 2011) applied in the sample NA11, revealed that the HEU-type zeolite presents characteristics of group 1 zeolite (clinoptilolite) and of group II (Intermediate heulandite). The mineral-chemistry of the zeolites was determined by SEM-EDS microanalyses. The chemical formula of the HEU-type zeolite (NA11) is $Ca_{1.8}K_{1.0}Mg_{0.7}Na_{0.5}Al_{6.4}Si_{29.5}O_{72}$ $21H_2O$, whereas that of pure heulandite (HEU1) is $Ca_{3.6}Na_{1.0}K_{0.2}Sr_{0.2}Ba_{0.1}Al_{8.1}Si_{27.6}O_{72}\cdot 21H_2O$. The uptake ability of the NA11 tuff sample, measured by the AMAS (Ammonium Acetate Saturation) method (Kantiranis *et al.*, 2011), was 231 meq/100g, while the corresponding value for the heulandite (HEU1 sample) 296 meq/100g. The cesium sorption ability of the two materials (500 mg/L $CsNO_3$ aqueous solutions of pH 2-12 labelled with ^{137}Cs) was determined, after equilibration for 24 hours and separation of the solid and liquid phase by filtration and centrifugation, using a gamma-ray spectroscopy (measurement of the 661 keV radiation emitted by ^{137}Cs).

Experimental results and conclusions

The experimental results showed that the cesium sorption ability of the HEU-type (clinoptilolite-heulandite) zeolitic tuff (sample NA11) was higher than this of the pulverized pure heulandite (HEU1) (Fig. 1). This is most probably due to the contribution of the nano/micro of the HEU-type zeolite (86 wt%) and the micas+clay minerals (4 wt%), as well as the meso/macro-pores of the zeolitic tuff to cesium cation sorption, while in the case of pure heulandite only the micro/nano-pores of the crystals contributed to the cesium removal from the solutions. The chemical composition of the zeolites (zeolite chemistry) can also influence their uptake ability. The cesium sorption ability was not significantly affected by the solution pH. The lower uptake value observed in the case of solutions with initial pH 2 is, most probably, due to the competition of the Cs^+- with H^+- cations. HEU type zeolites exhibit an amphoteric character having the ability to neutralize the solutions acting either as a proton acceptor or as a proton donor (Fig. 2). Cesium is present in aqueous solutions of pH 2-12 always in Cs^+ cationic form.

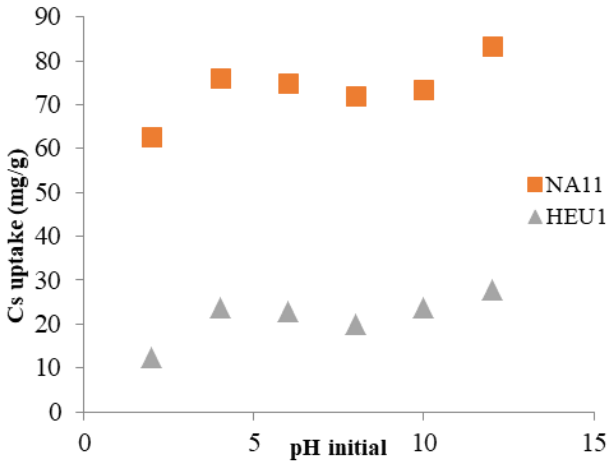

Fig 1. Variation of Cs uptake capacity of zeolitic tuff (NA11) and of pure crystals of heulandite (HEU1) in accordance with the initial pH of the solutions.

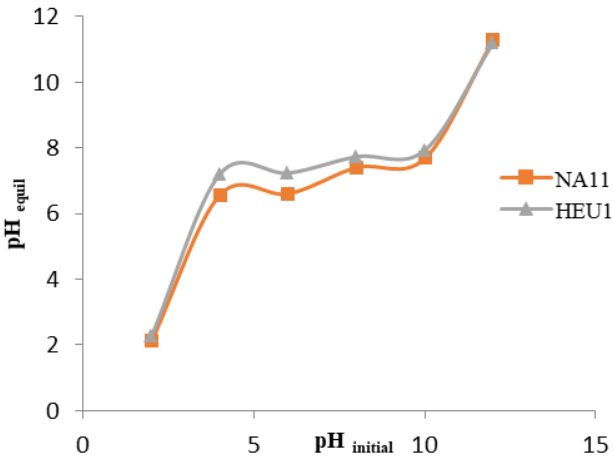

Fig 2. Variation of pH in the solutions after using the zeolitic tuff (NA11) and the pure crystals of heulandite (HEU1), in comparison with initial pH of the Cs traced aqueous solutions.

References

Baerlocher, Ch., McCuster, L.B., Olson, D.H., 2007. Atlas of zeolite framework types. Amsterdam, Elsevier, 301p.

EU Regulation No 651/2013. Commission Implementing Regulation (EU) No 651/2013 of 9 July 2013 concerning the authorization of clinoptilolite of sedimentary origin as a feed additive for all animal species and amending Regulation (EC) No 1810/2005.

Filippidis, A., 2016. Applications of the Hellenic Natural Zeolite (HENAZE) and specifications of zeolitic tuffs. Bull. Geol. Soc. Greece, 50(4), 1809-1819.

Filippidis, A., Kantiranis, N., 2007. Experimental neutralization of lake and stream waters from N. Greece using domestic HEU-type rich natural zeolitic material. Desalination, 213, 47-55.

Filippidis, A., Kantiranis, N., Papastergios, G., Filippidis, S., 2015a. Safe management of municipal wastewater and sludge by fixation of pollutants in very high quality HEU-type zeolitic tuff. J. Basic & Applied Research Intern., 7(1), 1-8.

Filippidis, A., Papastergios, G., Kantiranis, N., Filippidis, S., 2015b. Neutralization of dyeing industry wastewater and sludge by fixation of pollutants in very high quality HEU-type zeolitic tuff. J. Global Ecology & Environment, 2(4), 221-226.

Filippidis, A., Kantiranis, N., Tsirambides, A., 2016a. The mineralogical composition of Thrace zeolitic rocks and their potential use as feed additives and nutrition supplements. Bull. Geol. Soc. Greece, 50(4), 1820-1828.

Filippidis, A., Tziritis, E., Kantiranis, N., Tzamos, E., Gamaletsos, P., Papastergios, G., Filippidis, S., 2016b. Application of Hellenic Natural Zeolite in Thessaloniki industrial area wastewater treatment. Desalination & Water Treatment, 57(42), 19702-19712.

Floros, G.D., Kokkari, A.I., Kouloussis, N.A., Kantiranis, N.A., Damos, P., Filippidis, A.A., Koveos, D.S., 2018. Evaluation of the natural zeolite lethal effects on adults of the bean weevil under different temperatures and relative humidity regimes. J. Economic Entomology, 111(1), 482-490.

Godelitsas, A., Misaelides, P., Filippidis, A., Charistos, D., Anousis, I., 1996. Uranium sorption from aqueous solutions on sodium-form of HEU-type zeolite crystals. J. Radioanal. Nucl. Chem., 208, 393-402.

Kalaitzis, A., Stoulos, S., Melfos, V., Kantiranis, N., Filippidis, A., 2019. Application of zeolitic rocks in the environment: assessment of radiation due to natural radioactivity. J. Radioanal. Nucl. Chem., 319, 975-985.

Kantiranis, N., Chrissafis, C., Filippidis, A., Paraskevopoulos, K., 2006. Thermal distinction of HEU-type mineral phases contained in Greek zeolite-rich volcaniclastic tuffs. European J. Mineralogy, 18(4), 509-516.

Kantiranis, N., Sikalidis, K., Godelitsas, A., Squires, C., Papastergios, G., Filippidis, A., 2011. Extra-framework cation release from heulandite-type rich tuffs on exchange with NH_4^+. J. Environmental Management, 92, 1569-1576.

Misaelides, P., 2011. Application of natural zeolites to the environmental remediation: A short review. Microporous Mesoporous Materials, 144, 15-18.

Misaelides, P., 2019. Clay minerals and zeolites for radioactive waste immobilization and containment: A concise overview. In: Mercurio, M., Sarkar, B. and Langella, A. (eds). Modified clay and zeolite nanocomposite materials: Environmental and pharmaceutical applications. Elsevier, Amsterdam, pp. 243-274.

Misaelides, P., Godelitsas, A., Filippidis, A., 1995a. The use of zeoliferous rocks from Metaxades-Thrace, Greece, for the removal of caesium from aqueous solutions, Fresenius Environ. Bull., 4, 227-231.

Misaelides, P., Godelitsas, A., Filippidis, A., Charistos, D., Anousis, I., 1995b. Thorium and uranium uptake by natural zeolitic materials. Sci. Total Environ., 173-174, 237-246.

Misaelides, P., Sarri, S., Kantiranis, N., Noli, F., Filippidis, A., de Blochouse, B., Maes, A., Breynaert, E., 2018. Investigation of chabazitic materials as Cs-137 sorbents from cementitious aqueous solutions. Microporous Mesoporous Materials, 266, 183-188.

Mitchell, S., Michels, N.L., Kunze, K., Perez-Ramirez, J., 2012. Visualization of hierarchically structured zeolite bodies from macro to nano length scales. Nature Chemistry, 4, 825-831.

Rajec, P., Macasec, F., Misaelides, P., 1999. Sorption of heavy metals and radionuclides on zeolites and clays. In: Misaelides, P., Macasek, F., Pinnavaia, T.J., Colella, C. (Eds.) Natural microporous materials in environmental Technology. Kluwer, Dordrecht, 353-363.

Vogiatzis, D., Kantiranis, N., Filippidis, A., Tzamos, E., Sikalidis, C., 2012. Hellenic Natural Zeolite as a replacement of sand in mortar: Mineralogy monitoring and evaluation of its influence on mechanical properties. Geosciences, 2, 298-307.

15th International Congress of the Geological Society of Greece
Athens, 22-24 May, 2019 | Harokopio University of Athens, Greece
Bulletin of the Geological Society of Greece, Sp. Pub. 7 Ext. Abs. GSG2019-139

Characterization of Nigeria Kaolin as Raw Material for the Ceramic Industry

D. Nifora[1], E. Gianni[1], J.E. Ogala[2], D. Papoulis[1], S. Kalaitzidis[1], K. Christanis[1], V. Angelatou[3], E.M. Panagiotara[3]

(1) Department of Geology, University of Patras, 1 Asklepiou Str., 26504 Rion, Greece. despina.nifora@gmail.com
(2) Department of Geology, Delta State University, P.M.B. 1, Abraka, Nigeria.
(3) Hellenic Survey of Geology and Mineral Exploration (HSGME), 1 Spyrou Loui Str., 13677 Acharnai, Greece

Introduction

Kaolin has attracted the interest of many researchers due to its physical and chemical properties, thus being considered as one of the most studied industrial rocks. Kaolinite [$Al_2Si_2O_5(OH)_4$] is the most common mineral of the rock, followed by halloysite, dickite and nacrite. Kaolin deposits can be classified as either primary, formed due to in situ hydrothermal alteration or weathering of granitic rocks, or secondary, formed by the erosion and re-deposition of primary deposits (Prasad et al., 1991). Kaolin can be used in a wide range of industrial applications including ceramics. These products are dinnerware, sanitaryware, tile, porcelain, pottery and also refractory items (Murray, 2006). Each application relies on a specific set of properties; thus, kaolin characteristics can strongly affect the quality of the product. (Papoulis, 2003). According to the ceramic industry classification, kaolin products are distinguished into low and high quality products, on the basis of the purity of raw material, as well as the particle size distribution of the clay (Bloodworth et al., 1993).

In the present work, kaolin from Oza-Nogogo area, southern Nigeria was studied for the first time, in order to assess the suitability of this raw material for the ceramic industry. The evaluation of its industrial usage potential was based on a particular set of requirements defined by Bloodworth et al. (1993).

Geological Setting

The kaolin occurrences of Oza-Nogogo area belong to Oligocene-Miocene Ogwashi-Asaba Formation (Reyment, 1965); they outcrop along with coarse sandstone, light to brown clays and interbedded lignite layers (Akpokodje et al., 1991). The Ogwashi-Asaba Formation consists of sediments deposited during the third and last cycle of Niger Delta Basin (Schluter, 2006). The kaolin occurrences are characterized as sedimentary kaolin, with very high kaolinite content and subordinate amounts of quartz (Emofurieta and Salami, 1988).

Materials and Methods

Twenty samples were collected from four outcrops in Iduneha, Ewan, Uvbe and Ewebi, exposed by streams, hand dug pits and quarries. X-Ray diffraction (Bruker D8 Advance) with Cu-Kα radiation (λ = 1.5418 Å) and Nickel filter was applied to determine the mineral content in the raw samples. Scanning Electron Microscopy (SEM) was performed using an InspectTM F50 of FEI, in order to study the texture and the individual anomalies of the crystal structure of kaolinite. The particle size distribution of the kaolin samples was determined via Mastersizer 2000 of Malvern Instruments. Due to the underestimation of the clay fraction with the Laser Scattering Method, the results were converted applying Di Stefano's et al. (2010) equations. Both brightness and whiteness were measured between 380 to 780 nm, by using a Carry 100 UV-Vis spectrophotometer of Varian, controlled by Cary WinUV software. The nitrogen sorption-desorption isotherms for the samples degassed at 200°C for 2 h, were obtained at 77 K, using Nova 2200e Surface area and Pore size analyzer of Quantachrome. Specific surface area was determined from Brunauer-Emmett-Teller (BET) isotherms, whereas pore volume and diameter were identified via Barrett-Joyner-Halenda (BJH) method. Atterberg limit tests were performed for the determination of the liquid limit (LL) and the plastic limit (PL). The plasticity Index (PI) was calculated from the arithmetic difference of the LL and PL values as derived from Casagrande apparatus.

Results

According to the results obtained by X-Ray diffraction, the kaolinite content is very high (up to 89%), while quartz is the main impurity usually not exceeding 10%. Other secondary minerals, in only a small number of samples and in trace amounts, are dolomite, anatase, illite and iron oxides.

The results of six representative kaolin samples are given in Table 1. The grain size distribution shows that the kaolinized samples of Iduneha, Uvbe and Ewebi display high contents of fine clay fraction (<2 μm), with average values of 51%, 54% and 46%, respectively, whereas kaolin sample of Ewan reveal the least clay content (41%). The aforementioned results can also be confirmed by SEM analysis. Representative SEM image is given in Fig 1. Pseudo-hexahedral crystals of kaolinite dominate in the kaolinized samples, whilst its particle size appears to be <2 μm. In addition, intense orientation is observed, which is a feature of sedimentary kaolin deposits.

Both kaolin samples of Iduneha and Uvbe show high brightness, exceeding 91%. Similar results are presented for whiteness, with the exception of sample L1/IDH/01, for which the color was not as white as it was in the other samples, due to its Fe_2O_3 content. The values for specific surface area of Iduneha kaolin, are higher (10.603-13.636 m^2/g) than the kaolin from Uvbe and Ewebi. The total pore volume of the samples is significantly small (0.03-0.08 cm^3/g) and the pore diameter ranges between 3.6-5 nm. High values of 32.3 nm and 33.3 nm were observed in the samples L1/IDH/04 and L5/UVB/01, respectively. The Plasticity Index is unusually high and is related to the forming conditions.

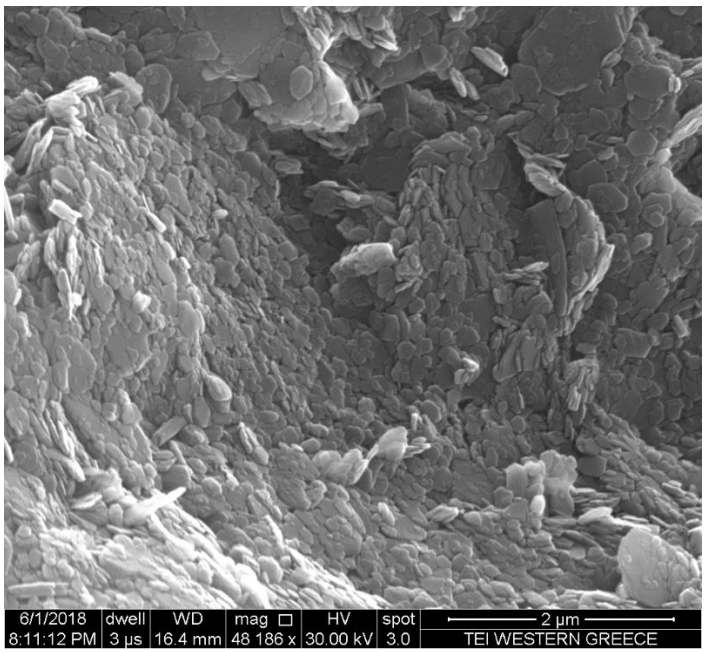

Figure 1. SEM image of a representative kaolin sample from Iduneha, showing hexahedral crystals of kaolinite.

Table 1. Results of physical properties of kaolin samples of Iduneha, Uvbe and Ewebi locations.

Location	Sample name	Grain size <2 µm	Brightness (%)	Whiteness (%)	SSA[1] (m^2/g)	Pore diameter (nm)	Pore volume (cm^3/g)	LL[2] (%)	PL[3] (%)	PI[4] (%)
Iduneha	L1/IDH/01	53	91.1	78.6	13.64	3.64	0.062	71.33	39.08	32.25
Iduneha	L1/IDH/04	43	94	85.4	12.59	33.25	0.078	98.31	44.29	54.02
Iduneha	L2/IDH/01	56	97.1	92.7	10.6	3.65	0.065	69.89	36.02	33.87
Uvbe	L5/UVB/01	50	-	-	9.39	32.27	0.05	-	-	-
Uvbe	L7/UVB/01	63	95.3	88.3	-	-	-	64.49	43.84	20.65
Ewebi	L9/EWE/01	40	-	-	9.29	3.61	0.062	53.86	41.29	12.57

1: Specific surface area, 2: Liquid limit, 3: Plasticity limit, 4: Plasticity Index

Conclusions

The kaolin samples obtained from the outcrops of Iduneha, Uvbe and Ewebi display similar properties. Taking into account the high content of kaolinite, the grain size being <2 µm, the high values of brightness and whiteness and the very light brown color, the kaolin of these areas meets the industrial set requirements for the manufacture of low-quality ceramics. Specifically, due to its surficial and thick strata, Iduneha is considered to have a significant economic interest. On the contrary, the Ewan occurrence is of inferior quality, and its exploitation could be an option only after beneficiation. However, for high-quality ceramic products, the studied kaolin samples fail to meet the industry's high standards.

References

Akpokodje, E.G., Etu-Efeotor, J.O. and Olorunfemi, B.N., 1991. The composition and physical properties of some ceramic and pottery clays of southeastern Nigeria. Journal of Mining and Geology, 2(1), 1-8.

Bloodworth, A.J., Highley, D.E. and Mitchell, C.J., 1993. Industrial Minerals Laboratory Manual-Kaolin. British Geological Survey.

Di Stefano, C., Ferro, V. and Mirabile, S., 2010. Comparison between grain size analyses using laser diffraction and sedimentation methods. Biosystems Engineering, 106, 205-215.

Emofurieta, W.O. and Salami, A.O., 1988. A comparative study of two kaolin deposits in southwestern Nigeria. Journal of Mining and Geology, 24(1&2): 15-20.

Murray, H.H., 2006. Applied Clay Mineralogy Occurrences, Processing and Application of Kaolins, Bentonites, Palygorskite-Sepiolite and Common Clays. Elsevier Science, 2, 1-180.

Papoulis, D., 2003. Mineralogical study, kaolinitization processes and properties of kaolins from Leucogia Drama and Kos Island. Ph.-D Thesis, University of Patras, p. 289.

Prasad, M.S., Reid, K.L. and Murray, H.H., 1991. Kaolin: processing, properties and applications. Applied Clay Science, 6, 87-119.

Reyment, R.A., 1965. Aspects of geology of Nigeria. University of Ibadan Press, p.145.

Schluter, T., 2006. Geological Atlas of Africa, Springer Science + Business Media, Germany, 255.

15th International Congress of the Geological Society of Greece
Athens, 22-24 May, 2019 | Harokopio University of Athens, Greece
Bulletin of the Geological Society of Greece, Sp. Pub. 7 Ext. Abs. GSG2019-150

The Mineralogical Composition of Samos Zeolitic Rocks and their Potential Use as Feed Additives and Nutrition Supplements

A. Filippidis, N. Kantiranis, C. Mitiglaki, A. Tsirambides
Aristotle University of Thessaloniki, Faculty of Sciences, School of Geology, Department of Mineralogy-Petrology-Economic Geology, 54124 Thessaloniki, Greece, anestis@geo.auth.gr, kantira@geo.auth.gr, michristi@geo.auth.gr, ananias@geo.auth.gr

Introduction and Objectives

Clinoptilolite of sedimentary origin with ≥80 wt% clinoptilolite, ≤20 wt% clay minerals, free of fibres and quartz, can be used as feed additive for all animal species (EU Regulation No 651/2013, Filippidis *et al*. 2016) and consequently as nutrition supplement. In humans and animals, inhaled or injected or swallowed, fibrous zeolites (mainly erionite and mordenite, and to a lesser extent roggianite and mazzite), as well as the SiO_2 minerals (quartz, cristobalite, tridymite), were found to be toxic, carcinogenic and highly pathogenic (Davis, 1993; Driscoll, 1993; Ross *et al.*, 1993).

The zeolitic rocks of Karlovasi-Marathokampos basin of Samos Island have been investigated for their mineralogy, petrology, geochemistry and possible industrial or environmental applications by many authors (e.g., Stamatakis, 1989; Pe-Piper & Tsolis-Katagas, 1991; Kantiranis *et al*., 2004, 2011; Filippidis *et al.*, 2005; Mitiglaki *et al*., 2015). Studies on the use of zeolitic rocks as feed additives in different animals show negative, neutral and positive effects on the production and quality of livestock products (e.g., Pond & Mumpton, 1984; Tserveni-Gousi *et al*., 1997; Yannakopoulos *et al*., 2000; Filippidis, 2010). In most studies the quality characteristics (EU Regulation No 651/2013, Filippidis *et al.*, 2016) of zeolitic rocks are not mentioned.

The aim of the present study is to determine the mineralogical composition by the X-Ray Diffraction (XRD) method, of fifteen samples of the zeolitic rocks from the Karlovasi-Marathokampos basin and evaluate their potential use as feed additives (in accordance with the EU Regulation No 651/2013) and as nutrition supplements (Filippidis *et al*., 2016).

Results and Conclusions

Since the EU Regulation No 651/2013 concerns the clinoptilolite of sedimentary origin, the examined 15 samples can be grouped in those containing clinoptilolite and those without clinoptilolite.

Concerning the clinoptilolite-bearing rocks (Table 1), two samples (S1, S11) contain the fibrous zeolite mordenite (20-21 wt%), five samples (S7, S9, S10, S12, S13) contain <80 wt% clinoptilolite (22-73 wt%), two samples (S4, S6) contain <80 wt% clinoptilolite (17-33 wt%) and >20 wt% clay minerals (27-42 wt%), one sample (S3) contains >80 wt% clinoptilolite (86 wt%) and all samples contain quartz (2-5 wt%). Considering this mineralogical composition (Table 1), none of the clinoptilolite-containing rocks meet the requirements of the EU Regulation No 651/2013, and thus they cannot be used as feed additives for all animal species and consequently as nutrition supplements, since all of them contain 2-5 wt% quartz, two of them 20-21 wt% mordenite (fibrous zeolite), nine of them <80 wt% clinoptilolite (17-73 wt%) and two of them >20 wt% clay minerals (27-42 wt%).

Table 1. Mineralogical composition (wt%) of the clinoptilolite-containing rocks from Karlovasi-Marathokampos basin of Samos Island.

Sample	Clinoptilolite	Mordenite	Analcime	Phillipsite	Micas	Clay minerals	Quartz	Feldspars	Amorphous	Tot.
S1	59	21	-	-	4	8	5	3	-	100
S3	86	-	-	-	2	2	2	8	-	100
S4	33	-	-	-	9	27	5	18	8	100
S6	17	-	-	27	2	42	2	10	-	100
S7	54	-	-	-	10	4	2	30	-	100
S9	43	-	-	-	14	11	2	26	4	100
S10	67	-	-	-	7	4	2	20	-	100
S11	59	20	-	-	4	8	4	5	-	100
S12	73	-	-	-	11	4	5	7	-	100
S13	22	-	29	-	8	15	2	24	-	100

Concerning the non clinoptilolite-bearing rocks (Table 2), one sample (S15) contains 62 wt% the fibrous zeolite mordenite, three samples (S2, S5, S14) contain 29-70 wt% analcime, one sample (S8) contains 63 wt% chabazite, two samples (S5, S8) contain >20 wt% clay minerals (23-29 wt%) and all samples contain quartz (2-6 wt%). Although the EU Regulation No 651/2013 refers to clinoptilolite of sedimentary origin, using the presence or absence of quartz and

fibrous minerals, we could evaluate the potential use of the non clinoptilolite-containing rocks, as feed additives and as nutrition supplements. Considering the mineralogical composition (Table 2), none of the mordenite, analcime and chabazite containing zeolitic rocks, can be used as feed additives for all animal species and consequently as nutrition supplements, since all of them contain 2-6 wt% quartz and one of them contains 62 wt% mordenite (fibrous zeolite).

Table 2. Mineralogical composition (wt%) of the non clinoptilolite-containing rocksfrom Karlovasi-Marathokampos basin of Samos Island.

Sample	Mordenite	Analcime	Chabazite	Micas	Clay minerals	Quartz	Feldspars	Amorphous	Tot.
S2	-	70	-	5	3	6	12	4	100
S5	-	29	-	6	29	3	30	3	100
S8	-	-	63	2	23	4	8	-	100
S14	-	68	-	4	2	6	11	9	100
S15	62	-	-	1	1	2	12	22	100

References

Davis, J.M.G., 1993. In vivo assays to evaluate the pathogenic effects of minerals in rodents, in: Guthrie, G.D.Jr., Mossman, B.T., (Eds.). Health Effects of Mineral Dusts. Mineralogical Society of America, Washington DC, Reviews in Mineralogy 28, 471-487.

Driscoll, K.E., 1993. In vitro evaluation of mineral cytotoxicity and inflammatory activity, in: Guthrie, G.D.Jr., Mossman, B.T., (Eds.). Health Effects of Mineral Dusts. Mineralogical Society of America, Washington DC, Reviews in Mineralogy 28, 489-511.

EU Regulation No 651/2013. Commission Implementing Regulation (EU) No 651/2013 of 9 July 2013 concerning the authorisation of clinoptilolite of sedimentary origin as a feed additive for all animal species and amending Regulation (EC) No 1810/2005.

Filippidis, A., 2010. Environmental, industrial and agricultural applications of Hellenic Natural Zeolite. Hellenic Journal of Geosciences 45, 91-100.

Filippidis, A., Kantiranis, N., Drakoulis, A., Vogiatzis, D., 2005. Quality, pollution, treatment and management of drinking, waste, underground and surface waters, using analcime-rich zeolitic tuff from Samos island, Hellas. 7th Hellenic Hydrogeological Conference, Athens, Greece, Proc., II, 219-224.

Filippidis, A., Kantiranis, N., Tsirambides, A., 2016. The mineralogical composition of Thrace zeolitic rocks and their potential use as feed additives and nutrition supplements. Bull. Geol. Soc. Greece 50(4), 1820-1828.

Kantiranis, N., Stamatakis, M., Filippidis, A., Squires, C., 2004. The uptake ability of the clinoptilolitic tuffs of Samos Island, Greece. Bull. Geol. Soc. Greece 36(1), 89-96.

Kantiranis, N., Sikalidis, K., Godelitsas, A., Squires, C., Papastergios, G., Filippidis, A., 2011. Extra-framework cation release from heulandite-type rich tuffs on exchange with NH4+. Journal of Environmental Management 92, 1569-1576.

Mitiglaki, C., Kantiranis, N., Filippidis, A., Stamatakis, M., 2015. Uptake ability of zeolitic tuffs with Clinoptilolite, Analcime, Phillipsite and Mordenite from Samos Island (in Greek with English abstract). Scientific Annals, School of Geology, Aristotle University of Thessaloniki 103, 51-54.

Pe-Piper, G., Tsolis-Katagas, P., 1991. K-rich mordenite from Late Miocene rhyolitic tuffs, Island of Samos, Greece. Clays & Clay Minerals 39, 239-247.

Pond, W.G., Mumpton, F.A., 1984. Zeo-Agriculture: Use of Natural Zeolites in Agriculture and Aquaculture. International Committee on Natural Zeolites, Brockport, New York, 305 p.

Ross, M., Nolan, R.P., Langer, A.M., Cooper, W.C., 1993. Health effects of various mineral dusts other than asbestos, in: Guthrie, G.D.Jr., Mossman, B.T., (Eds.). Health Effects of Mineral Dusts. Mineralogical Society of America, Washington DC, Reviews in Mineralogy 28, 361-407.

Stamatakis, G.M., 1989. A boron-bearing potassium feldspar in volcanic ash and tuffaceous rocks from Miocene lake deposits, Samos Island, Greece. American Mineralogist 74, 230-235.

Tserveni-Gousi, A.S., Yannakopoulos, A.L., Katsaounis, N.K., Filippidis, A., Kassoli-Fournaraki, A., 1997. Some interior egg characteristics as influenced by addition of Greek clinoptilolitic rock material in the hen diet. Archiv fur Geflugelkunde 61(6), 291-296.

Yannakopoulos, A., Tserveni-Gousi, A., Kassoli-Fournaraki, A., Tsirambides, A., Michailidis, K., Filippidis, A., Lutat, U., 2000. Effects of dietary clinoptilolite-rich tuff on the performance of growing-finishing pigs, in: Colella, C., Mumpton, F.A., (Eds.). Natural Zeolites for the Third Millennium, Napoli, De Frede, 471-481.

15th International Congress of the Geological Society of Greece
Athens, 22-24 May, 2019 | Harokopio University of Athens, Greece
Bulletin of the Geological Society of Greece, Sp. Pub. 7 Ext. Abs. GSG2019-163

Application of the XRF-core scanning technique in the study of late Quaternary palaeoclimatic changes within the southern Red Sea

F. Paraschos[1], H. Kaberi[1], D. Sakellariou[1], M. Geraga[2], S. Sergiou[2]

(1) Institute of Oceanography, Hellenic Centre for Marine Research (HCMR), Athens-Sounio 46.7km, Mavro Lithari, 19013 Anavyssos, Attiki, Greece, fparaskos@hcmr.gr

(2) University of Patras, Department of Geology, Laboratory of Marine Geology and Physical Oceanography 26 504, Patras, Greece

Introduction and Objectives

Non-destructive techniques provide a continuous analysis of sediment cores and constitute an essential tool in the reconstruction of past environmental and climatic conditions. XRF-core scanning in particular can provide a high-resolution record of element intensities, the ratios of which can be used in order to decipher palaeoenvironmental characteristics. One of the main aims of this research, which was carried out within the framework of the ERC-funded DISPERSE project (Bailey et al., 2012), was the application of the XRF-core scanning technique in order to investigate the palaeoceanographic and palaeoclimatic conditions that prevailed in the southern Red Sea during the late Quaternary. The Red Sea, one of the youngest oceanic basins on earth also described as an 'ocean in the making', presents a strong significance for both earth scientists and archaeologists alike. One of the reasons the Red Sea has received much attention in the last decades can be attributed to the fact that the basin is viewed as an archive of past sea-level changes (e.g., Trommer et al., 2010 and references therein). These sea-level fluctuations played an important role in controlling the environmental conditions developed within the basin on a glacial-interglacial timescale (e.g., Rohling et al., 2008a). The Red Sea and especially its southern corridor, has also been a subject of study in the field of archaeology as it is considered to have been a pathway for the dispersal of the modern human (*H. Sapiens Sapiens*) out of Africa during the Pleistocene (Bailey et al., 2019 and references therein). This study presents the preliminary results revealed through the various elemental ratios of two sediment cores retrieved from the continental shelf off the Farasan Islands (Saudi Arabia).

Materials and methods

Two distinct areas within the continental shelf off the Farasan Islands were surveyed during the DISPERSE-Farasan cruise on board the R/V Aegaeo in 2013. The first core (FA09) was retrieved from survey area 1, which is located on the upper slope-outer continental shelf, whereas the second one (FA14) from the inner continental shelf, located between the Farasan Islands and the Arabian Peninsula (Sakellariou et al., 2019). Both cores were retrieved via gravity coring with 3-5m long barrels, photographed and sedimentologically described. The cores were afterwards scanned with the use of the AVAATECH XRF core scanner system at the CORELAB laboratory of the University of Barcelona, at 2mm resolution, in three runs at 10, 30 and 50kV in an X-ray tube. Six samples were also retrieved from specific depth intervals in both cores for chronological dating via ^{14}C AMS analysis. Five samples of about 10 mg of hand-peaked *Gs ruber* individuals were taken from core FA09, while one sample of benthic *Cibicides sp* specimens were retrieved from the FA14 core due to a lack of planktonic foraminiferal assemblages. Samples were analysed at the Scottish Universities Environmental Research Centre laboratories (SUERC).

Results and discussion

Preliminary results were drawn from the relative changes of the elemental profiles observed in both cores, the ratios of which are used as proxies of environmental and hydrological conditions. The 266 cm long FA09 core presents two visually distinct parts separated by a sharp interface at 129.5 cm b.s.f., or 15332 BP. Within the upper 0-120 cm b.s.f there is an increase in the Ca/Fe ratio (Figure 1), which is used as a proxy of marine Ca in comparison to terrigenous Fe (Richter et al., 2006); and can therefore suggest a transition from a glacial period of low biogenic production and high terrigenous inputs (downwards of 120 cm b.s.f) to an interglacial period of higher biogenic productivity (upwards of 120 cm b.s.f). This observation is further supported by a decrease in the Sr/Ca (Figure 1) log-ratio within the same depth interval which is also a proxy of biogenic Ca inputs. Ratios of the terrigenous elements K, Si, Fe to the carbonate Ca (Figure 1) have been used as proxies for aeolian dust input (Hanebuth and Henrich, 2009) and show increased values below 130 cm b.s.f supporting the theory that the sediments below 130 cm b.s.f were deposited during the arid Last Glacial Maximum (LGM). In terms of proxies for palaeoproductivity, according to Thomson et al. (2006) Br/Cl (Figure 1) may reveal increased organic matter inputs. Within this core, Br/Cl shows an increase between 110-130 cm b.s.f, which also coincides with the visually identified sapropel layer between 115-130 cm b.s.f. Finally, increased amounts of Sr, which is used as a proxy of high salinity by Arz et al. (2001b), were found below 130 cm b.s.f. The 293 cm long FA14 core also presents two visually distinct units separated by a 7cm thick transition layer. The upper layer is found between 0-225 cm b.s.f while the lower one below 230.5 cm b.s.f or 9027 BP. Within this core the Ca/Fe ratio (Figure 2) slightly increases from about 240 cm b.s.f upwards with a broad peak at about 210 cm b.s.f indicating increased marine productivity in the upper interglacial part. The Br/Cl ratio (Figure 2) exhibits increasing values from around 230 cm b.s.f upwards therefore, indicating a higher input of biogenic matter. Similarly to FA09, increased amounts of Sr (Fig. 2) are also present within the lower glacial unit of this core, below 230 cm b.s.f.

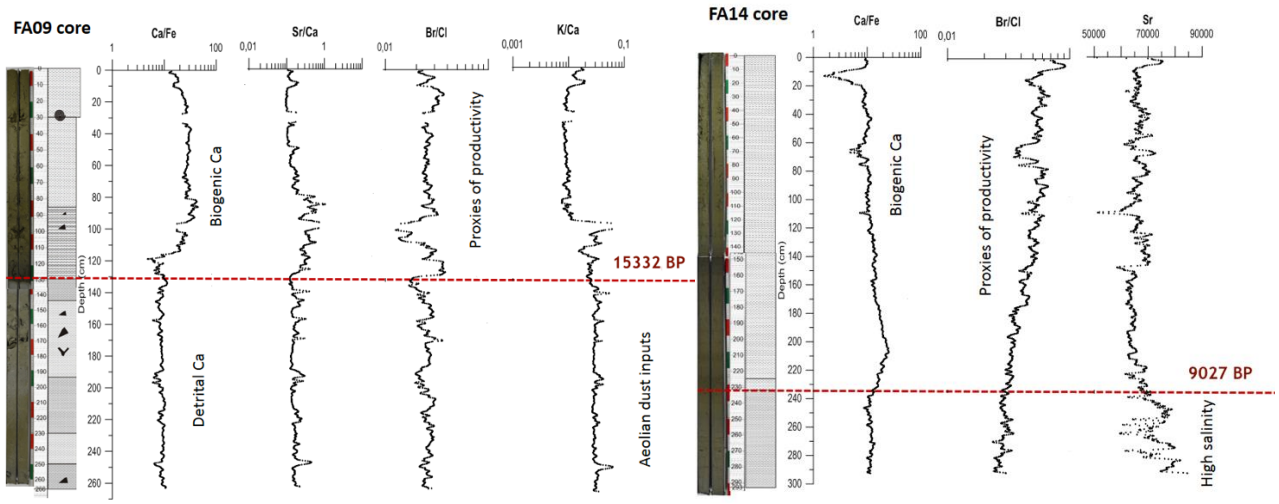

Figure 1, 2. Diagnostic elemental ratios for FA09 and FA14 cores. The dotted red lines depict the presumed transition between the Last Glacial Maximum (LGM) and interglacial sedimentation.

Conclusions

Application of the XRF-core scanning technique resulted in a preliminary qualitative description of the palaeoenvironmental conditions that prevailed during the sediment deposition in the upper slope (FA09 core) and inner shelf (FA14 core) of the Farasan Islands. One of the main conclusions drawn was that the transition from the LGM environment to the current interglacial marine setting did not happen simultaneously in both locations due to the distinct morphological characteristics of each basin. Both basins presented increased salinity during the LGM as well as decreased marine productivity and biogenic carbonates. The basin within survey area 2 (FA14 core) presented higher salinity values and as a result it can be presumed that during the low sea levels of the LGM it was completely isolated. Transitioning into the interglacial period marine productivity and biogenic carbonates increased whereas salinity decreased. It is apparent that through the vertical distribution of various diagnostic elemental ratios many conclusions can be drawn concerning depositional environments. Ongoing geochemical studies will assist in the calibration and establishment of this non-destructive technique in palaeoenvironmental research.

Acknowledgements

This research is funded by the European Research Council through Advanced Grant 269586 DISPERSE under the 'Ideas' Specific Programme of the Seventh Framework Programme. The authors would like to thank the Saudi Commission for Tourism and National Heritage (SCTH) for permission to undertake fieldwork. S. Sergiou thanks General Secretariat for Research and Technology (GSRT) and the Hellenic Foundation for Research and Innovation (HFRI) for funding support. We would also like to thank the captain and crew of the R/V AEGAEO for their continuous efforts to ensure the smooth running of the scientific operation during the offshore survey work.

References

Arz, H.W., Pätzold, J., Moammar, M.O., Röhl, U., 2001b. Late Quaternary climate records from the Northern Red Sea: results on gravity cores retrieved during the R/V METEOR Cruise M44/3. J King Abdulaziz Univ. Mar Sci 12, 101–113.

Bailey, G.N., King, G.C.P., Devès, M., Hausmann, N., Inglis, R., Laurie, E., Meredith-Williams, M., Momber, G., Winder, I., Alsharekh, A., Sakellariou, D., 2012. DISPERSE: dynamic landscapes, coastal environments and human dispersals. Antiquity 86, 334. http://antiquity.ac.uk/projgall/bailey334/

Hanebuth, T.J.J and Henrich, R., 2009. Recurrent decadal-scale dust events over Holocene western Africa and their control on canyon turbidite activity (Mauritania). Quat Sci Rev 28, 261-270.

Sakellariou, D., Rousakis, G., Panagiotopoulos, I., Morfis, I., Bailey, G., 2019. Geological structure and Late Quaternary geomorphological evolution of the Farasan Islands continental shelf, southern Red Sea, SW Saudi Arabia. In: N. M. A. Rasul and I. C. F. Stewart (eds.), Geological Setting, Palaeoenvironment and Archaeology of the Red Sea.

Bailey, G.N., Williams, M.M., Alsharekh, A., Hausmann, N., 2019. The Archaeology of Pleistocene Coastal Environments and Human Dispersals in the Red Sea: Insights from the Farasan Islands. In: N. M. A. Rasul and I. C. F. Stewart (eds.), Geological Setting, Palaeoenvironment and Archaeology of the Red Sea.

Richter, T.O., Van der Gaast, S., Koster, B., Vaars, A., Gieles, R., De Stigter, H., De Haas, H., vanWeering, T.C.E., 2006. The Avaatech XRF core scanner: technical description and applications to NE Atlantic sediments. In: Rothwell, R.G. (Ed.), New Techniques in Sediment Core Analysis. Special Publication, vol. 267. Geological Society, London, pp. 39-50.

Thomson, J., Croudace, I.W., Rothwell, R.G., 2006. A geochemical application of the ITRAX scanner to a sediment core containing eastern Mediterranean sapropel units. In: ROTHWELL, R.G. (ed.) New Techniques in Sediment Core Analysis. Geological Society, London, Special Publications, 267, 65-77.

Trommer, G., Siccha, M., Rohling, E. J., Grant, K., van der Meer, M. T. J., Schouten, S., Hemleben, C., Kucera, M., 2010. Millennial-scale variability in Red Sea circulation in response to Holocene insolation forcing, Paleoceanography, 25, 3203.

15th International Congress of the Geological Society of Greece
Athens, 22-24 May, 2019 | Harokopio University of Athens, Greece
Bulletin of the Geological Society of Greece, Sp. Pub. 7 Ext. Abs. GSG2019-168

Tracing the depositional microenvironment and related genetic mechanisms of Fe-rich palygorskite and Mg-Fe-smectite in the Velanida clay deposit, western Macedonia, Greece

K. Vythoulkas[1,2], M. Stamatakis[2], A. Argyraki[2], K. Kouli[2], V. Zotiadis[3]

(1) GEOHELLAS S.A., 8A Pentelis Street, 17564, Palaio Faliro, Greece, kvythoulkas@geohellas.com (2) National and Kapodistrian University of Athens, Panepistimiopolis Zografou, 15784 Athens, Greece. (3) Edafomichaniki S.A., Em. Papadaki Street, 14121 Neo Irakleio, Greece

The Velanida clay deposit composed of Fe-rich palygorskite and Mg-Fe-smectite rich clays, is situated within the so called "Ventzia" basin, located approximately 7 km southwest of the town of Eani in Kozani prefecture, Greece. This clay deposit lays unconformably on ultramafic rocks of the Vourinos ophiolitic complex and Mesozoic limestones of the Pelagonic Unit. The clay sediments were deposited in a fluvial-lacustrine rift basin formed during the Upper Pliocene – Lower Pleistocene period and grade east into the upper layers of the "Servia" Neogene basin that consists primarily of magnesium rich carbonates, dolomitic marlstone and sandstone (Stamatakis, 1995). According to a generic model by Kastritis *et al.*, (2003), the initial sediment supply into the basin was mainly fine-grained serpentine sands and Mg-Fe-smectite clays that eroded from the saprolite bodies formed on the Vourinos ophiolite complex and the smectite-bearing sands of the Mesohellenic trench. During the closure of the basin sediment supply shifted, producing a high energy detrital deposit composed of carbonates mostly derived from the Triassic crystalline limestones located to the north of the deposit.

Fe-rich palygorskite and Mg-Fe-smectite rich clays from the deposit were characterized by combining geological (stratigraphy), mineralogical, geochemical, sedimentological and micropaleontological data to better understand the depositional microenvironment and their related genetic mechanisms. Methods utilized for the current study included X-ray diffraction (XRD), scanning electron microscopy (SEM) coupled by energy dispersion spectrometry (EDS), chemical analysis and micropaleontological investigation.

Stratigraphy data based on the evaluation of over 100 exploratory boreholes reveal the presence of three distinct Mg-rich clay layers, alternating with gravelly clays, with a total thickness of approximately 50 - 70 m that dip gently to the southeast at angles ranging from 5º to 10º. The clay-rich layers include from the bottom of the sequence: 1) a green/brownish Mg-Fe smectite rich layer (A1) with a total thickness of 30 to 40 m, 2) a greyish palygorskite-rich layer (A2) with a total thickness of approximately 15 m, and 3) a greyish/greenish white or brownish purple mixed palygorskite-smectite layer (A3) with a total thickness of nearly 20 m. Carbonate concretions composed of calcite – dolomite mixtures are observed at the base of the A2 layer, mainly in globular form less than 1 cm wide. The overburden material consists of overlying Pleistocene carbonate sediments whereas the interburden material consists of intercalating clastic sediments such as micro-conglomerates and loose sand of serpentine origin and sandy clays of serpentine and smectite origin.

Mineralogical analysis by XRD was conducted on representative clay samples collected from the exploratory boreholes. The main mineral phases identified are palygorskite or /and Mg-smectite while serpentine, dolomite, calcite and quartz are accessory phases. Mineralogical data in combination with sedimentological and stratigraphy data determine a general, lateral grading in the Velanida deposit that portrays palygorskite rich clays in the center grading to mixed palygorskite-smectite clays and to smectite rich clays that alternate with sandy clays and serpentine sands towards the outer rim of the deposit. Coarser detrital sediments of serpentine sand and gravel, and smectite clayey sands were deposited at the outward part of the deposit.

The SEM study revealed the presence of several forms of palygorskite lath assemblages regarding the length or the orientation of the fibers, the density and the intergrowth between them and the void spaces in skeletal textures of laths. Moreover, palygorskite laths have been observed to develop on the surface of Fe-Mg-smectite flakes or to intergrow with rhombohedral dolomite crystals. All the above are indicative of the deposition micro-environment conditions related to palygorskite formation mechanisms (Garcia-Romero *et al.*, 2013).

Chemical analysis was performed on about 50 representative clay samples collected from exploratory boreholes for main oxides and trace elements. Geochemical analysis of chemical data was completed by plotting the relative concentrations of major oxides on ternary diagrams as well as by statistical analysis for the preliminary evaluation of possible geochemical reactions during deposition/diagenesis of the clays. Concerning major oxides, Velanida palygorskite clays exhibit low Al_2O_3 (4.3 % on average) and high MgO (12.7 % on average) and Fe_2O_3 content compared to typical palygorskite clays from Attapulgus clay deposits of Georgia and Florida, USA. Although Fe-rich palygorskites are scarce (Suarez *et al.*, 2011), the Fe_2O_3 content of palygorskite from the Velanida clay deposit is high ranging from 11.2 to 14.6 %.

Micro-paleontological data were co-evaluated, concerning Mg-clays genesis, to explore a probable link to a climatic change from a humid subtropical climate to a more arid or semi-arid climate of the Upper Pliocene and to provide insights into the general paleo-environmental conditions and the depositional environment of the clay deposit. Representative samples of palygorskite and smectite rich clays were pretreated following standard palynological procedures to prepare them for palynological-palynofacies analysis. The protocol followed included reaction of the sediment with strong acids in repeated steps, to remove the inorganic clasts, acetolysis and finally sieving the residue to collect the less than 7 μm fraction. Recovered palynomorphs include pollen, fungal remains, algal spores, as well as microscopic charcoal particles.

Pinus, *Cedrus*, *Picea* and *Tsuga* are some of the tree pollen recovered, while herb vegetation includes Ericaceae and Poaceae.

According to the findings of the present study combined with an extensive review of the international literature regarding palygorskite formation, three distinct genetic processes are considered with respect to the Velanida palygorskite mineral assemblage: 1) diagenetic formation through the full expense of Mg-smectite clays as documented in the Carrion lacustrine basin of central Spain (Sanchez *et al.*, 1995), in the calcretes of the Duero and Tajo basins from central Spain (Rodas *et al.*, 1994), in a Mg-rich environment of the Neogene Madrid basin from Spain (Pozo *et al.*, 2016) and in the Attapulgus region from southern Georgia-northern Florida, USA (Moll, 2001), 2) pedogenesis related processes such as incomplete dissolution of Mg-smectite and precipitation as identified in soils of Maharashtra, India (Hillier *et al.*, 2008) and in the Chinese Loess Plateau of northwest China (Xie *et al.*, 2013) and 3) chemical precipitation from solutions rich in Mg, Si and Al as revealed in the Tertiary lacustrine formation of Jbel Rhassoul, Morocco (Chahi *et al.*, 1993), in the Cretaceous paleosols of the Bauru Basin, Brazil (Silva *et al.*, 2018) and in the fluvial-lacustrine Serinhisar-Acıpayam basin of western Anatolia, Denizli, Turkey (Akbulut *et al.*, 2003). Combined action of the above processes cannot be excluded, similarly to palygorskite formation in SW Eskisehir, Turkey where chemical precipitation in an alkaline lake environment rich in Al and Fe under semiarid or arid conditions and transformation from saponite during diagenesis, have been suggested as the main processes, (Yeniyol, 2012). In our study the main mechanisms of Velanida palygorskite formation were probably both, complete diagenetic transformation of Mg-smectite, more evident in the clay layer A2, and partial dissolution of Mg-smectite followed by precipitation of palygorskite as manifested in the mixed palygorskite-smectite clays of layer A3. Chemical precipitation from saturated solutions rich in Mg, Si and Al was much more limited and local.

Acknowledgements

We would like to thank GEOHELLAS S.A. for the financial support of this study, G. Kacandes and G. Kastritis (GEOHELLAS S.A.) for critical review of this abstract, and V. Skounakis of the NKUA for assistance in the SEM study.

References

Akbulut, A., Kadir, S., 2003. The geology and origin of sepiolite, palygorskite and saponite in Neogene lacustrine sediments of the Serinhisar-Acipayam basin, Denizli, SW Turkey. Clays and Clay Minerals, 51, 279-292.

Chahi, A., Duplay, J., Lucas, J., 1993. Analyses of palygorskites and associated clays from the Jbel Rhassoul (Morocco): chemical characteristics and origin of formation. Clays and Clay Minerals, 41, 401-411.

Garcia-Romero, E., Suarez, M., 2013. Sepiolite–palygorskite: Textural study and genetic considerations. Applied Clay Science, 86, 129-144.

Hillier, S, Pharande, A.L., 2008. Contemporary pedogenic formation of palygorskite in irrigation induced, saline-sodic, shrink-swell soils of Maharashtra, India. Clays and Clay Minerals, 56, 531-548.

Kastritis, I.D., Kacandes, G.H., Mposkos, E., 2003. The palygorskite and Mg-Fe smectite clay deposit of the Ventzia basin, western Macedonia, Greece, in: Eliopoulos, D. et al., (Eds), Mineral exploration and sustainable development, 891-894.

Moll, W.F., 2001. Baseline studies of the clay minerals society source clays: geological origin. Clays and Clay Minerals, 49, 374-380.

Pozo, M., Carretero, M.I., Galan, E., 2016. Approach to the trace element geochemistry of non-marine sepiolite deposits: Influence of the sedimentary environment (Madrid Basin, Spain). Applied Clay Science, 131, 27-43.

Rodas, M., Luque, F.J., Mas, R., Garzon, M.G., 1994. Calcretes, palycretes and silcretes in the Paleogene detrital sediments of the Duero and Tajo basins, central Spain. Clay Minerals, 29, 273-285.

Sanchez, C. and Galan, E., 1995. An approach to the genesis of palygorskite in a Neogene-Quaternary continental basin using principal factor analysis. Clay Minerals, 30, 225-238.

Silva, M.L., Batezelli, A., Ladeira, F.S.B., 2018. Genesis and paleoclimatic significance of palygorskite in the cretaceous paleosols of the Bauru Basin, Brazil. Catena, 168, 110-128.

Stamatakis, M. G., 1995. Occurrence and genesis of huntite-hydromagnesite assemblages, Kozani, Greece – important new white fillers and extenders. Transactions-Institution of Mining and Metallurgy, 104, B179-186.

Suarez, M., Garcia-Romero, E., 2011. Advances in the crystal chemistry of sepiolite and palygorskite, in: Galan, E., Singer, A. (Eds.), Developments in palygorskite-sepiolite research a new outlook on these nanomaterials, 33-55.

Xie, Q., Chen, T., Zhou H., Xu X., Xu H., Ji J., Lu H., Balsam W., 2013. Mechanism of palygorskite formation in the Red Clay Formation on the Chinese Loess Plateau, northwest China. Geoderma, 192, 39-49.

Yeniyol, Y., 2003. Geology and mineralogy of a sepiolite-palygorskite occurrence from SW Eskisehir (Turkey). Clay Minerals, 47, 93-104.

15th International Congress of the Geological Society of Greece
Athens, 22-24 May, 2019 | Harokopio University of Athens, Greece
Bulletin of the Geological Society of Greece, Sp. Pub. 7 Ext. Abs. GSG2019-185

Genesis and geotectonic setting of the Mt Papikion pluton (Central Rhodope, Greece)

A. Drakoulis[1], A. Koroneos[1], T. Soldatos[1], L. Papadopoulou[1]

(1) Aristotle University of Thessaloniki, University Campus, 54124, Thessaloniki, Greece, alexdr@geo.auth.gr

The evolution of the Rhodope massif has been extensively studied and its basement in the Greek part has been divided into two tectonic units: the Lower Tectonic Unit (LTU), also known as Pangaion, and the Upper Tectonic Unit (UTU) also known as Sidironero. The LTU is exposed as tectonic windows in the UTU. In the eastern Rhodopes, LTU is exposed as a string of four separated domes: the Chepinska, Arda, Kesebir-Kardamos, and Biela Reka (Burg, 2012).

The Mt. Papikion pluton stretches East-West from Iasmos to Komotini, and South-North from the Xanthi-Komotini fault to the Greek-Bulgarian border. The pluton, with characteristic gneissic texture, covers about 100 km^2, intrudes the SW parts of Kesebir-Kardamos Dome (Figure 1), and it is in contact with gneisses to NE and marbles to SW, representing the lower and the intermediate unit of Kesebir-Kardamos Dome, respectively (Bonev *et al.*, 2006).

In this paper we focus on the genesis and the geotectonic setting of the Mt. Papikion pluton.

Mt. Papikion pluton consists mainly of five rock types which have been classified on the basis of field observations, mineralogical composition and Q'-ANOR classification. These types are hornblende diorite (Hbl-Dr), biotite hornblende diorite (Bt-Hbl-Dr), hornblende granodiorite (Hbl-Grd), biotite hornblende granodiorite (Bt-Hbl-Grd) and biotite granodiorite (Bt-Grd).

Based on field observations, isotopes and trace elements behavior, evolution of the plutonic rocks can be attributed to an assimilation with simultaneous fractional crystallization process (AFC) (Figure 2). The rock types of the Mt Papikion pluton are essentially the result of the fractional crystallization process of two dioritic melts having small geochemical differences, which assimilate the rocks into which they intrude, namely gneiss and meta-SnGr (meta-syenogranite). The model proposed on the basis of trace elements and verified by isotopes takes into consideration two initial dioritic magmas. The bulk distribution coefficients calculated by the AFC models are in agreement with the crystallization of plagioclase + K-feldspar + hornblende + biotite + apatite + zircon + allanite + titanite + magnetite, as determined by the variation of the major elements, trace elements and rare earth elements. The deviations that many of the samples of the Mt Papikion pluton show from these curves are probably due to the fact that these rocks do not represent pure melts but are the result of an incomplete separation between the residual liquid and the crystalline solid.

U-Pb method in zircons gave an age of 236±8 Ma (Drakoulis *et al.*, 2013) which considered as the age of crystallization as well as the age of the pluton intrusion, suggesting a magmatic episode in the Upper-Middle Triassic. Despite the fact that the pluton is located in the Rhodope Massif, it differs from the extended Eocene-Miocene magmatism of the area and it is even very different from that of Xanthi, which is located only few kilometers west. Plutons of similar age are not mentioned in the literature for the Rhodope Massif, while older ages have been reported for metagranites. However, plutons of similar ages (Poli *et al.*, 2009; Bonev et *al.*, 2018) have been found in the Serbo-Macedonian Massif which is part of the UTU.

The presence of basic rocks in Mt. Papikion pluton, suggests that a mantle component had a significant role in the genesis and evolution of the pluton. This feature in combination with petrotectonic and spider diagrams, suggest a volcanic arc magmatism. The lower unit of the Kardamos Dome consists of high metamorphic grade rocks, orthogneiss and migmatites, which also suggests its continental origin. The pluton of Mt Papikion intrudes mainly the orthogneiss, which indicates an environment of an active continental margin, in accordance to the geochemical data.

The pluton's emplacement occurs in the Middle Triassic. Geochemical characteristics show that the intrusion took place in an active continental margin. During the Middle Triassic, as various researchers state, the ocean of Paleo-Tethys closed and the ocean plate subducted under individual parts of Eurasian continental blocks (active continental margins) (Fig. 3).

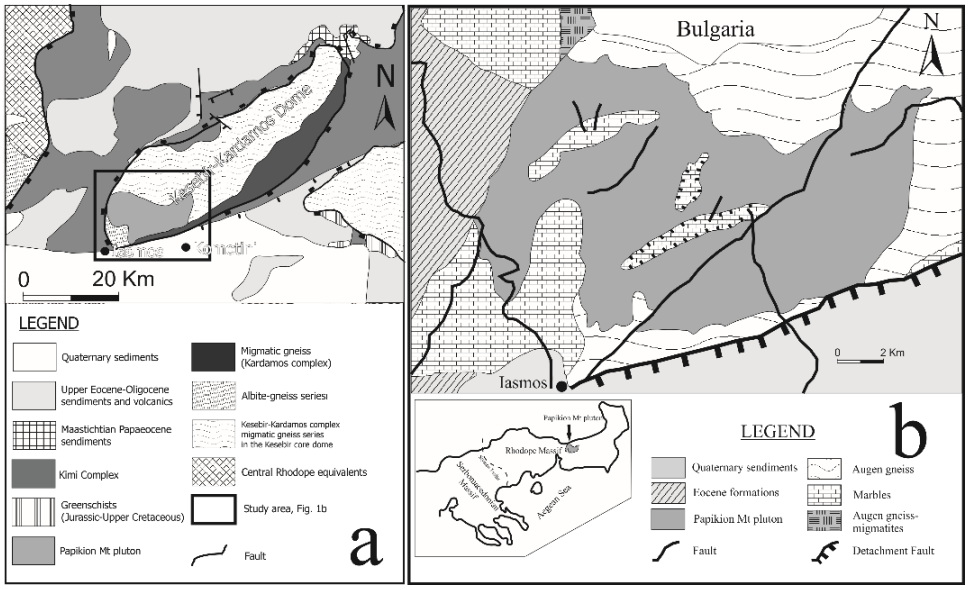

Figure 1. a: Geological map of Kesebir-Kardamos Dome (modified after Bonev *et al.*, 2006), b: Geological map of Mt Papikion pluton (modified after Dimadis and Zachos, 1986).

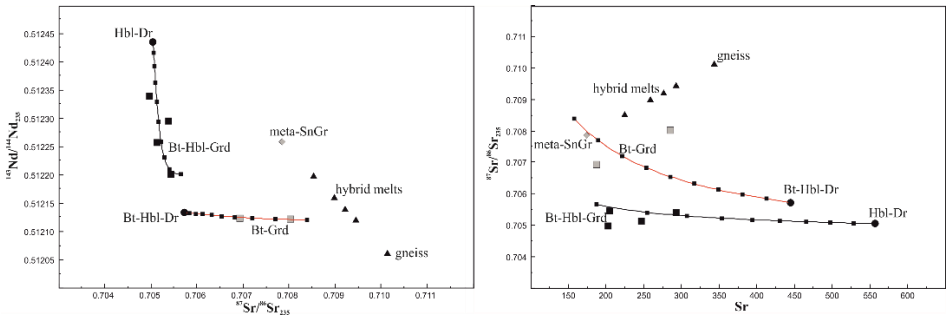

Figure 2. $^{143}Nd/^{144}Nd_{235}$ vs $^{87}Sr/^{86}Sr_{235}$ and $^{87}Sr/^{86}Sr_{235}$ vs Sr plots. Isotope modelling of AFC process of the Mt Papikion pluton evolution.

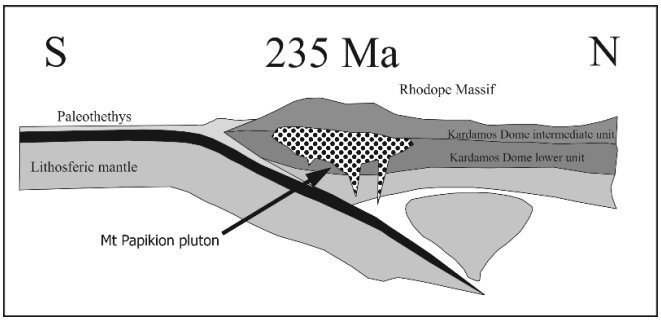

Figure 3. Geotectonic setting of Mt Papikion pluton emplacement (Active continental margin).

References

Bonev, N., Burg, J.-P., Ivanov, Z., 2006. Mesozoic-Tertiary structural evolution of an extensional gneiss dome–the Kesebir-Kardamos dome, eastern Rhodope (Bulgaria-Greece). Int. J. Earth. Sci., 95 (2), 318-340.

Bonev, N., Moritz, R., Borisova, M., Filipov, P., 2018. Therma-Volvi-Gomati complex of the Serbo-Macedonian Massif, Northern Greece: A Middle Triassic continental margin ophiolite of Neotethyan origin. Journal of the Geological Society, DOI: https://doi.org/10.1144/jgs2017-130.

Burg, J-P, 2012. Rhodope: From Mesozoic convergence to Cenozoic extension, in: Skourtsos E., Gordon S. Lister (Eds.), The Geology of Greece. Review of petro-structural data in the geochronological frame Journal of the Virtual Explorer, Electronic Edition, ISSN 1441-8142, 42, paper 1.

Dimades, E., Zachos, S. 1986.Geological map of Rhodope 1:200.000. IGME.

Drakoulis, A., Koroneos, A., Poli G., Soldatos, A., Papadopoulou, L., Murata, M., Eliwa, H., 2013. U-Pb zircon dating of the Mt. Papikion pluton (Central Rhodope, Greece): New constraints on the evolution of Kesebir-Kardamos Dome. Acta Vulcanologica 25, 1-2, 83-98.

Poli, G., Christofides, G., Koroneos, A., Soldatos, T., Perugini, D., Lagone A., 2009. Early triassic granitic magmatism – Arnea and Kerkini granitic complexes – in the Vertiskos unit (Serbo-macedoniam massif, north-eastern Greece) and its significance in the geodynamic volution of the area. Acta Vulcanologica, 20/21, 4770.

15th International Congress of the Geological Society of Greece
Athens, 22-24 May, 2019 | Harokopio University of Athens, Greece
Bulletin of the Geological Society of Greece, Sp. Pub. 7 Ext. Abs. GSG2019-188

Textural, Mineralogical and Geochemical Assessment of the Pikrolimni Lake Sediments (Kilkis district, Northern Greece) and suitability for use in pelotherapy

E. Sofianska[1], K. Athanasoulis, D. Tarenides, N. Xirokostas, M. Gaga

Hellenic Survey of Geology and Mineral Exploration, 1 S.Louis st., 13677, Acharnes, Athens, Greece, esofianska@igme.gr

Mud therapy has been used since ancient periods for medical or cosmetic purposes. Pelotherapy is the application of thermal muds (peloids) for recovering muscle-bone-skin pathologies (Veniale et al. 2007). Peloid muds are fine grained sediments, produced by different geological and biological processes. Because of their positive and beneficial effect on human organisms their mixture with water could often be used for mud baths and cataplasms. Nowadays, pelotherapy is being more and more focused on specific pathologies and treatments. However, not all muds can be used for mud therapy, whereas natural occurrences of suitable thermal muds are going exhausted. To be suitable for pelotherapy, certain qualities of peloids are necessary. Textural, mineralogical and geochemical characteristics of a virgin mud are critical factors ruling its quality for use as peloid mud in pelotherapy. Special attention was given to potentially toxic elements (PTE) namely As, Cd, Cr, Cu, Hg, Ni, Pb, Zn etc., because of their hazardous effect on human health (Carretero et al., 2010; Rebelo et al., 2011).

The present research was conducted on the Pikrolimni Lake sediments (PLS). Pikrolimni Lake is located in the Kilkis district, near Thessaloniki (23 km), in northern Greece. It is a small shallow lake up to 1.5 m depth, and it is well known as a pelotherapy center. PLS are used for the preparation of peloid mud, but no detailed data exist on their characteristics.

The aim of this investigation was to assess the texture, mineralogy and geochemistry of PLS. Chemical results were compared with reported Earth's upper crust average shale (Li, 2000) as well as with different muds used for medical purposes. The index of geo-accumulation (Igeo) and the iron normalized enrichment factor (EF) were used for the characterization of PTE contamination levels. The results of this investigation aim at helping to develop suitable processes for making the PLS suitable for therapeutic uses.

Three composite samples were prepared by mixing of least 10 sub-samples collected from representative bottom surfaces 5x10 m of the lake. Portions of the sediment samples were used for grain size, mineralogical and geochemical analyses. The grain size composition was performed according to the ASTM D 422-63 and ASTM 2217-85.

X-ray powder diffraction (XRD) analysis was used for the study of the mineralogical composition of the sediments. Bulk samples and the separated clay fraction (<2μm) in oriented, glycolized and heated samples were used. The major and minor element oxides were determined by X-ray fluorence analysis (XRF), whereas the concentrations of PTE were determined by inductively coupled plasma mass spectrometry (ICP-MS). All the analytical work was conducted at the Laboratories of the Institute of Geology and Mineral Exploration (IGME).

Textural analyses showed that the sediment samples are composed of 73.10% sand, 23.62% silt and 3.27% clay, and are classified as sandy loamstones (Curtis 2005) This means that a sieving is necessary to improve the quality of the sediments for application in pelotherapy.

XRD analyses revealed that the PLS are composed of high average quantities of quartz (59.3%) and clay minerals (19.7%), followed by muscovite (12.0%), albite (8.0%) and carbonates (1%). The clay minerals present are mainly kaolinite, with minor montmorilonite, and illite.

The chemical composition of PLS showed an increased SiO_2 content varying between 63.44 and 70.35% (average value 66.97%), and a lower Al_2O_3 varying between 8.86% and 12.60% (average value 10.72%), expressing the mineralogical composition of them. In comparison with the chemical composition of the average shale the PLS have significantly higher SiO_2 and lower Al_2O_3 (58.39% and 15.12%, respectively). This is attributed to the fact that the PLS samples have a larger content of quartz and a lower content of clay minerals. They also have lower Fe_2O_3 (3.41%) and higher Na_2O (2.61%) than the average shale (6.75% and 1.29%, respectively. A lower percentage of K_2O (1.60%) in PLS, in relation to that of the average shale (3.21%), is due to their lower content of illite. The concentrations of MnO, MgO, TiO_2 and P_2O_5 is comparable with those referred for the average shale. The Na_2O/CaO ratio is<1, confirming the presence of the typical non-swelling 2:1 clay minerals (El-Hinnawi and Abayazeed, 2012).

The analyzed PTE in PLS (Table 1) were found to be higher for Pb, As, Ni, Cr and Zn and lower for Co and Cu in comparison to average shale. The calculated *Igeo* values, on the basis of average shale composition, showed moderate contamination for Pb and As and no contamination for Ni, Zn, Cr, Co, Cu for the PLS. The *EF* values for Ni, Zn, Cr, Co, and Cu ($EF \leq 1$) denoted no enrichment that is a natural origin of them. The minor enrichment found for As and Pb ($1 < EF < 3$), must be associated with anthropogenic activities. Pb and As were classified into the first group of heavy metals that should be essentially absent from peloids because they are known as human toxicants or environmental hazardous (Rebelo *et al*., 2011). However, many examples of peloid muds applied to pelotherapy are referred to contain higher levels of these heavy metals (Quintela *et al*., 2012; Rizo *et al*., 2013).

In conclusion, on the basis of the texture the PLS can be used as virgin clays in pelotherapy only after sand size particles could be separated by sieving, before any potential application. It is an advantage for PLS that the most PTE are within

normal ranges. The minor enrichment of PLS in Pb and As is probably of no significant concern for human health in case of their application in pelotherapy.

Table 1. Summary of heavy metals data for the Pikrolimni Lake sediments

Trace elements	Range (mg/kg)	Average (mg/kg)	Average shale	EF	Description of enrichment	Igeo	Description of contamination
As	24-42	33,33	13	1,92	Minor enrichment	0,77	Moderate
Co	9-12	10,67	19	0,42	No enrichment	-1,42	Uncontaminated
Cr	80-92	85,67	90	0,71	No enrichment	-0,66	Uncontaminated
Cu	29-33	31,00	45	0,51	No enrichment	-1,12	Uncontaminated
Ni	46-52	49,00	50	0,73	No enrichment	-0,61	Uncontaminated
Pb	30-35	32,67	20	1,22	Minor enrichment	0,12	Moderate
Zn	85-110	95,33	95	0,75	No enrichment	-0,58	Uncontaminated

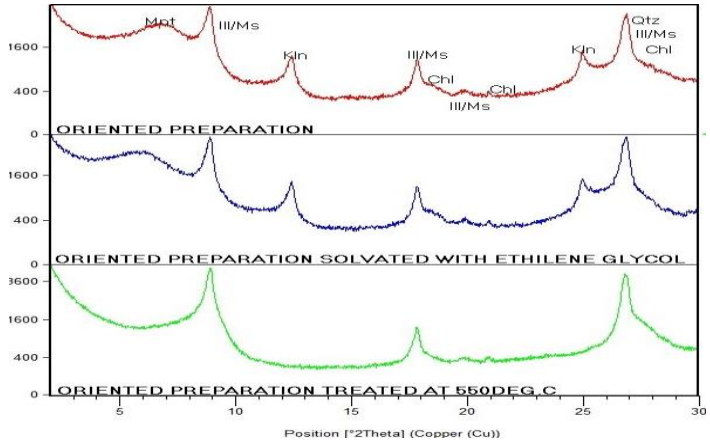

Fig.1. XRD patterns of Pikrolimni Lake sediments (Ill/Ms-Illite/Muscovite, Kln-Kaolinite, Mnt-Montmorillonite, Chl-Chlorite, Q-Quartz).

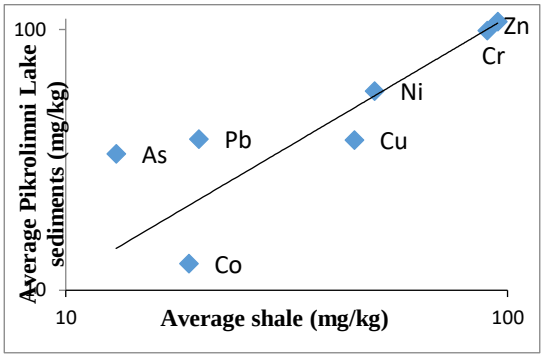

Fig. 2, Relationship between average trace elements in PLS and average shale

A further investigation is needed to study the concentration of these metals in a derivative peloid mud from the PLS and to determine the mobility and bioavailability of the metals. These properties are among the most important for the suitability of a peloid mud for pelotherapy.

Acknowledgements

This research was financially supported by the IGME.

References

Carretero, M.I., Pozo, M., Martín-Rubí, J.A., Pozo, E., Maraver, F., 2010. Mobility of elements in interaction between artificial sweat and peloids used in Spanish spas. Applied Clay Science 48, 506–515

Curtis, J.O. 2005. Electromagnetic Poser Attenuation in Soils. ERDC/EL TR-05-5. Vicksburg, MS: U.S. Army Engineer Research and Development Center.

El-Hinnnawi, E., Abayazeed, S.D., 2012, The Suitability of some Egiptian smectitic clays for mud therapy. Journal of Applied Science 12, 480-485.

Li, YH.A., 2000. A compendium of geochemistry. Princeton: Princeton University Press.

Quintela, A., Terroso, D., Da Silva, E. F., & Rocha, F., 2012. Certification and quality criteria of peloids used for therapeutic purposes. Clay Minerals 47, 441–451.

Rebelo, M., Viseras C., Lopez Galindo, A., Rocha F., Fereira da Silva, E., 2011. Characterization of Portuguese geological materials to be used in medical hydrology. Applied Clay Science 51, 258-66.

Rizo, O.D., Rudnikas, A.G., Rodrigues, K.D., Padila, D.B., 2000. Assessment of historical heavy metal content in healing muds from San Diego (Cuba) using nuclear analytical techniques. Nucleaus 53, 19-23.

Veniale, F Battero, A., Jobstraibizer, P.G., Setti M., 2007. Thermal muds: Perspectives of innovations. Applied clay science 36, 141-147.

15th International Congress of the Geological Society of Greece
Athens, 22-24 May, 2019 | Harokopio University of Athens, Greece
Bulletin of the Geological Society of Greece, Sp. Pub. 7 Ext. Abs. GSG2019-193

Rare-Earth Minerals within Phyllite-Quartzite Series of SE Alagonia Area (Peloponnese)

G. Economou[1], D. Tsagas[1], A. Photiades[1]
(1) EAGME, Olympic Village, Acharnae, Greece, dop@igme.gr, dirgen@igme.gr, fotiadis@igme.gr

The Rare Earth Elements (REEs) have recently moved into the spotlight since the European Commission were characterized them as critical elements. The wide use of REEs in a variety of modern applications set in motion many exploration projects for new potential REE-bearing resources. In Greece, also there are prominent locations which demonstrate REE enrichments giving the opportunity for further research. In the frame of the current research work, REE-bearing minerals where found to be present within the Phyllite-Quartzite Series of SE Alagonia Area (Peloponnese).

The study area extends to the south-eastward parts of Alagonia village, in the NW slopes of the Taygetos Mt., and geologically, consists of metamorphic nappe pile that took place during the plastic deformation of the Phyllitic-Quartzitic series and its thrusting westward on the top of the Plattenkalk series in Miocene times (Xypolias & Doutsos 2000; Jolivet et al., 2010). Furthermore, the Phyllite–Quartzite series dominated by schists and metapelites, and a lower unit of the Plattenkalk series consisting of multi-colored crystalline platy Mesozoic limestone topped by meta-flyschoidal sequence of the lower Oligocene. Due to the intercontinental subduction events in Oligocene times, both the Plattenkalk series, as the deeper metamorphic unit of the external Hellenides, and the Phyllite–Quartzite series, underwent successively HP/LT metamorphic episodes, the former during late Oligocene-lower Miocene times (Thee & Seidel 1991), and the latter in Lower Miocene 19-24 My (Panagos et al., 1979; Seidel et al., 1982, 2006).

In particular, the Phyllite–Quartzite series in the area of Alagonia, over 500 m thick, due to penetrate ductile deformation, consists of a wide range of dark-grey coloured sequence of phyllite–schist rocks (metashales and/or metamudstones) cutting by quartz veinlets (pressure dissolution). Besides, this lithological sequence is affected by stretching lineation indicating top-to-the-W and/or top-to-the-WSW sense of shear, and contains of pseudo-intercalations, boudins and shear-bands of blueschists within greenschists (chloritoid, albite), mica-schists, metaquartzite, quartz-pebble metaconglomerate, marble, serpentinite, and MORB metavolcanic rocks (Skarpelis, 1982).

Phyllite and mica-schist samples were characterized using different mineralogical techniques in order to quantify the modal mineralogy and the REE composition of REE-bearing phases. More specifically measurements were performed using polarized microscopy (Leica DMLP) under reflected and transmitted light, scanning electron microscopy (SEM) with a JEOL-JSM 5600 for semi-quantitative evaluation of minerals and finally X-ray diffraction (XRD).

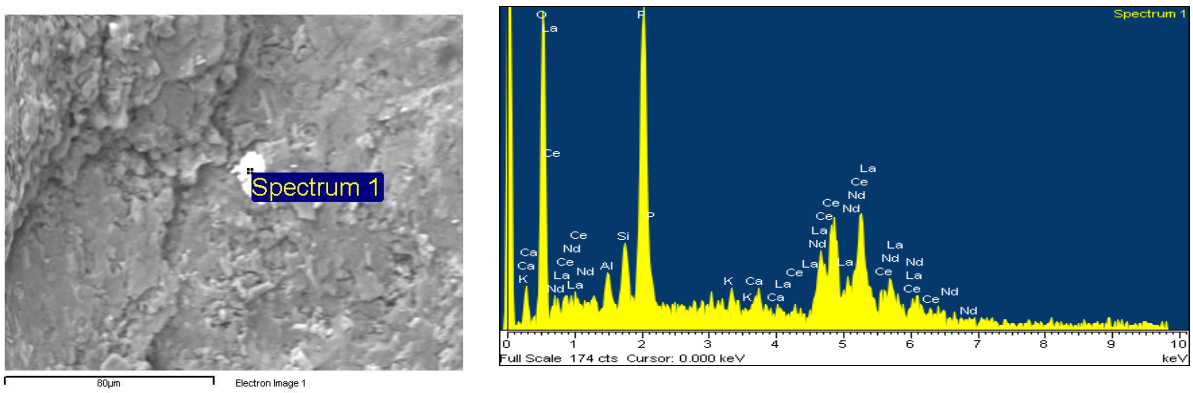

Figure 1. SEM Quantitative evaluation of monazite by SEM (I.G.M.E., Mineralogy – Petrography Lab.)
(Al_2O_3 : 2.50%**, SiO_2 :** 3.15%**, P_2O_5 :** 30.13%**, K_2O :** 0.95%**, CaO :** 1.73%**, La_2O_3 :** 17.42%**, Ce_2O_3 :** 31.94%**, Nd_2O_3:** 12.05%, Total: 99.87%)

The **phyllite sample,** which is black in color due to the high chlorite presence, characterized by its intense schistosity indicating metamorphic layering and by a fine-grained mineral content. In fine-layers the mineral phases are distinguished by **quartz**, in elongated recrystallized assemblages, associated with muscovite-flakes and scattered magnetite. Furthermore, it was determined by the measurements the presence of **muscovite,** micritic and microsparitic **calcite**, **rhipidolite** as Fe-rich chlorite, and **albite** as elongated hypidiomorphic crystals. Besides, the **REE-bearing phases, which** appear as gangue minerals are represented mainly by **monazite** (Fig. 1) and in lesser extend **allanite** (Fig. 2) and **apatite.** The latter contributes to the elevated phosphorus content. Zircon, magnetite, titanium-rich phases (rutile and sphene) as well are the minor mineral phases.

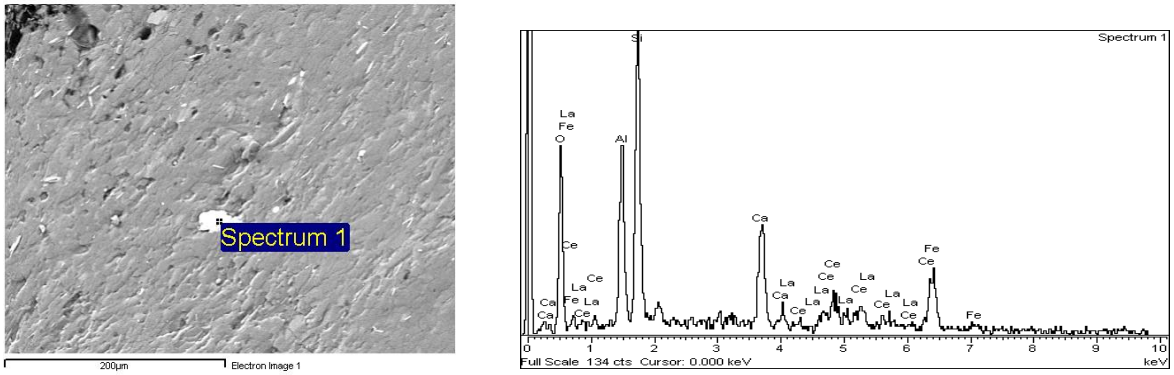

Figure 2. Semi-Quantitative evaluation of allanite by SEM (I.G.M.E., Mineralogy – Petrography Lab.)
(Al_2O_3 :19.85 %**, SiO_2 :** 35.25%**, CaO :**12.16%**, FeO :**15.96%**, La2O**3 : 5.09**, Ce_2O_3** :11.22 %, **Total**: 99.53)

On the other hand, the **mica-schist** sample reveals a medium-grained grayish sample with foliated texture, which is also presented in banded layers. They provided the following mineral assemblage, such as, **quartz**, in elongated recrystallized forms, associated with muscovite-flakes and scattered magnetite; mica, consisting mainly of **muscovite** related to **paragonite** components, chlorite, under compositions of **clinochlore** and **rhipidolite** (iron-rich member), and **albite** as elongated hypidiomorphic crystals. Moreover, the **rare-earth minerals** appear as gangue minerals consisting mainly of **allanite-monazite** mineral phases, **allanite** and **apatite**, and many titanium-rich minerals; monazite, zircon and magnetite are accessory minerals. We signalize that paragonite as common mineral in blueschist facies rocks along with other sodic minerals (e.g. glaucophane) retrograded to greenschist facies, where paragonite and glaucophane are transformed into chlorite and albite.

We accepted that the various types of rare-earth minerals are associated with hydrothermal mineralizations where affected metavolcanic rocks. The studied samples could be associated with the protolith of the Phyllite–Quartzite series derived from a rift sequence of Permian-Triassic age, which took place in Apulia with its progressive expansion and basalt eruptions (Seidel et al., 1982); or these rare-earth mineralizations would be related with an accreted Palaeotethyan oceanic crust (Stampfli et al., 2001).

Obviously, the presence of rare-earth minerals in Alagonia area is a promising target locality to survey of sedimentary placers in recent river gravels, such as the Neda River, that would be survived by physical and chemical weathering of a primary deposit and then transported by water to a new location and deposited.

References

Jolivet, L., Trotet, F., Monie, P., Vidal, O., Goffe, B., Labrousse, L., Agard, Ph., Ghorbal, B., 2010. Along-strike variations of *P–T* conditions in accretionary wedges and synorogenic extension, the HP–LT Phyllite–Quartzite Nappe in Crete and the Peloponnese. Tectonophysics, 480:133-148.

Panagos, A.G., Pe-Piper, G., Piper, D.J.W., Kotopouli, C. N., 1979. Age and stratigraphic subdivision of the Phyllite series Krokee region Peloponnese, Greece. N. Jb. Geol. Paläont. Monatshefte, 1979, 181–190.

Seidel, E., Kreuzer, H., Harre, W., 1982. A late Oligocene-Early Miocene high-pressure belt in the External Hellenides. Geol. Jahrb. E23:165-206.

Seidel, M., Zacher, W., Schwarz, W.H., Jaeckel, P., Reischmann, T., 2006. A Late Carboniferous age of the gneiss of Potamos (Kythira Island, Greece) and a new consideration on geodynamic interpretations of the Western Hellenides. N. Jb. Geol. Paläont. Abh., 24:325–344.

Skarpelis, N., 1982. Metallogeny of massive sulphides and petrology of the External Metamorphic Belt of the Hellenides (SE Peloponnesus). PhD thesis, University of Athens.

Stampfli, G., Mosar, J., Faure, P., Pillevuit, A., Vannay, J.-C., 2001. Permo-Mesozoic evolution of the western Tethys realm: the Neotethys East Mediterranean basin connection, in: Ziegler, P., Cavazza, W., Robertson, A.H.F., Crasquin-Soleau, S. (Eds), Peri-Tethys Memoire, 5. Peri-Tethyan Rift-Wrench Basins and Passive Margins. Memoires du Museum National d'Histoire Naturelle, 51-108.

Theye, T., Seidel, E., 1991. Petrology of low-grade high pressure metapelites from the External Hellenides (Crete Peloponnese). A case study with attention to sodic minerals. Eur. J. Mineral, 3:343-366.

Xypolias, P., Doutsos, T., 2000. Kinematics of rock flow in a crustal-scale shear zone, implication for the orogenic evolution of the southwestern Hellenides. Geol. Mag., 137/1:81–96.

15th International Congress of the Geological Society of Greece
Athens, 22-24 May, 2019 | Harokopio University of Athens, Greece
Bulletin of the Geological Society of Greece, Sp. Pub. 7 Ext. Abs. GSG2019-227

Evaluation of the impact of a landfill on the soil physicochemical parameters

E. Koutsopoulou[1], D. Papoulis[1], P. Tsolis-Katagas[1]
(1) University of Patras, 26504 Rion, Greece, ekoutsop@upatras.gr

Introduction

Although proper waste management nowadays includes collection, transport, treatment and finally disposal of waste together with monitoring and regulation, landfilling is still widely used as a waste management method for municipal solid waste. However, landfills if not properly managed, give rise to air and water pollution and may severely affect the environment due to leachate leakage and contaminant transport in the surrounding environment which can cause numerous contamination problems long after disposal has ceased. Landfill leachate may contaminate the natural soil and groundwater if allowed to migrate without appropriate engineered facilities to mitigate its effect on the natural environment.

The aim of the study was to evaluate the environmental risks associated with the waste disposal facility in the municipality of Zakythos and the extent of the leachate adverse impacts on the natural soil environment.

Materials and Methods

Samples were collected around the landfill and from sediments from a stream system, in the vicinity of the waste disposal site. The mineralogical composition of all samples was determined by XRD and bulk sample chemical analyses for major and trace elements were performed with INAA and ICP-MS. Surface soil samples were also collected down gradient of the landfill and analysed to determine some physicochemical parameters which are usually considered indicators of pollution from solid waste disposal. Determination of the physicochemical parameters was performed in soil extracted solutions according to Handbook of Soil Analysis (Pansu and Gautheyrou, 2006). Chloride (Cl^-) was measured using the $AgNO_3$ method by Hach® titration kits while sulphate (SO_4^{2-}), nitrate (NO_3^-), nitrite (NO_2^-) and ammonium (NH_4^+) were determined using a spectrophotometer (Hach® DR/4000). pH and Electrical Conductivity (EC) were measured according to 9045D EPA (Environmental Protection Agency) and USDA, National Soil Survey Handbook (2011) methods respectively.

Results and Discussion

Clays and clay minerals are widely used in environmental applications due to their ability for adsorption and removal of heavy metal contaminants, organic and biological cations and non-ionic organic compounds (Koutsopoulou et al., 2010, Schoonheydt et al., 2018). The determination of the clay mineralogy of the clayey material used in a waste disposal site is a key factor in controlling the contaminant transport in the surrounding environment which can cause numerous problems long after disposal has ceased. X-ray diffraction patterns of random powder mounts revealed the presence of quartz, calcite, plagioclase, traces of gypsum and clay minerals in all samples. The clay fraction (<2μm) of the samples is dominated by smectite, chlorite, illite, serpentine and mixed-layer chlorite-smectite. X-Ray Diffraction patterns of the <2 μm fraction of samples collected around the landfill are shown in Figure 1. Chemical analyses showed that the highest values of heavy metals such as As, Cu, Zn and Pb are evident in the stream sediments (Koutsopoulou et al., 2013). The pH values calculated range between 7.7 and 8.8 for all samples which do not exceed the permissible WHO limits and EC values range between 120μS/cm and 2750μS/cm with the highest values found in the stream sediments. Chloride values ranged between 20 and 400 mg/L and sulphates between 19 and 2000 mg/L. Chloride is usually considered as a tracer around landfill sites; the presence of sulphates, however could also be attributed to the dissolution of gypsum present in most of the samples. The mean values of some of the physicochemical parameters determined are given in Figure 2. The comparison of mean soil extraction values with surface runoff water and rainwater shows that stream sediments are becoming enriched in most of the analyzed physicochemical parameters. The ammonium concentration of the soil extractions and the surface runoff water display elevated values that exceed the EE drinking water guidelines (0.2 mg/L). Ammonium in soils and surface water is usually a marker of bacterial, sewage or animal waste pollution and could be attributed to contamination from the landfill site (Koutsopoulou et al., 2013). The mean nitrite concentration (0.7 mg/L) of the soil extractions and the surface water is also an indicator of contamination from the landfill.

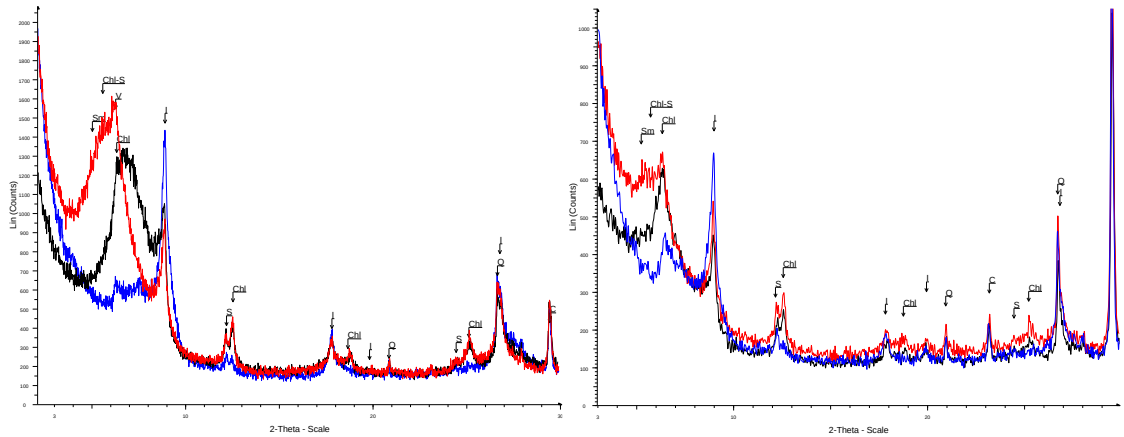

Figure 1. X-Ray diffraction patterns of the <2 μm fraction of the samples. Sm: smectite, Chl: chlorite, I: illite, S: serpentine, Chl-S: mixed layer chlorite-smectite, Q: quartz, C: calcite.

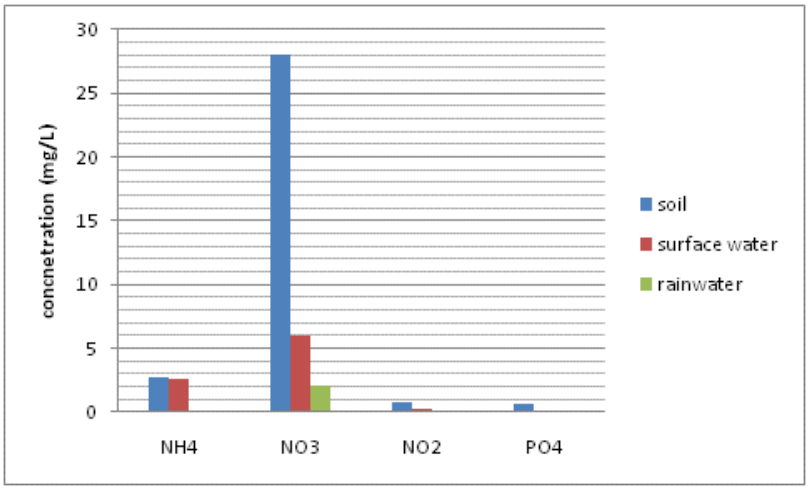

Figure 2. Mean chemical composition of soil extractions, surface runoff water and rainwater in mg/L.

Conclusions

The environmental impact of the landfill in the downstream area was evaluated. The mineralogical composition of the samples collected from the landfill site revealed the presence of abundant clay minerals (i.e. smectite) which are widely used as natural clay barriers in waste disposal sites. The mean chemical composition of the soil extractions and surface runoff waters show that stream sediments are becoming enriched in most of the analyzed physicochemical parameters. The concentrations of the aforementioned physicochemical parameters in the soil samples exceeded the average permissible concentrations and are considered as human induced contamination from the landfill.

Acknowledgements

This research was funded by the University of Patras through the 'K. Karatheodoris' basic research funding scheme.

References

Koutsopoulou, E., Papoulis, D., Tsolis-Katagas, P., and Kornaros, M., 2010. Clay minerals used in sanitary landfills for the retention of organic and inorganic pollutants. Applied Clay Science 49, 372-382.

Koutsopoulou, E., Katsanou, K., Papoulis, D., Zagana, E., Tsolis-Katagas, P., 2013. Environmental assessment of contaminants in a downstream area of a landfill, Bulletin of the Geological Society of Greece, 47, 972-980.

Lambert, J.F., 2018. Organic Pollutant adsorption on clay minerals, in: Schoonheydt, R., Johnston, C.T., Bergaya, F., (Eds.), Surface and Interface Chemistry of Clay Minerals, Developments in Clay Science, vol. 9, 195-244.

Pansu, M., Gautheyrou, J., 2006. Handbook of Soil Analysis. Mineralogical, Organic and Inorganic Methods. Springer-Verlag, Berlin, Heidelberg. 995 pp.

USDA, National Soil Survey Handbook, 2011. United States Department of Agriculture, Part 618, Soil Properties and Qualities.

15th International Congress of the Geological Society of Greece
Athens, 22-24 May, 2019 | Harokopio University of Athens, Greece
Bulletin of the Geological Society of Greece, Sp. Pub. 7 Ext. Abs. GSG2019-232

Numerical simulation of the Kallianos Au-Ag-Te-bearing ore fluid flow along the CBU detachment, Attico-Cycladic Metallogenetic Massif

M. Fitros[1,3], S.F. Tombros[2], S. Kokkalas[3]

(1)Mineralogical Museum of Lavrion, Attica, Hellas michalis.fitros92@gmail.com
(2)Regional Directorate of Primary and Secondary Education in Western Greece, PDEDE, 25A Akti Dimaion, 26222, Patras, Hellas
(3)Department of Geology, University of Patras, Rion, 26500, Patras, Hellas

Abstract

The Kallianos deposit is located in south Evia at the northern part of the Attico-Cycladic Metallogenetic Massif and consists of carbonate-replacement and vein-type ores. The Au-Ag-Te vein mineralization associates with sixteen ore-bearing syntaxial quartz-I and -II type veins that intersect the schists and marbles of the Cycladic Blueschist Unit. The veins comprise two hypogene ore stages which involve the deposition of stage I-pyrite, and stage II-chalcopyrite, galena and tellurides. Zones of muscovite-chlorite alteration surround the quartz-I and -II type veins.

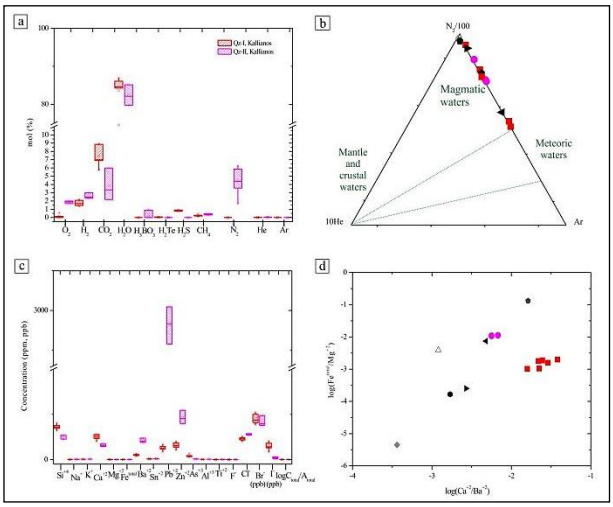

Figure 1. Fluid chemistry of the Kallianos ore fluids: (a). Box-and-whisker plot for the L-V fluid inclusions displaying their gaseous phase content (in mol fractions %) in quartz-I and quartz-II for Kallianos ore fluids, (b).Ternary N2, He and Ar diagram of fluid inclusion gaseous compositions. End-member gaseous fluid compositions and compositional ranges are from Wilkinson (2001), (c). Box-and-whisker plot for the L-V fluid inclusions showing the liquid phase content (in ppm and ppb) in quartz-I and quartz-II, and (d). Log(Ca+2/Ba+2) versus log(Fetotal/Mg+2) plot for the fluid inclusion liquid phase. In this plot for comparison, we have also added data from Plaka, Daskalio, vein 80 and Sounio, Lavrion, Aspros Kavos, Makronisos and Volax, Tinos. The magmatic values are from Williams-Jones et al. (2010).

Bulk chemical analyses of the quartz-I and quartz-II veins and related sulfides from Kallianos suggest that they are enriched in Au, Ag and Mo. They also display Th/U values ≤ 7.8, $(La/Sm)_N$ ratios of ~ 0.2 to 0.7 and moderate negative Ce/Ce* and Eu/Eu* anomalies. Raman and chromatographic analyses suggests ore-fluid gaseous phase contains mostly CO_2, N_2, and H_2S, minor H_3BO_3, O_2, H_2, CH_4, and H_2Te and traces of He and Ar (Fig 1a, b). Bulk composition of the ore fluid liquid phase indicates that Cl^- is the dominant anion in the ore solution and Si^{+4}, Mg^{+2}, Ba^{+2}, Pb^{+2}, $Fe^{+2(total)}$ and Zn^{+2} the dominant cations (Fig. 1c). Stage I-ore fluid bears $log(Ca^{+2}/Ba^{+2})$ values in respect to the stage II-ore fluid which is characterized by higher $log(Fe^{total}/Mg^{+2})$ values (Fig. 1d). He, Ar and Ne isotope compositions were also obtained from fluids extracted from the same samples. Their $^3He/^4He$, $^{40}Ar/^{36}Ar$, $^{20}Ne/^{22}Ne$ and $^{21}Ne/^{22}Ne$ compositions range from 0.02-0.08 R_A, 1139-1809, 8.94-9.71 and 0.05-0.15, respectively (Figs. 2a, b). A magmatic origin is deduced for the ore fluids in equilibrium with quartz-I and -II based on measured noble gas isotopic compositions.

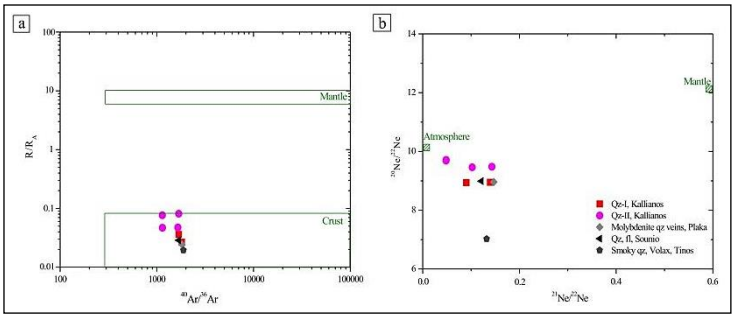

Figure 2. Helium, argon and neon isotopes: (a). R/RA versus 40Ar/36Ar, and (b). 20Ne/22Ne versus 21Ne/22Ne isotopic compositions of primary fluid inclusions in vein quartz from Kallianos ores. For comparison we have also analyzed inclusions from molybdenite quartz veins from Plaka, and quartz crystals from a fluorite vein from Sounio. The "Mantle", "Crustal" and "Atmosphere" fields are from Ballentine and Burnard (2002).

The Upper Continental Crust-normalized REE profiles of the Kallianos quartz veins and vein-type ores appear mildly enriched in the LREE relative to HREE. The Kallianos REE patterns, share many common features to the granodiorite of Plaka and related aplites, carbonate-replacement and vein-type ore deposits (Berger et al., 2013). Moreover, these REE patterns have some similarities with the Tinos leucogranite, aplites and smoky quartz from Volax and quartz veins from Panormos Bay (Tombros et al., 2007, 2010). However, Tinos REE patterns appear with some differences in their LREE patterns relatively to Kallianos.

On the N_2-He-Ar plot (Fig. 1b) the gaseous phase of both stage I and II ore fluids plots in the magmatic waters field. The linear trend observed on the same plot (i.e., on the N_2-Ar join, Fig. 1b) indicates simple cooling of the ore fluids. The Kallianos ore fluids, based on noble gases isotopic compositions resemble to both Lavrion and Tinos ore fluids, even Tinos has lower $^{20}Ne/^{22}Ne$ isotopic values (Fig. 2a, b). Fluid chemistry of the liquid phase suggests that the Kallianos ore fluids mainly plot close to the ore fluids exsolved from the Plaka granodiorite (Lavrion), and more infrequently close to Tinos (Fig. 1b and d). Moreover, in the $\log(Ca^{+2}/Ba^{+2})$ versus $\log(Fe^{total}/Mg^{+2})$ plot the quartz-II ore fluid lies on the mixing line defined between Tinos and Lavrion end-members (Fig. 1d).

An important issue addressed in our study is that a possible magmatic source is indicated from the bulk geochemistry of the quartz-I and-II veins, fluid chemistry and noble gas isotopic compositions (Figs. 1, 2). In order to estimate the possible distance from where the ore fluid could have been exsolved and then transported, we have applied a convective heat-transfer flow model. This model considers as sources the Lavrion and Tinos granitoids, which are the closest to the Kallianos ores (e.g., currently at ~60 and 85 km). It is also based on steady-state fluid flow and simple cooling of the ore fluids, using as a pathway the CBU secondary detachment between the schists and marbles. In the fault damage zone the driving flow mechanism was horizontal fluid convection that resulted in the fluctuations of temperature of the ore-fluid over distance and time. For the simplest case (fluid velocity $\approx 9 \cdot 10^{-3}$ km/Ma, by analogy to Panormos Bay, Tinos, Tombros, 2011), the equation is: $T(x) = x\ln t + bv\left(\frac{x_0 - t_0 \ln t}{T_0}\right)x$ (1).

Modelling parameters are T(x) = 230ºC, t = 2 Ma for Plaka's granodiorite, Lavrion and 4 Ma for Volax, Tinos, and x_0 = 0, i.e., the Plaka and Volax sites. At t_0 = 9.4 Ma, the ore fluid from Lavrion (T_0 = 460ºC, P ≤ 200 bars, salinity of ~ 55 wt. % equivalent NaCl, Bonsall et al., 2011) or at t_0 = 10 Ma, the fluid from Tinos (T_0 = 320ºC, P ≤ 200 bars, salinity of ~ 5 wt. % equivalent NaCl, Tombros et al., 2007) commenced to flow in the fault zone. Pressures obtained from fluid inclusions for Kallianos are P ~ 125 bars, nevertheless, the temperatures are lower due to the greater distance from the granitoid source and simple cooling of the ore fluids. Solving equation (1) for distance, we conclude that if the fluid moved in the marbles-schist interface it would have flown for a distance of 22.4 to 27.6 km away from Plaka, Lavrion or 23.9 to 29.4 km away from Volax, Tinos.

Based on our geochemical results and numerical simulation of temperature over distance we examine two possible scenarios about the source of the Kallianos ore fluids. The first involves the granodiorite of Plaka in Lavrion area. Bradley et al. (2013) reported that Attica and Evia have experienced ~ 25º ± 6.5º of post-Middle Pliocene clockwise rotation which is linked to acceleration of the Aegean subduction slab retreat and the subsequent initiation of the Evia and Corinth Gulf rifting. In a pre-rotational setting at ~ 9 to 8 Ma the areas of Kallianos, Plaka-Sounio in Attica could have been at a distance of ≤ 20 to 25 km, i.e., the calculated distance that the ore fluid had travelled along the CBU detachment or the WCDS. The second scenario implicates the Tinos leucogranite as a source of the ore fluids exsolved from Volax site. In a similar case at Panormos Bay, Tinos (Tombros et al., 2007, 2010), the Au-Ag-Te mineralization was linked to the volatile evolution of the Tinos pluton, which at surface is ~ 16 km from the leucogranite. Channelized flow at depth may have occurred along the damage zone of the detachment interface between the BU marbles and the CBU or alternatively along the contact between the CBU and the UCU. However, for the Au-Ag-Te bearing ore fluid originated from Tinos the calculated distance that the ore fluid may had moved along the CBU detachment or the NCDS was ~ 24 to 30 km. It seems that Tinos leucogranite could only have promoted mineralization up to Panormos Bay, as recommended by Tombros et al. (2007, 2010). Herein, we propose that Kallianos is an outlier or satellite ore deposit of the Lavrion hydrothermal system with Plaka's granodiorite as the major source for the Au-Ag-Te ore fluids. A possible subsurface pluton with similar characteristics cannot be excluded but there are not any data for its presence so far.

References

Ballentine, C.J., Burnard, P.G., 2002. Production, release and transport of noble gases in the continental crust. Reviews in Mineralogy and Geochemistry 47, 481-538.

Berger, A., Schneider, D.A., Grasemann, B., Stockli D., 2013, Footwall mineralization during Late Miocene extension along the West Cycladic Detachment System, Lavrion, Greece. Terra Nova 25, 181-191.

Bonsall, T.A., Spry, P.G., Voudouris, P., Tombros, S., St. Seymour, K., Melfos, V., 2011. The geochemistry of carbonate-replacement Pb-Zn-Ag mineralization in the Lavrion District, Attica, Greece: Fluid Inclusion, stable isotope, and rare earth element studies. Economic Geology 106, 619-651.

Tombros, S.F., 2011, Fluid flow and mass exchange calculations on the Panormos Bay Au-Ag-Te hydrothermal system, Tinos Island, Greece, in: Macías, B., Guajardo, F., (Eds.), Rock Chemistry, Nova Science Publishers Inc, 131-143.

Tombros, F.S., St. Seymour, K., Williams-Jones, A.E., 2010. Explanation and conditions of formation of the high tellurium contents in the early and late base metals stages of the epithermal polymetallic Ag-Au-Te mineralization, Tinos Island, Hellas. Economic Geology 105, 1097-1111.

Tombros, F.S., St. Seymour, K., Williams-Jones, A.E., Spry, P.G., 2007. The genesis of epithermal Au-Ag-Te mineralization, Panormos Bay, Tinos Island, Cyclades, Hellas (Greece). Economic Geology 102, 1269-1294.

Wilkinson, J.J., 2001. Fluid inclusions in hydrothermal ore deposits. Lithos 55, 229-272.

Williams-Jones, A.E., Samson, I.M., Ault, K.M., Gagnon, J.E., Fryer, B.J., 2010. The genesis of distal zinc skarns: Evidence from the Mochito deposit, Honduras. Economic Geology 105, 1411-1440.

15th International Congress of the Geological Society of Greece
Athens, 22-24 May, 2019 | Harokopio University of Athens, Greece
Bulletin of the Geological Society of Greece, Sp. Pub. 7 Ext. Abs. GSG2019-234

Exhumation of the high-pressure northwestern Cyclades, Aegean: New thermodynamic data from Penteli mountains

A.L. Holm[1], I. Baziotis[2], S. Klemme[1], J. Berndt[1]

(1) University of Muenster, Muenster, Germany, a_holm04@uni-muenster.de (2) Agricultural University of Athens, Iera Odos str. 75, 11855, Athens, Greece

Introduction

The Attic-Cycladic Crystalline Belt (ACCB) is one of the well-studied regionally metamorphosed provinces (under high-pressure/low-temperature conditions) worldwide (e.g., Ring *et al*., 2010). It is formed as a result of major extensional collapse of the Alpine orogenic belt in the Aegean that resulted from the collision between the Eurasian plate and Gondwana-derived fragments in the Cenozoic (e.g., Jolivet and Brun, 2010). The ACCB underwent high-pressure/low temperature (HP/LT) blueschist to eclogite facies metamorphism in the period ca. 50–40 Ma, and greenschist-amphibolite facies overprint in ca. 25–20 Ma (e.g., Laurent *et al*., 2017 and references therein). The northwesternmost extension of ACCB is represented by Penteli area where two major units are exposed: the upper tectonic unit (UTU) and lower tectonic unit (LTU). In this study, we focus on metapelitic lithologies and provide new geothermobarometric data (pseudosections) that constrain peak and post-peak P-T evolution of the LTU of Penteli area in western ACCB.

Analytical Methods

We have performed detailed characterization of 10 metapelitic samples for their texture and mineral chemistry. Major element compositions on minerals were determined in polished thin sections (Fig. 1) using a JEOL JXA 8900 Superprobe EPMA equipped with four wavelength-dispersive spectrometers at the Agricultural University of Athens (Athens, Greece). All analyses were performed with an accelerating voltage of 15 kV, 15 nA, focused beam for all minerals except for beam sensitive minerals where the beam was slightly defocused (5 μm diameter). Counting times were 20 s on peak and 10 s on background positions. Natural mineral standards used were quartz (Si), corundum (Al), diopside (Ca), jadeite (Na), olivine (Mg), fayalite (Fe), spessartine (Mn), orthoclase (K), ilmenite (Ti), chromite (Cr), apatite (P) and Ni-oxide (Ni) obtained from the Smithsonian Institute.

Whole-rock major element concentrations were determined on fused beads, using the X-ray fluorescence (XRF) wavelength spectrometer (Panalytical PW-2400) of the accredited according to ELOT EN ISO/IEC 17025:2005 biogeochemical laboratory of the Hellenic Centre for Marine Research. Major elements were determined as oxides following the procedure described in Karageorgis *et al*. (2005).

Results

The LTU schists are pervasively foliated and are divided into five types (based on the predominant matrix assemblage): calcite-chlorite-garnet (type-I), chloritoid-phengite (type-II), chlorite-phengite (type-III), paragonite-chlorite-phengite (type-IV) and paragonite-chloritoid-phengite (type-V) schists. The type-I schists and marbles are the predominant lithologies in the Penteli LTU. Mineral assemblages of type-I contain calcite + quartz + chlorite + phengite + albite + garnet ± zircon ± apatite ± titanite ± opaques. The paragonite-bearing schists (type-IV and type-V) contain aligned chlorite, phengite and chloritoid grewing in the main foliation; paragonite may occur as inclusions in chloritoid, too. In type-II and V, chloritoid porphyroblasts host chlorite + phengite inclusions.

The K-rich white micas are mainly phengites with Si ranging from 3.126 to 3.526 a.p.f.u.. The celadonite component ranges from 5.9 to 36.2%, pyrophyllite from 7.1 to 34.9% and paragonite is up to 15%. The X_{Mg} [X_{Mg}=Mg/(Mg+Fe)] of chlorites is in the range of 0.41–0.70, and the Si content of 2.51–2.84 a.p.f.u.. The clinochlore component ranges from 34 to 62% and the daphnite from 26 to 52%. The chloritoid is rich in iron with X_{Fe} [Fe^{2+}/(Mn + Mg + Fe^{2+})] in the range of 0.77–0.95 The paragonite composition is relatively homogeneous, and Si content ranges from 2.928 to 3.097 a.p.f.u., while X_{Na} [X_{Na}=Na/(Na+K)] from 0.878 to 0.980. Detailed mineral chemistry data can be found in Baziotis *et al*. (2019).

P-T pseudosections – Modeling approach

We used the bulk-rock compositions of three different rock types (II, III and IV) as an analogue for the representative rock types in this study. Pressure-Temperature isochemical phase diagrams (pseudosections) were calculated in the system SiO_2–TiO_2–Al_2O_3–MgO–MnO–FeO –Fe_2O_3–CaO–Na_2O–K_2O–H_2O, employing Perple_X software (ver. 6.8.6; 2019, Connolly, 2005, 2009) over the P-T range 0-14 kbar and 300-600 ºC. The thermodynamic database of Holland & Powell (1998, updated 2002) was used for minerals. Solid solution models are included in the latest version of Perple_X: Gt(HP) for garnet (Powell and Holland, 1998), Omph(HP) for clinopyroxene (Holland and Powell, 1996), Pheng(HP) for phengite (Powell and Holland, 1999), Bio(HP) for biotite (Powell and Holland, 1999), Chl(HP) for chlorite (Holland *et al.*, 1998), Pl(h) for plagioclase, Ep(HP) for epidote (Powell and Holland, 1998), Ctd(HP) for chloritoid (White *et al.*, 2000), Act(M) for amphibole (Massonne and Willner, 2008), Mica(M) for K white mica (Massonne and Willner, 2008), Stlp(M) for stilpnomelane (Massonne and Willner, 2008), Pu(M) for pumpellyite (Massonne and Willner, 2008), and an ideal solid-solution model IlGkPy for ilmenite. Reflecting the selected solution models, Mn is considered as incorporated in garnet and ilmenite, thus precludes the possibility of garnet over -stability. The fluid phase was assumed to be pure H_2O, initially

in excess.

A caveat required by the pseudosection computations is the choice of the bulk-rock composition. In calculations based on whole-rock analysis (XRF method), the derived phase assemblage is assumed to represent equilibrium over the scale of a hand–specimen; for fine-grained rocks like those obtained from LTU of Penteli, the XRF compositions may represent a good proxy of the effective composition. Paralyzer operated under Matlab environment was used to run the build file (v1.6. Mark Caddick). Finally, we employed the WERAMI software (in Perple_X) to compute compositional and modal isopleths for specific solid solutions as was the PyWERAMI software for projection of the calculated isopleths.

Our pseudosection approach provides a unique frame of P-T conditions for a specific bulk-rock composition, but also serves as an ideal tool to derive the peak and post-peak metamorphic evolution. The variability of the rock composition even on a very small scale (hand-specimen or smaller) as clearly seen along the intense foliation can be depicted for different stable assemblages. Further, because mineral compositions are also controlled by bulk chemistry under various P-T conditions, each isopleth corresponding to different mineral solid solutions is also uniquely determined in terms of P-T values, range, and slope. Each was calculated separately for each rock type. We should note, that even though the phase assemblages depend on the fluid phase evolution (e.g., Wei and Clarke, 2011; Baziotis *et al*., 2017), it is not the goal of the current study and we will apply such exercise on a future paper.

In the computed pseudosections, the main reactions, represented by a few univariant reactions, several narrow divariant, and wider trivariant, quadrivariant and quinivariant fields, delimit the stability fields of chloritoid (ctd), chlorite (chl), epidote (ep), garnet (gt), zoisite (zo), plagioclase (pl), albite (ab), stilpnomelane (stp), omphacite (omp), actinolite (act), biotite (bi) and phengite (phg). Pumpellyite (pu) was not stable. Based on both observed (thin sections) and calculated mineral assemblages, a P-T history was derived from the different pseudosections for the three rock types. Detailed pseudosection calculations will be presented at the meeting.

Discussion and Conclusions

We provide new constraints from pseudosection modelling of three rocks from the LTU of Penteli, part of the northwestern extension of the ACCB. Data gathered from mineral compositions and assemblages, textural relationships, Perplex_X calculations (P-T pseudosections, isopleths) demonstrate that these rocks underwent HP/LT metamorphism. The studied LTU rocks underwent similar high-P/low-T conditions of formation, in which a distinct post-peak history characterized by heating along a clockwise P-T path is suggested; such rocks probably recrystallized within a subduction channel environment. The post peak T history is almost identical with the path proposed for the Syros rocks (see Laurent *et al*., 2018). Both areas (Penteli and Syros) are characterized by heating during exhumation continuously from P~12 kbar, and then by cooling from P~8 kbar and onward. In this case, then the present position may suggest either a mechanism which incorporates lateral extension of ~ 100 km or the two areas where part of the same heterogeneous (Syros reached much deeper parts; ~35–40 difference for their maximum depth recorded in the two units) subduction/exhumation system but at different places in the horizontal scale (Baziotis *et al*., 2019).

Acknowledgements

We greatly thank Dr. A. Karageorgis for performing the XRF analyses at the Hellenic Centre for Marine Research (HCMR).

References

Baziotis, I., Tsai, C.H., Ernst, W.G., Jahn, B.M., Iizuka, Y., 2017. New P–T constraints on the Tamayen glaucophane-bearing rocks, eastern Taiwan: Perple_X modelling results and geodynamic implications. Journal of Metamorphic Geology 35(1), 35-54.

Baziotis, I., Proyer, A., Mposkos, E., Windley, B., Boukouvala, I., 2019. Exhumation of the high-pressure northwestern Cyclades, Aegean: New PT constraints, and geodynamic evolution. Lithos 324, 439-453.

Connolly, J.A.D., 2005. Computation of phase equilibria by linear programming: tool for geodynamic modelling and its application to subduction zone decarbonation. Earth and Planetary Science Letters 236, 524–541.

Connolly, J.A.D., 2009. The geodynamic equation of state: what and how. Geochemistry, Geophysics, Geosystems 10, doi: 10.1029/2009GC002540 (Q10014).

Holland, T., Powell, R., 1998. An internally consistent thermodynamic data set for phases of petrological interest. Journal of metamorphic Geology 16(3), 309-343.

Jolivet, L., Brun, J.P., 2010. Cenozoic geodynamic evolution of the Aegean. International Journal of Earth Sciences 99, 109–138.

Karageorgis, A.P., Anagnostou, C.L., Kaberi, H., 2005. Geochemistry and mineralogy of the NW Aegean Sea surface sediments: implications for river runoff and anthropogenic impact. Applied Geochemistry 20(1), 69–88.

Laurent, V., Huet, B., Labrousse, L., Jolivet, L., Monie, P., Augier, R., 2017. Extraneous argon in high-pressure metamorphic rocks: distribution, origin and transport in the Cycladic Blueschist Unit (Greece). Lithos 272, 315–335.

Massonne, H.J., Willner, A.P., 2008. Phase relations and dehydration behaviour of psammopelite and mid-ocean ridge basalt at very-low-grade to low-grade metamorphic conditions. European Journal of Mineralogy 20(5), 867-879.

Powell, R., Holland, T., Worley, B., 1998. Calculating phase diagrams involving solid solutions via non-linear equations, with examples using THERMOCALC. Journal of metamorphic Geology 16(4), 577-588.

Powell, R., Holland, T., 1999. Relating formulations of the thermodynamics of mineral solid solutions; activity modeling of pyroxenes, amphiboles, and micas. American Mineralogist 84(1-2), 1-14.

Ring, U., Glodny, J., Will, T., Thomson, S., 2010. The Hellenic subduction system: High pressure metamorphism, exhumation, normal faulting, and large-scale extension. Annual Review of Earth and Planetary Sciences 38, 45–76.

Wei, C.J., Clarke, G.L., 2011. Calculated phase equilibria for MORB compositions: a reappraisal of the metamorphic evolution of lawsonite eclogite. Journal of Metamorphic Geology 29, 939-952.

White, R.W., Powell, R., Holland, T., Worley, B.A., 2000. The effect of TiO_2 and Fe_2O_3 on metapelitic assemblages at greenschist and amphibolite facies conditions: mineral equilibria calculations in the system K2O-FeO-MgO-Al_2O3-SiO_2-H_2O-TiO_2-Fe_2O_3. Journal of Metamorphic Geology 18(5), 497-511.

15th International Congress of the Geological Society of Greece
Athens, 22-24 May, 2019 | Harokopio University of Athens, Greece
Bulletin of the Geological Society of Greece, Sp. Pub. 7 Ext. Abs. GSG2019-246

Carbon Mineralization into Nesquehonite-Based Building Materials.

Vasilios Skliros[1], Filio Daskalaki[1], Petros Tsakiridis[1], Maria Perraki[1]

(1) National Technical University of Athens, School of Mining and Metallurgical Engineering, 9 Heroon Politechniou St., 15780, Zografou (Athens), Greece, sklirosbill@metal.ntua.gr

Carbon dioxide sequestration (CCS) is considered to be the future for the reduction of the industrial carbon emissions (Baena-Moreno *et al.*, 2019). Nesquehonite synthesis has been proposed as a promising permanent storage of CO_2 emission under low pressure conditions, with competitive properties as building material.

In this work, we study the cementitious characteristics of nesquehonite synthesized in high alkaline environment and under low-pressure conditions by reaction of gaseous CO_2 with Mg-chloride solution, as following:

$$MgCl_2 \cdot 3H_2O + CO_{2(g)} + H_2O \rightarrow MgCO_3 \cdot 3H_2O_{(s)} + 2H^+$$

A saturated Mg^{2+} solution was used for its synthesis, at a temperature of 25°C and pH 9.3. During the reaction, since the pH tended to reduce, a continuous input of NH_3 solution of high concentration (35%) was required to keep the pH in alkaline values (Ferrini *et al.*, 2009). The NH_3 solution didn't react with the products and was easily separated by using a vacuum pump. Nesquehonite synthesized herein was subsequently studied by means of X-Ray Diffraction, optical microscopy (Fig. 1), scanning electron microscopy (Fig. 2), FT-IR and Raman spectroscopic methods. Synthesized nesquehonite forms elongated fibers, exhibiting transparent to translucent diaphaneity and vitreous luster. FT-IR and Raman spectroscopy revealed the presence of OH^- and CO_3^{2-} in the crystal structure of nesquehonite.

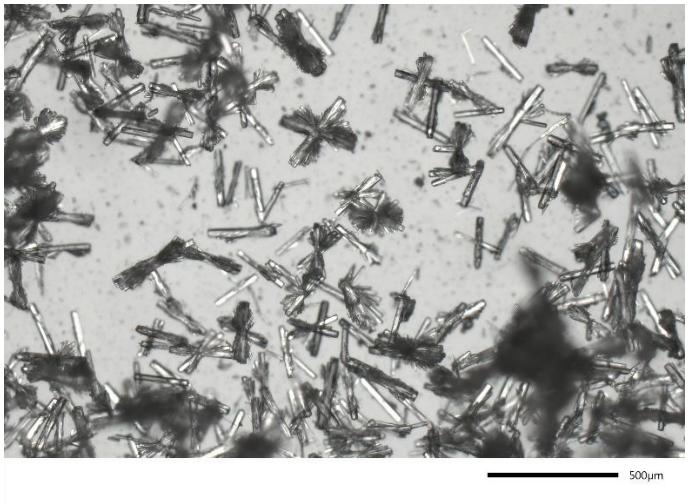

Figure 1. Photomicrograph of nesquehonite synthesized herein under transmitted polarizing light.

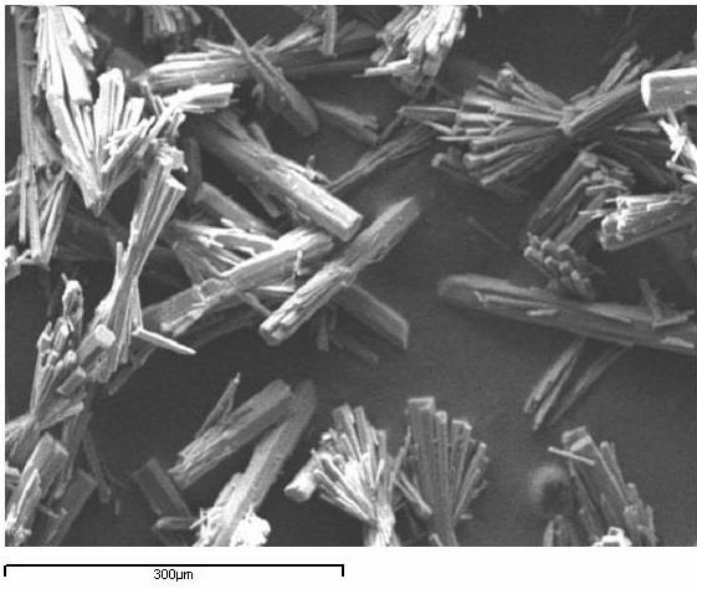

Figure 2. Secondary electron image of nesquehonite synthesized herein.

After being synthesized, nesquehonite was examined for its cementitious characteristics, by mixing it with reactive magnesia, standard aggregate sand and water to create a mortar. The new mortar was cast into 5x5x5 silicone mold and cured in water for 28 days (Fig. 3a). The sample achieved a compressive strength of 14 MPa after 28 days (Fig. 3b). Subsequently, it was studied by means of X-Ray Diffraction and FT-IR spectroscopy. XRD results indicated the presence of Mg(OH), which was formed after reactive magnesia hydration. FTIR study revealed the stability of CO_3^- in the binder of the mortar.

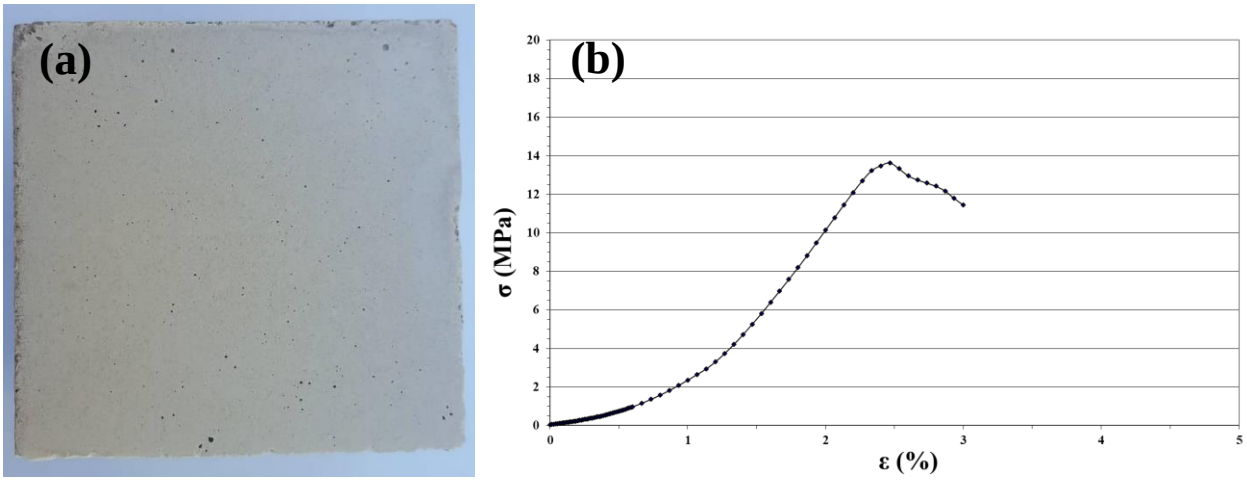

Figure 3. (a) Photomacrograph of the mortar sample and (b) comprehensive strength of the sample achieved herein.

As shown, a permanent storage of CO_2 might be achieved by CO_2 mineralization into a new nesquehonite-based "green" mortar with competitive properties. This method might be a part of Carbon Capture, Utilization, and Storage (CCUS) technologies to remove CO_2 from the flue gas and from the atmosphere by providing a safe, permanent and useful storage option.

References

Baena-Moreno, F. M., Rodríguez-Galán M., Vega F., Alonso-Fariñas F., Vilches Arenas L. F., Navarrete B 2019. Carbon Capture and Utilization Technologies: A Literature Review and Recent Advances, Energy Sources, Part A: Recovery, Utilization and Environmental Effects 41.

Ferrini, V., De Vito, C., Mignardi S. 2009. Synthesis of Nesquehonite by Reaction of Gaseous CO2 with mg Chloride Solution: Its Potential Role in the Sequestration of Carbon Dioxide, Journal of Hazardous Materials 168, 832-837.

15th International Congress of the Geological Society of Greece
Athens, 22-24 May, 2019 | Harokopio University of Athens, Greece
Bulletin of the Geological Society of Greece, Sp. Pub. 7 Ext. Abs. GSG2019-247

Precipitation of $MgCO_3 \cdot 3H_2O$ from aqueous solutions: the role of Mg^{2+}:CO_3^{2-} concentration ratio, pH and temperature

Vasilios Skliros[1], Panagiotis Papazotos[1], Filio Daskalaki[1], Petros Tsakiridis[1], Maria Perraki[1]

(1) National Technical University of Athens, School of Mining and Metallurgical Engineering, 9 Heroon Politechniou St., 15780, Zografou (Athens), Greece, sklirosbill@metal.ntua.gr

Synthetic nesquehonite ($MgCO_3 \cdot 3H_2O$), a promising building material (Glasser *et al.*, 2016), as recently gained interest as mineralization product of carbon capture and storage (CCS). The main advantage of nesquehonite in being a potential permanent storage solution for CO_2 emissions is that at least 30% of its structure consist of CO_3^{2-} (Ferrini *et al.*, 2009).

PHREEQC geochemical software has been recently proposed to be a useful tool in modeling CCS mineralization products (Liu *et al.*, 2019).

The aim of this study is to investigate the thermodynamic kinetics of CO_2 mineralization and to determine the precipitation of nesquehonite in the MgO-CO_2-H_2O system applying the geochemical software PHREEQC (Parkhurst & Appelo, 1999, v. 3), and using data from laboratorial experiments. Nesquehonite was synthesized herein by mixing a rich in Mg^{2+} aqueous solution with a rich in CO_3^{2-} one, at a temperature of 25 °C and pH 9.3, according to the following reaction:

$$Mg^{2+} + CO_{2\,(g)} + 4H_2O \rightarrow MgCO_3 \cdot 3H_2O_{\,(s)} + 2H^+ \quad (1)$$

Since during the reaction, pH was continuously decreasing, an additional input of alkaline solution (NH_3) was required to keep pH in alkaline values (Ferrini *et al.*, 2009).

An important controlling factor of the amount of Magnesium (Mg)-carbonate minerals crystallized and precipitated by CO_2 mineralization is the CO_3^{2-} concentration in the solution reactant (Ferrini *et al.*, 2009).

For simulating the nesquehonite synthesis experiments with the geochemical software PHREEQC, Minteqv4 thermodynamic database (Allison *et al.*, 1991) was used. Saturation Index (SI) of $MgCO_3 \cdot 3H_2O$ was calculated under different thermodynamic conditions in order to better study the precipitation/dissolution reactions of $MgCO_3 \cdot 3H_2O$.

SI of the solution is given by the equation:

$$SI = Log\ (IAP / K_{SP}),$$

where IAP is the ion activity product; K_{SP} is the equilibrium constant. When SI value is 0 the solution is in equilibrium with the mineral phase; when the SI value is >0 the solution is oversaturated, resulting in mineral precipitation, and when SI value is <0, the solution is undersaturated indicating that dissolution is required to reach equilibrium.

The parameters evaluated herein were Mg^{2+}:CO_3^{2-} concentration ratio, pH and temperature. The precipitation/dissolution reaction of $MgCO_3 \cdot 3H_2O$ was investigated in a range of pH from slightly acidic to strong alkaline pH values (5-14) (Figure 1) and temperature values from 10°C to 80°C (Figure 2). Calculations were performed for 1.5M solution of Mg^{2+}.

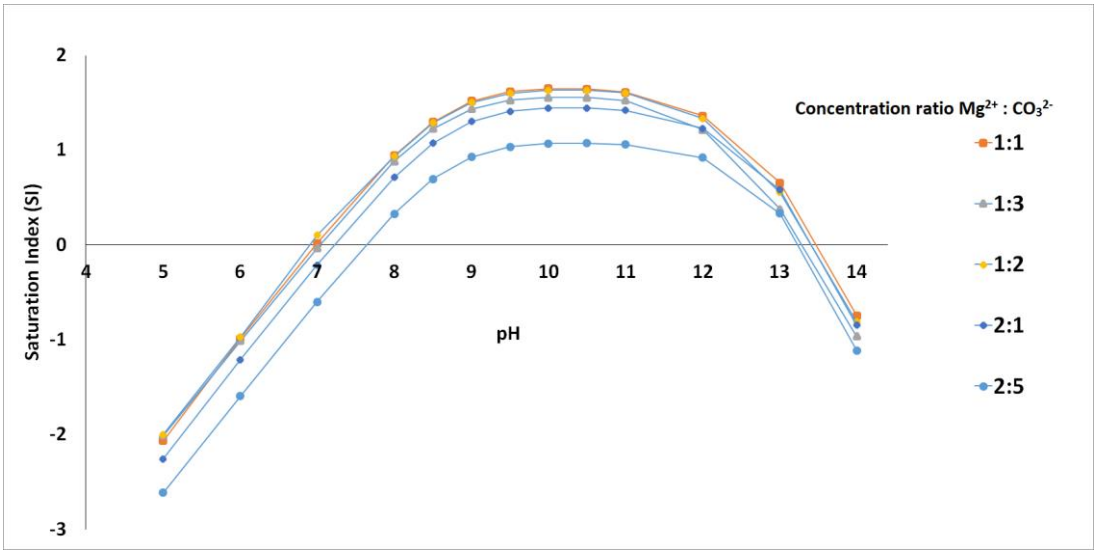

Figure 1. Saturation Index of $MgCO_3 \cdot 3H_2O$ in various pH (T=25°C) and concentrations of Mg^{2+} and CO_3^{2-}.

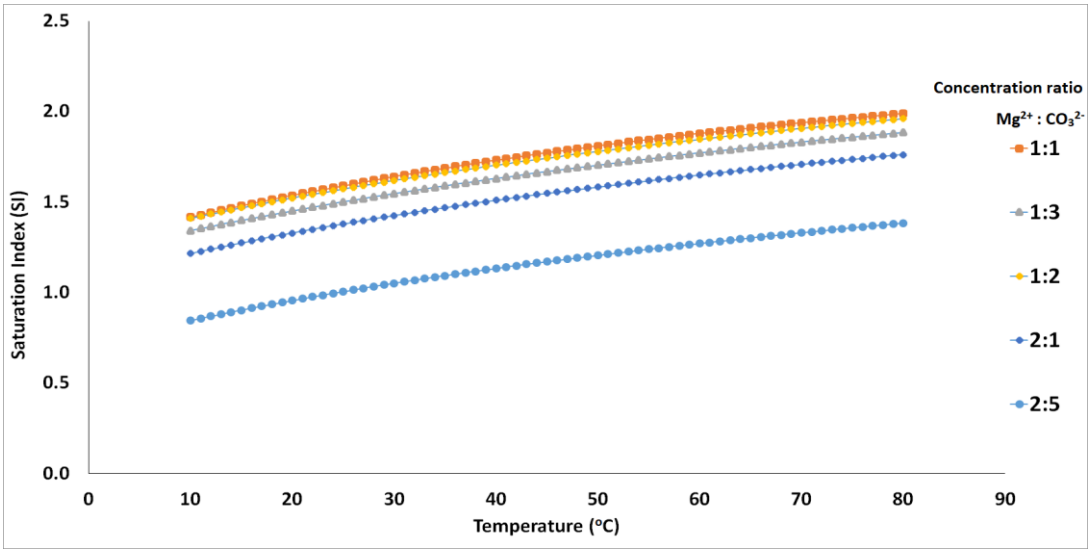

Figure 2. Saturation Index of $MgCO_3 \cdot 3H_2O$ in various temperatures (pH 9.3) and concentrations of Mg^{2+} and CO_3^{2-}.

$MgCO_3 \cdot 3H_2O$ precipitation may potentially take place in a range of thermodynamic conditions (Figures 1, 2) under different ratio concentrations of Mg^{2+} and CO_3^{2-}. $MgCO_3 \cdot 3H_2O$ precipitation occurs from pH 7 to pH 13 in a temperature range from 10°C to 80°C, under different Mg^{2+}:CO_3^{2-} concentration ratio.

The higher the Mg^{2+}:CO_3^{2-} concentration ratio of the initial solution is, the higher SI is. SI exhibits the highest value in slightly alkaline to alkaline pH conditions (pH 9.5-10). SI values in slightly acid to neutral (pH<7) and strong alkaline (pH>13.5) pH conditions are <0 indicating dissolution of nesquehonite (Figure 1). SI exhibits an upward inclined trend line with temperature increase (Figure 2) since K_{SP} is highly dependent on temperature. As shown, the effect of temperature is less significant compared to the effect of pH.

PHREEQC modeling of nesquehonite synthesis indicates that $MgCO_3 \cdot 3H_2O$ precipitation might occur in higher pH and temperature conditions than those referred to in previous studies.

References

Allison J.D., Brown D.S., Novo-Gradac K.J. 1991 MINTEQA2/PRODEFA2, A geochemical assessment model for environmental systems, Version 3.0 User's Manual, Environmental Research Laboratory, Office of Research and Development, US Environmental Protection Agency, EPA/600/3- 91/021, Athens, Georgia, 30605, 92.

Glasser, F. P., Jauffret, G., Morrison, J., Galvez-Martos, J. , Patterson, N., Imbabi, M. S. 2016 Sequestering CO 2 by mineralization into useful nesquehonite-based products, Frontiers in Energy Research, 4.

Ferrini, V., De Vito, C., Mignardi, S. 2009 Synthesis of nesquehonite by reaction of gaseous CO2 with Mg chloride solution: Its potential role in the sequestration of carbon dioxide. Journal of Hazardous Materials, 168, 832–837.

Liu, B., Zhao, F., Xu, J., Qi, Y. 2019 Experimental investigation and numerical simulation of CO_2-brine-rock interactions during CO_2 sequestrtion in a deep saline aquifer, Sustainability, 11, 317.

Parkhurst D.L., Appelo C.A.J. 1999. User's guide to PHREEQC-A computer program for speciation, batch-reaction, one-dimensional transport, and inverse geochemical calculations: U.S. Geological Survey Water-Resources Investigations Report 312, 99-4259.

15th International Congress of the Geological Society of Greece
Athens, 22-24 May, 2019 | Harokopio University of Athens, Greece
Bulletin of the Geological Society of Greece, Sp. Pub. 7 Ext. Abs. GSG2019-249

Quality Assessment of Eocene Limestones in Zakynthos Island, Western Greece, for Industrial Uses

M. Kati, E. Chioti, P. Voudouris, K. Gkoutzioupa

National and Kapodistrian University of Athens, Faculty of Geology and Geoenvironment, Department of Mineralogy and Petrology, GR-15784 Athens, Greece, kati@geol.uoa.gr

Introduction and Geological Background

Limestones are extremely valuable raw materials with a wide variety of chemical and industrial uses which are determined by their physical and chemical properties. The latter, in turn, directly depend on their depositional processes and environments but, also on the post-depositional (diagenetic) alterations that they have undergone. So, the geological, mineralogical and petrographic observations of the limestones are necessary to predict the chemical properties of the end products which can be produced from them (Freas *et al*., 2006). Accordingly, Eocene Limestones from Zakynthos Island were examined in order to establish certain qualitative characteristics which could contribute to their assessment for various industrial uses. The studied limestones are part of the carbonate succession of the Paxos (or Pre-Apulian) tectonic unit that crops out on the Ionian Islands, in western Greece, and represents the foreland of the Hellenides. After the Early-Middle Jurassic rifting, the Paxos unit functioned as an isolated carbonate platform which received exclusively and almost uninterruptedly calcareous sediments until the Oligocene, when it was completely foundered. The older rocks of the Paxos unit exposed on Zakynthos are of Upper Cretaceous age, constituting the Vrachionas mountain range, a calcareous anticline with a NNW-SSE treding axis. The Eocene Limestones, as well as all the younger formations, occur mostly on the eastern sides of the Vrachionas, constituting an east-dipping monocline (Fig.1A).

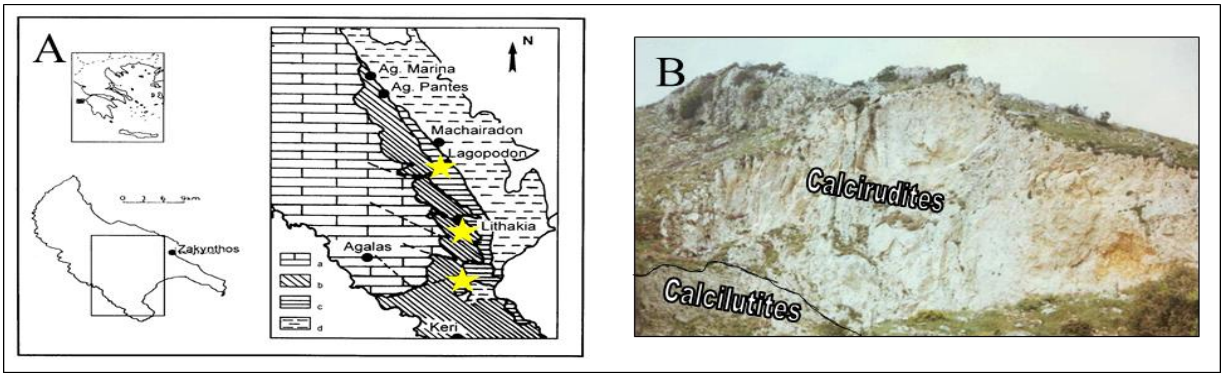

Figure 1. A. Simplified geological map (after IGME, 1980 and Accordi & Carbone, 1992) and the localities of the studied material, (a.Cretaceous, b.Eocene, c.Oligocene, d.Miocene). B. The two main lithofacies of Eocene Limestones (Lagopodon).

Material and Methods

Fieldwork included detailed facies analysis in three old quarries in central Zakynthos (Fig. 1A) and sampling of more than 50 selected samples. Polished slabs and thin sections were prepared of all the samples that were also stained with Alizarin red S and Potassium ferricyanide. The depositional and diagenetic characteristics were examined using transmitted light microscopy while the mineralogical composition of the non-carbonate material was determined through X-ray diffraction (XRD) analysis of the insoluble residue of the <30μm and <2μm fractions of selected samples, subsequent to their treatment with H_2O_2 to remove any organic matter. Chemical analysis of selected samples was performed using X-ray fluorescence spectrometry (XRF) technique.

Results

Two main lithofacies were identified: a) thinly to medium bedded calcilutites with alternating whitish and light-brown beds and some scattered chert nodules and b) massive to very thickly bedded white to very pale grey calcirudites (Fig 1B). The calcilutites comprise pelagic-hemipelagic carbonate deposits and are mainly represented by pelagic foraminiferal mudstones to wackestones (Fig. 2a), often with burrows, and fine-grained bioclastic packstones with abundant transported neritic skeletal fragments. Mineralogical study revealed that they consist mainly of non-ferroan low-magnesian calcite while their insoluble residue consists mostly of a-quartz (microquartz) and less clay minerals (smectite, illite, kaolinite and vermiculite) (Table 1). Chemical analysis showed CaO content of 54.75% (corresponding to limestone with 97.71% $CaCO_3$), MgO 0.63%, SiO_2 0.14% while the percentacges of all other oxides are in the range of <0.10% to negligible (Table 2). The calcirudites constitute very coarse-grained, polygenetic limestone breccias, with a grain-supported fabric, very poor sorting and without internal sedimentary structures. They consist of numerous reefal blocks (Fig. 2b) and bioclastic lithoclasts (Fig. 2c), originating from the platform-margin and shelf, and minor pelagic

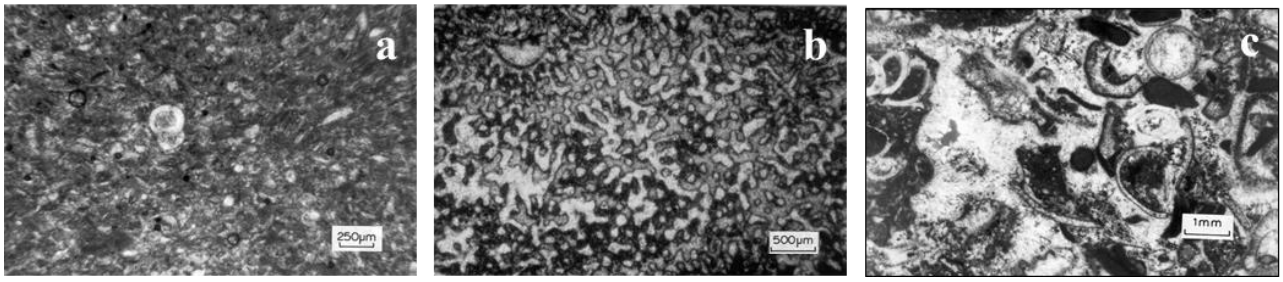

Figure 2. Characteristic lithotypes of the studied Eocene limestones: a. pelagic mudstone-wackestone b. coral boundstone c. bioclastic grainstone-rudstone.

intraclasts of similar composition to their minimal matrix (pelagic wackestone). Facies analysis and petrographic study clearly showed that they constitute resedimenented limestones deposited mainly by debris flows at the base of a carbonate slope environment (Kati, 2006). Despite their clastic nature, they show great mineralogical homogeneity, the dominant mineral being the above low-Mg calcite. Their insoluble residue, although qualitatively and quantitatively is almost the same with that of the calcilutites, comprises mainly clay minerals and less a-quartz (Table 1). Their chemical composition showed CaO rates from 55.15-55.75% (corresponding to limestone with $CaCO_3$ from 98.5-99.1%), while of the other oxides only MgO is most abundant (0.51-0.68%) and the percentages of the remaining are < 0.05%. It should be noted that the organic content was essentially negligible in both lithofacies and dolomitization phenomena are entirely lacking.

Table 1. Semi-quantitative analysis of clastic insoluble residue (x = small amounts, xx = moderate, xxx = large, xxxx = almost pure, IR = insoluble residue).

Sample/ Lithofacies	Kaolinite	Illite	Smectite	Vermiculite	Illite/Smectite	a-Quartz	IR (%)
ZK-1 / calcilutite						xxxx	1.80
ZK-2 / calcilutite	x	x	xx	x		x	0.18
ZK-3 / calcilutite	x	x	xxx			x	0.18
ZK-4 / calcilutite	x	x	x	x		xx	0.08
ZK-5 / calcirudite	xx		xxx			x	1.44
ZK-6 / calcirudite	x		xxx			x	0.18
ZK-7 / calcirudite	x	x	xx	x	xx	x	0.66

Conclusions

Based on their carbonate content, the two lithofacies constitute ultra-high-calcium limestones (more than 97% $CaCO_3$) (Oates, 1998) which are considered suitable for many high-value chemical and industrial uses. The two lithofacies, however, are diversified as to type, size and origin of their constituent grains, as well as their depositional mechanisms and diagenetic paths, resulting in differentiation of their chemical purity. Specifically, although calcilutites display the greatest homogeneity in their primary constituents, their qualitative characteristics appear to have been affected by the presence of detrital clays that arrived in their depositional setting, and also from extensive phenomena of silicification during diagenesis. Their carbonate content (<98.5% $CaCO_3$) classifies them as "high purity limestones" (Cox *et al*., 1977) that can be used in cement manufacture, fertilizer industry, in metallurgy, for flue-gas desulphurization, in various environmental uses, etc. The calcirudites (limestone breccias), despite the considerable heterogeneity in their components show better quality characteristics in relation to calcilutites. The origin of most of their clasts and their early lithification are directly reflected in their mineralogical and chemical composition. Their impurities probably represent only clay minerals of detrital origin, since other main diagenetic alterations were not observed. Therefore, the studied breccias with $CaCO_3$ content >98.5% ("very high purity limestones") can be used in applications even of higher value, as in production of lime, fillers and pigments in paper, paint and plastics industries and pharmaceutical uses.

References

Accordi, G., Carbone, F., 1992. Lithofacies map of the Hellenide Pre-Apulian zone (Ionian Islands, Greece). Cons. Nazion. Ricer., Spec. Publ., 27p., Roma.

Cox, F.C., Bridge, McC., Hull, J.H., 1977. Procedure for the assessment of limestone resources. Mineral Assessment Report 30, Institute of Geological Sciences, London.

Freas, R.C., Hayden, J.S., Pryor Jr, C.A., 2006. Limestone and Dolomite, in: Kogel, J.E., Trivedi, N.C., Barker, J.M., Krukowski, S.T. (Eds), "Industrial Minerals and Rocks. Commodities, Markets, and Uses", 7th Edition, Society for Mining, Metallurgy, and Exploration, Inc., 581- 597.

Kati, M., 2006. Facies analysis and depositional mechanisms of the Eocene limestone breccias of the Preapulian Zone, Zakynthos Island, western Greece. Bull. Geol. Soc. Greece, vol. XXIX/II, pp. 19-38.

Oates, J.A.H., 1998. Lime and Limestone. Chemistry and Techology, Production and Uses. Wiley-VCH.

15th International Congress of the Geological Society of Greece
Athens, 22-24 May, 2019 | Harokopio University of Athens, Greece
Bulletin of the Geological Society of Greece, Sp. Pub. 7 Ext. Abs. GSG2019-254

Mineralogical and Geochemical Study of the Contact Aureole of the Sithonia Plutonic Complex, Elia Area, Chalkidiki Peninsula, N. Greece

A. Stamatiadis[1], L. Papadopoulou[1], A. Koroneos[1], T. Soldatos[1]

(1) Department of Mineralogy-Petrology-Economic Geology, School of Geology, Aristotle University of Thessaloniki, Thessaloniki 541 24, Greece, arisstam17@gmail.com

The extensive magmatic activity that took place in the area of northern Greece during the Tertiary is represented by numerous igneous rocks that are found at the regions of the Rhodope Massif, the Serbo-Macedonian Massif and the Circum-Rhodope Belt (Christofides et al., 2001). The Sithonia Plutonic Complex is a part of that magmatic activity and is located at the Sithonia Peninsula, which constitutes the middle "leg" of the "three-legged" Chalkidiki Peninsula. This intrusion occupies the largest part of the Sithonia Peninsula, except for the central-western and the southernmost parts, where the magmatic body intrudes into the rocks of the Serbo-Macedonian Massif and the Circum-Rhodope Belt. It consists of various petrographic types, including granite and granodiorite, but also pegmatite and aplite dykes that interrupt both the magmatic body and the country rocks. This pluton has caused contact aureole phenomena to the country rock of these regions, forming a narrow belt about 100 m width.

At the area of Elia, which is the study area, two-mica granite and leucogranite are found to be in contact with the meta-sediments of the Mellisochori Formation (former Svoula Flysch) that mainly consists of dark phyllites (metapelites) passing upward into calcareous siltstones and (meta-) sandstones, whereas the most common lithology is formed by platy to massive calcareous (meta-) sandstones and minor quartzites (Meinhold et al., 2013). The studied rocks consist of yellowish to brownish calcareous metapsammites with intercalations of grey metapelites.

The metamorphic mineral assemblages are located in sites between metapsammites and metapelites, or inside the former, as lenticular, "boudinage" bodies possibly indicating that the thermal content was transferred from the pluton to the country rocks through a fluid flow mechanism (Fig. 1).

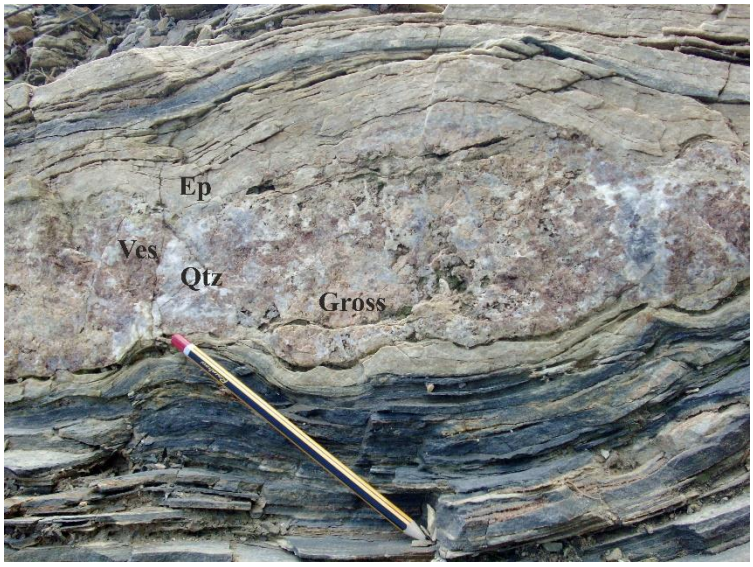

Figure 1. Lenticular body developed among metapsammite layers. Qtz=Quartz, Ves=Vesuvianite, Gross=Grossular, Ep=Epidote.

The mineralogy assemblage consists of quartz, clinozoisite, epidote, garnet, pyroxene, vesuvianite, calcite, titanite and plagioclase, while amphibole, zircon, K-feldspar, apatite, chlorite, biotite, allanite and opaques are also present. Garnet is characterized as grossular, containing an andradite component $[(Ca,Na,Mg)_3(Al,Fe,Mn)_2(Si,Al)_3O_{12}]$ and no obvious chemical difference in composition was recognized from core to rim. Vesuvianite is represented by the chemical formula $[(Ca_{18.8},Na_{0.4},K_{0.1})_{19.2}(Al_{10.1},Fe^{+}_{21.7},Mg_{0.7},Ti_{0.2},Mn_{0.1})_{12.8}Si_{17.9}O_{68}(OH)_{10}]$. It is characterized as high-grade metamorphosed, P4/nnc symmetry vesuvianite and is often found with garnet. Pyroxenes' composition corresponds to diopside $[En_{27.9}Fs_{22.8}Wo_{49.4}]$, while amphiboles' composition to ferroedenite. Plagioclase's composition ranges from andesine to bytownite $[Or_{0\text{-}6.3}Ab_{23.8\text{-}56.6}An_{40.9\text{-}75.8}]$ and K-feldspars are found in small quantity, with composition $[Or_{96.2}Ab_{3.2}An_{0.6}]$. Minerals of the epidote-group, mostly clinozoisite, are present in most parts of the entire contact aureole (Fig. 2).

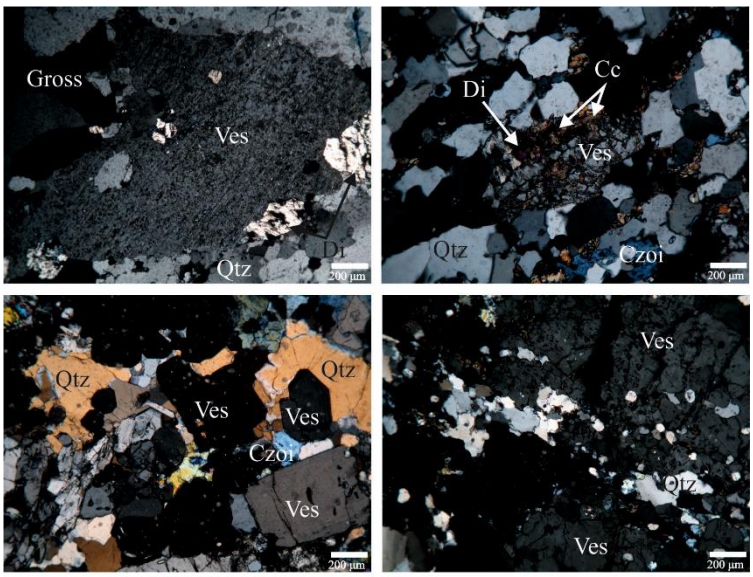

Figure 2. Representative microscopic images of the mineral assemblages (Nicols +). Qtz=Quartz, Ves=Vesuvianite, Gross=Grossular, Czoi=Clinozoisite, Di=Diopside, Cc=Calcite.

According to Kockel et al. (1977) the conditions under which the contact aureole was developed ranged from 500 to 540°C, based on mineral assemblages. The participation of calcsilicate minerals, especially vesuvianite, in the paragenesis of the contact aureole rocks is an indication of fluid-present processes. Another notable observation is the absence of wollastonite, a common calcsilicate mineral in thermal metamorphosed rocks, leading to the assumption that the temperature of the studied paragenesis did not exceed 600ºC which is the critical value for the stability of wollastonite-bearing assemblages (Timon et al. 2007). On the other hand, the vesuvianite-bearing assemblages are stable in temperatures above 480ºC, so a temperature range of 500-600ºC at pressures not exceeding 6 kbar (Trommsdorff 1968, Bogoch et al. 1997), with the participation of H_2O-rich and CO_2-poor fluids as formation conditions could be acceptable. Also, the presence of mineral assemblages at specific sites and the lenticular shape of the metamorphic bodies could reveal the possible pathways of fluids deriving from the magmatic body as well as the places where metamorphic reactions occurred.

In addition, Christofides et al. (2007) have determined for the two-mica granite, which is the plutonic type that intrudes into the studied metamorphic rocks, a crystallization depth of about 15 km, corresponding to a pressure of 4,5 kbar. Such calcsilicate rocks containing vesuvianite, but not wollastonite, are common constituents of many medium-grade contact aureoles. Actually, the observations of this study are in agreement with other studies that deal with the conditions of the Sithonia Plutonic Complex emplacement.

References

Bogoch R., Kumarapeli, S., Matthews A. 1997. High-pressure K-feldspar-vesuvianite bearing assemblage in the central metasedimentary belt of the Grenville Province, Saint Jovite area, Quebec. Canadian Mineralogist, 35, 1269-1275.

Christofides G., Koroneos A., Soldatos T., Eleftheriadis G., Kilias A. 2001. Eocene magmatism (Sithonia and Elatia plutons) in the Internal Hellenides and implications for Eocene-Miocene geological evolution of the Rhodope massif (Northern Greece). In: Downes, H., Orlando, V. (Eds.), Tertiary Magmatism in the Dinarides Acta Vulcanologica, 13, 73-89.

Christofides G., Perugini D., Koroneos A., Soldatos T., Poli G., Eleftheriadis G., Del Moro, A., Neiva A.M. 2007. Interplay between geochemistry and magma dynamics during magma interaction: An example from the Sithonia Plutonic Complex (NE Greece). Lithos, 95, 243-266.

Kockel F., Mollat H., Walther H. 1977. Erlauterungen zur geologischen Karte der Chalkidiki und angrezender Gebiete 1:100.000. Bundesanstalt fur Geowissenschaften und Rohstoffe, Hannover.

Meinhold G., Kostopoulos D. 2013. The Circum-Rhodope Belt, northern Greece: Age, provenance, and tectonic setting. Tectonophysics, 595-596, 55-68.

Timon S.M., Moro M.C., Cembranos M.L., Fernández A., Crespo J.L. 2007. Contact metamorphism in the Los Santos W skarn (NW Spain). Mineralogy and Petrology, 90, 109-140.

Trommsdorff V. 1968. Mineralreaktionen mit Wollastonit und Vesuvian in einem Kalksilikatfels der alpinen Disthenzone (Claro, Tessin). Schweizerische Mineralogische und Petrographische Mitteilungen, 48, 655-666.

15th International Congress of the Geological Society of Greece
Athens, 22-24 May, 2019 | Harokopio University of Athens, Greece
Bulletin of the Geological Society of Greece, Sp. Pub. 7 Ext. Abs. GSG2019-256

The contribution of Visible Near Infrared Reflectance spectroscopy to colour determination: the case of the experimental ceramic briquettes

G. Karountzou[1], V. Xanthopoulou[1,2], I. Iliopoulos [1,3]

(1) Department of Geology, University of Patras, 26504, Patras, Greece, g.karountzou@upnet.gr
(2) Laboratory of Electron Microscopy and Microanalysis, University of Patras, 26504 Patras, Greece
(3) ERAAUB, Facultat de Geografia i Història, Departament d'Història i Arqueologia

Introduction

The aim of this study is to investigate and determine the colour changes in experimental ceramic briquettes through different states (from unfired to be fired at 1050ºC) using Visible Near Infrared Reflectance Spectroscopy (VNIR). Initially the studied material was examined in terms of colour following the ordinary method of Munsell Chart (2000). Reflectance spectroscopy has been defined as a technique that uses the excitation energy in the Visible-Near Infrared (350-2500nm) wavelength regions of the electromagnetic spectrum to identify minerals. The Visible Near Infrared spectroscopy (VNIR) contributed to a more accurate determination of colour, since we can obtain tristimulus values from visible region. The main factors which are responsible for the colour changes is the presence of different minerals as well as the conditions during firing. The mineralogical determination was performed by X-ray Powder Diffraction (XRPD) in order to identify and confirm all the primary minerals and the neoformed mineralogical phases as a result of the firing regime.

Materials and Methods

The experimental briquettes were prepared using clayey raw materials (n=4) which were collected from Achaea and Corinth (Northern Peloponnese, Greece) and were fired at three different temperatures (700, 900 and 1050ºC) under oxidizing conditions**.**

Different techniques (X-ray diffraction and VNIR spectroscopy) were performed to investigate the mineralogical composition and evaluate the colour changes. The mineralogy of the unfired and fired materials was studied by XRPD using a BRUKER D8 ADVANCE diffractometer. Spectral curves and colorimetry data of samples were obtained using a SpecTERRA SM-3500 Spectral Evolution portable spectrometer. The calibration was performed using a standard white reference plate. Visual observation of the unfired and fired samples was performed by following the Munsell colour chart (2000). The VNIR region detects effects due to several different electronic processes including crystal field, charge transfer, colour centers and conduction band transitions. Fe-oxide minerals are easily detected in the VNIR region (350–2500 nm) since most electron transitions are caused by various kinds of iron oxides (Fang *et al*., 2018). The process which was been followed for the colour evaluation of the experimental briquettes is based on the transformation of the visible spectra (350-780 nm) to values X, Y, Z according to the International Commission on Illumination (CIE, 1931). Then these values were converted to Munsell and CIE L * a * b * notations using the Munsell Conversion Program (Wallkillcolour, 2019).

The spectra were taken and focused on the visible region (350 to 780 nm) for the colour determination. Thereafter transformed into tristimulus values X, Y, Z according to the International Commission on Illumination (CIE, 1931) using the software DarwinSp by SpecTERRA (Version 1.2). Transformation into absorption spectra was performed (A=log1/R) to the original spectra curves. Savitzky-Golay algorithm was applied for background noise reduction and then 2nd derivative was calculated using the software Origin Pro 9.0.

Results

The examined samples were differentiated in terms of composition based on XRPD and VNIR results. The first sample (C4) is characterized as calcareous clayey raw material due to the abundant participation of calcite; the second one (C13) is rich in calcite and dolomite and is characterized as calcareous-dolomitic whereas the rest of the samples (C9 and HS45) are calcite-free and are characterized as siliceous (Xanthopoulou, 2019). The newly formed mineralogical phases developed in the calcareous and calcareous dolomitic samples are larnite, which was formed at 700ºC and diopside and gehlenite which appeared at 900ºC. Hematite is the newly formed mineral after the firing of the siliceous samples at 700ºC to 1050ºC and using 2nd derivative to original spectra (Fig. 1a) the relevant absorption band is visible near 550nm (Deaton & Balsam 1991).VNIR spectrometer results were obtained into tristimulus values X, Y, Z (Fig. 1a) according to the International Commission on Illumination (CIE, 1931) and then converted into Munsell colour notations.

Discussion

The colour of the unfired siliceous sample HS45 was yellowish brown and during firing obtained a reddish yellow hue-yellow red (700ºC), a light red hue (900ºC) and at the highest temperature (1050ºC) obtained a red hue. This is due to the low Ca concentration which allows hematite formation. On the other hand, the sample C9 was reddish brown at the unfired state and during firing the hue became darker red (1050ºC). Hematite formed at 900 ºC and is responsible for the

reddish hue.

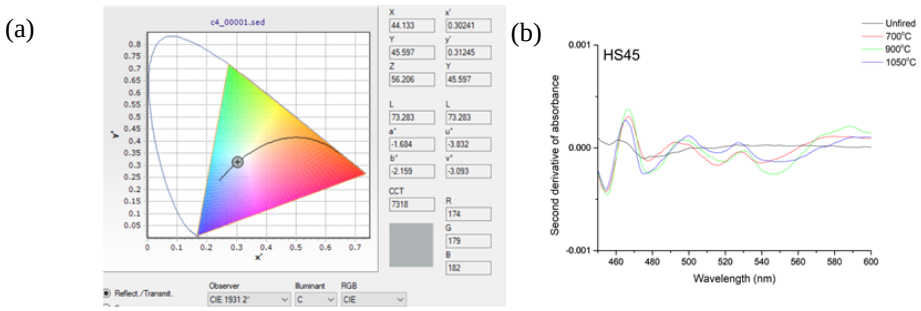

Figure 1. (a) Illustration of colorimetry results obtained using DarwinSp software and (b) Plot of 2nd derivative absorbance

On the contrary, Ca-rich samples exhibit different hues due to the formation of Ca-silicates minerals. The colour of sample C4 was gray and during firing (700ºC) it transformed to very pale brown (900ºC) and at the highest temperature to pale yellow (1050ºC). XRPD results showed the formation of gehlenite at 900 ºC which is responsible for the buff colour (Molera *et al*., 1998). Sample C13 originally had a pale yellow colour and during firing obtained a light gray hue (700-900ºC) and at higher temperature obtained a darker pale yellow colour (1050ºC). The formation of diopside during firing is related to the yellowish and creamy colours. The creamy colours are also related to the decomposition of calcite, the development of pyroxenes and to the low presence of iron oxides (Molera *et al*., 1998). VNIR results specifically for sample C9, contributed to a further discrimination among the firing temperatures, a fact that it was not evitable by visual observation as it is displayed in Fig. 2.

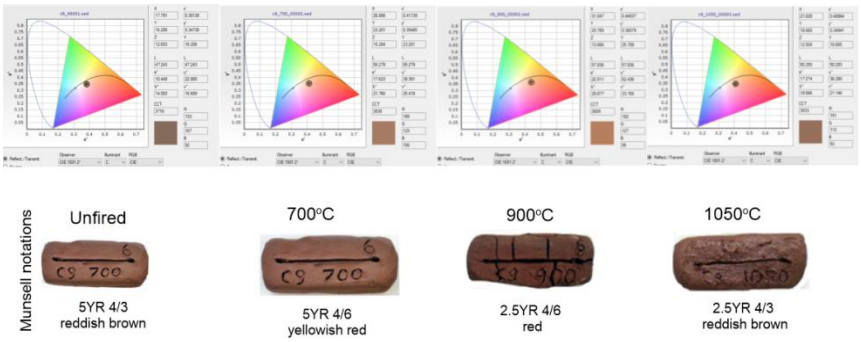

Figure 2 Colorimetry display (above) and munsell notations (below) for sample C9 in all temperatures

Conclusion

VNIR spectra results are obtained into numerical data and thus we acquire a quantitative measurement of colour. On the contrary the Munsell soil chart has limited number of chips for colour determination and offers a qualitative measurement of colour by the visual observation which is considered as a subjective perception among each observer. The use of the NIR spectrometer may provide an alternative untrained approach that can produce results not only for colour coordinates but also about the reflectance spectra, which contain more information about mineral identification.

References

Cornell, R. M., Schwertmann U., 2003. The Iron Oxides: Structure, Properties, Reactions, Occurrences and Uses, 2nd ed, WILEY-VCH GmbH & Co. KGaA.

Darwin Sp Application Software User Manual Version 1.2, 2012

De Bonis, A., Cultrone, G., Grifa, C., Langella, A., Leone, A. P., Mercurio, M., Morra, M., 2017. Different shades of red: The complexity of mineralogical and physicochemical factors influencing the colour of ceramics. Ceramics International 43, 8065–8074.

Fang, Q., Hong, H., Zhao, L., Kukolich, S., Yin, K., Wang, C., 2018. Visible and Near-Infrared Reflectance Spectroscopy for Investigating Soil Mineralogy: A Review. Journal of Spectroscopy2018, 3168974.

Kreimeyer, R., 1987. Some notes on the firing colour of clay bricks. Applied Clay Science 2(2), 175-183.

Molera, J., Pradell, T., Vendrell-Saz, M., 1998. The colours of Ca-rich ceramic pastes: Origin and characterization. Applied Clay Science 13(3), 187-202.

Munsell Conversion Program version 2019, http://wallkillcolor.com

Munsell Soil Colour Charts, 2000. Revised Washable Edition.

Murphy, R.J., Monteiro, S.T., 2013. Mapping the distribution of ferric iron minerals on a vertical mine face using derivative analysis of hyperspectral imagery (430-970 nm), ISPRS Journal of Photogrammetry and Remote Sensing 75, 29-39.

Szalai, Z., Kiss, K., Jakab, G., Sipos, P., Belucz, B., Németh, T., 2013. The use of UV-VIS-NIR reflectance spectroscopy to identify iron minerals. AstronomischeNachrichten 334(9), 940-943.

Xanthopoulou, V., 2019. Assessment of clayey raw material suitability for ceramic production in Nothern Peloponnese: An archaeometric approach, School of Natural Sciences, Department of Geology. Ph.D. Thesis, University of Patras, Patras, 104 p.

Zhang, X. L., Wu, G. J., Zhang, C. L., Xu, T. L. and Zhou, Q. Q., 2015. What's the real role of iron-oxides in the optical properties of dust aerosols? Atmospheric Chemistry and Physics 15(21), 12159-12177.

15th International Congress of the Geological Society of Greece
Athens, 22-24 May, 2019 | Harokopio University of Athens, Greece
Bulletin of the Geological Society of Greece, Sp. Pub. 7 Ext. Abs. GSG2019-260

Petrographic and geochemical characteristics of mantle peridotites of Edessa ophiolite (North Greece)

A. Rogkala[1], P. Petrounias[1], P.P. Giannakopoulou[1]

(1) Section of Earth Materials, Department of Geology, University of Patras, 265 04, Patras, Greece, katerinarogkala@gmail.com

Abstract

The Edessa ophiolite represents remnants of an oceanic lithosphere obducted onto Palaeozoic-Mesozoic marble and schists during Upper Jurassic to Lower Cretaceous (Decourt *et al.*, 1977, Michailidis, 1990). The ophiolitic rocks include several tectonic units that are considered to be the northwards continuation of the Veria-Naousa ophiolite (Pe-Piper and Piper, 2002, Saccani *et al.*, 2008, Rogkala *et al.*, 2017). Petrographic, geological and geochemical evidence indicates that this ophiolite complex consists of both mantle and crustal suites (Rogkala *et al.*, 2019). It includes serpentinised harzburgite with high degree of serpentinisation, lherzolite, diorite, gabbro, diabase and basalt. This study presents new data on petrographic characteristics and geochemical compositions of mantle peridotites from this ophiolite, especially serpentinised harzburgite and minor lherzolite. The serpentinised harzburgite displays dark green colour and local relic pyroxenes with moderate to intense mantle deformation features, such as banding and foliation. Locally, it encloses lenses, pods or elongated bodies (up to few meters) of chromitite, which according to their texture and mode of occurrence, are classified as massive and disseminated podiform bodies. Moderately lherzolite is an infrequent, medium-grained rock, which is characterised by greenish black to dark green colour and conchoidal fracture. It occurs as relic, irregular bodies up to a few meters, surrounded by harzburgite. Local lherzolite slivers are repeated in the mantle domain of Edessa due to a series of imbricated thrusts occurring through the area.

The petrographic description of the serpentinised harzburgite and lherzolite has been conducted in polished-thin sections from 35 samples, which have been collected throughout the whole exposure. The serpentinised harzburgite has been intensively serpentinised. The primary mineralogy constitutes less than 5% of the mode and comprises clinopyroxene, Cr-spinel and chromite (Figure 1a). Clinopyroxene appears as subhedral porphyroclasts. The Cr-spinel crystals and chromite are subhedral to euhedral and scanning electron microscopic observation revealed that infrequently they show an irregular distribution of ferritchromite and Cr-bearing magnetite compositional areas, at their rims. Serpentine is the main alteration product showing mesh, ribbon, bastite and intersertal textures. Chlorite and magnetite are also products of hydrothermal alteration of the serpentinised harzburgite. Lherzolite displays mainly porphyroclastic texture (Figure 1b). Its primary mineralogy includes olivine (40-60 vol%), orthopyroxene (30-40 vol%), clinopyroxene (5-25 vol%) and spinel (up to 5 vol%). Rare Fe-Ni-Co sulphides with Cu coexist with spinel. Olivine displays porphyroclastic grains and smaller neoblasts. Orthopyroxene porphyroclasts exhibit local kink-bands, undulatory extinction and exsolution lamellae of clinopyroxene. Olivine and orthopyroxene porphyroclasts surrounded and partly replaced by neoblastic olivine (Figure 1b). Clinopyroxene occurs as porphyroclastic and neoblastic grains in the recrystallised matrix (Figure 1b). Spinel is of aluminous composition and forms subhedral to euhedral grains with lobate boundaries, which veined and surrounded by a rim of garnet and sulphides. Various serpentine, chlorite, tremolite and magnetite are observed due to subsequent hydrothermal alteration.

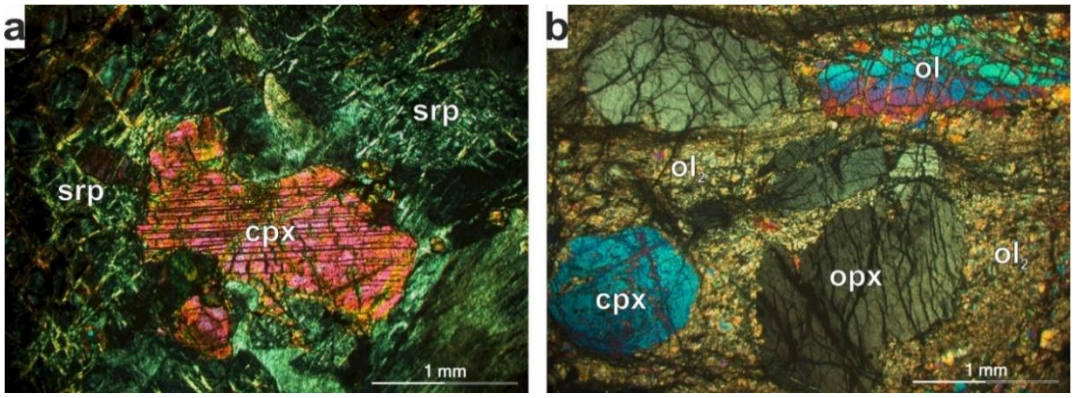

Figure 1. Textural characteristics of mantle peridotites from Edessa ophiolite: a) Photomicrograph of porphyroclastic clinopyroxene in serpentinised harzburgite surrounded by serpentine, b) Photomicrograph of porphyroclastic olivine, clinopyroxene and orthopyroxene in lherzolite surrounded by neoblastic olivine (cpx: clinopyroxene, srp: serpentine, ol: olivine, ol_2: neoblastic olivine, opx: orthopyroxene).

Major, trace and rare earth elements data from the mantle peridotites from the Edessa ophiolite were performed at Bureau Veritas Mineral Laboratories at Vancouver (Canada). Major element analyses were carried out using an XRF spectrometer and a sequential spectrometer (ICP-ES). Trace elements and rare earth elements were determined on totally digested samples by inductively coupled plasma-mass spectrometry (ICP-MS) in the same laboratory. Detection limits for major and trace elements range from 0.01 wt.% to 0.04 wt.% and from 0.01 ppm to 10 ppm, respectively. The analytical

precision calculated from replicate analyses is better than 3% for most major elements and better than 5% for trace elements. Lherzolite is richer in SiO_2, TiO_2, Al_2O_3 and CaO than the serpnetinised harzburgite. Low CaO and Al_2O_3 contents in serpentinised harzburgite are consistent with low clinopyroxene abundance. The serpentinised harzburgite shows higher Mg# [100*Mg^{2+}/(Mg^{2+}+Fe^{2+})] ranging from 82.27 to 84.79 than the lherzolite (82.33-83.74). Trace element abundances are also highly variable among the mantle peridotites. More specifically, lherzolite is richer mainly in V, Sc, Ga and Y compared to the harzburgite. On the other hand, the serpentinised harzburgite exhibits higher Co, Zn, Ni and Cr abundances than the lherzolite. The total rare earth element (REE) inventory of the Edessa peridotites is variable, ranging between 0.20 to 4.74 ppm. They exhibit a more limited range of heavy REE (HREE = Er + Tm + Yb + Lu = 0.00-1.04 ppm) abundances compared to that of light REE (LREE = La + Ce + Pr + Nd = 0.20-2.50 ppm) and middle REE (MREE = Sm + Eu + Gd + Tb + Dy + Ho = 0.00-1.88 ppm). Lherzolite displays higher REE concentrations with respect to serpentinised harzburgite. Lherzolite is characterised by relatively LREE-depleted primitive mantle-normalised REE patterns, exhibiting a nearly linear increase from LREE to HREE (Figure 2). Most of them bear resemblance to abyssal peridotites in terms of primitive mantle-normalised REE profiles (Niu, 1997), especially in MREE and HREE segment. The serpentinined harzburgite shows higher depletion in MREE and HREE compared to abyssal peridotites, whereas their REE patterns reaching up to and below to the field of SSZ-type peridotites (Figure 2).

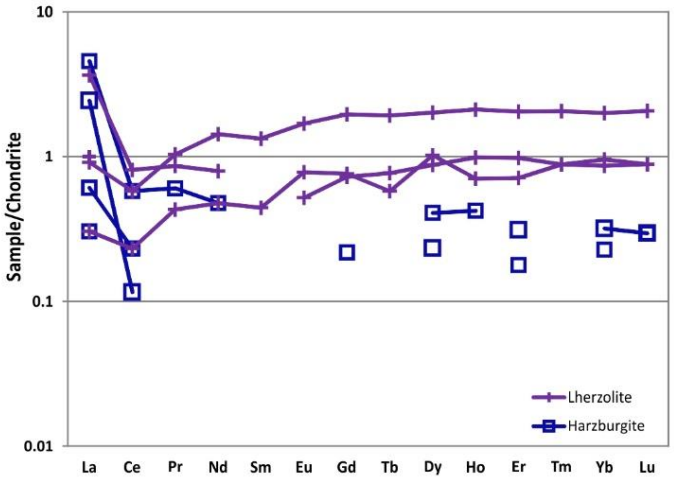

Figure 2. Chondrite-normalised REE patterns of peridotites and from the Edessa ophiolite. Normalising values are after McDonough and Sun (1995).

Lherzolite formed by low to moderate degrees of partial melting and subsequent melt-rock reaction in an oceanic spreading setting. On the other hand, refractory harzburgite formed by high degrees of partial melting in a supra-subduction zone (SSZ) setting. Petrographical characteristics and geochemical compositions of the mantle peridotites suggest that the Edessa oceanic mantle evolved from a typical mid-ocean ridge (MOR) oceanic basin to the mantle wedge of a SSZ. This scenario explains the higher degrees of partial melting recorded in harzburgite, as well as the overprint of primary geochemical characteristics in the Edessa peridotites.

Acknowledgements

We kindly thank M. Kalpogiannaki for her assistance with the construction of the geological map. A. Rogkala was financially supported by the Greek State Scholarship Foundation (IKY) during her Ph.D. study. This research is co-financed by Greece and the European Union (European Social Fund- ESF) through the Operational Programme «Human Resources Development, Education and Lifelong Learning» in the context of the project "Scholarships programme for post-graduate studies - 2nd Study Cycle" (MIS-5003404), implemented by the State Scholarships Foundation (IKY).

References

Decourt, J., Aubouin, J., Savoyat, E., et al.: 1977. Le sillon mésohellénique et la zone pélagonienne, Bulletin de la Société géologique de France, 1, 32-70.

McDonough, W.F., Sun, S.S., 1995. The composition of the Earth. Chemical Geology, 120, 223-253.

Michailidis, K.M., 1990. Zoned chromites with high Mn-contents in the Fe-Ni-Cr-laterite ore deposits from the Edessa area in Northern Greece. Mineralium Deposita 25, 190-197.

Niu, Y., 1997. Mantle melting and melt extraction processes beneath ocean ridges: evidence from abyssal peridotites. Journal of Petrology, 38, 1047-1074.

Pe-Piper, G., Piper, D.J.W., 2002. The igneous rocks of Greece. The anatomy of an orogeny. Gebrueder Borntraeger, Berlin/Stuttgart, 573.

Rogkala, A., Petrounias, P., Tsikouras, V., Hatzipanagiotou, K., 2017. New occurrence of pyroxenites in the Veria-Naousa ophiolite (north Greece): Implications on their origin and petrogenetic evolution. Geosciences, 7 (4), 92.

Rogkala, A., Petrounias, P., Tsikouras, B., Giannakopoulou, P.P., Hatzipanagiotou, K., 2019. Mineralogical evidence for partial melting and melt-rock reaction processes in the mantle peridotites of Edessa ophiolite (north Greece). Minerals, 9, 120.

Saccani, E., Photiades, A., Santato, A., Zeda, O., 2008. New evidence for supra-subduction zone ophiolites in the Vardar zone of northern Greece: implications for the tectonomagmatic evolution of the Vardar oceanic basin. Ofioliti, 33 (1), 65-85.

15th International Congress of the Geological Society of Greece
Athens, 22-24 May, 2019 | Harokopio University of Athens, Greece
Bulletin of the Geological Society of Greece, Sp. Pub. 7 Ext. Abs. GSG2019-266

Application of Near-Infrared Spectroscopy for the identification of rock mineralogy

M. Kokkaliari[1], I. Iliopoulos[1]

(1) Department of Geology, University of Patras, 2650 Patras, Greece, kokkaliari_m@upnet.gr

Introduction

In the present study, a variety of different rock samples characterized by hydrous minerals, from Kos Island, South-East Aegean, were used to produce reflectance spectra in the VIS-NIR region. The spectroscopic analysis is supported with petrographic analysis accompanied with microphotography and X-Ray Powder Diffraction analysis, aiming at first level to classify the samples into the main rock types, and secondly to contribute to the mineralogical recognition. Through this study we attempt to examine the spectral characteristics of these different lithotypes and the way that the mineralogy could affect the absorption features of each spectrum. Even though the spectral data may be difficult sometimes to be interpreted due to lacking available extensive spectral libraries, the NIR spectroscopy can be a useful tool for direct and on-site identification of the rock mineralogy. The absorption features are a result of energy-matter interactions caused by molecular vibrations at specific frequencies. The evaluation of these features allows as to determine which functional group participates in the structure of the mineral. The major spectral features in the NIR region is a result mostly of water and hydroxyl groups vibrations such as Al-OH, Fe-OH, Mg-OH (Clark et al., 1990). However, several different parameters (such as grain size, color, mineralogy, texture, water content etc.) can affect the spectroscopic properties of the samples resulting in spectral variability (Clark, 1999).

Geological Setting

Kos Island (Dodecanese) is located in the eastern edge of the Aegean Volcanic Arc (Pe-Piper and Piper 2005). The geologic structure of the island is composed of various lithologies spanning the three main categories of rock classification: magmatic, metamorphosed and sedimentary rocks (Drinia et al. 2010, Soder et al. 2016, Kalt et al. 1998). Significant events for the petrologic evolution of Kos were the two episodes of magmatism, whose products are mainly found in the western part of the island (dating at ~ 3.5 Ma and ~ 161 ka, respectively). Particularly, the ~161 ka magmatic event caused the largest Quaternary eruption (>60 km^3) in the Mediterranean and the formation of the voluminous, unwelded Kos Plateau Tuff (KPT; Allen, 2001).

Materials and Methods

The sampling performed on Kos (Iliopoulos et al., 2016) comprised a range of different lithologies and the main rock types included in this study are actinolite schist, clay schist, cataclasite, monzodiorite, diorite, and altered diorite. Petrographic thin sections were prepared and studied by means of polarizing microscope (Zeiss AxioScope A.1) in order to determine the mineral phases and classify them in the three main rock types. The detailed petrographic analysis provided additional information for the texture of the sample, the particle size and the metamorphic conditions. The mineralogy of the samples was verified by means of X-Ray Powder Diffraction (BRUKER D8 Advance). The reflectance spectroscopy (SM-3500 Spectral Evolution portable spectrometer) was applied in contact with a smooth, clean surface of the hand samples. The samples did not pre-processed in order to achieve as much as possible of the realistic conditions in the field. The methods discussed above were applied at the Research Laboratory of Minerals and Rocks, Department of Geology, University of Patras.

Data Analysis and Conclusions

Each sample from Kos Island for this study, was examined for its petrological characteristics and a semi-quantification was determined from the XRPD analysis (Table 1).

Table 1. Major mineral identification and the semi-quantitative analysis of the studied samples ('-': not detected; 'tr': traces; '+': few; '++': common; '+++': frequent; '++++': abundant; '+++++': dominant). Mineral abbreviations are according to Whitney & Evans, 2010.

	AS1	AS8	AS14	L4	SP3	PPY4	PPY6
Lithotype	**altered diorite**	**altered diorite**	**actinolite schist**	**clay schist**	**cataclasite**	**monzodiorite**	**diorite**
qz	tr	tr	Tr	++	++++	+	tr
pl	+	++	++	+	++	++++	++++
afs	-	-	-	tr	tr	+	+
hbl-act	+++++	+++++	++++	-	-	+++	++
ep-zo	+	++	tr	-	-	-	-
ilt-bt-ms	-	-	+	++++	++	+	++
chl	tr	tr	++	+++	tr	tr	tr

Monzodiorite is an inequigranular, coarse-grained sample (PPY4) with porphyroid, poikilitic texture, comprising quartz, plagioclase, alkali-feldspar, hornblende and minor biotite. Sample PPY6, has a more dioritic composition with biotite and hornblende being more abundant. The predominant mineral of altered diorites (samples AS1, AS8) is hornblende, forming coarse-grain phenocrysts (up to 6 mm) in a fine-grained matrix with plagioclase, and its saussiritization products epidote and chlorite. The cataclasite sample (SP3) has a cataclastic texture and consists of quartz, plagioclase, muscovite and minor alkali-feldspar and chlorite. The clay schist sample (L4) is fine-grained and has a grano-nematoblastic texture comprising chlorite, muscovite, quartz and plagioclase and minor alkali-feldspar. The L4 sample comes from pelitic protolith and has undertaken low grade metamorphism (chlorite zone according to Barrow metamorphism). The actinolite schist (sample AS14) has a grano-lepidoblastic texture forming hornblende and plagioglase porphyroblasts in a chlorite – mica matrix. The following conclusions were drawn during the preparation of the study:

- The NIR spectra of altered diorites (samples AS1, AS8) are dominated by the zoisite and amphibole absorption features, however the percentage participation of the minerals plays an important role.
- In the case of sample AS8, where the epidote is more abundant in the sample, the spectrum illustrates the epidote absorption features more detailed, whereas the spectrum of AS1 illustrates the amphiboles absorption features, with broader characteristics though, due to the presence of epidote.
- The epidotes are good reflectors for NIR spectroscopy even though they are fine-grained, saussiritization products.
- The spectra from PPY4 is characterized by the presence of hornblende which dominates the sample, with characteristic doublet features at ~2330 and ~2390 nm. As the biotite participation increases (PPY6 sample), even though the spectrum is characterized by the hornblende absorption features, it has a positive slope and a small sharp feature at ~2250 nm, indicative of biotite.
- The spectrum obtained from the cataclasite (SP4) is characterized by broad rounded absorption features at ~1900 and ~2200 nm and that could indicate the presence hydrous, Al-rich minerals, like illite and muscovite. However, due to small percentage of phyllosilicate minerals and their brittle crystallinity as opposed to the siliceous minerals (quartz and feldspars), the characteristic absorption features in higher wavelengths (> 2300 nm) are subdued. Only a small, sharp feature at ~2290 indicate the presence of chlorite.
- The clay schist spectrum (sample L4) is characterized by the absorption features of mica. The intense absorption feature at ~2200nm is characteristic for illite-muscovite.
- The actinolite schist spectrum (sample AS14) is characterized by absorption features both of amphibole (~2400 nm) and chlorite (~2250 and ~2300 nm).
- Relatively light colour to transparent siliceous minerals such as quartz and feldspars do not exhibit any intense absorption features. The most noticeable effect is the increasing reflectance of the sample respectively to the percentage participation of these minerals.
- The broad absorption feature at ~1100 nm is characteristic for the presence of iron in oxides and hydroxides.

Acknowledgments

Maria Kokkaliari is a PhD student and is financially supported by the "General Secretariat for Research and Technology (GSRT)" and the "Hellenic Foundation for Research and Innovation (HFRI)", at the University of Patras.

References

Allen, S.R., 2001. Reconstruction of a major caldera-forming eruption from pyroclastic deposit characteristics: Kos Plateau Tuff, eastern Aegean Sea. Journal of Volcanology and Geothermal Research 105, 141–162.

Clark, R.N., King, T.V.V., Klejwa, M., Swayze, G.A., Vergo, N., 1990. High spectral resolution reflectance spectroscopy of minerals. J. Geophys. Res. Solid 95, 12653-12680.

Clark, R. N., 1999. Spectroscopy of rocks and minerals, and principles of spectroscopy. Remote Sensing for the Earth Sciences: Manual of Remote Sensing, 3, 3–58.

Drinia, H., Koskeridou, E., Antonarakou, A., Tzortzaki, E., 2010. Benthic Foraminifera Associated with the Zooxanthellate Coral Cladocora in the Pleistocene of the Kos Island (Aegean Sea, Greece): Sea Level Changes and Palaeoenvironmental Conditions. Bulletin of the Geological Society of Greece, Proceedings of the 12th International Congress Patras, May, 2010

Kalt, A., Altherr, R., & Ludwig, T., 1998. Contact Metamorphism in Pelitic Rocks on the Island of Kos (Greece, Eastern Aegean Sea): a Test for the Na-in-Cordierite Thermometer. Journal of Petrology 39, 663–688.

Iliopoulos, I., Passa, S. & Moulo, K., 2016. Geological expedition on Kos Island, Greece (5th –8th November, 2015): Preliminary Results. SELAP Project. Department of Geology, University of Patras, Greece. Technical Report 16.1

Pe-Piper G, Piper DJW, 2005. The South Aegean active volcanic arc: relationships between magmatism and tectonics. Devel Volcanol 7, 113–133.

Soder, C., Altherr, R., & Romer, R. L., 2016. Mantle metasomatism at the edge of a retreating subduction zone: Late neogene lamprophyres from the Island of Kos, Greece. Journal of Petrology 57, 1705–1728.

Whitney, L., Evans, W., 2010. Abbreviations for names of rock forming minerals. American Mineralogist 95, 185-187.

15th International Congress of the Geological Society of Greece
Athens, 22-24 May, 2019 | Harokopio University of Athens, Greece
Bulletin of the Geological Society of Greece, Sp. Pub. 7 Ext. Abs. GSG2019-267

Geological Aspects of the Zeolitic Tuffs of Petrota region, Evros, Northeastern Greece

M. Vavelidis[1], K.Giouri[1], E.Michailidou[1], L.Papadopoulou[1], G. Christidis[2], A. Karetou[1], C.L.Stergiou[1]

(1) Department of Mineralogy-Petrology-Economic Geology, Aristotle University of Thessaloniki, 54124, Thessaloniki, Greece, e-mail: vavelidi@geo.auth.gr
(2) School of Mineral Resources Engineering, Technical University of Crete, 73100, Chania, Greece

Two zones of zeolitictuffs are located approximately 2 km westwards and northwestwards of Petrota village at Evros region, northeastern Greece. During the recent decades several detailed publications have been published on the mineralogy, geochemistry, quality characteristics and applications of these zeolitic tuffs (Kantiranis et al., 2006; Favvas et al., 2016; Filippidis, 2016).The present study is an attempt toreview and also add new data on the geological aspects of the zeolitic tuffs regarding their mineralogical and structural features.

The geological background of the region is composed by Mesozoic phyllites, schists, and gneisses of the Rhodope Massif which are overlaid by Upper Eocene to Oligocene sedimentary series of the Evros molassic basin (Caracciolo et al., 2012, 1978; Kilias et al., 2015). The younger regional stratigraphy includes Pliocene to Quaternary loose conglomerates and alluvial deposits of the Evros and Ardas rivers (Andronopoulos, 1978).

According to Andronopoulos (1978) and Caracciolo et al. (2012) the regional molassic rocks of Upper Eocene age are subdivided as follows (Fig. 1): the lower Komara Series, which mainly consists of conglomerates and coarse-grained sandstones with local intercalations of clays and marls, the middle Pentalofos Sequence of volcano-sedimentary origin, the Upper Sandstone Serieswith fine-grained sandstones and thin clayey intercalations and the younger transgressive limestone. Overlying Oligocene marl limestone and sandstones with marl intercalations constitute the stratigraphy of the molassic basin.

Hydrothermally altered rhyolites and rhyolitic tuffs, as well as polymictic loose breccias and cohesive grit-breccias build up the Pentalofos Sequence (Andronopoulos, 1978; Marantos et al., 2006) (Fig. 1). The rhyolites and the rhyolitic tuffs appear silicified, kaolinitized and locally zeolitized. Their most extensive occurrence is found in the west of Petrota village near the Greek-Bulgarian borders.In addition, rhyolites appear also as small intrusions within the loose breccias formation. According to Ivanova et al. (2000) the Petrota area is located at the southeastern part of the Sheinovets caldera, which mostly extends at the adjacent Bulgaria. According to stratigraphic data, the timeline of the volcanic activity in the Bulgarian part spreads between Priabonian and Rupelian (34.2 to 32.8 Ma), while in the Greek part K/Ar dating of the rhyolites revealed that the volcanic activity continued up to 20.7±1.6 Ma (Ivanova et al., 2000; Barbieri et al., 2001). The loose breccias formation is characterized by large, unconsolidated, angular and unsorted blocks of schists, pegmatites and volcanic material comprising fragments of rhyolites and lava flows. Grits and cobbles of chloritized schist, quartz, lava shards and rhyoliteare located within the cohesive breccias formation. The formation appears in massive, thick-bedded layers of sandstones including thin intercalations, or lenses, of tuffs which are composed byfine clayey-silicic material, kaolinite and layers of zeolitized silicic material. Pyroclastic flows set in a shallow marine environment contributed significantly in the formation of these rocks. In addition, Marantos et al. (2006) report the presence of a tuff-ring volcanic center in the region (Fig. 1).

The spatial distribution of the cohesive grit-breccias formation largely corresponds to the occurrence of the two zones of zeolitic tuffs (Fig. 1). The two zones start at the hilly area near Petrota village and develop towards the west (Kokkalo-Omega) and the northwest (KM-Gazomilos) spreading for 2.5 km and 1.4 km and covering areas of approximately 0.33 km^2 and 0.13 km^2, respectively. Clinoptilolite and mordenite are the two zeolite minerals which are found throughout the two zeolitic zones. Quantitative and qualitative analysis of 31 bulk surface samples from the two zoneswas performed by X-Ray diffraction. According to the results, the presence of clinoptiloliteat the first zone ranges between 54wt%and 80wt%, while at the second zone it ranges between 52wt% to 80wt%. Mordenite was determined in 14 samples ranging from 0.3wt% to 15.3wt%.The mineralogical composition of the samples includes quartz, opal, analcime, biotite, chlorite, smectite, kaolinite, and goethite, while hornblende, sanidine, anorthoclase and plagioclase are also found in the polymictic samples. It should be mentioned that Filippidis and Tsirambides (2012)while summarizing the zeolite presence of the tuffs in the Petrota area, they mention that at Drista location (KM-Gazomilos zone) clinoptilolite-heulandite contents reach up to 95wt%,with an average of 89wt%.

Structurally the zeolitic tuffs appear mostly in gently dipping beds. At the Kokkalo-Omega zone the beds are exposed atthe steep, south-facing,stream area of the hill range running from Petrota village to Omega location as well as along an amphitheatric slope at the northern hillside near Omega (Fig. 1). The zeolitic tuffs appear both as thin beds (<10 cm in width) and as lenses of fine-grained material in coarser-grained beds. The zeolitic beds appear between more massive beds of sandstones (up to 50 cm in width). The general direction of these beds starts as E-W and continues as NNW-SSE, while they dip in average 17°N-NE. Major tectonic feature of the area is a NW-SE trending and SW dipping fault which crosscuts the zone of the zeolitic tuffs. Throughout the KM-Gazomilos zone the development of the zeolitic bedsfollows the morphological gradient of the northeast-facing hill slopes. Thus, significant vertical exposures of zeolitic tuffs are missing from this area. Most of the zeolitic beds exposures can be observed in streams perpendicular to the hill slopes morphology. The zeolitic beds range from less than 10 cm up to 20 cm in width and they are less polymictic than the zeoliticbeds of the Kokkalo-Omega zone. They trend in a SE-NW direction, likewise a major fault which separates this

zone in two parts regarding the dipping of the beds. Consequently the beds of the hilly western part dip in average 45º SW, while these of the plain eastern partdip in average 10ºNE. At the southern part of this zone, near KM location, the beds dip between 58º to 82º SW-SSW. The steeper dipping of the beds at this location is the result of the anticlinal exposure of phyllites which belong to the metamorphic basement of the Rhodope Massif.

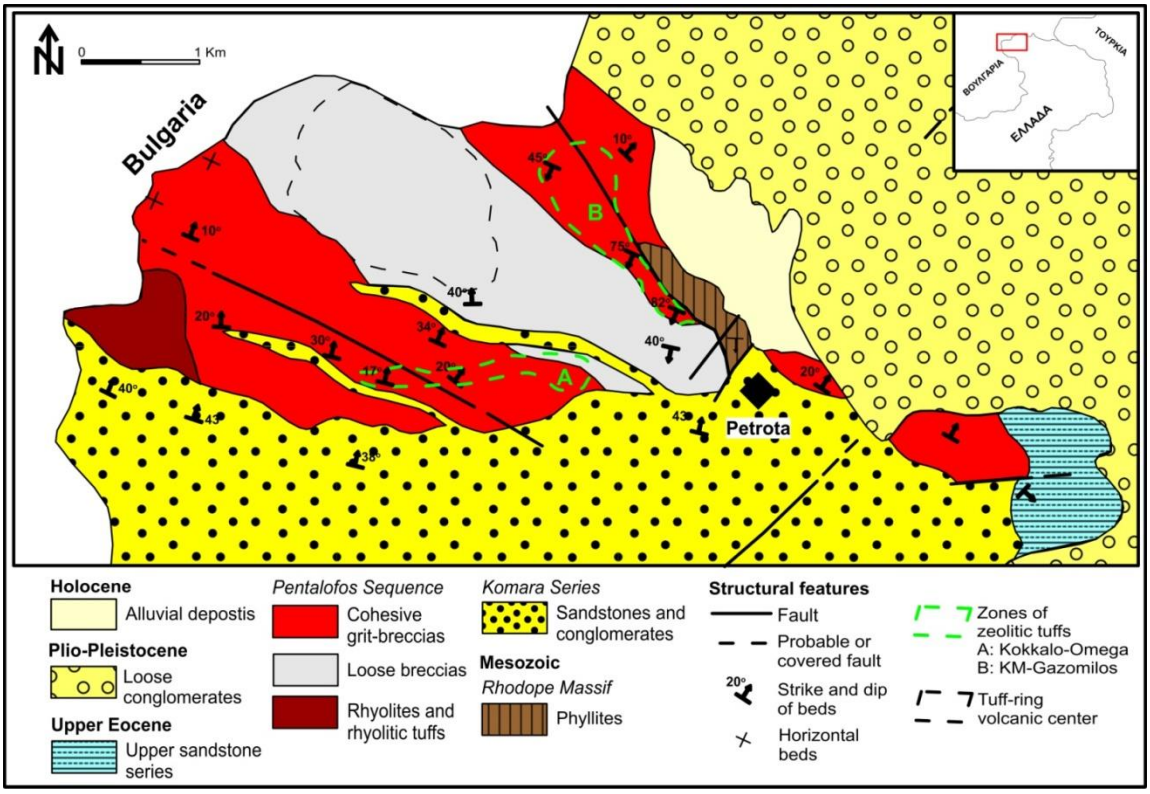

Figure 1. Geological map of the Petrota area, demonstrating the development of the zeolitic tuffs zones and the suggested tuff-ring volcanic center (Andronopoulos, 1978; Marantos et al., 2006).

Acknowledgements

The first author would like to acknowledge Zeolite Petrota Industrial and Commercial S.A. “O Lithoxoos” for their support on field survey logistics.The field survey was carried out at exploration concessions of the company. The School of Mineral Resources Engineering (Technical University of Crete)and MSALabs are acknowledged for their assistance at the analytical research.

References

Andronopoulos B., 1978. Ormenio, Geological Map of Greece 1:50.000. IGME Publications, Athens.

Barbieri, M., Castorina, F., Masi, U., Garbarino, C., Nicoletti, M., Kassoli-Fournaraki, A., Filippidis,Mignardi, S., 2001. Geochemical and isotopic evidence for the origin of rhyolites from Petrota (Northern Thrace, Greece) and geodynamic significance. Chemie Der Erde-geochemistry 61(1), 13-29.

Caracciolo, L., Von Eynatten, H., Tolosana-Delgado, R., Critelli, S., Manetti, P.,Marchev, P., 2012. Petrological, geochemical, and statistical analysis of Eocene–Oligocene sandstones of the Western Thrace Basin, Greece and Bulgaria.Journal of Sedimentary Research 82(7), 482-498.

Favvas, E.P., Tsanaktsidis, C.G., Sapalidis, A.A., Tzilantonis, G.T., Papageorgiou, S.K., Mitropoulos, A.C., 2016. Clinoptilolite, a natural zeolite material: structural characterization and performance evaluation on its dehydration properties of hydrocarbon-based fuels. Microporous and Mesoporous Materials 225, 385-391.

Filippidis, A., 2016. Applications of the Hellenic Natural Zeolite (HENAZE) and specifications of zeolitic tuffs. Bulletin of the Geological Society of Greece 50(4), 1809-1819.

Filippidis, A.,Tsirambides, A., 2012. Quality characteristics of the Greek zeolites, environmental, industrial, agricultural and aquacultural uses of Hellenic natural zeolite: A review. Scientific Annals, School of Geology, Aristotle University of Thessaloniki, Special Volume 101, 125-133 (in Greek with English abstract).

Ivanova, R., Stoykova, K.,Yanev, Y., 2000. Acid pyroclastic rocks from the Sheinovets caldera, Eastern Rhodopes: Lithostratigraphy, characteristics and age. Geochemistry Mineralogy Petrology 37, 47-56.

Kantiranis, N., Chrissafis, C., Filippidis, A., Paraskevopoulos, K.M., 2006. Thermal distinction of HEU-type mineral phases contained in Greek zeolite-rich volcaniclastic tuffs. European Journal of Mineralogy 18(4), 509-516.

Kilias, A.D., Vamvaka, A., Falalakis, G., Sfeikos, A., Papadimitriou, E., Gkarlaouni, C.H., Karakostas, B., 2015. The Mesohellenic Trough and the Paleogene Thrace Basin on the Rhodope Massif, their Structural Evolution and Geotectonic Significance in theHellenides. Journal of Geology and Geosciences 4, 198.

Marantos, I., Michail, C., Koshiaris, G., 2006. Study of the zeolitic alteration in Petrota Tertiary volcaniclastic rocks, Thrace area, NE Greece. Geoscience 124, 126.

15th International Congress of the Geological Society of Greece
Athens, 22-24 May, 2019 | Harokopio University of Athens, Greece
Bulletin of the Geological Society of Greece, Sp. Pub. 7 Ext. Abs. GSG2019-270

Mineralogical and Petrographic study of magnesite and its host rocks at Mantoudi area of N. Euboea, Greece

V. Stergiou[1], P. Lampropoulou[1], P. Petrounias[1], P.P. Giannakopoulou[1], A. Rogkala[1], K. Hatzipanagiotou[1]
(1) University of Patras, Department of Geology, GR-26504, Rio Patras, Greece, vstergiou94@gmail.com

The present work deals with the mineralogical and petrographic study of Greek magnesite and its host rocks at the area of Mantoudi of N. Euboea of Greece which belongs to the Pelagonian Zone. The magnesite deposits of N. Euboea which are hosted by Alpine type ultramafic rocks are the major magnesite producing areas of Greece.

Greece is a EU country with a significant mineral resources background in terms of quality, quantity and variety of ores and minerals. The Greek Mining/Metallurgical Industry (GMMI) constitutes an important sector of the economic activity of the country as it supplies essential raw materials for primary industries and various downstream users. One of the abundance of ores is magnesite, which is used in several industrial applications as fertilizer, filler in rubber materials, in colour industries etc (Haben, 2002, Skliros, 2013). Nevertheless the main uses of magnesite are the production of caustic magnesia and other basic refractory materials. (Newman, 1997, Lampropoulou, 2003).

The last 100 years the intensive exploitation of magnesite ore of this area led to the significant reduce of the resources and simultaneous increase of the total cost of the production. The Greek industry should be remaining to the forefront of the developments. In this direction the continuous research for new industrial applications of magnesite and its products is demanded. Moreover the host rocks of magnesite (waste after exploitation) could be a new direction to their utilization contributing to the circular economy. Nowadays, TERNA MAG is a magnesite and magnesia producer, member of GEK TERNA GROUP, one of the leading business groups in Greece. It exploits the world-class magnesite deposits in the northern part of Euboea Island.

In this work, samples of magnesite and its host rocks collected from Gerorema and Babakas mining areas in order to be studied. They have been analysed by petrographic microscopy, X-ray Diffractometry (XRD) and Scanning Electron Microscopy with EDS system (SEM-EDS). Gerorema is the main metalliferous area where magnesite is mined in underground mining and characterized from high-purity, boron-free and low-iron, calcium and silicon impurities. (Gartzos, 1985). The results of the petrographic features, textures characteristics and mineralogical compositions are presented here.

According to the results magnesite of Gerorema area, characterized as microcrystalline to cryptocrystalline while sometimes veins of crystalline magnesite have been detected in peridotites (Figure 1). The host rocks of this area are ultramafic rocks of dunite, harzburgite, lherzolite as well as serpentinite. Through the polarizing microscope and the respective XRD pattern the pure cryptocrystalline magnesite rock (consisted of about 90% magnesite) is indicated in Figure 2.

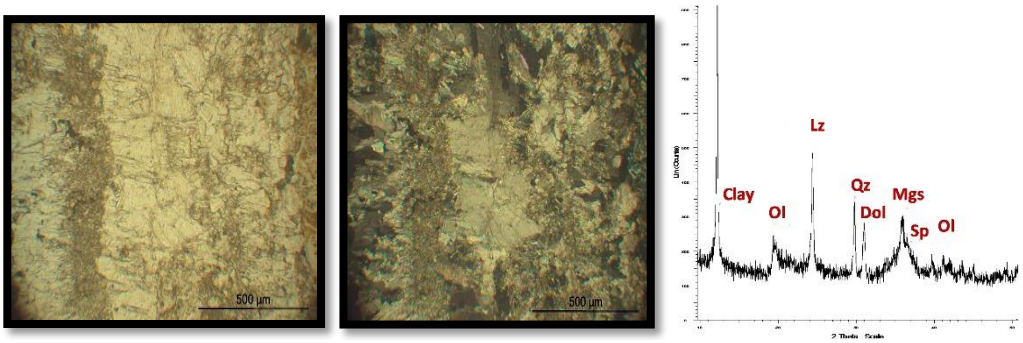

Figure 1. Petrographic microscopy analysis (parallel Nicols left and cross right) and respective XRD pattern of crystalline magnesite in the form of veins. Dol: dolomite; Lz: lizardite; Mgs: magnesite; Ol: olivine; Qz: quartz; Sp: spinel

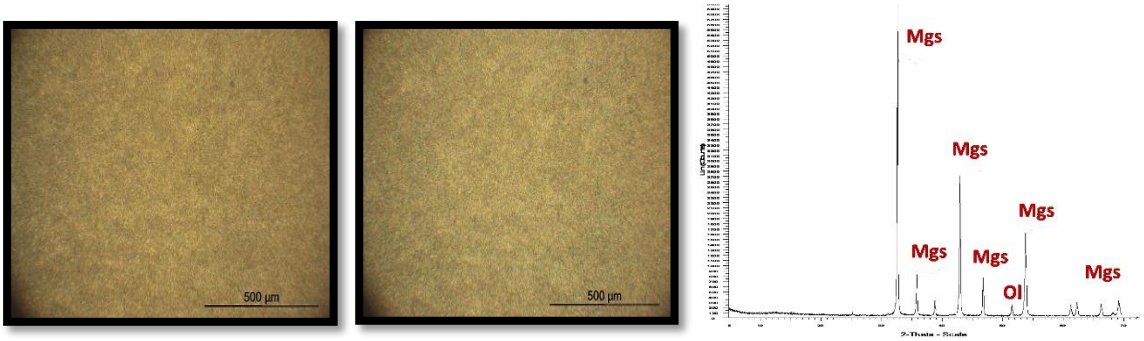

Figure 2. Petrographic microscopy analysis (parallel Nicols left and cross right) and respective XRD pattern of pure microcrystalline to cryptocrystalline magnesite. Mgs: magnesite; Ol: olivine

In case of Babakas area the results indicated that pure cryptocrystalline magnesite is hosted in ultramafic rocks, especially of serpentinized harzburgite. (Figure 3).

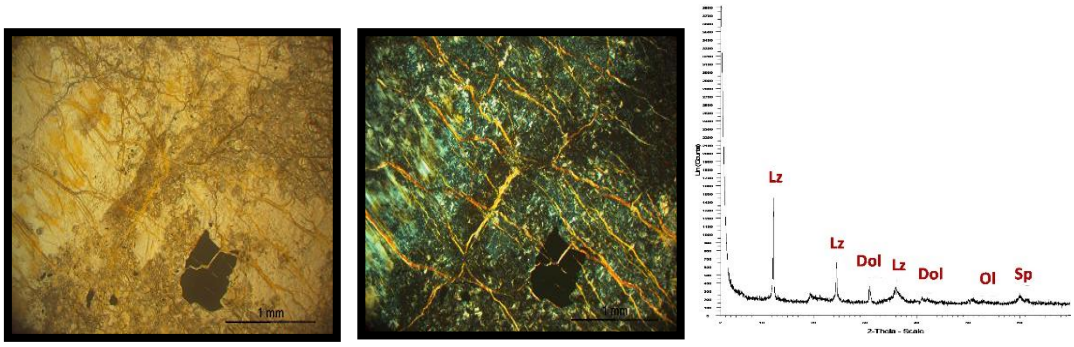

Figure 3. Petrographic microscopy analysis and respective XRD pattern of serpentinized harzburgite. Dol: dolomite; Lz: lizardite; Ol: olivine; Sp: spinel

This work introduced the idea of the synergy of these rocks, (without extensive enrichment) in several tested mixtures as raw materials for the production of new alternative low cost ceramics or aggregates, contributing further to the industrial development, save energy and economy.

Acknowledgements

The authors wish to thank Dr. A.K Seferlis of the Laboratory of Electron Microscopy and Microanalysis, University of Patras for his assistance with the microanalyses and SEM observations. Special thanks to the TERNA MAG for their excellent collaboration in the course of this research.

References

Harben, P.W., 2002. The Industrial Minerals HandyBook - A Guide to Markets, Specifications, & Prices, 4th Edition, Industrial Minerals Information Services, UK.

Skliros, V., Lampropoulou, P.G., Tsikouras, B., Hatzipanagiotou, K., Christogerou A., Angelopoulos, G.N., 2013. Characterization of a new laboratory ceramic product from industrial by-products as raw materials and caustic magnesia as additive. Proceedings of the 13th International Congress of Geological Society of Greece, vol. XLVII, Chania, Greece, p.2050.

Lampropoulou, P.G., 2003. Mineralogical study and properties of basic refractories and new synthesized magnesia-spinel compositions derived from magnesite of N. Evian, Greece Ph.D. Thesis, University of Patras, Greece, 250 p.

Gartzos, E., 1986. On the genesis of cryptocrystalline magnesite deposits in the ultramafic rocks of northern Euboea, Greece. Ph.D. Thesis, University of Athens, Greece.

15th International Congress of the Geological Society of Greece
Athens, 22-24 May, 2019 | Harokopio University of Athens, Greece
Bulletin of the Geological Society of Greece, Sp. Pub. 7 Ext. Abs. GSG2019-278

Application of Natural and Synthetic Microporous Materials for Engine Oil Leakages Treatment: A Comparative Study

K. Koukouza[1], C. Vasilatos[1], M. Stamatakis[1]

(1) Department of Geology and Geoenvironment, National and Kapodistrian University of Athens, Panepistimiopolis Zografou, 15784 Athens, Greece, vasilatos@geol.uoa.gr

We live in the era of growing industrialization and development of automotive industry. Those terms are undeniably related to an increasing demand for materials like crude oil and petroleum products. The everyday use, transportation and distribution of those substances unfortunately leads to an increase in the potential risks such as oil spills. Oil contamination is recognized as one of the major environmental issues nowadays with many consequences on the environmental and human health (Carmody et al., 2007). The removal of oil leakages can be made by oil absorption process techniques using various absorbents. Natural mineral sorbents offers satisfactory results because of the ease of their use, their stability, their need for specific surface area and their low cost. Their remarkable performance is based on their ability to absorb and immobilize the substances without releasing them under pressure (Franus et al., 2014). The microporous structure and the sorption property that zeolites exhibit, make them a promising material for the removal of petroleum substances.

Sorbents can be classified as hybrid systems, as they can be employed for active removal as well as for containment, and are particularly effective in recovering traces of oil from both land and water (Carmody et al., 2007). Also, sorbents are a class of materials which sorb oil either by absorption or adsorption. Past few decades have seen elaborate exploration of synthetic organic, inorganic, and natural organic sorbents, with a greater interest in the latter materials (Adebajo and Frost, 2003). Earlier observations (Franus et al., 2014) showed the potential use of synthetic zeolites as sorbents of petroleum substances as individual so as additives for enhancing the product. Also, the use of expanded perlite in combating oil spills have been examined (Roulia et al., 2002). Owing to their relative abundance, and due to the biodegradability of some of these, use of mineral sorbents has gained traction lately. However, no study has considered the comparison of natural and synthetic materials.

The goal of this study was to indicate the probability of microporous materials, examined globally, in order to compare and ensure the best possible solution with regard to the absorption of petroleum products. By comparing different grain sizes and most of all different materials we can have a comprehensive picture of their potential use. Both on the basis of the composition and on the basis of the structure of each material, behaves differently, as a result it has a different capacity in terms of absorption in general and in particular in petroleum products.

Three bulk samples of natural zeolites derived from different locations and one sample of synthetic zeolite derived from hydrothermal processing of fly ash (Koukouzas et al., 2009, 2010, Itskos et al., 2015) were used. Particularly, natural zeolite samples were derived from the Greek islands of Samos and Kimolos (Z-SAM and Z-KIM), and Pitigliano, Tuscany Italy (Z-IT), whereas the fly ash was derived from Meliti Power Plant Station (SYN-Z). For comparison of the absorption capacity of the samples, a calcareous diatomite bulk sample was used, originating from Mytilinii, Samos Island, Greece (DIAT).

For the study, five different grain fractions of each natural zeolite material (s1 > 1mm, 1mm< s2 >500μm, 500μm< s3 >250μm, 250μm< s4 >63μm and s5 <63μm) were used in order to determine the most suitable grain size for such application. With regard to the petroleum products, were used two types of oil: (1) High viscosity oil (SHELL HELIX HX5 20W-50) and (2) Low viscosity engine oil used in SEM Siemens-5000 instrument.

The mineral composition of the sorbents was investigated by X-ray diffraction. The particle size distribution and specific surface area was measured with a laser particle-size analyzer. The specific surface area refers to the total area of the unit mass of the material. It is an important indicator for evaluating the adsorption capacity. The experimental procedure was the standard test method for oil absorption by spatula. In particular, 3g of each solid absorbent material was placed on a 12x12 glazed surface and then the addition of the oil was made from the bottle drop by drop (using the glass tube) and after each addition was thoroughly mixed the oil and the sorbent by rubbing with the spatula. Continuing the addition of the oil till exactly enough oil has been incorporated to produce a very stiff paste that does not break or separate. The experiments were carried out in 3 repetitions.

Textural parameters such as BET surface area, pore volume, average pore width and the results of oils sorption of the investigated sorbents are summarized in the Table 1. The results of oil absorption capacity using the low viscosity oil were similar.

The results indicate that the sorption capacity of the investigated materials is controlled mainly by the textural parameters of the materials, especially specific surface area and diameters of pores. The studied zeolites differed in the contribution of micro- and mesopores in the surface and diameters of mesopores. In general, lower specific surface area and smaller grain fractions leads to lower oil absorption.

By comparing all the samples tested it's evident that the material with the best absorption capacity was the natural zeolite from the island of Kimolos and especially the grain fraction <63μm that was able to sorb 1.8ml/g of high viscosity oil. That high sorption capacity may be related to the larger surface area.

According to the literature data (e.g. Georgiadis & Stamatakis, 2009) all zeolite materials tested, could be assumed as functional in terms of their sorption capacity, with the finest grain fraction of Kimolos natural zeolite sample (Z-KIM s5) exhibiting the best performance.

Table 1. Textural parameters and absorption capacity for the high viscosity engine oil SHELL HELIX HX5 20W-50

Sample	Grain size	Absorption capacity (ml/g)	BET Surface Area (m^2/g)	Average pore width (Å)	Single point adsorption total pore volume (cm^3)
Z-KIM (s1)	>1mm	0.2			
Z-KIM (s2)	1mm – 500μm	1.0			
Z-KIM (s3)	500μm - 250μm	1.4			
Z-KIM (s4)	250μm - 63μm	1.5			
Z-KIM (s5)	<63μm	**1.8**	22.4	1365.9	0.8
Z-IT (s1)	>1mm	0.4			
Z-IT (s2)	1mm – 500μm	1.3			
Z-IT (s3)	500μm - 250μm	1.4			
Z-IT(s4)	250μm - 63μm	**1.7**	20.0	2368.6	1.2
Z-IT (s5)	<63μm	1.3			
Z-SAM (s1)	>1mm	0.3			
Z-SAM (s2)	1mm – 500μm	1.1			
Z-SAM (s3)	500μm - 250μm	1.2			
Z-SAM (s4)	250μm - 63μm	**1.4**	18.5	114.8	0.9
Z-SAM (s5)	<63μm	1.0			
SYN-Z		**1.4**	18.6	1412.3	0.9
DIAT		0.9			

It can be conclude that the narrow pores are less accessible for viscous substances and macromolecular substances such as oils. As far as the mineral composition is concerns, the result showed that oil absorption was highest by the natural clinoptilolite and motmorillonite mixture of the Kimolos sample). Diatomite was characterized by the lowest sorption capacity with respect to the tested substances. Notably, the analyses also indicate the potential use of synthetic zeolites from lignite fly ash for the removal of oil spills.

Acknowledgements

The Centre for Research & Technology, Hellas (Chemical Process & Energy Resources Institute), is thanked for providing the lignite fly ash and for the BET analysis. National and Kapodistrian University of Athens is acknowledged for supporting this work.

References

Adebajo M.O., Frost R.L., Kloprogge J.T., Carmody O., Kokot S., 2003. Porous Materials for Oil Spill Cleanup: Areview of Synthesis and Absorbing Properties. Journal of Porous Materials 10, 159-170.

Camody O., Frost R., Xi Y., Kokot S., 2008. Selected adsorbent materials for oil-spill cleanup. Athermoanalytical study. Journal of Thermal Analysis and Calorimetry 91, 809-816.

Franus M., Brander L., Franus W., 2014. Use of zeolite mixtures for the removal of petroleum products. 4th International Conference Industrial and Hazardous Waste Management, Crete, Greece.

Georgiades G.N., Stamatakis M.G., 2009. Clayey Diatomite from a Deposit in Central Greece. A Multifunctional Raw Material for Absorption and Insulation. Refractories WORLDFORUM 2, 150-165.

Itskos, G., Koutsianos, A., Koukouzas, N., Vasilatos, C., 2015. Zeolite development from fly ash and utilization in lignite mine-water treatment. International Journal of Mineral Processing 139, 43-50.

Koukouzas, N., Vasilatos, Ch., Itskos, G., Moutsatsou, A., 2009. Characterization of CFB-coal fly ash zeolitic materials and their potential use in wastewater treatment. 2009 World Coal Ash Conference, Lexington, Kentucky, USA, 12p.

Koukouzas, N., Vasilatos, C., Itskos, G., Mitsis, I., Moutsatsou, A., 2010. Removal of heavy metals from wastewater using CFB-coal fly ash zeolitic materials. Journal of Hazardous Materials 173(1-3), 581-588.

Roulia M., Chassapis K., Fotinopoulos CH., Savvidis TH., Katakis D., 2003. Dispresion and sorption of oils spills by emulsifier-modified expanded perlite. Spill Science & Technology Bulletin 8, 425-431.

15th International Congress of the Geological Society of Greece
Athens, 22-24 May, 2019 | Harokopio University of Athens, Greece
Bulletin of the Geological Society of Greece, Sp. Pub. 7 Ext. Abs. GSG2019-283

The contribution of Near Infrared Spectroscopy for the characterization of calcite-rich rocks

M. Kokkaliari[1], I. Iliopoulos[1]

(1) Department of Geology, University of Patras, 2650 Patras, Greece, kokkaliari_m@upnet.gr

Introduction

The subject addressed in the present contribution is related to the application of Near Infrared Spectroscopy on calcite-rich rocks for mineralogical identification. Calcite is an abundant mineral in many geological environments. Depending on their $CaCO_3$ and $MgCO_3$ content carboniferous sedimentary rocks are differentiated into limestones, dolomites and the in-between categories. In addition, calcite is frequently the main cementing substance between the siliceous grains of sandstones, which are clastic sedimentary rocks, composed mostly of quartz, feldspars, clay minerals and also include fragments of breccias and conglomerates. Furthermore, calcite is the main constituent of marbles, which are crystalline rocks used as structural stones according to their quality. The use of NIR spectroscopy is an easy and straightforward method that can determine the mineralogical composition of carbonate rocks. The aim of the present work is to compare the spectral signatures of Near Infrared region for different lithotypes, with a semi-quantitative mineralogical determination and their petrographic study. For this reason, limestones, marbles and calcitic sandstones were used to determine how the participation of other minerals influence the spectral features obtained.

Materials and methods

The samples analyzed were collected from Astypalaia (AST7, AST9A2, AST10, AST12, AST25, AST26) and Kos Island (PPY3, PKR1, PKR5, KF4) in the Aegean Sea, Greece. The two islands have completely different lithologies. The geologic structure of Astypalaia Island comprises both Alpine and post-Alpine formations (Marnelis & Bonneau, 1977; Marnelis, 1986). Due to extended deformation mechanism, Astypalaia Island can be divided in two areas, with the eastern part consisting of Santonian-Maastrichtian limestones, and the central and western part of the Island mainly consisting of flysch deposits. On the other hand, Kos Island geological structure, consists of a range of lithologies that cover the main tree categories of rock types (magmatic, metamorphic and sedimentary) (Drinia et al. 2010, Soder et al., 2016, Kalt et al., 1998). For the petrographic analysis, thin sections were prepared and studied using polarized microscope (Zeiss AxioScope A.1) in order to determine the mineralogical composition of each sample and their textural characteristics. Furthermore, through X-Ray Powder Diffraction analysis (BRUKER D8 Advance) the mineralogy of the samples was verified, and a semi-quantification was performed. The Near Infrared spectra were acquired on the smooth and clean surface hand specimens with a SM-3500 Spectral Evolution portable spectrometer. Furthermore, the Cathodoluminescence method (Reliotron III Cathodoluminescence system attached on a Leitz Wetzlar Orthoplan Microscope), provided us more information about the mineralogy of the sample, that was not perceptible through normal observation, during the petrographic analysis. The methods discussed above were applied at the Research Laboratory of Minerals and Rocks, Department of Geology, University of Patras.

Results and Conclusions

The calcitic sandstones are rocks rich in siliceous grains of quartz and feldspars cemented together with micritic calcite. Their mineralogical composition is supplemented by clay minerals, which give the samples a yellowish color. The micro-brecciated limestone is rich in metallic and siliceous minerals and has channel-like porous. The spectra have small, sharp absorption features ~1400nm and a shoulder-like feature at 2200 nm which represent the presence of clay minerals in the sample.

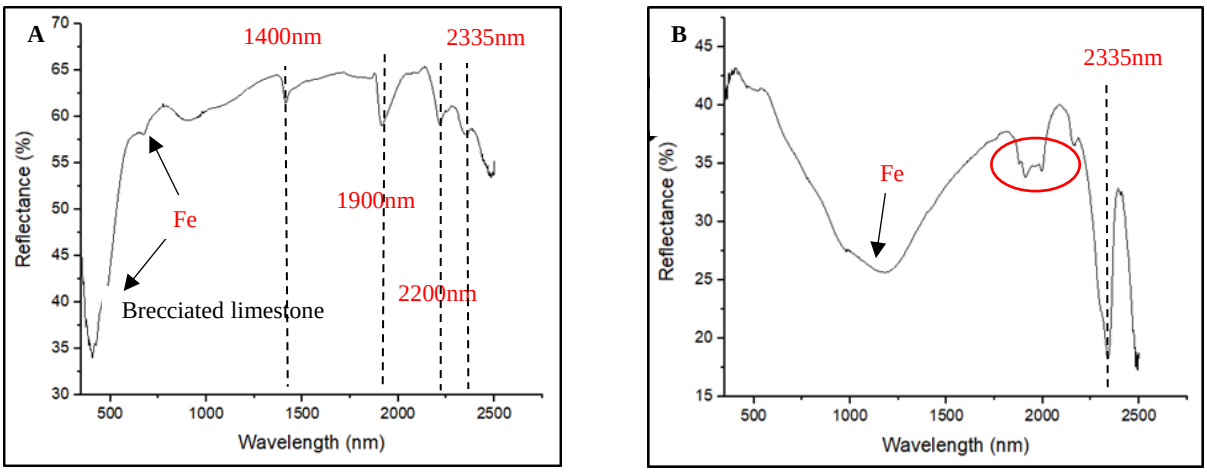

Figure 1. A) Representative spectrum from brecciated limestone (sample AST12), B) Representative spectrum from a marble (sample PKR5)

Also, the ~1900 nm absorption feature is deep and rounded and indicate unbound water in the structure of the samples (figure 1A). The characteristic absorption feature of calcite at ~2340nm is small and not distinctive for the sample and could be confused with absorption features of clay minerals. An important role for the shape of the spectrum plays the presence of metallic minerals which characterizes the reflectance of the spectrum. The fossiliferrous micritic limestone is a non-cohesive formation with visible microscopically porosity, with channels-like porous and consists of micritic calcite and bioclasts and endoclasts in a small percentage. The spectrum is characterized by the major absorption feature of calcite in ~2340nm but also by the ~1400 and ~1900 nm rounded features which indicates the presence of water. The marbles are coarse-grained samples with the typical granoblastic texture, comprising calcite and minor wollastonite, diopside and hedenbergite. The spectra are characterized by the major absorption feature of calcite at ~2340nm (figure 1B), by the characteristic doublet feature at ~1.890 and ~2000 nm (see red circle in figure 1B) and by a broad absorption feature at ~1100nm.

According to the above study, the following conclusions were drawn:

- Calcite, when present in small proportions, is difficult to be identified and usually present similar absorption features with chlorites and mica.
- Quartz and feldspars are featureless in the Near Infrared region, however their percentage contributes to the overall reflectance of the sample
- The percentage of clay minerals in the sample strongly influence the absorption features of the sample and may subdue the absorption features of calcite, when is present in small amounts.
- When dolomite is present in small amounts in the mineralogy of the lithotype, it cannot be discriminated from calcite. However, when dolomite dominates, the absorption features are shifted to smaller wavelengths.
- A possible difference among marbles and limestones could be the presence or absence of broad absorption features at ~1400 and ~1900 nm. However, in the case of well crystalized limestones, this argument might not be representative.
- The reflectance variations of the spectra caused by the grain size of the minerals does not affect the position of the absorption features.
- Absorption features at the visible range of the electromagnetic spectrum are caused by the presence of ferrous minerals.
- The broad absorption feature at ~1100nm is caused by the presence of ferrous iron either substituting Ca^{2+} in calcite, or due to the presence of ferrous minerals like diopside on hedenbergite, in the case of marbles.
- The spectra of these lithologies even though address to a specific mineral, the calcite, do not add any information for the conditions of formation of these rocks, or for their crystallinity.

Acknowledgments

Maria Kokkaliari is a PhD student and is financially supported by the "General Secretariat for Research and Technology (GSRT)" and the "Hellenic Foundation for Research and Innovation (HFRI)", at the University of Patras.

References

Drinia, H., Koskeridou, E., Antonarakou, A., Tzortzaki, E., 2010. Benthic Foraminifera Associated with the Zooxanthellate Coral Cladocora in the Pleistocene of the Kos Island (Aegean Sea, Greece): Sea Level Changes and Palaeoenvironmental Conditions. Bulletin of the Geological Society of Greece, Proceedings of the 12th International Congress Patras, May, 2010

Kalt, A., Altherr, R., & Ludwig, T., 1998. Contact Metamorphism in Pelitic Rocks on the Island of Kos (Greece, Eastern Aegean Sea): a Test for the Na-in-Cordierite Thermometer. Journal of Petrology 39, 663–688.

Marnelis, P., Bonneau, M. 1977. Stratigraphie et structure de l'île d'Astypalea (Dodécanèse, Grèce), in: Kallergis, G. (Ed.) VI. Colloquium on the geology of the Aegean region, 1, 323−332.

Marnelis, P. 1986. Geological Map of Greece, 1:50.000, Astipalaia Sheet. Institute of Geological and Mining Research, Athens.

Soder, C., Altherr, R., & Romer, R. L., 2016. Mantle metasomatism at the edge of a retreating subduction zone: Late neogene lamprophyres from the Island of Kos, Greece. Journal of Petrology 57, 1705–1728.

15th International Congress of the Geological Society of Greece
Athens, 22-24 May, 2019 | Harokopio University of Athens, Greece
Bulletin of the Geological Society of Greece, Sp. Pub. 7 Ext. Abs. GSG2019-288

Mineralogical and Geochemical features of Upper Cretaceous Ni-laterite and Karstic-Nickel ores from Lokris (Continental Greece): implications for burial depth

M. Ramadani[1], C. Gianniou[1], P. Stamatis[1], N. Sofis[1], M.E. Damoulianou[1], S. Kalaitzidis[1]
(1) Department of Geology, University of Patras, 26504 Rio Greece; corresponding author: skalait@upatras.gr

Introduction

The Ni-laterite and laterite derived sedimentary ores in Greece are a major source of nickel, which nowadays is regarded as a metal of strategic significance. The exploitable deposits with an average Ni-content in the order of 0.9-1.4%, are mainly located in Lokris area, Euboea and Kastoria, and the metallurgical facility that produces a ferronickel alloy is located at Larymna. In Continental Greece and Euboae only laterite derived sedimentary Fe-Ni ore deposits are under exploitation, whereas Ni-laterite ores are sub-economic. Lateritization took place in Cretaceous times, resulting in extensive development of Ni-lateritic profiles. Lateritization was followed in Late Cretaceous by erosion of weathering crusts, transport of the lateritic material and submarine deposition as a clastic sediment during transgression of the sea, either on ultramafic rocks (secondary deposits) or in karstic traps of limestones (Karstic Nickel deposits) (Albandakis,1980; Eliopoulos and Economou-Eliopoulos, 1999; Skarpelis, 1999; 2005).

In this study the mineralogical and geochemical characteristics of selected Ni-lateritic profiles and sedimentary Fe-Ni-deposits from the broader area of Lokris are discussed, towards a more comprehensive interpretation of the environment of deposition and the diagenetic evolution of the ores.

Geological Settings

Geologically the area of Lokris belongs to the Sub-Pelagonian geotectonic zone, which in the broader studied area consists of Triassic-Jurassic dolomites and limestones, Upper Jurassic ophiolite formations, Upper Cretaceous limestones and flysch sediments. The Ni-laterites in the area were formed during the Lower-Late Cretaceous by the intense weathering of the ultramafic-mafic sequences of these ophiolite rocks under tropical/subtropical and hence humid environment (Albandakis, 1980; Eliopoulos and Economou-Eliopoulos, 1999; Skarpelis, 2000).

Materials and Methods

Samples were taken from the Ni-laterite profile of Metochi area, where exploratory works have been carried out, as well as along four vertical profiles at the Nissi, Kopaida and Agios Ioannis (North Sector) and Villes Karstic-Nickel deposits, which represent allochthonous lateritic deposits, deposited over the karstified limestone.

Polished blocks and thin sections were prepared from a series of ore lithologies, as well as of the transgressive Cretaceous limestones. Ore petrography was carried out by combined optical microscopy, Scanning Electron Microscope and X-ray diffraction using a Bruker D8 Advance X-Ray diffractometer. The transgressive bituminous limestones were also examined under a LEICA DMRX microscope, fitted with an MPV reflectance measurement unit. Major and minor element analyses were conducted using a RIGAKU ZSX PRIMUS II spectrometer.

Results and Discussion

The general mineralogical and geochemical characteristics of each studied profile can be summarized as follows:

Metochi Ni-laterite profile: displays an *in situ* lateritic zonation above the ultramafic bedrock, the latter consisting mainly of lizardide and diopside. However, evidences of small-scale reworking of the material were also traced in the upper parts. The Ni-rich lithologies are mainly the clayey layers, consisting of mixed-layered clays and chamosite, containing Ni up to 0.64 wt.%.

Villes profile, Ag. Ioannis area: mineralization is of karstic type, overlying the Jurassic limestones. The lower parts are characterised by the predominance of silicates, in the form of quartz (silcrete fragments) and mixed-layered clays, and hematite, whereas carbonates and iron-oxides show enrichment towards the upper parts. The argillaceous layers contain less than 1 wt.% Ni, whereas the hematite-kaolinite rich layers in the upper part of the profile display up to 3.6 wt.% Ni and 1.5 wt.% Cr.

Nissi profile, Ag. Ioannis area: mineralization is of karstic type, with a fine-grained sedimentary mixture of calcite, magnetite, boehmite, and garnierite, occupying the lower parts displaying 1.4 wt.% Ni and 415 mg/kg Co. The overlain layer shows a coarser and more brecciated character, with significant occurrence of angular chromite and quartz grains. Towards the middle and upper parts of the profile silicates in form of mixed-layered clays and Fe-oxides, mainly as pelloids, are predominant. Nickel concentration ranges between 0.5-1 wt.% and this of Co between 415-459 mg/kg. The overlying carbonate rock represents a marly bituminous limestone, with frequent occurrence of hematite, chromite and pyrite grains. Within this layer, apart from bituminite-like material, well preserved macerals of the vitrinite group were traced, providing evidences for their indigenous nature. The random reflectance values of the indigenous vitrinite population ranges between 0.75-0.82% (Fig. 1), with these values corresponding to the middle catagenesis maturation stage, providing indications for the burial depth of the studied profiles.

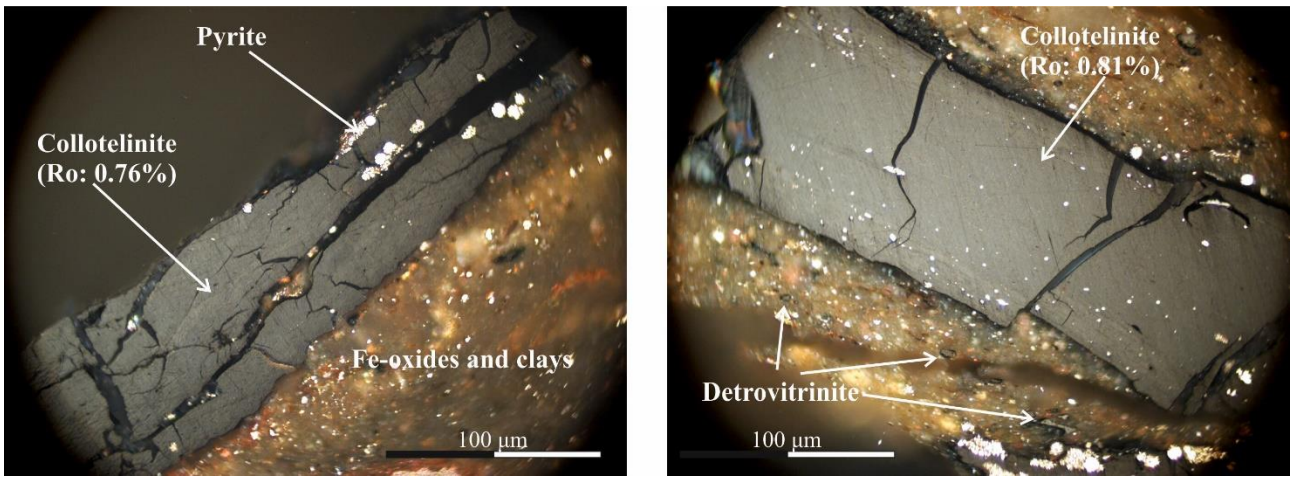

Figure 1. Photomicrographs of the Cretaceous bituminous limestone, overlying the Nickeliferrous karstic ore in Nissi deposit, showing telovitrinite particles and the respective reflectance values; white light, using oil immersion.

Kopaida profile: karstic type mineralization with an argillaceous prevailing sedimentary facies. The main mineralogical assembly of the clay-rich strata consists of hematite, goethite, chlorite, kaolinite, quartz, chamosite and boehmite. Within the more massive Fe-rich strata, magnetite, chromite and asbolane are more evident. Nickel values range from 0.95-1.3 wt.% and those of Co between 411-566 mg/kg.

North Section profile: the mineralogical assembly consists mainly of hematite, goethite, chromite, chlorite, magnetite, kaolinite, chamosite and boehmite. The lower part is a coarse brecciated facies, whereas towards the upper parts finer sedimentary facies prevail. Nickel values range from 0.3 to 0.5 wt.% and those of Co between 302-483 mg/kg.

Conclusions

The sedimentological and mineralogical features of the studied profiles confirm the prevailing allochthonous nature of the Ni-rich horizons and are in accordance with the previous studies. The comparative study of the different deposits demonstrates also that the formation of Karstic Nickel ore-types took place in variable depositional environments with fluctuations in the hydrological regimes and the transportation and/or the depositional modes of the clastic material. The presented data reveal that in most cases coarser material was deposited at the base getting finer towards the top. In some places, evidences of terrestrial plant input suggest shallow, relatively anoxic environment at least during the initial deposition stage of the overlying carbonates.

Acknowledgements

The authors would like to thank the Geological Team of LARCO GMMSA for the access to sampling sites and assistance during field work. The Laboratory of Electron Microscopy and Microanalysis, of the Faculty of Natural Sciences, University of Patras, is gratefully acknowledged for the support in SEM studies and the XRF analyses.

References

Albandakis N., 1980. The nichel-bearing iron ores in Greece. UNESCO IGCP 169 Int. Symp. Metallog. Mafic Ultramafic Complexes 1, 194-213.

Eliopoulos D.G, Economou-Eliopoulos M., 1999. Geochemical and mineralogical characterization of Fe-Ni and bauxitic-laterite deposits of Greece. Ore Geology Reviews 16 (2000) 41–58.

Skarpelis N., 1999. Lateritic weathering crusts as a source of ferruginous spheroidal particles of sedimentary nickeliferous iron ores, Greece. Bull. Acad. Serbe Sci. & Arts, 39, 213-224.

Skarpelis N., 2000. Sedimentary nickeliferous iron ores and lateritic weathering crusts in SW Balkan Peninsula: mineralogical textural relationships and genesis. Proc.1st Conf. Greek Comm. Econ. Geol. Miner. Geoch., 398-412 (in Greek).

Skarpelis N., 2005. Laterization processes of ultamafic rocks in Cretaceous times: The fossil weathering crusts of mainland Greece. J. Geoch. Explor., 88, 325-328.

15th International Congress of the Geological Society of Greece
Athens, 22-24 May, 2019 | Harokopio University of Athens, Greece
Bulletin of the Geological Society of Greece, Sp. Pub. 7 Ext. Abs. GSG2019-296

Borate and Sulphate Salt Deposits of the Late Miocene Basin of Karlovasi, Samos Greece

C. Klitorakis[1], M. Stamatakis[1]

(1) Department of Geology and Geoenvironment, National and Kapodistrian University of Athens, Panepistimioupoli Zografou, 15784 Athens, Greece. stamatakis@geol.uoa.gr

The present graduate study refers to the research of the borate and the sulphate deposits of the Late Miocene basin of Karlovassi, west Samos Island, Greece.

Borates, which are the main objective of the research, are the most important economic source of boron. This happens due to the fact, that boron is extremely dispersed in nature, averaging 10ppm in earth's crust (Anovitz and Grew, 1996). As a result, there are relatively few occurrences where the element is sufficiently concentrated to be economic.

Samos Island is located in the eastern part of the Aegean Sea and neighbors with the coast of Asia Minor-Turkey.

The Karlovassi basin which is the main area of the research, is one of the two biggest sedimentary basins of Samos and has a North-South direction. Furthermore, the basement rocks of the basin are mainly marbles and limestones (Papanikolaou 1979). To be more specific, the basin was filled with basalt conglomerates, evaporites, marls, claystones and limestones. The Karlovasi basin has been predominated by hot and dry conditions during Late Miocene. These conditions led to the formation of a saline and alkaline lake (Stamatakis, 1986, 1989b). As it is known, borate salts and boric acid enrichments of supergene type occur mostly within recent playas-saline flats associated with volcanic emanations and hot springs (Helvaci, 2015). This criteria, along with older field and laboratory data on the occurrence of borates and celestine in the lake (Stamatakis and Economou, 1996), lead us to investigate in detail the Karlovassi basin, to locate any considerable amount of borate deposits that may be economically exploitable.

For that reason, the aim of this study was to determine the borate deposits of this basin and draw the conclusions on the genesis and possible importance of the borates existed in that area.

The borate mineral that has been found the most, is colemanite-$Ca_2B_6O_{11}$•5(H_2O) (Figure 1). Furthermore, ulexite is also present in some cases in smaller amounts with the form of needle-like crystals, with approximately 0.2mm size. Additional, celestine and barite crystals were found in the form of fissure fillings crossing the colemanite groundmass. Barite occurs rarely, covering celestine, as a fine-grained thin film of a few microns in thickness. Secondary calcite occurs replacing colemanite in micro and macro scale.

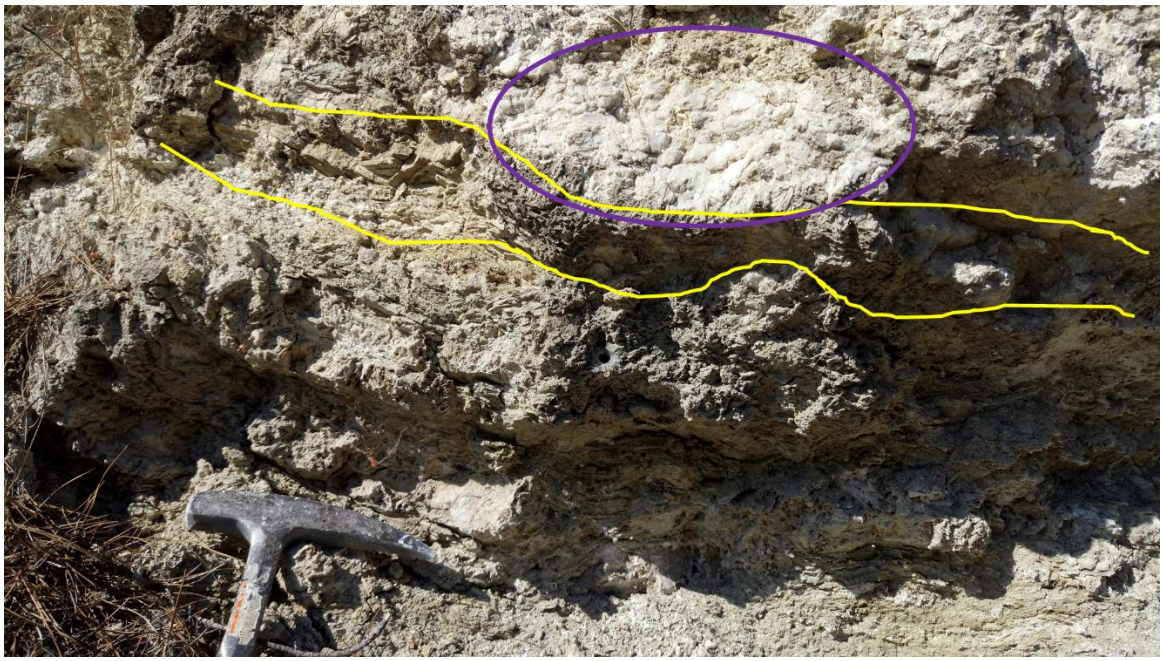

Figure 1. Characteristic colemanite crystals (purple circle) and laminated layer of clay (yellow lines)

In the context of the present study, several depositional information, fieldwork observations and analytical lab results are presented. The field work included the sampling and investigation of the relationship of the borates with the host rocks. Moreover the analytical lab tests that have been carried out on the geological samples from the basin of Karlovasi were:

- X-ray diffraction (XRD), which helped the identification of the mineral phases
- Scanning Electron Microscope (SEM), which yields flexibility in the analysis of the geometry and composition of the microstructure of the individual mineral phases and their relationship

- Optical Microscope Analysis (LM), which helped the identification of minerals in each rock sample through observation under magnification using both crossed and uncrossed nicols
- Inductively Coupled Plasma Optical Emission Spectrometry (ICP-OES), which is predominant in the analysis of major and trace elements
- Stereoscopic microscope analysis, which helped to capture characteristic photographs providing very important information about the macro-structure of the mineral assemblages of the specimens

All of the above tests were necessary in order to identify the presence of the borate and the sulphate minerals and the related minerals as well.

Afterwards, conclusions about the studied area and the depositional model are presented. Some of them are:

- The Karlovasi basin is continental type and during Late Miocene it was a playa lake like environment similar to that of the Neogene basins of western Anatolia, Turkey.
- The borate and sulphate deposits relate with the hydrothermal activity due to volcanism which took place in Late Miocene
- The host rocks of the deposits are the tuffaceous rocks rich in Authigenic K-feldspar and zeolites and dolomitic claystone
- The intense weathering of borate minerals in the basin of Karlovasi was reinforced by large-scale tectonic events that caused fractures in the sedimentary rocks of Upper Miocene and thus to the host rocks of the boron deposits. These data, combined with the rare occurrences of boron-bearing bodies found in this study, lead us to the conclusion that the probability of maintaining large borate mining bodies is limited
- The only part of the basin which may have prosperity of further research by performing a drilling project is its NE part, where the Upper Miocene siliceous limestone-porcelanite cap rock is still preserved and may protect the borates from strong weathering that occurs in the rest of the basin.

Acknowledgements

I would like to thank Dr. Ioannis Mitsis for his advice and assistance in the XRD analysis. My grateful thanks are also extended to Dr. Charalampos Vasilatos for his help in doing the SEM data analysis, to Mr. Vasileios Skounakis, who helped me prepare the SEM samples coefficient and to Dr. Athanasios Karalis, chief of Imerys Industrial Minerals S.A., for his support in the ICP measurements. Last but not least, I would like to acknowledge the support provided by my family during the preparation of my undergraduate study.

References

Anovitz, L. M., and Grew, E. S., 1996. An introduction. In Mineralogy, Petrology and Geochemistry of Boron. Mineral. Soc. Amer., Reviews in Mineralogy, Vol. 33, Ch. 1, pp. 1-40.

Garrett D. (1998) Borates. Handbook of Deposits, Processing, Properties, and Use. London: Academic Press

Helvacı, C., 2015, Geological Features of Neogene Basins Hosting Borate Deposits: An Overview of Deposit and Future Forecast, Turkey. Bull. Min. Res. Exp., 151: pp 169-215

Helvaci C., Stamatakis M., Zagouroglou C. & Kanaris J. (1993). Borate minerals and related authigenic silicates in northeastern Mediterranean Late Miocene continental Basins. Exploration and Mining Geology V. 2, 14-22

Helvaci, C. (1978) A review of the mineralogy of the Turkish borate deposits. Mercian Geology, 6, 257 -270

Papanikolaou D., 1979. Unites tectoniques and phases de deformation dans l'ile de Samos, Mer Egee, Grece. Bull. Soc. Geol De France, XXI, no: 6, p. 745-752

Stamatakis, M.G., 1986 Boron distribution in hot springs, volcanic emanations, marine evaporites and in volcanic and sedimentary rocks of Cenozoic age in Greece Ph. D. thesis, University of Athens, Athens, Greece

Stamatakis M., 1989a Boron-bearing K-feldspar in volcanic ash and tuffite from Miocene lake deposits, Samos Island, Greece. Am. Mineralogist, v.74, p.230-235

Stamatakis M., 1989b, Authigenic silicates and silica polymorphs in the Miocene saline-alcaline deposits of the Karlovasi basin, Samos, Greece. Econ. Geol., v.84, p.788-798.

Stamatakis M.G. & Economou G.S. 1991. A colemanite and ulexite occurrence in Late Miocene saline--alkaline lake of west Samos, Greece. Economic Geology, 86, 166-172.

15th International Congress of the Geological Society of Greece
Athens, 22-24 May, 2019 | Harokopio University of Athens, Greece
Bulletin of the Geological Society of Greece, Sp. Pub. 7 Ext. Abs. GSG2019-297

Study of the chromite mineralization associated to ophiolites from Tinos Island, Attico-Cycladic Massif

M. Kokkaliari[1], E. Koutsopoulou[1], S. F. Tombros[2], K. St. Seymour[1]

(1) Department of Geology, University of Patras, Rion, 26500, Patras, Greece, kokkaliari_m@upnet.gr

(2) Regional Directorate of Primary and Secondary Education in Western Greece, PDEDE, 25A Akti Dimaion, 26222, Patras, Greece

Tinos chromitites appear in the ophiolite complex of Mount Tsiknia. The host rocks to the chromite orebodies are mostly serpentinites, meta-dunites, -peridotites, with minor -pyroxenites and locally-gabbros. Tinos Island is part of Cyclades Blueschist Unit (CBU), a nappe overlying a Pre-Alpidic anatectic basement covered by meta-volcanic and meta-sedimentary rocks (Bröcker and Franz, 2005; Rabillard et al., 2015). The whole sequence is underlain by the lowermost Basal Unit (BU), which comprises of Late-Triassic to -Cretaceous neritic meta-dolomites and -flysch (Xypolias et al., 2012), and overthrusted by an ofiolite slice (Katzir et al., 2000). These rocks have been metamorphosed at eclogite to blueschist facies conditions (Brichau et al., 2010) 53-40 Ma, and retrograded at greenschist to amphibolite facies at ≥ 25 and ~ 12 Ma (Bolhar et al., 2010). The whole sequence is intruded by a ~14 to 18 Ma monzogranite to granodiorite pluton, (Brichau et al., 2007), and a peripheral to it a boron- and fluorine-rich leucogranite (Mastrakas and St. Seymour, 2000), at the eastern part of the island. The intruded pluton resulted in contact metamorphism (Stolz et al., 1997) of pyroxene- and amphibole-hornfels and pyroxene-garnet skarns in the inner zone of the aureole, and albite-epidote hornfelses in the outer zone. The aim of the present work was to study the lithotypes, paragenesis and petrochemistry of Tinos chromitites of the host rocks. In combination with the mineral chemistry of chromite we also attempted to outline their genetic environment.

Materials and Methods

Sampling included the ultramafic host rocks, i.e., serpentinites, meta-dunites, -peridotites, -pyroxenites, -gabbros and greenschists as well as the chromitites of the ophiolite complex. From these samples a total of 48 polished and thin sections have been studied with optical microscopy, Scanning Electron Microscopy (SEM) and selected samples have been analyzed for their major and trace elements.

Results and Discussion

The mineral chemistry of the Tinos chromite indicates that chromite was in equilibrium with boninite melts originated from a Supra-Subduction Zone (SSZ), i.e., in a depleted mantle wedge. The chromites of Tinos have compositions which in the ternary Cr-Fe^{3+}-Al classification diagram of Stevens (1994) plot mostly in the field of Al-chromite and only a few samples in the field of Fe-chromite. The latter may represent the re-equilibrated margins of chromite grains. In the binary classification diagram for spinels the Tinos samples extend in the fields of Mg-chromite and chromite sensu strictu (figure 1). The ultramafic host rocks are dunites and harzburgites, characteristic rocks for the lithology of 'depleted mantle'.

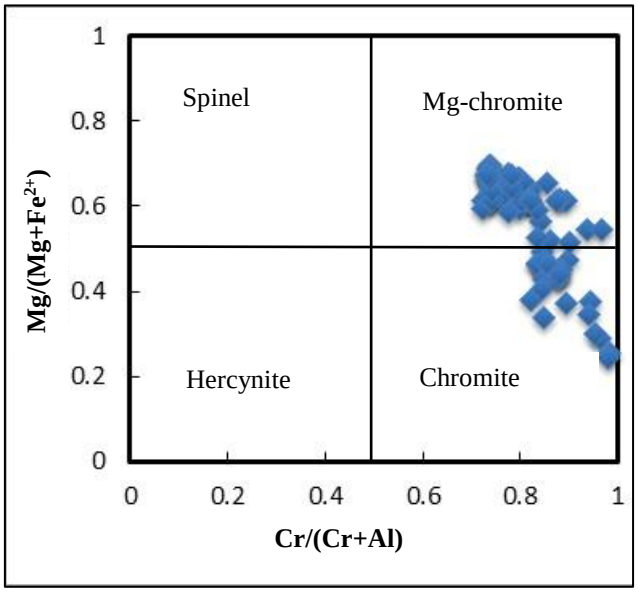

Figure 1. Analyzed chromites from the chromites of the ophiolithic complex in Mount Tsiknia on the Mg / (Mg + Fe^{+2}) vs. Cr / (Cr + Al) diagram.

A detailed petrographic study was carried out in order to examine the texture of the chromite crystals (figure 2A) and the presence of other metallic phases. Base metal sulfides such as pyrite, pyrrhotite, chalcopyrite, heazlewoodite have been identified which initially may have been in equilibrium with the ultramafic magma. However, the presence of galena, sphalerite, wurtzite and base metals antimonites (figure 2B) i.e., tennantite and alloys, as well as native Ni and Pb is probably linked to the metasomatic and/or hydrothermal processes, related to the emplacement of the neighboring Tinos composite granodiorite-leucogranite.

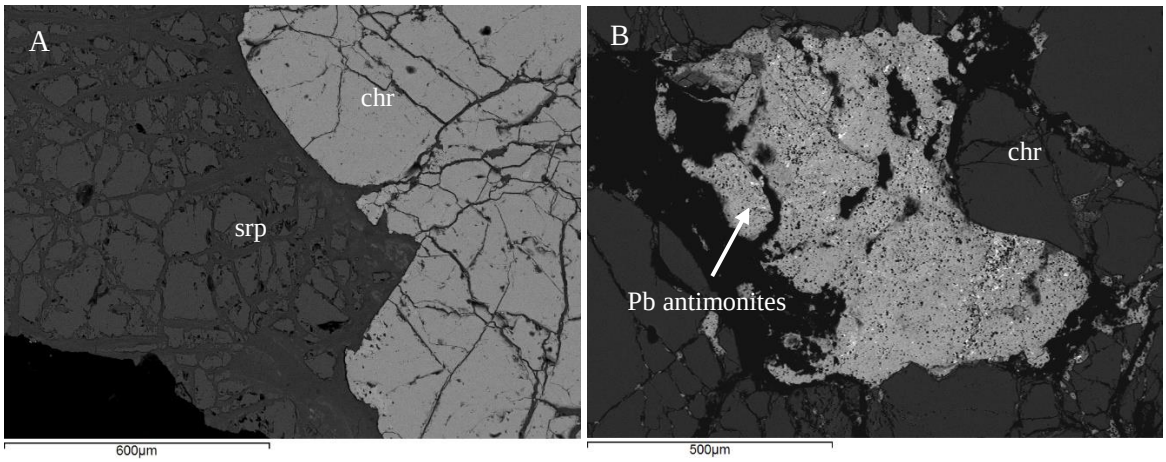

Figure 2. A) Chromite crystals in contact with the serpentinized mass, B) Pb-antimonites that appear to occupy the crystals of chromite. chr: chromite, srp: serpentine.

Conclusions

The following conclusions were drawn during the preparation of the study:

- The ultramafic host rocks are dunites and harzburgites, typical of 'depleted mantle'.
- Ore phases in intergrowths with chromite were identified, specifically of basic metal, sulfides and alloys, whether of primary or secondary origin.
- Tinos mineralization is related to the emplacement of Tinos composite granodiorite-leucogranite.

References

Bolhar, R., Ring, U., Allen, C.M., 2010. An integrated zircon geochronological and geochemical investigation into the Miocene plutonic evolution of the Cyclades, Aegean Sea, Greece: Part 1: Geochronology. Contributions of Mineralogy and Petrology 160, 719-742.

Bröcker, M., Franz, L., 2005. P-T conditions and timing of metamorphism at the base of the Cycladic blueschist Unit, Greece: the Panormos window on Tinos re-visited Neues Jarhbuch für Mineralogie Abhandlungen 181, 91-93.

Brichau, S., Thomson, S., Ring, U., 2010. Thermochronometric constraints on the tectonic evolution of the Serifos detachment, Aegean Sea, Greece. International Journal of Earth Sciences (Geol. Rundsch) 99, 379-393.

Brichau, S., Ring, U., Carter, A., Monié, P., Bolhar, R., Stockli, D., Brunel, M., 2007. Extensional faulting on Tinos Island, Aegean Sea, Greece: how many detachments? Tectonics 26, TC4009, doi:.org/10.1029/2006TC001969.

Katzir, Y., Avigad, D., Matthews, A., Garfunkel, Z., Evans, B.W., 2000. Origin, HP/LT metamorphism and cooling of ophiolitic mélanges in southern Evia (NW Cyclades), Greece. Journal of Metamorphic Geology 18, 699-718.

Mastrakas, N., St. Seymour, K., 2000. Geochemistry of Tinos granite: A window to the Miocene microplate tectonics of the Aegean region. Neues Jarhbuch für Mineralogie Abhandlungen 175, 295-315.

Rabillard, A., Arbaret, L., Jolivet, L., Le Breton, N., Gumiaux, C., Augier, R., Grasemann, B., 2015. Interactions between plutonism and detachments during metamorphic core complex formation, Serifos Island (Cyclades, Greece). Tectonics 34, 1080-1106.

Stolz, J., Engi, M., Rickli, M., 1997. Tectonometamorphic evolution of SE Tinos, Cyclades, Greece. Schweizerische Mineralogische et Petrographische Mitteilungen 77, 209-231.

Xypolias, P., Iliopoulos, I., Chatzaras, V., Kokkalas, S., 2012. Subduction and exhumation related structures in the Cycladic Blueschists: insights from Evia Island (Aegean region, Greece). Tectonics 31, TC2001, doi: 10.1029/2011TC002946.

15th International Congress of the Geological Society of Greece
Athens, 22-24 May, 2019 | Harokopio University of Athens, Greece
Bulletin of the Geological Society of Greece, Sp. Pub. 7 Ext. Abs. GSG2019-383

Mineralogical and Geochemical Investigation of Sb-bearing minerals from Greek ores

E. Tzamos[1], G. Grieco[2], M. Bussolesi[2], A. Xenidis[3], A. Zouboulis[4], A. Godelitsas[1]

(1) Department of Geology and Geoenvironment, National and Kapodistrian University of Athens, Zografou Campus, 15784, Athens, Greece, tzamos@geo.auth.gr
(2) Department of Earth Sciences, Università degli Studi di Milano, via Botticelli n.23, 20133, Milano Italy
(3) School of Mining and Metallurgical Engineering, National Technical University of Athens, Zografou Campus, 15780, Athens, Greece
(4) Department of Chemistry, Aristotle University of Thessaloniki, University Campus, 54124, Thessaloniki, Greece

Critical Raw Materials (CRMs) are those raw materials that are economically and strategically important for the European economy, but have a high-risk associated with their supply. It is important to note that these materials are not classified as 'critical' because these materials are considered scarce, rather they are classified as 'critical' because (http://criticalrawmaterials.org/critical-raw-materials) : (1) they have a significant economic importance for key sectors in the European economy, such as consumer electronics, environmental technologies, automotive, aerospace, defense, health and steel, (2) they have a high-supply risk due to the very-high import dependence and high level of concentration of set critical raw materials in particular countries and (3) there is a lack of (viable) substitutes, due to the very unique and reliable properties of these materials for existing, as well as future applications.

Sb is classified as a Critical Raw Material (CRM) in all relevant official EU reports (e.g. European Commission, 2017). Applications of Sb include flame-retardants, alloys, pigments, semiconductors, pharmaceuticals etc. (e.g. Grund *et al.*, 2006) and according to the latest EC report (2017), Sb has the third highest supply risk for the EU industry after the two categories of rare earth elements (LREEs and HREEs). Sb metal is recovered from ore primarily by pyrometallurgical techniques. Hydrometallurgical processing is suitable for some ores containing precious metals (Grund *et al.*, 2006).

According to Arvanitidis (2011) Sb ores in Greece are formed and found in veins at various areas of Rhodope, Thessaloniki and Chios Isl.. The concentration of Sb in these veins varies between 1 and 2.5wt.% and secondary mineral phases occurring with Sb minerals include Pb, Fe, Cu, Ag and Au sulphides. The indicative reserves of Sb from these areas are 2,400 tones and further research is required at these occurrences for the determination of their potential. According to Klocho (2019), worldwide reserves are 1,500,000 tones (rounded). Major Sb deposits are found China (reserves 480,000 tones), Russia (350,000 recoverable tones), Bolivia (reserves 310,000 tones), Australia (reserves 140,000 tones) and Turkey (reserves 100,000 tones) (Klocho, 2019). China is the main global supplier with a share of 87% of the world production (European Commission, 2017).

The most promising Sb occurrence in Greece is found in the mixed sulphide ore deposits of Kassandra mining district (NE Chalkidiki). This is clearly depicted in the concentration of Sb in the concentrates produced from these mines: Sb is found having a concentration of 712.9 ppm in the Py-AsPy concentrate from Olympias, 748.2 ppm in the ZnS concentrate from Stratoni and >2000 ppm in the PbS concentrate from Stratoni (Tzamos *et al.*, 2019).

Although Sb is a CRM present in many localities from Greece, detailed studies regarding the mineralogy and geochemistry of Sb minerals and ores of Greece have not yet been made. Thus, the scope of the present study is to report new results concerning the mineralogy and the chemistry of these minerals from different Greek localities.

For the present study, twelve (12) Sb-bearing ore samples from Lachanas (Thessaloniki), Chios Isl., Kassandra mining district (Olympias and Stratoni, Chalkidiki) were concerned. Polished sections were mounted from each sample and were examined in optical microscope (Fig. 1). After examination in optical microscope, scanning electron microscopy (SEM) images and microprobe analyses (EPMA) were obtained using a JEOL 8200 electron probe micro-analyzer equipped with a wavelength dispersive spectrometer (WDS). Analytical conditions were: 15kV accelerating voltage, 15 nA beam current, 2 μm beam diameter with a counting time of 20 s on the peaks and 10 s on the background. The approximate detection limit was 0.01 wt.% for each element.Also, four (4) representative samples were analyzed for their concentration in trace elements using Perkin Elmer ICP-OES/MS after standard fusion and acid-digestion.

Microscopic study of polished sections under the optical microscope and SEM, revealed the presence of stibnite in Olympias (sample O1), stibnite (sample M1) and boulangerite along with galena, pyrite and sphalerite (sample M2) in Stratoni, boulangerite in Lachanas (sample K1), stibnite (sample C4) and valentinite (sample C5) in Chios. Microprobe analyses showed that all Sb-bearing minerals have typical concentration regarding their content in major elements.

Table 1 presents the results of the chemical analyses for some trace elements analyzed. Elevated concentrations of samples of samples M1, M2 and O1 in Ag, Mn, Cd and Sn is attributed to the presence other mineral phases (e.g. galena) micro-inclusions and impurities, along with Sb minerals.

Regarding other trace elements, sample M2 shows an unusual high concentration in Bi (1610 ppm), sample M1 has an elevated concentration of Se (10 ppm) and sample K1 contains significant amount of Hg (10.08 ppm). Moreover, Tl shows enrichment in three out of the four analyzed samples: 92 ppm in sample M2, 15.12 ppm in sample O1 and 8.80 ppm in sample K1. Elevated concentrations in Bi, Se, Hg, and –especially- Tl and their geochemical significance are part of our ongoing research concerning the Sb ores of Greece along with research on the development of methods for the extraction of Sb from mixed sulphide concentrates.

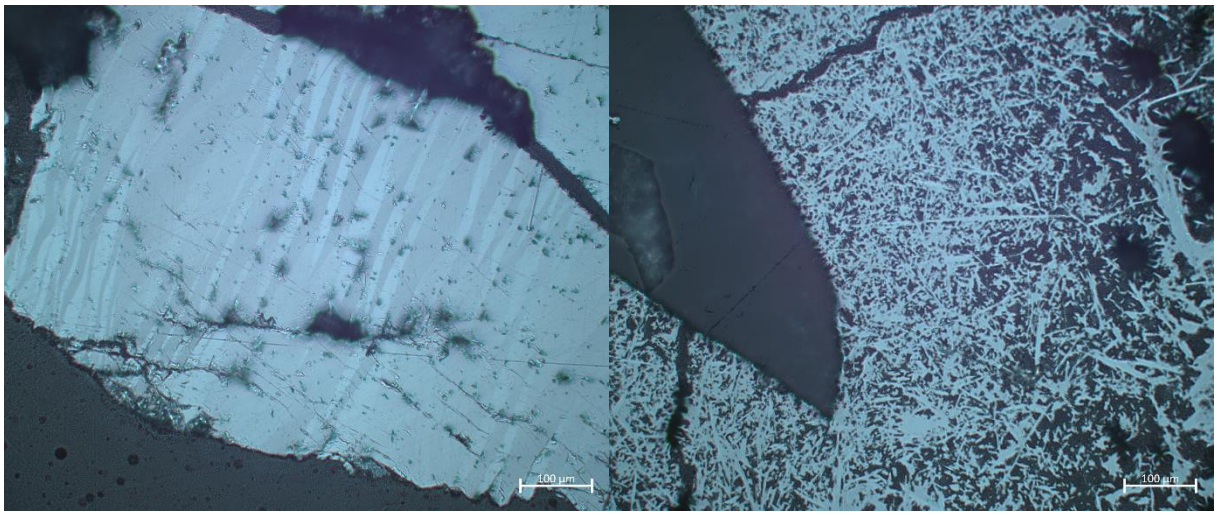

Figure 1. Stibnite (left-sample M1) and boulangerite (right-sample M2) from Stratoni, reflected light (N //).

Table 1. Trace element concentrations of the studied samples.

Element	Mo	Ag	Mn	Cd	Bi	Sn	Se	Te	Tl	Hg
Unit	ppm	ppm	ppm	ppm	ppm	ppm	ppm	ppm	ppm	ppm
Detectionlimit	0.05	20	1	0.02	0.04	0.1	0.3	0.05	0.05	0.01
Sample M1 (Stratoni)	<0.05	26759	63	0.94	0.69	15.7	10.0	0.05	0.58	0.37
Sample M2 (Stratoni)	0.12	>200000	428	21.85	1609.67	69.7	0.8	2.74	92.00	0.22
Sample K1 (Lachanas)	<0.05	1391	3	0.74	6.73	0.2	<0.3	<0.05	8.80	10.08
Sample O1 (Olympias)	0.29	70047	3074	8.17	4.20	83.7	0.7	0.17	15.12	n/a[1]

1: n/a = not analyzed

Conclusions

- Sb (considered as a Critical Raw Material) is reported to have potential for exploitation from Greek ores, especially from the Kassandra mining district were new methods for its extraction from the mixed sulphide concentrates must be developed
- Sb-bearing minerals found in Greek relevant ores are antimonite, stibnite, boulangerite and valentinite with typical chemical composition in major elements.
- Mineral samples hand-picked and analyzed with ICP-ES/MS were found to have elevated concentrations in various trace elements (Bi, Se, Hg and Tl) with ongoing research aiming to reveal the significance of this fact.

Acknowledgements

This research is implemented through IKY scholarships programme and co-financed by the European Union (European Social Fund - ESF) and Greek national funds through the action entitled ”Reinforcement of Postdoctoral Researchers”, in the framework of the Operational Programme ”Human Resources Development Program, Education and Lifelong Learning” of the National Strategic Reference Framework (NSRF) 2014 – 2020.

References

Arvanitidis, N., 2011. Reserve potential of Greek non-energy minerals. http://nikolaosarvanitidis.eu/?p=234 (accessed on 21/03/2019- in Greek).

European Commission, 2017. Study on the review of the list of Critical Raw Materials. Written by: Deloitte Sustainability, British Geological Survey, Bureau de Recherches Géologiques et Minières, Netherlands Organisation for Applied Scientific Research, 93p.

Grund, S.C., Hanusch, K., Breuning, H.J., Wolf, H.U., 2006. Antimony and antimony compounds, in: Ullmann's Encyclopedia of Industrial Chemistry, Wiley-VCH, Weinheim.

http://criticalrawmaterials.org/critical-raw-materials (accessed on 21/03/2019)

Klocho, K., 2019. Antimony. U.S. Geological Survey, Mineral Commodity Summaries, February 2019, 22-23.

Tzamos, E., Papadopoulos, A., Grieco, G., Stoulos, S., Bussolesi, M., Daftsis, E., Vagli, E., Dimitriadis, D., Godelitsas, A., 2019. Investigation of trace and critical elements (including actinides) in flotation sulphide concentrates of Kassandra mines (Chalkidiki, Greece). Geosciences (under review).

15th International Congress of the Geological Society of Greece
Athens, 22-24 May, 2019 | Harokopio University of Athens, Greece
Bulletin of the Geological Society of Greece, Sp. Pub. 7 Ext. Abs. GSG2019-385

Rare Earth Elements in the Black Sands From Coastal Cliffs Sedimentary Deposits, of Aggelochori Area

S. Lazaridis[1], A. Kipourou-Panagiotou[1], A. Papadopoulos[1], N. Kantiranis[1], A. Koroneos[1], K. Albanakis[1]
(1) Aristotle University of Thessaloniki, University Campus, 54124, Thessaloniki, Greece, slazarid@geo.auth.gr

Introduction

Coastal sands are a result of weathering of nearby rocks. The erosion and deposition can be a result of either the sea waves, or of the action of the local streams and rivers. Black coastal sands are a result of the action of sea waves that separate the heavy (black) from the light (white) minerals. The heavy fraction of the black sands is mainly consisted of titanite, rutile, monazite, xenotime, zircon, magnetite, illmenite and allanite. Sometimes, the concentration of such minerals allows their economic exploitation either for economic metals or Rare Earth Elements (REE). Some heavy minerals being resistant in chemical weathering are exclusively enriched in REEs, such as monazite, xenotime and allanite. The light fraction is consisted of common minerals like quartz, feldspars, calcite and other minerals found in the nearby rocks (Pohl, 2005; Ridley, 2013). Previous research has been done about the coastal black sands found in Greece. Most of them are focused at northern Greece (Pe and Panagos, 1979; Pergamalis et al., 2001; Papadopoulos et al., 2014; 2015; 2016; 2018; Tzifas et al., 2017). The study area belongs to the Axios Zone. Particularly, in the narrower area metamorphic rocks intruded by felsic igneous rocks and their sedimentary counter parts in the presence of Neogene – Quarternary formations are found (Filippidis et al., 1997 and references there in).

Objectives

Filippidis et al. (1997) provided a mineralogical and radiological study of the studied sands. In this study, the main objectives are to provide additional mineralogical information. Moreover, the chemical content, exclusively focusing on the REEs is also studied in order to give the economic importance of these sands. The REE concentrations of the studied sands are compared to those of black sands exhibiting elevated REE contents from Kavala and Sithonia (Papadopoulos *et al.*, 2014; 2016). Finally, primary effort to study the source rocks of these sands is attempted by comparing the REE patterns of the black sands with the REE patterns of neighbouring granitic rocks (Fanos and Monopigado).

Methods

Four samples (5 kg each) collected from a coastal slope at height of five meters above sea level at a distance of 30 meters from each other, in order to examine a horizon of black sand formed in the recent geological period. The samples have been washed with clean water to remove any shells and algae and dried at the oven at 50 degrees for 48 h. The 4, 2, 1, 0.063 mm sieves have been used to obtain the grain size distribution of the samples. For minerals separation, representative 15 – 20 g of the 1 – 0.063 mm of each sample have been selected. Hand magnet was used to remove magnetite. Afterwards, the magnetic (I >1.70 mA) and non-magnetic (I <1.70 mA) fractions have been obtained by using a magnetic separator. 0.5 g from each magnetic fraction was pulverized, in order to get the semi-quantitative mineralogical composition with P-XRD. Then, the sample being the most enriched in zircon (sample AGG-3) was selected for chemical analyses. In particular, the whole rock and the fractions >4, 4-2, 2-1, 1-0.063 mm as well as the magnetic and non-magnetic fractions of 1-0.063 mm grain size have been pulverized and analyzed for their major elements content with XRF and trace elements content by ICP-MS at MS Analytical laboratories, Canada.

Results

According to Schlee (1973), samples AGG-1, 2, 4 are classified as gravels and sample AGG-3 as gravel sediment, indicating probable fluvial transport and deposition environment (Venetikidis, 2012). The main mineral constituents are quartz, feldspars and phyllo-silicates. Minor quantities of magnetite and titanite have been found. Traces of pyroxenes, amphiboles and dolomite as well as heavy minerals such as zircon, hematite and illmenite are present.

The ΣREE (ppm) of the samples was 75.14 for the whole rock (w.r.) and 99.66, 76.00, 54.72 and 73.46 for the fractions >4 mm, 4-2 mm, 2-1 mm and 1-0.063 mm respectively. For the magnetic separated samples,the I>1.70 fraction has 283.95 ppm while the I <1.70 fraction has 39.88 ppm.

The whole rock (w.r.) REE patterns, have been compared to the REE patterns of black sands from Kavala and Sithonia, displaying elevated REE concentrations (Papadopoulos *et al.*, 2014; 2016) (Fig. 1). In order to assume the source rock, the whole rock REE patterns are compared with those of local granitic rocks (Fanos and Monopigado) (Michail *et al.*, 2016 and references therein and Koroneos, 2009 respectively) (Fig. 2).

Conclusions

Excluding several common silicates, like quartz and feldspars, the main REE bearing minerals are zircon and titanite. The ΣREE content of the studied samples are below but close to the average value of the Sithonia sands, but well below those of Kavala sands. The REE pattern of the w.r. is quite similar to those of Monopigado and Fanos granitoids. The presence of ultrastable detrital non opaque heavy minerals like zircon and titanite along with the unstable amphiboles and pyroxenes and the stable to moderate stable opaque heavy minerals hematite and ilmenite is suggestive for mineralogical immaturity

and thus relatively limited sediment transportation. Furthermore, the absence of the characteristic pinkish feldspars of Fanos pluton, implies that the source rock of the studied sediment could possibly be the Monopidado pluton. Further investigation is imperative, in order to determine the source rock.

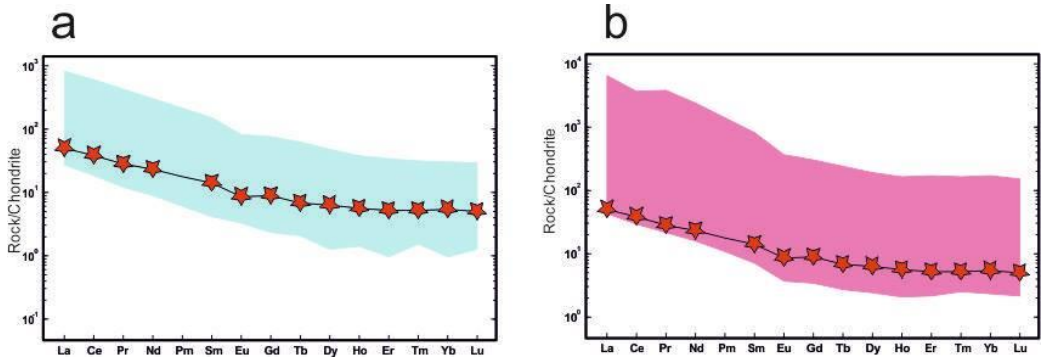

Figure 1. Comparison of the black sands (w.r.) REE pattern with those of (a) Sithonia and (b) Kavala

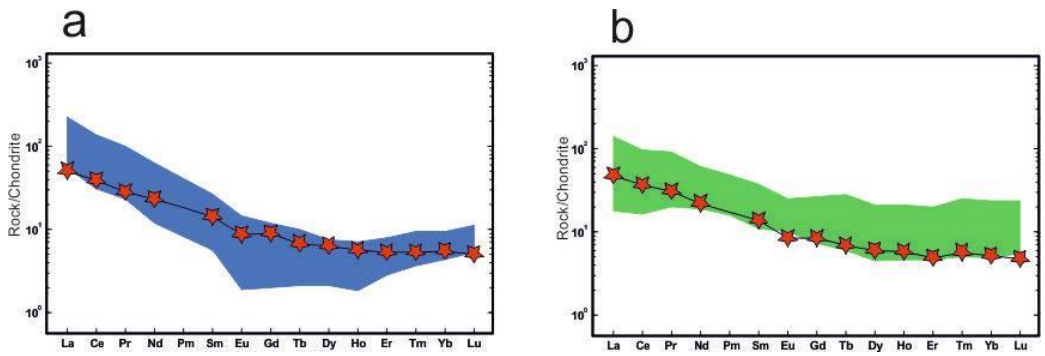

Figure 2. Comparison of the black sands (w.r.) REE pattern with the REE whole rock pattern from (a) Fanos and (b) Monopigado granitic rocks.

References

Filippidis, A., Misaelides, P., Clouvas, A., Godelitsas, A., Barbayiannis, N., Anousis, I., 1997. Mineral, chemical and radiological investigation of a black sand at Touzla Cape, near Thessaloniki, Greece. Environmental Geochemistry and Health 19, 83-88.

Koroneos, A., 2009. Petrogenesis of the Upper Jurassic Monopigadon pluton related to the Vardar/Axios ophiolites (Macedonia, northern Greece) and its geotectonic significance. Chemie der Erde 70, 221-241.

Michail, M., Pipera, K., Koroneos, A., Kilias, A., Ntaflos, T., 2016. New perspectives on the origin and emplacement of the Late Jurassic Fanos granite, associated with an intra-oceanic subduction within the Neotethyan Axios-Vardar Ocean. International Journal of Earth Sciences. Doi 10.1007/s00531-016-1321-4.

Papadopoulos, A.,Christofides, G., Koroneos, A., Hauzenberger, C., 2015. U, Th and REE content of heavy minerals from beach sand samples of Sithonia Peninsula (northern Greece). NeuesJahrbuch für Mineralogie – Abhandlungen (Journal of Mineralogy and Geochemistry) 192/2, 107-116.

Papadopoulos, A., Christofides, G., Pe-Piper, G., Koroneos, A., Papadopoulou, L., 2014. Geochemistry of beach sands from Sithonia Peninsula (Chalkidiki, Northern Greece). Mineralogy and Petrology.Doi 10.1007/s00710-014-0351-5.

Papadopoulos, A.,Koroneos, A., Christofides, G., Papadopoulou, L., 2016. Geochemistry of beach sands from Kavala, Northern Greece. Italian Journal of Geosciences.Doi 10.3301/IJG.2016.01.

Pe, G.G., Panagos, A.G., 1979. Heavy mineralogy of river and beach sands, continental Greece.NeuesJahrbuch für Mineralogie 136, 254–261.

Pergamalis, F., Karageorgiou, D.E., Koukoulis, A., Katsikis, I., 2001. Mineralogical and chemical composition of sand ore deposits in the seashore zone N. Peramos-L. Eleftheron (N. Greece). Bulletin of Geological Society of Greece XXXIV/3, 845–850.

Pohl, W., 2005. Economic Geology: Principles and Practice. Wiley- Blackwell, Chichester, 663 p.

Ridley, J., 2013. Ore Deposit Geology. Cambridge University Press, New York, 409 p.

Tzifas, I.T., Misaelides, P., Godelitsas, A., Gamaletsos, P.N., Nomikou, P., Karydas, A.G., Kantarelou, V., Papadopoulos, A., 2017. Geochemistry of coastal sands of Eastern Mediterranean: The case of Nisyros volcanic materials. Chemie der Erde. http://dx.doi.org/ 10.1016/j.chemer.2017.07.002.

Schlee, J., 1973. Atlantic continental shelf and slope of the United States: sediment texture of the northeastern part. U.S. Geol. Surv., Prof. Pap.529-L, p. 64

Venetikidis, D.A., 2012. Sedimentary and petrologic study of Quaternary clastic sediments of Mygdonia basin at Platanorema site, Lagkadikia. MSc Thesis 92 p.

15th International Congress of the Geological Society of Greece
Athens, 22-24 May, 2019 | Harokopio University of Athens, Greece
Bulletin of the Geological Society of Greece, Sp. Pub. 7 Ext. Abs. GSG2019-391

Mineralogical and Geochemical Study of the Zeolitized Volcaniclastic Rocks of Petrota region, Evros Prefecture, Northeastern Greece

E. Michailidou[1], M. Vavelidis[1], L. Papadopoulou[1], N. Kantiranis[1]

(1) Department of Mineralogy, Petrology, Economic Geology, Aristotle University of Thessaloniki, 54124, Thessaloniki, Greece, elenimichailidou@yahoo.gr

Introduction

The present study has been carried out to determine the mineralogical and geochemical composition of the zeolitized pyroclastic flow deposits in the Petrota area of Evros prefecture, in northeastern Greece, further to the previous studies that have been conducted in the surrounding area (Kirov *et al.*, 1990; Stamatakis *et al.*, 1996, 1998; Barbieri *et al.*, 2001; Marantos *et al.*, 2006; Filippidis *et al.*, 2016). The broader area is located near the Greek-Bulgarian border and it belongs geotectonically to the eastern Rhodope massif (Kirov *et al.*, 1990; Barbieri *et al.*, 2001). According to Stamatakis *et al.* (1996, 1998), the zeolitic tuffs that rest on the pre-Cenozoic basement, extend on a horizon of 15km in length and 100m in depth and they were deposited in a supra to infra-littoral environment during the Eocene. Their origin is considered epiclastic and it is suggested that they were transported from their initial to their current location through water. Although most of the zeolite occurrences are characterized as sedimentary type, in rare occasions, due to mixed sulphide and gold mineralization, the zeolite formation is related to hydrothermal alteration (Stamatakis *et al.*, 1996, 1998; Barbieri *et al.*, 2001; Filippidis *et al.*, 2016).

Analytical techniques

In order to determine the mineralogical composition of the zeolite-rich tuffs, 6 thin-polished sections were prepared and studied under a light polarizing microscope and using Scanning Electron Microscopy (SEM) connected to an Energy Dispersive Spectrometer (EDS). The major and trace elements of 12 representative samples were identified by the X-ray fluorescence (XRF) method and 4 Acid digestion ICP-MS analysis, respectively. Furthermore, X-ray powder diffraction (XRD) analysis was performed on 12 randomly oriented powder samples to define the minerals present in the zeolitic tuffs.

Results

Petrographically, most samples present a typical porphyritic texture, containing phenocrysts of primary minerals and metamorphic fragments of different sizes and shapes. Feldspars (sanidine and plagioclase) are the dominant minerals and they appear in phenocrysts with clear zoning and twinning. Although most analytical methods indicate that quartz is abundant in all samples, its presence microscopically isn't represented by phenocrysts. Biotite phenocrysts are abundant and exhibit strong pleochroism with pale to deep brown colour. Amphiboles are observed as primary minerals in the igneous rock, but also as components of the metamorphic fragments. Most amphibole crystals appear brown with intense pleochroism under plane-polarized light. In the sample collected from the Mavri Petra region the amphibole phenocrysts display a distinctive light blue colour. Zeolites can be observed under the microscope mostly in tabular shapes within altered feldspars. As a result of the argillic alteration during zeolitization, clay minerals, such as celadonite, can be found scattered in the altered volcanic groundmass. The mineral assemblage of the metamorphic fragments is dominated by quartz, K-feldspar, plagioclase, micas (muscovite and biotite), amphibole and garnet.

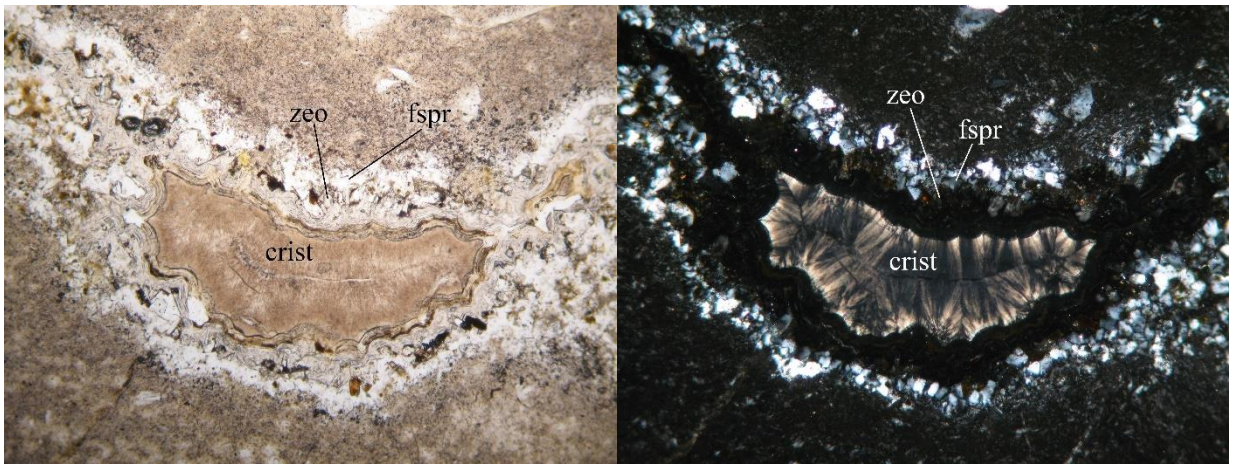

Figure 1. Microphotographs of a cristobalite formation (crist), surrounded by a microcrystalline aggregation of feldspars (fspr) and zeolites (zeo), under plane-polarized (left) and cross polarized light (right) (Mavri Petra region, Evros prefecture).

The mineral phases mentioned above were confirmed by X-ray powder diffraction (XRD). The dominant zeolite in the area of interest is clinoptilolite, while there are some random occurrences of mordenite in small amounts. XRD data also

reveal the presence of quartz, along with its high-temperature polymorph, cristobalite (Fig. 1).

Observation under the Scanning Electron Microscope (SEM) indicates that the dominant minerals are feldspar and zeolite. The groundmass of the investigated samples has undergone diagenetic alteration and zeolites appear as pseudomorphs of plagioclase crystals or as tabular zeolitic aggregations. The glass shards of the porphyritic texture are also partially or fully altered, and cristobalite formations (Fig. 2) appear as a result of the transformation that took place in an open hydrological system (Stamatakis *et al.*, 1998; Kassoli-Fournaraki *et al.*, 2000). Micas are widespread in all the investigated locations, mostly represented by biotite and muscovite. Biotite is observed both in the parental volcanic rock and the metamorphic fragments hosted in it, whilst muscovite is solely a component of the latter. Amphiboles and pyroxenes have also been detected, with amphiboles prevailing in quantity and size (Fig. 2, amp). Additional minerals that have been identified in small amounts are epidote, garnet, titanite, apatite, zircon, ilmenite, magnetite and rutile.

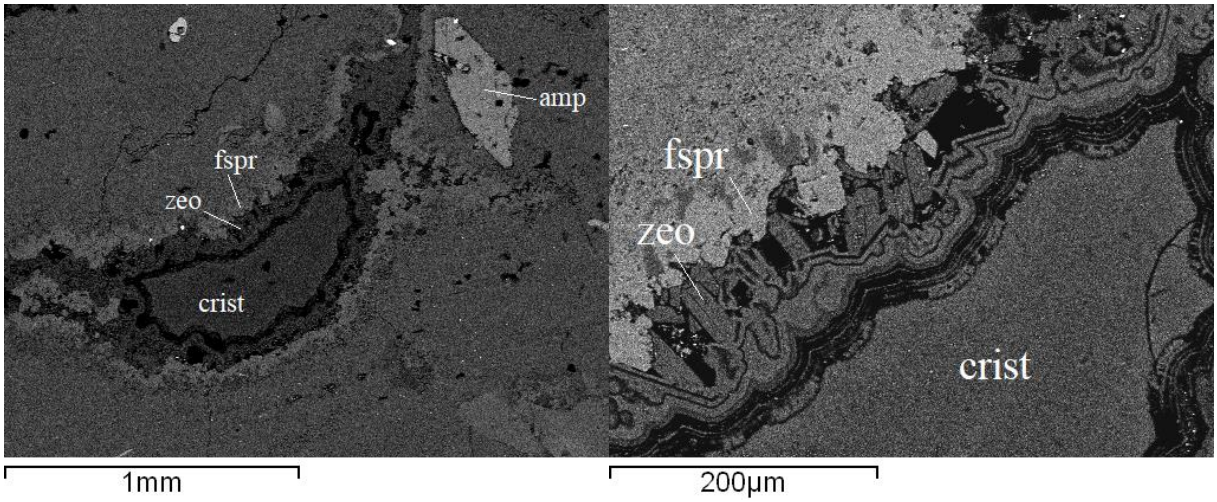

Figure 2. Detailed illustration of the tabular zeolitic crystals (zeo) and the partially altered feldspars (fspr) surrounding the cristobalite formation (crist) of Fig. 1, as displayed under the Scanning Electron Microscope (SEM).

Chemical analysis of major elements using the X-ray fluorescence (XRF) method has indicated that SiO_2 concentrations range from 67,05 to 71,29 wt%, while Al_2O_3 from 11,29 to 14,12 wt% and K_2O from 1,88 to 4,45 wt%. The rest of the elements appear in minor amounts.

Additionally, 12 representative samples of the same area were analyzed through 4 Acid digestion ICP-MS method in order to define the concentrations of 45 trace elements, including some rare earth elements (La, Ce, Y, Nb, Sc). The overall concentrations for La range from 13.5 to 32.8 ppm, for Ce from 27 to 60 ppm, for Y from 8.4 to 19.5 ppm, for Nb from 14.9 to 25.8 ppm and for Sc from 1 to 4 ppm. The Mavri Petra region, exhibits the highest concentrations in Cu (3.1 ppm), Pb (72.2 ppm), Mn (476 ppm), V (32 ppm), P (0.048 %) and second highest in W (150.4 ppm). The analyzed concentrations of U in two samples of the Palaeokklisi region appear to be 18.9 and 21.8 ppm, relatively high in comparison to the rest that vary from 2.9 to 9.8 ppm. Northwestern of the Palaeokklisi area, close to the Greek-Bulgarian boarder, the concentrations of Sr appear to be high (872 ppm) compared to 55 to 350 ppm in the other locations.

Acknowledgements

The authors wish to thank MSc student A. Stamatiadis and PhD candidate N. Kipouros for the preparation of the thin-polished sections. They are also most grateful to E. Sotiroudis for his great assistance during field work and sampling.

References

Barbieri, M., Castorina, F., Masi, U., Garbarino, C., Nicoletti, M., Kassoli-Fournaraki, A., Filippidis, A., Mignardi, S., 2001. Geochemical and isotopic evidence for the origin of rhyolites from Petrota (Northern Thrace, Greece) and geodynamic significance. Chemie Der Erde-geochemistry 61(1), 13-29.

Filippidis, A., 2016. Applications of the Hellenic Natural Zeolite (HENAZE) and specifications of zeolitic tuffs. Bulletin of the Geological Society of Greece 50(4), 1809-1819.

Filippidis, A., Kantiranis, N., Tsirambides, A., 2016. The mineralogical composition of Thrace zeolitic rocks and their potential use as feed additives and nutrition supplements. Geological Society of Greece.

Kassoli-Fournaraki, A., Stamatakis, M., Hall, A., Filippidis, A., Michailidis, K., Tsirambides, A., and Koutles, Th., 1997. The Ca-rich clinoptilolite deposits of Pentalofos, Thrace, Greece. In Abstracts 5th Int. Conf. Occurrence, Properties and Utilization of Natural Zeolites – "Zeolite '97" (De Frede, Napoli, Italy), 178-180.

Kirov, G.N., Filippidis, A., Tsirambides, A., Tzvetanov, R.G., and Kassoli-Fournaraki, A., 1990. Zeolite-bearing rocks in Petrota Area (Eastern Rhodope massif, Greece). Geologica Rhodopica, 500-511.

Marantos, I., Michael, C., Kosharis, G., 2006. Study of the zeolitic alteration in Petrota Tertiary volcaniclastic rocks, Thrace area, NE Greece. Geoscience 124, 126.

Stamatakis, M.G., Hall, A., Hein, J.R., 1996. The zeolite deposits of Greece. Mineral. Deposita 31, 473-481.

Stamatakis, M.G., Hall, A., Lutat, U., and Walsh, J.N., 1998. Mineralogy, origin and commercial value of the zeolite-rich tuffs in the Petrota-Pentalofos area, Evros Count, Greece. Estudios Geologicos 54, 3-15.

SPECIAL SESSION

T4.S1 Geochemical mapping for environmental and resource management

Conveners: **Ar. Argyraki, (NKUA)**
A. Liakopoulos (IGME)
A. Demetriades (IUGS-CGGB)

Jointly organized by the IUGS Commission on Global Geochemical Baselines (CGGB), the Society for Environmental Geochemistry and Health and the EuroGeoSurveys Geochemistry Expert Group

15th International Congress of the Geological Society of Greece
Athens, 22-24 May, 2019 | Harokopio University of Athens, Greece
Bulletin of the Geological Society of Greece, Sp. Pub. 7 Ext. Abs. GSG2019-014

Environmental Contamination of Soils by Cadmium, Associated with Former Zn-Pb Ore Mining Activity in the Upper Silesia Region (southern Poland)

A. Pasieczna[1], A. Konon[1], I. Wysocka[1]

(1) Polish Geological Institute National Research Institute, Rakowiecka 4, 00-975 Warsaw, Poland, irena.wysocka@pgi.gov.pl

Due to the fact that Cd is classified as a potentially harmful element with respect to soil biological activity, plant metabolism and the health of humans and animals, there is concern over anthropogenic accumulations of Cd in the environment. It has no essential biological function, but it tends to accumulate in plants and aquatic biota, with consequent problems of toxicity. It is toxic to humans through the inhalation of dust, causing lung damage, and may cause cancer from long-term exposure, being also teratogenic and embryocidal.

As soil is the main disposal and landfill receptor for different types of wastes, it is of great importance to carry out research, which provides the necessary data on the element content in the Earth's surface materials. Systematic geochemical mapping is a very effective tool of showing the geographical distribution of the elements, and environmental geochemical baseline data are urgently required to inform policy-makers and to provide a sound basis for environmental legislation and resource management.

The study area is located in southern Poland (in the Polish part of the Upper Silesian Coal Basin). It is a part of the Palaeozoic Variscan structure cut by numerous faults. The stratigraphic section is represented by the Triassic, Neogene and Quaternary systems (Wilanowski *et al*., 2009). The deposits of Zn and Pb ores, exploited in the past occurring in the Triassic ore-bearing dolomite were characterised as the largest and richest Zn and Pb ore deposits in the world (Szuwarzyński, 1996; Viets *et al*., 1996; Paulo and Strzelska-Smakowska, 2000). For many years, the most important sectors in the study area were coal mining and Fe metallurgy, as well as Zn metallurgy in the past. The analysed area shows a diverse relief, locally highly modified as a result of industrial activity. There are many landfills of slag and mining waste near historical and present-day metal smelters.

Since 1996, a detailed geochemical mapping project for this region (scale 1:25,000) has been conducted by the Polish Geological Institute. Until 2019, 17 map sheets have been completed and published in the form of separate atlases. The main objectives of this project were the investigation of the environmental impacts of industry on soil contamination by potentially hazardous elements (including Cd) and assessment of the degree of soil contamination.

The obtained research results allowed determination of the geochemical baseline of Cd in the region, controlled by natural factors, and indication of anthropogenically contaminated areas. The anthropogenic factors were associated mainly with former mining, processing and metallurgical industry of Zn-Pb ore, Fe smelting, as well as hard coal mining and energy industry.

The study was performed on soil samples from two depth intervals: 0−30 cm (topsoil 22,663 samples) and 80−100 cm (subsoil 19,307 samples), collected with a density grid of 16 samples/km^2. Content of Cd in soil was determined by the inductively coupled plasma optical emission spectroscopy (ICP-OES) after sample digestion in hot *aqua regia* solution.

Analysed topsoil samples had a wide range of such properties as pH (from very acidic to alkaline), TOC content (0.05–55.9%) and particle size distribution (from sandy to clay soil) showed their significant transformation. Anthropogenic transformations have led to so significant changes in the chemical composition of the soil in relation to the parent rocks that the basic geochemical features of the original rocks in the topsoil are very poorly visible. In areas of mining activity, around historical and modern metallurgical plants, as well as near mine heaps and waste dumps there are numerous anthropogenic anomalies of Ag, As, Cd, Cr, Cu, Fe, Hg, Ni, Pb and Zn. The obtained results indicated great variation in Cd content in topsoil (<0.5–2,107 mg/kg; mean 4.3 mg/kg) and subsoil (<0.5–747 mg/kg; mean 2.2 mg/kg). Strong anomalies for Cd (Fig. 1), as well as for Ag, As, Pb and Zn, are observed in the areas of historical Zn-Pb ore mining, former Zn smelters, and modern Fe industry. About 25% of topsoil samples contained more than 4 mg/kg of Cd (Pb >144 mg/kg and Zn >419 mg/kg). About 25% of subsoil samples contained more than 0.7 mg/kg of Cd (Pb >33 mg/kg and Zn >101 mg/kg).

The anthropogenic pollution sources in the natural environment encompass metallurgy of Fe and non-ferrous metals, chemical and metal industries, mining of coal and its large-scale burning in power plants, historical exploitation and smelting of Pb-Zn ore, the impact of industrial waste (heaps of gangue and slag, settling ponds for sludge coal mud, mine water discharges), urbanisation and transport.

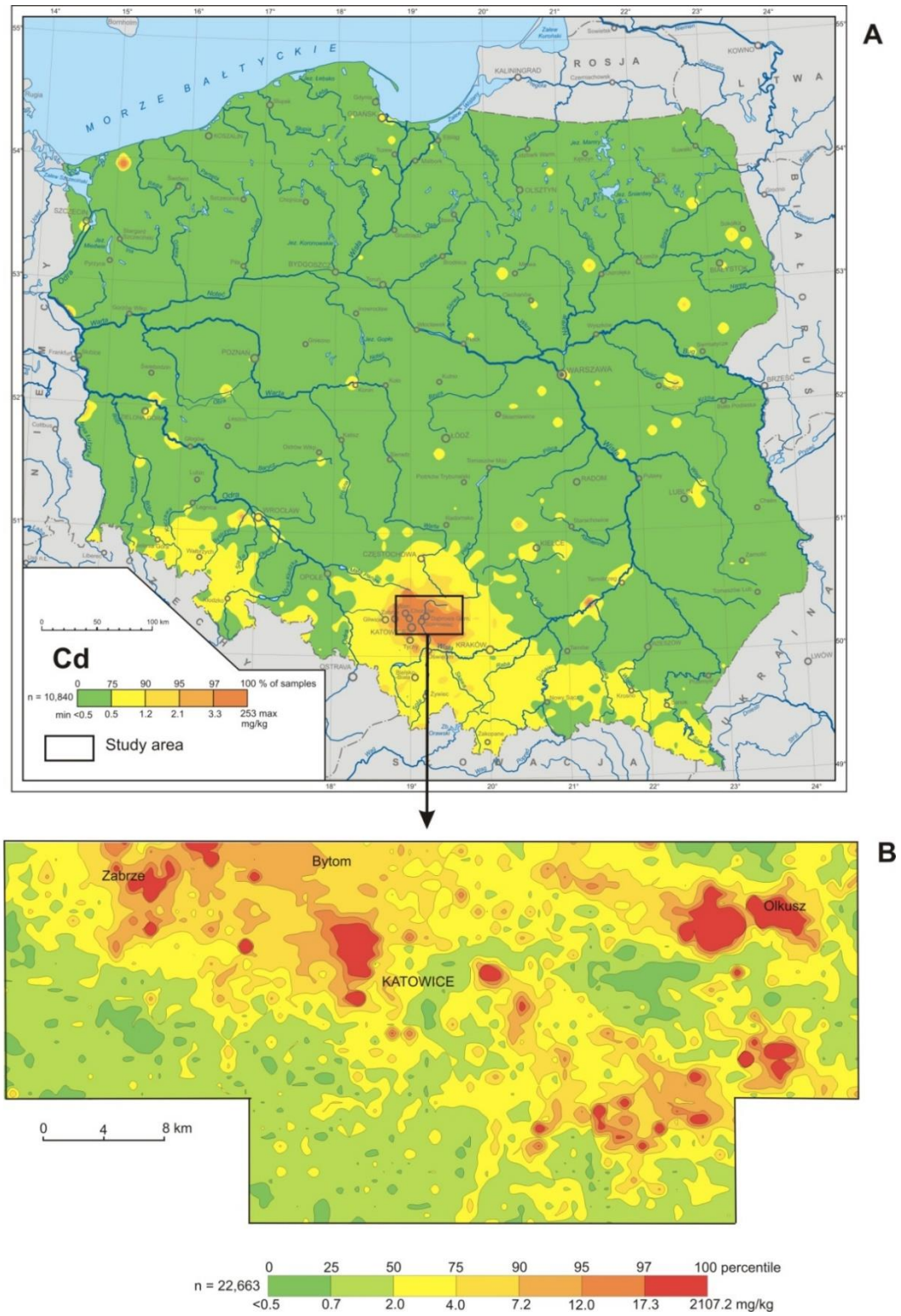

Figure 1. Cadmium content in topsoil samples (0-30 cm) of Poland (A) and Upper Silesia Region (B).

References

Paulo, A., Strzelska-Smakowska, B., 2000. Ores of non-ferrous and precious metals, ed. Uczelniane Wyd. Naukowo-Dydaktyczne AGH Kraków (in Polish).

Szuwarzyński, M., 1996. Ore bodies in the Silesian-Cracow Zn–Pb ore district, Poland. Prace Państwowego Instytutu Geologicznego 154, 9-24.

Viets, J.G., Leach, D.L., Lichte, F.E., Hopkins, R.T., Gent, C.A., Powell, J.W., 1996. Paragenetic and minor- and trace-element studies of Mississippi Valley type ore deposits of the Silesian-Cracow district, Poland. Prace Państwowego Instytutu Geologicznego 154, 51-71.

Wilanowsk,i S., Krieger, W., Żaba, M., 2009. Explanations to the Geological map of Poland, Zabrze sheet, scale 1:50,000. Państwowy Instytut Geologiczny, Warszawa (in Polish).

15th International Congress of the Geological Society of Greece
Athens, 22-24 May, 2019 | Harokopio University of Athens, Greece
Bulletin of the Geological Society of Greece, Sp. Pub. 7 Ext. Abs. GSG2019-032

Application of Dual Isotopes ($\delta^{15}N$, $\delta^{18}O$) to Determine Nitrate Contamination Sources in Cr(VI)-impacted Groundwater of Central Greece Aquifers

E. Kelepertzis[1], K. Pyrgaki[1], A. Argyraki[1], F. Botsou[2], P. Boeckx[3], I, Megremi[1], S. Karavoltsos[2], M. Dassenakis[2]

(1) Department of Geology and Geoenvironment, National and Kapodistrain University of Athens, Athens, Greece, kelepert@geol.uoa.gr
(2) Department of Chemistry, National and Kapodistrain University of Athens, Athens, Greece
(3) Isotope Bioscience Laboratory-ISOFYS, Ghent University, Gent, Belgium

High nitrate (NO_3^-) concentrations in groundwater occur in many areas around the world, largely as a result of excessive application of fertilisers, animal manure and inappropriate sewage management. A series of recent publications have established that naturally-occurring Cr(VI) is prevalent in groundwater associated with ultramafic aquifers in Greece (*e.g.*, Kaprara *et al.*, 2015). There is some evidence that increased NO_3^- in alluvial aquifers of agricultural areas may exacerbate the mobilisation of Cr(VI) via intensive groundwater recharge through the vadose zone and associated increased contact with Cr-containing minerals or nitrification of ammonium in fertilisers (Mills *et al.*, 2011). Coupled nitrogen and oxygen isotopes of NO_3^- have proven useful in providing detailed information regarding the NO_3^- sources and transformations in groundwater systems. Here, we applied the combined use of the $\delta^{15}N$ and $\delta^{18}O$ in NO_3^- in groundwater systems in Greece, previously identified to contain elevated Cr(VI) concentrations (*e.g.*, Pyrgaki *et al.*, 2016), with the aim to determine the NO_3^- sources and examine the possible linkage of N cycling to Cr(VI) mobilisation. The porous aquifers from Schinos, Central Evia and Thiva regions have served as prime examples where both anthropogenic NO_3^- contamination and ultramafic-derived Cr(VI) affect groundwater chemistry.

A total of 28 groundwater samples from productive wells and bores were collected from the three study areas during November 2017 (dry period): 9 samples from Schinos (borehole depth ranging from 4 to 55 m), 13 samples from Evia (depth ranging from 4 to 250 m) and 6 samples from Thiva (depth ranging from 150 to 250 m). Concentrations of dissolved NO_3^- and Cr(VI) were determined after well-established international protocols for water sampling, handling, preservation and analysis. The $\delta^{15}N$ and $\delta^{18}O$ of NO_3^- were analysed using the bacterial denitrification method. Hexavalent Cr concentrations for this specific data set ranged from 10 to 112 μg/l in Thiva, 12 to 121 μg/l in Schinos and 11 to 189 μg/l in Evia. Nitrate concentrations showed a different distribution, with the highest concentrations determined in Evia (median 120 mg/l, range from 18 to 334 mg/l), followed by those in Thiva (median 66 mg/l, range from 21 to 151 mg/l) and Schinos (median 46 mg/l, range from 9 to 70 mg/l). The isotopic composition of NO_3^- for the whole data set ranged from 2.4 ‰ to 21 ‰ for $\delta^{15}N$, and from -0.73 ‰ to 15.3 ‰ for $\delta^{18}O$. Potential sources of NO_3^- in the studied aquifers include the application of synthetic fertilisers and manure in the agricultural fields of Evia and Thiva regions, and the existence of residential waste cesspools in Schinos and Evia areas. The NO_3^- isotope ratios in most studied water samples fall in the compositional range of NH_4^+ in fertiliser, soil N and manure/septic waste (Fig. 1). The soil N cannot be considered to be the main origin of NO_3^- because NO_3^- concentrations were much higher than expected concentrations produced by the mineralisation of soil organic N. A cluster of samples from Schinos and Evia exhibited $\delta^{15}N$ values close to or higher than 8‰, falling in the field of animal and/or human waste; especially for Schinos, and given the absence of intensive agricultural practices in this area, it is deduced that domestic sewage is the main source of NO_3^- in groundwater. On the other hand, isotope data indicated that nitrification of NH_4^+-based fertilisers is responsible for the high NO_3^- concentrations measured in groundwater from Thiva, and partially from Evia. The high $[NO_3^-]/[Cl^-]$ ratios identified in these water samples signified that chemical fertilisers are the principal source of dissolved NO_3^-.

No clear relationship could be established between Cr(VI) and NO_3^- in this study, when the entire data set was taken into account; several samples with elevated Cr(VI) concentrations exhibited low NO_3^- concentrations and vice versa. Nonetheless, we found a significantly positive correlation between these solutes in the case of Schinos groundwater system (r=0.83, p=0.005) which might indicate an enhanced Cr(VI) generation when sewage wastes interfere with Cr-containing ultramafic source material. For Evia and Thiva groundwater samples, the nitrification of NH_4^+ in fertilisers, as evidenced by the isotope data of $\delta^{15}N$ and $\delta^{18}O$ in NO_3^-, could be responsible for the production of environmentally relevant amounts of Cr(VI) because the increased concentrations of H^+ may increase the mobility of Cr(III) and its subsequent oxidation on Mn oxides (Mills *et al.*, 2011). Although, it is difficult to support a direct link between the isotope data and Cr(VI) concentrations (Fig. 1), it appears that the process of nitrification, either from human/animal waste or synthetic fertilisers, trigger the geochemical occurrence of geogenic Cr(VI) in groundwater. Both NO_3^- and Cr(VI) occur primarily in oxic groundwater, deduced by the high Eh and dissolved oxygen (DO) values measured in the samples, providing a deciding geochemical environment that promotes the persistence of these constituents in solution. Locally in the aquifer, decreasing DO concentrations along flowpaths favour the process of denitrification. This is evident in one groundwater sample from Schinos ($\delta^{15}N$ and $\delta^{18}O$ values of 21.5 ‰ and 15.3 ‰, respectively) that exhibited the lowest Cr(VI) concentration (8 μg/l) determined in the data set. The results of this study assist in the clear identification of NO_3^- contamination origin and provide science-based information to the general public and municipal key stakeholders for a more effective water management planning.

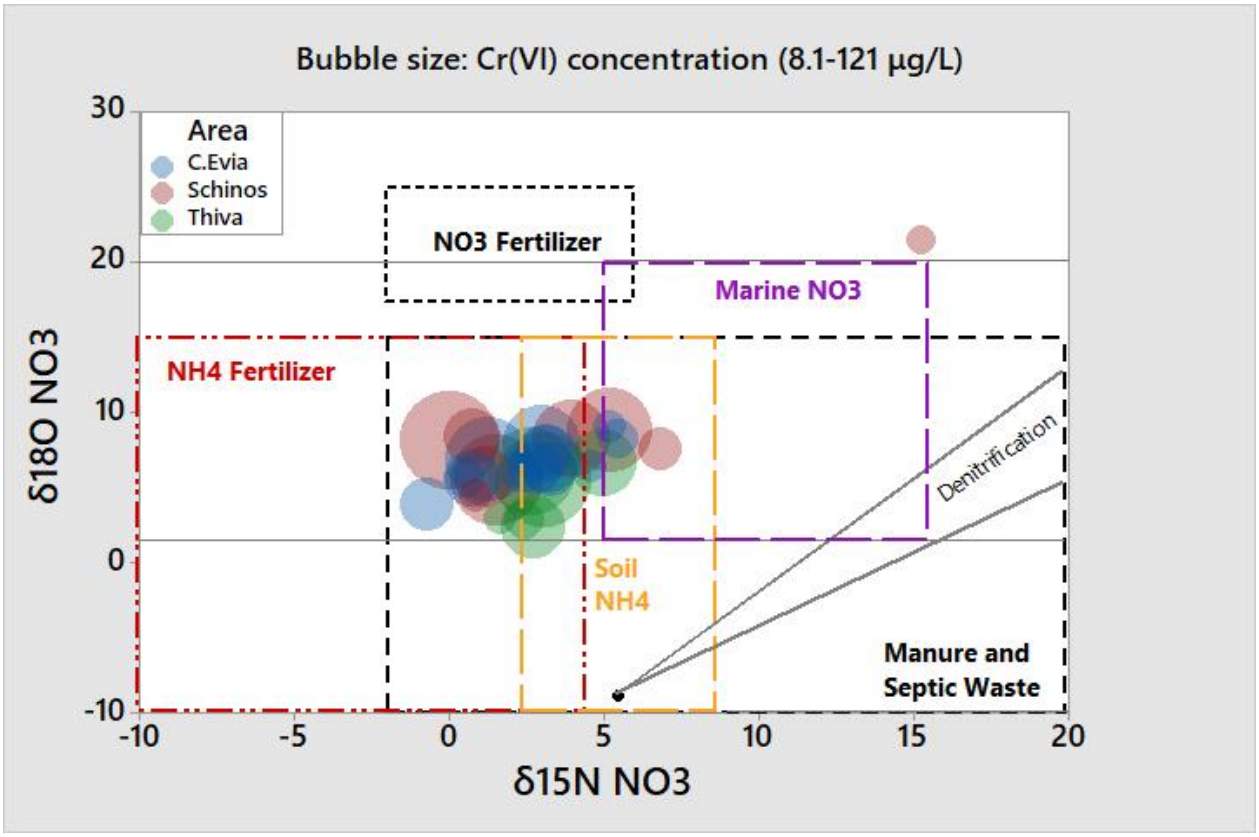

Figure 1. Isotopic values of NO_3^- for the studied groundwaters along with graduated symbol plot of Cr(VI) concentrations. Typical ranges of δ^{15}N-NO_3^- and δ^{18}O-NO_3^- values for different nitrate sources were taken from Kendall and Aravena, (2000).

Acknowledgements

The present work was co-funded by the European Union (ERDF) and Greek national funds through the Operational Program "Competitiveness, Entrepreneurship and Innovation", under the ERANETMED 1st Joint Call on Water Resources (project acronym: CrITERIA/ project code: T3EPA-00004).

References

Kaprara, E., Kazakis, N., Simeonidis, K., Coles, S., Zouboulis, A.I., Samaras, P., Mitrakas, M., 2015. Occurrence of Cr(VI) in drinking water of Greece and relation to the geological background. Journal of Hazardous Materials 281, 2-11.

Kendall, C., Aravena, R., 2000. Nitrate isotopes in groundwater systems, in: Cook, P.G., Herzeg, A. (Eds.), Environmental tracers in Subsurface Hydrology. Kluwer Academic Publishers, Boston, 261-297.

Mills, C.T., Morrison, J.M., Goldhaber, M.B., Ellefsen, K.J., 2011. Chromium(VI) generation in vadose zone soils and alluvial sediments of the southwestern Sacramento Valley, California: A potential source of geogenic Cr(VI) to groundwater. Applied Geochemistry 26, 1488-1501.

Pyrgaki, K., Argyraki, A., Kelepertzis, E., Paraskevopoulou, V., Botsou, F., Dassenakis, E., Skourtsos, E. 2016. Occurrence of hexavalent chromium in the ophiolite related aquifers of Loutraki and Schinos areas. Bulletin of the Geological Society of Greece 50, 2261-2270.

15th International Congress of the Geological Society of Greece
Athens, 22-24 May, 2019 | Harokopio University of Athens, Greece
Bulletin of the Geological Society of Greece, Sp. Pub. 7 Ext. Abs. GSG2019-046

European-wide Data on Arsenic Concentrations in Agricultural Soils, Waters and Crops (AgriAs Project)

T. Tarvainen[1], T. Hatakka[1], K. Loukola-Ruskeeniemi[1]

(1) Geological Survey of Finland, P.O.Box 96, 02151 Espoo, Finland, timo.tarvainen@gtk.fi

Arsenic is a toxic and carcinogenic substance. According to WHO, the greatest threat to public health from As originates from contaminated groundwater. Food is another notable pathway for As exposure in humans. There are numerous As-related publications and reports, but many of them focus on As problems in South-East Asia or are limited to groundwater or contaminated soil. The AgriAs project (http://projects.gtk.fi/AgriAs/index.html; Water-JPI 2017) has focused on European data on agricultural soils and the quality of related surface water and groundwater.

The AgriAs project has summarised European-wide databases and publications on As concentrations in soil and water. This was followed by a literature review and a questionnaire on national-level data sources of As concentrations in agricultural soil and water. A web-based AgriAs questionnaire on national and large-scale regional data sources on As in soil, surface water, groundwater and crops in Europe was sent to 23 countries. The general findings, concerning As concentrations in crops, were summarised from the literature. Following the assessment of data availability, a list of major data gaps was reported.

Reimann *et al.* (2009) have provided a comprehensive summary of the European-wide availability of data on As concentrations in soil and water. More up-to-date information on national and regional data sources were identified from the AgriAs questionnaire. The questionnaire revealed that regional-scale data are available on As concentrations in soil and surface water. These data can provide a detailed insight into the European-wide anomalies found in the FOREGS (Salminen *et al.*, 2005), Baltic Soil Survey (Reimann *et al.*, 2003), GEMAS (Reimann *et al.*, 2014; Tarvainen *et al.*, 2013, 2014) and LUCAS surveys (Tóth *et al.*, 2016a, b).

There are quite extensive European-wide data sets on As concentrations in agricultural soil, but more detailed regional mapping at the national level is needed, especially in those areas where anomalously high As concentrations in topsoil have been discovered. According the AgriAs questionnaire and literature study, European-wide data as well as nationwide data on As concentrations in crops are entirely lacking. There is no up-to-date map of As concentrations in European groundwater related to agricultural sites. European-wide or large-scale regional databases very seldom combine As concentrations in agricultural topsoil with concentrations in adjacent surface water or groundwater.

According to the European-wide soil geochemical data, two study sites of the AgriAs project in Verdun (France) and in Freiberg (Saxony, Germany) represent anomalous As areas (Fig. 1). Arsenic anomalies can be either geogenic or anthropogenic, or the anomalies can be a combination of naturally high As concentration and long history of mining and metallurgy like the study site in Freiberg. The study site near Verdun (France) represents anthropogenic anomaly: it is a chemical ammunition breaking-down facility of the interwar period converted into agricultural land. Thus, the two test sites can be used to develop and demonstrate the objectives of the AgriAs project: develop recommendations/guidelines for sustainable management of As risks together with stakeholders; to demonstrate As removal technologies in Verdun and Freiberg to assess their technological and economic feasibility; and apply biological tools to manage ecological, environmental and human risks.

Acknowledgements

AgriAs is co-funded by EU and the Academy of Finland, L'Agence nationale de la recherché (France), Bundesministerium für Ernährung und Landwirtschaft (Germany) and Forskningsrådet FORMAS (Sweden) under the ERA-NET Cofund WaterWorks2015 Call.

References

Reimann, C., Siewers, U., Tarvainen, T., Bityukova, L., Eriksson, J., Gilucis, A., Gregorauskiene, V., Lukashev, V., Matinian, N.N., Pasieczna, A., 2003. Agricultural Soils in Northern Europe: A Geochemical Atlas. Geologisches Jahrbuch, Sonderhefte, Reihe D, Heft SD 5, Schweizerbart'sche Verlagsbuchhandlung, Stuttgart, 279 p.

Reimann, C., Matschullat, J., Birke, M., Salminen, R., 2009. Arsenic distribution in the environment: The effects of scale. Applied Geochemistry 24, 1147–1167.

Reimann, C., Birke, M., Demetriades, A., Filzmoser, P., O'Connor, P. (Eds.), 2014. Chemistry of Europe's Agricultural Soils. Part A: Methodology and Interpretation of the GEMAS Data Set. Geologisches Jahrbuch (Reihe B 102), Schweizerbarth, Hannover, 528 p.; http://www.schweizerbart.de/publications/detail/isbn/9783510968466.

Salminen, R. (Chief-Ed.), Batista, M.J., Bidovec, M. Demetriades, A., De Vivo, B., De Vos, W., Duris, M., Gilucis, A., Gregorauskiene, V., Halamic, J., Heitzmann, P., Lima, A., Jordan, G., Klaver, G., Klein, P., Lis, J., Locutura, J., Marsina, K., Mazreku, A., O'Connor, P.J., Olsson, S.Å., Ottesen, R.-T., Petersell, V., Plant, J.A., Reeder, S., Salpeteur, I., Sandström, H., Siewers, U., Steenfelt, A., Tarvainen, T., 2005. Geochemical Atlas of Europe. Part 1 – Background Information, Methodology and Maps. Geological Survey of Finland, Espoo, Finland, 526 pp.; http://weppi.gtk.fi/publ/foregsatlas/.

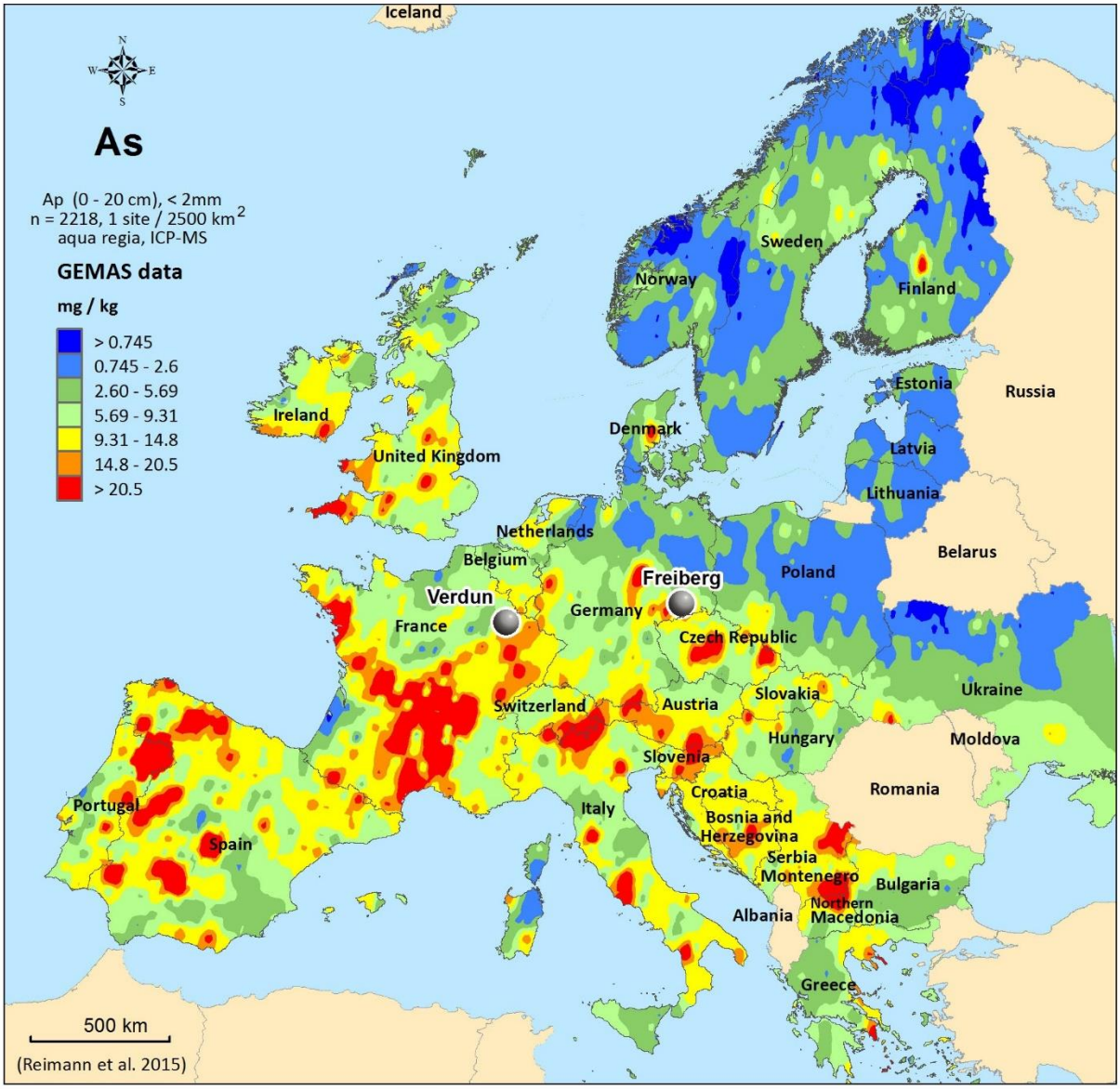

Figure 1. Geochemical map showing the distribution of As in GEMAS agricultural soil (hot *aqua regia* extraction) and the AgriAs project study sites in Verdun (France) and in Freiberg (Saxony, Germany).

Tarvainen, T., Albanese, S., Birke, M., Ponăvič, M., Reimann, The GEMAS Project Team, 2013. Arsenic in agricultural and grazing land soils of Europe. Applied Geochemistry 28, 2–10.

Tarvainen, T., Birke, M., Reimann, C., Ponăvič, M., Albanese, S., 2014. Arsenic anomalies in European agricultural and grazing land soil, in: Reimann, C., Birke, M., Demetriades, A., Filzmoser, P., O'Connor, P. (Eds.), Chemistry of Europe's Agricultural Soils. Part B: General Background Information and Further Analysis of the GEMAS Data Set. Geologisches Jahrbuch (Reihe B103), Schweizerbarth, Hannover, 81-88.

Tóth, G., Hermann, T., Szatmári, G., Pásztor, L., 2016a. Maps of heavy metals in the soils of the European Union and proposed priority areas for detailed assessment. Science of the Total Environment 565, 1054-1062.

Tóth, G., Hermann, T., Da Silva, M.R., Montanarella, L., 2016b. Heavy metals in agricultural soils of the European Union with implications for food safety. Environment International 88, 299-309.

Water-JPI, 2017. Water JPI, Challenges for a changing world. http://www.waterjpi.eu/index.php?option=com_content&view=article&id=79&Itemid=686

15th International Congress of the Geological Society of Greece
Athens, 22-24 May, 2019 | Harokopio University of Athens, Greece
Bulletin of the Geological Society of Greece, Sp. Pub. 7 Ext. Abs. GSG2019-064

Soil Geochemical Baselines of Ni on a Continental, National and Local Scale

T. Hatakka[1], T. Tarvainen[1]
(1) Geological Survey of Finland, P.O.Box 96, 02151 Espoo, Finland, tarja.hatakka@gtk.fi

Introduction

The abundances of the chemical elements in the Earth's surface materials are relevant to agriculture, soil fertility, forestry, animal and human health, industrial pollution, mineral resource potential, setting of environmental standards, water quality and land-use planning. Systematic environmental geochemical baseline data are necessary to inform policy makers and to provide a sound basis for legislation. Geochemical baseline mapping provides background information for environmental assessment.

Results

The Geological Survey of Finland (GTK) has experience in geochemical mapping on a continental scale (Fig. 1), a national scale, a regional scale (Fig. 2) and even on a local scale within urban areas. Since 2016, GTK has carried out soil geochemical baseline mapping around mining areas. A large Ni anomaly related to greenstone belt can be detected on the European scale and the national scale geochemical maps in Finnish Lapland. In the European-wide FOREGS map (Fig. 1) and on the regional scale geochemical map (Fig. 2), the Ni concentrations in subsoil within the anomaly zone of Finnish Lapland are 40 – 100 mg/kg. In 2016, GTK took soil samples at 35 sites of the Kevitsa Ni mining area surroundings (Fig. 3). The Ni concentrations were 18 – 228 mg/kg in subsoil and the calculated upper limit of baseline variation for Kevitsa mining area surroundings was 110 mg/kg. Thus, even the European-wide geochemical map provided a good estimate for the soil geochemical baseline for this anomalous zone. However, the much higher concentrations of potentially harmful elements have been found on the local scale baseline mapping around other mining area surroundings, which are not so clearly detected on a European scale.

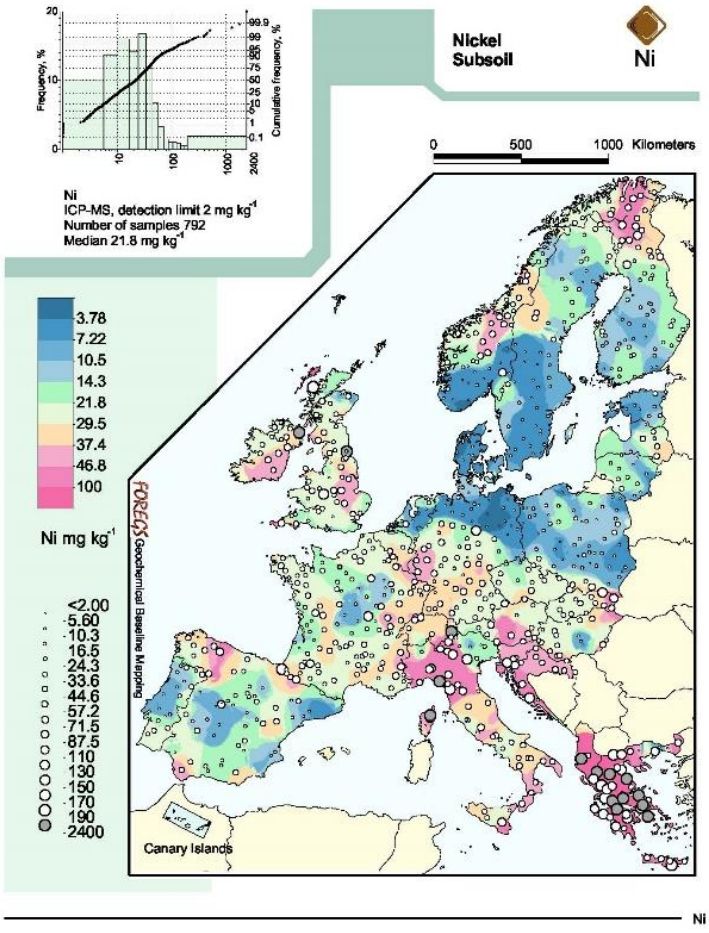

Figure 1. Geochemical map showing the distribution of Ni in subsoil (<2 mm grain size, total dissolution) in Europe. FOREGS Geochemical mapping (Salminen *et al.*, 2005).

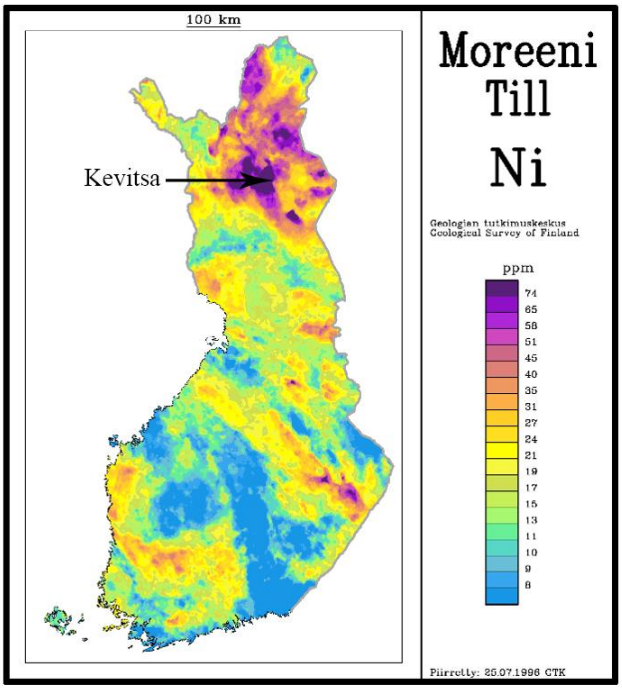

Figure 2. Geochemical map showing the distribution of Ni in glacial till (<0.06 mm grain size, *agua regia* extraction) in Finland on a regional scale (Salminen, 1995).

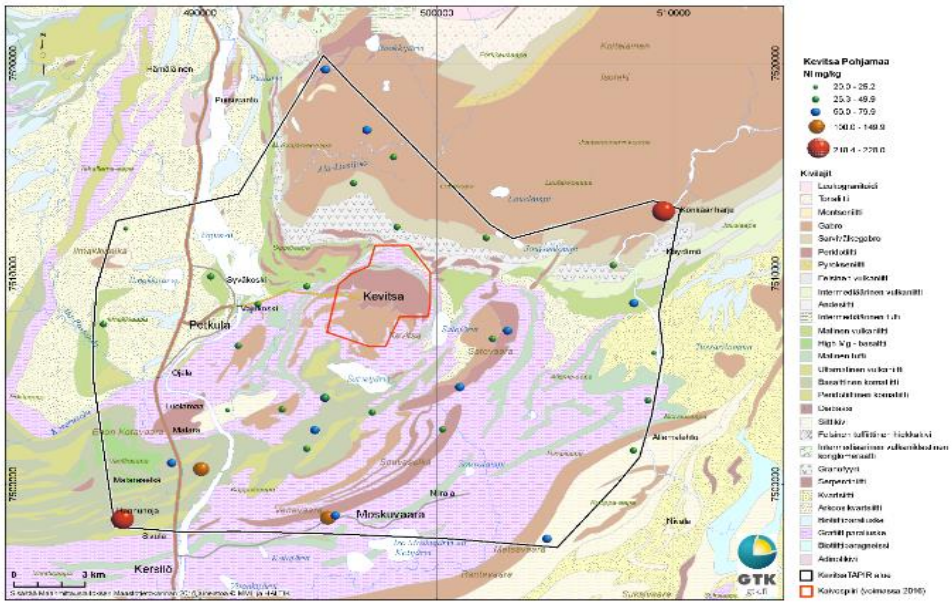

Figure 3. Geochemical map showing the distribution of Ni in soil parent material (<2 mm grain size, *aqua regia* extraction) in Kevitsa, Sodankylä, Finland.

Acknowledgements

This work is funded by the Geological Survey of Finland project 50402-200302.

References

Salminen, R. (Ed.), 1995. Alueellinen geokemiallinen kartoitus Suomessa vuosina 1982 – 1994. Geologian tutkimuskeskus. Tutkimusraportti 130. Geological Survey of Finland. Report of Investigation 130.

Salminen, R. (Chief-Ed.), Batista, M.J., Bidovec, M. Demetriades, A., De Vivo, B., De Vos, W., Duris, M., Gilucis, A., Gregorauskiene, V., Halamic, J., Heitzmann, P., Lima, A., Jordan, G., Klaver, G., Klein, P., Lis, J., Locutura, J., Marsina, K., Mazreku, A., O'Connor, P.J., Olsson, S.Å., Ottesen, R.-T., Petersell, V., Plant, J.A., Reeder, S., Salpeteur, I., Sandström, H., Siewers, U., Steenfelt, A., Tarvainen, T., 2005. Geochemical Atlas of Europe. Part 1 – Background Information, Methodology and Maps. Geological Survey of Finland, Espoo, Finland, 526 p.; http://weppi.gtk.fi/publ/foregsatlas/.

15th International Congress of the Geological Society of Greece
Athens, 22-24 May, 2019 | Harokopio University of Athens, Greece
Bulletin of the Geological Society of Greece, Sp. Pub. 7 Ext. Abs. GSG2019-065

GEMAS: Geochemical Mapping of Mg in Agricultural Soil of Europe and its Criticality Assessment

Ph. Négrel[1], A. Ladenberger[2], C. Reimann[3], M. Birke[4], A. Demetriades[5], M. Sadeghi[2]

(1) BRGM, Laboratories Division, Orléans, France, p.negrel@brgm.fr.
(2) Geological Survey of Sweden, Uppsala, Sweden.
(3) Geological Survey of Norway, Trondheim, Norway.
(4) Bundesanstalt für Geowissenschaften und Rohstoffe, Stillweg 2, 30655 Hannover, Germany.
(5) Institute of Geology and Mineral Exploration (IGME), 1 Spirou Louis St., Olympic Village, Acharnae, 13677 Athens, Hellas (retired).

Introduction

Agricultural soil (Ap-horizon, 0–20 cm) samples were collected from a large part of Europe (33 countries, 5.6 million km^2) as part of the GEMAS (GEochemical Mapping of Agricultural and grazing land Soil) project (Reimann *et al.*, 2014a, b). The survey area includes a diverse group of soil parent materials with varying geological history, a wide range of climate zones, and landscapes. The chemical composition of soil represents largely the primary mineralogy of the source bedrock, with superimposed effects of the last glaciation, pre- and post-depositional chemical weathering, formation of secondary products such as clays, and element mobility (Négrel *et al.*, 2015), or continental-scale distribution of elements (Reimann *et al.*, 2014a; Ladenberger *et al.*, 2015).

Magnesium is the eighth most abundant element in the Earth's upper continental crust (UCC), with an estimated elemental abundance of 14,955 mg/kg (Rudnick and Gao, 2003). Magnesium is essential for all organisms, not toxic under normal circumstances and is a key plant nutrient and essential for photosynthesis in plants. It is used in industry, for example, in transport (automotive, aircraft, train), consumer electronics (laptop, mobile phone, tablet), steel industry, titanium and zirconium production, pharmaceutical and agricultural chemical production and medical implants. Magnesium may also be a preference material in all light-weight vehicle concepts, hydrogen storage and advanced battery technology. Currently, Mg, as alloying element, is essential for the aluminium industry. The worldwide primary Mg production in 2016 was around 878 Kt, and 85% of global demand was supplied by China. Magnesium's criticality is not based on geographical lack of raw material in Europe, rather on trade issues, since China's low-cost production and export policy made primary production in Europe redundant. The last smelter in Europe was closed in 2001, since European based smelters were unable to compete with low-cost Chinese production, and as a result European primary demand depends mainly on import from China. Worldwide demand is expected to increase in the next decade. In particular, the development of R&D technologies could significantly affect the long-term demand for Mg. The overall results of the 2017 criticality assessment, classified critical raw materials with respect to economic importance versus supply risk, identified 26 raw materials as critical (European Commission, 2017), comprising Mg and elements like Sb, Nb and Ge.

The demand for 'critical' element resources activated all efforts to find new deposits and possibilities to extract them from mines throughout the world. The GEMAS data set offers European scale results for several so-called high-tech elements, and almost all listed on the Critical Raw Materials list by the European Commission (2017). Here, one of the major elements of the UCC, Mg, is used as a test critical element. The geochemical distribution of Mg in agricultural soil of Europe turns out to be a useful starting tool for identifying potential areas for the occurrence of new resources of high-tech elements.

Materials and methods

Agricultural soil samples were collected in 33 European countries at an average density of 1 site per 2500 km^2, covering an area of about 5.6 million km^2 (Reimann *et al.*, 2014a, b). The methods for GEMAS sampling, sample preparation and analysis for major and trace elements were described in detail in Reimann et al. (2014a). Agricultural soil (Ap; 2108 samples) was collected from the ploughing layer of an agricultural arable field at a depth of 0–20 cm. Each sample (ca 3.5 kg) corresponds to a composite of five sub-samples taken from the corners and centre of a 10 × 10 m square. All composite samples were sieved to <2 mm, and milled to less than 63 μm for analysis by wavelength dispersive X-ray fluorescence spectrometry (WD-XRF). A series of project standards and replicates of project samples were used to monitor trueness, repeatability and accuracy, detection limits and QC (Reimann *et al.*, 2011). Samples were also investigated using *aqua regia* and MMI® extraction followed by ICP-MS multi element analysis not showed here.

Results and Discussion

Less than 5% of the 2108 samples of agricultural soil, analysed for Mg by XFR, are lower than the 50 mg/km detection limit. The median for Mg in the Ap samples in Europe is around 5488 mg/kg and the maximum close to 126,638 mg/kg. Compared to the UCC total Mg average, the median Mg concentration, measured by XRF, is substantially lower in the European agricultural soil samples (ratio median Ap/UCC = 0.367); this may suggest a possible overestimation of the UCC value; it may be also an indication of an overall depletion of the important plant nutrient Mg in agricultural soil. The combination plot histogram - density trace one-dimensional scattergram-boxplot (Fig. 2a) shows the Mg univariate

data distribution. The one-dimensional scattergram and boxplot highlight the existence of a substantial number of outliers in the Mg distribution. The density trace and histogram are overall symmetrical in the log-scale. Liming and use of Mg fertilisers are the strongest anthropogenic interferences on natural Mg-cycles. Given the major human interference with Mg in agricultural soil, the map of Mg still clearly depicts geological process (Fig 2b). The southern limit of the last glaciation is thus still visible as a concentration break on the map, but the median Mg concentrations between northern and southern Europe are not as contrasted, as for many other elements (Reimann *et al.*, 2014a, b). Basically, areas underlain by limestone (e.g., eastern and southern Spain), dolomite (Alps) and mafic/ultramafic rocks (Hellas, Norway, Finland) appear as large Mg anomalies on the map. The Central Scandinavian Clay Belt is also visible as a Mg anomaly on the map, as well as the occurrence of Mg-silicates in northern Europe.

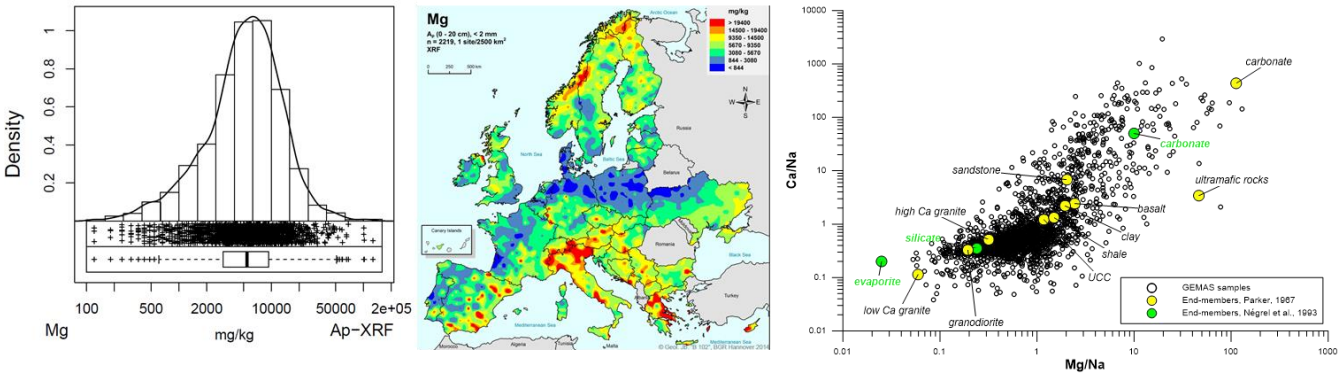

Figure 2. (a) Combination plot of histogram, density trace, one-dimensional scattergram and boxplot of the Mg distribution in European Ap samples following XRF analysis; (b) map of XRF total Mg concentrations; (c) Ca/Na versus Mg/Na ratios in Ap samples, with average values for the main lithological end-members (Parker (1967) for basalt, high and low Ca granite, clay, shale, sandstone, carbonate, ultramafic rocks and granodiorite; Négrel et al. (1993) for silicate, carbonate, evaporite).

Soil chemical composition represents to a large extent the primary mineralogy of the source bedrock, with superimposed effects of glaciation, pre- and post-depositional chemical weathering, formation of secondary products such as clays, and element mobility. Therefore, in soil, Mg, like Al and K, is often retained in weathering profiles, while Na and Ca are rapidly leached as dissolved ions. Comparison of Ca and Mg geochemical pattern, in relation to general Na distribution in soil, allows discrimination between carbonate and silicate parent materials and among various siliciclastic components (low Ca granite, sandstone and ultramafic rocks).

With the knowledge that the most important Mg mineral resources are hosted by ultramafic lithologies and their weathering/alteration products (magnesite), carbonate rocks (dolomite) and chemical deposits (carnallite), GEMAS Mg anomalies can be used to look for potential regions for more detailed Mg exploration.

Acknowledgements

The GEMAS project is a cooperative project of the EuroGeoSurveys Geochemistry Expert Group with Eurometaux companies, and a number of outside organisations (e.g., Alterra, The Netherlands; Norwegian Forest and Landscape Institute; Research Group Swiss Soil Monitoring Network, Swiss Research Station Agroscope Reckenholz-Tänikon, several Ministries of the Environment and University Departments of Geosciences, Chemistry and Mathematics in a number of European countries and New Zealand; ARCHE Consulting in Belgium; CSIRO Land and Water in Adelaide, Australia).

References

European Commission, 2017. Study on the review of the list of Critical Raw Materials: Criticality assessments. Brussels, 13.9.2017, COM(2017) 490 final, 92 p.

Ladenberger, A., Demetriades, A., Reimann, C., Birke, M., Sadeghi, M., Uhlback, J., Andersson, M., Jonsson, E., the GEMAS Project Team, 2015. GEMAS: Indium in agricultural and grazing land soil of Europe – its source and geochemical distribution patterns. Journal of Geochemical Exploration 154, 61–80.

Négrel, Ph., Allègre, C.J., Dupré, B., Lewin, E., 1993. Erosion sources determined from inversion of major, trace element ratios and strontium isotopic ratios in river water: the Congo Basin case. Earth and Planetary Sciences Letters 120, 59-76.

Négrel, Ph., Sadeghi, M., Ladenberger, A., Reimann, C., Birke, M., the GEMAS Project Team, 2015. Geochemical fingerprinting and sources discrimination in soils and sediments at continental scale. Chemical Geology 396, 1-15.

Parker, R.L., 1967. Composition of the Earth's crust. U.S. Geological Survey Professional Paper 440-D, 17 p.

Reimann, C., Demetriades, A., Eggen, O.A., Filzmoser, P., 2011. The EuroGeoSurveys GEochemical Mapping of Agricultural and grazing land Soils project (GEMAS): Evaluation of quality control results of total C and S, total organic carbon (TOC), cation exchange capacity (CEC), XRF, pH, and particle size distribution (PSD) analysis. NGU Report no. 2011.043, 90 p.

Reimann, C., Birke, M., Demetriades, A., Filzmoser, P., O'Connor, P. (Eds.), 2014a. Chemistry of Europe's agricultural soils (A): Methodology and interpretation of the GEMAS dataset. Geologisches Jahrbuch, Schweizerbarth, Stuttgart, 528 p.

Reimann, C., Birke, M., Demetriades, A., Filzmoser, P., O'Connor, P. (Eds.), 2014b. Chemistry of Europe's agricultural soils (B): General background information and analysis of the GEMAS dataset. Geologisches Jahrbuch, Schweizerbarth, Stuttgart, 352 p.

Rudnick, R.L., Gao, S., 2003. Composition of the Continental Crust. In: Holland, H.D., Turekian, K.K. (Eds-in-chief), Treatise on Geochemistry Volume 3: Rudnick, R.L. (Ed.), The Crust. Elsevier-Pergamon, Oxford, 1-64.

15th International Congress of the Geological Society of Greece
Athens, 22-24 May, 2019 | Harokopio University of Athens, Greece
Bulletin of the Geological Society of Greece, Sp. Pub. 7 Ext. Abs. GSG2019-066

FOREGS, EGG and GEMAS: European Continental-scale Geochemical Projects for Environmental and Resource Management

A. Demetriades[1], T. Tarvainen[2], C. Reimann[3], Ph. Négrel[4], A. Ladenberger[5], M. Birke[6], M. Sadeghi[5]

(1) Institute of Geology and Mineral Exploration (I.G.M.E.), 1 Spirou Louis St., Olympic Village, Acharnae, 13677 Athens, Hellas (retired), alecos.demetriades@gmail.com
(2) Geological Survey of Finland, Espoo, Finland
(3) Geological Survey of Norway, Trondheim, Norway
(4) BRGM, Laboratories Division, Orléans, France
(5) Geological Survey of Sweden, Uppsala, Sweden
(6) Bundesanstalt für Geowissenschaften und Rohstoffe, Hannover, Germany

Introduction

In Europe, three continental-scale geochemical projects were carried out at different times to fulfil a variety of purposes and uses. The first, the FOREGS Geochemical Atlas of Europe was carried out from 1997 to 2006, with the publication of a two-volume atlas (Salminen *et al.*, 2005; De Vos, Tarvainen *et al.*, 2006), as a contribution to the Global Geochemical Baselines project of the International Union of Geological Sciences for the establishment of the European Global Geochemical Reference Network (Darnley *et al.*, 1995). It covered 26 countries and an area of 4.25 million km^2. The second, European Groundwater Geochemistry (EGG) project was carried out from 2007 to 2010, with the publication of a one-volume atlas (Reimann and Birke, 2010); this rather unique cost-effective project used as sampling medium bottled mineral water as a proxy to the geochemistry of groundwater. The third, GEMAS (GEochemical Mapping of Agricultural and grazing land Soil), was carried out from 2008 to 2014, with the publication of a two-volume atlas (Reimann *et al.*, 2014a, b); it covered 33 European countries and an area of 5.6 million km^2.

Materials and methods

In the FOREGS Geochemical Atlas of Europe project, samples of stream sediment (n=799), stream water (n=807) and residual soil (top 0-25 cm; n=845; bottom >75 cm; n=788) were collected from drainage basins of <100 km^2 in area, and floodplain sediment (top 0-25 cm; n=743) from drainage basins of 1000-6000 km^2 in area; the average density of each sampling medium was approximately 1 sample/4700 km^2. Methods of sample collection, sample preparation, laboratory analysis, quality control procedures and data processing are described in Salminen, Tarvainen *et al.* (1998) and Salminen *et al.* (2005). The EGG project bottled mineral water samples were purchased from supermarkets (n=884), and the analytical, quality control and data processing procedures are described in Reimann and Birke (2010). The field methods used in the GEMAS project for the sampling of agricultural soil (0-20 cm; n=2108), and grazing land soil (0-10 cm; n=2023), laboratory methods and quality control procedures are described in detail in EGS GEG (2008) and Reimann *et al.* (2014a).

Results and discussion

As Li is an important critical element for future sustainable technologies according to UNEP (2009), but is not yet in the list of critical materials of the European Commission (2017), it is used as an example. The geochemical maps of Li in agricultural soil from the GEMAS project (Figs. 1a), and Li in floodplain sediment from the FOREGS project (Fig. 1b) display overall similar patterns. The most striking feature on all geochemical maps is the discrete element concentration break at the maximum extent of the last glaciation, a feature that is even shown on the map of Li in bottled mineral water from the EGG project (Fig. 1c). The agricultural soil, floodplain sediment and bottled mineral water maps, display overall lower Li values to the north of this break compared to those in the south. Hence, there are at least two distinctly different Li background ranges at the continental-scale.

Comparing the geochemical maps with the Li mineralisation and mineral deposits map from the ProMine Mineral Database (Fig. 1d), the FOREGS, GEMAS and EGG project continental-scale geochemical maps exhibit overall anomalous or elevated concentrations in the vicinity of most of these occurrences. From the mineral exploration point of view, the anomalous samples shown on the bottled mineral water Li map (Fig. 1c) should be of even greater interest, as they depict the geochemistry at depth. It is stressed that in all projects the objective was to map the geochemical background element variation. However, all three geochemical maps (Fig. 1) show many areas that warrant more detailed surveys for the delineation of areas of mineral potential for Li.

In conclusion, the results of the three continental-scale geochemical surveys demonstrate the variable geochemical background across Europe. It needs to be defined for each determinand in each sample medium. For environmental impact studies a site-specific background level will need to be established. Further, all data sets can be used for area selection for more detailed mineral exploration.

Acknowledgements

FOREGS, EGG and GEMAS are cooperative projects of the EuroGeoSurveys Geochemistry Expert Group.

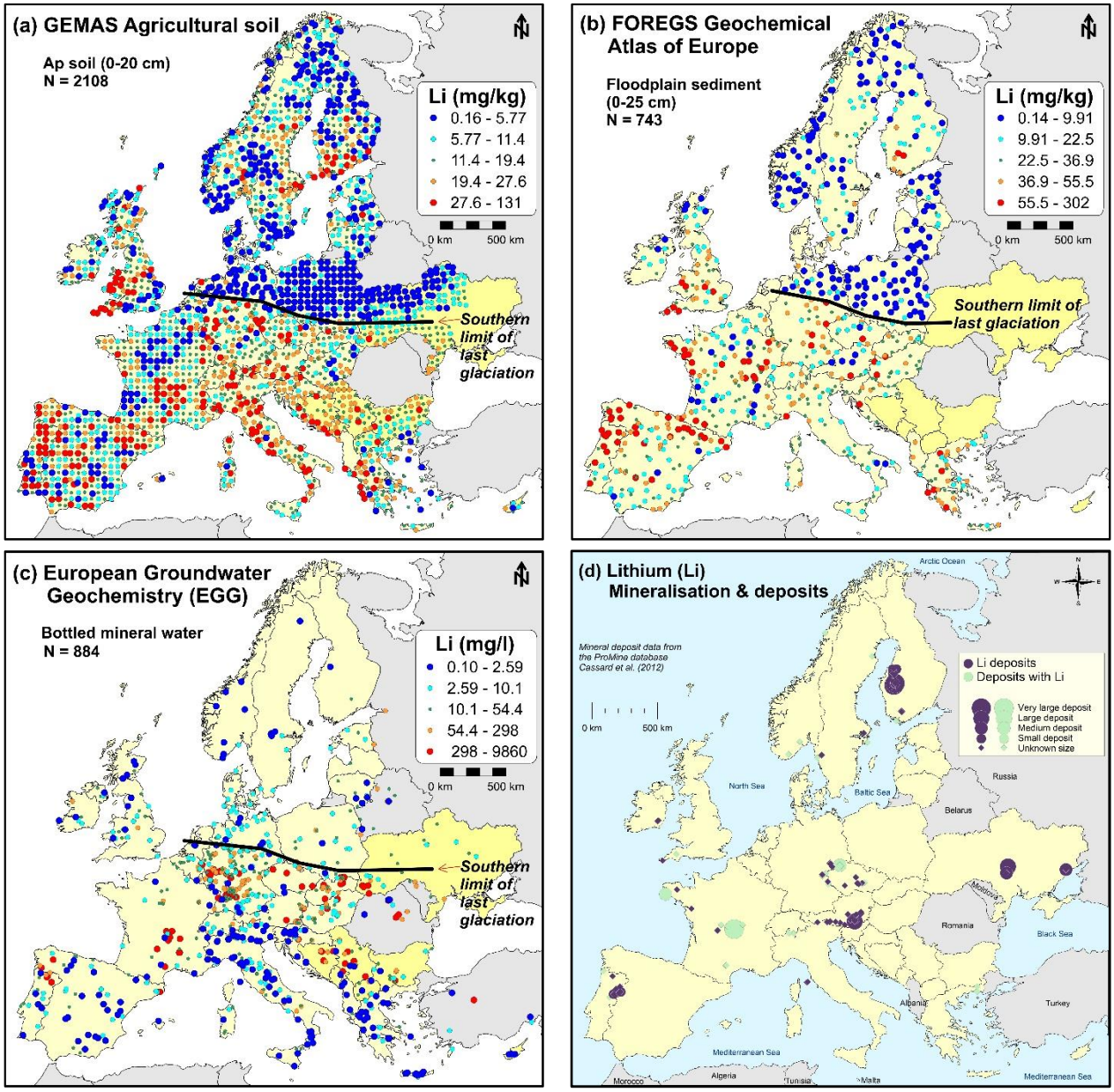

Figure 1. Geochemical maps showing the distribution of Li in (a) GEMAS agricultural soil (hot *aqua regia* extraction); (b) FOREGS floodplain sediment (total), and (c) EGG bottled mineral water; (d) Li mineral deposit map from the ProMine Mineral database (http://minerals4eu.brgm-rec.fr/); pale yellow indicates the 26 countries covered by FOREGS, and darker yellow the additional 6 countries covered by GEMAS (Albania was covered by FOREGS and EGG but not by GEMAS).

References

Darnley, A.G. *et al.*, 1995. A Global Geochemical Database for Environmental and Resource Management. Recommendations for International Geochemical Mapping – Final Report of IGCP Project 259. Earth Science Report 19. UNESCO Publishing, Paris, 122 p.; http://globalgeochemicalbaselines.eu.176-31-41-129.hs-servers.gr/datafiles/file/Blue_Book_GGD_IGCP259.pdf.

De Vos, W., Tarvainen, T. *et al.*., 2006. Geochemical Atlas of Europe. Part 2 - Interpretation of Geochemical Maps, Additional Tables, Figures, Maps, and Related Publications. Geological Survey of Finland, Espoo, 618 p; http://weppi.gtk.fi/publ/foregsatlas/.

EGS GEG, 2008. EuroGeoSurveys geochemical mapping of agricultural and grazing land in Europe (GEMAS) – Field manual. Geological Survey of Norway, Trondheim, NGU report 2008.038, 46 p.; http://www.ngu.no/upload/Publikasjoner/Rapporter/2008/2008_038.pdf.

European Commission, 2017. Study on the review of the list of Critical Raw Materials: Criticality assessments. Brussels, 13.9.2017, COM(2017) 490 final; 92 p.; http://doi.org/10.2873/876644.

Reimann, C. and Birke, M. (Editors), 2010. Geochemistry of European Bottled Water. Borntraeger Science Publishers, Stuttgart, 268 p.; http://www.schweizerbart.de/publications/detail/artno/001201002#.

Reimann, C., Birke, M., Demetriades, A., Filzmoser, P., O'Connor, P. (Eds.), 2014a. Chemistry of Europe's agricultural soils (A): Methodology and interpretation of the GEMAS dataset. Geologisches Jahrbuch, Schweizerbarth, Stuttgart, 528 p.

Reimann, C., Birke, M., Demetriades, A., Filzmoser, P., O'Connor, P. (Eds.), 2014b. Chemistry of Europe's agricultural soils (B): General background information and analysis of the GEMAS dataset. Geologisches Jahrbuch, Schweizerbarth, Stuttgart, 352 p.

UNEP, 2009. Critical metals for future sustainable technologies and their recycling potential. UNEP, DTI/1202/PA, Paris, 81 p.

Salminen, R., Tarvainen, T. *et al.*, 1998. FOREGS Geochemical Mapping Field Manual. Geological Survey of Finland, Espoo, Guide 47, 36 p.; http://tupa.gtk.fi/julkaisu/opas/op_047.pdf.

Salminen, R. *et al.*, 2005. Geochemical atlas of Europe. Part 1 – Background information, methodology and maps. Geological Survey of Finland, Espoo, 525 p.; http://weppi.gtk.fi/publ/foregsatlas/.

15th International Congress of the Geological Society of Greece
Athens, 22-24 May, 2019 | Harokopio University of Athens, Greece
Bulletin of the Geological Society of Greece, Sp. Pub. 7 Ext. Abs. GSG2019-067

URGE: The EuroGeoSurveys Geochemistry Expert Group's Urban Geochemistry projects

Alecos Demetriades[1], Christopher C. Johnson[2], Manfred Birke[3], Anna Ladenberger[4]

(1) Institute of Geology and Mineral Exploration (I.G.M.E.), 1 Spirou Louis St., Olympic Village, Acharnae, 13677 Athens, Hellas (retired), alecos.demetriades@gmail.com
(2) GeoElementary, Derby, United Kingdom
(3) Bundesanstalt für Geowissenschaften und Rohstoffe, Hannover, Germany
(4) Geological Survey of Sweden, Uppsala, Sweden.

Introduction

Given the fact that by 2050 more than 80% of the European population will be living in cities, the quality of the urban environment is becoming an important issue in the 21st century. Since the industrial revolution, with a peak after the Second World War, the urban environment has been contaminated with many inorganic toxic elements and organic compounds, which are being emitted by a wide variety of human activities (industry, traffic, domestic heating, coal and oil combustion, incineration, construction activities, *etc.*), and often accumulate in urban soil (Johnson *et al.*, 2011).

Although the negative long-term health related hazard of certain elements, such as Pb, has been known since ancient Hellenic times, little or no precautions were taken to protect the workers and the environment. Industries were, and often still are haphazardly distributed within the urban layout. Since, the 1970s a conscious attempt is being made in many countries to develop industrial facilities outside the residential, commercial, and recreational parts of cities. Within the urban structure remain, however, the brownfield sites, and the problems associated with the need of their remediation and redevelopment in order to reduce the pressure on greenfield sites.

Since many health-related problems are linked to the state of the urban environment (Fig. 1a), European citizens want to be aware of the geochemistry of the land their houses are built on. Moreover, it is especially important that the chemical quality of soil in public places, such as schoolyards, parks, playgrounds, kindergartens, recreation areas, and workplaces is known. Estate agents need to know the quality of the land they are marketing, and insurance brokers the potential risks to their customers.

With the frequent occurrence of highly contaminated soil in urban areas, a conscious management of soil excavation, transport, and redistribution within a city is another important issue. Urban soil is generally contaminated to a variable degree, depending on its location relative to a pollution source.

Knowledge about soil contamination, geochemical background concentrations, and detailed spatial element distribution is thus becoming a key issue in urban planning. Hence, the increasing interest to map the current chemical state of topsoil (Fig. 1b), and house dust (Fig. 1c) and to define potential risks to human health (Fig. 1d). This knowledge helps to complete still missing comparable geochemical data sets about urban ecosystems. Additionally, such information is urgently needed by decision-makers, local and regional authorities, planners, house buyers, and town administrations, for finding innovative and practical solutions for sustainable urban development and securing human health at a satisfactory level of risk. In fact, multidisciplinary cooperation takes on a completely new dimension in the tackling of urban problems, caused by contaminating activities, *i.e.*, applied geochemists work alongside public health officers, urban planners, medical doctors, *etc.* Hence, the need for the production of a harmonised urban geochemical database of high quality and integrity for multipurpose use (Figs. 1b, c, d).

Urban geochemistry projects of the EuroGeoSurveys Geochemistry Expert Group

The Geological Surveys of Europe have the task of providing high quality geochemical databases for the management of the environment and mineral resources. They have also a long-standing history in urban geochemical surveys, hence the publication of a textbook '*Mapping the Chemical Environment of Urban Areas*' (Johnson *et al.*, 2011) by members of the EuroGeoSurveys Geochemistry Expert Group. The Group has also published several urban geochemistry case studies in a form of topical publication (Demetriades *et al.*, 2018). Although the results of urban geochemistry surveys, carried out in different European countries, are of good quality, they are, however, incompatible, because of different sampling, sample preparation and analytical methods. In order to produce comparable urban geochemistry data across Europe, a harmonised methodology must be followed. For this purpose, an urban geochemistry manual was written and published in 2015 (Demetriades and Birke, 2015a), and two large bulks of reference samples prepared at the Geoanalytical Laboratories of the State Geological Institute of Slovak Republic. Due to wide interest in the quality of the urban environment, another comprehensive manual was written and published in 2015 (Demetriades and Birke, 2015b), following a request by the European Commission COST Action (TU1206) project 'SUB-URBAN – '*A European network to improve understanding and use of the ground beneath our cities*'. This manual describes the procedure of (i) sampling topsoil, subsoil, house dust, attic dust, road dust or sediment, atmospheric particulates and bio-indicators, including human tissues, (ii) sample preparation, (iii) laboratory analysis, (iv) quality control, (v) data conditioning, and (vi) data processing and map plotting.

EuroGeoSurveys recognising the importance of the urban environment have established an Urban Geology Expert Group in order to tackle all the urban issues from the geosciences perspective. It is, therefore, highly probable that the urgently needed harmonised urban geochemical databases will be developed in the next few years.

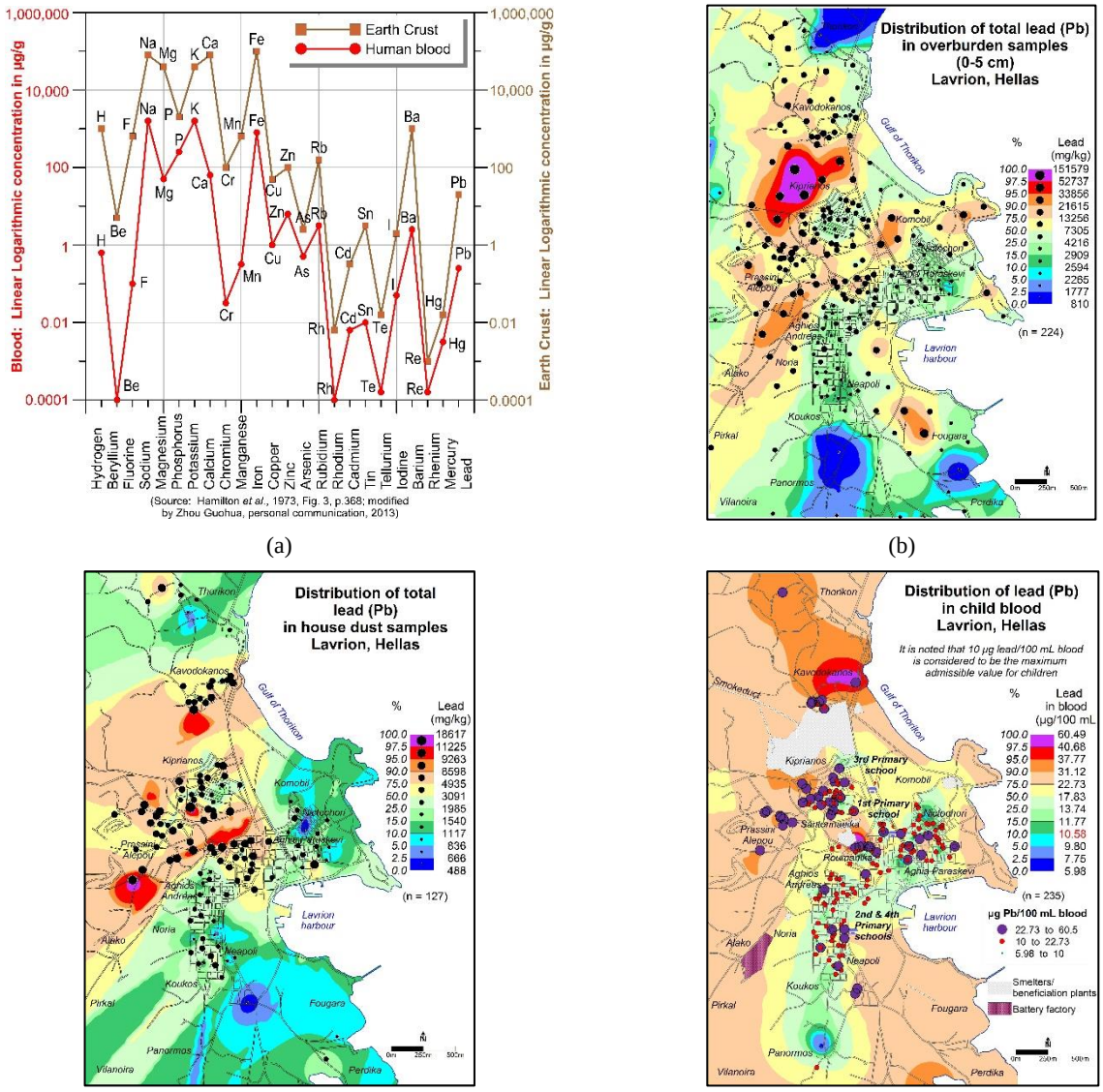

Figure 1. (a) Graph showing relationship between selected element concentrations in Earth Crust and human blood (Demetriades *et al.*, 2018, Fig. 1, p.2); (b) distribution of total Pb in overburden, Lavrion, Hellas (Demetriades, 2011, Fig. 25.8, p.444); (c) distribution of total Pb in house dust, Lavrion, Hellas (Demetriades, 2011, Fig. 25.9, p.445), and (d) distribution of Pb in child blood, Lavrion, Hellas (Demetriades, 2011, Fig. 25.10, p.447).

References

Demetriades, A., 2011. The Lavrion urban geochemistry study, Hellas. Chapter 25, In: C.C. Johnson, A. Demetriades, J. Locutura, R.T. Ottesen (Eds.), Mapping the chemical environment of urban areas. Wiley-Blackwell, John Wiley & Sons Ltd., Chichester, West Sussex, U.K., 424-456; http://doi.org/10.1002/9780470670071.

Demetriades, A., Birke, M., 2015. Urban Topsoil Geochemical Mapping Manual (URGE II). EuroGeoSurveys, Brussels, 52 p.; http://www.eurogeosurveys.org/wp-content/uploads/2015/06/EGS_Urban_Topsoil_Geochemical_Mapping_Manual_URGE_II_HR_version.pdf.

Demetriades, A., Birke, M., 2015. Urban Geochemical Mapping Manual: Sampling, Sample preparation, Laboratory analysis, Quality control check, Statistical processing and Map plotting. EuroGeoSurveys, Brussels, 162 p.; http://www.eurogeosurveys.org/wp-content/uploads/2015/10/Urban_Geochemical_Mapping_Manual.pdf.

Demetriades, A., Johnson, C.C., Birke, M. (Guest Eds.), Urban Geochemical Mapping: The EuroGeoSurveys Geochemistry Expert Group's URGE project. Special Issue, Journal of Geochemical Exploration 187, 213 p.

Demetriades, A., Johnson, C.C., Birke, M., 2018. Editorial: Urban Geochemical Mapping: The EuroGeoSurveys Geochemistry Expert Group's URGE project. In: Demetriades, A., Johnson, C.C., Birke, M. (Guest Eds.), Urban Geochemical Mapping: The EuroGeoSurveys Geochemistry Expert Group's URGE project. Special Issue, Journal of Geochemical Exploration 187, 1-5. https://doi.org/10.1016/j.gexplo.2017.10.024.

Hamilton, E.J., Minski, M.J., Cleary, J.J., 1973. The concentration and distribution of some stable elements in healthy human tissues from the United Kingdom: an environmental study. Sci. Total Environ. 1(4), 341–374; http://dx.doi.org/10.1016/0048-9697(73)90024-7.

Johnson, C.C., Demetriades, A., Locutura, J. and Ottesen, R.T. (Eds.), 2011. Mapping the Chemical Environment of Urban Areas. Wiley-Blackwell, John Wiley & Sons Ltd., Chichester, West Sussex, UK, 616 p.; http://eu.wiley.com/WileyCDA/WileyTitle/productCd-0470747242.html.

15th International Congress of the Geological Society of Greece
Athens, 22-24 May, 2019 | Harokopio University of Athens, Greece
Bulletin of the Geological Society of Greece, Sp. Pub. 7 Ext. Abs. GSG2019-076

Urban Geochemical Surveys in Hellas

S. Tassiou[1], A. Liakopoulos[1], A. Demetriades[2]

(1) Hellenic Survey of Geology and Mineral Exploration, 1 Spirou Louis St., Olympic Village, Acharnae, 13677 Athens, Hellas, stassiou@igme.gr
(2) IUGS Commission on Global Geochemical Baselines, P.O.Box 640 47, Zografou, 15710 Athens, Hellas

Introduction

Urban soil is generally contaminated to a variable degree depending on its proximity to potential contaminating sources. Traffic is one of the main sources of urban contamination, *e.g.*, Pb from the use of leaded petrol, Zn and Cd from tyre wear, Sb from brake pads, and the platinum group elements (PGEs) from the wear of catalytic converters, are some typical elements that often reach high concentrations in the urban environment. Lead was also a key ingredient in white paint, and in towns with a high proportion of white wooden houses very high concentrations were found in soil. Crematoria can or have emitted mercury (Hg). Coal, lignite and heavy oil fired electrical power and heating stations emit S, Ag, V, U, Br and Ba. The use of impregnated wood may have resulted in high concentrations of As, Cr and Cu, especially in kindergartens (nursery schools) and playgrounds. Building materials (plaster and paint) may also contain high concentrations of organic contaminants, especially polychlorinated biphenyls (PCBs), which again end-up in urban soil. Coal and wood burning, the use of diesel fuel, and the production of coke, all lead to the emission of polycyclic aromatic hydrocarbons (PAHs). There exist countless other sources of local contamination in towns, and there is thus every reason to be concerned about the quality of the urban environment, and the suitability of soil for sensitive land uses, such as schools, playgrounds, parks and vegetable gardens. Contaminated urban soil may contaminate indoor dust and, therefore, lead to an increased human exposure to inorganic and organic toxic chemicals. Consequently, the distribution of contaminants in urban soil needs to be documented and made known to city administrations to avoid costly mistakes in land use planning, and further spreading of highly contaminated materials.

Urban geochemistry projects

The Institute of Geology and Mineral Exploration (presently the Hellenic Survey of Geology and Mineral Exploration) realised the significance of carrying out systematic urban geochemical mapping surveys to assist urban authorities and other stakeholders in sustainable land use planning. The first multi-sample media urban survey was carried out in 1989-1992 in Aghios Constaninos (Kamariza) and Lavrion, municipalities to the south-east of Athens, which were centres of mining and smelting activities from ancient to recent times (Hatzigeorgiou-Stavrakis and Vergou-Vichou, 1992). Samples of garden soil (n=187), house dust (n=159) and road dust (n=169) were collected, analysed and studied. The health-related hazards affecting the local population were documented by cross-sectional epidemiological studies.

The second multi-sample media urban geochemical survey was carried out in the Lavrion urban and suburban area (1994-1999), and is considered to be the most comprehensive urban geoscientific project that has ever been carried out, not only in Hellas but globally (Demetriades, 1999; NTUA, 1999). It was a collaborative project between the Institute of Geology and Mineral Exploration and the National Technical University of Athens, and was coordinated by the Municipality of Lavreotiki. Apart from the geochemical results in overburden samples (n=224) and house dust (n=127), different thematic maps were compiled at a scale of 1:5000: (a) metallurgical processing wastes and representative samples (n=62) collected and analysed, (b) parent rocks and representative samples (n=140) collected and analysed, (c) land use, (d) property ownership, and (e) hazard and risk. The geochemistry of the subsurface, and the quality of ground water, were studied by sampling of drill cores and boreholes/wells, respectively. Further, the chemical results of human tissues, such as human blood from 235 children, deciduous teeth (n=82) and 24-hour urine (n=65) showed that the contaminants have entered the human body and affected human health and, especially, of children. The end products were (a) an integrated environmental management plan for the remediation of the different types of metallurgical processing wastes and contaminated overburden, and (b) measures for the protection of the local inhabitants.

As multi-sample media urban geochemical surveys are costly, it was decided to carry out in other towns systematic surface soil (0-10 cm) multi-element geochemical surveys using a regular sampling grid of 500x500 m. Six towns have been mapped up to now, and these are (i) Nafplion (Fig. 1a; Vassiliades, 2008a; Tassiou, 2009a), (ii) Sparti (Fig. 1b; Vassiliades, 2008b; Tassiou, 2009b), (iii) Drama (Fig. 1c; Vassiliades, 2008c; Tassiou, 2009c), (iv) Thrakomakedonaes (Fig. 1d; Vassiliades, 2008d; Tassiou, 2009d), (v) Volos (Tassiou and Kaminari, 2016; Tassiou *et al.*, 2016), and (vi) Igoumenitsa (Gerouki and Liakopoulos, 2016; Gerouki and Sgouros, 2016), with the collection of 144, 206, 176, 173, 205 and 135 soil samples, respectively. In order to produce compatible and harmonised urban geochemical databases all samples were analysed by the same hot *aqua regia* analytical method at the same commercial laboratory.

References

Demetriades, A. (Ed.), 1999. Geochemical atlas of the Lavrion urban area for environmental protection and planning. Vol. 1: Explanatory text, 365 p.; Vol. 1A: Figures and Tables, 210 p.; Vol. 1B, Appendix reports, 176 p.; Vol. 2: Geochemical atlas, 199 p.; Vol. 4: Environmental management plan for the rehabilitation of soil in the Lavrion urban area, 155 p. LIFE Programme Contract No: 93/GR/A14/GR/4576, Soil rehabilitation in the Municipality of Lavrion. Open File Report E-8272, Institute of Geology and Mineral Exploration, Athens, Hellas.

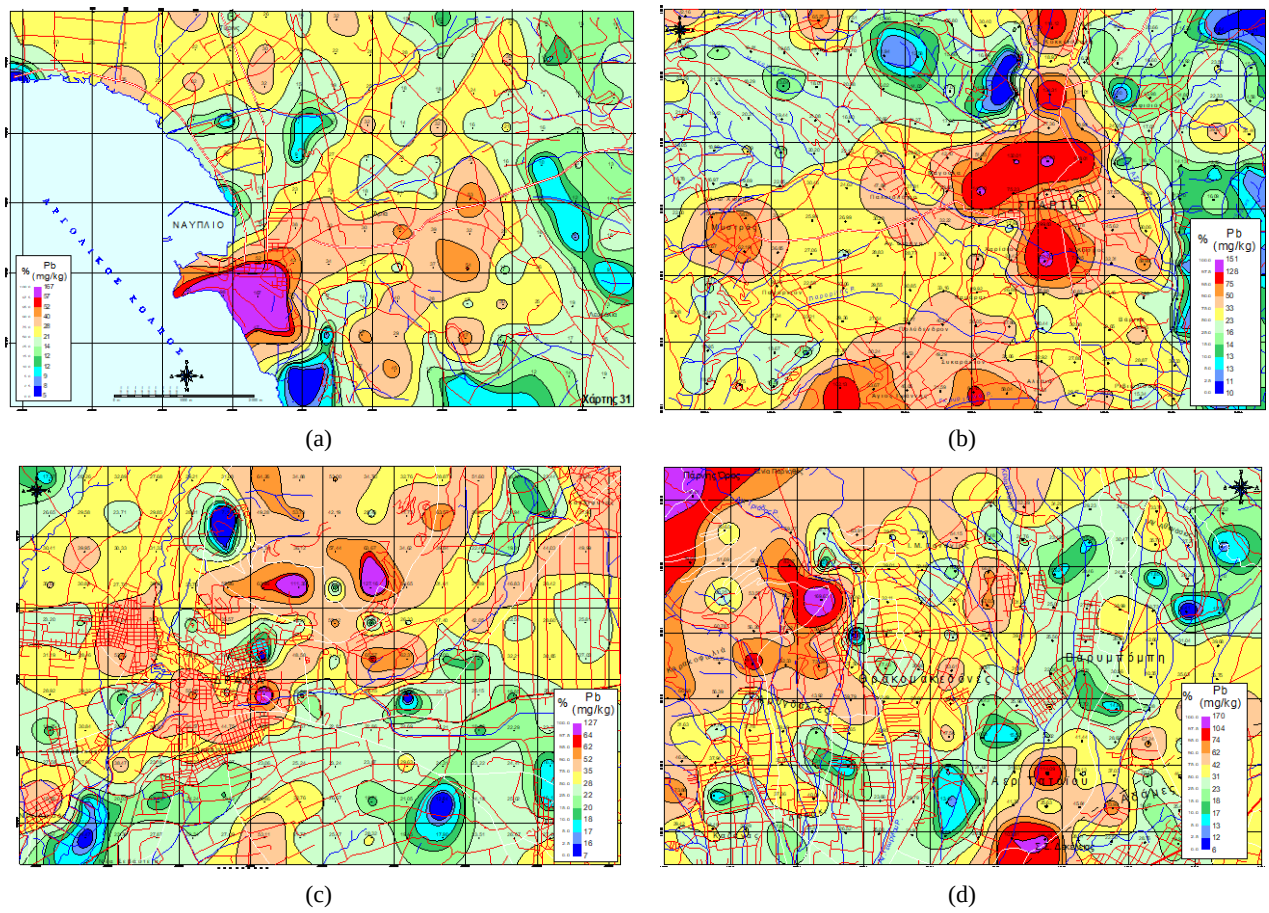

Figure 1. (a) Geochemical distribution maps of Pb in surface soil (0-10 cm) in (a) Nafplion (Vassiliades, 2008a); (b) Sparti (Vassiliades, 2008b); (c) Drama (Vassiliades, 2008c); (d) Thrakomakedhonaes (Vassiliades, 2008d).

Gerouki, F., Liakopoulos, A., 2016. Environmental geochemical study of urban-suburban area of Igoumenitsa. Vol. A: Interpretative text. Open File Report E11137, Institute of Geology and Mineral Exploration, Athens, Hellas, 150 p.

Gerouki, F., Sgouros, D., 2016. Environmental geochemical study of urban-suburban area of Igoumenitsa. Vol. B: Geochemical maps. Open File Report E11138, Institute of Geology and Mineral Exploration, Athens, Hellas, 53 p.

Hatzigeorgiou-Stavrakis, P., Vergou-Vichou, K., 1992. Environmental geochemical survey in the area of Lavrion and Aghios Constantinos (Kamariza), Attiki. Open File Report E-6778, Institute of Geology and Mineral Exploration, Athens (in Greek with an English abstract).

NTUA, 1999. Environmental characterisation of Lavrion site – Development of remediation techniques. Vol. 3, LIFE Programme Contract No: 93/GR/A14/GR/4576, Soil rehabilitation in the Municipality of Lavrion. National Technical University of Athens, Greece. Open File Report E-8272, Institute of Geology and Mineral Exploration, Athens, Hellas.

Tassiou, S., 2009a. Environmental geochemical study of urban-suburban area of Nafplion. Vol. A: Interpretative text. Open File Report E10258, Institute of Geology and Mineral Exploration, Athens, Hellas, 123 p.

Tassiou, S., 2009b. Environmental geochemical study of urban-suburban area of Sparti. Vol. A: Interpretative text. Open File Report E10304, Institute of Geology and Mineral Exploration, Athens, Hellas, 127 p.

Tassiou, S., 2009c. Environmental geochemical study of urban-suburban area of Drama. Vol. A: Interpretative text. Open File Report E10282, Institute of Geology and Mineral Exploration, Athens, Hellas, 127 p.

Tassiou, S., 2009d. Environmental geochemical study of urban-suburban area of Thrakomakedonaes. Vol. A: Interpretative text. Open File Report E10230, Institute of Geology and Mineral Exploration, Athens, Hellas, 132 p.

Tassiou, S., Kaminari, M., 2016. Environmental geochemical study of urban-suburban area of Volos. Vol. A: Interpretative text. Open File Report E11135, Institute of Geology and Mineral Exploration, Athens, Hellas, 257 p.

Tassiou, S., Kaminari, M., Sgouros, D., 2016. Environmental geochemical study of urban-suburban area of Volos. Vol. B: Geochemical maps. Open File Report E11136, Institute of Geology and Mineral Exploration, Athens, Hellas, 53 p.

Vassiliades, E., 2008a. Environmental geochemical study of urban-suburban area of Nafplion. Vol. B: Geochemical maps. Open File Report E10257, Institute of Geology and Mineral Exploration, Athens, Hellas, 47 p.

Vassiliades, E., 2008b. Environmental geochemical study of urban-suburban area of Sparti. Vol. B: Geochemical maps. Open File Report E10303, Institute of Geology and Mineral Exploration, Athens, Hellas, 47 p.

Vassiliades, E., 2008c. Environmental geochemical study of urban-suburban area of Drama. Vol. B: Geochemical maps. Open File Report E10281, Institute of Geology and Mineral Exploration, Athens, Hellas, 47 p.

Vassiliades, E., 2008d. Environmental geochemical study of urban-suburban area of Thrakomakedonaes. Vol. B: Geochemical maps. Open File Report E10230, Institute of Geology and Mineral Exploration, Athens, Hellas, 47 p.

15th International Congress of the Geological Society of Greece
Athens, 22-24 May, 2019 | Harokopio University of Athens, Greece
Bulletin of the Geological Society of Greece, Sp. Pub. 7 Ext. Abs. GSG2019-081

Field-portable X-Ray Spectrometry as Rapid Measurement Tool for Environmental Geochemical Investigations in Former Mining Areas: The Case of Kirki Mines (Greece)

A. Liakopoulos[1], B. Lemiere[2], V. Laperche[2]

(1) Hellenic Survey of Geology and Mineral Exploration, Sp. Loui 1, Olympic Village Acharnai 13677, aliakopoulos@igme.gr
(2) BRGM, 3 avenue Claude Guillemin, BP 36009, 45060 Orléans Cedex 2, France

Introduction

Geochemical environmental monitoring, as a prerequisite for environmental risk assessment, is crucial in abandoned mining and mineral processing sites, where one of the most important environmental problems is associated with the disposal of extraction wastes, as well tailings, directly into streams or at their edge, the generation of acid mine drainage and the resulting environmental pollution of soil, stream and floodplain sediment, surface and ground water. However, in most cases, environmental monitoring is severely restricted, due to lack of funds and, consequently, environmental geochemists need of a cost-saving alternative method to classical laboratory analysis programmes, dealing efficiently with remote or harsh field conditions. Nowadays, portable X-ray fluorescence (pXRF) analysers are a key technique for investigating a wide range of fields (Lemiere, 2018). The technique introduces the acquisition of real–time measurements in the field, making possible the real-time geochemical mapping of areas by identifying elements of interest and gaining an understanding of the trends in elemental soil or sediment pollution.

This paper explores the potential for a wider use of Field Portable X-Ray Fluorescence Spectroscopy instruments (pXRFs) in geochemical environmental assessment by using as case study the abandoned Kirki mine area in north-eastern Greece. The results demonstrated that handheld XRF analyser in the Kirki mine area is a rapid and practical tool for fast, real-time and cost-effective environmental surveys for potential hazardous element dispersal in a short period of time.

The former mining area of Kirki (Aghios Philippos) is located in the gently mountainous part of Thrace, in the north-eastern part of Greece, situated at 22 km to the NNW of Alexandroupolis (NE Greece, Fig.1). First mining works dated since 1880. More recently, the area has been intensively mined during two period: (a) from 1973 to 1982 by the private company 'Kirki Mines Inc.', with underground mining, and (b) from 1989 to 1998 with surface mining operation by 'Evros Mines Co', (Papassiopi *et al.*, 2009; Liakopoulos *et al.*, 2010). Ores were beneficiated by flotation in the plant located near the railway, 5 km south of the mine. Lead and zinc were the main commodities, along with copper and precious metals. A total of 250,000 tons of Pb-Zn ore were processed, whereas galena and sphalerite concentrates were exported to Balkan and Central European smelters (Arikas *et al*., 2007; Triantafylidis *et al*.; 2016). Mining and ore beneficiation for Cu, Zn and Pb ceased in 1998 and no remediation action was taken (Liakopoulos *et al*., 2010; Triadafylidis *et al*., 2016). Tailings and impoundments were exposed to atmospheric conditions and their chemical, mineralogical, physical and geotechnical characteristics were affected. Climate, which can be an important destabilising factor, is harsh in the Kirki area, with hot and dry conditions during summer, and cold, rainy and windy days in the winter (temperate Mediterranean continental climate). Drainage from the Kirki mine is collected by the Kirkalon stream, joining a small river, Eirini, near the plant (Fig. 1), which reaches the sea near Alexandroupolis through a cultivated plain overlying an aquifer used for water supply.

Method

The field portable X-Ray fluorescence (pXRF) unit used was a NITON™ XLt792WY equipped with an X-ray miniaturized tube (40 kV/50mA max.), multifilter configuration with the ability to determine 22 elements (Mn, Fe, Co, Ni, Cu, Zn, As, Se, Pb, Hg, Rb, Sr, Cd, Ag, Sn, Sb; Cr, V, Ti, Sc, Ca and K) in optimum matrix conditions (Lemiere *et al*., 2006). The spectrometer was factory calibrated for the analysis of bulk and/or of soil samples in field, as well as in laboratory conditions. The pXRF unit was used either (a) directly in contact with the soil, sediment or rock target, (b) on-site on a roughly homogenised soil or sediment sample, and/or (c) a near-site location where sample drying, sieving and milling was possible in order to allow sample preparation to be close as possible to laboratory conditions. Methods (a) and (b) were suitable for target identification and sample selection whereas method (c) provided quantitative results (US EPA, 1998). A total of 635 measurements were performed with the pXRF spectrometer during two field trips, including on-site measurements on a roughly homogenised sediment sample as well as analyses in laboratory-controlled conditions. For verification of field results, a total of 39 sediment samples, analysed by pXRF laboratory conditions, were analysed by ICP-MS at OMAC laboratory in Ireland.

Results – discussion

The relationship between field and laboratory XRF data, is good for Pb, Zn and Cu, and poor for As (Fig. 2). The latter is due to high Pb concentration in Kirki samples, resulting in strong Pb interference, as the As-Kα line is overlapped by the Pb-Lα line. For the geochemical conditions of Kirki, the pXRF field measurements are satisfactory for mapping reliably Zn, Pb and Cu contamination, whereas high As can be interpreted in terms of As contamination probability. Serious Pb, Cu and Zn pollution has been recorded in Kirkalon stream sediments as well as at the upper part of Eirini River (Fig. 3&4), whereas extremely high concentrations of Pb, Cu and Zn were found in stream sediments close to the Aghios Philippos mine and also near the tailing dumps area. Downstream of the ore-beneficiation plant

contamination levels decrease gradually and it is markedly lower when the river crosses the alluvial formations of the Alexandroupolis plain.

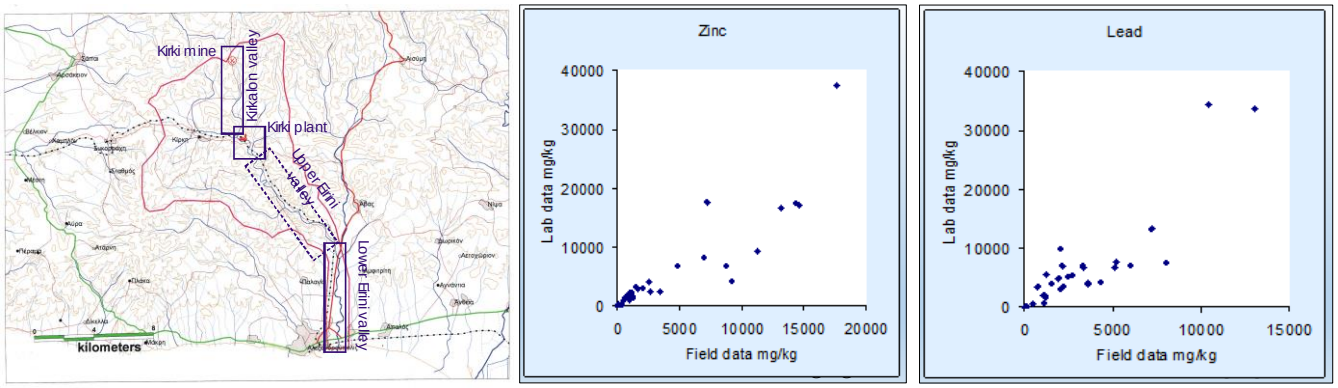

Figures 1 & 2: (left) Map of study area; (right) Relationship between Pb and Zn pXRF and Laboratory measurements.

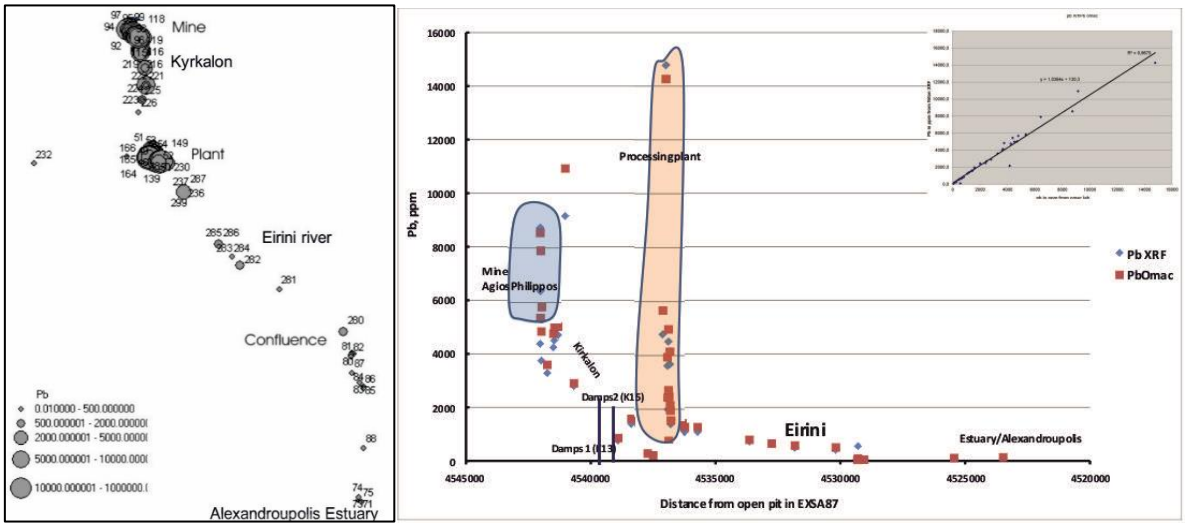

Figures 3 & 4: (left) Cartographic distribution of pXRF Pb measurements along Kirkalon and Eirini rivers from Kirki to sea, which have been obtained by on-site measurements on a roughly homogenised sediment; (right) plot shows analyses performed under lab conditions on pre-treated samples and results are compared with data obtained by ICP-MS.

Conclusion

In the Kirki mine area case study, we took advantage of pXRF as a compositional analysis technique, used as part of environmental monitoring processes, since it was straightforward to use, did not require laborious sample preparation, it was cost-effective, providing higher sampling density data sets and real-time or near real-time decision support for operational decisions.

Acknowledgements

The research was a part of the work carried out by I.G.M.E. in the framework of project 65231 with the support of EU Structural Funds (3rd Community Support Framework, Ministry of Development, Operational Programme 'Competitiveness' (O.P.C.), project 65231) realised in 2002–2009.

References

Arikas, K., Asfahani, N., Nowak, A., Goetz, D., 2007. The Kirki mine in Evros Prefecture, NE Greece, and considerations on the environmental impact - Part I: geochemical and mineralogical study of the tailing ponds and mineral concentrates. Mining and Metallurgical Annals 17(1-2), 21–50.

Lemière, B., 2018. A review of pXRF (field portable X-ray fluorescence) applications for applied geochemistry. Journal of Geochemical Exploration 188, 350–363.

Lemière, B., Crouzet, C., Liakopoulos, A., Michael, C., Romaidis, J., 2006. Test and feasibility of the implementation of monitoring tools for mining and industrial applications on the Kirki mining area (Greece) – Final report E9949, BRGM/RC-54499-FR Open File B.R.G.M.-I.G.M.E. report, Institute of Geology and Mineral Exploration, Athens, Greece, 125 p.

Liakopoulos, A., Lemiere, B., Michael, C., Crouzet, C., Laperche, V., Romaidis, I., Drougas, I., Lassin, A., 2010. Environmental impacts of unmanaged solid waste at a former base metal mining and ore processing site (Kirki, Greece). Waste Management Research 28(11), 996–1009.

Papassiopi, N., Mylona, E., Xenidis, A., Paspaliaris, I., Liakopoulos, A., Angellatou, V., Drougas, J., 2009. Assessment of major acid generation sources in the mining site of Agios Filippos, Kirki, GR. Proceedings of the 3rd International Conference on Advances in Mineral Resources Management and Environmental Geotechnology (Amireg), 333 p.

Triantafyllidis, S., Loupasaki, C., Tsangaratos, P., 2016. Geochemical modeling-based rehabilitation proposal for abandoned sulfidic flotation mill tailings, Kirki, Thrace, NE Greece. Environmental Earth Sciences 75:1403, 1-19.

US EPA, 1998. Environmental Technology Verification Report, Field Portable X-ray Fluorescence Analyzer, Niton XL Spectrum Analyze. Report EPA/600/R-97/150; https://archive.epa.gov/nrmrl/archive-etv/web/pdf/01vr_niton.pdf.

15th International Congress of the Geological Society of Greece
Athens, 22-24 May, 2019 | Harokopio University of Athens, Greece
Bulletin of the Geological Society of Greece, Sp. Pub. 7 Ext. Abs. GSG2019-083

Application of Phosphates in Mine Affected Soils Increases Arsenic Availability for Plant Uptake: Preliminary Results

I. Zafeiriou[1], G. Kalyvas[1], D. Ioannou[1], I. Massas[1]

(1) Agricultural University of Athens Iera Odos 75, 11875, Athens, Greece, j.zafeiriou@gmail.com

Background and objectives

Arsenic is an element that can cause toxicity even at low concentrations jeopardizing human and animal health (Shankar *et al.*, 2014). Assessment of pedo-environmental factors that affect the geochemical behaviour of As, especially mobility and bioavailability of the element, provides substantial information that may be applied for the restoration of contaminated soil using phytoremediation techniques. Among factors regulating As uptake by plants is the concentration of phosphates in soil since P and As oxyanions show similar geochemical behaviour (Strawn, 2018). According to relevant literature, the As hyperaccumulator plant *Pteris vittata*, can accumulate from some hundred up to some thousand mg of As per kg of dry weight, depending on soil properties and experimental conditions (Danh *et al.*, 2014). No study, however, systematically questioned the optimum As:P molar ratio in soil in relation to the ability of *P. vittata* to accumulate As under field conditions.

In the present work, batch experiments were conducted aiming to: (a) comparatively evaluate As mobilisation in two highly contaminated mine soil samples following the application of phosphates either in the form of a commercial triple superphosphate fertiliser (TSP) or in the form of $NH_4H_2PO_4$, (b) study As desorption behaviour in the two soil samples and (c) estimate a TSP agronomic dose that can safely enhance As removal from soil in case of phyto-remediation scenario.

Materials and Methods

Two topsoil samples were collected from the wider area of Lavrion (Attica, Greece) and analysed for their physicochemical properties (Page, 1982) (Table 1). To study the desorption of As in the presence of P in these soil samples, a two factor experiment in three replicates was applied (P source X P rate). Stock solutions of varying phosphate concentrations (2.36-88.88 mg/l) were prepared by dilution of appropriate amounts of TSP (0-46-0) in deionised water, of TSP in 0.01 M $NaNO_3$ electrolyte solution and of $NH_4H_2PO_4$ in 0.01 M $NaNO_3$ electrolyte solution. One gram of air dried soil was weighed into a series of 50 ml falcon tubes and 20 ml of solution containing the appropriate phosphorous concentrations (P rates) from each P source were added. The tubes were gently shaken at 125 rpm for 24 hours in a reciprocal shaker placed in an incubator with standard temperature of 22 ± 1^0C and centrifuged for 5 min at 2200 rpm afterwards. The supernatants were filtered through a Whatman paper No 42 and As and P concentrations determined by hydride generator Varian model VGA 77 and Shimadzu UV-1700 spectrophotometer, respectively.

Table 1. Physicochemical soil properties and As fractions obtained according to Wenzel *et al.* (2001) sequential extraction protocol (SEP). W1: non-specifically sorbed; W2: specifically sorbed; W3: sorbed on amorphous and poorly crystalline hydrous oxides of Fe and Al; W4: sorbed on well-crystallised hydrous oxides of Fe and Al; W5: residual.

Soil properties			Soil properties (mg/kg)			Fraction	S.E.P. (mg/kg)	
Parameter	Soil 1	Soil 2	Parameter	Soil 1	Soil 2		Soil 1	Soil 2
Clay (g/kg)	328	230	Fe_d	41.5	45.3	W1	5.0	4.1
Silt (g/kg)	220	210	Fe_o	4.8	7.0	W2	104	64.3
Sand (g/kg)	458	560	Al_d	728	575	W3	313	645
pH (1:1)	8.0	7.7	Al_o	2390	1098	W4	241	394
$CaCO_3$ (g/kg)	115	64	As total	852	1745	W5	106.0	303
Act. $CaCO_3$ (g/kg)	27	3	P total	733	1061			
O.M. (g/kg)	22	52	P inorganic	391	796			
CEC (cmol./kg)	30	27	P organic	342	265			
			P available	10.7	11.0			

Results and Discussion

The soil samples are alkaline and medium textured with similar pH values and available P content. However, in soil 1 carbonates, active carbonates and amorphous Al contents are much higher than in soil 2, while soil 2 exhibits higher organic matter and amorphous Fe oxides contents (Table 1). Total As concentration is very high in both soil samples but over two-times in soil 2 (852 vs 1745 mg/kg). Most As was found in W3 and W4 fractions, showing that As in the studied soil is preferentially bound to Fe oxides and especially to amorphous and poorly crystalline hydrous oxides of Fe.

Both P source and P rate significantly affected As extraction from the tested soil samples. The significant differences between the P sources can be mainly attributed to the presence of $NaNO_3$ in equilibrating solutions that probably assisted the ability of phosphates to extract As from both soil samples (Smith *et al.*, 2002), and not to differences between TSP and $NH_4H_2PO_4$ extracting efficiency. Increased phosphates rate application resulted to higher As concentrations in the equilibrium solutions, but different As desorption patterns for the two soil samples were observed (Fig. 1). In soil 1, by increasing the P rate, As desorption constantly and significantly increased in relation to the preceding P rate. For soil 2, increasing P rates did not always produce significant differences in As desorption. Though in soil 2 maximum As desorption was obtained by the highest P rate, and an almost steady extracting ability of added phosphates concentrations was observed from the 3rd P rate and onwards. Arsenic amounts extracted from the tested soil samples ranged between 8 and 64.4 mg/kg for soil 1 and between 16.5 and 35.3 mg/kg for soil 2. Considering that the initial As concentration that could be extracted by phosphates was 108.6 and 68.4 mg/kg for soil 1 and 2, respectively (sum of W1 and W2 fractions, Table 1), it is very clear that within 24 hours of equilibration more than 50% of non-specifically and specifically sorbed As (highest P rate) was replaced by phosphates. Interestingly, the lowest P rate showed much lower As desorption from soil 1, in spite that the potentially available As concentration was higher compared to soil 2 (Table 1). The observed As desorption hysteresis in soil 1 compared to soil 2, can be attributed to the higher Al amorphous oxides content in soil 1 that show high P adsorption capacity reducing the extracting ability of phosphates at low concentrations or/and to easily exchangeable by phosphates As forms in soil 2.

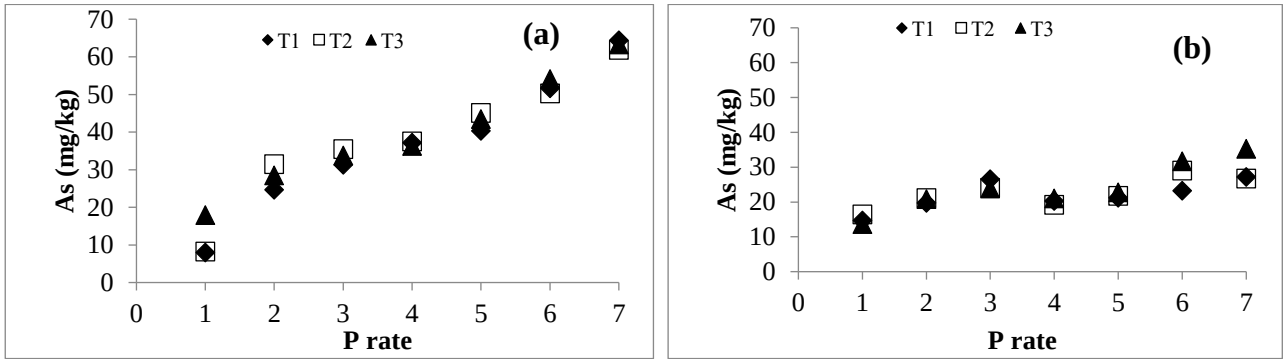

Figure 1. As desorption from (a) Soil 1, and (b) Soil 2. T1:TSP in water; T2:TSP in 0.01 M $NaNO_3$; T3: $NH_4H_2PO_4$ in 0.01 M $NaNO_3$. P rates (mg/l); 1: 2.36, 2: 6.77, 3: 11.08, 4: 15.9, 5: 22.0, 6: 40.6, 7: 88.9.

Recently, by growing *P. vittata* in pots containing a soil from the same area with very high As concentration, Kalyvas *et al.* (2018) found that the maximum extraction ability of the plant ranged from 42 to 73% of available As in the tested soil (W1+W2 fractions). Compared to the results of the present study and independently from the P source, the highest P rate liberated up to 59% and 52% of available As from soil 1 and 2, respectively, suggesting that released As can be up taken by *P. vittata*. However, the maximum adsorbing capacity of both soil samples for P, do not exceed 550 mg/kg in the case of TSP in water (data not shown). For phytoremediation purposes, and to avoid possible leaching of excess As and P, an application rate of 500 mg P/kg as TSP in the studied soil samples appears as a safe recommendation. This application rate leads to the liberation of approximately 40 and 30% of available As in the solution of soil 1 and 2, respectively, that could safely be up taken by *P. vittata* if no antagonism between As and P in the rizosphere of the plant occurs.

Conclusions

The findings of this preliminary work propose that the application of a relatively high TSP dose in the As polluted soil can increase the availability of As for plant uptake without raising great environmental concerns. Nevertheless, pot experiments are needed to thoroughly study the effect of different phosphate fertiliser rates on the ability of *P. vittata* to extract As from the studied soil samples by avoiding As and P leaching due to excess concentrations in soil solution.

References

Danh, L.T., Truong, P., Mammucari, R., Foster, N., 2014. A critical review of the arsenic uptake mechanisms and phytoremediation potential of *pteris vittata*. International Journal of Phytoremediation, 16(5), 429-453.

Kalyvas, G., Tsitselis, G., Gasparatos, D., Massas, I., 2018. Efficacy of EDTA and olive mill wastewater to enhance As, Pb, and Zn phytoextraction by *pteris vittata* L. from a soil heavily polluted by mining activities. Sustainability, 10(6), 1962.

Page, A.L. (Ed.), 1982. Methods of soil analysis, Part 2: Chemical and Microbiological Properties. 2nd edition, American Society of Agronomy, Madison, WI.

Shankar, S., Shanker, U., Shikha, 2014. Arsenic contamination of groundwater: A review of sources, prevalence, health risks, and strategies for mitigation. The Scientific World Journal, ID 304524, 18 p.

Smith, E., Naidu, R., Alston, A. M., 2002. Chemistry of inorganic arsenic in soils: II. effect of phosphorus, sodium, and calcium on arsenic sorption. Journal of Environmental Quality 31(2), 557-563.

Strawn, D.G., 2018. Review of interactions between phosphorus and arsenic in soils from four case studies. Geochemical Transactions, 19(1), 10 p.

Wenzel, W.W., Kirchbaumer, N., Prohaska, T., Stingeder, G., Lombi, E.,Adriano, D.C., 2001. Arsenic fractionation in soils using an improved sequential extraction procedure. Analytica Chimica Acta 436(2), 309-323.

15th International Congress of the Geological Society of Greece
Athens, 22-24 May, 2019 | Harokopio University of Athens, Greece
Bulletin of the Geological Society of Greece, Sp. Pub. 7 Ext. Abs. GSG2019-102

Geochemical Survey Database of Hungary – Concept, Development and Application

D. Tolmacs[1]

(1) Mining and Geological Survey of Hungary, Columbus Str. 17–23, Budapest, Hungary, tolmacs.daniella@mbfsz.gov.hu

Introduction

Developing a geochemical baseline database through systematic sampling and chemical analysis is a key area of applied geochemistry. It is essential to define the geochemical baseline for the near-surface geological media in order to assess the current state of the environment and to provide information on mineral resources. For this purpose, in the last three decades, many low-to-high sampling density geochemical surveys were conducted at the one-time Geological Survey of Hungary (currently known as the Mining and Geological Survey of Hungary). Until recently, the large amount of geochemical data, produced by these surveys, was dispersed throughout published literature and maps, but has not been collected and collectively interpreted. Our mission was to develop a geochemical database and to implement revision and interpretation of these archive data. The database currently contains data of more than 30 surveys, including the National Survey, the regional surveys of mountains, many large-scale local programmes, and data from three pan-European projects, *i.e.*, FOREGS Geochemical Atlas of Europe (Salminen *et al*., 2005; De Vos, Tarvainen *et al*., 2006), EGG - European Groundwater Geochemistry (Reimann and Birke, 2010), and GEMAS - Geochemical mapping of agricultural and grazing land soil (Reimann *et al*., 2014a, b).

Brief history of geochemical surveys in Hungary

Geochemical surveys in Hungary for a long time aimed to assist mineral exploration. At the beginning of the 1990s, however, the potential environmental application of geochemical mapping was recognised. The main objective of the first country-scale National Survey in the one-time Geological Institute of Hungary was to define the geochemical baseline values for the most important potentially toxic and essential elements. The programme was based on floodplain sediment, and for this approximately 200 sampling sites had been designated (Ódor *et al.*, 1997). The National Survey was the base for the first version of the Geochemical Atlas of Hungary. This survey was soon expanded to the regional-scale survey of the mountainous areas; in this survey, approximately 4 km^2-large catchment basins were designated in the mountainous regions of the country and at the outlet point of each basin one stream sediment sample was collected. The second version of the Geochemical Atlas of Hungary was the result of the integration of the National Survey and the regional surveys. These two important programmes were followed by many smaller (local, linear, gap-filler) mapping programmes, most of which were conducted for a specific purpose. The Survey also participated in several important EU-scale and EuroGeoSurveys projects, *e.g.*, FOREGS, EGG and GEMAS (Salminen *et al.*, 2005; De Vos, Tarvainen *et al*., 2006; Reimann and Birke, 2010; Reimann *et al.*, 2014a, b).

Concept and development of the Geochemical Survey Database of Hungary

The initial idea behind the Geochemical Atlas of Hungary was that it can be regularly expanded by new surveys. However, by 2015 it became evident, that there was not a single, transparent database available from which a new atlas can be compiled. Moreover, old files and GIS maps did not meet compliance with modern requirements. Thus, we decided to revise all geochemical programmes to clarify objects and methodology.

The work mostly included the processing of huge number of digital and paper databases and maps, as well as publications and project reports. Work was pulled back by the fact that much information was missing and since data were originated from multiple places, there was a lot of contradiction in connection with sample numbering, coordinates, *etc*. Moreover, both in the National Survey and in the survey of the mountainous regions, there have been a large number of composite samples, the material of which had been collected from different locations.

Altogether, data of 34 surveys have been gathered, resulting in *ca*. 2500 samples, 1000 subsamples and 3000 rows of analytical data. The sample index map of the database was published online on the website of the Mining and Geological Survey of Hungary in 2017 (Fig. 1).

Discussion

The harmonisation and collective interpretation of data shows that the original intention of integrating these surveys into one atlas cannot be accomplished. Differences have been shown between scale, sampled media, analytics and analysed parameters. Application of data for environmental and mineral exploration purposes is possible and has been achieved at regional and local scale in mountains, whereas no reliable data is available from the hilly lands and lowlands at a sufficient scale. Based on our findings, it is concluded that a reliable country-scale geochemical atlas for multiple application is to be accomplished only through the implementation of a new national survey.

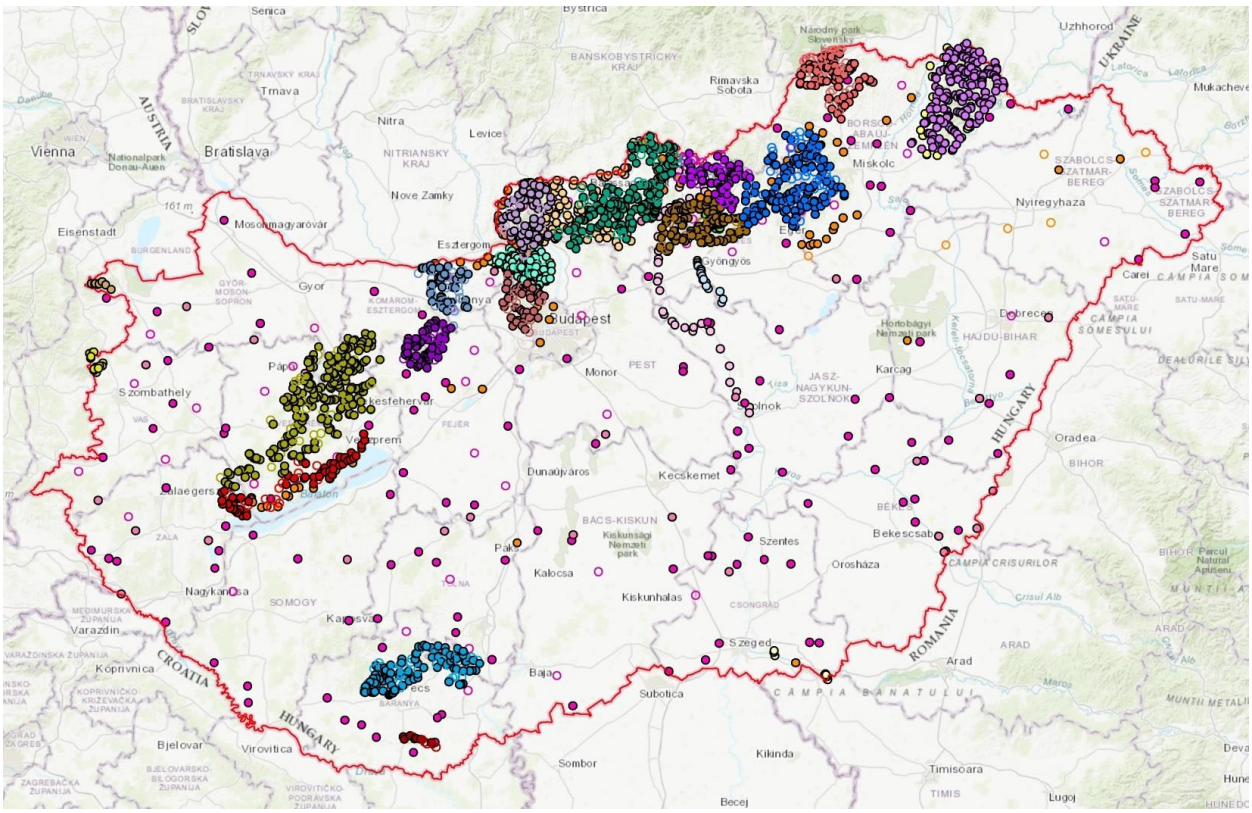

Figure 1. Geochemical Survey Database of Hungary – Sample index map

References

De Vos, W., Tarvainen, T. (Chief Eds.), Salminen, R., Reeder, S., De Vivo, B., Demetriades, A., Pirc, S., Batista, M.J., Marsina, K., Ottesen, R.T., O'Connor, P.J., Bidovec, M., Lima, A., Siewers, U., Smith, B., Taylor, H., Shaw, R., Salpeteur, I., Gregorauskiene, V., Halamic, J., Slaninka, I., Lax, K., Gravesen, P., Birke, M., Breward, N., Ander, E.L., Jordan, G., Duris, M., Klein, P., Locutura, J., Bel-lan, A., Pasieczna, A., Lis, J., Mazreku, A., Gilucis, A., Heitzmann, P., Klaver, G., Petersell, V., 2006. Geochemical Atlas of Europe. Part 2 - Interpretation of Geochemical Maps, Additional Tables, Figures, Maps, and Related Publications. Geological Survey of Finland, Espoo, 692 p.; http://weppi.gtk.fi/publ/foregsatlas/.

Ódor L., Horváth I., Fügedi U., 1997. Low-density geochemical mapping in Hungary, in: Marsina, K., Vrana, K. (Eds.), Environmental Geochemical Baseline Mapping in Europe. Special Issue, Journal of Geochemical Exploration, 60(1), 55-66.

Reimann, C., Birke, M. (Eds.), 2010. Geochemistry of European Bottled Water. Borntraeger Science Publishers, Stuttgart, 268 p.; http://www.schweizerbart.de/publications/detail/artno/001201002#.

Reimann, C., Birke, M., Demetriades, A., Filzmoser, P., O'Connor, P. (Eds.), 2014a. Chemistry of Europe's agricultural soils – Part A: Methodology and interpretation of the GEMAS data set. Geologisches Jahrbuch (Reihe B 102), Schweizerbarth, Hannover, 528 p.; http://www.schweizerbart.de/publications/detail/isbn/9783510968466.

Reimann, C., Birke, M., Demetriades, A., Filzmoser, P., O'Connor, P. (Eds.), 2014b. Chemistry of Europe's agricultural soils – Part B: General background information and further analysis of the GEMAS data set. Geologisches Jahrbuch (Reihe B 103), Schweizerbarth, Hannover, 352 p.

Salminen, R. (Chief-Ed.), Batista, M.J., Bidovec, M., Demetriades, A., De Vivo, B., De Vos, W., Duris, M., Gilucis, A., Gregorauskiene, V., Halamic, J., Heitzmann, P., Lima, A., Jordan, G., Klaver, G., Klein, P., Lis, J., Locutura, J., Marsina, K., Mazreku, A., O'Connor, P.J., Olsson, S.Å., Ottesen, R.T., Petersell, V., Plant, J.A., Reeder, S., Salpeteur, I., Sandström, H., Siewers, U., Steenfelt, A., Tarvainen, T., 2005. FOREGS Geochemical Atlas of Europe, Part 1: Background Information, Methodology and Maps. Geological Survey of Finland, Espoo, 526 p.; http://weppi.gtk.fi/publ/foregsatlas/.

15th International Congress of the Geological Society of Greece
Athens, 22-24 May, 2019 | Harokopio University of Athens, Greece
Bulletin of the Geological Society of Greece, Sp. Pub. 7 Ext. Abs. GSG2019-121

Development of a GIS Story Map for Improved Communication of the ERANETMED CrITERIA Project Results on Cr(VI)-Impacted Water Bodies of the Mediterranean

S. Potamousis[1], A. Argyraki[1], K. Pyrgaki[1], E. Kelepertzis[1], F. Botsou[2], I. Megremi[1]

(1) Department of Geology and Geoenvironment, National and Kapodistrian University of Athens, Panepistimiopolis Zographou, Athens, Greece, potamousis.st@gmail.com
(2) Department of Chemistry, National and Kapodistrian University of Athens, Athens, Greece

Geographic Information Systems (GIS) is an upcoming digital technology, which provides the opportunity to share geospatial data globally. This key feature makes it essential for the communication between the (geo)scientific world and the general audience. Story Maps are an innovative communication technique developed by ESRI© (2012) and achieved a breakthrough in this field. They are interactive maps that combine multimedia content and text that can be displayed on various screen sizes. Individuals have constantly wanted to include geographic information into their lives for things as locating discoveries or registering property (Sui and Goodchild, 2001). GIS Story Maps combine geospatial data with photos, video, audio, and text to visualise a theme or sequential events. Therefore, a Story Map contributes to spatial organisation of GIS data in a reading-pleasant way, while it is widely available in a cloud-based software platform (ArcGIS Online) accessible by anyone, beyond institutions, on the World Wide Web (Scott *et al*., 2016). Thus, it is a tool for public engagement as it can effortlessly be shared via social media or embedded within a website.

One of the objectives of the ERANETMED CrITERIA project is to provide a dialogue platform for public or private water managers and local communities of areas where the groundwater resources are impacted by hexavalent Cr, mainly as a result of the geological setting. Such areas in central-eastern Mediterranean region and Oman are included as case studies in the project. The ultimate aim is to guide water stakeholders towards a sustainable way of water usage by taking into account water pressures as well as climate change (Pyrgaki *et al.*, 2018). Extended water sampling and analysis have been implemented in the study areas on a seasonal basis and have provided a rich data set with respect to water quality data. These have subsequently been interpreted in conjunction with the European Union water standards, as well as other factors including precipitation and land use. Within this context a Story Map is being developed in order to accommodate the produced data in a comprehensive way and present them in a memorable and compelling character that combines analytical and artistic characteristics.

The creation of the Story Map involved selection of a template appropriate for the end recipients and an interesting, memorable and comprehensive title. Then, a proper base map had to be chosen, in which various layers can be added depending on what is analysed. Specifically, a global terrain map has been selected and information layers concerning geology, sampling points, boreholes, urban/industrial/rural areas have been added. Symbols on the map are explained either on a legend or in text. Also, multiple graphs, additional maps and other data have been adjusted on the story, such as in the form of carefully designed custom pop ups. These included Piper diagrams with explanation of water type and links to geology, climate concerning charts, elemental concentration ratios, and historical statistics whenever available. Furthermore, hyperlinks for videos, websites and email addresses have been added to provide all necessary information to concerned stakeholders.

All of the above, aim to provide helpful information to the local stakeholders and water managers. Story Maps act as a valuable tool, able to bring people closer to the GIS technology and its capabilities, more to draw their attention on a specific issue like the water administration and awaken them from vital issues' unawareness.

Acknowledgements

The present work was co-funded by the European Union (ERDF) and Greek national funds through the Operational Programme 'Competitiveness, Entrepreneurship and Innovation', under the ERANETMED 1st Joint Call on Water Resources (project acronym: CrITERIA/ project code: T3EPA-00004).

References

ESRI©, 2012. Telling stories with maps: A white paper. Retrieved from https://learn.arcgis.com/en/arcgis-book/chapter3/.

Pyrgaki, K., Argyraki, A., Hatzaki, M., Kelepertzis, E., Botsou, F., Megremi, I., Di Palma, L., Paternoster, M., Zissimos, A., Christou, A., Hatipoglu Bagci, Z., Moraetis, D., Dermatas, D., 2018. Assessing groundwater quality of Cr(VI) impacted water bodies along a climate gradient from Central- East Mediterranean to Oman. MEDCLIVAR 2018 Conference, University of Belgrade, Serbia.

Scott, M.S., Edwards, S., Dayan, S., Nguyen, T., Cragle, J., 2016. GIS Story Maps: A Tool to Empower and Engage Stakeholders in Planning Sustainable Places. Institute for Public Administration (IPA), University of Delaware, 69 p.

Sui, D.Z., Goodchild, M.F., 2001. GIS as media? International Journal of Geographical Information Science 15(5), 387-390.

15th International Congress of the Geological Society of Greece
Athens, 22-24 May, 2019 | Harokopio University of Athens, Greece
Bulletin of the Geological Society of Greece, Sp. Pub. 7 Ext. Abs. GSG2019-125

Fate of Trace Elements in Urban Surface Drainage Deposits of the Athens Basin, Greece

P. Kourgia[1], A. Argyraki[1], E. Dassenakis[2], M. Skoullos[2], V. Paraskevopoulou[2]

(1) Department of Geology and Geoenvironment, National & Kapodistrian University of Athens, Panepistimiopolis Zographou, 15784 Athens, Greece, b.kourgia@gmail.com
(2) Department of Chemistry, National & Kapodistrian University of Athens, Panepistimiopolis Zographou, 15784 Athens, Greece

Introduction

Urban deposits (road dust and gully sediment) are reflective of a wide range of anthropogenic activities, and are a useful medium for evaluating the level and distribution of trace element contaminants in the surface environment. The drainage system of cities plays an important role in terms of capturing and/or releasing trace element contaminants to the receiving aquatic bodies (Duzgoren-Aydin *et al.*, 2014). Monitoring of the urban environment of Greece's capital, Athens, provided important information about how trace element concentrations behave between seasons and how they contribute to the urban pollution. Chemical partitioning of contaminants in both road dust and gully sediment can, therefore, be useful to evaluate the long-term fate of contaminants in the urban system. Urban sediment samples have been collected and analysed from different altitudes within the Athens basin, based on the hydrographic network of the area.

Sampling and analysis

A total of 26 urban sediment samples were collected and analysed for 33 elements following hot *aqua regia* dissolution and measured by Inductively Coupled Plasma Emission Spectroscopy. Soil organic carbon content, soil pH and grain-size distribution and magnetic susceptibility measurements have been determined, and mineralogical analysis by powder X-ray diffraction was also performed in order to identify possible factors explaining the variability of elemental concentrations. The BCR sequential extraction protocol (Ure, 1992; Ure *et al*., 1993) was subsequently applied to a set of ten selected samples with the highest concentrations of trace elements (Cd, Co, Cr, Cu, Ni, Pb, Zn). Seasonal sampling at selected sampling sites over one year was also performed, followed by determination of the reactive content of trace elements after extraction with dilute (0.43 M) HNO_3 at room temperature (Rodrigues *et al*., 2010) and measurement by Flame Atomic Absorption Spectroscopy.

Results and discussion

Basic statistical parameters of *aqua regia* concentrations of As, Cd, Co, Cr, Cu, Fe, Mn, Ni, Pb and Zn in sediment samples are tabulated in Table 1. With the exception of Co and As, both maximum and median values were found to be much higher in this work than those presented for Athens topsoil in a previous study (Kelepertzis and Argyraki, 2015).

Table 1. Statistical summary of *aqua regia* extractable concentrations of major and trace elements for the investigated sediment samples from Athens basin (n = 26), and comparison with topsoil values reported by Kelepertzis and Argyraki (2015; Table 1, p.66).

Element	This study (n = 26)		Kelepertzis and Argyraki (2015) (n = 45)	
	Range	Median	Range	Median
As (mg/kg)	8 – 18	12.5	4.4 – 227	27.1
Cd (mg/kg)	0.5 – 2	0.93	0.09 – 2.35	0.37
Co (mg/kg)	6 – 14	8	8.7 – 52.8	14.5
Cr (mg/kg)	54 – 193	215	21.1 – 558	82.4
Cu (mg/kg)	43 – 640	98.2	15.1 – 316	59.2
Fe (%)	1.03 – 2.56	1.72	0.99 – 4.06	2.35
Mn (mg/kg)	269 – 648	390	246 – 2810	564
Ni (mg/kg)	43 – 112	69.7	25.4 – 762	94.5
Pb (mg/kg)	44 – 3092	267	9.6 – 823	106
Zn (mg/kg)	147 – 1469	598	37.2 – 783	146

Cluster analysis performed on the results identified two major groups of elements based on a >43.6% criterion of similarity. The first cluster contains elements of geogenic origin including Co, Fe, Mn and Ni. The parameters of soil organic carbon, magnetic susceptibility, Cu and Cr are grouped together in a second cluster showing similarity level >65%, while a third cluster groups together Pb, Zn and Cd and is interpreted as anthropogenic. Sequential extraction results support this grouping as the anthropogenic elements tend to be released in the first two extraction steps. Cadmium and Zn are the only trace elements showing significant association with the exchangeable fraction, reaching 40%, suggesting that they are the most susceptible elements to mobilisation during runoff. Moreover, Cu and Pb are largely associated with the oxidisable fraction. Trace element fractions identified as showing larger associations with the reducible and oxidisable fractions will continue to be vulnerable to mobilisation as a result of changes in ambient pH

and/or redox conditions (Robertson *et al*., 2002). No significant seasonal variation has been observed for all the studied elements, except Cd which displayed significantly lower concentrations during the December sampling period.

Soil and dust in cities and towns that are contaminated by trace elements, of anthropogenic origin, represent a potential risk for the residents through several pathways (Kelepertzis *et al*., 2013). Urban surface drainage deposits are the main sinks where dust, urban soil and anthropogenic sediments can be trapped. Briefly, it was documented that the type and extent of contamination in the surface environment of the Athens basin reflects the characteristics of prevalent anthropogenic activities, and that traffic-related activities are the primary sources of contaminants in the city.

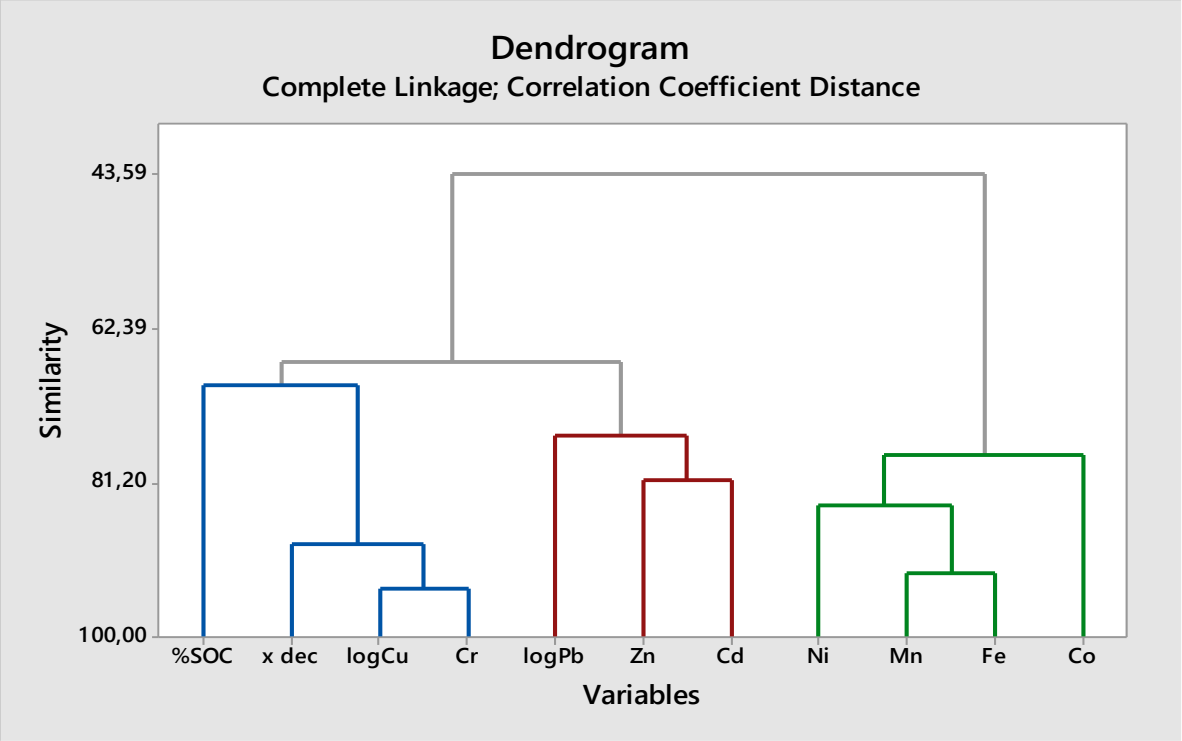

Figure 1. Dendrogram showing grouping of measured parameters in surface drainage deposits of the Athens Basin.

Acknowledgements

The research work was supported by the Hellenic Foundation for Research and Innovation (HFRI) and the General Secretariat for Research and Technology (GSRT), under the HFRI PhD Fellowship grant (GA. no. 1225/14677).

References

Duzgoren-Aydin, N.S., Wong, C.S.C., Song, Z.G., Aydin, A., Li, X.D., You, M., 2006. Fate of heavy metal contaminants in road dusts and gully sediments in Guangzhou, SE China: A chemical and mineralogical assessment Human and Ecological Risk Assessment 12, 374-389.

Kelepertzis, E., Argyraki, A., 2015. Geochemical associations for evaluating the availability of potentially harmful elements in urban soils: Lessons learnt from Athens, Greece. Applied Geochemistry 59, 63-73.

Kelepertzis, E., Stathopoulou, E., 2013. Availability of geogenic heavy metals in soils of Thiva town (central Greece). Environmental Monitoring and Assessment 185, 9603-9618.

Robertson, D.J., Taylor, K.G., Hoon, S.R., 2003. Geochemical and mineral magnetic characterisation of urban sediment particulates, Manchester, UK. Applied Geochemistry 18, 269-282.

Rodrigues, S.M., Henriques, B., Ferreira da Silva, E., Pereira, M.E., Duarte, A.C., Römkens, P.F.A.M., 2010. Evaluation of an approach for the characterization of reactive and available pools of twenty potentially toxic elements in soils: Part I – The role of key soil properties in the variation of contaminants' reactivity. Chemosphere 81, 1549–1559.

Ure, A.M., Quevauviller, Ph., Muntau, H., Griepink, B., 1992. B. EUR report. CEC Brussels, 14763, 1992:85.

Ure, A.M., Quevauviller, Ph., Muntau, H., Griepink, B., 1993. Speciation of heavy metal in soils and sediments. An account of the improvement and harmonisation of extraction techniques undertaken under the auspices of the BCR of the Commission of the European Communities. International Journal of Environmental Analytical Chemistry 51, 135-151.

15th International Congress of the Geological Society of Greece
Athens, 22-24 May, 2019 | Harokopio University of Athens, Greece
Bulletin of the Geological Society of Greece, Sp. Pub. 7 Ext. Abs. GSG2019-145

Distribution of Trace Elements in Old Lignite Disposal Sites and Potential Impact on the Local Environment, Oropos Basin, Northern Attika

E. Karampetsou[1], L. Arvaniti[1], K. Kollias[2], C. Stouraiti[1], E. Kampouroglou[1]

(1) Department of Geology & Geoenvironment, Division of Economic Geology & Geochemistry, NKUA, Panepistimiopolis 15784, Athens, Greece, ekarampetsou2@gmail.com
(2) School of Mining & Metallurgical Engineering, Laboratory of Metallurgy, NTUA, Zografos 157 80, Athens, Greece

The Oropos Basin was one of the most important lignite-bearing areas in Greece. The lignite deposits in the area of Mavrosouvala, between Markopoulo and Milesi, has been known since 1830 and mining activity in the area lasted for about a century. Numerous waste lignite and spoil heaps have been neglected ever since. Previous research in the area has underlined geogenic contamination of potentially toxic elements in the groundwater and the Neogene sediments bedrock of this basin (Stamatis *et al.*, 2011; Kampouroglou and Economou-Eliopoulos, 2016; Kampouroglou *et al.*, 2017). However, the environmental impact of the neglected lignite wastes has not been evaluated so far. The aim of this research was to sample mining wastes from different disposal sites and perform mineralogical and geochemical analysis. Characterisation of samples includes semi-quantitative mineralogical analysis by SEM/EDS analysis and XRD, bulk waste geochemical analysis for major and trace elements by XRF and ICP-MS and LECO methods.

Based on field observations and the bulk analysis the mine waste material is characterised as highly heterogeneous consisting of variable amounts of waste lignite, soil and waste rock. Total sulphur concentration (LECO measurements) in the all the waste types including the waste rock is high, *i.e.*, from 3.5 up to 10.7 wt.% associated with a high pyrite content (Fig. 1). Organic carbon also shows high variability from 0.1 to 19 wt.%. According to SEM/EDS analysis the sulphides (pyrite, sphalerite) and montmorillonite host significant amounts of As in the waste lignite whereas goethite is the main carrier of As in the waste rock (dolomitic limestone).

Ashing of lignite waste and then dissolution by nitric acid in closed vessels (and microwave heating) was performed in order to minimise loss of volatile elements during the open vessel acid attack at high temperatures. Trace element concentration of the digests were measured by ICP-MS. The total Fe concentration in the lignite waste (XRF analysis) ranges from 5.1 to 7.9 wt.%, being probably associated with the abundance of pyrite; it is also possible to participate in clay minerals (montmorillonite). The average concentration of As, Cr, Co, and Ni in the lignite ash is higher than the respective ash concentration of the main Greek lignite deposits (Table 1). The determination of As in the ash samples is considered accurate, since the digestion test was performed in closed vessels (Lachas *et al.*, 1999).

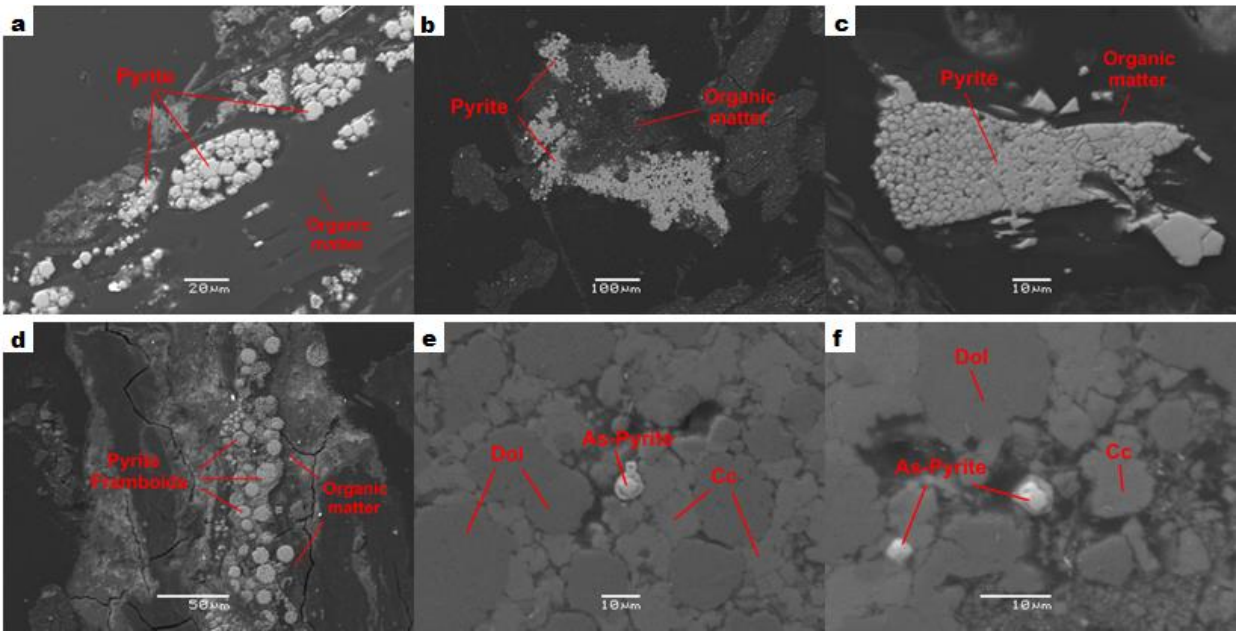

Figure 1. Pyrite occurrence as framboids in the lignite waste (a-d) and As-pyrite in the dolomitic limestone host rock (e-f).

Table 1. Concentrations in ppm of trace elements and iron of lignite waste (bulk analysis by XRF) and lignite ash (ICP-MS analysis) from Oropos basin. For comparison, lignite ash from the main lignite deposits of Greece are shown (Foscolos *et al.*, 1989, 1998).

Element	Oropos Lignite waste (dried bulk, n=3)	Oropos Lignite ash	Ptolemaida/Amyntaio ash	Megalopoli ash	Drama ash
Fe (wt.%)	5.1 – 7.9	4.3	-	-	-
As	80 – 119	168	23.5 – 104	20 – 30	102 – 606
Ba	74 – 544	-	612 – 852	487 – 700	425 – 1323
Cd	2 – 7	2	<3.3	<1.8	<2.1
Cr	610 – 640	535	234 – 591	236 – 351	50 – 290
Co	102 – 216	132	18 – 35	25 – 53	9 – 25
Cu	56 – 98	50	140 – 220	165 – 194	25 – 110
Mo	<15	-	18 – 29	10 – 33	46 – 712
Mn	195 – 576	185	304 – 1172	319 – 531	168 - 1273
Ni	643 – 2752	1842	229 – 651	215 – 226	57 – 246
Pb	14.7 – 40	20	50 – 67	56 – 66	50 – 119
U	15 – 40	-	21 – 97	12 – 13	33 – 313
V	188 – 344	219	267 – 348	227 – 282	116 – 737
Y	21 – 41	-	24 – 26	35 – 47	28 – 298
Zn	116 – 194	83	57 – 98	110 – 185	50 – 242

High concentrations of Cr and Ni ranging from 234 to 591 ppm and 229 and 651 ppm, respectively, have also been recorded in the ash from Ptolemaida – Amyntaio lignite basin (Papanikolaou *et al.*, 2004).

The paste pH test (1 part solid:1 part water) was used to determine the acidic nature of the waste samples and ranged from 2.7 to 4.9. Samples having a paste pH of <4.0 are considered potentially acid forming (PAF), and these samples contain significant acidic sulphate salts. Preliminary results of acid-base accounting tests (ABA) showed Neutralisation Potential Ratio (NPR) values <1and Net Neutralisation Potential (NNP) <-20 kg $CaCO_3$/t indicating potential acid generation from the mine waste material. These conditions could enhance metal leachability and cause an increased risk for the local water and soil.

Acknowledgements

We would like to thank V. Skounakis from the Department of Geology and Geonvironment, NKUA, for performing the SEM/EDS analysis.

References

Alexakis, D., Gamvroula, D., 2014. Arsenic, chromium, and other potentially toxic elements in the rocks and sediments of Oropos Kalamos Basin, Attica, Greece. Applied and Environmental Soil Science ID718534, 8 p.

Foscolos, A.E., Goodarzi, F., Koukouzas, C.N., Hatziyannis, G., 1989. Reconnaissance study of mineral matter and trace elements in Greek lignites. Chemical Geology 76, 107-130.

Foscolos, A.E., Goodarzi, F., Koukouzas, C.N., Hatziyannis, G., 1998. Assessment of environment impact of coal exploration and exploitation in the Drama basin, Northeastern Greek – Macedonia. Energy Sources 20, 795-820.

Kampouroglou, E., Economou-Eliopoulos, M., 2016. Assessment of the environmental impact by As and heavy metals in lacustrine travertine limestone and soil in Attica, Greece: Mapping of potentially contaminated sites. CATENA 139, 137-166.

Kampouroglou, E., H. Tsikos, Economou-Eliopoulos, M., 2017. Carbonate stable isotope constraints on sources of arsenic contamination in Neogene tufas and travertines of Attica, Greece. Open Geosciences 9(1), 577–592.

Lachas, H., Richaud, R., Jarvis, K.E., Herod, A.A., Dugwell, D.R., Kandiyoti, R., 1999. Determination of 17 trace elements in coal and ash reference materials by ICP-MS applied to milligram sample sizes. The Analyst 124, 177–184.

Papanicolaou, C., Kotis, T., Foscolos, A., Goodarzi, F., 2004. Coals of Greece: a review of properties, uses and future perspectives. International Journal of Coal Geology 58(3), 147-169.

Stamatis, G., Alexakis, D., Gamvroula, D., Migiros, G., 2011. Groundwater quality assessment in Oropos-Kalamos basin, Attica, Greece. Environmental Earth Sciences 64(4), 973–988.

15th International Congress of the Geological Society of Greece
Athens, 22-24 May, 2019 | Harokopio University of Athens, Greece
Bulletin of the Geological Society of Greece, Sp. Pub. 7 Ext. Abs. GSG2019-161

Seasonal and Temporal Variation of the Piezometric Level in the Alluvial Aquifer of Loutraki (Korinthia), with the Use of GIS Mapping Techniques

K. Pyrgaki[1], P. Krassakis[1], V. Gemeni[1], N. Koukouzas[1], A. Argyraki[2], K. Voudouris[3]

(1) Centre for Research and Technology, Hellas (CERTH), 52 Egialias St., 15125 Maroussi, Athens, pyrgaki@certh.gr.
(2) Department of Geology and Geoenvironment, National University of Athens, Panepistimioupolis, Ano Ilissia, Athens, Greece.
(3) Lab of Engineering Geology & Hydrogeology, Dept. of Geology, Aristotle University of Thessaloniki, Greece.

According to the European groundwater directive (2006/118/EC), groundwater bodies must be protected from qualitative and quantitative degradation. According to the 1st revision of the National Water Management Plan for the River Basin District of Attica, the groundwater body of Loutraki is characterised by a good qualitative and quantitative status. The water demand (mainly for drinking purposes) of Loutraki is covered exclusively by the alluvial aquifer located at the southern part of the basin. It is estimated that the annual groundwater abstractions from the alluvial aquifer are approximately 2.5 million m^3. During the summer, the groundwater abstractions are doubled as Loutraki is a popular touristic resort and this causes an additional pressure on the aquifer. Within such a framework, the scope of the present study is to assess the variation of groundwater level between the wet and dry season as well as to compare the present and the past piezometric level for the studied part of the aquifer by using Geographical Information Systems. Several researchers have used GIS techniques for the assessment of groundwater-level fluctuation (Tiwari *et al*., 2017).

Loutraki basin is located at the south-east part of Korinthiakos Gulf in the North-east Peloponnese (Fig. 1) and covers an area of approximately 53.3 km^2. The maximum elevation in the basin is 1368 m a.s.l., while the mean elevation is 470 m a.s.l. The climate is temperate with a dry summer and rainy winter and a mean annual temperature of 18.2ºC. The alluvial aquifer covers an area of 7.45 km^2 with a maximum water level depth of 150 m (Kounis and Vitoriou-Georgouli, 2003). The delineation of the groundwater body of Loutraki is depicted in Fig. 1. The thickness of the unsaturated zone increases gradually from the western to the eastern part of the aquifer and ranges from zero to 125 m while the maximum thickness of the saturated zone is approximately 200 m. Hydraulic conductivity ranges from 2×10^{-4} to 5.2×10^{-5} m/s and the transmissivity from 1.6×10^{-2} to 4.3×10^{-3} m^2/s (Stamatis and Voudouris, 2000).

The present study assembles new data (2017) and existing unpublished data (2009), which were acquired by the Municipal Directorate for Water and Sewage of Loutraki – Agioi Theodoroi on groundwater level/piezometric head of the alluvial aquifer. The groundwater level depth in 14 boreholes was recorded during the wet season in April 2017 and the dry season in September 2017 (Fig. 1). The delimitation of the study area was performed based on the geographical distribution of the boreholes and it is estimated at 6.4 km^2 (Fig. 2) covering only a small part (12%) of the basin. The borehole depths range from 20 to 220 metres with a gradual depth increase towards the north-eastern part of the alluvial aquifer. Four piezometric maps were produced using ESRI's ArcGIS 10.4 software by using the Spatial Analyst toolbox and Inverse Distance Weight (IDW) interpolation technique. IDW was selected as opposed to kriging interpolation due to the imbalanced spatial distribution of the measurement points across the study area. Further, the root mean squared error (RMSE) indicator by IDW was lower in comparison to the difference between observed and calculated values.

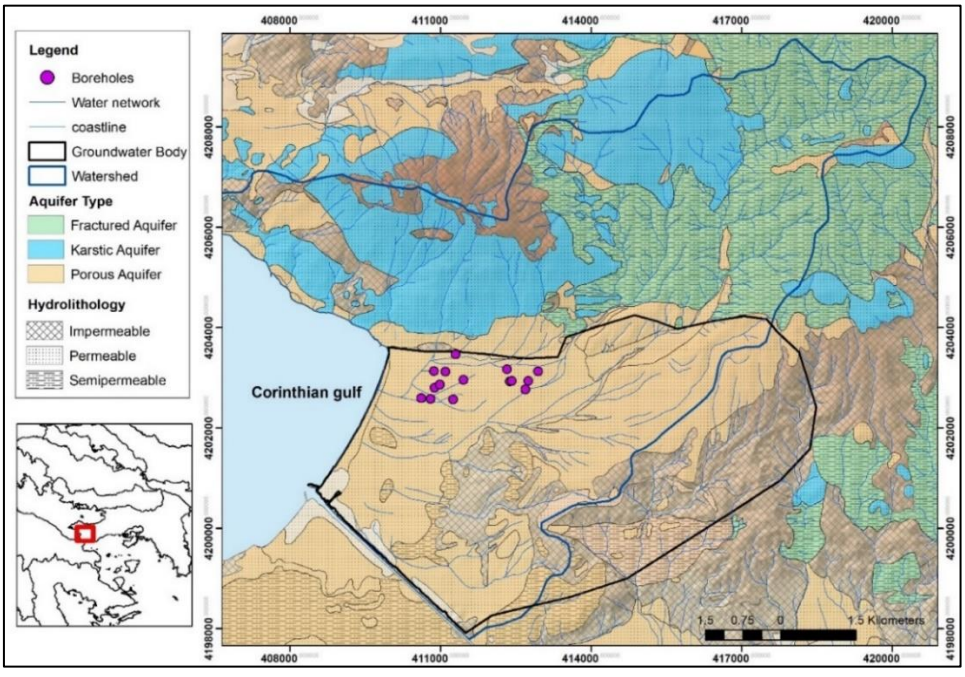

Figure 1. Hydrolithological map of Loutraki basin and groundwater monitoring boreholes.

The aquifer is under unconfined conditions in the upstream part, transforming in confined conditions in the coastal part. Groundwater recharge occurs through infiltration of rainfall and torrents. Limited recharge originates from the upstream boundary of the aquifer via fractured rocks. Groundwater flow has a direction from north-east to south-west, and the piezometric head ranges from higher than 12.73 m to below sea level (<-0.48 m) (Fig. 2). A seasonal variation of the piezometric head between wet and dry seasons of both 2009 and 2017 is noted by comparing the maps. During the dry season (Fig. 2a, c), the piezometric head decreases reaching negative values near the coastal zone at the south-west part of the basin. This is attributed to increased groundwater abstractions during the summer months. No significant variations were observed between the wet and dry seasons of 2009 and 2017. This indicates that the quantitative status of the aquifer remained relatively stable within the 8-years period. However, it must be highlighted that the risk of sea water intrusion in the coastal zone is high during the dry season. This is also proved by the fact that electrical conductivity and chloride concentrations increase near the coastal zone (Pyrgaki *et al*., 2016). Therefore, water managers must take measures in order to avoid aquifer overpumping during summer months in order to minimise the risk of sea water intrusion in the coastal part of the aquifer system.

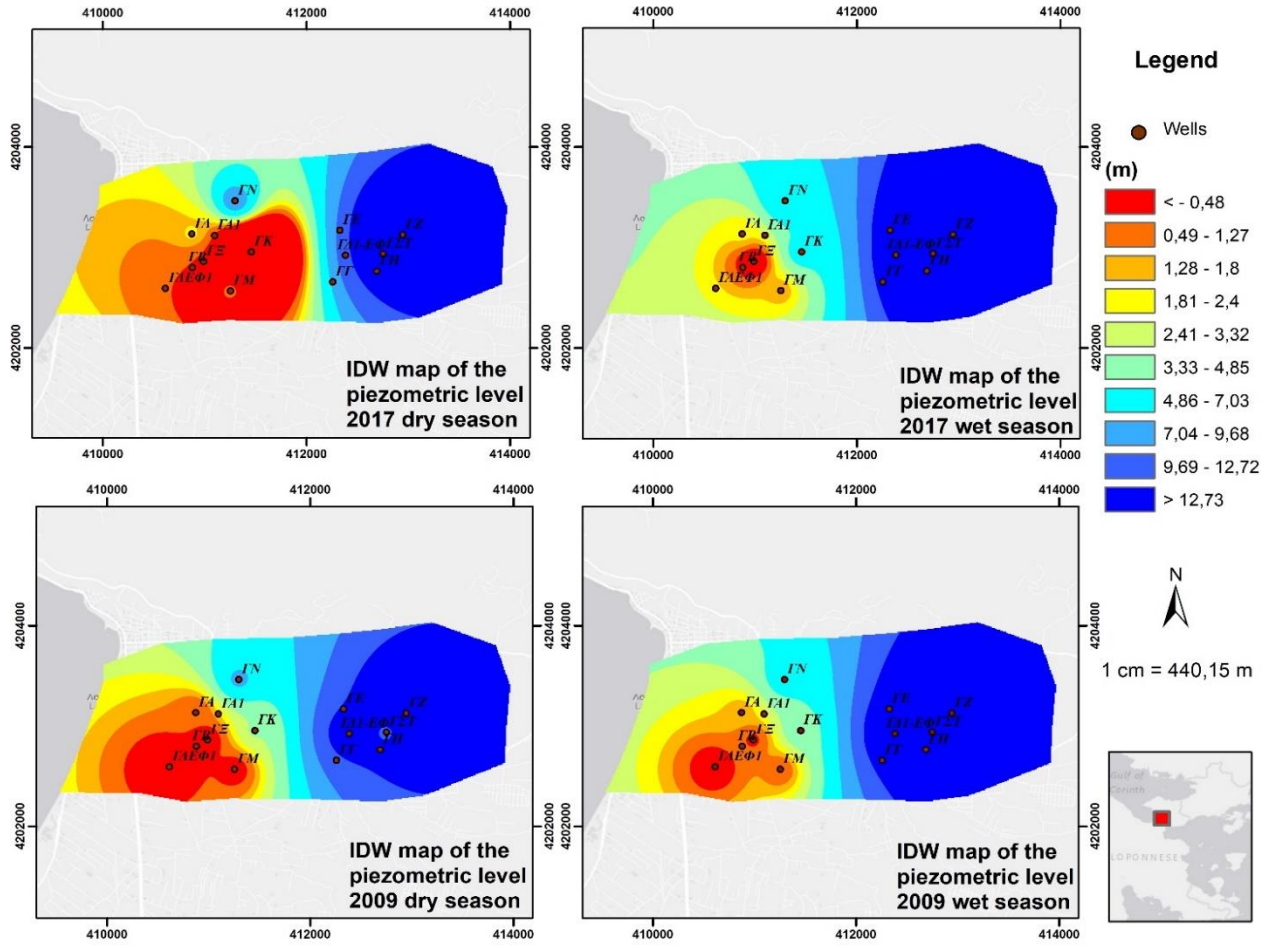

Figure 2. Piezometric maps of the alluvial porous aquifer of Loutraki during the dry (a), wet (b) season of 2017, and dry (c) and wet (d) season of 2009.

Acknowledgements

The authors would like to thank the Director of the Municipal Directorate for Water and Sewage of Loutraki – Agioi Theodoroi, Mr. Anastasios Mastrantonakis, and its technical staff for providing access to the Municipal boreholes and their help during water level measurements, as well as for providing existing groundwater level data.

References

Kounis, D., Vitoriou-Georgouli, A., 2003. Hydrogeological survey regarding the hydrological balance of the metallic aquifer of Loutraki area. Institute of Geology and Mineral Exploration (IGME). Unpublished Technical Report, Athens (in Greek).

Pyrgaki, K., Argyraki, A., Kelepertzis, E., Paraskevopoulou, V., Botsou, F., Dassenakis, E., Skourtsos, E., 2016. Occurrence of hexavalent chromium in the ophiolite related aquifers of Loutraki and Schinos areas. Bulletin of the Geological Society of Greece 50, 2261-2270.

Stamatis, G., Voudouris, K., 2000. Delineation of protection zones according to hydrogeological criteria: the case study of Loutraki alluvial aquifer. Digital Library of Theophrastus, Mineral Wealth Journal 116, 13-36 (in Greek).

Tiwari, A.K., Nota, N., Marchionatti, F., De Maio, M., 2017. Groundwater-level risk assessment by using statistical and geographic information system (GIS) techniques: a case study in the Aosta Valley region, Italy. Geomatics, Natural Hazards and Risk 8(2), 1396-1406.

15th International Congress of the Geological Society of Greece
Athens, 22-24 May, 2019 | Harokopio University of Athens, Greece
Bulletin of the Geological Society of Greece, Sp. Pub. 7 Ext. Abs. GSG2019-231

Environmental Impact of Mn Mining Wastes on the Accumulation of Potential Hazardous Elements in Soil and Crop Grains in Western Drama Plain, Macedonia, Northern Greece

E. Sofianska[1], K. Michailidis[1]

(1) Hellenic Survey of Geology and Mineral Exploration, 1 Sp. Louis st., 13677 Acharnes, Athens, Greece, esofianska@igme.gr

Chronic exposure of humans to a contaminated terrestrial ecosystem is a matter of general health concern (Adriano, 2001). Potential hazardous elements (PHEs) represent a serious threat to the environment in general, and can have adverse effects on plants, animals and humans (Alloway, 2005; Kabata-Pendias and Mukherjee, 2007; Abreu *et al.*, 2014).

Active or abandoned mining areas can be significant sources of PHEs contamination for the surrounding areas, including agricultural land (*e.g.*, Navarro *et al*., 2008). Specifically, excessive accumulation of PHEs in cultivated topsoil (0-20cm) around mining areas, results in their elevated uptake by food crops, thus posing great concern because of potential human health risk, at least to local inhabitants, via the food chain (*e.g.*, Zhuang *et al.*, 2009). Therefore, in recent years increasing attention has been paid to the issue of excessively high levels of PHEs in agricultural soil, near mining areas (*e.g.*, Hua *et al.*, 2018), and the transfer and accumulation of PHEs in the soil-plant system became a popular research topic (*e.g.*, Wang *et al*., 2017).

The present study was conducted in the western part of Drama plain (WDP) of Macedonia, Northern Greece, at an effort to assess the potential human health risk via the dietary route, probably coming from toxic PHEs dispersed from an abandoned Mn mine. The results are expected to raise awareness among the public on the safety of consuming food products grown at particular sites of WDP. Mining and mineral processing activities at the well-known 25km Kato Nevrokopi Mn mine of Drama district (an abandoned mine since 1994), have generated enormous piles of mine wastes (tailings, low grade ore, ore concentrate) deposited within the Xiropotamos stream valley, without any safety measures for the environment. Their erosion and downstream transport by the Xiropotamos stream resulted in the dispersion of the mine wastes and their deposition on the land of WDP. Thus, around the stream, the alluvial soil has attained a black colour due to mixing with the mine wastes (Sofianska, 2013). WDP constitutes an agricultural area producing mainly cereals. The corn–wheat rotation system is the dominant cropping pattern. Therefore, information about the concentration of PHEs in agricultural soil and cultivated food crops in WDP is very important for assessing health risk on the local population. The purpose of the study was to assess the concentration of PHEs and their spatial distribution in the soil of WDP. A control site, unaffected from mine wastes, was selected for comparison. The contamination levels of soil and the ability of plants to accumulate PHEs were estimated by means of the pollution load index (*PLI*) and the bio-accumulation factor (*BAF*), respectively.

Paired soil and plant (corn–wheat) grain samples were collected and analysed for Mn, Pb, Zn, Cu, Cd and As by inductively coupled plasma mass spectrometry (ICP-MS), after leaching with hot aqua regia, at the certified ACME Analytical Laboratories of Canada. The results of the research (Table 1) were as follows: PHEs concentrations in the WDP soil samples exceed significantly the average composition of agricultural soil worldwide. Locally, the concentrations of all analysed PHEs exceed soil quality standards (Kabata-Pendias, 2011). The reported PHEs are hosted in the Mn mine ore minerals, and were also found in the WDP soil samples (Sofianska, 2013). Spatially, the higher PHEs concentrations were found on the agricultural land along both sides of the Xiropotamos stream, and their levels in soil generally decreased with distance from the stream. The concentration trend of PHEs (average values) in the studied soil samples is Mn>Pb>Zn>As>Cu>Cd. Average values of *PLI*, calculated on the basis of the maximum permissible limits for agricultural soil (Chiroma *et al*., 2014), follow the order Mn>As>Pb>Cd>Zn>Cu. Based on *PLI* values, soil in the study area is on average characterised as very strongly contaminated by Cu, slightly polluted by Zn and Cd and very strongly polluted by Mn, Pb and As.

The concentration of PHEs (average values) in the wheat and corn grains follow the trend Zn>Mn>Cu>Cd>As>Pb and Zn>Mn>Cu>Pb>As>Cd, respectively. Among the studied PHEs, Cd concentration in wheat grains (4 sites out of 11) and Pb in corn grains (2 sites out of 9) were found to exceed the permissible limits, whereas all other PHEs in both types of grain were within the acceptable levels for food consumption as suggested by the World Health Organization (WHO). The concentration of PHEs in grain samples were affected by their concentrations in the soil substrate, as well as by the plant species, as recorded in other investigations (*e.g.*, Wang *et al.*, 2017). Specifically, the concentration of Mn, Pb, Zn, Cu, and As in crop grains increased with increasing PHEs concentrations in soil, whereas those of Cd have the opposite trend.

BAF values of food crops for the considered PHEs were below 1. They displayed the order Pb<Mn<As<Cd<Cu<Zn for wheat, and Pb<As<Mn<Cd<Cu<Zn for corn, and they tend to decrease rapidly with increasing PHEs in soil, a finding consistent with previous studies (*e.g.*, Wang *et al*., 2017). It is worth noting that *BAF* values are the highest in the control site, where the *PLI* are the lowest for the PHEs.

Paired wheat and corn plants grown in the same soil substrate displayed different accumulation and translocation patterns. Wheat plants have a higher ability to transfer soil Mn, Zn, Cu, Cd and As in their grains than corn, while corn grains accumulate higher amounts of Pb.

In conclusion, the WDP agricultural soil is strongly affected by PHEs due to the dispersion of the mine wastes from the

25km Mn mine. The reported results for the crop grains for all PHEs were found on average to be within the standards set by WHO. Given that there are land sites where Cd or Pb accumulation in food crops may pose a health risk to the local population through the consumption of wheat or corn, it is proposed either to take necessary measures as, for example, remediation of contaminated soil or to avoid planting these cereals in the particularly contaminated land sites.

Table 1. Basic statistical data of PHEs measured in the soil–crop system of western Drama plain.

Sample type/Parameter	Mn (mg/kg) mean/range	Pb (mg/kg) mean/range	Zn (mg/kg) mean/range	Cu (mg/kg) mean/range	Cd (mg/kg) mean/range	As (mg/kg) mean/range
Surface soil	25,180 730–13,013	844 45–1996	486 59–2140	92 13–153	6 1.5–27.5	224 10–1077
World agricultural soil[1]	488	27	70	38.9	0.41	6.83
Max.permissible limit for soil[1]	2000	100	300	100	3	20
Pollution load index (PLI)	12.6 0.35–65.1	8.44 0.45–20	1.62 0.20–17.3	0.92 0.13–1.53	1.99 0.17–9.17	11.2 0.50–53.9
Wheat grain composition	37.7 28–46	0.071 0.01–0.15	37.6 22.7–67.9	5.14 3.81–6.98	0.18 0.03–0.39	0.13 <0.1–0.3
Corn grain composition	5.78 4.00–11.0	0.31 0.05–1.09	22.9 18.9–33.3	1.59 1.25–2.66	0.011 <0.01–0.03	0.014 0.1–0.3
Max.permissible limit for food[2]	500	0.30	100	73	0.20	–
BAF[3] corn ($x10^{-4}$)	29.6 0.88–85.4	9.69 1.37–10.8	1211 240–3305	298 44–985	136 2.76–938	27.4 3.21–100
BAF wheat ($x10^{-4}$)	125 4.81–283	4.01 0.16–12.8	1725 564–3847	1096 352–1626	709 19.9–1950	30.5 3.54–154

[1]Kabata-Pendias, (2011); [2]Chiroma*et al*., (2014); [3]Bio-accumulation factor

References

Abreu, M.M., Bech, J., Carvalho, L.C., Santos, E., 2014. Potential hazardous elements fluxes from soil to plants and the food chain, in: Bini, C., Bech, J. (Eds.), PHES, Environment and Human Health. Springer, Dordrecht, 309–337.

Adriano, D., 2001. Trace elements in terrestrial environments: biogeochemistry, bioavailability and risks of metals. Springer-Verlag, New York, 867p.

Alloway, B., 2005. Bioavailability of elements in soil, in: Selinus O., Alloway B., Conteno J., Finkelman R., Fuge R., Lindh U., Smedley P. (Eds.), Essential of medical geology impacts of the natural environment on public health. Elsevier Inc., 347–372.

Chiroma, T.M., Ebewele, R.O., Hymore, F.K., 2014. Comparative assessment of heavy metals in soil, vegetables and urban grey water used for irrigation in Yola and Kano. International Refereed Journal of Engineering and Science 3, 1–9.

Hua, C., Yang, X, Liu, Y., Tan, X., Yang, Y., 2018. Spatial distributions, pollution assessment and qualified source apportionment of soil heavy metals in a typical mineral mining city in China. Sustainability 10, 3115-3124.

Kabata-Pendias, A., Mukherjee, A., 2007. Trace Elements from Soil to Human. Springer, Berlin, 550p.

Kabata-Pendias, A., 2011. Trace Elements in Soils and Plants. CRC Press Inc., Boca Raton, Florida, 505 p.

Navarro, M., Pérez-Sirvent, C., Martinez-Sanchez, M., Vidal, J., Tovar, P., Bech, J., 2008. Abandoned mine sites as a source of contamination by heavy metals: a case study in a semi-arid zone. Journal of Geochemical Exploration 96, 183–193.

Sofianska, E., 2013. Geochemical assessment of soil, water and plant contamination in the western Drama basin, associated with former Mn exploitation in the broader area. Experimental remediation of contaminated soils. PhD thesis Aristotle University of Thessaloniki, Greece, 453p.

Wang, S., Wu, W., Liu, F., Liao, R., Hu, Y., 2017. Accumulation of heavy metals in soil-crop systems: a review for wheat and corn. EnvironmentalScience and Pollution Research 24, 15209–15225.

Zhuang, P., McBride, M., Xia, H., Li, N., Li, Z., 2009. Health risk from heavy metals via consumption of food crops in the vicinity of Dabaoshan mine, South China. Science of the Total Environment 407, 1551–1561.

15th International Congress of the Geological Society of Greece
Athens, 22-24 May, 2019 | Harokopio University of Athens, Greece
Bulletin of the Geological Society of Greece, Sp. Pub. 7 Ext. Abs. GSG2019-253

Detection of Engineered, Incidental, and Natural Nanoparticles in Marine Waters in the Proximity of Islands

A. Gondikas[1], T. Kalampaliki[1], A. Dura[1], P.M. Chronakis[2], P. Nomikou[1], A. Godelitsas[1], S. Pergantis[2], Th. J. Mertzimekis[1], M. Hassellov[3]

(1) National and Kapodistrian University of Athens, School of Science, Faculty of Geology and Geoenvironment, Athens, Greece, agondikas@geol.uoa.gr
(2) University of Crete, Department of Chemistry, Heraklion, Greece
(3) Gothenburg University, Department of Marine Sciences, Gothenburg, Sweden

In the past few decades, there has been a strong drive towards understanding the potential environmental impact of nanotechnology (Wiesner *et.al.*, 2006), which has produced a vast number of publications studying the eco-toxicity and, to a lesser extent, the reactivity and transformation of nanoparticles (NPs) in the environment. Although size distributions and number concentrations of the NPs are of paramount importance in such studies, these parameters are often neglected (Baalousha *et.al.*, 2013). Experimental studies for the determination of real-world size distributions and number concentrations of nanoparticles and their dynamics are still scarce. Furthermore, scientific interest is focused on the potential environmental impact of engineered nanoparticles (ENPs), following their release from nano-enabled products; e.g., Ag, Cu, TiO_2 ENPs. In comparison, less attention is being given to incidental nanoparticles (INPs), i.e., nanoparticles that are unintentionally produced due to anthropogenic activities; e.g., plastic particles. In contrast, naturally occurring colloids (particles in the size range of 1 to 1000 nm) have been studied for decades. However, natural nanoparticles (NNPs), such as iron oxides, have been detected and characterised either as a few individual particles, or as part of the 'colloidal fraction' in natural samples. Therefore, there is a shortage of information on the abundance of ENPs, INPs, and NNPs. Identifying differences in their physicochemical characteristics would allow proper source appointment to nanoparticles, facilitate risk assessment and regulation of the nanotechnology industry, and improve our understanding of the role of nanoparticles in the global cycling of elements. Moreover, recent regulatory recommendations (2011/696/EU and EPA-HQ-OPPT-2010-0572) call for the need to characterise nanoparticles based on number concentrations and size distributions; a paradigm-shift away from the conventional mass-based evaluation of solid materials. As a result, the occurrence of natural and anthropogenic nanoparticles in the environment need to be re-evaluated on the basis of population dynamics, i.e., changes of particle number and size with time. The lack of standardised protocols for measuring these properties is weakening regulatory efforts and has created an uneven playing field for nanoparticle manufacturers and processors, hindering investments in research and development. It is, therefore, necessary to develop measurement protocols that will simplify the regulatory field, and thus unlock investment spending for nanoparticles manufacturers, which in turn will help create job opportunities, support the production of environmentally responsible nano-enabled products, and contribute towards the economic growth of the EU.

Nanometrology is critical for enforcing regulations on nano-enabled products and for determining their environmental impact. Environmental nanometrology unavoidably deals with materials of poorly-defined properties and in complex matrices (von der Kammer *et.al.*, 2012), in which nanoparticles may undergo significant transformations (Louie *et.al.*, 2014). It is, therefore, imperative to develop appropriate sampling and analysis protocols to understand the environmental dynamics of these materials. Stabilising agents and separation techniques may be necessary to prevent artefacts, such as aggregation, dissolution, and loss of material. Furthermore, analysis of nanoparticles in an environmental matrix is a challenging task for two reasons: first, the complexity of the matrix may hinder the performance of analytical equipment and second, there are no straightforward guidelines to distinguish ENPs from NNPs or INPs (Wagner *et.al.*, 2014).

In order to differentiate between ENPs, NNPs, and INPs, two approaches can be followed. First, analysis of the bulk solid material and use of specific handles (such as elemental ratios, crystal phases, isotope ratios, etc.) to identify the material in question. This approach requires the presence of significantly high amounts of nanoparticles in the sample. Second, nanometrology offers information specifically for nanoparticles, however it is hindered by the complexity of sample handling. Recent technological advancements have drastically improved nanometrology. For example, efforts to minimise artefacts for electron microscopy analysis (e.g., by using stabilisers), the development of single-particle inductively coupled plasma – mass spectrometry (spICPMS) (Pace *et.al.*, 2011), and single particle chronoamperometry (Tschulik *et.al.*, 2013) for the determination of particle number concentrations and size distributions. These analytical techniques, although not yet developed to their full potential, make it possible to measure composition, number concentrations, and size distributions of nanoparticles suspensions. In combination with appropriate sampling and sample treatment methods, these techniques will be applied to the characterisation of nanoparticles in a real-world environment in this work. Such information would be essential for (1) the regulation of ENPs, (2) studying the environmental implications of ENPs and INPs, and (3) understanding the role of NNPs in the global cycle of elements and pollutants.

The overarching goal of this project is to compare the physicochemical characteristics and population dynamics of engineered, incidental, and natural nanoparticles in the marine environment, in the proximity of an island. Marine waters and sediments are hosts to several potential sources of nanoparticles, both anthropogenic and natural. A few examples are the release of nanoparticles from ship paints, wastewater, food, sunscreens, and cosmetics, the precipitation of particles from volcanic and hydrothermal vent activity, and the deposition of particulate fuel combustion by-products and

atmospheric particles on the water column. Although several nano-enabled products for use in the marine environment are already commercialised (e.g., ship paints), information of the fate of nanoparticles in marine water systems is limited. The primary objective of this research project is to produce analytical handles for detecting and characterising ENPs, INPs, and NNPs, while exploring the applicability of advanced environmental nanometrology techniques in marine water systems. It is aimed to (1) optimise sampling techniques for the marine environment, (2) develop methods of analysis, which will tackle difficulties posed by the characteristics of the system (e.g., high salinity, low concentration), (3) measure element-specific nanoparticle populations, (4) identify key descriptors for differentiating nanoparticles based on their source, taking advantage of seasonal variations of these sources, and (5) integrate the gathered information into large-scale databases that will facilitate risk assessment of ENPs. For the purposes of this project, a unique location, the Island of Santorini, Greece, has been identified, which hosts an unusually large variety of sources for ENPs, INPs, and NNPs in a partially enclosed system.

Santorini is part of the active Aegean Volcanic Arc in the South Aegean Sea (Megalovassilis *et.al.*, 2015), a volcano-tectonic line along the subduction zone between the European and African plates. It is the top part of a volcano that is submerged under water and its circular shape forms a natural barrier that partially isolates the waters of the volcanic Caldera from the rest of the Aegean Sea (Nomikou *et.al.*, 2014); there exist only three shallow openings on the North-West and South-West parts of the Caldera with a maximum depth of 390 m. Its unique seabed morphology is likely to act as a natural trap for anthropogenic and natural nanoparticles. In addition, the island has a relatively small area (approx. 20 km^2), but receives an excessive number of tourists during the summer season. Tourist arrivals by cruise ships, ferry boats, or airplanes lie in the range of 1,500,000 – 2,000,000 per tourist season (April – October), while permanent population on the island is less than 25,000 people. The drastic population increase during the tourist season offers an opportunity to study natural sources of nanoparticles, prior to the tourist season, and anthropogenic sources during the tourist season.

Environmental concentrations of nanoparticles are currently being modelled based on information of their production and use. However, these models have not been validated due to the lack of real-world environmental measurements (Nowack *et.al.*, 2015). Such measurements are scarce and typically focus on one element of interest. This work aspires to set a standard for detecting nanoparticles in natural waters and applying state-of-the-art environmental nanometrology techniques for measuring time-resolved number concentrations and size distributions of these materials. High-frequency recorded CTD data in the water column over the Santorini caldera will be used to create depth profiles of oceanographic properties such as conductivity, temperature and salinity. These data will be combined with NP measurements to determine the particle population dynamics, i.e., changes of number and size over time and space.

Acknowledgements

This project has received funding from the Hellenic Foundation for Research and Innovation (HFRI) and the General Secretariat for Research and Technology (GSRT), under grant agreement No 1317.

References

Baalousha, M., Lead, J., 2013. Nanoparticle dispersity in toxicology. Nature Nanotechnology 8, 308–309.

Louie, S., Ma, R., Lowry, G.V., 2014. Transformations of nanomaterials in the environment. Frontiers of Nanoscience 7, 55-87.

Megalovassilis, P., Godelitsas, A., 2015. Hydrothermal influence on nearshore sediments of Kos Island, Aegean Sea. Geo-Marine Letters 35, 77−89.

Nomikou, P., Parks, M.M., Papanikolaou, D., Pyle, D.M., Mather, T.A., Carey, S., Watts, A.B., Paulatto, M., Kalnins, M.L.,.Livanos, I., Bejelou, K., Simou, E., Perros, I., 2014. The emergence and growth of a submarine volcano: The Kameni islands, Santorini (Greece). Journal of Geophysical Research 1-2, 8-18.

Nowack, B., Baalousha, M., Bornhöft, N., Chaudhry, O., Cornelis, G., Cotterill, J., Gondikas,A., Hassellöv, M., Lead, J., Mitrano, D.M., von der Kammer, F., Wontner-Smith. T., 2015. Progress towards the validation of modeled environmental concentrations of engineered nanomaterials by analytical measurements. Environmental Science: Nano 2(5), 421-428.

Pace, H.E., Rogers, N.J., Jarolimek, C., Coleman, V.A., Higgins, C.P., Ranville, J.F., 2011. Determining transport efficiency for the purpose of counting and sizing nanoparticles via single particle inductively coupled plasma mass spectrometry. Analytical Chemistry 83(24), 9361–9369.

Tschulik, K., Haddou, B., Omanovic, D., Rees, N.V., Compton, R.G., 2013. Coulometric sizing of nanoparticles. Cathodic and anodic impact experiments open two independent routes to electrochemical sizing of Fe_3O_4 nanoparticles. Nano Research 6, 836–841.

von der Kammer, F., Ferguson, P.L., Holden, P.A., Masion, A., Rogers, K.R., Klaine, S.J., Koelmans, A.A., Horne, N., Unrine, J.M., 2012. Analysis of engineered nanomaterials in complex samples. Environmental Toxicology and Chemistry 31(1), 33−49.

Wagner, S., Gondikas, A., Neubauer, E., Hofmann, T., von der Kammer, F., 2014. Spot the difference: Engineered and natural nanoparticles in the environment—Release, behavior, and fate. Angewandte Chemie International Edition 53, 12398–12419.

Wiesner, M., Lowry, G.V., Alvarez, P., Dionysiou, D., Biswas, P., 2006. Assessing the Risks of Manufactured Nanomaterials. Environmental Science & Technology 40(14), 4336–4345.

15th International Congress of the Geological Society of Greece
Athens, 22-24 May, 2019 | Harokopio University of Athens, Greece
Bulletin of the Geological Society of Greece, Sp. Pub. 7 Ext. Abs. GSG2019-255

Variability and Enrichment of Metals in Soils and Sediments along Karvounoskala Stream (NE Chalkidiki, Northern Greece)

A. Karetou[1], M. Vavelidis[1], K. Giouri[1], N. Kantiranis[1], L. Papadopoulou[1], C.L. Stergiou[1]

(1) Department of Mineralogy-Petrology-Economic Geology, School of Geology, Aristotle University of Thessaloniki, 54124 Thessaloniki, Greece, akaretou@geo.auth.gr

The occurrence of metals in the environment originates from various sources including natural processes, as well as anthropogenic activities. Geochemical ratios of metals in soils are based on the chemical and mineralogical associations in the natural environment. Metals mostly adsorb and accumulate in sediments than water or suspended solids. Hence, sediments act as a metals sink in the aquatic environments (Salomons *et al*., 1984; Zhang *et al.*, 2016).

The present study focuses on element (As, Cd, Cr, Cu, Ni, Pb, Sb, Zn) enrichment along the Karvounoskala stream, which is located near Stratoni village and discharges in Ierissos Gulf. The wider area has a long history concerning the mining activities of Greece (Chalkidiki Peninsula). Geologically, the study area belongs to the Kerdylia formation, part of the Serbomacedonian massif. In this region, the Stratoni granodiorite intrudes marbles, biotite- and hornblende-biotite-gneisses and amphibolites, which are overlain by alluvial deposits (Kockel *et al.*, 1977; Vavelidis *et al*., 1983).

Nine samples were in total collected downstream Karvounoskala stream as follows: 5 soils and 4 sediments. After they were transferred to the laboratory, the samples were dried at 50˚C for 48h in order to remove the moisture. The whole soil and sediment samples were pulverised in a mortar to achieve a homogeneous sample of particle size <0.063 mm. Total element concentrations were determined by Inductively Coupled Plasma-Atomic Emission Spectroscopy (ICP-AES) and compared to the global average composition of shales (Turekian *et al*., 1961). Element enrichment was assessed by using the following geochemical indices: enrichment factor (EF), contamination factor (Cf), geo-accumulation index (I_{geo}) and contamination degree (Cd) (Salomons *et al*., 1984; Müller, 1969; Hakanson *et al*., 1980; Sakan *et al*., 2009). For the calculation of these indices, the concentration of each studied element is normalised against a reference element. In this study, Al was used as a reference element, since it revealed low variability. Total Al content in soil and sediment samples was determined by X-Ray Fluorescence (XRF).

According to the results of this study, element concentrations in soil followed the order Pb >Zn > As > Cu > Cr > Sb > Ni > Cd. Geochemical maps were plotted within a GIS environment. The map presenting the variation of Pb concentrations in the studied samples is illustrated in Fig. 1.

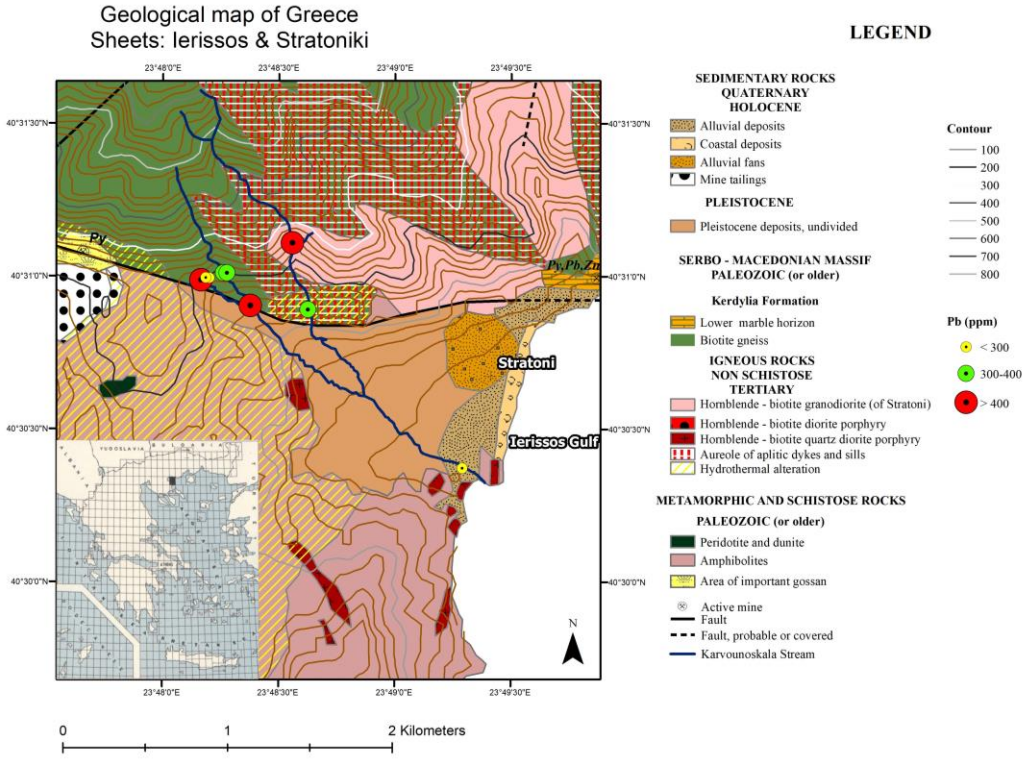

Figure 1. Variation of Pb concentrations in the studied samples along Karvounosklala stream.

Concerning the EF values, Cd revealed the highest (43.96), followed by Pb (32.72), Sb (12.85), As (11.39), Zn (2.55), Cu (1.66), Ni (0.38) and Cr (0.28). According to these values, soil samples revealed very strong enrichment in Pb and Zn, strong enrichment in Sb and As and minor enrichment in Zn, Cu, Ni and Cr. I_{geo} values indicate that in the soil

samples Cd levels (4.47-4.85) range from heavily to extremely contaminated, and Pb (0.14-4.43) ranges from uncontaminated-moderately contaminated to heavily-extremely contaminated. A wider range is exhibited by Sb levels (2.15-3.08) since the soils are characterised from moderately-heavily to heavily contaminated. For As ([-0.96]-2.90) and Zn ([-1.32]-0.79) the soils are practically uncontaminated to moderately-heavily contaminated, and for Zn ([-1,32]-0,79) and Cu ([-1.91]-0.17) the soils are practically uncontaminated to uncontaminated-moderately contaminated. The Cr and Ni levels are below 0, demonstrating no contamination. Contamination degree (Cd) values indicate very high contamination for Cd, Pb, Sb and As, while low contamination is indicated for Zn, Cu, Cr and Ni (Fig. 2).

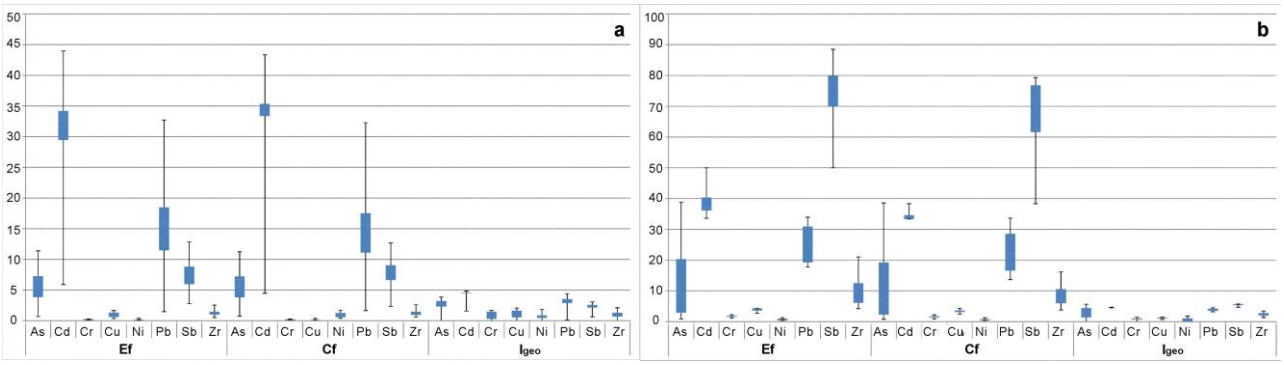

Figure 2. Variation of the geochemical indices, as they were calculated for (a) soil and (b) sediment samples.

Regarding the sediment samples, their element content presented minor differentiation with respect to the soil samples, following the order Zn > Pb > As > Cu > Cr > Sb > Ni > Cd. The highest EF value was recorded at 88.5 for Sb, followed by As (38.8), Cd (50.0), Pb (33.9), Zn (21.1), Cu (4.30), Cr (2.22) and Ni (1.27). Therefore, sediment samples exhibited extremely strong enrichment in Sb, very strong enrichment in As, Cd and Pb and strong enrichment in Zn. Moderate enrichment was revealed for Cu, while the sediments had a minor enrichment in Ni and Cr. I_{geo} values in the sediments presented similar distribution with the respective ones in the soils, indicating that sediment samples are heavily to extremely contaminated with regard to Sb (4.68-5.72), Cd (4.47-4.68) and Pb (3.19-4.49). A wider range is exhibited by As ([-0.96]-4.68), since the samples are characterised from practically uncontaminated to moderately contaminated. Moreover, Zn (1.34-3.43), Cu (0.70-1.51) and Cr ([-0.85]-0.55) levels range from moderately to heavily contaminated, uncontaminated-moderately to moderately contaminated and uncontaminated to uncontaminated-moderately contaminated, respectively. The Ni levels are below 0, indicating no contamination. Contamination degree (Cd) values suggest that the highest contamination in sediments is indicated by Sb, Cd, Pb, As and Zn. Moderate contamination is indicated by Cu, while signs of low contamination were shown by Cr and Ni (Fig. 2).

In general, soil and sediment compositions appear rather uniform. This is expected, since both are derived from the weathering of the rocks in the study area. The studied elements originate from the weathering of the surrounding geological formations, as well as from the element occurrences that they host. All samples are partly enriched in Sb, Pb, As, Cd and Zn due to the presence of polymetallic sulphides, Fe-Mn oxides and slags in the soils and sediments. Traces of Cr and Ni are attributed to amphibolite occurrences (Karetou *et al.*, 2018).

Acknowledgements

The first author (A. Karetou) would like to thank Hellas Gold S.A. for performing the chemical analyses of the samples.

References

Hakanson, L., 1980. An ecological risk index for aquatic pollution control. A sedimentological approach. Water research 14, 975-1001.

Karetou, A., Vavelidis, M., Giouri, K., Kantiranis, N., Papadopoulou. L., 2018. Mineralogical composition and grain size distribution in samples along Karvounoskala stream (NE Chalkidiki, Northern Greece), in: Neubauer F. *et al*. (Eds.), Abstract volume of the XXI International Congress of the Carpathian Balkan Geological Association (CBGA), Salzburg, September 10-13. Geologica Balcanica, p. 177.

Kockel, F., Mollat, H., Walther H., 1977. Erlauterungen zur Geologischen Karte der Chalkidiki und angrenzender Gebiete 1:100.000 (Nord-Griechenland). Bundesanstalt fur Geowissenschaften und Rohstoffe.

Müller, G., 1969. Index of geoaccumulation in sediments of the Rhine River. GeoJournal 2, 108–118.

Sakan, S.M., Djordjevi´c, D.S., Manojlovi´c, D.D., Polic, P.S., 2009. Assessment of heavy metal pollutants accumulation in the Tisza river sediments. Journal of Environmental Management 90, 3382–3390.

Salomons, W., Förstner, U., 1984. Metals in the Hydrocycle. Springer, Berlin, Germany, 349 p.

Turekian, K.K., Wedepohl, K.H., 1961. Distribution of the elements in some major units of the Earth's crust. Geological Society of America Bulletin 72, 175-192.

Vavelidis, M., Pernicka, E., Wagner, G., 1983. Studies in Pb-Ag and Au occurrences in northeastern Chalkidiki (Greece), European Journal of Mineralogy 61, 212-213.

Zhang, Z., Juying, L., Mamat, Z., Qing, F.Y., 2016. Sources identification and pollution evaluation of heavy metals in the surface sediments of Bortala River, Northwest China. Ecotoxicology and Environmental Safety 126, 94–101.

15th International Congress of the Geological Society of Greece
Athens, 22-24 May, 2019 | Harokopio University of Athens, Greece
Bulletin of the Geological Society of Greece, Sp. Pub. 7 Ext. Abs. GSG2019-272

Single Particle Electrochemistry for Detecting Nanoparticles in Water Environments

Th. Kalampaliki[1], A. Godelitsas[1], P. Nomikou[1], A. Gondikas[1]

(1) National and Kapodistrian University of Athens, Scholl of Science, Faculty of Geology and Geoenvironment, Athens, Greece, tkalampa@gmail.com.

In the past few decades scientific interest is focused on the potential impact of nanoparticles (NPs) in human health and the environment. Naturally occurring NPs are present throughout the Earth's crust including oceans, lakes, rivers, groundwater and hydrothermal vents. NPs are also formed in the lithosphere, which is comprised of rocks, soils, magma or lava and the biosphere, which covers micro-organisms and higher organisms, including humans (Hochella *et al.*, 2015). During a single eruption event more than 30 million tonnes of ash, may be released to a height of tens of kilometres and reach the stratosphere, where volcanic ash NPs may spread worldwide and affect multiple areas for years (Ermolin *et al.*, 2018).

Further, the environment contains the so called incidental nanoparticles, *i.e*., those that are unintentionally produced from human activities (*e.g*., through friction and combustion processes). These particles are the by-products of human activities and generally have varying sizes and shapes. Many of the processes that generate incidental NPs are frequent activities, such as diesel engines or large-scale mining. Also, wear and corrosion processes release particles and molecular precursors to air and water, which can produce incidental NPs (Westerhoff *et al*., 2018).

Engineered NPs, on the other hand, are a relatively new type of NPs and recent concerns have been placed that they may induce adverse environmental and human health effects. They are specifically designed and synthesised in order to be used as ingredients in commercial goods. A few examples of products containing NPs are ship paints, food, sunscreens, and cosmetics.

In aquatic systems, NPs may undergo various geochemical and biological processes and may negatively impact aquatic ecosystems (Zhao *et al.*, 2013). It is, therefore, essential to understand and investigate the fate and behaviour of NPs in the marine environment and examine their biological effects on organisms. The fate and the behaviour of NPs in sea water depends on physicochemical characteristics, such as salinity, composition, organic matter, *etc*. Microscopic and spectroscopic techniques are often used to characterise NPs. The particle size and shape, aggregation/agglomeration state, surface chemistry, chemical composition, and dissolution state are examples of key NP physicochemical characteristics.

Several state-of-the-art analytical techniques, namely, transmission electron microscopy (TEM), atomic force microscopy (AFM), and dynamic light scattering (DLS), are widely applied to characterise NPs. The advanced microscopic methods (*e.g*., TEM, AFM, *etc*.) can generally provide accurate dimensions of NPs that are free from artefacts, but these techniques suffer from low analysis speed and high operating costs. Light scattering is strongly influenced by particle radius, aggregates contaminants (*e.g*., dust) that might mask the signal of NPs (Solokov *et al.*, 2017). Therefore, there is a necessity for producing analytical handles for detecting and characterising engineering and natural NPs, while exploring the applicability of advanced environmental nanometrology techniques in marine water systems.

Here, we present a new detection strategy, based on the Faradaic charge transfer when NPs impact an electrode (Tschulik *et al.*, 2013). The direct detection of particle collisions at electrodes is a recent field and presents several competitive advantages over the state-of-the-art methods. It is characterised by high sensitivity, high frequency of measurements, high selectivity, ability to measure non-opaque samples, and has the potential to be developed into a portable device for conducting direct, spatially resolved measurements.

In this technique, a microelectrode is kept under suitable electrochemical control and is introduced into a suspension containing nanoparticles. When a nanoparticle arrives at the electrode due to Brownian motion, electron tunnelling between the particle and the electrode occurs. Upon contact and depending on the applied potential, an electrochemical reaction is triggered: the nanoparticle can be electrochemically reduced or oxidised, or can mediate (catalyse) a charge transfer process giving a transient current that appears as a 'spike' or a 'step' in the chronoamperometric scan (Fig. 1).

The number of atoms in the nanoparticle can be derived from the detected electrical charge using Faraday's 1st Law (the amount of charge passed through an electrode during an impact is determined by its size). The charge (Q) resulting from the oxidation or reduction of a particle impacting the electrode can be subsequently calculated from the area under the current intensity signal:

$$Q = \int I \mathrm{d}t = ezN$$

where I is the current, t the spike duration, e the electronic charge, z the average number of exchanged electrons per reduced or oxidised formula unit of the NP and N the number of reduced NP units.

Under the assumption of spherical geometry, the effective radius of the particle can be ascertained:

$$r = \sqrt[3]{\frac{3MQ}{4\pi e N_A z \rho}}$$

where r is the radius of the nanoparticle, M is the molar mass, F is the Faraday constant, z is the number of electrons

transferred per atom in the particle, and ρ is the density of the nanoparticle. Time-resolved measurements of the electrochemical signal provide information about the rate of agglomeration and/or dissolution of NPs (Tschulik *et al.*, 2013; Katelhon *et al.*, 2016).

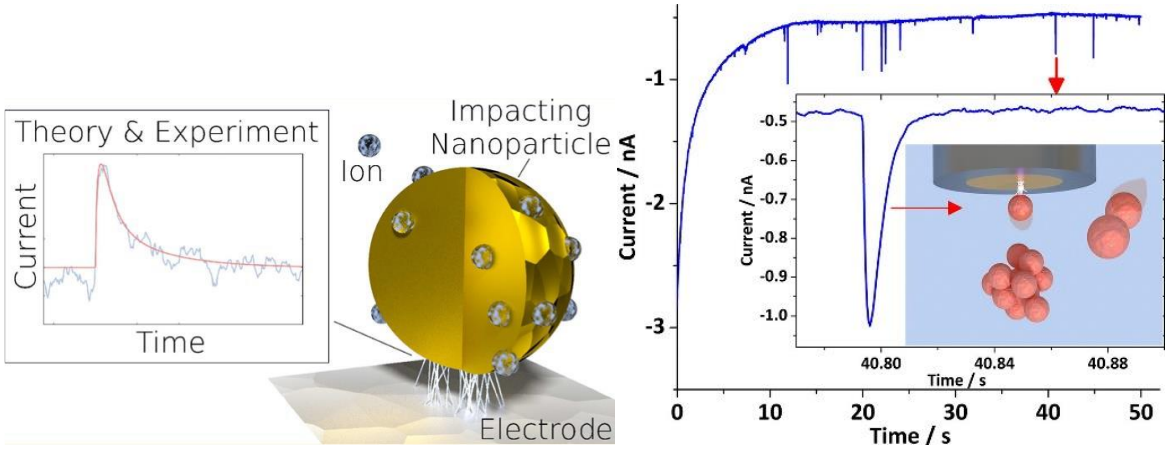

Figure 1. Schematic of an electron tunnelling between particle and electrode during a 'nano-impact' (left); A chronoamperogram recorded at a gold microelectrode with dispersed NPs at an applied potential of -0.4V (right) (Katelhon *et al.*, 2016).

Acknowledgements

This project has received funding from the Hellenic Foundation for Research and Innovation (HFRI) and the General Secretariat for Research and Technology (GSRT), under grant agreement No 1317.

References

Ermolin, M.S., Fetodov, P.S., Malik, N.A., Karandashev, V.K., 2018. Nanoparticles of volcanic ash as a carrier for toxic elements on the global scale. Chemosphere 200, 16-22.

Hochella, M.F., Spencer, M.G., Jones, K.L., 2015, Nanotechnology: nature's gift or scientists' brainchild? Environmental Science Nano 2, 114-119.

Katelhon, E., Feng, A., Cheng, W., Eloul, S., Bachelor-McAuley, C., Compton, R.G., 2016. Understanding nano-impact current spikes: Electrochemical doping of impacting nanoparticles. The Journal of Physical Chemistry 120, 17029–17034.

Solokov, S.V., Eloul, S., Katelhon, E., Bachelor-McAuley, C., Compton R.G., 2017. Electrode-particle impacts: a users guide. Physical Chemistry Chemical Physics 19(1), 28-43.

Tschulik, K., Haddou, B., Omanovic, D., Rees, N.V., Compton, R.G., 2013. Coulometric sizing of nanoparticles. Cathodic and anodic impact experiments open two independent routes to electrochemical sizing of Fe_3O_4 nanoparticles. Nano Research 6, 836–841.

Westerhoff, P., Atkinson, A., Fortner, J., Wong, M.S., Zimmerman, J., Gardea-Torresdey, J., Ranville, J., Herckes, P., 2018. Low risk posed by engineered and incidental nanoparticles in drinking water. Nature Nanotechnology 13, 661-669.

Zhao, J., Wang, Z., Dai, Y., Xing, B., 2013. Mitigation of CuO nanoparticle-induced bacterial membrane damage by dissolved organic matter. Water Research. 47, 4169–4178.

15th International Congress of the Geological Society of Greece
Athens, 22-24 May, 2019 | Harokopio University of Athens, Greece
Bulletin of the Geological Society of Greece, Sp. Pub. 7 Ext. Abs. GSG2019-274

Combining Geochemical Mapping with Mineralogical and Chemical Data for Improved Interpretation of Elemental Mobility in the Urban Environment

A. Argyraki[1], E. Kelepertzis[1]

(1) Department of Geology and Geoenvironment, National and Kapodistrian University of Athens, Panepistimiopolis Zographou, 15784, Athens, Greece, argyraki@geol.uoa.gr

The environmental impact of urban development is a major concern of our times and the management of contaminated urban areas is a significant societal challenge at global scale with legal, financial and possible human health implications as over 50% of the global population resides in cities. Potentially harmful elements (PHEs) including trace metals and metalloids are always high in the agenda of urban environmental studies because of: a) their multiple industrial, domestic, medical and technological applications that have led to their wide distribution in urban environments, and b) their non-degradable character. An increasing body of scientific evidence suggests that measuring the total concentration of PHEs in soil and other environmental compartments in big cities does not provide an effective basis for the evaluation of potential adverse effects to humans and the environment, and tends to overestimate the risks and induce unnecessary remediation costs (Cipullo *et al*., 2018 and references therein). Rather, the elemental mobility and bioaccessibility of the contaminants have a central role in understanding human exposure, as the chemical structure of PHEs and associated mineral phases affect their solubility in physiological fluids and influence the absorption capacity of the human body. Risk-based environmental management decisions can also be impaired due to the fact that exposure to contaminant mixtures is often overlooked and receptor population vulnerabilities that can be profound in big cities are not taken into account. Here, we present results from a series of studies concerning the urban environment of Athens (Greece) with the aim to demonstrate how geochemical mapping at different spatial scales, combined with chemical methods and mineralogy can provide insights for better interpretation of PHEs environmental mobility. The ultimate aim is to contribute to improved planning and management of the urban development of Athens, the capital city of Greece with a population of over 3 million people.

Initially, a geochemical baseline study of surface soil, based on a systematic sampling survey covering the Greater Athens and Piraeus area, was implemented (Argyraki and Kelepertzis, 2014). The near total concentrations of the major elements Fe, Al, K and Ca, and PHEs Ni, Cr, Co, Mn, As, Pb, Zn, Cu, Cd, Sb and Sn were determined. Principle Component Analysis and Cluster Analysis, combined with analysis of soil heterogeneity and spatial variability, were implemented in order to distinguish the sources of elements and their classification as geogenic or anthropogenic. The geochemical maps, showing the overall spatial distribution patterns of elemental concentrations, were plotted using a GIS and the Inverse Distance Weighted (IDW) interpolation method with a power of 2. Geographically Weighted Regression was used to evaluate the spatial correlations between the studied elements. It was found that the major factor controlling variability of the chemical composition of surface soil is the bedrock chemistry, resulting in a significant enrichment in concentrations of Ni, Cr, Co and possibly As. Anthropogenic influences are also significant, controlling elements that are typical of human activities, i.e., Pb, Zn, Cu, Cd, Sb, and Sn. The highest concentrations of the classical urban contaminants are observed in the surface soil from roadside verges and in the older parts of the city, as well as the densely populated areas. Spatial distribution patterns of PHEs demonstrated an increase in concentrations of the anthropogenic PHEs towards the city core (Fig. 1). The *aqua regia* extracted (pseudo-total), potentially phytoavailable, mobilisable, orally bioaccessible and reactive pools of PHEs were subsequently operationally defined by applying adequate chemical reagents on 45 urban top-soil samples (Kelepertzis and Argyraki, 2015). Despite the elevated pseudototal concentrations of geogenic elements (Ni, Cr, As and Co) in Athens soil, their availability is limited because of their sequestration in stable mineral phases. The pseudototal content of the anthropogenic group of elements (Pb, Zn, Cu, Cd) is the predominant factor controlling their availability. An association between available fractions of this group of elements and amorphous Fe oxides has been observed based on detailed mineralogical analysis of soil grains by Scanning Electron Microscopy-Energy Dispersive Spectroscopy (SEM-EDS) (Fig. 2). The study of Pb isotopic ratios in selected soil and house dust samples indicated that Pb in Athens soil is a mixture of local soil background Pb with high $^{206}Pb/^{207}Pb$ ratios, and Pb derived from the re-suspension of particulates deposited from past vehicular exhaust emissions of leaded petrol with a low $^{206}Pb/^{207}Pb$ ratio (Kelepertzis *et al.*, 2016). House dust exhibits anthropogenic enrichment of vehicular traffic-related Pb, Zn and Cu in relation to the urban soil. Furthermore, anthropogenic PHEs in house dust were found to be associated with the magnetic fraction that is enriched in magnetite (Kelepertzis *et al.*, 2019). Examination of selected spherules (size >30 μm) by electron back scatter diffraction (EBSD) in a Field Emission SEM instrument produced pattern image quality maps that helped to verify the magnetite crystal phases, while the focused ion beam (FIB) technique confirmed the high-temperature industrial origin of the magnetite spheres (Fig. 3). Such spherical particles have also been identified in the exterior soil indicating that they are ubiquitous in the urban chemical environment of Athens. The similarity in the Pb isotope results and the microstructure of particles between the urban soil and the house dust material suggests that these two environmental sampling media share common industrial and traffic-related sources.

We conclude that combining data of geochemical mapping from micro- to macro-scale with chemical data and detailed mineralogical observations can provide invaluable information for further studies of exposure assessment and environmental management in urban areas.

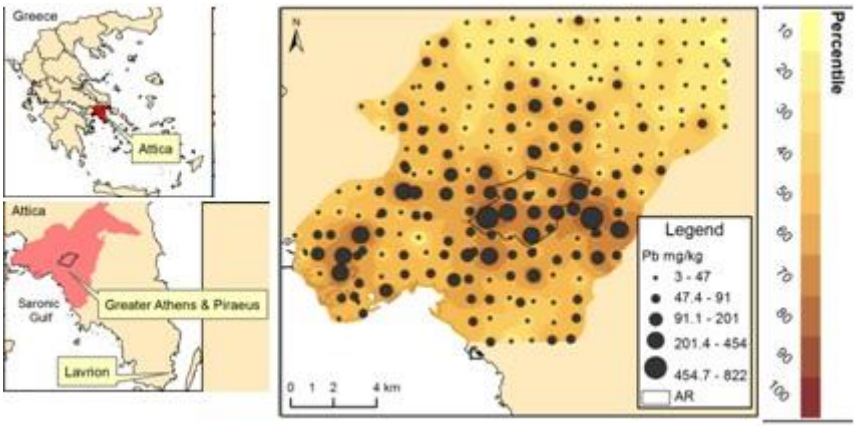

Figure 1. Lead distribution in Athens soil. AR denotes the centre of the city.

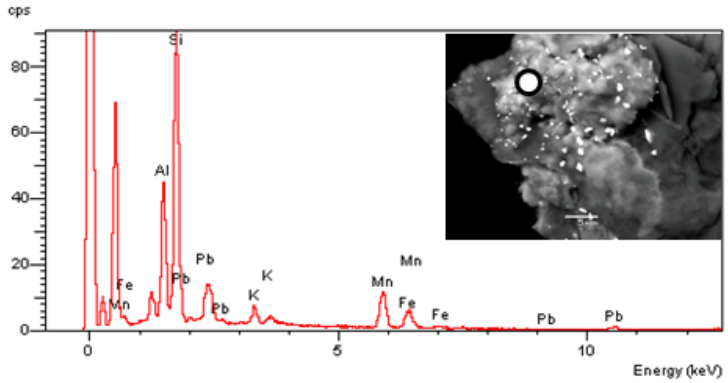

Figure 2. Microphotograph of PHE-bearing soil grain showing Mn-Fe oxide phase (bright) enriched in Pb and Sb.

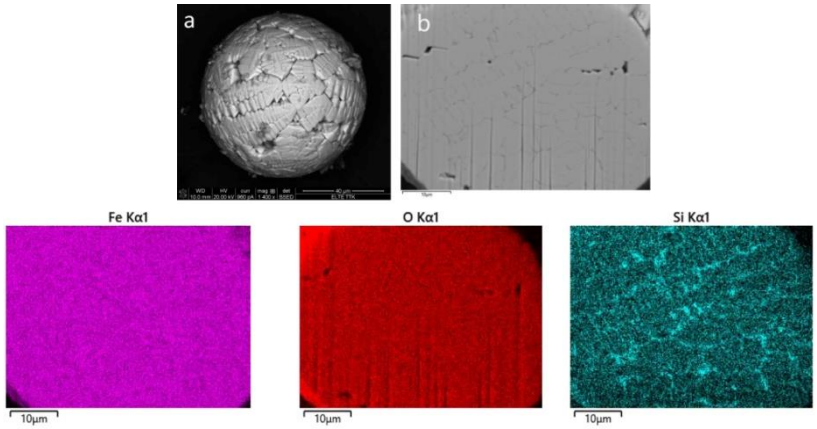

Figure 3. FIB-SEM images of an anthropogenic magnetite sphere in house dust and corresponding EDS elemental mapping.

Acknowledgements

We acknowledge the graduate and postgraduate students of the Department of Geology and Geoenvironment, NKUA, that have contributed to this research through their dissertation projects.

References

Argyraki, A., Kelepertzis, E., 2014. Urban soil geochemistry in Athens, Greece: The importance of local geology in controlling the distribution of potentially harmful trace elements. Science of The Total Environment 482–483, 366–377.

Cipullo, S., Prpich, G., Campo, P., Coulon, F., 2018. Assessing bioavailability of complex chemical mixtures in contaminated soils: Progress made and research needs. Science of the Total Environment 615, 708–723.

Kelepertzis, E., Argyraki, A., Botsou, F., Aidona, E., Szabo, A., Szabo, C., 2019. Tracking the occurrence of anthropogenic magnetic particles and potentially toxic elements (PTEs) in house dust using magnetic and geochemical analyses. Environmental Pollution 245, 909-920.

Kelepertzis, E., Komarek, M., Argyraki, A., Sillerova, H., 2016. Metal(loid) distribution and Pb isotopic signatures in the urban environment of Athens, Greece. Environmental Pollution 213, 420-431.

Kelepertzis, E., Argyraki, A., 2015. Geochemical associations for evaluating the availability of potentially harmful elements in urban soils: Lessons learnt from Athens, Greece. Applied Geochemistry 59, 63-73.

15th International Congress of the Geological Society of Greece
Athens, 22-24 May, 2019 | Harokopio University of Athens, Greece
Bulletin of the Geological Society of Greece, Sp. Pub. 7 Ext. Abs. GSG2019-339

Decoupled Geochemical Behaviour of Tl, Au, As in Sea-floor Massive Sulphides, Kolumbo Arc-volcano: Evidence from LA-ICP-MS Elemental Mapping of Arsenian Pyrite

N. Zegkinoglou[1], S.P. Kilias[1], M. Keith[2], D.J. Smith[2], P. Nomikou[1], P. Polymenakou[3]

(1) Department of Geology and Geoenvironment, National and Kapodistrian University of Athens, Athens 15784, Greece, nikolaoszegkinoglou@yahoo.com
(2) School of Geography and Geology, University of Leicester, Leicester LE1 7RH, UK
(3) Hellenic Centre for Marine Research, Heraklion 71003, Crete, Greece

Thallium (Tl) is considered as toxic for human and animal organisms, microorganisms and plants (Peter and Viraraghavan, 2005; Karbowska, 2016). Thallium is redox active and has two oxidation states (Tl1+ and Tl3+), while Tl1+ is believed to be the most common in Tl minerals (Xiong, 2007; George et al., 2019); monovalent Tl (Tl1+), believed to be the most common in Tl minerals (Xiong, 2007; George et al., 2019), is very mobile, and potentially released into the environment under a range of physicochemical conditions, being easily transported in aqueous form due to its high solubility (Peter and Viraraghavan, 2005).

Recent studies of terrestrial ore deposits have demonstrated the ability of pyrite to host concentrations from a few ppm up to weight per cent (e.g., ≤3.5 wt%) levels of Tl (Zhou et al., 2005; D' Orazio et al., 2017; George et al., 2018; 2019; Muntean et al., 2011). Regardless its potential to release Tl into the environment under a range of physicochemical conditions, the speciation of Tl in pyrite is not very well understood. Metal incorporation in pyrite is complex (e.g., Deditius et al., 2014; Deditius and Reich, 2016), and it has not been evidently shown whether Tl enters the crystal structure of pyrite or tends to occur as micro- to nano-particles of Tl-bearing phases. It has been suggested that the occurrence of Tl+ in pyrite is coupled with the presence of Sb3+ and As3+. More specifically, the occurrence of Tl in As-pyrite (Tl+-bearing nanoparticles or structurally bound Tl) is strongly reliant on As contents (Deditius and Reich, 2016). Moreover, Tl+ can be lattice-bound in pyrite by a simple coupled heterovalent substitution, i.e., $2Fe^{2+} \leftrightarrow Tl^{+} + Sb^{3+}$ (D' Orazio et al. 2017; George et al., 2018). However, more recent studies (George et al., 2019) have questioned the model of a coupled Tl+ and Sb3+ substitution, suggesting that Tl+ could occur in structural defects in pyrite.

Understanding the pathways and processes of the mineralogical sequestration of Tl and other minor elements (e.g., As, Sb, Hg, etc.) is key to economic factors in SMS environmental impact, as well as prospecting and extraction. Consequently, investigation is required of how the minor elements (e.g., Tl, As, Sb) are distributed among key ore minerals and accessory SMS phases, and how this distribution is changed during precipitation, later recrystallisation (dissolution–reprecipitation), and sea water weathering (halmyrolysis). The Kolumbo shallow submarine arc-volcano, located in the 5 Ma-to-present Hellenic Volcanic Arc (HVA) in Greece, hosts an active hydrothermal system currently forming polymetallic SMS mineralisation, the only known SMS deposit associated with continental margin volcanism (Kilias et al., 2013). Polymetallic sulphide-sulphate (baryte) chimneys are uniquely enriched in Tl (mean: 510 ppm; max.: >1,000 ppm) and Sb (mean: 8330 ppm; max.: 2.2 wt.%) (±Hg, As, Au, Ag, Zn). The maximum concentrations of Kolumbo Tl (>1,000 ppm), are the highest reported from modern SMS deposits located on arc volcanoes, which rarely exceed 100 ppm (Monecke et al., 2016). Consequently, Kolumbo is an ideal natural laboratory to investigate the deportment of potentially toxic Tl (and other metal contaminants, As, Sb) in the Aegean Sea.

The studied sulphide-sulphate chimneys exhibit concentric mineral zones, formed at successive stages of chimney growth (Kilias et al., 2013): a lithified inner sulphide-sulphate core (ISSC) mantled by an outer As-sulphide layer (OAsL), which in turn is covered by a Fe-rich crust (SFeC) (Kilias et al., 2013). Pyrite is the dominant sulphide mineral in the ISSC, followed by marcasite, sphalerite, galena, Sb-Pb-sulphosalts, and minor, chalcopyrite, anglesite, Al-silicates, and Sb-Zn-sulphosalts. The OAsL consists chiefly of amorphous orpiment (As_2S_3)-like, and realgar (AsS)-like As-sulphides, stibnite, and Pb-Sb (-As) sulphosalts, in a baryte matrix, and rare opal; the OAsL is overgrown by amorphous ferrihyhydrite-like Fe-oxyhydroxides (SFeC).

Here we report LA-ICP-MS trace element analyses and maps showing the concentration, distribution and zonation of Tl, Au, As, Sb, and Mo in: (1) primary colloform-crustiform and moss textured pyrite (Py 1 – up to: 131 ppm Au; 5870 ppm As; 64,600 ppm Sb; 22 ppm Mo, and 10,140 ppm Tl); (2) later recrystallised (dissolution–reprecipitation) fine-grained pseudobladed pyrite (Py 2) – (up to: 65 ppm Au; 13,290 ppm As; 36,100 ppm Sb; 7.8 ppm Mo, and 2390 ppm Tl); (3) euhedral zonal pyrite (Py 3) – (up to: 54 ppm Au; 17,870 ppm As; 11,580 ppm Sb; 2.2 ppm Mo, and 1163 ppm Tl); and (4) sphalerite (Sph) – (up to: 40 ppm Au; 3920 ppm As; 29,700 ppm Sb; 12.1 ppm Mo, and 7470 ppm Tl) from the 'inner' ISSC zone; (5) colloform pyrite (Py1A) – (up to: 58.3 ppm Au; 7930 ppm As; 10.6 ppm Mo; 46,800 ppm Sb, and 1661 ppm Tl); (6) orpiment (As_2S_3)-type As-rich sulphides ('As_2S_3') – (up to: 861 ppm Au; 90 ppm Mo; 12,300 ppm Sb, and 82,200 ppm Tl); (7) stibnite (Stb) – (up to: 64 ppm Au; 21,800 ppm As; 94 ppm Mo, and 21,800 ppm Tl), and Sb-Pb sulphosalts – (up to: 89.5 ppm Au; 6550 ppm As; 14 ppm Mo, and 1381 ppm Tl) from the 'outer' OAsL zone. Ablation profiles for As, Sb, Tl and Au can be either irregular or smooth, indicating both lattice substitutions and nanoparticle inclusions (e.g., George et al., 2019). ISSC pyrite and sphalerite, are particularly rich in Tl (≤10,140 ppm, Py1; ≤2390 ppm, Py2; ≤1163 ppm, Py3; 7470 ppm, Sph), Sb (≤64,600 ppm, Py 1; ≤29,700 ppm), and As (≤17870 ppm, Py 3; 3920 ppm), and Stb in Tl (≤21,800 ppm) and As (≤21,800 ppm); Au may be present above 100 ppm in Py 1(≤131 ppm), and

above 800 in 'As2S3' (≤861 ppm), and Mo may be present above 20 ppm in Py1 (≤22 ppm), As2S3 (≤90 ppm) and Stb (≤94 ppm). LA-ICP-MS analyses show good correlation of Tl and Sb (R2 = 0.52) in Py1; Tl and Mo in Py1 (R2 = 0.86); Py2 (R2 = 0.82) and Py1A (R2 = 0.57); Sb and Au in sphalerite (R2 = 0.76), and, Tl and As in stibnite (R2 = 0.52). Concentrations of Au, Sb, Mo and Tl drop significantly from Py1 to Py3, and further to Sph, in the ISSC, while, in the OAsL the opposite trend is observed, i.e., Au is increased in Py1A and 'As2S3', and, Mo and Tl are enriched in 'As2S3' and stibnite, compared to the respective ISSC sulphide phases; Sb is generally comparatively decreased in the OAsL.

Trace element mapping using LA-ICP-MS of colloform Py1 reveals a marked compositional zoning with respect to Tl, As, Sb, Au and Mo (also Pb and Ag). Based on the LA-ICP-MS mapping, Tl shows no clear correlative relationship with Au or As, but only with Sb and Mo. This is supported by interelement Tl vs Au, and Tl vs As trends, which show no correlation (R2 = 0.20 R2 = 0.13, respectively).

Our findings suggest that:

1. During the growth of each zone sequence, *i.e.*, ISSC, OAsL, sulphide assemblages and their trace elements are modified by redox processes, overprinting fluids, recrystallisation, exsolution of metastable phases, or boiling, during initial precipitation and later recrystallisation (a dissolution–reprecipitation process); as a result a large proportion of these elements (Au, Sb, Mo and Tl) are expelled possibly as composite nano-particles (George *et al.*, 2019), causing a zone refinement of the elements present in the various formed chimney minerals, strongly supporting zone refinement to be indispensable for polymetallic chimney growth at Kolumbo.
2. Observed decoupled behaviour between Tl and Au, Tl and As, and coupled behaviour between Tl and Sb (at least in colloform Py1), contradicts the paradigm of strong dependence of Tl uptake on As and Au contents of pyrite (Deditius and Reich, 2016), as it has also been before documented for Au and Cu for the Kolumbo SMS mineralisation (Zygouri *et al.*, 2018). In addition, statistically significant coupled behaviour exists between Tl and Mo in Py1 and Py2.
3. The incorporation of Tl into colloform pyrite seems to be facilitated by the presence of Sb, and not As that generally facilitates Au incorporation (Zygouri *et al.*, 2018) in the Kolumbo hydrothermal vent system. Our results corroborate that Tl is possibly incorporated in Py1 mainly in micro- to nano-particles (NPs) of other Tl-bearing phases, possibly Tl-stibnite, with important implications from an economic and environmental point of view.

Acknowledgements

The "SeaBioTech" EU-FP7 project (Grant No. 311932) is thanked for funding the sampling.

References

D'Orazio, M., Biagioni, C., Dini, A., Vezzoni, S., 2017. Thallium-rich pyrite ores from the Apuan Alps, Tuscany, Italy: constraints for their origin and environmental concerns. Mineralium Deposita 52, 687–707.

Deditius, A.P., Reich, M., 2016. Constraints on the solid solubility of Hg, Tl, and Cd in arsenian pyrite. American Mineralogist 101, 1451–1459.

Deditius, A.P., Reich, M., Kesler, S.E., Utsunomiya, S., Chryssoulis, S.L., Walshe, J., Ewing, R.C., 2014. The coupled geochemistry of Au and As in pyrite from hydrothermal ore deposits. Geochimica et Cosmochimica Acta 140, 644–670.

George, L.L., Biagioni, C., D'Orazio, M., Cook, N.J., 2018. Textural and trace element evolution of pyrite during greenschist facies metamorphic recrystallization in the southern Apuan Alps (Tuscany, Italy): initiation of Tl-rich sulphosalt melt formation. Ore Geology Reviews 102, 59–105.

George, L.L., Biagioni, C., Lepore, G.O., Lacalamita, M., Agrosì, G., Capitani, G.C., Bonaccorsi, E. and 'Acapito, F., 2019. The speciation of thallium in (Tl, Sb, As)-rich pyrite. Ore Geology Reviews 107, 364–380.

Karbowska, B., 2016. Presence of thallium in the environment: sources of contaminations, distribution and monitoring methods. Environmental monitoring and assessment 188(11), 640.

Kilias, S.P., Nomikou, P. et al., 2013. New insights into hydrothermal vent processes in the unique shallow-submarine arc-volcano, Kolumbo (Santorini), Greece. Scientific Reports 3, 2421; DOI:10.1038/srep02421.

Large, R.R., Maslennikov., V.V., Robert, F., Danyushevsky, L.V., Chang,Z., 2007. Multistage sedimentary and metamorphic origin of pyrite and gold in the Giant Sukhoi Log deposit, Lena Gold Province, Russia. Economic Geology 102, 1233–1267.

Monecke, T., Petersen, S., Hannington, M.D., Grant, H., Samson, I.M., 2016. The minor element endowment of modern sea-floor massive sulfide deposits and comparison with deposits hosted in ancient volcanic successions, in: Verplanck, P.L., Hitzman, M.W. (Eds), Rare Earth and Critical Elements in Ore Deposits. Reviews in Economic Geology 18, 245–306.

Muntean, J.L. et al., 2011. Magmatic–hydrothermal origin of Nevada's Carlin-type gold deposits. Nature Geoscience 4(2), 122.

Peter, A.L.J., Viraraghavan, T., 2005. Thallium: a review of public health and environmental concerns. Environment International 31(4), 439–501.

Xiong, Y., 2007. Hydrothermal thallium mineralization up to 300 °C: a thermodynamic approach. Ore Geol. Rev. 32, 291–313.

Zhou, T.F., Fan, Y., Yuan, F., Wu, M.A., Hou, M.J., Voicu, G., Hu, Q.H., Zhang, Q.M., Yue, S.C., 2005. A preliminary geological and geochemical study of the Xiangquan thallium deposit, eastern China: the world's first thallium-only mine. Mineralogy and Petrology 85, 243–251.

Zygouri, E., Kilias, S.P., et al., 2018. LA-ICP-MS evidence for coupled geochemistry of Au, Cu and As in As-pyrite from modern sea-floor massive sulphides, Kolumbo arc-volcano, Greece, in: Santoro, L. et al., Abstracts from the 2017–2018 Mineral Deposits Studies Group meeting, Applied Earth Science, 127(2), 46-79, DOI: 10.1080/25726838.2018.1487425.

SPECIAL SESSION

T4.S2 Insights into the Nature of the Earth's Upper Mantle approached from the study of Ophiolites and Volcanic Rocks

Conveners: **Petros Koutsovitis (CERTH)**
Theodoros Daflos (Univ. Wien)
Andreas Magganas (NKUA)

15th International Congress of the Geological Society of Greece
Athens, 22-24 May, 2019 | Harokopio University of Athens, Greece
Bulletin of the Geological Society of Greece, Sp. Pub. 7 Ext. Abs. GSG2019-085

Internal lithospheric rotation at the initiation of rift-drift: an example of proto-transform era tectonics from the Vourinos Ophiolite, Greece

Anne Ewing Rassios
Institute of Geology and Mineral Exploration Region of West Macedonia, Greece, rassannie@gmail.com

The initial concept and recognition in outcrop of a "petrologic moho" was established within the Vourinos ophiolitic complex of northern Greece (Jackson et al 1974). Follow-up work documented the contact between mantle tectonite and an ultramafic-mafic cumulate suite as one of an intrusional topography (Rassios 1981; Harkins et al 1980). The orientation of the petrologic moho and that of stratotectonic "upping" (based on magmatic layering and fractionation patterns) was observed to be at nearly a 90° rotation to that of the dominant lithospheric mantle -> magmatic -> oceanic sedimentary profile. While early research by the aforementioned investigators documented ductile and magmatic structural fabrics in great detail, the block rotation of the petrologic moho unit was assumed to be via a non-exposed Tertiary (?) brittle fault system. Such a fault system was not observed even during detailed explorationist investigation of the area during the 1980's and 1990's.

A synthesis of this early research within a modern framework of ductile lithospheric deformation reveals a fabric continuity that suggests this rotation occurred in near-ridge crest ductile conditions. Evidence towards this interpretation includes:

- Continuity of ductile mineral fabric (lineation and foliation) within the magmatic and restite tectonite peridotite within the petrologic moho section and between the petrologic moho section and regional mantle tectonite.
- Parallel orientation of sub solidus mineral enlargement between exposures within the neighboring sub-moho Aetoraches chrome mine and cumulus grains within the magmatic section of the petrologic moho area.

The mechanism of this rotational deformation could be ascribed to proto-transform era tectonism (Garya 2012) or complex deformation within transtensional-transpressional zones between transfer faults (Dewey et al 1998).

i) Several fragments of flaser gabbro were observed in the 1970's research in contact with the north west border of the magmatic section of the petrologic moho area. Today we recognize these could mark the trace of a high temperature (transform) fault;
ii) the cumulate rocks of the petrologic moho section trace magmatic evolution towards troctolite rather than gabbronorite as elsewhere at Vourinos (Rassios 1981). This, in a modern consensus framework, could also be a transform-related phenomenon;
iii) Vourinos is dominated by Cr-rich chromite and chrome ores. The only occurrence of Al-rich chrome ores within the Vourinos mantle section crop out within the nearby Kissavos locality. These Al-rich ores might be related to transform fault-related hydrous magmatic activity concurrent to sub-ridge crest crystallization.

The direct observation of oceanic transform fault systems is difficult: oceanic topographic maps of the "google earth" type show a thick network of such faults at ridge crests, directly implying the coexistence of active ridge crest lithospheric generation with transform fault initiation. Rare instances of transform faults have been documented from ophiolites (eg Troodos-Cyprus, Domokos-Greece) that cut through various lithospheric levels. We believe that at Vourinos, the rotation in ductile conditions of a block of approximately 3 km^3 is probably associated with this early ridge crest – transform era. If so, this shows the possible nature of the initiation of transforms at depths about 10km below the ridge crest system.

References

Dewey J, Holdsworth R, and Strachan R,. Transpression and transtension zones. Geological Society, London, Special Publications 1998, v.135; p1-14.
Gerya, T. (2012) Origin and models of oceanic transform faults. Tectonophys., 522-523, 34-56.
Harkins, M., Green, H., and Moores, E., 1980. Multiple intrusive events documented from the Vourinos ophiolite complex, northern Greece. Am. Journ. Sci. 280-A, 284-290.
Jackson, E.D., Green, H.W., and Moores, E.M., 1975, The Vourinos ophiolite, Greece: cyclic units of lineated cumulates overlying harzburgite tectonite: Bulletin of the Geological Society of America, v. 86, p. 390–398.
Rassios, A., 1981. Geology and Evolution of the Vourinos Complex, Northern Greece. PhD. Thesis, Univ. of Calif. (Davis), 499 pp.

15th International Congress of the Geological Society of Greece
Athens, 22-24 May, 2019 | Harokopio University of Athens, Greece
Bulletin of the Geological Society of Greece, Sp. Pub. 7 Ext. Abs. GSG2019-118

Rodingitized Gabbroic Rocks in Vavdos Ophiolite, West Chalkidiki, North Greece

A. Sideridis[1], L. Papadopoulou[2], B.Tsikouras[3] and P. Tsitsanis[4]

(1) University of Patras, Faculty of Science, School of Geology, Sector of Earth Materials, University Campus, 26504, Rion, Greece, alkis.sideridis@gmail.com
(2) Aristotle University of Thessaloniki, Faculty of Science, School of Geology, Sector of Mineralogy-Petrology-Economic Geology, University Campus, 54 124, Thessaloniki, Greece
(3) Universiti Brunei Darussalam, Faculty of Science, Physical and Geological Sciences, Jalan Tungku Link, BE 1410 Gadong, Brunei Darussalam
(4) Independent scholar, Makedonias 21, 63 200, Nea Moudania, Greece

Introduction

Rodingite is an infrequent lithology in Greek ophiolites (e.g. Hatzipanagiotou & Tsikouras, 2001; Tsikouras et al., 2013). In this paper rodingitized gabbroic rocks, from the Vavdos ophiolite (Innermost Hellenic Ophiolitic Belt) are studied for the first time. They are hosted in the crustal section of the ophiolite, consisting of gabbroic rocks. The rodingitized rocks appear as whitish a) in dikes cross-cutting gabbronorite or b) as contact zones between massive gabbronorite and peridotites. Rodingites typically are related to serpentinization demonstrating the paragenesis diopside + garnet ± vesuvianite (e.g. Hatzipanagiotou et al., 2003; Tsikouras et al., 2009). This is not the case in the present study; therefore the petrography, mineral chemistry and geochemistry of the rodingitized occurrences will be studied, in order to determine their protolith and the events that led to their greenschist-like paragenesis.

Geological Setting

Vavdos ophiolite is part of a dismembered ophiolite complex of west Chalkidiki, which is part of the NW-SE trending Innermost Hellenic Ophiolitic Belt (Bebien et al., 1986). The ophiolite is obducted on the metamorphic Serbomacedonian Massif at the SW and it is bounded by the Chortiatis Magmatic Suite and the Circum Rhodope Belt at the NE (e.g. Meinhold et al., 2009). Peridotite and pyroxenite consist the mantle section and the transitional zone of the ophiolite, respectively. Mafic rocks dominate the crustal section and they are distinguished into four categories: a) massive gabbronorite, b) gabbronorite dike intruding the massive counterpart, c) diabase and d) two types of rodingitized gabbroic rocks (rodingites). The first type forms dikes intruding gabbronorite (vein rodingite) and the second occurs as a narrow zone at the contact of gabbronorite with peridotites (massive rodingite).

Materials and methods

Mineral chemical analyses of one gabbronorite (b147) and five rodingitized gabbros (samples in Table 1) were carried out at the Scanning Microscope Laboratory, A.U.Th., using a JEOL JSM-6390LV Scanning Electron Microscope (SEM) equipped with an Energy Dispersive Spectrometer (EDS) INCA 250 with 20kV accelerating voltage and 0.4 mA probe current. Pure Co was used as an optimization element. For SEM observations, the samples were coated with carbon – average thickness of 200 Å – using a vacuum evaporator JEOL-4X. Whole rock geochemical analyses of two massive gabbronorites (b147, b153) and six rodingites (samples in Table 1 plus b5a), for REE concentrations were performed at ActLabs (Ontario, Canada) using the 4b-INAA package (method described in http://www.actlabs.com/).

Petrography and mineral chemistry

The adcumulate massive gabbronorites are subhedral to anhedral with granular and in places subophitic texture. Magnetite with embayed boundaries is commonly surrounded by tschermakite and chlorite. The rodingites demonstrate relict textures similar to gabbronorite including blasto-granular and blasto-subophitic textures. The leucocratic matrix mainly consists of clinozoisite that forms symplectites with quartz. Hornblende, actinolite and lesser chlorite and tremolite, comprise the mafic minerals. The opaque minerals (magnetite, ilmenite) are skeletal in texture and are exsolved from actinolite and chlorite$_{ex}$ (exsolved chlorite). There is also a case of an embayed almandine rich garnet corona around this exsolution. These gulfs are filled with clinozoisite. No primary plagioclase or pyroxene was observed. Rodingites' parageneses are listed in Table 1. Vein rodingites show a wider range in the total iron content of clinozoisite (0.46 to 9.76 wt %), while the massive counterparts do not exceed the 3.58 wt %. Low total iron contents in clinozoisite are consistent with actinolite and tremolite abundance, while elevation of the iron corresponds to hornblende dominance in the rodingitized gabbros.

Geochemistry

The REE concentration patterns of massive gabbronorites and rodingites demonstrate many similarities and they are divided in three groups. The first group includes massive rodingites and gabbronorites and is characterized of spoon-like LREE patterns and flat HREE profiles with a strong positive Eu anomaly. Fractionated LREE slopes and a positive Eu anomaly coupled with flat HREE profiles correspond to the second group, comprised of vein rodingites and their rodingitized wallrock. The third group includes one sample of vein rodingite demonstrating slightly fractionated LREE and an unfractionated HREE profile with a notable negative Eu anomaly. The geochemical affinities of the studied rocks

display a spatial distribution, with the first group, consisting of massive rodingites and gabbronorites, occurring at the south of the ophiolite whilst the rest groups (vein rodingites) are located to the north of it.

Table 1 Paragenetic characteristics of the rodingitized samples, M: massive rodingite, V: vein rodingite and MV: vein rodingite's country rock.

samples	type	paragenesis
b32b	MV	clinozoisite + actinolite + tremolite + hornblende + chlorite + magnetite + pyrite + rutile + titanite + quartz
b5b	V	clinozoisite + actinolite + hornblende + tremolite + epidote + titanite + zircon + ilmenite + pumpellyite
b5c2	V	clinozoisite + actinolite + hornblende + chlorite + ilmenite + $chlorite_{ex}$ + garnet + albite + titanite + chalcopyrite + quartz
b4a3	M	actinolite + clinozoisite + chlorite + albite + titanite + spinel + pyrite + quartz
b4	M	hornblende + clinozoisite + actinolite + chlorite + tourmaline + pumpellyite + spinel + quartz

Discussion and conclusions

Rodingites are associated with massive gabbronorite either as dikes or as narrow zones adjacent to a gabbronorite-peridotite contact. Their textures are reminiscent of gabbronorite textures, thus indicating the latter (or other genetically related lithologies), as the most likely protolith. The gabbronorite and rodingite REE patterns demonstrate great resemblance; well defined positive Eu anomalies and unfractionated HREE. All Eu anomalies are considered as magmatic feature that was inherited to the metasomatic rocks. Vavdos rodingites paragenesis is different from the rest of the diopside + garnet ± vesuvianite bearing Greek counterparts. They are hosted in massive gabbronorite, unlike the other Greek rodingites, which are closely associated with ultramafic lithologies, being either their hosts or protoliths. Bach and Klein (2009) studied the formation of rodingites at mafic/ultramafic boundaries. They concluded that serpentinization fluids that had previously weakly reacted with gabbroic rocks will be able to crystallize grossular + diopside ± chlorite (200-300 ^{o}C). However, when fluids had time to react with gabbroic rocks, garnet was replaced by either epidote or prenhite and diopside by tremolite. In the extreme case of fluid's total modification after interacting with gabbro, the ideal paragenesis would be: albite + actinolite + chlorite + epidote. The aforementioned mineral replacements were identified in this paper; garnet was replaced by clinozoisite, tremolite is closely related to actinolite. Based on this assumption, actinolite dominated rodingites, with the lowest amounts of total iron in clinozoisite were produced from fluids, which had largely equilibrated with the country gabbronorite. The wide range of clinozoisite's total iron contents observed in the vein rodingites (one sample is garnet bearing) could depict the modification of the metasomatic fluid while reacting with the gabbronorite.

References

Bach, W. & Klein, F. 2009. The petrology of seafloor rodingites: Insights from geochemical reaction path modeling. Lithos, vol. 112, no. 1-2, pp. 103-117.

Bebien, J., Dubois, R. & Gauthier, A. 1986. Example of ensialic ophiolites emplaced in a wrench zone: innermost Hellenic ophiolite belt (Greek Macedonia). Geology, vol. 14, no. 12, pp. 1016-1019.

Hatzipanagiotou, K. & Tsikouras, B. 2001. Rodingite formation from diorite in the Samothraki ophiolite, NE Aegean, Greece. Geological Journal, vol. 36, no. 2, pp. 93-109.

Hatzipanagiotou, K., Tsikouras, B., Migiros, G., Gartzos, E. & Serelis, K. 2003. Origin of rodingites in ultramafic rocks from Lesvos Island (NE Aegean, Greece). Ofioliti, vol. 28, no. 1, pp. 13-23.

Meinhold, G., Kostopoulos, D., Reischmann, T., Frei, D. & BouDagher-Fadel, M.K. 2009. Geochemistry, provenance and stratigraphic age of metasedimentary rocks from the eastern Vardar suture zone, northern Greece. Palaeogeography, Palaeoclimatology, Palaeoecology, vol. 277, no. 3-4, pp. 199-225.

Tostevin, R., Shields, G.A., Tarbuck, G.M., He, T., Clarkson, M.O. & Wood, R.A. 2016. Effective use of cerium anomalies as a redox proxy in carbonate-dominated marine settings. *Chemical Geology*, vol. 438, pp. 146-162.

Tsikouras, B., Karipi, S., Rigopoulos, I., Perraki, M., Pomonis, P. & Hatzipanagiotou, K. 2009. Geochemical processes and petrogenetic evolution of rodingite dykes in the ophiolite complex of Othrys (Central Greece). Lithos, vol. 113, no. 3-4, pp. 540-554.

Tsikouras, B., Karipi, S. & Hatzipanagiotou, K. 2013. Evolution of rodingites along stratigraphic depth in the Iti and Kallidromon ophiolites (Central Greece). Lithos, vol. 175-176, pp. 16-29.

15th International Congress of the Geological Society of Greece
Athens, 22-24 May, 2019 | Harokopio University of Athens, Greece
Bulletin of the Geological Society of Greece, Sp. Pub. 7 Ext. Abs. GSG2019-153

Serpentinization and Ca-metasomatism of the Rodingite Dykes Intruding Ultramafic Olistostromes of Kimi Flysch, Evia Island (Greece)

C. Karkalis[1,2], A. Magganas[1], P. Koutsovitis [2].

(1) Department of Geology and Geoenvironment, National & Kapodistrian University of Athens, Panepistimiopolis, Athens, GR-15784

(2) Centre for Research & Technology Hellas, Chemical Process and Energy Resources Institute (CERTH/CPERI), 52 Egialias street, Athens GR-151 25

Background

In Kimi region (Evia island, Greece) the Maestrichtian-Paleocene flysch is composed by sedimentary rocks (sandstones, shales, cherts), intercalations of Upper Cretaceous limestone (Robertson, 1990), as well as olistostromes of serpentinized peridotites. The ultramafics are strongly associated with rodingite dykes, ophicalcites and talc schists. Rodingites appear as veins with horizontal (E-W) or NNE-SSW direction. They are composed by three distinct concentric zones, characterized by specific mineral assemblages. The ultramafic host rocks consist of two thin irregular zones of successive metasomatized serpentinite and chloritite near the contact with the rodingite dykes.

Aims and Objectives

The present study aims to investigate the relation between serpentinization and rodingitization, as well as the physicochemical conditions under which Ca-metasomatism affected the exhumed mantle rocks of Kimi. For the purpose of this study the following methods were followed: a) Field work emphasized on the ophiolitic ultramafic rocks intruded by rodingite dykes. b) Mineralogical analyses c) Whole rock chemical analyses d) Stable O-C isotopic analyses of calcite e) Data processing.

Results

Petrographical and geochemical investigation of the rodingite rocks included the study of their marginal, transitional and core zones. As calcite occurs in some of the studied samples, rodingites were further divided into two groups, corresponding to non-carbonated (Group-I) and carbonated (Group-II) dykes. Their texture ranges from cryptocrystalline to microcrystalline, usually porphyroblastic including idiomorphic (hydro)garnet and vesuvianite porphyroblasts. In both rodingite groups, chlorite and/or diopside predominate in the marginal zones, whereas vesuvianite and/or garnet are the main mineral phases of the core zones. Tranistional zones include all the aforementioned minerals in various and unequal amounts. Accessory minerals include relict spinel, prehnite, epidote, apatite, allanite, amphibole, dolomite, quartz and opaque Fe-Ti oxides.

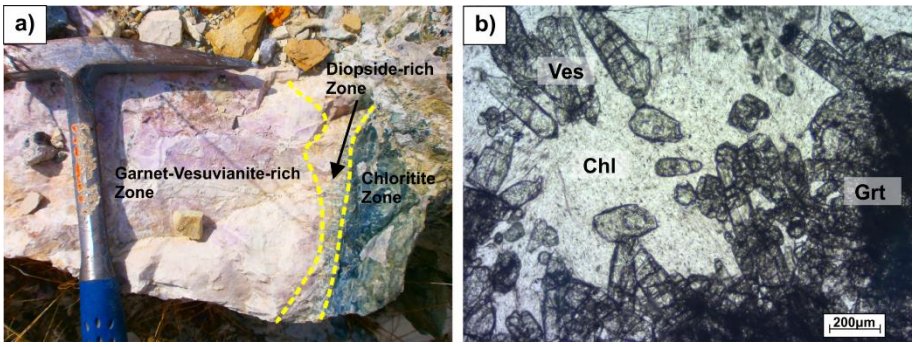

Figure 1. a. Macroscopic image of rodingite dyke b. Rodingite photomicrograph (PPL) consisting of chlorite (Chl) – garnet (Grt) matrix with vesuvianite porphyroblasts.

Calcite appears in the form of veins or within cavities in the rodingite groundmass. Garnet is mainly classified as (hydro)grossular, whereas a few (hydro)andradite crystals also occur. Chlorite is classified mostly as penninite, whereas clinopyroxene is classified as diopside. Ultramafic rocks are divided into serpentinized peridotites, metasomatized serpentinites and chloritites. Serpentinitic rocks include mostly serpentinite, bastite grains, garnet porphyroblasts, as well as relict pyroxene grains with accessory spinel. Regarding their whole rock chemistry, rodingites are mainly CaO enriched and depleted in SiO_2 and total alkalies, whereas their LOI contents are quite high. The carbonated rodingites (Group-II) show significant enrichment in light rare earth elements (LREE). Stable isotopic data in calcite crystals of the rodingite, ophicalcite and red mudstone samples present a wide range of $\delta^{13}C$ and $\delta^{18}O$ VPDB contents. Metasomatized serpentinites show higher CaO and SiO_2 contents compared to those of chloritites.

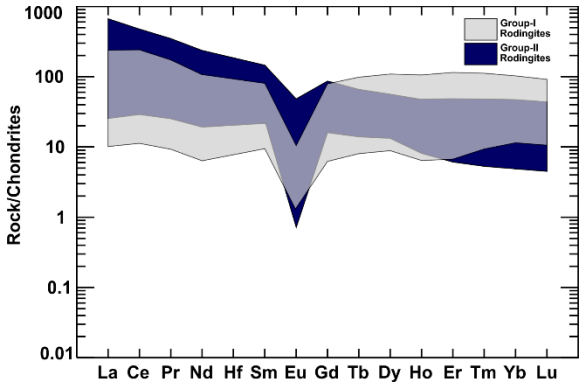

Figure 2. CN-normalized REE patterns [after McDounough and Sun (1995)] of Group-I and Group-II rodingites.

Discussion and Conclusions

Rodingitization is strongly associated with serpentinization, evolved under alkaline conditions, in a Supra Subduction Zone (SSZ) within the closing oceanic basin (Robertson, 1990). The occurrence of three distinct zones within the rodingite dykes corresponds to gradual fluid infiltration with H2O/rock ratio and CO2/H2O ratio increasing, and T decreasing towards their cores. Ultramafics are characterized by a transition from an outer metasomatized zone to an inner chloritic rim near the contact with the rodingite dykes. Rodingitization likely evolved into two metasomatic events characterized by different XCO2 conditions. Vesuvianite was formed at a late stage of the first metasomatic event under Ca2+/OH- rich fluids and low CO2/H2O ratio (Hatzipanagiotou et al., 2003; Li et al., 2004; Li et al., 2008; Koutsovitis et al., 2013). The occurrence of additional calcite in some the rodingite dykes corresponds to a second metasomatic event of higher XCO2 conditions. The CaO enrichment and SiO2-alkali depletion is associated with clinopyroxene and anorthite breakdown dissolution during serpentinization (Frost et al., 2008). LREE enrichment is significantly higher in carbonated rodingites, indicating the presence of carbonic-LREE complexes in the metasomatic fluids, whereas Zr mobility can be associated with the presence of PO43--LREE and LREE-OH- complexes (Aja et al., 1995; Veyland et al., 2000). REE are hosted within monazite and allanite. Stable isotope data indicate the participation of hydrothermal and seawater fluids. The closure of the oceanic basin is accompanied by the formation of Kimi flysch and the incorporation of the ultramafic olistostromes.

References

Aja, S.U.,Wood, S.A., Williams-Jones, A.E., 1995. The aqueous geochemistry and the solubility of some Zr-bearing minerals. Applied Geochemistry, 10, 603–620.

Frost, B.R., Beard, J.S., McCaig, A., Condliffe, E., 2008. The formation of micro-rodingites from IODP hole U1309D: key to understanding the process of serpentinization. Journal of Petrology, 49, 1579–1588.

Hatzipanagiotou, K., Tsikouras, B., Migiros, G., Gartzos, E., Serelis, K., 2003. Origin of rodingites in ultramafic rocks from Lesvos island (NE Aegean, Greece). Ofioliti, 28, 13–23.

Koutsovitis, P., Magganas, A., Pomonis, P., Ntaflos, T., 2013. Subduction-related rodingites from East Othris, Greece: Mineral reactions and physicochemical conditions of formation, Lithos, 172-173, 139-157.

Li, X.P., Rahn, M., Bucher, K., 2004. Metamorphic Processes in Rodingites of the Zermatt-Saas Ophiolites, International Geology Review, 46, 28–51.

Li, X.P., Rahn, M., Bucher, K., 2008. Eclogite facies metarodingites: phase relations in the system SiO2–Al2O3–Fe2O3–FeO–MgO–CaO–CO_2–H_2O: an example from the Zermatt-Saas ophiolite, Journal of metamorphic Geology, 26, 347–364.

Robertson, A.H.F., 1990. Late Cretaceous oceanic crust and Early Tertiary foreland basin development, Euboea, Eastern Greece. Terra Nova, 2, (4), 333-339.

Tsikouras, B., Karipi, S., Rigopoulos, I., Perraki, M., Pomonis, P., Hatzipanagiotou, K., 2009. Geochemical processes and petrogenetic evolution of rodingite dykes in the ophiolite complex of Othrys (Central Greece). Lithos, 113, 540–554.

Veyland, A.,Dupont, L., Rimbault, J., Pierrard, J.-C., Aplincourt, M., 2000. Aqueous Chemistry of Zirconium (IV) in Carbonate Media. Helvetica Chimica Acta, 80, 414–427.

15th International Congress of the Geological Society of Greece
Athens, 22-24 May, 2019 | Harokopio University of Athens, Greece
Bulletin of the Geological Society of Greece, Sp. Pub. 7 Ext. Abs. GSG2019-154

Metasomatism of Triassic ultramafic cumulates and lavas in Othris, Greece

P. Koutsovitis[1,2], A. Magganas[2], Th. Ntaflos[3], N. Koukouzas[1].

(1) Centre for Research & Technology Hellas, Chemical Process and Energy Resources Institute (CERTH/CPERI), 52 Egialias Str., Athens GR-15125
(2) National & Kapodistrian University of Athens, Faculty of Geology and Geoenvironment, Department of Mineralogy and Petrology, Panepistimioupolis, Athens, GR-15784
(3) University of Vienna, Department of Lithospheric Research, Althanstr. 14, Vienna, A-1090.

Cumulate wehrlites, ultramafic lavas, and associated mafic dykes and pillow-lavas outcrop within a Middle-Late Triassic igneous and sedimentary sequence in Othris, Central Greece. These rocks have been variably affected by metasomatic and metamorphic processes (Figure 1). Ultramafic rocks (wehrlites and ultramafic lavas) are serpentinized in processes that are restricted (moderate alteration) or pervasive, forming serpentinites. Balanced lizardite/antigorite ratios suggest that serpentinization took place under conditions that reached greenschist facies. Most trace element concentrations were relatively decreased during serpentinization. Local rodingitization is characterized by the formation of hydrogarnets, secondary diopside, chlorite, pumpellyite and prehnite. This metasomatic mineral assemblage replaced cumulus clinopyroxene as well as primary accessory plagioclase. Rodingitization occurred with diffusive mass transfer of CaOH+ species under relatively mildly oxidizing physicochemical conditions, along with fluid solutions with an increased CO2/H2O ratio.

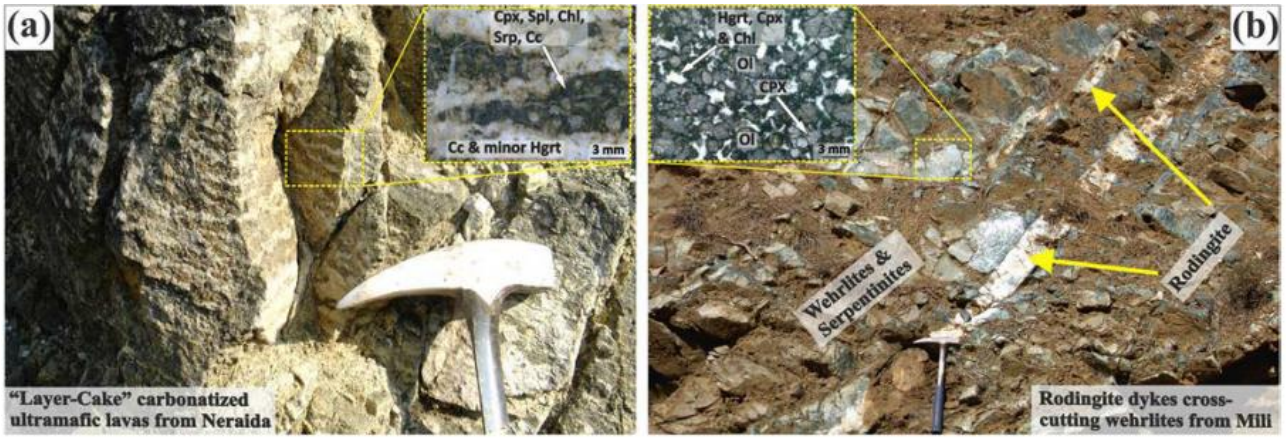

Figure. 1. (a) "Layer-cake" carbonatized ultramafic lavas from the region of Neraida. Enclosed is a stereoscopic image of a polished hand specimen displaying the penetration of calcite. (b)Rodingite dykes crosscutting partially serpentinized and rodingitized wehrlites. Enclosed is a stereoscopic image of a polished hand specimen of a partly rodingitized wehrlite displaying the occurrence of hydrogarnet. (Figure 1 is Figure 2 of Koutsovitis et al. 2018).

Rodingites formed as a result of extensive metasomatism that replaced protolithic boninitic dykes intruding wehrlites. The metasomatic hydrous fluids responsible for this process were relatively alkaline, occurring under low to moderate P-T conditions (180-320 °C, P≈2-5 kbar), in conditions of increased fO2. Rodingites experienced desilification, and rodingitization also resulted in variable decreases and less often increases in trace element concentration.

Carbonation processes affected ultramafic lavas; the most intense carbonation is exposed in the Neraida locality where it has created "layer-cake" structures within the lavas. Metasomatic carbonation was caused by shallow-level continuous circulation of Ca-rich fluids too low in temperature to significantly affect clinopyroxenes. The restricted occurrence of serpentine and hydroandradite indicates that carbonation occurred in association with low-grade serpentinization and rodingitization processes. The metasomatic phenomena documented herein are related to subduction settings and more specifically to the seafloor exhumation of the mafic–ultramafic rocks in the fore-arc area.

We have calculated that serpentinization and rodingitization of wehrlites began within relatively moderate temperature and pressure conditions (~350 °C, P≈6 kbar), with rodingitization processes in both wehrlites and rodingites progressing during further continuous cooling of circulating hydrothermal fluids at shallower depths. The final metasomatic stage is represented by carbonation processes.

References

Koutsovitis, P., Magganas, A., Ntaflos, T., Koukouzas N. 2018. Rodingitization and carbonation, associated with serpentinization of Triassic ultramafic cumulates and lavas in Othris, Greece. Lithos, 320-321, 35-48.

15th International Congress of the Geological Society of Greece
Athens, 22-24 May, 2019 | Harokopio University of Athens, Greece
Bulletin of the Geological Society of Greece, Sp. Pub. 7 Ext. Abs. GSG2019-173

The Mirdita Eastern Ophiolite, Albania: Non-metasomatized Spinel-harzburgites whithin the Suprasubduction Ophiolite of Tropoje

T. Ntaflos[1], K. Onuzi[2], C. Hauzenberger[3], A.H.N. Rice[4], P. Proßegger[1], N. Mekshiqi[2], G. Kaza[2]

(1) University of Vienna, Dept. of Lithospheric Research, Austria theodoros.ntaflos@univie.ac.at
(2) Institute of Geo-Sciences, Energy, Water and Environment, Tirana, Albania
(3) Geocenter - Petrology & Geochemistry, NAWI Graz, Austria (4) University of Vienna, Dept. of Geodynamics & Sedimentology, Austria.

The Mirdita ophiolites in northern Albania are divided into the Western Mirdita Ophiolite (WMO), with MORB geochemical affinities, and the Eastern Mirdita Ophiolite (EMO), for which suprasubduction geochemical affinities have been reported (Beccaluva et al., 2005). Ultramafic massifs in the WMO are often plagioclase bearing lherzolites/harzburgites whereas those in the EMO are strongly depleted spinel harzburgites.The Tropoje ultramafic-mafic complex, which forms the northernmost part of the EMO, consists of spinel harzburgites, dunites, wherlites, orthopyroxenites and gabbros (Fig. 1).

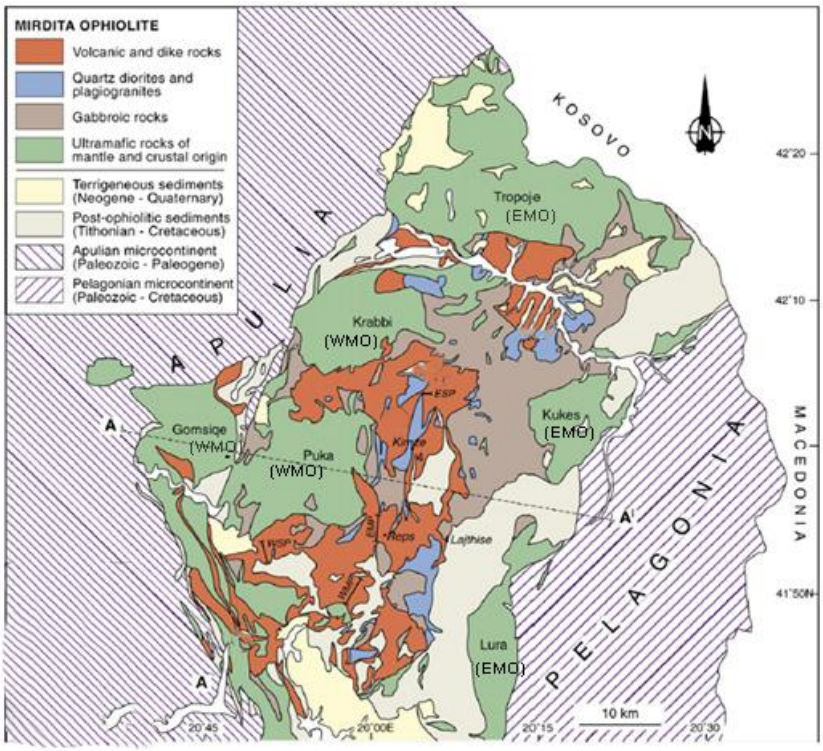

Figure 1. Geological map of northern Albania modified after Dilek et al., 2007. WMO: Western Mirdita Ophiolite, EMO: Eastern Mirdita Ophiolite.

The spinel harzburgites, which experienced variable degrees of serpentinization, are coarse- to medium-grained. One of the most striking features of the Tropoje ultramafic rocks is an outcrop of exceptionally fresh coarse- to medium-grained spinel harzburgites. While occasionally the peridotites exhibit a weak foliation, the prevalent texture is protogranular. Olivine is mainly coarse-grained (up to 6 mm size), typically showing kink-bands that frequently contain submicron-sized spinel exsolution lamellae. Both orthopyroxene and clinopyroxene, with grain size up to 3 mm and 1.5 mm, respectively, carry very thin exsolution lamellae of the other pyroxene. The olivine inclusions in coarse-grained orthopyroxene show evidence for reaction of a percolating melt with dunites (Fig. 2). Spinel, up to 1 mm in size, is interstitial between boundaries of the associated silicates and its composition indicates that the Tropoje peridotites are strongly depleted in basaltic components.

The rock-forming minerals (olivine, orthopyroxene and clinopyroxene) are all highly magnesian and chemically homogenous. The magnesium numbers (Mg#=100xMg/[Mg+Fe]) for olivine and orthopyroxene are fairly homogeneous and vary within the narrow range of 90.9-91.6 and 91.5-91.7, respectively. The clinopyroxene is exceptionally highly magnesian, with Mg# ranging between 93.6 and 95.4. In both orthopyroxene and clinopyroxene, the Al_2O_3 contents range from 0.95 to 1.75 and from 0.62 to 2.27 wt%, respectively. Spinel shows a considerable variation in $Al_2O3$and Cr_2O3. The range in Cr# (Cr#=100xCr/[Cr+Al]) is 51.7-69.2, but no compositional variations have been observed between core and rim.

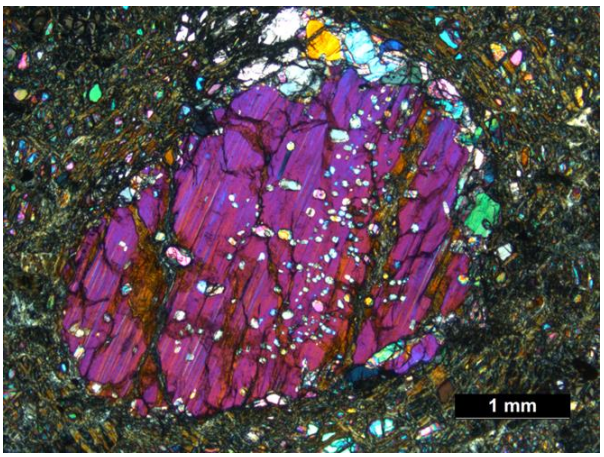

Figure 2. Coarse-grained opx with olivine inclusions: evidence for rock-melt interaction

The silicate minerals are strongly depleted in trace elements. LA-ICP-MS analyses of clinopyroxenes show that the LREE are below detection limit whereas the ratio of (Tb/Yb)N range from 0.10 to 0.15 and Lu is around 0.5xPM.Equilibrium temperatures calculated at a pressure of 1.5 GPa are relatively low, ranging between 620 and 830◦C.The lowest temperature corresponds to the most residual peridotite, in which the clinopyroxene has the highest Mg# (95.4) and the spinel the highest Cr# (69.2).The spinel-harzburgites from these exceptional fresh outcrop have experienced high degrees of partial melting. Applying the method of Hellebrand (2001) to samples containing spinel with Cr# < 60 yields around 20% partial melting. The overall strong depletion in trace elements and prominent depletion of the LREE in clinopyroxenes as well as the absence of hydrous phases is not consistent with a suprasubduction origin as it has been suggested for the Tropoje ultramafic massif.

References

Beccaluva, L., Coltorti M., Saccani, E., Sienna, F., 2005. Magma generation and crustal accretion as evidenced by suprasubduction ophiolites of the Albanide-Hellenide Subpelagonian Zone. The Island Arc 14,551-563.

Dilek, Y., Furnes, H., Shallo, M., 2007. Suprasubduction zone ophiolite formation along the periphery of Mesozoic Godwana. Godwana Research, 11, 453-475.

Hellebrand, E., Snow, J.E., Dick, H.J.B. Hofmann, A.W. 2001. Coupled major and trace elements as indicators of the extent of melting in mid-ocean-ridge peridotites. Nature, 410, 677-681.

15th International Congress of the Geological Society of Greece
Athens, 22-24 May, 2019 | Harokopio University of Athens, Greece
Bulletin of the Geological Society of Greece, Sp. Pub. 7 Ext. Abs. GSG2019-264

New Insights into the Tectonic Evolution of the UAE-Oman Ophiolite Suite

S. Kim[1], S. Kwon[1,2], Y. Jang[3], S. Kokkalas[4]

(1) Department of Earth System Sciences, Yonsei University, Seoul 03722, Republic of Korea
(2) School of Earth Sciences, The Ohio State University, Columbus, OH 43210, USA
(3) Geological Research Division, Korea Institute of Geoscience and Mineral Resources, Daejeon 34132, Republic of Korea
(4) Department of Geology, University of Patras 26500, Patras, Greece

The United Arab Emirates (UAE)-Oman ophiolite, a thrust sheet of Tethyan oceanic lithosphere that was emplaced onto the formerly passive continental margin of Arabia, is the largest and most well studied ophiolite with excellent preservation of the ocean plate stratigraphy of the obducted oceanic crust with related igneous and metamorphic rocks (Goodenough et al., 2014). Thus, the area provides a wonderful natural laboratory to study the subduction-obduction and their related processes in the mantle wedge at a convergent boundary (e.g., Searle and Cox, 2002; Rioux et al., 2013; Goodenough et al., 2014; Spencer et al., 2017; Joun et al., 2018). The UAE ophiolite belt preserves large slices of complete ocean plate stratigraphic section from mantle, lower crust, sheeted dikes, and pillow lavas of mid-ocean ridge basalt affinity, namely phase 1 magmatism, with intercalated pelagic sediments lying on top of the fault bounded metamorphic sole (Nicolas et al., 2000). This earlier oceanic crust is intruded by phase 2 magmatic rocks that consist of high-level gabbro, dolerite, basalt, pyroxenite, wehrlite and tonalite (Goodenough et al., 2014) with hydrous SSZ geochemical affinity (e.g., Rioux et al., 2013; Haase et al., 2016). Isotopic ages suggest that both magmatic activities are overlapped in the range of ca. 98.6 to 94.5 Ma (Rioux et al., 2016; Joun et al., 2018). These age spans are younger than about 5 Ma from the oldest age of the ophiolite. Apart from the magmatic history that formed the ophiolite crust, the obduction and exhumation history of the Semail ophiolite has been studied by various workers based on the nature of HP-metamorphism beneath the ophiolite complex (Searle and Cox, 2002; Styles et al., 2006). They reported a relatively wide range of ages from ca. 96 Ma (U-Pb ages, Rioux et al., 2016), ca. 92.4 – 94.9 Ma (Ar-Ar ages, Hacker and Gnos, 1997), ca. 89 – 101 Ma (K-Ar ages, Gnos and Peters, 1993). These ages are older than about 6 Ma compared with the youngest estimated ophiolite obduction age of ca. 93 to 83 Ma (Jacobs et al., 2015). These ages were suggestive of a subducting plate origin with crustal slices stacked below the overriding plate during the obduction (e.g. Searle et al., 2015).

However, we have reported the weighted mean age of ca. 91.8 Ma from the garnet metagabbro in Masafi metamorphic sole that is ca. 3 Ma younger to the protolith ages of ca. 94.5 and 94.9 Ma which are inferred from the oscillatory zoned zircons (Rioux et al., 2013), and is overlapped with previously reported metamorphic ages from the UAE ophiolite belt (Styles et al., 2006; Searle et al., 2015). The U/Pb ratios yield protolith ages of ca. 93.6 Ma for the olivine websterite sample and ca. 90.6 and 91.2 Ma for the tonalite samples. The same grains for the garnet metagabbro, phase 2 tonalite, and olivine websterite yield all positive ε_{HF} (t) values range from 5.6 – 10.0 for the ages 89 – 96 Ma, 5.1 – 10.0 for the age of 87 – 92 Ma, and 12.6 – 22.6 for the age of 89 – 96 Ma. These results indicate that the garnet metagabbro from this study originated from the mantle wedge, thus the overriding plate, formed through the metasomatism of depleted mantle with fluid derived from the subducting plate, rather than the subducted slab that has been interpreted as the origin of garnet amphibolite in general, although the positive ε_{Hf} value of the tonalite indicates the interaction during this mantle metasomatism as indicated by earlier research (Joun et al., 2018).

Acknowledgements

We would like to thank Khalifa University and the Ministry of Energy, UAE for providing the field permissions for this research. This research was supported by the KIGAM research project (Development of IOR/EOR technologies and field verification for carbonate reservoir in UAE), funded by the Ministry of Science and ICT, Korea to S. Kwon.

References

Gnos, E., Peters, T., 1993. K-Ar ages of the metamorphic sole of the Semail ophiolite; implications for ophiolite cooling history. Contributions to Mineralogy and Petrology 113, 325-332.

Goodenough, K.M., Thomas, R.J., Styles, M.T., Schofield, D.I., MacLeod, C.J., 2014. Records of ocean growth and destruction in the Oman-UAE ophiolite. Elements 10, 109-114.

Haase, K.M., Freund, S., Beier, C., Koepke, J., Erdmann, M., Hauff, F., 2016. Constraints on the magmatic evolution of the oceanic crust from plagiogranite intrusions in the Oman ophiolite. Contributions to Mineralogy and Petrology 171, 1-16.

Hacker, B.R., Gnos, E., 1997. The conundrum of samail: explaining the metamorphic history. Tectonophysics 279, 215-226.

Jacobs, J., Thomas, R.J., Ksienzyk, A.K., Dunkl, I., 2015. Tracking the Oman ophiolite to the surface - New fission track and (U-Th)/He data from the Aswad and Khor Fakkan Massifs, United Arab Emirates. Tectonophysics 644, 68-80.

Joun, H., Kokkalas, S., Tombros, S., 2018. Recycled oceanic crust as a source for tonalite intrusions in the mantle section of the Khor Fakkan block, Semail ophiolite (UAE). Geoscience Frontiers, https://doi.org/10.1016/j.gsf.2018.09.006

Nicolas, A. Ildefonse, B., Boudier, F., Lenoir, X., Ben Ismail W., 2000. Dike distribution in the Oman-United Arab Emirates ophiolite. Kluwer Academic Publishers 21, 269-287.

Rioux, M., Garber, J., Bauer, A., Bowring, S., Searle, M., Kelemen, P., Hacker, B., 2016. Synchronous formation of the metamorphic sole and igneous crust of the Semail ophiolite: New constraints on the tectonic evolution during ophiolite formation from high-

precision U-Pb zircon geochronology. Earth and Planetary Science Letters 451, 185-195.
Rioux, M., Bowring, S., Kelemen, P., Gordon, S., Miller, R., Dudás, F., 2013. Tectonic development of the Samail ophiolite: high-precision U-Pb zircon geochronology and Sm-Nd isotopic constraints on crustal growth and emplacement. Journal of Geophysical Research: Solid Earth 118, 2085e2101.
Searle, M.P., Cox, J., 2002. Subduction zone metamorphism during formation and emplacement of the Semail ophiolite in the Oman Mountains. Geological Magazine 139, 241-255.
Searle, M.P., Waters, D.J., Garber, J.M., Rioux, M., Cherry, A.G., Ambrose, T.K., 2015. Structure and metamorphism beneath the obducting Oman ophiolite: evidence from the Bani Hamid granulites, northern Oman mountains. Geosphere 11, 1812-1836.
Spencer, C.J., Cavosie, A.J., Raub, T.D., Rollinson, H., Jeon H., Searle, M.P., Miller, J.A., McDonald, B.J., Evans, N.J., the Edinburgh Ion Microprobe Facility (EIMF), 2017. Evidence for melting mud in Earth's mantle from extreme oxygen isotope signatures in zircon. Geology, vol.45, 975-978, doi:10.1130/G39402.1.
Styles, M.T., Ellison, R.A., Phillips, E.R., Arkley, S., Schofield, D.I., Thomas, R.J., Goodenough, K.M., Farrant, A.R., McKervey, J.A., Crowley, Q.G., Pharoah, T.C., 2006. The geology and geophysics of the United Arab Emirates, vol. 2. Geology, Ministry of Energy, United Arab Emirates, Abu Dhabi, p. 351.

15th International Congress of the Geological Society of Greece
Athens, 22-24 May, 2019 | Harokopio University of Athens, Greece
Bulletin of the Geological Society of Greece, Sp. Pub. 7 Ext. Abs. GSG2019-380

First report of Fe inclusions in olivine: olivine from the magnesite-hosting ultramafic rocks of Gerakini, Chalkidiki, Northern Greece

E. Tzamos[1,2], , G. Grieco[3], E. Pagona[4], A. Papadopoulos[2], M. Bussolesi[3], M. Mitrakas[4], A. Zouboulis[2]

(1) North Aegean Slops SA, Thessaloniki, Greece, tzamos@chem.auth.gr
(2) Laboratory of Chemical and Environmental Technology, Section of Chemical Technology and Industrial Chemistry, School of Chemistry, Aristotle University of Thessaloniki, 54124 Thessaloniki, Greece
(3) Department of Earth Sciences, Università degli Studi di Milano, via Botticelli n.23, 20133, Milano Italy
(4) Chemical Engineering Department, Schoolf of Engineering, Aristotle University of Thessaloniki, 54124, Thessaloniki, Greece

Magnesite ore deposits are closely associated with ophiolitic ultramafic rocks -more specifically dunites and chartzburgites. Dunites consist mainly of olivine (>90% v/v), whereas in chartzburgites the main mineral phases are olivine and pyroxenes (ortho- and clino-). These rocks can be altered at several extents due to serpentinization, and their primary minerals are altered to different mineral phases (mainly serpentine) but even in cases of extended serpentinization, relics of the primary minerals remain unaltered.

The mineral olivine belongs to the orthorhombic crystal system have a general chemical formula: X_2SiO_4, where X=Mg, Fe. The ratio of magnesium to iron varies between the two endmembers of the solid solution: forsterite (Mg_2SiO_4) and fayalite (Fe_2SiO_4). Compositions of olivine are commonly expressed as molar percentages of forsterite (Fo) and fayalite (Fa).

Synthesis of olivine in laboratory experiments has shown that, depending on the physico-chemical conditions, Mg and Fe can be substituted in small extend by other bivalent cations (e.g. Zn, Ni, Mn) (Nord *et al.*, 1982, Annersten *et al.*, 1982, 1984a, 1984b, Ericsson *et al.*, 1986).

Geologically, Gerakini area belongs to the ophiolitic sequence of Western Chalkidiki. In Gerakini the –serpentinized-ultramafic formations hosts numerous magnesite ore deposits. Currently, magnesite is being mined at Gerakini by the company “Grecian Magnesite SA”.

The main scope of this work is to provide new data about Fe inclusions found in olivine grains from the Gerakini ultramafic rocks. This is the first such report in Greece and –to the best of our knowledge- worldwide.

For the present study several rock samples (serpentinized dunites and chartzburgites) were taken from the Rachoni open pit mining site located at the Gerakini mining district. Thin-polished sections were mounted from each sample and were examined both in optical microscope (transmitted and reflected light). Mineral chemistry was determined with a JEOL 8200 electron microprobe equipped with a wavelength dispersive system (SEM-WDS). The system was operated using an accelerating voltage of 15 kV, a sample current on brass of 15 nA, a counting time of 20 s on the peaks and 10 s on the background. A series of natural minerals were used as standards.

In one of the studied samples (W5), the examination in the SEM revealed a very rare phenomenon: olivine grains in one particular area of the examined section had inclusions (Figure 1). EDS and WDS analyses from the inclusions showed that they consist solely of Fe.

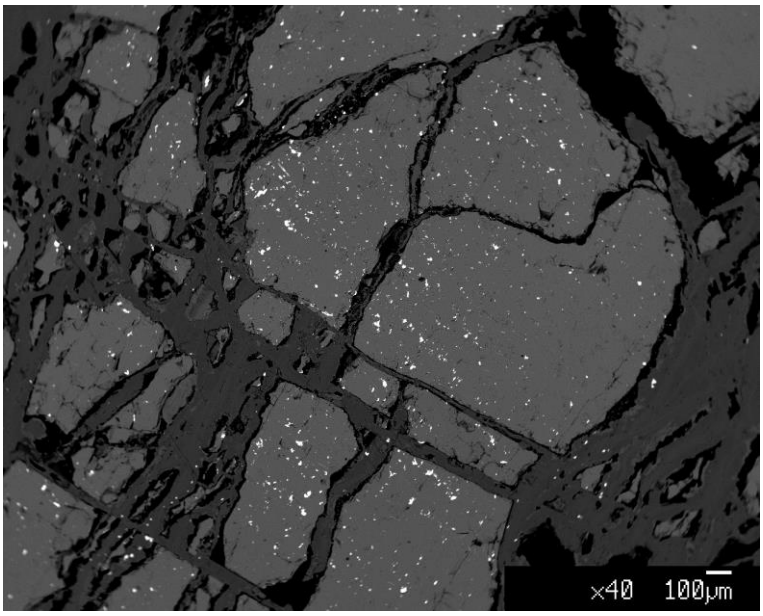

Figure 1. Back Scattered Electron (BSE) image from sample W5 showing Fe inclusions (white) in olivine relics (light grey). Dark grey is serpentine matrix.

The study of the mineral chemistry of olivines from sample W5 (Table 1) did not reveal any notable differences between olivines hosting Fe inclusions and those not. All olivines are high forsteritic and Fo content in both cases has a constant value of 0.90 ($Fo_{0.90}Fa_{0.10}$). Also, NiO content of olivines is rather low (<0.44wt.%), but no Ni alloys were found during the microscopic study of the sections.

Table 1. Mineral chemistry of olivine grains from sample W5. Analyses No 22-26 are from olivines with Fe incusions, whereas analyses No 31-35 are from olivines without inclusions.

Analysis No	22	23	24	25	26	31	32	33	34	35
SiO_2	41.59	41.51	41.75	41.30	41.16	41.65	41.75	41.31	41.31	41.74
TiO_2	0.01	0.04	0.05	0.01	0.05	--	--	--	0.01	--
Al_2O_3	--	--	--	0.04	--	--	--	--	0.02	0.02
Cr_2O_3	--	0.01	--	--	--	--	0.04	--	0.04	0.03
FeO	9.04	8.98	8.94	9.03	8.96	9.17	8.97	9.01	8.89	8.94
MnO	0.12	0.15	0.15	0.15	0.10	0.08	0.13	0.11	0.10	0.14
MgO	49.66	50.00	49.58	49.60	49.61	49.73	49.74	49.84	50.06	49.38
NiO	0.36	0.39	0.41	0.44	0.32	0.36	0.29	0.36	0.38	0.39
CaO	0.03	0.03	0.02	0.03	0.03	0.03	0.02	0.01	0.01	0.01
Total	100.82	101.11	100.90	100.60	100.23	101.03	100.93	100.65	100.83	100.65
Fo	0.90	0.90	0.90	0.90	0.90	0.90	0.90	0.90	0.90	0.90

The Fe inclusions must have segregated from magmas prior to or along with crystallization of olivine. The segregation of these inclusions, although minor amount, could result in Fe depletion in the evolved magmas (Bai *et al.*, 2017). Of course, subsolidus equilibration between olivine and chromite (Mg^{2+} diffusion from chromite to olivine and Fe^{2+} from olivine to chromite at subsolidus temperature) is the most probable factor controlling the olivine chemical composition and its high Fo content.

Conclusions

During the microscopic and mineral chemistry investigation of the studied samples, Fe inclusions in olivine were found in olivine grains of one of the samples. These inclusions must have crystallized prior to or along with olivine grains. The high Fo content of olivines in the studied samples is attributed –mainly- to subsolidus equilibration between olivine and chromite and –to some extend- to the formation of these inclusions.

Acknowledgements

This research has been co-financed by the European Union and Greek national funds through the Operational Program Competitiveness, Entrepreneurship and Innovation, under the call RESEARCH – CREATE – INNOVATE (project code:T1EDK-03543).







References

Annersten, H., Adetunji, J., Filippidis, A., 1984a. Cation ordering in Fe-Mn silicate olivines. American. Mineralogist, 69(11/12), 1110-1115.

Annersten, H., Ericsson, T., Filippidis, A., 1982. Cation ordering in Ni-Fe olivines. American Mineralogist, 67(11/12), 1212-1217.

Annersten, H., Filippidis, A., 1984b. Cation ordering in Ni-Fe olivines: reply. American Mineralogist, 69(1/2), 164.

Bai, Y., Su, B.-X., Chen, C., Yang, S.-H., Liang, Z., Xiao, Y., Qin, K.-Z., Malaviarachchi, S.P.K., 2017. Base metal mineral segregation and Fe-Mg exchange inducing extreme compositions of olivine and chromite from the Xiadong Alaskan-type complex in the southern part of the Central Asian Orogenic Belt. Ore Geology Reviews, 90, 184-192.

Ericsson, T., Filippidis, A., 1986. Cation ordering in the limited solid solution Fe_2SiO_4-Zn_2SiO_4. American Mineralogist, 71(11/12), 1502-1509.

Nord, A.G., Annersten, H, Filippidis, A., 1982. The cation distribution in synthetic Mg-Fe-Ni olivines. American Mineralogist, 67(11/12), 1206-1211.

15th International Congress of the Geological Society of Greece
Athens, 22-24 May, 2019 | Harokopio University of Athens, Greece
Bulletin of the Geological Society of Greece, Sp. Pub. 7 Ext. Abs. GSG2019-381

Iron oxidation state in Greek Cr-ore minerals

E. Tzamos[1], A. Douvalis[2], A. Rassios[3], M. Bussolesi[4], G. Grieco[4], A. Papadopoulos[5], A. Godelitsas[1]

(1) Department of Geology and Geoenvironment, National and Kapodistrian University of Athens, Zografou Campus, 15784, Athens, Greece, tzamos@geo.auth.gr
(2) Physics Department, University of Ioannina, 45110, Ioannina, Greece
(3) Institute of Geology and Mineral Exploration, 50100, Kozani, Greece
(4) Department of Earth Sciences, Università degli Studi di Milano, via Botticelli n.23, 20133, Milano Italy
(5) Laboratory of Chemical and Environmental Technology, School of Chemistry, Aristotle University of Thessaloniki, 54124 Thessaloniki, Greece

Although electron microprobe analysis (EMPA) is the most common analytical method for the study of mineral chemistry, it cannot recognize the multiple oxidation states of transitional metals and, as a sequence, the Fe^{2+}/Fe^{3+} ratio is calculated stoichiometric. In the case of spinels, this calculation method is applied assuming a proportion of 1 bivalent and 1 trivalent cation per 4 oxygens, thus ignoring the possibility of non-stoichiometry due to Fe^{3+} excess and cation vacancies in the lattice (Quintilani *et al.*, 2006).

For the determination of the actual Fe oxidation states in minerals, ^{57}Fe Mössbauer spectroscopy (MS) has be proven to be a very effective method (Wood and Virgo, 1989, McCammon *et al.*, 1998, Sobolev *et al.*, 1999, Quintilani *et al.*, 2006). The determination of the actual oxidation states of Fe and the attribution of Fe^{2+} and Fe^{3+} to the tetrahedrally and octahedrally coordinated T and M sites is spinels has been proven to be accurately calculated by the application of MS (e.g., Andreozzi *et al.*, 2001, Hålenius *et al.*, 2002, Quintilani *et al.*, 2006). Furthermore, since Fe ratios of Cr-spinels are used for the estimation of fO_2 by the Ballhaus *et al.* (1990) oxygen geobarometer and for the estimation of equilibrium temperatures by the Ballhaus *et al.* (1991) geothermometer, the determination of the actual oxidation states of Fe and their use in these estimations is valuable for the accurate reconstruction of the thermo-oxidative history Cr-spinels host rocks.

The aim of this study is to present new MS data of spinels (chromites) from Vourinos ophiolitic sequence chromitites and compare the actual Fe oxidation states calculated by MS with the stoichiometric calculations based on EMPA.

Four chromitite samples from three mining sites of Vourinos chromite mining district were used for this study: Xerolivado-Skoumtsa (2 samples), Aetoraches (1 sample) and Rizo (1 sample). All samples were examined in transmitted and reflected light optical microscopes. Mineral chemistry was determined with a JEOL 8200 electron microprobe equipped with a wavelength dispersive system (SEM-WDS). The system was operated using an accelerating voltage of 15 kV, a sample current on brass of 15 nA, a counting time of 20 s on the peaks and 10 s on the background. A series of natural minerals were used as standards. The approximate detection limit is 0.01 wt.% for each element. For each sample, 4-6 of unaltered Cr-spinel cores were analyzed and their compositions averaged to produce a statistical result. The samples were crashed, grained and, with the use of magnetic separator, chromite was separated from the other mineral phases present. These almost pure (>90 wt.%) chromite samples were analyzed by means of ^{57}Fe Mossbauer spectroscopy.

Fe^{2+} and Fe^{3+} cations based on four oxygen and the Fe^{3+}/Fe^{2+} and $Fe^{3+}/\Sigma Fe$ ratios calculated by different approaches are presented in Table 1, whereas MS spectra acquired for the four samples is presented in Figure 1.

Table 1. Calculations of Fe^{2+} and Fe^{3+} cations and Fe^{3+}/Fe^{2+} and $Fe^{3+}/\Sigma Fe$ ratios for the studied samples.

Sample		XER5	XER10	RIZ3	AET4
Parameter	Method				
Fe^{2+} cations based on 4 (O)	EMPA	0.348	0.359	0.338	0.330
Fe^{3+} cations based on 4 (O)	EMPA	0.085	0.048	0.069	0.053
Fe^{3+}/Fe^{2+}	EMPA	0.246	0.135	0.205	0.161
$Fe^{3+}/\Sigma Fe$	EMPA	0.197	0.119	0.170	0.139
Fe^{3+}/Fe^{2+}	MS	0.250	0.140	0.330	0.200
$Fe^{3+}/\Sigma Fe$	MS	0.200	0.120	0.250	0.170

Comparison between spinel Fe^{3+} contents calculated by EMPA and measured by MS show significant differences: Fe^{3+} contents calculated by EMPA range between 11.9 to 19.7% of total Fe, whereas Fe^{3+} contents measured with MS range between 12 and 25%. In addition, the values of Fe^{3+}_{MS} content is higher in all samples compared to the Fe^{3+}_{EMPA} content. The differences observed in the Fe^{3+} contents by the different approaches are due to non-stoichiometry. MS can reveal

the Fe^{3+} excess of Cr-spinels while the EMPA approach cannot (Bosi *et al.*, 2004). Fe^{3+} excess is attributed the fact that during Cr-spinel oxidation, the only cations involved are Fe^{2+} and Fe^{3+}. During this process, tetrahedrally coordinated Fe^{2+} oxidized to Fe^{3+} with the formation of a cation vacancy in the T site (Quintilani *et al.*, 2006).

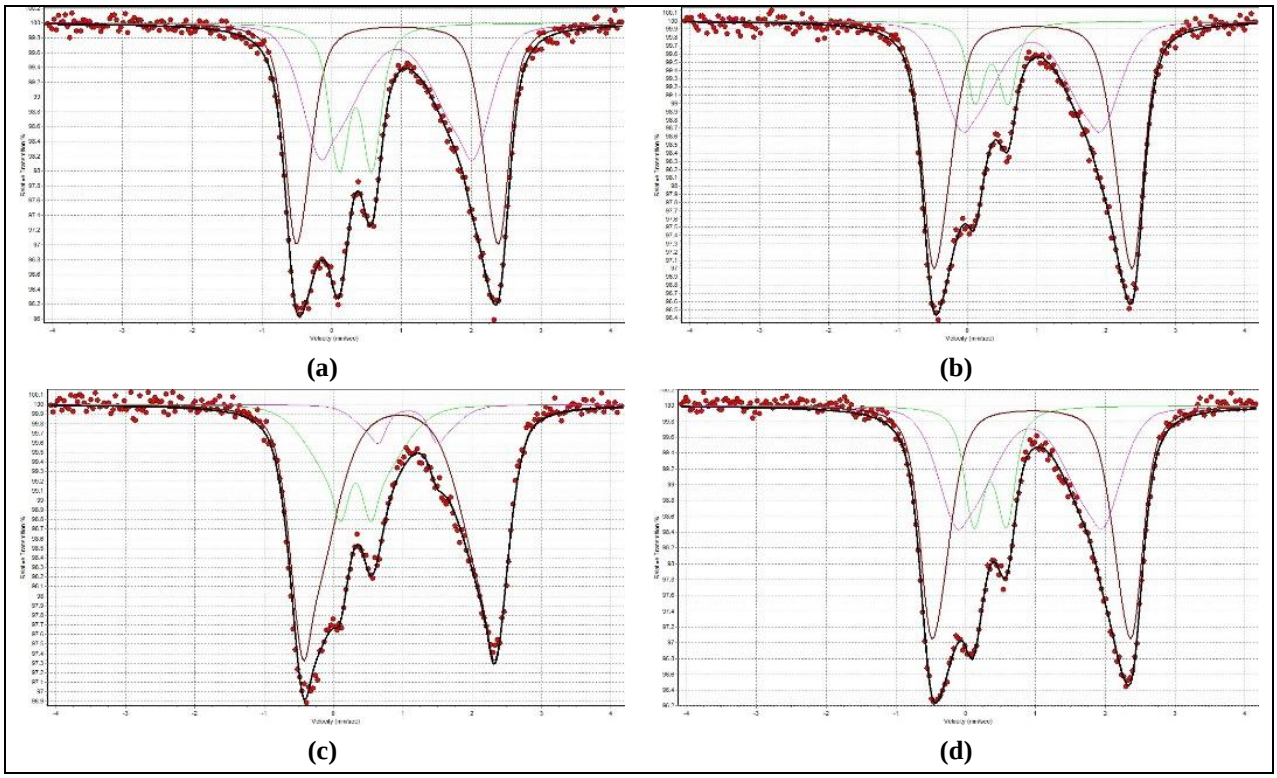

Figure 1. MS spectra of Vourinos Cr-spinel samples recorded at 77 K: (a) XER10, (b) XER5, (c) RIZ3 and (d) AET4.

The difference is slight in samples from Xerolivado-Skoumtsa (Southern Vourinos-samples XER5 and XER10) and significant in samples from Northern Vourinos (Rizo-sample RIZ3 and Aetoraches-sample AET4). This fact implies higher oxidation degrees (Bosi *et al.*, 2004) for Northern Vourinos Cr-spinels than of those from Southern Vourinos were oxidation seems to be insignificant, implying a relation between the degree of oxidation and provenance.

Ongoing research is targeting the further investigation of the latter remark and the estimation of the geothermo-barometric conditions via the accurate quantification of Fe^{3+} that has been revealed by MS measurements.

Acknowledgements

This research is implemented through IKY scholarships programme and co-financed by the European Union (European Social Fund - ESF) and Greek national funds through the action entitled ”Reinforcement of Postdoctoral Researchers”, in the framework of the Operational Programme ”Human Resources Development Program, Education and Lifelong Learning” of the National Strategic Reference Framework (NSRF) 2014 – 2020.

References

Andreozzi, G.B., Hålenius, U., Skogby, H., 2001. Spectroscopic active $^{IV}Fe^{3+}$-$^{VI}Fe^{3+}$ clusters in spinel-magnesioferrite solid solution crystals: a potential monitor for ordering in oxide spinels. Physics and Chemistry of Minerals, 28, 435-444.

Ballhaus, C., Berry, R.F., Green, D.H., 1990. Oxygen fugacity controls in the Earth’s upper mantle. Nature, 349, 437-449.

Ballhaus, C., Berry, R.F., Green, D.H., 1991. High pressure experimental calibration of the olivine-orthopyroxene-spinel oxygen geobarometer: implications for the oxidation state of the upper mantle. Contributions to Mineralogy and Petrology, 107, 27-40.

Bosi, F., Andreozzi, G.B., Ferrini, V., Lucchesi, S., 2004. Behavior of cation vacancy in kenotetrahedral Cr-spinels from Albanian eastern belt ophiolites. American Mineralogist, 89, 1367-1373.

Hålenius, U., Skogby, H., and Andreozzi, G.B. (2002) Influence of cation distribution on the optical absorption spectra of Fe^{3+}-bearing spinel s.s.-hercynite crystals: evidence for electron transition in $^{VI}Fe^{2+}$-$^{VI}Fe^{3+}$ clusters. Physics and Chemistry of Minerals, 29, 319-330.

McCammon, C.A., Chinn, I.L., Gurney, J.J., McCallum, M.E., 1998. Ferric iron content of mineral inclusions in diamonds from George Creek, Colorado determined using Mössbauer spectroscopy. Contributions to Mineralogy and Petrology, 133, 30-37.

Quintilani, M., Andreozzi, G., Graziani, G., 2006. Fe^{2+} and Fe^{3+} quantification by different approaches and fO_2 estimation for Albanian Cr-spinels. American Mineralogist, 91, 907-916.

Sobolev, V.N., McCammon, C.A., Taylor, L.A., Snyder, G.A., Sobolev, N.V., 1999. Precise Mössbauer milliprobe determination of ferric iron in rockforming minerals and limitations of electron microprobe analysis. American Mineralogist, 84, 78-85.

Wood, B.J., Virgo, D., 1989. Upper mantle oxidation state: Ferric iron contents of lherzolite spinels by ^{57}Fe Mössbauer spectroscopy and resultant oxygen fugacities. Geochimica et Cosmochimica Acta, 53, 1277-1291.

15th International Congress of the Geological Society of Greece
Athens, 22-24 May, 2019 | Harokopio University of Athens, Greece
Bulletin of the Geological Society of Greece, Sp. Pub. 7 Ext. Abs. GSG2019-382

Mineralogical and Geochemical Investigation of the Alteration of Ultramafic Magnesite-Hosting Rocks from Gerakini (Chalkidiki, Northern Greece)

A. Papadopoulos[1], E. Tzamos[1,2], E. Pagona[3], G. Grieco[4], A. Kasinos[5], E. Tziritis[2,6], M. Mitrakas[3], A. Zouboulis[1]

(1) Laboratory of Chemical and Environmental Technology, Section of Chemical Technology and Industrial Chemistry, School of Chemistry, Aristotle University of Thessaloniki, 54124 Thessaloniki, Greece, argpapad@geo.auth.gr
(2) North Aegean Slops SA, Thessaloniki Greece
(3) Chemical Engineering Department, School of of Engineering, Aristotle University of Thessaloniki, 54124, Thessaloniki, Greece
(4) Department of Earth Sciences, Università degli Studi di Milano, via Botticelli n.23, 20133, Milano Italy
(5) Grecian Magnesite SA, Gerakini, Greece
(6) Hellenic Agricultural Organization "Demeter", Soil and Water Resources Institute, Sindos, Greece

Background

Magnesite is closely associated with ophiolitic ultramafic rocks, more specifically dunites and chartzburgites, which can be altered at several extents due to different alteration episodes (e.g. serpentinization, carbonitization-silicification). In Northern Greece, the main magnesite ore deposits are located at Chalkidki area, more specifically, at Vavdos, Gerakini, Ormilia, Poligiros and Agia Paraskevi. Currently, magnesite is being mined at Gerakini and Ormilia sites by "Grecian Magnesite SA' mining company. The study area of Gerakini hosts the ophiolitic sequence of Western Chalkidiki.

Objective

Previous researchers have already provided mineralogical and geochemical data about ultramafic host rock-types, as well as magnesite (e.g. Papadopoulos, 2007, Skliros, 2013). In this study, the main objectives are to provide additional mineralogical and geochemical information, aiming to elucidate the mineralogical and geochemical differences of the different ultramafic lithological host rock-types, reveal their alteration history and thus to contribute to the understanding of magnesite formation.

Methods

For the present study, seven (7) rock samples were taken from the Rachoni open pit mining site located at the Gerakini mining district. Thin-polished sections were mounted from each sample and were examined both in optical microscope and by means of scanning electron microscopy (SEM). Mineralogical composition of the collected samples was determined by X-Ray Diffraction (XRD) whereas supplementary information on the composition was received by Thermo-Gravimetric and Differential Thermal Analysis (TG-DTA) and Fourier-Transformed Infrared Spectroscopy (FT-IR). The chemical composition of the samples was determined by FUS-ICP-MS.

Results

The studied samples can be divided into three different categories based on the degree and type of alteration they have undergone.

The mineral assemblages of quartz+carbonates(dolomite+calcite)+spinels+chlorite, as well as the enrichment in SiO_2 and CaO (Table 1) content of samples W1 and W2 are typical of listwanites. Listwanites are silica-carbonate-rich products of low-grade metasomatic processes after mafic and ultramafic rocks (Tsikouras *et al.*, 2006 and references therein). More specifically, hydrothermal circulation of a CO_2-rich fluid phase in a high water/rock ratio (Koutsovitis and Magganas, 2013) favor the formation of listwanites. The silification-carbonization reactions may well be responsible for the liberation of MgO from serpentine, suggesting an alternative source of Mg responsible for the magnesite formation.

Sample W3 is consisted of vermiculite+quartz+serpentine+talc+amphibole+plagioclase+chlorite+magnesite. Notably, also small grains of zircon and monazite were observed with SEM. The extended presence of vermiculite indicate that this sample has undergone clay alteration apart from serpentinization (Serelis *et al.*, 2004).

Samples W4, W5, W6 and W7 mainly consist of olivine+serpentine+pyroxenes+spinels+magnetites+carbonates (magnesite+dolomite+calcite). These rocks are all typical magnesite-hosting serpentinites having undergone various degrees of serpentinization with their protoliths being dunites and hartzburgites.

The chemical analyses of the studied samples are in agreement with the mineralogical investigation and the classification of these rocks in three different categories.

Table 1. Chemical composition of major and minor oxides in studied samples.

Sample		W1	W2	W3	W4	W5	W6	W7
SiO_2	(wt.%)	64.92	65.31	40.63	41.8	37.22	35.02	36.63
Al_2O_3	(wt.%)	10.74	1.23	2.68	0.55	0.32	0.24	0.34
$Fe_2O_{3(t)}$	(wt.%)	1.88	7.23	5.76	8.34	8.5	7.9	8.18
MnO	(wt.%)	0.035	0.106	0.107	0.117	0.147	0.112	0.119
MgO	(wt.%)	8.42	5.82	33.32	45.16	43.86	41.91	42.21
CaO	(wt.%)	3.95	7.44	1.52	0.54	0.47	0.3	0.47
Na_2O	(wt.%)	2.95	0.05	0.1	< 0.01	< 0.01	< 0.01	< 0.01
K_2O	(wt.%)	0.38	0.06	0.01	< 0.01	< 0.01	< 0.01	< 0.01
TiO_2	(wt.%)	0.078	0.051	0.045	0.007	0.004	0.003	0.004
P_2O_5	(wt.%)	0.02	0.04	0.02	0.01	0.01	< 0.01	< 0.01
LOI	(wt.%)	6.87	12.47	15.96	3.5	9.49	14.43	12.35

Regarding the content of the samples in rare earth elements (REE), samples W4, W5, W6 and W7 contain very low REE concentrations, which is a typical characteristic of serpentinized ultramafic rock. On the contrary, the chondrite-normalized patterns of samples W1, W2 and W3 reveal higher REE concentrations, especially LREE.

Conclusions

Considering the mineralogical and geochemical composition of the rock-types, serpentinization, carbonitization-silicification and clay alteration can be distinguished. Carbonatization-silicification suggests additional Mg source for the formation of magnesite. Ongoing research aims to the better understanding of the geologic history of the ultramafic rocks of the broader Gerakini-Ormilia area along with the magnesite ore formation at these localities.

Acknowledgements

This research has been co-financed by the European Union and Greek national funds through the Operational Program Competitiveness, Entrepreneurship and Innovation, under the call RESEARCH – CREATE – INNOVATE (project code:T1EDK-03543).







References

Koutsovitis, P., Magganas, A., 2013. Mineralogy and geochemistry of listwanite occurrences from the Othris ophiolite, Greece. EGU General Assembly, Vienna, Austria., Geophysical Research Abstracts, 15, EGU2013-12712.

Papadopoulos, A., 2007. Production and applications of commercial types of Klisoura bauxite and Gerakini magnesite. M.Sc. Thesis, Aristotle University of Thessaloniki, 130p. (in Greek)

Serelis, K., Gartzos, E., Tsaousidou, P., 2004. Investigation of the alterations of the ultramafic rocks hosting magnesite ores at N. Evia. Proceedings of the 10th International Congress, Thessaloniki, Greece, Bulletin of the Geological Society of Greece, XXXVI, 377-386. (in Greek)

Skliros, V., 2013. Investigation of the formation conditions of Vavdos and Gerakini (Central Chalkidiki) magnesite occurences and environmental applications utilization study. M.Sc. Thesis, University of Patras, 186 p. (in Greek).

Tsikouras, B., Karipi, S., Grammatikopoulos, T., Hatzipanagiotou, K., 2006. Listwaenite evolution in the ophiolite melange of Iti Mountain (continental Central Greece). European Journal of Mineralogy, 18, 243-255.

GENERAL SESSION

T5 Geomorphology, Quaternary Geology and Geoarchaeology

Conveners: **Niki Evelpidou (NKUA)**
Efthymios Karymbalis (HUA)

Co-organized by the Committee for Geomorphology and Environment, G.S.G.

15th International Congress of the Geological Society of Greece
Athens, 22-24 May, 2019 | Harokopio University of Athens, Greece
Bulletin of the Geological Society of Greece, Sp. Pub. 7 Ext. Abs. GSG2019-051

The Mavrovouni-1 cave in the flysch of Gavrovo-Tripolis Zone (SW Greece)

P. Karoutsos[1], G. Lazaridis[2], G. Iliopoulos[1]

(1) Department of Geology, University of Patras, 26504, Rio, panoskaroutsos@hotmail.com
(2) Aristotle University of Thessaloniki, Department of Geology, Laboratory of Geology and Palaeontology, 54124, Thessaloniki, Greece

Among several thousands of caves that have been reported in Greece, there are hundreds that have developed in non-carbonate lithology (i.e. Lazaridis et al., 2016 and cited references) and non-pure carbonates, such as breccias and conglomerates (i.e. Vlastaridis et al., 2014). Caves formed in flysch sediments have not identified previously in Greece and even in countries with thousands of recorded karst caves, only few examples are known (i.e. Pavuza, 2013).

The aim of this study is to document the morphology of the Mavrovouni-1 cave formed in flysch deposits and set the basis for further investigation in caves in this lithology and their speleogenesis.

Location and geology

The cave is located at 119 m above sea level (a.s.l.) at the Mavrovouni hill (287 m s.a.l.), which lies between the low mountains of Klokova (1038 m a.s.l.) to the East and Varasova (917 m a.s.l.) to the West. Its entrance (N 38.357470˚, E 21.661114˚) was artificially opened during road construction works.

In the broader area an Upper Eocene flysch formation that consists of three series of sandstones, conglomerates and shales crops out. These rocks belong to the Gavrovo-Tripoli Zone with a total thickness of about 700 m. Furthermore, they overlay almost 900 m thick limestones of Upper Cretaceous and Paleocene-Middle Eocene age (IGME 1991). The cave has been formed in SW dipping beds of polimictic conglomerates with well-rounded cobbles of carbonates and cherts that are alternating with lenses of shales and sandstones.

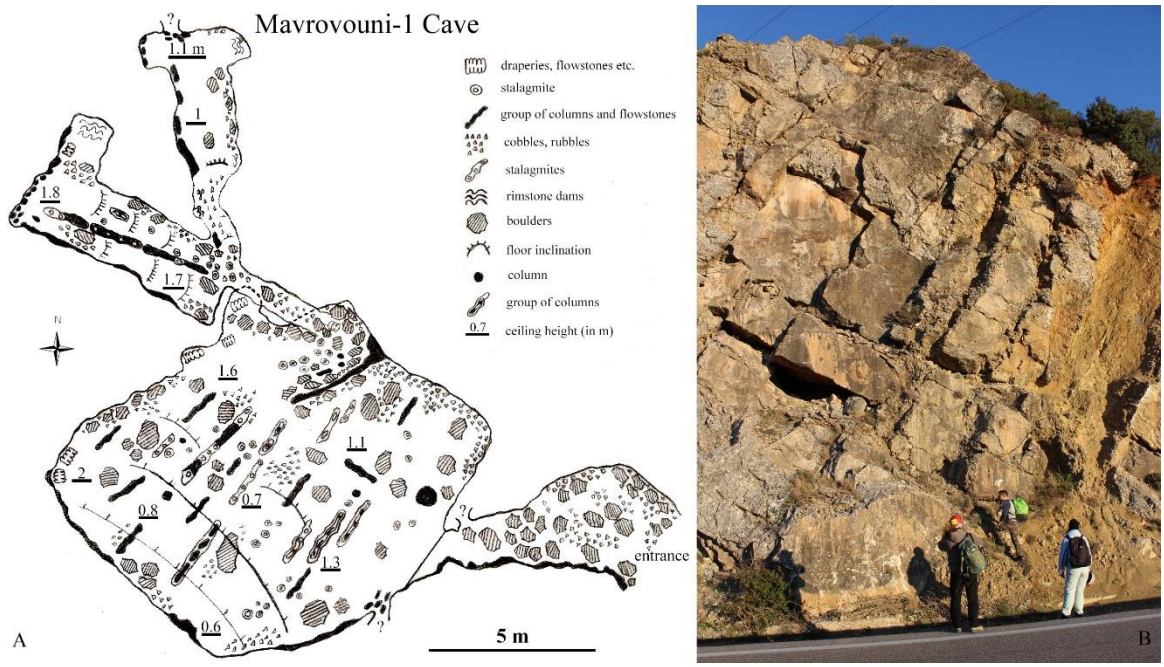

Figure 1. Mavrovouni-1 Cave: A. ground-plan; B. the cave entrance on the section with conglomerates and shales.

Cave description

A detailed survey of the Mavrovouni-1 cave resulted in the ground-plan of figure 1 (for methods see Kalogeropoulos et al., 2008; Trimmis, 2018 and references cited). The cave area is about 140 m2 and total passage length is almost 50 m. It consists of a main chamber that is connected to smaller elongated corridors. The entrance corridor is an about ENE-WSW 9 m long passage that leads to the main chamber that is accessible after climbing a three meters high wall. The main chamber is an about 10x10 m space of low height ranging from 0.6 to 2 m. The chamber is connected through a narrow passage at the NW edge to a bifurcating corridor. The latter consists of a 7 m long ascending part towards the West and another 7 m long descending part towards the NNW. The height of this part ranges from 1.4 to 1.8 m.

The side walls and the cave-ceiling are characterized by the absence of typical dissolutional features (see i.e. Lauritzen and Lundberg, 2000; Gunn, 2004; Ford and Williams, 2007; White and Culver, 2005) and they form planar surfaces. Furthermore, the floor is covered by boulders.

The cave is moderately decorated mainly with common types of speleothems, such as stalagmites, stalactites, coralloids, draperies, soda-straws, flowstones, rimstone dams, shelfstones, some less common such as the eccentrics and the rarely reported yet in Greece cave-blisters (see Hill and Forti, 1997 for nomenclature). However, most of the speleothems are

dry and some of them corroded. It worth's to mention that the largest columns, stalagmites and stalactites were formed along NE-SW and NW-SE directions due to their relation with rock discontinuities.

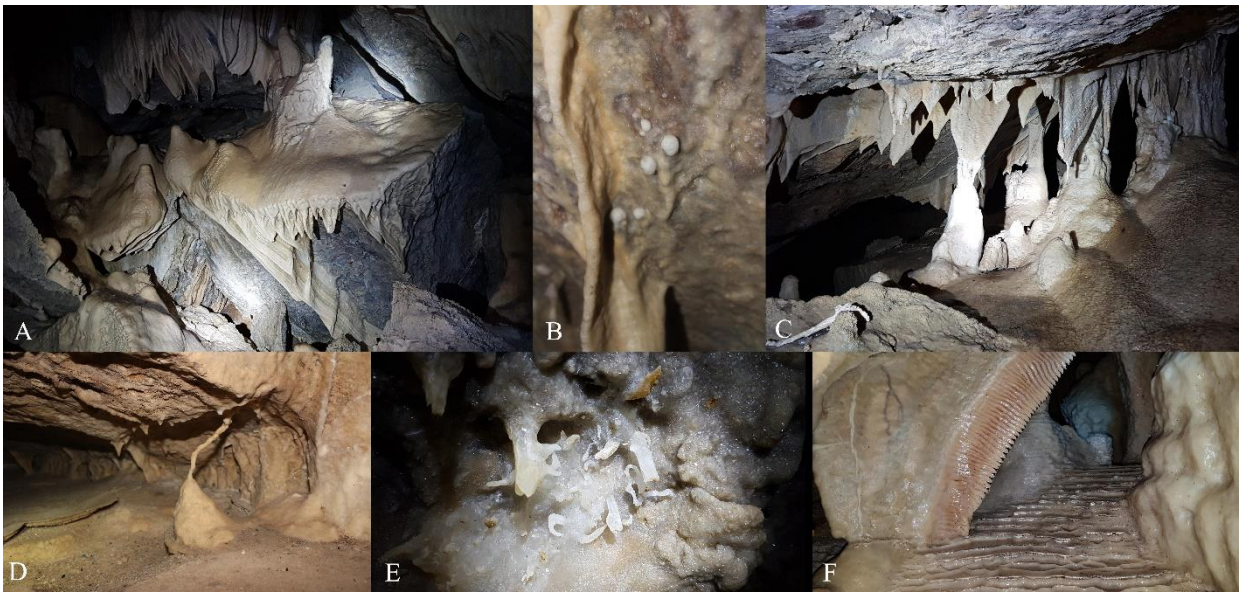

Figure 2. Speleothems from Mavrovouni-1 Cave: A. flowstone and stalagmites on collapsed boulders; B. Cave blisters (diameter ~1cm); C. columns, stalagmites and draperies along joints; D. a deflected stalactite connected to a stalagmite in a dry pool; E. eccentrics; F. drapery and rimstone dams.

Concluding remarks

- The Mavrovouni-1 cave has been mainly formed along a NW-SE direction that is more or less parallel to the strike of the bedding. Joint-controlled walls and ceiling are also related to breakdown morphology that appears in the cave.
- Commonly caves found in Flysch have been developed by tectonics and have a crevise morphology (i.e. Pavuza, 2013; Lenart et al., 2014). However, the Mavrovouni-1 cave is morphologically differentiated by crevises and resembles typical karst cavities. The presence of speleothems is indicative of the conglomerate's solubility by the seepage water. Thus, a dissolution process succeeded by breakdown is plausible.
- Some of the speleothems found in the cave are rarely reported in Greece, such as the cave-blisters (see also Sotiros Cave in Athens; V. Athanassopoulos in Lazaridis [coordinator, 2019]).
- Although, flysch outcrops are not attractive to cave exploration and survey due to the scarcity of cavernous forms, the future study of flysch caves in Greece should first focus in their discovery and identification in the field. Mavrovouni and the surroundings is a promising area for such a research.

Acknowledgments

We thank the geology students and cavers Kyriaki Fellachidou, Alkiviadis Sideridis and Xenofon Simos for their assistance during the field work.

References

Ford, D., Williams, P.D., 2007. Karst hydrogeology and geomorphology. John Wiley and Sons Inc.

Gunn, J., 2004. Encyclopedia of Caves and Karst Science. Taylor and Francis Inc. Hill, C.A., Forti, P., 1997. Cave minerals of the world (2nd ed.). 1-463, National Speleological Society.

IGME, 1991. Sheet Thermon, scale 1:50.000.

Kalogeropoulos, I., Lazaridis, G., Tsekoura, A., 2008. Methodology of cave mapping: comparing routings. 4th Pancretan Speleological Symposium. Hellenic Speleological Society, Rethymnon, Crete, Greece

Lazaridis, G., Trimmis, K.-P., Karadimou, G., Kalogeropoulos, I., Papaioannou, I. Ch., 2016. Geological exploration of the Kastanophyto Cave, Greece. Proceedings of the VII International Scientific Correspondence Conference. Speleology and Spelestology. Nabereznye Chelny.

Lazaridis G. (coordinator). Speleothems in Greece. Web [accessed 15/3/2019]. http://speleothems.weebly.com/

Lenart, J., Pánek, T., & Dušek, R. (2014). Genesis, types and evolution of crevice-type caves in the flysch belt of the Western Carpathians (Czech Republic). Geomorphology, 204, 459-476.

Pavuza, R. 2013. Caves in the Austroalpine Flysch. Newsletter UIS-Comm. Pseudokarst, 23: 7-13.

Trimmis, K.P., 2018. Journal of Archaeological Science: Paperless mapping and cave archaeology: A review on the application of DistoX survey method in archaeological cave sites. Reports 18, 399-407.

Vlastaridis, J., Lazaridis, G., Eleftheriadis, E., 2014. Caves and speleology of Sintiki, in Municipality of Sintiki: the area and its history. Sidirokastro, Serres, Greece.

White, W. B., Culver, D. C. 2005. Encyclopedia of caves, Elsevier Amsterdam (The Netherlands).

15th International Congress of the Geological Society of Greece
Athens, 22-24 May, 2019 | Harokopio University of Athens, Greece
Bulletin of the Geological Society of Greece, Sp. Pub. 7 Ext. Abs. GSG2019-052

Cupola-related morphology of the Mesolakkia Caves, Greece

G. Lazaridis[1], K. Fellachidou[1], S. Efraimidou[1]

(1) Aristotle University of Thessaloniki, Department of Geology, Laboratory of Geology and Palaeontology, 54124, Thessaloniki, Greece, geolaz@geo.auth.gr

Cupola is a term that describes dome-shaped solution cavities and they are accompanied by several features such as terraces, cusps, pendants, pillars, rock bridges etc. Their formation has been attributed to a number of processes summarized by Osborne (2004) and thus they are considered as polygenetic (Dublyansky, 2013).

A brief description of the Mesolakkia caves along with a data set with cupola dimensions and images are given. Furthermore, the process of speleogenesis is discussed on the basis of the morphological observations.

Methods

The study of the Mesolakkia caves is based on their morphological features. They are surveyed in two and three dimensions using standard and paperless speleological mapping techniques (i.e. Kalogeropoulos *et al.*, 2008; Trimmis, 2018 and reference therein). Laser distance meter and Suunto compass were used. Rock discontinuities measured with a Clar compass. Identification and interpretation of morphological features follow Lauritzen and Lundberg (2000), Gunn (2004), Ford and Williams (2007), White and Culver (2005) and of speleothems follow Hill and Forti (1997).

Cave description and morphology

Three caves have been found to be opened in the marble of the Pangeon Unit (Rila-Rhodope Massif). These are the Disakia Cave, Small Disakia Cave and Disakia shelter-cave, considered all together part of a uniform cave system, called below Disakia Cave System (DCS).

Disakia Cave: is a relatively small cave. Its entrance is a 3m deep pothole. It consists of (Fig. 1) small rooms and fracture-guided passages of NW-SE direction that are interconnected to each other with small SW-NE passages and windows. Some passages are characteristically high and narrow (Fig. 1F). There is also a number of abruptly terminating passages.

The predominant solution feature noticed are the cupolas that are formed in side-walls and mainly the ceiling. Most of them found to be unrelated to rock fractures and generally wide. Thus, their horizontal diameters appear to be larger than that of the vertical axis. Inside these concave features corroded speleothems, such as stalactites, flowstone and draperies are commonly present. Their length (largest horizontal diameter) ranges from 0.51 to 2.20 m and their width from 0.36 to 1.9 m. Their height is only 0.15 to 0.90 m. Their mean shape is 0.97x0.80x0.48 m. Apart from the small-scale cupolas, there are some cupola-like rooms. In addition terraces, notches, cups, pendants and similar forms are also present.

Cave decoration consists of calcite speleothems that in most cases appear to be corroded or damaged and broken by visitors. It is worth to mention that the cave, and especially its deepest parts display numerous inscriptions with mainly names and in some cases dates. They seem to be of the 20th and 21st centuries but the presence of older inscriptions cannot be excluded since a detailed record of them is pending.

Table 1. Small-scale cupola measurements from the Disakia Cave.

Length(cm)	60	125	120	60	61	51	220	92	83
Width(cm)	36	100	100	57	49	36	190	74	81
Height(cm)	37	90	50	37	27	35	60	15	80

Small Disakia Cave: The entrance of this cave is a small opening on a steep escarpment. Close to the entrance the passage is short and partially filled with fine-grained sediment. In the deepest part there are two rooms interconnected to each other with a small window-like passage, located about two meters higher than the cave floor. The last room is the largest one and displays cupolas and related forms that cut evenly the bedrock and speleothems. The floor in filled with guano.

Disakia shelter-cave: Between the above mentioned caves there is a small cavity presently forming a shelter-cave. This small cave remnant has a diameter of few meters and its walls and ceiling consist a chain of cupolas (Fig. 1D).

Discussion

In the absence of geochemical evidence in DCS, the interpretation of speleogenesis can be grounded only on morphological criteria. In the broader area there are both epigene and hypogene caves (Lazaridis, 2017). DCS consists of chambers interconnected with passages and blind galleries that form a ramiform pattern in ground-plan (see Palmer, 2000). This pattern is indicative of phreatic speleogenesis and genetically placed between spongework and network caves, that means caves formed in mixing zones by aggressive waters of low flow velocity (diffusion dominates) and caves formed mainly related to hydrothermal activity (Dublyansky, 2013). Orientation of passages is strongly affected by discontinuities of the bedrock and especially the more or less vertically dipping groups of joints. Meso-scale features, such as pendants, pillars, cups, terraces, ridges, notches and the predominant forms cupolas that occur on the bedrock are

probably related to the main phase of speleogenesis. Small-scale cupolas and the related solution features that intersect vadose speleothems indicating a post-phreatic process due to condensation corrosion. Other, vadose dissolution forms and forms developed in concentrated lateral flow, such as scallops, are absent in DCS.

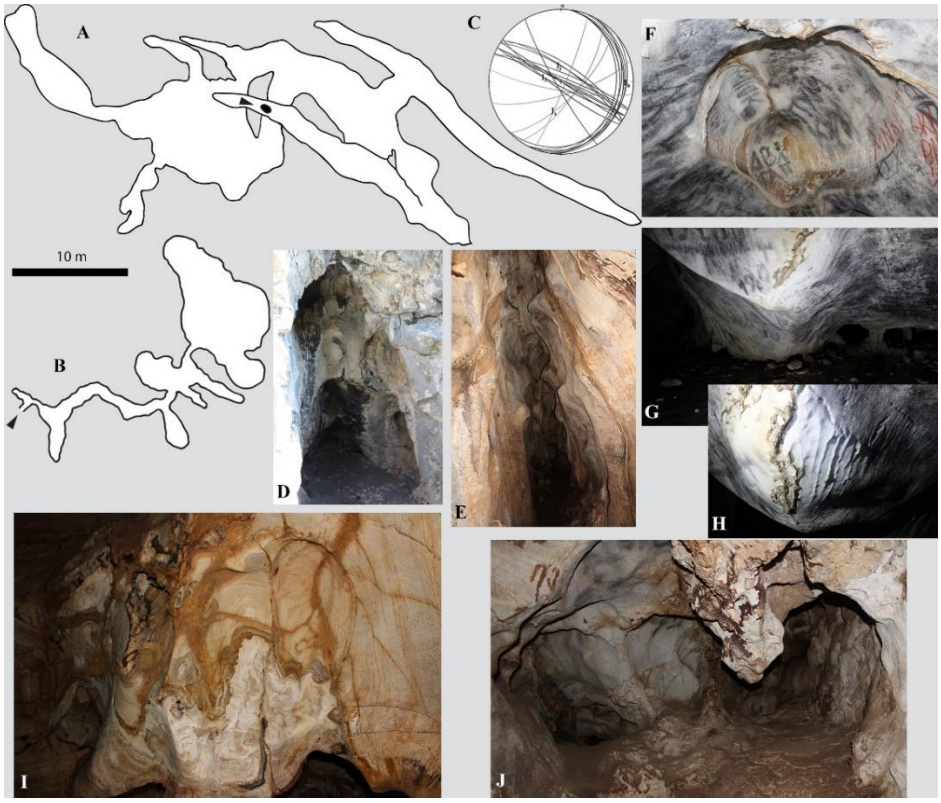

Figure 1. A. Ground-plan of Disakia cave; B. ground-plan of small Disakia cave; C. Schmidt diagram of rock discontinuities; D. view of Disakia shelter-cave; E. narrow and high fracture guided passage in Disakia cave with cusps and terraces related to cupolas; F. typical flat and wide cupola in Disakia cave; G. cusp and ridge separating cupola-shaped rooms in Disakia cave; H. detail of corrosion on the wall of G; I. cupola that evenly intersects the rock and speleothems in small Disakia cave; J. pendant and partitions in small Disakia cave.

Concluding remarks

The meso scale cupolas that form chambers and (e.g. Disakia shelter-cave) and the cave pattern indicate a phreatic origin and dissolution by convecting water bodies. A relation to the hydrothermal speleogenetic phase that has been affected the area (Lazaridis, 2017) cannot be excluded.

Small-scale cupolas and the corroded speleothems are due to condensation corrosion that is post-phreatic but not necessarily distinguished from the speleogenetic process; i.e. hydrothermal speleogenesis.

Further speleological exploration and geological investigation in the broader area could provide more evidence for the speleogenesis.

Acknowledgements

We thank the members of the Kavala's speleological group for indicating the cave entrances and accompanying us during the field work. The MA Architect, Iraklis Kalogeropoulos is thanked for his contribution in the cave survey.

References

Dublyansky, Y.V., 2013. Karstification by geothermal waters, in: Shroder J., Frumkin A. (Eds.), Treatise on geomorphology. Academic Press, San Diego, (6): 57–71.

Ford, D., Williams, P.D., 2007. Karst hydrogeology and geomorphology. John Wiley and Sons Inc.

Gunn, J., 2004. Encyclopedia of Caves and Karst Science. Taylor and Francis Inc. Hill, C.A., Forti, P., 1997. Cave minerals of the world (2nd ed.). 1-463, National Speleological Society

Kalogeropoulos, I., Lazaridis, G., Tsekoura, A., 2008. Methodology of cave mapping: comparing routings. 4th Pancretan Speleological Symposium. Hellenic Speleological Society, Rethymnon, Crete, Greece
http://ese.edu.gr/media/seminars/sem_notes/hartografisi/survey_methods.pdf

Lauritzen, S., Lundberg, J., 2000. Solutional and erosional morphology of caves., in: Klimchouk, A., Ford, D.C., Palmer, A.N., Dreybrodt, W. (Eds.), Speleogenesis. Evolution of Karst Aquifers. Huntsville: National Speleological Society.

Lazaridis, G., 2017. Hypogene Speleogenesis in Greece., in: Klimchouk, A., Palmer, A.N., De Waele, J., Auler, A.S. & Audra, P. (Eds.), Hypogene Karst Regions and Caves of the World. Springer, 225-239.

Osborne, R.A.L., 2004. The troubles with cupolas. Acta Carsologica, 33: 9-36. Davis, G.H., Reynolds, S.J., Kluth, C.F., 2011.

Trimmis, K.P., 2018. Journal of Archaeological Science: Paperless mapping and cave archaeology: A review on the application of DistoX survey method in archaeological cave sites. Reports 18, 399-407.

White, W. B., Culver, D. C. 2005. Encyclopedia of caves, Elsevier, Amsterdam (The Netherlands).

15th International Congress of the Geological Society of Greece
Athens, 22-24 May, 2019 | Harokopio University of Athens, Greece
Bulletin of the Geological Society of Greece, Sp. Pub. 7 Ext. Abs. GSG2019-053

Drawing a paragenetic cave passage in MatLab

G. Lazaridis[1], D. Voulanas[2]

(1) Aristotle University of Thessaloniki, Department of Geology, Laboratory of Geology and Palaeontology, 54124, Thessaloniki, Greece, geolaz@geo.auth.gr
(2) Aristotle University of Thessaloniki, Department of Geology, Laboratory of Engineering Geology and Hydrogeology, 54124, Thessaloniki, Greece

Paragenesis (Roth (1937; Renault 1958; 1968; Ford 1971; Ford and Ewers, 1978; Lauritzen and Lauritsen 1995; Bella and Bosák, 2015) is a poorly understood process of cave passage upwards enlargement that results in a variety of geomorphological features. It is observed in phreatic cave systems, when groundwater velocity reduces resulting in permanent deposition of transported sediment that protects the lower part of the passage from dissolution (only negligible dissolution has been observed; i.e. Vaughan, 1998). Theoretically the process is limited upwards to the water table. Such passages are known from caves in carbonates, gypsum and salt (i.e. Frumkin, 1998; Pasini 2009, 2012). Paragenesis has been considered related to periglacial environments (Farrant and Smart, 2011; Lauritzen, 2013).

Although, most authors consider paragenesis as a result of dissolution, others (Roth, 1937; Kunský, 1950) a result of mechanical erosion and Pasini (1975, 2009), uses the term "erosion" sensu lato, including mechanical erosion, physical dissolution and corrosion. Farrant and Smart (2011) reviewed the role of alluvation and paragenesis in speleogenesis. However, direct observation on paragenetic processes is obscured either by sediment filling or by their phreatic nature.

The aim of this study is to geometrically reproduce the cross-section shape of a paragenetic canyon in order to investigate the controlling factors of the process.

Methods

In order to investigate the development of a paragenetic passage a geometric perspective is applied in Matlab. The first step starts with the cross section of a circular phreatic passage and the following steps represent the sum of three agents, deposition, corrosion, and corrasion that act simultaneously on the perimeter of the cross section. At the first step, deposits cover the half of the passage height and shields the lower part from corrosion and corrasion. This is an assumption in order to simplify the computations. Although dissolution occur on the covered by sediment passage and within the sediments, its action has been found to be negligible in comparison with the rest passage (Vaughan, 1998) and thus it is ignored. Corrosion acts isotropically at the wet perimeter of the fully flooded passage and actually it is set at a well-accepted maximum of 0.1 mm/year. Corrasion is considered to act upwards due to buoyancy of suspended load. A heterogeneous flow regime with stratification and formation of a bottom layer, mainly stationary is assumed. The abrasion by suspended sediment and kinetic energy flux are estimated according to Anderson (1986); for the relation of suspended sediment and flow velocity a data series from the Blue Hole spring, Central Kentucky, USA is used (Reed et al., 2010). Sediment supply is considered uninterrupted.

Illustration of the passage development done in MATLAB environment, attempting to describe the geometrical evolution of the points and the ceiling trace seen in Figure 2. The passage width at each step n is defined as the intersection of the sediment level and the cave ceiling (flooded part of the passage cross section) of the n-1 step. The ceiling is traced as the sum of corrosion and corrasion. Both agents are related to fluid velocity. Sediment level is set as a pseudo-random percentage of the water-filled part of the passage at n-1 step.

Results

The cross-section of the passage is drawn first as the result of dissolution that gave a continuously widening upwards passage. This shape differs significantly from what is the canyon-like shape of a paragenetic passage. Then the calculation is repeated with the contribution of erosion *sensu lato* that acts upwards. In this case the result resembles a paragenetic canyon. This is due to the high rate of erosion that is higher than that of dissolution. Furthermore, the rate of erosion *s.l.* is only indicative since the data for the suspended load come from a spring during flood. However, a key point on these results is that dissolution is directly related to flow velocity, whereas abrasion scales with flow velocity to the fifth power (Whipple et al., 2000). The results are intriguing and largely based on the initial assumptions for the calculations. However, there are some studies on abrasion and dissolution rates in cave passages, such as Newson (1971). In the Cheddar cave in Mendip dissolution is found to be 75 times higher than abrasion, except of years of significant flooding events where abrasion was two times higher than dissolution. Although this seems to be insignificant it is the result of mainly only one flooding event in a year, whereas paragenesis takes place in phreatic fully flooded caves, where these conditions are permanent. Cooper et al. (2014) have similarly shown the paragenesis as the result of dissolution and mechanical erosion.

Conclusions

- A cross section of a paragenetic canyon is drawn in MatLab by using geometrical relations of passage's key points, equations for abrasion process and empirical data.
- This concept supports that paragenetic canyon is explained by high erosion s.l. rate.
- In contrary to dissolution, which is directly proportional to flow velocity, abrasion scales with flow velocity to the fifth power.

- Flood-like conditions favour paragenesis, as it is shown by the necessity for high abrasion rates.

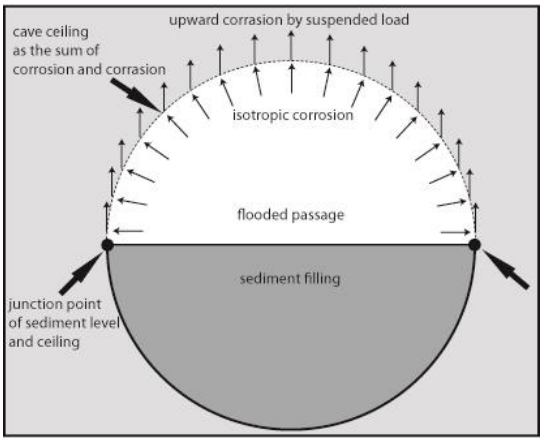

Figure 1. Sketch showing the basic concept of geometric development of a phreatic passage during paragenesis.

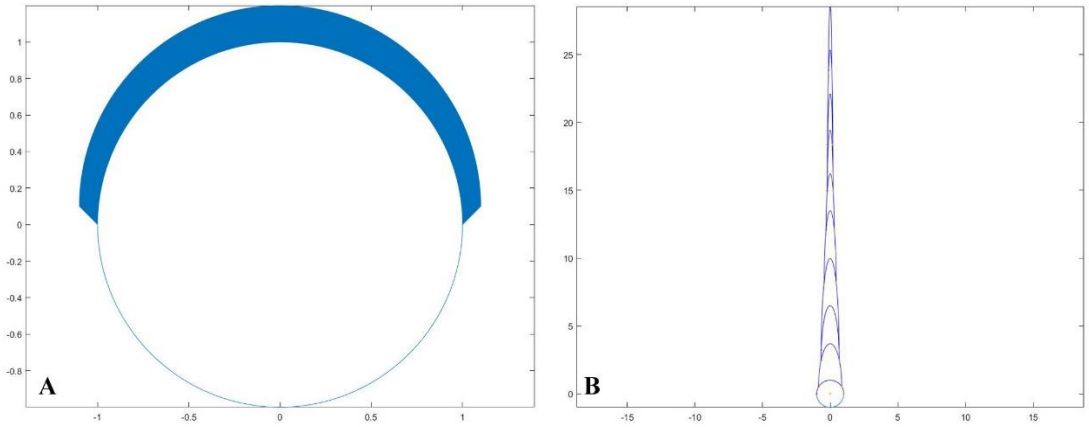

Figure 2. Modification of passage cross-section due to A. corrosion for a duration of 1000 years and B. abrasion and corrosion for a duration of 10 years.

References

Bella, P. and Bosák, P., 2015. Ceiling erosion in caves: early studies and Zdeněk Roth as author of the concept. Acta Carsologica, 44(1).

Cooper, M. P., Perne, M., Covington, M. D., 2014. Simple shear stress approximations and a first step in modeling mechanical erosion in caves. 2014 GSA Annual Meeting in Vancouver, British Columbia, 2014.

Farrant, A., 2004. Paragenesis. Encyclopedia of Caves and Karst Science. Fitzroy Dearborn. New York, 569-571.

Farrant, A. R., Smart, P. L. 2011. Role of sediment in speleogenesis; sedimentation and paragenesis. Geomorphology, 134, 79-93.

Ford, D., 1971. Geologic structure and a new explanation of limestone cavern genesis. Transactions of the Cave Research Group of Great Britain, 13, 81-94.

Frumkin, A., 1998. Salt cave cross-sections and their paleoenvironmental implications. Geomorphology, 23, 183-191.

Ford, D. C., R. O. Ewers, 1978. "The development of limestone cave systems in the dimensions of length and depth." Canadian Journal of Earth Sciences 15(11): 1783-1798.

Kunský, J., 1950: Kras a jeskyně. - Přírodovědecké nakladatelství, 163 pp., Praha.

Lauritzen, S.-E. Paragenesis: The “Royal Mark” Of Subglacial Speleogenesis. 16th International Congress of Speleology, 2013 Brno. 366 - 367.

Lauritzen, S., A. Lauritsen 1995. "Differential diagnosis of paragenetic and vadose canyons." Cave and Karst Science 21(2): 55-59.

Newson, M. D., 1971. A model of subterranean limestone erosion in the British Isles based on hydrology. Transactions of the Institute of British Geographers, 55-70.

Pasini, G., 1975. Sull’importanza speleogenetica dell’“Erosione antigravitativa”. Le Grotte d’Italia, 12, 297-326.Pasini, G., 2009. A terminological matter: paragenesis, antigravitative erosion or antigravitational erosion? International Journal of Speleology, 38, 4.

Pasini, G., 2012: Speleogenesis of the “Buco dei Vinchi” inactive swallow hole (Monte Croara karst sub-area, Bologna, Italy), an outstanding example of antigravitative erosion (or “paragenesis”) in selenitic gypsum. An outline of the “post-antigravitative erosion”. - Acta Carsologica, 41, 1, 15–34.

Renault, P., 1958: Eléments de spéléomorphologie karstique. - Annales de Spéléologie, 13, 1–4, 23–48.

Renauly, P. 1968. Contribution à l'étude des actions mécaniques et sédimentologiques dans la spéléogenèse. Annales de spéléologie, 530-596.Vaughan, K., 1998. A Quantitative Analysis of Interstitial Fluid-Chemistry and Limestone Dissolution Rates within the Clastic Sediment of a Karst Aquifer Conduit, Mammoth Cave, Kentucky.

Whipple, K.X., Hancock, G.S. and Anderson, R.S., 2000. River incision into bedrock: Mechanics and relative efficacy of plucking, abrasion, and cavitation. Geological Society of America Bulletin, 112(3), pp.490-503.

15th International Congress of the Geological Society of Greece
Athens, 22-24 May, 2019 | Harokopio University of Athens, Greece
Bulletin of the Geological Society of Greece, Sp. Pub. 7 Ext. Abs. GSG2019-054

Paleo-hydrology of the Stefanina Cave (Greece)

G. Lazaridis[1], K. Fellachidou[1]

(1) Aristotle University of Thessaloniki, Department of Geology, Laboratory of Geology and Palaeontology, 54124, Thessaloniki, Greece, geolaz@geo.auth.gr

The hydrological conditions and development of the epigenetic Stefanina Cave and the maximum paleo-flow discharge in its main passage are investigated on the basis of cave pattern, passage geometry and scallop length.

Scallops are small-scale morphological features that form asymmetric dissolution pockets due to turbulent flow of a solvent over a soluble surface. Caves are ideal environment for the formation of scallops that indicate forced flow of unsaturated water along a pressure head. In deep-phreatic setting, where dissolution takes place by convecting water bodies, scallops are absent. Furthermore, these pockets are also indicators of flow direction due to their asymmetry and a reverse relationship between their size and the flow velocity of the fluid (Curl, 1966; Curl, 1974; Lauritzen, 1989).

The Stefanina Cave or Lakkia Cave (N40.78183 E23.61357 WGS84; Fig.1) is located NE of the Stefanina Village at about 850 m above sea level (a.s.l.) in the northern slope of the Neromanna stream. The area consists of metamorphic rocks such as marbles and gneisses in alternations that belongs to the almost 3 km thick Kerdylion Series of the Serbomacedonian Massif. The cave is opened in the "upper marble horizon" (20-350 m thick) with white marble (coarse crystalline thick layered), bluish crystalline limestone (fine-grained, thin bedded) intercalated with schists, amphibolites and gneisses.

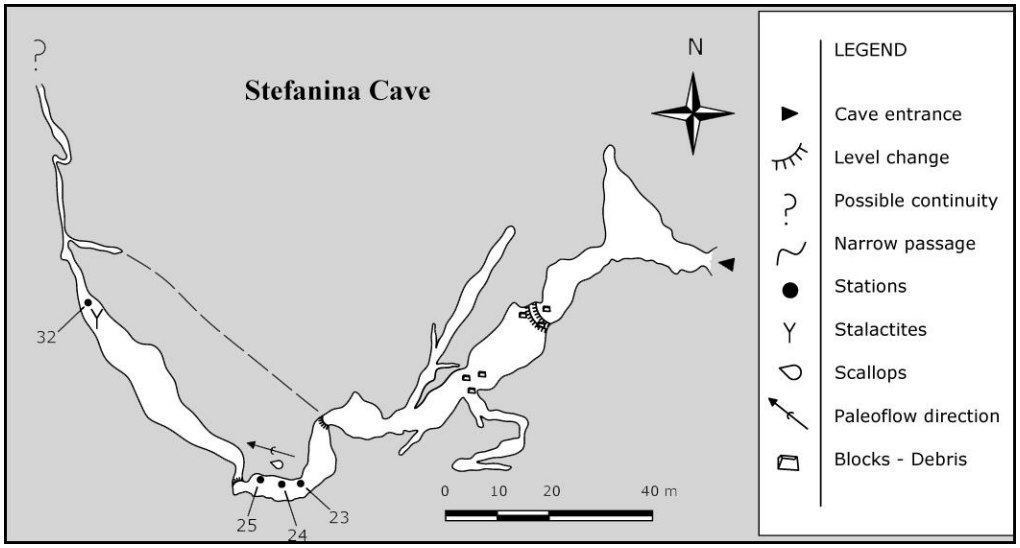

Figure 1. Ground-plan of the Stefanina Cave

Methods

The cave surveyed according to standard cave techniques (i.e. Kalogeropoulos *et al*., 2008; Trimmis, 2018 and reference therein). Rock discontinuities were measured with CLAR compass. Terms and morphological descriptions of caves can be found in Lauritzen and Lundberg (2000), Gunn (2004), Ford and Williams (2007), White and Culver (2005). The gathered data were processed in the spreadsheet program ScallopEx (Woodward and Sasowsky, 2009). The calculations run for 5°C water temperature. The estimated flow velocities were statistically analysed in the software PAST 3.2 (Hammer *et al*., 2001).

Description and results

The explored part of the Stefanina Cave is 210 m long and covers an area of 1250 m^2. Total passage length is 325 m and forms a branchwork horizontal pattern (Palmer, 2000). The height difference between the entrance and the deepest explored part is about 30 m, giving a hydraulic gradient about 0.2. At about 120 m from the entrance a meandering vadose canyon is formed and sediment fill has been eroded revealing the carbonate bedrock. After that point the conduit forms a keyhole passage in cross section and becomes gradually narrow and more canyon like (Fig. 2).

In figure 1 survey stations 23-25 where scallops measured are depicted. In addition, a number of measurements are taken between and after these stations. In total about 400 scallops where measured in 30 locations, at different heights inside the passage. The estimated peak flow velocity ranges from 0.4 to 2.7 m/s (mean=1.32; s=0.46, n=30; Fig. 2E). The null hypothesis of normal distribution cannot be rejected. The highest and lowest values appear as outliers. However, the smaller values have been found inside the meandering canyon at locations inside of bends, where lower values are expected. Based on these values and the dimensions of the passage measured from the cross sections, a peak flow discharge equal to 2.2 m^3/s is estimated.

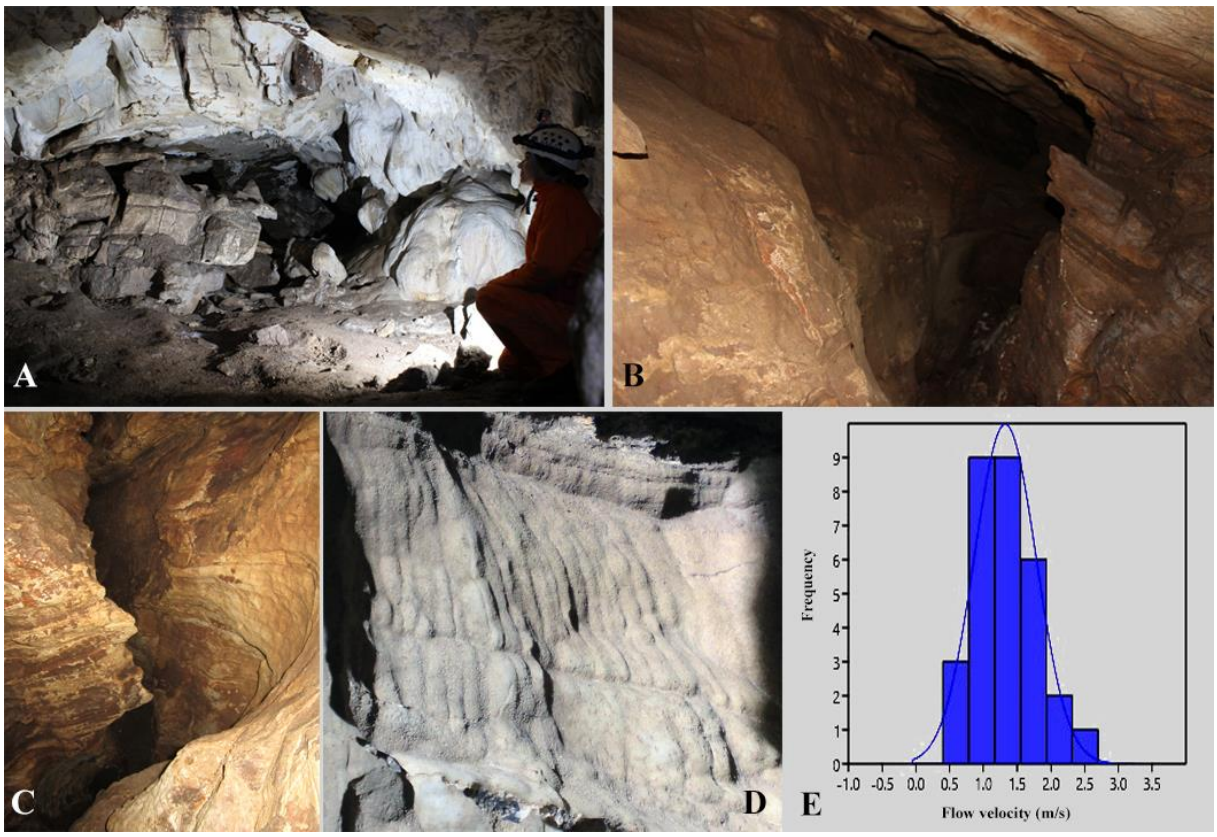

Figure 2. A. View of the main passage at the upstream part of the cave; B. Keyohole section with the phreatic upper and the vadose canyon power part; C. bend in the meandering channel; D. wall detail with scallops; E. histogram with scallop-based estimations of flow velocity in the area of survey stations 23-25.

Concluding remarks

- The Stefanina Cave has a branchwork pattern in ground-plan that is commonly related to recharge via karst depressions (Palmer, 2000). The passages are both curvilinear and angular, related to foliation and fractures, respectively. It is mainly developed along the foliation of the host rock.
- The cross section in the upstream part of the cave indicates a phreatic passage.
- The keyhole cross section found in that canyon passage at about the middle part of the explored cave, is indicative of a second stage of developed after water table drop.
- The peak discharge estimated in the keyhole cross section is indicative for that area and it is expected to be higher further inside the cave due to the existence of lateral passages.

References

Curl, R.L., 1966. Scallops and Flutes. Transactions Cave Research Group of Great Britain, 7(2): 121-160.

Curl, R.L., 1974. Deducing Flow Velocity in Cave Conduits from Scallops. National Speleological Society Bulletin, 36(3): 22.

Ford, D., Williams, P.D., 2007. Karst hydrogeology and geomorphology. John Wiley and Sons Inc.

Hammer, Ř., Harper, D.A.T., & Ryan, P.D., 2001. PAST: Paleontological Statistics Software Package for Education and Data Analysis–Palaeontol. Electron, 4: 9.

Kalogeropoulos, I., Lazaridis, G., Tsekoura, A., 2008. Methodology of cave mapping: comparing routings. 4th Pancretan Speleological Symposium. Hellenic Speleological Society, Rethymnon, Crete, Greece
http://ese.edu.gr/media/seminars/sem_notes/hartografisi/survey_methods.pdf

Lauritzen, S.E., 1989. Scallop Dominant Discharge. Proceedings of the 10th International Congress of Speleology, Budapest, Hungary, 123-124.

Lauritzen, S., Lundberg, J., 2000. Solutional and erosional morphology of caves. Klimchouk, A., Ford, D.C., Palmer, A.N., Dreybrodt, W. (eds.) Speleogenesis. Evolution of Karst Aquifers. Huntsville: National Speleological Society.

Lazaridis, G., 2017. Hypogene Speleogenesis in Greece. In: Klimchouk, A., Palmer, A.N., De Waele, J., Auler, A.S. & Audra, P. (eds.) Hypogene Karst Regions and Caves of the World. Springer, 225-239.

Palmer, A., 2000. Hydrogeologic control of cave patterns. Speleogenesis: Evolution of Karst Aquifers. Huntsville: National. Speleological Society, 77-90.

Trimmis, K.P., 2018. Paperless mapping and cave archaeology: A review on the application of DistoX survey method in archaeological cave sites. Journal of Archaeological Science: Reports 18, 399-407.

White, W.B., Culver, D.C., 2005. Encyclopedia of caves, Elsevier Amsterdam (The Netherlands).

Woodward, E., Sasowsky, I.D. 2009. A spreadsheet program (ScallopEx) to calculate paleovelocities from cave wall scallops. Acta Carsologica, 38(2-3): 303-305.

15th International Congress of the Geological Society of Greece
Athens, 22-24 May, 2019 | Harokopio University of Athens, Greece
Bulletin of the Geological Society of Greece, Sp. Pub. 7 Ext. Abs. GSG2019-057

Coastal Geoelectrical Survey at the Ancient Harbor of Lechaion (Greece)

John D. Alexopoulos, Spyridon Dilalos, Georgia S. Mitsika
NKUA, Department of Geology and Geoenvironment, Panepistimiopolis, Zografou, Greece, jalexopoulos@geol.uoa.gr

Introduction – Location - Geology

The study area is located at coastal area of the Ancient Harbor of Lechaion, at the area of the outer harbor moles (Figs. 1-2), in order to investigate a possible extension of the existing ancient settlements. It is located on the southeastern coast of the Corinthian Gulf, 3km to the west of the modern city of Corinth, Greece. The construction of the Ancient Harbor dates to the 6th-7th century BC and archaeological evidence suggest that its use continued throughout the Roman period (Rothaus, 1995; Stiros *et al*., 1996).

Lechaion harbor site lies in the southern coastal area of the Lechaion Gulf (Fig. 1). The broader area comprises alluvial and coastal deposits including loose materials, sands, pebbles and gravels (Papanikolaou *et al.,* 1998). The geophysical survey was carried out in an area lying approximately 3 km west of the modern city of Corinth and consisting of recent beach deposits including sands and gravels (Papanikolaou *et al*., 1998). They are cohesive at places making up beach rocks.

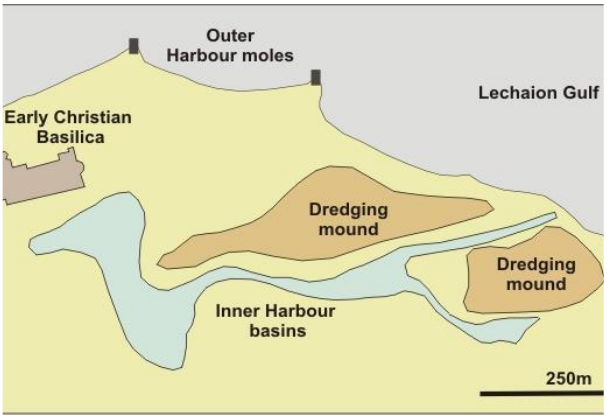

Figure 1. The Ancient Harbor of Lechaion (Minos-Minopoulos *et al.*, 2013) and location of the study area.



Figure 2. Location of the ERT sections

Geoelectrical research

Three (3) profiles were carried out (Fig. 2) by applying the Electrical Resistivity Tomography technique, which is indicated for the investigation of buried archaeological settlements (Alexopoulos *et al.,* 2014). The total length of investigation was 224 meters. Section "Lexaio-1" was 96 meters while sections "Lexaio-2" and "Lexaio-3" were 64m length each one. The roll-along technique was applied in order to reach the desired length and depth of investigation. The Wenner array was chosen with minimum electrode spacing equal to 0,40 meters. A total number of 3.610 data points were collected from all three ERT sections, investigating the subsurface resistivity distribution. The instrument used for the field measurements was the ABEM Terrameter Unit, supported by the Lund Imaging System.

The resistivity data points that were collected during the field campaign were processed with Res2DInv Software (Geotomo). During the processing, the software tries to minimize the misfit error of an arbitrary model, checking the raw data points. The inversion process is continuously repeated until the minimum possible misfit is reached. The robust inversion was used, as the most appropriate for such geoenvironments and targets.

During the set-up of the two geoelectrical lines, the coordinates of each electrode have been determined using Differential Global Positioning System (*dGPS*) and Real-Time Kinematics (RTK) technique. The topographic relief must be taken under consideration in such investigations and should be embodied in the inversion procedure of the ERT measurements. The geodetic system used for the coordinates was the local (Greek) EGSA'87 (Datum GGRS'80).

Results and Discussion

In Section 2 (Fig. 3), a dominant geoelectrical formation of low resistivity (<50 Ohm.m) has been investigated, from the depth of 2m up to the maximum depth of investigation which is equal to almost 6,0 meters. At shallow depths (<2 meters), resistant formations (500-2000 Ohm.m) have been determined along the section (Fig.3-red dashed rectangulars). It should be mentioned that along the main resistant formation (17,0-40,6m.) the highest resistant zones are adumbrated clearly (reddish colors) illustrated with almost sharp boundaries.

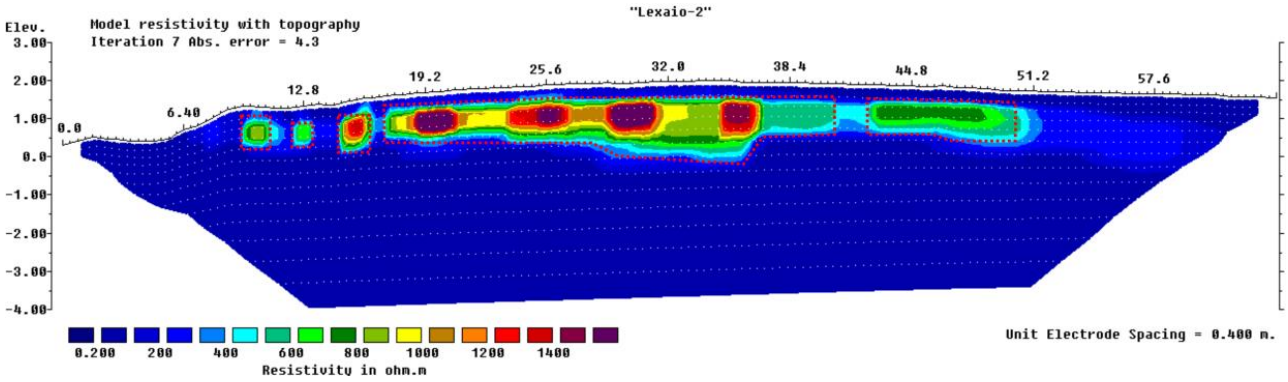

Figure 3. The resistivity model of Section-2 (7 iterations, RMS=4.3%) in scale 1:2.

In Section 3 (Fig. 4), even though the general image is similar, the resistant formations are quite bigger in size. The dominant geoelectrical formation of low resistivity (<100 Ohm.m) has also been investigated, extending mainly from the depth of 2,5 meters to the maximum depth of investigation which is equal to almost 6,0 meters. In this section, between 38,4-51,0 meters the aforementioned conductive formation is interrupted by a relatively resistant zone with values close to 400 Ohm.m. At depths less than 3,0 meters, highly resistant formations (550-6500 Ohm.m) have been determined along the section (Fig.4-red dashed rectangulars). It should be mentioned that two main resistant formations have been investigated (5,6-28,6m. and 30,0-64,0m), from depths 0,2-1,8m. and 0,4-4,0m equally. Along the first main resistant formation the highest resistant zones (>1500 Ohm.m) are adumbrated clearly (purplish colors) and are illustrated with almost sharp boundaries. Concerning the second major resistant zone, almost all the resistivity values are above 2000 Ohm.m (purplish colors). The geoelectrical boundaries here are also quite sharp and clear.

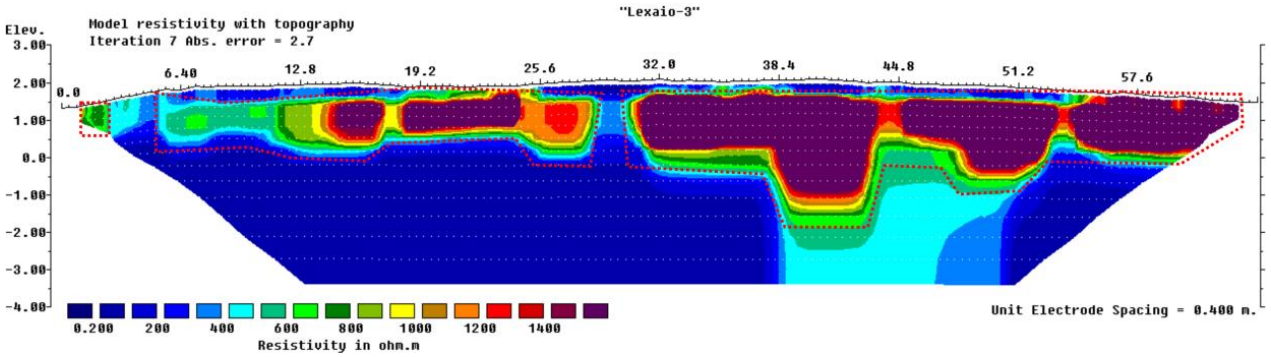

Figure 4. The resistivity model of Section-3 (7 iterations, RMS=2.7%) in scale 1:2.

Conclusions

The results of the geoelectrical survey seem to adumbrate some zones (Figs. 3-4, reddish & purplish colors) that could be interpreted as archaeological remains of the coastal installations of the ancient foreharbor. These are presented and discussed by Mourtzas *et al.* (2014) in the context of the geoarchaeological approach of the ancient harbor of Lechaion.

Acknowledgements

The authors would like to thank Mr. Spyridon Mavroulis and Ms. Helen Kaplanidi for their contribution in the field campaign.

References

Alexopoulos, J.D., Dilalos, S., Tsatsaris, A., Mavroulis, S., 2014. ERT and VLF measurements contributing to the extended revelation of the ancient town of Trapezous (Peloponnesus, Greece). In: *Near Surface Geoscience 2014-20th European Meeting of Environmental and Engineering Geophysics*, Doi: 10.3997/2214-4609.20141974.

Papanikolaou, D., Logos, E., Lozios, S., Sideris, Ch., 1998. Neotectonic Map of Greece, Sheet Corinth, scale 1:100.000, Earthquake Planning & Protection Organization, 90p.

Minos-Minopoulos, D., Pavlopoulos, K., Apostolopoulos, G., Dominey-Howes, D., Lekkas, E., 2013. Preliminary results of investigations of possible ground deformation structures in the early Christian basilica, ancient Lechaion harbour, Corinth, Greece. *Bulletin of the Geological Society of Greece*, 47(4), 1769-1778, http://dx.doi.org/10.12681/bgsg.11056

Mourtzas, N.D., Kissas, C., Kolaiti, E., 2014. Archaeological and geomorphological indicators of the historical sea level changes and the related palaeogeographical reconstruction of the ancient foreharbour of Lechaion, East Corinth Gulf (Greece). *Quaternary International*, 332, 151-171, https://doi.org/10.1016/j.quaint.2012.12.037

Rothaus R., 1995. Lechaion, western port of Corinth: A preliminary archaeology and history. *Oxford Journal of Archaeology*, 14(3), 293-306, https://doi.org/10.1111/j.1468-0092.1995.tb00065.x

Stiros, S., Pirazzoli, P., Rothaus, R., Papageorgiou, S., Laborel, J., Arnold, M., 1996. On the Date of Construction of Lechaion, Western Harbour of Ancient Corinth, Greece. *Geoarchaeology: An International Journal*, 11(3), 251-263.

15th International Congress of the Geological Society of Greece
Athens, 22-24 May, 2019 | Harokopio University of Athens, Greece
Bulletin of the Geological Society of Greece, Sp. Pub. 7 Ext. Abs. GSG2019-060

Cavernous forms in Mandres Quarry (Kilkis, Greece)

N. Kargopoulou[1], G. Lazaridis[1], A. Karakosta[1]

(1) Aristotle University of Thessaloniki, Department of Geology, Laboratory of Geology and Palaeontology, 54124, Thessaloniki, Greece, ntkargop@geo.auth.gr

A small limestone quarry (~0.4 hectares) is located in a low hill in the vicinity of Mandres village, in Kilkis Prefecture (N. Greece). It is 1.2 km east to the village, at about 180 m above sea level (N40.88426 E22.92365). A number of small cavities and cavernous forms are found during commercial works in the NE part of the quarry (Fig. 1). They are opened in carbonates (limestones and dolomite) of Middle to Upper Triassic age (Carnian-Anisian) that are overlain by quartzites. These rocks belong to the Deve Koran-Doubia Unit of the Circum-Rhodope geotectonic zone (Kockel & Ioannides, 1979; Kaufmann *et al*., 1976; Mountrakis, 2010) that is tectonically placed upon the calcareous flysch of Svoula Unit. The age of the latter is younger than Upper Triassic. These Alpine rocks crop out at higher altitudes and they are surrounded by quaternary sediments. Although the largest cave in the area, the Agios Georgios show cave (Kilkis town), is opened in these carbonates, our knowledge about caves and speleogenesis in the area is quite limited.

Methods

The cavities are surveyed according to standard cave techniques (i.e. Kalogeropoulos *et al*., 2008; Trimmis, 2018 and reference therein). Rock discontinuities were measured with CLAR compass. Terms and morphological descriptions of caves can be found in Lauritzen and Lundberg (2000), Gunn (2004) Ford and Williams (2007) White and Culver (2005).

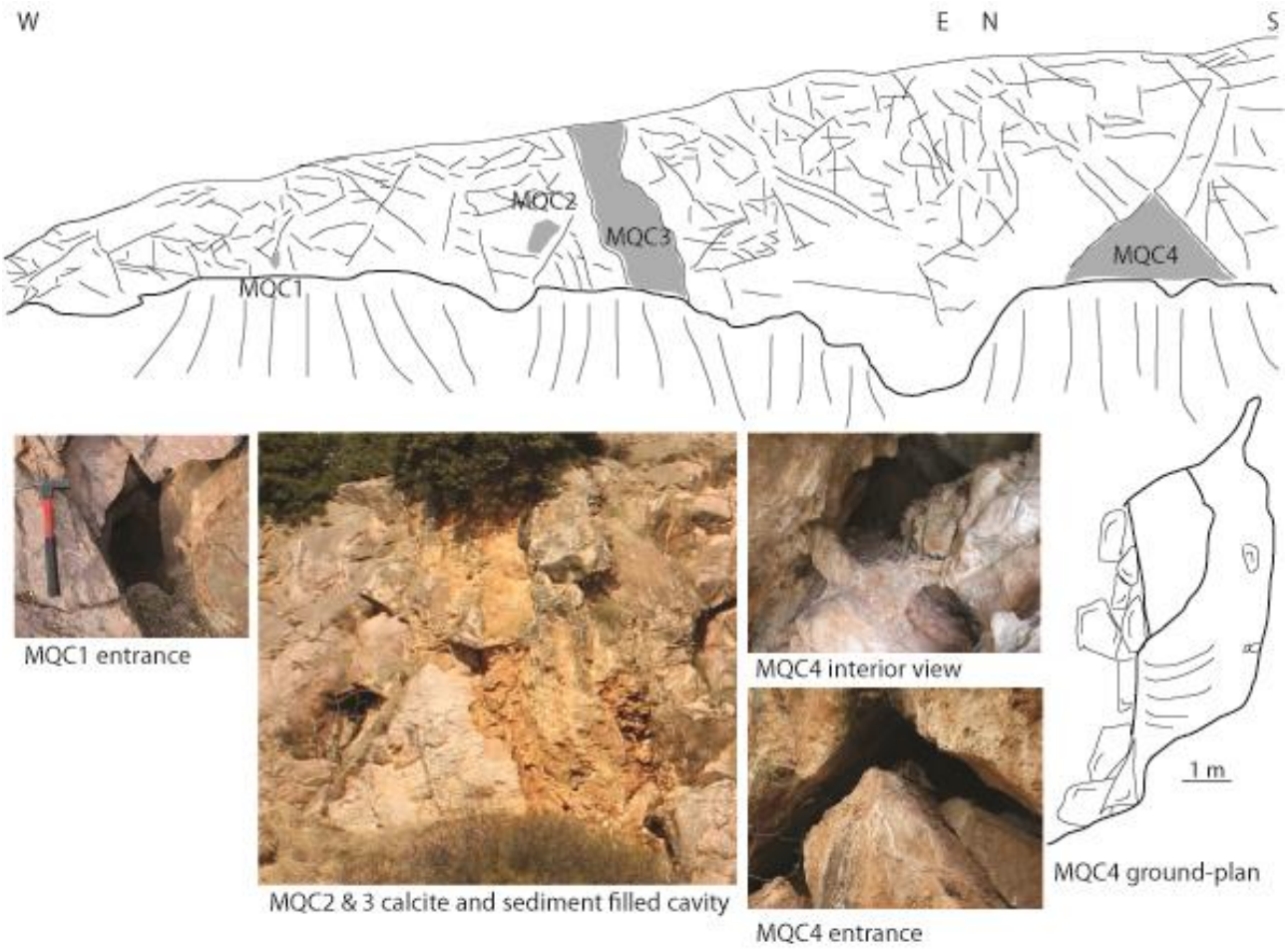

Figure 1. Sketch of the quarry escarpment in Mandres, with the cave entrances depicted and ground plan of the largest cavity.

Description and results

The cavities found in the Mandres Quarry (MQC: Mandres Quarry Cavity) are mainly fracture guided by N-S and E-W discontinuities. Their length reaches about 6m and the largest one (MQC4) is located in the eastern escarpment and covers an area of ~30 m^2. In the latter, the ceiling and the side-walls coincide with rock discontinuities and are probably related to breakdown that affects the original morphology. Its NE part, however, displays a dissolutional passage that is abruptly terminated. It is poorly decorated with few common speleothems such as stalagmites, flowstone and coralloids. This is

commonly the case in all the cavities found in the quarry that are mainly decorated with coralloids. The only exception is a fracture-guided cavity at the northern escarpment that is almost totally filled with thick calcite layers, flowstones, coralloids. The central part of the cavity is partially filled with fine-grained red sediment.

All in all the caves are characterized by minimum dissolutional forms of small-scale that means the information about speleogenesis comes from passage-scale forms. The high and narrow, symmetrical and fracture guided passages are indicative of phreatic speleogenesis. This is in agreement with the absence of vadose marks. Furthermore, the orientation, the shape and the filling of the passages in these cavities is similar to those found in the Agios Georgios cave and its surroundings (i.e. in the Quarry to the north of the cave). The latter is considered to have been developed by hypogene speleogenesis (Lazaridis, 2017).

Conclusions

- A number of small cavities with similar morphological features is investigated and recorded in detail.
- Their meso-scale morphology is phreatic and identical to the hypogene caves of the area and thus they probably have been developed under similar conditions.
- This group of cavities provides new information and expands the area that has been affected by the processes of hypogene speleogenesis in the carbonates of the Circum-Rhodope Zone.

References

Ford, D., Williams, P. D. 2007. Karst hydrogeology and geomorphology, John Wiley & and Sons IncInc.

Gunn, J. 2004. Encyclopedia of Caves and Karst Science, Taylor and& Francis Inc.

Kaufmann, G., Kockel, F., and Mollat, H., 1976. Notes on the stratigraphic and paleogeographic position of the Svoula Formation in the Innermost Zone of the Hellenides (northern Greece). Bulletin de la Societe Geologique de France 18, 225-230

Kalogeropoulos, I., Lazaridis, G., Tsekoura, A., 2008. Methodology of cave mapping: comparing routings. 4th Pancretan Speleological Symposium. Hellenic Speleological Society, Rethymnon, Crete, Greece http://ese.edu.gr/media/seminars/sem_notes/hartografisi/survey_methods.pdf

Kockel F., Ioannides K., 1979. Geological Map of Greece, Kilkis sheet. Scale 1:50.000, Institute of Geology and Mineral Exploration, Greece.

Lauritzen, S., Lundberg, J. 2000. Solutional and erosional morphology of caves. Klimchouk, A., Ford, D. C., Palmer, A. N., Dreybrodt, W. (eds.) Speleogenesis. Evolution of Karst Aquifers. Huntsville: National Speleological Society.

Lazaridis, G. 2017. Hypogene Speleogenesis in Greece. In: Klimchouk, A., Palmer, A. N., De Waele, J., Auler, A. S. & Audra, P. (eds.) Hypogene Karst Regions and Caves of the World. Springer, 225-239.

Mountrakis, D. 2010. Geology and Geotectonic Evolution of Greece. University Studio Press Inc, Greece, p. 374 (in greek)

Trimmis, K. P. 2018. Paperless mapping and cave archaeology: A review on the application of DistoX survey method in archaeological cave sites. Journal of Archaeological Science: Reports 18, 399-407.

White, W. B., Culver, D. C. 2005. Encyclopedia of caves, Elsevier Amsterdam (The Netherlands).

15th International Congress of the Geological Society of Greece
Athens, 22-24 May, 2019 | Harokopio University of Athens, Greece
Bulletin of the Geological Society of Greece, Sp. Pub. 7 Ext. Abs. GSG2019-061

Documenting condensation corrosion in Agios Georgios cave (Kilkis, Greece)

A. Karakosta[1], G. Lazaridis[1], N. Kargopoulou[1]

(1) Aristotle University of Thessaloniki, Department of Geology, Laboratory of Geology and Palaeontology, 54124, Thessaloniki, Greece, karakosta@geo.auth.gr

The Agios Georgios show cave is located at a small hill in the town of Kilkis (N. Greece). It has been formed in the Middle- Upper Triassic limestones that belong to the Deve Koran-Doubia subzone of the Circum-Rhodope geotectonic zone (i.e. Mountrakis, 2010 and references therein).

Morphologically the cave is an 800 m^2 2-dimensional maze with narrow and high fracture-guided passages (Fig. 1). Some chambers are mainly formed due to breakdown. Even though the entrance of the cave is artificially opened, there were multiple entrances in the past. These are nowadays obscured by sediment filling of Late Pleistocene age, as it is indicated by large mammal fossils (Tsoukala, 1992).

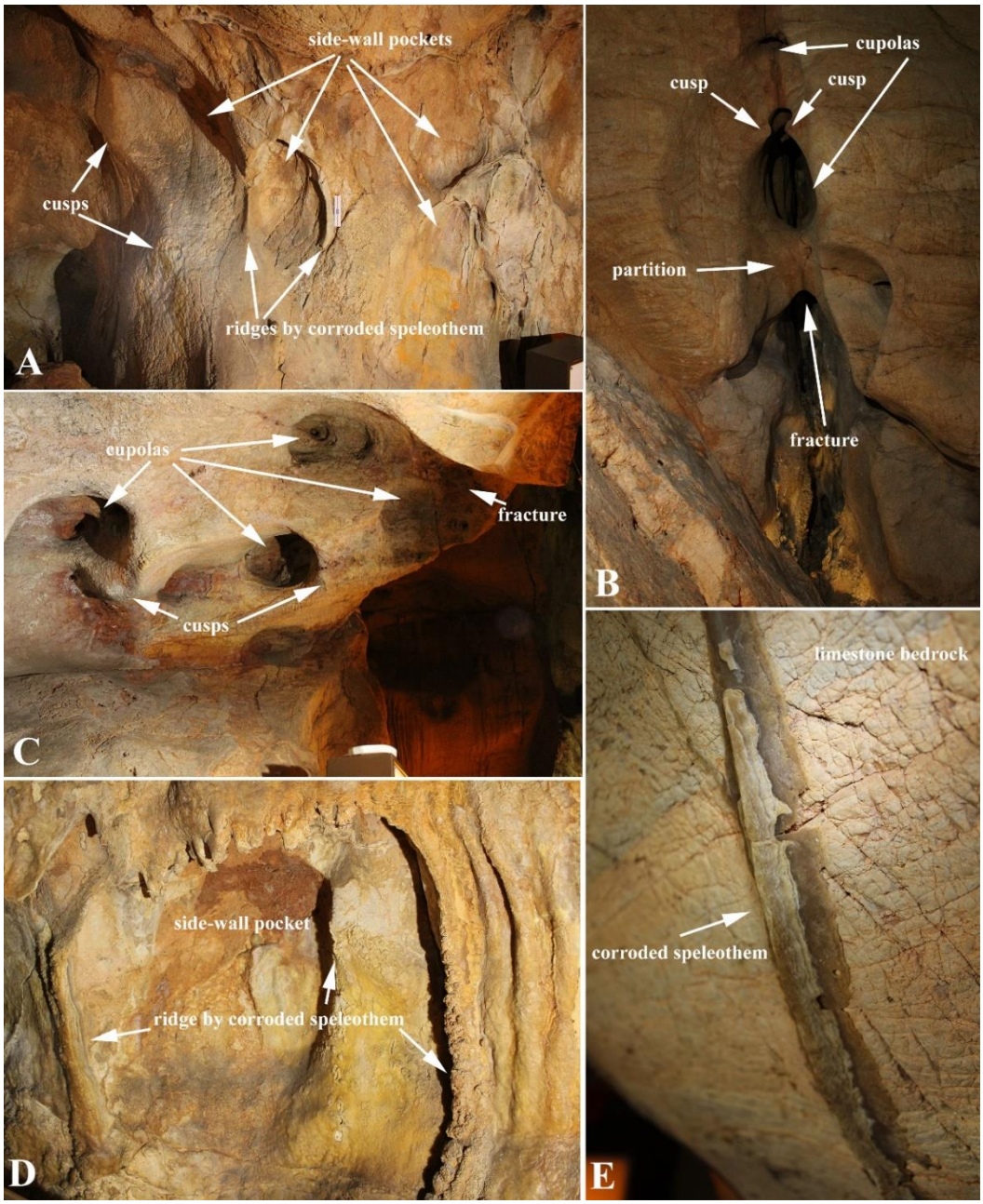

Figure 1. Characteristic condensation corrosion features of Agios Georgios show cave. A. Solution-smoothed wall with cupolas, cusps and corroded speleothems that delimit cupolas. B. Fracture-guided cupolas on the ceiling of a narrow passage and accompanying forms. C. Ceiling cupolas along bedding and a more susceptible to solution bed in limestone. D. Wall-pockets and corroded speleothems. E. Solution-smoothed wall and remnant of corroded speleothem.

Regarding the (chemical) depositional forms the cave appears moderately decorated. The predominant speleothem in Agios Georgios cave is the coralloids with globular or button-like shape. Other speleothems recorded in the cave are stalactites, stalagmites, columns, draperies, flowstones, eccentrics and shields. A number of studies has been done on stalactites and stalagmites to investigate the paleo-environment of the cave (Antonelou, 2007; Antonelou *et al*., 2010; Dotsika *et al*., 2010; Ifandi, *et al*., 2015).

Meso- and small-scale morphology includes cupolas, cusps, partitions, echinoliths, rock bridges and pendants (Figure 1). Some of these dissolutional forms, such as the cupolas, partitions etc., are polygenetic (e.g. Dublyansky, 2013), causing difficulties in the interpretation of speleogenesis. Especially in the broader area of Agios Georgios cave, it has been already noticed that these dissolutional forms are developed over both the speleothems and the limestone (Lazaridis, 2017). This observation dates their formation as post-speleogenetic and means that although the origin of the cave has been considered hydrothermal-phreatic (Lazaridis, 2017), many of the cupolas and related forms have developed when the cave drained and after the deposition of speleothems by seepage water. Thus, these features are the result of condensation corrosion, which is a process of bedrock and speleothem removal from film water that condenses on the rock-mineral substrate, when their temperature is below dew point of cave air (e.g. Dreybrodt *et al*., 2005).

The aim of this study is to document the dissolutional forms by condensation corrosion, their distribution in the cave and set some questions for further investigation.

Condensation corrosion morphology

The related to condensation corrosion features are widespread all over the cave. However, the significant extend of coralloids in the area that is known as “second floor”, obscures the observation of dissolutional forms. Their dimensions range from few centimeters up to the passage diameter. They are either side-wall pockets (Fig. 1A, D) or ceiling cupolas (Fig. 1B). Accompanying forms, such as cusps and partitions do exist (Fig. 1B, C). Some of them are fracture guided (Fig. 1B). In general they contribute in the formation of solution-smoothed walls or boneyard morphology on the ceiling.

Conclusions

- This study provided a detailed documentation of condensation corrosion morphology in Agios Georgios cave and verified previous report of the process (Lazaridis, 2017).
- The morphological features that are observed are quite similar to those described in other caves (e.g. Dublyansky and Spötl, 2014) and have been attributed to condensation corrosion.
- Since Agios Georgios is a show cave, the study of condensation corrosion is crucial because visitors could affect the cave climate and enhance that process.
- Among others, in our future goals is to create a data-set with dimensions of these dissolutional forms, measure and estimate the amount of dissolution and possibly the rate, to correlate their formation to the environmental conditions and check if the process is still active.

Acknowledgments

We thank the geology student and caver Kyriaki Fellachidou for her assistance during the field work.

References

Antonelou, A., 2007. Study of speleothems from Agios Geogios Cave, Kilkis prefecture: Investigation of paleoclimatic environmental conditions using stable isotopes of C and O. MS. Thesis, University of Patras, Patras, 183 p.

Antonelou, A., Tsikouras, B., Papoulis, D., Hatzipanagiotou, K., 2010. Investigation of the formation of speleothems in the Agios Georgios Cave (N. Greece). Bulletin of the Geological Society of Greece 43, 876-885.

Dotsika, E., Psomiadis, D., Zanchetta, G., Spyropoulos, N., Leone, G., Tzavidopoulos, I., Poutoukis, D., 2010. Pleistocene palaeoclimatic evolution from Agios Georgios Cave speleothem (Kilkis, N. Greece). Bulletin of the Geological Society of Greece 43, 886-895.

Dreybrodt, W., Gabrovšek, F., Perne, M., 2005. Condensation corrosion: a theoretical approach. Acta Carsologica, 34(2), 317-348.

Dublyansky, Y.V., 2013. Karstification by geothermal waters, in: Shroder J, Frumkin A, (Eds.), Treatise on geomorphology. Academic Press, vol 6, 57–71.

Dublyansky, Y.V., Spötl, C., 2014. Morphological effects of condensation-corrosion speleogenesis at Devils hole ridge, Nevada, in: Klimchouk, A., Sasowsky, I.D., Mylroie, J., Engel, S.A., Summers Engel, A., (Eds.), Hypogene cave morphologies, Karst Waters Institute Special Publication, 18, 36-43.

Ifandi, E., Tsikouras, B., Papoulis, D., Hatzipanagiotou, K., Antonelou, A., 2015. A new microenvironment for the formation of clay minerals: the example of authigenic halloysite-7Å and gibbsite in a stalactite from Agios Georgios Cave, Kilkis, north Greece. International Journal of Speleology, 44(3), p. 10.

Lazaridis, G., 2017. Hypogene Speleogenesis in Greece, in: Klimchouk, A., Palmer, A.N., De Waele, J., Auler, A.S., Audra, P. (Eds.), Hypogene Karst Regions and Caves of the World, Springer 14, 225-239.

Mountrakis, D., 2010. Geology and geotectonic evolution of Greece, University Studio Press.

Tsoukala, E.S., 1992. The Pleistocene large mammals from the Agios Georgios cave, Kilkis (Macedonia, N. Greece). Geobios, 25(3), 415-433.

15th International Congress of the Geological Society of Greece
Athens, 22-24 May, 2019 | Harokopio University of Athens, Greece
Bulletin of the Geological Society of Greece, Sp. Pub. 7 Ext. Abs. GSG2019-088

Geomorphological and Sedimentological Setting of the Filiouris River Wave Dominated Delta

E. Tzelepi[1], S. Doani[1], K. Koliadimou[1], K. Vouvalidis[1]

(1) Aristotle University of Thessaloniki, School of Geology, Department of Physical and Environmental Geography, 54124, Thessaloniki, Greece, efitzelepi@geo.auth.gr, doanisofia@geo.auth.gr, koliadim@geo.auth.gr, vouval@geo.auth.gr

Extended Abstract

The aim of the present research is to study the sedimentological record of fluvial and coastal landforms of the Filiouris River wave dominated delta plain, during Holocene. Filiouris River crosses the Rhodope plain and flows into Thracian sea (North Aegean), southwards the Komotini City, creating a deltaic plain. Concerning its geological setting, Filiouris is located at the Thracian basin which is one of the widest basins of North Aegean created on the Rhodope geotectonic Massif, Strandja and Sakarva Massifs (Mountrakis, 2010). The Neogene and Quaternary sediments, 1-2 km thick, cover the lower part of Filiouris River basin. Sampling took place on the west side of the Filiouris River plain, between the coastline and Mitrikos Lake. A total of 12 samples were collected and stored in plastic bags (Figure 1). The sampling positions were conducted by portable GPS device. The map was produced using ArcGIS software, the topographical map from Hellenic Military Geographical Service (H.M.G.S.) and the geological map from I.G.M.E. The sediment samples were analyzed in the Physical Geography Lab of Aristotle University of Thessaloniki. Each sample was dried at 90° C and weighted using a precision balance. Organic matter was removed from all the samples using H_2O_2 (10%) and then particle size analysis was performed. Eight samples were sieved for the fractions of particles -2.00 phi to 4.00 phi (Table 1) while four fine grained samples were analyzed by the use of the pipette method (Table 2)(Folk, 1974). Grain size statistical analysis was performed using GRADISTAT Version 8.0 (Blott, 2010) software and the triangular graphs according to Shepard (1954), Folk (1956) and Folk et al. (1970).

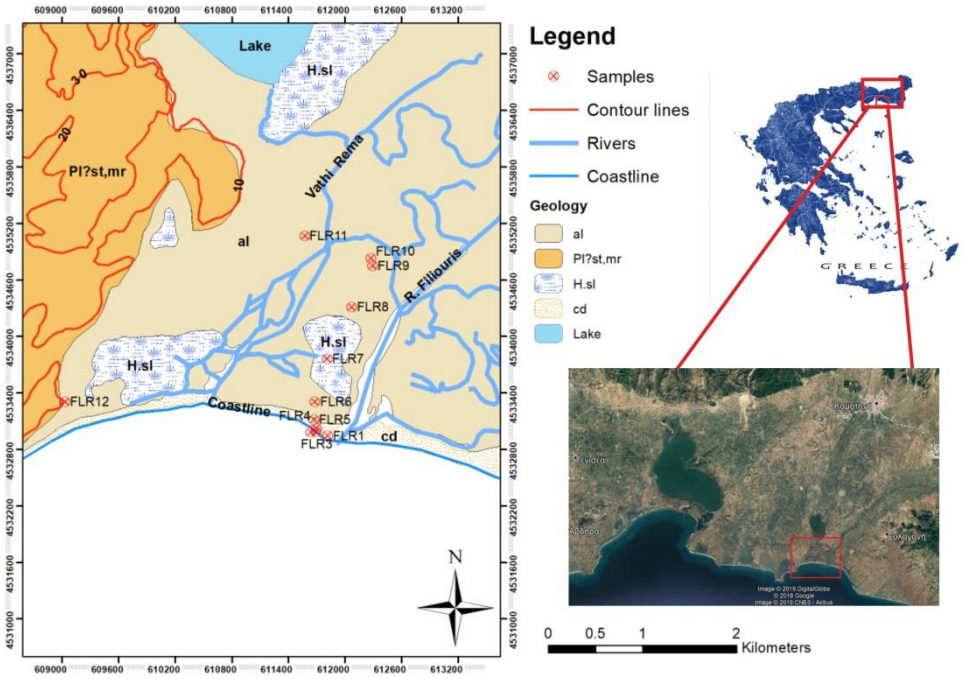

Figure 1.Geomorphological map based on IGME map Xilagani, 1:50.000, Datum: D_GGRS_1987, GRS_1980 and sampling locations.

Table 1. Summary of Grain size analysis results by sieving method.

Sample Name	M	σ	sk	k	Type
FLR1	1,251	0,615	-0,175	0,986	Medium Sand-Moderately Well Sorted
FLR2	0,981	0,547	0,120	1,155	Coarse Sand- Moderately Well Sorted
FLR3	1,255	0,685	0,027	0,949	Medium Sand-Moderately Well Sorted
FLR4	2,043	0,526	-0,035	1,053	Fine Sand-Moderately Well Sorted
FLR5	2,198	0,458	0,027	1,022	Fine Sand-Well Sorted
FLR6	1,311	0,701	-0,084	1,071	Medium Sand-Moderately Sorted
FLR8	1,910	0,517	0,154	1,135	Medium Sand-Moderately Well Sorted
FLR11	1,118	0,721	-0,005	1,180	Medium Sand-Moderately Sorted

Table 2. Summary of Grain size analysis results by pipette method.

Sample Name	Sand	Silt	Clay	Type
FLR7	77,8%	10,9%	11,3%	Muddy Sand
FLR9	74,4%	12,4%	13,2%	Muddy Sand
FLR10	7,2%	40,7%	52%	Mud
FLR 12	59,7%	28,1%	12,2%	Silty Sand

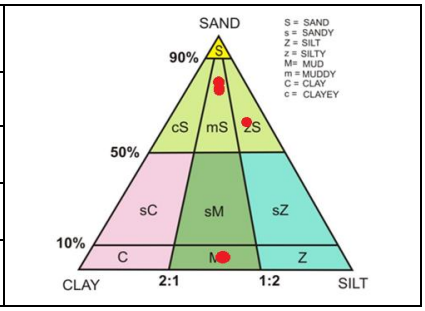

According to the grain size analysis (Table 1 & 2), samples FLR1, FLR2, FLR3 have been deposited in a current coastal depositional environment and they are supermature sediments. Sample FLR4 indicates a transition from coastal to mainly Aeolian depositional environment. Sample FLR5 has an aeolian origin and indicates the present day coastal dune formation. Sample FLR6 was collected further northwards. However, it has similar sedimentary characteristics with samples FLR1, FLR2 and FLR3 and it could be assumed as coastal. Sample FLR7 consists of silty clayey fine-grained sand (77.8%). The sample has been collected from a small temporary marsh of Filiouris Plain. The high content in fine-grained sand is probably indicative of a former dune environment. The high content of silt and clay has been apparently reinforced because of the current marshy environment. Sample FLR8 has similar sedimentological and macroscopic characteristics with FLR4. Sample FLR9 consists mainly of fine-grained sand (74.40%) with silt and clay, while sample FLR10 is mostly silty clay and indicative of a marshy environment. It is very likely that the origin of these two samples is highly related to the fluvial action of the Filiouris River in the vicinity of the old river channel before human intervention. Sampling position of FLR11 sample is the most remote in relation with the present day coastline. Despite the long distance from the coastline, its sedimentological characteristics and the presence of marine mollusks indicates coastal sediment. Finally, the sample FLR12 consists of silty sand and there is a correlation established not only by the presence of the adjacent marshy environment but also by the pre-existing river deposition.

From the sedimentological characteristics of the sampling locations, we can conclude that there is a succession of coastal and aeolian depositional environments from South to North. The former coastline was located on the area of sample's FLR11 location and was gradually shifted towards its current location (coastline). Regarding their positions, the sediments are very well sorted indicating a wave reworking process. Additionally, it indicates a step forward delta progradation. The coastline of Filiouris River is a wave dominated deltaic coast with a succession of coastal and aeolian landforms.

References

BLOTT J. S. (2010): GRADISTAT Version 8.0 A Grain Size Distribution and Statistics Package for the Analysis of Unconsolidated Sediments by Sieving or Laser Granulometer.

Folk, R.L. and Ward, W.C., 1957.Brazos River bar [Texas]; a study in the significance of grain size parameters. Journal of Sedimentary Research, 27(1), pp.3-26.

Folk, R.L., 1974. Petrology of sedimentary rocks: Austin. Texas, Hemphill, 182.

Folk, R.L., Andrews, P.B. and Lewis, D., 1970.Detrital sedimentary rock classification and nomenclature for use in New Zealand. New Zealand journal of geology and geophysics, 13(4), pp.937-968.

Kilias, A.D., Vamvaka, A., Falalakis, G., Sfeikos, A., Papadimitriou, E., Gkarlaouni, C.H. and Karakostas, B., 2015. The Mesohellenic Trough and the paleogene Thrace basin on the Rhodope massif, their structural evolution and geotectonic significance in the Hellenides. JGeolGeosci, 4(198), p.2.

Mountrakis, D., 2010. Geology and geotectonic evolution of Greece. Thessaloniki, University. (In Greek)

Shepard, F.P. (1954) Nomenclature Based on Sand-Silt-Clay Ratios. Journal of Sedimentary Research, 24, 151-158.

15th International Congress of the Geological Society of Greece
Athens, 22-24 May, 2019 | Harokopio University of Athens, Greece
Bulletin of the Geological Society of Greece, Sp. Pub. 7 Ext. Abs. GSG2019-114

Archaeomagnetic investigations in the Eastern Mediterranean: New directional data and archaeomagnetic dating in Cyprus

E. Tema[1,2], I. Hedley[3,4]

(1) Dipartimento di Scienze della Terra, Università degli Studi di Torino, via Valperga Caluso 35, 10125 Torino, Italy, evdokia.tema@unito.it
(2) ALP-Alpine Laboratory of Palaeomagnetism, Peveragno, Italy
(3) Mineralogy Department, Earth and Environmental Sciences Section, Université de Genève, Switzerland
(4) Laboratoire de Paléomagnétisme, Musée de Préhistoire des gorges du Verdon, 04500 Quinson, France

Introduction

Improving the temporal and spatial distribution of the archaeomagnetic reference data is necessary to increase the reliability and accuracy of current geomagnetic field models and to provide information on the past evolution of the Earth's magnetic field. Even though Europe is characterized by the highest density of archaeomagnetic data compared to other continents, there are still some geographical areas that are poorly covered by reliable and high-quality geomagnetic field records, such as the Eastern Mediterranean. Actually, apart from Greece and Bulgaria that have a long history of archaeomagnetic investigations, and Israel that has recently published a catalogue with archaeomagnetic directions, the available directional data from Turkey, Cyprus, Syria and Lebanon are still scarce. In this study we present new directional archaeomagnetic results from four archaeological sites in Cyprus, and also explore the feasibility of archaeomagnetic dating in the island.

Materials and Methods

The material studied comes from four archaeological sites situated at Idalion (35.02º N, 33.45º E), Malloura 35.03º N, 33.02º E), Marki-Alonia (35.02º N, 33.33º E) and Agios Georgios Hill, Lefkosia (35.16º N, 33.35º E). In all cases baked clays from ancient hearths were sampled, after being oriented in situ using a magnetic as well as a sun compass, and an inclinometer. Sampling was carried out by gluing 25 mm diameter polycarbonate discs on the cleaned surface of the baked clay, using small quantities of instant adhesive (Fig. 1). Between 7 and 19 independently oriented samples were collected from each structure.



(a) **(b)**

Figure 1. Photos of the hearths sampled at the archaeological sites of a) Idalion and b) Agios Georgios (PA.SY.DY, structure 13). Archaeomagnetic sampling was performed using plastic discs glued on the baked clay and in situ oriented using a compass and an inclinometer.

Standard alternating field (AF) demagnetization procedures were applied to stepwise demagnetize the samples and isolate the Characteristic Remanent magnetization (ChRM) acquired during the last heating of the baked clay. Thermal demagnetization was not possible due to the plastic discs used during sampling.

Results

The results obtained after demagnetization are very well defined for all of the structures studied, with linear orthogonal projection diagrams. Mean directions were calculated assuming a Fisherian distribution based on at least 7 independently oriented samples for each baked clay structure (Fig. 2). The new directions coming from the sites of Marki-Alonia and Agios Georgios can be used as reference points to improve the directional dataset of Cyprus, as they have a well-defined independent dating. The baked clay sampled at Marki-Alonia is dated at 2300-2000 BC while the structure sampled at Agios Georgios (PA.SY.D.Y, structure 13) is dated at 305-107 BC. The hearth sampled at Idalion can be dated at 1200-700 BC but for the moment no other archaeological evidences are available to better constrain its dating. Finally, for the hearth studied at Mallura (MLR2) a reliable archaeological date is not at present available.

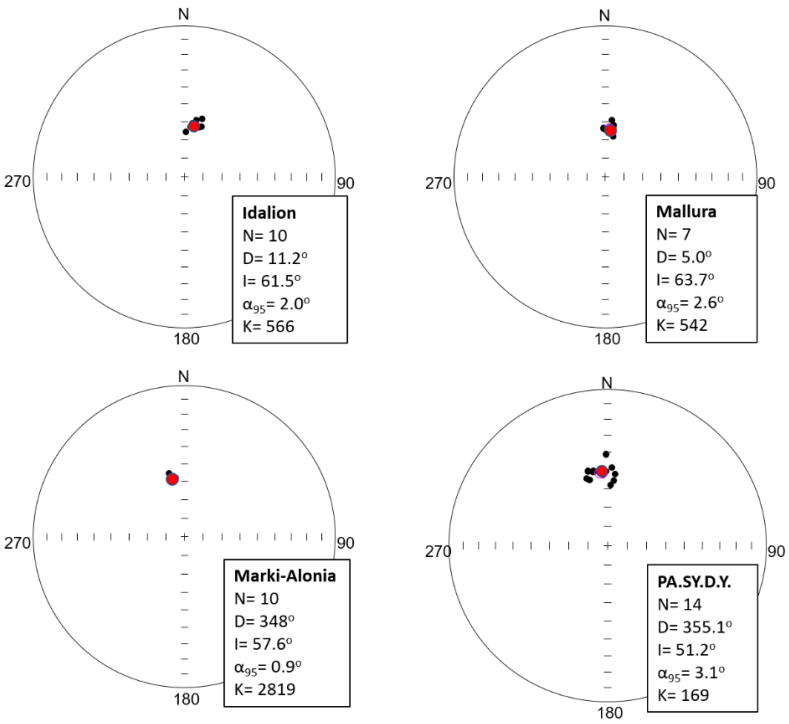

Figure 2. Equal area projections of the ChRM directions at sample level, together with the mean direction (red dot). D and I are the mean declination and inclination; α_{95} is the 95% angle of confidence; K is the precision parameter; N is the number of independently oriented samples considered for the calculation of the mean direction.

The data obtained from Marki-Alonia and Agios Georgios were compared with other available data from Cyprus (Tema et al., 2018) and nearby areas (Brown et al., 2015; Shaar et al., 2018), as well as with global geomagnetic field models. Instead, the directions from Idalion and Mallura that were not well dated, have been used for the archaeomagnetic dating of these two structures after comparison with the predictions of the SHA.DIF.14k (Pavón-Carrasco et al., 2014) global geomagnetic field model. It would appear that the Idalion structure was heated for last time in an interval 925-819 BC, if the 1200-700 BC time period is considered, while the Mallura hearth was used for the last time at 853-782 BC or 712-610 BC, taking into consideration the last millennium BC in the calculation of its age at 95% of probability.

Conclusions

Four new well-defined archaeomagnetic directions from Cyprus are presented. Two of them come from well dated archaeological structures, while for the other two data the available archaeological dating is poor. These two structures were therefore archaeomagnetically dated after comparison with the predictions of the SHA.DIF.14k model calculated at the geographic coordinates of the sites. The results obtained show that archaeomagnetic dating in Cyprus is possible, but the enrichment of the local dataset with new data is still necessary to improve the reliability of the global models' predictions in the area.

Acknowledgements

We would like to sincerely acknowledge all the archaeologists that have collaborated during the sampling of the structures studied for their availability, collaboration, sampling permission as well as for all the useful information they provided us regarding the sites, the materials studied and their dating.

References

Brown, M.C., Donadini, F., Korte, M., Nilsson, A., Korhonen, K., Lodge, A., Lengyel, S.N. & Constable, C.G., 2015. GEOMAGIA50.v3: 1. General structure and modifications to the archeological and volcanic database. Earth Planets Space, 67:83, doi:10.1186/s40623-015-0232-0.

Pavón-Carrasco, F.J., Osete, M.L., Torta, J.M., De Santis, A., 2014. A geomagnetic field model for the Holocene based on archaeomagnetic and lava flow data. Earth Planet. Sci. Lett., 388, 98-109.

Shaar, R., Hassul, E., Raphael, K., Ebert, Y., Segal, Y., Eden, I., Vaknin, Y., Marco, S., Nowaczyk, N., Chauvin, A., Agnon, A., 2018. The first catalog of archaeomagnetic directions from Israel with 4000 years of geomagnetic secular variations. Frontiers in Earth Science, 6:164. Doi: 10.3389/feart.2018.00164.

Tema, E., Hedley, I., Fasnacht, W., Peege, C., 2018. Insights on the geomagnetic Secular Variation in the Eastern Mediterranean: First directional data from Cyprus. Phys. Earth Planet. Int., 285, 1-11.

15th International Congress of the Geological Society of Greece
Athens, 22-24 May, 2019 | Harokopio University of Athens, Greece
Bulletin of the Geological Society of Greece, Sp. Pub. 7 Ext. Abs. GSG2019-129

Assessing Bedload in Vouraikos River, NW Peloponnese, Greece

S. Karalis [1], A. Iordanou [2], G. Karakostas [2], K. Charatsis [2] and E. Karymbalis [1]

(1) Harokopio University, Department of Geography, 70 El. Venizelou Av., Kallithea, Greece, 17671, skaralis@hua.gr
(2) University of West Attica, Department of Survey and Geoinformatics Engineering, Egaleo, Greece, 12243

Introduction

Vouraikos River and its watershed has been the subject of an on-going Ph.D research (of the first author) initiated in 2012, and aimed at quantifying and modelling sediment transport, with emphasis in bedload transport. In this abstract we briefly present the results of a 5-year long measurements program, regarding bedload transport.

Study Area

Vouraikos River is located in the northwestern Peloponnese and drains an area of 284 km^2. The southern part of its catchment consists of geological formations of Mesozoic age (mainly limestones, but also cherts and flysch layers which belong to the geotectonic zone of Olonos-Pindos and. The northern part is dominated by Late Pliocene to Quaternary fluvial and lacustrine Gilbert type fan-delta conglomerates (Bornovas and Rondoyanni, 1983). The climate of the north Peloponnese is coastal Mediterranean (Köppen: Csb) with mean annual temperature 14.5 °C, mean temperature of the coldest month 10.6 °C and mean temperature of the warmest month 26.4 °C (Katsafados et al., 2012). Rainfall exhibits a gradient ranging from more than 1500 mm of rain over the mountains of central Peloponnese to less than 450 mm at the seashore of the Gulf of Corinth. The main channel of Vouraikos river is made up, in general, by two distinct parts; It is characterised by a tranquil, slow flow in the valley of Kalavryta (gentle slope), while, after its exit from the valley (approximately downstream of the bridge of Kerpini), its slope increases and it becomes a roaring watercourse within a v-shaped, steep valley, until almost the village of Zachlorou. About 1 km upstream of the village of Zachlorou, the v-shaped, steep valley becomes a gorge, for which this river is widely known.



Figure 1.Panoramic view of the stream, downstream of the Pliatsikouras bridge station. The piles of gravels that can be seen in the left bank are supplied by a tributary. Occasionally, this sediment is shovelled and piled overbank.

In the study site (Pliatsikouras Bridge) the stream can be classified broadly as plain bed type. Not far downstream, as its slope increases, it becomes a step – pool type. The average slope is 1.5%. The principal sediment sources are fluvial, hillslope and debris flows while sediment storage is mainly overbank. These features can be seen in Fig. 1.

Methods and data

Bedload samplings were carried out with the use of a Helley-Smith sampler with a 15cm square opening. Sediments traps were also employed, but were abandoned at a later stage since their operation is very problematic under large discharges. On the contrary, the existence of the low bridge gave us the opportunity to use the Helley-Smith sampler, even in near-bankfull discharges. Sediment transport measurements were concurrent with flow velocity and water discharge measurements that, inter alia, revealed the at-a-station hydraulic geometry. Grainsize distributions (GSD) of surface bed material and the substrate were acquired from such gravelometric surveys as pebble counts and shovel (bulk) samplings (Karalis et al., 2016). Main geometric features of the river reach, such as slope, width and plan course were made available from a complete topographical survey of the reach that we performed, stretching about 400 m. upstream of the station. Two ten-years period hydrographs (1980-1990 and 2004-2014) were made available to us, courtesy of the Public (once) Power Corporation (DEH), that has been monitoring the river from a station(Zachlorou) just 2 Km downstream of Pliatsikouras Bridge. Rainfall and temperature data on a daily base were made available to us also by DEH.

Results

We compared our measurements against the outcome of some of the bedload equations included in B.A.G.S. (Bedload Assessment for Gravel-bed Streams) software, made by the United States Forest Service (Wilcock et al., 2009). Three equations were chosen from BAGS, in particular the ones that employ surface material distributions (Parker 1990, Wilcock 2001, Wilcock – Crowe 2003). Another equation, that has been developed for the Little Granite Creek, in Wyoming, USA, by Ryan & Emmett (2002) was also considered, due to the fact that it gave results very close to our

measurements. Finally, we developed a site-calibrated equation -Wclb2- based on the procedure outlined by Wilcock (2001).

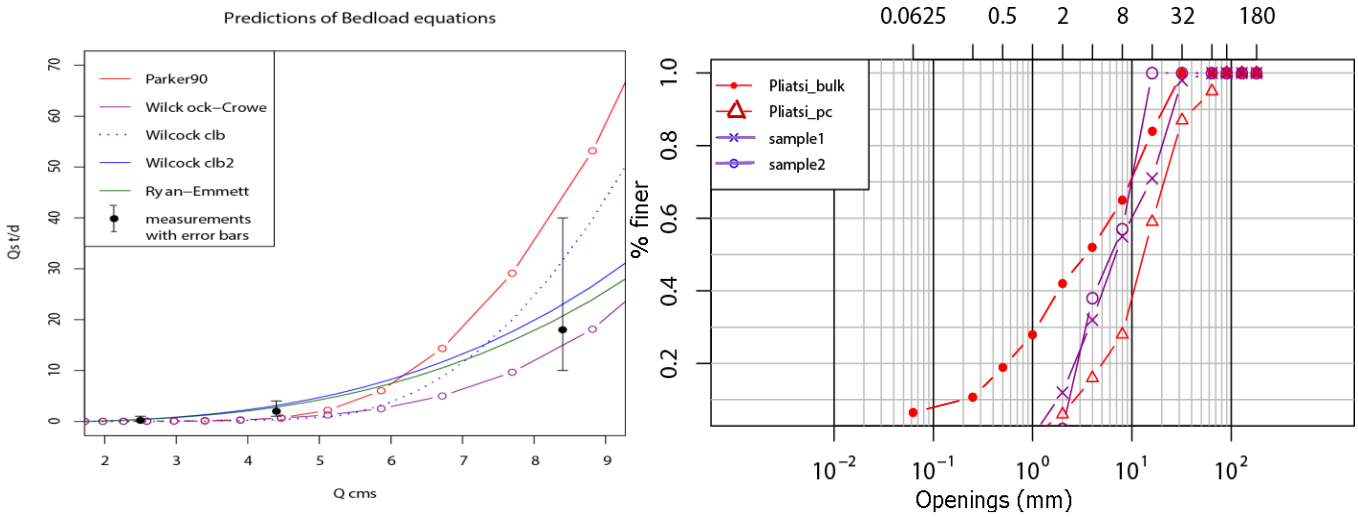

Figure 2. Left: predictions of 5 bedload equations against measurements. Right: GSD's of two different sampling methods of bed material (pebble count and bulk sample) along with GSD of two bedload samples, at the site. Error bars in measurements span from twice to half of the measured quantity.

Other well-known equations like Meyer – Peter & Muller, Kalinske, Einstein – Brown, Karim – Kennedy, Engelund & Hansen and Ackers – White were also tried. Only Ackers – White gave results close to our measurements, while all others seriously overestimated sediment load, by as much as 4-5 times.

Conclusions

As we can see (Fig.2, Left), with the exception of Parker90 equation, all others fall within a relatively short distance from our measurements. Another important point to note is the discharge at which the curve lifts above the x-axis, that is, the discharge above which we have some noticeable bedload transport. All equations are sensitive mainly in the size of surface material that will be used for the calculations (D50). As we see in Fig.2 (Right), bedload samples are somehow closer to the GSD obtained by pebble counts, but this is also due to the fact that Helley-Smith cannot trap sediments smaller than a few millimeters. The fact that we were able to sample near bankfull discharge (~8cms) was very favorable to the integrity of our estimations. An encouraging fact though, is that in the long term (a decade), all equations (except Parker90) predict the same mass of dislocated material, as we can see in Table 1, below.

Table 1. Mean annual bedload discharge from 5 equations in metric tonnes, for two periods

Q mean daily (cms)	*Ryan-Emmet*	*Wilcockclb*	*Wilcockclb2*	*Parker 90*	*Wilcock-Crowe*
A period 1980-1990:2,57	*2229*	*2008*	*2223*	*4862*	*2090*
B period 2004-2014:1,66	*693*	*882*	*1393*	*1958*	*1030*

The above values represent a percentage of 8-10% of the total load and happen mainly in the 4-month period from December to March of each year (unpublished Ph.D. results). Overall, our results seem reasonable. We can conclude that, given good quality hydrological, topographic and sedimentological data, these three equations from BAGS can give credible results. The most critical point is the choice of D50.

References

Bornovas, I.& Rondoyanni, Th. (1983) Geological Map of Greece,. Scale 1:500,000. Institute of Geology and Mineral Exploration.

Karalis S., Aytousmis A., Iordanou A.,Karakostas G.,Charatsis K., and Karymbalis E. (2016) Obtaining and testing coarse grain size distributions from photographic grid counts. Bulletin of the Geological Society of Greece, vol. L, 2016, Proceedings of the 14th Intern. Conference, Thessaloniki.

Katsafados, P., Kalogirou, S., Papadopoulos, A. and Korres, G. (2012). Mapping Long-Term Atmospheric Variables over Greece. Journal of Maps, 8, 181-184.

Ryan, S., & Emmett, W. (2002). The Nature of Flow and Sediment Movement in Little Granite Creek Near Bondurant, Wyoming. United States Department of Agriculture Forest Service Rocky Mountain Research Station General Technical Report

Wilcock P. (2001). Toward a practical method for estimating sediment-transport rates in gravel-bed rivers. Earth Surf.Process. Landforms 26, 1395–1408.

Wilcock P., Pitlick J. and Yantao C. (2009). Sediment Transport Primer: Estimating Bed-Material Transportin Gravel-bed Rivers. United States Department of Agriculture-Forest Service Rocky Mountain Research Station General Technical Report.

15th International Congress of the Geological Society of Greece
Athens, 22-24 May, 2019 | Harokopio University of Athens, Greece
Bulletin of the Geological Society of Greece, Sp. Pub. 7 Ext. Abs. GSG2019-131

Estimating Suspended Sediment Transport through Transparency Tube in Vouraikos River, NW Peloponnese, Greece

S. Karalis [1], A. Iordanou [2], G. Karakostas [2], K. Charatsis [2] and E. Karymbalis [1]

(1) Harokopio University, Department of Geography, 70 El. Venizelou Av., Kallithea, Greece, 17671, skaralis@hua.gr
(2) University of West Attica, Department of Survey and Geoinformatics Engineering, Egaleo, Greece, 12243

Introduction

Vouraikos River and its watershed has been the subject of an on-going Ph.D research (of the first author) initiated in 2012, and aimed at quantifying and modelling sediment transport. In this abstract we briefly present the results of a 5-year long measurements program, regarding suspended sediment transport. In particular, we discuss - and strongly encourage - the use of a transparency tube, a cheap and easy to use turbulometer (Anderson and Davic, 2004, Dahlgren et al.,2004), as a reliable alternative to more sophisticated and expensive instrumentation for monitoring sediment transport in rivers and streams.

Study Area

Vouraikos River is located in the northwestern Peloponnese and drains an area of 284 km^2. The southern part of its catchment consists of geological formations of Mesozoic age (mainly limestones, but also cherts and flysch layers which belong to the geotectonic zone of Olonos-Pindos. The northern part is dominated by Late Pliocene to Quaternary fluvial and lacustrine Gilbert type fan-delta conglomerates (Bornovas and Rondoyanni, 1983). The climate of the north Peloponnese is coastal Mediterranean (Köppen: Csb) with mean annual temperature 14.5 $^{\circ}$C. Rainfall exhibits a gradient ranging from 1500 mm of rain over the mountains to less than 450 mm at the seashore of the Gulf of Corinth. The drainage metwrk of Vouraikos directly drains extensive area of the Chelmos Mountain that retains snow for most of the year.

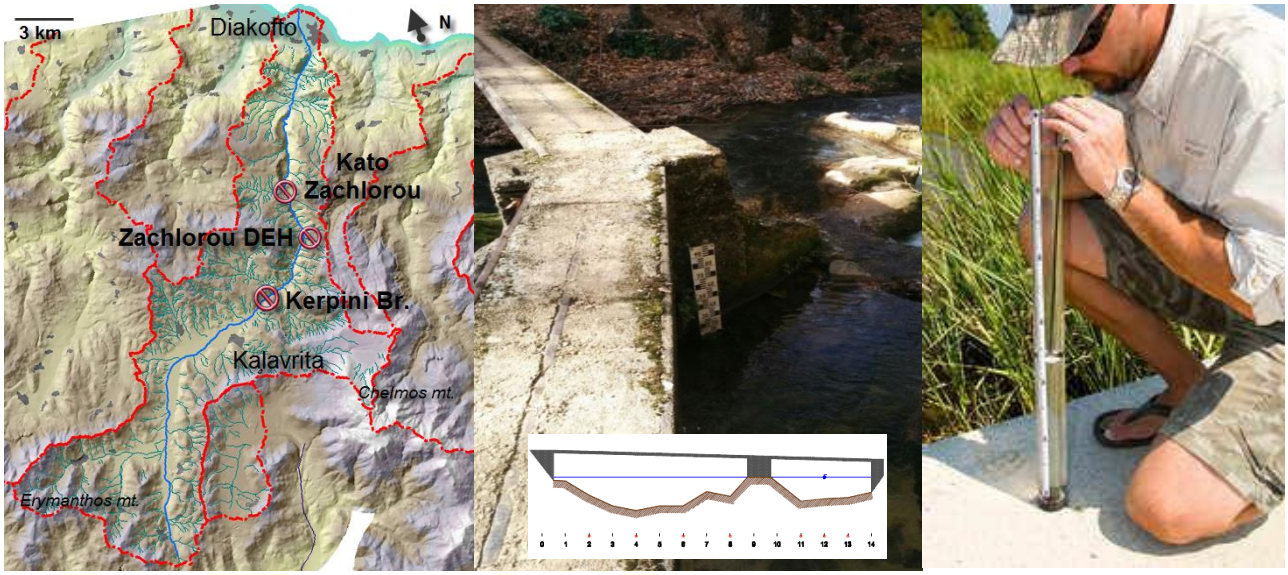

Figure 1.Left, a general map of the basin. Middle, the low bridge at Kato Zachlorou where measurements were conducted and (below) cross section of the channel. The stadia can be seen in the middle pier. Right, the use of the transparency tube is simple: one empties the tube until the mark in its bottom cup can be clearly seen, and then records the water height.

In the study site (Kato Zachlorou Bridge, Fig.1) the stream drains an area of 187 km^2 and it can be classified broadly as step – pool type. The stream is carved in the bedrock and the average slope is 2%. The principal sediment sources are fluvial and hillslope material while, due to the nature of the stream at the site, there is no sediment storage except from small sand pockets.

Methods and data

Two distinct periods of transparency tube daily measurements were conducted by a local collaborator, stretching about 2.5 months each. These periods were from 21/12/2015 to 26/02/2016 and from 25/2/2018 to 30/04/2018. Nine water samples were taken with a DH48 sampler lowered from the bridge, at high and low waters, which were later analyzed in the laboratory of Physical Geography of Harokopio University by drying in the oven and weighting the collected sediment. Discharge was estimated by the rating curve for the site. While the use of the transparency tube is rather simple, its main defect is the subjectivity of the observer when he decides that he “sees clearly” the black and white pattern at the cup. Because this point was not clearly agreed upon with the observer, the first period’s measurements were not considered trustworthy. Due care was taken, stressing that point to the observer before the beginning of the second period of the measurements, that yielded much more reliable results (Fig.2). A turbulometer reading – SSC curve was constructed and

was given an analytic expression (exponential) and extrapolated through the full range of the readings (0-60 centimeters).These measurements also yielded a sediment rating curve (Discharge – Suspended Sediment Concentration, SSC) for the site (Fig.2). In addition to the above, two ten-years period stage hydrographs (1980-1990 and 2004-2014) were made available to us, courtesy of the Public (once) Power Corporation (DEH), that has been monitoring the river through a hydrometric station (Zachlorou DEH), just 1.5 Km upstream. Rainfall and temperature data on a daily base were made available, also by DEH. We converted these stage hydrographs to discharge hydrographs with the use of our own rating curve for the site (10 points at Zachlorou DEH) and were thus able, using our sediment rating curve, to make a rough estimation of the suspended sediment load that had been transported during these periods. Another equation, developed by Ryan & Emmett (2002) for the Little Granite Creek, in Wyoming USA, was also considered, due to the fact that –regarding bedload - it gave results very close to our measurements, but also because these streams present significant similarities.

Results

The results can be seen in Figure 2. In the right panel we can see the time series of the second period of turbulometer measurements. Along with the discharge line we can see two lines of SSC, one from the turbulometer readings and the other from the sediment rating curve. It is clear that the turbulometer SSC is much more sensitive to the sediment load, since it depicts the peak in SSC caused by the flood of the 26th of February, while the next day, when the available sediment has been depleted, the SSC returns to low values even though the discharge is still high. An encouraging fact is that these two curves, despite their differences, yield the same, more or less, amount of sediment for the given period.

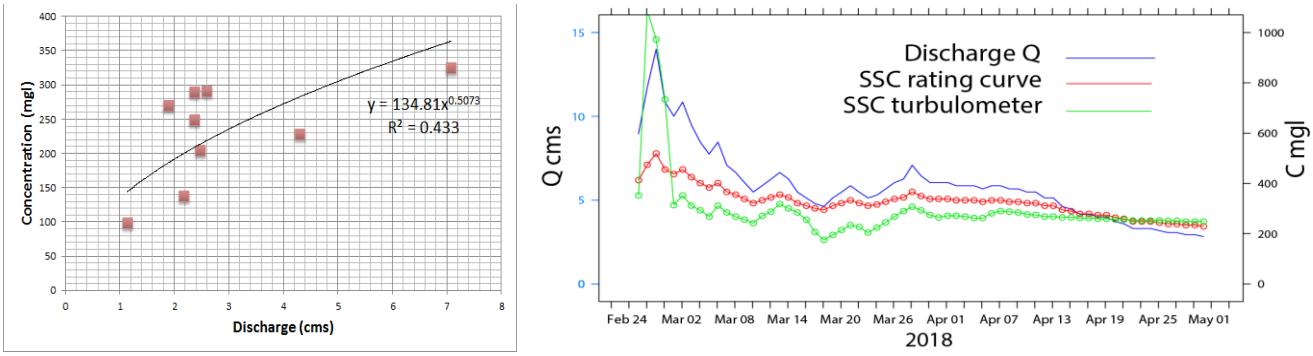

Figure 2.Left: the sediment rating curve used. Right: Time series of second period's measurements.

When applied over the two ten-year periods, the rating curve gives values of suspended sediment transport that range from 27 thousand metric tonnes per year for the first period (1980-1990) to about 13 thousand tonnes for the second period (2004-2014), with an average of 22 thousand tonnes. The maximum annual transport is estimated to be about 68 thousand tonnes for the hydrologic year of 1983. Ryan & Emmets' equation predicts much lower values, an average of 7 thousand tonnes. The bulk of the transport takes place mainly in the 4-month period from December to March. If we set on to calculate the transported material per km^2 based on the above values, we are faced with the difficulty of estimating the contributing basin area. Morphologically Vouraikos river is made up, in general, by four distinct parts (Sabot and Maroukian, 1989); The *mountainous* part that drains into the valley of Kalavryta (*upper*), while, after its exit from the valley (bridge of Kerpini), its slope increases and it becomes a roaring watercourse within a v-shaped, steep valley (*lower*), which, then, finally reaches the sea (*beachfront*) creating a fan. So, if we accept only the area downstream of Kerpini as contributing area (17 km^2) we come up with 1300 t/y/km^2. If we accept the whole of the basin at the site (187 km^2), we come up with just 120 t/y/km^2.

Conclusions

The use of a simple transparency tube turbulometer, is able, if locally calibrated, to assess total suspended solids and turbulence in rivers with acceptable accuracy. This method should be adopted by our governmental agencies as a cheap alternative for assessing sediment transport and even water quality, especially these days when the budgets for monitoring and research are dramatically reduced.

References

Anderson P. and Davic R.,(2004). Use of Transparency Tubes for Rapid Assessment of total suspended solids and turbulence in Rivers.Lake and Reserv. Manage. 20(2):110-120.

Bornovas, I.& Rondoyanni, Th. (1983) Geological Map of Greece,. Scale 1:500,000. Institute of Geology and Mineral Exploration.

Dahlgren R., V.Niewenhuyse E. and Litton G., 2004. Transparency tube provides reliable water quality measurements.http://CaliforniaAgriculture.ucop.edu.

Ryan, S., & Emmett, W. (2002). The Nature of Flow and Sediment Movement in Little Granite Creek Near Bondurant, Wyoming. United States Department of Agriculture Forest Service Rocky Mountain Research Station General Technical Report

Sabot V. and Maroukian H. (1989). River discharge and Stream Channel Changes Along a Torrent in Northern Peloponnesus, Greece. 2nd International Conference on Geomorphology. Frankfurt, Main.

15th International Congress of the Geological Society of Greece
Athens, 22-24 May, 2019 | Harokopio University of Athens, Greece
Bulletin of the Geological Society of Greece, Sp. Pub. 7 Ext. Abs. GSG2019-156

Human-induced Landslides in Northern Euboea Island, Central Greece

G. Gaitanaros[1], H. Skilodimou[1], G. Bathrellos[1]

(1) Section of Geography and Climatology, Department of Geology and Geoenvironment, National and Kapodistrian University of Athens, University Campus, 15784, Zografou, Athens, Greece; georgegaitan95@gmail.com

Introduction

Landslides can be triggered by a variety of physical factors (Bathrellos *et al.*, 2017). Additionally, human activities such as deforestation of slopes, removal of slope support in road cuts, alteration of surface runoff paths, have become important triggers for landslide manifestation (Skilodimou *et al.*, 2018).

The scope of the present study is to identify the influence of human activities on landslide occurrences. To accomplish this scope, the existing landslides along with anthropogenic factors such as road network and land use were used. Statistical analysis and GIS were applied to process and evaluate the landslides and factors. Thus, the spatial distribution landslides and their relation to roads and land use were determined.

Study area

The study area is located in the northern part of Euboea Island, in central Greece. The island is separated from the continental Greece through Euboean Gulf (Figure 1a). The region covers an area of about 93 km^2 and its altitude varies from 0 to 960m. The morphology of the area comprises a northern mountainous land with very steep slopes reaching an altitude of 960 m asl; an intermediate semi-mountainous land with lower altitudes and steep slopes; and a southern coastal area of limited extent with low altitudes and gentle slopes. The drainage networks of the area flow with a main direction from N to S and discharge into the North Euboean Gulf (Figure 1b).

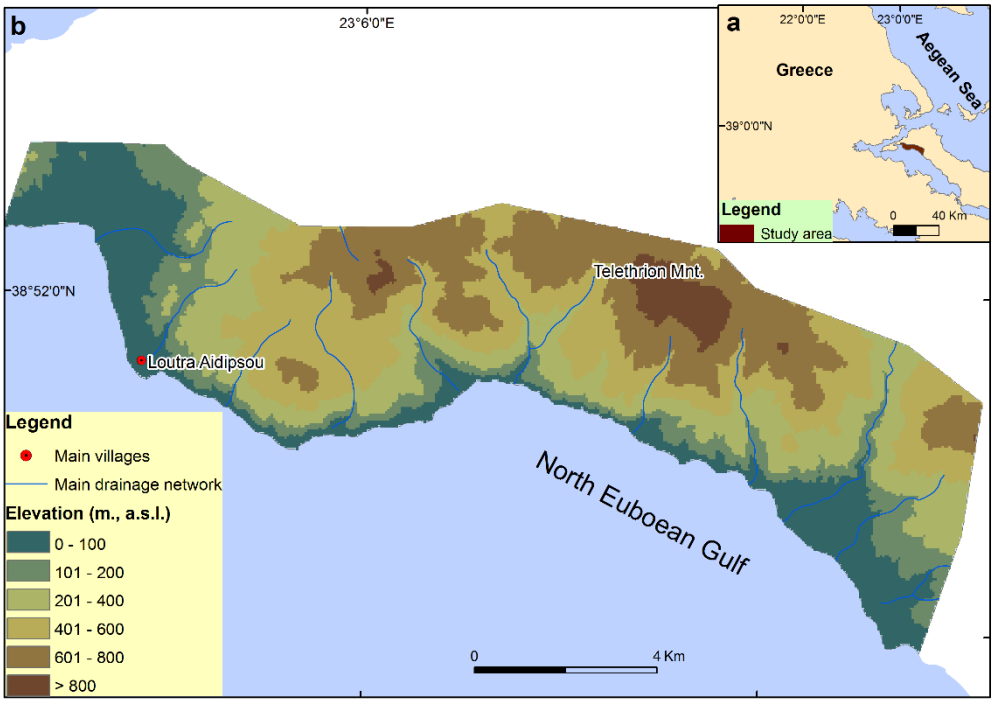

Figure 1. a) Location map of the study area; b) the elevations of the study area, the drainage network, and the main settlements.

Data and Methods

The existing landslides, provincial and rural road network along with land use of the study area are taken into consideration. To accomplish the scopes of the study nine buffer zones of increasing length measured around to each type the road network and five categories of land use were created. The number of landslide events, which were located in each class of each factor was determined. The relative frequency of landslides and the frequency ratio were calculated. The relative frequency of landslides is the ratio between the number of landslide that located in each category of factor and the total landslide events of the study area. To determine the frequency ratio, the area ratio for each category to the total area was computed. Finally, the frequency ratio for each category was calculated by dividing the relative frequency of landslide events to the area ratio.

Results

Table 1 shows the results of the statistical analysis. The relative frequency of landslides reaches its maximum value within

the first 50m of distance from any given provincial and rural road and decreases in distances beyond 50 m from roads. Table 1 presents the computed frequency ratio of landslide events for each buffer zone of both types of road network. According to Lee and Pradhan (2006), the frequency ratio values > 1, indicate strong relationship between landslides and the given buffer zone. The frequency ratio values show that buffer zones with distances smaller than / or equal to 50 m from provincial and rural roads is strongly related to landslide manifestation. In the case of land use, the majority of landslides are located in cultivated areas. The frequency ratio values are > 1 in cultivated land and in bare area, showing a strong relation to slope failures**.**

Table 1. Frequency and frequency ratio values of landslide occurrences into each category of each type of road network and land use.

Provincial roads network buffer zone (m)	**Area (m^2)**	**Area %, (a)**	**Landslides**	**Landslides %, (b)**	**Frequency ratio (b/a)**
10	3,918,733	4	3	12	2,7
25	5,587,498	6	5	19	3,2
50	8,414,607	9	8	31	3,4
75	7,447,923	8	2	8	0,9
100	6,590,960	7	1	4	0,5
150	10,955,038	12	0	0	0,0
200	8,858,134	10	0	0	0,0
300	13,252,325	14	0	0	0,0
>300	27,698,912	30	7	27	0,9
Total	92,736,734	100	26	100	1,0
Rural roads network buffer zone (m)					
10	2757475	3	1	4	1,3
25	3996804	4	2	8	1,8
50	6188115	7	3	12	1,7
75	5630217	6	1	4	0,6
100	5089316	5	0	0	0,0
150	8878116	10	0	0	0,0
200	7472717	8	0	0	0,0
300	12013350	13	0	0	0,0
>300	40710624	44	19	73	1,7
Total	92736734	100	26	100	1,0
Land use					
Urban area	1605997	5	3	12	2,2
Cultivated area	25478977	46	13	50	1,1
Forest	31084154	6	1	4	0,7
Shrubby area	34216126	42	2	8	0,2
Bare area	365310	1	7	27	24,6
Total	92736734	100	26	100	2,2

Conclusions

The frequency of landslides increases in close proximity to roads. A 100m wide zone along with any type of road corridors is strongly correlated with landslide events. The extensive cultivated land and the bare area of the study area are strongly related to landslide activity.

References

Bathrellos, G.D., Skilodimou, H.D., Chousianitis, K., Youssef, A.M., Pradhan, B. 2017. Suitability estimation for urban development using multi-hazard assessment map. Sci. Total Environ *575*, 119–134.

Lee, S., Pradhan, B. 2006. Probabilistic landslide hazards and risk mapping on Penang Island, Malaysia. J. Earth Syst. Sci 115 (6), 661–672.

Skilodimou, H.D., Bathrellos, G.D., Koskeridou, E., Soukis, K., Rozos, D. 2018. Physical and anthropogenic factors related to landslide activity in the Northern Peloponnese, Greece. Land 7(3), 85, doi: 10.3390/land7030085.

15th International Congress of the Geological Society of Greece
Athens, 22-24 May, 2019 | Harokopio University of Athens, Greece
Bulletin of the Geological Society of Greece, Sp. Pub. 7 Ext. Abs. GSG2019-157

Granite tafoni in Chalkidiki, Greece

K. Chitoglou[1], G. Lazaridis[1]

(1) Aristotle University of Thessaloniki, Department of Geology, Laboratory of Geology and Palaeontology, 54124, Thessaloniki, Greece, geolaz@geo.auth.gr

Sithonia Peninsula in Chalkidiki is an area dominated by the Sithonia Plouton occurrence and its characteristic geomorphic appearance of granite weathering. In the area of the Akti Kalogrias beach there is a significant number of cavities and surface potholes. Granite caves and tafoni formations have been described from several areas in Greece, such as Serres, Kavala (Lazaridis and Pipera, 2008), Fthiotida (Modianaki 2012) Naxos and Tinos (Evelpidou et al. 2010 and references therein), Paros and Ios (Hejl, 2005).

Several opinions, and sometimes controversial, can be found in literature about the formation of caves in granite rocks. The main processes that have been described in order to interpret their development (i.e. vidal romani, 1989; 1990; Cambell 1997; Twidale 2008; Uña Alvarez 2008; Romani 2008, Groom et al. 2015; Klimchouk 2017): 1. eolian deflation; 2. weathering through insolation; 3. frost action; 4. wetting and drying; 5. chemical and salt weathering; 6. biological decay; 7. gravitational forces (imposed by large boulder resting on an outcrop and causing crystal strain at the point or point of contact, eventually leading to rock basins on the outcrop and tafoni on the underside of the boulder); 8. microclimatic conditions; 9. exfoliation; 10. haloclasty [this category emracing crystal growth, hydration expansion and osmotic pressure]; endogenous processes.

In the present study two adjacent locations in Akti Kalogrias have been recorded in detail in order to describe the type of the cavities on the basis of their location and morphology, and to discuss their origin.

Methods

Track and cave positions are recorded with a Garmin GPSmap 60GSx and the track's length and area are estimated by MapSource software (v. 6.13.7 Garmin). Each cavity was labeled, morphologically categorized, measured and documented. Some of the cavities were surveyed in detail.

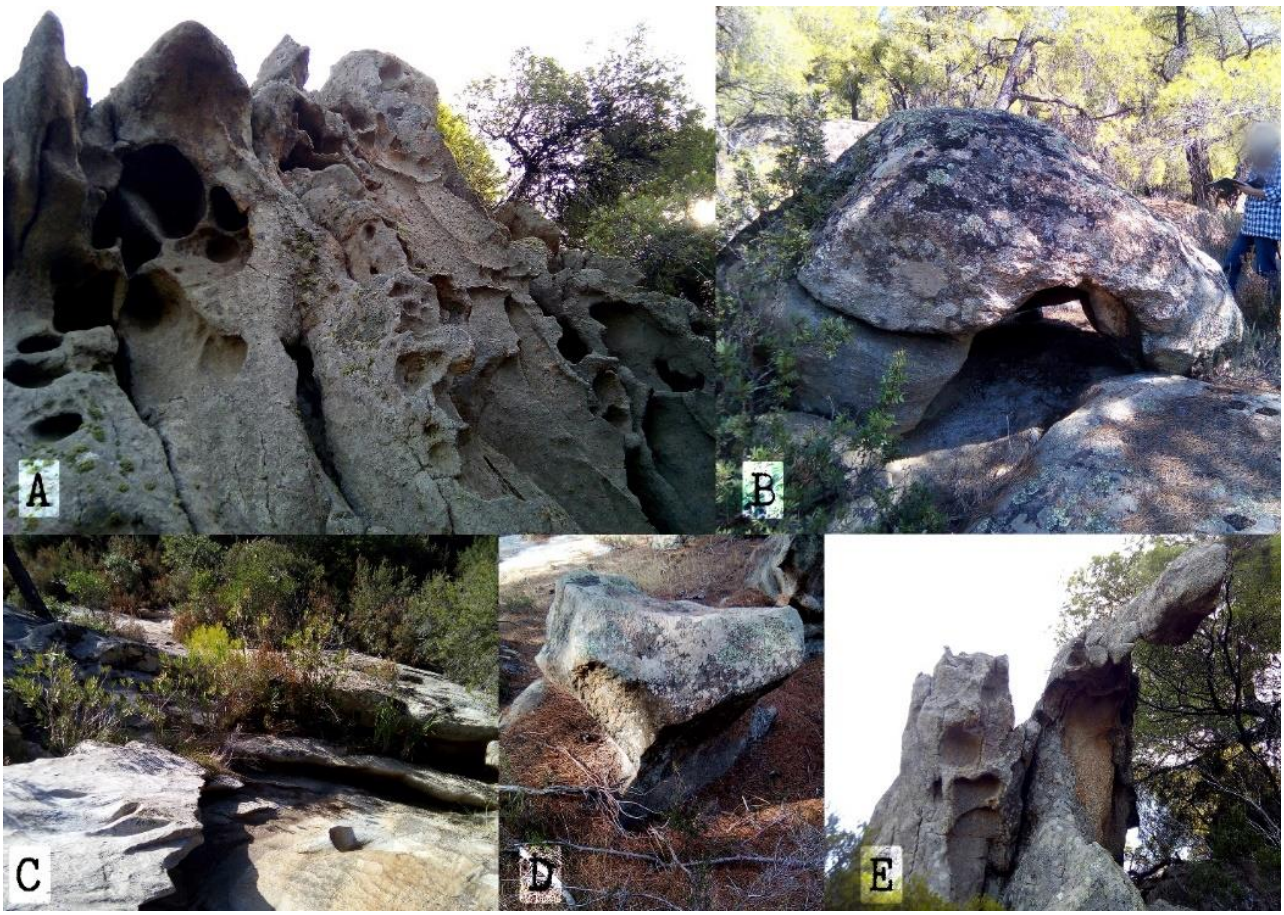

Figure 1. Morphological categories of tafoni in Akti Kalogrias area: A. tafone formed in the side of the rock host with honeycombed erosion; B. tafone formed in the base of the rock form; C. tafone develobed among discontinuities; D. a mushroom-like form; E. a complex tafone form.

Results

Their dimensions do not exceed 8 m. Their dimensions range along horizontal axis from 0.9m to 8m (mean 2.4 m); vertically (height) from 0.2 m to 3.0 m (mean 1,2 m); and their depth ranges from 0,15 m to 4.1 m with (1.2 m).

Morphologically they can be distinguished in 5 categories that groups cavities with similar number of openings, their location in relation to the boulder and any discontinuities. These categories are the following (Figure 1): 1.tafoni that are formed in the side part of the rock; 2. tafoni that are formed in the base or at the above a horizontal discontinuity and the erosion continues at the inside of the host rock and sometimes resembles a "tortoise shell" form; 3. tafoni that are formed between discontinuities; 4.tafoni that are formed in the base and around of the host rock giving a "mushroom-like shape to that; and 5. combination of the above-mentioned groups. Honeycomb erosion is observed in tafoni from various categories but mainly in basal, and side-wall tafoni.

Regarding their spatial distribution, two parameters are estimated: the number of cavities larger than 0.5 m found in the surveyed area; and number of cavities divided to the walked distance. These two parameters are 1/284 cavities/m^2 and 1/52 cavity/m^2 for the first area and 1/520 cavities/m^2 and 1/72 cavity/m^2 for the second area, respectively. In total, the two areas covered 21.500 m^2 and 3 km of distance that means 1/407 cavity/m^2 and 1/63 cavity/m.

The hypothesis that a preferred orientation exists was checked with directionality tests. The possibility of random orientation cannot be rejected. The logarithm of the cavity volume and the boulder that hosts the cavity are moderately correlated (n=22).

There are 3 main discontinuities recorded in the area (J_1: 126/85, J_2: 237/85 and J_3: 320/20). Their density decreases from J_3 to J_1. Among 43 tafoni, 21% is formed in boulders that are not *in situ*. Regarding the *in situ* tafoni, 29%, 18% and 35% are associated with the discontinuities J_1, J_2 and J_3, respectively. In 21% the cavities are formed along the combination of J_1, and J_3 discontinuities. In 38% of *in situ* there is no obvious relation to discontinuities.

Concluding remarks

With this work the tafoni weathering morphology in Sithonia is described qualitatively and quantitatively. Despite that large caves are commonly unexpected in this setting, it seems that these forms occur in large numbers. This means relatively high values in the estimated parameters. The results is expected to be used for comparisons with other granite tafoni occurrences.

References

André, M.F. and Hall, K., 2005. Honeycomb development on Alexander Island, glacial history of George VI sound and palaeoclimatic implications (two step cliffs/Mars Oasis, W Antarctica). Geomorphology, 65(1-2), 117-138.

Campbell, E.M., 1997. Granite landforms. Journal of the Royal Society of Western Australia, 80, 101.

Evelpidou N, Leonidopoulou D, Vassilopoulos A. 2010. Tafoni and alveole formation. An example from Naxos and Tinos Islands, in: Natural Heritage from East to West,Springer, Berlin, Heidelberg ,35-42.

Groom, K.M., Allen, C.D., Mol, L., Paradise, T.R. and Hall, K., 2015. Defining tafoni: Re-examining terminological ambiguity for cavernous rock decay phenomena. Progress in Physical Geography, 39(6), 775-793.

Hejl E. A pictorial study of tafoni development from the 2nd millennium BC. Geomorphology. 2005 Jan 3;64(1-2),87-95.

Huinink, H.P., Pel, L. and Kopinga, K., 2004. Simulating the growth of tafoni. Earth Surface Processes and Landforms: The Journal of the British Geomorphological Research Group, 29(10), 1225-1233.

Klimchouk, A., 2017. Types and settings of hypogene karst. In Hypogene Karst Regions and Caves of the World. Springer, Cham,1-39.

Lazaridis, G. and Pipera, K., 2008. Preliminary report on granite caves in Greece. Cadernos do Laboratorio Xeolóxico de Laxe: Revista de xeoloxía galega e dohercínico peninsular, (33), 101-113.

Modianaki, Z., Evelpidou, N., Stamatopoulos, L. and Stamatakis, M., 2012. Tafoni formation at Theologos (Fthiotida, Greece). Revista de Geomorfologie, 14.

Romaní JR. 2008. Forms and structural fabric in granite rocks. Cadernos do Laboratorio Xeolóxico de Laxe: Revista de xeoloxía galega e do hercínico peninsular. (33), 175-98.

Vidal Romaní, J.R., 1989. Geomorfología granítica en Galicia (NW España). Cadernos do Laboratorio Xeolóxico de Laxe: Revista de xeoloxía galega e dohercínico peninsular, 13, 89-163.

Romaní, J.R.V. and Twidale, C.R., 1998. Formas y paisajes graníticos. Universidade da Coruña.

Twidale, C.R. and Bourne, J.A., 2008. Caves in granitic rocks: types, terminology and origins. Cadernos do Laboratorio Xeolóxico de Laxe: Revista de xeoloxía galega e do hercínico peninsular, 33, 35-57.

Uña Álvarez, De, E., 2008. Description and nomenclature of the tafoni features (cavernous rock forms). Research approaches in granite terrains. Cuadernos Lab. Xeolóxico de Laxe (Coruna), 33, .65-82.

Uña Álvarez, De, E., and Vidal-Romaní JR. 2008. Some minor features (tafoni, cavernous forms) in the granite terrains of Los Riojanos (Pampa de Achala, Sierra Grande de Córdoba, República Argentina). Geometric and morphologic properties. Cadernos Laboratorio Xeolóxico de Laxe. 2008,33,3-99.

15th International Congress of the Geological Society of Greece
Athens, 22-24 May, 2019 | Harokopio University of Athens, Greece
Bulletin of the Geological Society of Greece, Sp. Pub. 7 Ext. Abs. GSG2019-158

Insights into Ceramic Technology of Roman-Late Roman Wares from Surface Survey in Sphakia Area, Crete through a petrographic and geochemical approach

A.-M. Pollatou[1], I. Iliopoulos[1,2], E. Nodarou[3]

(1) Department of Geology, University of Patras, Patras, Greece, katerinapollatou0@gmail.com
(2) ERAAUB, Facultat de Geografia i Història, Departament d'Història i Arqueologia, Universitat de Barcelona, Barcelona, Spain
(3) INSTAP Study Center for East Crete, Pacheia Ammos, Crete, Greece

Background

Sphakia is a diverse and moutainous region in SW Crete, Greece. Today it is rather remote and marginal but in the Roman and late Roman times large ports grew in the area resulting in an unprecedented economic boom. This is reflected in the pottery that was uncovered during the Sphakia Survey Project with significant quantities of vessels, especially amphorae and fine decorated pots, some identified as Cretan, others as possible off-island imports.

Objectives

The aim of this project is to investigate the firing technology of various types of pottery through the evaluation of the sintering of the ceramic pastes and the identification of the new formed mineral phases. This study is complemented by petrographic description, mineralogical determination (XRPD) of the ceramic fabrics, and chemical analysis (SEM-EDS). The outcome of this integrated study combining archeological information and archaeometric data is hoped to shed new light on issues such as the identification of Cretan production against potential imports from off-Cretan centers and local imitations of foreign prototypes.

Methods

A total of 101 ceramic sherds were analyzed through mineralogical and petrographic techniques. Petrographic analysis was performed on thin sections prepared from sherds using a Zeiss AxioScope A.1 polarizing microscope. Fresh fractures of the ceramic sherds were examined in scanning electron microscope (SEM). The analysis was performed on gold coated specimens using a JSM JEOL 6300 SEM equipped with an Energy Dispersive X-ray spectrometer (EDS) in the Laboratory of Electron Microscopy and Microanalysis at the University of Patras, Greece. The mineralogy of all studied samples was determined by means of X-ray Powder diffraction (XRPD) using a Bruker D8 Advance diffractometer in the Department of Geology, University of Patras.

Results

The petrographic assessment helped us to establish five fabric groups and two loners. The ceramic shapes recognized include fine drinking and serving vessels such as bowls, cups, dishes, plates and transport vessels, mainly amphorae. In spite of their qualitative similarities in terms of their content in aplastic inclusions, the textural differences observed through Optical Microscopy helped us identify the following fabric groups (Fig. 1):

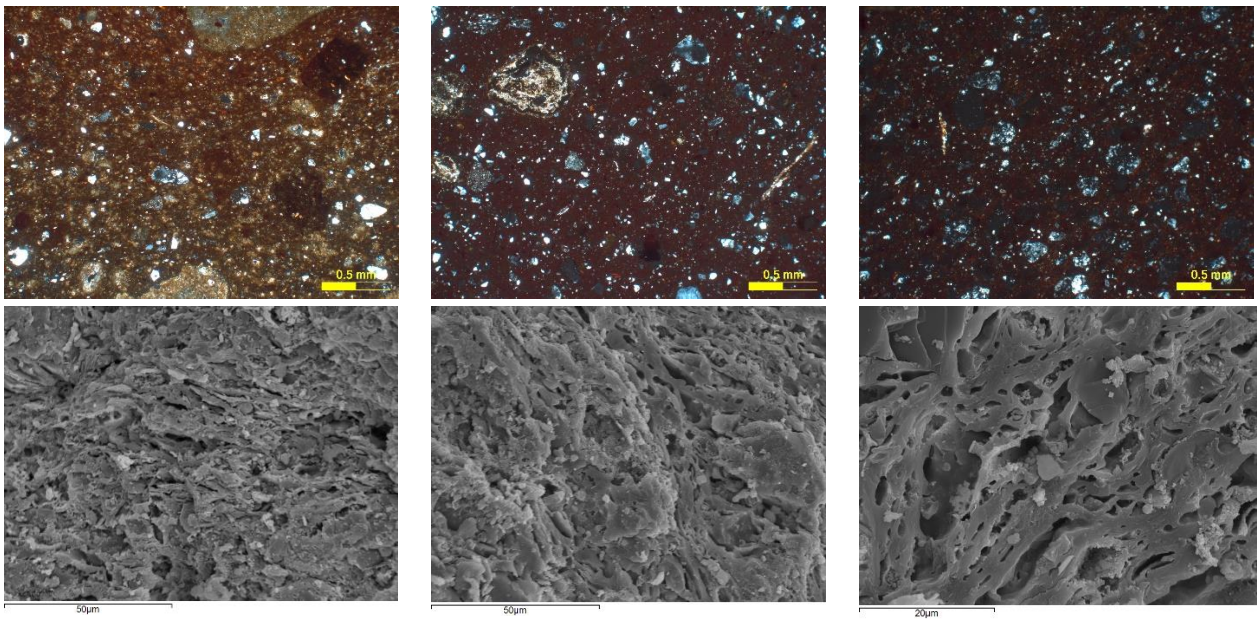

Figure 1. Characteristic photomicrographs (upper row) in crossed Nicols and secondary Electron SEM micrographs (lower row) of representative samples from groups A, B, C (samples 58, 83, 23).

- Group A: Micritic limestone + biotite ± chert
- Group B: Quartz + polycrystalline quartz + micritic calcite extensively decomposed
- Group C: Quartz + polycrystalline quartz
- Group D: Quartz + polycrystalline quartz + mica + micritic calcite extensively decomposed
- Group E: Quartz + white mica + brownish mica
- Loner 1: Quartz + white mica + brownish mica + subrounded volcanic fragments (diabase; hyalophyric) + sub-anglular plagioclase
- Loner 2: Quartz + brownish mica

XRPD and SEM/EDS allowed the establishment of the firing regime, and the overall pyrotechnology available to the ancient potters. The mineralogical groups identified through XRPD are presented in Table 1. The preliminary SEM/EDS results allowed the chemical characterization of the various petrographic groups and corroborative evidence for the firing temperatures obtained through XRPD. Thus, Group A and loners are non-calcareous (CaO<6%) and present low firing temperatures (Cultrone *et al.* 2001), while Groups C and E are calcareous (CaO>6%) and present higher firing temperatures. The remaining groups present a variability of firing temperatures and chemical compositions. As to clay microstructure (Maniatis *et al.* 1981) the preliminary results indicate that fabric group A exhibits initial vitrification (IV) with isolated smooth surfaces, fabric group B presents continuous vitrification (CV) with a continuous smooth vitrified layer visible across the sample, and group C presents extended vitrification (V) with deformed phyllosilicates.

Table 1. Classes created according to the same mineralogical assemblages and firing temperatures as estimated through the XRPD analysis. Abbreviations are according to Whitney & Evans, 2010.

Classes	Mineralogical assemblages	Equivalent Firing Temperatures
I	qz+ ilt± ab± cal± an± or	<850
II	qz+ an+ hem± mul	>850
IIIa	qz+ an+ ilt+ px+ hem± or± anl	~850-950
IIIb	qz+ an+ ilt+ gh+ px+ hem± or	~850-950
IV	qz+ an+ gh+ px+ hem	~950-1000
V	qz+ an+ px+ hem+ gh± or± cal	~950-1000
VI	qz+ an+ px+ hem	>1000

Conclusions

To sum up, this study deals with pottery that was produced in or reached this remote part of Crete in an era of intense circulation and sea trade in the Mediterranean. Archaeometric analysis including thin section petrography, XRPD, and SEM/EDS allowed an integrated technological study of the ceramic vessels. Several mineralogical and chemical groups were established indicative of different technologies of manufacture in terms of clay recipes and pyrotechnologies. This approach offered new insights on ancient potter's choices and practices as well as on the origin of the final product.

Acknowledgements

We would like to thank Drs J. Moody and J. Francis for entrusting us with the analysis of the Sphakia pottery; the personnel of the X-ray Diffraction Laboratory and the Laboratory of Electron Microscopy and Microanalysis of the University of Patras is gratefully acknowledged for conducting the analyses.

References

Cultrone, G., Rodriguez-Navarro, C., Sebastian, E., Cazalla, O., De La Torre, M.-J., 2001. Carbonate and Silicate Phase Reactions during Ceramic Firing. Eur. J. Mineral, 13, 621-634.

Maniatis, Y., Tite, M, 1981. Technological Examination of Neolithic- Bronze Age from Central- Southeast Europe and from the Near East. Journal of Archaeological Science, 8, 59-76.

Whitney, L., Evans, W., 2010. Abbreviations for names of rock forming minerals. American Mineralogist, Volume 95, 185-187.

Bulletin of the Geological Society of Greece, Sp. Pub. 7 Ext. Abs. GSG2019-159

Volcanic eruption signatures in speleothem archives of Santorini

Katerina Theodorakopoulou1, Konstantinos Kyriakopoulos1, Constantin.D.Athanassas 2, Evangelos Galanopoulos1, George Economou 3, Fanis Mavridis 4, Andreas Darlas 4

1Department of Geology and Geoenvironment, National and Kapodistrian University of Athens, Greece, katheo@phys.uoa.gr
2 Department of Geological Sciences, National Technical University of Athens (NTUA), Greece
3 Institute of Geology and Mineral exploration, Athens, Greece
4 Ephorate of Palaeoanthropology and Speleology, Athens, Greece

Speleothems are useful in detecting past geoenvironmental events and, specifically, variations in their chemical composition on the level of trace elements, constitutes a proxy of volcanic eruptions, enabling both the dating and the assessment of their effects. (Frisia et al., 2005)

Several geochemical studies on speleothems have identified well documented volcanic eruptions in the Mediterranean and the Near East, such as the Minoan eruption of Santorini, the Campanian Ignimbrite eruption, as well eruptions from Nisyros and Etna volcanoes etc. (Fleitmann et al. 2009; Bar-Matthews eta al. 1999; Verheyden et al.2008; Badertscher et al. 2014; Gençalioğlu-Kuşcu et. al, 2018). In the speleothem record, volcanic eruptions are generally identified in the carbonate laminae by sharp spikes in the amount of specific major and trace elements. Typically, high concentrations of S, Br, Bi, Zi, Ba, Mo etc can be indicative of volcanic activity (Frisia et al., 2005; Wynn et al., 2008; Bobrowski et al. 2003; Badertscher et al. 2014).

This study attempts to clarify possible 'signatures' of past volcanic eruptions in speleothems of Santorini. The Santorini volcano has shown significant explosive activity over the last 2 million years, which has not only altered the landscape, but also affected the civilizations of prehistoric and historical ages in east Mediterranean region.

Contrary to mainland, karstic systems in Santorini are poor and limited to the carbonate post- alpine sediments to the south-east. Carbonate rocks are exposed on the Profitis Ilias Mountain and Mesa Vouno mainly. (Heiken and McCoy, 1984). The most important cave is the Zoodochos Pigi, in the southeast part of the island in the vicinity of Ancient Thera. The presence of a permanent spring inside the cave, had been of immense value to the inhabitants of the Archaic city, as testified through the abundance of Archaic inscriptions (Hiller von Gaertringen et al.1904). Despite the poor decoration, speleothems such as flowstone abound in the cave.

During examination of the speleothem deposits in Zoodochos Pigi, we encountered charcoal trapped within the flowstone on a sharp boundary between bioturbated deposits to the bottom and undisturbed CaCO3 precipitation right above it (Fig.1).The unprecedented discovery of charcoal atop a bioturbated horizon shows evidence of sudden cessation of human activity in the cave in far- off times.

In order to explore the nature and the timing of the event, material enveloping the charcoal was submitted for mineralogical and geochemical analysis through optical and electron scanning microscopy (SEM-EDS), as well as XRD analysis, whereas the C-14 dating of the charcoal itself is underway.

Profiling of the chemical composition of the flowstone in the interface of the bioturbated (lower) horizon and the flowstone laminae, yielded several minerals and inclusions, exotic to typical flowstone composition, such as apatite, ilmenite, muscovite, FeS2 and Bi, Zi, Cu, Ni and Zn S, Ba oxides. (Fig.2). The presence of these minerals tails off sharply upwards going over typical (carbonate) flowstone mineralogy with calcite as the main mineral phase. Specifically elements such as Bi, Ba, S, Zi are associated with volcanic eruptions (Bobrowski et al. 2003).

In conclusion, this is the first analysis that has ever disclosed a volcanic eruption in the so far poorly speleothem record of Santorini. Chronological correlation on the basis of radiocarbon dating with the well documented timeline of eruptions of Santorini, as well as assessment of the possible wide - ranging effects on the local-to-regional environment and archaeological record of the said eruption is underway and yet to be announced shortly.



Figure 1. Santo-1 sample.

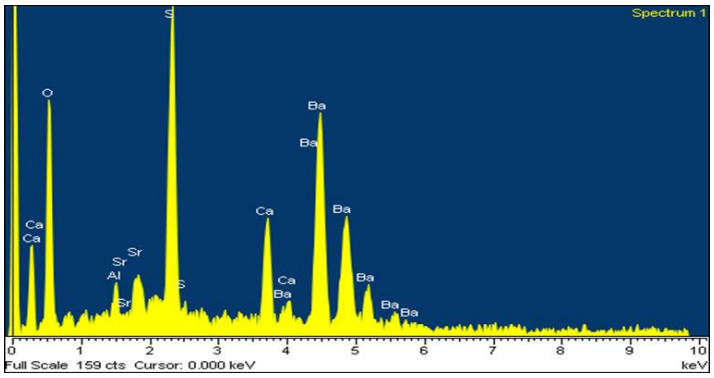

Figure 2. SEM-EDS analysis with high concentrations of S and Ba.

Acknowledgements

Katerina Theodorakopoulou is a post-doctoral fellow of the State Scholarships Foundation (IKY) at the Department of Geology and the Geoenvironment, University of Athens. This study is funded by this post-doctoral fellowship.

References

Bar-Matthews, M., Ayalon, A., Kaufman, A. and Wasserburg, G.J., 1999. The Eastern Mediterranean paleoclimate as a reflection of regional events: Soreq cave, Israel. Earth and Planetary Science Letters, 166(1), pp.85-95.

Badertscher, S., Borsato, A., Frisia, S., Cheng, H. Edwards, R.L., Tüysüz, O., Fleitmann, D. 2014. Speleothems as sensitive recorders of volcanic eruptions–the Bronze Age Minoan eruption recorded in a stalagmite from Turkey. Earth and Planetary Science Letters, 392, 58-66

Bobrowski, N., Honninger, G., Galle, B., Platt, U. 2003. Detection of bromine monoxide in a volcanic plume. Nature, 423, 273–276.

Gençalioğlu-Kuşcu, G., & Uslular, G. (2018). Geochemical characterization of mid-distal Nisyros tephra on Datça peninsula (southwestern Anatolia). Journal of Volcanology and Geothermal Research, 354, 13-28.

Fleitmann, D., Cheng, H., Badertscher, S., Edwards, R.L., Mudelsee, M., Gokturk, O.M., Fankhauser, A., Pickering, R., Raible, C.C., Matter, A., Kramers, J., Tüysüz, O. 2009. Timing and climatic impact of Greenland interstadials recorded in stalagmites from northern Turkey. Geophysical Research Letters, 36, 19.

Frisia, S., Borsato, A., Fairchild, I.J., Susini, J., 2005. Variations in atmospheric sulphate recorded in stalagmites by synchrotron micro-XU and XANES analyses. Earth and Planetary Science Letters, 235, 729-740

Heiken, G. and McCoy, F. (1984) Caldera Development during the Minoan Eruption, Thira, Cyclades, Greece. Journal of Geophysical Research, 89, 8441-8462

F. Hiller von Gaertringen et al., 1904. Thera. Untersuchungen, Vermessungen und Ausgrabungen in den Jahren 1895, 1898, 1902

Wynn, P., Fairchild, I., Baker, A., Baldini, J., McDermott, F. 2008. Isotopic archives of sulphate in speleothems. Geochimica et Cosmochimica Acta, 72, 10, 2465-2477.

Verheyden, S., Nader, F.H., Cheng, H.J., Edwards, L.R. and Swennen, R., 2008. Paleoclimate reconstruction in the Levant region from the geochemistry of a Holocene stalagmite from the Jeita cave, Lebanon. Quaternary Research, 70(3), pp.368-381

15th International Congress of the Geological Society of Greece
Athens, 22-24 May, 2019 | Harokopio University of Athens, Greece
Bulletin of the Geological Society of Greece, Sp. Pub. 7 Ext. Abs. GSG2019-160

Chronological constraints of pyroclastic deposits on Anafi Island, (Cyclades, Greece): Are they Minoan?

Katerina Theodorakopoulou[1], Konstantinos Kyriakopoulos[1], Kostas Stamoulis[2], Magali Rizza[3], Roberto Sulpizio[4], M. Cihat Alçiçek[4], Constantin D. Athanassas[6]

1 Department of Geology and Geoenvironment, National and Kapodistrian University of Athens, Greece, katheo@phys.uoa.gr
2 University of Ioannina-Archaeometry Center, Greece
3 Centre Européen de Recherche et d'Enseignement des Géosciences de l'Environnement, Aix-en-Provence, France
4 Department of Earth and Geo-environmental Sciences, University of Bari Aldo Moro, Italy,
5 Department of Geology, Pamukkale University, Denizli, Turkey
6 Department of Geological Sciences, School of Mining and Metallurgical Engineering, National Technical University of Athens, Greece

This study attempts to clarify whether formerly-documented pyroclastic deposits (Keller et al. 2014, McCoy and Dunn, 2002) belong to the Minoan eruption of Santorini or an earlier event. The 'Minoan' eruption, occurred in the 17th century BCE (1627–1600 BCE, Friedrich et al., 2006) and had widespread impacts on the civilization of the Aegean an Eastern Mediterranean (Marinatos, 1939).

Anafi Island could be a key site for the dispersal of Minoan tephra as it is the most nearby island of Santorini. Despite its proximity, only a few spots with pyroclastic deposits have been found on the island (Keller et al. 2014, McCoy and Dunn, 2002). The occurrence of tephra layers of the Minoan eruption on Rhodes, Kos and western Turkey (Keller, 1980; Eastwood et al., 1999), suggests that Anafi must have covered by Minoan tephra, which was probably eroded and swept away afterwards (Keller et al., 2014).

In recent years, a debate has sparked regarding the relation of the Anafi deposits to the Minoan eruption. McCoy and Dunn (2002) associated the thick pumice deposits on Anafi with the Minoan eruption, suggesting "a far larger (Minoan) eruption than previously thought". In contrary, Keller et al.(2014), after geochemical determination of glass composition by electron microbe analysis on the samples from Anafi, pointed out a strong geochemical similarity with those analyzed from LP2 eruption of Thera at 172 ka, as has been determined by Druitt et al. (1999), excluding any correlation with the Minoan eruptive phase.

In this study we attempt to settle the debate of the tephra chronology on Anafi on the basis of numerical dating and specifically by applying the OSL dating method to colluvial deposits that bracket the pumice deposits, reported by McCoy and Dunn (2002) and Keller et al. 2014. It is noted that it's the first time that the pyroclastic deposits of Anafi will be chronologically constrained, providing indirectly the provenance (Minoan or of an earlier eruptive phase) of the pyroclastic deposits.

Our field survey aimed to collect samples from two pumice deposits on Anafi, already studied by Keller et al. (2014) and and McCoy and Dunn (2002, 2004) at Prassa and Vounia, in the western and central part of the island accordingly. We collected 2 samples for OSL dating from the colluvial deposits that cover the pumice layer (Fig 1), as the base of the pumice deposits is not exposed in the section. The sample preparation was carried out at the Department of Geology and Geoenvrionment, University of Athens and aimed at extracting quartz grains from the sampled colluvia. OSL measurements were carried out at the OSL dating laboratories at CEREGE, Aix-Provence, France and the Archaeometry Center, University of Ioannina, Greece.

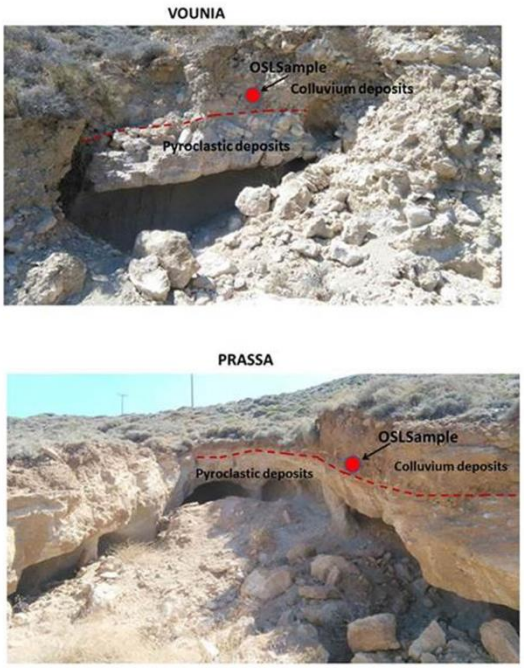

Figure 1. Sampling sites for OSL dating of Anafi Island. Localities: a) Vounia and b) Prassa. Red dot=OSL sample.

The results derived by the application of OSL dating, demonstrated that the colluvium above the pumice deposition at Prassa was dated about 21.04 ka and in Vounia about 29 ka. According to our new chronological framework from the two sites at Vounia and Prassa, we conclude that tephra deposits in Anafi could not be of Minoan origin as McCoy and Dunn (2002) have suggested, given that the age of the stratum above ranges between 21 ka- 29.ka. The age form Prassa, coincides well with the Cape Riva eruption of Santorini at about 21.8 ± 0.4 ka (Druitt, 1999). On the other hand, we could not unquestionably exclude its LP2 origin as suggested by Keller et al. (2004) as we did not date the base of pyroclastic deposits.

More geochemical and chronological analyses on pyroclastic deposits are needed, for the more efficient determination of their provenance and for the better understanding of the effects of Minoan eruption in the Aegean and eastern Mediterranean.

Acknowledgements

Katerina Theodorakopoulou is a post-doctoral fellow of the State Scholarships Foundation (IKY) at the Department of Geology and the Geoenvironment, University of Athens. This study is funded by this post-doctoral fellowship. Dating of the deposits was supported through the ENVI-Med/Mistrals (Acronym: Med-HolVol), granted to CEREGE, France.

References

Druitt, T.H., Edwards, L., Mellors, R.M., Pyle, D.M., Sparks, R.S.J., Lanphere, M., Davies, M.,Barriero, B., 1999. Santorini volcano. Geol. Soc. Lond. Mem. 19, 1-165.

Eastwood, W.J., Pearce, N.J.G., Westgate, J.A., Perkins, W.T., Lamb, H.F., Roberts, N., 1999. Geochemistry of Santorini tephra in lake sediments from Southwest Turkey. Glob.Planet. Chang. 21, 17–29.

Keller, J., Gertisser, R., Reusser, E. and Dietrich, V., 2014. Pumice deposits of the Santorini Lower Pumice 2 eruption on Anafi island, Greece: Indications for a Plinian event of exceptional magnitude. Journal of Volcanology and Geothermal Research, 278,120-128.

Marinatos, S., 1939. "The Volcanic Destruction of Minoan Crete." Antiquity 13, 425–439.

McCoy,F.W.,Dunn,S., 2002.Modelling the climatic effects of the LBA eruption of Thera: new calculations of tephra volumes may suggest a significantly larger eruption than previously reported (abstract). Proceedings of the Chapman Conference on Volcanism and the Earth's Atmosphere, American Geophysical Union, Santorini, Greece, 21–22.

15th International Congress of the Geological Society of Greece
Athens, 22-24 May, 2019 | Harokopio University of Athens, Greece
Bulletin of the Geological Society of Greece, Sp. Pub. 7 Ext. Abs. GSG2019-166

Beachrock development as an indicator of paleogeographic evolution, case of Akrotiri Peninsula, Cyprus

M. Polidorou [1], G. Saitis[1], N. Evelpidou[1,]

(1) National & Kapodistrian University of Athens, Faculty of Geology & Geoenvironment, Panepistimioupolis Zografou, Athens, Greece, mpolidorou@geol.uoa.gr, saitij@geol.uoa.gr, evelpidou@geol.uoa.gr

Akrotiri Penisnsula is located west of Limassol at the Southern end of the Island of Cyprus. It covers an area of approximately 100Km². The development of the peninsula started with the deposition of calcareous marls in to the Episkopi grabben during the Miocene which resulted the Akrotiri High in the form of an isolated island. The maritime space between the Akrotiri Island and the mainland eventually closed during the Quaternary and several geomorphic features were developed. Beachrocks identified at three continuous pocket beaches at the southwest part of the Akrotiri peninsula. Detailed GNSS measurements and GIS analysis revealed that the area is uplifted. A direct relationship between the development of the beachrocks and the paleogeographic evolution of the area is apparent. Additionally, results from Petrographic, mineral and sedimentary analysis on beachrock samples are indicating a continuous supply of material from the nearby Kouris River. A gradual reduction of the sediment granulometry consists the beachrock is observed. Also the transition of the texture of the samples from non-uniform to uniform is observed. The sample mineralogy varies eg quartz, alkaline feldspars, carbonate minerals, ortho and clino pyroxenes, serpentinites, hornblende, muscovite. A reduction in the contribution of overbearing minerals (according to their hardness) was observed from North to Southern beachrock slabs and the increase of carbonates, quartz and feldspart. It should be noted that there is a strong participation of fossils fragments were a number of them was preserved in good condition. SEM-EDX analysis were conducted and showed that the micritic and sparitic crystals of cement are consisted by High Magnesium Calcite +(>4 mol% CaCO3 or 1.2 wt.). The cement agent forms an isopachous coating around the sediment grains and with meniscus forms connect all the sedimentary particles which leads to the formation of a high density beachrock slabs.

15th International Congress of the Geological Society of Greece
Athens, 22-24 May, 2019 | Harokopio University of Athens, Greece
Bulletin of the Geological Society of Greece, Sp. Pub. 7 Ext. Abs. GSG2019-174

Palaeogeographic reconstruction of the Strymonikos Gulf (N. Aegean Sea, Greece) during the Last Glacial Maximum, based on high resolution seismic data

E. Benetou[1], D. Sakellariou[2], G. Rousakis[2], I. Morfis[2], I. Panagiotopoulos[2], I. Livanos[2], Chr. Ioakim[3], I. Zananiri[3], A. Karageorgis[2], S.E. Poulos[1]

(1) Department of Geology and Geoenvironment, National & Kapodistrian University of Athens, Panepistimioupolis-Zografou, 15784, Attiki, Greece, evben@geol.uoa.gr
(2) Institute of Oceanography, Hellenic Centre for Marine Research, Anavyssos 46th km, 19013 Anavyssos, Greece.
(3) Institute of Geology and Mineral Exploration, 1 Spirou Louis St., Olympic Village, 13677 Acharnae, Greece.

Introduction

Sequence stratigraphy is the key for many studies in shallow marine environments, indirectly indicating the prevailing conditions in the recent geological past. This method, combined with the bathymetric data, can give valuable information about the geologic evolution, capturing significant sedimentary structures, also derived from the alternating interglacial and glacial periods during the Quaternary. Thus, this method based on the high resolution seismic data is a particularly useful one for the investigation of the seabed morphology and substrate sequences formed during the last transgression after the end of the Pleistocene (Last Glacial Maximum), when the sea level was roughly 120m below its present level.

Objectives

The primary aim of the present study is the palaeogeographic reconstruction of the Strymonikos Gulf at the Last Glacial Maximum (LGM), focusing on the identification of the palaeo-riverbeds of the Strymon and Nestos rivers and the palaeo-shoreline.

Methods

A hydrographic survey was conducted by the Hellenic Centre for Marine Research and the Institute of Geology and Mineral Exploration, in the frame of YPOTHER project (NSRF 2007-2013), in July 2015 (Ioakim et al. 2016), which included high resolution multibeam (SeaBeam 2120) bathymetric mapping of a submarine area extending over 1200 nm, in combination with seismic profiling of the same area, covering 250 nm (3.5 kHz system – GeoAcoustics Ltd). Data processing and imaging was achieved by using the software package SB Interpreter of Triton Imaging while the maps were created using the ArcMap of ESRI.

Results

From the analysis and interpretation of the seismic profiles from the Strymonikos Gulf two seismic Units (A and B) were identified. The seismic character of Unit A includes transparent horizons and are associated with fine-grained deposits, which chronologically are related with the transgression after the Last Glacial Maximum and during Holocene. The seismic Unit B includes chaotic horizons without continuity, possibly representing coarser material. Unit B underlies Unit A and is deposited during the LGM. The interface between the Units A and B is an unconformity.

The palaeo-riverbed of Strymon was found at water depths of approximately 110-115 m. It was 2 - 3.5 km wide and the river was flowing southwards from southeast of Loutra Eleftheron. The palaeo-riverbed of Nestos was mapped on the 60-70 m deep platform between Thassos Island and Nea Peramos. The beds of the two palaeo-rivers are located on two platforms, separated by a 40-50 m high fault-controlled southwest-facing scarp, extending from Loutra Eleftheron to the North until west of Thassos to the South. This fault scarp divides the Strymonikos plateau in two parts, the lower eastern plateau where the paleo-Strymon river flowed and the western Plateau where the paleo-Nestos river did. The path of palaeo-Nestos was found to have shifted from its present position, within a canal of 1-1.5 km wide and surprisingly, in water depths of 60-65 m. Also, during this period the position of the palaeo-shoreline was 20-30 km (locally up to 40 km) seawards from its present position.

In the study area, syn-sedimentary tectonic activity is demonstrated by the 3-5 m offset of secondary active normal faults, affecting the Upper Pleistocene-Holocene sedimentary sequences. In addition, the existence of a fault scarp in the NE-SW direction (observed in the eastern part of the Strymonikos) is most likely the subaqueous extension of the active fault zone of Kavala-Xanthi-Komotini, which is responsible for the formation of the Strymonikos Gulf.

Conclusions

The neotectonic activity and the post glacial transgression play a crucial role in the configuration of the Strymonikos Gulf since the Late Quaternary. The palaeogeographic reconstruction showed that Nestos palaeo-river was falling into Strymon palaeo-river. The bathymetric difference of 50-55 m between the two riverbeds indicates the existence of an amazing landscape with impressive waterfalls. Finally, the position of the shoreline during the LGM is observed at distances >20 km seawards from its present position and at water depths of 121-135 m.

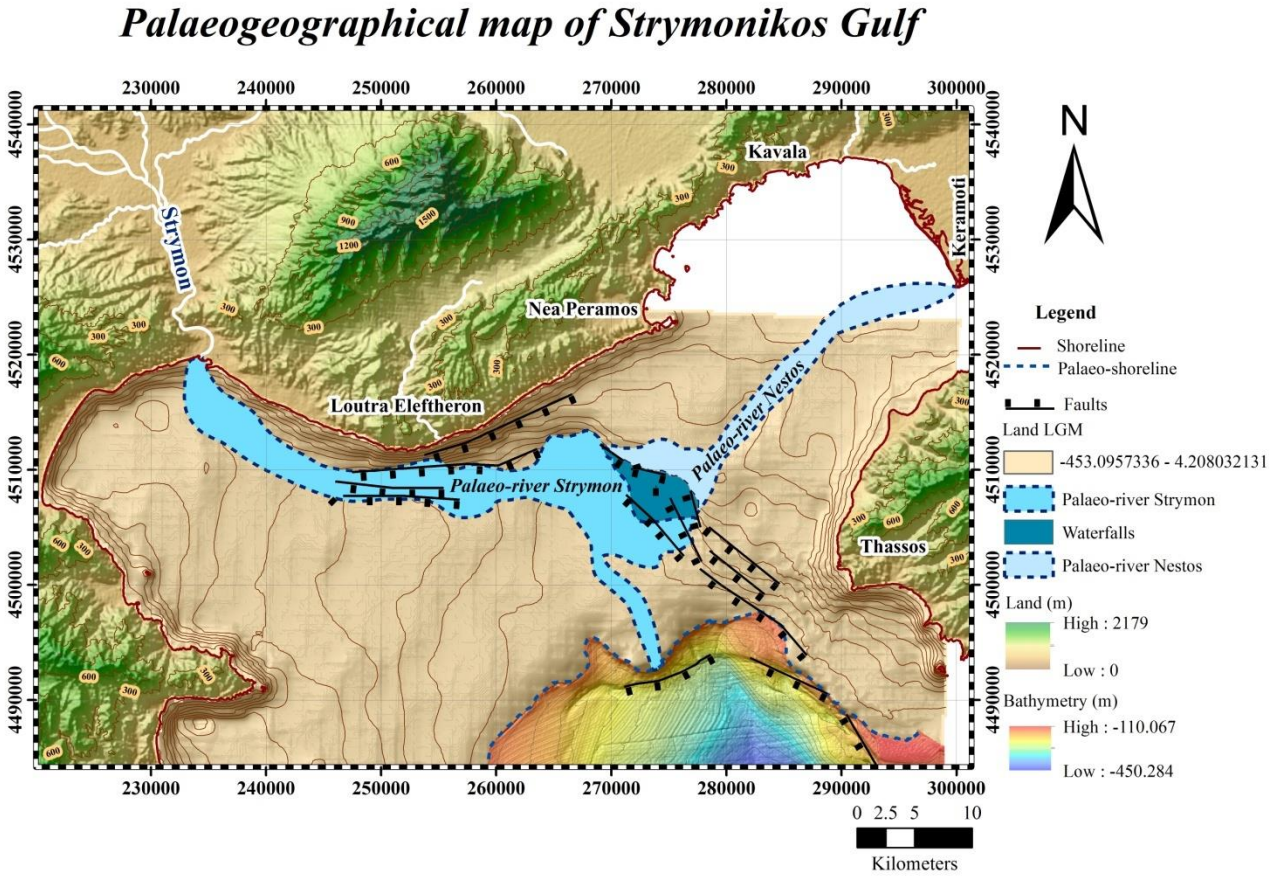

Fig. 1: Reconstruction of palaeo-shoreline and Strymon and Nestos paleo-rivers during the Last Glacial Maximum.

References

Catuneanu, O. (2002). Sequence stratigraphy of clastic systems: concepts, merits, and pitfalls. *Journal of African Earth Sciences*, *35*(1), 1-43.

Ioakim, Chr., Zananiri, I., Zimianitis, E., Efthymiou, G., Vakalas, I., Giamali, Chr., Valaouris, A., Drosopoulou, E., Gkintoni, E., Economou, G., Papatrechas, Chr., Tarenidis, D., Koutsovitis, P., Xirokostas, N., Sakalis, M., Spiropoulos, V., Patsis, P., Tsapara, E., Karagiorgis, A., Roussakis, G. & NCMR researchteam (2016). Final report of marine geological and sedimentaryresearch in theAegeanSea: Deliverablesof YPOTHER project. IGME, NSRF 2007-2013/ Operational Programme Competitiveness& Entrepreneurship/ Project Marine Geology and Mineral Research Study along the Coastline between Chalkidiki and Kavala, and the Caldera of Santorini, Athens, pp. 339 (in Greek).

Mountrakis, D. M., & Tranos, M. D. (2004). The Kavala-Xanthi-Komotini fault (KXKF): a complicated active fault zone in Eastern Macedonia-Thrace (Northern Greece). In *5th International Symposium on Eastern Mediterranean Geology, Thessaloniki, Greece*, Vol. 2, pp. 857-860.

Perissoratis, C., & Conispoliatis, N. (2003). The impacts of sea-level changes during latest Pleistocene and Holocene times on the morphology of the Ionian and Aegean seas (SE Alpine Europe). *Marine Geology*, *196*(3-4), 145-156.

Perissoratis, C., & Mitropoulos, D. (1989). Late Quaternary evolution of the northern Aegean shelf. *Quaternary Research*, *32*(1), 36-50.

15th International Congress of the Geological Society of Greece
Athens, 22-24 May, 2019 | Harokopio University of Athens, Greece
Bulletin of the Geological Society of Greece, Sp. Pub. 7 Ext. Abs. GSG2019-189

A geophysical approach to the archaeological excavation of Plasi Marathon (Attika, Greece)

N. Souglakos[1], J.D. Alexopoulos[1], N. Voulgaris[1], S. Dilalos[1], G.S. Mitsika[1], M. Petrakis[2], G. Vavouranakis[2,] P. Valavanis[2], Y. Papadatos[2]

(1) National and Kapodistrian University of Athens - Department of Geology and Geoenvironment, Panepistimiopolis, Zografou, Greece, nsouglak@geol.uoa.gr
(2) National and Kapodistrian University of Athens - Department of History and Archaeology, Panepistimiopolis, Zografou, Greece

Introduction

Many researchers have presented that ground penetrating radar (GPR) is a subsurface survey method indicated to acquire important preliminary information in various geological subsurface investigations, but also in archaeological and cultural heritage studies (Conyers, 2016). GPR stands out among the geophysical methods applied in archaeology, given the fact that it is a non-destructive practical field technique. GPR results can be presented as bi-dimensional profiles (2D) and three-dimension images (3D), in the form of block diagrams, fence-diagrams and volume/depth-slices. Especially the amplitude maps (e.g., depth-slices maps) allow the identification of areas with high or low amplitude of specific deep reflectors. Therefore, they can be used to identify buried targets and their dimensions, allowing the reconstruction of the subsurface in 3D (Porsani *et al*., 2010).

Geophysical survey

A combined GPR and ERT survey was performed during the summer of 2018, in the excavation of the Department of History and Archaeology of the NKUA at Plasi Marathon (Attica). On the basis of the walls of the Classical period already revealed in 2017 and the geoenvironmental conditions of the study area, the main objective of this study is to assess the existence of possible architectural remains in unexcavated parts of the site, particularly in an indicated area of 655 m^2. The existence of architectural remains would be of particular importance for the archaeologists in order to plan the next steps of the project but also to understand the density of habitation in the area. The revealed architectural remains in the adjacent excavation trenches were found in a mean depth of 0.5 m and the walls have a mean width of 0.5m.

A MALA 250 MHz shielded antenna was used for the field measurements. Single-fold exploratory GPR profiles were initially carried out at the site with a horizontal spacing between the parallel profiles equal to 2 m, in order to create a 2x2 m grid. Therefore, thirty-four (34) GPR profiles were carried out (Fig.1), with a total length of 610 m, using the following specifications: i) Time sampling rate Δt=512, ii) Time window W_t=196 ns and iii) spatial sampling rate Δx_s=0.02 m. The GPR data were processed with REFLEXW software, using the following package of filters: Subtract-mean (Dewow), Time-Zero Correction, Background Removal, Bandpass Filter, Deconvolution, Migration and final Hilbert Transformation-Envelope (Goodman and Piro, 2013; Porsani *et al.*, 2010). The obtained radargrams are presented in the form of fence-diagrams in Fig. 1. This simultaneous view of multiple radargrams allows us to identify the presence of the reflectors and their distribution within each radar section (Imposa *et al*, 2018). At this fence-diagram (Fig. 1), we can observe numerous reflections, sometimes fairly pronounced, located at depths between 0.25 m and 0.85 m. Many detectable reflections appear isolated, observed with a fairly small extension within each single scan, probably generated by objects with rather small dimensions. However, in the context of the fence diagram analysis, it was observed that these isolated reflectors often show a lateral continuity.

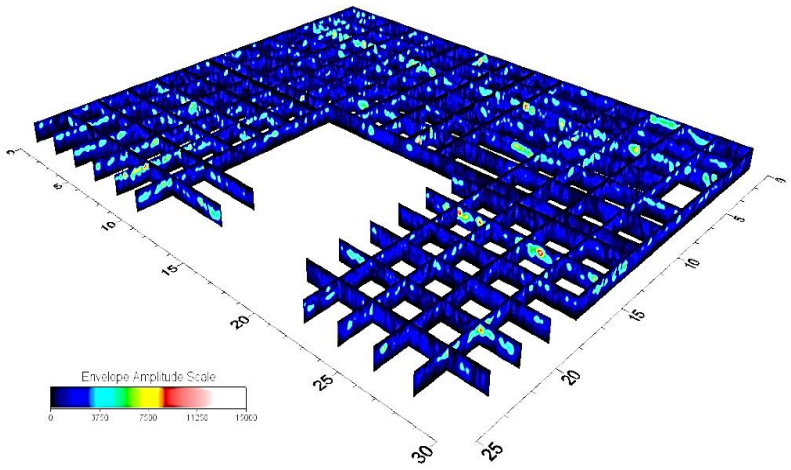

Figure 1. Fence diagram of the thirty-four (34) GPR profiles in the survey grid.

Beyond this, twenty (20) electrical resistivity tomography (ERT) sections were carried out, with a total length 413 m, in a 3x3 m grid and electrode spacing 0.25 m. An ABEM Terrameter system was used for the field measurements. The processing of the ERT data was performed with Res2DInv software. The robust inversion method is indicated for the

ERT processing (Alexopoulos *et al.*, 2014), since it provides results with sharper edges, similar to the shape of ancient domestic structures. For all the acquired ERT and GPR profiles, the coordinates were determined with dGPS (TOPCON Hiper-Pro).

Discussion and Results

The volume/depth-slices illustrated in Fig. 2 were obtained through the interpolation of the radar scans, derived from the processed data. These slices show the variation of the reflected signal amplitude distribution at different depths/volumes (Zhao *et al.*, 2013; 2015). The most reflective zones are illustrated in green and red colors.

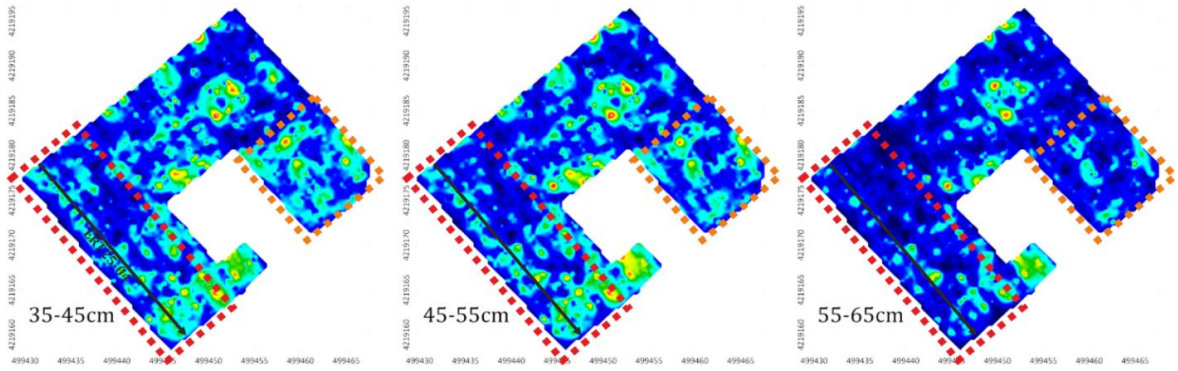

Figure 2. Volume/depth slices of the GPR data, with a depth range of 0.35–0.65 m.

After a careful analysis of each radargram, we obtained three slices for depths between 0.35 and 0.65 meters (Fig. 2), where the areas characterized by high amplitude values (reflection strength) are illustrated. In many cases, these areas do not show a lateral continuity probably due to the existence of targets with limited extension. These outcomes seem to enhance the results obtained from the previous analysis (Fig.1). In the SW area of these slices (Fig.2-red dotted zone) and in a smaller part at the SE area (Fig.2-orange dotted zone), additional areas that are characterized by high amplitude values but are not identified by the previous analysis, are now observed. These areas display continuity in depth, suggesting the possible presence of significant targets that may correspond to buried archaeological remains. The validity of the results will be tested during the excavations of 2019-2020, but they suggest a rather dense pattern of habitation, implying that Plasi could have been the location of the ancient demos of Marathon.

The inversion results (Fig.3) of the acquired ERT profiles, have also adumbrated areas of higher resistivity (Fig.3-reddish and purplish colors, ERT 25-04 positioned in Fig.2) that probably correspond to buried architectural remains.

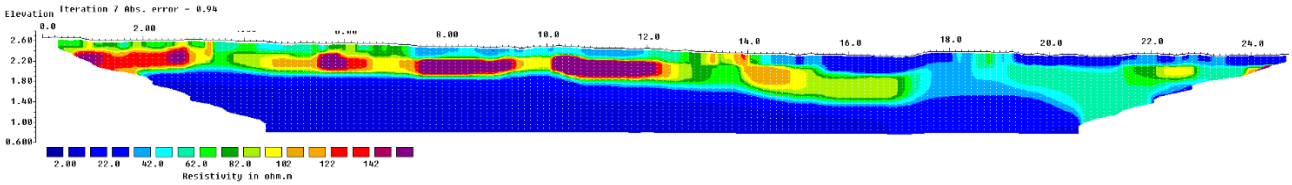

Figure 3. Inversion model of ERT 25-04 cross-section (RMS=0.94%), with electrode spacing 0.25m.

Acknowledgements

The authors would like to thank Mr. Konstantinos Mimmidis, Ms. Ioanna Liaskou, Mr. Athanasios Petras, Mr. Dimitrios Kastoras & Mr. Athanasios Kyrkos for their contribution during the acquisition of the field measurements and Terra-Marine Company for the kind supply of supplementary geophysical equipment.

References

Alexopoulos, J.D., Dilalos, S., Tsatsaris, A., Mavroulis, S., 2014. ERT and VLF measurements contributing to the extended revelation of the ancient town of Trapezous (Peloponnesus, Greece). In: Near Surface Geoscience 2014-20th European Meeting of Environmental and Engineering Geophysics, 5p, Doi: 10.3997/2214-4609.20141974.

Conyers, L.B., 2016. Interpreting Ground-penetrating Radar for Archaeology. Routledge.

Goodman, D. and Piro, S., 2013. GPR Remote Sensing in Archaeology (9). Springer, New York.

Imposa, S., Grassi, S, Patti, G., Boso, D., 2018. New data on buried archaeological ruins in Messina area (Sicily-Italy) from a ground penetrating radar survey. Journal of Archaeological Science: Reports, 17, 358–365, https://doi.org/10.1016/j.jasrep.2017.11.031

Porsani, J.L., de Matos Jangelme, G., Kipnis, R., 2010. GPR survey at Lapa do Santo archaeological site, Lagoa Santa karstic region, Minas Gerais state, Brazil. Journal of archaeological science, 37(6), 1141–1148, http://dx.doi.org/10.1016/j.jas.2009.12.028

Zhao, W., Forte, E., Pipan, M., Tian, G., 2013. Ground penetrating radar (GPR) attribute analysis for archaeological prospection. Journal of Applied Geophysics, 97, 107-117, https://doi.org/10.1016/j.jappgeo.2013.04.010

Zhao, W., Forte, E., Levi, S.T., Pipan, M., Tian, G., 2015. Improved high-resolution GPR imaging and characterization of prehistoric archaeological features by means of attribute analysis. Journal of Archaeological Science, 54, 77–85

15th International Congress of the Geological Society of Greece
Athens, 22-24 May, 2019 | Harokopio University of Athens, Greece
Bulletin of the Geological Society of Greece, Sp. Pub. 7 Ext. Abs. GSG2019-198

Recording Extraction Sites of Inert Materials in the Upper Reaches of Pinios River, Western Thessaly, Central Greece

S. Papalambrou[1], G. D. Bathrellos[1], H. D. Skilodimou[1]

(1) Department of Geography and Climatology, Faculty of Geology and Geoenvironment, National and Kapodistrian University of Athens, University Campus, ZC. 15784, Zografou, Athens, Greece; pap.sotos95@gmail.com, gbathrellos@geol.uoa.gr, hskilodimou@geol.uoa.gr

Introduction

On a global scale, the combined forces of urbanization and the rapidly expanding industry have increased the stress in natural environment and resulted morphological changes in landforms. The continuous and rapid progress of urbanization around the world and the consequent need for mineral sources has largely destroyed many formerly natural ecosystems (Tsolaki-Fiaka *et al.*, 2018). Extraction of inert materials from rivers is and will remain of great economic importance for Europe. Nevertheless this economic activity can have both immediate and long-term consequences for channel stability (Wishart *et al.*, 2008).

The scope of the present study is to record and map the location of the extraction sites of inert materials from rivers. It is an attempt to illustrate the landscape changes and especially the depositional environments in hydrographic networks due to extraction activity.

Study area

The study area is the upper reaches of Pinios River, which is located in Western Thessaly, at the west part of the fertile plain of Thessaly in central Greece. Its course starts at the northwestern part of the Trikala prefecture, from the confluence of Ion and Malakasiotis rivers. It is surrounded by mountainous areas which enclose its drainage basin and form its watershed. The altitudes of its drainage basin vary from 74 to 2,204 m a. s. l. The major tributaries of the upper reaches of Pinios River are: Ion river to the north, Malakasiotis, Klinovitikos Portaikos, rivers to the west and south and Lithaios river to the east. They drain large, heterogeneous areas, through extensive hydrographic networks (Figure 1).

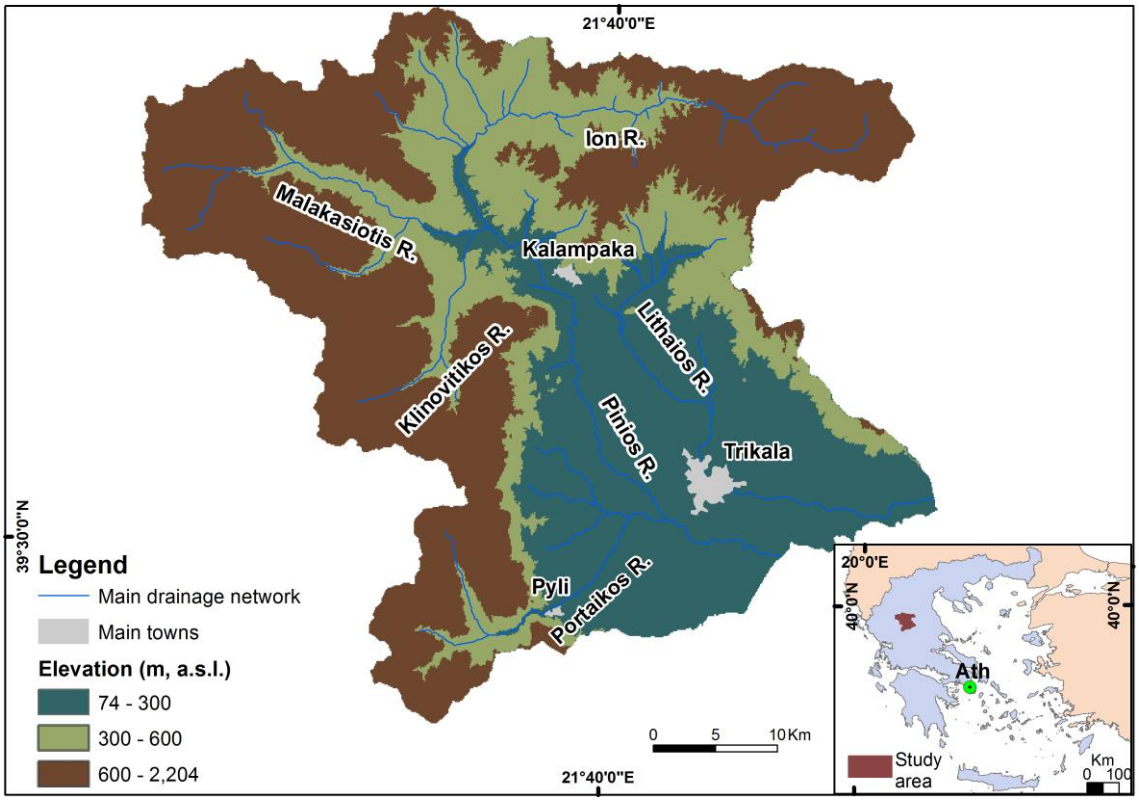

Figure 1. The location map of the study area; the elevations of the study area, the drainage network, and the main towns area (Ath, stands for the city of Athens).

Data and Methods

As a first step the locations of extraction sites of inert materials were recognized on satellite image. The next step was the verification of the location by field work. Geomorphological mapping was undertaken at a scale of 1: 5,000 in the upper reaches of Pinios River. It involves the determination of elements such as rivers, fluvial deposits and erosion. For the purpose of the present work, some morphometric parameters of the extraction sites of inert materials such as altitudes, area and volume of the removal materials were calculated. The type of removal materials was recognized. Additionally, the impacts of the extraction activity in the river systems were observed.

Results

A total number of 18 sites of extraction of inert materials in Pinios River and its tributaries were recorded and mapped (Table 1). Moreover, Table 1 shows their altitude, the area of extraction, the volume and the type of removal materials.

Table 1. The sites of extraction of inert materials in Pinios river and its tributaries, their altitude, the area of extraction, the volume and the type of removal materials.

ID	River	Altitude (m)	Area (m^2)	Volume (m^3)	Extraction material
1	Ion	260	7,730	19,325	Sand
2	Ion	260	1,360	2,720	Sand
3	Ion	260	7,200	10,800	Sand
4	Ion	260	2,200	3,300	Sand
5	Malakasiotis	310	1,030	1,030	Silt-Sand-Pebble
6	Malakasiotis	302	1,500	750	Sand-Pebble
7	Klinovitikos	291	12,500	10,000	Pebble-Sand
8	Klinovitikos	290	5,000	15,000	Pebble
9	Portaikos	198	1,300	2,600	Gravel
10	Portaikos	216	15,000	40,500	Gravel
11	Portaikos	186	5,000	10,000	Gravel
12	Pinios	227	15,300	35,190	Pebble
13	Pinios	219	40,000	68,000	Sand-Pebble
14	Pinios	185	5,900	38,350	Sand-Gravel-Pebble
15	Pinios	185	7,240	8,688	Sand-Gravel
16	Pinios	167	111,200	667,200	Sand-Gravel-Silt
17	Pinios	157	18,000	144,000	Sand-Pebble
18	Pinios	91	470	376	Silt
	Total		257,930	1,077,829	

The total area of the extraction sites reaches up to 257,930 m^2 and the total volume of removal materials are 1,077,829 m^3. The types of the removal materials are mainly sand and gravel. The extractions from the tributaries of Pinios river include mainly coarse grained materials. The removal materials come either from the riverbed or from the banks of the river and its terraces. In many cases the extractions have caused changes to channel morphology and bank erosion. Today, many of the extraction sites are inactive.

References

Tsolaki-Fiaka, S., Bathrellos, G.D., Skilodimou H.D. 2018. Multi-criteria decision analysis for abandoned quarry restoration in Evros Region (NE Greece). Land, 7 (2), 43, doi: 10.3390/land7020043.

Wishart, D., Warburton, J., Bracken, L. 2008. Gravel extraction and planform change in a wandering gravel-bed river: The River Wear, Northern England. Geomorphology, 94(1-2), 131-152.

15th International Congress of the Geological Society of Greece
Athens, 22-24 May, 2019 | Harokopio University of Athens, Greece
Bulletin of the Geological Society of Greece, Sp. Pub. 7 Ext. Abs. GSG2019-214

Western Lefkada Shoreline Displacement Rates Based on Photogrammetric Processing of Remote Sensing Datasets from Various Sources

A. Roufi[1], Emm. Vassilakis[1], S. Poulos[1]

(1) Faculty of Geology & Geo-environment, NKUA, Panepistimioupolis, Zographou, 15784, Greece, amaliaroufi@gmail.com

The aim of this study is to calculate the displacement rates of the coastline at the western part of the island, which is characterized of the escarpment coast. The shape of this coastal zone is caused mainly by tectonism which is very frequent in this wider area (Valkaniotis *et al.*, 2018). The western coast of the island from Cape Agios Ioannis (NW) to the southernmost point of the peninsula, Cape Doukato is steep and precipitous, as a result of the high seismicity of the Ionian Sea area (Bornovas, 1964). Along this side of the island, several landslides and rock falls are observed. The situation changes only at the northern part of the island, with a distinctive coastal landform over the narrow zone called "Zostiras" (Leivaditis & Verikiou - Papaspyridakou, 1986).

This work was conducted using two different types of data. Historical analogue panchromatic aerial images of high resolution (Zuidam and Van Zuidam-Cancelado, 1979) and contemporary digital high resolution multi-spectral satellite images were combined for extracting the coastline at the time period of acquisition. The acquisition of the aerial photographs took place during 1945 and 2010, while the satellite images where acquired during 2016, 2017 and 2018 (Figure 1). In all cases the images were digitally processed and optically optimized in order to produce a highly accurate representation of the shoreline at each time period. All the data were imported in a Geographic Information System platform, where they were subjected into comparison and geo-statistical analysis (Tsokos *et al.*, 2018). Several transects were drawn normally to the coast and the distance between them was set at every 200 m as the relative displacement of the coastline was calculated for each one of them.

In a way to achieve this, an extension of the ESRI ArcGIS v.10.6.1 software was employed as published by USGS and named Digital Shoreline Analysis System v.5 (DSAS). The DSAS extension (Thieler *et al.*, 2009) lets the user define a constant straight line in a specific distance from the shoreline and take transects perpendicular to it among the evolving coastlines. The measurements give quantitative information on the change of the position of the shoreline, as well as more useful statistical data. Even if this seems to be an arbitrary value, it worked rather sufficiently at this almost 12 km long segment of the shoreline as it can be characterized as rather curvy and either a smaller value would result an oversampled area with transects intersect each other mixing the calculations or a larger value would result quite sparse transect locations without any representative outcome.

Spatial classification of the calculated displacement rate

According to the geostatistical analysis results, the entire 42km shoreline was segmented into 8 areas, regarding the overall evolution of the coast throughout the studied time period. The basement rocks seem to play a very important role and therefore the dominant rock type for each segment is also mentioned below.

1. *Ag. Giannis:* The area is eroded from 0.11 to 1.06 m/yr. The geology of the area consists of contemporary coastal formations (Holocene) and limestone Pantokrator (L. Triassic).
2. *Ag. Nikitas:* There is a progradation of 0.02 to 0.27 m/yr in the Pantokrator limestones that crop out at the area, which seems to have been affected by the recent earthquakes of 2003 and 2015.
3. *Kathisma - Avali:* Erosion of the order of 0.01 to 0.54 m/yr is observed in contemporary coastal formations (Holocene) and Vigla limestones (E. Senonian)
4. *Chortata - Komilio:* At this area the progradation is larger as it reaches 0.52 m/yr. The outcrops consist of carbonates (Jurassic to Paleocene limestones). The earthquake of 2003 caused several falls of boulder size rocks from the existing terraces, forming a wider coastal zone.
5. *Dragano – Athani:* At this area there we observed also erosion (0.01 to 0.26 m/yr) and deposition (0.04 to 0.37 m/yr). In both cases the basement consists of limestones (L. Jurassic), whilst the eroded zone is covered by talus scree (Pleistocene) forming a slope of 65°-70°.
6. *Egremnoi:* We observed erosion varying from 0.02 to 0.29 m/yr simultaneously with deposition of 0.06 to 0.59 m/yr. The eroded formations are contemporary coastal deposits (Holocene) or limestones (L. Cretaceous). During the earthquakes of 2003 and 2015 massive rock falls were observed along the steep slopes. This fact is repeated after every major earthquake in these areas, due to the high elevation and steep slopes.
7. *Porto-Katsiki:* The L. Cretaceous limestones that crop out in this area are eroded with a rate from 0.04 to 0.49 m/yr.
8. *Krimnoi:* Coastal erosion reaching 0.66 m/yr was calculated along this shoreline segment.

Processing and Results

The described methodology introduces a simple but very convenient way of combining a dataset containing all the available shoreline traces throughout a given time period, in order to quantify its displacement rate for certain segments and therefore evaluate the risk or vulnerability of a coastal zone. We suggest that all kinds of remote sensing data (with

similar spatial resolution) could be included in this change detection procedure and the objective difficulty should be how far back in time one could find reliable datasets and hence increase the reliability of the methodology. The most labored issue would be to make all the collected datasets free from distortions and consequently comparable to each other, combine them in a Geographic Information System platform and finally determine and quantify the shoreline displacement rate and especially the erosion rate at certain segments.

By employing the methodology described above, at the area of investigation we have calculated the displacement rate of the coastline position over the past 75 years. The rates of change that were calculated were not homogeneous along the full length of the coastline. Specifically, the average value of the rate of receding is 10 cm/year, while extreme values of order 1 m/year were also observed, increasing the riskiness of specific positions. In those positions it has been estimated that the shoreline has receded over 55 m in the last 75 years and is strongly affected by the earthquake activity along with the human intervention in some cases. In conclusion we calculated that the extreme coastline displacement values reach the 1.06 m/yr (erosion) and 0.59 m/yr (progradation). The combination of geological formations and intense seismicity seems to be the main factor leading to these results.

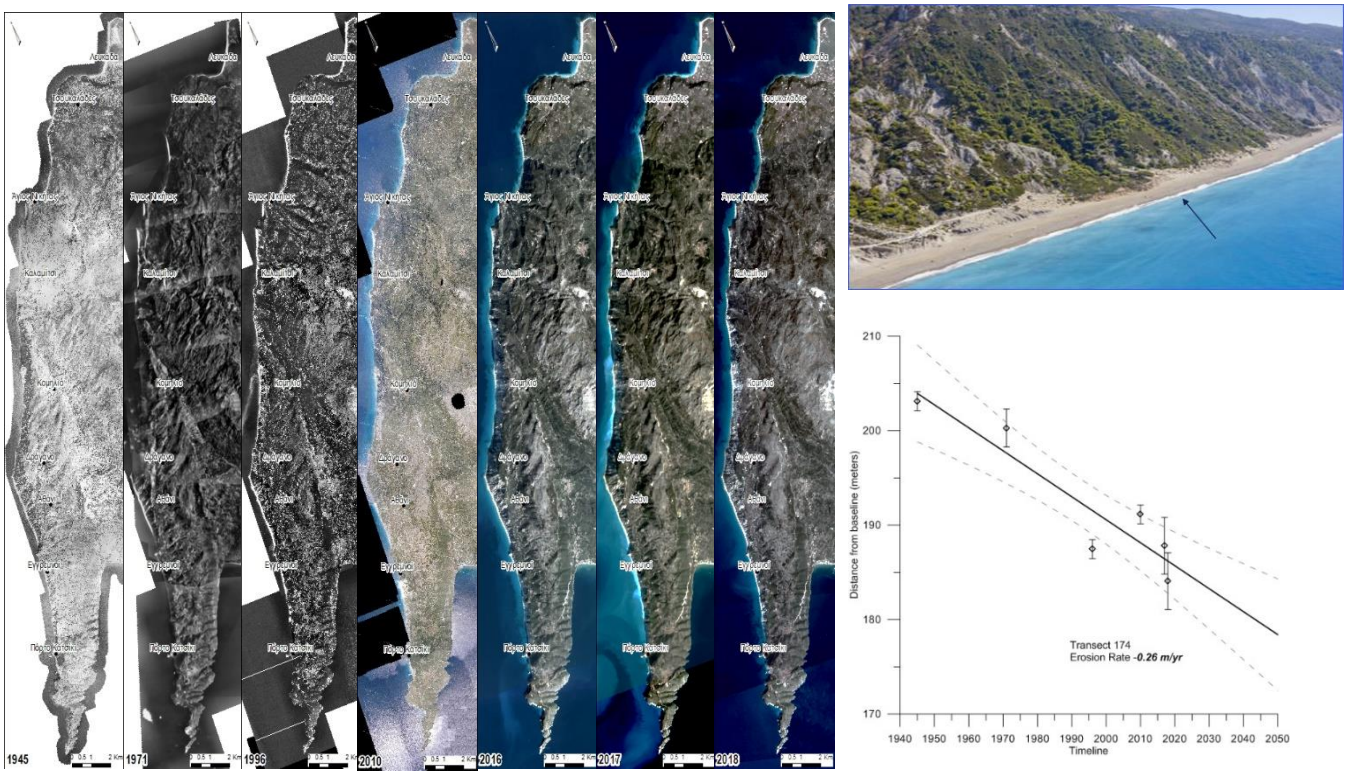

Figure 1. Datasets used for this study, representing the western part of Lefkada Isl. for the years 1945, 1971, 1996, 2010, 2016, 2017, 2018. The black arrow points at the location where section 174 corresponds (upper right) and below the coastline displacement rate diagram, calculating erosion of the order of 0.26 m/yr for the same section.

References

Bornovas, J., 1964. Geological Map of Greece 1:50.000, Sheet Lefkas. I.G.M.E., Athens.

Leivaditis, G., Verykiou – Papaspyridakou, E., 1987. Coastal sedimentary conditions that led to the formation of the "Zostira" in the city of Lefkada. 1st Panhellenic Geographic Conference, Athens, p. 229-231 (in Greek).

Rondoyanni, Th., Tsiambaos, G., 2008. The Aghios Nikitas - Athani active fault and the geological hazard of Lefkada island. 3rd National Conference of Earthquake Engineering and Engineering Seismology, Athens, p. 1961.

Thieler, E., Himmelstoss, E., Zichichi, J., Ergul, A., 2009. Digital Shoreline Analysis System (DSAS) version 5-An ArcGIS extension for calculating shoreline change. vol 2008-1278. U.S. Geological Survey.

Tsokos, A., Kotsi, E., Petrakis, S., Vassilakis, E., 2018. Combining series of multi-source high spatial resolution remote sensing datasets for the detection of shoreline displacement rates and the effectiveness of coastal zone protection measures. Journal of Coastal Conservation, 22, 431-441

Valkaniotis, S., Papathanassiou, G., Ganas, A., 2018. Mapping an earthquake-induced landslide based on UAV imagery; case study of the 2015 Okeanos landslide, Lefkada, Greece. Engineering Geology, 245, 141-152.

Van Zuidam, R., and F. Van Zuidam-Cancelado 1979. Terrain analysis and classification using aerial photographs: a geomorphological approach, 310 pp., International Institute for Aerial Survey and Earth Sciences (ITC).

15th International Congress of the Geological Society of Greece
Athens, 22-24 May, 2019 | Harokopio University of Athens, Greece
Bulletin of the Geological Society of Greece, Sp. Pub. 7 Ext. Abs. GSG2019-269

Assessment of the Evinos Delta Recent Shoreline Changes (Gulf of Patras, Western Greece)

E. Karymbalis[1], C. Gallousi[1], A. Cundy[2], K. Gaki-Papanastassiou[3], I. Tsodoulos[1], K. Tsanakas[1] V.D. Batzakis[1], D. Papanastassiou[4] I. Liapis[1], H. Maroukian[3]

(1) Department of Geography, Harokopio University, 70, El. Venizelou Str., 17671 Kallithea, Athens, Greece, karymbalis@hua.gr
(2) Ocean and Earth Science, National Oceanography Centre, Institution, University of Southampton, University Road, SO17 1BJ, Southampton, United Kingdom
(3) Section of Geography and Climatology, Department of Geology and Geoenvironment, National University of Athens, Panepistimioupolis, 15784, Athens
(4) Institute of Geodynamics, National Observatory of Athens, 20048 Athens

Introduction

River deltas are dynamic and complex depositional landforms, shaped by the competition between marine and fluvial processes (Coleman and Wright, 1975). River deltas crucially depend on sustained sediment supplies in order to maintain delta shoreline position and to balance subsidence. Because they are increasingly starved of sediment trapped behind dam reservoirs, many of the world's river deltas are becoming vulnerable to accelerated erosion, losing large tracts of land and becoming more exposed to flooding and sea-level rise (Ericson et al., 2006). In Greece the most distinctive shoreline changes concern beach zones of low lying coastal plains (mainly river deltas) and are mainly associated with severe decline or even elimination of fluvial sediment discharge due to river damming and uncontrolled sand and gravel mining activities from the lower reaches of the rivers.

The principal objective of this study is to quantify the post 1945 changes of the shoreline of the Evinos River delta in Western Greece using geo-referenced aerial photographs, a detailed Digital Elevation Model (DEM) and Landsat imagery. Quantitative assessment of recent delta shoreline changes is a part of the coastal monitoring that helps significantly in long-term predictions of shoreline positions, which is particularly useful for the design of future shoreline management and development strategies.

Study Area

The Evinos River delta is located on the northern shore of the Gulf of Patras. It covers an area of about 92 km^2 and belongs to one of the most significant ecosystems in Western Greece, the Messologi wetland, which is protected by the Ramsar Convention. According to Galloway's (1975) proposed delta classification it should be classified among those deltas affected by fluvial sediment supply and wave activity.

The formation of the Evinos delta is the result of the combination of suitable conditions for delta formation during the late Holocene. Climatic conditions within the drainage basin (high mean annual precipitation) along with the geology (presence of highly erodible formations) and morphology (relatively steep slopes in the upper reaches) of the catchment are characteristics favorable for weathering and erosion. Large amounts of sediments supplied by erosion are transported down the valley of the river to the coast. In addition, the bathymetry (maximum depth no more than 130 m) and tectonic features of the Gulf of Patras (the rate of tectonic subsidence during the Holocene is 0.4 mm/yr (Ferentinos et al., 1985)) in addition to the extremely low tidal range have permitted sediment accumulation in the area of the river mouth. According to the geomorphological map of the delta, constructed by Maroukian and Karymbalis (2004), the deltaic plain is crossed by four groups of abandoned distributaries. The coastline of the eastern palaeo-lobe consists of low cliffs and gravel beaches while the western coastal zone of the delta is characterized by a series of beach ridges which have built up an oblong area that protects Klisova lagoon from the Gulf of Patras. The Klisova lagoon is the result of the natural compaction of deltaic sediments after the shifting of the main channel to the east. The main channel of the Evinos River crossing the deltaic plain has been artificially aligned since 1959 while a dam has been constructed in the upper reaches of the catchment in 1997 in order to supply Athens with potable water.

Methodology

In order to detect and quantify diachronic changes of the Evinos delta shoreline, comparative observations of the coastlines of 1945, 1969, 2016 have been made utilizing GIS techniques. The coastlines of 1945 and 1996 have been digitized from georeferenced aerial photo-mosaic obtained from the Hellenic Millitary Geographical Service (HMGS) while the source for the most recent coastline of 2016 was the detailed DEM of the Hellenic Cadastre. This comparison allowed us to identify areas of progradation and parts of the fan-delta plain that are being eroded as well as to quantify cumulative progradation and erosion for the time periods 1945-1969 and 1945-2016 respectively. Using the 1945 digitized shoreline, 532 measurement sites were created every 50 m using an automated procedure. Coastal retreat or progradation was calculated for the intervals between the dates of the imagery by measuring the distance separating the two shorelines (in vector format) perpendicular to the older shoreline.

Remote sensing is becoming a highly effective and efficient coastline detection technique. Even if the accuracy of the coastline detection depends on the spatial resolution of the remote sensing images, the medium-resolution images such as Landsat TM, have been widely used to detect coastlines (Gens, 2010). Thus in an attempt to quantify land loss and/or

land gain for the time periods between 1993, 2002 and 2018, the broader deltaic area of the mouth of the river was divided into three parts (Figure 1) and three Landsat TM images, acquired on July 1993, August 2002 and August 2018 respectively, with a spatial resolution of 30 m, were collected. Image preprocessing was conducted on these three TM images, including radiometric correction, registration and precise geometric corrections. To distinguish coastal temporal variations, only Bands 5 and 4 of Landsat 5-7 and Landsat 8 images were used respectively.

Results and Conclusions

The comparative analysis of the 1945, 1969 and 2016 delta shorelines shows that the main process along a significant part of the delta front is intense erosion. In particular the coastline of the eastern abandoned part of the delta is retreating since 1945. The coastal geomorphic features of this part of the delta (exposed coastal sections of eroded delta deposits along low cliffs - up to 1.5 m high - and abandoned meandering channels now being eroded) as well as the presence of collapsed shoreline houses are indicative of erosive processes. The main cause of the east delta erosion are the exposition of the shoreline towards the predominant waves and long-shore currents (Piper et al., 1982) in addition to the lack of sediment supply since 1959 after the artificial closing of the river mouth. It is estimated that the area of the pre-1959 mouth has retreated for about 600 m since 1945. The only area where the delta progrades today is west of the present river mouth which consists of dynamic, gradually changing sandy barriers.

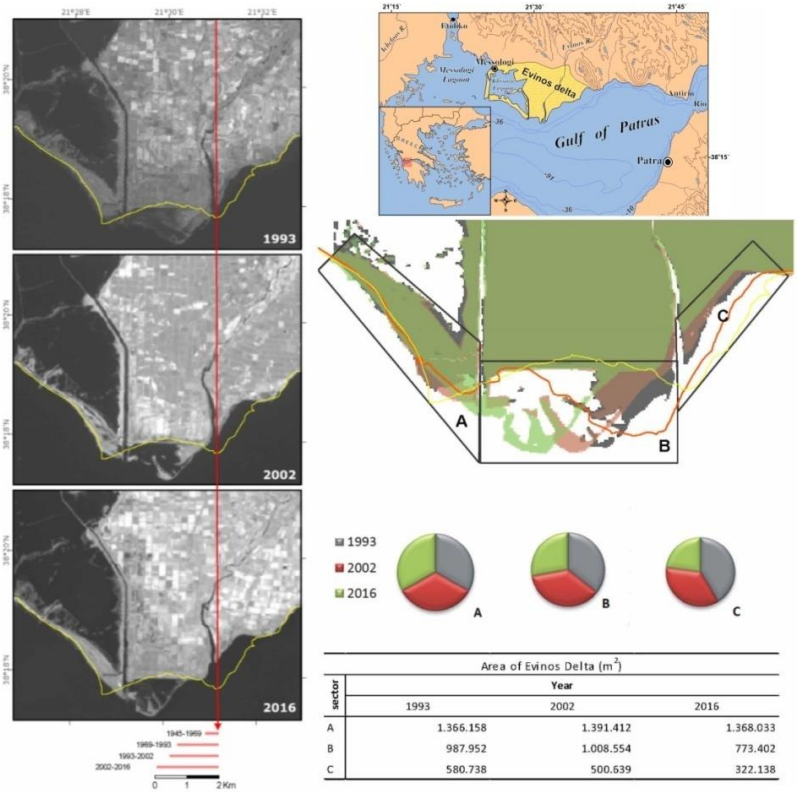

Area of Evinos Delta (m^2)

sector	Year		
	1993	2002	2016
A	1.366.158	1.391.412	1.368.033
B	987.952	1.008.554	773.402
C	580.738	500.639	322.138

Figure 1. Land loss and/or land gain for three parts of the Evinos River delta estimated by Landsat TM images.

The comparative analysis of Landsat TM images showed a significant land loss for the broader area of the active delta and the part of the delta east of the present river mouth, especially after 2002 (Figure 1). Land loss is primarily associated with severe decline of fluvial sediment discharge due to the construction of the dam (in 1997) in the upper reaches of the river. Another important reason for the erosion is the uncontrolled sand and gravel mining activity from the distributary channel of the river.

References

Ericson, J., Vörösmarty, C.J., Dingman, S.L., Ward, L.G, Meybeck, M., 2006. Effective sea-level rise in deltas: Causes of change and human dimension implications. Global & Planet. Change 50, 63-82.

Coleman, J.M., Wright, L.D., 1975. Modern river deltas. Variability of processes and sand bodies, in: Brousard, M.L. (Ed.), Deltas, models for exploration. Houston Geological Society, 99-149.

Galloway, W.E., 1975. Process framework for describing the morphological and stratigraphic evolution of deltaic depositional systems, in: Brousard, M.L. (Ed.), Deltas, models for exploration. Houston Geological Society, 87-98.

Gens, R., 2010. Remote sensing of coastlines: detection, extraction and monitoring. International Journal of Remote Sensing 31, 1819-1836.

Piper, D.J.W., Panagos, A.G., Kontopoulos, N., Spiliotopoulou, M., 1982. Coastal processes and morphology, Gulf of Patras, Greece. Z. Geomorph. N.F. 26, 365-374.

Ferentinos, G., Brooks, M., Doutsos, T., 1985. Quaternary tectonics of the Gulf of Patras, western Greece. J. Struct. Geol. 7, 713-717.

Maroukian, H., Karymblis, E., 2004. Geomorphic evolution of the fan-delta of the Evinos River in western Greece and human impacts in the last 150 years. Z. Geomorph. N.F. 48/2, 201-2017.

15th International Congress of the Geological Society of Greece
Athens, 22-24 May, 2019 | Harokopio University of Athens, Greece
Bulletin of the Geological Society of Greece, Sp. Pub. 7 Ext. Abs. GSG2019-276

Geomorphology of the Kerinitis River fan-delta (North Peloponnese, Greece)

D. Griva[1], A. Faka[1], I. Tsodoulos[1], V.D. Batzakis[1], M. Andreou[1], E. Karymbalis[1], S. Karalis[1]
(1) Department of Geography, Harokopio University, 70, El. Venizelou Str., 17671 Kallithea, Athens, Greece

Introduction

Deltas and fan-deltas are important geomorphic and sedimentary environments, acting as major sinks for fluvial sediments in the coastal zone, as important ecological systems, and as foci for urban and agricultural development. River deltas are relatively complex systems and subject to a range of fluvial, climatic, tectonic and sea-level controls (Coleman and Wright, 1975). The size and shape of a delta is controlled by the balance between watershed processes that supply sediment and coastal-marine processes (mainly wave activity, long-shore currents and tides) which redistribute that sediment. The size, geometry, and location of the receiving basin also play an important role in the evolution of fan-delta (Coleman and Wright, 1975).

The present study aims at a better understanding of the prevailing processes which contributed to the recent geomorphic evolution of the Kerinitis River fan-delta, located in the North Peloponnese (Central Greece), during the Late Holocene through geomorphological mapping and fieldwork. One of the objectives of this study was to assess mean shoreline change rates along the apron of the fan-delta using remote sensing data and GIS techniques.

Study Area

The fan-delta of the Kerinitis River is located along the southern coast of the western Gulf of Corinth and has been prograding in deep waters since the deceleration of sea-level rise during the upper Holocene like all the fan-deltas of the broader area of the northern Peloponnese. It has an area of 6.16 km^2 and the mean slope of its plain is 0.03.

The Kerinitis River drains an area of 80.84 km^2. The drainage basin is relatively elongated along a S.SW-N.NE trending axis and reaches an elevation of 1760 m in its southeastern end. Lithologically, the basin consists of 53.23 % limestones, 9.25 % cherts, 7.13 % flysch and 30.39 % Plio-Pleistocene deposits (mainly conglomerates and marls). Hence a significant area of the catchment is occupied by easily erodible geological formations. The general climatic conditions of the study area are typical of the temperate Mediterranean. The mean annual precipitation ranges from 800 mm near the coastline to more than 1200 mm in the southernmost highlands.

The receiving basin (Gulf of Corinth or the Corinth Rift) is one of the most active neotectonic features of the Eastern Mediterranean. It is a "back arc" elongated graben, formed by normal faulting associated with an approximately N-S crustal extension (Armijo *et al.*, 1996). The fan delta lies on the hanging wall of the Eliki fault, which is the most prominent fault appearing to control the westernmost sector of the Gulf (Koukouvelas *et al.*, 2001). The Gulf of Corinth can be characterized as a microtidal environment with an average mean tidal range of 0.15 m. Wave climate is primarily wind driven with offshore mean significant wave heights average heights < 0.3 m according to the output of the wave model (POSEIDON program).

Methodology

In order to determine the dominant processes responsible for the evolution and configuration of the fan-delta, detailed geomorphological mapping was carried out, which includes the identification and depiction of the dominant landforms of both the fan-delta plain (such as modern distributary channels, natural levees, abandoned channels, etc.) and the fan-delta coastal front (sandy and pebbly beaches, low cliffs, etc.). Mapping has been performed using a 5X5 resolution DEM obtained from the Hellenic Cadastre. The initial identification of the landforms is mainly based on the analysis of the DEM utilizing Esri ArcGIS 10. Additionally, study of old maps and interpretation of a series of geo-referenced aerial photos (taken in 1996) as well as Google Earth images were an invaluable source of information for the recognition of the fan-delta features. Data were organized into a Geographic Information System (GIS) spatial geodatabase using Esri ArcGIS 10. Field control was necessary to avoid mistakes made from the analysis of the DEM as well as from the interpretation of both aerial photos and Google Earth images. During the extensive field survey the entire deltaic area was examined following the traditional protocol of geomorphological mapping, verifying all the features and landforms identified during the initial phase of the research.

For the study of the recent changes of the fan-deltas shoreline, comparative observations of the coastlines of 1945, 1969, 1996, 2009 and 2017 have been made. The coastlines of 1945 and 1996 have been digitized from georeferenced aerial photo-mosaic obtained from the Hellenic Millitary Geographical Service (HMGS) and the Greek Ministry of Agriculture respectively. The coastlines of 1969 and 2009 have been derived from the topographic diagrams of the HMGS and the detailed DEM of the Hellenic Cadastre while the most recent coastline of 2017 has been obtained from digitization in Google Earth. This comparison allowed us to identify areas of progradation and parts of the fan-delta plain that are being eroded as well as to estimate mean annual progradation and erosion rates for the last 72 years. Using the 1945 digitized shoreline, 322 measurement sites were created every 10 m using an automated procedure. Coastal retreat or progradation was calculated for the intervals between the dates of the imagery by measuring the distance separating the two shorelines (in vector format) perpendicular to the older shoreline. These distances were then divided by the number of years to provide average annual coastal retreat or accretion rates.

Results and Conclusions

The active distributary of Kerinitis River has a braided pattern. It crosses the western part of the deltaic plain flowing parallel with the east Eliki fault segment for about 1.15 km and then turns to the east following a S.SW-N.NE flow direction for 1.2 km and flows into the Gulf of Corinth (Figure 1). Numerous presently inactive abandoned linear distributaries were recognized across the fan-delta plain. Old maps of the area along with aerial photographs of 1996 as well as the detailed DEM of the area have been particularly useful in identifying and mapping these traces of the abandoned river courses. A palaeochannel has been identified flowing along the east Eliki fault segment leading to the eastern border of the fan-delta. According to Pavlides et al. (2004) it corresponds to the main channel of the river before 1500 AD. A 1700 AD Venetian map of the area (Dokos and Panagopoulos, 1993) indicates that the course of the main channel during that period was similar to the recent one while a topographic map of Schmidt's (1879) (after a major 1861 earthquake during which the east Eliki fault segment was broadly ruptured for about a distance of 13 km and a vertical displacement up to 1 m occurred) shows the main channel flowing east of its present course (Pavlides *et al.*, 2004). These observations show a migration of the river after the 1861 event towards the central portion of the east Eliki fault segment but then the main channel changed its course flowing along its present position, which is similar with its 1700 AD path (Figure 1). The above mentioned changes of the main channel indicate that Kerinitis River appears to have been strongly affected by tectonic movements related to the westward propagation of the east Eliki fault segment.

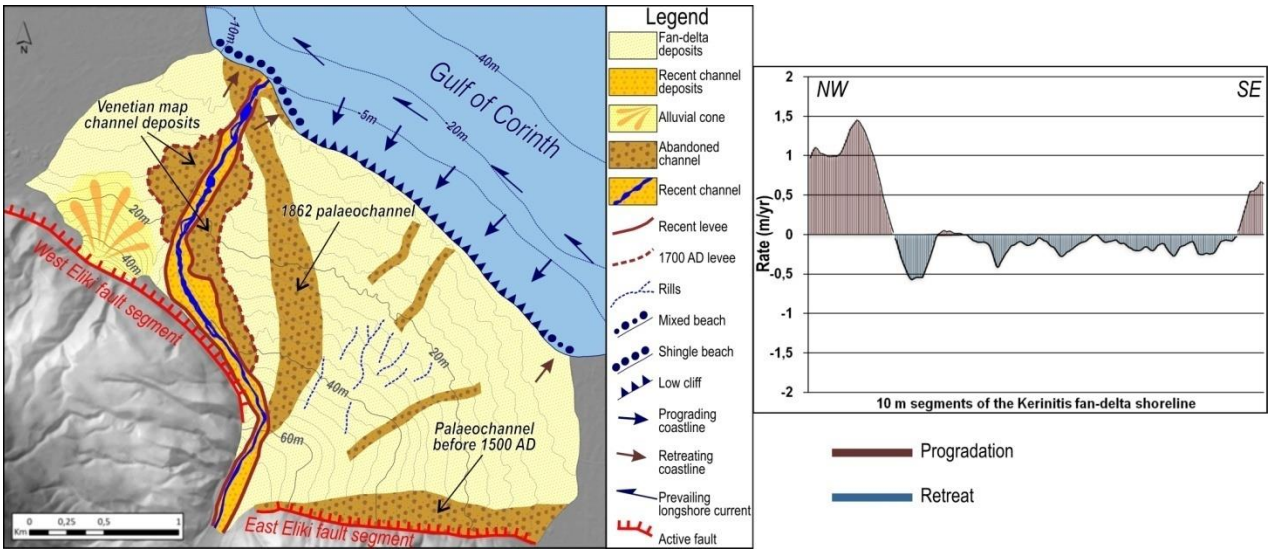

Figure 1. Geomorphological map of the Kerinitis River fan-delta and diagram showing progradation and retreat rates (in m/yr) estimated along the fan-delta shoreline for the time period between 1945 and 2017.

The comparable analysis of the 1945 and 2017 fan-delta shorelines shows that the main process along a significant part of the fan-delta front is intense and rapid erosion. Progradation (with a maximum mean rate of +1.46 m/yr) is observed only at the area around the presently active mouth of the river and at the easternmost edge of the fan-delta (Figure 1). A significant segment of the fan-delta shoreline is currently undergoing erosion with a maximum mean rate of -0.57 m/yr for the time period between 1945 and 2017. Evidence of coastal retreat is the appearance of a low cliff along the coastline due to the erosion of the top soil surface layer of the fan. Additionally, the presence of destroyed structures (designed to protect the coastline), along the central fan-delta apron indicates intense erosion.

References

Armijo, R., Meyer, B., King, G., Rigo, A., Papanastassiou, D., 1996. Quaternary evolution of the Corinth Rift and its implications for the Late Cenozoic evolution of the Aegean. Geophys. J. Int. 126(1), 11-53.

Coleman, J.M., Wright, L.D., 1975. Modern river deltas. Variability of processes and sand bodies, in: Brousard, M.L. (Ed.), Deltas, models for exploration. Houston Geological Society, 99-149.

Dokos, K., Panagopoulos, G., 1993. The Venetian Land Registry of Vonitsa. Educational Institute Agricultural Bank of Greece, Athens.

Koukouvelas, I., Stamatopoulos, L., Katsanopoulou, D., Pavlidis, S., 2001. A palaeoseismological and geoarchaeological investigation of the Eliki fault, Gulf of Corinth, Greece. Journal of Structural Geology 23, 531-543.

Pavlides, S.B., Koukouvelas, I.K., Kokkalas, S., Stamatopoulos, L., Keramydas, D., Tsodoulos, I., 2004. Late Holocene evolution of the East Eliki fault, Gulf of Corinth (Central Greece). Quaternary International 115-116, 139-154.

Schmidt, J., 1879. Studien uber Erdbeben, Carl Schottze, Leipzig, 68-83.

15th International Congress of the Geological Society of Greece
Athens, 22-24 May, 2019 | Harokopio University of Athens, Greece
Bulletin of the Geological Society of Greece, Sp. Pub. 7 Ext. Abs. GSG2019-298

Compositional Characterization of Prehistoric Pottery from Kephala Vasilikis, Ierapetra Crete (Greece)

E. Pantazi[1], I. Iliopoulos[1,2], E. Nodarou[3]

(1) Department of Geology, University of Patras, Patras, Greece, elepan0912@gmail.com
(2) ERAAUB, Facultat de Geografia i Història, Departament d'Història i Arqueologia, Universitat de Barcelona, Barcelona, Spain
(3) INSTAP Study Center for East Crete, Pacheia Ammos, Crete, Greece

Introduction.

In the present study petrographic and mineralogical techniques are employed for the compositional characterization of a ceramic assemblage from the site of Kephala Vasilikis, situated on the northern part of the Ierapetra Isthmus in east Crete. The aim is to investigate the provenance of the raw materials and the technology of manufacture of the ceramics.

Geological and archaeological setting.

The geology of Vasiliki is characterized by marine formations of Miocene age with lithologies varying from marl and sandstone to conglomerate. To the east of Vasiliki extend the alluvial deposits of the Ierapetra Isthmus dating to the Holocene (Papastamatiou, 1959). Archaeological excavations undertaken in the area of Vasiliki have brought to light evidence for human occupation spreading from the earliest prehistory to Roman times. The site under study is situated on the small hill of "Kephala" near the modern village. It is an advantageous position overlooking the Isthmus and the north-south passage. Excavation by Th. Eliopoulos (1994-1996) uncovered part of a Minoan settlement dating to the "Dark Ages", i.e. the Late Minoan (LM) IIIC/Early Geometric period (ca. 1200 BC). The main building of the multi-room complex bears strong evidence for ritual use, the most prominent find being the figurines of the "goddess with upraised arms" (Eliopoulos 1998). Although this is a single-phase architectural complex, excavation revealed vestiges of a much earlier occupation level dating to the Final Neolithic/Early Minoan I (FN/EM I) period. The pottery is very fragmentary but due to its early date it is of great interest because it confirms continuity of occupation in the area.

Samples and methods.

A total of 72 pottery samples were analyzed using petrographic and mineralogical techniques. The majority of the samples date to the LM IIIC which is the main period of occupation and comprises domestic vessels (cooking pots, jugs, basins, pithoi), fine wares (cups, bowls, kylikes) as well as parts of ritual figurines from the shrine. A smaller part of the sampled pottery comes from the earlier strata and comprises small- and medium-sized open vessels of FN/EM I date. For the petrographic analysis we used thin sections which were studied under a Zeiss AxioScope A.1 polarizing microscope. Also, for the mineralogical analysis we used a Bruker D8 Advance X-ray powder diffractometer (XRPD). All the analyses were carried out in the Department of Geology at the University of Patras, Greece.

Results and discussion.

The petrographic analysis established six main fabric groups (Table 1) and a few loners. Fabric groups A and B are coarse-grained consisting of igneous rocks, namely granites and granodiorites with the associated rocks and minerals.

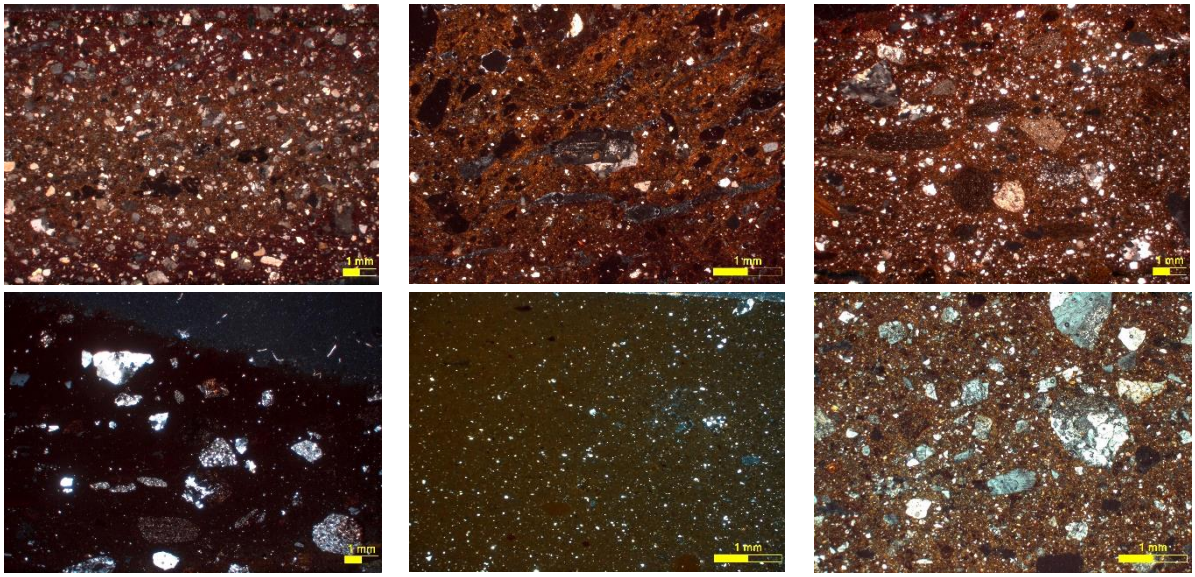

Figure 1. Upper row: Petrographic fabrics A (left), B (center) and C (left). Lower row: Petrographic fabrics D (left), E (center) and F (right).

This geology is not compatible with a strictly local origin, rather is attested in the northern part of the Isthmus, in the area of the Gulf of Mirabello (Papastamatiou, 1959, Nodarou & Moody, 2014). Fabric group C is also coarse-grained and contains metamorphic rocks, namely phyllites and quartzites, compatible with the Phyllite-Quartzite series outcropping on the north-eastern part of the Isthmus. Fabric group D is characterized by a fine matrix with coarse inclusions of phyllite, sandstone, and serpentine. This composition is compatible with the Ophiolite series and the Flysch mélange of the south coast (Liard, 2017, Liard et al., 2018). Fabric group E is characterized by a very fine matrix and is devoid of non-plastics. Finally, fabric group F is coarse-grained and comprises gabbros, diorites, and some phyllite fragments and is most likely connected to fabric group A. Among the loners it is worth mentioning one that is compatible with the local geology: it is a semi coarse fabric with micritic limestone and bioclasts.

Table 1. The petrographic fabric groups and their main characteristics.

Fabric group (code)	Fabric group (full name)	Main coarse Inclusions	Comments
A	Granite-granodiorite	Quartz, plagioclase, feldspars, biotite, chert fragments, sandstones fragments	Altered plagioclase and feldspars.
B	Granite-granodiorite-grog	Quartz, feldspars, plagioclase, chert fragments, phyllite fragments	High porosity, altered plagioclase and feldspars.
C	Metamorphic phyllite	Quartz, feldspars, chert fragments, quartzite fragments, igneous fragments	Some of the samples have quartz-rich matrix.
D	Ophiolite-bearing	Quartz, chert fragments, phyllite fragments, sandstones fragments	Pure clay paste.
E	Fine-very fine	Quartz, feldspars, chert fragments	Pure clay paste.
F	Diorite-gabbro	Quartz, calcite, plagioclase, feldspars, amphiboles, chert fragments, phyllite fragments	Altered plagioclase.

The mineralogical analysis was conducted on 25 representative samples from all the petrographic fabric groups. Five different classes were established on the grounds of their mineralogical composition. Quartz and plagioclase are present in all classes. Two classes are characterized by the presence of newly formed mineral phases: diopside and gehlenite, indicating that these samples were fired in higher temperatures (850-950 ^{o}C). On the contrary the absence of neo-formed phases in the rest of the classes possibly indicates that those samples were either fired in lower temperatures (<850 ^{o}C) or their chemical composition inhibited the formation of any new phase.

Conclusions.

The analysis of the ceramic material from Kephala Vasilikis demonstrated that the pottery consumed at the site was not strictly local, rather it was imported from different areas on the north and the south coast. The majority was produced with raw materials connected with the acid igneous rocks of the Gulf of the Mirabello, whereas the rest was connected with the Phyllite-Quartzite series on the northeastern part of the Isthmus and the Ophiolites of the south coast.

Fabric group B is tempered with grog and characterizes the FN/EM I pottery. This is a well-known clay “recipe” of the Early Bronze Age and is encountered in many sites in east Crete.

The next step of this study is to examine the samples with Scanning Electron Microscopy (SEM) in order to investigate the chemical composition of the clay pastes and establish the firing temperatures.

Acknowledgements

We would like to thank the excavator Th. Eliopoulos for entrusting us with the material from the site and the X-ray Diffraction Laboratory of University of Patras for conducting the XRD analyses.

References

Eliopoulos, T., 1998. A Preliminary Report on the Discovery of a Temple Complex of the Dark Ages at Kephala Vasilikis, in V. Karageorghis & N. Stampolidis (eds.) Eastern Mediterranean. Cyprus-Dodecanese-Crete, 16th-6th cent. B.C., Athens, 301-313.

Liard, F., 2017. Production and trade of pottery in the so-called “South Coast” fabric in Bronze Age Crete. Current interpretations and recent findings at Malia, northern Lassithi. Journal of Archaeological Science 21, 973-982.

Liard, F., Pomonis, P., Koutsovitis, P., Gait, J. Stamatakis, M., 2018. Ophiolites Associated with Pottery Production in Bronze Age Crete. Archaeometry 60, 731-749.

Nodarou, E. & J. Moody 2014. “Mirabello” fabric(s) forever: an analytical study of the granodiorite pottery of the Vrokastro area from the Final Neolithic period to Modern times. In Molloy, B.P.C. and Duckworth, C.N. (eds.) *A Cretan Landscape Through Time: Priniatikos Pyrgos and Environs.* BAR International Series 2634, 91-98. Oxford, Archaeopress.

Papastamatiou, I., 1959. Geological Map of Greece: 1:50 000, Kalo Chorio sheet. Institute for Geology and Subsurface Research.

15th International Congress of the Geological Society of Greece
Athens, 22-24 May, 2019 | Harokopio University of Athens, Greece
Bulletin of the Geological Society of Greece, Sp. Pub. 7 Ext. Abs. GSG2019-313

Revealing Historical Thermo- and Oligo - metallic Springs of Western Crete

Emmanouil Manoutsoglou[1], Nikolaos Spanoudakis[1], Paraskevi Garantzioti[1], Marialena Asproudi[1], Georgios Papanikolaou[1], Anastasia Vardali[1], Nikolaos Kallithrakas-Kontos[1]

(1) School of Mineral Resources Engineering, Technical University of Crete, University Campus, Akrotiri, Chania, Greece, emanout@mred.tuc.gr

Abstract

In this work, we present a brief description of hydro-chemical data from mineral springs reported in a historical study (Lekkas, 1938). The springs are located in different stratigraphical level and lithological units that outcrop in western Crete. These springs were monitored during the last three years. The outcomes of this monitoring work add to the existing knowledge, which is figured in the map of IGME (Figure 1). Athanassoulis et al., 2009 studied springs in most areas of Greece except Crete and the Ionian islands due to decreased interest and a small number of thermal springs. As shown in the map, four cold springs were recorded in Crete (Figure 1), although no further reference for Crete is mentioned in the technical report.

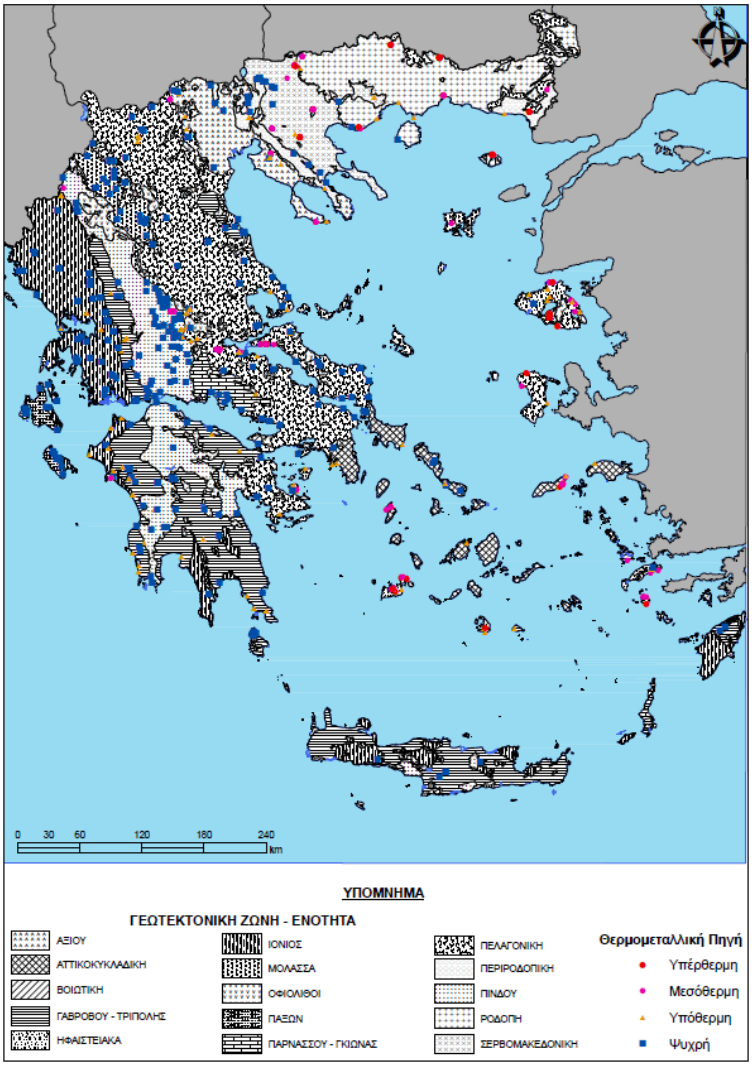

Figure 1. Geological map of IGME presenting the geotectonic zones of Greece and the distribution of thermal and mineral springs within them (after Athanassoulis et al. 2009)

As mentioned in the historical study on the thermal and mineral waters of Greece (Lekkas, 1938), Crete has 101 mineral springs most of which are saline or ferrous (Figure 2). Although, many of them were used as healing springs during the Ancient, Roman and Byzantine era, they faded into oblivion because the main concern of the authorities were focused in providing drinkable water to every settlement, city and more recently to the touristic infrastructures of the island as a result of the growing demands.

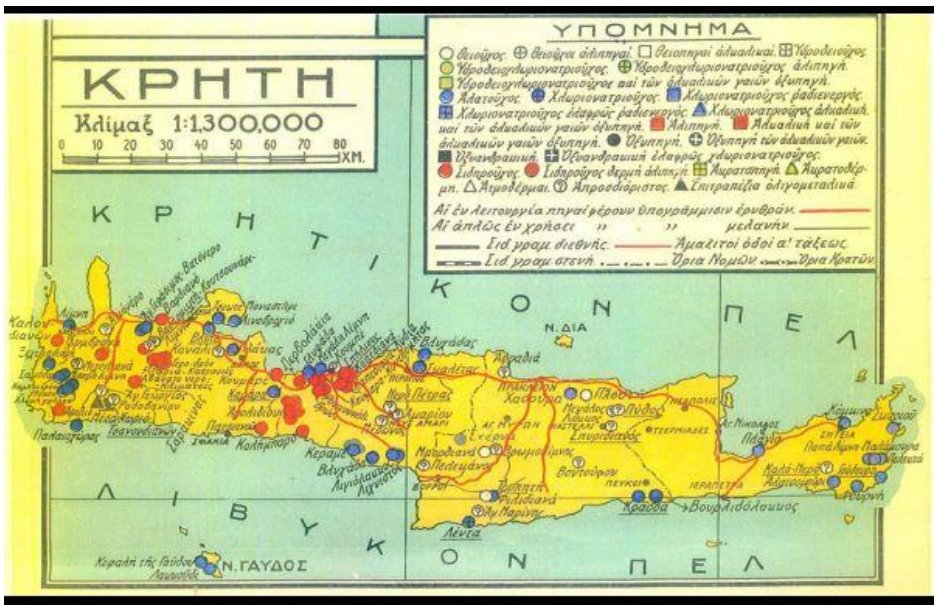

Figure 2. Distribution of thermal and metallic springs of Crete (after Lekkas, 1938)

Water samples were collected during, at least two wet and two dry periods in order to monitor and study the fluctuations in the physical characteristics but also their mineral content. The temperature (*T*), the pH the electrical conductivity (EC), and the total dissolved solids (TDS) of water samples were measured *in situ* by portable instruments. The samples were filtered, with 0.45μm filters and were stored in HDPE bottles. The aliquots for major and trace metal analyses were preserved by acidification with 2% HNO_3. The analysis of cations and trace-elements was carried out by ICP-MS (7500cx, Agilent Technologies), while the analysis of anions was carried out by phasmatophotometry (Hach DR2800).

(i) The springs hosted in the Phyllite Nappe are namely, Ksinonero, Temenia, Arelio and Moustakos:

The **Ksinonero** spring water is cold (14ºC, approximately) has pH equal to 3.2 and is connected with ferric depositions at its discharge. The concentration of dissolved iron (Fe) varies from 4 to 6g/l.

The historical healing springs of **Temenia** (Mesa Chorio and Tzanoudiana) are the only springs of Chania and Western Crete that have been recognized and utilized as healing springs with the Royal Decree of 31 August 1957, as diuretic. The temperature of the water of Mesa Chorio spring varies from 14.1-19.3°C, is slightly acidic (pH 5.7-6.4) and has very low TDS (50 mg/L to 140 mg/L).

The water of **Arelio** spring is cold (17º C), and lightly acidic (pH 6.3-6.8), and has very low TDS (50 mg/L). Periodically it contains Copper (Cu) up to 0.3 mg/L. During the Ottoman occupation, Bey's were transferring the water to the city of Chania, using large glass containers (Lekkas, 1938).

Moustakos spring has outlet temperature that varies from 18.7 to 22.5 ºC, pH varies from 5.3 to 6, and has also very low TDS (50-70 mg/L). Periodically, it has high manganese (Mn) content up to 1347 μg/L and iron (Fe) up to 0.2 mg/L.

(ii) The springs hosted in the Neogene formations are namely Kyrali, Lissos and Kares.

The **Kyrali** spring, located near to the Frangokastello fortress, is coastal and hosted under a relatively large alluvial fan. Moreover, is warm (21-27ºC) and connected with travertine depositions. Also, it contains fluorine (F) up to 0.2 mg/L. The remains of a round shaped pool in the sea, indicates that the warm water was used for bathing.

Lisssos spring is well known since the ancient era, as it is located to the Asklepius Temple of the homonymous ancient city. The water is hypothermic (20-22ºC), has near neutral pH that varies from 7.1 to 7.4, and relatively low TDS which varies from 200-400 mg/L. Periodically it contains up to 200 μg/L of zinc (Zn).

Kares Springs have outlet temperature 18.5-20 ºC, neutral pH and TDS that varies from 380-400 mg/L. The main dissolved constituents are HCO_3 (380 mg/L, approx.) and SO_4 (200 mg/L, approx.). Moreover the water contains 0.6 mg/L of dissolved fluorine (F) but also small quantities of trace elements including Li, Mo, Sr, etc.

The main characteristics of the waters that discharge from springs in the Phyllite Nappe are their very low TDS and the slightly acidic pH, except from the Ksinonero spring water which is extremely acidic. On the other hand the springs hosted in the Neogene formations exhibit extreme characteristics including travertine deposition or high content in dissolved trace elements.

Acknowledgements

We would like to thank the director of the laboratory of Hydrochemical Eng. and Remediation of Soil, Prof. N. Nikolaides and the stuff, Mrs Maria-Liliana Saru and Dr Stella Voutsadaki for the chemical analysis of the water samples.

References

Lekkas, N. 1938. The 750 mineral springs of Greece, Athens, 292 pp., (in Greek).

Athanassoulis, C., Vakalopoulos, P., Xenakis, M., Persianis, D., Taktikos, St. 2009. Integrated Quantitative and Qualitative Study of the Thermal Waters of Greece. Technical Report, IGME, Athens, 350pp. and Supplementary 243pp., (in Greek).

15th International Congress of the Geological Society of Greece
Athens, 22-24 May, 2019 | Harokopio University of Athens, Greece
Bulletin of the Geological Society of Greece, Sp. Pub. 7 Ext. Abs. GSG2019-329

Reconstructing the prehistoric landscape of Sikourio and Elatia intra-mountain basins, Thessaly, Greece

Sotiris Valkaniotis[1], Antonis Manakos[2], George Toufexis[3], Agathe Reingruber[4]

(1) Trikala, Greece, valkaniotis@yahoo.com
(2) Thessaloniki, Greece
(3) Diachronic Museum of Larissa, 41222 Larisa, Greece
(4) Free University of Berlin - Institute of Prehistoric Archaeology, 14492 Berlin, Germany

Extended Abstract

Mt Olympus (2919 m.a.s.l.) and Mt Ossa (1978 m.a.s.l.) form the northeastern boundaries of the Thessalian Plain in Central Greece, separating the plain from the Aegean Sea. At the lower slopes of Mt Olympus and Mt Ossa, a series of intra-mountain basins develop between the lower eastern Thessalian Plain and the main mountain blocks. The most prominent of these basins is Sikourio basin, separated from the Larisa plain by the Chassambali chain of hills. Sikourio basin is nowadays connected to another complex of smaller basins forming the Elateia basin. These intra-mountain basins probably were formed during the post-orogenic extension of Middle Tertiary (Caputo & Pavlides, 1993; Kilias, 1995). Today, Sikourio and Elateia basins are hydrologically connected to the Pinios river basin through the Kalamitsa drainage that flows towards northwest into the main Pinios river body. The river Xerias drains a large part of Mt Ossa and flows to the south towards the remnants of the lake Bara Toibasi in the southern part of Sikourio basin (Fig.1). Kalamitsa River and its smaller tributaries drain the largest part of Sikourio and Elateia basins, forming a steep gorge at Magoula Bounarbasi, near Kispelochori. Through small sinkholes around Bara Toibasi Lake, a result of karstification, lake water infiltrates and feeds the karstic aquifer developed inside the limestone formations. This karstic aquifer connects hydraulically both the surficial and the ground water of Sykourio basin with the springs that are found at the border of the bedrock formations of Chassambali hills and the East Thessalian alluvial aquifer, to the south of Sykourio basin.

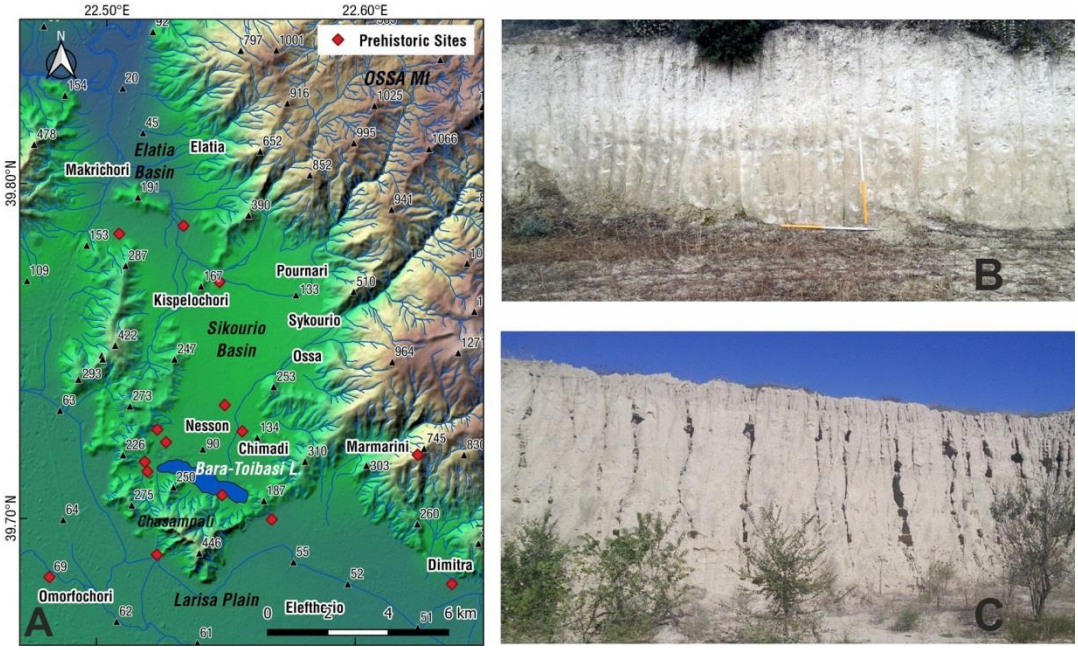

Figure 1. A) Overview map of Sikourio & Elateia basins. Prehistoric sites marked with red. Bara Toibasi Lake is shown with its extent from 1945, before recent irrigation & drainage modifications. B) Lacustrine sediments, northern part of Sikourio basin near Magoula Bounarbasi. C) Plio-Pleistocene lake sediments exposed at the abandoned quarries near Kalochori.

The hydrological conditions affected greatly the behaviour of human groups since prehistoric times. Permanent settlements were founded here already during the Neolithic Age – some of them forming in the course of many centuries (ca. 6000 calBC to ca. 4500 calBC) several meter high mounds (e.g. Nessonis II or Magoula Bounarbasi). Additionally, thanks to systematic surveys, a number of flat sites were detected, mainly in the area of the former lake Bara Toibasi (Fig. 1). Our working hypothesis is that these sites relate to the lake and were founded close to its former shores. We interpret Bara Toibasi Lake as a remnant of an older larger lake inside Sikourio basin. This lake is different from the ancient Lake Nessonis that extended in the Larisa plain south of Girtoni and from the Lake Karla south of Eleftherio (Gallis, 1992; Caputo et al. 1994, Reingruber et al. in print). Lacustrine (lake) sediments are exposed in large abandoned clay quarries around Bara Toibasi Lake, while in this study we document more outcrops to the northern part of Sikourio basin, with additional indications of probable extensive lacustrine sedimentation also in Elateia basin (Fig.1). These extensive

lacustrine sediments are indicators of a wider lake system that existed inside Sikourio and Elateia basins from Pliocene (?) up to Late Pleistocene-Holocene and are covered by recent alluvial sediments from the Xerias fan and secondary fans around the basin borders.

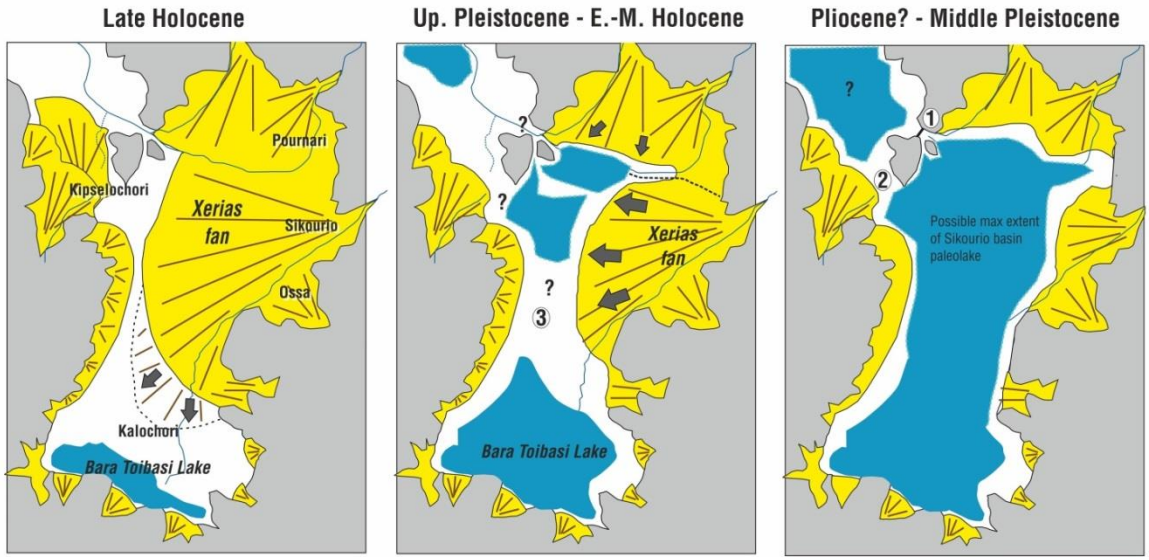

Figure 2. Proposed paleogeographic evolution of Sikourio basin and the proto-Sikourio lake system. The basin infill by the rapidly expanding Xerias fan, together with the fast draining through Bounarbasi (1) and Kipselochori (2) gorges, led to the confinement of Sikourio/Bara Toibasi Lake to the southernmost part of the basin. The westward expansion of Xerias fan closed the basin at the center (3) and created a hydrological divide between the northern and southern part.

Bara Toibasi Lake was previously considered as a product of hanging-wall subsidence of a proposed eastwards segment of Girtoni fault (Caputo 1990; Caputo et al., 1994). Using geological, geomorphological and archaeological observations, we propose the existence of a proto-Sikourio lake that covered Sikourio basin during Late Neogene - Quaternary. The draining of the lake was facilitated by a) the expansion of the Xerias fan that covered the central part of the basin and b) the lake outflow towards Elateia basin through Bounarbasi gorge and probably along Kipselochori area. Xerias fan expansion and lake draining led to the creation of Bara Toibasi Lake at the southern part of Sikourio that remains disconnected hydrologically with the northern part (Fig. 2). Sediment and water supply towards the northern part of proto-Sikourio lake/basin was probably affected by changes in the mountain catchments at Mt Ossa and identified large paleo-landslides that temporarily blocked drainage towards the lake/basin. Bounarbasi gorge opening and lake outflow is estimated to have taken place before the Mesolithic period and the beginning of the Holocene, probably around or shortly after the Last Glacial Maximum (LGM, ~24-16ka BP). Neolithic sites at the southern Sikourio basin are found around the estimated paleo-shoreline of Bara Toibasi. Draining through the karstic aquifers of Chassambali hills and a probable lower water supply through Xerias River led to the shrinkage of Bara Toibasi from the Neolithic era up to today. Conditions in Elateia basin are more complex; the Elateia basin complex includes a series of small closed connected intra-mountain basins that were cut through by Pinios River during Late Quaternary, as the Pinios River eroded through Olympus-Ossa mountain range and exited towards the Aegean Sea. While lacustrine sedimentation is present in Elateia basin, its previous connection with the Sikourio basin is under investigation.

Acknowledgements

We would like to thank the Ephorate of Antiquities in Larissa for granting us the permission to conduct investigations in the Basins of Sikourio and Elateia, and the German Research Foundations for the financial support (DFG, German Research Foundation - Project number RE 1699/2-1).

References

Caputo, R., 1990. Geological and structural study of the recent and active brittle deformation of the Neogene-Quaternary basins of Thessaly (Greece). Scientific Annals 12, Aristotle University of Thessaloniki, 252 pp.

Caputo, R., Pavlides, S., 1993. Late Cainozoic geodynamic evolution of Thessaly and surroundings (central-northern Greece). Tectonophysics 223, 339-362.

Caputo, R., Bravard, J.P., Helly, B., 1994. The Pliocene-Quaternary tecto-sedimentary evolution of the Larissa-Plain (Eastern Thessaly, Greece). Geodinamica Acta 7(4), 219-231.

Gallis, I.K., 1992. Atlas of Prehistoric Settlements in Eastern Thessaly Plain. Etairia Istorikon Erevnon Thessalia, Larisa, Greec, 240pp. (in Greek)

Kilias, A., 1995. Tectonic Evolution of the Olympus-Ossa Mountains: Emplacement of the Blueschists Unit in Eastern Thessaly and Exhumation of Olympus-Ossa Carbonate Dome as a Result of Tertiary Extension (Central Greece). Mineral Wealth 96, 7-22.

Reingruber, A., Toufexis, G., Valkaniotis, S., Manakos, A., in print. The Basins of Sykourio and Elateia in northeastern Thessaly: an attempt at reconstructing the (pre)historic landscape. AEThSE: 6th Archaeological Meeting of Thessaly and Central Greece, March 1-4 2018, Volos, Greece.

15th International Congress of the Geological Society of Greece
Athens, 22-24 May, 2019 | Harokopio University of Athens, Greece
Bulletin of the Geological Society of Greece, Sp. Pub. 7 Ext. Abs. GSG2019-354

New documentary sources regarding the large earthquake (~M7) and its associated tsunami of 8 November 1905 in Mt Athos, Northern Greece

Ioanna Triantafyllou[1], Gerassimos A. Papadopoulos[2], Efthymios Lekkas[1]

(1) National and Kapodistrian University of Athens, Department of Geology and Geoenvironment, Panepistiomiopolis Zografou Campus, 15784 Athens, Greece
ioannatriantafyllou@yahoo.gr
(2) International Society for Prevention & Mitigation of Natural Hazards, Athens, Greece, 10681

Abstract

Mt Athos, Northern Greece, is a monastic community with life since ~1000 AD, a UNESCO worldwide cultural heritage site that repeatedly hit by large earthquakes. On 8 November 1905 Mt Athos suffered a lot from an earthquake which shook the Balkan peninsula and had estimated magnitude ranging from 6.8 to 8.3. However, this important event remains little known since only very few documentary sources have been utilized so far. We collected a set of new documentary sources, ignored so far by the seismological community, including contemporary press reports, letters and manuscripts. Based on these sources we reconstructed the earthquake impact field and organized a data base which contains assignment of macroseismic intensity in 42 observation points, at epicentral distances up to ~660 km, and an identification of several sites where a variety of co-seismic ground failures were reported, the most important being landslides and sizable rockfalls. From magnitude-intensity relationships based on data of instrumental Greek earthquakes, macroseismic magnitude of ~7 equivalent to Ms was estimated, which is close to the most recent, reliable instrumental estimates of ~7.2. The examined sources revealed for the first time that earthquake-triggered landslides occurred in the southern tip of Mt Athos producing a local but powerful tsunami of ~3 m run-up. Eleven persons were reportedly killed.

Previous studies

The first scientific material regarding the 1905 earthquake was published in the Annals of the National Observatory of Athens (NOA) (Eginitis, 1910), where it was briefly reported that damage was caused in Iviron Monastery. Several years later, Critikos (1932, 1933) reported that damage was also caused in towns and villages of the area, while the earthquake was felt in the Balkan peninsula as far as Athens (Greece), Sofia and west coast of Black Sea (Bulgaria), Bucharest (Romania), Gulf of Adramition (NW Turkey) and Bari (eastern Italy). The same author, based on the macroseismic information published by Eginitis (1910), estimated that the epicentral (maximum) intensity reached at X degree in the 10-grade Rossi-Forel scale, which in the Mercalli-Modified (MM) scale (Wood and Neumann, 1931) corresponds to degree X-XII (Richter, 1958), which very likely is an exaggeration as one may conclude from a variety of documentary sources collected and analyzed by us. Sieberg (1932) dated the event on 9 November 1905, likely on local time, and reported on it very briefly. He has been, however, the only author that tried to draw isoseismals although based only on very few intensity observation points. Galanopoulos (1955) reported also very briefly on the destruction caused by the earthquake.

A prominent historian (Kadas, 1996) found and published a marginal note written in a religious book. The note, which is already known in the seismological community (e.g. Papazachos and Papazachou, 2003), says that due to the earthquake many people died and several monasteries were damaged greatly.

The 1905 earthquake has been included in several descriptive and/or parametric earthquake catalogues but there is confusion as regards the earthquake origin time. As an instance, Kárnik (1969) listed two large earthquakes occurring on 8th November 1905, one at 21.41 GMT and another at 22.06 GMT. An explanation may come out from the records of the Agamennone-type seismograph installed at Athens station in 1898. This seismograph, which was an instrument of intermediate response period introduced by G. Agamennone, Professor of Seismology in Rome, recorded the first seismic wave arrival of the 1905 earthquake at 23.41.54 local time (21.41.54 GMT). This may explain why many authors adopted origin time at 21.41.

The instrumental sources collected by ISC and used to analyze the 1905 event does not include any observation regarding the event in Kárnik (1969) catalogue at 8 Nov. 1905, 21:41. However, European stations offer plenty of measurements for the event at 22:06 which is very likely the correct origin time of the Athos main shock occurring on 8 November 1905. Then, the local time would be 9 November 1905 at 00:06, which likely justifies the dating by Sieberg (1932).

Various estimates of the 1905 earthquake epicenter are consistent with only small deviations from the most recent one calculated in the ISC-GEM (2018) catalogue. Various catalogues, however, provided widely divergent magnitude estimates ranging between 6.8 and 8.3 depending on the different magnitude scales and estimation methods used. Aiming to contribute in resolving the ambiguity regarding the earthquake magnitude we calculated a macroseismic magnitude.

New documentary sources

To further study the 1905 earthquake and tsunami we collected and evaluated a wealth of new information from a variety of documentary sources which remained unknown to the seismological tradition so far. The sources collected include contemporary press reports, manuscripts from Mt Athos and NOA archives, as well as various letters, articles and books containing descriptions about the earthquake and its associated phenomena and impact. From the documentary sources a data base was organized that documents the earthquake impact in both the built and natural environment. Seismic

intensities were assigned in 42 observation sites.

Contemporary press reports

We collected a set of seven contemporary press reports (CPRs) from newspapers published in Athens as well as in Thessalia Province, Central Greece. The relevant reports have been the closest to the event with publication time ranging from 27 October to 7 November 1905 [O.S.], i.e. from 9 to 20 November 1905 [N.S.]. A short review of some Thessalia Province newspaper reports was published by Papaioannou (2018).

NOA manuscript

After the establishment of the Institute of Geodynamics at NOA as the seismological service of the country in 1892, its scientific staff started the systematic record of earthquakes occurring in Greece from 1892 up to 1915 inclusive. The earthquakes were listed in chronological order in an unpublished manuscript called "Book of Earthquakes". In "Book of Earthquakes, Vol. 2", covering the time period from 1899 to 1915, there is a short section about the 1905 Athos earthquake.

Manuscripts from Mt Athos archives

We were able to collect two valuable manuscripts which are archived in Mt Athos monasteries. The first (ATHMS-1), dated 1 [O.S.]/14 [N.S.] November 1905, was written by an eyewitness monk named Avimelech Mikragiannanitis and was published later in a religious book by Bishop Rodostolos Chrysostomos (2004) (BOOK-1). However, the manuscript remained unknown to the seismological community so far. The second document (ATHMS-2) is an unpublished manuscript of the Codex (p.185) of Kafsokalivion monastery written in Mt Athos during 1915. A photograph of the manuscript was kindly provided to us by Father Patapios who currently gets monastic life at that monastery.

Letters

Bishop Chrysostomos Lavriotis (1905), being an eyewitness of the 1905 earthquake, sent a comprehensive letter to the Ecumenical Patriarch Joachim III in Constantinople (Istanbul) narrating the destructive effects of the earthquake in Athos. The letter (LETT-1) dated 3 [O.S.] /16 [N.S.] November 1905 was published in a contemporary religious journal and later reproduced in BOOK-1. Of relevance is also a postscript (LETT-2) dated 4 [O.S.]/17 [N.S.] November 1905 and inserted at the end of LETT-1.

Books and articles

The author of BOOK-1, in addition to publishing the valuable manuscript ATHMS-1, performed also an investigation of personal accounts among survivors of the 1905 catastrophic event. The results are included in BOOK-1 too. Useful information can also be found in a religious book by Kaloutsis (2000) (BOOK-2). Of interest is also an article (ART-1) published in a local journal by an eminent archaeologist (Mylonas, 1995).

Regardless the seismotectonic interpretation of the 1905 earthquake, it remains a key event for better understanding the hazards associated with earthquakes and related phenomena, such as landslides, rockfalls and tsunamis, in an important worldwide cultural heritage site like Mt Athos.

Conclusions

From the examination of the documentary sources regarding the 8th November 1905 large earthquake we concluded that this event caused extensive damage, mainly in the south part of Mt Athos. In addition important ground failures, particularly massive landslides and rockfalls were produced by the earthquake. Part of the landslide mass entered the sea and generated a 3 m high local tsunami. The maximum seismic intensity assigned was as high as IX-X (MM).From the seismic intensity field we calculated earthquake magnitude ~7.

References

Galanopoulos, A.G., 1955. The seismic geography of Greece, Ann. Geol. Pays Hellen. 6, 83–121

Eginitis, D., 1910. Catalogue des tremblements de Terre observes en Gréce pendant les années 1904-1908, Ann. de L' Observatoire Nat. d' Athènes 10, 560-585.

Critikos, M. N., 1932. Sur la Seismicité de Macédoine, Ann. de L' Observatoire Nat. d' Athènes 12, 149-159.

Critikos, M. N., 1933. Sur la Seismicité de Macédoine, Gerl. Beitr. zür Geophysik 40, 371-379.

Kadas, S. N. 1996. Marginal notes in codecis of Dionysiou monastery, Mt Athos, Edition by Dionysiou monastery, Mt Athos, 417 pp. (in Greek).

Kaloutsis, S.D. 2000.The Virgin Mary of Mirtidiotissa. 4th edition, Kythira, 126 pp. (in Greek).

Mylonas, P.M., 1995. Nineteenth century representational paintings and photographs of Athos monasteries and their interpretation. Archaeology, 54, 6-19 (in Greek with Engl. Abstr.).

Papaioannou, I., 2018. The seismic activity in Thessalia from 1900 to 1950. Thessaliko Imerologio, 73, 289-314 (in Greek).

Papazachos B.C., Papazachou, C., 2003. The Earthquakes of Greece, Ziti Publications, Thessaloniki, pp. 273 (in Greek).

Richter, Ch., 1958. Elementary Seismology. Freeman, San Francisco, CA, 768 pp.

Sieberg, A., 1932. Untersuchungen über Erdbeben und Bruchschollenbau im östlichen Mittelmeergebiet: Ergebnisse einer Erdbebenkundlichen Orientreise. Denksschr. Mediz. Naturwiss. Gesellsch. z. Jena, (Jena) 8, 3-13, 95.

Wood, H. O., Neumann, F., 1931. Modified Mercalli Intensity Scale of 1931, Bull. Seism. Soc. Am. 21, 277-283.

15th International Congress of the Geological Society of Greece
Athens, 22-24 May, 2019 | Harokopio University of Athens, Greece
Bulletin of the Geological Society of Greece, Sp. Pub. 7 Ext. Abs. GSG2019-356

Assessment of the Geomorphic Impacts of the Flash Flood Event of 15 November 2017 along the Shore of Eleusis Bay (Attica, Greece)

D. Griva[1], I. Parcharidis[1], E. Karympalis[1]
(1) Harokopio University, Dep. of Geography, El. Venizelou 70, 17671, Athens, Greece, gp218304@hua.gr

Greece experiences a variety of catastrophic weather events that are frequently followed by severe consequences on social and economic activity. Flash floods have caused tremendous loss of life and property over the past decades (Papagiannaki et al., 2013). The most deadly flood in Greece in the last 40 years occurred on November 15th 2017 in the western part of the region of Attica. A high intensity convective storm with orographic effects reaching up to 300 mm in 8 hours (200mm in only 3 hours) locally in a small area (18 km x 4 km zone) of the western and southern slopes of Pateras mountain caused flash floods along the streams of Agia Aikaterini, Soures and Koulouriotiko with extensive damages in the towns of Mandra and Nea Peramos and the loss of 24 people. Basin-average precipitation rates reached 57 mm/h over Soures stream, 41 mm/h over Agia Aikaterini stream and 140 mm/h in the core of the storm. It is noteworthy that a hydrological simulation study resulted in discharge values about 115 m^3/s and water level values exceeding 3 m in Soures and Agia Aikaterini streams which caused the flash flooding around the Mandra area (Varlas et al., 2019).

The most severely affected by the extreme flash flood event area is the western part of the Thriassion plain in west Attica. Thriassion plain hosts one of the largest industrial units in Greece including refineries, metallurgical industries, factories, shipyards as well as the waste landfill of the Attica prefecture. It covers a total area of 812.95 km^2 and is bounded by Pateras Mountain (1016 m) to the west, Parnitha mountain (1413 m) to the north and Aigaleo Mountain (468 m) to the east while the southern border of the plain is the Eleusis Bay. The Bay of Eleusis is a small and deep basin between the north coast of Salamina Island and the mainland. It has a coastline of approximately 15 km and receives the sediment load of a series of streams that drain the surrounding mountainous area. The upper reaches of the streams have relatively steep slopes resulting in high stream erosion capacity and transfer ability. Due to very high water flow velocities during the event (since in certain areas the terrain was very steep) and bottom shear stresses, the flash flood caused significant soil erosion and carried away not only large quantities of solids (practically it was a mud-flow), but also extremely large and heavy objects, such as buses and cars. Additionally, debris flows occurred along the steep coastal fan of the Koulouriotiko Stream which passes through the settlement of Nea Peramos.

In this study images from Copernicus Sentinel 2 and Planetscope Dove microsatellites are used. For this purpose images before and after the flood event in the area have been collected also only one Planetscope image dated 15/11/2017 which is the only one in which a part of the coastal zone is displaced due to cloudiness.

Sentinel 2 is part of the Copernicus mission having in constellation A (lunch on 23 June 2015) & B (lunch on 7 March 2017) satellites, sharing the same orbital plane at an altitude of 786 km and featuring a short repeat cycle of 5 days at the equator optimized to mitigate the impact of clouds for science and applications. The Sentinel-2 mission includes 13-spectral band multispectral optical imager with different resolution (down to 10 m) and a swath width of 290km. The data of the constellation of two satellite units can support the build-up and frequent update of globally consistent background reference maps to be used for impact assessments.

Concerning Planetscope optical multispectral satellite images, LEO (low earth orbit) SSO (SunSynchrnous Orbit), with pixel size (after orthorectified) 3 meters, were used covering the study area. Ortho Scenes products (3B) are radiometrically-, sensor- and geometrically-corrected products that are projected to a cartographic map projection. These products are projected to UTM coordinates and orthorectified using GCPs and fine-scale DEMs to a positional accuracy of <10 m RMSE. PlanetScope is a constellation of 120 smaller CubeSats known as ‘doves’ (dimensions 10 cm × 10 cm × 30 cm) built and operated by Planet, and launched in groups called ‘flocks’. PlanetScope imagery has four bands, blue (Band 1, 455–515 nm), green (Band 2, 500–590 nm), red (Band 3, 590–670 nm) and near infrared (Band 4, 780–860 nm) and a ground spatial resolution of 3.7 m, having a field-ofviewontheEarthsurfaceof20-30kilometer (Altena et al. 2017).

Research based on optical satellite images are simple to interpret and easily or free obtainable. Furthermore, absorption of infrared wavelength region by water and its strong reflectance by vegetation and soil make such images an ideal combination for mapping the spatial distribution of land and water. These characteristics of water, vegetation and soil make the use of the images that contain visible and infrared bands widely used for coastline mapping (DeWitt, et al., 2002). All images are georeferenced and spectral processing techniques (radiometric indices) have been applied in order to delineate the boundary land-water and then detect coastal changes producing multitemporal thematic maps based on the above optical data. In addition the Idepix ((Identification of Pixels) processor, integrated in the SNAP s/w, has been used which provides a pixel classification into properties such as clear/cloudy, land/water, snow, ice etc. although some limitations and weaknesses are presented. Finally Sentinel 1 OCeaN (OCN) data have been used dated 19-11-2017 (morning and night records) in order to collect knowledge about wind velocity and direction. The OCN product (OWI component) is a gridded estimate of the surface wind speed and direction at a height of 10 m above the ocean surface.
In order to process of Sentinel 2 Sentinel 1 (OCN) and Planetscope images the open ESA’s software SNAP, the ENVI and the open software QGIS were used.

The main objective of this study is to identify the effects of the 15 November 2017 flash flood event along the north shore

of Eleusis Bay using remote-sensing observations. These effects concern mainly the deposition of large amounts of sediments transported by the streams that flow into the Eleusis Bay.

References

Altena, B., Mousivand, A., Mascaro J., Kaab, A., (2017). Potential and limitations of photometric reconstruction through a flock of DOVEcubesats. The International Archives of the Photogrammetry, Remote Sensing and Spatial Information Sciences, Volume XLII-3/W3,doi.org/10.5194/isprs-archives-XLII-3-W3-7-2017

DeWitt, H., Weiwen Feng, J.R., (2002). Semi-Automated construction of the Louisiana coastline digital land-water Boundary using landsat TM imagery, Louisiana's Oil Spill Research and Development Program, Louisiana State University, Baton Rouge, LA 70803.

Papagiannaki, K., Lagouvardos, K., Kotroni, V., 2013. A database of high-impact weather events in Greece: A descriptive impact analysis for the period 2001–2011. Nat. Hazards Earth Syst. Sci. 13, 727–736.

Varlas, G., Anagnostou, N., Spyrou, C., Papadopoulos, A., Kalogiros, J., Mentzafou, A., Michaelides, S., Baltas, E., Karymbalis, E., Katsafados, P., 2019. A multi-platform hydrometeorological analysis of the flash flood event of 15 November 2017 in Attica, Greece. Remote Sensing 11(1), 45

15th International Congress of the Geological Society of Greece
Athens, 22-24 May, 2019 | Harokopio University of Athens, Greece
Bulletin of the Geological Society of Greece, Sp. Pub. 7 Ext. Abs. GSG2019-362

Flood hazard assessment of the Kerinitis River catchment, North Peloponnese, Greece

A. Kakonas[1], E. Karymbalis[1], C. Chalkias[1], N. Evelpidou[2]

(1) Department of Geography, Harokopio University, 70, El. Venizelou Str., 17671 Kallithea, Athens, Greece, gp217305@hua.gr
(2) Section of Geography and Climatology, Department of Geology and Geoenvironment, National University of Athens, Panepistimiopolis, 15784, Athens, Greece

Introduction

Floods are among the most dangerous natural hazards affecting the development of an area. In Greece, many drainage basins are relatively small with steep slopes, configured by steep streams with braided main channel morphology. These systems are usually dry, but experience extreme flash flood events of low frequency, but high magnitude. Such exceptionally high runoff may be a source of significant damage to human infrastructure. Despite the importance of these floods, the hydrological analysis of ephemeral streams in Greece has been especially difficult due to the lack of discharge gauges.

The aim of this study is to present a flood hazard assessment and mapping methodology for the Kerinitis River drainage basin which is located in the North Peloponnese. Additionally, the simulation of a flash flood event along the main channel of the river caused by an extreme rainfall event, similar to the storm that took place on January 11th and 12th, 1997 above the nearby catchment of Xerias River, using a surface GIS-based runoff model was attempted. The application of this modeling led to the direct runoff hydrograph along the Kerinitis main channel at the outlet of the basin (the apex of the fan-delta). The proposed methodologies are based on the application of GIS with the integration of various data concerning the study area.

Study area

Kerinitis is an ephemeral river with a dendritic drainage network, located in northwestern Peloponnese. Its drainage basin has an area of 82.94 km^2. It is a relatively elongated catchment along a S.SW-N.NE trending axis and reaches an elevation of 1760 m in its southeastern end. Lithologically, the basin consists of 53.23 % limestones, 9.25 % cherts, 7.13 % flysch and 30.39 % Plio-Pleistocene formations (mainly conglomerates sandstones and marls). The main channel follows a S.SW-N.NE flow direction for about 22.98 km and discharges into the Gulf of Corinth. At the mouth of the river, a fan-delta has developed covering an area of about 6.2 km^2. The broader area of the Northern Peloponnesus experiences a typical Mediterranean climate, with annual temperature averaging 13°C. The mean annual precipitation in the basin ranges between 600 mm in the northern coastal region and 700 mm in the southern mountainous region. Rainfall is distributed relatively unevenly with about 75% of it occurring between the months of October and March. The river has flooded on numerous occasions especially downstream from the national highway that connects Athens with Patras near the apex of the fan-delta.

Methodology

For the Kerinitis catchment flood hazard assessment and mapping, a multi criteria model was applied. The model was based on criteria / factors controlling the water route when drainage system capacity is exceeded by high runoff. The selected factors include the morphological slope, the elevation, the mean annual rainfall, the flow accumulation, the distance from the main channels of the streams, the hydro-lithology of the geological formations and the land use. Morphological slope values were obtained from the slope map which was produced by a detailed (5m X 5m resolution) Digital Elevation Model (DEM) of the Greek Cadastre. The same DEM was also used to calculated flow accumulation. The geological formations of the study area were derived from the 1:50,000 scale geological map of the Institute of Geology and Mineral Exploration of Greece while land-use data were obtained from CORINE land cover 2018. Each factor was divided into five classes with specific boundary values. Integer numbers, ranging from 1 to 5, were assigned to every class with 1 representing very low physical vulnerability and rank 5 indicating very high physical vulnerability to flood hazard. To estimate the final weights for each factor the Analytic Hierarchy Process (AHP) method was applied. It is a multi-criteria decision making technique, which provides a systematic approach for assessing and integrating the impacts of various factors, involving several levels of dependent or independent, qualitative as well as quantitative information (Chalkias, 2015).

For the calculation of the maximum discharge at the outlet of the Kerinitis River catchment (caused by an extreme weather event similar to the storm that took place on January 11th and 12th, 1997, above the nearby catchment of Xerias River), the GIS-based unit hydrograph derivation method was adopted. According to this concept, the definition of isochrones (flow traveling to the watershed outlet) at time intervals is the key point for the construction of time-area diagrams (Chow *et al*., 1988). Hence a routing model (Du *et al*., 2009) has been implemented in ESRI ArcGIS10 environment. The topography of the land surface (DEM) is one of the most fundamental elements for this simulation (Karymbalis *et al*., 2012). DEM-based surface hydrological analysis was the first step in order to execute the rainfall-runoff model. DEM analysis led to various derivatives such as slope (surface analysis), flow direction, flow accumulation and flow length. Since the methodology adopted is based on the concentration time, calculations were carried out for the travel time of water within the catchment for both channel and overland flow. In order to separate these two types of water flow a

suitable threshold on flow accumulation was selected. Having the flow accumulation and the various grids of rainfall the discharge at the channel of the river was calculated. Furthermore by using the appropriate equations both the channel and overland flow travel velocities for each cell off the basin was estimated and the travel time in each cell was computed from the travel distance. In order to design the isochrones for the rainfall event it was necessary to reclassify values of travel time. Finally, a convolution technique was implemented to construct the direct runoff hydrograph at the apex of the Kerinitis River fan-delta.

Results and Conclusions

The results of the flood hazard assessment are depicted on the map of Figure 1a. The study area was classified into five zones corresponding to areas of very high, high, moderate, low and very low flood hazard. It is obvious that flood prone areas (of high and very high physical vulnerability to flood hazard) are distributed mostly along the main channels of the Kerinitis River and its major tributaries. Particularly prone to floods are the overbank areas along the lower reaches of the Kerinitis main channel. The fact that the same area is also marked as highly prone to floods at the maps constructed for the study area in the frame of the assessment and management of flood risks by the Greek Ministry of Environment and Energy shows the validity of the proposed methodology. Additionally, the fan-delta plain downstream of the National highway is also of high vulnerability due to the low relief and the high discharge of the river at the apex of the fan in case of extreme rainfall events. Significant part of the highly and very highly vulnerable area is occupied by economically important cultivated land while most of the settlements of the catchment are located in flood prone areas.

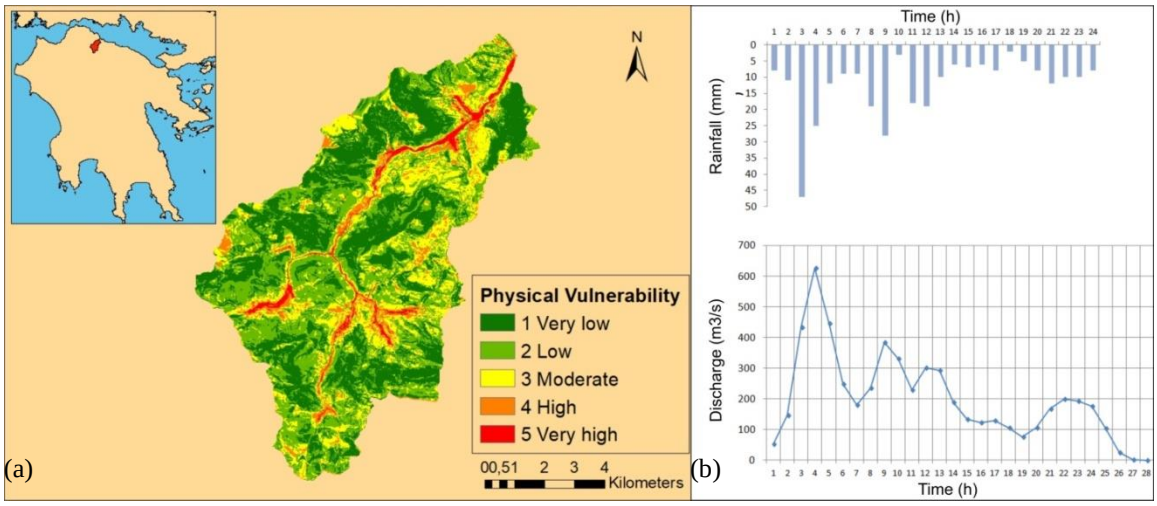

Figure 1. (a - left) Flood hazard assessment map of the Kerinitis River catchment and (b - right) direct hydrographs of the river at the apex of the fan-delta for the extreme rainfall event. 1 hourly stream discharges were obtained from the GIS-based hydrological analysis. The hydrograph includes also the 1 hourly mean rainfall above the catchment area.

Figure 1b displays a combined diagram of the hydrograph produced by the applied model that corresponds to the outlet of the catchment with the hyetograph temporally defined for the total duration of the event (x-axis). The analysis of the model-derived hydrograph for the Kerinitis River is relatively simple since the base flow at this part of the main channel is usually very low. The shape of the produced hydrograph is typical of a flash flood. It is sharp, with a relatively short time base and steeply rising limbs for each of the four peaks. The hyetograph, in the form of an upper axis histogram, is comprised of the hourly accumulated precipitation, over the entire catchment area. The model-derived hydrograph follows the mean rainfall pattern above the basin with four discharge peaks. The diagram shows that the basin's response to the precipitation is very quick. The first peak (~630 m^3/sec) occurred almost one hour after the first precipitation maximum (47 mm) and corresponds to the maximum discharge. We did not manage to validate the model since there are no gauging records in the study area. However, the findings of the proposed methodology are in agreement with the results of previous studies in catchments with similar characteristics (Karymbalis *et al.*, 2012, Tsanakas *et al.*, 2016).

References

Du, J., Xie, H., Hu, Y., Xu, Y., Xu, C.Y., 2009. Development and testing of a new storm runoff routing approach based on time variant spatially distributed travel time method. Journal of Hydrology 369(1-2), 44-54.

Chalkias, C. 2015. Spatial Multicriteria Analysis - Weighted Cartographic Overlay, in: Chalkias, C., Gkousia, M. (Eds), Γεωγραφική ανάλυση με την αξιοποίηση της γεωπληροφορικής. [ebook in Greek] Hellenic Academic Libraries, 67-92.

Chow, V., Maidment, D., Mays, L., 1988. Applied Hydrology, McGraw-Hill Education.

Karymbalis, E., Katsafados, P., Chalkias, C., Gaki-Papanastassiou, K., 2012. An integrated study for the evaluation of natural and anthropogenic causes of flooding in small catchments based on geomorphological and meteorological data and modeling techniques: The case of the Xerias torrent (Corinth, Greece). Zeitschrift für Geomorphologie 56 (1), 45–67.

Tsanakas, K., Gaki-Papanastassiou, K., Kalogeropoulos, K., Chalkias,C., Katsafados, P., Karymbalis, E., 2016. Investigation of flash flood natural causes of Xirolaki Torrent, Northern Greece based on GIS modeling and geomorphological analysis. Natural Hazards 84(2), 1015-1033.

15th International Congress of the Geological Society of Greece
Athens, 22-24 May, 2019 | Harokopio University of Athens, Greece
Bulletin of the Geological Society of Greece, Sp. Pub. 7 Ext. Abs. GSG2019-368

The Use of Water in Asclepieia

Paraskevi Garantzioti[1], Nikolaos Spanoudakis[1], Emmanouil Manoutsoglou[1]

(1) School of Mineral Resources Engineering, Technical University of Crete, University Campus, Akrotiri, Chania, Greece, pgarantzioti@isc.tuc.gr, nspanoud@mred.tuc.gr, emanout@mred.tuc.gr

Introduction

The use of water for therapeutic purposes has been known in Greece since the ancient times. The ancient Greeks were the pioneers in the use of warm and cold baths, especially for the hygiene and cleanliness of the body, as well as for the treatment of various diseases. Asclepius was one of the greatest healers of ancient Greece. Cult places for the healing god are uninterruptedly frequented in the Greek world, from the late Classical to the late Imperial period and enjoyed great popularity especially during the Hellenistic and Roman times (Melfi, 2010, Lioulias, 2010). The most characteristic of Asclepius therapeutic practice was the "ritual", the main part of which was the water, followed by special diet, hygiene and purification rules.

The importance of water in ritual of Egkoimisis and Purity

The location of Asclepieia next to thermal springs is connected with physical therapy. They have been located some distance from the urban settlement, in or near a grove, next to natural springs or the sea. Still, most of the Asclepieia were built in holy places and were considered sacred by the people before their devotion to Asclepius (Chatzinikolaou, 1999, Panagiotidou, 2014). The temples were often protected, located in concavities or in open valleys and hills with water streams, which were passed through the temples and were considered shelters (Vincent, 2009). Dedicated to Asclepius, the Asclepieia were not only temples of worship but also medical care centers. Scattered throughout the ancient world, they were over 300 in number, the largest and most famous being those of Trikke, Epidaurus, Kos, Athens, Corinth, Pergamon and Lebena. Data from ancient literary sources, such as the comedy "Plutus" by Aristophanes and the works of Pausanias, Strabo, Plutarch, Lucian of Samosata and others, and also archeological findings from some of the largest Asclepieia, provide valuable information about the operation of these holy institutions (Christopoulou-Aletra et al., 2010). At Asclepieia, the daily rituals were performed by priests, while the cities organized celebrations dedicated to Asclepius (Panagiotidou, 2014). During the consecration, the priests entered into the *Avaton*, which was connected to water springs and practiced the treatments as the patients slept (Economidou, 2015). According to Aristophanes, water had an important role in the ritual of incubation (Egkoimisis). There are abundant natural elements of Asclepieia, including those related to slumbers, springs, wells, fountains, small and big cisterns for complete immersion of the body and other water containers. Also, it is not at all clear what kind of water was used exclusively for Egkoimisis, and if the water available near *Avaton* was intended for cleaning or hydrotherapy or both. The only valid conclusion is that the water at the entrance of a sanctuary was mainly intended for the symbolic cleansing required for those visiting any Greek sanctuary, not only Asclepieia - as suggested by Hippocrates. Usually, outside from the sanctuary (and possibly at a distance from the entrance), there was a small basin serving as a local cleansing bath, since, according to the sacred laws of Asclepius, visitors had to be washed from impurities caused by various activities before entering the sanctuary (Renberg, 2017).

Role Of Water In The Sanctuaries Of Asclepius

Asclepieia were located next to springs, in holy places, so as to supply the temple with water. The landscape, combined with the holy waters and the groves, had a direct influence on people's health, releasing them from stress and other factors. Patients were relaxing to retrieve their vision or voice or to be cured from breast and foot disorders. In addition, the water was not only medical and beneficial to patients, but even to those who were healthy (Panagiotidou, 2014). Asclepieia were built around springs, e.g. the Asclepieion of Epidaurus and Pergamon, which were built in forest valleys next to springs. Also, the Asclepieio of Lebena, which was built on the southern coast of Crete in a landscape dominated by the harbor and a spring, and the Asclepieio of Kos, which was built near hot springs, with thermal baths (Panagiotidou, 2014), while the Asclepieion of Gortyn was situated beside the river Loussios.

Bathing facilities were found in almost all the sanctuaries of Asclepius, such as in Dion, the Asclepieio of Veria and others. The statue of Health was found in Kelepouri, to the south of the sanctuary of Asclepios, where a bath complex was excavated. At the same time, it is not unlikely that the abundance of water in these areas have also been used for healing purposes, resulting from the large number of bathing facilities that were excavated in the area, combined with the particularly intense worship of Asclepius in the city. Four bath complexes have emerged from the city of Dion including the large *Thermae* (Figure 1): (i) the big thermae near the southern entrance of the city, (ii) the so-called forum thermae in the NE corner of the respective complex, (iii) the thermae of the main road to the east of the sanctuary, and (iv) finally the so-called thermae of the eastern road located in the south of the Dionysus mansion (Lioulias, 2010).



Figure 1. Aerial photography of the great thermae complex at Dion (http://odysseus.culture.gr/h/2/eh251.jsp?obj_id=976)

In addition, the existence of baths is also concerned in the case of Asclepieion of Veria in which it is believed that there should be a set of bathing facilities. Excavations have revealed special architectural elements, as well as statues that indicate the quality of its construction (Lioulias, 2010).

Conclusions

It is generally accepted that Asclepieia in ancient Greece offered health care, combining experimental therapeutic methods with a variety of religious elements. The holistic approach they used to treat patients was based on the healing properties of the natural environment: knowledge of the life force of the sun, water, minerals, rocks, and knowledge of the properties of medicinal plants. What is now at the core of modern hospital design seems to have been a well-established practice in ancient Greek therapeutic centers. This is evident in the careful selection of the location of sanctuaries of Asclepius, which did not lack running water, and in some cases also healing springs (Christopoulou-Aletra et al., 2010). We can conclude that the importance of "heilig water", which was used for natural and spiritual purification, while offering treatment to patients through its properties, was fundamental in the general holistic philosophy and function of Asclepieia.

References

Chatzinikolaou, M., 1999. The Asklepieion of Kos. Department of Social Medicine, School of Medicine History, Ph.D. Thesis University of Athens, 373 p.

Christopoulou-Aletra, H., Togia, A., Varlami, C., 2010. The “smart” Asclepieion: A total healing environment, Archives of Hellenic Medicine, 27(2):259-263.

Ekonomidou, E., 2015. The Asklepieion in the sanctuary of Hippolytus at Troizina, Faculty of Philosophy, Department of History and Archeology, Ph.D. Thesis, University of Athens, 487 p.

Lebidaki, M., E., 2003. Small sacred buildings in the Asklipieion of Epidaurus, Faculty of Philisophy, Department of History and Arschaeology, Ph.D. Thesis, University of Athens, 435 p.

Lioulias, S., 2010. The devotion of Asclepios in Macedonia. Faculty of Philosophy, Department of History and Archeology, Department of Archeology, M.Sc. Thesis, Aristotle University of Thessaloniki, 243 p.**]**

Panagiotidou, O., 2014. Disease and Treatment in the Sanctuaries of Asklepios: A cognitive approach, Faculty of Theology, Theological School, Ph.D. Thesis, Aristotle University of Thessaloniki, 304 p.

Renberg H., G., 2017. Where Dreams May Come: Incubation Sanctuaries in the Greco-Roman World, Volume I, Leiden.

Vincent, E., 2009. Therapeutic Benefits of Nature Images on Health, Department of Environmental Design and Planning, Ph.D. Thesis, Clemson University, 263 p.

15th International Congress of the Geological Society of Greece
Athens, 22-24 May, 2019 | Harokopio University of Athens, Greece
Bulletin of the Geological Society of Greece, Sp. Pub. 7 Ext. Abs. GSG2019-370

Geomorphological and Sedimentological Dynamic Processes at the Semi-Closed Bay Plati Gialo (Sifnos Isl.)

A. Petropoulos[1], V. Kapsimalis[2], N. Evelpidou[1], Ch. Anagnostou [2]

(1) Department of Geology and Geoenvironment, National and Kapodistrian University of Athens, Panepistimiopolis, 15784 Athens, Greece, alexpetrop@geol.uoa.gr , evelpidou@geol.uoa.gr
(2) Institute of Oceanography, Hellenic Centre for Marine Research, 46.7 km Athens-Sounio Avenue, Mavro Lithari, 19013 Anavyssos, Greece, kapsim@hcmr.gr, chanag@hcmr.gr

Study Area

Platis Gialos Bay located at the Southern part of Sifnos Isl. and his length is determined at 1.000 m, with SE direction. The coast of Platis Gialos Sifnos has been under erosion and permanent coastal retreat for several years, especially at the central and west part of the beach. The main causes of coastal erosion are anthropogenic.

Methodology

This paper focuses most intently on the geomorphological and sedimentological dynamic processes of the Bay which forming the current situation. For this reason a number of tasks took place in order to determine the level of disturbances of this dynamic equilibrium. This study included two phases of survey for two different periods (summer/winter). The first phase deals with the geomorphological and sedimentological coast characteristics, and includes: i) long-term geomorphological evolution of the coastal zone through the analysis of satellite images (Google Earth), in order to estimate the intensity of coastal erosion. ii) topographic sections at the surface of the coastal zone, through D-GPS (Spectra Precision SP80 GNSS Receiver), perpendicular to the coastline, iii) sediment sampling in the subaerial coastal area, iv) analytical recording and mapping of the summer and winter shorelines via the D-GPS, v) the situation of the potential feeders of the shore with materials, necessary for the formation of an alluvial beach, and vi) recording of land uses (Fig.1). The second phase, includes the geomorphological and sedimentological characteristics of the marine area, in particular: i) topographic sections of the bottom surface until the depth of 1.5 m, through D-GPS, perpendicular to the coastline ii) sediment sampling in the subaquatic marine area, iii) data of the numerical recomposition of the wind and wave conditions of the study area, iv) bathymetric eco-sonar data (Lowrance LCX-15MT), v) side-scan single beam eco-sounder (StarFish 450), to determine the seabed morphological features of the bay and, vi) substrate component mapping (Fig. 1).

Laboratory analyzes were followed by the methods of dry granulometry, in order to categorize it, in different types on the basis of Folk & Ward (1957) method through GRATISTAT (v.8) software.

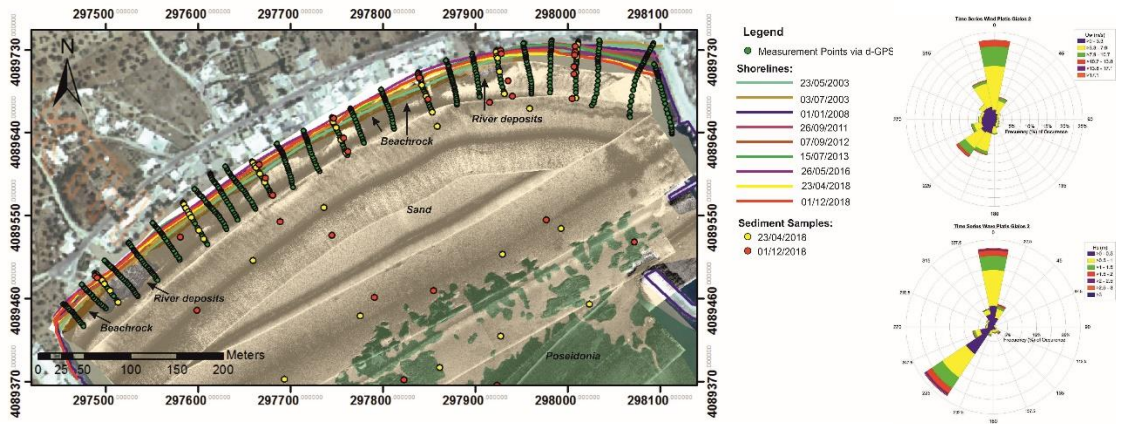

Figure 1. Thematic Map of the study area. Coastlines of different periods, sampling locations, topographic sections, and substrate component mapping are displayed. The next picture displays the time series from 1995 until 2004 for the wind and wave conditions of the study area.

Results

The results of sediment analyses were represented in thematic maps, showing the D50, Mz, Sk, Ku of the sediments. Most of the sediments from the land were characterized (by Folk & Ward, 1957) as Sand (125 – 250 μm) at the summer and as Slightly Gravelly Sand to Gravelly Sand (125 – 500 μm) at the winter, while marine sediments were characterized as Slightly Gravelly Sand (63 – 250 μm) both at summer and winter. Also, slope surface, slope orientation, the roughness of sub-bottom and substrate component mapping are illustrated. Bay presents relatively gentle slopes and shallow depths (with the maximum measured depth, -48 m), with small variations between winter and summer profile (Fig. 2).

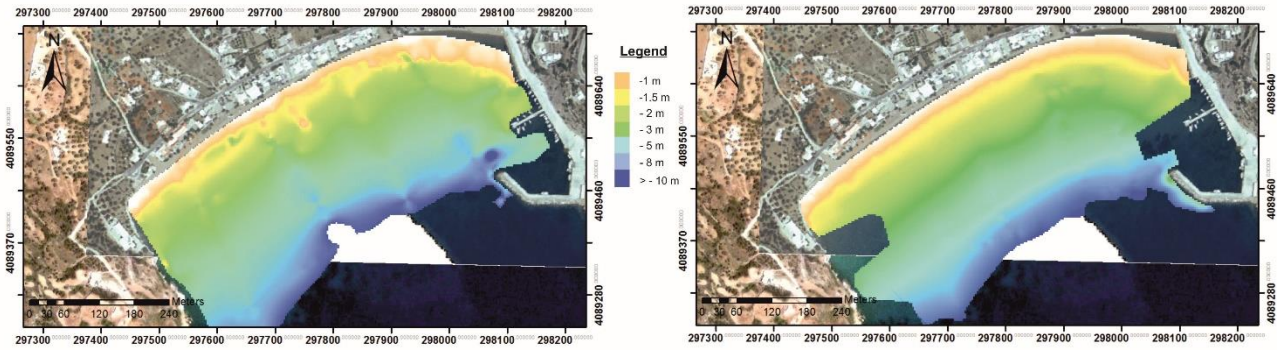

Figure 2. Bathymetric maps in two different seasonal periods. In the left image, bathymetry responds in the winter period, while the right image represents the summer period.

The interpretation of the results determines the morphodynamic condition of the study area, providing a comprehensive view of geomorphological and sedimentological characteristics of the Semi-Closed Bay Plati Gialo and the current prevailing conditions. Our ascertainment is that our study area, mainly the western and central part of it, are under erosion the last 10 years and especially due to the construction of the fishing shelter and the anthropogenic intervention in the natural mechanism of sediment supply from the torrents, in contrast with the eastern part, where the coastal deposition reaches the 26 m (Fig. 3).

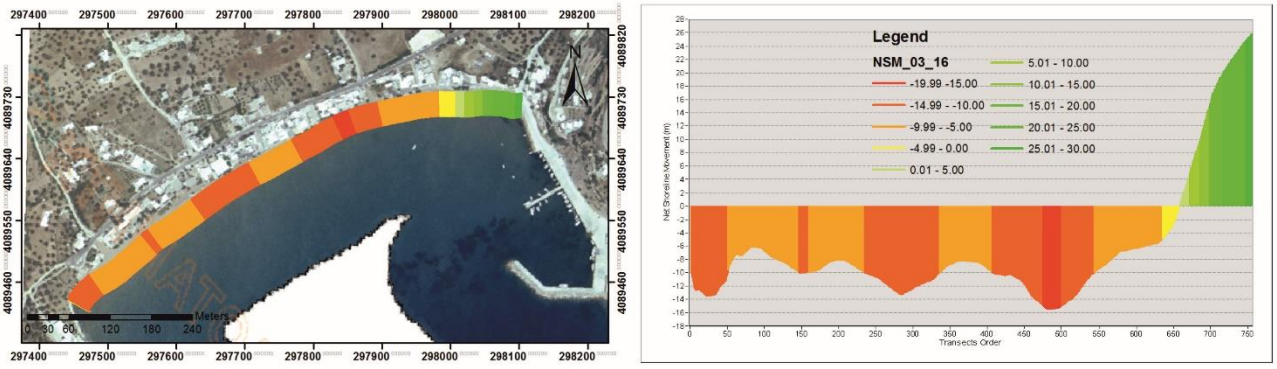

Figure 3. The picture displays the size of coastal erosion and coastal deposition at the coast of Platis Gialos from 2003 to 2016 using the add-on application Digital Shoreline Analysis System (DSAS) in the software ArcMap 10.3 (Thieler et al. 2009).

Discussion

The exposition of the coast to the southern waves, the reduced sediment supply from local fluvial network and the construction of the fishing shelter, are mainly responsible for the coastal retreat. Based on the premise that human has to adapt to nature and not nature to human, we propose "soft" shore interferences, like a gradually and monitory nourishment of the coast with appropriate sediment (quality and size - carbonate gravel of 0.5 - 4 mm in size), in order to bring back the previous morphodynamic balance of the beach of Platis Gialos. Beach nourishment preserves beach resources and avoids the negative effects of hard structures. Instead, beach nourishment creates a “soft” technique by creating a larger sand reservoir, pushing the shoreline seaward.

Acknowledgements

Many thanks to Prof. Seraphim Poulos for the disposal of scientific equipment. I would also like to thanks General Secretariat for Research and Technology (GSRT) and the Hellenic Foundation for Research and Innovation (HFRI) for finance support.

References

Folk, R.L. and Ward, W.C. (1957): Brazos River bar: a study in the significance of grain size parameters, Journal of Sedimentary Petrology, vol. 27, pp. 3-26.

Thieler, E.R., Himmelstoss, E.A., Zichichi, J.L. and Ergul, A. (2009): Digital Shoreline Analysis System (DSAS), Version 4.0 — An ArcGIS Extension for Calculating Shoreline Change: U.S. Geological Survey Open-File Report 2008–1278.

15th International Congress of the Geological Society of Greece
Athens, 22-24 May, 2019 | Harokopio University of Athens, Greece
Bulletin of the Geological Society of Greece, Sp. Pub. 7 Ext. Abs. GSG2019-372

Coastal and Marine geomorphological and environmental study of St. George bay, Western Naxos, Greece

A. Giannikopoulou[1], N. Evelpidou[1], I. Baziotis[2], M. Salomidi[3], A. Karkani[1]

(1) Section of Geography and Climatology, Department of Geology and Geoenvironment, National and Kapodistrian University of Athens, Panepistimiopolis, Zografou, Athens 15784, Greece, katagiann.geol.uoa.gr
(2) Department of Natural Resources Management and Agricultural Engineering, Laboratory of Mineralogy and Geology, Agricultural University of Athens, 11855 Athens, Greece
(3) Hellenic Center for Marine Research (HCMR), 46.7 km Athens-Sounio, 19013 Anavyssos, Greece

In order to study the geomorphological and environmental characteristics of St. George bay, western Naxos, Greece (Fig. 1), a series of 14 beachrock samples were collected and examined. Two transections of the bay, based on field measurements, were designed, in order to provide a deeper understanding of the beachrock development setting. Detailed recording of the beachrocks was accomplished through scuba diving, using a sonar device, measuring tapes, GPS device and Dive Computer.

Special attention was given to the cement, as to extract information about the conditions of formation of the beachrocks. Thin sections from the beachrock samples were studied through petrographic microscope in order to investigate their basic characteristics and to obtain information about their basic petrographic and mineral composition. Scanning Electron Microscopy (SEM) alongside with Energy Dispersive Spetrometry (EDS) were used for elemental analysis of the beachrock samples and their cement and Raman spectroscopy was used for identification of the cement crystal structure. For better interpretation of the results, the suggested tool, by Mauz *et al.* (2015), for reconstructing relative sea level in the far-field was used.

In order to estimate the ecological status of the bay, a study of the macroalgae of the area was also accomplished. Macroalgae sampling of two different methods was conducted, destructive (conventional samples) and non-destructive (photographic samples). 57 conventional samples were collected throughout the beachrock reef. These samples were prepared into herbariums and were identified in the best taxonomic level possible using stereoscope and microscope. Photographic samples were taken from the southwestern and northeastern part of St. George bay, from different types of bedrock (beachrocks, granodiorite, aeolianite) for comparison reasons. The percentages of different types of surface coverage (algal, sediment coverage) were counted for each sample, using the program Adobe Photoshop CS6. Finally, a statistical analysis of the data from the photographic samples was conducted, using the program PRIMER 5, in order to have a better evaluation of the algae data. The depth and coordinates of each conventional and photographic sample were recorded.

The results regarding the beach rock samples indicate that their formation took place under meteoric and marine vadose zone conditions. Certain results indicate that the development of the beachrocks took place during a sea level rise. Finally, macroalgae statistical analyses indicated that there are no significant differences between beachrocks and other rocks as substrates and the overall ecological status of St. George bay can be characterized as good, according to the Ecological Evaluation Index (EEI, Orfanidis *et al.*, 2003).

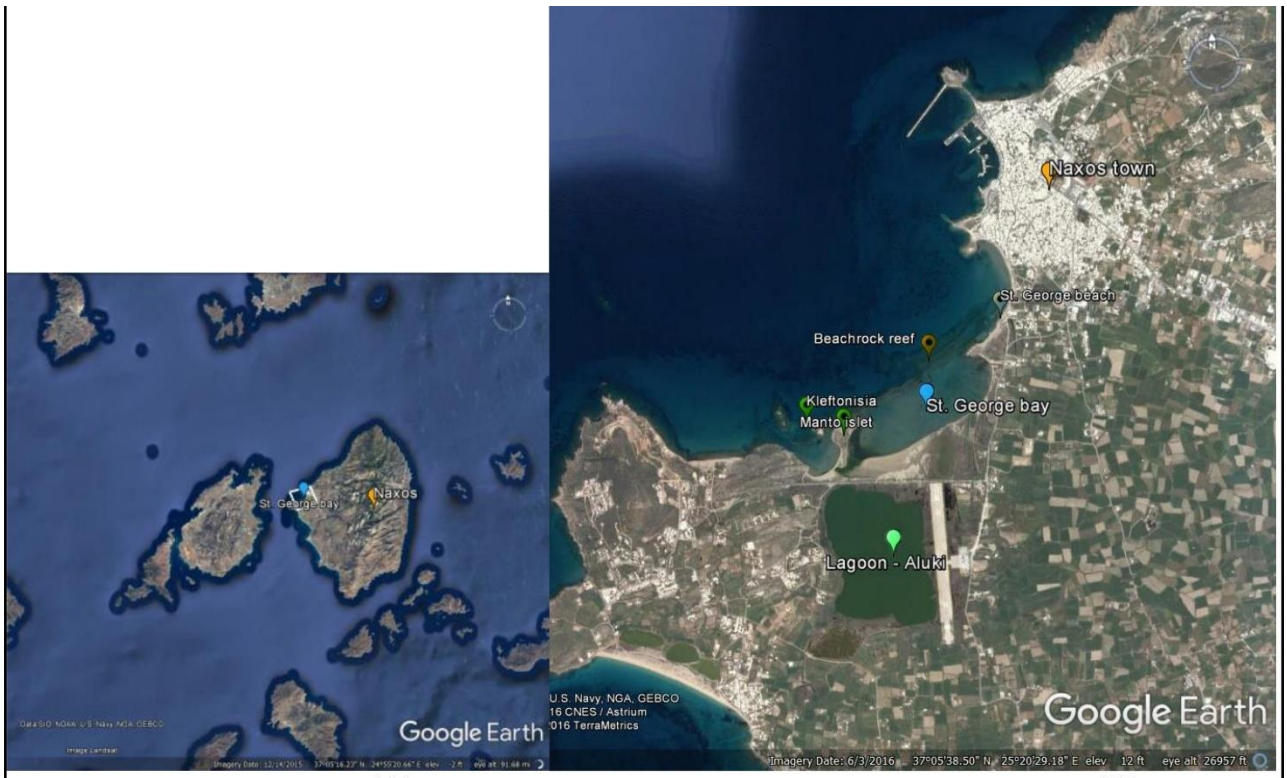

Figure 1 Geographical setting of study area: (A) Naxos island, (B) St. George bay (Google Earth images).

Acknowledgements

Eleni Kitinou (Hellenic Center of Marine Research), Pantelis Patsis (Institute of Geology &Mineral Exploration) and Anna Mauridou (Center for Research &Technology, Hellas) are thanked for their contribution in laboratory works. Nikos Tsoukalas (Center for Research &Technology, Hellas) and Elias Chatzitheodoridis (National Technical University of Athens) are also thanked for their support during laboratory works. Finally Manolis Lykouropoulos, Sophia Kagkani and Charalambos Kioses are thanked for their assistance and support during fieldwork.

References

Mauz, B., Vacchi, M., Green, A., Hoffmann, G., & Cooper, A., 2015. Beachrock: a tool for reconstructing relative sea level in the far-field. Marine Geology, 362, 1-16.

Orfanidis, S., Panayotidis, P., Stamatis, N., 2003. An insight to the ecological evaluation index (EEI). Ecological Indicators, 3(1), 27–33.

15th International Congress of the Geological Society of Greece
Athens, 22-24 May, 2019 | Harokopio University of Athens, Greece
Bulletin of the Geological Society of Greece, Sp. Pub. 7 Ext. Abs. GSG2019-373

A minerochemical cement study of a beachrock slab: The case study of Peristeria, Salamis Island.

G. Saitis[1], N. Evelpidou[1], S. Kawasaki[2], E. Koutsopoulou[3], A. Komi[1]

(1) National and Kapodistrian University of Athens, Panepistimioupoli, Athens, Greece, saitij@geol.uoa.gr
(2) University of Hokkaido, Kita 8, Nishi 5, Sapporo, Hokkaido, Japan
(3) Institute of Geology and Mineral Exploration, Acharnes, Athens, Greece

Introduction

Beachrocks are consolidated sedimentary formations and are composed of coastal sediments, which are cemented through the precipitation of carbonates. The lithification takes place in the intertidal zone and can include various sediments, such as sands and gravels of clastic and biogenic origin. This study deals with the cements' mineralogical and geochemical features of a beachrock outcrop and its aim is the contribution for further understanding on the cementation process of beachrocks. (e.g. Vieira and Ros, 2007; Vousdoukas et al., 2007; Karkani et al., 2017).

Study Area

The site of study is a beachrock outcrop at Peristeria area of Salamis Island which is located at the southeast of the island, 13 km from the city of Salamis. In the coastal area a stream that provides fresh water. The anthropogenic impact is highly evident as there are a number of constructions (basketball court, small piers). The beach has an orientation from East to West and its sediment is characterized as gravely sand. The beachrock slab covers an area of 1.36 Km^2 with a length 453m and maximum width of 50m (Figure 1). The examined beachrock has a mean dip of 13.5^o seawards.The beachrock mean height (from sea level) is 50 cm and it continues at about 1.5m below sea level. The outcrop has no evidence of vertical to shoreline (channels) erosion but a sea intrusion at its Eastern part. There the sea erodes the beachrock from the landward part and Contributes to new sediment accumulation.

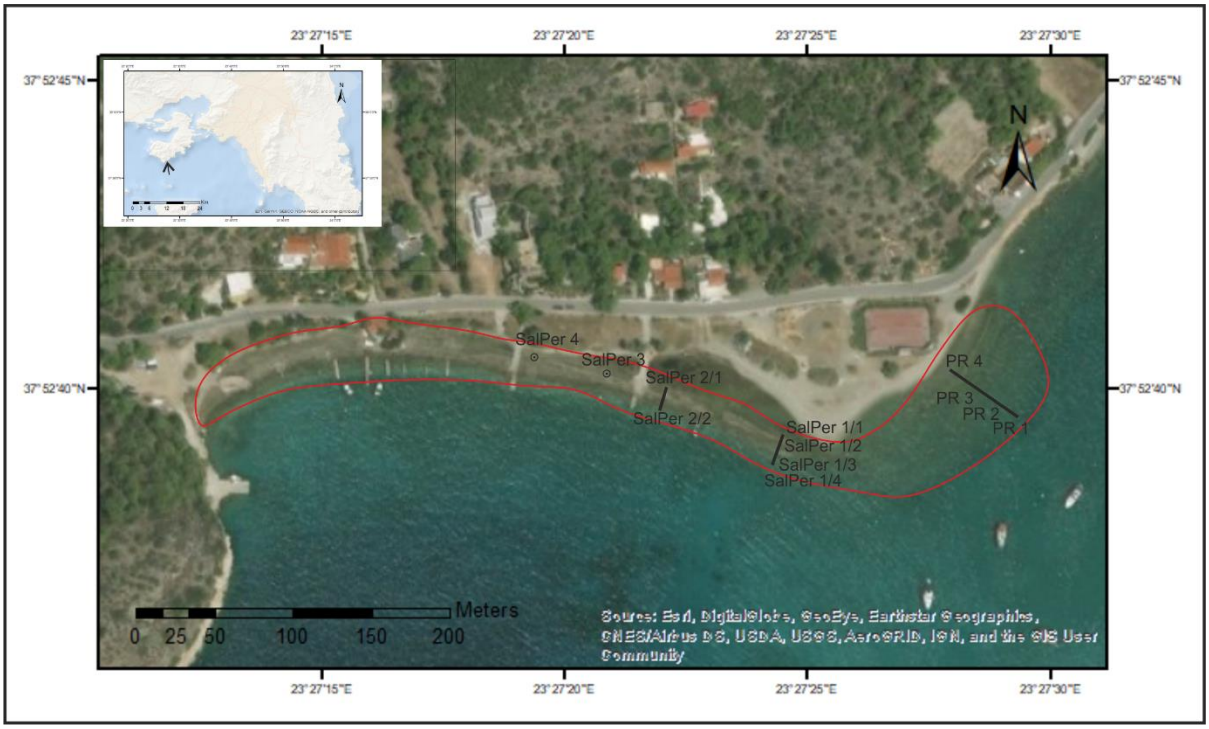

Figure 1. The red circled area indicates the beachrock slab, the lines indicates the morphology transects section and samples (code SalPer and PR) of the beachrocks.

Methodology

During the fieldwork detailed mapping of the beachrock slab was performed measuring width, height/depth with respect of the sea level. Additionaly, 12 samples were collected derived by the front and the end of the slabs and sediment bedding. Thin sections were prepared from the beachrocks and samples were studied for their mineralogical and morphological features with a petrographic polarized microscope and confirmed with Scanning Electron Microscope (SEM). Additionally, bulk material was examined for the mineralogical and geochemical composition with X-Ray diffraction (XRD) and Energy Dispersive X-ray Florescence Spectroscopy (XRF).

Results and Discussion

From the analysis of the beachrock samples, High Magnesium Calcite [$(Ca,Mg)CO_3$] cement in micritic form is most common (7% wt of MgO in samples) with microfossils. Sparitic formation of cement indicated a well grown crystallization or cement precipitation in the meniscus of sediment by mixing sea water and fresh ground water with higher influence by the marine phase. During the polarized and scanning electron microscopy needles of aragonite have been also observed which reveals a low energy coastal environment. Peristeria beachrock mineralogy is evenly distributed between Mg-calcite, Quartz and Calcite. SEM and XRD analysis also revealed the participation of clay minerals in the matrix cement in full accordance with the mineralogical results that showed the presence of clay minerals in the beachrocks (Figure 2).

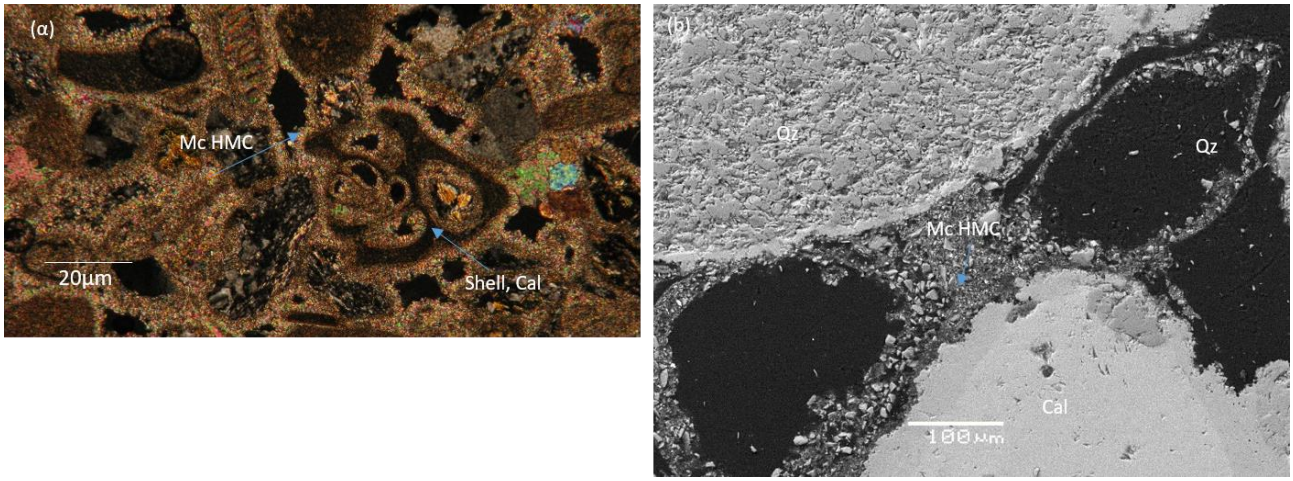

Figure 2. (a) Polarized microscopy, the samples are characterized by micritic and sparitic HMC cement that coat Quartz and shell fragment. (b) SEM analysis, micritic cement coat Calcite and Quartz grains and matrix of HMC and fine particles (e.g. clay minerals) cement, is observed.

Conclusion

The Peristeria beachrock outcrop has a very compact and thick morphology with a variety of sediment particles. An alternation in precipitation events seems to have taken place which initiates with a mixed environment of sea water and fresh ground water, was later succeeded with a period of saturation from sea water and lastly with a mixed sea/fresh water environment. The prevalence of the sea water influence in the precipitation of the cement could be due to a sea level rise, for a time period, and then followed by a sea level retreat.

References

Karkani, A., Evelpidou, N.,Vacchi, M., Morhange, C., Tsukamoto, S., Frechen, M., Maroukian, H., 2017. Tracking shoreline evolution in central Cyclades (Greece) using beachrocks. Marine Geology, 388, 25-37. ISSN 0025-3227. https://doi.org/10.1016/j.margeo.2017.04.009.

Vieira, M.M., Ros, L.F.d., 2007. Cementation patterns and genetic implications of Holocene beachrocks from northeastern Brazil. Sediment. Geol., 192 (3–4), 207–230.

Vousdoukas M.I., Velegrakis A.F., Plomaritis T.A., 2007. Beachrock occurrence, characteristics, formation mechanisms and impacts. Earth-Science Reviews, 85, 23–46.

15th International Congress of the Geological Society of Greece
Athens, 22-24 May, 2019 | Harokopio University of Athens, Greece
Bulletin of the Geological Society of Greece, Sp. Pub. 7 Ext. Abs. GSG2019-374

Sedimentological and geomorphological study of Vravrona Beach, East Attica.

A. Komi[1], A. Petropoulos[1], N. Evelpidou[1], S. Poulos[1], V. Kapsimalis[2]

(1) National and Kapodistrian University of Athens, Panepistimioupoli, Athens, Greece, akomi@geol.uoa.gr
(2) Hellenic Center of Marine Research, Anavyssos, Greece

This study focuses on the sedimentological and morphological features of Vravrona Beach, East Attica, in order to determine the seasonal changes in the textural group classification of the costal sediments, as well as, changes in coastline position (Fig. 1). Additionally, Vravrona Beach has been chosen for the assessment of a potential coastal erosion, using the Coastal Vulnerability Index (CVI) through GIS technology, since several incidents of erosion have been identified during the past decades in the broader area of East Attica (Dimou et al., 2010).

For the composition of the beach profile in seasonal scale, cross sections were conducted along the beach from landward to seaward until approximately 10 m from the coastline. Beach width as well as the current coastline position for each season were measured with a differential GPS (DGPS). The land use at the landward upper limits of the study area were also measured. Along selected cross sections, sediment sampling was also conducted during January 2018 for the composition of the winter profile of the study area and during September 2018 for the composition of the summer profile of the study area.

Sedimentological analyses were based on grain size distribution for the analysis of unconsolidated sediments by sieving and statistical parameters such as sorting, skewness, mean and kurtosis were calculating using GRADISTAT v. 0.4 software in order to determine the sedimentological features of the study area and the transport mechanism at the time of deposition. The textural group of the samples was also determined by Folk and Ward (1957) classification.

The grain size analysis of the samples, collected between the upper limit of the beach and the coastline during summer period, show that the majority of grains is described as slightly gravelly sand and gravelly sand, but during the winter period the grains are between gravely sand and sand. The samples collected from the coastline until approximately 10 m seaward are mainly described as slightly gravelly sand and sandy gravel for both sampling seasons (Fig. 2).

DGPS measurements of coastline position indicate changes that varies between 4.38 m to 7.41 m with a maximum value at 8.27 m. In agreement to field observations, DGPS measurements indicate an accumulation of sediments at the northern part of the beach during the winter period, while during summer period there is an accumulation of sediments at the southern part of the beach.



Figure 1. Vravrona Beach, East Attica.

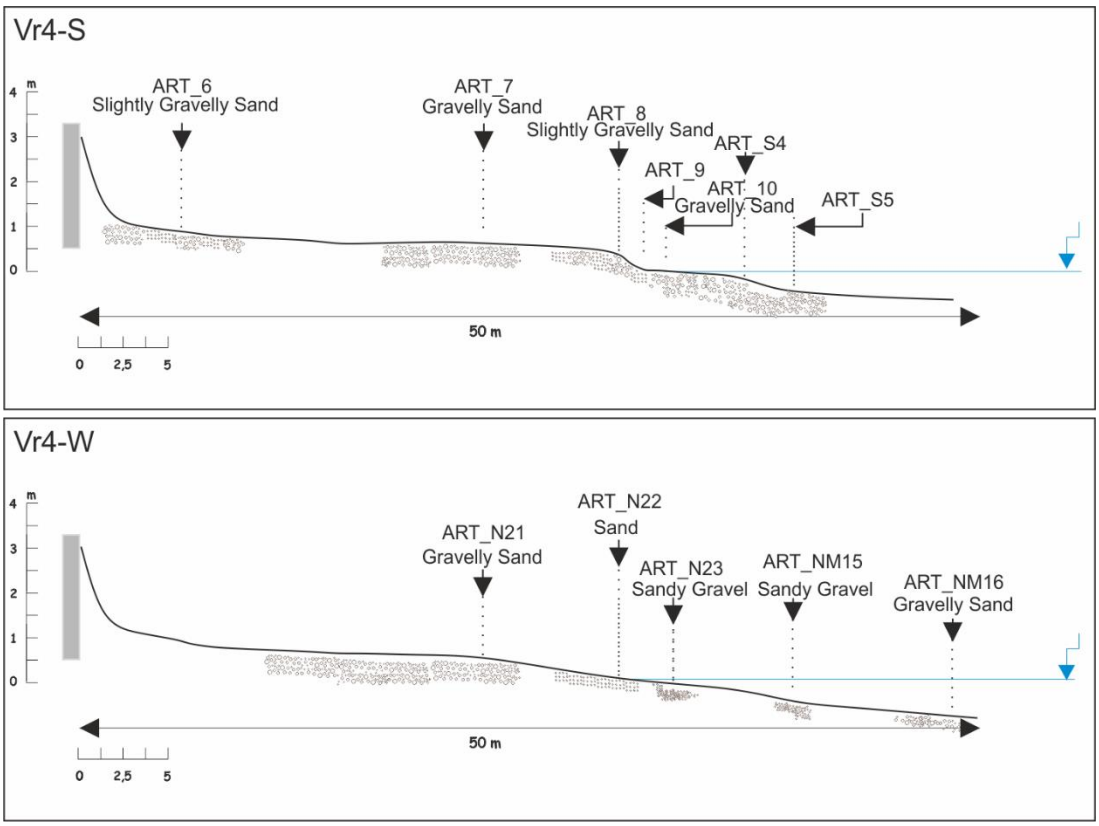

Figure 2. The above figure corresponds to the summer (top) and winter (bottom) profile of the cross section Vr4-S which is located at the southern part of the beach. The figure indicates the topography of the beach and the arrows point the collected sediments samples.

References

Dimou, A., Vassilakis, E., Antoniou, V., Evelpidou, N., 2010. An assessment of the coastal erosion at marathon East Attica (Greece). Proceeding of 10th International Congress of Hellenic Geographical Society, 1579-1587.

Folk, R.L. and Ward, W.C. (1957). Brazos River bar: a study in the significance of grain size parameters. Journal of Sedimentary Petrology, 27, 3-26.

Pantusa, D., D'Alessandro, F., Riefolo, L., et al., 2018. Application of a Coastal Vulnerability Index.
A Case Study along the Apulian Coastline, Italy. Water 2018, 10, 1218

Sammut, S., Gauci, R., Drago, A., Gauci, A., Azzopardi, J., 2017. Pocket beach sediment: A field investigation of the geodynamic processes of coarse-clastic beaches on the Maltese Islands (Central Mediterranean). Marine Geology 387 (2017) 58–73

SPECIAL SESSION

T6/T6.S1 Geo-Energy: From Exploration to Technological Advances and Sustainability

Conveners: **Yannis Bassias (HHRM)**
Spyros Bellas (HHRM)

JCo-organized by the Hellenic Hydrocarbon Resources Management (HHRM)

HHRM
HELLENIC HYDROCARBON RESOURCES MANAGEMENT

15th International Congress of the Geological Society of Greece
Athens, 22-24 May, 2019 | Harokopio University of Athens, Greece
Bulletin of the Geological Society of Greece, Sp. Pub. 7 Ext. Abs. GSG2019-043

Salt Layer Velocity Modelling in the East Mediterranean Basins

A. El-Bassiony[1], T. Martin[2], K. Shrimpton[2]

(1) PGS, Public Free Zone, Cairo, Egypt, ahmed.elbassiony@pgs.com
(2) PGS, Surrey, Weybridge, United Kingdom

Introduction

Recent large sub-salt discoveries in east Mediterranean waters have steered the focus on imaging beneath complex salt structures, where the main challenge is to correctly illuminate the sub-salt section. This involves optimizing acquisition parameters as well as building an accurate subsurface geological model. Only limited regions in the east Mediterranean are covered by multi-azimuth surveys; most of the 3D surveys available are narrow-azimuth. A lack of data diversity degrades the imaging of sub-salt zones even when using accurate subsurface models.

Optimal model building for depth imaging involves the application of many complimentary imaging technologies to mitigate assumptions in any singular process (Whitmore, 2016, and Brandsberg-Dahl et al., 2017). Illumination issues in the east Mediterranean are primarily caused by the complex interaction of shales and salt. The geometry of the salt layer and the velocity contrast across neighbouring lithologies determine the illumination and imaging quality beneath the salt layer. Using accurate interpretation of the top and base salt, and inserting a reliable velocity in the model, enhances the sub-salt imaging. This work focuses on the salt layer model building in three zones across the east Mediterranean Sea and the optimization of the salt/shales, and salt/carbonates velocities to enhance the sub-salt imaging and improve the reliability of amplitude data.

Velocity Model Building Methods in the East Mediterranean

The main challenge in imaging the pre-Messinian section is the Messinian salt section. The distribution of salt in the two major basins; the Herodotus and the Levant, is interrupted primarily by detrital deposits from the Nile Delta. At the basin margins the salt body geometry changes from a horizontal bedding in a compressive regime, to a more diapiric system closer to the cone of the Nile Delta. Away from the diapiric region, in both the Levant and Herodotus basins, the salt layer shows complex intra-salt reflectivity. Despite this, a constant velocity layer flattens the structure of the base of salt (BOS) (El-Bassiony et al., 2018). In regions where the BOS shows clear salt velocity variations, a variable salt velocity was imbedded. Feng and Rashef (2018) showed that the intra-salt reflectivity takes the form of thin clay beds with much lower velocities than salt, as recorded by well logs. Bell et al. (2018) approached the variable salt velocity modeling by comparing the variation of the gather flatness at BOS (gamma field) with the RMS amplitude map extracted in the salt section (Figure 3a and 3b). This showed that the salt has a lower average velocity where there was significant intra-salt reflectivity. The salt layer was split into clean and dirty regions, where the clean salt velocity that flattened the gathers was 4350 m/s, and the dirty salt velocities varied depending on the salt thickness. This yielded a velocity model that both flattened the base-salt reflector and improved the flatness of the intra-salt events (Figure 3c). In some areas, the salt layer is completely intruded by an inflow of the shales. For velocity insertion, the modeling of this complex intercalated shales/salt is a required but challenging task for the interpreter. The Messinian salt layer velocity changes from 4200 m/s in the Herodotus basin to 4300 m/s in the Levant basin. The pre-Messinian flood velocity starts from 2400 m/s s with a gradient k=0.2 m/s/m, where the detrital Miocene section are present. The starting velocity increases to 2700 – 4000 m/s in locations characterized by carbonate build-ups that reach the salt layer base (Figure 4). The model inside the carbonate built-up progresses has a gradient of 1.0-3.0 m/s/m, where the maximum velocity are 5000 m/s.

Case studies

West Egypt

PGS MultiClient data library includes 17500 line km of 2D offshore West Egypt and around 6000 sqkms of 3D acquisition over the 2D data (Figure 1). The two 3D surveys acquired offshore Matruh City cover the shallow Matruh Canyon and a deeper survey in the Herodotus Basin. The shallow area covered the Matruh Basin where no salt layer is present, while the deeper survey revealed the compressive salt layer with high pressure Miocene turbidites intrusions from beneath the salt. Figure 2A shows an example from the deeper West Egypt 3D survey. The high pressured turbidites beneath the salt layer have completely intruded the salt, forming a pillar cutting through the entire salt layer, leaving a mushroom-like shaly deposits above the salt top. The depth model included these contrasts using an inserted gradient velocity for the shale intrusions simulating the compaction differences between the sediments above and beneath the salt.

Cyprus - Eratosthenes Sea Mount

Salt and carbonate structural plays are important in recent hydrocarbon discoveries in the northern edge of the Herodotus basin. Data southwest of the Eratosthenes Sea Mount (ESM), was acquired using dual sensors streamers over an area of 6000 sq.km bordering Cyprus and Egypt (Figure 1). The water layer was built using a TS function, while the post-salt section was built from the PSTM velocities and followed by a sequence of TTI wavelet-shift tomography updates (Sherwood et al., 2011).

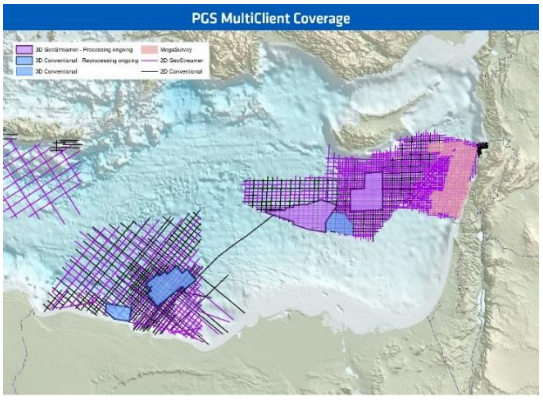

Figure 1. East Mediterranean map showing the PGS 2D and 3D MultiClient data acquired using dual-sensor streamers and conventional acquisition (Widmaier and Lie, 2016).

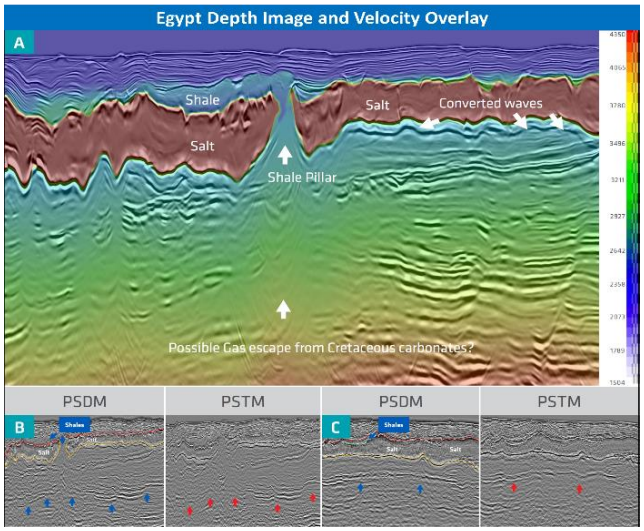

Figure 2. Different examples of shales/salt interactions in Egypt's West Med. 3D deep acquisition survey.

Using quantitative metrics to measure gather flatness, the inserted salt velocity showed localized errors at the BOS. This is shown in Figure 3a. A variable salt velocity was inserted according to Bell et al. (2018). The pre-salt sequence was split into four components (Figure 3d); a slower carbonate/sediment package with a velocity of 2600 m/s; a mid-carbonate (3500 m/s); an older carbonate cap with a velocity of 4500 m/s at the top increasing to 5500 m/s as it transitions to the carbonate basement (Fig. 3d). Global tomographic updates augmented the initial model optimizing gather flatness. The final images show a variable carbonate environment; a faster velocity at the carbonate barriers/reefs, and slower shallower velocities representing carbonate build-ups, which are very similar to the Zohr field.

Lebanon

PGS acquired a 2D survey comprising 9000 line km of dual-sensor data and 10000 sq. km of 3D data from offshore Lebanon. The salt layer showed good consistency using a higher interval velocity than those used in the Egyptian region. A salt velocity of 4300 m/s flattened the gathers at the BOS (Figure 4). A pre-salt model was inserted in this region using 2400 m/s as the starting velocity at the BOS and a gradient of 0.2 m/s/m, while closer to the continental shelf, the gradient increased to 0.3 m/s/m. Figure 4 shows an example from the Lebanon area. Analogous to the ESM example, a carbonate starting velocity of 4000 m/s was used, with a gradient of 0.1 m/s/m away from the continental shelf. Nearer the shelf, the carbonate velocities changed laterally to the carbonate basement value of 5000 m/s.

Conclusions

Salt layer complexity in the East Mediterranean sea contributes to uncertainties in the imaging of the Pre-Messinian salt sequence. Accuracy of the interpretation of the salt sediment contacts is vital, as is a reliable velocity estimation for both salt and sediments. Regions of the east Mediterranean Sea, show variable salt velocities as well as disparate deeper carbonate sequences. Resolving accurate velocities for these deep sediments requires accurate salt layer modeling.

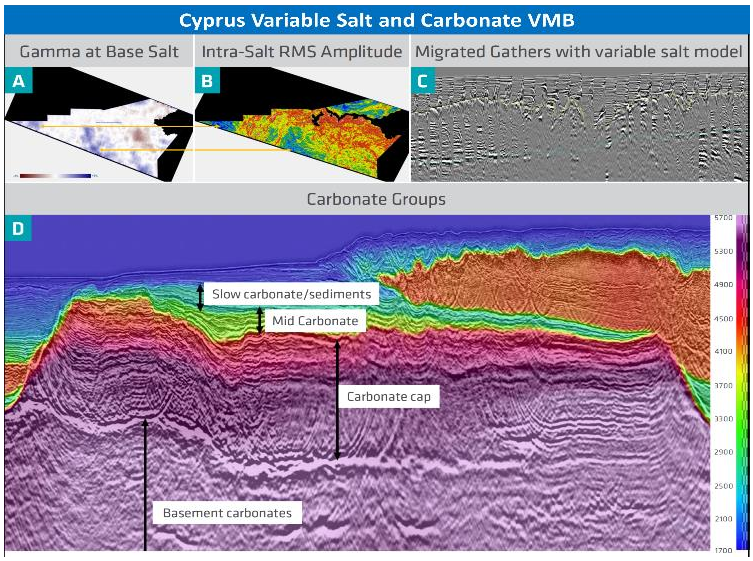

Figure 3. Southwest the ESM showing spatially variable salt velocity and vertical different carbonate groups.

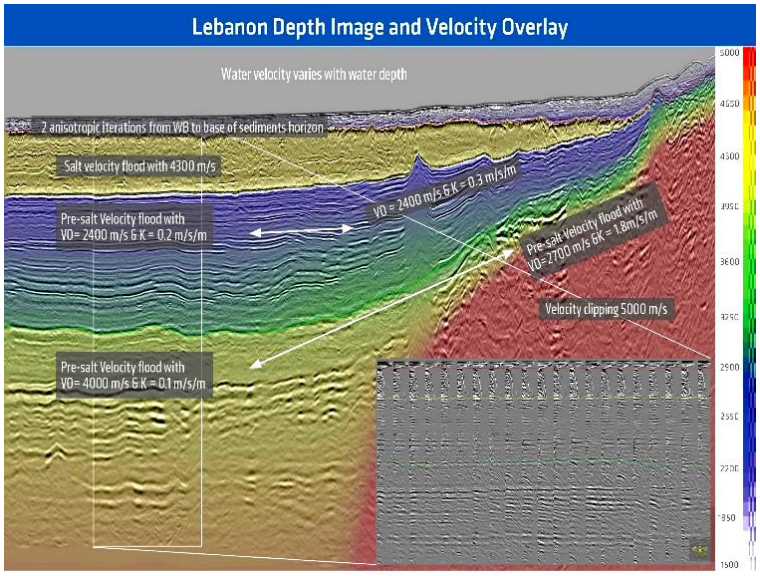

Figure 4. Example from offshore Lebanon showing a constant salt velocity, and a laterally varying gradient for the pre-Messinian section.

Acknowledgements

The authors wish to thank PGS MultiClient for the authorization to show examples from the different surveys acquired by PGS throughout the eastern Mediterranean. Grateful thanks is also given to the PGS Cairo and Weybridge imaging team for providing the case studies.

References

Bell, M., Asnaashari, A., Fairhead, S., Powell, W., 2018. Imaging and Evaluating Complex Pre-Salt Carbonate Environments: An Eastern Mediterranean Sea Velocity Model Build Case Study. Extended Abstract PETEX 2018.

Brandsberg-Dahl, S., Chemingui, N. and Valenciano, A., 2017. FWI for model updates in large-contrast media. The 15th International Congress of the Brazilian Geophysical Society & EXPOGEF, 308-312

El-Bassiony, A., Kumar, J. and Martin, T., 2018. Velocity model building in the major basins of the eastern Mediterranean Sea for imaging regional prospectivity: The Leading Edge, **37**(7), 519-528.

Feng, Y. E., and Reshef, M., 2016. The Eastern Mediterranean Messinian salt-depth imaging and velocity analysis considerations. Petroleum Geo Science, Thematic set: Messinian Salinity Crises, **22**, 333–339

Sherwood, J., Jiao, J., Tieman, H., Sherwood, K., Zhou, C., Lin, S., Brandsberg-Dahl, S., 2011. Hybrid tomography based on beam migration. SEG Technical Program Expanded Abstracts.

Whitmore, N., 2016. Extending the 3D primary image with multiples and mirrors. SEG Technical Program Expanded Abstracts, 4901-4905.

Widmaier, M. and Lie, Ø., 2016. Experiences with Dual-Sensor Towed Streamer Acquisition and Imaging in the Eastern Mediterranean. The 12th Middle East Geosciences Conference and Exhibition, Extended abstract.

15th International Congress of the Geological Society of Greece
Athens, 22-24 May, 2019 | Harokopio University of Athens, Greece
Bulletin of the Geological Society of Greece, Sp. Pub. 7 Ext. Abs. GSG2019-077

New Structural and Petroleum System Models of the Ionian Zone, North-Western Greece

Pablo Hernández[1], Rubén Pérez[1], Juan Pablo Pita[1], Adriana Ponte[1], Bibianaubio[1], Ylva Malmcrona[1], Alan Chambers[1], Antonio Martín[1], Lorenzo Cascone[1], Takis Konstantopoulos[2], Konstantinos Nikolaou[2]

(1) Repsol Exploration, C/Mendez Alvaro 44, 28045 (Madrid), Spain; p.hernandez@repsol.com
(2) Energean Oil & Gas, Kifissias Ave 32, Marousi 151 25 (Athens), Greece

The existence of active petroleum systems in Western Greece has been known since the 5th century B.C. (Karakitsios, 2013), when the Keri oil seep was documented by Herodotus in Zakynthos. In more recent times, over 5000km of 2D seismic data have been acquired and over 40 exploratory wells have been drilled in the western Greece onshore area, in search of commercial hydrocarbon accumulations. Success has been limited to date, largely due to the complexity of the shallow geology and surface topography, which results in a poor subsurface seismic image. In 2014, Energean Oil & Gas started a new phase of exploration activities in the area, encouraged by oil discoveries in the Mesozoic carbonates at Katakolon in NW Peloponessos (Greece) and Shpiragu, Ballsh and Cakran in Albania. While these discoveries confirm the hydrocarbon potential of NW Greece, much work is required to enhance our subsurface models and improve our geological understanding of the area.

NW Greece lies on the external part of the Dinaride-Hellenide fold and thrust belt, next to the boundary with the Apulian platform. This orogen is traditionally divided in 5 different units:

- Pre-Apulian zone, which consists of Triassic to Miocene deposits that characterize the transition zone between the Ionian basin and the Apulian platform.
- Ionian basin, characterized by Triassic evaporates, Jurassic to Eocene carbonates with minor shales and Oligocene flysch.
- Gavrovo / Kruja zone, which contains shallow water carbonates in the Eocene and Cretaceous. No older formations have been drilled yet or outcrops exist in the area.
- Distal Pindos / Crasta-Cukali, which represents the envelope between the Gavrovo zone to the West and the Pelagonian nappe in the East. It contains Mesozoic deep sea sediments and Upper Cretaceous to Eocene flysch.
- Pindos unit, characterized by oceanic domain sediments and ophiolitic rocks. Despite the still undergoing discussion on the origin of this unit, it is generally accepted that it was created during the opening of the Pindos Ocean in the Jurassic and obducted during the closure of the Neotethys Ocean (Papanikolaou, 2009).

Several structural models have been proposed in the past with significant implications for the deep and shallow prospectivity, since the Filiates-1 well (1966) drilled Cenozoic sediments below Triassic evaporites. One group of authors believe that several imbricates of Ionian basin are detaching one on top of the other with the Triassic evaporites acting as the major detachment in the area (Pieri, 1990). Permian sediments and basement remain unknown due to lack of well penetrations and outcrops. The alternative theory argues that the Ionian basin could be overthrusting the Apulian platform (Velaj, 2015).

In this review, we focus on the northernmost part of the Ionian Basin in Greece (Fig. 1) where four new structural sections have been constructed based on detailed surface geological data, well information and vintage 2D seismic. Our study integrates published and non-published information in order to build a consistent structural model that allows the definition of the major structural elements across the region.

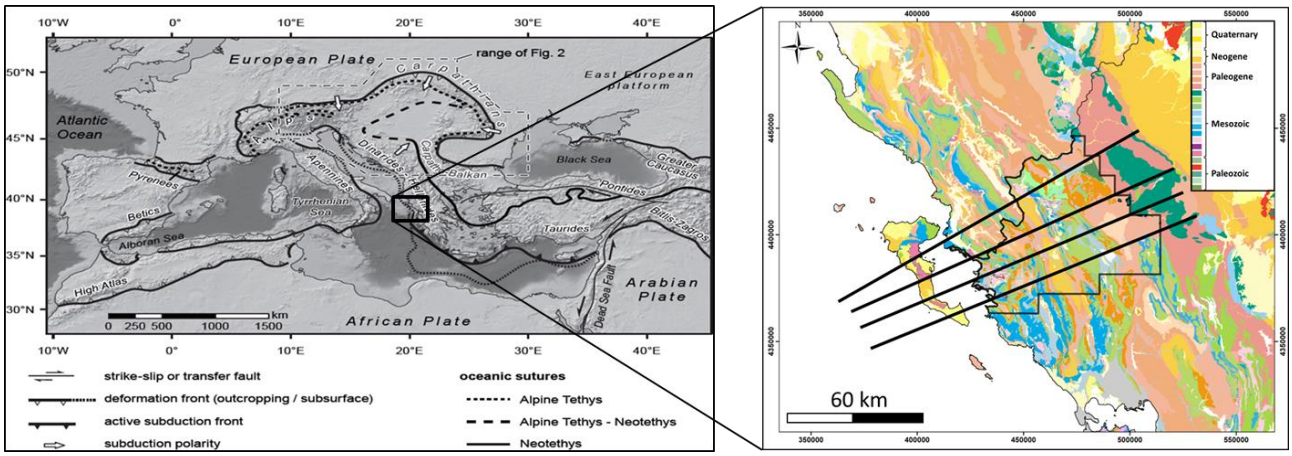

Figure 1. Circum-Mediterranean orogenic belt and geological map of the Hellenide fold and thrust belt and Ionian basin (modified from Cavazza *et al.*, 2013).

Our interpretation (Fig 2) is consistent with gravity and magnetic modeling, and also balanced and sequentially restored. This interpretation reflects the clear influence of salt tectonism since the early Jurassic, similar to what has been documented in Albania (Bega *et al*., 2017). The main processes affecting this restoration are: tectonic loading, erosion, decompaction, flexural isostasy, thermal subsidence and shortening from Oligocene times. The results of this restoration have been used for the construction of a 2D thermal maturity model. This modelling exercise shows that the burial and maturation history of the potential petroleum sources are strongly influenced by the kinematics of the deformation and thus, the onset of expulsion is modelled to become younger towards the West.

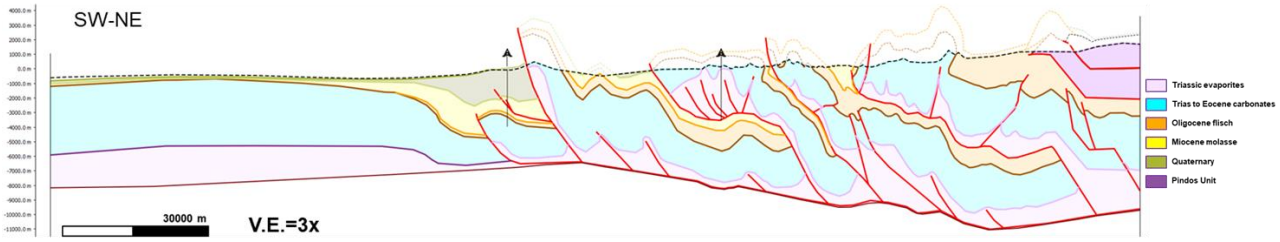

Figure 2. Regional structural section with SW-NE orientation.

Despite the high uncertainties that remain in the area, we believe that this work will help to understand the evolution of the Hellenide fold and thrust belt. In the near future, this will be done with the support of new seismic coverage being acquired at present times.

References

Bega, Z., Soto, J.I., 2017. The Ionian Fold-and-Thrust Belt in Central and Southern Albania: A Petroleum Province with Triassic Evaporites. Permo_Triassic Salt Provinces of Europe, North Africa and the Atlantic Margins. pp 517-538.

Cavazza, W., Wezel, F.C., 2003. The Mediterranean region – a geological primer. Episodes, Vol.26, no.3, pp. 160-168.

Karakitsios, V., 2013. Western Greece and Ionian Sea Petroleum Systems. AAPG Bulletin, v.97, no.9, pp. 1567-1595.

Papanikolaou, D., 2009. Timing of tectonic emplacement of the ophiolites and terrane paleogeography in the Hellenides. Lithos, Vol. 108, pp. 262-280.

Pieri, M., 1990. Structural model of Western Greece (Epiros and Akarnania). Public Petroleum Corporation of Greece.

Velaj, T., 2015. The structural style and hydrocarbon exploration of the subthrust in the Berati Anticlinal Belt, Albania. Journal of Petroleum Exploration and Production Technology, v.5, Issue 2, pp. 123-145.

15th International Congress of the Geological Society of Greece
Athens, 22-24 May, 2019 | Harokopio University of Athens, Greece
Bulletin of the Geological Society of Greece, Sp. Pub. 7 Ext. Abs. GSG2019-101

Co-combustion of Lignite and Solid Wastes from Olive Oil Industry

A. Vasileiadou[1,2], S. Zoras[1], A. Dimoudi[1], A. Iordanidis[2], V. Evagelopoulos[2]

(1) Department of Environmental Engineering, Faculty of Engineering, Democritus University of Thrace, 67100 Xanthi, Greece, E-mail: agvasileiadou@gmail.com
(2) Department of Geotechnology and Environmental Engineering, Western Macedonia University of Applied Sciences, Kila, 50100 Kozani, Greece

Municipal, industrial and agricultural solid wastes continuously increase along with the human development. The management of such wastes is of major importance since it is associated with severe environmental impact. Until recently, in Greece the main solid waste management-treatment is landfill. Other waste management approaches include composting and recycling of wastes in the concept of circular economy, that are still in early stages in Greece.

The participation of municipal solid waste (MSW) in the energy production under the so-called "waste-to-energy" scheme is gaining ground globally. The thermal processing technologies commonly used worldwide are incineration (combustion), pyrolysis and gasification. The benefit of the thermal treatment of wastes is triple: decreasing the waste volume, turning them into harmless material and producing energy. In Greece, the energy recovery from wastes by combustion has been recently regarded as a potential solution for the proper management of municipal solid wastes, due to its low cost and simple procedure (Athanasiou et al., 2015; Vamvuka et al., 2016).

Olive oil industry solid waste is a recalcitrant waste and poorly biodegradable due to its relative high lignin content. Thus, common biological treatment is not sufficient for the management of olive oil waste. Olive oil waste have been utilized for bio-compounds recovery (Nunes et al., 2019) as well as alternative fuel (Morvová, 2017) and biogas production (Afif et al., 2019). The biogas production and product valorization are in general expensive and rather sophisticated processes. On the other hand, thermal processes are simple and have relatively low cost.

The objective of this study is the investigation of the co-combustion of lignite with olive oil solid waste at different proportions as a potential alternative fuel with higher Gross Calorific Value (GCV).

Two olive oil waste samples: a) extracted olive pomace (EOP) and b) olive stone (OLS) were collected from an olive mill in Katerini, Greece. Lignite (LIG) sample was collected from the mines of the Western Macedonia area, Greece. All samples were firstly air-dried for two weeks. Then, the samples were ground to size less than one millimeter (<1 mm). Eventually, they were dried in an oven at 80 ^{o}C for 24 hours. Raw EOP and OLS, and raw lignite as well as 3 different blends at proportions (waste-lignite) 30-70, 50-50 and 70-30 were prepared by mixing. Gross Calorific Values were determined in a Leco AC-500 isoperibol bomb calorimeter according to ASTM D 5865-13 standard (ASTM D 5865-13, 2013). Proximate analysis (moisture, ash, volatile matter and fixed carbon) of the samples was performed in a Leco TGA 701 device according to the ASTM D 7582 (ASTM D 7582-15, 2015).

In Figure 1 the results of proximate analysis are presented. It is obvious that OLS and EOP samples exhibit much higher volatile content and much less ash percentage compared to lignite sample. High volatile matter is translated to higher heating capacity. This becomes apparent from the Gross Calorific values that are presented in Table 1. EOP has a GCV much higher than lignite and OLS exhibits almost double GCV compared to the respective value of lignite.

Thus, it can be concluded that blends of lignite with solid waste from olive oil industry appears to be very attractive as alternative fuel. However, further studying is required in order to estimate and compare emission and pollutant capacity issues of such wastes.

Table 1. Gross Calorific Values (GCV) of all samples (EOP: extracted olive pomace, OLS: olive stone, LIGA: lignite)

Sample ID	GCV (MJ/Kg)
EOP	19.63
EOP70 LIG30	17.02
EOP50 LIG50	15.78
EOP30 LIG70	14.28
OLS	22.30
OLS70 LIG30	18.96
OLS50 LIG50	18.58
OLS30 LIG70	13.54
LIGA	12.68

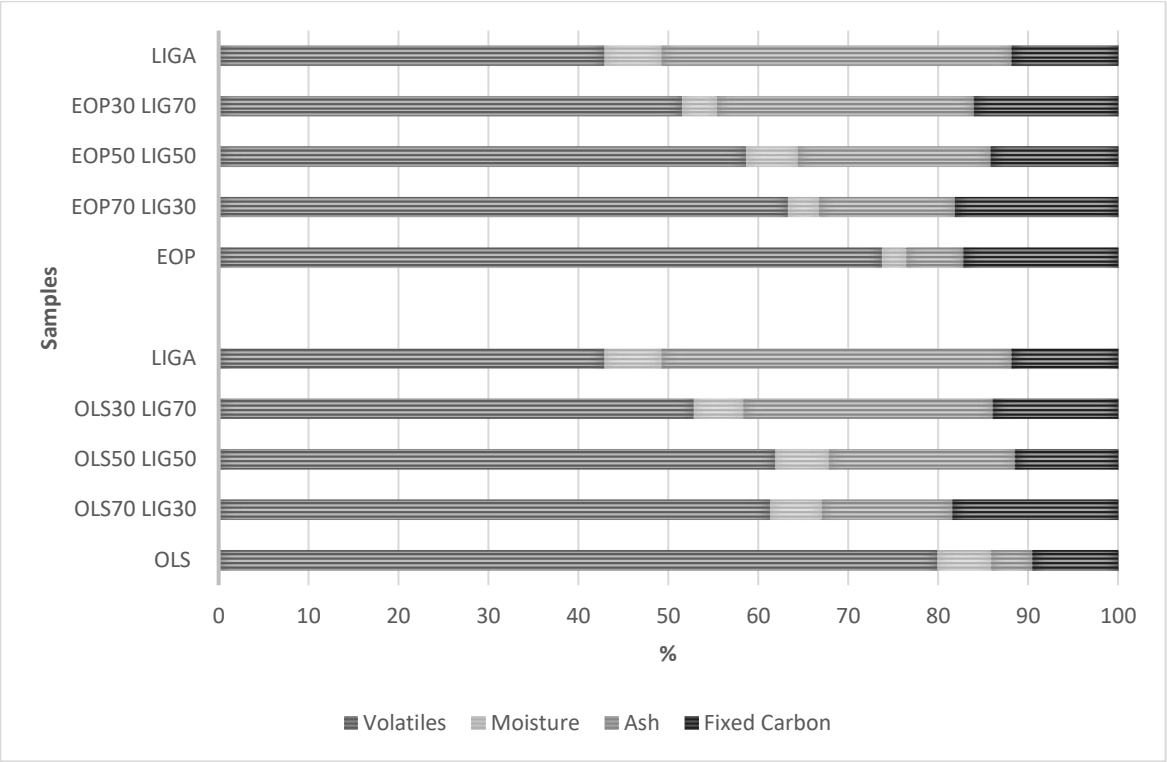

Figure 1. Proximate Analysis of the raw pre-dried samples and their blends (EOP: extracted olive pomace, OLS: olive stone, LIGA: lignite)

Acknowledgements

This research is co-financed by Greece and the European Union (European Social Fund- ESF) through the Operational Programme «Human Resources Development, Education and Lifelong Learning» in the context of the project "Strengthening Human Resources Research Potential via Doctorate Research" (MIS-5000432), implemented by the State Scholarships Foundation (IKY).

References

ASTM D 7582-15, 2015. Standard Test Methods for Proximate Analysis of Coal and Coke by Macro Thermogravimetric Analysis. ASTM International, West Conshohocken, PA.

ASTM D 5865-13, 2013. Standard Test Method for Gross Calorific Value of Coal and Coke. ASTM International, West Conshohocken, PA.

Afif, R. A., Linke, B., 2019. Biogas production from three-phase olive mill solid waste in lab-scale continuously stirred tank reactor. Energy 171, 1046-1052.

Athanasiou, C., Tsalkidis, D., Kalogirou, E., Voudrias, E, 2015. Feasibility analysis of municipal solid waste mass burning in the Region of East Macedonia – Thrace in Greece. Waste Management & Research 33(6), 561–569.

Morvová, M., Onderka, M., Morvová, M. Jr., Morva, I., Chudoba, V., 2019. Pyrolysis of Olive Mill Waste with On-line and Ex-post Analysis. Waste and Biomass Valorization 10, 511-520.

Nunes, M.A., Pawlowski, S., Costa, A.S.G., Alves R. C., Oliveira, M.B.P.P., Velizarov, S., 2019. Valorization of olive pomace by a green integrated approach applying sustainable extraction and membrane-assisted concentration. Science of The Total Environment 652, 40-47.

Vamvuka, D., Tsamourgeli, V, Zaharaki D. Komnitsas, K., 2016. Potential of poor lignite and Biomass blends in energy production. Energy Sources, Part A: Recovery, Utilization, And Environmental Effects 38, 2079-2085.

15th International Congress of the Geological Society of Greece
Athens, 22-24 May, 2019 | Harokopio University of Athens, Greece
Bulletin of the Geological Society of Greece, Sp. Pub. 7 Ext. Abs. GSG2019-148

Diagenetic Processes into the Reservoir of the Oil Field of Prinos-Kavala Basin, Macedonia, Greece

I. Ioakeimidis[1], N. Kantiranis[1], A. Georgakopoulos[1], P. Kiomourtzi[2], A. Tsirambides[1]

(1) Aristotle University of Thessaloniki, School of Geology, Department of Mineralogy-Petrology-Economic Geology, 54124 Thessaloniki, Greece, iioakimidis@hotmail.com, kantira@geo.auth.gr, ageorgak@geo.auth.gr, ananias@geo.auth.gr
(2) Energean, 32 Kifissias Ave. Artina Center, 151 25 Marousi, Athens, Greece, pkiomourtzi@energean.com

Introduction

Diagenetic processes begin immediately after the deposition of a clastic sediment and continue until the time of anchimetamorphism. All processes are gradual with increasing temperature and pressure. Diagenetic changes depend on the burial depth, the temperature, the chemical composition of the interstitial water and the type of the clastic constituents and cements. The factors that affect the degree of compaction of the components of a clastic sediment are the depth, the size of the grains, the type of clay minerals, the organic matter content, and various geochemical factors. The reduction of porosity and the deposition of cement material restrict the circulation of the fluids, particularly in sandstones, and negatively affect the oil reservoirs. In addition, the burial depth of the sediment is important because it can drastically reduce porosity, especially at depths >5 km (Chamley, 1989; Weaver, 1989; Boggs, 2009).

The most impressive mineralogical conversion during burial diagenesis is that of smectite to illite. The conversion is made in a solid state or by dissolution and recrystallization. At the conversion of smectite into illite dehydration occurs associated directly with the formation of hydrocarbons. The abundance of smectite favours the formation of hydrocarbons. However, the content of a sediment as a storage site in hydrocarbons is inconsistent with the amount of clay minerals found in it. The conversion of smectite into illite begins at temperatures of about 80°C and is accompanied by the production of large quantities of water. The mixed phases chlorite / smectite and chlorite / vermiculite may be formed during early or middle diagenesis. The proportion of chlorite layers in this mixed phase increases with increasing temperature, analogous behaviour to the increase of illite layers in the mixed phase illite / smectite (Tsirambides, 1983; Weaver & Associates, 1984; Nadeau et al., 1985; Chamley, 1989; Weaver, 1989; Lindgreen et al., 1991).

Most of the organic material in the clastic sedimentary rocks is sapropel deposited in lake, lagoon and marine environments with particularly low oxygen levels. Oxygen deficiency leads to anaerobic and reductive conditions which inhibit the oxidation and bacterial degradation of organic matter. This sapropel consists mainly of phytoplankton, zooplankton, seeds, pollen and residual particles of higher plants in rot. During burial diagenesis the organic material undergoes a series of important changes from the combined effect of biochemical and chemical agents. These diagenetic processes destroy most of the organic material and convert the remainder into an insoluble mass, the kerogen. Most of the organic material in shales and mudrocks is kerogen. The average concentration of organic carbon in shales and mudrocks is 1.0-2.2%. Some black shales contain significantly more organic carbon reaching 10% or more, while oil-bearing shales can contain 25% or more organic material (Tissot & Welte, 1984; Boggs, 2009).

From the study of diagenetic processes, significant conclusions can be drawn for the textural, mineralogical and chemical changes that occurred in a clastic sedimentary rock and vice versa. In addition, the extent to which these processes have affected other rock features, such as porosity and permeability, is particularly important when assessing the ability of a formation to function as a reservoir of water, gas or oil.

Results and discussion

Miocene clastic sediments taken from onshore drilling cores (depths 1,780-3,500 m) in the Nestos-Eastern Thassos basin indicated that they have been subjected to early diagenesis (Tsirambides et al., 1998).

The first exploration drilling in the Prinos-Kavala basin took place at the end of 1973 and since then 51 drillings have been carried out with an average depth of 3,000 m (Kiomourtzi, 2016). Today, there are 12 active production wells and 2 intake wells in the region. Crude oil production began in early 1981, initially with 8,000-10,000 barrels / day and peaked at 27,500 barrels / day in 1985. Since then, production has dropped significantly to 1,200 barrels / day. The first filling well, the PA-35, was successfully launched and started production in 2010, at a rate of 1,000 barrels / day to date, confirming the dynamic model of exploitation of the company that manages this field (Ioakeimidis, 2015).

The Prinos-Kavala basin began to form in the Lower Miocene and was gradually filled with clastic materials coming from the regional downfalls mainly in the northern part of the basin, as well as with the deposition of the Nestos River load, that flows to the northeast of the basin. Due to the high pressure of the overlying beds and the presence of cement material, the porosity is gradually reduced and the degree of compaction increases in the clastic sediments of Prinos-Kavala basin. Samples originated at depths >1000 m have been subjected to early diagenesis, while those originated at depths >2,600 m present clear characteristics of middle diagenesis. Late diagenesis processes are completed at greater depths under certain conditions. Such conditions were not detected in the examined basin (Ioakeimidis, 2015).

The total percentage of cement materials in the examined samples ranges between 5.5 wt% and 21.9 wt%. In particular, the carbonates are in the range 3.4 wt% to 14.3 wt%. The sum of organic matter and MnO2 ranges between 1.1 wt% and

4.5 wt% and the sum of Fe oxides and hydroxides ranges between 0.7 wt% and 3.4 wt%. The vertical distribution of the three cement materials measured is similar. The distributions are least differentiated in their intermediate regions, while the maximum and minimum curves are identical. This fact probably reflects the change of the sedimentation conditions (e.g., deposition environment, climate) with intense feeding conditions (minimum curves), alternating with milder conditions (maximum curves), the composition and the texture of the sediments, the physicochemical characteristics of interstitial water and finally the diagenesis conditions (Ioakeimidis, 2015).

The most important changes observed are the progressive conversion of smectite to illite or chlorite through their mixed phases of S/I and S/Ch, as well as the gradual increase in the degree of crystallinity of these two minerals. These changes are more pronounced in the <2 μm grain fraction, where clay minerals prevail. The changes in the percentages of illite, chlorite, sum of smectite + smectite/illite and kaolinite with depth in the clay fraction (<2 μm) are very evident. Illite and chlorite percentages range from 5 wt% to 24 wt% and from 2.7 wt% to 13.2 wt%, respectively, while their trend lines with depth are strongly increasing. The expanded clay minerals (smectite + smectite/illite) percentage ranges between 3.2 wt% and 11.2 wt%, while their trend line with depth is clearly increasing. The kaolinite percentage ranges from 0.1 wt% to 1.3 wt%, while its trend line with depth indicates a clear decrease (Ioakeimidis, 2015).

Clay mineral transformations with depth constitute significant tools in the estimation of the diagenesis stage and in extend in the hydrocarbon potential of the clastic sediments into the Prinos-Kavala reservoir. The conversion of swelling clay minerals into illite requires the circulation of solutions rich in K+ ions, starts at temperatures of 70-95oC depending on the geothermal gradient and is completed at temperatures up to 200oC. Taking into account the average geothermal gradient (30oC/km), this means an average burial depth of 2-4 km. At higher temperatures and depths, kaolinite is converted to illite and chlorite. These observations are in very good agreement with the chart trends of the clay fraction of the examined samples taken from depths of 2,635-2,960 m.

Another important indicator for assessing the evolution of diagenesis of a clastic sediment is the increase in crystallinity of illite structure with depth (Kübler, 1967; Weaver & Associates, 1984; Jaboyedoff et al., 2001). In the studied sediments the illite crystallinity gradually increases with depth with crystallinity index values varying from 8.41 mm to 5.33 mm. The average value of the illite crystallinity index is 7.9 mm, very close to that given by Weaver & Associates (1984) for middle diagenesis (7.2 mm). Two samples with values 3.16 mm and 3.25 mm, respectively, belong to illites that have undergone late diagenesis. The variance of illite crystallinity with depth according to Jaboyedoff et al. (2001) shows a slight decrease, i.e. a gradual reduction in the width of the illite peak (001) at half its height in both parallelly oriented and glycolated samples. The values of this index range between 2.11 and 1.24 (Ioakeimidis, 2015).

Conclusions

The oil-bearing Prinos-Kavala basin is 8 km west of Thassos and has a surface area of about 500 km2. In this basin hydrocarbons are trapped in sandstone and mudstone pores and are found at an average depth of 2,700 m. Among the clay minerals illite is the main phase showing a prominent increase with depth from 5 wt% to 24 wt%. Chlorite exhibits similarly a clear increase with depth from 2.7 wt% to 13.2 wt%. The expanded clay minerals (smectite + smectite / illite) also exhibit an increasing trend from 3.2 wt% to 11.2 wt%. The opposite trend is shown for kaolinite with a noticeable reduction in its content. Taking into account the detailed mineralogical analysis and the degree of illite crystallinity, it is concluded that the studied sediments have been subjected to middle diagenesis processes. This stage coincides with the "oil window" of temperatures 60-120oC (aprox. 2-4 km depth) reinforcing the dynamic formation of hydrocarbons in the Prinos-Kavala basin.

References

Boggs, S., Jr., 2009. Petrology of Sedimentary Rocks, 2nd edn. University of Oregon.

Chamley, H., 1989. Clay Sedimentology. Springer-Verlag, Berlin.

Ioakeimidis, I., 2015. Study of the diagenetic processes into the reservoirs of the oil field of Prinos-Kavala basin (Greece). Master Thesis, School of Geology, Aristotle University, Thessaloniki, 145 p. (in Greek with English summary).

Jaboyedoff, M., Bussy, F., Kübler, B., Thelin, Ph., 2001. Illite "Crystallinity" revisited. Clays & Clay Minerals 49(2), 156-167.

Kiomourtzi, P., 2016. Depositional environments and hydrocarbon potential basins in the North Aegean Sea. PhD Thesis, School of Geology, University of Patras, Patra, 529 p. (in Greek with English summary).

Kübler, B., 1967. La crystallinité de l'illite et les zones tout à fait supérieures du metamorphisme, in: Etages tectoniques, Colloque de Neuchâtel 1966, Edition de la Baconnière, Neuchâtel, Switzerland, 105-121.

Lindgreen, H., Jacobsen, H., Jakobsen, H.J., 1991. Diagenetic structural conversions in North Sea Jurassic illite/smectite. Clays & Clay Minerals 39(1), 54-69.

Nadeau, P.H., Wilson, M.J., McHardy, W.J., Tait, J.M., 1985. The conversion of smectite to illite during diagenesis: evidence from some illitic clays from bentonites and sandstones. Mineralogical Magazine 49, 393-400.

Tissot, B.P., Welte, D.H., 1984. Petroleum Formation and Occurrence, 2nd edn. Springer-Verlag, Berlin.

Tsirambides, A., 1983. Granulometric, mineralogical and oxygen isotope study of Neogene sediments from drilling cores of Nestos River delta. Ph.D. Thesis, School of Geology, Aristotle University, Thessaloniki, 187 p. (in Greek with English summary).

Tsirambides, A., Georgakopoulos, A., Filippidis, S., 1998. Prinos Basin: Sedimentological study of drill cuttings for carbonate origin. Unpublished report, Thessaloniki, 11 p.

Weaver, C.E., 1989. Clays, Muds, and Shales. Developments in Sedimentology 44, 1st edn. Elsevier, Amsterdam.

Weaver, C.E., Associates, 1984. Shale-Slate Metamorphism in Southern Appalachians. Developments in Petrology 10. Elsevier, New York.

15th International Congress of the Geological Society of Greece
Athens, 22-24 May, 2019 | Harokopio University of Athens, Greece
Bulletin of the Geological Society of Greece, Sp. Pub. 7 Ext. Abs. GSG2019-191

Preliminary Geothermal Investigation Northwest of Lake Kerkini, Strymon Basin (Macedonia, Northern Greece)

A. Arvanitis[1]

(1) Hellenic Survey of Geology and Mineral Exploration, 1 Sp. Louis St.,13677, Acharnae, Greece, arvanitis@igme.gr

The investigated area is located in the Strymon basin (Macedonia, Northern Greece), which constitutes a typical post-orogenic graben of primary geothermal interest due to its favorable geological and tectonic conditions and the identified low enthalpy fields at the basin margins. Taking into account the existence of the Lithotopos-Iraklia low enthalpy (temperature) geothermal field east of Lake Kerkini (Strymon basin), a preliminary geothermal exploration was conducted by I.G.M.E. (nowadays Hellenic Survey of Geology and Mineral Exploration) northwest of Lake Kerkini. The exploration process included collection and evaluation of geological, tectonic and geophysical data, wellhead and downhole temperature measurements, water sampling and analyses from selected wells and geochemical assessment of groundwater (Kougoulis *et al.*, 2005).

The basement of the explored area is mainly composed of various types of gneisses, amphibolites, amphibolite gneisses, schists, gneiss-schists, and pegmatite-aplite veins (small outcrops of meta-ultrabasic rocks and marbles) and belongs to the Serbo-Macedonian Massif (Vertiskos Unit). Granitoids have intruded the Vertiskos Unit. The Upper Permian/Lower Triassic Kerkini Granitic Complex (granites and granodiorite) intrudes this Unit northwest of the investigated area. The crystalline basement is covered by Neogene (Pliocene)-Quaternary terrestrial, fluvio-terrestrial, fluvio-torrential and fluvial marsh sediments consisting of pebbles, gravels, sandstones, clays and sands. Quaternary complex alluvial fans are developed along the southern margins of the Kerkini Mountains (north of the investigated area). Scree and talus cones occur at the base of the Kroussia Mountains, northwest of Lake Kerkini (Staikopoulos *et al.*, under publication; Ioannides *et al.*, under publication).

The main fault systems are oriented in NW-SE, NE-SW and E-W directions. The large high-angle NW-SE normal fault located along the longitudinal axis of Lake Kerkini is an important tectonic structure between basement and basin sediments which delineates the western margin of the Strymon basin and affects the geothermal conditions of the area. Another major tectonic structure is the E-W fault zone, which is located along the base of the Kerkini Mountains, related to the active N-S extensional stress field and bounds the northern margin of the Strymon basin. A number of faults in the above-mentioned directions are covered by the basin sediments.

The hydrogeological behavior of the geological units depends on their lithology and tectonic features. The basement is composed of impermeable metamorphic and granitic rocks but the intense fracturing and faulting create a secondary permeability and favor water circulation. The Neogene-Quaternary sediments are characterized as permeable - semipermable formations. Alluvial fans, scree and talus cones have high permeability and host good water-yielding aquifers due to their coarse-grained character and significant groundwater recharge with surface water. Several cold springs occur at the Kerkini Mountains yielding small to moderate quantities of water.

Geoeletrical survey involving a series of Vertical Electric Soundings (VES) with the Schlumberger array was carried out by I.G.M.E. north of Lake Kerkini in 1985 (Nikolaidis and Theodoridis, 1986). Geoeletrical sections oriented in N-S direction constructed from VES points. The interpretation and evaluation of these geoelectrical measurements have resulted in the following conclusions: (a) The resistivity values of the Neogene sediments overlying the basement range between 9 and 390 Ω.m due to the presence of clays, fine-grained and coarse-grained deposits. (b) Higher resistivity values of the Neogene sediments occur in the area south of the Kerkini Mountains. North of Lake Kerkini their values are lower than those northward (foothills of the Kerkini Mountains). (d) The alluvial fans, scree and talus cones show higher resistivity values (90-1,300 Ω.m) related to the grain-size distribution of deposits and the presence of water-bearing strata. (d) The total thickness of the Neogene and Quaternary sediments reaches 700m north of Lake Kerkini. (e) Significant basement subsidence associated with E-W normal faults has been identified in the foothills of the Kerkini Mountains. (f) North of the village of Kerkini, the basement has subsided steeply by about 300m (from 150 to 450m depth) due to normal fault activity. This normal fault can be considered to be a possible northwestward extension of the large high-angle NW-SE normal fault which is located along the longitudinal axis of Lake Kerkini and delineates the western margin of the Strymon basin. In general, the area is intensely tectonized and small-scale horst and graben structures have been formed.

Water temperature measurements were performed at the wellhead of 26 existing irrigation and water-supply wells, 30-162m deep, during their pumping. These wells are fed by water-bearing strata consisting of sands, gravels and pebbles intercalated with clay layers. The wellhead temperature values range between 14.6 and 22.0ºC. The maximum temperature of 22ºC was measured at the wellhead in well A-52, 81m deep (Figure 1), located in the village of Kerkini. Except for the wellhead temperature measurements, downhole temperature measurements were conducted in wells A-128, A-130 and A-131 (Figure 1). In well A-130, the temperature of 21.2ºC was recorded at depth of 121m (Kougoulis *et al.*, 2005). Taking into account that the mean annual air temperature of the area is 15.2ºC, the average geothermal gradient for the total depth is calculated to be 4.96ºC/100m. This value is higher than the normal geothermal gradient of 3ºC/100m.

Based on the distribution of the wellhead water temperature measurements, the corresponding isothermal curves were constructed (Figure 1). A geothermal anomaly is identified in the area of the village of Kerkini. The isothermal curves

trend SE-NW following the direction of the NW-SE western marginal fault of the basin. These curves remain open toward Lake Kerkini indicating the southeastward continuation of the geothermal anomaly. Considering that the isothermal curves in the neighboring Lithotopos-Iraklia low enthalpy geothermal field have characteristic NW-SE elongated shapes coinciding with the direction of the marginal fault (Karydakis *et al.*, 2005), it can be assumed that the observed small geothermal anomaly northwest of Lake Kerkini is a continuation of the above-mentioned field.

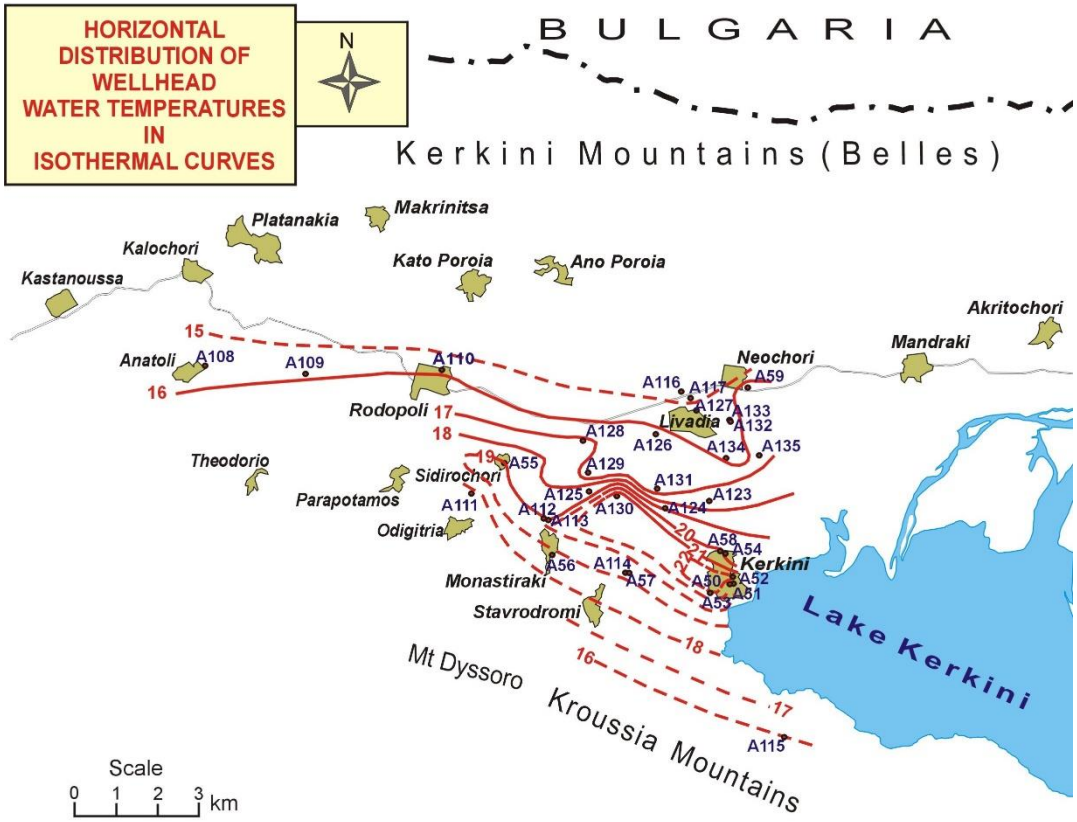

Figure 1. Distribution of isothermal curves based on the wellhead temperature measurements northwest of Lake Kerkini.

Water sampling and analyses from 10 selected wells were carried out (Kougoulis *et al.*, 2005). These water samples are classified as Na,Mg-HCO_3, Na,Mg-HCO_3SO_4, Na,Ca-HCO_3SO_4, Mg,Ca-HCO_3 and Mg-HCO_3 types. The coldest water sample (T=14.6ºC) from well A-116, 100m deep, has very low TDS (0.29 g/l), shows an almost neutral character (pH: 7.27) and belongs to Mg,Ca-HCO_3 type. The water sample from well A-53, 100m deep, having a temperature of 21.5ºC, TDS content of 0.54 g/l and showing an alkaline character (pH: 8.20) is classified as Na,Mg-HCO_3 type. Wells A-123, A-111, A-112, A-124, A-113, A-130, A-58 and A-52, 58-162 m deep, yield waters of 17.5-21.0ºC which belong to the following hydrochemical types: Mg,Ca-HCO_3, Na,Ca-HCO_3SO_4, Mg-HCO_3 and Na,Mg-HCO_3SO_4. These waters are characterized by low EC (440-680 μS/cm) and TDS (0.27-0.49 g/l) values and have a neutral to slightly alkaline pH (7.05-8.0). The plot of Na+K vs. Ca+Mg shows two main water groups: Group I (samples A-52, A-58, A-116, A-123, A-124, A-130) consists of waters of 14.6-21.0ºC with elevated concentrations of Ca+Mg (63.2-100.8 mg/l) and low concentrations of Na+K (13-23.8 mg/l). Group II (samples A-53, A-111, A-112, A-113) consists of waters of 17.9-21.5ºC with moderate concentrations of Ca+Mg (57.1-69.8 mg/l) and Na+K (59-133 mg/l).

The preliminary geothermal investigation northwest of Lake Kerkini has shown that a small positive geothermal anomaly controlled by the western marginal NW-SE fault occur in this area. The vicinity of the area with the Lithotopos-Iraklia low enthalpy geothermal field and the shape of the isothermal curves indicate the need for further systematic geothermal exploration.

References

Ioannides, K., Latsoudas C., Papaphilippou E., Lolou U. (under publication). Basic Geological Map of Greece: KASTANOUSA - POROIA map sheet, 1:50,000 scale. IGME, Athens.

Karydakis, G., Arvanitis, A., Andritsos, N., Fytikas, M., 2005. Low Enthalpy Geothermal Fields in the Strymon Basin (Northern Greece). Proceedings, World Geothermal Congress 2005, Antalya, Turkey, p. 12.

Kougoulis, C., Koutsinos, S., Arvanitis, A., Kolios, N., 2005. Exploration and identification of geothermal Fields in the Axios - Doirani area. Report, Institute of Geology and Mineral Exploration (I.G.M.E.), Thessaloniki, 11-56.

Nikolaidis, M., Theodoridis, T., 1986. Geoelectrical survey in the Strymon basin. Report, Institute of Geology and Mineral Exploration (I.G.M.E.), Athens, p. 9 + maps

Staikopoulos, G., Antoniades, P., Maltzaris, F. (under publication). Basic Geological Map of Greece: KERKINI map sheet, 1:50,000 scale. IGME, Athens.

15th International Congress of the Geological Society of Greece
Athens, 22-24 May, 2019 | Harokopio University of Athens, Greece
Bulletin of the Geological Society of Greece, Sp. Pub. 7 Ext. Abs. GSG2019-197

Potential CO_2 storage sites in Greece – A review

N. Koukouzas[1], V. Gemeni[1]
(1) Centre for Research and Technology, Hellas (CERTH), 52 Egialias St., 15125 Marousi, Athens, Greece, gemeni@certh.gr

The New Policy Scenarios (NPS), released by the International Energy Association (IEA), which incorporate existing energy policies as well as an assessment of the results likely to stem from the implementation of announced policy intentions, have identified a slight increase, compared to the previous years, to the CO_2 emission worldwide. On the other hand, according to the Organisation for Economic Co-operation and Development (OECD) and the IEA report "CO_2 Emissions from Fuel Combustion" (IEA, 2018), the CO_2 emissions in Greece since 2012 and up to 2016 (last published data) have been decreased from 7000 to 5900 tonnes/cappita.

Based on the strategy paper that was published by the European Commission (EC, 2018), the use of carbon capture and storage (CCS) technologies is "still necessary" to achieve long-term climate goals. Taking this into account and the continued high fossil fuel dependency of the Greek power sector, the potential for CCS opportunities within Greece should be investigated as a way of mitigating the greenhouse gases, in line with other options.

Different potential sites for CO_2 storage have been identified in Greece with total storage capacity in deep saline aquifers and hydrocarbon fields estimated at 2190 Mt. The total effective storage capacity in aquifers alone in Greece was estimated to be around 184 Mt (Hatziyannis, 2009). The aforementioned CO_2 storage capacity concerns the Tertiary sedimentary basins of Prinos, West Thessaloniki and a part of the Mesohellenic Trough (Hatziyannis, 2009) (Figure 1).

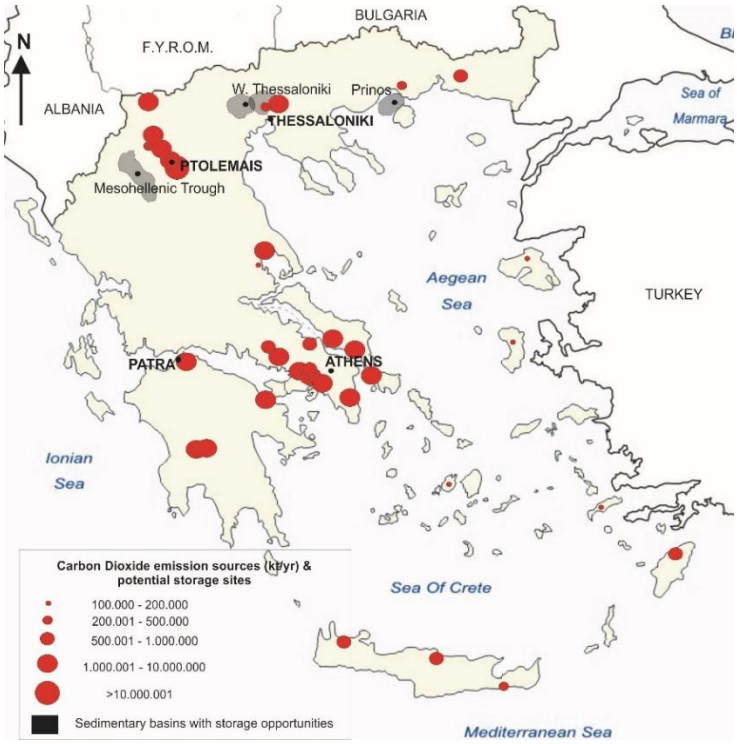

Figure 1. CO_2 emission sources and potential storage sites in Greece

Based on available information, Koukouzas et al. (2009) have conducted a Basin-Scale Assessment (Bachu et al., 2007), identify the best Basin for a potential CO_2 storage. The authors concluded that the tectonically stable offshore Prinos Basin has favourable characteristics for CO_2 geological storage as well as sufficient storage potential to take in the total amount of CO_2 produced by the nearby Komotini gas fired power station (0.7 Mt/year CO_2) for several decades. In addition, the offshore location of the potential reservoir and seal units increases the transportation costs but it is countered by the well-established infrastructure framework within 30–40 km of the coast (pipelines, wells and platforms).

The onshore Thessaloniki Basin appears to have very good technological and economic potential for CO_2 storage. Favourable factors include limited faulting, optimal depth ranges for CO_2 storage capacity, and relatively low drilling costs within the closures identified. It appears to have the capability to store all the regional stationary CO_2 emissions (one cement plant and one refinery with its 400 MW Combined Cycle Gas Turbine Unit emitting in total around 1.9 Mt CO_2/year) or the total lifetime.

The CO_2 storage potential of the Mesohellenic Trough is unclear due to sparse drilling across the basin although suitable reservoir and seal units appear to be present at appropriate depths, but the extensive faulting should be considered as a

potential risk. Tasianas and Koukouzas (2015), have examined further the area for its potential in storing CO_2. According to their research, CO_2 storage can take place in the Pentalofos sandstone (Figure 2), a reservoir extending throughout the entire MT and it is located below the Tsotylli Formation (Fm) caprock (Zelilidis et al. 2002).

More specifically, the geological modelling conducted in the Mesohellenic Trough, allowed the assessment of the CO_2 storage potential and provided an estimation of the CO_2 storage capacity for the Pentalofos reservoir. The Pentalofos formation is also capped by an effective cap rock, the Tsotylli Formation, and can be, thus, potentially be used as a storage area for CO_2 regionally. According to the geological model, the deepest point where the CO_2 can be stored corresponds to the base of the Tsarnos formation, at 2544 m depth. The estimated amount of potential CO_2 storage is up to 1435 Gt.

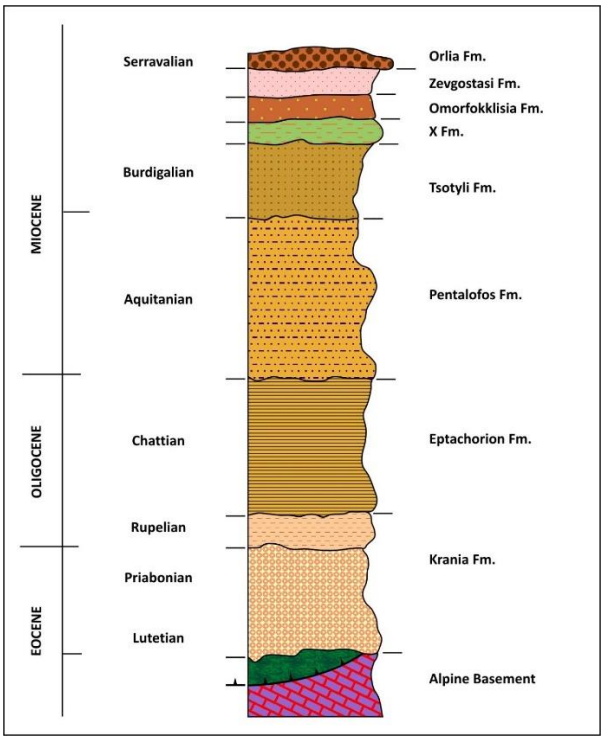

Figure 2. Stratigraphic column of Mesohellenic Trough

In addition to the geological modelling, geochemical experiments and modelling were also conducted for the Mesohellenic Trough, which support the fact that Pentalofos and Tsotyli sandstone formations are suitable for the long-term storage of CO_2 produced in the neighbouring lignite-fired power plants, at least in terms of mineralogy and geochemistry.

To conclude, the large-scale implementation of CCS at large point sources of CO_2 in Greece would reduce the national CO_2 emissions by 25–28%. The geological settings of the Tertiary and Neogene-Quaternary sedimentary basins in Greece appear to provide a promising option for CCS implementation. The identified potential reservoirs and overlying seal units occur within approximately 100 km of the significant stationary CO_2 emissions in NW Greece, which is favourable in terms of infrastructure costs. Continued optimisation of the models used, combined with more information on the structural properties of the potential reservoirs of the sedimentary basins, could help in their further evaluation as a potential storage structures for CO_2.

References

International energy Association (IEA), 2018. CO_2 Emissions from Fuel Combustion 2018, IEA, Paris

European Commission (EC), 2018. A Clean Planet for all A European strategic long-term vision for a prosperous, modern, competitive and climate neutral economy, Brussels, Belgium.

Hatziyannis, G., 2009. Country updates: Greece. In: Vangkilde-Pedersen T, editor. WP2 Report –Storage capacity. EU GeoCapacity –Assessing European Capacity for Geological storage of Carbon Dioxide. Project no. SE6-518318., 144-147

Koukouzas, N., Ziogou, F., Gemeni, F., 2009. Preliminary assessment of CO_2 geological storage opportunities in Greece. International Journal of Greenhouse Gas Control, 3, 502–513.

Koukouzas, N., Kypritidou, Z., Purser, G., Rochelle, C.A., Vasilatos, C., Tsoukalas, N., 2018. Assessment of the impact of CO_2 storage in sandstone formations by experimental studies and geochemical modeling: The case of the Mesohellenic Trough, NW Greece. International Journal of Greenhouse Gas Control, 71, 116-132.

Tasianas, A., Koukouzas, N., 2015. Assessing the Potential of the Mesohellenic Trough and Other Sites,in Greece, for CO_2 Storage. World Multidisciplinary Earth Sciences Symposium (WMESS2015), Procedia Earth and Planetary Science, 15, 607 – 612

Zelilidis, A., Piper, D.J.W., Kontopoulos, N., 2002. Sedimentation and basin evolution of the Oligocene-Miocene Mesohellenic basin, Greece. Aapg Bull, 86, 161-182.

15th International Congress of the Geological Society of Greece
Athens, 22-24 May, 2019 | Harokopio University of Athens, Greece
Bulletin of the Geological Society of Greece, Sp. Pub. 7 Ext. Abs. GSG2019-251

Near-seafloor Geohazards Analysis of the Western Patraikos Block, offshore western Greece

E. Tripsanas[1], D. Sakelariou[2], G. Rousakis[2], A. Stathopoulou[1], N. Lykakis[1]

(1) Hellenic Petroleum, Exploration & Production of Hydrocarbons S.A., 4A Gravias, Marousi 15125, Greece, etripsanas@helpe.gr
(2) Institute of Oceanography Hellenic Centre for Marine Research, 47th km Athens-Sounio Ave 19013, Anavyssos, Greece

Extended Abstract

Western Patraikos Block (WPB) was awarded to Hellenic Petroleum in 2012 for Hydrocarbon exploration activities. Extensive geological and geophysical analysis resulted in the identification of multiple potential leads, and one of them is planned to be tested by an exploration well in 2020. As a consequence, several environmental, oceanographic, and geological studies have been conducted in the region in order to ensure negligible impact on the marine environment and safe drilling procedures, namely: 1) side-scan-sonar images and multibeam bathymetry for the identification and mapping of seafloor characteristics (e.g. slope gradients, sedimentary structures), benthic biocommunities, and shipwrecks, cables and other human made objects, 2) analysis of ultra-high-resolution seismic-reflection data (sparker and chirp sub bottom profiles) for the identification and mapping of recent landslides and shallow faults, and 3) examination of a high-resolution 3D PSDM (pre-stack depth migration) seismic cube in order to define lithostratigraphy, fault mapping, and potential drilling hazards in the upper 1000 m of the sedimentary column. This work aims to present the key results from the various studies with ultimate goal to define areas of environmental, archeological, and geohazards risk, which should be treated with caution during drilling activities.

The bathymetry of the broader WPG was derived from the PSDM volume (Fig. 1A) and it was complemented by high-resolution (15 m grid) multibeam bathymetric data in selected areas of interest (AOI). Two major morphological settings comprise the WPB. An extensive shelf zone to the east, which represented a delta plain depositional setting during the low sea-level stand (~ 120 m below present sea level) of the last glacial maximum (LGM) (18 – 27 ka B.P.) (Fig. 1A). The lithology of such a depositional setting is anticipated to range from thick (> 1 m), paralic and river sand packages to lagoonal and flooding plain mud deposits. Shallow marine mud deposits characterize this area during high sea-level stands. The transition to the basin floor to the west occurs through a steep (5° - 15° and only locally up to 32°) delta slope (Fig 1D, E). Parallel, continuous to semi-continuous reflections in ultra-high and high-resolution seismic-reflection profiles indicate that mud-dominated sediments characterize late Quaternary deposits on the basin floor (Fig 1C).

A deep-tow system (DEEP-TOW 2000, Geoacoustics /Kongsberg), flying 30 m above the seafloor was used in selected areas of interest (AOI) for the acquisition of ultra-high resolution data (side scan sonar and chirp sub bottom profiler), in order to identify and map in detail on the seafloor structures and/or objects with dimensions down to 0.3 m. Through this dataset was possible to examine the presence of benthic biocommunities (e.g. corals), shipwrecks and archeological artifacts, cables, and sedimentary structures (e.g. sediment waves, expulsion features) that might impose issues on safe drilling procedures with respect to the environment. The seafloor in the AOI is smooth in the vast majority of its extension, with no benthic biocommunities or man-made structures and objects. However, the presence of extensive and widespread NW – SE and SW – NE lineations on the side-scan-sonar images reveal intense scouring of the seafloor through intense trawling activity in the area (Fig 1B).

Ultra-high resolution seismic-reflection profiles and sediment cores indicate that Holocene (high sea-level stand during the last 10 ka), sediment failures on the delta slope, although common, are of local-scale with limited run off distances (a few hundred meters) with a recurrence time interval of a few to several hundred years. On the other hand, sediment failures and gravity flow deposits during the LGM were abundant and of larger run off (a few to several km). This discrepancy is attributed to the direct river-sourced sediment discharge at the shelf edge during this low sea-level stand, resulting in the formation of thick, loose and easy to fail piles of sediment at a high gradient slope setting. Two large, mass-transport complexes at the southern and northern part of the basin floor are dated to have occurred during the LGM, based on their burial by a 10 – 20 m thick cover of hemipelagic mud. On the contrary, the entrapment of most river-sourced sediments at the shallower parts of the shelf to the east during the Holocene high sea-level stand resulted in lower sedimentation rates at the slope, and thus in more resilient to failure sediment packages.

The seismic-reflection profile in Figure 1C, extracted from the available 3D PSDM seismic cube, shows the existence of a major unconformity at the base of the Pliocene – Pleistocene section, which is interpreted to represent the areal exposure of the area during the Messinian Salinity Crisis, during which the sea-level had dropped over 1 km below the present sea level. Clastic sedimentation dominates in the overlying Pliocene – Pleistocene section, which consists of two seismic sequences, named as lower marine sequence (LMS) and upper progradational wedge sequence (UPWS). The LMS consists of continuous to semi-continuous, mid to high-amplitude seismic reflections, and it is interpreted to represent mud-dominated hemipelagic deposits interbedded in places by a few turbiditic channel sand packages. The UPWS comprises several foreset packages in the eastern part of the WPB. Those foreset geometries are interpreted as delta complexes of the Achelous River during low sea-level stands. Foreset packages transit westwards to bottom set packages, these being interpreted to comprise mud-dominated prodeltaic and marine depositional settings.

Given the current 3D seismic survey, faulting within the Pliocene – Pleistocene section is not common, and, where present, are of low displacement and occur within deformed strata by Late Neogene diapirism (Fig 1A, C). It is interesting that diapirism has absolutely no surface expression at the eastern part of the WPB, whereas it has a distinct seafloor

expression, in the form of elongated bulges, at the western basinal part of the WPB. This discrepancy on the seafloor imprint of the diapiric activity is attributed to much higher sedimentation rates and more efficient burial at the eastern parts of the WPB due to their proximity to the mouth of the Achelous River. Seafloor bulges at the basin floor related to diapirism are commonly characterized by steep flanks (2.5° – 10°), whereas Neogene faulting might also have in places seafloor expression. Ultra-high- and high-resolution seismic-reflection profiles indicate that infrequent (recurrence e period of 100s of years), local-scale (a few to several hundred meters long) failures occur along the flanks of the seafloor bulges formed by the uplifted diapirs at the western part of the WPB.

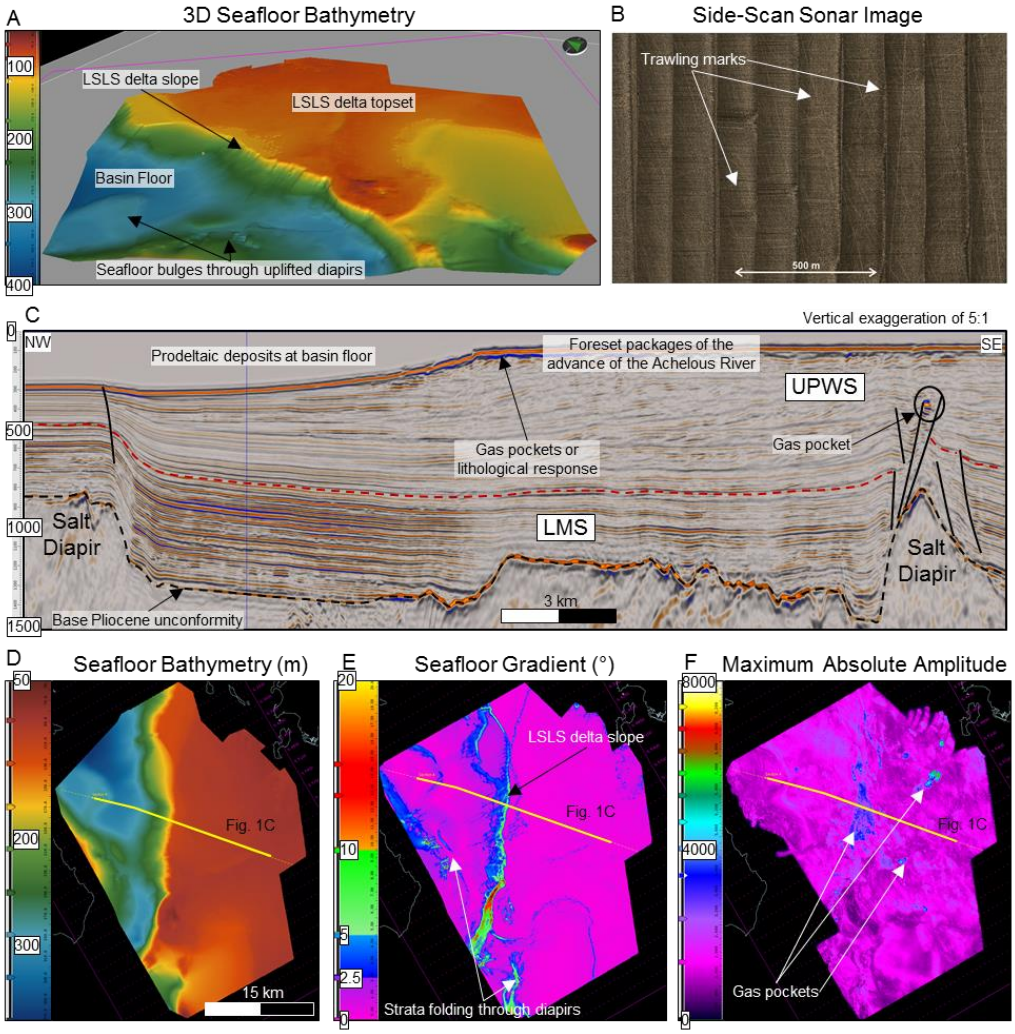

Figure 1. (A) Three dimensional representation of the bathymetry of the area of interest, showing key morphological characteristics. (B) Side-scan image showing a very smooth seafloor, which has been significantly scoured by trawling activities. (C) Seismic-reflection profile reveals that the Pliocene – Pleistocene section consists of a lower marine (LMS) and an upper progradational wedge sequence (UPWS). (D – F) maps of bathymetry, seafloor dip-angle, and maximum absolute amplitude from the UPWS showing areas of steep slopes (> 5°) and potential gas pockets, which have to be avoided during drilling. Steep slopes occur mostly at low sea-level stand (LSLS) delta slopes of the last glacial maximum (18 – 27 ka BP) and locally around areas of diapirism.

The presence and extension of shallow gas pockets in the Pleistocene section of the WPB was investigated through the generation of amplitude maps from the UPWS. Extremely high amplitude values are commonly associated to the presence of shallow gas accumulations, whose distribution and dimensions can be variable (Fig. 1C, F). In this manner, areas of high probability of encountering shallow gas pockets have been identified and mapped. The presence of (small <10 m in diameter and 1 – 2 m deep), circular depressions above such a zone of amplitude anomalies suggests the development of expulsion features (pockmarks), and thus, supports their interpretation as shallow gas pockets.

In conclusion, it is evident that through such a detailed and extensive work the WPB region has been properly evaluated, resulting in the identification and mapping of areas which either for potential geohazards issues (e.g. seafloor gradient, Neogene faults, slope stability, gas pockets), or environmental aspects (benthic biocommunities, shipwrecks, cables) have to be treated with caution and respect.

Acknowledgements

We would like to acknowledge the Spyros Mpelas from Hellenic Hydrocarbon Resources Management (HHRM), Karen Ware from RPS Energy, and Edison exploration team for their significant contribution in the organization, deployment, and completion of this extensive and in depth work.

15th International Congress of the Geological Society of Greece
Athens, 22-24 May, 2019 | Harokopio University of Athens, Greece
Bulletin of the Geological Society of Greece, Sp. Pub. 7 Ext. Abs. GSG2019-336

Combined CO_2 Geological Storage and Geothermal Energy Utilization in Greece

A. Arvanitis[1], N. Koukouzas[2], P. Koutsovitis[2], D. Karapanos[2], E. Manoukian[2]

(1) Hellenic Survey of Geology and Mineral Exploration, 1 Sp. Louis St., 13677, Acharnae, Greece, arvanitis@igme.gr
(2) Centre for Research and Technology Hellas/Chemical Process and Energy Resources Institute, Marousi, Greece

CO_2 injection and storage in deep geological formations can contribute to the exploitation of geothermal potential. CO_2 has significant advantages compared to water, due to certain favorable physical, chemical and thermophysical properties. Several proposals for the use of CO_2 in geothermal energy exploitation have been formulated but they still remain at an initial research stage (Arvanitis *et al.*, 2018):

- Supercritical CO_2 utilization as working fluid (heat transmission fluid) in Enhanced Geothermal Systems (EGS), where the natural permeability and/or fluid content is limited and insufficient. In EGS, fluid is injected from surface at high pressure into high-temperature deep rocks through wells under carefully controlled conditions to re-open the pre-existing natural fractures and flow through them into production wells extracting heat from the high-temperature rock formations. Supercritical CO_2 can be used as a working fluid instead of water or brine to recover the geothermal heat from the reservoir, due to specific thermodynamic advantages against water; e.g.: larger expansivity and compressibility, lower viscosity, higher mobility, larger flow velocity for a given pressure gradient, different enthalpy behavior in relation to pressure and temperature, higher heat extraction rates, less effective as a solvent for rock minerals (Brown, 2000; Pruess, 2006).
- Supercritical CO_2 injection into a deep saline aquifer and formation of "CO_2 Plume Geothermal" (CPG), which displaces native fluids and extracts heat from the geothermal reservoir. CPG involves pumping supercritical CO_2 into deep, naturally porous, permeable geologic reservoirs overlaid by low-permeability caprocks. The injected CO_2 absorbs heat from the reservoir, buoyantly rises to the surface, and drives a power generation system. The CO_2 is then cooled and re-injected into the reservoir. The produced CO_2 mass fraction depends on the stratigraphic positions of highly permeable layers which also affect the pore-fluid pressure drop across the reservoir. CPG systems provide viable geothermal energy resources for electricity production, even in regions with relatively low geothermal temperatures and heat flow rates, where suitable reservoirs exist (Randolph and Saar, 2011), leading to expansion of geothermal energy utilization. These systems are capable of achieving improvements in heat extraction efficiencies well above those accomplished by replacing water with CO_2 as the working fluid in EGS. Supercritical CO_2 has a large mobility (inverse kinematic viscosity) and thermal expansibility compared to water, resulting in the formation of a strong thermosiphon that typically eliminates parasitic pumping requirements (Garapati *et al.*, 2014). Traditional water-based geothermal development requires three geologic Conditions: (1) significant amounts of water, (2) a permeable formation to allow water extraction/reinjection, and (3) sufficient subsurface temperatures. EGS seeks to artificially generate Condition 2 and supply (water-based EGS) or avoid (CO_2-based EGS) Condition 1, thereby expanding geothermal heat mining prospects. On the other hand, CPG provides an alternative working fluid (avoiding Condition 1) with high mobility compared to water, thus expanding the range of usable natural-formation permeabilities (Condition 2). Similarly, CO_2 lowers minimum thresholds of economically and technologically viable subsurface temperatures (Condition 3), as its high mobility enhances heat extraction efficiency. Numerical simulations have indicated that CPG systems provide higher geothermal energy extraction rates significantly improving heat energy recovery over water-based systems (Randolph and Saar, 2011).
- A hybrid two-stage thermal energy recovery approach (initially brine and then brine and CO_2) from a deep saline aquifer. After the CO_2 injection, during the first stage, formation brine is pumped out to relieve the pressure. During the second stage and as CO_2 reaches the production wells, CO_2 and brine are produced together as working fluids. The produced brine can be used either for freshwater production by desalination (reverse osmosis), or as saline cooling water or even as injected water into adjacent EGS (Buscheck *et al.*, 2012).
- CO_2 utilization as a pressure-support fluid in order to create artesian pressures for CO_2 and brine production as working fluids. This can be achieved by developing a pattern of horizontal wells at reservoir bottom depths of 2.5-5 km and creating at least 4 concentric rings, consisting of inner ring brine/CO_2 producers, CO_2 injectors, brine reinjectors and outer-ring brine producers (Buscheck *et al.*, 2013).
- CO_2 dissolution in a saline aquifer and energy recovery of CO_2-rich hot brine through a geothermal doublet system (production and injection wells). This new approach involves (Kervévan *et al.*, 2017): (i) CO_2 capture with innovative technology based on the CO_2 dissolution in water (Pi-CO_2 technology), (ii) extraction of aquifer's brine through a production well, (iii) heat recovery through a surface heat exchanger system, and (iv) re-injection of the cooled brine through the injection well, which will be linked to the new Pi-CO_2 technology.

Potential sites suitable for CO_2 geological storage in Greece have been studied (CERTH, IGME), with efforts was made to assess their storage capacity. The following sites and formations have been proposed:

- Miocene sandstone reservoirs, more than 1,600 m deep, in the hydrocarbon (oil and gas) fields of Prinos and South Kavala, with a total capacity of 35 Mt CO_2

- Oil reservoirs in Kallirachi (wider offshore Prinos basin), with a storage capacity of 30 Mt CO_2
- Upper Jurassic-Lower Cretaceous limestones in the Epanomi gas field (south of Thessaloniki), at a depth of 2,600m, with a capacity of 2 Mt CO_2
- Fractured Cretaceous-Eocene limestones in the hydrocarbon (oil and gas) fields of Katakolo (West Peloponnese), with a storage capacity of 3.2 Mt CO_2.
- Deep saline aquifers of Miocene age in the offshore Prinos basin, with an average depth of 2,400m, an area of 800km^2, an average thickness of 260m, an average porosity of 18% and estimated capacity of 1,350 Mt CO_2.
- Deep (900-2,400m) saline aquifers within the Eocene formations in the wider onshore basin of Thessaloniki (Central Macedonia), including the Loudias and Alexandria structural traps as well as the deeper clean sandstone bed, with an average porosity of 8-10% and a total storage capacity of 640 Mt CO_2.
- The sedimentary formations of the Mesohellenic Trough (NW Greece), with an average depth of 1,000m, average porosity of 10%, average thickness of 300m and a storage capacity of 216 Mt CO_2.

In the Thessaloniki onshore basin as well as in the Mesohellenic Trough, where a potential of CO_2 geological storage in saline aquifers has been assessed, temperature measurements in deep hydrocarbon exploration boreholes have given the following results:

- Thessaloniki Basin: The temperature of 65ºC (Horner Correction) was recorded in borehole ALEXANDRIA-1 at 1,705m depth, within the ophiolithic bedrock. In borehole LOUDIAS-1, the temperatures of 74ºC and 83ºC were measured at depths of 1,520m and 2,614m respectively, within Eocene-Oligocene sediments. Temperatures of 73ºC, 76ºC and 79.5°C have been recorded at depths of 3,130m, 3,629m and 2,745m, within Paleogene (Eocene-Oligocene) sediments, in boreholes KORYFI-1, KLEIDI-1 and AEGINIO-1 respectively (Karytsas, 1990).
- Mesohellenic Trough: In borehole NEAPOLIS-2, a temperature of 49°C (uncorrected value) has been measured at a depth of 1,126m in the Senonian formations. In borehole NEAPOLIS-1, the temperature of 50°C has been recorded at 600m depth, on the roof of the Senonian limestones (Karytsas, 1990). However, in 1998, the temperature of 23°C was recorded at 605m depth in an exploration borehole drilled by the Institute of Geology and Mineral Exploration.

The offshore Prinos basin is located in the Gulf of Kavala and the available thermometric data have no significance, since the geothermal potential cannot be exploited. To the Northeast, the Nestos River Delta basin can be considered as its onshore extension. Hydrocarbon exploration boreholes N-1, N-2 and N-3 were drilled in the Nestos River Delta basin and the temperatures of 115ºC, 127ºC and 138ºC have been recorded at depths of 2,970m, 3,104m and 3,601m respectively, within the Miocene sediments. Additionally, the temperature of 122°C has been measured at the bottom of the geothermal exploration borehole N-1G (NW of the village of Eratino), 1,377m deep, in the metamorphic basement.

Considering that to date there are no studies on the implementation of EGS in Greece, it is considered more feasible to combine CO_2 geological storage and geothermal energy utilization in deep saline aquifers by mainly applying CPG technology. Among the studied CO_2 geological storage sites in deep aquifers, the Thessaloniki basin has been recognized as having an extensive geothermal potential of moderate temperatures (up to 89ºC). Bearing in mind that a CPG system provides greater power and more extensive thermal extraction over water-based systems, it is obvious that the case of the Thessaloniki basin requires further study so that CPG technology can optimize its geothermal potential.

References

Arvanitis A., Koukouzas N., Gemeni V., Koutsovitis P., 2018. Contribution of CO_2 Geological Storage to the Geothermal Energy Exploitation. 11th National Conference on Renewable Energy Sources, Institute of Solar Technology, Thessaloniki, Greece, Volume A, 493-507.

Brown, D. W., 2000. A Hot Dry Rock Geothermal Energy Concept Utilizing Supercritical CO_2 Instead of Water. 25th Workshop on Geothermal Reservoir Engineering, Stanford University, Stanford, California, USA, SGP-TR-165, p.6.

Buschek, T.., Chen, M., Sun, Y., Hao, Y., Elliot, T., 2012. Two-Stage, Integrated, Geothermal-CO_2 Storage Reservoirs: An Approach for Sustainable Energy Production, CO_2-Sequestration Security, and Reduced Environmental Risk. Lawrence Livermore National Laboratory (LLNL), Livermore, CA, USA, 20 p.

Buscheck, T., Chen, M., Lu, C., Sun, Y., Hao, Y., Celia, M.., Elliot, T., Choi, H., Bielicki, J., 2013. Analysis of Operational Strategies for Utilizing CO_2 for Geothermal Energy Production. 38th Workshop on Geothermal Reservoir Engineering Stanford University, Stanford, California, SGP-TR-198, p. 12.

Garapati, N., Randolph, J. B., Saar, M. O., 2014b. Total Heat Energy Output From, Thermal Energy Contributions To, and Reservoir Development of CO_2 Plume Geothermal (CPG) Systems. 39th Workshop on Geothermal Reservoir Engineering, Stanford University, Stanford, California, SGP-TR-202, p. 12.

Karytsas, C., 1990. Inventory of Low-Enthalpy Geothermal Resources Discovered Through Deep Oil and Gas Exploration Wells. Final report for contract DG XVII 7030/ETD/89-6, Centre for Renewable Energy Sources, Pikermi, Greece, 139 p., Appendix

Kervévan, C., Beddelem, M.-H., Galiègue, X., Le Gallo, Y., May, F., O'Neil K., Sterpenich. J., 2017. Main Results of the CO_2-DISSOLVED Project: First Step toward a Future Industrial Pilot Combining Geological Storage of Dissolved CO_2 and Geothermal Heat Recovery. Energy Procedia, 114, 4086-4098

Pruess, K., 2006. Enhanced Geothermal Systems (EGS) Using CO_2 as Working Fluid - A Novel Approach for Generating Renewable Energy with Simultaneous Sequestration of Carbon. Geothermics, 35, 351-367

Randolph, J. B., Saar, M. O., 2011. Combining Geothermal Energy Capture with Geologic Carbon Dioxide Sequestration. Geophysical Research Letter, 38, L10401, p 7.

15th International Congress of the Geological Society of Greece
Athens, 22-24 May, 2019 | Harokopio University of Athens, Greece
Bulletin of the Geological Society of Greece, Sp. Pub. 7 Ext. Abs. GSG2019-357

Multi-scale Fracture Network Characteristics in a Carbonate Reservoir Outcrop Analogue: Insights from µCT data in Core Plugs and Thin Sections.

S. Kokkalas[1*], S. Nizamuddin[2], S. Vega[3]

(1) Department of Geology, University of Patras 26500, Patras, Greece
(2) ADNOC Research & Innovation Center, Khalifa University, Abu Dhabi, UAE
(3) Centro de Geociencias, Universidad Nacional Autonoma de Mexico, Mexico

Motivation-Objectives

Most carbonate fractured reservoirs show high variation in lithology, diagenesis, fracture intensity, orientation and connectivity. This high degree of heterogeneity can have a significant impact on reservoir quality and sustainability of production. Outcrop analogues are key elements in the understanding of reservoir architecture and heterogeneity (Jones et al., 2015). Subsurface data represent an extremely small fraction of the reservoir complexity, while most times are not being representative for full fracture networks. This fact often leads to misinterpretation of well data and poor reservoir modelling. Outcrop analogue studies can significantly improve the understanding of fracture characteristics and their impact on fluid flow in hydrocarbon reservoirs. Capturing fracture data across multiple scales requires a range of different methods and appropriate technologies (Jones et al., 2015). We applied this strategy combining traditional fieldwork and digital data capture in a pilot study at a key outcrop along the Cretaceous Wasia and Thamama Group contact, in Ras Al-Khaimah (UAE), since these are regionally important fractured reservoirs.

Methods

Modern methods of digital acquisition, including terrestrial LiDAR or photogrammetry, are particularly adept at capturing detailed geometrical and geospatial attributes over wide areas. Their main advantage is that they result in more robust datasets over a larger scale-range, particularly for fracture heights, lengths, spacing, clustering, termination and connectivity. The acquired 3D point cloud data were used to extract a very detailed fracture network from the studied outcrop, including fracture orientations and 1D fracture density along two ~ 180 m long scanlines.

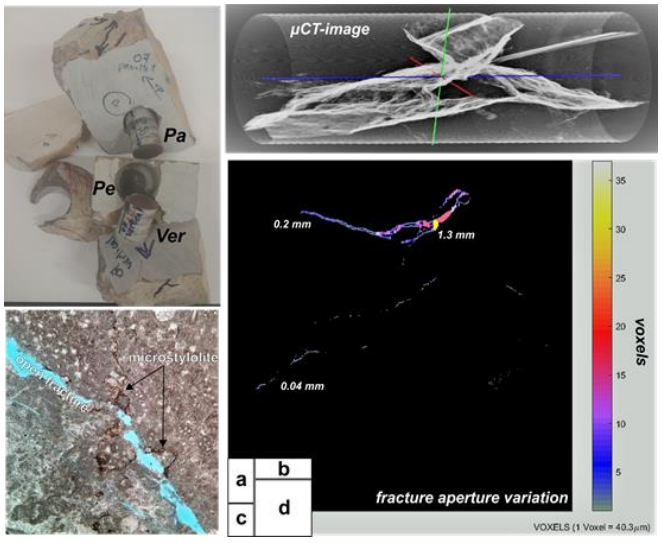

Figure 1a. Lab image showing the three-orthogonal plug-size cores drilled from the rock samples collected from the outcrop. b) High resolution micro-CT image from the examined core plugs, showing the detailed geometry of the microfractures and their overlapping setting. c) Microscopic image showing a mud-dominated packstone with an open fracture offsetting a brown-black colored microstylolite. d) Aperture variation along a fracture calculated from a 2D µCT image.

Additionally, large rock samples were collected along these two scanlines and plug-sized samples were drilled along three orientations orthogonal to each other, with one plug normal to the bedding and two along the bedding and orthogonal to each other (Fig. 1a). The core-plugs were analyzed with the technique of 3D X-Ray Computed Micro-Tomography (µCT). This is a non-destructive technique that allows to acquire images of the interior of the sample, in high resolution and high contrast, allowing to elaborate a 3D reconstruction (Fig. 1b). As in a tomography, numerous sections (e.g. 2000-4200) of the sample are captured in 2D to reconstruct with precision and detail the object in 3D. Moreover, thin sections were made from selected plug samples providing 2D information with a much higher detail in order to examine the microfractures distribution, aperture and filling.

µCT data scan details and processing

Standard samples (1.5´diameter x 3´length) were drilled from the outcrop rock samples. The plug-size samples were scanned using Xradia-520 Versa equipment from Zeiss, available with a maximum 160 kV high-energy and micro-focused X-ray tube. The device is equipped with a 2048 x 2048 pixels, noise suppressed, charge coupled detector assembly, having an innovative dual-stage system for getting high contrast images. For all samples, projections between

2651 and 4601 were taken. The distance of source and detector from the sample was chosen to be 73 mm and 50 mm respectively. This resulted in a pixel size (or voxel) of 40.39 microns. After scanning, the data were reconstructed (i.e. create a 3D image using all the 2D radiogram projections) using devices´ included reconstruction software.

The plug-size samples obtained from the outcrops had very low porosity, ranging from 0.21 to 3.65%, except for 2 samples that displayed porosity of 7%. Hence, it can be concluded that the fracture porosity plays a major role in these tight carbonates and this was one of the aims of this study. In order to obtain features from the 2D images we chose to apply a simple binary segmentation, by recording the range of pixel intensity values that represent the fractures in all slices of the sample. In order to better visualize the fractures in the 2D slice, a MATLAB code was written to segment the pixel intensity values that represent the fractures and assign those pixels white coloring, while the remaining pixels of the matrix in the slice are given a black color. All the segmented slices were loaded in the Vol-View software (open software), to visualize the segmented slices in 3D. This 3D view showed in great detail the fracture network distribution inside the samples (Fig. 1b).

Core-plug thin sections descriptions

Microscopic petrographic analysis showed that most of the rock samples can be classified as mud or grain dominated packstones with forams, echinoderms, bivalve fragments and sporadically Lithocodium-Bacinella green algae. Microstylolites and wispy seams are common, while most of the hairline fractures are straight and have several tip to tip overlapping segments filled often with calcite cement. Few fractures are open or partially filled with silt. Characteristic is that some younger open fractures cross-cut the earlier microstylolitic surfaces (Fig. 1c), while others are developed parallel to the stylolites.

Aperture Width Calculations

The aperture width clearly varies along the fractures (Fig. 1d), implying that is meaningless to assign a single aperture value for fractures in reservoir models. Therefore, an aperture width distribution over the 2D slice or along the full sample would be ideal. In this study, we calculated aperture width by measuring the distance normal to the fracture walls; i.e. by measuring the number of pixels lying between the two fracture walls. The full slice aperture distribution is displayed with a color scale in figure 1d and by multiplying the aperture distribution with the micro-CT scan resolution, we can obtain the fracture aperture in μm or mm. In the example of Fig. 1d, representing one of our most fractured samples, the fracture aperture ranges from 0.2-0.6 mm, with a maximum value of around 1.2 mm often located in the overlap zone or relay zone formed between the individual segments.

3D Fracture Intensity

Estimating the 3D volumetric fracture intensity (P_{32}) is a quite challenging task and most often is estimated indirectly from the 1D P_{10} or 2D P_{21} fracture intensity (Wang, 2005). The 3D fracture intensity (P_{32}) can be expressed as the area of fracture per unit volume of rock mass:

fracture density (m^{-1}) = fracture surface area (m^2) / sample volume (m^3) (Singhal and Gupta, 2010)

The fracture surface area is determined by counting the voxels in the complex fracture network in all slices of the sample and multiplying it with the pixel size to get the surface area of the fracture (m^2). This surface area is divided by the sample volume (m^3) to obtain the fracture density of the sample (units in m^{-1}). The fracture intensities P_{32} calculated from various scales and resolutions ranges from 0.75-3 m^{-1} with laser scanning ($P_{10} \rightarrow P_{32}$), 9-20 m^{-1} from field measurements ($P_{10} \rightarrow P_{32}$) to 12-35 m^{-1} (actual average P_{32} values from μCT data). It is important to note that the P_{32} fracture intensity obtained by μCT is expected to be much higher than the calculated values from other techniques, since this method is highly sensitive to distinct fracture orientation and size distribution, as well as due to the higher level of detail available in the μCT scan. This is also the underlying reason why it represents a true intensity indicator in the context of DFN modelling.

Conclusions

Application of this integrated microstructural methodology in a pilot field outcrop reservoir analogue provides a mean to gain high resolution data, forming a key input in reservoir geo-modelling workflows. The produced digital 3-D analogue, from the outcrop scale down to the core plug and thin section scale, provides essential data for the spatial representation of the reservoir heterogeneities, illustrating the complexity of fractured-carbonate reservoirs. Fracture parameters being quantified across a wide range of scales, and combined with elastic mechanical properties of the carbonate layers represent an ideal basis for the calibration of multi-scale fractured reservoir models.

Acknowledgements

We would like to thank the Petroleum Institute and ADNOC for funding this research project, as well as the ADNOC Research and Innovation Centre at Khalifa University for the permission to use the μCT equipment.

References

Jones, R.R., Long, J.J., Kokkalas, S., Daniels, S.E., Oxlade, D.M., Gilment, S.R., Woods, C.E., Wilkinson, M.W., 2015. Improved Multi-Scale Fracture Models Based on Quantitative Analysis of Outcrop Analogues. Third EAGE Workshop on Iraq. DOI: 10.3997/2214-4609.201414364

Singhal, B.B.S., Gupta, R.P., 2010. Applied Hydrogeology of Fractured Rocks, 2nd ed. Springer Science & Business Media B.V.

Wang, X., 2005. Stereological interpretation of rock fracture traces on borehole walls and other cylindrical surfaces. Ph.d., Virginia Polytechnic Institute and State University.

SPECIAL SESSION

T7/T7.S1 Natural Hazards under Climate Change Impact

Conveners: **C. Loupasakis (NTUA)**
Ch. Anagnostopoulou (AUTH)
E. Zervas (HOU)

15th International Congress of the Geological Society of Greece
Athens, 22-24 May, 2019 | Harokopio University of Athens, Greece
Bulletin of the Geological Society of Greece, Sp. Pub. 7 Ext. Abs. GSG2019-004

Lower Ionospheric turbulence variations during the recent activity of Etna Volcano, Sicily in December 2018

M.E Contadakis[1]., D. N. Arabelos[1], E.M.Scordilis[2]

(1) Department of Geodesy and Surveying, Aristotle University of Thessaloniki, Greece, kodadaki@eng.auth.gr (2) Department of Geophysics, Aristotle University of Thessaloniki, Greece

Introduction

Mount Etna is located close to the eastern coast of Sicily (λ = 14.99 ºE, φ=37.75 º N). With a height of ~3330m, it is considered as the highest volcano of Europe's mainland while it is classified among the most active volcanos globally. Its activity has started back in the middle Pleistocene and it is characterized as a composite volcano (cone-shaped mountain). Its eruptions are mostly of strombolian type (moderate bursts of expanding gases). The last eruption of Etna volcano took place on 24 December 2018 while two days later (26 December, 02:19 UTC) an earthquake of M=4.8 occurred ~15km to the ESE of the volcano, causing damage to the nearby city of Catania. In this paper, we investigate the ionospheric turbulence from TEC observations before and during this recent activity of Etna's Volcano.

Observational Data

To this purpose we use the TEC estimates provided by IONOLAB (http://www.ionolab.org) (Arikan et al. 2009) for 5 mid latitude GPS stations of EUREF network which cover epicentral distances from the active area ranging from 359.083km to 2327.287km, for the periods between 07/11/2018 to 05/01/2019. The selected GPS stations have about the same latitude and are expected to be affected equally from the Equatorial Anomaly as well as from the Auroral storms. Fig. 1 displays the locations of the five GPS stations (blue triangles) and the epicentre of the main shock. The IONOLAB TEC estimation system uses a single station receiver bias estimation algorithm, IONOLAB-BIAS, to obtain daily and monthly averages of receiver bias and is successfully applied to both quiet and disturbed days of the ionosphere for station position at any latitude. In addition, TEC estimations with high resolution are also possible (Arikan et al. 2009). IONOLAB system provides comparison graphs of its TEC estimations with the estimations of the other TEC providers of IGS in its site. In this work only TEC estimations in perfect accordance among all providers were used. The TEC values are given in the form of a Time Series with a sampling gap (resolution) of 2.5 minutes.

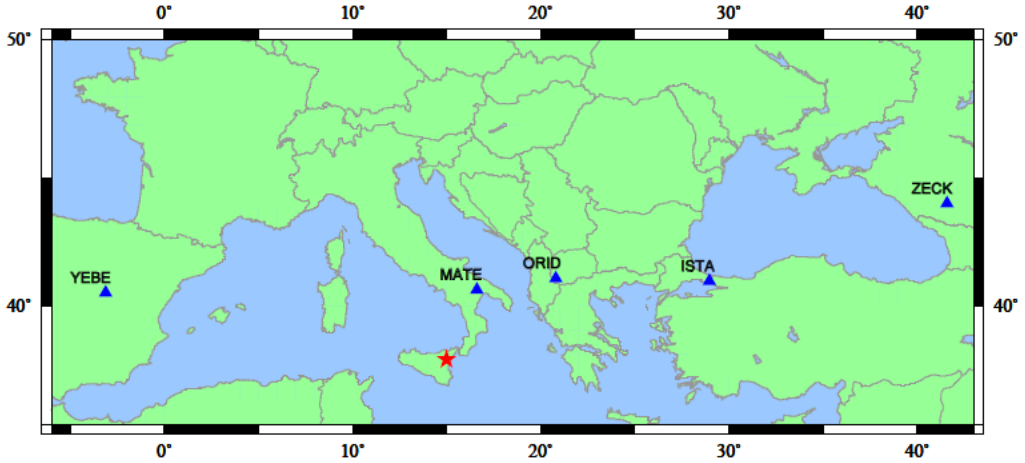

Figure 1. The sites of the EUREF Stations (blue triangles) and the Etna Volcano (red star).

Data Analysis

The observational data, which constitute a time series are analysed using Fast Fourier Transform analysis. From the slop of the logarithmic power spectrum diagram of a segment we can recognize whether the contributed variations to the spectrum are random or periodical. If they are random the slop will be 0, which correspond to the white noise, or -2 which correspond to the Brownian walk, otherwise the slop will be different the so called Fractal Brownian walk. This means that we can trace the presence of periodical variations in the logarithmic power spectrum of TEC variations. This method was successfully applied in our previous work (Contadakis et al. 2015) in order to find the frequency content of TEC turbidity. It is realized that the upper frequency limit f_o of the spectrum of TEC variations increases as we approach the source of the ionospheric turbidity modulation, in our case the earthquake preparation activity.

Results and discussion

The results of this investigation are summarized in Figures 2 and 3, and indicate that the High- Frequency limit f_o, of the ionospheric turbulence content, increases as the site and the moment of the Volcano event occurrence is approaching.

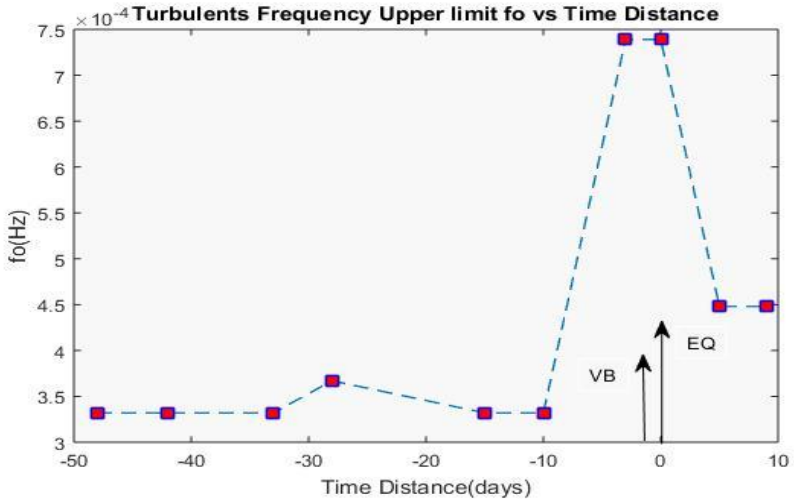

Figure 2 Ionospheric Turbulent Frequency Upper limit, f_o. The arrows indicate the time of the eruption and of the earthquake occurrence.

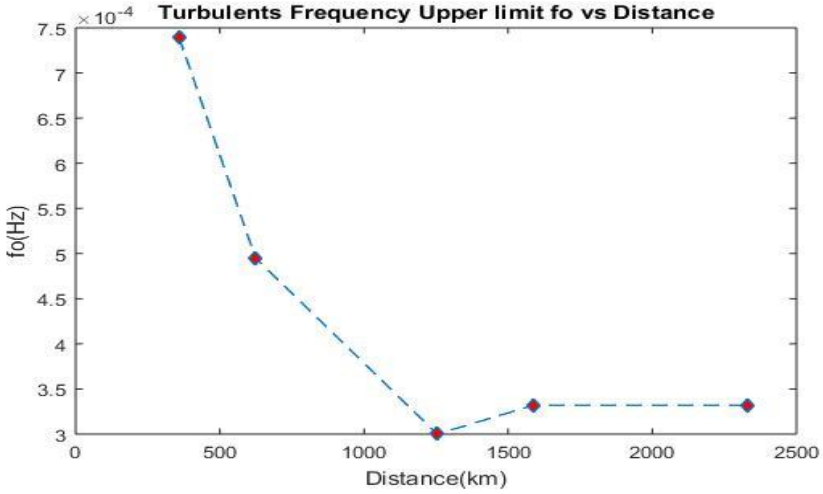

Figure 3 Turbulent Frequency Upper limit, f_o, over the Network stations around the eruption days

We conclude that the LAIC mechanism (Hayakawa 2011) through acoustic or gravity waves could explain this phenomenology. That is, tectonic activity during the volcano eruption produces anomalies at the ground level, which propagate upwards in the troposphere as Acoustic or Standing gravity waves. These Acoustic or Gravity waves affect the turbidity of the lower ionosphere, where sporadic Es-layers may appear too, and the turbidity of the F layer. Subsequently the produced disturbance starts to propagate in the ionosphere's wave guide. Thus, observing the frequency content of the ionospheric turbidity we will notice a decrease of the higher limit of the turbitity frequency band, as a result of the differential frequency attenuation of the propagating wave.

References

Arikan, F.,Yilmaz, A., Arikan, O., Sa Yin, I. Gurun, M.,Yildirim, S.A., 2009. Space Weather Activities of IONOLAB Group: TEC Mapi, Geoph. Res. Abstr., Vol 11.

Contadakis, M.E., Arabelos, D.N., Vergos, G., Spatalas, S. D., Scordilis, E.M., 2015.TEC variations over the Mediterranean before and during the strong earthquake (M = 6.5) of 12th October 2013 in Crete, Greece, Physics and Chemistry of the Earth, Volume 85, p. 9-16.

Hayakawa, M., 2011.On the fluctuation spectra of seismo-electromagnetic phenomena, Nat. Haz Earth Sys. Sci., 11,301-308.

15th International Congress of the Geological Society of Greece
Athens, 22-24 May, 2019 | Harokopio University of Athens, Greece
Bulletin of the Geological Society of Greece, Sp. Pub. 7 Ext. Abs. GSG2019-011

Catastrophic Volcano Explosive Eruptions: Causes and Mechanisms

E. Sharkov

Institute of Geology of Ore Deposits, Petrography, Mineralogy and Geochemistry (IGEM) RAS, Staromonetny per., 35, Moscow, Russia, e-mail: sharkov@igem.ru

How and why catastrophic explosive volcano eruptions occur? These explosions are accompanied by the ejection of vast amounts of gases and pyroclastic material, glowing clouds, surges, etc., and lead to great human and material losses, as well as exerting a significant, in some cases, long-term impact on the Earth's atmosphere and climate. It is assumed that this phenomenon is considered with degassing of magmas in relatively shallow transitional magma chambers beneath volcanoes, i.e. decreasing of gas solubility in the melt due to decrease of temperature and pressure. If the melt is saturated in volatiles, it can spontaneously expel the gas, i.e., begins to resurgent (retrograde) boiling. The scale of this process evidently depends on initial volatiles saturation in the melt and its energy state related to the formation and growth of gas bubbles in the melt because it is energy-consuming process (Sharkov, 2004). However, it is not clear yet why does magma degassing occasionally lead to catastrophic explosions which can last 2–4 months.

Most geologists suggest that catastrophic explosions are related to an abrupt increase of magma volume in shallow chambers owing to degassing. The relevant models suggest the following causes of explosions: groundwater penetration into magma chamber, collapse of volcanic cone, emplacement of gas-saturated basaltic magma into dacite magma chamber, penetration of magma chamber by fractures–conduits, etc. Unfortunately, none of these models explains the vast scale and long duration of the process, as well as specific mechanism of the large-scale bubble formation required for such explosions. The above phenomena actually can affect the eruption style in some cases; however, they cannot cause the catastrophic scale. All these hypotheses consider the explosion itself, but do not explain the high gas content in melts and the mechanism of practically simultaneous separation of gas bubbles in a significant volume. We believe that the process is mainly controlled by kinetic factors, because the formation of a new interface requires significant energy consumption. This is typical of any phase transition, including resurgent boiling of melt, which is considered here. Therefore, the formation of numerous nuclei of a new phase (crystals, melt, or gas) in the previously homogeneous medium can occur only after an energy barrier is overcome. Then, the process proceeds without problems, since it operates within the stability field of the new phase. The formation of a few nuclei owing to fluctuations cannot be developed to a large-scale process, because the increase of an existing bubble-melt interface is energetically more favorable than the formation of a new one. Therefore, for example, local decompression because of a fracture in the chamber's roof, can cause the growth of group of bubbles or lead to local magma foaming during filling of this fracture.

According to experimental data (Fluids, 1991), the solubility of water and CO_2 in mafic and felsic melts increases with pressure up to 3 GPa without extremes (Fig. 1). Unlike water, CO_2 solubility significantly depends on the melt composition, being the lowest in the felsic and intermediate magmas. In other words, water should be the dominant component of the gas phase in rhyolites and dacites of calc-alkaline series, typical for convergent tectonic settings, whose eruptions are typically catastrophic. The experimental data also indicate that water solubility in the melts remains nearly constant during pressure decrease to about 0.1 GPa and then abruptly decreases. Unlike water, the CO_2 solubility gradually decreases with decreasing pressure, and only weakly depends on the initial $CO_2/(CO_2 + H_2O)$ ratio.

From this follows that subduction-related water-bearing andesite–dacite magmas can become oversaturated in H_2O owing to abrupt pressure decrease under shallow conditions in peripheral chambers of volcanoes at depths of 3–4 km. In this case, melt in the magma chamber presents a "blasting" mixture, which is ready to explode at any moment owing to rapid degassing. Seismic observations show that the upper magma chambers beneath the most andesite–dacite volcanoes are located at these depths (2–8 km) (Macdonald, 1972). Hence, such situations frequently occur in nature.

However, as follows from experimental data, even the water-oversaturated melt cannot boil spontaneously without any additional impact or can boil only by scoria formation, as it takes place during the eruption of intraplate basalts. Large-volume separation of gas bubbles requires a mechanical shock-type impact: the melt must be abruptly compressed and subsequently decompressed (Stolper, 1982). In this case, gas bubbles begin to form over the entire magma volume in chamber. We believe that this mechanism can be applied to catastrophic volcanic eruptions. The volatile-saturated melt in a shallow chamber can explode owing to a strong earthquake, when pressure abruptly increases in the compression front and abruptly decreases in the subsequent expansion front. So, presence of volatile-rich magma as well as some energy pulse behaving as a "trigger," which causes the rapid and extensive formation of gas phase nuclei, are necessary for a catastrophic explosion.

This mechanism is especially efficient during a series of earthquakes, which usually precede catastrophic explosions; resurgent boiling begins at the moment when the energy barrier is overcome. During a further (stronger) impact, many homogeneously scattered gas bubbles are formed in magma. It is highly improbable that the entire chamber volume is spanned by this process, since pressure in the chamber can increase downward to 0.15–0.3 GPa (Macdonald, 1972), thus blocking further formation of bubbles. However, this pressure is sufficient for explosion and ejection of the material. At the moment of explosion, the magma chamber is impacted by the explosion-related shock wave, which is followed by the expansion front, thus again allowing large-volume degassing and a new explosion, and so on.

Such a mechanism determines the layer-shape resurgent boiling zone related to frontal propagation of shock waves. However, in any case, this zone, owing to explosions, will migrate downward, primarily develop at the shallower sections of the magma chamber, and gradually remove the melt from it. If the chamber has a significant vertical extent, it can be emptied to depths of about 5–6 km, since the melt at larger depths may be undersaturated in H_2O and retrograde boiling will stop. Calderas can form owing to the chamber emptying, and the volcano will become inactive until the formation of a new chamber by water-saturated magma replenishment, after which the process can repeat.

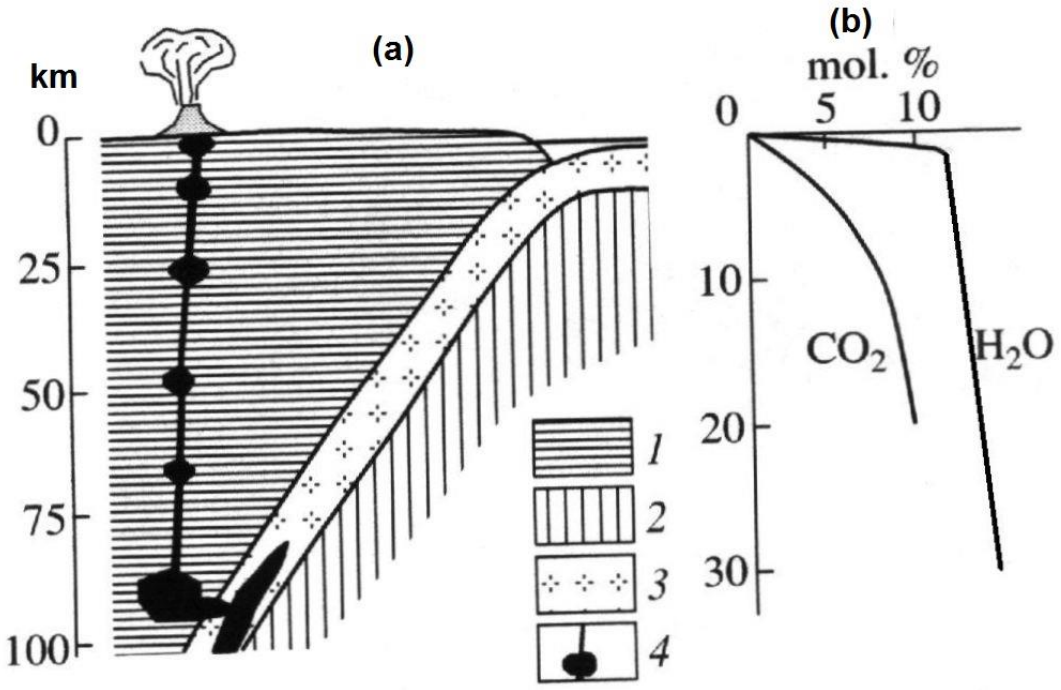

Fig. 1. Scheme illustrating the structure of the magmatic systems related to subduction zones at the active margins of continents and oceans. (a) Structure of the system: (*1*) continental lithosphere, (*2*) oceanic lithosphere, (*3*) subducted plate, (*4*) magma chamber. (b) Variations of H_2O and CO_2 solubility in silicate melt versus pressure (simplified after (Fluids, 1991).

Such a mechanism determines the layer-shape resurgent boiling zone related to frontal propagation of shock waves. However, in any case, this zone, owing to explosions, will migrate downward, primarily develop at the shallower sections of the magma chamber, and gradually remove the melt from it. If the chamber has a significant vertical extent, it can be emptied to depths of about 5–6 km, since the melt at larger depths may be undersaturated in H_2O and retrograde boiling will stop. Calderas can form owing to the chamber emptying, and the volcano will become inactive until the formation of a new chamber by water-saturated magma replenishment, after which the process can repeat.

References

Sharkov, E.V., 2004. Role of the energy of interface formation in the melting and retrograde boiling. Geochemistry Intern., 42(10), 950-961.

Fluids and Redox Reactions in Magmatic Systems, 1991. Ed. by A. A. Kadik (Nauka, Moscow,) (in Russian)

Macdonald, G. A., Volcanoes (Prentice Hall, Englewood Cliffs, 1972; Mir, Moscow, 1975).

Stolper, E. 1982. The Speciation of Water in Silicate Melts. Geochim. Cosmochim. Acta 46, 2609–2620.

15th International Congress of the Geological Society of Greece
Athens, 22-24 May, 2019 | Harokopio University of Athens, Greece
Bulletin of the Geological Society of Greece, Sp. Pub. 7 Ext. Abs. GSG2019-026

Climate Change and its Impact on the Recent Geological Past and today; the Role of Earth Scientist

Constantine Perissoratis
perissoratis@yahoo.gr

Introduction

In the last years the impacts of the climate change are repeatedly discussed and /or analyzed in either daily news or scientific presentations. Therefore we have to describe this subject and discuss the changes are expected to take place today or at the near future.

History of Quaternary – Holocene cold / warm climate periods. Regional setting

The Earth has undergone in the last about 500 000 years four significant climate changes. This time includes three cold periods, lasting about 100 000 years each, with a warm period between them, lasting about 12 000 years (Chappel and Shackleton, 1986). Today we are living in the last warm period that started about 12.000 years ago and is expected to end in about 2.000 years from now (Fairbanks, 1989) when the next cool period will start again. The cause of these cycles is the variability of the solar radiation reaching the earth.

One of the first areas to be studied were, two areas in Greece the greater city of Thessaloniki, in Thermaikos Gulf, northwestern Aegean as an estuarine, (Georgas and Perissoratis, 1989), and the Rhodes Island, southeastern Aegean, as an insular sector (Perissoratis, et al., 1996). According to the expected impacts, a series of actions were proposed, described and presented to the local and regional organizations. The main suggestions were referring to the impacts expected from two scenarios, as depicted by the IPCC working Group for southern Europe (Gue et al 1991). In the first scenario by the year 2030 it is expected a temperature increase of 1,8°C and sea level rise by 18cm (+/- 10cm) and, in the second scenario, by the year 2100, the estimations were respectively increase 3° C and 65 cm (+/- 35cm),

Predictions of future increases in Earth temperature and sea level rise.

Sea level increases as a result of a future temperature increase was and has been in research continuously by many researchers. At the same time the study of the sea level rise, especially in the last two hundred years and, further earlier, in the last two thousand years has been carried out. Thus according to Jevrejeva et al (2006) the sea level during the periods years 1850 to 2000 the global sea level rise was in the order of 20 mm/year, while according to Grinsted et al (2009) during the last 2000 years the minimum sea level rise was about 15mm/year and the maximum on 23mm/year. These estimations are within the known estimations during the Holocene period. As for the future estimations, for the year 2100 both ideas are different as it is presented in fig 1. The IPCC model consider a rise of 35 cm , that is a rate of 35mm/year while that of Grinsted et al, (2009) the expected rise will be to about 1.2 m that is 120 mm/year, an increase of the order of 3.5 times.

The impact by using the future predictions and the suggested actions

The above overestimations that certainly are based in hypotheses, without related to the presence of an ongoing event, and have been used by many research groups that deal with the expected impacts. As a consequence they usually suggest the carrying out of the necessary actions very soon. This is mainly because the predictions and the impacts if publicized are useful method for impressing the greater public, via the various media, and especially in western counties. In Greece particular two extensive analyses on the forthcoming impacts of the expected climatic change was carried out recently. In 2009 the National Bank of Greece established and funded the Committee on Impacts of the Expected Climate Change in Greece, that presented its reports in 2015 (CCISC, report 2015), presented and published in daily newspapers. The conclusions and suggestions of this committee were based, among other impacts, on an expected 1 m sea level by the end of 2100. As a conclusion a series of actions to be carried out soon was suggested. Otherwise the impacts will be disastrous, estimating also the economic cost.

Similar ideas in Greece were also presented by diaNEOsis a non-profit research organization that studied, among other, the impacts of climate change in the Greece economy (Georgakopoulos, 2017). The study, partly presented in daily newspapers and available to the public, considers the IPCC 2007 report and the values from 20 to 59 cm by the year 2100 as very moderate and accepts a sea level rise from 0.80 m to 2.0 meters. The study suggests a transition by 2050s to the low carbon economy, organizing meetings for the future impacts but, mainly, within the next four years, special plans for the Tourism and Agricultural sector. No evaluation of costs for these actions were presented.

It is well accepted that tourism is the main economic source of Greece. Therefore, the predicting by these studies that eventual impacts of an eventual climatic change will take place soon in Greece, the impression for the ordinary people are very negative and disappointed.

Even more very often many physical events that have been taking place in Greece , are related to consequences of the climate change without any scientific explanation, as was the case in the disastrous fire it the Mati location nearby Athens (23 July, 2018, with over 100 people dead).

Disaster amendment and mitigation policies – Conclusions

The impacts on the human environment are from natural events, that are mainly Coastal Erosion, Earthquakes, Tsunamis, Floods, and Active Faults The earth scientists have already knowledge and experience on the impacts of these natural events and have to deal with these regardless of the eventual climate change. At the same time the increased use, for various purposes, of the coastal region by the human population, in many aspects, degrade the coastal zone. The alternation of cool and warm periods in the latest geological past, are still ongoing, and all the available scientific knowledge should be used to see, in a more clear way, the impacts in an eventual climate change. An event that has not been recorded yet.

In conclusion since the natural events will always happen in human life, they require relevant actions both before and/or after their occurrence

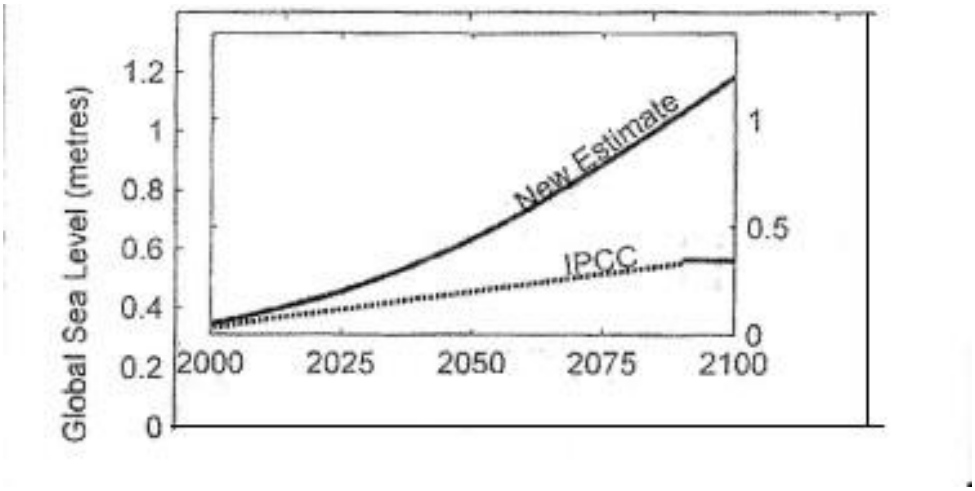

Figure 1. Global sea level (Grinsted et al. 2009) depicting the expected change between years 2000 to 2100 (2009 New Estimate) and IPCC (2007).

References

Chappell, J., and Shackleton, N. J. (1986). Oxygen isotopes and sea level. Nature (London) 324, 137 – 140.

Climate Change Impacts Study Committee of Bank of Greece, (2015): National Climate Change Adaptation Strategy, (NCCAS,), The environmental, economic and social impacts in Greece Chapters 1-5, 465 pages. Chapter 1The climate of the Eastern Mediterranean and Greece: Current and future mean sea levels Chapter 3, The cost of climate change in Greece.

Georgakopoulos, Th., 2017: The impact of climate change in the Greek Economy, diaNEOsis, Research and Policy Institute, in: info@diaNeosis.org, Articles/Nature, Athens, August 2017.

Georgas, D. and Perissoratis, C., (1989). Implications of future climate changes on the Inner Thermaikos Gulf: In: Implications of the Climate changes, UNEP, J.Milliman, et al eds, ch. 13, p.495-534, Arnold Press, London.

Grinsted,A., J.C.Moore, and S. Jevrejeva (2009), Reconstructing sea level from paleo and projected temperatures 200 to 2100 AD, Clim. Dyn., doi:10.1007/s00382- 008-0507-2.

Jevrejeva, S., A. Grinsted, J. C. Moore, and S. Holgate (2006), Nonlinear trends and multiyear cycles in sea level records, J. Geophys. Res., 111, C09012, doi: 10.1029/2005JC003229.

Meehl, G.A., T.F. Stocker, W.D. Collins, P. Friedlingstein, A.T. Gaye, J.M. Gregory, A. Kitoh,R. Knutti, J.M. Murphy, A. Noda, S.C.B. Raper, I.G. Watterson, A.J. Weaver and Z.-C. Zhao: Global Climate Projections. In: Climate Change 2007: The Physical Science Basis. Contributionof Working Group I to the Fourth Assessment Report of the Intergovernmental Panel on Climate Change [Solomon, S., D. Qin, M. Manning, Z. Chen, M. Marquis, K.B. Averyt, M. Tignor and H.L. Miller (eds.)]. Cambridge University Press, Cambridge, United Kingdom and New York, NY, USA. (2007)

Perissoratis, C., Georgas, D., Alexiadou, M.C., Dikaiakos, G., Lascaratos, A., Leontaris, S., Margaris N. and Tsakiri K., (1996). Implications of Expected Climatic changes for the island of Rhodes. In Implications of the Climatic changes, L. Jeftic et al. Edts, v. 2, p. 57-142, Arnold Press, London.

15th International Congress of the Geological Society of Greece
Athens, 22-24 May, 2019 | Harokopio University of Athens, Greece
Bulletin of the Geological Society of Greece, Sp. Pub. 7 Ext. Abs. GSG2019-056

The Contribution of Geophysical Survey to Seismic Hazard Mapping at Farsala basin (Greece)

John D. Alexopoulos, Spyridon Dilalos, Georgia S. Mitsika, Haralambos Kranis, Efthymis Lekkas

National and Kapodistrian University of Athens - Department of Geology and Geoenvironment, Panepistimiopolis, Zografou, Greece, jalexopoulos@geol.uoa.gr

Introduction – Geology

The study area is located at the broader area of Farsala (East Thessaly) and more specifically between the city of Farsala and its railway station. The main target of the geophysical survey was to investigate the subsurface litho-stratigraphic structure in order to assess the existence of two (2) possible fault zones. These zones were proposed in the primary Neotectonic Map of the area of Farsala, scale 1:25.000 (Fig. 1), produced by the Section of Dynamic Tectonics & Applied Geology of National Kapodistrian University of Athens in 2016, in the context of the Seismic Hazard Mapping of the Farsala broader area.

The alpine formations are mostly observed at the southern and eastern part of the greater study area. The late Cretaceous Limestones and Dolomitic Limestones (L-DL) seem to dominate (Fig.1). They are observed as mid-plated to un-plated with marly intercalations. Moreover, the ophiolite formations exist (Fig.1), which consist of peridotites and serpentinites, underlying the limestones. The existing ophiolite masses overlay the Jurassic Schists, which consist of clayey schists-cherts with conglomerates and limestone intercalations.

The post-alpine formations cover the broader part of the Farsala basin. The inner part is covered with fine-grained alluvial deposits comprised of clays, silts and sands (Fig.1). The outer areas of the basin, where the geophysical measurements were carried out, are covered with the proximal phases of scree and consist of clays, grains and sand alterations (Fig.1). The foothills of the area are covered by the semi-cohesive scree and talus cones (Fig.1).

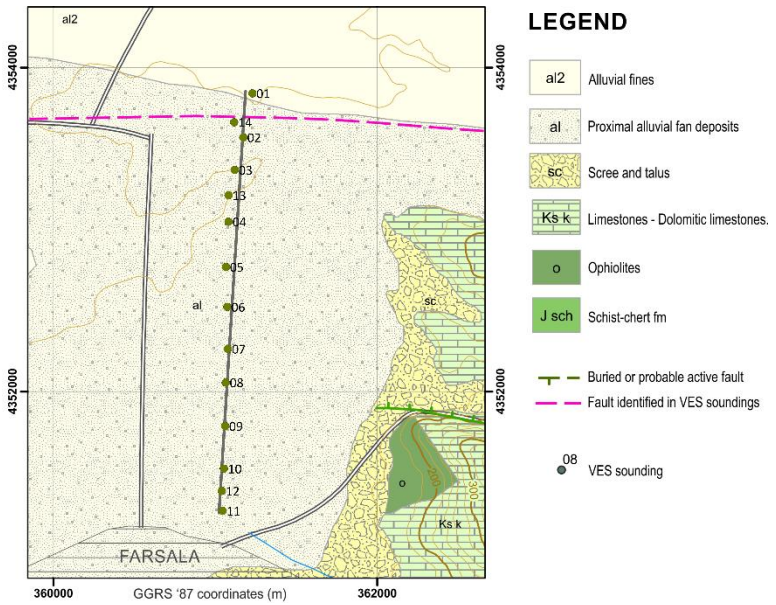

Figure 1. Updated Neotectonic Map (Division of Dynamic Tectonics & Applied Geology, 2016), with modified fault traces based on the results of the survey.

Geoelectrical research

Fourteen (14) vertical electrical resistivity soundings (VES) were conducted, using the *Schlumberger* array, along a N-S profile and total length of 2590 m. It is a method indicated for such geological investigations (Alexopoulos and Dilalos, 2010). The maximum current electrode spacing (AB) was equal to 1000 m. An *ABEM Terrameter* system was used for the field measurements.

The geophysical data were processed by applying the automatic method of Zohdy and Bisdorf (Zohdy, 1989), composing a "multilayer" model. Beyond that, the commercial software package IX1D by Interpex was used for the calculation of the "layered" model. The qualitative representation and adumbration of the general subsurface structure is shown in Figure 2, where the distribution of (true) resistivity is observed, based on the results of the multi-layered models (Zohdy, 1989). Therefore, between the VES 01-14-02, the resistivity distribution changes rapidly, almost in vertical direction, implying the existence of a lateral zone of geoelectrical discontinuity. Below VES 02-03-13, we observe a geoelectrical formation

of high resistivity values (>200 Ohm.m), at shallow depths (<50m). Beyond that, from VES 05 to the southern end of the section a smooth, horizontal resistivity distribution is shown, with low resistivity values (5-15 Ohm.m) dominating in the upper part.

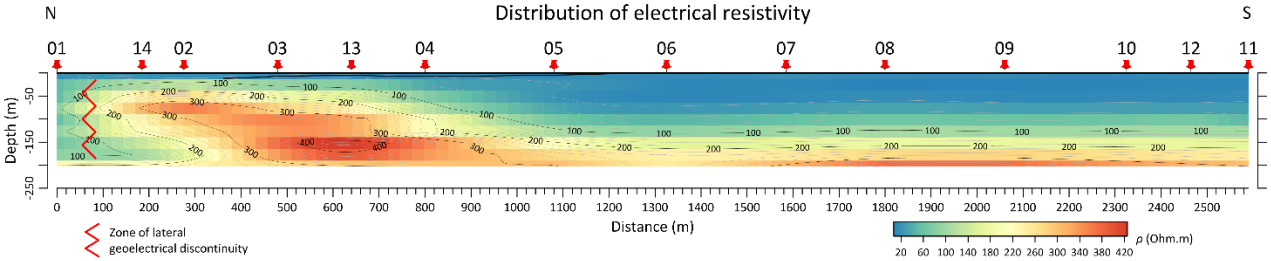

Figure 2. Distribution of (true) electrical resistivity

Interpretation and Discussion

The evaluation of the geoelectrical processing and the correlation with the geology of the area gives an overall image of the subsurface geological structure. The results of this procedure are illustrated in Figure 3, with a maximum depth of investigation equal to 200 meters. The boundaries of three different geological formations can be observed in this geological-geoelectrical section (Fig.3). Between VES 01 and 14, a lateral zone of tectonic discontinuity that clearly interrupts the subsurface layers was identified. The throw of this zone, based on the offset of the top of the carbonates, is almost 150 m, with the northern block downthrown with respect to the southern one.

Below VES 14-02-03-13-04, the cohesive L-DL formation, with high resistivity values (240-500 Ohm.m) was identified at depths less than 25 m. The overlying formation is considered to be the semi-cohesive scree (ρ=30-60 Ohm.m). Furthermore, between VES 14 and 02 and at depths more than 150 m, the schist-chert formation has been investigated. Below VES 05 and 05, the top boundary of Limestones-Dolomitic Limestones dips smoothly to the south, down to the depth of 100 m. From this point and up to the southern end of the profile, the top boundary of the L-DL formation is almost horizontal, at depths between 50-80 m. Across the whole section, the L-DL formation is covered by 20-100 m thick alluvial deposits of varying lithological composition (ρ=9-59 Ohm.m). These deposits have been suggested to host local aquifers (Rozos and Tzitziras, 2002).

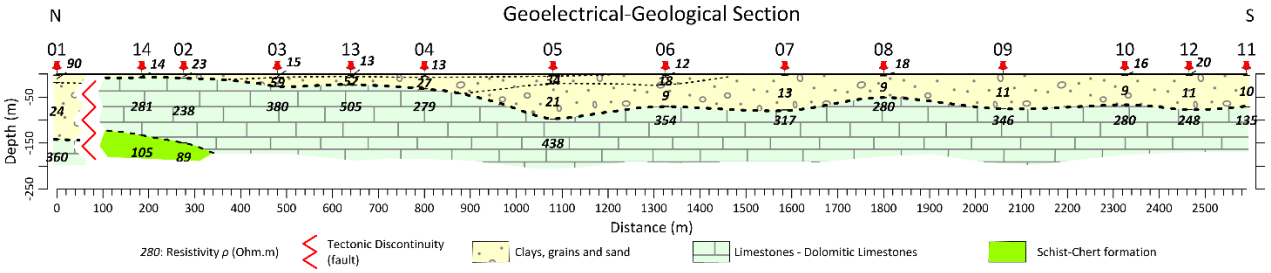

Figure 3. Geological interpretation of the geophysical section

Conclusions

Based on the geological interpretation of the geophysical survey (Fig. 3), the primary Neotectonic map of the area was modified. More specifically, the southern fault zones (Fig.1-green line) has been restricted to the edges of the hill area, since there is no geophysical evidence for its occurrence along the profile (as it was initially indicated). Additionally, the northern fault line (Fig.1-pink line), seems to have been relocated between the location of the soundings 01 and 14, with an estimated width of the zone equal to 120 meters. The verification of this fault zone, with similar characteristics to the ones of the local active fault zones of the area, implies but not necessarily proves its activity level.

Acknowledgements

The authors would like to thank Ms. Eyagelia Kalaboki and Ms. Augousta Salomidi for their contribution during the acquisition of the field measurements. The study was funded by SARG-NKUA, research account 70/3/13532.

References

Alexopoulos, J.D. and Dilalos, S., 2010. Geophysical research for geological structure determination in the region of South Mesogheia (Attica). Bulletin of the Geological Society of Greece, 43(4), 1898-1906, http://dx.doi.org/10.12681/bgsg.11381

Neotectonic Map of Scale 1:25.000, 2016. Project: Seismic Hazard Mapping for the greater area of Farsala. Division of Dynamic Tectonics & Applied Geology, National Kapodistrian University of Athens

Rozos, D. and Tzitziras, A., 2002. Report of the Engineering geological examination of ground water in Farsala area. Institute of Geology and Mineral Exploration (IGME).

Zohdy, A.A.R., 1989. A new method for the automatic interpretation of Schlumberger and Wenner soundings curves. Geophysics, 54 (2), 245-253, http://dx.doi.org/10.1190/1.1442648

15th International Congress of the Geological Society of Greece
Athens, 22-24 May, 2019 | Harokopio University of Athens, Greece
Bulletin of the Geological Society of Greece, Sp. Pub. 7 Ext. Abs. GSG2019-140

The 21 July 2017, Kos-Bodrum tsunami intensity mapping: Applying the integrated Tsunami Intensity Scale (ITIS2012)

M. Gogou[1], N.-E. Katsetsiadou[1], E. Lekkas[1], E. Andreadakis[1]

(1) National and Kapodistrian University of Athens, Faculty of Geology and Geoenvironment, Panepistimiopolis, Zografou, Athens, Greece mgogou@geol.uoa.gr

Introduction

On July 21, 2017 (22:31 UTC), a Mw 6.6 earthquake occurred off-shore the Kos Island, Greece. The epicenter is located in the marine area between Kos Island and the Turkish coasts in Gokova Bay. Shortly after the earthquake, tsunami waves hit the south-east coast of Kos and the coast of Mugla province in the Gokova Bay area.

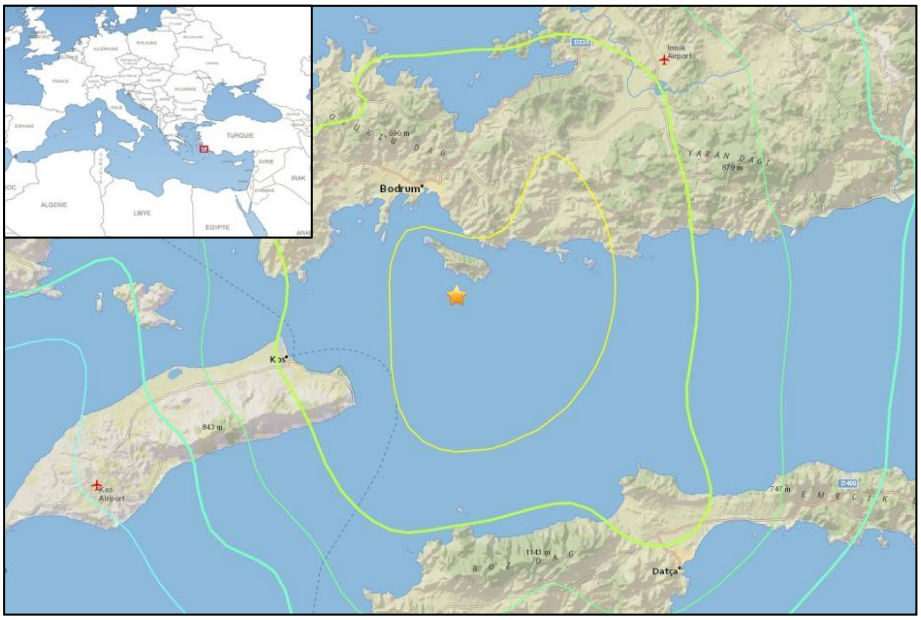

Figure 1. Interactive map for earthquake on July 21 (USGS map)

Methods

In order to assess the tsunami intensity, data regarding the tsunami impact and gathered from multiple sources on both the coastal zone of Kos and the eastern coast of Turkey, have been recorded, assigned against the ITIS2012, and mapped using ArcGIS. Interpolation methods have been used in order to display the impact zoning in the inundated areas.

Primarily collected data (autopsy, photo material, drone recordings, witnesses' testimonials) along with the web published data and preliminary scientific reports have been mapped and evaluated against ITIS2012.

Data collected from 48 different points around the tsunami affected area. Most of them are located in or closed to city of Kos (Greece) and city of Bodrum (Turkey).

Results

The results show limited, yet notable impact on each one of the ITIS2012 categories, escalating among the middle grades of the Scale, and classifying the event as a middle-intensity tsunami.

The max intensity for Bodrum area in Turkey is estimated at VII/XII grade as for the same tsunami the max intensity for Kos area in Greece is estimated at VI/XII grade. This can be attributed to different morphology, possible different distance, different wave direction or coastal land use.

Table 1. Tsunami intensity numbers based on IT IS_{2012} grade scale.l

$ITIS_{2012}$ Categories	Grade scale for Kos Port (GREECE)	Grade scale for Bodrum (TURKEY)
Physical Quantities	VI	VII
Impact on humans	V	V
Effects on mobile objects	VI	VII
Impact on infrastructure	VI	VII
Geoenvironmental Effects	V	VII
Effects on structured environment	VI	VII

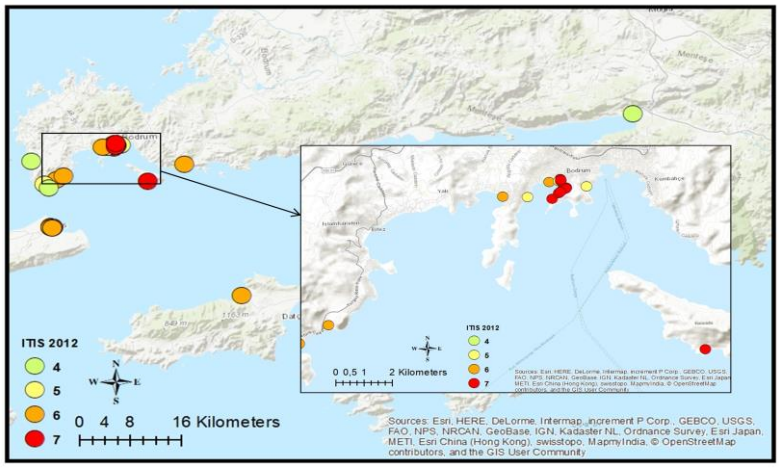

Figure 2. Kos-Bodrum tsunami intensity mapping.

Conclusions

Earthquake activity in Aegean Sea can easily generate tsunami waves and affect coastal humans and human activity.

Applying the ITIS Scale to a middle-intensity event for the first time, showed that the individual $ITIS_{2012}$ criteria successfully complemented each other creating an excellent zoned or point map.

The main criteria categories that mostly defined e a medium-impact tsunami are: a) Quantities, b) Impact on human & c) mobile objects

However needed direct field observation and direct data collect for better quality on every ITIS2012 category.

References

Lekkas, E., Emmanuel Andreadakis, E., Irene Kostaki, I., Kapourani, E. 2013. A Proposal for a New Integrated Tsunami Intensity, Scale (ITIS-2012). Bulletin of the Seismological Society of America, Vol. 103, No. 2B, pp. 1493–1502

Yalçıner, A.C., Annunziato, A., Papadopoulos, G., Dogana, G.G., Gulera, H.G., Cakird, T.E., Sozdinlere, C.O., Ulutasf, E., Arikawag, T., Suzenh, L., Kanoglui, U., Gulera, I., Probstb, P., Synolakis, C. 2017. The 20th july 2017 (22:31 utc) Bodrum/Kos earthquake and tsunami;

Dimova, L., Raykov, R. 2018. Numerical simulations of the earthquake-induced tsunami of July 20, 2017 (Mw=6.6) in Bodrum-Kos, Aegean Sea. Review of the Bulgarian geological society, vol. 79, part 1, 2018, p. xx–xx

Heidarzadeh, M., Necmioglu, O., Ishibe, T., Yalciner, A.C. 2017. Bodrum–Kos (Turkey–Greece) Mw 6.6 earthquake and tsunami of 20 July 2017: a test for the Mediterranean tsunami warning system. Geoscience Letter, Official Journal of the Asia Oceania Geosciences Society (AOGS) 4:31

Katsetsiadou, A.N. 2014. Applying the Integrated Tsunami Intensity Scale ($ITIS_{2012}$) on Ishinomaki Bay Coast after 2011 Tohuku, Japan mega-event. MSc Thesis, University of Athens

15th International Congress of the Geological Society of Greece
Athens, 22-24 May, 2019 | Harokopio University of Athens, Greece
Bulletin of the Geological Society of Greece, Sp. Pub. 7 Ext. Abs. GSG2019-141

Floodplain Mapping using Hydraulic Simulation Hec-RAS in G.I.S: A case study for Rafina basin (Attica, Greece) based on February 2013 storm event.

M. Andreou[1], S. Karalis[2], D.-V. Batzakis[2], E. Karymbalis[2]

(1) National and Kapodistrian University of Athens, Geology and Geoenvironment Department, University Campus-Zografou, Athens GR 15784, mrandreou204@gmail.com
(2) Harokopio University of Athens, Geography Department, Eleftheriou Venizelou Ave., 70, Kallithea, Greece

Introduction

Floodplain mapping is a basic tool for flood risk assessment (Correia et al., 1998). The coupling of hydraulic modeling Hec-RAS (Hydrological Engineering Center's River Analysis System) and G.I.S (Geographical Information System) has become a very effective tool in the field of flood risk prediction and management. Mapping the floodplain zones of a stream or a river is an important exercise related to both land-planning and river basin management (Yang et al., 2006).

The drainage basin of Rafina was mainly an agricultural region until the decade of 80s. According to the demographic data of the Greek Statistical Service (Hellenic Statistical Authority, 2015), population has increased about 3.5 times the last 30 years. Extreme fire events, roads constructions and uncontrolled building construction during that period of time were the triggering point of the following high rate urbanization. Flood history data has pointed out that flood events frequency increased during the above period. The conversion of agricultural and forest land use to urban and mixed-urban land use, strengthened the vulnerability of the drainage basin.

Information gathered from governmental organizations, emergency agencies, the press and field observations along with geologic, geomorphologic evidence, land use and hydraulic simulation by using Hec-Ras along the final 4km of the main stream, were stored, structured and analyzed in GIS platform, resulting ultimately flood plains delineation. A severe storm event on 22/02/2013 was taken as a case for the modeling framework.

Study Area

The study area is situated in East Attica approximately 15km east of Athens (Greece), consisting of a small catchment drained by Megalo Rema torrent. In terms of geomorphology, Megalo Rema basin (area 115km^2) consists of Pedeli mountain (920m a.s.l.) on the north and Ymmitos mountain (620m a.s.l.) on the northwest, draining into a low lying south part (max elevation 300m). The slope range is between 0° – 44.4^o and the mean slope is 6.3^o. The main channel of M.Rema torrent is a sixth-order stream (Strahler) which reaches the sea near to the Port of Rafina, to south Evoikos Golf, passing through a small valley where settlements of the municipalities of Geraka, Pallini, Peania and Rafina are situated. The land use is urban-mixed, urban and agricultural. The catchment is a small, flash flood basin drained by ephemeral watersources with an asymmetric drainage network (Fig.1A). The research of the flood history gives an Average Frequency of floods events 1Flood Event/2.7yrs during the last 27 years (Andreou, 2016).

Methodology

In this study delineated floodplain areas along the final 4km of the main stream M.Rema, by using ArcGIS version 10.0, Hec-GeoRas extension version 5 and hydraulic simulation Hec-GeoRas version 4.1. The accuracy of the results is defined by the geometric input data (Casas et al., 2006), in order to ensure the model precision we used a DEM (.dwg file) 1:500 scale. Two hundred cross-sections cutlines were created by HEC GeoRas, 1 cross-section cutline /20m, as input geometric data for the hydraulic simulation in HEC-RAS model (Fig.1B). Steady flow analysis is applied to manage the calculation of water surface profiles.

The steps that were followed between ArcGIS, Hec-GeoRas and Hec-Ras are described in Fig.2.

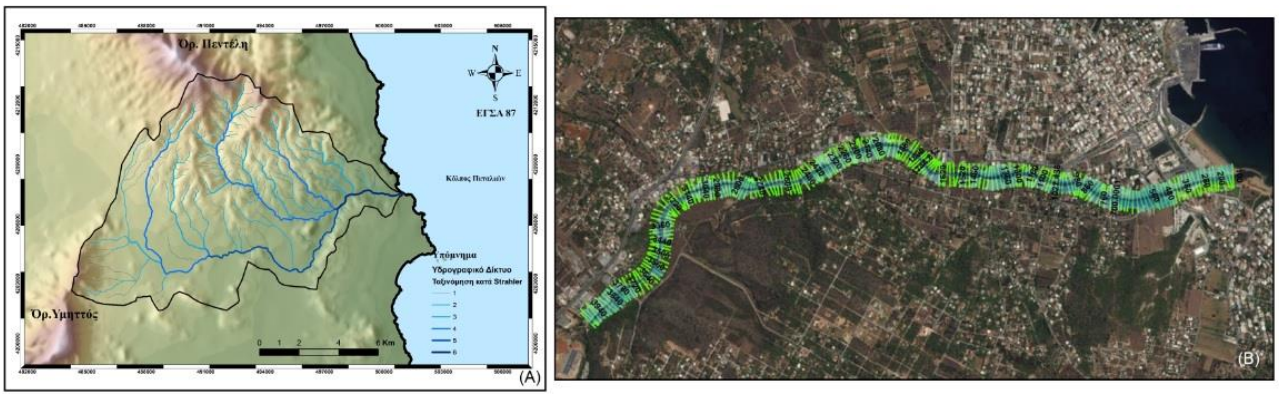

Figure 1: (A) Dem-Drainage Network, (B) Cross-sections cutlines along the final 4km of the main channel of M.Rema torrent.

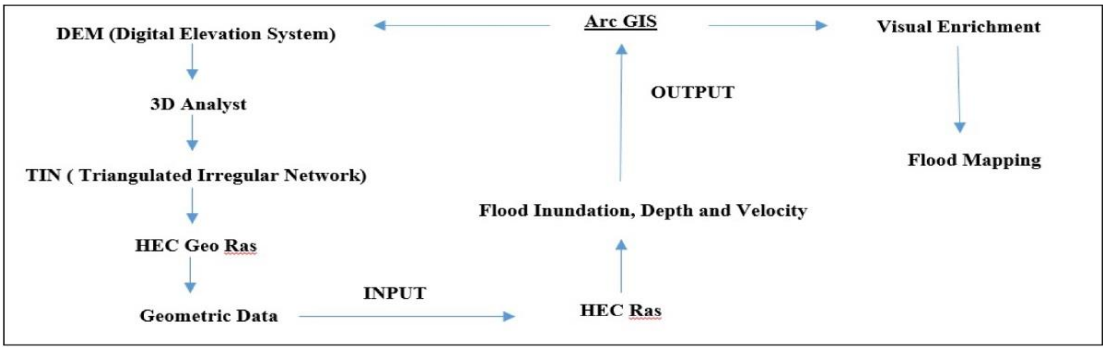

Figure 2: Steps in model design, using ArcGIS (geometric data-land use data) as INPUT data to HEC-Ras model and visualization the OUTPUT data by using GeoRAS extension (RAS Mapping) in ArcGIS.

Land-use data were obtained by Corine 2000 (CLC 2000), Ilots 2012(CLC 2012) land cover and field observation. Manning's n values were derived from the manual of the hydraulic model (HEC-Ras Hydraulic Reference Manual, 2010). The flood plain delineation exercises applied in the study were repeated for three discharges values: (A) discharge value of the storm event on 22/02/2013, Q_1=150m^3/s, (B) discharge value for return period 25 years Q_2=300m^3/s (Lazaridis – Nalmpantis, 2004), (C) discharge value for return period 50 years Q_3=600m^3/s (Tsakiris, 2007) (Fig.3).

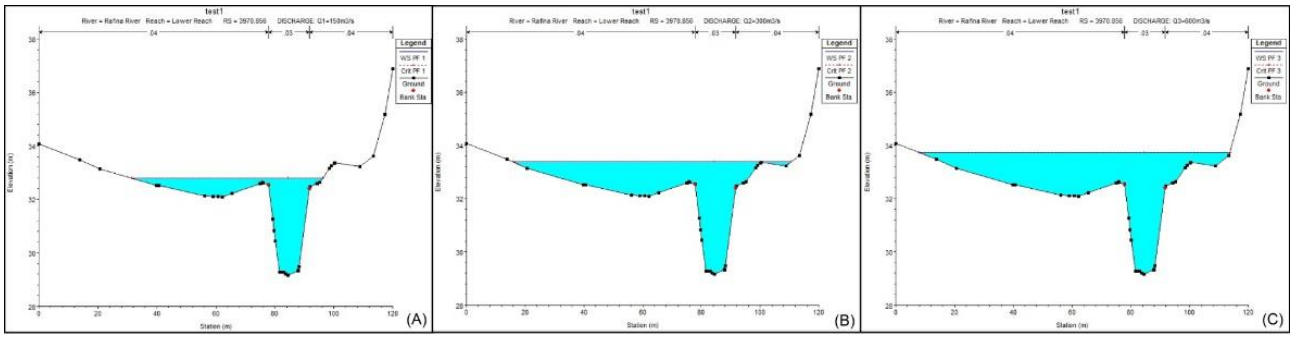

Figure 3: Cross section of 3970m, (A) profile1 Q_1=150m^3/s, (B) profile1 Q_2=300m^3/s, (C) profile1 Q_2=600m^3/s

Results

The results of the hydraulic simulation (HEC-RAS) for Q_1 profile fully correspond to the recorded construction's damages of the storm event on 22/02/2013, 43% of the 200 cross-sections cutlines are located in floodplain zones. The percentage of the cross-sections cutlines that are located in floodplain zones is 83% and 97% for Q_2 and Q_3 correspondingly.

High vulnerability areas are bounded by cross section ranges 4000m.-3700m. and 1000m.-100m. for Q_1 profile, 4000m. – 3680m., 3460m.-3260m., 3120m.-1920m., 1760m.-1280m. and 1220m.-0m for Q_2 profile. As concerns Q_3 profile the evaluation is that the whole distance (4km) presents high rate of vulnerability.

References

Andreou, M., 2016. Flood Risk Assessment of M.Rema (Rafina) Basin with the use of Geographical Information System (G.I.S). Msc Thesis, National Kapodistrian University of Athens, Faculty of Science, Department of Geology & Geo-environment, pp 57.

Casas, A., Benito, G., Thorndycraft, V.R., Rico. M., 2006. The topographic data source of digital terrain models as a key element in the accuracy of hydraulic flood modeling. Earth Surf. Process. Landforms 31, 444-456.

Correia, F.N., Rego F.C., Saraiva M.G., Ramos I., 1998. Coupling GIS with Hydrologic and Hydraulic Flood Modelling. Water Resources Management 12: 229-249.

HEC-Ras Hydraulic Reference Manual 2010, Version 4.1, US Army Corps of Engineers, Hydrologic Engineering Center. Chapter 3, pp 14-16

Hellenic Statistical Authority 2015. Population and Building Census 2011.

Lazaridis, L., & Nalpmpantis, I., 2004. Flood protection of Rafina Basin. Flood protection of Attica Conference, Athens T.E.E.

Tsakiris, P., 2007. Methodogiacal Approach to Flood Protection under the new prescription, Athens NTUA.

Yang, J., Townsend, R. D., & Daneshfar, B., 2006. Applying the HEC-Ras model and GIS techniques in river network floodplain delineation. Canadian journal of Civil Engineering, Vol. 33 No. 1: pp 19-28.

15th International Congress of the Geological Society of Greece
Athens, 22-24 May, 2019 | Harokopio University of Athens, Greece
Bulletin of the Geological Society of Greece, Sp. Pub. 7 Ext. Abs. GSG2019-176

Assessing Building Vulnerability to Tsunami Hazard in Kamari, Santorini, Greece

D.-V. Batzakis[1], L.-M. Misthos[2], G. Voulgaris[3], I. Tsodoulos[1], K. Tsanakas[1], M. Andreou[1], E. Karymbalis[1]

(1) Harokopio University of Athens, Geography Department, 70 Eleftheriou Venizelou Ave., Kallithea, Greece, mpatzakis@hua.gr
(2) National Technical University of Athens, School of Mining and Metallurgical Engineering, 9 Iroon Polytechniou Str., Zografou Campus, Greece
(3) Reitaku University, Faculty of Foreign Studies, 2-1-1 Hikarigaoka, Kashiwa, Japan

Introduction

Thera Island (Santorini) is an area susceptible to tsunamis, due to its geotectonic position within the broader geodynamic setting of Greece. Thera neighbours major fault zones in the South Aegean basin and constitutes the most active volcanic structure of the Hellenic Volcanic Arc. Seismicity and volcanic activity, in combination with submarine landslides triggered by them, are the main causes of tsunamis in the entire Aegean Sea. The subduction zone located south of Thera Island, is a major tsunamigenic area, since some of the largest known earthquakes have generated tsunamis. Characteristic events as those of 365 and 1303 AD, which were followed by two earthquakes of M8 or higher, greatly affected the coasts of the East Mediterranean Sea (Papazachos and Papazachou, 2003; Papadopoulos et al., 2014).

Aside from seismicity originated sea waves, tsunamis caused by submarine landslides, triggered mainly by earthquakes can also affect the Aegean Sea area, producing extensive run-ups, such as the 1956 AD event which impacted several islands of the Cyclades island complex (Dominey-Howes et al., 2000a). Moreover, volcanic activity has been linked to one of the largest tsunamis in the Mediterranean Sea, that initiated the decline of the Minoan Civilization in the Late Bronze Age (Cita and Aloisi, 2000; McCoy and Heiken, 2000). Likewise, a tsunami with run-ups exceeding 10 m, was produced by the collapse of the Columbo submarine volcano cone in 1650 AD, in the NE of Thera, affecting the Cyclades islands as well (Dominey-Howes et al., 2000b).

The aforementioned events have caused significant loss of life and construction damage in the past. There is a high likelihood for similar events to take place and affect the coasts of the Aegean Sea, once more, in the near future. Furthermore, the disaster risk is now significantly higher due to increased exposure of the buildings as a result of economic and touristic growth in Aegean Islands. In this regard, the purpose of the study is to assess building vulnerability to tsunami, in order to aid the coastal societies raising their resilient status.

Study Area

This study focuses on the eastern coast of Thera Island, as its geomorphology and human presence amplify the necessity of its vulnerability assessment. In terms of disaster management, the coastal settlement of Kamari poses the highest physical, social and economic relative exposure to natural hazards. According to the Hellenic Statistical Authority (2015), Kamari stands as the town with the highest population density (433 residents/ km^2) hosting 10% (1,344 residents) of the total island population. The number of buildings in Kamari amounted to 849. The majority is used as residential dwellings (55%), tourist facilities (21%) and commercial stores (15%). Furthermore, the presence of critical facilities including hospitals, schools and the airport increases the risk. With a coastline length of 2 km and maximum elevation of 50 m, the number of the vulnerable buildings to tsunami increases.

Methodology

In order to achieve the objective of this research, which is to quantify the buildings stock's vulnerability, a 'worst-case run-up scenario' was developed, based on scientific research that links tsunami run-up to earthquake magnitude, as presented in the literature (see Iida, 1963). Considering the history of tsunamis in the Aegean Sea (e.g. Maramai et al., 2014), a 10 m run-up tsunami – caused by a M8 earthquake – was assumed. To create the inundation and the run-up heights scenario in Thera, a 5 m resolution Digital Elevation Model, provided by National Cadastre & Mapping Agency S.A. (2016), was utilized.

The scale of the vulnerability assessment was set on the level of human settlement, which was selected based on the degree of relative exposure to the hazards. The calculations of the relative vulnerability of buildings in Kamari, were conducted via the application of the PTVA-3 analytic model (Dall'Osso et al., 2009) and the results were visualized using GIS software. The PTVA-3 model calculates each building's numerical index, referred to as the Relative Vulnerability Index (RVI) which ranges from 1 (Minor) to 5 (Very High). The model takes into account a weighted summation of two different components: the vulnerability of the carrying capacity of the building structure which is linked to the horizontal hydrodynamic force associated with water flow, and; the vulnerability of different building components due to their prolonged contact with water. The produced cartographic layers indicate the spatial distribution of the relative vulnerability of the buildings, in correlation with the inundation depth and their use. To apply the PTVA-3 model in Kamari, a field survey was conducted in order to catalogue the necessary attributes of the buildings for the application of the model.

Results

The results indicate that 423 out of 849 buildings are located within the inundation zone. The different RVI classes are distributed in a linear pattern according to the inundation depth. The buildings that have "Average" to "Very High" RVI

scores are clustered in water depths that exceed 5 m. In contrast, buildings with "Minor" to "Moderate" RVI scores are clustered in the lower water depths of up to 4 m. In specific, 68 buildings –16% of the total of the inundated buildings – obtained a RVI score of "Minor", 44 (10%) scored as "Moderate", 96 (23%) scored "Average", 140 (33%) scored "High", and 75 (18%) scored as "Very High". Figure 1c portrays the distribution of the building RVI scores within the inundation zone.

Finally, by correlating the main use of buildings with the RVI score, 50% of the dwellings are characterized by "High" and "Very High" scores, while the corresponding percentage for buildings occupying tourist facilities is 43%. However, the stores and food outlets are both characterized as having "Very High" scores – 76% and 83% respectively – which is explained by the substantial touristic growth of the coastal front. The abovementioned results reveal that after a tsunami event, the possibility of damage in economic and touristic facilities is high, leading to the loss of local comparative advantage of the settlement.

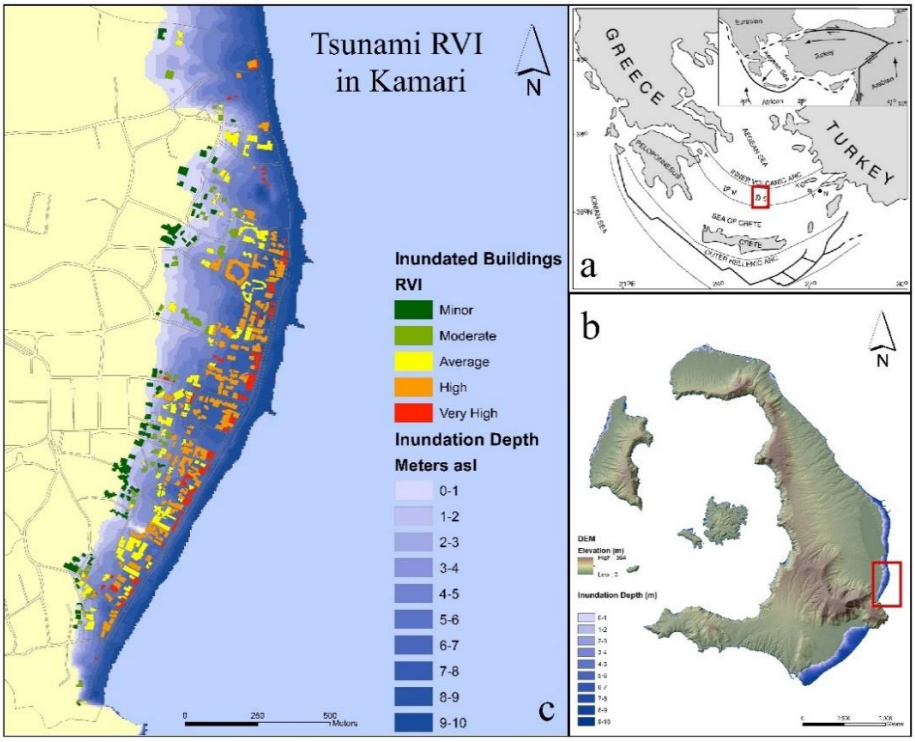

Figure 1. (a) The geodynamic framework of the Hellenic Arc (Dominey-Howes, 2004). (b) Map of the inundation zone according to the 10 m run-up scenario and the location of the study area. (c) Map of building RVI score distribution as a result of the application of the PTVA-3 model in Kamari.

References

Cita, M.B., Aloisi, G., 2000. Deep–sea tsunami deposits triggered by the explosion of Santorini (3500 y BP), eastern Mediterranean. Sedimentary Geology 135:181-203.

Dall'Osso, F., Dominey-Howes, D., 2009. A method for assessing the vulnerability of buildings to catastrophic (tsunami) marine flooding. Report prepared for the Sydney Coastal Councils Group Inc. pp.138.

Dominey-Howes, D., Cundy, A., Croudace, I., 2000a. High energy marine flood deposits an Astypalaea Island, Greece: possible evidence for the AD 1956 southern Aegean tsunami. Marine Geology 163:303-315.

Dominey-Howes, D., Papadopoulos, G., Dawson, A.G., 2000b. Geological and Historical Investigation of the 1650 Mt. Columbo (Thera Island) Eruption and Tsunami, Aegean Sea, Greece. Natural Hazards 21, 83-96.

Dominey-Howes, D., 2004. A re- analysis of the Late Bronze Age eruption and tsunami of Santorini, Greece, and the implications for the volcano–tsunami hazard. Journal of Volcanology and Geothermal Research 130:107-132.

Hellenic Statistical Authority (2015). Population and Building Census 2011.

Iida, K., 1963. Magnitude, energy and generation mechanisms of tsunamis and a catalogue of earthquakes associated with tsunamis. Tsunami Meeting at the 10th Pacific Science Congress, International Union of Geodesy and Geophysics Monograph No. 24, pp. 7-18.

Maramai, A., Brizuela, B., Graziani. L., 2014. The Euro-Mediterranean Tsunami Catalogue. Annals of Geophysics 57(4):s0435.

McCoy, F.W., Heiken, G., 2000. Tsunami Generated by the Late Bronze Age Eruption of Thera (Santorini), Greece. Pure and Applied Geophysics 157:1227-1256.

National Cadastre & Mapping Agency S.A. (2016). Digital Elevation Model, Thera Island.

Papadopoulos, G., Gràcia E., Urgeles, R., Sallares, V., De Martini, P.M., Pantosti, D., González, M., Yalciner, A.C., Mascle, J., Sakellariou, D., Salamon, A., Tinti, S., Karastathis, V., Fokaefs, A., Camerlenghi, A., Novikova, T. and Papageorgiou, A., 2014. Historical and pre-historical tsunamis in the Mediterranean and its connected seas: Geological signatures, generation mechanisms and coastal impacts. Marine Geology 354:81–109.

Papazachos, B. C., Papazachou, C. B., 2003. The Earthquakes of Greece, Ziti Editions, Thessaloniki, 286 pp. (in Greek).

15th International Congress of the Geological Society of Greece
Athens, 22-24 May, 2019 | Harokopio University of Athens, Greece
Bulletin of the Geological Society of Greece, Sp. Pub. 7 Ext. Abs. GSG2019-221

Inventory of Earthquake-Induced Rock Falls and Taluses in Skolis Mountain in Northwest Peloponnese, Greece

A. Litoseliti[1], I. Koukouvelas[1], K. Nikolakopoulos[1], V. Zygouri[1]
(1) University of Patras, Department of Geology, Rion 26504, Patras, Greece, aspalit87@gmail.com

Abstract

The 2008 Movri Mountain earthquake Mw=6.4 was a destructive earthquake, affecting a significant part of the NW Peloponnese. The earthquake triggered serious ground hazards (surface ruptures, liquefactions, rock falls) and extensive damage to buildings along a 30 km long by 20 km wide area (fig. 1). This study is based on the data base compiled after the earthquake, enriched by remote sensing data that cover a time period of 72 years. The analysis is focused to the west slope of the Skolis Mountain, Western Greece. In this slope we mapped by field work and remote sensing rock fall occurrence and evolution over the last 72 years (fig. 2). We also recognized that over this period the rock falls increase their width, or their length. The terms of width and length are defined along strike or down slope the Skolis Mountain respectively. To improve the reliability of our rock fall evolution model, two different methods have been applied: a) temporal and spatial distribution and b) statistical analysis of rock fall sites, across the Skolis Mountain, over the period from 1945 to 2017. Our rock fall inventory includes 10 time intervals, based on aerial photo interpretation. Analysis and mapping are implemented in a Geographic Information System (ArcGIS). Overall, pre- and post- Movri Mountain earthquake mapping shows significant size changes in rock fall sites and dispersal of boulders (fig. 3). Most of the fallen boulders are characterized by almost rectilinear fall paths. Taluses developed at the base of the slope are supplied by a narrow channel that consisted of small blocks of rocks and boulders. During the Movri Mountain earthquakes rock fall channels migrated upwards and downwards, along pre-existing rock fall deposits. Our analysis shows that the local seismicity appears to have a crucial control on Skolis slope processes influencing rock mass strength resulting in the occurrence of reactivated and newly formed rock falls (fig. 2). These observations are significant for proposing a mechanism of taluses inflation and the isolated boulders tracks for the identification and mitigation of hazard in an area prominent to rock falls.

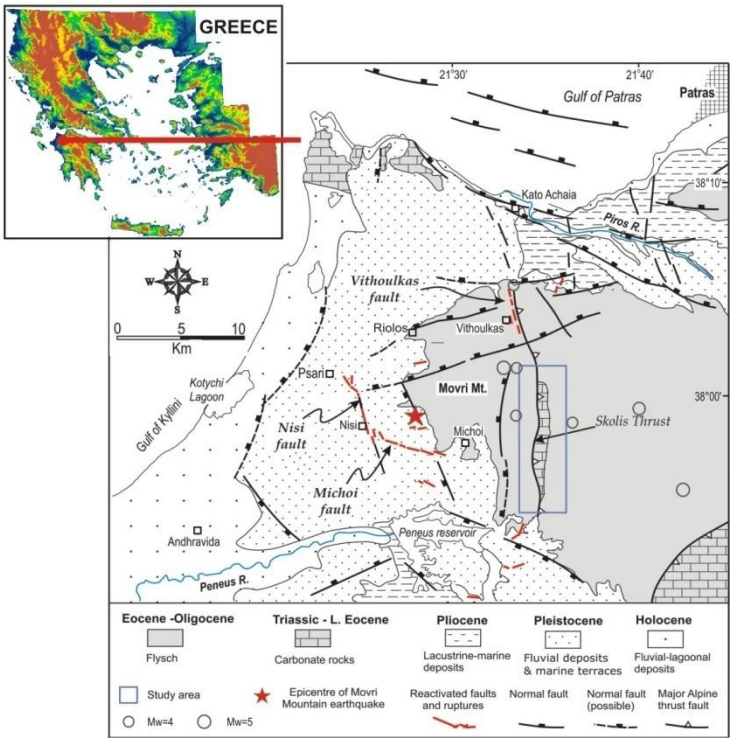

Figure 1. Map of the studied area showing lithology, active faulting and surface ruptures of the 2008 earthquake. The seismicity sequence after the 2008 earthquake is reproduced from www.gein.noa.gr.

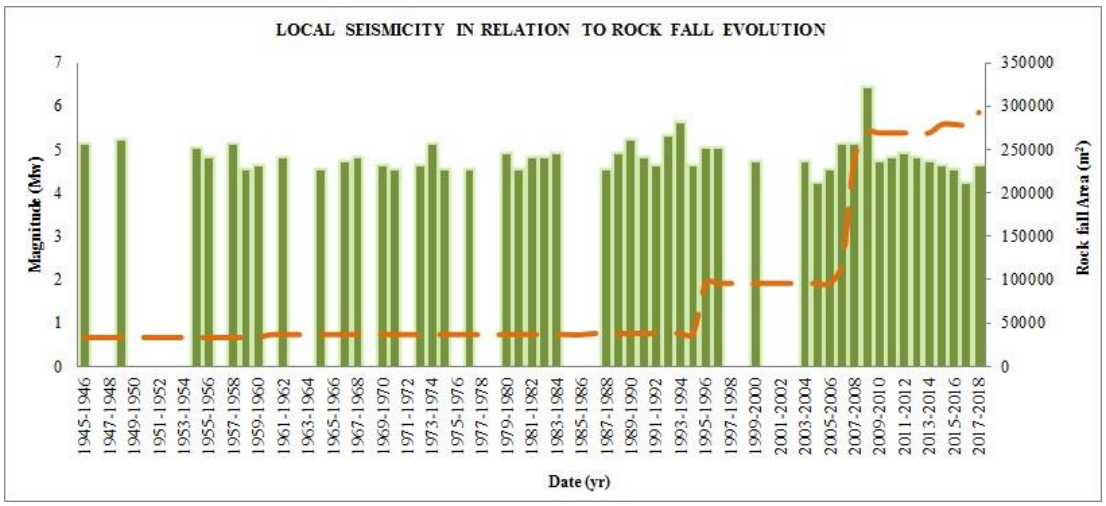

Figure 2. Diagram of seismicity in Skolis Mountain region that affected the size of rock falls over the period 1945 - 2017. The green columns represent the magnitude and the dashed orange line the evolution of the rock fall area. The range of the affected area is defined by the range of the map in figure 1.



Figure 3. Steep rock cliffs of the Skolis Mountain and Helicopter post-earthquake views of rock-falls and taluses.

References

Kokkalas, S., Kamberis, E., Xypolias, P., Sotiropoulos, S., Koukouvelas, I., 2013. Coexistence of thin- and thick-skinned tectonics in Zakynthos area (western Greece): insights from seismic sections and regional seismicity. Tectonophysics 597–598, 73–84.

Koukouvelas, I., Kokkalas, S., Xypolias, P., 2010. Surface deformation during the Mw 6.4 (8 June 2008) Movri Mountain earthquake in the Peloponnese, and its implications for the seismotectonics of western Greece. Int. Geol. Rev. 52, 249–268.

Koukouvelas, I., Litoseliti, A., Nikolakopoulos, K. and Zygouri, V., 2015. Earthquake triggered rock falls and their role in the development of a rock slope: The case of Skolis Mountain, Greece. Eng. Geol. 191, 71-85.

15th International Congress of the Geological Society of Greece
Athens, 22-24 May, 2019 | Harokopio University of Athens, Greece
Bulletin of the Geological Society of Greece, Sp. Pub. 7 Ext. Abs. GSG2019-262

Development of a Comprehensive Seismic Risk Model for Heraklion (Crete)

K. Michalaki, I. Kassaras

Section of Geophysics & Geothermics, Department of Geology and Geoenvironment, National and Kapodistrian University of Athens, Panepistimiopolis, 15784 Athens, Greece, katemichalaki@gmail.com

Seismic risk is determined by the combination of the probability of occurrence of a specified level of ground motion in a specified period of time (seismic hazard), the degree of damage expected to occur in structures after an earthquake (seismic fragility) and the assets exposed in a given area (economic exposure). Seismic risk assessment can provide critical information to stakeholders for the development of efficient risk reduction measures. However, in many cases observed ground motions are found to be underestimated by seismic hazard maps, due to lacking experience of strong earthquakes near urban areas and hence a questionable awareness of building stock endurance. In this work we present a physical risk model for the old part of Heraklion city (Crete). Crete is located in one of the most seismically active domains of eastern Mediterranean, marking the tip of the southern Hellenic subduction zone. Crete is considered also to be of high importance for the Greek tourism, estimated that contributes at around 47% of the GDP.

Heraklion, is the third most populated city of Greece. It is situated at the north-central coastal area of Crete, thus it is prone to strong earthquakes as manifested by the seismic history of the area (Papadopoulos, 2011) and the presence of several active faults in its vicinity. During the history of the city, several shallow and intermediate depth damaging earthquakes have occurred. Although instrumental and historical evidence does not indicate that Heraklion was damaged by earthquakes triggered by nearby shallow faults producing adverse effects to the city, a future incident cannot be excluded (Papazachos, 1995). According to the effective Greek seismic code (EAK-2000), Heraklion belongs to seismic hazard zone II for which predicted peak ground acceleration is PGA=0.24g. However, the above consists only an abstract approach, neglecting local conditions that may largely alter the effects of natural phenomena at a site. Therefore, a modern plan taking into account local conditions is required to facilitate effective interventions and mitigation policies.

To this aim, we develop a comprehensive seismic assessment by combining the exposure and vulnerability model of the old part of Heraklion city with the SHARE seismic zones (Giardini *et al*., 2014) and site response deduced from geotechnical data and microtremors measurements in order to acquire both probabilistic and deterministic earthquake loss assessments. The GEM OpenQuake-engine (OQ - www.globalquakemodel.org/openquake) was used to identify the regions with the highest risk within the target site, the most vulnerable assets, and the expected economic losses for a number of return periods and also for the most hazardous seismic sources in the vicinity of the city. The public-private Global Earthquake Model (GEM) foundation is an international pioneer that hosts an open initiative to develop state-of-the-art, widely accepted datasets, models and open-source tools/software for seismic risk assessment.

The herein work is organized as following. Path-effects were assumed after empirical GMPEs; site effects were approximated by experimental Horizontal to Vertical Spectral Ratios - HVSRs (Nakamura, 1989) obtained during an in-situ survey of microtremors measurements (ASPIDA, 2015) and geotechnical data (Auto-Seismo-Geotech, 1998). The census exposure model was available by EPANTYK (2009) and the corresponding fragility/vulnerability functions from the OpenQuake-platform (www.globalquakemodel.org/oq-platform). To assess the impact of soil response, the loss model was calculated with and without taking into account site amplification functions. Results were mapped using GIS tools.

Fig. 1 presents the resolved Probabilistic Seismic Hazard Assessment (PSHA) for the old city of Heraklion using OQ, SHARE Area Sources (AS), attenuation laws from the literature and site amplification. Site amplification was approximated by V_{S30}, derived from ambient noise HVSR (ASPIDA, 2015) and geotechnical borehole NSPT measurements (Auto-Seismo-Geotech, 1998). V_{S30} was obtained by inversion of the HVSR curves using ModelHVSR (Herak, 2008) and empirical relations (Tsiambaos & Sabatakakis, 2011) for the two data types, respectively. Probabilistic PGA values were found to range from about 370 to 470 cm/s^2, somewhat higher than values predicted in the global maps of the SHARE project (http://www.efehr.org/en/hazard-data-access/hazard-maps) calculated for rock conditions (V_{S30}=800 m/s), being of the order of 350 cm/s^2. Moreover, these are significantly larger than the value of 0.24 g predicted for the area by the national seismic code (EAK-2000). Fig. 2 illustrates the outcome of a scenario-damage calculation regarding a M_w6.5 earthquake on a N-S trending, east-dipping normal fault source located west of Heraklion (SHARE-GRCS740 fault source). The scenario, appears relatively amenable for the building stock implying a small percent (6%) of the buildings prone to undergo extensive damage or collapse, corresponding to 220 buildings out of the ~4000 ones in the target site available from the census data. In conclusion, the ongoing analysis manifests a robust methodology that yields consistent seismic risk assessments, which could be of use of stakeholders towards decisions on mitigation measures.

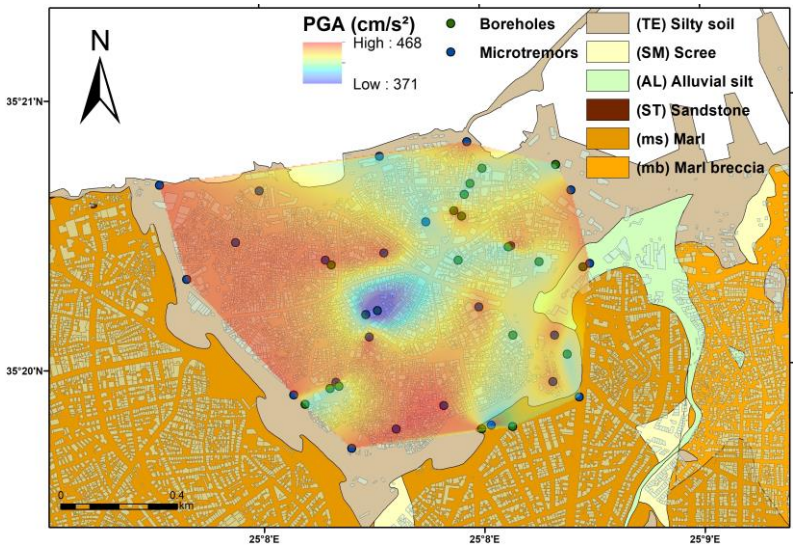

Figure 1. PSHA for the old Heraklion city using OQ, SHARE-AS and site amplification. PGA is calculated for 10% probability of exceedance within the next 50 years. Geology and buildings' footprints are also plotted.

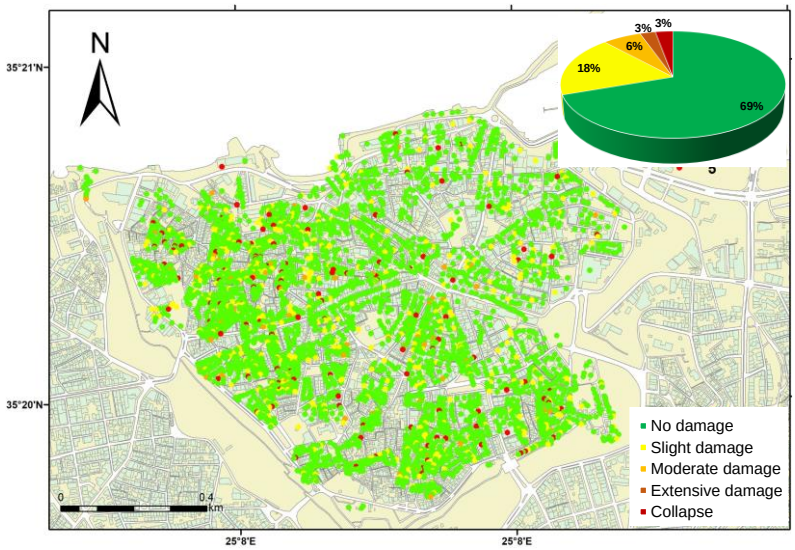

Figure 2. Damage distribution in Heraklion for an M_w6.5 scenario earthquake.

Acknowledgements

We would like to acknowledge G. Giannaraki, S. Mourloukos, P. Stoumpos, for their valuable help that greatly contributed in the current research. We thank A. Ganas and D. Kazantzidou-Firtinidou for discussions. I.K. thanks ASPIS-KRIPIS (MIS-448326) and HELPOS - Hellenic Plate Observing System" (MIS 5002697) research projects.

References

ASPIDA, 2015: Infrastructure Upgrade for Seismic Protection of the Country and Strengthen Service Excellence through Action, project MIS-448326, implemented under the Action, Development Proposals for Research Bodies-ASPIS-KRIPIS (in Greek).

Auto-Seismo-Geotech, 1998. Automated geotechnical program for the prevention and mitigation of seismic risk of seismic prone cities in the framework of analytical microzonation studies titled: Geological Survey of the Heraklion Crete area, H3A, Ministry of Development-GSRT, EPET II (in Greek).

Boore, D.M., 2003. Simulation of ground motion using the stochastic method. Pure Appl Geophys 160, 635–676.

EAK-2000 (2003) Greek National Building Code, Earthquake Protection and Planning Organization of Greece. EPPO Publ., Athens.

EPANTYK (2009) Development of GIS software for the representation of the structural wealth of the municipalities of the country and of its structural vulnerability in buildings block level. YP.ES.A, H.D, KEDKE, TEE, pp 39 (in Greek)

Giardini, D., Woessner J., Danciu L., 2014. Mapping Europe's Seismic Hazard, EOS, 95(29), 261-262.

Herak, M., 2008. ModelHVSR–A Matlab tool to model HVSR of ambient noise. Computer & Geosciences, 34, 1514-1526.

Milutinovic, Z., Trendafiloski, G., 2003. An advanced approach to earthquake risk scenarios with applications to different European towns. ReportWP4: vulnerability of current buildings, Risk-UE. EC, Brussels, DOI: 10.1007/978-1-4020-3608-8_23.

Nakamura, Y., 1989. A method for dynamic characteristics estimation of subsurface using microtremor on the ground surface. QR RTRI, 30, 25-33.

Papadopoulos, G.-A., 2011, A seismic history of Crete, First Ed., Ocelotos Public., Athens.

Papazachos, V., 1995. Faults of the big earthquakes (Ms>8.0) in the Hellenic arc, Proc. XV Congress of the Carpatho-Balcan, Geological Association, Athens, Greece.

Tsiambaos, G., Sabatakakis, N., 2011. Empirical Estimation of Shear Wave Velocity from In Situ Tests on Soil Formations in Greece, Bull. Engineering Geology and the Environment, 70, 291-297.

15th International Congress of the Geological Society of Greece
Athens, 22-24 May, 2019 | Harokopio University of Athens, Greece
Bulletin of the Geological Society of Greece, Sp. Pub. 7 Ext. Abs. GSG2019-286

SCR Calculation Using a Fault Specific Earthquake CAT Model Compared with the EIOPA Standard Formula

G. Deligiannakis[1], I. Papanikolaou[1], A. Zimbidis[2], I. Kakouris[3]

(1) Mineralogy-Geology Laboratory, Department of Natural Resources Development and Agricultural Engineering, Agricultural University of Athens, 75 Iera Odos Str., 118-55 Athens, Greece, gdeligian@aua.gr
(2) Department of Statistics, Athens University of Economics and Business, 76 Patission Str., 10434, Athens, Greece
(3) Prudential Actuarial Solutions Ltd, 148, Momferatou Str., 11475, Athens, Greece

Introduction

According to the new Solvency II EU Directive, each insurance company specifies the required capital, in order to ensure that it will be able to meet its obligations over the following year, with a probability of at least 99.5%. In order to accurately calculate the Solvency Capital Requirements (SCR) for earthquake perils, insurance companies can utilize either the Standard Formula (SF) as defined in technical papers approved by the European Insurance and Occupational Pensions Authority (EIOPA), or an internal Earthquake CAT model. The SF is based on past earthquake events and their corresponding insured losses, thus inheriting problems related to the incompleteness and the inhomogeneity of the historical records and lower spatial resolution of hazard (e.g. Grützner *et al.*, 2013; Papanikolaou *et al.*, 2015). Furthermore, it incorporates rough assumptions so that it can fit every insurance company in EU, only by adjusting the country factor, the risk zone weights and the correlation matrix for all Catastrophe Risk Evaluation and Standardizing Target Accumulations (CRESTA) zones in each country (European Commission, 2010).

Methodology

A newly developed Synthetic Stochastic Earthquake Catastrophe model is applied in the Region of Attica, Greece. It consists of three basic modules: Hazard, Vulnerability (including the Exposure) and Loss modules. We use a fault specific seismic hazard assessment approach for the Hazard Module, in order to address problems related to the historical records incompleteness, aiming on the reconstruction of a more complete earthquake catalogue over a larger period of time (~15,000 years, i.e. during the Holocene), obtain higher spatial resolution and calculate more realistic source locality distances. The method of seismic hazard mapping from geological fault throw-rate data was firstly introduced by Papanikolaou (2003) and Roberts *et al.*, 2004. It is based on an active faults database with 24 faults that are long enough to produce surface ruptures and can sustain damage in the Attica mainland in case of earthquake rupture, affecting the Attica Region (Deligiannakis *et al.*, 2018) (Fig. 1).

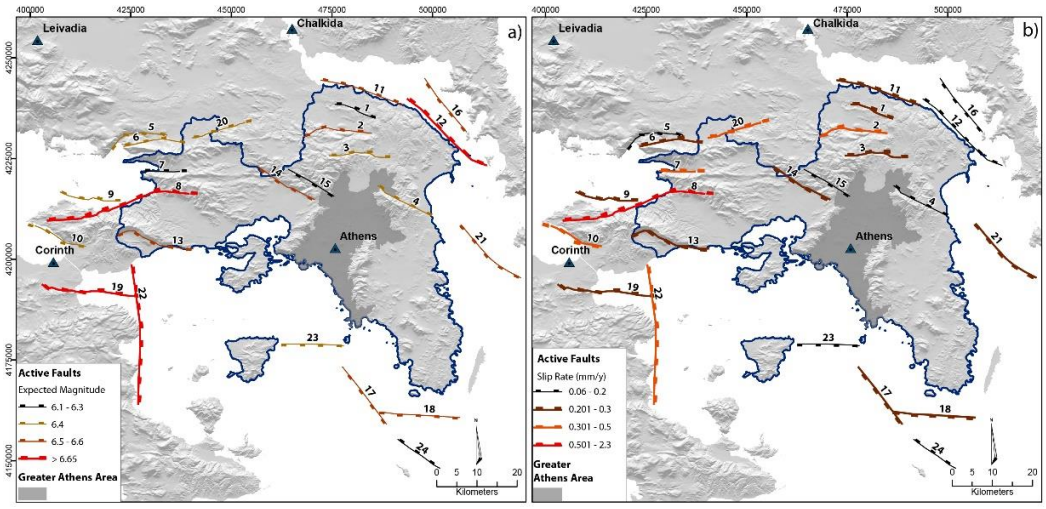

Figure 1. Map of active faults that can sustain damage within the region of Attica. Different colors and represent the maximum expected magnitude (a) and different slip-rate categories (b).

Epicenters induced by fault modeling, along with the catalogue events are stochastically simulated in order to project the future earthquakes. Attenuation relationships and amplification/attenuation factors based on the surface geologic conditions are then applied to each epicenter, in order to simulate future earthquake scenarios (Fig. 2, Left) and assess spatial distribution of the MM Intensity. The structural damage in buildings and the corresponding loss is computed using the Vulnerability Module, which is based on existing values (e.g. Sauter & Shah, 1978; Degg, 1992) (Fig. 2, Right). For the calculation of the SCR (Loss Module), a large dataset of simulated earthquake events is composed. The corresponding losses are either ranked in descending order, so that the appropriate arranged value can be selected, or a theoretical distribution is fitted over the whole sample of simulated losses.

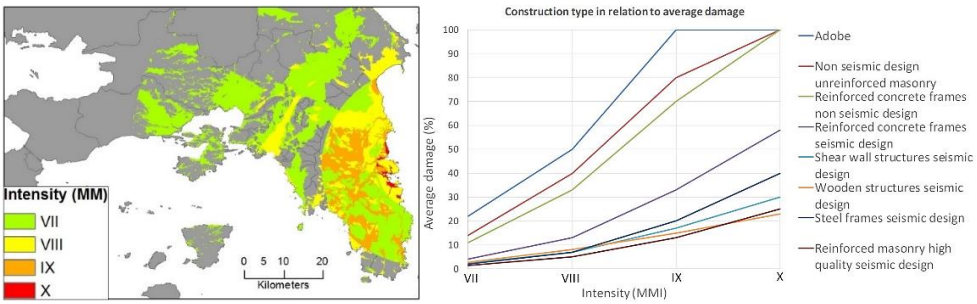

Figure 2. Left: Simulated earthquake event related to an active fault offshore eastern Attica. The modelled epicentre of the M6.6 event. Right: Vulnerability curves for different construction types, in relation to the Modified Mercalli intensity scale.

Results - Conclusion

Overall, for the whole Attica Region buildings inventory, the SCR calculated using the SF is overestimated by 15% compared to the hereby presented EQ CAT Risk Model. However, in 7 out of 10 CRESTA Zones in Attica, the SCR calculated by the SF was 3 – 57% higher, while in the remaining 3 cases it was 19 – 49% lower. These variations result from the differences on the spatial analysis, the local site conditions and the variations in seismic intensity recurrences throughout the same CRESTA Zone. For example, in CRESTA Zone "14" (Figure 3, left) the postal codes with low or zero intensity VIII recurrence are the ones with the largest insured values and thus the Earthquake CAT Model estimates a 57% lower SCR than the SF. Similarly, our model calculates the smallest SCR for the CRESTA Zone "16", compared to the rest of the CRESTA Zones of Attica. Nevertheless, there are still some Postal Codes within that Zone that have experienced intensity VIII and even IX in low recurrence (Figure 3, right). However, this CRESTA Zone is attributed to an extremely low CRESTA relativity factor (0.6), which seems to result in an SCR 55% lower than our model.

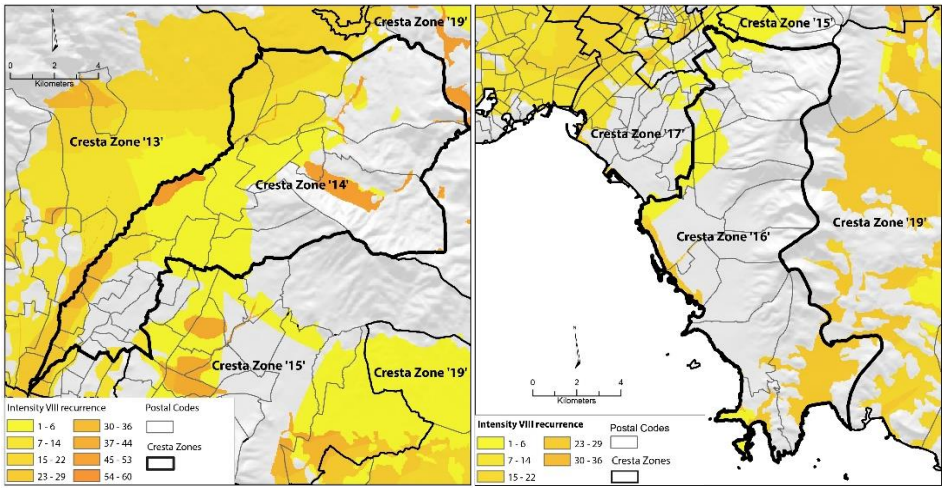

Figure 3. Fault Specific Seismic hazard map of the CRESTA Zone '14' (left) and "16" (right). Color variations show how many times the localities in the map have received enough energy to shake at intensity VIII over the past 15kyrs

Acknowledgements

We would like to thank the Bank of Greece for their support during the model development.

References

Degg, M.R., 1992. The ROA Earthquake Hazard Atlas project: recent work from the Middle East, in: McCall, G.J.H., Laming, D.J.C., Scott, S.C. (eds), Geohazards: Natural and man-made, 93-104.

Deligiannakis, G., Papanikolaou, I.D., Roberts, G., 2018. Fault Specific GIS Based Seismic Hazard Maps for the Attica Region, Greece. Geomorphology 306, 264-282.

European Commission, 2010. QIS5 technical specifications – Calibration Paper. CEIOPS-SEC-40-10, p. 92.

Grützner, Ch., Barba, S., Papanikolaou, I., Perez-Lopez, R., 2013. Earthquake Geology: science, society and critical facilities. Annals of Geophysics 56, 683-688.

Papanikolaou, I.D., 2003. Generation of high-resolution seismic hazard maps through integration of earthquake geology, fault mechanics theory and GIS techniques in extensional tectonic settings. Ph.D. Thesis, University of London, London, 437 p.

Papanikolaou, I.D., Van Balen, R., Silva, P.G., Reicherter, K., 2015. Geomorphology of Active Faulting and seismic hazard assessment: New tools and future challenges. Geomorphology 237, 1-13.

Roberts, G.P., Cowie, P., Papanikolaou, I., Michetti, A.M., 2004. Fault scaling relationships, deformation rates and seismic hazards: An example from the Lazio-Abruzzo Apennines, central Italy. Journal of Structural Geology 26, 377-398.

Sauter, F. & Shah, H.C., 1978. Studies on earthquake insurance. Central American Conference on Earthquake Engineering, San Salvador, El Salvador, p. 265-271.

15th International Congress of the Geological Society of Greece
Athens, 22-24 May, 2019 | Harokopio University of Athens, Greece
Bulletin of the Geological Society of Greece, Sp. Pub. 7 Ext. Abs. GSG2019-330

Landslides induced by the 2017 Lesvos (North Eastern Aegean Sea) earthquake and engineering measures for landslide disaster mitigation

E. Skourtsos[1], S. Lozios[1], K. Soukis[1], B. Antoniou[1], E. Andreadakis[1], S. Mavroulis[1], Ch. Filis[1], N.-I. Spyrou[1], I. Lialiaris[1], V. Alexoudi[1], N. Voulgaris[1], E. Lekkas[1]

(1) National and Kapodistrian University of Athens, Department of Geology and Geoenvironment, Panepistimiopolis Zografou, 15784, Athens, Greece, eskourt@geol.uoa.gr

Introduction

Landslides induced by the 2017 Lesvos Earthquake (North Aegean Sea, Greece) are presented along with their controlling factors and the engineering measures for landslide disaster mitigation. All presented data were derived from the research program applied in the earthquake-affected areas of southeastern Lesvos Island and conducted by the authors.

The 2017 June 12 Mw 6.3 Lesvos earthquake

On June 12, 2017 (12:28 GMT) an Mw 6.3 earthquake struck Lesvos Island (Northeastern Aegean, Greece) with focal depth of about 13 km and epicenter located offshore Plomari town (southeastern Lesvos). The main shock was generated by the rupture of the northern margin of the offshore Lesvos basin located between Lesvos Island in the north, Chios Island in the south and İzmir bay in the east (Papadimitriou et al. 2018). As regards the geodynamic setting, the North Aegean constitutes an extensional zone south of the North Anatolian dextral strike-slip fault zone and north of the Hellenic Trench (e.g. Le Pichon and Angelier, 1981). The small scale uplift of the Aegean area enables Anatolia to move with increasing velocity towards WSW resulting in the formation of the İzmir bay and the offshore Lesvos basin, which is bounded by E-W striking normal faults (Mascle and Martin 1990).

Earthquake environmental effects

Among the impact on public health (1 casualty and 15 injured people) and on the built environment (structural and non-structural damage in buildings), the earthquake also generated secondary environmental effects comprising mainly slope movements, ground cracks and a small-scale tsunami (Lekkas et al., 2017, Mavroulis et al., 2018). Slope movements were observed in several sites of the affected area resulting in partial damage to the road network including cracks and craters in the asphalt pavement and deformation of road protection barriers as boulders bounced across the roads, damage to adjacent building structures and related facilities and temporary or permanent traffic disruption (Mavroulis et al., 2018).

Factors controlling the earthquake-induced landslides

The observed slope movements are mainly attributed to pre-existing instability conditions formed in geotechnically unstable areas and landslide zones, presence of active faults forming intense relief with high and abrupt slopes and scarps, as well as suitable geometry of beds and discontinuities dipping towards the free face of slopes. Moreover, the eastern part of Lesvos Island is characterized by an arid to semi-humid climate, which is accompanied by relatively large surplus of water during the winter period (Karras, 1973). On the other hand, the western part of Lesvos Island is characterized by semi-arid climate with a small surplus of water during the winter period and high potential of evapotranspiration. The prevailing winds are northern and the southern winds follow. The distinction of the island into different climatic types reveals the difference in the occurrence of landslide phenomena between the two parts, with the eastern part having more landslide phenomena that the western one.

Local geological and morphological setting and types of the observed earthquake-induced slope movements

The research team conducted a detailed mapping of the sites affected by the earthquake-induced slope movements by combining not only the classical geological and geotechnical mapping but also modern and innovative mapping techniques including Unmanned Aerial Vehicles (UAV).

The observed slope movements were classified into:

- Wedge detachments, planar slides, toppling failures or movements due to combination of these slope movements attributed to the synergy of bedding, schistosity and fractures.
- Rotational landslides and failures of the soil, of the weathering mantle and of the surficial parts of the loose rockmass of the schists and pyroclastic rocks.

Slope movements were observed in the Agios Isidoros, Akrassi and Mesotopos areas and along Plomari – Melinta – Palaiochori road network.

Agios Isidoros and Plomari – Melinta – Palaiochori areas are composed of alpine formations including blueschists and marbles of Carboniferous age. These series also comprise carbonaceous metaconglomerates and large masses of greenschists. The affected areas are characterized by intense morphological slopes and morphological discontinuities, which locally are equal to or larger than 100 %, while the majority of the affected areas are characterized by slopes varying mainly from 51 to 100% and secondarily from 11 to 50 %. During the 2017 earthquake, rockfalls, planar slides and wedge failures occurred in Agios Isidoros and Plomari – Melinta – Palaiochori areas.

Akrassi area is located east of the homonymous village and along the road network leading from Akrassi to Plomari. This

area comprises Neogene ignimbrites lain unconformably over marbles, schists and ophiolites. Ignimbrites are composed of massive sheets with strong cohesion with flat surface overlying eroded surfaces of alpine formations. This area is characterized by intense morphology and slopes varying mainly from 51 to 100 % and secondarily from 11 to 50 %. During the 2017 earthquake, the generated slope movements in Akrassi included rockfalls and landslides.

Mesotopos area is located east of the main provincial road leading from Agra to Mesotopos. Ii is comprised by lava layers and pyroclastic rocks. During the 2017 earthquake, rockfalls were generated and affected the part of the aforementioned road.

Proposed engineering measures for the landslide disaster mitigation

The proposed engineering measures for the landslide disaster mitigation include the following:

- Removal of hanging, unstable and isolated rock blocks or of the loose rockmass
- Cleaning of the landslide materials accumulated behind retaining walls in order to create space for future slope movements and accumulation of mobilized material.
- Construction of concrete retaining walls along the base of natural or artificial slopes
- Simple and quick construction of gabion walls with flexibility to withstand foundation movement and with space behind them in order to receive and safely sustain loads of mobilized material
- Support and reinforcement anchors along with fastening of wire meshes over slopes with highly fractured, brecciated and loose rockmass
- Construction of concrete retaining walls along with landslides and rockfalls protection fenches on their top
- Excavation of horizontal benches into slope face for protection from rockfalls and the reduction of tensional forces in the surface rock and of surface erosion rates
- Construction of dynamic rockfall barriers
- Combinations of systems often provide the most effective solutions

Acknowledgements

The North Aegean Prefecture is acknowledged for the founding of this study in the frame of the "Applied research for management of landslide hazard in the earthquake affected area of Lesvos".

References

Karras, G. (1973). Climate classification of Greece based on Thornthwaite. PhD Thesis, University of Athens, 1-200.

Le Pichon, X. Angelier, J., 1981. The Aegean Sea. Philosophical Transactions of the Royal Society of London. A 300, 357-372.

Lekkas, E., Mavroulis, S., Skourtsos, E., Andreadakis, E., Antoniou, V., Kranis, C., Soukis, K., Lozios, S., Alexoudi, V., 2017. Earthquake environmental effects induced by the 2017 June 12, Mw 6.3 Lesvos (North Aegean Sea, Greece) earthquake. In Clark K. et al. (eds.): PATA DAYS 2017: 8th International INQUA Meeting on Paleoseismology, Active Tectonics and Archaeoseismology, 13-16 November 2017, Blenheim, New Zealand, Handbook and Programme, 228-231. ISBN 978-1-98-853036-9. http://dx.doi.org/10.21420/G2H061

Mascle, J. and Martin, L., 1990. Shallow structure and recent evolution of the Aegean Sea: A synthesis based on continuous reflection profiles: Marine Geology, 94, 271-299, https://doi.org/10.1016/0025-3227(90)90060-W

Mavroulis, S., Andreadakis, E., Antoniou, V., Skourtsos, E., Lekkas, E. (2018). Geodynamic phenomena and ESI 2007 intensities of the 2017 June 12, Mw 6.3 Lesvos (North Aegean Sea, Greece) earthquake. Geophysical Research Abstracts, 20, EGU2018-9254, EGU General Assembly 2018.

Papadimitriou, P., Kassaras, I., Kaviris, G., Tselentis, G.-A., Voulgaris, N., Lekkas, E., Chouliaras, G., Evangelidis, C., Pavlou, K., Kapetanidis, V., Karakonstantis, A., Kazantzidou-Firtinidou, D., Fountoulakis, I., Millas, C., Spingos, I., Aspiotis, T., Moumoulidou, A., Skourtsos, E., Antoniou, V., Andreadakis, E., Mavroulis, S., Kleanthi, M. (2018). The 12th June 2017 Mw=6.3 Lesvos earthquake from detailed seismological observations. Journal of Geodynamics, 115, 23-42, https://doi.org/10.1016/j.jog.2018.01.009

15th International Congress of the Geological Society of Greece
Athens, 22-24 May, 2019 | Harokopio University of Athens, Greece
Bulletin of the Geological Society of Greece, Sp. Pub. 7 Ext. Abs. GSG2019-343

Primary and secondary effects of the September 2018 Mw 7.5 Palu (Sulawesi Island, Indonesia) earthquake and their impact on the natural and built environment of Palu Bay area

S. Mavroulis[1], M. Gogou[1], E. Lekkas[1], P. Carydis[2]

(1) Section of Dynamic Tectonic Applied Geology, Department of Geology and Geoenvironment, National and Kapodistrian University of Athens, Panepistimiopolis, 15784, Athens, Greece, smavroulis@geol.uoa.gr
(2) National Technical University of Athens, Athens, Greece

On September 28, 2018, at 10:21 UTC [18:02:44, WITA (Indonesia Central Standard Time)], an earthquake occurred in the western part of Sulawesi Island (Indonesia) and more specifically on the coastal Lende area. It was assessed as M 7.5 [United States Geological Survey (USGS)] or M 7.7 [Indonesian Agency for Meteorology, Climatology and Geophysics (BMKG)]. The main shock is located onshore at a distance of 61 km north of Palu city and at depths of about 10 km.

It was preceded by a foreshock with magnitude M 6.1 generated at 07:00 UTC [15:00, WITA (Indonesia Central Standard Time)] and located 55 km NNW of Palu at a depth of about 18 km (USGS). The fault plane solutions of the main shock demonstrated an almost N-S striking left lateral strike slip fault (USGS, GCMT, CPPT, IPGP, GFZ) in the very complex tectonic environment of the Southeastern Asia. Based on the spatial distribution of aftershocks, it is estimated that the fault length was over 150 km (Sassa and Takagawa, 2018).

The affected Sulawesi Island is a K-shaped island located within the highly seismic active triple junction area between the Australian, Philippine and Sunda plates, which is composed of small rotating blocks bounded by active faults (Socquet et al., 2006). It is composed of four rapidly rotating crustal blocks: (1) the Makassar block, located in the southwestern part of Sulawesi, (2) the North Sula block, located in the northeastern part of Sulawesi, (3) the East Sulawesi block is pinched between the Makassar block and the North Sula block and (4) the Manado block, located at the northeastern end of the island (Socquet et al., 2006).

14 earthquake-induced tsunamis were recorded for Sulawesi Island between 1820 and 1982 (Soloviev et al., 1992). Since 1927, the Makassar Strait sustained the destructive effects of seven tsunamis (Prasetya et al., 2001). They are attributed to earthquakes involving main tsunamigenic tectonic structures comprising the Palu-Koro fault, which constitutes part of the Central Sulawesi fault system (Prasetya et al., 2001). In the case of the September 2018 earthquake, the most affected area was the Palu depression (Lekkas et al., 2018), along the boundary between the Makassar and the North Sula blocks. The most affected parts of Palu depression included the coastal areas of the Palu Bay and more specifically the onshore Palu valley, in the east of the Palu-Koro fault, which is considered as the causative fault based on the primary EEE observed on the field (Lekkas et al., 2018) and the analysis of teleseismic data and synthetic-aperture radar and satellite optical images (Bao et al., 2019).

The environmental effects induced by the 2018 Palu earthquake are classified into primary and secondary effects (Lekkas et al., 2018). The primary earthquake environmental effects (EEE) include coseismic surface ruptures in the Palu City area, while the secondary EEE included tsunami waves, liquefaction phenomena and ground cracks in the Palu Bay area (Lekkas et al., 2018).

The coseismic surface ruptures directed parallel and in an en echelon arrangement to the causative fault and resulted in deformation and destruction of the road network and buildings respectively. The deformed asphalt pavements as well as the adjacent damaged buildings along with the perimeter walls and railings reveal left lateral offset, which is in coincidence with the causative Palu-Koro fault.

The liquefaction phenomena occurred in Balaroa and Petobo districts and along a riverbed south of Bilomaru, located SE of Palu City. They comprised liquefaction- and lateral spreading-initiated flow that have resulted the total destruction of Balaroa and Petobo neighborhoods in Central Palu, which were swallowed up in a wave of mud resulting in thousands of dead, injured and missing people.

The ground cracks were observed as tension cracks close to sites with gravitational movements and lateral spreading and are attributed to the ground shaking.

Among the most impressive EEE, the 2018 Palu earthquake triggered a tsunami that struck the western coastal part of the Central Sulawesi Province extending from Magapa area to Palu Bay located north and south of the earthquake epicenter respectively. The tsunami struck several settlements along the aforementioned coastal area with the Palu Bay being the worst affected area. The coastal part of Palu City was devastated. The destructive waves arrived up to 10 minutes after the generation of the earthquake. This fact allowed little to no time for early warning and left no time to the local population for early evacuation resulting in many fatalities and huge economic damage. The evacuation started as soon as the tsunami approached the coast.

With inundation depth ranging from 2 to 5m locally and inundation distance of hundreds of meters, the waves devastated the Talise beach in Palu City, the Dongala village at the western tip of the Palu bay as well as all many villages along the coast of Palu bay claiming the life of thousands and resulting in heavy impact on buildings, infrastructures, mobile objects and the environment. It is mainly attributed to the synergy of coseismic seabed displacement, submarine landslides and

liquefied gravity flow within Palu bay. Factors enhancing the tsunami destructive characteristics and losses along the coastal areas of Palu Bay include: (a) the close proximity of the affected area to the epicenter of the main shock and to tsunamigenic source resulting in tsunami arrival times shorter than 10 minutes, low dispersion and cause extreme run-up, (b) the local bathymetry and seabed morphology, which is characterized by a very steep rise from the seafloor of North Makassar Straits with water depth of about 2500 m to the western coast of the Central Sulawesi province, (c) the coastal configuration of the affected area, which is composed of gulfs and a gently concave coastline that created a wave-guide, funneling effects on the tsunami wave energy, amplification of tsunami height and run up and enhanced damage along the coast of Palu Bay, (d) both local bathymetry and coastal configuration resulted in wave refraction and reflection.

As regards the earthquake impact on the building stock, the earthquake caused non-structural and structural damage mainly in Palu city. Multistory reinforced concrete (R/C) hotels and malls suffered heavy structural damage resulting in partial or total collapse. The ground floor of the buildings collapsed, while the upper floors behaved as rigid bodies, resulting in toppling of the damaged structures. In contrast, wooden and steel-frame buildings suffered mainly non-structural damage by the earthquake ground motion. Severe structural damage were observed in monumental structures such as mosques.

In the liquefaction-affected areas, the level of building destruction was almost complete with many buildings of all types being compressed together and wrecked into a soil and debris zone resulting in significant loss of life.

In the tsunami affected areas, all wooden structures founded along the coastal front were totally washed away by the wave pressure and only their concrete foundations were left in place. In villages along the western coast of Palu Bay, some wooden structures with wooden foundation were detached from their foundations and transferred inland but not destroyed.

The R/C buildings suffered typical tsunami-induced damage in the ground floor and in the first floor due to tsunami water pressure and impact with floating debris. Punching failure of brick infill walls under out-of-plane tsunami pressures were observed in the form of large circular openings in infill walls. Flexural failures of columns within their midheights are attributed to impact forces generated by floating debris.

Based on our field survey on the tsunami affected area and on all already published official reports on the tsunami impact, the Integrated Tsunami Intensity Scale (ITIS 2012) is applied for the Palu tsunami. Tsunami quantities and the impact on humans, mobile objects, coastal infrastructure, the natural environment and buildings were taken into account for the tsunami intensity assessment. The maximum assigned intensity is XII.

Acknowledgements

This study was partially funded by the Environmental, Disaster and Crises Management Strategies Post graduate Program of the Department of Geology and Geoenvironment of the National and Kapodistrian University of Athens.

References

Bao, H., Ampuero, J.-P., Meng, L., Fielding, E.J., Liang, C., Milliner, C. W. D., Feng, T., Huang, H. (2019). Early and persistent supershear rupture of the 2018 magnitude 7.5 Palu earthquake. Nature Geoscience, 12, 200-205, https://doi.org/10.1038/s41561-018-0297-z

Lekkas, E., Carydis, P., Mavroulis, S. (2018). The September 2018 Mw 7.5 Palu (Sulawesi Island, Indonesia) earthquake and tsunami disaster – Scientific Report (Version 1.0). Newsletter of Environmental, Disaster and Crisis Management Strategies, 9. Available at https://edcm.edu.gr/images/docs/2018/Newsletter_2018_9_Indonesia_EQ.pdf

Prasetya, G.S., de Lange, W.P., Healy, T.R., 2001. The Makassar Strait Tsunamigenic Region, Indonesia. Natural Hazards, 24, 295-307, https://doi.org/10.1023/A:1012297413280

Socquet, A., Simons, W., Vigny, C., McCaffrey, R., Subarya, C., Sarsito, D., Ambrosius, B., Spakman, W., 2006. Microblock rotations and fault coupling in SE Asia triple junction (Sulawesi, Indonesia) from GPS and earthquake slip vector data. Journal of Geophysical Research, 111, B08409, http://doi.org/10.1029/2005JB003963

Soloviev, S.L., Go, C.N., Kim, K.S., 1992. Catalog of tsunamis in Pacific. Academy of Sciences of the USSR, Moscow, Translated by Amerind Publishing Co. Pvt. Ltd., New Delhi

15th International Congress of the Geological Society of Greece
Athens, 22-24 May, 2019 | Harokopio University of Athens, Greece
Bulletin of the Geological Society of Greece, Sp. Pub. 7 Ext. Abs. GSG2019-346

Active faults controlling spatial distribution of environmental effects and building damage induced by the February 6, 2018, Mw 6.4 Hualien (Eastern Taiwan) earthquake

S. Mavroulis[1], E. Lekkas[1], P. Carydis[2]

(1) Section of Dynamic Tectonic Applied Geology, Department of Geology and Geoenvironment, National and Kapodistrian University of Athens, Panepistimiopolis, 15784, Athens, Greece, smavroulis@geol.uoa.gr
(2) National Technical University of Athens

The island of Taiwan is located at the convergent plate boundary between the Philippine Sea plate and the Eurasian plate (Shyu et al. 2005). It is the product of the ongoing collision between the Eurasian continental margin and the Luzon volcanic island arc, part of the Philippine Sea plate (e.g. Shyu et al. 2005, 2016). Currently, Taiwan is experiencing a double suturing. The Luzon volcanic arc is colliding with the Hengchun forearc ridge in the south, which is in turn colliding with the Eurasian continental margin. In the north both sutures are unstitching. As a result, Taiwan is composed of three lithospheric pieces of Taiwan: the Eurasian continental margin, the continental sliver, and the Luzon arc (e.g. Shyu et al. 2005, 2016).

The two sutures are producing separate neotectonic belts along the western and eastern part of the island. Each collision belt matures and then decays progressively from south to north resulting in discrete steps, manifested as seven distinct neotectonic domains along the western belt and four along the eastern belt. Each domain define a distinctive assemblage of active structures (Shyu et al. 2005, 2016). Characteristic examples of neotectonic domains in the eastern part of Taiwan are the Hualien and Ryukyu domains, which comprise active faults capable of producing earthquakes with magnitudes varying from 7.0 to 8.0. As it is shown from the study of historical and recent seismicity of the island, the eastern part has been often struck by large and destructive earthquakes in 1811 (M=7.5), 1815 (M=7.7), 1882 (M=7.5) and 1951 (M=7.5).

On February 6, 2018, an Mw 6.4 earthquake hit eastern Taiwan with epicenter close to the coastal area north of Hualien city and focal depth around 10 km. The main shock caused 17 casualties and 285 injured in the Hualien City. The most affected area was Hualien city with VII maximum intensity. This area is composed of metamorphic rocks of the Central Range overlain by sediments of the Longitudinal Valley, which are in turn overlain by alluvial deposits. Hualien city occupies an area founded on sediments of the Longitudinal Valley overlain by recent alluvial deposits. One of the major active faults of Taiwan, the Meilun fault, disrupts these recent formations. Moreover, it ruptured in the October 1951 earthquake and produced up to ~1.2 m of coseismic vertical offsets and up to ~2 m of sinistral offsets (Hsu 1955; Bonilla 1975, 1977). The onshore length of the fault is less than 10 km. This length appears to be too short considering that the 1951 earthquake had a magnitude of 7.3 (Hsu, 1962). Therefore, the fault may extend further offshore to the north (Shyu et al. 2005).

The scientific team visited the 2018 earthquake-affected area in Eastern Taiwan and conducted a field macroseismic survey and a geological reconnaissance in order to assess the earthquake impact on the natural environment and the building stock in Hualien County and to study the factors controlling the distribution of the observed earthquake environmental effects (EEE, Lekkas et al., 2018).

As regards building damage, the earthquake caused almost identical heavy structural damage, comprising collapse of the ground floors and tilting, to 6 multistory buildings in Hualien City, while the rest of the building stock suffered light non-structural damage or no damage at all. The common damage characteristic of the inspected buildings was the decomposition of the concrete in the columns of the ground floor due to crashing, resulting in failure of columns and the subsequent tilting, while the upper floors of the structures were left intact. The observed damage is the result of the synergy of the prevailing special ground conditions at each site, the effects of the vertical component of the earthquake ground motion on the performance of concrete and reinforcement of damaged buildings, the parameters of the ground shaking as well as the type, design and construction characteristics of the affected buildings. The earthquake also caused damage to infrastructures of Hualien. Cracks indicating left lateral displacement were observed in the superstructure of a bridge.

Taking into account the distribution of building damage and the geological setting of Hualien city, it is concluded that all damage was arranged along or close to the Meilun fault that runs right underneath Hualien with a length of 5 km and a strike direction of N20°-55°E.

As regards the EEE, secondary EEE comprising ground cracks, liquefaction phenomena and slope movements were generated. Ground cracks were observed in several sites in Hualien city characterized by different direction and offsets. They indicated dextral or sinistral stike-slip offset and extension or compression. It is significant to note that they were observed close to the damaged buildings. Liquefaction phenomena included ground cracks accompanied by ejection of sand-water mixture that covered parts of the asphalt pavement in the area east of Hualien airport and outside of the perimeter wall of the military base. Slope movements were generated along steep slopes associated with faults as well as along the high and steep slopes of the Taroko Gorge located north of Hualien city.

Based on the distribution of the EEE in Hualien city, it is concluded that ground cracks and liquefaction phenomena were also observed close to or along the Meilun fault.

Taking into account the application of radar interferometry techniques by several research teams and the detection of

permanent ground dislocation of tectonic origin in Hualien city (Yen et al., 2018; Huang and Huang, 2018), it is concluded that the eastern coastal part of the city located east of the Meilun fault is characterized by remarkably large uplift and northeastward displacement, while its western part located west of the Meilun fault is subsided and southwestwards displaced. Thus, the resulted displacement discontinuity coincides with the already mapped Meilun fault.

In conclusion, the spatial distribution of the environmental effects (ground cracks and liquefaction phenomena) and the building damage induced by the February 6, 2018, Mw 6.4 Hualien (Eastern Taiwan) earthquake is strongly related to and controlled by the Meilun fault which runs right underneath Hualien City.

Moreover, the observed damages resulted from the synergy of several factors comprising the soil characteristics, the effects of the vertical component of the earthquake ground motion, the construction type and the presence of the Meilun fault, which strongly affected the mechanical properties of the surficial sediments and the bedrock along or close to its trace.

Acknowledgements

All funding for this work was provided by the Environmental, Disaster, and Crisis Management Strategies Master Degree Program of the Department of Geology and Geoenvironment of the National and Kapodistrian University of Athens.

References

Bonilla, M.G., 1975. A Review of Recently Active Faults in Taiwan. Open File Rep (75-41, 58 pp.) U. S. Geol. Surv., Menlo Park, Calif.

Bonilla, M.G., 1977. Summary of Quaternary faulting and elevation changes in Taiwan. Mem. Geol. Soc. China, 2, 43-55.

Hsu, T.L., 1955. Earthquakes in Taiwan. Quart. J. Bank Taiwan 7 (2), 148-164 (in Chinese).

Hsu, T.L., 1962. Recent faulting in the Longitudinal Valley of eastern Taiwan. Mem. Geol. Soc. China 1, 95-102.

Huang, M.-H., Huang, H.-H., 2018. The complexity of the 2018 Mw 6.4 Hualien earthquake in east Taiwan. Geophysical Research Letters, 45, 13249-13257. https://doi.org/10.1029/2018GL080821

Lekkas, E., Mavroulis, S., Carydis, P. (2018). The February 6, 2018 Mw 6.4 Hualien (Eastern Taiwan) earthquake. Newsletter of Environmental, Disaster, and Crises Management Strategies, 6, ISSN 2653-9454. Available at: https://edcm.edu.gr/images/docs/2017/Newsletter_2018_2_Taiwan_EQ.pdf

Shyu, J.B.H., Chen, C.-F., Wu, Y.-M., 2016. Seismotectonic characteristics of the northernmost Longitudinal Valley, eastern Taiwan: Structural development of a vanishing suture. Tectonophysics, 692 (B), 295-308, https://doi.org/10.1016/j.tecto.2015.12.026

Shyu, J.B.H., Sieh, K., Chen, Y.-G., 2005a. Tandem suturing and disarticulation of the Taiwan orogen revealed by its neotectonic elements. Earth Planetary Science Letters, 233, 167-177, https://doi.org/10.1016/j.epsl.2005.01.018

Shyu, J.B.H., Sieh, K., Chen, Y.-G., Liu, C.-S., 2005b. Neotectonic architecture of Taiwan and its implications for future large earthquakes. Journal of Geophysical Research, 110, B08402. http://dx.doi.org/10.1029/2004JB003251

Yen, J.-Y., Lu, C.-H., Dorsey, R.J., Kuo-Chen, H., Chang, C.-P., Wang, C.-C., Chuang, R.Y., Kuo, Y.-T., Chiu, C.-Y., Chang, Y.-H., Bovenga, F., Chang, W.-Y., 2018. Insights into Seismogenic Deformation during the 2018 Hualien, Taiwan, Earthquake Sequence from InSAR, GPS, and Modeling. Seismological Research Letters, 90 (1): 78-87, doi: 10.1785/0220180228

15th International Congress of the Geological Society of Greece
Athens, 22-24 May, 2019 | Harokopio University of Athens, Greece
Bulletin of the Geological Society of Greece, Sp. Pub. 7 Ext. Abs. GSG2019-347

Boundary and Estimation of the Flood Development Velocity Using Unmanned Aerial Vehicle (UAV)-Derived Imagery and Ground Observations: The Case of the 2017 Mandra Flash Flood in Greece

N-I. Spyrou[1], E-S. Stanota[1], M. Diakakis[1], E. Andreadakis[1], G. Deligiannakis[2], E. Lekkas[1]

(1) Department of Geology and Geoenvironment, Zografou Athens, Greece, nspyrou@geol.uoa.gr
(2) Agricultural University of Athens, Athens, Greece

Background

The use of Unmanned Aircraft Vehicle (UAV) can make a decisive contribution to response to hydro-meteorological natural disasters increasingly affecting the Mediterranean region. UAVs can be used to identify, study and recover environmental impacts, as well as to improve data monitoring and recording using on board innovative sensors. The UAV in disaster management provides direct and detailed impact recording even in inaccessible areas. It also provides images and maps of enhanced resolution, especially on flash flood phenomena, in the case of which the spatial and temporal scales of occurrence do not favor traditional monitoring processes. The flash flood of west Attica on November 15 2017 has caused enormous damage on human and natural environment and a tragic loss of 24 people. The complexity of impacts typology and its distribution in space, highlighted the need to study the event, in terms of evolution and mapping of its extent and physical characteristics. The analysis with the use of UAV produced detailed flood extent and provided a comprehensive description of the characteristics of floodwaters within the flooded area.

Objectives

The research team studied the area during the flood and the day after, using a combination of ground and aerial observations with the aid of an unmanned aerial vehicle (UAV). The aim of this study is to identify different types of flood extent indicators, including mudlines, debris lines and others, based on collected imagery, which were recorded and lead to flood boundary delineation across the inundated area. In this work, the rate of flood development velocity is also estimated using the data which were collected through aerial and ground observations, including snapshots with specific timeframe. This study shows how aerial observations can improve the accuracy of defining the extent of floods and the speed of their deployment that in turn is very useful for risk mitigation efforts. UAV flights took place a few hours after the flood of November 15, 2017 and on November 16, 2017. The flood affected the western part of Attica in the city of Mandra and Nea Peramos and reached 300 mm in 13 hours causing 24 deaths and extensive damage to property and infrastructure.

Methods

- Research was carried out with ground and aerial observations on the flight of a UAV. Photos and videos were captured using the UAV in several flights, as well as ground observations and images.
- The collected data were analysed and processed and the collected images were georeferenced.
- The types of high - water marks were studied, categorized. The depth and the extent of the flood were assessed.
- The estimation of the water flow rate was based on the hydraulic head and the flow of objects on the water surface was based on videos and photos material which taken during the flood.
- In order to evaluate the characteristics of the flow and its speed, video snapshots, images of terrestrial and aerial observations that were selected, were analyzed. This data involved flowing obstacles such as trees, buildings and other facilities.
- Regarding the estimation of the water velocity, the variation of the water level on the same position at different times was also studied.

Results

According to the analysis of the collected data from the combined use of the aerial and ground observations [Fig 1], we achieved the accurate estimation of the flood extent and the definition of its characteristics. These characteristics were related with the boundaries, the depth and the speed of the flood. In this study the types of the flood boundaries were analyzed and categorized. The speed of the water during the flood reached 10 m / s, the depth reached 4.2 m and the flood area was 4.03 km^2.



Figure 1. Display of the flood boundaries in the industrial area of Mandra with the use of UAV.

Conclusions

The UAV allowed the collection of aerial photographs in an extended area during flood flows despite that a large portion of it was inaccessible due to road closures and safety issues. This way a large part of the useful data was captured in short time during and after the flood. Especially in the case of flash floods which are characterized by a rapid rise and withdrawal of floodwaters, it is virtually impossible for a field survey team to reach different parts of the inundated area and make ground observations during the actual phenomenon. As flood effects and flood marks of all kinds (e.g. high water marks, flood deposits) were removed during cleanup efforts in the days following the disaster, there was limited time to cover the whole affected area with detailed ground observations. In this case, the integration of aerial observations in post-flood analysis provided guidance to intensify ground observations at key locations where it was needed, in time before crucial evidence disappeared. This work demonstrated that the combination of aerial and ground observations allowed an accurate reconstruction of the 2017 flood, contributing to flood extent and water depth determination, peak discharge estimation and detailed mapping of impacts. The approach is considered to have several advantages connected with the collection of data during flash flood investigations and is capable of providing a holistic overview of multiple aspects of a flood that can be valuable to both science and civil protection. Aerial observations can act as an extra point of observation that accompanies the traditional ground-based field survey and fits well in the opportunistic nature of this type of studies.

References

Diakakis, M, Andreadakis, Nikolopoulos, E.I., Spyrou, N.I., Gogou, M.E., Deligiannakis, G., Katsetsiadou, N.K., Antoniadia, Z., Melaki, M., Georgakopoulos, A., Tsaprouni, K., Kalogiros, J., Lekkas, E. (2018). An integrated approach of ground and aerial observations in flash flood disaster investigations. The case of the 2017 Mandra flash flood in Greece. International Journal of Disaster Risk Reduction, Elsevier, 33, pp 290-309.

Suzette, M. K. (2016). Identifying and Preserving High-Water Mark Data. Chapter 24 ofSection A, Surface-Water Techniques Book 3, Applications of Hydraulics, USGS.

Gaume, E., Borga, M., 2008. Post-flood field investigation in upland catchment after major flash flood: proposal of a methodology and illustrations, Journal of flood Risk Management, 1 (4), 175-189.

15th International Congress of the Geological Society of Greece
Athens, 22-24 May, 2019 | Harokopio University of Athens, Greece
Bulletin of the Geological Society of Greece, Sp. Pub. 7 Ext. Abs. GSG2019-348

Debris Flow on a Fully Activated Intramontane Fan during the Flash Flood of Mandra. UAS-aided Field Mapping of Katsimidi Fan

E. Ezat[1], K.Z El Ajouz[1], Emm. Andreadakis[1], M. Diakakis[1], A. Georgakopoulos[1]

(1) Department of Geology and Geoenvironment, National and Kapodistrian University of Athens, Greece, elezat@geol.uoa.gr

Post-flood investigations contribute greatly to the hazard assessment in areas where catastrophic sedimentary processes are associated with extreme floods, through the analysis of the dominant sedimentary processes of the fans (Crosta & Frattini, 2004; Gaume & Borga, 2008). Structure from Motion techniques, and the use of Unmanned Aircraft Systems (UAS) in general, have been increasingly proved useful to post flood surveys (Andreadakis, Kapourani, Diakakis, Papaspyropoulos, & Filis, 2017; Tamminga, Eaton, & Hugenholtz, 2015). During November 2017, an extremely intense rainfall took place in West Attica. The highest precipitation levels were recorded on the high altitude areas west of Mandra and Nea Peramos. This resulted in extreme floods in the region that reached the towns, bringing destruction and 24 fatalities. The huge volume of surface runoff that reached 170 m^3/s and 4 m in height above the ground surface in some spots (Diakakis et al., 2018), reactivated old landforms on which a large portion of Mandra was built, resulting in houses, factories and roads being seriously damaged. The present research focused on the intramontane alluvial fan of Katsimidi stream, a tributary of Agia Ekaterini stream that caused the disaster in Mandra settlement, and at a 4 km distance upstream (west). It can be considered a prime example of reactivation of a fan of Pleistocene origin, accompanied by a debris flow, in which boulders larger than 1 meter in diameter were detached and transported along the streambed and finally deposited over the fan surface (Figure 1). The aim of the study was mapping of the flood features on the fan in explicit detail, with the aid of photogrammetry mapping by an Unmanned Aircraft Vehicle. The procedure included a number of flights programmed and executed through the Pix4D capture software for 3D maps, and processing, firstly in the Pix4D mapper software, and then in the ArcMap software of ESRI. In the first phase of modeling, through processing of 591 images, producing more than 7000 matches per image and a final cloud of more than 41 million points, the 3d model of the fan was produced, along with the orthophotomosaic and Digital Surface Model of the area.



Figure 1. Flood deposits in the streambed, near the apex (left). Boulders on the fan surface downstream (right)

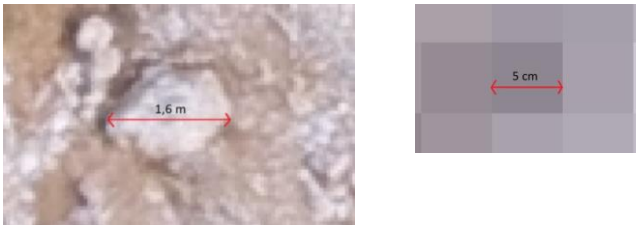

Figure 2. Left: Boulder characterizing extremely high energy flow. Right: Spatial resolution of UAV images

These products were introduced to the ArcMap environment, and a further processing producing the slope map of the area. Linear erosion was delineated with the aid of the orthomosaic and the slope map, followed by outlining of the flood deposits outcrops and areas of recently exposed bedrock. The outcome was a first map of erosion/deposition features. Further analysis taking into account the dominant visible clast size within the deposit polygons, lead to classification of deposition areas by dominant clast size (Figure 3). The resulting map (Figure 3), shows the following:

a) Larger diameter clasts (boulders larger than 50cm in diameter) were mainly deposited near the apex of the fan and along the main axis of flow of Katsimidi stream.

b) Bedrock exposure is located mainly along the local flood extent boundary
c) The size of clasts is reduced from the apex to the foot of the fan and from the axis of flow to the sides
d) Most of the coarse flood deposits are buffered by the forested area at the foot of the fan, permitting transportation only along corridors through the vegetation, and prevented from entering Agia Ekaterini stream.

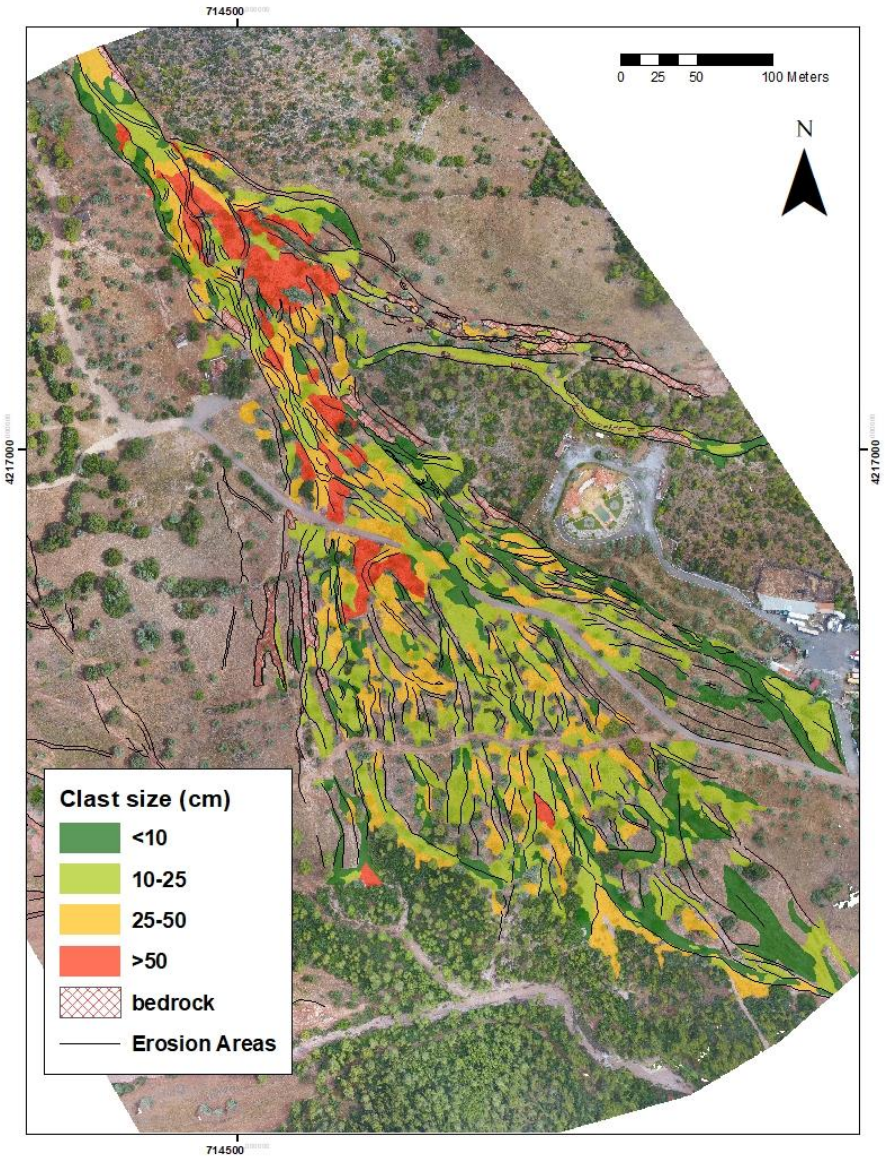

Figure 3. Linear erosion, bedrock exposure and flood deposition areas classified by clast size in Katsimidi fan.

This work demonstrates the applicability and value of imagery from small Unmanned Aircraft Systems in post flood surveys, as far as geomorphological impact and detailed mapping of small areas is concerned. Imagery should be collected with flights immediately after the disaster, and thus they help preserve all mapping data, which are usually soonafter altered or vanished, especially where restoration works are urgently needed, or when a following event should occur. In this way, research buys time to examine thoroughly and revisit virtually the disaster scene without leaving the lab, and more importantly, without missing any information from the field, not to mention the potential for explicitly detaild mapping, depending only on the initial ground sampling distance, which is adjusted through flight altitude.

References

Andreadakis, E., Kapourani, E., Diakakis, M., Papaspyropoulos, K., & Filis, C. (2017). Unmanned Aircraft Systems (UAS) in Post-Flood Surveys. The Case of Laconia Floods 2016. In 11th International Hydrogeological Congress of Greece. Athens.

Crosta, G. B., & Frattini, P. (2004). Controls on modern alluvial fan processes in the Central Alps, Northern Italy. Earth Surface Processes and Landforms, 29(3), 267–293. http://doi.org/10.1002/esp.1009

Diakakis, M., Andreadakis, E., Nikolopoulos, E. I., Spyrou, N. I., Gogou, M. E., Deligiannakis, G., … Lekkas, E. (2018). An integrated approach of ground and aerial observations in flash flood disaster investigations. The case of the 2017 Mandra flash flood in Greece. International Journal of Disaster Risk Reduction. http://doi.org/10.1016/J.IJDRR.2018.10.015

Gaume, E., & Borga, M. (2008). Post-flood field investigations in upland catchments after major flash floods: proposal of a methodology and illustrations. Journal of Flood Risk Management, 1(4), 175–189. http://doi.org/10.1111/j.1753-318X.2008.00023.x

Tamminga, A. D., Eaton, B. C., & Hugenholtz, C. H. (2015). UAS-based remote sensing of fluvial change following an extreme flood event. Earth Surface Processes and Landforms, 40(11), 1464–1476. http://doi.org/10.1002/esp.3728

SPECIAL SESSION

T7.S2 New advances in InSAR and GNSS techniques and their applications for geohazards

Conveners: **A. Ganas (NOA)**
P. Elias (NOA)
S. Valkaniotis,
M. Foumelis (BRGM)
P. Kourkouli (ICEYE)

15th International Congress of the Geological Society of Greece
Athens, 22-24 May, 2019 | Harokopio University of Athens, Greece
Bulletin of the Geological Society of Greece, Sp. Pub. 7 Ext. Abs. GSG2019-152

The GLab to support the geohazards community – experience of the Geohazards Exploitation Platform initiative of the European Space Agency

Th. Papadopoulou[1], Ph. Bally[2], M. Foumelis[3], F. Pacini[4], F. Provost[2], M. Leonardi[5]

(1) ARGANS Ltd., 260 Pin Montard str., Sophia Antipolis, France, tpapadopoulou@argans.co.uk
(2) European Space Agency (ESA), Largo Galileo Galilei 1, Frascati, Italy
(3) BRGM – French Geological Survey, 3 av. Claude-Guillemin, Orleans, France
(4) Terradue s.r.l., via Giovanni Amendola 46, Roma, Italy, (5) RHEA Group c/ ESA, Largo Galileo Galilei 1, Frascati, Italy

Abstract

The Geohazards Lab is an initiative developed within the framework of the Committee on Earth Observation Satellites (CEOS) Working Group on Disasters (WG Disasters) to enable a greater use of Earth Observation (EO) data and derived products to assess geohazards and their impact. The aim is to establish an inclusive and comprehensive process to optimize the use of EO technologies starting from the needs of national and local decision-makers in political and socio-economic sectors relevant to Disaster Risk Management (DRM).

The Geohazards Lab is based on a group of interoperable platforms with federated resources to animate and support the geohazards user community. It is originated by the European Space Agency (ESA), with the support of several other CEOS space agencies and partners, including the Italian Space Agency (ASI), the French Space Agency (CNES) and the German Space Research Centre (DLR), as well as several research institutes including BRGM, INGV, CNR-IREA, CNRS-EOST, NOA, NORUT and IGME.

Based on the success demonstrated during the CEOS Seismic Hazards Pilot activity, the Geohazards Exploitation Platform (GEP, geohazards-tep.eo.esa.int) continues to contribute in the CEOS Geohazards Lab initiative. The GEP is an activity originated by ESA in November 2015 and led by Terradue, to support the geohazards community exploiting satellite EO data to assess geohazard risks. It provides a data delivery mechanism, on-line processing tools and services and an e-collaboration environment to exploit EO data to assess geohazards and their impact. Conventional InSAR services (e.g. DIAPASON and SNAP S-1 DInSAR service), advanced InSAR services (e.g. InSAR SBAS of CNR-IREA), optical on-demand services (e.g. MPIC OPT, ALADIM and DSM OPT of the University of Strasbourg/CNRS EOST) and optical systematic services (e.g. INGV's STEMP for surface temperature mapping, NOVELTIS and INGV's VEGAN services for hot spot and vegetation vigor mapping) have been made available or are currently under integration. New platform functionalities are under implementation, such as the alerting system for automatic deformation mapping that shall trigger the services available on GEP based on seismic events polled from external systems e.g. the EMSC, USGS pager and Copernicus EMS.

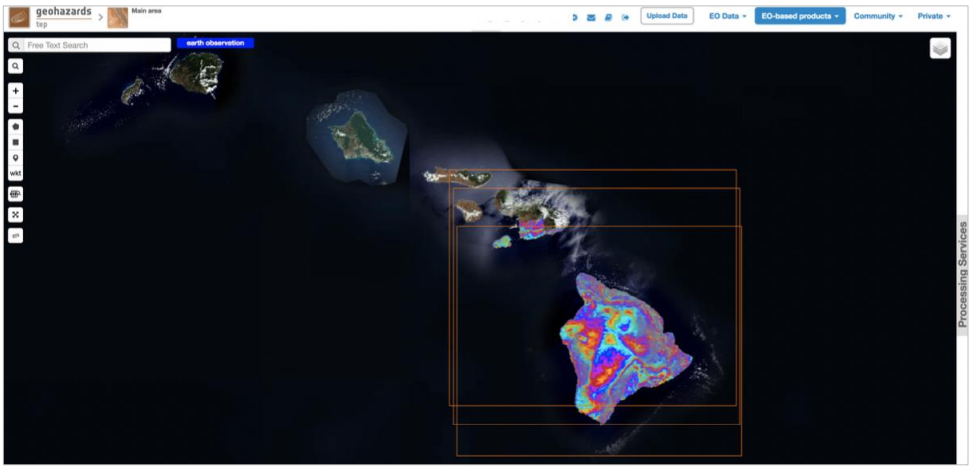

Figure 1. Preview of the Geohazards Exploitation Platform showing InSAR products over Hawaii generated systematically using DLR's S-1 High-Resolution InSAR Browse. Contains modified Copernicus Sentinel-1 data).

The Geohazards Lab envisages building a collaborative framework with expert geoscience centres and users to achieve a greater adoption of EO methods. Its goals are to support the exploitation of online hosted processing capabilities with a focus on cloud processing solutions, define consensus methods in liaison with experts to harmonize EO based products and establish a methodological approach to support the generation of reference ground deformation measurements in support to historical hazard analysis. Focusing on the harmonization of EO based products, the Geohazards Lab intends to coordinate with other available capabilities such as for instance the European Plate Observing System (EPOS), the Norwegian Ground Motion Service (NGMS), the Supra National Ground Motion Service (SNGMS) and the Geohazards Office (initiated by BRGM) to support a scientific animation activity and to work on common guidelines for standards and formats of EO based terrain motion measurements.

The Geohazards Lab supports users with EO expertise from geoscience centres who are the priority intermediaries with end users from local and regional DRM organizations. Users from both the EO and non-EO community can benefit from this effort as it will facilitate (i) the broader use EO products sharing common standards by EO practitioners, (ii) the interoperability of results obtained by different data provides within or outside EO processing platforms and (iii) an easier end-product interpretation by decision makers.

15th International Congress of the Geological Society of Greece
Athens, 22-24 May, 2019 | Harokopio University of Athens, Greece
Bulletin of the Geological Society of Greece, Sp. Pub. 7 Ext. Abs. GSG2019-196

Three-dimensional visualization of Santorini caldera wall point cloud displacements

M. Foumelis[1], T. Dewez[1], E. Papageorgiou[2]

(1) BRGM – French Geological Survey, Address, Orleans, France, m.foumelis@brgm.fr
(2) Aristotle University of Thessaloniki, 54124, Thessaloniki, Greece

Slope instabilities along steep caldera walls of active volcanoes pose a significant hazard, especially when the human factor is also present. Synthetic Aperture Radar (SAR) interferometry is a well-established geodetic imaging technique for monitoring ground displacements.

The circular shape of calderas introduces some restrictions for the global visualization of point-like displacement measurements, dictating the inspection, independently of each approximate linear segment of the terrain slopes.

In the present study, Persistent Scatterers Interferometry (PSI) ground displacements from Copernicus Sentinel-1 mission are manipulated in such a way to "unfold" and visualize the entire caldera walls on a single vertical planar surface. Point cloud analysis tools, originated from Terrestrial Laser Scanning (TLS) techniques, are explored for the manipulation of PSI point clouds in three-dimensional space and projection into pre-selected planes.

Such approach simplifies the actual inspection of the caldera walls, while allowing building a geospatial link between coordinates of the selected planar projection and the actual geolocation grid. Furthermore, the view of PSI in unfolded elevation grids is more effective, in particular to render displacement induced by gravity.

It is demonstrated that the utilization of advanced analysis and visualization tools throughout disciplines can improve the assessment of the SAR interferometric results and lead to a more effective decision making process.

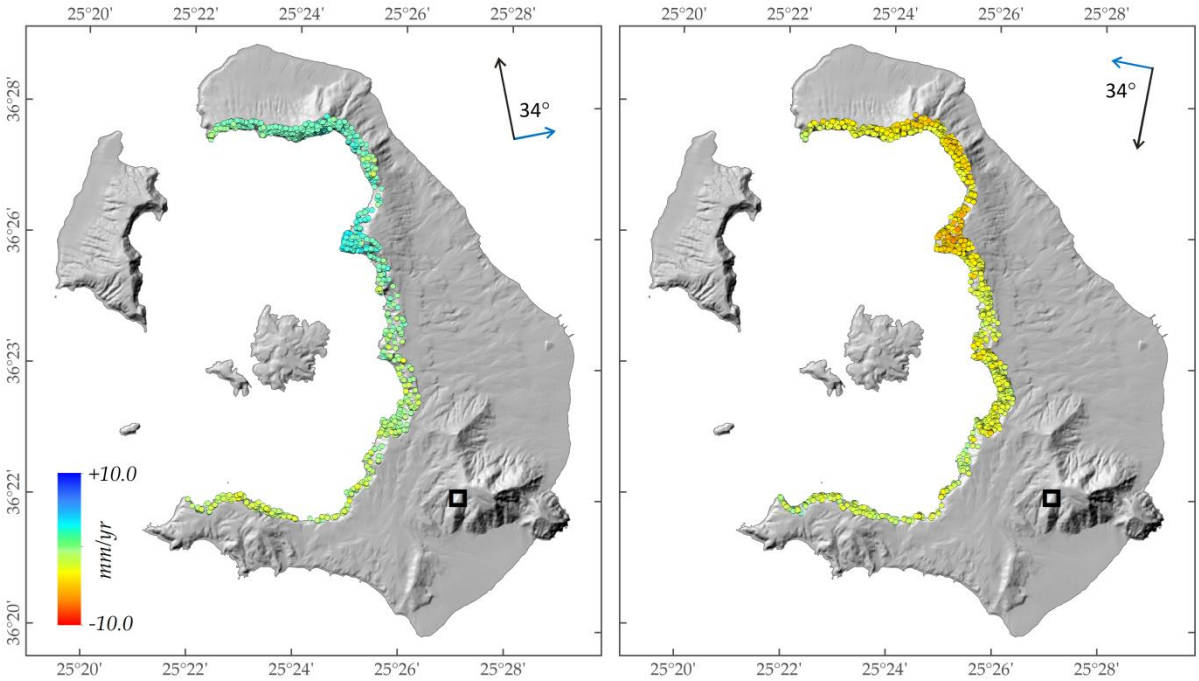

Figure 1. PSI displacement rates along the Santorini caldera walls from ascending (left) and descending (right) acquisition geometries. Reference point marked as square.

References

Antoniou, A.A., Lekkas, E., 2010. Rockfall susceptibility map for Athinios port, Santorini Island, Greece. Geomorphology 118, 152-166.

Antoniou, V., Lappas, S., Leoussis, Ch., Nomikou, P., 2017. Landslide sisk assessment of the Santorini Volcanic Group. In Proceedings of the 3rd International Conference on Geographical Information Systems Theory, Applications and Management (GISTAM 2017), 131-141.

Buckley, S.J., Ringdal1, K., Naumann1, N., Dolva, B., Kurz1, T.H., Howell, J.A., Dewez, T.J.B., 2019. LIME: Software for 3-D visualization, interpretation, and communication of virtual geoscience models. Geosphere 15(1), 222-235.

Dewez, T.J.B., Stewart, I.S., 2015. From digital elevation models to 3-D deformation fields. In book: Monitoring and Modelling Dynamic Environments, doi: 10.1002/9781118649596.ch12.

Foumelis, M., Trasatti, E., Papageorgiou, E., Stramondo, S., Parcharidis, I., 2013. Monitoring Santorini Volcano (Greece) breathing from space. Geophysical Journal International, doi: 10.1093/gji/ggs135.

Lekkas, E., 2009. Landslide hazard and risk in geologically active areas. The case of the caldera of the Santorini (Thera) volcano island complex (Greece). 7th Asian Regional Conference for IAEG, International Association for Engineering Geology (IAEG), Chengdu, China, p. 417-423.

Lekkas, E., 2014. Landslide hazard and risk in geologically active areas. The case of the caldera of the Santorini (Thera) volcano island complex (Greece), National University of Athens, Faculty of Geology & Geoenvironment, p. 7.

Papageorgiou, E., Foumelis, M., Mouratidis, A., Papazachos, C., 2018. Sentinel-1 monitoring of Santorini Volcano post-unrest state. IEEE International Geoscience and Remote Sensing Symposium (IGARSS 2018), Valencia, Spain, p. 4.

Papageorgiou, E., Foumelis, M., Trasatti, E., Ventura, G., Raucoules, D. & Mouratidis A., 2019. Multi-sensor SAR geodetic imaging and modelling of Santorini volcano post-unrest response. Remote Sensing 11(3), 259, https://doi.org/10.3390/rs11030259.

15th International Congress of the Geological Society of Greece
Athens, 22-24 May, 2019 | Harokopio University of Athens, Greece
Bulletin of the Geological Society of Greece, Sp. Pub. 7 Ext. Abs. GSG2019-200

RHETICUS: Insightful Geo-Analytics for Detecting Ground Instabilities and Monitoring Critical Infrastructures

Yiota Spastra[1], Stelios Bollanos[1], Giuseppe Forenza[2], Antonello Aiello[2]

(1) Planetek Hellas EPE, 44 Kifisias Avenue, 15125 Maroussi, Athens, Greece, e-mail: info@planetek.gr
(2) Planetek Italia s.r.l. Via Massaua 12, I-70132 Bari, Italy, e-mail: info@planetek.it

Abstract

Rheticus® is an automatic cloud-based geoinformation service platform, designed to deliver fresh and accurate data and information for monitoring the evolution of the Earth's surface. The platform, provides information by means of graphic indicators, dynamic diagrams and pre-set reports. The provided information allow users to immediately perform assessment operations over areas of interest.

Rheticus® Displacement represents a revolutionary model concept (through subscription) in monitoring critical infrastructure with the use of SAR data and the persistent scatter technique (PS), designed for users with high expectations in the value of information and its user friendliness provision.

More specifically, Rheticus® Displacement provides accurate information to monitor over time, through Multi-Temporal SAR Interferometry (MTInSAR) analysis, movements occurring across landslide features or structural weaknesses that could affect buildings or infrastructures. Using European Copernicus Sentinel-1 (S1) open data images and MTInSAR techniques, the service is complementary to traditional survey methods, providing a long-term solution to slope instability and geohazards monitoring.

The service update is guaranteed through the use of satellite images, mapping data and environmental information available online as open data. The service is updated with the availability of fresh incoming data, and the refresh rate can range from monthly to daily frequency depending on the service characteristics.

Rheticus® Displacement is a turnkey vertical web service for the continuous monitoring via satellite of instability phenomena affecting transportation infrastructures (roadways, railways, including bridges and tunnels) and/or their nearby areas, caused by structural defeats or ground displacements such as landslides or subsidence phenomena.

In this presentation, we focus on the great challenge of land and infrastructure monitoring as the key activity to ensure people's safety, environmental protection and the safeguarding of assets at all stages of the life cycle of infrastructures, from design to production, management and maintenance.

15th International Congress of the Geological Society of Greece
Athens, 22-24 May, 2019 | Harokopio University of Athens, Greece
Bulletin of the Geological Society of Greece, Sp. Pub. 7 Ext. Abs. GSG2019-323

Mapping deformation due to moderate/strong seismic events with Geohazards TEP - An overview of year 2018

Sotirios Valkaniotis[1], Athanassios Ganas[2]
(1) Trikala, 42131 Greece, valkaniotis@yahoo.com
(2) Institute of Geodynamics, National Observatory of Athens, Greece, aganas@noa.gr

Extended abstract

Since 2015 ESA provides early access to an on-line processing platform for satellite data, the Geohazards Exploitation platform or GEP https://geohazards-tep.eu/ GEP aims to support the exploitation of satellite EO for geohazards. It follows the Supersites Exploitation Platform (SSEP), originally initiated in the context of the Geohazard Supersites & Natural Laboratories initiative (GSNL). The Geohazards platform has been expanded to address broader objectives of the geohazards community. In particular it is a contribution to the CEOS Working Group - Disasters to support its Seismic Hazards Pilot and terrain deformation applications of its Landslide & Volcano Pilots. GEP is sourced with elements – data, tools, and processing including INSAR – relevant to the Geohazards theme and related exploitation scenarios. It offers the following advantages: a) Rapid on-demand production as soon as satellite data are available (within few hours up to a few days) b) Semi-automatic production: the user can manipulate certain parameters, versatility in date and frame selections and c) Does not require advanced knowledge of methodologies from the user perspective, but enables a greater choice of products than pure automatic pipelines. The Geohazards TEP product analysis permits the user to obtain results on: a) Primary surface faulting and deformation, b) Earthquake Environmental Effects (sec. faulting, triggered ruptures, landslides), c) Coherence shadows and multi-temporal coherence evaluation and d) Line-of-Sight (LOS) displacement (InSAR data) and 2D horizontal displacement (Optical data).

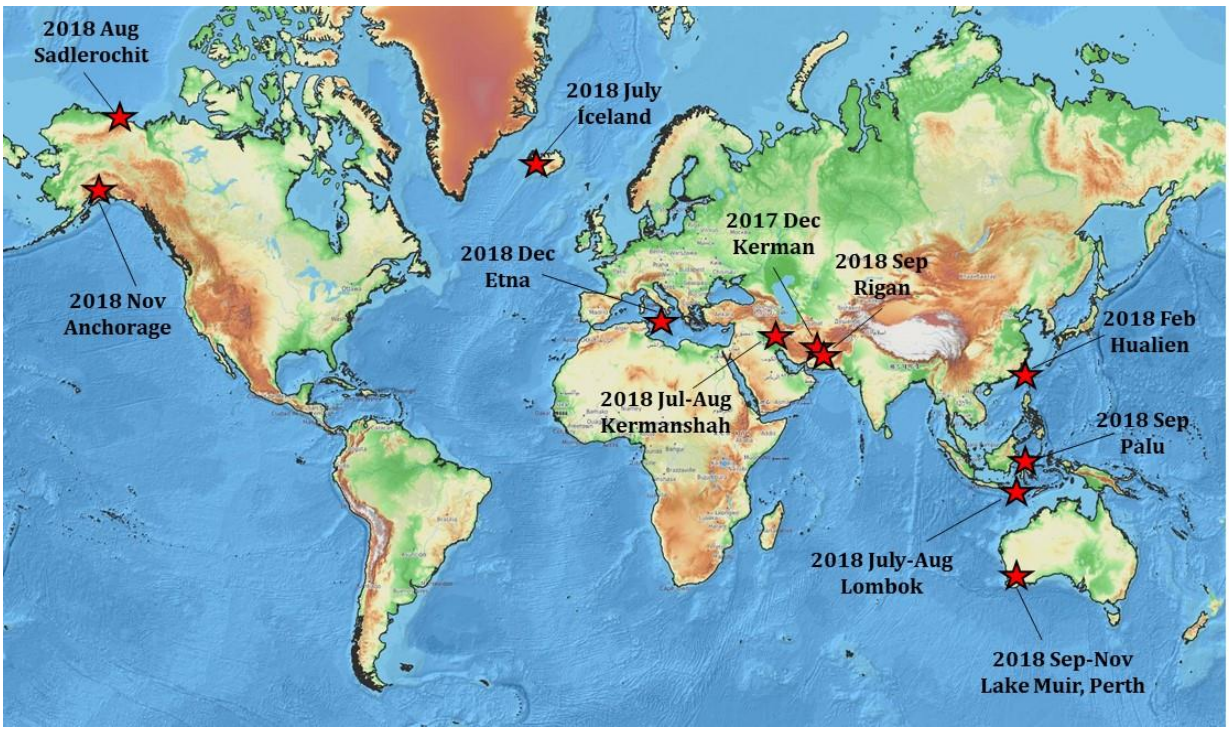

Figure 1. A) Global relief map showing the location of the 2018 seismic events examined in this study (red stars).

Geohazards TEP provides an effective platform to study earthquakes using InSAR & optical analysis. The Sentinel-1 and GEP tools (SNAP, DIAPASON, GMTSAR, MPIC-OPT etc.) captured surface deformation due to many strong events during 2018, with a threshold as low as M_W 4.9 (Catania, Italy Dec 26 2018). The semi-automatic nature of GEP platform is extremely useful to a Geoscientist End-User, with versatility in parameters and product selection. It was also demonstrated that optical displacement data (Sentinel-2/MPIC-OPT) are not an alternative to SAR geodesy, but have a complimentary role, for better capturing near-fault displacement than InSAR.

We examine the most significant shallow earthquake events between December 2017 and December 2018 (Fig. 1). The GEP tools and Sentinel1/2 imagery products are used to identify and examine earthquake surface ruptures, co-seismic landslides and other earthquake environmental effects. The majority of moderate/strong shallow events were identified in Sentinel-1 InSAR products and examples are presented for each single event or earthquake sequence (Fig. 2). Using

GEP we identified coseismic deformation of moderate-magnitude events like Perth, Australia and Catania, Italy (Valkaniotis 2018), strong earthquake sequences with multiple events like Lombok, Indonesia (Ganas et al. 2018), as well as in large plate boundary events such as the M_W 7.5 Palu, Indonesia earthquake (Valkaniotis et al. 2018). In addition, optical image correlation from Sentinel-2 imagery through the MPIC-OPT service (Stumpf et al. 2017) assisted in measuring near-fault large displacements, where InSAR is difficult to be applied due to lack of correlation and lack of coherence.

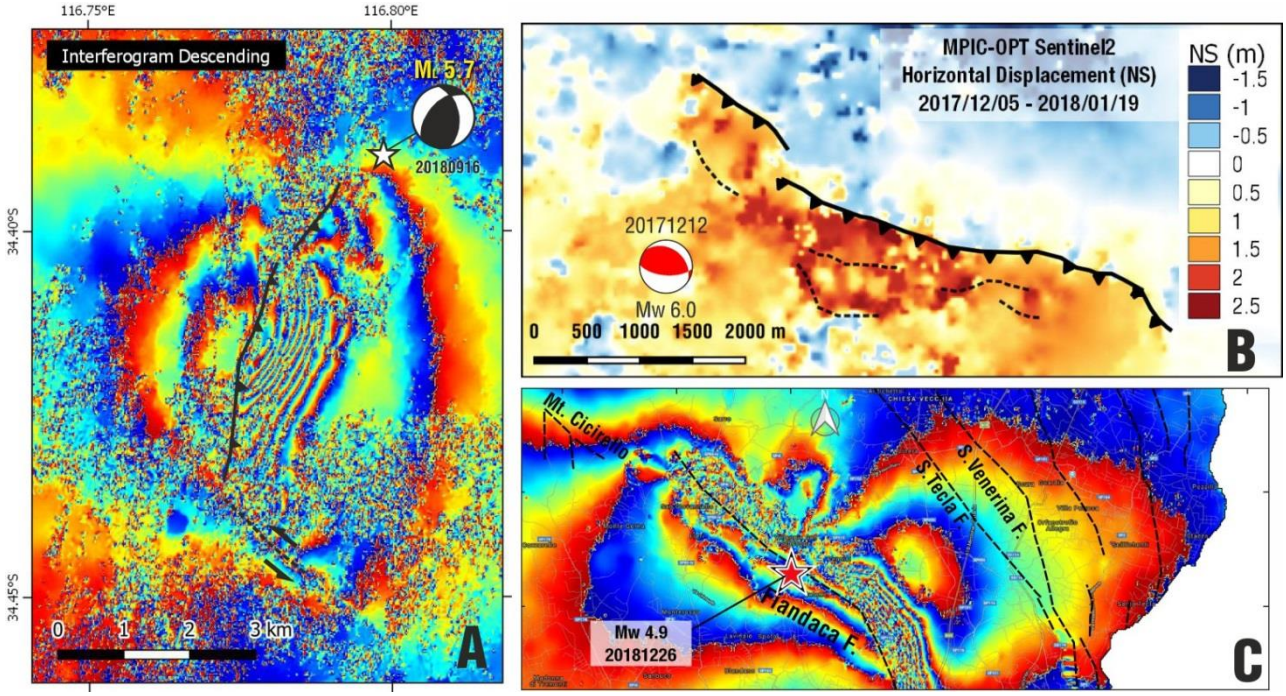

Figure 2. A) Coseismic interferogram of the M_L 5.7 Sep 16 2018 Lake Muir, AUS earthquake with surface faulting along a reverse/oblique fault. B) Horizontal displacement (N-S component) from Sentinel-2 optical images of the M_W 6 Dec 12 2017 earthquake in Kerman, SE Iran. C) Co-seismic interferogram of the Dec 26 2018 M_W 4.9 Catania, Italy earthquake at the SE flank of Etna volcano. Each color fringe on interferograms represent ~2.8 cm of displacement.

Acknowledgements

We thank Michael Foumelis, Panagiotis Elias and Pierre Briole for comments. Access to pre-operational Geohazards Exploitation Platform (geohazards-tep.eo.esa.int) was granted under the Early Adopters Program (National Observatory of Athens - Corinth Rift Laboratory).

We acknowledge support of this research by the project "HELPOS - Hellenic Plate Observing System" (MIS 5002697) which is implemented under the Action "Reinforcement of the Research and Innovation Infrastructure", funded by the Operational Programme "Competitiveness, Entrepreneurship and Innovation" (NSRF 2014-2020) and co-financed by Greece and the European Union (European Regional Development Fund).

References

Brito, A. and Caumont, H. 2015. The Geohazards Exploitation Platform. EO Science 2.0 , Frascati - Italy, 12-14 October 2015 http://doi.org/10.5281/zenodo.32032

Ganas, A. Tsironi, V. and Valkaniotis, S. 2018. A preliminary report on the 2018 Lombok region - Indonesia earthquakes. Online report submitted to EMSC on 9 August 2018, 14p
https://www.emsc-csem.org/Files/news/Earthquakes_reports/Lombok%20earthquake%20report%20GTV%209-8-2018.pdf

Stumpf, A., Malet, J.-P. and Delacourt, C. 2017. Correlation of satellite image time-series for the detection and monitoring of slow-moving landslides. Remote Sensing of Environment, 189, 40-55 https://doi.org/10.1016/j.rse.2016.11.007

Valkaniotis, S., Ganas, A., Tsironi, V., Barberopoulou, A., 2018. A preliminary report on the M7.5 Palu earthquake co-seismic ruptures and landslides using image correlation techniques on optical satellite data. Special report submitted to EMSC on 19 October 2018 http://doi.org/10.5281/zenodo.1467128

Valkaniotis, S. 2018. Differential Interferogram of the September 16 2018 Mw 5.3 earthquake Lake Muir, Perth, Australia. http://doi.org/10.5281/zenodo.1464715

15th International Congress of the Geological Society of Greece
Athens, 22-24 May, 2019 | Harokopio University of Athens, Greece
Bulletin of the Geological Society of Greece, Sp. Pub. 7 Ext. Abs. GSG2019-324

The October 25, 2018 M6.7 Zakynthos earthquake sequence (Ionian Sea, Greece): fault modelling from seismic and GNSS data and implications for seismic strain release along the western Hellenic Arc

Athanassios Ganas[1], Pierre Briole[2], George Bozionelos[3], Panagiotis Elias[4], Sotiris Valkaniotis[5], Varvara Tsironi[1], Alexandra Moshou[1] and Nikoletta Andritsou[1,3]

(1) Institute of Geodynamics, National Observatory of Athens, aganas@noa.gr barbara.tsir@gmail.com
(2) ENS/CNRS, PSL Research University, Laboratoire de Géologie, Paris, France briole@ens.fr
(3) National and Kapodistrian University of Athens, Faculty of Geology and Geoenvironment gbozionelos@geol.uoa.gr
(4) IAASARS, National Observatory of Athens, Greece pelias@noa.gr
(5) Koronidos Str., 42131 Trikala, Greece valkaniotis@yahoo.com

Extended abstract

We present preliminary analysis of the fault model and the shallow earthquake sequence offshore Zakynthos (Ionian Sea, Greece; Fig. 1) that was initiated by the October 25, 2018 $M_{w(NOA)}$=6.7 earthquake (event no 15 in Fig. 1). We use geodetic and seismological data (phase data and moment tensor solutions from NOA) to identify the geometry and kinematics of the fault plane using linear inversion techniques in elastic half-space. First, we analysed the time series of fourteen (14) permanent GNSS stations located around the epicentre, two of them (ZAKU, ZAKY) being located on the island of Zakynthos and one (STRF) on the small island of Strofades. The stations are equipped with dual-frequency geodetic receivers and belong to several networks such as NOANET (Ganas et al., 2008; 2013), HxGN SmartNet Greece, Uranus (Greece) and RING (INGV). The GNSS data are processed using the GIPSY 6.4 software. This software uses a Precise Point Positioning processing strategy (Zumberge et al., 1997). We found that cm-size co-seismic horizontal offsets were recorded by the continuous GPS stations operating at both Zakynthos and Strofades islands. Secondly, for the broader region of Zakynthos, 2335 earthquakes were relocated using phases from the NOA online catalogue for the period 23 October 2018 - 17 January 2019, applying the nonlinear location algorithm NonLinLoc (Lomax et al., 2000). Thirdly, we processed Sentinel-1 SAR (C-band) data. Despite the large magnitude of the mainshock (M6.7), the surface deformation in Zakynthos is not clearly visible with differential InSAR because of the offshore occurrence of the earthquake. In various co-seismic interferograms we see small co-seismic displacements within 1 fringe (28 mm). This small visible signal is not consistent with the slip-model predictions, based on the GPS inversion models (Fig. 2). We attribute the "reduced" InSAR signal in tropospheric effects that mask most of onshore deformation. We then modelled the co-seismic displacements by assuming that the earthquake corresponds to a homogenous slip on a rectangular fault buried in an elastic half space, and we use the formalisms of Okada (1992). The best fitting fault has a centroid at 6.5 km depth which is shallower than most seismological estimates (for example, the 12-15 km of GEOSCOPE). The GPS inversion product indicates that the 25 October 2018 earthquake was due to the activation of one reverse fault with a total length of about 30 km (see green rectangle in Fig. 1), at depths 5-15 km. The fault-dip direction is also retrievable from GNSS data inversion with a low-angle (25°), eastern-dip. Therefore, we propose that the M6.7 event occurred along a N-S striking seismic fault which is located on the African-Aegean plate interface (i.e. along the megathrust).

As the October 25, 2018 event occurred along the Hellenic megathrust it signifies the high degree of seismic coupling in this region of the Hellenic Arc (i.e. Laigle et al., 2002). It also highlights the "strong" nature of the subducting slab with the occurrence of "locked" patches under the Ionian seafloor that fail during large, reverse-slip earthquakes (see Fig. 1 where 6 such events are shown near Zakynthos). In addition, the data from the recent, strong seismic events of the western Hellenic arc (1976 Zakynthos, 1997 Strofades, 2018 Zakynthos; events 7, 10 and 15 in Fig. 1) point to a sequence of a low-angle events along the plate interface with most of co-seismic deformation taken up by the upper (Aegean) plate (plate transport and uplift).

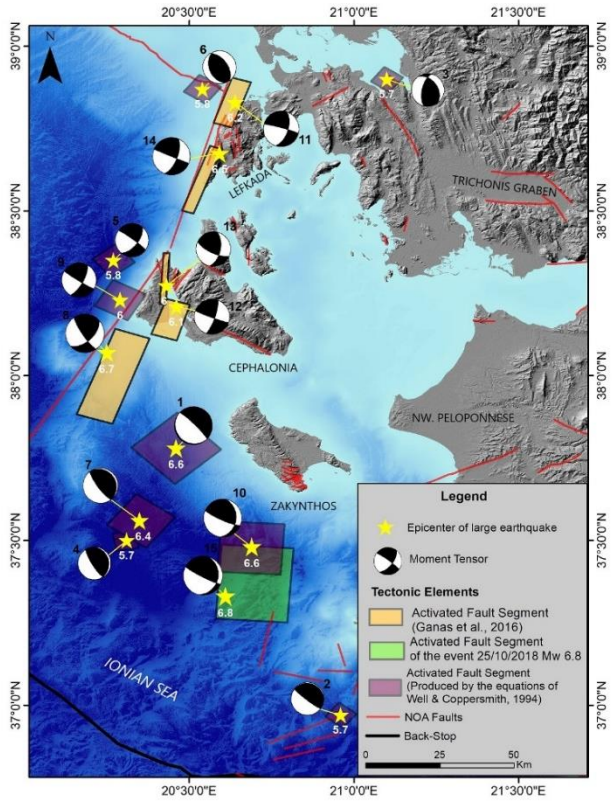

Figure 1. Overview relief map of western Greece showing the location of the offshore strong seismic events since 1959 (shaded rectangles).

Acknowledgements

We thank Nikos Roukounakis, Panagiotis Argyrakis and Nicola D' Agostino for comments. We thank the private Greek networks (Smartnet, Tree) for GNSS data and the NOA analysis group for seismic phase data. We acknowledge support of this research by the project "HELPOS - Hellenic Plate Observing System" (MIS 5002697) which is implemented under the Action "Reinforcement of the Research and Innovation Infrastructure", funded by the Operational Programme "Competitiveness, Entrepreneurship and Innovation" (NSRF 2014-2020) and co-financed by Greece and the European Union (European Regional Development Fund).

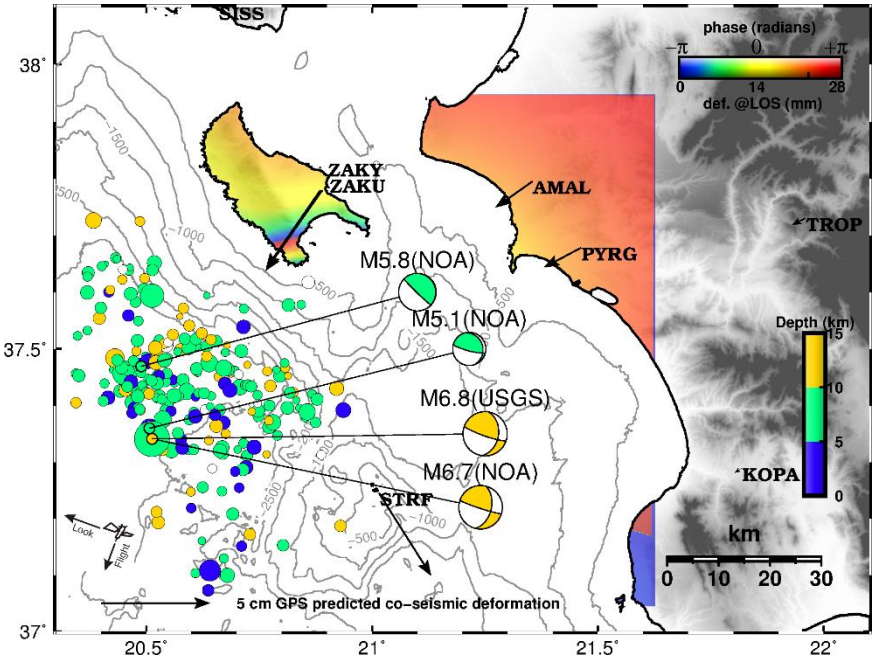

Figure 2. Modelled co-seismic S1 interferogram. Descending orbit.

References

Ganas, A., G. Drakatos, S. Rontogianni, C. Tsimi, P. Petrou, M. Papanikolaou, P. Argyrakis, K. Boukouras, N. Melis and G. Stavrakakis, 2008. NOANET: the new permanent GPS network for Geodynamics in Greece. Geophysical Research Abstracts, Vol. 10, EGU2008-A-04380

Ganas, A., Marinou A, Anastasiou D., Paradissis D., Papazissi K., Tzavaras P., Drakatos G. 2013. GPS-derived estimates of crustal deformation in the central and north Ionian Sea, Greece: 3-yr results from NOANET continuous network data. Journal of Geodynamics, 67, 62– 71. http://dx.doi.org/10.1016/j.jog.2012.05.010

Laigle, M. Hirn, A. Sachpazi, M. and Clément, C., 2002. Seismic coupling and structure of the Hellenic subduction zone in the Ionian Islands region, Earth and Planetary Science Letters, volume 200, Issues 3–4, Pages 243-253, https://doi.org/10.1016/S0012-821X(02)00654-4

Lomax, A., Virieux, J., Volant, P., Thierry-Berge, C., 2000. Probabilistic earthquake location in 3D and layered models. In: Thurber, C.H., Rabinowitz, N. (Eds.), Advances in Seismic Event Location. Kluwer Academic Publishers, Dordrecht/Boston/London, pp. 101–134.

Okada Y., 1992. Internal deformation due to shear and tensile faults in a half space, Bull. Seism. Soc. America, 82, 1018–1040.

Zumberge, J. F., M. B. Heflin, D. C. Jefferson, M. M. Watkins, & F. H. Webb, 1997. Precise point positioning for the efficient and robust analysis of GPS data from large networks, J. Geophys. Res., 102(B3), 5005-5018.

SPECIAL SESSION

T7.S3 The Geohazard supersites initiative with emphasis on the Greek supersite (Enceladus)

Conveners: **Spyros Lalechos (EPPO)**
Thomas Salonikios (EPPO)

15th International Congress of the Geological Society of Greece
Athens, 22-24 May, 2019 | Harokopio University of Athens, Greece
Bulletin of the Geological Society of Greece, Sp. Pub. 7 Ext. Abs. GSG2019-039

Structural Stability Risk Assessment for Nafplio and Lavrion part of the EnCeladus hellenIc Supersite

C. Kontopoulos[1], V. Charalampopoulou[1], C. Saroglou[2], C. Spyrakos[2], C. Maniatakis[2]

(1) Geosystems Hellas S.A., Athens, Greece, mail@geosystems-hellas.gr
(2) National Technical University of Athens, Zografou Campus, Greece

This study aims to highlight the potential of structural stability risk assessment for the areas of Nafplio and Lavrion part of the EnCeladus hellenIc Supersite under the terms of the research project STructural stABiLity risk assEssment (STABLE). The project will introduce a strategy and select most efficient methods and tools for harmonization of data, criteria and indicators to be addressed for tracking of impact of environmental changes on tangible cultural heritage (CH) assets, buildings and monuments, including structural deterioration processes at a city/village scale. The material and structural properties of heritage buildings, with special attention to foundation conditions, will be the focus of interest in order to assess their behaviour when exposed to ground motions.

These valuable information need to be complemented, calibrated and tested with ground data (e.g. geotechnical information), site scale monitoring (e.g. ground monitoring stations, laser scanners et c.) and risk forecasting models (earthquake) to derive end-user driven products (e.g. hazard, vulnerability and risk maps). The target customers of the project are the public bodies in charge to preserve the CH, Urban Planners, Academic Communities and private enterprises active in the specific sector. The project addresses the design and development of an IT service platform, combining advanced satellite technologies with existing ground-based data and risk forecasting modelling for the long term and continue monitoring and update of structural stability of the architectural heritage and in particular of historical centers affected by geo-hazards. The platform will provide alert models (geotechnical/structural risk forecasting models) based on a fixed infrastructure where technical parameters, gathered in the GIS environment (EO products, ground-based data, documentation etc.), are implemented for each test site. The platform will offer information in support to prevention of damage at CH in the form of regularly updated maps of element at risk, allowing to follow and predict the evolution of a risk, and consequently being able to give information usable for a priori actions before damages or disaster can occur. This information will enable the authorities responsible for the preservation of CH sites to carry out an effective planning and implementation policy of preventive maintenance and drastically improve the resilience factor of the CH asset. STABLE aims to bring together the excellence of Research Centers and SMEs with interdisciplinary skills built around CH but ranging from Civil and Geo-technical engineering, to Information Technology and remote sensing. The project implements knowledge exchange and interdisciplinary actions, to go forward in research towards novel techniques and improved monitoring and managing tools specifically developed for CH.

More specifically, the objectives of STABLE are the following:

- Obj-1: Collection of data from different monitoring techniques, such as satellite, terrestrial and autonomous airborne inspection systems as well as ground techniques, to perform the monitoring of CH sites and related surrounding areas, thus integrating novel remote sensing technologies.
- Obj-2: Definition of risk modelling systems enabling the forecast of structural stability of CH in different scenarios of seismic movements. More specifically, the objective will focus on the use of novel models taking advantage of data derived from satellite and ground-based techniques, for the definition of ad-hoc risk models of the structural stability of the CH and its resilience to different earthquakes scenarios.
- Obj-3: Development of a web-GIS tool for risk analysis of structural stability of CH integrating risk forecasting models with ground and remote sensing datasets. Demonstration activities will be carried out in the selected test cases in order to validate the approach.
- Obj-4: Address the importance of new technologies for sites monitoring and management with specific focus on the viability and sustainability of future commercial services based on the technologies improved, developed and verified in Obj-1 to Obj-3.
- Obj-5: Push innovation through the development of an initial research and training network that will focus its activities on the development, effective integration and increased utilization of existing and innovative technologies in the field of structural stability of CH.
- Obj-6: Provide researchers and professionals with the opportunity to go beyond the current state-of-the-art in the specific field, through a multidisciplinary and international approach based on a wide spectrum of technological tools and methods that can contribute to a more effective CH preservation and conservation.
- Obj-7: Build up specific complementary and market oriented skills to allow the European researchers and professionals to face the new challenge in terms of technology development and future services and improve their ability to face new opportunities in the emerging markets.

In order to carry out the demonstration and validation of the platform, 2 Greek case studies have been selected: i) the old city center of Nafplio and ii) the ancient Lavrion. Both are located in the area of the EnCeladus hellenIc Supersite.

Acknowledgements

This work was prepared in the framework of the STructural stABiLity risk assEssment project (STABLE), H2020-MSCA-RISE-2018 with Grant Agreement number: 823966.

Land subsidence due to the overexploitation of the aquifer at the Valtonera village

Ploutarchos Tzampoglou[1], Constantinos Loupasakis[2]

(1) Department of Civil and Environmental Engineering, University of Cyprus, Nicosia, Cyprus. tzampoglou.ploutarchos@ucy.ac.cy
(2) School of Mining and Metallurgical Engineering, National Technical University of Athens, 9, Heroon Polytechniou Str., 157 80, Zografou, Athens, Greece

This research focus on land subsidence due to the overexploitation of the aquifer in the village of Valtonera. The area of interest is located in the Amyntaio basin at Florina prefecture. The systematic overexploitation of the aquifer by both the open pit coal mine and the wells for irrigation purposes have led to a significant drawdown of the ground water level, during the last decades (Tzampoglou and Loupasakis, 2016). The hydrogeological and tectonic setting of the site in conjunction with the geotechnical parameters of the formations, trigger extensive land subsidence and surfaces ruptures. In detail, two parallel ruptures with NE-SW direction have been noticed which are causing significant damage to infrastructure farmlands and road network. The main objects of this research are the simulation of the failure mechanism and the calculation of the differential vertical displacements using the Plaxis three-dimensional finite element code.

Regarding the geotechnical and tectonic setting, the Valtonera village is intersected by a probable fault which extends with NNE - SSW direction. It is worth to mention that due to the fault offset, the thickness of the Perdikas formation at the SE'ern side is increased. The geological stratigraphic (Figure 2A) is composed of (from the new ones to the older ones):

Alluvial deposits: They consist of silty-clay with sand. Besides the fact that they present high compression index, their occurrence near to the surface lead to the conclusion that the ground water level drop does not influence them.

Perdikas formation: It consist of alternating layers of silty-clayey sand, sandy silty-clay, sandy gravels and organic silty-clay. Its present high compression index, especially for the sandy silty-clays and the organic silty-clays horizons. So, it is susceptible for the activation of land subsidence.

Proastio formation: It consist of alternating horizons of silty-clayey sand, sandy silty-clays, sandy gravels and organic silty-clays. Besides its high compression index, their contribution to the land subsidence mechanism is downgrade due to the fact that the participation of clay horizons to this formation is small (Tzampoglou and Loupasakis, 2017)

The soil data parameters can be summarize in Table 1(Tzampoglou and Loupasakis, 2017).

Table 1. Soil data set parameters

	Alluvial Deposits	Perdikas' Formation				Proastio Formation			
		Silty clayey sand Upper Strata (till 40m)	Sandy silty clay Upper Strata (till 40m)	Silty clayey sand Dipper Strata (till 90m)	Sandy silty clay Dipper Strata (till 90m)	Silty clayey sand Upper Strata (till 90m)	Sandy silty clay Upper Strata (till 90m)	Silty clayey sand Dipper Strata (till 160m)	Sandy silty clay Dipper Strata (till 160m)
v	0.30	0.30	0.30	0.3	0.30	0.30	0.30	0.3	0.3
γ_{unsat} (kN/m^3)	22.56	20.04	18.16	20.04	18.16	19.92	19.02	19.92	19.02
γ_{sat} (kN/m^3)	24.05	22.16	21.49	22.16	21.49	22.63	22.45	22.63	22.45
C (kN/m^2)	121.9	78.0	91.4	78.0	93.8	91.4	45.1	0.0	45.1
φ (^{0})	28.8	20.0	27.4	20.0	24.3	27.4	25.0	41.0	25.0
Kx (m/day)	0.09	2.94	0.16	2.94	0.16	5.66	0.63	5.66	0.63
Ky (m/day)	0.09	2.94	0.16	2.94	0.16	5.66	0.63	5.66	0.63
Kz (m/day)	0.09	2.94	0.16	2.94	0.16	5.66	0.63	5.66	0.63
Eoed (kN/m^2)	7596	7059	9756	12724	13590	15416	18156	27646	22720
Eref (kN/m^2)	5643	5244	7247	9452	10095	11452	13487	20537	16877

As for the hydrogeological data, evaluating the drawdown contour lines between May 1992 (Dimitrakopoulos, 2001) and May 2016, the maximum level drop reaches the 70 m at the perimeter of the mine and decrease as moving away from it. In the village of Valtornera the level drop varies from 10 to 20 meters. It should be noticed that isolated depression cones can be identified at the southeast of the village due to the overexploitation of for irrigation purposes.

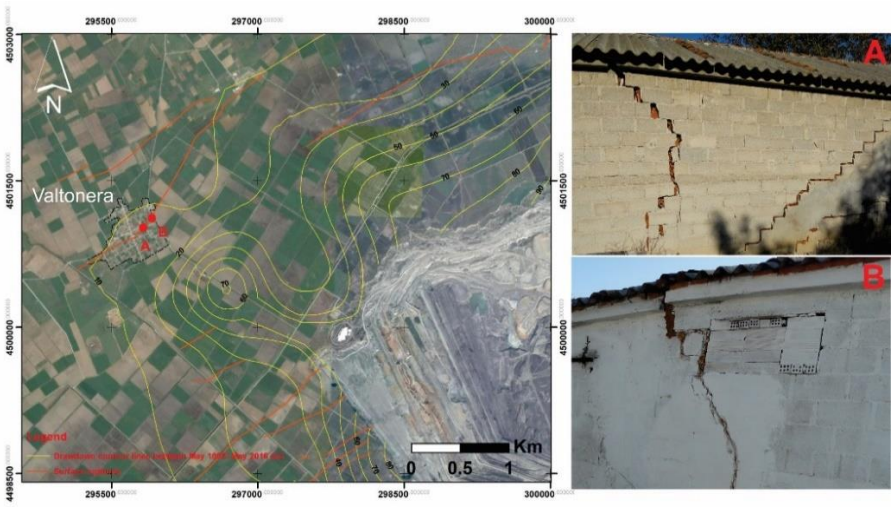

Figure 1. Distribution of the surface ruptures at the Valtonera village in relation with drawdown contour lines.

In order to simulate the land subsidence mechanism by using PLAXIS finite element geotechnical code, highlighting the important role of the ground water level drop, certain assumptions have been made. Firstly, six calculations steps were carried out, in order to gradually drawdown the aquifer from 0 to a level of -60 m. Furthermore, the Perdikas and the Proastio formation were divided into upper and dipper horizons aiming to increase the values of compressibility index in accordance to the stratigraphy depth, while the coarse grain and the fine grain horizons of these formations were set to be equally distributed. Finally, the simulations were conducted by applying the "consolidation analysis" while the constitutive law selected, was the Mohr–Coulomb model.

Taking into account the simulation analysis results, it seems that the vertical displacements increase proportional to the drawdown of the aquifer. The maximum vertical displacements have been noticed at the part where the formation of Perdikas increases. Furthermore, the differential vertical displacement increases in accordance to the level drop, reaching (for level drop around -60m) the value of 0.097 m (Figure 2B). This price is not high due to the fact that the fault doesn't border the aquifer and the Perdikas formation extends at both sides of the fault. It should be noticed that the results of the finite elements analysis are in agreement with the recorded surfaces ruptures offset (Figure 1).

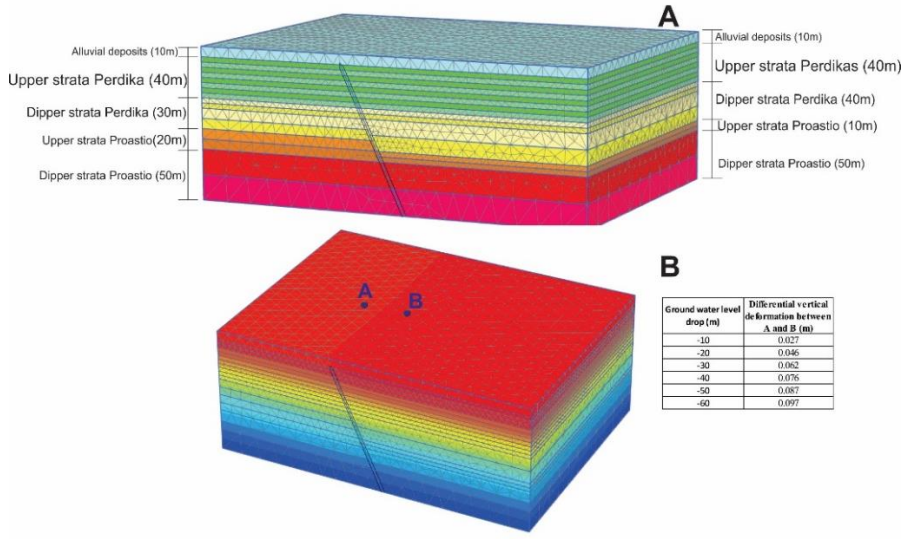

Ground water level drop (m)	Differential vertical deformation between A and B (m)
-10	0.027
-20	0.046
-30	0.062
-40	0.076
-50	0.087
-60	0.097

Figure 2. A. Simplified 3D simulation model of the site at the village of Valtonera, B. The results of deferential vertical displacements due to the level drop of the aquifer.

Acknowledgements

The authors wish to thank Prof. Gerolymos N. and the laboratory of Soil Mechanics of the National Technical University of Athens for providing us Plaxis 3D (2016).

References

Dimitrakopoulos, D., 2001. Hydrogeological conditioning of Amyndeon mine. Problems during exploitation and overcoming them. Phd Thesis, National Technical University of Athens, Athens.

Tzampoglou, P., Loupasakis, C., 2016. New data regarding the ground water level changes at the Amyntaio basin-Florina Prefecture, Greece. Bulletin of the Geological Society of Greece. 50, 1006-1015.

Tzampoglou, P., Loupasakis, C., 2017. Evaluating geological and geotechnical data for the study of land subsidence phenomena at the perimeter of the Amyntaio coalmine, Greece. International Journal of Mining Science and Technology. 28, 61-612.

15th International Congress of the Geological Society of Greece
Athens, 22-24 May, 2019 | Harokopio University of Athens, Greece
Bulletin of the Geological Society of Greece, Sp. Pub. 7 Ext. Abs. GSG2019-335

Deformation Monitoring of the Wider Area of Kaparelli - Plataies with the Contribution of Multitemporal SAR Interferometry and Copernicus Earth Observation Images

R. Mina[1], S.Lozios[1], K.Soukis[1], I.Parcharidis[2]

(1) National and Kapodistrian University of Athens, Athens, Greece, rozalia2vagxe@gmail.com
(2) Harokopio University of Athens, Athens, Greece

Characterizing active faults and quantifying their activity are major concerns in Greece. Geodetic measurements including GPS and leveling have provided valuable observations of crustal deformation. The GPS network, with stations generally spaced less than 10 km apart, could highlight mainly regional and in some cases local displacements. However, these measurements do not provide the high spatial resolution needed to detect in detail surface creep on individual faults.

Monitoring of active faults in areas of high exposure both building store and population is of great importance, providing useful information to assess seismic hazards and risks.

Our study area is located in the Beotian geographic department of Greece (Kaparelli – Plataies area) and ends up in the eastern Gulf of Corinth (Kalamaki bay). Surface topography and geomorphology of the Corinth Gulf are clearly associated with seismic activity along large normal faults. The 1981 earthquake sequence, which was characterized by shallow earthquakes (<10km) and magnitudes greater than 6 (Abercrombie et al., 1995), and especially the third shock, ruptured the Kaparelli fault which was activated during that period and produced extensive ground deformation. The fault is characterized as a complex fault zone due to its numerous fault segments. It is a south dipping normal fault with an active fault plane dipping at about 45o. This fault is a segment of a greater normal fault zone that is situated to the north of Parnitha Mountain in Central Greece. Recent geological data (Drakatos et al., 2005) showed that the Kaparelli area forms the boundary between fast-slipping normal faults in Corinth-Perachora regions and slow-slipping faults in Viotia, Attica.

Spaceborne Synthetic Aperture Radar (SAR) interferometry is a technique that produces 3D topographic data of Earth's surface directly from two SAR images (Bamler and Hartl, 1998). An extension of the basic technique, called differential SAR interferometry (DInSAR), allows measurements of land deformation and it has various applications in the fields of volcanology, cartography, crustal dynamics, slope instabilities and land subsidence. Using large stacks of SAR images acquired over the same area, long deformation time series can be analyzed using multi-temporal differential SAR interferometry techniques like Permanent Scatterers Interferometry (PSI) (Ferretti et al., 2001), Small Baseline Subset (SBAS) (Berardino et al., 2002), Interferometric Point Target Analysis (IPTA) (Werner et al., 2003), Stanford Method for Persistent Scatterers (StaMPS) (Hooper et al., 2004), Coherent Pixel technique (CPT) (Blanco-Sanchez et al., 2008). Multi-temporal DInSAR is nowadays a well-documented technique for the characterization of ground motions over large spatial areas and is capable of detecting movements with metric resolution and millimetric accuracy.

The area of interest is a part of the Corinthian Gulf characterized by active tectonism and seismic activity.

The main purpose of this paper is to detect potential displacement along the Kaparelli fault and its strands by the synergy of MTInSAR and geological field observations. Concerning MTInSAR a rich dataset of 92 ascending and 55 descending SLC Sentinel 1 A & B scenes covering the period October 2014 to November 2018 were processed using the SARPROZ s/w following the Persistent Scatterers Interferometry technique (PSI). Field observations include a fault scarp height model (based on field data) and a map of the main ruptures' traces (based on field measurements, using Field Move Clino app).

Combining interferometric results and geological field work can lead to a better understanding of a fault's movement and the ground deformation that it causes and thus contribute to seismic hazard assessment. Although monitoring concerns a short period few patterns of low rate of deformation are detected and an attempt to associate them with the local tectonism.

References

Abercrombie, R, E., Main, I, G., Douglas, A., Burton, P, W. The nucleation and rupture process of the 1981 Gulf of Corinth earthquakes from deconvolved broad-band data, Geophvs. J . Int., v. 120, p. 393-405, 1995

Bamler, R., Hartl, P., 1998. Synthetic aperture radar interferometry. Inverse problems, 14(4), R1.

Benedetti, L., Finkel, R., King, G., Armijo, R., Papanastassiou, D., Ryerson, F, J., Flerit, F., Farber, D., Stavrakakis, G. Motion on the Kaparelli fault (Greece) prior to the 1981earthquake sequence determined from 36Cl cosmogenic dating, Terra Nova, v. 15, p. 118–124, 2003.

Berardino, P., Fornaro, G., Lanari, R., & Sansosti, E., 2002. A new algorithm for surface deformation monitoring based on small baseline differential SAR interferograms. IEEE Transactions on Geoscience and Remote Sensing, 40(11), 2375-2383.

Blanco-Sanchez, P., Mallorquí, J. J., Duque, S., & Monells, D., 2008. The coherent pixels technique (CPT): An advanced DInSAR technique for nonlinear deformation monitoring. *Pure and Applied Geophysics*, 165(6), 1167-1193.

Drakatos, G., Petro, L., Ganas, A., Melis, N., Kostak, B., Kontny, B., Canon, S., Stercz, M., Monitoring of strain accumulation along active faults in the eastern gulf of corinth: instruments and network setup, Acta Geodyn. Geomater.Vol.2, No.1 (137), 13-23, 2005.

Hatzfeld, D., Karakostas, V., Ziazia, M., Kassaras, I., Papadimitriou, E., Makropoulos, K., Voulgaris, N., Papaioannou, C. Microseismicity and faulting geometry in the Gulf of Corinth (Greece), Geophys. J. Int., v. 141, p. 438–456, 2000.

Ferretti, A., Fumagalli, A., Novali, F., Prati, C., Rocca, F., & Rucci, A., 2011. A new algorithm for processing interferometric data-stacks: SqueeSAR. *IEEE Transactions on Geoscience and Remote Sensing*, *49*(9), 3460-3470.

Werner, C., Wegmuller, U., Strozzi, T., & Wiesmann, A., 2003. Interferometric point target analysis for deformation mapping. In Geoscience and Remote Sensing Symposium, 2003. IGARSS'03. *Proceedings. 2003 IEEE International* (Vol. 7, pp. 4362-4364). IEEE.

15th International Congress of the Geological Society of Greece
Athens, 22-24 May, 2019 | Harokopio University of Athens, Greece
Bulletin of the Geological Society of Greece, Sp. Pub. 7 Ext. Abs. GSG2019-379

Monitoring of Seabed Fluid Flow through Underwater Benthic Observatories. Environmental and Geohazard Assessment. Case studies from Patras and Katakolo Harbours

D. Christodoulou[1], S. Kordella[1], G. Papatheodorou[1], G. Etiope[2], G. Marinaro[2], A. Chalari[3], Gatsou M.[1]

(1) Laboratory of Marine Geology & Physical Oceanography, Department of Geology, University of Patras, University Campus, Rio, Patras, Greece, dchristo@upatras.gr
(2) National Institute of Geophysics and Volcanology, Sezione Roma 2, Rome, Italy, (3) Silixa Ltd., Elstree, Hertfordshire, United Kingdom

Introduction

Hydrocarbon seeps, mainly methane (CH_4) of microbial and thermogenic origin, formed during sediment burial. Seabed fluid determines a wide range of fluids (gases and liquids) passing from seabed sediments to seawater. The significance of seabed fluid flow goes beyond the geosciences, since they have a major impact to marine ecology and chemistry, representing also an important greenhouse gas source for the atmosphere (e.g., Etiope, 2004; Papatheodorou et al., 2007; Etiope and Ciccioli, 2009). Moreover gas seeps could be a geo-hazard for the social community, the constructions and the industry.

The link between gas emission and seismicity has been the subject of a wide number of multidisciplinary studies. Mellors et al. (2007) found significant statistical correlations between large earthquakes (M > 5.5) and the eruption of mud volcanoes. Signals recorded by Ocean Bottom Seismometers (OBSs) were explained as due to bubbles coming from gas seepage at the seafloor (Tary et al., 2012). Embriaco et al. (2013), suggested a link between seismic energy release and methane seepage using data from a multiparametric benthic observatory along the North Anatolian Fault in the Sea of Marmara.

Two major harbour in Western Greece, have been established over active, intense gas seepage areas, Patras Harbour (Christodoulou et al., 2003) and Katakolo Harbour (Etiope et al., 2006). Laboratory of Marine Geology & Physical Oceanography, participating among others, in three EU projects, has been used underwater benthic observatories for seepages activity monitoring.

Geological Setting

In Patras Gulf, a pockmark field has been developed in soft, layered Holocene silts, showing episodes of gas venting from the Pleistocene/Holocene interface which forms a gas accumulative horizon (Christodoulou et al., 2003; Papatheodorou et al. 1993). It is one of the most well documented pockmark field regarding its activity and the relationship with seismicity. On July 14th, 1993 an earthquake of magnitude M=5.4 on Richter scale was recorded in the active Patras graben. In a temperature recording station in the pockmark field, the temperature increased anomalously on three occasions prior to the earthquake and the earthquake occurred just after the last peak of increased temperature. Furthermore, it was noted that some pockmarks few days after the earthquake were still venting gas bubbles as is indicated by the extremely high reflectivity plumes shown on the sonographs (Hasiotis et al., 1996). On June 2008, after a major earthquake of MW=6.4R, which occurred on the Northwestern Peloponnese and for a period of fifteen days, gas plumes were recorded in the water column above pockmarks and methane measurements showed high concentrations of dissolved methane in the water column all over the pockmark field (Christodoulou et al., 2009).

Katakolo is one of the most productive thermogenic gas seepage zones in Europe and the biggest methane seep ever reported in Greece. The gas seepage takes place over an extended area in the Katakolo harbour and along two main normal faults off the harbor. Based on side scan sonar sonorgraphs at least 823 gas bubble (10-20 cm in diameter) plumes escaping over an area of 94,200 m^2 were recorded, at depths ranging from 5.5 to 16 m. The gas consists mainly of methane and has H_2S levels of hundreds to thousands ppmv, and shows significant amounts of other light hydrocarbons like ethane, propane, iso-butane and C_6 alkanes. Due to the shallow depth, more than 90 % of CH_4 released at the seabed enters the atmosphere and the gas seeps may produce severe geohazards for people, buildings and construction facilities due to the explosive and toxicological properties of methane and hydrogen sulfide, respectively (Etiope et al., 2005; 2006; 2013; Christodoulou, 2010).

Methodology and Results

In Patras Gulf gas monitoring module (GMM) has been developed for continuous and long-term measurements of seabed gas seepage integrated with seawater physical parameters data. GMM equipped by three semiconductor methane sensors, an H_2S electrode microsensor and a CTD SBE-37-SI Microcat (Sea Bird) for measurements of temperature, conductivity (C), temperature (T), and depth (D, or pressure, P) sampled every 10 minutes (Marinaro et al., 2006). GMM was deployed at the base of a large pockmark, at a water depth of 42 m.

Recordings were carried out in two consecutive campaigns over a period of about 6.5 months. This was the first long-term monitoring ever done on gas leakage from pockmarks by means of CH_4+H_2S+T+P sensors. The results showed frequent T and P drops associated with gas peaks, more than 60 events in 6.5 months, likely due to intermittent, like pulsation, seepage. Decreases in temperature below an ambient T, were associated with short-lived pulses (10-60 min) of increased CH_4+H_2S concentrations. This seepage "pulsation" can either be an active process driven by pressure build-up in the pockmark sediments, or a passive fluid release due to hydrostatic pressure drops induced by atmospheric

wind.

A newer version of GMM, equipped among others sensors, with a current meter, deployed at the eastern part of the Katakolo harbor at water depth of -7m, where intense gas seepage and oxygen concentration reductions have been identified during preparatory surveys. GMM monitoring lasted 3.4 months (101 days).

From detailed observation of the GMM parameters (CH_4, O_2, temperature, turbidity, current speed and direction) and wind speed obtained from the local meteorological station, 8 main periods were observed when dissolved oxygen concentration decreases and reaches hypoxic up to quasi-anoxic levels. Within these 8 periods, 54 short term (scale of hours) hypoxia events and 43 short term CH_4 peaks were observed, which in more than 95% of cases were followed by O_2 decrease. Current speed in combination to elevated CH_4 concentrations appeared to be the key factor responsible for the hypoxia and quasi-hypoxia events. When current speed is relatively steady and low (<4 cm/s) for a considerable amount of time (>4 h) and at the same time CH_4 concentration rises, dissolved oxygen concentration lingers at hypoxic levels and may even reach quasi-anoxic levels. The longest event of continuous hypoxia was almost 2 days, which was coupled with low current speed and elevated CH_4 concentrations.

At the same place a prototype fiber-optics-based monitoring system implemented both a distributed temperature sensor (DTS) and an intelligent distributed acoustic sensor (iDAS) of Silixa, Ltd. As far as we know, this was the first time that DTS and iDAS were used in marine environment. The iDAS system makes it possible to observe the acoustical signal along the entire length of an unmodified optical cable, detecting bubble plumes and allowing seepage detection and quantification. The DTS system can measure temporal variations of the gas plumes. A large metal pyramid frame was constructed, where fiber optic cable wrapped, and deployed on the seabed.

The preliminary analysis and interpretation of the collected data showed that the lower temperature values indicate gas leakage points. The cooler monitoring points are, at the same time, the points with the smallest typical daytime temperature deviations. Furthermore, a certain spatial pattern and a systematicity has been observed regarding the location of the colder monitoring points. This indicates possible permanent leakage points. iDAS data (acoustic footprint of the bubbles upon escape) is in agreement with the spatial temperature distribution of the DTS. Confirmation of these possible gas escapes also results from submarine optical reception of the fiber-optics-based monitoring system. Small local earthquakes of 1.3 to 2.8R, during the experiment, do not appear to affect the leaks.

Acknowledgements

The surveys presented in this chapter were carried out within the framework of three European Union funded projects (ASSEM, contr. EVK3-CT2001-00051, PYTHAGORAS II. Social Funds, HYPOX project EC Grant 226126, ENV.2008.4.1.2.1, FP7).

References

Christodoulou, D., 2010. Geophysical, geotechnical, sedimentological and remote sensing monitoring of active pockmark fields in high seismicity region, Western Greece. PhD Thesis, University of Patras. 296p.

Christodoulou, D., Papatheodorou, G., Fakiris, E., Etiope, G., Ferentinos, G., 2009. The activation of the Patras gulf pockmark field triggered by the June 8, 2008 earthquake. In Proceedings of 9th Panhellenic Symposium of Oceanography and Fisheries, p. 3-8.

Christodoulou, D., Papatheodorou, G., Ferentinos, G., Masson, M., 2003. Active seepage in two contrasting pockmark fields in Patras and Corinth Gulfs, Greece. Geo-Marine Letters 23,194-199.

Embriaco, D., Marinaro, G., Frugoni, F., Monna, S., Etiope, G., Gasperini, L., Polonia, A., Del Bianco, F., Namik Çağatay, M., Ulgen, U.B., Favali, P., 2013. Monitoring of gas and seismic energy release by multiparametric benthic observatory along the North Anatolian Fault in the Sea of Marmara (NW Turkey). Geophysical Journal International, 196 (2), pp. 850-866.

Etiope, G., Christodoulou, D., Kordella, S., Marinaro, G., Papatheodorou, G., 2013. Offshore and onshore seepage of thermogenic gas at Katakolo Bay (Western Greece). Chemical Geology 339, 115-126.

Etiope, G., Ciccioli, P., 2009. Earth's degassing – A missing ethane and propane source. Science, 323, 5913, 478.

Etiope, G., 2004. GEM – Geologic Emissions of Methane, the missing source in the atmospheric methane budget. Atmospheric Environment, 38, 19, 3099-3100.

Etiope, G., Papatheodorou, G., Christodoulou, D., Favali, P., Ferentinos, G., 2005. Gas Hazard Induced by Methane and Hydrogen Sulfide Seepage in the NW Peloponnesus Petroliferous Basin (Greece). Terrestial, Atmospheric and Oceanic Sciences 16, 897-908.

Etiope, G., Papatheodorou, G., Christodoulou, D., Ferentinos, G., Sokos, E., Favali, P., 2006. Methane and hydrogen sulfide seepage in the NW Peloponnesus petroliferous basin (Greece): origin and geohazard. AAPG Bulletin. 90, 701-713.

Hasiotis, T., Papatheodorou, G., Kastanos, N. Ferentinos, G., 1996. A pock-mark field in the Patras Gulf (Greece) and its activation during the 14/7/1993 seismic event. Marine Geology 130,333-344.

Marinaro, G., Etiope, G., Lo Bue, N., Favali, P., Papatheodorou, G., Christodoulou, D., Furlan, F., Gasparoni, F., Ferentinos, G., Masson, M., Rolin, J-F., 2006. Monitoring of a methane-seeping pockmark by cabled benthic observatory (Patras Gulf, Greece). Geo-Marine letters 26, 297-302.

Mellors, R., Kilb, D., Aliyev, A., Gasanov, A. & Yetirmishli, G., 2007. Correlations between earthquakes and large mud volcano eruptions, Journal of Geophysical Research, 112, B04304.

Papatheodorou, G., Hasiotis, T., Ferentinos, G., 1993. Gas charged sediments in the Aegean and Ionian Seas, Greece. Marine Geology 112, 171-184.

Papatheodorou G., Christodoulou D., Geraga M., Etiope G., Ferentinos G (2007) "The pockmark field of the Gulf of Patras: An ideal natural laboratory for studying seabed fluid flow" In: ZELILIDIS, A., PAPATHEODOROU, G. and GERAGA, M. (eds.): Sedimentology of western and central Greece from recent to Triassic. 25th IAS Meeting of Sedimentology, Patras, 2007, Field Trip Guidebook, p. 43-62.

Tary, J.B., Geli, L., Guennou, C., Henry, P., Sultan, N., Cagatay, M.N. & Vidal, V., 2012. Micro-events produced by gas migration and expulsion at the seabed: a study based on sea bottom recordings from the Sea of Marmara, Geophysical Journal International, 190, 993–1007.

15th International Congress of the Geological Society of Greece
Athens, 22-24 May, 2019 | Harokopio University of Athens, Greece
Bulletin of the Geological Society of Greece, Sp. Pub. 7 Ext. Abs. GSG2019-384

Response of Monumental Buildings during the Seismic Sequence in Peloponnesus Greece. Relation Parameters between Records and Analysis Seismic Loads

Thomas N. Salonikios

Institute of Engineering Seismology and Earthquake Engineering, Cosmos Offices, 5 Ag. Georgiou Str, Patriarchica Pylaia, 55535 Thessaloniki, Greece, salonikios@itsak.gr

In this work the response of the build environment, after four strong earthquakes, is observed in Peloponnesus, Greece. Particularly the research is focused on monumental and other masonry buildings with load carrying masonry walls. This response is correlated with the recorded accelerations of the ITSAK accelerograph network. These records are postprocessed and numerical values of effective accelerations and of spectral accelerations are given for comparison reasons. The considered earthquakes are Kythera Eq., Koroni Eq., Leonidio Eq. and Achaia – Ilia Eq. At the location of each record, various levels of accelerations were recorded. These values vary from low to high. The response of the build environment was examined and recorded by visual inspections from ITSAK research groups, at the stricken areas. The buildings under research are subdivided in five categories. In the first category are classified buildings with mudbrick masonry walls and clay mortar. The second category contains buildings with stone masonry walls and clay mortar. In third category are classified buildings with stone and/or brick masonry walls and lime mortar. In the fourth category are classified the temple buildings and the surrounding structures. In the fifth category are classified castles, ancient ruins and other structures build with stone and masonry walls with or without mortar. For Kythera, Koroni and Leonidio Eqs were observed only cracks on masonry buildings while for Achaia-Ilia Eq were additionally observed total and partial collapses.

It was found that in masonry buildings that are subjected to strong earthquakes first damages appear as cracks at the top floor. Probably this may attributed to the insufficient connection of the wooden roof with the walls. Also at the top storey the axial load of the piers are low and also the spandrels are not well wedged. The bell towers are usually constructed in contact with the building of the main temple. In these cases damages appear at the bell towers at the location of the top of the temple. This is justified by the consideration of the different way of oscillation of the two structural systems. Temple structural system is stiffer than the bell tower structural system. In many masonry buildings the distress and deformation of the walls are close to the failure values. This happen, mostly due to the absence of maintain in combination with antiquity. For these reasons after an earthquake usually appear cracks at the walls due to additional forces and deformations.

From the field observations and by the use of the postprocessed earthquake records, resulted that the analysis seismic accelerations for monumental masonry buildings should be significantly lower than the recorded ones. In this work are given scientifically validated reasons for the reduction of analysis seismic loads by the reassessment of material properties and appropriate values are proposed. Also case studies are given, from the analysis of different monumental masonry buildings that are simulated by finite element models and the considered assumptions are approved.

References

ITSAK – Civil Engineer Department of U.Patras – UCLA, (2008), “Preliminary Report on the Principal Seismological and Engineering Aspects of the Mw=6.5 Achaia-Ilia (Greece) Earthquake on 8 June 2008” Report for Web Dissemination. http://research.eerc.berkeley.edu/projects/GEER/GEER_Post%20EQ%20Reports/Greece_2008/greece_2008_index.html

Karantoni, F.V., Fardis, M.N., (1992), “Computed versus observed seismic response and damage of masonry buildings”, Journal of Structural Engineering, ASCE, Vol.118, No.7, pp. 1804-1821.

GENERAL SESSION

T8 Marine Geology and Oceanography

15th International Congress of the Geological Society of Greece
Athens, 22-24 May, 2019 | Harokopio University of Athens, Greece
Bulletin of the Geological Society of Greece, Sp. Pub. 7 Ext. Abs. GSG2019-025

Alterations of the Coastal Zone in Kamari Beach (Santorini Island, Cyclades Greece)

V. Chondraki [1*], V. Kapsimalis [2], S. Poulos [1], P. Nomikou [1], D Vandarakis.[2], S. Petrakis [1]

(1) Section of Geography & Climatology, Department of Geology and Geoenvironment, National and Kapodistrian University of Athens, Panepistimiopolis Zografou, Attiki 15784, Greece (*v.chondraki@gmail.com)
(2) Hellenic Centre for Marine Research, (HCMR), 46,7 km Athens Sounio ave., P.O. Box 712, P.C. 19013 Anavyssos, Attica, Greece

Introduction

The present study focuses on the mapping of the coastal and submarine morphology of the Kamari coastal zone in Southeast Santorini Island. Furthermore, its aim is to illustrate the physiographic features and the displacement of the coastal area for the period 1945-2016. By collecting and processing spatial data, aerial photographs and satellite images, habitat and several vulnerability maps were created, in order to determine the erosion processes of the coastal area. Kamari is a popular tourist attraction with a coastal area at risk, due to its extensive urban development. In order to protect the coastal area, 4 groins and 2 detached parallel breakwaters were constructed in 1991.

Methods

In order to create the habitat map, bathymetric and echo-sounding data was collected with the use of a Side-Scan Sonar and processed through Sonar Wiz (version6) software. For the study of the historical coastline displacement during the 70-year period (1945-2016), coastlines from aerial photographs and satellite images were georeferenced, digitized and compared with the use of ArcGIS 10.4. Moreover, marine surficial sediment samples were collected and granulometric analysis was carried out in order to understand the sedimentary processes that take place in the area.

Results

From 1945 to 2016, Kamari coastline has retreated by 18.5 m. In general, the coastal zone presents a variation in the volume of sediment deposition, as the rate of erosion is quite large. Specifically, during the first 15 years, an enormous rate of erosion has been observed, which, at some areas, exceeds 52m. For the next 13 years (1960-1973), the deposited sediment has advanced in some areas at the coastline by more than 38m. The start of a corrosive course of the coast is observed during the period of 1978-2003. Groins and breakwaters were constructed in 1991, which decreased the erosion rate in the area. However, during the following years the beach has stabilized against erosion. In 2012 a disastrous storm hit the area of Kamari, causing catastrophic damages. Finally, during the period 2015-2016 the beach presents an average retreat of approximately 4 m when maximum retreat accounts as much as 26.8 m and a maximum accretion of 15.4 m.

Main Conclusions

Due to the high rate of human activity, the coastal zone of Kamari has been heavily influenced. Undoubtedly, the construction of the breakwaters was a catalyst factor which contributed to the reduction of erosion rate. However, although the sediment supply is sufficient, the rate of erosion is rising rapidly and the beach's ability to recover almost non-existent. The intense annual winds and waves in the area, extensive settlement development and inadequate infrastructure exacerbate the erosion.

15th International Congress of the Geological Society of Greece
Athens, 22-24 May, 2019 | Harokopio University of Athens, Greece
Bulletin of the Geological Society of Greece, Sp. Pub. **7** Ext. Abs. GSG2019-187

High-Resolution AUV Mapping of Kolumbo submarine volcano, Santorini, Greece

P. Nomikou[1], M. Hannington[2], S. Petersen[2], S. Wind[3], V. Heinath[2], S. Lange[2], M. Rothenbeck[2], L. Triebe[2], E. Wenzlaff[2]

(1) Department of Geology and Geoenvironment, National and Kapodistrian University of Athens, Panepistimioupoli Zografou, 15784 Athens, Greece
(2) GEOMAR Helmholtz Centre for Ocean Research Kiel, Wischofstrasse 1-3, 24148 KIEL, Germany
(3) University of Ottawa, Department of Earth and Environmental Sciences, Ottawa, Canada

An important component of volcanic activity in the southern Aegean Sea is focused along a linear feature known as the Christiana-Santorini-Kolumbo (CSK) rift (Nomikou et al., 2018). Running in a NE-SW direction, it hosts a number of volcanic centers of late Pliocene to Pleistocene age as part of the overall east-west trending Hellenic subduction zone south of the island of Crete. Natural hazards from the CSK rift pose significant threats to the eastern Mediterranean region. They include earthquakes, subaerial or submarine volcanic eruptions, gas release from volcanoes, tsunami inundation of neighboring coastlines due to eruptions or submarine landslides, and potential aviation impacts from volcanic ash plumes.

Kolumbo volcanic chain lies just off the northeast coast of Santorini the consisting of 25 submarine cones and craters (Nomikou et al., 2012; Hooft et al., 2017), that extend in a NE-SW direction along the floor of Anhydros basin. The largest of these is Kolumbo crater, a 3 km diameter cone with a 1700 m wide crater, a rim as shallow as 18 m below sea level, and a flat crater floor 505 m below sea level. Kolumbo is currently the most active and dangerous submarine volcano in the Mediterranean Sea and its crater floor hosts a high-temperature hydrothermal field with active massive sulphide deposition of potential economic significance (Kilias et al., 2013). The 1650 eruption had significant impacts in the southern Aegean area. At least seventy people, who were in the sea offshore or along the NE coast of Santorini died, from asphyxiation by acidic gases. A large tsunami on 29 September caused widespread damage on Santorini and elsewhere within a 150 km radius (Ulrova et al., 2016).

The first detailed bathymetric map of the Kolumbo volcano was produced in 2001 using the 20 kHz SB2120 swath system on R/V Aegean (Nomikou et al., 2012; 2013). Bathymetric data were also acquired on-board the R/V Marcus Langseth using the Simrad Kongsberg EM122 12 kHz multibeam echo sounder in 2015. For the first time, high resolution AUV (Autonomous Underwater Vehicle) data were collected during POS510 cruise, in 7 missions of AUV Abyss (GEOMAR) (Hannington et al., 2017), under the framework of the collaborative project "ANYDROS: Rifting and Hydrothermal Activity in the Cyclades Back-arc Basin". The goal of this project was to understand the initiation of arc rifting and associated back-arc hydrothermal activity. The focus was on the CSK rift system and Santorini-Kolumbo volcanic line, one of the few places in today's oceans where submarine rifting of a continental margin arc can be studied in its earliest stages.

We present a new bathymetric map of Kolumbo volcano based on AUV bathymetry with 2m resolution which helps to map: a) the abrupt inner slopes of Kolumbo caldera, b) the active vent field at the northern part of the crater floor (485m depth), c) the lava dykes in the inner slopes, d) the mass wasting deposits in the inner slopes, e) the curvelinear scarps with inward dipping faces at the W-NW base of Kolumbo's flanks (faults and/or remnant crater rims).

Using developed autonomous underwater vehicles (AUVs) with capabilities to map the seafloor with higher resolution than is possible with hull-mounted or towed sonar systems so as to identify seafloor geomorphological characteristics and produce detailed morphotectonic and hazard maps of active volcanic areas.

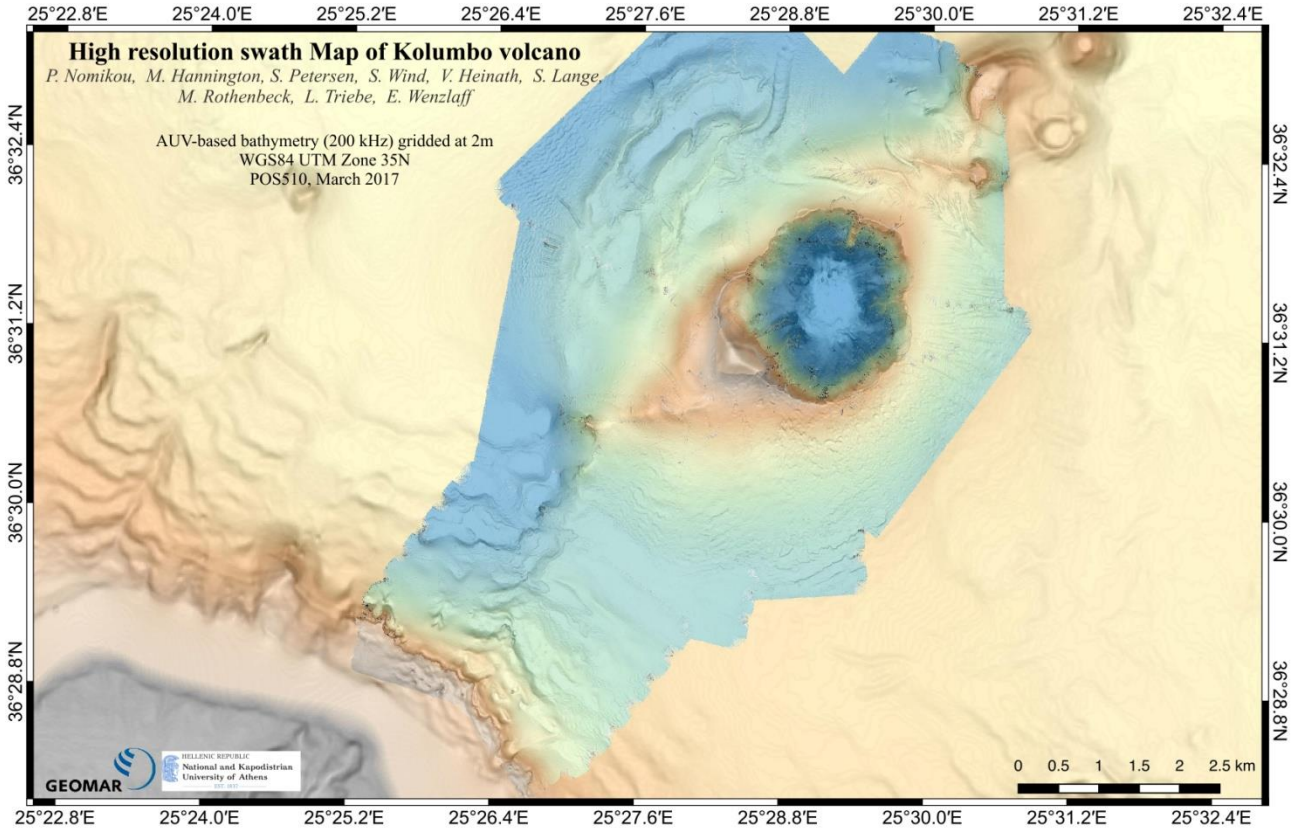

Figure 1. AUV multibeam compilation from 7 dives on Kolumbo volcano and Kolumbo line northeast of Santorini.

Acknowledgements

We thank the ship's captain and crew and science officers of the R/V Poseidon for their indispensable contribution to collecting swath datasets. For the data processing, visualization, and bathymetric maps we used the freely available software packages MBsystem and QGIS. We acknowledge funding from the "RESEARCH-CREATE-INNOVATE" of the "Competitiveness, Entrepreneurship and Innovation (EPANEK)", NSRF 2014-2020, R.G. 15336 (Research project: VIRTUAL DIVER) for the Department of Geology and Geoenvironment.

References

Hannington, M., et al., 2017, Rifting and Hydrothermal Activity in the Cyclades Back-arc Basin: Cruise Report of RV Poseidon, POS510, Catania-Heraklion 06.03.17-29.03.17, 361 p.

Hooft, E.E.E., et al, 2017. Backarc tectonism, volcanism, and mass wasting shape seafloor morphology in the Santorini-Christiana-Amorgos region of the Hellenic Volcanic Arc. Tectonophys. 712-713, 396–414.

Kilias SP., et al., 2013. New insights into hydrothermal vent processes in the shallow submarine arc-volcano, Kolumbo, Greece. Nature Scientific Reports, 3, 2421.

Nomikou, P., et al., 2012. Submarine Volcanoes of the Kolumbo volcanic zone NE of Santorini Caldera, Greece. Glob. Planet. Change, 90–91, 135-151.

Nomikou, P., et al., 2013. Submarine volcanoes along the Aegean volcanic arc. Tectonophysics, 597, 123–146.

Nomikou, P. et al. 2018. Expanding extension, subsidence and lateral segmentation within the Santorini - Amorgos basins during Quaternary: Implications for the 1956 Amorgos events, central - south Aegean Sea, Greece. Volume 722, 2 January 2018, Pages 138-153. Tectonophysics.

Ulvrova M., et al. 2016. Source of the tsunami generated by the 1650 AD eruption of Kolumbo submarine volcano (Aegean Sea, Greece). Journal of Volcanology and Geothermal Research 321, 125–139.

15th International Congress of the Geological Society of Greece
Athens, 22-24 May, 2019 | Harokopio University of Athens, Greece
Bulletin of the Geological Society of Greece, Sp. Pub. 7 Ext. Abs. GSG2019-213

CTD data profiling to assess the natural hazard of active submarine vent fields: the case of Santorini Island

A. Dura[1], T.J. Mertzimekis[2], E. Bakalis[2,3], P. Nomikou[1], A. Gondikas[1], M.D. Hannington[4], S. Petersen[4]

(1) Department of Geology and Geoenvironment, National Kapodistrian University of Athens, Zografou Campus, 15784, Athens, Greece, andura@geol.uoa.gr
(2) Department of Physics, National Kapodistrian University of Athens, Zografou Campus, 15784, Athens, Greece
(3) Department of Chemistry "G. Ciamician", University of Bologna, Italy
(4) GEOMAR - Helmholtz Centerfor Ocean Research Kiel, 24148 Kiel, Germany

Abstract

Almost three quarters of known volcanic activity on Earth occurs in underwater locations. The presence of active hydrothermal vent fields in such environments is a potential natural hazard for the environment, the society, and the economy. Despite its importance for risk assessment and risk mitigation, monitoring of the activity is impeded by the remoteness and the extreme conditions of underwater volcanoes. Kolumbo underwater volcano, 7 Km NE of Santorini island, featuring an active hydrothermal vent field, which has shown near–explosive dynamics in the recent years (Carey et al., 2013). CTD (conductivity, temperature, depth) time series from an earlier expedition in 2010–2011 (Bakalis et al., 2017), which investigated mainly the northern part of the vent field, have been used to develop an advanced mathematical model based on the Generalized Moments Method to describe the underlying mechanisms governing the hydrothermal vent activity. The model was further tested successfully in the inactive caldera near Nisyros Island (Dodecanese, Greece) (Bakalis et al., 2018).

The submerged volcanic activity of Santorini and the large difference of population present on the island between the winter and summer seasons, all within a partially enclosed system, make Santorini and its nearby active hydrothermal vent fields (e.g. Kolumbo) an ideal place for detailed investigation. The main objective of this work is to study high–frequency recorded CTD data in the water column over the Santorini caldera and the active neighboring hydrothermal vent fields. The data will be used to create depth profiles of the oceanographic properties such as conductivity, temperature and salinity and map their anomalies over active vents.

In 2017, GEOMAR in collaboration with the National and Kapodistrian University of Athens, used an Autonomous Underwater Vehicle (AUV) to investigate the evolution of the NE–trending Santorini–Kolumbo line, where it also collected CTD data. The mission lasted 25 days, 19 of which were onboard operations. Detailed CTD 3D profiles have been reconstructed from the raw data to study Kolumbo's active hydrothermal vent field and Santorini's vent field (Camilli et al., 2015) to a full extent. Here we present the results from the 15-hour survey held on the 25th March 2017, during the POS510 expedition targeting the Santorini vent field located in the North Basin of the Santorini Caldera, as seen in Figure 1.

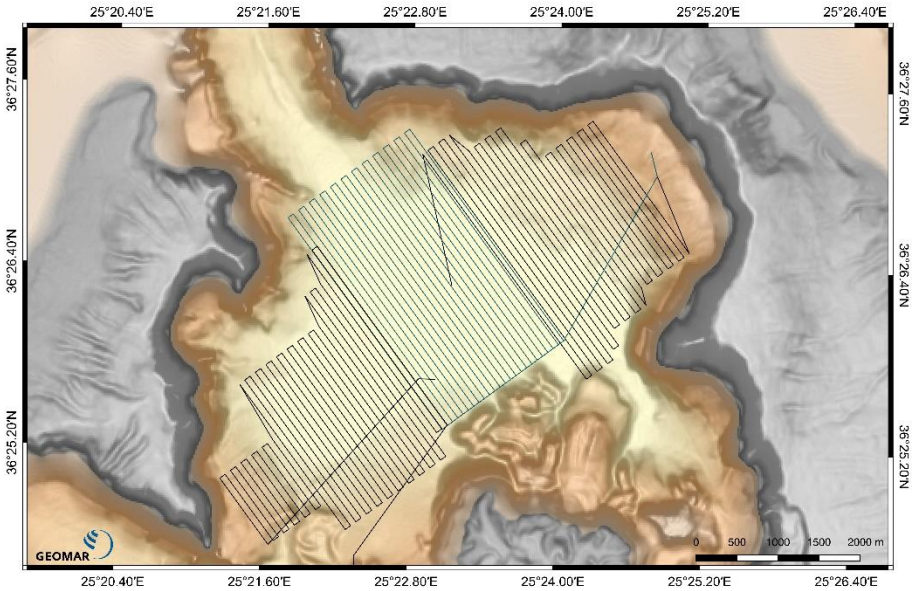

Figure 1. The area of the North Basin of the Santorini caldera that was surveyedwith AUV during POS510. (Nomikou et al., 2014; Hannington, M., et al., 2017).

In Figure 2, the depth profiles of the Temperature (T), Conductivity (C), Salinity (S) and Sound Velocity(V) are presented, respectively. The change in temperature seems to follow a typical open–ocean CTD profile, with higher

values near the surface and the thermocline zone, which tend to become smaller as the depth reaches its maximum values near the seafloor and above the vent field. This behavior is evident in the profiles of salinity, conductivity and sound velocity, as well. However, an anomaly emerges at the depth of 350m in the C and S profiles, as the CTD sensor is placed directly above the vent sources, as can be seen at the profiles recorded between 250 and 350 m. The anomaly is attributed to existing vent activity, which is not so intense as to change the local thermodynamics of the system and have a significant impact on the T profiles, but is recorded in the high–sensitivity C and S sensors, indicating that hydrothermal fluids are entering the water column from the crust in a weak, but continuous fashion.

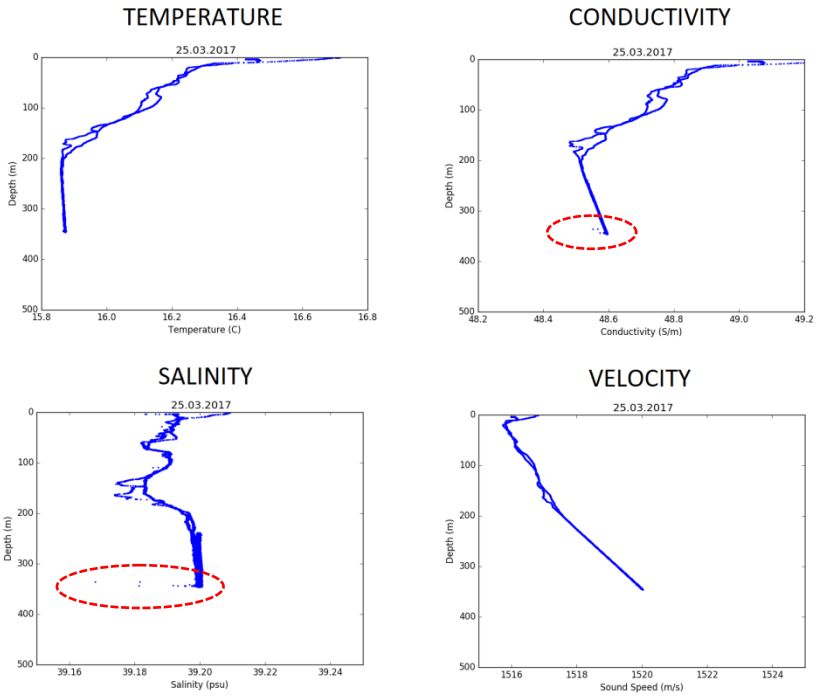

Figure 2. Temperature, Conductivity, Salinity and Sound Velocity profiles according to the 25-3-2017 survey in the North Basin of Santorini.Anomalies in the profiles are circled with dashed ovals.

As the present results are the first ones produced from this expedition, they provide strong motivation for further investigation. CTD anomalies in depth profiles will be fully documented, while a 2D map of vent activity will be constructed from measurements at constant depth of AUV operation. These stepsare crucial towards developing a supervised machine–learning algorithm able to provide a reliable description of the dynamic conditions over the hydrothermal vent field in near–real–time fashion and potentially provide the means to predict explosive conditions. The impact on developing appropriate mechanisms and policies to avoid the associated natural hazard is expected to be immense.

Acknowledgements

This project has received funding from the Hellenic Foundation for Research and Innovation (HFRI) and the General Secretariat for Research and Technology (GSRT), under grant agreement No 1317. We thank the captain and the crew of the R/V Poseidon and GEOMAR for their contribution in collecting the CTD data.

References

Bakalis, E., et al., 2017. Breathing modes of Kolumbo submarine volcano (Santorini, Greece), Sci. Rep. 7, 46516.

Bakalis, E., Mertzimekiset al., 2018. Temperature and Conductivity as Indicators of the Morphology and Activity of a Submarine Volcano: Avyssos (Nisyros) in the South Aegean Sea, Greece, Geosciences 8, 193.

Camilli R., et al., 2015. The Kallisti Limnes, Carbon Dioxide-Accumulating Subsea Pools. Scientific Reports 3:2421.

Carey S., et al., 2013. CO_2 Degassing from Hydrothermal Vents at Kolumbo Submarine Volcano, Greece and the Accumulation of Acidic Crater Water. Geology 9:1035-1038.

Hannington, M., et al., 2017. Rifting and Hydrothermal Activity in the Cyclades Back-arc Basin: Cruise Report of RV Poseidon, POS510, Catania-Heraklion 06.03.17-29.03.17, 361 p.

Nomikou P., et al., 2014. The emergence and growth of a submarine volcano: The Kameni islands, Santorini (Greece). GeoResJ 1–2:8–18.

15th International Congress of the Geological Society of Greece
Athens, 22-24 May, 2019 | Harokopio University of Athens, Greece
Bulletin of the Geological Society of Greece, Sp. Pub. 7 Ext. Abs. GSG2019-275

A detailed bathymetric and sedimentology study of the Volos Gulf

I. Zananiri[1], D. Mitropoulos[1], I. Vakalas[1], S. Maroulakis[1], V.Barsaki[1] & E. Zimianitis[1]
(1) Hellenic Survey of Geology & Mineral Exploration, Spirou Loui 1, 13677 Acharnae, Greece; izanan@igme.gr

Background and Objectives

The Hellenic Survey of Geology and Mineral Exploration (HSGME, former IGME), in the frame of the "National Strategic Reference Framework 2007 – 2013", Operational Program "Competitiveness and Entrepreneurship", implemented the project "Geological and multidisciplinary mapping in strategic and business scales for the selection of development, environmental and cultural targets (GEOCHART)". During the elaboration of this project, marine geology research (Zananiri et al. 2016) was carried out at around the broader Volos urban area (Fig. 1); the scope of this research was to define the present day situation of the gulf, establishing a detailed bathymetry, and to study the palaeogeographic evolution during the Upper Quaternary.

Method and Measurements

Bathymetric data were gathered with an AIRMAR EchoRangeSmartTM Sensor (200 kHz), resolution 0.01m, for a total of 72166 points, accounting to 146.8 km. The seismic profiles were acquired, using a Geoacoustics3.5 kHz 10KW high-resolution shallow seismic system, along 60 parallel lines in WSW – ENE and NNW – SSE direction (Fig. 1), track spacing of 200m for a total of 116.8 km. Finally, surface sediment samples (upper 10 – 20 cm) of both fine- and coarse-grained material were collected (58 samples), with a Dietz LaFond bottom grab sampler (Fig. 1), in order to study their distribution and properties along the gulf's bottom surface, and to complement the acoustic response data. The samples, after the appropriate laboratory preparation, were used for sedimentology analysis. The acquired data were assembled and interrogated using Geographic Information Systems (GIS); to accomplish this task a Personal Geodatabase was created, including all available information for the broader study area: local geology, topographic features, aerial imagery and hydrogeological data and incorporating all new data: bathymetry, granulometry, morphology, sampling etc (Zananiri et al. 2018).

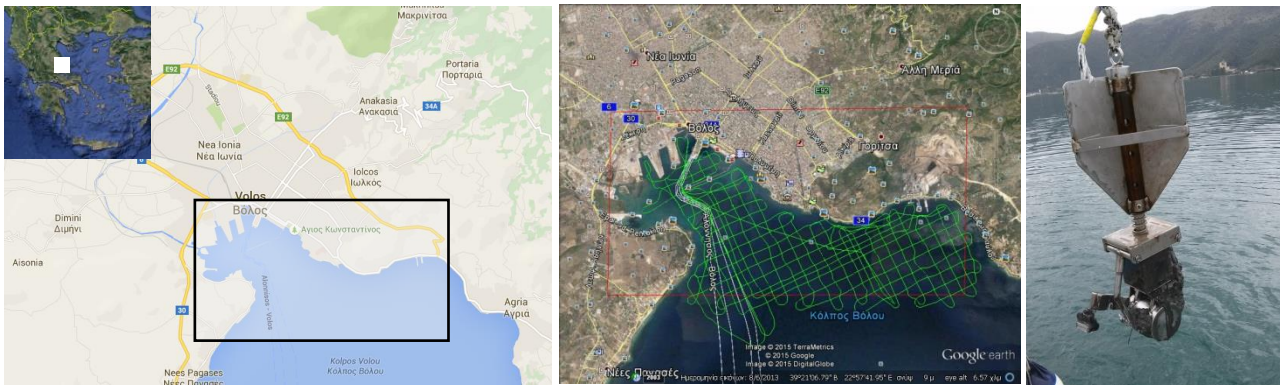

Figure 1. The location of Volos Gulf and main topographic features of the broader study area (left), seismic profiling (middle) and acquisition of grab samples (right).

Results and Conclusions

The detailed depth recording around the study area allowed the elaboration of a high resolution bathymetry map (Fig. 2), scale 1:5000, with contours drawn every 2m. In general the Volos Gulf is characterized by regular seafloor morphology, with a maximum depth of 44m and maximum slope at ~20°. Higher slopes, as expected, are located in coastal areas, following the morphology of the terrain, with some local ridges at the eastern part. Along the base of the latter, as well as in more central areas, creep or sedimentation phenomena are observed in the form of small landslides.

Seismic penetration in most parts was satisfactory, down to 40m, while limited in certain areas, possibly due to the extensive presence of organic matter or biogenic gas within the sediments. Seafloor appears as a continuous reflector (R0), weak in deep areas, intense and prolonged in the shallow; its behaviour being mainly attributed to the nature of the sediments that cover it. The digital processing of the seismic data allowed the mapping of a major unconformity (R1), defined by a strong reflector which extends throughout almost the entire area of the Volos gulf and ranges in depth between 0 to 40m below present-day seafloor (Fig. 2). This reflector is regular, in general, with a smooth morphological relief in the shallow areas and in the central part of the bay, with locally observed erosional features, such as palaeo-channels, river beds and human activity traces (deepening corridor, port works etc).

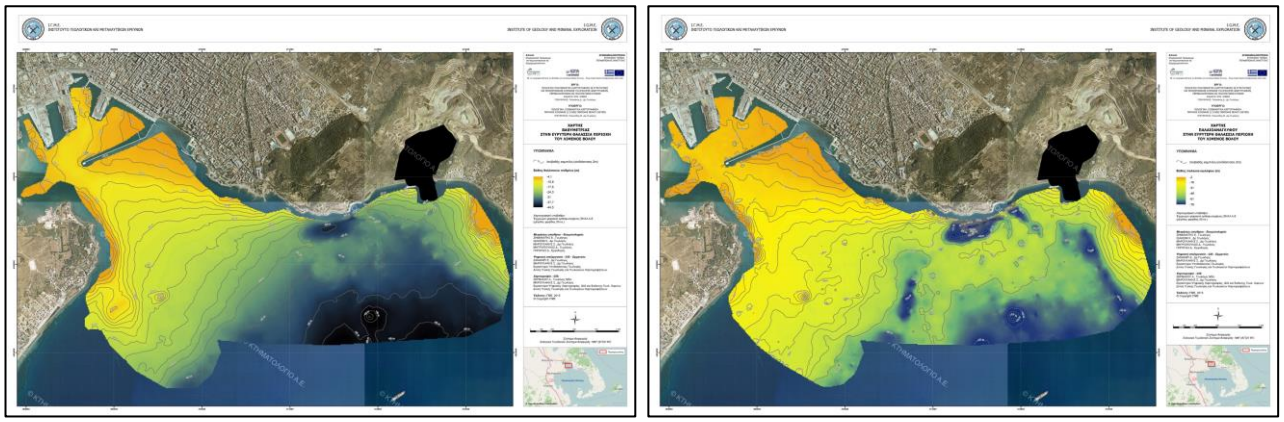

Figure 2. Bathymetry map (left) and palaeomorphology of the seafloor (right) for the study area.

Grain size distribution of seafloor sediments (Fig. 3) shows that fine fractions dominate most of the study area, with frequent presence of gravel. Locally sediments appear coarser, while a narrow sandy zone is observed at the port entrance. Sediment statistics denote that a stable, low energy, environment prevails in the area, where fine sediments can remain for long periods of time in suspension and even be transported by low energy streams to the more distal coastal areas. In the eastern part of the gulf the sediments are coarser, with increased gravel involvement, suggesting a higher energy environment where the sediments are transported and deposited mainly by rivers (Barsaki 2014) and streams.

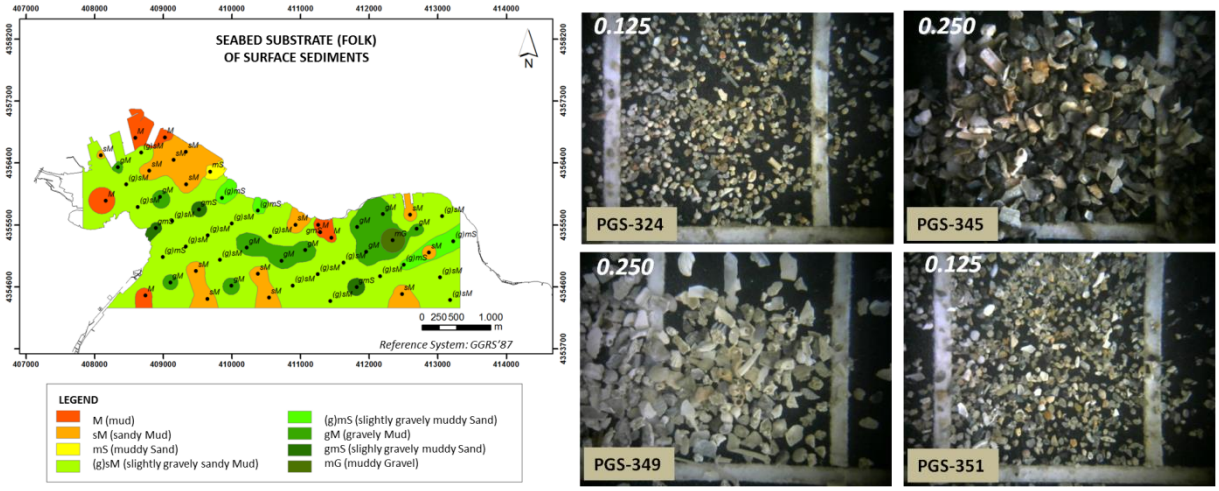

Figure 3. Grain size distribution of surface samples (left) and representative optical microscopy images (right)

Microscopic examination of the samples (Fig. 3) shows compositional variations the sand fraction from surface sediments at the port of Volos and the wider marine area. These variations concern both the type of minerals and the percentage of biogenic constituents involved. The studied sediments appear elsewhere leukocratic and elsewhere with greater involvement of dark-colored minerals, which – in addition to the presence or absence of biogenic components – reflects the type of material involved in sedimentation of the seabed and is directly linked to lithology (Tselepidis et al. 2015) of the wider region (carbonate and shale rocks).

References

Barsaki V., 2014: Flood risk assessment using GIS in the wider basin of the region of Volos, N. Magnesia, IGME Publications (in Greek), 56 pp.

Tselepidis V., Galanakis D. & Georgiou Ch., 2015: Geological and Neotectonic study of the urban and sub-urban area of Volos, IGME Publications (in Greek), 75 pp.

Zananiri I., Mitropoulos D., Maroulakis S., Zimianitis V., Vakalas I., Tassiou S., Kaminari M. & Efthimiou G., 2016: Reporting of the results of a bathymetry and sedimentary survey of the seafloor at the port of Volos and the broader marine area, IGME Publications (in Greek), 297 pp.

Zananiri I., Valaouris A., Vakalas I., Zimianitis V. & Drosopoulou E., 2018 : The IGME Marine geo-information system : integrating international standards towards INSPIRE-compliancy, IMDIS 2018 Book of Abstracts, Bolletino di Geofisica, Vol. 59 (1), p. 244-245

GENERAL SESSION

T9 Engineering Geology, Hydrogeology and Environmental Geology

15th International Congress of the Geological Society of Greece
Athens, 22-24 May, 2019 | Harokopio University of Athens, Greece
Bulletin of the Geological Society of Greece, Sp. Pub. 7 Ext. Abs. GSG2019-006

A semi-empirical approach for the prediction of trajectories in rockfalls

P. Asteriou, G. Tsiambaos
National Technical University of Athens, Greece, paster@central.ntua.gr

Rockfalls constitute a significant natural hazard that manifests as a sudden and violent downward movement of rock blocks. The design and implementation of appropriate mitigation measures rests on the estimation of the possible trajectories. Once the block comes in contact with a slope, depending on the kinematic state and the contact geometry, it might rebound resulting in a new parabolic trajectory. Alternate response types to rebound are rolling, sliding or a combination thereof. The rebound, which controls the post-impact part of the trajectory, is calculated according to the coefficients of restitution (COR) which are overall values that take into account all of the characteristics of the impact and describe the change in the block's velocity magnitude. Normal COR (n_{COR}) is defined as $n_{COR}=-v_{nr}/v_{ni}$, and Tangential COR (t_{COR}) is defined as $t_{COR}=v_{tr}/v_{ti}$, where *v* is the velocity and the subscripts *n*, *t* define its components (normal and tangential to the slope surface respectively), whereas as the subscripts *i* and *r* denote the impact and rebound stage.

COR estimation in practical applications is based on some suggestive values, which depend solely by the slope surface material. In addition, CORs are adjusted to the impact velocity applying some scaling methods that are also empirically derived. A detailed overview of COR definitions, suggested COR values and the scaling methods can be found in Asteriou & Tsiambaos (2018). However, the rebound is affected by many parameters: (i) the strength, stiffness, roughness and the inclination of the slope; (ii) the strength, stiffness, mass and shape of the block, and; (iii) the translational and rotational velocity, the collision angle and the configuration of the block during impact (Labiouse & Heidenreich, 2009). Therefore, selecting the COR values just by the material type consisting the slope can lead to significant simplifications.

It becomes apparent that a better method for selecting the COR is necessary. To attain this necessity, a semi-empirical method is presented hereafter, which considers: (i) the material types of both the slope surface and the block; (ii) the block mass and its incident velocity, and; (iii) the collision angle.

Methodology

An extensive experimental study was designed in order to examine the COR values with respect to the aforementioned parameters and to establish a correlation between them. The equipment required for conducting impact tests in the laboratory includes a block, an impact surface, a release mechanism and a data acquisition system.

Block shape has been found to have a significant effect on the rebound trajectory due to the configuration of the block at impact (Asteriou & Tsiambaos, 2016). When the block has an irregular shape, the impact configuration varies significantly between tests, introducing stochastic effects. To eliminate these effects, the tests were performed using spherical blocks and flat impact surfaces. The blocks were cast in silicon molds by two different artificial materials, namely a high-strength cement grout and an epoxy resin, with diameters of 3, 4, 5 and 6cm. Additionally, blocks were formed from intact specimens of a fine-graded marble and a quartizic sandstone, with diameters in the aforementioned range. Impact surfaces were created for all materials used. Each impact surface was the top side of a 5-cm-thick rectangular plate with 15cm sides that was fixed to a massive dead weight base to ensure the preservation of momentum during the impact. The physical and mechanical properties of these materials were determined according to the ISRM suggested methods, in order to correlate them with the response of the blocks at impact.

Two release mechanisms were developed. The first was used to conduct free-fall tests and consisted of an arm that held the block in the desired height by suction that was produced from a vacuum pump. The second mechanism involved an inclined tube with adjustable length and inclination, so as to control the incident translational velocity and the collision angle. The block was inserted into one side and released from the other towards the impact surface, after sliding and rolling through the tube, which also generated a random angular velocity.

The trajectories were recorded with a high-speed digital video camera at a frame rate of 500fps and a resolution of 440×330 pixels. The camera was installed 1m from the impact surface. A high-contrast background was installed to make the block visually distinguishable. An in-house machine vision algorithm was developed to track the motion and analyse the trajectory, providing all the necessary experimental data.

In total, over one thousand impact tests were performed organised in three stages. In the first stage, in order to assess the effects of material type, block mass and incident velocity, blocks from all material types and all sizes were released by free-fall, from various heights to impact on surfaces consisting of the same material. In the second stage, similar tests were performed, but the blocks impacted on surfaces of a different material type to assess the effect of impacts between different materials. Finally, in the third set, oblique impact tests were performed to study the effects of the collision angle and the angular velocity. A detailed documentation of the aforementioned testing campaigns (apparatuses, procedure, material properties, data acquisition and results) can be found in Asteriou & Tsiambaos (2018) and Asteriou (2018).

Research outcomes

In the first stage, the free-fall drops were performed from heights ranged from 0.1 to 4.5m, resulting in incident velocities (v_{ni}) ranging from 1.3 to 9.3ms^{-1}. Irrespectively of the material type, the results indicated that n_{COR} reduces with an increase in incident velocity and that for a given v_i, an increase in mass decreases n_{COR}. However, the rate of change differed for

each material tested, indicating that the rebound is also affected by the material type. A significant correlation was extrapolated when assessing the n_{COR} values, derived from the experimental testing, with the incident momentum (M_{ni}). The response (Figure 1) was well described by a hyperbolic function of the form:

$$n_{COR} = f(R)M_i^a + 1 \quad (1)$$

where R is the Schmidt hammer hardness value, which has been found to be the material property that correlates better with n_{COR} (Asteriou *et al.*, 2012). This was anticipated since the mechanical analogues of both the Schmidt hammer test and the free-fall impact tests resemble many similarities.

Eq.1 yields one when the incident momentum is very low, which corresponds to perfectly elastic collision and to yields to a negative n_{COR} value when R is very small, which corresponds to the case of a perfectly plastic collision. Both situations are in accordance to the principals described in impact mechanics.

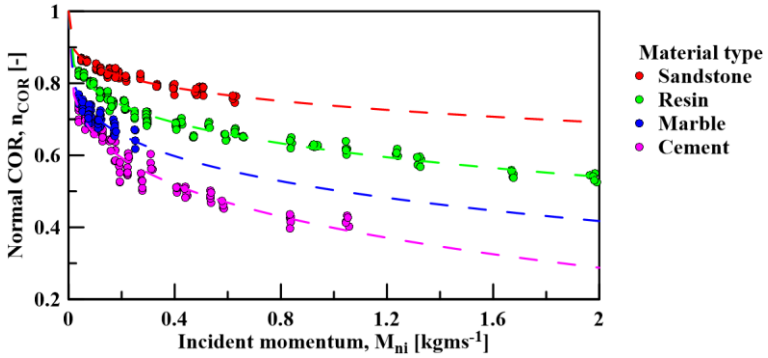

Figure 1. Normal COR as a function of incident momentum from the first testing stage

In the second testing stage, further tests were conducted by letting the spheres impact on a surface of a different material. It was seen that n_{COR} is affected by the material type of the impact surface, since n_{COR} was found to be increased as the surface became harder. This effect is quantified by calculating n_{COR} from Eq.1 with the Schmidt hardness of the block (R_b) and by introducing the correction factor c_{rh} defined as:

$$c_{rh}=2R_b/(R_s+R_b) \quad (2)$$

Where R_s is the Schmidt hardness of the impact surface. Eq. 2 yields to one when R_s equals R_b, which corresponds to the test conditions applied in the first testing stage.

In the third testing stage the effects of impact angle and angular velocity were examined by conducting inclined impact tests. The sandstone, marble and cement materials were used along with all block sizes, achieving velocity magnitudes in the range from 1.9 to 6.6ms^{-1}, impact angles from 20 to 65°, and angular velocities between 100 and 400s^{-1}.

The results verified the previous findings (i.e. n_{COR} decreases with the intensity of the impact and increases as the materials become harder) and that n_{COR} decreases as the impact angle tends to 90°, which has been noted in many relevant studies. However, the angular velocity did not have any effect on n_{COR}. Also, these results verified that the semi-empirical model that was extrapolated form the previous testing stages is applicable for inclined impacts as well, given that the normal component of the incident momentum is used. The relative error in the estimation of n_{COR} for oblique impacts using Eq. 3 is limited to ±15%, which is significantly lower compared to what found in relevant literature. On its final form, the semi-empirical model for the estimation of n_{COR} is:

$$n_{COR} = c_{rh}\,[(0.027R_b-1.536)M_{ni}^{0.244} + 1] \quad (3)$$

None of the investigated parameters posed any measureable effect on t_{COR}. This is in line with the findings in relevant literature. Thus, t_{COR} is assumed to be primarily affected by the roughness of the impact surface in combination with the block shape, which form the contact geometry. This justifies the limited scatter in t_{COR} values in this study, since all tests were performed with spherical blocks impacting on planar surfaces, leading to repeatable impact configuration between tests.

Acknowledgements

This post-doctoral research was carried out with a scholarship granted by the State Scholarships Foundation of Greece (IKY) under the act "Supporting Post-Doctoral Researchers" of the Operational Program "Human Resources Development, Education and Life Lifelong Learning" (Thematic Priority Axes 6, 8, 9) and is co-funded by the European Social Fund (ESF) and the Greek Government.

References

Asteriou, P. Tsiambaos G., 2018. Effect of impact velocity, block mass and hardness on the coefficients of restitution for rockfall analysis. Int J Rock Mech Min Sci, 106, 41-50

Labiouse, V., Heidenreich, B., 2009. Half-scale experimental study of rockfall impacts on sandy slopes. Nat Hazards Earth Syst Sci, 9(6): 1981–1993.

Asteriou, P., Tsiambaos G., 2016. Empirical model for predicting rockfall trajectory direction. Rock Mech Rock Eng, 49(3): 927–941.

Asteriou, P., 2018. Effect of impact angle and rotational motion on the coefficients of restitution for rockfalls. Geotec Geol Eng.

Asteriou, P., Saroglou, H., Tsiambaos, G., 2012. Geotechnical and kinematic parameters affecting the coefficients of restitution for rock fall analysis. Int J Rock Mech Min Sci, 54. 103–113

15th International Congress of the Geological Society of Greece
Athens, 22-24 May, 2019 | Harokopio University of Athens, Greece
Bulletin of the Geological Society of Greece, Sp. Pub. 7 Ext. Abs. GSG2019-007

A New Software Tool for the Analysis of Rockfalls

P. Asteriou
National Technical University of Athens, Greece, paster@central.ntua.gr

Rockfalls are gravitationally driven geomorphic processes that occur rapidly on steep rocky slopes. They can have disastrous effects on human activities and infrastructure and therefore constitute a significant natural hazard. However, due to the complex nature of the phenomenon, the available analysis methods incorporate assumptions that can lead to oversimplifications, since limited parameters are taken into account. This paper presents a new software tool for rockfall trajectory modeling. The software allows the user to choose the analysis method, selecting from: a) the lump-mass model; b) some recently proposed semi-empirical methods; and c) a new neural network algorithm that is trained with the data acquired from an extensive laboratory and field investigation, previously performed by the author (Asteriou, 2016). First, the software is presented and then the well-documented rockfall incident in Ponti, following the Mw=6.5 Lefkada earthquake in 2015, is briefly described and analysed with the software. The outcomes are commented and compared to the actual trajectory. Some interesting remarks on the reliability and accuracy of these methods are discussed.

Rockfall Software Structure

The software was developed in MatLab. The user interacts with the software through the Graphical User Interface (GUI) environment, resulting to a user-friendly application. In order to perform an analysis, the user must go through four stages; a) Model creation; b) Definition of parameters; c) Computation; and d) Interpretation. At the first stage, the user defines slope's geometry by importing an excel spreadsheet containing the vertex coordinates of each segment, input the vertex coordinates in the GUI environment or draw the slope manually with the cursor. Then, the detachment point is defined in the GUI manually or with the cursor. At the next stage, the user selects the analysis method and defines the parameters required by the selected analysis method in pop-up windows (such as: CORs, slope roughness, initial velocity and others). The computation (stage c) is performed according to what defined at the previous two stages. Finally, at the last stage, the trajectory is depicted and all necessary data (block velocity, kinetic energy, and rebound height) are available both graphically and in a tabular environment. After each stage has been completed the settings are automatically saved allowing to start-over the analysis in any stage and modify any parameter in order to assess different scenarios and compare the results.

Overview of the Available Analysis Methods

During a rockfall the block can travel through the air, roll or slide on the slope surface and impact onto the slope. While the block is travelling through the air, its motion is calculated by the ballistic trajectory equations. Following the projectile motion, the block will impact the slope and it will either rebound and revert to a new parabola, or slide on the slope surface. When the block is in contact with the slope, sliding or rolling is calculated according to Statham (1976). The rolling/sliding distance depends on the tangential velocity, the slope angle and the friction/roughness of the slope. The rebound can be assessed with one of the following methods:

- The lump-mass model, which is used in the majority of similar software due its simplicity. The response to the impact is described by the coefficients of restitution (CORs), which are assumed to be overall parameters that take into account all the characteristics of the impact. In practice, COR values are obtained by some indicative values that are provided as guidelines, which depend solely by the material that constitutes the slope surface.
- Some empirical models found in literature, which originate from back-analysis of real rockfall events (i.e. Wyllie, 2014) and from experimental testing (i.e. Giacomini *et al.*, 2012; Asteriou and Tsiambaos, 2018). These model are used to estimate the appropriate CORs taking into account more parameters, such as the impact velocity and angle, the material type and others.
- A neural network algorithm developed especially for this software that is based on the data acquired in Asteriou (2016). In general, a neural network is a computing model whose layered structure resembles the networked structure of neurons in the brain. A neural network learns from data, so it can be trained to forecast future events. The model used for the software is a deep learning multi-layered network that was trained by more than 3000 laboratory and field tests.

Analysis of the Ponti Rockfall

On 17 November 2015, an earthquake (Mw 6.5) struck the island of Lefkada and triggered a number of rockfalls. In Ponti village, a limestone block was detached at an elevation of 500m, rolled approximately for 250m, impacted 22 times on the slope and finally impacted a family residence, penetrated two brick walls and killed a person inside the house. The slope overhanging the residence has its peak at 600m and an average slope angle of approx. 40° and the house rests at an elevation of 130m. The block was nearly cubical with 1.4-m-sides and its volume was approximately $2m^3$.

The rock path and the impact points on the slope were identified by a field survey, performed using an unmanned aerial vehicle (UAV) with an ultrahigh definition (UHD) camera, which produced a high-resolution orthophoto and a digital terrain model (DTM) of the slope (Saroglou *et al.*, 2018). Figure 1 illustrates the plan view of the slope (top), its cross-

section (bottom), and the actual trajectory impact points are depicted by the red vertical lines. Hereafter, a back-analysis of the Ponti event is presented using an example of each method available in the software.

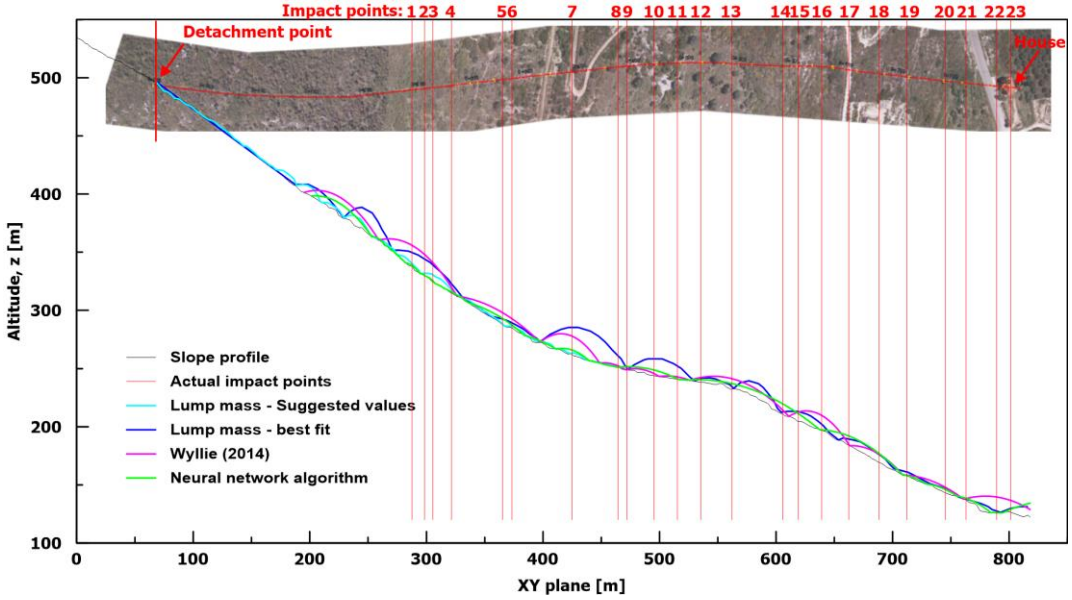

Figure 1. Plan view and cross section along the block's path.

First, the lump mass model is assessed using with the CORs suggested in literature (bedrock outcrops: n_{COR}=0.35 and t_{COR}=0.85). The falling rock primarily rolls on the slope and stops much earlier than its actual runout distance (Fig.1 – cyan path). In order to approach more closely the actual trajectory various CORs combinations were examined. The best match occurs with n_{COR}=0.60 and t_{COR}=0.85, which corresponds to bedrock (Fig.1 – blue path). 14 impacts occur instead of the actual 22, their positions significantly differ from the actual ones and the bounces are unrealistically high (up to ~25m) according to the observations of Volkwein *et al.* (2011).

Using the CORs estimated from the empirical model proposed by Wyllie (2014), the trajectory (Fig.1 - magenta line) consists of 12 impacts points, which are randomly positioned compared to the actual positions on the slope. However, the rebound heights are more realistic compared to the previous analysis presented, with a maximum bounce of ~12m.

Finally, the neural network algorithm provides the best estimate of the trajectory. It consists of 16 impacts with the slope, but again in different locations compared to the actual ones (Fig1. Green path). The trajectory is more shallow and realistic in terms of bounce heights, as the maximum rebound is ~6m.

Conclusions

In this study, a well-described rockfall event was analyzed with the aid of a newly developed software in order to assess various rockfall trajectory analysis methods. In addition, this software is equipped with a neural network algorithm that is trained with numerous experimental data. The results indicate that the classical lump-mass model approach, which is to estimate the CORs solely by the slope material and to consider them as constants, does not provide realistic paths and leads to excessive rebound heights. The trajectory is better appraised when CORs are calculated with semi-empirical models because CORs vary according to the impact conditions considered by the model. Finally, the neural network algorithm results to the most realistic path, since more parameters are involved to estimate CORs and in the same time the user has less parameters to choose. On the other hand, the main disadvantage of this neural network algorithm is its 'black box' nature, meaning that there is limited justification on how the output is reached and limiting understanding on the features that affected this output.

Acknowledgements

This post-doctoral research was carried out with a scholarship granted by the State Scholarships Foundation of Greece (IKY) under the act "Supporting Post-Doctoral Researchers" of the Operational Program "Human Resources Development, Education and Life Lifelong Learning" (Thematic Priority Axes 6, 8, 9) and is co-funded by the European Social Fund (ESF) and the Greek Government.

References

Asteriou, P., 2016. Investigation of the geotechnical parameters which control rockfalls. Ph.D. Thesis, NTUA, Athens, 691 p.

Asteriou, P., Tsiambaos, G. 2018. Effect of impact velocity, block mass and hardness on the coefficients of restitution for rockfall analysis. Int J Rock Mech Min Sci., 106, 41–50.

Giacomini, AK., Thoeni, C., Lambert, S., Booth, Sloan, SW. 2012. Experimental study on rockfall drapery systems for open pit highwalls. Int J Rock Mech Min Sci., 56, 171–181.

Statham, I., 1976. A scree slope rockfall model. Earth Surface Processes 1.1, 43–62.

Saroglou, C., Asteriou, P., Zekkos, D., Tsiambaos, G., Clark, M., Manousakis, J., 2018. UAV-based mapping, back analysis and trajectory modeling of a coseismic tockfall in Lefkada island, Greece. Nat. Hazards Earth Syst. Sci., 18, 321–333.

Wyllie, DC. 2014. Calibration of rock fall modeling parameters. Int J Rock Mech Min Sci., 67, 170–180.

Volkwein, A., Schellenberg, K., Labiouse, V., Agliardi, F., Berger, F., Bourrier, F., Dorren, LKA., Gerber, W., Jaboyedoff, M. 2011. Rockfall characterisation and structural protection – a review. Nat. Hazards Earth Syst. Sci., 11, 2617–2651.

15th International Congress of the Geological Society of Greece
Athens, 22-24 May, 2019 | Harokopio University of Athens, Greece
Bulletin of the Geological Society of Greece, Sp. Pub. 7 Ext. Abs. GSG2019-015

Documentation of the failures triggered by the July 20, 2017 Bodrum-Kos, Aegean Sea Mw=6.6 earthquake

G. Papathanassiou[1] S. Valkaniotiss[2], Sp. Pavlides[3]

(1) Democritus University of Thrace, Dept. Civil Engineering, Xanthi, Greece gpapatha@civil.duth.gr
(2) Trikala, Greece
(3) Aristotle University of Thessaloniki

Extended abstract

On July 20, 2017 at 22:31 UTC (01:31 local time) a shallow earthquake of Mw6.6 magnitude occurred in Gökova Bay at a depth of ≈10Km (Fig. 1). The epicenter of the earthquake, located between Bodrum, Turkey and the island of Kos, Greece, SE Aegean Sea. In particular, according to Kandilli Observatory and Earthquake Research Institute (KOERI) the epicenter was at 36.9620ºN 27.4053ºE, while according to the National Observatory of Athens (NOA) at 36.9643ºN 27.4332ºE. The fault plane strikes N280°E and dips to the north with an angle of about 40 degrees in a nearly E-W direction with surface deformation that reached about 20cm onshore islet Karaada (Ganas et al. 2017, Karasözen et al. 2018). Preliminary inversion results of geodetic data, as constrained by InSAR observations, suggest that the upper edge of the fault (14km length and 12km width) is offshore (near the Gökova ridge bathymetric feature) at a shallow depth (2±0.5km - Ganas et al. 2017, Karasözen et al. 2018).

The recorded acceleration at the city of Bodrum, which is located at an epicentral distance of 12 km was 158.76 cm/sec^2. Based on the preliminary distribution of peak ground acceleration (PGA), provided by ITSAK, 2017, the PGA values at the city of Kos and cape Louros were estimated as 0.2 g and 0.25 g, respectively (ITSAK, 2017).

The primary goal of this study was to document the earthquake-induced secondary effects and to provide quantitative data regarding the characteristics of the liquefaction related phenomena at the island of Kos. In order to achieve this, a post-earthquake field survey conducted on 13-14 August, 2017.

Based on the field observations, it can be summarized that the earthquake caused damages to the building stock of the town of Kos, mainly to Ottoman and Venetian-era constructions, including partial collapses that killed two people and seriously injured several others (Papathanassiou et al., 2019). Damages were also reported in the city of Bodrum. Focusing on the island of Kos, the most remarkable type of environmental effects is the liquefaction related phenomena that induced severe damages to the port facilities and to the custom building at the new port of Kos, and at the old harbor of the city. Moderate liquefaction-induced structural failures were induced at the marina of Kos, while at cape Louros ejected material due to liquefaction covered more than 450m^2 (Papathanassiou et al., 2019). Furthermore, a tsunami wave was reported indicating that the generation of tsunami-related phenomena e.g. flooding and structural damages is likely in the Aegean Sea. In particular, the tsunami effects were observed at the south coast of Bodrum peninsula and at the northeast coast of Kos Island, with a maximum run-up measured at 1.9 m at Bodrum area (Yalçıner et al., 2017). Small-scale size rockfalls were reported in the southern part of the island of Kos.

Taking into account the quantitative characteristics of the earthquake-induced secondary effects e.g. liquefaction phenomena and tsunami, the macroseismic intensity was evaluated by applying the Environmental Seismic Intensity (ESI-07), a scale based only on environmental effects introduced by Michetti et al. (2007). Thus, according to Papathanassiou et al. (2019), the macroseismic intensities at the coastal area of cape Louros and the at waterfront area of the city of Kos were assessed as VIII taking into account i) the dimensions of liquefaction manifestations in the former case, ii) the lateral spreading and subsidence at the port and at the old harbour of the city of Kos, and iii) the characteristics of the generated tsunami documented by Yalciner et al. [4]. Details regarding the liquefaction related phenomena are presented in sections 5.1 and 5.2 in this article.

The secondary goal of this study is to investigate in detail a lateral spreading site, located at the old harbor of the city of Kos. This was achieved by performing traditional ground measurements as well as an image-based survey following the Structure from Motion (SfM) technique in order to virtually measure the deformation. The novelty of this study is related to the fact that the applied SfM technique for measuring the lateral spreading displacement was based on a simple handheld digital camera instead of a UAV. Comparing the obtained measurements by these two methods, it is resulted that the deviation of the measurements on horizontal axis e.g. width of cracks, between the virtual (SfM-based) and the manually field observations is less than 1%. Thus, it can be concluded that the SfM-based technique provide reliable data regarding the lateral displacement and accordingly, could be used for the purposes of a rapid post-earthquake field survey (Papathanassiou et al., 2019).



Figure 1. (upper left) Earthquake-induced ground failures at the cape Louros (photo taken by G. Papathanassiou on August 13, 2017), upper right) liquefaction manifestations at the area of marina that is used as a dry dock and for the maintenance and repairs of sailboats and yachts Louros (photo taken by G. Papathanassiou on August 13, 2017), lower left)) lateral spreading phenomena induced damages to custom building (photo taken by G. Papathanassiou on August 14, 2017), lower right)) failure at the new port of Kos (photo taken by G. Papathanassiou on August 14, 2017).

References

Ganas A, Elias P, Valkaniotis S, Briole P, Kapetanidis V, Kassaras I, Barberopoulou A, Argyrakis P, Chouliaras G, Moshou A.2017. Co-seismic deformation and preliminary fault model of the July 20, 2017 M6.6 Kos earthquake, Aegean Sea; 2017. https://www.emsc-csem.org/Files/event/606346/Kos_report_30-7-2017.pdf

ITSAK, 2017. Earthquake Mw6.6 July 21, 2017, Preliminary report, ITSAK, OASP; 2017. Thessaloniki, 20 pages (in Greek) - http://www.itsak.gr/uploads/news/earthquake_reports/EQ_COS_20170721_M6.6.pdf

Karasözen, E., Nissen, E., Büyükakpınar, P., Cambaz, M.D., Kahraman, M., Ertan, E.K., Abgarmi, B., Bergman, E., Ghods, A., Özacar, A.A., 2018. The 2017 July 20 Mw 6.6 Bodrum–Kos earthquake illuminates active faulting in the Gulf of Gökova, SW Turkey. Geophys. J. Int., 214 (1), 185-199 https://doi.org/10.1093/gji/ggy114

Michetti AM, Esposito E, Guerrieri L, Porfido S, Serva L, Tatevossian R, Vittori E, Audemard F, Azuma T, Clague J, Comerci V, Gurpinar A, McCalpin J, Mohammadioun B, Mörner NA, Ota Y, Roghozin, E. 2007. Intensity Scale ESI 2007. Mem. Descr. Carta Geol d'Italia. 74, Rome; 2007

Papathanassiou G., Valkaniotis S., Pavlides S. 2019. The July 20, 2017 Bodrum-Kos, Aegean Sea Mw=6.6 earthquake; preliminary field observations and image-based survey on a lateral spreading site, Soil Dynamics and Earthquake Engineering, 116, 668-680, https://doi.org/10.1016/j.soildyn.2018.10.038

Yasuda S, Morimoto I, Kiku H, Tanaka T. 2004. Reconnaissance report on the damage caused by the three Japanese earthquakes in 2003. In proceedings of the 11th ICSDEE and 3rd ICEGE. Berkeley CA USA;1:14-21.

Yalçıner A, Annunziato A, Papadopoulos G, Dogan G, Guler H, Cakir T, Sozdinler C, Ulutas E, Arikawa T, Suzen L, Kanoglu I, Guler I, Probst P, Synolakis C. 2017. The 20th July 2017 (22:31UTC) Bodrum/Kos earthquake and Tsunami; Post Tsunami Field Survey Report. 2017; http://users.metu.edu.tr/yalciner/july-21-2017-tsunami-report/Report-Field-Survey-of-July-20-2017-Bodrum-Kos-Tsunami.pdf

15th International Congress of the Geological Society of Greece
Athens, 22-24 May, 2019 | Harokopio University of Athens, Greece
Bulletin of the Geological Society of Greece, Sp. Pub. 7 Ext. Abs. GSG2019-030

Evaluation of the Liquefaction Hazard at the western side of the city of Thessaloniki Based on Data Provided by in – Situ Tests

D. Efstathiadou[1], G. Papathanassiou[2], V. Marinos[1], An. Anastasiadis[3]

(1) Department of Geology, Aristotle University of Thessaloniki, 54124, Thessaloniki, Greece, efstadeppie@gmail.com
(2) Department of Civil Engineering, Democritus University of Thrace, Xanthi, Greece
(3) Department of Civil Engineering, Aristotle University of Thessaloniki, 54124, Thessaloniki, Greece

Extended abstract

Soil liquefaction is the phenomenon in which a loose saturated soil layer suddenly loses its strength as a result of seismic vibration and instantly behaves as a liquid. Historically, earthquake-induced liquefaction events have occurred in Japan (1964 Niigata), Alaska (1964 Prince William Sound), Taiwan (1999 Chi - Chi), Washington (2001 Tumwater) and Greece (2014 Cephalonia) to name a few.

In the wider area of Thessaloniki three geological formations are present (Chortiatis magmatic suite, sedimentary rocks of Neogene and Quaternary deposits). The area is of great interest due to the recent geological deposits and the existence of seismogenic areas in near vicinity. The last century two moderate events occurred triggering failures to the manmade environment at the city of Thessaloniki.

For the purposes of this study, data from 64 geotechnical boreholes (figure 1) have been collected and analyzed. In particular, the liquefaction susceptibility per soil layer has been examined according to the criteria of Bray and Sancio (2006); based on the values of Plasticity index (PI), liquid limit (LL) and water content (wc). Afterwards, the factor of safety of susceptible to liquefaction soil layers was computed following the procedure recommended by Youd et al. (2001).

The aim of this study is to develop a map showing the value of the critical peak ground acceleration that should be generated, adopting a seismic scenario of M_w = 6.6, in order to classified a site as liquefiable at the central and western part of Thessaloniki. In order to achieve this, two published models of liquefaction hazard are adopted that were developed by taking into account the Liquefaction Potential Index (LPI); the first model was presented by Toprak and Holzer (2003) and the second one by Papathanassiou (2008).

According to Toprak and Holzer (2003) sand boils are likely to occur where LPI =5 and lateral spreading phenomena will occur where LPI =12, while according to Papathanassiou (2008) the possibility of liquefaction surface evidences is more than 50% for LPI>14.

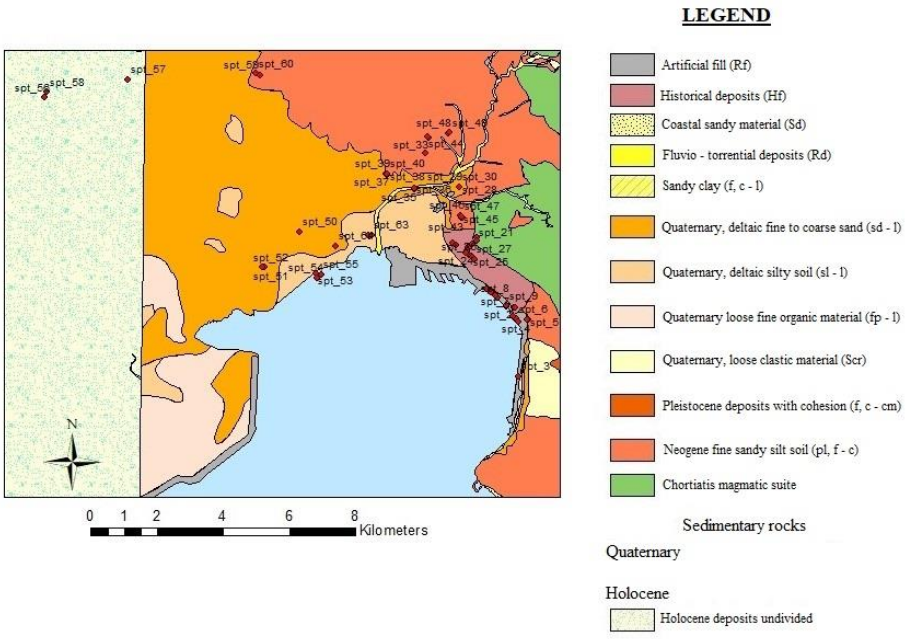

Figure 1 Map with the 64 boreholes that have been analyzed.

As an outcome, it is concluded that the liquefaction hazard is relatively high at the area of Kalohori and at the coastal area and at the western region of Thessaloniki, and that the consequences may be quite important for the manmade environment. At these areas, sand boils are likely to occur according to Toprak and Holzer (2003) when the PGA values

ranges between 0.1 and .0.3g for a scenario of M_w = 6.6.

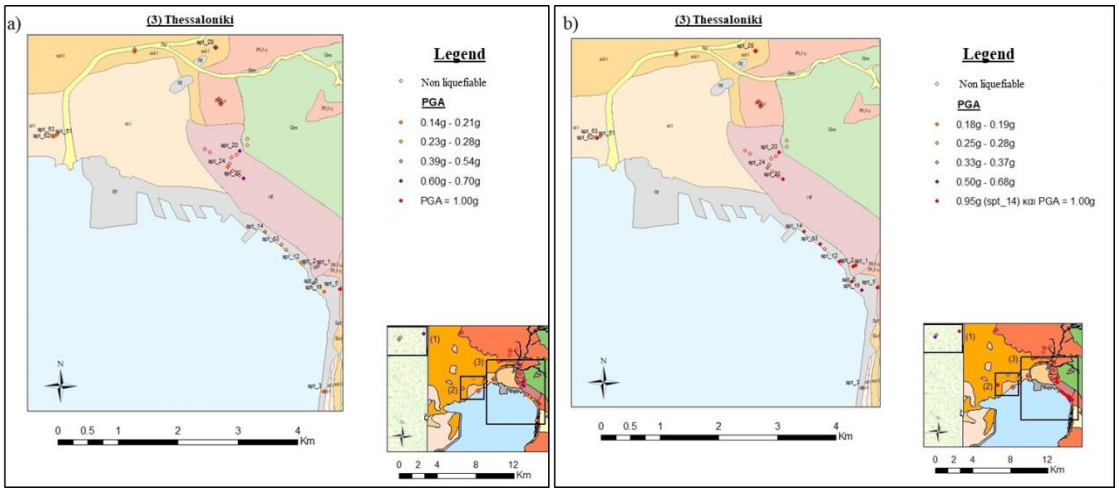

Figure 2 PGA map of Thessaloniki for the classification model of a) Toprak and Holzer (2003) and b) Papathanassiou (2008)

According to the model of Toprak and Holzer (2003), the thickness of the liquefiable soils varies between 0.50m and 4.00m at the coastal area and the western region of Thessaloniki while at the Kalohori area ranges between 3.50m and 6.85m, reaching at some sites 8.40m. Regarding the model of Papathanassiou (2008), the thickness of the liquefiable soils varies between 0.50m and 4.00m at the coastal area, while at the western region of Thessaloniki ranges between 5.00m and 9.00m and at the Kalohori area ranges between 3.50m and 5.15m.

In addition, this study shows that the classification model of Toprak and Holzer (2003) is more conservative than the one suggested by Papathanassiou (2008).

Acknowledgements

The author would like to A. Kokkala, PhD. candidate for providing the data that were used in this study.

References

Bray, J.D. and Sancio, R.B. (2006) 'Assessment of the liquefaction susceptibility of fine - grained soils', Journal of Geotechnical and Geoenvironmental Engineering, pp. 1165 - 1177.

Papathanassiou, G. (2008) 'LPI - based approach for calibrating the severity of liquefaction - induced failures and for assessing the probability of liquefaction surface evidence', Elsevier, pp. 94 -104.

Toprak, S. and Holzer, T.L., 2003. Liquefaction Potential Index: Field Assessment, J. of Geotech. And Geoenvironmental Eng., Vol 129, No 4, pp. 315-322.

Youd, T.L., Idriss, I.M., Andrus, R.D., Arango, I., Castro, G., Christian, J.T., Dobry, R., Finn, W.D.L., Harder, L.F., Hynes, M.E., Ishihara, K., Koester, J.P., Liao, S.S.C., Marcurson, I.W., Marti, G.R., Mitchell, J.K., Moriwaki, Y., Power, M.S., Robertson, P.K., Seed, R.B. et al. (2001) 'Liquefaction resistance of soils: summary report from the 1996 NCEER and 1998 NCEER/NSF workshops on evaluation of liquefaction resistance of soils', Journal of Geotechnical and Geoenvironmental Engineering, pp. 817 - 833.

15th International Congress of the Geological Society of Greece
Athens, 22-24 May, 2019 | Harokopio University of Athens, Greece
Bulletin of the Geological Society of Greece, Sp. Pub. 7 Ext. Abs. GSG2019-044

Vulnerability of critical infrastructures to rock fall hazard: the case of the Wastewater Treatment Facility of Tolo, Greece.

V. Kontogianni, N. Spanou, N. Nikolaou

Hellenic Survey for Geology and Mineral Exploration, 1st S.Loui str., Acharnes, 13677, Greece; villy@igme.gr

The nature and extent of the risk associated with rockfall in steep terrains is a function of the local terrain conditions such as the structure of the rock, the slope stability and the geological processes that lie underground. Furthermore, climate, and weather-related phenomena can alter the local conditions and affect an area's risk. These variables make the assessment of hazard more difficult, especially when specific infrastructures are situated at the site and support measures are required to be adopted. The HSGME has performed numerous studies on rockfall hazard assessment at cliffs of broken, faulted or jointed rock. Among them there exist cases of steep bedrock layers undercut by activities of man for infrastructures developments, mining works etc. In these last cases humans and infrastructures are subjected to serious threat from detached falling rocks (Konstantopoulou et al., 2015). The available support systems for mitigating this risk have the ability either to stabilize the slope or to dissipate the kinetic energy of falling rock. Due to the lack of an official design code, these systems are designed primarily by experience and engineering judgment which often makes the design rather conservative.

In this study, assessment of rockfall hazard along a 300m long manmade cliff at Tolo, Naflio (Greece) is presented. The area is of specific interest due to fact that the foot of the 10 to 110m high cliff hosts the local wastewater treatment plant (WTP) of Tolo, consisting of clarifiers, aeration tanks and other supplementary infrastructures. The WTP plant was decided to be situated at the specific site, a few meters from the seaside of Tolo, to minimize wastewater transportation cost for disposal to the sea.

Geology of the site

According to the Geological Map (sheet 'Nafplion', IGME, 1970; scale 1:50.000) the area consists of Triassic limestone. Tectonically the area is dominated by folds, thrusts and faults, mainly normal that contribute to the morphological structure of the wider area of the trench of Argolis. The limestone rock mass is blocky to thickly bedded, moderately fractured. Randomly intersecting discontinuities include bedding, joint systems, fractures and open cracks caused by blasting practices during the preparation of the site for the facility construction. Also, several overhanging rocks were detected along the cliff (Figure 1).

Stability analysis of the rock cliff

Stability analysis of the cliff required evaluation of the rock structure. The compressive strength of the rock material ranges between 13.8-28.3MPa, based on experimental tests performed at the Lab. *Lithos* of IGME. Furthermore, detailed in situ evaluation of the rock mass characteristics (RQD parameter, spacing of discontinuities, condition of discontinuities and groundwater conditions) permitted the estimation of the Rock Mass Rating (RMR, Bieniawski, 1989) ranging between 52 and 70, corresponding to fair to good quality rock mass. Yet, the contoured plot of the rock discontinuities orientation (presented by poles) is shown in Figure 2 (*Schmidt net)*. Kinematic analysis of slope concerning three critical slopes along the cliff were carried out using the Dips v.5.1 software (Rocscience) taking into consideration the orientation of discontinuities and the shear strength of the potential sliding surface (angle of friction). The results indicated that several wedges of dimensions 0.2m^3 to 36m^{3}are free to slide or topple along all the three critical slopes.



Figure 1: Left: Extended fractured rock slope close to one of the clarifiers of the facility. Right: Overhanging rocks.

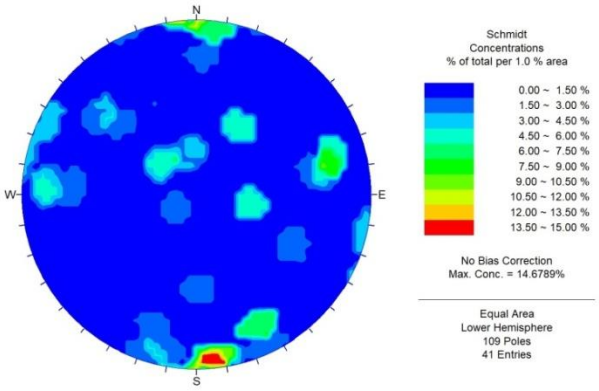

Figure 2: Contoured plot of 109 poles of discontinuity orientation of the examined rock and their concentrations (Schmidt stereonet projection, Dips v.5.1).

Rockfall Hazard Assessment

The outcomes of the stabilty analysis confirm that the various parts of the WTP are subjected to rockfall instabilities. The associated rockfall hazard varies depending on the height of the slope, as well as on the thickness of the inner zone and was considered to be medium to high (Figure 3) suggesting the need of remedial measures. Based on the indentified characteristics of potentially unstable rock mass, analyses of the motion of detached rocks were conducted with Rocfall 4.0 software (Rocscience) on the most critical profiles close to the facility parts. As anticipated, rockfall trajectories suggest that all the facility parts (buildings, tanks etc) are at risk, and also provide evidence that certain types of measures, as for instance mechanical removal of overhanging rocks or installation of fence that require a certain spatial margin between the slope and the facility to be protected, should be excluded for the necessary margin does not exist. Given this conclusion, the remaining suitable measures proposed for the site is wire mesh and rock bolts installation of specific characteristics.

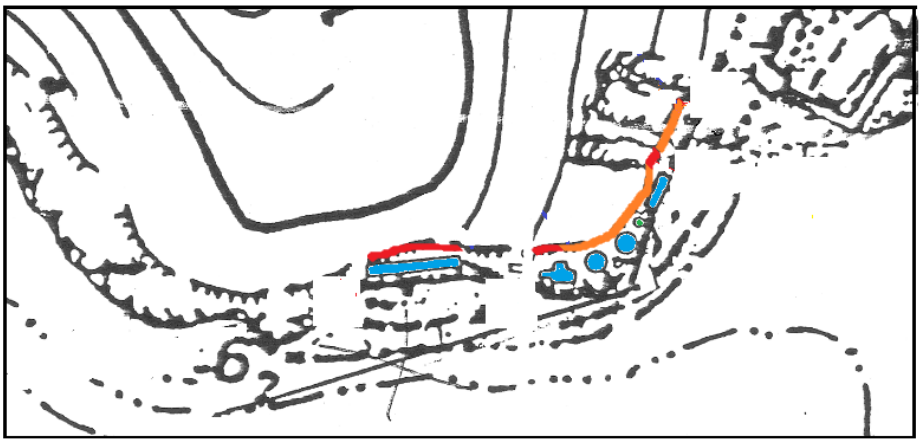

Figure 3: Rockfall hazard map along the WTP of Tolo. Orange line indicates the length of the cliff need to be supported (medium risk). Red lines correspond to locations of extended overhanging rocks of high risk. The facility parts are drawn in blue (the background map is a topographic map provided by the Municipality of Nafplio).

Acknowledgements

This study is part of the work done for the contract between IGME and Municipality of Nafplio, for the study of the stabilization of rock slopes at the Wastewater Treatment Plant of Tolo, in 2017.

References

Bieniawski, Z. T., 1989. Engineering rock mass classifications: a complete manual for engineers and geologists in mining, civil, and petroleum engineering. Wiley-Interscience. pp. 40–47.

G. Konstantopoulou, N. Spanou, V. Kontogianni, 2015. Rockfall at the Arvanitia Pathway, Nafplio, Greece: Protection of the Site with Respect to Its Unique Natural Beauty and Archaeological Interest. Engineering Geology for Society and Territory - Volume 8: Preservation of ntural heritage. Lollino G. et al. (editors), chapter 75, Springer Int. Publ., 431-436.

IGME, 1970. Geological Map of Greece, scale 1:50.000, Sheet 'Nafplion' by Tataris, A, Kallergis, G. and Kounis, G. Athens.

15th International Congress of the Geological Society of Greece
Athens, 22-24 May, 2019 | Harokopio University of Athens, Greece
Bulletin of the Geological Society of Greece, Sp. Pub. 7 Ext. Abs. GSG2019-045

Ground settlements and tilting of buildings due to tunneling - evidence from geodetic surveys in the Athens Metro

V. Kontogianni[1], S. Stiros[2]

(1) Hellenic Survey for Geology and Mineral Exploration, 1st S. Loui str., Acharnes, 13677, Greece; villy@igme.gr

(2) Dept of Civil Engineering, Patras University, Patras 26500, Greece; stiros@upatras.gr

The excavation of tunnels produce ground settlements ("ground loss") which result in subsidence, tilting and occasionally damage to overlying structures. The above is known since many decades ago (Terzaghi, 1942) and till now systematic recording of ground deformation is a common practice for decision making about the development of the excavation or about measures for ground and/or structures stabilization. In this study we summarize geodetic monitoring data from tilting of two brick chimneys in the Technopolis area and ground subsidence at Sepolia area during the construction of the Athens Metro in 1997 and 2003, respectively.

Evidence of ground/structures deformation at the Athens Metro excavation

Tilting of chimneys at Technolopis (Gazi) area

The geological conditions of the Athens Metro consist of the local flysch, which is deformed and foliated and in its upper parts is highly weathered. An up to 70m wide tunnel influence zone (zone of extension of the settlement trough above the tunnel axis) was predicted on the surface. This zone includes Technopolis site dominated by three historical brick chimneys (Figure 1).

Systematic monitoring of the chimneys aimed to detect any movements of the order of a few mm during the tunnel excavation in depth as Papastamos et al. (2015) described in detail. Horizontal dislocation of the top of the chimneys provided evidence about chimneys' tilting, a critical parameter for decision making about the progress of the construction. Maximum amount of tilting was recorded to be 7.5‰ for K1, while the value of the remnant tilting was of the order of 5‰. Despite the fact that 2‰ tilting is regarded to be a threshold for the structural integrity of buildings of different types (Harris et al. 1999; Burland et al. 2001), the Gazi chimneys, survived a much larger amount of tilting without damage. The explanation is that chimneys' geometrical and structural characteristics enabled them to behave as isolated, slender structures subjected only to rigid-body rotation around the vertical axis. The distortion of the chimneys is apparently free from differential settlements which are the most common cause of structural damage.

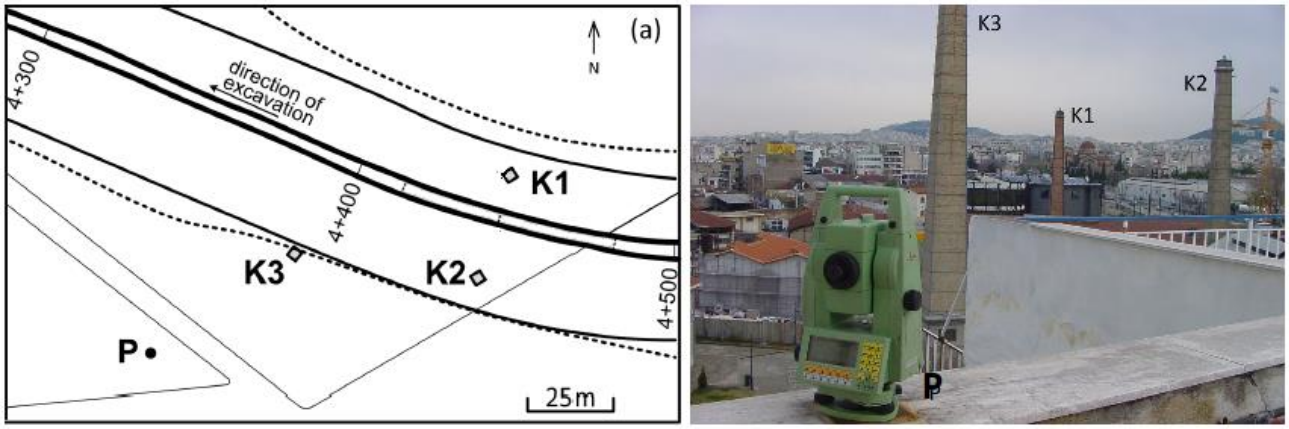

Figure 1: Left: Location map of the Technopolis area on which the tunnel and its influence zone are shown. The location of the three chimneys K1, K2 and K3, and of the monitoring point P are also shown. Right: View of the three chimneys from the fixed monitoring point P.

Ground subsidence at Sepolia area

Extension of the Athens Metro from Sepolia to Ag. Antonios met the Athenian schist and alluvia (locally overlying) and the excavation technique applied was mechanical excavation using a TBM.

The monitoring project of the ground and structures was based on systematic leveling of hundreds of control points on the ground surface and buildings within the assumed area of influence above the tunnel opening. The recorded total ground subsidence, shown in Figure 2, forms contours with higher values reaching 24mm above the tunnel axis, a pattern that confirms the Gaussian trough model. However, the pattern of ground subsidence indicates that the settlement trough is not uniform, both at the transversal direction and along the tunnel axis. This is due to three independent reasons: *first*, local conditions, as for instance natural voids in the ground altering the state of stresses at the opening vicinity, *second*, tunnel construction details involving time of installation of the lining, pause of excavations etc.;

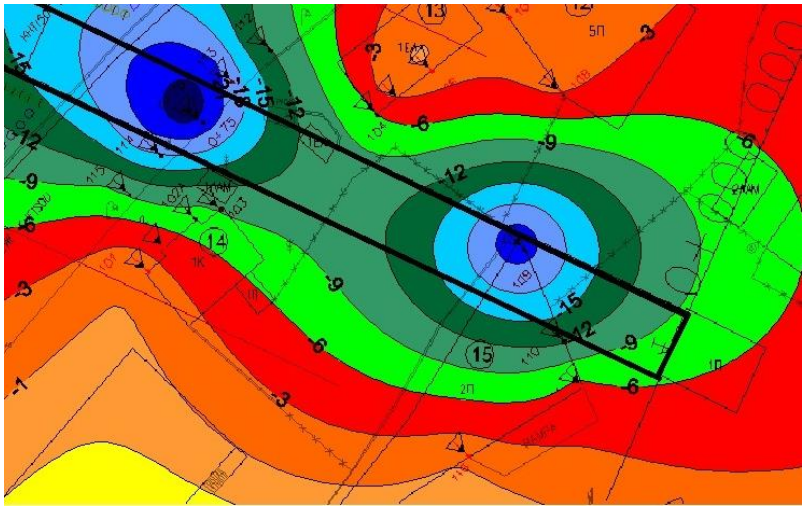

Figure 2: Total ground subsidence observed during the excavation of line 2 of the Athens Metro (at Sepolia area) in contour form. Subsidence ranges up to 24mm. Tunnel is marked by a rectangular.

and *third*, the state of the ground surface, being either a greenfield or built, with the later state consisting of a mixed system of ground and structure increasing the natural stiffness of the ground and consequently diminishing the surface subsidence.

Conclusions

Geodetic monitoring data from two brick chimneys in the Technopolis area during the construction of the Athens Metro suggest that the chimneys suffered a high amount of tilting though without any damage. Later, geodetic monitoring data from the ground subsidence at Sepolia area during tunneling for the Athens Metro reveal that the profile of the settlement trough on the ground surface was not uniform, both at the transversal direction and along the tunnel axis.
The interpretation of the monitoring records of the above projects led to the conclusion that they both deviate from idealized cases, subsequently verifying that urban excavation remains a challenge for geologists and engineers and geodetic monitoring is an invaluable tool tightly linked to safety in constructions.

Acknowledgements

We thank Attiko Metro for providing data which were kept confidential for more than a decade.

References

Burland, J.B., Standing, J.R. & Jardine, F.M. 2001. *Building responces to tunneling – Case studies from construction of the Jubilee Line Extension. London.* Vol. 2, Case studies. London: Thomas Telford.

Harris, D.I., Mair, R.J., Burland, J.B. & Standing, J.R. 1999. Compensation grouting to control tilt of Big Ben Clock Tower. *Geotechnical Aspects of Underground Construction in Soft Ground*, Balkema, 225-232.

Papastamos, G., Stiros, S., Saltogianni, V. Kontogianni, V., 2015. 3-D strong tilting observed in tall, isolated brick chimneys during the excavation of the Athens Metro. *Applied Geomatics* 7, 115-121.

Terzaghi, K. 1942. Shield tunnels of the Chicago Subway. Journal of the Boston Society of Civil Engineers, 29(3), 163-210.

15th International Congress of the Geological Society of Greece
Athens, 22-24 May, 2019 | Harokopio University of Athens, Greece
Bulletin of the Geological Society of Greece, Sp. Pub. 7 Ext. Abs. GSG2019-075

Irrigation water consumptive use changes in South Ptolemais lignite bearing hydrogeological basin (Greece) using NDVI remotely sensed data

G. Louloudis[1], N. Stathopoulos[1]

(1) Public Power Corporation S.A. of Greece, Mines Central Department, 29 Chalkokondili str., 10432 Athens, Greece

The present paper is a good example of using remote sensing data for temporal and spatial land use and in specific vegetation changes determination. In this case study of Sarigiol basin (South Ptolemais lignite bearing basin, Greece), irrigation water consumption assessment was correlated with the Normalized Difference Vegetation Index (NDVI). For this analysis two satellite images for the dates 26/07/2007 (Landsat-5) and 15/07/2018 (Landsat-8) were used.

Landsat-5 and Landsat-8 satellite images consist of quantized and calibrated digital numbers (DN) representing the multi-spectral image data. In order for the images to be appropriately used in various applications and analyzes, digital pixel values must initially be converted to Reflectance or Radiance values at the Top of the Atmosphere (TOA). This process is called Radiometric calibration.

The digital values of the spectral bands of the satellite images in the visible, near and mid infrared range of the spectrum are converted to TOA Reflectance with algorithms provided by the Landsat official website (the calibration coefficients are provided in the metadata file of the images).

The Normalized Difference Vegetation Index (NDVI) indicates the existence of vegetation in the area of interest and is the most widespread and acceptable of vegetation indices. Its calculation is made by utilizing the Near-Infrared (NIR) and Red spectral bands, calibrated in TOA Reflectance values, according to the following equation (Rouse et al., 1973):

$$NDVI = \frac{NIR - RED}{NIR + RED}$$

NDVI ranges between -1 and 1, with the value 0 being the limit of vegetation and the values approaching 1 reflecting the younger and healthier vegetation. Figure 1 and Figure 2 below show the NDVI values of the areas of interest for the dates 26/07/2007 and 15/07/2018. These dates have been chosen for both the quality of satellite images and the fact that for these years there are data, recording electrical consumption of irrigation water pumping, which represent water consumption for various areas of the Sarigiol basin.

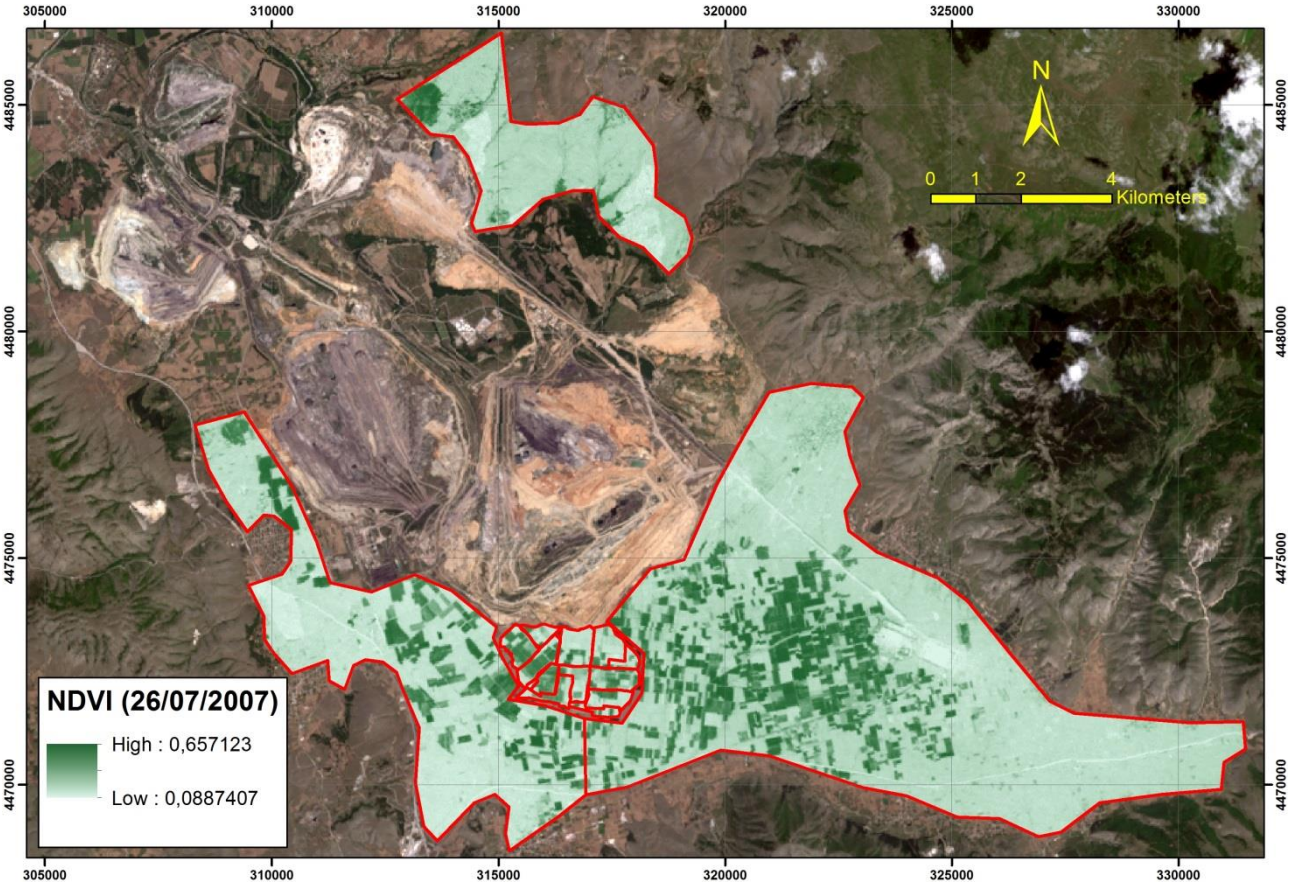

Figure 1. NDVI – July 26, 2007.

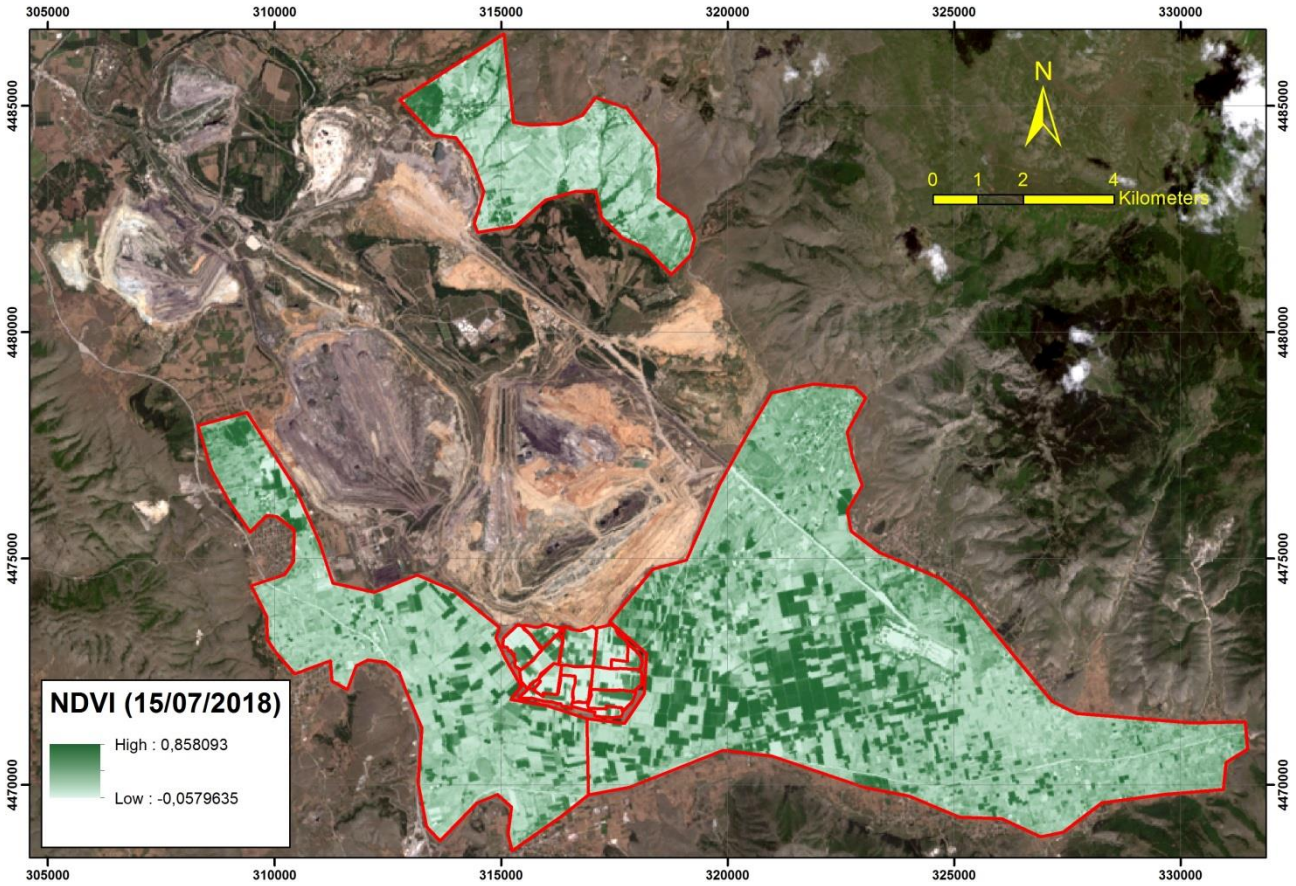

Figure 1. NDVI – July 15, 2018.

The linear regression analysis between NDVI (2007 satellite image) average values for the agricultural areas of interest and known water consumption for these areas (estimated by electric power consumption of irrigation pumps) produced the following equation:

$$y = 1.647 * x - 0.313 \text{ , with } R^2 = 0{,}7896 \qquad \text{(Louloudis et al, 2019)}$$

Where:

y: mean annual water consumption (m^3/m^2)

x: NDVI average values

Additional to this the linear regression analysis between NDVI2007 and NDVI2018 for same regions is the following:

NDVI2018=NDVI2007*0.571+0.286 with R^2=0.85

Applying the previous equations to the average NDVI values (15 July 2018) satellite image the irrigation water consumption was estimated at 35.000.000 m^3 for the year 2018 with mean annual consumption 0.73 m^3/m^2. An analogous estimation was deduced introducing to Blaney Criddle water consumptive use crop coefficient Kc calculated by the following equation:

Kc=1.18*NDVI+0.05 (Masahiro, 2005)

Applying the previous equation to the average NDVI values of 0.57 returns a coefficient Kc equal to 0.72.

The study concludes that there is an annual increase of 1.000.000 m^3 for irrigation use. The results reinforce the arguments of Public Power Corporation of Greece (PPC) that the amount of water that is being pumped for lignite exploitation water inrush and geotechnical protection purposes, is negligible in comparison with the water consumption for irrigation and therefore the water balance of Sarigiol aquifer is mainly affected by farmers water pumping.

References

Rouse Jr, J.W., Haas, R.H., Schell, J.A. and Deering, D.W., 1973. Monitoring the vernal advancement and retrogradation (green wave effect) of natural vegetation.

Gemitzi A., I.V., Angelou 2017. Vegetation changes in Natura 2000 sites in Greece using remote sensing data, 15Th International Conference on Environmental Science and Technology, Rhodes, Greece

Myneni R.B., F.G., Hall, P.J., Sellers and Marshak A.L., 1995. The Interpetation of Spectral Vegetation Indexes. IEEE Transactions on Geoscience and Remote Sensing

Koumantakis J., K., Lioni, 2012. Groundwater Sarigiol Kozani basin potential with to South lignitebearing Mine Field. Third part Present state of groundwater resources in Sarigiol, NTUA, Athens.

Louloudis G., N.Stathopoulos, G., Kasfikis, 2019. Special hydrogeological study of Ptolemais Mines, PPC Internal Report, Athens.

Masahiro T., R., Allen, and Trezza R., 2005. Calibrating Satellite Based Vegetation Indices to Estimate Evapotraspiration and Crop coefficients, J. Irrig. Drain Eng., U.S.A.

15th International Congress of the Geological Society of Greece
Athens, 22-24 May, 2019 | Harokopio University of Athens, Greece
Bulletin of the Geological Society of Greece, Sp. Pub. 7 Ext. Abs. GSG2019-086

Thermal Remote Sensing for Water Outflows Detection and Determination of the Role of Lineaments in Underground Hydrodynamics of Evia Island/Central Greece

L. Athanasiadou[1], E. Psomiadis[1], G. Stamatis[1]

(1) Laboratory of Mineralogy & Geology, Department of Natural Resources Management & Agricultural Engineering, Agricultural University of Athens, Iera Odos 75, Athens, Greece, karkjul83@gmail.com

Abstract

The coastal karst system of Evia Island, which is developed due to the extended presence of carbonate formations, discharges into the sea in many different locations having a direct relation to the tectonic system of the area. Thermal infrared remote sensing has been proved its capability in monitoring thermal differentiations of coastal water plumes. The aim of this work is to locate the fresh water outflows through remote sensing and specific with the use of Landsat's 8 thermal images and how this karstification process is controlled by the lineaments of the area.

Introduction

The study area is the island of Evia, which extends along the South-Eastern mainland of Sterea Hellas in Central Greece; covers an area of 3684 Km^2. Part of the Evia Island's is covered by carbonate formations creating a coastal karst base level which is a consequence of Alpine Orogeny's tectonic movements and of the vertical eustatic movements in the Quaternary period. Coastal aquifers have the tendency to discharge their subsurface flow into the sea through coastal or submarines springs, which appear in tectonic discontinuities.

Having as a goal to detect and map this significant groundwater discharge Landsat-8 (L8) thermal infrared (TIR) data have been used for monitoring of the cold-water plume patterns in the coastal areas (Gibbons *et al*., 1989). The thermal infrared bands of L8 provide temperature measurements at a spatial resolution of 30 m and permit the study of surface temperature characteristics (Parcharidis *et al.,* 1998). It is known that various surface objects reflect the radiation in different ways depending on surface properties. The use of thermal bands is based on the fact that all physical surfaces absorb the electromagnetic radiation according to their texture, their orientation and their heat capacity and they emit it accordingly to the environment (Parcharidis *et al.,* 1998; Migiros *et al*., 2005).

Geological setting of the study area

The tectonic evolution of the Evia region and its surroundings has formed the geomorphology of the island. The intense tectonic movements during the Quaternary period as well as the consequence of Alpine orogenic activities were leaded to strongly karst development. Coastal and submarines karst springs were revealed in many areas of Evia (Katsikatsos *et. al.,* 1976b). From geological point view, Evia consists of the following units (Katsikatsos, 1992): (a) The unit of Central and Northern Evia and Skyros belong to Pelagonian zone which overthrust on the unit of Southern Evia and is composed of: 1) Paleozoic crystallized formations, 2) Neo-Paleozoic semi-metamorphosed clastic formations, 3) Formations of Lower-Middle Triassic (clastic formations, volcanic rocks and limestones), 4) Limestones of Middle – Upper Jurassic, 5) Masses of ophiolites that are overthrusted on the Upper Cretaceous limestones and 6) Flysch sediments, (b) The unit of Almyropotamos consists of Mesozoic to Middle-Eocene coarse-grained marbles of great thickness, passing upwards into metaflysch and schists intercalate in the entire thickness of these marbles, (c) The unit of Southern Evia which is metamorphosed and overthrust on the flysch of Almyropotamos unit and Comprise: 1) Tsakaioi unit consisting of schist and amphibolite including large bodies of serpentine, 2) Styra unit consisting of thin plate marble, sipoline, quartizite and amphibolitic schist and 3) Ochi unit is consists of glaucophane schist, large bodies of amphibolite and manganese microquartzite. Moreover, ophiolitic rocks were developed at the base of the Styra – blueschist nappe on top of the Mesozoic – Eocene unit of Almyropotamos (Papanikolaou, 2009) and (d) The Post alpine sediments which include Alluvial and Neogene sediments.

Materials and Methodology

The geospatial data that were used for the research was: 1) 18 topographic maps at 1:50.000 scale of the Hellenic Geographic Service, 2) 12 geologic maps at 1:50.000 of Institute of Geology and Mineral Exploration, 3) satellite images of Landsat 8 with various dates from 2013 to 2018, and 4) image analysis software's (ENVI v.5.5 - Harris Geospatial Solutions, USA and European Space Agency and ArcGIS v.10.5.1, Environmental Systems Research Institute, Redlands, CA, USA). Thermal images were processed using ENVI program for conversion DN to temperature (Celsius degrees), following the steps outlined in the handbook of USGS (2016). L8 contains two thermal bands (Band 10, high gain and Band 11, low gain) with resolution 30m which record the scattering of infrared radiation from the sea surface. Band 10 was selected, because acquisition in high gain was provided greater radiometric resolution (sensitivity). Brightness temperatures (in Kelvin) are computed as follows (Where: $K1$ and $K2$ = Calibration constants, in Kelvin. ENVI reads these values from the Landsat metadata):

$$T = \frac{K2}{\ln\left(\frac{K1}{L_\lambda} + 1\right)}$$

Then, the new images were imported to ArcMap 10.5.1. Bilinear interpolation, density slicing and temperature supervised classification were used. With the same program, topographic and geologic maps were edited. Finally, combing thermal images with geological maps and tectonic lineaments, sea surface temperature (SST) maps had been created.

Results

The fresh water outflows are more diluted and cooler in relation to sea water, and spread upwards to the sea-surface, creating characteristic water plumes (Astaras, 2001). At thermal images, the darkest tones correlate with the lowest temperatures which are related to the fresh cold water outflows. In many coastal areas of Evia Island (Metoxi, Xalkida, Marmari, Limni, Vlaxia, Vathiremma, Aliveri) the phenomenon was clearly detected. More specifically, at Limnionas-Xalatzas area the appearance and quantity of outflows' is more clear and higher (figure 1).

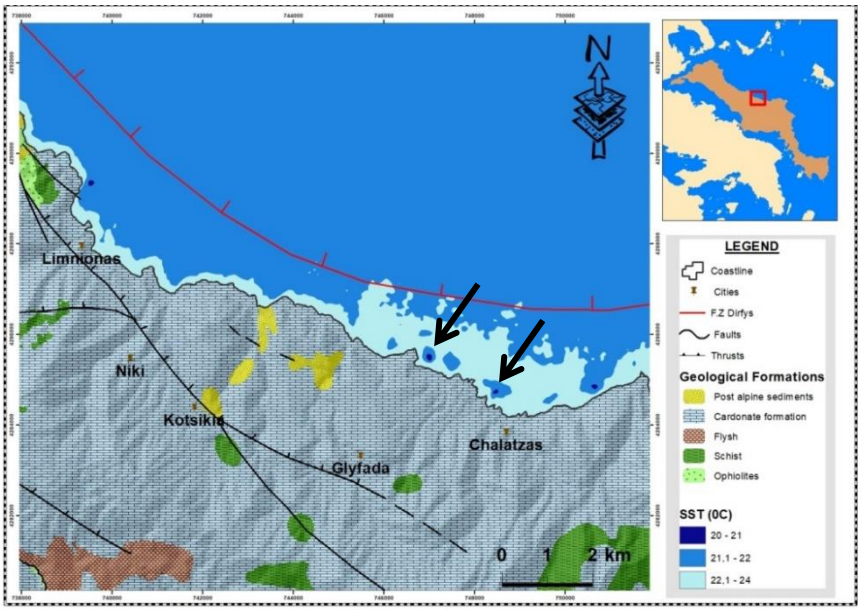

Figure 1. Water outflows mapped on July image of L8 (03/07/2013 – dry period). The outflows are appeared clearly (black arrows show the fresh water outflows).

Conclusion

Remote Sensing is possible to identify fresh water outflows based on thermal anomalies in sea surface. In this research Landsat 8 TIRS (high gain) images were used (from 2013 to 2018) to detect the fresh water plumes into the sea. G.I.S was utilized to combine geologic and topographic maps with thermal images having as a purpose of creating classified sea surface temperature maps (SST) and investigate the relation of water outflows with the tectonic lineaments of the study area.

References

Astaras, T., 2001. The present state remote sensing applications to multitemporal monitoring of the environment, with emphasis to delineation of coastal plain areas suffering from salt water encroachment (intrusion) and to detection of water discharge in coastal rocky (mainly carstic) environment. Future prospects. A keynote lecture presented at the 9th MCM of COST 621 Meeting in Venice, Italy, March 22-24, 2001

Gibbons, D.E., Wukelic, G.E., Leighton, J.P., Doyle, M.J. 1989. Application of Landsat Thematic Mapper data for coastal thermal plume analysis at Diablo Canyon. Photogrammetric Engineering and Remote Sensing 55: 903-909.

IGME - Institute of Geology and Mineral Exploration, Department of Geological Maps, 12 Maps Sheets, 1:50.000 Scales.

HAGS - Hellenic Army Geographic Service, 18 Map Sheets, 1:50.000 Scales.

Katsikatsos, G., Mercier, Vergely, J. P., 1976b. La fenetre d Attique. Cyclades et des fenetres metamorphiques des Hellenides internes (Grece). C.R Acad. Sc. Paris, 283, D., 1614 -1616, Paris

Katsikatsos, G., 1992. Geology of Greece, Study and Teaching, University of Patras.

Migiros, G., Psomiadis, E., Papanikolaou, I., Karamousalis, T., Stamatis, G., 2008. Groundwater coastal discharge of the karstic system of the Mani Peninsula, Southern Peloponnesus-Greece. Proceedings of the 8th International Congress of Hydrogeology, Vol. 1, p. 317-326.

Papanikolaou, D., 2009. Timing of tectonic emplacement of the ophiolites and terrane palegeography in the Hellenides, Lithos, 108, 262–280.

Parcharidis, I., Psomiadis, E., Stamatis, G., 1998. Using Landsat TM images to study karstic phenomenon. ITC Journal, 1998-2, p.118-123, Netherland.

USGS - U.S. Geological Survey, Department of the Interior (2016). Landsat 8 (L8) data users hand book, Version 2.0, EROS Sioux Falls, South Dakota.

15th International Congress of the Geological Society of Greece
Athens, 22-24 May, 2019 | Harokopio University of Athens, Greece
Bulletin of the Geological Society of Greece, Sp. Pub. 7 Ext. Abs. GSG2019-097

New assumptions in regards to the geological setting of the Minyans draining works of the Copais plain

Michaela-Maria Karathanou-Nicholaidi[1], Constantinos Loupasakis[1], Paraskeyas Tsangaratos[1], Elissavet Chatzicharalampous[1]

(1) School of Mining and Metallurgical Engineering, National Technical University of Athens, 9, Ir. Polytechniou str., 15780, Polytechnioupoli, Zografou, Athens, Greece, nicholaidi_micha@hotmail.com

Introduction

For the first time in history lake Copais, the largest lake in Greece (250,000 acres), was partly desiccated by works completed by the Minyans around 2000B.C. Its desiccation has been a very important issue because this was the method used to develop these acres and cultivate tis land, while in parallel avoiding disease caused by stagnant waters of the lake.

The study area

Copais today is a plain with 95 meters average altitude. The plain is occupied by Pliocene deposits., while rocks like neritic limestone, flysch, dolomite and peridotite protrude. The limestone is karstified presenting numerous sinkholes. The rivers which traverse Copais are the Melanas, the Beotian Kifisos, the Erkina and the Potza river.

Ancient draining works

Minyans tried to desiccate part of Copais Lake. They constructed waterproof embankments (from clay and large & small limestone rocks) in order to join B. Kifisos with Melanas river and then limit the water and guide it to the sinkholes in the northeast part of the lake. In this part of the plain there are numerous sinkholes able to drained a big amount of the water. Later, Minyans tried to used two of these sinkholes to construct a tunnel which would have transferred larger amounts of water from the lake, but they never finished the construction. Furthermore, along the boundaries of the lake they constructed more embankments in order to desiccate and cultivate the fertile land which was covered by the lake's water. The areas surrounded and protected by the embankments always included sinkholes for drainage in case of flooding. Castle Gla and Acropolis of Agios Ioannis have been constructed on top of protruding limestone, they were enclosed by walls andthey were having strategic role as storing places of the harvest crop.



Figure 1. Sinkhole which used for entrance of the tunnel

Extra suggestions from those of Knauss's theory

- Knausse's assumption that ancient settlements were located next to castle Gla, don't seem to be valid. The reason is that this place was often flooded. This is apparent from the fact that the settlement is located near the area where the waters of the rivers end up and for this reason castle Gla is located on top of a protruding limestone hill and surrounded by sinkholes excluded from the fortification walls of the castle. In addition, one extra embankment behind the castle, on a higher level- proves that the entire area was flooding.
- There was one more Acropolis (of Agios Ioannis) near the sinkholes where the rivers Melanas and B. Kifisos end up. This acropolis had a similar operation with castle Gla. This ancient Acropolis came up from recent excavations.
- Minyans desiccated parts by protecting them with embankments. As aforementioned this areas always included sinkholes for drainage in case of flooding.



Figure 1. Sinkhole which used for entrance of the tunnel

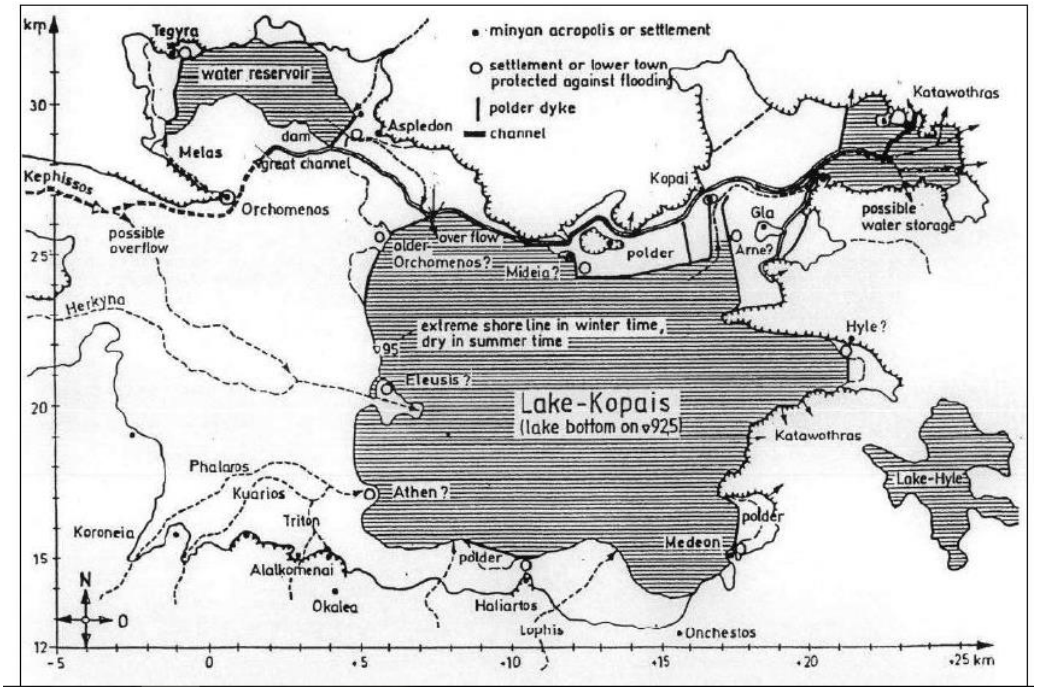

Figure 3. Boiotia, Copais-basin, flooding conditions at the end of the Middle Helladic period (Knauss, 1991)

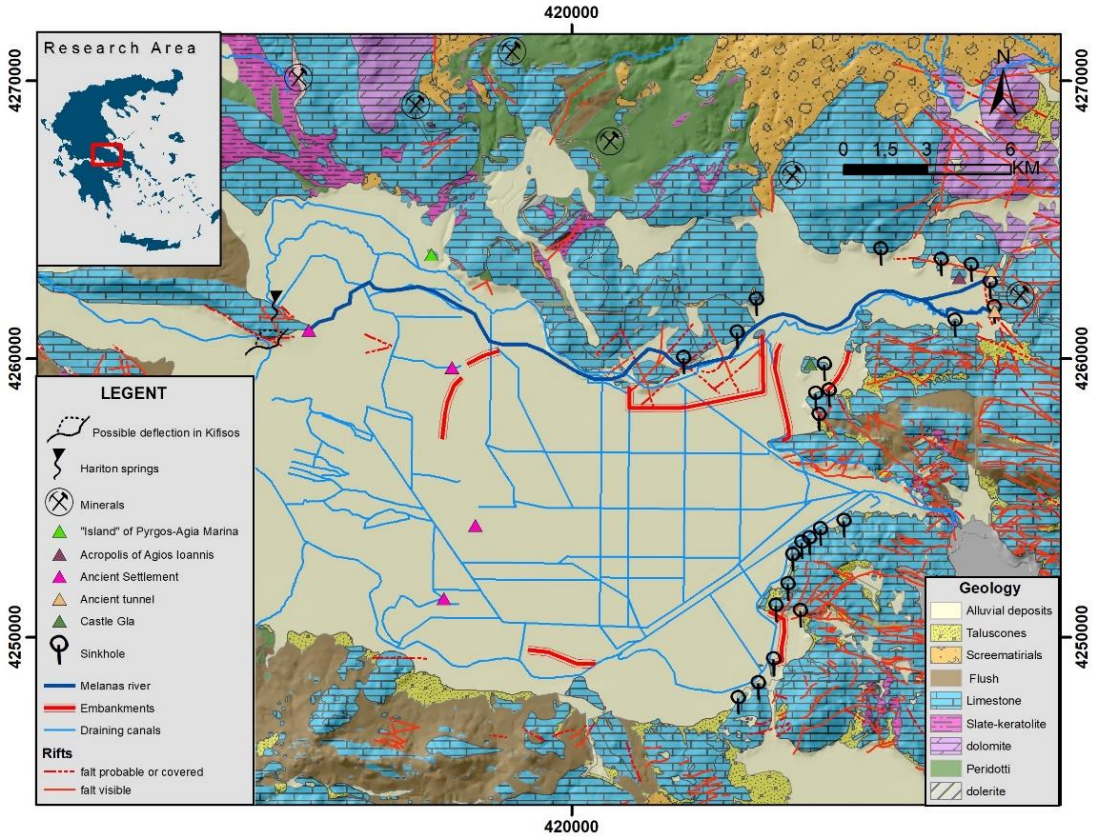

Figure 4. Boiotia-Copais, suggestion about ancient works by Minyans (used maps Atalandi, Vagia & Larymna from I.G.M.E.)

References

Knauss, 1991, Arkadian and Boiotian Orchomenos, Centres of Mycenaean hydraulic engineering, Irrigation and Drainage Systems 5: 363-381. Kluwer Academic Publishers. Printed in the Netherlands

N.Skoulikidis, E.Dimitriou & I.Karaouzas, 2018, Springer-Verlag GmbH Germany, The rivers of Greece, Evolution, Current status and perspectives, Springer

N. Mamassis, S. Moustakas, and N. Zarkadoulas, Representing the operation of ancient reclamation works at Lake Copais in Greece, Water History, doi:10.1007/s12685-015-0126-x, 2015.

I.G.M.E. 1965, 1970, 1978, Geological Map of Greece, Sheets Atalanti, Vagia & Larymna, Scale 1:50.000. IGME Athens.

15th International Congress of the Geological Society of Greece
Athens, 22-24 May, 2019 | Harokopio University of Athens, Greece
Bulletin of the Geological Society of Greece, Sp. Pub. 7 Ext. Abs. GSG2019-098

Nitrate Exchange Capacity of Greek Palygorskite and Sepiolite for their Potential Application in Water Treatment

C. V. Lazaratou[1], I. E. Triantafyllidou[2], D. Vayenas[2], D. Papoulis[1]

(1) Department of Geology, University of Patras, 26504 Patras, Greece, lachristie93@gmail.com
(2) Department of Chemical Engineering, University of Patras, 26504 Patras, Greece

Introduction

Palygorskite and sepiolite are the only 2:1 clay minerals characterized by fibrous morphology and 2:1 ribbons structure. Both minerals have similar structures, except from palygorskite's shorter b dimension where two Si-O group chains exist, instead of three in case of sepiolite (Moreira et al., 2017). The change in the orientation of the chains is responsible for the interruption of the octahedral layers, and that leads to the existence of empty channels. In order to have charge balance, in the free space can enter variable amounts of either cations or anions which can be exchanged along with zeolitic water (Galan 1996). Their structure, basal spacing as well as crystal morphology and dimensions are the main causes of their high specific surface area and adsorption capacity, which in combination with their abundance and low – cost, enable them as cost-effective adsorbents for a variety of contaminants from water systems.

The aim of this study is the Anion Exchange Capacity (AEC) evaluation of Greek fibrous clay minerals, in order to be exploited for water treatment, as environmental-friendly and low-cost adsorbents. Initial experiments to determine the effect of nitrate initial concentration, adsorbent's dosage and contact time have been carried out. Specifically, palygorskite from Grevena (Western Macedonia, Greece) and sepiolite from Corinth (Peloponnese, Greece) are used for the crucial nitrate removal from water without any modification that increases cost. Nitrate (NO_3^-) presence in groundwater is quite common, especially at the areas with nitrogenous fertilizers oversupply, as almost the 20% of the N-fertilizers leaches into the groundwater, in nitrate form (Lu et al., 2019), making it a widespread water contaminant. Nitrate in high concentration levels consist a threat to the ecosystem, as can contribute to eutrophication and infant's disease methaemoglobovinemia (Capodici et al., 2018), making its remediation with cost-effective and non-toxic methods a significant topic.

Materials and Methods

Palygorskite from Ventzia basin (Grevena/Western Macedonia, Greece) and sepiolite from Solomos village (Corinth/ Peloponnese, Greece) were used for a series of batch experiments. The particular palygorskite deposit is exploited by Geohellas S.A. and was diagenetically formed through the smectite - silica rich solutions interaction (Kastritis et al., 2003) while the sepiolite occurrence was recently discovered by Papoulis et al., (2018) between WNW- and ENE-trending active faults. Samples were fractionated in order to obtain powder sedimentation (< 50μm) and were characterized by XRD, FTIR, SEM and BET that conducted at several laboratories of University of Patras.

Batch kinetic experiments were carried out to examine the adsorption process, for various adsorbent dosage (i.e. 0.4, 0.8, 1.6 and 4 g) in various NO_3^- concentrations (i.e. 15, 30 and 50 mg/L) for both palygorskite and sepiolite. 250 ml conical flasks were employed, filled with 200 ml of the examined NO_3^- concentration and adsorbent dose and were agitated mechanically for 40 min. Samples were taken in various time intervals (i.e. 2.5, 5, 10, 15, 20, 30 and 40 min). The experiments were conducted in room temperature and there was no pH adjustment. Samples were centrifuged at 5.500 rpm for 3 min and filtered through 0.45 μm Whatman filters. For every time interval, and using the proper sample dilution, NO_3^- concentration was measured to a spectrophotometer (Hach-Lange UV-VIS) using a calibration curve at 220 nm according to the Standard Methods for the Examination of Water and Wastewater (APHA, 1998). The removal efficiency (%) of each clay mineral was determined based on equation (1).

$$\textit{Removal efficiency} = \frac{c_0 - c_f}{c_0} \% \quad (1)$$

Where c_0 is the initial nitrate concentration and c_f is the final nitrate concentration after adsorption process.

Results

Palygorskite X-Ray Diffraction pattern showed all its characteristic peaks including at10.4 and 20 Å, meanwhile the 6 Å peak is referred to the smectite mineral saponite which co-exist with palygorskite at Grevena's deposit. Sepiolite presents no impurities at all, or at least bellow detection limits, as it can be seen by its diffraction pattern with its characteristic peak at 7.2 Å. The FT-IR spectra confirmed XRD results. According to SEM observations the clay minerals' fibrous morphology was verified, while according to BET analysis the specific surface area for palygorskite and sepiolite was estimated at 210 m^2/g and 234 m^2/g respectively. Batch kinetic experiments, for both fibrous clay minerals, indicated similar characteristics and behavior for nitrate removal. Specifically, in case of palygorskite the increase of adsorbent's dosage at 4 g, compared to 0.4 and 0.8 g, results to an increased nitrate removal for all the

examined concentrations. Specifically for 15 mg/L, minimum and maximum removal reached up 8 and to 20% respectively. Nevertheless the maximum nitrate removal for all dosages is not contact time depended, as in all cases after 15 minutes the adsorbed nitrate concentration almost reaches plateau (Fig. 1a). With initial nitrate concentration increase to 30 and 50 mg/L the nitrate removal capacity of 4 g palygorskite is degrading to 17.6% and 12% respectively, while the other masses' efficiency is even lower. Sepiolite presents similar behavior with palygorskite, as the 4 g dosage is the preferable mass to eliminate all studied nitrate concentrations within 15-20 min. However, sepiolite found to be a better adsorbent for the higher concentration levels of the pollutant, as the 22.6 % and 24.2% of 30 mg/L and 50 mg/L nitrate respectively can be removed, compared to the 15% removal for 15 mg/L nitrate (Fig. 1b).

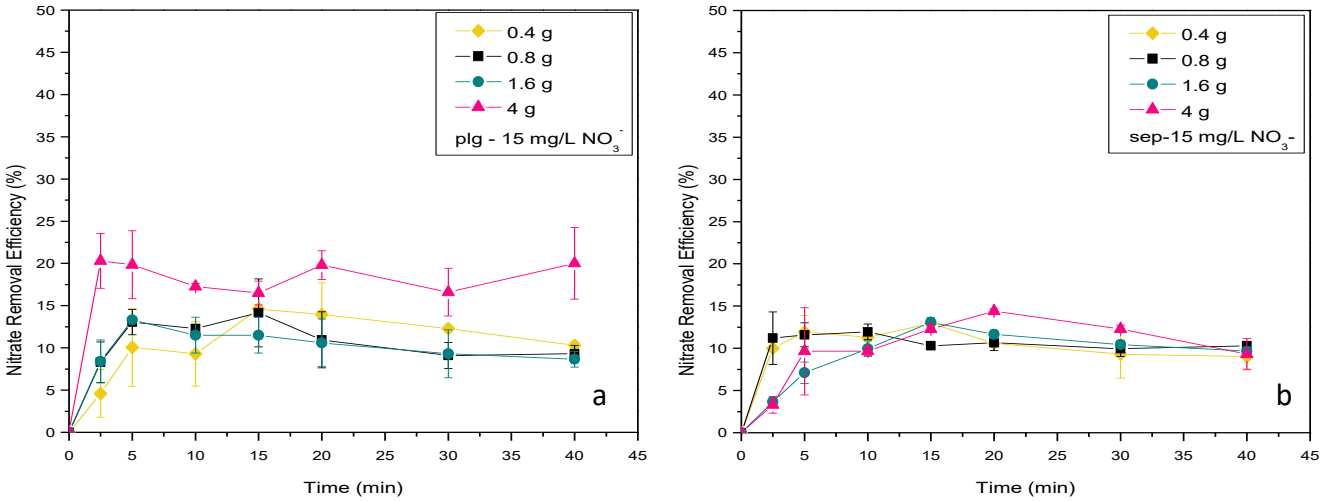

Figure 1. Nitrate removal at 15 mg/L for all dosages for a) palygorskite and b) sepiolite.

Conclusions

Nitrate consist a threatening pollutant for humans health and marine ecosystems, making its removal or degradation from water systems crucial. Palygorskite from Grevena (Greece) and sepiolite from Corinth (Greece) proved to be promising anionic adsorbents depending on the pollutant's initial concentration, the adsorbent dosage and contact time. Palygorskite is more efficient adsorbent at low nitrate concentration levels, in contrast to sepiolite, which nitrate removal efficiency is positively correlated with the initial concentration increase. The adsorbent's mass had impact especially on palygorskite's removal capacity and less on sepiolite's, as the highest examined mass were the most efficient in both cases within 15-20 minutes. However, the maximum removal efficiency through adsorption process for both palygorskite and sepiolite found to be not sufficient for the main nitrate removal mechanism. The possible application of Greek clay occurrences seems promising for pre- or post- water treatment, in combination with more effective but costly technologies, such as biological denitrification or electrochemical methods, in order to gain nitrate remediation via a hybrid and possible more efficient system. Nevertheless, further study needs to be conducted regarding co-existing ions, and clay minerals potential modification or combination with other materials.

Acknowledgements

Special thanks to laboratory of Environmental System's team, at Chemical Engineering Department, University of Patras for their help in batch experiments and the UV-VIS analysis.

References

APHA, AWWA, WPCF.1998. Standard Methods for the Examination of Water and Wastewater, 20th edn. Washington, DC.

Capodici, M., Avona, A., Laudicina, V. A., & Viviani, G. (2018). Biological groundwater denitrification systems: Lab-scale trials aimed at nitrous oxide production and emission assessment. Science of the Total Environment, 630, 462-468.

Galan, E. (1996).Properties and applications of palygorskite-sepiolite clays, Clay Minerals, 31(4), 443-453.

Kastritis, I.D., Mposkos, E. & Kacandes, G.H., (2003).The palygorskite and Mg-Fesmecite clay deposits of the Ventzia basin, western Macedonia, Greece. In Eliopoulos et al. (Eds), Millpress, Roterdam, Mineral exploration and Sustainable Development-Proceedings of the 7th SGA Meeting. 891-894.

Lu, J., Bai, Z., Velthof, G.L, Wu, Z., Chadwick, D., & Ma, L. (2019).Accumulation and leaching of nitrate in soils in wheat-maize production in China. Agricultural Water Management, 212, 407-415.

Moreira, M. A., Ciuffi, K. J., Rives, V., Vicente, M. A., Trujillano, R., Gil, A., de Faria, E. H. (2017). Effect of chemical modification of palygorskite and sepiolite by 3-aminopropyltriethoxisilane on adsorption of cationic and anionic dyes. Applied Clay Science, 135, 394-404.

Papoulis, D., Panagiotaras, D., Tsigrou, P., Christoforidis, K. C., Petit, C., Apostolopoulou, A., Koukouvelas, I. (2018).Halloysite and sepiolite - TiO_2 nanocomposites: Synthesis characterization and photocatalytic activity in three aquatic wastes. Materials Science in Semiconductor Processing, 85, 1-8.

15th International Congress of the Geological Society of Greece
Athens, 22-24 May, 2019 | Harokopio University of Athens, Greece
Bulletin of the Geological Society of Greece, Sp. Pub. 7 Ext. Abs. GSG2019-105

Hydrogeochemical and hydrodynamic characterization of Aghia Sub-Basin, Thessaly, Central Greece

E. Tziritis[1], V. Pisinaras[1], C. Doulgeris[1], K. Skordas[2], A. Panagopoulos[1]

(1) Hellenic Agricultural Organization "Demeter", Soil and Water Resources Institute, Sindos 57400, Thessaloniki, Greece, e.tziritis@swri.gr
(2) Department of Ichthyology and Aquatic Environment, School of Agricultural Sciences, University of Thessaly, Fitokou street, 38446 Volos, Greece.

The Aghia Sub-Basin (ASB) is located at the eastern boundary of the River Pinios Basin and covers an area of approximately 45 km^2 (Fig. 1). According to the hydrolithological map presented in Fig. 1b, there are three dominant hydrolithological units identified: 1. Fractured formations of low- to medium-permeability (HA2) consisted mainly of gneiss, gneiss-schists, and ultrabasic formations (amphibolites and prasinites). Within these units, groundwater flow occurs predominantly through their tectonically driven fractures (secondary porosity) and to a lesser extent through the primary porosity. 2. Alluvial deposits of variable permeability (HP1) consisted mainly of recent deposits of variable texture, including lateral screes that fill the basin at the southern plain part of Aghia sub-basin watershed in which a groundwater system of medium potential is formed. 3. Old talus cones and scree of variable permeability (HP4) favor direct infiltration of precipitation compared with the alluvia.

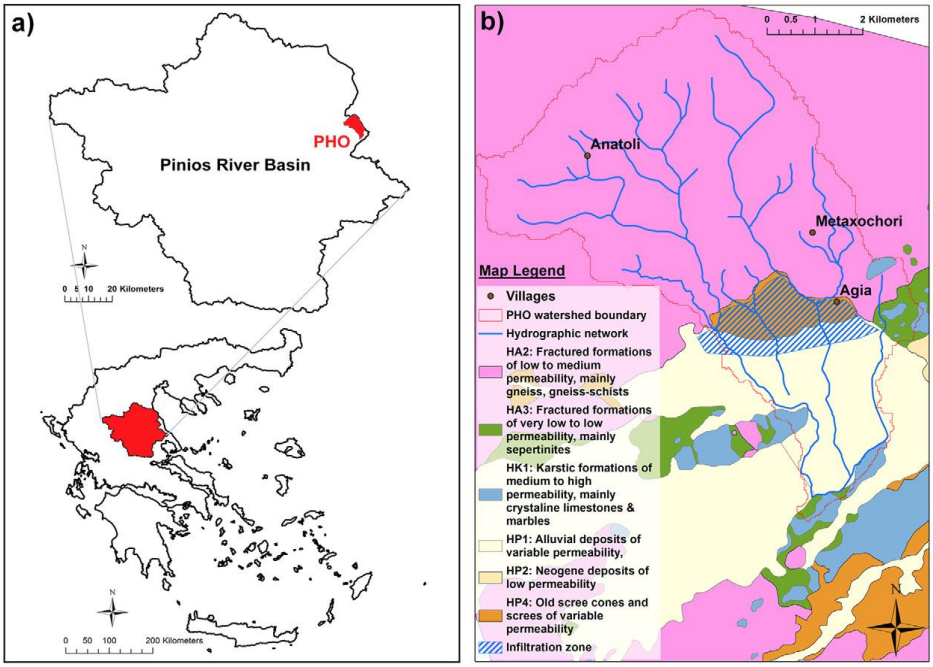

Figure 1: Location of ASB and hydrolithological map (after Pisinaras et al., 2018)

According to previous hydrogeological studies (Hellenic Ministry of Agricultural Development and Food, 2012), lateral crossflows from the adjacent weathered crystalline rock formations at the northern parts of the basin (HA2) and the extensive transition zone that has developed along the same front of the basin (HP4), constitute the major groundwater recharge mechanism of the aquifer system that develops within the alluvium (HP1). Direct recharge through precipitation is important at the infiltration– transition zone (HP4) and occurs over the entire extent of the basin; however, its importance is reduced considerably there. The mountainous weathered crystalline rock formations (HA2) are not used for water production, and therefore no production wells exist in this system.

The overexploitation of groundwater reserves, especially along the downstream southern part of the area, is indicated by the fact that the localized artesian phenomena reported in the past decades (Hellenic Ministry of Agricultural Development and Food, 2012) do not occur any longer, except for a limited number of cases and periods over exceptionally wet hydrological years. Regarding water resources management status, irrigation constitutes the major water consumer for the watershed, and demands are almost exclusively covered by groundwater. According to Tziritis et al. (2016), agriculture constitutes a dominant factor for the hydrogeochemical conditions of the wider area, as reflected by the locally high NO_3 concentrations observed in the alluvial groundwater system. Moreover, the irrational irrigation practices applied, are reflected by locally increased salinization, which is attributed to irrigation water return.

Two groundwater sampling campaigns (n=24) were conducted in June and October 2017, corresponding to the wet and dry hydrological periods, respectively. Totally 22 parameters (physicochemical, major-minor ions, trace elements) in situ and at the accredited laboratory of the Soil and Water Resources Institute (SWRI). Results (median values) revealed

that groundwater is circum-neutral (pH=7.3), and EC is 508 μS cm–1, indicating good quality for irrigation water. The dominant cation is Ca^{2+}, followed by Mg^{2+} and Na^{+}, in descending order. The dominant anion in groundwater is HCO_3^-, followed by NO_3^- and Cl^-. The presence of nitrates among the dominant anions is indicative of the anthropogenic impact due to agricultural activities; however, its median concentration is relatively low (17 mg L^{-1}), and the impact is mainly observed locally (concentrations up to 86.5 mg L^{-1}). The concentrations of heavy metals/metalloids are low and fall within the typical margins of natural groundwater (Hem, 1985). No significant variations were observed among the two sampling periods. Nevertheless, sulfates are rather low in the first period, probably indicating a temporal reducing environment affecting their concentration.

All groundwater samples have the same water type (Ca-HCO_3), which is evident from their common hydrodynamic characterization, which classifies them as recharge waters. Their common hydrogeochemical signature is also clearly identified in the Piper diagram in Fig. 2. These observations are in line with the geological and hydrogeological regime of the ASB, confirming that the area constitutes a recharge window, where the lateral crossflows from the metamorphic bedrock recharges the alluvium plain through a general north–south direction. Along the same direction, EC values and NO_3^- concentrations increase with distance from the transition zone. Hence, EC values vary from 0.49 to 0.62 mS cm–1 and NO_3^- concentrations from 8.8 to 31.5 mg L^{-1}, which may suggest the contribution of excellent water quality lateral crossflows from the transition zone to the alluvial groundwater system.

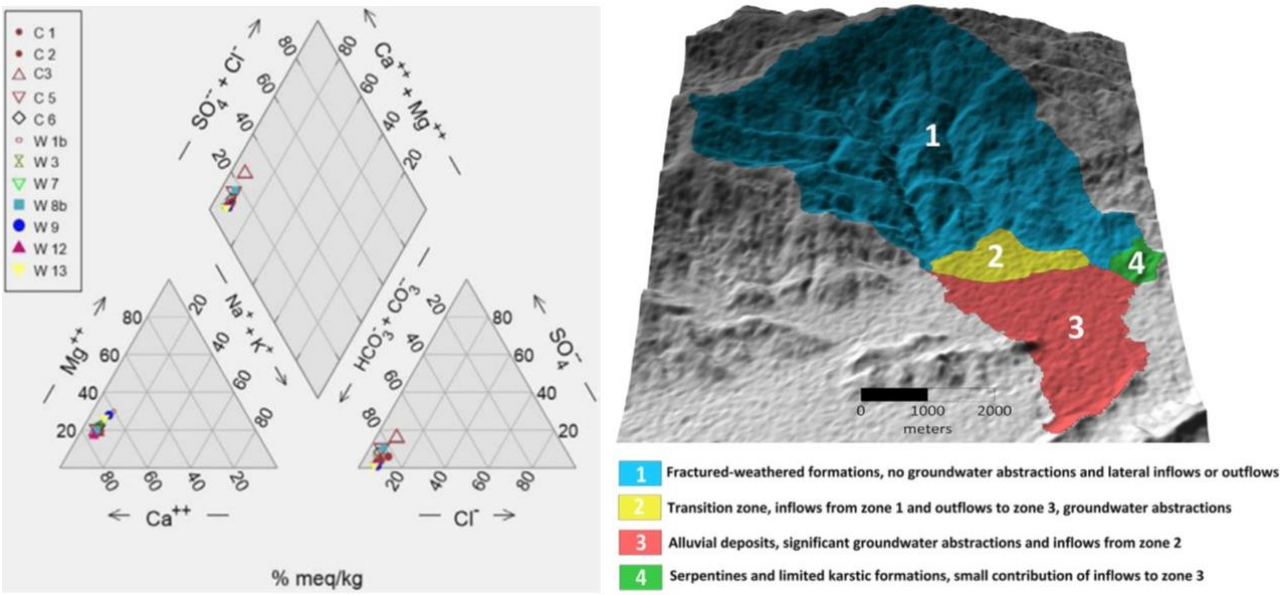

Figure 2: Piper diagram for groundwater samples (average values of periods) and spatial distribution of the major hydrodynamic zones in ASB.

Based on the calculated saturation indices (logQ/K) for the main mineral phases expected, calcite and dolomite are oversaturated in all samples; hence, these phases are the main precipitates that are deposited in the aquifer matrix. The molar ratios of Ca/HCO3 of all samples are <0.5 (range 0.28–0.38). Considering the overall geological regime, the primary source of calcium is possibly attributed to the ion exchange process (Hounslow, 1995; Tziritis et al., 2016). Specifically, Na+, which is enriched in solute due to metamorphic rocks, exchanges with Ca2+, which is hosted in Ca-rich feldspars such as anorthite (CaAl2Si2O8). This process also explains the relatively low Na+ concentrations in groundwater, contradictory to those expected according to bedrock geology. Calcium may also originate from the weathering of Ca-rich silicate minerals (e.g., diopsidic pyroxene [CaMgSi2O6]), which are abundant in the metamorphic bedrock.

Based on the combined evidences of hydrogeology and hydrogeochemistry, 4 different hydrodynamic zones (Z) may be identified (Fig.2). Specifically, Zone 1 is composed by fractures-weathered formation, with no groundwater abstractions and lateral crossflows. Zone 2 is a transition zone with groundwater abstractions, which receives inflows from Z1 and discharges outflows to Z3. Zone 3 is consisted of alluvial deposits, with significant groundwater abstractions and inflows from Z2. Finally, Zone 4 is mainly composed by serpentines and limited karst formations and a relatively small contribution of inflows to Z3.

References

Hellenic Ministry of Agricultural Development and Food. 2012. Preliminary engineering and geological study for the construction of a reservoir in the Prefecture of Larissa, Agiokampos "Livadotopos" site, Athens

Hem, J. 1985. Study and interpretation of the chemical characteristics of natural water. U.S. Geological Survey, Water Supply Paper 2254.

Tziritis, E., K. Skordas, and A. Kelepertzis. 2016. The use of hydrogeochemical analyses and multivariate statistics for the characterization of groundwater resources in complex aquifer system. A case study in Amyros River basin, Thessaly, central Greece. Environ. Earth Sci. 75:339. doi: 10.1007/s12665-015-5204-y.

Hounslow, A.W. 1995. Water quality data—analysis and interpretation. CRC Press.

Pisinaras, V., Panagopoulos, A., Herrman, A., Bogena, H.R., Doulgeris, C., Ilias, A., Tziritis, E., Wendland, F. 2018. Hydrologic and geochemical research at Pinios Hydrologic Observatory: Initial results. Vadose Zone Journal 17:180102, https://doi.org/10.2136/vzj2018.05.0102

15th International Congress of the Geological Society of Greece
Athens, 22-24 May, 2019 | Harokopio University of Athens, Greece
Bulletin of the Geological Society of Greece, Sp. Pub. 7 Ext. Abs. GSG2019-107

The Use of Environmental Stable Isotopes at the Tirnavos Alluvial Basin (Central Greece)

I. Vrouhakis[1,2], E. Tziritis[2], A. Panagopoulos[2], C. Kulls[3], G. Stamatis[1]

(1) Agricultural University of Athens, Sector of Geological Sciences, Mineralogy and Geology Laboratory, Iera Odos 75, Athens, Greece, ivrouhakis@yahoo.gr
(2) Hellenic Agricultural Organization "Demeter", Soil and Water Resources Institute, Sindos 57400, Thessaloniki, Greece
(3) Technische Hochschule Lubeck, Monkhofer Weg 239, Lubeck, Germany

Introduction

Oxygen and hydrogen isotopes are widely used as conservative groundwater tracers because their values remain constant as long as there are no phase changes or fractionation along the flow path (Clark and Fritz, 1997). The isotopic composition of precipitation depends on local conditions and various environmental factors such as temperature, distance from the sea or continentality, latitude, altitude, amount and season (Sharp, 2007). The composition of these tracers reveals useful information such as the origin and mixing of groundwater, the degree of mixture of surface, meteoric and ground water, the salinization of groundwater and others. $\delta^{18}O$ values can be used to identify the source of groundwater, as well as to determine the mean altitude of recharge (Matiatos *et al*., 2010). In order to facilitate interpretation of data the expected mean $\delta^{18}O$ value of direct recharge at the local altitude can be plotted (Leibundgut *et al*., 2011).

Geological-hydrological characteristics

Tirnavos sub-basin forms the north-eastern part of the eastern Thessaly plain of Central Greece. It is filled by Quaternary alluvial deposits that are bounded along the SW part of the basin by Neogene marls and sandy-clay deposits. At the western margins karstified marbles of middle-upper Cretaceous crop out. The crystalline bedrock of the Pelagonian unit composed by Mica-schists of Upper Paleozoic and Gneisses of Paleozoic age form the northern boundary of the sub-basin (Figure 1). Two major springs emerge at the contact of the karstified system with the alluvial deposits. Pinios and Titarisios Rivers flow across the sub-basin which hydrologically is part of the Pinios River Basin. The Quaternary deposits host an unconfined aquifer near the talus cones of Titarisios at NW, which towards the central parts of the basin converts to a system of a phreatic and a deeper confined aquifer, separated by a sequence of clay layers (Panagopoulos, 1996). Despite the limited potential of the phreatic aquifer nowadays, its importance is paramount as it forms an effective buffer zone that protects the confining units from deep percolation of anthropogenic origin pollutants, especially of agricultural origin. Also, the marbles of the west margin of the basin host a karstic aquifer of great potential. This karstic aquifer and the Titarisios River are the main recharge sources of the alluvial basin aquifer system. Agriculture is the dominant land use in the study area, covering approximately 16.000ha (71% of the gross area) (Alexandridis *et al*., 2014).

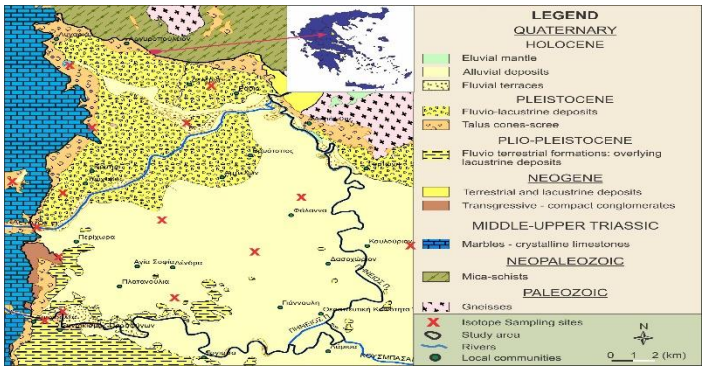

Figure 1. Geological map of the study area (based on Panagopoulos, 1996)

Methods and Results

The purpose of this study is to examine the isotopic composition of the typical alluvial aquifer system of Tirnavos sub-basin and compare it with the isotopic composition from previous studies for the wider region. Sampling was performed at April (isotope and hydrochemical analyses) and September (isotope analyses) of 2018, that are representative for the dry and wet hydrological periods, respectively. Sampling network consisted of 34 wells, 2 springs and 6 surface water sites from Pinios and Titarisios Rivers. Fifteen (15) and eleven (11) samples were collected for isotopic analyses over the first and second periods, respectively. Based on the analytical results, the Local Groundwater Isotope regression Line (LGIL) was compiled and plotted along with the Global MWL, Greek MWL and Thessaly MWL, as depicted in Figure 2A. Isotope values of $\delta^{2}H$ and $\delta^{18}O$ are expressed as the difference between the measured ratios of the sample and reference divided by the measured ratio of the reference, which is expressed as the VSMOW values (Vienna-Standard Mean Ocean Water). The isotopic ratio of $\delta^{18}O$ in the study area ranges between -9.8‰ and -6.9‰ with an average value of -8‰. This value almost coincides with the average value recorded from spring waters of Thessaly

which is -8.29‰ (Dotsika *et al*., 2010). Similarly, the isotopic ratio of δ^2H ranges between -66.2‰ and -47.5‰ with an average value of -51.3‰ which is almost the same with the average value recorded in Thessaly which is -51.1‰, on the basis of the aforementioned reference. Based on these observations, the isotope composition of groundwater for Tirvanos sub-basin seems to fit perfectly with the obtained levels from the previous study on Thessaly region. The function that express the LGIL which is $\delta^2H=6.71\delta^{18}O$ +2.09 compared to Thessaly MWL ($\delta^2H=6.48\delta^{18}O$ +1.7) presents similar slope (6.71 and 6.48) and little higher value of the d-excess (2.09 and 1.7). Generally, the deuterium excess is primarily controlled by kinetic effects associated with evaporation of water at the surface of the oceans or inland and increases with an increase in the moisture deficit of the oceanic air masses (Sharp, 2007). Differences in d-excess arise as a consequence of varying temperature, relative humidity and wind speed at the sea surface, where global atmospheric moisture mainly originates, as well as from admixture of recycled continental vapour (Dotsika *et al*., 2010, Tziritis, 2011). Hence, the value of d-excess (close to 2) in the study area compared to the GMWL value (10) could probably be attributed to the environmental conditions. The projection of δ^2H and $\delta^{18}O$ ratios for surface and ground waters in a common plot (Figure 2B) defines the Local Surface Isotope regression Line for the study area (y=5.06x-9.95). Although the number of surface water sites could have been larger, the slope of the regression line (5.06) and the d-excess value (-9.95) do indicate the effect of the evaporation on these surface receivers. It could also be argued that due to the difference in the isotopic ratio between groundwater and surface water, there seems to be no (or not significant) hydraulic interaction between them.

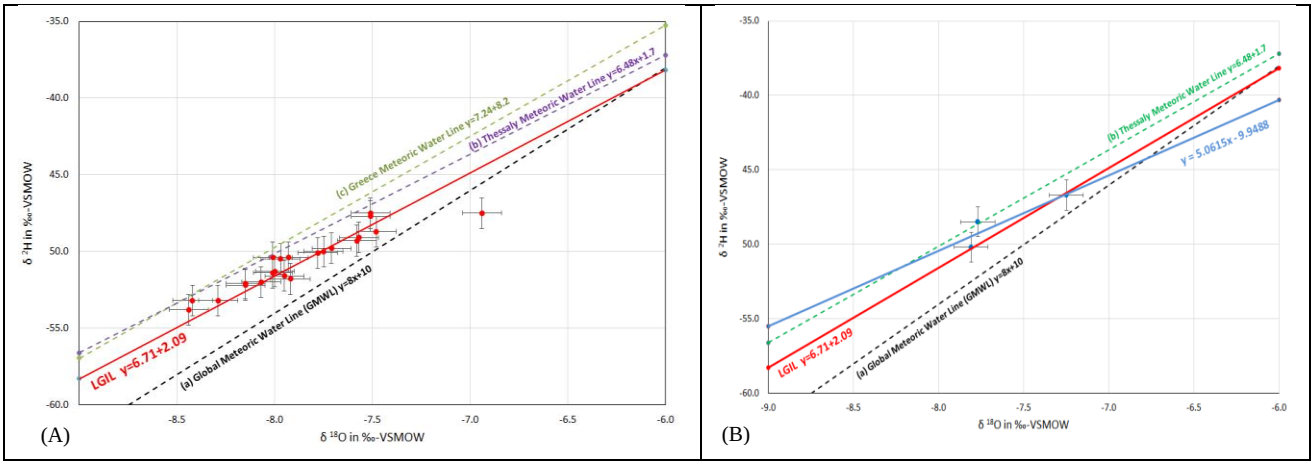

Figure 2. (A) Local Groundwater Isotope regression Line (Tirnavos sub-basin) along with (a) GMWL (Craig, 1961), (b) Thessaly Meteoric Water Line (Dotsika et al., 2010) (c) Greece Meteoric Water Line (Argiriou & Lykoudis, 2006) (B) Local Groundwater Isotope regression Line compared to Local Surface Isotope regression Line (blue line)

Conclusions

The isotopic composition of Oxygen (^{18}O) and Deuterium (^2H) were defined for the alluvial aquifer system of Tirnavos sub-basin. For this purpose, totally 26 samples for both groundwater and surface waters were collected in two sampling periods. Results were plotted and the Local Groundwater Isotope Line and Local Surface Isotope Line were compiled. The slope and the d-excess values compared to the Thessaly Meteoric Water Line (Dotsika *et al*., 2010) showed no significant deviations; thus, demonstrating that the study area follows the general composition of the wider region isotopic ratio. The low value of d-excess compared to the GMWL value may be attributed to the environmental conditions. Regarding to the Local Surface Isotope Line, the slope of the regression line and the d-excess value show the effect of the evaporation on these surface receptors.

References

Alexandridis, T., Panagopoulos, A., Galanis, G., Alexiou, I., Cherif, I., Chemin, Y., Stavrinos, E., Bilas, G., Zalidis, G., 2014. Combining remotely sensed surface energy fluxes and GIS analysis of groundwater parameters for irrigation assessment. Irrigation Science 32, 127-140.

Argiriou, A. A., Lykoudis, S., 2006. Isotopic composition of precipitation in Greece. Journal of Hydrology 327(3-4), 486-495.

Clark, I.D., Fritz, P., 1997. Environmental Isotopes in Hydro-geology. New York: CRC Press.

Craig, H., 1961. Isotopic variations in meteoric waters. Science 133, 1702-1803.

Dotsika, E., Lykoudis, S., Poutoukis, D., 2010. Spatial distribution of the isotopic composition of precipitation and spring water in Greece. Global and Planetary Change 71(3-4), 141-149.

Matiatos, I., Alexopoulos, A., Zouridakis, N. Use stable isotopes in the determination of the mean altitude of recharge and the investigation of function mechanism of spring waters in Argolis peninsula. 12th Int. Congress of the Geological Society of Greece, Patra, Greece, Volume XLIII, No 4, p.1792.

Leibundgut, Christian, Piotr Maloszewski, and Christoph Külls. Tracers in hydrology. John Wiley & Sons, 2011.

Panagopoulos, A., 1996. A methodology for groundwater resources management of a typical alluvial aquifer system in Greece, School of Earth Sciences. Ph.D. Thesis, University of Birmingham, 46p.

Sharp, Z., 2007. Stable isotope Geochemistry. Pearson Education, USA, pp. 344.

Tziritis, E., 2011. Stable isotope study of a karstic aquifer in Central Greece. Composition, variations and controlling factors. In Advances in the research of aquatic environment, Springer, Berlin, Heidelberg, 193-200.

15th International Congress of the Geological Society of Greece
Athens, 22-24 May, 2019 | Harokopio University of Athens, Greece
Bulletin of the Geological Society of Greece, Sp. Pub. 7 Ext. Abs. GSG2019-147

Quality Control of the Suitability of Specific Igneous Rocks for Use as Aggregates in Road Pavement Layers

V. Boumpoulis[1], G. Mouzoulas[1], N. Depountis[1], N. Sabatakakis[1]

(1) Department of Geology, Laboratory of Engineering Geology, University of Patras, 265 04 Patras, Greece, geo11086@upnet.gr

This research focuses on accessing the suitability of specific igneous rocks for their potential use as aggregates in road pavement layers. During the current research several quality control tests were carried out on andesite and dacite rocks, obtained from the areas of Methana and Agioi Theodoroi, approximately 60 Km West of Athens.

The quality control test were conducted under the specific guidelines of Hellenic Technical Specifications ELOT and EN <European Standards> for aggregate properties' determination, while the procedure was referred to the estimation of the following parameters:

- Geometrical properties (grain size analysis, flakiness index and sand equivalent value)
- Physical properties (apparent density and water absorption)
- Mechanical properties (Micro - Deval index, Los Angeles Abrasion Value, Aggregate Impact Value)

The laboratory testing results led to the general conclusion that the samples obtained from the andesite and dacite rocks cannot be used as aggregates in road pavement layers, due to their high Los Angeles Abrasion Values (LAAV). High values of LAAV represent a low strength in mechanical corrosion and crush and contribute to the low quality of these geomaterials as aggregates. Only the sample obtained by a basaltic andesite outcrop proved to be suitable for use as aggregate in road pavement layers.

Introduction

Aggregate materials are necessary for the preparation of concrete and mortars, construction of road pavement layers, road embankments, bituminous mixtures, track ballast, drainage and filter materials, and as armour stones. At the same time they are increasingly used in various environmental applications such as, protection of soils from erosion, filters for water purification, stability of natural and artificial slopes, and stabilization of landslides. (Koukis *et al*, 2007).

In road construction, the aggregate materials must be healthy and of high strength. Specifically those used on the bituminous mixtures should have high strength and resistance to friction and impact, as well as a high polishing resistance index. Aggregate specifications are becoming increasingly stringent for materials used in the upper road pavement layers (bases), designed to support high,localised loading. The upper road pavement layers are also subject to greater influence from other external factors, such as atmospheric temperature (Hill *et al*, 2001).

A description of the general requirements of geomaterials used as aggregates in bases and subbases of road pavements are described below. The subbase layers consist of layers, which are placed on the substrate or in the rehabilitation layer, while the base layers are located between the subbase and the surface asphalt layers. Aggregates materials used for bases and subbases should meet certain requirements to ensure satisfactory stability under repeated vehicle loads. Generally, the aggregates used for bases and subbases have to satisfy the requirements of the European Standards EN-13242:2002 «Aggregates for unbound and hydraulically bound materials for use in civil engineering work and road» as well as the Hellenic Technical Specifications ELOT 1501-05-03-05-01.

Methods and materials

In the current research, laboratory tests were conducted on samples of igneous rocks adapted from the areas of Methana and Agioi Theodoroi (Figure 1). These rocks consist the main outcrops of these areas and are mainly constituted by andesites and dacites.

Initially, block samples were collected from the outcrop of the referred geological formations (total block sample weight per site over 50kg). After the collection, pieces of rocks were broken into smaller size in the lab for further processing in the rock crusher. Then, with the help of the crusher and the appropriate setting, particles of 14 mm diameter and smaller were created. Finally, by using the appropriate sieves, the necessary quantity of the required material for each laboratory test was collected.

Results

For the quality control of aggregates' suitability, laboratory tests were carried out in the materials above, in terms of their physical, geometric and mechanical properties. In particular, the following tests were performed: Flakiness Index (I_F), Sand equivalent (SE), Water Absorption (W_a), Apparent Density (ρ_a), Micro-Deval (MD), Los Angeles Abrasion Value (LAAV), Aggregate Impact Value (AIV) and uniaxial compression test.

The results of the laboratory tests performed are shown in Table 1

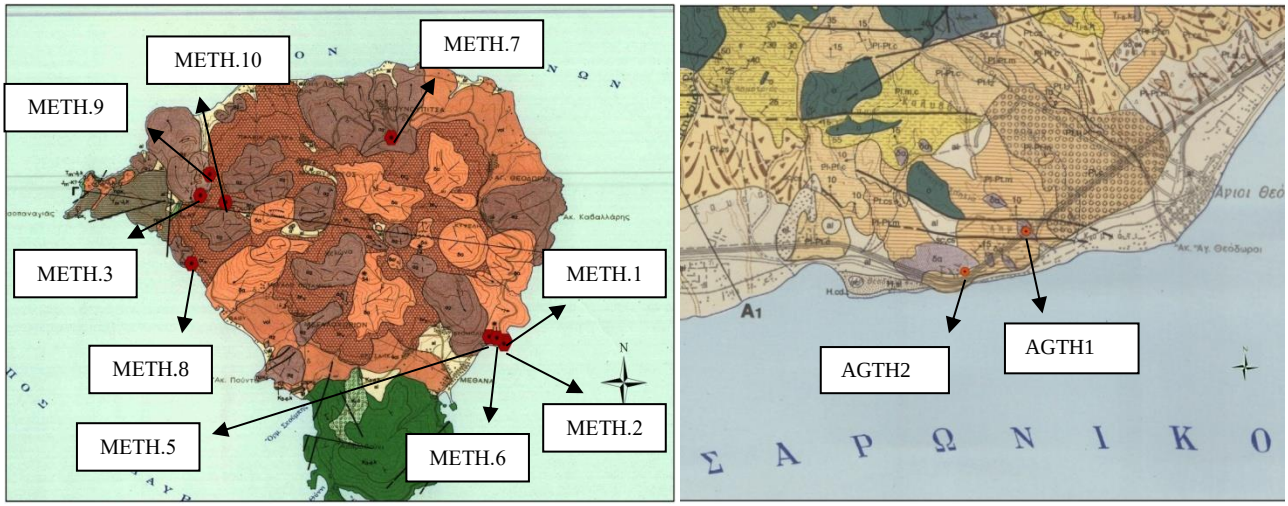

Figure 1: Map of the rock sampling area (Methana and Agioi Theodoroi, Issue sheet Sofikon and Methana, 1979-1981).

Table 1: Results of laboratory tests.

Rock samples	Aggregate test							
	I_F(%)	SE(%)	ρ_a(g/cm^3)	Wa(%)	MD(%)	LAAV(%)	AIV(%)	σ_c(MPa)
METH.1 (andesite)	12	76	2.78	3.56	18.02	54.17	32.65	50-86
METH.3 (andesite)	15	76	2.57	3.01	25.08	54	39.38	
METH.8 (andesite)	12	79	2.62	4.39	18.16	46.31	32.35	
METH.9 (andesite)	16	71	2.19	5.3	31.49	51	41.59	
METH.7 (basaltic andesite)	6	79	3.14	0.45	3.78	15.3	17.84	110
METH.2 (dacite)	7	77	2.70	3.36	44.64	43	26.5	25-50
METH.5 (dacite)	15	73	2.35	5.04	52.32	67.9	37.07	
METH.6 (dacite)	9	57	2.23	3.27	26.54	58.56	28	
METH.10 (dacite)	19	76	2.20	5.44	57.1	73	45	
AGTH1 (dacite)	10	81	2.64	3.65	26.87	37.08	28.3	
AGTH2 (dacite)	16	74	2.19	5.54	54.6	75.3	41	
Specification limits for road pavement layers (ELOT)	**≤35 (coarse aggregate)**	**>40% (fine aggregate)**	-	-	-	**≤40 (base) ≤50(subbase)**	-	
European Standards EN-13242:2002	**≤50**	**-**	**≥2**	**<0,5**	**≤50**	**≤60**	**≤38**	

Conclusion

According to the Hellenic Technical Specifications ELOT 1501-05-03-05-01 and the European Standards EN-13242:2002 «Aggregates for unbound and hydraulically bound materials for use in civil engineering work and road» only the basaltic andesite outcrop (**METH.7)** proved to be suitable for use in road bases and subbases**.**

References

Hellenic Technical Specifications ELOT 1501-05-03-05-01, 2009. Road pavement layers with unbound aggregates.

Hill A., Dawson A., Mundy M., 2001. Utilisation of aggregate materials in road construction and bulk fill. Journal of Resources, Conservation and Recycling, Volume 32, Issues 3–4, Pages 305-320, doi.org/10.1016/S0921-3449(01)00067-2.

Koukis, G., Sabatakakis N., 2007. Geology of technical works, technical book published by «Papasotiriou», 623 pages.

15th International Congress of the Geological Society of Greece
Athens, 22-24 May, 2019 | Harokopio University of Athens, Greece
Bulletin of the Geological Society of Greece, Sp. Pub. 7 Ext. Abs. GSG2019-167

A methodology to delineate protection zones in karst aquifers: The case of municipality of Kozani, North Greece

N. Kazakis[1], M.M. Ntona[1], M. Bannenberg[1], E. Gavrilidou[1], S. Lappos[2], Voudouris K.[1]

(1) Aristotle University of Thessaloniki, Department of Geology, Laboratory of Engineering Geology & Hydrogeology, GR54124 Thessaloniki, Greece, kazakis@geo.auth.gr
(2) DEYA Kozanis, 2nd Km EO Kozani- Thessaloniki, Kozani, Greece

Carbonate rocks in Greece occupy about 35% of the surface area of Greece and are mainly located in the western, central and southern parts of the country. The carbonate rocks can be divided into sedimentary formations (limestones and dolomites) and metamorphic rocks (marbles). They mainly date from the Triassic to the Cretaceous periods, whereas marbles have a Paleozoic-Mesozoic age. Within the carbonate rocks are hosted karst aquifers which are the main supply source for domestic use in many sites of Greece. However, integrated management plans of karst aquifers in Greece are only focused on extraction limitations, while detailed monitoring, vulnerability assessment and modelling are neglected. According to the EU Directives and new Greek legislation of management plans of aquifers in Greece require the determination of protection zones of springs and wells used for domestic uses.

The delineation of protection zones is not a straightforward and one-dimensional process. It should be a part of an integrated management plan of the aquifer system (Burgess and Fletcher, 1998). The process is much more difficult dealing with karst aquifer due to their anisotropy and uncertainty of their structure and function. A sustainable management of karst aquifers includes the following steps (Biava et al., 2014; Kazakis et al., 2018):

a) Detailed hydrogeological observations (temporal and spatial data).
b) Data analysis applying advanced statistical methods.
c) Application of integrated models depending.
d) Vulnerability and risk assessments.

Although in Greece, many studies deal with statistical analysis of karst systems (Panagopoulos and Lambrakis, 2006), vulnerability assessment (Kazakis et al., 2015; Nanou and Zagana, 2018) and time series analysis (Manakos et al., 2019) there is a methodological gap for the delineation of protection zones in Greek karst aquifers. It is pointed out that karst aquifers are highly vulnerable to pollution, precisely because of their specific structure (Biava et al., 2014).

In this study we suggest a methodological approach for the delineation of protection zones in karst aquifers. The process includes basic hydrogeological research, hydrochemical and isotopic analysis, statistical analysis, simulation process, and vulnerability and pollution risk assessment. Obviously, the delineation of the protection zones of the karst systems constitute the final step and maybe the most important step for the sustainability of the systems. In this study we provide the methodological framework in simple research steps in order to delineate protection zones to karst aquifers. This protocol has been developed during the study of four karst aquifers in the municipality of Kozani, in western Macedonia, north Greece (Fig. 1). The water demands of the municipality are covered by exploiting of these karst aquifers. Hence, the sustainability of these hydrosystems is of the outmost importance for the water security of the area. The suggested methodology to delineate protection zones in karst aquifers includes the following research steps:

Literature review: A detailed literature review of the existing geological and hydrogeological studies is essential for the delineation of protection zones. The literature review could provide the initial hydrogeological conceptual model of the karst aquifer, the missing data and determine the field work.

Data base development and digitization in Geographic Information System (GIS) environment: All available maps (geological, geomorphological, hydrogeological) including geological and hydrogeological information should be digitized. Hence, a data base can be created in G.I.S. environment in order to elaborate and analyse the various spatial data and create the corresponding thematic maps.

Hydrogeological observation: The hydrogeological research includes field measurements, data collection and analysis. More specific, field measurements include: a) hydrogeological-geological mapping of karst features, springs, aquifer boundaries, faults using both field measurements, satellite images and UAS (DRONE) images, b) geophysical research applying electrical resistivity tomographies in order to determine the structure of the aquifer, c) hydrochemical analysis to determine the quality of groundwater, and d) isotopic analysis of stable isotopes and tritium in order to determine the recharge zones and groundwater age.

Statistical analysis: The statistical analysis includes methods such as cross-correlation, autocorrelation and phase function of rainfall and discharge of the karst aquifer. The main contribution is to understand the functioning of the hydrosystem and determine the lag time of the system.

Modelling: The modelling process contributes in the prediction and exploitation of the quantities of the system. The modelling process include both lumped (e.g. Karstmod) and spatial models (e.g. Modflow-CFP).

Groundwater vulnerability and pollution risk assessment: The vulnerability and pollution risk assessment are the final step to delineate protection zones and suggest land use changes. The PaPRIKa method and the corresponding

plugin have been widely used for the vulnerability assessment of karst aquifers (Ollivier et al., 2019) and hence, it has been included in the suggested methodological approach.

The holistic approach of the suggested methodology can ensure high reliability in the delineation of protection zones in karst aquifers. It can be adopted in different hydrosystems according to the data availability. Additionally, the integrated approach of this method ensures the reliability of the results and the social acceptance of the protection zones. It should be mentioned that the application of different methods give different results as regards to the extension of the protection zones. Hence, the proposed methodology would be benefit by improvement in hydrological data monitoring and the application of isochrones method to compare the results.

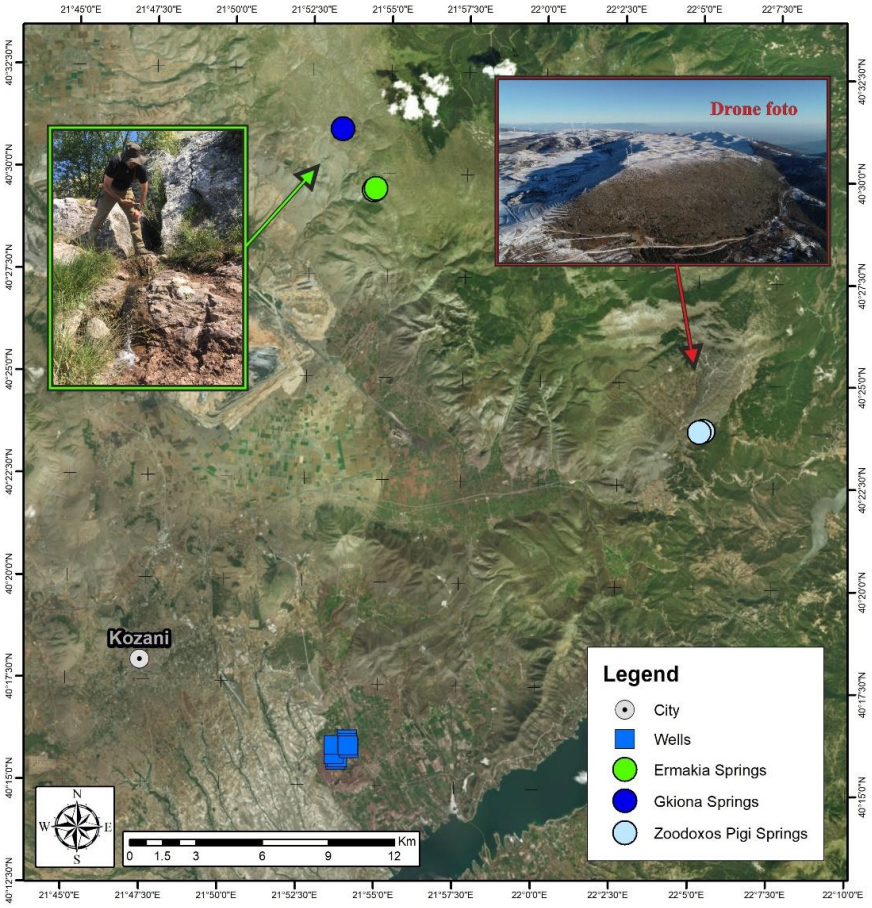

Figure 1. Karst aquifer systems in the Kozani region.

Acknowledgements

This research was carried out within the framework of the project entitled "Development of a methodology for the protection and integrated management of karst aquifers supplying the Municipality of Kozani with drinking water", Scientific Coordinator: Dr. Kazakis Nerantzis. It was funded by the Water and Sewage Management Company of Kozani (DEYAK).

References

Biava, F., Consonni, M. et al. (2014). Delineation of protection zones for the main discharge area of the Gran Sasso aquifer (central Italy) through an integrated geomorphological and chronological approach. J. of Water Resource and Protection 6, 1816-1832.

Burgess, D.B., Fletcher, S.W. (1998). Methods used to delineate groundwater source protection zones in England and Wales. Groundwater pollution, Aquifer recharge and Vulnerability. Geological Society, London, Special publications 130, 199-210.

Kazakis, N., Oikonomidis, D., Voudouris, K., (2015). Groundwater vulnerability and pollution risk assessment with disparate models in karstic, porous and fissured rock aquifers using remote sensing techniques and GIS in Anthemountas basin, Greece. Environmental Earth Science 74:7, 6199-6209.

Kazakis, N., Chalikakis, K., Mazzilli, N., Ollivier, C., Manakos, A., Voudouris, K. (2018). Management and research strategies of karst aquifers in Greece: literature overview and exemplification based on hydrodynamic modelling and vulnerability assessment of a strategic karst aquifer. Sci Total Environment 643, 592-609.

Manakos, A., Ntona, M., Kazakis, N., Chalikakis, K. (2019). Enhanced characterization of the Krania-Elassona structure and functioning allogenic karst aquifer in central Greece. Geosciences 9(1), 15; https://doi.org/10.3390/geosciences9010015.

Nanou, E.A., Zagana, E. (2018). Groundwater vulnerability to pollution map for karst aquifer protection (Ziria Karst System, Southern Greece). Geosciences 8, 125.

Ollivier, C., Chalikakis, K., Mazzilli, N., Kazakis, N., Lecomte, Y., Danquigny, C., Emblanch, C. (2019). Challenges and limitations of karst aquifer vulnerability mapping based on the PaPRIKa method; application to a large European karst aquifer (Fontaine de Vaucluse, France). Environments (in press).

Panagopoulos, G., Lambrakis, N. (2006). The contribution of TSA to the study of the hydrodynamic characteristics of the karst systems: application on two typical karst aquifers of Greece (Trifilia, Almyros Crete). J. Hydrology 329, 368–37.

15th International Congress of the Geological Society of Greece
Athens, 22-24 May, 2019 | Harokopio University of Athens, Greece
Bulletin of the Geological Society of Greece, Sp. Pub. 7 Ext. Abs. GSG2019-178

Assessment of Rockfall Risk along Kakia scala road, Greece

K. Mazarakis[1], K. Diamantis[2]

(1) School of Science, Faculty of Geology and Geoenvironment, National and Kapodistrian University of Athens, University, Campus- Zografou 15784, Athens, Greece, mazarakis.konst@gmail.com
(2) Department of Civil Engineering, University of West Attica, 28 Ag. Spiridona Str., 12243, Athens, Greece

Introduction - Objective

Rockfall phenomena often occur at highway road cuts in mountainous terrain. It's a common type of fast-moving landslide and represents a major hazard in mountain areas worldwide. They can cause human lives' loss and extensive damage to the human structures (especially roadways and houses). Rockfalls are dependent on the site conditions (both topographic and geological structure), climate, tectonic, human activities as well as seismic loading (Hoek and Bray, 1981; Koukis et al., 1994; Guzzetti et al., 1996; Marinos and Tsiambaos, 2002). As far as Greece is concerned, Rockfall is considered as the most frequent (55%) landslide type (Koukis et al., 1994; Marinos and Tsiambaos, 2002) and usually occurs after heavy rainfalls or earthquake events.

The main objective of the research is the rockfall risk assessment in the "Kakia Scala" region using Rockfall Hazard Rating System (R.H.R.S). The study area is a typical example with high impact of rockfalls. It is part of the *"Patra–Athens–Thessaloniki-Evzoni (P.A.TH.E.)"* motorway one of the most major highways in Greece and for this reason the importance of a reliable rockfall risk assessment is crucial. Eight representative sites (A-H) were examined, and the Rockfall Hazard Rating System was calculated according to Pierson et al. (1990).

Geology-Tectonics-Seismicity

"Kakia Skala" area mainly consists of Alpine formations that belong to the Sub-Pelagonian geotectonic unit. A carbonate (limestone and dolomitic limestone) sequence of Middle-Upper Triassic age constitutes the basement of this area (Gaitanakis et al., 1984). A transgressive sequence of Cretaceous limestones – marly limestones overlies them. Finally, this sequence passes upward to post-alpine formations (Late Pleistocene screes and cone - shaped screes, talus cones, alluvial Deposits, marls, clays, Fig 1). The present research focusses on the limestones because rockfalls occur only on them.

The study area is mostly affected by normal faults which have an East–West to ENE-WSW direction while the inclination fluctuates from 45° to 75° (sometimes until 85° or seldom 90°). On the other hand a smaller number of secondary faults with NE–SW direction are met (Mettos et al., 1988). This great fault zone mostly occurs in limestone and dolomitic limestone of the Middle-Upper Triassic. Many faults go through the fault zone, but the "Kakia Skala" main fault can easily be recognized. This happens because it has been activated many times in the past and its plane has become much more smooth and impressive. Although "Kakia Skala" is not considered to be highly seismic, the high seismicity of the eastern "Corinthian gulf" (next to it) has a great influence on it. Some researchers (Mettos et al., 1988; Rondoyanni and Papadakis, 1992; Makris et al., 2004) mentioned that the "Kakia Skala" fault is of great importance and possible to be approximately related with an earthquake of Ms=6.5 Richter. Earthquakes of this size are likely to cause a significant movement along the crack and cause rockfalls.

Methods - Results

In order to assess the exposition to the risk associated with Rockfalls and the remediation works, many classification systems were designed for highway slopes. One of the most widely used methods is the Rockfall Hazard Rating System (RHRS, by Pierson et al., 1990). It is an approach that leads to an immediate and relatively user-friendly way of scoring the hazard level of the examined rock slope. In the scoring procedure, several critical parameters concerning the geological and the geometrical features are evaluated (slope height, the ditch effectiveness, average vehicle risk, percent of decision sight distance, roadway width, structural condition, friction, difference in erosion rates, block size, volume of rockfall per event, climate and presence of water on slope, rockfall history). Each parameter contributes to the overall hazard associated to a score of 3, 9, 27 or 81 following an exponential increase in the form of $y=3^x$. According to the literature data, slopes with a rating of less than 300 can be considered as slopes with low risk while slopes with a rating greater than 500 are identified for urgent remedial action (slopes of high hazard level). In this study eight representative sites (A-H, Fig 1) were examined and the Rockfall Hazard Rating System values were calculated for each section. As it was listed in Table 1, the Rockfall Hazard Rating System (R.H.R.S) gives values between 378 and 603. Along the study area, the most dangerous sites are F (603) and G (504). Both of them present high risk and so measurements must be taken. The best site is H (378) and it is characterised as moderate.

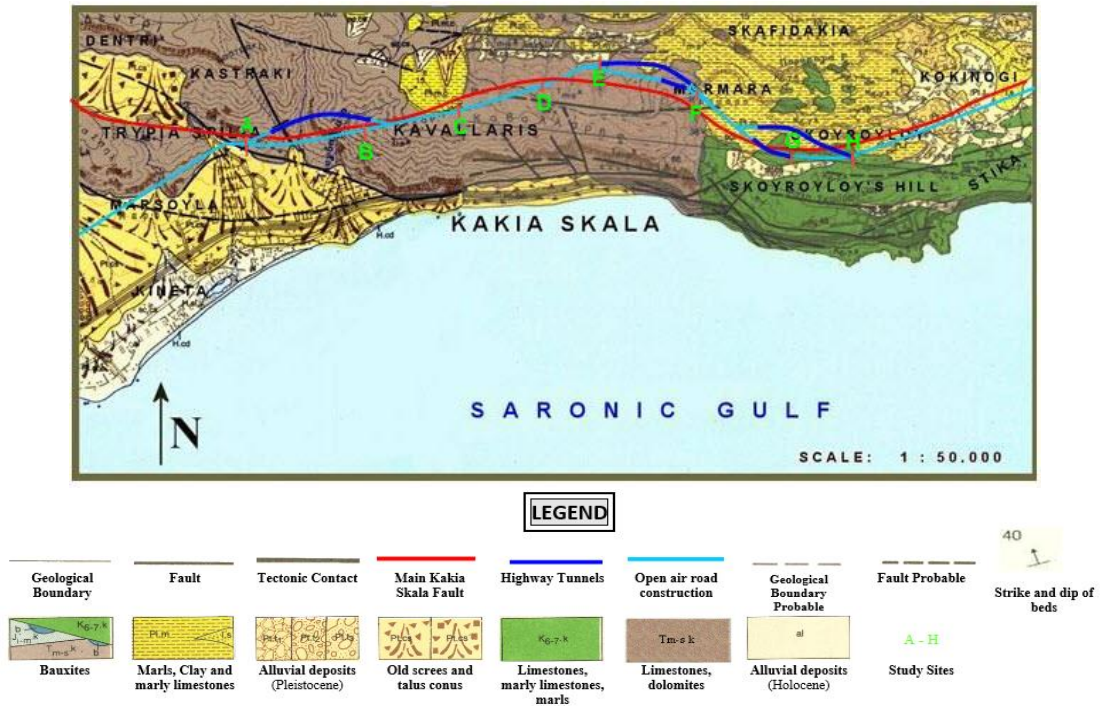

Figure 1. Geological Map of the "Kakia Skala" area (Geological mapping: I.G.M.E. 1976)

Table 1. The rating of each site and their classification according to RHRS

Site	Rating	Classification
A	423	Moderate
B	459	Moderate
C	486	Moderate
D	477	Moderate
E	441	Moderate
F	603	High
G	504	High
H	378	Moderate

Conclusions

To sum up, this research mainly attempts to study the assessment of Rockfall Risk in the "Kakia Skala" area, which is part of the one of the most major highways in Greece. For this reason, the Rockfall Hazard Rating System (R.H.R.S) values were calculated for eight sites. The study demonstrates that the R.H.R.S fluctuates between 378 and 603 and the most dangerous sites are F (603) and G (504). Both of them present high risk and so urgent remedial actions must be taken. The best site is H (378) and it is identified as moderate.

References

Hoek, E., Bray, J., 1981. Rock Slope Engineering, third ed. Institution of Mining and Metallurgy, London.

Gaitanakis, P., Mettos, A., Koutsouveli, A., Rondoyanni, Th., 1984. Geological map of Greece scale 1:50.000, Megara sheet. IGME ed, Athens.

Guzzetti, F., Cardinali, M., Reichenbach, P., 1996. The influence of structural setting and lithology on landslide type and pattern. Environmental and Engineering Geosciences 2, 531–555.

Koukis, G., Tsiambaos, G., Sabatakakis, N., 1994. Slope movements in the Greek territory: A statistical approach, Proceedings 7th International Congress, IAEG, Lisboa, Portugal, p.4621-4628.

Makris, J., Papoulia, J., Drakatos, G., 2004. Tectonic deformation and microseismicity of the Saronikos Gulf, Greece. BSSA 94, 3920–3929.

Marinos, P., Tsiambaos, G., 2002. Earthquake triggering rock falls affecting historic monuments and a traditional settlement in Skyros island, Greece. Proceedings of the International Symposium Landslide risk mitigation and protection of cultural and natural heritage Kyoto, Japan, p. 343-346.

Mettos, A., Rondoyanni, T.H., Bavay, P.H., 1988. The Pleistocene deposits of the Sousaki – Agioi Theodori (Corinthia). Stromatography and deformation. Bulletin Geol. Soc. Greece XX/2, 91-111.

Pierson, L.A., David, S.A., Van Vickle, R., 1990. Rockfall Hazard Rating System Implementation Manual. Oregon Federal Highway Administration (FHWA), Report FHWA-OR-EG-90–01, FHWA, U.S. Dep. of Transp.

Rondoyanni, T.H., Papadakis, I., 1992. Evaluation of the faults at Revithousa island - Neotectonic Research. Unpublished Report IGME, Athens.

15th International Congress of the Geological Society of Greece
Athens, 22-24 May, 2019 | Harokopio University of Athens, Greece
Bulletin of the Geological Society of Greece, Sp. Pub. 7 Ext. Abs. GSG2019-183

Investigation of Seawater Intrusion Zone in the Coastal Area Stavros-Vrasna Using Hydrogeological and Geophysical Methods

D.G. Zerva[1], K. Voudouris[1], G. Vargemezis[2], P.Tsourlos[2]

(1) Aristotle University of Thessaloniki, Department of Geology, Lab. of Engineering Geology & Hydrogeology, 54124 Thessaloniki, Greece, d.zerva2009@gmail.com
(2) Aristotle University of Thessaloniki, Department of Geology, Lab. of Applied Geophysics, 54124 Thessaloniki, Greece

Abstract

The survey was conducted in Stavros-Vrasna area which is located in northern Greece at the eastern part of the prefecture of Thessaloniki and covers 11.27 km^2. Groundwater sampling took place during the dry season, and the samples were analyzed. Moreover, geophysical survey by the application of geoelectrical tomography method has been conducted. Six (6) geoelectrical tomographies were measured in order to determine the electrical resistivity of underground. The results show 3 different lithological types of aquifers: a) Sedimentary, b) Karstic and c) Fractured. The dominant groundwater aquifer is porous, and most part of it, is confined. In the area of Vrasna, a salinity zone has been detected by geoelectrical survey at a quite large distance from drinking wells, enough to not allow any affection. In opposition with the results of hydrochemical analysis, in the area of Stavros an early stage of seawater intrusion has been detected at the W_St1 well by the geophysical survey.

Since the needs of the entire area especially during summer period are limitedly satisfied, mapping of possible salinity zones is very crucial to avoid the quality degradation of the groundwater caused by new drillings in these zones.

Introduction

Salinization (or seawater intrusion) is a widespread phenomenon that concerns coastal aquifers. The reasons of salinization are many and can be related to each other. The climatic change (Ferguson et al., 2012) which results in the rise of the sea-level, the over extraction caused by the increased irrigation needs, the urbanization increase of coastal areas (Neumann et al., 2015), the touristic development (Garcia et al., 2003), even the impact of topography and the aquifer recharge have led to a numerous of studies and approaches.

The objective of this study is to determine the extent of seawater intrusion in the coastal area of Stavros-Vrasna by the use of Electrical Resistivity Tomography (ERT), as a 2D resistivity method, in conjunction with hydrochemical data.

Methodology

Groundwater samples were collected from 17 waterwells and physicochemical parameters of Electrical Conductivity (E.C.), Total Dissolved Solids (T.D.S), active acidity (pH) and temperature (T) have been measured. Moreover, the samples from 11 hydrowells were analyzed by hydrochemical methods and the main ions were measured (Mg^{2+}, Ca^{2+}, Na^+, K^+, HCO_3^-, NO_3^-, SO_4^{2-} and Cl^-) and ionic ratios Mg/Ca, Cl/HCO_3, Na/Cl, (Ca+Mg)/(Na+K), Na/K, SO_4/Cl and Na/Ca have been calculated (Fig. 1).

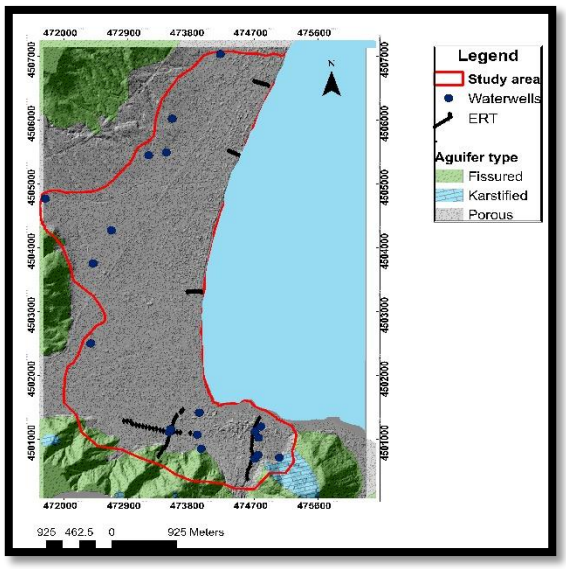

Figure 1. Map of study area.

Six Electrical Resistivities Tomographies (ERT) were measured. Three ERT of 1000 m each were conducted in Stavros and three of 230 m each in Vrasna. Two types of arrays were used, Dipole-dipole and Multiple Gradient.

Results

Throughout the coastal aquifer, the temperature, pH and electrical conductivity with the total dissolved solids are within the normal range. According to the ionic ratio of Na^+/Cl^-, seawater intrusion does not occur, while the high concentrations of Na^+ indicate either the weathering of alkaline formation nor possible sewages. Nevertheless, the geophysical survey reveals, in Stavros area, the potential hazard for seawater intrusion at W_St1 well (Fig. 2).

Moreover, the geophysical survey revealed 5 potential waterwell locations for the avoidance of the W_St1 well further charge and defined that the salinization zone of Vrasna is far from drinking well's locations. Additionally, the lithostratigraphy of the coastal aquifer in the area of Vrasna has been determined (Fig. 3).

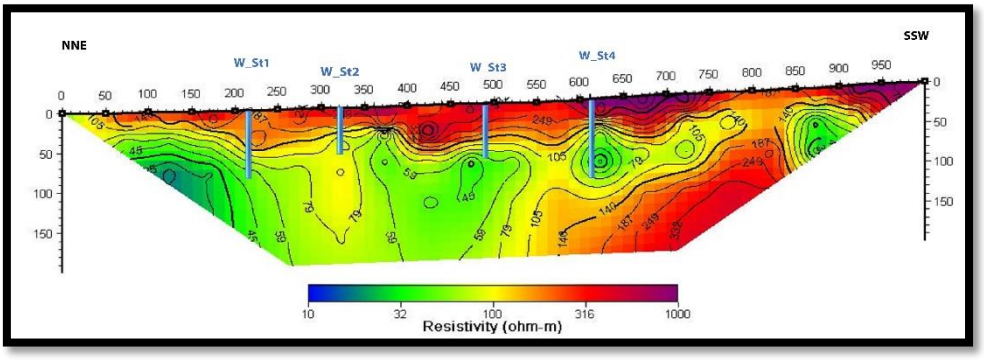

Figure 2. Electrical Resistivity Tomography (ERT) St1.

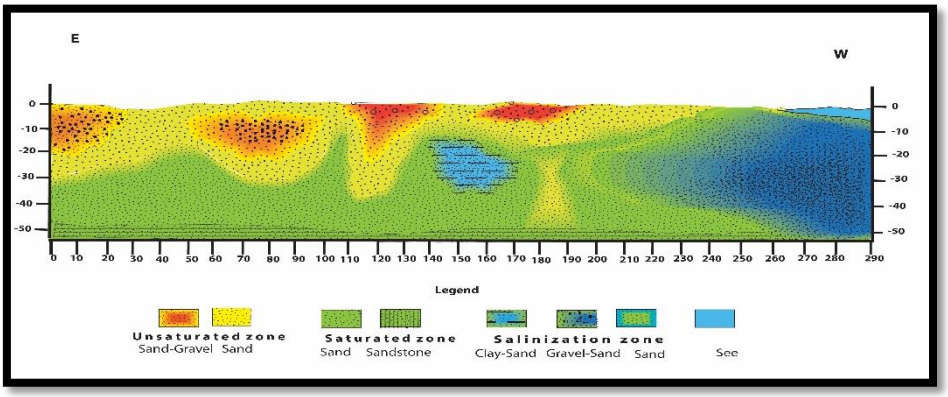

Figure 3. Hydrolithogeophysical section Vr3 (Vrasna).

Acknowledgement

This paper forms a part of the Master study carried out by the first author. The author would like to thank the Stavros Community's President, Mr Chris Golidakis and the public servants of Municipality of Volvi, Mrs Argiro Katrantzi and Mr George Itsios, for their help and support.

References

Ferguson, G., Gleeson, T. (2012). Vulnerability of coastal aquifers to groundwater use and climate change.

Garcia, C., & Servera, J. (2003). Impacts of Tourism Development on Water Demand and Beach Degradation on the Island of Impacts of Tourism Development on Water Demand and Beach Degradation on the Island of Mallorca (Spain). Tourism, 287–300. https://doi.org/10.1111/j.0435-3676.2003.00206.x.

Neumann, B., Vafeidis, A. T., Zimmermann, J., & Nicholls, R. J. (2015). Future coastal population growth and exposure to sea-level rise and coastal flooding - A global assessment. PLoS ONE, 10(3). https://doi.org/10.1371/journal.pone.0118571.

15th International Congress of the Geological Society of Greece
Athens, 22-24 May, 2019 | Harokopio University of Athens, Greece
Bulletin of the Geological Society of Greece, Sp. Pub. 7 Ext. Abs. GSG2019-194

The effect of the degree of saturation on shear strength of sandy soils. The example of Geni Tzami of Edessa, Northern Greece

D. Papatsikourakis[1], N. Chatzigogos[1], Th. Makedon[1]
(1) Aristotle University of Thessaloniki, Thessaloniki, Greece, dpapatsik@geo.auth.gr

Introduction/Setting

In order to investigate the foundation's conditions of a construction, it is important to determine the mechanical characteristics of the subsoil and specifically the determination of its shear strength and compressibility. In cases where sandy soils undergo fluctuations in their moisture content, the determination of their shear strength should take into account their behavior in unsaturated conditions (Fredlund & Rahardjo, 1993). This requires, shear tests of soil specimens (in this case direct shear tests) performed with control of the degree of saturation. The present paper presents the subsoil's mechanical behavior in the Geni Tzami of Edessa under conventional tests as well as tests in unsaturated conditions. The city of Edessa is located in Almopia which is the western sub-zone of the broader Axios geotectonic zone in Central Macedonia. The Geni Tzami is founded on the Quaternary formations of the city which are mainly aluvial deposits and cones of fluvial deposits from the underlying travertines of Edessa (Figure 1).

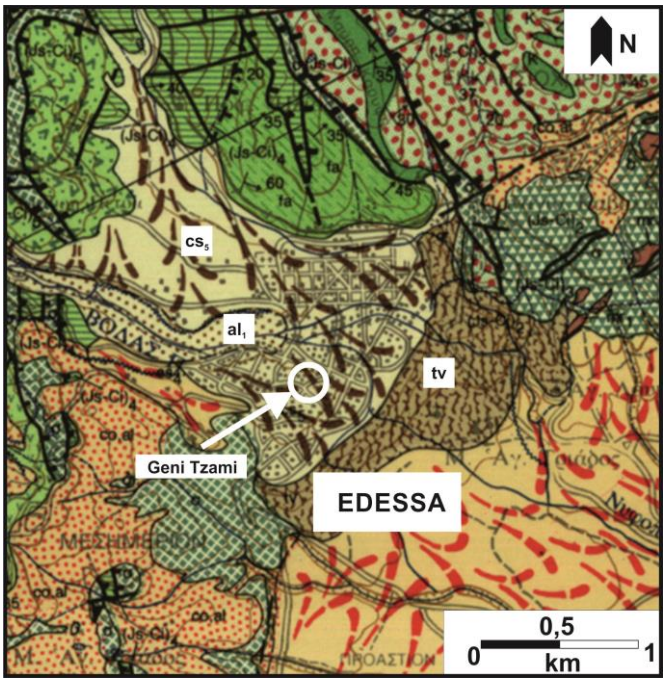

Figure 1. The geology of the city of Edessa (Quaternary): al_1, alluvial deposits cs_5 cones of fluvial deposits, tv: travertines

Methodology

The restoration of Geni Tzami included a core sampling 15m borehole for the geological and geotechnical investigation of the foundation conditions. The results of the coring showed an interchange between sand and silty sand layers with variable fines content and a small percentage of gravels. The groundwater conditions were dry during the drilling but a low potential groundwater table might develop during the wet season in the coarser deposits. The mechanical properties of the soil samples (c' and φ') were estimated using both empirical relationships from the N_{SPT} values and a specific laboratory testing experimental program. Till recently the production of reliable experimental data for the unsaturated behavior of granular soils using the axis translation technique was difficult. This was due to the lack of sophisticated laboratory equipment for non cohesive soils since most of the used devices required cohesive specimens. The device used for this experimental programwas the GDS unsaturated back-pressure shear boxof the Laboratory of Engineering Geology & Hydrogeology of A.U.TH. (Figure 2).Since the foundation soil is mostly under partially saturated conditions the soil specimens were tested for shear strength via consolidated drained shear tests under their natural moisture content and in saturated condition so as to obtain a more accurate picture of the actualin situ shear strength.The unsaturated conditions were simulated using the axis translation technique by applying constant pore-air and pore-water pressure in order to control the matric suction in the samples.

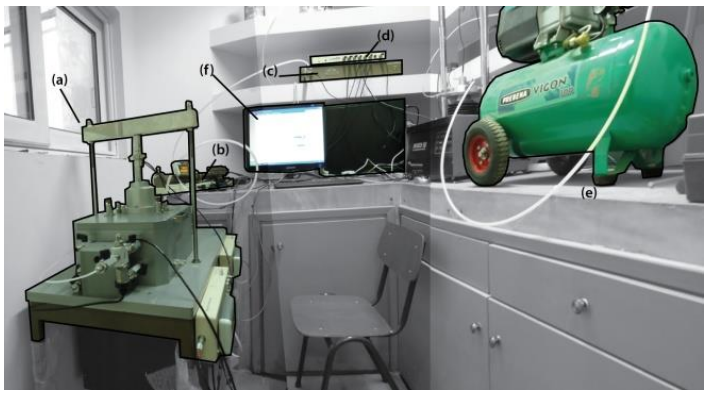

Figure 2. The GDS unsaturated back-pressure shear box of the Laboratory of Engineering Geology & Hydrogeology of A.U.TH.

The mechanical behavior of unsaturated soils depends on the characteristic for each soil type angle φ^b as well as the relationship between the soil suction and the degree of saturation as described by the soil water characteristic curve (SWCC) (Fredlund et. al. 2013).

Results/Conclusions

The test results showed:

- An increase of soil shear strength with the reduction of the degree of saturation.
- An increase of the percentage of shear strength variation between saturated and unsaturated conditions with reduced axial stress (Figure 3).
- An observed cohesion of c'=23,5° under natural moisture content while φ remains almost stable under both conditions. Cohesion presentsanincrease with reduced degree of saturation depending on the matric suction values and the angle φ^b (Figure 4).
- The value of φ^b was estimated as φ^b=11,08° using the SWCC to obtain a matric suction value of u_a-u_w=120 kPa for moisture content m=11.20%. This value is in accordance with similar experimental values in the literature.

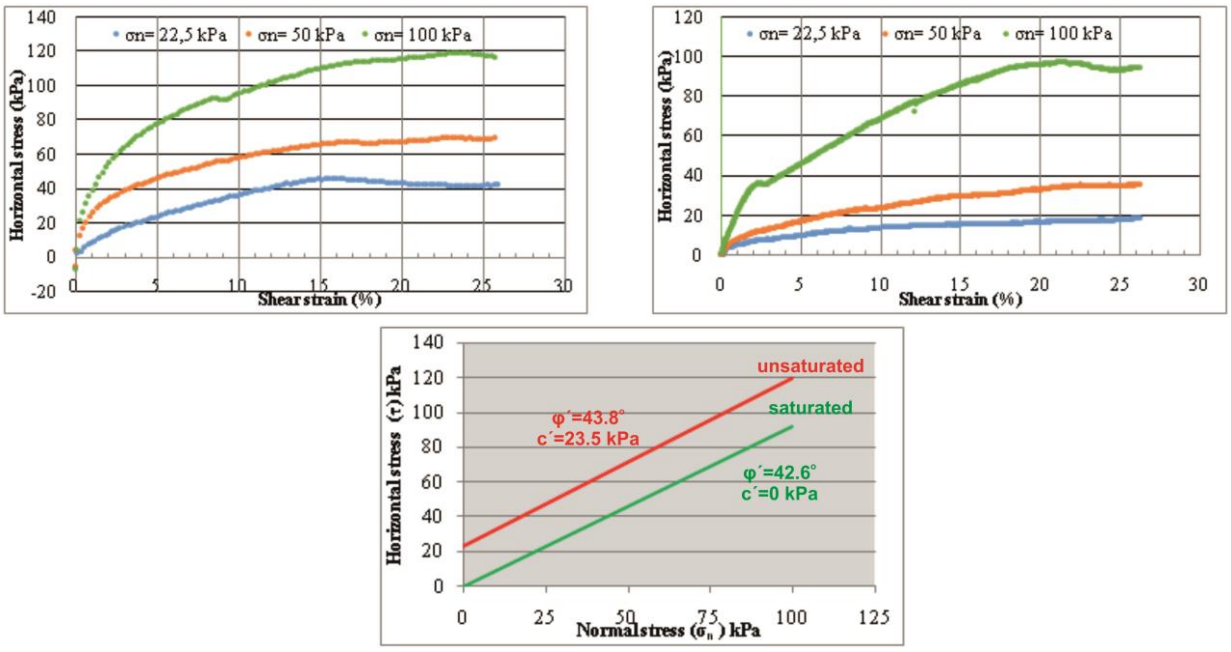

Figure3. Left: Horizontal stress – shear strain diagram for unsaturated conditions. Right: Horizontal stress – shear strain diagram for saturated conditions. Bottom: Mohr – Coulomb failure envelopes for unsaturated and saturated conditions.

References

Fredlund, D.G., & Rahardjo, G. 1993. Soil mechanics for unsaturated soils. John Wiley & Sons.

Fredlund, D.G. &Houston, S.L. 2013. Interpretation of soil-water characteristic curves when volume change occurs as soil suction is changed. Taylor & Francis Group, London.

15th International Congress of the Geological Society of Greece
Athens, 22-24 May, 2019 | Harokopio University of Athens, Greece
Bulletin of the Geological Society of Greece, Sp. Pub. 7 Ext. Abs. GSG2019-209

Hydrochemical characteristics of the Oropos coastal aquifers, Attica, Greece

D. Hermides[1], D. Zachariadis[1], G. Stamatis[1]
(1) Agricultural University of Athens, 75 Iera Odos St., Athens, Greece, dermides@aua.gr

This article deals with the hydrochemistry of coastal aquifers of the Oropos plain, Attica, Greece (Fig. 1). The geological structure of the study area is complex consisted of: (i) alpine sediments of Permo-Triassic volcanosedimentary and carbonate rocks, ophiolites and Cretaceous limestone and flysch (Katsikatsos, 2000); and (ii) post-alpine lacustrine, lagoon and torrential Miocene sediments, Pleistocene conglomerate/breccia and clay and Holocene clay, sand and conglomerate (Parginos et al., 1989, Perissoratis, 1989; Mettos, 1992). The Oropos plain is a NE-SW oriented neotectonic depression affected by W-E, NE-SW and NW-SE striking tectonic and neotectonic faults (Papanikolaou et al., 1986; Perissoratis, 1989; Papanikolaou *et al*., 1989) as well as by the Pleistocene sea level fluctuations (Lambeck 1996). The interaction of tectonic and stratigraphic factors combined with eustatic changes established a complex hydrogeological regime where successive unconfined and confined aquifers have been formed. In total, four aquifers occur in the study area (Dounas et al., 1980; Pagounis 1994). The upper aquifer occurs in the Holocene sediments which is unconfined and locally confined. The second aquifer, which is confined, occurs in the Pleistocene sediments. The third aquifer occurs in the Miocene conglomerate and the last one in the Mesozoic carbonate.

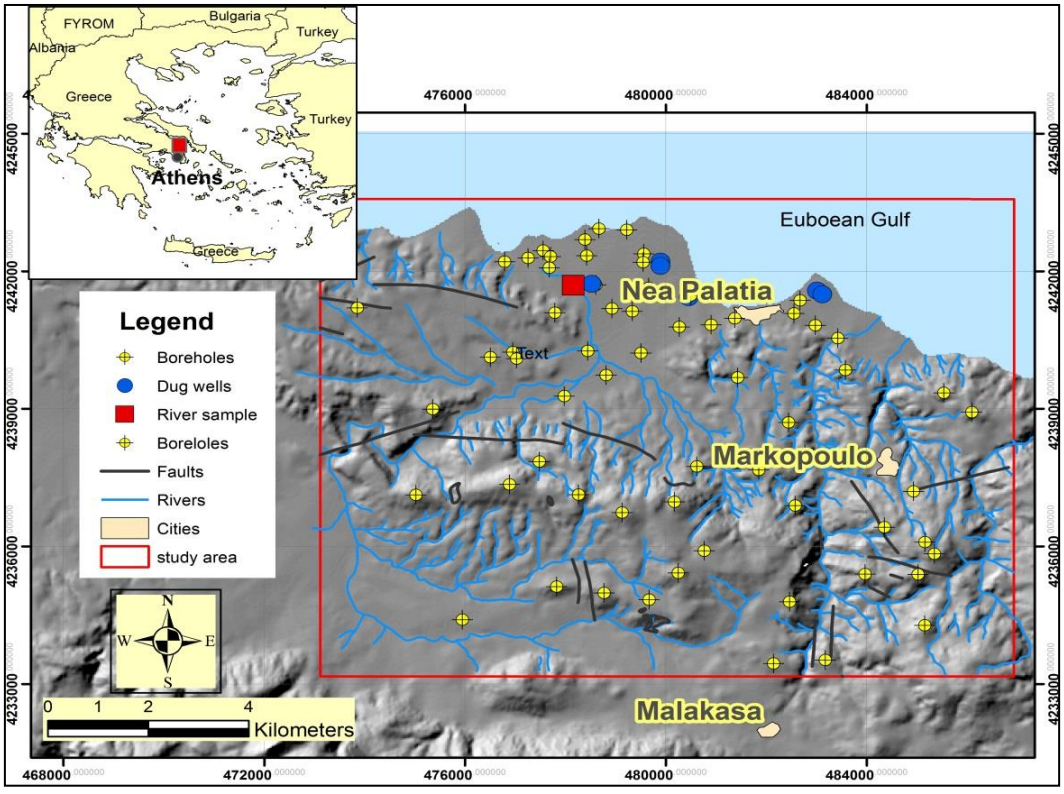

Figure 1. Study area.

The objective of this article was to highlight the occurrence of good quality groundwater which is hosted in the confined aquifer of the Pleistocene sediments located adjacent to the coastline of the Oropos plain.

The hydrochemistry of Oropos groundwaters has been investigated using major and heavy metal constituents. Groundwater samples from 36 wells and one sample from Asopos River surface water were collected. Physico-chemical characteristics of Temperature T (oC), pH and Electrical Conductivity EC (μS/cm) were measured in situ. The method of titration was used for Ca^{2+}, Mg^{2+}, HCO_3^-, and Cl^- determination and Hack Dr 3000 Spectrophotometer was used for NO_3^-, PO_4^{3-}, NH_4^+ and SiO_2 determination. The concentration of Na^+ and K^+ was determined using the CORNING Flame Photometer 410. Heavy metals Sr, Cd, Cu, Fe, Mn, Ni, Pb, Cr VI και Zn were determined using AAS GBS 908 Atomic Absorption Spectrophotometer. Ion balance error was better than 5%.

Hydrochemistry of groundwaters in the Holocene, Miocene and Mesozoic sediments indicated seawater influence. Electrical conductivity (EC) values ranged between 526 and 3770 μS/cm with a median at 2098 μS/cm. Chlorides ranged between 31 and 993 mg/l with a median at 260 mg/l. On the contrary, groundwater quality of the Pleistocene

conglomerate was very good. The EC values which ranged between 766 and 971μS/cm with a median at 854 μS/cm and chlorides which ranged between 95 and 163 mg/l with a median 121 mg/l led to the conclusion that this coastal aquifer is protected from seawater intrusion, despite the fact that it is located adjacent to the coastline. The NO_3^- and PO_4^{3-} concentrations were increased in the agricultural area which is attributed to fertilizers. Most of the heavy metal concentration such as Cd, Fe, Pb and Ni exceeded the EU limits which they have been determined at 82, 2500, 817, 217 μg/lit respectively. Groundwaters were categorized into 2 main water types based on the expanded Durov diagram (Fig. 2) (Lambrakis, 1991): (i) the first group was mainly depicted on the field 2 indicating fresh groundwater of Ca-Mg-HCO3 type; and (ii) the second group was depicted on the field 8 that is Ca-Mg-Cl type indicating reverse cation exchange of old Na-Cl waters (Lloyd, *et al.* 1985). The Asopos River surface sample was projected on the field 9 indicating Na-Cl type contaminated by seawater. Based on the Piper diagram most of the samples showed Ca-Mg-Na-HCO3 type and some samples showed no dominant type which means mixing processes are in progress.

It is worth mentioned that the Pleistocene aquifer resources represent a reserve of good quality water which needs to be properly managed.

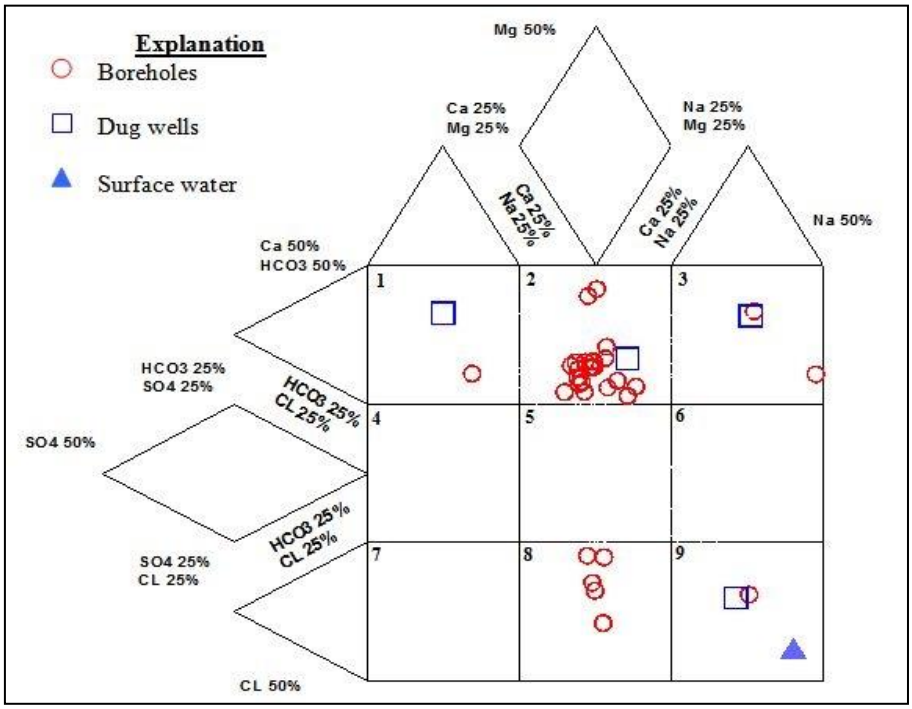

Figure 2. Expanded Durov diagram showing the classification of the Oropos groundwaters

References

Dounas, A., Kallergis, G., Morfis, A., Pagounis, A., 1980. Hydrogeological research of brackish karstic springs at Ag. Apostoloi of Kalamos, Nr 31 IGME Athens

Katsikatsos, G., 2000. Geological map of Greece scale 1:50.000, ‘‘Eretria’’ sheet, IGME publication, Athens

Lambeck, K., 1996. Sea Level change and shore-line evolution in Aegean Greece since Upper Palaeolithic time, Antiquity, 70/269, p 588-611.

Lambrakis, N., 1991. Elaboration of the hydrochemical data by PC, Mineral Wealth Vol.74:53-60 (In Greek). [Journal Article]

Lloyd, J.W., Heathcote, J.A., 1985. Natural inorganic hydrochemistry in relation to groundwater, Clarendon Press Oxford p. 294. [

Mettos, A., 1992. Geological and paleogeographic study of continental Neogene and Quaternary formation of NE Attica and SE Biotia Ph.D. Thesis University of Athens 270 p. [

Pagounis, M., 1994. Hydrogeological research of Viotia Prefecture, IGME, Hydrological Hydrogeological research-water reserves determination, Volume I and II Athens.

Parginos, D., Bornovas, I., Mauridis, A., Mettos, A., 1989. Geological map of Greece scale 1:50.000, ‘‘Chalkida’’ sheet, IGME publication, Athens

Papanikolaou, D., et al., 1989. Submarine tectonic map of S. Euboean Gulf, ed. OASP-HCMR-TDTEG

Papanikolaou, D., Mariolakos, H., Lekkas, E., Lozios, S., 1986. Morphotectonic observations in Asopos basin and Oropos coastal zone, Contribution to Neotectonics of N. Attica, Bulletin of EGE volume XX p. 251-267.

Perissoratis, K., Mettos, A., Van Andel, T., 1989. Stratigraphy and Tectonics of S. Euboean Gulf and the wide Neogene basin, Bulletin of EGE volume XXIII/1 p. 209-221.

15th International Congress of the Geological Society of Greece
Athens, 22-24 May, 2019 | Harokopio University of Athens, Greece
Bulletin of the Geological Society of Greece, Sp. Pub. 7 Ext. Abs. GSG2019-212

Hazard identification of the Mediterranean Temporary Mountain Pond ecosystems in Central Greece: A Geo-environmental approach

C. Vasilatos[1], M. Anastasatou[1], P. Pomonis[1], J. Alexopoulos[1], E. Vassilakis[1], M. Stamatakis[1]

(1) National and Kapodistrian University of Athens, Panepistiomiopolis, 15784, Zografou, Athens, Greece, vasilatos@geol.uoa.gr

Mediterranean Temporary Ponds (MTPs) are shallow water bodies which are characterized from a short wet period and their small size (Zacharias et al., 2007). MTPs of Europe have are under an effective protection status, as a result of their identification as a priority habitat (Annex I code 3170*) in the EU Directive 92/43/EEC (Habitats' Directive). These ponds are very delicate ecosystems regarding their hydrological and geochemical characteristics. Due to their small size, they are open to random destruction or other unpredictable dangers. Although small in size, MTPs are complex ecosystems where topography, soil, water and hydrological conditions and microorganisms are closely connected (Zacharias et al., 2007; Stamatakis et al., 2015). The conservation and restoration of such ecosystems is very difficult because of their unique characteristics. The most common threats for MTPs include destruction of the hosting area through human and animal pressures, hydrological disturbance, fire and generally changes in ecological conditions resulting in an increase of competitive plants, nutrition influx, toxic contaminants and wastes, sedimentary deposit filling, exotic-invasive fauna and flora and negative effects from domesticated or hunted fauna (Dimitriou et al., 2006).

The study was carried out in the MTPs area of the National Forest Park of Mt. Oiti (GR2440004) and Mt. Kallidromo (GR2440006). The National Forest Park of Mt. Oiti covers an area of 7.210 ha, extends at altitudes of 400-2.116 m and encompasses a small network of four temporary ponds (TPs) of natural origin. The protected area of Mt. Kallidromo extends at altitudes of 43–1.393 m. and includes several streams which are tributaries of Spercheios River. Mt Kallidromo covers an area of 6.685ha and also encompasses a small network of three temporary ponds. Overall, the survey has included seven small and independent MTPs of high altitude in the areas of Mt. Oiti (Louka, Livadies, Greveno and Alikaina) and Mt. Kallidromo (Nevropolis, Mourouzos and Souvala) (Figs 1, 2).

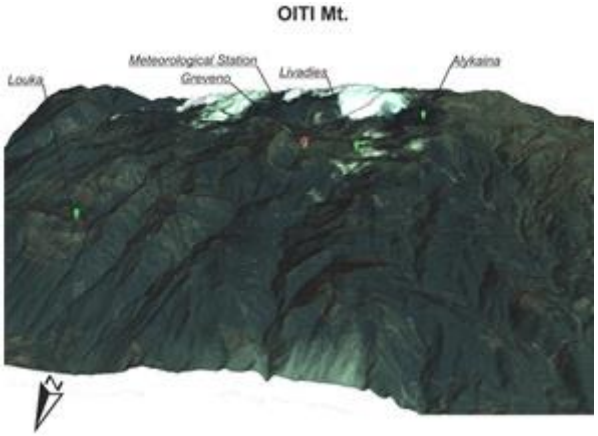

Figure 1. Locations of the studied MTPs of Mt. Oiti, on a Digital Elevation Model (Alexopoulos et al., 2015).



Figure 2. Locations of the studied MTPs of Mt. Kallidromo on a Digital Elevation Model (Alexopoulos et al., 2015).

The current study aims to present a dataset of the geo-environmental parameters in order to assess the potential hazards for these priority habitats. Furthermore, it is also worth mentioning that MTPs are unevenly studied, regarding their geological, hydrological, hydrochemical, geochemical and mineralogical characteristics and this work provides a first report on an integrated evaluation of these parameters regarding the qualitative and quantitative risk identification of the MTPs in Central Greece (Alexopoulos et al., 2015; Delipetrou et al., 2015; Stamatakis et al., 2015; Vasilatos et al., 2015).

A 3-year sampling campaign took place at the temporary ponds (TPs) of the Mt. Oiti and Kallidromo, over two different time periods, autumn and spring, by doing so, we ensured that the data were representative and comparable to the conditions during the wet and the dry period (Stamatakis et al., 2015). Bottom sediments and water samples were collected from each pond. Sampling was carried out at the bottom of the outer part of the habitat, from designated sampling points, with a maximum uppermost of 15cm and side inspection of the plant communities.

The analytical methods used on the sediments consist of granulometric characterization, mineralogical analysis (powder XRD), chemical analysis of major and trace elements (ICP-AES and ICP-MS) and organic matter determination (Stamatakis et al., 2015). Water measurements include pH, Eh, conductivity and TDS values and were performed in situ. The water samples were also analyzed for NO_2^-, NO_3^-, NH_4^+, PO_4^{3-}, HCO_3^- and SO_4^{2-} (Stamatakis et al., 2015).

Regarding mineralogical analysis, Kallidromo bottom sediment samples revealed high participation of quartz and clay minerals, mostly montmorillonite. High clay mineral participation in Kallidromo, results in mostly fine gained fractions.

Oiti samples consist of quartz. However, albite, iron-rich smectites and clay minerals have also been defined. Furthermore, in terms of granulometry, Oiti samples composed mostly of sand.

The studied MTPs develop hydrochemical fluctuations as a result of annual hydrological changes. The MTPs of Mt.Oiti present very low dissolved salts concentrations. On the other hand, ion concentrations in Mt. Kallidromo MTPs are higher due to its geological background. The geochemical results and the water chemistry coupled with temporal analysis indicated that precipitation (meteoric water) is the main mechanism for the Mt. Oiti MTPs formation. Hydrochemistry suggests that there is no interaction between the ponds and the geological background. On the other hand, Mt. Kallidromo MTPs show a strong affection to the local geological background, exhibiting higher Fe concentrations compared to those of Mt. Oiti. Fe presence is related to high concentrations of As and Co, which indicate a strong correlation to the geological formations of the area. pH variation is controlled by processes such as photosynthesis and oxidation of organic matter. These processes can succeed one another in short time. Bottom sediment samples from Mt. Oiti present high concentrations of SiO_2 in comparison to the Kallidromo samples, but show lower Fe_2O_3, MgO and CaO rates. Trace elements in the samples from the Oiti bottom sediments show lower Ni numbers, but all the other trace elements are in comparable numbers. The MTPs present sporadic sensitivity regarding ammonium and phosphate ions, derived from decomposition of organic matter (mostly cattle feces in Oiti and cattle and horse feces in Kallidromo). Pb enrichment noticed in the second sampling campaign of Nevropoli pond in Mt. Kallidromo, which might come from buckshot during hunting activity in the area. The same enrichment determined to the respective bottom sediment sample.

The morphology of Mt. Oiti and Mt. Kallidromo MTPs is unaffected from anthropogenic factors. Animal manures affect the nutritional status of the examined Mediterranean Temporary Ponds. It is noticed that animal manures increase the area's fertility and could result in the invasion of competitive flora species that might reduce the endemic flora of the ponds.

A monitoring procedure would be important for this type of ecosystems (Vasilatos et al., 2015). This procedure may be implemented based on the geological, hydrochemical and geochemical parameters of the MTPs. Some of the parameters that need monitoring are: i) the pond surface area, ii) the climatic conditions, iii) the anion and cation levels, ammonia and phosphorus concentrations, iv) water pH, Eh and conductivity together with total dissolved salts and oxygen saturation in the pond's water and v) the fluctuation of the organic matter in the bottom sediments.

Acknowledgements

This work was supported by the EU frame of LIFE11 NAT/GR/1014 "FOROPENFORESTS". National and Kapodistrian University of Athens is acknowledged for supporting this work.

References

Alexopoulos, J.D., Vassilakis, E., Dilalos, S., Mavroulis, S., Farangitakis, P., Michelioudakis, D., 2015. Geoenvironmental, hydrogeological and geochemical study of the areas of temporary ponds (3170*), Technical Report. Action A2, LIFE11 NAT/GR/1014 'ForOpenForests', Vol. A, p. 3-149.

Delipetrou P., Dimitriadis I., Zikos A., Sarika M., Georghiou K. 2015. Base study and interannual variation of temporary pond (3170*) communities in Mt. Oiti and Mt. Kallidromo. Part A: Flora and Deliverable A.3.1.a for the project LIFE11 NAT/GR/2014 - ForOpenForests. National and Kapodistrian University of Athens - HSPN, p. 67.

Dimitriou, E., Karaouzas, I., Skoulikidis, N., Zacharias, I., 2006. Assessing the environmental status of Mediterranean temporary ponds in Greece. Ann Limnol-Int J Lim. 42(1), 33–41.

Directive 2009/147/EC Of The European Parliament And Of The Council of 30 November 2009 on the conservation of wild birds, 2009, Official Journal of the European Union L 20, p. 7-25.

European Commission, 2003. Interpretation manual of European Union habitats directive. Natura 2000, Nature and biodiversity, EUR 25, 32-3.

Stamatakis, M.G., Vasilatos, Ch., Anastasatou, M., Antonopoulou, S., 2015. Geoenvironmental, hydrogeological and geochemical study of the areas of temporary ponds (3170*), Technical Report. Action A2, LIFE11 NAT/GR/1014 'ForOpenForests', Vol. B, 150-310.

Vasilatos, Ch., Anastasatou, M., Stamatakis, M.G., 2015. Suggested protocol for the monitoring of the Hydrogeochemical Indicators in the context of Action D2 and After-Life integration. Action A2 - Geoenvironmental, hydrogeological and geochemical study of the areas of temporary ponds (3170*), LIFE11 NAT/GR/1014 'ForOpenForests', 26 p.

Zacharias, I., Dimitriou, E., Dekker, A., Dorsman, E., 2007. Overview of temporary ponds in the Mediterranean region: Threats, management and conservation issues. Journal of Environmental Biology. 28(1), 1-9.

15th International Congress of the Geological Society of Greece
Athens, 22-24 May, 2019 | Harokopio University of Athens, Greece
Bulletin of the Geological Society of Greece, Sp. Pub. 7 Ext. Abs. GSG2019-229

Thessalia Plain, a Long Term Problem for Managing Water Resources with Multiple Versions

P. Sampatakakis[1], M. Stefouli[1], P. Krassakis[2], N. Koukouzas[2], S. Kazana[2]

(1) Hellenic Survey of Geology and Mineral Exploration, Spyrou loui 1, C Entrance, Olympic village, 13677, Acharnae, Attiki
(2) Centre for Research and Technology, Hellas (CERTH), 52 Egialias St., 15125 Maroussi, Athens

As one of the world's largest users of fresh water resources, irrigated agriculture has a profound effect on the water cycle, water availability, distribution of water, and water quality. Irrigated croplands are essential contributors– they comprise 15% of arable land yet provide 36% of food (FAOSTAT Statistical Database, http://www.fao.org/statistics/en/). However, they are also large consumers of fresh water resources. Despite high yields and relatively low risk (relative to rain fed lands), the large amounts of water used for irrigation often conflict with competing demands. In semi-arid lands these conflicts are exacerbated by already strained resources, climate change, and population growth. Accurate information on agricultural water needs and withdrawals at appropriate spatial and temporal scales remains a key limitation to joint water and land management decision-making. Addressing these problems require assessments of irrigation practices to ensure that farms are currently using water efficiently and the development of tools to facilitated additional water saving strategies at farm to irrigation district scales. These assessments and tools could be implemented by using medium resolution remote sensing data, which are being increasingly used to monitor, manage, and forecast agriculture water use at different spatial scales.

The coverage of the water needs of the Thessalia plain remains a landmark issue for the country and the local and central authorities. The area under consideration is unique: Numerous research programs and studies, concerning the management of water resources, have been realized. The major irrigation projects have been designed since 1925 up to contemporary times. The scientific community has presented different estimates in relation to the reserves and the real needs. This paper does not attempt to approximate the size of water needs, nor does a reassessment of inventories. It is undertaking a review of the possibility of further exploiting local water resources.

The most recent updates to the water balance carried out by IGME, add significant new results have been derived from the major hydraulic parameters. It must be emphasized that the above mentioned hydraulic parameters consist a vital criterion for the most suitable selection of the technical interventions which must be followed. The output will determine the technical interventions that can be carried out in order to upgrade the underground water reserves through artificial enrichment.

Summarizing, a key element of the present work is that underground aquifers are easily amenable to artificial enrichment at depths of <100 m in the selected region of Thessalia Basin. Aim of the study is to introduce the following points:

a) The selection of a pilot area is located in Thessalia plain, (Figure 1) which has high water permeability (region of the stream sediment cones). In addition, 23 cone areas are presented in the 1:50,000 scale IGME geological maps, of total surface area of 12.9 km^2 which have been analysed.
b) Applying mild forms of "artificial enrichment", utilizing the local hydrographic network and working in shallow aquifers, "peripheral hydraulic loading". Different hydrologic parameters have been estimated using the Digital Elevation Model of Ktimatologio S.A. with 5 m. resolution: Bifurcation Ratio, Length Ratio Drainage Density, Constant of Channel Maintenance, Length of Overland Flow Stream Frequency, Basin Length, Elongation Ratio, Basin Relief, Relief Ratio, Ruggedness Number and Mean Stream Slope. Furthermore, basins directly related with their outflow to the cones that have been selected. Actually, 62% of all basins have an altitude that varies between 138 to 414 meters, while 98.86% of the total area of the basin includes slopes that vary between 0 to 35 degrees.
c) A total length of 815 km for the streams running the area have been mapped and analysed, 190 km are directly related with their flow to cones (Figure 1). A number of basins of a total area of 73. 6 km^2 contribute to surface flows towards the sedimentary cones. Drainage density of basins varies between 0.0024 to 6.29.
d) No disturbance to existing land uses by the development of technical enrichment interventions. Land uses are effectively monitored using medium resolution satellite data.
e) Exploitation of surface run-offs in non-flood time periods to avoid accumulation of sediment within the enrichment channels.
f) Using a combination of satellite and vector data in appropriate and homogenized geospatial databases to monitor and support the operation of these mild technical projects. This is possible after the estimation of significant environmental indicators on a weekly basis (NDVI, NDWI, Chlorophyll A, e.t.c), which are directly related to the status of the crops.

It could be generally agreed that results of the present work are important and critical for the sustainable artificial enrichment of ground water aquifers. Furthermore, remote sensing techniques can be used to support watershed implementation plans to satisfy future water needs.

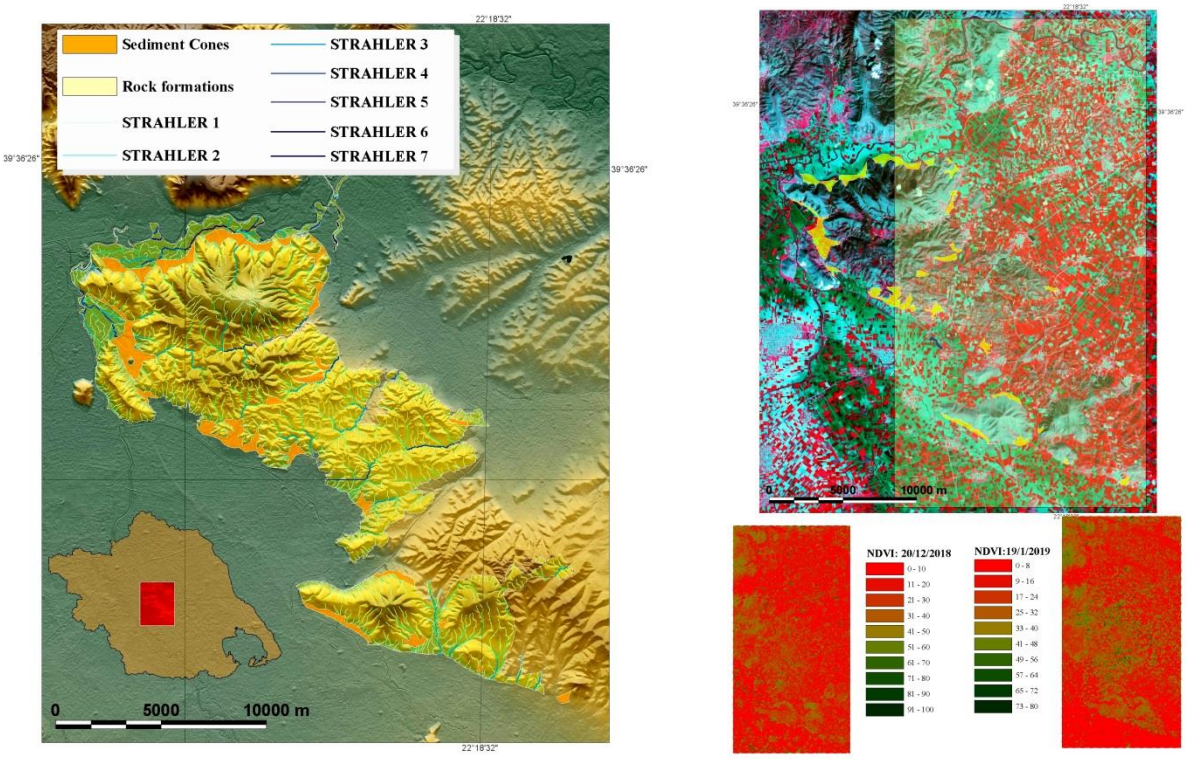

A **B**

Figure 1. A: Map of the study area located in Thessalia plain, in which sediment cones, rock formations and drainage network are presented. B: Landsat image of April 2017 of the pilot area of study. NDVI estimates of 20/12/2018 and 19/1/2019 Sentinel 2 images for the area (transparent polygon). Monitoring is supported.

Acknowledgements

The authors would like to thank Ktimatologio S.A. for providing the Digital Elevation Model of the study area.

References

Bornovas, I., Filipakis, N. 1969. Geological Map of Greece 1:50.000, Sheet Farsala. I.G.M.E., Athens.
Bornovas, I., Filipakis, N. 1969. Geological Map of Greece 1:50.000, Sheet Sofhades. I.G.M.E., Athens.
Plastiras, V., Filipakis, N. 1985. Geological Map of Greece 1:50.000, Sheet Larisa. I.G.M.E., Athens.
ESA scientific Data Hub https://scihub.copernicus.eu/dhus/#/home.
FAOSTAT Statistical Database (http://www.fao.org/statistics/en/).
USGS Explorer website (https://earthexplorer.usgs.gov).

15th International Congress of the Geological Society of Greece
Athens, 22-24 May, 2019 | Harokopio University of Athens, Greece
Bulletin of the Geological Society of Greece, Sp. Pub. 7 Ext. Abs. GSG2019-239

Chromium-manganese redox couple resulting in elevated Cr^{6+} concentration in groundwater of the Psachna basin, Central Euboea, Greece

P. Papazotos[1], E. Vasileiou[1], M. Perraki[1]

(1) School of Mining and Metallurgical Engineering, Division of Geo-sciences, National Technical University of Athens, 9 Heroon Polytechniou St., 15773 Zografou, Greece, papazotos@metal.ntua.gr

Chromium (Cr) includes two main species in natural aquatic systems, the trivalent (Cr^{3+}) and the hexavalent (Cr^{6+}) one (Richard and Bourg, 1991). The speciation of Manganese (Mn) in aquatic environment is controlled by the prevailing physical and chemical conditions, which includes mainly two oxidation states, the soluble divalent (Mn^{2+}) and the insoluble tetravalent (Mn^{4+}) manganese (Homoncik *et al.*, 2010). Mn mobility, speciation and concentration are controlled by the physical parameters of pH, redox potential (Eh), dissolved oxygen (DO) and also by the aqueous solution chemistry (Homoncik *et al.*, 2010).

Mn-oxide minerals, in which trivalent manganese (Mn^{3+}) and/or Mn^{4+} is accommodated, such as birnessite (Fendorf *et al.*, 1992), pyrolousite (Eary and Rai, 1987), asbolane-type (Fandeur *et al.*, 2009), lithiophorite-type (Fandeur *et al.*, 2009) and cryptomelane (Feng *et al.*, 2007) have been reported to act in rocks and soils as natural oxidizing agents for the redox transformation of Cr^{3+} into Cr^{6+} in three (3) main steps (Amacher and Baker, 1982; Eary and Rai, 1987; Richard and Bourg, 1991):

(1) Adsorption of Cr^{3+} on the surface sites of MnO_2,
(2) Oxidation of Cr^{3+} to Cr^{6+} by surface Mn^{4+},
(3) Desorption of the reaction products, Cr^{6+} and Mn^{2+} in the aqueous solution

The oxidation reaction takes place according to the following equation:

$$Cr^{3+} + 1.5\ \delta MnO_2(s) + H_2O \rightarrow HCrO_4^- + 1.5Mn^{2+} + H^+ \quad (1)$$

The amount and the surface area of Mn-oxides are crucial factors and control the oxidation rate of Cr^{3+}, which is initially very fast, but through the time it slows down considerably (Eary and Rai, 1987). In addition, the oxidation rate of Cr^{3+} is highly dependent pH values (Amacher and Baker, 1982).

The aim of this research is to examine the speciation of dissolved Mn in groundwater of the Psachna basin, according to pH and Eh conditions, in order to investigate the oxidation of Cr^{3+} into Cr^{6+}.

The Psachna basin - an ultramafic dominated environment- is located in the central part of Euboea Island; the main land use is agriculture. The geological formations of the Psachna basin are the carbonate rocks (limestones, dolomites), the ultramafic/mafic rocks (serpentinites, peridotites, diabases), the Fe-Ni ore deposits and post-Alpine sediments of Neogene and Quaternary age. The main aquifer system of the study area is developed into Quaternary sediments of ultramafic and carbonate origin. A large set of major ions and trace elements of thirty-four (34) groundwater samples were analysed and presented herein. The physical parameters (electrical conductivity-EC, DO, pH and Eh) were measured in-situ immediately after samples were collected according to YSI Professional Digital Sampling System (ProDSS); The analyses of major ions were determined by atomic absorption spectrometry (Ca^{2+}, Mg^{2+}, Na^+ and K^+), by titrimetry (Cl^- and HCO_3^-) and by turbidimetry (SO_4^{2-}) and the analyses of trace elements were performed at Analytical Laboratories of Bureau Veritas Commodities Canada Ltd, by means of inductively coupled plasma mass spectrometry (ICP-MS).

pH ranges from 7.21 to 8.27 (mean 7.64) indicating slightly alkaline conditions; Eh varies from 135.7 mV to 291 mV (mean 254.7 mV) suggesting an oxidative geological environment. The results of this study showed high concentrations of Cr (up to 161.5 μg L^{-1}), Cr^{6+} (up to 131.1 μg L^{-1}) and NO_3^- (up to 540 mg L^{-1}) in groundwater. The majority of the groundwater samples (70%) analysed herein, exceed the limit of 50 μg L^{-1} for Cr concentration in drinking water of World Health Organization (WHO, 2011). The remarkable extreme values of NO_3^- are over 10 times higher than the guideline value of 50 mg L^{-1} (WHO, 2011) and indicate the intense agricultural activities accompanied by extensive use of Nitrogen-bearing fertilizers. The concentrations of Mn (up to 25.53 μg L^{-1}) are below the guideline value (50 μg L^{-1}) for drinking water of WHO (2011).The oxidation of Cr^{3+} in natural aquatic environment is a process mainly attributed to the Mn oxides (Eary and Rai, 1987; Richard and Bourg, 1991). pH-Eh plots in the Pourbaix diagram for Mn (1966) revealed, that Mn^{2+} dominates, even at low concentration, in the groundwater samples of the Psachna basin (Fig. 1). Besides, Economou-Eliopoulos *et al.*, (2014) identified Mn-oxide minerals (birnessite, asbolane and cryptomelane) in the Euboea soils, which combined with the presence of Mn^{2+} in groundwater supports the natural oxidation mechanism of Cr^{3+} into Cr^{6+} by Mn oxides.

The weak to moderate correlation coefficients and the non-linear relationship between physical parameters (DO, EC, pH and Eh) and Mn concentrations indicate an unclear mechanism that is related to the Mn solubility and the spatial distribution of Mn concentrations in groundwater of the Psachna basin. The elevated concentrations of Cr^{6+} (up to 131.1 μg L^{-1}) may be attributed to the oxidation of Cr^{3+} by the redox couple of Mn^{2+}/Mn^{4+}. An additional external oxidant agent is likely to affect the water system synergistically with Mn redox couple increasing the Cr^{6+} concentrations.

Previous studies showed that DO could oxidize Cr^{3+} into Cr^{6+}, but the oxidation rate is very slow and enables Cr^{3+} to take part in faster reactions such as sorption or precipitation (Eary and Rai, 1987). Therefore, oxidation of Cr^{3+} by DO seems to be unlikely in soils. An additional potential redox couple except for Mn^{2+}/Mn^{4+} is NO_2^-/NO_3^- , which could make possible the redox transformation of Cr^{3+} into Cr^{6+} in natural aquatic environments (Richard and Bourg, 1991; Stamatis *et al.*, 2011). Spatial distribution maps of Cr^{6+} and NO_3^- support a possible link between these two parameters; this hypothesis is strengthened by the strong correlation coefficient between NO_3^- and Cr^{6+} (r=0.68). However, the exact mechanism that the presence of NO_3^- results in increased Cr^{6+} concentration in groundwater has yet to be defined.

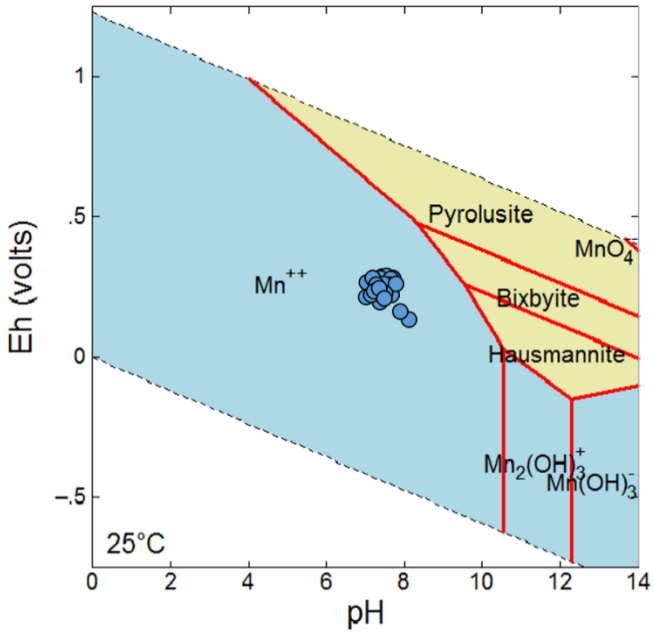

Figure 1. Eh-Ph diagram (Pourbaix, 1966) of the system Mn-O-H.

References

Amacher M. C., Baker D. E., 1982. Redox reactions involving chromium, plutonium and manganese in soils. Final Report DOE/DP/04515-1, Pennsylvania State University, Institution for Research on Land and Water Resources.

Eary, L. E., Rai, D., 1987. Kinetics of Chromium(III) Oxidation to Chromium(VI) by Reaction with Manganese Dioxide. Environmental Science and Technology.]

Economou-Eliopoulos, M., Frei, R., Atsarou, C., 2014. Application of chromium stable isotopes to the evaluation of Cr(VI) contamination in groundwater and rock leachates from central Euboea and the Assopos basin (Greece). Catena

Fendorf, S. E., Fendorf, M., Sparks, D. L., Gronsky, R., 1992. Inhibitory mechanisms of Cr(III) oxidation by δ-MnO2. Journal of Colloid and Interface Science.

Feng, X. H., Zhai, L. M., Tan, W. F., Liu, F., He, J. Z., 2007. Adsorption and redox reactions of heavy metals on synthesized Mn oxide minerals. Environmental Pollution.

Homoncik, S. C., MacDonald, A. M., Heal, K. V., Ó Dochartaigh, B. É., Ngwenya, B. T., 2010. Manganese concentrations in Scottish groundwater. Science of the Total Environment.

Pourbaix, M., 1966. Atlas of electrochemical equilibria in aqueous solutions (English edition). Pergamon press, Oxford.

Richard, F. C., Bourg, A. C. M., 1991. Aqueous geochemistry of chromium: A review. Water Research.

Stamatis, G., Alexakis, D., Gamvroula, D., Migiros, G., 2011. Groundwater quality assessment in Oropos-Kalamos basin, Attica, Greece. Environmental Earth Sciences.

World Health Organization (WHO). (2011): Guidelines for drinking water quality, World Health Organization Geneva, 4th Edition.

15th International Congress of the Geological Society of Greece
Athens, 22-24 May, 2019 | Harokopio University of Athens, Greece
Bulletin of the Geological Society of Greece, Sp. Pub. 7 Ext. Abs. GSG2019-248

Predicting Soil Erosion Rate Before and After Wildfires: The Case of Pineios dam drainage basin

M. Michalopoulou[1], K. Kavoura[1], N. Depountis[1], N. Sabatakakis[1]
Department of Geology, University of Patras, University campus 26504, Rio, Greece, geo12088@upnet.gr

Introduction

One of the most significant outcomes of soil erosion in drainage basins is the extensive deposition of sediment within dam's water-reservoirs. This procedure could lead to an increased aggradation rate in the dam's water-reservoir which results in a reduced water storage capacity. World widely, soil erosion is calculated with the use of the Revised Universal Soil Loss Equation (RUSLE) adopted in a Geographical Information System (GIS) framework. In the current study, RUSLE and GIS were used for predicting soil erosion rate of Pineios dam drainage basin, before and after the wildfires of August 2007 occurred in the Ilia regional unit; thus examining the aggradation rate in the dam's water-reservoir. Factors that control RUSLE equation were imported in the GIS framework and applied on a Digital Elevation Model (DEM) map of Pineios River basin with 85m accuracy. Soil erosion rates were calculated before and after the wildfires by using as a dependent variable the cover management factor C, which is strongly influenced by large destructive fires.

Description of the study area

Pineios dam is located in the Ilia regional unit, Western Greece and its name comes from the homonymous river. It is one of the longest earth-filled dams in Greece. The Pineios River basin occupies an area of 1026 km^2, whereas the dam's drainage basin occupies an area of 673.41 km^2 (Figure 1). Surface water run-off from the dam's drainage basin is collected to a large water reservoir that occupies an area of 19.87 km^2. Pineios dam has a length of 2175 m, a height of 50 m, an absolute crest height of +101 m and is constructed with an impermeable clayey core. Its reservoir has been designed to collect 415*10^6 m^3 of surface water. The upper and lower height of water in the reservoir is +93 m and +65 m, respectively. The reservoir started to fill in with water after the completion of the dam's construction in 1967 (Depountis *et al.*, 2018).

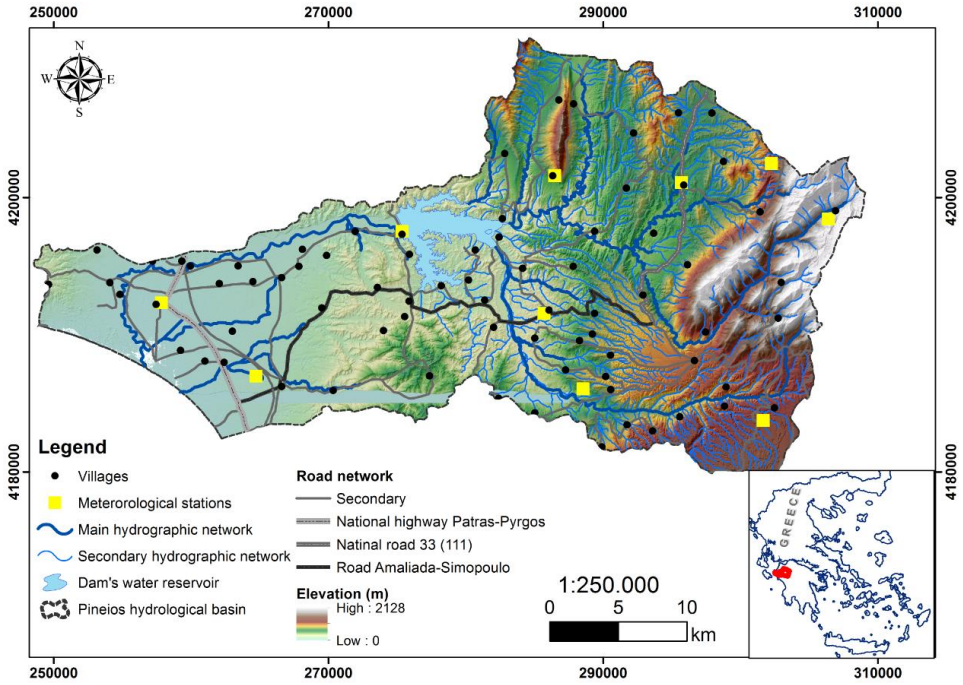

Figure 1. Digital Elevation Model (DEM) map of Pineios River basin.

The RUSLE equation

Revised Universal Soil Loss Equation (Renard *et al.*, 1997) is based on the Universal Soil Loss Equation, USLE (Wischmeier and Smith, 1978), with soil erosion rates calculated by the following formula: **SE = R*K*L*S*C*P. SE** is the computed average soil loss per unit area expressed in tones/ha/year, **R** is the rainfall-runoff erosivity factor expressed in MJ.mm.ha^{-1}.h^{-1}.year, **K** is the soil erodibility factor expressed in t.h.MJ^{-1}.mm^{-1}, **L** is the slope length factor, **S** is the slope steepness factor, **C** is the cover management factor and **P** is the erosion control practice factor. In the current research R factor was calculated by using rainfall data from the seven (7) meteorological stations located in the dam's drainage basin, K factor was calculated by applying the appropriate erodibility factors in each of the geological formations prevailing in the area of interest, L and S factors were calculated by using a Digital Elevation Model (DEM) map with

85m accuracy (Figure 1). P factor was set to 0,5 taking into consideration that a high percentage of the study area is devoted to agricultural land such as olive groves, complex cultivation patterns, non-irrigated arable land, land principally occupied by agriculture, with significant areas of natural vegetation, which means that erosion control techniques are implemented indirectly, mainly with terraces (Koulouri, 2004). Finally the dependent variable C which stands for the cover management factor was set to different values before and after the wildfires of 2007 by modifying appropriately land uses from the Corine data base.

Soil erosion rate before and after the wildfires

By applying the RUSLE equation in the GIS framework, with the assumption that LS factor's equation equals to LS = (FlowAccumulation*CellSize/22.13)$^{0.6}$(Sin(Slope*0.01745)/0.09)$^{1.3}$*1.3 (Mitasova and Mitas, 2001) and C factor has been increased by an average value of 35.29 % due to wildfires, the following soil erosion rate maps are produced before (a) and after (b) the wildfires. In detail, the raster files that represent the six factors of RUSLE were multiplied in order to create a new raster image. Therefore, a composite predictive soil erosion rate map was created, with the soil loss given in t/ha. Soil erosion rate before the wildfires calculated as SE(a)=80 t/ha/year, whereas after the wildfires SE(b)=104 t/ha/year; thus, an increase of 30% in soil loss occurred due to the wildfires.

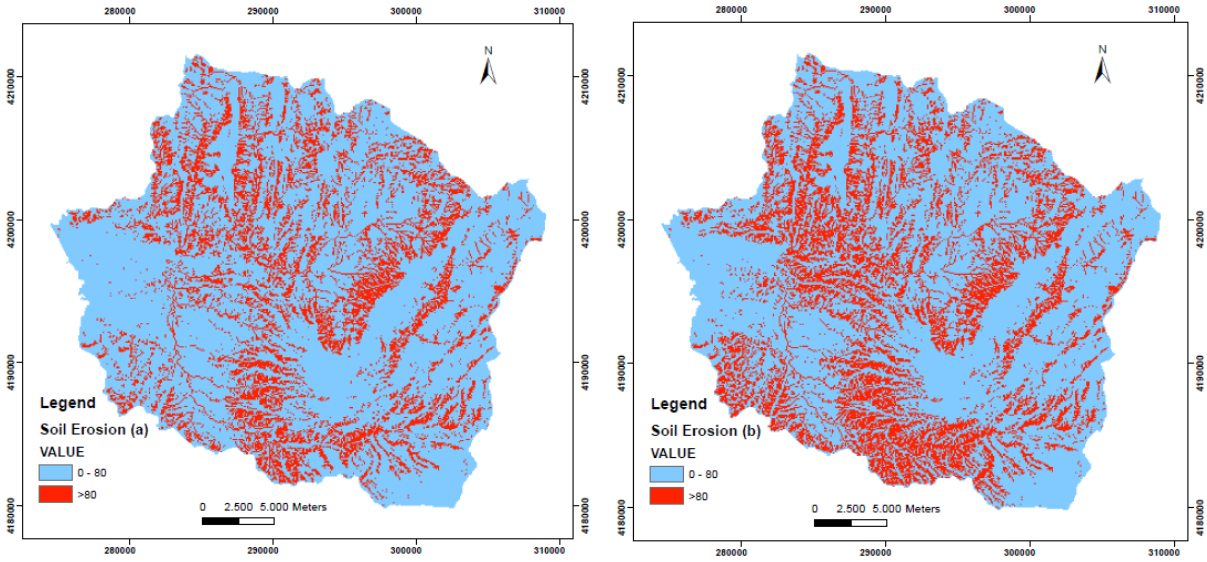

Figure 2. Soil Erosion (SE) rate map of the basin of Pineios dam before (a) and after (b) the wildfires of 2007.

Conclusion

With the use of RUSLE equation and GIS framework, soil erosion rate of Pineios dam drainage basin was calculated as SE(a)=80 t/ha/year and SE(b)=104 t/ha/year, before and after the wildfires of 2007, respectively, by using a DEM with 85m accuracy. This reflects to an increase in soil erosion of 30% and the controlling factor for this increase is basically the cover management factor C. A significant amount of this soil loss volume has been deposited for the last 50 years in the water reservoir of Pineios dam. This volume has to be verified with measurements in the thickness of the reservoirs deposited material in order to validate the accuracy of the results obtained with the use of RUSLE equation.

Acknowledgements

This research was carried out under the support of the "Pineios Water Supply Unit". The authors wish to express their sincere appreciation to its generous support.

References

Depountis, N., Vidali, M., Kavoura, K., Sabatakakis, N., 2018. Soil erosion prediction at the water reservoir's basin of Pineios dam, Western Greece, using the Revised Universal Soil Loss Equation (RUSLE) and GIS. WSEAS Transactions on Environment and Development, 14: 457-463. E-ISSN: 2224-3496.

Renard, K.G., Foster, G.R., Weesies, G.A., McCool, D.K., Yoder, D.C., 1997. Predicting soil erosion by water: a guide to conservation planning with the Revised Universal Soil Loss Equation (RUSLE), Agriculture Handbook, No.703, USDA-ARS.

Wischmeier, W.H., Smith, D.D., 1978. Predicting rainfall erosion losses, a guide to conservation planning, Agriculture Handbook, No. 537.

Mitasova, H. and L. Mitas, 2001. Multiscale soil erosion simulations for land use management, in Landscape Erosion and Evolution Modeling (edited by R.S. Harmon and W.W. Doe III), Springer US, New York, 321-347.

Koulouri, M., 2004. Soil water erosion and land use change in the Mediterranean: abandonment of traditional extensive cultivation. Ph.D. Thesis. Department of Environmental Studies, University of the Aegean, 218 p.

15th International Congress of the Geological Society of Greece
Athens, 22-24 May, 2019 | Harokopio University of Athens, Greece
Bulletin of the Geological Society of Greece, Sp. Pub. 7 Ext. Abs. GSG2019-258

Imaging Industrial Pollution Using Electric Resistivity Tomography (ERT). Preliminary Results from Thessaloniki Tanneries (Greece)

A. Atzemoglou
Hellenic Survey for Geology and Mineral Exploration (HSGME), 1 Fragon str., 54626 Thessaloniki, Greece. matzem@thes.igme.gr

Introduction

Pollution from organic and inorganic pollutants is very frequent in places with industrial activity. The existence of pollution plumes in shallow or even in deeper aquifers is inevitable. Pollution can be due to raw materials that are used during treatment of industrial products, during the storage of intermediary products and from the remains (wastes). The cost of risk assessment for the polluted regions, with the existing geochemical environmental techniques, is judged expensive, time-consuming and does not provide results for the entire region.

Imaging of the pollution of waters in rural regions, recording the pollution in places of industrial wastes deposition, imaging of salination of underground water regions, imaging of the water-bearings stratum pollution from petroleum products and other environmental problems have been identified using lot of geophysical techniques. The fast cover with dense network of measurements in the entire region that offers the possibility of extension is one of the main advantages of the geophysical methods. In opposition, the geochemical techniques cover parts of the polluted area with specific samplings and chemical analyses.

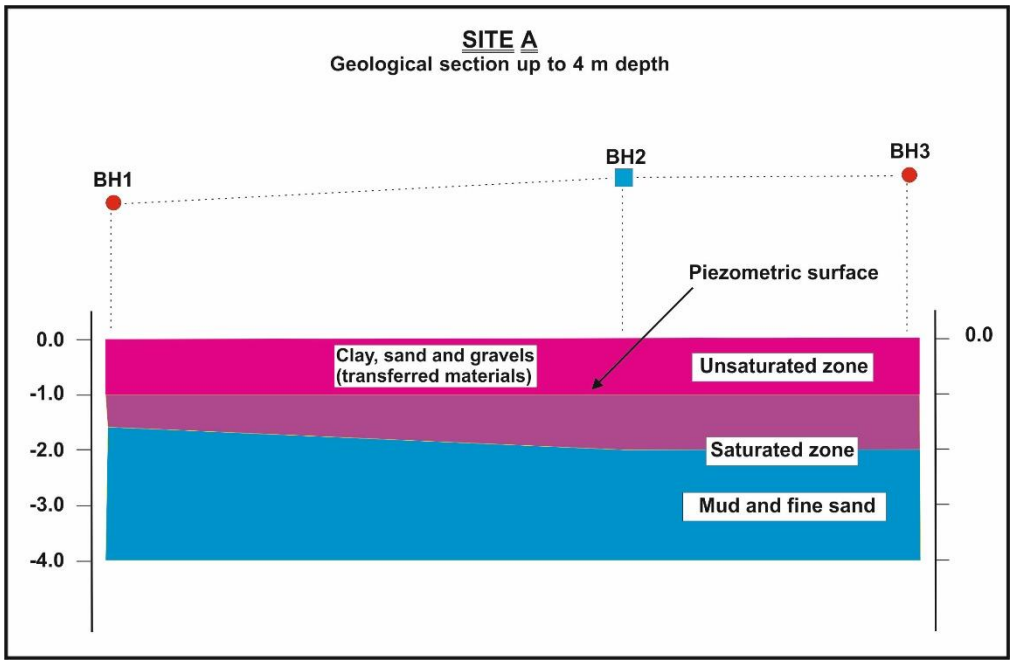

Figure 1. Geological section of site A according to boreholes BH1, BH2 and BH3.

Geological and hydrogeological setting

The tanneries of Thessaloniki established in 1970. Then they were developed arbitrarily. Surface channels with polluted liquids, storage of dangerous chemical substances without particular precautions etc. had resulted the pollution of subsoil and underground waters and the progressive demission of the environment.

The geophysical research was realized in 3 selected places A, B and C. The geological and hydrogeological conditions in region A, as these were recorded the shallow drillings (BH1, BH2 and BH3) are as follow: Unconsolidated geological formations (sediments) up to 5 m in depth, consisting of sands, fluvial and torrential deposits, red clays with limestone conglomerates (figure 1). Underground water measurements showed that the pH values are normal and the electric conductivity values are between 3,41 and 6,95 mS / cm. Low concentration values (0,5 - 6,8 mg/l) of free oxygen prove the existence of organic pollutants.

The chromium (Cr^{+3}), the zinc (Zn) and the arsenic (As) are the inorganic pollutants in the soil and the dichloromethane and the acetone are main organic.

The chromium (Cr^{+3}) is also observed in the underground water while the petroleum products (TPH) are main organic pollutants (Atzemoglou et al. 2003).

Geophysical research and results

We applied the electric resistivity tomography (ERT) at the region of tanneries of Thessaloniki (Greece), aiming at the investigation of subsoil and underground water in-depth up to 5 meters. The research was realized with the LUND system of ABEM that supports many electrode configurations and 42 electrodes (max.). Data were initially plotted in pseudosections and bad quality data points were rejected. Subsequently the data were processed using a non-linear 2-D inversion scheme and the results of the region A are showed in figure 2.

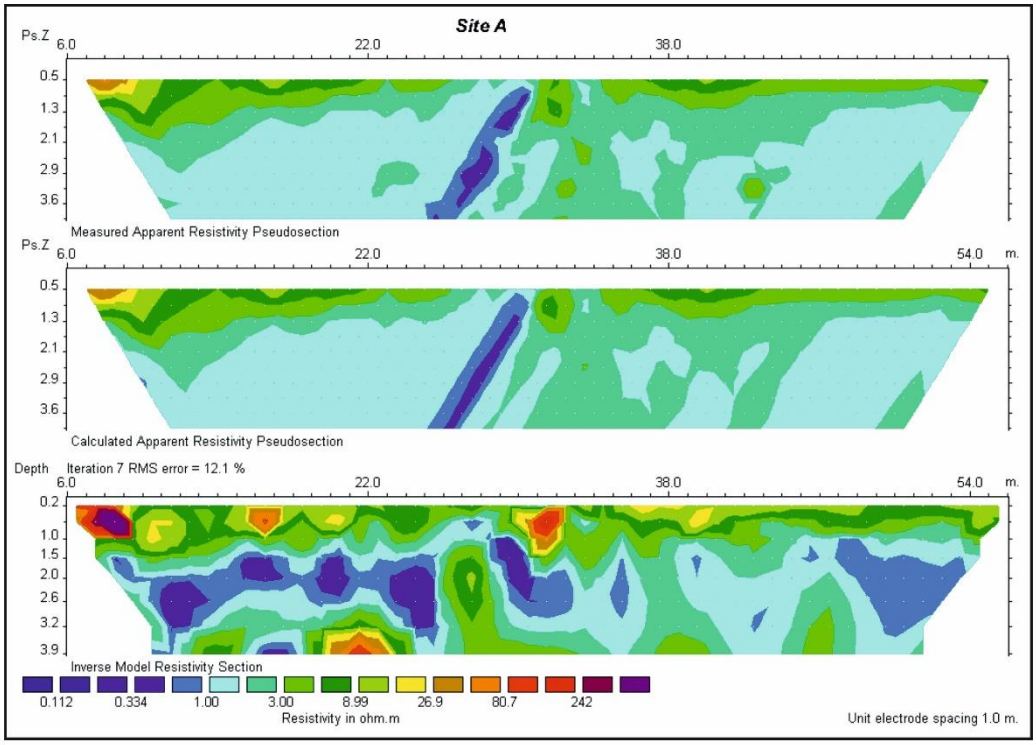

Figure 2. Inversion of geoelectrical measurements in region A.

The geophysical identification of the pollutants present in the underground water depends mainly on the contrast between the rock porosity properties, when it is saturated with water, and when it contains various humid pollutants. The rock resistivity depends also from the rock's electronic conductivity and the electrolytic (ionic) conductivity of the water contained in their pores. Thus the measurement of resistivity is decisive. The organic and inorganic substances can cause decrease of the resistivity of the materials. This decrease could be referred to the increase of the total dissolved salts (TDS) found in the rock.

The content of soil samples in chromium, at 1-meter depth, is 5 to 10 mgr/l and is lower (1%) than the surface chromium values. That content does not influence considerably to the electronic conductivity. The content of samples of water in chromium reaches the 0,2 mgr / l percentage that according to relation TDS and conductivity (Driscoll, 1986) cannot increases the conductivity of water above 0,4 mS/cm. If we take into consideration that the measured conductivity of water is 3.000 until 7.000 mS/cm (salination), we could conclude that the effect of Cr concentration to electric resistivity measurements is very small. With the same reasoning, the content in hydrocarbons of petroleum products does not affect the measurements of electric resistivity. The content in NaCl in studied region is too high (noise) that the previous concentrations does not affect decisively to measured resistivity values.

References

Atzemoglou, A., Skianis, G. (2003). Geophysical research in Thessaloniki tanneries, IGME, internal report. (text in Greek).
Driscoll, F. (1986). Groundwater and wells. Mower House publications.

15th International Congress of the Geological Society of Greece
Athens, 22-24 May, 2019 | Harokopio University of Athens, Greece
Bulletin of the Geological Society of Greece, Sp. Pub. 7 Ext. Abs. GSG2019-261

The artificial increase of microroughness of various recycled materials used as aggregates in concretes contributes to the increase of the final concrete strength

P.P. Giannakopoulou[1], P. Petrounias[1], A. Rogkala[1], M. Kalpogiannaki[1]

(1) Section of Earth Materials, Department of Geology, University of Patras, 265 04, Patras, Greece, peny_giannakopoulou@windowslive.com

Abstract

This study examines different types of recycled materials such as beer green glass and waste tile used in different mixtures in order to prepare concrete specimens and more specifically their effect on concrete strength and how their microroughness influences the mechanical strength of the produced concrete specimens. Concrete, a mixture of cement, aggregates and water, is the most used man-made material and has numerous civil engineering applications (Jackson, 1981, Neville, 2005, Taylor, 1994). Aggregates are the major constituents of concrete, typically occupying between 70% and 80% of its volume. The rapid growth of the construction industry has led to environmental problems caused by excessive mining and usage of natural resources such as aggregate and cements (Mo *et al.*, 2016). Therefore there is a need to improve the reuse value of waste materials. Since the usage of conventional aggregates is not environmental friendly and causes depletion of natural resources (Medina *et al.*, 2012), a variety of waste materials such as clay, waste glass, asphalt, waste tile and plastic wastes have been recycled and used as aggregate in concrete blocks. In concrete, most observed faults either in the case of waste glasses or in the cases of asphalt and tiles are due to their smooth surfaces (Abdallah *et al.*, 2014, Meng *et al.*, 2018) which are responsible for the extended cracks and detachments along the rims of the aggregate particles with the cement paste, limiting the final concrete strength (Petrounias *et al.*, 2018). The surface texture of the recycled materials was studied by using Secondary Electron Images. Since the microroughness of materials used as aggregates in concretes plays severe role on their final strength as it is responsible for the adequate bonding between the cement paste and the aggregate particle, artificial increase of microroughness of the recycled materials specimens was carried out using quartz primer for coating the recycled materials three times, one every 24 hours. Normal concrete cube specimens (150×150 mm) were made from the different mixtures containing recycled materials. The recycled materials were crushed through standard sieves and separated into the size classes of 2.00-4.75, 4.45-9.5 and 9.5-19.1 mm and then washed before their used in concrete specimens. These specimens were tested in a compression testing machine. After the compressive strength test, the quality cohesion between the cement paste and the aggregate particles in concretes were examined. The concrete strength ranged from 14 to 20 MPa. The lowest compressive strength values were observed in concrete specimens made by mixtures containing exclusively glass as aggregates (Fig. 1a). On the other hand, concretes made by mixtures of glass with primer and tile with primer present the highest compressive strength values.

Table 1. Compressive strength of concrete specimens of different mixtures of recycled materials (*glass with primer in the small class and tile with primer in the other two classes, ** tile with primer in the big class and glass with primer in the two small classes).

Sample	Compressive strength of concrete (MPa)
Glass	14
Glass with primer	15
Tile	17
Tile with primer	17.5
Glass with primer and tile with primer*	20
Glass with primer and tile with primer**	18

The results of the compressive strength test of the concrete specimens are in accordance to the artificial given microroughness of the recycled materials used as aggregates in concretes. The artificial increase of microroughness seems to positively contribute to all strength values of the studied concrete specimens. The observations of the surface texture of the recycled aggregates show glassy to smooth surfaces for the studied glass, tile and smooth to almost rough for the studied glass and tile grains which have been coated with quartz primer. In general, the quartz primer, as high adherence material, gave microroughness to the recycled materials used as aggregates in concrete specimens and hence increased their final strength. More specifically, among the various produced concrete specimens, these made by the mixture of glass coated with quartz primer in the smaller class and tile coated with quartz primer in other two classes, attributed to the highest concrete strengths (Fig. 1b).

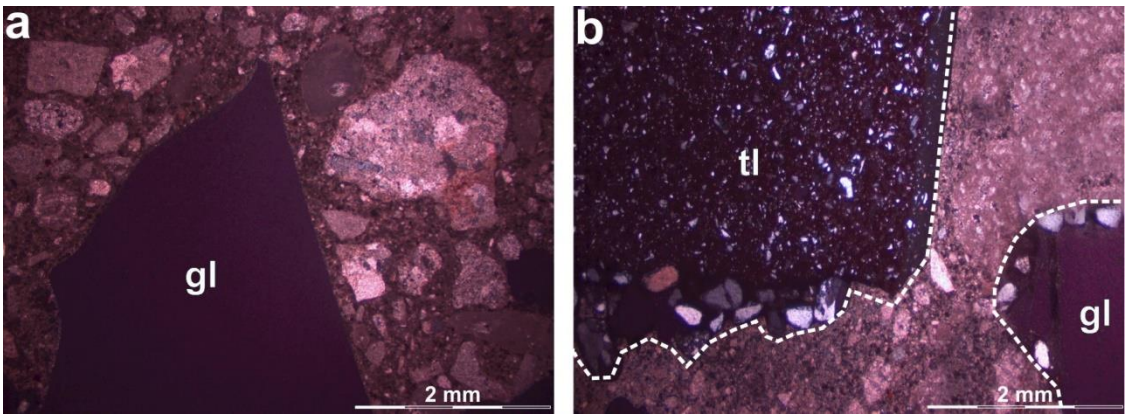

Figure 1. Photomicrograph of concrete specimen in crossed nicols showing a. glass as aggregate, b. mix of beer green glass with quartz primer and tile with quartz primer as aggregates. gl: glass, tl:tile.

This is due both to the artificial increase of and to the optimum interlocking of grains which has been created from the combination of glass coated with quartz primer in the small class tile coated with quartz primer in the bigger classes. Subsequently, concrete specimens made by mixture of tile coated with quartz primer in the bigger class and glass coated with quartz primer in the smaller classes attributed in lower but satisfactory strength. The lower strength is attributed to greater participation of glass coated with quartz primer in concrete specimens. However, its satisfactory strength is due to the artificial increase of microroughness of the aggregate particles as well as due to the good interlocking of grains. The main conclusions of this work are the above:

- The artificial increase of microroughness of the used recycled materials used as aggregates in concretes seems to be determinant factor for the final concrete strength.
- The mixture of glass coated with quartz primer in the small class and tile coated with quartz primer in other two classes due to the optimum cohesion between the cement paste and the aggregate particle as well as due to interlocking of grains lead to the optimum mixture of recycled materials in concretes.

Acknowledgements

The authors wish to thank Dr. Drakopoulos of the Foundation for Research and Technology-Hellas (FORTH) Institute of Chemical Engineering and High Temperature Chemical Processes (ICE/HT) Rio-Patras, Greece and A.K Seferlis of the Laboratory of Electron Microscopy and Microanalysis, University of Patras for his assistance with the microanalyses and SEM micrographs.

References

Abdallah, S., Fan. M. 2014. Characteristics of concrete with waste glass as fine aggregate replacement. International Journal of Engineering and Technical Research. 2, 11-17.

Jackson, N. 1981. Civil Engineering Materials, Macmillan Press Ltd, London.

Medina, C., De Rojas, M.S., Frías, M. 2012. Reuse of sanitary ceramic wastes as coarse aggregate in eco-efficient concretes. Cement. Concrete. Composites. 34 (1), 48-54.

Meng, Y., Ling, T.G., Mo, K.H. 2018. Recycling of wastes for value-added applications in concrete blocks: An overview. Resources, Conservation & Recycling. 138, 298-312.

Mo, K.H., Alengaram, U.J., Jumaat, M.Z., Yap, S.P., Lee, S.C. 2016. Green concrete partially comprised of farming waste residues: a review. Journal of Cleaner Production. 117, 122-138.

Neville, A.M. 2005. Properties of Concrete, ELSB 5th Edition, Pearson Education Publishing Ltd. London.

Petrounias, P., Giannakopoulou, P.P., Rogkala, A., Stamatis, P.M., Tsikouras, B., Papoulis, D., Lampropoulou, P., Hatzipanagiotou, K. 2018. The Influence of Alteration of Aggregates on the Quality of the Concrete: A Case Study from Serpentinites and Andesites from Central Macedonia (North Greece). Geosciences 8, 115.

Taylor, G.D. 1994. Materials in Construction. Second Edition, Longman Group Ltd, Longman House, Burnt Mill.

15th International Congress of the Geological Society of Greece
Athens, 22-24 May, 2019 | Harokopio University of Athens, Greece
Bulletin of the Geological Society of Greece, Sp. Pub. 7 Ext. Abs. GSG2019-265

The impact of secondary phyllosilicate minerals on concrete strength produced from mafic and ultramafic aggregate rocks

M. Kalpogiannaki[1], P. Petrounias[1], A. Rogkala[1], P.P. Giannakopoulou[1], P. Pomonis[2], B. Tsikouras[3], K.Hatzipanagiotou[1]

(1) Section of Earth Materials, Department of Geology, University of Patras, 265 04, Patras, Greece, maria.kalpogiannaki@gmail.com
(2) Department of Geology and Geoenvironment, National and Kapodistrian University of Athens, Panepistimioupolis Zografou, 15784 Athens, Greece,
(3) Physical and Geological Sciences, Faculty of Science, Universiti Brunei Darussalam, Jalan Tungku Link, Gadong BE1410, Bandar Seri Begawan, Brunei Darussalam

Abstract

The aim of this study is to highlight the impact of the secondary phyllosilicate minerals in mafic and ultramafic rocks used as aggregates on concrete strength and more specifically the influence of microroughness of the aggregates in the adherence of the cement paste. The studied aggregate samples used for the production of concrete, were collected from ophiolite complexes in Central Macedonia. Quantitative petrographic analysis indicates that the tested samples display various percentages of secondary phyllosilicate minerals. Mineral quantification of the studied rock samples was performed by using the Rietveld method on bulk samples. The ocean-floor metamorphism variably affected the collected ultramafic and mafic samples. During this process primary minerals from ultramafic and mafic rocks are often altered to secondary ones as a result of the ocean-floor metamorphism process. Chlorite is the dominant secondary phase in mafic rocks, such as diabase, gabbro and basalt which attributes to their low microroughness and to unfavorable interfaces between cement paste and aggregate particles. On the other hand, in ultramafic rocks, such as serpentinized peridotites, serpentine, chlorite and talc seem to be the dominant secondary phases. Additionally, ultramafic aggregates are characterized by low microroughness contributing on de-bonding between the aggregate particles and the cement paste. Phyllosilicates constitute an important group of minerals which includes serpentine, chlorite, micas, and clay minerals. The basic structure of the phyllosilicate minerals is based on interconnected six-member rings of $SiO4^{-4}$ tetrahedral that extend outward in infinite sheets. Several researchers have highlighted the impact of secondary phyllosilicate minerals on the engineering properties of various igneous aggregates (Petrounias *et al*., 2018b). More specifically, Petrounias et al. (2018b) proposed two petrographic indexes M_{ph} and U_{ph}. The petrographic index M_{ph} which is the sum of the phyllosilicate minerals in mafic samples is describing by the following equation M_{ph}= Chlorite (%). On the other hand, the petrographic index U_{ph} (%) which is the sum of the secondary phyllosilicate minerals present in ultramafic rocks is describing by the following equation: U_{ph} = Serpentine (%) + Chlorite (%) + Talc (%).

Concrete is the most used man-made material and comprises a mixture of mortar, aggregates and water (Jackson, 1981). Usually, aggregate is considered as inert filler, which accounts for 60 to 80% of the volume and 70 to 85% of the weight of concrete. Aggregates are divided into natural stone aggregates (sand and gravel) and crushed aggregates (crushed stones). The quality of aggregate, including its long-term durability and resistance to cracking, influence the properties of both fresh and hardened concrete. The inhomogeneous structure of concrete can be described as a three-phase system consisting of hardened cement paste, aggregate and the interface between aggregate particles and cement paste. Many researchers investigate the relationship between the percentages of different mineralogical compositions of aggregates and the final compressive strength of concrete. Several researchers (Petrounias *et al.,* 2018a, Petrounias *et al.,* 2018c) investigating various igneous rocks from Greece concluded that the secondary products of serpentinites and andesites largely influence their mechanical properties, which definitely have an adverse effect on their performance as concrete aggregates. However, a research gap is identified concerning the effect of these minerals on the produced concretes by different type of mafic aggregates.

Representative mafic and ultramafic rocks were collected from the Veria-Naousa and Edessa ophiolite complexes and were prepared normal concrete cube specimens. The Veria-Naousa ophiolite complex in northern Greece belongs to the Almopias subzone of the Axios geotectonic zone. It consists, from base to top, of serpentinised lherzolite and harzburgite, which are cut by scarce pyroxenite dykes, gabbro, diabase and pillow basalt (Rogkala *et al.,* 2017). The Edessa ophiolite represents remnants of oceanic lithosphere, which was thrust out of one basin during the Upper Jurassic to the Lower Cretaceous time (Rogkala *et al,* 2019). It is intensively tectonized and consists of several tectonic units.

Mafic and ultramafic aggregates used in order to prepare concrete specimens using normal Portland cement (CEM II 32.5N), which is conformed to EN 197-1. Potable tap water, free of impurities such as salt, silt, clay and organic matter, with pH = 7.0, was used for mixing and curing the concrete. In order to keep a consistent composition for all the concrete specimens, we adopted the principle of maintaining the same volume of aggregate per m^3 of the mixture. The proportions of the concrete mixtures, by mass, were 1/6/0.63 cement, aggregate and water ratio. The mineralogical characteristics of aggregates were examined in thin sections with a polarizing microscope and their mineralogical composition was also determined by XRD analysis and was calculated using the Rietveld refinement method. Normal concrete cubes specimens (150 mm × 150 mm) were prepared according to ACI-211.1-91. The compression test of concrete was elaborated according to BS EN 12390-3:2009. After the compressive strength test, the textural characteristics of concretes were examined. Thin sections were studied in a polarizing microscope according to ASTM C856–17. In a next stage, 3D

depiction of thin sections of the concrete specimens was carried out (Fig. 1) showing the adherence between the aggregates and the cement paste as well as the microroughness of the aggregate particles.

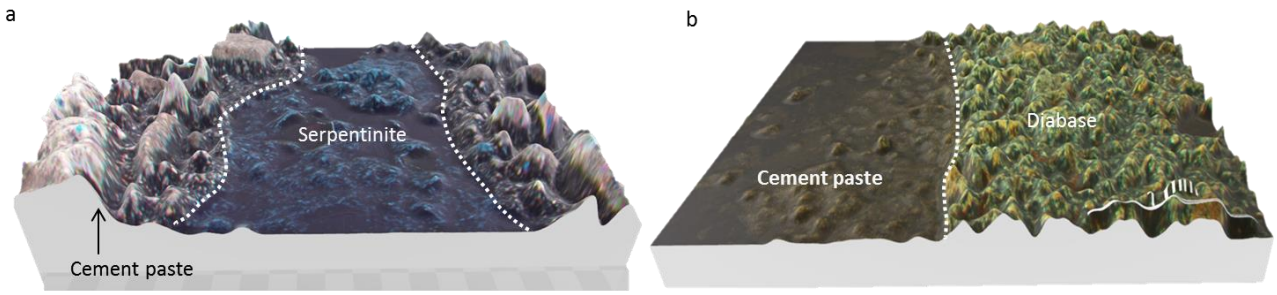

Figure 1. 3D depiction of thin sections of concrete specimens: a. ultramafic rock (serpentinite) used as aggregate, b. mafic rock (diabase) used as aggregate

The influence of secondary phyllosilicate minerals on concrete strength is confirmed by the correlation between the (UCS_{con}) strength of concrete and the percentage of secondary phyllosilicate minerals contained in the tested mafic and ultramafic rocks. Regression analysis is the commonest statistical method for the investigation of the interdependence of the physical and mechanical parameters. Figure 2 shows that as the percentage of serpentine, talc and chlorite in ultramafic rocks as well as the percentage of chlorite in mafic rocks increases, the yield strength of the produced concrete decreases. This is partly due to the ability of the phyllosilicate minerals to absorb water in their structure. In order to perform the regression analysis under a single correlation, U_{Ph} values were used as representative phyllosilicate values in ultramafic rocks and M_{Ph} values as representative phyllosilicate values in mafic rock formations. The function that links the above sizes is possible to describe by the following relation:

$$UCS_{con}= -0{,}0667* (U_{Ph}/M_{Ph})+31{,}246,\ R^2=0{,}82.$$

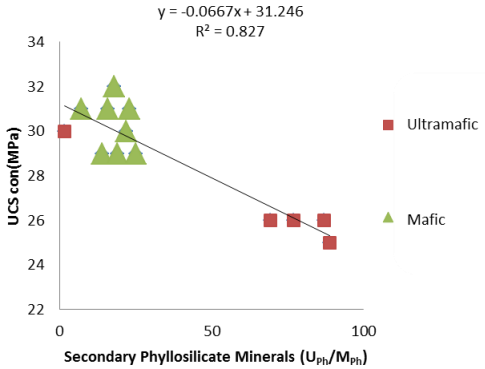

Figure 2. Secondary phyllosilicate minerals of mafic (M_{Ph}) and ultramafic rocks (U_{Ph}) respectively plotted against the strength of the produced concretes (UCS_{con}).

To conclude, as the percentage of secondary phyllosilicate minerals like serpentine, chlorite and talc increases the compressive strength of the produced concretes decreases respectively as more cracks, detachments and de-bonding between the aggregates containing the secondary phyllosilicate minerals and the cement paste.

References

Jackson, N. 1981. Civil Engineering Materials, Macmillan Press Ltd, London.

Petrounias, P., Giannakopoulou, P.P., Rogkala, A., Lampropoulou, P., Koutsopoulou, E., Papoulis, D., Tsikouras, B., Hatzipanagiotou, K. 2018b. The Impact of Secondary Phyllosilicate Minerals on the Engineering Properties of Various Igneous Aggregates from Greece. Minerals. 8, 329.

Petrounias, P., Giannakopoulou, P.P., Rogkala, A., Stamatis, P.M, Lampropoulou, P., Tsikouras, B., Hatzipanagiotou. K. 2018c. The effect of petrographic characteristics and physico-mechanical properties of aggregates on the quality of concrete. Minerals, 8 (12), 577. doi.org/10.3390/min8120577.

Petrounias, P., Giannakopoulou, P.P., Rogkala, A., Stamatis, P.M., Tsikouras, B., Papoulis, D., Lampropoulou, P., Hatzipanagiotou, K. 2018a. The Influence of Alteration of Aggregates on the Quality of the Concrete: A Case Study from Serpentinites and Andesites from Central Macedonia (North Greece). Geosciences 8, 115.

Rogkala, A., Petrounias, P., Tsikouras, B., Giannakopoulou, P.P., Hatzipanagiotou, K., 2019. Mineralogical evidence for partial melting and melt-rock interaction processes in the mantle peridotites of Edessa ophiolite (north Greece). Minerals 9 (2), 120.

Rogkala, A., Petrounias, P., Tsikouras, B., Hatzipanagiotou, K. 2017. New occurrence of pyroxenites in the Veria-Naousa ophiolite (north Greece): Implications on their origin and petrogenetic evolution. Geosciences, 7, 92, doi:10.3390/Geosciences7040092.

15th International Congress of the Geological Society of Greece
Athens, 22-24 May, 2019 | Harokopio University of Athens, Greece
Bulletin of the Geological Society of Greece, Sp. Pub. 7 Ext. Abs. GSG2019-268

Remediation of pH values and removal of Fe from Agios Philippos Kirkis mine through a new experimental electric device using low cost mineral raw materials

P. Petrounias[1], A. Rogkala[1], P.P. Giannakopoulou[1], P. Lampropoulou[1]

(1) Section of Earth Materials, Department of Geology, University of Patras, 265 04, Patras, Greece, Geo.plan@outlook.com

Abstract

This study focuses on both the remediation of the pH values and the removal of toxic load of Fe from pit lakes from Agios Philippos Kirkis mines (southern of Alexandroupoli, Evros Prefecture, Greece) by using a combination of economically and environmentally friendly mineral raw materials such as sterile aggregates (serpentinite, andesite), industrial rocks (magnesite), other natural and organic materials (peat and biochar) in a new experimental electric device. As raw materials for the consolidation of an important acid mine drainage, mainly sterile materials were used which resulted in the execution of laboratory tests to assess such as aggregates, based on sustainable disposal and reuse of sterile materials (serpentine, andesite, magnesite, peat and biochar). The treatment of polluted industrial waste water remains a topic of global concern since waste water discharged from municipalities, communities and industries must ultimately be returned to receiving waters or to the land (Weber *et al.*, 1991). Acid mine lakes have been formed worldwide and are responsible for numerous water quality problems, which severely limit their beneficial uses and may constitute an environmental risk both in the water body itself and downstream environments and water resources (Salmon *et al.*, 2008, Schindler, 1986, Geller, 1998, Geller *et al.*, 2009). Pit lakes or mining lakes, which are unique water bodies, such as this at Agios Philippos form in many places of the world as a consequence of opencast mining. When the activity ceases, the open pit is back filled with groundwater and surface water. The rate of filling is depended on climatic and geologic conditions, as well as the regional hydrologic characteristics. Assessment of the environmental risks of pit lake development is imperative for the mining industry and the public, especially in cases of high sulphidation deposits characterized by high concentrations of heavy metals (Plumlee, 1999).

Various mineral raw materials have been used as chemical reagents for the neutralization of pH, as well as for the removal of heavy metals. Several researchers have used experimental columns of batch type to examine the effect of various mineral raw materials. However, a research gap has been observed concerning the remediation of this phenomenon by using electrical driven flow forced device. The up to now proposed approaches for the remediation of this phenomenon include high cost techniques (Amarasinghe and Williams, 2007). For these reasons, in this study a new experimental electric forced device is proposed with the use of low cost mineral raw materials for achieving remediation of industrial waste water.

The basic concept for the construction of the experimental electrical device was the simulation of a standard continuous water recirculation system of the treated acidic runoff, in filters with a combination of mineral raw materials. The filters were filled with certain percentages of the selected mineral raw materials. Furthermore, 50 liters of waste water from the pit lake of Agios Philippos were placed into the experimental device. From the beginning of the experimental process periodic measurements of pH values of water were made. During the experimental process, sporadic samples of water were taken for geochemical analysis which it took place after the completion of the experimental process. In the experimental electrical device the combined use of mineral raw materials such as serpentinite, andesite, magnesite, peat and biochar as remediation agents of the acidic effluents of the selected lake with continuous water circulation, was evaluated. The variation of the pH values during the operation of the experiment is listed in Table 1. The pH values showed a continuously increasing trend from the first till the fourth day of the experiment, when pH reached the maximum value of 6.93. The infection of the pH curve after the fourth day indicates a general stability of pH at slightly reduced values of around 6.5–6.8 maintaining a steady trend with very small fluctuations.

Table 1. Results of geochemical analyses of the sediment sample deriving from the Agios Philippos mine.

Day	**1st**	**1st**	**1st**	**2nd**	**3rd**	**4th**	**4th**	**5th**	**6th**	**7th**
	Day(11:00)	Day(11:00)	Day(11:00)	Day	Day	Day(10:00)	Day(19:00)	Day	Day	Day
pH	2.99	3.79	4.70	6.04	6.45	7.13	6.65	6.57	6.54	6.82
T_{water} (°C)	25.2	26.0	29.0	28.0	29.0	37.6	37.8	39.8	38.0	37.6

Regarding the pH adjustment, the experimental device was particularly effective. This happened due to the participation of magnesite and serpentinite which were very effective in pH remediation (Teir *et al.*, 2006). In this study, the serpentinite may release magnesium ions while also engaging more H^+. The increase in pH can be attributed mainly to the adsorption of H^+ cations on the surface of serpentine crystals as the structure of serpentine consists of silicon tetrahedral which is combined with magnesium. Moreover, the studied serpentinite presents an important advantage in contrast to other lithotypes concerning the specific reaction surface. The Pliocene andesite had positively effected on the normalization of pH values due to its chemical composition, but is less effective than serpentinite and magnesite.

The results of the water geochemical analysis during the 7-day operation of the device suggest that the referred combination yielded satisfactory results with respect to the remediation of the removal of Fe.

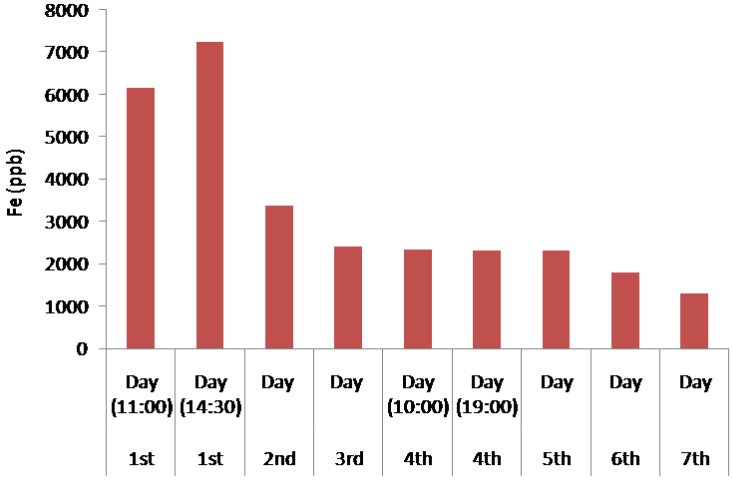

Figure 1. Histogram of Fe concentration in the treated water waste during the continuous water flow operation.

Fig. 1 illustrates the concentration of Fe in the water during the seven days of experiment. An increase in the concentration of Fe in the first day is observed explaining by the initial leaching of Fe from the serpentinite and the andesite, which contain small percentages of Fe, as well as to the contamination from the metallic parts of the pumps, as highly acidic solutions, like the initial treated water, promote solubility in the aerobic condition due to the oxidation of Fe^{2+} to Fe^{3+} through an increased oxidation potential and the temporarily increased its concentration until the pH increases. In the second day (pH> 4.5), there was a strong decrease in Fe concentration in the solution.

Acknowledgements

The authors wish to thank M. Kalpogiannaki for her assistance with the construction of the geological map.

References

Amarasinghe, B.M.W.P.K., Williams, R.A. 2007. Tea waste as a low cost adsorbent for the removal of Cu and Pb from wastewater. Chemical Engineering Journal. 132(1–3), 299–309.

Geller, W., Klapper, H., Salomons, W. 1998. Acidic Mining Lakes. Springer Verlag, Berlin, Heidelberg.

Geller, W., Koschorreck, M., Wendt-Potthoff, K., Bozau, E., Herzsprung, P., Büttner, O., Schultze, M. 2009. A pilot-scale field experiment for the microbial neutralization of a holomictic acidic pit lake. Journal of Geochemical Exploration. 100 (2–3), 153-159.

Plumlee, G.S. 1999. The environmental geology of mineral deposits. Plumlee, G.S. & Logsdon, M.J. (eds.), Reviews in Economic Geology, 6A. The Environmental Geochemistry of Mineral Deposits. Part A: Processes, Techniques, and Health Issues, Society of Economic Geologists. 71-116.

Salmon, S.U., Oldham, C., Ivey, G.N. 2008. Assessing internal and external controls on lake water quality: limitations on organic carbon-driven alkalinity generation in acidic pit lakes. Water Resources Research. 44, W10414.

Schindler, D.W. 1986. The significance of in-lake production of alkalinity. Water Air Soil Pollut. 30, 931-944.

Teir, S., Eloneva, S., Fogelholm C., Zevenhoven, R. 2006. Stability of calcium carbonate and magnesium carbonate in rainwater and nitric acid solutions. Energy Conversion and Management. 47, 3059-3068.

Weber, W.J., McGinley, P.M., Katz, L.E. 1991. Sorption phenomena in subsurface systems: concepts, models and effects on contaminant fate and transport. Water Research. 25(5), 499–528.

15th International Congress of the Geological Society of Greece
Athens, 22-24 May, 2019 | Harokopio University of Athens, Greece
Bulletin of the Geological Society of Greece, Sp. Pub. 7 Ext. Abs. GSG2019-277

Large Shear Box Testing on weathered zone of Flysch. The Case Studies of Panagopoula and Karya Landslides

S. Anagnostopoulou[1], N. Depountis[1], N. Sabatakakis[1]
(1) Department of Geology, Patras University, 26504 Patras, Greece, geo09008@upnet.gr

Abstract

This paper describes the landsliding behavior of highly weathered and tectonically decomposed flysch in characteristic landslides in Western Greece, focusing on its mechanical parameters, such as shear strength. Generally, the most serious landslide movements in Western Greece are often observed in the upper weathered zone of flysch and they often constitute translational and composite landslides.

Large shear box tests were performed on selected samples of weathered flysch zone, under different moisture and density conditions. Three varying normal stresses were applied in each sample to determine the effects upon shear resistance and displacement. The results show that an increase of moisture content ensue an appreciable decrease in apparent friction angle. Furthermore, a dilatant behavior in dense samples was exhibited in contrast with the loose ones. A clear effect of composition - structure as well as moisture - density is also observed on the shear strength variation.

Introduction

During the last decade, an increase of 25% of landslide phenomena has been recorded in the country, as a result of human activities, increasing urbanization and uncontrolled use of land areas that are vulnerable to landslides (Sabatakakis *et al*., 2012). Many of these landslides have been occurred in weathered flysch, a critical landslide-prone geological formation that have been reactivated in recent decades due to intense and prolonged rainfall. In this study, representative landslides, i.e., Panagopoula and Karya landslides, are examined and focusing on the mechanical behavior of the weathered flysch through shear strength tests.

Panagopoula comprises an extensive instability zone, including composite fault-related slides, located in the Gulf of Corinth, where periodically induced landslide events have been interspersed with creep activity (Koukis *et al*., 2009, Kavoura *et al*., 2016). In 1971 and 1972, translational and rotational slides occurred, affecting the transportation lines over about 250 m. The slides took place on structurally sheared and weathered flysch sediments and are still locally active in smaller areas (Sabatakakis *et al*., 2015).

Karya village, belongs to Municipality of Patras located about 12 km away from the city center and cited close to the edge of Panachaikon Mountain, with an altitude of 250m a.s.l. Significant failures were recorded in 1961, 1999 and 2001 including earth flows and translational slides on weathered flysch and mainly due to prolonged rainfalls (Sabatakakis *et al*., 2005, Koukis *et al*., 2007).

Methods

This paper presents the results of two series of large shear box tests on typical highly weathered and decomposed flysch formation, obtained from Panagopoula and Karya sites.

The soil samples were coming from exploratory boreholes as well as from flysch outcrops in characteristic sites of the extended landslide zones. Classical laboratory tests were conducted to determine moisture content, grain size distribution and Atterberg limits.

The Large Shear Box 300 (VJT2780A) apparatus (Fig.1) was used. From each type of weathered flysch, a series of tests were performed on prepared specimens with different water content and density in order study the effects of these parameters on the shear strength characteristics. Specimens were tested on dry, wet (partially saturated) and fully saturated conditions. Loose and dense specimens were also prepared to represent surficial and deeper zone of weathering.

Direct shear tests were performed on flysch sample grain fraction passing through the sieve No. 4 (<4.75mm) in accordance with ASTM standards (2004). Tests were performed using large shear box (300mm square about 160mm thick), soil samples under certain density - moisture conditions and three different normal stresses. The weathered flysch samples collected from the failure zone (weak zone) were classified according to USCS as clayey sands (SC) of medium plasticity with a small presence of well-graded gravels and a moisture content of 16-18%.



Figure 1. Large Shear box apparatus.

The different consolidation loads were left for one day in case of saturated conditions, whereas for a couple of hours until stabilization in case of dry tests. The shearing rate of the samples was very low in order to assure that no significant amount of pore water pressure would be developed at any stage of the test. All tests were regulated with the criteria to stop when the accumulated shear strain (γ) reached 10%.

Conclusions

Instability phenomena are very common in the weathered and tectonically highly sheared flysch, causing serious problems in many places in Western Greece. Large Shear laboratory tests in the weathered zone of flysch of representative flysch-prone landslides, show a definite decrease in the effective friction angle within the increase in water up to saturation state. Significant differences are also observed in the failure envelops of dense and loose conditions.

Acknowledgements

This research was co-financed by the European Union (European Social Fund-ESF) and Greek national funds through Operational Program NSRF 2014-2020.

References

ASTM (2004) Standard Test Method for Direct Shear Test of soils Under Consolidated Drained Conditions D3080-04.

Kavoura, K., Sabatakakis, N., Tsiambaos, G., 2016. Long term ground displacements due to a large landslide in western Greece. Landslides and Engineered Slopes. Experience, Theory and Practice – Aversa et al. (Eds) CRC Press 2016, Pages 1177–1181. doi: 10.1201/b21520-142.

Koukis, G., Sabatakakis, N., Lainas, S., 2007. Soil suitability estimation for housing purposes in landslide-prone areas. The case of karya village, Patras, W.Greece. Bull of Geological Society of Greece, [Proceedings of 11th International Congress, Vol.XXX, 1683 – 1694.

Koukis, G., Sabatakakis, N., Ferentinou, M., Lainas, S., Alexiadou, X., Panagopoulos, A., 2009. Landslide phenomena related to major fault tectonics: rift zone of Corinth Gulf, Greece. Bulletin of engineering geology and the environment. 68.2: 215-229. doi: 10.1007/s10064-008-0184-8.

Sabatakakis N, Koukis G, Mourtas D, 2.005: Composite landslides induced by heavy rainfalls in suburban areas: City of Patras and surrounding area, western Greece. Landslides 2(3): 202 – 211. doi: 10.1007/s10346-005-0002-3

Sabatakakis, N., Koukis, G., Vassiliades, E., Lainas, S., 2012. Landslide susceptibility zonation in Greece. Natural Hazards 65(1):523 – 543. doi: 1007/s11069-012-0381-4.

Sabatakakis, N., Tsiambaos, G., Rondoyianni, R., Papanakli, St., Kavoura, K., 2015. Deep - seated structurally controlled landslides of Corinth Gulf rift zone, Greece: The case of Panagopoula landslide. [Proceedings of 13th ISRM Congress, Innovations of Applied and Theoretical Rock Mechanics - ISBN: 978-1-926872-25-4, paper 651.

15th International Congress of the Geological Society of Greece
Athens, 22-24 May, 2019 | Harokopio University of Athens, Greece
Bulletin of the Geological Society of Greece, Sp. Pub. 7 Ext. Abs. GSG2019-285

Spatial and Temporal Distribution of Precipitation in Northern Peloponnese

A. Mylonas[1], E.A. Nanou[1], K. Perdikaris[1], M.K. Petropoulou[1], A.M. Giannakea[1], E. Zagana[1]

(1) Laboratory of Hydrogeology, Department of Geology, University of Patras, 26504 Rion, Patras, Greece
geo12097@upnet.gr

Background

Climate is a constant changing variable, affecting urban development and ecosystems. The Mediterranean, due to complex topography and atmospheric circulation patterns (Tyrlis *et al*., 2013), presents intense susceptibility to climatic changes (Goubanova *et al.*, 2007). As a part of the eastern Mediterranean basin, the climate and the precipitation regime of Greece has piqued the interest of many researchers (Livada *et al.*, 2008, Nastos *et al.*, 2008, Dotsika *et al.*, 2010, Karavitis *et al.*, 2011). Following the same pattern, precipitation and temperature in Peloponnese vary according to regional characteristics.

Precipitation is one of the most important climatic variables in the water cycle and the information it provides is critical for understanding the hydrological balance (Hatzianastassiou *et al.*, 2008). The precipitation regime is significantly affected by the topography of each region. According to Voudouris *et al.* (2007), the estimation of the annual rainfall distribution in Korinthia prefecture, NE Peloponnese, is controlled by the physiography of the area. However, in the present study, the method that was followed for the spatial analysis, does not take into consideration the variation of precipitation according to the elevation, because this was not possible for such an extended area characterized by a complicated morphology.

Objectives

The main aim of the present study is the construction of a high resolution map that depicts the spatial distribution of precipitation, as well as the observation of the temporal distribution in the study area, in order to recognize variations throughout the years.

Methods

Daily rainfall time series from 33 meteorological stations, corresponding to the hydrological years 1985-2015, were processed and the mean annual precipitation was estimated, as well as the minimum and maximum values recorded in each station. The locations of the observation posts were subsequently digitized in ArcGIS 10.1, and each corresponding mean annual rainfall value was inserted. The spatial distribution map resulted from the Inverse Distance Weighting (IDW) interpolation tool. For the temporal distribution, the stations in the eastern, central and western part of the area were compared in groups, as well as all together.

Results

The precipitation regime presents distinct differentiations in northern Peloponnese. The eastern and northeastern sections of the study area present the lowest values, ranging from 468 to 647 mm/year, while, moving toward the west mean annual rainfall values increase. The highest values, from 1068 to 1505 mm/year, appear in the S-SW region. During the period 1985-2015, the hydrological years 1989-1990 and 1998-1999 were recorded as the driest and wettest years respectively, by the majority of the meteorological stations in northern Peloponnese. It is also observed that 2006-2007 was a dry year for the eastern and central parts of the study area, while 2013-2014 was documented as a very wet hydrological year for the eastern and western regions. Generally, almost all stations, with very few exceptions, seem to have an increased tendency in precipitation over the considered time period. Finally, it is worth mentioning, that the highest and lowest annual precipitation values were recorded by Kastania station in 2000-2001 (2842 mm) and Halkeio station in 1999-2000 (196.1 mm) respectively.

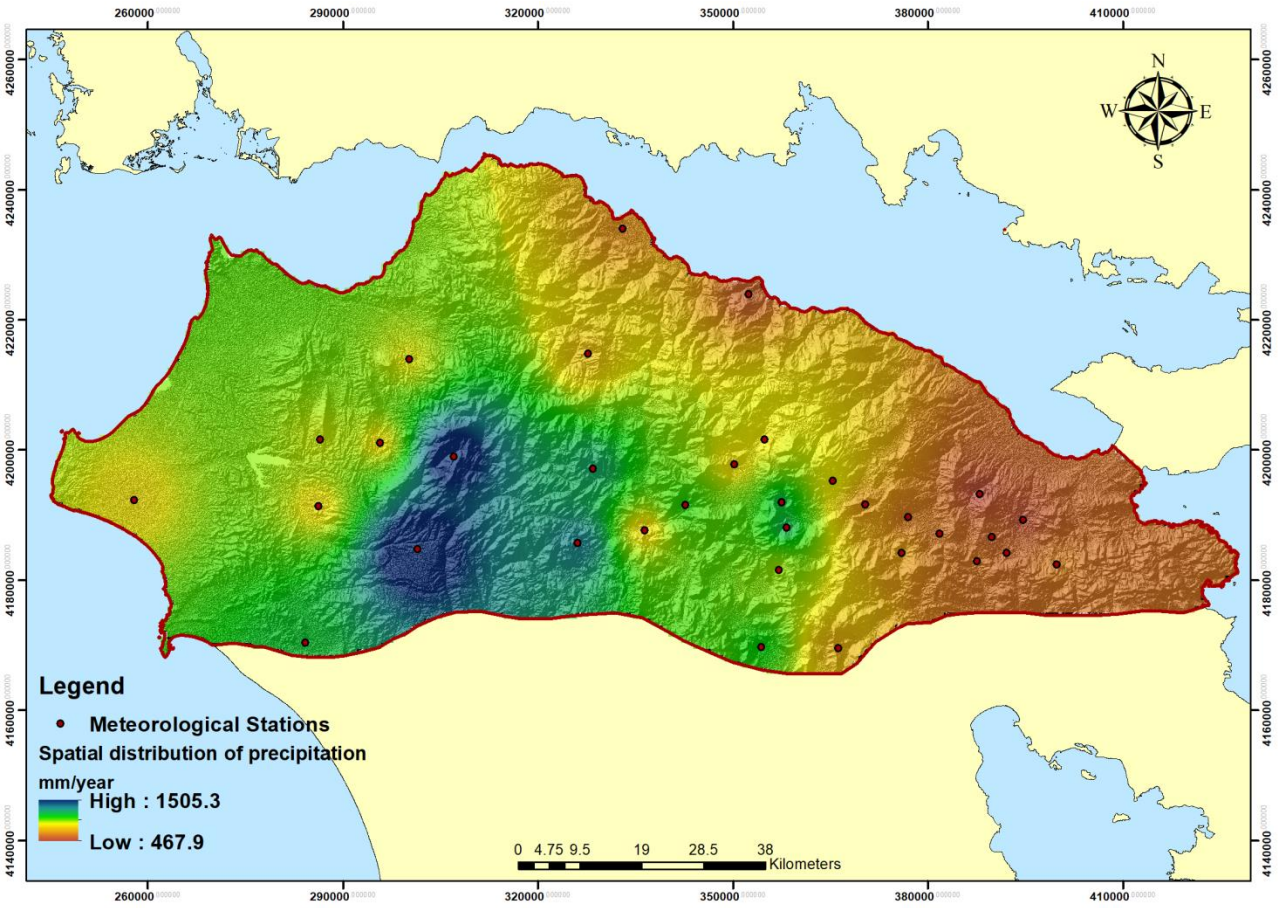

Figure 1. Spatial distribution of precipitation

Acknowledgements

The authors wish to thank the Special Secretariat for Water, Ministry of Environment and Energy, as well as the Western Greece Waters Directorate, Decentralized Administration of Peloponnisos, Western Greece and Ionion, for the precipitation data that they provided.

References

Dotsika, E., Lykoudis, S., Poutoukis, D., 2010. Spatial distribution of the isotopic composition of precipitation and spring water in Greece. Global and Planetary Change 71, 141-149. **[**

Goubanova, K., Li, L., 2007. Extremes in temperature and precipitation around the Mediterranean basin in an ensemble of future climate scenario simulations. Global and Planetary Change 57, 27-42.

Hatzianastassiou, N., Katsoulis, B.D., Pnevmatikos, J., Antakis, V., 2008. Spatial and Temporal Variation of Precipitation in Greece and Surrounding Regions Based on Global Precipitation Climatology Project Data. Journal of Climate 21, 1349-1370.

Karavitis, C.A., Alexandris, S., Tsesmelis, D.E., Athanasopoulos, G., 2011. Application of the Standardized Precipitation Index (SPI) in Greece. Water 3, 787-805.

Livada, I., Charalambous, G., Assimakopoulos, M.N., 2008. Spatial and temporal study of precipitation characteristics over Greece. Theoretical and Applied Climatology 93, 45– 55.

Nastos, P.T., Zerefos, C.S., 2008. Decadal changes in extreme daily precipitation in Greece. Advances in Geosciences 16, 55-62.

Tyrlis, E., Lelieveld, J., Steil, B., 2013. The summer circulation over the eastern Mediterranean and the Middle East: influence of the South Asian monsoon. Climate Dynamics 40, 1103-1123

Voudouris, K., Mavrommatis, T., Antonakos, A., 2007. Hydrologic balance estimation using GIS in Korinthia prefecture, Greece. Advances in Science and Research 1, 1-8.

15th International Congress of the Geological Society of Greece
Athens, 22-24 May, 2019 | Harokopio University of Athens, Greece
Bulletin of the Geological Society of Greece, Sp. Pub. 7 Ext. Abs. GSG2019-292

Landslide susceptibility assessment in Northern Epirus using a deterministic approach

D. Loukidis[1], I. Vakalas[2], N. Loukidis[2], C. Gallousi[2], I. Tsodoulos[2]

(1) Department of Civil and Environmental Engineering, University of Cyprus, Kallipoleos 75, 1678 Nicosia, Cyprus, e-mail: loukdis@ucy.ac.cy
(2) Ionia Labs S.A. Soil & Rock Mechanics Laboratory, Pavlou Mela 13, Nea Ionia, Athens, Greece

Introduction

Epirus is a region having a high density of active landslides and numerous areas prone to slope instabilities due to its particular geology and large annual precipitation. In such conditions, blasting operations performed in the context of seismic surveys have to be planned in such a way that there is no risk of triggering ground instabilities or generating significant ground deformations. Herein, we present a summary of a methodology for landslide susceptibility assessment developed and applied in the context of the seismic survey operations in the Ioannina hydrocarbon exploration block. The project took place under the supervision of Repsol and Energean Oil & Gas Joint Venture, which have been awarded the specific block.

The study area covers an extensive part of Northern Epirus (Fig. 1), which is dominated by carbonate and clastic sedimentary rocks. Of particular importance are the outcrops of the flysch of the Ionian Zone, as well as the outcrops of Posidonia shales and Miocene marls, which all are characterized by low strengths. The study was implemented in three stages: a) preliminary desktop analysis, b) field survey, data collection and sampling and c) evaluation of ground failure hazard using a deterministic approach.

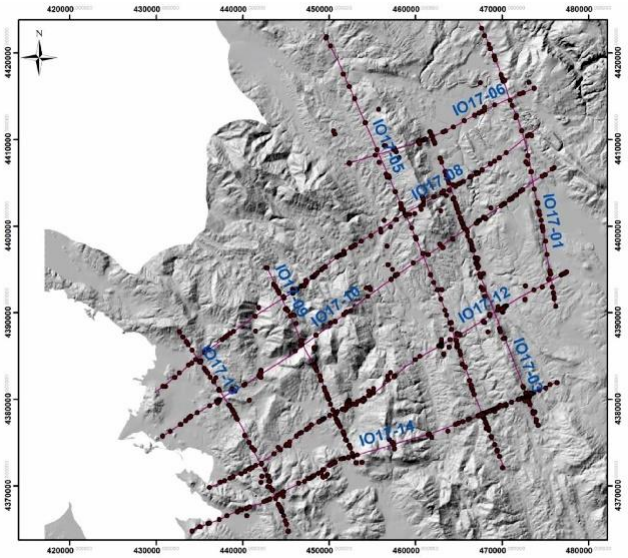

Figure 1: Extent of seismic lines. Circles represent points of data collection and sampling.

Methodology

Considering the large extent of the seismic lines (400km total length), a GIS-based preliminary screening procedure was first applied in order to identify areas of low landslide susceptibility and exclude them from subsequent detailed analysis. This consisted of calculating the topographic/bedding plane intersection angles (Meentemeyer & Moody 2000) within 200m from the seismic lines, combined with geological map data and examination of satellite photos for land use and infrastructure, in order to assign a risk classification score. The preliminary screening allowed for an optimized fieldwork planning given a specific timeframe and resources.

Based on the screening stage, a field survey took place in which more than 700 points along the seismic lines were accessed in order to produce the geotechnical input necessary for the landslide susceptibility computations. Field work included dip measurements for bedding planes and two major joint sets (if present), characterization of discontinuity condition (weathering, coating), joint roughness coefficient (JCR) assignment, rock mass characterization using GSI and Schmidt hammer tests for the estimation of the unconfined compression strength. In a limited number of locations, rock samples were collected for further strength testing in the lab.

The landslide susceptibility computations were done using a multimodal deterministic approach (Fell et al. 2008), in which three slope stability indicators were computed at each point of a 15m x 15m grid by making simplifying idealizations regarding slope geometry and assuming ground uniformity. The indicators were: a) the static factor of safety *FS*, b) the critical seismic acceleration a_c, and c) the permanent displacement $d_{perm,eq}$ caused by a reference earthquake event. Similarly to the work of Grant et al. (2016), the following modes of failure were considered: i) rotational sliding, ii) planar sliding along bedding planes, and iii) wedge failure along two discontinuities (one being the

bedding planes). Equivalent Mohr-Coulomb rock mass strength parameters (cohesion, friction) were estimated based on the GSI classification (Hoek et al. 2002). For structureless rock masses (e.g. Miocene marls), strength parameters were estimated based on the available technical literature. For rotational failures, mathematical expressions were used which were derived from the charts of Michalowski (2002) and Loukidis et al. (2003) for the *FS* and a_c calculation, respectively. The final *FS* and a_c values were set to be the minimum among the examined failure modes. Having established a_c at each grid point, $d_{perm,eq}$ was calculated using formulas based on Newmark sliding block considerations (e.g. Jibson 2007). Three scenarios of groundwater regime were examined, namely pore water coefficient values 0, 0.2 and 0.4. Fig. 2 presents a sample of the outcome of deterministic approach computations for a seismic line segment.

Finally, the landslide susceptibility mapping was followed by detailed design of the blasting operations (shothole locations, depth and weight of explosive charges) in collaboration with Repsol S.A. personnel. The operations planning was made by taking into account, along with the seismic refraction resolution requirements, computations of the permanent displacement $d_{perm,blast}$ caused by blasting, applying the necessary degree of conservatism.

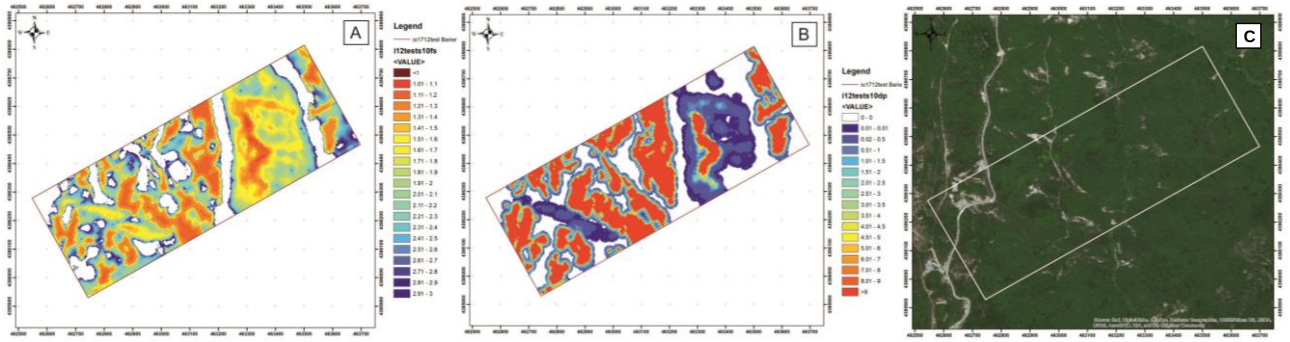

Figure 2: Example results: Maps of a) static FS, b) $d_{perm,eq}$ (in cm) and c) satellite image of a sector along line I7012.

Results

According to the analysis, 45% of the areas were identified as low risk, 34% as moderate risk and 21% as high risk. Line IO1701 (Fig. 1) exhibited the lowest susceptibility, while Line IO1705 was the line of highest susceptibility, with substantial number of natural landslides located in small distance from the line corridor. Generally, the seismic line segments that cross the western slope of Kassidiaris Mountain are located in an area of significant active landslide events, e.g. Aetopetra, Lavdani landslides. All quantitative slope stability indexes point out to the fact that sectors dominated by flysch and Miocene marls present the highest susceptibility for ground failures. The results of the study were incorporated in the blasting operations planning, targeting in preventing development of permanent displacements that would trigger landslide events under any real circumstances by canceling shotholes in high risk locations or reducing the explosive charges.

Acknowledgements

Ionia Labs would like to thank Repsol S.A. and Energean Oil & Gas S.A. for the funding and supervision of the project. Especially, Ionia Labs would like to thank Dr. Takis Konstantopoulos of Energean Oil and Gas S.A. for his support during the geological survey and especially for his help in the optimization of the routing plan. We would also like to thank Dr. Constantinos Tzimeas of Energean Oil & Gas (currently at Repsol S.A.) and Mr. Willy Hernandez of Repsol S.A for the effective administrative support. Finally, we would like to acknowledge the constructive comments of Mr. Juan Pablo Pita Gutiérrez, Mr. Harald Stockhausen and Mrs. Irene García Saiz of Repsol S.A. which helped to enhance the methodological approach.

References

Fell, R., Corominas, J., Bonnard, C., Cascini, L., Leroi, E., Savage, W. 2008. Guidelines for landslide susceptibility, hazard and risk zoning for land-use planning. Engineering Geology, 102, 99-111.

Grant, A., Wartman, J., Abou-Jaoude, G. 2016. Multimodal method for coseismic landslide hazard assessment. Engineering Geology, 212, 146-160.

Hoek, E., Carranza-Torres, C. and Corkum, B. 2002. Hoek-Brown criterion –2002 edition. Proc. NARMS-TAC Conference, Toronto, 2002, 1, 267-273.

Jibson, R.W. 2007, Regression models for estimating coseismic landslide displacement: Engineering Geology, 91, 209-218.

Loukidis, D., Bandini, P., Salgado, R. 2003. Stability of seismically loaded slopes using limit analysis. Géotechnique, 53(5), 463-480.

Meentemeyer, R.K., Moody, A. 2000. Automated mapping of conformity between topographic and geological surfaces. Computers & Geosciences, 26(7), 815-829.

Michalowski, R.L. 2002. Stability charts for uniform slopes. Journal of Geotechnical and Geoenvironmental Engineering, 128(4), 351-355.

15th International Congress of the Geological Society of Greece
Athens, 22-24 May, 2019 | Harokopio University of Athens, Greece
Bulletin of the Geological Society of Greece, Sp. Pub. 7 Ext. Abs. GSG2019-334

Hydrogeological conditions and water resources management of Ios Island, Cyclades, Greece

Christos Filis[1], Emmanuel Skourtsos[1], Apostolos Alexopoulos[1], Spyridon Lekkas[1]

(1) National and Kapodistrian University of Athens, Department of Geology and Geoenvironment, Panepistimiopolis Zografou, 15784, Athens, Greece, chfilis@geol.uoa.gr

The Cyclades islands have been experiencing over time problems of water scarcity, due to limited water resources. The last decades precipitation over the south Aegean islands displays generally a larger variance and has a tendency of becoming dryer, compared to long-term climatic normal (Nastos & Zerefos, 2010) because of climate changes. Reduced precipitation can affect the sustainability, quantity and quality of water resources. The natural shortage of water resources is exacerbated by increasing water consumption for human needs, such as the expansion of irrigated land and the development of urban, industrial and touristic areas.

These conditions reinforce the necessity to improve water management in order to ensure the necessary quantity of water supply. This necessity becomes stronger in areas with complex geological setting, with relatively small aquifers and tangential (with hydraulic communication) to the sea, where overpumping and the expected minimum natural renewal due to the dry climate, leads to a significant drawdown in water table, resulting sometimes in the salinization of groundwater.

The municipal water supply of Ios Island has been reinforced by a series of projects and interventions, mainly focusing to the summer period due to tourism where water demand surpasses by far water availability, consisting of:

- New deep boreholes.
- Construction and operation of the water reservoir of Mylopotamos with a total capacity of 215,000m^3.
- Construction and operation of Mylopotas desalination plant with a total capacity of 1,000m^3/day.

Given the climate change that has taken place in recent years, there is a continuous quantitative and qualitative degradation of Ios Island water resources. Indicatively, it is reported that it has been recorded:

- Partial or total recession of springs discharges.
- Significant drawdown of wells and boreholes water tables.
- The water reservoir of Mylopotamos was totally empty in 2000 and 2018, due to the prolonged drought.

The Ios Island almost entirely comprises of metamorphic rocks and Quaternary formations unconformably cover them (Van Der Maar & Jansen, 1981). The metamorphic rocks are including the dominant unit of the Cycladic Blueschist Unit (CBU) which is located mainly in the north part of the island and in scattered outcrops in the south. The CBU is tectonically overlying the Cycladic Basement Unit which constitutes the Variscan basement and is demonstrated in the central and south part of the island.

Three main aquifer systems developed on Ios Island include (Kourmoulis, 1980; Papadopoulos & Stergiopoulos, 2000; JV of Aegean Watersystems, 2005; Giannoulopoulos & Lappas, 2010):

- The shallow aquifer system in porous Quaternary formations.
- The karstic aquifer system in the carbonate rocks of the Cycladic Blueschist Unit (CBU).
- The aquifer system (both shallow and deep) in the fractured hard rocks mainly of the Cycladic Basement Unit.

Precipitation is the direct recharge of the three aforementioned aquifer systems. It should be mentioned, that the overlying, shallow aquifer system is also indirectly recharged from the streams runoff during the winter months and from the formations of the Cycladic Blueschist Unit (CBU) and mainly of the Cycladic Basement Unit (augengneiss and garnet-mica schists). However, even this indirectly recharge depends on the precipitation.

The shallow, porous aquifer system of Mylopotas, Manganari, Psathi, Koumbara and Kato Kambos is encountering continuous quantitative and qualitative degradation, due to restriction of precipitation during the winter months and overpumping during the summer months.

The karstic aquifer system of the north part is being discharged in the Aegean Sea and therefore, it is not of particular hydrogeological interest.

The aquifer system in the fractured hard rocks mainly of the Cycladic Basement Unit occurs in the weathered zone (shallow) and in the fractured zone (deep) of the garnet-mica and the augengneiss and is encountering continuous and over time quantitative degradation since:

- The great majority of small springs which discharge the weathered zone has suffered partial or total recession through the years, due to the restriction of the precipitation and the prolonged drought.
- The time fluctuation from 1976 until today of the springs discharges, named Epano Desi, Kato Desi, Psathi and Aghia Theodoti, which discharge the fractured zone of the augengneiss shows both continuous recession and flow, covering even today the water supply of some settlements. It should be mentioned, that in the recharge areas (hydrogeological basins) of the aforementioned springs there are no wells and boreholes and therefore, their

continuous discharge recession is due to restriction of the precipitation and the prolonged drought.

- The time fluctuation from 2005 until today of the fractured zone water table of the augengneiss shows drawdown which exceeds 35 meters in the west and southwest of Kastro or Pyrgos and is almost 15 meters in the south margin of the Mylopotas alluvial basin.

In conclusion, a continuous quantitative and qualitative degradation of Ios Island water resources is being recorded which is the result of both the restriction of precipitation during the winter months and therefore of the limited recharge and the overpumping during the summer months of the three main aquifer systems. Furthermore, the direct consequence of the climate change is the often occurrence of extreme hydrometeorological phenomena that favors the runoff instead of infiltration which leads to the restriction of the recharge of the three main aquifer systems.

For the sustainable water resources management of the Ios Island new projects must be planned, such as:

- Artificial recharge for both the shallow, porous aquifer system and the aquifer system (shallow and deep) in the fractured hard rocks mainly of the Cycladic Basement Unit.
- Construction and operation of new water reservoirs.
- Construction and operation of new desalination plants.

References

Giannoulopoulos, P., Lappas, J., 2010. Recording and valuation of the hydrogeological characteristics of underground waters and aquifer systems of Greece. River Basin District of the Aegean Island (14), IGME, Athens.

JV of Aegean Watersystems, 2005. Development of tools for the water resource management of the hydrological district of Aegean islands. Issue 19 – Ios Island. Ministry of Development, Athens.

Kourmoulis, N., 1980. Hydrogeological investigation of the Cyclades islands – Ios. Hydrological and Hydrogeological Investigations, No. 42, IGME, Athens.

Nastos, P., Zerefos, Ch., 2010.Climate Change and precipitation in Greece. Hellenic Journal of Geoscience, 45, 185-192.

Papadopoulos, N., Stergiopoulos, K., 2000. Drought study of Sifnos – Ios islands, Prefectural Government of Cyclades, Technical Service Department, Athens.

Van Der Maar, P.A., Jansen, J.B.H., 1981. Geological Map of Greece, "IOS" Sheet, IGME, Athens.

15th International Congress of the Geological Society of Greece
Athens, 22-24 May, 2019 | Harokopio University of Athens, Greece
Bulletin of the Geological Society of Greece, Sp. Pub. 7 Ext. Abs. GSG2019-340

The use of geochemical ratios in groundwater quality assessment: the case of the Thriassion Plain Attica, Greece

P. Makri[1], D. Hermides[2], M. Psychogiou[3], A. Ermidou[2]

(1) National and Kapodistrian University of Athens, Department of Geology and Geoenvironment, Panepistimiopolis, Zografou 157 84, pmakri@geol.uoa.gr
(2) Agricultural University of Athens

Hydrochemical diagrams aim at interpreting any evolution occurring in the groundwater systems. This paper is an effort to assess the groundwater quality and the geochemical processes using a diagram based on Chadha's work (Chadha, 1999), who classifies natural waters, documenting Piper's and extended Durov's diagrams. The example of hydrochemical analyses were given from groundwater samples of Thriassion Plain. The study area (Figure 1) is located 25 km west of Athens and has undergone uncontrolled urban and industrial development. Geologically, it is dominated by alpine sediments represented by Palaeozoic volcano-sedimentary complex, Triassic phyllites and sandstone, limestones, dolomitic limestones and dolomites, and Cretaceous limestones. Post-alpine sediments of Neogene-Quaternary marls, clay and marly limestones conglomerates as well as Holocene clay, sands and gravels have filled in the basin (Katsikatsos et al., 1986). The post alpine tectonic activities (Papanikolaou et al., 1999) combined with the Pleistocene sea level fluctuations (Lambeck, 1996) is responsible for the current landscape: firstly a sequel of Pliocene to Lower Pleistocene movements gave born to the main neotectonic fault of Mt. Parnes (Lekkas, 2001; Mariolakos et al., 2001) at the northern edge of the study area. Later, in M. Pleistocene the extension fault of Aspropyrgos defined the basin of Eleusis; this activity goes on to date. As a result, a complex hydrogeological regime has been established in which a multi-layered confined aquifer system has been formed (Hermides, 2018).

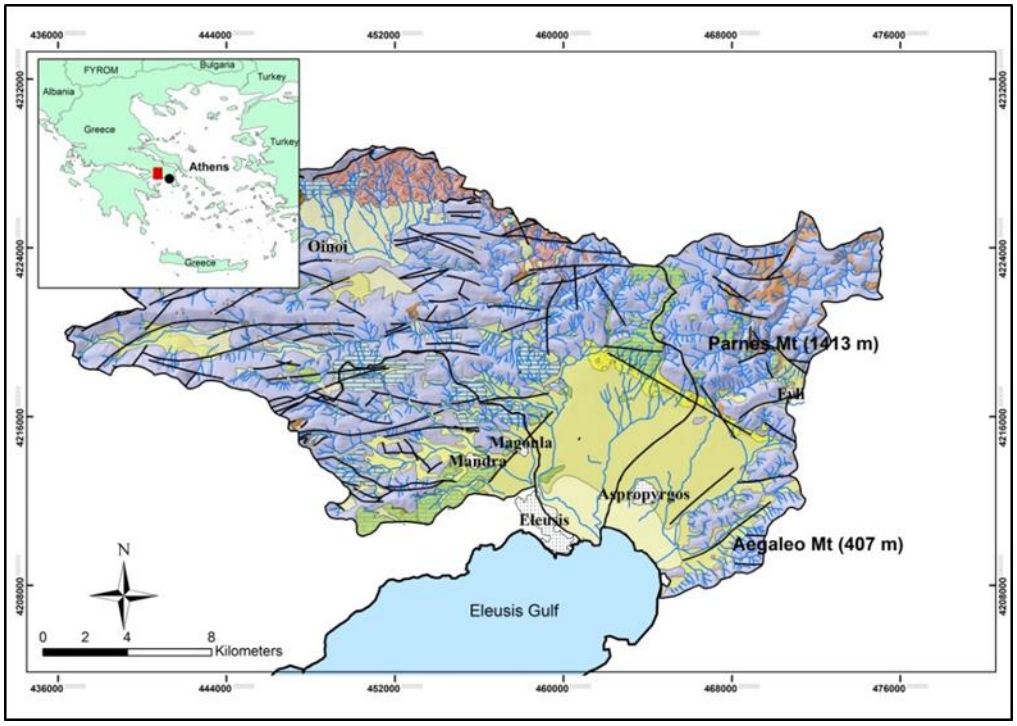

Figure 1.The study area

To attend our objective, sampling of 45 wells and boreholes along with measurement of basic physico-chemical parameters took place. The target anions Cl^- , SO_4^{-2} and cations Ca^{+2}, Mg^{+2}, Na^+, K^+, were identified with Ion Chromatography, while the HCO_3^- anion was characterized with titration. Then, hydrochemical sections, XY diagrams, distribution maps of ionic ratios as well as Gibbs diagrams (Gibbs, 1971) were used to identify origin of salinity and geochemical processes. Based on the relationship between TDS (meq/l) and Na/Na+Ca, $Cl/Cl+HCO_3$ meq/l ratios these diagrams have shown that evapotranspiration (ET) and rock-water interaction that dominate the study area play an important role to the increase of groundwater salinity. All data were illustrated on a Chadha diagram (Figure 2) to interpret groundwater geochemical processes: this diagram uses simple spreadsheets excel file. Concentration meq/l % of (Ca+Mg)-(N+K) and HCO_3^- ($Cl+SO_4$) are displayed onto X and Y axes respectively. The diagram is divided into 8 fields. The geochemical processes that occur in groundwater such as mix of fresh water with modern seawater (red dashed line and arrow 3 in Figure 2), refreshening (arrow1), mix of fresh water with aged water and possible ancient seawater influence (arrow 2), reverse cation exchange (double arrow 4) and base ion exchange are mainly presented in the fields 5, 6, 7, 8. The interpretation of the produced diagram highlights the stratigraphic factors and especially the

clay strata occurrence that have isolated fresh groundwater from seawater. The abundant occurrence of clay deposits to the depth of the plain work as barriers to sea intrusion. Good quality groundwater has been identified which confirms the role of clay strata, showing evolution of saline to fresh water.

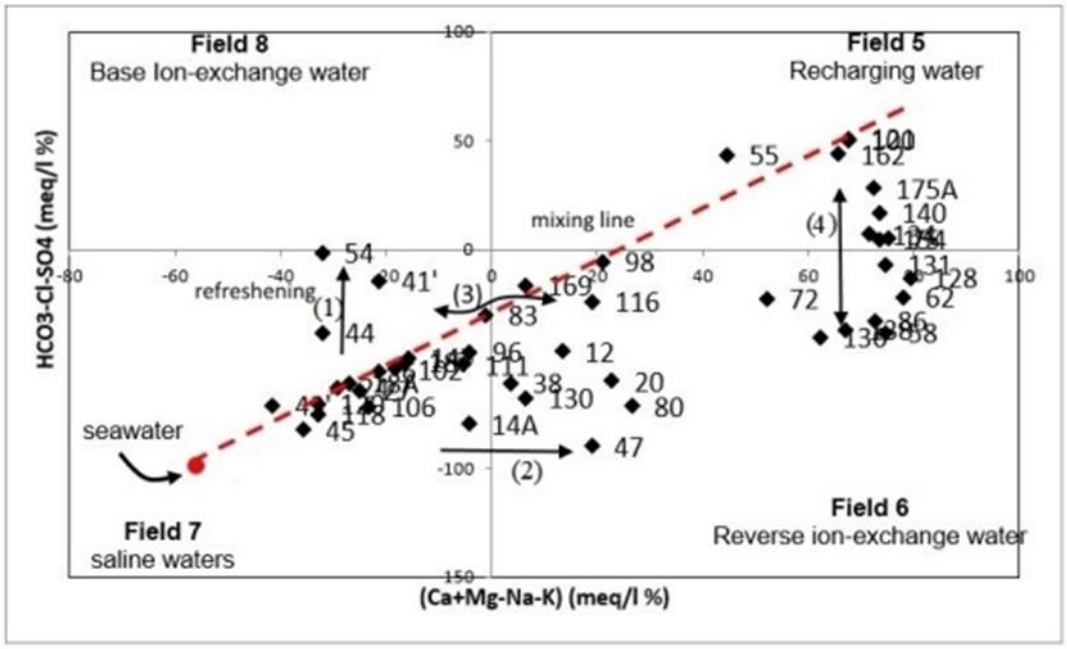

Figure 2: The geochemical processes in the groundwater illustrated on a Chadha diagram. Dashed line represents the mix of modern seawater with modern fresh water. Arrows represent hydrogeochemical processes as follows: (1) refreshening, (2) reverse cation exchange of aged seawater, (3) reverse cation exchange of modern seawater, (4) reverse cation exchange of aged fresh water. Double direction of the arrows means that the position of the sample shifts depending on the season time.

References

Gibbs, R.J., 1970. Mechanisms controlling world water chemistry. Sci. J. 170:795–840.

Hermides, D., 2018. Hydrogeological conditions of the Thriassion Plain basin with emphasis on the geohydraulic characteristics of the aquifers and the groundwater quality. PhD thesis, Agricultural University of Athens, pp 283.

Katsikatsos, G., Mettos, A., Vidakis, M., Dounas, A., Pomoni, F., Tsaila-Monopolis, S., Skourtsi-Koroneou, V., 1986. Geological map of Greece, in scale 1:50.000, ‘‘Athina-Elefsis’’ sheet, IGME publication, Athens.

Lambeck K (1996) Sea Level change and shore-line evolution in Aegean Greece since Upper Palaeolithic time. Antiquity 70(269):588–611.**]**

Lekkas, E., 2001. The Athens earthquake (7 September 1999): Intensity distribution and controlling factors. Engineering Geology, Publ. Elsevier Science Ltd., Vol.59, 297-311.

Mariolakos, H., Theocharis, D., 2001. Shifting shores in the Saronic Gulf during the last 18,000 years and the Kychreia paleolimni. Proceedings of the 9th International Conference, Athens, Bulletin of Hellenic Geological Society XXXVI 1: 405-413.

Mariolakos, H., Fountoulis, I., Sideris C., Chatoupis, T., 2001. Morphoneotectonic structure of Parnes’ Mt of Attica Proceedings of the 9th International Congress, Athens, Bulletin of the Geological Society of Greece, XXIV/1, 183-190.

Papanikolaou D, Lekkas E, Sideris Ch, Fountoulis I, Danamos G, Kranis CH, Lozios L (1999) Geology and tectonics of Western Attica in relation to the 7-9-99 earthquake. Newsletter of E.C.P.F.E., Council of Europe, 3: 30–34.

15th International Congress of the Geological Society of Greece
Athens, 22-24 May, 2019 | Harokopio University of Athens, Greece
Bulletin of the Geological Society of Greece, Sp. Pub. 7 Ext. Abs. GSG2019-351

Geo-environmental impact on the aquifer systems of the wider fire-affected area (August 2017) on Kythira Island, Greece

Christos Filis[1], Nikolaos Karalemas[1], Emmanuel Skourtsos[1], Haralambos Kranis[1], Stelios Lozios[1], Varvara Antoniou[1], Michael Diakakis[1], Spyridon Mavroulis[1], George Danamos[1], Emmanuel Vasilakis[1], George Mallinis[2], Ioannis Lialiaris[1], Eythimios Lekkas[1]

(1) National and Kapodistrian University of Athens, Department of Geology and Geoenvironment, Panepistimioupolis Zografou, 15784, Athens, Greece, chfilis@geol.uoa.gr
(2) Demokritus University of Thrace, Department of Forestry and Management of the Environment and Natural Resources, Orestiada, 68200, Greece

Three main aquifer systems developed on Kythira Island include (Pagounis, 1981; Pagounis & Gertsos, 1984, Danamos, 1991; Koumantakis *et al.*, 2006):

- The porous aquifer system in Neogene and Quaternary formations.
- The karstic aquifer system in the carbonate formations of the Pindos and Tripolis units.
- The aquifer system (both shallow and deep) in the fractured hard rocks mainly of the Phyllites – Quartzites unit.

The main discharge of the aquifer systems takes place in coastal and submarine brackish springs around the island, except for its northern part where the Phyllites – Quartzites unit outcrops and its central part where springs of small capacity discharge the carbonate formations of the Pindos unit.

The municipal water supply of Kythira has been reinforced by a series of projects and interventions, focusing on the summer touristic period, when water demand surpasses by far water availability, mainly consisting of new deep boreholes. Precipitation is the direct recharge of the three aforementioned aquifer systems while indirectly lateral discharge occurs in places between adjacent and tangential aquifer systems and from the streams runoff as well.

On August 4, 2017 a shrub, rather a forest fire broke out close to the island hospital; it expanded rapidly due to strong winds blowing in the area and raged out of control for four days, inducing considerable damage. The size of the fire-affected area was about 20km^2, 16km^2 mainly of shrub and 4km^2 of agriculture land.

For the detailed evaluation of the geo-environmental impact of the aforementioned fire to the aquifer systems of the Kythira Island concerning the quantitative and qualitative degradation seventeen municipal water points were finally selected for further hydrogeological study.

The water points monitoring network were used in September 2017, June 2018 and October 2018 for measurements of the water tables heads and springs discharges while water samples were collected and chemical, trace elements and microbiological analysis were carried out.

The impact of the fire on the quantity of the aquifer systems of the wider fire-affected area could not be fully clarified and there was indirect evidence of their recharge (it remains unknown its rate compared to the recharge before the August 2017 fire) during the three field trips such as:

- Fluctuation of the measurements of the water table heads.
- Fluctuation of the measurements of springs discharges.
- Fluctuation of the measurements of boreholes hydrometers.
- Changes to the hydrochemical facies of the Piper's, Durov's and Stiff's diagrams of the collected water samples.

The results and the evaluation of the chemical and trace elements showed that there was no impact of the fire on the quality of the wider fire-affected area aquifer systems. However, microbiological analysis from the Mylopotamos spring showed qualitative degradation, due to human activities in the wider area preexisting the August 2017 fire (Pagounis, 1981).

For the sustainable water resources management of the wider fire-affected area new projects were proposed in order to prevent phenomena that favors the runoff instead of infiltration which lead to the restriction of the recharge of the three main aquifer systems, such as works of artificial recharge.

References

Danamos, G., 1991. Contribution to the geology and hydrogeology of the Kythira Island. PhD Thesis, National and Kapodistrian University of Athens.

Koumantakis, I., Vassiliou, E., Psychogios, K., Dimitrakopoulos, D., Markantonis, K., 2006. The important role of nappe tectonics in the coastal aquifers. The case study in the island of Kythira (Greece). Proceedings of the 8th conference on limestone hydrogeology, Switzerland.

Pagounis, M., 1981. Hydrogeological investigation of the island of Kythira. Hydrological and Hydrogeological Investigations, No. 36, IGME, Athens.

Pagounis, M., Gertsos, T., 1984. Hydrogeological investigation of the island of Kythira. Hydrological and Hydrogeological Investigations, No. 42, IGME, Athens.

15th International Congress of the Geological Society of Greece
Athens, 22-24 May, 2019 | Harokopio University of Athens, Greece
Bulletin of the Geological Society of Greece, Sp. Pub. 7 Ext. Abs. GSG2019-365

General Hydro-electric Masterplan of Tekhuri River, in Georgia – The importance of the local engineering geological conditions

N. Kazilis[1], M. Kazilis[1]

(1) Geodata Engineering S.p.A.- Greek Branch, Theodorou Litsa 9, Thermi 57001, Thessaloniki, Greece, Town, email: nka@geodata.it

A Feasibility Study Layout Masterplan of the Tekhuri River located on the south-west slopes of Caucasus Mountains, in North-west Georgia, had been prepared in 2015. That Masterplan included five (nr. 5) individual hydro-electric projects containing five (nr. 5) dams (one rockfill type embankment dams with central clay core and four of the RCC gravity type dam), their height varied between minimum 23m over to 47m without taking into account the foundations excavations. In addition, the full initial project, included five (nr. 5) headrace tunnels, of diameter ranging between 2.5m to 4.0m with their lengths ranging between 3.6 over to 5.0km linking the reservoirs with the relevant provided five (nr. 5) power houses downstream, of total then provided installed of 112MW. The prevailing engineering geological conditions of the three upstream dam and their reservoirs are geologically characterized by the presence of a volcano-sedimentary folded sequence of, thick to medium layered, sandstones, siltstones, mudstones, andesitic lavas and tuffs. From the engineering geological point of view, the aforementioned sequence is characterized by relatively high strength, generally low deformability and low permeability, that practically secure both the dam and reservoir feasibility. However, the two downstream dams and their reservoirs geologically develop over karstic limestone formations outcrops which from the engineering geological aspect are characterized by very high permeability, with serious potential reservoir water-tightness and associated dam stability problems. In the beginning of 2016, a private investing company undertook the carrying out of the missing designs and the submission of the relevant application to get the permission for the implementation of the whole cascade hydro project to the Georgian Authorities. Within the obligations of the application procedure for obtaining the relevant concession permission by the Georgian authorities, there was carried out the necessary Feasibility Study by a local (Georgian) consulting company. The candidate Developer for the concession contract, just before the submission of the official application to the Georgian authorities, assigned to an Austrian consultancy the carrying out of the Technical Due Diligence Study of the Feasibility Study of the project which had been carried out by the local Georgian consultancy, focusing in particular on the Hydrological, Hydraulic, Geological and Geotechnical and the Energy aspects of the design. Within the framework of the Due Diligence study, a Greek team of Geologists and Geotechnical Engineers from the Greek branch office of an Italian consultancy based in Thessaloniki, Greece, undertook the geological and geotechnical part of the aforementioned study. In the presentation, there are described, first, the unsuccessful ways of the input and the essential incorporation of the geological information in the Feasibility Planning and Design of the Project Masterplan and in general, all of the hydroelectric projects in Georgia. Then, there are presented the final evaluation of the proven "non-feasible" of some of the provided dams and reservoirs of the previously developed project Masterplan. Finally, there are presented the Masterplan modifications based on the geological proposals to be in full alignment of the hydrological, hydraulic and energy considerations of the project, in order to achieve the technical and financial feasibility of the General Masterplan of the Hydro-electric Development of the river Tekhuri in the area of the South Caucasus mountains of Georgia.

15th International Congress of the Geological Society of Greece
Athens, 22-24 May, 2019 | Harokopio University of Athens, Greece
Bulletin of the Geological Society of Greece, Sp. Pub. 7 Ext. Abs. GSG2019-393

Statistical approach of groundwater quality parameters at Almopia basin, Macedonia, North Greece.

C. Mattas[1], T. Kaklis[1], N. Veranis[2], G. Soulios[1]

(1) School of Geology, AUTH, P.C. 54124, Thessaloniki, Greece, cmattas@geo.auth.gr
(2) IGME, Perevou 39, P.C. 54352, Thessaloniki, Greece

Introduction

The aim of this work is to present the groundwater quality characteristics and to identify the hydrochemical processes of the central alluvial part of the Almopeos river basin that administratively belongs to Almopia Municipality (Macedonia, North Greece) and covers an area of 240 km^2. The main geological formations that outcrop in the river basin are gneisses, schists, marbles, ophiolitic rocks, volcano-sedimentary series, limestones and flysch. The central part that constitutes the study area, is covered by sediments that are mainly composed of: clayey, clayey-sandy, clayey-gravely depositions, clay-sand-gravel material, colluvial deposits, conglomerates and pyroclastic volcanic material. A system of successive confined and unconfined aquifers is developed in these sediments. The main anthropogenic activities that have impact on the environment in the area are agriculture and livestock farming. There are also a few food processing units and touristic activities at Pozar thermal springs area. The main cultivations are fruit bearing trees and irrigated crops (such as maize, clover, vineyards, sunflower). Regarding the hydrogeological regime of the study area, the alluvial aquifers are recharged by the precipitation and lateral by the mountainous karstic formations that surround them (Mattas et al 2017). Groundwater level measurements that were implemented by I.G.M.E. during the decades of 1980, 1990 and 2000 recorded a continuous water level drawdown but this trend seems to reverse according to measurements that were implemented by the authors of this work in the year 2017 (Mattas et al 2017).

Materials and methods-Results-Discussion

A total of 52 groundwater samples were collected over the dry and wet periods of the years 2004 to 2007 by I.G.M.E.. In situ measurements of the physicochemical parameters (EC, pH) took place and chemical analyses for the main ions (Ca, Mg, Na, K, HCO_3, Cl, SO_4 and NO_3) were performed. We chose to study the data from this period, since during these three years there were not significant changes regarding the hydrogeological-climate conditions or the exploitation regime of the water resources. The available hydrochemical data were statistically processed with classical methods and the joint use of multivariate statistical methods. The Pearson method, the R-mode factor analysis and K-means cluster analysis were used to investigate the relation between the parameters in order to identify the prevailing hydrogeological procedures that determine the hydrochemical regime of the area. All mathematical and statistical computations were made using the Microsoft Excel 2010 and IBM SPSS statistics 20 software.
The results of the conventional statistical process are presented in Table 1. According to these results, the majority of

Table 1. Summary statistics of the groundwater samples quality characteristics.

(n=52)	pH	EC	Ca	Mg	Na	K	HCO_3	Cl	SO_4	NO_3
MEAN	7,54	423,25	53,10	16,18	9,15	2,69	219,70	10,23	27,41	9,65
MIN	6,77	140,4	22,44	0,97	3	1	62,22	3,54	9,3	0
MAX	8,11	1369	206,17	44,76	62	6	835,7	113,47	70	47,08

the samples correspond to typical good quality waters since these values do not exceed the maximum permissible limit for drinking or irrigation purposes. The Pearson coefficient is a statistical tool to show the degree of dependency of one variable with the other and is used to measure and establish the relationship between two variables. According to the results presented in Table 2, Pearson coefficient has revealed a high correlation between EC-Ca–Mg–HCO_3, which is expected as EC is a dependent variable and depends on the values of ions that determine the composition of water. This correlation is attributed to the dissolution of karstic rocks. Additionally, a high correlation was observed between Na-Cl and pH-SO_4. This is probably due to the existence of the geothermal field that is developed at the western boundaries and the central part of the alluvial plain (Arvanitis et al 2008). The R-Factor analysis resulted in three (3) factors as it is illustrated in Table 3 that interpret 74.726% of the total variance. The Kaiser-Meyer-Olkin coefficient is 0.604 (>0.5), and hence the method is valid. Electrical Conductivity, Ca, Mg and HCO_3 participate in Factor 1. These variables are associated to the procedures of carbonate rocks dissolution by water and Factor 1 has positive value in the northwestern and eastern boundaries of the area (Figure 1) where lateral recharge of the alluvial aquifers from karstic rocks take place. In Factor 2 pH, Na and Cl participate and it has positive values (Figure 1) mainly at the western boundaries and could be attributed to the existence of the geothermal field. K and SO_4 participate in the Factor 3 showing positive values at the north and western parts of the basin. This could be explained by the existence of the geothermal field at the western boundaries and due to agricultural activities. The K-means cluster analysis groups the samples according to their similarities. A subjective decision must be taken by the researcher regarding the final number of groups and in this case study three groups were selected. The results are shown in Table 4. The samples of the first group mainly appear at the western boundaries of the study area that lateral recharge of aquifers from mountainous rocks takes place and the samples of the second group at the eastern boundaries following groundwater flow that passes through the sediments of the plain

part of the basin. The third group includes one sample with different water quality compared to the other samples close to an area that a geothermal spring exists.

Table 2. Pearson correlation matrix of Almopeos river basin.

n=52	EC	pH	Ca	Mg	Na	K	HCO_3	Cl	SO_4	NO_3
EC	1	-0,215	**0,884**	**0,754**	0,57	0,041	**0,859**	0,491	0,412	0,414
pH	-0,215	1	-0,121	-0,032	-0,452	0,129	-0,093	-0,499	**0,089**	-0,027
Ca	**0,884**	-0,121	1	0,51	0,36	-0,072	**0,857**	0,271	,246	0,295
Mg	**0,754**	-0,032	0,51	1	0,258	0,263	**0,73**	0,248	0,456	0,347
Na	00,57	-0,452	0,36	0,258	1	0,100	0,31	**0,897**	,217	0,101
K	0,041	0,129	-,072	0,263	0,100	1	0,007	0,119	0,331	0,012
HCO_3	**0,859**	-0,093	**0,857**	**0,73**	0,310*	0,007	1	0,204	0,185	0,272
Cl	0,491	-0,499	,271	0,248	**0,897**	0,119	0,204	1	0,286	0,003
SO_4	0,412	**0,089**	,246	0,456	0,217	0,331	0,185	0,286	1	0,355
NO_3	0,414	-0,027	0,295	0,347	0,101	0,012	0,272	,003	0,355	1

Table 3. Varimax rotation factor loadings.

	Component		
	1	2	3
EC	0,906	0,373	0,119
pH	-0,004	-0,736	0,257
Ca	0,889	0,193	-0,112
Mg	0,764	0,077	0,381
Na	0,235	0,888	0,157
K	-0,071	0,015	0,816
HCO_3	0,928	0,117	-0,060
Cl	0,130	0,922	0,219
SO_4	0,330	0,079	0,743
NO_3	0,503	-0,101	0,228

Table 4. Final Cluster centers.

	Component		
	1	2	3
EC	299,02	555,69	1369,00
pH	7,55	7,55	7,02
Ca	40,39	64,00	206,20
Mg	10,72	22,62	44,76
Na	5,83	12,48	39,00
K	2,57	2,90	2,0
HCO_3	160,49	274,96	835,7
Cl	5,79	14,86	46,09
SO_4	23,94	32,27	29,30
NO_3	6,24	14,96	0,44

References

Arvanitis A., Kolios N., Koutsinos S. (2008). Geothermal exploration in the Almopia basin (Macedonia, Northern Greece). Proceedings of 8th International Hydrogeological Congress of Greece, volume 2, p. 443-454.

Mattas C., Veranis N., Kaklis T., Voudouris K., Soulios G. (2017). Groundwater level flctuation of the alluvial aquifer in Almopia basin (Macedonia) correlated with groundwater abstraction. Proccedings of the 11th International Hydrogeological Congress, Athens, Greece, p. 291-298

GENERAL SESSION

T10 Geology and Society: Geo-environmental education and Sustainability, Geological Heritage

15th International Congress of the Geological Society of Greece
Athens, 22-24 May, 2019 | Harokopio University of Athens, Greece
Bulletin of the Geological Society of Greece, Sp. Pub. 7 Ext. Abs. GSG2019-001

Underground coal mining in Central Europe in the mid. 19th century: a literary documentation by Zola's "Germinal"

A. Iordanidis, I. Kapageridis, A. Asvesta

Department of Geotechnology and Environmental Engineering, Western Macedonia University of Applied Sciences, Kila, 50100 Kozani, Greece, andior@teiwm.gr

Germinal is considered to be one of the ten greatest novels in the French language and is a story of a miner's strike, taking place in a coal mining area in northern France in the mid. 1800's (Zola, 2004). The novelist, Emile Zola, lived himself for several months in this area, thus providing accurate descriptions of the miners' life. This literary work provides indeed important information on the history of coal mining in Central Europe during the 19th century. Zola, being a naturalist novelist, addresses in an explicable way all aspects of coal mining (legislation, labour types, health and safety issues, environmental problems, mining conditions, mineral processing etc.), which could be very useful for educational purposes. All the information mentioned above is emphasized in our study.

The contribution of coal utilization in the so-called industrial revolution is indisputable. The **industrialization** of a coal mining area is evenly described in the following parts, comprising sugar refineries, flour mills, blast furnaces, construction and cable works, glass factories and coke-ovens: *Over in Montsou the Fauvelle sugar refinery was still working; the Dutilleul flour mill and the factory at Bleuze that made cables for the mines were managing to keep going; the Sonneville construction works had received only a third of its usual number of orders; of the three blast-furnaces the ironworks in Machiennes only two were lit; at the Gagebois glass factory there was a threat of a strike; only two batteries of coke-ovens still going; …the blast furnaces and the coke-ovens. These last, batteries of a hundred slanting chimneys, stood all in a line like ramps of red flame; nineteen pits they have, with thirteen producing coal and six for drainage or ventilation. Ten thousand workers, concessions stretching over sixty-seven communes, a production level of five thousand tons a day, a railway linking all the pits, and workshops and factories.*

Founding and Management of coal mines resemble the modern ones as seen in Zola's descriptions: *concession-holders were to found the Anzin Mining Company; people were busy taking soil samples; companies were set up and concessions were materialized overnight; the new mines that he had to be abandoned after long months of toil, mine-shafts closed by rock-falls, miners drowned by sudden floods, hundreds of thousands of francs draining away down a few holes in the ground; problems of managing the business, the panicking shareholders, the tussles with the hereditary landowners of ancient estate; After establishing the company, the pits were beginning to yield meagre returns; almost ruined with the ferocity of the competition of other Companies; A settlement had been reached between the three concessions and they were amalgamated; a distribution of shares; the total capital value represented a sum of nearly three million francs; faced with the crisis, the Company had been forced to reduce its costs, naturally the workers were the ones to tighten their belts; the Company would gradually whittle their wages down; Coal had been piling up at the pit-heads for two months now, since all factories were idle; the Company didn't lay off its workers because it would be ruinous not to maintain its plants; a strike would bring its workforce to heel and leave it less well paid than before.*

Different types of colliers are illustrated in several parts of the book (Figure 1): *the **hewers** were wedged between the face and the ceiling and kept grazing their elbows as they extracted the coal; Each afternoon the **shifters** came and fetched the rubble left at the end of each tunnel by the **hewers** and then disposed of it in the cavities where the seam had already been mined; Simple **pit-boy** to start with, then **putter** once I was strong enough to push the tubs, and then **hewer** for eighteen years; **Banksmen** of each deck would drag the tubs out and replace them with others; The **onsetters** were busy wheeling the full tubs roughly across the cast-iron flooring; After that they put me on **maintenance** work, filling in seams, repairing the roads; they had to bring me up and give me surface job...they made me a **driver**; The **engineman** standing by the operating lever was listening out for the signal bells; a large white **horse**, pulling a train of coal tubs; Each full tub reached the surface marked with a special token so that the **checkweighman** could credit it to the appropriate team of miners; The haulage roadway had not yet been widened by the **stonemen**; a full tub could only just pass underneath, with the **putters** having to get down on their knees and push so as not to crack their skulls open; The tubs of coal came directly from the pit-head and were then emptied out by **tripplers** on to the screens; To the right and left from these chutes, the **women and girls** who did the screening; a **deputy** shining his lamp in their faces; A **stoker** shovelling coal into one of the boilers that powered the drainage-pump; which the **engineers** had had no inkling of despite their extensive knowledge of the terrain*. All these categories of mine workers are clearly elucidated by Bulman and Redmayne (1906).

The **mine machinery** on the surface along with **coal processing** plant are also illustrated in the following novel fragments (Figure 2): *The screening-shed with its asphalt roof; the headgear over the pit-shaft; the huge engine house and the square tower containing the drainage pump; The winding-engine was setback some twenty-five metres from the shaft and housed at a higher level; working at full steam and producing every one of its four-hundred horse power; The engine would start up each time a cage departed and the spools-two enormous wheels measuring ten metres in diameter, around the hubs of which two steel cables wound unwound in opposite directions; did the screening equipped with a rake and shovel; the clean coal fell through funnels down into the railway wagons standing on the line beneath the shed.*

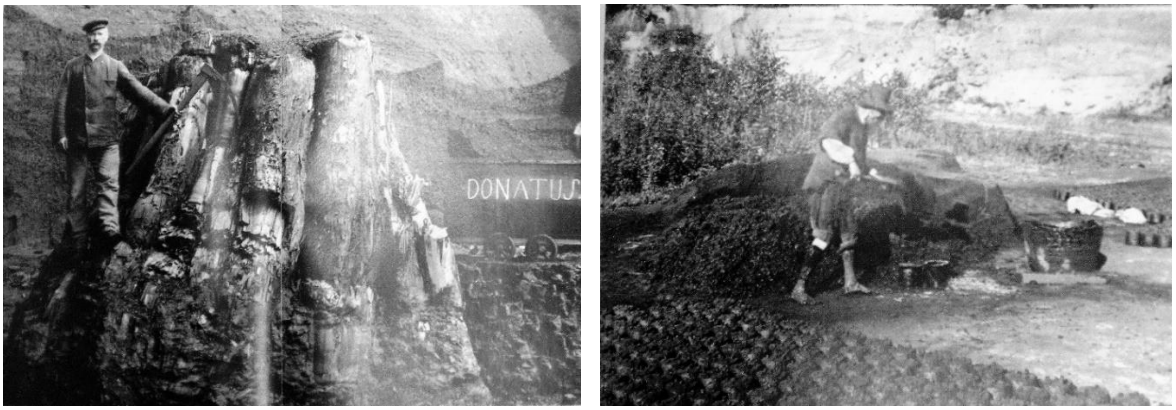

Figure 1. A collier standing next to a mega xylite trunk (left) and hand-made manufacturing of briquettes (right).

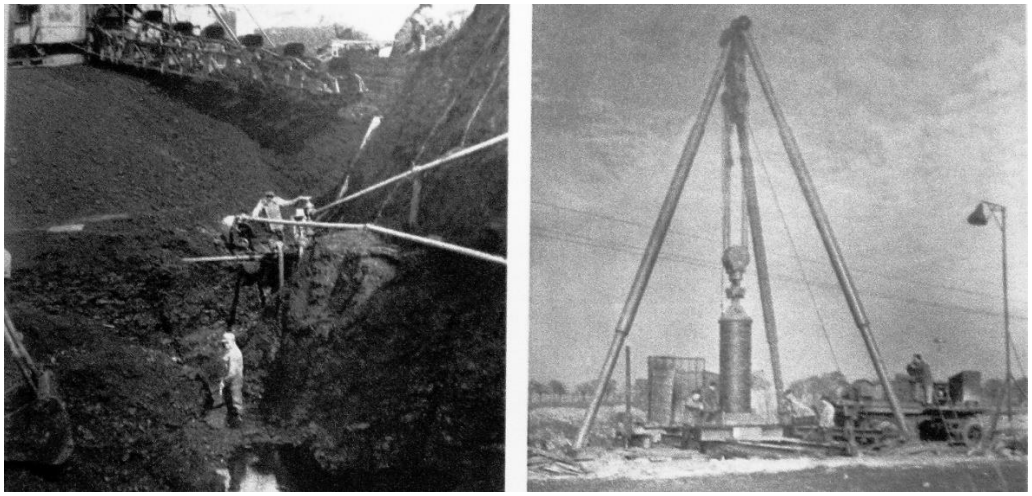

Figure 2. Coal mine with primitive excavators and drainage problems (left) and a drainage pump (right).

The **mining techniques** and the **working conditions** in the underground coal mine are described as follows: *Five hundred and fifty-four metres deep, but there are four loading-bays on the way down; The shaft itself is divided vertically into three sections by wooden planks. In the middle are the cages, on the left is the emergency shaft where there are ladders; the miners crossed pit-bottom, a cavity hewn out of the rock, which was reinforced with masonry vaults; oak props supported the roof and retained the crumbling rock behind a wooden framework; Ventilation doors open with a bang and then slowly closed again; the temperature reached thirty-five degrees; there was no circulation of air, and the suffocating atmosphere was potentially fatal; Each man hacked into the shale bedrock, digging it out with his pick; they had to drag themselves forward on their elbows and knees and were quite unable to turn round without banging their shoulders; the atmosphere became even more poisonous from the asphyxiating firedamp.*

Health problems and **accidents** of the miners and their families connected to coal exploitation are often emphasized by Zola: *The old man spat black phlegm; It's the water that's got under my skin, what with getting soaked all the time down at the coal-face; with his frail limbs and huge joints, swollen from scrofula; soaked to the skin and shivering, their lungs a prey to the pneumonia; the anaemia that was gradually eating away at them; They've dragged me out of there three times now, barely in one piece. Once with my hair all signed, once full to the gills with earth, and once with my belly full of water, all swollen like a frog's; a rock-fall it was, completely flattened him, swallowed him whole, bones, flesh, blood, the lot. Two of his uncles and then, later on, his own three brothers had all lost their lives down there.*

Environmental pollution caused by coal exploitation is depicted in quite a few parts of *Germinal*: *The spoil-heap was already covered in grass, while at the other end it was being eaten away by an internal fire, which had been smouldering for a year now and gave off a thick pall of smoke; beneath a dun-coloured sky; the road were coated in mud, the thick, glutinous mud of coal-mining regions that looks as black as liquid soot; factory buildings with tall chimneys that belched out soot and filthied what remained of the countryside.*

Overall, it is evident that substantial information is inhered from this literary work, Zola's *Germinal*, regarding coal mining in the mid. 19th century in Central Europe. The latter is not only important for comprehending the history of coal mining, but may be useful for teaching mining subjects in educational institutes.

References

Bulman, H.F., Redmayne, R.A.S., 1906. Colliery Working and Management, 2nd Ed. London (first published in 1896).
Zola, E., 2004. Germinal, Penguin Books Ltd (first published in 1885).

15th International Congress of the Geological Society of Greece
Athens, 22-24 May, 2019 | Harokopio University of Athens, Greece
Bulletin of the Geological Society of Greece, Sp. Pub. 7 Ext. Abs. GSG2019-049

Lesvos Petrified Forest: the fascinating colours of the silicified trunks

A. Iordanidis[1], J. Garcia-Guinea[2], N. Zouros[3], A. Asvesta[1]
(1) Department of Geotechnology and Environmental Engineering, Western Macedonia University of Applied Sciences, Kila, 50100 Kozani, Greece andior@teiwm.gr & aiordanidis@yahoo.co.uk
(2) Museo Nacional Ciencias Naturales, CSIC, Abascal 2, 28006 Madrid, Spain
(3) Department of Geography, University of the Aegean, 81100 Mytilene, Greece

The Lesvos Petrified Forest was formed by silicification process of plants during the Lower Miocene era, when intense volcanic activity occurred in that region. It is situated in the western part of Lesvos island (NE Greece) and consists of hundreds of standing and lying fossilized tree trunks, covering an area of 150 km^2. It is one of the most important natural heritage monuments in the world and in 2004 the area was included in the Global Geoparks Network (Zouros, 2010). The Natural History Museum of the Lesvos Petrified Forest is the management body of Lesvos Geopark.

The numerous visitors of this geopark are impressed by the fascinating colours of the fossilized trunks. A palette of vivid colours is often evident in the silicified stems (Figure 1). Variable colours are noticed not only in fossil plants from the same locality, but within a sole fossil plant itself.

Several factors affect the distribution of different colours within the fossilized plants: the nature of pyroclastic rocks and the hydrothermal solutions produced during the volcanic activity; the silicification process itself (replacement of cell-wall structure or void filling, i.e. permineralization process); the possibility of a multi-stage petrification and the subsequent mobility of chemical elements therein; the palaeoenvironmetal conditions (hydrology, pH, Eh etc.); the type of species and the variability of plant tissues within the same species.

The aim of the present study is the investigation of the origin of these natural colourants by determining the chemical and mineral abundance of fossil plant samples.

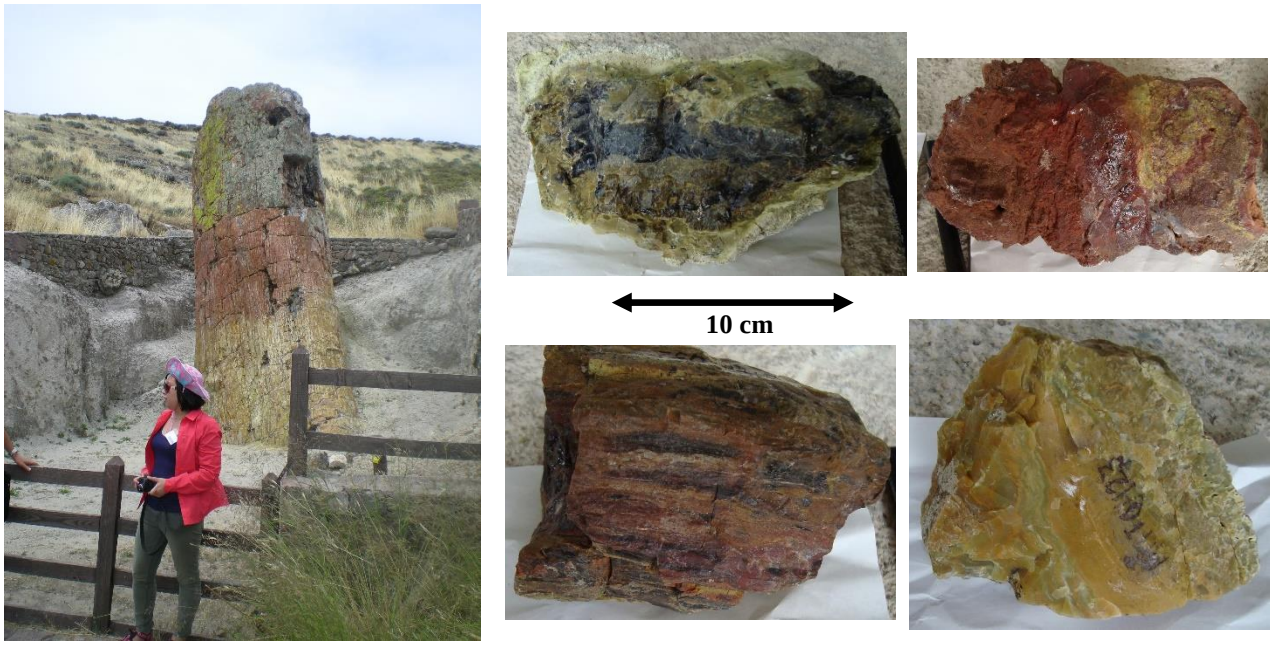

Figure 1. The famous, longest –world record awarded- standing fossilized tree from Lesvos geopark, showing three characteristic chromatic zones [left] and macroscopic images of four representative silicified plant samples [right].

Seventeen fossil plant samples were collected from the Sigri pyroclastic formation within the Lesvos Petrified Forest. Polished block sections of each sample were prepared for analytical purposes. A Philips QUANTA 200 Environmental Scanning Electron Microscope (ESEM), coupled with an Oxford INCA Energy 200 Energy Dispersive System (EDS) was used for imaging and chemical (both in area and spot) analyses. For the Raman spectroscopy, a Thermo Scientific DXR Raman Microscope with a 780 nm laser beam was employed. The power value of the sample irradiation was ranging from 6 mW to 12 mW. The average spectral resolution in the Raman shift range of 100-3000 cm^{-1} was 5cm^{-1} (grating 400 lines/mm, spot size 2μm).

The main colours determined are black, milky white, transparent white, green, red, orange, brown and yellow. The presence of black carbon was clearly estimated in the black zones by the characteristic Raman spectra bands at 1378 and 1536 cm^{-1} (Figure 2). However, pure silica was only detected by EDS in the black colour of some samples. Thus, black colour is attributed either to the relicts of organic matter in the silicified sample or may simply be related to the low reflectance of translucent silica oxides (Musteo & Acosta, 2016).

Raman spectroscopy confirmed the presence of opal in milky white and quartz in transparent white colours. Quartz was revealed with its intensive band at 465 cm^{-1} and the secondary bands at 123, 203 and 497 cm^{-1}, while opal showed a characteristic hump between 200 and 500 cm^{-1}, with distinct strong peaks at 350, 784 and 1590 cm^{-1} (Iordanidis et al., 2014). The EDS analysis of green, yellow, orange, brown and red colours revealed that iron (Fe) is the primary colourant, with the intensity of colour proportional to the abundance of that element. Consequently, lower concentrations of Fe were found in the green colour, while higher contents of iron were determined in the red colour and intermediate contents for orange, brown and yellow tints (Sileo, 1979). Similarly, the presence of iron oxides and hydroxides was determined in the red/orange/brown/yellow and green colours by Raman spectroscopy (Figure 2) and particularly hematite (Fe_2O_3) for the red hue, lepidocrocite [γ-FeO(OH] for the green colour and goethite [α-FeO(OH)] or mixtures of the aforementioned iron oxides/hydroxides for the brown/orange/yellow tints (Musteo & Acosta, 2016). Hematite showed characteristic bands at 223, 296, 402, 658 and 1315 cm^{-1}, goethite presented peaks at 243, 298, 389, 550, 681 and 1298 cm^{-1} and lepidocrocite displayed characteristic bands at 170, 256, 285, 440, 525 and 694 cm^{-1}.

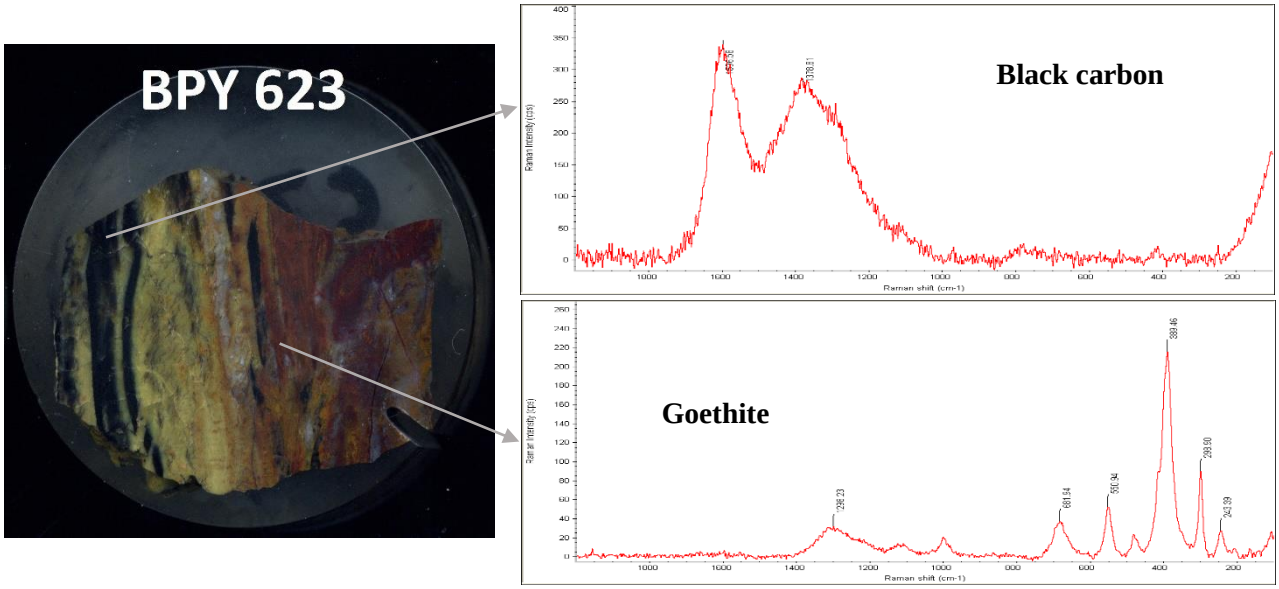

Figure 2. Polished block section of the BPY 623 fossil plant sample, showing characteristic black, white, green, yellow, brown, orange and red colours [left] and the Raman spectra of black carbon and goethite determined in the black and brown areas respectively [right].

Trace amounts of the chemical elements Mn, Ti, V, Hg, Ba, REE were also detected by EDS. Some of these trace elements, such as Mn and Ti are known as natural colourants (Sileo, 1979). However, they were determined in all colour hues and therefore could not be consider as colour creators. It should also be noted that the chemical analysis of this study refers to a spot or area (up to some hundreds of μm^2) EDS analysis and not to a bulk sample analysis.

In conclusion, the complementary use of ESEM-EDS and Raman microscopy techniques provided significant information on the natural colourants, accountable for the fascinating colours of the fossilized stems from Lesvos petrified forest.

Acknowledgements

This research received support from the SYNTHESYS Project (ES-TAF-5318), which http://www.synthesys.info/ is financed by European Community Research Infrastructure Action under the FP7 "Capacities" Programme at the Museo Museo Nacional de Ciencias Naturales (CSIC), Madrid, Spain.

References

Iordanidis, A., Garcia-Guinea, J., Strati, A., Gkimourtzina, A., 2014. A comparative study of pigments from the wall paintings of two Greek Byzantine churches. Analytical Letters 4(16), 2708-2721.

Mustoe, G., Acosta, M., 2016. Origin of Petrified Wood Color. Geosciences 6 (2), 25.

Sileo, A.C., 1979. Geochemistry of silicified wood and associated sediments, Petrified Forest National Park, Arizona. Chemical Geology, 26, 151-163.

Zouros, N., 2010. Lesvos Petrified Forest geopark, Greece: Geoconservation, Geotourism and Local development. Journal of Parks, Protected Areas and Cultural sites 27, 19-28.

15th International Congress of the Geological Society of Greece
Athens, 22-24 May, 2019 | Harokopio University of Athens, Greece
Bulletin of the Geological Society of Greece, Sp. Pub. 7 Ext. Abs. GSG2019-058

A survey of show caves in Greece

A. Zacharoudi [1], G. Lazaridis[1]

(1) Aristotle University of Thessaloniki, Department of Geology, Laboratory of Geology and Palaeontology, 54124, Thessaloniki, Greece, geolaz@geo.auth.gr, +302310998554

About 30 show caves exist in Greece, which are scattered in both the mainland and the islands. Some of them are temporarily closed to the public due to maintenance reducing their number to 25. Show caves are the most important geotouristic feature according to Cigna and Forti (2013). They exist for at least 400 years and provide an income to more than 100 million people around the world (Cigna and Forti, 2013). In any case a viable development is crucial for any show cave and their environments.

This study investigates the status and the conditions of show cave development in Greece from the perspective of a geologist.

Methods

In order to collect data a survey has been created with questions based on the UIS Management Guidelines for Show Caves (see Cigna and Forti, 2013) about the suggested prerequisites of show cave development. In addition to that form, a second one has been added with information about the cave visitors per year and a number of fields related to the dimensions and geology of each cave.

The questions were of varied content about the cave visitors, the materials that have been used, the ideal lighting that have no effect in the biology and climate of the cave, the cave monitoring of parameters such as temperature, humidity or carbon dioxide, and how these data are treated and interpreted.

Results

In total 25 completed forms provided information about the conditions of cave development in Greece.

Regarding the entrance to the caves, the natural entrance is used in 56%, in which it has been opened and modified in 43%. Independently of whether an artificial entrance is used or not, a double set of doors it is used in only 28%.

The materials used in the caves are commonly compatible with the cave environment. However, at least in 21% non-compatible materials have been used and in other cases compatible materials have been used in a way that has a negative effect on the cave environment.

The pathway is only in less than 21% a continuous route, which means that visitors use another exit and do not repeat parts of the route. This results in twice the time spend in cave that has a negative impact on the cave environment. The group size varies from 8 to unlimited persons and depends only to the cave size. Furthermore, the breaks between groups vary from 5 minutes to unlimited, and depends on the visitors per day.

The lights along the pathways is a parameter that show improvement of the Greek show caves. Many of them have already installed proper lighting and others have included such changes in their plans. However, in 52% of the caves the lights are on during the working hours, independently of the visitors' presence.

The cave environment is monitored in only 40% of the Greek show caves for the parameters of temperature and humidity (unknown instrument precision) and only 28% report a carbon dioxide monitoring system. However, none of them reported a use of these records or scientific staff responsible for the data evaluation. Furthermore, only occasional collaboration with geologists has been reported and mainly with the Ephorate of Paleoanthropoloy and Speleology (Ministry of Culture and Sports) and with some Universities. The guides are part-time staff and they are mainly shelf-educated on speleological subjects (this may include also the attendance of seminars in speleological clubs). The aim in cave management are in most cases the advertisement of the cave (76%), the protection and conservation of each environment (20%) and new employment (4%). The visitor volume ranges for about 40% with data available, from 2.500 to 200.000 providing more than half a million euros income.

Concluding remarks

On the basis of this survey, the Greek show caves are important geotouristic destinations. However, it seems that Greek show caves do not conform perfectly to the standards of UIS Management Guidelines for Show Caves and the related literature (Cigna and Burri, 2000; Gillieson, 2009; 2011; Cigna and Forti, 2013; Cigna 2016). Entrance-related problems may be a closed natural entrance or an artificial one without an efficient air lock system. Pathways that doubles the visitors' stay inside the cave, combined with group size and frequency based on demand instead of environmental studies, is also a potential hazard. In addition, the absence of monitoring systems and scientific staff makes difficult the evaluation of the conditions in each cave.

Acknowledgements

We would like to thank all the people who work in the show caves for their good-will to help in the survey and the Ephorate of Palaeoanthropology and Speleology, Ministry of Culture and Sports for the provided information.

References

Cigna, A.A., 2016. Tourism and show caves. Zeitschrift für Geomorphologie, Supplementary Issues 60, 217-233.

Cigna, A. A., Burri, E., 2000. Development, management and economy of show caves. International Journal of Speleology 29, 1.

Cigna, A. A., Forti, P., 2013. Caves: the most important geotouristic feature in the world. Tourism and Karst areas 6, 9-26.

Gillieson, D. S., 2011. Management of caves. Karst management. Springer.

Gillieson, D., 2009. Caves: processes, development and management, John Wiley and Sons.

15th International Congress of the Geological Society of Greece
Athens, 22-24 May, 2019 | Harokopio University of Athens, Greece
Bulletin of the Geological Society of Greece, Sp. Pub. 7 Ext. Abs. GSG2019-069

Geology and the Aztecs: How the Ore Deposits of Mesoamerica Influenced the Socioeconomic Development of an Empire, from its Emergence to its Downfall

Argyrios Periferakis[1]

(1) National and Kapodistrian University of Athens, Department of Geology and Geoenvironment, University Campus, Athens, Greece, argyrisperiferakis@gmail.com

Introduction

The oldest major settlement of Mesoamerica, Teotihuacan, was built mainly from pyroclasts extracted via quarry tunnels, from the basaltic flows underlying the superficial volcanic tuffs, for approximately 300 years, between 150 BC and 150 AD. These tunnels are still in existence today and were subsequently used by the inhabitants of the city for ritualistic and burial purposes (Manzanilla *et al.*, 1996). Another such example is the city of Xochicalco, where there are tunnels originally used for limestone mining. So, from an early stage, the indigenous populations of Mesoamerica build their major settlements in places where there was a relatively easy procurement of building materials, and constructed the buildings virtually on top of the quarry tunnels, which were then converted to other purposes. The Aztecs themselves claimed their descent from the Toltecs, which in turn believed themselves to be ancestors of the inhabitants of Teotihuacan (Pemberton, 2011). As far as metallurgy and use of processed metal objects is concerned, modern research maintains that metalworking was introduced gradually in Mesoamerica through maritime trade with South America, and more specifically with Ecuador between 650 and 700 AD (Hosler, 2009; and references therein). In this research we present a general description of the metallogeny of Mesoamerica, and we document how the Aztecs mined for or collected as tribute gold, silver, copper, turquoise, jadeite and obsidian, how the availability of such commodities shaped their civilisation and how in the end lead to their demise.

Metallogeny of Central America

The oldest ore deposits of the area date back to the Proterozoic (Camprubi, 2009), but here the main interest is in the metallogenic province of the Pacific margin, which is the greatest silver province of the world (Camprubi, 2009). The intense Mesozoic to Cenozoic magmatism resulted in a host of porphyry and epithermal deposits, as well as skarn deposits. Many surface manifestations of porphyry deposits were mined for Cu and Au. Examples of such deposits are San Juan Mazatlán in Oaxaca, Tiámaro in Michoacán, Bacamari and La Azulita in Sinaloa, Caborca, El Promontorio, La Mariquita and El Alacrán in Sonora and many others (Camprubi, 2009; and references therein). For most of these deposits there is no evidence proving that they were the locus of Aztec mining activity but it is reasonable to assume that quarrying of some scale must have taken place in some of them, although tunnels are yet to be discovered or have since collapsed. Uncommonly, for such an extensive metallogenic province, there are very few high sulfidation epithermal deposits, while intermediate sulfidation epithermal deposits are dominant. Many such deposits are Ag/Au-rich or polymetallic, while high sulfidation deposits cluster in the NW Mexico (Camprubi, 2009).

Mining and Use of Obsidian within the Aztec Society

Perhaps the most well known rock coming to mind when seeing Aztec murals, weapons and everyday tools, is obsidian. Indeed, it can be argued that it was the most important natural resource of the Mesoamerican indigenous populations, since it was first exploited by the Olmecs (Pastrana & Domínguez, 2009). The physical properties of obsidian, namely its sharpness, durability and predictable cleavaging, made it an excellent material for a number of uses. The main sites for obsidian extraction, of the Aztec Empire, were Sierra de las Navajas, Otumba, Paredón, Tulancingo and Pico de Orizaba. The extraction of obsidian could be accomplished directly from the available outcrops, or via shallow trenches, open pits and tunnels. Obsidian was used for the creation of most implements of everyday life, be it weapons, ritual tools, everyday tools, jewels, vases and sculptures. Such was the importance of obsidian for the Aztecs that every source was assiduously exploited, while need for continuous mining and processing of obsidian lead to the gradual delineation of distinct socioeconomic strata, i.e. miners, knappers and obsidian traders.

Copper Mining and Importance for the Aztec Civilisation

Archaeological research has discovered remnants of ancient quarries in Zocotallan, Cerro del Aguilar, Tasco and in the Zapotec country (Phillips, 1925). Ayutla and Ayutlan in Jalisco and Inguaran and Bastan in Michoacán are settlements associated with copper mining and processing, while similar settlements have been found in the area of Guerrero (Hosler, 2009). However, the Aztecs did not most probably have any knowledge of bronze, as exhibited by the chemical analyses of various copper objects found in Mesoamerican archaeological sites (Phillips, 1925). While the metallurgy of the Aztecs was pretty advanced, they never progressed to the Bronze Age *sensu stricto*, as they did not intentionally use tin in conjunction with copper to produce bronze. It appears that the main focus of Aztec in particular and Mesoamerican metalworkers in general was to alloy Cu with other metals to produce religious and ornamental items which would be durable and shiny having a yellowish golden colour.

Use of Ornamental Stones and Minerals

The two principal ornamental minerals of the Aztecs, which shall be examined here, were turquoise and jadeite. Turquoise $[Cu(Al, Fe^{3+})_6(PO_4)_4(OH)_8 \cdot 4H_2O]$ was used in a variety of applications, from jewelry and ornaments, to

mosaics, shields and knife handles, for the upper echelons of the Aztec society. Current research (Thibodeau *et al.*, 2018) indicates that turquoise most probably was mined in SW Mesoamerica, from locations in West and Central Mexico, where copper mining has also been documented (Hosler, 2009). Since turquoise forms in the oxidation zones of copper deposits, it is reasonable to assume that in many cases turquoise and copper were extracted from the same mines. Regarding jadeite $[Na(Al, Fe^{3+})Si_2O_6]$ was used by almost every Precolombian civilisation of Mesoamerica in some form or another. In the case of the Aztecs, jadeite had acquired a mythical status and was restricted only to upper social classes, as they valued jadeite even more than gold and silver. The sources of jadeite are believed to be the Motagua River Valley in modern-day Guatemala and the Balsas Valley in Guerrero, while possibly more sources remain to be identified (Howard, 2001).

Gold and Silver in the Aztec Society

The abundance of gold and gilded items used and possessed by the Aztecs is described by many historians and chroniclers of the 16th and 17th centuries, and is verified by archaeological discoveries. According to descriptions by Cortés and Pizarro, the gold of the Aztec Empire came from Çoçolan, Malinaltepec, Tenis, Tochtepec, Zacatula and Xaltepec. The majority of gold was extracted from placer deposits and the term «placer» itself is most probably of Spanish origin and refers to deposits of detrital and residual material, such as sand or gravel, which contain a valuable mineral as a result of weathering and preferential mechanical accumulation (Yeend & Shawe, 1989). The descriptions of the Aztecs to the Spanish, about gold procurement, present gold mining as little more than picking gold grains from the sand which they gathered from the bottom of riverbeds. The need to furnish with gold and gilded items the upper echelons of their society lead to the creation of a separate and elite class of goldsmiths. Silver is a different story altogether, as it appears to have waded its way through the Aztec society and metalworking tradition through marketing networks.

Discussion and Conclusions

In effect, the existence of many different valuable minerals and rocks, and the constant need of the upper socioeconomic classes of the Aztecs for a display of precious ornate jewels and accessories lead to the formation of different professional classes of craftsmen, who occupied a distinct spot in the social fabric of the Aztec Empire. However, gold did not have a monetary value and it is interesting to observe that entire civilisations of Mesoamerica, who had regulated their everyday life without using any metal implements, shifted their focus on associating available metals with ornamental, religious and ritualistic maters (Hosler, 2009). This is a clear formative effect of geology, as had ore deposits of particular metals not existed, a whole aspect of the Aztec civilisation – and the preceding and contemporary ones for that matter – would be significantly different if it had existed at all. Additionally, the constant demand of the Aztec society for precious stones, which could not be found in their entirety within the borders of the Aztec Empire, lead to an ever increasing need for expansion, and therefore constant warfare. However, the display of wealth, and especially of gold, or of gilded items was the catalyst of the Aztecs' downfall by Cortés and his conquistadors (Pemberton, 2011). Interestingly, the presence of gold and silver contributed in altering the perception of the Spanish about the association between land ownership and wealth. In the Old World, the ownership of arable lands meant a steady income, roughly commensurate with the productivity of said agricultural expanses. However, the conquistadors virtually destroyed local societies, and as a result local production capacity (Harrasta, 2014). So, the conquest of more land was simply the means to an end, namely in acquiring gold and silver. The influx of enormous amounts of gold to Europe in the end had negative effects for European economies, since it caused a rapid drop in the nominal value of gold, and, since currency at the time was based on a country's gold reserves, widespread inflation. Despite that, the Spanish economy was, in the short term, benefited, since it overcompensated for the partial devaluing of its gold reserves by the huge increase in the net amount of gold available (Harrasta, 2014). A more far reaching consequence of the real and imaginative wealth of Mesoamerica in particular and the New World in general, was the Treaty of Tordesillas in 1494, the race for colonisation and the eventual war between England and Spain, in 1588 (McKee, 1987).

References

Camprubi, A., 2009. Major metallogenic provinces and epochs of Mexico, SGA News 25, 1-32.

Harrasta, J., 2014. El Dorado, the Search for the Fabled City of Gold, Charles River Editors.

Hosler, D., 2009. West Mexican Metallurgy: Revisited and Revised, Journal of World Prehistory 22, 185-212.

Howard, K., 2001. Jadeite, Canadian Institute of Gemology.

Manzanilla, L., López, C., Freter, A., 1996. Dating Results from Excavations in Quarry Tunnels behind the Pyramid of the Sun at Teotihuacan, Ancient Mesoamerica 7, 245-266.

McKee, A., 1987. From Merciless Invaders, The Defeat of the Spanish Armada, 2nd Edition, Grafton Books.

Pastrana, A., Domínguez, S., 2009. Cambios en la estrategia de la explotación de la obsidiana de Pachuca: Teotihuacan, Tula y la Triple Alianza, Ancient Mesoamerica 20, 129-148.

Pemberton, J., 2011. Conquistadors, Searching for El Dorado: The Terrifying Spanish Conquest of the Aztecs and Inca Empires, Futura.

Phillips, G., 1925. The Metal Industry of the Aztecs, American Anthropologist 27, 550-557.

Thibodeau, A., López Luján, L., Killick, D., Berdan, F., Ruiz, J., 2018. Was Aztec and Mixtec turquoise mined in the American Southwest? Science Advances 4, doi: 10.1126/sciadv.aas9370.

Yeend W., Shawe, D., 1989. Gold deposits in the Virginia City-Alder Gulch District, Montana, in: Yeend W., Shawe D., Wier K. (Eds), Geology and Resources of Gold in the United States, U.S. Geological Survey, Bulletin 1857, pp. G1-G13.

15th International Congress of the Geological Society of Greece
Athens, 22-24 May, 2019 | Harokopio University of Athens, Greece
Bulletin of the Geological Society of Greece, Sp. Pub. 7 Ext. Abs. GSG2019-070

The Influence of Ore Deposits to the Development and Collapse of the Inca Civilisation between the 15th and the 16th Century

Argyrios Periferakis[1]

(1) National and Kapodistrian University of Athens, Department of Geology and Geoenvironment, University Campus, Athens, Greece, argyrisperiferakis@gmail.com

Introduction

In South America, covering mostly the area of modern day Peru, the most developed sociopolitical entity of the Precolumbian Americas, started as the small city-state of Cusco. At the height of its power, the Inca Empire covered vast expanses of land from Ecuador to the North to Chile to the South, while the Andes formed its Eastern frontier. The population of the Empire at that time is estimated at around $16 \cdot 10^6$ people (Pemberton, 2011). While the economic system of the Incas did not include any concept of money and was based on mutual trade, the role of precious metals, namely silver and gold, as well as of other metals and minerals was pivotal in establishing distinct social strata and a domestic trading network. The Incas built upon an already rich pre-existing tradition of mining and metallurgy, which was assimilated from the peoples they conquered. By capitalising on mineral wealth and relatively advanced ore extraction and processing techniques, they created a civilisation which is remembered as being amongst the wealthiest in historical record. Of course, such sumptuousness was to prove the undoing of the Incas, as it drove the relentless Spanish conquest. In this research the quantification of the cumulative effect of the availability of different ores in the socioeconomic fabric of the Incas is attempted, so as to demonstrate how geology shaped the Age of Discovery.

Geological Setting and Ore Deposits of the Andean Cordillera

The Andes constitute the richest source of mineral wealth in the New World and are characterised by a rich metallurgical tradition since 700 BC (Cooke *et al.*, 2009). In terms of metallic ores, the Andes represent one of the richest orogenic belts, and are a source for many metals, such as Sb, Be, Bi, Cu, In, Mo, Pt, Re, Tr, Al, W, Zn and Sn. The Fe-Cu skarn deposits of the Andahuaylas-Yauri zone in Peru, are associated with quartz monzonite stocks and also contain native Au. At the Northern and Southern ends of the Andean belt there are a lot of copper deposits, dating from the Upper Palaeozoic to the Pleistocene. Most porphyry copper deposits are related to dacitic-granodioritic porphyry stocks (Oyarzún, 2000). Within modern day Peru – in the centre of the erstwhile Inca Empire – there are numerous Cu ± (Fe, Au, Zn) skarn deposits, Cu-Fe manto-type deposits, and widespread Cu vein deposits, which are considered to be the first exploited copper source (Oyarzún, 2000; and references therein). As far as Au deposits are concerned, there are epithermal Au-Ag veins, Au quartz veins, Au placer deposits, Au skarn deposits and Cu ± Au porphyry deposits in Ecuador and Peru (Noble & Vidal, 1996). In the Western Cordillera, in modern day Peru and Chile, there are numerous deposits of Ag, either in primary or secondary form and as inclusions of Ag-minerals in galena (Bellido & Montreuil, 1972). Tin is found in Tertiary deposits related to sub-volcanic intrusive bodies, which crosscut Palaeozoic clastic formations (Sillitoe *et al.*, 1975).

Gold and Silver in the Context of the Inca Society

The main source of gold of the Incas can be traced back to placer deposits, which were the first to be exploited by man. However, both porphyry and vein deposits are known to have been exploited. In general, the Inca Empire had abundant gold resources within its borders, both in its central part, in modern day Peru, as well as in Ecuador, Chile and Colombia (Petersen, 1970). While native gold was extracted from quartz veins, placer deposits in Peru were exploited at the valleys of Rio Chinchipe, Rio Mariñón, Rio Santiago de Montaña, Rio Aguarrica, Rio Morona and Rio Chachapoyas. It must be mentioned that a substancial percent of Incan gold ornaments where not made of pure gold. Rather, using a depletion gilding treatment (Petersen, 1970) objects made from a Cu-Au-Ag alloy were given an even superficial golden layer. Interestingly, due to the importance of gold and silver extraction, and for purposes of production intensification the Inca employed the mit'a labour system, using *«mitmaqkunas»* – the Inca term for resettled labourers – which in conjunction with local labourers lead to the creation of mining micro-communities in fairly remote places, such as those recently investigated in the Atacama Desert. This is an excellent early example of how local ore availability has social and economic consequences on a regional scale. As far as Ag is concerned it was exploited both in its native form, from Ag-bearing veins, and also extracted from complex ores. The Inca Empire also had access to Cerro Rico de Potosí, which was until fairly recent times the world's richest silver mine (Cooke *et al.*, 2009).

Use and Mining of Mercury, Copper and Tin

Cinnabar (HgS) and native mercury occurrences of Colombia, Chile and Ecuador have been known since ancient times and one of the largest cinnabar deposits in the world is found at Huancavelica in Peru (Brown, 2001; and references therein). Cinnabar had various cosmetic and ornamental uses in the Inca society in addition to its use for pigment manufacturing, while native mercury was mined between 1400 BC and 1450 AD, reaching its peak around the time of the Incas. However, as the health hazards associated with mercury, which was also used for silver amalgamation, were

realised, the Incas abandoned its use. It is tempting to assume that the coexistence of exploitable gold deposits and exploitable mercury deposits made it possible to produce such vast amounts of gold and silver plated objects. Copper was the earliest metal used in smelting, as evidenced by the copper slags, dated between 900 and 700 BC, which were found in the Highlands of Bolivia. The Incas made extensive use of alloys, namely arsenic bronze and tin bronze, which are alloys of arsenic and copper and tin and copper respectively (Cooke *et al.*, 2009), while evidence of bismuth bronze have been found at Machu Pichu; the existence of Cu-Au and Cu-Ag-Au alloys has also been noted (Cooke *et al.*, 2009). Tin was obtained from the *altiplano* – the Andean Plateau – where cassiterite (SnO_2) occurrences are abundant and it was widely used throughout the Inca Empire. It is still doubtful if the Incas knew of the existence of tin as a pure element, despite using it, in the form of cassiterite, to create alloys (Petersen, 1970).

Discussion and Conclusions

Within the context of the Inca civilisation, it is possible to approach ore mining and processing as a formative factor of social and economic differentiation, which in turn had ritual and religious connotations, as noted by van Gijseghem *et al.* (2013). A principal aspect of any empire's economical policy is the acquisition of revenue, which drives imperial expansion, which in turn leads to a further increase in revenue, in a circular scheme repeated so often in the course of human history. Revenue was extracted by taxation, tribute and plunder, and by intensification of productive activities. The latter can be achieved by infrastructure improvements, technological innovations and new production methods, and local socioeconomic reform. All such measures result in the symbolic and political integration of provinces, which will in turn expedite road construction, administrative infrastructure establishment and as such the imperial control structure will be physically and notionally expanded. From the abovementioned reasoning it becomes evident that the need to increase the influx of ores, and especially of precious metals, was a cardinal factor if not in fuelling directly the expansion of the Inca Empire, then in accelerating the assimilation of provinces rich in specific resources. This trend continued up until the Spanish conquest in 1532, when the abundance of ore deposits was to be in essence the cause of the Empire's collapse. After the discovery of America by Christopher Columbus in 1492, Spain and Portugal, the two great seafaring nations of the 15th and 16th centuries divided the as yet undiscovered or otherwise unexplored world in two, with the Treaty of Tordesillas (McKee, 1987). What followed was arguably one of the most frantic exploration attempts in the history of mankind, influenced in a not inconsiderable degree by tales of immeasurable wealth and of the existence of El Dorado (Harrasta, 2014). However, such vast amounts of treasure were a mixed blessing. On one hand, Spain used them to expand her empire, her military and her navy. On the other hand, it was often that despite the massive influx of precious metals, the Spanish Crown was not capable to pay the soldiers guarding it. Ultimately, the existence of the undefended Spanish galleons off the Peruvian coast prompted the legendary raiding voyage of Sir Francis Drake in 1577 which, in tandem with other covert or apparent acts of hostility paved the way for the war of 1588 between the two nations (McKee, 1987). Of how and why the discovery of the Americas transformed the existing *status quo*, historical conclusions have been reached long ago. What has not been adequately put forth, however, is the importance of the «geological background» in the existential battle of the contemporary nascent empires and colonial powers. For can it be said that had the Americas not possessed such phenomenal natural wealth the Spanish Empire would have so rapidly flourished? Or is it a foregone conclusion that even if such ore deposits existed, albeit being not accessible by the indigenous populations which would consequently be relatively poor, the Spanish would have rushed to such a frenetic conquest, especially given the fierce native resistance and the adverse environmental and geomorphological conditions? It can be therefore concluded that the fortuitous discovery of a new continent so rich in natural wealth was the fulcrum of colonialism and expansionism of the Old World, shaping the course of human history for centuries. It is, accordingly, evident how the interplay between man and geology is a formative factor of human history.

References

Brown, K., 2001. Worker's health and colonial mercury mining at Huancavelica (Perú), The Americas, The Academy Franciscan History 57, 467-469.

Cooke, C., Balcom, P., Biestar, H., Wolfe, A., 2009. Over three millennia of mercury pollution in the Peruvian Andes, Proceedings of the National Academy of Sciences 106, 8830-8834.

Harrasta, J., 2014. El Dorado, The Search for the Fabled City of Gold, Charles River Editors.

McKee, A., 1987. From Merciless Invaders, The Defeat of the Spanish Armada, 2nd Edition, Grafton Books

Noble, D., Vidal, C., 1994. Gold in Perú, SEG Newsletter 17, 7-17.

Oyarzún, J., 2000. Andean metallogenesis: a synoptical review and interpretation, in: Cordani, U., Milani, E., Thomas Filho, A., Campos, D. (Eds.), Tectonic Evolution of South America, 725-753.**]**

Pemberton, J., 2011. Conquistadors, Searching for El Dorado: The Terrifying Spanish Conquest of the Aztecs and Inca Empires, Futura.

Petersen, G., 1970. Minería y Metalurgia en el Antiquo Perú, Arquelógicas 12, Publicaciones del Instituto de Investigaciones Antropologícas, Museo Nacional del Antropología y Arqueología

Sillitoe, R., Halls, C., Gran,t J., 1975. Porphyry tin in Bolivia , Economic Geology, vol. 70, pp. 913-927.

van Gijseghem, H., Vaughn, K., Whalen, V., Linares Grados, M., Olano Canales, J., 2013. Economic, Social, and Ritual Aspects of Copper Mining in Ancient Peru: An Upper Ica Valley Case Study, in: Tripcevich, N., Vaughn, K. (Eds.), Mining and Quarrying in the Ancient Andes, Sociopolitical, Economic, and Symbolic Dimensions, 275-298.

15th International Congress of the Geological Society of Greece
Athens, 22-24 May, 2019 | Harokopio University of Athens, Greece
Bulletin of the Geological Society of Greece, Sp. Pub. 7 Ext. Abs. GSG2019-071

Lavrion from Ancient Greece to the Present Day: A Study of how an Ore Deposit Shaped History

Argyrios Periferakis[1], Nikolaos Paresoglou[2]

(1) National and Kapodistrian University of Athens, Department of Geology and Geoenvironment, University Campus, Athens, Greece, argyrisperiferakis@gmail.com
(2) Université de Caen, Département d'Histoire, Archéologie et Patrimoin, Esplanade de la Paix, Caen, France

Introduction

The carbonate replacement ore deposit of Lavrion and the methods through which Ancient Athenians and subsequently Romans mined for silver have been the subject of many detailed researches. Also, many authors have correlated the course of Athens in Antiquity with the profits gained from the exploitation of Lavrion. In addition, contemporary researchers have written about the crisis that came about in the 1870s and its repercussions in Greek economy. Here, we attempt to present a collective assessment of the impact of this, the most famous ore deposit of European Antiquity, in the course of the Greek Nation through the ages.

Geology of the Ore Deposit of Lavrion

The diversity of the ore deposits of Lavrion is well known, and the ore is preferentially concentrated between contacts of rocks with different permeability.The Kamariza ore district, which was mined in ancient times (Gelaude *et al.*, 1996) is a carbonate replacement system whose development is attributed to the exhumation and formation of a Miocene metamorphic core-complex, in the Atticocycladic Crystalline belt. The ore bodies at Kamariza occur as infillings along fracture zones and faults and also as massive stratabound replacement sulfide bodies and chimneys. The fractures and faults were the pathways for the ascending mineralising fluids (Voudouris *et al.*, 2008). The minerals of the carbonate replacement system are pyrite, arsenopyrite, sphalerite, galena and chalcopyrite. The ores are enriched in As, Sb, Ag, Bi, Sn and Au. Galena is the principal carrier of Ag, with enrichment reaching up to 3000 gr/t (Voudouris *et al.*, 2008). This, in brief, is the nature of the ore deposit mined in antiquity and in modern times.

Lavrion and its Importance in Antiquity

It is not precisely known when the first mining activities at Lavrion occurred. Archaeological finds of the Minoan Era indicate that this happened around 3000 BC. Organised mining activities are believed to have started around the 8th century BC, with silver production starting around the 7th century BC (Economopoulos, 1996). In the 5th and the 4th century BC silver production reached its peak. The mines of Lavrion were controlled by the City of Athens and were leased to private contractors, who paid for exclusive mining rights of smalls sections of the galleries. Slaves were also used to mine for galena inside the galleries. To extract silver from lead ore a two step process is necessary; initially the ore is smelted and silver-rich lead is produced while the remaining slag is discarded. In the second part of the process, the so-called «cupellation» the lead is ignited and burned in a furnace with a strong influx of air. Then only pure silver remains at the bottom of the furnace. Thus, 99 % pure silver is produced while large amounts of litharge, the monoxide of lead, are discarded (Rehren, 2000).

In part, the income generated from the mines made possible the construction of the temples at Acropolis. Colonated temples were amongst the most expensive buildings in antiquity, not to mention the cost of the metopes, the murals, the statues and the towering gold-ivory statue of Athena Promachos itselt (Stuttard, 2013). Combined with the tribute of the Delian League, the income from Lavrion made Athens the wealthiest city-state in the Ancient World.

The creation of the vast Athenian fleet in 482 BC was the result of the Lavrion mining activities, and was initiated following a public dispute over the exploitation of a recently discovered silver vein at the mines. With the generated wealth directed to the addition of 100 triremes the Athenian fleet now reached the unprecedented number – for a single Greek city-state – of 200 triremes manned with trained oarsmen and hoplites. Two years later, during the naval battle of Salamis, the Greek fleet numbered around 380 triremes, of which more than half were the triremes of Athens.

The wealth generated by the mining activities at Lavrion was one of the main factors of Athenian strategic dominance during much of the Peloponnesian War. In peacetime, Athens maintained and manned a fleet of about 300 triremes, building 20 new each year, as old ships were in constant need of replacement. Such a fleet was manned by 60000 seamen and supported by 20000 dockyard workers. Each ship needed one talent to be constructed and an additional one for crew wages and ship maintenance for each month at sea. During one naval campaigning season – 8 months – having around 2/3 of its ships at sea, the city had to pay around 1600 talents – more than twice the annual tribute of the whole Delian League. Undoubtedly, paying for an entire ship and its crew – around 200 men – entailed a sizeable expense. Such a large fleet enabled Athens to coerce more than 200, mostly maritime, city states, to join its alliance. Athens entered into the war with a reserve of 5000 talents. Not until the last stages of the war did the Lacedemonians succeed in disrupting the mining activities and thus cutting off Athens from the last major source of its income. The income from the mines allowed the Athenians to sustain a fleet out of all proportion to the realistic capacity of any city state of the era. Supplemented by smaller navies of other members of the Delian League it gave Athens an insurmountable advantage. Even after the complete disaster and the loss of most of the Athenian fleet at Sicily in 413 BC Athens was able to rebuild her fleet. All in all, Athens built and lost two entire fleets during the Peloponnesian War

and went on to fight for 27 years (Davis Hanson, 2005). The mining activities at Lavrion continued well into the Late Roman period with more advanced mining techniques involving drainage procedures for extending the galleries below the water table.

Interim Years and Mining in the 19th and 20th Centuries

Despite the absence of mining activity since Roman times, the existence and possible economic potential of the mines did not go completely unnoticed. British explorer G. Wheler who visited Attica during 1675-1676 reports that there were older people remembering a lead mine in the area, which was abandoned for fear that it would be taxed by the Ottomans. In fact, the same people reported that there were traces of silver within the lead mined. In 1790, the British explorer Hawkins reported that there might be economic potential in mining the Ag-Pb ores at Lavrion. German surveyors brought by the Greek Government in 1835 and 1841 gave conflicting opinions about the possibility of exploiting any ore at Lavrion and what ores could be exploited.

The ancient slags remaining at Lavrion since Antiquity were recognised as economically important by the geologist A. Kordellas in 1860. Since the nascent Greek State did not have the organisational and financial capacity to found a State Mining Company, in 1864 Jean-Baptiste Serpieri founded the Italian-French Company Roux-Serpieri-Fressynet C.E. This year marks the creation of the modern day Lavrion. However, despite acquiring the lease of some 15000 acres from the Greek State, the Company also bought illegally heaps of slags from the Municipality of Keratea, without permission from the State. Besides this, the Company expropriated all kinds of slags found in the area, with no State permission and ignoring courts' decisions. The Italian-French company behaved with a cavalier attitude, more reminiscent of a colonial affair. This behaviour enraged the Greek State while the ambassadors of France and Italy issued a proclamation defending the company's interests. In the end, the appearance of French warships of Lavrion resulted in Greece accepting an unprofitable settlement. In 1873 Roux-Seprieri-Fressynet C.E. was bought by the Bank of Constantinople's co-owner Andreas Syggros, and was renamed to Lavrion Metallurgy Company. Many people rushed to buy the new companies' shares only to discover soon enough that many of them were fakes. This triggered a downfall of the shares' price and ultimately a collapse of the Stockmarket. Thousands of individuals soon discovered that they had worthless stocks at their hands, having spent thousands of drachmas to no real gain. In addition, the Company actually decreased its slag production output and Syggros successfully blackmailed the State to lessen the annual tribute of the Company to State. The stockmarket crisis and the significant reduction in state profits from the mines of Lavrion were amongst the contributing factors for the bankruptcy of the Greek State in 1893. Meanwhile, Serpieri founded the Compagnie Française du Laurium which acquired the sole right of exploitation of the area's underground mineral wealth. As the amount of slags was exhausted in 1917 the Greek company was forced to close, while the French Company continued its activities until 1977 (Dermatis, 1994).

Conclusions

By the aforementioned we have demonstrated the significance of the presence of Lavrion throughout the Greek history as another example of how geology and history intertwine. It can be stated with certainty that had this ore deposit not existed Ancient Athens in particular and Ancient Greece in general would have followed radically different historical courses. For it can be considered as a sacrosanct principle that to civilisation and war making, these two driving forces of human history, a steady influx of money is a prerequisite. From the military exploits of Ancient Athenians who checked the Persian invasion time and again to the exquisite temples at Acropolis, the mark of Lavrion's ore deposit is resplendent. In modern times, the mineral wealth of the area became the locus of initially international and subsequently national enterprising and corporations. It shaped the international relations of Greece with France and Italy through the 1860s to the 1880s and was one of the major steps leading to the financial crisis of 1893. This then is the complete story of the importance of Lavrion for Greece, a tumultuous saga of ever increasing mining profits and their management and allocation.

Acknowledgements

We are deeply indebted to Mr. Iordanis Paresoglou for his invaluable interest in our research and for the rare sources which he provided. We are also thankful for his incisive comments on the matters regarding the historical aspect of Lavrion in ancient and modern times.

References

Davis Hanson, V., 2005. A War Like No Other, How the Athenians and Spartans Fought the Peloponnesian War, Random House Editions.

Dermatis, G., 1994. Scenery and Monuments of Laureotiki, Publication of the Municipality of Laureotiki.

Economopoulos, J., 1996. Mining Activities in Ancient Greece from the 7th to the 1st Centuries BC, Mining History 3, 109-114.

Gelaude P., van Kalmthout P., Rewitzer C., 1996, Laurion, The Minerals in the Ancient Slags, Janssen Print.

Rehren T., 2000, Roads to riches: making good the silver ore at Lavrion in Greece, Archaeology International 4, 31-34.

Stuttard, D., 2013. Parthenon, Power and Politics on the Acropolis, The British Museum Press.

Voudouris, P., Melfos, V., Spry, P.G., Bonsall, T.A., Tarkian, M., Solomos, C., 2008. Carbonate-replacement Pb-Zn-Ag±Au in the Kamariza area, Lavrion, Greece: Mineralogy and thermochemical conditions of formation, Mineralogy and Petrology 94, 85-106.

Wheler, G., 1682. A Journey into Greece, vol. 6, William Cademan, Robert Kettlewell and Awnsham Churchill Eds.

15th International Congress of the Geological Society of Greece
Athens, 22-24 May, 2019 | Harokopio University of Athens, Greece
Bulletin of the Geological Society of Greece, Sp. Pub. 7 Ext. Abs. GSG2019-072

Radionuclides in Rocks and Associated Health Hazards: Examples from Norway and India

Argyrios Periferakis[1]

(1) National and Kapodistrian University of Athens, Department of Geology and Geoenvironment, University Campus, Athens, Greece, argyrisperiferakis@gmail.com

Introduction

After 1960 the association between radiation and adverse health effects has come to the foreground. Epidemiological research indicates that even low doses of radiation over an appreciable amount of time are distinctly connected to a quantifiable increase in cancer incidence rate. Such low and constant doses of radiation often come from natural sources, namely from the rocks exposed on the surface of the area, or from the drinking water of the aquifers contained within radioactive rocks. Here cancer incidence data from areas with high background radiation and radioactive water sources in India and Norway is examined, so as to demonstrate the correlation between geology and public health hazards.

Radiation and Associated Induced Damage on DNA

In nature, uranium, thorium, radium and radon are the most common sources of ionizing radiation. These radioactive elements tend to concentrate in highly fractionated magmas, so they are commonly found in acidic rocks, such as granites. Uranium exists in three naturally occurring isotopes, $^{234}_{92}$U, $^{235}_{92}$U, $^{238}_{92}$U, of which the latter is the most abundant in nature and has a half life of $4.51 \cdot 10^9$ years. Thorium can be found in nature in 30 different isotopes, but the most stable one is $^{232}_{90}$Th with a half life of $13.9 \cdot 10^9$ years. As far as radon ($^{222}_{86}$Rn) is concerned, it is derived from the parent radionuclide $^{226}_{88}$Ra, which has a half life of 1620 years, and is a member of the $^{238}_{92}$U decay series (Banks *et al.*, 1995). While radon is chemically inert, being a noble gas, it accumulates in groundwaters and more importantly becomes airborne, thus being quite a potent radiation source. Based on the half life values mentioned it becomes evident that even rocks of Precambrian age, containing sizeable amounts of uranium or thorium will be significantly radioactive. All of these radioactive elements emit alpha, beta and gamma radiation during their decay series, which is potentially hazardous to humans, depending on the dose, the dose rate and the time span of exposure.

It is a general axiom that the rate of mutagenesis depends upon the dose rate and the total absorbed dose of ionising radiation. For a given dose and dose rate, the biological effects also depend upon the linear energy transfer (LET), a quantity used to describe the «quality» of radiation (Hall, 1991). As far as radiation protection is concerned, and regarding low LET radiations, experimental results indicate that the same dose delivered in a protracted period of time results in reduced biological effects. This is known as the dose rate effect or DRE, which however only applies to low and intermediate LET radiations (Hall, 1991). Even so, for some types of cells, at different ranges of low dose rates, an inverse DRE is observed, meaning that even low background radiation doses may be quite more dangerous than originally thought, in some cases. Low and intermediate LET radiations, such as electrons, positrons and photons, cause a small number of ionizations per unit of distance traversed into matter. Gamma radiation, i.e. photons, causes mostly indirect effects in cells. Indirect effects are those associated with the molecules produced during water radiolysis. Such molecules are the hydroxyl radicals and other free radicals, which interact with and damage DNA and other biomolecules. However, newer data (Goodhead, 1994) indicate that even low LET radiations cause some degree of focused damage on DNA, creating small clusters of double strand breaks (DSB) which may not always be repaired by the cell, thus leading either to cellular death or to proliferation of potentially cancerous cells. High LET radiations, like alpha radiation, i.e. helium nuclei, deposit a high amount of energy in fewer cells, leading to significant DNA damage, and cellular death. In contrast to photons or electrons, where most irradiated cells survive, alpha radiation leads to a higher percentage of cellular death, albeit surviving cells may have a higher carcinogenic potential, due to more significant DNA damage (Hall, 1991). The consequences are understandably more far reaching if the mutations happen, and are not repaired, in germ line cells, instead of somatic ones. The continued exposure of individuals to even low LET radiations and dose rates not only is hazardous for inducing more and more damage, but for hindering DNA repair by N-glycosylases, endonucleases and purine imidazole-ring cyclases (Téoule, 1987).

Cancer Incidence and Background Radiation in India and Norway

Looking at the annual cancer incidence rate map in the states of India, for the last 26 years (Dhillon *et al.*, 2018) it can be observed that there are significant differences between the rates of different regions. If such a map is correlated with the geology of India, it can be observed that areas, which comprise carbonatites, are also characterised by relatively elevated cancer incidence rates. Interestingly, if the cancer incidence map of India (Dhillon *et al.*, 2018) is overlaid upon the isodose map of India (Sankaran *et al.*, 1986) it can be observed that areas characterised by elevated background radiation levels roughly correspond to areas with elevated cancer incidence rates. Recent research on the carbonatites of Tamil Nadu indicates background radiation well in excess of the safe background radiation exposure levels. One other relative example is the region of Kerala, where much of the soil contains almost 10 wt. % thorium and uranium oxides (Chougaonkar *et al.*, 2004), exhibits the highest cancer incidence rate in India. It is reported that the maximum outdoor dose in this region is 39.1 mSv/a, which is higher than the maximum allowed for a radiation worker,

where the limit is 20 mSv/a, and around 13 times the mean human background radiation exposure, which is about 3 mSv/a (Brenner *et al.*, 2003). Another study in the region of Kerala (Forster *et al.*, 2002) proved that the background radiation of the area accelerates point mutations in mitochondrial DNA. By implication, the amount of radiation absorbed could lead also to mutagenesis in the nuclear DNA of the cells, potentially leading to changes in gene expression, in protein structure and functionality and higher risk of cancer incidence.

Norway is an example comparable to India, due to the existence of rocks of comparable age and also of carbonatites of comparable geochemical characteristics. Looking at the cancer incidence rate map of Norway (Patama *et al.*, 2014), it can be deduced that higher cancer incidence rate correspond roughly with locations where there are outcrops of the Precambrian basement, which are mainly granites and gneisses, containing relatively high amounts of radionuclides, leading to elevated levels of background radiation. In addition, Cambrian shales in some areas of Norway are characterised by elevated uranium levels. The potential for adverse health effects has been studied in the Fen carbonatite complex in Telemark (Sundal & Strand, 2004). There are about 350 dwellings in the area which according to measurements are characterised by increased radiation emission. The carbonatites in the area contain the highest amounts of Th ever recorded in a bedrock in Norway. Both the indoor and outdoor radiation values are higher in the areas where the carbonatite is exposed. Another acute problem in Norway is the concentration of radon in groundwater. According to extensive sampling by Banks *et al.* (1995) groundwaters in gneissic and porphyry rocks have radon levels exceeding the maximum acceptable threshold of 100 Bq/lt, with some samples approaching 1000 Bq/lt. Samples from the granite in Iddefjord have a radon concentration of 8500 Bq/lt. Already radon exposure has been estimated to account for around 10 to 20 % of lung cancer cases in Norway (Banks et al., 1995). Samples from the same area also exceed the safe thorium and uranium concentrations.

Discussion and Conclusions

The association between background radiation and health effects has long been established. However, there is no large scale research correlating cancer incidence with background radiation attributable to geological factors at a national or even continental level. How the soil formed by such radioactive rocks contributes to the introduction of radionuclides in the food chain has not been examined here, but this is surely another contributing factor to the dose received by the locals, which has to be studied extensively. In any case it is demonstrated how cancer incidence rates in a national level do exist, at least partially, as a function of background radiation and by implication of regional geological setting.

There is still a lot of research to be undertaken on how exactly different radioactive rocks affect public health, and how governmental public health policies should be formulated taking notice of the petrological and geochemical characteristics of each particular area. In these last decades the effects of radiation on nucleic acids have been thoroughly studied, although there are still many questions and uncertainties, regarding cell sensitivity in particular cell cycle phases and radiation-induced cell signalling and its ramifications for the survival of complex cellular systems. Finally, it would be useful to assess how prolonged relatively small doses of radiations inhibit the function of DNA repair enzymes. By combining such research data it will hopefully be possible to quantify the effects of background radiation at different levels in multicellular organisms in general and humans in particular.

References

Banks, D., Røyset, O., Strand, T., Skarphagen, H., 1995. Radioelement (U, Th, Rn) concentrations in Norwegian bedrock groundwaters, Environmental Geology 25, 165-180.

Chougaonkar, M., Eappen, K., Ramachandran, T., Shetty, P., Mayya, Y., Sadasivan, S., Venkat Raj, V., 2004. Profiles of doses to the population living in the high background radiation areas in Kerala, India, Journal of Environmental Radioactivity 71, 275-297.

Dhillon, P., Mathur, P., Nandakumar, A., Fitzmaurice, C., Anil Kumar, G., Mehrota, R., Shukla, D., Rath, G., Gupta, P., Swaminathan, R., Thakur, J., Dey, S., Allen, C., Badwe, R., Dikshit, R., Dhaliwal, R., Kaur, T., Kataki, A., Visweswara, R., Gangadharan, P., Dutta, E., Furtado, M., Varghese, C., Bhardwaj, D., Muraleedharan, P., Odell, C., Glenn, S., Bal, M., Bapsy, B., Bennett, J., Bodal, V., Chakma, J., Chakravarty, S., Chaturvedi, M., Das, P., Deshmane, V., Gangane, N., Harvey, J., Jayalekshmi, P., Jerang,, K., Johnson, S., Julka, P., Kaushik, D., Khamo, V., Koyande, S., Kutz, M., Langstieh, W., Lingegowda, K., Mahajan, R., Mahanta, J., Majumdar, G., Manoharan, N., Mathew, A., Nene, B., Pati, S., Pradhan, P., Raina, V., Rama, R., Ramesh, C., Sathishkumar, K., Schelonka, K., Sebastian, P., Shackelford, K., Shah, J., Shanta, V., Sharma, J., Shrivastava, A., Tawsik, S., Tyagi, B., Vaitheeswaran, K., Vallikad, E., Verma, Y., Zomawia, E., Lim, S., Vos, T., Dandona, R., Srinath Reddy, K., Naghavi, M., Murray, C., Swaminathan, S., Dandona, L., 2018. The burden of cancers and their variations across the states of India: the Global Burden of Disease Study 1990-2016, The Lancet Oncology 19, 1289-1306.**]**

Forster, L., Forster, P., Lutz-Bonengel, S., Willkom, H., Brinkmann, B., 2002. Natural radioactivity and human mitochondrial DNA mutations, PNAS 99, 13950-13954.

Goodhead, D., 1994, Initial events in the cellular effects of ionizing radiations: clustered damage in DNA, International Journal of Radiation Biology 65, 7-17. **[**

Hall, E., 1991. Weiss Lecture, International Journal of Radiation Biology 59, 595-610.

Patama, T., Engholm, G., Klint, Å, Larønningen, S., Ólafsdóttir, E., Christensen, N., Storm, H., Pukkala, E., 2014. Small-area based map animations of cancer incidence in the Nordic countries with new entities, 1971-2010, Nordic Cancer Union, astra.cancer.fi/cancermaps/Nordic_18.

Sandal A., Strand T., 2004. Indoor gamma radiation and radon concentrations in a Norwegian carbonatite area, Journal of Environmental Radioactivity 77, 175-189.

Sankaran, A., Jayaswal, B., Nambi, K., Sunta, C., 1986. U, Th and K Distributions Inferred From Regional Geology and the Terrestrial Radiation Profiles in India, Bhabha Atomic Research Centre.

Téoule, R., 1987. Radiation-induced DNA damage and its repair, International Journal of Radiation Biology 51, 573-589.

15th International Congress of the Geological Society of Greece
Athens, 22-24 May, 2019 | Harokopio University of Athens, Greece
Bulletin of the Geological Society of Greece, Sp. Pub. 7 Ext. Abs. GSG2019-073

The Importance of Emery in the Cultural, Social and Economic Development of Naxos Island, Cyclades, Greece

Argyrios Periferakis[1]

(1) National and Kapodistrian University of Athens, Department of Geology and Geoenvironment, University Campus, Athens, Greece, argyrisperiferakis@gmail.com

Introduction

The establishment of permanent habitation in Naxos Island, since Prehistory, is strongly linked to the exploitation of the Islands' natural resources. In ancient times, the population of the island tended not to endeavour so much to engage in a seafaring trade like other populations from islands in the Aegean. In general, a sizeable proportion of Naxians remained restricted to agricultural or mining activities and trading activities between different communities. It is entirely possible that the amplitude of agricultural produce and the income generated from emery export lead to the development of a relatively different and somewhat isolationist culture, which is also reflected on the folklore of the island. In this research the aim is to delineate the effect of emery exploitation in the socioeconomic development of the Island from Ancient Greece to the present day, demonstrating how geology contributed to the formation of an insular community.

Geology of Naxos Island and Emery Formation

Naxos is the largest island of the Cyclades complex and belongs to the Atticocycladic belt of the Hellenides. The Island comprises a metamorphic core complex intruded by a granodiorite during Late Meiocene. Sedimentary rocks and ophiolites are tectonically emplaced upon the granodiorite and the metamorphic rocks. The metamorphic rocks of the island are believed to have been affected by at least four metamorphic events. The emery deposits of the Island are the results of bauxites' metamorphosis. There are widespread metabauxite deposits in Naxos, most of which have a lenticular shape. They are found most commonly inside marbles and sometimes in sheet-like form inside schists. The tectonic deformation is evident and it is believed that the metabauxite lenses were an initially more or less continuous body, torn apart by tectonic procedures (Feenstra, 1985). There is still no consensus on the exact emery reserves of Naxos or the initial amount of emery reserves prior to any exploitation. The general term «emery» is used to describe any rock rich in corundum. The Greek term for emery is *«smyris»*, and is derived from the port of Smyrna, which was the focal point for emery distribution in ancient times. On the other hand, the term «emery» is derived from the Emeri peninsula, where the emery mines of Naxos are located. The principal mineral of emery, corundum, is believed to have been named from the corruption of the Indian word *«kauruntaka»* which was used to describe the same mineral (Holroyd & McCracken, 1996).The most common mineral assemblage of emery worldwide comprises corundum (Al_2O_3), magnetite ($Fe^{2+}Fe_2^{3+}O_4$), hematite (Fe_2O_3), hercynite ($Fe^{2+}Al_2O_4$), and trace impurites such as mullite $\left[Al_{(4+2x)}Si_{(2-2x)}O_{(10-x)}\right]$, titania, silica and magnesia. The typical quality of «commercial grade» emery contains less that 10 wt. % silica and is therefore rich in corundum. The commercial grade emery of Naxos contains around 50-80 wt. % corundum and a sizeable percent of FeTi-oxides, while margarite $\left[CaAl_2(Al_2Si_2O_{10})(OH)_2\right]$ is the most common silicate mineral (Feenstra, 1985).

Regional Use and Export of Naxian Emery from Ancient Greece to the 18th Century

The first documented use of emery in tool manufacturing is during the Neolithic period. It is believed that emery was of crucial importance in the creation of the famous Cycladic statues which are amongst the most well known artefacts of the Cycladic Civilisation. Emery is described also in the work of Theophrastus, *«Peri Lithon»* (Bourdakou, 1997). While under the scope of this research it is difficult to quantify the exact effect of emery exploitation in the economy of ancient Naxos, it is remarkable that Naxos was so wealthy so as to maintain a fleet of four triremes, which took part in the naval battle of Salamis in 480 BC, at a time when most Aegean Islands did not have the ability to maintain even a single warship (Papadopoulos, 1961). In 466 BC Naxos was destroyed by Athens and subsequently very little evidence of the development of Naxian economy is available. No mention of emery mining or export is made during Roman times or the Byzantine era. In 1207 AD Naxos and other Cycladic Islands were conquered by the Venetians, who established the Duchy of the Aegean, with the Island of Naxos as its capital. The first reappearance of emery in historical texts can be traced in 1304, when in Venetian texts it is mentioned that emery was transported to Crete and then on to Venice in small amounts for as yet unspecified uses (Slot, 2008). It was Italian traders who exported emery after 1625 AD, first transporting it with small ships to the port of Smyrna, from where it was transported by ship to other European ports, or by roads to locations in the interior of Asia Minor (Zevgolis, 1947). During this period emery was used for cleaning rusted sword blades. In 1665 C. Huygens mentions that the use of emery dust from Naxos is indispensable in cleaning telescope lenses. It may be no overstatement that had emery from Naxos not existed then lenses of such accuracy would not have been developed at such an early stage (Slot, 2008). During the 18th century, along with its other notable use, emery dust was used for the abrasion of heavy duty sailmaking needles. The alternative was to use a hammer to perfect the shape of every needle individually but this was more time consuming and raised the price of the needles. The emery mines in the NE of the Island, between the gulfs of Moutsouna and Lyona, were exploited by the villages of Apeiranthos, Koronos, Danakos, Mesi, Skado and Keramoti. The inhabitants of these villages alone had been granted exclusive exploitation rights, both by the preceding Venetian administration and by the Ottomans (Glezos, 1989). During the Ottoman occupation of Naxos, there was no tax imposed on emery mining or

export as it was not considered valuable enough. Only in 1824 did the Ottomans impose such a tax and this lead the people of Naxos closer to joining the revolution in the ongoing War of Greek Independence.

Emery in the Economic and Political Life of the Greek State

Worldwide demand for emery reached its peak around the end of the 19th century, following the Industrial Revolution. During the same period, the incremental increase of the iron industry lead to a widespread demand for emery. Emery, whether natural or artificial, is essential for the abrasion of steel tools and machine parts. Among the major emery deposits worldwide in Bavaria, America and Asia Minor, the emery of Naxos stands out in having the highest corundum percentage. This means that comparatively to other emeries, the Naxian emery has the highest value as an abrasive. The importance of this mineral resource for the national economy was recognised early enough by the nascent Greek State which, between 1845 and 1920, regulated the commercial exploitation of emery through a series of «mining law edicts». During those years and afterwards, the quarries belonged to the Hellenic State, which conceded the right for their exploitation to the inhabitants of the Municipalities of Koronis and Apeiranthos. In the first decades of the 20th century, Naxos did not have any ports suitable for loading deep draught cargo ships, and emery was transported using smaller boats to Syros, where it was then transhipped to larger cargo ships. The cost of transporting emery to Syros was borne by the Greek State. It was deemed necessary for the emery mines to be state-controlled, for the better organisation of production, as well as for marketing reasons. At the same time, the State lacked the funds necessary to expand the mining tunnels and finance the proper maintenance and improvement work so as to ensure their structural integrity. In 1922 it was decided to build an aerial cable railway system, so as to alleviate the cost of transporting emery from the mines to the loading station at Moutsouna Bay. Up until then miners had been transporting bags full of emery from the mines to the Bay, on their backs or using donkeys. In 1923, it was decreed that emery would be sold directly to foreign markets, with no mediators, with a fixed percentage of the profits being used for infrastructural improvements. Along with the aerial railway system, wharfs and storehouses were built in Moutsouna Bay, so as to gather and load the emery to barges directly for export, obviating the need, and the associated cost, for transport to Syros. This aerial cable railway system was constructed between 1926 and 1929, for the easier transportation of emery, from the mines, to the bay of Moutsouna; it remained in operation until 1982 when it was replaced by trucks which took advantage of the improving road network. Today, the mining of emery has practically come to an end. The development of artificial abrasives, which are much cheaper than emery, after the 1970s, signalled the gradual decline and eventual halting of systematic mining in the Island. The much greater purity and physicochemical uniformity of synthetic abrasives and their lower cost does not leave any market share for the emery of Naxos.

Discussion and Conclusions

From the aforementioned it becomes evident that the existence of exploitable emery deposits has been a key factor in shaping the economy and even the culture and the society of the Island. Since antiquity, Naxos had a robust and growing economy which was in large part attributed to its mineral wealth. During the Venetian and Ottoman occupations, the economic importance of emery lead to its exploitation; this was then systematised by the Greek State. For over 2000 years the inhabitants of NE Naxos have maintained their mining rights over the quarries. Over the years, emery miners became a distinct socioeconomic class of the island, while the need for exporting emery gave rise to an extensive trading network, between Naxos, Syros and Smyrna, and other major ports. The economic value of emery was an important contribution to the Greece's gross domestic product up until the 1970s. There is no doubt that without emery Naxos would not have been such a wealthy Island in Ancient times, and would maybe have relied more on commerce. This would in turn have resulted in development of coastal communities with different folklore, traditions and social classes. In addition, in a state level, it is doubtful that the developing Greek State, between 1831 and 1940 would have maintained a viable import-export balance, without the significant profits of emery trade. This is one characteristic example of how ore deposits can be instrumental in shaping the cultural and socioeconomic profile of small insular societies and at the same time in influencing state economy.

Acknowledgments

I am deeply indebted to Mr. Iordanis Paresoglou for his kind interest in this research and his valuable comments and perspective into the history of Naxos Island. I am also thankful for his providing of historical sources and relative material. This research would have been impossible without his assistance.

References

Bourdakou, E., 1997. Ancient Greek Terminology – The Problem of the Naxian Earth, ELETO, Athens, Greece, 187-195.

Feenstra, A., 1985. Metamorphism of Bauxites on Naxos, Greece. Ph.D. Thesis, Instituut voor Aardwetenschappen, Rijksuniversiteit te Utrecht, Utrecht, 23, 33p.

Glezos, P., 1989. The State Exploitation of the Naxian Emery – The Collaborative Mining of the Mineral and the «Reconstruction», Aperathitika 1.IV, 69-108.

Holroyd, W., McCracken, D., 1994. Emery, in: Carr D. (Ed.), Industrial Minerals and Rocks, 6th Edition, Society for Mining, Metallurgy and Exploitation Inc., 425-428

Papadopoulos, N., 1961. The Naval Battle of Salamis, Bookshop of Estia.

Slot, B., 2008. The «original Naxian emery» in international economy (14th-19th century), Flea 19, 17-19. **[**

Zevgolis, A., 1989. History of the Naxian Emery, Aperathitika 1.IV, 61-68

15th International Congress of the Geological Society of Greece
Athens, 22-24 May, 2019 | Harokopio University of Athens, Greece
Bulletin of the Geological Society of Greece, Sp. Pub. 7 Ext. Abs. GSG2019-074

The Yukon Gold Rush: Early Examples of the Socioeconomic and Environmental Impact of Mining

Argyrios Periferakis[1]

(1) National and Kapodistrian University of Athens, Faculty of Geology and Geoenvironment, University Campus, Athens, Greece, argyrisperiferakis@gmail.com

Introduction

The Gold Rush of the late 19th and early 20th century was a momentous historical and social event. However, it was also one of the first instances of large scale mining in a remote and yet relative virgin area. The negative effects of mining on the landscape, the flora and the fauna of Yukon in general and Klondike in particular are one of the earliest examples of the environmental impact of extensive and unregulated mining. In the event, the Canadian authorities proved totally unprepared to handle the massive influx of people, issuing miner's certificates without restrictions to aspiring prospectors and allowing them free use of a given site by the river, with no restrictions on tree cutting and fishing. In 1898 alone, 34364 miners' certificates were issued by the authorities. There were two main ways which were followed by individuals and organised groups of people. The seaborne route started from either Seattle or Victoria, to the northwest, in Nome, where then people boarded boats to sail upstream in the Yukon River, all the way to Dawson City. Overland routes started when the prospectors arrived by boat at Skagway and Dyea, and then followed already established trails. Others came through more northern routes staying at all times inside the Canadian borders. In any case, at some point prospectors would have to use either a canoe or a boat – either carried with them during the journey or constructed on the spot – to arrive in Dawson via Yukon River or one of its tributaries. Then began the race to find and claim an area to mine and then the arduous task of placer mining. Following the first report of gold in 1896, the next ten years would mark one of the most radical transformations of local society and environment.

Geology of Au Ore Deposits in the Klondike area

The gold found in the placer deposits in Klondike is characterised by limited dispersion and originates from the erosion of orogenic gold mineralisation in the Klondike Schists. This mineralising event occurred after regional compressional deformation in the Jurassic, approximately 100 my after a Permian metamorphic event (MacKenzie *et al.*, 2008). Since their discovery, more than a century ago, the goldfields of the wider area have produced around 311 tonnes of gold. The bench and creek placers are fluvial in origin, and their age ranges from Pliocene to Holocene. The goldfields rest upon medium-grade and high-grade metasedimentary rocks, metaigneous rocks of the Yukon-Tanana terrane, and a small amount of ultramafic rocks of the Slide Mountain Terrane. The orogenic gold mineralisation comprises discordant mesothermal quartz veins (Lowey, 2006). Their mineralogy is characterised by anhedral milky quartz, with minor amounts of carbonate, barite, muscovite, pyrite and galena (Rushton *et al.*, 1993), while reported gold grades of up to 9 Kgr/ton have been reported. Gold recovered from the placer deposits of the area manifests in many different forms, from large nuggets to very small grains actually floating on the water. This gold is almost entirely detrital in origin and its source are the aforementioned auriferous quartz veins. The placers themselves are fluvial in origin and their formative mechanisms were controlled by tectonics and climate. A prolonged period of weathering combined with isostatically compensated exhumation turned the quartz veins in a quartz-rich residuum that was then reworked in the Au gravel deposits of the Klondike area. The lower level gravel deposits are richer in Au due to successive circles of aggradation and incision which were related to reconcentration of the placer gold (Lowey, 2006).

Placer Mining Methods

Usually, in order to get to the gravels containing gold grains, the soil covering them had to be removed. But since the soil, averaging around 2-3 m, was frozen it had to be thawed. This was achieved by lighting numerous fires and when the soil was sufficiently softened it was removed using shovels and buckets. Upon reaching the gravel layer, the miners used mercury in the sluice boxes. Mercury amalgamates with gold and can be used to separate it from the ore. It is subsequently removed during the refining process. Another method was hydraulic mining, which involved using the water of the rivers and streams to strip the overburden of the gravel. Usually, hydraulic concessions were issued, involving 5 mile lengths of the river. The water was transported by wooden flumes or canals and the heated to increase its pressure. In this way, pressurised jets of water were directed against gravel and vegetation on the walls of the river streams. Some companies also employed dredging using suitably modified riverboats. In this way it was possible to recover gold even from submerged riverbeds. This method destroyed the topography of riverbeds, and also in many cases altered the flow of streams or created small lakes. Moreover, the use of mercury during dredging contributed to the pollution of both land and water.

Environmental Impact

The uncontrollable influx of miners in the years following 1896 resulted in severe degradation to the local environment. In particular, the forests of the area were almost destroyed, since the mass of incoming aspiring gold diggers needed copious amounts of wood for building and boat construction, for cooking and for heating purposes, for boat building, as steamship and locomotive fuel and for infrastructural improvements. Collateral damage by accidental fires destroyed

the forests even more. In less than two years, the vast majority of trees had been cut down, radically altering the local landscape. This deforestation resulted in poor water retention properties by the soil, exponentially increasing flash flood probability, and also in a lower water table. Dredging and the melting of the permafrost by fires altered the vegetation and the topography of the area permanently (Willis, 1997). Furthermore, mercury remains in the soil and in the river water to this day, further endangering a host of animal species. Besides these negative effects, intense hunting and fishing almost destroyed the local fauna, altering the balance of the ecological system, creating interrelated side effects that would persist for decades. Finally, for sanitation reasons, waste from Dawson City was emptied on the Yukon River, exacerbating the environmental degradation.

Socioeconomic Consequences

From the many thousands of people who, upon hearing about stories of unprecedented wealth, set for the area of Yukon, less than half would eventually arrive and an even smaller percentage would actually find gold. Amongst the miners who would persevere through successive harsh winters, coupled with inadequate diets and virtually non-existent sanitary conditions, many would fall victim to a host of diseases, and most notably typhoid fever. Of particular interest is the extensive appearance of scurvy in miners, which further denotes the malnourishment of the people and their negligence for their health. In addition, as the Gold Rush was associated with the seasonal movement of large masses of people, overland or through the river network, there was a cyclic seasonal spread of pathogens, and the emergence of diseases not normally existing in the area. Such was the nature of malaria, which affected many of the people in the area during the Gold Rush (Highet, 2008). Also notable is the transience of miners in the area during the Gold Rush. Most aspiring gold miners rushing to the area of Klondike did not believe that they would stay there more than one or two years. The notion of finding gold in the river streams, via digging and panning, appealed to many relatively poor men who aimed at coming back home with a small fortune with a relatively meagre monetary investment. In reality, not all could find a promising place to stake a mining claim and a good percentage of arriving prospectors worked in pre-established claims, or found employment in other posts in the city (Brand, 2003). Gradually, after 1906, larger companies would buy most private expanses in the creeks and use more large scale and sophisticated dredging methods. In any case, individuals usually lacked the money and technical knowledge necessary to exploit in full their small claims. Thus in the space of ten years there was an almost complete industrialisation of the gold digging process. The state favoured such an outcome, since it was easier to regulate larger companies, and in fact, environmental pollution and degradation were significantly lessened by the application of more effective methods – dredging however would continue unabated until 1966. The expansion of the City of Dawson itself and the acquiring of large tracks of land by westerners had another negative side-effect: the native populations of the area – the Tagish, Tutchone and Han Indians – gradually disappeared from the area. These Indians were ravaged by diseases and faced starvation as overhunting resulted in the disappearance of most animals and overfishing and dredging lead to the fish disappearing from streams and rivers (Willis, 1997). The creation of an extensive mining community within the space of two years meant that more permanent infrastructural ameliorations were necessary. Roads and railways were constructed and regular boat trips from Seattle and Victoria were established, to transport the myriads of prospectors and supply Dawson. Like Dawson, Skagway and Dyea, other towns along the miner migration trails grew from small settlements and ports having no docking facilities, to large scale cities, in a matter of one or two years, due to influx of passing miners and people associated with the rendering of services. Such towns were in the beginning initially lawless and it was a while before the state managed to impose law and order.

Conclusions

In effect, the expansion of Western culture and associated socioeconomic organisation spread through the vast territories of Canada and the USA through the emergence of local capitalist economies, which were then gradually linked to the wider national socioeconomic network. In assessing the effects of the Gold Rush, it is evident how geology had a formative effect on the creation of a new socioeconomic fabric in an area quite distant and marginal in respect to state interventionism, state control and Western culture in general. The existence of the Klondike gold deposits sparked a torrent of social mobility and proved the focal point for the urbanisation and industrialisation of much of NW Canada. In studying the history of the Gold Rush, the transition from individual to corporate mining also becomes evident. One of the cardinal points of this story however is the danger to man and environment alike, if mining is left unregulated by the state and comprehensive environmental restoration and sustainable mining schemes are not enforced. Today, 113 years after the end of the tumultuous period of the Gold Rush, the damage to the environment and wildlife is still evident.

References

Highet, M., 2008. Gold Fever: Death and Disease During the Klondike Gold Rush, 1898-1904, M.Sc. Thesis, University of Manitoba, Winnipeg, 176-179 p.**]**

Lowey, G., 2006. The origin and evolution of the Klondike goldfields, Yukon, Canada, Ore Geology Reviews 28, 431-450.

MacKenzie, D.J., Craw, D., Mortensen, J., 2008. Orogenic gold mineralisation in the Klondike goldfield, Canada: Implications for gold exploration in the Otago Schist, AusIMM New Zealand Branch Conference, Wellington, New Zealand, pp. 279-289.

Rushton, R.W., Nesbitt, B.E., Muehlenbachs, K., Mortensen, J.K., 1993. A fluid inclusion and stable isotope study of Au quartz veins in the Klondike district, Yukon Territory, Canada: a section through a mesothermal vein system, Economic Geology 38, 647-678.

Willis, B., 1997. The Environmental Effects of the Yukon Gold Rush 1896-1906: Alterations to Land, Destruction of Wildlife, and Disease, University of Western Ontario, Ontario, 102-105 p.

15th International Congress of the Geological Society of Greece
Athens, 22-24 May, 2019 | Harokopio University of Athens, Greece
Bulletin of the Geological Society of Greece, Sp. Pub. 7 Ext. Abs. GSG2019-094

Geological and mining history of Serifos Island, Greece: current state and perspectives for protection of mineralogical and petrological geotopes

N. Vlachopoulos[1], P. Voudouris[1]

(1) National and Kapodistrian University of Athens, Department of Geology & Geoenvironment, Panepistimiopolis, 15784 Athens, Greece, nvlahopoulos@gmail.com, voudouris@geol.uoa.gr

Geology

The Serifos island, located in the south Aegean Sea, represents a multiple mineralized district including intrusion-hosted, skarn, carbonate-replacement and vein-type ores. Serifos belong to the metamorphic core complex of the Attic-Cycladic Crystalline Belt, which represents a polymetamorphic terrane within the Alpidic orogen of the Hellenides. The Serifos mineralization is related with the emplacement of I-type plutonic rocks, controlled by extensional kinematic conditions, when the metamorphic core complexes reached near-surface levels. The Serifos granodiorite is considered to be synchronous with Miocene extensional detachment faulting, and intruded schists and marbles causing an extensive contact metamorphic aureole.

Serifos' mines history

The mines exist on the island since the 3.000 BC. Mines continued to work during the Roman times while it was the Venetians later on that systematically organized the mining operations in the island. However, due to the frequent attacks of pirates, the mining activity stopped for a long time. A new company appeared in 1880, the French interests "Serifos-Spiliazeza and in 1884 the company commissioned by contract the operation of the iron ore mines to the German mineralogist Emile Grohmann. When Grohmann undertook the operation of the mines, the headquarters of the company were transferred in Mega Livadi where a two-story neoclassical building, with architectural elements of the "Ziller" style were created, ruins of which still stand at the end of the beach today. Mega Livadi was the main iron ore export harbor of Serifos, equipped with all the necessary sorting and shipment facilities (Fig. 1).



Figure 1. (a) Mega Livadi (b) the Headquarters of the iron ore mines

The economy of the island boomed but the working conditions in the mines were awful for the miners. The safety measures were inadequate and many of the workers died in work accidents. A strike broke out on August 7th 1916, when the miners refused to load a cargo ship. The workers stopped working and demanded better working conditions and an eight-hour work per day rule. A fatal fight between the strikers and the police forces in August 21th, 1916, ended with the death of four workers and decades of them were injured. However, the union achieved the 8-hour work-day in the mines that was officially established by the Greek State in 1925. The iron ore mines were finally cease operations in 1965 when the Gromman's heirs found richer mines in South Africa and abandoned the mines of Serifos, as a result of the depletion of stocks, the high costs of relatively small-scale exploitation, but mainly as a result of the collapse in iron ore prices worldwide. The Ministry of Culture declared as historical monuments the Headquarters of the mines, the loading bridge in Megalo Livadi, the loading bridge in Koutalas, the workers' residencies as well as any kind of equipment that remains to provoke memories both of the flourishing of the island in another era, and of the tragic events of 1916.

Mineralogical and petrological Geotope

Serifos, is not only famous because of the mining activity during the past, it shows also unique mineralogical and petrological features: Its very rare and worldwide known skarn minerals (e.g. garnets, quartz and its green variery called prase, ilvaite; Fig. 2), attracted scientists and mineral collectors from all over the world. The SW part of Serifos island including the Agia Marina - Koutalas, Mega Livadi - Koundouro and Avessalos subaereas, displays all the criteria necessary to be characterized as a mineralogical and petrological Geotope. The Avessalos area is the best site in the world in respect to the mineral green quartz (prase). The crystal forms, intergrowths and sizes (up to 40cm) of green

quartz specimens from this locality are spectacular. The area is characterized by a granatitic ((Fig. 2a) and hedenbergitic skarn and by the development of huge geodes filled by prograde and retrograde skarn minerals. In the Neroutsika location in Avessalos area two forms of prase are observed the first variety refers to very deep green colored crystals accompanied by iron roses. The second variety refers to double-coloured crystals of prase-amethyst. The transition between **t**hese two crystals is abrupt within the same crystal, where prase occurs at the base and amethyst at the top of the crystal. The amethysts are transparent and of gemstone quality. In the southern part of Avessalos area large geodes, containing unique quartz crystals, not only in respect to their quality but also for their crystal forms, reflecting very special growth conditions, occur. Rare combinations of prase-amethyst scepter crystals contain phase alternations, including transitions from prase towards amethyst and finally to prase even within a single composite crystal. Scepters include both normal and reverse forms. Calcite-prase intergrowths, abundant within the southern Avessalos geodes, were found for the first time in Serifos island: Calcite crystals, either as rhomboeder, or in platy forms alternate with the prase suggesting contemporaneous deposition probably during boiling processes. The Agia Marina area is characterized by splendid occurrences of andraditic garnets in association with quartz crystals (Fig. 2b). The garnets (up to 5cm in size) accompany quartz and hematite in quartz veins crosscutting hornfelsic gneiss or hedenbergitic skarn. The Kondouros area is characterized by hedenbergitic skarn including the best ilvaite crystals worldwide. Geodes within the skarn are filled by idiomorphic crystals of ilvaite, hematite (iron roses), quartz and calcite. The ilvaite crystals replace hedenbergite, forming radial aggregates reaching sizes up to 50cm (Fig. 2c).



Figure 2. (a) Garnet associated with hedenbergite (Neroutsika); (b) Quartz (Agia Marina); (c) Ilvaite crystals replacing hedenbergite (Koundouro).

Geotourism - Geotouristic development

Geotourism, the tourism through earth features and monuments, is an alternative way of tourism that includes wondering in nature, experiencing the monuments of geology, landscape, environment, history and culture of an area. All these can be found in abundance at the Serifos Island. The geotouristic development of mineralogical and petrological geotopes at Serifos, ensures the preservation of the geological heritage of Serifos Island and also offers the opportunity for sustainable development. Special geo-trails have been developed in order to discover the natural, geological and cultural treasure of the island. Geo-trails have been mapped using modern Geographical Information Systems, as below:

- **Mega Livadi – Koundouros.** Koundouros' area is characterized by hedenbergitic skarn including the best ilvaite crystals worldwide. Mega Livadi area could be described as an outdoor mining museum, with underground mining galleries, iron rails, semi-destroyed bridges, wagons and a loading bridge compose a unique scenery. At the nearby bay of Almiros you can see, near the sea, the mineral water springs.
- **Agia Marina- Koutalas.** Agia Marina area is characterized by splendid occurrences of andraditic garnets in association with quartz crystals. Koutalas' area is characterized by the operations of mining activity such as rail systems, ore transport, wagons and the workers' residencies.
- **Avessalos.** Avessalos' area is the best site in the world in respect to the mineral green quartz (prase). The crystal forms, intergrowths and sizes (up to 40cm) of green quartz specimens from this locality are spectacular.
- **Chalara** with iconic mining infrastructure.
- **Miners pathway.** The hiking trail leading from "Giftika" area to Ano Chora, was the road that the miners used to take, in order to reach the western areas of the island and get to work. It was built in 1858, it is still well-preserved and it constitutes one of the most beautiful paths of the island.

The Serifos geotopes belong to the Greek mineralogical and geological heritage and can be considered as mineralogical treasures, unique throughout world. They deserve to become part of the European Natural Geoparks, following a policy which enhances the natural mineral wealth, so as to protect and promote it.

References

Salemink, J., 1980. On the Geology and Petrology of Serifos island (Cyclades, Greece). Ann. Geol. Pays Hell., 30, 342-365, Utrecht, Nederlands.

Voudouris, P., Katerinopoulos, A., Christofalou, F., and Kassimi, G., 2007. Serifos island, Aegean Sea/Greece: a worldwide unique mineralogical and petrological geotope. ProGeo News, 1, 7-8

15th International Congress of the Geological Society of Greece
Athens, 22-24 May, 2019 | Harokopio University of Athens, Greece
Bulletin of the Geological Society of Greece, Sp. Pub. 7 Ext. Abs. GSG2019-151

Urban Geology in Central-Europe – Concept and Practice in Budapest

G. Halupka[1], A. Csörghe-Andó[1]
(1) Mining and Geological Survey of Hungary, 1145 Budapest, Columbus street 17-23., Hungary, halupka.gabor@mbfsz.gov.hu

In the past decades a regular urban geological research program has been initiated in the Hungarian state geological research institute (present official name: Mining and Geological Survey of Hungary, 'MBFSz').

Budapest, capital of Hungary was chosen as target area, because of its complex environmental, social effects which have an extensive interaction with the geological environment under the city. Moreover lots of archive data of previous on-field detections are also available here, which provides an excellent reference base for a comprehensive comparison.

Here we present a comprehensive (a) and a small-scale, multi-location aspect (b) of this research program.

Two aspects of the urban geological program are presented here, as follows:

a) An overview of the detailed urban geology research program, on example of 21st district of Budapest;

b) A special sub-research, targeting urban parks' physical features, including underlying shallow geology, soil-temperature and soil-moisture content measurements.

a.) Research program concerning 21st district of Budapest follows a general method which was used in case of other districts of the capital, in the past years. The method is not equal with putting a general geological map under the city in GIS, but much more a detailed relation revealing process among different natural (geological, hydrogeological etc.) and manmade features (street network, built-up areas, green sites etc.), based on archive and fresh on-field data, laboratory examination of soil and groundwater samples, detecting groundwater levels. Using modern data processing tools, we have compiled multi-thematic map-series, accompanied by an explanatory report. Since one map-series contains 15-20 basic and derived, computed themes, a comprehensive, scientific analyses and investigation based picture of the district can be provided for leaders, decision makers, and stakeholders of municipalities.

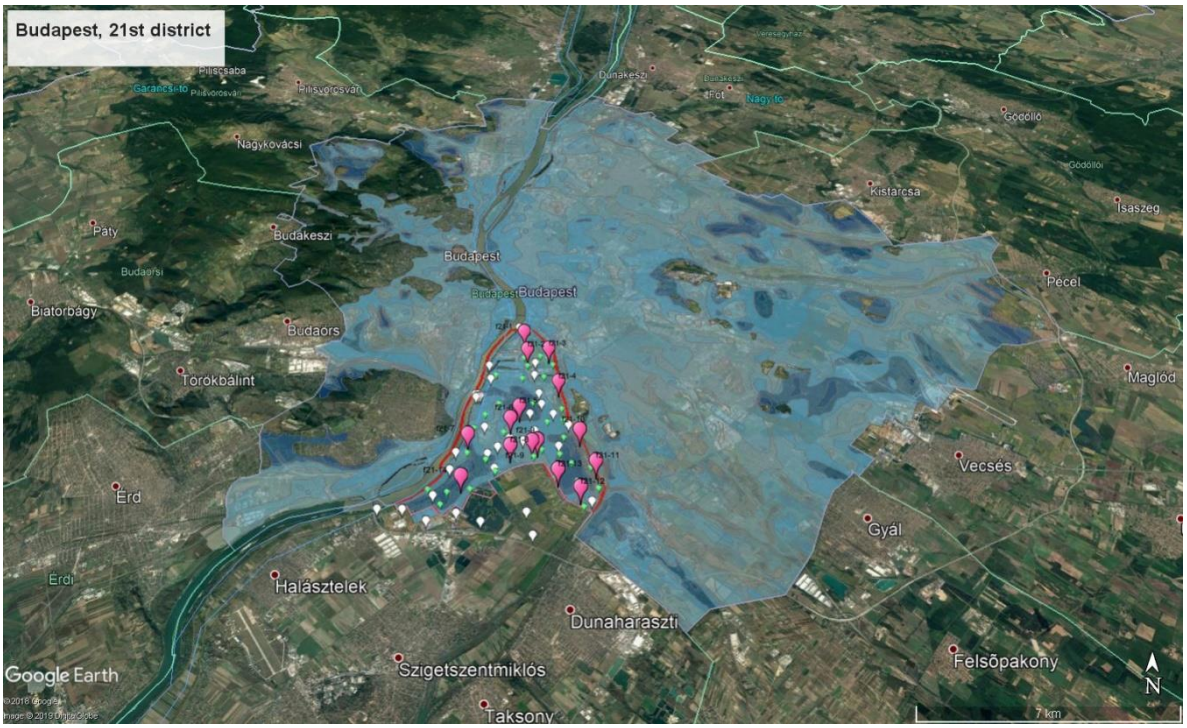

Figure 1. A Google Earth draft of Budapest, capital of Hungary, with on-field research (sampling) points of 21st district, and distribution of groundwater.

b.) The objective of the sub-research is to understand better natural processes, interactions among natural and human factors, and so: long-term sustainability of the urban parks. Role of the parks in everyday life of a city should be more and more important in mirror of the climate change, especially if their social relevance is also considered. If we approach this role, it is essential to find a clear connection between the natural and human factors; to interpret properly needs of a park for the society, and needs of the society for a park. A systematic

observation of natural factors of a park can be a strong support to get closer to this connection.
In our sub-research, a more than 2.5-year long dataset of air and soil temperature, soil moisture content, and precipitation is available for now, gained by manual data collecting, with weekly frequency. However, in one of the detected parks (Park 3, 'Honvéd tér') new, automated soil temperature meters have been installed at the beginning of this year, providing data from 4 points of the park, 7 different subsurface levels, hour by hour. This tool provides much higher data-resolution, both in time and space. First results of comparison of the two, different time-scale datasets will be presented.

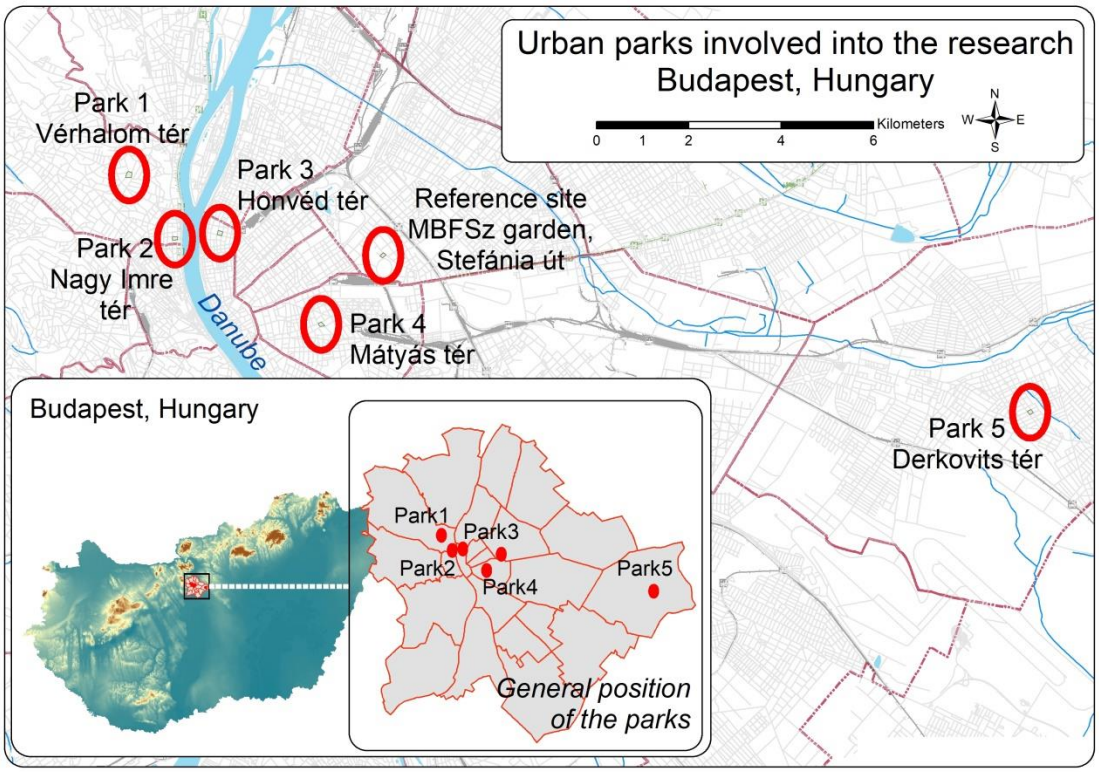

Figure 2. Position of urban parks of Budapest involved into the research.

Acknowledgements

This research is supported by the Mining and Geological Survey of Hungary.

15th International Congress of the Geological Society of Greece
Athens, 22-24 May, 2019 | Harokopio University of Athens, Greece
Bulletin of the Geological Society of Greece, Sp. Pub. 7 Ext. Abs. GSG2019-195

Geo-biodiversity and cultural environment of Nisyros volcano

V. Antoniou[1], P. Nomikou[1], E. Zafeirakopoulou[1], P. Bardouli[1], T. Ioannou[1]

(1) Department of Geology and Geoenvironment, National and Kapodistrian University of Athens, Panepistimioupoli Zografou, 15784 Athens, Greece

Story maps are widespread as an interactive tool used for science and spatial data communication, information and dissemination. A web-based application using story mapping technology is here presented to show the walking paths and routes of Nisyros volcano, Dodecanese, Greece (Figure 1). A tailored story map that combines thematic webmaps, scenes (3D webmaps), narrative text and multimedia content was created to highlight the geological and cultural environment of Nisyros. The webmaps and scenes were entirely created by a Geographic Information System (GIS) having a great impact on web-based visual presentations.

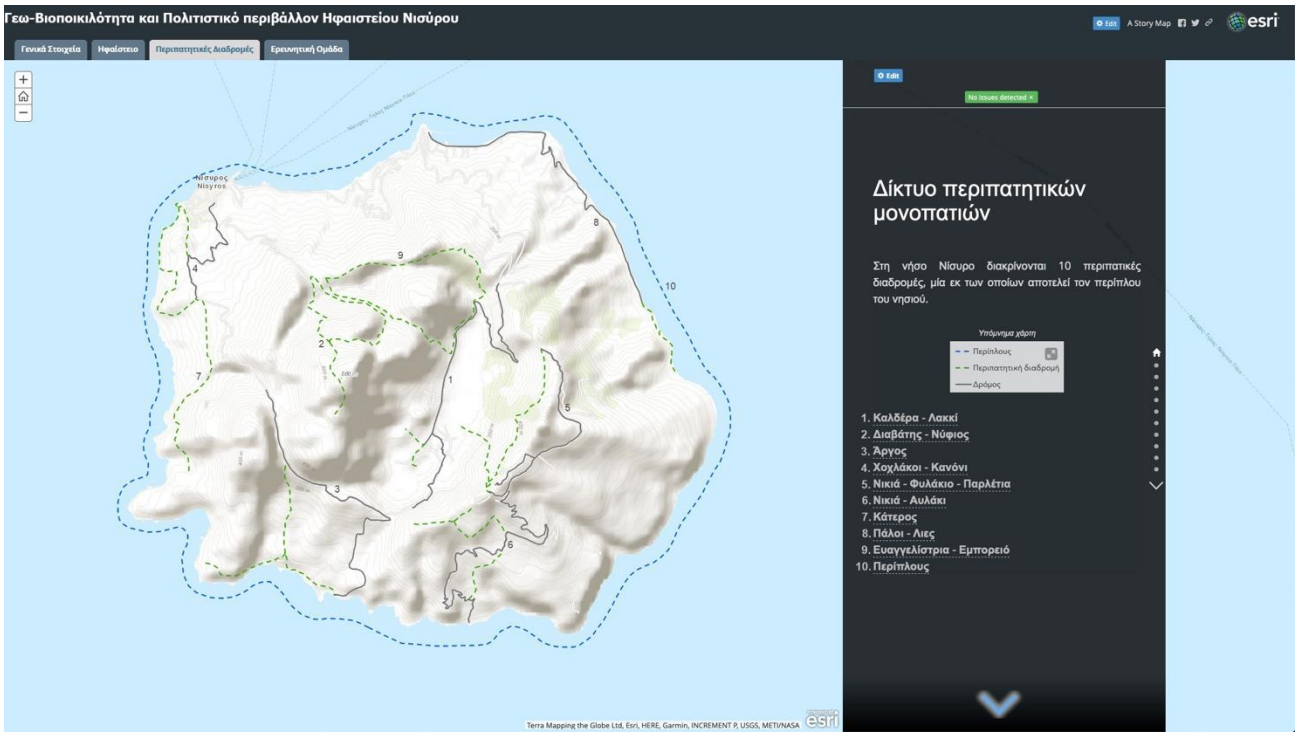

Figure 1. Walking paths and routes of Nisyros Volcanic Island (1. Kaldera - Laki, 2. Diavatis - Nifios, 3. Argos, 4. Hohlaki - Kanoni, 5. Nikia – Filakio - Parletia, 6. Nikia-Avlaki, 7. Kateros, 8. Pali-Lies, 9. Emporios – Laki - Evagelistria, 10. Circumnavigation, ---- path, — road)

The island of Nisyros was selected as it presents unique characteristics. It is one of the smaller islands of Dodecanese islands in the eastern Aegean Sea covering an area of 42 km2 and having an almost circular shape with a total width of 8.5 km and a coastal circumpherence of about 25 km,. It is composed of Quaternary volcanic rocks with a central caldera diameter of approximately 2.8 km surrounded by volcanic domes and thick lavas averaging about 550 m height with Profitis Ilias mountain having the maximum altitude of 698 m (Nomikou & Papanikolaou, 2011).

The history of Nisyros is strongly connected to the volcano, and impresses the visitors with its steaming hydrothermal craters, intensive smell of sulphur and fumarolic gases and hot springs on its northern and southern shores (Dietrich, 2018). Due to its volcanic morphology and geographical position, in the southeast corner of the Aegean Sea, which make it a rather inaccessible island, the cultural and historical heritage of the island have been unchanged in time. Nisyros Island combines the volcanic history and natural beauty with the splendor of art and civilization, expressed through prehistoric and historic locations and monuments. The interpretations vary regarding the names of the island: Porphyris, Kisiris and Nisyros. The first references are present from Early Neolithic times, in the form of relicts from the “Cycladic and Minoan” civilizations. Historical records start from the Hellenistic epoch continuing through Roman, Byzantine, Venetian and Ottoman eras till modern times (Dietrich, 2018). All these periods bequeath to the island plenty of churches, monasteries with hagiographic frescoes, castles, caves and spas.

In the presented application, the aim was to present the geodiversity, the cultural environment and the biodiversity (unique flora and fauna) along the paths of the volcano. Using Story Maps, this relative new geographical approach, having open source code, provides many possibilities, as it is easy to be used both from the developer and from the end user and allows integration of new functions combining many scientific fields in order to disseminate and understand scientific findings to broader non-technical audiences (Janicki et al., 2016; Wright et al., 2014). Furthermore it is

responsive, and it can be also as interactive as the developer wishes. Users can navigate easily through the content, using either the sequence of the predefined tabs or jumping from one to another according to their will.

The developed application can be an ideal way for presenting the geological, geomorphological and historical contents of other places, especially places which can be characterized as geotopes or protected areas worldwide (e.g. Natura 2000 areas) (Antoniou et al, 2018). Finally, as Nisyros volcano portrays a geotope, this application provides a quick access of the available information to a wide audience, developing the interest and possibly motivating the public to learn more about the volcanic landscape of Nisyros, or even to visit it.

Acknowledgements

This work was supported by "Business of Public Benefit-Municipality of Nisyros", in the framework of the Applied Research Program 'Path network of Nisyros: Recording and Enhancement via contemporary media of online digital cartography" of National Kapodistrian University of Athens (NKUA).

References

Antoniou, V., Ragia, L., Nomikou, P., Bardouli, P., Lampridou, D., Ioannou, T., Kalisperakis, I. and Stentoumis, C., 2018. Creating a Story Map Using Geographic Information Systems to Explore Geomorphology and History of Methana Peninsula. ISPRS Int. J. Geo-Inf. 2018, 7(12), 484.

Dietrich W., 2018. Geography, Nature and Habitation of Nisyros Volcano. Editors: Dietrich, Volker Jörg, Lagios, Evangelos (Eds.), p. 1-12. Hardcover ISBN 978-3-319-55458-7

Janicki, J., Narula, N., Ziegler, M., Guénard, B. and Economo, E.P., 2016. Visualizing and interacting with large-volume biodiversity data using client–server web-mapping applications: The design and implementation of antmaps. org. Ecological Informatics, 32, 185-193.

Nomikou P. & Papanikolaou D. 2011. Extension of Active Fault Zones on Nisyros Volcano across the Yali-Nisyros Channel based on Onshore and Offshore data. Marine Geophysical Research, Special issue on «Seafloor Mapping for Geohazard Assessment», DOI 10.1007/s11001-011-9119-z.

Wright, D.J., Verrill, A., Artz, M. and Deming, R., 2014. Story maps as an effective social medium for data synthesis, communication, and dissemination. In Proceedings of the Fall Meeting 2014, San Francisco, CA, USA, 15–19 December 2014.

15th International Congress of the Geological Society of Greece
Athens, 22-24 May, 2019 | Harokopio University of Athens, Greece
Bulletin of the Geological Society of Greece, Sp. Pub. 7 Ext. Abs. GSG2019-259

New digital applications to promote the geological heritage of Cretan UNESCO Geoparks under GEOIN project

C. Fassoulas[1], S. Staridas[2], E. Nikolakakis[1], E. Perakis[3]

(1) Natural History Museum, University of Crete, Uni campus Voutes, Crete, Greece, fassoulas@nhmc.uoc.gr
(2) Staridas Geography, Skordylon 56, Heraklion Crete, Greece
(3) Sitia Geopark, Municipality of Sitia, Crete, Greece.

Geosites are outcrops with significant geological value that can contribute to the restoration of the geological evolution of an area (Gray, 2004). All together constitute the geological heritage of a territory. Areas of outstanding geological value including geosites of international significance that are under a holistic conservation and management plan for the local sustainable development can be nominated as UNESCO Global geoparks (UGGp). Since 2015 Crete hosts two among the five UNESCO Global geoparks of Greece, those of Psiloritis and Sitia. Core aim of the UGGps is the conservation and promotion of geological heritage and incorporation them with other natural and cultural values for the development of geotouristic activities (UNESCO, 2019). In addition, geoparks have to develop educational and training activities to inform visitors and inhabitants on the value of their natural environment and raise awareness on critical geological issues and geohazards.

Under the GEOIN project (www.geo-in.eu) that supports the Geotourism in insular Geoparks of Greece and Cyprus, the Natural History Museum of the University of Crete has undertaken the development of three web-based applications to promote geoheritage, support visitors' needs and educate through entertainment, at Psiloritis and Sitia UGGps. The first application is a web-gis based interactive map of each of the two areas. It has been scheduled to be compatible with desktop and mobile devices connected with the web, but are also used for static digital displays with touch screens. This WebGIS application is separated in two distinct parts, the map panel on the left and the side panel on the right, which interact with each other. The side panel is further distinguished in major units, each one of them comprising points of interest and other information related to the geological, environmental, cultural and religious heritage of the two geoparks. Clicking upon every unit will add the correspondent layers on the map panel, while the content of that unit slides down as an accordion. All the information is presented as an interactive list in harmony with the map. When clicking on a point on the map, the side panel automatically scrolls until the equivalent information appear on top and vice versa, when clicking on a specific information on the side panel, the map zooms in to that location. The geosites of the two UGGps of Crete have been assessed and categorized in various types following international standards and procedures (Fassoulas *et al.*, 2011; Fassoulas *et al.*, 2013). Based on these categories the geosites are presented in the application both in the core map and the interpretation part offering simple information of their type and features and an accompanying image (Figure 1). This application may be used thus as a geography book with interactive chapters and to perform a virtual tour in the Psiloritis and Sitia Geoparks.

The second application comprises the development of Storytelling maps for Psiloritis and Sitia geoparks. Story telling maps are widely used nowadays for the complete and interactive presentation of a story using various multimedia means such as videos, animations, spherical panoramas and images (ESRI 20019). A good example for the use of Story maps to interpret and promote geological heritage using web-gis tools is the Santorini Volcano Story map produced by Staridas (2018) that received the First place at the 2019 ESRI contest for the Travel, Recreation and Destination category. One story telling map has been produced for each of Psiloritis and Sitia UGGps that presents the geological heritage of the areas along selected routes. Each map is built up with data gathered from the two geoparks but also data acquired during the project such as, earth based and aerial spherical panoramas that combine site interpretation information through text, sketches and animations. Scrolling down through the various chapters of the story telling maps, information is displaced at the left part of the web page, while interactive maps alternate with videos, images and animations appear at the other side, to fully present the geological content of each route.

The third application developed, is the e-geodiscover educational application. This is developed as an app compatible with android devices that can be downloaded for free and stored in a mobile device to run, even without Wi-Fi access. The educational approach is based on the treasure handing games, forcing users to discover an area using a digital map with location tracked through the device's gps, identify geosites and other locations of natural and cultural importance, and select the correct answer in selected spots. The proximity of the device in a predefined buffer zone around a spot area is identified by the gps permitting the pop up of introductory information for the site and then of predefined answers in the form of simple phrases, images, or true/false options. Correct response within three tries enables the appearance of complementary information about the site and guidance to discover the next. The application has the ability to trace players' response and can count the first provided answer per site to evaluate the total performance of the player at the end. The applications have been scheduled along three of the geo-routes of the two geoparks; the Migias and Gonies trails at Psiloritis, and the Upper Zakros trail at Sitia.

All applications will be hosted at and accessed from the new geoparks websites that are under development. These application not only contribute in the promotion of the geological heritage of each geopark, increase of their visibility and attract visitors of young ages, but being web-based can serve the needs of future visitors to schedule and design their trip in the two geoparks. Moreover, these applications can serve the needs of disabled people, especially those with mobile

disabilities, to visit remote sites being inaccessible to them, explore the nature and geology values of the two geoparks from their home places, and possibly trigger them to visit other accessible places of the two areas. Finally, as all applications will be also available at geopark's info centers, and educational facilities, will strengthen the provided environmental education and enrich their didactic methodologies.

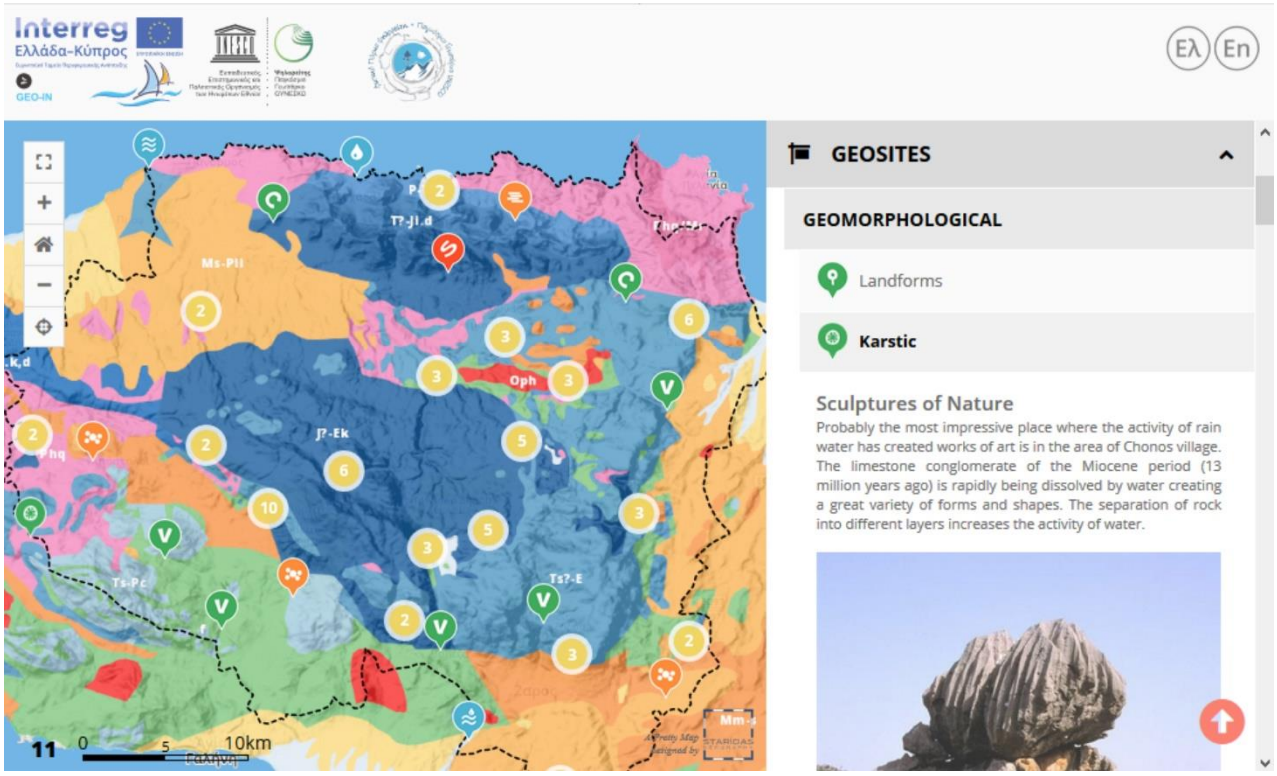

Figure 1. Image of the Interactive web-map for Psiloritis UNESCO Global Geopark presenting a simplified geological map with location of geosites and information at the right part on the Geomorphological, Karstic geoisties.

Acknowledgements

GEOIN project was financed under the INTERREG Greece – Cyprus 2014-2020 framework.

References

ESRI, 2019. Arc-gis story maps. https://storymaps.arcgis.com/en/

Fassoulas C., Mouriki D., Dimitriou-Nikolakis P. & Iliopoulos G. 2011. Quantitative assessment of geotopes as an effective tool for geoheritage management. GEOHERITAGE, DOI 10.1007/s12371-011-0046-9

Fassoulas C., Staridas S., Perakis V. & Mavrokosta C., 2013. Revealing the geological heritage of eastern Crete through the development of Sitia Geopark, Bull. Geol. Soc. Greece, Proc. Vol. XLVII, No 2, 1004-1016.

Gray, M. 2004. Geodiversity: valuing and conserving abiotic nature. Wiley, West Sussex

Staridas S., 2018. The Volcano of Santorini: A story map. https://www.esri.com/en-us/arcgis/products/esri-story-maps/contest/winners-gallery/2018-winners/

UNESCO, 2019. International Geosciences and Geoparks program, UNESCO, Paris, (http://www.unesco.org/new/en/natural-sciences/environment/earth-sciences/unesco-global-geoparks/)

15th International Congress of the Geological Society of Greece
Athens, 22-24 May, 2019 | Harokopio University of Athens, Greece
Bulletin of the Geological Society of Greece, Sp. Pub. 7 Ext. Abs. GSG2019-263

The time period before humans. An Educational Program of the Natural History Museum of Philekpaideftiti Etaireia

F. Tripolitsiotou[1], H. Drinia[2], A.Antonarakou[2]

(1) Natural History Museum of Philekpaideftiti Etaireia, 1 str Arsaki, p. Psychiko Athens, Greece, tripolitsiotou.f@e-arsakeio.gr
(2) Geology Department, Athens, Greece, cntrinia@geol.uoa.gr, aantonarakou@geol.uoa.gr

In the present work, an attempt has been made to highlight the contribution of the Museums of Natural Sciences to the teaching of the Geosciences through designing and presenting an educational program whose subject is derived from the field of Geology and specifically from Palaeontology and Historical Geology, aiming at understanding the geological time and its comparison with historical time. For this purpose, three different models of depicting geologic time have been designed, for the construction of which participated a group of pupils. In addition, an attempt of designing 3d visualization of microfossils and 3d printing is presented.

Introduction

The knowledge gained in informal learning environments is particularly important (Hann & Jackson 1995), taking into consideration the fact that in such environments there is a change in attitudes to the subjects under study, psychomotor skills are developed and the social interaction between the team members is promoted (Ioannidou et al 2002) Thus, school teachers choose visits to museums when they think that they are linked to curriculum subjects and are educationally relevant to the pupils' age.

Several museums try to make their educational programs be directly linked to the school curriculum (Allard & Boucher, 1998). This cooperation can be achieved at various levels, such as the complementary level where the museum complements school education. (Koliopoulos, 2005)

The Museum of Natural History of Philekpaideftiti Etaireia is considered to be a Museum of this type, which is located within the area of the Arkakeia Schools in Psychiko. The aim of this Museum is to make the Museum become a school and its target is to offer knowledge through experiential education programs which are linked to the curriculum of the subjects, depending on the pupils age and as it is suggested by the Analytical Program of Studies (Tripolisitsou et al., 2018)

The educational program presented in the present work is entitled: "The Time period before humans", and was designed and carried out in this Museum. The program which is still in progress takes place in 3 stages and so far it has been attended by 250 students aged 9-15 years as well as individual adults.

Methodology

Prior to the design of the educational program " The Time period before humans ", a survey had been conducted among 450 students concerning pupils of the 4th grade of primary school to the 2nd grade of Senior High School who responded to a question about the geological time on the geologic time scale, in order to collect data on whether students are able to understand geological time.

The objective questions we have posed based on the results of geological time research are as the following:

- What are the mental representations of the students in relation to geological time, how do they perceive it?
- What is the relationship between geological and historical time?
- Can the participants categorize the fossil organisms into basic categories? (bivalves, gastropods, corals ..)
- After completing the training program which they attended, which ideas do they express about fossils, and geological time?

Table1: Teaching Model

Before	Classroom	Preparation	Submit Study Subject	Was the form of the Earth always the same as we see it today?
During	Museum	Implementation	Subject study and data collection	Attendance of Educational program - knowledge enrichment and activities. Collection of data in the Museum
After	Classroom	Extension	Analysis and synthesis	Discussion and knowledge building

In this training program, the Allard & Boucher, (1998) & Paquin (1995) teaching model is applied (Table 1).

In addition to this teaching model, the Pre-Post teaching model is also used, according to which the participants fill in a questionnaire before starting the program and the same one immediately after its completion in order to record the students' initial ideas on the theme of geological time.

Description of the program

Initially, the students at the Museum fill in a questionnaire aiming at recording their initial ideas on fossilization and understanding of geological time.

Then through interactive presentation and fossilization models they learn about fossils and the ways of fossilization. Furthermore, there are activities based on experiential learning aiming at the identification and classification of fossils. For this purpose, models of depicting geological time have been designed for the acquaintance and understanding of the geological ages, giving emphasis on the Phanerozoic Eon. The students observe the fossilized exhibits of the Museum and examine fossils that belong to the museum exhibits as they are able to touch them. In addition, by using geological time models, participants try to understand the minimality of historical time as compared to the duration of geological time.

With the help of a group of seven students, enlarged 3-dimensional models of microfossils have been designed using computer programs aiming at getting students to get acquainted with the fossils, since they can touch and observe them in a better way.

Conclusions

The final questionnaire as well as the students' comments show that there is a positive response to the program and an understanding of geological time depending on the pupils' age. The older the age the better and the understanding of geological time.

An unexpected positive outcome is that the students are impressed with the extent of geological time and are concerned about the impact of human activities on the environment during the time of human existence on Earth.

References

Allard, M & Boucher, S (1998). Eduquer au musée. Un modèle theorique de pédagogie muséale. Cahiers du Québec.

Hann, K. and Jackson, R. (1995). Learning from experiences: approaches to research in the informal sector. European Conference on Research in Science Education, Leeds UK

Koliopoulos D., (2004) Teaching Approach in Physical Museums, Metaichmio pub

Paquin M, (1995) Modèle didactique d'utilization d'instutition culturelles quebecoises a des fins educatives. Loisir et Societe Education p.81.

Tripolitsiotou F, Drinia H., Antonarakou A, (2018). Searching for the lost paleontological thesaurus. An educational program of the Natural History Museum of Phileakpaideftiki Etaireia. Neos pedaegogos proceedings, pp 778-785.

15th International Congress of the Geological Society of Greece
Athens, 22-24 May, 2019 | Harokopio University of Athens, Greece
Bulletin of the Geological Society of Greece, Sp. Pub. 7 Ext. Abs. GSG2019-281

The Gamila Peak Spherical Concretions and the Oxia Hanging Valley at the Vikos-Aoos Geopark

C.L. Stergiou[1], A. Chatzipetros[2], T. Telbisz[3], A. Mindszenty[4]

(1) Department of Mineralogy, Petrology, Economic Geology, Faculty of Geology, Aristotle University of Thessaloniki, 54124 Thessaloniki, Greece, e-mail: christer@geo.auth.gr
(2) Department of Geology, Faculty of Geology, Aristotle University of Thessaloniki, 54124 Thessaloniki, Greece
(3) Department of Physical Geography, Eötvös University, Pázmány Péter sétány 1/C, 1117 Budapest, Hungary
(4) Department of Physical and Applied Geology, Eötvös University, Pázmány Péter sétány 1/C, 1117 Budapest, Hungary.

Vikos-Aoos Geopark is part of the European and Global Geopark Networks of UNESCO since 2010 and it is located at the NW part of the Pindus Mountain Range at Epirus Region, northwestern Greece. The Geopark extends in an area of 1.200 km^2 from the area of Northern Pindus National Park to the Greek-Albanian borders. The area is characterized by a mountainous continuous and rugged terrain which is interrupted by steep gorges, elongated narrow valleys, and alluvial plains. Smolikas (Geros peak: 2637 m a.s.l.) and Tymfi (Gamila peak: 2497 m a.s.l.) Mountains host the highest peaks of the Geopark, while Vikos and Aoos Gorges as well as Konitsa plain control the lower relief morphology. Except of the major geological, geomorphological, and natural aspects, the Geopark hosts also significant cultural aspects. Sixty one traditional settlements belonging to the municipalities of Zagori and Konitsa, most of which are protected culturally and architecturally, are found within the Geopark area. These settlements bear a total population of 9954 inhabitants (Hellenic Statistical Authority, 2018). Nevertheless, 6362 of these inhabitants reside at Konitsa town, thus the Geopark area could be characterized as depopulated (Telbisz et al., 2019). In these publication we further discuss on the special geological aspects of the Vikos-Aoos Geopark, the Gamila peak spherical concretions and the Oxia hanging valley which are located at the Tymfi mountain massif, based on the recent publications made by authors (Chatzipetros and Stergiou, 2016; Telbisz et al., 2019).

The Tymfi mountain massif belongs to the Ionian geotectonic Zone of Greece. Jurassic to Cretaceous dolomites and limestones, Cretaceous to Upper Eocene limestones, and the Upper Eocene to Lower Miocene flysch formation characterize the local stratigraphy. Plenty of chert intercalations are found within the dolomites and the limestones as beds or as nodules. These sedimentary series constitute a continuous stratigraphy which is largely exposed due to the Vikos and Aoos Gorges incisions at the Tymfi anticline. The S-SW tilting, low-angle anticline of Tymfi has a NNW-SSE axial direction and it was formed under the Paleogene-Neogene folding and the later structural reconstruction of the area by ENE-WSW trending faults (Astraka and Konitsa faults) (Galanakis et al., 2007; Chatzipetros and Stergiou, 2016). Along with the structural features, an old glaciokarst and an active karst system had actively shaped the geomorphology of the Tymfi mountain massif since Pliocene resulting in a well karstified mountainous terrain. Voidomatis River constitutes the tributary where large amounts of subsurface and surface waters are drained.

The Gamila peak spherical concretions were described for the first time by Telbisz et al. (2019) (Fig. 1). They are found on the pathway (approximately at 2100 m a.s.l.) to Gamila peak in large collapsed rocky scraps, in limestone boulder sections or as boulders. They have spherical to elongated shapes ranging in diameter from 0.10 to 1 m and concentric zones. These zones are made of alternating fine-grained siliceous material and carbonate cement enriched in bioclastic material. Microscopic study revealed that the matrix of the concretions is both carbonatic and siliceous (Telbisz et al., 2019). Regarding their formation it could be suggested that their diagenesis is characterized by an early and imperfect carbonate cementation, and by a simultaneous massive precipitation of SiO_2 in the intergranular space. Although that the origin of the SiO_2-rich solutions is yet unknown it may be assumed that their origin is the dissolute siliceous bioclasts and to a lesser extent some external fluids enriched in SiO_2-rich (Telbisz et al., 2019). Concretions of various sizes and shapes are found worldwide in different sedimentary rock types. The Gamila peak spherical concretions resemble to the spherical concretions found at Lower Eocene Drunka limestone formation at Egypt. Nevertheless, their complete mineralogical, geochemical and genesis interpretation needs further investigation.

Limestone pavements, shafts, and remnants of moraines and periglacial rock glaciers found in large U-shaped depressions and in higher cirques characterize the glaciokarst morphology (Waltham, 1978; Telbisz et al., 2019). Based on the description of these features Hughes et al. (2007) identifies three glacial stages; an early plateau glacier and outlet glaciers stage, a middle cirque and valley glaciers stage, and a third cirque glaciers stage. These stages are dated respectively at 430 ka BP, at 140 ka BP, and at 110 ka BP (Hughes et al., 2007). The Oxia hanging valley is another remnant of the glaciokarst of Tymfi. It was identified by Chatzipetros and Stergiou (2016) and mapped by using an Unmanned Aerial Vehicle (Fig. 2). The aerial scans covered the entire length of the valley, as well as its exit to the Vikos Gorge. The valley has a total length of 3.24 km and runs across the western part of the Tymfi mountain massif in a SW-NE direction. Eocene limestones form the lithological basement of the valley. The surrounding geomorphology is characterized by a typical karst plateau and several tributaries draining this plateau end at the valley. The valley starts at 1332 m a.s.l. in a slightly uplifted block of the mountain massif and exit to Vikos Gorge approximately at 1305 m a.s.l. after covering approximately 3.20 km of distance. The exit of the valley has a U-shape and it is located approximately at 670 m above the bed of the gorge. From the other side of the uplifted block and towards SE there is another V-shaped valley (1.9 km in length) starting at 1327 m a.s.l. and ending approximately at 1000 m a.s.l. near Ano Pedina village.



Figure 1. A fractured spherical concretion in a limestone boulder section on the pathway to Gamila peak (Photo: T. Telbisz).



Figure 2. An aerial photograph taken by the DJI Phantom 3 Professional UAV which was used to scan the Oxia hanging valley. A dashed line highlights the exit of the hanging valley to Vikos Gorge. (Photo: A. Chatzipetros).

References

Chatzipetros, A. Stergiou, C., 2016. Morphotectonic indications of uplift from the Vikos Gorge area using UAV: Preliminary results. Tectonics and Structural Geology Committee of the Geological Society of Greece, 1st TSG Meeting, Athens, Greece.

Galanakis, D., Paschos, P., Rondoyanni, T., Georgiou, C., 2007. Neotectonic Activity of Konitsa Area and the 1996 Earthquakes. Hellenic Journal of Geosciences 42, 57-64.

Hughes, P.D., Woodward, J.C. Gibbard, P.L., 2007. Middle Pleistocene cold stage climates in the Mediterranean: new evidence from the glacial record. Earth and Planetary Science Letters 253, 50–56.

Hellenic Statistical Authority (ELSTAT), 2018: Available from: http://www.statistics.gr/statistics/pop [Accessed 26/3/2018].

McBride, E.F., Abdel-Wahab, A. El-Younsy, A.R., 1999. Origin of spheroidal chert nodules, Drunka Formation (Lower Eocene), Egypt. Sedimentology 46, 733–755.

Telbisz, T., Stergiou, C.L., Mindszenty, A., Chatzipetros, A., 2019. Geological and Geomorphological Characteristics of Vikos Gorge and Tymphi Mountain (Northern Pindos National Park, Greece) and Karst-Related Social Processes of the Region. Acta Carsologica 48(1), 29-42.

Waltham, A.C., 1978. The caves and karst of Astraka, Greece. Transactions of the British Cave Research Association 5, 1–12.

15th International Congress of the Geological Society of Greece
Athens, 22-24 May, 2019 | Harokopio University of Athens, Greece
Bulletin of the Geological Society of Greece, Sp. Pub. 7 Ext. Abs. GSG2019-299

Geosites' Evaluation Methodology As A Tool for Geoconservation

I. Valiakos[1], N. Zouros[1,2], K. Bentana[1]

(1)Natural History Museum of the Lesvos Petrified Forest, Sigri, Lesvos Island, Greece, lesvospf@otenet.gr
(2) University of the Aegean, Department of Geography, University Hill, Mytilini, Greece

In many countries, protection measures have been introduced for specific geological monuments and protected areas have been created that include sites of special geological - geomorphological value, but the management of these areas has not had as priority the protection of geological - geomorphological sites.

In Greece until recently the elements of the abiotic environment were referred to in Law 1650/1986 as objects of protection without being subject to management. The locations containing special geological monuments are mainly protected in the context of the archaeological or forestry legislation. As a result, there was a lack of protection of geological - geomorphological sites. Law 1650/1986 and especially law 3937/2011, which regulate the management of protected areas and biodiversity conservation include provisions on the conservation of biodiversity. In Law 3937/2011 for the first time the concept of geosites and geoparks are introduced into the Greek legal order.

The subject of this paper is the presentation of an integrated methodology and criteria for the evaluation of geosites that constitute the basic unit of the geological and geomorphological heritage and the use of this methodology for the implementation of an integrated geo-conservation policy. A special point is the incorporation of the methodology of quantitative evaluation of the geosites and its results as a basic tool for the management of the geoparks of Greece, as well as for its application in a geopark internationally.

An essential component of the research was the development and implementation of the geosites' assessment methodology that assessed the locations and structures of geological and geomorphological interest in Lesvos Island UNESCO Global Geopark in order to define the priorities for protection, promotion and management and ultimately select those sites which are exploited in the context of the different actions of the Geopark of Lesvos in the fields of awareness raising, education and tourism.

Taking advantage of the data collected, the criteria necessary for the creation of a framework for the evaluation of geosites and the definition of parameters for a system of evaluation of the geosites of Greece were defined.

In conclusion, the main results of the research carried out are:

- the proposal for an integrated methodology for the evaluation of geosites and the use of this methodology for the implementation of an integrated geo-conservation policy.
- the incorporation of the methodology of quantitative assessment of the geosites and its results as a basic tool for the management of geoparks of Greece, as well as for its application in geopark internationally.

References

Brilha, J. (2016). Inventory and Quantitative Assessment of Geosites and Geodiversity Sites: a Review, Geoheritage, pp. 119-134

Giusti, C., Gonzalez-Diez, A. (2000). A methodological approach for the evaluation of impacts on sites of geomorphological interest (SGI), using GIS techniques, International Archives of Photogrammetry and Remote Sensing, XXXIII, Supplement B7, pp. 47-53

Reynard, E. (2004). L'évaluation des géotopes géomorphologiques en Suisse, Paysages géomorphologiques, Séminaire de 3ème cycle CUSO 2003, Université de Lausanne, Institut de géographie (Travaux et Recherches n° 27), pp. 138- 149.

Theodosiou-Drandaki, I. (1999). Criteria for geosites selection. In: proceedings of the 1st meeting on geological-geomorphologic heritage conservation. Hermoupolis, Syros island, 13-15.7.06.

Zouros, N., Valiakos, I. (2010). Geoparks management and assessment. Bulletin of the Geological Society of Greece, 2010, Proceedings of the 12th International Congress, Patras, May, 2010,Vol. XLIII – No 2, pp. 965-975.

15th International Congress of the Geological Society of Greece
Athens, 22-24 May, 2019 | Harokopio University of Athens, Greece
Bulletin of the Geological Society of Greece, Sp. Pub. 7 Ext. Abs. GSG2019-300

The Role Of The Educational Activities Of Temporary Exhibitions: The Case Of The Temporary Exhibition Of The Natural History Museum Of The Lesvos Petrified Forest "Gaias' Memories: UNESCO Global Geoparks Of Greece - Cyprus"

K. Bentana[1], N. Zouros[1,2], I. Valiakos[1]

(1) Natural History Museum of the Lesvos Petrified Forest, Sigri, Lesvos Island, Greece, lesvospf@otenet.gr (2) University of the Aegean, Department of Geography, University Hill, Mytilini, Greece

The educational role of a Museum, as well as its goals, are changing and differentiating both in time and in terms of the needs of the time that it is going through. The educational activities of the Museums are confronted with new facts and new challenges and are called upon to take on new roles. The Natural History Museum of the Lesvos Petrified Forest, by expanding its role, has designed and presented to the public a series of temporary exhibitions aiming at enhancing its contact with the public and especially students and young people, as well as its visibility and especially new findings and activities of.

In this context, the Natural History Museum of the Lesvos Petrified Forest drew up the periodic exhibition "Gaias' Memories: UNESCO Global Geoparks of Greece - Cyprus". The exhibition began its tour from Athens and the Eugenides Foundation and then is scheduled to travel to Cyprus, Crete and Lesvos. The exhibition is complemented by educational and informative activities aiming at acquainting visitors of all ages with the UNESCO Global Geoparks, the impressive geological and natural monuments that host the Geoparks of Greece and Cyprus, the geological and natural processes that created the landscapes in conjunction with time and shaped the background for the development of the variety of modern natural ecosystems and culture from prehistory to the present day.

The aim of the work is to investigate the role of the educational activities taking place at the temporary exhibition "Gaias' Memories: UNESCO Global Geoparks of Greece - Cyprus" of the Natural History Museum of the Lesvos Petrified Forest for the development of the contact with the public and the approach of new groups.

References

Zouros, N., Pavlides, S., Soulakellis, N., Chatzipetros, A., Vasileiadou, K., Valiakos, I., Bentana, K. (2009). Usıng actıve faults for raısıng publıc awareness and sensıtısatıon on seısmıc hazard: a case study from Lesvos Geopark, NE Aegean sea, Greece. Proceedings of the VIII European Geoparks Conference.

Zouros, N., Valiakos, I., Bentana, K. (2017a). Alternative tourism activities in Lesvos island UNESCO Global Geopark, 14th EGN Conference, Abstracts Volume, Ponta Delgada, Azores, p. 42.

Zouros, N., Valiakos, I., Bentana, K. (2017b). Lesvos island UNESCO Global Geopark: Raising visibility and promotion, 14th EGN Conference, Abstracts Volume, Ponta Delgada, Azores, p. 42.

Zouros, N., Valiakos, I., Gribilakos, G., Plougarlis, A., Bentana, K., Rozakis, V., Agiasoti, M., Tsalkitzi, O. (2015). New fossil findings in the petrified forest of Lesvos along the new Kalloni - Sigri road. "The forest under the road" a new travelling exhibition of the Lesvos geopark, European Geoparks conference 3rd-6th September 2015, Abstracts volume, p. 123.

15th International Congress of the Geological Society of Greece
Athens, 22-24 May, 2019 | Harokopio University of Athens, Greece
Bulletin of the Geological Society of Greece, Sp. Pub. 7 Ext. Abs. GSG2019-308

Geosites – Geoparks of Greece: Conservation of Geological Heritage and Sustainable Development

E. Moraiti[1], I. Zananiri[2] & S. Staridas[3]

(1) Hellenic Survey of Geology & Mineral Exploration, Spirou Loui 1, 13677 Acharnae, Greece; moraiti@igme.gr
(2) Hellenic Survey of Geology & Mineral Exploration, Spirou Loui 1, 13677 Acharnae, Greece; izanan@igme.gr
(3) Hellenic Survey of Geology & Mineral Exploration, Spirou Loui 1, 13677 Acharnae, Greece; now at: Staridas Geography, Heraklion, Crete; staridasgeography@gmail.com

Geosites can be considered as the "book of the Earth", enclosing the geological history of each region, and therefore their preservation and promotion is crucial. However, during their study a question that arises is "based on which elements can a site be characterized as a *geotope* (Stürm 1994, Wiedenbein 1994)", comprising a key element of the "geological heritage"? It is noteworthy that the characterization, evaluation and interpretation of geotopes is a dynamic concept, and, apart from their conservation and management, educational and informative issues have to be taken into account. Similarly, for geoparks the proposed definitions encompass not only the geological and geomorphological elements found in nature, but also the plan for protecting and conserving them in a sustainable way.



Figure 1. Characteristic geosites from Greece.

Greece, located in the convergence space of two tectonic plates, is characterized by an active tectonic regime and a complex geological structure, exhibiting a variety of geological formations, landforms, geological processes (past or emerging), that are of particular scientific or educational interest, while many of those have high cultural and tourist value (Fig. 1).

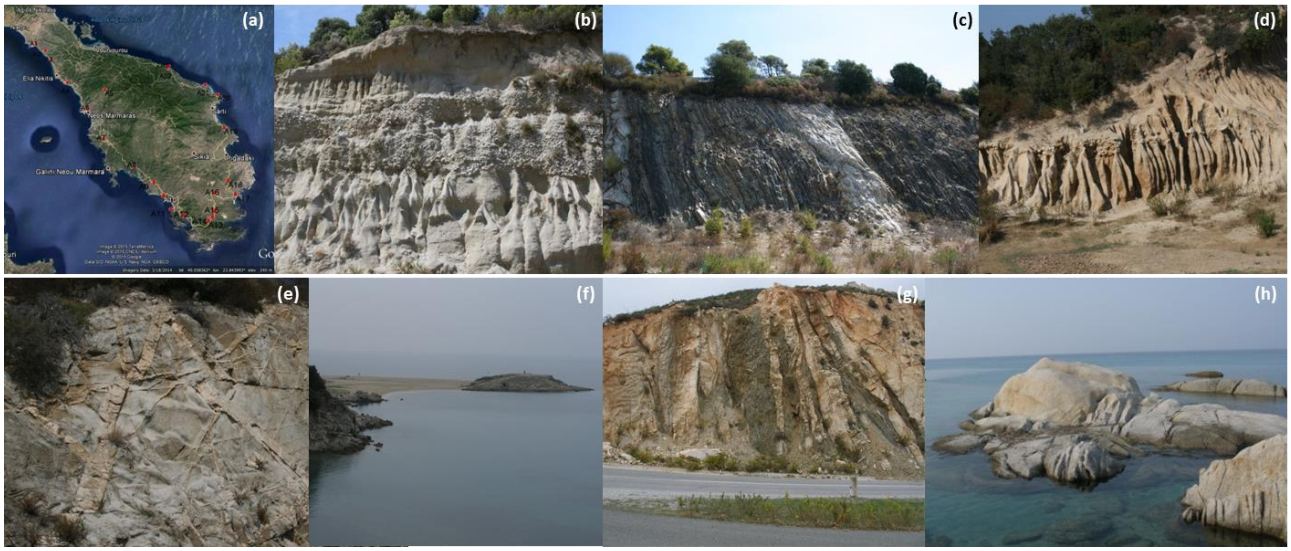

Figure 2. A designated geotrail (a) in Sithonia peninsula (N. Greece) and characteristic geosites: Neogene sediments with characteristic erosional forms (b, d), tectonic contact of the Sithonia granitoid and rocks of the Circum-Rhodope belt (c, g), tectonism and pegmatite/quartz dykes, tombolo geomorphology (f) and coastal features (h) (Zananiri 2016).

Thus, the need for detailed recording of those sites is imminent in order to preserve their scientific, educational and environmental value; moreover, towards promotion of the Hellenic geological heritage, areas which fulfill the necessary conditions and potential must be highlighted and specific tasks may be designed: geotrail mapping, thematic networks of geosites, geo-tourism promotion, and establishment of geoparks.

A first attempt to record the "monuments of nature" was made in 1982 by the Institute of Geology and Mineral Exploration (now Hellenic Survey of Geology & Mineral Exploration-HSGME). The recording and promotion of the Hellenic geosites continued more systematically from 1995 until today, with the elaboration of several projects (2nd CSF, 3rd CSF, NSRF 2007-2013), carried out by the Department of Geology and Geological Mapping (Drandaki 2009, Theodosiou 2010, Moraiti 2016 and references therein). In this context more than 1400 sites have been recorded in the Greek territory, many of which have been classified as of "National Importance" and form the basis of the relevant national registry compiled by the Working Group of the Ministry of Environment and Energy. Moreover, geotrails have been thoroughly mapped in 9 areas (e.g. see Fig. 2), while several more are planned.

The HSGME database – updated and complemented by additional data in the frame of the ongoing "GEOINFRA" project (NSRF 2014-2020) – will function as a source of information for every use: public/private sector, local authorities, and the broader public, at a national and international level, towards the development, planning and conservation of nature, environmental education and tourism. Prominent geotopes and designated geotrails will be available for browsing through an online interface (Fig. 3) and smartphone applications, comprising a useful supplement for the promotion of geotourism.

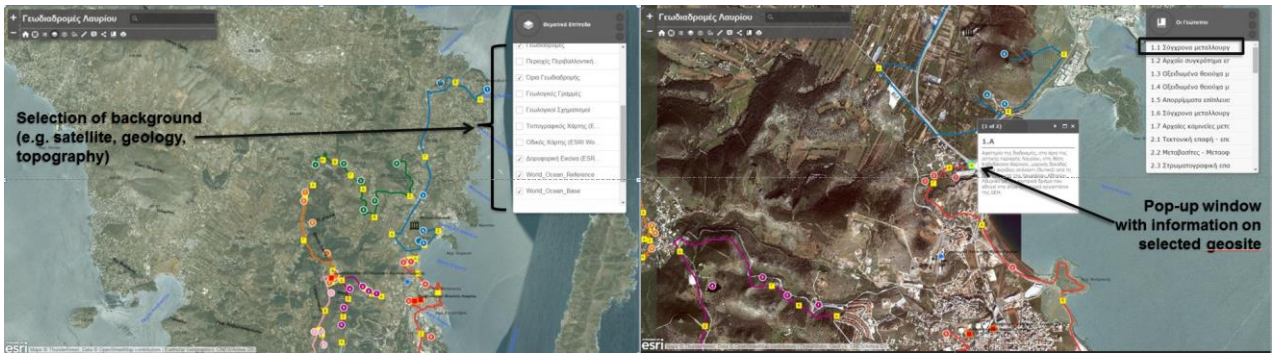

Figure 3. Browsing the geotrails of Lavrion through an online interface (Moraiti & Staridas 2015)

Finally, the development and management of proposals for geoparks in selected areas, could be implemented by the local councils or other relevant entities, ensuring preservation of the geological heritage and provide socioeconomic benefits to local communities.

Drandaki I., 2009. 3rd C.S.F. Project: Geosites- Geoparks, contribution to sustainable development. IGME Publications (in Greek), pp. 40.

Moraiti E., 2016. A thorough report on the IGME database of geosites – geoparks. IGME Publications (in Greek), pp. 166.

Moraiti E. & Staridas S., 2015. Thematic geotrails of the Lavreotiki geopark: planning and aspirations. Abstract and oral presentation – Workshop for the Lavreotiki geopark 10/06/2015, IGME Publications (in Greek), pp. 61.

Stürm B., 1994. The geotope concept: geological nature conservation by town and country planning. In: O'Halloran D., Green C., Harley M., Sanley M. & Knill J. (eds). Geological and Landscape Conservation. Geological Society, London, 27-31.

Theodosiou I., Athanassouli E., Epitropou N., Janikian Z., Kossiaris G., Michail K., Nicolaou E., Papanikos D., Paschos P., Pavlidou S. & Vougioukalakis G., 2010. Geotrails in Greece, Bulletin of the Geological Society of Greece, Proceedings of the 12th International Congress, XLIII (2), p.939-947.

Wiedenbein F.W., 1994. Origin and use of the term "geotope" in German–speaking countries. In: O'Halloran D., Green D., Harley C., Stanley M., Knill J. (eds), Geological and Landscape Conservation. Geological Society, London: 117–120.

Zananiri I., 2016. Geotrails of Chalkidiki: a travel through geology, history and mining activities. IGME Publications (in Greek), pp. 147.

15th International Congress of the Geological Society of Greece
Athens, 22-24 May, 2019 | Harokopio University of Athens, Greece
Bulletin of the Geological Society of Greece, Sp. Pub. 7 Ext. Abs. GSG2019-364

Geotourism as a tool for the protection and promotion of the Cave of Galaxidi

P. Karamani[1], H. Drinia[2], G. Panagiaris[3]

(1) National and Kapodistrian University of Athens, Lab. of Museum Studies, Panepistimiopolis, 15784 Athens, Greece, nagia00@hotmail.com
(2) National and Kapodistrian University of Athens, Department of Geology and Geoenvironment, Panepistimiopolis, 15784 Athens, Greece, cntrinia@geol.uoa.gr
(3) University of West Attica, Department of Conservation of Antiquities and Works of Art, Ag. Spiridonos str., 12210, Athens, Greece, gpanag@teiath.gr

Introduction

Geotourism has rapidly developed in the last two decades. One of its most popular segments is cave geotourism (e.g. Garofano 2003, 2010). Transforming a cave into a tourist attraction, or show cave, is complex and it requires modifying the unwelcoming raw underground space. The first step needed to start the process of transformation of a natural cave into a show cave is to recognize its value. This step requires the understanding of both their aesthetic and scientific aspects (Garofano & Govoni, 2012).

Galaxidi is a coastal town on the northern coast of the Corinthian Gulf and belongs to the extended municipality of Delphi, Fokida that is located in the region of Central Greece. The Cave of Galaxidi, also known as “Karkaros” is located on the central square of Galaxidi, known as square of Nicholas Mamas. Before 1940, the cave served as an improvised "dump", since from a hole at the top of the rock the inhabitants were usually throwing old objects. Observing the physical properties of the cave (stable temperature), the inhabitants of Galaxidi used it for many years as a refrigerator. In 1965, two Australians turned the cave from refrigerator for cheeses to a disco. In 1980, following a Ministerial Decision by Melina Merkouri on the Protection of Caves, according to which caves are included in the category of Monuments and are considered an integral part of the country's cultural heritage the function of the cave as a place of entertainment was terminated. Since then, the cave remains closed to visitors.

The general purpose of this study is to establish the cave of Galaxidi as a cultural organization aiming to the enrichment of the lives of people by promoting research, knowledge and enjoyment through an integrated experience that will be offered to the widest possible audience within and outside of this unique geo- monument. More specific objectives are the presentation of the cave as geological formation, as well as an interest pole of paleontological, archaeological, historical, folklore and aesthetic aspect.

Activities and materials developed to promote the geological heritage

The cave of Galaxidi has an outstanding potential to promote geotourism and education in Earth Sciences. Its location and accessibility can attract the arrival of a large number of visitors each year. This great potential, however, has not been exploited owing to the abandonment of the cave for many years.

As part of the overall redevelopment and reuse of the cave, it is necessary to carry out a series of actions such as site plan, rock mechanics study, removal of all movable components, removal of all wiring etc, aimed at its remediation. The collaboration of scientific staff (geologists, conservationists) is necessary in any work so as not to cause further damage.

Approach & Involvement of the local community

Community engagement took place in two stages:1st stage: Meeting with the community, its needs and its specific features, presentation of the project to the community, assignment of tasks, participation in the interview process. 2nd stage: Creating a stable, timeless relationship with the community of Galaxidi (Karamani et al., 2019).

Proposal for cultural and environmental promotion of the cave

Considering that the tourist development of caves due to their particularly sensitive and closed ecosystems should in principle be avoided, a mild tourist development is proposed based on the specific features of the cave and with taking into consideration its protection (Papathanasoglou & Painessi, 2006). All the suggestions of re-emergence and re-use were largely shaped by the limitations and possibilities posed by the monument.

The cave system can be divided into four thematic sections while before the entrance of the cave there is an introductory text preceded for the history of the cave.

Section 1: Caves and Mythology

- Nymphs and Caves
- The birth of Jupiter
- The birth of Mercury

Section 2: Cave and Philosophy

- Allegory of Plato's Cave

Section 3: The cave in the memories of the inhabitants

- The Galaxidians narrate - Photographic archive

- Guests “leave” their own thoughts

Section 4: Caves and Environmental Education

- The uses of caves over time

- The development of environmental awareness through educational actions

A number of actions will enhance the communication character of the Cave including logo, banner suspension, creation of a vendor, creation of a website and social networking pages, inauguration invitations, inauguration events.

Conclusions

The case of Galaxidi Cave exemplifies the work necessary in order to promote education in Earth Sciences and promote the appreciation and conservation of important geosites and geoheritage in general. This study showed that the social approach is mandatory. The local population has to be involved in the project, and training is crucial for the improvement of scientific outreach and guidance, where local communities play a central role. Galaxidi Cave constitutes an excellent example of promotion of Earth Sciences education in issues related to geoheritage.

Acknowledgements

The authors would like to express their gratitude to the Municipality of Galaxidi for the hospitality they offered during the study. The research is part of the postgraduate research of the senior author in the framework of the Postgraduate Program “Museum Studies”.

References

Garofano, M., 2003. Geoturismo. Scoprire le bellezze della terra viaggiando, DPS edizioni, Genova, 7, 39.

Garofano, M., 2010. Geotourism. The geological attractions of Italy for tourists, Geoturismo edizioni, Genova, 5, 34-36, 73-74, 103.

Garofano, M. & Govoni, D., 2012. Underground Geotourism: A Historic and Economic Overview of Show Caves and Show Mines in Italy, Geoheritage. 4. 10.1007/s12371-012-0055-3.

Karamani, P., Drinia, H., Siakas, S., Panagiaris, G., 2018. Study of cultural and environmental promotion of the cave of Galaxidi, ECHOPOLIS INTERNATIONAL 2018 «Nature and culture-based strategies and solutions for cities and territories : an idea whose time has come !», 26-28 November, 2018, Athens, Greece

Papathanasoglou, A. & Painessi, M., 2006. Caves and their protection. Independent Authority, Athens, Greece.

15th International Congress of the Geological Society of Greece
Athens, 22-24 May, 2019 | Harokopio University of Athens, Greece
Bulletin of the Geological Society of Greece, Sp. Pub. 7 Ext. Abs. GSG2019-376

Geopark of Aghios Nikolaos – Neapolis, Lakonia, Peloponnese

E. Moraiti[1] and A. Alexopoulos[1]

(1) Hellenic Survey of Geology & Mineral Exploration, Spirou Loui 1, 13677 Acharnae, Greece; moraiti@igme.gr
(2) University of Athens, aalexopoulos@geol.uoa.gr

Along the coast near Neapolis (Peloponnese, Greece) a vast amount of cylindrical and cone-shaped tube like structures can be found within the quarternary und neogene coastal arenitic limestones (Fig. 1).



Figure 1. The Petrified forest of Agios Nikolaos.

The microscopic anatomical study and the large number of samples studied resulted in finding components fossilized palm trees, coniferous and broadleaf trees.At the same time highlighting the uniqueness of the Geopark which epkalyptetai of fossiliferous marine sediments, such as Bryozoans, red algae, molluscs, echinoderms and other categories of animal fossils, giving particular attention to the emergence of the Geopark.

All these tubes have to be interpreted as dissolution pipes. The former explanation as “petrified forest” can no longer be maintained. Dissolution pipes are syngenetic karst formations, which can be verified in many young coastal sediments in the Mediterranean as well as worldwide. It can be shown, that the genesis of dissolution pipes is closely related to an intense root growth. Fossilized root structures (rhizoliths, rhizocretions, etc.) are mainly concentrated in places of dense tube distributions as well as along young tectonic fissures. At different places along the coast near Aghios Nikolaos many fracture structures accompanied by rhizoliths can be demonstrated running parallel to the coast for distances of several hundred meters. At the Peninsula of Palaeokastro south of Neapolis dissolution Pipe fields can be clearly identified even in satellite images. Within many different rhizoliths unambiguous cell structures can be detected.



Figure 2. Stereopair of a cluster of pipes at Ag. Nikolaos “Petrified Forest” (left); Stereopair of a cluster of pipes at “The Petrified Forest”, Cape Bridgewater, western Victoria – note the cemented rims (right).

The interpretation of the tube forms near Aghia Marina as “petrified forest” is no longer tenable but this does not affect the high geological value of the Geopark of Aghios Nikolaos-Korakas. Due to the very good outcrop conditions in the area of Neapolis, the development of a young tectonically controlled coast with its arenitic sediments und with its different karst phenomena can be a tangible experience.

The focused solution process seems a better hypothesis for general interpretation of both isolated pipes, and the dense fields of pipes which are a distinctive feature of dune limestones throughout the world. Note that the four alternative modes of focusing water flow discussed above are not presented as mutually exclusive hypothesises—all could act, either together or separately, according to the local situation in any area.

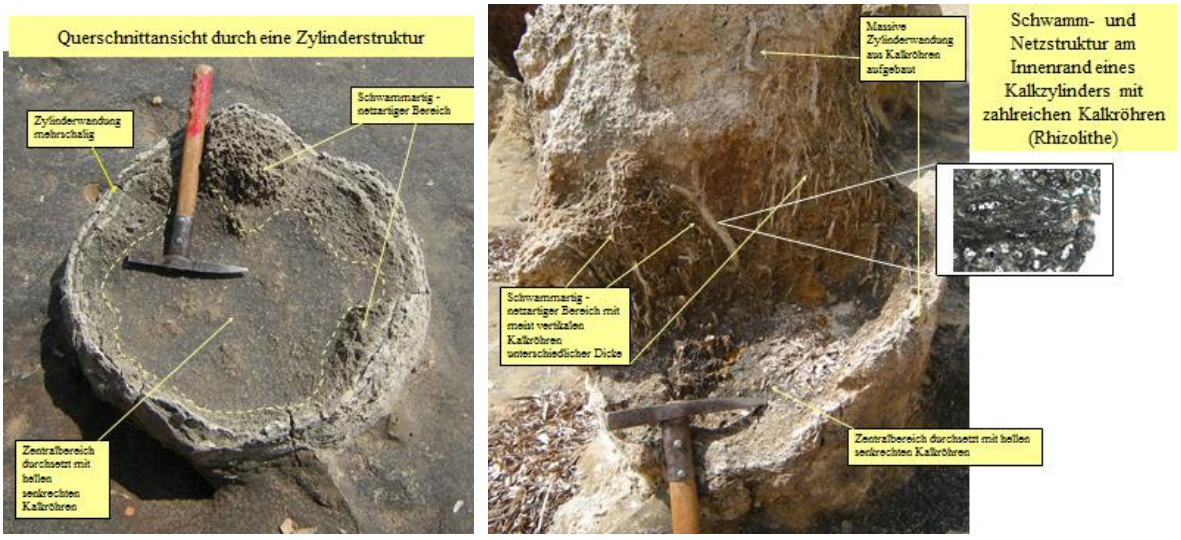

Figure 3: Cross-sectional view through cylinder structure of pipes at "The Petrified Forest".

Rhizomorphs are common in dune sands and form around small roots growing through the sand. Such roots would preferentially follow the organic-rich soils that fill the solution pipes and branch out from them. Thus, rhizomorphs could be called petrified roots, but the pipes are not petrified trunks.

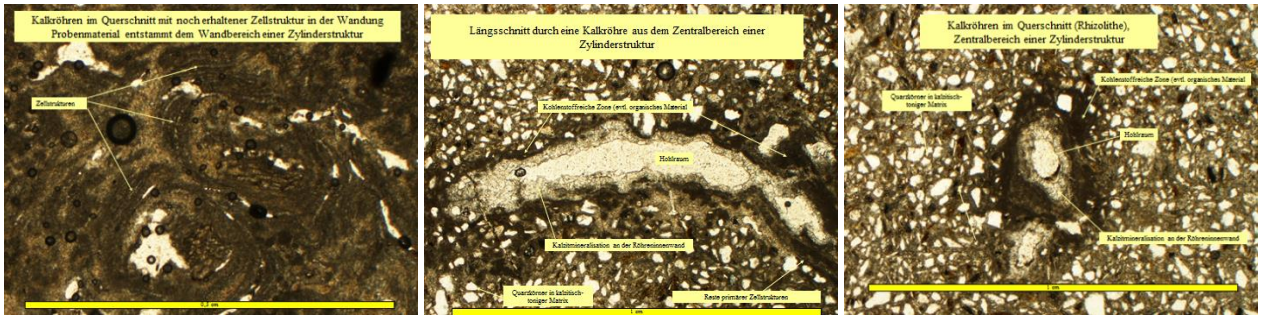

Figure 4. Thin sections of cylinder structure of pipes at "Petrified Forest".

The Geopark of Aghios Nikolaos represents with its dissolution pipes pseudo forest and with the high concentration of various fossil root structures a nationwide unique selling proposition. Its value and its significance as a national Geotope is on the same level as the other world famous petrified forests.

References

Brink A.B.A., Partridge T.C., 1980: The nature and genesis of solution cavities (Makondos) in Transvaal cave breccias. Palaeontology Africa 23: 47-49.

Coetzee F., 1975: Solution pipes in coastal aeolianites of Zululand and Moçambique. Transactions of the Geological Society of South Africa 78: 323-333.

Gardner R.A.M., 1983: Aeolianite. In: Goudie AS., Pye K. (Eds.), Chemical sediments and geomorphology.Academic Press, London, 265-300.

Grimes K.G., 1994: The South-East Karst Province of South Australia. Environmental Geology 23:

Grimes K.G., 2001: Karst features of Christmas Island (Indian Ocean). Helictite 37, 2: 41-58.

Grimes K.G., 2002: Syngenetic and Eogenetic Karst:an Australian viewpoint. In: Gabrovšek F. (Ed.), Evolution of Karst: from Prekarst to Cessation.Inštitut za Raziskovanje Krasa, ZRC SAZU, Postojna, 407-414.

Grimes K.G., 2004: Solution Pipes or Petrified Forests? Drifting sands and drifting opinions! The Victorian Naturalist 121, 1: 14-22.

Herwitz S.R., 1993: Stemflow influences on the formation of solution pipes in Bermuda eolianite Geomorphology 6: 253-271.

Jacobson G.J., Hill P.J., Ghassemi F., 1997: Geology and Hydrogeology of Nauru Island. In: Vacher H.L.,

Lowry D.C., 1973: Origin of the Pinnacles. AustralianSpeleological Federation Newsletter 62: 7-8.

Lundberg J., Taggart B.E., 1995: Dissolution pipes in northern Puerto Rico: an exhumed paleokarst.Carbonates and Evaporites 10, 2: 171-183.

White S., 2000: Syngenetic Karst in Coastal Dune Limestone: A Review. In: Klimchouk A.B.,

15th International Congress of the Geological Society of Greece
Athens, 22-24 May, 2019 | Harokopio University of Athens, Greece
Bulletin of the Geological Society of Greece, Sp. Pub. 7 Ext. Abs. GSG2019-377

Support techniques for the preservation of Poliphimos cave in Maronia, Thrace – Greece

B. Christaras[1], Th. Chatzigogos[2], A. Dimitriou[1], N. Chatzigogos[1], Th. Makedon[1], D. Vogiatzis[1], S. Filippidis[1] & E. Moraiti[3]

1 Lab. of Engineering Geology, Dept. of Geology, School of Geology, AUTH. 54621 Thessaloniki, christar@geo.auth.gr
2 Lab. of Soil Mechanics & Foundations, School of Civil Engineering, AUTH, hatz@geo.civil.auth.gr
3 Hellenic Survey of Geology & Mineral Exploration, Spirou Loui 1, 13677 Acharnae, Greece; moraiti@igme.gr

Abstract

The cave is located in a distance of 5 km from Maronia Town, near Komotini City, in Thrace – Eastern Greece. It is considered as an important natural monument which unfortunately has not already developed. According to the Greek mythology, Cyclope Poliphimos is considered that was living in the cave. According to the archaeological research, the cave was used as living and religious site, from the Neolithic until the Byzantine period. The cave is 2000 m long and covers an area of 10.000 m^2, according to Petrohilou, A. (1984), who investigated the cave for first time. The present study was a part of a project, of touristic development of the cave, included in the 3rd EU Framework Program. For this purpose, the stability conditions and the more appropriate protection measures of the cave were determined (Christaras et al. 2004[1]).

The area consists of compact coarse-grained karstic limestone which is traversed by faults of NNW-SSE to NW-SE and E-W directions. The cave is formed in low depth and for this reason, the stability is determined by discontinuities of the following directions: kl1: 089/68, kl2: 344/80, kl3: 246/75 and kl4: 041/77 while he bedding is almost horizontal (Fig. 1). The spacing between the discontinuities changes from 20 to 100 cm, their length appears to be more than 1 m and their dip is close to vertical. The majority of the discontinuities are opened and filled with calcite carbonate. The above mentioned geometrical features in conjunction to the practically horizontal bedding of the limestone form probably unstable blocks on the roof of the cave (Fig. 1). Wedge failures could also be created according to our observations. The RQD of the rock mass is estimated 75-90, the compressive strength 35-60 MPa and the RMR is 61-70, according to Bieniawski (1989).



Fig. 1. Failure on the roof, along bedding.

Table 1: Proposed support measures

Section	Potential wedges	Arrangement and length of rock bolts	Safety Factors after bolting
152-151	kl1-kl3-ss2	2.0 x 2.5 m – L=3 m	2.24
	kl1-kl2-ss2	2.0 x 2.5 m – L=3 m	2.04
154-153	kl1-kl2-ss2	2.0 x 2.0 m – L=3 m	3.32
	kl1-kl3-ss2	2.0 x 2.0 m – L=3 m	2.00
156-155	kl1-kl3-ss2	2.0 x 2.0 m – L=3 m	2.33
158-157	kl1-kl3-ss2	2.0 x 2.0 m – L=5 m	2.21
	Kl2-kl3-ss2	2.0 x 2.0 m – L=5 m	2.51
160-159	kl1-kl3-ss2	2.0 x 2.0 m – L=5 m	2.31
	Kl1-kl2-ss2	2.0 x 2.0 m – L=5 m	2.14
162-161	kl1-kl3-ss2	2.0 x 2.0 m – L=5 m	1.97
151-150	kl1-kl3-ss2	2.0 x 2.5 m – L=3 m	2.45

The tectonic data were elaborated, using UNWEDGE software, in order to determine the unstable wedges or blocks. For this purpose, the following pairs of values were used: a) c = 10 t/m^2, φ = 30° b) c = 16 t/m^2, φ = 30°. The geometry of the blocks formed by the combination of the vertical discontinuities with the horizontal bedding creates potential unstable blocks, falling from the roof. The sides of the cave seem to be stable.

For the reinforcement support of the roof, an arrangement of stainless pre-tensioned self-drilling rockbolts is suggested (2X2m and 2X2.5m, length 3m and 5m [Table 1, Fig. 2]) as the optimum scenario of intervention, giving safety factors >2 .

According to our investigation, we arrived to the following conclusions:

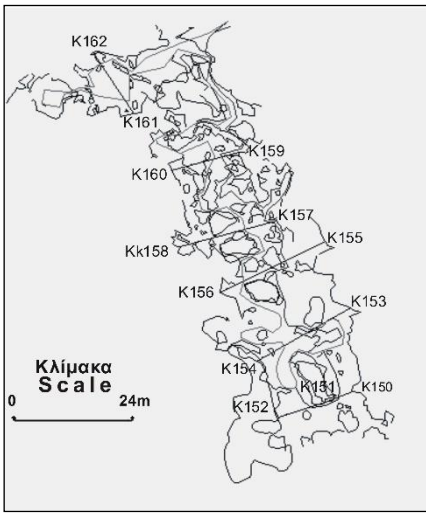

Fig. 2. The studded cross-sections.

1. As the thickness of the overlying layers is small, the stability analysis was only based on the probable creation of unstable wedges due to the tectonic system and not to a stress pattern due to the load of the overlaying layers.
2. The probable unstable wedges are mainly observed at the roof of the cave, creating either falling or sliding blocks
3. The proposed support measures take into account the specific conditions and the monumental character of the cave.
4. The safety factors, after the application of the proposed support measures, are generally enough high (SF>2), having using relatively moderate admissions and mechanical characteristics for the rock mass.
5. For the reinforcement support of the roof, an arrangement of stainless pre-tensioned self-drilling rockbolts is suggested (2X2m and 2X2.5m, length 3m and 5m [Table 1]) as the optimum scenario of intervention, giving safety factors >2.

Acknowledgements

The present research was funded by the 3rd EU framework program and the District of Eastern Macedonia and Thrace.

References:

Bieniawski, Z.T. (1989). Engineering rock mass classification. New York: Wiley.

Christaras, B., Chatzigogos, Th., Dimitriou, An., Chatzigogos, N., Makedon, Th., Filippides, S. (2004). Stability of Polifimos cave, in Maronia City of Thrace, N. Grrece, Bull. Geol. Soc. Gr., vol. XXXVI/4, Thessaloniki, pp. 1892-1901.

Petrohilou, A. (1984). The caves of Greece. Ekdotiki Athinon Ltd.

SPECIAL SESSION
ROUNDTABLE DISCUSSION

T10.S1. Highlighting, Protection and management of Geosites and management of Geosites

Conveners: **N. Zouros (Univ. Aegean)**
E. Moraiti (IGME)
Ch. Fassoulas (Nat. His. Mus. Crete)
P. Paschos (IGME)

Co-organized by the Committee for Conservation and Promotion of GeoHeritage, G.S.G.



15th International Congress of the Geological Society of Greece
Athens, 22-24 May, 2019 | Harokopio University of Athens, Greece
Bulletin of the Geological Society of Greece, Sp. Pub. 7 Ext. Abs. GSG2019-301

A catalogue of national importance geosites in Greece

N. Zouros[1], C. Fasoulas[2], E. Moraiti[3], P. Paschos[3], G. Iliopoulos[4].

1. University of Aegean
2. University of Crete
3. Hellenic Survey for Geology and Mineral Exploration (H.S.G.M.E.)
4. University of Patras

Greece is characterized by a complex geological setting and evolution and was subjected to a variety of geological and geomorphological processes, resulting in a high geodiversity. As a result a large number of spectacular landscapes and rock outcrops form today a great number of geosites, some of them indicative and representative of the geological evolution of Greece, characterized thus as of national importance.

In spite of their intrinsic value for the natural and human environment and the legal framework created by the L.1650/1986 for the protection of the environment and especially its revision law 3937/2011, till now the majority of geosites has not been awarded any kind of legal protection due to their scientific, educational and aesthetic value.

The Committee for the Conservation and Enhancement of the Geological Heritage of the Geological Society of Greece took an initiative in October 2016 and invited all its members to identify and register in form proposals of geosites which present special geological interest and needs for protection. In December 2018 a special committee was created by the Ministry of Environment and Energy aiming to a proposal of measures for the protection of the geological heritage. Among the proposal was the establishment of a catalogue of the 100 geosites of national importance as a first step for the protection of the most important geosites of Greece.

The Committee for the Conservation and Enhancement of the Geological Heritage of the Geological Society of Greece contributed to this effort with the submission of a catalogue including 108 geosites. This Catalogue was formed taking into account the existing geosites catalogues: the geosite catalogue of IGME (2016), the Atlas of Geological Monuments of the Aegean (2002), the catalogues of the five areas recognized as UNESCO Global Geoparks, published scientific papers as well as the list of the geosites submitted by the Committee members.

The catalogue includes the following geosite categories:

a. Geomorphological geosites

b. Stratigraphic geosites

c. Tectonic geosites

d. Palaeontological geosites

e. Mining geosites

f. Petrological geosites

g. Volcanic geosites

h. Human made geosites

To select the sites which were included in the Catalogue six criteria have been used: 1) scientific and educational value (integrity, rarity, representativeness, and exemplarity); 2) natural beauty and aesthetic value; 3) cultural value; 4) geodiversity; 5) potential threats and protection needs (legal protection, vulnerability); and 6) potential for use (recognizability, geographical distribution, accessibility, and potential for generating economic activities).

The proposed catalogue is a first effort for the legal protection of the important geological heritage sites of Greece and should be further developed and increased.

SPECIAL SESSION

T10.S2. New Developments in Science Education. Science with and for Society

Conveners: **Assi Antonarakou (NKUA)**
Zaharoula Smyrnaiou (NKUA),
Hara Drinia (NKUA)
Kiki Makri (NOA)

Co-organized by the Geodidactics of Geoscience Committee, G.S.G.

GEOLOGICAL SOCIETY OF GREECE
COMMITTEE OF GEOSCIENCES DIDACTICS

15th International Congress of the Geological Society of Greece
Athens, 22-24 May, 2019 | Harokopio University of Athens, Greece
Bulletin of the Geological Society of Greece, Sp. Pub. 7 Ext. Abs. GSG2019-055

Development skills through responsible research and innovation educational practices

P. Argyri
National Kapodistrian University of Athens, Zografou, Athens, Greece, argiry@gmail.com

Secondary education faced the challenge of integration Responsible, Research and Innovation (RRI). Involving students and teachers in reflecting on the role of research and innovation (R&I) fosters sustainable interactions between schools, researchers, industry and civil society organizations, both in formal and informal learning. On the other hand, following challenges of priorities set by the European Commission, school has to include innovative educational learning activities for development students' skills being in interaction with society and workplaces. This means that teaching science is not only about implementing inquiry learning activities in classroom, but it has to highlight the importance of science, research and innovation to young peoples' lives and prepare them to become responsible citizens. This paper presents the learning scenario of earthquakes as inquiry process including RRI components, as proposal to educational community for rebranding the way of teaching science in classroom.

Introduction. Why Responsible Research & Innovation?

It is the ambition of the European Union (EU) to ensure that research and innovative ideas can be turned into products and services that create jobs and prosperity, as well as help preserve the environment and meet the societal needs of Europe and the world. To achieve this, the European institutions, its Member States and private business actors invest considerable monetary and human resources into Research, Development & Innovation (RRI). The need to gear the innovation process to societal needs is reflected in many high-level policies, strategies and programming documents, such as the objective of the EU 2020 strategy to create smart growth or the Horizon 2020 programme that defines tackling societal challenges as one of the main priorities (European Commission (2010a). In the same terms, in 2007, under the seventh framework programme for research & technological development (FP7), of exploratory learning and teaching. 'Science and Society' became 'Science in society (SiS)' with the main objective to foster public engagement and a sustained two-way dialogue between science and civil society. (It) touches mainly upon civil society engagement in Research & Innovation, supported by further activities enabling easier access to scientific results, better uptake of the gender equality and ethics dimension in R&I, and formal and informal education to science.

RRI and Science education

Science education has a very critical role for the implementation of the new paradigm of RRI where a new relationship between science and society is to be established. Teachers faced the challenge of ensuring tomorrow's researchers and citizens have the necessary knowledge and skills to fully participate and take responsibility in the research and innovation process. RRI inspires all levels of science education to adopt an inquiry approach to science. Such as, formal and non-formal providers can use new tools and methods in order to integrate responsibility and responsiveness within RRI, so educational programs combine Science, Technology, Engineering, Mathematics and – moreover Arts and Computing (STEAM [6] and STEM+C [8]) with social, economic and ethical principles.

The deliberate involvement in students' scientific and technological research procedures is considered an essential requirement towards the development of scientific and technological literacy. On the other hand, RRI for students' scientific literacy is essential to foster responsible citizens. Young learners have natural-born curiosity, full of questions and wonder. Science education must help learners develop scientific thinking and challenge students to build a base of knowledge and skills for solving problems with increasingly in-depth solutions with sophisticated explanations along their lives. Teaching science is creativity preparation for the cultivation of students' scientific skills in the way of critical thinking, to acquire an important role in the development of the various sectors of human activity.

The integration of inquiry based science learning (IBSL) methods into the socio-scientific inquiry-based learning (SSIBL) approach represents an opportunity to introduce RRI into science education at schools. The SSIBL approach in STEM classes, supports both the development of scientific literacy and the acquisition of key skills for STEM such as inquiry and critical thinking skills. These practices can be easily integrated into any type of school activity. The integration of Responsible Research and Innovation (RRI) principles in educative contexts can be strongly beneficial for students, as it supports them in the development of critical thinking and collaborative learning skills while accommodating multidisciplinary and stronger student engagement. Hence, it is essential to lay out principles that will help on the implementation of RRI in teaching and learning activities in schools.

Under this framework, teachers should use high-quality vocational training opportunities and access to educational resources, feedback and re-organization of teaching practices and methods that provide RRI in Science classroom. The use of digital repositories of European projects that provide educational material, research studies and reports, good practices, free of charge, seminars on the integration of innovative teaching practices in the classroom on science (mathematics, biology, physics, chemistry, geography, astronomy, mechanics, robotics etc.) are a driving force for following RRI at primary and secondary education. The overall aim of this paper is to identify the RRI potential in the teaching-learning scenarios with the characteristic examples of earthquakes.

Earthquakes as inquiry learning process

Following the steps of an inquiry learning process for development citizen skills, at the observation phase students recall their knowledge for lithospheric plates; observe and compare maps that present the limits of them and the distribution of earthquakes; identify that the recording site of earthquakes are related to the limits of lithospheric plates; interpret data presented on maps. After the introduction, they are able to make reasonable hypotheses based on evidence of maps and their prior knowledge; they justify their assumptions, based on the morphology of the lithosphere they observe on the maps. The activities of why an earthquake occur, follow the study of what happen on an earthquakes. At the investigation, phase students study a) the types of seismic waves b) the characteristics of waves c) the propagation of seismic waves in the Earth's layers. Through access to the real data of the seismographs, students try estimate the distance between the epicenter of an earthquake and a station and not the exact location of the epicenter. Thus, you can draw a circle to represent the distance on a map. The center of the circle is the location of station and the radius of the circle corresponds to the distance between the station and the epicenter of the earthquake. The epicenter of the earthquake will be located to the point where all three circles intersect. Moreover statistical analysis through the recording data from at least 5 center-stations that record earthquakes nearby; record the areas that have experienced earthquakes of more than 5 degrees of the Richter scale; record when and where has the largest earthquake took place in the course of the last years; which areas are exhibited intense seismic activity, and so on. At the conclusion phase students make decisions of preventive measures, should we take for earthquakes and how could react to the time of the earthquake.

Earthquakes as RRI initiative

Through the specific project School Study Earthquakes (https://sse-project.eu/) engages students in employing real-problem solving skills, handling and studying situations, and participating in meaningful and motivating science inquiry activities. The RRI component of the project lies in the fact that students deal with real seismic data that they have acquired themselves while they have to communicate their findings to the local communities. In countries like Greece, Italy and Bulgaria the phenomenon is rather common. Surveys in the field demonstrate that the general public is not well informed on the necessary measures that have to be applied to minimize the impact of the natural phenomenon. A complicated geophysical phenomenon like the earthquake is possible to be studied in the classroom with the use of a simple instrument and results can be obtained with the combination of data from the collaborating schools.

Conclusion

Students take the role of researchers in employing real-problem-solving skills, handling and studying situations, and participating in meaningful and motivating science inquiry activities, understand how to manage real data and are able to know the importance of working and experimenting with this type of information, reflecting on the need to provide full mechanisms for scientific research.

References

EC (2010a): Communication from the Commission: Europe 2020 - A strategy for smart, sustainable and inclusive growth. Brussels, 3.3.2010, COM(2010) 2020final.

15th International Congress of the Geological Society of Greece
Athens, 22-24 May, 2019 | Harokopio University of Athens, Greece
Bulletin of the Geological Society of Greece, Sp. Pub. 7 Ext. Abs. GSG2019-096

New Scientific Approaches in the Construction of Meaning- The role of SWAF in Educational Design

Z. Smyrnaiou

National and Kapodistrian University of Athens, Faculty of Philosophy, Pedagogy and Psychology, Panepistimiopolis, Athens, Greece zsmyrnaiou@ppp.uoa.gr

Abstract: The CREATIONS EU Program aims at creating and producing innovative teaching approaches being recognized as best practices in the European community, by observing the scientific framework of creativity and combining science and art. Responsible Research and Innovation and the principles of Science with and for Society act as a catalyst to new developments on Science Education. In this paper a demonstrator entitled "The Ghost Particle" is presented. This scenario is framed by the scientific, pedagogical framework of Effective Learning Environments, Creativity and Inquiry-Based Approach, the principles of the European Framework of Responsible Research and Innovation and is in line with the Creations Features and the principles of Science with and for Society.

Introduction

Worldwide challenges- A need for a renewed approach on Science teaching models

Over the last few years, there is a need both from political decisions and scientific paradigms to redefine teaching methods and reform educational systems. Nowadays educational systems but also all the members of a school community face lots of challenges (Smyrnaiou et al.2017, 2018). These challenges are firstly relevant to the educational practices and the purposes of school education and they can be categorized in: a) student lack of motivation, b) the scientific outflow, c) old or inappropriate teaching methods and d) difficult scientific notions.

Fostering the principles of Science with and for Society

Europe is confronted with major socio-economic challenges which significantly affect its common future (Hazelkorn et al.2015). These challenges must be tackled in innovative and multi-disciplinary ways based on research and new smart technologies, processes and methods, social innovation mechanisms, coordinated actions and policies that will anticipate or influence major evolutions for Europe. In order to understand, analyze and build inclusive, innovative and reflective societies, Europe requires a response which unfolds the potential of shared ideas for the European future to create new knowledge, technologies and capabilities (Rocard et al., 2007). The aim is to gain a greater understanding of the societal changes in Europe and their impact on social cohesion, and to analyze and develop social, economic and political inclusion and positive inter-cultural dynamics in Europe and with international partners (Owen et al., 2012). New theories in science education focus on developing a pedagogical framework that builds on the essential features of creative learning including exploration, dynamics of discovery, student-led activity, engagement in scientifically oriented questions, priority to evidence in responding to questions, formulations of evidence-based explanations, connection of explanations to scientific knowledge, and communication and justification of explanations. The Science with and for Society principles (SWAFS) are important in addressing the European societal challenges tackled by Horizon 2020 (European Commission, 2012) building capacities and developing innovative ways of connecting science to society. It will make science more attractive, increase society's appetite for innovation, and open up further research and innovation activities. It allows all societal actors (researchers, citizens, policy makers, business, third sector organizations etc.) to work together during the whole research and innovation process in order to better align both the process and its outcomes with the values, needs and expectations of European society.

The Responsible Research and Innovation Principles (RRI)

Responsible Research and Innovation (RRI) seeks to involve society in discussing how science and technology can help create the kind of world we want for generations to come. Education and innovation are the key aspects. The RRI framework promotes a transparent process where innovators need to be mutually responsive. With the aim of building an open classroom and innovation system of learning that tackles societal challenges. However, parallel to the large positive impact on human welfare and wellbeing, science and technology sometimes create new risks and ethical dilemmas. RRI involves society in discussing how science and technology can help create the kind of world and society we want for generations to come (Smyrnaiou et al, 2017, 2018). The principles of RRI, according to the European Commission are:

1. Governance addresses the responsibility of policymakers to prevent harmful or unethical developments in research and innovation.
2. Public Engagement implies that societal challenges should be framed on the basis of widely representative social, economic and ethical concerns and common principles on the strength of joint participation of all societal actors - researchers, industry, policymakers and civil society
3. Gender Equality addresses the underrepresentation of women.
4. Science Education faces the challenge to better equip future researchers and other societal actors with the necessary knowledge to fully participate and take responsibility in the research and innovation process.
5. Open Access states that RRI must be both transparent and accessible free.

6. Ethics respects fundamental rights and the highest ethical standards in order to ensure increased societal relevance and acceptability of research and innovation outcomes.

7. Sustainability: RRI indicators contribute to sustainable growth, as the scientific knowledge function as an ecosystem and its effects on well- being.

8. Social justice refers to a) the relationship between the researchers and the research subjects and b) the participation of social groups in benefits arising from research.

CREATIONs European Research Programme

In the framework of the European Project CREATIONS (http://creations-project.eu/), 16 partners from ten European countries develop creative approaches based on Art for an engaging science classroom. CREATIONS will establish a pan-European network of scientists, teachers, artists and students with the aim to improve the skills of young people in STEM (science, technology, engineering, mathematics) and to pool talent to scientific careers. The aims of CREATIONS Program are to give students and teachers opportunities to experiment with many different places, activities, personal identities, and people and simulate the work of the scientist and researcher in the classroom. It promotes a better understanding of how science work and enhances students' science related career aspirations. The program encourages and empowers science teachers to affect change by implementing and promoting inquiry-based science teaching and learning.

The Ghost Particle Demonstrator

This pedagogical scenario implements the Inquiry Based Science Education (IBSE) approach as an effective educational framework that aspires to attract students to an authentic scientific search and search process. In their effort students will be supported by computational models and simulations that contribute to the explanation and assimilation of demanding scientific concepts (Smyrnaiou, et al., 2012). Students' involvement with HYPATIA (Kourkoumelis et al.2014) enables them to study the fundamental particles of matter and their interactions through the observation of graphic representations / realizations of the products by particle collisions. These products are derived from "events" detected by the ATLAS detector in the new, world-wide, LHC accelerator located in Geneva at the European CERN Particle Physics Laboratory. Students 'commitment to role play / dramatization is based on physical representation of transport (Smyrnaiou et al.2016). In addition, the scenario was implemented through the application of the CLIL (Content and Language Integrated Learning) approach, with the main objective of highlighting the communicative approach (interactive approach, argumentation) adopted in foreign language teaching to discover learners' learning and engagement in scientific environments (Lemke,2009). Students act as scientists and develop research questions. In the context of the scenario, students are involved in manipulating experiments with computer-based simulations. The scenario has already been applied to a public school targeting high school students aged 12 to 14. Three teachers from different disciplines participated in the scenario implementation: (1) Physics teacher, (2) English teacher to implement the CLIL approach, (3) Artist Teacher. The script took place within four weeks - a two-hour lesson each week - and was completed with student presentations on the subject area of the history of particle physics, the principles of neutrinos and how the current detectors worked. In addition, the students created an artistic exhibition with their work on the arts to promote their perceptions of subatomic particles and their respective principles.

References

Hazelkorn, E., Ryan, C., Beernaert, Y., Constantinou, C. P., Deca, L., Grangeat, M. & Welzel-Breuer, M. 2015. Science Education for Responsible Citizenship: Report to the European Commission of the Expert Group on Science Education.

Kourkoumelis, C. and Vourakis, S. 2014. HYPATIA-An online tool for ATLAS event visualization. Physics Education, 49, (1), 21-32.

Lemke, J.L. 2009. Teaching All the Languages of Science: Words, Symbols, Images, and Actions.

Owen, R., Macnaghten, P., & Stilgoe, J. 2012. Responsible research and innovation: From science in society to science for society, with society. Science and public policy, 39(6), 751-760.

Rocard, M., Csermely, P., Jorde, D., Lenzen, D., Walberg-Henriksson, H., & Hemmo, V. 2007. Science Education NOW: A renewed pedagogy for the future of Europe, Brussels: European Commission. Luettu.

Smyrnaiou, Z., Moustaki, F., Yiannoutsou, N., & Kynigos, C. 2012. Interweaving meaning generation in science with learning to learn together processes using Web 2.0 tools. Themes in Science & Technology Education, 5(1/2), 27-42.

Smyrnaiou Z., Georgakopoulou E., Sotiriou M., Sotiriou S. 2017a. The Learning Science Through Theatre initiative in the context of Responsible Research and Innovation. Journal on Systemics, Cybernetics and Informatics (JSCI), 15 (5), 14-22.

Smyrnaiou Z., Sotiriou M., Sotiriou S. & Georgakopoulou E. 2017b. Multi- Semiotic systems in STEMS: Embodied Learning and Analogical Reasoning through a Grounded- Theory approach in theatrical performances. WSEAS transactions on Advances on Engineering Education, 14, 99-114.

Smyrnaiou, Z., Sotiriou, M., Georgakopoulou E., Papadopoulou, E. 2016. Connecting Embodied Learning in educational practice to the realization of science educational scenarios through performing arts, International Conference "Inspiring Science Education", Athens.

Smyrnaiou Z., Georgakopoulou E., Sotiriou M., Sotiriou S. 2018. Constructing Scientific Notions: Students' and Teachers' Conceptual Change through a Responsible Research and Innovation Initiative, Co-Create! 2018, Co-creation of curricula, tools and educational scenarios for building soft competences for personal development, and employability, Science Centre AHHAA in Tartu, Estonia.

The Directorate-General for Research and Innovation of the European Commission. 2012. "Responsible research and innovation - Europe's ability to respond to societal challenges".

15th International Congress of the Geological Society of Greece
Athens, 22-24 May, 2019 | Harokopio University of Athens, Greece
Bulletin of the Geological Society of Greece, Sp. Pub. 7 Ext. Abs. GSG2019-099

Earth Observation for Earth System Science Education: the MICE activity

P. Asimakopoulou[1], P. Nastos[1], E. Vassilakis[1], A. Antonarakou[1]

(1) Department of Geology and Geoenvironment,National and Kapodistrian University of Athens, University Campus- Zografou, Athens, Greece, passimak@geol.uoa.gr

Abstract

Developing educational material based on satellite remote sensing technologies, information and methods, is a key trend in modern pedagogy of Earth System Sciences. Here, we present "MICE", a classroom activity on **M**elting **IC**e **E**ffects, that utilizes remote sensing information to demonstrate the value of Earth Observation (EO) as a context to teach the STEM (Science, Technology, Engineering and Mathematics) school curriculum. The activity focuses on the subject of polar ice melting as a main climate change effect and the different impact of land and sea ice melting on sea level rise. Students, have the opportunity to discover the above experimentally and subsequently, to observe the diachronic change on polar ice through sequences of satellite images and discover the positive climate feedback on global warming. The activity was translated and adapted to the Greek curriculum from the freely available classroom resources of the European Space Agency (ESA, "Teach with Space" collection). MICE, has been enriched with Greek scientific material, including up-to-date information on climate impacts, localized for the extended region. As part of an evolutionary process, the activity was pilot-tested with 6th grade primary school students and adjusted according to the trial findings. This work is considered as the first step towards the development of original Greek educational material that will utilize EO and climate change as the context to teach STEM school curriculum, capitalizing on the pedagogical role satellite remote sensing and inquiry-based teaching methods, can play.

Introduction

Recent trends in Science Education include the development of modern educational techniques and material to teach the STEM school curriculum. At the European level, the main instrument to provide space-related material to the primary and secondary education community is the European Space Education Resource Office (ESERO) of ESA. ESERO aims at bringing Earth Observation (among other themes) to the classroom, by targeting mainly the teachers' community, as the key actors for realizing qualitative STEM education. Towards this goal, ESERO supports the education community by providing material and classroom resources based on Earth Observation (EO) and geared towards science. One of the venues used by ESERO to effectively disseminate the modern educational material towards the teachers are the annually-organized "ESA summer and autumn teacher workshops". These workshops are inspired by real and actual ESA space missions and programmes to provide teachers with unique material demonstrating how space can be utilized to teach STEM curricular subjects in school.

In the same context, the European Copernicus EO Programme acts as an effective multiplier for the development and optimization of EO-related education activities, through the provision of free information content and advanced IT open resources that can directly impact teaching and learning systems by providing insights of our planet, never available before. The incorporation of Copernicus data and information in all levels of education is an ongoing effort which has been initiated with the establishment of the Copernicus Academy Network.

Both the tools and information content provided by Copernicus and the ESA-ESERO educational materials and resources, need translation and proper adaptation to the Greek educational ecosystem and curriculum. Here, we demonstrate such an adaptation of an ESERO educational activity for Greece. In the following paragraphs we provide an overview of the activity and the conclusions drawn from its pilot application.

Activity description and pilot application

As a starting point for the development of the educational activity, we applied a bottom-up approach to gather the teachers' views, needs and interests on the subject EO utilization in STEM education. For this purpose, we constructed a survey, gathering educators' opinions on (a) the preferred activities' duration (short 20'-30' or longer 90' and above), (b) the preferred activities' morphology (worksheet based, multimedia based, experiment based, etc.) and (c) the preferred subjects of interest as far as natural or man-made disasters are concerned. The mapping process of educators' views, requirements, needs and subjects of interest, is an on-going one, aiming to acquire an extended sample over time and to record related trends.

The sample of teachers is drawn from the schools visiting the three museums of the faculty of Geology and Geoenvironment of NKUA (Mineralogy and Petrology Museum, Paleontology Museum and the Zoological Museum). Visiting Schools come from all over the Attika region and ever further away. Based on the preliminary results of the teachers' survey, climate change and subsequent impacts (melting polar ice, sea level rise, greenhouse effect) are high on teachers' preferences.

This survey drove us to select an existing thematically-related classroom activity from the freely available ESA classroom

resources, entitled “The ice is melting – How can we investigate the effects of melting ice” (ESA-ESERO, 2017), as a starting point for utilizing best practices and space-related themes for teaching Earth System Sciences.

Following that, the activity was translated to Greek and linked to the Greek curriculum (following Antoniou et al., 2014). Then it was enriched with Greek pedagogical and scientific content both on the student worksheets and the teacher’s guide. Up-to-date information on climate change issues has been integrated from the latest report of the Intergovernmental Panel on Climate Change (IPCC), including information on the expected climate imparts over Greece (Guilyardi et al., 2018; Zerefos, 2011). As a next step, the activity was pilot tested with two classes of 6th grade students (42 students in total) from the 4th primary school of Geraka. Pupils worked in groups of 4 for 90’ in total. This pilot application provided important feedback that helped us review and improve the material as discussed in the next section.

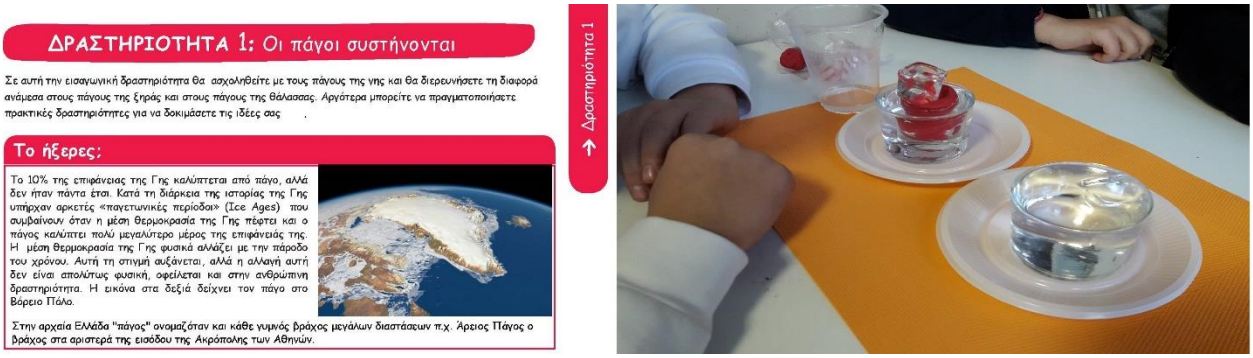

Figure 1. Sample from the MICE activity (left) and the student trials (right)

Discussion and Conclusions

Based on the pilot trial findings, we conclude that the MICE’s cognitive goals are successfully achieved in the classroom, while students’ interest is maintained at a high level. The use of satellite images as learning tools throughout the student worksheets, found to have a positive effect on deeper comprehension of the physical processes involved at a global scale. At the same time, the use of diachronic archives of satellite imagery, facilitated better understanding of the dynamic evolution of such phenomena under climate change (Galani, 2016). As far as the evolution of the activity per se, the student trials provided valuable practical feedback that has already been incorporated in order to improve the material, such as revised teacher guidelines and other practical alterations for ensuring the success of the experiments and other hands-on exercises.

These encouraging trial results along with the teachers’ positive survey feedbacks, paves the way for the development of similar material to address more Earth System Science phenomena, focusing on hot topics such as climate change and natural disasters (e.g. floods, forest fires, oil spills, algal blooms, desert dust outbreaks, volcanic eruptions etc.).

ESA ESERO thematic educational material, along with the free and open information, data and tools provided by the Copernicus ecosystem, provide a first-class opportunity for educational exploitation of these resources.

Acknowledgments

PA acknowledges the ESA ESERO for giving her the opportunity to participate in 2018’s Teacher’s Workshop in ESA/ESTEC premises and the Copernicus Academy network for supporting this work. The authors thank the teachers and students that participated in the activity trials (4th primary school of Geraka)

References

Antoniou, N., Dimitriadis, Panagiotis Kampouris, K., Papamihalis, K., & Paptsimba, L., 2014. Physiscs textbook for the 2nd grade of High School. OEDB - School Textbooks Publishing Organization. Retrieved from http://ebooks.edu.gr/modules/ebook/show.php/DSGYM-B200/530/3507,14384/

Zerefos, C., 2011. Foreword and Summary of "THE ENVIRONMENTAL, ECONOMIC AND SOCIAL IMPACTS OF CLIMATE CHANGE IN GREECE", Climate Change Impacts Study Committee (CCISC) - Bank of Greece. Retrieved from http://www.bankofgreece.gr/BoGDocuments/1.6.2011%20Foreword%20and%20summary%20of%20the%20findings%20of%20the%20Report.doc

ESA-ESERO., 2017. The ice is melting - How can we investigate the effects of melting ice. Retrieved November 26, 2018, from http://www.esa.int/Education/Teachers_Corner/The_ice_is_melting_How_can_we_investigate_the_effects_of_melting_ice_Teach_with_space_PR13

Galani, L., 2016. Thematic development and extension of Greek Geography Curriculum via the use of satellite images in the classroom. In D. Psillos, A. Molohidis, & M. Kallery (Eds.), Proceedings of 9th Hellenic Conference of ENEFET (pp. 884–891). Thessaloniki, Greece: Aristotle University of Thessaloniki. https://doi.org/ISBN: 978-960-243-702-5

Guilyardi, E., Lescarmontier, L., Matthews, R., Point, S. P., Rumjaun, A. B., Schlüpmann, J., & Wilgenbus, D., 2018. IPCC Special Report-Global Warming of 1.5°C- Summary for Teachers. Office for Climate Education OCE,Paris, p. 24. Retrieved from http://www.oce.global/wp-content/uploads/2018/12/ST1.5_OCE_LR.pdf?fbclid=IwAR2iwLND3quDab49rY6vdXCjGMJ3PHMtpuTUGIuBNQipHM1WSNUx3483uQY.

15th International Congress of the Geological Society of Greece
Athens, 22-24 May, 2019 | Harokopio University of Athens, Greece
Bulletin of the Geological Society of Greece, Sp. Pub. 7 Ext. Abs. GSG2019-233

Analysis of *Tyrannosaurus* representations in cinema

G. Lyras[1], M. Basias[1]

(1)National and Kapodistrian University of Athens, Faculty of Geology and Geoenvironment, Panepistimiopolis, 15784 Zografos, Greece, glyras@geol.uoa.gr

Background and Objectives

Dinosaurs have been the subject of numerous films (Debus, 2016). Despite that nearly all films belong to the science fiction genre, their importance to the promotion of vertebrate palaeontology is rather significant. One of the most famous and frequently shown dinosaurs is *Tyrannosaurs rex*. In this contribution, we examine the accuracy of the *Tyrannosaurus* depictions in films. We do so by applying a geometric morphometric analysis of images from films and actual specimens.

Methods

The depictions of *Tyrannosaurus* used in this analysis are profile images selected from 15 movies ranging from 1918 to 2018. Only images displaying a side profile of the head were selected. Some images were mirrored with Adobe Photoshop, in order to have the correct orientation. Those images were compared with photographs of *Tyrannosaurus* skulls seen from the lateral side. We selected a set of seven landmarks that could be identified both on the anatomical features of the skulls and on the film images. The landmarks on the skulls were the following: (1) most caudal point of the tooth row; (2) most rostral point of the tooth row; (3) point of maximum curvature of the rostal part of the premaxilla; (4) the most ventral point of the nasals; (5) highest point of the postorbital bone; (6) highest point of parietal bone; (7) center of the orbit. The landmarks of the tooth row (landmarks 1 and 2) could be easily identified on most film images. For landmarks 3 to 6, we assumed a negligible thickness of soft tissues covering the skull at those points. Because the eye is filling approximately 65% of the orbit (Stevens, 2006), the eye is considered here as the homologous landmark of center of the orbit (landmark 7). Because in the available film images the mouth is opened at various degrees, we did not collect any landmark on the mandible. Landmark coordinates were digitized using tpsDig2 v.2.17 (Rolf, 2015). For the general Procrustes analysis, principal component analysis, and visualization of shape variation along principal components, we used MorphoJ software (Klingenberg, 2011).

Results and Conclusions

The representation of *Tyrannosaurus* in films has changed over time. From 1918 till the 1980s the cinematographic head of *Tyrannosaurus* had an outline which was, unlike actual *Tyrannosaurus*, high over the antorbital fenestra. Despite the fact that the cranial anatomy of *Tyrannosaurus* was well known since 1908, film makers delayed in applying this knowledge into their creations. As a matter of fact, only after the 1990s, films presented a more realistic depiction of the *Tyrannosaurus* head. Although some recent dinosaur movies present outdated representations of dinosaurs, the last decade's trend indicates that as paleontologists continue to make new discoveries about dinosaurs, the way we see them in the cinema will also change.

References

Debus, A. 2016. Dinosaurs ever evolving: The changing face of prehistoric animals in popular culture. McFarland & Company.

Klingenberg, C.P. 2011. MorphoJ: an integrated software package for geometric morphometrics. Molecular Ecology Resources, 11: 353-357.

Rohlf, F.J. 2015. The tps series of software. Hystrix, the Italian Journal of Mammalogy, 26(1): 9-12.

Stevens, K.A. 2006. Binocular vision in theropod dinosaurs. Journal of Vertebrate Paleontology, 26: 321-330.

15th International Congress of the Geological Society of Greece
Athens, 22-24 May, 2019 | Harokopio University of Athens, Greece
Bulletin of the Geological Society of Greece, Sp. Pub. 7 Ext. Abs. GSG2019-325

Preliminary results of evaluation of educational program "Peri Anemon & Ydaton"

K. Makri[1], E. Galanaki[1], I. Koletsis[1], V. Kotroni[1], K, Lagouvardos[1]
(1) National Observatory of Athens, I. Metaxa & V. Pavlou, 15236 Penteli, Greece, kikimakri@noa.gr

Introduction

The research team of METEO Gr at the National Observatory of Athens has implemented an educational program for secondary schools named "Peri Anemon & Ydaton" since 2016. The content of the educational program is in line with the curriculum of the Middle and High Schools and its structure is based on the constructive model of Driver and Oldham (Driver, 1986).
The curriculum aims to provide to students acquisition of knowledge on severe weather phenomena, with emphasis on their impact on individuals and the society. The curriculum has an interdisciplinary as well as a holistic character. The interdisciplinary approach ensures the synthesis of knowledge, concepts and approaches from different sciences, natural and human, with the aim to unify the knowledge (Flogaiti, 2006). The evaluation of an educational program is a prerequisite as it helps to improve the program and determine if the program meets their stated goals. The purpose of this paper is to present the preliminary results of the evaluation of the educational program "Peri Anemon & Ydaton".

Methodology

Evaluation is a systematic process of collecting, analyzing and interpreting information to determine the extent to which students achieve instructional objectives (Gronlund, 1990). In the evaluation process, the first step is to determine the objective of evaluation and to quantify the achievement of the educational goals. The program "Peri Anemon & Ydaton" aims to present and discuss the weather phenomena, which affect students in the Mediterranean area, emphasizing in the severe weather phenomena and the related protection measures.
The main objectives of the program are the explanation of the following weather phenomena:

A. the creation of cyclonic and anticyclonic systems
B. the formation of the cold and warm fronts
C. the water cycle and the creation of clouds
D. the stability and the instability in the atmosphere
E. the cloud classification
F. the creation of thunderstorms
G. the creation of cloud-to-ground lightning strikes
H. the formation of tornadoes.

The dominant tool for teaching strategies is the didactic tool of the model, since the student can confirm or reject his perceptions about the development of the weather phenomena. Furthermore, the students can discover the factors that influence the meteorological phenomena, such as the creation of high intensity rainfall and thunderstorm, the formation of a tornado and the creation of lightning, while developing psychomotor skills. During the educational program, the cooperative approach is applied to ensure students' cooperation. In parallel, modern teaching tools (educational videos, interactive tablet applications, experimental devices) are implemented, aiming at the experiential approach of knowledge. For the above objectives, Bloom's taxonomy was used, while the program targets 8 overall goals.
A multiple-choice questionnaire with 20 questions pertaining to the whole cognitive approach is used as an evaluation tool. To ensure student's participation in the evaluation, the questionnaire is given as a software application and students are informed of their success score at the completion of the questions. In this paper, we used the results of the 257 questionnaires completed by Middle and High Schools students, from all over the area of Greece.

Conclusions

Among the 257 questionnaires completed by the students and analysed, the correct responses **average is 67%.** The number of the sample can be characterized as satisfactory in order to obtain reliable results. The total percentage of correct answers was calculated in relation to the ***relative frequency percentage*** **(pi**) and the ***cumulative frequency percentage*** **(Pi),** as indicators of evaluation (Figs. 1, 2). A total of 78% of the sample provided answers with an accuracy exceeding 50% (Fig. 1).
To assess the achievement of the above eight (8) learning objectives, twenty (20) questions formed the questionnaire and were categorized by objective (A to H) as follows: **A:** Q1, 2, **B**: Q3, 4, 5, **C:** Q7, 8, 18. **D:** Q6, **E:** Q9, 10, **F:** Q13, 14, 15, 16, 20, **G:** Q12, 19, **H:** Q11, 17. Every question is an evaluation criterion relevant to the cognitive goal. The main preliminary results of the educational evaluation of the program are presented in Figures 1 and 2.

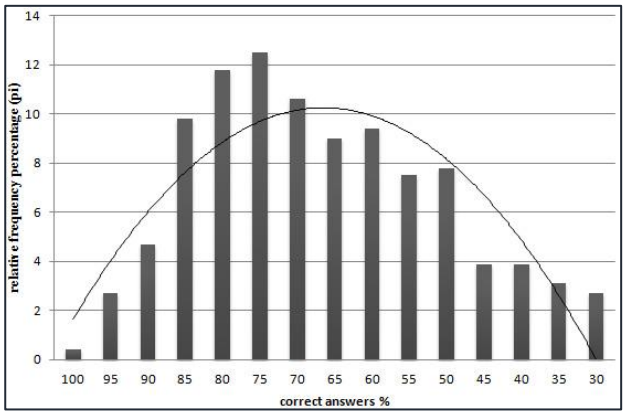

Figure 1: Relative frequency of correct answers (pi)

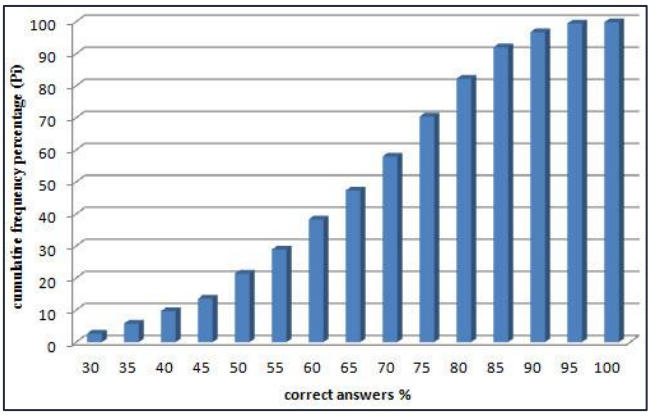

Figure 2: Cumulative frequency of correct answers (Pi)

Fig. 1 presents the relative frequency of correct answers, while Figure 2 presents the cumulative frequency of correct answers. For the analysis of the above results, the assumption that the 5/10 grade (or 50%) is considered successful was adopted. As it is obvious from Figure 1, the majority of students gave correct answers from 50% - 85%, proving that the educational program achieves its educational goals, at a satisfactory level. The percentage of correct answers in the range of 50 - 70 % ranged from 8-10 %. The corresponding percentage of correct answers from 70% - 85% was 10-12%, showing that this is the dominant range of students with correct answers. On the contrary, the percentage of correct answers which ranges of 30- 45% and 90% - 100% was less than 5%. The percentage of students with correct answers follows a Gauss distribution (Fig.1), revealing that the sample is representative, and that the questionnaire was built according to the educational programme and the average cognitive level.

Figure 2 shows that the cumulative percentage of correct answers with a success rate lower than 35 % is less than 6%. The percentage of correct answers with a success rate lower than 45% is 13,6%, while the corresponding percentage for success rates lower than 50%, 60%, 70% and 80% are 21,4%, 38,3%, 58% and 82%, respectively. Consequently, it is once again shown that the predominant range of students with correct answers is 50-85%.

The obtained results prove that the overwhelming majority of students had successfully answered to the questions, consistently to a normal (Gauss) distribution (Spiegel, 2000). Based on the above preliminary results of evaluation of the educational program "Peri Anemon & Ydaton", it is evident that the program is achieving at a great extent its cognitive goals. It should be noted that the evaluation is underway and it will be completed by May 2019.

References

Driver, R., Oldham, V., 1986. A constructivist approach to curriculum development in science, Studies in Science Education, 18, 105-122

Gronlund, N.E. and Linn, R.L. (1990) Measurement and Evaluation in Teaching. McMillan Company, New York.

Flogaiti, E. (2006). Education on Environment and Sustainability, Hellenic Grammata, ISBN 978-960-9552-26-4.

Fraenkel R. Jack & Wallen E. Norman (2009). How to Design and Evaluate Research in Education. McGraw-Hill, ISBN 978-0-07-352596-9.

Matthews, M.R. (1994). Science Teaching: The Role of History and Philosophy of Science. New York: Routledge Press.

Spiegel, M & Stephens, L, 2000.Θεωρία και Προβλήματα Στατιστικής. 3η έκδοση. Αθήνα: Εκδόσεις Τζιόλα. ISBN 960805012X.

15th International Congress of the Geological Society of Greece
Athens, 22-24 May, 2019 | Harokopio University of Athens, Greece
Bulletin of the Geological Society of Greece, Sp. Pub. 7 Ext. Abs. GSG2019-345

INNOVEXPO: Interactive Presentation of Geomyths and their Geological Background

E. Koskeridou[1], I. Mariolakos[1], N. Skoulikidis[2], G. Lyras[1], D. Thivaiou[1], C. Psarras[1], G. Katopodis[3], A. Plessa-Valadaki[3], S. Plessas[1], I. Papadopoulos[3], E. Vretzaki[3], G. Pehlivanides[3], S. Tsafaras[3]

(1) National and Kapodistrian University of Athens, Faculty of Geology and Geoenvironment, Department of Hist. Geology-Paleontology, Athens, Greece, ekosker@geol.uoa.gr
(2) Hellenic Centre for Marine Research, P.C. 19013 Anavyssos, Attika Greece
(3) TETRAGON SA, 2B, Karaiskaki str. 54641, Thessaloniki, Greece

The scientific analysis of myths can identify hidden references to geological events in narratives previously viewed as imaginary products of creative storytelling. Although this is the case in mythologies around the World (Vitaliano, 1973), the body of myths originally told by the ancient Greeks is of particular interest (e.g. Mariolakos, 2018). Their mythology has an extensive influence on the culture of Western civilization and is widely known to the public. Here we present our ongoing 3-year project that focuses on the geomythology of ancient Greece. The project, which is entitled INNOVEXPO, aims to the development of innovative applications, incorporating scientifically substantiated content will combine scientific research with the creative industry, to develop multiple levels of interpretation, documentation and content acquisition. As a result, we will develop a prototype methodology, in order to form a complex grid of and their original methodology of interconnection, for the enrichment and interactive presentation of exhibitions.

Myths, including geomyths, consist of narratives and stories that lack a material representation. Many previous exhibitions on mythology were designed around objects of material culture inspired by myths (e.g. depictions of heroes and mythical battles). Here we decided to apply a different approach, one that will present myths directly, while minimizing the use of objects of material culture. In order to do so we will use innovative technological applications that act as expressive and conceptual tools for the design of modern museographic practices (Figs 1 and 2). At the same time, it will be easy transportable and adaptable to the specific needs of each exhibition space. Furthermore, we experiential, cognitive, sensory and aesthetic experience.

We are currently investigating Greek myths and their potential geological background as a means to discover the references to geological phenomena. This complex project will be the basic model infrastructure for the interactive presentation of exhibitions, contributing to the promotion and dissemination of multidimensional themes of culture, tourism and other thematic areas. Results can be presented in museums, cultural centers and tourist organizations.

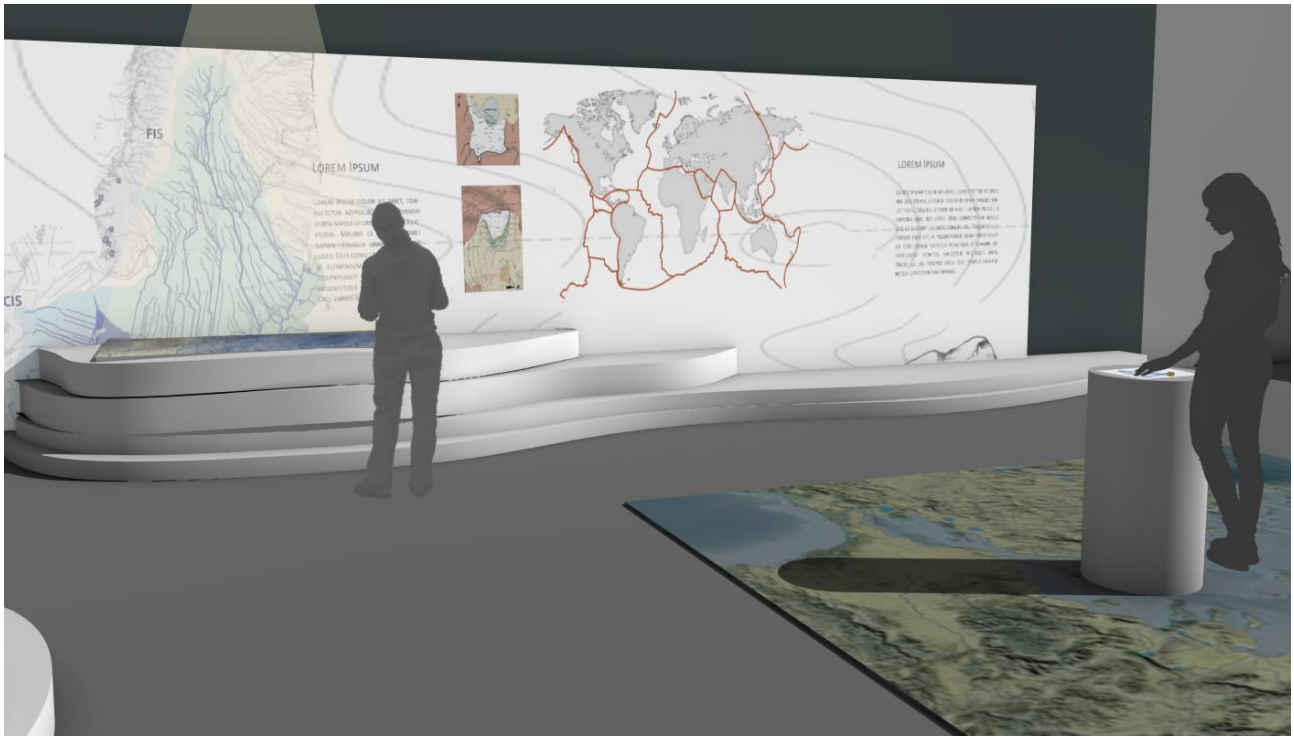

Figure 1. Conceptual design of the INNOVEXPO exhibition.

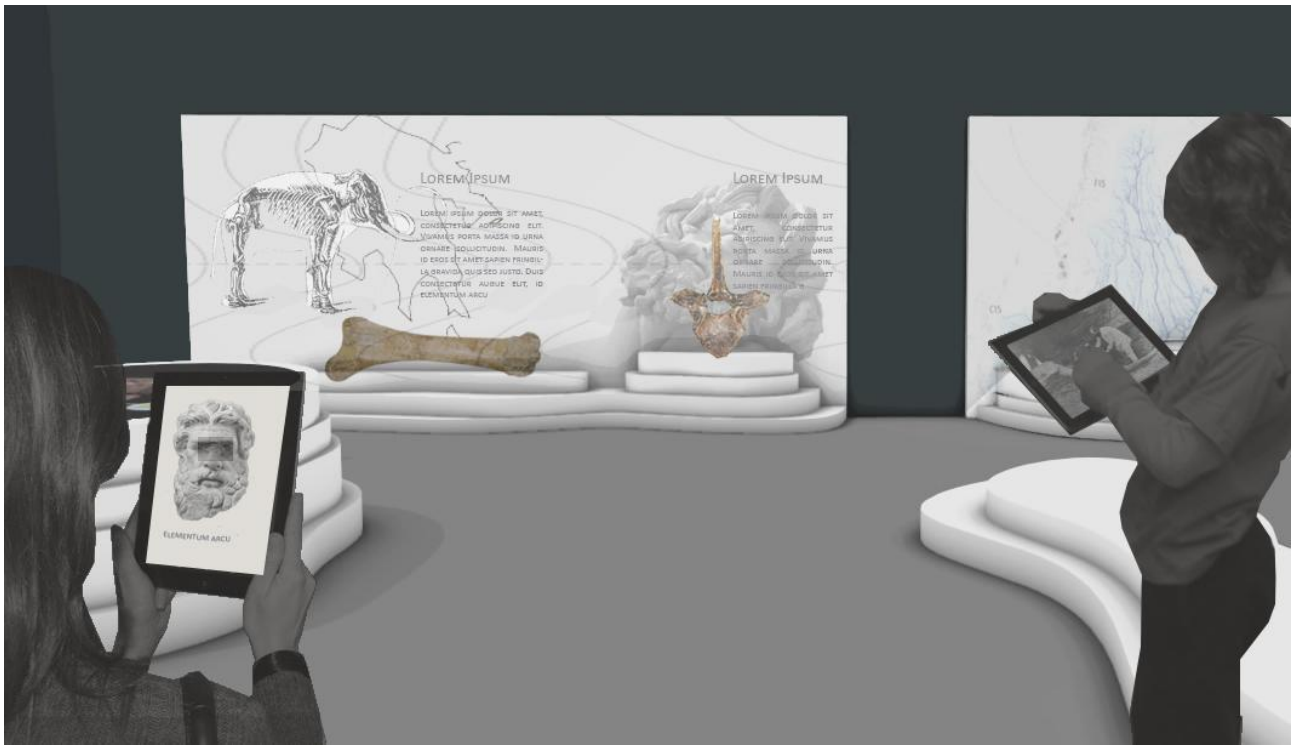

Figure 2. Conceptual design of the INNOVEXPO exhibition.

Acknowledgement

This research has been co-financed by the European Regional Development Fund of the European Union and Greek national funds through the Operational Program Competitiveness, Entrepreneurship and Innovation, under the call RESEARCH – CREATE – INNOVATE (project code: T1EDK-02363)

References

Mariolakos, I., 2018. Mariolakos I. (2018). Ancient Greece and Water: Climatic Changes, Extreme Events, Water Management,and Rivers in Ancient Greece. In: N. Skoulikidis, E. Dimitriou, I. Karaouzas (eds.) The Rivers of Greece. Springer, Series: The Handbook of Environmental Chemistry, 3-30.

Vitaliano, D.B., 1973. Legends of the Earth. Indiana University Press.

15th International Congress of the Geological Society of Greece
Athens, 22-24 May, 2019 | Harokopio University of Athens, Greece
Bulletin of the Geological Society of Greece, Sp. Pub. 7 Ext. Abs. GSG2019-359

Designing an Educational Scenario Aiming to Teach the Concept of Geological Time to Secondary Education Students with Visual Disabilities

K. Marmarinos[1], A. Antonarakou[1], H. Drinia[1], F. Antoniou[1]

(1) National & Kapodistrian University of Athens, University Campus- Zografou, Athens, Greece, kmarmarinos@geol.uoa.gr

Introduction

The understanding of the enormous amount of time in which the Earth has been formed and evolved is one of the most difficult concepts not only for students but for people of all ages (Dodick & Orion, 2003). The difficulty in understanding the geological time is due to its vast scale of events that go beyond everyday experience, as human existence on Earth is very small compared to the temporal scale of the geological events on it (Dodick & Orion, 2006; Trend, 1998).

Despite all the difficulties described above the concept of the geological time is taught in the secondary education of Greece as it is necessary for students to understand not only the long-term geological changes but also other processes that occur slowly on the planet, including climate change, oceanography, paleontology, evolutionary biology and cosmology (Dodick, 2007; Dodick & Orion, 2006; Nam, Karahan & Roehrig, 2016; Ravachol & Orange, 2012).

Given that in the context of equal opportunities, visually impaired people should have access to the same information as their sighted peers (Aldrich & Sheppard, 2001), Geology teachers are also called to teach geological time to students with visual impairments. The challenge for them is even bigger as in that case visual representations are not an option.

Options-Aim

For students with visual impairments learning is possible through touch (Millar & Al-Attar, 2004). Appropriately designed educational scenarios involving hands-on activities can be used to further enhance teaching (Simone, 2007) and make it in a funy and enjoyable way (Howe, 2006).

Inspiration

Inspiration resources are successful efforts made by researchers to teach concepts related to geological time to students with visual impairments including:

- The haptic exploration of actual fossils or replicas, which may include placing them in the correct chronological order (Neuhauser, 2011; Perkins School for the Blind, 2016; Richard, 1967; Travis, 1990; Wild, Hilson, & Farrand, 2013).
- The use of materials of different texture that simulate a stratigraphic sequence (Neuhauser, 2011; Ratajeski, 2017).

Other inspiration resources are scenarios made for normal vision students like the linear representation of the geological time on the human hand (Borel, 2014) or the proposals for the representation of stratigraphic strata using simple materials in order to teach the principle of superposition. Those ideas have been adapted adequately for students with visual impairments.

Description

A variety of specific haptic educational objects or activities is proposed to be used to teach and stimulate the interest of students with visual impairments in geological time. These haptic educational objects or activities are easily made with low cost materials and do not require much time for their construction. The construction details and teaching scenarios directions are also provided.

The Examples are designed for personalized instruction and include: Haptic comparison of recent and fossilized sea cells, haptic exploration of a fictional dinosaur footprint made in clay, simulation of a stratigraphy sequence with pieces of fabric, simulation of a drilling core, simulation of geological timeline in the students hand and the placement of animal toy models in the correct chronological order.

References

Aldrich, F. K., & Sheppard, L. (2001). Tactile graphics in school education: perspectives from pupils. British Journal of Visual Impairment, 19(2), 69–73.

Borel, B. (2014). The Greatest Animal War. Nautilus, (17). Retrieved from http://nautil.us/issue/17/big-bangs/the-greatest-animal-war

Dodick, J. (2007). Understanding Evolutionary Change within the Framework of Geologic Time. McGill Journal of Education, 42, 245–264.

Dodick, J., & Orion, N. (2003). Cognitive Factors Affecting Student Understanding of Geologic Time. Journal of Research in Science Teaching, 40, 415–442. Retrieved from https://stwww1.weizmann.ac.il/geogroup/wp-content/uploads/sites/24/2016/10/jrst_article.pdf

Dodick, J., & Orion, N. (2006). Building an understanding of geological time: A cognitive synthesis of the "macro" and "micro" scales of time. In C. A. Manduca & D. W. Mogk (Eds.), Earth and Mind: How Geologists Think and Learn about the Earth (pp. 64–92). Geological Society of America. Retrieved from https://pdfs.semanticscholar.org/de3d/f52f16e01956e531e2ab80bc9ca40a5bdb53.pdf

Howe, M. (2006). A new approach to teaching those with Disabilities : EMBed methodology and the visually disabled. The Triple Helix.

Millar, S., & Al-Attar, Z. (2004). External and body-centred frames of reference in spatial memory: Evidence from touch. Perception

and Psychophysics, 66(1), 51–59.
Nam, Y., Karahan, E., & Roehrig, G. (2016). Native American Students' Understanding of Geologic Time Scale: 4th-8th Grade Ojibwe Students' Understanding of Earth's Geologic History. International Journal of Environmental & Science Education, 11(4), 485–503.
Neuhauser, K. (2011). Privilege on Teaching a Totally Blind Student Physical and Historical Geology. In The Geological Society of America (GSA) Annual Meeting. Minneapolis. Retrieved from https://gsa.confex.com/data/handout/gsa/2011AM/Paper_192703_handout_252_0.pdf
Perkins School for the Blind. (2016). Forensic Geology Lab: Digging Through the Sands of Crime. Retrieved June 8, 2018, from http://www.perkinselearning.org/accessible-science/activities/forensic-geology-lab-digging-through-sands-crime
Ratajeski, K. (2017). Examples of Tactile Aids for Teaching Introductory Geology Students with Visual Disabilities. Earth Educators Rendezvous, Albuquerque, [Poster].
Ravachol, D. O., & Orange, C. (2012). Scientific knowledge and learning in biology and geology: Between phenomenon and event. In C. Bruguiere, A. Tiberghien, & P. Clement (Eds.), E-Book Proceedings of the ESERA 2011 Conference: Science learning and Citizenship (part 1) (pp. 58–64). Lyon, France: European Science Education Research Association.
Richard, B. (1967). Teaching Introductory Geology to a Blind Person. Journal of Geological Education, 15(4), 152–153.
Simone, N. (2007). Adapting Hands-On Science Programs for Students with Disabilities. CSIRO Education. Worcester Polytechnic Institute. Retrieved from http://www.wpi.edu/Pubs/E-project/Available/E-project-042907-213933/unrestricted/IQP-HXA-A073-CSIRO.pdf
Travis, J. (1990). Geology and the Visually Impaired Student. Journal of Geological Education, 38, 41–49.
Trend, R. (1998). An investigation into understanding of geological time among 10- and 11-year-old children. International Journal of Science Education, 20(8), 973–988.
Wild, T. A., Hilson, M. P., & Farrand, K. M. (2013). Conceptual Understanding of Geological Concepts by Students With Visual Impairements. Journal Of Geoscience Education, 61, 222–230.

15th International Congress of the Geological Society of Greece
Athens, 22-24 May, 2019 | Harokopio University of Athens, Greece
Bulletin of the Geological Society of Greece, Sp. Pub. 7 Ext. Abs. GSG2019-360

Using 3D-printed models to improve pupil comprehension of fossil foraminifera

A. Antonarakou[1], G. Lyras[1], Z. Smyrnaiou[2], E. Besiou[1], A. Nikolopoulos[1], S. Zarkogiannis[1], A. Gramba[1]

(1) National and Kapodistrian University of Athens, Faculty of Geology and Geoenvironment, Panepistimiopolis, Zografos, Greece, aantonar@geol.uoa.gr
(2) National and Kapodistrian University of Athens, Faculty of Philosophy, Pedagogy and Psychology Panepistimiopolis, Zografos, Greece, zsmyrnaiou@ppp.uoa.gr

Background and Objectives

The use of visual models in natural sciences is a commonplace. Physical scale-models of organisms, organs and cells are frequently seen in classrooms and lecture halls. Foraminifera are not an exception to this. D'Orbigny, the scientist who named the group in 1839, was the first to create a set of three-dimensional scale-up models of foraminifera (Miller, 2002). His aim was to make foraminifera available to everybody without entailing the necessity of observing them under the microscope (Heron-Allen, 1917). Since then, several scientists and artists have reproduced scale models of foraminifera (Miller, 2013). However, most of them are treated as museum objects. The reason behind this is simple: foraminifera have complex shapes that are difficult to massively reproduce without loosing the fine detail of the original. Therefore many teaching models of foraminifera usually lack detail and have an unnatural look.

The recent development of three dimensional printing technologies enables us to create low cost, yet highly accurate objects. Although 3D printing has been around for decades, only the last years it became affordable to the common consumer. This study examined the impact of a modeling-based instructional intervention on students in primary / early secondary school using different tools: 3D printing, museum objects and microscope images that support modeling. Our aim is to evaluate the use of tactile models could help pupils understand images from the microscope.

Theoretical Framework

The literature of the science education offers important data to the scientific modelling. Many researchers agree that modeling should be the main technique of teaching sciences (Mellar et al., 1994). For science education, it is especially important that students learn how to develop models and how to draw explanations of natural phenomena (Coleman, 1998). The modeling process in Sciences' teaching has been studied via the use of different pedagogic tools: objects from everyday life used for the experiments and technology-based learning environments. The results show that the advantages of different pedagogic tools can contribute to the act of learning the sciences' concepts taking into consideration the cognitive processes that are involved in the modelling (Smyrnaiou & Weil-Barais, 2005; Smyrnaiou & Dimitracopoulou, 2007).

Models can play a role in the learning process when we ask students to construct models. In this "*learning by modeling*" students are required to construct an external model with the objective to make the model behave as similar as possible as the real system (Penner, 2001). We speak also of "*learning from models*" when students can interact with the model. Students' learning processes center around the exploration of this model by changing values of input variables and observing resulting values of output variables. In this process they experience rules from the domain or (re-) discover (aspects) of these rules (de Jong, 2006). Finally, both ways of using models can be combined in what we will call "*model-based inquiry learning*".

Gerard Vergnaud (1987) has proposed, in a constructivist aspect, a general theoretical framework (schema) which emphasises to the relationships that the student has to construct in order to be able to understand and interpret situations, to communicate their purpose and to make predictions, inferences, etc. He emphasises the role of the student's actions and cognitive resources in the elaboration of knowledge, within a constructivist approach. He distinguishes three functioning registers: a) the register of actions on real objects; the register of mental representations; the register of symbolic representations (maths, language, etc.).

Methods

Specimens of *Globigerinoides ruber* were scanned on a XMCT system (Friedrich-Alexander Universitat Erlangen-Nurnberg, Erlanger, Germany). The specimens were scanned at 80kV, detector array size of 2000*1336, 1500 projections/360º, 2,5s/projection) slice thickness. The 3D reconstruction and visualization of the CT data was performed in AVIZO (www.vsg3d.com). The created 3D meshes were prepared for printing in Autodesk Meshmixer (www.meshmixer.com) and Slic3r (https://slic3r.org). The models were printed on a Prusa i3 MK2S fused filament fabrication printer. Two types of polylactic acid (PLA) filament were used: light gray and semitransparent. The models were printed as complete shells, with the exception of one model, whose shell was sliced in half so that its internal structure can be observed. All printed models were 200 times larger than natural size.

We set up an installation with binocular microscopes, foraminifera pictures and 3D models. The fundamental concepts micropalaeontology and using microscopes were explained to the pupils. After that, the pupils were asked to examine foraminifera under the microscope. Then they were given the models and were asked to examine the foraminifera under the microscope again.

The research was set out to explore students' descriptions and manipulations while being exposed to the different

mediums: symbolic objects; real objects. Furthermore, students' models while using "3D printer" and microscope were explored. Finally, the extent to which the combination of the two mediums enhanced students' understanding was investigated.

Results and Conclusions

At the end of the session, the pupils were asked to evaluate the 3D models. In particular the pupils were given a short survey that had the following statements. Nearly all pupils have never used a microscope before and only a small percentage of them (24%) had ever seen a 3D printed object. The 3D printed models helped to the better understanding of the foraminifera structure (97%). However, most pupils were mostly impressed by the microscope itself rather than the 3D models.

In many cases 3D printing is used as a support technology in teaching including printing of scale up models of microscopic objects (see for an overview, Ford and Minshall, 2018). As expected, our foraminifera models helped pupils underhand the fine details of the foraminifera shell. The models do not replace the experience of the real object (as that is seen through a microscope), but do contribute to the better understanding of the subject. Fused filament fabrication 3D printing enables scientists to cheaply create teachable objects of high quality. Our experiment demonstrated that the use of objects that are increased in scale, makes them more accessible, and helps the underfunding of microscopic organism and structures. Similar projects in the future should be more complex and thus capitalize on the growing affordability of 3D printing.



Figure 1. A pupil examining a foram under a microscope (left) and looking at a 3D model of the same organism (right).

References

Coleman, E.B., 1998. Using explanatory knowledge during collaborative problem solving in science. Journal of the Learning Sciences, 7(3&4), 387-427.

de Jong, T., 2006. Computer simulations - Technological advances in inquiry learning. Science, 312, 532-533.

Ford, S., Minshall, T., 2018. Invited review article: Where and how 3D printing is used in teaching and education. Additive Manufacturing, 25, 131-150.

Heron-Allen, E., 1917. Presidential address, 1916- 1917: Alcide d'Orbigny, his life and his work. Journal of the Royal Microscopical Society, 1917, 1- 105.

Mellar, H., Bliss, J., Boohan, R., Ogborn, J., Tompsett, 1994. Learning with Artificial Worlds: Computer Based Modeling in the Curriculum, The Falmer Press, London.

Miller, C.G., 2002. Micropalaeontological models at the Natural History Museum, London. The Geological Curator 7(7), 263-274.

Miller, C.G., 2013. A brief history of modelling Foraminifera: from d'Orbigny to Zheng Shouyi. The Micropalaeontological Society, Special Publications, Geological Society, London, 337-349.

Penner, D.E., 2001. Cognition, computers, and synthetic science: Building knowledge and meaning through modelling. Review of Research in Education, 25, 1-37.

Smyrnaiou, Z., Weil-Barais, A., 2005. Évaluation cognitive d'un logiciel de modélisation auprès d'élèves de collège, Didaskalia, 27, 133-149.

Smyrnaiou, Z., Dimitracopoulou A., 2007. Inquiry learning using a technology-based learning environment. Proceedings of 8th International Conference on Computer Based Learning, Heraklion, Crete, 90-100.

Vergnaud, G., 1987. Les fonctions de l'action et de la symbolisation dans la formation des connaissances chez l'enfant. In Piaget J., Mounoud P., Bronckart J.P., Psychologie, Encyclopédie de la Pléïade, Paris, Gallimard, pp. 821-844.

15th International Congress of the Geological Society of Greece
Athens, 22-24 May, 2019 | Harokopio University of Athens, Greece
Bulletin of the Geological Society of Greece, Sp. Pub. 7 Ext. Abs. GSG2019-361

Urban Geology: Educational Proposal for Geosience: A Case Study From the Inner City of Athens, Greece

G. Kontokostas[1], A. Antonarakou[1], M. Fountopoulou[2], H. Drinia[1], S. Lozios[1]

(1) National and Kapodistrian University of Athens, Department of Geology and Geoenvironment, Panepistimiopolis, Zografos, Greece, geokon@geol.uoa.gr
(2) National and Kapodistrian University of Athens, Department of Philosophy, Pedagogy and Psychology Panepistimiopolis, Zografos, Greece, mafoun@ppp.uoa.gr

Background and Objectives

The limited exploitation and low understanding of geological notions, in modern education in physical sciences, motivated the design of research procedures about the understanding of rock formations, of recognizing rocks, of informing about geological potential, using techniques entailed in the scientific/educational methodology by inquiry, suggesting educational walking paths through historical center of Athens.

From the geological point of view, the basin of Athens is bounded to the east by Mountain Hymettus which is built by metamorphic alpine formations (marbles and schists), constituting the lower tectonic unit, and to the west by the overlying tectonic unit of Mountains Egaleo and Poikilo, which include non-metamorphic formations like limestones, volcanosedimentary sequences and ophiolites. The tectonic contact of these two units includes a low gradient detachment fault.

The major part of the basin is covered by neogene and quaternary formations (terrestrial, marine and lake deposits of conglomerates, sandstones, marls and pelitic rocks, but also laterally extended debris and scree deposits).

Below the neogene formations, small alpine low-grade metamorphic rock formations (crystalline limestones and phyllites) are emerging forming small individual hills (Tourkovounia, Lycabettus, Acropolis, Philopappus etc.), overlying both the metamorphic formations of Hymettus and the non-metamorphic formations of Egaleo.

In this paper, the geology of the city of Athens and in particular the area of the inner city (historic center) is mainly studied. The designed geological walk trail is a practical endorsement, where the students will use fieldwork skills to identify a range of rocks and geological materials in the built environment and can also be informed about geological features of the area. Someone would think that urban area is poor for geological study and contains few useful geological data. This thought derives from the fact that primary surface of a city has been built and sharpened artificially, streets have been constructed, hydrographic networks have been shaped and hide, natural surface has been degraded.

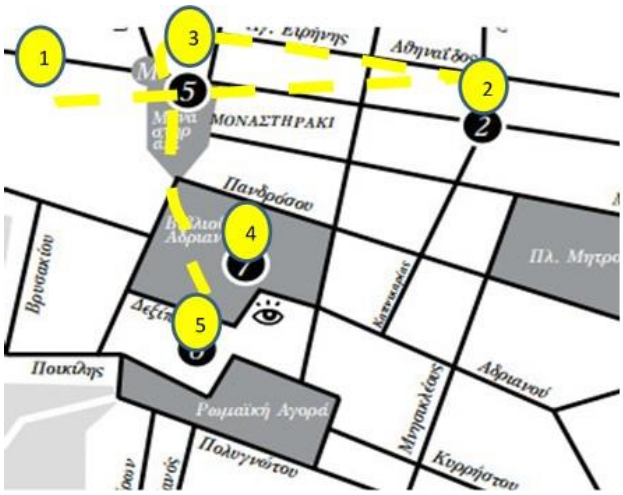

Figure 1. The walk trail: (1) Monastiraki (2) Kapnikarea (3) Pantanassa (4) Library of Hadrian (5) Roman Market.

Research Methology

This work is an attempt to follow research steps forth by inquiry – based learning: a) trigger of interest, b) reminding of basic knowledge/formulation of hypotheses, c) experimentation/trials d formulation of conclusions, e) applications/generalization according to learning.

We designed the walk trail: Syntagma- Monastiraki-Kapnikarea-Pantanassa-Library of Hadrian -Roman Market (Fig. 1) and we pursued the educational research with an experimental group of students of secondary school of Attica.

Results and Conclusions

The results of our research were compared with a control group of students of secondary school of Attica who visited our paleontology museum in Faculty of Geology and Geoenvironment of School of Science of National & Kapodistrian University of Athens. We noticed that students' understanding, creativity, cooperation and critical thinking were spectacularly improved. They learned about the Eridanus River, they could recognize white marble of Pendeli, grey Hymettus' marble, green marble of Karystos, granites and limestones with fossils. The most interesting point of the research was when the students realized that the complexity of the natural world arises from the combinations of few simple procedures.

Acknowledgements

The authors would like to thank the Director of Paleontology-Geology Museum, Professor Vassileios Karakitsios.

15th International Congress of the Geological Society of Greece
Athens, 22-24 May, 2019 | Harokopio University of Athens, Greece
Bulletin of the Geological Society of Greece, Sp. Pub. 7 Ext. Abs. GSG2019-390

Characteristics of students' alternative ideas on geodynamic phenomena and factors controlling their development

Athanasia Bakopoulou[1], Assimina Antonarakou[1], Alexandra Zambetakis-Lekkas[1]

(1) National and Kapodistrian University of Athens, Department of Geology and Geoenvironment, Panepistimiopolis Zographou, 15784 Athens, Greece, abakopoulou@geol.uoa.gr

We analyze Greek students' alternative ideas, both initial and synthetic, on geodynamic phenomena. More specifically, we present students' concepts on Earth structure, earthquake occurrence, volcano formation and relief change. An indicative curriculum and textbook evaluation is attempted in order to specify their involvement in concept construction. A new synthetic mental model on earthquake occurrence is revealed. New synthetic alternative ideas on geodynamic phenomena are presented. Finally, (a) the characteristics of initial and synthetic alternative ideas on geodynamic phenomena are outlined separately, and (b) the factors that control their development are highlighted and grouped, hoping that their revelation will lead to the decomposition of alternative ideas.

15th International Congress of the Geological Society of Greece
Athens, 22-24 May, 2019 | Harokopio University of Athens, Greece
Bulletin of the Geological Society of Greece, Sp. Pub. 7 Ext. Abs. GSG2019-394

Literacy in Geosciences among Students: An In-Depth Study into Greek Secondary Education

M. Psychogiou[1], K. Louvaris[1], K. Georgiou, A. Antonarakou[2] and H. Drinia[2]

(1) Hellenic Ministry of Education, Athens, Greece mpsychogiou@geol.uoa.gr, klouvari@geol.uoa.gr katerinageorgiou@gmail.com
(2) National and Kapodistrian University of Athens, Department of Geology and Geoenvironment, Athens, Greece aantonar@geol.uoa.gr, cntrinia@geol.uoa.gr

Literacy in Geosciences has been the topic of a number of researchers worldwide (Happs, 1985; Dove, 1997; Sharp et al, 1995; Ford, 2005; Lillo, 1994). Nevertheless, this report is incomplete as far as Greek students are concerned. Ioannidou & Vosniadou (2001) conducted a research regarding misconceptions about Earth's inner layers where they detected several incomplete or erroneous ideas on part of the students. But what exactly are misconceptions and why are they important when it comes to science teaching? The definition provided by Osborne et al. (1983) describes a misconception as a conception which differs significantly from that which is commonly agreed by the scientific community. The theory of conceptual change supports that, in order for the new knowledge to be acquired, there needs to be a reorganization of the existing knowledge (Read, 2004). This process might be impeded by the deep-rooted misconceptions and educators need to apply specific instruction for successful outcomes. According to Posner et al. (1982), the four following conditions must be met in order for conceptual change to occur:

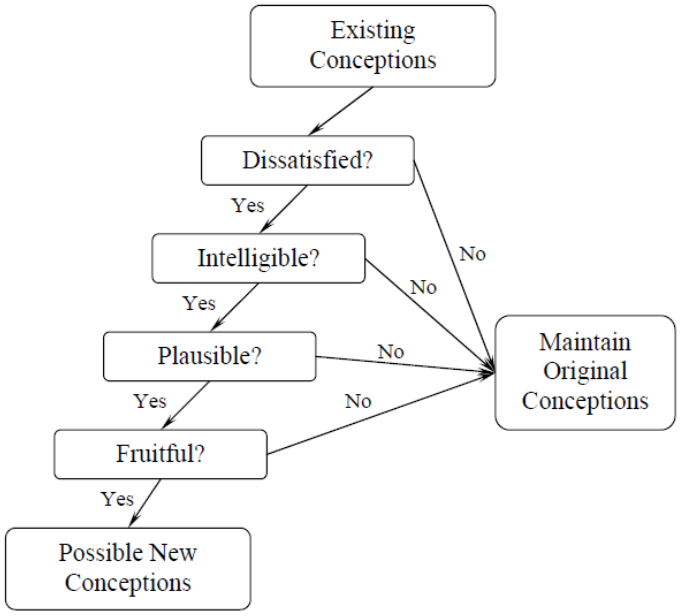

Figure 1. Posner et al.'s (1982) Conceptual Change Model – adapted from Dole & Sinatra (1998).

The position of Greece in the geodynamic model of our planet makes it unique as far as the natural phenomena are concerned, but most importantly about the natural disasters that this country has been plagued with (Nivolianitou, 2011). Greece is number one region in Europe as far as seismic activity is concerned and also ranks in the sixth position on a global scale (Tsapanos and Burton, 1991). There are 5 active volcanoes, as it is reported in the Index for Risk Management 2018 (INFORM 2018) that could possibly affect the population, and recent floods and wildfires have claimed a considerable number of lives. According to UNDRR (United Nations office for Disaster Risk Reduction) and their International Data base, the most frequently occurring disasters in Greece are floods, earthquakes, wildfires, storms, extreme temperatures, and some others, with earthquakes having the highest mortality rate. As Shaw et al. (2011) mention, "[I]t has been widely acknowledged that education takes on a pivotal role in reducing disasters and achieving human security in the attempt to achieve sustainable development" (p. 1). This is the main reason why it is of utmost importance to record the existing conceptions of schoolchildren in Greece regarding natural phenomena, their genesis, and ways to protect against them and consider revising the existing educational practices if need be.

The responses included in this paper were collected during the school years 2015-2019 from junior and senior high schools in Athens and Lamia, two densely populated cities in Greece. Students were asked to complete certain questionnaires in order to carry out an evaluation of their literacy in geological issues regarding the Earth, the genesis of volcanoes and earthquakes, the formation of mountains as well as of the different types of rocks, the importance of fossils, and water resources. The results that were obtained were rather disappointing, with students aged between 14-16 holding severe misconceptions about basic geological concepts or seriously lacking relevant knowledge. Only 13% of the students were able to identify the key components of a map, 15% could draw a fairly accurate sketch of earth's interior or name the different layers. The most common mistakes were that they drew the layers' proportions incorrectly and only 20% were

able to name “core”, “mantle”, and “crust”; and when they did, they mostly mentioned “inner and outer crust or mantle”, they described the core as being in a gas or liquid state and the mantle in a solid state. A mere 30% were correct about the way the rocks were formed and where this procedure takes place. Most of them regarded rocks as static, unchangeable elements of the Earth and only 40% recognized that rocks are comprised of minerals. Additionally, while 60% of the students knew how volcanoes are formed, only 14% were able to provide a definition of what an active volcano is, and approximately one third could recognize more than half of the volcanoes in the pictures they were shown. Less than 10% answered correctly about the formation of mountains while there was also an answer provided by a student who claimed that they are formed as a result of mountain reproduction. Only 36% actually realize that a mountain could have been formed at the bottom of an ocean. They also hold a lot of misconceptions about fossils. They do not recognize that microfossils exist or their role in forming rocks. When the students were asked to justify the existence of marine fossils on the mountains, more than half of them supported that it happened due to the receding of the sea rather than the formation of the fossiliferous rocks at the bottom of an ocean and their displacement because of plate tectonics. A vast majority of the students were not able to identify folds, stratification, foliation or to distinguish between gravels and pebbles or magma and lava. As far as the water is concerned, 60% of the students believe that the water resources are depleting - which might be the case only for fresh-water and additionally, more than half of them hold the misconception that once the water from rain enters the ground it is of no use to humans.

All in all, this research reveals the depth of students’ illiteracy regarding geological issues, even though some concepts are currently taught in secondary education in Greece. One obvious reason for this might be that the inclusion of geological units in the science curriculum is fragmented and inadequate and another that all science lessons are taught mostly as lectures in teacher-centered environments with few hands-on activities and not enough lab experiments or field trips. Geology is a science which is better understood through an experiential way and it is imperative that the education stakeholders reconsider the current teaching approaches.

References

Dove J., (1997). Student ideas about weathering and erosion. *International Journal of Science Education, 19*(8), 971–980.

Ford, D.J. (2005). The challenges of observing geologically: third graders’ descriptions of rock and mineral properties. *Science Education 87*, 276-295.

Happs J. C., (1985). Regression on learning outcomes: some examples from the Earth Sciences. *European Journal of Science Education, 7*(4), 431–443.

INFORM (2018). *Index for Risk Management*. Inter-Agency Standing Committee Task Team for Preparedness and Resilience and the European Commission. Retrieved from http://www.inform-index.org

Ioannidou, I., & Vosniadou, S. (2001). The development of knowledge about the composition and layering of the earth’s interior. *Nea Paedia, 31*, 107–150 (in Greek).

Lillo J. (1994). An analysis of the annotated drawings of the internal structure of the Earth made by students aged 10-15 from primary and secondary schools in Spain. *Teaching Earth Sciences, 19*(3), 83–87.

Nivolianitou Z. (2011), The use of Virtual Reality in the mapping of risk for operators dealing with hazardous tasks, *9th International Conference on Information Communication Technologies in Health*, July 14 – 16, Samos, Greece

Osborne, R. J., & Wittrock, M. C. (1983). Learning science: A generative process. *Science Education 67*, 489–508.

Posner, G. J., Strike, K. A., Hewson, P. W., and Gertzog, W. A. (1982). Accommodation of a scientific conception: Towards a theory of conceptual change. *Science Education 66*, 211–217.

Read, J. R. (2004). Children’s Misconceptions and Conceptual Change in Science Education. Available from http://acell.chem.usyd.edu.au/Conceptual-Change.cfm

Sharp J. G., Mackintosh M. A. P. & Seedhouse P., (1995). Some comments on children‘s ideas about Earth structure, volcanoes, earthquakes and plates. *Teaching Earth Sciences, 20*(1), 28–30.

Shaw, R. Takeuchi, Y, Gwee,Q.Y, & Shiwaku, K. (2011), Disaster Education: An Introduction. In Shaw,R. Takeuchi, Y, Gwee,Q.Y, & Shiwaku, K. (Eds.) *Disaster Education Community, Environment and Disaster Risk Management, vol 7*, (pp. 1 - 22). Emerald Group Publishing Limited.

Tsapanos, T.M. & Burton P.W. (1991). Seismic hazard evaluation for specific seismic regions of the world, *Tectonophysics, 195*, 153-169.

SPECIAL SESSION

T11.S1 Innovative Sensing Techniques for Geohazards

Conveners: **V. Marinos (AUTH)**
C. Loupasakis (NTUA)
E. Vassilakis (NKUA)

15th International Congress of the Geological Society of Greece
Athens, 22-24 May, 2019 | Harokopio University of Athens, Greece
Bulletin of the Geological Society of Greece, Sp. Pub. 7 Ext. Abs. GSG2019-016

Application of Structure-from-Motion (SfM) technique for measuring near-field earthquake-induced failures; case studies from Greece

S. Valkanioits[1], G. Papathanassiou[2], Ath. Ganas[3]

(1) Koronidos 9, Trikala, Greece, valkaniotis@yahoo.com
(2) Democritus University of Thrace, Dept. Civil Engineering, Xanthi, Greece
(3) Institute of Geodynamics, National Observatory of Athens

Extended abstract

Documentation of earthquake environmental effects (surface ruptures, landslides etc.) is a very critical issue, since based on the accuracy of the provided information, protection and mitigation measures can be designed. However, it is well known that mapping these features is not always feasible due to several adverse factors e.g. near-vertical slopes, coastal cliffs, imposing high risk to human surveys. In order to overcome this issue and to quantitatively describe the earthquake-induced geological failures e.g. landslides and liquefaction-induced lateral spreading, remote sensing techniques were applied during the last two decades such as Interferometric Synthetic Aperture Radar (InSAR), Light Detection and Ranging (LiDAR) and photogrammetric surveys. The latter one, a photogrammetric survey, is frequently conducted by use of Unmanned Aerial Vehicles (UAV), such as multicopters equipped with webcams, digital cameras and other sensors (Colomina and Molina, 2014; Lindner et al., 2016; Rossi et al., 2017, Yu et al., 2017). UAVs provide a convenient remote sensing platform for post-earthquake surveys given their ability to collect ultra-high-resolution imagery in short time over terrain that is often difficult to access. Using the Structure from Motion (SfM) image processing technique, a 3D point cloud can be created by intersecting the matched features between the overlapping, offset images. Point clouds from optical images enable the detailed representation of complex 3D surfaces, better editing and classification of the dataset and creation of further products like orthophotos, DSMs, DTMs, textured models etc. Comparison between different point cloud sets enables highly accurate change detection analysis, using recently developed matching algorithms. This work presents the mapping of earthquake-induced failures from two strong and shallow earthquakes occurred on November 17, 2015 onshore Lefkada (Mw 6.5; Ganas et al. 2016; Papathanassiou et al. 2017) and July 20, 2017 offshore Kos (Mw 6.6; Papathanassiou et al. 2019) , Greece. In the latter case, the SfM-based technique was applied using a ground-based digital camera, while in the former one a UAV DJI Phantom 3 was used. The Lefkada case study focuses on a deep-seated landslide triggered at the coastal area of Athani village (Okeanos site), SW Lefkada that induced severe damages to a recently constructed luxury hotel, while the Kos case study deals with the lateral spreading reported in the old harbor of the city.

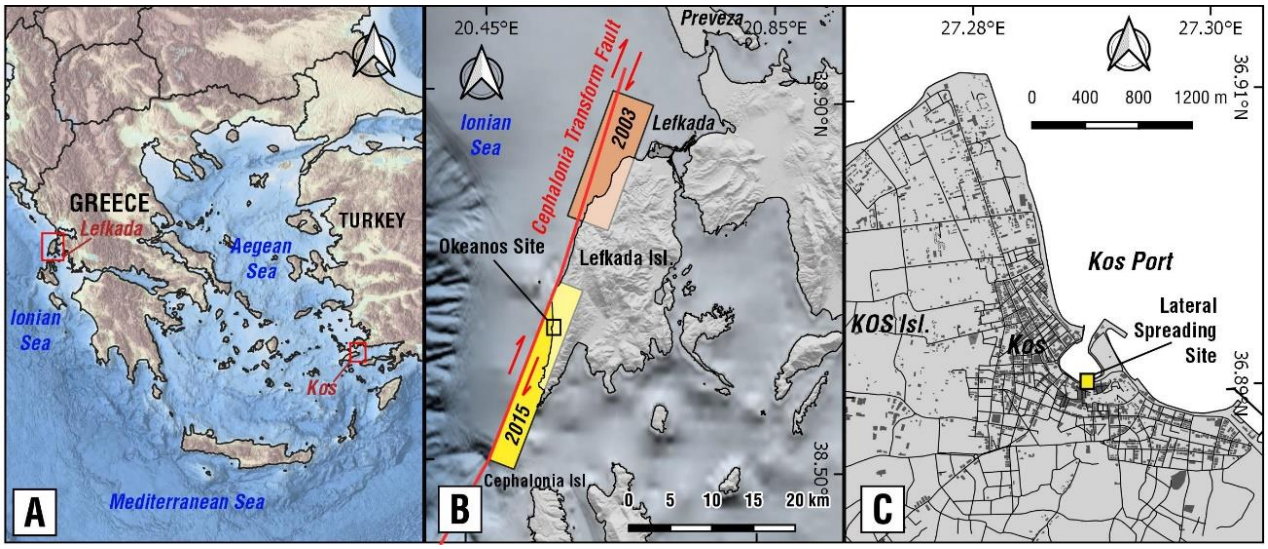

Figure 1. A) Overview map of Greece showing the location of the two case study sites. B) Relief map of Lefkada Island with the location of the Okeanos landslide site. The 2015 earthquake rupture extent is shown with a yellow polygon (Ganas et al. 2016). C) Map of Kos city with the location of the lateral spreading site.

The outcomes arisen by this study are that i) in the case of Okeanos landslide, the extraction of a detailed point cloud enabled the high-resolution modeling of the landslide at a site with challenging conditions such as limited accessibility and complex relief. It was demonstrated that both change analysis and volumetric calculation for co-seismic landslides demand a pre-event detailed point cloud set that can be co-registered and compared with the post-event set. Coastal areas are usually covered by multi-temporal aerial imagery in working scales (1:5K – 1:30K) that can be used to extract point

clouds suitable as a reference (Valkaniotis et al., 2018).

Regarding the effects mapped on Kos, it was found that the SfM-based technique provides reliable data (on horizontal axis) for documenting and modeling lateral displacement features and accordingly, could be used for the purposes of a rapid post-earthquake field survey (Papathanassiou et al., 2019). Furthermore, this technique can be applied even with a low-cost ground-based technique e.g. a simple hand-held digital camera. However, it cannot be characterized as satisfactory on vertical axis since a 12% deviation exists between the measurements obtained by these two techniques (SfM and traditional one), and some caution should be applied when using SfM-based technique.

Acknowledgements

We thank Nikos Grendas and Elisavet Kollia for field support.

We acknowledge support of this research by the project “HELPOS - Hellenic Plate Observing System” (MIS 5002697) which is implemented under the Action “Reinforcement of the Research and Innovation Infrastructure”, funded by the Operational Programme "Competitiveness, Entrepreneurship and Innovation" (NSRF 2014-2020) and co-financed by Greece and the European Union (European Regional Development Fund).

References

Colomina, I., and Molina, P., 2014. Unmanned Aerial Systems for Photogrammetry and Remote Sensing: A Review. ISPRS Journal of Photogrammetry and Remote Sensing, 92, 79-97

Ganas, Athanassios, Panagiotis Elias, George Bozionelos, George Papathanassiou, Antonio Avallone, Asterios Papastergios, Sotirios Valkaniotis, Issaak Parcharidis, Pierre Briole, 2016. Coseismic deformation, field observations and seismic fault of the 17 November 2015 M = 6.5, Lefkada Island, Greece earthquake, Tectonophysics, 687, 210-222, ISSN 0040-1951, http://dx.doi.org/10.1016/j.tecto.2016.08.012

Lindner, G., Schraml, K., Mansberg, R., Hübl, J., 2016. UAV monitoring and documentation of a large landslide. Applied Geomatics, 8, 1-11.

Papathanassiou George, Sotiris Valkaniotis, Athanassios Ganas, Nikos Grendas, Elisavet Kollia, 2017. The November 17th, 2015 Lefkada (Greece) strike-slip earthquake: Field mapping of generated failures and assessment of macroseismic intensity ESI-07, Engineering Geology, 220, 13-30, http://dx.doi.org/10.1016/j.enggeo.2017.01.019.

Papathanassiou G., Valkaniotis S., Pavlides S. 2019. The July 20, 2017 Bodrum-Kos, Aegean Sea Mw=6.6 earthquake; preliminary field observations and image-based survey on a lateral spreading site, Soil Dynamics and Earthquake Engineering, Volume 116, January 2019, Pages 668-680, https://doi.org/10.1016/j.soildyn.2018.10.038

Rossi G., Tanteri L., Tofani V., Vannoci P., Moretti S., Casagli N., 2017. Use of multicopter drone optical images for landslide mapping and characterization. Nat. Hazards Earth Syst. Sci. Discuss., doi:10.5194/nhess-2017-46.

Valkaniotis S., Papathanassiou G., Ganas Ath. 2018. Mapping an earthquake-induced landslide based on UAV imagery; case study of the 2015 Okeanos landslide, Lefkada, Greece, Engineering Geology, vol. 245, pp. 141-152

Yu, M., Huang, Yu., Zhou, J., Mao, L., 2017. Modeling of landslide topography based on micro-unmanned aerial vehicle photography and structure-from-motion. Environ Earth Sci., 76, 520 doi:10.1007/s12665-017-6860-x

15th International Congress of the Geological Society of Greece
Athens, 22-24 May, 2019 | Harokopio University of Athens, Greece
Bulletin of the Geological Society of Greece, Sp. Pub. 7 Ext. Abs. GSG2019-034

Object-Based Characterization and Semantic Labeling of Landslide and Rockfall phenomena using UAV photogrammetry

E. Karantanellis[1], V. Marinos[1], E. Vassilakis[2]

(1) Laboratory of Engineering Geology & Hydrogeology, Aristotle University of Thessaloniki, 54124, Thessaloniki, Greece
skarantanellis@gmail.com
(2) National and Kapodistrian University of Athens, 15772, Athens, Greece.

A variety of remote sensing tools have been extensively used in the past years for landslide detection and mapping purposes. In addition, detection and mapping of landslide and rockfall events using remote sensing products has been proved to be an effective approach to provide landslide inventories (Scaioni *et al*., 2014). However, most of the studies are lacking valuable semantic information about landslide elements and how they react with the surrounding environment; natural and man-made primitives. In addition, post classification object-based approaches have been proved to result in better accuracies compared with the pixel-based (Martha *et al*., 2011). Lately, innovative close-range remote sensing technology such as Unmanned Aerial Vehicle (UAV) photogrammetry and Terrestrial Laser Scanning (TLS) are widely applied in the field of geoscience due to their efficiency in collecting data about terrain morphology rapidly. Their main advantage stands on the fact that conventional methods are mainly collecting point measurements such as compass measurements of bedding and fracture orientation only from areas that were accessible. Aerial platforms are capable to overcome technical issues such as potential occlusions and unfavorable incidence angles due to their ability to capture imagery from multiple positions and with different angles. Nowadays, UAVs tend to be more flexible and powerful tools for landslide and rockfall investigations compared to TLS, due to their low-cost and ease of transportability in harsh environments but also with technology advances such as maintaining of Real Time Kinematic (RTK) positioning. An important factor of their usefulness is their capability to offer unprecedented spatial resolution over wide inaccessible areas, maintain a variability of different sensors (optical, laser, thermal, multispectral) and great ability to reach remote areas and acquire data as close as the user defines. UAVs applications are widely used in post-disaster situations for emergency support, in infrastructure monitoring, in natural resources management, in geohazard monitoring etc. (Corominas *et al*., 2016; Vassilakis *et al*., 2019). The latter proves that UAV market has been rapidly growing over the last decade and in future more applications will be introduced in the public. Thus, rapidness and efficiency of Structure-from-Motion (SfM) technology in landslide management provides numerous advantages such as creating landslide inventory maps providing 3D information of large areas.

This research aims to demonstrate the applicability of UAV technology for automated semantic labeling in managing landslide and rockfall hazard in mountainous environments during emergency situations. SfM photogrammetry in addition to high accuracy RTK-GNSS ground control point establishment, is used to provide detailed 3D point clouds describing the surface morphology of the landslide and rockfall elements. Specifically, two test sites were exploited, a detailed UAV survey took place in a landslide case site, on Santorini island and specifically in Red Beach which constitutes one of the most touristic places on the island. In addition, a rockfall test site namely as «Proussos», near one of the most visited and famous Monasteries in the territory of Evritania prefecture, in Greece, was investigated via detailed UAV flight plans. The latter site is formed as an unstable steep slope across the main road network, on which continuous failures and road cuts appear after heavy rainfall events (Figure 1). The Red Beach test site is located on Santorini island, which in turn represents one of the most unique geological structures as it is formed around the caldera of an active volcano. Moreover, rockfalls and landslides are widespread phenomena due to the orientation and steepness of the cliffs (Karantanellis *et al*., 2019) which are mainly formed as high elevated lava domes (>50 m) with loose material inside, extruded by sticky, slow-flowing dacite lava due to continuous coastal erosion.

The proposed methodology was divided in five main working phases. The first phase includes designing and execution of an optimal UAV flight planning in order to collect accurate 3D data. The current step is crucial in order to provide complete and precise model at the later processing stages. During the second phase, the pre-processing and raw data preparation such as point cloud filtering and elimination of ambiguities is taking place, while at the next phase an image segmentation using the 3D point cloud RGB information is created. The main task was focused on identifying the specific landslide elements by using an object-based approach. Object-Based Image Analysis (OBIA) is an image analysis technique, remarkably developed during the last decade, since recent advances in computer vision and machine learning with the main task to automatically replicate human interpretation to identify objects in remote sensing images brought impressive results (Blaschke, 2010). It is only during the last decade, that OBIA methods have proved to outperform the pixel ones such as elimination of false positives which are missed by pixel-based approaches (Keyport *et al*., 2018). A sequence of image-based processes was applied, including multi-scale object segmentation, spectral, morphometric and contextual information extraction aiming to detect the landslide among other features. The latter is mainly developed as a knowledge-driven ruleset to serve for identifying individual landslide objects based on their morphometric and spectral parameters. The next phase was set up for object classification in meaningful and homogeneous landslide classes (e.g. scarp, depletion zone, accumulation zone) which are spatially connected by introducing contextual information in the ruleset. The validation of the results represents the final phase, which is based on accuracy assessment against a digitized

landslide map and field observations. The resulted models were used as reference to detect and characterize 3D landslide features and provide detailed identification of hazardous regions.

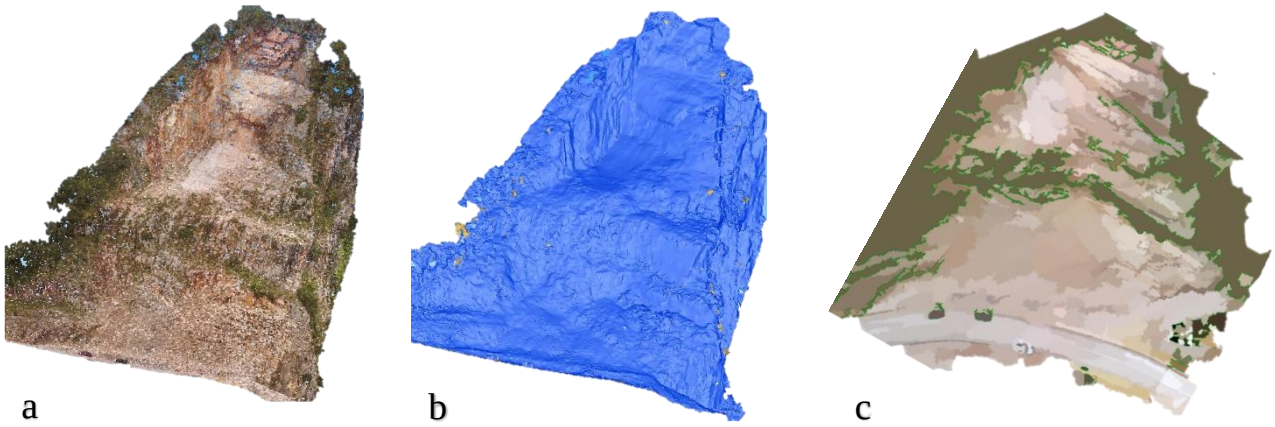

Figure 1. a) 3D point cloud of Proussos case site, b) 3D mesh model of Proussos case site, c) 3D point cloud segmentation and classification – OBIA initial result

The proposed methodology presents the effectiveness and efficiency of UAV platforms to acquire accurate photogrammetric datasets from intense relief environments and complex surface topographies by providing a holistic assessment and characterization of the failure site based on semantic classification of the landslide and rockfall objects. Results have demonstrated the capabilities of combining UAV platforms with computer-based methods for rapid and accurate identification of valuable semantic information subjectively and even from inaccessible areas of the landslide and rockfall body.

Acknowledgements

This research is co-financed by Greece and the European Union (European Social Fund- ESF) through the Operational Programme "Human Resources Development, Education and Lifelong Learning" in the context of the project "Strengthening Human Resources Research Potential via Doctorate Research" (MIS-5000432), implemented by the State Scholarships Foundation (IKY).

References

Blaschke, T., 2010. Object based image analysis for remote sensing. ISPRS Journal of Photogrammetry and Remote Sensing 65, 2-16.

Colomina, I., Molina, P., 2014. Unmanned aerial systems for photogrammetry and remote sensing: A review. ISPRS Journal of Photogrammetry and Remote Sensing 92, 79-97.

Karantanellis, E., Marinos, V., 2019. Multitemporal Landslide Mapping and Quantification of Mass Movement in Red Beach, Santorini Island Using Lidar and UAV Platform. IAEG/AEG Annual Meeting Proceedings, San Francisco, California, USA, p. 163-169.

Keyport, R. N., Oommen T., Martha T. R., Sajinkumar K.S., Gierke J.S., 2018. A comparative analysis of pixel- and object-based detection of landslides from very high-resolution images. International Journal of Applied Earth Observation Geoinformation 64, 1-11.

Martha T., Kerle N., Van Westen C., Jetten V., Kumar K.V. 2011. Segment Optimization and Data-Driven Thresholding for Knowledge-Based Landslide Detection by Object-Based Image Analysis. IEEE Trans Geosci Remote Sensing 29 (12), 4928-4943

Scaioni, M., Longoni L., Melillo V., Papini M., 2014. Remote Sensing for Landslide Investigations: An Overview of Recent Achievements and Perspectives. Remote Sensing 6, 9600-9652.

Vassilakis, E., Foumelis, M., Erkeki, A., Kotsi, E., Parcharidis, I., Lekkas, E., 2019. Multitemporal Surface Deformation Analysis of Amyntaio Slide (Greece) using Remotely Piloted Airborne System and Structure-from-Motion photogrammetry. 4th Joint International Symposium on Deformation Monitoring, Athens.

15th International Congress of the Geological Society of Greece
Athens, 22-24 May, 2019 | Harokopio University of Athens, Greece
Bulletin of the Geological Society of Greece, Sp. Pub. 7 Ext. Abs. GSG2019-171

Engineering Geological Mapping of Earthquake-Induced Landslides in south Lefkada Island, Greece Using UAV; Applications and Limitations

N. Grendas[1], V. Marinos[1], G. Papathanassiou[2], A. Ganas[3], S. Valkaniotis[4]

(1) Aristotle University of Thessaloniki, School of Geology, Faculty of Sciences, 541 24, Thessaloniki, Greece, ngrendas@gmail.com
(2) Democritus University of Thrace, Department of Civil Engineering
(3) National Observatory of Athens, Institute of Geodynamics, Lofos Nymfon, Athens 118 10, Greece, aganas@noa.gr
(4) Trikala, Greece

Introduction

A strong, shallow depth, earthquake (Mw=6.5) occurred onshore Lefkada island on November 17, 2015 with the focal depth estimated at 10 Km (Ganas et al., 2016). Lefkada has been repeatedly struck by earthquakes during the last century (1911-2015). The surface magnitude (Ms) of instrumentally recorded earthquakes ranges between 5.3 and 6.4. (Papathanassiou et al., 2005; 2017). The 2015 seismic fault is a near-vertical strike-slip fault running along the western coast, which is part of the CTF zone (Cephalonia Transform Fault). Landslides and ground cracks were mainly reported at the western part of the island, inducing structural damages. High severity slope failures occurred at Egremnoi and Gialos areas that both are located at western coastal regions. This study aims to investigate the engineering geological conditions at those areas assigned based on GSI classification, and assess the characteristics and physical quantities (eg. type, area-m2, volume-m3) of the instabilities. In order to achieve this, a field survey was conducted in July 2016 and landslide characterization was conducted in Eggremnoi and Gialos areas with the use of UAV imagery in relation with engineering geological mapping (Grendas et al., 2018). Furthermore, types and dimensions of slope failures were evaluated in order to estimate the total volume of the mass movement. Structure-from-Motion models produced by UAV images (using Agisoft Photoscan software) permitted the accurate and detailed identification and mapping of co-seismic failures. Moreover, all the field data from the engineering geological mapping, have been digitized and rasterized at 5 m grid spacing using ArcGIS (Figure 2). The outcome of the present study is the precise calculation of the area-m2 and volume-m3 regarding the slope failures and the correlation among the pre mentioned failures with the existing engineering geological conditions (Figure 2, Figure 3). The limitations of UAV surveys at the specific region are also presented.

Materials and Methods

Photogrammetry is called the “technique which is used in order to be received 3D data via 2 or multiple photos of the same object, captured from different angle” (Vasuki et al., 2014). Unmanned aerial systems (UAS) have been described by different names (e.g. aerial robots) but the most common title is UAV (Unmanned Aerial Vehicle) or more simply “drones” (Colomina & Molina, 2014, Siebert & Teizer, 2014). The Digital Surface Model (DSM) of Gialos area was constructed by UAV images. We performed the UAV surveys with a DJI Phantom 3 Professional quadcopter that acquired 12MP digital images. The main advantages of a UAV survey in the study sites were:

- Surveying of remote and/or inaccessible areas.
- Rapid data acquisition and wide area coverage.
- Extraction of very high resolution topography that can facilitate volumetric calculations

Regarding Eggremnoi and Gialos areas, 144 and 139 photos of 12MP were captured and analyzed respectively, via Agisoft Photoscan Pro, producing detailed point clouds (Figure 1). DSM/orthophoto maps of the sites were also constructed (Grendas et al., 2018).

Discussion and conclusions

The use of a UAV sensor made possible the mapping of landslide boundaries as well as the mapping of some structures that were not visible from the ground during the field investigation. On the other hand, during field investigation, the determination of landslide typology is possible but not the mapping of exact boundaries. Areas with dense plant cover are not available to use as long as the correct capturing of the terrain is not possible. This is in contrast to other imaging methods in which the removal of vegetation canopy is feasible (e.g. LIDAR). Towards the interpretation of Gialos site, vegetation cover was sparse and most of the structures and landslides were visible, in contrast with Eggremnoi site where dense and high vegetation was present, diminishing ground surface visibility. However, it must be noted that the peripheral segments of DEMs present quite large deformation (due to poor overlapping), an issue that leads to non-feasible editing and interpretation.

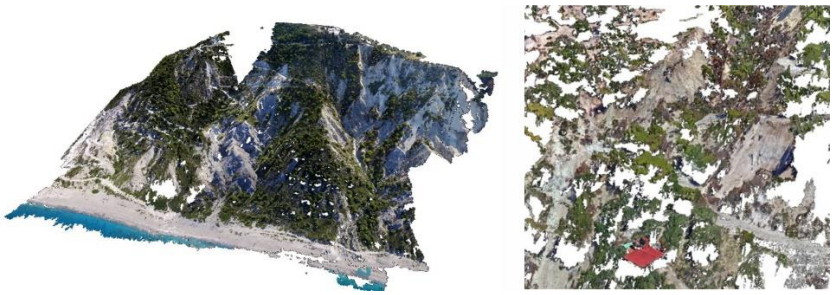

Figure 1. Structure-from-Motion models (point cloud) of the study sites from acquired UAV imagery. Left: Gialos site. Right: Close-up of Gialos site model, where frequent gaps in coverage are visible due to dense vegetation

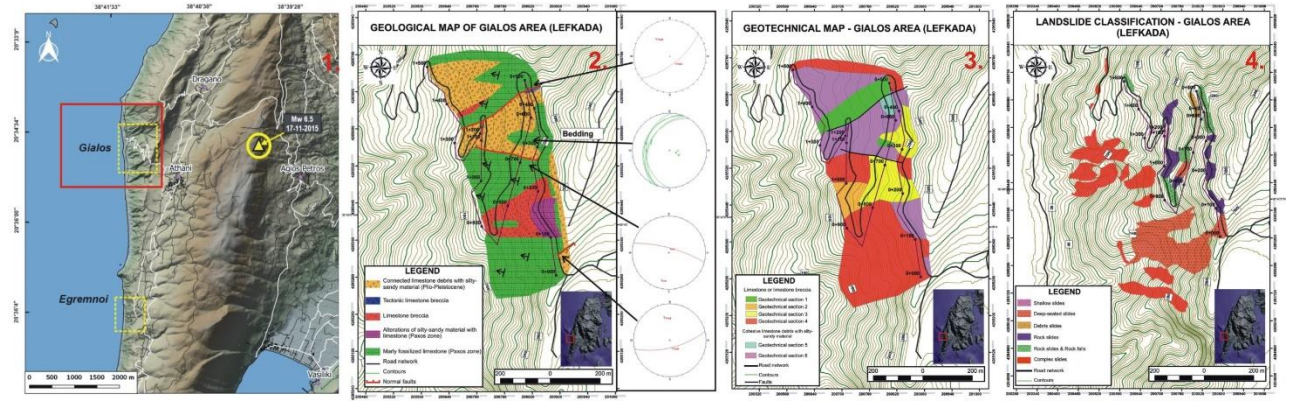

Figure 2. 1: Shaded relief map of Lefkada showing Gialos area (red square) 2: Geological map of Gialos area 3: Engineering geological map. 4: Landslide classification map produced according to DEM model

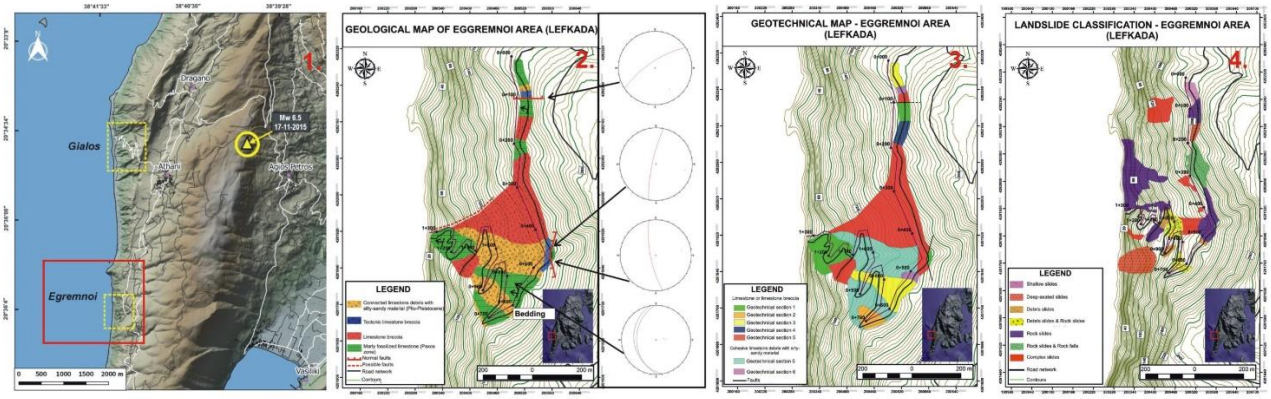

Figure 3. 1: Shaded relief map of Lefkada showing Eggremnoi area (red square) 2: Geological map of Eggremnoi area 3: Engineering geological map. 4: Landslide classification map produced according to DEM model

References

Colomina I., Molina P., 2014. Unmanned aerial systems for photogrammetry and remote sensing: A review. ISPRS Journal of Photogrammetry and Remote Sensing 92, pp. 79–97.

Ganas A., Elias P., Bozionelos G., Papathanassiou G., Avallone A., Papastergios A., Valkaniotis S., Parcharidis I., Briole P., 2016. Coseismic deformation, field observations and seismic fault of the 17 November 2015 M = 6.5, Lefkada Island, Greece earthquake, Tectonophysics, 687, 210-222, ISSN 0040-1951, http://dx.doi.org/10.1016/j.tecto.2016.08.012.

Grendas N., Marinos V., Papathanassiou G., Ganas A., Valkaniotis S., 2018. Engineering geological mapping of earthquake-induced landslides in south Lefkada Island, Greece; evaluation of the type and characteristics of the slope failures. Environmental Earth Sciences (2018) 77:425, https://doi.org/10.1007/s12665-018-7598-9.

Papathanassiou G., Valkaniotis S., Ganas A., Grendas N., Kollia E., 2017. The November 17th, 2015 Lefkada (Greece) strike-slip earthquake: Field mapping of generated failures and assessment of macroseismic intensity ESI-07, Engineering Geology, 220, 13-30, http://dx.doi.org/10.1016/j.enggeo.2017.01.019.

Papathanassiou G, Pavlides S, Ganas A (2005) The 2003 Lefkada earthquake: Field observations and preliminary microzonation map based on liquefaction potential index for the town of Lefkada. Engineering Geology, 82, 12– 31.

Siebert S., Teizer J., 2014. Mobile 3D mapping for surveying earthwork projects using an Unmanned Aerial Vehicle (UAV) system. Automation in Construction, 1–14.

Vasuki Y., Holden E.-J., Kovesi P., Micklethwaite S., 2014. Semi-automatic mapping of geological Structures using UAV-based photogrammetric data: An image analysis approach. Computers & Geosciences, v. 69, 22-32.

15th International Congress of the Geological Society of Greece
Athens, 22-24 May, 2019 | Harokopio University of Athens, Greece
Bulletin of the Geological Society of Greece, Sp. Pub. 7 Ext. Abs. GSG2019-175

Ground Truth Validation of Land Subsidence Phenomena Identified by DinSAR Techniques at the Coastal Zone of N. Faliro, Moschato and Kallithea Municipalities

A. Kaitantzian[1], C. Loupasakis[1], I. Parcharidis[2], C. Maroufidis[1]

(1) School of Mining and Metallurgical Engineering, National Technical University of Athens, 9, Heroon Polytechniou Str., Athens, Greece, ankait@metal.ntua.gr
(2) Department of Geography, Harokopio University of Athens, 70, El. Venizelou Str., Athens, Greece

Land subsidence is considered among the most frequent geological hazard that usually occurs as a consequence of a number of phenomena, namely: natural compaction of unconsolidated fine - grained deposits, groundwater over - exploitation, peat - oxidation and collapse of underground cavities (Ziaie *et al.*, 2009). The effects of the land subsidence include damages to building structures as well as loss of functionality of linear and point infrastructures (pipeline and road network deformations, well-casing failures and protrusion etc.) (Osmanoğlu *et al.*, 2011; Cigna *et al.*, 2012).

The main purpose of the current study is to investigate land subsidence in the coastal zone of the N. Faliro, Moschato and Kallithea municipalities, by means of advanced DinSAR techniques and to identify the main causes of the observed ground deformations that contribute to the development of the surface fractures affecting the site.

Detecting, measuring and monitoring land subsidence is important for the urban and infrastructures planning as well as for the risk management. Repeat-pass space-borne SAR interferometry (InSAR) is a unique tool for large-scale monitoring of surface deformation at a low cost and great precision (Massonnet & Feigl, 1998) and particularly for land subsidence regardless of its cause (Dixon *et al.*, 2006; Herrera *et al.*, 2009; Osmanoglu *et al.*, 2011; Chaussard *et al.*, 2013).

The application advanced DinSAR techniques for the detection of land motion phenomena revealed that the area extending between the outlets of the Kiffisos and Ilisos rivers is affected by subsidence with LOS deformation rates of -1.5 to -6.9 mm/yr during the period 1992 - 2001 and of -1.5 to -3mm/yr for the period 2002-2010 (Fig.1a,b).

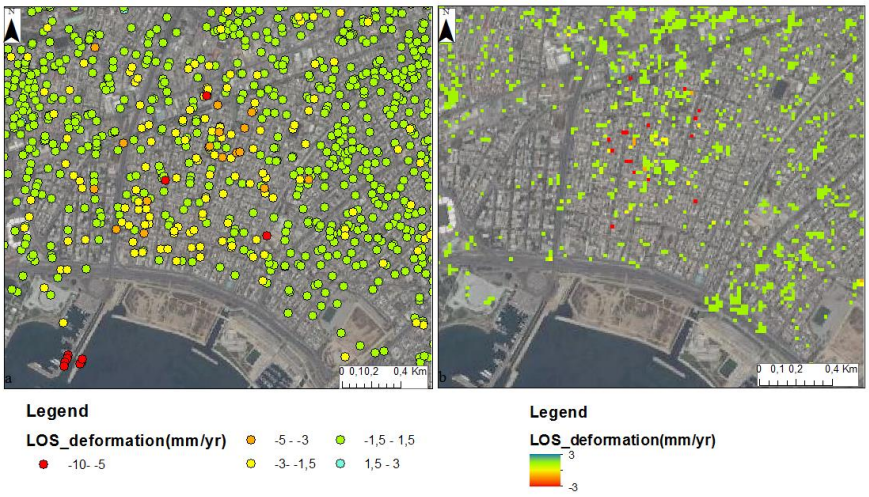

Figure 1. a) Velocities from 1992 to 2001 as derived by the PSI analysis of ERS1&2 data b) Velocities from 2002 to 2010 as derived by the SVD analysis of ENVISAT data.

In order to further validate and interpret these results, field observations have been conducted exploited. The surface ruptures extent mainly at the area between the riverbeds of Kiffisos and Ilissos Rivers, leading to differential displacements. The visible traces of subsidence affect pavements and numerous buildings (Fig.2).



Figure 2. Field evidence of ruptures in the study area. Coordinates are in UTM WGS84 (projected). Damages witnessed at building (point 1), pavement (point 2) and natural terrain (point 3).

The outcomes of the performed analysis indicated that the land subsidence phenomena in the study area could be attributed primarily to the natural compaction of the fine grained alluvial deposits. Furthermore, the overexploitation of groundwater reservoir cannot be entirely excluded.

Acknowledgments

The European Space Agency (ESA) through the Terrafirma project has funded the SAR imagery processing. The authors gratefully acknowledge the German Space Agency - DLR (German) for having processed SAR data for the area.

References

Cigna, F., Osmanoğlu, B., Cabral-Cano, E., Dixon, T. H., Ávila-Olivera, J.A., Garduño-Monroy, V.H., DeMets, C., Wdowinski, S., 2012. Monitoring land subsidence and its induced geological hazard with Synthetic Aperture Radar interferometry: A case study in Morelia, Mexico. Remote Sensing of Environment 117, 146–161.

Chaussard, E., Amelung, F., Abidin, H., Hong, S.H., 2013. Sinking cities in Indonesia: ALOS PALSAR detects rapid subsidence due to groundwater and gas extraction. Remote Sensing of Environment 128, 150-161.

Dixon, T.H., Amelung, F., Ferretti, A., Novali, F., Rocca, F., Dokka, R., Sella, G., Kim, S.W., Wdowinski, S., Whitman, D., 2006. Subsidence and flooding in New Orleans - a subsidence map of the city offers insight into the failure of the levees during Hurricane Katrina. Nature 441, 587-588.

Herrera, G., Fernandez, J.A., Tomas, R., Cooksley, G., Mulas, J., 2009. Advanced interpretation of subsidence in Murcia (SE Spain) using A-DInSAR data modelling and validation. Natural Hazards Earth System Science 9, 647-661.

Massonnet, D., Feigl, K.L., 1998. Radar interferometry and its application to changes in the Earth's surface. Reviews of Geophysics 36, 441-500

Osmanoğlu, B., Dixon, T. H., Wdowinski, S., Cabral-Cano, E., Jiang, Y., 2011. Mexico City Subsidence Observed with Persistent Scatterer InSAR. Journal of Applied Earth Observation and Geoinformation 13(1), 1–12.

Ziaie, A., Kumarci, K., Ghanizadeh, K.R., Mahmodinejad, A., 2009. Prediction of earth fissures development in Sirjan. Res J Environ Sci 3, 486-496.

15th International Congress of the Geological Society of Greece
Athens, 22-24 May, 2019 | Harokopio University of Athens, Greece
Bulletin of the Geological Society of Greece, Sp. Pub. 7 Ext. Abs. GSG2019-181

Rock Mass Characterization Using Lidar Terrestrial Laser Scanner for Rockfall Susceptibility Assessment in Perissa Area (Santorini)

I. Farmakis[1], V. Marinos[2], E. Karantanellis[2] G. Papathanasiou[3]

(1) Queen's University, K7L 2N8, Kingston, ON, Canada, i.farmakis@queensu.ca
(2) Aristotle University of Thessaloniki, 54124, Thessaloniki, Greece
(3) Democritus University of Thrace, Xanthi, 67100, Greece.

Rockfalls consist one of the most dominant geological hazards in mountainous rocky regions with the potential to turn catastrophic if occurs in the anthropogenic environment. Due to that fact, the identification of the possible locations to produce the phenomenon is of high importance. Susceptibility is the parameter describes these locations and the qualitative and quantitative assessment of it is necessary for the timely treatment of a possible rockfall occurrence. However, this approach requires some critical rock mass characteristics to be known. These ones that govern the phenomenon and so the more detailed acquisition of them increases the calculations reliability. Such data acquisition can be achieved by implementing conventional mapping methods as well as remote sensing techniques like LiDAR (Light Detection and Ranging) scanners. The LiDAR technology is extremely preferred the last decades in the field of Geosciences, providing many advantages against the pre-existing methods (Abellán et al., 2009; Lato et al., 2009; Kromer et al., 2018).

In the current study, LiDAR technology was implemented to extract the appropriate parameters can be used for the rockfall susceptibility assessment. The study area was the limestone slopes in Perissa area at the southeastern part of Thera island at Santorini complex. After data processing, joint orientation parameters, joint spacing and block volumes were extracted. Parameters which are usually either statistically or at confined areas estimated considering homogeneous rock mass in them respect. The extra element this methodology provides is the creation of spatial distribution maps of the above-mentioned parameters, taking into account the fluctuation of their values along the slopes. Thus, the produced result can be used in the spatially-specific susceptibility assessment without considering each slope or formation as an entire susceptibility mapping unit. The data processing is extensively analyzed step by step providing the reader with the desirable view of the whole procedure. Finally, the results produced by the current methodology are validated and interpreted according to in-situ records and measurements as well as manually extracted measurements on the point clouds.

Study area

In particular, the study area is part of the internal Hellenic Volcanic Arc and geologically belongs to the Atticocyladian geotectonic zone's bedrock. Located on the southeastern part of Thera, represents one of the two pre-alpine bedrock exposures on the island, and specifically the indigenous unit, as the rest is covered by the later volcanic activity's products. Perissa's cliffs belong to the wider carbonate formation of Profitis Ilias that consists of Early Cretaceous recrystallized limestones which compose the semi-metamorphosed bedrock of the Atticocycladian zone and specifically the South Cyclades Unit. The landscape of the coastal Perissa area is in general very steep with dipping up to 70 degrees, heights up to 50 m and face towards the SW and SSW.

Data acquisition

The LiDAR data was obtained by using an Optech ILRIS-3D long-range terrestrial laser scanner and the survey planning aimed to acquire a dense and high-resolution dataset for the detailed mapping of all necessary parameters required in the direction of rockfall susceptibility. In specific, five predefined scan locations were used to cover the different slopes formed along the entire cliff with the most feasible overlapping, given the buildings that exist in a small distance from the slopes, in order to minimize the orientation bias and occlusion effect. The obtained point clouds were merged and geo-referenced by utilizing on-slope-placed targets and their absolute coordinates measurements taken from a total station as they were easily identified within the dataset due to the high resolution. The entire dataset consists of more than 15 million points.

Methodology

The proposed methodology initially aims to the orientation estimation of the individual slopes formed along the cliff as well as the discontinuity sets, following aproaches proposed by Riquelme et al., 2014. Sequentially, joint spacing values are extracted for each discontinuity set according to Riquelme et al., 2015 and based on these geometric parameters the block volume distribution is estimated. Furthermore, a spatial distribution map (Figure 1) for each of the above-mentioned parameters is created providing the desirable spatial information which a further analysis could be based on in order to produce a spatial-aimed result rather than a single susceptibility value for each individual slope. Current methodology's implementation was carried out by using CloudCompare and ArcGIS software as well as numerous Matlab algorithms on DSE software package.

Results

Principal discontinuity sets orientations extracted from the used semi-automated methodology are presented and

compared with the conventional compass measurements taken in-situ. Furthermore, statistics, graphs and maps illustrate the distribution of each discontinuity set orientation, spacing value, as well as the block volume, are listed.

It is commonly accepted that the block volumes formed along a slope are the very critical parameter for the rockfall susceptibility assessment. Moreover, further space-resolved stability analyses for the susceptible-defined areas can be carried out utilizing the spatial distribution maps produced by this methodology. The authors also utilized the extracted orientation data in order to create the corresponding stereoplot to each slope and detect the governing failure mechanism on each of them. The parameters being extracted from the proposed LiDAR data processing methodology are spatially independent and display fluctuations along the cliffs. Thus, the main aftermath earned here is the fact that the rock masses are not represented realistically when being treated as homogenous and isotropic in respect of parameters such as joint spacing and/or block volumes. Sequentially, susceptibility is not represented any more by a specific value for an entire slope or a formation considered as a united mapping unit. Contrariwise, it can be changing defining the more and the less susceptible areas along the slopes. That fact leads the focus of interest, for additional analysis, only to certain areas and prevents the consumption of unnecessary funds and time in the entire united unit investigation.

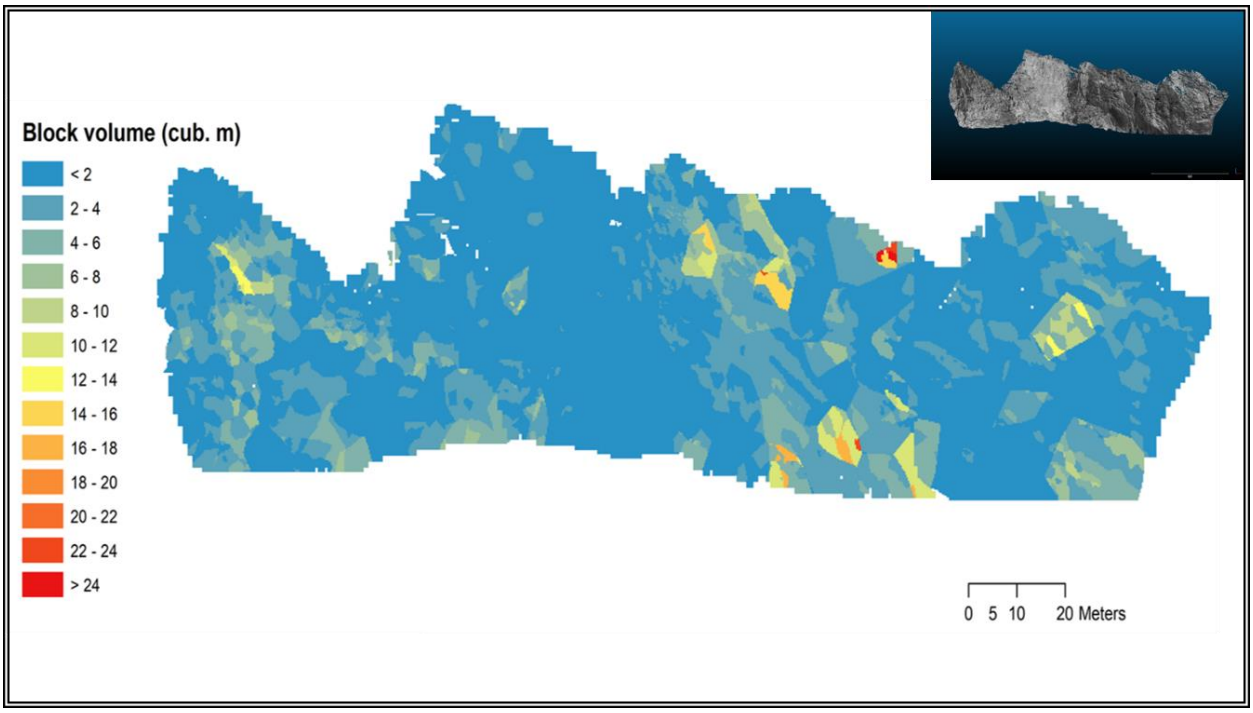

Figure 1. Potential block volume spatial distribution map.

References

Abellán, A., Jaboyedoff, M., Oppikofer, T., Vilaplana, J.M., 2009. Detection of millimetric deformation using a terrestrial laser scanner: Experiment and application to a rockfall event. Nat. Hazards Earth Syst. Sci. 9, 365–372. https://doi.org/10.5194/nhess-9-365-2009

Kromer, R.A., Rowe, E., Hutchinson, J., Lato, M., Abellán, A., 2018. Rockfall risk management using a pre-failure deformation database. Landslides 15, 847–858. https://doi.org/10.1007/s10346-017-0921-9

Lato, M., Hutchinson, J., Diederichs, M., Ball, D., Harrap, R., 2009. Engineering monitoring of rockfall hazards along transportation corridors: Using mobile terrestrial LiDAR. Nat. Hazards Earth Syst. Sci. 9, 935–946. https://doi.org/10.5194/nhess-9-935-2009

Riquelme, A.J., Abellán, A., Tomás, R., 2015. Discontinuity spacing analysis in rock masses using 3D point clouds. Eng. Geol. 195, 185–195.

Riquelme, A.J., Abellán, A., Tomás, R., Jaboyedoff, M., 2014. A new approach for semi-automatic rock mass joints recognition from 3D point clouds. Comput. Geosci. 68, 38–52.

15th International Congress of the Geological Society of Greece
Athens, 22-24 May, 2019 | Harokopio University of Athens, Greece
Bulletin of the Geological Society of Greece, Sp. Pub. 7 Ext. Abs. GSG2019-184

Slope Stability Monitoring of the Urban Boundary Layer of Hills in Athens City by Means of MTInSAR

Kazana[1] S., Krassakis[1] P., Chen[2] F., Parcharidis[3] I., Koukouzas[1] N., Lekkas[4] E.

(1) Centre for Research and Technology, Hellas (CERTH), 52 Egialias St., 15125 Maroussi, Athens, kazanageol@yahoo.gr
(2) Institute of Remote Sensing and Digital Earth, Chinese Academy of Sciences, Beijing, China
(3) Harokopio University of Athens, Athens, Greece
(4) National & Kapodistrian University of Athens, Athens, Greece

In many urban areas of the world, the issues associated with rocky slope instability are numerous, ranging from first-time rapid rockfalls to reactivated slow rock mass slides and from minor, localized failures to broader catastrophic events. A variety of factors, such as the topography, geological - geotechnical structure of the formations and environmental conditions control the occurrence of slope failures (Chowdhury and Flentje, 2011). The growth of urban population is responsible for inevitable expansion of urban centres adjacent to hazardous hilly regions. As a result, stability concerns arise for the safety of humans and the infrastructure. The need to predict and prevent these slope failures is critical. Despite the extremely slow rates of hillslope movements, imperceptible to the optical observation, the cumulative displacement over a period of time may cause considerable risk to manmade structures and increase vulnerability. Although authorities have general restrictions prohibiting building on slopes exceeding a certain degree of incline, other effects triggering slope instability should also be considered in mass movement assessments when projecting a complete urban growth plan.

In recent years, integrated remote sensing techniques based on space-based SAR interferometry techniques could become the key method to identify and predict slope instabilities. Since 90's differential repeat-pass interferometry radar (DInSAR) based on SAR images processing has proven an interesting tool for the measurement and observation of ground deformation (Massonnet and Rabaute, 1993). Nowadays, using large stacks of SAR images acquired over the same area, long deformation time series can be analysed using multitemporal differential SAR interferometry techniques which overcome several limitations of repeat-pass interferometry. The most important advantage of the method is the ability to construct maps of yearly rates of ground displacement or the change to the rates at millimetric scale. Space-based SAR interferometry techniques could become an effective tool for prediction of slope instabilities and identification of locations, where potential slope failures may appear and human interventions could cause instability (Di Martire et al. 2012, Burns S.F. 2015).

The main purpose of this study is the slope stability monitoring of Athens city hills. In the case of Athens progressive residential development has been taking place bellow the shadow of steep rocky hills of the city centre. It is worth mentioning that some of the most renowned ancient monuments in the city are founded on these hills.
The Athens Basin represents a complex neotectonic asymmetric graben bounded by NNE-SSW marginal faults (Papanikolaou et al., 2004). The basin is surrounded by the mountains of Aegaleo, Parnitha, Pendeliko and Hymettus. The southern and south-western part of the basin is open towards the Saronikos Gulf forming a shoreline of about 47 km. A number of historical hills are distributed within the basin, Acropolis, Nymphs, Philopappou, Pnika, Areopagus, Lycabettus and Tourkovounia. Based on the comparative evaluation of the geological maps and the available literature it is summarized that the Athens hilltops are formed by light to dark grey, thickly bedded to massive and occasionally medium bedded, recrystallized Upper Cretaceous limestone with numerous joints and karstic cavities. These limestone masses are a member of the upper calcareous horizon of the lithostratigraphic series of the alpine formations that were overthrusted the "Athens Schist" formation that constitute the basement of many parts of Athens Basin. The limestones overlie a marly horizon which covers the Athens Schist series, including schists, shales, sandstones, marls and limestones (Koukis and Sabatakakis, 2000). In places the limestone hills are covered by post-alpine deposits. The neotectonic structure of the broader Athens area comprises a number of major tectonic fractures with E-W and NW-SE strike direction (Papanikolaou et al., 2004). It can be determined that the limestone outcrops were subjected to a NNE-SSW tensile tectonic stress field which formed faults, mainly normal throughout the calcareous mass. Although the limestones have excellent mechanical characteristics they are fractured by numerous joint sets and are intensively weathered forming karstic fissures often 0.5 to 2 m wide and in case of Tourkovounia the voids reach 15m width (Karfakis and Loupasakis, 2006). The karstificated fractured zones represent areas of slope instability and may cause differential settlements of structures and even the failure of the foundation of residences.

Taking into consideration all these points Athens hillslopes' monitoring is an indispensable and essential issue due to its nature to provide support for slope stability risk assessment in urban and suburban cases.
The current research work aims to examine the contribution of high resolution radar satellite images and specifically TerraSAR-X stripmap in the mapping of low rate land displacement over the urban boundary layer of hills in Athens city by means of MTInSAR for the period 2012-2016. In addition, DEM and DEM-derived spatial models have been created and used. Analysis of the results shows that generally the urbanised slopes in Athens hills are stable. Patterns of displacement are locally observed and are of minor importance. Nonetheless, a more detailed knowledge of the local conditions of the limestone outcrops is needed by fieldwork. The methodologies applied proved an effective way to describe the potential behavior of the rock mass with respect to the probability of occurrence of slope displacements.

References

Burns, S.F. (2015). Urban Landslides: Challenges for Forensic Engineering Geologists and Engineers. In: Lollino G., Manconi A., Guzzetti F., Culshaw M., Bobrowsky P., Luino F. (eds) Engineering Geology for Society and Territory - Volume 5. Springer, Cham

Chowdhury, R. and Flentje, P., (2011). Practical reliability approach to urban slope stability. 11th International Conference on Applications of Statistics and Probability in Civil Engineering. August. ETH Zurich, Switzerland. CRC Press/Balkema

Di Martire, D., De Rosa, M., Pesce, V., Santangelo, M.A., Calcaterra, D. (2012). Landslide hazard and land management in high-density urban areas of Campania region, Italy. Nat Hazards Earth Syst Sci 12(4):905–926

Karfakis, J. and Loupasakis, C. (2006). Geotechnical characteristics of the formation of "Tourkovounia" Limestones and their influence on urban construction - City of Athens, Greece. IAEG2006 Paper number 794. The Geological Society of London.

Koukis, G., Sabatakakis, N. (2000). Engineering geological environment of Athens, Greece. Bul Eng Geol Environ. 59(2):127-135.

Marinos, G.P., Katsikatsos, G., Georgiades-Dikaioulia, E., Mirkou, R. (1971). The Athens' Schists Formation I: Stratigraphy and Structure. Ann Géol Pays Hell. 23:183-216. (In Greek).

Massonnet, D. and Rabaute, T. (1993). Radar interferometry: Limits and potential. IEEE Transactions on Geoscience and Remote Sensing, 31(2), 455±464

Papanikolaou D., Bassi E.-K., Kranis H. and Danamos G. (2004). Paleogeographic evolution of the Athens basin from upper Miocene to present. Bulletin of the Geological Society of Greece vol. XXXVI, p.

15th International Congress of the Geological Society of Greece
Athens, 22-24 May, 2019 | Harokopio University of Athens, Greece
Bulletin of the Geological Society of Greece, Sp. Pub. 7 Ext. Abs. GSG2019-203

3D rock thickness extraction by combining Point Clouds of different origin. Case Study: The roof of Koutouki Cave Peania, Greece

A. Konsolaki[1], Emm. Vassilakis[1], V. Giannopoulos[2], G. Kontostavlos[3], G. Psaltakis[4]

(1) Remote Sensing Laboratory, Faculty of Geology & Geo-environment, NKUA, Panepistimiopolis, Zographou, 15784, Greece, alikikons@geol.uoa.gr
(2) Ministry of Culture, Ephorate of Palaeoanthropology and Speleology, Ardittou 34b, Athens, 11636, Greece
(3) Board Member of Hellenic Speleological Society, Sina 32, Athens, 10672, Greece
(4) Landmark-Loutridis Co., Vouliagmenis Ave. 248, Ag. Dimitrios, 17343, Greece

The purpose of this research is to combine two state-of-the-art technologies in surveying for extracting the rock thickness above a cavity. By combining Lidar technology for indoor surveying and photogrammetric processing of Unmanned Aerial Systems (UAS – drones) data, we managed to calculate and project with high accuracy the rock thickness of the roof of the underground environment of Koutouki Cave (Peania, Greece).

Usually, cave systems are complex and unique because of their distinctive geometry and compound geomorphology along with natural harsh conditions such as constrained accessibility, limited light, high humidity and possible existence of water. Such environments make mapping difficult and further complicated (Kershaw, 2012). Nowadays, the state-of-the-art in surveying of open surface is based on LiDAR technology. Lately, similar technology has started to be used for indoor surveying and consequently in cave mapping, especially where the underground space allows it.

Our research was based on the use of a recently released piece of equipment introducing a lightweight mobile handheld laser scanning system (GeoSLAM ZEB – REVO) that has the ability to produce a quite dense point cloud within an underground cavity. The x, y, z point cloud is generated while the operator walks through the cave (Zlot and Bosse, 2014). The specifications of this equipment include a 360º rotation, a (class 1 eye safe) 100Hz laser – making 100 rotations per second with the collection of 43,200 points per second. The maximum effective range is around 25-30m for indoor environment and data over 30m are usually excluded.

Scanning the Cave

The testing was held at "Koutouki" cave which is situated on the north – eastern side of Hymittos mountain in Athens and stretches at an altitude of 510m, within the Jurassic thick bedded marbles of Attica Geotectonic Unit (Lekkas and Lozios, 2000). It is the biggest and most popular show cave of Attica (*37º56,8'N, 23º49,7'E*).

Wearing a backpack and holding the Zeb - Revo device the scanning process of Koutouki Cave was established in less than 25 minutes, following the main corridor – touristic route. Even in narrow spaces outside the main route where larger systems require a survey tripod, the mobile device was still effective. The entire cave contains many geomorphological features such as speleothems which are included in the scan. The technical entrance, as well as the outdoor space in the surrounding area were also scanned, requisite for the later geo-referencing procedure. The physical entrance of the cave is a 38m cavern where the range of the handheld laser scanner (maximum indoor range 30m) can't reach. The final point cloud contained more than 80 million of points representing the entire show cave, including the shaded areas and chambers, which are not visible or able to be visited by any guest walking on the visitor's aisle.

Open Surface surveying with UAS

The open to the air surface of the area of interest was extracted with the implementation of a rotor-wing UAS during the field surveys. It was used to collect high-resolution natural colour images with its built-in camera (with 3.61 mm focal length) bundled on a two-axis gimbal.

The UAS platform is equipped with a Geodetic Navigation Satellite System (GNSS) antenna which provides quite good precision especially for the horizontal positions of which may be used for the alignment of the images captured during the survey (Fonstad *et al.*, 2013). Despite this we used 8 ground control points (GCPs) the coordinates of which were measured with high precision equipment (Real Time Kinematics GNSS) for maximizing the accuracy of the products, since the main objective was the combination of these outcomes with the previously mentioned under surface point clouds (Fugazza *et al.*, 2018). The flight was programmed at an average flight elevation of 120 m and a total of 36 aerial photographs were acquired for the photogrammetric processing afterwards, based on the Structure-from-Motion photogrammetric methodology (Westoby *et al.*, 2012; Granshaw, 2018).

Processing and Results

After the collection of the data we had to geo-reference the point clouds, in order to transform the registered point clouds from their local coordinate system to the Hellenic Geodetic Reference System (GGRS'87) (Mugnier, 2002). The reliability of the methodology is accomplished by measuring the geodetic coordinates of at least three non-collinear signalized markers outside the cavity system using Global Navigation Satellite Systems (Galley et al., 2015). The post processing of the data follows the registration and point cloud geo-referencing. The initial step in the post processing is to generate a triangular 3D – mesh by using the CloudCompare v2.10.2 software (Girardeau-Montaut, 2011) (Figure 1).

Both point clouds of the cave and the open surface above the cave were processed to produce several Digital Surface

Models (DSMs) in order to make quantification analysis of the terrain by using a GIS platform. The point cloud data of Koutouki cave were partitioned into the ceiling (roof), including the stalactites and the floor (ground), including the stalagmites and columns of the cave. In addition, the point cloud was filtered by erasing the noise, including the points generated by the human presence, the technical entrance of the cave, the commercial route containing the stairs, the railings and the concrete, along with noise generated by the equipment.

Once the point cloud was cleaned, both ground and ceiling points clouds were used to create two separate DSMs with spatial analysis of 0.05m using the natural neighbor triangulation method. Additionally, after the photogrammetric processing of the aerial photographs we created a dense 3D point cloud which led to a Digital Surface Model (DSM) with spatial analysis of 0.06 m.

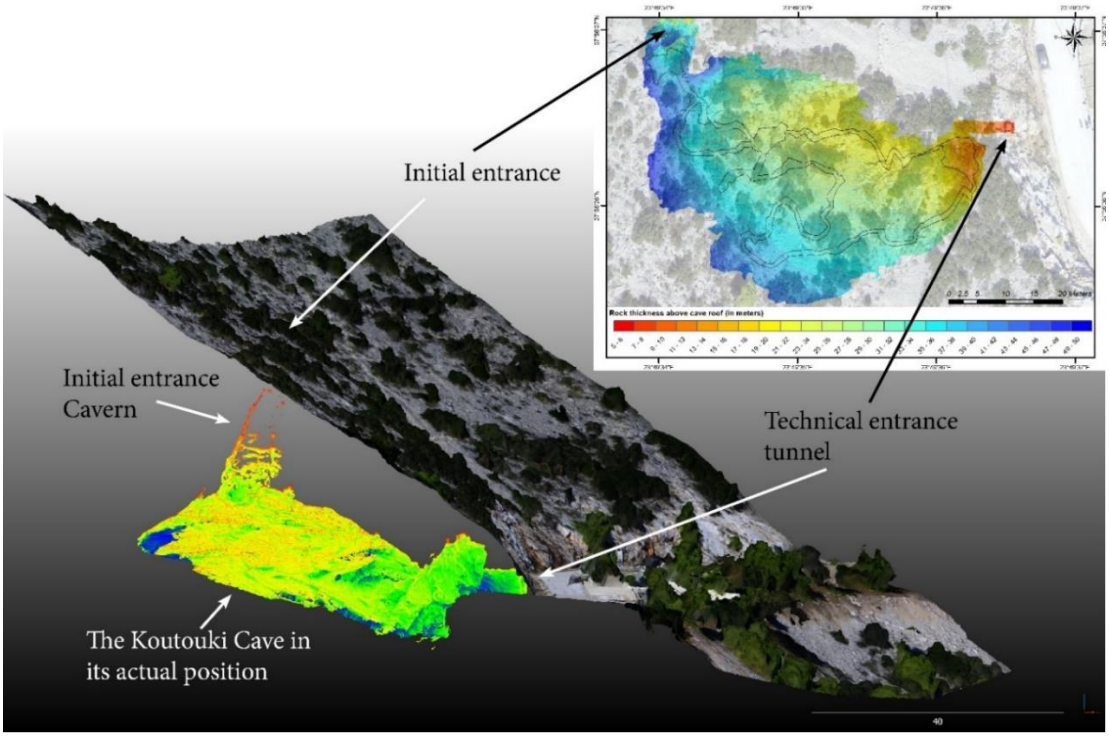

Figure 1. 3D visualization of the combined data of the underground triangular mesh of Koutouki Cave and the open-to-the-air surface relief. The inset is a map view of the cave showing the rock thickness distribution above the cave roof.

The information that was derived by the DSMs is sufficient to proceed to the generation of the rock thickness above the roof of Koutouki Cave by using GIS map algebra and subtracting the DSM of the ceiling from the open surface DSM. The result of this procedure led to the calculation of the rock thickness above the roof of Koutouki Cave with very high accuracy and resolution, which varies from 5.38 m (at the technical entrance, to the east) to 48.57 m (at the westernmost parts of the cave) with a mean rock thickness of 30 m.

Acknowledgements

The authors are grateful to the Ephorate of Palaeoanthropology and Speleology of the Ministry of Culture and especially to its Director A. Darlas, for giving the allowance to the scientific team in order to scan the Cave. Special thanks to Landmark-Loutridis company for supporting this research effort by letting us use the equipment and provide us the GeoSLAM – REVO point cloud data.

References

Fonstad, M., Dietrich, J., Courville, B., Jensen, J., Carbonneau, P., 2013. Topographic structure from motion: a new development in photogrammetric measurement. Earth Surface Processes and Landforms, 38, 421-430.

Fugazza, D., Scaioni, M., Corti, M., D'Agata, C., Azzoni, R.S., Cernuschi, M., Smiraglia, C., Diolaiuti, G.A., 2018. Combination of UAV and terrestrial photogrammetry to assess rapid glacier evolution and map glacier hazards. Nat. Hazards Earth Syst. Sci., 18, 1055-1071.

Granshaw, S.I., 2018. Structure from motion: origins and originality. The Photogrammetric Record, 33, 6-10.

Girardeau-Montaut, D., 2011. CloudCompare - Open Source project. Available from http://www.cloudcompare.org/ [accessed 28 February 2019].

Kershaw, B., 2012. Managing the survey information of the caves of Judbarra / Gregory National Park, Northern Territory. Helictite, 41, 87-94.

Lekkas, S. and Lozios, S., 2000. Tectonic Structure of Mount Hymittos. Ann. Geol. de Pays Helleniques, 38, 47-62.

Mugnier, C., 2002. Grids and datums: The hellenic republic. Photogramm. Eng. Remote Sens., 68, 1237–1238.

Westoby, M.J., Brasington, J., Glasser, N.F., Hambrey, M.J., Reynolds, J.M., 2012. 'Structure-from-Motion' photogrammetry: A low-cost, effective tool for geoscience applications. Geomorphology, 179, 300-314.

Zlot, R., Bosse, M., 2014. Three-Dimensional Mobile Mapping of Caves. Journal of Cave and Karst Studies, 76, 191-206.

15th International Congress of the Geological Society of Greece
Athens, 22-24 May, 2019 | Harokopio University of Athens, Greece
Bulletin of the Geological Society of Greece, Sp. Pub. 7 Ext. Abs. GSG2019-220

Rockfalls Dynamics Analysis and Mass Movement Characterization based on Multi-Temporal UAV and LiDaR surveys in "Apothikes" area, Santorini Island, Greece

I. Konstantinidis[1], E. Karantanellis[1], V. Marinos[1]

(1) Laboratory of Engineering Geology & Hydrogeology, School of Geology, Aristotle University of Thessaloniki, 54124, Thessaloniki, Greece, ioakekonst@geo.auth.gr

During the last decade, there has been an increasing demand in geo-engineering society for automatically monitored areas susceptible to landslide and catastrophic rockfall events. Traditional methods were supplemented, mostly by in-situ observational methods held by experts or by point-based approaches such as inclinometers and GPS measurements. Lately, we were given the opportunity to apply active sensors such as Terrestrial Laser Scanning (TLS) technology or passive ones such as Unmanned Aerial Vehicle (UAV) photogrammetry, as a result of the introduction of innovative remote sensing technologies as a common practice. This change has led to more accurate, precise and time-effective local scale modelling of the landslide event. Specifically, Structure from Motion (SfM) methodology enabled the production of ultra high-resolution orthomosaic and Digital Terrain Models (DTMs) of hazardous regions, via detailed point clouds. The current research demonstrates a powerful approach to precisely foresee potential rockfall hazards in the area of interest, based on a multi-temporal change detection procedure in time intervals in order to prevent any undesired consequence via the integration of innovative remote sensing tools and the suitable analysis of their results.

The investigated site is located in Santorini Island, Greece and is called "Apothikes". Specifically, the area is situated in the southern part of the island, east of the Akrotiri village, on a road that leads to the only beach that lays inside the caldera region. Various rockfall incidents of significant magnitude have been recorded in the slope over the years, mainly connected with external triggering factors and especially occurring after heavy rainfall. These rockfalls have caused numerous destructions on the road and have concluded to its temporary disruption in the past. These blocks are not only confined along the road but can also reach the seacoast. The significance of this specific region in which the research is held originates from the notable human activity (hotel, residences) that takes place at the top of the slope as well as the restlessness tourist activity during the year which is especially observed in the area of the beach located directly under the prone area. Specifically, "Apothikes" comprise one of the most tourist destinations in the whole island. Consequently, it is indispensable to provide accurate and precise precognitions of any potential rockfall hazard because of their significant environmental and commercial impacts.

In general, the volcanic complex of Santorini belonged to the volcanic arc of South Aegean and is the most active globally. The commission of this complex is based lengthwise in two main volcano-tectonic lines with a NE-WS strike. The area is geologically characterized by successive alternations of volcanic beds of strong ignimbrite and soft layers of pyroclastic materials with different engineering properties. The morphology consists of very steep slopes (≤80°) with highly steep dip discontinuities (76°-90°) which have significant persistence. All these parameters constitute to differential erosion and undercut in the base of the slope which develop tensile tenses and eventually lead to the loss of the rockmass cohesion and finally the failure of the previously suspended unstable blocks of ignimbrite (≤4m³) from a notable height (≅15m). The main failure mode comprises rock pillar detachment followed by toppling or planar sliding failure, which result to their fragmentation. The fallen blocks reveal fresh surfaces and as a result, the laterally blocks exhibit a lack of confining stress. Consequently, new cracks begin to emerge and the same process accelerates.

Analytically, in this particular case, multi-sensor fusion and multitemporal change detection techniques were performed among three different datasets derived from i) a Terrestrial Laser Scanner (TLS) during summer 2014 and ii) a UAV platform during summer of 2018 and spring of 2019 respectively. The aim of this procedure is to monitor and characterize topographical changes between different epochs for robust modelling of the rockfall's dynamics. The proposed approach of multi-sensor change detection was accomplished with the correlation of the 3 multi-epoch models in order to quantify the rockfall's displacements with computer-based methods. With the results of this comparison it was possible to classify the whole investigated area into sub-regions based on rockfall susceptibility.

In order to precisely predict potential rockfall hazards in the area we proceed to a trajectometry simulation in the prone sub-regions. The produced Digital Surface Model (DSM), from the latest acquired dataset, was converted to hillshade via QGIS3.0. The prone blocks, that we have already spot, was analyzed and their potential trajectories was specified in both 3D and 2D display. This analysis gave us the capability to estimate the outcome (energy, velocity, height and travel time) of any potential rockfall event pre and post the implementation of remedial measures. It gives us confidence that through this in-depth risk assessment we can mitigate potential miscarriages of the protection measurements that can be possibly applied in these certain sub-regions.

To conclude, all these innovative remoting sensing technologies provide the researcher many benefits compared to conventional methods. For instance, they pose great data transferability, completeness, precision and accuracy in the research study. Additionally, due to their capabilities they can produce holistic region measurements, which constitutes very important parameter for the whole geo-engineering society in order to scale up research area without degrading the measurement quality. At last, it is important to highlight UAV ability to eliminate user's risk to get harmed in order to gain access in some inaccessible areas via their remoted technology. This study demonstrates that, they could be

considered as a valuable supplemental tool in engineering geology to investigate the quantification of rockfall hazard via a multitemporal change detection analysis and to create an accurate potential failure mechanism model. However, it is significant to mark the importance of fieldwork, site investigation and the geological judgment of the researcher because it is essential to be able to test the validation and the quality of the obtained information.

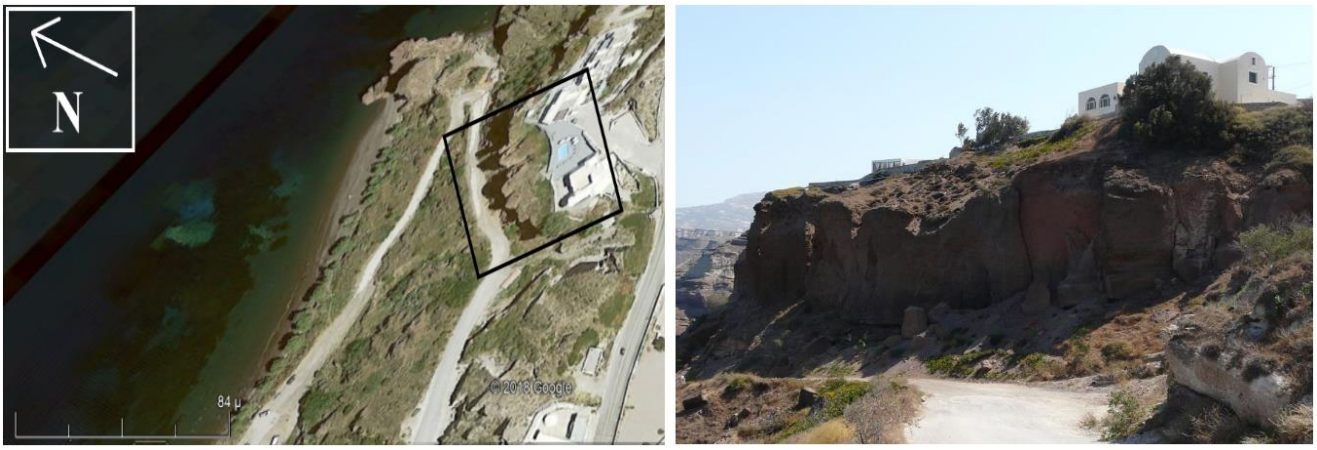

Figure 1. A satellite image of the investigated site "Apothikes" via Google Earth and a close-up image (Marinos et al., 2014) of the prone sub-region that is marked in the first figure.

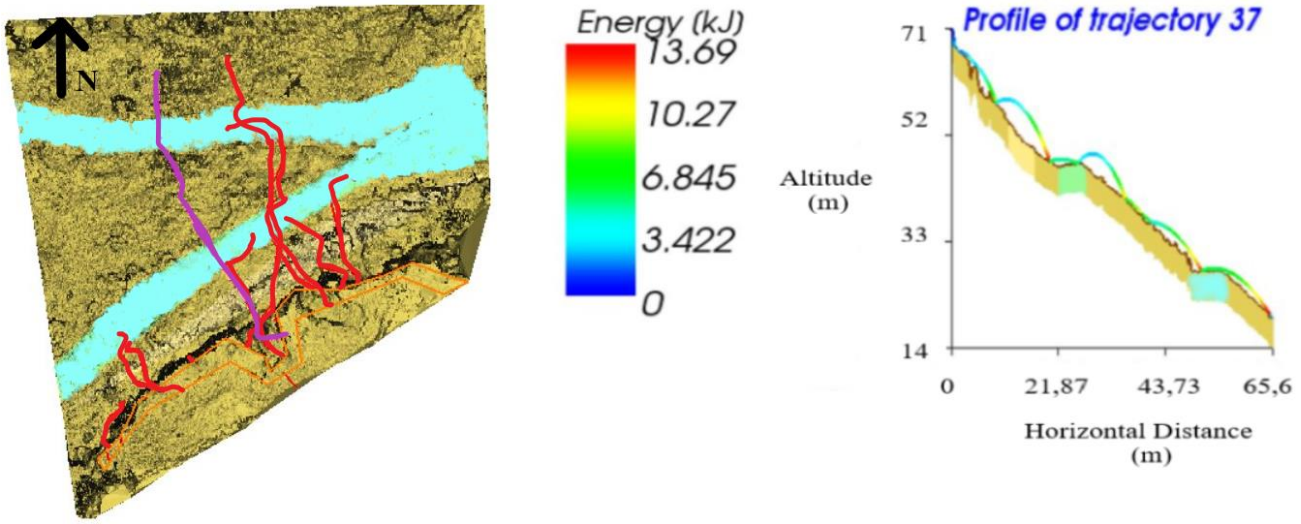

Figure 2. Example of a trajectory analysis (purple one) with energy output that have been applied in the prone sub-region of Figure 1. With light blue color is highlighted the road that leads to the beach.

References

Giordan, D., A. Manconi, A. Facello, M. Baldo, F. dell'Anese, P. Allasia, and F. Dutto, 2014, Brief Communication "The use of UAV in rock fall emergency scenario". Natural Hazards Earth System Sciences Discussions, 2, pp 4011–4029

Lucieer, A., S. M. de Jong, D. Turner, 2014, Mapping landslide displacements using Structure from Motion (SfM) and image correlation of multi-temporal UAV photography. Progress in Physical Geography, Vol. 38(1), pp 97–116.

Marinos, V., S. Paulidis, G. Pantazis, E. Lamprou, G. Prountzopoulos, P. Asteriou, G. Papathanasiou, T. Kaklis, 2014. Geological Research, Risk Estimation and Remedial Measures Suggestion for the Landslide Events in Kokkini Paralia and in the area of Apothikes, Municipality of Thira.

Mountrakis, D. 2010. Geology and Geo-tectonic Evolution of Greece, pp 132-143.

Turner D., Arko Lucieer, Steven M. de Jong, 2015, Time Series Analysis of Landslide Dynamics Using an Unmanned Aerial Vehicle (UAV). Remote Sensing, 7, pp 1736-1757.

Zieher, T., I. Toschi, F. Remodino, M. Rutzinger, Ch. Kofler, A. Mejia-Aguilar, R. Schlögel, 2018, Sensor- and Scene Guided Integration of TLS and Photogrammetric Point Clouds for Landsliding Monitoring. The International Archives of the Photogrammetry, Remote Sensing and Spatial Information Sciences, Volume XLII-2.

15th International Congress of the Geological Society of Greece
Athens, 22-24 May, 2019 | Harokopio University of Athens, Greece
Bulletin of the Geological Society of Greece, Sp. Pub. 7 Ext. Abs. GSG2019-223

Landslide Change Detection Based on Multi-Temporal Digital Elevation Models of Ropoto, Central Greece

A. Vassou[1], E. Karantanellis[1], V. Marinos[1]

(1) Laboratory of Engineering Geology & Hydrogeology, Faculty of Geology, Aristotle University of Thessaloniki, Greece, vassouna@gmail.com

Introduction

A landslide constitutes a significant natural hazard that includes mass movement of soil, rocks and/or mud due to the pull of gravity, most of them occurring gradually, but some may be abrupt. It is a phenomenon which most of the times it is not predictable and unfortunately unavoidable and can cause significant casualties and immeasurable economic losses, effecting many aspects of human life. Extensive rainfall, earthquakes, unfavorable geology and human intervention are some potential triggering factors that can induce a landslide event. According the aforementioned, it is necessary to mitigate the landslide hazard to ensure optimum security. As a result, new methodologies are required to develop a better perception of landslide hazards. With the recent advances of technology, various remote sensing methods have been developed providing useful topographic data. In the current study, detailed imagery data has been obtained by using Unmanned Aerial Vehicles (UAV). The UAVs, also known as drones, are aircrafts where are capable of taking high-resolution images and producing via photogrammetric software, precise 3D point cloud, Digital Surface Models and respective Orthophoto. Valuable data source with extended applications on surveillance, inspection, mapping and 3D imaging are now available. The purpose of this study is to investigate and detect potential topographic changes of a mega-landslide by using multi-temporal UAV data. The landslide is induced at the community of Ropoto and constitutes a great risk while a large part of the village has been affected (approximately 280m wide and 750m long) (Figure 1). Ropoto village, belongs to the Municipality of Trikala in the Central part of Greece and according to the geological map (1:50.000), with the title “Mouzakion”, belongs to the geotectonic zone of Pindos (Mountrakis, 1985). The geology of the area of interest consists of the following formations: Paleocene-Eocene flysch formations (transition flysch units in this case) that present a high heterogeneity (sandstones, conglomerates, limestones, siltstones, shales, marls), transition beds consisted of thick-bedded limestones with sandstone and shale (M. Maastrichtian-L. Paleocene) and the thin-bedded limestone formation (Turonian-M. Maastrichtian). The tectonic development of the Ropoto area affected all of the formations and mainly the newer ones (flysch and transition formations), thus isoclinal folds and thrust faults were created. Flysch has thus suffered from compressional forces being highly deformed. Shear zones and smaller faults are also present in the site specific area due to this tectonic disturbance. These geological characteristics produced very weak rock masses which presented the landslide. Brittle rock formations, such as limestones here, created very permeable zones, so very high pore water pressure is often developed triggering the landslide. The latter, explains the water presence between the flysch and thick-bedded limestone formations covered by scree. Consequently, the landslide occurred after 12 hours of intense rainfall within the weathered mantle of flysch depth of the transition beds. As a result, the greater part of the central village infrastructure massively collapsed.

Methodology

For the detection of surface deformation due to landsliding, field investigation is requisite and typically involve field mapping to characterize the geomorphological conditions. Additionally, there is a number of factors that need to be continuously assessed: the extent of the landslide, detection of fissure structures, topography of the land and the rate of displacements that could be related to the fracture (Niethammer et al. 2010). The latter, depending on the scale of the problem, can take valuable time while rough terrain can constitute access restrictions, therefore the assessment of the landslide is deficient. In order to understand the mechanism of the landslide, horizontal and vertical displacements should be measured. A number of remote sensing methods are valuable tools towards this assessment. Therefore, except the visual interpretation, high resolution images were captured by the UAV while it provides ultra-high spatial resolution and accuracy that is needed to monitor temporal changes. At the community of Ropoto, several movements have been recorded during the last decades. First movement occurred in 1963, while the last episodic large landslide happened in 2012. Ever since the landslide is evolving gradually without perceivable movements. In this survey, in order to detect these changes multi-temporal digital elevation models of the area we quantified and compared.

Initially, for change the detection assessment, pre-disaster data is required. The reference data is provided by the Land Registry of Greece where Digital Elevation Models (DEM) - LSO (Large Scale Orthophotos) were created with the use of aircrafts equipped with high-end optical sensors between 2007 and 2009 with pixel resolution of 5 m. Those digital elevation models are specialized database that represents the topographic relief of a surface between points of known elevation. By interpolating known elevation data from sources such as ground surveys and photogrammetric data capture, a rectangular digital elevation model grid can be created. By setting these multi-temporal photogrammetric products under two different procedures, two similar results were given, while according to the visual interpretation they displayed the same volume of movement. In the first procedure the value of the second one has being subtracted from the value of the first one on a cell-by-cell basis and the second one calculates the area and the volume of the region between a surface and a reference plane. As a result, we have two DEM’s of difference involving quantifying volumetric change between these

multi-temporal photogrammetric products showing parts with gain or loss material (Figure 2). Especially the crown and the foot of the landslide demonstrate major amount of material removal. On the other hand, several other parts of the landslide reveal an unexpected increment.

Concluding, Ropoto landslide constitute an active landslide that shows gradually evolving movements through the years. As so, the continuous monitoring of the landslide in 6 months' period, it is required to determine the extent, magnitude and style of landslide movement, for risk and even emergency risk management assessments. Last but not least, the need of implementing Unmanned Aerial Vehicles (UAV) in landslide risk assessments is constantly increasing while they provide a safe, quick and potentially more accurate way of inspecting large scale and difficult to access areas, requiring minimal human resources. However, in order to process these results, the contribution and critical evaluation of an expert is obligatory.



Figure 1: Aspect of Ropoto landslide: a) 2016-Google earth, b) 2018-Image.

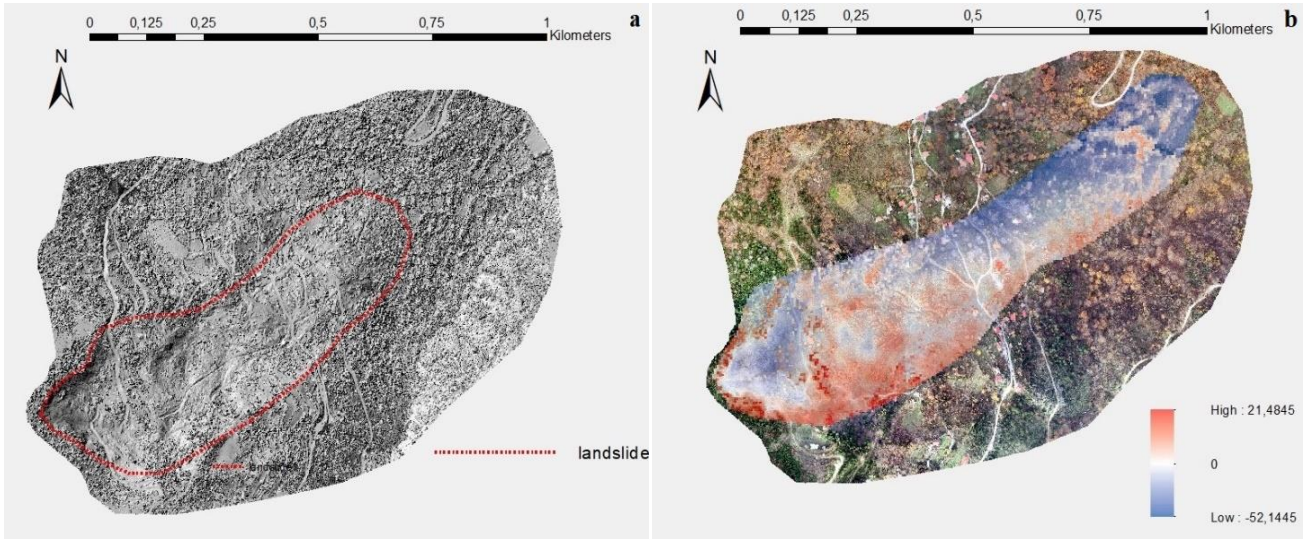

Figure 2: a) DEM of Ropoto-Hillshade , b) DEM of Difference of Ropoto

References

Mountrakis, D.M., 2010.Geology and geotechnical evolution of Greece, 1st.University Studio Press.

Williams, R., 2012. DEMs of Difference. Geomorphological Techniques, 17

Niethammer, U., Rothmund, S., James, M.R., Travelletti, J., Joswing, M. 2010. UAV-Based Remote Sensing of Landslides. International Archives of Photogrammetry, Remote Sensing and Spatial Information Sciences, Vol. XXXVIII, Commission V Symposium, Newcastle upon Tyne, UK.

Jaukovic, I.C, Hunter, A.J., 2016. Unmanned Aerial Vehicle: A new tool for landslide risk assessment. Proceedings of the 11th ANZ Young Geotechnical Professionals Conference – 11YGPC Queenstown, New Zealand.

15th International Congress of the Geological Society of Greece
Athens, 22-24 May, 2019 | Harokopio University of Athens, Greece
Bulletin of the Geological Society of Greece, Sp. Pub. 7 Ext. Abs. GSG2019-225

UAV Point Clouds for Semi-Automated Rockfall Hazard Assessment: a Post-Failure Application of a Novel Method in Plomari, Lesvos Island

E. Lymperis[1], E. Karantanellis[1], V. Marinos[1]
(1) University of Thessaloniki, University Campus, Faculty of Sciences, Thessaloniki, Greece, geo.elymperis@gmail.com

Abstract

Rockfalls constitute an abrupt type of landslide process with manifold impact at local level, on economy and mostly on a human modified environment. Over the past few decades, urban expansion in hazardous areas and development of modern transportation and energy infrastructure, combined with a global demand for higher safety standards, have rendered the assessment of rockfall hazard most urgent than ever. In this context, up to date, rapid automated and accurate mapping of rockfall characteristics is key to identifying hazardous areas and proposing mitigation measures in an efficient manner. The current study proposes a novel, semi-automated approach to detect rockfall hazard from detailed 3D point clouds and highlights the significance of UAV application in the landslides domain. A case study of a recent rockfall event, triggered by heavy rainfall in Plomari, Lesvos island is presented. The event occurred within the boundaries of the settlement and induced damage on several houses, forcing 37 people to evacuate the proximal area. Data was collected shortly post-failure with a commercial UAV platform and implemented in producing a high-resolution 3D point cloud from which block geometry measurements of sliding slope have been provided in relation with the geometrical characteristics of the main discontinuity surfaces and the slope morphology. Field measurements and laboratory tests of the rock joint strength were contributed for the analysis of the slope stability of the rock blocks. A practical, qualitative hazard assessment system is proposed, based on parameterization of corresponding rock discontinuity factors detected in terms of point cloud analysis. Results have demonstrated the capabilities of combining UAV platforms with computer-based methods for rapid and accurate identification of discontinuity parameters, objectively, and even in inaccessible areas of the rockfall body. These capabilities

Introduction

Rockfalls present a substantial increase in their spatial and temporal distribution over the last decade especially in developed societies with severe impact on infrastructure and livehood. The latter has a direct link with the tremendous increase of population in urban areas where built-up zones extended in landslide and rockfall prone areas (Glade et al., 2005). Geo-information techniques and remote sensing have played a vital role in the interpretation and understanding of landslide and rockfall kinematics. A variety of sensors and techniques have been implemented in the field, demonstrating a relationship between the desired application and the method of choice. Lately, Unmanned Aerial Vehicles (UAVs) are widely applied in harsh environments for utra-high resolution data acquisition and accurate 3D surface reconstruction (Nex et al., 2015). Their ability to collect data subjectively from different orientation angles and inaccessible steep rock faces, with very low operational cost and reduced risk for the surveyor make UAVs an integral tool for landslide assessment and rockmass characterization. The collected imagery is taking full advantage of Structure from Motion (SfM) technique with Multi-View Stereo (MVS) to build a 3D point cloud as well as a Digital Surface Model (DSM) and an orthophoto of the area. This work aims to point out the applicability of UAVs in detecting and characterizing rockfall hazard on mountainous environment based on photogrammetric 3D point clouds derived from low-cost UAVs. The acquisition survey aims to produce topographic-grade accurate 3D data from which reliable, valuable geotechnical information can be extracted in an effective manner. The focus of this study was mainly on geometric discontinuity information retrieval, specifically, orientation and and spacing of the main joint sets, through block volume measurements in 3D space. Field measurements were also exploited to assess the mechanical characteristics of the discontinuities as well as to cross-correlate the data derived from the UAV. The acquired discontinuity properties were parameterized and included in a formulated Hazard Index to provide concrete and accurate rockfall hazard analysis.

Methodology

The approach discussed involved the quantification of rock discontinuity characteristics; five major joint set properties were implemented in the hazard assessment system, namely: Joint Set Spacing, Orientation (dip/dip direction), Roughness, Joint Wall Compressive Strength and Persistence. A morphology factor was also introduced. All the data used in this study were collected shortly after the rockfall event of November 24, 2018. A commercial UAV platform with a built-in optical sensor was used to collect imagery. A total of 200 images were used to construct a dense point cloud of 20 million points (2100 points/m^2). Manual measurements were also made on the accessible foot of the slope using conventional equipment (compass clinometer, profilometer, Schmidt hammer, measure tape). For the hazard assessment process, Orientation and Spacing and Morphology have been derived from block volume measurements made on the obtained point cloud, while Roughness, Wall Strength and Persistence have been imported as-is from the manual survey. The data derived from the point cloud has been post-validated via the respective manual measurements. The hazard zonation has been categorized in three main qualitative fields, namely: i) *High*, where areas have a greater possibility to fail, ii) *Moderate* and iii) *Low*, where areas have a lesser possibility to fail. A novel qualitative hazard matrix has been developed, taking consideration on the aforementioned properties: each joint set property, except for the orientation, has been parameterized accordingly, to a Low-Moderate-High order. A multi-criteria process has been

implemented to calculate a formulated Hazard Index (H.I.) in a GIS environment. The slope is sectioned in parts(planes), for each of which a separate H.I. is calculated, based on its discrete parameter values. The final product of the hazard assessment process is a hazard map, which includes an outline of the slope divided in polygons, each assigned a color according to its calculated H.I.

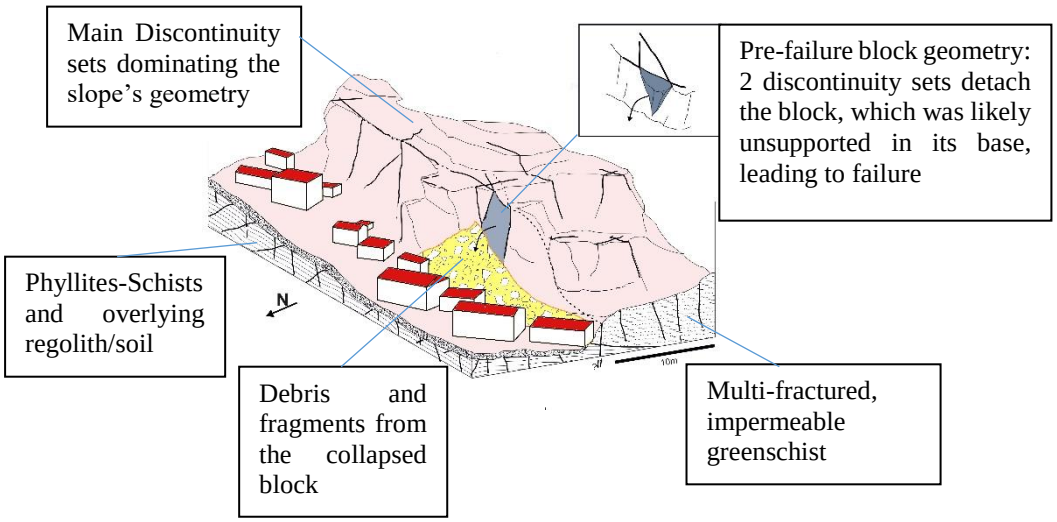

Figure 1: Conceptual block model of the case area

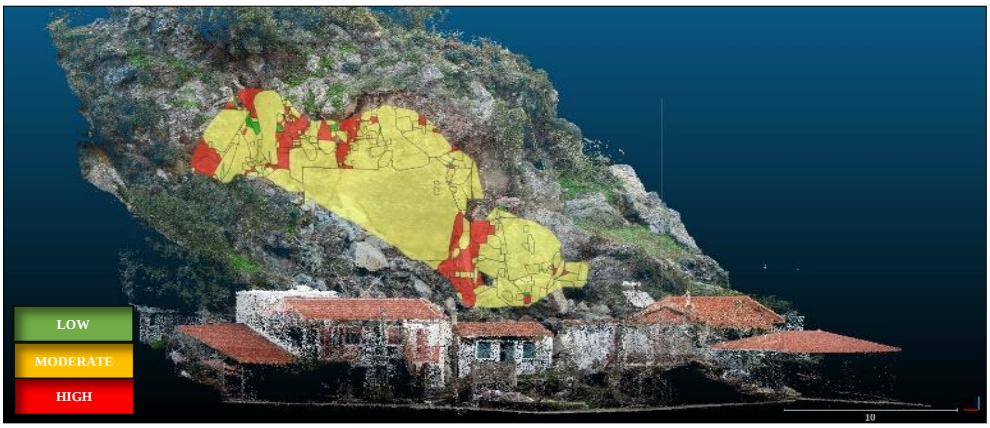

Figure 2: Hazard map overlaid on the point cloud of the failure slope.

Conclusions

Rapid rockfall mapping is important in post-disaster situations. UAVs, in combination with field investigations, have limitless advantages for emergency situations, in specific rockfall management, due to their clear benefits over conventional methods of collecting surface measurements, in harsh environments. Their main contribution in such cases, is the combined ability to provide holistic 3D topographic data in a time efficient manner and with minimized human exposure. The five selected parameters (Roughness, Wall Compressive Strength, Spacing and Persistence) tuned in the proposed Hazard Index revealed good results in comparison with the in-situ investigations and raised expectations for the discussed approach. At a subsequent time, the proposed method will be implemented in different case studies to validate its transferability in different rockfall scenarios. In addition, machine learning algorithms will be tested for exporting discontinuity properties in an automated and subjective way without user interaction.

Acknowledgements

This research is co-financed by Greece and the European Union (European Social Fund-ESF) through the Operational Programme «Human Resources Development, Education and Lifelong Learning» in the context of the project "Strengthening Human Resources Research Potential via Doctorate Research" (MIS-5000432), implemented by the State Scholarships Foundation (IKY).

References

Glade, T., Anderson, M., & Crozier, M. J., 2005. Landslide Hazard and Risk. (T. Glade, M. Anderson, & M. J. Crozier, Eds.). Chichester, West Sussex, England: John Wiley & Sons, Ltd

Nex, F., Gerke, M., Remondino, F., Przybilla, H.-J., Bäumker, M., Zurhorst,A., 2015. ISPRS Benchmark for multi-platform photogrammetry, Joint ISPRS conference 2015, Munich, Germany

15th International Congress of the Geological Society of Greece
Athens, 22-24 May, 2019 | Harokopio University of Athens, Greece
Bulletin of the Geological Society of Greece, Sp. Pub. 7 Ext. Abs. GSG2019-236

Landslide Investigation Using UAV Photogrammetric Methods Within Marly Formations in Open Pit Lignite Mines in Northern Greece.

F. Paraskevopoulos-Tsiakiris[1], E. Karantanellis[1], V. Marinos[1]

(1) Laboratory of Engineering Geology & Hydrogeology, School of Geology, Aristotle University of Thessaloniki, 54124, Thessaloniki, Greece, parafoti@geo.auth.gr

Energy production in Greece greatly depends on lignite combustion, therefore exploitation of the indigenous deposits is of great importance. Lignite mainly comes from open pit mines, in whom marly formations are usually found overlaying the lignite accumulation. Due to poor geotechnical parameters, mine's unique geometry (high temporary slopes in steep angles), combined with the pore water pressure from heavy rainfalls behaving as triggering mechanism, as a result landslide phenomenon often occur. The current research takes advantage of Unmanned Aerial Vehicles and their capabilities to detect, map and with the appropriate process, analyze and discover the basic engineering geological principles (type of failure, triggering mechanism, volume etc.) governing these failures.

Specifically, two mine areas have been examined, both of them have undergone rehabilitation (Marinos 2012). The first one is in Florina and the second in Kozani prefecture. These two districts according to the geotectonic units of Greece appertain to Pelagonian nappe and moreover belong in the upper and in the lower part of the elongated intermontaine Florina-Ptolemais-Kozani tectonic graben respectively (Pavlides *et al.*, 1986).

Research was initiated with data collection from the in-situ investigation of the mining areas. The UAV, bearing a high-resolution camera with a GPS tracker, was set to fly in a pre-determined flight path to map the plain view of each mine. Meanwhile a thorough field survey to recognize and assess the basic geological and geometrical factors regulating the landslides like marl's bed dip/dip direction, discontinuity surfaces, geometrical characteristics of landslides, faults, etc. was executed.

The Digital Surface Model, Point Cloud and finally Orthomosaic with the contribution of a photogrammetric software was created taking consideration of the desired Ground Sampling Distance (GSD). Methodology continued with the creation of topographic parameters such as Hillshade, Aspect, Slope. With an accurate manual mapping in GIS environment of the Orthomosaic obtained in each case, two individual landslides were identified at Florina's mine in Amyntaio (Figure 1) and 147 in total at Kozani's mine in Prosilio (Figure 2).

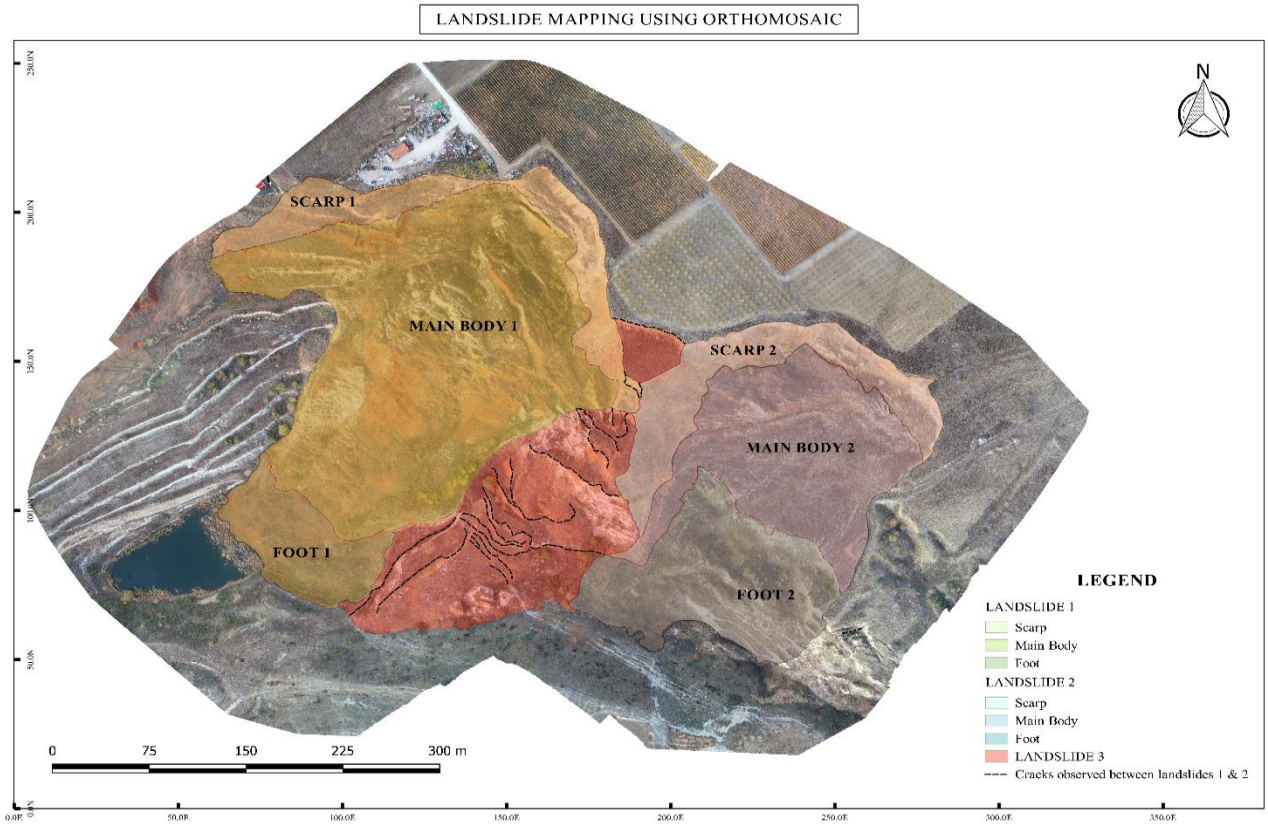

Figure 1. Map based on the Orthomosaic depticting two landslides within marly formations in Florina's mine in Amyntaio area, each with its individual characteristics. The pink color corresponds to the possible union between landslide 1 & 2 into a massive one.

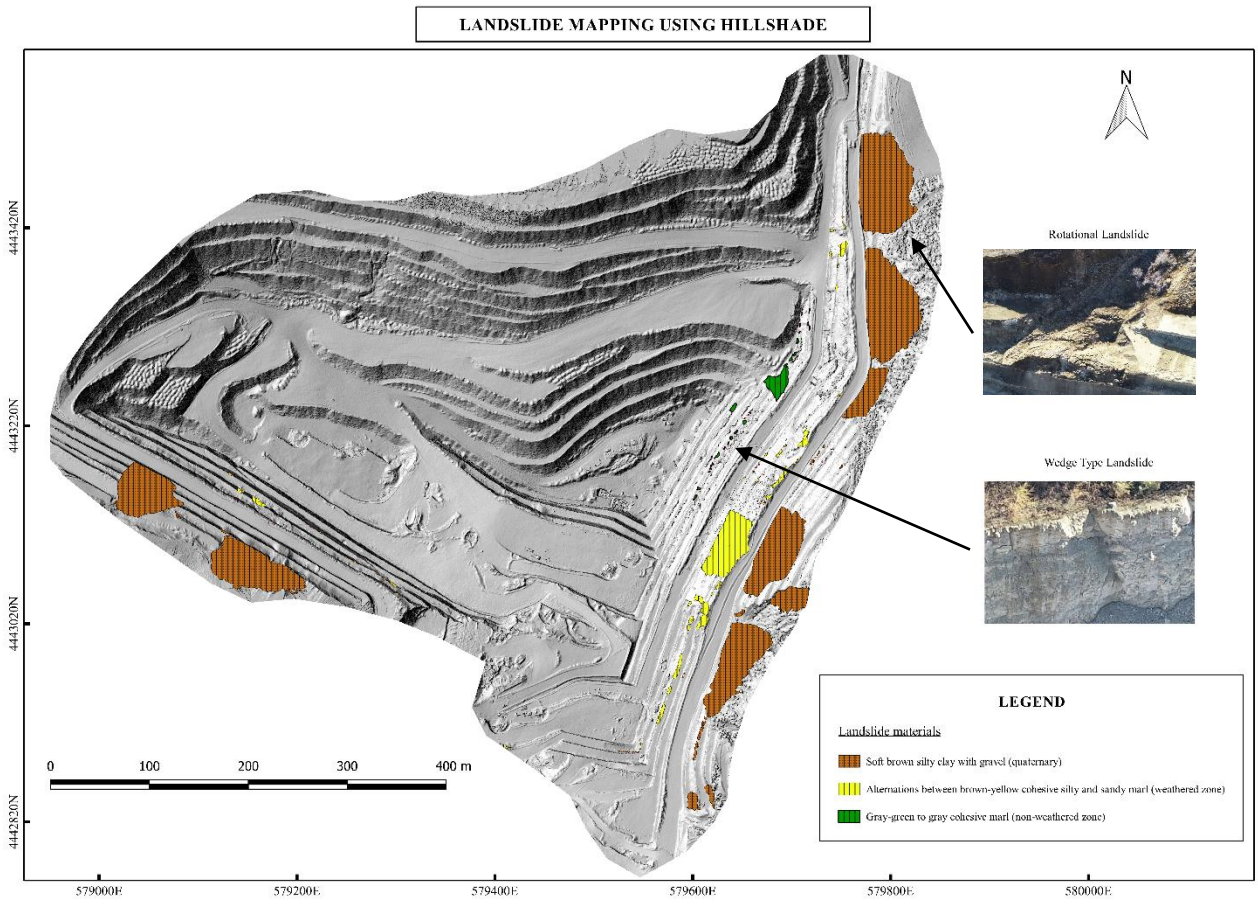

Figure 2. Map based on the Hillshade which depicts the 147 different landslides found in the upper parts of the mine within almost exclusively marly formations in Kozani's mine, in Prosilio area.

Furthermore, taking into account information derived from the interpretation of the aforementioned topographic tools it was made possible to calculate the fundamental data for each landslide such as slope orientation and dip, discontinuities orientation and dip and finally propose a failure mechanism matching those given by the in-situ investigation. Last but not least, through the application of the prementioned photogrammetric program it was made able to identify and export the volume of each slide with a very good correlation to reality as it was verified by actual data.

Finally, for the Amintaio open pit the responsible failure mechanism is the rotational one for both slides. In the Prosilio open pit from the 147 known landslides 109 were identified as rotational and 38 as wedge type failures. Volumetric analysis showed materials movements ranging from 0.28m³±30.00% to 531.71m³±0.74% for the mapped landslides in the area of interest.

Concluding, the aim of the research is to designate an effective and simultaneously low-cost method of detecting, monitoring and assessing landslide phenomena. This attribute comes to absolute need regarding open pit mines, where a 24/7 surveillance is essential because of marl's highly susceptibility to failures. UAV usage checks all the above criteria when it comes in conjunction with proper geological knowledge can truly provide remarkable results.

References

Marinos, P., 2012. Autopsy report in slope stability in METE corporation mine located in Prosilio in Kozani area.

Pavlides, S.B., Mountrakis, D.M., 1986. Neotectonics of the Florina – Vegoritis – Ptolemais Neogene Basin (NW Greece): an example of extensional tectonics of the greater Aegean area. Ann. Geol. Pays Hell. 33 (1), 311 – 327.

15th International Congress of the Geological Society of Greece
Athens, 22-24 May, 2019 | Harokopio University of Athens, Greece
Bulletin of the Geological Society of Greece, Sp. Pub. 7 Ext. Abs. GSG2019-271

New technologies for landslide monitoring. Examples from the Greek territory

K. Nikolakopoulos[1], A. Kyriou[1], I. Koukouvelas[1]
(1) University of Patras, Department of Geology, Rio, 26504, Greece, knikolakop@upatras.gr

Abstract

Active landslides can be monitored using many different methods such as classical geotechnical measurements including inclinometers, topographical survey measurements with total stations or Global Navigation Satellite Systems (GNSS) receivers. Newer methods include Airborne Light Detection and Ranging (LiDAR) systems, Terrestrial Laser Scanners (TLS), photogrammetric techniques using airphotos or high resolution satellite images, Differential Interferometry using radar images (DInSAR). A recently emerged methodology is the computer vision technique using data from Unmanned Aerial Vehicles (UAVs). The advantages and drawbacks of those different methodologies for landslide monitoring are described and analyzed in several studies highlighting the existence of a high resolution and accurate representation of the relief as a prerequisite in order to achieve a proper displacement identification (Nikolakopoulos et al., 2017; Nikolakopoulos et al., 2018; Nikolakopoulos and Koukouvelas, 2017; Kyriou and Nikolakopoulos, 2016; Kyriou and Nikolakopoulos, 2018). Additionally, all the studies agreed that a key point in active landslide monitoring is the performance of repeated surveys, as the transient geomorphology of the sliding area changes resulting in the requirement of precise mapping over time. The current study presents the exploitation of new technologies including TLS, UAV and DInSAR for landslide monitoring that were applied in different sites within the Greek territory.



Figure 1. Landslide mapping with UAV at Analipsi village, Western Peloponnese. Orthomosaic is the resulting product of each flight campaign. Image A: a historical image of Google Earth. Image B: the orthoimage of the last campaign (3/11/2016).

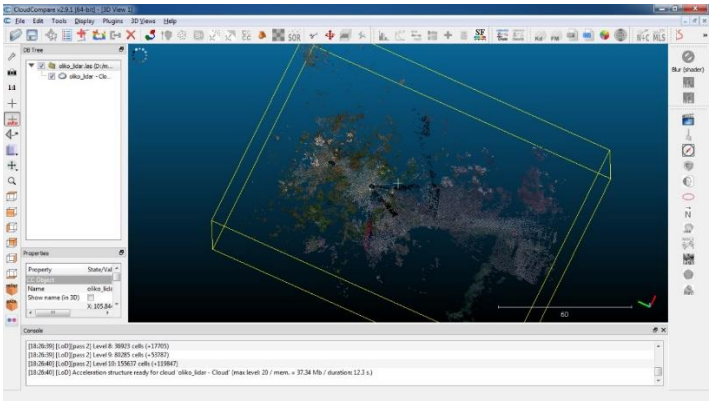

Figure 2. Moira landslide mapping with Terrestrial Laser Scanner. Point cloud generated from the TLS measurements.

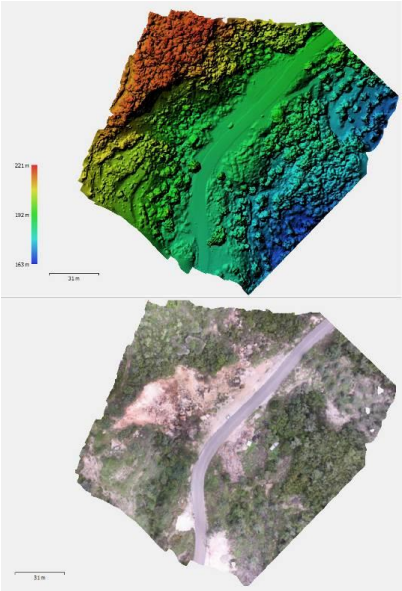

Figure 3. Landslide Mapping with UAV. Top image: DSM with 4cm spatial resolution from the Agios Petros landslide in Lefkada. Bottom image: the respective orthophoto with a spatial resolution of 2cm.

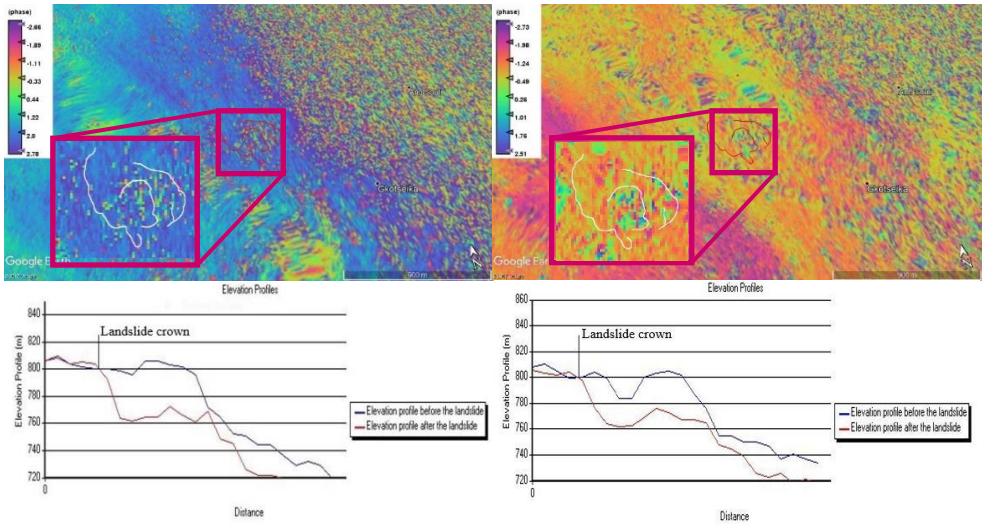

Figure 4. Top images: Interferograms displaying the ground deformation caused by the landslide is mapped (alterated colors within the landslide boundaries). Bottom images: Elevation profiles of interferometric DSMs showing the relief change at Moira area after the landslide.

References

Kyriou Aggeliki, Nikolakopoulos Konstantinos, 2018, A synergy of radar and optical data of Copernicus programme for landslide mapping, Proc. SPIE 10790, Earth Resources and Environmental Remote Sensing/GIS Applications IX, 107900G, doi: 10.1117/12.2325622.

Kyriou Aggeliki, Nikolakopoulos Konstantinos, 2018, Assessing the suitability of Sentinel-1 data for landslide mapping. European Journal of Remote Sensing, vol. 51, No. 1, 402–411, https://doi.org/10.1080/22797254.2018.1444944

Kyriou S. Aggeliki, Nikolakopoulos G. Konstantinos, 2016, Sentinel-1 data for the detection and mapping of landslides. a case study from Western Peloponnese, Greece, Proc. 'Living Planet Symposium 2016', Prague, Czech Republic, 9–13 May 2016 (ESA SP-740)

Nikolakopoulos G. Konstantinos, Antonakakis Antonis, Kyriou Aggeliki, Koukouvelas Ioannis, Stefanopoulos Panagiotis, 2018, Comparison of terrestrial laser scanning and structure-from-motion photogrammetry for steep slope mapping, Proc. SPIE 10790, Earth Resources and Environmental Remote Sensing/GIS Applications IX, 107900F, doi:10.1117/12.2326175

Nikolakopoulos G. Konstantinos, Kavoura Katerina, Depountis Nikolaos, Kyriou Aggeliki, Argyropoulos Nikolaos, Koukouvelas Ioannis, Sabatakakis Nikolaos, 2017, Preliminary results from active landslide monitoring using multidisciplinary surveys. European Journal of Remote Sensing Vol. 50 (1) p. 280-299. Vol. 50 (1) p. 280-299, http://dx.doi.org/10.1080/22797254.2017.1324741.

Nikolakopoulos G. Konstantinos, Koukouvelas K. Ioannis, 2017, Emergency response to landslide using GNSS measurements and UAV, Proc. SPIE 10428, Earth Resources and Environmental Remote Sensing/GIS Applications VIII, 1042816, doi: 10.1117/12.2278728

15th International Congress of the Geological Society of Greece
Athens, 22-24 May, 2019 | Harokopio University of Athens, Greece
Bulletin of the Geological Society of Greece, Sp. Pub. 7 Ext. Abs. GSG2019-282

Rockfall Analysis and Protection Measures Recommendations at Eptahori Village, Epirus, Greece

Avgerinou P.[1], Marinos V.[1], Papathanasiou G.[2]

(1) Aristotle University of Thessaloniki, Department of Geology, 54124 Thessaloniki, Greece, peli.avg@gmail.com
(2) Democritus University of Thrace, Department of Civil Engineering

This paper deals with a rockfall analysis in the northern steep slope at Eptahori Village, Epirus, Greece, which exhibits extended rockfall instabilities along its face, placing the village at the base of the slope at high risk. Along the examined slope, numerus older rockfall events were recorded. These rockfalls were caused by toppling of overhanging sandstone blocks formed by large tension cracks that were generated due to the erosion of the weak siltstone layers. The geological setting of the study area consists of molassic formations of "Eptahori" and "Pentalofo" units and more particularly by thick sandstone beds ("Pentalofos" unit) on the upper part of the slope, underlied by thin siltstone layers ("Eptahori" unit), which continues to the base of the slope. The structure of the rock mass is blocky, developed by bedding orientation NW – SE, dipping to the slope, which consists the main joint set of the rock mass as well by sub-vertical joints with orientation NNW – SSE within the thick sandstone layers (Figure 1). These joints act as tension cracks along the slope due to the loss of support of the eroded material. These joints are widened due to the high rate of atmospheric precipitation that enters these open discontinuities of the rock mass and to the temperature changes, creating significant unstable blocks along the slope.



Figure 1. (a) Face log of the slope to SW, (b) Major planes of the rock mass in Schmidt projection, (c) Resulting point cloud from LiDAR scanning

The objective of this paper is to assess the engineering geological model of the rockfall events, to evaluate the degree of rockfall hazard along the face of the slope and finally propose the protection structures along the slope. A detailed field survey of the geological and engineering geological conditions was executed during July – August 2018 along with field measurements. Moreover, terrestrial laser scanning (Light Detection and Ranging – LiDAR) (Fig. 1c) as well as Unmanned Aerial Vehicle (UAV) flights above the study area were made. According to the resulting images and the generated point clouds, the slope morphology and block structures were precisely determined. The unstable zones were also detected and volume measurements of hanging blocks were carried out so as to develop the engineering geological model of the slope and evaluate the behavior of the formations prior to rockfall.

Rockfall analysis were conducted by developing rockfall trajectory simulation models using RAMMS: Rockfall (RApid Mass Movement Simulation), which stands out to be a usefull and advanced modelling software in simulation of rockfall trajectories in three dimensions. According to these models, all the potential rockfall trajectories along the face of the slope were examined and the trajectories evaluated with high risk were analyzed, estimating the worst-case scenario of rockfall along the slope. Moreover, the parameters of motions of rocks were determined by the simulation results. The resulting model parameters were calibrated according to restitution coefficients in order to improve simulation results. The simulation model was developed by an accurate and detailed Digital Surface Model (DEM) of the terrain of the slope created by the high resolution resulting point cloud data set of LiDAR scanning. The input parameters of the model concerning the type of terrain and vegetation at the slope as well the best-fit simulation of rock bodies were determined in accordance with detailed field observation data (Fig. 2).

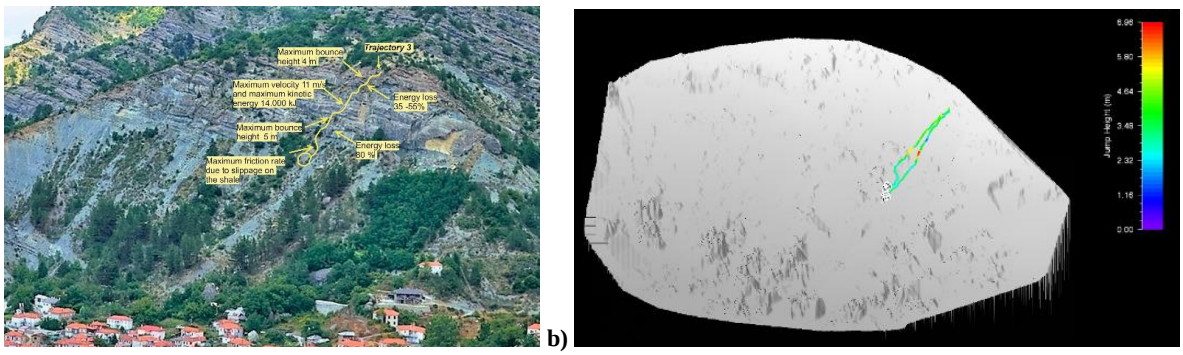

a) b)

Figure 2. Simulation model of potential rockfall trajectory along the slope (a) displaying parameters of motion of rock, (b) in RAMMS: Rockfall.

According to the rockfall simulation model, the blocks develop an average jump height of 3 to 4 m with a local maximum of 8 m during bouncing at sandstone benches, where the velocity of the rocks range from 5 to 8 m/s reaching a maximum of 15 m/s. During their motion, the rocks develop high kinetic energy rates (8.000 – 12.000 kJ), which are reduced, as indicated by the values of the restitution coefficients, when sliding on the shale layers of the base of the slope. During this contact, friction forces are developed and provoke the absorption of high amount of kinetic energy. The trajectories are hence stopped at the base of the slope or continue with reduced velocity towards the toe of the slope, placing the residential zone at high risk. The rockfall potential along the slope was assessed as medium to high hazard degree, based on the rock mass quality, the volume of blocks, the history of older rockfalls, the steepness of the slope and the presence of unstable blocks.

A series of protection measures – both active and passive – are proposed in order to reduce the hazard to the lowest possible level. Active structures aim to decrease the probability of failure by surface drainage of the slope by construction of drainage ditches and protection measures (e.g. sprayed polymer coatings) from the erosion of the siltstone members. Passive protection structures are strongly proposed as effective measures in order to retain falling blocks and absorb impact energy (Fig. 3). In particular, the measures proposed are:

- Dynamic rockfall barriers (or flexible catch fences) constructed in two lines at the toe of the slope, up to a height of 3 m and energy absorption capacity of up to 10,000 kJ for the first line and a height of up to 2 m and energy absorption capacity of up to 8,500 kJ for the second line. Of course, these very high energies concern the worst-case scenario of the analysis.
- Ditches (rock traps) constructed in front of barriers 2 to 5 m wide with depth up to 1 m filled with soil material for the absorption of average energy of 10,000 kJ.



Figure 3. Recommended construction sites of dynamic rockfall barriers and ditches at the toe of the slope.

Acknowledgements

The authors acknowledge with thanks RAMMS development team at WSL Institute for Snow and Avalanche Research SLF in Davos and especially Marc Christen, project Leader for providing the software. We appreciate the assistance of residents at Eptahori village for their help throughout field work.

References

Asteriou, P. et al., 2013. Rockfalls: influence of rock hardness on the trajectory of falling rock blocks. Bulletin of Geological Society of Greece, 13th International Congress, Chania, Greece XLVII. http://dx.doi.org/10.12681/bgsg.11033

Jaboyedoff, M. et al., 2012. Use of LIDAR in landslide investigations: a review. Nat Hazards, 5–28. doi:10.1007/s11069-010-9634-2

SLF/WSL, E. Z., RAMMS::ROCKFALL User Manual, RAMMS (RApid Mass Movement Simulation): http://ramms.slf.ch/ramms/

Van Westen, C. et al., 2006. Landslide hazard and risk zonation—why is it still so difficult? Bulletin of Engineering Geology and the Environment, 65, 167–184. doi:10.1007/s10064-005-0023-0

Vazaios, I. et al., 2014. LiDAR as input for Discrete Fracture Networks: A comparison of automated and manual joint mapping using a scanned surface model. Canadian Geotechnical Society, GeoRegina, Regina, SK, Sept-Oct.

15th International Congress of the Geological Society of Greece
Athens, 22-24 May, 2019 | Harokopio University of Athens, Greece
Bulletin of the Geological Society of Greece, Sp. Pub. 7 Ext. Abs. GSG2019-284

T-LIDAR Applications for Studying Active Faults and Extracting Deformation Rates in Greece

I. Papanikolaou[1], K. Reicherter [2], S. Schneiderwind[2], J. Mason[2], G. Deligiannakis[1], S. Mechernich[3], T. Wiatr[2]

(1) Mineralogy-Geology Laboratory, Department of Natural Resources Development and Agricultural Engineering, Agricultural University of Athens, 75 Iera Odos Str., 118-55 Athens, Greece. Email: i.pap@aua.gr
(2) Institute of Neotectonics and Natural Hazards, RWTH Aachen, Lochnerstrasse 4-20, 52056 Aachen, Germany
(3) Institute of Geology and Mineralogy, University of Cologne, Zülpicher Strasse 49b, 50674 Köln, Germany

Introduction

Fault specific approaches are of decisive value for seismic hazard assessment by providing quantitative assessments through measurement of geologically recorded slip on active faults (Wesnousky, 1986). The geometry and kinematics of active faults are important for locating and characterizing the seismic sources. In addition, the long-term prediction of future earthquakes can be achieved through the study of the cumulative patterns of slip on active faults. Fault slip-rates that govern earthquake recurrence can be extracted from dated geologic and/or geomorphic indicators offset by faults, covering a time span that generally encompasses a large number of earthquake cycles. Terrestrial Light Detection and Ranging (T-LIDAR) is nowadays a major tool for earthquake geology and seismic hazard assessment by providing high spatial resolution (Papanikolaou et al. 2015). Resolution usually ranges from several cm to a few mm, depending on the distance to the target. T-LIDAR has been early used for studying the fault geometry and quantifying the fault plane characteristics. The Arkitsa fault Plane in Central Greece plane was one of the first worldwide applications and the first one in Greece by Jones *et al.*, 2009.

Methodology

Over the last few years we have implemented a large number of T-LIDAR studies for several active faults in Greece, introducing also some pioneer methodologies. These include: a) the extraction of kinematic data for the Spili fault in Crete (Wiatr *et al.*, 2013), b) the extraction of fault slip-rates based on the height of postglacial fault scarps in the Lastros Fault (Mason *et al.*, 2016), c) tracing of paleoevents based on the reflectivity and roughness changes along the scarp, (Wiatr *et al.*, 2015), d) tracing of paleoevents from fault plane weathering features, combined with Cosmogenic isotope dating offering info regarding both the slip and date of past events (Mechernich *et al.*, 2018), e) the combined use of LiDAR multispectral analysis with GPR (Ground Penetrating Radar) in paleoseismic trenching, (Schneiderwind *et al.*, 2016) using as an example the Kapareli trench site (Kokkalas *et al.*, 2007,) f) the identification of undiscovered paleoshoreline notches in the Perachora Peninsula adding more info regarding local tectonic movements (Schneiderwind *et al.*, 2017).

Results & Discussion

Kinematic indicators were accurately calculated on the Spili fault scarp in Crete (Fig. 1), where the percentage threshold error of the individual vector angle is lower than 3% for the dip direction and dip for planes.

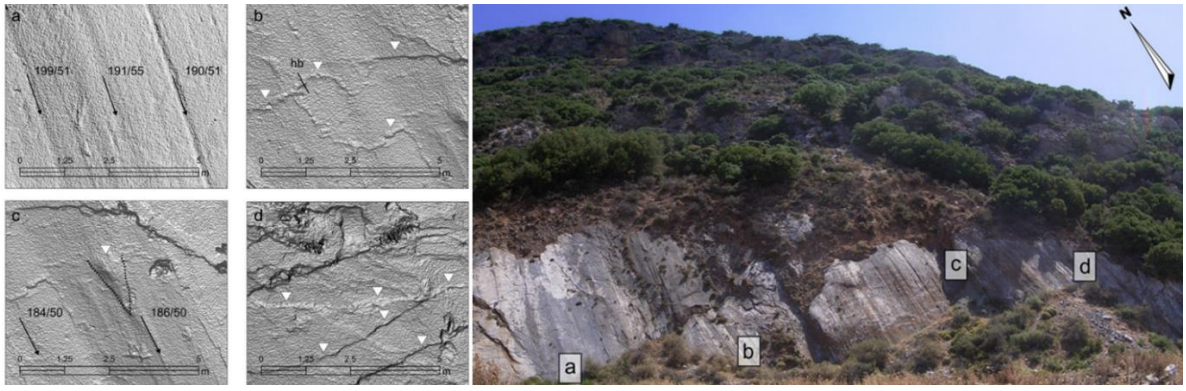

Figure 1. Kinematics indicators on the bedrock fault plane of the Spili fault, after Wiatr *et al.*, 2013.

Vertical displacements along a 1.3km long scanned segment of the Lastros fault in Crete were accurately determined using a T-LIDAR induced 3D model of the fault scarp, yielding a slip rate of 0.69±0.15mm/y (Fig. 2, left). T-LIDAR backscatter analyses at the Pisia fault scarp, along with Cosmogenic ^{36}Cl isotope dating, provided evidence for at least 6 paleoearthquakes (Fig. 2, right). The combination of laser scanning with GPR provided a 3D visualisation of a paleoseismic trench site in Kapareli, showing that trench stratigraphy and logging can be made using both techniques. Moreover, data from terrestrial laser scanning of coastal cliffs enhanced the recognition of tidal notches and supported palaeoseismic studies by providing spatial information and exact measurements of horizontal movements (Fig. 3).

All the above applications in Greece strongly imply that T-LIDAR is a major tool for earthquake geology and tectonic geomorphology, by offering quantitative data on the fault geometry, fault kinematics and deformation rates.

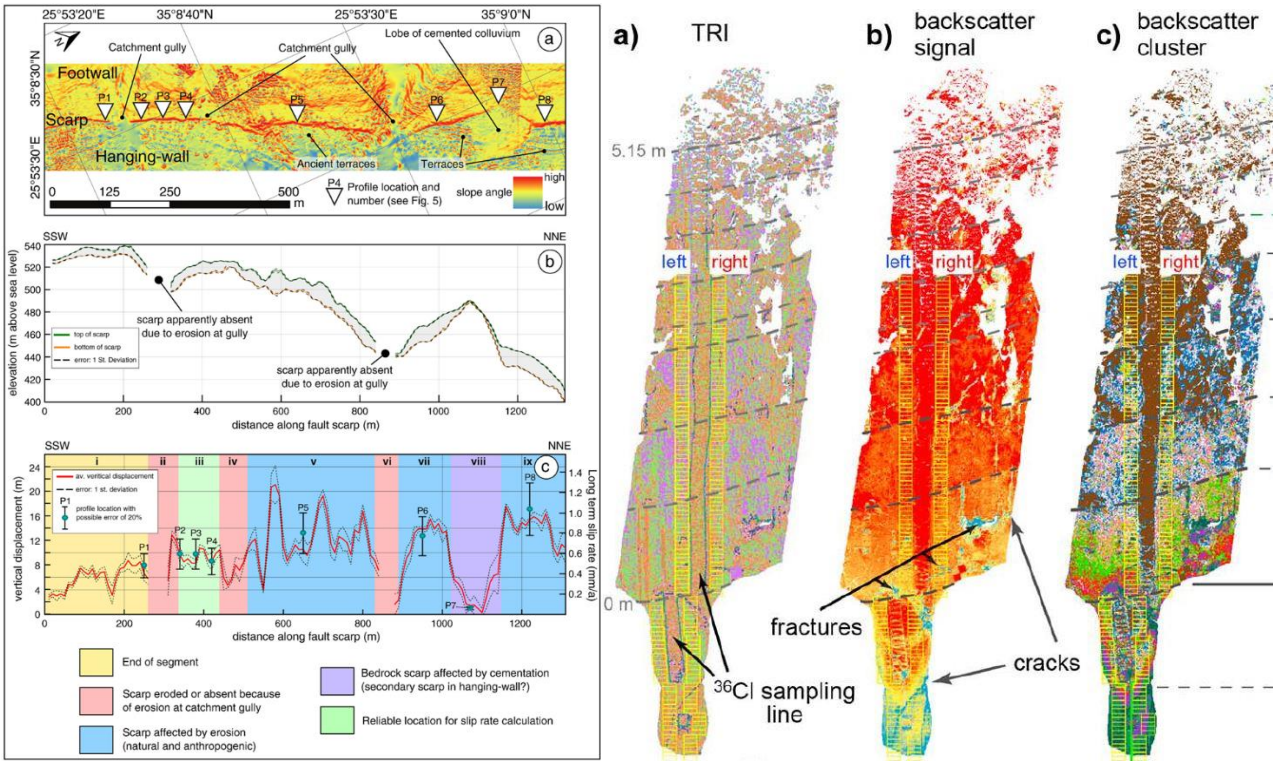

Figure 2. Left: The Lastros fault scarp geometry in relation to the postglacial rates of movement, after Mason *et al.*, 2016. Right: Surface characteristics of the Pisia fault scarp, based on T-LIDAR scanning, after Mechernich *et al.*, 2018.

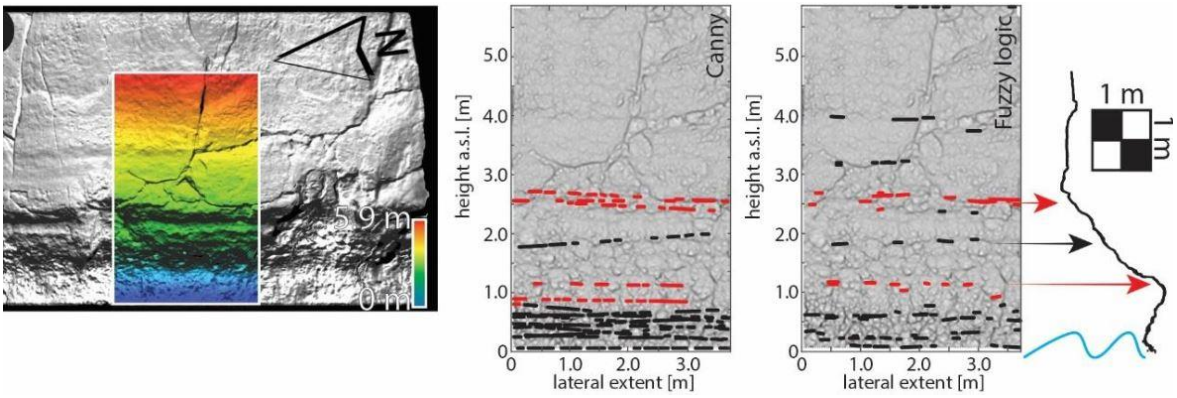

Figure 3. T-LIDAR scanned coastal cliff at Perachora peninsula, after Schneiderwind *et al.*, 2017.

References

Jones, R.R., Kokkalas, S., McCaffrey, K.J.W., 2009. Quantitative analysis and visualization of nonplanar fault surfaces using terrestrial laser scanning (LIDAR)-the Arkitsa fault, central Greece, as a case study. Geosphere 5, 465–482.

Kokkalas, S., Pavlides, S., Koukouvelas, I., Ganas, A., Stamatopoulos, L, 2007. Paleoseismicity of the Kaparelli fault (eastern Corinth Gulf): evidence for earthquake recurrence and fault behavior. Italian Journal of Geosciences 126, 387-395.

Mason, J., Schneiderwind S., Pallikarakis, A., Wiatr T., Mechernich, S., Papanikolaou, I., Reicherter, K., 2016. Fault structure and deformation rates at the Lastros-Sfaka Graben, Crete. Tectonophysics 683, 216–232.

Mechernich, S., Schneiderwind, S., Mason, J., Papanikolaou, I.D., Deligiannakis, G., Pallikarakis, A., Binnie, S.A., Dunai, T.J., Reicherter, K., 2018. The Seismic History of the Pisia Fault (Eastern Corinth Rift, Greece) From Fault Plane Weathering Features and Cosmogenic 36Cl Dating. Journal of Geophysical Research: Solid Earth 123, 4266-4284.

Papanikolaou, I.D., Van Balen, R., Silva, P.G., Reicherter, K., 2015. Geomorphology of Active Faulting and seismic hazard assessment: New tools and future challenges. Geomorphology 237, 1-13.

Schneiderwind, S., Boulton, S.J., Papanikolaou, I., Reicherter, K., 2017. Innovative tidal notch detection using TLS and fuzzy logic: Implications for palaeo-shorelines from compressional (Crete) and extensional (Gulf of Corinth) tectonic settings. Geomorphology 283, 189-200.

Schneiderwind, S., Mason, J., Wiatr, T., Papanikolaou, I., and Reicherter, K., 2016. 3-D visualisation of palaeoseismic trench stratigraphy and trench logging using terrestrial remote sensing and GPR – a multiparametric interpretation. S. Earth 7, 323–340.

Wesnousky, S.G., 1986. Earthquakes, quaternary faults and seismic hazard in California. J. Geophys. Res. 91, 12587–12631.

Wiatr T., Reicherter K., Papanikolaou I., Fernández-Steeger T., Mason J., 2013. Slip vector analysis with high resolution t-LiDAR scanning. Tectonophysics 608, 947-957.

Wiatr, T., Papanikolaou, I., Fernández-Steeger, T., Reicherter K., 2015. Bedrock fault scarp history: Insight from t-LiDAR backscatter behavior and analysis of structure changes. Geomorphology 228, 421–431.

15th International Congress of the Geological Society of Greece
Athens, 22-24 May, 2019 | Harokopio University of Athens, Greece
Bulletin of the Geological Society of Greece, Sp. Pub. 7 Ext. Abs. GSG2019-333

Fast-moving landslides mapping contribution using Sentinel-2

I. Gougoustamos[1], I. Parcharidis [1], C. Loupasakis [3]
(1) Harokopio University/Dep. Of Geoggraphy,El. Venizelou 70, 17676 Athens, Greece, johnniegougos@gmail.com
(2)National Technical University of Athens, School of Mining and Metallurgical Engineering, Department of Geological Sciences, Zographou Campus, GR-157 80 Athens, Greece

According to the World Atlas of Natural Hazards (McGuire, 2004), landslides are the most frequent and widespread natural hazard on Earth. They can occur on any terrain, particularly hilly and mountainous areas and mostly given the suitable conditions of soil or bedrock, groundwater, and the angle of slope (Varnes, 1978). Landslides can be characterized by low probability of evolution into a catastrophic event but can have very large direct and indirect impacts on man-made structures (Klose et al., 2014). Mapping of existing landslides in areas of known slope instability produces maps that can potentially deliver knowledge for landslide risk management strategies. Landslide activity maps represent a shortcut in the assessment of the hazard related to slope movements (Parise and Wasowski 1999), and show the areal extent of slope subject to failure, probable maximum extent of ground movement and highlight areas where more detailed studies should be conducted.

"Traditional" ground motion monitoring methods are based on field surveys. These methods include mainly geodetic/levelling measurements and Global Positioning System (GPS) networks, extensometers etc. However these methods of ground deformation monitoring except that provide information only about a few points present furthermore many disadvantages, such as high costs, time consuming and most of the monitoring systems require installation by experts of special equipment which in many cases is impossible nor are they able to produce knowledge of the past (retrospective products).

Earth Observation (EO) satellites, a non-invasive source of knowledge, host a diverse range of sensor types that utilize different parts of the electromagnetic spectrum (optical and radar sensors), a very rich archive of scenes and different techniques to provide a range of measurements from space offers several opportunities to map and monitor natural and human-induced Earth hazards from space (Cigna, 2018). Specifically, for landslides the ability to quantify them from space using repeat imagery depends, in principle, on the precision of the method used, the total displacement between two data acquisitions, the rate of displacement, and the existence of corresponding features in phase data (for radar) or amplitude data (for radar and optical sensors) that can be tracked over time (Delacourt et al., 2007, Kääb and Leprince 2014). Since 90's differential repeat-pass interferometry radar (DInSAR) based on SAR images processing has proven an interesting tool for the measurement and observation of ground deformation (Massonnet and Rabaute., 1993). The basic idea of the method is the analysis of the phase of the reflected wave radar from two or more images which cover the same region to observe ground displacement.

In recent years using large stacks of SAR images acquired over the same area, long deformation time series can be analysed using multitemporal differential SAR interferometry techniques which overcomes several limitations of repeat-pass interferometry. These coherent methods exploit either permanently coherent Persistent Scatterers (PSs) or temporally coherent Distributed Scatterers (DSs) known by names Persistent or Permanent Scatterer Interferometry (Ferretti et al., 2001, Werner et al., 2003) and Small Baseline Subset (Berardino et al., 2002) Both techniques have been widely applied for monitoring of slope instability with millimetric precision (Raucoules et al., 2013, Casagli et al., 2017). The most important advantage of the method is the ability to construct maps of yearly rates of ground displacement or the change to the rates. Nevertheless, significant difficulties are found when using this technique. These difficulties are related to the large variability of slope (steep and rough topography typical of landslide-prone areas) instabilities in terms of mechanisms of movement, failure geometries, size of unstable areas and deformation rates causing phase ambiguity problems and signal decorrelation. Additionally, in regions with strong topographic relief presented local atmospheric variations can in many cases lead to strong atmospheric phase artifacts; all these parameters , often obstract the interferometric preprocessing, making it difficult to estimate surface displacements (Hanssen 2001, Delacourt et al., 2003, Strozzi et al. 2005).

Monitoring and measurement of landslide activity using optical satellite sensors is also an efficient method which has been used since the end of 70's (Sauchyn and Trench 1978) mainly based on visual interpretation.The increasing of Very High Resolution (VHR) optical sensors, since beginning of 2000, led to the increase of new methods to monitoring land motion including landslides although that optical images are strongly dependent on atmospheric conditions. The methods can be split into two categories, pixel-based and object-based, both containing techniques applicable to single and multitemporal images and frequently making use of additional data. In recent years and from the beginning of the anvailability of high resolution optical data different methods with processing differentiation and in order to improve the accuracy of the measurements under different conditions have been developed.

The current research work aims to examine further contribution of medium resolution of free optical satellite images and specifically Sentinel 2 in the mapping of landslide of moderate and/or rapid velocity of travel regardless of the cause induced them in three different area specifically in USA (Yakima County, WA), Italy (Ponzano, Central Italy) and Greece (Amyntaio, Northern Greece). Also validate the results based on knowledge derived from other sources of knowledge. For the purpose of this study the normalized cross-correlation (NCC) method of image matching was used (Debella-Gilo and Kääb 2010, Heid and Kääb, 2012).

15th International Congress of the Geological Society of Greece
Athens, 22-24 May, 2019 | Harokopio University of Athens, Greece
Bulletin of the Geological Society of Greece, Sp. Pub. 7 Ext. Abs. GSG2019-363

Monitoring Surface Deformation Combining Optical and Radar Sentinel Data: The New Zealand Case

E. Kalamatianou[1], C. Tourlakidis[1], A. Fylaktos[1], P. Krassakis[2], I. Gougoustamos[1] I. Parcharidis[1]

(1) Harokopio University of Athens, El. Venizelou str.70, 17676 Kallithea, gp217306@hua.gr
(2) Centre for Research and Technology Hellas / Chemical Process and Energy, Resources Institute (CERTH/CPERI), Egialias str. 52, GR-151 25, Maroussi, Attica

The New Zealand region lies in the southwest Pacific Ocean overlapping a distinct belt of volcanic and earthquake activity that surrounds the Pacific Ocean. This is known as the "Ring of Fire". New Zealand lies on the boundary between the Pacific and Australian plates. To the north of New Zealand and beneath the eastern North Island, the thin and dense Pacific plate moves down beneath the thicker and lighter Australian plate. Within the South Island the plate margin is marked by the Alpine Fault where the plates are moved horizontally. Plate movement results in volcanic activity mainly in the North Island as well as earthquakes that are felt throughout the country (Graham, 2008). On November 14, 2016, a large magnitude [Mw] 7.8 earthquake struck the northeastern part of the South Island of New Zealand. The Kaikoura earthquake, named after the coastal town near the epicenter, had associated surface rupture on more than 20 mapped faults (Stirling et al. 2017), caused widespread crustal deformation (both uplift and subsidence), and triggered more than 10,000 landslides in the complex topography of the affected area (Dellow et al., 2017). Because of this, the earthquake has been described as the "most complex earthquake ever studied" (Jibson et al. 2018). Seismological evidence suggest that the main Kaikoura earthquake of Mw 7.8 was relatively rare for New Zealand with long recurrence intervals (Beavan et al. 2010).

Since the 1990's differential repeat-pass interferometry radar (DInSAR) based on SAR SLC images processing has proven an interesting tool for the measurement and observation of ground deformation (Massonnet and Rabaute., 1993). The basic idea of the method is the analysis of the phase of the reflected wave radar from two or more images which cover the same region in order to observe ground displacement. DInSAR has been widely used to identify ground deformation caused by different natural and anthropogenic phenomena. Many studies are motivated by the potential of SAR interferometry to be applied on a wide range of applications related to seismotectonics. The utilization of an appropriate interferometric dataset allows measuring the various components of the seismic cycle, namely the pre-seismic, co-seismic, and post-seismic deformation (Stramondo et al. 2009; Papanikolaou ei al. 2010, Briole et al. 2015).

Nevertheless, significant difficulties are found when using this technique. These difficulties are related to the large variability of slopes (steep and rough topography of prone areas), failure geometries, size of earthquake-prone areas and deformation rates causing phase ambiguity problems and signal decorrelation. Additionally, in regions with strong topographic relief presented local atmospheric variations can lead to strong atmospheric phase artifacts in many cases; all these parameters, often obstruct the interferometric pre-processing, making it difficult to estimate surface displacements (Hanssen 2001).

This paper aims to combine Sentinel SAR SLC and GRD images from Sentinel 1 satellite in order to overcome the above constrains of DInSAR. This is dome merging results about co-seismic displacement detection from SLC images and measurement from Sentinel 1 GRD data processing. There were used two images, one pre-seismic (Master) sensed on November3rd 2016 and one post-seismic (Slave) sensed on December 3rd 2016. Both SLC and GRD images were acquired on the same days, as the Level-1 Sentinel 1 products provide Single Look Complex images and Ground Range Detected images simultaneously. Level-1 focused data are the generally available products intended for most data users. Level-1 products can be either Single Look Complex (SLC) or Ground Range Detected (GRD). Each acquisition mode can potentially generate Level-1 SLC and GRD products. GRD resolutions will depend on the mode and the level of multi-looking. The SLC images were used in order to measure the displacement through the conventional interferometry technique (two passes plus DEM interferometry). The GRD images were used to enhance the results of the InSAR technique, which could not measure extreme surface displacement such as landslides. For that matter the Offset tracking method was used. Offset Tracking is a technique that measures feature motion between two images using patch intensity cross-correlation optimization. It is widely used in glacier motion estimation Level-1 Ground Range Detected (GRD) products consist of focused SAR data that has been detected, multi-looked and projected to ground range using an Earth ellipsoid model such as WGS84. The ellipsoid projection of the GRD products is corrected using the terrain height specified in the product general annotation. The terrain height used varies in azimuth but is constant in range (Lu & Veci, 2016). All referred methods were done with SNAP, the open source software for SAR image processing provided by ESA.

In order to combine the results of both methods a supervised classification was done in ArcGIS software provided by ESRI. The InSAR technique provides displacement results in millimeters, but the Offset-tracking technique provides results in millimeters per day, so we processed the latter results so they have the same units with displacement. All results were combined in one readable map to provide the total displacement of the affected area in Kaikoura.

References

Barrell, DJA, Litchfield, NJ, Townsend, DB, Quigley, M, Van Dissen, RJ, Cosgrove, R, Cox, SC, Furlong, K, Villamor, P, Begg, JG, Hemmings-Sykes, S, Jongens, R, Mackenzie, H, Noble, D, Stahl, T, Bilderback, E, Duffy, B, Henham, H. Klahn, A, Lang, EMW, Moody, L, Nicol, R, Pedley, K and Smith, A. 2011. Photographic Feature–Strike-slip ground surface rupture (Greendale Fault) associated with the 4 September 2010 Darfield earthquake, Canterbury, New Zealand. Quarterly Journal of Engineering Geology and Hydrogeology, 44: 283–291.

Briole, P., Elias, P., Parcharidis, I., Bignami, C., Benekos, G., Samsonov, S., Kyriakopoulos, C., Stramondo, S., Chamot-Rooke, N., Drakatou, M.L. & Drakatos, G., (2015). The seismic sequence of January-February 2014 at Cephalonia Island (Greece): constraints from SAR interferometry and GPS, Geophysical Journal International., 203, 1528-1540.

Dellow S. et al., (2017) Bulletin of the New Zealand Society for Earthquake Engineering, Vol. 50, No. 2, 106-116

Dowrick, DJ. 1998. Damage and intensities in the magnitude 7.8 1931 Hawkes Bay, New Zealand, earthquake. Bulletin of the New Zealand Society for Earthquake Engineering, 31: 139–163.

Graham, I.J. (ed.) 2008, A continent on the move: New Zealand: Geoscience into the 21st Century: Geological Society of New Zealand, Miscellaneous Publication, v. 124, pp. 1–388.

Hanssen, R.F. 2001 Radar interferometry: data interpretation and error analysis. In Remote Sensing and Digital Image Processing; Kluwer Academic: Dordrecht, Netherlands,

Jibson, R.W., Allstadt, K.E., Rengers, F.K., and Godt, J.W., (2018), Overview of the geologic effects of the November 14, 2016, Mw 7.8 Kaikoura, New Zealand, earthquake: U.S. Geological Survey Scientific Investigations Report 2017–5146, 39 p., https://doi.org/10.3133/sir20175146.

Lu J., Veci L., Sentinel 1 Toolbox, Offset Tracking Tutorial, Copyright © 2016 Array Systems Computing Inc. http://www.array.ca

Massonnet , D.; Rabaute, T. 1993 Radar interferometry: limits and potential. IEEE Trans. Geosci. Remot. Sen., 31, 455-464.

Papanikolaou, I.D., Foumelis, M., Parcharidis, I., Lekkas, E.L. &Fountoulis, I.G., (2010). Deformation pattern of the 6 and 7 of April 2009, Mw=6.3 and Mw=5.6 earthquakes in L' Aquila (Central Italy) revealed by ground and space based observations. Natural Hazards and Earth System Sciences 10, 73-87.

Quigley, M, Villamor, P, Furlong, K, Beavan, J, Van Dissen, R, Litchfield, N, Stahl, T, Duffy, B, Bilderback, E, Noble, D, Barrell, D, Jongens, R and Cox, S. 2010. Previously unknown fault shakes New Zealand's South Island. Eos, Transactions, American Geophysical Union, 91(49): 469–471.

Stirling, M.W. & Litchfield, Nicola & Villamor, Pilar & Van Dissen, Russ & Nicol, Andy & R. Pettinga, Jarg & Barnes, Philip & Langridge, Rob & Little, Tim & Barreil, D.J.A. & Mountjoy, Joshu & Ries, William & Rowland, J & Fenton, Clark & Hamling, I & Asher, Cameron & Barrier, Andrea & Benson, Adrian & Bischoff, Alan & Zinke, Robert. (2017). The Mw7.8 2016 Kaikōura earthquake: Surface fault rupture and seismic hazard context. Bulletin of the New Zealand Society for Earthquake Engineering. 50. 73-84.

Stramondo S, Chini M, Bignami C, Salvi S, Atzori S (2009) X-, C-, and L-Band DInSAR Investigation of the April 6. Abruzzi Earthq IEEE Geosci Remote S 8(1):49–53.

15th International Congress of the Geological Society of Greece
Athens, 22-24 May, 2019 | Harokopio University of Athens, Greece
Bulletin of the Geological Society of Greece, Sp. Pub. 7 Ext. Abs. GSG2019-392

Comparative study of landslide mapping on UAV and TLS derived point-clouds: A case study in Anilio, Greece

C.Kritikou[1], E. Karantanellis[1], V. Marinos[1]

(1) Laboratory of Engineering Geology & Hydrogeology, School of Geology, Aristotle University of Thessaloniki, 54124, Thessaloniki, Greece, fkritikos@geo.auth.gr

Introduction

Landslide phenomena pose a major threat to humans and the environment. Due to the complex nature of landslides, a thorough investigation is essential in order to identify and study such disastrous phenomena. The incorporation of innovative tools, such as Unmanned Aerial Vehicles and Terrestrial Laser Scanners is proved to be very effective in the investigation process, in terms of precision, and time-efficient. Moreover, the use of remote sensing techniques in landslide surveys provides information that covers a variety of applications, such as landslide identification and mapping, monitoring, susceptibility and hazard assessment (Scaioni M. et al., 2014). This study, by employing both a UAV Photogrammetry and a Terrestrial Laser Scanning approach for data acquisition, focuses on landslide identification and mapping in a vegetated area and provides a comparative analysis of the mapped landslide features on both, UAV and TLS-derived, point-clouds. It is noted that besides the use of these tools, a field investigation was conducted, in order to evaluate the results derived from the point-clouds.

Study area

The study area is located in Anilio village, in the prefecture of Epirus, Greece. According to the geotectonic zonation of Greece, the area appertains to the zone of Olonos-Pindos, which is composed of Mesozoic carbonate and siliciclastic rocks and Tertiary flysch formations. Pindos flysch consists mainly of sandstones, siltstones and their alternations repeated in several thrust sheets with NW-SE direction. Flysch, in general, is characterized by heterogeneity, presence of members with low strength and a complex structure due to folding, shear zones and discontinuities (Marinos et al., 2015). Therefore, its behaviour in slope stability is controlled by these factors in connection with the regional setting, such as morphological and groundwater conditions. The area of interest is formed entirely in a flysch environment, with siltstone formations being predominant, and strongly tectonized by numerous thrusts, being in very close proximity to the Pindos ophiolite nappe, resulting in the degradation of the original rock mass quality.

Methodology

In order to collect the information, a combination of methods was applied. During a visit in the study area, alongside with in-situ investigation, data were collected using an Unmanned Aerial Vehicle and a ground-based LiDAR system. A series of overlapping high resolution images of the area of interest were acquired by the UAV following a predefined flight path. UAV photogrammetry was used in combination with the Structure from Motion technique, as very detailed 3D models can be obtained from overlapping imagery with SfM algorithms (Lucieer et al., 2014). UAV imagery was used in the SfM workflow in a software environment and was automatically processed, resulting in the generation of a point-cloud, a Digital Surface Model (DSM) and an orthomosaic. Consequently, a hillshade map was produced, where two main landslides in the region of Anilio are depicted (Figure 1). Furthermore, data were collected by a TLS using the Time of Flight principle for ranging. In order to cover the whole scene and avoid occluded areas, several scans from different points of view are needed (Jaboyedoff et al., 2018). For that purpose, scans were conducted from two different positions. Later, with the aid of a point-cloud processing software (CloudCompare 2.10.2), point-clouds from the multiple scans were used as input and were manually merged in order to generate a single point-cloud of the landslide area.

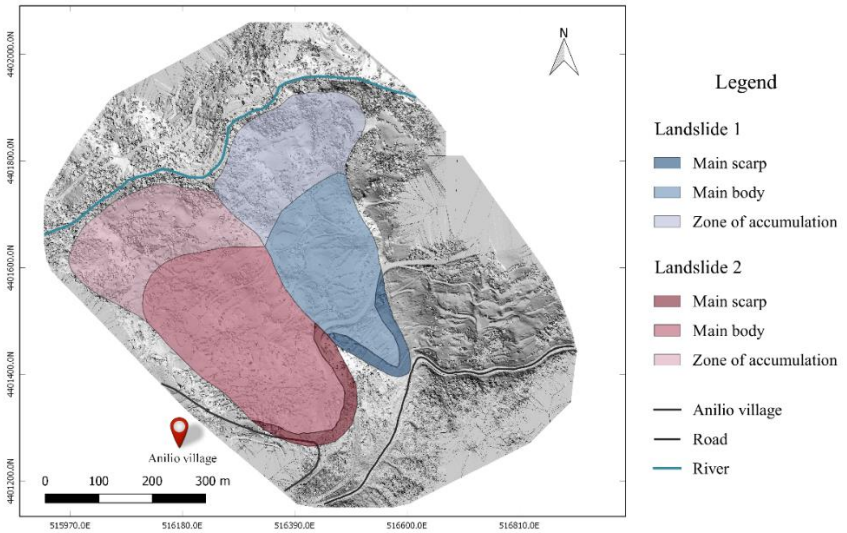

Figure 1. Hillshade map depicting two main landslides in the region of Anilio.

Results

The two point-clouds, one derived from UAV data and one derived from TLS data (Fig. 2), were used in order to detect geomorphological features of typical landslides, such as scarps, depressions and zones of uplift. These features were identified and mapped on both point-clouds and were later compared. An accuracy assessment of the resulted segments was conducted in order to verify the efficiency of each approach in a densely vegetated area. The main difference between the two methods, which reflects on their derivatives, lies in the fact that the UAV method uses a passive sensor and LiDAR technology uses an active sensor. More specifically, the laser scanner acts as a source of illumination, emitting laser beams, whereas the UAV camera, as a passive sensor, can only capture the scene lit by natural light. This means that, LiDAR technology offers an advantage in landslide studies in vegetated areas as it can penetrate vegetation and reach the ground surface. However, this may not be possible in areas with dense tree canopy and vegetation, but such features can be removed from a TLS point-cloud in a software environment. As a result, the TLS derived point-cloud (Fig. 2a) is free of colour and consists of ground points, from the reflection of the ground surface, and non-ground points, from the reflection of trees and vegetation which can be manually removed. The UAV derived point-cloud is colour coded, meaning each point has an RGB value attributed to it and is not free of vegetation as it is produced by imagery processing (Fig. 2b). This means it is not easy to identify the geomorphological features of the landslide. Even if filters are applied, to extract the vegetation, or if they are manually removed, shadows will be still shown in the point-cloud.

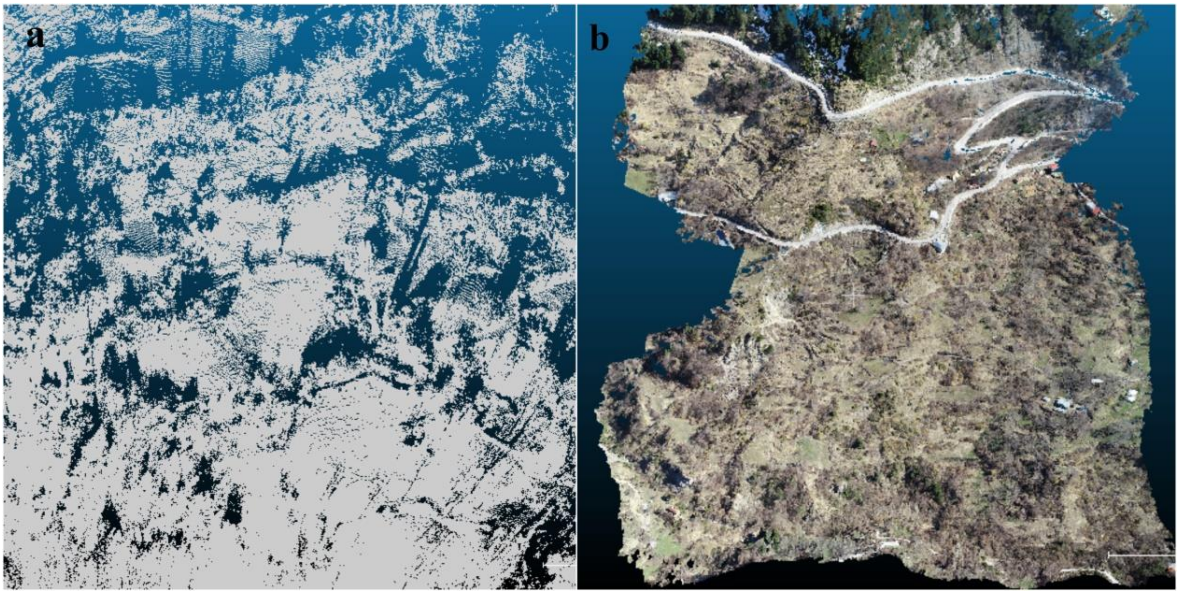

Figure 2. a)TLS-derived and b)UAV-derived point-cloud of the area of interest.

References

Jaboyedoff M., Abellán A., Carrea D., Derron M. H., Matasci B. and Michoud C., Mapping and Monitoring of Landslides Using LIDAR. In book: Natural Hazards: Earthquakes, Volcanoes, and Landslides, (2018)

Lucieer, A., Jong, S. M. de, & Turner, D. (2014). Mapping landslide displacements using Structure from Motion (SfM) and image correlation of multi-temporal UAV photography. Progress in Physical Geography: Earth and Environment, 38(1), 97–116.

Marinos V., Papathanassiou G., Vougiouka E., Karantanellis E. (2015). «Towards the Evaluation of Landslide Hazard in the Mountainous Area of Evritania, Central Greece». Engineering Geology for Society and Territory, Lollino et al. (eds.), Published by Springer – Volume 2, pp.989-993, DOI: 10.1007/978-3-319-09057-3_173

Scaioni, M.; Longoni, L.; Melillo, V.; Papini, M. Remote Sensing for Landslide Investigations: An Overview of Recent Achievements and Perspectives. Remote Sens. 2014, 6, 9600-9652.

SPECIAL SESSION

T11/T11.S2 Geoinformatics: Remote Sensing, Information Technology and Intelligent Methods in Geosciences

Conveners: **Ch. Roumpos (T.U. Crete)**
I. Kapageridis (TEI W. Macedonia)
M. Galetakis (T.U. Crete)

15th International Congress of the Geological Society of Greece
Athens, 22-24 May, 2019 | Harokopio University of Athens, Greece
Bulletin of the Geological Society of Greece, Sp. Pub. 7 Ext. Abs. GSG2019-002

RUS Copernicus Service: Cloud Computing, Support and Training for Sentinel Users.

G. Karadimou[1], B. Bonneval[1], F. Palazzo[1], S. Rémondière[1], T. Šmejkalová[1], M. Castro-Gómez[1], C. Gilles[1], E. Guzzonato[2], B. Mora[2].

(1) Serco Italia S.p.A, Via Sciadonna 24-26, 00044, Frascati (Rome), Italy, Georgia.Karadimou@serco.com
(2) CS SI, 5 rue Brindejonc des Moulinais, 31506, Toulouse, France

Offering systematic open and free Earth observation data at global coverage (and with an observational continuity ensured for decades), the Copernicus satellite constellation is a game-changer for many different applications, including climate monitoring, environmental changes (atmospheric, marine, land), agriculture, forestry, natural hazards and many others. However, the exploitation of remote sensing data is often computationally heavy and knowledge demanding.

With the aim to tackle these issues the RUS Copernicus (Research and User Support for Sentinel Core Products) project, funded by the European Commission and managed by the European Space Agency (ESA), started operations in October 2017. The service is offered free of charge and is operated by CSSI and its partners: Serco Italia SPA, Noveltis, Along-Track, and CS Romania. The main aim of RUS is to enable and increase the uptake of Copernicus data and support R&D activities within Europe. The service provides not only powerful computational environment (up to 40 cores for processing and 50 TBytes of storage capacity) - in the form of customized Linux based Virtual Machines (VMs) preinstalled with a wide variety of open source toolboxes - but also EO expertise and support for application-specific data selection, processing and visualization as well as algorithm development and scaling-up to large amount of Sentinel products. Moreover, users can install additional proprietary tools and SW in case they hold a valid license. The service is exclusively foreseen for training, research and R&D (no commercial use) and is currently available only to the residents of EU ("Copernicus citizens").

Apart from ICT resources and user support, RUS Copernicus has implemented an extensive training programme, led by Serco Italia SPA, and open to everyone (from students to decision-makers and professionals). It is designed to fit users' needs at all levels of expertise regardless their location or the topic of interest. The training programme covers a wide portfolio of applications and consists of three main pillars: 1) Face-2-Face training (generally up to 2 days in duration, for max. 45 participants); 2) Webinars (regular monthly webinars, special webinars, up to 500 participants); 3) E-learning. All trainings/resources are free and exploit only open source software in order to facilitate repeatability for users (even users not registered for a free RUS VM).

By January 2019, more than 2,000 people have participated in RUS training events and the recorded webinars count more than 28,000 views on the dedicated RUS YouTube channel. Additional 1,200 users are registered to the E-learning portal, which enables them to learn and test their knowledge in EO at their own pace.

15th International Congress of the Geological Society of Greece
Athens, 22-24 May, 2019 | Harokopio University of Athens, Greece
Bulletin of the Geological Society of Greece, Sp. Pub. 7 Ext. Abs. GSG2019-035

Spatiotemporal Variability of Water Table Levels in Al Ain Region, United Arab Emirates

A. Abuelgasim and M. Elkamali

National Water Center, Department of Geography and Urban Planning, United Arab Emirates University, Al Ain, UAE, a.abuelgasim@uaeu.ac.ae

Abstract

Management of groundwater recourses has been one of the most critical challenges facing human beings in the past few decades. Mapping groundwater levels and fluctuations provide a valuable source of information for various applications of human and urban activities as well as their impact on the environment. Al Ain region in the United Arab Emirates has been facing serious problems with the depletion of its groundwater resources in the past few decades. This problem has been intensified by the rising urban population, and expansion in agricultural activities. It has been judged to be prudent to continuously monitor groundwater levels from different observations well. Such study shall be useful for integrating water resources management, planning groundwater development, and sustainable water resources for agricultural and urban utilization. The water table levels from different observation wells around Al Ain city were interpolated using deterministic and stochastic interpolation techniques to predict the spatial distribution of water levels for the period between 2014 to 2017. It has been observed that groundwater level ranges from 2 m inside Al Ain city to 154 m at Remah district western of Al Ain city. The fluctuations of the groundwater level during the mentioned period will be presented and discussed. Furthermore, the study will provide the necessary steps in generating a hydrogeological model for sustainable water resources management.

In the Arabian Peninsula and particularly in United Arab Emirates (UAE) groundwater is a major source of fresh water supply particularly to agriculture. More recently, the socio-economic development, the high population growth and expansion in agriculture have placed enormous strains on the limited available water resources. Achieving sustainable water use and management practices is thus of vital importance. The development of an integrated water management strategy based on the long-term monitoring of changes in groundwater storage and its seasonal dynamics is a first step towards this goal.

Groundwater level in Abu Dhabi, United Arab Emirates (UAE) has been continuously subject to changes in both level and salinity. Due to the arid characteristics of the region, the enormous water consumption to meet the intensive urbanization and expansion processes comes mainly from the groundwater and desalinization plants. In addition, demands from agriculture, domestic and industrial sectors participate with more than 65% of the water consumption mainly from groundwater resources. A decrease of the groundwater level by as much as 80 m has been reported in some areas in Abu Dhabi emirate. Furthermore, the arid climate in UAE with less than 100 mm a year in average combined with the high evaporation rate (2-3 m/year) and the low groundwater recharge (4% of total annual water use) are more contributing to the scarcity of these resources.

Water wells in the study area offer information about depth to water provided from Environmental Agency of Abu Dhabi, some of these wells are productive wells which they use for farming and some are observation wells to monitor water table dynamics. Information obtained from both types of wells were used for studying aquifers parameters (permeability, porosity, storativity, so on), groundwater exploration, and furthermore for investigating land surface deformations. In recent years deterministic and stochastic interpolation techniques have been utilized to predict the spatiotemporal variability of water table levels inside the GIS environment. The benefit of using GIS environment that is providing better use of interpolation techniques to predict the spatiotemporal variations. This paper is focusing in identifying the variations of water table levels over space and time in Al Ain region to provide better understanding of groundwater dynamics in the study area.

Both stochastic and deterministic techniques provide a means for studying the spatiotemporal variability of water levels from close points. Stochastic interpolation methods import the spatial variability of the variable by using the spatial autocorrelation property, while deterministic interpolation methods use the values of the variable only. Stochastic interpolation techniques use both statistics and mathematical functions for interpolation, while deterministic interpolation techniques use only mathematical functions. The main methods of deterministic interpolation available in GIS software include triangulation with linear interpolation, Inverse Distance Weighted (IDW), spline and spline modified.

Stochastic methods have the capability of producing a prediction surface, but they can also provide some measure of the certainty or accuracy of the predictions. Ordinary kriging is a stochastic method that is common in GIS analysis tools. Kriging is similar to IDW (deterministic method) in that it weights the surrounding measured values to derive a prediction for each location. However, the weights are based not only on the distance between the measured points and the prediction location but also on the overall spatial arrangement among the measured points.

When using Kriging interpolation technique, the spatial autocorrelation is studied using the empirical semi variogram to investigate that close points are mores similar than far away points. Empirical semi variogram has variety of models that use to fit the plotting between semi-variance and the distance between points. The best fit model should be selected carefully because it will affect the prediction surface.

The provided water table levels data were in form of depth to water in meter with lithological description. These data were processed in ArcGIS software package to create point map showing the spatial distribution of water wells. In order to generate interpolated surface using stochastic technique the Geostatistical wizard of ArcGIS has been used to utilize interpolated surface of water table levels. Geostatistical wizard allows to construct and manipulate semi-variogram model to optimize the interpolation process and Kriging type used was Ordinary Kriging. Generating interpolation surface using Kriging method provide additional benefit of creating standard deviation surface to evaluate the accuracy of the interpolated surface. On the other hand, the interpolated surface using deterministic technique was generated using IDW method. A comparison between both methods have been conducted.

This study showed that depth to water increased during May to November (drought season) and return to decrease between December to April (rainy season). Interpolated surfaces generated from stochastic interpolation technique showed higher accuracy than surfaces generated from deterministic interpolation technique. Standard deviation surface maps from Kriging method showed a consistent value to consider the generated surface as optimum results. The trend of water table levels during this period showed a significant decrease and this can be result of the consistent drop in rainfall at the study area between 2014-2017 coupled by increase in groundwater withdrawals.

Acknowledgements

This work is supported by a grant from the National Water Centre of the United Arab Emirates University under Grant number 31R155-Research Centre- NWC -3-2017.

15th International Congress of the Geological Society of Greece
Athens, 22-24 May, 2019 | Harokopio University of Athens, Greece
Bulletin of the Geological Society of Greece, Sp. Pub. 7 Ext. Abs. GSG2019-036

Land Surface Deformations Using SAR Interferometry: Past, Present, and Future Trends

M. Elkamali, and A. Abuelgasim

National Water Center, Department of Geography and Urban Planning, United Arab Emirates University, Al Ain, UAE, 201890072@uaeu.ac.ae.

Synthetic Aperture Radar Interferometry (InSAR) has played an essential role in monitoring changes of Earth's surface in the last few decades (Pepe et al., 2016). This technology relies on measuring the phase difference between two or more complex values SAR images acquired at different times and/or different orbital positions. Primarily, the distributions of the receiving/transmitting antennas will define the interferometric distributions. Mono-static InSAR involves two antennas to produce three interferometric distributions; these are i) across-track interferometry, which acquires SAR images at the same time from different positions, ii) along-track interferometry that acquires SAR images at different times but from the same position, and iii) repeat-pass across-track interferometry that acquires SAR images at different times and from different positions.

The SAR data availability increased rapidly in the recent years operated with various SAR instruments over different platforms, which archived SAR data acquired from different wavelengths, look angle geometries, and acquisition modes. Using different wavelengths allow to reach a different level of information, such as different level of penetration, the longer the wavelength, the stronger the penetration. Satellites use a various wavelength; AIRSAR uses P-band (65 cm), ALOS uses L-band (23 cm), while ERS-1/-2 RADARSAT ENVISAT uses C-band (5 cm), and TerraSAR-X and COSMO-SkyMed use X-band (3 cm). SAR images acquired with different look angle geometries over the same period could allow retrieving complete 3D displacements. Different acquisition modes are available; the main differences are in the way of scanning the Earth's surface like generating a narrow swath when using Stripmap mode, a wide swath from ScanSAR mode, or viewing the scene from multiple angles when using Spotlight mode.

Since SAR systems operate in side-looking geometry and the antenna is not pointed perpendicular to the nadir point but perpendicular to the travel direction, the displacement value measured will be in the RADAR Line-Of-Sight (LOS) direction. Measurements value in LOS direction is composed of vertical, easting and northing components. Decomposing displacement measurement in LOS direction requires multiple angle SAR scenes, but still retrieving the deformation of northing component is very difficult. This because most of the recent SAR satellites operate at near-polar orbits (parallel to N-S direction), so the viewing geometries are blind to N-S displacements. Raucoules et al. (2013b) retrieved 3D deformation from displacement components from azimuth and LOS direction along both ascending and descending orbits obtained by the correlation for each point of the processing grid affected by a certain quality. Another study by used Differential Global Navigation Satellite System (DGNSS) to retrieve the whole 3D deformation named East, North, and Up components.

InSAR techniques have restrictions and limitations that should be considered particularly spatial and temporal decorrelations. These decorrelations occur due to the large gap between two acquisitions in time or space, respectively. There are other limitations such as; surface displacement which depends on the system, surface physical properties, atmospheric condition, and the software used. Some restrictions might vary according to the landcover of the study area. For instance, the InSAR technique depends on finding coherent (stable) pixels during the deformation time to measure surface displacement. Therefore, it is easy to find coherent pixels over urban or mountain areas, but there is an effect of high buildings and mountains on Radar signal; however, it is hard to find coherent pixels over vegetated areas.

This research provides a comprehensive review of the applications of InSAR technology in properly identifying land surface deformations. The review is primarilyfocused on the applications of this technology to different land cover types. Land cover types studied in this research were desert, glaciers, mountain, rural, vegetation, and urban.

Desert area is characterised by similar targets which have less decorrelation to shorter radar wavelengths. Performing PSI on X-band or C-band to observe ground displacement over desert areas is very efficient because there is a great possibility to obtain high PS density. Glacier surfaces are displaying relative faster motion than other landscapes, so there is no significant difference between various radar frequencies for detecting glacier surface motion. In order to detect surface deformation using InSAR technique over mountainous terrain, all available SAR data is applicable (ENVISAT C-band, TerraSAR X-band, ALOS L-band, COSMOSkyMed X-band, and Sentinel-1A C-band).

Rural areas have some aspects from urban areas and others from desert areas. SAR data used for detecting surface deformation over rural areas were found as; ENVISAT C-band, ALOS L-band, TerraSAR X-band, ERS1/2 C-band, and Sentinel-1A C-band. Land surface deformations over vegetation surface considered as the most difficult one due it is high temporal correlation. To reduce this effect multiple SAR data from all available sources is required to over come this error. So most of the studies used a combination between ERS-1/2 C-band, ALOS L-band, Sentinel-1 C-band, TerraSAR X-band, COSMOSkyMed X-band, and ENVISAT C-band.

Most of the scholarly studies in the related literature on retrieving surface deformation over urban areas used more than one radar wavelength because finding coherent pixels are more feasible over urban areas.

Acknowledgements

This work is supported by a grant from the National Water Centre of the United Arab Emirates University under Grant number 31R155-Research Centre- NWC -3-2017.

15th International Congress of the Geological Society of Greece
Athens, 22-24 May, 2019 | Harokopio University of Athens, Greece
Bulletin of the Geological Society of Greece, Sp. Pub. 7 Ext. Abs. GSG2019-084

Potential of Sentinel-2 data on detecting hydrothermal alteration using clustering: the case of Nisyros caldera (Greece).

A. Tompolidi[1,2], O. Sykioti[1], K. Koutroumbas[1], S. Xenaki[1], I. Parcharidis[2]

(1) Institute for Astronomy, Astrophysics, Space Applications and Remote Sensing, National Observatory of Athens, V. Pavlou & I. Metaxa, Penteli, Greece, atompolidi@noa.gr
(2) Harokopio University of Athens, E. Venizelou Avenue 70, Kallithea, Greece

The aim of this study is to investigate the potential of detecting and mapping hydrothermal alteration from Sentinel-2 data, using an innovative clustering algorithm, as well as the interpretation of the resulting clusters using spectral indices (SIs) linked to the hydrothermal alteration within the caldera of Nisyros.

Geological setting

Nisyros is a small, almost circular, island, which constitutes the youngest volcano of the South Aegean Active Volcanic Arc (SAAVA) with a central caldera depression of 4km diameter (Fig. 1a). The volcanic edifice, entirely formed during the Late Quaternary, lies above an Alpine basement of Mesozoic limestones and is characterized by calc-alkaline series (from basaltic andesitic to rhyolitic composition) (Francalanci *et al*., 2005). In historical times, several hydrothermal eruptions took place in the south-eastern part of the caldera generating hydrothermal craters. Nowadays, various fumarolic fields are present in the hydrothermal crater area (Gorceix synthem) with the major fumarolic vents to be located in the craters of Stephanos, Polybotes (Micros Polybotes and Megalos Polybotes) and Phlegethon and the minor fumarolic vents in the Kaminakia craters area (Marini *et al.*, 2002). In these areas, steam-heated, acid sulfate hot waters are formed, due to O_2-driven oxidation of H_2S to H_2SO_4, where ascending hydrothermal gases condense, in shallow groundwaters or surface waters. These acidic solutions react with the host rocks and form advanced argillic alteration.

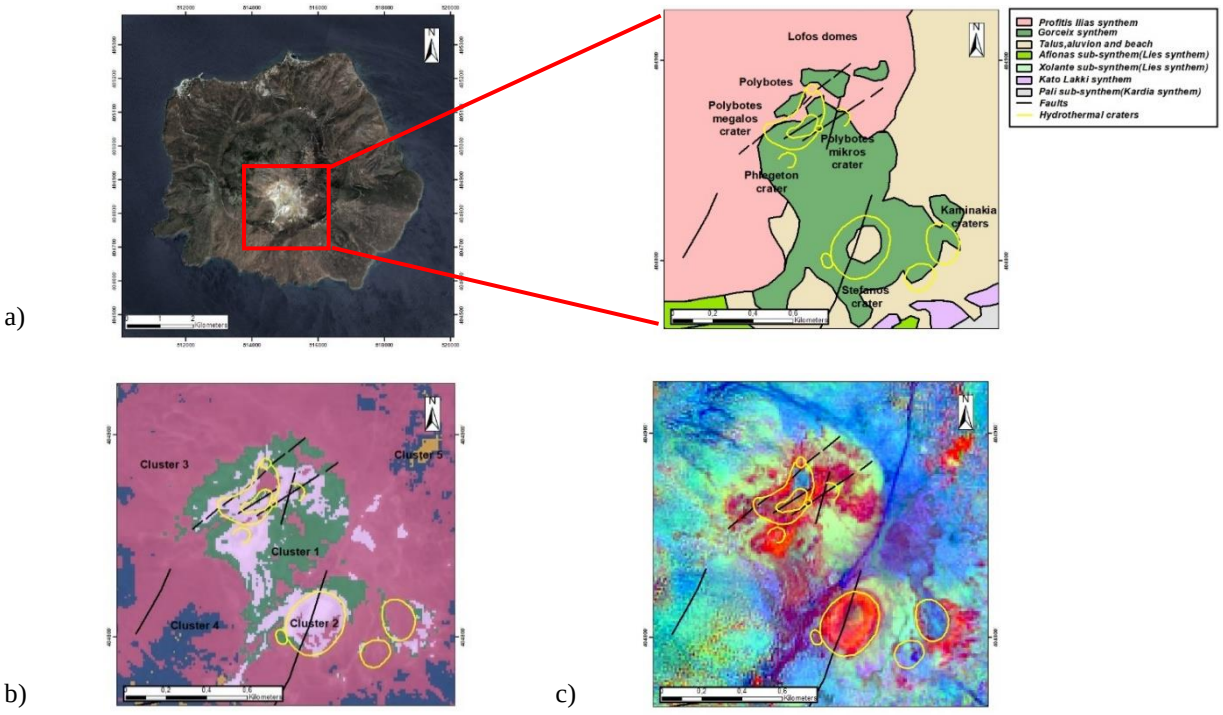

Figure 1. a) Left: Nisyros island. The red rectangle shows the location of hydrothermal alterations within the caldera. Right: Simplified geological map of Nisyros caldera (1:10.000) by Volentik *et al.*, 2005, b) Clustering map and c) Color composite map of the spectral indices around the hydrothermal field within the caldera of Nisyros (R:Hydroxyl-bearing alteration index, G: All iron oxides index, B: Ferric iron oxides index).

Materials

Recent studies have shown the capabilities of Sentinel-2 MSI data in geological and lithological mapping (Van der Meer *et al*., 2014, Ge *et al*., 2018). For the purpose of this study, a Sentinel-2A MSI L1C image was used, acquired on 22/7/2017. The image has been atmospherically corrected with the Sen2Cor tool within ESA's SNAP software. The resulting bottom-of-the-atmosphere reflectance dataset, consisting of 12 spectral bands with 10m spatial resolution, was then subset to the caldera area.

Methodology

The adopted methodology consists of the following processing steps: a) Projection of the data on the space spanned by the first three principal components. b) Application of the Online GAPCM (O-GAPCM) clustering algorithm on the projected data. The O-GAPCM is a possibilistic clustering algorithm, which has the ability to recover the true number of clusters, while, in addition, it can identify hyperellipsoidally-shaped clusters, formed in the feature space (Xenaki *et al.*, 2018). c) Comparison of the clustering results with the georeferenced simplified geological map of Nisyros (1:12.500) (Volentik *et al.*, 2005), in order to investigate whether the hydrothermal alteration area of the Gorceix synthem is identified. d) Interpretation of the clusters covering the Gorceix synthem and the surrounding area, using the hydroxyl-bearing alteration (SI-i), the all iron oxides (SI-ii) and the ferric iron oxides (SI-iii) spectral indices (Van der Werff & Van der Meer, 2016).

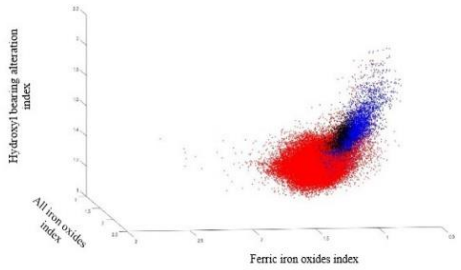

Figure 2. 3D-plot of the three clusters covering the Gorceix synthem (Cluster 1 (blue), Cluster 2 (black)) and the surrounding area (Cluster3 (red)) resulting by the O-GAPCM algorithm space spanned by the three spectral indices.

Results

The O-GAPCM algorithm has produced five clusters within the Nisyros caldera (Fig. 1b). In the sequel, we focus on the following three clusters: Clusters 1 and 2, which according to the simplified geological map exhibit significant overlap (69%) with the hydrothermal area (Gorceix synthem) (Fig. 1a) and Cluster 3, which covers the surrounding area. As shown in Figs. 1b-1c, Clusters 1 and 2 differ from Cluster 3, in terms of hydroxyl-bearing alteration (SI-i), all iron oxides (SI-ii) and ferric iron oxides (SI-iii) presence. Cluster 3 is mainly characterized by the presence of iron (both ferric and all iron oxides), which is in accordance with Seymour and Lalonde (1991). In particular, all iron oxides (west of the Gorceix synthem) are mainly detected on post-calderic dacitic lava domes (Profitis Ilias synthem) and ferric iron oxides (east of Gorceix synthem) on lacustrine intracalderic deposits (talus, aluvion and beach) (Fig. 1a). In contrast, Clusters 1 and 2 exhibit stronger hydroxyl-bearing alteration than Cluster 3 (Fig. 2). Focusing on Clusters 1 and 2, the former is characterized by a strong presence of both all iron oxides and hydroxyl-bearing alteration, while the latter is mainly characterized by strong hydroxyl-bearing alteration (Fig. 1c). Concluding, Sentinel-2 data seem to contain the necessary spectral information for the detection of hydrothermal alterations in a geothermal volcanic environment, which can be extracted using clustering methods. Current investigations include the examination of the mineralogical content of the alteration zones inside the Nisyros caldera, utilizing Sentinel-2 and/or other multispectral data.

Acknowledgements

We acknowledge support of this work by the project “PROTEAS II” (MIS 5002515), which is implemented under the Action “Reinforcement of the Research and Innovation Infrastructure,” funded by the Operational Programme “Competitiveness, Entrepreneurship and Innovation” (NSRF 2014–2020) and co-financed by Greece and European Union (European Regional Development Fund). The authors would like to thank Dr G. E. Vougioukalakis, for providing additional field information on Nisyros.

References

Francalanci, L., Vougioukalakis, G.E., Perini, G. and Manetti, P., 2005. A West-East Traverse along the magmatism of the south Aegean volcanic arc in the light of volcanological, chemical and isotope data. In *Developments in Volcanology* (Vol. 7, pp. 65-111). Elsevier.

Ge, W., Cheng, Q., Tang, Y., Jing, L. and Gao, C., 2018. Lithological classification using sentinel-2A data in the Shibanjing ophiolite complex in inner Mongolia, China. *Remote Sensing*, *10*(4), p.638.

Marini, L., Gambardella, B., Principe, C., Arias, A., Brombach, T. and Hunziker, J.C., 2002. Characterization of magmatic sulfur in the Aegean island arc by means of the δ34S values of fumarolic H2S, elemental S, and hydrothermal gypsum from Nisyros and Milos Islands. *Earth and Planetary Science Letters*, *200*(1-2), pp.15-31.

Seymour, K.S. and Lalonde, A., 1991. Monitoring oxygen fugacity conditions in pre-, syn-and postcaldera magma chamber of Nisyros volcano, Aegean island arc, Greece. *Journal of Volcanology and Geothermal Research*, *46*(3-4), pp.231-240.

Van der Meer, F., Hecker, C., van Ruitenbeek, F., van der Werff, H., de Wijkerslooth, C. and Wechsler, C., 2014. Geologic remote sensing for geothermal exploration: A review. *International journal of applied earth observation and geoinformation*, *33*, pp.255-269.

Van Der Werff, H. and Van Der Meer, F., 2016. Sentinel-2A MSI and Landsat 8 OLI provide data continuity for geological remote sensing. *Remote sensing*, *8*(11), p.883.

Volentik, A., Principe, C., Vanderkluysen, L. and Hunziker, J., 2005.Explanatory notes on the "Geological Map of Nisyros Volcano (Greece)". In: Hunziker JC, Marini L (eds): The geology, geochemistry and evolution of Nisyros Volcano (Greece). Mémoires de Géologie (Lausanne), No.44 : 7–25.

Xenaki, S.D., Koutroumbas, K.D. and Rontogiannis, A.A., 2018. A Novel Online Generalized Possibilistic Clustering Algorithm for Big Data Processing. *In the 26th European Signal Processing Conference (EUSIPCO)*, Rome, Sept. 2018.

15th International Congress of the Geological Society of Greece
Athens, 22-24 May, 2019 | Harokopio University of Athens, Greece
Bulletin of the Geological Society of Greece, Sp. Pub. 7 Ext. Abs. GSG2019-123

Application of Variable Lag Variography on Directions Derived Using k-Means Clustering of Sample Pairs

I. Kapageridis
Technological Educational Institute of Western Macedonia, Koila, Kozani, Greece, ioannis.kapageridis@gmail.com

Abstract

Variography is an important step in any geostatistical resource estimation study. Calculation and modelling of experimental variograms using samples from irregular sampling patterns is a painful and time-consuming task. The more random the sampling pattern is, the more difficult it becomes to find directions and basic spacings (lags) that have a high enough number of sample pairs to produce reliable variogram points. Even after the application of directional and spacing tolerances, fixed lag variography can fail to produce interpretable experimental variograms that can be used to derive a model of the underlying structure. Finding directions that produce interpretable variograms can also be a fairly difficult task, even with the interactive and dynamic interfaces that most modern geostatistical packages provide. Variable Lag Variography (VLV) based on k-means clustering of sample pairs has been successfully used in the past to address the deficiencies of applying fixed lags and lag tolerances to irregularly spaced data. Sample pairs are grouped into clusters based on their sample distance, with the centre of each group representing a single variogram point lag, and the maximum difference in the group from this centre representing the particular variogram point lag tolerance. The study presented in this paper, takes the concept of variogram sample pair clustering one step further, using a k-means clustering process to derive the most populated directions in the sampling space. Sample pairs are first grouped into clusters based on their azimuth and plunge. Each cluster has a centre representing a particular azimuth and plunge (direction), and a radius representing azimuth and plunge tolerances. In these automatically produced directions, VLV is then applied to produce the experimental variogram, making maximum usage of the available sample pairs. This two-step automated approach can significantly reduce the time and effort required in producing the most interpretable experimental variograms from a set of irregularly spaced samples.

1. Standard Calculation of Experimental Variograms

Most geostatistical software packages follow this concept. As shown in Figure 1a (for a 2D case), for a particular direction chosen, a search area is defined using some direction tolerance which can be controlled both horizontally and vertically (Deutsch *et al.* 1992). Some packages use the same direction tolerance in both cases while others allow for separate tolerances to be applied for azimuth and plunge. These tolerances are allowed to expand the search area as the separation distance increases up to a maximum distance (bandwidth) from the direction vector. This way, the search area begins as a cone of circular or elliptical section (depending on whether the azimuth and plunge tolerances are different), and then becomes a cylinder of similar section to the cone, once the maximum distance from the direction vector is reached. Some packages allow for a separate maximum distance to be applied horizontally and vertically.

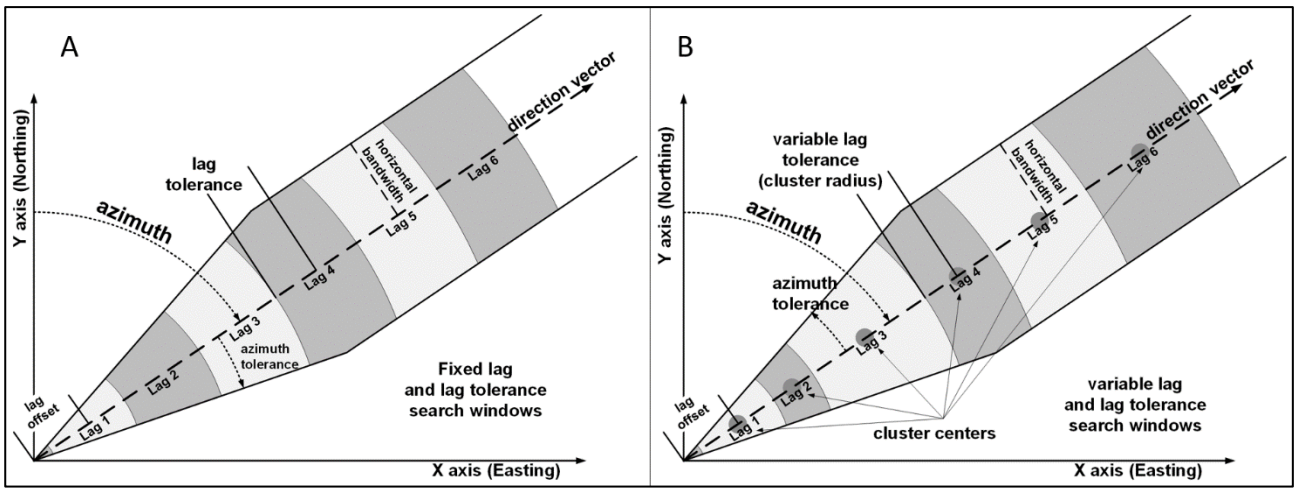

Figure 1. (A) Standard sample pair selection and (B) variable lag sample pair selection based on k-means clustering.

2. k-Means Clustering of Variogram Directions – Step 1

k-means clustering is a method originally used in signal processing, commonly used for cluster analysis in data mining. k-means clustering groups *n* observations into *k* clusters, with each observation assigned to the cluster with the nearest mean. The term "k-means" was introduced by MacQueen in 1967. The standard algorithm was first proposed by Lloyd in 1957, while Forgy published essentially the same method in 1965. A more efficient version was proposed by Hartigan

and Wong in 1975 and 1979. It is an iterative algorithm that is performed in steps. Before any iteration, the clusters are initially centred on an equal number of observations. These observations can be chosen using different methods. Iterations involve two steps. In the first step, each observation is assigned to the cluster whose mean yields the least within-cluster sum of squares. The second step involves the calculation of the new means to be the centroids of the observations in the new clusters. The algorithm converges when there is no change in the assignments. IBM SPSS Statistics was used to provide the k-means clustering functionality in this study.

In this study, drillhole samples from an underground tungsten mine with a fairly irregular drilling pattern were used to form pairs for variography purposes. The separating distance, azimuth and plunge of each pair vector were calculated. Sample pairs were grouped into clusters using k-means based on their azimuth and plunge. The produced clusters represented the most populated (with sample pairs) directions in 3D space. The average azimuth and plunge of each cluster constituted the variogram direction, and the difference of the average and the maximum azimuth and plunge of each cluster were considered as the azimuth and plunge tolerances for each direction. The produced directions were not following a fixed angle step, while the tolerances of each direction were different and specific to that direction.

Variable Lag Variography – Step 2

VLV has been introduced by the author as a way to automatically adjust lag parameters to match the spatial distribution of sample locations and improve the resulting experimental variogram (Kapageridis, 2015). As shown in Figure 1b, sample pairs selected for a particular direction using standard criteria or the clustering process described in the previous section, are grouped into clusters based on the 3D distance between their samples. Variography parameters using k-means clustering in VLV are represented by the resulting clustering information:

- *Lag offset*: the average separation of the first cluster (first variogram point).
- *Lag*: the average separation of each cluster (each variogram point) - different for each variogram point.
- *Lag tolerance*: the maximum distance of the pairs classified in a specific cluster from that cluster's center - different for each variogram point, not a fixed value.
- *Pair count*: the number of pairs classified in each cluster.

Figure 2 shows an example of an experimental variogram calculated using the standard method based on fixed lag and lag tolerances (dashed), and an experimental variogram calculated using VLV (solid). The direction in which the variogram was calculated is the same in both cases and was one of the directions derived using the clustering method described in Step 1 (azimuth 54º and plunge -19º). The improvement in the interpretability of the variogram using VLV is clear.

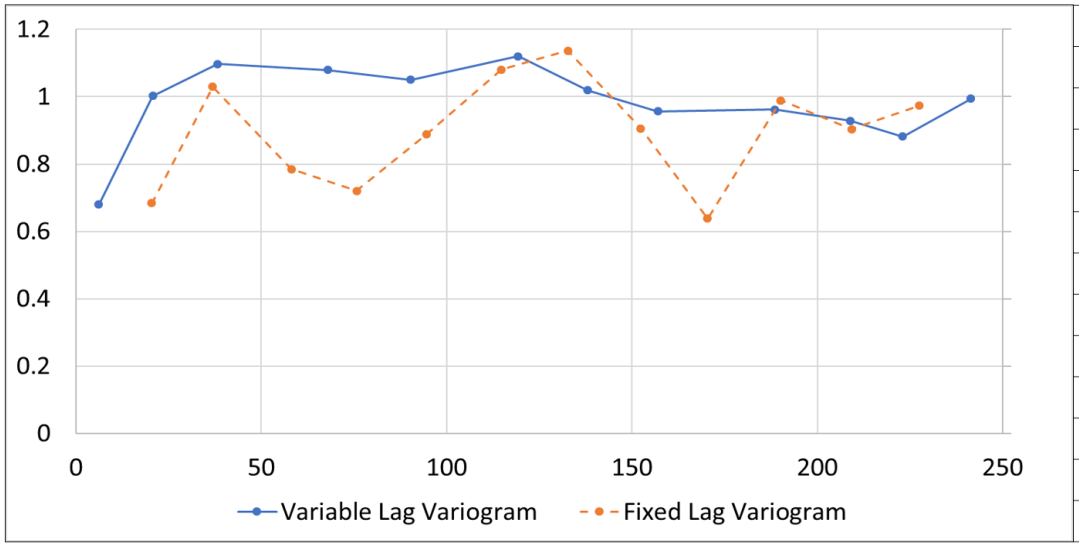

Point	VLV	Fixed Lag
1	7694	294
2	5244	723
3	3172	1707
4	7697	3356
5	9707	3661
6	9633	3772
7	5457	2826
8	6034	3618
9	4084	873
10	3858	2326
11	3874	2263
12	3180	2065

Figure 2. Fixed and variable lag variogram calculated in the same direction, and corresponding numbers of sample pairs.

References

Deutsch, C.V., and Journel, A.G. 1992. GSLIB - Geostatistical Software Library and User's Guide, Oxford University Press.

Forgy, E.W. 1965. Cluster analysis of multivariate data: efficiency versus interpretability of classifications. Biometrics 21: 768–769.

Hartigan, J. A. 1975. Clustering algorithms. New York: John Wiley and Sons.

Hartigan, J. A.; Wong, M. A. 1979. Algorithm AS 136: A K-Means Clustering Algorithm. Journal of the Royal Statistical Society, Series C 28 (1): 100–108.

Kapageridis, I. 2015. Variable Lag Variography Using k-means Clustering. Computers & Geosciences, Volume 85, Part B: 49-63.

Lloyd, S. P. 1982. Least square quantization in PCM. Bell Telephone Laboratories Paper. IEEE Transactions on Information Theory 28 (2): 129–137.

McQueen, J. B. 1967. Some Methods for classification and Analysis of Multivariate Observations. Proceedings of 5th Berkeley Symposium on Mathematical Statistics and Probability 1. University of California Press. pp. 281–297.

15th International Congress of the Geological Society of Greece
Athens, 22-24 May, 2019 | Harokopio University of Athens, Greece
Bulletin of the Geological Society of Greece, Sp. Pub. 7 Ext. Abs. GSG2019-192

Raw materials' detection using hyperspectral remote sensing techniques. Case study W. Milos, Greece

Th. Valsamidis[1], V. Karathanassi[2], P. Kolokoussis[2], V. Andronis[2]

(1) National Kapodistrian University of Athens, Department of Geology and Geoenvironment, Panepistimioupoli, Zografou, Greece, theovalsam@geol.uoa.gr
(2) National Technical University of Athens, School of Rural and Surveying Engineering, Heroon Polytechniou 9, Zografou, Greece

Introduction

The goal of this research is to evaluate the potential of using hyperspectral airborne data for geological mapping, focusing on rock formations, ore deposits and raw materials identification, hence formations with a significant economic value. Moreover, it aims at identifying the limitations and the key factors in the process. Finally, this work can act as a compass for young scientists that want to combine outcomes from hyperspectral remote sensing methods and techniques with classic geological mapping techniques, as in this paper the linear spectral unmixing steps of the hyperspectral data are outlined.

Study Area

The study area of this research is the western part of Milos Island, situated in the southwestern corner of the Cyclades islands in the Aegean Sea, Greece. This area is a part of the Natura 2000 network and the natural habitat of protected species, like the Mediterranean seal and the Milos' red viper (Liordos et al., 2017). It is also characterized by the existence of very few small villages and hamlets, active or abandoned quarries and extractions sites and a lot of vegetation.

Milos Island is a part of the active Hellenic volcanic arch and is characterized by calc-alkaline mafic rocks, the most common being andesites, dacites, rhyolites, obsidians and tuffs (Alfieris et al., 2013). Apart from those, the island is one of the most densely mineralized areas in the Aegean Sea, containing economically viable occurrences of both metallic and non-metallic minerals, with reported exploitation since antiquity. These include perlite, bentonite, kaolin, deposits of manganese and barite.

Materials

The hyperspectral images, which have been used in this work for the identification and characterization of the island's surface deposits, have been acquired with a Digital Airborne Imaging Spectrometer (DAIS) 7915 sensor that has 79 spectral bands between 0.5 – 14 μm. (Ganas et. al, 2002). The hyperspectral imagery has 5m spatial resolution, is comprised of 4 independent strips N-S oriented with side overlap of 20% and it was acquired on the 25th of August 1998. Apart from the airborne image, the ASTER GDEM has been also used during orthorectification and atmospheric correction in order to minimize the geometric and atmospheric errors. Due to lack of ground measurements, geological maps of the Institute of Geology and Mineral Exploration (IGME) have been used as the main source of ground truth information, regarding the island formations. USGS Spectral Signatures have been downloaded for these formations as well.

Methods and Results

Prior to the implementation of the spectral unmixing, preprocessing took place in order for the data to be homogenous and free of radiometric or geometric errors. Atmospheric correction using ATCOR4 was carried out for the elimination of the atmospheric effects and the estimation of the real surface reflectance. Orthorectification using GDEM and at least 15 ground control points for each image strip has also been carried out leading to a single mosaic image.

The first step of the unmixing procedure is the dimensionality reduction. More specifically Principal Component Analysis (PCA) and Minimum Noise Fraction (MNF) were used for this purpose. The PCA method demonstrated that almost all information is concentrated in the first four PCA bands. Aiming at the same purpose, the MNF method was implemented, resulting to 16 MNF bands containing substantial information.

The lack of matching between the hyperspectral image spectra and USGS standard signatures for various rock formations led to the selection of spectral targets either from the user using auxiliary sources or by applying endmember extraction techniques, which is the second step of the spectral unmixing. In the manual selection, both training and validation data were selected by the user using the geological map of IGME, due to the lack of in situ measurements. Three main ore deposits that had distinct spectral signatures among them were selected. Namely, two or three pure outcrops of kaolin, barite and pozzolan were manually selected for training areas and another couple or trio (depending on the area) that were used for evaluation.

Regarding the automatic extraction of endmembers, three different extraction algorithms were implemented; the embedded in the ENVI program Pixel Purity Index (PPI) method, the Simple Endmember Extraction (SEE) method (Andreou et al., 2011) and the N-FindR algorithm (Winter, 1999). These three methods were tested for two different scenarios, the first including a mask in the aquatic environment and the second a wider mask covering water and dense vegetation areas. The result of this procedure was the extraction of 14 and 16 endmembers (for the sea mask and the mixed masked respectively) through the PPI method and 13 endmembers for the other two algorithms. These endmembers

were compared with the user's targets, in order to identify those that correlated best to each raw material. The assessment was carried out measuring the spectral angle difference between the extracted and the reference spectral signature.

The aggregate result (Table 1) was 6 cases (3 different extraction methods with 2 different masks applied for each one), where the total number of endmembers, the closest endmember (number) to each material's signature and a mean score as a credibility index were identified.

Table 1. Summary table comparing endmembers

Endmember extraction method	Number of endmembers	Barite best endmember	Barite best score	Kaolin best endmember	Kaolin best score	Pozzolan best endm.	Pozzolan best score	Mean best score
N-FindR (sea mask)	12	12	0.829	11	0.884	7	0.854	0.856
N-FindR (sea+veg mask)	13	3	0.791	6	0.906	10	0.794	0.830
PPI (sea mask)	17	17	0.838	1	0.925	8	0.830	0.864
PPI (sea+veg mask)	16	9	0.864	1	0.843	11	0.839	0.867
SEE (sea mask)	13	13	0.834	4	0.952	12	0.798	0.861
SEE (sea+veg mask)	13	12	0.825	6	0.952	12	0.824	0.867

It is observed that:

- SEE (sea+veg) assigned two different materials for the same endmember.
- The PPI method outperformed.
- SEE (sea mask) produced satisfactorily results, and detected kaolin with the highest accuracy.

In order for the automatic extraction of endmembers to be accurate, the endmembers must be discrete, hence to have wide angle differences. The methods that fulfilled this criterion were PPI and N-FindR, due to the fact that only a few endmembers display an angle difference <0.1. Moreover, the 3 endmembers of the materials of interest, presented wide angle differences with the rest endmembers

The final step of the spectral unmixing was the creation of abundance maps for each of the three aforementioned materials (barite, kaolin, pozzolan). For this, three methods, the Constraint Linear Spectral Unmixing method (CLU), Mixture Tuned Match Filtering (MTMF) and Network Based Method (NBM) (Karathanassi et. al., 2011), have been applied. Among these, CLU and NBM produced the most accurate maps.

Discussion and Conclusions

The current study had a high difficulty level in terms of mapping due to the wide vegetation areas in Western Milos that hid a wide variety of formations and hinder a complete geological mapping. Another burden was the quite similar formations, since the volcanic island of Milos is characterized by mafic rocks and volcanic tuffs, formations that need in situ mineralogical analysis and higher resolution data, making it quite difficult to be correctly identified with the current remote sensing dataset.

Nevertheless, every endmember extraction methodology tested was successful as it managed to produce pure endmembers that matched the user's endmembers and have wide spectral angle differences between them thus making them easily distinguishable.

Regarding the abundance mapping of the pure raw materials, the most reliable method was the NBM method, with the CLU being second in terms of accuracy.

To sum up, the utility of hyperspectral data in identifying ore deposits is unambiguous, especially when talking about areas with difficult access. It is clear that in order to achieve a high level of accuracy, in situ measurements are prerequisite. Furthermore, an ideal case would be a sensor whose spectral resolution would match the USGS spectral library, so that every mineral in the area could be matched with a mineral of the spectral library.

Acknowledgements

We wish to thank Dr. Athanassios Ganas for supplying the airborne hyperspectral raw data.

References

Alfieris, D., Voudouris, P., Spry P. G., 2013. Shallow submarine epithermal Pb–Zn–Cu–Au–Ag–Te mineralization on western Milos Island, Aegean Volcanic Arc, Greece: Mineralogical, geological and geochemical constraints. Ore Geology Reviews 53, 159-180.

Andreou, D., Karathanassi, V., 2011. 3rd workshop on using principal component analysis for endmember extraction. Hyperspectral Image and Signal Processing: Evolution in Remote Sensing (WHISPERS), Lisbon, Portugal

Ganas, A., Ferrier, G. 2002. Mapping epithermal gold in Milos using DAIS Hyperspectral data. Mineral Wealth 122, 37-46

Karathanassi, V., Sykas, D., Topouzelis, K., 2011. Development of a Network-Based Method for Unmixing of Hyperspectral Data. IEEE Transactions on Geoscience and Remote Sensing (3), 1-11

Liordos, V., Kontsiotis, V. J., Anastasiadou, M., Karavasis, E., 2017. Effects of attitudes and demography on public support for endangered species conservation. Science of The Total Environment 595, 25-34.

Winter, M. E., 1999. N-FINDR: an algorithm for fast autonomous spectral end-member determination in hyperspectral data, SPIE 3753, Imaging Spectrometry V

15th International Congress of the Geological Society of Greece
Athens, 22-24 May, 2019 | Harokopio University of Athens, Greece
Bulletin of the Geological Society of Greece, Sp. Pub. 7 Ext. Abs. GSG2019-199

Detection of Chromite Minerals Using Spectral Linear Unmixing on Sentinel-2 Imagery.Case study: Ingessana Hills, Blue Nile Province, Sudan.

A. Anifadi[1, 2], O. Sykioti[3], E.Vassilakis[1]

(1) National &Kapodistrian University of Athens, Department of Geology & Geoenvironment, Panepistimiopolis Zografou Athens GR15784, aanyfant@geol.uoa.gr
(2) LARCOG.M.M.S.A.,
(3) Institute for Astronomy, Astrophysics, Space Applications & Remote Sensing, National Observatory of Athens, Vas. Pavlou & I. Metaxa, 15 236 Penteli, Greece

Introduction

The Ingessana hills in the southern Blue Nile of Sudan consist of serpentinised and highly silicified dunites in contact with the intruding Bau granite. The observed chromite mineralization zones are associated with NE-SW trending shear-zones. The mineralization associated with ophiolitic belts includes podiform chromite, asbestos, talc, and base metal (Cu, Ni, Co) mineralization. We applied Linear Spectral Unmixing algorithmon a 10m spatial resolution Sentinel-2 images in ordertodetect and map the chromite mineralization and the associated mineralization of ophiolitic belts. The resulting abundance maps show the capabilityof Sentinel-2 for detailed mineral mapping and detection of potential chromite ore depositlocations.

Background and Object

The study area is located at the Ingessana Hills, in Blue Nile Province of Sudan (Fig. 1). The dominant basement rocks consist of serpentinised hartzburgites and dunites with metadolerite, epidiorite and gabbro surrounded by psammopelitic metamorphic rocks and cropping out around the hill (Fig.1). The chromite mineralization is mainly concentrated in the western side of the Ingessana Hills as lenses, veins, in irregular patches and disseminated deposits, in the serpentinites and talc carbonate rocks of the dunite –peridotite gabbro (Ibrahim, 2003). The lenses and the veins generally strike NNW with steep dips.

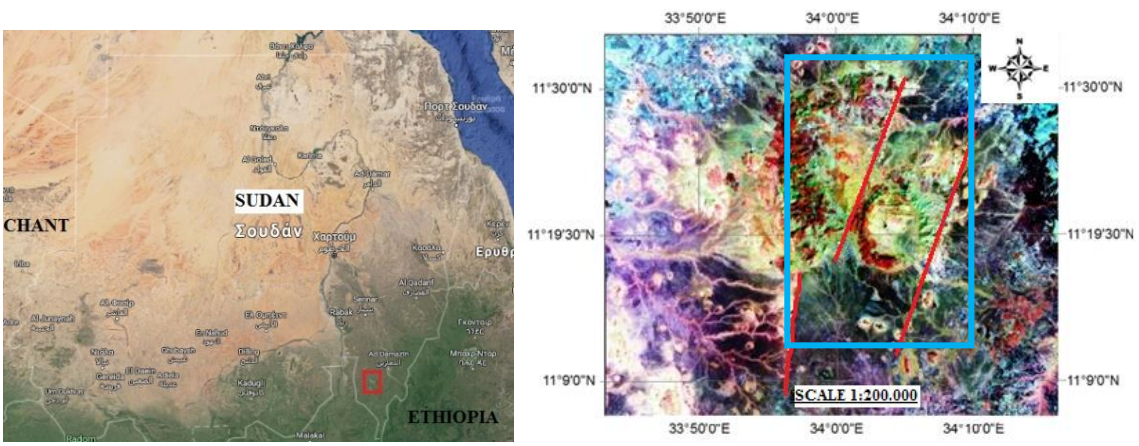

(a) (b)

Figure 1. (a) The red box indicates the location of the study area in Sudan. (b) Colour composite of the mosaic Sentinel-2 image after equalization stretching of the study area [R:12 (2,19μm), G:8A (0,86μm), B:3 (0,56μm)]. The red lines correspond to the main faulting. The cyan box represents the area of the abundance images that are shown in Fig.2.

Methodology

In this study, we used two adjacent Sentinel 2 (S2B) images Level 1C, acquired on19/02/2019 and on 29/02/2019. After atmospheric correction, the two images were mosaicked (Fig.1). The output reflectance image has 12 spectral bands and 10m spatial resolution.We then performed Linear Spectral Unmixing (LUN). The LUN approach assumes that the reflectance of each pixel is a linear combination of the spectral signature of each material (endmember) present in the pixel (Keshava & Mustard, 2002) and determines its relative abundance, based on its spectral characteristics. Compliant to the geology of the area, the spectral signatures of talc, chlorite, chromite, limonite, hematite, antigorite, epidote, quartz, tremolite, chrysotile and dolomite were retrieved from the USGS Spectral Library. We applied a Least Squares LUN with a positivity constraint. The abundance map for each endmember was calculated (Fig. 2). The abundance values were then normalized between 0 and 1.

Results and Conclusions

Chromite is detected west and east of the Ingessana Hills (Fig. 3). The easternmost outcrops of chromite are accompanied by high limonite abundances, indicating that they are rich in iron (Fig. 2a, b). Limonite has also been detected at an extended area aligned to the NE - SW faulting of the Ingessana Hills. Antigorite, seems to have the same spatial extentwith chromite (fig.2c), while chrysotile (fig.2d) is detected at the fringes of serpentinised rocks in contact with meta-sediments. The proposed areas for further investigationare presented in fig.3.The results are in a good agreement with literature, unpublished reports and with the geological map, including locations of current mining sites.

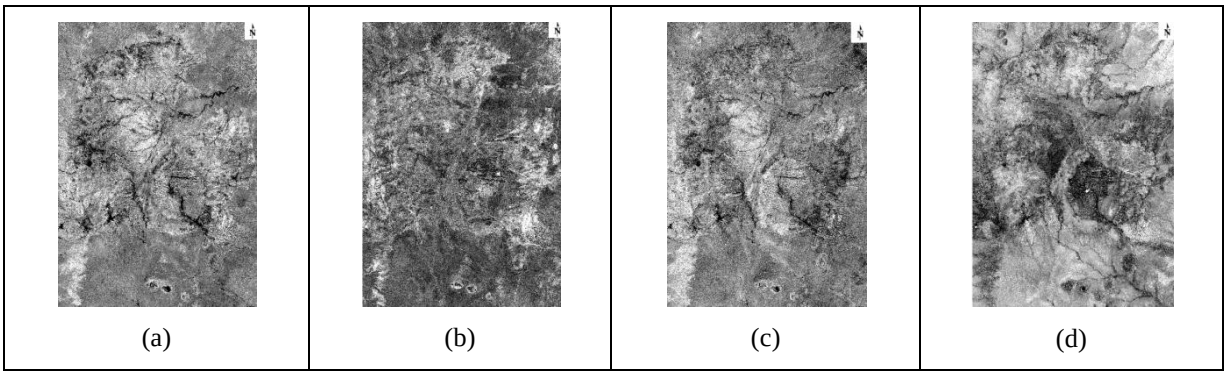

Figure 2.Spectral Linear Unmixing (LUN) result. Abundance images of (a) chromite, (b)limonite, (c) antigorite, (d) chrysotile. Black and white areas correspond to low and high mineral abundances correspondingly.

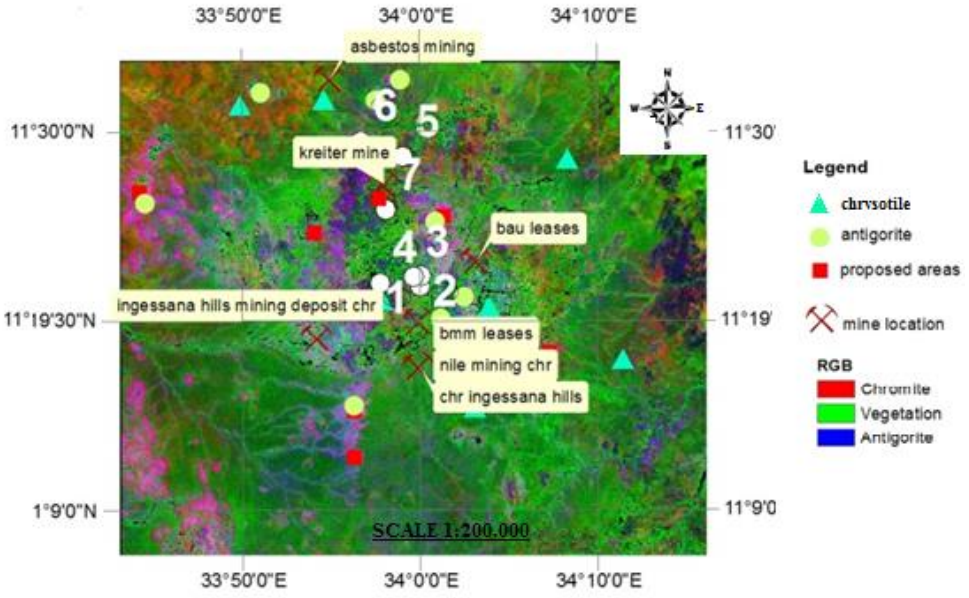

Figure 3.CCF image of the abundances of: R: Chromite G:Vegetation B:Antigorite. The proposed locations for further investigation are shown (red squares).

References

Babiker I. M., 1982. The chromatiferous ultrabasic rocks of Jebal El Ingessana, Eastern Sudan. Precambrian Research Volume 16, Issue 4, p.p. A44-A45.

Ibrahim M., 2003. Information about Ingessana Hills artisanal Gold Mining Sites chosen for the environmental and health assessment. Global Mercury project Eg/GLO/01/G34.

Keshava N. and Mustard J.F., 2002. Spectral unmixing, IEEE Signal Process., vol. 19, no. 1, pp. 44–57.

Mohamed-Ali M.A., Simos J., Kheiralla K.M., 2017. Chromite exploration using electrical resistivity tomography in Ingessana Hill, Blue Nile, state Sudan. Proceedings of 119th the IIER International Conference, Putrajava, Malaysia, 4th – 5h September 2017.

Yassin A., Khalil F. A.,Gadir A. S., 1984. Explanatory note to the Geological Map at the scale 1.200.000 of the DemographicRepublic of the Sudan.Department of Energy and Mining Geological & Mineral resources Department, Bulletin 35.

15th International Congress of the Geological Society of Greece
Athens, 22-24 May, 2019 | Harokopio University of Athens, Greece
Bulletin of the Geological Society of Greece, Sp. Pub. 7 Ext. Abs. GSG2019-205

Applying Machine learning and GIS in landslide susceptibility assessment. The case of Krikeliotis water basin, Evritania, Greece

A.Tsampa[1], P.Tsangaratos[2,3]

(1) School of Science & Technology, Hellenic Open University, Parodos Aristotelous 18, 26335 Patra, std115817@ac.eap.gr, tsampa.areti@gmail.com
(2) School of Science & Technology, Hellenic Open University, Parodos Aristotelous 18, 26335 Patra, tsaggaratos.paraskevas@ac.eap.gr
(3) School of Mining and Metallurgical Engineering, National Technical University of Athens, 9, Ir. Polytechniou str., 15780, Zografou, Athens, Greece, ptsag@metal.ntua.gr

Landslides are considered as one of the most disastrous natural hazards worldwide which are responsible for adverse affects on the natural and human environment. The non-linear and complex nature of the physical but also man-made processes which leads to the evolution of landslides makes the prediction of landslides a very difficult task (Pourghasemi *et al.*, 2018). Landslide susceptibility assessments are the main investigation tool capable of providing valuable information concerning the relation between landslides and landslide-related variables but also the main investigation tool for zoning landslide prone areas (Tien Bui *et al.*, 2017). Nowadays, it is common practice to apply Machine learning algorithms along with Geographic Information Systems (GIS) so as to develop landslide susceptibility models. Numerous applications are found in the literature involving fuzzy logic algorithms, artificial neural networks and neuro-fuzzy models, ensemble tree-based models and evolutionary population based algorithms (Hong *et al.*, 2017; Pham *et al.*, 2018; Pourghasemi *et al*., 2018; Chen *et al.*, 2019). In this context, the main purpose of the present study was to produce a predictive spatial model for landslide susceptibility by using Machine Learning methods and GIS. In particular, a Random Forest (RF) model (Dou *et al.*, 2019) was used as the base learning algorithm for the development of the predictive spatial model whereas the management of the landslide related variables were achieved using GIS. The developed methodology involved several phases. During the first phase nine spatial variables related to landslide phenomena were selected and the data of 85 landslide events were analyzed. Analytically, the elevation, the slope angle, slope aspect, the distance from the river network, the profile curvature, the plan curvature, the Topographic Wetness Index, the geological formations and the distance from the tectonic features were the nine variables identified as most important and relevant to the landslide phenomena recorded in the research area. The second phase involved classifying each variable and weighting them according to the results obtained by the method Weight of Evidence. The third phase involved a multi-collinearity analysis in order to identify the existence or not of correlations between the landslide-related variables and to decide their usage and the application of the Learning Vector Quantization (LVQ) algorithm, so as to evaluate the predictive ability of the variables. During the third phase, the initial database was separated into training (70% of the total number of incidence) and validating (the remaining 30%) subsets. The last phase involved the implementation of the RF model and the construction of the landslide susceptibility map, whereas to evaluate the performance of the developed methodology the area under the success and predictive curve (AUC) were used. The water basin of the Krikeliotis river located in the Municipality of Evritania, Greece was selected as a test site to evaluate the predictive performance of the developed methodology whereas several R packages were used, based on R a language and environment for statistical analysis and graphical presentation (R Core Team, 2017), whereas ArcGIS 10.3.1 (ESRI, 2013) was used for accessing the spatial data and generating the landslide susceptibility maps. Based on the results of the multi-collinearity analysis all variables were used during the analysis, since no serious collinerarity was detected, whereas the LVQ algorithm evaluated as the most important and critical variable the variable associated with the geological formations, followed by the altitude and the morphological gradient (Table 1).

Table 1. Results of multi-collinearity analysis and importance based on LVQ algorithm.

Landslide variables	Variance Inflation Factor	Tolerance Index	Importance (LQV)
Geology formations	1.719	0.581	0.75
Distance from tectonic features	1.146	0.872	0.59
Distance from river network	1.396	0.716	0.51
Elevation	1.391	0.719	0.74
Slope angle	1.752	0.570	0.73
Slope aspect	1.140	0.876	0.61
TWI	1.899	0.526	0.68
Plan curvature	1.515	0.660	0.53
Profile curvature	1.093	0.914	0.52

During the study a grid search technique was used so as to set the optimal structural parameters *mtry* (number of variables used in each model) and *ntree* (number of produced trees) used by the RF model. For the *mtry* parameter it was set to 7 and for the *ntree* parameter it was set to 2000. According to the results of the RF model, the most important variables based on the Mean Decrease Accuracy and the Mean Decrease Gini was the elevation and the geological formations. Figure 1 illustrates the produced by the RF model landslide susceptibility map in which the 21.36% of the study area is characterized as very high susceptible, the 24.90% as high susceptibility, while the 34.19% as low and very low landslide susceptibility. Furthermore, by analyzing the training and validation data, the RF model showed an AUC value of 0.8670 and 0.7851, respectively, whereas the relative landslide density for the very high susceptible zone was 0.8460 when using the training subset and 0.7242 when using the validation subset.

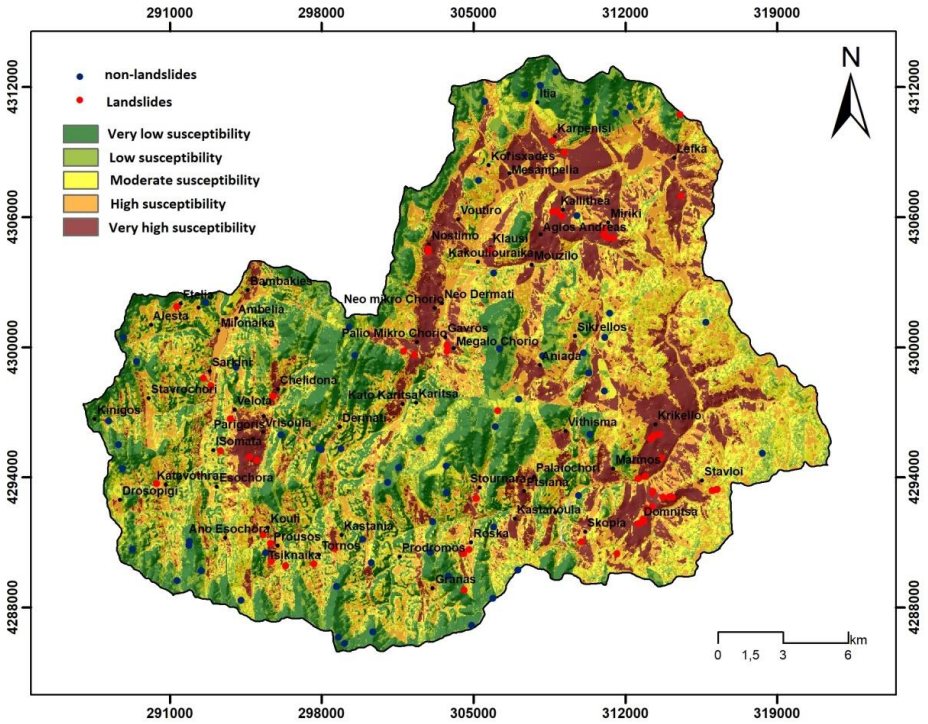

Figure 1. Landslide susceptibility based on RF model.

As a concluding remark one can highlight the fact that the identification of areas characterized by very high landslide susceptibility achieved by this study and also similar studies could be considered as a basic process that should precede any implementation of infrastructure development projects since it provides crucial information and knowledge concerning the mechanism responsible for landslide phenomena.

References

Chen, W., Panahi, M., Tsangaratos, P., Shahabi, H., Ilia, I., Panahi, S., Li, S., Jaafari, A., Ahmad B.B., 2019. Applying population-based evolutionary algorithms and a neuro-fuzzy system for modeling landslide susceptibility. Catena 172, 212-231.

Dou, J., Yunus, A. P., Tien Bui, D., Merghadi, A., Sahana, M., Zhu, Z., Chen, C.-W., Khosravi, K., Yang, Y., Pham, B. T., 2019. Assessment of advanced random forest and decision tree algorithms for modeling rainfall-induced landslide susceptibility in the Izu-Oshima Volcanic Island, Japan. Sci. Total Environ. 662, 332-346.

ESRI, 2013. ArcGIS Desktop: Release 10.1 Redlands, CA: Environmental Systems Research Institute.

Hong, H., Ilia, I., Tsangaratos, P., Chen, W., Xu, C., 2017. A hybrid fuzzy weight of evidence method in landslide susceptibility analysis on the Wuyuan area, China. Geomorphology 290, 1–16.

Pham, B.T., Shirzadi, A., Tien Bui, D., Prakash, I., Dholakia, M.B., 2018. A hybrid machine learning ensemble approach based on a radial basis function neural network and rotation Forest for landslide susceptibility modeling: a case study in the Himalayan area, India. Int. J. Sediment Res. 33(2), 157-170.

Pourghasemi, H.R.,Yansari, Z.T., Panagos, P., Pradhan, B., 2018. Analysis and evaluation of landslide susceptibility: a review on articles published during 2005–2016 (periods of 2005–2012 and 2013–2016). Arab. J. Geosci. 11, 193. https://doi.org/10.1007/s12517-018-3531-5.

R Core Team, 2017. R: A Language and Environment for Statistical Computing, R Foundation for Statistical Computing, Vienna, Austria, https://www.R-project.org.

Tien Bui, D., Tuan, T.A., Hoang, N.-D., Thanh, N.Q., Ngugen, D.B., Liem, N.V., Pradhan, B., 2017. Spatial prediction of rainfall-induced landslides for the Lao Cai area (Vietnam) using a hybrid intelligent approach of least squares support vector machines inference model and artificial bee colony optimization, Landslides 14(2), 447-458.

15th International Congress of the Geological Society of Greece
Athens, 22-24 May, 2019 | Harokopio University of Athens, Greece
Bulletin of the Geological Society of Greece, Sp. Pub. 7 Ext. Abs. GSG2019-206

Improving the efficiency of artificial neural networks for ore reserve estimation by employing suitable training methods

M. Galetakis, I. Oikonomidou, A. Vasileiou and A. Soultana
School of Mineral Resources Engineering, Technical University of Crete, Chania, Greece, galetaki@mred.tuc.gr

Introduction

Ore reserve estimation is traditionally developed using a model of selected deposit attributes, created by discretizing them into small blocks. Among these attributes, the thickness and the grade are the most critical for the ore reserve estimation. The thickness and the quality characteristics of the deposit are determined by several factors related to the usually complicated geological process which led to the deposit formation. Many of these factors are not well known and cannot be brought easily into a conventional mathematical model. Any attempt to model the geometrical and quality characteristics of a deposit inevitably requires simplifications and assumptions of the spatial variation. The existing methods are mainly based on either geometrical reasoning or statistical techniques and generally assume that the spatial distribution of the modelled parameters is a function of distance.

Artificial Neural Networks (ANNs) have provided a new approach for the estimation of the reserves of a deposit. Since the ANNs are not only trainable nonlinear dynamic systems but also adaptive model-free estimators, no assumption concerning the spatial variation of the deposit attributes need to be made. The basic approach for developing ANN model for the ore reserve estimation is to train the model using an existing borehole data set and appropriate learning methods (Wu and Zhou, 1992; Galetakis, 1999; Kapageridis, 2005; Samanta and Bandopadhyay, 2009; Li et al., 2010).

The way that available data are divided into training, testing, and validation subsets can have a significant influence on the performance of an ANN (Tahmasebi et al., 2011). This study presents methods for dividing borehole data into these subsets considering spatial and quality criteria. These methods are compared with the conventional approach commonly used in the literature, which involves an arbitrary division of the data.

Artificial Neural Networks

Artificial neural networks (ANNs) are nonlinear dynamic systems consisting of a large number of highly interconnected processing units, called artificial neurons or simply neurons, which are organized into a hierarchy (layers of neurons). Their architecture and operation are inspired by our understanding the biological structure of neurons and the operation of the human brain (Galetakis et al., 2002).

Basically, three entities characterize a neural network: the characteristics of individual neuron, the network topology and the learning strategy. Each processing unit (neuron) receives one or more inputs and delivers a single output. The neuron consists of an input function (a summation function) the result of which is fed to activation function which in turn determines the output. The topology of the network is the manner in which neurons are organized and connected. Neurons are combined to form layers which can be connected fully or partially. When the output from every neuron of a particular layer is connected to every neuron in the next layer the network is fully connected otherwise it is partially connected. Associated with each connection between these processing units, there is a weight value defined to represent the connection strength. Each network has an input layer, which accepts the input data to the network, an input layer which delivers the network response and the intermediate layers which represent the hidden features of the problem (Rumelhart et al., 1986).

Feedforward networks are those in which the output from neuron can only feed forward, while feedback networks are those in which the output from a neuron can be directed back as an input to any neuron. Learning methods for neural networks can be classified into supervised and unsupervised. The most commonly used supervised method for feedforward neural networks is the backpropagation.

Ore reserve estimation by ANNs

Estimating the grade and the reserves of a deposit is a particularly critical stage in the planning process of exploitation. The methods used vary depending on the type of the ore, the planned method of exploitation, the required degree of precision and the number and type of the data obtained from the exploration stages. In this study the estimation of the grade and reserves of a copper deposit was conducted by using a feedforward ANN.

The examined cooper deposit is located in the state of Arizona and is described in detail by Hustrulid and Kuchta (2006). It is low-grade porphyry type cooper deposit that has been explored with 40 vertical boreholes of varying depth. In each borehole assays, at an average spacing of 1.5m, were analyzed for the determination of % content of Cu. Borehole assay data were regularized into composites of equal length used then for grade and reserves estimation.

The used feedforward ANN, as shown in Figure 1, had an input layer with 3 neurons, a hidden layer of *m* neurons and an output layer with one neuron. The coordinates of each composite sample were used as inputs, while the content (%) in Cu is used as the output. The optimal number *m* of hidden layer neurons was evaluated during training, while bias

(a_o, b_o) and momentum factor were also used to improve the accuracy of the estimation and to accelerate the training process respectively.
Three different training methods were used. The first training method was the conventional approach which involves the random division of the entire data set into training, testing, and validation subsets. The second training method involves initially the division of the data set into subgroups corresponding to the elevations of the planned benches for the exploitation of the deposit. Subsequently each subgroup was divided into training, testing, and validation subsets using the conventional approach. The third training method include two steps: first the assignment of weights to samples based on their grade (% Cu) and then their division into training, testing and validation randomly. These weights represent samples impact on the training process of the ANN.
To avoid overtraining of neural networks, both the early stopping technique and the control of the number of neurons on the hidden layer were used. A comparative evaluation of these ANN methods and the Kriging was then performed.

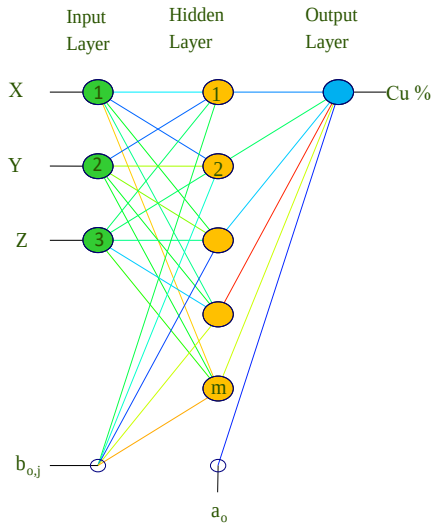

Figure 1. Structure of multiple-layer feedforward network used for ore reserve estimation.

Discussion of results-Conclusions

The obtained results were compared to those of the Kriging method and showed that the ANNs trained either with the first or the second method performed mainly as global estimators. These networks showed the general trend of the variation of the Cu content in the studied area. The large number of samples with low Cu grade have affected the neural network training and led to an underestimation of the Cu content. Neural networks trained with the third method have shown that they can depict both local and global variations in Cu content in the studied area, performing equally to Kriging method.

Acknowledgements

The research leading to these results has received funding from the Special Research Funds Account (ELKE) of the Technical University of Crete (Project code 81792). The presented results reflect only the authors' view and the funding authority is not liable for any use that may be made of the information contained therein.

References

Galetakis M., 1999. Application of Artificial Neural Networks in Solving Problems Related with Open Pit Mine Planning and Design, Mineral Wealth, 113, 47-56.

Galetakis, M., Theodoridis, K., and Kouridou, O., 2002, Lignite quality estimation using ANN and adaptive neuro-fuzzy inference systems (ANFIS), APCOM, p. 425–431.

Hustrulid, W., Kuchta, M., 2006. Open Pit Mine Planning & Design:CSMine software package, 2nd ed. Taylor and Francis/Balkema.

Kapageridis I., 2005. Input space configuration effects in neural network-based grade estimation, Computers and geosciences, 112, 704-717.

Li X., Xie Y., Guo Q. and Li L., 2010, Adaptive ore grade estimation method for the mineral deposit evaluation, Mathematical and computer modeling, 52, 1947-1956.

Rumelhart, D., Hinton, G., Williams R., 1986. Learning internal representations by error propagation, Parallel distributed processing, 1, MIT Press, Cambridge, Mass., 318-362.

Samanta, B. and Bandopadhyay, S., 2009. Construction of a radial basis function network using an evolutionary algorithm for grade estimation in a placer gold deposit, Computers and geosciences, 35, 1592-1602.

Tahmasebi, P. and Hezarkhani, A., 2012. A hybrid neural networks-fuzzy logic-genetic algorithm for grade estimation, Computers and geosciences, 42, 18-27.

Wu X. and Zhou, Y., 1992. Reserve estimation using neural network techniques, Computers and geosciences, 19(4), 567-575.

15th International Congress of the Geological Society of Greece
Athens, 22-24 May, 2019 | Harokopio University of Athens, Greece
Bulletin of the Geological Society of Greece, Sp. Pub. 7 Ext. Abs. GSG2019-235

Applying Weight of Evidence method in landslide susceptibility assessments

G.Diamandopoulou[1], I.Ilia[2,3]

(1) School of Science & Technology, Hellenic Open University, Parodos Aristotelous 18, 26335 Patra, std115797@ac.eap.gr, giolanta_d@hotmail.com
(2) School of Science & Technology, Hellenic Open University, Parodos Aristotelous 18, 26335 Patra, ilia.ioanna@ac.eap.gr
(3) School of Mining and Metallurgical Engineering, National Technical University of Athens, 9, Ir. Polytechniou str., 15780, Zografou, Athens, Greece, gilia@metal.ntua.gr

Landslides are the result of a number of natural processes that contribute decisively to the evolution of Earth's surface. It has been reported that due to the interaction of landslide phenomenon with the man kind activities they are considered as one of the most dangerous natural hazards, with serious repercussions on the economic and social development of an area, and also in some case the loss of human lives. According to Kjekstad and Highland (2008) landslides are the 7th more destructive natural hazard responsible for the 17% of deaths caused by natural disasters. According to Brabb (1985), 90% of the losses caused by a landslide could be avoided, if the landslide risk is recognized and evaluated prior to the occurrence of the incident. In this direction, in recent years, a systematic effort is being made towards mapping the areas which are prone to landslides by implementing various methods and techniques (Pourghasemi *et al*., 2018). A decisive impetus to this effort have been made by the implementation of Geographic Information Systems (GIS) along with the introduction of sophisticated methods, expert based, statistical, probabilistic or deterministic, that are capable to provide valuable information concerning the relation between landslides and geo-environmental variables (Hong *et al.*, 2017; Tien Bui *et al.*, 2017). In this context, the main purpose of the present study was to produce a landslide susceptibility map based on a probabilistic method, Weight of Evidence, within a GIS framework and also to perform a sensitivity analysis so as to identify the response of the model to small changes in the weights of the selected conditioning factors (Ilia and Tsangaratos, 2016). In order to evaluate the efficiency of the WofE model, Selinoundas river basin, located at Achaia County, Greece has been selected as an appropriate test site. ArcMap 10.1 software (ESRI, 2013) was used for accessing the data and for producing the landslide susceptibility map, whereas data and information obtained from bibliographic references and previous studies regarding the landslide activities in the region were the main source of data (Tsagas, 2011; Tsangaratos *et al.*, 2015; Polykertis and Chalkias, 2018).

In more details, the methodology which was followed during the present study included four stages of analysis. During the first stage a total of 37 landslide locations were used as training data and 9 landslide conditioning factors were selected, namely: elevation, slope, aspect, profile curvature, plan curvature, geology, topographic wetness index (TWI), distance from rivers and distance from faults. The second stage involved classifying each variable and weighting them according to the results obtained by the method Weight of Evidence. The third stage involved the construction of the landslide susceptibility map, whereas to evaluate the performance of the developed methodology the area under the success curve (AUC) was used. The fourth stage involved the implementation of a sensitivity analysis.

Based on the implementation of the WofE model concerning the conditioning factors, slope, profile curvature and elevation are shown to influence more the landslides spatial distribution, while geology is proved to be the most sensitive factor in changes according to the sensitivity analysis. The variable geology, shows the highest fluctuation concerning the relative landslide density that reaches the 7.05% within the zone of moderate susceptibility, 9.71% within the high susceptibility zone and 3.42% within the very high susceptibility zone. This could be attributed to the fact that the scale of the geological maps that were used as the primary source may not had been ideal for the purpose of analysis. Valuable information about the extent of each geological formation may be missing, however, the overall evaluation of the variable do not suggest removing it from the analysis. Figure 1 illustrates the landslide susceptibility map produced by the WofE model depicting the basin area in five susceptibility zones: very low, low, moderate, high and very high susceptibility. The performance of the model has been evaluated by estimating the AUC value which was estimated to be 0.78, indicating a satisfactory classifying ability.

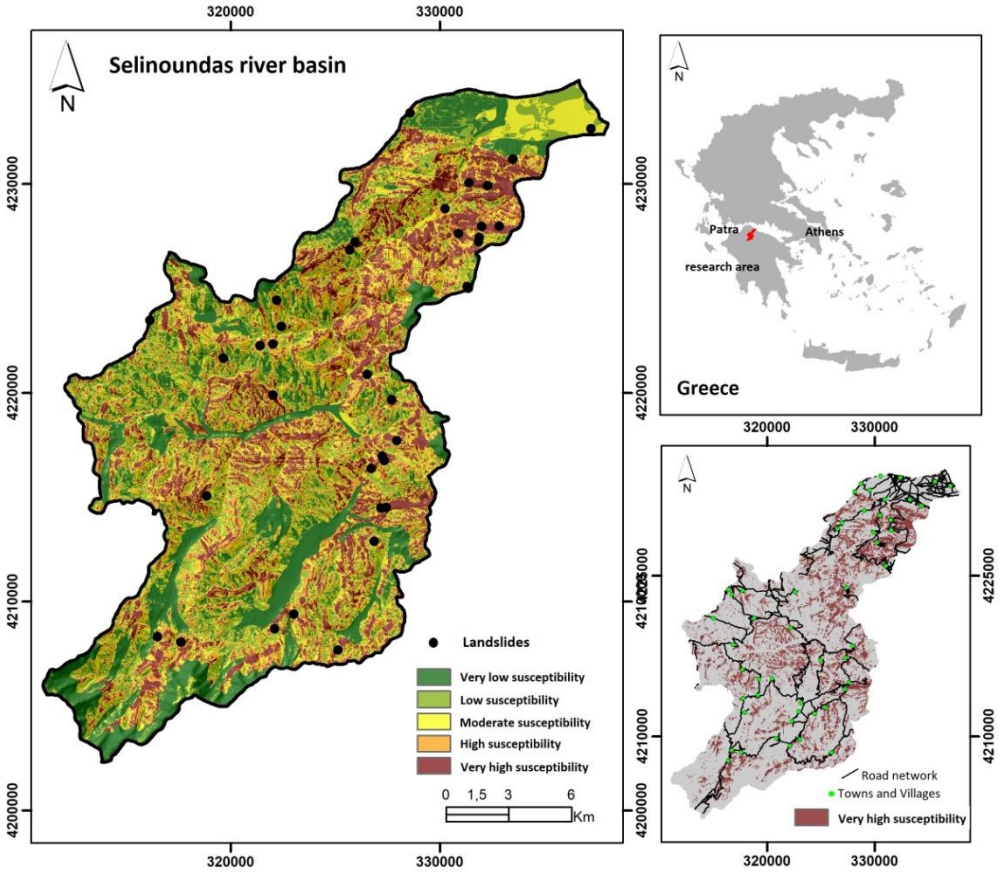

Figure 1. Landslide susceptibility based on WofE model.

According to the landslide susceptibility map, the main part of the basin area, including villages and parts of the road network, is classified in the zones of high and very high susceptibility indicating that there is an urgent need for prevention and protection measures to be taken. Furthermore, given the large area of the basin which is characterized by high and very high susceptibility as well as the high cost of constructing mitigation structures, the creation of a risk map based on the produced landslide susceptibility map is of first priority so as to implement targeted actions and appropriate prevention measures.

References

Brabb, E.E., 1984. Innovative approaches to landslide hazard and risk mapping, Proceedings of the 4th International Symposium on Landslides, 16–21 September, Toronto, Ontario, Canada (Canadian Geotechnical Society, Toronto, Ontario, Canada), 1:307–324.

ESRI, 2013. ArcGIS Desktop: Release 10.1 Redlands, CA: Environmental Systems Research Institute.

Hong, H., Ilia, I., Tsangaratos, P., Chen, W., Xu, C., 2017. A hybrid fuzzy weight of evidence method in landslide susceptibility analysis on the Wuyuan area, China. Geomorphology 290, 1–16.

Ilia, I., Tsangaratos, P., 2016. Applying weight of evidence method and sensitivity analysis to produce a landslide susceptibility map. Landslides 13(2), 379–397.

Kjekstad, O., Highland, L.M., 2008. Economic and social impacts of landslides, in Sassa, D., and Canuti, P., eds., Landslides—Disaster risk reduction: Berlin, Springer- Verlag, p. 573–587.

Polykretis, C., Chalkias, C., 2018. Comparison and evaluation of landslide susceptibility maps obtained from weight of evidence, logistic regression, and artificial neural network models. Nat. Hazards, 93(1), 249-274.

Pourghasemi, H.R.,Yansari, Z.T., Panagos, P., Pradhan, B., 2018. Analysis and evaluation of landslide susceptibility: a review on articles published during 2005–2016 (periods of 2005–2012 and 2013–2016). Arab. J. Geosci. 11, 193. https://doi.org/10.1007/s12517-018-3531-5.

Tien Bui, D., Tuan, T.A., Hoang, N.-D., Thanh, N.Q., Ngugen, D.B., Liem, N.V., Pradhan, B., 2017. Spatial prediction of rainfall-induced landslides for the Lao Cai area (Vietnam) using a hybrid intelligent approach of least squares support vector machines inference model and artificial bee colony optimization, Landslides 14(2), 447-458.

Tsagas, D., 2011. Geomorphological observations and gravitational movements in North Peloponnese. Ph.D., Thesis, Athens.

Tsangaratos, P., Loupasakis, C., Rozos, D., Ilia, I., 2015. Landslide susceptibility assessments using the k-Nearest Neighbor algorithm and expert knowledge. Case study of the basin of Selinounda river, Achaia County, Greece.SafeChania 2015: The knowledge triangle in the Civil Protection Service Center of Mediterranean Architecture, Chania, Crete, Greece, 10-14 June 2015.

15th International Congress of the Geological Society of Greece
Athens, 22-24 May, 2019 | Harokopio University of Athens, Greece
Bulletin of the Geological Society of Greece, Sp. Pub. 7 Ext. Abs. GSG2019-242

Leave-one-out cross validation method in hydrogeochemistry using GIS: A case study of Schinos village, NE Peloponnese, Greece

P. Papazotos[1], I. Polychroni[2], E. Vasileiou[1], M. Perraki[1]

(1) School of Mining and Metallurgical Engineering, Division of Geo-sciences, National Technical University of Athens, 9 Heroon Polytechniou St., 15773 Zografou, Greece, papazotos@metal.ntua.gr
(2) Department of Geology and Geoenvironment, Laboratory of Climatology and Atmospheric Environment, National and Kapodistrian University of Athens, Panepistimiopolis 15784, Zografou, Greece

Interpolation methods categorized either as deterministic or as geostatistical, are based on known values in order to estimate unknown values for any data. They are mostly used for generating spatial distribution maps. Deterministic interpolation methods are based on mathematical equations. The most common deterministic methods are inverse distance weighting (IDW) and radial basis function (RBF) (Varouchakis and Hristopoulos, 2013; Bhunia *et al.*, 2018). Geostatistical interpolation methods are based on statistics of the measured points by means of semivariogram. They quantify the distance among neighboring points. Some of the most important and widely used geostatistical methods in the scientific field of geology are kriging techniques (Krige, 1951; Matheron, 1963). The most frequently used sub-types of kriging are ordinary kriging (OK), simple kriging (SK), universal kriging (UK) and empirical Bayesian kriging (EBK) (Varouchakis and Hristopoulos, 2013; Bhunia *et al.*, 2018).

The aim of the present study is to propose the optimum interpolation method by comparing the main deterministic (IDW and RBF) and the geostatistical (OK, SK, UK and EBK) methods on the basis of the parameter of electrical conductivity (EC) in the coastal aquifer of Schinos village, NE Peloponnese, Greece. This study will contribute to reducing the uncertainties in the spatial distribution maps of the hydrogeochemical parameters.

The Schinos village is located in NE Peloponnese, Greece and belongs to the Corinth prefecture. The main aquifer system in the area is a granular unconfined alluvial coastal aquifer consisting of sands, gravels and conglomerates of ultramafic and carbonate origin; it is characterized by deterioration of quality due to the seawater intrusion and high concentrations of nitrate (NO_3^-) and hexavalent chromium (Cr^{6+}) (Papadopoulos and Lappas, 2014; Pyrgaki *et al.*, 2016).

A total of twenty (20) groundwater samples were collected from irrigation wells in the alluvial aquifer of Schinos village during the period of November to December 2016. The evaluation of the best interpolated method was achieved by performing the cross validation method, which uses the total number of samples and estimates the value of a known position by means of leave-one-out sample, so there is one measured and one estimated value. This procedure was repeated for the twenty (20) groundwater samples and for all the methods examined herein (IDW, RBF, OK, SK, UK and EBK). Geostatistical methods were performed with semivariogram using Gaussian-model-function, since it produced the most favorable outcome. The root-mean-square error (RMSE) and the mean absolute error (MAE) are two approaches to quantify the predictive performance of different interpolation methods and were calculated using ArcGIS 10.3. The equations for the estimation of RMSE and MAE are:

$$\mathrm{RMSE} = \sqrt{\frac{\sum (Z_i - Z)^2}{n}}$$

$$\mathrm{MAE} = \frac{1}{n}\sum_{i=1}^{n} | Z_i - Z |$$

Where Z_i is the predicted value, Z is the measured value, and n is the total number of observations.

EC constitutes one of the most representative parameter for groundwater quality, since it is a significant indicator of groundwater quality and presents strong to very strong correlation coefficients with the majority of major ions and the total dissolved solids (TDS) (R^2=0.90). Furthermore, elevated values of EC, which are directly associated with increased concentrations of Cl^-, usually reveal a seawater intrusion regime into the aquifer making explicit the qualitative degradation of the groundwater in the study area (Papadopoulos and Lappas, 2013). EC values in the Schinos village range from 972 to 3943 μS cm^{-1} with a mean of 2032.35 μS cm^{-1} and a median of 2017.5 μS cm^{-1}. 95% of the samples have EC > 1000 μS cm^{-1}. The EC has set a maximum guideline value of 2500 μS cm^{-1} in drinking water according to World Health Organization (WHO, 2011).

The physical parameter of EC was interpolated using deterministic (IDW and RBF) and geostatistical methods (OK, SK, UK and EBK). The IDW method was estimated for three (3) different weighting power (1,2,3), since these weights could affect significantly the results. Spatial distribution maps of EC present different spatial patterns for each interpolation method. According to RMSE, the most appropriate deterministic and geostatistical methods are in decreasing order IDW1>IDW2>IDW3>RBF, and UK>SK>OK>EBK, respectively. Lower value of RMSE indicates the better interpolation method. According to MAE, the most appropriate deterministic and geostatistical methods are in decreasing order IDW2>IDW3>IDW1>RBF and SK>UK>OK>EBK, respectively. Lower value of MAE suggests more precise results. Data treatment and cross validation method revealed, that the best interpolation methods for generating spatial distribution maps of EC are RBF and EBK for deterministic and geostatistical methods, respectively. The

method with the lowest values of RMSE and MAE was the EBK suggesting that this is the most suitable interpolation method (Figure 1), as also stated by Hussain *et al.*, 2014.

The optimum interpolation methods for estimating the spatial variability of the values of EC in the coastal aquifer of Schinos village are geostatistical methods using GIS techniques. Selecting the most appropriate interpolation method is a complex process due to the variability of the examined parameters and the high number of manually-adjusted parameters, which are dependent on the user's experience. The most crucial factors are: the magnitude and the spatial distribution of the dataset (dependence of the distance), the interpolated qualitative or quantitative parameter since some methods are more suitable for datasets with extreme values (e.g. NO_3^-, Cr^{6+}), while others are proper for datasets without outliers (e.g. EC, TDS and the majority of major ions).

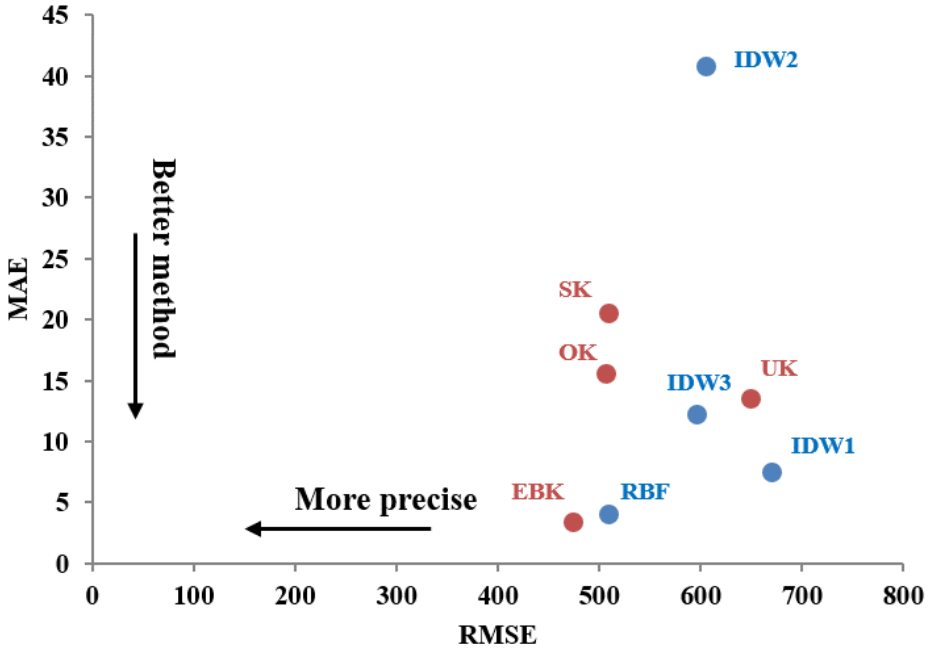

Figure 1. RMSE and MAE for deterministic (blue circles) and geostatistical (red circles) interpolation methods for the groundwater samples in the Schinos village.

References

Bhunia, G.S., Shit, P.K., Maiti, R., 2018. Comparison of GIS-based interpolation methods for spatial distribution of soil organic carbon(SOC). Journal of the Saudi Society of Agricultural Sciences, 17 (2), 114–126.

Hussain, I., Shakeel, M., Faisal, M., Soomro, Z.A., Hussain, T., 2014. Distribution of total dissolved solids in drinking water by means of Bayesian kriging and gaussian spatial predictive process water quality. Exposure Health, 6 (4), 177–185.

Krige, D., 1951. A statistical approach to some basic mine valuation problems on the Witwatersrand. Journal of the Chemical, Metallurgical and Mining Society of South Africa, 52, 119–139.

Matheron, G., 1963. Principles of geostatistics. Economic Geology, 58, 1246–1266.

Papadopoulos, K., Lappas, I., 2014. Groundwater quality degradation due to Cr6+ presence in Schinos area, prefecture of Corinth, Central Greece. 10th International Hydrogeological Congress of Greece, Thessaloniki.

Pyrgaki, K., Argyraki, A., Kelepertzis, E., Paraskevopoulou, V., Botsou, F., Dassenakis, E., Mitsis, I., Skourtsos, E., 2016. Occurrence of hexavalent chromium in the ophiolite related aquifers of Loutraki and Schinos Areas. Bulletin of the Geological Society of Greece, 50 (4), 2261-2270.

Varouchakis, E.A., Hristopulos, D.T., 2013. Comparison of stochastic and deterministic methods for mapping groundwater level spatial variability in sparsely monitored basins. Environmental Monitoring Assessment, 185, 1–19.

World Health Organization (WHO), 2011. Guidelines for drinking water quality, World Health Organization Geneva, 4th Edition.

15th International Congress of the Geological Society of Greece
Athens, 22-24 May, 2019 | Harokopio University of Athens, Greece
Bulletin of the Geological Society of Greece, Sp. Pub. 7 Ext. Abs. GSG2019-306

Retrieving Geomorphological information from Oblique Landscape Photographs. A robust method based on Geoinformatics

C. Chalkias[1], K. Kalogeropoulos[1], E. Papadias[1]
(1) Harokopio University, Department of Geography, El. Venizelou 70, 17671, Athens, Greece, xalkias@hua.gr

Background

Maps, illustrations and photographs of landscapes have been essential methods to visualize and analyse Earth features and processes (Dykes, 2008). The creation of traditional geomorphological mapping requires intensive fieldwork, qualitative interpretations of remotely sensed imageries (e.g. aerial photographs) and topographic maps, as well as quantitative assessments using detailed orthophotomaps or/ and satellite images (Verstappen, 2011). In most of the cases, oblique landscape photographs are used only for the general interpretation of the area under investigation.

Objectives

In this study, we present a new method for the generation of geomorphological information from various landscape oblique photographs with the use of an open freely available tool, the WSL monoplotting tool. In order to test this method we used historical photographs as well as recent oblique photographs from unmanned aerial vehicles (UAVs – Drones). Another aim of this paper is to evaluate the limitations, the prerequisites and the assumptions of the proposed method.

Methods

1. The use of historical landscape photographs and the WSL monoplotting tool.

Landscape is been under continuous changing by natural but also human powers through time. Although historical photographs contain valuable information about these changes, in most cases extraction of accurate spatial data is either very difficult and demanding, or not possible at all. Monoplotting tool, developed by WSL (Bozzini et al. 2012), offers a solution aiming to produce georeferenced vector data directly from pictures which then can be integrated in traditional GIS procedures and systems. For testing the tool we utilized a picture taken in 1937 from the temple of Poseidon at Cape Sounio, Greece. The tool requires also a georeferenced map and a Digital Elevation Model (DEM). With the use of Monoplotting tool we digitized various landforms from the Historical photograph as well as elements recognized in modern images. The results have rather acceptable accuracies (~ 5m - 50m). Inaccuracies were produced due to: a) difference between the spatial resolution of the basemap and the DEM, b) inaccuracies in the evaluation of control points and c) due to inaccuracies in the identification of real location of the shooting point of the historical photograph which is probably the main challenge of the method.



Figure 1. Digitizing of a landform from historical photograph within the environment of Monoplotting tool.

2. The use of oblique images from of modern UAVs - drones to create detailed geomorphological datasets.

The recent years the unmanned aerial vehicles (UAVs-Drones) have overwhelmed the market and have become widely available, by being cheaper. They permit an operative observing of large areas in a very short time compared to conventional techniques (Jordan, 2015; Madjid et al., 2018). Thus, drones have become an important tool for scientists and researchers around the world and they are used for many purposes besides military like archaeology, farming-precision agriculture, natural disasters management, structural safety inspections and geographic mapping. An aspect of this last use of drone is the Geomorphological / Landform mapping. They can provide a broad, aerial perspective of a

variety of earth features (Tziavou et al., 2017). The proposed methodology consists of the following steps: a) Construction of a trigonometric network, the points of which will act as ground control points (GCPs), in the photographs that the low-cost drone will take. The points should cover as far as possible the entire study area, and will be accurately measured with the proper GPS equipment b) The next step is the use of drone in order to take various oblique photographs of the study area, c) selection of the proper images in order to include the landforms under investigation d) Import of these images into the WSL Monoplotting Tool, e) linkage between oblique images and background rectified image with the use of the GCP and g) digitizing of the landforms and export to a GIS platform.

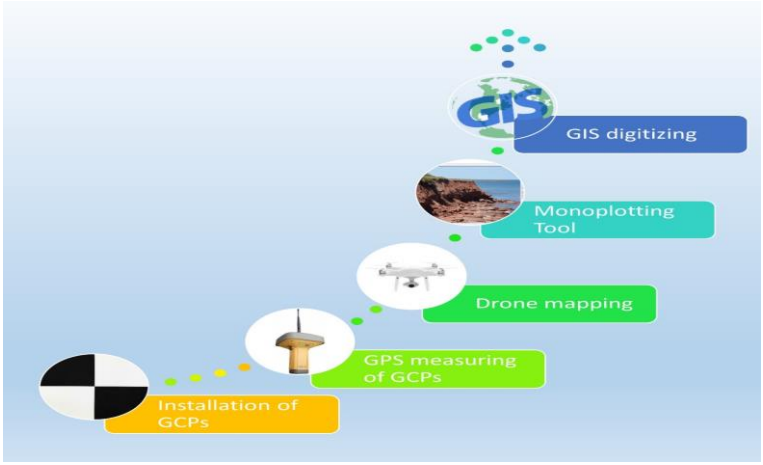

Figure 2. Digitizing landforms from UAV captured oblique images.

Results - Conclusions

The results are promising and the methods can be used to retrieve geomorphological information from historical photographs and thus to illustrate geomorphological changes as well as to create relatively low-cost recent geospatial datasets with the used of UAVs. The potential uses of the method are numerous including in general gemorphological mapping and evaluation of past landforms in order to analyze and visualize Earth surface features and processes. Given the increasing interest in using historical photography, and with the recent high use of Geoinformatics in Earth Sciences, the proposed method can be used to accurately classify landscape photographs in order to evaluate earth procedures and changes.

The article concludes that the proposed approach has a huge potential, although some limitations exist relating to the accuracy of the results as well as the pre-required information about the photographs of the landscape.

References

Bozzini, C., Conedera, M., Krebs, P., 2012. A new monoplotting tool to extract georeferenced vector data and orthorectified raster data from oblique non-metric photographs. International Journal of Heritage in the Digital Era 1: 499–518.

Dykes, A., P., 2008. Geomorphological maps of Irish peat landslides created using hand-held GPS. Journal of Maps 2008: 258-276.

Jordan, B., 2015. A bird's-eye view of geology: The use of micro drones/UAVs in geologic fieldwork and education. GSA Today, 25 (7), doi: 10.1130/GSATG232GW.1.

Madjid, M.Y.A., Vandeginste, V., Hampson, G., Jordan, C.J., Booth, A.D., 2018. Drones in carbonate geology: Opportunities and challenges, and application in diagenetic dolomite geobody mapping. Marine and Petroleum Geology, doi: 10.1016/j.marpetgeo.2018.02.002.

Tziavou, O., Pytharouli, S., Souter, J., 2017. Unmanned Aerial Vehicle (UAV) based mapping in engineering geological surveys: Considerations for optimum results.. Engeo(2017), doi:10.1016/j.enggeo.2017.11.004.

Verstappen, H., T., 2011. Old and new trends in Geomorphological and Landform Mapping. In: Geomorphological Mapping: Methods and applications. Smithm M., J., Paron P., Griggiths J. (Eds). Elsevier: London, 13-38.

15th International Congress of the Geological Society of Greece
Athens, 22-24 May, 2019 | Harokopio University of Athens, Greece
Bulletin of the Geological Society of Greece, Sp. Pub. 7 Ext. Abs. GSG2019-375

A Risk-based analysis of Engineering Geology Failures in Pipeline Corridors Investigations

P.–M. Spanidis[1], C. Roumpos[2], K. Liakoura[2]

(1) ASPROFOS Engineering S.A., Division of Project Management, 284 El. Venizelou str., 17675 Athens, Greece.
(2) Public Power Corporation S.A. of Greece, Mines Central Department, 29 Chalkokondili str., 10432 Athens, Greece

.

Pipelines are safe and environmentally friendly means for transportation of oil and gas over long distanced areas. The investigation of the terrestrial corridors within which the pipeline systems are developed is a multidisciplinary and multitasking process of high complexity. This process is iterative and starts with examinations in a wide '*corridor of interest'* and then narrows down to a more defined route at each engineering/design stage insofar more data is acquired to a final zone (also known as: '*Right of Way'*-ROW) that is finally identified as appropriate for the pipeline erection/construction. The scope of this process is the performing of an integrated assessment of various corridor alternatives by considering critical environmental, geological, geotechnical, social factors and natural hazards as well. For this reason, teams consisting of experts from various disciplines of science and technology (managers, geologists, environmentalists, archaeologists, sociologists, surveying engineers, piping designers, etc.) make all necessary evaluations to produce appropriate assessments from which the most advantageous corridor can be demonstrated and selected in relation to criteria of technical feasibility, constructability, safety, environmental compliance, cost effectiveness, public acceptance and permitting.

The Engineering Geology investigation constitutes a significant and sensitive part of that process. The objective of geological investigation is the analysis of the consistency of stratigraphic and soil formations, the geographic, terrain and landform features and the determination of soil geotechnical properties within the corridors under examination. The interpretation of geological layouts and laboratory results from tests performed on material collected from boreholes and site tests, constitute an instrument providing inputs valuable for the structural designs of the buried pipeline sections. These inputs derived from investigations of pipeline route encroachments of instable/loose formations, active faults, erosive or rocky sites, steep slope locations, soils prone to buoyancy or liquefaction and water crossings. Even important for the quality and efficiency of the pipeline design studies is the consideration of historical seismic data and determination of the seismic action parameters in determining the earthquake effects to the pipeline body at the wider areas where the alternative corridors are to be developed.

The investigation of pipeline corridors is a combination of desktop studies, extended field surveys as well as soil sampling and laboratory testing works. It is common practice the route corridor investigations to be performed in the early stage of the pipeline projects, where various supply chain scenarios are under examination and the technical philosophy of the pipeline system at hand has not yet come to a level of solid technical maturity. This fact combined with a number of other factors such as, managerial deficiencies, lack of appropriate expertise, low cost investigations, tight time schedules, non-completely developed project organization and planning schemes and low reliability baseline data/studies, might generate failures with potential effects to the quality of the engineering and design studies. In terms of the Engineering Geology, these failure risks represent any low quality/reliability data of surface/subsurface geology, hydrogeology, tectonics and seismicity, which, once they have inserted in the designs and calculations of other technical/technological studies, generate risks inserting the entire pipeline project time and cost overruns.

There are several types of Engineering Geology failure causes observed pipeline route corridors investigations with crucial impact in the elaboration of basic and detailed engineering studies (topographical, civil, mechanical, pipeline crossing design, structural and stress analysis). The main categories of risk generating failures are:

(a) Incomplete or low performance site surveys: refers to failures in field data collection, improper fieldworks logistics, omissions in visiting areas of geological/geotechnical/hydrogeological concern, inadvertent soil sampling and drilling works, insufficient experience of site personnel, inappropriate evaluation of crossings morphology, non-availability of field instrumentation/equipment, reactions of local communities, landowners or stakeholders reactions against the geotechnical research, permitting dysfunctions and weather conditions;
(b) Desktop Analysis failures: refers to failures related to inappropriate spatial analysis of baseline geographical data of the under evaluation corridors, lack of remotely sensed and satellite imagery/spectral data, limitations of GIS/software capabilities, IT equipment and hardware defects, time elapsing in transforming conventional mapping products to digital form, etc.;
(c) Poor scientific background and evidence: refers to non-availability of previous substantial geological studies and surveys, misuse/misinterpretation of baseline maps, satellite imagery and remote sensing products and ortho-photo-rectified maps, poor literature reviews and scientific knowledge acquisition;
(d) Managerial dysfunctions: refers to failures caused by budgetary limitations, lack of managerial capabilities, poor planning, organizational limitations, non-finalized project scope definition, unjustified delays in decision-making, uncontrolled delays in obtaining permissions, lack of interface management and poor quality controls;

In view of the above, some reasonable research questions are raising up: is there any method of analyzing the nature of Engineering Geology failures and quantifying the associated risks? Is there any instrument of representing those failures into an ontology enabling probabilistic estimation(s) of risk failures? Are there any methods of examining risk-based scenarios analysis developed as a tool for project management improvement in pipeline contexts?

The objective of this paper is to suggest a methodology aiming to the better understanding/management of Engineering Geology failures based on application of quantitative methods and structured according to the following main tasks:

(i) Understanding, identification and classification of Engineering Geology Failures that insert risks in multidisciplinary investigations of pipeline route assessments;
(ii) Developing a Risk-based analysis of Engineering Geology failures using the Analytical Hierarchy Process (AHP) technique for obtaining the probability of occurrence of failure risk factors/sub-factors based on knowledge aggregation and empirical evidence of pipeline route experts and engineering geologists (see Table-1);
(iii) To represent the identified failure causes in a Fault Tree Analysis (FTA) ontology enabling a top-down and bottom-up probabilistic analysis (see Figue-1);

The methodology is supported by a Case Study showing how the results of probabilistic analysis produced by the AHP and the FTA ontology provides an integrated approach of estimating time and cost overruns using the Expected Value (EV) function in engineering geology investigations. The methodology is advised as a low cost and soft computing solution, however, its techno-economic views and limitations have to be considered.

Table-1: Probabilities of Failure Risks - AHP results

Reciprocal Matrix

Main Failure Risks		*R1*	*R2*	*R3*	*R4*
SITE SURVEY FAILURES	*R1*	**1,00**	3,50	1,50	3,00
DESKTOP FAILURES	*R2*	0,29	**1,00**	0,50	0,43
POOR EVIDENCE FAILURES	*R3*	0,67	2,00	**1,00**	1,67
MANAGERIAL DEFICIENCIES	*R4*	0,33	2,33	0,60	**1,00**

Normalized Matrix

Main Failure Risks		*R1*	*R2*	*R3*	*R4*	*WRi*
SITE SURVEY FAILURES	WR_1	0,44	0,40	0,42	0,49	***0,436***
DESKTOP FAILURES	WR_2	0,13	0,11	0,14	0,07	***0,112***
POOR EVIDENCE FAILURES	WR_3	0,29	0,23	0,28	0,27	***0,267***
MANAGERIAL DEFICIENCIES	WR_4	0,15	0,26	0,17	0,16	***0,185***
		1,00	**1,00**	**1,00**	**1,00**	**1,000**

WR_i: Weight of Risk Factors $\quad \sum WR_i = 1;\ 0 < WR_i < 1$

Consistency control

CI =	0,086	RI =	0,9	CR =	0,023 < 0,10

CI: Consistency index
RI: Random Index
CR: Consistency Ratio

Figure-1: FTA Ontology

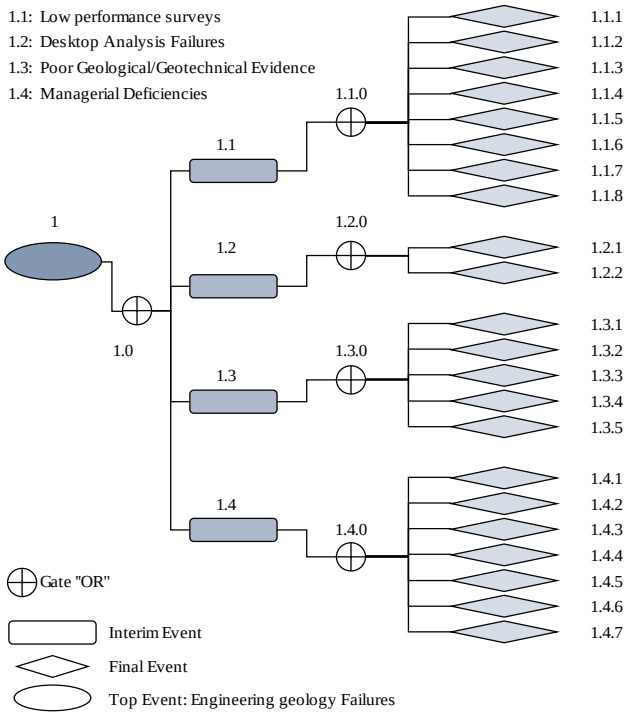

References

Botsis, C., Anagnostidis, G., Sariyiannis, A., Kokavesis, N. (2004) An Overview of the Seismic Verification Analyses performed for Natural Gas Pipeline Networks, Seismic Engineering, PVP, 486

Dawotola, A., Van Gelder, P. H. A. J. M., Vrijling, J. K., (2009). Risk Assessment of Petroleum Pipelines using a combined Analytical Hierarchy Process – Fault Tree Analysis (AHP-FTA), Proceedings of the 7th International Probabilistic Workshop, Delft

De F. S. M. Russoa, R., Camanhob, R., (2015). Criteria in AHP: a Systematic Review of Literature, Procedia Computer Science 55 pp. 1123 – 1132

Dey, P.K. (2006) Integrated project evaluation and selection using multiple-attribute decision making technique, International Journal of Production Economics, 103, 90-103

O' Rourke, T. D., Palmer, M. C., (1996). Earthquake Performance of Gas Transmission Pipelines. Earthquake Spectra, vol.(12), No.3, pp. 493-527

Reddy, D. V., (2010). Engineering Geology, Vikas Publishing House, PVT, LTD

Saaty, T. L., (2008). Decision making with the Analytic Hierarchy Process, International Journal of Services and Sciences, vol.(1) No.1, pp. 83-98

Vessely, W. E., Goldberg, F. F., Roberts, N. H., Haasl, D. F., (1981). Fault Tree Handbook, NUREG-0492, US Nuclear Regulatory Commission, Washington DC, 20555.

GENERAL SESSION

T12 Atmospheric Sciences

15th International Congress of the Geological Society of Greece
Athens, 22-24 May, 2019 | Harokopio University of Athens, Greece
Bulletin of the Geological Society of Greece, Sp. Pub. 7 Ext. Abs. GSG2019-012

Indoor and Outdoor Air Pollution Monitoring Developments in the Municipality of Thessaloniki – Preliminary Actions from Three European Funded Projects

G. Papastergios[1,2], P. Tzoumaka[3], A. Kelessis[3]

(1) Dpt. of Operational Planning & Monitoring of Structural Funds, Municipality of Thessaloniki, Vas. Georgiou A' 1, 54636, Thessaloniki, Greece, g.papastergios@thessaloniki.gr
(2) Dpt. of Mineralogy-Petrology-Economic Geology, Aristotle University of Thessaloniki, 131 Egnatia St. Thessaloniki 54124, Greece, gpapaste@geo.auth.gr
(3) Dpt. of Environment, Municipality of Thessaloniki, Kleanthous 18, 54642, Thessaloniki, Greece

Introduction

In 2014 Thessaloniki was selected to join the 100 Resilient Cities (100RC) network. Since then, the Municipality of Thessaloniki has developed its resilience strategy based on 8 city values (Social Cohesion, Local Identity & Heritage, Environmental Management, Health and Wellbeing, Youth Empowerment, Multi-stakeholder Engagement, Technology Adaptation, Economic Prosperity), which represent the city's identity and guide about future planning. Within the aforementioned strategy, Urban Resilience is described as "the capacity of cities to function, so that people living and working in cities - particularly the poor and vulnerable – survive and thrive no matter what stresses or shocks they encounter". However, a number of, more or less, similar definitions, for Urban Resilience, can be found in the literature (i.e., 100 RCs 2018, Meerow et al., 2016, Spaans and Waterhout 2017).

Environmental Management is one of the key values of Thessaloniki's Resilience Strategy and Thessaloniki has engaged into several activities supporting this value. Within this context, air pollution is one of the main environmental concerns of the Municipality of Thessaloniki. Therefore, the Municipality established a Network of 6 Air Pollution and 9 Meteorological Monitoring Stations, in order to monitor air pollutants and meteorological parameters, since 1990 (Kassomenos et al., 2011; Kelessis et al., 2006; Tzoumaka, et al., 2008; Vouitsis et al., 2015). The stations are distributed within the limits of the Municipality and cover a wide range of air pollution station types, according to the EU relevant directives. At these stations some fundamental meteorological parameters are also measured.

The monitoring and recording of the measurements of the Municipal Network is systematic on 24 hour basis. The air pollutants measured are particulate matter (PM_{10} and $PM_{2.5}$), carbon monoxide (CO), sulphur dioxide (SO_2), ozone (O_3), nitrogen monoxide NO and nitrogen dioxide (NO_2). All the analyzers are compliant with the EU standards for air quality monitoring and are frequently calibrated. Additionally, measurements of BTEX have been performed at two sites and their monitoring has been added to the monitoring schedule. The meteorological parameters measured are ambient temperature, relative humidity, wind velocity, wind direction and atmospheric pressure.

Having all of the above in mind, the aim of the present work is to present the current developments regarding indoor and outdoor air monitoring actions that the Municipality of Thessaloniki has taken in order to increase its resilience towards values described in its strategy such as Environmental Management, Health and Wellbeing and Technology Adaptation.

Study area and Project(s) Description and Goals

The study area is located in northern Greece and includes the Municipality of Thessaloniki, which is the 2nd largest municipality in Greece with 325.000 inhabitants. The past years the Municipality of Thessaloniki has developed short-term (5 year operational program) and long-term (Thessaloniki 2030, Resilience Strategy) strategies, in which has set several environmental issues as top priorities. In the previous years, the Municipality of Thessaloniki was a partner-beneficiary in more than 45 projects that received funding, either from National Regional or Sectoral Programmes or from other funding tools with a total, initial budget that was over 100 mil. Euros. Building on this experience, the Municipality continued becoming a partner in proposals, seeking funding from various sources; thus, seeking to add knowledge to issues that are considered crucial for the Municipality, such as air pollution, digital services, resilience and others. These proposals were built upon the partnerships of previous years and resulted in several of the proposals being accepted for funding, concerning various sections (i.e., mobility, migration etc.). Three of these projects are dealing with issues such as outdoor air pollution, indoor air pollution, IoT, governance, co-creation and resilience, in general. These projects are entitled CUTLER, AIRTHINGS and LIFE SMART IN'AIR and are described below.

The full title of the **CUTLER** project is "*Coastal Urban developmenT through the LEnses of Resiliency*" and is funded under the Horizon 2020 Programme. The project's total budget is 5,080,125.00 €, while the Municipality of Thessaloniki has 241,250.00 € assigned to its budget. The project's duration is 36 months and the consortium consists of 15 partners from Greece, Ireland, Belgium, Turkey, Germany, and Finland. CUTLER project is strongly connected with the concept of Urban Resilience. With this project an effort is being made to shift the existing paradigm of policy making, which is largely based on intuition, towards an evidence-driven approach enabled by big data. The Municipality of Thessaloniki is the lead partner in Work Package 9 and as a pilot action, the Municipality has chosen to use the CUTLER platform to design, implement, monitor, and evaluate a new Controlled Parking System (CPS) in the 1st, 3rd and 5th Municipal Districts of the city. The Dpt. of Environment of the Municipality has a large dataset regarding the air quality of the city (SO_2, PM_{10}, CO, NO, NO_2, O_3), which is available through its open data portal and it will be

used to make a first assessment of the new CPS on the air quality of the city. The platform that will be developed by the technical partners of the project will be used to evaluate the environmental impact of the new CPS on the quality of the ambient area. This will be achieved by examining and comparing air pollutants' trends for selected periods, first with Key Performance Indicators (KPIs) and finally with an Air Quality Index adapted for the urban Thessaloniki area. The final environmental goal will be to provide evidence to decide if there has been an improvement, deterioration or no change of state in the environmental conditions due to the proposed parking policy.

The full title of the project **AIRTHINGS** is "*Fostering resource efficiency and climate change resilience through community based Air Quality Internet of Things*". The project is funded under the Balkan – Mediterranean 2014-2020 – Interreg V-B" (BalkanMed) Programme. The total budget of the project is 1,417,322.66 €, out of which 227,390.00 € are assigned to the budget of the Municipality of Thessaloniki. The project has a duration of 24 months and its consortium consists of 5 partners from Greece, Cyprus, Albania, and FYROM. Under the AIRTHINGS project, three important technologies will be disseminated among the Balkan countries: (i) IoT Sensors Grid: A grid of 91 IoT Sensors will be distributed and will start measuring air quality in the cities of Sofia (22), Thessaloniki (22), Cyprus (19), Tirana (17) Skopje (11), (ii) Open Data Platform for sharing online information obtained from the sensors, and (iii) 61 chimney filters (chimney filter reduces PM emissions with 60% on average). All the above actions will help the project partners to combine state of the art technologies and know-how into synergic unity that will result in sustainable development and urban resilience. Relying on the community-based approach the partners will pilot demonstrate the capabilities of new real-time monitoring node network, thus providing local communities with information which is not being available previously.

The full title of the project **LIFE SMART IN'AIR** is "*Smart indoor air monitoring network to reduce the impacts of pollutants on environment and health*". The project is funded under the LIFE 2014 - 2020 Programme. Its total budget is 3,919,777.00 €, while the Municipality's budget is 63,001.00 €. The duration of the project is 50 months and the consortium consists of 10 partners from Greece, France, Spain, Portugal, Belgium, and Bulgaria. The project's main objective is to provide a complete and smart solution to monitor and improve In Air Quality (IAQ). This will be done through innovative micro-analysers for BTEX and formaldehyde connected to a user-friendly web and smartphone interface to easily treat the data, link them with risks on human and environment health and implement actions to reduce this pollution. The project will demonstrate a method that hasn't been applied and tested before: sensitive, fast and easy-to use micro-analysers for real-time detection of 2 types of hazardous Volatile Organic Compounds (VOCs): formaldehyde and BTEX (Benzene, Toluene, Ethylbenzene and Xylenes). These microanalysers will be connected to a user interface for data interpretation (e.g. link between pollutants concentrations and alert and health) and implementation of practical measures for improving IAQ. The Municipality of Thessaloniki will use its expertise to implement the demonstration of the LIFE SMART IN'AIR project in one school. It will be responsible to use chemical data monitored by the micro-analyzers to improve the indoor air quality of the school and to implement good practices. The Municipality will also be involved in the communication and dissemination activities.

Concluding remarks

With air pollution being one of the first environmental problems to be addressed by the EU, clean air is considered essential to good health. Hence, all available information and understanding of the air quality issue is essential part of tackling it with efficiency. The 3 funded projects that the Municipality of Thessaloniki is a partner of, are trying to provide complete knowledge regarding a sensitive matter, and all future accomplishments that will come through their successful implementation will be a step forward towards a better understanding of the problem, an increase in the city's resilience and in the well being of the city's population.

Acknowledgements

The project "*Coastal Urban developmenT through the LEnses of Resiliency* - **CUTLER**" has received funding from the Horizon 2020 Programme of the European Union (Ref.: 770469). The project "*Fostering resource efficiency and climate change resilience through community based Air Quality Internet of Things* - **AIRTHINGS**" has received funding from the Balkan – Mediterranean 2014-2020 – Interreg V-B" (BalkanMed) Programme (Ref.: 5019199). The project "*Smart indoor air monitoring network to reduce the impacts of pollutants on environment and health* - **LIFE SMART IN'AIR**" has received funding from the LIFE Programme of the European Union (Ref.: LIFE17 ENV/FR/000330).

References

100 RCs (Resilient Cities). 2018. The EU Resilience Prospectus. Available on line at www.100resilientcities.org, last access November 2018.

Kassomenos, P.A., Kelessis, A., Paschalidou, A.K., Petrakakis, M. 2011. Identification of sources and processes affecting particulate pollution in Thessaloniki, Greece. Atmospheric Environement 45, 7293-7300.

Kelessis, A.G., Petrakakis, M.J., Zoumakis, N.M. 2006. Determination of benzene, toluene, ethylbenzene and xylenes in urban air of Thessaloniki, Greece. Environmental Toxicology 21(4), 440-443.

Meerow, S., Newell, J.P. and Stults, M. 2016. Defining urban resilience: A review. Landscape and Urban Planning 147, 38-49.

Spaans, M. and Waterhout, B. 2017. Building up resilience in cities worldwide – Rotterdam as participant in the 100 Resilient Cities Programme. Cities 61, 109–116.

Tzoumaka, P.N., Kelessis, A.G., Petrakakis, M.J., Samara, C., Papagiannopoulos, N.M., Zoumakis, N.M., Tzourelis, G. 2008. Experimental measurements of C2-C5 and C6-C10 in urban area of Thessaloniki, Greece, Fresenius Environmental Bulletin, 17,10a, 1594-1600.

Vouitsis, I., Amanatidis, S., Ntziachristos, L., Kelessis, A., Petrakakis , M., Stamos, I., Mitsakis E., Samaras, Z., 2015. Daily and seasonal variation of traffic related aerosol pollution in Thessaloniki, Greece, Atmospheric Environment 122, 577-587.

15th International Congress of the Geological Society of Greece
Athens, 22-24 May, 2019 | Harokopio University of Athens, Greece
Bulletin of the Geological Society of Greece, Sp. Pub. 7 Ext. Abs. GSG2019-078

High Altitude Meteorological Observations in Central Greece

G.S. Mitsika[1], S. Dilalos[1], P.T. Nastos[1], J.D. Alexopoulos[1], P. Delipetrou[2], K. Georghiou[2]

(1) NKUA, Department of Geology and Geoenviroment, Panepistimiopolis, Zografou, g.mitsika@geol.uoa.gr
(2) NKUA, Department of Biology, Panepistimiopolis, Zografou, Greece

Introduction

Data availability is severely limited in high-altitude regions (Shea *et al.*, 2015) mainly due to the remoteness and difficulty in accessing the sites. However, high mountain ecosystems are among the most sensitive environments to changes in climatic conditions occurring on global, regional and local scales (Ruiz *et al.*, 2008). Due to significant warming observed globally during the recent century, the international scientific community has focused more attention to understand the cause and effect interaction on the ecosystems and their individual components to climate changes (Borgaonkar *et al.*, 2011). In many mountain regions of the world, high altitudes appear to experience a stronger warming than the surrounding lowlands (Vuille, 2011) and that the warming is more closely related to an increase in daily minimum temperature than a change in the daily maximum (Diaz and Bradley, 1997; Beniston, 2006; Giambelluca *et al.*, 2008).

Objectives

The main objective of this study is to evaluate the variability of meteorological parameters measured by two high altitude meteorological stations (OITI and KALLIDROMO) that have never been analyzed before, located in two mountainous Natura 2000 sites of Central Greece, in the Region of Sterea Ellada (Figure 1). The stations were settled in the framework of the Project: Conservation of priority forests and forest openings in "Ethnikos Drymos Oitis" and "Oros Kallidromo" of Sterea Ellada. The data sets recorded in the meteorological stations cover the periods 2014-2018. OITI is a weather station located in site Greveno, National Forest Park of Mt. Oiti (38°49'26.00"N - 22°16'57.00"E - 1896 m). KALLIDROMO is a weather station located in site Gravia, Mt. Kallidromo (38°44'29.87"N - 22°28'12.00"E - 998 m). The National Park of Mt. Oiti extends at altitudes of 400 – 2116 meters and includes most of the highest peaks of the mountain (except the highest, Pyrgos, at 2152 m). The Mt. Kallidromo extends at altitudes of 43–1393 meters.



Figure 1. Map presenting the sites of OITI and KALLIDROMO meteorological stations (left image). The right image presents the snowy OITI station during its installation on December 2013.

Results

The meteorological parameters of Air Temperature (ºC), Relative Humidity (%), Precipitation (mm), Photosynthetically Active Radiation – PAR (μmol/m²s), Barometric Pressure (mbar), Wind-Direction (°), Wind Speed (m/s) and UVA (W/m²) were analyzed. For OITI station we analyzed the additional parameters of Soil Temperature (°C), Soil Moisture (vol%) and Hourly ETo (mm). Only the graphs for the Air Temperature and Precipitation covering the period January 2014 - December 2018 are presented in this study in Figures 2 & 3 respectively.

The measurements of OITI show that the coldest month is January (–2.03 ºC) and the warmest is July (15.2 ºC). The measured extreme values are: -18.1 ºC (January 9, 2017) for the minimum Air Temperature and 28.3 ºC (June 30, 2017) for the maximum Air Temperature. Also the mean PAR value is 339 (μmol/m²s), the minimum 0 and the maximum 2795 (μmol/m²s). The mean Precipitation value is 69.1 mm with an extreme value of 307 mm to be measured in

September 2018. Finally the mean Relative Humidity value is 75.5%

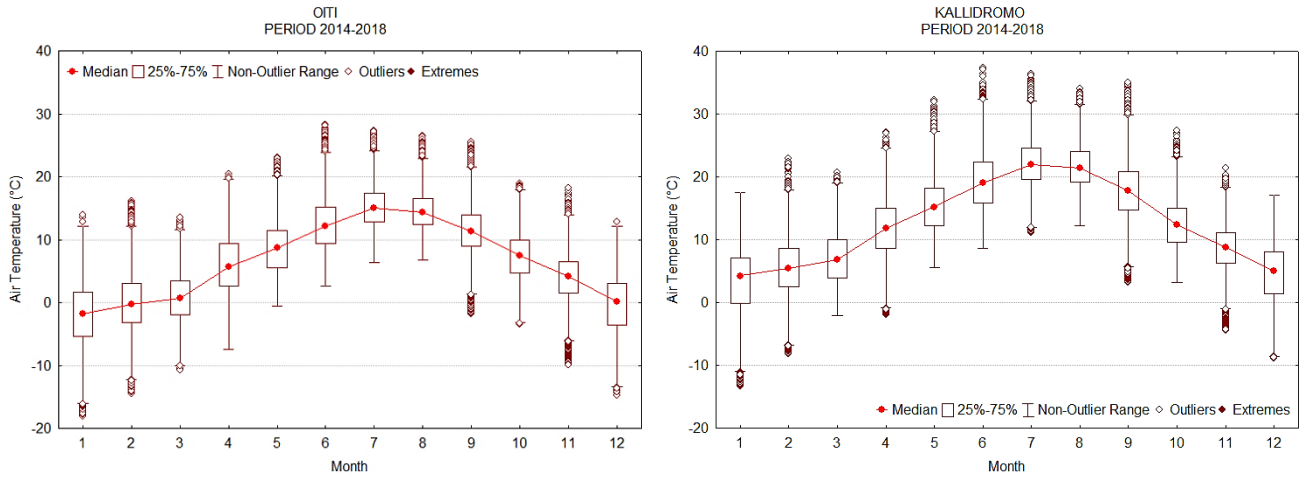

Figure 2. Air Temperature graphs for OITI (left) and KALLIDROMO (right) weather stations.

The measurements of KALLIDROMO show that the coldest month is January (3.49 ºC) and the warmest is July (22.1 ºC). The measured extreme values are: –13.3 ºC (January 8, 2017) for the minimum Air Temperature and 37.3 ºC (June 30, 2017) for the maximum Air Temperature. The mean PAR value is 192 (μmol/m²s), the minimum 0 (μmol/m²s), the maximum 1,354 (μmol/m²s). The mean Precipitation value is 66.2 mm and the Relative Humidity value is 72%.

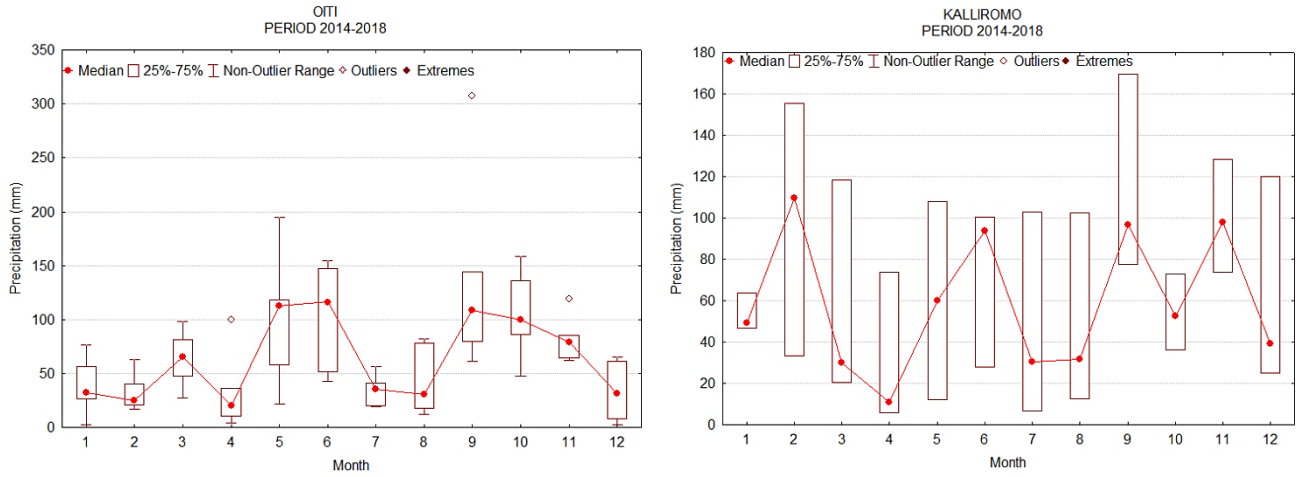

Figure 3. Precipitation graphs for OITI (left) and KALLIDROMO (right) weather stations.

Acknowledgements

This work was funded in the context of LIFE11 NAT/GR/1014 “FOROPENFORESTS” project.

References

Beniston M., 2006. Mountain weather and climate: a general overview and a focus on climatic change in the Alps. Hydrobiologia, 562, 3–16.

Borgaonkar H.P., Sikder A.B., Ram S. 2011. High altitude forest sensitivity to the recent warming: A tree-ring analysis of conifers from Western Himalaya, India. Quaternary International - QUATERN INT. 236. 158-166. 10.1016/j.quaint.2010.01.016.

Diaz H.F., Bradley R.S., 1997. Temperature variations during the last century at high elevation sites. Climatic Change, 36, 253–279.

Giambelluca T.W., Diaz H.F., Luke M.S.A., 2008. Secular temperature changes in Hawai’i. Geophysical Research Letters, 35, L12702.

Ruiz D., Moreno H.A., Gutiérrez M.E., Zapata P.A., 2008. Changing climate and endangered high mountain ecosystems in Colombia, Science of The Total Environment, Volume 398, Issues 1–3, Pages 122-132, ISSN 0048-9697, https://doi.org/10.1016/j.scitotenv.2008.02.038.

Shea J.M., Wagnon P., Immerzeel W.W., Biron R., Brun F., Pellicciotti F. 2015 A comparative high-altitude meteorological analysis from three catchments in the Nepalese Himalaya, International Journal of Water Resources Development, 31:2, 174-200, DOI: 10.1080/07900627.2015.1020417

Vuille M., 2011. Climate Variability and High Altitude Temperature and Precipitation. In: Singh V.P., Singh P., Haritashya U.K. (eds) Encyclopedia of Snow, Ice and Glaciers. Encyclopedia of Earth Sciences Series. Springer, Dordrecht

15th International Congress of the Geological Society of Greece
Athens, 22-24 May, 2019 | Harokopio University of Athens, Greece
Bulletin of the Geological Society of Greece, Sp. Pub. 7 Ext. Abs. GSG2019-291

Understanding Wake Capture Effect of the Ice Particle Aggregation Process with the Use of 3D-printed Analogues

D. Mitropoulos[1], M. McCorquodale[2], C. Westbrook[3]

(1) University of Reading, Reading, United Kingdom, mitropoulos.dim@outlook.com
(2,3) University of Reading, Reading, United Kingdom

Background

The interactions of ice crystals in a cloud has raised the interest of researchers since the 1950's. With the progress of aviation technology scientists were able to climb high in the troposphere with an airplane and measure the properties of clouds. One of these properties is the habit of ice crystals and how they interact together. With this data in hand, later experiments with ice crystal analogues could be done in a controlled environment of a laboratory, that gave the researchers the chance to compare the behaviour of real ice particles and modelled analogues of them and then form parameterisations that can predict this behaviour. The importance of Reynolds number is its universality, which means that it can describe the flow pattern of an object at different scales. Also, for the purpose of this study, Reynolds number helps to identify the validity of the laboratory ice particle analogue experiments with the ice particles in the atmosphere. Various dimensional and physical parameters for both areas (atmosphere and laboratory) give ratios (Reynolds numbers) of the same order. Consequently, the behaviour of an ice crystal in the atmosphere resembles the behaviour of the modelled analogues in the laboratory. Such behaviour could be fluttering motions of the crystals. Aggregation is the process where two same or different ice crystals are clumping together (Ambaum 2010). The forces that act on ice particles that sediment, which means that they fall only due to the force of gravity (no wind advection or turbulence) are the weight of the particle (w), the buoyant force (B) and the drag force (Fd). Also, terminal velocity (Vt) is very important for the aggregation process as many aggregation models use the parameterisation that all crystals and aggregates fall with their own terminal velocity.

Objectives

The aggregation of ice crystals is an important microphysical process within ice clouds, giving rise to large ice crystals with complex shapes. Aggregation occurs through the collision of ice crystals that sediment within a cloud at different constant velocities which in the literature are called terminal velocities. Current parameterisations in climate models and radar ice content retrievals enable us to estimate the terminal velocity of individual ice crystals. The validity of these parameterisations diminishes as ice crystals approach each other because of the interaction of the trailing particle (upper particle) with aerodynamic forces that are produced in the wake of the leading particle (lower particle) as they sediment through the atmosphere. The impact of the forces that act on each particle during their trajectory is currently little understood, limiting our knowledge of the aggregation process and how efficient actually is. Also, this research aims to expand this knowledge and offer greater understanding of these interactions in order to reduce the uncertainty of ice content and snowfall parameterisations as ice clouds, for example cirrus clouds, cover 1/3 of the atmosphere (Baran 2004) and cirrus clouds affect the solar and infrared energy budget due to their high albedo (reflectivity) and cause heating in the upper troposphere and cooling below (Fu and Liou 1993). It should be made clear that in most climate models, their aggregation processes essentially ignore the interaction of the falling crystals, for example, the wake capture of the trailing crystal and its abrupt acceleration near the aggregation point. In other words, they accept that the two crystals are falling their own constant speeds (terminal velocities).

Methods

To investigate the interaction of two ice particles in a controlled environment and specifically the wake capture of the trailing crystal by the leading crystal laboratory methods are used. The laboratory experiments include a cylindrical tank which is filled with a glycerol and water mixture, a tool for releasing crystals simultaneously and the 3D crystal analogues. Also, for the capturing of the video footage and for the measurement of the terminal velocities and the separation of the crystals a camera and the MATLAB software (mathworks.com) are used respectively. With more details, the cylindrical tank is made by plexiglass and its dimensions are 28cm in diameter and 60cm in height. The height of the tank is adequate for the crystals to reach their terminal velocity, when they are released independently, and aggregation most of the times which is depended by the type, the size and the initial separation of the crystals. Additionally, the width (28cm) of the tank gives the ability to eliminate any drag from the wall of the tank due to high viscosity even for relatively low Reynolds numbers (for example Re=120) (Fidleris and Whitmore 1961). At the bottom of the tank there is a metal mesh which is connected to a wooden handle and helps to retrieve the sedimented particles. The mixture in the tank is consisted by a part of glycerol (in this case it is 40%) and a part of water (60%). This mixture helps to achieve a range of Reynolds numbers which are similar to the ice particles falling in the atmosphere.

Results

In figure 1 and table 1 we see that the increase in velocity of the trailing particle is influenced by its diameter. There is an increase of velocity when diameter of the particle becomes smaller. Also, all types of particles follow this trend (parallel to each other) except type G particle. This is because there is less data (sometimes the crystals were aggregating too early before they enter the field of view of the camera) for the trailing crystal with D=0.74cm and because aggregation only

occurred at 1.6cm initial separation (even less data) and this results in higher uncertainty of that particular crystal. Additionally, the trend lines (Figure 1) cannot be defined accurately because of the few measurements and more particle sizes are needed to be tested, for that reason the trends are chosen subjectively. However, the abrupt acceleration in the area of wake capture is experienced in all the particle experiments that have been made and that shows that aggregation possibility is much higher than when the particles fall with steady velocities (terminal velocity) like in most aggregation models parameterisations (Lin et al. 1983; Locatelli and Hobbs 1974; Pruppacher and Klett 2012).

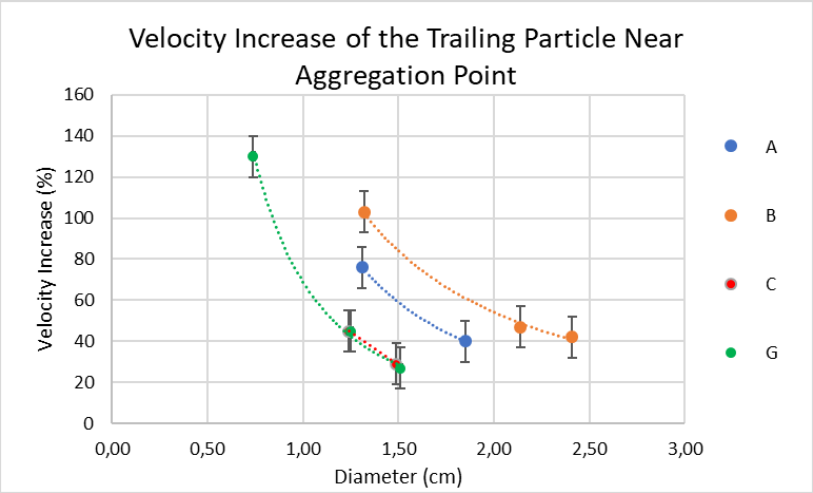

Figure 1. Velocity increase of the trailing particle in relation with its terminal velocity (individually released) near aggregation point. Uncertainty of velocity increase: ± 10%. Uncertainty of diameter is too small to be plotted.

Table 1. Velocity increase in relation to terminal velocity (individually released) at near aggregation point. For B and G particles, two trailing crystals were tested with the larger particle of each type.

Leading Particle		**A (R)** Re=258	**A (r)** Re=140	**B (R)** Re=443	**B (r)** Re=397	**C (R)** Re=255	**C (r)** Re=192	**G (R)** Re=310	**G (r)** Re=234
Trailing Particle	Re	140	258	397	443	192	255	234	310
	r/R	0.71	0.71	0.89	0.89	0.83	0.83	0.83	0.83
	V increase	**76%**	**40%**	**47%**	**42%**	**45%**	**29%**	**45%**	**27%**
	Re			175				89	
	r/R			0.55				0.49	
	V increase			**103%**				**130%**	

Conclusions

The acceleration of the leading particle in the wake capture area is examined and it is found that the acceleration starts after the release of the particles. Although, in the area of reduced pressure the acceleration is steady (on condition that the particles are going to aggregate – initial separation < aggregation threshold), in the area of wake capture the acceleration increases until aggregation. This acceleration in the wake capture is affected by the ratio of diameters of the leading (R) and the trailing (r) particles r/R. The smaller the r/R ratio the higher the increase of the velocity of the trailing crystal. It is observed that the highest increase of velocity of a particle relative to its terminal velocity (when it is released isolated) was measured to be 130% near aggregation point.

References

Ambaum, M. H. P., 2010: Thermal Physics of the Atmosphere. John Wiley & Sons, 254 pp.

Baran, A. J., 2004: On the scattering and absorption properties of cirrus cloud. Journal of Quantitative Spectroscopy and Radiative Transfer, 89, 17–36.

Fu, Q., and K. N. Liou, 1993: Parameterization of the Radiative Properties of Cirrus Clouds. J. Atmos. Sci., 50, 2008–2025

Fidleris, V., and R. L. Whitmore, 1961: Experimental determination of the wall effect for spheres falling axially in cylindrical vessels. Br. J. Appl. Phys., 12, 490.

Lin, Y.-L., R. D. Farley, and H. D. Orville, 1983: Bulk Parameterization of the Snow Field in a Cloud Model. J. Climate Appl. Meteor., 22, 1065–1092.

Locatelli, J. D., and P. V. Hobbs, 1974: Fall speeds and masses of solid precipitation particles. Journal of Geophysical Research, 79, 2185–2197.

Pruppacher, H. R., and J. D. Klett, 2012: Microphysics of Clouds and Precipitation: Reprinted 1980. Springer Science & Business Media, 1079 pp.

AUTHOR INDEX

Abuelgasim	Abdelgadir	763	765														
Adedeji	Olumide Akinwale	201															
Agiadi	Konstantina	114															
Aidona	Elina	30	43	85													
Aiello	Antonello	577															
Alçiçek	Cihat	486															
Alexopoulos	John D.	178	179	181	203	464	491	550	635	657	701	789					
Alexoudi	Vasiliki	563															
Aligizaki	Katerina	83															
Almpanakis	Konstantinos	392															
Alsaif	Manar	157	194														
Anagnostopoulou	Sofia	651															
Anagnostou	Christos	515															
Anastasakis	George	99	145	147	149												
Anastasatou	Marianthi	635															
Anastasiadis	Anastasios	605															
Anastasiadis	Aris	103	552	564	570	572											
Andreadi	Maria	326															
Andreou	Maria	499	554	556													
Andritsou	Nikoletta	580															
Andronis	Vasileios	770															
Anestoudis	Dennis	165															
Angelatou	Vassiliki	342															
Angeliki	Zacharoudi	670															
Anifadi	Alexandra	772															
Anthymidis	Marios	211															
Antonarakou	Assimina	99	105	106	115	139	141	143	149	691	712	719	721	723	724	725	
Antoniou	Varvara	564	661	687													
Antoniou	Faye	719															
Arabas	Agnieszka	77															
Arabelos	Dimitrios	544															
Aravadinou	Eirini	188															
Aravani	Foteini	312															
Ardabili	Omid	338															
Argyraki	Ariadne	434	399	419	424	434											
Argyri	Panagiota	708															
Arvaniti	Lamprini	422															
Arvanitis	Apostolos	533	539														
Asimakopoulou	Panagiota	712															
Asproudi	Marialena	503															
Asteriou	Pavlos	599	601														
Asvesta	Argyro	292	294	666	668												
Athanasiadou	Laoura	613															
Athanassas	Constantin	484	486														
Athanassoulis		352															
Atzemoglou	A.	643															
Avgerinou	Pelagia	752															
Avramidis	Pavlos	51	123	127	129												
Bakalis	Evangelos	594															
Bakopoulou	Athanasia	724															
Baksheev	Ivan	316															
Bally	Philippe	575															
Bannenberg	Matthias	625															
Bardouli	Pavlina	687															
Barsaki	Vassiliki	596															
Basias	Michail	714															
Bassiakos	Yannis	91	93	166													
Bassias	Yiannis	161	163														
Bassukas	Dimitris	129															
Bathrellos	George	478	493														
Batzakis	Vassilios Dimitrios	497	499	554	556												
Baumann	Karl-Heinz	101															
Baziotis	Ioannis	360	517														
Bellas	Spyros	133															
Benammi	Mouloud	30															
Benetou	Evangelia	489															
Bentana	Konstantina	695	696														
Berndt	Jasper	360															
Besiou	Evangelia	139	721														
Billia	Alexandra-Maria	251															
Birke	Manfred	405	407	409													
Bismayer	Ulrich	316															
Bitharis	Stylianos	172	198														
Boeckx	Pascal	399															
Bohnhoff	Marco	190															
Bollanos	Stelios	577															
Bonev	Nikolay	32															
Bonneval	Béatrice	762															
Borst	Anouk	314															
Botsou	Fotini	399															
Bougiouris	Angelos	147															
Boukouras	Kostas	275															
Boumpoulis	Vasileios	623															
Bountzis	Polyzois	226	239														
Bourli	Nicolina	117	125	135	137												
Bozionelos	George	580															

Bracchi	Valentina Alice	95										
Briole	Pierre	255	580									
Bussolesi	Micol	390	451	449								
Calabrese	Sergio	324	330	332								
Caputo	Riccardo	183										
Cardellini	Carlo	324										
Carluccio	Roberto	220										
Carras	Nicolaos	20										
Carter	Gareth D.O.	73	75									
Carydis	Panayotis	566	568									
Castro Gómez	Miguel	762										
Chailas	Stelios	209	217	277								
Chalari	Athena	587										
Chalkias	Christos	511	782									
Chamilaki	Eleni	117										
Charalampopoulou	Vasiliki	583										
Charatsis	Kostas	474	476									
Chatzaras	Vasileios	188										
Chatzicharalampous	Elissavet	615										
Chatzigogos	Nikolaos	631	703									
Chatzigogos	Theodoros	703										
Chatzipetros	Alexandros	693	198	172	174							
Chatzipetros	Alexandros											
Chatzis	Nikoloas	211										
Chatzopoulos	Georgios	283										
Cheilaris	Sophia	108										
Chen	Fulong	738										
Chioti	Eleni-Maria	366										
Chitoglou	Krystallia	480										
Chondraki	Vasileia	45	591									
Chorozoglou	Dimitris	241	224	230								
Chousianitis	Konstantinos	275										
Christanis	Kimon	342										
Christaras	Vassilios	703										
Christidis	Georgios	336	376									
Christodoulou	Dimitris	587										
Christoforidis	Christoforos	43										
Chronakis	Michael	428										
Console	Rodolfo	220	228	232								
Contadakis	Michael	544										
Corselli	Cesare	95										
Csörghe-Andó	Anita	685										
Cundy	Andrew	497										
Cvetkoska	Aleksandra	73										
Dadashzadehahari	Hooman	338										
Dafnis	Pavlos	159										
D'Alessandro	Walter	324	330	332								
Damoulianou	Maria-Elli	384										
Danamos	George	661										
Danelian	Taniel	34										
Darlas	Andreas	484										
Dasenakis	Manos	65										
Daskalaki	Filio	362	364									
Daskalopoulou	Kyriaki	324	330	332								
Dassenakis	Manos	399										
Delagas	Michalis	152										
Deligiannakis	Georgios	159	754	562	570							
Delipetrou	Pinelopi	789										
Demetriades	Alecos	405	407	409	411							
Depountis	Nikolaos	623	641	651								
Dewez	Thomas	576										
Diakakis	Michalis	570	572	661								
Diamantis	Konstantinos	627										
Diamantopoulou	Georgia	778										
Dietrich	Volker	217										
Dilalos	Spyridon	550	464	789	203	491						
Dimakopoulos	Georgios	49										
Dimitriadis	Sarantis	294										
Dimitriou	A	703										
Dimiza	Margarita	43	47	65	79	81	83	87	95	101	103	108
Dimopoulos	Nikolaos	125										
Dimou	Vasiliki-Grigoria	47	83									
Dimoudi	Argyro	529										
Diz	Paula	73										
Djiba	Aliou	316										
Doani	Sofia	470										
Doğan Külahcı	Güllü Deniz	320										
Doulgeris	Charis	619										
Douvalis	Alexios	451										
Doxa	Chrysa	170										
Drakoulis	Alexandros	350										
Drinia	Hara	691	139	141	105	24	719	723	699	725		
Dura	Ana	594	428									
Durand	Virginie	190										
Economou	George	484	354									
Efraimidou	Stella	458										

Efstathiadou	Despoina	605					
Efstathiou	Angeliki	222					
El Ajouz	Konstantinos Zouher	572					
El Bassiony	Ahmed	524					
Eleni	Koutsopoulou	388					
Elias	Panagiotis	255	580				
Elkamali	Muhagir	763	765				
Emmanouilidis	Alexandros	51	123	127	129		
Ermidou	Aikaterini	659					
Etiope	Giuseppe	587					
Evageopoulos	Vasileios	529					
Evangelidis	Christos	275					
Evelpidou	Niki	488	511	515	517	519	521
Everest	Jeremy D.	73	75				
Evgenakis	Manolis	43					
Ezat	Eleftheria	572					
Faka	Antigoni	499					
Farmakis	Ioannis	736					
Fassoulas	Charalampos	689	706				
Fatourou	Eugenia	108					
Faucher	Agathe	194	157				
Fellachidou	Kyriaki	458	462				
Filipov	Petyo	32					
Filippaki	Eleni	91	166	93			
Filippidis	Anestis	298	314	328	340	344	
Filippidis	Sokratis	703					
Filis	Panagiotis	63					
Filis	Christos	657	661	564			
Finch	Adrian	314					
Fitros	Michalis	358					
Forenza	Giuseppe	577					
Fouache	Eric	45					
Foumelis	Michael	575	576				
Fountopoulou	Marisa	723					
Foutrakis	Panagiotis	147					
Francke	Alex	41					
Frey	Eberhard	69					
Fylaktos	Asimakis	757					
Gaga		352					
Gagliano	Antonina Lisa	300					
Gaitanaros	George	478					
Gaki-Papanastassiou	Kalliopi	497					
Galanaki	Elissavet	715					
Galanakis	Dimitrios	143					
Galanidou	Nena	79					
Galanopoulos	Evangelos	484					
Galetakis	Michail	776					
Gallousi	Christina	497	655				
Gamaletsos	Platon	328					
Ganas	Athanassios	728	732	275	253	578	580
Garantzioti	Paraskevi	503	513				
Garcia-Guinea	Javier	292	668				
Gartzos	Efthimios	217					
Gatsou	Maria	587					
Gavrilidou	Elisavet	625					
Gemeni	Vasiliki	424	535				
Georgakopoulos	Andreas	531					
Georgakopoulos	Argyris	572					
Georghiou	Kyriacos	789					
Georgiou	Sofia	43					
Georgiou	Katerina	725					
Georgoulas	Eleftherios	125					
Geraga	Maria	346	73	75	77		
Gerogiannis	Nikolaos	188					
Giannakea	Artemis Maria	653					
Giannakopoulou	Panagiota P.	372	645	647	649	378	
Gianni	Eleni	342					
Giannikopoulou	Aikaterini	517					
Gianniou	Constantina	384					
Giannopoulos	Vassilios	740					
Giaourtsakis	Ioannis	49					
Giaourtsakis	Ioannis	61	63				
Gilles	Chloé	762					
Giouri	Katerina	430	376				
Giovenzana	Francesca	95					
Gkamaletsos	Platon	314					
Gkaniatsa	Georgia	99					
Gkeme	Anastasia	30					
Gkoutzioupa	Konstantina	366					
Godelitsa	Athanasios	432	314	328	428	451	390
Gogou	Marilia	552	566				
Gogou	Alexandra	65	77	101			
Gondikas	Andreas	594	428	432			
Gorini	Christian	161					
Gougoustamos	Ioannis	756	757				
Gouliotis	Leonidas	205	165	168			

Gramba	Alexia	721									
Grasset	Laurent	30									
Grendas	Nikolaos	732									
Grendas	Ioannis	215									
Grieco	Giovanni	449									
Grieco	Giovanni	451	453	390							
Grigoryan	G.	34									
Griva	Diamantina	499	509								
Gueydan	Frédéric	194	157								
Guy	Franck	30									
Guzzonato	Eric	762									
Hadjiefthymiades	Stathes	271									
Halupka	Gábor	685									
Hannington	Mark	592	594								
Harzhauser	Mathias	24									
Hassellov	Martin	428									
Hatakka	Tarja	401	403								
Hatzidimitriou	Panagiotis	215									
Hatzipanagiotou	Konstantin	647	378								
Hauzenberger	Christoph	445									
Hedley	Ian	472									
Heinath	Verena	592									
Hengesh	James	159									
Hermides	Demetrios	633	659								
Hernandez	Pablo	527									
Hollender	Fabrice	215									
Holm	Anja Lisa	360									
Ilia	Ioanna	778									
Iliopoulos	George	456	39	49	53	55	57	59	69	125	89	706
Iliopoulos	Ioannis	334	137	370	374	382	501					
Iliopoulos	Aggelos	230									
Ioakeim	Chrysanthi	489									
Ioakeimidis	Ioakeim	531									
Ioannou	Dafni	415									
Ioannou	Theodora	687	666	292	668	529					
Iordanou	Alexandros	474	476								
Jang	Yirang	447									
Johnson	Christopher	409									
Jolivet	Marc	157									
Jorrisen	Frans J.	35									
Kaberi	Helen	346									
Kafousia	Nefeli	114									
Kaitantzian	Agavni	734									
Kaklis	Triantafillos	663									
Kakonas	Andreas	511									
Kakouris	Iraklis	562									
Kalaitzidis	Stavros	342	384								
Kalamatianou	Efi	757									
Kalampaliki	Theodora	428	432								
Kallithrakas-Kontos	Nikolaos	503									
Kalogeras	Ioannis	213									
Kalogeropoulos	Kleomenis	782									
Kalpogiannaki	Maria	645	647								
Kalyvas	Georgios	415									
Kampouridis	Panagiotis	39	49	63							
Kampouroglou	Evdokia	422									
Kanellopoulos	Christos	334									
Kantiranis	Nikolaos	113	328	340	531	344	430	392	394		
Kapageridis	Ioannis	666	768								
Kapetanidis	Vasileios	237	259	265	267	269	271	249	285	287	289
Kapsimalis	Vasilios	45	591	119	515	521					
Karadimou	Georgia	762	85								
Karakaisis	George	279									
Karakitsios	Vasileios	114	139	143							
Karakonstantis	Andreas	267	249	285	287	289					
Karakosta	Anastasia	466	468								
Karakostas	Vassilis	220	239	241	228	232	243	245			
Karakostas	George	474	476								
Karakostas	Christos	211									
Karalemas	Nikolaos	661									
Karalis	Sotirios	474	476	554	499						
Karamani	Panagiota	699									
Karamitros	Ioannis	275									
Karampetsou	Eleftheria	422									
Karanika	Konstantina	53									
Karanikolas	Dimitris	89									
Karantanellis	Efstratios	730	736	742	744	746	748	759			
Karapanos	Dimitrios	539									
Karathanassi	Vasileia	770									
Karathanou Nicholaidi	Michaela Maria	615									
Karatsolis	Boris-Theophanis	87									
Karavoltsos	Sotirios	399									
Karen	Seymour St.	388									
Karetou	Athanasia	430	376								
Kargopoulos	Nikolaos	39	49	63							
Kargopoulou	Nikoleta	466	468								

Karimbalis	Efthimios	554								
Karkalis	Christos	442								
Karkani	Eleana	517								
Karmis	Petros	205								
Karountzou	Georgia	370								
Karoutsos	Panagiotis	456								
Karymbalis	Efthymios	474	476	556	497	499	509	511		
Kasama	Takeshi	314								
Kasinos	Andreas	453								
Kassaras	Ioannis	267	269	271	249	560	287	289		
Kati	Marianna	113	366							
Katopodis	George	717								
Katsara	Anthi	316								
Katsetsiadou	Katerina Navsika	552								
Katsigera	Anna	103								
Kaviris	George	237	259	261	263	265	267	249	251	287
Kavoura	Katerina	641								
Kawasaki	Satoru	519								
Kazakis	Nerantzis	625								
Kazana	Stavroula	738	637							
Kazantzaki	Maria	93	91	166						
Kazantzidou-Firtinidou	Danai	271								
Kazili	Maria	662								
Kazilis	Nikolaos	662								
Keith	Manuel	436								
Kelepertzis	Efstratios	399	434							
Kelessis	Apostolos	787								
Kementzetzidou	Despina	273								
Kilias	Adamantios	153	436							
Kim	Soujung	447								
Kiomourtzi	Paschalia	531								
Kipourou-Panagiotou	Afroditi	392								
Kiratzi	Anastasia	279								
Kirdis	Stamatis	63								
Kkallas	Charalampos	207	211							
Klemme	Stephan	360								
Klitorakis	Charalampos	386								
Kokkalas	Sotirios	358	447	541						
Kokkaliari	Maria	137	374	382	388					
Kokotini	Marianna	39								
Kolendrianou	Maria	57								
Koletsis	Ioannis	715								
Koliadimou	Kalliopi	470								
Kollias	Konstantinos	422								
Kolokoussis	Polychronis	770								
Komi	Apostolia	519	521							
Kondopoulou	Despina	198								
Konidaris	George	28								
Konon	Agnieszka	397								
Konsolaki	Aliki	740								
Konstantinidis	Ioakeim	742								
Kontakiotis	George	114	139	141	99	105	143	147	106	
Kontakos	Kiriakos	275								
Kontogianni	Villy	607	609							
Kontokostas	George	723								
Kontopoulos	Christos	583								
Kontopoulos	Nikolaos	55								
Kontostavlos	Giorgios	740								
Kordella	Stavroula	587								
Korkmaz	Aslıhan	320								
Koroneos	Antonios	350	392	368						
Koskeridou	Efterpi	139	141	24	106	717				
Kosmidou	Vasiliki	131	161	133						
Kostis	Andreas	141								
Kostoglou	Anastasios	239	241	245						
Kostopoulos	Dimitris	28	30							
Kostopoulou	Sofia	55	121							
Kostopoulou	Vassiliki	21								
Kotroni	Vassiliki	715								
Koufos	George	28	30	37						
Koukousioura	Olga	43	45	47	83	85	103			
Koukouvelas	Ioannis	55	558	750						
Koukouza	Konstantina	380	444	424	738	535	637	539		
Kouli	Katerina	41	348	65	73	75	85			
Koumoutsakou	Olga	149								
Koumoutsea	Ioanna	63								
Kourgia	Paraskevi-Maria	420								
Kourliaftis	Giannis	119								
Kourouklas	Christos	228	230							
Kouskouna	Vassiliki	261	263							
Koutroumbas	Konstantinos	766								
Koutsopoulou	Eleni	356	519							
Koutsovitis	Petros	442	444	539						
Kozanoglou	Caterina	77								
Kranis	Haralambos	170	179	196	251	550	661			
Krassakis	Pavlos	424	738	637	757					

Kritikou	C.	759										
Ktenidou	Olga-Joan	213										
Kuells	Christopher	621										
Kwon	Sanghoon	447										
Kynigopoulou	Zoi	30										
Kyriakopoulos	Konstantinos	484	486	217								
Kyriakoulis	Ioannis	106										
Kyrikou	Styliani	41										
Kyriou	Aggeliki	750										
Ladenberger	Anna	405	407	409								
Lagaria	Anna	87										
Lagios	Evangelos	209	281	217								
Lagouvardos	Kostas	715										
Lampropoulou	Paraskevi	649	378									
Lange	Sabine	592										
Laperche	Valérie	413										
Lappos	Sokratis	625										
Lazaratou	Christina Vasiliki	617										
Lazaridis	Georgios	318	456	458	460	462	670	466	468	480		
Lazaridis	Stilianos	392										
Lazos	Ilias	198	172	174	176							
Le Maitre	Anne	30										
Leicher	Niclas	41										
Lekkas	Efthymis	550	552	738	564	657	256	566	568	570	661	507
Lekkas	Spyridon	178										
Lemiere	Bruno	413										
Leonardi	Marco	575										
Less	Gyorgy	47										
Li Vigni	Lorenza	324	330	332								
Liakopoulos	Alexandros	411	413									
Liakopoulos	Spyros	275										
Liakopoulou	Dionysia	97										
Liakoura	K.	784										
Lialiaris	Ioannis	564	661									
Lianou	Vasiliki	99										
Liapi	Eleni	89										
Liapis	Ioannis	497										
Ligkovanlis	Stefanos	57										
Lin	Aiming	166										
Litoseliti	Aspasia	558										
Livas	Agis	113										
Loukidis	Dimitrios	655										
Loukidis	Nikolaos	655										
Loukola-Ruskeeniemi	Kirsti	401										
Louloudis	George	611										
Loupasakis	Constantinos	615	584	734	756							
Louvaris	Kostas	725										
Lozios	Stylianos	564	586	661	723							
Lykakis	Nikolaos	537										
Lymperis	Evriviades	159										
Lymperis	Efstathios	746										
Lyras	Georgios	714	717	721								
Magganas	Andreas	442	444									
Maggini	Massimiliano	183	631	703								
Makri	Kyriaki	715										
Makri	Panayota	659										
Makrodimitras	Georgios	131	133	163								
Makropoulos	Kostas	237	259									
Malinverno	Elisa	87	95	101								
Mallinis	George	661										
Mallouchou	Myrto	110										
Manakos	Antonis	505										
Mangira	Ourania	239	230	232	243							
Maniakas	Ioannis	57										
Maniatakis	Charilaos	583										
Manoukian	Eleonora	539										
Manoutsoglou	Emmanouil	503	513									
Mantzouka	Dimitra	24										
Marantos	Ioannis	336										
Maravelis	Aggelos	117	121									
Margaris	Basil	279										
Margariti	Eirini	110										
Marinaro	Giuditta	587										
Marinos	Vassilios	605	730	732	736	742	744	746	748	752	759	
Mariolakos	Ilias	717										
Marion de Procé	Solène	45										
Marmarinos	Konstantinos	719										
Maroufidis	Constantinos	734										
Maroukian	Hampik	497										
Maroulakis	Spiros	596										
Martin	Tony	524										
Martinez-Garzon	Patricia	190										
Mason	Jack	754										
Massas	Ioannis	415										
Mattas	Christos	663										
Mavridis	Fanis	484										

Mavrogonatos	Constantinos	316	334						
Mavroulis	Spyridon	564	256	566	568	661			
Mazarakis	Konstantinos	627							
McCorquodale	Mark	791							
McNeill	Lisa C.	73	75						
Mechernich	Silke	754							
Megremi	Ifigeneia	399	334						
Melfos	Vassilios	312	322	176					
Merceron	Gildas	30							
Merle	Didier	106							
Mertzimekis	Theodoros	428	594						
Messaris	Gerasimos	51							
Miaritis	Kostantinos	65							
Michailidis	Dimitrios	39							
Michailidis	Ioannis	43	83	108					
Michailidis	Kleopas	426							
Michailidou	Eleni	376	394						
Michalaki	Katerina	560							
Michalopoulou	Maria	641							
Michas	Georgios	247	234	75					
Migiros	George	81							
Mikellidou	Ioulietta	67							
Milker	Yvonne	35							
Millas	Christos	237	259						
Mina	Rozalia	586							
Mindszenty	Andrea	693							
Misaelides	Panagiotis	328	340						
Misailidis	Ioannis	261	263						
Misthos	Loukas-Moysis	556							
Mitiglaki	Christina	344							
Mitrakas	Manasis	449	453						
Mitropoulos	Dimitrios	791	596						
Mitsika	Georgia S.	550	464	789	491				
Moforis	Leonidas	143							
Mora	Brice	762							
Moraiti	Evgenia	697	706	701	703	181			
Mortyn	Graham P.	139	105						
Moshou	Alexandra	580							
Mouzoulas	George	623							
Mpotziolis	Chrysanthos	121							
Murru	Maura	220	228	232					
Mylonas	Anastasios	653							
Mytiglaki	Christina	340							
Nanou	Eleni Anna	653							
Nastos	Panagiotis T.	789	712						
Navrozidou	Valentini	83							
Negrel	Philippe	405	407						
Nifora	Despoina	342							
Nikitas	Anastasios	108							
Nikolakakis	Emanouel	689							
Nikolakopoulos	Konstantinos	558	750						
Nikolaou	Nikolaos	607							
Nikolaou	Konstantinos	165	205						
Nikolopoulos	Athanasios	721							
Nishiwaki	Takafumi	166							
Nizamuddin	Syed	541							
Nodarou	Eleni	482	501						
Noli	Fotini	340							
Nomikou	Paraskevi	592	591	687	594	428	79	432	436
Ntaflos	Theodoros	444	445						
Ntokos	Dimitrios	155							
Ntokou	Panagiota	155							
Ntona	Maria-Margarita	625							
Ntzanis	Epameinondas	51							
Oflaz	Sabire Asli	73							
Ogala	Jude Etunimonuwa	342							
Oikonomidou	Ioanna	776							
Oikonomopoulos	Konstantinos	163							
Onuzi	Kujtim	445							
Pacini	Fabrizio	575							
Pagona	Evagelia	449	453						
Paipoutlidi	Katerina	336							
Palazzo	Francesco	762							
Pallikarakis	Aggelos	81							
Panagiaris	George	699							
Panagiotara	Eleni Maria	342							
Panagiotaras	Dionisios	129							
Panagiotopoulos	Konstantinos	41	73	75					
Panagiotopoulos	Ioannis	101							
Panagopoulos	Andreas	619	621						
Panagopoulos	George	205	165						
Panagopoulos	Anestis	159							
Panou	Areti	273							
Pantazi	Eleanna	501							
Papadatos	Yiannis	491							
Papadias	Evaggelos	782							

Papadimitriou	Panayotis	237	259	265	267	271	249	285	287	289		
Papadimitriou	Eleftheria	220	239	241	224	226	228	230	232	243	245	
Papadimitriou	Nikolas	161	163									
Papadopoulos	Ilias	717	283									
Papadopoulos	Gerasimos	507										
Papadopoulos	Argyrios	449	328	451	453	392						
Papadopoulou	Lambrini	113	300	312	318	322	440	350	368	430	376	394
Papadopoulou	Penelope	53	59									
Papadopoulou	Theodora	575										
Papageorgiou	Elena	576										
Papagkikas	Konstantinos	316										
Papaioannou	Alexandros	65										
Papaioannou	Christos	211										
Papalambrou	Sotiris	493										
Papanastassiou	Dimitris	497										
Papanikolaou	Ioannis	159	79	81	754	562						
Papanikolaou	Dimitrios	71	79									
Papanikolaou	Georgios	503										
Papastergios	Georgios	787										
Papathanasiou	George	732	736	752	603	728	605					
Papatheodorou	George	77	587									
Papatsikourakis	Dimitrios	631										
Papazachos	Costas	207	211									
Papazotos	Panagiotis	639	780	364								
Papoulis	Dimitrios	617	342	356								
Pappa	Filothei	310										
Pappa	Irena	69										
Paradisopoulou	Parthena	273										
Paraschos	Francesca	346										
Paraskevopoulos-Tsiakiris	Fotios	748										
Parcharidis	Issaak	766	734	738	756	586	509	757				
Paresoglou	Nikolaos	675										
Parinos	Constantine	65	77	101								
Partheniou	Eleni	253										
Pasadakis	Nikolaos	117										
Paschos	Panagiotis	706										
Pasieczna	Anna	397										
Patruno	Stefano	67										
Pavlides	Spyros	168	172	174	198	603						
Pavlopoulos	Kosmas	45	103									
Pavlou	Kyriaki	249	281	285	287	289						
Pechlivanidou	Sofia	75										
Pehlivanides	George	717										
Perakis	Evangelos	689										
Perdikaris	Konstantinos	653										
Perdikatsis	Vasileios	336										
Perez	Ruben	527										
Pergantis	Spiros	428										
Peridis	Savvas	125										
Periferakis	Argyrios	671	673	675	677	679	681					
Perissoratis	Constantine	548										
Perraki	Maria	639	780	362	364							
Petersen	Sven	592	594									
Petika	Eftychia	322										
Petrakis	Manolis	491	591									
Petropoulos	Alexandros	515	521									
Petropoulou	Melina Kondylia	653										
Petrounias	Petros	372	645	647	649	378						
Peyron	Odile	41										
Pfanz	Hardy	332										
Phillips	Marcie Purkey	73										
Photiades	Adonis	20	354									
Pikridas	Christos	198	172	176								
Pisinaras	Vasilios	619										
Plastiras	Chris-Alexander	30										
Plessas	Spyros	717										
Plessa-Valadaki	Aikaterini	717										
Polidorou	Miltiadis	488										
Pollatou	Aikaterini-Maria	482										
Polychroni	Iliana	780										
Polymenakou	Paraskevi	436										
Pomoni-Papaioannou	Fotini	21	47									
Pomonis	Antonis	263										
Pomonis	Panagiotis	647	635									
Pontikes	Yiannis	314										
Popoola	Olatunde Isaiah	201										
Potamousis	Stylianos	419										
Poulos	Serafim	119	495	521	591							
Prevedouros	Ioannis	127										
Proßegger	Peter	445										
Provost	Floriane	575										
Psaltakis	Giannis	740										
Psarra	Stella	87										
Psarras	Christos	106	717									
Psomiadis	Emmanouil	613										
Psychogiou	Maria	659	725									

Pyrgaki	Konstantina	399	419	424				
Raicheva	Raia	32						
Ramadani	Maria	384						
Rassios	Anne	451	439					
Ravani	Alexandra	87						
Reicherter	Klaus	35	81	754				
Reimann	Clemens	405	407					
Reingruber	Agathe	505						
Rémondière	Sylvie	762						
Rice	Alexander Hugh	445						
Riller	Ulrich	35						
Rizza	Magali	486						
Rogkala	Aikaterini	372	645	647	649	378		
Rondoyanni	Theodora	93						
Rothenbeck	Marcel	592						
Roufi	Amalia	495						
Roumpos	C.	784						
Rousakis	Grigorios	77	537					
Roussiakis	Socrates	49	39	61	63	97		
Rovithis	Emmanouel	211						
Sabatakakis	Nicholas	623	641	651				
Sadeghi	Martiya	405	407					
Saitis	Giannis	488	519					
Sakelariou	Dimitrios	537	192	346	194	489	196	
Sakellariou	Nikolaos	261	263					
Sakkas	Georgios	261	263	271				
Sakkas	Vassilis	209	281	217	253	170		
Salomidi	Maria	517						
Salonikios	Thomas	589						
Samios	Michalis	275						
Sampatakakis	Panagiotis	637						
Saroglou	Charalampos	583						
Savini	Alessandra	95						
Schmiedl	Gerhard	35						
Schneiderwind	Sascha	754						
Scordilis	Emmanuel	544						
Seferlis	Miltiadis	83	43					
Sergiou	Spyros	346	75					
Sharkov	Evgenii	546						
Shillington	Donna S.	73	75					
Shrimpton	Kevin	524						
Sideridis	Alkiviadis	440						
Skampa	Elisavet	101						
Skandalos	Panagiotis	39	63					
Skilodimou	Hariklia	478						
Sklavounou	Stamatina	63						
Skliros	Vasilios	362	364					
Sklodimou	Hariklia	493						
Skordas	Konstantinos	619						
Skoulikidis	Nikolaos	717						
Skourtsos	Emmanuel	564	657	661	178	179		
Skovolas	S.	168						
Šmejkalová	Tereza	762						
Smith	Daniel	436						
Smyrnaiou	Zacharoula	710	721					
Sofianska	Emilia	352	426					
Sofis	Nikolaos	384						
Sokos	Eftimios	275						
Soldatos	Triantafyllos	350	368					
Sotiriadis	Ioannis	285						
Souglakos	Nikolaos	491						
Soukis	Konstantinos	564	586					
Soulios	Georgios	663						
Soultana	Athanasia	776						
Spanidis	P.-M.	784						
Spanou	Natalia	607						
Spanoudakis	Nikolaos	503	513					
Spastra	Yiota	577						
Spingos	Ioannis	237	259	267	249	251	285	287	289
Spry	Paul G.	316						
Spyrakos	Constantine	583						
Spyrou	Nafsika-Ioanna	564	570					
Stamatakis	Michael	348	635	380	386			
Stamatiadis	Aristeidis	368						
Stamatis	Georgios	613	621	633				
Stamatis	Panagiotis	384						
Stamoulis	Kostas	486						
Stanota	Eirini-Spyridoula	256	570					
Staridas	Spyridon	689	697					
Stathopoulos	Nick	611						
Stathopoulou	Aikaterini	537						
Stathopoulou	Elizabeth	110						
Stauropoulou	Chrysanthi	117						
Stavrakakis	Spyros	101						
Stefouli	Marianthi	637						
Stergiou	Christos	430	376	693	176			

Stergiou	Vasiliki	378														
Stiros	Stathis	186	609													
Stouraiti	Christina	422														
Sulpizio	Roberto	486														
Svorligkou	Georgia	39	49	61	63											
Sykioti	Olga	766	772													
Syrides	Georgios	47	85													
Tarenidis		352														
Tarvainen	Timo	401	403	407												
Tassiou	Sofia	411														
Tatar Erkül	Sibel	320														
Telbisz	Tamás	693														
Tema	Evdokia	472														
Theodor	Marc	35														
Theodorakatou	Dimitra	271														
Theodorakopoulou	Katerina	484	486													
Theodorou	Georgios	39	49	63												
Theodoulidis	Nikolaos	215														
Thivaiou	Danae	24	717													
Titschack	Jürgen	35														
Tokmaktsi	Eleni	89														
Tolmács	Daniella	417														
Tombros	Stylianos Fotios	358	388													
Tompolidi	Athanasia-Maria	766														
Toufexis	Georgios	505														
Tourlakidis	Christos	757														
Triantafyllidis	Stavros	302	304	306	308	310										
Triantafyllou	Ioanna	507														
Triantaphyllidou	Irene Eva	617														
Triantaphyllou	Maria	43	45	47	65	67	71	77	79	81	83	87	95	101	103	108
Triebe	Lars	592														
Trikalinou	Georgia	196														
Tripolitsiotou	Fani	691														
Tripsanas	Efthymios	537														
Tsafaras	Spyros	717														
Tsagas	Dimitrios	354														
Tsakalos	Evangelos	91	166	93												
Tsakiridis	Petros	362	364													
Tsaklidis	George	226														
Tsampa	Areti	774														
Tsampouraki-Kraounaki	Konstantina	192														
Tsanakas	Konstantinos	556	497													
Tsangaratos	Paraskeyas	615	774													
Tsiambaos	George	599														
Tsikouras	Basilios	440	647													
Tsirambides	Ananias	296	298	531	344											
Tsironi	Varvara	580														
Tsitsanis	Pavlos	440														
Tsodoulos	Ioannis	556	497	499	655											
Tsolis-Katagas	Panagiota	356														
Tsoni	Maria	53	55	59	89											
Tsoukalas	Nikolaos	63														
Tsourlos	Panagiotis	205	629													
Tsourou	Theodora	95	34	24	108											
Turkmen	Taylan	190														
Tzamos	Evangelos	449	451	453	390											
Tzampoglou	Ploutarchos	584														
Tzanis	Andreas	222	209	277	170											
Tzedakis	Chronis	79														
Tzelepi	Efi	470														
Tzifas	Ioannis	314	328													
Tziritis	Evangelos	619	621	453												
Tzortzi	Marianthi	57														
Tzortzopoulou	Maria	108														
Tzoumaka	Paraskevi	787														
Tzouxanioti	Maria	263														
Unkel	Ingmar	123														
Vachard	D.	34														
Vakalas	Ioannis	596	655	25												
Valavanis	Panos	491														
Valiakos	Ilias	695	696													
Valkaniotis	Sotiris	603	728	732	578	580	168	505								
Vallianatos	Filippos	247	234	283												
Valsamidis	Theophilos	770														
Vandarakis	Dimitrios	119	45	591												
Vardali	Anastasia	503														
Varesis	Alexandros	145														
Vargemezis	George	205	629													
Varol	Elif	320														
Vasilatos	Charalampos	326	635	380												
Vasileiadou	Agapi	529														
Vasileiou	Anthoula	776														
Vasileiou	Eleni	639	780													
Vasiliadis	Georgios	243														
Vassilakis	Emmanuel	730	712	119	772	740	635	495	661							
Vassilopoulou	Spiridoula	271	281													

Vassou	Athanasia	744				
Vavelidis	Michael	430	376	394		
Vavlas	Nikos	279				
Vavouranakis	George	491				
Vayenas	Dimitrios	617				
Vega	Sandra	541				
Ventouzi	Chrisanthi	207				
Veranis	Nikos	663				
Vlachopoulos	Nikolaos	683				
Vlachos	Evangelos	69				
Vogiatzis	Dimitris	703				
Voudouri	Maria-Olga	318				
Voudouris	Panagiotis	316	683			
Voudouris	Konstantinos	424	625	629		
Voudouris	Panagiotis	366	176			
Vougioukalakis	George	334				
Voulanas	Dimitrios	460				
Voulgaris	Nicholas	237	259			
Voulgaris	Gerasimos	556				
Voulgaris	Nicholaos	249	491	564	287	
Vouvalidis	Konstantinos	470	85			
Vretzaki	Eleni	717				
Vrouhakis	Ioannis	621				
Vythoulkas	Konstantinos	348				
Wagner	Bern	41				
Weinkauf	Manuel F. G.	35				
Wenzlaff	Emanuel	592				
Westbrook	Christopher	791				
Wiatr	Thomas	754				
Wind	Sandra	592				
Wysocka	Irena	397				
Xanthopoulou	Vayia	370				
Xenaki	Spyridoula	766				
Xenidis	Anthimos	390				
Xirokostas		352				
Xypolias	Paris	188				
Yousefi	Fazilat	300				
Zafeirakopoulou	Effrosyni	687				
Zafeiriou	Ioannis	415				
Zagana	Eleni	653				
Zambetakis-Lekkas	Alexandra	34	21	724		
Zampakis	Petros	51				
Zananiri	Irene	596	697	25		
Zarkogiannis	Stergios	105	721			
Zaxariadis	Dinitrios	633				
Zegkinoglou	Nikolaos	436				
Zelilidis	Avraam	117	121	125	135	137
Zerva	Dimitra	629				
Zervopoulou	Anna	174				
Zidianakis	Giannis	89				
Zimbidis	Alexandros	562				
Zimianitis	Vaggelis	596				
Zoras	Stamatios	529				
Zotiadis	Vassilis	348				
Zouboulis	Anastasios	449	453	390		
Zouros	Nikolaos	292	668	695	696	706
Zygouri	Vasiliki	558				



ΕΓΕ 2019

15th International Congress of the Geological Society of Greece

Athens, 22-24 May 2019

EXPLORING AND PROTECTING OUR LIVING PLANET EARTH

15th International Congress

Athens
22-24 May 2019
Harokopio University

of the Geological Society of Greece

ORGANIZER:

National and Kapodistrian University of Athens

Co-ORGANIZERS

Harokopio University of Athens

Geotechnical Chamber of Greece

www.gsg2019.gr